SPRINGER
REFERENCE

PHILIPPE HUMBERT
FERIAL FANIAN
HOWARD I. MAIBACH
PIERRE AGACHE
EDITORS

Agache's Measuring the Skin

Non-invasive Investigations, Physiology, Normal Constants

Second Edition

Springer

Agache's Measuring the Skin

Philippe Humbert • Ferial Fanian
Howard I. Maibach • Pierre Agache
Editors

Agache's Measuring the Skin

Non-invasive Investigations, Physiology, Normal Constants

Second Edition

With 644 Figures and 157 Tables

Springer

Editors

Philippe Humbert
Department of Dermatology
University Hospital of Besançon
Besançon, France

Ferial Fanian
Center for Study and Research on the Integuments
Department of Dermatology
University Hospital of Besançon
Besançon, France

Howard I. Maibach
Department of Dermatology
School of Medicine
University of California
San Francisco, CA, USA

Pierre Agache (deceased)
Department of Dermatology
University Hospital of Besançon
Besançon, France

The original French edition Physiologie de la peau et explorations fonctionnelles cutanées was published by Editions Médicales Internationales, Paris, 2000

ISBN 978-3-319-32381-7 ISBN 978-3-319-32383-1 (eBook)
ISBN 978-3-319-32382-4 (print and electronic bundle)
DOI 10.1007/978-3-319-32383-1

Library of Congress Control Number: 2016958724

Printed on acid-free paper

This Springer imprint is published by Springer Nature
The registered company is Springer International Publishing AG
The registered company address is: Gewerbestrasse 11, 6330 Cham, Switzerland

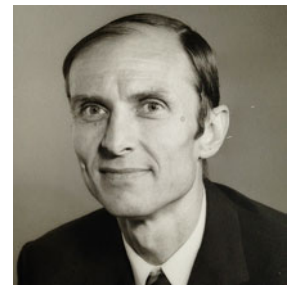

"This textbook is dedicated to the memory of its creator, Professor Pierre Agache, whose fingerprints are visible in every page".

Foreword

We live in a world of rapidly increasing information. The journalists and academicians often speak about this in a negative sense – utilizing the word "overload."

Many readers understand the overload phenomena and its impact on their daily life and work. Few of us can master the rapidly increasing data of the Information Age.

The Googles of the universe have aided us greatly in dealing with information overload.

It is divided into the pre- and post-computer age and has been expedited greatly by electronic searching and indexing. The Google world is attempting to ameliorate unmet need-indexing and electronic availability of the world's book collections.

In spite of all of these electronic advances and aids, we remain indebted to the rare scholar – in this case the late Pierre Agache – for his seminal contributions in the previous edition of this book.

Professor Agache was a dedicated, thoughtful, and disciplined scholar – making the previous edition one of the most valuable reference textbooks for anybody working in the dermatologic space, including the skin, hair, nails, and their other organ involvements.

This edition builds upon the work of Pierre's work.

We have in this edition – the current edition – a technology that Pierre did not have available.

The Springer organization has arranged so that this book will be updated – almost on a daily basis – when needed. The reader is now able to get updates in both electronic and print-on-demand versions.

We greatly appreciate the creativity and assistance of Dr. S. Klemp for making this available. We also thank the Springer team for their skilled assistance in their editorial process.

Your editors appreciate corrections and suggestions and can be readily reached by email and telephone.

Howard I. Maibach

Preface

Measuring the Skin: A New Look in Dermatology

Measuring the skin succeeds now to looking at the skin or inspecting the skin.

Many clinicians limited their diagnosis in dermatology on the only description of skin signs and skin lesions. The fundamental functions of the skin were not considered except through the aspect of the skin. For example, loss of barrier function was deducted of the dryness pattern of the skin. The development of cosmetology with new active ingredients which are enable to modify the skin physiology by targeting cell and their nucleus functions, has led the biometrologists to create the new instrumental devices to accurately assess the imperceptible modifications of the skin.

Since the skin is an organ which can be easily analyzed by looking, touching and smelling to evaluate some of its patterns such as roughness/smoothness, dryness/moisture, Stiffness/sagging, elasticity, extensibility, resistance, radiance/dullness, temperature and etc., it is now appreciated to be able to assess quantitative measurements, to visualize through the skin and inthe skin different structures such as dermis, vessels, appendages, etc.

The real development of methods to measure the skin took place during the 1970s. Indeed, in the last fifty years, the knowledge on the skin physiology and anatomy has been significantly developed in such a manner we are not able to imagine correctly the problems existed many years ago.

Up to these last years, histology remained the gold standard for morphological investigation of the skin, although biopsy may alter the original morphology. Advances in ultra-sound and optics provide nowadays a true in vivo analysis of the skin with precise and accurate signification, leading to the non-invasive optical biopsies. These progresses have many clinical applications in different fields of the medicine such as cancer diagnosis.

Thus a new semiology was born, requiring to be familiar with new patterns and signs. Healthy images at different anatomic sites as well as pathological data regularly appear in the field of biometrology, and need to be known by young researchers and dermatologists.

The data and images given by new technologies could be now available for the practitioners and physiologists which were reserved only to engineers and researchers in the past,. These methods give the possibility of repetitive histometric measurements of the same skin site.

Inflammatory diseases, blistering dermatosis and skin tumors are easily explored using new sophisticated methods, and the treatment effects can be evaluated. Since biometrology permits to follow the effects of such active principles, it is necessary to enter in the field of cutaneous pharmacology.

Another domain which interests the pharmacists, cosmeticians, doctors, researchers and also the people is skin aging. Indeed, skin appearance is changing with age, not only in terms of wrinkles and loss of elasticity, but also in terms of its moisture and radiance. Biometrological assessment allows to determine the mechanisms between intrinsic and extrinsic factors which are involved in skin aging process. The quality of the barrier function of the skin is assessed by numerous methods more and more sophisticated, allowing to have knowledges on the skin hydration in different levels. Further, new technologies such as RAMAN method helps to determine the qualitative and quantitative constitution of the skin; The non-invasive imaging technologies significantly improve the diagnosis and also clinical management of skin conditions while giving the dermatologist and closely related specialists, the new ways for assessing and exploring the skin in its unknown and invisible parts.

The aim of this new edition of Measuring the skin is to provide the doctor, the researcher, the cosmetician and all person who is involved in assessing the skin, with the tools and their usefulness to characterize the skin. In none of other field of medicine does such a book exist. Indeed, due to it superficial location and simple approach the skin is the target of every measure, every device, and all of its function have been explored. When written for the first time by Prof. Pierre Agache and myself in 2004, we didn't imagine at that time that a new edition will bring so many new information, and disclose so new fields of investigation.

This book has vocation to be the professional basic book of each of you, who wants to know how to characterize such skin property, and wants to know more on new skin physiology developments. In memory of my mentor, I am proud to follow him in this skin specialty he contributed to create and to develop.

Philippe Humbert

Acknowledgments

We would never have been able to finish this work without the help of our colleagues.

The authors would like to express their deepest gratitude to the persons listed below for their valuable help and support:

- Adeline Jeudy, Thomas Lihoreau, Sophie Mac-Mary, Jean-marie Sainthillier, Alexandre Guichard and Ahmed Elkhyat for their help to update the table of contents and the new authors according to the recent publications.
- Dr. Makan Rahshenas for his great help to carry out the correspondance with authors
- Isabelle Bruey for her assistance in bibliography
- Agnès Fontaine and Brigitte Boissenin for their precious help to organise the work meetings.
- Elisabeth Homassel for her valuable help in english translation of some chapters.
- Dr. Hui Xiaoying and Tita F. Reyes and other colleagues of Pr. Maibach in San Francisco who helped us a lot in updating process.
- Deep thanks to the Springer team who followed the redaction process patiently and efficiently.
- In memory of Pr. Xuemin Wang, Vice-Chairman of Shanghai Skin Disease Hospital, who has written two wonderful chapters on microbiology of the skin in this edition. Unfortunately he expired on February 2016 without having the opportunity to see the outcome.
- Special thanks to Mr. Emmanuel Leclerc, editorial director and Mrs. Sylvie Cortes, Edition Department assistant at « Lavoisier » editing house in Paris who dedicated the all legal autorisations to Springer for the upcoming edition of this textbook.
- Finally a no-name appreciation to all secretaries, colleagues, collaborators and medical and university staffs who helped the authors/co-authors during this long project.

Phillippe Humbert
Ferial Fanian
Howard I. Maibach

Introduction

Ferial Fanian

Readers of the previous edition of this book have relied on it to aid them in measuring all parameters of the skin through the appreciable work of Pierre Agache and Philippe Humbert. After the heart-rending death of Pierre Agache in 2003, the first edition was published on 2004 by Springer which was a modified complete translation of the french version edited by him and published in 2000 by Lavoisier (Physiologie de la peau et explorations fonctionnelles cutanées).

Unfortunately the second version was delayed according to several administrative reasons till I have been asked on 2011 to start this big project. Although it was a noticeable major job, it was my great honnor to work with the well known authors and also the two great editors, Howard Maibach and Philippe Humbert who always made me the fruitful suggestions and were my enthusiastic supporter through out this long project.

I would like to appreciate all of the respected authors and editors and also all of my friends and colleagues which are named in acknowledgment.

I would like to express my special thanks to Doctor Aude Agache, the esteemed daughter of Professor Agache who did kindly help the team to carry out all administrative steps successfully.

At the end, I would like to dedicate this work to my mother and father, Saeideh Bashirazami and Mohamadali Fanian, which are my first and permanent encouraging teachers to study more and more, to my dear Professors, Yahya Dowlati and Alireza Firooz who gave me the scientific view and motivated me always to go on even in the hard moments, and finally to my husband, Massoud Salari, who was always at my side cheering me up and supporting me through the happy and unhappy moments and also my son, Sepanta Salari, who understood patiently my busy time during this hard project.

Procedure

The table of the contents was modified in order to add the most updated technologies in skin physiology, biometrologie, biophysics, imaging and clinical scoring. The authors have been selected according to the most recent published articles in each field.

Comparing to the first edition with 84 chapters and 784 pages, this new edition contain 160 chapters and 1652 pages which can cover the most of the researchers' needs in this domain.

Fortunately, this volume has been selected to become part of the SpringerReference portfolio, which now comprises over 400 major reference works and almost 500,000 entries/chapters online. This means it will not only be a static printed book, but it will have a "living" update version online which is very important for this book because of its gadget like nature.

Contents

In the first section, we have considered an anatomic approach for the chapter titles : you will start with the surface of the skin and then you will go deeper by leafing the pages. Then you would discover the different measuring techniques according to the functional approach : Mechanical, Photoprotection and sensory function of the skin. Furtherly, you will find the standard scoring scales (which will be more completed for the next edition) and the book finishes with skin maps.

We have kept most of the precious chapters of Pierre Agache whose scientific value still remain intact even after 10 years.

All of the reader's precious comments are welcome.

On behalf of the editors, I would like to invite all of the researchers who are interested to introduce the new methods in the global domain of "Measuring the Skin", to contact the editors.

Contents

Volume 1

Volume 2

About the Editors

Philippe Humbert
Department of Dermatology
University Hospital of Besançon
Besançon, France

Professor Humbert has been elevated to the grade of Professor of University in 1993, at the age of 34 years. Specialist in Dermatology as well in internal Medicine, Allergology and clinical Immunology, and skin oncology, he performed a Ph.D. in cutaneous Pharmacology.

During his position of head of the Department of Dermatology in the University Hospital of Besançon from 1993 to 2015, he developed a clinical department with all the specialties of Dermatology, i.e., Allergology, Surgery, Laser, Internal Medicine, Oncology, pediatric Dermatology, Photobiology, Biometrology.

During the same period, he created the Laboratory of Cutaneous Biology in which news skin models are developed as well as cell cultures (keratinocytes, fibroblasts, melanocytes. . .) which are used as pharmacological models.

On a clinical point of view, he created the CERT (Center for Investigation and Research on the Skin) in which, with a team of engineers, doctors, pharmacists, technicians, he performss clinical studies for evaluation of cosmetics or drugs.

In this field of biometrology, he was elected as President of the ISBS (International Society for Bioengineering and Imaging of the Skin) from 2005 to 2010 (he organized indeed the International Meeting of ISBS in Besançon in 2009), as well as President of the International Society of Cutaneous Pharmacology. He was President of ESCAD in 2011.

His bibliography includes more than 350 publications and five books.

Professor Philippe Humbert received the Award of the French Society of Dermatology, of the French Society of Dermatological Research, as well the French Society of Cosmetology.

Known for his humanism and generosity, Professor Philippe Humbert welcomes many students or professors coming from abroad, and he was proud to contribute to teach six famous Chinese Professors. He collaborates with many universities over the world. Believing in the creativity of his students, he helped them to assess three innovative start ups in the domain of skin biometrology (Skinexigence^{R}), skin biology (Bioexigence^{R}), and skin pharmacology (Proviskin^{R}).

Student of Pr Agache, his Editor position is the way to honor his mentor, and to contribute to his artwork.

Ferial Fanian
Center for Study and Research on
the Integuments
Department of Dermatology
University Hospital of Besançon
Besançon, France

Ferial Fanian is a French-Persian dermatologist working in Research Centre of Department of Dermatology of Besançon, France (CERT). She has a remarkable experience on laser applications in dermatology while she was always working as a researcher in biometrology of the skin.

She is also familiar with optical Biopsy methods particularly with in vivo Confocal Microscopy and that is why she is the board member of ICNI group (Non-Invasive Cutaneous Imaging thematique Group) at French Society of Dermatology. She was working on melanocytes activity and morphology through her PhD thesis. She has also obtained two academic fellowship in « Laser and Cosmetic Dermatology » and also « Innovative Chronic Wound Healing » in 2012 and 2013 in France.

Actually, she is the reviewer or invited author for several English and French scientific journals in the field of dermatyology, aesthetic medicine and biometrology such as JEADV, Archives of Dermatology, Journal of Cosmetic Dermatology, Case Reports in Dermatological Medicine, Medical Staff Dermatologie, Réalités Thérapeutiques en Dermato-Vénérologie.

Research Interests
Advances and Emerging Techniques in Dermatology
Anti-Aging
Cosmetic Dermatology
Invasive and Non-Invasive Methods in Dermatology
Investigative Dermatology

Howard I. Maibach
Department of Dermatology
School of Medicine
University of California
San Francisco, CA, USA

Present Title: Professor

EDUCATION	DEGREE
Tulane University, New Orleans, LA	A.B.
Tulane University, New Orleans, LA	M.D.
USPHS, Hospital of the University of Pennsylvania	Resident/Fellow

HONORARY DEGREES	DEGREE	YEAR
L'Universite de Paris-Sud, France	Ph.D.	1985
Université Claude Bernard Lyon 1, France	Ph.D.	2008
University of Southern Denmark	M.D.	2010

Dr. Howard Maibach joined the University of California Faculty in 1961 as Assistant Professor, and is currently Professor of Dermatology.

Dr. Maibach, an expert in contact and occupational dermatitis, sees patients at the Environmental Dermatoses Clinic, which is part of the Dermatology Clinic at UCSF. His most active fields of research are dermatopharmacology, dermatotoxicology, and environmental dermatoses. He has been doing human subject research for 45 years.

He has been on the editorial board of more than 30 scientific journals. His bibliography includes more than 2790 publications and 100 books.

He is member of 19 professional societies, including the American Academy of Dermatology (AAD), San Francisco Dermatological Society (SFDS), North American Contact Dermatitis Group (NACDG), American Contact Dermatitis Society (ACDS), International Contact Dermatitis Research Group (ICDRG), Society of Toxicology (SOT), European Environmental and Contact Dermatitis Research Group (EECDRG), and the Internal Commission on Occupational Health. He is a consultant to government, academia, and industry worldwide.

Dr. Howard Maibach was honored as the 2013 recipient of The Master Dermatologist Award by The American Academy of Dermatology's 71st Annual Conference held in Miami, Florida. This prestigious award recognizes an Academy member's significant contributions to the field of dermatology and to the American Academy of Dermatology.

In March 2015, The International League of Dermatological Societies (ILDS) awarded Dr. Maibach their 2014 ILDS Certificate of Appreciation in recognition of his outstanding contribution to dermatology, both nationally and internationally, through his work, research, publications, and teaching in the USA and over 60 countries.

Contributors

Ahlam Abdou Department of Dermatology, Ibn Sina Hospital, Rabat University Hospital, Rabat, Morocco

Denise M. Adams Hemangioma and Vascular Malformation Center, Cincinnati Children's Hospital Medical Center, Cincinnati, OH, USA

Department of Pediatrics, College of Medicine, Cincinnati Children's Hospital Medical Center, Cincinnati, OH, USA

Yasser Afifi Private Clinic, Rabat, Morocco
e-mail: yaafifi@yahoo.fr

Pierre Agache Department of Dermatology, University Hospital of Besançon, Besançon, France
e-mail: aude.agache@free.fr; ferial.fanian@chu-besancon.fr; ferial.fanian@cert-besancon.com

Marina Agozzino San Gallicano Dermatological Institute, Rome, Italy
e-mail: ardigo@ifo.it

Tamara Al-Bader Oriflame Skin Research Institute, Stockholm, Sweden

Oriflame R&D Ltd, Bray, Co Wicklow, Ireland

Department of Medical Sciences, Dermatology and Venereology, Uppsala University, Uppsala, Sweden

Peter Altmeyer Department of Dermatology and Allergology, Ruhr University Bochum, Bochum, Germany

Hajar Amarouch Department of Dermatology, Ibn Sina Hospital, Rabat University Hospital, Rabat, Morocco

Marco Ardigò San Gallicano Dermatological Institute, Rome, Italy
e-mail: ardigo@ifo.it

Lars Arendt-Nielsen Department of Health Science and Technology, Faculty of Medicine, Center for Sensory-Motor Interaction (SMI), Aalborg University, Aalborg, Denmark

---

Pierre Agache: deceased.

Javier Arnáiz Lastras Faculty of Sciences for Physical Activity and Sport (INEF), Universidad Politécnica de Madrid, Madrid, Spain

Sophia Arndt Department of Dermatology, Venereology and Allergology, Center of Experimental and Applied Cutaneous Physiology, Charité - Universitätsmedizin Berlin, Berlin, Germany

Philippe Assouly Centre Sabouraud, Saint-Louis Hospital, Paris, France
e-mail: philippe.assouly@orange.fr

Sébastien Aubry University Hospital of Besançon, Besançon, France

Department of Radiology, I4S Laboratory, INSERM EA4268, University of Franche-Comte, Besançon, France
e-mail: radio.aubry@free.fr

Luis Bagatolli Membrane Biophysics and Biophotonics group/MEMPHYS Center for Biomembrane Physics, Department of Biochemistry and Molecular Biology, University of Southern Denmark, Odense, Denmark

Nawel Baghdadli L'Oréal Research and Innovation, Aulnay-Sous- Bois, France

P. Bahadoran Department of Dermatology, Nice CHU Hôpital Pasteur, Nice Cedex 3, France
e-mail: Philippe.BAHADORAN@unice.fr

Chiara Baldini Dipartimento di malattie muscolo-scheletriche e cutanee, U.O. Reumatologia, Pisa, Italy
e-mail: c.baldini@med.unipi.it

Mathurin Baquié Scientis Pharma SA, Geneva, Switzerland

Robert Baran Nail Disease Center, Cannes, France
e-mail: baran.r@wanadoo.fr

Gladimir V. G. Baranoski Natural Phenomena Simulation Group, University of Waterloo, Waterloo, ON, Canada
e-mail: gvgbaran@cs.uwaterloo.ca

André O. Barel Faculty of Physical Education and Physiotherapy, Vrije Universiteit Brussel, Brussel, Belgium
e-mail: anbarel@vub.ac.be

Fernanda Naspolini Bastos Universidade Luterana do Brasil, Canoas, Brazil

Jean-Claude Beani Clinique Universitaire de Dermato-Vénéréologie, Photobiologie et Allergologie, Pôle Pluridisciplinaire de Médecine, CHU de Grenoble, Grenoble, France
e-mail: jeanclaudebeani@gmail.com; jcbeani@chu-grenoble.fr

Philippe Benech Faculté de Médecine Secteur Nord, UMR 7259 (NICN) CNRS – Aix-Marseille Université, Marseille, France
e-mail: philippe.benech@univ-amu.fr

Bruno A. Bernard L'Oréal Research and Innovation, Clichy, France
e-mail: bbernard@rd.loreal.com

Jean-claude Bernengo Non Invasive Technologies, Paris, France
e-mail: bernjc@free.fr

Jacques Bittel Cepa, CNRS, Strasbourg Cedex, France

Stefano Bombardieri Dipartimento di malattie muscolo-scheletriche e cutanee, U.O. Reumatologia, Pisa, Italy
e-mail: s.bombardieri@int.med.unipi.it

S. Boutefnouchet Unité de Préparation et de Contrôles des Médicaments, Service Pharmaceutique – Groupement Hospitalier Edouard Herriot-Hospices Civils de Lyon, Lyon cedex 03, France

Emilie Brenaut Department of Dermatology, University Hospital of Brest, Brest, France

Mª Julia Bujan Faculty of Medicine and Health Science, Universidad de Alcalá de Henares, Campus Universitario, Ctra. Barcelona, Madrid, Spain

Shona A. Burkes Skin Sciences Program, Division of Plastic Surgery, Department of Surgery, Cincinnati Children's Hospital Medical Center, College of Medicine, University of Cincinnati, Cincinnati, OH, USA

James L. Winkle, College of Pharmacy, University of Cincinnati, Cincinnati, OH, USA

Francisco M. Camacho School of Medicine, Medical-Surgical Dermatology Department, Hospital Universitario Virgen Macarena, University of Seville, Seville, Spain
e-mail: fmcamacho@us.es; camachodp@medynet.com

Victor Candas Ex Research Director at CNRS, Strasbourg Cedex 2, France
e-mail: v.candas@orange.fr

Massimiliano Cazzato Dipartimento di malattie muscolo-scheletriche e cutanee, U.O. Reumatologia, Pisa, Italy
e-mail: m_cazzato@virgilio.it

Tenn F. Chen Natural Phenomena Simulation Group, University of Waterloo, Waterloo, ON, Canada
e-mail: t4chen@cs.uwaterloo.ca

Audris Chiang UC Irvine School of Medicine, Berkeley, CA, USA

Department of Dermatology, University of California, San Francisco, CA, USA
e-mail: audrisc@uci.edu

Peter Clarys Faculty of Physical Education and Physiotherapy, Vrije Universiteit Brussel, Brussel, Belgium
e-mail: pclarys@vub.ac.be

Carol Courderot-Masuyer Bioexigence, Besançon, France
e-mail: bioexigence@wanadoo.fr

Razvigor Darlenski Department of Dermatology and Venereology, Tokuda Hospital Sofia, Sofia, Bulgaria
e-mail: darlenski@gmail.com

Maxim E. Darvin Department of Dermatology, Venereology and Allergology, Center of Experimental and Applied Cutaneous Physiology, Charité – Universitätsmedizin Berlin, Berlin, Germany
e-mail: maxim.darvin@charite.de

J. P. Delage U688 Physiopathologie mitochondriale, Université Victor Segalen-Bordeaux 2, Bordeaux Cedex, France

Alessandra Della Rossa Dipartimento di malattie muscolo-scheletriche e cutanee, U.O. Reumatologia, Pisa, Italy
e-mail: a.dellarossa@ao-pisa.toscana.it

Heinrich Dickel Department of Dermatology and Allergology, Ruhr University Bochum, Bochum, Germany
e-mail: h.dickel@klinikum-bochum.de

Valentina Dini Department of Dermatology, University of Pisa, Pisa, Italy

Stéphane Diridollou L'Oreal Research and Innovation, Chevilly, Larue, France
e-mail: sdiridollou@rd.loreal.com

Van Neste Dominique Skinterface Tournai and Brussels' Hair Clinic, Tournai, Belgium
e-mail: info@skinterface.be

Yahya Dowlati Center for Research and Training in Skin Diseases and Leprosy, Tehran University of Medical Sciences, Tehran, Iran
e-mail: dowlatiy@yahoo.com

Peter D. Drummond School of Psychology and Exercise Science, Murdoch University, Perth, WA, Australia
e-mail: p.drummond@murdoch.edu.au

L. Duteil CPCAD (Centre de Pharmacologie Clinique Appliquée à la Dermatologie), Hôpital L'ARCHET 2, Nice Cedex 3, France
e-mail: philippe.BAHADORAN@unice.fr

Vanessa Ecarnot CERT, Department of Dermatology, CHRU Besançon, Besançon, France

Claudia El Gammal Dermatology, Medical Care Center, Diakonie Klinikum Jung-Stilling, Siegen, Germany

Stephan El Gammal Dermatological Clinic, Diakonie Klinikum Bethesda, Freudenberg, Germany
e-mail: stephan@ElGammal.de

Ahmed Elkhyat Center for Research and Studies on the Integument (CERT), Department of Dermatology, Clinical Investigation Center (CIC BT506), Besançon University Hospital, INSERM UMR1098, FED4234 IBCT, University of Franche-Comté, Besançon, France
e-mail: aelkhyat@chu-besancon.fr

Ramona Enea L'Oréal Research and Innovation, Aulnay-Sous- Bois, France

Françoise Falson ISPB-Faculté de Pharmacie, University of Lyon, Lyon, France
e-mail: francoise.rieg-falson@univ-lyon1.fr

Ferial Fanian Center for Study and Research on the Integuments, Department of Dermatology, University Hospital of Besançon, Besançon, France
e-mail: ferial.fanian@chu-besancon.fr; ferial.fanian@cert-besancon.com; fanian@gmail.com

Ismael Fernández-Cuevas Faculty of Sciences for Physical Activity and Sport (INEF), Universidad Politécnica de Madrid, Madrid, Spain
e-mail: ismael.fernandez@upm.es

Hugo Ferreira Faculty of Sciences, Institute of Biophysics and Biomedical Engineering, Universidade de Lisboa, Lisboa, Portugal

Davide Filingeri Environmental Ergonomics Research Centre, Loughborough Design School, Loughborough University, Loughborough, UK
e-mail: davidefilingeri@hotmail.it

Alireza Firooz Center for Research and Training in Skin Diseases and Leprosy, Tehran University of Medical Sciences, Tehran, Iran
e-mail: firozali@sina.tums.ac.ir

Joachim W. Fluhr Department of Dermatology, Charité – Universitätsmedizin Berlin, Berlin, Germany
e-mail: Joachim.Fluhr@charite.de

Annette Friedrich Department of Dermatology, Venereology and Allergology, Center of Experimental and Applied Cutaneous Physiology, Charité - Universitätsmedizin Berlin, Berlin, Germany

Bernard Gabard Lörrach, Germany
e-mail: b.gabard@iderma.ch

Thilo Gambichler Department of Dermatology and Allergology, Ruhr University Bochum, Bochum, Germany

Parisa Gazerani Department of Health Science and Technology, Faculty of Medicine, Center for Sensory-Motor Interaction (SMI), Aalborg University, Aalborg, Denmark
e-mail: gazerani@hst.aau.dk

Edgar Gentilhomme French Army Health Research Department, La tronche, France
e-mail: edgargentilhomme@crssa.net

Nicola Gerrett Institute of Sport and Exercise Science, University of Worcester, Worcester, UK
e-mail: n.gerrett@worc.ac.uk

Marion Ghibaudo L'Oréal Research and Innovation, Aulnay-Sous- Bois, France

E. Gilbert EA 4169 "Aspects Fondamentaux, Cliniques et Thérapeutiques de la Fonction Barrière Cutanée", Laboratoire de Pharmacie Galénique Industrielle – Faculté de Pharmacie., Université Claude Bernard Lyon 1, Lyon cedex 08, France

Johanna M. Gillbro Oriflame Skin Research Institute, Stockholm, Sweden

Oriflame R&D Ltd, Bray, Co Wicklow, Ireland

Department of Medical Sciences, Dermatology and Venereology, Uppsala University, Uppsala, Sweden
e-mail: johanna.gillbro@oriflame.com

Pedro Gómez Carmona Faculty of Sciences for Physical Activity and Sport (INEF), Universidad Politécnica de Madrid, Madrid, Spain

Salvador Gonzalez Dermatology Service, Memorial Sloan-Kettering Cancer Center, New York, NY, USA

Medicine Department, Alcalá University, Madrid, Spain

G. S. Goriparthi Department of Pharmaceutics, UCL School of Pharmacy, London, UK

Alexandros Goulioumis Department of Anesthesiology, Intensive Care and Pain Therapy, The Knappschaftskrankenhaus Dortmund, Dortmund, Germany

Marcella Guarrera Department of Health Sciences-Section of Dermatology, University of Genoa, Genoa, Italy
e-mail: guarrera@unige.it

Alexandre Guichard Center for Research and Studies on the Integument (CERT), Department of Dermatology, Clinical Investigation Center (CIC INSERM 1431), Besançon University Hospital; INSERM UMR1098, FED4234 IBCT, University of Franche-Comté, Besançon, France
e-mail: guichard.alexandre@gmail.com

J. C. Guimberteau Institut Aquitain de la Main, Bordeaux-Pessac, France
e-mail: adf.guimberteau@wanadoo.fr

Stefan F. Haag Department of Dermatology, Venereology and Allergology, Center of Experimental and Applied Cutaneous Physiology, Charité - Universitätsmedizin Berlin, Berlin, Germany

Farhaan Hafeez Department of Dermatology, University of California, San Francisco, San Francisco, CA, USA
e-mail: farhaanhafeez@gmail.com; farhaan.hafeez@yale.edu

Marek Haftek Laboratoire de Recherche Dermatologique, EA 4169, Faculté de Médecine et de Pharmacie, Université Claude Bernard Lyon 1, Lyon, France
e-mail: marek.haftek@univ-lyon1.fr

Eva Hagforsen Oriflame Skin Research Institute, Stockholm, Sweden

Oriflame R&D Ltd, Bray, Co Wicklow, Ireland

Department of Medical Sciences, Dermatology and Venereology, Uppsala University, Uppsala, Sweden

Steffi Hansen Department Drug Delivery, Helmholtz Institute for Pharmaceutical Research Saarland (HIPS), Helmholtz Center for Infection Research, Saarbruecken, Germany
e-mail: steffihansen@web.de

Farina Hashmi School of Health Sciences Research, University of Salford, Manchester, UK
e-mail: F.Hashmi@salford.ac.uk

Hournaz Hassanzadeh Center for Research and Training in Skin Diseases and Leprosy, Tehran University of Medical Sciences, Tehran, Iran
e-mail: hasanzadeh.hoornaz92@gmail.com

Kathryn L. Hatch Department of Agricultural and Biosystems Engineering, University of Arizona, Tucson, AZ, USA
e-mail: khatch@ag.arizona.edu

George Havenith Environmental Ergonomic Research Centre, Loughborough Design School, Loughborough University, Loughborough, UK
e-mail: G.Havenith@lboro.ac.uk

Trinh Hermanns-Lê Laboratory of Skin Bioengineering and Imaging (LABIC), Liège University, Liège, Belgium

Service de Dermatopathologie, CHU du Sart Tilman, Liège, Belgium

Department of Dermatopathology, Unilab Lg, University Hospital of Liège, Liège, Belgium
e-mail: Trinh.hermanns@chu.ulg.ac.be; Trinh.le@ulg.ac.be

Camile L. Hexsel Brazilian Center for Studies in Dermatology, Porto Alegre, Brazil

Doris Hexsel Brazilian Center for Studies in Dermatology, Department of Dermatology, Pontificia Universidade Catolica do Rio Grande do Sul (PUC-RS), Porto Alegre, RS, Brazil
e-mail: doris@hexsel.com.br

Simon Hodder Environmental Ergonomics Research Centre, Loughborough Design School, Loughborough University, Loughborough, UK
e-mail: S.Hodder@lboro.ac.uk

Golara Honari Department of Dermatology, Stanford School of Medicine, Redwood City, USA
e-mail: Honari@stanford.edu

Magdalena Hoppel Department of Pharmaceutical Technology and Biopharmaceutics, Faculty of Life Sciences, University of Vienna, Vienna, Austria
e-mail: magdalena.hoppel@univie.ac.at

Philippe Humbert Department of Dermatology, University Hospital of Besançon, Besançon, France
e-mail: philippe.humbert@univ-fcomte.fr

Alia Arif Hussain Department of Dermatology, Roskilde Hospital, University of Copenhagen, Roskilde, Denmark
e-mail: alia.arif.hussain@gmail.com

Soeren Jaspers Research and Development, Beiersdorf AG, Hamburg, Germany
e-mail: Soeren.Jaspers@beiersdorf.com

Gregor B. E. Jemec Department of Dermatology, Roskilde Hospital, University of Copenhagen, Roskilde, Denmark
e-mail: gbj@regionsjaelland.dk

Adeline Jeudy Research and Studies Center on the Integument (CERT); Clinical Investigation Center (CIC BT506), Department of Dermatology, Besançon University Hospital, Besançon, France
e-mail: ajeudy@chu-besancon.fr

Jessica W. Y. Jor Auckland Bioengineering Institute, University of Auckland, Auckland, New Zealand
e-mail: j.jor@auckland.ac.nz

Jakob Mutanu Jungersted Department of Dermatology, University of Copenhagen, Copenhagen, NV, Denmark
e-mail: jungersted@gmail.com

Raphaela Kästle Department of Dermatology and Allergology, General Hospital Augsburg, Augsburg, Germany

Karsten König Department of Biophotonics and Laser Technology, Saarland University, Saarbruecken, Germany

JenLab GmbH, Jena, Germany
e-mail: k.koenig@blt.uni-saarland.de

Jeanette Kamphowe Department of Dermatology and Allergology, Ruhr University Bochum, Bochum, Germany

Behrooz Kasraee Scientis Pharma SA, Geneva, Switzerland
e-mail: behroozkasraee@yahoo.com

Rachid Kechidi University Hospital of Besançon, Besançon, France
e-mail: r.kechidi@live.fr

Katsuko Kikuchi Department of Dermatology, Tohoku University Graduate School of Medicine, Sendai, Japan
e-mail: kkikuchi@med.tohoku.ac.jp

Victoria Klang Department of Pharmaceutical Technology and Biopharmaceutics, Faculty of Life Sciences, University of Vienna, Vienna, Austria
e-mail: victoria.klang@univie.ac.at

Fanny Knorr Department of Dermatology, Venereology and Allergology, Center of Experimental and Applied Cutaneous Physiology, Charité - Universitätsmedizin Berlin, Berlin, Germany
e-mail: fanny.knorr@charite.de

Laurence Kocher Service d'Explorations Fonctionnelles Neurologiques, Centre Hospitalier Lyon Sud, Hospices Civils de Lyon, Pierre-Bénite, France
e-mail: laurence.kocher@chu-lyon.fr

Nikiforos Kollias Johnson & Johnson Consumer and Personal Products Worldwide, Skillman, NJ, USA

Charles B. Kromann Department of Dermatology, Roskilde, Zealand University Hospital, University of Copenhagen, Copenhagen, Denmark
e-mail: charles.kromann@gmail.com

Oliver Kuss Institute for Biometry and Epidemiology, German Diabetes Center, Leibniz Institute for Diabetes Research at Heinrich Heine University Düsseldorf, Düsseldorf, Germany

Jürgen Lademann Department of Dermatology, Venereology and Allergology, Center of Experimental and Applied Cutaneous Physiology, Charité – Universitätsmedizin Berlin, Berlin, Germany
e-mail: juergen.lademann@charite.de

Cheng-Che Eric Lan Department of Dermatology, Kaohsiung Medical University, Kaohsiung, Taiwan

Helene M. Langevin Department of Neurological Sciences, University of Vermont, College of Medicine, Burlington, VT, USA
e-mail: helene.langevin@med.uvm.edu

Anna-Christina Lauer Department of Dermatology, Venereology and Allergology, Center of Experimental and Applied Cutaneous Physiology, Charité - Universitätsmedizin Berlin, Berlin, Germany

Youssef Lboutounne CIC-BT CHU, Besançon, France
e-mail: youssef-lboutounne@hotmail.fr

Won-Soo Lee Department of Dermatology, Institute of Hair and Cosmetic Medicine, Yonsei University Wonju College of Medicine, Wonju, Gangwon-Do, Republic of Korea
e-mail: leewonsoo@yonsei.ac.kr

Christina Lee Johnson & Johnson Consumer and Personal Products Worldwide, Skillman, NJ, USA
e-mail: CLee56@its.jnj.com

Jackson Leong Dermatology Department, University of California, San Francisco, San Francisco, CA, USA
e-mail: jacksonleong@gmail.com

Dominique Leroy Dermatologist, Department of Dermatology, University Hospital centre, Caen, France
e-mail: dominique.leroy10@wanadoo.fr

Li Li Department of Dermatology, West China Hospital, Sichuan University, Chengdu, China

Yuanhong Li Department of Dermatology, No.1 Hospital of China Medical University, Shenyang, People's Republic of China
e-mail: liyuanhong@vip.sina.com

Thomas Lihoreau Center for Research and Studies on the Integument (CERT), Department of Dermatology, Clinical Investigation Center (CIC INSERM 1431), Besançon University Hospital; INSERM UMR1098, FED4234 IBCT, University of Franche-Comté, Besançon, France
e-mail: tlihoreau@chu-besancon.fr

Shari R. Lipner Department of Dermatology, Weill Cornell Medical College, New York, NY, USA
e-mail: shl9032@med.cornell.edu

Caterina Longo Dermatology and Skin cancer Unit, Arcispedale Santa Maria Nuova-IRCCS, Reggio Emilia, Italy
e-mail: longo.caterina@gmail.com

Gustavo S. Luengo L'Oréal Research and Innovation, Aulnay-Sous- Bois, France
e-mail: gluengo@rd.loreal.com

Sophie Mac-Mary Skinexigence SAS, Bioparc, Besançon, France
e-mail: smac@skinexigence.com

Howard I. Maibach Department of Dermatology, School of Medicine, University of California, San Francisco, CA, USA
e-mail: maibachh@derm.ucsf.edu

M. Malathi Department of Dermatology, Jawaharlal Institute of Post Graduate Medical Education and Research, Gorimedu, Puducherry, India
e-mail: mmalathi.dr@live.com

George Man Department of Dermatology, Dermatology Service, Veterans Affairs Medical Center San Francisco, University of California San Francisco, School of Medicine, San Francisco, CA, USA
e-mail: georgeisman@gmail.com

Mao-Qiang Man Department of Dermatology, Dermatology Service, Veterans Affairs Medical Center San Francisco, University of California San Francisco, School of Medicine, San Francisco, CA, USA
e-mail: mqman@hotmail.com

Joao Carlos Marins Human Performance Laboratory – LAPEH, Universidade Federal de Viçosa (Brazil), Minas Gerais Código, Viçosa, Brazil

Slaheddine Marrakchi Department of Dermatology, Hedi CHAKER Hospital, Sfax, Tunisia
e-mail: slaheddine.marrakchi@tunet.tn

Alain Mavon Oriflame Skin Research Institute, Stockholm, Sweden

Oriflame R&D Ltd, Bray, Co Wicklow, Ireland

Department of Medical Sciences, Dermatology and Venereology, Uppsala University, Uppsala, Sweden

Sylvie Meaume Department of Geriatrics, Wound Care Unit, Rothschild Hospital, Paris, France
e-mail: sylvie.meaume@rth.aphp.fr

Annette Mehling BASF Personal Care and Nutrition GmbH, Düsseldorf, Germany
e-mail: annette.mehling@basf.com

Martina C. Meinke Department of Dermatology, Venereology and Allergology, Center of Experimental and Applied Cutaneous Physiology, Charité – Universitätsmedizin Berlin, Berlin, Germany
e-mail: martina.meinke@charite.de

Eve Merinville Oriflame Skin Research Institute, Stockholm, Sweden

Oriflame R&D Ltd, Bray, Co Wicklow, Ireland

Department of Medical Sciences, Dermatology and Venereology, Uppsala University, Uppsala, Sweden

Shahram F. Mevaloo Health Studies Group, Center for Strategic Research, I.R.I Ministry of Sport and Youth, Tehran, Iran
e-mail: sfaradjzadeh@yahoo.com

G. Milcovich Department of Pharmaceutics, UCL School of Pharmacy, London, UK

Laurent Misery Department of Dermatology, University Hospital of Brest, Brest, France
e-mail: laurent.misery@chu-brest.fr

Hiroyasu Mizuno L'OREAL, KSP Research and Innovation center, Kawasaki, Japan

Mette Mogensen Department of Dermatology and Venereology, Bispebjerg Hospital, University of Copenhagen, Copenhagen, Denmark
e-mail: mogensen.mette@gmail.com

Garrett Moran Oriflame Skin Research Institute, Stockholm, Sweden

Oriflame R&D Ltd, Bray, Co Wicklow, Ireland

Department of Medical Sciences, Dermatology and Venereology, Uppsala University, Uppsala, Sweden

Marta Mosca Dipartimento di malattie muscolo-scheletriche e cutanee, U.O. Reumatologia, Pisa, Italy
e-mail: marta.mosca@med.unipi.it

D. Moyal La Roche-Posay Laboratoire Dermatologique, Asnieres Sur Seine, France
e-mail: dominique.moyal@loreal.com

S. Murdan Department of Pharmaceutics, UCL School of Pharmacy, London, UK
e-mail: s.murdan@ucl.ac.uk

Patrice Muret Engineering and Cutaneous Biology Laboratory, UMR 1098, University of Franche-Comte, Besançon, France

Clinical Pharmacology Department, University Hospital, Besançon, France
e-mail: patrice.muret@univ-fcomte.fr; p1muret@chu-besancon.fr

Shohreh Nafisi Department of Chemistry, Central Tehran Branch, IAU, Tehran, Iran

Department of Dermatology, University of California, San Francisco, CA, USA
e-mail: drshnafisi@gmail.com

Martyn P. Nash Auckland Bioengineering Institute, University of Auckland, Auckland, New Zealand

Department of Engineering Science, University of Auckland, Auckland, New Zealand

Yves Neveux Livernon, France
e-mail: yves.neveux@free.fr

Poul M. F. Nielsen Auckland Bioengineering Institute, University of Auckland, Auckland, New Zealand

Department of Engineering Science, University of Auckland, Auckland, New Zealand

Jesper B. Nielsen Department of Public Health, University of Southern Denmark, Odense, Denmark
e-mail: jbnielsen@health.sdu.dk

Thomas A. Nielsen Department of Health Science and Technology, Faculty of Medicine, Center for Sensory-Motor Interaction (SMI), Aalborg University, Aalborg, Denmark

Mia Nilsson Oriflame Skin Research Institute, Stockholm, Sweden

Oriflame R&D Ltd, Bray, Co Wicklow, Ireland

Department of Medical Sciences, Dermatology and Venereology, Uppsala University, Uppsala, Sweden

Lars Norlén Department of Cell and Molecular Biology (CMB), Karolinska Institutet, and Dermatology Clinic, Karolinska University Hospital, Stockholm, Sweden
e-mail: lars.norlen@ki.se

Yacine Ouzzahra Institute for Health and Behaviour, University of Luxembourg, Walferdange, Luxembourg
e-mail: Yacine.Ouzzahra@uni.lu

Lídia Palma CBIOS – Research Center for Health Science and Technologies, Universidade Lusófona, Lisbon, Portugal

Salvatore Panduri Department of Dermatology, University of Pisa, Pisa, Italy

Matthew D. Parker Auckland Bioengineering Institute, University of Auckland, Auckland, New Zealand

David D. Pascoe School of Kinesiology, Auburn University, Aubur, Al, USA
e-mail: Pascodd@auburn.edu

Paola Pasquali Dermatology Department, Pius Hospital de Valls, Valls, Spain
e-mail: pasqualipaola@gmail.com

J. Pauchot Orthopedic Surgery, Traumatology, Plastic Aesthetic, Reconstructive Surgery, and Hand Surgery Department, EA 4268, IFR 133 INSERM I4S, Besançon University Hospital, Besançon, France
e-mail: julien.pauchot@gmail.com

Giovanni Pellacani Dermatology Unit, University of Modena and Reggio Emilia, Modena, Italy

Gérald E. Piérard Laboratory of Skin Bioengineering and Imaging (LABIC), Liège University, Liège, Belgium

Service de Dermatopathologie, CHU du Sart Tilman, Liège, Belgium
e-mail: Gerald.pierard@ulg.ac.be

Claudine Piérard-Franchimont Laboratory of Skin Bioengineering and Imaging (LABIC), Department of Clinical Sciences, Liège University, Liège, Belgium
e-mail: Claudine.franchimont@ulg.ac.be

Fabrice Pirot EA 4169 "Aspects Fondamentaux, Cliniques et Thérapeutiques de la Fonction Barrière Cutanée", Laboratoire de Pharmacie Galénique Industrielle – Faculté de Pharmacie., Université Claude Bernard Lyon 1, Lyon cedex 08, France

Unité de Préparation et de Contrôles des Médicaments, Service Pharmaceutique – Groupement Hospitalier Edouard Herriot-Hospices Civils de Lyon, Lyon cedex 03, France
e-mail: fabrice.pirot@univ-lyon1.fr

Johan L. Du Plessis Occupational Hygiene and Health Research Initiative, North-West University, Potchefstroom, South Africa
e-mail: Johan.DuPlessis@nwu.ac.za

Anne Potter L'Oréal Research and Innovation, Aulnay-Sous- Bois, France

Pascale Quatresooz Laboratory of Skin Bioengineering and Imaging, Department of Dermatopathology, University Hospital of Liège, Liège, Belgium

Department Histology, University of Liège, Liège, Belgium
e-mail: Pascale.quatresooz@chu.ulg.ac.be

Ali Rajabi-Estarabadi Center for Research and Training in Skin Diseases and Leprosy, Tehran University of Medical Sciences, Tehran, Iran
e-mail: dralirajabi@yahoo.com

Adriana Rakowska Department of Dermatology, Medical University of Warsaw, Warsaw, Poland
e-mail: adriana.rakowska@gmail.com

Loïc Rambaud French Institute for Public Health Surveillance, Saint Maurice, France
e-mail: l.rambaud@invs.sante.fr; l-rambaud@wanadoo.fr

Alfredo Rebora Department of Health Sciences-Section of Dermatology, University of Genoa, Genoa, Italy

Pascal Reygagne Centre de Santé Sabouraud, Hôpital Saint Louis, Paris, France
e-mail: p.reygagne@centresabouraud.fr

Corinne Reymermier BASF Beauty Care Solutions France S.A.S, Lyon, France
e-mail: corinne.reymermier@basf.com

Jean de Rigal L'Oréal Recherche, Chevilly Larue, France
e-mail: jderigal@rd.loreal.com; jderigal@bbox.fr

Francis J. Ring Medical Imaging Research Unit, University of South Wales, Pontypridd, UK
e-mail: efring@glam.ac.uk

Mª Angélica Roberto Plastic Surgery Service, Rua José António Serrano, Lisboa, Lisbon, Portugal

Luís Monteiro Rodrigues CBIOS – Research Center for Health Science and Technologies, Universidade Lusófona, Lisbon, Portugal

Department of Pharmacological Sciences, Universidade de Lisboa – School of Pharmacy, Lisbon, Portugal
e-mail: monteiro.rodrigues@ulusofona.pt; monteirorodrigues@sapo.pt

Marco Romanelli Department of Dermatology, University of Pisa, Pisa, Italy
e-mail: m.romanelli@med.unipi.it

Catarina Rosado Universidade Lusófona (CBIOS – Research Center for Health Science and Technologies), Lisbon, Portugal

K. Roussel CPCAD (Centre de Pharmacologie Clinique Appliquée à la Dermatologie), Hôpital L'ARCHET 2, Nice Cedex 3, France

L. Roussel EA 4169 "Aspects Fondamentaux, Cliniques et Thérapeutiques de la Fonction Barrière Cutanée", Laboratoire de Pharmacie Galénique Industrielle – Faculté de Pharmacie., Université Claude Bernard Lyon 1, Lyon cedex 08, France

Patricia Rousselle Tissue Biology and Therapeutic Engineering Unit, Institute of Protein Biology and Chemistry, UMR 5305 – CNRS, University of Lyon, Lyon, France
e-mail: patricia.rousselle@ibcp.fr

Lidia Rudnicka Department of Dermatology, Medical University of Warsaw, Warsaw, Poland
e-mail: lidia.rudnicka@dermatolodzy.com.pl

Mark W. Rutland KTH, Royal Institute of Technology, Stockholm, Sweden
e-mail: mark@kth.se

Eduardo Ruvolo Johnson & Johnson Consumer and Personal Products Worldwide, Skillman, NJ, USA
e-mail: eruvolojr@gmail.com

Jean-Marie Sainthillier Skinexigence, Besançon, France
e-mail: jmsainthillier@skinexigence.com

D. Salmon EA 4169 "Aspects Fondamentaux, Cliniques et Thérapeutiques de la Fonction Barrière Cutanée", Laboratoire de Pharmacie Galénique Industrielle – Faculté de Pharmacie., Université Claude Bernard Lyon 1, Lyon cedex 08, France

Unité de Préparation et de Contrôles des Médicaments, Service Pharmaceutique – Groupement Hospitalier Edouard Herriot-Hospices Civils de Lyon, Lyon cedex 03, France
e-mail: damien.salmon01@chu-lyon.fr

Osvaldo Santos Faculty of Medicine, Public Health Preventive Medicine Institute and Environmental Health Institute, Universidade de Lisboa, Lisbon, Portugal

Elke Sattler Department of Dermatology, Ludwig Maximilian University Munich, Munich, Germany

E. Sawaya Institut Aquitain de la Main, Bordeaux-Pessac, France

Julia J. Scarisbrick Department of Dermatology, Queen Elizabeth Medical Centre, University Hospitals Birmingham NHS Foundation Trust, Queen Elizabeth Hospital, Birmingham, UK
e-mail: juliascarisbrick@doctors.net.uk

Monika Schäfer-Korting Institute of Pharmacy, Pharmacology and Toxicology, FreieUniversität Berlin, Berlin, Germany

Sabine Schanzer Department of Dermatology, Venereology and Allergology, Center of Experimental and Applied Cutaneous Physiology, Charité - Universitätsmedizin Berlin, Berlin, Germany
e-mail: sabine.schanzer@charite.de

Richard K. Scher Department of Dermatology, Weill Cornell Medical College, New York, NY, USA
e-mail: scherri@med.cornell.edu

Christian Schulze Research and Development, Beiersdorf AG, Hamburg, Germany
e-mail: Christian.Schulze@beiersdorf.com

Hamm-Ming Sheu Department of Dermatology, National Cheng Kung University College of Medicine and Hospital, Tainan, Taiwan
e-mail: hmsheu@mail.ncku.edu.tw

Manuel Sillero Quintana Faculty of Sciences for Physical Activity and Sport (INEF), Universidad Politécnica de Madrid, Madrid, Spain

Henrique Silva CBIOS – Research Center for Biosciences and Health Technologies, Universidade Lusófona, Lisboa, Portugal

Department of Pharmacological Sciences, Universidade de Lisboa – School of Pharmacy, Lisbon, Portugal

Iqbaljit Singh Department of Dermatology, UCSF, Fremont, CA, USA
e-mail: gill1606@gmail.com

Mariana Soirefmann Dermatology Department, Pontificia Universidade Catolica do Rio Grande do Sul (PUC-RS), Porto Alegre, Brazil

Zhenhhua Song L'Oréal Research and Innovation, Aulnay-Sous- Bois, France

Aleksandr B. Stefaniak Centers for Disease Control and Prevention, National Institute for Occupational Safety and Health, Morgantown, WV, USA
e-mail: AStefaniak@cdc.gov

Tomasz J. Stefaniak Department of General, Endocrine and Transplant Surgery, Medical University of Gdansk, Gdansk, Poland
e-mail: wujstef@gumed.edu.pl

Markus F. C. Steiner GO Health Services, NHS Grampian, Aberdeen, UK
e-mail: m.steiner@abdn.ac.uk; m.steiner@nhs.net

Andrew J. Taberner Auckland Bioengineering Institute, University of Auckland, Auckland, New Zealand

Department of Engineering Science, University of Auckland, Auckland, New Zealand

Hachiro Tagami Department of Dermatology, Tohoku University Graduate School of Medicine, Sendai, Japan
e-mail: hachitagami@ybb.ne.jp

Liliana Tavares CBIOS – Research Center for Health Science and Technologies, Universidade Lusófona, Lisbon, Portugal

Devinder Mohan Thappa Department of Dermatology and STD, The Jawaharlal Institute of Postgraduate Medical Education and Research, Pondicherry, Puducherry, India
e-mail: dmthappa@gmail.com

Lotte Themstrup Department of Dermatology, Roskilde Hospital, University of Copenhagen, Roskilde, Denmark
e-mail: lotte.themstrup@gmail.com

Pierre Treffel Pharmaceutical laboratory, Codexial Dermatologie, Vandœuvre-lès-Nancy, France
e-mail: Pierre.treffel@codexial-dermatologie.com

Jui-Chen Tsai Institute of Clinical Pharmacy and Pharmaceutical Sciences, National Cheng Kung University, College of Medicine, Tainan, Taiwan

Claudia Valenta Department of Pharmaceutical Technology and Biopharmaceutics, Faculty of Life Sciences, University of Vienna, Vienna, Austria
e-mail: claudia.valenta@univie.ac.at

Daniel Varchon Laboratoire de Mécanique Appliquée R. Chaléat, University of Franche-Comté, Besançon, France
e-mail: daniel.varchon@univ-fcomte.fr

Céline Viennet Engineering and Cutaneous Biology Laboratory, UMR 1098, University of Franche-Comte, Besançon, France
e-mail: celine.viennet@univ-fcomte.fr

Martine Vigan Department of Dermatology, University Hospital of Besancon, Besançon, France
e-mail: martine.vigan@gmail.com

Marty O. Visscher Skin Sciences Program, Division of Plastic Surgery, Cincinnati Children's Hospital Medical Center, Cincinnati, OH, USA

Department of Surgery, College of Medicine, University of Cincinnati, Cincinnati, OH, USA
e-mail: marty.visscher@gmail.com

Michael Vogt Institute for High Frequency Techniques of the Ruhr-University, Bochum, Germany

Xuemin Wang Shanghai, China

Hans-Jürgen Weigmann Department of Dermatology, Venereology and Allergology, Center of Experimental and Applied Cutaneous Physiology, Charité - Universitätsmedizin Berlin, Berlin, Germany
e-mail: hweinet@alice-dsl.net

Julia Welzel Department of Dermatology and Allergology, General Hospital Augsburg, Augsburg, Germany
e-mail: julia.welzel@klinikum-augsburg.de

Xuemin Wang: deceased.

Alexander Witkowski Dermatology Unit, University of Modena and Reggio Emilia, Modena, Italy

Ximena Wortsman Department of Radiology and Department of Dermatology, Institute for Diagnostic Imaging and Research of the Skin and Soft Tissues, Clinica Servet, Faculty of Medicine, University of Chile, Santiago, Chile
e-mail: xworts@yahoo.com

Perry Xiao School of Engineering, London South Bank University, London, UK
e-mail: xiaop@lsbu.ac.uk

Sang Woong Youn Department of Dermatology, Seoul National University Bundang Hospital, Seongnam, Gyeonggi-do, South Korea
e-mail: swyoun@snu.ac.kr

Chao Yuan Department of Skin and Cosmetic Research, Shanghai Skin Disease Hospital, Shanghai, China
e-mail: dermayuan@163.com

Hamed Zartab Center for Research and Training in Skin Diseases and Leprosy, Tehran University of Medical Sciences, Tehran, Iran

Tissue Engineering and Wound Healing Lab, Department of Surgery, Division of Plastic Surgery, Brigham and Women's Hospital – Harvard Medical School, Boston, USA
e-mail: hzartabmd@yahoo.com; hzartab@partners.org; hzartabmd@gmail.com

The Human Skin: An Overview

1

Pierre Agache, Thomas Lihoreau, Sophie Mac-Mary, Ferial Fanian, and Philippe Humbert

Contents

Pierre Agache: deceased.

P. Agache • P. Humbert
Department of Dermatology, University Hospital of Besançon, Besançon, France
e-mail: aude.agache@free.fr; ferial.fanian@chu-besancon.fr; ferial.fanian@cert-besancon.com; philippe.humbert@univ-fcomte.fr

T. Lihoreau (✉)
Center for Research and Studies on the Integument (CERT), Department of Dermatology, Clinical Investigation Center (CIC INSERM 1431), Besançon University Hospital; INSERM UMR1098, FED4234 IBCT, University of Franche-Comté, Besançon, France
e-mail: tlihoreau@chu-besancon.fr

S. Mac-Mary
Skinexigence SAS, Bioparc, Besançon, France
e-mail: smac@skinexigence.com

F. Fanian
Center for Study and Research on the Integuments, Department of Dermatology, University Hospital of Besançon, Besançon, France
e-mail: ferial.fanian@chu-besancon.fr; ferial.fanian@cert-besancon.com; fanian@gmail.com

P. Humbert et al. (eds.), *Agache's Measuring the Skin*,
DOI 10.1007/978-3-319-32383-1_1

Keywords
Human skin • Body temperature control • Chemical barrier • Elasticity • Hydration • Immune function • Mechanical protection • Microcirculation • Self-maintenance and self-repair • Sensory function • Sexual function • Skin appendages • Topographical variations

1 A Few Figures About the Skin

Area: 1.8 m^2
Average thickness: 1.2 mm
Average volume: 3.5 dm^3 = 0.035 m^3
Weight with blood: 4.7 kg
Weight without blood: 4.2 kg
Ratio area/thickness = 150,000

The skin participates in many physiological and pathological events and processes of the human organism, owing to its large area of contact with the internal milieu, but also to its volume and variety of tissues. The cutaneous expression of internal diseases is frequent, varied, and often specific.

2 Skin Structure

The general structure of the skin is a stratified tissue whose four layers are, from the top to the bottom, the stratum corneum (8–20 µm thick, could go up to 1.5 mm on palms and soles), the viable epidermis (30–80 µm), the dermis (1–2 mm), and the hypodermis or subcutis (0.1 to several cm) (Fig. 1). Each of these layers has its own physiology, functions, and evolution along life.

2.1 Annexes

The skin is a heterogeneous organ (dead tissue, epithelium, connective tissue, muscles, etc.), and furthermore it harbors four types of independent mini-organs, also called skin appendages:

– The nails, growing at a speed of 3 mm/month on hands and 1–1.5 mm/month on feet, with this speed decreasing with age (Scher and Daniel 2007)
– The pilosebaceous follicles and hair: between 90,000 and 130,000 on the scalp, with a terminal hair diameter of 40–120 µm, depending of the phototype; 60–100 hair fall per day, and they grow at a speed of 0.35–0.44 mm/day, (1 cm/month, 12 cm/year) (Blume-Peytavi 2008; Guichard et al. 2013)
– The eccrine sweat glands (three millions)
– The apocrine sweat glands (armpit, perineum)

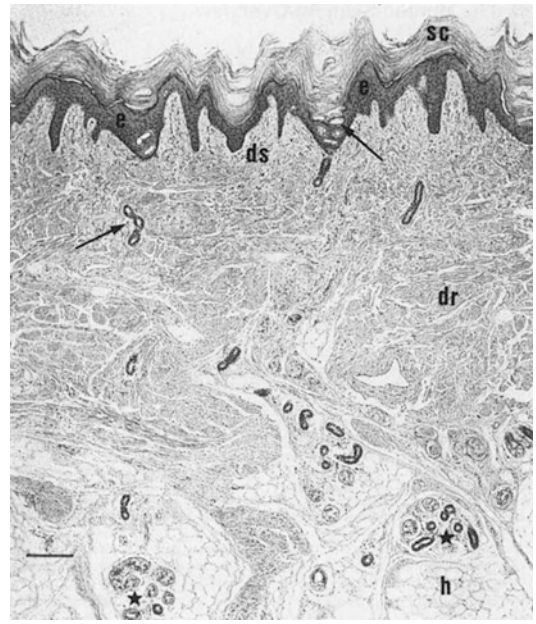

Fig. 1 A vertical section of the plantar skin. *dr* reticular dermis. *ds* superficial dermis. *e* viable epidermis, *h* hypodermis and adipose tissue, *sc* stratum corneum. *Stars* coiled part of sweat glands (both secretory segment and lower duct). *Arrows* sweat ducts. Note the large skin thickness (1.8 mm, in other sites it would be close to 1 mm), the absence of pilosebaceous follicles, the large thickness of the stratum corneum, and the great number of sweat glands. In vivo dimensions were about 15 % larger. Bar = 200 µm (From Degos and Civatte 1977)

2.2 Variations

Topographical variations in its structure and functions are considerable: the scalp, the skin of the face, the dorsal skin of the hands and feet, the

palms and soles, the armpits, and the perineum have their own anatomy, functions, and reactivity (Tagami 2008; Sandby-Møller et al. 2003; Waller and Maibach 2006).

To briefly give some examples, in usual temperature and hygrometric atmosphere conditions (20–22 °C, 40–60 %), skin sebum excretion could vary from 0 (arms, legs, etc.) to more than 200 μg/cm^2 (greasy subjects forehead), and hydration index could go from 10 (dry skin on the legs) to 100 (well-hydrated skin on the forehead, without unity).

Aging (intrinsic or extrinsic) is obviously modifying skin structure (Lévêque and Agache 1993):

- Hydration presents maximum values between 20 and 40 and then regresses.
- Elasticity is the mechanical property that better reflects skin aging: it decreases and becomes oriented with age, is sun exposure dependent, and more important on women, and its values decrease from head to feet.
- Skin microrelief, roughness, and wrinkles are not involving on the whole body in the same manner, again depending on topology (gravity, expressions, etc.) or environmental factors (sun, tobacco, etc.), along life (Guinot et al. 2006);
- Microcirculation: capillary density, structured at the beginning even if variable in density in different body areas (mean of 60–70/mm^2), could worse until a disorganized (orientation), heterogeneous (size, shape of the capillaries) network, characterized by a density of 30/mm^2 or less.

The skin characteristics are also function of **sex** and **ethnicity** of the subject; it could even be dependent on the **side of the face** (Mac-Mary et al. 2010) or **environmental factors** (season, weather, etc.) (Fanian et al. 2013).

Due to these important variations, parameters previously cited appear in publications in comparison before and after a treatment, rather than compared to "normal" or "pathologic" values.

3 Skin Functions

3.1 Specific

- Self-maintenance and self-repair (but there is no repair of appendages)
- Mechanical protection: resistance to frontal and tangential shocks, attenuation of external pressures, body external shape maintenance through reversible deformations, adhesion of the palms and soles to objects in the hand and on the ground
- Chemical barrier: limitation of foreign substances penetration, prevention of water and endogenous fluid loss
- Protection against ultraviolet rays
- Protection against environmental pathogenic microorganisms
- Social and psychological function through the physical aspect and mimic

3.2 Exerted in Cooperation with Other Organs

- Sensory function: tactile senses, perception of temperature and pain and even of light (popliteal region) (Campbell and Murphy 1998)
- Body temperature control: especially regulation of heat gains and losses
- Immune function: the skin is the first line of information and defense in the process of immunity, especially "delayed immunity"
- Ossification: synthesis of provitamin D (vitamin D is responsible for the intestinal absorption of calcium)
- Sexual function: conversion of testosterone into more active dihydrotestosterone

References

Blume-Peytavi U. Hair Growth and disorders: with 85 tables. Springer: Berlin; 2008.

Campbell SS, Murphy PJ. Extraocular circadian phototransduction in humans. Science. 1998;279:396–9.

Degos R, Civatte J, editors. Dermatologie. Paris: Flammarion; 1977.

Fanian F, Mac-Mary S, Jeudy A, Lihoreau T, Messikh R, Ortonne J, Sainthillier JM, Elkhyat A, Guichard A, Hejazi K, Humbert P. Efficacy of micronutrient supplementation on skin ageing effects and seasonal variation. Clin Interv Aging. 2013;8:1–11.

Guichard A, Humbert P. Développement et déploiement d'une expertise trichologique au sein du service de Dermatologie du CHRU de Besançon. Thèse d'exercice en pharmacie, Université de Franche-Comté, 2013.

Guinot C, Latreille J, Mauger E, Ambroisine L, Gardinier S, Zahouani H, Gue´henneux S, Tschachler E. Reference ranges of skin micro-relief according to age in French Caucasian and Japanese women. Skin Res Technol. 2006;12:268–78.

Lévêque JL, Agache P. Aging skin, properties and functional changes. Dekker: New york; 1993.

Mac-Mary S, Sainthillier JM, Jeudy A, Sladen S, Williams C, Bell M, Humbert P. Assessment of cumulative exposure to UVA through the study of asymmetrical facial skin aging. Clin Interv Aging. 2010;5:277–84.

Sandby-Møller J, Poulsen T, Wulf HC. Epidermal thickness at different body sites: relationship to age, gender, pigmentation, blood content, skin type and smoking habits. Acta Derm Venereol. 2003;83: 410–3.

Scher RK, Daniel CR. Onychologie. Diagnostic, traitement, chirurgie. 3rd ed. Paris: Elsevier; 2007.

Tagami H. Location-related differences in structure and function of the stratum corneum with special emphasis on those of the facial skin. Int J Cosmet Sci. 2008;30:413–34.

Waller J, Maibach H. Thickness of aging skin. Cosmet Toiletries. 121(11). Nov 2006; 295–299.

Measurements of the Human Skin: Why and How?

2

Pierre Agache

Contents

This chapter was originally published under the ISBN 978-3-540-01771-4 with the following book title Measuring the Skin. The content has not been changed.

Pierre Agache: deceased.

P. Agache (✉)
Department of Dermatology, University Hospital of Besançon, Besançon, France
e-mail: aude.agache@free.fr; ferial.fanian@chu-besancon.fr; ferial.fanian@cert-besancon.com

P. Humbert et al. (eds.), *Agache's Measuring the Skin*, DOI 10.1007/978-3-319-32383-1_2

Keywords
Gaussian distribution • Good measuring practice • Interval scales • Comparative measurements • MKSA system • Nominal scale • Nongaussian series • Ordinal scale • Parametric evaluation • Sequential analysis • Standard deviation • Taguchi designs

In experimental sciences, measuring phenomena is a key point, since it is through the quantitative evaluation of an effect related to a given cause that the law of phenomena can be founded. (Bernard 1984)

1 The Relevance of Measurements

Metrology is the science of measurement, of evaluation of its requirements, limitations, and interpretations. The primary reason for using metrology in cutaneous noninvasive investigations is its role as a major source of progress, not only because impressions are replaced by objective facts and qualitative descriptions by quantitative assessments, but also because new situations are unveiled. Even the simplest phenomenon becomes complex when measured; one starts from one fact and then discovers its possible components and variations, which induces new hypotheses and opens a pathway for new knowledge. Physics in the past could only progress through the development of measurement methods. The remarkable advances in human physiology during the nineteenth century, which preceded modern medicine and allowed it to progress, came about because of a double process of discovery and quantification. Skin metrology provides many examples. The measurement of sebum secretion with a view to correcting the removal of lipid from the surface quickly showed that the measured phenomenon was not the one expected, but rather the partial emptying of a follicular reservoir, the existence of which had previously been ignored. The measurement of epidermal turnover in psoriasis provided a leap forward in understanding the disease.

Biological phenomena are changeable and difficult to quantify. At first glance, observation may prevail over measurement, but the notion of dimension is required to investigate a structure and the magnitude of change. The pathologist must decide whether, in the visualized skin section, the tissue components are modified in dimension and number by a pathological process. Furthermore, normal characteristics vary depending on the anatomical site, which has not yet been quantified; consequently, the pathologist remains unable to reach a conclusion unless major changes are seen. When the noninvasive anatomical or functional investigations are quantitative, they provide a measure with low subjectivity. The clinician evaluating a new medication would like to rapidly and accurately assess treatment efficacy; this goal can be reached only by quantification of clinical symptoms. Accordingly, it is necessary to know whether the measure is accurate (degree of precision and variability) and if it truly reflects the targeted phenomenon.

Numerical results of blood sample examinations is standard practice. It is likely to be the same for most clinical symptoms in the years to come. This is possible today in the detection and substantiation of subtle changes (e.g., aging (Escoffier et al. 1989; Larnier et al. 1994)) or the effect of a therapy on a chronic disease such as scleroderma (Humbert et al. 1993). The last decade of progress in molecular genetics has emphasized the considerable benefit that the collection of data provided by everyday medical practice might generate, and in years to come practitioners will certainly be involved in collecting and processing this data. Such information requires classification, substantiation, and treatment using statistical parameters. A few nondermatological specialties also utilize skin measurements, e.g., in physiology (endocrinology, body temperature regulation, immunology, etc.), where the skin is an effector organ readily examined noninvasively because of its accessibility. It is also the case for cosmetology research, where innocuousness and efficacy criteria may become visually unattainable because of their subtlety, and require instrumental measurements for assessment.

2 Types of Measurements

Before choosing an appropriate evaluation method, it is necessary to look at the nature of the data. If they relate to individuals or categories, hence with no possibility of converting them into numbers, the evaluation mandates a nominal scale. If the data can be translated into numbers, but on a scale where intervals are unknown or uneven, they can only be ranked. Finally, if the variation is measured on a continuous scale with even intervals, then the traditional evaluation is used: the so-called parametric evaluation (Siegel 1956).

2.1 Nominal Scale

This is the only means of measuring categories, facts or states, named by a word or an expression, and not put into numbers, for example, aggravation, desquamation, over 60-year-old subjects, etc. The nominal scale uses a number or the percentage of a total. If the measured category is part of a series, it can be replaced by a number for easier presentation, but without ranking.

A percentage should be presented with its uncertainty margins, thus its standard deviation (SD). The latter is calculated by the formula $SD = [p(1 - p)/n]^{1/2}$, where p is the percentage (from 0 to 1) and n the total number of data. The confidence interval for an occurrence by chance of less than 5 % is that between two standard deviations on each side of p. Tables of 5 % confidence intervals can be found in statistics textbooks. A close evaluation can be obtained using an abacus (Fig. 1).

2.2 Ordinal Scale

The ordinal scale provides only a ranking. This type of scale should be selected for two reasons: either the data are part of a discontinuous series, thus one cannot apply a number to them, or they come from a continuous series, but on an unknown scale on which it is not known if the distances between the measured objects are equal or proportional: only the rank is identified. For instance, nonexistent, slight, good, and very good improvements can be rated 0, 1, 2, 3, knowing that 3 does not mean that the improvement was 3 times better than 1. To describe series of this type, the adequate parameters are the median and the extreme values. Graduated scales should be avoided (especially when the series is made up of averages) because they may be mistakenly used for parametric measurements instead of being more accurately applied to ranking measurements. This type of classification is particularly indicated in psychosensorial evaluations in which the phenomenon under study varies discontinuously, or continuously but with unknown intervals.

2.3 Interval Scale

Interval scales are most commonly used in evaluation for numbers in a continuous series. Units may be changed if the scale is the same (e.g., temperature in the same series can be converted from Celsius into Fahrenheit degrees and vice versa). If the data have a gaussian (or normal) distribution, they can be described by the mean and its standard error (i.e., the standard deviation of the mean); otherwise the adequate parameters are the median and the extreme values. If it is previously known that the studied parameter has a gaussian distribution, one can surmise that the means of samples equal to or greater than 30 are also normally distributed. In a comparative evaluation, it is often possible that each subject is its own reference; this avoids the interindividual source of variation (important in biology) and makes it possible to use statistical tests for matched pairs.

2.3.1 Opposition Method

The opposition method, also called the zero method, is used to obtain a higher degree of precision than a direct measurement. The rationale is to measure only the difference between the unknown quantity and another very close and already precisely known value. The measure of

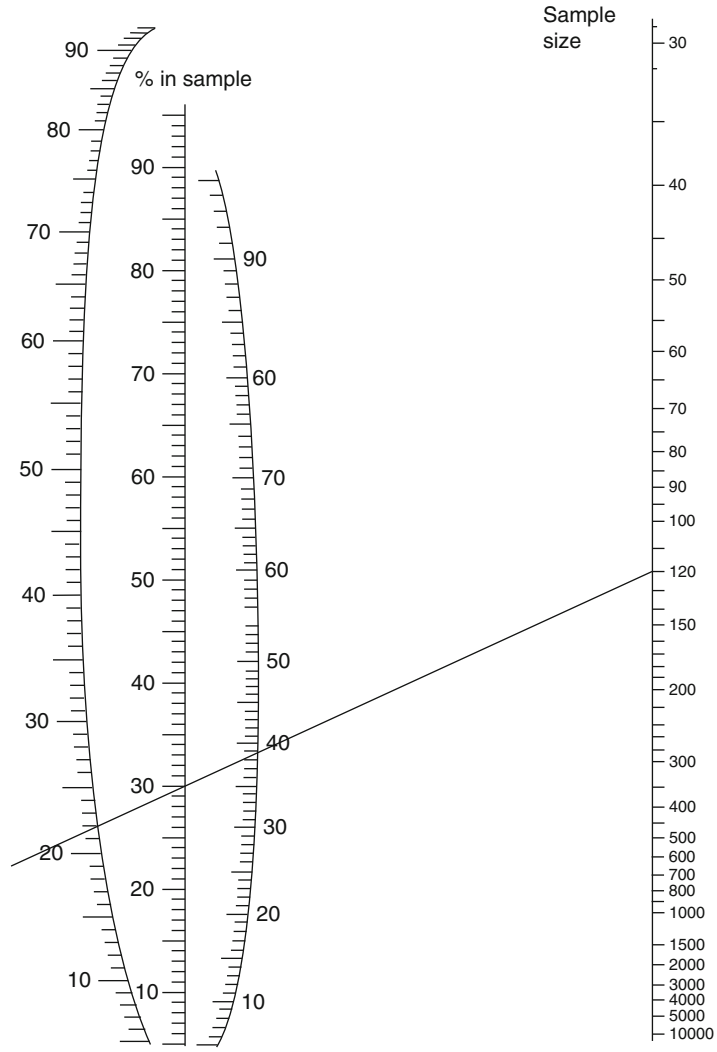

Fig. 1 Confidence interval of a percentage when the probability of a greater or lower number occurring by chance only is limited to 5 %. As shown, if the sample size is 120, the 5 % confidence interval of 30 % is 22–39 %. If the sample size is 40, the 5 % confidence interval of 30 % is 18–47 %

the difference can be more precise because it deals with a much smaller quantity. Consequently its precision, related to the initial value to be measured, becomes more accurate. For instance, to weigh sebum laid on a glass slide, the slide is placed on one pan of a pair of scales and a standard mass of a similar weight known with great precision (e.g., a glass slide without sebum) is placed on the other. Then a weight is added on the lighter side to make up the difference and this difference is then measured. The International Bureau of Weights and Measures has scales designed for this type of differential weighing.

2.3.2 Psychosensorial Evaluations

For the psychosensorial evaluations in which the studied phenomenon is believed to vary in a continuous and uniform way (equal intervals), a nongraduated linear scale is used for each measurement. Generally this measurement consists of a 10-cm-long horizontal line, with zero on the left end and ten on the right; the measurement is indicated by a small vertical stroke. Graduated scales are less suitable because they tend to distort the scoring by favoring values close to the graduations, with the operator influenced by the value indicated. However, operators should be well

aware of the scale extremes (zero and ten), which sets the limits of the measure; consequently its variability is lessened. Another way to decrease variability is to replace the absolute measurement by a comparative measurement: the objects to be compared are placed next to each other so that they are perceived almost simultaneously; the nearer they are in time and space, the more accurate the measurement is. Operator training is also important.

3 Selecting the Suitable Unit

The units can be either arbitrary (e.g., millimeters on the linear scales used for psychosensorial measures), or arbitrarily linked to international physical units (e.g., skin blood flow measured in volts by the Doppler), or absolute (e.g., skin blood flow measured by the epicutaneous xenon clearance in milliliters per minute per 100 g soft tissue). Physical units are always better than arbitrary units, and absolute units are preferred to those of other associated physical phenomena (e.g., measuring stratum corneum water depletion in milliliters per square centimeter per hour, as compared to decreased electrical impedance). Creating dermatological or biological units should be avoided when it is possible to use internationally approved units so that skin structure and properties remain within the physics of all other materials for easier comparison and the opportunity to use the laws of physics and chemistry for interpretation, thus considerably increasing the benefit of the measurements, also necessary for scientific progress.

We recommend measurements in units of the *Système International d'Unités* (SI), also called the MKSA system, the four fundamental units of which are the meter (m), the kilogram (kg), the second (s) and the ampere (A). Skin area is commonly measured in square centimeters, its thickness in millimeters, etc. For the derived units, the conversion between the centimeter-gram-second (CGS) system, MKSA, or other systems is often a source of error. See conversion tables in ▶ Chap. 160, "Correspondence Between International System Units (MKSA) and CGS Units."

4 Data Presentation

Faced with a variation or a distribution, the first step to prepare is a graphic representation: a curve or a histogram. The eye appreciates at once a series of features necessary for the interpretation and the processing of the information, for example, the gaussian or nongaussian characteristic of a distribution, the linear or nonlinear character of a relation, and the absolute level of a measure. Misunderstandings often stem from skipping this step.

When studying a histogram, the first question is "Does it fit a well-known distribution?" because the processing and interpretation of the data is then easier. A gaussian distribution, bell-shaped and symmetrical, means that data are independent of each other and that the distribution most probably results only from their summation. A distribution with two peaks may correspond to two interpenetrated gaussian curves. To rapidly check if a distribution is gaussian, the use of gaussometric graph paper (or gaussologarithmic if the abscissa is in logarithms) is suitable: it provides a quick calculation of the adjustment to this type of distribution. An asymmetrical histogram may indicate a binomial distribution. A substantial asymmetry suggests a Poisson distribution (a particular case of binomial distribution). An asymmetrical distribution can sometimes be transformed into a gaussian one by using the logarithm of the data.

Showing a variation through a mathematical function (of time or any other parameter) indicates major progress in data interpretation, if the variable has an anatomical or functional meaning. This makes it possible to use the function in other situations, sometimes to generalize its use, with further progress in knowledge. However, a purely descriptive mathematical model (i.e., when variables are devoid of biological meaning) is of minimal interest. The linear function speaks for itself and is one of the most profitable functions through the calculation of the slope and intercepts with the axes. It can be deduced from an exponential function by taking the logarithm of the data, and from any other function by replacing x on the x-axis with a power of x (e.g., for $y = a + b/x$, $1/x$ is put on the x-axis).

5 Precision of Measures

In a common parametric measurement, the highest level of accuracy is desirable, even if ultimately the decimals are rounded for convenience. Only the significant figures must be mentioned. Sampling uncertainty should always be mentioned, together with the observed variation.

5.1 Calculation of the Maximum Experimental Error in Measurements

To predict the maximum possible error in a measure of combined quantities from the separate measure of each quantity, the standard rules are:

- The absolute error Δy on a sum $y = u + v$ is the sum of the errors on each component $\Delta y = \Delta u + \Delta v$.
- The absolute error Δy on a difference $y = u - v$ is the sum of the errors on each component $\Delta y = \Delta u + \Delta v$.
- The absolute error Δy on a product $y = uv$ corresponds to the formula $\Delta y = u\Delta v + v\Delta u$. The relative error $\Delta y/y = \Delta u/u + \Delta v/v$.
- The absolute error Δy on a quotient $y = u/v$ corresponds to the formula $\Delta y = (u\Delta v + v\Delta u)/v^2$. The relative error $\Delta y/y = \Delta u/u + \Delta v/v$.

Note that these errors (Δu, Δv, etc.) are experimental errors on crude data and have no relation to statistical errors which are dealt with in the following paragraphs.

5.2 Variation in a Gaussian Distribution

In a gaussian distribution, the mean (m) must be presented with its uncertainty limits (i.e., either standard deviation and number of data, or standard error of the mean). The standard deviation (SD) must be mentioned with the number of observations (n) because the confidence interval it indicates (95 % confidence interval ranges between two standard deviations on each side of m) differs with the number of measurements. The standard error could either be mentioned (SD divided by the square root of the number of observations), as in the error bars of a graph of means. If the data are logarithmic, the mean must be geometrical (n^{th} root of the product of n data). In the case of a percentage, both the SD and the number of data should be mentioned.

5.3 Variation in an Atypical Distribution

If the histogram does not show a gaussian distribution, it should be described using the median instead of the mean, i.e., the value under and above which 50 % of the observations are found. The variability around this value is indicated in the quartiles, which are the values under which 25 %, 50 %, and 75 % of the observations are made. One can also mention the centiles (or percentiles), the 80th centile being the value under which 80 % of the data are found.

The constant search for precision must not be sterilizing. An isolated mean, a separate percentage, a graph with no mention of variation are only indicators, but are always preferable to the text alone.

6 Comparative Measurements

One purpose of a measurement is to compare the obtained value to others, to ascertain whether the observed difference is true, or rather to calculate the probability that it might originate from chance alone. The methods chosen vary according to the type of measurement.

6.1 Comparison of an Isolated Value (x) to a Gaussian Series of More than 30 Numbers

Its distance to the mean of the series determines the probability for the value x to belong to this reference population by chance alone. For a

distance of 1 SD, the probability is 15.9 %, for two SDs 2.3 %, and for three SDs 0.13 %. The exact probability is the total area (=1) under the Gauss curve minus the part of that area beyond x on the x-axis. It can be found in gaussian curve tables, where it has to be divided by 2 since the value of x is located on one side of the mean (one-tailed test).

6.2 Comparisons of Two Series of Measurements

6.2.1 Gaussian Series or Series Larger than 30

Use the test of comparison of variances (statistics manuals: F tables), followed by the usual parametric tests of comparison of means.

Series with Variances (s^2) Not Significantly Different

– Independent samples n_a and n_b are ≥ 30; use the formula:

$$\in = (m_a - m_b)/\left({s_a}^2/n_a + {s_b}^2/n_b\right)^{0,5}$$
$$\text{with degree of freedom } (df) = n_a + n_b - 2$$

– Independent samples n_a and n_b are <30; use the formula:

$$t = \frac{m_a - m_b}{\sqrt{\left(\frac{1}{n_a} + \frac{1}{n_b}\right)\frac{s_a^2(n_a - 1) + s_b^2(n_b - 1)}{n_a + n_b - 2}}}$$
$$\text{with } df = n_a + n_b - 2$$

– Matched samples: the calculation is made on the paired differences (n pairs): use the formula:

$$t \ (\text{or} \in) = m.n^{0.5}/s, \ \text{where}$$
$$df = n - 1 \ \text{and}$$
$$m = \text{the mean of differences.}$$

The parameter (distance to the mean, calculated in standard deviation) is the same for the three situations, but it is called $\in$ or t depending on the size of each sample (30 or <30, respectively).

Series with Significantly Different Variances (s^2)

The same formulas are used but the number of degrees of freedom used to refer to the probability table must be modified according to the formula of Welch's G test,

$$\frac{1}{ddl} = \frac{1}{n_a - 1}\left[\frac{s_a^2}{n_a s^2}\right] + \frac{1}{n_b - 1}\left[\frac{s_b^2}{n_b s^2}\right]$$

the global variance s^2, calculated by the equation: $s^2 = {s^2}_a/n_a + {s^2}_b/n_b$

The threshold value of parameter t depends on the risk α and the one-tailed or two-tailed character of the hypothesis to be checked.

6.2.2 Nongaussian Series

Nonparametric tests should be used, for example:

– Comparison of two nominal-type series: χ^2 test
– Comparison of two independent ordinal-type series: Mann and Whitney test
– Comparison of two matched ordinal-type series: Wilcoxon's matched pairs signed-ranks tests
– Comparison of two independent interval-type series: randomization test for two independent samples (Siegel 1956)
– Comparison of two matched interval-type series: randomization test for matched pairs (Siegel 1956) (the most powerful nonparametric test)

6.3 Simultaneous Comparison of Several Sets of Measurements

- Gaussian series: one-way variance analysis (ANOVA)
- Nongaussian series:
  – Nominal type series: #χ^2 test
  – Independent ordinal- or interval-type series: Kruskal-Wallis variance analysis (Siegel 1956)
  – Matched ordinal- or interval-type series: Friedman's variance analysis (Siegel 1956)

7 Minimizing the Number of Measurements

7.1 Sequential Analysis

When observing the sequential *chance* occurrence of two types of events in order to know if one type is more probable than the other, intuitively one feels the most probable is the one that happens more often. Indeed, when the difference in occurrences increases, at one point it becomes statistically significant at the 5 % probability level (or any level chosen in advance). On a graph showing the sequence of events, each one marked by an oblique dash in a specific direction (e.g., upward for one series, downward for the other), a broken line is obtained, the global direction of which leans toward the direction of the most probable event. The limits the line would cross when the difference is significant can then be drawn on each side of the central line. As soon as this happens, the experiment can be stopped (Fig. 2) (Whitehead 1997).

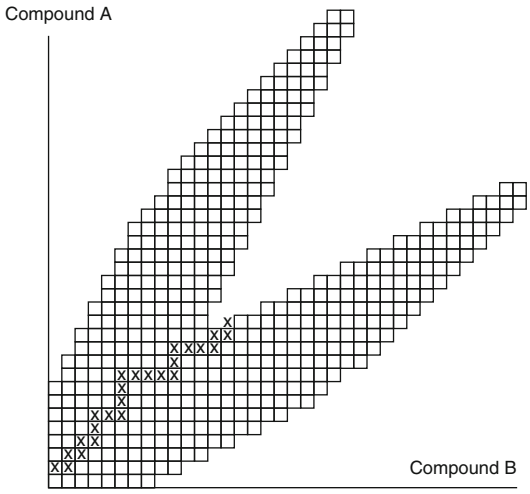

Fig. 2 Sequential trial. In the first patient, compound A was more effective than compound B, thus the first *vertical box* above the *black* one was checked. In the second patient, compound B was more effective than compound A, thus the next *horizontal box* was checked. In this example, the exit lies between the two wings of the grid, indicating no significant difference in effectiveness between the two compounds. Significance would be indicated by an exit at the exterior side of the wings

These limits can be computed using mathematic formulas which can be found in the book of Armitage et al. signalled at the end of this chapter.

7.2 Taguchi Designs

Taguchi designs are the most widely used experimental plans aimed at reaching the desired result with a minimum of experiments Taguchi and Wu (1980). For example, for the study of the effect of three parameters, each having two possibilities, it is possible to carry out four experiments instead of eight corresponding to the possible combinations. Among the categories of plans, the main types are:

- Designs with two parameters, each having two modes (L4 designs)
- Designs with three to five parameters, each having two modes (L8 designs)
- Designs for parameters with three modes (L9 designs)
- Designs allowing the combination of one parameter with two modes with parameters with three modes (L18 designs)
- Crossed designs, i.e., combining controlled parameters (as in the above designs) with so-called external parameters that are not under control.

8 Good Measuring Practice

Any measurement, especially in biology, has a degree of uncertainty, due to the nature of the measured phenomenon, as well as the measuring device and the operator. The reliability of a measurement can only be obtained if these last two factors are under control.

Equipment on the market must comply with technical standards. However, with time, performance may weaken, due to climatic, magnetic or other factors; we recommend placing the equipment on a test bench at regular intervals (for instance every year) in order to check the accuracy of its technical performance. For example, when a

device uses several pressures, are the displayed pressures correct? Does a cast meant to last several years lose its shape with time? It may be wise to check the device completely every year by measuring the equivalent skin standard. For example, the reliability of an ultrasound imaging device is checked by measuring the thickness of the layers of a stratified material. These methods are rarely used but should become common practice. Indeed, it is difficult to find standard materials that are reliable over prolonged periods. Manufacturers should assist users on this matter.

Most errors are caused by the operator and not the equipment. They tend to occur if the operator does not systematically ask: Have I read thoroughly and understood the instruction manual? Have I followed the recommendations? It is not possible to be a good operator instantly; patience, a critical mind, and experience are necessary.

The second question is related to the conditions in which the measurement is taken. Environmental conditions: temperature and relative humidity of the room must always be noted. Other conditions are specific to the type of measurement (e.g., for thermography). Physiological conditions related to the subject should be respected: minimum of 15 min acclimation to the room temperature, rest, relaxation (made easier when the test is noninvasive), thermal comfort, absence of sweating. A third question arises when subjects are their own controls: is the test site appropriate? Symmetry is no guarantee (Treffel et al. 1994), neither is proximity (Panisset et al. 1992). The random permutation of control and active sites obviates this problem. Finally a mandatory procedure is to always write down the date and hour, the environmental conditions, and an identification mark of the tested subjects, including the control subjects. Good practice in metrology implies that a manual or computerized logbook be kept with each device.

A rational catalog of possible errors sources is (Serup 1994):

1. Study design (strategic error)
2. The measuring device (technical error)
3. The use of the device (performance error)
4. Measuring conditions (inadequate laboratory facilities)
5. Selection and preconditioning of test subject (subject-related error)
6. Data acquisition, storing, and handling (data error)
7. Reporting and publication policies (explanatory mistake)

Even when these rules are observed, it is useful to know the results obtained by others. It often happens that the values given by a device in a laboratory group are not exactly the same as those given by similar equipment in another group. When new equipment is implemented, the operating team should check the reliability of their measurements on the same subjects, and know the variation coefficient (standard deviation/mean) of the measured parameters in a sample of at least 30 people. This is also essential in order to forecast the number of subjects (belonging to the tested sample) that will have to be recruited in comparative studies using this method.

For two independent samples, this number is given by the formula:

$$N \geq 2\left[\left(\in_{\alpha} + \in_{\beta}\right)s/\Delta\right]^2$$

where $\in_{\alpha}$ is the accepted limit probability for considering as true a difference Δ that does not exist (risk α): usually one takes $\in_{\alpha} = 1.96$ for a $\leq$5 % risk of error. And $\in_{\beta}$ is the risk of ignoring a real difference Δ (risk β): usually the chosen figure is: $\in_{\beta} = 1.28$ for a $\leq$10 % risk of error.

If the samples are matched (i.e., if subjects are their own controls) the formula is:

$$N \geq \left[\left(\in_{\alpha} + \in_{\beta}\right)s/\Delta\right]^2$$

Misinterpretation is forgivable. Mistakes are often made because of ignorance of what is actually measured. Upon obtaining results, the operator must ask the following two questions:

1. Beyond the object that is officially measured, what is the real phenomenon, e.g., the so-called sebum excretion rate? Possible answers are:
   - The follicular reservoir excretion rate
   - The sebaceous gland secretion rate

- The absorbing paper absorption rate
- The stratum disjunctum absorption rate

or what is the measuring method rationale, e.g., skin thickness measurement by ultrasound. The possible answer is the time for the ultrasound to go forward and backward divided by its *assumed constant* speed.

2. What is the measurement unit and why? For example, the cutaneous blood flow is measured in volts by the Doppler because an absolute calibration of the device has not been possible. A bias in the measurement technique may also alter the interpretation. It can be caused by subject and/or operator subjectivity or biased sample selection. The former problem is circumvented by using a single- or double-blind protocol, the latter by randomization of the sample or the sites so as to cancel unknown physiological variation (always use an algorithm-generated list of random numbers).

9 Conclusion

The following procedure should be followed by the operator:

1. Ascertain the reliability and accuracy of the equipment.
2. Meticulously follow all the manufacturer's instructions for using the equipment.
3. Set up the laboratory so that the material and physiological conditions of a precise measurement are routinely ensured.
4. Systematically record the above-mentioned elements on a specific logbook.
5. Determine the variance of the equipment's measures, preferably before the method is used routinely.

Acknowledgments The author thanks Mrs. Mariette Mercier, Professor of Statistics at the Faculty of Medicine and Pharmacy of Besançon (France), who kindly revised this chapter and provided the information about Welch's test.

References

Bernard C, editor. Introduction à l'étude de la médecine expérimentale. Paris: Flammarion; 1984. p. 185. Paris, 1865.

Escoffier C, De Rigal J, Rochefort A, Vasselet R, Lévêque J-L, Agache P. Age-related mechanical properties of human skin: an in vivo study. J Invest Dermatol. 1989;93:353–7.

Humbert P, Dupond JL, Agache P, et al. Treatment of scleroderma with oral 1,25-dihydrovitamin D3: evaluation of skin improvement using non-invasive techniques. Acta Derm Venereol. 1993;73:449–51.

Larnier C, Ortonne JP, Venot A, Faivre B, Beani JC, Thomas P, Brown TC, Sendagorta E. Evaluation of cutaneous photodamage using a photographic scale. Br J Dermatol. 1994;130:167–73.

Panisset F, Treffel P, Faivre B, Brunet-Lecomte P, Agache P. Transepidermal water loss related to volar forearm sites in humans. Acta Derm Venereol. 1992;72:4–5.

Serup J. Bioengineering and the skin: from standard error to standard operating procedure. Acta Derm Venereol Suppl. 1994;185:5–8.

Siegel S, editor. Nonparametric statistics for the behavioral sciences. London: McGraw-Hill; 1956.

Taguchi G, Wu Y, editors. Introduction to off line quality control. Nagoya: Central Japan Quality Control Association; 1980.

Treffel P, Panisset F, Faivre B, Agache P. Hydratation, transepidermal water loss, pH and skin surface parameters: correlations and variations between dominant and non-dominant forearms. Br J Dermatol. 1994;130:325–8.

Whitehead J. The design and analysis of sequential clinical trials. 2nd ed. Chichester: Wiley; 1997.

Suggested Reading

Altman DG, editor. Practical statistics for medical research. London: Chapman & Hill; 1993.

Armitage P, Berry G, editors. Statistical methods in medical research. 2nd ed. Oxford: Blackwell Scientific Publications; 1987.

Bailar JC, Mosteller F, editors. Medical uses of statistics. Waltham: NEJM Books; 1986 (This is a general statistical handbook devoted to biologists and physicians, and written in simple language that would be understood even by readers who had no education in biostatistics).

Beyer WH, editor. Handbook of tables for probability and statistics. 2nd ed. Boca Raton: CRC Press; 1968.

Box GEP, Hunter WG, Hunter JS, editors. Statistics for experimenters. New York: Wiley; 1978.

Salsburg DS, editor. The use of restricted significance tests in clinical trials. Berlin/Heidelberg/New York: Springer; 1992.

Chronobiology of the Skin: Cutaneous Clocks and Biorhythms

3

Annette Mehling and Corinne Reymermier

Contents

Keywords
Biorhythms • Chronobiology • Circadian • Clocks • Skin

1 Introduction

Cognizance of time and its influence on the recurring behavioral patterns of plants and animals dates back many centuries (reviewed by Reinberg and Smolensky 1983; Moser et al. 2006; Halberg et al. 2001). The study of the rhythmic time-based relationships found in biological systems has been coined chronobiology – the science of investigating and objectively quantifying phenomena and mechanisms of the biological time structure, including the rhythmic manifestations of life (American Association for Medical Chronobiology and Chronotherapeutics, www.aamcc.net/glossary.htm). Chronobiological rhythms have a profound influence on organisms by providing the temporal structure for biological processes. To "tell time," most living organisms use timekeeping mechanisms known as "biological clocks." These "clocks" coordinate our physiological and behavioral functions, thereby optimizing the adaptations to and interactions with our environment. In the last decades, hundreds of different clocks/cycles have been identified sparking renewed interest in chronobiology. In addition, the awareness of the implications of chronobiological effects has increased, and it is now

A. Mehling (✉)
BASF Personal Care and Nutrition GmbH, Düsseldorf, Germany
e-mail: annette.mehling@basf.com

C. Reymermier
BASF Beauty Care Solutions France S.A.S, Lyon, France
e-mail: corinne.reymermier@basf.com

P. Humbert et al. (eds.), *Agache's Measuring the Skin*,
DOI 10.1007/978-3-319-32383-1_3

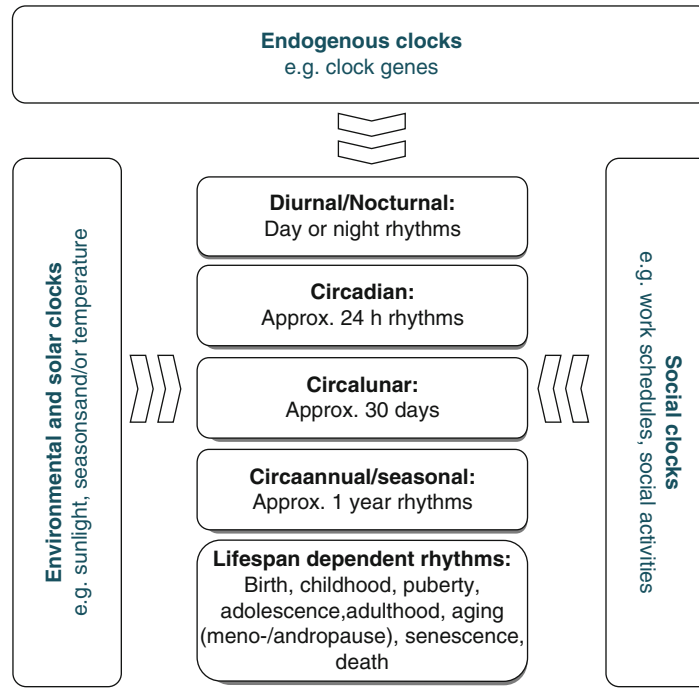

Fig. 1 Schematic representation of typical chronobiological rhythms and the clocks influencing them

recognized that these have true mechanistic and therapeutic implications (e.g., chronotherapy; reviewed by Kaur et al. 2013; Librodo et al. 2012). A short description of typical chronobiological rhythms is depicted in Fig. 1.

While the underlying science of biological oscillators is intricate and complex and therefore not entirely understood, our master clocks are most likely set according to the world's most reliable timekeeper: the sun. The circadian rhythm, the daily cycle, is probably the most pronounced and therefore the best researched. Light is assumed to be the most important zeitgeber, the external stimuli which entrain the rhythms and govern the synchronization of the circadian rhythm. Circadian timekeeping systems in mammals are organized into a complex hierarchical network of oscillators with the suprachiasmatic nucleus (SCN) of the hypothalamus acting as the principal pacemaker. The SCN receives light signals from specialized cells in the retina, the retinal ganglion cells, which entrain the SCN to light-dark cycles via glutaminergic innervation and/or photoreceptive systems based on melanopsin. This in turn triggers circadian rhythms, e.g., via the release of the hormone melatonin or adrenocorticotropic hormone (ACTH; Berson et al. 2002; Hastings et al. 2003; Luboshitzky 2000), which influences the peripheral clocks ubiquitously found in human cells. Although the exact functions are not yet well elucidated, it is reasonable to assume that the peripheral clocks are then responsible for the physiological fine-tuning leading to optimized responses to environmental and internal occurrences and processes. Biological periodicities can also be governed by other environmental cues, e.g., by the lunar cycle, but also by daily social rhythms, e.g., work. Interestingly, if left undisturbed, the "free-running" circadian rhythm in humans is approximately 25 h (possibly reflecting lunar influences as secondary synchronizers as this time period corresponds to the orbit time of the moon and with it, the tidal peaks that occur every 12 h and 25 min). One aspect that should not be forgotten is that life itself is a biological rhythm. Malfunctions of the biological clocks can lead to various disorders, including hypertension, sleep, psychosomatic disorders, and a number of chronobiological rhythms most likely out of phase in the elderly population

(Mishima et al. 2000; Pagani et al. 2011; Chang and Guarente 2013).

Skin is the interphase of the body and its environment. As such, it plays a critical role in the adaptation of processes to maintain the body's homeostasis. Although seasonal variations and phases inherent to life also play a role (e.g., reviewed by Mehling and Fluhr 2006), in the following, an overview will be given on chronobiological effects found in the skin with the main focus being on circadian rhythms (in this context including ultradian rhythms, etc.) and skin clocks.

2 Functional Chronobiological Rhythms of the Skin

Among the initial systematic and comprehensive studies actually focusing on the natural "healthy," chronobiological effects found in the skin function were the studies conducted by Yosipovitch et al. (1998) and Le Fur et al. (2001). Yosipovitch et al. conducted a study comparing the rhythmicity of the skin surface parameters: skin pH, skin surface moisture, skin barrier function (via transepidermal water loss, TEWL), and skin temperature. Measurements were conducted at four different locations (forehead, forearm, upper back, and shin) on seven women and nine men at 2-h intervals over a period of 24 h under well-controlled conditions. Discernible rhythms for TEWL, temperature, and pH were observed at most sites. Using TEWL as a measure of skin barrier function, the skin barrier showed an improved status in the morning which decreased toward the evening. This was not correlated with an increase in skin temperature, although skin temperature was also elevated at night. No significant differences were observed for skin hydration although capacitance was slightly higher around 4 p.m. In a later study, Yosipovitch et al. (2004) also investigated the effects of cortisone treatment of irritated and nonirritated skin on the circadian rhythms of blood flow, skin temperature, and TEWL. Blood flow exhibited circadian and ultradian rhythms with a significant correlation found to skin temperature but not TEWL. Blood flow was highest in the late afternoon/early evening and before onset of sleep and lowest in the morning.

Le Fur et al. (2001) studied time-dependent rhythms of the face and volar forearm skin over a time span of 48 h every 4 h under standardized environmental conditions. In addition to the skin parameters reported by Yosipovitch et al., sebum secretion was also measured. Salivary cortisol levels as surrogate markers for plasma cortisol were assessed to ensure that the volunteers were synchronized. In general, these results corroborated those found by Yosipovitch et al. Circadian rhythms were detected for sebum excretion (face), transepidermal water loss (face and forearm), skin temperature (forearm), pH (face), and capacitance (forearm). In addition, ultradian rhythms with periods of 8 h were found for sebum excretion, of 8 and 12 h for transepidermal water loss (face and forearm), and of 12 h for skin temperature (forearm). Skin pH was highest in the morning, sebum secretion peaked around midday, skin temperature of the forearm (but not face) was lowest around midday and exhibited two peaks at 4:00 p.m. and 4:00 a.m., and skin barrier function (cheek) as assessed by TEWL was lowest at 8:00 a.m. and 4:00 p.m.

Denda and Tsuchiya (2000) investigated the recovery of the skin barrier function (via TEWL measurements) of the volar forearm skin at various time points in the course of a day (30 h). Skin surface temperature peaked at 2:00–3:00 a.m. and remained slightly elevated throughout the morning. Following skin barrier disruption via tape stripping, recovery rates assessed via TEWL and measured 1 h after tape stripping exhibited time-dependent effects with decreased recovery rates found between 20:00 and 23:00 h in comparison to measurements made at other time points. During this time, there was no significant correlation to skin temperature. The basal TEWL values were observed at about 03:00 h (33.6 °C and 0.30 mg/cm^2/h) indicating that the time-dependent differences in cutaneous barrier repair are independent of changes in skin temperature.

"Out-of-sync" clocks have also been implicated in atopic dermatitis, psoriasis, contact

hypersensitivity, and skin cancer (Wood and Hrushesky 1996; Gelfant et al. 1982; Li et al. 2013; Takita et al. 2013; Gaddameedhi et al. 2011; Cermakian et al. 2013; Muñoz-Hoyos et al. 2007). Cutaneous immune responses to allergens differ throughout the day, e.g., Reinberg et al. (1965) observed that there is a circadian variation to the reactivity to skin tests. Zak-Nejmark et al. (2006) et al. studied skin reactivity of healthy and atopic individuals to histamine and observed that healthy individuals have the lowest reactivity at night. In contrast atopic individuals exhibit the highest reactivity at night. Histamine binding to lymphocytes and neutrophils also displayed variations between day and night. As atopics tend to suffer more from itching at night and asthma is also increased at night, this may have implications for chronotherapeutic approaches. Circadian processes may play a role in the exacerbation of skin cancer. Mice exhibited a fivefold increase of invasive squamous cell carcinoma when irradiated with UVB at 4:00 a.m. than at 4:00 p.m. Low-dose UVB has been reported to downregulate clock genes and to alter their expression, thereby modulating circadian rhythms (Kawara et al. 2002). Maintaining the proper balance between light and dark and the resulting beneficial (e.g., vitamin D production) or damaging effects (e.g., photodamage) of UV (reviewed by Desotelle et al. 2012) may have a pronounced impact on cellular functioning and susceptibility to skin cancer. Downregulation of clock genes has been observed in skin tumor biopsies indicating a possible role in protective role in cutaneous tumorigenesis (Lengyel et al. 2013), possibly attributable to aberrant cellular responses to DNA damage, including repair, checkpoints, and apoptosis. Clock genes play a role in hair cycling, beard hair follicles have endogenous clocks lined to PER1 and PER3, and clock gene dysfunction may play a role in age-related alopecia (Watanabe et al. 2012; Geyfman and Andersen 2010). These are but a few examples of chronobiological rhythms playing a role in cutaneous processes.

Differences in the circadian rhythms of skin function have been observed. These may be attributable to the time intervals used to assess the parameters. In some studies, parameters were measured every 2 h, in others every 4 h, etc. Depending on the sampling time, and the circadian rhythms exhibited by the organism, ultradian rhythms can be identified or certain circadian rhythms being missed. Other parameters, such as ambient temperature and humidity as well as season, may also lead to masking of the natural biorhythms or to different entrainments. Gender (e.g., menstrual cycle of women), age (children tend to have longer sleep phases, whereas aged people most likely have defective clocks), etc., may also play a role.

3 Cutaneous Clocks

Although circadian rhythms are entrained by the external time cues that are primarily governed by the solar day, circadian oscillations are also generated at the cellular level and occur in most cells of the body. These molecular clocks are not always directly linked to the cues given by the SCN, and cell autonomous clockworks can be found. These may be linked to physiological and metabolic processes that are not directly associated with the solar day, e.g., metabolic processes linked to food uptake or temperature variations as potential zeitgeber. The orchestration of the oscillations is governed by an intricate network of transcriptional and translational feedback loops. Among the most prominent examples are the positive transcriptional regulator genes *Clock* (Circadian Locomotor Output Cycles Kaput) and *Bmal*1 (brain and muscle aryl hydrocarbon receptor nuclear translocator-like protein-1) which drive the expression of the target genes such as the *Period* (*Per*) 1–3 genes and the genes *Cryptochrome* (*Cry*) 1 and 2. Autoregulatory negative feedback loops occur via the formation of PER/CRY protein complexes which in turn block the transcription factor CLOCK/BMAL1 and thereby inhibit their own transcription. How does this occur? The positive arm of the regulatory feedback loop is formed by the heterodimer CLOCK/BMAL1 which binds to the E-box sequences of targets genes such as *Per, Cry, ROR* (retinoid-related orphan receptor), and

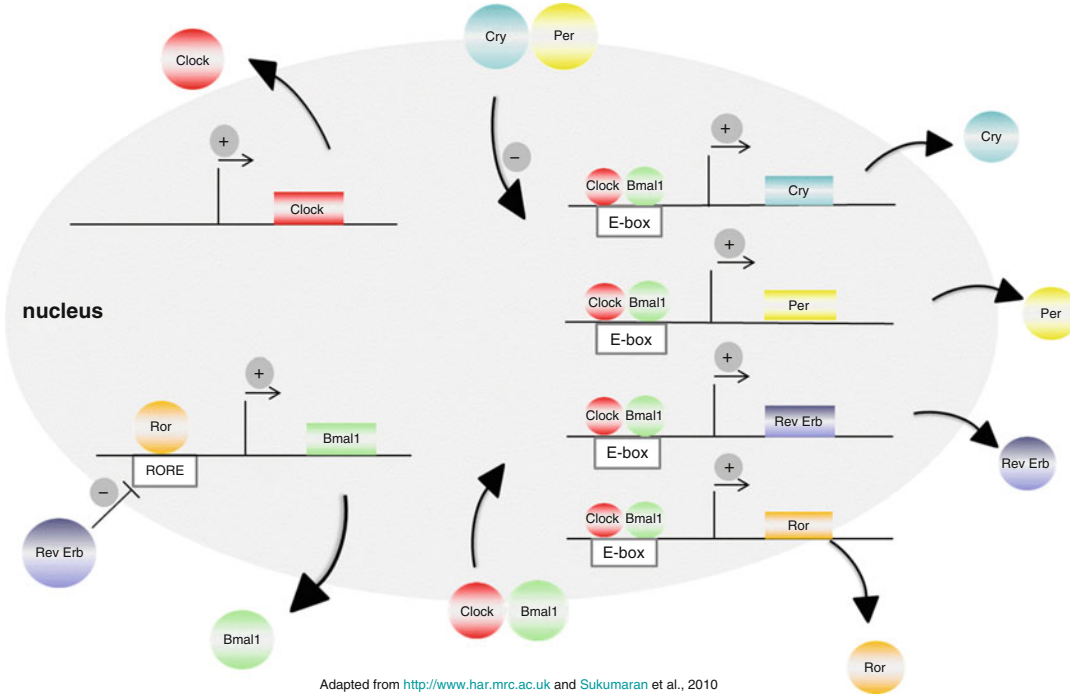

Fig. 2 Example of feedback mechanisms regulating cellular rhythms. In the cytoplasm, Clock and Bmal1 associate as a heterodimer before their translocation to the nucleus where they are able to bind to the E-box sequences of target genes such as PER, CRY, ROR and REV ERB in order to stimulate their transcription. CRY and PER are transcription factors which form the negative regulatory loop. They are able to heterodimerize in the cytoplasm before their translocation in the nucleus where they are able to inhibit the action of CLOCK/BMAL1 complex. Moreover, the nuclear receptor transcription factors ROR and REV-ERB have opposite control on *Bmal*1 gene. In turn ROR up-regulates and REV-ERB down regulates the expression of Bmal1 by binding to the RORE element present in the upstream region of the *Bmal*1 gene

REV-ERB (orphan nuclear receptor), thereby stimulating their transcription. The gene products, CRY and PER, can then form heterodimers which subsequently function as repressive transcription factors by inhibiting CLOCK/BMAL1 induced transcription, thereby forming the negative arm of the regulatory feedback loop. Further "oscillation" is achieved in that the expression of *Bmal1* is regulated by the nuclear receptor transcription factors ROR and REV-ERB. ROR upregulates and REV-ERB downregulates the expression of *Bmal1* by binding to the RORE element present in the upstream region of the *Bmal1* gene (Fig. 2). In addition, TIM (timeless protein) can control PER stabilization in the cytoplasm by binding to specific domains in order to coregulate their subcellular localization and to protect PER from degradation or to activate the repression of CLOCK/BMAL1 function (Sukumaran et al. 2010). Cellular clockworks such as these are also found in the skin, and it is estimated that up to 10 % of the genes exhibit a circadian rhythmic expression (Desotelle et al. 2012).

Expression of the human clock genes, *Clock, Tim, Per1, Cry1,* and *Bmal1,* is found in both the oral mucosa and skin and is typically aligned with the circadian profiles controlled by the SCN. The patterns are strongly correlated with the expression patterns found in mice suggesting that the skin itself may be an additional pacemaker in circadian rhythms (Bjarnason et al. 2001). The expression of the genes *Per1, Cry1,* and *Bmal1* peaks in the morning, late afternoon, and at night. In addition, the expression of the cell cycle proteins of the mucosa

coincides with the expression of some clock genes, e.g., with *Per*1 expression occurring at the same time as the G_1 phase, indicating an interaction of the gene products. Cultured human skin cells, e.g., keratinocytes and fibroblasts, as well as the keratinocyte cell line HaCaT and the melanoma A375 have been shown to exhibit expression of the circadian clock genes *Clock* and *Per1* (Zanello et al. 2000). HaCaTs have robust circadian expression patterns which correlate well with those found in vivo as does the murine fibroblast cell line NIH3T3. In a recent study, Spörl et al. (2011) investigated the effects of temperature cycles on the rhythmicity of the cutaneous clocks. As Yosipovitch et al. (1998) already reported for human skin, temperature is an effective zeitgeber for the cellular clocks, e.g., *Per2* (both primary keratinocytes and cultured cell lines), thereby linking them to the physiological influences given by environmental cues. Rhythmic PER2 expression has also been described by Tanioka et al. (2009) who observed an essential role of this protein in generating circadian oscillations in the peripheral clocks. Temperature can even be used to entrain the cells. Interestingly, a circadian transcription of *Insig2a* was also observed. This gene is pivotal for cholesterol homeostasis and with it for keratinocyte differentiation, cornified envelope development, and skin barrier function. If there is a cholesterol deficiency, sterol regulatory element binding proteins (SREBPs) are released and activate de novo synthesis of cholesterol (e.g., via *Hmgcr*) or enhance its uptake (e.g., via *Ldl* receptor gene products), whereby both genes also intriguingly exhibit circadian rhythms. The same group recently employed genome-wide transcriptional profiling in which whole genome microarrays were used to characterize gene expression profiles in human suction blister epidermis during the course of a day (Spörl et al. 2012). Over 300 genes exhibited diurnal daytime-dependent expression, many of which were also found in vitro. Among these, Krüppel-like factor 9 (*Krf9*) exhibited a profound circadian rhythms which was cortisol dependent and linked to keratinocyte differentiation and proliferation.

The proliferation HaCaT cells has also been reported to be influenced by melatonin – the secretion of which has a pronounced circadian rhythm itself (Hipler et al. 2003; Fischer et al. 1999). Clock gene expression in HaCaT cells is modulated by low-dose UVB irradiation (Kawara et al. 2002) suggesting that expression in circadian clock genes in keratinocytes is influenced by solar irradiation via melatonin-independent mechanisms. These studies give further indication that skin processes follow chronobiological patterns and exposure of the skin to UV irradiation and/or light may possibly be involved in the circadian rhythm regulation via modulation of clock gene expression. The observation that skin cancer is also controlled by circadian rhythms, e.g., as nucleotide excision repair genes follows circadian patterns (Gaddameedhi et al. 2011; Sancar et al. 2010), further points to the important role chronobiological processes have on organisms.

4 Conclusions

The skin barrier function is essential in protecting the body against water loss, pathogens, and xenobiotics. The studies described above suggest that skin has a pronounced circadian rhythm. An interpretation of the observed time-dependent patterns is that they are suggestive of skin adapting to boost its protective functions during the day to ward off environmental threats; during evening and night processes are then directed at regeneration. As skin seems to be more reactive and permeable toward late afternoon and evening, these effects can possibly be used to optimize delivery and efficacy of both cosmetic and medical actives. Clocks are found on the cellular/molecular level in cells throughout the body indicating a profound importance for the fine-tuning needed to maintain the body's homeostasis when adapting multitude of different environmental and cellular cues. The concepts of chronopharmaceutics and chronocosmetics are not just obscure imaginings – they have a justified role in designing more efficacious and targeted approaches to pharmaceutical and skin care regimens.

References

Berson DM, Dunn FA, Takao M. Phototransduction by retinal ganglion cells that set the circadian clock. Science. 2002;295:1070–3.

Bjarnason GA, Jordan RC, Wood PA, Li Q, Lincoln DW, Sothern RB, Hrushesky WJ, Ben-David Y. Circadian expression of clock genes in human oral mucosa and skin: association with specific cell-cycle phases. Am J Pathol. 2001;158:1793–801.

Cermakian N, Lange T, Golombek D, Sarkar D, Nakao A, Shibata S, Mazzoccoli G. Crosstalk between the circadian clock circuitry and the immune system. Chronobiol Int. 2013;30:870–88.

Chang HC, Guarente L. SIRT1 mediates central circadian control in the SCN by a mechanism that decays with aging. Cell. 2013;153:1448–60.

Denda M, Tsuchiya T. Barrier recovery rate varies time-dependently in human skin. Br J Dermatol. 2000;142:881–4.

Desotelle JA, Wilking MJ, Ahmad N. The circadian control of skin and cutaneous photodamage. Photochem Photobiol. 2012;88:1037–47.

Fischer TW, Wigger-Alberti W, Elsner P. Melatonin in dermatology. Experimental and clinical aspects. Hautarzt. 1999;50:5–11.

Gaddameedhi S, Selby CP, Kaufmann WK, Smart RC, Sancar A. Control of skin cancer by the circadian rhythm. Proc Natl Acad Sci U S A. 2011;108:18790–5.

Gelfant S, Ozawa A, Chalker DK, Smith Jr JG. Circadian rhythms and differences in epidermal and in dermal cell proliferation in uninvolved and involved psoriatic skin in vivo. J Invest Dermatol. 1982;78:58–62.

Geyfman M, Andersen B. Clock genes, hair growth and aging. Aging (Albany NY). 2010;31:122–8.

Halberg F, Cornélissen G, Otsuka K, Katinas G, Schwartzkopff O. Essays on chronomics spawned by transdisciplinary chronobiology. Witness in time: Earl Elmer Bakken. Neuro Endocrinol Lett. 2001;22:359–84.

Hastings MH, Reddy AB, Maywood ES. A clockwork web: circadian timing in brain and periphery, in health and disease. Nat Rev Neurosci. 2003;4:649–61.

Hipler UC, Fischer TW, Elsner P. HaCaT cell proliferation influenced by melatonin. Skin Pharmacol Appl Skin Physiol. 2003;16:379–85.

Kaur G, Phillips C, Wong K, Saini B. Timing is important in medication administration: a timely review of chronotherapy research. Int J Clin Pharm. 2013;35:344–58.

Kawara S, Mydlarski R, Mamelak AJ, Freed I, Wang B, Watanabe H, Shivji G, Tavadia SK, Suzuki H, Bjarnason GA, Jordan RC, Sauder DN. Low-dose ultraviolet B rays alter the mRNA expression of the circadian clock genes in cultured human keratinocytes. J Invest Dermatol. 2002;119:1220–3.

Le Fur I, Reinberg A, Lopez S, Morizot F, Mechkouri M, Tschachler E. Analysis of circadian and ultradian rhythms of skin surface properties of face and forearm of healthy women. J Invest Dermatol. 2001;117:718–24.

Lengyel Z, Battyáni Z, Szekeres G, Csernus V, Nagy AD. Circadian clocks and tumor biology: what is to learn from human skin biopsies? Gen Comp Endocrinol. 2013;1:67–74.

Li WQ, Qureshi AA, Schernhammer ES, Han J. Rotating night-shift work and risk of psoriasis in US women. J Invest Dermatol. 2013;133:565–7.

Librodo P, Buckley M, Luk M, Bisso A. Chronotherapeutic drug delivery. J Infus Nurs. 2012;35:329–34.

Luboshitzky R. Endocrine activity during sleep. J Pediatr Endocrinol Metab. 2000;13:13–20.

Mehling A, Fluhr JW. Chronobiology: biological clocks and rhythms of the skin. Skin Pharmacol Physiol. 2006;19:182–9.

Mishima K, Okawa M, Hozumi S, Hishikawa Y. Supplementary administration of artificial bright light and melatonin as potent treatment for disorganized circadian rest-activity and dysfunctional autonomic and neuroendocrine systems in institutionalized demented elderly persons. Chronobiol Int. 2000;17:419–32.

Moser M, Frühwirth M, Penter R, Winker R. Why life oscillates–from a topographical towards a functional chronobiology. Cancer Causes Control. 2006;17(4):591–9.

Muñoz-Hoyos A, Espín-Quirantes C, Molina-Carballo A, Uberos J, Contreras-Chova F, Narbona-López E, Gutiérrez-Salmerón MJ. Neuroendocrine and circadian aspects (melatonin and beta-endorphin) of atopic dermatitis in the child. Pediatr Allergy Immunol. 2007;18:679–86.

Pagani L, Schmitt K, Meier F, Izakovic J, Roemer K, Viola A, Cajochen C, Wirz-Justice A, Brown SA. Eckert A serum factors in older individuals change cellular clock properties. Proc Natl Acad Sci U S A. 2011;108:7218–23.

Reinberg A, Smolensky MH. Introduction to chronobiology, Biological rhythms and medicine topics in environmental physiology and medicine. 1983. Springer New York, p. 1–21. doi 10.1007/978-1-4613-9496-9.

Reinberg A, Ghata J, Sidi E. Circadian reactivity rhythms of human skin to histamine or allergen and the adrenal cycle. J Allergy. 1965;36:273–83.

Sancar A, Lindsey-Boltz LA, Kang TH, Reardon JT, Lee JH, Ozturk N. Circadian clock control of the cellular response to DNA damage. FEBS Lett. 2010;584:2618–25.

Spörl F, Schellenberg K, Blatt T, Wenck H, Wittern KP, Schrader A, Kramer A. A circadian clock in HaCaT keratinocytes. J Invest Dermatol. 2011;131:338–48.

Spörl F, Korge S, Jürchott K, Wunderskirchner M, Schellenberg K, Heins S, Specht A, Stoll C, Klemz R, Maier B, Wenck H, Schrader A, Kunz D, Blatt T, Kramer A. Krüppel-like factor 9 is a circadian transcription factor in human epidermis that controls proliferation of keratinocytes. Proc Natl Acad Sci U S A. 2012;109:10903–8.

Sukumaran S, Almon RR, DuBois DC, Jusko WJ. Circadian rhythms in gene expression: relationship

to physiology, disease, drug disposition and drug action. Adv Drug Deliv Rev. 2010;62:904–17.
Takita E, Yokota S, Tahara Y, Hirao A, Aoki N, Nakamura Y, Nakao A, Shibata S. Biological clock dysfunction exacerbates contact hypersensitivity in mice. Br J Dermatol. 2013;168:39–46.
Tanioka M, Yamada H, Doi M, Bando H, Yamaguchi Y, Nishigori C, Okamura H. Molecular clocks in mouse skin. J Invest Dermatol. 2009;129:1225–31.
Watanabe M, Hida A, Kitamura S, Enomoto M, Ohsawa Y, Katayose Y, Nozaki K, Moriguchi Y, Aritake S, Higuchi S, Tamura M, Kato M, Mishima K. Rhythmic expression of circadian clock genes in human leukocytes and beard hair follicle cells. Biochem Biophys Res Commun. 2012;425:902–7.
Wood PA, Hrushesky WJ. Circadian rhythms and cancer chemotherapy. Crit Rev Eukaryot Gene Expr. 1996;6:299–343.
Yosipovitch G, Xiong GL, Haus E, Sackett-Lundeen L, Ashkenazi I, Maibach HI. Time-dependent variations of the skin barrier function in humans: transepidermal water loss, stratum corneum hydration, skin surface pH, and skin temperature. J Invest Dermatol. 1998;110:20–3.
Yosipovitch G, Sackett-Lundeen L, Goon A, Huak CY, Goh CL, Haus E. Circadian and ultradian (12 h) variations of skin blood flow and barrier function in non-irritated and irritated skin – effect of topical corticosteroids. J Invest Dermatol. 2004;122:824–9.
Zak-Nejmark T, Nowak IA, Kraus-Filarska M. Circadian variations of histamine binding to lymphocytes and neutrophils and skin reactivity to histamine in atopic and healthy subjects. Arch Immunol Ther Exp (Warsz). 2006;54:283–7.
Zanello SB, Jackson DM, Holick MF. Expression of the circadian clock genes clock and period1 in human skin. J Invest Dermatol. 2000;115:757–60.

The Skin Surface Ecosystem: A Presentation

4

Thomas Lihoreau and Pierre Agache

Contents

Keywords
Skin surface • Microbiome • Microbiota • Microflora • Microbiology • Stratum corneum • Ecosystem • Bacteria • Dysbiosis

The skin surface is an ecosystem: its ground is the desquamating uppermost stratum corneum (the *stratum disjunctum*) and the living part is the resident bacterial and mycotic flora, continuously proliferating in a complex environment made of lipids of sebaceous and epidermal origin, desmosomal and intercellular enzymatic protein degradation, transepidermal water, and sweat. The part played by physicochemical phenomena (surface tension, electrochemistry) is considerable. This ecosystem constantly regenerates and remains stable in spite of the daily sloughing out of one *stratum disjunctum* layer, i.e., about a third of the ecosystem thickness. Its part in the skin physiology is essential and subject of lots of works in the last years, involving experts in dermatology, microbiology, immunology, and molecular and genomic fields.

1 Skin Relief

The relief of the skin surface (also referred to as microrelief, microtopography, skin surface texture, skin roughness) varies according to the anatomic site and their own characteristics. It is formed by the association of the furrows, the follicular orifices or sweat pores, and the slightly

Pierre Agache: deceased.

T. Lihoreau (✉)
Center for Research and Studies on the Integument (CERT), Department of Dermatology, Clinical Investigation Center (CIC INSERM 1431), Besançon University Hospital; INSERM UMR1098, FED4234 IBCT, University of Franche-Comté, Besançon, France
e-mail: tlihoreau@chu-besancon.fr

P. Agache
Department of Dermatology, University Hospital of Besançon, Besançon, France
e-mail: aude.agache@free.fr; ferial.fanian@chu-besancon.fr; ferial.fanian@cert-besancon.com

P. Humbert et al. (eds.), *Agache's Measuring the Skin*,
DOI 10.1007/978-3-319-32383-1_4

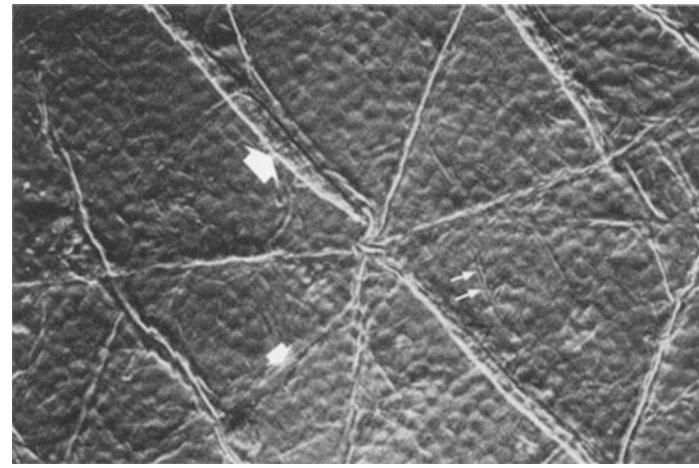

Fig. 1 Volar forearm skin surface. *Thick arrow*: first-order furrow. *Middle-sized arrow*: second-order furrow. *Small arrows*: third-order furrows. In between furrows are easily recognized the bumps made by corneocytes (corneocyte pavement). Scanning electron micrograph (Courtesy of Dr Boleslav Turek)

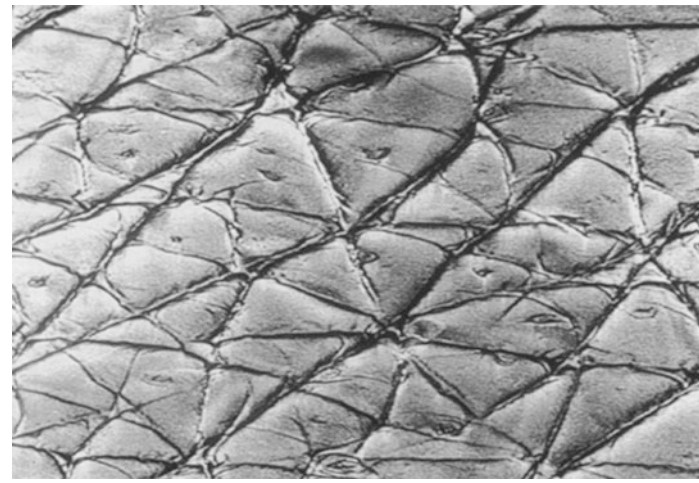

Fig. 2 Volar forearm skin surface. Sweat duct orifices are seen on some plateaus. Scanning electron micrograph (Courtesy of Dr Boleslav Turek)

protruding corneocytes (Fig. 1). On most sites, the main furrows, called primary lines (Wolf 1940; Hanusova 1938; Tring and Murgatroyd 1974), are 70–200 μm deep and follow two directions at least and delimit plateaus of variable shapes according to the area (Chinn and Dobson 1964; Sarkany and Caron 1965). The follicular orifices are located at the junction of these furrows, whereas the eccrine sweat pores (Figs. 2 and 3) are preferentially on the plateaus (Johnson et al. 1970) or in more superficial furrows, called secondary lines, and 20–70 μm deep. The third type of furrows roughly separates groups of corneocytes and is inconstant.

This network of furrows is present at birth (Tchernoff 1985) and its depth increases with age until puberty (Makki et al. 1984). In adults, it is less deep in women (Makki et al. 1984). On the face, small wrinkles (depth 0.2–1 mm) and deeper wrinkles (depth >1 mm) appear with age. On other zones, the deepest furrows increase, the small furrows disappear, and the skin surface becomes distended (Makki et al. 1984; Corcuff et al. 1983; Zahouani and Vargiolu 2004). The main function of the furrows is mechanical. By (partly) smoothing out they allow the extension of the skin surface and the epidermis. Their anatomical distribution

reflects at each site the direction of the mechanical constraints sustained by the skin. On the volar forearm, the resistance to this smoothing action represents approximately 50 % of the resistance of the whole skin to stretching (Panisset et al. 1993). The furrows also act as channels for the sebum and sweat flowing and retention. They preferentially trap and keep the substances applied on the skin: they are possibly preferential sites of percutaneous absorption.

On the palms and soles, the furrows draw curvy shapes which form the dermatoglyphs. The plateaus are replaced by concentric ridges on top of which sweat pores are located at regular intervals (Fig. 4). This type of relief seems specifically adapted to the need to adhere to the ground and objects. This is achieved by three factors: the dermatoglyphic drawing, the constant moisturizing of the crests by a slow although continuous sweat secretion which considerably increases the friction coefficient (Highley et al. 1977), and finally the sudden sweat secretion of the palms and soles in the event of a psychological stress (psychogenic sweating). This function was crucial for primitive humans who lived naked in the savanna. For a probably similar reason, the palms and soles have no pilosebaceous follicles: the sebum, like any fatty substance, and the hairs reduce the friction coefficient (Elkhyat et al. 2014).

2 Microbiology of the Skin Surface

One major aspect of the skin surface ecology is the presence of a resident bacterial (more than 10^{10} bacteria living on our skin), mycotic (and probably viral) flora; its presence and normal behavior are essential to ensure a healthy skin (Kloos 1981). Numerous researches focus on understanding the role of these microbes in human health and

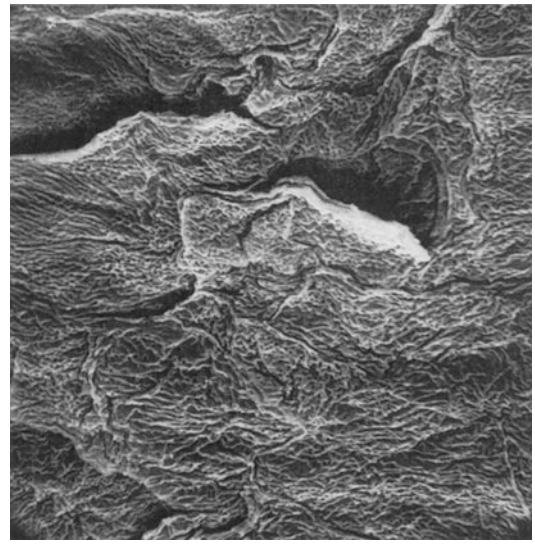

Fig. 3 Sweat duct orifice. Scanning electron micrograph of a Silflo replica. X 2000. (Laboratory of Skin Biophysics, Besançon)

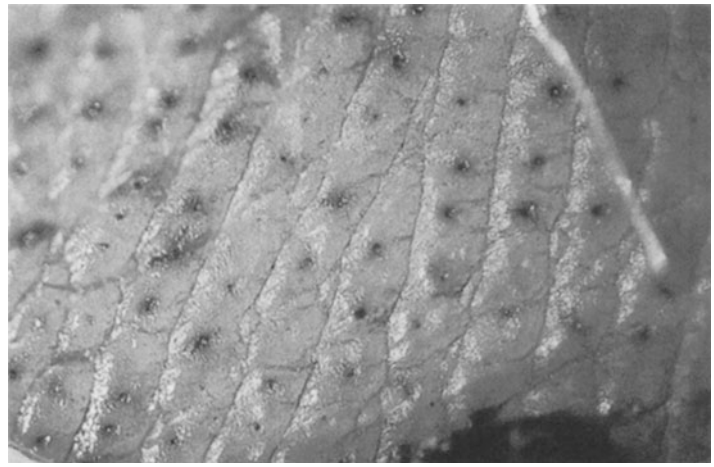

Fig. 4 Finger pad skin surface. Orthophtaldialdehyde-dyed sweat orifices are located on the concentric ridges (Laboratory of Skin Biophysics, Besançon)

diseases; this field of research received support from institutions such as US National Institutes of Health that initiated in 2007 the Human Microbiome Project (HMP, www.hmpdacc.org) and use now advanced and high-level technologies, like metagenomic sequencing for genetic characterization of skin microbiota (Schloss 2014) or molecular gene profiling to identify the species or phylotypes (Dekio et al. 2005).

2.1 Skin Flora Behavior

Research over the last years has provided data on the nature and the taxonomy of the resident species (Table 1). Most of these microorganisms live in colonies adhering to the squames, mainly in the furrows of the skin surface, in the pilosebaceous infundibula, and inside the *stratum disjunctum*.

The permanently *resident* character of the typical skin flora (micrococci, *P. acnes*, aerobic corynebacteria, *Pityrosporum*) implies its continuous proliferation in situ, regulated by the nutrients found in the area (especially lipids), humidity, pH, and probably other factors such as temperature, partial oxygen and carbon dioxide pressure, and exposure to ultraviolet rays. The bacterial spectrum depends primarily on local factors. For example, the density (number of microorganisms per surface unit) is almost constant. It reproduces itself quickly after scratching, bathing, or washing and even after disinfection (Johnston et al. 1987). A bath a day or no washing for 3 weeks will not make any difference (Hartmann 1990).

The *temporarily resident* character (transient flora) applies to potentially pathogenic (*S. aureus, C. minutissimum*, Gram-negative bacteria (*Proteus, Klebsiella, Pseudomonas aeruginosa, Escherichia coli*), non-lipophilic yeast (*levure*) (*C. albicans*), dermatophytes) microorganisms. They either come from the environment or invade the skin from adjacent areas (nasal vestibules, rectum). They do not proliferate, except if local or immune conditions are favorable. Accordingly their preferred location is in folds (armpits,

Table 1 Bacteria found on healthy skin

1. **Gram+ cocci**
They produce a catalase which differentiates them from streptococci. There are two main genera:
Staphylococci, able to ferment glucose under anaerobic conditions. They include mainly *S. albus* (coagulase negative) with its 9 species: the main species are *S. epidermidis, S. hominis*, *and S. saccharolyticus*, distinguished by their phenotype and their DNA (Kloos 1981). They are ubiquitous, i.e., found almost everywhere on the integument
S. aureus (coagulase +) is sometimes found steadily on healthy skin, especially in nasal vestibules (nasal carriage). It belongs to the transient resident flora
Micrococci (strictly aerobic) have 8 species, distinguished by their phenotype, their possible genetic transformation, and partly by their DNA (Kloos 1981; Marples 1981). They are ubiquitous
2. **Aerobic corynebacteria** (Tring and Murgatroyd 1974; Pitcher and Jackman 1981)
These are club-shaped sticks, are Gram+, and do not produce spores. Cultures under UV light emit a coral fluorescence. They are also characterized by the presence of arabinose and corynemycolic acid in their wall. On the skin some are responsible for a sour pungent smell. There are two categories:
Non-lipophilic in vitro (perineum, axilla):
C. minutissimum
C. xerosis
Brevibacterium epidermidis (responsible for the unpleasant foot odor due to the production of CH_3SH)
Lipophilic in vitro:
C. lipophilicus (toe webs, perineum, axilla)
C. jeikeium (also called *Corynebacterium JK*) and *C. urealyticum* (also called *Corynebacterium D2*) are part of the transient resident flora
3. **Propionibacteria**
These are anaerobic corynebacteria in vitro. They are lipophilic as well as lipolytic and are found on the seborrheic areas and in the pilosebaceous follicles
P. acnes = *C. parvum* (immune enhancer)
P. granulosum
P. avidum (proteolytic)
4. **Gram-negative bacteria** (Somerville and Noble 1970)
Acinetobacter calcoaceticus (axilla, toe webs)
The transient resident flora includes *Pseudomonas, Proteus,* and *Klebsiella*: located in the axilla, nostrils, groin, perineum, and toe webs
5. **Yeasts**
Pityrosporon (P. ovale = *P. orbiculare* = *Malassezia furfur*), lipophilic and lipolytic, is abundant on seborrheic areas

(*continued*)

Table 1 (continued)

Non-lipophilic yeasts of rectal origin (*Candida*, *Rhodotorula*, *Torulopsis*, *Cryptococcus*) belong to the transient resident flora of the perineum
6. **Dermatophytes**, transiently resident, come from the environment : *Trichophyton rubrum, T. interdigitale, Epidermophyton floccosum, Microsporon*

perineum, between toes), and they are found in some individuals only and in diseased skin. They are generally few in number ("*S. aureus* carriage" applies if density is over 10^6 bacteria/cm^2). In some cases, the skin *transient flora* comes from the environment (contamination in hospital wards, sinks); for example, Gram-negative bacilli are abundant in vases and flower pots; group B streptococci may be of pharyngeal or rectal origin.

The neonate skin is colonized through vaginal contact, and then within the next 3 days following birth, the flora diversifies (*S. epidermidis* especially appears), due to the transition from an aqueous and sterile environment of the womb to a gaseous one, characterized by constant microbial interactions and bacterial colonization (Capone et al. 2011). Infant and young children skin harbors mainly micrococci, white staphylococci, corynebacteria, frequently Gram-negative bacteria, streptococci (during the period of hyposeborrhea between the ages of 6 months and 6 years), and *S. aureus* (colonization of the nasal vestibule), these proportions evolving over the first years; early microbial colonization is important for the development of skin barrier and immune functions and widely for the systemic immune system. In older people there is a global flora decrease, especially of propionibacteria.

2.2 Topographical Variations

The major importance of the environment in the proliferation of microorganisms is shown from topographical variations. Even among healthy individuals, differences in location and quantity of microbes have been described (ethnicity, skin pH, age, BMI); these fluctuations are not being yet fully explained, even if diet, hygiene, environment, host physiology, genetics, and early microbial exposure are implicated (Schommer and Gallo 2013; Grice and Segre 2011; Grice et al. 2008). Thanks to genomic and molecular recent approaches, relying on sequence analysis of the 16S ribosomal RNA gene (present in all bacteria and archaea), it seems that not dominant but low-abundance organism's composition could allow to better differentiate each individual (Schloss 2014).

The skin is confronted to an important diversity of parameters that could influence its surface characteristics; furthermore and depending on the body site, a wide variety of cell types can be encountered (Sanford and Gallo 2013).

Three types of habitat for microbes are distinguished. The *fatty habitat* (scalp, face, shoulders, thorax) is marked by the importance of the sebum secretion, triglycerides being necessary to the development of propionibacteria and Pityrosporum. Thus the density in *P. acnes* varies in parallel with the "sebum excretion rate" changes with age or isotretinoin treatment (Leyden et al. 1991). The sebaceous lipids inhibit *Streptococcus pyogenes* and hydrophilic species (Tables 3 and 4); thus, surprisingly, occlusion on the scalp does not alter the flora nor increase the bacterial density (Leyden et al. 1991). The *humid habitat* applies to the body creases where the transcutaneous water loss cannot be evacuated and the easier corneocyte degradation facilitates supply of protein, which is the selective nutrient of dermatophytes. The other hairless sites correspond to the *dry habitat*, where dryness is responsible for a low bacterial density. To these three habitats should be added the nostrils (*nasal vestibule*) which play an important role in the skin colonization.

The distribution of the main species on the main body sites is presented in Tables 2, 3, and 4. This is only an outline, since differences can be found on quite close sites and depend on skin thickness, folds, density of hair follicles, and glands. For example, inside the sebaceous follicle, Pityrosporum are found at the ostium, white staphylococci at the supra-infundibulum level, and anaerobic propionibacteria (*P. acnes*) in the infra-infundibulum.

2.3 Proliferation

Continuous proliferation is mandatory for the resident flora because of the stratum corneum desquamation which daily removes approximately one cell layer. The *stratum disjunctum*, daily preserved through the decay of one stratum compactum layer, and especially the pilosebaceous infundibula constitute the reservoir.

Table 2 Topographical variations of the skin flora

1. **Oily habitat** (seborrheic)
Scalp: Pityrosporum > propionibacteria (*P. acnes* > *P. granulosum* > *P. avidum*) > white staphylococci (*S. epidermidis, S. hominis*)
Other areas : propionibacteria > Pityrosporum > white staphylococci
2. **Wet habitat**
Axilla: aerobic corynebacteria, *P. avidum* > *P. granulosum, P. acnes*, white staphylococci (*S. epidermidis, S. hominis*), *Acinetobacter calcoaceticus* (Chinn 1964), ± *S. aureus*, Gram-negative bacilli
Groin: aerobic corynebacteria, *P. avidum*, white staphylococci ± Gram-negative bacilli
Perineum: white staphylococci ± *S. aureus*, Gram-negative bacilli, group B streptococci
Interdigital: *P. avidum*, aerobic corynebacteria, *Acinetobacter calcoaceticus* (Johnston et al. 1987), ± Gram-negative bacilli, *C. minutissimum*
3. **Dry habitat**
Upper limbs: white staphylococci (*S. epidermidis, S. hominis, S. haemolyticus*), lipophilic corynebacteria
Lower limbs: white staphylococci
Hands (impossible to sterilize): white staphylococci ± *S. aureus* (in dermatologists), corynebacteria of the JK group (in oncologists), Gram-negative bacilli, candidas
4. **Nasal vestibules**:
P. avidum, *Staphylococcus epidermidis*, aerobic corynebacteria ± *S. aureus* (20 % of permanent carriers), Gram-negative bacilli

The main growth factors are the available nutrients, humidity, and heat. This explains the high microbiological density increases (Tables 3 and 4). A 24-h occlusion increases by 1,000 the bacterial density: an increased number of staphylococci and micrococci appear first and then non-lipophilic diphtheroids and Gram-negative bacilli. Moisture is essential for the development of *C. albicans*. In the tropical jungle environment, non-lipophilic corynebacteria and Gram-negative bacilli proliferate. However seasons have little effect in temperate countries. For premature babies, the high relative humidity and temperature of incubators imply a risk of proliferation of *P. aeruginosa* on the umbilical stump.

Unfavorable or selection factors are also present. The sweat, through its lactic acid, inhibits some colonies of micrococci and staphylococci. *P. acnes* (and acne) proliferates through a small increase of the skin surface pH (from 5.5 to 6.0), but staphylococci do not (Korting and Schmid 1995). A pH $\leq$5.0 inhibits *Brevibacterium epidermidis* (Korting and Schmid 1995). There are specific substrates for each bacterial adhesin (e.g., *S. aureus* adheres to fibronectin and fibrinogen by teichoic acid and protein A).

Some bacteria inhibit the proliferation of exogenous microorganisms (bacterial interference). Pityrosporum (by production of phenylethyl alcohol) and aerobic corynebacteria inhibit most of the Gram-negative bacteria. *S. epidermidis* inhibits *S. pyogenes* and some colonies of micrococci. The eradication of the resident flora favors the prolonged life of *S. aureus,* however without any effect on *Candida albicans, S. pyogenes*, and *P. aeruginosa*. Dermatophytes produce penicillin and streptomycin (hence the selection of resistant

Table 3 Skin flora regional variations (bold typed: site typical figures)

Scalp (Ref. Leyden et al. 1991)	Forehead without P	Limb extremities with P		Upper	Lower
Total number/cm^{2a}	1 **10^6**	1,2 **10^6**	4,4 **10^6**	1,7 10^3	4,4 10^3
Cocci %	23.1	18.1	7.2	**93.1**	**87.8**
Lipophilic C %	2.3	0.9	0.02	3.9	5.0
Non-lipophilic C %	0	0.1	0	0	7.1
Propionibacteria %	27.5	6.1	**83.5**	3.0	0.01
Pityrosporum %	**46.7**	**73.9**	9.2	0	0

P Pityriasis capitis
[a]Geometric mean

Table 4 Skin flora regional variations (bold typed: site typical figures)

Axilla (Ref. Leyden et al. 1991)	Toe webs		Perineum	Normal	With Dphyt
	Odorless	With odor			
Total number/cm^{2a}	4,8 10^3	1,3 $\mathbf{10^6}$	4,3 $\mathbf{10^7}$	1,4 $\mathbf{10^7}$	2,9 $\mathbf{10^7}$
Cocci (cfu/cm^2)	**86.6**	25.7	14.2	22.7	12.9
Lipophilic C %	10.9	**54.7**	**58.0**	**75.1**	**78.1**
Non-lipophilic C %	0.3	**16.9**	**26.4**	2.1	8.8
Propionibacteria %	1.1	2.4	0	0	0
Gram-negative bacilli %	1.1	0.3	7.7	0.05	0.06
Candidas %	0	0	0.06	0.02	0.02
Dermatophytes (prevalence %)	0	0	0	0	84.6

Dphyt dermatophytes
[a]Geometric mean

cocci). Bacteria of the *Brevibacterium* genus inhibit the dermatophytes (by production of methanethiol).

What is the effect of skin cleansing (Brandberg and Andersson 1981)? Absence of washing, even for a week, does not increase the total number of microorganisms. Excess washing has little or no effect either. A shower causes a local and transient reduction in microbial count on denser areas and an increase in density on the lower ones, probably through colony breaking and dispersion. Washing with an antiseptic can induce an apparently total disappearance of the flora, but it does not last. One possible mechanism of this resistance is the formation of bacterial clusters covered by a protecting film (biofilm). Testing the efficacy of washings, antiseptics, and disinfectants has been addressed recently by Kramer (1999).

2.4 Role of Skin Flora?

- The resident skin flora plays a fundamental part as a barrier against colonization by pathogenic or harmful species. This effect is enhanced by the physiological desquamation: squamous conditions favor the carriage of pathogenic bacteria. Microorganisms may also have a role in the immune system by educating the billions of T cells found in the skin (Grice and Segre 2011) or helping protect against allergy or inflammation (Fyhrquist et al. 2014).
- Propionibacteria transform the sebum triglycerides into free fatty acids – one of the characteristics of the physicochemical environment of the skin surface. They contribute to its acidity and its low surface energy.
- *Propionibacterium acnes* is an immunity enhancer. In the 1970s, under the name *Corynebacterium parvum*, it has been used to improve the late hypersensitivity in melanoma patients. It is possible that this effect be exerted through percutaneous absorption of some bacterial products which modulate the cytokine production by skin viable tissues.

2.5 Pathology

Abnormal high or low rates, absence, deregulations, or presence of new resident species in skin flora could have pathological consequences not only on the skin but also widely on the whole organism.

"Dysbiosis" is the dedicated term for an imbalance of microorganisms and exists in much pathology, but it is not clear whether and in which proportions this phenomenon is a cause or a consequence of the concerned disease (Schommer and Gallo 2013; Grice and Segre 2011; Grice et al. 2008), more so because of complex and dynamic interaction networks between microorganisms and host.

In this context and in a more or less accurate and well-known way, diseases related to

microorganism ecosystem dysfunction have been described (Zeeuwen et al. 2013):

- In atopic dermatitis, flares are associated with colonization and infection by *S. aureus* but also with defects in some epidermal functions as well as environmental factors.
- In seborrheic dermatitis ("dandruff" on the scalp), the presumptive target of fungicides that are efficient against the pathology is *Malassezia* spp. (that is however also found in healthy skin) and *M. restricta* and *M. globosa* for dandruff.
- No microorganisms have been directly linked to chronic plaque psoriasis, especially given that genetic factors are known to be implied; however, potential differences have been detected in the microbiome between psoriatic and normal skin (diversity and staphylococcus (Fry et al. 2014a, b)), probably due to a breakdown – not yet identified – in the immune tolerance to the skin microbiome.
- Acne inflammatory disorder is associated with damage caused by *P. acnes* bacterium (one of the lipophilic microorganisms that are increased at puberty) in the pilosebaceous unit, and it appears that pathological follicles contain *P. acnes*, *Staphylococcus epidermidis*, and *Corynebacterium* (*P. acnes* only in healthy follicles) (Murillo and Raoult 2013).
- A mite named *Demodex*, existing on healthy skin, is significantly increased on the skin of papulopustular rosacea patients. *Demodex* could take an advantage of microbiome ecosystem shift due to genetic but also immune and age variations and express some antigen inducing the inflammatory immune response (Yuan et al. 2014; Lacey et al. 2007).
- *S. epidermis* is usually commensal but in some cases uses the indwelling medical devices to cause nosocomial infection and disease.
- Infections in chronic wounds could also be due to commensal microorganisms (species implicated not being well identified), taking the opportunity to invade the skin presenting defects in its barrier function and participating in healing difficulties (Canesso et al. 2014).
- Current works are also studying the role of microbiome in sensitive skin syndrome, herpes viruses, or specific areas like scalp microbiome (alopecia areata, seborrheic dermatitis dandruff, pediculosis capitis).

Thus, a better knowledge of skin microbiome and interactions with many other factors is still necessary to understand and identify the skin disorders associated with an imbalance and to adapt new diagnostic or therapeutic approaches, including manipulation of skin microbes. For in vitro research, skin substitute will have to take into account microbiome of the tissue it claims to replace, as well as antiaging medicine is interested in understanding the role of microbiome in sagging or wrinkle development.

3 Chemicophysical Status

3.1 pH

The skin surface acidity, discovered by Heuss in 1892, was later highlighted by Schade and Marchionini (1928) who underlined its protection feature and called it the "acidic mantle." By the way, it controls the resident flora to a great extent and prevents the skin colonization by pathogenic species (Marchionini and Hausknecht 1938; Korting et al. 1987). It may also favor corneodesmosome decay and desquamation because the stratum corneum hydrolases have an optimal pH of 5.6 (Öhman and Vahlquist 1993). The value of the skin pH is between 4.2 and 6.1 and its distribution between these values is Gaussian, except on the forehead (Braun-Falco and Korting 1986; Zlotogorski 1987). Findings related to difference with gender are contradictory (Zlotogorski 1987; Dikstein and Zlotogorski 1989; Elhers et al. 2001). Diurnal variation was advocated, with a peak about midday (Yosipovitch et al. 1998), but it may be related to climatic influence (Elhers et al. 2001) (see Annex 4, circadian rhythms).

There are "physiological holes in the acidic mantle" (Marchionini and Hausknecht 1938), where the pH is closer to 7. These sites are the axilla, perineum, interdigital areas, toe webs, and

legs. Even on the uncovered body most of which are acidic, local pH differences contribute to the existence of a particular flora. On the forehead, it is slightly lower than on the cheeks (Zlotogorski 1987; Dikstein and Zlotogorski 1989). In a cross-over comparative study on the effect of the prolonged use of alkaline soaps and acidic detergents on the forehead pH and flora, Korting et al. (1987) and Schmid and Korting (1995) showed that a small increase in pH (from 5.5 to 6.0) activated the proliferation of *P. acnes* without changing that of staphylococci and at the same time exacerbated acne. Inversely, a similar pH decrease would improve acne significantly ($p < 0.00001$).

The origin of the skin acidity depends on the content in free fatty acids of the surface ecosystem (Ansari 2014). Any cleansing of the skin, even with a soap with a higher acidity than the skin, increases the pH (Korting et al. 1987; Gfatter et al. 1997). Stratum corneum stripping is associated with a steep pH rise (Öhman and Vahlquist 1998). In newborn babies, the skin pH lies between 6 and 7 and the skin surface free fatty acid content is lower than in adults (Braun-Falco and Korting 1986; Gfatter et al. 1997; Behrendt and Green 1958; Beare et al. 1960). On day 1 pH was found higher than in adults in all body sites (soles, back, abdomen, palms, forearm, forehead): mean 7.1 ± 0.17 versus 5.7 ± 0.16, respectively ($n = 44$). By the second day the pH decreased although keeping statistically different from adult values (Beare et al. 1960). The latter was attained only by the fourth day of life. Can sweat (pH between 4.0 and 6.8) be responsible in part for the surface acidity? It seemingly has no influence on the basal level; the sites with higher pH are those of continuous sweating.

On the buccal mucosae, pH is usually close to 7, with a maximum on the hard palate (see ▶ Chap. 156, "Main Skin Biological Constants") (Yosipovitch et al. 2000).

3.2 Skin Surface Tension

The formation of droplets, or conversely the spreading of a liquid over a surface, depends on liquid-solid interfacial energies (Fig. 5). When the droplet remains stable, its contact angle θ obeys Young's equation: $\Gamma_{sv} = \Gamma_{sl} + \Gamma_{vl} \cos\theta$, where Γ_{sv}, Γ_{sl}, and Γ_{vl} are respectively the interfacial energies solid-vapor, solid-liquid, and vapor-liquid. Generally the vapor element is the air and is not mentioned, hence the simplified formula $\Gamma_s = \Gamma_{sl} + \Gamma_l \cos\theta$, where Γ_s is the surface energy of the solid, Γ_l the surface tension of the liquids, and Γ_{sl} the interfacial energy solid-liquid. When $\Gamma_s < \Gamma_l + \Gamma_{sl}$, no droplet is formed, but the liquid spreads out over the solid, up to making (theoretically) a single molecular layer. In this case, it is considered that $\cos\theta = 1$. The hydrophobicity or hydrophilicity of a surface is mainly connected to the interfacial energy Γ_{sl}.

The overall skin surface is hydrophobic. As such, a water droplet placed on the volar forearm (wettability of the skin test (Elkhyat et al. 2014)) persists over 15 min. This property, long known (Jacobi 1949), is characterized by a low surface wetting critical tension (i.e., the maximal surface tension of a liquid still able to completely spread out over that surface) 27.5 ± 2.4 dyn/cm on the volar forearm (water has a surface tension of 72.8 dyn/cm and olive oil 32 dyn/cm) (Elkhyat et al. 1996). In that respect, the skin surface is

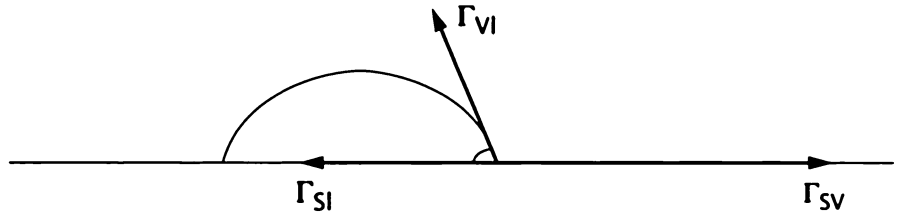

Fig. 5 A theoretical profile of a drop at equilibrium on a solid surface. Vectors are those of interfacial energy. By definition, the contact angle is always inside the drop. $\ni_{sv}$, $\ni_{sl}$, and $\ni_{vl}$ are the solid-vapor, solid-liquid, and vapor-liquid interfacial energies, respectively

similar to plastic substances. Its surface free energy on the forearm is 38.7 ± 6.4 mJ/m^2, somewhat higher than that of plastic substances, with an apolar component of 35.6 ± 5.8 mJ/m^2, a basic polar component of 4.2 ± 3.0 mJ/m^2, and an acidic polar component of 0.8 ± 0.7 mJ/m^2. The skin surface, from an electrochemical viewpoint, is therefore mainly monopolar basic (Mavon et al. 1997).

On seborrheic areas the skin surface is less hydrophobic, its wetting critical tension being beyond 50 dyn/cm. This higher value is related to the high amount of sebum; a cleansing of the forehead with ether reduces it to 29 dyn/cm (Elkhyat et al. 1996). Similarly, on the forehead the surface free energy (42.5 ± 3.9 mJ/m^2) is higher than on the forearm because of the greater part of basic polar component (28.3 mJ/m^2) in turn linked to the high amount of free fatty acids in the sebum (Mavon et al. 1997). Degreasing and dehydrating the forehead with ether decrease both the surface free energy and the basic polar component.

The skin hydrophobia contributes to its low permeability. Thus the sweat has enough time to evaporate and so play its role in thermoregulation. In profuse sweating, the sweat in excess drips down but does not form an emulsion with the sebum. Even in more stable and prolonged conditions, and in vitro, no sebum-sweat emulsion could be shown, although the surface tensions of both liquids are close (less than 2 dyn/cm apart), and the interfacial tension is only 1.1 dyn/cm (Mavon 1997).

Finally surface tension, because of the enormous forces it generates, has a major role in the adherence of microorganisms to their support (corneocytes, hairs), in the spontaneous sebaceous excretion, and in skin surface regreasing after cleansing (▶ Chap. 13, "Sebaceous Physiology").

4 Social and Cultural Function

Although it has often been overlooked in publications because of its "non-organic" nature, the social and cultural function of the skin is considerable. It involves ethnic, racial, age-related, and "apparent health" considerations and influences the psyche of each individual. It participates in self-consciousness and in the image which is projected toward the others. This function relies on the skin relief, optical properties, color, and mechanical properties. Desquamation on dry skin is much more visible than on oily skin. The stratum corneum translucency softens an irregular surface relief or small wrinkles (Creidi et al. 1994), hence the higher reliability of instrumental measurements of this relief. In the same way, to reduce wrinkle visibility, an oily cosmetic is better than an opaque makeup. The translucence of the whole stratum corneum also contributes to a better visibility of the underlying bloodstream and favors a radiant complexion. Furthermore, the variations in the mechanical behavior of the stratum corneum depend on the hydration of its superficial layers; in this area, microfractures due to very dry conditions generate an unpleasant tight feeling in healthy subjects and pruritus in atopic subjects.

References

Ansari SA. Skin pH and skin flora. In: Handbook of cosmetic science and technology. 4th ed. Boca Raton, CRC Press; 2014. pp. 163–74.

Beare JM, Cheeseman EA, Gailey AAH, Neill DW, Merrett JD. The effect of age on the pH of the skin surface in the first week of life. Br J Dermatol. 1960;72:62–6.

Behrendt A, Green M. Skin pH pattern in the newborn infant. J Dis Child. 1958;95:35–41.

Brandberg A, Andersson I. Preoperative whole body disinfection by shower bath with chlorhexidine soap: effect on transmission of bacteria from skin flora. In: Maibach HI, Aly R, editors. Skin Microbiology: relevance to clinical infection. New York: Springer; 1981. p. 92–7.

Braun-Falco O, Korting HC. Der normale pH-Wert der menschlichen Haut. Hautarzt. 1986;7:126–9.

Canesso MC C, Vieira AT, Castro TBR, Schirmer BGA, Cisalpino D, Martins FS, Barcelos, LS. Skin wound healing is accelerated and scarless in the absence of commensal microbiota. J Immunol. 2014;193:5171–80.

Capone KA, Dowd SE, Stamatas GN, Nikolovski J. Diversity of the human skin microbiome early in life. J Invest Dermatol. 2011;131(10):2026–32.

Chinn HD, Dobson RL. The topographic anatomy of human skin. Arch Dermatol. 1964;89:267–73.

Corcuff P, De Rigal J, Lévêque JL, Makki S, Agache P. Skin relief and aging. J Soc Cosmet Chem. 1983;34:177–90.

Creidi P, Faivre B, Agache P, Richard E, Haudiquet V, Sauvanet JP. Effect of a conjugated oestrogen (Premarin) cream on ageing facial skin. A comparative study with a placebo cream. Maturitas. 1994;19:211–23.

Dekio I, Hayashi H, Sakamoto M, Kitahara M, Nishikawa T, Suematsu M, Benno Y. Detection of potentially novel bacterial components of the human skin microbiota using culture-independent molecular profiling. J Med Microbiol. 2005;54(Pt 12):1231–8.

Dikstein S, Zlotogorski A. Skin surface hydrogen ion concentration (pH). In: Lévêque J-L, editor. Cutaneous investigation in health and disease: non invasive methods and instrumentation. New York: Marcel Dekker; 1989. p. 49–58.

Ehlers C, Ivens UI, Moeller UM, Senderovitz T, Serup J. Females have lower skin surface pH than men. A study on the influence of gender, forearm site variation, right/left difference and time of the day on the skin surface pH. Skin Res Technol. 2001;7:90–4.

Elkhyat A, Mavon A, Leduc M, Agache P, Humbert P. Skin critical surface tension: a way to assess the skin wettability quantitatively. Skin Res Technol. 1996;2:91–6.

Elkhyat A, Fanian F, Mac-Mary S, Guichard A, Lihoreau T, Jeudy A, Humbert P. Skin wettability and friction. In: Handbook of cosmetic science and technology. 4th ed. Boca Raton, CRC Press; 2014. pp. 337–44.

Fry L, Baker BS, Powles AV, Fahlen A, Engstrand L. Is chronic plaque psoriasis triggered by microbiota in the skin? Br J Dermatol. 2013;169:47–52.

Fry L, Baker B, Powles A, Engstrand L. Psoriasis is not an autoimmune disease? Exp Dermatol. 2015; 24:241–4.

Fyhrquist N, Ruokolainen L, Suomalainen A, Lehtimäki S, Veckman V, Vendelin J, Alenius H. Acinetobacter species in the skin microbiota protect against allergic sensitization and inflammation. J Allergy Clin Immunol. 2014;134:1301–9.

Gfatter R, Hackl P, Braun F. Effects of soap and detergents on skin surface pH, stratum corneum hydration and fat content in infants. Dermatology. 1997;195:258–62.

Grice EA, Segre JA. The skin microbiome. Nat Rev Microbiol. 2011;9(4):244–53.

Grice EA, Kong HH, Renaud G, Young AC, Bouffard GG, Segre JA, et al. A diversity profile of the human skin microbiota. Genome Res. 2008;18(7):1043–50.

Hanusova S. Hautrelieftypen (Skin relief types). Arch Klin Exp Dermatol. 1938;208:1–23.

Hartmann AA. Composition of the skin flora. In: Braun-Falco O, Korting HC, editors. Skin cleansing with synthetic detergents. Berlin: Springer; 1990. p. 83–6.

Highley DR, Coomey M, DenBeste M, Wolfram LJ. Frictional properties of skin. J Invest Dermatol. 1977;69:303–5.

Jacobi O. Neue Erkenntnisse über die hygroskopischen Eigenschaften und die Benetzbarkeit der Keratinsubstanz. Kolloid Z. 1949;114:88–103.

Johnson C, Dawber R, Shuster S. Surface appearances of the eccrine sweat duct by scanning electron microscopy. Br J Dermatol. 1970;83:655–60.

Johnston DH, Fairclough JA, Brownt EM, Morris R. Rate of bacterial recolonization of the skin after preparation: four methods compared. Br J Surg. 1987;74:64.

Kloos WE. The identification of *staphylococcus* and *micrococcus* species isolated on human skin. In: Maibach HI, Aly R, editors. Skin microbiology. Relevance to clinical infection. New York: Springer; 1981. p. 3–12.

Korting HC, Schmid MH. The concept of the acid mantle of the skin: its relevance for the choice of skin cleansers. Dermatology. 1995;191:276–80.

Korting HC, Kober M, Müller M, Braun-Falco O. Influence of repeated washings with soap and synthetic detergents on pH and resident flora of the skin of forehead and forearm. Acta Derm Venereol. 1987;67:41–7.

Kramer A. Hand disinfection and antiseptics of skin, mucous membranes and wounds. In: Gabard B, Elsner P, Surber C, Treffel P, editors. Dermatopharmacology of topical preparations. Berlin: Springer; 1999. p. 121–34.

Lacey N, Delaney S, Kavanagh K, Powell FC. Mite-related bacterial antigens stimulate inflammatory cells in rosacea. Br J Dermatol. 2007;157(3):474–81.

Leyden JJ, Nordstrom KM, McGinley KJ. Cutaneous microbiology. In: Goldsmith LA, editor. Physiology, biochemistry and molecular biology of the skin. 2nd ed. New York: Oxford University Press; 1991. p. 1403–24.

Makki S, Agache P, Mignot J, Zahouani H. Statistical analysis and three-dimensional representation of the human skin surface. J Soc Cosmet Chem. 1984;35:311–25.

Marchionini A, Hausknecht W. Säuremantel der Haut und Bakterienabwehr. 1. Mitteilung. Die regionäre Verschiedenheit der Wasserstoffionenkonzentration der Hautoberfläche. Klin Wochenschr. 1938;17:663–6.

Marples RR. Coagulase-negative staphylococci: classification and problems. In: Maibach HI, Aly R, editors. Skin microbiology. Relevance to clinical infection. New York: Springer; 1981a. p. 13–8.

Marples RR. Newer methods of quantifying skin bacteria. In: Maibach HI, Aly R, editors. Skin microbiology: relevance to clinical infection. New York: Springer; 1981b. p. 45–9.

Mavon A. Energie libre de surface de la peau humaine, in vivo: Une nouvelle approche de la sehorrhee. Besançon: Thèse Sciences de la Vie et de la Santé; 1997.

Mavon A, Zahouani H, Redoules D, Agache P, Gall Y, Humbert P. Sebum and stratum corneum lipids increase human skin surface free energy as determined from contact angle measurements: a study on two anatomical sites. Colloids Surf B: Biointerfaces. 1997;8:147–55.

Murillo N, Raoult D. Skin microbiota: overview and role in the skin diseases acne vulgaris and rosacea. Future Microbiol. 2013;8(2):209–22.

Öhman H, Vahlquist A. In vivo studies conceming a pH gradient in human stratum corneum and upper epidermis. Acta Derm Venereol. 1993;74:375–9.

Öhman H, Vahlquist A. The pH gradient over the stratum corneum differs in X-linked recessive and autosomal dominant ichthyosis: a clue to the molecular origin of the "Acid Skin Mantle"? J Invest Dermatol. 1998;111:674–7.

Panisset F, Varchon D, Pirot F, Humbert Ph, Agache P. Evaluation du module d'Young du stratum corneum in vivo. Congrès Annuel de Recherche Dermatologique, Nîmes, 14–16 Oct 1993.

Pitcher DG, Jackman PGH. The current status of aerobic cutaneous coryneform bacteria. In: Maibach HI, Aly R, editors. Skin microbiology. Relevance to clinical infection. New York: Springer; 1981. p. 19–28.

Sanford JA, Gallo RL. Functions of the skin microbiota in health and disease. Semin Immunol. 2013;25(5):370–7.

Sarkany L, Caron GA. Microtopography of the human skin. Studies with metal-shadowed replicas from plastic impressions. J Anat. 1965;99:359–64.

Schade H, Marchionini A. Der Säuremantel der Haut (nach Gaskettenmessung). Klin Wochenschr. 1928;7:I2–4.

Schloss PD. Microbiology: an integrated view of the skin microbiome. Nature. 2014;514(7520):44–5.

Schmid MH, Korting HC. The concept of acid mantle of the skin: its relevance for the choice of skin cleansers. Dermatology. 1995;191:276–80.

Schommer NN, Gallo RL. Structure and function of the human skin microbiome. Trends Microbiol. 2013;21 (12):660–8. and Consortium, T. H. M. P. Structure, function and diversity of the healthy human microbiome. Nature. 2012;486(7402):207–14.

Somerville DA, Noble WC. A note on the gram negative bacilli of human skin. Eur J Clin Biol Res. 1970; l5:669–71.

Tchernoff M. Le relief de la surface cutanée chez le nouveau-né. Etude quantitative. (Skin surface relief in Neonates. A quantitative study). Med.Thesis N° 85–124, Besançon; 1985.

Tring FC, Murgatroyd LB. Surface microtopography of normal human skin. Arch Dermatol. 1974;109:223–6.

Wolf J. Das Oberflächenrelief der menschlichen Haut (Skin surface relief in man). Z Mikr Anat Forsch. 1940;47:351–400.

Yosipovitch G, Xiong GL, Haus E, Sackett-Lundeen L, Ashkenazi I, Maibach HI. Time-dependent variations of the skin barrier function in humans: transepidermal water loss, stratum corneum hydration, skin surface pH, and skin temperature. J Invest Dermatol. 1998;110:20–3.

Yosipovitch G, Maayan-Metzger A, Merlob P, Sirota L. Skin barrier properties in different body areas in neonates. Pediatrics. 2000;106:105–8.

Yosipovitch G, Kaplan I, Calderon S, David M, Chan YH, Weiinberger A. Distribution of mucosal pH on the bucca, tongue, lips and palate: a study in healthy volunteers and patients with lichen planus, Behcet's disease and Burning Mouth syndrome. Acta Derm Venereol. 2001;81:178–80.

Yuan C, Wang XM, Guichard A, Lihoreau T, Mac-Mary S, Khyat L, Ardigo M, Humbert P. Comparison of reflectance confocal microscopy and standardized skin surface biopsy for three different lesions in a pityriasis folliculorum patient. Br J Dermatol. 2015;172:1440–2.

Zahouani and Vargiolu. Skin line morphology: tree and branches. In: Handbook of Measuring the skin. 1st edn. Berlin: Springer; 2004. pp. 40–59.

Zeeuwen PLJM, Kleerebezem M, Timmerman HM, Schalkwijk J. Microbiome and skin diseases. Curr Opin Allergy Clin Immunol. 2013;13(5):514–20.

Zlotogorski A. Distribution of skin surface pH on the forehead and cheek of adults. Arch Dermatol Res. 1987;279:398–401.

Skin Color and Pigmentation

5

L. Duteil, K. Roussel, and P. Bahadoran

Contents

L. Duteil (✉) • K. Roussel
CPCAD (Centre de Pharmacologie Clinique Appliquée à la Dermatologie), Hôpital L'ARCHET 2, Nice Cedex 3, France
e-mail: philippe.BAHADORAN@unice.fr

P. Bahadoran
Department of Dermatology, Nice CHU Hôpital Pasteur, Nice Cedex 3, France
e-mail: Philippe.BAHADORAN@unice.fr

P. Humbert et al. (eds.), *Agache's Measuring the Skin*,
DOI 10.1007/978-3-319-32383-1_5

1 Introduction

The color of the skin is a commonly used parameter to assess different aspects and conditions of the skin. It depends mainly on its pigment content, on the spectrum of the illuminating light, and on the quality of the cutaneous surface. When light impinges on the skin, a few percents are directly reflected by the surface (specular reflection) whereas entering photons are either absorbed or scattered by different molecules and structures present in the cutaneous layers. The pigments of the skin, also called chromophores, are mainly represented by melanin in the epidermis and by hemoglobin in the dermis. Other molecules such as bilirubin, amino acids, nucleic acids, porphyrins, and carotenoids (endogenously produced) may participate at different levels to the absorbing and reflecting process of the light. The pigmentation of the skin is related to the melanin amount in the keratinocytes. The various contents of melanin in the keratinocytes produce the wide spectrum of human skin color found in the different human races. Two classes of melanins are found in humans: the eumelanins which are brown to black pigments and the phaeomelanins which are yellow to reddish-brown (Fitzpatrick et al. 1979). Melanin absorbs in a decreasing manner from ultraviolet (UV) (highest absorption) to visible light domain. On the other hand, hemoglobin in the dermal microvasculature contributes to the overall skin color with a red dominant for oxygenated hemoglobin and bluish red for reduced

hemoglobin. Here again, the hemoglobin contribution to the skin color depends on the melanin amount in the keratinocytes which acts as a neutral filter; it is readily visible in fair-skinned people, and practically not observable in deeply melanized skin (Stamatas et al. 2008; Diffey and Robson 1992).

The need for assessment of the skin color and pigmentation extends from the dermatocosmetology domain (including sunscreens, skin pigmenting or depigmenting products, antiaging agents, and makeup evaluations) to the clinical dermatology for the characterization of the various types of skin pigmented lesions. Although the human eye is able to distinguish between hundreds of colors, the results of visual assessment remain subjective and qualitative with a poor reproducibility in time.

Since the last decades, several objective methods and technologies have been developed (Taylor et al. 2006; Takiwaki et al. 1994; Fullerton et al. 1996) to measure skin color and some were proposed as commercially available devices. Two main types of skin color investigation systems are coexisting. One is based on different approaches of analysis of reflected light by the skin which gives only spectral information. The second is based on the skin imaging technologies which offers, besides the color and spectral aspects, spatial information taking into account, for example, the lesion borders or heterogeneity on a large skin area (e.g., the whole face). The first and oldest type of systems is based on the spectrophotometric analysis of the reflected light by the skin, the illuminating light being either a continuous spectrum (white light) (Andersen and Bjerring 1990; Lock-Andersen et al. 1998a) or single bands specific of absorption of melanin and hemoglobin (Lock-Andersen et al. 1997; Feather et al. 1988). The reflectance tristimulus CIE colorimetry (Weatherall and Coombs 1992; Piérard 1998) allows expressing the color of the skin in a three-dimensional space. These objective methods are easy to use but have the inconvenience to produce color information only on small areas (0.5–1 cm^2). They are very useful in skin pharmacology where only the information on skin erythema and pigmentation intensities are needed on small test surfaces.

With the progress of the optical instrumentation, of the digital imaging techniques, and the development of dedicated image analysis processing, the spatial component of the skin color can be integrated in the measurement (Alghamdi et al. 2012; Liu et al. 2012). Recent development of dermoscopy has been shown to improve the diagnostic accuracy of pigmented skin lesions (Celebi et al. 2009). Some of these techniques, such as the multispectral imaging taking into account the combination of spectral and spatial information, aim to determine the severity of skin pathologies. Finally, thanks to the improvement of digital image processing technology and to the high quality of the available video camera, techniques of epiluminescence microscopy such as dermoscopy and reflectance confocal microscopy (RCM) (Smith and MacNeil 2011) represent very promising tools allowing the dermatologist to perform a very accurate noninvasive diagnosis of pigmented skin lesions.

2 Visual Assessment of Skin Color and Pigmentation

The eye is the first diagnostic tool for the dermatologist. Color perception is the result of radiant electromagnetic radiations in the “visible” wavelength range 400–700 nm collected by the eye and interpreted by the brain. Thus, color perception includes physical and psychophysiological aspects. The human eye is known to have a high power of discrimination between colors including shades and hues (Wassermann 1971; Bornstein 1968). The evaluation of skin pigmentation by visual examination depends not only on the subjective perception of colors by the observer but also on the nature of the illuminant and on the geometric position of the observer relative to the skin surface. Moreover, visual memory concerning colors is not stable in time making repetitive evaluations not reliable.

Various scales and indexes have been developed to reduce potential interobserver variability

and enable more objective assessment of skin pigmentation. For example, in the case of melasma, the severity index of melasma MASI (Kimbrough-Green et al. 1994) is calculated on the basis of area (A) of involvement, darkness (D) of melasma, and homogeneity (H) of the hyperpigmentation.

Using a standardized environment and grading skin color with either standard color references such as Munsell standards or very precise rating scales or color charts (Taylor et al. 2006; de Rigal et al. 2007) may lead to reliable visual color assessments.

3 Reflectance Tristimulus CIE Colorimetry

Colorimetry tristimulus system is based on the following two principles: the first is that each color can be matched by a suitable mixture of three selected light radiations; the second is that if two colors are matched by three radiations, the mixture of these two colors is found additive by suitable optical means. In 1931, the "Commission Internationale de l'Eclairage (CIE)" standardized the color mixture characteristics of an "average observer" and developed a standard framework for a color specification. The standard observer is represented by functions which were determined from data obtained from series of observers matching the color at each wavelength from 400 to 700 nm with appropriate mixtures from three primary light sources. In this system, each color is defined with a set of three tristimulus primary values (X: red content, Y: green content, Z: blue content). The drawback of the CIE 1931 color system is that equal distances in the chromaticity diagram do not represent equal differences in color as perceived by the human eye. This was corrected in the CIE 1976 L* a* b* color system which more closely represents the human eye sensitivity to color. The L*, a*, b* coordinates are also calculated from the X, Y, and Z tristimulus primary values. In the L*a*b* color space, L* is the lightness ranging from 0 (black) to 100 (white), a* is the balance between red (positive values) and green (negative values) and b* is the balance between yellow (positive values) and blue (negative values).

Based on the accumulation of numerous measurements of skin color using colorimetry (Chardon et al. 1993; Chardon et al. 1991) have shown that all the different types of basal skin color (stable state) for a selected body site (the back, for example) are located inside a vertical arched volume in the L*a*b* color space (Fig. 1). In this volume, the points of color are distributed from top to bottom as a function of the natural melanic pigmentation intensity with the nonmelanized skin (albino) at the top and very dark skin at the bottom. The points constitute the melanization axis which structure the volume along its longer axis and are distributed in its section as a function of the hue and chroma afforded by the natural skin pigment mixing (melanin, hemoglobin, carotenoids, etc.). Figure 1 indicates also that the direction of color changes in the volume depends of the skin pigment involved in the reaction related to the skin color variation. For example, following an UVA irradiation, the induced Immediate Pigment Darkening (IPD) does not follow the melanization axis but a different direction due to the fact that IPD is the bluish coloration generated by photo-oxidized melanins already present in the skin. This bluish color is expressed by a decrease of the b* component. On the other hand, the induction of an erythema translates the skin color point outside the melanization axis toward the colorimetric coordinate of hemoglobin (L*≈45, a*≈45, b*≈18).

Since the Caucasian skin has a yellow/orange aspect, the constitutional pigmentation is well described in the L* versus b* plane. Thus, sectors of skin color categories have been delineated (Chardon et al. 1991) to correspond roughly to the skin phototypes (Fitzpatrick 1988). The sectors are delimited by radii originating from $L^* = 50$ and $b^* = 0$ and constitute defined angles with the b* axis. Therefore, a subject can be characterized by the so-called individual typology angle (ITA°) which is calculated by

$$\mathrm{ITA}^\circ = \mathrm{Arctangent}\left((L^* - 50)/b^*\right) \times 180/\Pi$$

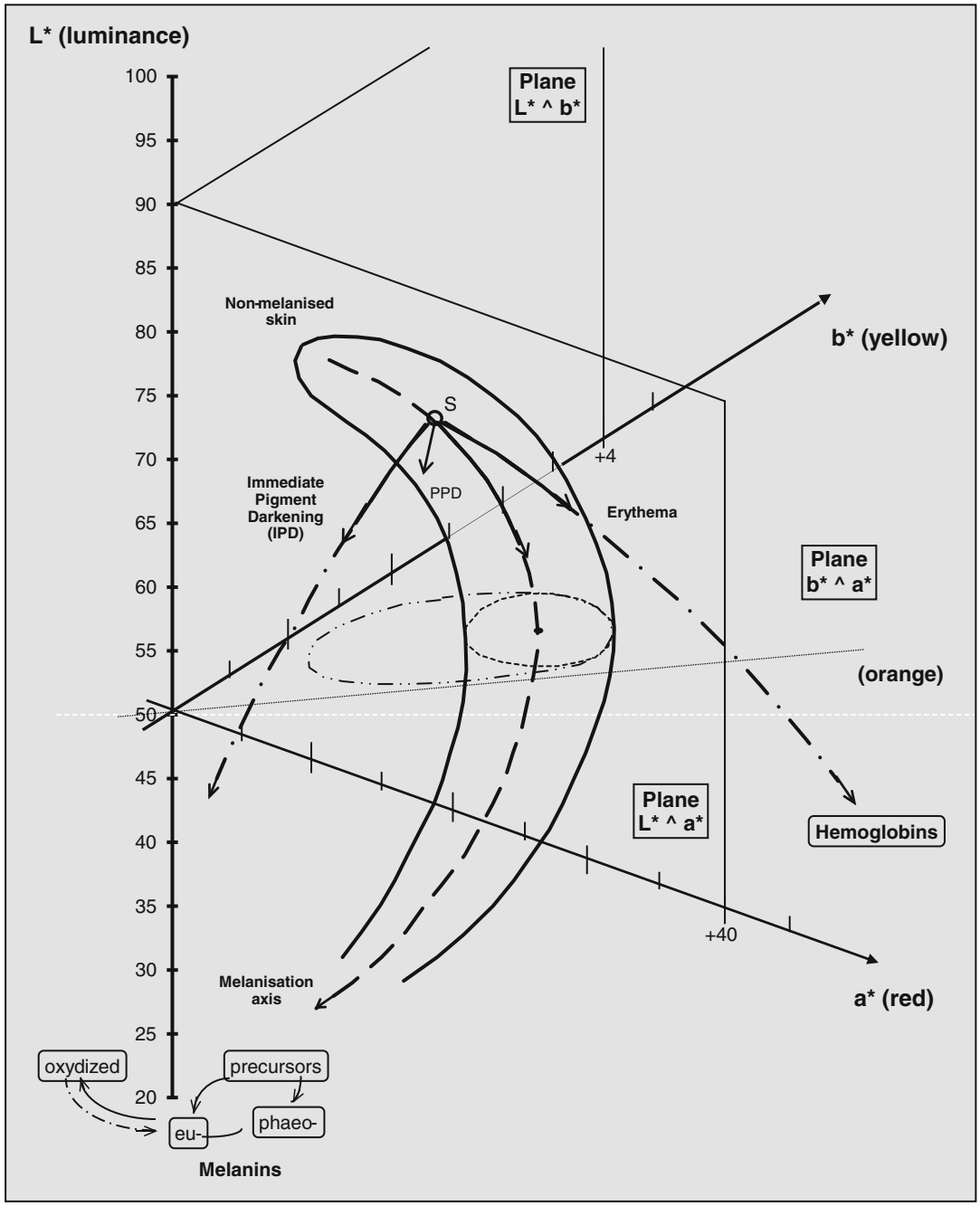

Fig. 1 The skin color volume in the CIE L*, a*, b* color space (With permission of A. Chardon et al. (1991))

The values proposed for the angles of skin category boundaries were

Very light skin > 55° > Light skin > 41° > Intermediate skin > 28° > Tanned skin > 10°.

It has been shown (Masson et al. 1992) that the use of ITA allows to determine the range of ultraviolet doses needed to induce a minimal erythema (Minimal Erythema Dose determination without prior irradiation).

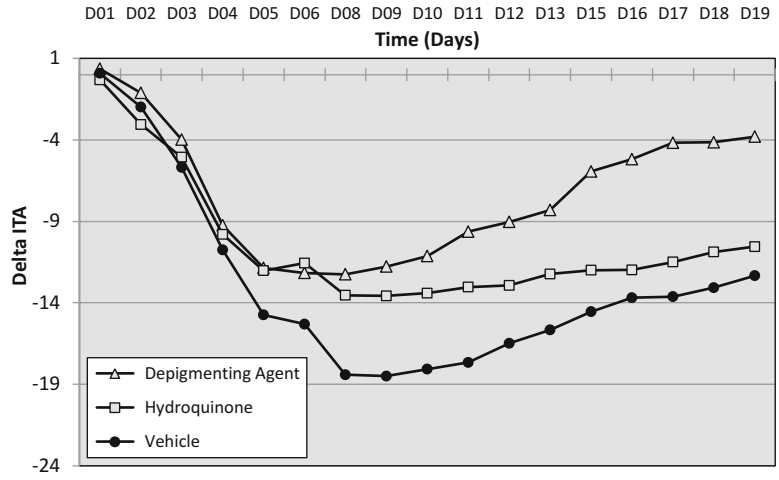

Fig. 2 Evolution of ITA angle (normalized to baseline before UV exposure) on UV induced pigmentation (UV exposure from D01 to D04, doses range 0.75–1.5 MED). Effect of a depigmenting agent compared to Hydroquinone and Vehicle (With courtesy of GALDERMA R&D Laboratories)

Colorimetry has been extensively used to assess the process of UV-induced hyperpigmentation (Park et al. 1999), skin typology (Roh et al. 2001), and photoprotection factors (Andreassi et al. 1990; Ferguson et al. 1996; Chardon et al. 1988; Moyal et al. 2000). Figure 2 illustrates the depigmenting treatment effect measured by the ITA angle on skin UV-induced pigmentation (4-day exposure with dose range 0.75–1.5 MED).

4 Reflectance Spectrophotometry

4.1 Reflectance Spectroscopy

The scanning reflectance spectroscopy (Andersen and Bjerring 1990; Stamatas et al. 2004) analyzes the spectrum of light reflected by the skin, typically between 400 and 700 nm, and allows to measure skin color in order to obtain information on skin chromophore content. The optical properties of the skin are determined by the spectral absorption, reflection, and scattering of the light as it strikes and penetrates the different cutaneous structures. The scanning reflectance spectrometers are built to measure the diffuse reflectance of the light, i.e., the part of the light which is modified by the absorption, reflection, and scattering processes inside the skin, and which is re-emitted from the skin. This technique is also called diffuse reflectance spectroscopy or DRS (Stamatas et al. 2004). The instrumental setup consists of: a light source such as a xenon short arc lamp or a tungsten halogen lamp, a measuring head which is an integrating sphere, an optical system (monochromator or equivalent) to decompose and analyze the light re-emitted by the skin, and a photodetector to measure the light intensity in the different bands of wavelength. A system of optical guides (bundles of optical fibers) conducts the light from the source to the skin and from the skin to the monochromator and the photodetector. In some handheld instruments (e.g., Minolta 2600d, Osaka, Japan), the distance between the light source and the skin surface is shorter (about 10 cm) and the reflected light is diffracted by a dual beam monochromator and measured by a photodiode array.

Different skin modeling simulations have been used to analyze spectral data (Häggblad et al. 2010; Meglinski and Matcher 2003). For example, the reflectance spectra of the human skin in visible and near-infrared (NIR) spectral region have been calculated using the Monte Carlo technique (Wang et al. 1995), and the specular and internal reflection on the medium surface is taken into account. Skin is represented as a complex inhomogeneous multilayered highly scattering and absorbing medium. The model takes into account variations in spatial distribution of blood, index of blood oxygen saturation, volume fraction of water, and chromophore content.

An example of skin DRS reflectance spectra (presented as absorption spectra) is illustrated in Fig. 3. On this figure, compared to the normal skin spectrum, the differences of a heavy pigmented skin lesion (lentigo) spectrum and a deeply vascularized lesion (raised red spot) are clearly observable. The amounts of melanin, oxy-Hb, and deoxy-Hb can be calculated from the DRS spectra using different models and algorithms. Pigmentation and erythema indexes can be also derived from these calculations. Figure 4 shows the melanin concentration obtained from reflectance spectra obtained in the same study as Fig. 2 using a tristimulus spectrophotometer (Konica Minolta CM 700d).

Wallace et al. (2000) aimed to document the optical reflectance (range 320–1100 nm) characteristics of pigmented skin lesions in order to evaluate their potential for improving the differential diagnosis of malignant melanoma from benign pigmented skin lesions. Characteristic differences in spectra from benign and malignant lesions were studied and showed significant differences between lesion groups classified by histology. This simple objective technique appeared to perform as well as the expert dermatologist and could improve the diagnostic accuracy of nonspecialists such as trainees and GPs.

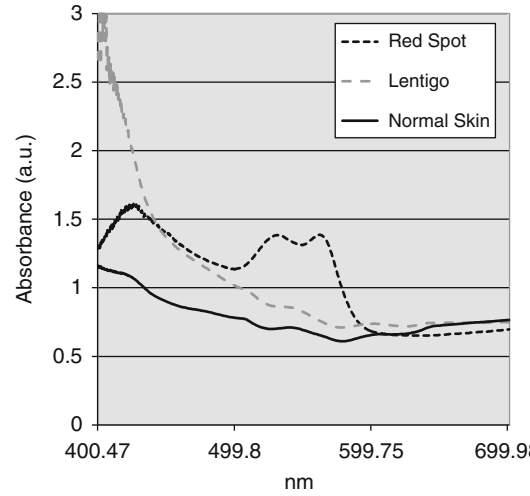

Fig. 3 DRS absorbance spectra (arbitrary unit) of three types of skin area: a pigmented lentigo (shape of typical melanin absorbance curve), a raised red spot (shape of typical hemoglobins absorbance curve, absorption peaks of oxyhemoglobin visible at 542–577 nm) and a normal skin area. Measurements performed with a Diffuse Reflectance Spectrometer (Canfield Scientific system, Fairfield, NJ, USA)

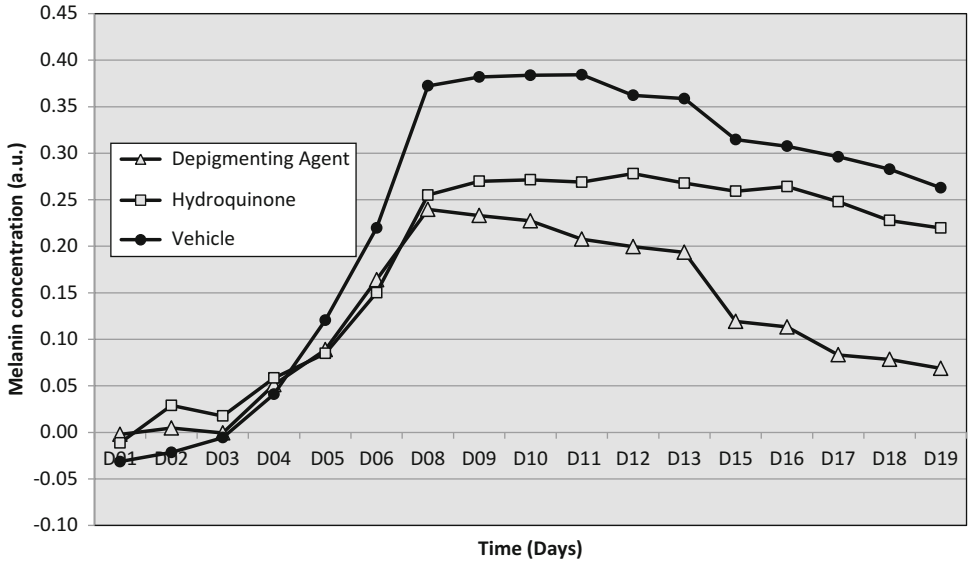

Fig. 4 Evolution of Melanin concentration on UV induced pigmentation (UV exposure from D01 to D04, doses range 0.75–1.5 MED). Effect of a depigmenting agent compared to Hydroquinone and Vehicle (With courtesy of GALDERMA R&D Laboratories)

4.2 Narrow-Band Reflectance Spectroscopy

The reflectance spectrophotometers are known to be expensive, cumbersome, and not well adapted for the routine clinical uses. Since the spectrophotometric measurements result often in the analysis of some specific narrow bands or peaks of spectra corresponding to the absorption bands of the main chromophores of the skin, the use of simpler and cheaper devices based on narrow-band analysis was developed.

The Mexameter MX16® (Courage-Khazaka, Elelectronik, Köln, Germany) is equipped with 16 light-emitting diodes (LED) arranged circularly and emitting at 568 nm (green), 660 nm (red), and 880 nm (infrared). The positions of emitter and receiver guarantee that only diffuse and scattered light is measured. As the quantity of emitted light is defined, the quantity of light absorbed by the skin can be calculated. The system is based on the principles described by Diffey and coworkers (1984). The melanin index (mx) is measured at two wavelengths (660 and 880 nm). These wavelengths have been chosen in order to achieve different absorption rates by the melanin pigments. For the erythema index (ex), two different wavelengths are used to measure the absorption capacity of the skin. One of these wavelengths corresponds to the spectral absorption peak of hemoglobin (568 nm) and the other wavelength (660 nm) has been chosen to avoid other color influences (e.g., bilirubin). The measuring area is 5 mm in diameter (0.2 cm^2). Other types of narrow-band spectrophotometers such as the DermaSpectrometer (Cortex Technology, Hadsund Denmark) are based on two LEDs whose bands are centered in the green (568 nm) and in the red (655 nm). The erythema index is also calculated from the ratio of red to green reflected light intensities. The melanin index is obtained from the inverse of reflected light intensity.

Several studies (Clarys et al. 2000; Tian et al. 2011) have been performed to compare narrow-band spectrophotometers to tristimulus colorimeter. The results showed both kinds of instruments are able to detect very small changes in skin color. The correlation between the instruments were found to be moderately good between L* and the melanin indexes and good between a* and the erythema indexes. A recent study performed on scars (Van der Wal et al. 2013) showed that the Mexameter, the Colorimeter, and the DSL II colorimeter provided reliable color data on normal skin and scars.

Various type applications of assessment of the cutaneous pigmentation by narrow-band spectrophotometers were performed including, for example, UV-induced pigmentation (Lim et al. 2008; Seitz and Withmore 1988), efficacy of depigmenting agent (Yoshimura et al. 2001; Hurley et al. 2002), and protection of vitiligo (Gniadecka et al. 1996; Park et al. 2006). Skin typology (Hermanns et al. 2001; Lock-Andersen et al. 1998b) and epidemiology (Lock-Andersen et al. 1998c) produced numerous subjects of works. In the retrospective skin cancer case–control studies, there are major difficulties to estimate sun exposure during lifetime of subjects because no suitable objective measurements are available.

5 Dermoscopy and Skin Imaging Systems

Dermoscopy (dermatoscopy, epiluminescence microscopy, incident light microscopy, skin surface microscopy) has become one of the major in vivo noninvasive diagnostic techniques used in the diagnosis of melanoma and other pigmented skin lesions (Celebi et al. 2009; Park et al. 2006). With the progress of both handheld optics and digital imaging techniques, recent development of dermoscopy has been shown to improve the diagnostic accuracy of pigmented skin lesions.

The technical setup consists of a magnifying optical system (surface microscope, stereomicroscope, handheld scope) allowing magnification of the lesion image. The lesion is covered with an immersion oil or any kind of liquid including water and alcohol in order to eliminate surface reflections of the illuminating light. This makes the stratum corneum translucent,

enabling the visualization of pigmented structures of the epidermis and of the dermal-epidermal junction and superficial papillary dermis which are impossible to observe with the naked eye. The vessels of the superficial vascular plexus can be also observed.

Various diagnostic systems have been proposed for assessing dermoscopic images. All systems take into account local and global features. For example, in the ABCD system used for the melanoma diagnosis, the investigator has to score asymmetry (A), borders (B), colors (C), and number of different dermoscopic structures (D). For all the diagnostic systems, the color aspect of the pigmentation of the lesion is crucial, including number of different colors, aspect of pigment networks, distribution of pigments, and shape margin of pigmented areas.

However, the use of dermoscopy is limited to experienced and trained dermatologists who show no more than 85 % of skin lesion detection rate. Since the last decade, numerous computerized image analysis models have been proposed in order to maximize the diagnostic accuracy, in particular in the field of lesion border detection (Celebi et al. 2009; Abbas et al. 2013; Garnavi et al. 2011), color quantification (Lee et al. 2012; Shakya et al. 2012), and pattern classification (Abbas et al. 2012).

Finally, the classical photography technique performed in Wood's light is also a useful method to visualize skin pigmentation (Fulton 1997; Garcia and Fulton 1996; Asawanonda and Taylor 1999). This technique is based on the filtering of the light emitted by the flash using UVA band pass filter. The hyperpigmented skin areas such as solar lentigos appear darker on the black-and-white image compared to "normal skin" due to the fact that melanin absorbs heavily in the UVA domain. On the other hand, depigmented lesions such as vitiligo macules are displayed as white areas on the skin (Paraskevas et al. 2005). Here again, the processing of that kind of images by dedicated gray levels analysis software could increase the objective quantification level of this technique.

6 Reflectance Confocal Microscopy: A New Tool to Measure Skin Color?

Reflectance confocal microscopy (RCM) is a recent skin imaging technique that allows in vivo, noninvasive, real-time, and almost histological visualization of the skin (Hofmann-Wellenhoff et al. 2012). Confocal microscopy is a technique that enables virtual optical sections through an object of interest. Confocal microscopy was first used in biology to visualize cellular organelles, and it was adapted recently for clinical practice, especially in dermatology. Reflectance means that the images are obtained by reflection of a laser by endogenous molecules. Since melanin is the strongest contrast agent in the skin, RCM is particularly suitable to investigate skin pigmentation. Paradoxically melanized structures look very bright on RCM images, a feature that can be easily seen on RCM sections of the dermal-epidermal junction, where bright (pigmented) keratinocytes surround dark (nonpigmented) dermal papilla (Fig. 5). Interestingly, based on morphological criteria, RCM can discriminate between the different pigment cell populations in the skin (Busam et al. 2001). The interest of RCM for the diagnosis of pigmented lesions, especially pigmented tumors, has largely been reported (Kang et al. 2010a). RCM is also interesting for the evaluation of pigmentation disorders such as vitiligo (Kang et al. 2010b, and Fig. 6) or melasma (Kang et al. 2010c). Regarding normal pigmentation, it was reported recently that RCM may help to quantify variations of skin pigmentation (Lagarrigue et al. 2012). One of the objectives of this work was to identify RCM parameters able to quantify in vivo epidermis pigmentation potentially applicable in clinical studies. The study included 111 healthy female volunteers with phototypes I–VI. The authors proposed an index called "papillary contrast" and defined as the difference in brightness between the cellular ring around the papilla zone and the central dermal papilla zone. The mean papillary contrast (PC) was estimated according to the following function (Figs. 5 and 6):

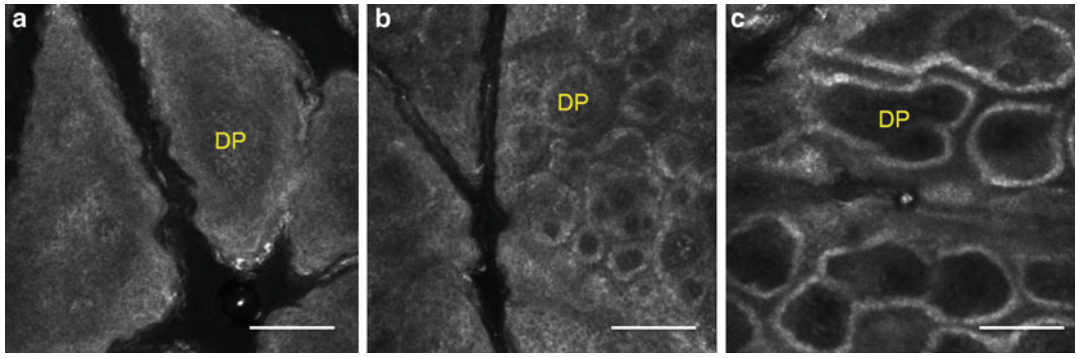

Fig. 5 RCM evaluation of normal pigmentation. Confocal images (500 × 500 μm) at the dermal epidermal junction presenting differences in the brightness of peri-papillar cells between skin phototypes II (**a**), III (**b**), and V (**c**). Scale bar: 125 μm. *DP* dermal papilla. Abdomen skin, non-exposed. Coll. P. Bahadoran

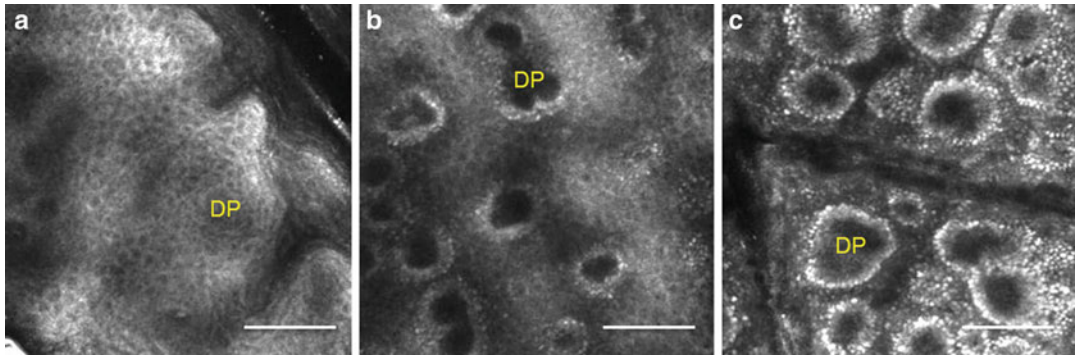

Fig. 6 RCM evaluation of pigmentation in vitiligo. Confocal images (500 × 500 μm) at the dermal epidermal showing increasing brightness of peri-papillar cells in vitiligo lesion (**a**), perilesional skin (**b**), and distant normal skin (**c**). Scale bar: 125 μm. *DP* dermal papilla. Abdomen skin, non-exposed (Adapted from: Kang et al. (2010b))

$$\mathrm{PC} = \frac{\sum \left(\overline{\mathrm{B\_ring}} - \overline{\mathrm{B\_center}}\right)}{\mathrm{Nb\_pap}}$$

where PC, papillary contrast; B_ring, brightness of the ring papilla; B_center, brightness of the central dermal papilla; and Nb_pap, number of papillae.

PC measured at the dermoepidermal junction appeared to be a reliable marker of epidermis pigmentation and showed a strong correlation with skin pigmentation assessed clinically using the Fitzpatrick's classification. However, additional studies comparing RCM with established methods of skin color measurement such as colorimetry are needed in the future to confirm the interest of this approach. Another limitation worth considering is the price of the RCM device ~100,000 euros, though it can be used for other purposes. Despite these limitations, RCM represents a significant advance in the field of pigment measurement since it might allow a quantification of melanin along with a morphological identification of melanized cells.

7 Spectral Imaging and Image Processing

Spectral imaging is the integration of spectroscopy with spatial measurement thus it extends the image into spectroscopy by allowing

measurement of the spectrum at each point of the image. As described before (see Sect. 5), spectroscopy yielded quantitative information and extended understanding of skin pigmentation. Images give morphological information such as lesion texture, borders, area. Spectral imaging of skin surface is then a way to extract both of these two crucial aspects of pigmented lesions.

The information captured by spectral imaging is similar to that acquired by the clinician. So spectral imaging provides global and sufficiently rich information to support diagnosis. In addition, this information is quantitative, objective, and reproducible. The spectral information is more detailed than information provided by human eye or contained in color images.

The human eye, like the dermatoscope (see Sect. 5), only has the capacity to capture in three spectral bands with its sensors for red, green, and blue (RGB). Multispectral imaging (MSI) can capture spectral information in wavelengths from several tens up to one hundred for Hyperspectral Imaging (HIS). The high definition of the skin spectral response which can be out of the visible light range offers a new possibility for identifying and quantitatively characterizing a cutaneous lesion leading to a more precise and robust diagnosis.

Even if different types of spectral imaging measurement are used, most of them imply a sequential capture.

Spectral imaging methods can be divided into four different methods. The wavelength-scan methods using preferentially variable filters measure the images one wavelength at a time. The spatial-scan methods using either a grating or a prism measure the whole spectrum at a time line by line. Time-scan methods are based on measuring interference of light. Interference is obtained using a Michelson system or other interferometer. At the end of the acquisition, the data is transformed to the actual spectral image by the Fourier transform. The fourth method measures the whole spectral image simultaneously, but compromises on spectral and spatial resolution. It consists of separating the CDD (charged coupled device) digital camera surface into several blocks, each of them capturing different wavelengths (Garini et al. 2006). The selection of the most appropriate method depends on the capture constraints (e.g., time, sample movement, resolution need). The larger the number of wavelengths or the higher the spatial resolution, the longer will be the capture.

Multispectral technology has been applied to dermatology mainly for noninvasive diagnosis of melanomas. It has also been proposed for analysis of bruised skin (Randeberg et al. 2006), vascular lesions, (Kuzmina et al. 2010), acne vulgaris (Fujii et al. 2008), and various pigmented lesions including melasma, (Prigent et al. 2012), naevi, and pigmented skin cancers (Diebele et al. 2012a).

For noninvasive melanoma diagnosis, band selection in spectral imaging has been tested.

Some authors have used a predefined set of bands (Dhawan et al. 2009; Kuzmina et al. 2010; Diebele et al. 2012b; Elbaum et al. 2001). However, these sets differ among publications (Elbaum) and could be debatable as they are based on the spectral information supposed (melanin and hemoglobin absorption spectra) and not actually contained in the spectral image capture without taking into account the global information provided by multispectral technology. Other authors have applied methods and algorithms derived from the image processing field (Garini et al. 2006).

The synthesis of multispectral information consists in reducing the quantity of data while keeping all pertinent information. The most favorable approach will be based on the analysis of the spectral information contained in each skin lesion capture. The proposed method consists of identifying the most relevant features allowing the description of the captured data.

The features can be estimated as a linear combination of the different wavelengths that can be assimilated to a “spectral print.”

The most currently used method is the independent component analysis (ICA) introduced in computerized skin analyses by Tsumura et al. (1999). The aim was to isolate the spectral components linked to melanin and hemoglobin chromophores using ICA. The principle was to obtain the spatially independent spectral components of the image expecting that some of these

independent features would correspond to certain molecules present in the skin.

Melanin and hemoglobin, the two principal chromophores involved in skin spectrum, are independently distributed. Tsumara et al. proved that the two features obtained by ICA correspond to these two skin chromophores representing the healthy skin spectral print.

ICA is commonly implemented to multispectral imaging seeking specific characterization of skin pigmented pathology, for example, for melasma diagnosis (Prigent et al. 2012).

A high number of different approaches have been proposed in the literature: implementation of statistical method based on Blind Source Separation (BSS) as Non-Negative Matrice factorization (NMF) to quantified melanin and hemoglobin (Galeano et al. 2012), band selection based on on machine learning algorithms Support Vector Machine (SVM) (Quinzán et al. 2013), geometric method.

Although further investigation is expected, multispectral imaging is an effective tool for capturing the information useful in dermatology.

8 Conclusion

Skin color and pigmentation can be assessed using a wide variety of techniques. The choice depends on the objectives of the investigator. Two main families of methods can be identified: the first is related to the measure of skin color and pigmentation as a whole, i.e., as it can be needed in clinical pharmacology, for example, where only the information on skin erythema or pigmentation intensities are needed on small test surfaces. The associated technologies are based on different approaches of analysis of reflected light by the skin and gives only spectral information. The second family concerns the diagnostic assessments of pigmented skin lesion in which the accurate measurement of hue and chroma of the substructures of the pigmented lesion are very important with integration of morphological components in the assessments. In that sense, dermoscopy has been shown to improve the diagnostic accuracy of pigmented skin lesions and some other techniques such as the multispectral imaging, taking into account the combination of spectral and spatial information, are still in development. Finally, thanks to the improvement of digital image processing technology and to the high quality of the available optics, techniques of epiluminescence microscopy such as dermoscopy and reflectance confocal microscopy represent very promising tools allowing the dermatologist to perform a very accurate noninvasive diagnosis of pigmented skin lesions.

References

Abbas Q, Celebi ME, Fondon GI. Computer-aided pattern classification system for dermoscopy images. Skin Res Technol. 2012;18:278–89.

Abbas Q, Fondon Garcia I, Celebi ME, Ahmad W, Mushtaq Q. Unified approach for lesion border detection based on mixture modeling and local entropy thresholding. Skin Res Technol. 2013;19:314–9.

Alghamdi MA, Kumar A, Taïeb A, Ezzedine K. Assessment methods for the evaluation of vitiligo. JEADV. 2012;26:1463–71.

Andersen PH, Bjerring P. Nonivasive computerized analysis of skin chromophores in vivo by reflectance spectroscopy. Photodermatol Photoimmunol Photomed. 1990;7:249–57.

Andreassi L, Casini L, Simoni S, et al. Measurement of cutaneous colour and assessment of skin type. Photodermatol Photoimmunol Photomed. 1990;7:20–4.

Asawanonda P, Taylor CR. Wood's light in dermatology. Int J Dermatol. 1999;38:801–7.

Bornstein M. Color and its measurements. J Soc Cosmet Chem. 1968;19:649–67.

Busam KJ, Charles C, Lee G. Halpern AC Morphologic features of melanocytes, pigmented keratinocytes, and melanophages by in vivo confocal scanning laser microscopy. Mod Pathol. 2001;14(9):862–8.

Celebi ME, Schaefer G, Iyatomi H, Stoecker WV. Lesion border detection in dermoscopy images. Comput Med Imaging Graph. 2009;33(2):148–53.

Chardon A, Dupont G, Hourseau C, et al. Colorimetric determination of sun-protection-factor. Poster. 15th IFSCC Congress. London. Preprints A/A24. 1988. p. 313–22, 9.

Chardon A, Cretois I, Hourseau C. Skin colour typology and suntanning pathways. Int J Cosmet Sci. 1991;13:191–208.

Chardon A, Moyal D, Bories MF, et al. Comparing suntans from actual sun using various SPF sunscreens. Cosmet Toiletries. 1993;79:9.

Clarys P, Alewaeters K, Lambrecht R, et al. Skin color measurements: comparison between three instruments:

the Chromameter®, the DermaSpectrometer® and the Mexameter®. Skin Res Technol. 2000;6:230–8.
de Rigal J, Abella ML, Giron F, Caisey L, Lefebvre MA. Development and validation of a new Skin Color Chart. Skin Res Technol. 2007;13:101–9.
Dhawan AP, D'Alessandro B, Patwardhan S, Mullani N. Multispectral optical imaging of skin-lesions for detection of malignant melanomas. Conf Proc IEEE Eng Med Biol Soc. 2009;2009:5352–5. doi:10.1109/IEMBS.2009.5334045.
Diebele I, Bekina A, Derjabo A, Kapostinsh J, Kuzmina I, Spigulis J. Analysis of skin basalioma and melanoma by multispectral imaging. Proc SPIE. 2012; 8427, Biophotonics: Photonic Solutions for Better Health Care III, 842732. 2012 June 1. doi:10.1117/12.922301.
Diebele I, Kuzmina I, Lihachev A, Kapostinsh J, Derjabo A, Valeine L, Spigulis J. Clinical evaluation of melanomas and common nevi by spectral imaging. Biomed Opt Express. 2012b;3(3):467–72.
Diffey BL, Robson J. The influence of pigmentation and illumination on the perception of erythema. Photodermatol Photoimmunol Photomed. 1992;9(2):45–7.
Diffey BL, Oliver RJ, Farr PM. A portable instrument for quantifying erythema induced by ultraviolet radiation. Br J Dermatol. 1984;III:663–72.
Elbaum M, Kopf AW, Rabinovitz HS, Langley RG, Kamino H, Mihm Jr MC, Sober AJ, Peck GL, Bogdan A, Gutkowicz-Krusin D, Greenebaum M, Keem S, Oliviero M, Wang S. Automatic differentiation of melanoma from melanocytic nevi with multispectral digital dermoscopy: a feasibility study. J Am Acad Dermatol. 2001;44(2):207–18.
Feather J, Ellis DJ, Leslie G. A portable reflectometer for the rapid quantification of cutaneous haemoglobin and melanin. Phys Med Biol. 1988;33:711–22.
Ferguson J, Brown M, Alert D, et al. Collaborative development of a sun protection factor test method: a proposed European standard. Int J Cosmet Sci. 1996;18:203–18.
Fitzpatrick TB. The validity and practicality of sun-reactive skin type I through VI (Editorial). Arch Dermatol. 1988;77:219–21.
Fitzpatrick TB, Szabo G, Seiji M, et al. Biology of the melanin pigmentary system (section 3, Chapter 14). In: Fitzpatrick TB, Eisen AZ, Wolff K, editors. Dermatology in general medicine. New-York: Mc Graw Hill; 1979. p. 131.
Fujii H, Yanagisawa T, Mitsui M, Murakami Y, Yamaguchi M, Ohyama N, Abe T, Yokoi I, Matsuoka Y, Kubota Y. Extraction of acne lesion in acne patients from multispectral images. Conf Proc IEEE Eng Med Biol Soc. 2008;2008:4078–81. doi:10.1109/IEMBS.2008.4650105.
Fullerton A, Fischer T, Lahti A, et al. Guidelines for measurements of skin colour and erythema. Contact Dermatitis. 1996;31:1–10.
Fulton JE. Utilizing the Ultraviolet (UV Detect) camera to enhance the appearance of photodamage and other skin conditions. Dermatol Surg. 1997;23:163–9.
Galeano J, Jolivot R, Marzani F. Quantification of melanin and hemoglobin in human skin from multispectral image acquisition: use of a neuronal network combined to a non-negative matrix factorization. Appl Comput Math, special issue on Applied Artificial Intelligence and Soft Computing. 2012;11(2):257–70.
Garcia A, Fulton JE. The combination of glycolic acid and hydroquinone or kojic acid for the treatment of melasma and related conditions. Dermatol Surg. 1996;22:443–7.
Garini Y, Young IT, McNamara G. Spectral imaging: principles and applications. Cytometry A. 2006;69A:735–47.
Garnavi R, Aldeen M, Celebi ME, Varigos G, Finch S. Border detection in dermoscopy images using hybrid thresholding on optimized color channels. Comput Med Imaging Graph. 2011;35:105–15.
Gniadecka M, Wulf HC, Mortensen N, et al. Photoprotection in Vitiligo and Normal Skin. Acta Derm Venereol. 1996;76:429–32.
Häggblad E, Petersson H, Ilias MA, Anderson CD, Salerud EG. A diffuse reflectance spectroscopic study of UV-induced erythematous reaction across well-defined borders in human skin. Skin Res Technol. 2010;16:283–90.
Hermanns JF, Petit L, Hermanns-Lê T, et al. Analytic quantification of phototype-related regional skin complexion. Skin Res Technol. 2001;7:168–71.
Hofmann-Wellenhoff R, Pellacani G, Malvehy J, Soyer HP, editors. Reflectance confocal microscopy for skin diseases. Berlin: Springer; 2012.
Hurley ME, Guevara IL, Gonzales RM, Pandya AG. Efficacy of glycolic acid peels in the treatment of melasma. Arch Dermatol. 2002;138:1578–82.
Kang HY, Bahadoran P, Ortonne JP. Reflectance confocal microscopy for pigmentary disorders. Exp Dermatol. 2010a;19(3):233–9.
Kang HY, le Duff F, Passeron T, Lacour JP, Ortonne JP, Bahadoran P. A noninvasive technique, reflectance confocal microscopy, for the characterization of melanocyte loss in untreated and treated vitiligo lesions. J Am Acad Dermatol. 2010b;63(5):e97–100. No abstract available.
Kang HY, Bahadoran P, Suzuki I, Zugaj D, Khemis A, Passeron T, Andres P, Ortonne JP. In vivo reflectance confocal microscopy detects pigmentary changes in melasma at a cellular level resolution. Exp Dermatol. 2010c;19(8):e228–33. doi:10.1111/j.1600-0625.2009.01057.x.
Kimbrough-Green CK, Griffiths CE, Finkel LJ, Hamilton TA, Bulengo-Ransby SM, Ellis CN, et al. Topical retinoic acid (tretinoin) for melasma in black patients. A vehicle-controlledclinical trial. Arch Dermatol. 1994;130:727–33.
Kuzmina I, Diebele I, Asare L, Kempele A, Abelite A, Jakovels D, Spigulis J. Multispectral imaging of pigmented and vascular cutaneous malformations: the

influence of laser treatment.Proc SPIE. 2010; 7376, Laser Applications in Life Sciences, 73760J. 2010 Nov 24. doi:10.1117/12.873701

Lagarrigue SG, George J, Questel E, Lauze C, Meyer N, Lagarde JM, Simon M, Schmitt AM, Serre G, Paul C. In vivo quantification of epidermis pigmentation and dermis papilla density with reflectance confocal microscopy: variations with age and skin phototype. Exp Dermatol. 2012;21(4):281–6.

Lee G, Lee O, ParkS MJ, Oh C. Quantitative color assessment of dermoscopy images using perceptible color regions. Skin Res Technol. 2012;18:462–70.

Lim S, Kim SM, Lee YW, Ahn KJ, Choe YB. Change of biophysical properties of the skin caused byultraviolet radiation-induced photodamage in Kore. Skin Res Technol. 2008;14:93–102.

Liu Z, Sun J, Smith M, Smith L, Warr R. Unsupervised sub-segmentation for pigmented skin lesions. Skin Res Technol. 2012;18:77–87.

Lock-Andersen J, Therkildsen P, de Fine Olivarius F, et al. Epidermal thickness, skin pigmentation and constitutive photosensitivity. Photodermatol Photoimmunol Photomed. 1997;13:153–8.

Lock-Andersen J, Gniadecka M, de Fine OF, et al. Skin temperature of UV-induced erythema correlated to laser Doppler flowmetry and skin reflectance measured redness. Skin Res Technol. 1998a;4:41–8.

Lock-Andersen J, Wulf HC, Knudstorp ND. Skin pigmentation in Caucasian babies is high and evenly distributed throughout the body. Photodermatol Photoimmunol Photomed. 1998b;14:74–6.

Lock-Andersen J, Knudstorp ND, Wulf HC. Facultative skin pigmentation in caucasians: an objective biological indicator of lifetime exposure to ultraviolet radiation ? J Med Invest. 1998c;44(3–4):121–6.

Masson P, Mérot F. Phototype and ITA° parameters as predictive for determination of MED and SPF in tanned or untanned subjects. Poster; Preprints 17th IFSCC congress, Yokohama, Oct 1992.

Meglinski IV, Matcher SJ. Computer simulation of the skin reflectance spectra. Computer Methods Programs Biomed. 2003;70:179–86.

Moyal D, Chardon A, Kollias N. UVA protection efficacy of sunscreens can be determined by the persistent pigment darkening (PPD) method (Part 2). Photodermatol Photoimmunol Photomed. 2000;16:250–5.

Paraskevas LR, Halpern AC, Marghoob AA. Utility of the Wood's light: five cases from a pigmented lesion clinic. Br J Dermatol. 2005;152:1039–44.

Park SB, Suh DH, Youn JI. A long-term time course of colorimetric evaluation of ultraviolet light-induced skin reactions. Clin Exp Dermatol. 1999;24:315–20.

Park ES, Na JI, Kim SO, Huh CH, Youn SW, Park KC. Application of a pigment measuring device –Mexameter – for the differential diagnosis of vitiligo and nevus depigmentosus. Skin Res Technol. 2006;12:298–302.

Piérard GE. EEMCO guidance for the assessment of skin colour. J Eur Acad Dermatol Venerol. 1998;10:1–11.

Prigent S, Descombes X, Zugaj D, Petit L, Dugaret AS, Martel P, Zerubia J. Skin lesion evaluation from multispectral images. Hal-00757039, version 1–26 Nov 2012 – INRIA research report no 8196 – Nov 2012, 20 p.

Quinzán I, Sotoca JM, Latorre-Carmona P, Pla F, García-Sevilla P, Boldó E. Band selection in spectral imaging for non-invasive melanoma diagnosis. Biomed Opt Express. 2013;4(4):514–9. doi:10.1364/BOE.4.000514. Epub 2013 Mar 4.

Randeberg LL, Baarstad I, Løke T, Kaspersen P, Svaasand LO. Hyperspectral imaging of bruised skin. Proc SPIE 6078, Photonic Therapeutics and Diagnostics II, 60780O. 2006 Feb 22. doi:10.1117/12.646557.

Roh K-Y, Kim D, Ha S-J, et al. Pigmentation in Koreans: study of the differences from Caucasians in age, gender and seasonal variations. Br J Dermatol. 2001;144:94–9.

Seitz JC, Withmore CG. Measurement of erythema and tanning response. The time course of UVB and UVC erythema. J Invest Dermatol. 1988;91:454–7.

Shakya NM, LeAnder RW, Hinton KA, Stricklin SM, Rader RK, Hagerty J, Stoecker WV. Discrimination of squamous cell carcinoma in situ from seborrheic keratosis by color analysis techniques requires information from scale, scale-crust and surrounding areas in dermoscopy images. Comput Biol Med. 2012;42:1165–9.

Smith L, MacNeil S. State of the art in non-invasive imaging of cutaneous melanoma. Skin Res Technol. 2011;17:257–69.

Stamatas GN, Zmudzka BZ, Kollias N, Beer JZ. Noninvasive measurements of skin pigmentation in situ. Pigment Cell Res. 2004;17:618–26.

Stamatas GN, Zmudzka BZ, Kollias N, Beer JZ. In vivo measurement of skin erythema and pigmentation: new means of implementation of diffuse reflectance spectroscopy with a commercial instrument. Br J Dermtol. 2008;159:683–90.

Takiwaki H, Overgaard L, Serup J. Comparison of narrowband reflectance spectrophotometric and tristimulus colorimetric measurements of skin color. Skin Pharmacol. 1994;7:217–55.

Taylor S, Westerhof W, Im S, Lim J. Noninvasive techniques for the evaluation of skin color. J Am Acad Dermatol. 2006;54:282–90.

Tian Y, Wang YX, Gu WJ, Zhang P, Sun YEY, Liu W. Physical measurement and evaluation of skin color changes under normal condition and post-ultraviolet radiation: a comparison study of Chromameter CM 2500d and Maxmeter MX18. Skin Res Technol. 2011;17:304–8.

Tsumura N, Haneishi H, Miyake Y. Independent component analysis of skin color image. J Opt Soc Am A. 1999;16:2169–76.

Van der Wal M, Bloemen M, Verhaegen P, Tuinebreijer W, et al. Objective color measurements; clinimetric

performance of three devices on normal skin and scar tissue. J Burn Care Res. 2013;34(3):187–94.
Wallace VP, Crawford DC, Mortimer PS, et al. Spectrophotometric assessment of pigmented skin lesions: methods and feature selection for evaluation of diagnostic performance. Phys Med Biol. 2000;45(3):735–51.
Wang L, Jacques SL, Zheng L. MCML – Monte Carlo modeling of light transport in multi-layered tissues. Comput Methods Programs Biomed. 1995;47 (2):131–46.
Wassermann HP. The colour of human skin. Spectral reflectance versus skin colour. Dermatologica. 1971;143:166–73.
Weatherall IL, Coombs BD. Skin color measurements in terms of CIELAB color space values. J Invest Dermatol. 1992;99:468–73.
Yoshimura K, Harii K, Masuda Y, Takahashi M, Aoyama T, Iga T. Usefulness of a narrow-band reflectance spectrophotometer in evaluating effects of depigmenting treatment. Aesthetic Plast Surg. 2001;25(2):129–33.

The Measurement of Skin Color

6

Behrooz Kasraee

Contents

Keywords

Skin color • Skin melanin content • Chromameter • CIE XYZ color space • CIELAB • CMYK model • Dermacatch • Dermaspectrphotometer • Mexameter • RGB color space • Skin colorimetry

The color of human skin is determined by its melanin content, its oxy- and deoxy-hemoglobin contents, and the amount of endogenous or exogenous pigments such as bilirubin and carotene (Andreassi et al. 1999). The measurement of skin color is of the utmost importance for many researchers and clinicians involved in dermatologic as well as cosmetic fields. The noninvasive measurement of epidermal melanin content is necessary for in vivo studies that implicate skin depigmentation and repigmentation. Skin erythema values are considered as an index of inflammation and dermal vascularity/vasodilatation and are utilized in the evaluation of therapeutic outcome in several dermatologic treatments. The first quantitative evaluation of skin color was accomplished in 1939 by Edwards and Duntley, who obtained colorimetric data specific for different types of skin pigmentation (Edwards and Duntley 1939). Other authors subsequently utilized similar instruments to evaluate the skin color of different ethnic groups. In the 80s, the calorimetric technology evolved greatly and sophisticated instruments suitable for dermatologic use became available (Andreassi et al. 1999).

B. Kasraee (✉)
Scientis Pharma SA, Geneva, Switzerland
e-mail: behroozkasraee@yahoo.com

P. Humbert et al. (eds.), *Agache's Measuring the Skin*,
DOI 10.1007/978-3-319-32383-1_6

It is important to note that although the in vitro color measurement can be reliably done by several colorimetric devices, the quantification of skin color "evolution" in vivo appears to be more complex, as in vivo fluctuations in erythema can affect melanin values and vice versa (Baquie and Kasraee 2014). Knowing that melanin absorbs light in a large range of wavelengths (including green, red, and near-infrared light), the confusion over the discrimination between melanin and erythema can easily occur by colorimetric devices.

To discriminate melanin from skin erythema, different technologies have been developed with a variable level of reliability. Some colorimeters are based on scanning reflectance spectrophotometry (Andreassi et al. 1999), and others rely on tristimulus (i.e., three specific wavelengths) colorimetry, such as Chromameter (Minolta) (Andreassi et al. 1999), or narrow-band simple reflectance colorimetry, such as Mexameter (Courage-Khazaka, Germany) (Andreassi et al. 1999; Baquie and Kasraee 2014).

In order to understand the different color measurement technologies, it is essential to know the different existing color models.

1 The RGB Color Space

The name of the model comes from the initials of the three additive primary colors, red, green, and blue. This is an additive color model in which red, green, and blue lights are added together in various ways to produce a broad array of colors. Today, the main purpose of the RGB model is the representation and display of images in electronic devices such as computers. It has also been used in conventional photography. Before the electronic age, the RGB color model already had a robust theory behind it, based on human perception of colors (International Color Consortium 2006).

RGB is a *device-dependent* color model, that is, different devices reproduce or detect a given RGB value differently, since the color elements and their response to the individual R, G, and B levels might differ from one manufacturer to another, or even in the same, device over time. Thus, RGB values do not define the same *color* across different devices (International Color Consortium 2006).

2 The CMYK Model

This is a subtractive color model in contrast to the additive RGB color model.

This model works by partially or entirely masking colors on a lighter, usually white, background and is the model used in color printing. The colors are cyan (C), magenta (M), yellow (Y), and key (K; black). The CMYK model is a device-dependent model (International Color Consortium 2006).

3 CIE-*L*a*b** (CIELAB)

This is the most complete color space specified by the International Commission of Illumination (French *Commission Internationale de l'éclairage*). It describes all the colors visible to the human eye and was created to serve as a device-independent model to be used as a reference (International Color Consortium 2006).

The three coordinates of CIELAB represent the lightness of the color ($L^* = 0$ yields black and $L^* = 100$ indicates diffuse white), its position between red/magenta and green (a^*, negative values indicate green while positive values indicate magenta), and its position between yellow and blue (b^*, negative values indicate blue and positive values indicate yellow) (Andreassi et al. 1999; International Color Consortium 2006).

4 CIE XYZ

The CIE XYZ color space encompasses all color sensations that an average person can experience. It serves as a standard reference against which many other color spaces are defined. The human eye has three kinds of cone cells, which sense

light, with spectral sensitivity peaks in short (*S*, 420–440 nm), middle (*M*, 530–540 nm), and long (*L*, 560–580 nm) wavelengths. These cone cells underlie human color perception under medium- and high-brightness conditions. The CIE model capitalizes on this fact by defining Y as luminance. Z is quasi-equal to blue stimulation, or the S cone response, and X is a mix (a linear combination) of cone response curves chosen to be nonnegative. The XYZ tristimulus values are thus analogous to, but not equal to, the LMS cone responses of the human eye (Andreassi et al. 1999; International Color Consortium 2006).

5 The Basis of Skin Colorimetry

The basis of investigation of optical properties of an object is recording the intensity of light which is reflected from its surface at many narrow-band wavelength(s) throughout the spectra of visible light (400–700 nm), namely, the reflectance spectrophotometry (Takiwaki 1998). The CIE-L*a*b* values are most commonly used for the quantification of skin color (Weatherall and Coombs 1992). There are several other formulas that are proposed and used by other authors (Dawson et al. 1980; Kollias and Baqer 1985; Feather et al. 1989; Andersen and Bjerring 1990) for the conversion of reflectance data into different indices that show relative amounts of epidermal melanin pigment as well as oxy- and deoxy-Hb in the superficial vascular plexus of the dermis (Takiwaki 1998). These indices are read according to the Dawson's theory, by calculating the reflectance or absorbance values of the skin measured at several wavelengths that are determined in order to enable the abstraction of information about the quantity of the targeted chromophore (Takiwaki 1998). In practical use, a reflectance spectrometer is expensive and cumbersome, as it necessitates the connection to a computer. Several portable opto-electronic instruments have thus been designed and become widely available (Serup and Agner 1990; Westerhof 1995; Takiwaki and Serup 1995; Feather et al. 1988; Pearse et al. 1990; Kopola et al. 1993).

6 Chromameter®

Chromameter (Minolta, Osaka, Japan) is a tristimulus colorimetric instrument based on scanning reflectance spectrophotometry. It contains a xenon lamp as the light source, photodetectors, a microcomputer, and colored filters that match the CIE colorimetric standard observer curves (Westerhof 1995). Color values in accordance with the CIE color systems (L*a*b, or XYZ) are calculated automatically with these instruments. To obtain data, the probe head is placed onto the skin and the shutter button is pushed gently. The results (L*a*b, XYZ or melanin index in more recent chromameters) are instantly displayed on the screen (Takiwaki 1998).

Chromameter has the following disadvantages:

- Skin color is easily influenced by pressure on the skin and orthostatic position of the device (Takiwaki et al. 1994; Queille-Roussel et al. 1991; Takiwaki and Serup 1994). To avoid the influences of differences in the manner of measurement, standardized guidelines for skin color measurement with these instruments have been proposed by Fullerton et al. (1996).
- The color of an object smaller than the opening of the probe head (8–11 mm) cannot be measured exactly (Takiwaki 1998).
- The evaluation of the pattern or distribution of skin color in a test area is not possible (Takiwaki 1998). The values obtained by chromameter indicate an average of the total test area. These problems may be solved by computer-assisted image analysis of digitized color pictures of an object (Takiwaki 1998). However, as the color of an object depends on the illumination and the characteristics of the device used to record the image such as a CCD (charge coupled devices), the color values obtained with software for image analysis are not absolute but should be considered as relative data, which are comparable only with those obtained using the same system and under the same situations (Takiwaki 1998).
- To the best of our knowledge, there are no data available at present to show whether or not the

melanin values obtained by chromameter can be falsely affected by changes in the levels of skin erythema and vice versa.

7 Derma-Spectrphotometer®

Derma-Spectrophotometer (DSM; Cortex Technology, Denmark) is a narrow-band skin colorimeter with a high intensity white LED as the light source. DSM can display skin color in L*a*b, RGB, CMYK, and XYZ color models and can also display melanin and erythema values. For ease of operation, the probe is equipped with a guiding light that illuminates the target prior to reading. The effect of pressure on color measurements is minimal due to the probe head design. However, as an important disadvantage, the environmental light can affect the measurements. It is not known whether changes in erythema can falsely affect melanin values measured by Derma-Spectrophotometer and vice versa. The device is more ergonomic than chromameter.

8 Mexameter® (Courage-Khazaka, Germany)

This narrow-band simple reflectance colorimeter analyzes an area of 20 mm^2, that is, a disk of 5 mm in diameter. The device contains 16 diodes positioned at the periphery of the photodetector (Baquie and Kasraee 2014). Diodes emit at 568, 660 and 880 nm, which respectively correspond to green, red, and infrared light. Photodetection of the reflected light after emissions in the green and red allows computing cutaneous hemoglobin content (i.e., erythema value with arbitrary units), while analysis of reflected light from wavelengths in the red and near-infrared provides values of skin melanin content (i.e., melanin value also with arbitrary units). L*a*b, RGB, or CMYK values are not displayed (Baquie and Kasraee 2014).

The color measurement is automatically performed when the probe head is placed on the skin surface and removed. A vertical and gentle movement is necessary to reassure a correct measurement (Baquie and Kasraee 2014). The disadvantages of Mexameter include the followings:

- Measurements can be affected by environmental light. Color measurements should therefore be done in a dark place.
- If the probe is not vertically placed on the skin surface or removed too rapidly, measurement accuracy can be affected.
- Measurements are affected by the pressure applied by the probe to the skin (Baquie and Kasraee 2014).
- A recent extensive study on Mexameter sensitivity and specificity confirmed that changes in skin erythema levels can falsely affect melanin values and vice versa (Baquie and Kasraee 2014).

A few clinical studies have compared the tristimulus and narrow-band colorimetric devices. Shriver and Parra found a strong correlation between the melanin index (MI) and L* value and concluded that both types of devices provide accurate measurements of skin and hair color in persons of European, Asian, and African-American ancestry (Shriver and Parra 2000).

In a comparison of the tristimulus chromameter and the narrow-band spectrophotometers and the Mexameter and the Derma-Spectrophotometer for the evaluation of various skin color changes (erythema, irritation, blanching, artificial, and UV tanning), it was found that the sensitivity and reproducibility of all devices were acceptable. The Mexameter showed the weakest sensitivity, but the day-to-day repeatability of melanin measurements was better for the narrow-band spectrophotometers (Clarys et al. 2000).

9 Dermacatch®

Dermacatch is a new colorimetric device recently developed by the Swiss company Colorix. Dermacatch is a visible-spectrum reflectance colorimeter that is made of a diode emitting in the "full visible light spectrum" (Baquie and Kasraee 2014). The photodetector measures the globally

reflected light to compute erythema as well as melanin values (with arbitrary units that differ from the Mexameter's units). The measured area covers a disk of 5.5 mm in diameter, that is, 24 mm^2.

An extensive in vitro and in vivo study, involving 18,000 measurements aimed at comparing the reproducibility, sensitivity, and specificity of Dermacatch versus Mexameter, showed that Dermacatch values were significantly more reproducible than Mexameter (Baquie and Kasraee 2014). Dermacatch was also shown to be more sensitive and specific than Mexameter in measuring melanin and erythema values in vivo (Baquie and Kasraee 2014). Changes in erythema levels did not affect melanin values and vice versa, that is, unlike Mexameter, Dermacatch could precisely discriminate the two parameters (Baquie and Kasraee 2014). It is claimed that the environmental light does not affect Dermacatch measurements; this, however, was not evaluated in the above-mentioned study. Disadvantages of Dermacatch are the followings:

- Measurement data are only displayed on the screen and cannot be printed out or automatically transferred to the computer.
- The color of an object smaller than the opening of the device (D: 5 mm) cannot be measured.

Recently bought by "Delfin technology", this device has been recently upgraded and commercialized to "SkinColorCatch".

10 Conclusion

Skin colorimetry remains a complex subject. Although the in vitro measurement of color (e.g., in color charts) by most colorimeters provides reproducible and reliable results, color measurement in biologic materials such as skin, in which parameters such as pigmentation, skin roughness, and especially skin erythema can readily change, is much more complicated. Taking into account that changes in each parameter can significantly, and falsely, affect the values obtained for other parameters, one should note that data obtained for skin color "evolution" in two different time points should be interpreted with considerable caution. New, more specific colorimeters that permit a more precise discrimination between melanin and erythema might help to resolve this problem.

References

Andersen PH, Bjerring P. Noninvasive computerized analysis of skin chromophores in vivo by reflectance spectroscopy. Photodermatol Photoimmunol Photomed. 1990;7:249–57.

Andreassi L, et al. Practical applications of cutaneous colorimetry. Clin Dermatol. 1999;13:369–73.

Baquie M, Kasraee B. Discrimination between cutaneous pigmentation and erythema: comparison of the skin colorimeters Dermacatch and Mexameter. Skin Res Technol. 2014;20(2):218–27

Clarys P, Alewaeters K, Lambrecht R, Barel AO. Skin color measurements: comparison between three instruments: the Chromameter, the DermaSpectrometer and the Mexameter. Skin Res Technol. 2000;6(4):230–238.

Dawson JB, Barker DJ, Ellis DJ, Grassam E, Cotterill JA, Fisher GW, Feather JW. A theoretical and experimental study of light absorption and scattering by in vivo skin. Phys Med Biol. 1980;25:695–709.

Edward A. Edwards and S. Quimby Duntley. The pigments and color of living human skin. Am J Anatomy. 1939;65:1–33.

Feather JW, Ellis DJ, Leslie G. A portable reflectometer for the rapid quantification of cutaneous haemoglobin and melanin. Phys Med Biol. 1988;33:711–22.

Feather JW, Hajizadeh-Saffar M, Leslie G, Dawson JB. A portable scanning reflectance spectrophotometer using visible wavelengths for the rapid measurement of skin pigments. Phys Med Biol. 1989; 34:807–20.

Fullerton A, Fischer T, Lahti A, Wilhelm KP, Takiwaki H, Serup J. Guidelines for measurement of skin colour and erythema. Contact Dermatitis. 1996;35:1–10.

International Color Consortium, Specification ICC.1:2004–10 (Profile version 4.2.0.0) Image technology colour management – architecture, profile format, and data structure, 2006.

Kollias N, Baqer A. Spectroscopic characteristics of human melanin in vivo. J Invest Dermatol. 1985;85:38–42.

Kopola H, Lahti A, Myllyla R, Hannuksela M. Two-channel fiber optic skin erythema meter. Opt Eng. 1993;32:222–6.

Pearse AD, Edwards C, Hill S, Marks R. Portable erythema meter and its application to use in human skin. Int J Cosmet Sci. 1990;12:63–70.

Queille-Roussel C, Pocet M, Scaffer H. Quantification of skin colour changes induced by topical corticosteroid preparations using the Minolta Chroma Meter. Br J Dermatol. 1991;124:264–70.

Serup J, Agner T. Colorimetric quantification of erythema -a comparison of two colorimeters (Lange Micro Color and Minolta Chroma Meter CR-200) with a clinical scoring scheme and laser-Doppler flowmetry. Clin Exp Dermatol. 1990;15:267–72.

Shriver MD, Parra EJ. Comparison of narrow-band reflectance spectroscopy and tristimulus colorimetry for measurements of skin and hair color in persons of different biological ancestry. Am J Phys Anthropol. 2000;112:17–27.

Takiwaki H. Measurement of skin color: practical application and theoretical considerations. J Med Invest. 1998;44:121–6.

Takiwaki H, Serup J. Variation in color and blood flow of the forearm skin during orthostatic maneuver. Skin Pharmacol. 1994;7:226–30.

Takiwaki H, Serup J. Measurement of erythema and melanin indices. In: Serup J, Jemec GBE, editors. Handbook of non-invasive methods and the skin. Boca Raton: CRC Press; 1995. p. 377–84.

Takiwaki H, Overgaard L, Serup J. Comparison of narrow-band reflectance spectrophotometric and tristimulus colorimetric measurements of skin color. Skin Pharmacol. 1994;7:217–25.

Weatherall IL, Coombs BD. Skin color measurements in terms of CIELAB color space values. J Invest Dermatol. 1992;99:468–73.

Westerhof W. CIE colorimetry. In: Serup J, Jemec GBE, editors. Handbook of non-invasive methods and the skin. Boca Raton: CRC Press; 1995. p. 385–97.

Discrimination Between Cutaneous Pigmentation and Erythema: Comparison of the Skin Colorimeters Dermacatch and Mexameter

7

Mathurin Baquié and Behrooz Kasraee

Contents

Keywords

Chromameter • Mexameter • Erythema • Melanin • Skin color • Reflectance colorimetry • Colorimeter • Quantification of skin color

1 Introduction

Defining skin color and monitoring its modulation under the influence of varying types of stimuli (such as drug or light test/treatment, exposure to irritants) is a highly indicative method in dermatocosmetic research as well as in day-to-day practice. However, quantification of skin color evolution appears to be complex, as in vivo fluctuations in erythema can affect melanin values and vice versa. Knowing that melanin absorbs light in a large range of wavelengths (including green, red, and near-infrared light), the confusion over the discrimination between melanin and erythema (i.e., redness of hemoglobin) can easily occur by colorimetric devices.

To discriminate melanin from skin erythema, different technologies have been developed with a variable level of reliability; some colorimeters are based on scanning reflectance spectrophotometry (Bjerring 1995; Anderson and Bjerring 1995; Wilhem and Maibach 1995; Clarys et al. 2000; Biniek et al. 2012), others rely on tristimulus (i.e., three specific wavelengths) colorimetry (such as Chromameter®, Minolta) (Clarys et al. 2000; Westerhof et al. 1986; Seitz and Whitmore 1988; Queille-Roussel et al. 1991; Chan and Li Wan Po

M. Baquié • B. Kasraee (✉)
Scientis Pharma SA, Geneva, Switzerland
e-mail: behroozkasraee@yahoo.com

P. Humbert et al. (eds.), *Agache's Measuring the Skin*,
DOI 10.1007/978-3-319-32383-1_7

1993; Waring et al. 1993; Westerhof 1995; Takiwaki and Serup 1995; Elsner 1995; Rubegni et al. 2002) or narrow-band simple reflectance colorimetry, e.g., Mexameter® (Courage-Khazaka) (Clarys et al. 2000; Farr and Diffey 1984, 1985; Diffey et al. 1984; Diffey and Farr 1991; Takiwaki et al. 1994; Anderson 1995; Erythema Meter 1999; DermaSpectrometer 1999; Mexameter MX 16 1999; Courage W, Khazaka G, 1999, Calculation of the melanin value and erythema value for the Mexameter, personal communication; Gabard et al. 1993; Draaijers et al. 2004). Recently, has been released a new colorimeter, Dermacatch® (Colorix), which uses the entire visible-spectrum reflectance. It is claimed to better discriminate between melanin and erythema. To evaluate its potential, Dermacatch® was compared with Mexameter®, one of the mostly used colorimeters in dermatological research. Sensitivity, specificity, and reproducibility of the respective erythema/melanin values of the two devices were first evaluated on standardized color charts. Then, the parameters were also analyzed on human volunteers before and after targeted exposure to different UVB doses and/or modulation of cutaneous erythema (through the application of topical vasodilator and vasoconstrictor agents).

2 Material and Methods

2.1 Instruments

2.1.1 Mexameter® M X16 (Courage-Khazaka, Germany)

This narrow-band simple reflectance colorimeter analyzes an area of 20 mm^2, that is, a disk of 5 mm in diameter. The device contains 16 diodes positioned at the periphery of the photodetector. Diodes emit at 568, 660, and 880 nm, which respectively correspond to green, red, and infrared light. Photodetection of the reflected light after emissions in the green and red allows computing cutaneous hemoglobin content (i.e., erythema value with arbitrary units), while analysis of reflected light from wavelengths in the red and near-infrared provides values of skin melanin content (i.e., melanin value also with arbitrary units).

2.1.2 Dermacatch® (Colorix, Switzerland)

The visible-spectrum reflectance colorimeter is made of a diode emitting in the full visible spectrum. The photodetector measures the globally reflected light to compute erythema as well as melanin values (with arbitrary units that differ from the Mexameter's units). The measured area covers a disk of 5.5 mm in diameter, that is, 24 mm^2.

2.2 In Vitro Measurements

The two colorimeters were tested on 67 colors of the wildly used Natural Colour System (NCS) color chart from the Scandinavian Colour Institute (Stockholm, Sweden). The selected colors covered notably the grey (i.e., from white to black), pink (i.e., from light pink to dark pink), red (i.e., from light red to dark red), beige (i.e., from light beige to dark beige), and brown (i.e., from light brown to dark brown) scales: NCS S 0300-N, NCS S 0500-N, NCS S 1000-N, NCS S 8000-N, NCS S 8500-N, NCS S 9000-N, NCS S 4000-N, NCS S 4500-N, NCS S 5000-N, NCS S 0505-Y20R, NCS S 1005-Y20R, NCS S 2005-Y20R, NCS S 3005-Y20R, NCS S 4005-Y20R, NCS S 5005-Y20R, NCS S 6005-Y20R, NCS S 7005-Y20R, NCS S 8005-Y20R, NCS S 8505-Y20R, NCS S 0505-Y50R, NCS S 1005-Y50R, NCS S 2005-Y50R, NCS S 3005-Y50R, NCS S 4005-Y50R, NCS S 5005-Y50R, NCS S 6005-Y50R, NCS S 7005-Y50R, NCS S 8005-Y50R, NCS S 0505-Y80R, NCS S 1005-Y80R, NCS S 2005-Y80R, NCS S 3005-Y80R, NCS S 4005-Y80R, NCS S 5005-Y80R, NCS S 6005-Y80R, NCS S 7005-Y80R, NCS S 8005-Y80R, NCS S 8505-Y80R, NCS S 3560-Y30R, NCS S 4550-Y30R, NCS S 3560-Y40R, NCS S 4550-Y40R, NCS S 3560-Y50R, NCS S 4550-Y50R, NCS S 3560-Y60R, NCS S 4550-Y60R, NCS S 3560-Y70R, NCS S 4550-Y70R, NCS S 0580-Y80R, NCS S 1080-Y80R, NCS S 0585-Y80R, NCS S 1085-

Y80R, NCS S 0580-Y90R, NCS S 1080-Y90R, NCS S 1085-Y90R, NCS S 1080-R, NCS S 6010-Y90R, NCS S 2565-R80B, NCS S 2565-G, NCS S 2070-G70Y, NCS S 0520-G80Y, NCS S 0530-G80Y, NCS S 0540-G80Y, NCS S 0550-G80Y, NCS S 0560-G80Y, NCS S 0570-G80Y, NCS S 0575-G90Y). On each color square, ten measures were collected with both colorimeters.

2.3 In Vivo Measurements

2.3.1 Analysis of Different Fitzpatrick Skin Colors

In vivo tests were performed on three groups of volunteers with, respectively, phototype II, III, and IV to validate the reliability of both devices. The analyzed area consisted of the proximal volar arm that was unexposed to UV light; ten measures were collected with both colorimeters.

2.3.2 Analysis of Cutaneous Erythema and Pigmentation

Twelve male volunteers of Fitzpatrick skin type III were recruited with an average age of 23. Approval from the local ethics committee as well as informed consent from the volunteers was collected prior to any experiment. Exclusion criteria were any sign, prior or during the experiment, of photosensitivity (e.g., drug-induced photosensitivity, diseases such as solar urticaria or auto-immune diseases), allergies to agents used during the tests, infection or inflammation of the skin, involvement in additional clinical test in parallel or within the preceding 3 months, or exposure to ultraviolet irradiation or intensive sunlight within 4 weeks before or during this study. All experiments were performed in the same room under controlled ambient conditions (temperature at 23 °C and relative humidity at 40 %). While each volunteer was acclimatized for 15 min prior testing, the skin area of interest was thoroughly cleansed with a neutral lotion and then rehydrated with an open application of Excipial cream (Spirig laboratories, Switzerland). For each time point and condition, measurements with both colorimeters were collected ten times on each specific skin area of interest. In parallel, images were taken with a dermatoscope (Handyscope, Fotofinder) at each site for expert visual assessment.

2.3.3 Erythema Induction on the Forearms

For each of the 12 volunteers, a skin area of 40 mm in diameter was treated on the volar aspect of each forearm with 5 mM methyl nicotinate cream (MNC) for 30 s under occlusion at 3 mg/cm^2. MNC cream was prepared through dissolution of methyl nicotinate (Sigma-Aldrich) in ethanol 70° following the dispersion of the solution in Excipial cream to obtain a final concentration of 5 mM MNC. Two control areas, selected on each volar forearm, were similarly treated with Excipial cream alone. No skin site was closer than 40 mm to the antecubital fossa or to the wrist. After the exposure time of 30 s, excess of the cream was removed. Measurements were collected before treatment (i.e., 0 min) as well as after 5 and 10 min. At each time point, 10 measurements were performed on each area with each colorimeter.

2.3.4 UVB Exposure on the Back

On each side of the volunteer's back at the level of vertebra L1, three squares of 20 mm in width were exposed to UVB at 450, 600, and 750 mJ/cm^2, respectively, through a unique treatment by Excimer Laser (Xtrac, Photomedex). Measurements by Dermacatch as well as Mexameter were done before treatment (i.e., day 0) as well as after 2, 7, and 14 days. For each treated area, a contiguous unexposed skin area was considered as the respective control site.

2.3.5 Erythema Reduction on the Back

Seven days after UVB exposure, one of the two skin areas exposed at 750 mJ/cm^2 as well as its contiguous unexposed site was treated with a dermocorticoid (0.05 % clobetasol propionate, Dermovate cream) at 3 mg/cm^2 for 18 h under occlusion. After the exposure time, excess of the cream was removed. Measurements were collected before treatment (i.e., 0 h) as well as after 18 h of exposure.

2.3.6 Erythema Induction on the Back

Fourteen days after UVB exposure, one side of the back was treated with 5 mM MNC for 30 s under occlusion at 3 mg/cm^2. UVB-exposed as well as contiguous unexposed skin areas were similarly treated. Measurements were collected before treatment (i.e., 0 min) and after 10 min. The rest of the protocol was identical to the experiment of erythema induction on the forearms.

2.4 Calculation and Statistics

Coefficient of determination (R^2) was considered in the case of the in vitro analysis when visually assuming that the darkening and reddening of the standard colors gradually increased and remained constant, respectively.

Correlation ratio (CR) to compare the values of the two colorimeters relied on the Pearson correlation.

Coefficient of variation (CV) was calculated as follows: (Mean value after treatment – Mean value before treatment)/Mean value before treatment × 100. Mean values corresponded to the average of the 10 repetitive measures from the same specific skin area at the same time point.

Multiple ANOVA analysis with Bonferroni correction was used to define the significance of the changes between conditions and time points.

3 Results

3.1 In Vitro Experiments

To define the reliability of the two colorimeters, initial tests were performed on an international standard, the NCS color chart. Colors of the chart were selected to visually show a gradual increase in darkness and a constant redness. When analyzing any type of colors, erythema values of Dermacatch remained constant, while those of Mexameter significantly fluctuated (Fig. 1a, c, and e). Regarding melanin values, Dermacatch values increased in a similar proportion to visual perception, while the increase of the Mexameter values was not consistent (Fig. 1b, d, and f). Therefore, the limited range of sensitivity of Mexameter triggered a weak correlation between the two devices (Table 1). However, the repeatability of values was high for both colorimeters (standard deviation values–SD–of Table 1) and was below the official SD mentioned by the providers (i.e., +/−10 arbitrary units of the value for both devices).

3.2 In Vivo Experiments

3.2.1 Analysis of Different Fitzpatrick Skin Colors

Contrary to the in vitro results that showed a poor specificity of Mexameter, the in vivo values of the two colorimeters provided a similar pattern of the three examined Fitzpatrick skin phototypes (i.e., type II, III, and IV) and were consistent with visual perception. However, the reproducibility of the data was slightly weaker with Mexameter even though the SD was below the official value (Fig. 2 and Table 2).

3.2.2 Erythema Induction on the Forearms

To determine if an increase in erythema was detectable by the colorimeters, forearms were treated with topical 5 mM MNC, a vasodilator. MNC was known to only induce a transient increase in redness; therefore, melanin values were expected to remain constant before and after MNC application, despite the homogenous increase in skin erythema. After 5 min of exposure, skin redness increased and reached a plateau according to both colorimeters and dermatoscopic evaluations. Noteworthy, Mexameter falsely measured a significant decrease in pigmentation that was inversely proportional to the increase in cutaneous redness. Thus, the melanin measurement with Mexameter appeared to be biased by the induced erythema modulation. In parallel, analysis of data from Dermacatch showed that its melanin values were not affected by this specific induced skin erythema (Fig. 3 and Table 3).

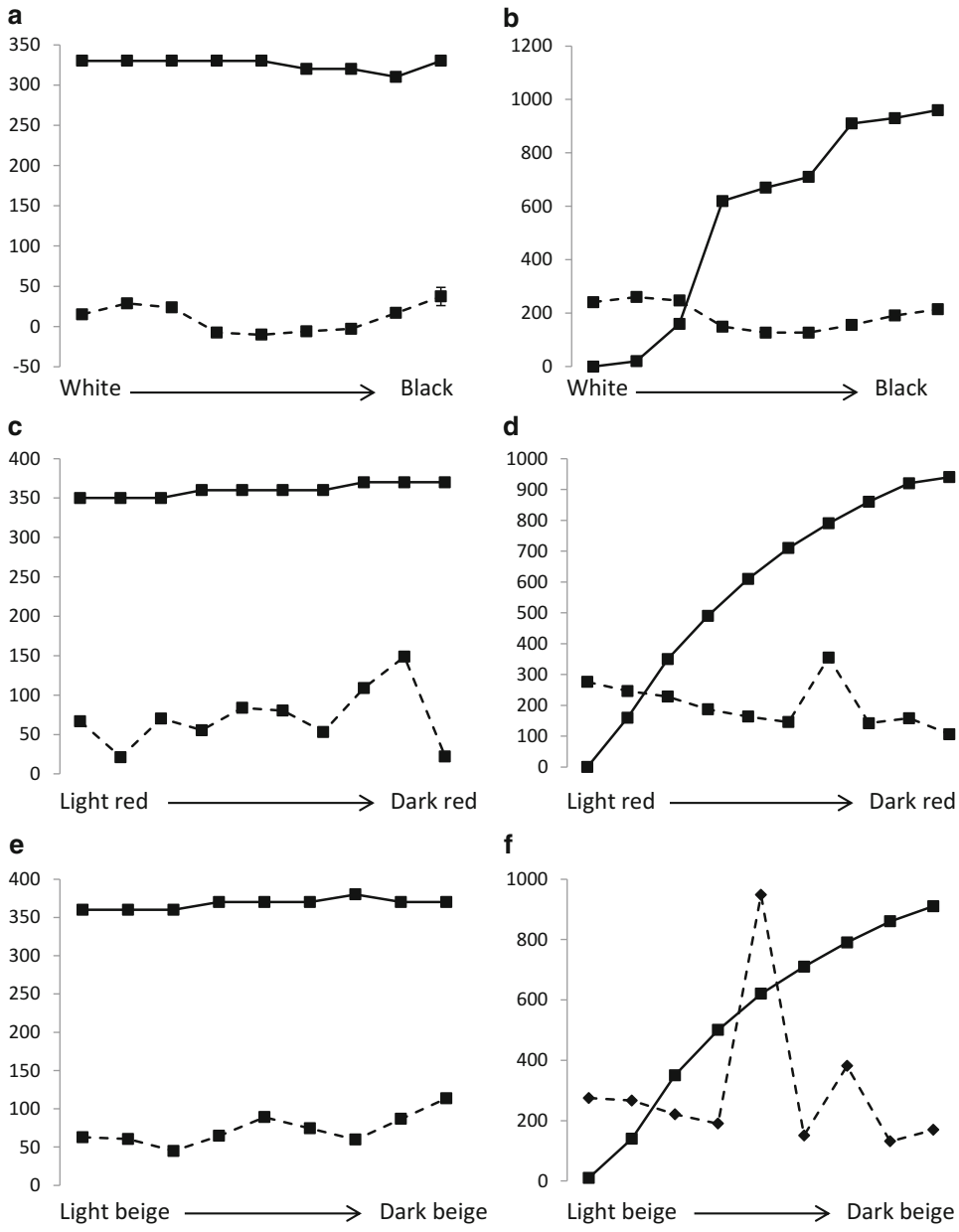

Fig. 1 Comparison of melanin and erythema values of the two colorimeters on the NCS color chart. Examples of erythema values (**a**, **c**, **e**) and melanin value (**b**, **d**, **f**) on colors ranging from *white* on the *left* side of the graph to *black* on the *right* side (**a**, **b**), *light red* to *dark red* (**c**, **d**), and light beige to dark beige (**e**, **f**). Mexameter values are depicted as a *dashed line* and Dermacatch values as *solid line*

3.2.3 UVB Exposure on the Back

According to visual perception through dermatoscopic images, skin erythema reached its maximum at day 2 following the UVB exposure on the volunteer's back and then gradually decreased. Moreover, the intensity of erythema seemed to be proportional to the applied UVB dose. Interestingly, both devices showed the

Table 1 In vitro reliability of melanin and erythema values of both colorimeters

	Melanin values		Erythema values	
	Dermacatch	Mexameter	Dermacatch	Mexameter
SD	0	2.7	0	2
R^2	0.949	0.259	0.891	0.105
CR	0.112		−0.135	

SD standard deviation, R^2 coefficient of determination, *CR* correlation ratio

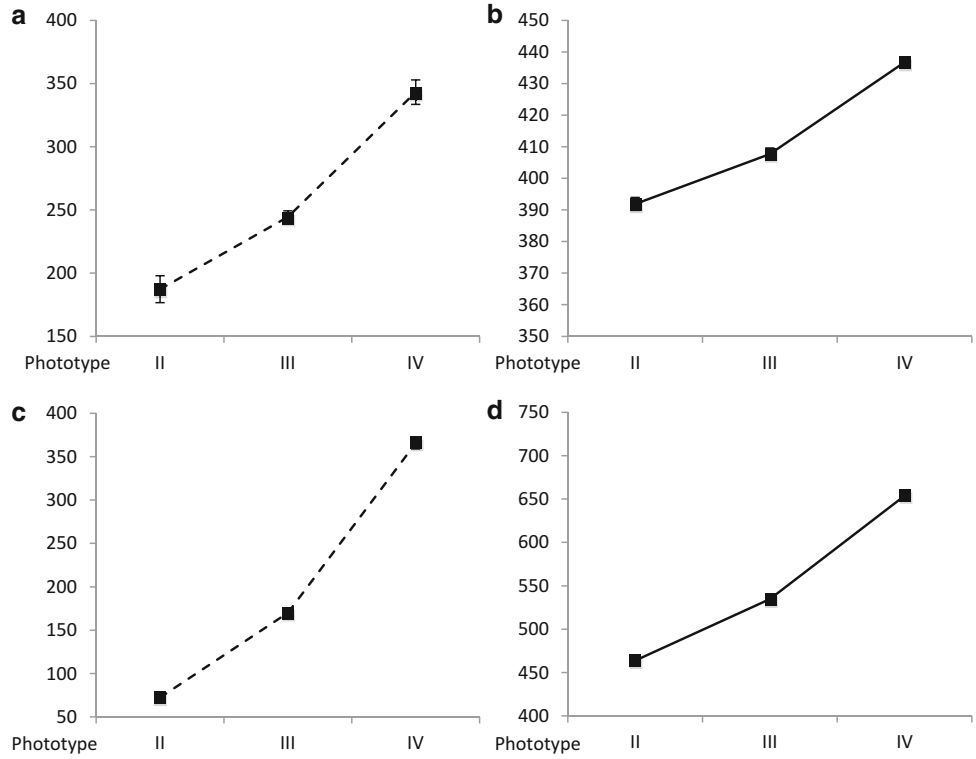

Fig. 2 Analysis of different Fitzpatrick skin colors. Erythema (**a**–**b**) and melanin values (**c**–**d**) from three groups of volunteers with phototype II, III, and IV, respectively, were provided by Dermacatch (**a**, **c**) and Mexameter (**b**, **d**)

Table 2 In vivo reliability of both colorimeters on different phototypes

	Melanin values		Erythema values	
	Dermacatch	Mexameter	Dermacatch	Mexameter
SD	2.1	4.1	1.8	8.4
CR	1		1	

SD standard deviation, *CR* correlation ratio

same pattern for erythema values, and this pattern was proportional to the applied dose of UVB.

In the case of melanin quantification, visual assessment considered an increase in pigmentation up to day 7, which appeared to be a plateau up to day 14. Dermacatch detected a slight increase in melanin values already at day 2, while Mexameter showed a false but significant decrease in melanin values at the same time point for the conditions at 600 and 750 mJ/cm^2

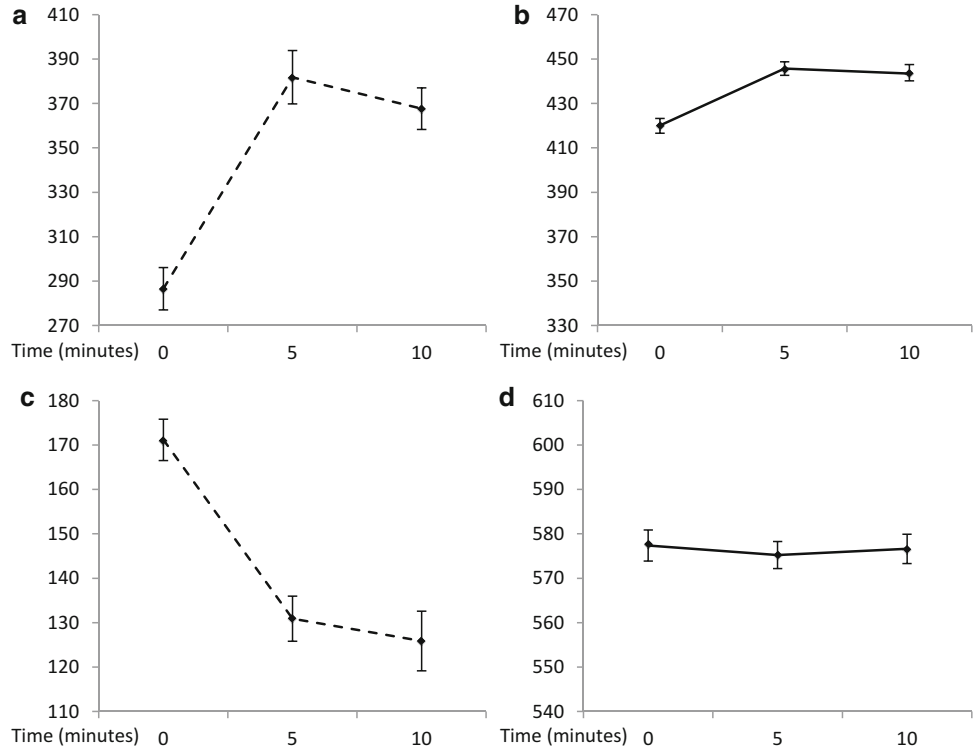

Fig. 3 Erythema induction on the forearms. Erythema (**a**–**b**) and melanin values (**c**–**d**) were provided by Dermacatch (**a**, **c**) and Mexameter (**b**, **d**) after a vasodilatation treatment of the forearm

Table 3 In vivo reliability of both colorimeters after erythema induction on forearms

	Melanin values				Erythema values			
	Dermacatch		Mexameter		Dermacatch		Mexameter	
Time (minutes)	5	10	5	10	5	10	5	10
CV	−0.37	−0.13	−23.5	−26.5	6.1	5.6	33.2	28.3
SD	3.3		5.5		3.4		3.2	
CR	0.70				1.0			

CV coefficient of variation, *SD* standard deviation, *CR* correlation ratio

of UVB. Some melanin values of Mexameter were thus consistently and significantly biased by the increase in skin erythema (Fig. 4 and Table 4).

3.2.4 Erythema Reduction on the Back

The following experiment consisted in analyzing the impact of a redness reduction on the melanin values. Seven days after UVB exposure, when the UVB-treated skin areas were already hyperpigmented but still erythematous, an UVB-exposed (i.e., 750 mJ/cm^2) as well as an unexposed portion of the back was treated with the vasoconstrictor Dermovate cream. After the exposure time of 18 h, skin erythema was slightly reduced according to both devices, which was confirmed by dermatoscopic images. The rate of erythema decrease measured by the two colorimeters was significantly similar regardless of the prior exposure of the skin to 0 or 750 mJ/cm^2 of UVB. Noteworthy, it appeared that Mexameter erroneously detected a significant reduction of pigmentation on the skin that had been previously exposed to UVB. However, such

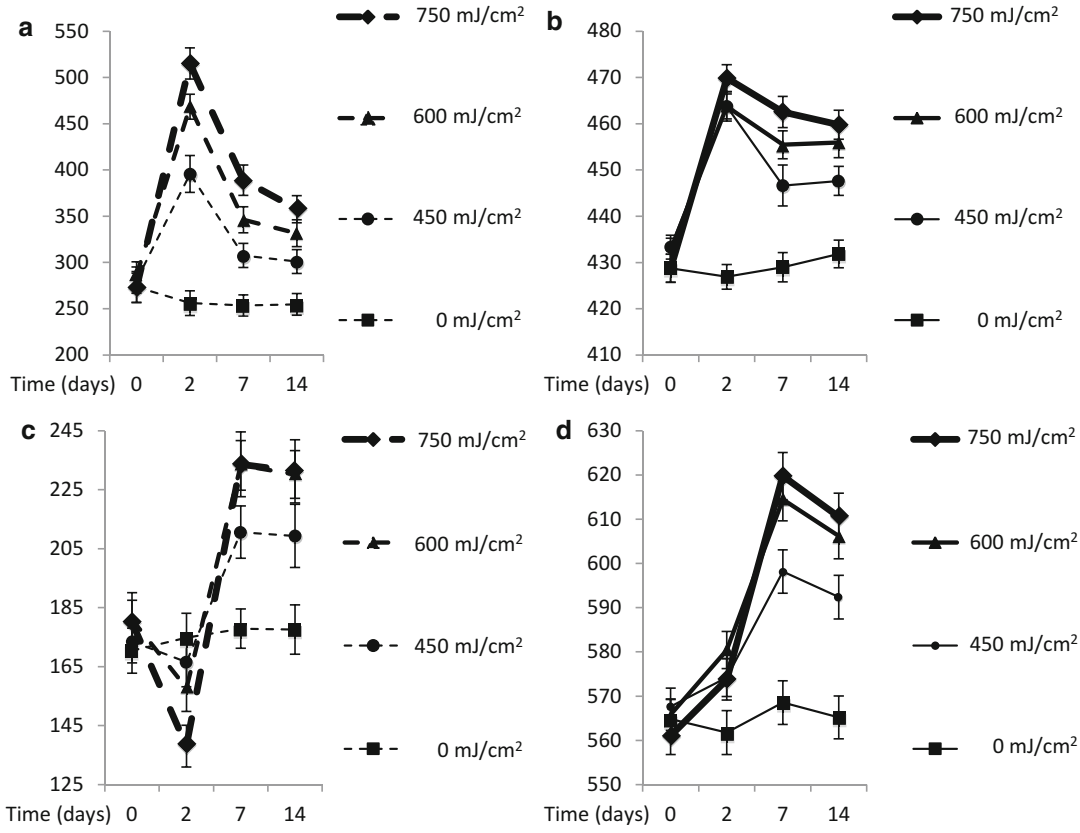

Fig. 4 UVB exposure on the back. Erythema (**a**–**b**) and melanin values (**c**–**d**) were collected by Mexameter (**a**, **c**) and Dermacatch (**b**, **d**) after a treatment of increasing doses of UVB (450, 600, and 750 mJ/cm^2) on the back

Table 4 In vivo reliability of both colorimeters after UVB exposure on the back

		Melanin values		Erythema values	
	mJ/cm^2	Dermacatch[a]	Mexameter[a]	Dermacatch[a]	Mexameter[a]
CV	750	2.3/10.5/8.8	−23.3/29.9/28.5	9.6/7.9/7.2	89.0/42.7/31.2
	600	2.6/8.6/7.1	−12.9/28.9/27.2	7.2/5.3/5.4	63.2/20.6/15.6
	450	1.1/5.4/4.4	−4.0/21.4/20.6	7.0/3.1/3.3	40.9/9.5/7.2
	0	−0.5/0.7/0.1	2.8/5.4/4.4	−2.4/0.1/0.7	−2.4/0.1/0.7
SD		4.7	8.5	3.1	14.6
CR	750	1		1	
	600	1		1	
	450	1		1	
	0	0.4		0.1	

CV coefficient of variation, *SD* standard deviation, *CR* correlation ratio
[a]The 3 CV values, respectively, correspond to the conditions at 2, 7 and 14 days compared to day 0

pigmentation reduction was not significant in the case of the skin not exposed to UVB. Finally, reproducibility of Mexameter values was found to be lower than that of Dermacatch (Fig. 5 and Table 5).

3.2.5 Erythema Induction on the Back

To further evaluate the false influence of skin erythema on melanin values, the UVB-exposed areas of the back as well as the adjacent unexposed regions of the back were treated with

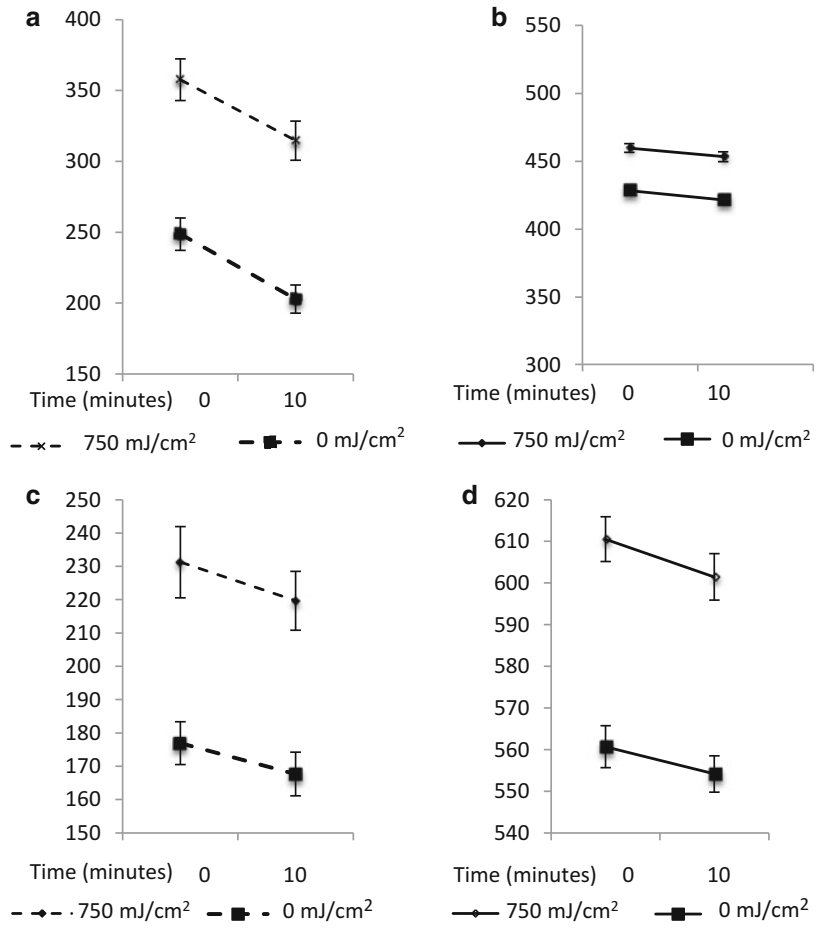

Fig. 5 Erythema reduction on the back. Erythema (**a**–**b**) and melanin values (**c**–**d**) were collected by Mexameter (**a**, **c**) and Dermacatch (**b**, **d**) after a vasoconstriction treatment on the back

Table 5 In vivo reliability of both colorimeters after erythema reduction on the back

		Melanin values		Erythema values	
	mJ/cm2	Dermacatch	Mexameter	Dermacatch	Mexameter
CV	750	−1.5	−5.0	−1.4	−12.0
	0	−1.2	−5.2	−1.6	−18.5
SD		5.1	8.1	3.2	12.5
CR		1.0		0.9	
		1.0		0.9	

CV coefficient of variation, *SD* standard deviation, *CR* correlation ratio

the vasodilator MNC on the 14th day following the UVB exposure. As confirmed by dermatoscopic images, melanin values remained constant before and after MNC application, despite the homogenous increase in skin erythema. Results from Mexameter showed that melanin values were significantly affected by the increased erythema. The incorrect diminution in pigmentation was inversely proportional to the degree of pigmentation of the tested area. In the case of Dermacatch, the increase in skin erythema did not affect melanin values. The latter remained constant before and after erythema induction regardless of the pigmentation status of the

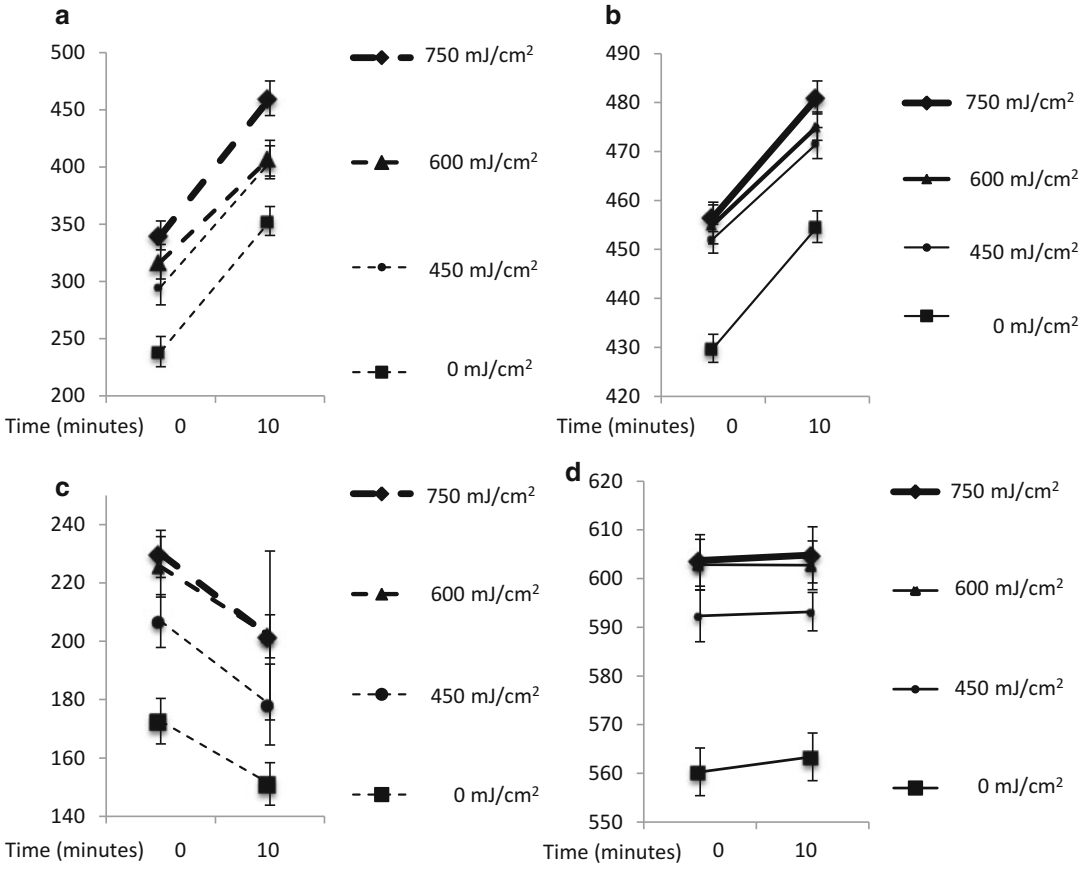

Fig. 6 Erythema induction on the back. Erythema (**a**–**b**) and melanin values (**c**–**d**) were provided by Mexameter (**a**, **c**) and Dermacatch (**b**, **d**) after a vasodilatation treatment of the back (exposed or not to the different doses of UVB)

studied area. Moreover, when quantified by Dermacatch, it appeared that the rate of erythema increase was significantly identical (based on the provider's criteria of the SD: ± 10 units) between the skin areas previously exposed to 0, 450, 600 or 750 mJ/cm^2 of UVB (increase of 20 units ± 5 units). Regarding Mexameter, some of its erythema values did not show a significantly similar rate of erythema increase (increase of 109 units ± 19 units when the provider's SD corresponded to ± 10 units). Finally, taken together Mexameter values showed a SD above the officially accepted value, which indicated a limited reproducibility of the device. In the same circumstances, Dermacatch SD was always below the limit defined by the providers (Fig. 6 and Table 6).

4 Discussion

Due to a partial overlap in wavelengths, colorimetric measurements of melanin can be falsely biased by a fluctuation in skin erythema and vice versa. Thus, an optimal skin colorimeter needs to be able to precisely discriminate between cutaneous melanin and erythema. The present study compared the new colorimeter Dermacatch with the reference device Mexameter in regard to (i) sensitivity to erythema and melanin detection as well as (ii) specificity of detecting changes in erythema or melanin, and (iii) reproducibility of melanin/erythema measurements.

Table 6 In vivo reliability of both colorimeters after erythema induction on the back

		Melanin values		Erythema values	
	mJ/cm^2	Dermacatch	Mexameter	Dermacatch	Mexameter
CV	750	0.2	−12.3	5.4	35.2
	600	0.1	−10.5	4.4	28.5
	450	0.1	−13.8	4.3	36.9
	0	0.6	−12.5	5.8	47.9
SD		5.0	11.6	3.2	14.3
CR	750	−1		1	
	600	1		1	
	450	−1		1	
	0	−1		1	

CV coefficient of variation, *SD* standard deviation, *CR* correlation ratio

In vitro evaluations showed a high level of reproducibility of both devices, which was in accordance with the technical data from the providers. However, the narrow-band technology of Mexameter showed a limited reliability especially in quantifying the darkening of the colors (e.g., from light pink to dark pink or light beige to dark beige).

In vivo, both colorimeters could reliably distinguish the different skin phototypes to the same extent. Moreover, a specific modulation in skin erythema, regardless of the pigmentation status, showed that Mexameter and Dermacatch erythema values were in accordance with visual perception. However, in the case of Mexameter, the rate of erythema increase after MNC treatment appeared to be erroneously influenced by its pigmentation status. In addition, Mexameter's melanin values were falsely affected by the erythema induction in all the three sets of experiments (i.e., vasodilatation of the normal skin, UVB exposure, and vasodilatation of the UVB-treated hyperpigmented skin). Mexameter showed significantly lower melanin values each time that the skin erythema was increased, and such a false decrease in melanin values was inversely proportional to the pigmentation level of the tested area. On the contrary, Dermacatch could reliably discriminate between skin erythema and melanin without any cross contamination.

Finally, the fact that Mexameter was at least two times less reproducible than Dermacatch increased the risk of a potential confusion over the detection of erythema or melanin fluctuations when using Mexameter.

Taken together, the analysis of more than 18,000 measurements performed in the present study showed that the sensitivity of both colorimeters was high. However, Dermacatch appeared to be a more reproducible device as well as a more specific colorimeter to discriminate pigmentation from cutaneous erythema.

References

Anderson PH. In vivo cutaneous assays to evaluate topical corticosteroids and nonsteroidal anti-inflammatory drugs using reflectance spectroscopy. In: Berardesca E, Elsner P, Maibach HI, editors. Bioengineering of the skin: cutaneous blood flow and erythema. Boca Raton: CRC Press; 1995. p. 281–91.

Anderson PH, Bjerring P. Remittance spectroscopy: hardware and measuring principles. In: Berardesca E, Elsner P, Maibach HI, editors. Bioengineering of the skin: cutaneous blood flow and erythema. Boca Raton: CRC Press; 1995. p. 231–41.

Biniek K, Levi K, Dauskardt RH. Solar UV radiation reduces the barrier function of human skin. Proc Natl Acad Sci U S A. 2012;109:17111–6.

Bjerring P. Spectrophotometric characterization of skin pigments and skin colour. In: Serup J, Jemec G, editors. In vivo examination of the skin: a handbook of non-invasive methods. Boca Raton: CRC Press; 1995. p. 373–5.

Chan SY, Li Wan Po A. Quantitative evaluation of drug induced erythema by using a tristimulus colour analysis. Skin Pharmacol. 1993;6:298–312.

Clarys P, Alewaeters K, Lambrecht R, Barel AO. Skin color measurements: comparison between three instruments: the Chromameter(R), the DermaSpectrometer

(R) and the Mexameter(R). Skin Res Technol. 2000;6:230–8.
DermaSpectrometer. Operation manual. Hadsund: Cortex Technology ApS; 1999.
Diffey BL, Farr PM. Quantitative aspects of ultraviolet erythema. Clin Phys Physiol Meas. 1991;12:311–25.
Diffey BL, Oliver RJ, Farr PM. A portable instrument for quantifying erythema induced by ultraviolet radiation. Br J Dermatol. 1984;111:663–72.
Draaijers LJ, Tempelman FR, Botman YA, Kreis RW, Middelkoop E, van Zuijlen PP. Colour evaluation in scars: tristimulus colorimeter, narrow-band simple reflectance meter or subjective evaluation? Burns. 2004;30:103–7.
Elsner P. Chromametry: hardware, measuring principles and standardization of measurements. In: Berardesca E, Elsner P, Maibach HI, editors. Bioengineering of the skin: cutaneous blood flow and erythema. Boca Raton: CRC Press; 1995. p. 247–52.
Erythema Meter. Operation manual. Andover: Diastron; 1999.
Farr PM, Diffey BL. Quantitative studies on cutaneous erythema induced by ultraviolet radiation. Br J Dermatol. 1984;111:673–82.
Farr PM, Diffey BL. The erythemal response of human skin to ultraviolet radiation. Br J Dermatol. 1985;113:65–76.
Gabard B, Juch R, Treffel P, Bieli E, Clarys P, Barel AO. Quantification of the skin blanching assay by color measurement with the Minolta Chromameter: influence of the vehicle and of the corticosteroid concentration. In: Brain KR, James VJ, Walter KA, editors. Prediction of percutaneous penetration methods, measurements, modelling, vol. 3b. Cardiff: STS Publishing; 1993. p. 511–9.
Mexameter MX 16. Operation manual. Koeln: Courage-Khazaka Electronic; 1999.
Queille-Roussel C, Poncet M, Schaefer H. Quantification of skin colour changes induced by topical corticosteroid preparations using the Minolta Chromameter. Br J Dermatol. 1991;124:264–70.
Rubegni P, Cevenini G, Stanghellini E, Andreassi M, Sbano P, Fabiani P, Andreassi L. A new device for objective assessment of skin type in Caucasians by violet light reflectance. Int J Cosmet Sci. 2002;4:187–93.
Seitz JC, Whitmore CG. Measurement of erythema and tanning responses in human skin using a tristimulus colorimeter. Dermatologica. 1988;177:70–5.
Takiwaki H, Serup J. Measurement of erythema and melanin values. In: Serup J, Jemec G, editors. In vivo examination of the skin: a handbook of non-invasive methods. Boca Raton: CRC Press; 1995. p. 377–84.
Takiwaki H, Overgaard L, Serup J. Comparison of narrow-band reflectance spectrophotometer and tristimulus colorimetric measurements of skin color. Skin Pharmacol. 1994;7:217–25.
Waring MJ, Monger L, Hollingsbee DA, Martin GP, Mariott C. Assessment of corticosteroid skin blanching: evaluation of the Minolta Chromameter CR-200. Int J Pharm. 1993;94:211–22.
Westerhof W. CIE colorimetry. In: Serup J, Jemec G, editors. In vivo examination of the skin: a handbook of non-invasive methods. Boca Raton: CRC Press; 1995. p. 385–97.
Westerhof W, Van Hasselt BA, Kammeijer A. Quantification of UV induced erythema with a portable computer controlled chromameter. Photodermatology. 1986;3:310–4.
Wilhem KP, Maibach HI. Evaluation of irritation tests by chromametric measurements. In: Berardesca E, Elsner P, Maibach HI, editors. Bioengineering of the skin: cutaneous blood flow and erythema. Boca Raton: CRC Press; 1995. p. 269–79.

The Architectural Behavior of the Skin

8

J. C. Guimberteau, J. P. Delage, and E. Sawaya

Contents

Keywords
Dermis • Epidermis • Hypodermis • Microfibrils • Polyedrons • Skin • Structural ontology

1 Introduction

The traditional approach treated the skin in the same way for at least 50 years. The skin is a protective membrane, a carpet that puts us in contact with the universe and provides information on possible attacks. All components of the skin are now clearly identified. The skin is made of palisade epidermal cells in ranks to better ensure our protection, below with a thick dermis to strengthen defenses (Fig. 1). But the dynamic aspects of the skin have been totally neglected.

As a plastic surgeon, I've always been very intrigued by simple phenomena, but still not very well explained and summarized under the term of ELASTICITY, SUPPLENESS, PLIABILITY, and FLEXIBILITY. How do all these elements adapt and link on each other during the movement, how does the skin move? (Fig. 2).

The skin, indeed, outside the traumatic event, always returns to its original state extemporaneously.

J.C. Guimberteau (✉) • E. Sawaya
Institut Aquitain de la Main, Bordeaux-Pessac, France
e-mail: adf.guimberteau@wanadoo.fr

J.P. Delage
U688 Physiopathologie mitochondriale, Université Victor Segalen-Bordeaux 2, Bordeaux Cedex, France

P. Humbert et al. (eds.), *Agache's Measuring the Skin*,
DOI 10.1007/978-3-319-32383-1_8

2 Materials and Methods

We will discuss from video observations realized during surgical procedures, under tourniquet. In order to clarify the comment, we will refer to the traditional anatomical layers distribution (Fig. 3).

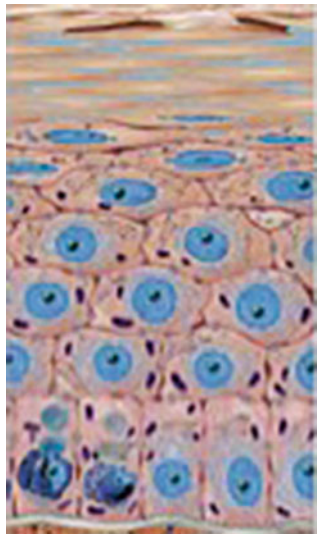

Fig. 1 Diagram of the skin as it is proposed in classical histological books

This study is done using a video endoscope and borescope contact magnifying, respectively, 25 and 80 times Karl Storz camera Image One connected to a fiber optic Tricam 221,030 and associated with a cold light source Xenon Nova 201,315 (Fig. 4). The sequences were recorded with a video recorder KIPRO AJA HDV 10 ^{E}.

For in vitro studies made by Prof. JP Delage (INSERM), the skin fragments were fixed by immersion in a 10 % solution of formaldehyde for 5 days and then rinsed in the water for 5 days. Then they were subjected to maceration (NaOH) using the technique described by Passerieux et al. (2006). They were macerated in 5 N NaOH solution at 18° for 5 days and then rinsed in the water again for 5 days. This technique allows the maintenance of the main collagen (Type 1). The preparation is then frozen, dehydrated, and pigmented at the gold and examined under a Philips electron microscope.

The classic description is that there is a thin epidermis consisting of cornified and stratified thick epithelium cells. The dermis is more fibrous and houses glands, blood vessels, follicles, and nerve endings or specialized sensory receptors.

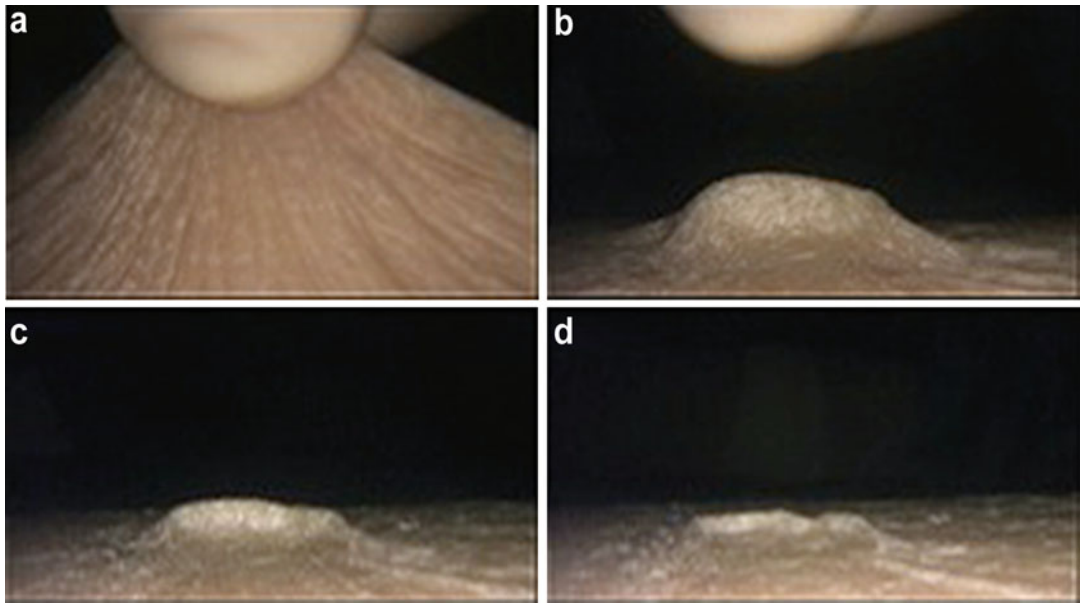

Fig. 2 (**a**–**d**) When we lift up the skin, we feel a little resistance to traction but the skin does not tear, and then, when we let go, it returns to its initial position, as if from memory (**a**, **b**, **c**, **d**)

Fig. 3 Use of endoscope during surgery

Aside from acting as a barrier to dehydration, infection, and physical damage, the skin has a major role in metabolism, sensation, and thermoregulation. But even if the cutaneous constitution is perfectly well defined, the following question remains: how does the skin move?

How do all these elements adapt and link on each other during movement?

3 Surface of the Epidermis

3.1 The Diversity of the Forms

The first observation which leads us to the main feature which is the skin morphology is varied (Fig. 5).

It is fascinating to see that the surface of the epidermis has many forms, and all of them come from the same basic polyhedric pattern.

The color can be very varied too. Skin color also exhibits many different tones: from white to very dark; the skin comes in many gradations.

But the diversity doesn't only concern color and pilosity. In the same person, depending on the anatomical zones, we can notice that these pseudopolyhedric forms can change into squares, into parallel cylinder ridges reminding us of sandhills, or into diamond-shaped pannels that look like waves.

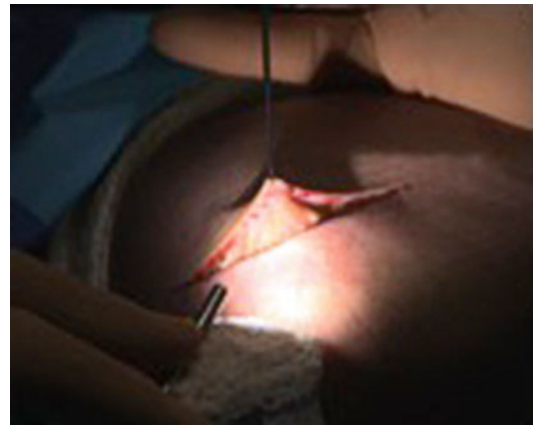

Fig. 4 Subcutaneous endoscopic exploration with a fiber optic and cold light

These forms can glow with youth or sag with age, wrinkle with the weather, or get thinner when people have lost weight.

We can see changes due to the person's activity, like in the palm of a heavy worker or the arch of the foot of a jogger, and inner intrinsic influences like dermatosis digging deep lines, nevus coloring pigmenting the surface, or stretch marks, fractures of the dermis that occur during pregnancy.

3.2 Polyhedrons with Different Shapes

The skin is varied but always remains woven by this polyhedric drawing framework, irregular, fundamental, simple, and yet rarely described in the literature (Fig. 6a, b).

Therefore, questions should be asked:

Why is the skin surface made of polyhedron shapes?
Why isn't the cutaneous surface perfectly smooth?

The epidermis, the most superficial layer, is a surface printed with these small, changing polyhedrons, all of them irregular and different, limited to three, four, or five sides, each side about 500 μ length, with lines about 50 μ wide between the polyhedrons.

Not one polyhedron looks like its neighbor, and its distribution is very irregular.

Fig. 5 (**a-f**) Differents shapes of the skin surfaces X2. (**a**) Shoulder skin surface (**b**) Palm of the hand (**c**) Pulp finger (**d**) Abdomen. Strecht marks (**e**) Thigh skin surface (**f**) Foot plantar surface

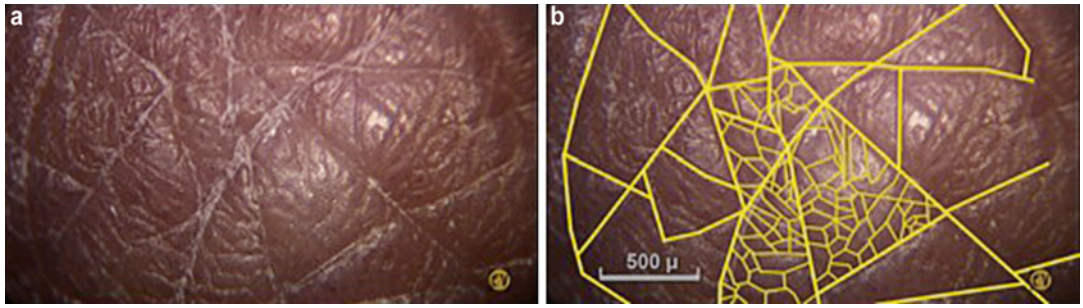

Fig. 6 (**a, b**) X3 Irregular polyhedrons at the skin surface. Each polyhedron is made of smaller polyhedrons which adjusts to its neighbour inside the bigger one

3.3 Complex Mosaic Pattern of Irregular Polyhedrons

These polyhedrons move in the three-dimensional space, and during their movements, we can notice changes even on their surface.

When the skin stretches and creases during everyday activities, these small polyhedrons move; their shape and aspect change, and when the forces are removed, they return to their initial state.

All the moments of our everyday lives induce these unperceivable yet unnoticed changes. Yet on closer observation, we do see those lines of force which change from vertical to horizontal and then blur out to appear again according to the strength of the pressure exerted.

These lines of force have got a physical reality. This diversity becomes more impressive as we draw the operating microscope closer, but then, it becomes more difficult to photograph and visualize because the depth of field is reduced, and the patient's fine movements from breathing and pulsations at rest are amplified.

Nevertheless, with careful study, we can see these changes, through video capture, especially by high magnification and filming in slow motion.

First, let's see the movement magnified ten times (Fig. 7a–d).

The polyhedrons are directed to the right. Let's press on the left, and they all move rapidly, apparently in a disordered manner; their forms change and the lines of force move to the left.

The response to the constraint, to the physical force applied, is obvious. The gymnastics agility of the polyhedrons, the apparent mechanical faculty ability to change forms and orientations, needs further investigation.

The shape of polyhedrons changes under the mechanical constraint. Lines of force are subject to stress.

The next sequence will clarify these movements, by drawing the microscope closer with 25 times magnifying power (Fig. 8a–d).

At rest, let's examine polyhedrons A, B, C, and D.

Let's pull downward lightly on the framework without changing the depth of field of the camera.

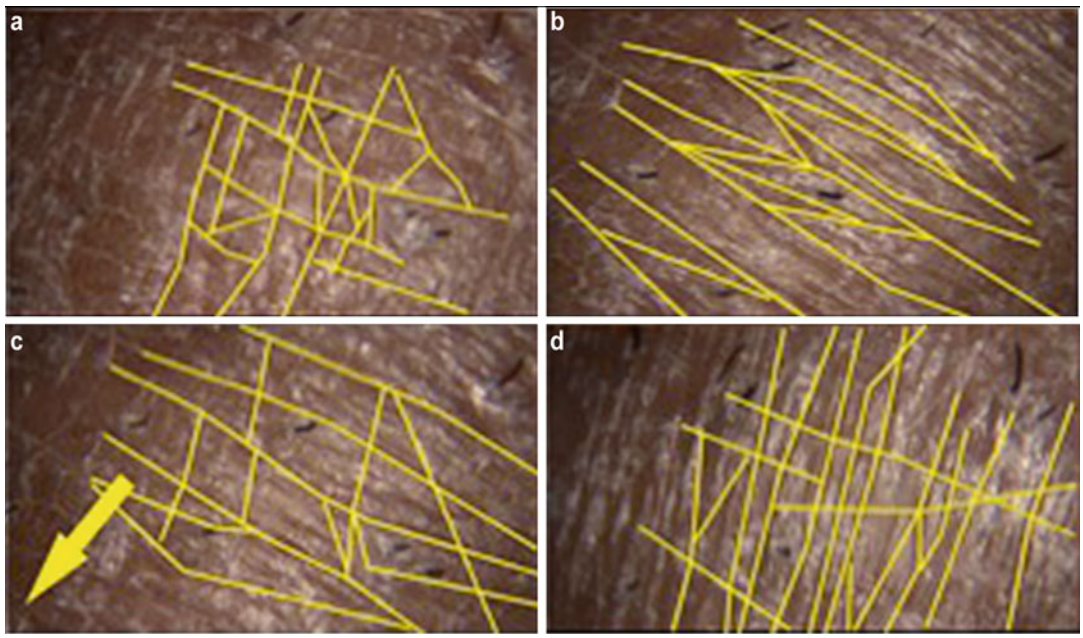

Fig. 7 (**a-d**) The response to the constraint, to the physical force applied, is obvious. The gymnastics agility of the polyhedrons, the apparent mechanical faculty ability to change forms and orientations

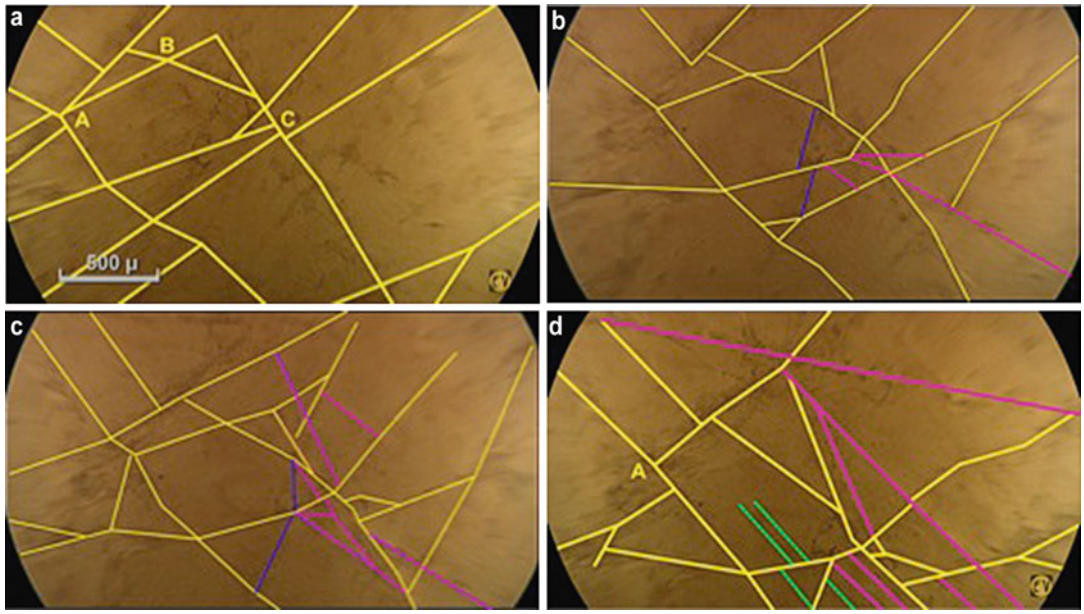

Fig. 8 (**a-d**) X3. Between a rest situation (**a**) and a local constraint to the right, polyhedrons shapes are changing and new lines are appearing

The elements B, C, and D are moving downward. The separation lines are only stretched.

But A remains rather static.

Then, as the traction exerted becomes stronger, new lines of force, E, F, and H, emerge, oriented in the direction of constraint, passing through existing structures. Then, as the traction becomes stronger, new lines appear colored in pink even slightly modifying the initial structural lines. Increasing constraint creates new lines here in green. The distance from A to C has increased by 15 %.

So we see stretching in the direction of the applied force with successive appearance of new lines of force added to the original ones, which look different and change the general shape.

Fig. 9 Moreover, inside each polyhedron , we can observe other subunits with varied dimensions and forms, Polyhedrons are fractalized

3.4 Polyhedrons Are Fractalized

Moreover, inside each polyhedron, we can observe other subunits with varied dimensions and forms, which remain inactive until the tension overwhelms the fibers and give rise to their final shape (Fig. 9).

We get the impression that there is a dynamic environment which has a higher organization with structural latent solutions. It is certainly a fractalization that makes the dispersion of the force easier. We are reminded of the phenomenon we have described in the sliding tissue around tendons.

These dynamic comportments based on fractal organization are a very fascinating phenomenon and can be easily observed in heavily exposed skin, like the skin of the palm, where the wrinkles are particularly visible.

Inside these polyhedrons, measuring 500 µ on each side, we can observe sub-polyhedrons of 50 µ, substructures, perfectly individualized on

the mechanical morphology and mechanical behavior, because each small polyhedron adjusts to its neighbor inside the bigger one.

Finally, these sequences show that, although these polyhedrons stretch and are transformed, their ridges move very little. We can already assume there are anchor points with the depth of the epidermis.

The hypothesis that each apex could be reinforced by fibrils like a pillar or a column is wrong, but one can get the impression that the shape of the epidermis depends on elements existing deep inside.

There is an intimate fibrillar morphodynamic architecture in the epidermis. This epidermis architecture is linked with and depends on elements existing deep inside.

Our epidermis is not like an even tile but like a chaotic mosaic.

So the cutaneous architecture is not inert; it is living under constraint.

4 The Cutting of the Epidermis and Dermis

4.1 The Skin Is Under Tissular Tension

This tissue tension is also obvious when we cut the skin, either the dermis or the aponeurosis (Fig. 10). There is an intrinsic, pre-existing constraint tissue tension as revealed by observation.

The edges of the skin spontaneously draw apart a few millimeters as soon as the surgeon makes an incision.

We are going to continue the exploration but this time using a contact endoscope.

This is an endoscope magnifying 25 times with simultaneous recording. An analysis of the sequences will be done at the same time, in order to keep the impressions of the moment intact.

Cutting through the epidermis and a part of the dermis enables us to confirm our early hypothesis and observations from the very beginning. We can find deep inside the dermis the fibrils which undoubtedly with their biomechanism infiltrate the extracellular matrix of the dermis. They penetrate it (Fig. 11).

Fibrils penetrate the dermis, and they exert a morphological influence on the shape of the skin surface of the epidermis.

But let's focus on our investigation. How do these microfibrils coming from the depth of the subcutaneous tissue turn into irregular polyhedrons at the surface of the skin?

The transverse cross section of the epidermis gives us a different impression with a view according to the lines of relief on the surface.

Sometimes they look like roman tiles (Fig. 12). Sometimes there are no lines of strain, but we can notice immediately as an obvious marker the limit between the epidermis and the dermis, at the level of the basement membrane, and the small vertical papillary vessels (Fig. 13a, b).

The epidermis is homogeneous, from its bottom to its surface, and the stratum corneum, its last element, also participates in its dynamic behavior which is global.

Fig. 10 (**a-b**) Tissue tension is also obvious when we cut the skin, either the dermis or the aponevrosis

Fig. 11 Deep inside the dermis, the fibrils undoubtedly, with their biomechanism infiltrate the extracellular matrix of the dermis

So the epidermis moves, but in addition, if we look closer, we can observe at the center of the epidermis a slightly convex network which curves downward as if attracted by something.

Thus, our original observations on the surface may have been confirmed by cutting the skin.

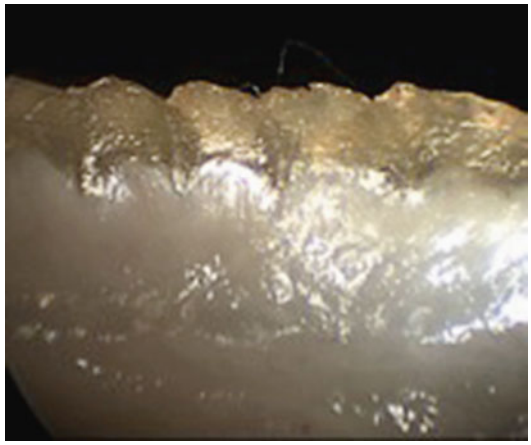

Fig. 12 The transverse cross section of the epidermis gives us a different impression with a view according to the lines of relief on the surface. Sometimes they look like roman tiles

The form of the epidermic surface is dictated deep inside, by tethers whose direction is random, but which is nearly vertical in this particular case.

Fibrils cross the lamina densa and the stratum basale and shape the epidermis and its surface. This physical link between the dermis and epidermis is evident with video. Moreover in this continuity, there is a slight time lag on the papillary crest line. The interrelationships are more complex than expected (Fig. 14a, b).

We have been able to identify these intraepidermic fibrous tethers.

So there are different axes which cross the epidermis, split it, and, by intersecting in space, make movement possible.

4.1.1 Back Home

But before going further, let's recapitulate.

The surface of the skin is made of polyhedrons fractalized into smaller units (Fig. 15).

Each polyhedron has got a shape determined, deep inside, by tethers whose organization is irregular, without visible order, but which tends to be vertical.

The epidermis is formed of a network of fibrils where the cells are situated in attractivity comfortably within these pseudopillars (Fig. 16a, b).

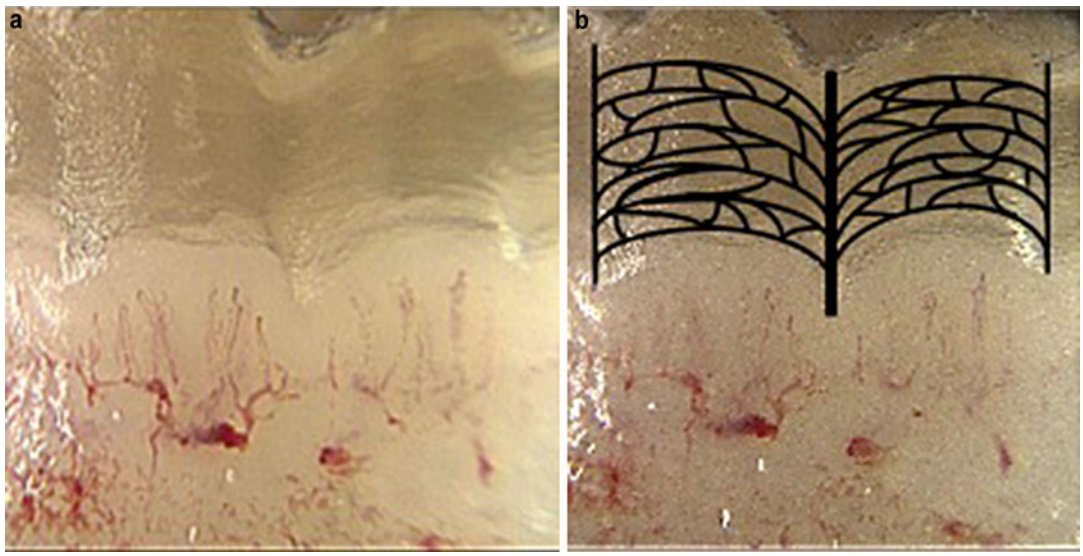

Fig. 13 Inter-polyhedrons grooves are in correspondence with converging lines deep to the dermis. Observation of the surface and of the cross-section (X50) of the epidermis highlights the harmonious relationship that exists between the cellular structures and the structures linking the furrows of the epidermis and the dermis

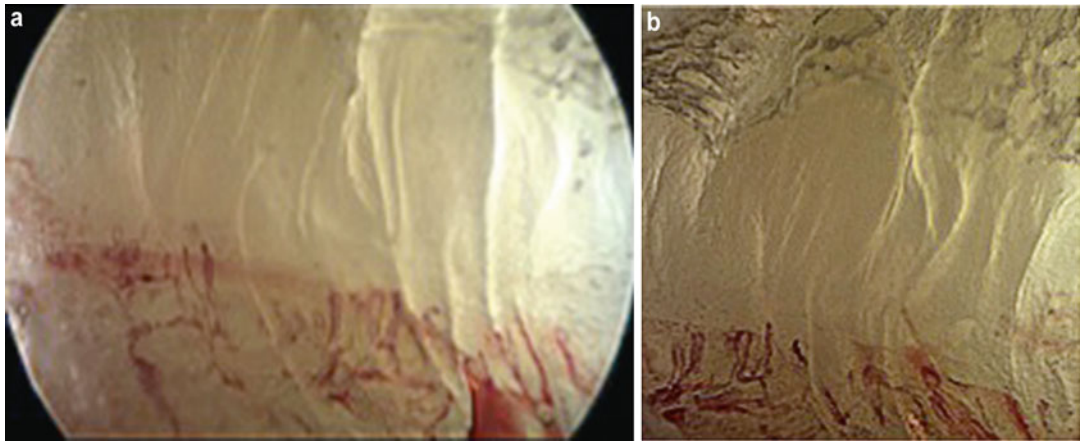

Fig. 14 (**a, b**) Fibrils cross the lamina densa, the stratum basale and shape the epidermis and its surface. This physical link between dermis and epidermis is evident with a video

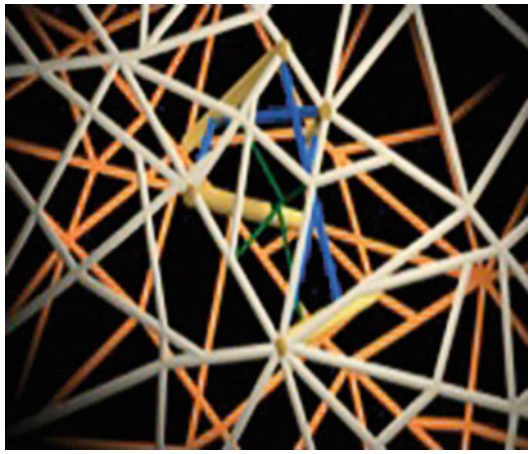

Fig. 15 The surface of the skin is made of polyhedrons fractalised into smaller units

At this level, everything is mobile, under tension, without disruption but without any blood vessels.

We will find the vascularization in the dermis.

5 Junction Between the Epidermis and Dermis

The dermis is not easy to film because with the tourniquet on, it is white and inexpressive (Fig. 17). And after reperfusion, it is entirely red and highly bleeding.

Cutting through the epidermis and a part of the dermis allows us to confirm our initial observations and the hypothesis that deep inside, microfibrils penetrate and infiltrate the matrix of the dermis where they exert a morphological influence on the shape of the dermis. How do these microfibrils, rooted as they are in the depths of the subcutaneous tissue, give rise to irregular polyhedrons at the surface of the skin?

In certain cross sections of the epidermis and dermis, you can see obviously the fibers which pass through the dermis, the basement membrane, and the epidermis and extend into the furrows between the epidermal polyhedrons. The dermis and the epidermis are shaped by these fibers (Fig. 18a–c).

Fibrils cross the lamina densa and the stratum basale and shape the epidermis and its surface. This physical link between dermis and epidermis is evident with video.

Bleeding occurs at the level called papillary dermis.

This zone is full of vessels which seem to end in small vertical loops, but which, in fact, form a real network under the epidermis (Fig. 19a, b).

The notion of papillary crests can thus be explained. At the surface of the dermis, it seems that the papillary vessels and their multifibrillar texture bump against the Malpighian layer and push it a little.

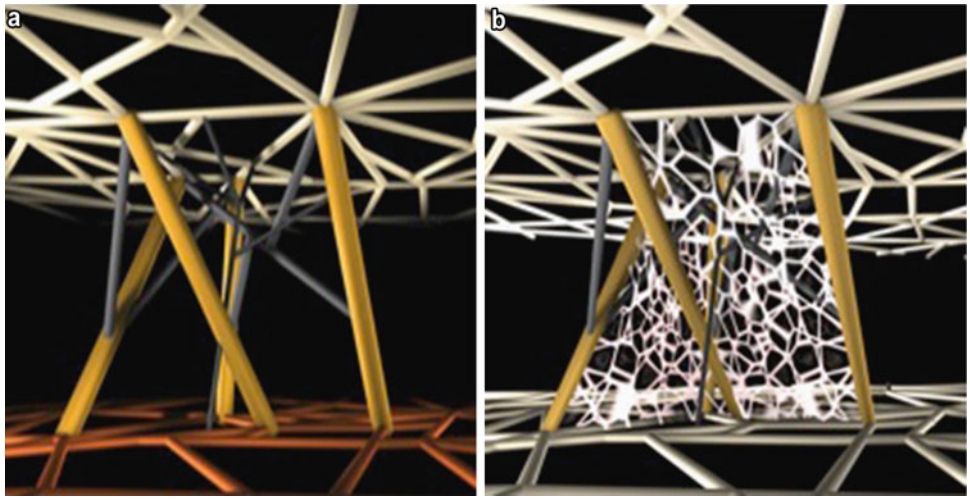

Fig. 16 (**a, b**) X50 Diagram explaining the fibrillar network of the epidermis framing the skin surface (**a**), linked with the dermis and embedding the epithelial cells (**b**)

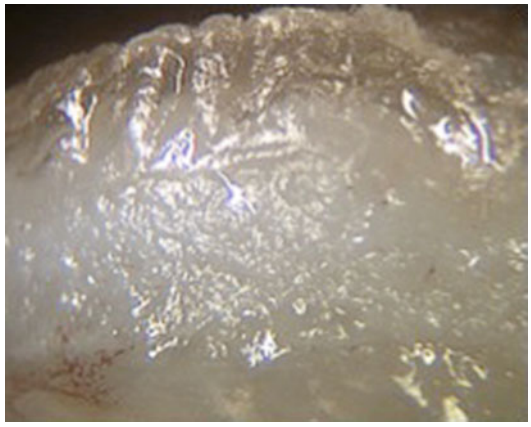

Fig. 17 The dermis is not easy to film because with the tourniquet on, it is white and inexpressive

The distribution of the papillary crests is irregular and occasionally in relation with the surface of the epidermis above (Fig. 20a, b).

What is the most surprising is that this vascular network coming from the dermis is moving with the depth of the epidermis, perfusing the undersurface.

Actually, if we watch these sequences carefully, we can see movements between the dermis and the epidermis.

Moreover in this continuity, there is a slight time lag between the papillary crest line and the surface of the epidermis. The interrelationships are more complex than expected. This is amazing, particularly when one takes into account the notion of a real tissue continuity, and if you focus now on the red spot, you can see the epidermis moving with the dermis with about half a second's delay (Fig. 21).

These crests papillae can be visible if the epidermic surface is rough, but they can sometimes be less prominent. There is a difference in mobility between the top of the papillary crest and the bottom inside the dermis (Fig. 22a–c).

6 The Dermis

So these framing fibers which model the shape of the epidermis also shape the surface of the dermis.

The same print with polyhedrons and lines will be observed, but it won't be an exact replica because the repartition of the axial fibers is irregular in the space (Fig. 23a, b).

The lines imprinted on the surface of the dermis as well as the epidermis also show close relationships with structures deeper than the dermis.

Thanks to the work of JP Delage, working with INSERM, after performing cross sections on the surface of the dermis every millimeter, we can reveal that these print ridges disappear when they are over 2 mm deep.

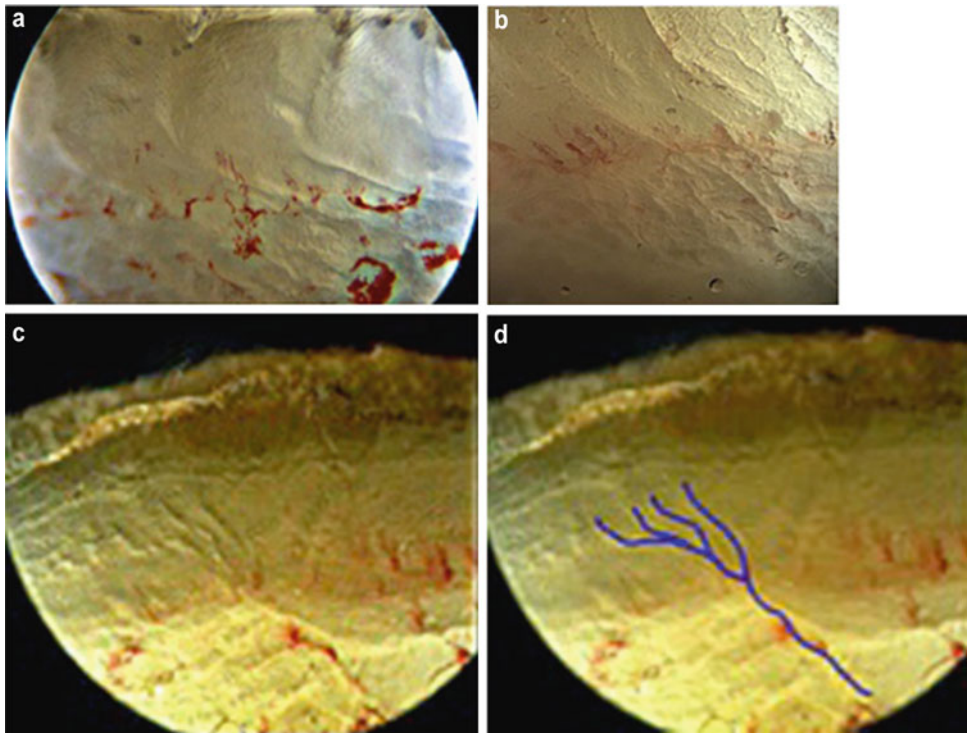

Fig. 18 (**a**) X25, (**b, c**) X20. Dermis cross section with evidence of the continuity of these fibers irregular in shapes and distributions

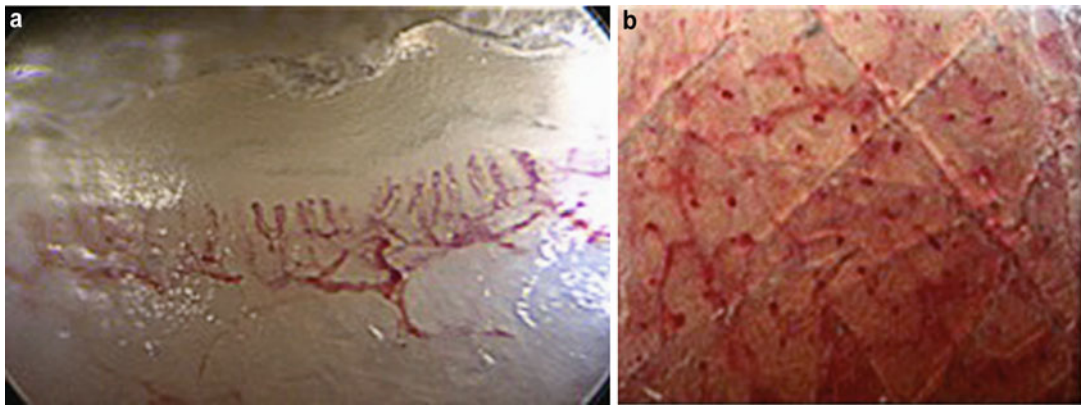

Fig. 19 (**a, b**) Papillary dermis. This zone is full of vessels which seem to end in small vertical loops arborizing (**a**), but which, in fact, form a real network under the epidermis perfusing the undersurface (**b**)

Beyond this depth, it seems that the extracellular matrix takes a different form (Fig. 24a, b). The mechanism structure of the medium central part of the dermis is difficult to explore since the structures are imbricated. Fibril repartition of collagen and elastin, which looks very chaotic, plays a leading part.

Yet other sections of the dermis also show the presence of tissue axes, apparently less scattered (Fig. 25a, b).

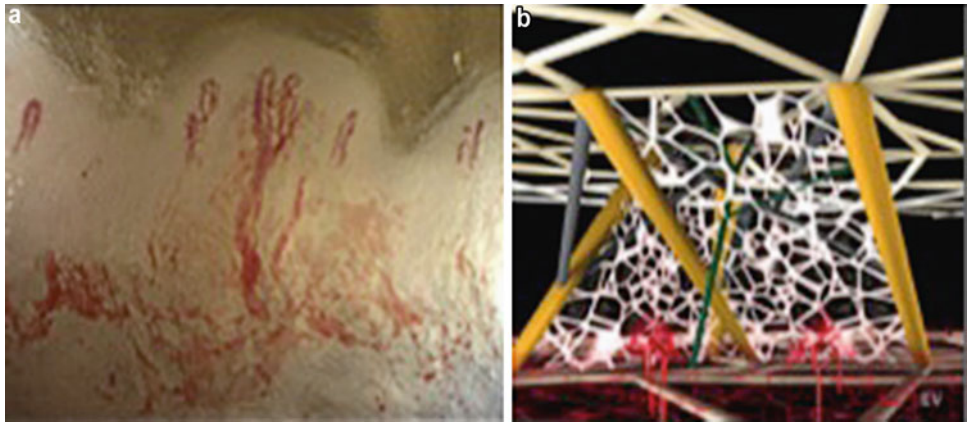

Fig. 20 (**a, b**) At the surface of the dermis, it seems that the papillary vessels and their multifibrillar texture bump against the Malpighian layer. (**b**) Diagram of the papillary zone

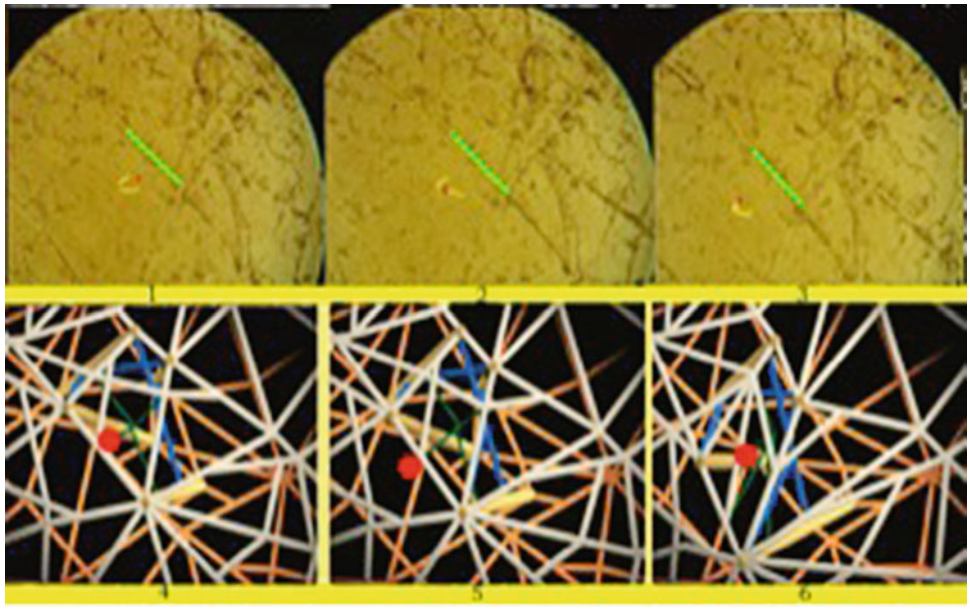

Fig. 21 (**a, b, c**) if you focus now on the red spot, you can see the epidermis moving with the dermis with about half a second's delay

These more axial fibrils could be the continuity of these microfibrillar and microvacuolar systems, which rise from the hypodermis and climb up to the dermis.

Sometimes, fibers are gathered in looking like balls or a basket-weave formation.

This suppleness, this mobility and possibility to recover the initial form, this fibrillar mechanism, obeys to the same rules as those observed in the tendon gliding system and simultaneously nests in its framing network epidermic cells, fibroblasts, all cellular constituents in this network thus linked all together.

We perceive a world of great mobility. What impresses us most is the general suppleness of the epidermis and the dermis, which can be folded and manipulated with no stratification and no separation in total tissular continuity and in this

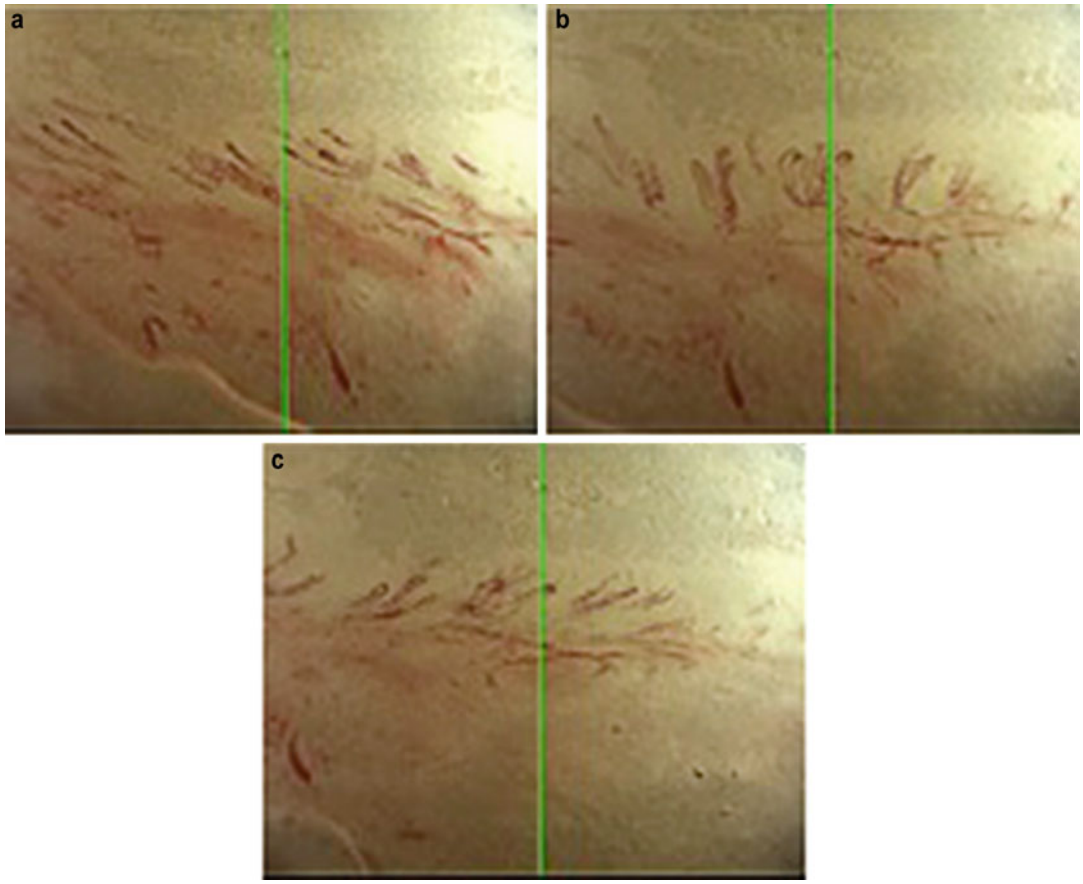

Fig. 22 (**a, b, c**) Cross section of the dermisn in vivo. This vascular network coming from the dermis is moving with the depth of the epidermis

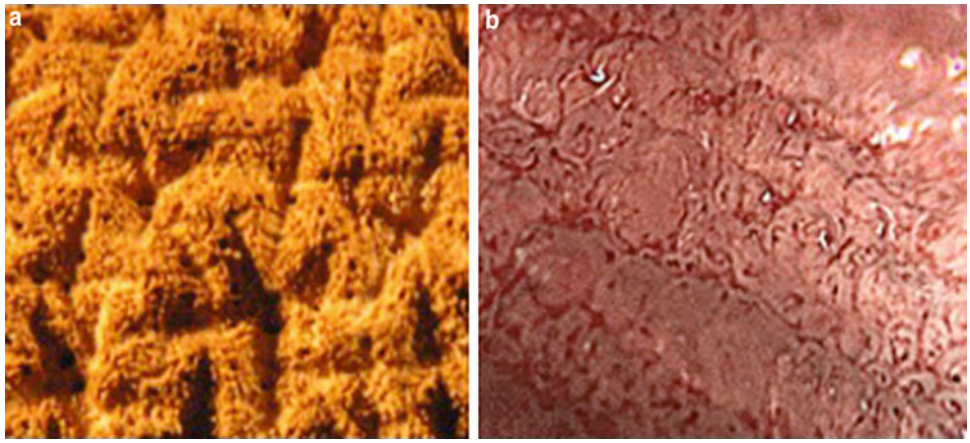

Fig. 23 (**a**) Dermis surface framed as the epidermis surface In vitro (Delage preparation) X25 (**b**) In Vivo after trauma

Fig. 24 (**a, b**) Cross sections on the surface of the dermis, every millimetre, we can reveal that these prints ridges disappear when they are over 2 mm deep

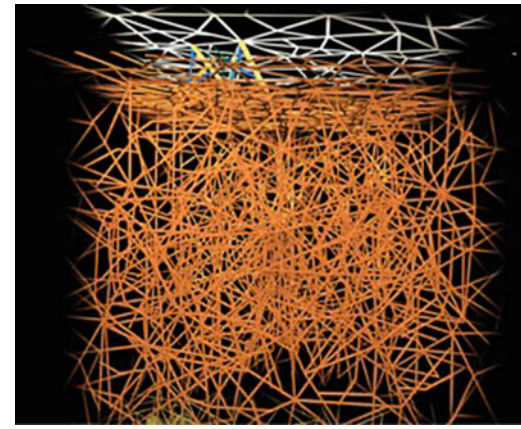

Fig. 26 Diagram. Dense and irregular fibrillar organisation of the dermis linking epidermis and hypodermis

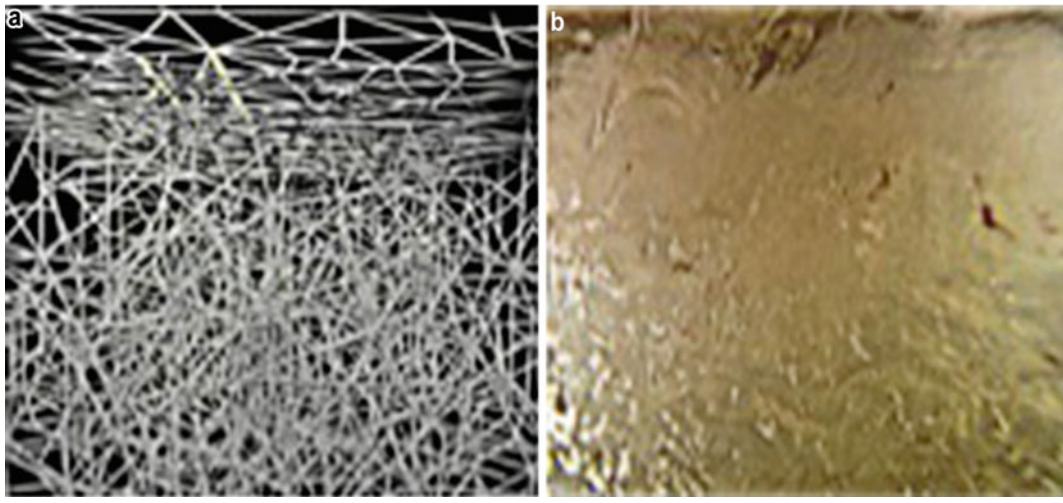

Fig. 25 (**a, b**) The mechanism structure of the medium central part of the dermis is difficult to explore since the structures are imbricated. (**a**) Diagram (**b**) in vivo cross section

interwoven maze where nerves and vessels could all exist (Fig. 26).

Then, the sequences showing the choreography of the polyhedrons, their connection to the depth of the dermis and agility, make sense.

7 The Hypodermis

Once the dermis and epidermis have been crossed, the connection to the hypodermis happens simply.

Again, there are no stratified and separate layers of the tissue between the reticular dermis and hypodermis layers. Fat lobules under tension rapidly bulge out between the superficial veins and emerge between the sectioned edges of the reticular dermis (Fig. 27).

The fat lobules are inlaid in the reticular dermis in total physical continuity through the fibrillar continuous network (Fig. 28).

Greater mobility of structures within the hypodermis is evident. The fat lobules are situated

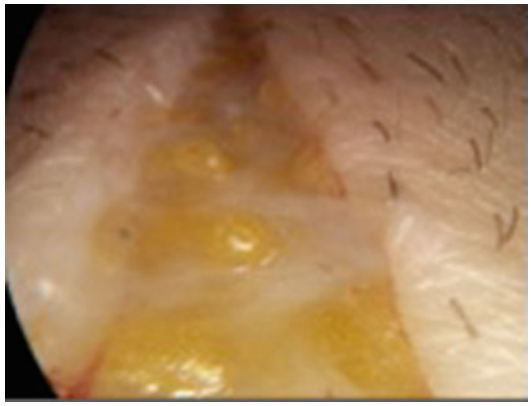

Fig. 27 Fat lobules under tension rapidly bulge out between the superficial veins and emerge between the sectioned edges of the reticular dermis

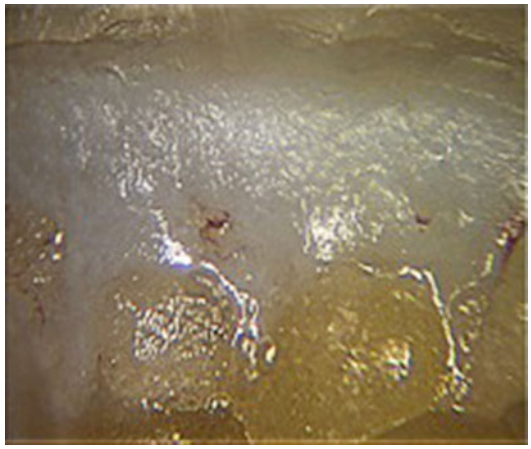

Fig. 28 The fatty lobules are Inlaid in the reticular dermis in total physical continuity through the fibrillar continuous network. There are not separated layers

between the blood vessels, below the dermis (Fig. 29), and look like little olive-shaped balloons, with widely variable dimensions ranging from approximately 100 μ to 1 cm in diameter. Their height varies from several millimeters to several centimeters. Although the size of the lobules varies considerably, they have a consistently smooth appearance and rounded shape (Fig. 30).

These lobules, containing millions of adipocytes, flatten, dilate, turn, and twist within the spaces that contain them, without separating or dissociating from each other. Fatty lobules display

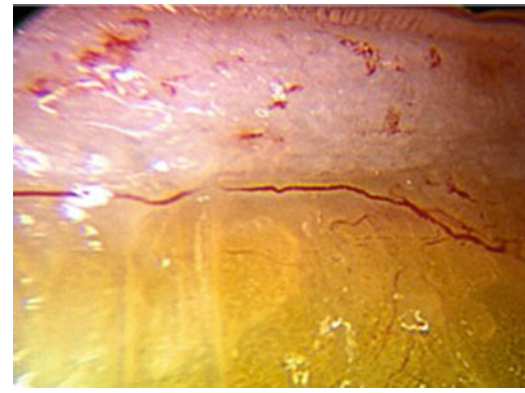

Fig. 29 Fibrillar and vascular continuity between the reticulous dermis and the hypodermis is total X10

Fig. 30 Fatty lobules are of very different dimensions and shapes X15

great mobility and tend to slip from the grip of the surgical forceps.

The fibrils that leave the dermis are continuous with those that enter the lobules – there is total fibrillar continuity. Fibrils are found between the lobules (Fig. 31a, b). They ensure mobility between them, penetrating them and merging with the intercellular structures.

They extend toward the superficial fascia. This influences the functional and morphological properties of the fatty tissue.

In this way the fibrils contribute to, and help to determine, the form of the lobules, framing the cells within them (Fig. 32).

The mobility of the adipocytes within the lobule during externally applied movement is fascinating. There is complete and total harmony between the cells.

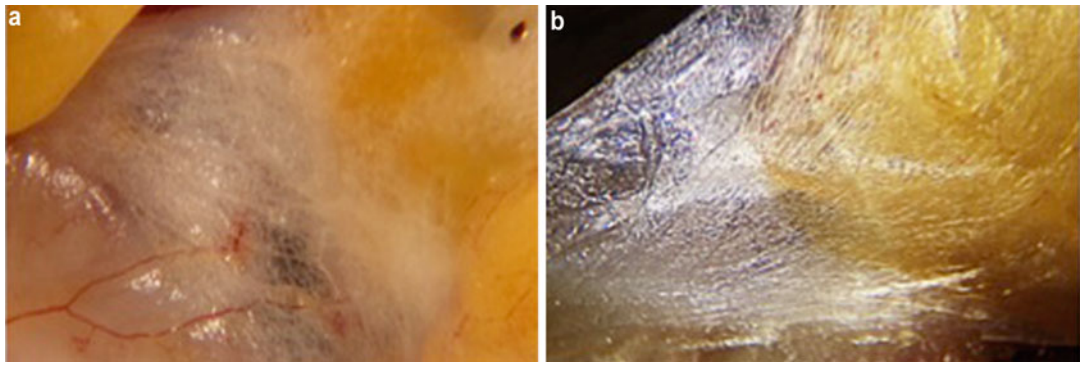

Fig. 31 (**a, b**) Fibers frame completely the shape of the fatty lobule. (**b**) Tissular continuum is total X45

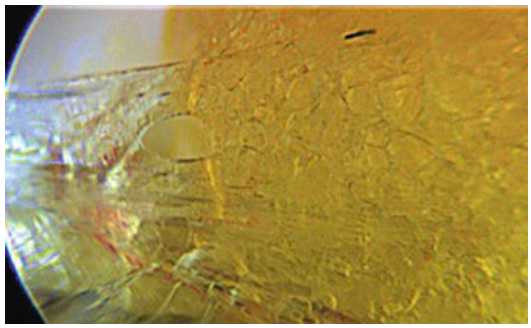

Fig. 32 Fibers penetrate the fatty lobules, helping to the adipocytes arrangements X60

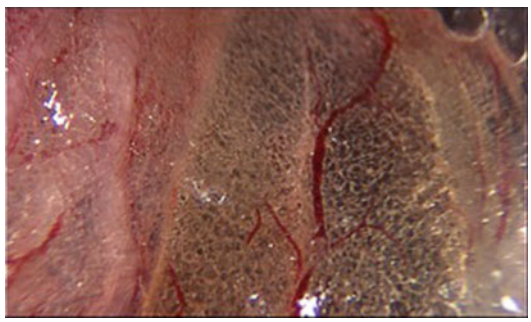

Fig. 33 Fatty lobules even close to each other can be with different colors X45

The adipocytes are not all exactly of the same color. Adipose tissue can be white in certain areas in some patients (Fig. 33). It also displays different shades of yellow, from pale yellow to bright buttercup, to tawny. From our study of tissue samples under the scanning electron microscope, it would seem that the brown cells are in fact immature multifunctional cells with big nuclei, which are also capable of producing collagen. We are only at the dawn of our understanding of this cellular diversity.

Situated within the hypodermis and continuous with the fibrillar system extending from the dermis, we find the superficial fascia. Very often, it is difficult to distinguish the superficial fascia from the hypodermis or to separate them surgically. The superficial fascia can be described as a fibrillar reinforcement and a densification of the fibrillar network, but it should not be thought of as a sheet separated from other structures. Some authors, a long time ago, have observed this continuity and have taken a more nuanced view of the concept of separate tissue layers within the body (Richet 1877).

Tissue continuity with adjacent structures is total. Its role could be to maintain stability of form by holding the rest of the hypodermis under tension. Cutting into this tissue leads to a marked widening of the gap formed by incision of the dermis.

Then what are the relationships with the subcutaneous area (Fig. 34)**?**

Relations with the subcutaneous have already been described in previous reports. The skin covers the slip system that we called the Multifibrillar Collagenic and Microvacuolar Absorbing System (MCVAS), namely, fibrillar system, encompassing microvacuoles and thanks to fibrillar and water movements can to

ensure the damped structural mobility without discontinuity in transmission of information and energy.

7.1 The MCVAS

We can say that these polyhedric forms of the cutaneous surface mirror the multifibrillar microvacuolar organization underneath, that the fibrillar continuity toward the surface thus shaped by the deep structures completely builds the architecture of the dermis and the epidermis.

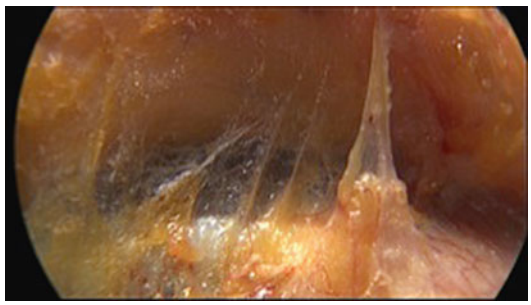

Fig. 34 Evidence of tissular and fibrillar physical continuity between, the hypodermis and the subcutaneous area

7.2 A Pattern Emerges (Fig. 35) (2, 3)

The cell belongs to this system; it is in this system, from the DNA nucleic helix to the cytoskeleton including the links to the integrins and neighboring cells directly or through this fascinating tissue.

Everything is in continuity; everything is connected; everything moves to fit; everything moves and always comes back to its previous position; everything moves and can be replaced; everything moves within the tissue continuity.

Therefore, the form can be described and interpreted.

Now, let's stitch suture the skin back but let's keep in mind that, from now on, nothing will be accounted for without considering this fractal and dispersed pattern tissue organization that can be found in lots of other fields all around us and which introduces the fact that mobility and adaptability in biology do not depend on order and proportionality.

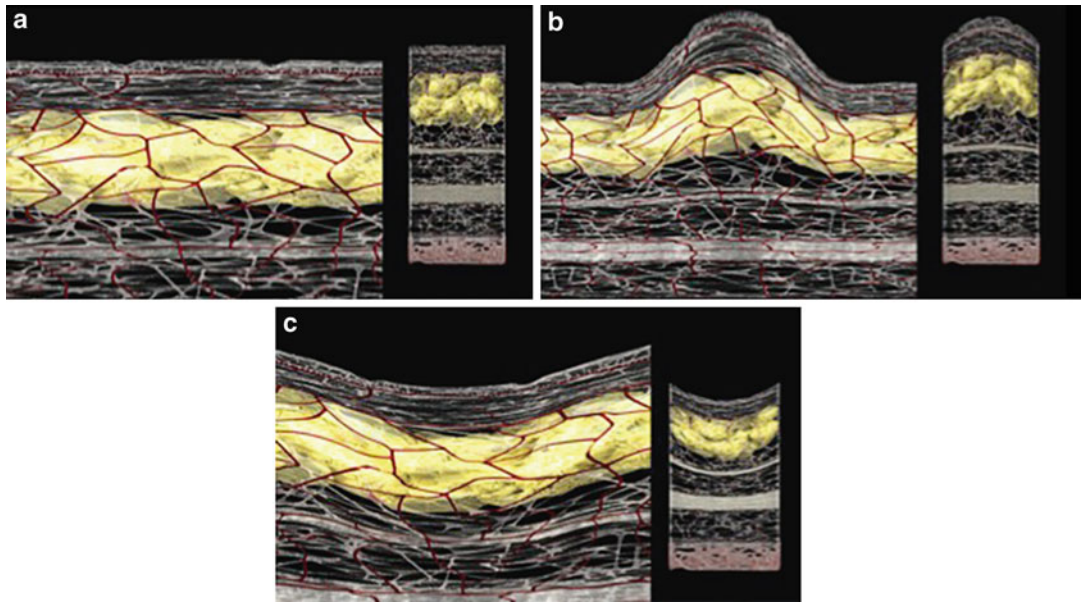

Fig. 35 The skin is part of the globality of the living matter and cannot and must not be regarded as a separated surface layer. We have to rethink the traditional layered vision

8 Conclusions

Skin is actually the area with the outside world report of a living matter. It is its component protection and its area information and exchange.

It is part of the globality of the living matter and cannot and must not be regarded as a separated surface layer.

References

Richet, A. (1877). Traité pratique d' anatomie (5th ed). Paris: Chamerot et Lauwereyns.

Passerieux, E., Rossignol, R., Chopard, A. et al. (2006) Structural organization of the perimysium in bovine skeletal muscle: junctional plates and associated intracellular subdomains. *J Struct Biol. 154*, 206–16. Texte.

Optical Properties of Skin Surface

9

Gladimir V. G. Baranoski and Tenn F. Chen

Contents

Keywords

Skin • Reflection • Transmission • Attenuation • Absorption • Scattering • Sieve effects • Detour effects • Fluorescence

Abbreviations

COHb	Carboxyhemoglobin
HHb	Deoxyhemoglobin
MetHb	Methemoglobin
NADH	Nicotinamide adenine dinucleotide
O_2Hb	Oxyhemoglobin
SHb	Sulfhemoglobin
UVR	Ultraviolet radiation

1 Introduction

The interactions of light with human skin are controlled by the intrinsic optical properties of this remarkable biological surface. In the case of visible light, these interactions result in attributes, such as hue and glossiness, that characterize its appearance. From a tissue optics perspective, it is difficult to find a material more complex than human skin, which explains the wide range of variations in skin appearance observed in the world population.

Light impinging on the skin surface can be reflected back to the environment or transmitted to its internal layers. The amount of reflected light is associated with the probability of reflection, which, in turn, depends on the local refractive index differences and the angle of incidence of

G.V.G. Baranoski (✉) • T.F. Chen
Natural Phenomena Simulation Group, University of Waterloo, Waterloo, ON, Canada
e-mail: gvgbaran@cs.uwaterloo.ca; t4chen@cs.uwaterloo.ca

P. Humbert et al. (eds.), *Agache's Measuring the Skin*,
DOI 10.1007/978-3-319-32383-1_9

the incoming light with respect to surface normal vector. The larger the angle of incidence and the local refractive index of the skin surface, the higher the probability of light being reflected.

Once light is transmitted into the skin tissues, it can be further attenuated by their constituents such as cells, fibers, and organelles. The mechanisms of light attenuation, namely, scattering and absorption, alter the spatial and spectral profiles of the light traveling within the various skin layers. Eventually, a portion of the traversing light may be propagated back to the environment.

In this chapter, we examine the optical properties of healthy human skin from a first-principles point of view. We focus on the main light-attenuation structures, or agents, acting within the cutaneous tissues. These agents can be loosely divided into two groups, namely, scatterers and absorbers. In the next sections, we review the roles of these agents with respect to their spatial and spectral action domains and discuss their interplay through light sieve and detour effects. We also concisely describe the roles of key light-emission (fluorescence) agents found in the skin tissues. The chapter closes with an overview of practical challenges related to the advance of research on skin optical properties.

2 Scattering Agents

The three main types of scattering occurring within the skin layers are reflective-refractive scattering, Mie scattering, and Rayleigh scattering (Baranoski and Krishnaswamy 2010). The occurrence of these forms of scattering is associated with different tissue constituents. The reflective-refractive scattering, or geometrical scattering, is largely controlled by the refractive index differences between large structures (e.g., cells) and the surrounding medium. For the most part, this type of scattering can be described using ray or geometrical optics. The Mie and Rayleigh scattering occurring within the skin tissues have been associated with the presence of small-scale light-scattering agents such as collagen fibers (Jacques 1996). In these types of scattering, the agents have dimensions on the same order of magnitude of the wavelength of the impinging light, or smaller in the case of Rayleigh scattering (McCartney 1976). The mathematical description of these forms of scattering is usually more involving, and it takes into account wave optics phenomena to determine the attenuation of the propagated light. In the case of Rayleigh scattering, shorter wavelengths are preferably attenuated, i.e., the light attenuation is inversely proportional to the fourth power of the wavelength of light (McCartney 1976).

The dry mass of the most superficial part of the skin, the horny layer or stratum corneum, is dominated by the presence of keratin (Swanbeck 1959). Keratin is a protein produced by the keratinocyte cells located in the epidermis (van de Graaff 1995). This process, known as keratinization, starts in the lower epidermal layers. Upon its completion, the keratinocytes have migrated to the stratum corneum, where they become dead cells, termed corneocytes, filled with keratin fibrils. Since the keratin fibrils are birefringent, i.e., their refractive index depends on the polarization and direction of propagation of the impinging light (Feynman et al. 1964), the skin surface can also present some degree ($\sim$20 %) of birefringence (Swanbeck 1959). In addition, the internal orientation of these fibrils within the corneocytes can asymmetrically affect the propagation of light by these cells (Swanbeck 1959).

The light reflected on the skin surface may be further spatially perturbed by the presence of microrelief structures and mesostructures (e.g., wrinkles) (Magnenat-Thalmann et al. 2002; Sandoz et al. 2004; Sohaib et al. 2013). The rougher the skin surface, the closer the distribution of the reflected light resembles that of a perfect Lambertian reflector. In addition, the presence of these structures can result in some adjacent points on the skin surface being blocked from the impinging light (shadowing effect) and others being blocked from view (masking effect). It is also worth noting that the presence of lipids, including native oily sebum, may reduce the apparent roughness of the skin surface and increase its glossiness.

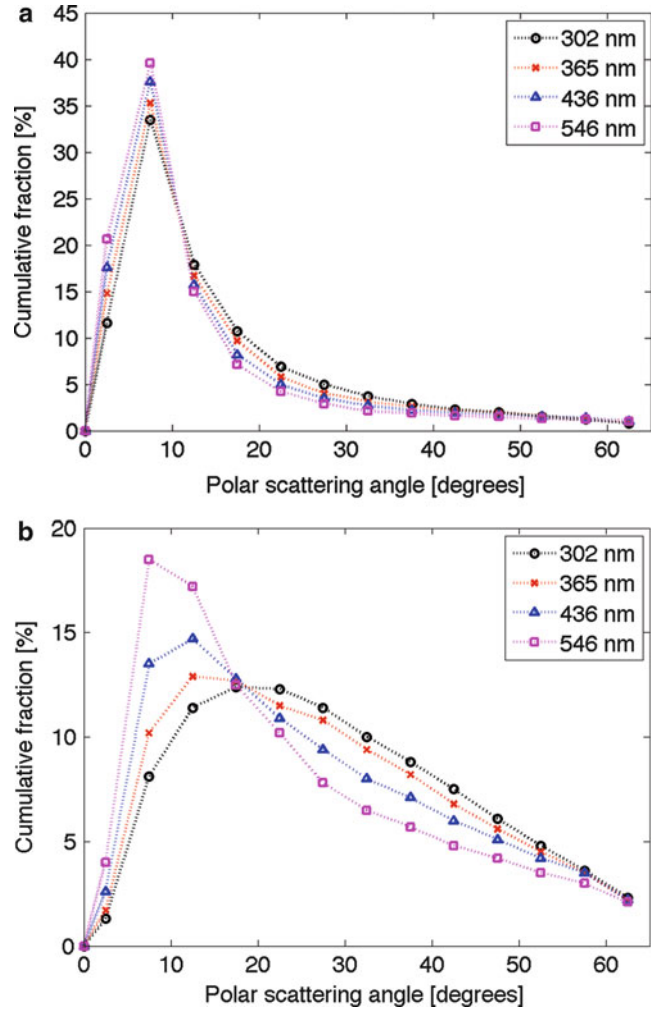

Fig. 1 Cumulative fractions of ultraviolet and visible light scattered by stratum corneum and epidermis samples of Caucasian subjects. (**a**) Stratum corneum. (**b**) Epidermis. Scattering data was measured by Bruls and van der Leun (1984) considering perpendicular irradiation and assuming azimuthal symmetry with respect to distribution of the scattered light

Below the stratum corneum, we find the epidermal tissues: stratum lucidum, a thin clear layer found only in the epidermis of the palms and soles (van de Graaff 1995), stratum granulosum, stratum spinosum, and stratum basale, the deepest epidermal layer. Scattering measurements by Bruls and van der Leun (1984) on Caucasian skin specimens resulted in a forward scattering behavior being observed for the stratum corneum and the epidermis of these specimens (Fig. 1). Although the portion of light going from one layer to another may be affected by the internal arrangement of the cells and their refractive index differences, one has also to take into account the scattering caused by other structures such as the melanosomes. These membranous organelles are packed with melanin, the most important photoprotective pigment present in human skin (Kollias et al. 1991). Accordingly, it is directly associated with the level of pigmentation of an individual (e.g., lightly, moderately, and heavily pigmented). Typically, the volume fraction of the epidermis occupied by melanosomes varies from 1.3 % for lightly pigmented specimens to 43 % (for darkly pigmented specimens) (Jacques 1996), with the melanin content of the melanosomes varying from 17.9 % to 72.3 % (Kollias et al. 1991).

The melanosomes, like other relatively small biological structures (Latimer 1984), can cause small angular deviations in the direction of light

propagation, which are associated with wave optics phenomena. It has been observed (Chedekel 1995) that as their size decreases from approximately 300 nm to a degraded particle form, known as melanin dust (Kollias et al. 1991), they go from a predominantly forward scattering to a more symmetrical scattering behavior. It is worth mentioning that some amount of melanin dust may be also present in the stratum corneum (Kollias and Baqer 1986), notably following physiological changes in the skin pigmentation due to exposure to ultraviolet radiation (Kollias 1995).

The skin melanosomes are usually found in the long filaments of the melanocyte cells and within the keratinocyte cells (Toda et al. 1972). Although these organelles are predominantly located in the stratum basale (Olson et al. 1973), under different stimuli, notably exposure to ultraviolet radiation (UVR), they can migrate to the upper layers (Kochevar et al. 2008) as part of a process of induced pigmentation commonly known as tanning (Lin and Fisher 2007). Besides an increase in the biosynthesis of melanin (melanogenesis (Chedekel 1995)), the tanning process may also result in a temporary thickening of the skin tissues (Lopez et al. 2004).

Below the epidermis, one finds another skin layer with different histological characteristics, namely, the dermis. The boundary between these layers is characterized by the presence of interdigitations of the dermis, known as dermal papillae, into the epidermis. The roughness of this epidermis-dermis interface is typically greater than the skin-air roughness (Federici et al. 1999). Due to the high-roughness condition of this interface, it has a significant impact in the scattering profile of light traveling between these layers.

The dermis can be further subdivided into two structurally distinct layers: the papillary dermis and the reticular dermis. These layers are essentially composed of irregular connective tissue with nerves, lymphatic vessels, and blood vessels, the larger ones occurring in the reticular dermis. This connective tissue, in turn, is mostly formed by collagen fibrils organized into fibers. Collagen is a protein molecule that makes up about 70 % of the dry weight of the dermis, and it is also birefringent (Anderson and Parrish 1982). Besides the collagen fibers, reticulum and elastin fibers can also be found in the dermis. Although these structures are believed to be responsible for Mie and Rayleigh scattering occurring within the dermis, the sources of these types of scattering, especially for Rayleigh scattering, have not yet been clearly identified.

Since the papillary dermis is characterized by the presence of small-scale collagen fibers and fibrils, while the thicker and more fibrous reticular dermis is characterized by the presence of large-scale collagen fibers, the working hypothesis is that Rayleigh scattering is more likely to be caused by the papillary structures (Jacques 1996). Despite open questions regarding the sources of these types of scattering in the dermal layers, their compound effect is the deeper penetration of longer wavelengths into the dermal layers (Anderson and Parrish 1981). Moreover, although scattering measurements by Jacques et al. (Jacques et al. 1987) on isolated dermis samples of Caucasian individuals revealed a forward-directed light traversing these samples (Fig. 2), it has also been observed that after a number of interactions, collimated light traveling within this tissue quickly becomes diffuse.

Eventually, the light traversing the dermis may reach the hypodermis. This adipose tissue consists mostly of fat cells that contain a number of smooth droplets of lipids whose size is large than that of typical tissue scatterers (Bashkatov et al. 2005). Nonetheless, light remission by large cellular structures in the hypodermis can further contribute for increasing the scattering of light within the dermis.

3 Absorption Agents

Once light is transmitted to the skin tissues, it is also attenuated by different absorbers present in these tissues. The amount of light absorbed in a given skin layer with respect to the spectral domains of interest, notably ultraviolet (100 to ~380 nm), visible (~380 to ~780 nm), and infrared (~780 to 3,000 nm) (CIE 2011; McCluney 1994), depends on the quantity, distribution, and

light extinction (absorption) spectra of the absorbers present in that layer. Although the occurrence of most absorbers found in human skin cannot be narrowed to a single layer, the absorption profile of each layer is usually associated with the presence of a specific set of absorbers. For example, in the stratum corneum, the absorption of light is mainly connected to the presence of keratin (Kölmel et al. 1990), uranic acid (Olivarius et al. 1997; Young 1997), and beta-carotene (Lee et al. 1975). Both keratin and uranic acid are characterized by a strong absorption behavior in the ultraviolet domain (Fig. 3), while beta-carotene is characterized by a more pronounced absorption behavior in the visible domain (Fig. 4).

In the epidermal layers, the absorption of light is mainly associated with the presence of two classes of melanin: eumelanin and pheomelanin (Chedekel 1995; Thody et al. 1991). These pigments are the main absorbers acting in the ultraviolet and visible domains (Chedekel 1995) and have a strong impact on the color of the skin surface (Alaluf et al. 2002c; Thody et al. 1991). Both are characterized by a relative broad

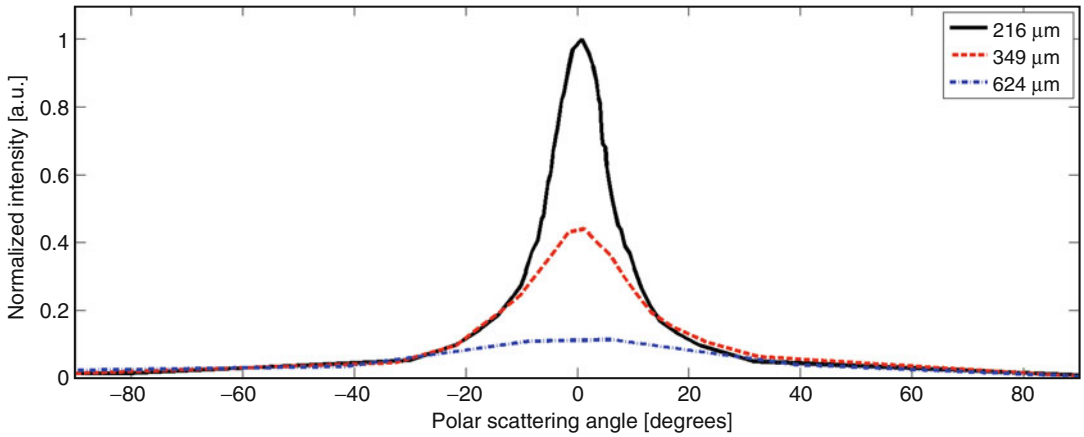

Fig. 2 Distribution of light (632.8 nm) scattered by dermis samples of various thicknesses obtained from Caucasian subjects. Scattering data was measured by Jacques et al. (1987) considering perpendicular irradiation and assuming azimuthal symmetry with respect to distribution of the scattered light

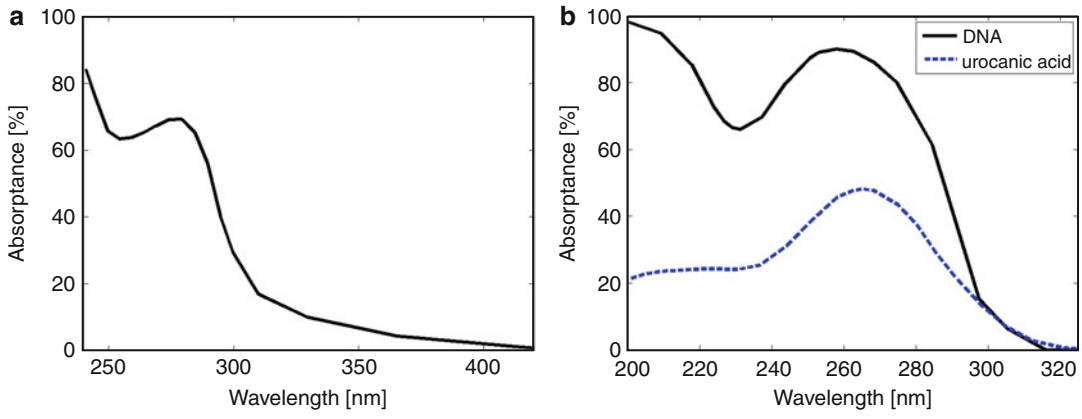

Fig. 3 Absorbers of light in human skin acting primarily in the ultraviolet domain. (**a**) Absorbance of keratin over a distance of 4 µm (Bendit 1966). (**b**) Absorbance of 50 µg/mL of DNA and 15 µmol/L of urocanic acid over a distance of 1 cm (Clendening 2002; Oudhia 2012; Sutherland and Griffin 1981; Young 1997)

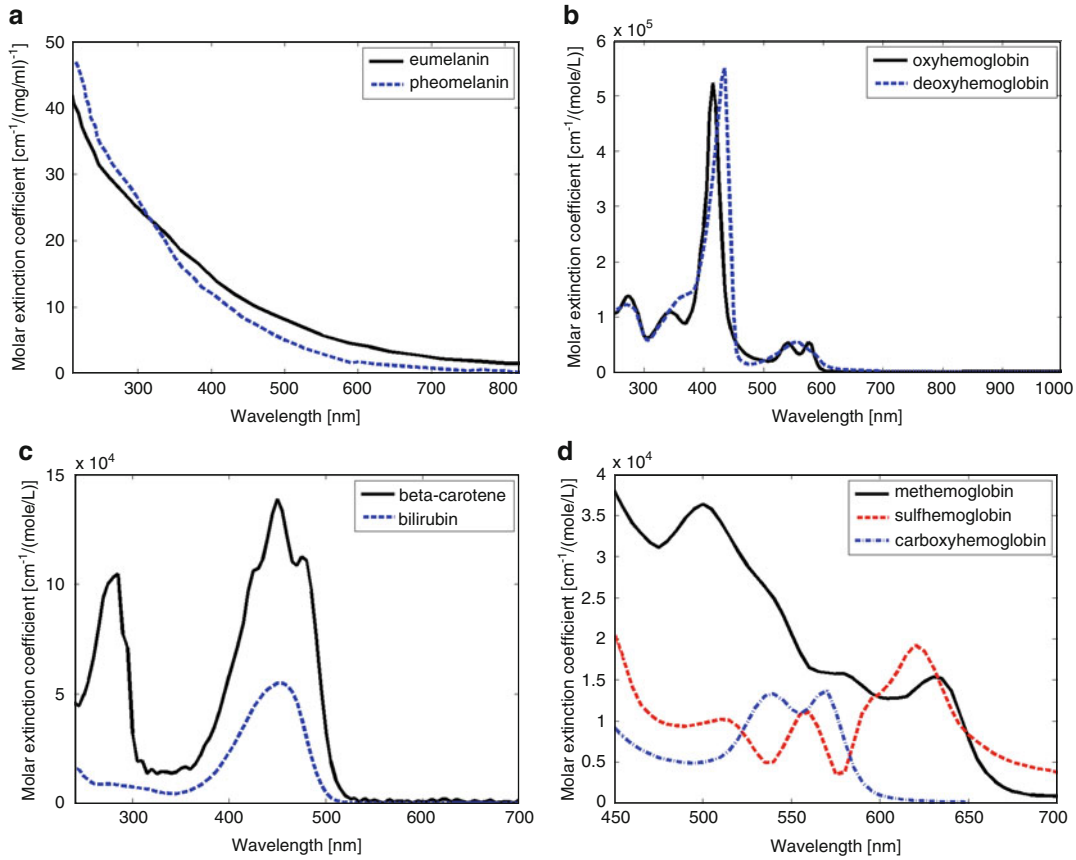

Fig. 4 Absorbers of light in human skin acting in the ultraviolet domain and visible domains. (**a**) Molar extinction coefficients of eumelanin and pheomelanin (Jacques 2001). (**b**) Molar extinction coefficients of functional hemoglobins (Prahl 1999). (**c**) Molar extinction coefficients of beta-carotene and bilirubin (Prahl 2001). (**d**) Molar extinction coefficients of dysfunctional hemoglobins (Randeberg et al. 2004; Siggaard-Andersen et al. 1972; Yarynovska and Bilyi 2006)

absorption spectrum (Fig. 4), with higher values for shorter wavelengths. Although, as mentioned earlier, melanin may be also found in the stratum corneum in the form of granules ("dust") under normal conditions (Kollias 1995; Kollias et al. 1991), the melanin absorption level is primarily associated with the amount of this pigment found in the epidermal layers (Jacques 1996).

The epidermal melanin pigmentation can be classified into two types: constitutive (determined by genetic factors) and facultative (induced to external stimuli, particularly UVR) (Anderson and Parrish 1982). The ratio between the volumetric concentration of pheomelanin and eumelanin present in human skin varies from an individual to another (Kollias and Baqer 1986; Parsad et al. 2003). The volumetric concentrations of eumelanin and pheomelanin, in turn, depend on the concentrations of these pigments in the melanosomes, which vary for different skin phototypes (Alaluf et al. 2002b; Hennessy et al. 2005).

Besides the melanins, the absorption profile of the epidermal layers with respect to shorter wavelengths may be also affected by the presence of beta-carotene (Alaluf et al. 2002a), keratin formed during the keratinization process (van de Graaff 1995), and DNA found in the epidermal cells (Sutherland and Griffin 1981; Young 1997). However, while the contribution of beta-carotene to light absorption is more significant in the visible domain, the contributions of keratin and DNA are practically exclusive to the ultraviolet domain (Fig. 3).

The volume fraction of blood in human tissue can vary from ∼0.2 % to ∼7 % (Flewelling 1995; Jacques 1996). In blood-perfused tissues, such as the dermis and hypodermis, spectral responses in the ultraviolet and visible domains are associated with variations in the concentration of blood-borne pigments, notably hemoglobin. Most of the oxygen carried by blood is reversibly bound to hemoglobin molecules stored in the erythrocytes (red blood cells). The oxygenated and deoxygenated states of hemoglobin correspond to its two functional forms, namely, oxyhemoglobin (O_2Hb) and deoxyhemoglobin (HHb), which tend to have a more pronounced effect on the absorption profile of human skin within the visible domain (Fig. 4).

An increase in the volume fraction of blood in the dermal tissues accentuates the influence of blood-borne pigments on the spectral responses of human skin. Such spectral variations may result from erythema, a condition in which a dilation of the dermal blood vessels caused by external stimuli induces a "redness" appearance around the stimulus site (Baranoski and Krishnaswamy 2010). Although different types of stimuli (e.g., mechanical, chemical, electrical, thermal) can trigger erythema, it has been most extensively investigated as an acute response to UVR (Diffey 1980).

In addition to the functional forms of hemoglobin, dysfunctional forms of hemoglobin that do not bind oxygen reversibly can also be present in the erythrocytes, namely, carboxyhemoglobin (COHb), methemoglobin (MetHb), and sulfhemoglobin (SHb) (Baranoski et al. 2012). Similar to their functional counterparts, the dysfunctional hemoglobins can contribute to the absorption of light within the visible domain (Fig. 4), albeit at a lower level. Normally, only small traces (<2 %) of COHb and MetHb are found in human blood (Cunnington et al. 2004; Haymond et al. 2005; Yarynovska and Bilyi 2006), while SHb is absent (Gharahbaghian et al. 2009; Yarynovska and Bilyi 2006). However, certain pathological conditions are associated with the presence of excessive amounts of dysfunctional hemoglobins in the bloodstream. In these cases, one of the symptoms is a "bluish" skin color (cyanosis), which is more apparent in the body extremities of individuals with a relatively low level of melanin pigmentation (Gopalacharand et al. 2005; Haymond et al. 2005).

Besides the different forms of hemoglobin, other blood-borne pigments, such as bilirubin (Rolinsky et al. 2001; Saidi 1992) and carotenoids, such as beta-carotene, alpha-carotene, lutein, zeaxanthin, and lycopene (Alaluf et al. 2002a; Sthal and Sies 2004), can also contribute to light

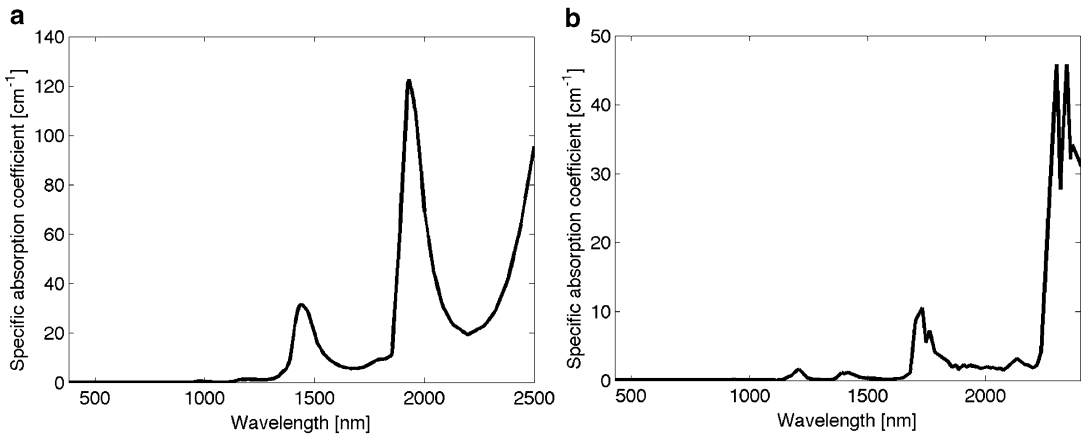

Fig. 5 Absorbers of light in human skin acting primarily in the infrared domains. (**a**) Specific absorption coefficient of water (Palmer and Williams 1974; Pope and Fry 1997). (**b**) Specific absorption coefficient of lipids (Altshuler et al. 2003; Prahl 2004; van Veen et al. 2004)

absorption in the dermal layers, especially in the visible domain (Fig. 4). Bilirubin is a pigment derived from the degradation of hemoglobin during the normal and abnormal destruction of red blood cells, and it is normally filtered out of the blood by the liver (Baranoski et al. 2012). If this organ is not working properly, an excessive quantity of this substance may be present in the bloodstream, resulting in a "yellowness" in the skin, a condition known as jaundice or hyperbilirubinemia (Rolinsky et al. 2001; Saidi 1992). Excessive amounts of carotenoids may also give the skin a "yellowness" appearance (Sthal and Sies 2004). Among the carotenoids found in human skin, beta-carotene and lycopene occur in larger quantities. They have similar absorption spectra, with a slight shift toward the red end of the light spectrum in the case of lycopene (Darvin et al. 2005).

In the infrared domain, the absorption of light in the skin layers is controlled by the presence of lipids (Williams et al. 1988) and water (Jacquez et al. 1955b). Both materials are characterized by broad absorption spectra in this domain (Fig. 3). Reflectance measurements by Jacquez et al. (1955a, b) illustrate the different skin spectral signatures that can be detected in the ultraviolet, visible, and infrared domains (Fig. 6). They depict some of the main spectral features of the skin surface. For example, one can observe that a low level of melanin pigmentation tends to make the characteristic "omega" shape around 500 nm (caused by the presence of oxyhemoglobin) more prominent. In addition, one can observe spectral features in the infrared domain that are directly associated with the bands of absorption maxima of lipids and water in that domain.

4 Detour and Sieve Effects

Although the spectral responses of human skin can be analyzed with respect to the different contributions of its scattering and absorption agents, such responses are in fact the result of their combined actions. For example, the skin spectral responses in the visible domain are largely determined by how much light is absorbed by melanin and hemoglobin. In their native state, these pigments are usually found in organelles (melanosomes) and cells (erythrocytes), respectively, which also scatter light. In addition, when light traverses a turbid medium such as human skin, refractive index differences between these structures and the surrounding materials may cause multiple external and internal reflections that increase the light optical path length. This phenomenon, referred to as detour effect (Fukshansky 1981; Rabinowitch 1951), increases the probability of the traversing light to interact with the pigment of interest. Conversely, light traversing

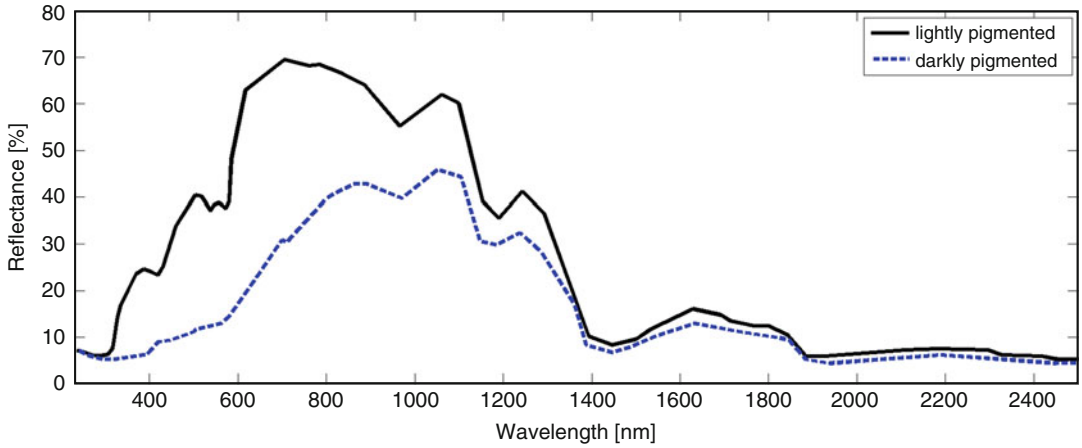

Fig. 6 Reflectance spectra of lightly pigmented and darkly pigmented skin specimens measured by Jacquez et al. (1955a, b) considering an angle of incidence equal to 16.75°

a turbid medium may not encounter a pigment-containing structure, a phenomenon referred to as sieve effect (Fukshansky 1981; Rabinowitch 1951).

While the detour effect increases the probability of light absorption by the pigment of interest (notably in bands of absorption minima (Butler 1964)), the sieve effect reduces the probability of light absorption (notably in bands of absorption maxima (Latimer and Eubanks 1962)) in comparison with a homogenous solution with equal concentration of this pigment (Lovell et al. 1999; Pittman 1986). The net result of these two effects depends on several factors such as the distribution and volume fraction of the pigment-containing structures in the medium and the pigment concentration within these structures (Fukshansky 1981; Kramer et al. 1951; Pittman 1986; Rabinowitch 1951). For example, the sieve effect tends to dominate in whole blood samples with a low hematocrit (cellular volume fraction), while the detour effect tends to dominate in samples with a high hematocrit (Lovell et al. 1999; Pittman 1986; Yim et al. 2012). In the case of human skin, sieve and detour effects are more prominently associated with the presence of the melanosomes. For this reason, in the remainder of this section, we briefly review the main factors affecting their size, shape, and distribution within the cutaneous tissues.

Under normal physiological conditions, the size, shape, and distribution of the melanosomes depend on the biophysical characteristics of the skin specimen. While darkly pigmented individuals present larger, longer, wider, and denser melanosomes (Olson et al. 1973; Szabó et al. 1969) individually dispersed (Hawk and Parrish 1982; Szabó et al. 1969; Toda et al. 1972), lightly pigmented individuals present smaller melanosomes (Olson et al. 1973; Szabó et al. 1969) that appear in groups, or aggregates, surrounded by a membrane-bound vesicle (Hawk and Parrish 1982; Szabó et al. 1969; Toda et al. 1972). A mixture of single and aggregate complexes of melanosomes may also be found in moderately pigmented individuals (Hawk and Parrish 1982; Olson et al. 1973). Observations by Olson et al. (1973) indicate that the presence of melanosome complexes is inversely proportional to the size of individual melanosomes.

Differences in the size and shape of skin melanosomes have been also associated with the class of melanin present in these organelles (Liu et al. 2005). Liu et al. (2005) have observed that eumelanin-containing melanosomes (eumelanosomes) found in black hair can usually have a shape of an oblate ellipsoid, while pheomelanin-containing melanosomes (pheomelanosomes) found in red hair can have a shape of an ellipsoid or closer to a perfect sphere, and they are generally smaller than those isolated from black hair. Experiments by Alaluf et al. (2001) involving heavily pigmented skin specimens have resulted in the same observation for skin pheomelanosomes, with their sphericity (given in terms of their long-to-short axis) ranging from 1.0 (perfectly spherical) to 6.0 (oblate, rod-shaped).

5 Fluorescence Agents

When electromagnetic radiation propagating at a certain wavelength is absorbed by a material, it may excite the orbital electrons of the atoms or molecules of this material to a higher quantum state. Upon return of these electrons to their ground state, they emit photons of light at another (usually longer) wavelength (Hunter and Harold 1987). This process, known as fluorescence, has a timescale of approximately 10^{-8} s or shorter (ANSI 1986). Endogenous materials that produce fluorescence upon excitation are called fluorophores. The key fluorescence properties of a fluorophore are its excitation and emission spectra, and the maxima of these spectra give the excitation-emission pair that characterizes that fluorophore (Kollias et al. 1998).

Within the human skin, we find mainly ultraviolet-induced fluorescence agents. These fluorophores include reduced nicotinamide adenine dinucleotide (NADH), keratin, collagen, elastin, aromatic amino acids (tryptophan and tyrosine), flavins, and porphyrins (Na et al. 2000, 2001; Sinichkin et al. 1998). The occurrence of fluorescence in human skin is associated with the main fluorophores present in its layers, namely, keratin (stratum corneum and epidermis), NADH

(epidermis), and collagen (dermis). Experiments by Ehlers et al. (2006) show that the fluorescence observed in the epidermal layers, notably in the stratum spinosum and stratum basale, has a slower decay characteristic than the keratinous stratum corneum and the collagen-rich dermis. Ehlers et al. (2006) have attributed this behavior to the presence of living cells in the former two skin layers.

Collagen is considered to be the main fluorophore contributing to the ultraviolet-induced autofluorescence of human skin (Sinichkin et al. 1998), with an excitation-emission maxima lower than excitation-emission maxima of keratin and NADH (Gilles et al. 2000; Na et al. 2000). Accordingly, the skin ultraviolet-induced autofluorescence is more pronounced within the dermal tissues (Anderson and Parrish 1982). It is worth noting that although melanin is a relatively low quantum yield fluorophore in the ultraviolet domain, experiments by Huang et al. (2006) indicate that natural melanins can exhibit significant fluorescence emission under near-infrared light excitation.

6 Challenges and Perspectives

Despite the importance of human skin and the advances in measurement technology, the current understanding of the optical properties of human skin is far from complete. Arguably the main obstacle is the lack of reliable and openly available measured data. For instance, the most useful measured dataset with respect to the scattering profile of the epidermis was obtained by Bruls and van der Leun (1984) in 1984 for specimens with similar biophysical characteristics (Caucasians) and considering a small set of illumination conditions. Since then, as examined by Baranoski et al. (2004, 2005), it has been often unduly generalized to represent the scattering of these tissues for skin specimens with different pigmentation levels and under a wide range of illumination conditions. Similar observations apply to the scattering of the dermis samples measured by Jacques et al. (1987).

Other significant examples of data barriers include the absorption spectra of the different absorbers present in the human skin. These datasets are obtained under in vitro conditions. Hence, they are bound to present significant qualitative and quantitative differences with respect to their in vivo counterparts. These differences are related not only to sieve and detour effects outlined earlier but also to experimental constraints such as the use of solvents during the preparation of dilute solutions of these absorbers for spectrophotometric measurements (Sardar et al. 2001). These procedures may alter the size and optical properties of the absorbing particles (Riesz et al. 2006). Currently, the chemical structure of key pigments, such as melanin, is still object of investigation, which makes the whole process of measuring their absorbing spectra even more difficult. In addition, the available measured absorption spectra for several absorbers found in the skin tissues are usually limited to specific spectral domains. Other examples of data scarcity include the refractive indices of different tissue constituents, which, when available, are usually provided as a single value measured at a specific wavelength.

Investigations of skin fluorescence are also impaired by data availability issues. For example, there are many fluorophores in human skin whose excitation-emission and quantum efficiency spectra are still object of investigation. This type of data is difficult to obtain since the fluorescence signal can be masked by the absorption of light by pigments such as melanin and hemoglobin (Na et al. 2001; Sinichkin et al. 1998). Moreover, fluorescence measurements may be further disturbed by environmental and physiological changes that may alter the molecular structure of the fluorophores and their spatial distribution (Na et al. 2000; Sinichkin et al. 1998).

In the last decades, a large body of work based on computer simulations have attempted to advance the current understanding of the optical properties of skin surfaces (Baranoski and Krishnaswamy 2010; Tuchin 2007). However, these simulations themselves are often limited by the scarcity of measured data to characterize the

scattering and absorption of different skin specimens. Furthermore, in order to be used in a predictive manner, these simulations need to be evaluated, which, in turn, requires comparisons of modeled data with measured data. Besides being also scarce, these datasets (e.g., reflectance and BRDF curves) rarely include characterization information (e.g., thickness, refractive indices) for the specimens employed in the measurements, which further impairs the proper evaluation of the simulations. It is important to note that the measurement of these specimens characterization parameters also involves sizable hurdles, not only under in vivo conditions (e.g., differences in water content from physiological levels to environmental levels (Chan et al. 2007)) but also under in vitro conditions (e.g., crystallization from freezing the tissue (Schaaf et al. 2010)).

Although one should not dismiss the contributions of computer simulations to the current understanding of skin optical properties, such computational efforts can lead to more substantial advances in skin tissue optics if paired with actual measured data. Hence, we believe that it is essential to strengthen the experimental basis in this area by enhancing quantitatively and qualitatively the measurement and dissemination of fundamental biophysical data associated with the optical properties of the skin tissues.

References

Alaluf S, Heath A, Carter N, Atkins D, Mahalingam H, Barrett K, et al. Variation in melanin content and composition in type V and type VI photoexposed and photoprotected human skin: the dominant role of DHI. Pigment Cell Res. 2001;14:337–47.

Alaluf S, Heinrich U, Stahl W, Tronnier H, Wiseman S. Dietary carotenoids contribute to normal human skin color and UV photosensitivity. J Nutr. 2002a;132:399–403.

Alaluf S, Atkins D, Barret K, Blount M, Carter N, Heath A. Ethnic variation in melanin content and composition in photoexposed and photoprotected human skin. Pigment Cell Res. 2002b;15:112–8.

Alaluf S, Atkins D, Barret K, Blount M, Carter N, Heath A. The impact of epidermal melanin on objective measurements of human skin color. Pigment Cell Res. 2002c;15:119–26.

Altshuler GB, Anderson RR, Manstein D, inventor; The General Hospital Corp., Palomar Medical Technologies, Inc., assignee. Method and apparatus for the selective targeting of lipid-rich tissues. United States Patent US 6605080 B1. 12 Aug 2003.

Anderson RR, Parrish JA. The optics of human skin. J Invest Dermatol. 1981;77(1):13–9.

Anderson RR, Parrish JA. Optical properties of human skin. In: Regan JD, Parrish JA, editors. The science of photomedicine. New York: Plenum Press; 1982. p. 147–94.

ANSI. Nomenclature and definitions for illuminating engineering. New York: Illuminating Engineering Society of North America; 1986. Report No.: ANSI/IES RP-6-1986.

Baranoski GVG, Krishnaswamy A. Light and skin interactions simulations for computer graphics applications. Amsterdam: Morgan Kaufmann; 2010.

Baranoski GVG, Krishnaswamy A, Kimmel B. An investigation on the use of data-driven scattering profiles in Monte Carlo simulations of ultraviolet light propagation in skin tissues. Phys Med Biol. 2004;49:4799–809.

Baranoski GVG, Krishnaswamy A, Kimmel B. Increasing the predictability of tissue subsurface scattering simulations. Visual Comput. 2005;21(4):265–78.

Baranoski GVG, Chen TF, Kimmel B, Miranda E, Yim D. On the noninvasive optical monitoring and differentiation of methemoglobinemia and sulfhemoglobinemia. J Biomed Opt. 2012;17(9):097005. -1-14.

Bashkatov AN, Genina EA, Kochubey VI, Tuchin VV. Optical properties of human skin, subcutaneous and mucous tissues in the wavelength range from 400 to 2000 nm. J Phys D Appl Phys. 2005;38:2543–55.

Bendit EG. Infrared absorption spectrum of keratin. I. Spectra of α-, β-, and supercontracted keratin. Biopolymers. 1966;4:539–59.

Bruls WAG, van der Leun JC. Forward scattering properties of human epidermal layers. Photochem Photobiol. 1984;40:231–41.

Butler WL. Absorption spectroscopy *in vivo*: theory and application. Annu Rev Plant Phys. 1964;15:451–70.

Chan D, Schulz B, Gloystein K, Müller HH, Rübhausen M. *In vivo* spectroscopic ellipsometry measurements on human skin. J Biomed Opt. 2007;12(1):014023. -1-6.

Chedekel MR. Photophysics and photochemistry of melanin. In: Zeise L, Chedekel MR, Fitzpatrick TB, editors. Melanin: its role in human photoprotection. Overland Park: Valdenmar Publishing Company; 1995. p. 11–22.

(CIE 2011) Commission Internationale de L'Eclairage. ILV: international lighting vocabulary, new. Vienna, Austria: CIE Central Bureau. 2011. Report No.: CIE S 017/E:2011.

Clendening B. UV Spectrophotometric analysis of DNA and RNA. Hofstra University; Hempstead, New York, USA; 2002.

Cunnington AJ, Kendrick SW, Wamola B, Lowe B, Newton CRJC. Carboxyhemoglobin levels in Kenyan

children with Plasmodium Falciparum malaria. Am J Trop Med Hyg. 2004;71(1):43–7.

Darvin ME, Gersonde I, Meinke M, Sterry W, Lademann J. Non-invasive *in vivo* determination of the carotenoids beta-carotene and lycopene concentrations in the human skin using the Raman spectroscopic method. J Phys D Appl Phys. 2005;38:2696–700.

Diffey BL. Ultraviolet radiation physics and the skin. Phys Med Biol. 1980;25(3):405–26.

Ehlers A, Riemann I, Anhut T, Kaatz M, Elsner P, König K. Fluorescence lifetime imaging of human skin and hair. In: Periasamy A, So PTC, editors. Multiphoton microscopy in the biomedical sciences VI. San Jose: SPIE; 2006. p. 60890N-1-10.

Federici JF, Guzelsu N, Lim HC, Jannuzzi G, Findley T, Chaudhry HR, Ritter AB. Noninvasive light-reflection technique for measuring soft-tissue stretch. Appl Optics. 1999;38(31):6653–60.

Feynman RP, Leighton RB, Sands M. The Feynman lectures on physics, vol. 1. Reading: Addison-Wesley Publishing Company; 1964.

Flewelling R. Noninvasive optical monitoring. In: Bronzino JD, editor. The biomedical engineering handbook. Boca Raton: IEEE Press; 1995. p. 1346–56.

Fukshansky L. Optical properties of plants. In: Smith H, editor. Plants and the daylight spectrum. London: Academic; 1981. p. 21–40.

Gharahbaghian L, Massoudian B, DiMassa G. Methemoglobinemia and sulfhemoglobinemia in two pediatric patients after ingestion of hydroxylamine sulfate. West J Emerg Med. 2009;10(3):197–201.

Gilles R, Zonios G, Anderson RR, Kollias N. Fluorescence excitation spectroscopy provides information about human skin *in vivo*. J Invest Dermatol. 2000;115 (4):704–7.

Gopalacharand AS, Bowie VL, Bharadwaj P. Phenazopyridine-induced sulfhemoglobinemia. Ann Pharmacother. 2005;39(6):1128–30.

Hawk JLM, Parrish JA. Responses of normal skin to ultraviolet radiation. In: Regan JD, Parrish JA, editors. The science of photomedicine. New York: Plenum Press; 1982. p. 219–60.

Haymond S, Cariappa R, Eby CS, Scott MG. Laboratory assessment of oxygenation in methemoglobinemia. Clin Chem. 2005;51(2):434–44.

Hennessy A, Oh C, Diffey B, Wakamatsu K, Ito S, Rees J. Eumelanin and pheomelanin concentrations in human epidermis before and after UVB irradiation. Pigment Cell Res. 2005;18:220–3.

Huang Z, Zeng H, Hamzavi I, Alajlan A, Tan E, McLean AI, et al. Cutaneous melanin exhibiting fluorescence emission under near-infrared light excitation. J Biomed Opt. 2006;11(3):034010. -1-6.

Hunter RS, Harold RW. The measurement of appearance. 2nd ed. New York: Wiley; 1987.

Jacques SL. Origins of tissue optical properties in the UVA, visible and NIR regions. In: Alfando RR, Fujimoto JG, editors. OSA TOPS on advances in optical imaging and photon migration. 2nd ed. Washington, DC: Optical Society of America; 1996. p. 364–9.

Jacques SL. Optical absorption of melanin. Oregon Medical Laser Center; Portland, Oregon, USA; 2001.

Jacques SL, Alter CA, Prahl SA. Angular dependence of HeNe laser light scattering by human dermis. Laser Life Sci. 1987;1(4):309–33.

Jacquez JA, Huss J, McKeehan W, Dimitroff J, Kuppenheim HF. Spectral reflectance of human skin in the region 235–700 μ. J Appl Physiol. 1955a;8:212–4.

Jacquez JA, Kuppenheim F, Dimitroff M, McKeehan W, Huss J. Spectral reflectance of human skin in the region 0.7–2.6 μ. J Appl Physiol. 1955b;8:297–9.

Kochevar I, Taylor R, Kritmann J. Fundamentals of cutaneous photobiology and photoimmunology. In: Wolff K, Goldsmith LA, Katz S, editors. Fitzpatrick's dermatology in general medicine. New York: McGraw Hill; 2008. p. 152–8.

Kollias N. The spectroscopy of human melanin pigmentation. In: Zeise L, Chedekel MR, Fitzpatrick TB, editors. Melanin: its role in human photoprotection. Overland Park: Valdenmar Publishing Company; 1995. p. 31–8.

Kollias N, Baqer A. On the assessment of melanin in human skin *in vivo*. Photochem Photobiol. 1986;43 (1):49–54.

Kollias N, Sayre RM, Zeise L, Chedekel MR. Photoprotection by melanin. J Photochem Photobiol B. 1991;9:135–60.

Kollias N, Gilles R, Moran M, Kochevar IE, Anderson RR. Endogenous skin fluorescence includes bands that may serve as quantitative markers of aging and photoaging. J Invest Dermatol. 1998;111(5):776–80.

Kölmel KF, Sennhenn B, Giese K. Investigation of skin by ultraviolet remittance spectroscopy. Brit J Dermatol. 1990;122:209–16.

Kramer K, Elam JO, Saxton GA, Elam Jr WN. Influence of oxygen saturation, concentration and optical depth upon the red and near-infrared light transmittance of whole blood. Am J Physiol. 1951;165(1):229–46.

Latimer P. A wave-optics effect which enhances light absorption by chlorophyll *in vivo*. Photochem Photobiol. 1984;40(2):193–9.

Latimer P, Eubanks CAH. Absorption spectrophotometry of turbid suspensions: a method of correcting for large systematic distortions. Arch Biochem Biophys. 1962;98:274–85.

Lee R, Mathews-Roth MM, Pathak MA, Parrish JA. The detection of carotenoid pigments in human skin. J Invest Dermatol. 1975;64:175–7.

Lin JY, Fisher DE. Melanocyte biology and skin pigmentation. Nature. 2007;445:843–9.

Liu Y, Hong L, Wakamatsu K, Ito S, Adhyaru B, Cheng C, et al. Comparison of structural and chemical properties of black and red human hair melanosomes. Photochem Photobiol. 2005;81:135–44.

Lopez H, Beer JZ, Miller SA, Zmudzka BZ. Ultrasound measurements of skin thickness after UV exposure: a

feasibility study. J Photochem Photobiol B. 2004;73:123–23.
Lovell AT, Hebden JC, Goldstone JC, Cope M. Determination of the transport scattering coefficient of red blood cells. In: Chance B, Alfano RR, Tromberg BJ, editors. Optical tomography and spectroscopy of tissue III. San Jose: SPIE; 1999. p. 175–82.
Magnenat-Thalmann N, Kalra P, Lévêque JL, Bazin R, Batisse D, Querleux B. A computational skin model: fold and wrinkle formation. IEEE Trans Inf Technol B. 2002;6(4):317–23.
McCartney EJ. Optics of the atmosphere: scattering by molecules and particles. New York: Wiley; 1976.
McCluney R. Introduction to radiometry and photometry. Boston: Artech House; 1994.
Na R, Stender I, Henriksen M, Wulf HC. Autofluorescence spectrum of skin: component bands and body site variations. Skin Res Technol. 2000;6:112–7.
Na R, Stender I, Henriksen M, Wulf HC. Autofluorescence of human skin is age-related after correction for skin pigmentation and redness. J Invest Dermatol. 2001;116 (4):536–40.
Olivarius FF, Wulf HC, Therkildsen P, Poulsen P, Crosby J, Norval M. Uranic acid isomers: relation to the body site, pigmentation, stratum corneum thickness and photosensitivity. Arch Dermatol Res. 1997;289:501–5.
Olson L, Gaylor J, Everett MA. Skin color, melanin, and erythema. Arch Dermatol. 1973;108:541–4.
Oudhia A. UV-VIS spectroscopy as a nondestructive and effective characterization tool for II-VI compounds. Recent Res Sci Technol. 2012;4(8):109–11.
Palmer KF, Williams D. Optical properties of water in the near infrared. J Opt Soc Am. 1974;64(8):1107–10.
Parsad D, Wakamatsu K, Kanwar AJ, Kumar B, Ito S. Eumelanin and phaeomelanin contents of depigmented and repigmented skin in vitiligo patients. Brit J Dermatol. 2003;149:624–6.
Pittman RN. In vivo photometric analysis of hemoglobin. Ann Biomed Eng. 1986;14(2):1416–32.
Pope RM, Fry ES. Absorption spectrum (380–700 nm) of pure water. II. Integrating cavity measurements. Appl Optics. 1997;36(33):8710–23.
Prahl SA. Optical absorption of hemoglobin. Oregon Medical Laser Center; Portland, Oregon, USA; 1999.
Prahl SA. PhotochemCAD spectra by category. Oregon Medical Laser Center; Portland, Oregon, USA; 2001.
Prahl SA. Optical absorption of fat. Oregon Medical Laser Center; Portland, Oregon, USA; 2004.
Rabinowitch EI. Light absorption by pigments in the living cell. In: Photosynthesis and related processes. 2nd vol. Part 1. New York: Interscience Publishers; 1951. p. 672–739.
Randeberg LL, Bonesrønning JH, Dalaker M, Nelson JS, Svaasand LO. Methemoglobin formation during laser induced photothermolysis of vascular skin lesions. Laser Surg Med. 2004;34(5):414–9.
Riesz J, Gilmore J, Meredith P. Quantitative scattering of melanin solutions. Biophys J. 2006;90:4137–44.
Rolinsky B, Küster H, Ugele B, Gruber R, Horn K. Total bilirubin measurement by photometry on a blood gas analyser: potential for use in neonatal testing at point of care. Clin Chem. 2001;47(10):1845–7.
Saidi IS. Transcutaneous optical measurement of hyperbilirubinemia in neonates [dissertation]. Houston: Rice University; 1992.
Sandoz P, Marsaut D, Armbruster V, Humbert P, Gharbi T. Towards objective evaluation of skin aspect: principles and instrumentation. Skin Res Technol. 2004;10:263–70.
Sardar DK, Mayo ML, Glickman RD. Optical characterization of melanin. J Biomed Opt. 2001;6(4):404–11.
Schaaf D, Eurell T, Johnson T. Cultured human keratinocytes for optical transmission measurement. J Biophoton. 2010;3(3):161–8.
Siggaard-Andersen O, Nørgaard-Pedersen B, Rem J. Hemoglobin pigments. spectrophotometric determination of oxy-, carboxy-, met-, and sulfhemoglobin in capillary blood. Clin Chim Acta. 1972;42(1):85–110.
Sinichkin YP, Utz SR, Mavliutov AH, Pilipenko HA. *In vivo* fluorescence spectroscopy of the human skin: experiments and models. J Biomed Opt. 1998;3 (2):201–11.
Sohaib A, Farooq AR, Atkinson GA, Smith LN, Smith ML, Warr R. *In vivo* measurement of skin microrelief using photometric stereo in the presence of interreflection. J Opt Soc Am A. 2013;30(3):278–86.
Sthal W, Sies H. Carotenoids in systemic protection against sunburns. In: Krisnky N, Mayne ST, Sies H, editors. Carotenoids in health and disease. Boca Raton: CRC Press; 2004. p. 201–11.
Sutherland JC, Griffin KP. Absorption spectra of DNA for wavelengths greater than 300 nm. Radiat Res. 1981;86:399–409.
Swanbeck G. On the keratin fibrils of the skin. J Ultra R. 1959;3:51–7.
Szabó G, Gerald AB, Pathak MA, Fitzpatrick TB. Racial differences in the fate of melanosomes in human epidermis. Nature. 1969;222:1081–2.
Thody AJ, Higgins EM, Wakamatsu K, Ito S, Burchill SA, Marks JM. Pheomelanin as well as eumelanin is present in human epidermis. J Invest Dermatol. 1991;97:340–4.
Toda K, Pathak MA, Parrish JA, Fitzpatrick TB. Alteration of racial differences in melanosome distribution in human epidermis after exposure to ultraviolet light. Nat New Biol. 1972;236:143–5.
Tuchin VV. Tissue optics light scattering methods and instruments for medical diagnosis. 2nd ed. Bellingham: The International Society for Optical Engineering; 2007.
van de Graaff KM. Human anatomy. 4th ed. Dubuque: William C Brown; 1995.
van Veen RLP, Sterenborg HJCM, Pifferi A, Torricelli A, Cubeddu R. Determination of VIS- NIR absorption coefficients of mammalian fat, with time- and spatially resolved diffuse reflectance and transmission

spectroscopy. In: Biomed Topical Meeting. Miami Beach: Optical Society of America; 2004. p. SF4.
Williams ML, Hincenbergs M, Holbrook KA. Skin lipid content during early fetal development. J Invest Dermatol. 1988;91:263–8.
Yarynovska IH, Bilyi AI. Absorption spectra of sulfhemoglobin derivatives of human blood. In: Cote GL, Priezzhev AV, editors. Optical diagnostics and sensing VI. San Jose: SPIE; 2006. p. 1–6.
Yim D, Baranoski GVG, Kimmel BW, Chen TF, Miranda E. A cell-based light interaction model for human blood. Comput Graph Forum. 2012;31(2):845–54.
Young AR. Chromophores in human skin. Phys Med Biol. 1997;42:789–802.

Microbiology of Skin Surface

10

Xuemin Wang, Chao Yuan, and Philippe Humbert

Contents

Keywords

16S rRNA • Acne vulgaris (AV) • Atopic dermatitis (AD) • Psoriasis vulgaris (PV) • Skin flora • Skin microbiome • Vulvar skin

1 Introduction

The human skin is the largest organ of the human body. It protects the underlying tissues and plays an important role as a frontline defense system against invading pathogens and external environmental factors. It is colonized by a unique and complex microbial ecosystem, including bacteria, fungi, and bacteriophages, some of which could become pathogenic under certain conditions. The skin microbiome is very complex. Hundreds of different microbial species reside on the whole surface of the skin. Its composition and distribution are uniquely different from the flora of other organs. There are always differences among different people and different areas of the skin on the same person. Recent 16S rRNA-based methods revealed the similar situations.

Skin flora are usually nonpathogenic. They are not harmful to their host and offer benefits. The benefits bacteria can offer include preventing transient pathogenic microorganisms from colonizing the skin surface, either by competing for nutrients, secreting chemicals against them, or stimulating the skin's immune system. The microbial composition and distribution of the human skin microbiota have been associated with multiple

Xuemin Wang: deceased.

X. Wang
Shanghai, China

C. Yuan (✉)
Department of Skin and Cosmetic Research, Shanghai Skin Disease Hospital, Shanghai, China
e-mail: dermayuan@163.com

P. Humbert
Department of Dermatology, University Hospital of Besançon, Besançon, France
e-mail: philippe.humbert@univ-fcomte.fr

P. Humbert et al. (eds.), *Agache's Measuring the Skin*,
DOI 10.1007/978-3-319-32383-1_10

skin diseases, including atopic dermatitis (AD), acne vulgaris (AV), psoriasis vulgaris (PV), rosacea, dandruff, seborrheic dermatitis, etc.

2 The Skin Flora

The human skin flora, more properly referred to as the skin microbiome, are the microorganisms which reside on the whole human skin. Most of studies have been upon those that reside upon the 2 m^2 of human skin (cf. the human microbiome). Many of them are bacteria of which there are around 1,000 species from 19 phyla upon the human skin. The total number of bacteria on an average human has been estimated at one trillion. Most are found in the superficial layers of the epidermis and the upper parts of hair follicles.

Staphylococcus epidermidis and other coagulase-negative staphylococci were used to have been regarded as the primary bacterial colonizers of the human skin (Grice and Segre 2011). Other microorganisms that are generally regarded as skin colonizers include coryneforms of the phylum Actinobacteria, for example, the genera *Corynebacterium*, *Propionibacterium*, and *Brevibacterium* and the genus *Micrococcus*. Gram-negative bacteria, with the exception of some *Acinetobacter* spp., are generally not isolated from the skin, but are thought to arise in cultures owing to contamination from the other organs, such as the gastrointestinal tract (Roth and James 1988). Non-bacterial microorganisms have also been isolated from the skin. The most commonly isolated fungal species are *Malassezia* spp., which are especially prevalent in sebaceous areas. The *Demodex* mites, such as *Demodex folliculorum*, *Demodex brevis*, etc., are regarded as part of the normal skin flora. The living of *Demodex* mites depended on the amount of sebum. They are much more prevalent following puberty and reside at sebaceous areas of the face. *Demodex* mites may also feed on epithelial cells lining the pilosebaceous unit or even on other microorganisms (such as *Propionibacterium acnes*) that inhabit the same space. The role of commensal viruses has not been published, and investigations are limited by the available molecular and microbiological means to identify and characterize viruses. Historically, culture-based approaches have been the standard for characterizing microbial diversity. It is now evident that only a minority of bacteria are able to thrive in isolation (Dunbar et al. 2002). Furthermore, hair follicles and sebaceous glands are the typical anoxic environments where some of anaerobic microorganisms reside.

2.1 Healthy Skin

The skin represents an interesting human habitat in which lifestyle and environmental factors shape the microbial community of different specific body sites. No taxa are ubiquitously present in every subject and body site, although targeted studies reveal that specific body sites are generally dominated by certain defining taxa.

The human skin is mainly comprised of Actinobacteria, Proteobacteria, and Firmicutes, some studies finding that more than 90 % of the microbiota of the forearm belonged to these phyla (Gao et al. 2007). The volar forearms of different subjects were found to only share 2 % of species-level operational taxonomic units (OTUs) (Gao et al. 2007), whereas the hands share 13 % of OTUs (Fierer et al. 2008). Estimates of species-level OTUs for skin sites include 246 for the volar forearm (Gao et al. 2007), more than 150 for the palms, and 113 for the inner elbow (Fierer et al. 2008). More than 50 % of sequences obtained from arm skin sites belong to *Propionibacterium*, *Corynebacterium*, *Staphylococcus*, *Streptococcus*, and *Lactobacillus* species (Grice et al. 2008).

2.2 Special Area Skin

The skin microbial community also plays an important role in the formation of body odor in, for instance, the vulva, axillae, etc. Few molecular-based researches were done on the axillary microbiome. Callewaert et al. (2013) detected the axillary microbiome of a group of 53 healthy subjects. A profound view was obtained of the

interpersonal, intrapersonal, and temporal diversity of the human axillary microbiota. Denaturing gradient gel electrophoresis and next generation sequencing on 16S rRNA gene region were combined and used as extent to each other. Two important clusters were characterized, where *Staphylococcus* and *Corynebacterium* species were the abundant species. Females predominantly clustered within the *Staphylococcus* cluster (87 %, $n = 17$), whereas males clustered more in the *Corynebacterium* cluster (39 %, $n = 36$). The axillary microbiota was unique to each individual. Left-right asymmetry occurred in about half of the human population.

The inter- and intraindividual differences in bacterial flora on the vulvar skin are known to exist. Aly et al. (1979) used a cultivation method to show that microbial counts are higher on the vulvar skin than on the forearm skin and that *S. aureus* normally inhabits the vulvar area. Brown et al. (2007) detected bacteria, such as *S. epidermidis*, *S. aureus*, *P. acnes*, *Lactobacillus* spp., *Prevotella* spp., etc., identified on the vulvar skin using the 16S rRNA gene-based clone library method. The number of total bacteria and the predominant species, such as *S. epidermidis* and *Lactobacillus* spp., were higher in the labia than those at other sites. There were only 60 % of subjects with *S. aureus* detected. *Prevotella* spp. were more predominant in the labial skin than in the vaginal skin (Mikamo et al. 1998). The species of the genus *Lactobacillus* are predominant in the labia minora of Japanese women, identified using the 16S rRNA gene-based clone library method (Shiraishi et al. 2011). *Prevotella* spp. were detected in the labia and groin of 95 % of Japanese subjects by another study (Miyamoto et al. 2013), so it is indicated that *Prevotella* spp. play a key role in vulvar skin conditions.

3 Skin Diseases

3.1 Atopic Dermatitis

Atopic dermatitis (AD) is a common, multifactorial, fluctuating, chronic inflammatory skin disease with a genetic predisposition. AD is often associated with atopic conditions such as asthma and IgE-mediated food allergy, which can be triggered by different allergens and various environmental factors. The relevance of the colonization of the skin with bacteria, such as *S. aureus*, and fungi, such as *Malassezia furfur*, *Pityrosporum orbiculare*, and *Candida albicans*, to AD has been controversial over the past few decades. Children with AD often have infective exacerbations which are treated with antibiotics and/or antiseptics.

The most common infective cause is *S. aureus* with a trend toward antibiotic resistance. *S. aureus* is one of the important microorganisms of normal skin flora. Bacterial skin flora of patients with AD differ from that of healthy people.

AD skin provides a favorable environment for colonization and proliferation of *S. aureus*. Skin colonization with *S. aureus* is more in the lesional skin than in nonlesional skin and is minimal in the skin of healthy children. All of these published data have shown that there are significant differences between *S. aureus* in the lesional skin and nonlesional skin ($P < 0.01$) (see Table 1).

Haslund et al. (2009) confirmed the important role of colonization with *S. aureus* as an aggravating factor in AD, as there was a significant correlation between the severity of AD and *S. aureus* skin colonization. The results of their study were in agreement with other results (see Table 2).

Several studies demonstrated that the colonization of the skin with superantigen-producing *Staphylococcus aureus* is associated with increased severity of AD. It has been shown that AD may be aggravated by the direct biological

Table 1 The colonization of *S. aureus* in AD skin (%)

Reference	Lesional skin	Nonlesional skin
Miyamoto et al. (2013)	65.0	30.0
Gomes et al. (2011)	57.0	43.0
Al-saimary et al. (2005)	69.7	30.3
Pezesk et al. (2007)	42.5	57.5
Hon et al. (2005)	48.5	51.5
Matsui et al. (2005)	86.0	14.0
Guzik et al. (2005)	100.0	0

Table 2 The relationship between severity of AD and skin colonization (%)

Severity	Gomes et al. (2011)	Haslund et al. (2009)
Mild	46.0	48.0
Moderate	*73.0*	52.0
Severe	*100.0*	77.5

action of bacteria or their products or by an immunological reaction to bacterial antigens or superantigens.

The studies (Hill 2011; Gomes et al. 2011; Pezesk et al. 2007; Guzik et al. 2005) had shown association between lesional skin *S. aureus* colonization rates with increasing age. The colonization rate in this study was 41.4 % (12 out of 29) in the youngest group, 81.8 % (18 out of 22) in the second group (>2–12 years), and 100 % (9 out of 9) in the third group (>12 years).

Malassezia species are confirmed to be involved in the development of skin lesions in AD; sometimes the response of adult AD to anti-inflammatory treatments is poor. Takahata et al. (2007) collected scale samples from skin lesions of 58 patients with AD in the head and neck regions (28 males and 30 females; 31 children and 27 adults), and fungal DNA was extracted from the samples directly. The number and identities of the *Malassezia* species were analyzed with high accuracy using a polymerase chain reaction-based culture-independent method. The in vivo level of anti-*Malassezia* IgE antibody was also assayed. The results had shown that *Malassezia restricta* was the predominant species in the children with AD, while both *M. restricta* and *M. globosa* predominated in the adults. The increased sensitization in terms of anti-*Malassezia*-specific IgE responses in the sera to both *M. globosa* and *M. restricta* from adults was comparable to that from children. There are some differences of the cutaneous *Malassezia* flora between adults and children with AD.

AD skin lesions are characterized by a Th-2 cell-mediated response to environmental antigens (Baker 2006). The increasing prevalence and severity of atopic diseases including AD over the last three decades have been attributed to decreased exposure to microorganisms during early life, which may result in an altered Th-1/Th-2 balance and/or reduced T cell regulation of the immune response. The patients with AD exhibit defects in innate and acquired immune responses resulting in a heightened susceptibility to bacterial, fungal, and other microorganism colonization, most notably colonization by *S. aureus*. Toxins produced by *S. aureus* exacerbate disease activity by both the induction of toxin-specific IgE and the activation of various cell types including Th-2 cells, eosinophils, and keratinocytes. Allergens expressed by the *Malassezia furfur* have also been implicated in disease pathogenesis in some of AD patients. Microorganisms play an influential role in AD pathogenesis, interacting with disease susceptibility genes to cause initiation and activation of disease activity.

The relevance of specific IgE antibodies for AD is still under discussion. Several experimental studies focus on a link between allergens and AD by IgE-independent mechanisms (Isolauri and Turjanmaa 1996). There is increasing evidence of a relationship between microorganisms and the deviation of immune responses. A high correlation between a positive patch test with milk and delayed-onset reactions due to milk provocation tests in children was found, while milk-specific IgE antibodies were relevant only for immediate-type reactions. Some clinical studies had shown that the IgE-mediated sensitization to *P. ovale* for the prediction of a therapeutic effect of ketoconazole in the treatment of AD using patch tests with *P. ovale* may be more useful. Positive patch test reactions to *P. orbiculare* have been demonstrated in atopic patients (Lindner et al. 2000). In the case of positive patch test results with food and mite allergens, patients may find relief by avoiding allergen exposure. The treatment of children with AD with specific probiotic bacteria strains reduces the eczema severity.

Allen et al. (2008) found that some clinical features are the special features of AD, such as miliaria of AD, which causes the itching, the most common symptom of this dermatitis, which occurred in areas of sweating, even in areas where patients did not realize they perspired. The epidemiological study results found that

sweating was a significant factor in exacerbating eczema. Miliaria arises from blockage of the eccrine sweat ducts. The material causes the blockage of duct. It is the film-like materials, which contain film-producing *S. epidermidis*, extracellular polysaccharide substance, and filaggrin-deficient stratum corneum. So the sweating and sweat retention are the important information of flare factors (Mowad et al. 1995). The subclinical miliaria provoked by film-producing *S. epidermidis* as part of a "double-hit" phenomenon (Serra et al. 1997) fits well in the pathogenesis of AD.

The microbiology of AD skin is dealt with the causes, mechanism, treatment, and prevention. This is the new insight to help us research and formulate the treatment strategy for AD.

3.2 Acne Vulgaris

Acne vulgaris (AV) is the most common, multifactorial, chronic inflammatory follicle disorder affecting much more individuals all over the world. It is a global disease that has no predilection for a specific race or gender. More than 60 % of the population suffers from AV at some point in their life. Four basic mechanisms contributing to acne are hormones, increased sebum production, changes inside hair follicles, and bacteria. The most commonly cited theory regarding the pathogenesis of acne states that increased sebum production leads to alterations in the lipid composition of hair follicles (Cunliffe 2002). Then *P. acnes* is a species of bacteria that implicated frequently and acts as the key player of the acnegenic microbes (Bruggemann et al. 2004). P acne is not only eliciting inflammatory lesion response but also the important pathogenesis of whole mechanism of disease. *P. acnes* can be recovered from skin surface as well as follicles on both normal and acne skin (Bruggemann et al. 2004). There is also no correlation between the number of *P. acnes* within a lesion and the clinical features of acne, both the types of lesion and severity of disease. But *P. acnes* is able to metabolize triglycerides into free fatty acids and glycerol, which is an immunological stimulant and/or a cytotoxic agent that leads to breakage in the follicular epithelium (Higaki et al. 2000). Other proposed *P. acnes* virulence factors include enzymes that are involved in adherence and colonization of the follicle (Cunliffe 2002). Another bacterial species detected frequently from pilosebaceous units and acne lesions are *S. epidermidis* and *Propionibacterium* species (*P. granulosum*). They are often significantly less abundant than *P. acnes* in acne lesions, but its abundance appears to correlate with clinical severity of acne. In addition to bacterial species, another microbial group is the fungal genus *Malassezia*, which has been implicated in the pathogenesis of seborrheic dermatitis and dandruff (Ro and Dawson 2005); their link to acne remains far more speculative.

3.3 Psoriasis Vulgaris

Psoriasis vulgaris (PV) is a common, chronic, relapsing/remitting, immune-mediated skin disease characterized by red, scaly patches, papules, and plaques, which usually itch. The skin lesions seen in psoriasis may vary in severity from minor localized patches to complete body coverage. The prevalence of psoriasis is around 2–4 % of the general population. The clinical characteristics are red, scaly patches on the skin. The manifestation of psoriasis includes hyperkeratosis, hyperproliferation of keratinocytes, infiltration of the skin by immune cells, and angiogenesis. The most commonly affected skin areas are elbows and knees.

Several bacterial species, including *S. aureus* and *Streptococcus pyogenes*, have been suggested to play a role in the pathogenesis of psoriasis. Fungi, including *M. furfur* and *Candida albicans*, have also been linked with the development of psoriatic skin lesions and play a role in the pathogenesis of PV.

The overall bacterial diversity of the microbiota in the psoriatic lesions is greater than in normal skin samples. There are significant differences in the distribution of the three major bacterial phyla in the human skin biota: Actinobacteria, Firmicutes, and Proteobacteria. Firmicutes are overrepresented in the lesion

Table 3 Distribution of dominant bacterial phylum in patient with PV (%) (Gao et al. 2008)

Bacteria	Nonlesional skin	Psoriatic lesional skin
Actinobacteria	47.6	37.3
Firmicutes	39.0	46.2
Propionibacterium	21.9	11.4

whereas the other two are underrepresented. The distribution of dominant bacterial phylum in lesional skin and nonlesional skin of patient with PV (%) is shown in Table 3.

3.4 Others

The genus *Malassezia* (*Pityrosporum*), recognized as a member of microbiological flora of the human skin, has been recently revised to include *Malassezia* species. The pityriasis versicolor (PV) is one of the common skin diseases caused by the *Malassezia* infection. The results of Salah's (Salah et al. 2005) study had shown *Malassezia globosa* was the predominant species in lesional skin of PV (65 %). It was isolated alone in 47 % of cases and associated in 18 % with *M. furfur* (13 %) or *M. sympodialis* (5 %). In the healthy skin, *M. globosa* was found alone in 7.77 % and associated in 15.54 % with *M. furfur* (4.44 %), *M. sympodialis* (4.44 %), *M. restricta* (3.33 %), and *M. slooffiae* (1.11 %). *M. globosa* presents the main species implicated in the pathogenicity of PV and *M. furfur* as the second agent of importance.

The vulvar skin is the special area of female. The bacterial population of vulvar skin is characterized by a high density of microorganisms that are related to flora of the vagina and urethra, such as *Lactobacillus* spp., or are common on other areas of the skin, such as *Staphylococcus epidermidis* and *Staphylococcus aureus*. Miyamoto et al. (2013) studied the vulvar skin of healthy Japanese women and understood microbes of the stratum corneum. A total of 40 subjects were quantified. The detection ratio and number of skin bacteria at the three test sites, labia and groin, mons pubis, and inner thigh, were taken. The labia and groin had significantly (>10-fold) more bacteria than the other sites. *Lactobacillus* spp. and *S. epidermidis* were the predominant species at all sites, followed by *S. aureus. Propionibacterium acnes* was present in almost all subjects but was less abundant than *S. aureus*, which was present in about 50 % of subjects. *Prevotella* spp. were detected in the labia and groin in almost all subjects but not in other sites.

Gardnerella vaginalis is one of the common skin diseases at the genital area. Myhre et al. (2002) took the samples from 278 (99 boys and 179 girls) out of 3,773 children, with a mean age of 5.63 years (range, 5.13–6.73), and found that at least one bacterial species was isolated from the genitals of 59 (33.9 %) girls. Most isolates (39 out of 99) were bacteria representing skin flora (staphylococci and coryneform organisms), with viridans streptococci and related organisms as the second most common group of isolates (31 out of 99). *S. anginosus* was the single most frequent bacterial species identified (17 isolates). *Streptococcus pyogenes* was isolated from the genitals of two girls, *Streptococcus pneumoniae* from one girl, and *Haemophilus influenzae* from eight girls. *G. vaginalis* was not isolated from the genitals in any girl, but the organism was isolated from the anal canal in three children. The results had shown that a large number of different aerobic organisms from children were identified from the genital area. *G. vaginalis* was rare and only isolated from the anal canal.

The skin flora is influenced by some system diseases (Arun and Palit 2003). Mean colony-forming units were 160.6, forearm, and 229.4, sternum ($P < 0.000$). In logistic regression analysis, patients in the medical intensive care unit were significantly more likely to have high counts on the arm (odds ratio, 2.48; 95 % confidence interval, 1.34–4.43; $P = 0.004$), and blacks were significantly more likely to have higher counts on the sternum when compared with other ethnic groups (odds ratio, 1.92; confidence interval, 1.18–3.11; $P = 0.009$). No differences were noted between inpatients or outpatients in prevalence of methicillin-sensitive *Staphylococcus aureus*, but inpatients were more likely to carry

methicillin-resistant *Staphylococcus aureus* (arm, $P = 0.007$; sternum, $P = 0.02$). Outpatients had a higher prevalence of micrococci and gram-negative bacteria at both skin sites (all $P < 0.01$) and yeast at the sternal site ($P = 0.007$). This comparison provides data to differentiate between effects of hospitalization and effects of chronic illness on skin flora.

4 Skin Flora Influence by Skin Surface pH

The acidic pH of the horny layer, measurable on the skin surface, has long been regarded as a result of exocrine secretion of the skin glands (Rippke et al. 2002). The "acid mantle" was thought to regulate the bacterial skin flora and to be sensitive primarily to skin-cleansing procedures. The pH of the deeper layers of the stratum corneum changes, as well as on the influence of physiological and pathological factors. The central role for the acidic milieu as a regulating factor in stratum corneum homeostasis is now emerging. This has relevance to the integrity of the barrier function, from normal maturation of the stratum corneum lipids to desquamation. Changes in the pH and the organic factors influencing it appear to play a role, not only in the pathogenesis, prevention, and treatment of irritant contact dermatitis but also of atopic dermatitis and ichthyosis and in wound healing. On the basis of these findings, a broader concept, exceeding the superficial "acid mantle" theory, has been formulated.

Microbiology of skin surface deals with skin health care and skin disease treatment and prevention. So healthy skin, abnormal skin and skin diseases, and the skin microbiome and its diversity all are being the hot topics of dermatology.

References

Allen HB, Jones NP, Bowen SE. Lichenoid and other clinical presentations of atopic dermatitis in an inner city practice. J Am Acad Dermatol. 2008;58:503–4.

Al-saimary IE, Bakr SS, Al-Hamdi KE. Staphylococcus aureus as a causative agent of atopic dermatitis/eczema syndrome (ADES) and its therapeutic implications. Internet J Dermatol. 2005;3(2):1.

Aly R, Britz MB, Maibach HI. Quantitative microbiology of human vulva. Br J Dermatol. 1979;101:445–8.

Arun C, Palit IA. The genus Malassezia and human disease. Indian J Dermatol Venereol Leprol. 2003;69:265–70.

Baker BS. The role of microorganisms in atopic dermatitis. Clin Exp Immunol. 2006;144:1–9.

Brown CJ, Wong M, Davis CC, et al. Preliminary characterization of the normal microbiota of the human vulva using cultivation-independent methods. J Med Microbiol. 2007;56:271–6.

Bruggemann H, Henne A, Hoster F, et al. The complete genome sequence of Propionibacterium acnes, a commensal of human skin. Science. 2004;305:671–3.

Callewaert C, Kerckhof FM, Granitsiotis MS, et al. Characterization of Staphylococcus and corynebacterium clusters in the human axillary region. PLoS One. 2013;8, e70538.

Cunliffe WJ. Looking back to the future – acne. Dermatology. 2002;204:167–72.

Dunbar J, Barns SM, Ticknor LO, et al. Empirical and theoretical bacterial diversity in four Arizona soils. Appl Environ Microbiol. 2002;68:3035–45.

Fierer N, Hamady M, Lauber CL, et al. The influence of sex, handedness, and washing on the diversity of hand surface bacteria. Proc Natl Acad Sci U S A. 2008;105:17994–9.

Gao Z, Tseng CH, Pei Z, et al. Molecular analysis of human forearm superficial skin bacterial biota. Proc Natl Acad Sci U S A. 2007;104:2927–32.

Gao Z, Tseng CH, Strober BE, et al. Substantial alterations of the cutaneous bacterial biota in psoriatic lesions. PLoS One. 2008;3, e2719.

Gomes PLR, Malavige GN, Fernando N, et al. Characteristics of Staphylococcus aureus colonization in patients with atopic dermatitis in Sri Lanka. Clin Exp Dermatol. 2011;36(2):195–200.

Grice EA, Segre JA. The skin microbiome. Nat Rev Microbiol. 2011;4:245–53.

Grice EA, Kong HH, Renaud G, et al. A diversity profile of the human skin microbiota. Genome Res. 2008;18:1043–50.

Guzik TJ, Bzowska M, Kasprowicz A, et al. Persistent skin colonization with Staphylococcus aureus in atopic dermatitis: relationship to clinical and immunological parameters. Clin Exp Allergy. 2005;35(4):448–55.

Haslund P, Bangsgaard N, Jarlov J, et al. Staphylococcus aureus and hand eczema severity. Br J Dermatol. 2009;161(4):772–7.

Higaki S, Kitagawa T, Kagoura M, et al. Correlation between Propionibacterium acnes biotypes, lipase activity and rash degree in acne patients. J Dermatol. 2000;27:519–22.

Hill SE, Yung A, Rademaker M. Prevalence of Staphylococcus aureus and antibiotic resistance in children with atopic dermatitis: a New Zealand experience. Australas J Dermatol. 2011;52:27–31.

Hon KL, Lam MC, Leung TF, et al. Clinical features associated with nasal Staphylococcus aureus colonisation in Chinese children with moderate-to-severe atopic dermatitis. Ann Acad Med Singapore. 2005;34 (10):602–5.

Isolauri E, Turjanmaa K. Combined skin prick and patch testing enhances identification of food allergy in infants with atopic dermatitis. J Allergy Clin Immunol. 1996;97:9–15.

Lindner MT, Johansson C, Scheynius A, et al. Positive atopic patch test reactions to Pityrosporum orbiculare in atopic dermatitis patients. Clin Exp Allergy. 2000;30:122–31.

Matsui K, Gilani SJ, Gonzalez M, et al. Staphylococcus aureus re-colonization in atopic dermatitis: beyond the skin. Clin Exp Dermatol. 2005;30(1):10–3.

Mikamo H, Kawazoe K, Sato Y, et al. Preterm labor and bacterial intra-amniotic infection: arachidonic acid liberation by phospholipase A2 of Prevotella bivia. Anaerobe. 1998;4:209–12.

Miyamoto T, Akiba S, Sato N, et al. Study of the vulvar skin in healthy Japanese women: components of the stratum corneum and microbes. Int J Dermatol. 2013;52:1500–5.

Mowad CM, McGinley KJ, Foglia A, et al. The role of extracellular polysaccharide substance produced by *Staphylococcus epidermidis* in miliaria. J Am Acad Dermatol. 1995;33:729–33.

Myhre AK, Bevanger LS, Berntzen K, et al. Anogenital bacteriology in non-abused preschool children: a descriptive study of the aerobic genital flora and the isolation of anogenital Gardnerella vaginalis. ACTA Paediatr. 2002;91:885–91.

Pezesk PFZ, Miri S, Ghasemi R, et al. Skin colonization with Staphylococcus aureus in patients with atopic dermatitis. Internet J Dermatol. 2007;5 (1). doi:10.5580/e93.

Rippke F, Schreiner V, Schwanitz HJ. The acidic milieu of the horny layer: new findings on the physiology and pathophysiology of skin pH. Am J Clin Dermatol. 2002;3:261–72.

Ro BI, Dawson TL. The role of sebaceous gland activity and scalp microfloral metabolism in the etiology of seborrheic dermatitis and dandruff. J Invest Dermatol Symp Proc. 2005;10:94–197.

Roth RR, James WD. Microbial ecology of the skin. Annu Rev Microbiol. 1988;42:441–64.

Salah SB, Makni F, Marrakchi S, et al. Identification of Malassezia species from Tunisian patients with pityriasis versicolor and normal subjects. Mycoses. 2005;48:242–5.

Serra E, Puig S, Otero D, et al. Confirmation of a double-hit model for the NF1 gene in benign neurofibromas. Am J Hum Genet. 1997;61:512–9.

Shiraishi T, Fukuda K, Morotomi N, et al. Influence of menstruation on the microbiota of healthy women's labia minora as analyzed using a 16S rRNA gene-based clone library method. Jpn J Infect Dis. 2011;64:76–80.

Takahata Y, Sugita T, Kato H, et al. Cutaneous Malassezia flora in atopic dermatitis differs between adults and children. Br J Dermatol. 2007;157:1178–82.

Evaluation of Skin Surface Flora

11

Xuemin Wang, Chao Yuan, and Philippe Humbert

Contents

Keywords

16S ribosomal RNA • Contact plates • Swabbing methods • Tape stripping • Detergent scrub technique • Microorganism sampling methods

1 Introduction

The microorganisms, such as bacteria, fungi, etc., on the skin have been identified mostly by culture based on the sampling methods. The composition and distribution of the microorganisms on the skin were not extensively described until culture-independent molecular methods have been used now. The main techniques in sampling the skin microorganisms include impression methods, swabbing methods, and washing methods and punch biopsy. Both swabbing and taping are simple, quick, and noninvasive. Other two methods are scraping and punch biopsy which are applied under certain situation. Scraping usually comprises significant amount of skin cells. Punch biopsy is invasive, and it can cover all layers of the skin microbiota. There are two kinds of specific sampling techniques for follicle of the skin. Each category included several techniques. For example, the impression methods included contact plates, pads, sellotape stripping, etc. The washing methods included the detergent scrub technique and the sterile bag technique. About these three different sampling techniques, such as swabbing, scraping, and punch biopsy, the

Xuemin Wang: deceased.

X. Wang
Shanghai, China

C. Yuan (✉)
Department of Skin and Cosmetic Research, Shanghai Skin Disease Hospital, Shanghai, China
e-mail: dermayuan@163.com

P. Humbert
Department of Dermatology, University Hospital of Besançon, Besançon, France
e-mail: philippe.humbert@univ-fcomte.fr

P. Humbert et.al. (eds.), *Agache's Measuring the Skin*,
DOI 10.1007/978-3-319-32383-1_11

results were shown that there was no difference of detection at all depths of the skin (Grice et al. 2008). There are special methods for follicular sampling methods. They are comedone extractor and cyanoacrylate glue.

2 Methods of Sampling

There are several sampling methods for microorganism of skin surface (Tiffany and Michael 2014). How to choose the method for applying it is depending on the numbers and types of bacteria (Grice et al. 2009).

For all surface sampling methods, adequate time must be needed after sample collection to allow the bacterial flora to reestablish before a further sample can be taken from the same site. Another way is sampling bacteria from adjacent sites or from identical sites on the right and left side.

2.1 Impression Methods

2.1.1 Contact Plates

The contact plates are specialized Petri dishes that are filled with different appropriate culture media until the agar surface is slightly concaved. The different bacteria should be under different culture conditions in suitable media. The common culture medium is fresh blood agar.

The contact plates are pressed firmly onto the skin to remove surface bacteria. One study was used to sample the medial surface of the forearm and midsternum because they are representative of the "dry" areas of the skin surface that are readily accessible and in contact with the environment (Larson et al. 2000). These are also frequent sites of intravenous (IV) catheterization (arm) or surgery (sternum). Generally the dominant arm was sampled, but in inpatients, attempts were made to avoid obtaining cultures near IV sites. When a mediastinal incision was present, the upper back was sampled rather than the sternum.

It is limited to one recovery medium. The facilitated colony counting is mainly a method to assess the results of this test. It only gives the estimation of the number of the microcolonies. The number of colonies (colony-forming units, CFU) is counted with a grid printed or glued on its base. It is not a quantitative way because there is no dispersal step to break down aggregates of cells into smaller colony-forming units.

However, these have severe limitations and should only be used if a specific organism is being sought or if low numbers of bacteria ($\leq$10 cm^2) are expected and they can all be cultured on the same medium. The method is suitable for isolating *S. aureus* from suspected infected eczema.

It is easy and quick to use on intact and broken skin. The method of contact plates can be employed for routine patient sampling. But it is not quantitative. Since these colonies are not dissociated, the density of CFUs obtained does not correspond to the density of bacteria on the skin.

2.1.2 Pads

The velvet pads are used to remove bacteria from the skin surface. The main advantage of it is that the sufficient microorganisms are removed to serially inoculate a number of different culture media. The method is very inefficient too, and only a small proportion of microorganisms are successfully transferred from the pad to the medium. Since mechanical rinsing could improve bacterial recoveries, the pads are no longer used directly to inoculate culture media. The quantitative estimate of bacterial numbers could be obtained.

2.1.3 Tape Stripping

Tape stripping is a common method for skin microbiological study since it could sample not only skin surface but also aerobic bacteria residing in the upper part of the epidermis. Mostly all areas of the skin contain numerous pilosebaceous follicles. Some microorganisms are pulled out from the upper portion of each duct so that the numbers of bacteria may not decline in subsequent strips, as they do in areas with few pilosebaceous units. The tape strips are inverted onto the surface of the culture medium. If the tape is removed, not all microorganisms are transferred to the culture media successfully. The combination of tape

stripping and contact plates is often used for skin sampling. The tape is used to remove successive sheets of epidermal cells, and the contact plates are used to remove the exposed bacteria.

2.2 Swabbing Methods

The swabbing methods included dry swabs and moist swabs. The dry swabs are associated with poor recoveries of viable organisms. The moist swabs are among the most versatile of skin sampling techniques. Normally the swab, fixed to an applicator, is soaked in phosphate buffer saline containing 2 % Tween 80 and 0.3 % lecithin or Williamson-Kligman washing fluid. A template delimiting the sampling area is put on the skin. The swab is vigorously rubbed inside the template. Then the buffer is inoculated to appropriate culture media. The number of colonies in each culture can be counted. If CFU density is too high, it makes counting impossible, and serial dilutions are done before inoculation. The sensitivity limit is 4 CFUs per template. The accurate quantitative results cannot be obtained by the swabbing methods.

There is no doubt that moist swabbing is the method of choice for skin surface sampling. It remains the most commonly used method for routine sampling of patients with diseases, infections, or wounds of the skin. It can detect the unknown pathogen of the above skin disease. They are semiquantitative. But the method can be used when few microorganisms are present or when the swabbed area can be accurately defined and the bacteria of interest are known to reside superficially. In other words, it inoculates several culture media with a single swab and thus makes it possible to detect the entire range of skin flora present, and finally bacterial counting is possible since the original colonies have been dissociated by shaking in the buffer and flora collection has been improved by the friction. Usually skin swabs could be collected both from skin lesions and non-lesional areas from patients with skin diseases (e.g., AD) and also from healthy control skin (Petry et al. 2014). Two skin swabs were taken from each patient for culture and sensitivity, one from the worst area of atopic dermatitis and the other from non-lesional skin. Also 15 skin swabs were taken from the skin of healthy children. Specific swabs for this method exist in various materials, such as polyvinyl alcohol foam, cotton, rayon, calcium alginate, etc. And they are commercially available. There are severe limitations, and for seeking the specific microorganism or the lower numbers of bacteria ($\leq$10 cm^2), they can be cultured on the same medium. They depend on the types of swab used, and the procedures are used to transfer microorganisms to the culture media. Several recovery media can be inoculated immediately, both in the clinic or laboratory. All types should be moistened by phosphate-buffered saline. The area of the sample site can be standardized by holding a template onto the skin surface. The swabs rub the studied area of skin surface firmly and repeatedly for several seconds to ensure adequate removal of microorganisms. For semiquantitative work, the swabs transfer to 1 ml of half-strength wash fluid and decimally diluted in the same. A fixed volume (usually 100 ml) of each dilution and the undiluted sample is then plated onto one or more suitable recovery media and spread with a sterile glass spreader. The correct use of swabs is the best or only possible methods of skin sampling. They are used for routine clinical or research sampling from any sites, e.g., the back, chest, forehead, shoulders, etc. The inoculum is put on the suitable medium for culture.

For research the swabbing techniques can be standardized, whether in intertriginous areas or on damaged skin whichever is interesting. It can be an identification of components of the aerobic skin flora of premature neonates.

2.3 Washing Method

2.3.1 The Detergent Scrub Technique

The detergent scrub technique is the most widely used for research purposes since this method could be standardized, quantitative, reproducible, and efficient (i.e., removes over 95 % of the aerobic bacteria present at the sample site). Several modifications and adaptations have appeared in different studies. A metal ring is held firmly

against the skin surface and the procedures are standardized, including the wash fluid, the amount, the time of rubbing, the collection of wash fluid, etc. There are several features of the scrub wash technique that are worthy of further comment. The wash fluid contains a mild detergent in order to facilitate dispersal of clumps of bacteria. Various modifications ford the survival of different skin bacteria in wash fluid with inconclusive results. It is best for individual investigators to estimate for themselves the survival time in wash fluid of those organisms of special interest to them. The sample site is chosen because the subungual space harbors large numbers of bacteria and is one of the most difficult sites to disinfect. Several recovery media can be employed.

The detergent scrub technique is more efficient in terms of number of microorganisms recovered or in reproducibility. For research purposes, and when quantitative data are required, the detergent scrub technique should be chosen. The major limitation of this technique is that it is fairly aggressive and cannot be used on sensitive or damaged skin, although several groups have used it to sample bacteria from eczema lesions. It is suitable for determining the proportion of the resident staphylococcal flora resistant to an antibiotic.

3 Follicular Sampling Methods

Until now, many researchers are still interested in the pathogenesis of pilosebaceous follicle for the living organisms. The methods that will be described below can be used to sample noninflamed lesions only and are not suitable for use with normal follicles or inflamed lesions.

3.1 Comedone Extractor

Open comedones are removed nontraumatically using a comedone extractor. It is the best method of sampling intrafollicular bacteria. Microcomedones are more common, but it is not easier than rapidly polymerizing cyanoacrylate glue. Both open comedones and microcomedones can be obtained noninvasively. This method for damaged follicles is not similar as the method for normal follicles. The standard procedure is as follows. The first step is sterilizing the skin surface with an isopropanol swab. Then the entire comedone is removed by the extractor. It is transferred by a sterile needle into a preweighed microcentrifuge. The amount of wash fluid is pipetted into the tube and the bacteria are dispersed from the comedone with the micro tissue grinder. The fluid according to the different treating procedure is then plated onto one or more selective or nonselective media as required. Bacteria can be counted and expressed as CFU per milligram wet weight of comedonal material. The detection limit is 4 CFU/comedo. However, it should be ensured that the whole of the comedone is removed from the skin because the distribution of bacteria in follicular ducts varies with depth. The density and composition of the microflora at the face could be tested. It is simple and quick procedure. It can study microflora of a single pilosebaceous unit. It can inoculate several recovery media.

3.1.1 Cyanoacrylate Glue

Rapidly polymerizing cyanoacrylate glue is used to remove thin sheets of stratum corneum. It could be quickly realized that follicular plugs are extracted from pilosebaceous follicles as the glue being pulled away from the skin surface. This method is very easy. It is not used for normal follicles. One drop of the glue is spread over an area of the skin and left to polymerize for 1 min. The second step is pressed on this glass slide over for 1 min and then the slide is slowly removed from the skin. It is then applied on top of the area of the skin and spread uniformly by inverting a glass slide over it and pressing down firmly. After several minutes, the slide is removed from the surface of the skin with the adherent sheet of both adhesive and follicular casts, which represent the contents of microcomedones and consist of a mixture of corneocytes, sebum, and microbes. The more standardized procedure uses a sterile glass sampler of known surface area instead of a slide and a sterile Teflon ring to delineate the

target area, which is extracted twice with glue. It can inoculate several recovery media.

Normal pilosebaceous follicles cannot be studied by either of these two methods, but only microdissected follicles from biopsies. It can collect the entire comedo or cyst because the flora of the follicular duct varies according to depth. It can count or analyze several samples because the flora can be very different from one follicle to another.

One commercial kit, such as Exolift®, included a patented dermal tape and cyanoacrylate glue. It is easier to use than glass slides or samplers, but is much more expensive. Whichever procedure is followed, only follicular bacteria will be enumerated since surface organisms are sequestered between the glue and the thin sheet of stratum corneum. The main problems with the use of cyanoacrylate glue are the high frequency of incomplete takes, when the glue fails to polymerize properly over part of the sample site, and the uncertainty of removing entire follicular casts. For obvious reasons, the method should not be used near the eyes.

3.1.2 Impact Factors

There are some important factors in determining the choice of sampling method, location of bacteria, type of the skin, type of bacteria, choice of sample site, efficacy of technique, reason for sampling, etc. The different growth media are suitable for recovery of resident skin bacteria and primary pathogens. For example, the *brain heart infusion* or *reinforced clostridial* agar containing 6 mg/l furazolidone is suitable for *Propionibacteria*; *heated blood* agar for *coagulase-negative staphylococci*; *mannitol* salt agar and *cysteine lactose electrolyte deficient* (*CLED*) *medium* for *S. aureus*; *fresh blood* agar containing 0.2 % w/v glucose, 0.3 % w/v yeast extract, 0.2 % v/v Tween 80, and 6 mg/l *furazolidone* for *aerobic coryneforms*; and *fresh blood* agar containing 0.0002 % crystal violet or 7.5 mg/l nalidixic acid and 17 units/ml *polymyxin B* for *group A beta-hemolytic streptococci*. Antibiotic sensitivity test can be done according to the Clinical and Laboratory Standards Institute (CLSI, 2011), using vancomycin, erythromycin, gentamicin, penicillin, ampicillin, fusidic acid, and flucloxacillin antibiotics (r1).

3.1.3 Application of New Techniques

Recently the molecular characterizations of the human surface skin microorganisms based on 16S ribosomal RNA analysis have been carried out on a large scale (Gao et al. 2007). For the fungi, such as yeast, the specific techniques of culture are used and the 18S ribosomal DNA analysis has been done. Molecular analyzing was used for some studies, not only qualitative but also quantitative. The polymerase chain reaction-restriction fragment length polymorphism method (PCR-RFLP) of *Malassezia* species, a part of the skin microflora of neonates, was applied. The results supported that neonates acquire *Malassezia* flora through direct contact with their mothers or hospital personnel (Mourelatos et al. 2007a). For quantitative analysis of *Malassezia*, the real-time polymerase chain reaction (PCR) assay could be used also (Mourelatos et al. 2007b). The dominant operational taxonomic units (OTUs) conducted often are captured by all these methods although the rare OTUs are different. Commensal bacteria play a crucial role in the development of the immune system in humans (Zomorodain et al. 2008).

The objectives of the evaluation of skin surface flora are to study the pathogenic flora carriage in patients, the effects of antibiotics and antiseptics on skin flora, the efficiency of skin disinfection methods, and the physiology of resident skin flora under different environmental conditions. So understanding the methods of evaluation, knowing its impact factors, and applying new techniques are the goals of achieving the aims.

References

Gao Z, Tseng CH, Pei Z, et al. Molecular analysis of human forearm superficial skin bacterial biota. Proc Natl Acad Sci U S A. 2007;104:2927–32.

Grice EA, Kong HH, Renaud G, et al. A diversity profile of the human skin microbiota. Genome Res. 2008;7:1043–50.

Grice EA, Kong HH, Conlan S, et al. Topographical and temporal diversity of the human skin microbiome. Science. 2009;324:1190–2.

Larson EL, Cronquist AB, Whittier S, et al. Differences in skin flora between inpatients and chronically ill outpatients. Heart Lung. 2000;29:298–305.

Mourelatos K, Eady EA, Cunliffe WJ, et al. Temporal changes in sebum excretion and propionibacterial colonization in preadolescent children with and without acne. Br J Dermatol. 2007;156:22–31.

Petry V, Lipnharski C, Bessa GR, et al. Prevalence of community-acquired methicillin-resistant Staphylococcus aureus and antibiotic resistance in patients with atopic dermatitis in Porto Alegre, Brazil. Int J Dermatol. 2014;6:731–5.

Tiffany CS, Michael AF. What lives on our skin: ecology, genomics and therapeutic opportunities of the skin microbiome. Drug Discov Today Dis Mech. 2014;9:1–10.

Zomorodain K, Mirhendi H, Tarazooie B, et al. Molecular analysis of Malassezia species isolated from hospitalized neonates. Pediatr Dermatol. 2008;3:312–6.

Measurement of Skin Surface Acidity

12

Measuring Skin pH

Razvigor Darlenski and Joachim W. Fluhr

Contents

Keywords

Skin pH • In vivo • Skin physiology • Flat glass electrode • Dye • Age • Gender

Abbreviations

β-Gluc Cer'ase	Beta glucocerebrosidase
CD	Cornedesmosome
FLIM	Fluorescence lifetime imaging
FFA	Free fatty acids
SC	Stratum corneum
sPLA2	Secretory phospholipase A2
TEWL	Transepidermal water loss

1 Core Messages

- Skin surface is characterized by acidic pH
- The acidic milieu is important for sustaining skin physiology namely epidermal barrier homeostasis, stratum corneum integrity and antimicrobial defence
- Among variety of methods for skin surface acidity investigation, the flat glass electrode remains the gold standard and most practical for in vivo measurement of cutaneous pH
- Subject-, instrument- and environment-related variables influence skin surface acidity measurements

R. Darlenski
Department of Dermatology and Venereology, Tokuda Hospital Sofia, Sofia, Bulgaria
e-mail: darlenski@gmail.com

J.W. Fluhr (✉)
Department of Dermatology, Charité – Universitätsmedizin Berlin, Berlin, Germany
e-mail: Joachim.Fluhr@charite.de

P. Humbert et al. (eds.), *Agache's Measuring the Skin*,
DOI 10.1007/978-3-319-32383-1_12

2 Introduction

The skin separates the inner part of our body against the potentially harmful environment. The skin barrier protects the human body against many external stressors namely physical stress (mechanical, thermal, UV radiation e.g.,), chemical stress (tensides, prolonged water exposure, solvents e.g.,) and environmental conditions (Elias and Choi 2005). The concept of acid mantle of the skin was introduced more than 80 years ago by Schade and Marchionini (1928). Today there is a growing body of evidence that the acidic nature of the outermost skin layers is a key factor in regulating epidermal barrier homeostasis, stratum corneum (SC) integrity and cohesion, as well as antimicrobial defence (Schade and Marchionini 1928; Fluhr et al. 2010; Fluhr and Elias 2002).

The striving for quantification and qualification dates since the ancient societies. Nowadays a demand for standardizing and unifying evaluation procedures in biomedical research is widely accepted. Different non-invasive methods for the in vivo investigation of the skin surface acidity have been developed in the past decades (Darlenski et al. 2009). Here we summarize the different measurement techniques for skin pH and we discuss the potential factors that influence pH measurements.

3 Role of Skin Surface Acidity for Epidermal Functions

The acidic pH of SC is essential for the formation of intact skin barrier. Although basal permeability barrier function is competent at birth (Behne et al. 2002), skin surface pH is neutral at birth both in humans and in various animal models (Fluhr et al. 2004a; Hardman et al. 1998; Visscher et al. 2000). Following acute barrier disruption by either tape stripping or acetone treatment, barrier recovery was markedly delayed in the newborn rats (Fluhr et al. 2004a). Further animal studies excluded a variety of exogenous and endogenous mechanisms previously thought to be implicated in post-natal SC acidification (Fluhr et al. 2004b). The results proved the central role for two endogenous mechanisms, the secretory phosholipase A2 pathway and sodium-proton exchanger, in the generation of the postnatal acid mantle. The functional consequences of neutral pH of SC included abnormal permeability homeostasis and defects in SC integrity, attributed respectively to the reduced beta glucocerebrosidase (β-Gluc Cer'ase) and increased serine proteases activity directly after birth (Fluhr et al. 2004a). Exogenous acidification of SC normalized barrier recovery kinetics and improved SC integrity (Fluhr et al. 2004a).

SC acidity is essential for the epidermal barrier recovery, the latter being delayed at a neutral pH, due to disturbance in processing secreted extracellular SC lipids, while lipid secretion remains unimpaired (Mauro et al. 1998). The impairment of the barrier homeostasis was attributed to the acidic pH optima of the key lipid-processing enzymes, i.e., β-Gluc-Cer'ase and acidic sphingomyelinase. Rising of the pH resulted in perturbations of lipid processing and in an impairment of the barrier homeostasis. Later it was shown that prolonged increase of pH leads to degradation of these enzymes by sustained serine proteases activity (Hachem et al. 2005). It was further demonstrated that prolonged increase of pH not only delays barrier recovery, but also increases basal transepidermal water loss (TEWL) (Hachem et al. 2005). It has been proposed that an acidic pH directly impacts lipid-lipid interactions in the SC extracellular lamellar bilayers (Bouwstra et al. 1999).

The acidity of the skin surface is also involved in the regulation of the corneocyte desquamation, respectively SC integrity and cohesion. The main enzymes, regulating the integrity/cohesion, kallikrein 5 (previously known as SC trypsin-like enzyme, SCTE) and kallikrein 7 (previously known as SC chymotrypsin-like enzyme, SCCE) exhibit normal-to-alkaline pH optima (Komatsu et al. 2005; Egelrud 2000). A superbase-induced elevation in SC pH resulted in reversible increase of the activity of these enzymes (Hachem et al. 2003). Moreover, these changes are followed by degradation of desmoglein 1 and reduction of the corneodesmosome-density, thus stimulating the process of desquamation (Hachem et al. 2003).

Acidification of skin surface results in improved lipid processing and inhibition of the degradation of corneodesmosomes (Hachem et al. 2010)

The acidic buffer system of the skin is essential for performing an unspecific antimicrobial protection as well as the regulation of the innate immunity (Drake et al. 2008). Elevation of the pH values is beneficial for growing pathogens on the skin surface, such as *Staphylococcus aureus* and *Candida albicans*, while normal flora predominantly grow best at acidic environment (Korting et al. 1990; Schmid-Wendtner and Korting 2006). The absence of an acidic SC at birth has been associated with an increased risk of bacterial and yeast infections in neonates (Leyden and Kligman 1978). The clinical importance of these findings is reflected in the pathophysiology of diaper dermatitis. The incomplete acidification of the SC, together with the ammonia-induced alkalization activates stool enzymes (trypsin, lipase), causing irritation and further perturbation of the skin barrier. Additional data on the role of skin surface acidity for antimicrobial protection can be found in the chapter on skin surface acidity of this book.

4 Measuring Methods

A variety of measuring methods for investigating skin surface acidity exist. The pioneering studies were performed by gas chain bell electrode (Schade and Marchionini 1928). Nowadays the most widely used devices are based on flat glass electrode (Fig. 1).

4.1 Flat Glass Electrode

Different companies have developed planar electrodes specialized for skin measurement. Any commercialized pH meter device fitted with a planar electrode can be used for the measurement of skin surface pH (Ehlers et al. 2001a). The contact site between the electrode and the skin covers an area of approximately 10 mm in diameter, and its use is considered as non-invasive. The flat glass

Fig. 1 Measurement of skin surface pH with flat glass electrode device Skin-pH-meter PH 905 (Courage and Khazaka electronic GmbH, Germany)

electrode measurements are widely used and considered as simple, non-cumbersome, and reproducible (Darlenski et al. 2009). The following practical consideration should be taken into account when performing the measurement:

- The electrode face (membrane) should not be brought into contact with hard objects. During short intervals between measurements, the electrode (or rather the electrode face) is best immersed in a KCl solution or in distilled water.
- Any kind of contamination of the electrode (e.g., by lipids or proteins) should be avoided or eliminated.
- Regular devise calibration is advised.
- Before application to the skin, the electrode must be dipped into distilled water to moisten the surface. Then, the flat electrode top is placed on the skin with slight pressure during the measurement.
- Excessive pressure on the probe should be avoided.
- Ambient temperature and sweating may affect the pH measurements. It is desirable to perform

measurements under controlled conditions (e.g., 20–22 °C) and the relative humidity between 40 % and 60 %.
- Volunteers should be relaxed and acclimatized to the measuring environment for 15–20 min.
- No cosmetic residue or excessive sebum should be left on the surface of the skin. In both cases, gentle dry wiping is advised for the removal. Cleaning must be avoided as it will greatly affect pH measurements (even pure water).
- A minimum period of 3–6 h should be awaited between the personal hygiene procedures of the subject and the measurements.

4.2 pH-sensitive Dyes

Certain dyes have a color that changes according to pH, e.g., bromthymol blue and carboxy-SNARF-1 marking (Wagner et al. 2003). Limitation include that pH spectra of some dyes are not adjusted to the acidic nature of SC as well as potential in vivo toxicity. Values obtained by flat glass electrode assessment were concordant with the ones estimated by fluorescent dye marking (Wagner et al. 2003).

4.3 Experimental Methods

Two-photon fluorescence lifetime imaging (FLIM) assess SC acidity by using fluorophore 2′,7′-bis-(2-carboxyethyl)-5-(and- 6)-carboxyfluorescein with a pH-dependent lifetime in the range of the expected values within SC (Hanson et al. 2002). It was shown that SC pH increases with depth. The authors hypothesized that the acid mantle results from the presence of aqueous acidic pockets within the lipid-rich extracellular matrix of SC (Hanson et al. 2002).

In vivo Raman confocal microscopy offers the possibility to measure quantitatively constituents within the depth of SC (Fluhr et al. 2010, 2012; Darlenski et al. 2009). Early studies showed that this method can detect urocanic acid isomers within the epidermis (Caspers et al. 2001). As discussed in detail in former chapters of this book, the histidine-to-urocanic acid pathway is one of the endogenous mechanisms for skin surface acidification. Lactic acid can be monitored by Raman spectroscopy in vivo and certain differences between newborns and adults exist in the profile of lactate (Fluhr et al. 2012). A pseudo-pH measurement is possible with in-vivo Raman microsprectroscopy.

5 Variables Influencing the Measurement

A wide number of variables influence the skin pH measurement and should be taken into account e.g., anatomical site, age, gender, race and circadian rhythms (Fluhr and Elias 2002; Darlenski et al. 2009; Darlenski and Fluhr 2012).

5.1 Age

Skin surface pH changes over age with the neonatal period being the most dynamic. We have shown that even in full-term neonates surface pH is around 6.5 and decreases within the first days after birth (Fluhr et al. 2012). This is in accordance with other publications (Schmid-Wendtner and Korting 2006; Ali and Yosipovitch 2013; Yosipovitch et al. 1998). A schematic overview on skin surface acidity differences within selected age groups (infants vs. adults) is presented in Fig. 2 (adapted from (Fluhr et al. 2012)). Acidification progresses throughout the first months, independently from the baby's birth weight. Being stable throughout the greater period of the lifespan, in elderly an increase in skin surface pH is observed. Subjects over 80 years of age have half a unit higher SC pH on both, the forehead and the cheek, than in younger adults (Zlotogorski 1987). A positive

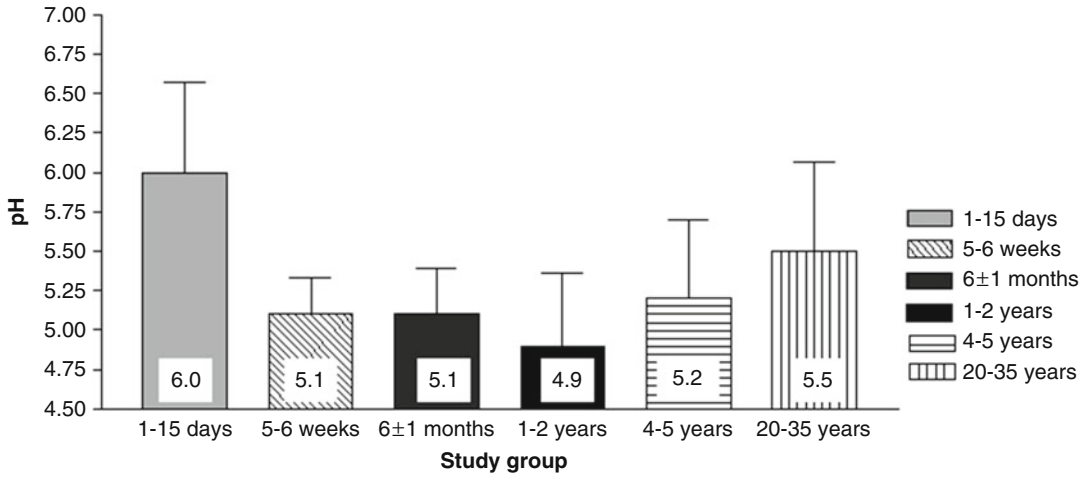

Fig. 2 Skin surface acidity in different age groups

correlation between age and pH was reported by other groups (i.e., higher pH at older age) (Thune et al. 1988).

5.2 Gender

No gender differences were noticed at the forehead and the cheek in a controlled study (Zlotogorski 1987). Other groups found higher values on the volar forearm of females (Yosipovitch et al. 1993a, b; Ehlers et al. 2001b). It is tempting to hypothesize that pH is under sex hormone regulation.

5.3 Race

Data on racial variances in skin surface acidity is controversial. The majority of studies show lower pH values in darker skin subjects at least in the upper parts of the SC (Berardesca et al. 1998; Gunathilake et al. 2009). Lower pH was associated with enhanced epidermal barrier function and higher SC integrity, linked to increased lamellar body density and epidermal lipid content (Gunathilake et al. 2009).

5.4 Circadian Rhythm

Diurnal variation in skin surface pH has been documented. Yosipovitch et al. reported SC pH maxima between 2.00 and 4.00 p.m. (Yosipovitch et al. 1998). Lowest pH values were witnessed around 4.00 a.m. with a plateau during daytime (Le Fur et al. 2001). A control under glucocorticoid hormones can be assumed.

5.5 Anatomical Site

Higher pH values at the intertriginous areas (axillae and inguinal region) were noted in 1938 and named "physiological gaps" in the acid mantle (Marchionini and Hausknecht 1938). Since then a lot of studies were performed on the anatomical variations in skin surface acidity. We have recently published a full body mapping of skin surface pH (Fig. 3) (Kleesz et al. 2012). No difference between the left and right arm was detected (Ehlers et al. 2001a; Treffel et al. 1994).

The role of other external factors such as skin cleansing, application of cosmetics and

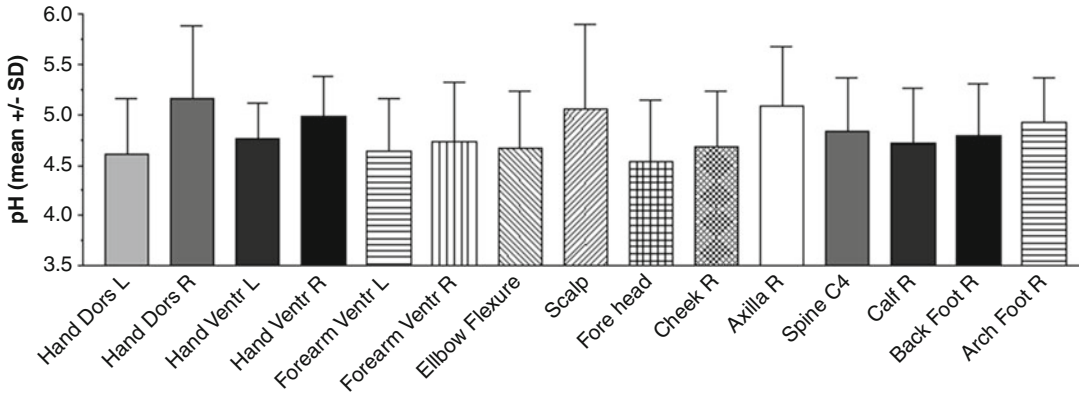

Fig. 3 Anatomical site variations in healthy adults. Abbreviations: *R* right, *L* left, *C4* region corresponding to the fourth cervical spine

concomitant skin disease has been discussed in detail in the chapter, devoted on skin surface acidity formation, of this book.

6 Conclusion

Measuring skin surface pH is possible in vivo by non-invasive and reproducible methods. Different variables influence pH values and should be taken into consideration prior to initiating skin physiology studies. Novel techniques such as Raman confocal microscopy should be challenged in a multicenter way in order to be introduced routinely in practice.

References

Ali SM, Yosipovitch G. Skin ph: from basic science to basic skin care. Acta Derm Venereol. 2013. doi:10.2340/00015555-00011531. epub ahead of print.

Behne MJ, Meyer JW, Hanson KM, Barry NP, Murata S, Crumrine D, Clegg RW, Gratton E, Holleran WM, Elias PM, Mauro TM. Nhe1 regulates the stratum corneum permeability barrier homeostasis. Microenvironment acidification assessed with fluorescence lifetime imaging. J Biol Chem. 2002;277:47399–406.

Berardesca E, Pirot F, Singh M, Maibach H. Differences in stratum corneum ph gradient when comparing white caucasian and black african-american skin. Br J Dermatol. 1998;139:855–7.

Bouwstra JA, Gooris GS, Dubbelaar FE, Ponec M. Cholesterol sulfate and calcium affect stratum corneum lipid organization over a wide temperature range. J Lipid Res. 1999;40:2303–12.

Caspers PJ, Lucassen GW, Carter EA, Bruining HA, Puppels GJ. In vivo confocal raman microspectroscopy of the skin: noninvasive determination of molecular concentration profiles. J Invest Dermatol. 2001;116:434–42.

Darlenski R, Fluhr JW. Influence of skin type, race, sex, and anatomic location on epidermal barrier function. Clin Dermatol. 2012;30:269–73.

Darlenski R, Sassning S, Tsankov N, Fluhr JW. Non-invasive in vivo methods for investigation of the skin barrier physical properties. Eur J Pharm Biopharm. 2009;72:295–303.

Drake DR, Brogden KA, Dawson DV, Wertz PW. Thematic review series: skin lipids. Antimicrobial lipids at the skin surface. J Lipid Res. 2008;49:4–11.

Egelrud T. Desquamation in the stratum corneum. Acta Derm Venereol Suppl (Stockh). 2000;208:44–5.

Ehlers C, Ivens UI, Moller ML, Senderovitz T, Serup J. Comparison of two ph meters used for skin surface ph measurement: the ph meter 'ph900' from courage & khazaka versus the ph meter '1140' from mettler toledo. Skin Res Technol. 2001a;7:84–9.

Ehlers C, Ivens UI, Moller ML, Senderovitz T, Serup J. Females have lower skin surface ph than men. A study on the surface of gender, forearm site variation,

right/left difference and time of the day on the skin surface ph. Skin Res Technol. 2001b;7:90–4.
Elias PM, Choi EH. Interactions among stratum corneum defensive functions. Exp Dermatol. 2005;14:719–26.
Fluhr JW, Elias PM. Stratum corneum ph: formation and function of the 'acid mantle'. Exog Dermatol. 2002;1:163–75.
Fluhr JW, Mao-Qiang M, Brown BE, Hachem JP, Moskowitz DG, Demerjian M, Haftek M, Serre G, Crumrine D, Mauro TM, Elias PM, Feingold KR. Functional consequences of a neutral ph in neonatal rat stratum corneum. J Invest Dermatol. 2004a;123:140–51.
Fluhr JW, Behne MJ, Brown BE, Moskowitz DG, Selden C, Mao-Qiang M, Mauro TM, Elias PM, Feingold KR. Stratum corneum acidification in neonatal skin: secretory phospholipase a2 and the sodium/hydrogen antiporter-1 acidify neonatal rat stratum corneum. J Invest Dermatol. 2004b;122:320–9.
Fluhr JW, Darlenski R, Taieb A, Hachem JP, Baudouin C, Msika P, De Belilovsky C, Berardesca E. Functional skin adaptation in infancy – almost complete but not fully competent. Exp Dermatol. 2010;19:483–92.
Fluhr JW, Darlenski R, Lachmann N, Baudouin C, Msika P, De Belilovsky C, Hachem JP. Infant epidermal skin physiology: adaptation after birth. Br J Dermatol. 2012;166:483–90.
Gunathilake R, Schurer NY, Shoo BA, Celli A, Hachem JP, Crumrine D, Sirimanna G, Feingold KR, Mauro TM, Elias PM. Ph-regulated mechanisms account for pigment-type differences in epidermal barrier function. J Invest Dermatol. 2009;129:1719–29.
Hachem JP, Crumrine D, Fluhr J, Brown BE, Feingold KR, Elias PM. Ph directly regulates epidermal permeability barrier homeostasis, and stratum corneum integrity/cohesion. J Invest Dermatol. 2003;121:345–53.
Hachem JP, Man MQ, Crumrine D, Uchida Y, Brown BE, Rogiers V, Roseeuw D, Feingold KR, Elias PM. Sustained serine proteases activity by prolonged increase in ph leads to degradation of lipid processing enzymes and profound alterations of barrier function and stratum corneum integrity. J Invest Dermatol. 2005;125:510–20.
Hachem JP, Roelandt T, Schurer N, Pu X, Fluhr J, Giddelo C, Man MQ, Crumrine D, Roseeuw D, Feingold KR, Mauro T, Elias PM. Acute acidification of stratum corneum membrane domains using polyhydroxyl acids improves lipid processing and inhibits degradation of corneodesmosomes. J Invest Dermatol. 2010;130:500–10.
Hanson KM, Behne MJ, Barry NP, Mauro TM, Gratton E, Clegg RM. Two-photon fluorescence lifetime imaging of the skin stratum corneum ph gradient. Biophys J. 2002;83:1682–90.
Hardman MJ, Sisi P, Banbury DN, Byrne C. Patterned acquisition of skin barrier function during development. Development. 1998;125:1541–52.
Kleesz P, Darlenski R, Fluhr JW. Full-body skin mapping for six biophysical parameters: baseline values at 16 anatomical sites in 125 human subjects. Skin Pharmacol Physiol. 2012;25:25–33.
Komatsu N, Saijoh K, Sidiropoulos M, Tsai B, Levesque MA, Elliott MB, Takehara K, Diamandis EP. Quantification of human tissue kallikreins in the stratum corneum: dependence on age and gender. J Invest Dermatol. 2005;125:1182–9.
Korting HC, Hubner K, Greiner K, Hamm G, Braun-Falco O. Differences in the skin surface ph and bacterial microflora due to the long-term application of synthetic detergent preparations of ph 5.5 and ph 7.0. Results of a crossover trial in healthy volunteers. Acta Derm Venereol. 1990;70:429–31.
Le Fur I, Reinberg A, Lopez S, Morizot F, Mechkouri M, Tschachler E. Analysis of circadian and ultradian rhythms of skin surface properties of face and forearm of healthy women. J Invest Dermatol. 2001;117:718–24.
Leyden JJ, Kligman AM. The role of microorganisms in diaper dermatitis. Arch Dermatol. 1978;114:56–9.
Marchionini A, Hausknecht W. Säuremantel der haut and bakterienabwehr. Klin Wochenschr. 1938;17:663–6.
Mauro T, Holleran WM, Grayson S, Gao WN, Man MQ, Kriehuber E, Behne M, Feingold KR, Elias PM. Barrier recovery is impeded at neutral ph, independent of ionic effects: implications for extracellular lipid processing. Arch Dermatol Res. 1998;290:215–22.
Schade H, Marchionini A. Der säuremantel der haut (nach gaskettenmessung). Klin Wochenschr. 1928;7:12–4.
Schmid-Wendtner MH, Korting HC. The ph of the skin surface and its impact on the barrier function. Skin Pharmacol Physiol. 2006;19:296–302.
Thune P, Nilsen T, Hanstad IK, Gustavsen T, Lovig Dahl H. The water barrier function of the skin in relation to the water content of stratum corneum, ph and skin lipids. The effect of alkaline soap and syndet on dry skin in elderly, non-atopic patients. Acta Derm Venereol. 1988;68:277–83.
Treffel P, Panisset F, Faivre B, Agache P. Hydration, transepidermal water loss, ph and skin surface parameters: correlations and variations between dominant and non-dominant forearms. Br J Dermatol. 1994;130:325–8.
Visscher MO, Chatterjee R, Munson KA, Pickens WL, Hoath SB. Changes in diapered and nondiapered infant skin over the first month of life. Pediatr Dermatol. 2000;17:45–51.
Wagner H, Kostka KH, Lehr CM, Schaefer UF. Ph profiles in human skin: influence of two in vitro test systems for

drug delivery testing. Eur J Pharm Biopharm. 2003;55:57–65.

Yosipovitch G, Tur E, Cohen O, Rusecki Y. Skin surface ph in intertriginous areas in niddm patients. Possible correlation to candidal intertrigo. Diabetes Care. 1993a;16:560–3.

Yosipovitch G, Tur E, Morduchowicz G, Boner G. Skin surface ph, moisture, and pruritus in haemodialysis patients. Nephrol Dial Transplant. 1993b;8:1129–32.

Yosipovitch G, Xiong GL, Haus E, Sackett-Lundeen L, Ashkenazi I, Maibach HI. Time-dependent variations of the skin barrier function in humans: transepidermal water loss, stratum corneum hydration, skin surface ph, and skin temperature. J Invest Dermatol. 1998;110:20–3.

Zlotogorski A. Distribution of skin surface ph on the forehead and cheek of adults. Arch Dermatol Res. 1987;279:398–401.

Sebaceous Physiology

13

Alireza Firooz, Hamed Zartab, and Ali Rajabi-Estarabadi

Contents

Keywords

Sebocyte • Sebum • Sebaceous • Receptors • Hormones • Wax ester • Squalene • Fatty acid

1 Sebaceous Glands and Sebocytes

The sebaceous gland is a holocrine system made of multiacini. Palms and soles are the only parts of the skin which do not have sebaceous glands. Sebaceous gland development is related to epidermis and hair follicles (Benfenati and Brillanti 1939; Montagna 1974; Thody and Shuster 1989; Deplewski and Rosenfield 2000).

2 Embryology

By week 13–15 of fetal development, it is possible to distinguish a gland arising from a hair follicle in a cephalocaudal direction. At 17 weeks, the gland has started making lipids and lipid droplets can be seen in the center of the gland (Fujita et al. 1972; Sato et al. 1977). The acini of the gland will attach to the common excretory duct; this duct begins as a cord composed of sebum-containing cells which will eventually rupture, forming the first pilosebaceous canal. The new acini will then

A. Firooz (✉) • A. Rajabi-Estarabadi
Center for Research and Training in Skin Diseases and Leprosy, Tehran University of Medical Sciences, Tehran, Iran
e-mail: firozali@sina.tums.ac.ir; dralirajabi@yahoo.com

H. Zartab
Center for Research and Training in Skin Diseases and Leprosy, Tehran University of Medical Sciences, Tehran, Iran

Tissue Engineering and Wound Healing Lab, Department of Surgery, Division of Plastic Surgery, Brigham and Women's Hospital – Harvard Medical School, Boston, USA
e-mail: hzartabmd@yahoo.com; hzartab@partners.org; hzartabmd@gmail.com

P. Humbert et al. (eds.), *Agache's Measuring the Skin*,
DOI 10.1007/978-3-319-32383-1_13

originate from the peripheral parts of the canal (Tosti 1974). Not all the acini in a unit are in the same stage of differentiation (Serri and Huber 1963).

3 Histology

In sebaceous glands, the most external layer is the basal layer and includes mitotically active small, flattened, or cuboidal cells comprising about 40 % of the gland. This layer is called the peripheral zone. The next layer is the maturation zone which also comprises about 40 % of the gland. Here, cells are larger and contain lipid droplets. Toward the center, there is the necrosis zone which comprises about 20 % of the gland. Its cells have stopped dividing and there is lipid accumulation; cells lose their subcellular structures, and when they reach to the duct, they are at their terminal differentiation so they rupture and release their content into the duct. The mechanism of lysis and rupture may include release of lysosomal enzymes. Desmosomes and tight junctions attach sebocytes to their surroundings. It takes about 21–25 days for sebocytes to renew (transit time) (Plewig and Christophers 1974). This transit time for the sebum which is in the canal is 14 h (Downing and Strauss 1982). The gland is surrounded by trabeculae of collagen-rich connective tissue. Those glands that are not associated with hair follicles are called free sebaceous glands. They include Meibomian (eyelids), Montgomery's (nipples), Tyson's (genitals), and ceruminous (ears) glands and Fordyce spots (oral epithelia) which secrete their contents directly to skin surface. Most of the sebaceous glands in humans are associated with hair follicles (Schneider and Paus 2010).

The most common ways of identifying sebocytes are using lipophilic dyes Oil Red O, Sudan IV, and Nile Red and also using immunostaining against lipid-associated proteins such as perilipin and adipophilin. They can also be detected using staining for fatty acid synthase, keratin 7, or other markers (Schneider and Paus 2010).

4 Physiology

A few hours after birth, sebum secretion increases and reaches a peak during the first week (Agache et al. 1980; Henderson et al. 2000). In humans, sebum is a major component of the vernix caseosa. In fetal and neonatal periods, sebum development is regulated by various factors including maternal androgens, steroid synthesis, growth factors, cell adhesion molecules, extracellular matrix proteins, intracellular signaling molecules, other hormones, cytokines, enzymes, and retinoids (Deplewski and Rosenfield 2000; Niemann et al. 2003). There is a correlation between maternal and neonatal sebum excretion rates which will be lost in the following weeks after the birth. The sebum level per unit of skin is in the same range as adults and the sequence of sebaceous transformation is identical to postnatal life. It seems that maternal hormones play an important role on glands. Androgens stimulate sebum secretion before birth (Agache et al. 1980; Henderson et al. 2000). After a slow reduction in the rate of sebum excretion, another increase happens with adrenarche (about the age of 9 years) and continues until the age of 17 years when it reaches adult range (Pochi et al. 1977). Contrary to the cycling growth of hair follicles, sebaceous gland growth is continuous. But in mice it has been shown that there are functional fluctuations such as changes in sebocyte apoptosis and also changes in the volume of sebaceous glands. These fluctuations are dependent upon hair cycle (Lindner et al. 1997).

The number of glands remains approximately constant throughout life, though their size increases as one ages (Fenske and Lober 1986; Zouboulis and Boschnakow 2001). The quality of glands is the same in normal adults and prepubertal and hypogonadal males, but the glands are bigger in normal adults (Serri and Huber 1963). It takes more than a week for sebocytes to synthesize and secrete sebum. As one gets older, sebaceous gland turnover will be slower (Plewig and Kligman 1978). Therefore, facial sebaceous glands undergo hyperplasia in older ages. There are some cofactors for sebaceous gland

hyperplasia such as immune suppression, ultraviolet radiation, and overexpression of aging-associated gene Smad7 and parathormone-related protein. On the other hand, c-Myc overexpression is associated with enhancement in sebum production. There are also differences between males and females in terms of their circulating levels of GH, IGF-1, 17β-estradiol, progesterone, DHEA, and testosterone (Makrantonaki et al. 2006; Zouboulis and Makrantonaki 2006). In women, sebum level tends to decrease after menopause. In males, no significant change occurs until the eighth decade (Zouboulis and Boschnakow 2001).

Sebocytes are components of sebaceous glands which synthesize and store lipid (Hong et al. 2008). Two of the signals for sebocyte development are β-catenin and lymphoid enhancer factor-1 (Lef-1). Stem cell progeny chooses the lineage according to the level of β-catenin (Niemann et al. 2003; Takda et al. 2006). Low levels stimulate epidermis and sebaceous gland formation, while high levels make the stem cell go toward making hair follicles. There are intracellular signaling molecules which control lineage differentiation. Examples of these molecules are transcription factor 3 (Tcf3), Lef-1, Indian hedgehog (IHH), and sonic hedgehog (SHH). SHH is needed for terminal hair lineage differentiation (Fuchs et al. 2001; Merrill et al. 2001; Nicolaides 1974; Niemann et al. 2002). IHH along with other molecules is involved in the development of sebocytes (Allen et al. 2003).

Sebaceous glands have different functions; they produce sebum, regulate cutaneous steroid synthesis and local androgen synthesis, interact with neuropeptides, synthesize certain lipids having antimicrobial effects, and have anti-inflammatory and pro-inflammatory effects (Zouboulis et al. 2002, 2003; Zouboulis 2000, 2001; Fritsch et al. 2001; Thiboutot et al. 2003; Wille and Kidonieus 2003a; Böhm et al. 2002). In humans, sebum contributes to maintain a functional epidermal barrier. Other exact roles of sebum in humans (such as protection against UV-B radiation and being a source of antioxidants especially vitamin E, anti- and pro-inflammatory substances, and antimicrobial peptides and pheromones) remain to be completely understood (Proksch et al. 2008; Zouboulis et al. 2008; Smith and Thiboutot 2008). There is some evidence suggesting that dietary factors may alter the output of sebocytes. Increased amount of fat or carbohydrate in the diet may increase sebum production, while decreased caloric intake might have the reverse effect. Variations in carbohydrates might also affect sebum composition (Llewellyn 1967; MacDonald 1964, 1967; Downing et al. 1972; Pochi et al. 1970).

5 Sebocytes Versus Adipocytes

The similarities of these two cells are as follows: large amounts of lipid accumulation, similar types of receptors, and partially similar enzymes involved in lipid production (Smith and Thiboutot 2008). The differences are as follows: lipid production, composition, and secretion differ in them. Besides, their origins are different: hair follicle keratinocytes for sebocytes and mesenchymal cells for adipocytes (Schneider and Paus 2010; Schneider et al. 2009).

6 What Is Sebum?

In mammals, sebaceous glands produce a mixture of relatively nonpolar lipids. It acts as a heat insulation layer and also a hydrophobic protection against overwetting. In many mammals sebaceous glands produce and deliver pheromones. In furry mammals it is also used for thermoregulation. It has different ingredients and functions in different species (Montagna 1974; Nikkari 1974; Pochi 1982; Wheatley 1956; Thody and Shuster 1989). For instance, sebaceous gland secretions of hamster skin lack squalene and wax esters found in human skin sebum (Ito et al. 1998). Sebum density at 4 °C (gcm^{-3}) is 0.90 ± 0.01 and its freezing point is between 15 °C and 17 °C (Burton 1970). Melting point of free fatty acids and triglycerides is between 20 °C and 30 °C (Dünner 1946). Sebum surface tension ($mN\ m^{-1}$ or dyne/cm) is 24.9 ± 2.6 between 26.5 and 31.0 °C. The sebum

viscosity 0 (*poise*) is 0.552 at 38 °C and 0.664 at 36 °C (Butcher and Coonin 1949) and about 0.5 at 30 °C (at about 30 °C some components become viscous and the sebum viscosity increases irregularly) (Burton 1970).

Human sebum is a mixture of sebaceous lipids and cell debris. It is made of wax esters (made from fatty acids and fatty alcohols), glycerides, squalene (an intermediate in cholesterol synthesis made through fusion of two molecules of farnesyl pyrophosphate by squalene synthase), cholesterol, cholesterol esters, and free fatty acids (Pappas et al. 2002). Their contribution to human sebum is as follows: triglycerides, diglycerides, and free fatty acids 57 %, wax esters 26–30 %, squalene 12–20 %, cholesterol esters 3–6 %, and cholesterol 1.5–2.5 %. This differs significantly from epidermal lipid components which are as follows: glycerides 30–35 %, free fatty acids 8–16 %, wax esters and squalene 0 %, cholesterol esters 15–20 %, and cholesterol 20–25 % (Schneider and Paus 2010; Smith and Thiboutot 2008; Picardo et al. 2009).

Squalene and some of the fatty acids are solely made by sebaceous glands (Pappas et al. 2002). In the human body, squalene and wax esters are only found in sebocytes (Schneider and Paus 2010). In vitro synthesis of squalene, wax esters, and cholesterol esters is less than their in vivo synthesis. However, this can be enhanced by using arachidonic acid (AA) and linoleic acid (LA) (Sanders et al. 1994; Zouboulis et al. 1998). Squalene may be a marker of sebocytes' terminal differentiation (Zouboulis et al. 1998). The squalene is a linear intermediate in the cholesterol synthesis pathway. It is not converted into lanosterol and this stops the completion of cholesterol synthesis and leads to accumulation of squalene; the reasons which might explain this are not crystal clear; however the possibilities may be overexpression or increased activity of the enzyme squalene synthase or decreased level or activity of other enzymes in the cholesterol synthesis pathway (Smith and Thiboutot 2008).

β-Oxidation of LA is a sebocyte-specific process and is related to the level of sebocyte differentiation (Pappas et al. 2002). Branched-chain fatty acids and lipids which are desaturated in a particular way are unique characteristics of sebum. The enzyme which catalyzes the sebocyte-specific desaturation is called Δ6 desaturase (fatty acid desaturase-2). This enzyme is mainly found in sebocytes which are differentiated. These cells are found in the suprabasal layers of sebaceous glands. Therefore, this enzyme can be regarded as a functional marker for activity and differentiation of sebocytes (Ge et al. 2003).

Palmitoleic (sapienic) and sebaleic acids are predominant fatty acids and are unique in humans (Nicolaides 1974; Pappas et al. 2002; Ge et al. 2003; Stewart et al. 1986a). Δ6 desaturase converts palmitic acid (16:0) to sapienic acid (16:1, Δ6). Sapienic acid represents about 25 % of total fatty acids. Sapienic acid can be further elongated by a 2-carbon unit and its further unsaturation produces sebaleic acid (18:0, Δ5,8). The ratio between Δ6 and Δ9 unsaturated fatty acids is suggested as an index for sebocyte maturation and their associated metabolic processes (Ge et al. 2003; Zheng et al. 1999). Palmitoleic acid has antibacterial activity against gram-positive bacteria like *P. acnes* (Wille and Kidonieus 2003b). Animal studies have suggested a new role for the sebocytes associated with the ability to secrete antibacterial proteins and sterol regulation (Nagai et al. 2005).

Sebum is abundant on the head, face, neck, shoulders, back, and anterior thorax except breasts. Around female nipples there are large sebaceous glands. On external genitalia, the amount of sebum is less and other areas have very few sebum. Palms and soles do not have any sebum (Emanuel 1938). Sebum lipid composition changes with age or the activity of the glands (Nikkari 1974; Ramasastry et al. 1970; Stewart and Downing 1985; Jacobson et al. 1985). There are differences in proliferation of sebaceous glands in different locations regarding their response to androgens, and this is due to their different sensitivities to androgen effects (Akamatsu et al. 1992).

The amount of surface sebum is expressed as casual level (CL) which is the amount of sebum

per unit of skin surface area (Agache 2004; Kim et al. 2006). Skin is classified into three different skin types in terms of individuals' subjective feelings being oily, normal, and dry. However, it has been proposed that people usually regard their skins drier than what is objectively measured on their facial skin. Therefore, simple subjective classification of skin type is not a useful method of classification (Youn et al. 2002). The maximum amount of CL is on the forehead (having usual values between 100 and 200 μg/cm^2 in adults with normal sebum secretion) and on the scalp. Hyposeborrhea is defined as CL less than 50 μg/cm^2 and hyperseborrhea is CL of more than 500 μg/cm^2 which is due to both more sebum production and higher density of sebaceous glands (Greene et al. 1970; Pierard 1987).

CL shows daily fluctuations: at night, there is a 6–7 % reduction which returns to the previous level in the morning (Mavon 1997). There are also seasonal fluctuations with about 30 % higher CLs at the beginning of the summer compared to autumn (Constans et al. 1985). This is not due to the increase in the number of secreting sebaceous glands (Piérard-Franchimont et al. 1990). Temperature also affects CL: at an external temperature of 40 °C, the sebum is very fluid and the CL and re-fatting rates are high, while at 10 °C, the sebum is solid and the CL is very low (Dünner 1946). Most of the sebum will probably undergo cutaneous absorption, with part of its components (especially squalene) being used by keratinocytes (Blanc et al. 1989).

7 Immortalized Sebocyte Lineages

SZ95 sebocytes are human sebaceous gland cell lines used for research involving the sebaceous gland. They are immortalized cell lines of sebocytes which can be cloned and have major characteristics of normal human sebocytes and can subsequently undergo apoptosis (Wróbel et al. 2003; Zouboulis 1992; Zouboulis et al. 1991, 1999). CCAAT/enhancer-binding protein transcription factors, galectin-12, resistin, and sterol regulatory element-binding protein 1 (SREBP1) are lipogenic factors which have been found in SZ95 sebocytes (Harrison et al. 2007). Another lineage of immortalized sebocytes is called SEB-1. They also have characteristic proteins of human sebaceous glands. Their cytoplasm can induce Oil Red O-positive lipid droplets (Thiboutot et al. 2003). E6E7 is another immortalized sebocyte lineage. Like the SZ95 lineage, E6E7 expresses k7 and involucrin and they respond to chemicals in a similar way (Lo Celso et al. 2008).

8 Sebocyte Receptors

Peptide hormones and neurotransmitter receptors are CRH receptors 1 and 2, melanocortin 1 (regulates inflammation) and 5 (marker of differentiation) receptors, μ-opiate receptors (bind β-endorphin and stimulate lipogenesis), VPAC receptors (bind vasoactive intestinal peptide), neuropeptide Y (NY) receptors (cytokine synthesis), calcitonin gene-related peptide (CGRP) (localized with substance P), cannabinoid receptors 1 and 2 (sebocyte differentiation), histamine-1 receptor (squalene synthesis regulation), insulin-like growth factor (ILGF)-1 receptor (lipid accumulation in sebocytes), and growth hormone (GH) receptors (increased differentiation and increased DHT effect on lipogenesis) (Zouboulis et al. 2002; Böhm et al. 2002, 2004; Deplewski and Rosenfield 1999; Dobrosi et al. 2008; Krause et al. 2007; Makrantonaki et al. 2004; Pelle et al. 2008; Seiffert et al. 2000; Ständer et al. 2005; Zhang et al. 2006).

Nuclear receptors (bind a hormone-specific hormone response element) include androgen receptors (increased proliferation) and other types of receptors. Androgen receptors have been found in sebaceous glands, eccrine glands, and hair follicle mesenchymal cells. In human skin, these receptors have been found with highest density on sebaceous glands. Both basal and differentiating sebocytes have androgen receptors and this shows that androgens play a role in sebocyte proliferation regulation and also in lipogenesis. Other nuclear receptors include

progesterone receptors (nuclei of basal sebocytes), estrogen receptors α (basal and early differentiated sebocytes) and β (basal and partially differentiated sebocytes) (increased polar lipids), retinoic acid receptors (RARs) α and γ (proliferation regulation), retinoid X receptor (possibly regulates lipogenesis), vitamin D receptor (proliferation regulation and cell cycle regulation, lipid content regulation, IL-6 and IL-8 secretion modulation), PPARs (increase lipogenesis and PGE2 release, increase cyclooxygenase-2 synthesis and IL-6 secretion), and liver X receptors (increase lipogenesis, decrease proliferation, decrease cyclooxygenase-2 and nitric oxide synthase) (Hong et al. 2008; Blaüer et al. 1991; Choudhry et al. 1992; Liang et al. 1993; Akamatsu et al. 1993; Alestas et al. 2006; Fimmel et al. 2007; Kim et al. 2001; Makrantonaki and Zouboulis 2007; Pelletier and Ren 2004; Reichrath et al. 1997, 2000; Russell et al. 2007; Schmuth et al. 2005; Schuler et al. 2005; Thornton et al. 2003, 2006; Tsukada et al. 2000; Zouboulis et al. 2007).

The vanilloid receptor is present in sebocytes which are differentiating and its ligand (capsaicin) decreases differentiation (Tóth et al. 2005).

9 Hormones and Sebaceous Glands

Sebocytes produce hormones including corticotropin-releasing hormone (CRH), androgens, estrogens, atRA, cortisol, vitamin D3, and eicosanoids (prostaglandins (PGs), prostacyclins, leukotrienes (LTs), and derivatives of AA) (Zouboulis 2000, 2005; Zouboulis et al. 2008). The skin has a corticotropin-releasing hormone (CRH)/proopiomelanocortin (POMC) system which can deal with signals with the potential to damage cells (Solminski et al. 2000). Nerves in the dermis and different cutaneous cells including sebocytes synthesize and release CRH in response to pro-inflammatory cytokines. CRH has receptors in sebocytes and when these receptors are activated, they lead to regulation of nonpolar lipids and expression of 3β-hydroxysteroid dehydrogenase-Δ (Deplewski and Rosenfield 2000) isomerase (Zouboulis et al. 2002). CRH stimulates the secretion of α-melanocyte-stimulating hormone, and this in turn reduces interleukin (IL)-8 synthesis in sebocytes in vitro (Böhm et al. 2002). In sebocytes, CRH directly upregulates conversion of dehydroepiandrosterone (DHEA) into testosterone using the enzyme 3β-Δ (Deplewski and Rosenfield 2000)-hydroxysteroid dehydrogenase (3β-HSD). Also, synthesis of neutral lipids and IL-6 and IL-8 is stimulated with CRH (Fritsch et al. 2001; Zouboulis et al. 2002; Krause et al. 2007). Different hormones including testosterone, estrogen, growth hormone, and others regulate expression of the abovementioned receptors. Adrenocorticotropic hormone induces cortisol secretion (Stewart et al. 1986b). All enzymes which are needed to transform cholesterol to steroids and adrenal precursors including dehydroepiandrosterone (DHEA) sulfate and DHEA are found in the skin (Zouboulis 2000; Thiboutot et al. 2003). Testosterone gets converted into 5α-dihydrotestosterone (DHT) using the enzyme 5α-reductase. The type I of this enzyme is the predominant type in sebaceous glands, sweat glands, and the epidermis. The highest activity is found on the sebaceous glands of the face and scalp (Luu-The et al. 1994; Thiboutot et al. 1995; Chen et al. 1998).

Animal studies have suggested that for terminal differentiation of sebocytes, DHT and peroxisome proliferator-activated receptor (PPAR) ligands should both be present (Rosenfield et al. 1998). PPARs in human sebocytes have a regulatory role on different lipid metabolic genes in sebocytes, mitochondria, peroxisomes, and microsomes (Fritsch et al. 2001; Zouboulis et al. 1998; Chen et al. 2003; Brun et al. 1996). Glucocorticoids can affect sebaceous glands. Patients suffering from adrenal insufficiency have reduced amounts of sebum secretion. Decreased levels of androgens might be an explanation for the mechanism of glucocorticoid action (Pochi et al. 1963; Goolamali et al. 1974). Estrogens show inhibitory effects on sebaceous activity, possibly through their inhibitory role on gonadotropin secretion or enhancement of binding between testosterone and its binding globulin

(Montagna 1974; Zouboulis and Boschnakow 2001; Zouboulis 2000; Strauss et al. 1962; Guy et al. 1996). Cortisol, estrogen, and atRA decrease differentiation while increasing proliferation and decreasing intracellular accumulation of neutral lipids (Wróbel et al. 2003; Harrison et al. 2007; Chen et al. 2006). Prolactin can affect sebaceous glands indirectly through its effect on increasing adrenal androgen production (Glickman et al. 1982). In the logarithmic phase of cell growth and differentiation, vitamin D3 is antiproliferative in SZ95 sebocytes. Also, in hamsters, it decreases lipogenesis (Sato et al. 2001; Schreiner et al. 2003). Lipogenesis can be regulated by all-trans retinoic acid and androgens in sebocytes of both hamsters and humans. Fibroblast growth factor (FGF), transforming growth factor (TGF)-α, and epidermal growth factor (EGF) have shown to be mitogenic in sebocytes of hamsters. TGF-α and FGF act as anti-lipogenic agents (Zouboulis et al. 1999; Sato et al. 2001; Akimoto et al. 2002). Inflammatory signals can be induced by eicosanoids in human sebocytes (Alestas et al. 2006). In patients with acne, nerves around sebaceous glands express substance P, though in acinar peripheral regions, undifferentiated sebocytes produce substance P inactivator neutral endopeptidase (Makrantonaki et al. 2004). Also in these patients, UV-induced fluorescence on the face has been reported to be correlated with casual sebum level. Distribution of fluorescence changes as age of onset differs and as the patient ages. The number and distribution of acne lesions are associated with amount and distribution of UV fluorescence (Choi et al. 2012).

References

Agache P. Sebaceous function assessment. In: Agache P, Humbert P, editors. Measuring the skin. Berlin: Springer; 2004. p. 281–9.

Agache P, Blanc D, Barrand C, Laurent R. Sebum levels during the first year of life. Br J Dermatol. 1980;103:643–9.

Akamatsu H, Zouboulis CC, Orfanos CE. Control of 5-α-dihydrotestosterone is dependent on the localization of the sebaceous glands. J Invest Dermatol. 1992;99:509–11.

Akamatsu H, Zouboulis CC, Orfanos C. Spironolactone directly inhibits proliferation of cultured human facial sebocytes and acts antagonistically to testosterone and 5-alpha-dihydrotestosterone in vitro. J Invest Dermatol. 1993;100:660–2.

Akimoto N, Sato T, Sakiguchi T, Kitamura K, Kohno Y, Ito A. Cell proliferation and lipid formation in hamster sebaceous gland cells. Dermatology. 2002;204:118–23.

Alestas T, Ganceviciene R, Fimmel S, Müller-Decker K, Zouboulis CC. Enzymes involved in the biosynthesis of leukotriene B_4 and prostaglandin E_2 are active in sebaceous glands. J Mol Med. 2006;84:75–87.

Allen M, Grachtchouk M, Sheng H, Grachtchouk V, Wang A, Wei L, et al. Hedgehog signaling regulates sebaceous gland development. Am J Pathol. 2003;163:2173–8.

Benfenati A, Brillanti F. Sulla distribuzione delle ghiandole sebacee nella cute del corpo umino. Arch Ital Dermatol. 1939;15:33–42.

Blanc D, Saint-Leger D, Brandt J, Constans S, Agache P. An original procedure for quantitation of cutaneous resorption of sebum. Arch Dermatol Res. 1989;281:346–50.

Blaüer M, Vaalasti A, Pauli SL, Ylikomi T, Joensuu T, Tuohimaa P. Location of androgen receptor in human skin. J Invest Dermatol. 1991;97:264–8.

Böhm M, Schiller M, Ständer S, Seltmann H, Li Z, Brzoska T, et al. Evidence for expression of melanocortin-1 receptor in human sebocytes in vitro and in situ. J Invest Dermatol. 2002;118:533–9.

Böhm M, Li Z, Ottaviani M, Picardo M, Zouboulis CC, Ständer S, et al. Beta-endorphin modulates lipogenesis in human sebocytes. J Invest Dermatol. 2004;123:A 10.

Brun R, Tontonoz P, Forman B, Ellis R, Chen J, Evans RM, et al. Differential activation of adipogenesis by multiple PPAR isoforms. Genes Dev. 1996;10:974–84.

Burton JL. The physical properties of sebum in acne vulgaris. Clin Sci. 1970;39:757–67.

Butcher EO, Coonin A. The physical properties of human sebum. J Invest Dermatol. 1949;12:249–54.

Chen W, Zouboulis CC, Fritsch M, Blume-Peytavi U, Kodelja V, Goerdt S, et al. Evidence of heterogeneity and quantitative differences of the type 1 5α-reductase expression in cultured human skin cells. Evidence of its presence in melanocytes. J Invest Dermatol. 1998;110:84–9.

Chen W, Yang C-C, Sheu H-M, Seltmann H, Zouboulis CC. Expression of peroxisome proliferator-activated receptor and CCAAT/enhancer binding protein transcription factors in cultured human sebocytes. J Invest Dermatol. 2003;121:441–7.

Chen W, Liao C, Hung C, Lin T, Sheu H, Zouboulis CC. Potent corticosteroids inhibit lipogenesis in sebaceous glands. Dermatology. 2006;213:264–5.

Choi CW, Choi JW, Park KC, Youn SW. Ultraviolet-induced red fluorescence of patients with acne reflects

regional casual sebum level and acne lesion distribution: qualitative and quantitative analyses of facial fluorescence. Br J Dermatol. 2012;166:59–66.
Choudhry R, Hodgins MB, Van der Kwast TH, Brinkmann AO, Boersma WJ. Localization of androgen receptors in human skin by immunohistochemistry: implications for the hormonal regulation of hair growth, sebaceous glands and sweat glands. J Endocrinol. 1992;133:467–75.
Constans S, Makki S, Petiot F, Agache P. Sebaceous levels from 6 to 15 years: comparison with pubertal events. J Invest Dermatol. 1985;84:454–5. Abstr.
Deplewski D, Rosenfield R. Growth hormone and insulin like growth factors have differentiation. Endocrinology. 1999;140:4089–94.
Deplewski D, Rosenfield RL. Role of hormones in pilosebaceous unit development. Endocr Rev. 2000;21:363–92.
Dobrosi N, Tóth B, Nagy G, Dózsa A, Géczy L, Nagy T, et al. Endocannabinoids enhance lipid synthesis in human sebocytes via cannabinoid receptor-2-mediated signaling. FASEB J. 2008;22:3685–95.
Downing DT, Strauss JS. On the mechanism of sebaceous secretion. Arch Dermatol Res. 1982;272:343–9.
Downing D, Strauss J, Pochi P. Changes in skin surface lipid composition induced by severe caloric restriction in man. Am J Clin Nutr. 1972;25:365–7.
Dünner M. Der Einfluss physikalischer Faktoren (Druck, Temperatur) auf die Talgabsonderung des Menschen. Dermatologica. 1946;93:249–71.
Emanuel SV. Quantitative determinations of the sebaceous gland's function, with particular mention of the method employed. Acta Derm Venereol. 1938;17:444–56.
Fenske NA, Lober CW. Structural and functional changes of normal aging skin. J Am Acad Dermatol. 1986;15:571–85.
Fimmel S, Saborowski A, Térouanne B, Sultan C, Zouboulis C. Inhibition of the androgen receptor by antisense oligonucleotides regulate the biological activity of androgens in SZ95 sebocytes. Horm Metab Res. 2007;39:149–56.
Fritsch M, Orfanos CE, Zouboulis CC. Sebocytes are the key regulators of androgen homeostasis in human skin. J Invest Dermatol. 2001;116:793–800.
Fuchs E, Merrill B, Jamora C, DasGupta R. At the roots of a never-ending cycle. Dev Cell. 2001;1:13–25.
Fujita H, Asagami C, Murata S, Murozumi S. Ultrastructural study of embryonic sebaceous cells, especially of their serum droplet formation. Acta Derm Venereol. 1972;52:99–115.
Ge L, Gordon J, Hsuan C, Stenn K, Prouty S. Identification of the δ-6 desaturase of human sebaceous glands: expression and enzyme activity. J Invest Dermatol. 2003;120:707–14.
Glickman SP, Rodenfield RL, Bergenstal RM, Helke J. Multiple androgenic abnormalities, including elevated free testosterone, in hyperprolactinemic women. J Clin Endocrinol Metab. 1982;55:251–7.
Goolamali SK, Plummer N, Burton JL, Shuster S, Thody AJ. Sebum excretion and melanocyte stimulating hormone in hypoadrenalism. J Invest Dermatol. 1974;63:253–5.
Greene RS, Downing DT, Pochi PE, Strauss JS. Anatomical variation in the amount and composition of human skin surface lipid. J Invest Dermatol. 1970;54:240–7.
Guy R, Ridden C, Kealey T. The improved organ maintenance of the human sebaceous gland: modeling in vitro the effects of epidermal growth factor, androgens, estrogens, 13-cis retinoic acid, and phenol red. J Invest Dermatol. 1996;106:454–60.
Harrison WJ, Bull JJ, Seltmann H, Zouboulis CC, Philpott MP. Expression of lipogenic factors galectin-12, resistin, SREBP-1 and SCD in human sebaceous glands and cultured sebocytes. J Invest Dermatol. 2007;127:1309–17.
Henderson CA, Taylor J, Cunliffe WJ. Sebum excretion rates in mothers and neonates. Br J Dermatol. 2000;142:110–1.
Hong I, Lee M, Na T, Zouboulis CC, Lee M. LXRα enhances lipid synthesis in SZ95 sebocytes. J Invest Dermatol. 2008;128:1266–72.
Ito A, Sakiguchi T, Kitamura K, Akamatsu H, Horio T. Establishment of a tissue culture system for hamster sebaceous gland cells. Dermatology. 1998;197:238–44.
Jacobson E, Billings JK, Frantz RA, Kinney CK, Stewart ME, Downing DT. Age-related changes in sebaceous wax ester secretion rates in men and women. J Invest Dermatol. 1985;85:483–5.
Kim M, Deplewski D, Ciletti N, Michel S, Reichert U, Rosenfield R. Limited cooperation between peroxisome proliferator-activated receptors and retinoid X receptor agonists in sebocyte growth and development. Mol Genet Metab. 2001;74:362–9.
Kim MK, Choi SY, Byun HJ, Choi SY, Byun HJ, Huh CH, et al. Evaluation of gender difference in skin type and pH. J Dermatol Sci. 2006;41:153–6.
Krause K, Schnitger A, Fimmel S, Glass E, Zouboulis CC. Corticotropin-releasing hormone skin signaling is receptor-mediated and is predominant in the sebaceous glands. Horm Metab Res. 2007;39:166–70.
Liang T, Hoyer S, Yu R, Soltani K, Lorincz AL, Hiipakka RA, et al. Immunohistochemical localization of androgen receptors in human skin using monoclonal antibodies against the androgen receptor. J Invest Dermatol. 1993;100:663–6.
Lindner G, Botchkarev VA, Botchkareva NV, Ling G, Van der Veen C, Paus R. Analysis of apoptosis during hair follicle regression (catagen). Am J Pathol. 1997;151:1601–17.
Llewellyn A. Variations in the composition of skin surface lipid associated with dietary carbohydrates. Proc Nutr Soc. 1967;26:11.
Lo Celso C, Berta M, Braun K, Frye M, Lyle S, Zouboulis CC, et al. Characterisation of bipotential epidermal progenitors derived from human sebaceous gland: contrasting roles for c-Myc and β-catenin. Stem Cells. 2008;26:1241–52.

Luu-The V, Sugimoto Y, Puy L, Labrie Y, Lopez Solache I, Singh M, et al. Characterization, expression, and immunohistochemical localization of 5-α-reductase in human skin. J Invest Dermatol. 1994;102:221–6.

MacDonald L. Changes in the fatty acid composition of sebum associated with high carbohydrate diets. Nature. 1964;203:1067–8.

MacDonald L. Dietary carbohydrates and skin lipids. Br J Dermatol. 1967;79:119–21.

Makrantonaki E, Zouboulis CC. Testosterone metabolism to 5α-dihydrotestosterone and synthesis of sebaceous lipids is regulated by peroxisome proliferators-activated receptor ligand linoleic acid in human sebocytes. Br J Dermatol. 2007;156:428–32.

Makrantonaki E, Oeff M, Fimmel S, Seltmann H, Orfanos CE, Zouboulis CC. Estrogen activity on human skin involves interaction with the insulin-like growth factor-I (IGF-I) signaling pathway. J Dtsch Dermatol Ges. 2004;2:544.

Makrantonaki E, Adjaye J, Herwig R, Brink T, Groth D, Hultschig C, et al. Age-specific hormonal decline is accompanied by transcriptional changes in human sebocytes in vitro. Aging Cell. 2006;5:331–44.

Mavon A. Energie libre de surface de la peau humaine in vivo: une nouvelle approche dela séborrhée. [Thèse Sciences de la Vie et de la Santé]. Besançon, No. 259706; 1997.

Merrill B, Gat U, DasGupta R, Fuchs E. Tcf3 and Lef1 regulate lineage differentiation of multipotent stem cells in skin. Genes Dev. 2001;15:1677–705.

Montagna W. An introduction to sebaceous glands. J Invest Dermatol. 1974;62:120–3.

Nagai A, Sato T, Akimoto N, Ito A, Sumida M. Isolation and identification of histone H3 protein enriched in microvesicles secreted from cultured sebocytes. Endocrinology. 2005;146:2593–601.

Nicolaides N. Skin lipids: their biochemical uniqueness. Science. 1974;186:19–26.

Niemann C, Owens D, Hulsken J, Birchmeier W, Watt F. Expression of DeltaNLef1 in mouse epidermis results in differentiation of hair follicles into squamous epidermal cysts and formation of skin tumours. Development. 2002;129:95–109.

Niemann C, Unden AB, Lyle S, Zouboulis CC, Toftgård R, Watt FM. Indian hedgehog and β-catenin signaling: role in the sebaceous lineage of normal and neoplastic mammalian epidermis. Proc Natl Acad Sci U S A. 2003;100 Suppl 1:11873–80.

Nikkari T. Comparative chemistry of sebum. J Invest Dermatol. 1974;62:257–67.

Pappas A, Anthonavage M, Gordon J. Metabolic fate and selective utilization of major fatty acids in human sebaceous gland. J Invest Dermatol. 2002;118:164–71.

Pelle E, McCarthy J, Seltmann H, Huang X, Mammone T, Zouboulis CC, et al. Identification of histamine receptors and reduction of squalene levels by an antihistamine in sebocytes. J Invest Dermatol. 2008;128:1280–5.

Pelletier G, Ren L. Localization of sex steroid receptors in human skin. Histol Histopathol. 2004;19:629–36.

Picardo M, Ottaviani M, Camera E, Mastrofrancesco A. Sebaceous gland lipids. Dermatoendocrinol. 2009;1:68–71.

Pierard GE. Rate and topography of follicular heterogeneity of sebum excretion. Dermatologica. 1987;175:280–3.

Piérard-Franchimont C, Piérard GE, Kligman AM. Seasonal modulation of sebum excretion. Dermatologica. 1990;181:21–2.

Plewig G, Christophers E. Renewal rate of human sebaceous glands. Acta Derm Venereol. 1974;54:177–82.

Plewig G, Kligman AM. Proliferative activity of the sebaceous glands of the aged. J Invest Dermatol. 1978;70:314–7.

Pochi P. The sebaceous gland. In: Maibach HI, Boisits EK, editors. Neonatal skin: structure and function. New York: Marcel Dekker; 1982. p. 67–80.

Pochi PE, Strauss JS, Mescon H. The role of adrenocortical steroids in the control of human sebaceous gland activity. J Invest Dermatol. 1963;41:391–9.

Pochi P, Downing D, Strauss J. Sebaceous gland response in man to prolonged total caloric deprivation. J Invest Dermatol. 1970;55:303–9.

Pochi PE, Strauss JS, Downing DT. Sebum, acne and androgens in children. Clin Res. 1977;25:531A [abstract].

Proksch E, Brandner JM, Jensen JM. The skin: an indispensable barrier. Exp Dermatol. 2008;17:1063–72.

Ramasastry P, Downing DT, Pochi PE, Strauss JS. Chemical composition of human skin surface lipids from birth to puberty. J Invest Dermatol. 1970;54:139–44.

Reichrath J, Mittmann M, Kamradt J, Müller S. Expression of retinoid-X receptors (-alpha, -beta, -gamma) and retinoic acid receptors (-alpha, -beta, -gamma) in normal human skin: an immunohistological evaluation. Histochem J. 1997;29:127–33.

Reichrath J, Classen U, Meineke V, DeLuca H, Tilgen W, Kerber A, et al. Immunoreactivity of six monoclonal antibodies directed against 1, 25-dihydroxyvitamin-D3 receptors in human skin. Histochem J. 2000;32:625–9.

Rosenfield RL, Deplewski D, Kentsis A, Ciletti N. Mechanisms of androgen induction of sebocyte differentiation. Dermatology. 1998;196:43–6.

Russell L, Harrison W, Bahta A, Zouboulis CC, Burrin J, Philpott M. Characterization of X receptor expression and function in uman skin and the pilosebaceous unit. Exp Dermatol. 2007;16:844–52.

Sanders D, Philpott M, Nicolle F, Kealey T. The isolation and maintenance of the human pilosebaceous unit. Br J Dermatol. 1994;131:166–76.

Sato S, Hiraga K, Nishijima A, Hidano A. Neonatal sebaceous glands: fine structure of sebaceous and dendritic cells. Acta Derm Venereol. 1977;57(4):279–87.

Sato T, Imai N, Akimoto N, Sakiguchi T, Kitamura K, Ito A. Epidermal growth factor and 1alpha, 25-dihydroxyvitamin D3 suppress lipogenesis in

hamster sebaceous gland cells in vitro. J Invest Dermatol. 2001;117:965–70.
Schmuth M, Ortegon A, Mao-Qiang M, Elias P, Feingold K, Stahl A. Differential expression of fatty acid transport proteins in epidermis and skin appendages. J Invest Dermatol. 2005;125:1174–81.
Schneider M, Paus R. Sebocytes: multifaceted epithelia cells: lipid production and holocrine secretion. Int J Biochem Cell Biol. 2010;42:181–5.
Schneider MR, Schmidt-Ulrich R, Paus R. The hair follicle as a dynamic miniorgan. Curr Biol. 2009;19: R132–42.
Schreiner EP, Wolff B, Winiski AP, Billich A. 6-(2-Adamantan-2-ylidene-hydroxybenzoxazole)-O-sulfamate: a potent non-steroidal irreversible inhibitor of human steroid sulfatase. Bioorg Med Chem Lett. 2003;13:4313–6.
Schuler C, Seifert M, Seltmann H, Zouboulis CC, Tilgen W, Reichrath J. The sebocytes as a new target for bioactive vitamin D analogues. J Invest Dermatol. 2005;124 Suppl 5:A42.
Seiffert K, Zouboulis CC, Seltmann H, Granstein R. Expression of neuropeptide receptors by human sebocytes and stimulatory effect of their agonists on cytokine production. Horm Res. 2000;53:102.
Serri F, Huber WM. The development of sebaceous glands in man. In: Montagna W, Ellis RA, Silver AF, editors. Advances in biology of skin, vol IV: sebaceous glands. Oxford: Pergamon; 1963. p. 1–18.
Smith KR, Thiboutot DM. Thematic review series: skin lipids. Sebaceous gland lipids: friend or foe? J Lipid Res. 2008;49:271–81.
Solminski A, Wortman J, Luger T, Paus R, Solomon S. Corticotropin-releasing hormone and propriomelanocortin involvement in the cutaneous response to stress. Physiol Rev. 2000;80:979–1020.
Ständer S, Schmelz M, Metze D, Luger T, Rukwied R. Distribution of cannabinoid receptor 1 (CB1) and 2 (CB2) on sensory nerve fibers and adnexal structures in human skin. J Dermatol Sci. 2005;38:177–88.
Stewart ME, Downing DT. Measurement of sebum secretion rates in young children. J Invest Dermatol. 1985;84:59–61.
Stewart M, Grahek M, Cambier L, Wertz P, Downing D. Dilutional effect of increased sebaceous gland activity on the proportion of linoleic acid in sebaceous wax esters and in epidermal acylceramides. J Invest Dermatol. 1986a;87:733–6.
Stewart ME, McDonnell MW, Downing DT. Possible genetic control of the proportions of branched-chain fatty acids in human sebaceous was esters. J Invest Dermatol. 1986b;86:706–8.
Strauss JS, Kligman AM, Pochi PE. Effect of androgens and estrogens on human sebaceous glands. J Invest Dermatol. 1962;39:139–55.
Takda H, Lyle S, Lazar A, Zouboulis CC, Smyth I, Watt F. Human sebaceous tumours harbor inactivating mutations in LEF1. Nat Med. 2006;12:395–7.
Thiboutot D, Harris G, Iles V, Cimis G, Gilliland K, Hagari S. Activity of the type I 5α-reductase exhibits regional differences in isolated sebaceous glands and whole skin. J Invest Dermatol. 1995;105:209–14.
Thiboutot D, Jabara S, McAllister JM, Sivarajah A, Gilliland K, Cong Z, et al. Human skin is a steroidogenic tissue: steroidogenic enzymes and cofactors are expressed in epidermis, normal sebocytes, and an immortalized sebocyte cell lines (SEB-1). J Invest Dermatol. 2003;120:905–14.
Thody AJ, Shuster S. Control and function of sebaceous glands. Physiol Rev. 1989;69:383–416.
Thornton M, Taylor A, Mulligan K, Al-Azzawi F, Lyon C, O'Driscoll J, et al. Oestrogen receptor-β is the predominant oestrogen receptor in human scalp skin. Exp Dermatol. 2003;12:181–90.
Thornton M, Nelson L, Taylor AH, Birch M, Laing I, Messenger A. The modulation of aromatase and estrogen receptor alpha in cultured human dermal papilla cells by dexamethasone: a novel mechanism for selective action of estrogen via estrogen receptor beta? J Invest Dermatol. 2006;126:2010–8.
Tosti A. Comparison of histodynamics of sebaceous glands and epidermis in man: a microanatomic and morphometric study. J Invest Dermatol. 1974;62:147–52.
Tóth I, Géczy T, Czifra G, Seltmann H, Paus R, Kovács L, et al. The vanilloid receptor 1 (RPV1) is expressed and functionally active on human SZ95 sebocytes. J Invest Dermatol. 2005;124 Suppl 5:A68 [Abstract].
Tsukada M, Schroder M, Roos T, Chandraratna R, Reichert U, Merk H, et al. 13-cis retinoic acid exerts its specific activity on human sebocytes through selective intracellular isomerization to all-trans retinoic acid and binding to retinoid acid receptors. J Invest Dermatol. 2000;115:321–7.
Wheatley VR. Sebum: its chemistry and biochemistry. Am Perfumer. 1956;68:37–47.
Wille JJ, Kidonieus A. Palmitoleic acid isomer (C16:1δ6) is the active antimicrobial fatty acid in human skin sebum. Skin Pharmacol Appl Skin Physiol. 2003a;16:176–87.
Wille J, Kidonieus A. Palmitoleic acid isomer (C16:1delta6) in human skin sebum is effective against gram-positive bacteria. Skin Pharmacol Appl Skin Physiol. 2003b;16:176–87.
Wróbel A, Seltmann H, Fimmel S, Müller-Decker K, Tsukada M, Bogdanoff B, et al. Differentiation and apoptosis in human immortalized sebocytes. J Invest Dermatol. 2003;120:175–81.
Youn SW, Kim SJ, Hwang IA, Park KC. Evaluation of facial skin type by sebum secretion: discrepancies between subjective descriptions and sebum secretion. Skin Res Technol. 2002;8:168–72.
Zhang L, Li W, Anthonavage M, Eisinger M. Melanocortin-5 receptor: a marker of human sebocyte differentiation. Peptides. 2006;27:413–20.
Zheng Y, Eliertsen K, Ge L, Zhang L, Sundberg J, Prouty S, et al. Scd1 is expressed in sebaceous glands

and is disrupted in the asebia mouse. Nat Genet. 1999;23:268–70.
Zouboulis CC. Human skin: an independent peripheral endocrine organ. Horm Res. 1992;54:230–42.
Zouboulis CC. Human skin: an independen peripheral endocrine organ. Horm Res. 2000;54:230–42.
Zouboulis CC. Is acne vulgaris a genuine inflammatory disease? Dermatology. 2001;203:277–9.
Zouboulis CC. Acne and sebaceous gland function. Clin Dermatol. 2005;22:360–6.
Zouboulis CC, Boschnakow A. Chrono- and photoaging of the human sebaceous gland. Clin Exp Dermatol. 2001;26:600–7.
Zouboulis CC, Makrantonaki E. The role of hormones in intrinsic aging. In: Gilchrest B, Krutmann J, editors. Skin aging. New York: Springer; 2006. p. 55–64.
Zouboulis CC, Xia L, Detmar M, Bogdanoff B, Giannakopoulos G, Gollnick H, et al. Culture of human sebocytes and markers of sebocytic differentiation in vitro. Skin Pharmacol. 1991;4:74–83.
Zouboulis CC, Xia L, Akamatsu H, Seltmann H, Fritsch M, Hornemann S, et al. The human sebocyte culture model provides new insights into development and management of seborrhoea and acne. Dermatology. 1998;196:21–31.
Zouboulis CC, Seltmann H, Neitzel H, Orfanos CE. Establishment and characterization of an immortalized human sebaceous gland cell line (SZ95). J Invest Dermatol. 1999;113:1011–20.
Zouboulis CC, Seltmann H, Hiroi N, Chen W, Young M, Oeff M, et al. Corticotropin-releasing hormone: an autocrine hormone that promotes lipogenesis in human sebocytes. Proc Natl Acad Sci U S A. 2002;99:7148–53.
Zouboulis CC, Fimmel S, Ortmann J, et al. Sebaceous gland. In: Hoath SB, Maibach HI, editors. Neonatal skin: structure and function. 2nd ed. New York: Marcel Dekker; 2003. p. 59–88.
Zouboulis CC, Chen W, Thornton M, Qin K, Rosenfield R. Sexual hormones in human skin. Horm Metab. 2007;39:85–95.
Zouboulis CC, Baron JM, Bohm M, Kippenberger S, Kurzen H, Reichrath J, et al. Frontiers in sebaceous gland biology and pathology. Exp Dermatol. 2008;17:542–51.

Measurement of Skin Surface Sebum

14

Alireza Firooz, Ali Rajabi-Estarabadi, and Hamed Zartab

Contents

A. Firooz (✉) • A. Rajabi-Estarabadi
Center for Research and Training in Skin Diseases and Leprosy, Tehran University of Medical Sciences, Tehran, Iran
e-mail: firozali@sina.tums.ac.ir; dralirajabi@yahoo.com

H. Zartab
Center for Research and Training in Skin Diseases and Leprosy, Tehran University of Medical Sciences, Tehran, Iran

Tissue Engineering and Wound Healing Lab, Department of Surgery, Division of Plastic Surgery, Brigham and Women's Hospital – Harvard Medical School, Boston, USA
e-mail: hzartabmd@yahoo.com; hzartab@partners.org; hzartabmd@gmail.com

P. Humbert et.al. (eds.), *Agache's Measuring the Skin*,
DOI 10.1007/978-3-319-32383-1_14

Keywords
Skin surface lipid • Sebum • Sebaceous gland • Assessment • Sebum excretion rate • Casual level

1 Utility

Many conditions can affect the function of sebaceous glands, so assessment of sebaceous function can be useful for evaluation of the pathogenesis of skin diseases, diagnosis of some diseases (such as hypoandrogenic syndromes), efficacy of skin and hair care products, and medical treatments.

2 What Can Be Assessed?

2.1 The Composition of Skin Surface Lipid (SSL)

The composition of the secreted sebum is an individual characteristic and depends on the person's age, his/her hormonal system, and function of body region (Wójcik et al. 2011). The SSL is composed of lipids originated from sebum and also lipids with epidermal origin (keratinocyte intercellular spaces). Lipids produced by the epidermal cells are an insignificant fraction of the total extractable surface lipid on areas rich in sebaceous glands. Lipids of epidermal origin fill the spaces between the cells, like mortar or cement. The sebaceous lipids are primarily nonpolar lipids as triglycerides, wax esters, and squalene, while epidermal lipids are a mixture of ceramides, free fatty acids, and cholesterol (Pappas 2009).

The sebaceous lipid mixture is highly complex and consists of triacylglycerols, diacylglycerols, and free fatty acids, which together account for 50–60 % of its composition. SSL also contains 20–30 % wax esters (WE), 10–16 % squalene, and 2–4 % cholesterol esters (Picardo et al. 2009). It is believed that free fatty acids which are present on the skin surface appear as a result of partial hydrolysis of triglyceride (Downing et al. 1969). Also the relative composition of sebum depends on the sampling method used. In particular, if the major components of sebum, triglycerides, are sampled before or after their modification by bacteria (which hydrolyze them to free fatty acids and glycerol) (Pappas 2009).

2.2 The Quantity of Sebum Excretion

2.2.1 Sebum Casual Level

The natural skin lipids spread as a nonuniform thin layer on the skin surface. This spontaneous layer is known as the "casual level" of skin surface lipids, expressed in μg/cm^2 (Rode et al. 2000a). It ranges from 100 to 700 μg/cm^2 on the forehead of normal adults. It is a static parameter, expressing the amount of SSLs present on an untreated skin surface (Clarys and Barel 1995). Sebaceous glands are scattered all over the body except for palms, soles, and the dorsum of the feet (Smith and Thiboutot 2007). The greatest number of the glands and the amount of sebum is on the face (T-zone, especially the forehead), back, and chest, and it may range from 400 to 900 glands/cm^2 (Thody and Shuster 1989). The number of active sebaceous glands and the amount of sebum per unit skin surface area (casual level) are different in different people, but the shape and distribution in a human body seem to remain constant during the life; however, their size changes – it grows with age (Pierard 1986; Zouboulis and Boschnakow 2001).

2.2.2 The Refatting Rate

Because of this thin layer of lipids, dirt and cell debris may stick to the skin. This contamination makes real-value sebum excretion measurements almost impossible. The dirt, cell debris, and droplets of excessive lipid can be removed from the skin surface with solvents. By removing the surface lipids, the skin is degreased or defatted, creating an opportunity for a real impression of the rate of sebum excretion. Refatting time is the time from defatting until casual level is reached. Washing gently with a detergent solution and then performing three wipes with alcohol is optimal

for degreasing the forehead, nose, and chin. For the cheek and upper back, it is sufficient to use a mild soap. Casual level is reached after 2 h in all seborrheic areas, irrespective of level of oiliness (Rode et al. 2000a).

2.2.3 The Secretion Rate

Measuring sebum secretion is the focus of constant attention of dermatologists, cosmetologists, and pharmacists as well as after cosmetic producers. We can do it with various methods which were already used in the past. Measurement of sebum excretion rate (SER) is tedious and time-consuming. It is now possible to measure SER 1 h after degreasing with a 70 % ethanol solution. The skin surface lipids (SSL) collected during this time have similar composition to those collected for up to 7 h. A qualitative and quantitative study of sebaceous excretion showed that the refatting kinetics obeyed the same mathematical law, independent of the subjects' individual SER (Saint-Leger and Cohen 1985).

2.2.4 The Sebum Replacement Time

The time required to recover CL after cleaning the sebum from the skin surface is called sebum replacement time. It is a time taking measurement and so difficult to manage which makes it less frequently used (Agache 2004).

2.2.5 The Density of Sebum-Rich Reservoirs

The number of spots over a plastic film is related to the density of sebum which exists in rich follicular reservoirs.

2.2.6 The Instant Sebum Delivery

This parameter presents the unpremeditated secretion of sebum from follicular reservoirs. It can be obtained using Sebufix tape on the skin surface for a few seconds.

2.2.7 The Follicular Excretion Rate

This measurement has been presented to estimate the delivery rate of sebum from follicular reservoirs.

2.3 Glandular Parameters

Glandular parameters include density, distribution, and level of activity of active sebaceous glands (Agache 2004).

3 Methods for Collecting Sebum

Various methods have been developed for collecting the SSL on the human skin, and although these were used in the past, these are still practical and operative.

3.1 Solvents

The technique is based on the solubility of the SSLs in solvents. For the measurement of SSL of hairless skin, it can be collected by scrubbing the skin surface with a degreased cotton pad, a polyurethane sponge, or a swab and then extracted with a solvent.

The cup method should be used for assessment of the amount of SSL per unit surface area (CL). In this method a hollow cylinder made of metal, glass, or plastic is placed on the skin. Then an exact amount of a solvent is poured into a cylinder and is collected after 1 or 2 min. Finally, the solvent is evaporated and the lipids weighted. Also the amount of the sebum collected through this method can be evaluated by high-performance thin-layer chromatography or densitometry (Piérard et al. 2000).

For collecting SSL from hairy skin, the best method is to rinse the hair with a solvent (e.g., ether). For separating the hairs and squames, it is filtered by using Whatman paper and then evaporated.

Unfortunately, in this method there is no control of the amount of sebum collected from follicular reservoirs which may have an influence on the results. On the other hand, the application of these solvents can alter the physiology and structure of the stratum corneum (SC); hence, this method is no longer recommended for assessing the amount of SSLs (Piérard et al. 2000).

The solvents most commonly used in studies are shown in Table 1. It seems the most

Table 1 Solvents for collecting SSL and their features

Solvents	Features
Ether (diethyl ether)	The most convenient, widely used, moderately polar
Ether-ethanol mixture	Extracts nearly all known lipids
Ethanol (EtOH)	Well tolerated
Petroleum ether	Leaves the polar group of free fatty acids and water
Hexane	Leaves the polar group of free fatty acids and water
Acetone	Difficult solving of waxes
Carbon tetrachloride	–
Methanol-chloroform mixture	Too aggressive for in vivo studies, produces epidermal damage

convenient and the best option is ether (Agache 2004).

3.2 Absorbent Paper Pads

One of the most widely used methods for measurement of sebum secretion rate is the cigarette paper which was introduced by Strauss and Pochi and improved by Cunliffe and Shuster (1969). This method has been applied for measuring sebum secretion rate and sebum glandular parameters (Agache 2004). The absorbent capacity of papers differs, and it is necessary to check that the saturation point will not be reached and the paper absorbs the different components equally.

For this purpose, the paper can be checked by using artificial sebum (Agache 2004; Blanc and Agache 1980). Artificial sebum has been used for studies on properties of the skin and hair. One study showed that a mixture of 17 % fatty acid, 44.7 % triglyceride, 25 % wax monoester (jojoba oil), and 12.4 % squalene is very similar to human sebum. It is stable on exposure to the atmosphere at 32 °C for at least 48 h, and it is also stable on storage at 4 or −20 °C, either dry or in chloroform/methanol solution for at least 6 months. This synthetic sebum could be useful in studies on cosmetic properties of the skin surface or hair, on penetration of chemicals into the skin, or in development of standardized tests of laundry detergent performance (Wertz 2009).

The skin is first cleansed to remove surface lipids. A previously extracted cigarette paper is then placed against the skin and held in place with an ace bandage. After a 3-h collection period, the cigarette paper is removed. Lipids are extracted from the paper using ethyl ether and quantified either by weighing or by quantitative thin-layer chromatographic analysis (Sisalli et al. 2006; Downing et al. 1982). When samples are extracted for quantitative analysis, an internal standard (e.g., methyl nervonate) can be added to the extraction solvent (Clarys and Barel 1995).

A combined method for cigarette absorbent paper is interposing the paper between the skin and a UV-light video camera (Visioscan VC 98, C + K Electronic, Cologne, Germany). After defined collecting time (45 s or more), pictures of the lipid droplets are analyzed by computerized image analysis.

3.3 Bentonite Gel

Bentonite has been used to adsorb sebum. Bentonite gel is a water suspension of 15.5 % bentonite clay and 0.2 % carboxymethyl cellulose (Collison et al. 1987; Jacobsen et al. 1985a). After washing the skin with soap and water and swabbing with an ethanol-soaked gauze pad, a thin layer of bentonite gel is applied to the skin. In initial studies, two 1.8-mm diameter circular disks of Dacron mesh were pressed into the bentonite, and these were covered with additional bentonite. At 3-h interval thereafter, the Dacron disks and adhering bentonite were replaced and sampling continued for 24 h. The amount of sebum adsorbed per disk over 3 h decreases steadily for about the first 12 h, after which the rate of sebum secretion becomes constant. The excess sebum secreted during the initial 12 h of

collection is interpreted as a reflection of a follicular reservoir. Only after this reservoir is depleted is the sustainable sebum secretion rate measurable (Harris et al. 1983).

This sustainable secretion rate is equal to the rate of synthesis in the glands. In later studies, bentonite was applied to the skin, and a rectangular piece of Dacron mesh large enough to cover most of the skin was pressed into the gel and covered with additional bentonite. After 7 h, the Dacron mesh on the forehead was replaced, and after another 7 h (to deplete the reservoir), the rectangular Dacron was replaced with two circular disks of Dacron for a final 3-h collection period, reflecting the sustainable rate of sebum secretion. The lipids were extracted from the bentonite into ethyl ether and analyzed by quantitative thin-layer chromatography. In a variant on this method, the final collection period after depletion of the follicular reservoir was extended to 9 h, and the extracted sebum was quantified gravimetrically (Harris et al. 1983).

The bentonite clay method seems to be sensitive to collect sebum in very low sebum conditions, but its major drawback is the fact that it takes at least 12 h for collecting the SSLs, making it the most cumbersome and time-consuming method (Stewart and Downing 1985).

3.4 Frosted Glass

Schaefer and Kuhn-Bussius demonstrated that sebum secretion could be measured by collecting it on a slide of frosted glass which was applied for 30 s on the skin and measuring the transparency. As sebum is adsorbed on the rough surface, it spreads and fills the microscopic pockets. This smoothes the surface and will result in less light scattering when the plate is illuminated with a beam of light. The relationship between the amount of adsorbed lipid and light transmission was quantified and shown to be nonlinear. Subsequently, several instruments based on this principle have become commercially available. The first of this is the Lipometer introduced by L'Oreal (Aulnay-sous-Bois, France). More recently, the Sebumeter has been made by Courage + Khazaka Electronic (Koln, Germany). These instruments allow measurement of the amount of sebum on the skin surface or the sebum secretion rate, which can be made easily within a few minutes. The important advantage of this method is that it bears no risk of uneven retrieval of the components. However, calibration can be difficult, and unless the sebaceous reservoir has been depleted, this will be the least accurate means for measuring sebum secretion rates (Saint-Leger et al. 1979). This method has been suggested for use in specific temperature and humidity. Also the surface of the glass must be cleaned and degreased before using. The skin surface temperature must be at least 30 °C because in lower temperatures some sebum components become semisolid and induce a change in optical density (Wójcik et al. 2011; Saint-Leger et al. 1979). This method is time-saving and highly reproducible and needs no trained scientific staff compared with previous techniques.

3.5 Plastic Film

3.5.1 Sebutape

The Sebutape© (CuDerm Corp., Dallas, Texas) consists of a hydrophobic polymeric white film (Kligman et al. 1986) and is used to measure the sebum secretion (Dobrev 2007; Clarys and Barel 1996) and evaluate the distribution of skin pores (Pierard 1986; Nordstrom et al. 1986). There are innumerable, tiny air cavities, and the surface is coated with a lipid-porous adhesive which enables the tape to be sealed to the skin during the period of collection. The film absorbs the sebum originating from the follicular openings. As sebum reaches the skin surface, it is rapidly absorbed into the film. As the air within the microcavities is displaced by sebum, the lipid-filled cavities become transparent to light. The output from each follicle forms a sharply defined spot; the size corresponds to the volume of the droplet. Sebum absorption by Sebutape is slow and perhaps incomplete because of the barrier of the glue (Saint-Leger and Cohen 1985).

First, the skin surface is ordinarily prepared by soap and water washing to remove debris and lipids. For greater accuracy, complete defatting can be obtained by wiping with a gauze pad soaked in hexane. The film is placed on the forehead for 1–3 h and then a computer image analysis is conducted. In the places where the sebaceous secretion has been absorbed, the film becomes transparent. Thanks to the placing of the film on the dark background, we can receive the pore patterns. These patterns can be assigned to one of five categories, referring to images provided by the manufacturer: prepubertal, pubertal, acne, mature, or senescent (Clarys and Barel 1995). Lipids which are examined with this method can be also extracted and then analyzed with thin-layer chromatography (Sisalli et al. 2006; Nordstrom et al. 1986).

The self-adhesive application of the Sebutape omits the difficult procedures encountered in the cigarette paper method and the former extraction methods. Moreover, the area under investigation is covered during the procedure, resulting in a more standardized collection. Compared with the cigarette paper technique, the Sebutape requires a shorter collection time, as most of the parameters can be determined after 1 h of collection and also, most of the evaluation methods described can be carried out on the same Sebutape: kinetic color measurement during the collection period, image analysis after the collection period, and quantitative and qualitative analysis after extraction of the lipids from the tape.

3.5.2 Sebufix F16

The Sebufix instrument is also commonly used. Here, like in the Sebutape, we use a polymer film to measure the activity of the sebaceous glands. The film is image analyzed with a UV-light video camera (Visioscan® VC 98, C + K Electronic, Cologne) device (Dobrev 2007). The Sebufix is thus very similar to the Sebutape; the only difference is the fact that in the case of the Sebutape, the film is placed on the selected area for 1–3 h and in the other for 30 s (Clarys and Barel 1996). Therefore, the Sebufix allows for measuring sebum secretion within a shorter period of time.

The method is not really quantitative because the relation between the surface of a spot and the quantity of sebum it contains is not known and several spots can rapidly coalesce. Accordingly, it cannot measure the CL, but it may provide an estimate of the refatting rate. It can display the distribution of the active sebaceous gland and the individual refatting rate of each gland (Saint-Leger and Cohen 1985).

3.5.3 Sebumeter SM 810

This device facilitates objective measurement of sebum from the skin surface areas and can be used to determine the level of sebum on the skin surface or the rate of its secretion (Knaggs et al. 1999; Tagami 2003; Schaefer and Kuhn-Bussius 1970; Bergler-Czop and Brzezińska-Wcisło 2010; Biro et al. 2003). It cannot, however, determine the state of the sebaceous glands (Son et al. 2008). In order to gather sebum secretion, the film is pressed to the skin or hairy skin or other areas of the body for 30 s. Then the film with the sebum gathered is subjected to a photometric analysis and gives the sebum index. The Sebumeter is a simple device, easy to operate, which can be used to make an objective classification of dry, normal, or oily skin (Nouveau-Richard et al. 2007; Youn et al. 2005; Kim et al. 2006) as well as to evaluate "the biological age" of the skin (Jacobsen et al. 1985b; Marrakchi and Maibach 2007; Firooz et al. 2012).

Nevertheless, one study has shown that a statistically significant difference was present between the oily and dry skin types. However, there were no statistical differences between oily and normal, and normal and dry skin types. So subjective skin type does not match the amount of sebum secreted. Thus, this simple and subjective classification is of very limited use and it should be reevaluated by using an objective and standardized measuring tool (Yong et al. 2002).

Compared with Lipometer® (L'Oreal, Aulnay-sous-Bois, France), the Sebumeter is more user-friendly and there is no need to clean the probe at each assessment. Thanks to its integrity, reproducibility, commercial availability, easy handling and operating, short measuring time, and numerical

values, the Sebumeter is now used in most of the sebum evaluation studies (Ambroisine et al. 2007; Lee et al. 2006; Cheng et al. 2007, 2009; Stinco et al. 2007; Akhtar et al. 2010).

3.5.4 Sebumeter SM 815(Cassette)

The measurement is based on grease-spot photometry. The Sebumeter cassette contains a mat synthetic tape, 0.1 mm thick. A special tape becomes transparent in contact with the sebum on the skin surface. For sebum determination, the measuring head of the cassette is inserted into the aperture of the device, where the transparency is measured by a light source sending light through the tape which is reflected by a little mirror behind the tape. A photocell measures the transparency. The light transmission represents the sebum content on the surface of the measuring area and is displayed in units from 0 to 350. The measuring time of 30 s is controlled by a clock set in the device. The measuring head of the cassette exposes a 64 mm^2 measuring section of the tape. For a measurement, the tape is moved forward by a trigger at the side of the cassette to expose a new section of tape. The used tape is rewound inside the cassette. The accuracy of this tool is about ± 5 %. It would be the best choice for assessment of SSLs on hairy skin and scalp skin.

3.5.5 Applications of Sebumeter

1. To objectively classify skin type as dry, normal, or oily (Firooz et al. 2007; Davari et al. 2008; Seirafi et al. 2009; Davoudi et al. 2010)
2. To study the effectiveness of hair and skin cosmetic products
3. To study sebaceous gland activity in different diseases
4. To assess the effectiveness of different kinds of treatment on skin diseases

3.6 Skin Surface Cast

This absorbing material is a mixture of plaster of Paris and water which gives a smooth paste. After degreasing of the skin surface by a solvent, it is spread over the skin and after 20 min will become solid. It is easily evaluated using a staining product. Osmic acid is a good material which has been used for this purpose (Sarkany and Gaylarde 1968).

4 Global Assessment of the SSL Casual Level

The casual level is a static parameter, expressing the amount of thin layer of SSLs when the skin surface remains untouched for several hours. The basis of global assessment of the SSL casual level is to sample the SSL on the skin surface in its spontaneous phase, at least 5 h after defatting and at least 24 h after application of a cosmetic product (Kligman 1963). If

Two methods have been defined for measurement of casual level.

4.1 Gravimetric Method

In case of sampling the sebum with solvent, the latter is evaporated under a nitrogen flow and the remaining sebum will be weighed. To ensure reliable outcomes, strict situation and precision are needed:

1. Sensitivity of scale: up to 0.01 mg
2. Clean field: protected from drafts
3. Field: placed on a special table or concrete base or a stone
4. Reduction of static electricity: by using aluminum containers
5. Stability: thermal stability and reduced relative humidity in the room and inside of the scale (where it is controlled by silica gel)

If the skin surface sebum is collected with filter paper, the initial and original method, which includes immersing the paper in a solvent for several hours, is used to extract lipids. Then the solvent is evaporated and the remaining lipid weighed. All the precision steps must be followed as above and also any contact with fingers must be avoided (Saint-Leger and Cohen 1985).

4.2 Photometric Method

All materials used for sampling the SSL (glass slide, Sebutape, Sebufix F16, Sebumeter tape) have a different sampling modulus, so they can collect only a part of the SSL. Their modulus depends on three main factors:

1. Capacity of the material for absorbing
2. The available area on the sensor
3. Skin surface lipid viscosity

Two factors influencing on the absorbing capacity of the material and the available area on the sensor include roughness and cleanliness of the slide. The main factor which influences on the SSL viscosity is temperature. It seems that repeated sampling on the same area avoids the feature bias in measurements.

5 Refatting Rate

5.1 Free Refatting Rate

The level of skin surface sebum 1 h after degreasing is called free refatting rate or sebum replacement rate. When the skin surface lipids are removed, the time which is needed to recover the entirety of sebum is about 3–4 h, although the half of it reforms in 30 min. But for this purpose, the initial rate which can be assessed during the first hour is applied as the free refatting rate (Agache 2004; Pie'rard-Franchimont et al. 2010).

5.2 Sebum Excretion Rate (SER)

Sebum excretion rate (SER) is a dynamic parameter expressing the speed of production of sebum in μg/cm^2/min. This rate is an indicator and quantifier of the activity of the sebaceous glands (Rode et al. 2000b). The duration of the definitive collection period is important because SER in the first hour after degreasing the skin is equal to the free refatting rate, and then it progressively decreases over the first hours to become stable after 9 h. SER of the first hour sampling usually ranges from 0.5 to 2.5 μg/cm^2/min on the forehead (Pie'rard-Franchimont et al. 2010). The measurement of SER can be done with filter paper, clay gel, Sebutape, and Sebumeter.

6 Density and Activity of Sebaceous Glands

6.1 Osmic Acid (OsO_4) Staining

The main factor of this method is that when OsO_4 is encountered with unsaturated fatty acids, it is reduced to osmium which shows a black color on the field. In these kinds of studies, first sebum is sampled by using an absorbent paper and then it is placed in a flask containing wool and a few drops of OsO_4. The follicular ostia, where the sebum is stored, are presented as black spots. The evaluation is achieved using densitometry or computerized image analysis (Lademann et al. 2001).

Table 2 The different parameters of sebaceous glands activity and the available methods for their assessment

Sebaceous gland parameter	Methods of assessment						
	Solvents	Absorbent pads	Bentonite clay	Sebutape	Sebumeter	Lipometer	Sebufix
Casual level	✓				✓	✓	
Sebum excretion rate	✓	✓			✓	✓	
Refatting rate							
Instant sebum delivery				✓			✓
Follicular excretion rate				✓			✓
Glandular parameter				✓			✓

6.2 Sebufix F16 and Sebutape

In this method, the sebum-loaded film is examined through the light. The available evaluation techniques for this purpose include densitometry, computerized image analysis, photometry, and colorimetry. Densitometry is the simple way to achieve the global quantification of transplant spots and is expressed in arbitrary units. All parameters related to glandular production such as the measurement of cumulated stained areas, the number of spots per cm^2, the average of the spots, and the distribution of the sebum spots versus their size are provided by computerized image analysis (Serup 1991).

The different parameters of sebaceous gland activity and the available methods for their assessment are summarized in Table 2.

References

Agache P. Sebaceous function assessment. In: Pierre G, Humbert P, editors. Measuring the skin. 1st ed. Heidelberg: Springer; 2004. p. 281–9.

Akhtar N, Khan BA, Mahmood T, et al. Formulation and evaluation of antisebum secretion effects of sea buckthorn w/o emulsion. J Pharm Bio Allied Sci. 2010;2:13–7.

Ambroisine L, Ezzedine K, Elfakir A, et al. Relationships between visual and tactile features and biophysical parameters in human facial skin. Skin Res Technol. 2007;13:176–83.

Bergler-Czop B, Brzezińska-Wcisło L. Assessment of the skin parameters – moisture, melanin content, pH and production of sebum in patients treated with oral isotretinoin: a preliminary report. Post Dermatol Alergol. 2010;27:83–9.

Biro K, Thaci D, Ochsendorf FR, et al. Efficacy of dexpanthenol in skin protection against irritation: a double-blind, placebo controlled study. Contact Dermatitis. 2003;49:80–4.

Blanc D, Agache P. Sebum excretion. Methods of measurement and influence of physical factors. Int J Cosmet Sci. 1980;2:243–50.

Cheng Y, Dong Y, Dong M, et al. Moisturizing and antisebum effect of cosmetic application on facial skin. J Cosmet Dermatol. 2007;6:172–7.

Cheng Y, Dong Y, Wang J, et al. Moisturizing and antisebum secretion effects of cosmetic application on human facial skin. J Cosmet Sci. 2009;60:7–14.

Clarys P, Barel A. Quantitative evaluation of skin surface lipids. Clin Dermatol. 1995;13:307–21.

Clarys PM, Barel AO. Sebumetry: a comparison between lipid collection techniques. Skin Res Technol. 1996;2:222.

Collison DW, Burns TL, Stewart ME, et al. Evaluation of a method for measuring the sustainable rate of sebaceous wax ester secretion. Arch Dermatol Res. 1987;279:266–9.

Cunliffe WJ, Shuster S. The rate of sebum excretion in man. Br J Dermatol. 1969;81:697–704.

Davari P, Gorouhi F, Jafarian S, Firooz A. A randomized investigator-blind trial of different passes of microdermabrasion therapy and their effects on skin biophysical characteristics. Int J Dermatol. 2008;47:508–13.

Davoudi SM, Sadr B, Hayatbakhsh MR, et al. Comparison of skin sebum and elasticity level in patients with sulfur mustard induced dermatitis and healthy controls. Skin Res Technol. 2010;16:237–42.

Dobrev H. Clinical and instrumental study of the efficacy of a new sebum control cream. J Cosmet Dermatol. 2007;6:113–8.

Downing DT, Strauss JS, Pochi PE. Variability in the chemical composition of human skin surface lipids. J Invest Dermatol. 1969;53:322–7.

Downing DT, Stranieri AM, Strauss JS. The effect of accumulated lipids on measurement of sebum secretion in human skin. J Invest Dermatol. 1982;79:226–8.

Firooz A, Gorouhi F, Davari P, et al. Comparison of hydration, sebum and pH values in clinically normal skin of patients with atopic dermatitis and healthy controls. Clin Exp Dermatol. 2007;32:321–2.

Firooz A, Sadr B, Babakoohi S, et al. Variation of biophysical parameters of the skin with age, gender and body region. Sci World J. 2012;2012:386936.

Harris HH, Downing DT, Stewart ME, et al. Sustainable rates of sebum secretion in acne patients and matched normal control subjects. J Am Acad Dermatol. 1983;8:200–3.

Jacobsen E, Billings JK, Frantz RA, et al. Age-related changes in sebaceous wax ester secretion rates in men and women. J Invest Dermatol. 1985;85:483–5.

Kim MK, Choi SY, Byun HJ, et al. Comparison of sebum secretion, skin type, pH in humans with and without acne. Arch Dermatol Res. 2006;298:113–9.

Kligman AM. The uses of sebum. In: Montagna W, Ellis RA, Silver AF, editors. The sebaceous glands. Oxford: Pergamon Press; 1963. p. 110–24.

Kligman AM, Miller DL, Mcginley KJ. Sebutape: a device for visualizing and measuring human sebaceous secretion. J Soc Cosmet Chem. 1986;37:369–74.

Knaggs H, Bajor J, Becker W. The Sebumeter and its use. Retinoids 1999;15:15–7.

Lademann J, Otberg N, Richter H, et al. Investigation of follicular penetration of topically applied substances. Skin Pharmacol Appl Skin Physiol. 2001;14:17–22.

Lee SM, Huh CH, Park KC, Youn SW. Effects of repetitive superficial peels on facial sebum secretion in acne

patients. J Eur Acad Dermatol Venereol. 2006;20:964–8.
Marrakchi S, Maibach HI. Biophysical parameters of skin: map of human face, regional and age-related differences. Contact Dermatitis. 2007;57:28–34.
Nordstrom KM, Schmus HG, McGinley KJ, et al. Measurement of sebum output using a lipid adsorbent tape. J Invest Dermatol. 1986;87:260–3.
Nouveau-Richard S, Zhu W, Li YH, et al. Oily skin: specific features in Chinese women. Skin Res Technol. 2007;13:43–8.
Pappas A. Epidermal surface lipids: special focus review. Dermatoendocrinol. 2009;1:72–6.
Picardo M, Ottaviani M, Camera E, et al. Sebaceous gland lipids. Dermatoendocrinol. 2009;1:68–71.
Pie'rard-Franchimont C, Quatresooz P, Pie'rard GE. Sebum production. In: Farage MA, Miller KW, Maibach HI, editors. Textbook of aging skin. Berlin: Springer; 2010. p. 343–52.
Pierard GE. Follicle to follicle heterogeneity of sebum excretion. Dermatologica. 1986;173:61–5.
Piérard GE, Piérard-Franchimont C, Marks R, et al. EEMCO guidance for the in vivo assessment of skin greasiness. The EEMCO group. Skin Pharmacol Appl Skin Physiol. 2000;13:372–89.
Rode B, Ivens U, Serup J. Degreasing method for the seborrheic areas with respect to regaining sebum excretion rate to casual level. Skin Res Technol. 2000a;6:92–7.
Rode B, Ivens U, Serup J. Degreasing method for the seborrheic areas with respect to regaining sebum excretion rate to casual level. Skin Res Technol. 2000b;6(2):92–7.
Saint-Leger D, Cohen E. Practical study of qualitative and quantitative sebum excretion on the human forehead. Br J Dermatol. 1985;113:551–7.
Saint-Leger D, Berrebi C, Duboz C, et al. The lipometre: an easy tool for rapid quantitation of skin surface lipids (SSL) in man. Arch Dermatol Res. 1979;265:79–89.
Sarkany I, Gaylarde P. A method for demonstration of the distribution of sebum on the skin surface. Br J Dermatol. 1968;80:744–6.
Schaefer H, Kuhn-Bussius H. A method for the quantitative determination of human sebum secretion. Arch Klin Exp Dermatol. 1970;238:429–35.
Seirafi H, Farsinejad K, Firooz A, et al. Biophysical characteristics of skin in diabetes: a controlled study. J Eur Acad Dermatol Venereol. 2009;23:146–9.
Serup J. Formation of oiliness and sebum output: comparison of a lipid-absorbent and occlusive-tape method with photometry. Clin Exp Dermatol. 1991;16:258–63.
Sisalli S, Adao A, Lebel M, et al. Sorptive tape extraction a novel sampling method for the in vivo study of skin. LC-GC Eur. 2006;19:33–9.
Smith KR, Thiboutot DM. Thematic review series: skin lipids. Sebaceous gland lipids: friend or foe? J Lipid Res. 2007;49:271–81.
Son T, Han B, Jung B, Nelson JS. Fluorescent image analysis for evaluating the condition of facial sebaceous follicles. Skin Res Technol. 2008;14:201–7.
Stewart ME, Downing DT. Measurement of sebum secretion rates in young children. J Invest Dermatol. 1985;84:59–61.
Stinco G, Bragadin G, Trotter D, et al. Relationship between sebostatic activity, tolerability and efficacy of three topical drugs to treat mild to moderate acne. J Eur Acad Dermatol Venereol. 2007;21:320–5.
Tagami H. Development of instruments for measuring the skin. J Jpn Med Assoc. 2003;129:1405–8.
Thody AJ, Shuster S. Control and function of sebaceous glands. Physiol Rev. 1989;69:383–416.
Wertz PW. Human synthetic sebum formulation and stability under conditions of use and storage. Int J Cosmet Sci. 2009;31:21–5.
Wójcik A, Budzisz E, Rotsztejn H. Skin surface lipids and their measurements. Post Dermatol Alergol. 2011;6:498–505.
Yong SW, Kim SJ, Hwang IA, Park KC. Evaluation of facial skin type by sebumeter secretion: discrepancies between subjective descriptions and sebum secretion. Skin Res Technol. 2002;8:168–72.
Youn SW, Na JI, Choi SY, et al. Regional and seasonal variations in facial sebum secretions: a proposal for the definition of combination skin type. Skin Res Technol. 2005;11:189–95.
Zouboulis CC, Boschnakow A. Chrono- and photoaging of human sebaceous gland. Clin Exp Dermatol. 2001;26:600–17.

Measurement of Skin Surface Hydration

15

Peter Clarys and André O. Barel

Contents

Keywords

Stratum corneum • Hydration • Electrical properties • Impedance • Capacitance • Measurement principle

1 Introduction

The presence of an adequate amount of water is an essential prerequisite for the maintenance of the normal structure and function of the stratum corneum. It has been known since many years that the electrical properties of the skin are related to the water content of the stratum corneum. Measurement of the total electrical resistance (impedance) of the skin to an alternating current of frequency F is the most widely used method for assessing the hydration state of the skin surface. The total impedance (Z) depends on two components, a resistance R and a capacitance C, as explained by a simple theoretical model where the skin is submitted to an electrical alternating circuit with a resistance in parallel with a capacitor (Lévêque and de Rigal 1983; Bernengo and de Rigal 2000; Tagami 2006; Barel and Clarys 2006; Gabard et al. 2006). As pointed out by many authors, the complex electrical impedance properties of the horny layer are dependent on the water content of this layer but also on a variety of other factors (ions, proteins, natural

P. Clarys (✉) • A.O. Barel
Faculty of Physical Education and Physiotherapy, Vrije Universiteit Brussel, Brussel, Belgium
e-mail: pclarys@vub.ac.be; anbarel@vub.ac.be

P. Humbert et al. (eds.), *Agache's Measuring the Skin*,
DOI 10.1007/978-3-319-32383-1_15

moisturizing factors, etc.). Many physical factors may play a role in impedance measurements: design of the oscillating electronic circuit and frequency of the electrical current, geometry of applied electrode on the skin (micrometer or millimeter distance between the electrodes), measuring depth of the electrical field in the skin, direct galvanic contact or not with the skin surface, pressure of application of the electrode, etc.

Comparative studies about the measuring capabilities of the various electrical methods have been published (Gabard et al. 2006; Clarys et al. 1999, 2012; Fluhr et al. 1999; Xia et al. 2009).

It is the aim of the present chapter to give an overview of the available commercial instruments but equally to discuss some recently developed devices used for the assessment of skin surface hydration.

2 Commercial Electrical Instruments

2.1 Corneometer CM 825

The principles and characteristics of this capacitance-based instrument manufactured by Courage-Khazaka have been published by several research groups (Barel and Clarys 2006; Gabard et al. 2006; Clarys et al. 1999, 2012; Fluhr et al. 1999; Xia et al. 2009; Corneometer CM 825, 2013; Heinrich et al. 2003). The instrument has a flat measuring probe with an interdigitating grid of gold-covered electrodes. During the measurement there is no direct galvanic contact of the electrode surface with the skin since the interdigitating grid is covered with a low dielectric vitrified material. The pressure of application of the measuring probe is lower than 1 N as assured by a spring system triggering the capacitance measurements. The frequency shifts from 0.95 MHz for a hydrated medium to 1.15 MHz for a dry medium. The variable total capacitance of the skin surface is converted in arbitrary units (a.u.) of skin hydration ranging from 20 (very dry) to 120 (well-hydrated) units. Skin penetration depth of the electrical current is about 45 mm.

2.2 DermaLab Moisture Unit

The instrument is based on skin conductance measurements and is manufactured by Cortex Technology (Gabard et al. 2006; Fluhr et al. 1999; DermaLab conductance instrument 2013), operating at a single frequency of 100 MHz and delivering impedance units between 0 and 10,000 μS. There are two moisture probes available: a classical flat-faced electrode for normal skin surface and a pin probe featuring eight pin electrodes for very dry and scaly skin and for scalp measurements. There is galvanic contact between the electrodes and the skin surface. A spring system assures a constant pressure of application of the probe on the skin surface (0.9 N) and triggers the measurement of impedance.

2.3 Moisture Meter

These more recent instruments are manufactured by Delfin Technologies. The technical description of these instruments and their use has been published (Alanen et al. 2004; Moisture Meter 2013). There are three types of instruments: the classical model Moisture Meter D operating at a frequency of 300 MHz, a compact and wireless model of Moisture Meter D (same frequency), and the new Moisture Meter SC, operating at 1.3 MHz. The Moisture Meter D instrument can be equipped with four different probes with different diameters of the measuring head. As a consequence measuring depths between 0.5 and 5.0 mm are obtained. Both versions of the Moisture Meter D deliver hydration data expressed as relative dielectric constant units. The Moisture Meter SC, fully portable and with wireless data transfer capabilities, is also equipped with a variable application force system ranging from 0 to

1.81 N. The measuring depth is 2 mm. This instrument delivers arbitrary dielectric constant data which are converted in water content (in percent).

2.4 Nova Dermal Phase Meter

These instruments are manufactured by Nova Technology Corporation, and technical descriptions of the system have been published (Gabard et al. 2006; Clarys et al. 1999; Fluhr et al. 1999; Nova DPM 9003 2013). The instruments measure impedance of the skin at preselected frequencies up to 1 MHz. The final readout is given in arbitrary DPM units. Different sizes of measuring probes are available: DPM 9103 external diameter of electrode 8.76 mm, DPM 9105 diameter 5.08 mm, and DPM9107 diameter 3.81 mm. Constant pressure of application is assured by means of a sensor switch spring system. Recently a handheld portable apparatus (Penguin) has been developed with a wireless transmission system of data. This model delivers also data concerning skin surface temperature and force of application of the probe.

2.5 Skicon 200 EX

This instrument is commercialized by ISB Company (Tagami 2006; Gabard et al. 2006; Clarys et al. 2012; O'Goshi and Serup 2007; co.jp, skicon 200 EX 2013). Technical descriptions of the most recent apparatus (Skicon 200 EX) have been published (co.jp, skicon 200 EX 2013). The Skicon 200 EX measures the impedance expressed in micro-siemens (μS) units, at a single frequency of 3.5 MHz. The measuring head consists of concentric interdigitating gold-covered electrodes with a gap of 200 mm between the electrodes. There is direct galvanic contact between the electrodes and the skin. Pressure application of the electrode on the skin surface is constant using a spring system (0.5 N) (Clarys et al. 2012).

3 Recently Developed Devices

Other more sophisticated experimental devices for measuring hydration and image hydration of the skin have been recently developed.

3.1 Opto-thermal Transient Emission Radiometry (OTTER)

This novel experimental infrared remote-sensing technology developed by Imhof et al. (1984) measures in vivo the opto-thermal emission at a wavelength of 13.1 mm. From the opto-thermal decay curves, a water distribution profile in the stratum corneum can be determined in vivo. However this rather expensive instrument has not been commercialized.

3.2 Skin Capacitance Imaging Systems

A nonoptical skin surface imaging system, based on the fingerprint-sensing technology, has been developed by the L'Oréal research group: skin capacitance imaging (SCI) (Lévêque and Querleux 2003). The sensor is composed of an array of capacitance microsensors. SCI images are acquired, and the capacitance values are transformed into a range of 256 gray levels to compose a nonoptical image. The mean gray level of the image represents the average skin surface hydration correlating well with the average capacitance values given by the Corneometer (Xhauflaire-Uhoda and Piérard 2009). This device remains experimental and is not commercially available.

Aqualmarger, a contact imaging instrument using silicon fingerprint sensors, has been recently developed by Biox Systems. The device with 256 × 300 capacitance-sensing pixels (5 μm resolution) has shown potentials for skin hydration imaging and skin surface microrelief measurements (Xiao et al. 2011).

Finally the Moisture Map MM 100 instrument developed by Courage-Khazaka became recently commercially available (Moisture Map MM 100 2014). This instrument is a device featuring a capacitance sensor based on the recording fingerprint technology (patent of L'Oréal on skin chip (Lévêque and Querleux 2003)). The image of the Moisture Map sensor of the skin surface represents graphical information on the mean surface hydration distribution and also the microtopography of the surface.

3.3 Confocal Raman Spectroscopy

Raman instruments are becoming commercially available, and in the typical in vivo Raman spectra obtained, the respective contributions of keratins and water can be discriminated (Caspers et al. 1998). As a consequence the percentage of water in the skin in function of depth can be determined from Raman spectra (Van Der Pol and Caspers 2009). Unfortunately these Raman spectroscopy instruments are rather expensive and not used for routine measurements.

4 Conclusions

Taking into account the comparative performances and the high degree of correlation between the instruments, the possibilities of in vitro calibration, the range of sensitivity, the depth of measurement, and the low coefficient of intra-person variability, it can be concluded in this chapter that the Corneometer, DermaLab, Moisture Meter, Nova Dermal Phase Meter, and Skicon are validated electrical instruments for assessing the hydration state of the horny layer. The recently developed but not always commercially available instruments allow the determination of additional stratum corneum properties.

Acknowledgments The authors are grateful to Dr. Bernard Gabard for his contribution to this chapter.

References

Alanen E, Nuutinen J, Nicklén K, Lahtinen T, et al. Measurement of hydration in the stratum corneum with the Moisture Meter and comparison with the Corneometer. Skin Res Technol. 2004;10:32–7.

Barel AO, Clarys P. Measurement of epidermal capacitance. In: Serup J, Jemec GB, Grove GL, editors. Handbook of non-invasive methods and the skin. Boca Raton: CRC Press; 2006. p. 337–44.

Bernengo JC, de Rigal J. Techniques physiques de mesure de l'hydratation du Stratum Corneum. In: Agache P, editor. Physiologie de la peau et explorations fonctionelles cutanée. Cachau: Editions Médicales Internationales; 2000. p. 117–62.

Caspers PJ, Lucassen GW, Wolthuis R, et al. In vitro and in vivo Raman spectroscopy of human skin. Biospetroscopy. 1998;4:S31–9.

Clarys P, Barel AO, Gabard B. Non invasive electrical measurements for the evaluation of the hydration state of the skin: comparison between the capacitance method (Corneometer), the conductance method (Skicon) and capacitive reactance method (Nova). Skin Res Technol. 1999;5:14–20.

Clarys P, Clijsen R, Taeymans J, Barel AO. Hydration measurements of the stratum corneum: comparison between the capacitance method (digital version of the Corneometer CM 825) and the impedance method (Skicon 200EX). Skin Res Technol. 2012;18:316–23.

co.jp, skicon 200 EX. 2013. www.ibs-hamamatsu. I.B.S. Co Ltd, Shizuoka-Ken.

Corneometer CM 825, 11. 2013. www.courage-khazaka.com. Courage-Khazaka, Cologne.

DermaLab conductance instrument. 2013. www.cortex.dk. Cortex Technology, Hadsund.

Fluhr JW, Gloor M, Lazzereni SL, Kleesz P, et al. Comparative study of five instruments measuring stratum corneum hydration (Corneometer CM 820 and CM 825, Skicon 200, Nova DPM 9003DermaLab) Part II. In vivo. Skin Skin Res Technol. 1999;5:171–8.

Gabard B, Clarys P, Barel AO. Comparison of commercial electrical measurement instruments for assessing the hydration state of the stratum corneum. In: Serup J, Jemec GB, Grove GL, editors. Handbook of non-invasive methods and the skin. Boca Raton: CRC Press; 2006. p. 351–8.

Heinrich U, Koop U, Leneveu-Duchemin MC, Osterrieder K, et al. Multicenter comparison of skin hydration in terms of physical, physiological, and product dependent parameters by the capacitive method (Corneometer CM 825). Int J Cosmet Sci. 2003;25:45–53.

Imhof RE, Birch DJ, Thornley FR, Gilchrist JT, et al. Opto-thermal transient emission radiometry. J Phys Sci Instrum. 1984;17:521–5.

Lévêque JL, de Rigal J. Impedance methods for studying skin moisturization. J Soc Cosmet Chem. 1983;34:419–28.

Lévêque JL, Querleux B. Skin Chip®, a new tool for investigating the skin surface in vivo. Skin Res Technol. 2003;9:313–47.

Moisture Map MM 100. 2014. www.courage-khazaka.de.

Moisture meter. 2013. www.delfintech.com. Delfin Technologies, Stamford.

Nova DPM 9003. 2013. www.novatechcorp.com. Nova technologies, Portsmouth.

O'Goshi KI, Serup J. Skin conductance: validation of the Skicon 200 EX compared to the original Skicon 100. Skin Res Technol. 2007;13:13–8.

Tagami H. Epidermal hydration: measurement of high frequency electrical conductance. In: Serup J, Jemec GB, Grove GL, editors. Handbook of non-invasive methods and the skin. Boca Raton: CRC Press; 2006. p. 329–36.

Van Der Pol A, Caspers PJ. Confocal Raman spectroscopy for in vivo skin hydration measurement. In: Barel AO, Paye M, Maibach HI, editors. Handbook of cosmetic science and technology. New York: Informa; 2009. p. 151–64.

Xhauflaire-Uhoda E, Piérard GE. Skin capacitance imaging. In: Barel AO, Paye M, Maibach HI, editors. Handbook of cosmetic science and technology. New York: Informa; 2009. p. 141–9.

Xia P, Cortea LI, Singh H, Zeng X. In vivo hydration – a comparison study of different measuring techniques. 2009. www.skin-forum.eu/posters.

Xiao P, Singh Hn Ou X, Caparnagiu AR, Kramer G, Imhof RE. In-vivo solvent penetration measurement using contact imaging and skin stripping. SCC Annual Scientific Meeting & Technology Showcase, New York. 2011.

Infant Skin Hydration

16

Marty O. Visscher

Contents

M.O. Visscher (✉)
Skin Sciences Program, Division of Plastic Surgery, Cincinnati Children's Hospital Medical Center, Cincinnati, OH, USA

Department of Surgery, College of Medicine, University of Cincinnati, Cincinnati, OH, USA
e-mail: marty.visscher@gmail.com

P. Humbert et al. (eds.), *Agache's Measuring the Skin*,
DOI 10.1007/978-3-319-32383-1_16

Keywords
Infant • Neonate • Premature • Skin barrier • Stratum corneum • Hydration • Transepidermal water loss • Innate immunity

1 Introduction

Optimum hydration is critical for stratum corneum (SC) function (Blank 1952; Gloor et al. 1998). Among the multiple functions affected by SC water content are desquamation, restoration of barrier integrity after wounding, acid mantle formation, microbial colonization, tactile discrimination, infection control, immunosurveillance, and protection against ultraviolet light and environmental irritants (Rawlings and Leyden 2009). Optimum hydration may be defined as the amount of SC water that achieves flexibility (biomechanics) while facilitating terminal differentiation, programmed cell death, and orderly corneocyte incorporation into the lower SC with balanced pH-dependent desquamation of the outer SC. Overhydration can cause maceration, disruption of the intercellular lipid bilayers, desmosomal degradation with creation of amorphous regions, corneocyte swelling, enhanced molecular transport, and increased permeability (Warner et al. 1999, 2003; Zimmerer et al. 1986), as well as irritation, inflammation,

and urticaria (Halkier-Sorensen et al. 1995; Hurkmans et al. 1985; Kligman 1996; Medeiros 1996; Rustemeyer and Frosch 1996; Willis 1973). Low hydration can cause dryness/scaling, aberrant desquamation via reduced enzyme activity, cracking, reduced flexibility, tightness, and itching. On balance, the SC water-handling properties must be sufficiently robust to respond to local, potentially disruptive forces, e.g., friction, heat, humidity, bathing, and topical product applications (Visscher et al. 2002). This chapter explores infant skin hydration for healthy full-term infants and premature babies and considers the factors that impact hydration after birth.

2 Fetal Skin Development

Water concentration varies throughout the SC (Warner et al. 1988) with lower hydration in the outermost layers, increasing with depth and decreasing at the lowest levels (Bouwstra et al. 2003). In vivo measurements with Raman spectroscopy indicate normal skin to be 25–30 % water, while hydrated SC is 45 % and dry skin ranging from 10 % to 15 % (Boncheva et al. 2009).

In contrast, the human fetus is immersed in a high-water environment of amniotic fluid during development. Epidermal cornification begins to occur around 23 weeks from head to toe and dorsal-ventral (25 week, abdomen) over the fetus and occurs in a programmatic fashion from head (initially, week 23) to toe and dorsal-ventral (week 25, abdomen) across the fetus, presumably under hormonal control (Hoath et al. 2006; Hardman et al. 1998). This is in contrast to skin cultures where cornification does not occur when the epidermis is covered with water and requiring dry conditions for SC formation (Supp et al. 1999). Vernix caseosa, a mixture of sebaceous gland secretions, lanugo, and desquamated epithelial cells, appears about the time of fetal cornification. It extrudes onto the epidermis through the hair shaft, spreads over the surface (Hardman et al. 1998), and, presumably, protects the epidermis from exposure to amniotic fluid via formation of a hydrophobic layer (Youssef et al. 2001). Although the mechanism is yet unknown, vernix may create a sufficiently dry environment for cornification.

3 Full-Term Infant Skin Hydration

3.1 Birth

Within minutes to hours after birth, full-term infant skin hydration varies with body site (chest, back, forehead), time under the radiant warmer, and the presence of vernix (Visscher et al. 1999a, 2005). Despite prolonged exposure to water during gestation, low skin hydration is consistently observed in full-term neonates within the first day after birth (Visscher et al. 1999b, 2000, 2005; Fluhr et al. 2012). In 30 healthy full-term infants, hydration decreased markedly in the first day and then increased during the first 2 weeks, unlike the mother's skin where hydration was relatively constant (Fig. 1). Water-binding ability also increased during the first 14 days. Water-handling properties of the upper inner thigh and buttocks were evaluated in 19 healthy full-term infants at birth (day 3 or 7) and months 1, 3, 6, 9, and 12. SC hydration for the thigh increased over the first month was relatively constant over 12 months and was lower than their mothers' values (Minami-Hori et al. 2014). Water holding capacity of thigh SC was higher for infants versus mothers, decreased during the first month and then remained constant.

These changes suggest that the SC is undergoing adaptive changes to the drier environment (Visscher et al. 2000). Abrupt humidity reduction in hairless mice increased DNA synthesis, decreased total free amino acids, and reduced filaggrin immunoreactivity, due to decreased epidermal keratohyalin granules induced by high

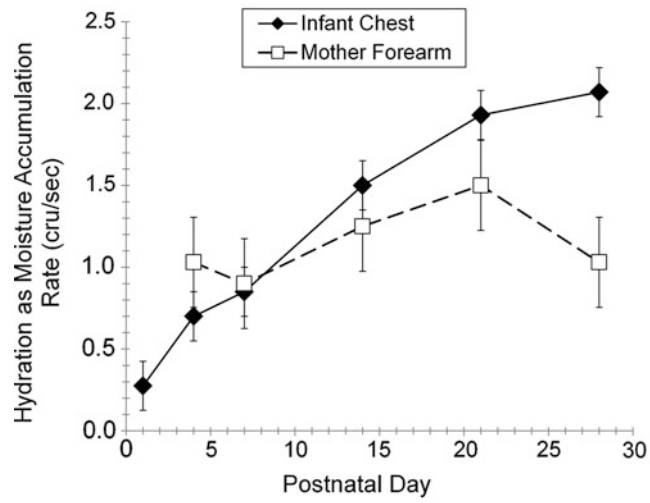

Fig. 1 Full-term skin hydration over the first month. In 30 healthy full-term infants, hydration decreased markedly in the first day and then increased during the first 2 weeks, unlike the mother's skin where hydration was relatively constant (Adapted from Visscher et al. 2000)

humidity and produced dry skin (Visscher et al. 1999b; Denda et al. 1998; Katagiri et al. 2003; Scott and Harding 1986). Low hydration may indicate an underdeveloped SC due to lack of transglutaminase activity (Rawlings and Matts 2005). However, this is unlikely since very low transepidermal water loss (TEWL) is consistently observed full-term newborn skin indicating a well-functioning epidermal barrier (Fluhr et al. 2012; Hammarlund et al. 1979; Ludriksone et al. 2014).

3.2 Vernix

Vernix covers newborn skin at birth and contains 80 % water. It is sometimes removed immediately after birth. Its potential hydrating effects were evaluated in parallel groups of full-term infants. Vernix was wiped off at delivery in one group and left on and allowed to rub in for another. The vernix-treated skin had significantly higher skin hydration at 4 h and 24 h after birth ($p < 0.05$) (Fig. 2a; Visscher et al. 2005). Skin pH values were lower in the vernix-treated group suggesting that vernix assists in acid mantle development (Fig. 2b; Visscher et al. 2005). Visual erythema was lower immediately after birth for the vernix group and dryness tended to be lower ($p = 0.10$).

3.3 Adaptation and Time

The full-term infant skin was significantly drier than the skin of older infants (1, 2, and 6 months) and the mothers (Nikolovski et al. 2008). Low SC hydration and dryness during the immediate postnatal period may result from several interacting factors including a lack of water-binding natural moisturizing factor (NMF) in the upper SC, via extraction into the amniotic fluid in utero (soaking effect) (Visscher et al. 2002; Robinson et al. 2010a) and/or to delayed or impaired filaggrin proteolysis at high humidity (Scott and Harding 1986). About 40 % of NMF consists of free amino acids (FAA) that result from proteolysis of filaggrin. FAA levels were measured for high-performance liquid chromatography analysis of the surface SC collected from the skin surface of newborn infants. The levels were extremely low at birth (in the absence of vernix), increased over the first month but remained markedly lower than typical adult levels (Fig. 3a;

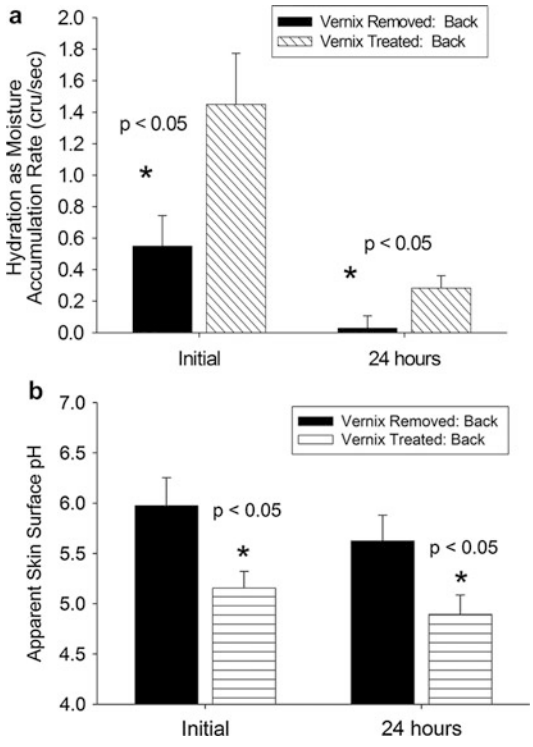

Fig. 2 (**a**, **b**) Effect of vernix on infant skin hydration. At birth, vernix was allowed to remain on the skin in one group of healthy newborns and removed from the other. The vernix-treated skin had significantly higher skin hydration at 4 h and 24 h after birth ($p < 0.05$) (**a**). Skin pH values were lower in the vernix-treated group suggesting that vernix assists in acid mantle development ($p < 0.05$) (**b**). From Visscher et al. 2005

Visscher et al. 2011). Vernix contains FAAs, and the relative amounts of histidine and glutamic acid were higher than expected from filaggrin proteolysis alone, indicating that vernix may contain other sources of soluble amino acids. Vernix-treated skin had significantly higher FAA levels 24 h after birth compared to skin with vernix removed, paralleling the higher skin hydration (Fig. 3b; Visscher et al. 2011). The higher FAAs in the vernix-treated skin are attributed to the vernix rather than to proteolysis of filaggrin in the upper stratum corneum secondary to a reduction in ambient humidity (Scott and Harding 1986).

To further examine the cause of low hydration, levels of FAA were measured across ten layers of neonatal foreskin and adult volar forearm skin. Neonatal foreskin was used as an in vitro control for newborn skin because FAA levels could be determined as a function of SC depth. FAAs were significantly lower across ten layers of neonatal foreskin compared to adult volar forearm skin. The arginine/citrulline ratio is relatively high in filaggrin, i.e., 8:1 (McKinley-Grant et al. 1989). To facilitate proteolysis to FAA, the filaggrin arginine residues must be deaminated to citrulline to allow separation from the intracorneocyte matrix (Chavanas et al. 2006; Kamata et al. 2009). Despite the depth in the tissue, citrulline levels were diminished relative to adults, and the ratio of arginine to citrulline was higher in foreskin. This suggests that filaggrin proteolysis to form FAA had not occurred in the uppermost layers of foreskin SC and, perhaps, that the newborn infant is not yet producing water-binding amino acids to hydrate the SC.

Additional information about SC hydration has been determined among infants aged 3–12 months and compared with adults using Raman confocal microspectroscopy. Water levels were higher in infants to a depth of 26 μm versus the same depth in adults, with the greatest difference at a depth of 10–14 μm (Nikolovski et al. 2008). Compared with adults, SC NMF levels were lower in infants in the outer 12 μm. Water content (mass percent) measured by Raman confocal microspectroscopy was lower throughout the SC for full-term newborns aged 1–15 days than older infants and adults. The level in the SC of 60 % water saturation was deeper for the youngest infants (Fluhr et al. 2012). One explanation of the lower levels in infants is that sphingomyelinase and B-glucocerebrosidase are not able to function under the conditions of acidity and hydration, resulting in an SC lipid matrix that is not fully competent due to the absence of specific hydrophobic components. An examination of NMF levels at an SC depth of 1–2 μm by attenuated total reflectance Fourier transform infrared spectroscopy showed no significant differences from birth to 12 months in a cohort of healthy full-term infants for either the upper inner thigh or the buttocks (Minami-Hori et al. 2014).

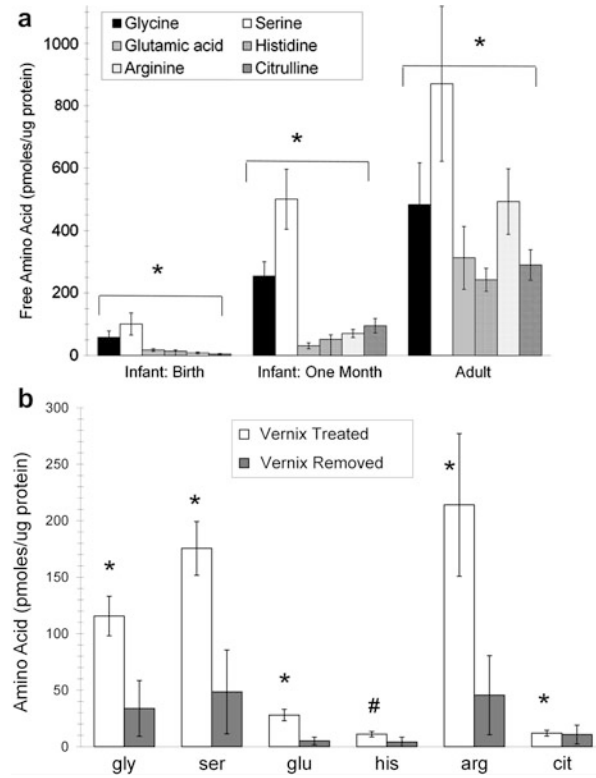

Fig. 3 (**a**, **b**) Free amino acid levels in infant skin. The free amino acid (FAA) component of natural moisturizing factor was measured from surface SC collected from newborn infants. The levels were extremely low at birth (in the absence of vernix), increased over the first month, but remained markedly lower than typical adult levels (**a**). *Indicates all groups different from each other ($p < 0.05$). Vernix-treated skin had significantly higher FAA levels 24 h after birth compared to skin with vernix removed, paralleling the higher skin hydration (**b**). *Indicates higher for a vernix-treated skin ($p < 0.05$). #Indicates lower for a vernix-treated skin ($p < 0.05$) (Figure 3b reprinted with permission from John Wiley and Sons)

4 Premature Infant Skin Hydration

4.1 Relevance

Premature infants are at increased risk for infection, a leading cause of mortality, due to an underdeveloped epidermal barrier with few cornified layers (Evans and Rutter 1986; Cartlidge 2000). Reduction in mortality is a global health priority. Implementation of evidence-based strategies for catheter insertion and maintenance of very premature infants significantly reduced infections, but to a lesser extent than expected (Kaplan et al. 2011). Poor skin integrity may be a predisposing factor for sepsis.

4.2 Birth, Effects of Gestational Age, and Adaptation

At 23 weeks GA, TEWL values can be as high as 75 g/m^2/h, and skin hydration is high as the SC is nearly absent (Sedin et al. 1983). By week 26, a few cornified layers have formed (TEWL of ~45 g/m^2/h), corresponding to a wounded skin surface (Evans and Rutter 1986; Cartlidge 2000). At 29 weeks, TEWL is 17 g/m^2/h and markedly higher than values of 5–6 g/m^2/h observed in full terms. To investigate the rate of SC maturation, hydration and TEWL were measured daily, over periods of up to 67 days, in ten very premature infants ranging from 23 to 32 weeks GA (most were <26–27 weeks) (Kalia et al. 1998) using low-frequency impedance spectroscopy to measure hydration (Fig. 4). Skin impedance was low in premature infants, indicating high levels of SC hydration and gradually decreased over time, i.e., ~70 days (Emery et al. 1991). Impedance values increased with increasing gestation. There was variability in the rate of change in hydration and TEWL, as shown for infants of 23 weeks' (Fig. 4a, b) and 26 weeks' GA (Fig. 4c, d), respectively. The time to reach normal (full-term) hydration (skin impedance of 200) was longer for the younger infant with increasing SC hydration and

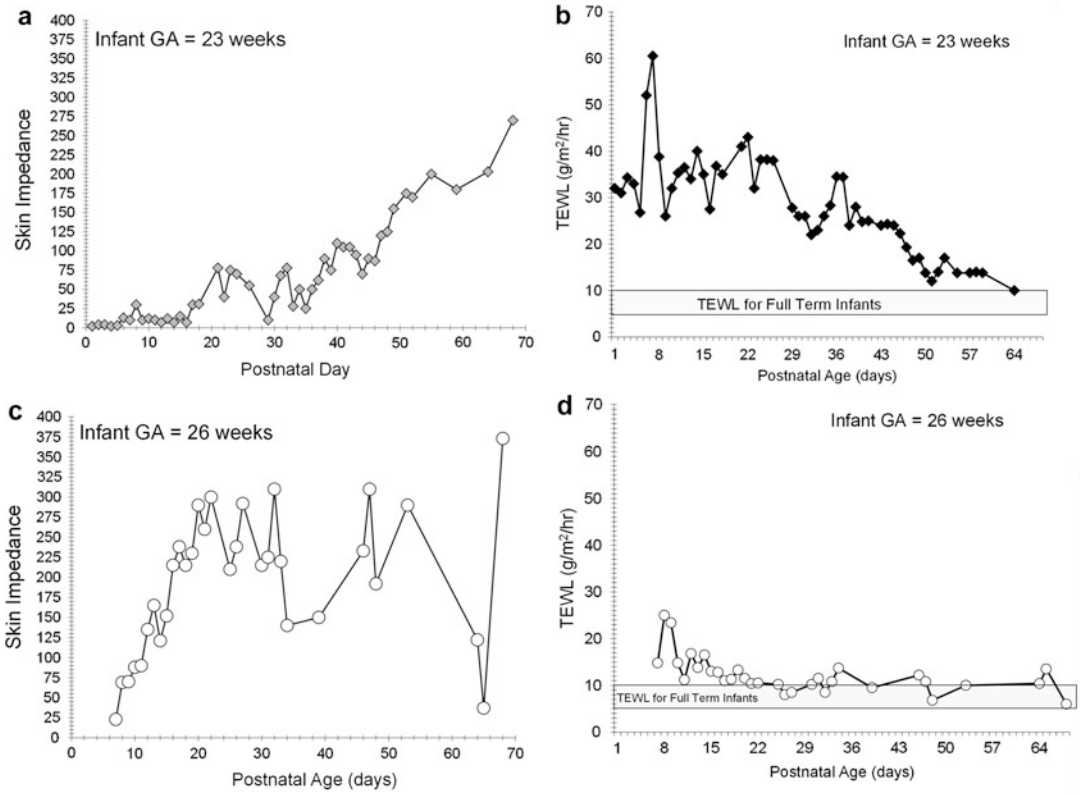

Fig. 4 (**a**, **b**, **c**, **d**) Stratum corneum maturation in premature infants. Hydration and TEWL were measured daily in ten very premature infants ranging from 23 to 32 weeks GA. Skin impedance was low in premature infants, indicating high SC hydration, and gradually decreased over time. There was variability in the rate of change in hydration and TEWL, as shown for infants of 23 weeks (**a**, **b**) and 26 weeks GA (**c**, **d**), respectively. The time to reach normal (full-term) hydration (skin impedance of 200) was longer for the younger infant with increasing SC hydration and decreasing TEWL over time. The profile differed for the 26-week infant as "normal" levels occurred more quickly (Adapted from Kalia et al. 1998)

decreasing TEWL over time. The profile differed for the 26-week infant as "normal" levels occurred more quickly. The time to complete SC maturation may be as long as 9 weeks postnatal age (Kalia et al. 1998; Harpin and Rutter 1983; Agren et al. 1998; Nonato et al. 2000).

SC hydration was inversely related to gestational age among 40 premature and full-term neonates (Okah et al. 1995). Skin hydration was measured daily from days 2–7 and then weekly for 7 weeks in 48 premature infants of 30–37 weeks GA (mean 34.4). Overall, hydration was constant over the period and higher for the abdomen and buttocks versus the leg and forehead (Kanti et al. 2014). SC hydration was significantly higher for the most premature subgroup, aged 30.3–33.7 weeks, but decreased over time versus the older groups which were 34.0–34.8 and 35–36.7 weeks GA. Skin hydration for the leg increased over time for infants 35–36.7 weeks.

One day after birth, SC hydration was significantly higher for infants <30 weeks gestational age than infants >30 weeks due to high amounts of water passing through the skin. Hydration values did not differ for infants 32–24 weeks GA versus full-term neonates (≥37 weeks GA). Hydration values on day 5 were significantly lower than on day 1 for infants less than

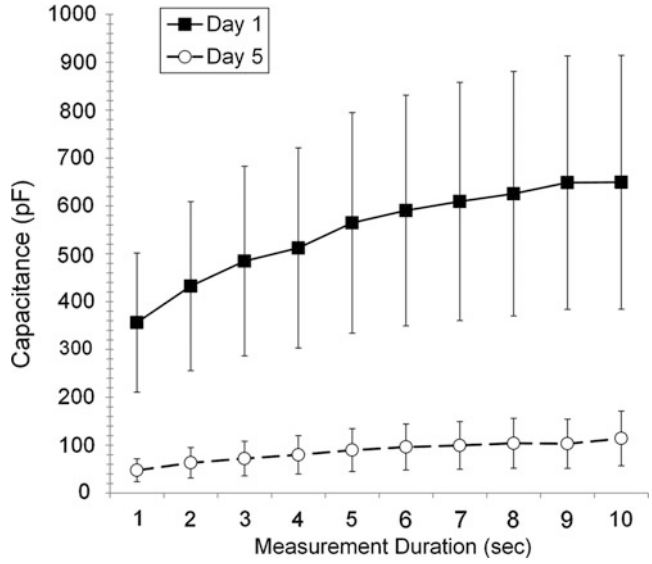

Fig. 5 Stratum corneum hydration in premature infants. One day after birth, SC hydration was significantly higher for infants <30 weeks gestational age than infants >30 weeks due to high amounts of water passing through the skin. Hydration values did not differ for infants 32–24 weeks GA versus full-term neonates (≥37 weeks GA). Hydration values on day 5 were significantly lower than on day 1 for infants less than 26 weeks GA, and environmental conditions (isolettes) were constant throughout the period (Adapted from Okah et al. 1995)

26 weeks GA, and environmental conditions (isolettes) were constant throughout the period (Fig. 5). This finding suggests that SC maturation is rapid for very premature infants once they are exposed to a dry environment (Harpin and Rutter 1983; Okah et al. 1995) (Agren et al. 2006). Very premature infants frequently exhibit an abnormal desquamation several weeks after birth, indicative of a hyperproliferative SC (Okah et al. 1995; Bodak and Bodemer 2002; Visscher et al. 2009). Humidity affects filaggrin proteolysis to form NMF which, in term, hydrates the skin (Rawlings et al. 1994). NMF levels are likely to be quite low under the conditions of rapid skin development for premature infants in low-humidity settings, based on results of newborn animal studies (Scott and Harding 1986).

5 Infants, Atopy, and Hydration

Atopic dermatitis is characterized by a compromised barrier, reduced ceramides and mutations of the filaggrin gene, and increased barrier permeability (Imokawa et al. 1991; Ponyai et al. 2008; Weidinger et al. 2006). Uninvolved atopic skin exhibits subclinical inflammation, reduced hydration, increased TEWL, and increased SC turnover (Tagami et al. 2006). The skin hydration of uninvolved, non-lesional skin on the cheek, chest, back, forearm, and leg of infants <12 months of age was significantly lower than comparable sites in a cohort of nonatopic infants of the same age (Matsumoto et al. 2007). Decreased hydration was also found in older cohorts and infants between 1–2 years and 2–4 years, versus their nonatopic counterparts.

6 Factors Influencing Infant Skin Hydration

Some of the "environmental" factors that impact infant SC hydration have been described above as the infant transitions from a wet environment during gestation to relatively drier surroundings after birth. Routine activities of daily living, such as water exposure (bathing), clothing (diapering),

and application of topical materials are expected to impact infant SC hydration as they do in adults.

6.1 Water Exposure: Bathing

With bathing, infant SC transitions from dry to wet and back to a dry environment, somewhat analogous to the transition from aqueous in utero conditions to much drier conditions at birth. Bathing in water for 10 min significantly decreased hydration, measured as the rate of moisture accumulation, friction, visual erythema, and visual dryness 15 min later (Visscher et al. 2002). The time of recovery to prebath hydration levels was not determined. Similarly, SC hydration decreased in adults who soaked for 10 min, and reductions in hydration persisted for more than 4 h (Visscher et al. 2003). Subsequent studies indicated that the reduction in SC hydration was associated with decreases in NMF measured in the upper SC (Robinson et al. 2010a, b). While the impact of water exposure on infant NMF has not been reported, similar findings are anticipated.

Fifty-seven healthy full-term newborns were either bathed with water or wiped with a water-soaked cloth twice weekly from days 7–28 weeks. SC hydration was higher on the abdomen and forehead for the bathing group than the water-wiped group, although SC hydration levels were lower than for older infants and adults (Garcia Bartels et al. 2009). However, it was not possible to determine whether the increases were due to adaptation or to the water exposure from each method. Healthy newborns ($n = 307$) were enrolled within 48 h of birth in a randomized trial to compare a cleanser versus water alone at least twice per week for 4 weeks. SC hydration did not differ for the two products over the study period (Lavender et al. 2013). The effects of bathing twice weekly with two liquid cleansers and water along were determined among three parallel groups of infants ($n = 180$ total) aged 1 day to <12 months. SC hydration increased versus baseline for the cleansers versus water after 1 week but returned to baseline levels at week two, with no evidence of dryness, erythema, or edema (Dizon et al. 2010). Infants and young children ($n = 125$), aged 1–36 months, used a liquid baby wash or a baby shampoo at least three times weekly or a baby lotion (and bathing) once daily over 4 weeks. Both the baby wash and baby lotion resulted in significantly increased SC hydration at weeks 1 and 4 (Coret et al. 2014). The increase was attributed to the skin care products although there was no untreated control to eliminate factors that could have increased hydration.

6.2 Diapers

SC hydration of diapered and non-diapered skin sites did not differ at birth (Visscher et al. 2000). Measurements were made 15 min after removing the diaper to avoid confounding effects of surface water. Diapered skin hydration increased significantly over the first two postnatal weeks and was higher than non-diapered skin on day 7, but the sites were not different by day 28. Diapered skin hydration increased from day 2–28 among 44 healthy newborns with values higher on the buttocks versus the leg (Garcia Bartels et al. 2012). Among 3–6-month-old infants, skin hydration was lower for diapered versus non-diapered skin 15 min after diaper removal, suggesting that the site difference continues over time (Visscher et al. 2002). Diaper SC hydration increased during the first month of life and then remained constant through the first year among 19 infants (Minami-Hori et al. 2014). The water holding capacity followed a similar pattern, diminishing in month one.

Disposable diaper technology has progressed significantly since it was first introduced, particularly with the development of water-vapor-permeable outer covers that reduce skin hydration and in diaper humidity (Counts et al. 2014). The severity of diaper dermatitis has decreased as a result of these advances (Odio and Friedlander 2000; Runeman 2008).

6.3 Effect of Humidity: Premature Infants

Groups of hairless mice were kept at high (90 % RH) and low (10 % RH) humidity for 5 days following acclimation at 40–50 % RH. Epidermal DNA synthesis increased, beginning 12 h after exposure to low humidity, but did not change at high humidity, even though TEWL values were comparable. SC hydration was significantly lower for the low-humidity group, suggesting that the decrease in SC hydration caused an increase in DNA synthesis (Sato et al. 1998). The effect of environmental humidity on skin barrier development in 22 premature infants aged 23–27 weeks was determined by varying the incubator humidity after 7 days at 85 % relative humidity (RH). Infants were then exposed to either 75 % or 50 % RH until day 28. Barrier integrity, measured as TEWL, decreased significantly from about 62 g/m^2/h at birth to about 33 g/m^2/h on day 7. The decrease at day 28 was significantly more pronounced at 50 % RH with a mean TEWL of 13 g/m^2/h versus 22 g/m^2/h at 70 %. Although SC hydration was not measured, values would likely be reduced, given the findings from the animal study. The influence of decreasing humidity at birth on filaggrin was determined using a newborn rat model (Scott and Harding 1986). Proteolysis occurred immediately after birth, and filaggrin was found in the lower stratum corneum only (Scott and Harding 1986). Proteolysis depended on the humidity at birth and was observed at ranges of 80–95 % RH, but not at 100 % RH.

References

Agren J, Sjors G, Sedin G. Transepidermal water loss in infants born at 24 and 25 weeks of gestation. Acta Paediatr. 1998;87:1185–90.

Agren J, Sjors G, Sedin G. Ambient humidity influences the rate of skin barrier maturation in extremely preterm infants. J Pediatr. 2006;148:613–7.

Blank IH. Factors which influence the water content of the stratum corneum. J Invest Dermatol. 1952;18:433–40.

Bodak N, Bodemer C. Cutaneous hydration of the premature and new born. Ann Dermatol Venereol. 2002;129:143–6.

Boncheva M, de Sterke J, Caspers PJ, Puppels GJ. Depth profiling of stratum corneum hydration in vivo: a comparison between conductance and confocal raman spectroscopic measurements. Exp Dermatol. 2009;18:870–6.

Bouwstra JA, de Graaff A, Gooris GS, Nijsse J, Wiechers JW, van Aelst AC. Water distribution and related morphology in human stratum corneum at different hydration levels. J Invest Dermatol. 2003;120:750–8.

Cartlidge P. The epidermal barrier. Semin Neonatol. 2000;5:273–80.

Chavanas S, Mechin MC, Nachat R, Adoue V, Coudane F, Serre G, Simon M. Peptidylarginine deiminases and deimination in biology and pathology: relevance to skin homeostasis. J Dermatol Sci. 2006;44:63–72.

Coret CD, Suero MB, Tierney NK. Tolerance of natural baby skin-care products on healthy, full-term infants and toddlers. Clin Cosmet Invest Dermatol. 2014;7:51–8.

Counts JL, Helmes CT, Kenneally D, Otts DR. Modern disposable diaper construction: innovations in performance help maintain healthy diapered skin. Clin Pediatr (Phila). 2014;53:10S–3.

Denda M, Sato J, Masuda Y, Tsuchiya T, Koyama J, Kuramoto M, Elias PM, Feingold KR. Exposure to a dry environment enhances epidermal permeability barrier function. J Invest Dermatol. 1998;111:858–63.

Dizon MV, Galzote C, Estanislao R, Mathew N, Sarkar R. Tolerance of baby cleansers in infants: a randomized controlled trial. Indian Pediatr. 2010;47:959–63.

Emery MM, Hebert AA, Aguirre Vila-Coro A, Prager TC. The relationship between skin maturation and electrical skin impedance. J Dermatol Sci. 1991;2:336–40.

Evans NJ, Rutter N. Development of the epidermis in the newborn. Biol Neonate. 1986;49:74–80.

Fluhr JW, Darlenski R, Lachmann N, Baudouin C, Msika P, De Belilovsky C, Hachem JP. Infant epidermal skin physiology: adaptation after birth. Br J Dermatol. 2012;166:483–90.

Garcia Bartels N, Mleczko A, Schink T, Proquitte H, Wauer RR, Blume-Peytavi U. Influence of bathing or washing on skin barrier function in newborns during the first four weeks of life. Skin Pharmacol Physiol. 2009;22:248–57.

Garcia Bartels N, Massoudy L, Scheufele R, Dietz E, Proquitte H, Wauer R, Bertin C, Serrano J, Blume-Peytavi U. Standardized diaper care regimen: a prospective, randomized pilot study on skin barrier function and epidermal il-1alpha in newborns. Pediatr Dermatol. 2012;29:270–6.

Gloor M, Bettinger J, Gehring W. Modification of stratum corneum quality by glycerin-containing external ointments. Hautarzt. 1998;49:6–9.

Halkier-Sorensen L, Petersen BH, Thestrup-Pedersen K. Epidemiology of occupational skin diseases in

Denmark: notification, recognition and compensation. In: Van der Valk PGM, Maibach HI, editors. The irritant contact dermatitis syndrome. Boca Raton FL: CRC Press; 1995. p. 23–52.

Hammarlund K, Nilsson GE, Oberg PA, Sedin G. Transepidermal water loss in newborn infants. II. Relation to activity and body temperature. Acta Paediatr Scand. 1979;68:371–6.

Hardman MJ, Sisi P, Banbury DN, Byrne C. Patterned acquisition of skin barrier function during development. Development. 1998;125:1541–52.

Harpin VA, Rutter N. Barrier properties of the newborn infant's skin. J Pediatr. 1983;102:419–25.

Hoath SB, Pickens WL, Visscher MO. The biology of vernix caseosa. Int J Cosmet Sci. 2006;28:319–33.

Hurkmans JF, Bodde HE, Van Driel LM, Van Doorne H, Junginger HE. Skin irritation caused by transdermal drug delivery systems during long-term (5 days) application. Br J Dermatol. 1985;112:461–7.

Imokawa G, Abe A, Jin K, Higaki Y, Kawashima M, Hidano A. Decreased level of ceramides in stratum corneum of atopic dermatitis: an etiologic factor in atopic dry skin? J Invest Dermatol. 1991; 96:523–6.

Kalia YN, Nonato LB, Lund CH, Guy RH. Development of skin barrier function in premature infants. J Invest Dermatol. 1998;111:320–6.

Kamata Y, Taniguchi A, Yamamoto M, Nomura J, Ishihara K, Takahara H, Hibino T, Takeda A. Neutral cysteine protease bleomycin hydrolase is essential for the breakdown of deaminated filaggrin into amino acids. J Biol Chem. 2009;284:12829–36.

Kanti V, Bonzel A, Stroux A, Proquitte H, Buhrer C, Blume-Peytavi U, Bartels NG. Postnatal maturation of skin barrier function in premature infants. Skin Pharmacol Physiol. 2014;27:234–41.

Kaplan HC, Lannon C, Walsh MC, Donovan EF. Ohio statewide quality-improvement collaborative to reduce late-onset sepsis in preterm infants. Pediatrics. 2011;127:427–35.

Katagiri C, Sato J, Nomura J, Denda M. Changes in environmental humidity affect the water-holding property of the stratum corneum and its free amino acid content, and the expression of filaggrin in the epidermis of hairless mice. J Dermatol Sci. 2003;31:29–35.

Kligman AM. Hydration injury to human skin. In: van der Valk PMH, editor. The irritant contact dermatitis syndrome. Boca Rotan: CRC Press; 1996. p. 187–94.

Lavender T, Bedwell C, Roberts SA, Hart A, Turner MA, Carter LA, Cork MJ. Randomized, controlled trial evaluating a baby wash product on skin barrier function in healthy, term neonates. J Obstet Gynecol Neonatal Nurs. 2013;42:203–14.

Ludriksone L, Garcia Bartels N, Kanti V, Blume-Peytavi U, Kottner J. Skin barrier function in infancy: a systematic review. Arch Dermatol Res. 2014;306:591–9.

Matsumoto T, Yuasa H, Kai R, Ueda H, Ogura S, Honda Y. Skin capacitance in normal and atopic infants, and effects of moisturizers on atopic skin. J Dermatol. 2007;34:447–50.

McKinley-Grant LJ, Idler WW, Bernstein IA, Parry DA, Cannizzaro L, Croce CM, Huebner K, Lessin SR, Steinert PM. Characterization of a cdna clone encoding human filaggrin and localization of the gene to chromosome region 1q21. Proc Natl Acad Sci U S A. 1989;86:4848–52.

Medeiros Jr M. Aquagenic urticaria. J Investig Allergol Clin Immunol. 1996;6:63–4.

Minami-Hori M, Honma M, Fujii M, Nomura W, Kanno K, Hayashi T, Nakamura E, Nagaya K, Miyauchi Y, Fujimura T, Hotta M, Takagi Y, Kitahara T, Takema Y, Iizuka H. Developmental alterations of physical properties and components of neonatal-infantile stratum corneum of upper thighs and diaper-covered buttocks during the 1st year of life. J Dermatol Sci. 2014;73:67–73.

Nikolovski J, Stamatas GN, Kollias N, Wiegand BC. Barrier function and water-holding and transport properties of infant stratum corneum are different from adult and continue to develop through the first year of life. J Invest Dermatol. 2008;128:1728–36.

Nonato LB, Lund CH, Kalia YN, Guy RH. Transepidermal water loss in 24 and 25 weeks gestational age infants. Acta Paediatr. 2000;89:747–8.

Odio M, Friedlander SF. Diaper dermatitis and advances in diaper technology. Curr Opin Pediatr. 2000;12:342–6.

Okah FA, Wickett RR, Pickens WL, Hoath SB. Surface electrical capacitance as a noninvasive bedside measure of epidermal barrier maturation in the newborn infant. Pediatrics. 1995;96:688–92.

Ponyai G, Hidvegi B, Nemeth I, Sas A, Temesvari E, Karpati S. Contact and aeroallergens in adulthood atopic dermatitis. J Eur Acad Dermatol Venereol. 2008;22:1346–55.

Rawlings AV, Leyden JJ. Skin moisturization. 2nd ed. New York: Informa Healthcare USA, Inc; 2009.

Rawlings AV, Matts PJ. Stratum corneum moisturization at the molecular level: an update in relation to the dry skin cycle. J Invest Dermatol. 2005;124:1099–110.

Rawlings AV, Scott IR, Harding CR, Bowser PA. Stratum corneum moisturization at the molecular level. J Invest Dermatol. 1994;103:731–41.

Robinson M, Visscher M, LaRuffa A, Wickett R. Natural moisturizing factors (nmf) in the stratum corneum (sc) 1: effects of lipid extraction and soaking. J Cosmet Sci. 2010a;62:13–22.

Robinson M, Visscher M, LaRuffa A, Wickett R. Natural moisturizing factors (nmf) in the stratum corneum (sc) 2: regeneration of nmf over time after soaking. J Cosmet Sci. 2010b;62:23–9.

Runeman B. Skin interaction with absorbent hygiene products. Clin Dermatol. 2008;26:45–51.

Rustemeyer T, Frosch PJ. Occupational skin diseases in dental laboratory technicians. (i). Clinical picture and causative factors. Contact Dermatitis. 1996;34:125–33.

Sato J, Denda M, Ashida Y, Koyama J. Loss of water from the stratum corneum induces epidermal DNA synthesis in hairless mice. Arch Dermatol Res. 1998;290:634–7.

Scott IR, Harding CR. Filaggrin breakdown to water binding compounds during development of the rat stratum corneum is controlled by the water activity of the environment. Dev Biol. 1986;115:84–92.

Sedin G, Hammarlund K, Stromberg B. Transepidermal water loss in full-term and pre-term infants. Acta Paediatr Scand Suppl. 1983;305:27–31.

Supp AP, Wickett RR, Swope VB, Harriger MD, Hoath SB, Boyce ST. Incubation of cultured skin substitutes in reduced humidity promotes cornification in vitro and stable engraftment in athymic mice. Wound Repair Regen. 1999;7:226–37.

Tagami H, Kobayashi H, O'Goshi K, Kikuchi K. Atopic xerosis: employment of noninvasive biophysical instrumentation for the functional analyses of the mildly abnormal stratum corneum and for the efficacy assessment of skin care products. J Cosmet Dermatol. 2006;5:140–9.

Visscher M, Maganti S, Munson KA, Bare DE, Hoath SB. Early adaptation of human skin following birth: a biophysical assessment. Skin Res Technol. 1999;5:213–20.

Visscher MO, Chatterjee R, Munson KA, Pickens WL, Hoath SB. Changes in diapered and nondiapered infant skin over the first month of life. Pediatr Dermatol. 2000;17:45–51.

Visscher MO, Chatterjee REJ, LaRuffa AA, Hoath SB. Biomedical assessment and instrumental evaluation of healthy infant skin. Pediatr Dermatol. 2002;19 (6):473–81.

Visscher MO, Tolia GT, Wickett RR, Hoath SB. Effect of soaking and natural moisturizing factor on stratum corneum water-handling properties. J Cosmet Sci. 2003;54:289–300.

Visscher MO, Narendran V, Pickens WL, LaRuffa AA, Meinzen-Derr J, Allen K, Hoath SB. Vernix caseosa in neonatal adaptation. J Perinatol. 2005;25:440–6.

Visscher MO, DeCastro MV, Combs L, Perkins L, Winer J, Schwegman N, Burkhart C, Bondurant P. Effect of chlorhexidine gluconate on the skin integrity at picc line sites. J Perinatol. 2009;29:802–7.

Visscher MO, Utturkar R, Pickens WL, LaRuffa AA, Robinson M, Wickett RR, Narendran V, Hoath SB. Neonatal skin maturation - vernix caseosa and free amino acids. Pediatr Dermatol. 2011;28(2):122–32.

Warner RR, Myers MC, Taylor DA. Electron probe analysis of human skin: determination of the water concentration profile. J Invest Dermatol. 1988;90:218–24.

Warner RR, Boissy YL, Lilly NA, Spears MJ, McKillop K, Marshall JL, Stone KJ. Water disrupts stratum corneum lipid lamellae: damage is similar to surfactants. J Invest Dermatol. 1999;113:960–6.

Warner RR, Stone KJ, Boissy YL. Hydration disrupts human stratum corneum ultrastructure. J Invest Dermatol. 2003;120:275–84.

Weidinger S, Illig T, Baurecht H, Irvine AD, Rodriguez E, Diaz-Lacava A, Klopp N, Wagenpfeil S, Zhao Y, Liao H, Lee SP, Palmer CN, Jenneck C, Maintz L, Hagemann T, Behrendt H, Ring J, Nothen MM, McLean WH, Novak N. Loss-of-function variations within the filaggrin gene predispose for atopic dermatitis with allergic sensitizations. J Allergy Clin Immunol. 2006;118:214–9.

Willis I. The effects of prolonged water exposure on human skin. J Invest Dermatol. 1973;60:166–71.

Youssef W, Wickett RR, Hoath SB. Surface free energy characterization of vernix caseosa. Potential role in waterproofing the newborn infant. Skin Res Technol. 2001;7:10–7.

Zimmerer RE, Lawson KD, Calvert CJ. The effects of wearing diapers on skin. Pediatr Dermatol. 1986;3:95–101.

Measurement of Skin Radiance

17

Adeline Jeudy, Vanessa Ecarnot, and Philippe Humbert

Contents

A. Jeudy (✉)
Research and Studies Center on the Integument (CERT); Clinical Investigation Center (CIC BT506), Department of Dermatology, Besançon University Hospital, Besançon, France
e-mail: ajeudy@chu-besancon.fr

V. Ecarnot
CERT, Department of Dermatology, CHRU Besançon, Besançon, France

P. Humbert
Department of Dermatology, University Hospital of Besançon, Besançon, France
e-mail: philippe.humbert@univ-fcomte.fr

P. Humbert et al. (eds.), *Agache's Measuring the Skin*,
DOI 10.1007/978-3-319-32383-1_17

Keywords
Skin radiance • Color • Texture • Photography • Clinical scoring

1 Introduction

Radiance, as an optical parameter defined by physics, can be measured in terms of the amount of light that is emitted from a particular object, such as light source. If we apply this definition to skin radiance, then when the skin reflects more incident light should look more radiant. However, skin radiance is more complex, is a psychophysical parameter, is the mirror of general health, both physical and psychological, and involves more than simply the quantity of light that is reflected from the skin (Matsubara et al. 2012; Petitjean et al. 2007a).

A gray skin, a "blotchy complexion," may reflect bad looks because of great fatigue, weariness, hormonal status, emotional states (sadness, stress, etc.), illness (dysfunction of vital organs such as the liver), nutrition deficiency or excess, tobacco, alcohol, pollution, seasons, etc. (Purdue and Hunt 1986; Middleton 1968; Monfrecola et al. 1998; Koh et al. 2002; Besné et al. 2003).

Inversely "peachy-colored skin" reflects a smooth, pink, and velvety skin with good health status. The complexion plays essential psychological and social roles (Petitjean 2006).

Many articles showed that the perception of aging is highly influenced by the skin tone uniformity (Nkengne et al. 2008; Puccetti et al. 2011; Fink and Matts 2008; Matts et al. 2007; Fink et al. 2012).

According to the literature, no precise definition and quantifiable description exist for skin radiance. It is difficult to list all constituting parameters and their relative proportions; they involve quite complicated surface and internal qualities of the skin (Jeudy et al. 2014).

When the light meets the skin surface, a small quantity (about 5 % (Takiwaki et al. 1997)) is reflected directly, while the major part penetrates to the different layers of the skin. The specular light gives its luminous aspect, whereas the back-scattered light (Fig. 1) gives the complexion (peachy-color). In other words, specular reflection explains the glow (depending on the nature and state of the surface of the skin), absorption phenomena explain its hue (depending on the skin's chromophore content), whereas diffusion phenomena define its saturation (depending mostly on the collagen content).

The skin radiance seems to be a balanced mixture of (Petitjean 2006):

- **Color**, which is mostly influenced itself by the skin microcirculation and inner skin structures
- **Light reflection**
- More globally **of texture** of the skin surface

Therefore, the related studies imply the quantification of each mentioned components.

2 Color

The skin color mainly depends on the melanin as well as the hemoglobin concentrations and their distributions; they absorb the light and affect subsurface reflection (Kim et al. 2015).

The melanin (brown) absorbs all wavelengths, but this absorption decreases considerably from purple to red, which makes the melanin look like a mixture of gray (global absorption) and yellow (significant absorption of blue light).

Hemoglobin looks red because it absorbs selectively the green light and therefore retrodiffuses a light where this complementary color is missing.

The importance of the distribution of color was observed by Matts et al. (2007), who found that in female skin, melanin evenness had a stronger effect on perceived age, health, and attractiveness than hemoglobin. Similarly, Fink et al. (2012) found that hemoglobin distribution in males was associated more strongly with health and attractiveness perception, whereas the evenness of melanized features was a stronger marker for age perception.

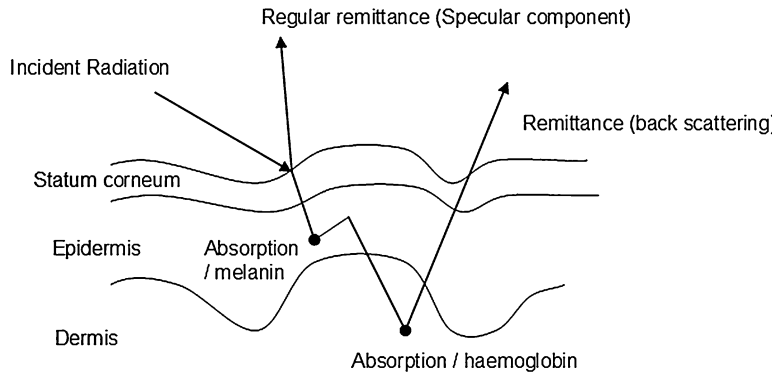

Fig. 1 Optical pathways in the skin (The layer is so thin in the stratum corneum and the epidermis that its contribution to remittance other than specular is minimal over the entire visible and near-infrared regions (Anderson and Parrish 1981))

The hemoglobin plays an important role in the skin radiance, which is usually perceived as "pink" skin. An indirect way to assess the radiance is to study consequently the skin microcirculation.

2.1 Assessment of Skin Microcirculation

The hemoglobin transports the oxygen inside the red globules: if oxygen is not enough, the face will be gray and dull. If the microcirculation is effectively stimulated, the light will more easily reflect the red blood cells at the source of the skin color.

The skin microcirculation is therefore an important factor of the dull complexion:

- Under stress, catecholamines are delivered in the skin, inducing vasoconstriction (and thus produce skin pallor) (Purdue and Hunt 1986; Sainthillier et al. 2002; Altemus et al. 2001).
- With tiredness (lack of sleep and/or intensive activity), the body reacts by sending more blood to vital organs and the cutaneous microcirculation is "sluggish" (Besné et al. 2003).
- With pollution and smoking, the microvessels lose their colors (grayish aspect of the skin) (Monfrecola et al. 1998; Koh et al. 2002; Besné et al. 2003; Petitjean et al. 2006; Raitio et al. 2004).
- With aging, papillar capillary loops disappear, inducing a loss in dermal nutritional vessel density and surface area for exchange (Li et al. 2006a).

Among the existing available techniques, capillaroscopy and videocapillaroscopy (Video Microscope Moritex Serie MS500, Perimed) allow direct visualization of the capillary network in vivo.

This optical device is made of a microscopic lens, a beam guide, and a CCD camera (Fig. 2).

The method used is based on the use of epiluminescence video microscopy. This device uses a halogen lamp as a light source. The light is conveyed to the target optical fiber. The incident light is generally lateral to increase the contrast, and on cold light.

The video microscope is connected to a computer with an operating system for the implementation of digital accurate quantitative measurements and a picture archiving.

Exploration is carried out directly on the skin after depositing a drop of oil to enhance skin transparency. An optical magnifying system is used to visualize its vascular network. Different levels of magnification can be used to assess the surface of the microvasculature structure as well

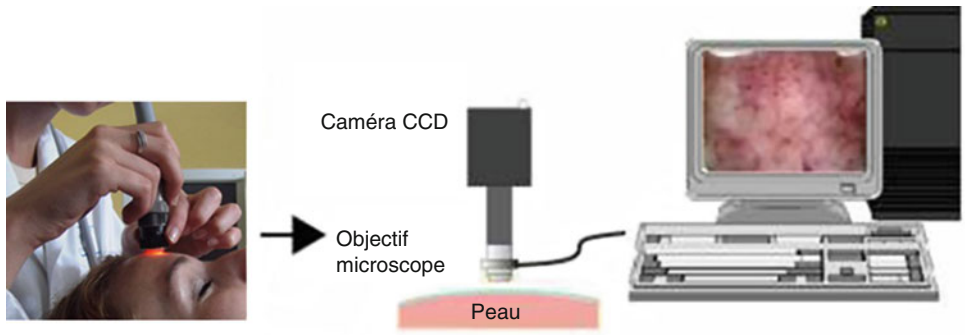

Fig. 2 Videocapillaroscopy device

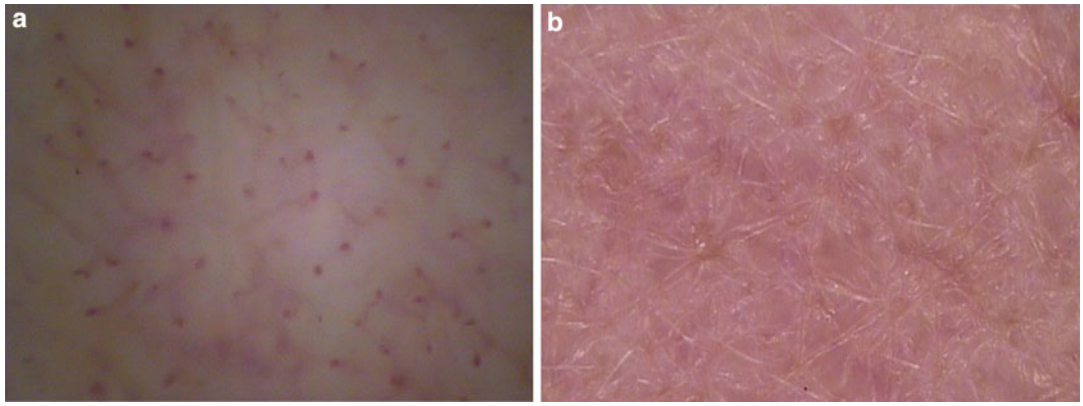

Fig. 3 (**a**) (1.73 mm^2) magnification of ×200 allows to quantify the vascularization network of the skin, whereas (**b**) (28 mm^2) a magnification of ×50 allows to quantify the skin redness

as its color (Fig. 3) (Humbert et al. 2005; Sainthillier et al. 2005).

With this assay system, you can access various parameters such as capillary diameters, lengths, surfaces, density, and intercapillary space.

Various magnifications are available: The lenses of ×200, ×100, and ×50 enable to explore of microcirculatory network for areas of 1–20 mm^2. The images are color coded and use RGB system (three layers red, green, and blue) and a resolution of 528 × 720 pixels.

The main advantage of this technique is its interactivity. The result of the capture and quality of the image can be checked immediately. Handling is easy thanks to the use of a computer, which is directly connected to the videocapillaroscope, and the whole data acquisition process is digitized.

2.2 Assessment of Skin Color

The most logical way to assess skin complexion is to study directly its color. In 2006, Taylor et al. described the different techniques available (Taylor et al. 2006). Among them, reflectance spectroscopy, chromameters, and narrowband reflectometers should be the most frequently used one. The latter are dedicated to the assessment of erythema or pigmentation (by measuring more specifically the skin chromophores) (Agache 2004a, b).

The color variations of the skin surface can be measured by reflectance spectroscopy (spectrocolorimeter (CM2600D, Konica Minolta Sensing) or chromameter (CR400, Konica Minolta Sensing). These devices have sensitivities corresponding to those of the human eyes, but the measurements are performed in standardized conditions using the same light source. The International Commission of Illumination (Commission Internationale de l'Eclairage) (CIE) has defined the spectral characteristics of several types of typical illuminants (the D65 corresponds to average daylight and is usually used as the reference) (Precise color communication 1998):

2.2.1 Chromameter CR 200 (Minolta)

With this instrument, the skin surface is illuminated by a pulsed xenon arc lamp. The light reflected perpendicular to the surface is collected for a tristimulus color analysis at 450, 560, and 600 nm, using the $L^*a^*b^*$ color system, as determined by the CIE (Robertson 1990). The L^* parameter expresses color brightness (varying between a value of 100 for a white surface and 0 for a black surface).

The a^* parameter represents changes along a red/green axis with changes from +60 for a red surface to −60 for a green surface. The b^*

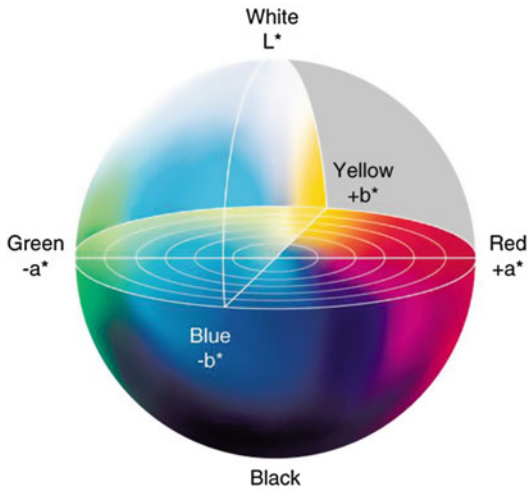

Fig. 4 $L^*a^*b^*$ color system

parameter changes from +60 for a yellow surface to −60 for a blue surface (Fig. 4).

The probe is applied on the skin surface simply by weight (651 g). With the standard equipment, the skin surface under the probe application is 1.77 cm^2 (diameter of 1.5 cm). The pressure of application on the skin is rather high, 368 g/cm^2. The instrument is calibrated using a white calibration plate (Clarys et al. 2000).

The skin radiance can therefore be described by a* which corresponds to the redness and L* which defines the luminosity.

However, additional information can be extracted, in order to qualify the skin color heterogeneity:

Color difference metric DeltaE =

$$\left[(L_1 - L_2)^2 + (a_1 - a_2)^2 + (b_1 - b_2)^2\right]^{1/2}$$

(Haeghen et al. 2000)

and/or vividness:

– Chroma $= \left((a*)^2 + (b*)^2\right)^{1/2}$ (Precise color communication 1998)

which are key factors in the problematics of dull complexion.

2.2.2 Mexameter M X16 (Courage-Khazaka)

The Mexameter (Courage & Khazaka MX18) measures the amount of melanin and hemoglobin in the skin.

In this instrument, 16 light emitting diodes circularly arranged emit light at three defined wavelengths 568 nm (green), 660 nm (red), and 880 (infrared). A photodetector measures the light reflected by the skin. The principle is based on the measurement of absorbed and reflected light at green and red wavelengths for hemoglobin and at red and near-infrared wavelengths for melanin. A melanin index is computed from the intensity of the absorbed and the reflected light at 660 and 880 nm, respectively. An erythema index is computed from the intensity of the absorbed and the reflected light at 568 and 660 nm, respectively.

The skin measuring area is 5 mm in diameter (surface 0.20 cm^2). The probe is applied on the skin surface with constant pressure using a spring: pressure of application on the skin is 91 g/cm^2 (Clarys et al. 2000).

The skin radiance can be described by erythema index, which corresponds to the redness.

2.2.3 Derma-Spectrometer (Cortex Technology)

This instrument's light emitting diodes emit light at two defined wavelengths: 568 nm (green) and 655 nm (red). A photodetector measures the light reflected by the skin. It measures the absorbed and reflected light at green wavelengths for hemoglobin and at red wavelengths for melanin. A melanin index and an erythema index are computed from the intensity of the absorbed and the reflected light at 568 and 655 nm, respectively. The skin measuring area is 6 mm in diameter (surface 0.28 cm^2). The probe is applied on the skin surface, simply by weight (640 g). The pressure of application on the skin is 158 g/cm^2. This instrument is calibrated using a black and white calibration plate (Clarys et al. 2000).

As Mexameter, the skin radiance can be described by erythema index which corresponds to the redness.

3 Reflection

The optical appearance of the skin such as radiance, glow, and shine can be quantified by determining the light-reflection profile of the skin. Understanding the optical-reflection characteristics by means of objective measurements is the first step in investigating these aspects of facial appearance.

The reflection of light from the skin is complicated by its multilayer structure. The stratum corneum, the outermost layer of the epidermis, is optically translucent and reflects partially incident light while allowing most of it to penetrate to deeper layers of the skin. As a result, the reflection from the skin is a mixture of specular surface reflection and diffuses subsurface reflection. It is therefore necessary to separate the surface and subsurface reflections from the skin to achieve a concept of the fundamental optical characteristics associated with its appearance (Matsubara 2012).

3.1 Assessment of the Skin Ability to Reflect the Light

The assessment of the light reflexion provides direct information on the skin radiance. It is generally admitted that radiant skin tends to act as a mirror, that is, to reflect rays in a specular manner, and dull skin tends to diffuse light more (Petitjean et al. 2007b).

3.1.1 Glossymeter

Courage and Khazaka had developed the **Glossymeter** to assess the quantity of specular and diffuse light reflected by the skin.

In the probe head containing parallel white light is created by the LEDs. Light is sent out at 0° and reflected by mirrors to 60° to the skin surface.

Part of the light is directly reflected in the same angle, so the angle of incidence is equal to the angle of reflection, and the other part of the light is absorbed by the surface and then scattered and reflected diffusely.

The Skin-Glossymeter GL 200 measures both the portion of directly reflected light, mirrored from the surface, which is related to the gloss and the scattered portion from the surface.

Two separate measurement channels measure the direct reflected light (again guided by a mirror in the same angle, i.e., at 120°) and the diffuse reflected (scattered) light degrees.

The scattered/diffuse reflected light is measured at 90° (completely vertically above the measured surface) under the assumption that light is scattered in the same way over all degrees.

The Skin-Glossymeter GL 200 is designed to assess the gloss of the skin surface. Skin, however, does vary not only in structure and brightness but also in color. With the DSC (Diffuse Scattering Correction), these facts are taken into account and the diffuse reflection light portion detected in the gloss measurement channel is eliminated, thus allowing to compare gloss measurements of different skin types.

3.1.2 SkinGlossMeter

The **SkinGlossMeter** is developed by Delfin Technology for measuring the specularly reflecting light from skin. In the SkinGlossMeter, the light beam reflects back at the same angle as it contacts the measured surface. This device does not measure scattered light.

As a light source, the instrument has a built-in 635 nm red semiconductor diode laser (superior reflective capabilities from the skin). The laser's spot size diameter at the surface level is 50 μm.

3.1.3 Brillanometer

Gillon et al. have also developed a specific contactless device (**brillanometry**) (Gillon et al. 2002). This device is for determination of both specular and diffuse light reflections continuously in numerous directions; it allows measurement of the skin gloss.

For skin optical measurements, an incident polarized-light beam is sent on the skin surface to be analyzed according to one direction, and the reflected beam is simultaneously measured in the same direction (Fig. 5). A small proportion of the light is reflected at the stratum corneum/air

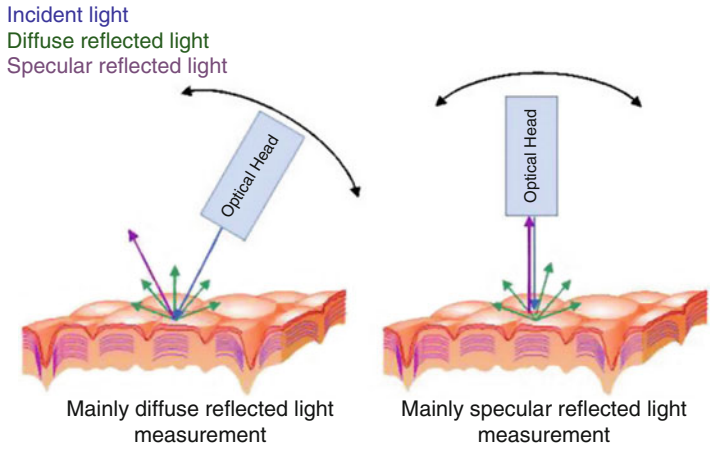

Fig. 5 Presentation of the two components of skin reflected light measurement. Variation of optical head positioning in numerous directions (Gillon et al. 2002)

interface, due to specular reflectance, which keeps the same polarization as incident light; this manifestation gives shining skin radiance if well moisturized and tightened.

On the contrary, diffuse reflected light is depolarized. This optical property allows separating both components of the light (specular and diffuse light reflections).

3.1.4 GonioLux

Recently, the Orion concept developed **GonioLux**, a device that measurement of light intensities re-emitted in all directions of space.

Parameters are expressed as a volume or quantity of re-emitted light in different directions of space:

- Spec.Vol. = Specular reflection
- Diff.Vol. = Diffused light (specular diffusion and back-scattered light after its absorption by the skin – relationship with the skin relief or iridescence)
- Left or right Aniso.Vol. = Anisotropy of all reflections (for 2 directions = Left and right)
- Tot.Vol. = total quantity of light re-emitted by the surface

Results can be expressed as a ratio of these different parameters.

3.1.5 Translucymeter

Optical measurement of subsurface reflection can be acquired using translucymetre (TLS850, Diastron Ltd, Andover, Hampshire, UK). TLS 850 is a contact translucency device in which light source has direct contact with the skin (Fig. 6). So it can measure only subsurface reflections (Kim et al. 2015).

A narrow beam from a RGB LED source illuminates the skin. Measurements can be performed using the "one color" mode of the LED, that is, either red, green, or blue.

Translucent materials like skin scatter light within deeper layers of the skin and a proportion of the scattered light are reflected back to the probe. The back-scattered light from the skin is collected by the fiber optic flathead (FOP).

The decrease in skin surface scattering increases light penetration into the deeper skin layers, resulting in an increase in skin transparency.

This collected light can be displayed in light levels on a PC depending on the distance of the sample illumination point.

The translucency value is composed of three parameters as follows: (Kim et al. 2015)

- The K value represents the amount of light detected by the probe as close to the light source as possible.
- The ALPHA value represents the rate of attenuation of the light level moving away from the source. A high ALPHA represents a rapid attenuation of light intensity.

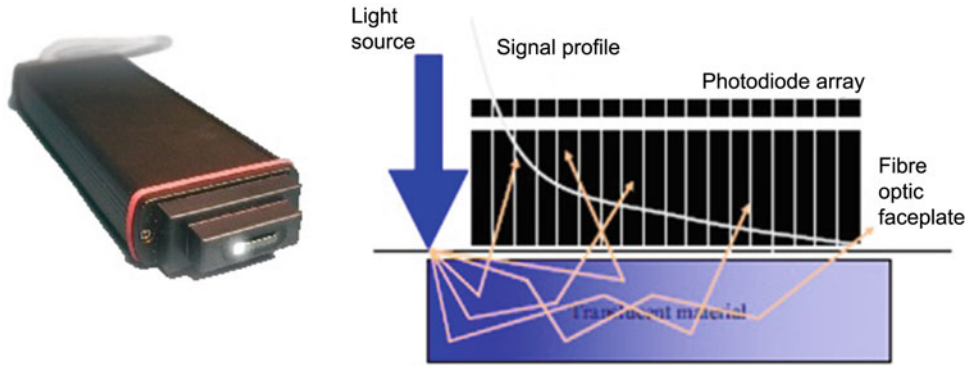

Fig. 6 Principle of tanslucymeter

- The AREA value represents the total amount of light scattered into the material.

4 Relief

This is in agreement with Fink and Matts (2008), who showed in 2008 that the surface **topography** cues had a significant influence on facial age perception and that the absence of facial discoloration is a key indicator of health, two attributes that are probably most influential in the evaluation of human facial attractiveness.

The relief of the skin produces different image contrasts depending on the brightness level of the surface (the same relief appears more easily in the case of a bright surface). When the skin surface is irregular, it absorbs light with difficulty and reflects it in many directions. This is particularly typical of dry and scaly skin (Jeudy et al. 2014).

Radiant skin is usually considered as smooth and homogeneous, without imperfections. Although innate, the microtopography of the skin is affected by the environment as well as aging and undergoes changes in quantity, depth, and direction (Pierard et al. 2004; Li et al. 2006b).

Profilometry (mechanical, transparency, or optical), initially developed for microtechniques, has been applied for many years to study the skin relief (Lagarde et al. 2001; Nardin et al. 2002; Lee et al. 2008; Makki et al. 1979).

4.1 Fringes Projection

One of the most up-to-date methods for the 3D evaluation of skin topography in real time is the digital fringe projection method. This method consists of a projector unit used for a digital projection of a striped pattern in a defined angle onto the skin in vivo and a camera used as a recording unit combined with a processing analysis unit (Fig. 7).

By analysis of the distortions of the striped pattern, it is possible to reconstruct the 3D structure of the skin precisely in an objective and reproducible manner (Luebberding et al. 2014).

Interestingly this in vivo technique allows to study the skin imperfections via the assessment of the volume and depth of the wrinkles and in particular the roughness and heterogeneity of the microrelief (dilated pores, comedones, fine wrinkles, etc.) (Fig. 8).

Currently, two such devices are available on the market: PRIMOS® (GFMesstechnik GmbH, Berlin, Germany) and DermaTOP® (Breukmann, Teltow, Germany). The main difference between them is in how the fringe patterns are produced: the PRIMOS® uses micromirrors with different PRIMOS® models available according to sampling sizes, while

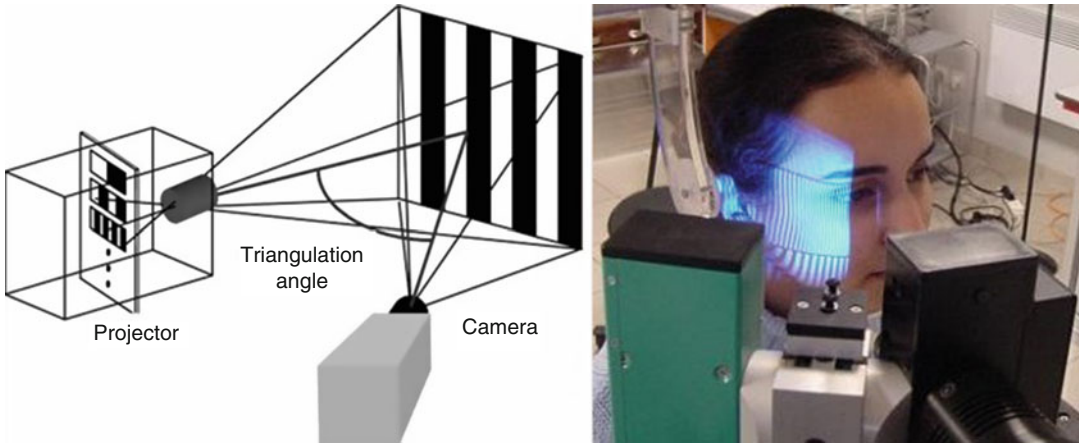

Fig. 7 Principle of fringe projection

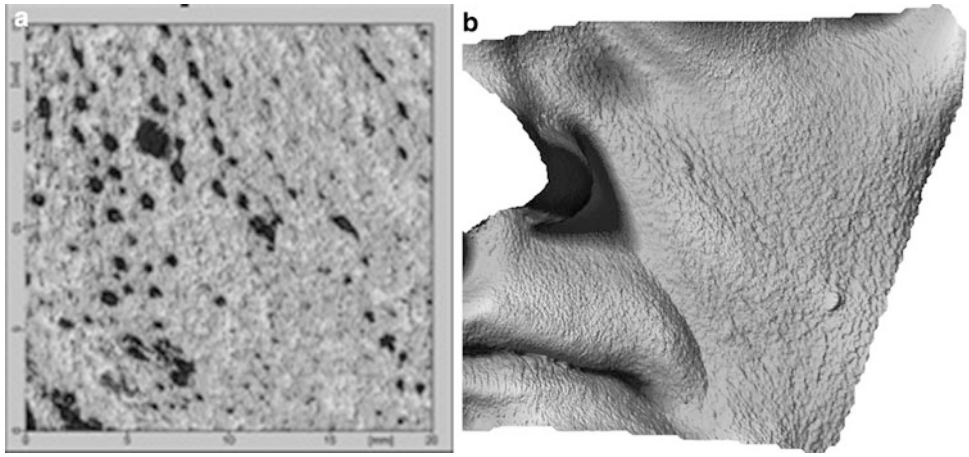

Fig. 8 3-D reconstructions obtained from the cheek (20 × 20 mm area), allowing to detect dilated pores (**a**), or from hemi-face (60 × 80 mm area) (**b**) allowing to quantify the roughness/heterogeneity of its relief (Jeudy et al. 2014)

DermaTOP® uses a template for the shadow projection and offers the option of measuring different sized areas using the same device. Similar performances are reported by both systems (Tchvialeva et al. 2010).

4.2 VisioScan

Skin microrelief parameters can be evaluated by VisioScan (Courage and Khazaka). This device uses a special high-resolution video camera that uses ultraviolet A light (proven to present no hazard to normal human skin) for uniform illumination of the skin and has been developed specially to study the skin surface directly, with SELS (Surface Evaluation of the Living Skin) software (Fig. 9).

The resulting images show the structure of the skin and the level of dryness, and the gray-level distribution of the image (in 256 grey levels) is used to evaluate the following skin microrelief parameters: maximum wrinkle depth (Rt), surface evaluation (SE) of skin

Fig. 9 Visio Scan and example of a resulting image

roughness (SEr), skin smoothness (SEsm; proportional to width and format of the wrinkles), and the number and width of the wrinkles (SEw) (Mercurio et al. 2013).

5 MultiFactors Assessments

5.1 Photography

Once calibrated and standardized, photography offers many applications to study skin complexion. It appears more appropriate to study texture or color heterogeneity than glowing aspect because of the influence of the light. The image can be easily disturbed by brightness induced by the flashlight or by the environment. The nature as well as the positioning of the light source and the posture of the subject are of major importance and must be taken into consideration to avoid visual artifacts (Raitio et al. 2004; Haeghen et al. 2000; Tanaka et al. 2008; Baret et al. 2006).

5.1.1 Polarized Photography

Polarized light photography provides more information than usual in terms of heterogeneity of structure.

For the measurement of skin-color or relief features, imaging systems equipped with two polarizing filters are widely used; the planes of polarization of the filters are oriented perpendicular or parallel to one another, and one filter is located in front of the source of illumination and the other is located front of the camera lens.

With the cross-polarized-light photography technique, the surface-reflection component from the skin, known as specular reflection, is removed, and only the subsurface reflection component from the skin is captured in the resulting image revealing the complexion (skin redness or paleness, color heterogeneity, etc.) (Fig. 10).

With the parallel polarized-light photography technique, the specular reflections are included in captured images, and in this case, details of the surface are enhanced (wrinkles, shininess, scaling) (Fig. 10) (Matsubara 2012).

With parallel polarization (C), only the reflected polarized lights pass (revealing the shininess and relief of the skin (Photograph D)).

Imperfections, which can be revealed by parallel polarization in photography, can be directly assessed thanks to profilometry.

5.1.2 SAMBA (Bossa Nova Technologies)

The application of systems of polarization of the light currently used in photographs has given the opportunity to Bossa Nova Technologies (Los Angeles, CA, USA), to develop a system called SAMBA a few years ago (McMullen and Jachowicz 2003). This whole-face image-capture-and-analysis system was used to measure the surface and subsurface reflections from the skin.

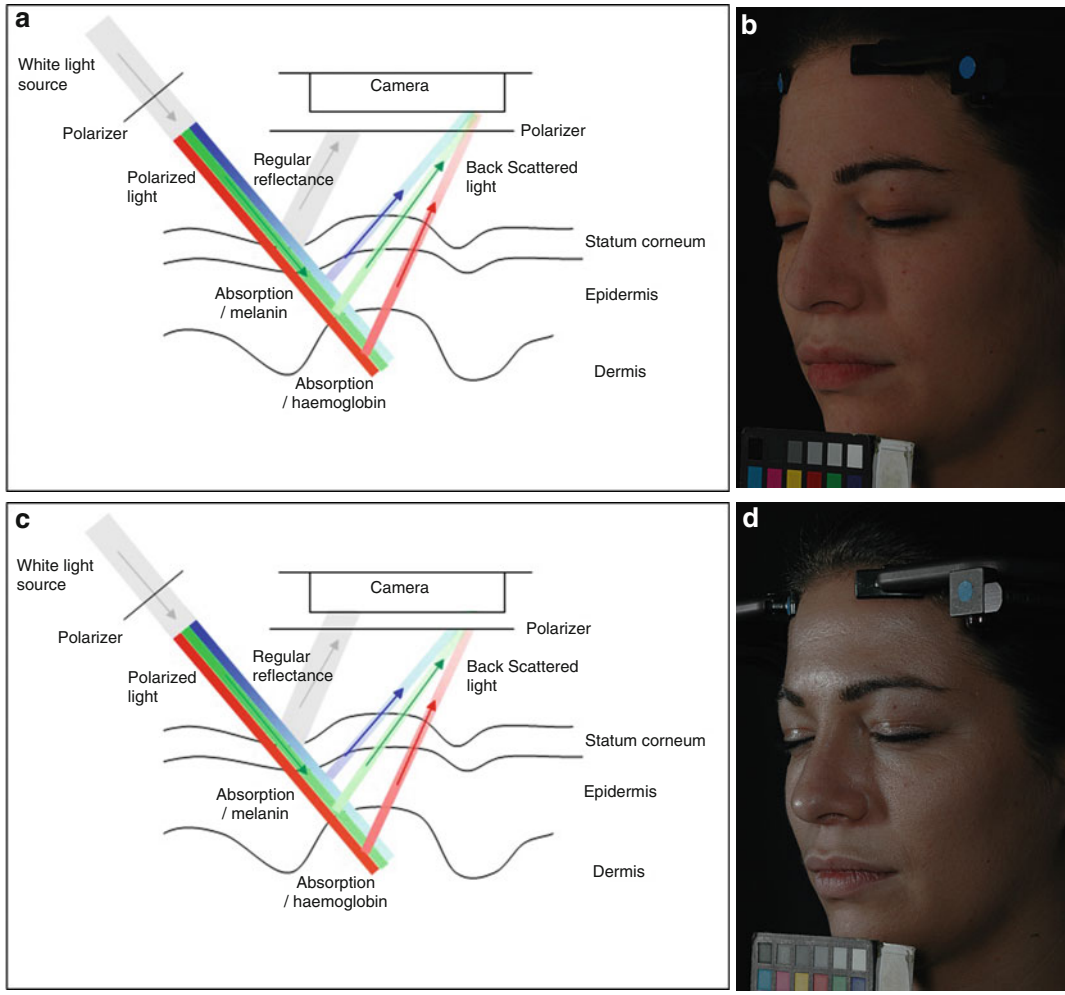

Fig. 10 Simplified schema of the principle of polarized-light photography. (**a**) With cross-polarization, only the back-scattered light reached the lens (revealing the complexion (Photograph (**b**))

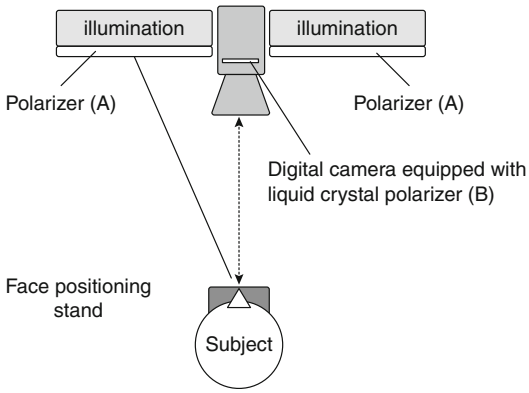

Fig. 11 Diagram of the SAMBA face-imaging system

This system consists of two illumination units, a high-resolution digital camera and a head-positioning stand (Fig. 11). Each illumination unit is equipped with a linear polarizing filter. The digital camera is also equipped with a liquid–crystal polarizer that can electrically flip its polarization angle from a direction that is parallel to the plane of polarization of the polarizing filters on the illumination units to one that is at 90° to it (crossed orientation) (Matsubara 2012).

The frequency of the flip is 4 Hz, and therefore, facial images for the two polarization states can be

Fig. 12 VISIA complexion analysis system

captured in very rapid succession. The facial position and angle in the parallel (P) and crossed (C) polarization images is therefore identical, and the corresponding pixels in the two images can be compared with one another by image processing to extract the surface-reflection component (Matsubara 2012).

5.1.3 VISIA (Canfield Imaging Systems)

The VISIA Complexion Analysis System (Canfield Imaging Systems, Fairfield, NJ, Fig. 12) generates a series of photographs using standard, ultraviolet, and cross-polarized lighting.

The system also analyzes the photographs to quantify the skin complaint and count the number of lesions, such a brown spots or dilated pores. VISIA uses standard flash lighting to identify spots, rhytides, texture, and pore.

Ultraviolet lighting is used to generate an ultraviolet spot image and a porphyrin image. The ultraviolet lighting takes advantage of the selective absorption of ultraviolet light by epidermal melanin in comparison with deeper melanin (Goldsberry et al. 2014).

5.2 Clinical Scoring

In 2006, Baret et al. organized a round table meeting with women (Baret et al. 2006). As a result of these exchanges, many items (including the skin grain, brightness, and color) were selected and studied in volunteers of different age groups from image analysis of video data of their face. Experts performed clinical scoring and then divided the volunteers in two groups: the young one, whose radiance was considered more dependent on skin luminosity and color ("rosy color"), and the old one, who was mainly characterized by irregular skin surface aspects and color variations.

These definitions corroborate the idea that radiance is multifactorial and naturally include an important subjective part.

DESCRIPTORS	ANTICIPATED OPTIMUM	SKIN EVALUATION
Red Pink	**Absence of red (unless the product contains an active ingredient to promote cutaneous micro-circulation)** 	*+/– red skin*
Beige	**Medium beige (unless the product is a make-up foundation)** 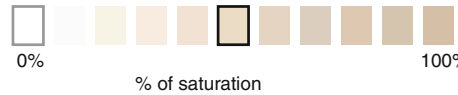	*+/– clear complexion*
Olive	**Absence of olive** 	*Less sallow complexion*
Light pink	**Optimal pinkness** 	*Pinker complexion*
Luminosity	**Optimal luminosity** 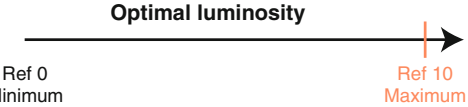	*More luminous skin*
Brightness	**Optimal brightness** 	*More uniform and regular skin*
Transparency	**Optimal transparency** 	*More transparent skin*

Fig. 13 C.L.B.T. parameters defining the complexion

As previously mentioned for photography, it is of great importance to perform the scoring in controlled conditions. The subjects have to be seated between "daylight" lamps and to wear white clothes as well as a white paper cap to avoid any influence from extrinsic colors and to stay at rest in a temperature-controlled room (Musnier et al. 2004).

In 2004, Musnier et al. organized a brainstorming session with several beauticians to develop a model of sensory evaluation of the skin radiance (Musnier et al. 2004). One hundred volunteers were also interviewed to self-appraise their complexion. The synthesis of the data allowed to determine four skin coloring descriptors and to construct a model "C.L.B.T.," based on the visual perception of skin color (C), luminosity (L), brightness (B), and transparency (T). Recently, this score was adapted to the Asian skin (Périn et al. 2007).

The "red-pink," "beige," "olive," and "light-pink" skin hues were determined to describe the various complexions' coloring. Skin hues are due to chromophores found within the skin in the form

of melanin (brown and yellow hues), bilirubin (yellow hue), or hemoglobin (bluish red hue). The perceived color depends largely on both the concentration of the various pigments and their distribution throughout the skin's thickness.

The visual evaluation of skin coloring by trained assessors is undertaken with the help of structured visual color scales presenting the spectrum of the four main facial hues (red-pink/beige/olive/light-pink). Each hue is saturated at 100 % and its color gradations were shown. The results are expressed in terms of color saturation percentages.

Skin luminosity was defined as the intensity of the light areas reflected on the salient areas of the face, while skin brightness was the combined uniformity of skin coloring and skin texture, and skin transparency was the possibility of seeing the vessels beneath the skin. Figure 13 presents the interpretations attributed to the different descriptors after the application of a cosmetic product designed to improve "complexion radiance."

The visual evaluation of luminosity, brightness, and transparency (the LBT descriptors) is made using visual analogical scales that range from "no luminosity/brightness/transparency" (limit 0) to "maximum luminosity/brightness/transparency" (limit 10) (Musnier et al. 2004).

Clinical scoring offers the possibility to evaluate the different parameters implicated in the skin radiance.

6 Conclusion

Finally, no instrument can quantify today the skin radiance globally, but there are devices which allow to assess its different components.

With contrast to the color, the glow remains difficult to quantify. The development of simulation systems would perhaps be one solution (Minami et al. 2007). Many terms are usually employed to characterize the skin radiance: shininess, brightness, glow, glare, gloss, etc. Shininess, brightness, and gloss refer to the reflection of light to something and are more frequently used to characterize seborrheic skin or to assess the effect of makeup on lips. Glare seems to evoke a shine with a dazzling light, whereas the glow associates an intense color with a slight shine. The glowing aspect of the skin has thus to be differentiated from its brightness, which is the characteristic of greasy skin and is inaesthetic. If gloss is what women expect for their hair, glow is a better representation of radiant skin. All these notions show a real need to define the skin radiance more accurately (Jeudy et al. 2014).

The assessment of skin radiance implies the study of the geometry of the light reflection as well as the interaction between the light (interaction with surface-relief/glow) and the color (interaction within the skin/complexion) (Petitjean 2006).

References

Agache P. Skin color measurement. In: Agache P, Humbert P, editors. Measuring the skin: non-invasive investigations, physiology, normal constants. Berlin: Springer; 2004a. p. 33–9.

Agache P. Assessment of erythema and palor. In: Agache P, Humbert P, editors. Measuring the skin: non-invasive investigations, physiology, normal constants. Berlin: Springer; 2004b. p. 40–59.

Altemus M, Rao B, Dhabbar FS, Ding W, Granstein RD. Stress-induced changes in skin barrier function in healthy women. J Invest Dermatol. 2001;117:309–17.

Anderson RR, Parrish JA. The optics of human skin. J Invest Dermatol. 1981;77:13–9.

Baret M, Bensimon N, Coronel S, Ventura S, Nicolas-Garcia S, Korichi R, Gazano G. Characterization and quantification of the skin radiance through new digital image analysis. Skin Res Technol. 2006;12:254–60.

Besné I, Clot JP, Misery L, Breton L. Stress et dermatologie, Chapter 18. In: Thurin JM, Baumann N, editors. Stress, pathologies et immunité. Paris: Médecine-Sciences Flammarion; 2003. p. 192–9.

Clarys P, Alewaeters K, Lambrecht R, Barel AO. Skin color measurements: comparison between three instruments: the Chromameter, the DermaSpectrometer and the Mexameter. Skin Res Technol. 2000;6(4):230–8.

Fink B, Matts PJ. The effects of skin colour distribution and topography cues on the perception of female facial age and health. J Eur Acad Dermatol Venereol. 2008;22:493–8.

Fink B, Matts PJ, D'Emiliano D, Bunse L, Weege B, Röder S. Colour homogeneity and visual perception of age, health and attractiveness of male facial skin. J Eur Acad Dermatol Venereol. 2012;26:1486–92.

Gillon V, Perie G, Schnebert S, Pauly G. A new method for contactless in vivo quantitative measurement of stratum corneum gloss attributes: influence of natural active ingredients. In: Marks R, Lévêque JL, Voegeli R, editors. The essential stratum corneum. London: Martin Dunitz; 2002. p. 331–4.

Goldsberry A, Hanke CW, Hanke K. VISIA system: a possible tool in the cosmetic practice. J Drugs Dermatol. 2014;13(11):1312–4.

Haeghen YV, Naeyaert JMAD, Lemahieu I, Philips W. An imaging system with calibrated color image acquisition for use in dermatology. IEEE Trans Med Imaging. 2000;19(7):722–30.

Humbert P, Sainthillier JM, Mac-Mary S, Petitjean A, Creidi P, Aubin F. Capillaroscopy and videocapillaroscopy assessment of skin microcirculation. Dermatological and cosmetic approaches. J Cosmet Dermatol. 2005;4:153–62.

Jeudy A, Mac-Mary S, Sainthillier JM, Lihoreau T, Fanian F, Humbert P. Skin radiance measurement. In: Barel AO, Paye M, Maibach HI, editors. Handbook of cosmetic science and technology. 4th ed. New York: Edition Informa Healthcare; 2014. p. 459–66.

Kim HJ, Baek JH, Eo JE, Choi KM, Shin MK, Koh JS. Dermal matrix affects translucency of incident light on the skin. Skin Res Technol. 2015;21 (1):41–6.

Koh JS, Kang H, Choi SW, Kim HO. Cigarette smoking associated with premature facial wrinkling: image analysis of facial skin replicas. Int J Dermatol. 2002;41 (1):21–7.

Lagarde JM, Rouvrais C, Black D, Diridollou S, Gall Y. Skin topography measurement by interference fringe projection: a technical validation. Skin Res Technol. 2001;7:112–21.

Lee HK, Seo YK, Baek JH, Koh JS. Comparison between ultrasonography (Dermascan C version 3) and transparency profilometry (Skin Visiometer SV600). Skin Res Technol. 2008;14:8–12.

Li L, Mac-Mary S, Sainthillier JM, Gharbi T, Degouy A, Nouveau S, De Lacharrière O, Humbert P. Age related-changes of the cutaneous microcirculation in vivo. Gerontology. 2006a;52:142–53.

Li L, Mac-Mary S, Marsaut D, Sainthillier JM, Nouveau S, Gharbi T, Lacharrière D, Humbert P. Age-related changes in skin topography and microcirculation. Arch Dermatol Res. 2006b;297:412–6.

Luebberding S, Krueger N, Kerscher M. Quantification of age-related facial wrinkles in men and women using a three-dimensional fringe projection method and validated assessment scales. Dermatol Surg. 2014;40 (1):22–32.

Makki S, Barbenel JC, Agache P. A quantitative method for the assessment of the microtopography of human skin. Acta Derm Venereol. 1979;59:285–91.

Matsubara A. Differences in the surface and subsurface reflection characteristics of facial skin by age group. Skin Res Technol. 2012;18(1):29–35.

Matsubara A, Liang Z, Sato Y, Uchikawa K. Analysis of human perception of facial skin radiance by means of image histogram parameters of surface and subsurface reflections from the skin. Skin Res Technol. 2012;18 (3):265–71.

Matts PJ, Fink B, Grammer K, Burquest M. Color homogeneity and visual perception of age, health, and attractiveness of female facial skin. J Am Acad Dermatol. 2007;57:977–84.

McMullen R, Jachowicz J. Optical properties of hair: effect of treatments on luster as quantified by image analysis. J Cosmet Sci. 2003;54:335–51.

Mercurio DG, Segura JH, Demets MB, Maia Campos PM, Mercurio D. Clinical scoring and instrumental analysis to evaluate skin types. Clin Exp Dermatol. 2013;38 (3):302–8.

Middleton JD. The mechanism of water binding in stratum corneum. Br J Dermatol. 1968;80:437–50.

Minami K, Kaneko T, Suzamwa T, Aosaki T, Nagatami N, Hotta H, Hori K. Changes in facial impressions by controlling the color of surface reflection from cosmetic foundations: appearance evaluation and formulation technique. IFSCC. 2007;10:111–7.

Monfrecola G, Riccio G, Savarese C, Posteraro G, Procaccini EM. The acute effect of smoking on cutaneous microcirculation blood flow in habitual smokers and nonsmokers. Dermatology. 1998;197(2):115–8.

Musnier C, Piquemal P, Beau P, Pittet JC. Visual evaluation in vivo of complexion radiance using the CLBT sensory methodology. Skin Res Technol. 2004;10:50–6.

Nardin P, Nita D, Mignot J. Automation of a series of cutaneous topography measurements from silicon rubber replicas. Skin Res Technol. 2002;8:112–7.

Nkengne A, Bertin C, Stamatas GN, Giron A, Rossi A, Issachar N. Influence of facial skin attributes on the perceived age of Caucasian women. J Eur Acad Dermatol Venereol. 2008;8:982–91.

Périn F, Saetun K, Pungpod P, Pram-On M, Périn V, Aroonrat N. A new method for the in vivo visual evaluation of the radiance of the Asian skin complexion. In: Conference of the Asian Societies of Cosmetics Scientists, Singapore, 7–9 Mar 2007.

Petitjean A. Approches biométrologiques de l'éclat du teint. Th: Sci. Vie Santé, Besançon 2006: 25-06-05.

Petitjean A, Mac-mary S, Sainthillier JM, Muret P, Closs B, Humbert P. Effects of cigarette smoking on the skin of women. J Dermatol Sci. 2006;42:259–61.

Petitjean A, Sainthillier JM, Mac-Mary S, Muret P, Closs B, Gharbi T, Humbert P. Skin radiance: how to quantify? Validation of an optical method. Skin Res Technol. 2007a;13(1):2–8.

Petitjean A, Sainthillier JM, Mac-Mary S, Muret P, Closs B, Gharbi T, Humbert P. Validation of technique measuring skin radiance. Skin Res Technol. 2007b;13:2–8.

Pierard GE, Uhoda I, Pierard-Franchimont C. From microrelief to wrinkles. An area ripe for investigation. J Cosmet Dermatol. 2004;2:21–8.

Precise Color Communication. Color control from perception to instrumentation. Japan: Konica Minolta Sensing; 1998.

Puccetti G, Nguyen T, Stroever C. Skin colorimetric parameters involved in skin age perception. Skin Res Technol. 2011;17:129–34.

Purdue GF, Hunt JL. Cold Injury: a collective review. J Burn Care Rehabil. 1986;7(4):331–42.

Raitio A, Kontinen J, Rasi M, Bloigu R, Röning J, Oikarinen A. Comparison of clinical and computerized image analyses in the assessment of skin ageing in smokers and non-smokers. Acta Derm Venereol. 2004;84:422–7.

Robertson AR. Historical development of CIE recommended color difference equations. Color Res Appl. 1990;3:167–70.

Sainthillier JM, Creidi P, Degouy A, Muret P, Montastier C, Hirt JP, Besné I, Breton L, Gharbi T, Humbert Ph. Topical application of a manganese gluconate preparation inhibits the effects of neosynephrin on the cutaneous microcirculation *(Poster)*. 20th World Congress of Dermatology, Paris, 1–5 July 2002.

Sainthillier JM, Gharbi T, Muret P, Humbert P. Skin capillary network recognition and analysis by means of neural algorithms. Skin Res Technol. 2005;11 (1):9–16.

Takiwaki H, Kanno Y, Miyaoka Y, Arase S. Computer simulation of skin color based on a multilayered skin model. Skin Res Technol. 1997;3:36–41.

Tanaka H, Nakagami G, Sanada H, Sari Y, Kobayashi H, Kishi K, Konya C, Tadaka E. Quantitative evaluation of elderly skin based on digital image analysis. Skin Res Technol. 2008;14(2):192–200.

Taylor S, Westerhof W, Im S, Lim J. Non invasive techniques for the evaluation of skin color. J Am Acad Dermatol. 2006;54:S282–90.

Tchvialeva L, Zeng H, Markhvida I, McLean D, Lui H, Lee T. Skin roughness assessment, Chapter 18. In: Domenico Campolo (ed.) New developments in biomedical engineering. In-Tech; 2010.

Analysis of Skin Relief

18

Jean-Marie Sainthillier, Sophie Mac-Mary, and Philippe Humbert

Contents

Keywords
Relief • Microrelief • Wrinkles • Roughness • Replicas • Fringe projection

1 Introduction

Although the skin is smooth, its surface is not even. Its relief is a succession of peaks and hollows organized in a relatively uniform pattern of deep and wide primary furrows (20–200 μm) and of finer and more superficial transversal secondary furrows (30–70 μm). Tertiary and quaternary lines are also observed but they can be studied only with high-resolution systems. The structure of microdepressions or microrelief forms the sides of more or less triangle-shaped plateaus on most of the body surface, except on the palms and soles (Fig. 1). This network has two roles: it gives the skin a protective mechanical stretching ability in the direction of the constraints the skin sustains and it is also useful for the evacuation and retention of sebum and sweat and to capture substances applied to the skin (Agache 2000; Agache and Humbert 2004; Bazin and Lévêque 2011).

The skin of the face has its own specificities: in addition to its microrelief, a locally more marked relief pattern is visible. It consists of a macrorelief made of fine wrinkles (depth between 0.2 and 1 mm) and wrinkles (>1 mm) which appear and develop with aging, more notably on the forehead (glabella wrinkle), the crow's foot area, and later on the cheeks. These wrinkles are the result of

J.-M. Sainthillier (✉)
Skinexigence, Besançon, France
e-mail: jmsainthillier@skinexigence.com

S. Mac-Mary
Skinexigence SAS, Bioparc, Besançon, France
e-mail: smac@skinexigence.com

P. Humbert
Department of Dermatology, University Hospital of Besançon, Besançon, France
e-mail: philippe.humbert@univ-fcomte.fr

P. Humbert et al. (eds.), *Agache's Measuring the Skin*,
DOI 10.1007/978-3-319-32383-1_18

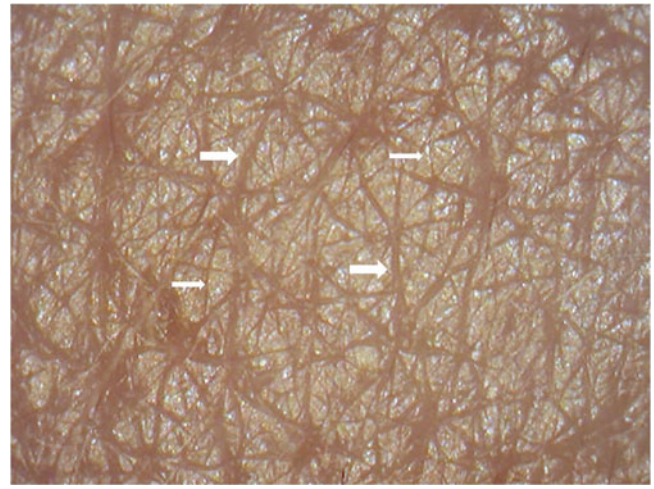

Fig. 1 Surface of cheekbone. *Thick arrows*: primary furrows. *Thin arrows*: secondary furrows

structure alterations in the epidermis, the dermis, and the hypodermis (Bazin and Lévêque 2011; Zahouani and Vargiolu 2000; Piérard et al. 2004).

Both types of relief are neither measured nor quantified with similar procedures because of their different scales (from several microns to a few millimeters, i.e., up to a factor 100). Furthermore their exploration requires different approaches which must take into account their localization and the resolution necessary to measure them.

The assessment of both micro- and macrorelief is described below for use in clinical research and the description is centered on an accurate and polyvalent technique to perform measurements both in vitro (on replicas) and in vivo: optical profilometry by fringe projection.

2 Profilometry and Fringe Projection

The techniques available to assess a surface and carry out its 3D reconstruction can be listed in five main groups: optical systems (by detection of reflected light, depending on depth and angle of relief), mechanical systems, laser profilometry, optical systems by transmission, and optical profilometry by fringe projection (Lagarde et al. 2001; Stout et al. 2000).

Interestingly, 2D imaging allows to measure the relief indirectly (it is called pseudo relief). The principle (either by camera or by photography) is to detect the contrast formed by the wrinkle and the adjacent skin. Generally the wrinkle appears dark inside a lighter area, and the intensity of the contrast corresponds to the depth and marked appearance of the wrinkle (Rosa Pena Ferreira et al. 2010; Russ 2007).

Mechanical profilometry was the first method developed and is based on a tactile detector able to measure a 2D profile or a 3D surface. It is mechanically connected to an inductive sensor which transforms the relief variations into an analogue signal.

Laser profilometry, based on dynamic focalisation or (simple or double) triangulation, uses the movement of a mobile lens or a spotlight reflected on a sensor to measure the height at each point of a sample surface.

Profilometry by transmission measures the variation of intensity of light shining through a replica. Applying the Beer-Lambert law, the absorption of light is linked to the transparency and therefore the thickness of the replica.

These systems are very different in terms of acquisition speed (from a few seconds to several minutes with mechanical systems), accuracy, and easiness of use. Laser profilometry and fringe projection profilometry are the only methods that can be used on the skin in vivo.

Profilometry by fringe projection is based on the principle of interferometry. It was originally

devised in the microtechnics industry and its application to the study of the skin was developed in the 1980s. From the 2000s, compact systems with specifically designed sensors and software were developed to study the skin relief. It became therefore possible to reduce the acquisition time, to remove or add some stages of processing and filtering while improving sensitivity.

The principle of fringe projection is to project structured light, i.e., a network of fringes, onto the investigated surface (Marsaut 2004). Fringes are deformed (modulated) by the relief. Several acquisitions with different phases of the projected network are recorded by a camera; after processing by a dedicated software, the tridimensional profile of the studied area is reconstructed within a few seconds (Takeda et al. 1982; Srinivasan et al. 1984; Hayashi et al. 1989). Two systems with CE certification are currently available: DermaTop Blue (Eotech in France) and Primos (GFM in Germany). Repeatability, reproducibility, and sensitivity of other very similar devices (Microtop) have already been shown (Lagarde et al. 2001).

The DermaTop device consists of a LED projector for the fringes and a CCD camera (Fig. 2). Three sets of objectives can be adapted to the system: an objective of great accuracy dedicated to the characterization of microrelief in vitro, an intermediary objective specifically designed to study facial wrinkles, and a wide-field objective for larger measurement areas of the nasogenian folds, the lips, or the cheeks. A fair compromise must be found between the size of the investigated area (which increases) and the precision of the measurement (which decreases) in relation to these objectives. Most examples and images presented in this chapter are issued from this device and illustrate the possibilities offered by various objectives in relation to the investigations.

Although data acquisition by fringe projection is fast (a few thousandths of second), processing and 3D reconstruction are complex. The whole procedure involves several steps: all the raw data of each subject (in absolute coordinates) are loaded, solved (by calculating the deformation of fringes from the sensor's parameters), and straightened while taking into account the global shape of the area. The surfaces are then registered (in relation to the first measure, i.e., at T0) by using the surface itself or fixed anatomical marks (in wide-field imaging). A region of interest is defined (of variable size but always smaller than the exploration field), then filtered, and finally projected onto a reference plan. This final projection constitutes what is called 3D topography and is the basis for calculation (micro- and macrorelief). The topography defined vertically and horizontally (by lateral resolution determined according to the sensor used) is expressed by a matrix where each point corresponds to a single height (scale in z).

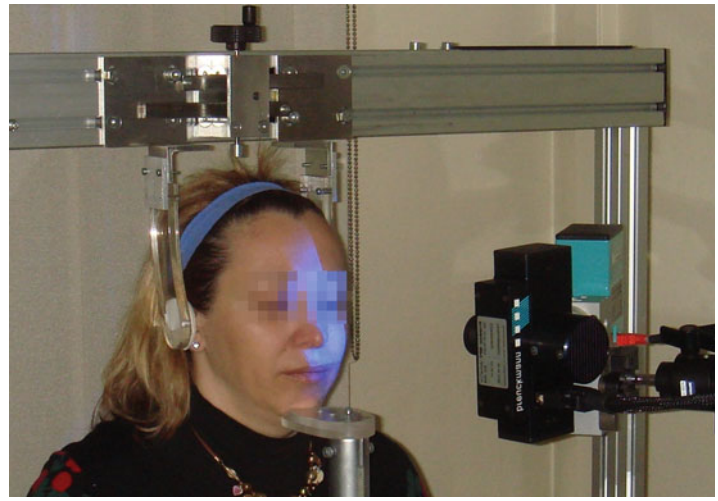

Fig. 2 Measurement of the cheekbone in vivo with Eotech system. The *blue* light covers the site where fringes are projected (left side of the subject's face). The sensor consists of a fringe projector (*black*) and a CCD camera (*green*) and is attached to a table where its position and the subject's position can be reproduced. Measurements are performed in a dark room to limit the influence of external light

3 Microrelief and Roughness

A rough surface is defined by its asperities and irregularities, uneven to the touch. Inversely a surface is deemed soft if its contact is pleasant because of its smoothness. Roughness is therefore linked to both sensorial and functional criteria: for example, a surface roughness accounts for its sensitivity to wear and tear or its adherence or sliding properties (Zani 2003).

Originally roughness is defined in two dimensions only. Standard measuring instruments developed from mechanical profilometry are contact systems composed of a mobile unit and a sensor that scans the sample according to predetermined direction and length. From the acquisition of a profile, various mathematical formulas are applied to extract parameters. It is difficult to apprehend roughness because it is a statistical parameter with a variety of possible definitions: means of heights of peaks, height of the highest peaks, wider amplitude between the height of a peak and the depth of a furrow, mean distance between several peaks, etc. No definition is actually more relevant than another and everything therefore depends on the intended application.

Paradoxically there is no standard to characterize surface states (roughness calculated directly in three dimensions on a surface). Calculation methods developed for profiles can however be adapted to surfaces by the addition of a supplementary dimension.

Based on our experience in this field, we have selected two robust and sensitive parameters: Sa and St. They are well-known, easy to calculate, and complementary because they allow for localized and global reading of the measured surface.

- **Sa** (in μm): arithmetic mean of the deviations of the surface to the mean plane
- **St** (in μm): dynamics = amplitude = difference in height between the highest peak and the lowest hollow of the surface

St is used to assess the quality of the calculated surface quickly and globally. Important variations of this parameter usually express acquisitions with noise, with the presence of aberrant points. Sa is a parameter sensitive enough to detect a change in microrelief, even of low amplitude (between 5 and 10 μm). Of course, other parameters exist and have been used successfully in the study of the skin surface (Zahouani et al. 1985; Mignot et al. 1987; Mignot 1986; Makki et al. 1979, 1984).

The distribution/orientation of the furrows can also be calculated under the form of a compass rose. The density of orientation in a determined angle corresponds to the number of elements of the furrows having this orientation. With this method it is possible to quantify the rate of anisotropy of the relief which is defined in the interval 0–100 % (0 % expresses the anisotropy rate of a perfectly isotropic surface and 100 % of a perfectly anisotropic surface) (Zahouani and Vargiolu 2004; Zahouani et al. 1998; Lagarde et al. 2005).

4 Wrinkles and Macrorelief

In terms of topography a volume combines two complementary quantities: negative quantity located in depth (absence of matter) and positive quantity located in height (presence of matter). The separation plane between both quantities corresponds to the mean plane.

Mathematical measurement of the volume of a wrinkle consists therefore in the assessment of the negative matter located under the mean plan, by integrating the three dimensions of the image, i.e., height, width, and depth (in mm):

$$\text{Volume} = \text{height} \times \text{width} \times \text{depth}.$$

Several methods are available to calculate the volume of a wrinkle. These approaches all use the mean plane and quantify the volume located beneath it (Sainthillier et al. 2009). They are however different in the way they define the calculation zone and are therefore more or less adapted in relation to the nature of the relief.

The calculated parameters are usually linked to the morphology of the wrinkle (its surface, volume, mean depth, etc.). Other more elaborated parameters can be defined to quantify the slope

of the wrinkle, its splay, and its fragmentation. However, the relevance of these parameters depends on their application to surfaces free of any perturbation, noise, or artifacts.

On the forehead (Fig. 3), the relief is usually flat and not very marked but covers a large surface, with one or two horizontal wrinkles frequently discontinued at their centre. The top of the glabella is sometimes visible on the most marked foreheads. In the assessment of this area, the calculation of the global volume will be preferred, taking into account all the wrinkles and fine wrinkles. This method is reliable only if the surface has absolutely no artifacts (they would distort the calculation).

On the crow's foot wrinkles (Fig. 4), the relief is more irregular and localized, with one or several independent wrinkles spreading like a fan from the eye canthus. Unlike evaluation on the forehead, the assessments of the crow's foot wrinkles are aimed at characterizing and following up a selected and clearly identified wrinkle, free of any artifact. A region of interest is defined in the shape of a polygon around the studied wrinkle or

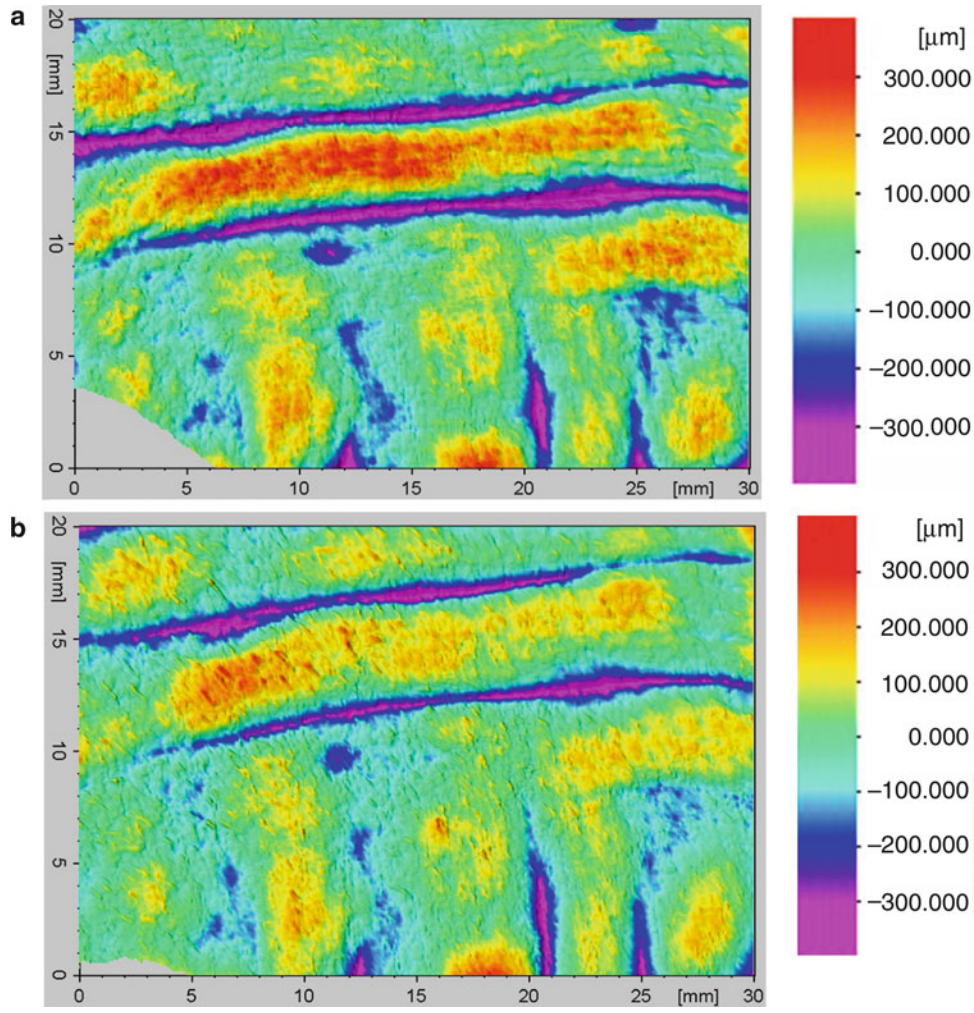

Fig. 3 In vivo acquisitions before/after treatment (*top/bottom*) on the forehead (30 × 20 mm). The *top* end of the glabella is visible in the lower part of the images. A few non measured points appear in the lower *left* corner. The calculated volume varies from 28.4 to 23.7 mm^3. The decrease is the result of the evolution of both horizontal wrinkles which become narrow and discontinued. The maximal depth varies from 0.95 to 0.79 mm

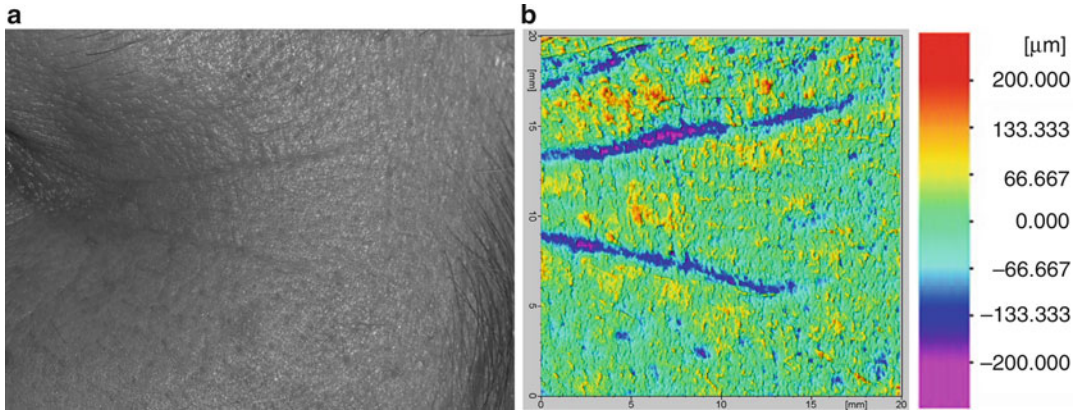

Fig. 4 In vivo acquisitions of crow's foot wrinkles (20 × 20 mm). *Top*: original image taken by the camera. *Bottom*: 3D topography. Two fine and discontinued wrinkles are visible. The region of interest has been defined at a distance from the eye canthus (the eyes were open during the acquisition process) and does not take into account the hair on the *right* and the eyebrows at the *top* of the image. The calculated volume is 7.7 mm^3 in this example

part of wrinkle. This polygon defines a binary mask inside which the volume is calculated. The polygonal shape is preferred to a rectangle in order to follow the curves of the wrinkle more accurately. Its geometrical characteristics and its position can be saved and applied to other surfaces in a perfectly comparable way at different times of measurement.

To quantify its volume, a relief is usually filtered (median filtering, Fourier transform, etc.), and a cutoff threshold may also be determined.

The aim of the filtering process is to separate the shape and the relief of the wrinkle from its intrinsic (micro)roughness. It is then possible to analyze separately both sets of data and to determine on which item the investigational ingredient or treatment is active.

Other areas such as the lips or nasogenian folds can be studied (Goldman et al. 2009). In this type of assessment, the main objective is not the measurement of the volume in itself but rather the comparison of shapes, by subtracting surfaces, by measuring local roughness, or by drawing profiles.

A complete acquisition of the lips can be made with a wide-field objective (Fig. 5). Imaging of this area is rather easy from the front but the repeatability of the measures can be an issue because the lips are naturally more or less contracted at the time of acquisition. Points which are not measured appear in the brightest areas or at the junction between the upper lip or the lower lip. It is possible to isolate an area of interest on one of the lips and to calculate roughness parameters locally (Sa and St). It is also possible to draw vertical profiles regularly spaced on the whole surface and to compare their curvature radius during the various acquisitions.

The wide-field objective can also be used to quantify the depth or width of nasogenian folds (Fig. 6). This type of measurement is a very interesting tool in the follow-up of the effects of a filler or an injection on the relief of the area. The acquisition is performed from a three fourth view of the area of the face under the eye. Its morphology is characterized by profiles drawn in a fan shape from the cheek and crossing the nasogenian fold (e.g., in relation to the quantity of injected product or the dermatologist's gesture).

Other facial sites can also be studied such as eye bags or jaw ptosis but experience on this type of assessment is currently not sufficient. A multisensor system (two sensors – fringes + CCD camera – placed at 45° around the subject) dedicated to 3D measurements of the whole face is available (AEVA, Eotech) (Fig. 7). It is used to measure facial ptosis or the curve of the breasts.

Besides the assessment of features of the face, fringe projection is also an interesting technique in the study of cellulite. The sensor is placed on an

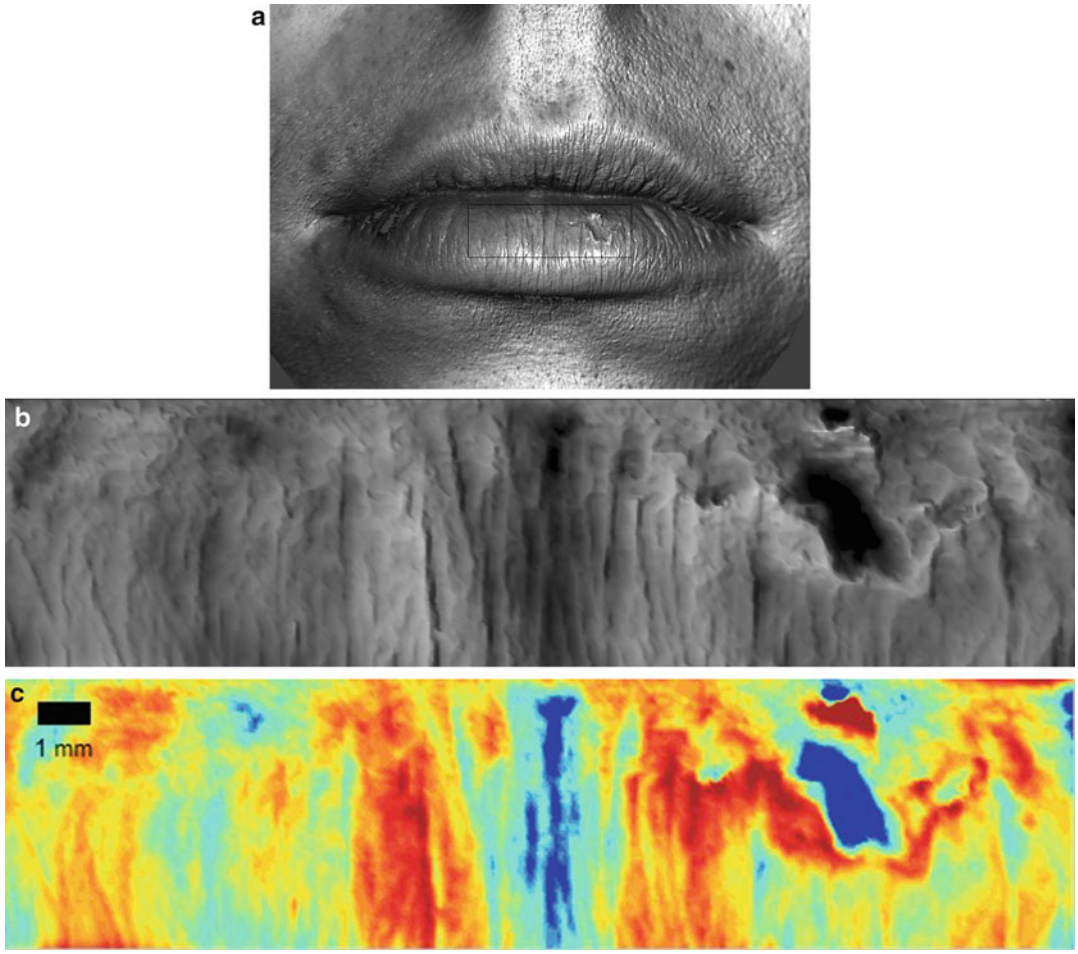

Fig. 5 *Top*: In vivo acquisition of lips (with camera texture) with wide field objective (80 × 60 mm). A few non measured points are visible in the lower part of the image, on the *right* and on the *left*. A small wound is visible on the lower lip. *Bottom*: a 20 × 5 mm region of interest has been extracted from the centre of the lower lip. Its microrelief is clearly visible, as well as the wound

adjustable tripod. Measurements are performed on the thigh and the volume of the dimples is analyzed. For obvious reasons the exact localization of the tested area (especially its height) and the position of the subject are essential for the quality and repeatability of this type of measurement.

5 Acquisition from Replicas

The technique of replicas is a simple process to reproduce a surface and is also a practical means to study it independently from its support (Lagarde et al. 2001). Replicas are made with silicon polymer (Silflo®, Monaderm, Monaco) which polymerizes at room temperature in contact with a specific catalyzer. It is harmless for the skin and mucosa. The product flows in the hollow parts of the skin, follows its relief perfectly, and within a few minutes becomes a negative cast reproducing the relief of the skin very finely.

Replicas can be made directly on the skin (Fig. 8) or with a rigid support (Cuderm, Dallas, USA) of standard size which delimitates the cast site. Silflo® is then applied with a syringe or a spatula.

Replicas must be made by trained staff to reduce the risk of having artifacts such as holes

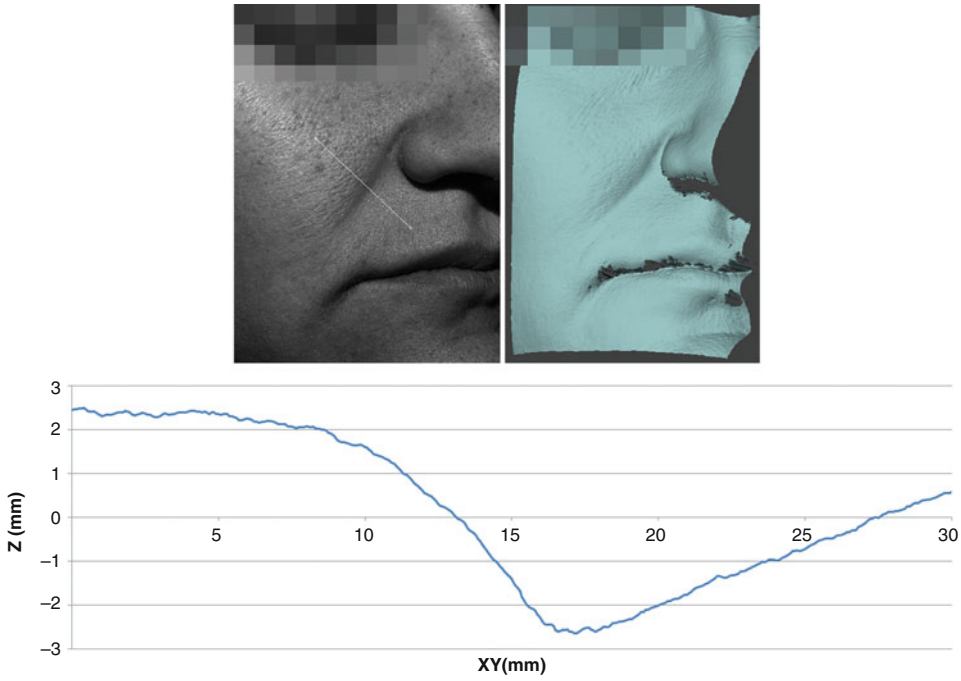

Fig. 6 In vivo acquisition of nasogenian fold with wide field objective lens (80 × 60 mm). On the *left*, image of the *right* side of the face, taken by the camera. On the *righ*t, in the corresponding 3D reconstructed image, non measured areas are visible (nostrils, lashes, lips folds) and appear like transparent tears (these points are not taken into account in calculation). These areas are located in dark zones that cannot be solved by the system. The section in white on the camera view has been drawn manually from the cheek. From this section it is possible to determine locally the depth of the fold which gets wider very progressively in a gradual slope toward the upper lip (*bottom* graph). It is therefore more difficult to calculate its width. In this type of approach the coordinates of the section must be saved for future applications on the same site on the various topographies of the subject (for example before and after injection)

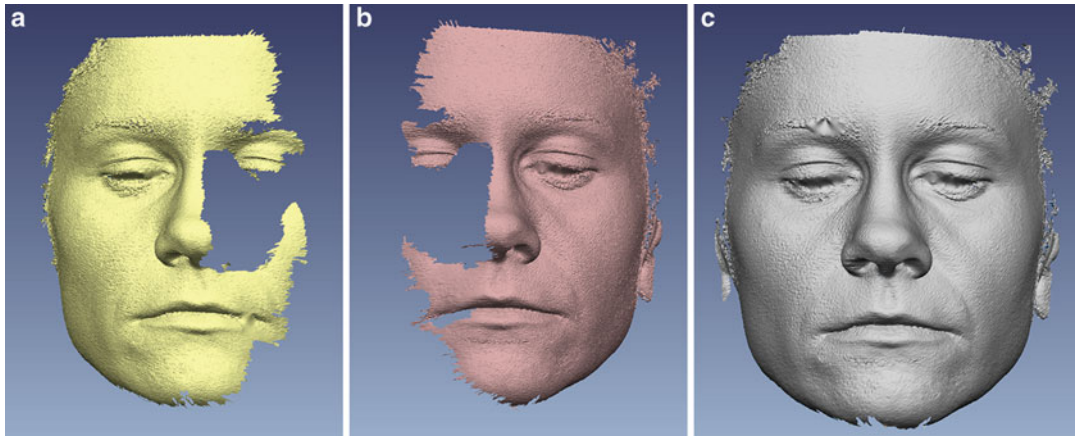

Fig. 7 Acquisition of the whole face with AEVA system. The final 3D reconstruction (*bottom*) results from the combination of 2 acquisitions of the *right* and *left* sides (2 images at the *top*). Side acquisitions are made one after the other, with the subject staying perfectly still. To ensure a global reconstruction of quality, both views must have overlapping zones to facilitate registration. The resolution of the periphery of the face is poor (especially the ears, hair, chin). Interpolation has been carried out on the eyebrows and the eyes

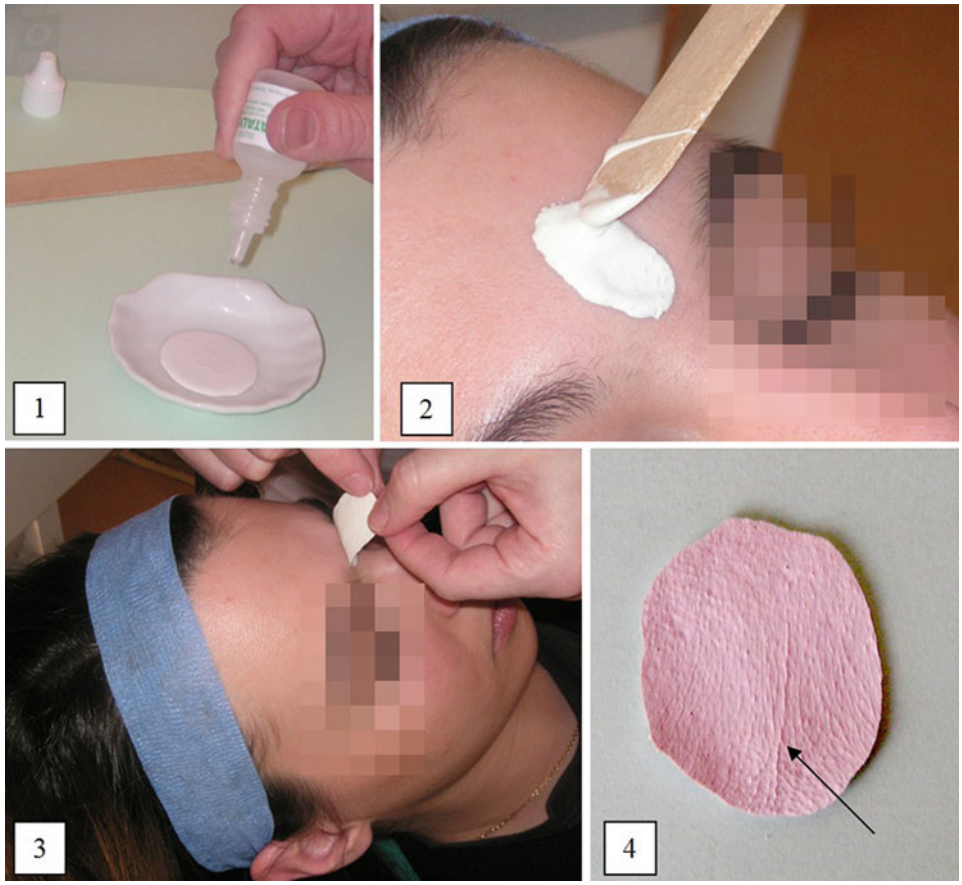

Fig. 8 Preparation of replica (**1**) A few drops of catalyser are added to Silflo® and the mixture is homogenized immediately before application. (**2**) Silflo® is spread on the skin with a spatula. (**3**) After a few minutes wait, the replica is gently removed. The negative relief of the subject's glabella (a very fine wrinkle in this example) is visible on the replica (**4**)

or bubbles. It is also necessary to check the subject's movements when the replica is produced. In theory, replicas can be made on any site on the body as long as the surface is relatively flat and without artifacts, but on the face the presence of many artifacts (hairs, vellus, pores, etc.) makes microrelief analysis rather difficult.

The accurate localization of the tested sites is essential to ensure that the same area is measured at each time of assessment according to the plan in the study protocol.

Microrelief is characterized using an objective with a high degree of precision, and the size of the region of interest is therefore reduced (10 × 10 mm). The replica is positioned on a flat surface under the sensor (its orientation is not relevant). Replicas made with the help of a support require, during computer processing, the application of an occlusion mask adapted to its shape (either round or rectangular). During the calculation of the topography, this binary mask delimitates automatically the inside of the cast excluding the edges.

Replicas are used not only to study microrelief (Fig. 9) but also to cast the wrinkles of the face, such as crow's feet (Fig. 10) or glabella (Fujimura et al. 2007; Takema et al. 1997). To compare the evolution of wrinkles or fine wrinkles over a period of time, measurements must be superimposed with accuracy. In this process called registration (also found in acquisitions in vivo), the various acquisitions are compared and then aligned, with the first acquisition

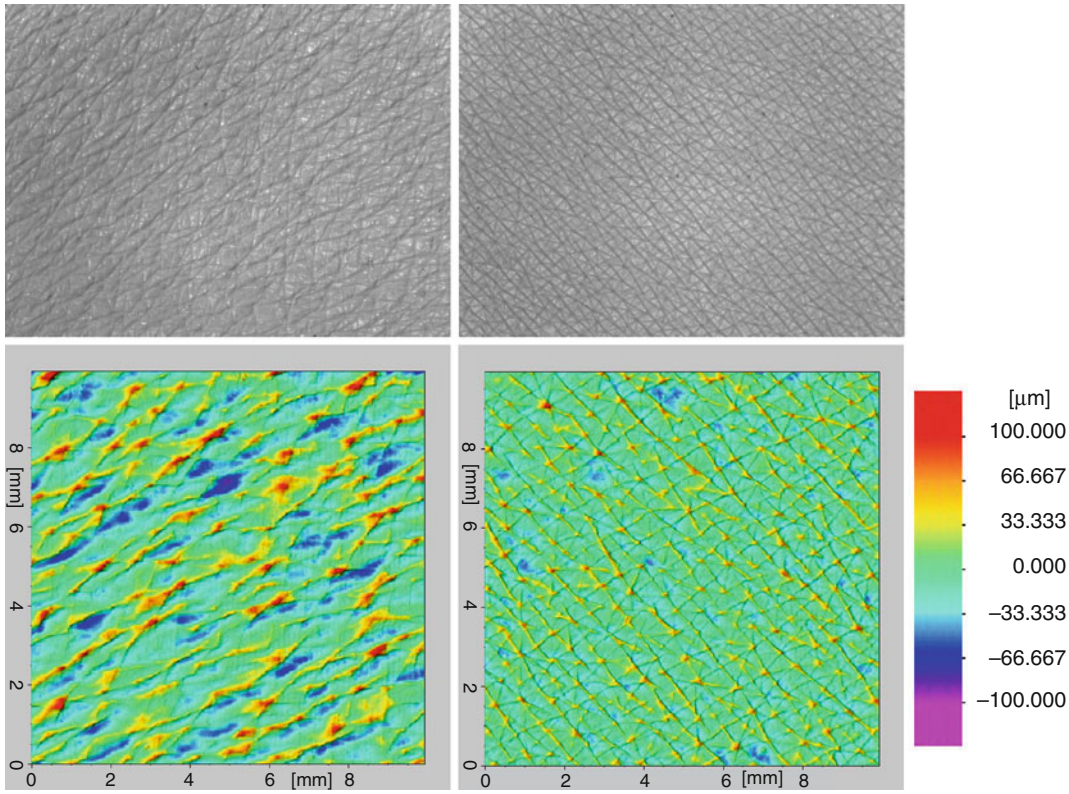

Fig. 9 Examples of microrelief from replicas of the forearm of an old subject (*left*) and a young subject (*right*). *Top*: Camera images of the replicas. *Bottom*: Corresponding topographic images (10 × 10 mm) defined at the centre of the replica. The altitude of the surfaces has been inversed for illustrative purposes. However the roughness parameters (Sa and St) are mathematically symmetrical. The microdepressionary network is clearly visible: coarse and anisotropic (*left*), or regular and isotropic (*right*). (*Left*: Sa = 22.1/St = 253.8 µm; *right*: Sa = = 14.4 /St = 178.3 µm)

(T0) being used as a reference. Registration is a delicate automated process (if acquisition is of poor quality, its alignment and the alignment of the following acquisitions are perturbed or even impossible). Analysis may then become complex and difficult when the number of acquisitions increases (>5).

The assessment of relief from replicas is interesting because it gives the opportunity to carry out cost-effective multicentric studies (devices for 3D imaging and analysis are expensive). If the replicas are of good quality, they can be digitized in very high resolution since there is no movement during acquisition. Their fair color accentuates the contrast of fringes and optimizes 3D reconstruction. Another advantage is the possibility to store them for future analysis.

6 In Vivo Acquisition

The possibility to assess wrinkles in vivo is one of the main advantages of fringe projection because it is a fast matricial measurement without contact that can be performed directly on the skin.

In vivo measurements are not as easy as they seem and require strict acquisition conditions. They must take into account slight movements of the subject (shaking, breathing) as well as dark or too bright areas of the skin where the contrast of fringes is lost. Therefore the 3D sensor is systematically associated with a positioning table where the subject can be in a reproducible and stable position although it may be uncomfortable (Fig. 2). A ball joint fixed on a rail supports the sensor which can rotate around the subject for

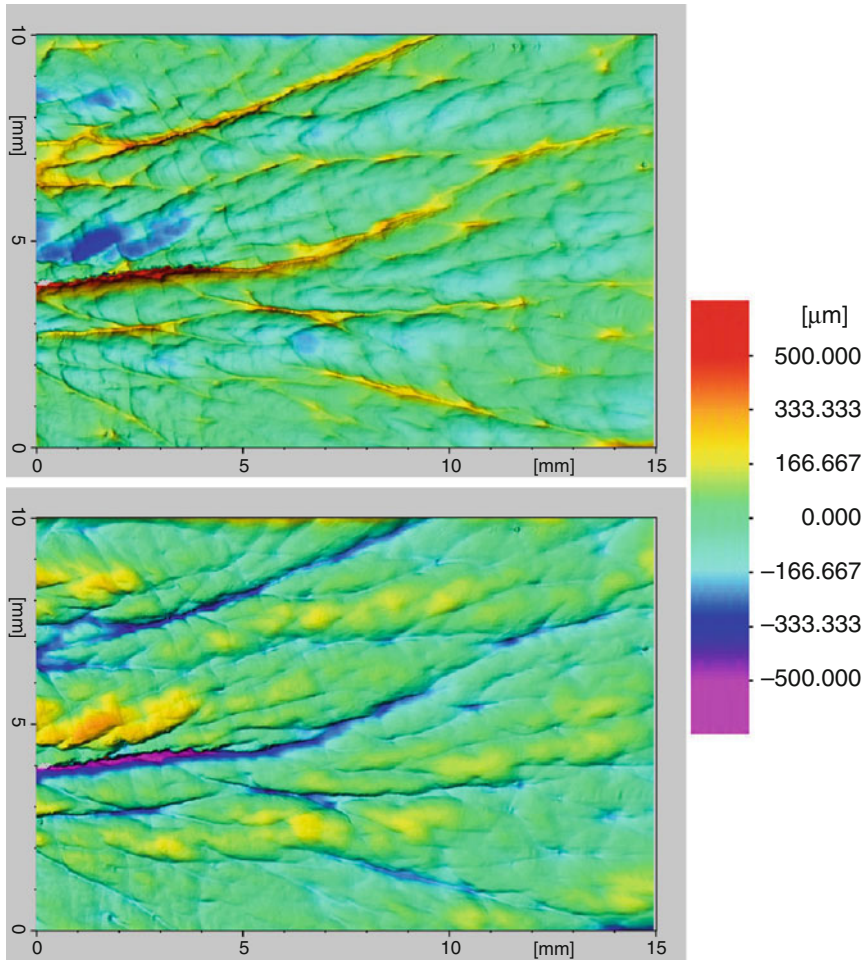

Fig. 10 Replicas of crow's foot wrinkles. *Top*: topography (15 × 10 mm) from the central part of the replica. *Bottom*: the same topography after inversion of altitudes. A few non measured points are visible at the start of the central wrinkle on the *left*. The calculated volume is 5.36 mm^3

full face, three fourth view, or profile measurements.

The subject is asked to fix a point and keep their eyes open for measurement of crow's foot wrinkles or eyes closed for measurement of forehead wrinkles. The procedure takes place in a dark room to ensure that the contrast of fringes is not perturbed by light.

In vivo measurements are also limited by the morphology of the studied site and by the depth of field which depends on the lateral resolution of the selected objective (from 6 to 40 mm). Possibilities of evaluation will be restricted on areas with important differences of levels (the eye, nose, etc.). This accounts partly for the fact that the use of a high-precision objective associated with low depth of field is not possible in vivo.

Noises present in in vivo acquisitions are materialized by aberrant or not measured points. They create breaches and more or less large distortions. Noises cannot always be detected during acquisition; they become really visible only when topography is processed. Adapted filtering (median filtering with large kernel) and filling by interpolation can compensate these perturbations to a certain extent.

The characterization of macrorelief in vivo opens very interesting perspectives in clinical evaluation. Associated with a positioning system (table or tripod), it is a reliable and polyvalent

measurement. Unlike replicas, several acquisitions can be carried out if a problem arises, on sites where it is not possible to make replicas (lips, for instance). Its main drawback however is that 3D acquisition in vivo generates more noises and requires more complex computer processing.

7 Conclusion

Fringe projection is a technique without contact to obtain accurate measurements of surfaces and it is therefore well adapted to the skin and its constraints. Added to the possibility to adapt the size of the measurement field to the studied object, it is a very interesting tool in clinical evaluation. Fringe projection is however not without drawbacks and restrictions. Like all methods of 3D digitization, it is still expensive and needs technical, practical, and computing competence.

3D digitization requires rigorous acquisition procedures to fix and document as exactly as possible the context in which the measurement is performed. The subjects are at the heart of the acquisition process by their position, attitude, posture, or expression which can strongly influence measurements.

References

Agache P. Physiologie de la peau et explorations fonctionnelles cutanées. Paris: Editions Médicales Internationales; 2000.

Agache P, Humbert P. Measuring the skin. Berlin: Springer; 2004.

Bazin R, Lévêque JL. Longitudinal study of skin aging: from microrelief to wrinkles. Skin Res Technol. 2011;17:135–40.

Fujimura T, Haketa K, Hotta M, Kitahara T. Global and systematic demonstration for the practical usage of a direct in vivo measurement system to evaluate wrinkles. Int J Cosmet Sci. 2007;29:423–36.

Goldman MP, Skover GR, Payonk GS. Three-dimensional imaging techniques in the assessment of facial volume augmentation. J Drugs Dermatol. 2009;8(12):1113–9.

Hayashi S, Mimura K, Nishijima Y. Changes in surface configuration of the skin caused by ageing and application of cosmetics; three-dimensional analysis according to a new system based on image analysis and Fourier transformation. Int J Cosmet Sci. 1989;11:67–85.

Lagarde JM, Rouvrais C, Black D, Diridollou S, Gall Y. Skin topography measurement by interference fringe projection: a technical validation. Skin Res Technol. 2001;7:112–21.

Lagarde JM, Rouvrais C, Black D. Topography and anisotropy of the skin surface with ageing. Skin Res Technol. 2005;11:110–9.

Makki S, Barbenel JC, Agache P. A quantitative method for the assessment of the microtopography of human skin. Acta Dermatovenerologica (Stockholm). 1979;59:285–91.

Makki S, Mignot J, Zahouani H, Agache P. Statistical analysis and three dimensional representation of human skin surface. J Soc Cosmet Chem. 1984;35:311–25.

Marsaut D. Ingénierie optique et microsystème silicium. Développement d'une instrumentation dédiée à la biologie cutanée. Thèse de Sciences, Université de Franche Comté, 2004.

Mignot J. Analyse du relief cutané: problèmes rencontrés. Solutions et perspectives. Les entretiens du CARLA, Tome VII, novembre 1986.

Mignot J, Zahouani H, Rondot D, Nardin P. Morphological study of human skin topography. Int J Bioeng Skin. 1987;3:177–96.

Piérard GE, Uhoda I, Piérard-Franchimont C. From skin microrelief to wrinkles. An area ripe for investigation. J Cosmet Dermatol. 2004;2:21–8.

Rosa Pena Ferreira M, Costa PC, Bahia FM. Efficacy of anti-wrinkle products in skin surface appearance: a comparative study using non-invasive methods. Skin Res Technol. 2010;16:444–9.

Russ JC. The image processing handbook. Boca Raton: CRC Press; 2007.

Sainthillier JM, Mac-Mary S, Humbert P. Analyses et représentations des rides par imagerie 2D. Ann Dermatol Venereol. 2009;136 suppl 6:S273–9.

Srinivasan V, Liu HC, Halioua M. Automated phase-measuring profilometry of 3-d diffuse objects. Appl Optics. 1984;23:3105–8.

Stout K, Blunt L. Three dimensional surface topography. Penton Press: London; 2000.

Takeda M, Ina H, Kobayashi S. Fourier-transform method of fringe-pattern analysis for computer-based topography and interferometry. J Opt Soc Am. 1982;72 (1):156–60.

Takema Y, Tsukahara K, Fujimura T, Hattori M. Age-related changes in the three-dimensional morphological structure of human facial skin. Skin Res Technol. 1997;3:95–100.

Zahouani H, Vargiolu R. Mesure du relief cutané et des rides. In: Agache P, editor. Physiologie de la peau et explorations fonctionnelles cutanées. Paris: Editions Médicales Internationales; 2000. p. 41–57.

Zahouani H, Vargiolu R. Skin line morphology: tree and branches. In: Agache P, Humbert P, editors. Measuring the skin. Berlin: Editions Springer; 2004. p. 40–59.

Zahouani H, Chuard M, Mignot J, Makki S, Agache P. Etude tridimensionnelle du relief cutané. Innov Technol Biol Med. 1985;6:447–60.
Zahouani H, Vargiolu R, Humbert Ph. 3D morphological tree representation of the skin relief: a new approach of skin imaging characterization. 20th IFSCC Congress, Cannes, 1998, vol 3. pp 69–79.
Zani ML. La mesure de rugosité ? Quelques normes. . . et plusieurs dizaines de paramètres. Mesures 758. Oct 2003.

Additional Information on Relief Analysis

Digital Surf, http://www.digitalsurf.fr/en/dsvisitefr.html.
SPIP™, Image Metrology Software for Microscopy. http://www.imagemet.com/

Other Profilometry Techniques Not Mentioned in This Article

Stereoscopic photography
Quantificare: http://www.quantificare.com/index.php?q=LifeViz_EsthetiqueFR
The 3D LifeWiz system is made of a compact camera. It is based on stereovision which gives perception of depth. Two systems are available: a global system for large visualisation of the neck and face and a more accurate system for localised visualisation of wrinkles or scars.
Image processing by projected shadow
http://www.monaderm.com/Appareil_scientifique.php?appareil=quantirides
http://www.monaderm.com/Appareil_scientifique.php?appareil=quantiline
Quantirides and Quantilines systems have been developed to analyze, quantify and characterize wrinkles and microrelief from Silflo® replicas. The negative print of wrinkles is placed under oblique light (35°) which generates projected shadows behind each wrinkle. Acquisition of this image and its shadows is performed via high resolution digital camera. The image is then analyzed with dedicated software.
Profilometry by contact
http://www.altimet.fr/fr/index.htm
This company develops a range of equipment (Altisurf) for the metrology of surfaces, more specifically devised for the microtechnics industry (tests on varnishes, characterization of ink deposits, textile textures. . .) and nanotechnics industry (materials and substrates, corrosion, adhesive. . .)

Influence of the Sebum and the Hydrolipidic Layer in Skin Wettability and Friction

19

Ahmed Elkhyat, Ferial Fanian, Ahlam Abdou, Hajar Amarouch, and Philippe Humbert

Contents

A. Elkhyat (✉)
Center for Research and Studies on the Integument (CERT), Department of Dermatology, Clinical Investigation Center (CIC BT506), Besançon University Hospital, INSERM UMR1098, FED4234 IBCT, University of Franche-Comté, Besançon, France
e-mail: aelkhyat@chu-besancon.fr

F. Fanian
Center for Study and Research on the Integuments, Department of Dermatology, University Hospital of Besançon, Besançon, France
e-mail: ferial.fanian@chu-besancon.fr; ferial.fanian@cert-besancon.com; fanian@gmail.com

A. Abdou • H. Amarouch
Department of Dermatology, Ibn Sina Hospital, Rabat University Hospital, Rabat, Morocco

P. Humbert
Department of Dermatology, University Hospital of Besançon, Besançon, France
e-mail: philippe.humbert@univ-fcomte.fr

P. Humbert et al. (eds.), *Agache's Measuring the Skin*,
DOI 10.1007/978-3-319-32383-1_19

Keywords
Human skin • Wettability • Water contact angle • Hydrophobic/hydrophilic balance • Sebum • Hydrolipidic layer • Friction coefficient

1 Introduction

Water changes the properties of human keratin fibers existing in the skin, hair, and nails (Barba et al. 2010). Examples are the sorption of water by stratum corneum, the spreading of water and lipidic liquids which influences skin absorption, thermal loss, as well as transcutaneous pressure of water vapor, carbon dioxide, and oxygen (Agache et al. 2004). The production of a sweat/sebum emulsion can also be influenced by these interactions as well as the behavior and effect of topical drugs or cosmetics on the skin (Agache et al. 2004).

Frequent washing increases brittleness of the nail (Uyttendaele et al. 2003), and chronic wetting and drying of nails may cause lamellar dystrophy (onychoschizia) (van de Kerkhof et al. 2005). Brittle nails affect about 20 % of the population, and women are affected twice as frequently as men (Lubach et al. 1986). Hydrophobicity of soft tissue surfaces in the human body, including those of the human oral cavity, has been described for decades as playing an important role in many biological processes, like cellular adhesion (Barba et al. 2010), contact inhibition, elasticity (Agache et al. 2004), tissue membranes functions, intracellular structures (Uyttendaele et al. 2003), and adhesion of infectious microorganisms (van de Kerkhof et al. 2005). Generally, tissues with absorption/exchange functions or, indeed, lubrication tend to be more hydrophilic. On the other hand, tissues requiring protection against pathogenic microorganisms or acids tend to be hydrophobic (Lubach et al. 1986).

From a fundamental point of view, wetting is an important phenomenon, because of its diverse applicability in everyday life. Friction and lubrication are intimately coupled to wettability.

In this chapter, we will first treat human skin wettability by showing effects of some treatments and applications on wettability parameters. Secondly, the skin friction coefficient will be studied through the effect of the surfaces hydrophobic/hydrophilic balance (Ho/Hi).

2 Human Skin Wettability

Wetting refers to the contact between a solid surface and a liquid; it depends on intermolecular interactions. The degree of surface wetting is evaluated through the measurement of contact angle. The wetting of the surface is the best, if it has the minimum contact angle (θ). When $\theta = 0°$, the surface wets completely; the opposite corresponds to $\theta = 180°$ (dewetting), and the partial wetting refers to θ ranging from 0 to 180° (Fig. 1).

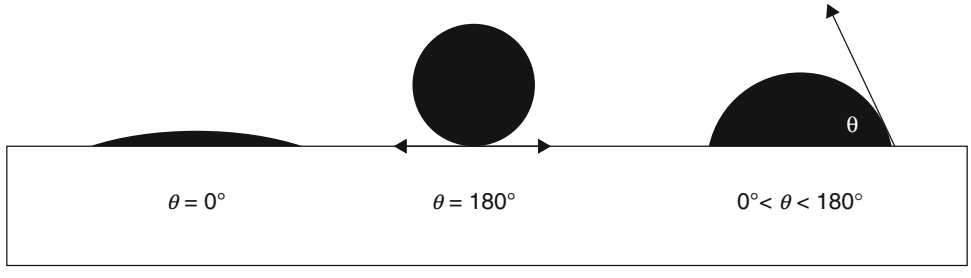

Fig. 1 Solid wettability: $\theta = 0°$: total wetting, $\theta = 180°$: non wetting = dewetting, 0° θ 180°: partial wetting, $0° < \theta < 180°$: partial wetting

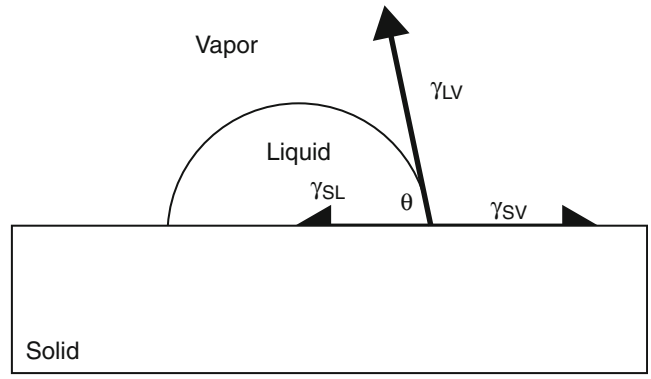

Fig. 2 Equilibrium of a liquid drop on a solid surface: contact angle and surface energy

2.1 Theory

2.1.1 Contact Angle and Superficial Energy (Fig. 2)

Young's equation (Eq. 1) (Young 1805) relates the surface tension between the liquid vapor (γ_{LV}), the solid vapor (γ_{SV}), and the solid-liquid (γ_{SL}) and the free surface energy by contact angle (θ). The general form of this equation for the solid-liquid-air system is

$$\gamma_{LV} \cos\theta = \gamma_{SV} - \gamma_{SL} - \pi_e \qquad (1)$$

where π_e (external pressure) = 0 for low energy solids (Fowkes 1964).

2.1.2 Critical Surface Tension (γ_c) and Hydrophobic/Hydrophilic Balance (Ho/Hi)

Critical Surface Tension

γ_c (Fig. 3): The definition of γ_c is based on an empirical relationship between the cosine of the contact angle and the surface tension of a series of homologous liquid (Eq. 2) (Zisman 1964)

$$\cos\theta = 1 - b\left(\gamma_{liquid} - \gamma_c\right) \qquad (2)$$

where γ_{liquid}, liquid surface tension (mJ/m^2). Note that a reduction of γ_c means an increase in the surface hydrophobia.

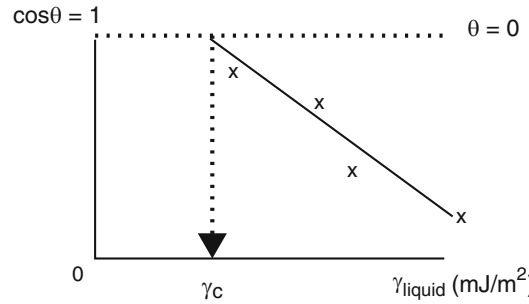

Fig. 3 Critical surface tension γ_c: total wetting condition (γ_{liquid} γ_c)

Hydrophobic/Hydrophilic Balance (Ho/Hi)

For decades, the surface hydrophobicity has been reported to play an important role in many biological processes, such as cellular adhesion, contact inhibition, elasticity, functionality of tissue membranes, functioning of intracellular structures, and adhesion of infectious microorganisms (Norris et al. 1999).

The skin hydrophobia balance (Ho/Hi) is quantified by a relationship between γ_c and the water surface tension (Eq. 3) (Elkhyat et al. 2001)

$$Hi = \gamma_c / \gamma_{H2O} \qquad (3)$$

where Hi is surface hydrophilia and Ho is surface hydrophobia.

This parameter is expressed by the ratio of its critical surface tension γ_c to the water surface tension γ_{H2O} normalized by the latter.

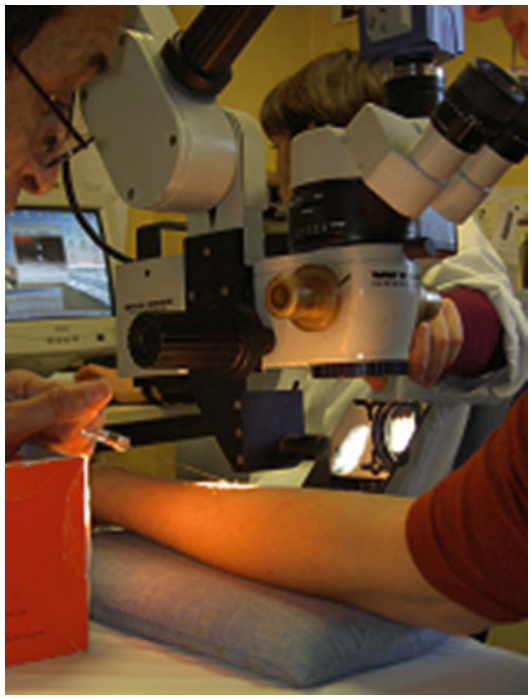

Fig. 4 Contact angle visualization and measurement: tool rests on the use of a mirror directed 45° to the skin "Profile drop method"

Free Surface Energy FSE (γ_s)

Free skin energy is a topical parameter that determines most of the surface properties such as adsorption, wetting, adhesion, etc. The γ_s of the solids cannot be directly measured, because of the very weak mobility of the molecular atoms. It is necessary to resort to indirect methods such as study of the interactions between a solid and a liquid. The γ_s is derived from the measurement of the contact angle of pure liquids, with known surface tension parameters.

Several approaches are mentioned in the literature; the two most commonly used for the skin are described below:

Geometric mean approach (Owens and Wendt 1969): The γ_s proportional to the intermolecular energy is the sum of the dispersion component γ_s^d and the polar component γ_s^p.

Acid-base approach (Van Oss et al. 1988; Good and Van Oss 1992): The γ_s can be expressed as the sum of Lifshitz-van der Waals γ_s^{LW} and acid-base γ_s^{AB} components $\gamma_s = \gamma_s^{LW} + \gamma_s^{AB}$. The acid-base components can be expressed as $\gamma_s^{AB} = 2\left(\gamma_s^+ . \gamma_s^-\right)^{1/2}$; the γ_s^+ and γ_s^- components indicate, respectively, the electron-acceptor and the electron-donor components.

2.2 Contact Angle Measuring

For the visualization and the measurement of the contact angle, we developed a tool especially designed for the wettability in vivo measurements (Fig. 4). This tool is based on the use of a mirror directed at a 45° angle to the skin (profile drop method).

A drop of test liquid is deposited on the skin surface using a microsyringe and inflated up to a final drop volume of 5 μl. The advancing contact angle of test liquids corresponds to the maximum value of the contact angle when the drop is inflated without moving the contact line.

The drop's image is recorded using a video camera (CDD-Iris, Sony, France) connected to a computer and mounted on a microscope (Wild Heerbrugg M650, Switzerland), with a magnification of ×16, fitted with a slanted mirror. After visualization and storage of the drop profile, the contact angle is measured using a program which can determine θ from the tangents of both sides of the drop. The influence of roughness and skin temperature on the contact angle is treated in the literature (Wenzel 1936; Neumann and Good 1979; Mavon et al. 1997). The temperature effects on the liquid in contact with the skin are minimized with the nature of the deposit (advancing contact angle) and with shortening the time of deposit (15–20 s).

In order to allow every researcher to be able to assess the skin wettability, a new device has just been developed which stands for drop shape analysis (Fig. 5). With this measuring procedure, a drop of liquid (mostly water) dribbled on the inner side of the lower arm. According to the wettability of the sample surface, the drop will take on a form depending on the surface tension. In order to interpret this form into a conclusive

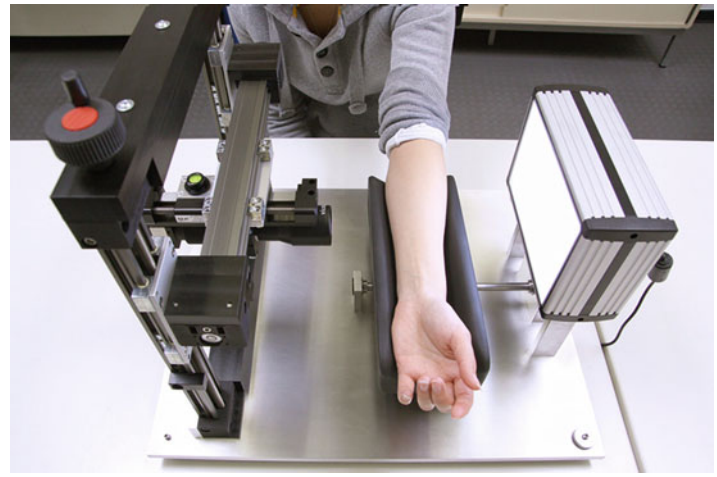

Fig. 5 Human skin wettability measurement: forearm rest with the new device

value for measurements, the drop's contact angle is determined.

This device has three basic components: (1) A black and white camera with a telecentric measuring lens adjustable with a small linear axes portal. (2) An arm rest with adjustable settling angle. The angle is set to position the lower arm on which the measurement is performed as horizontal as possible. This setting prevents the drop to run or disintegrate, and both sides of the contact angles are the same on each side of the drop if the contact area is positioned horizontally. (3) Software: The software allows the adjustment of the arm in a horizontal position, the calculation of the drop angle, and saving of pictures and data.

2.3 Data Analyses

2.3.1 Water Contact Angle θ_w

Water is an important factor for normal skin function. When the water content decreases, the skin becomes dry, itchy, and uncomfortable. The spreading degree of a water drop on the skin surface is an indication of its hydrophobic (Ho) or hydrophilic (Hi) properties.

Skin: Water spreads differently on skin. On the volar forearm, a poor site in sebum, water forms a semi hydrophobic contact angle ($\theta_w = 80°-91°$) (Mavon et al. 1997; Elkhyat et al. 2004a, b; Schott 1971). On the forehead, rich site in sebum, water spreads over ($\theta_w = 57°-73°$) (Afifi et al. 2006; Fotoh et al. 2007; Mavon et al. 1998). A study of ten different sites (Afifi et al. 2006) was confirmed that the skin with poor sebaceous lipids is a hydrophobic surface ($\theta_w = 91°-102°$). On the rich sebaceous zones, the skin becomes hydrophilic ($\theta_w = 60°-85°$) (Fig. 6). Fotoh et al. (Fotoh et al. 2007) showed that the forehead skin wettability is significantly different ($p < 0.05$) between Black people (Africans or Caribbeans) ($\theta_w = 71°$) and Mixed races (African or Caribbean) ($\theta_w = 67°$) and Caucasians ($\theta_w = 67°$). The water contact angle θ_w was recently measured on the forehead of 60 children (aged 7–11), and the results showed a $\theta_w = 87°$ higher than adults indicating the skin is more hydrophobic than adults. Note that the sebum level measured on these children was particularly low (17 μg/cm^2) (Lodge 2007; Mac-Mary et al. 2012a).

Nail: The in vivo evaluation of the nails shows that human nail is a hydrophilic surface with a $\theta_w = 65°$ (Fig. 7). No significant difference has been found between different ethnicities (France, China, Iran, Morocco) or different sexes (Elkhyat et al. 2010).

2.3.2 Critical Surface Energy γ_c and Hydrophobic/Hydrophilic Balance (Ho/Hi)

The skin hydrophobia increases by decreasing γ_c. Just like θ_w, the critical surface tension (γ_c) values show that in the presence of sebum, the skin is less hydrophobic. On the forearm, γ_c is about

Fig. 6 Human skin wettability: effect of sebum on hydrophobic/hydrophilic balance

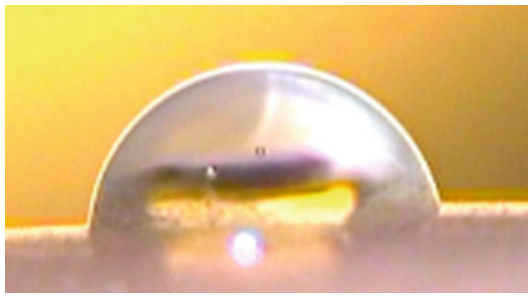

Fig. 7 Nail: hydrophilic surface with water contact angle = 65°

26–27.5 mJ/m^2 (Rosemberg et al. 1973; El-Shimi and Goddard 1973; Ginn et al. 1968; Adamson et al. 1968; Elkhyat et al. 1996), and on the forehead, as a rich site in sebum, γ_c increases (33.2 mJ/m^2) indicating an increasing of skin wettability. According to Eq. 3, the percentage of hydrophobia Ho of the forearm is between 62 % and 64 %, while the presence of sebum on the forehead reduces the skin hydrophobia to 54 %.

2.3.3 Surface Free Energy (γ_s)

The surface wettability increases with increasing γ_s.

The γ_s value of the skin at the forearm is approximately 38.5 mJ/m^2 (Elkhyat et al. 2001; Mavon et al. 1997), while on the forehead, it ranges between 42 and 46 mJ/m^2 according to the skin type (oily, normal, dry skin) (Mavon et al. 1998). The use of the acid-base approach shows that the forehead (sebum-rich area) is a strongly monopolar basic surface ($\gamma_s^- = 26$ mJ/m^2) and that the forearm (sebum-poor area) is a

weakly basic surface ($\gamma_s^- = 4$ mJ/m^2) (Mavon et al. 1998). The γ_s increasing on the forearm is noticed by the increasing of the apolar component γ_s^{LW} (+10 mJ/m^2).

2.4 Effects of Some Treatments (Table 1)

The skin hydrophobia increases with the increase of θ_w and γ_c and decrease of γ_s (Elkhyat et al. 2001; Mavon et al. 1998).

2.4.1 Degreasing and Washing

Skin: Degreasing with organic solvents or washing with soap and water increases considerably the skin hydrophobia. This effect is observed by increasing the water contact angle θ_w (+10–15°) while reducing the free surface energy γ_s and the critical surface energy γ_c (Mavon et al. 1998). The initial skin hydrophilia of the forehead was found 2 h later after degreasing, time required for the reconstitution of the sebum current level (Mavon et al. 1998).

Nail: The degreasing of the nails with organic solvents also increases its hydrophobia (θ_w = +25°) (Fig. 8) (Elkhyat et al. 2010).

Hair: Virgin hair shows a mean thickness of 1.1 nm. The outermost layer of virgin hair surface is primarily made of a fatty acid called 18-methyleicosanoic acid (18-MEA), which strongly contributes to the hydrophobicity (θ_w = 103°) and lubricity of virgin hairs (Lodge 2007). Due to its hydrophobicity, the virgin hair surface is lacking of any water film, and therefore, the water film thickness measured on the surface is very low. Damaged hair, however, is slightly hydrophilic due to the removal of the fatty acid layer during damaging process (θ_W = 50°−80°) (Lodge 2007).

2.4.2 Application of Moisturizers (Cream, Thermal Water)

Our skin needs an adequate daily fluid intake to replenish the water stock in the dermis (dehydration will induce the loss of skin elasticity and increasing the skin folds). On the other hand, the skin should renew the hydrolipidic film essential for the appearance and also for the barrier function of the epidermis. Applying a moisturizer on the face of 60 children for 1 week showed a significant decrease in θ_w angle (−10°) indicating an increase in skin hydration (+15 arbitrary unit) (Mac-Mary et al. 2012a, b).

Table 1 Human skin wettability

	Volar forearm		Forehead	
	No treated	Degreasing "ether"	No treated	Degreasing "ether"
θ_w	80° (Wenzel 1936); 84° (Neumann and Good 1979)	92° (Neumann and Good 1979);101° (Fowkes 1964)	57–73° (Elkhyat et al. 2004b); 60° (Elkhyat et al. 2004a)	84° (Fowkes 1964)
	88° (Fowkes 1964); 91° (Mavon et al. 1997)		67–71° (Schott 1893–1895)	
γ_c	26 (Afifi et al. 2006); 26.8 (Fotoh C et al. 2007)	21.6 (Mac-Mary et al. 2012a)	33.2	22.4
	27 (Mavon et al. 1998); 27.5 (Lodge 2007; Mac-Mary et al. 2012a) 30.6 (Neumann and Good 1979)			
Ho	62 % (Elkhyat et al. 2001)	70 % (Elkhyat et al. 2001)	54 %	69 %
γ_s	38.5 (Fowkes 1964; Elkhyat et al. 2001)	32.4 (Fowkes 1964)	42–46 (Elkhyat et al. 2004b)	34.5 (Fowkes 1964)

θ_w: Water contact angle, Ho: Surface hydrophobicity; γ_c: Critical surface tension (in mJ/m^2); γ_s: Surface free energy (in mJ/m^2)

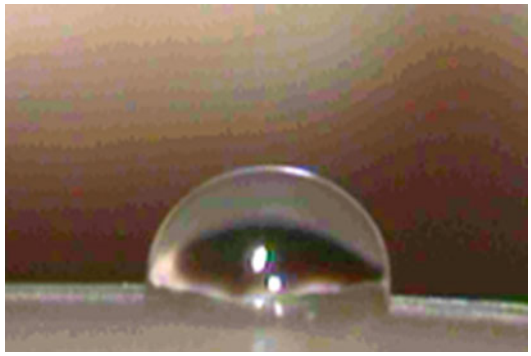

Fig. 8 Nail: degreasing effects: contact angle improvement (90°)

The effect of moisturizers is also noticed by increasing the critical surface energy (γ_c) and free surface energy γ_s. The application of thermal water reduces the skin hydrophobia by reducing the θ_w (−10°). This effect disappears 30 min after application (Elkhyat et al. 2004a).

2.4.3 Other Applications

Nutritional supplement provides comprehensive care of the skin envelope of the healthy individual and well-being as well. The effect of a nutritional supplement on the dryness in postmenopausal women has been shown with decreasing the contact angle which was initially hydrophobic (Humbert et al. 2005). The presence of mucus layer makes the surface of the pork tongue significantly more hydrophilic (more wettable). This effect is noted by decreasing the angle θ_w (−27°) and increasing the energy γ_s (+11 mJ/m^2) (Ranc et al. 2006).

2.5 Discussion

The skin wettability study shows clearly the role of hydrolipidic layer on the skin hydrophobia. The suppression or the alteration of this layer increases the skin hydrophobia. This capacity of the cutaneous lipids to increase skin wettability was attributed to the free fatty acids, especially to those existing in the sebum. By increasing the amount of squalene and paraffin in sebum, skin wetting was found to be increased (Gloor et al. 1973).

The in vivo quantification of physicochemical parameters of wetting nails has a potential value in the field of researches. The practical interest of drug penetration through transungual barrier function places these studies increasingly at the center of attention. The choice of intermediate films, including antifungals and varnishes, depends on the knowledge of these parameters.

3 Human Skin Friction Coefficient

The frictional behavior of the skin in contact with different materials plays a critical role in the sensory perception of them. The friction is extremely important in our perception of cosmetic application such as antiaging cream and moisturizers (Gee et al. 2005). The consumer exposure of the wide majority of cosmetic products is limited to dermal contact. While touching an object, a contact happens between our skin and the object; then the tribological properties of such a contact influence how an object is perceived. Sensory perception is an important factor in the decision-making process of consumers (Bongaerts et al. 2007).

The friction coefficient is the measurement of the level of sliding between two surfaces. The initial force to start the slide is called the "dynamic friction coefficient," while the force necessary to continue this is called the "kinetic friction coefficient." A high friction coefficient represents a weak slide, while a low friction coefficient indicates a good slide.

The review of the published literature on the skin friction shows a wide range of measured values of μ (Table 2). These differences indicate that the assessment of the friction coefficient of the skin is a highly complex problem. It involves skin elasticity, skin anisotropy, micro-topography, anisotropy of the skin relief leading to variation in testing conditions, and individual differences in measuring techniques. This last point can divide the test apparatus into two types of designs: one called incorporate linear motion, wherein a probe is pressed onto the surface and dragged across the skin in a straight line, and the other design is rotational and consists of a probe pressed onto

Table 2 Human skin friction coefficient (μ) – literature data

Author	Sliding material	Motion of test	μ	Ref
Comaish et al.	Teflon[(1)] nylon[(2)] polyethylene [(3)] wood[(4)]	Linear	0.2[(1)]–0.45[(2)]–0.3[(3)]–0.4[(4)] forearm	Comaish and Bottoms (1971)
Kenins	Different wool fabrics	Linear	0.32–0.48: dry skin	Kenins (1994)
			0.48–1.23: wet skin (forearm, finger)	
El-Shimi	Steel (rough[a], smooth[b])	Rotational	0.2–0.4[a]	El-Shimi (1977)
			0.3–0.6[b] (volar forearm)	
Highley et al.	Nylon	Rotational	0.19–0.28 (volar forearm)	Highley et al. (1977)
Cua et al.	Teflon	Rotational	0.34 (forehead)	Cua et al. (1990)
			0.26 (volar forearm)	
			0.21 (palm), 0.12 (abdomen)	
			0.25 (upper back)	
Asserin et al.	Ruby	Linear	0.7 (volar forearm)	Asserin et al. (2000)
Elkhyat et al.	Teflon[(1)]	Linear	0.18[(1)]–0.42[(2)]–0.74[(3)] (volar forearm)	Elkhyat et al. (2004b)
	Steel[(2)]			
	Glass[(3)]			
Elsner et al.	Teflon	Rotational	0.48 (volar forearm)	Elsner et al. (1990)
			0.66 (vulva)	
Sivamani et al.	Steel	Linear	0.56 (normal skin: dorsal finger)	Sivamani et al. (2003a)
			0.50 (isopropyl alcohol exposure: dorsal finger)	
			0.2 (normal skin in vitro)	
			0.3 (water exposed skin in vitro)	
Sivamani et al.	Steel	Linear	0.4–0.6 (volar forearm)	Sivamani et al. (2003b)
Derler et al.	Textile sample	Linear	0.27–0.7 (finger)	Derler et al. (2007)
Egawa et al.	Finger print		0.4 (volar forearm)	Egawa et al. (2002)
Lodén et al.	Steel	Rotational	0.55 (dorsum of the hand)	Lodén et al. (1992)
			1.1 (lower back)	
			0.65 (volar forearm) respectively in atopic skin	
			0.4 – 0.65 – 0.55	
Fotoh et al.	Steel	Linear	0.7–0.9 forehead	Fotoh C et al. (2007)

and rotated against the skin surface. The friction coefficient does not vary significantly with gender but varies considerably among the anatomical sites of the body (Cua et al. 1990; Elsner et al. 1990; Sivamani et al. 2003a); the age effect was also measured (Asserin et al. 2000; Elsner et al. 1990; Sivamani et al. 2003a). The friction coefficient is influenced by load (Asserin et al. 2000; Sivamani et al. 2003a; Koudine et al. 2000; Ramalho et al. 2007); however, it is increased due to water application (El-Shimi 1977; Asserin et al. 2000; Sivamani et al. 2003b). On the other hand, the application of petrolatum and glycerine on the forearm and on the hand decreases the friction coefficient immediately, and this effect lasts for at least 1 h after application (Ramalho et al. 2007). The application of isopropyl alcohol (Sivamani et al. 2003a) and

washing with soap (Egawa et al. 2002) will dry the skin and decrease its friction coefficient. The finger has a friction coefficient (μ) ranged from 0.27 to 0.70 and varying among individuals due to different states of skin hydration (Derler et al. 2007). Recently, our group (Fotoh et al. 2007) showed a significant difference ($p < 0.05$) of μ measured on the forehead depending on the ethnic affiliation. In 2004 (Elkhyat et al. 2004b), we showed the influence of the hydrophobic and hydrophilic characteristics of sliding and slider surfaces on μ. In this study, the wettability parameters for six surfaces (volar forearm, Teflon, silicone impression material [Silflo], vinyl polysiloxane impression material resin, steel, and glass) were measured, and their influences were compared to the friction coefficient μ.

The tribometer was developed and validated (Elkhyat et al. 2004b; Fotoh et al. 2007; Ranc et al. 2006; Asserin et al. 2000) to characterize the friction properties between skin in vivo and different sliding surfaces. A sliding ball of 10 mm diameter was pressed on the ventral forearm with a constant normal load (F_N) of 0.1 N and then moved at a constant velocity of 0.5 mms^{-1}. In order to maintain surfaces as flat as possible, a short sliding distance of 10–15 mm was selected.

In this study, we showed that if the skin is rubbed against a hydrophobic surface such as Teflon, the friction coefficient (μ) is lower than when rubbed against a hydrophilic surface such as glass or steel: so the hydrophobic surfaces have the lowest friction coefficient.

4 Discussion

Frictional properties of human skin depend not only on the skin itself including its texture, suppleness, smoothness, and its dryness or oiliness (Lodén et al. 1992) but also on its interaction with external surfaces and the outside environment (Zhang and Mak 1999).

In this chapter, we saw the role of the skin hydrophobia in the skin friction coefficient. The largest hydrophobicity of the abdomen explains its lowest friction coefficient compared to the forehead measured by Cua et al. (1990). Water application decreases the skin hydrophobia and consequently increases its friction coefficient measured by Egawa et al. (2002) and Sivamani et al. (2003b). The decrease of μ after degreasing (isopropyl alcohol) (Sivamani et al. 2003a) or after washing with soap and water (Egawa et al. 2002) is quite normal; indeed, these treatments increase the skin hydrophobia (Table 1), while the increased skin hydrophobia with aging or in atopic skins leads to low μ as reported in the literature (Asserin et al. 2000; Lodén et al. 1992).

The role of the surface lipids was speculated as one possible factor contributing to the frictional properties of the skin, and the correlation between μ and the skin lipid content was evaluated: Cua et al. (1995) showed that the skin lipid content plays a role in the frictional properties of the skin. Moreover, in the skin, the friction resistance depends on hydrophilic and lipophilic elements present on the cutaneous surface. Fotoh et al. (2007) assumed that the hydrophilic/hydrophobic balance of the cutaneous hydrolipidic film is different between the different ethnic groups studied. Black women could have a decreased skin friction coefficient as well as an increased cutaneous hydrophobicity comparatively to Mixed-race and Caucasian women.

5 General Conclusion

The exploitation of these parameters should allow to classify the different types of the skin according to their affinity with water, which is of major importance in biology as in cosmetology. These data should also be possible to guide the cosmetic formulation to discriminate the emulsions which cannot spread properly on the skin. Investigation of skin frictional properties is relevant to several research areas, such as skin physiology, skin care products, textile industry, human friction-dependent activities, and skin friction-induced injuries (Zhang and Mak 1999). Friction of skin forms an integral part of tactile perception and plays an important role in the objective evaluation of consumer-perceptible skin attributes (Wolfram 1983).

6 Conclusion

In cosmetic researches, the structure and the physicochemical properties of the skin, the nail, and the hair are of great interest. Studies of physicochemical parameters of wetting the skin bring a new look at the interactions between the formulations and keratin (or skin).

Up to now, these parameters are known as a fundamental tool to orient better the formulations. An average of evaluating certain activities or medicated cosmetics and knowledge of the physicochemical parameters of wetting the skin surface can provide useful information in the field of hygiene, cosmetics, and topical medications.

To date, the study of bio-tribological properties of human skin has attracted much attention, which is attributed to its importance in human daily life. A good understanding of skin friction is generally believed to have not only the potential benefits for the performance of conducting tasks but also the prevention of pain and discomfort (for instance, a good understanding of the mechanism between skin and various materials could help in avoiding the chance of getting blisters on the foot) (Liu et al. 2013).

References

Adamson AW, Kunichika K, Shirlev F. Dermatometry for coeds. J Chem Educ. 1968;45:702–4.

Afifi Y, Elkhyat A, Hassam B, et al. Mouillabilité de la peau et peau séborrhéique. In: Uhoda E, Paye M, Pierrard GE, editors. Actualités en Ingénierie Cutanée, vol. 4. Paris: ESKA; 2006. p. 111–7.

Agache P, Elkhyat A, Mavon A. Measurement of skin surface wettability. In: Agache P, Humbert P, editors. Measurement of the skin: non-invasive investigations, physiology, normal constants. Berlin: Springer; 2004. p. 87–91.

Asserin J, Zahouani H, Humbert P, et al. Measurement of the friction coefficient of the human skin in vivo. Quantification of the cutaneous smoothness. Colloids Surf B: Biointerfaces. 2000;19:1–12.

Barba C, Martí M, Manich AM, Carilla J, Parra JL, Coderch L. Water absorption/desorption of human hair and nails. Thermochem Acta. 2010;503–504:33–9.

Bongaerts JHH, Fourtouni K, Stokes JR. Soft-tribology. Lubrication in a compliant PDMS-PDMS contact. Tribol Int. 2007;40(10–12):1531–42.

Comaish S, Bottoms E. The skin and friction: deviations from Amonton's laws, and the effects of hydration and lubrication. Br J Dermatol. 1971;84:37–43.

Cua A, Wilheim KP, Maibach HI. Friction properties of human skin: relation to age, sex and anatomical region, stratum corneum hydration and transepidermal water loss. Br J Dermatol. 1990;123:473–9.

Cua AB, Wilhelm KP, Maibach HI. Skin surface lipid and skin friction: relation to age, sex and anatomical region. Skin Pharmacol. 1995;8:246–51.

Derler S, Schrade U, Gerhardt LC. Tribology of human skin and mechanical skin equivalents in contact with textiles. Wear. 2007;263:1112–6.

Egawa M, Oguri M, Hirao T, et al. The evaluation of skin friction using a frictional feel analyzer. Skin Res Technol. 2002;8:41–51.

Elkhyat A, Mavon A, Leduc M, et al. Skin critical surface tension. A way to assess the skin wettability quantitatively. Skin Res Technol. 1996;2:91–6.

Elkhyat A, Agache P, Zahouani H, et al. A new method to measure in vivo human skin hydrophobia. Int J Cosmet Sci. 2001;23:347–52.

Elkhyat A, Courderot-Masuyer C, Mac-Mary S, et al. Assessment of spray application of Saint Gervais water effects on skin wettability by contact angle measurement comparison with bidistilled water. Skin Res Technol. 2004a;10:283–6.

Elkhyat A, Courderot-Masuyer C, Gharbi T, et al. Influence of the hydrophobic and hydrophilic characteristics of sliding and slider surfaces on friction coefficient: *in vivo* human skin friction comparison. Skin Res Technol. 2004b;10:215–21.

Elkhyat A, Lihoreau T, Humbert P. Nail: hydrophobic/lipophilic balance: wettability and friction coefficient. Skin Res Technol. 2010;16:483.

El-Shimi AF. In vivo skin friction measurements. J Soc Cosmet Chem. 1977;28:37–51.

El-Shimi A, Goddard ED. Wettability of some low energy surfaces. J Colloid Interface Sci. 1973;48:242–8.

Elsner P, Wilhelm D, Maibach HI. Frictional properties of human forearm and vulvar skin: influence of age and correlation with transepidermal water loss and capacitance. Dermatologica. 1990;181:88–91.

Fotoh C, Elkhyat A, Mac-Mary S, et al. Characterization of cutaneous specificities of young women African and Caribbean, black and mixed-race living under temperate climate. Abstract of papers, 21st World Congress of Dermatology, Buenos Aires, 30 Sept–5 Oct 2007.

Fowkes FM. Attractive forces at interfaces. Ind Eng Chem. 1964;56:40–52.

Gee MG, Tomlins P, Calver A, et al. A new friction measurements system for the frictional component of touch. Wear. 2005;259:1437–42.

Ginn ME, Noyes GM, Jungermann E. The contact angle on water on viable human skin. J Colloid Interface Sci. 1968;26:146–51.

Gloor M, Franz P, Friedrich HC. Untersuchungen über die Physiologie der Talgdrüsen und über den Einflub der

Hautoberflaschenlipide auf die benetzarkeit der Haut. Arch Derm Fors. 1973;248:79–88.

Good RJ, Van Oss CJ. The modern theory of contact angles and the hydrogen bond components of surface energies. In: Schrader ME, Loeb GI, editors. Modern approaches to wettability: theory and application. New York: Plenum Press; 1992. p. 1–27.

Highley DR, Coomey M, Denbeste M, et al. Frictional properties of skin. J Invest Dermatol. 1977;69:303–5.

Humbert Ph, Mac-Mary S, Creidi P, Elkhyat A, Sainthillier JM, Heidet-Hommeau V, Montastier C. A double-blind placebo-controlled clinical trial to demonstrate the efficacy of nutritional supplement on dry skin conditions. Satellite symposium of the 14th Congress of the European Academy of Dermatology and Venereology, London, 12–16, 2005.

Kenins P. Influence of fiber-type and moisture on measured fabric-to-skin friction. Text Res J. 1994;64:722–8.

Koudine AA, Barquins M, Anthoine PH, et al. Frictional properties of skin: proposal of a new approach. Int J Cosmet Sci. 2000;22:11–20.

Liu X, Lu Z, Lewis R, Carre MJ, Matcher SJ. Feasibility of using optical coherence tomography to study the influence of skin structure on finger friction. Tribol Int. 2013;63:34–44.

Lodén M, Olsson H, Axéll T, et al. Friction, capacitance and transepidermal water loss (TEWL) in dry atopic and normal skin. Br J Dermatol. 1992;126:137–41.

Lodge, RA. B.S. Wetting behavior and surface potential characteristics of human hair (A Thesis). The Ohio State University. 2007.

Lubach D, Cohrs W, Wurzinger R. Incidence of brittle nails. Dermatologica. 1986;172:144–7.

Mac-Mary S, Elkhyat A, Sainthillier JM, Jeudy A, Perrot K, Lafond S, Predine O, Mermet P, Tarrit C, Humbert. Specific cosmetic for children: an in vivo randomized single-blind study of efficacy in 7- to 12-year-old children. 27ème Congrès de l'International Federation of Societies of Cosmetic Chemists. 15–18 Oct 2012, Johannesburg, Afrique du Sud.

Mac-Mary S, Elkhyat A, Sainthillier JM, Jeudy A, Perrot K, Lafond S, Predine O, Mermet P, Tarrit C, Humbert P. Skin properties of 7- to 12-year old children. 27ème Congrès de l'International Federation of Societies of Cosmetic Chemists. 15–18 Oct 2012, Johannesburg, Afrique du Sud.skin.

Mavon A, Zahouani H, Redoules D, et al. Sebum and stratum corneum lipids increase human skin surface free energy as determined from contact angle measurements: a study on two anatomical sites. Colloids Surf B: Biointerfaces. 1997;8:147–55.

Mavon A, Redoules D, Humbert P, et al. Changes in sebum levels and skin surface free energy components following skin surface washing. Colloids Surf B: Biointerfaces. 1998;10:243–50.

Neumann AW, Good RJ. Techniques of measuring contact angles. Colloids Surf Sci. 1979;11:31–91.

Norris DA, Puri N, Labib ME, et al. Determining the absolute surface hydrophobicity of microparticulates using thin layer wicking. J Control Release. 1999; 59:173–85.

Owens DK, Wendt R. Estimation of the surface free energy of polymers. J Appl Polym Sci. 1969;13:1741–7.

Ramalho A, Silva CL, Pais A, et al. In vivo friction study of human skin: influence of moisturizers on different anatomical sites. Wear. 2007;10:1044–9.

Ranc H, Elkhyat A, Servais C, et al. Friction coefficient and wettability of oral mucosal tissue: changes induced by a salivary layer. Colloids Surf A: Physicochem Eng Aspect. 2006;276:155–61.

Rosemberg A, William R, Cohen G. Interaction involved in wetting of human skin. J Pharm Sci. 1973;62:920–2.

Schott H. Contact angles and wettability of human skin. J Pharm Sci. 1971;60:1893–5.

Sivamani RK, Goodman J, Gitis NG, et al. Coefficient of friction: tribological studies in man-an overview. Skin Res Technol. 2003a;9:227–34.

Sivamani RK, Wu G, Gitis NV, et al. Tribological testing of skin products: gender, age, and ethnicity on the volar forearm. Skin Res Technol. 2003b;9:1–7.

Uyttendaele H, Geyer A, Scher RK. J Drugs Dermatol. 2003;2:48–9.

van de Kerkhof PC, Pasch MC, Scher RK, Kerscher M, Gieler U, Haneke E, Fleckman P. J Am Acad Dermatol. 2005;53:644–51.

Van Oss CJ, Good RJ, Chaudhury MK. Additive and non additive surface tension components and interpretation of contact angles. Langmuir. 1988;4:884–91.

Wenzel RN. Resistance of solids surfaces to wetting by water. Ind Eng Chem. 1936;28:988–94.

Wolfram LJ. Friction of skin. J Soc Cosmet Chem. 1983;34:465–76.

Young T. An essay on the cohesion of fluids. Phil R Soc (London). 1805;95:65–87.

Zhang M, Mak AFT. In vivo friction properties of human skin. Prosthet Orthot Int. 1999;23:135–41.

Zisman WA. Contact angle, wetting, adhesion. In: Fowkes FM, editor. Advanced chemical, vol. 43. Washington, DC: American Chemical Society; 1964. p. 1–51.

Skin Friction Coefficient

20

George Man and Mao-Qiang Man

Contents

Keywords

Skin friction coefficient • Aging • Gender • Stratum corneum

1 Measurement of Skin Friction Coefficient

The skin friction coefficient represents the skin resistance against the movement of an object on the skin surface. The coefficient of friction (μ) is calculated as the ratio of the friction force over the normal load. The normal load and friction force are expressed in newtons (N), and the coefficient of friction is dimensionless $\mu = F_{friction}/F_{normal}$ (Naz et al. 2014). Many devices, including a triaxial quartz force plate (Kistler, Winterthur, Switzerland) (Derler et al. 2007; Gerhardt et al. 2008), Revolt SkinTribometer (Veijgen et al. 2013a, b), Frictiometer® FR 770 (Courage-Khazaka, Cologne, Germany) (Zhu et al. 2011; Neto et al. 2013), and Measurement Technologies Skin Friction Meter (Aca-Derm Inc., California, USA) (Zhang and Mak 1999), are available for the measurement of skin friction coefficients. The principle and methods of these devices are similar. For Courage-Khazaka Frictiometer® FR 770, the flat tip of the probe is made of Teflon. The tip surface area contacting the skin is 2 cm^2. The normal force level is 0.7 N and rotation speed is 255RPM. During measurement, the Frictiometer® FR 770 probe is connected to an MPA5 unit which is linked to a computer. The skin friction

G. Man (✉) • M.-Q. Man
Department of Dermatology, Dermatology Service, Veterans Affairs Medical Center
San Francisco, University of California San Francisco, School of Medicine, San Francisco, CA, USA
e-mail: georgeisman@gmail.com; mqman@hotmail.com

P. Humbert et.al. (eds.), *Agache's Measuring the Skin*,
DOI 10.1007/978-3-319-32383-1_20

coefficient will be displayed on a computer monitor upon placing the probe on the surface of the skin. The unit for skin friction coefficient is arbitrary unit (au).

2 Factors That Influence Skin Friction Coefficient

2.1 External Determinants of Skin Friction Coefficient

2.1.1 Material

As stated above, the skin friction coefficient represents resistance of the skin against the movement of an object on the surface of the skin. Thus, the type of material in contact with the skin can affect the skin friction coefficient. For instance, among bamboo viscose, polytetrafluoroethylene, and cotton/polyester (50 %/50 %), cotton/polyester yielded the highest friction coefficient (0.43 ± 0.04 for cotton/polyester; 0.38 ± 0.04 for bamboo viscose; 0.30 ± 0.04 for polytetrafluoroethylene) when sliding on the inner forearm at the normal load of 14.6 ± 1.3 N (Gerhardt et al. 2009). The skin friction coefficient on the fingertip pad is lower for aluminum in comparison with rubber hoses (0.6 for aluminum and 0.9 for hoses), especially at a lower level of normal force (Seo and Armstrong 2009). Among aluminum, nylon, silicone, cotton, and pelite, silicone induced the highest skin friction coefficient (Zhang and Mak 1999). The skin friction coefficient is positively correlated with the surface energy of the material against the skin (Veijgen et al. 2013b). The skin friction coefficient is also different between sheet and knitted materials (Comaish and Bottoms 1971).

2.1.2 Temperature

Regarding the impact of ambient temperature on skin friction coefficients, the results are controversial. Both static and dynamic skin friction coefficients were positively correlated with ambient temperature (Veijgen et al. 2013a, b). In contrast, another study demonstrated that skin friction coefficients on the porcine skin were higher at room temperature than that at 45 °C (Hills et al. 1994). Nevertheless, these evidences suggest that the ambient temperature can affect skin friction coefficients. Hence, it is necessary to maintain a consistent ambient temperature when measuring skin friction coefficients.

2.1.3 Normal Force

Several studies showed that the normal force had a negative impact on skin friction coefficient (Veijgen et al. 2013b; Seo and Armstrong 2009; Koudine et al. 2000; Bobjer et al. 1993; Sivamani et al. 2003). For example, when the normal force levels ranged from 1 to 1,000 g, both dynamic and static skin friction coefficients on the abdomen decreased as normal force increased (Comaish and Bottoms 1971). Another study demonstrated a sharp reduction in the static skin friction coefficient in the forearm when the normal force levels were increased from 10 to 100 mN, while the dynamic skin friction coefficient only slightly declined (Koudine et al. 2000). Further reduction of the normal force levels from 200 to 800 mN only induced a minimum reduction in both the static and dynamic skin friction coefficients (Koudine et al. 2000). Seo et al. (Seo and Armstrong 2009) reported that the skin friction coefficient on the fingertip pad in contact with aluminum was 0.6 ± 0.4 at the normal force level of 1.6 ± 0.7 N, while skin friction coefficient was 0.4 ± 0.3 at the normal force level of 10.8 ± 1.3 N. But a further increase in the normal force level to 19.6 ± 1.9 N did not cause an additional reduction in the skin friction coefficient (0.4 ± 0.2). A negative correlation of the skin friction coefficients with the normal force was also demonstrated on various body sites (Zhang and Mak 1999).

2.1.4 Contact Surface Area

The surface of the skin in contact with the material can also affect the skin friction coefficient. Generally, the skin friction coefficient in the normal skin increases as the contact area increases (Comaish and Bottoms 1971; Bobjer et al. 1993; Warman and Ennos 2009). But following topical treatment of the skin with either paraffin oil or lard, skin friction coefficient was negatively correlated with contact area (Bobjer et al. 1993). In addition, the type of material in contact with the skin influences the relationship between the skin

friction coefficient and the contact area. For example, the skin friction coefficient was positively correlated with the contact surface area when in contact with polythene, whereas the skin friction coefficient did not vary with the contact surface area when in contact with wool (Comaish and Bottoms 1971).

2.2 Internal Determinants of Skin Friction Coefficient

2.2.1 Age

The association of the skin friction coefficient with age is inconclusive. Although studies showed that both dynamic and static skin friction coefficients varied significantly with ages (Veijgen et al. 2013a, b), no differences in the skin friction coefficients between young and aged subjects have also been demonstrated (Cua et al. 1990, 1995; Elsner et al. 1990). Our studies demonstrated that the skin friction coefficients in both males and females changed over their lifetimes, particularly in females (Fig. 1; Zhu et al. 2011). As shown in Fig. 1a, skin friction coefficient on both the canthus and the dorsal hand of females gradually increased before the age 40 years and then declined over lifetime, while on the forehead, skin friction coefficient positively correlated with age (Fig. 1a, $R^2 = 0.03506$, $p < 0.001$). In males, skin friction coefficient on the forehead and canthus did not change dramatically over the lifetime (Fig. 1b). But skin friction coefficient on the dorsal hand of males increased from age 0 to 40 and remained unchanged thereafter. Collectively, these data suggest that the association of the skin friction coefficient with age is body site and gender dependent.

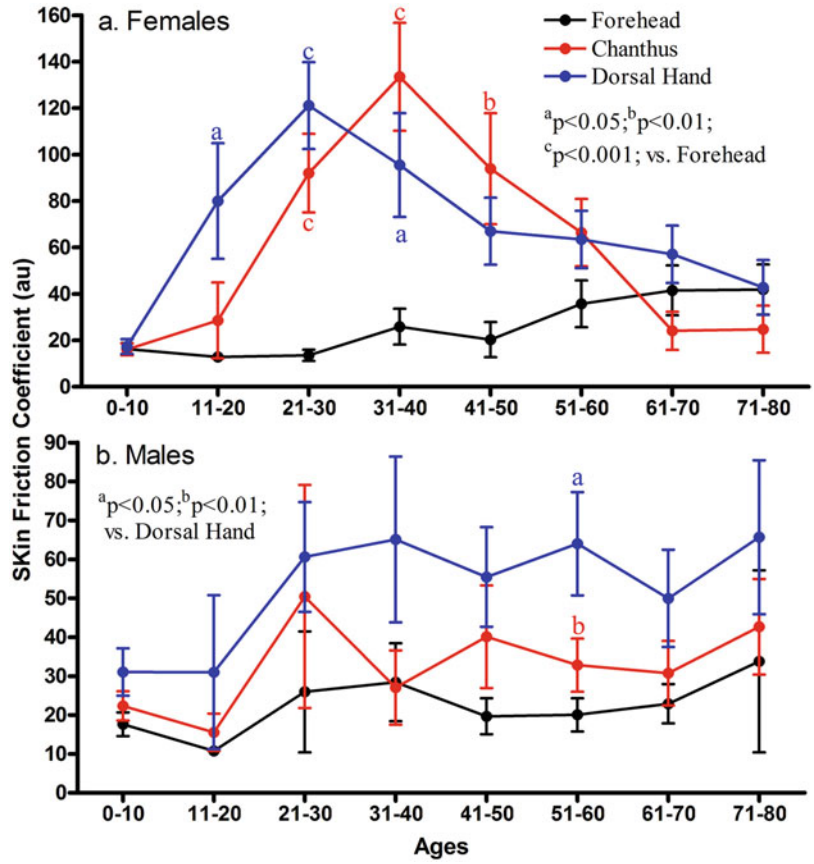

Fig. 1 Skin friction coefficient varies with age and body sites (this figure is modified from previous publication (Zhu et al. 2011)). (**a**) In females; (**b**) In males. Significant differences between body sites are shown in the figures. $N = 300$ for males and $N = 333$ for females

2.2.2 Body Sites

It is generally accepted that the skin friction coefficient varies with body sites although some study showed no significant variation among body sites (Zhang and Mak 1999). On the upper limbs, both static and dynamic skin friction coefficients vary significantly among the midventral forearm, middorsal forearm, index finger pad, and dorsal hand (Veijgen et al. 2013b). Both static and dynamic skin friction coefficients are higher on the index finger pad than on the dorsal forearm (Veijgen et al. 2013a). Our study showed that the canthus displayed a higher skin friction coefficient than the forehead (Fig. 1). The skin friction coefficients were lower on the forehead than on the dorsal hand (Fig. 1). But another study demonstrated that the forehead exhibited the highest skin friction coefficient (Fig. 2). Skin friction coefficients also vary among fingers (Warman and Ennos 2009). The variation of skin friction coefficient with body site is gender dependent (Fig. 1a vs. Fig. 1b).

2.2.3 Gender

The gender differences in skin biophysical properties including skin friction coefficient have been well documented (Zhu et al. 2011; Cua et al. 1990; Man et al. 2009; Choi et al. 2007; Marrakchi and Maibach 2007), although some studies showed no gender differences in skin friction coefficient on various body sites (Gerhardt et al. 2008; Veijgen et al. 2013a; Cua et al. 1990, 1995). Our recent study in a large Chinese population showed that there were differences in skin friction coefficients between males and females (Fig. 3). The gender differences in skin friction coefficients are age and body site dependent. For example, on the forehead, there was no difference in skin friction coefficient between males and females (Fig. 3a). In contrast, on the canthus and the dorsal hand, skin friction coefficients in females significantly differed from males (Fig. 3b, 3c). The biggest differences between males and females occurred at 31–60 years old on the canthus (Fig. 3b) and at 20–30 years old on the dorsal hand (Fig. 3c). Skin friction coefficients on the dorsal hand of males aged 0–10 years were significantly higher than those in females (Fig. 3c). Thus, the discrepant results from different studies could be in part due to the differences in subject ages and body sites.

2.2.4 Stratum Corneum Hydration

The impact of stratum corneum hydration on skin friction coefficients has been extensively studied. Skin friction coefficients in both males and females were linearly correlated with skin stratum corneum hydration. Moisturization of the skin induced a more dramatic increase in the skin friction coefficient in females than in males (Gerhardt et al. 2008), suggesting that the influence of skin hydration on skin friction varies with gender. The impact of moisturizers on skin friction coefficient

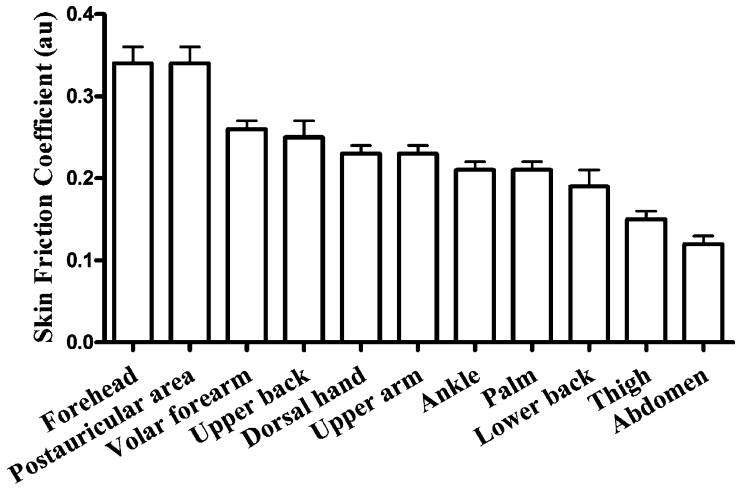

Fig. 2 Variation of skin friction coefficient with body sites (this figure is modified from previous publication (Cua et al. 1995)). $N = 29$

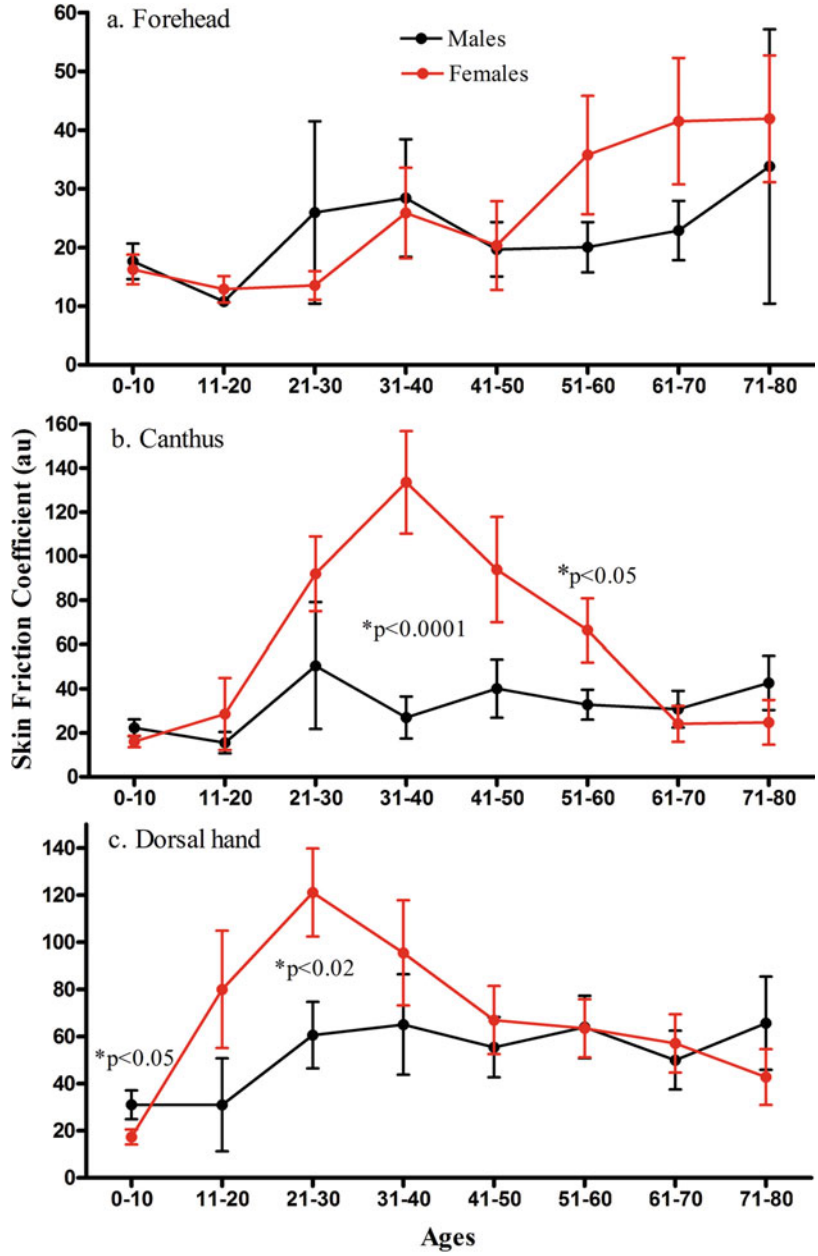

Fig. 3 Comparison of skin friction coefficient between females and males (this figure is modified from previous publication (Zhu et al. 2011)). (**a**) Depicts the differences between males and females on the forehead, (**b**) on the canthus, and (**c**) on the dorsal hand. Significant differences are shown in the figure

varies with their properties. For example, skin friction coefficient increased immediately after the addition of water to the skin and returned to normal level within 10–15 min (Sivamani et al. 2003; Highley et al. 1977; Nacht et al. 1981). Skin friction coefficients were raised up to twofold following topical application of moisturizers (creams) and remained elevated for up to 4 h (Sivamani et al. 2003). Mineral oil, petrolatum, and glycerin could cause an initial reduction in the skin friction coefficient, followed by a marked increase (Highley et al. 1977; Nacht et al. 1981). The relationship between skin friction coefficient and skin hydration varies with gender and body sites. One study showed that skin friction coefficients were positively correlated with skin hydration on the forehead and dorsal forearm, but not on the abdomen, upper back, and

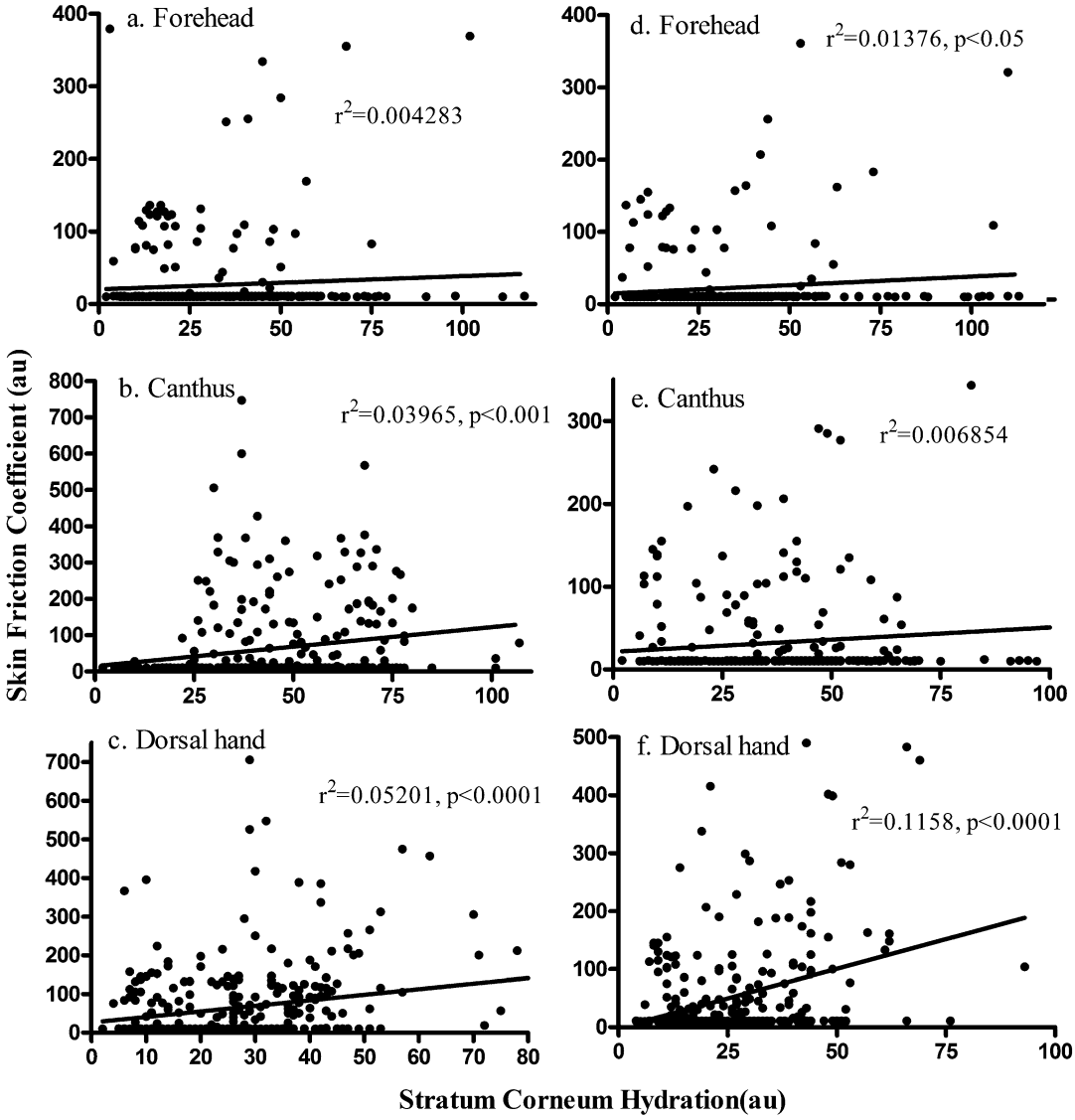

Fig. 4 Correlation of skin friction coefficient with stratum corneum hydration. (**a**, **b,** and **c**) represent the correlation of skin friction coefficient with stratum corneum hydration in females, while (**d**–**f**) are in males. Statistical significances are shown in the figures

postauricular area (Cua et al. 1990). Our study has demonstrated that the skin friction coefficients on the forehead were positively correlated with skin hydration in males, but not in females (Fig. 4a vs. Fig. 4d). In contrast, on the canthus, skin friction coefficients were positively correlated with skin hydration in females, but not in males (Fig. 4b vs. Fig. 4e). In subjects with atopic dermatitis, the correlation of skin friction coefficients with skin hydration was only found on the volar forearm and lower back, but not on the dorsal hand (Lodén et al. 1992).

2.3 Other Determinants

Besides the external and internal factors described above, there are many other determinants that can

affect the skin friction coefficient. Studies have shown that air humidity can positively impact both static and dynamic skin friction coefficients (Veijgen et al. 2013a), while skin temperature, hair on the skin, and evening measurement have a negative effect on the skin friction coefficients (Veijgen et al. 2013a, b). Regarding the relationship of epidermal permeability barrier function measured by transepidermal water loss (TEWL) to skin friction coefficients, studies showed that TEWL levels were associated with skin friction coefficients on the thigh and the palm in normal subjects (Cua et al. 1990) and on the lower back in atopic subjects (Lodén et al. 1992). Topical application of 10 % sebum decreased static skin friction coefficient between the skin and polythene, but increased static skin friction coefficient between the skin and wool (Comaish and Bottoms 1971). In normal human, skin friction coefficient between the skin and Teflon (polytetrafluoroethylene-based product) was linearly correlated with skin surface sebum content (Cua et al. 1995). Sweat could increase the skin friction coefficient, too (Bobjer et al. 1993). In females, the skin friction coefficient on the forearm was significantly higher in premenopause than postmenopause (Elsner et al. 1990). Additionally, the movement speed of the object on the skin was positively correlated with skin friction coefficient (Zhang and Mak 1999).

3 Summary

Skin friction coefficients can easily be measured. Since there are many internal and external factors that can affect the value of skin friction coefficient, a consistent environment and measurement device would be required in order to obtain comparable results. Age, gender, body site, and skin condition should be considered in the interpretation and comparison of the results.

References

Bobjer O, Johansson SE, Piguet S. Friction between hand and handle. Effects of oil and lard on textured and non-textured surfaces; perception of discomfort. Appl Ergon. 1993;24:190–202.

Choi EH, Man MQ, Xu P, Xin S, Liu Z, Crumrine DA, Jiang YJ, Fluhr JW, Feingold KR, Elias PM, Mauro TM. Stratum corneum acidification is impaired in moderately aged human and murine skin. J Invest Dermatol. 2007;127:2847–56.

Comaish S, Bottoms E. The skin and friction: deviations from Amonton's laws, and the effects of hydration and lubrication. Br J Dermatol. 1971;84:37–43.

Cua AB, Wilhelm KP, Maibach HI. Frictional properties of human skin: relation to age, sex and anatomical region, stratum corneum hydration and transepidermal water loss. Br J Dermatol. 1990;123:473–9.

Cua AB, Wilhelm KP, Maibach HI. Skin surface lipid and skin friction: relation to age, sex and anatomical region. Skin Pharmacol. 1995;8:246–51.

Derler S, Schrade U, Gerhardt L-C. Tribology of human skin and mechanical skin equivalents in contact with textiles. Wear. 2007;263:1112–6.

Elsner P, Wilhelm D, Maibach HI. Frictional properties of human forearm and vulvar skin: influence of age and correlation with transepidermal water loss and capacitance. Dermatologica. 1990;181:88–91.

Gerhardt LC, Strässle V, Lenz A, Spencer ND, Derler S. Influence of epidermal hydration on the friction of human skin against textiles. J R Soc Interface. 2008;5:1317–28.

Gerhardt LC, Lenz A, Spencer ND, Münzer T, Derler S. Skin-textile friction and skin elasticity in young and aged persons. Skin Res Technol. 2009;15:288–98.

Highley KR, Coomey M, DenBeste M, Wolfram LJ. Frictional properties of skin. J Invest Dermatol. 1977;69:303–5.

Hills RJ, Unsworth A, Ive FA. A comparative study of the frictional properties of emollient bath additives using porcine skin. Br J Dermatol. 1994;130:37–41.

Koudine AA, Barquins M, Anthoine PH, Aubert L, Lévêque JL. Frictional properties of skin: proposal of a new approach. Int J Cosmet Sci. 2000;22:11–20.

Lodén M, Olsson H, Axéll T, Linde YW. Friction, capacitance and transepidermal water loss (TEWL) in dry atopic and normal skin. Br J Dermatol. 1992; 126:137–41.

Man MQ, Xin SJ, Song SP, Cho SY, Zhang XJ, Tu CX, Feingold KR, Elias PM. Variation of skin surface pH, sebum content and stratum corneum hydration with age and gender in a large Chinese population. Skin Pharmacol Physiol. 2009;22:190–9.

Marrakchi S, Maibach HI. Biophysical parameters of skin: map of human face, regional, and age-related differences. Contact Dermatitis. 2007;57:28–34.

Nacht S, Close JA, Yeung D, Gans EH. Skin friction coefficient: changes induced by skin hydration and emollient application and correlation with perceived skin feel. J Soc Cosmet Chem. 1981;32:55–65.

Naz S, Jamil AW, Sherani FS. Skin friction coefficient as a parameter for temperament assessment: a review. Int J Sci Tech Res. 2014;3:178–81.

Neto P, Ferreira M, Bahia F, Costa P. Improvement of the methods for skin mechanical properties evaluation through correlation between different techniques and factor analysis. Skin Res Technol. 2013;19:405–16.

Seo NJ, Armstrong TJ. Friction coefficients in a longitudinal direction between the finger pad and selected materials for different normal forces and curvatures. Ergonomics. 2009;52:609–16.

Sivamani RK, Goodman J, Gitis NV, Maibach HI. Friction coefficient of skin in real-time. Skin Res Technol. 2003;9:235–9.

Veijgen NK, Masen MA, van der Heide E. Variables influencing the frictional behaviour of in vivo human skin. J Mech Behav Biomed Mater. 2013a;28:448–61.

Veijgen NK, van der Heide E, Masen MA. A multivariable model for predicting the frictional behaviour and hydration of the human skin. Skin Res Technol. 2013b;19:330–8.

Warman PH, Ennos AR. Fingerprints are unlikely to increase the friction of primate fingerpads. J Exp Biol. 2009;212:2016–22.

Zhang M, Mak AF. In vivo friction properties of human skin. Prosthet Orthot Int. 1999;23:135–41.

Zhu YH, Song SP, Luo W, Elias PM, Man MQ. Characterization of skin friction coefficient, and relationship to stratum corneum hydration in a normal Chinese population. Skin Pharmacol Physiol. 2011; 24:81–6.

Dermoscopy: Basic Knowledge of an Innovative Imaging Tool

21

Alexander Witkowski, Giovanni Pellacani, Salvador Gonzalez, and Caterina Longo

Contents

Keywords

Dermoscopy • Melanoma • Nevi • Diagnosis • Basal cell carcinoma • Algorithm • Inflammatory skin disease • Trichoscopy • Infectious skin disease

List of Abbreviations

ELM	Epiluminescence microscopy
LPLK	Lichen planus-like keratosis
RCM	Reflectance confocal microscopy

1 Introduction

Dermoscopy, also known as epiluminescence microscopy (ELM) or dermatoscopy, is the non-invasive examination of the skin with a device that permits improved visualization of surface and subsurface structures enabling the clinician to recognize morphologic features that are not perceived by naked eye examination (Argenziano et al. 1999, 2002). With the ability to visualize a new dimension of colors and microstructures, the dermatoscope increases the clinician's sensitivity and specificity when differentiating benign from malignant skin lesions and recently has been shown to improve the recognition of a growing number of skin diseases in general dermatology (Argenziano et al. 2009). ELM also forms a link between macroscopic clinical observation and

The authors have no conflict of interest to disclose.

A. Witkowski • G. Pellacani
Dermatology Unit, University of Modena and Reggio Emilia, Modena, Italy

S. Gonzalez
Dermatology Service, Memorial Sloan-Kettering Cancer Center, New York, NY, USA

Medicine Department, Alcalá University, Madrid, Spain

C. Longo (✉)
Dermatology and Skin cancer Unit, Arcispedale Santa Maria Nuova-IRCCS, Reggio Emilia, Italy
e-mail: longo.caterina@gmail.com

P. Humbert et al. (eds.), *Agache's Measuring the Skin*,
DOI 10.1007/978-3-319-32383-1_21

microscopic dermatopathology allowing the clinician to increase their confidence in clinical judgment (Argenziano et al. 2003). Dermoscopy maximizes early detection while minimizing the unnecessary excision of benign skin tumors proving that this modality can be used to both lower unnecessary healthcare expenditures and more importantly decrease mortality of melanoma (Alexandrescu 2009).

2 Tools

The dermatoscope is a handheld monocular optical system that enables magnification (10×) of the skin surface with the aid of an illumination system, either polarized or nonpolarized. Polarized devices allow for unobstructed viewing of vascular and chrysalis structures and do not require the use of immersion fluid such as mineral oil, alcohol, or water. Nonpolarized devices require immersion fluid and provide better viewing of pseudocysts, blue-gray dots, and blue-white veil/structures. Most current commercially available devices utilize LED illumination and provide the ability to switch between polarized and nonpolarized viewing (Argenziano et al. 2002; Wang et al. 2008; Liebman et al. 2012). Digital dermoscopy is the process of attaching a dermatoscope to a digital camera system that allows for easy photographic documentation, high-definition capture of lesions for enlarged view on a computer screen, and storage for patient follow-up (Argenziano et al. 2009, 2003; Soyer et al. 2012, 2001; Salerni et al. 2012; Niederkorn et al. 2011). Videodermoscopy aids in monitoring high-risk patients who present with a plethora of pigmented skin lesions that need to be followed up regularly and is also useful in the examination of hair disorders. Skin lesions can be magnified up to 120×, and mole mapping software allows for organized quantification and localization of lesions (Ross et al. 2006a). Both digital dermoscopy and videodermoscopy can take advantage of the ability to consult a second opinion via teledermatology (Malvehy and Puig 2002). Dermoscopy is also useful in aiding reflectance confocal microscopy (RCM) as the structures viewed in dermoscopy allow for determining mapping location in RCM, both with correlating histopathologic features (Bassoli et al. 2010).

3 Colors

Dermoscopy allows for in-vivo evaluation of colors of the epidermis, dermal-epidermal junction, and papillary dermis that are not easily viewed with traditional naked eye examination. Colors play a key role in the evaluation of skin lesions as the color perceived by the viewer is relative to the location of melanin (chromophore) and other pigment in the skin. Black correlates to melanin located in the stratum corneum and the upper epidermis, light to dark brown in the epidermis, gray to gray-blue in the papillary dermis, and steel-blue in the reticular dermis. Blue color represents melanin deposition deeper in the skin layers. Red color is associated with an increased number or dilation of blood vessels, trauma, or neovascularization. White color is a result of regression or scarring (Braun et al. 2005; Reisfeld 2000).

4 Structures

The use of dermoscopy permits the visualization of a variety of structures that aid the clinician in assessing both melanocytic and non-melanocytic lesions (Soyer et al. 2001, 2012). They include the presence or absence of pigment network, local features, and vascular structures (Stolz et al. 2002; Menzies et al. 2003; Braun et al. 2005; Reisfeld 2000; Malvehy et al. 2007; Ferrara et al. 2002; Haliasos et al. 2010). The six most common morphologic types of vascular structures include comma vessels, dotted vessels, linear-irregular vessels, hairpin vessels, glomerular vessels, and arborizing vessels (Table 1) (Zalaudek et al. 2010a, b).

Table 1 List of the main vascular pattern as seen in dermoscopy

Vessel type (new terminology)	Description	Diagnostic significance
Comma vessels (linear curved)	Coarse vessels that are slightly curved, barely branching, and variable in both size and caliber	Mainly in melanocytic nevi, especially dermal nevi
Dotted vessels (dots)	Tiny red dots densely aligned next to each other	Spitz nevi, sometimes in seborrheic keratosis, rarely in thin AHM
Linear irregular vessels (linear straight; linear serpentine)	Linear, irregularly shaped, sized, and distributed red structures	Pyogenic granuloma and melanoma
Hairpin vessels (linear looped)	Vascular loops sometimes twisted and bending, usually surrounded by a whitish halo when seen in keratinizing tumors	Common in seborrheic keratosis and melanoma
Glomerular vessels (linear coiled)	Tortuous capillaries often distributed in clusters mimicking the glomerular apparatus of the kidney	Bowen disease; intraepidermal carcinoma
Arborizing vessels	Stem vessels of large diameter branching irregularly into fine terminal capillaries. Vessel color is bright red	Frequently in BCC
Crown vessels (linear serpentine)	Groups of orderly bending, scarcely branching vessels located along the border of the lesion	Sebaceous hyperplasia

4.1 Melanocytic Lesions (Criteria)

4.1.1 Pigment Network

Pigment network is made up of pigmented network lines and hypopigmented holes, which correspond to the presence or absence of melanotic pigment in the cells of the basal layer of the epidermis. Network lines correlate histologically to rete ridges that are thick and contain an abundance of melanin. Network holes correlate histologically to the suprapapillary plate that is thinner and contains less melanin deposition. The pigmented network can be typical or atypical (Johr 2002). The network may not be visible if the rete ridges are short or less pigmented. Areas devoid of any network type corresponding to the flattening of rete ridges are called structureless areas.

The pigment network can be observed individually or in combination of the any of the following patterns: reticular pattern, globular pattern, homogeneous pattern, and starburst pattern. Reticular pattern is the most common global pattern found in melanocytic lesions. It appears as a grid of line segments, honeycomb-like, and in different shades of black, brown, or gray. Globular pattern consists of variously sized, round to oval structures. Homogeneous pattern is characterized by diffuse, uniform, structureless color filling most of the lesions. Starburst pattern is characterized by the presence of pigmented streaks and/or dots and globules in a radial arrangement at the periphery of a melanocytic lesion (Soyer et al. 2012; Braun et al. 2005; Johr 2002; Argenziano et al. 1998, 2011a).

4.1.2 Broadened Network

Broadened network is defined as localized pigment network in which the line segments are thickened and irregular (Johr 2002).

4.1.3 Atypical Pigment Network

Atypical pigment network is described as black, brown, or gray thickened and irregular line segments anywhere in the lesion. In melanoma it typically presents as a sharp cutoff or demarcation of the pigment network at the periphery of the lesion. The term "atypical" network has been recently defined as the presence of different type of network within a given lesion (Soyer et al. 2012; Johr 2002; Argenziano et al. 1998, 2011a).

4.1.4 Dots

Dots are defined as small, round structures less than 0.1 mm in diameter which may be black,

light or dark brown, gray, or blue-gray (Stolz et al. 2002; Menzies et al. 2003; Malvehy et al. 2007). Black dots originate from pigment accumulation in the stratum corneum and the upper epidermis. Brown dots correspond to focal melanin accumulations at the dermo-epidermal junction. Blue-gray dots, also known as granules, dust-like dots, or "peppering," are caused by accumulation of loose melanin or fine melanin particles in melanophages or free in the deep papillary or reticular dermis (Ferrara et al. 2002; Zalaudek et al. 2009; Soyer et al. 2000; Stoecker et al. 2011).

4.1.5 Globules

Globules are defined as symmetrical, round to oval, well-demarcated structures that may be black, brown, blue, or red. They are larger than dots and correspond histologically to nests of pigmented benign or malignant melanocytes, clumps of melanin, and/or melanophages situated usually in the lower epidermis, at the dermal-epidermal junction, or the papillary dermis (Stolz et al. 2002; Menzies et al. 2003; Braun et al. 2005; Reisfeld 2000; Malvehy et al. 2007; Ferrara et al. 2002; Zalaudek et al. 2009; Soyer et al. 2000). In benign lesions they have relatively homogenous size and shape with even distribution and generally central localization. In comparison, malignant lesions present with globules of varying size and shape with asymmetric peripheral localization (Stoecker et al. 2011; Kittler et al. 2000).

4.1.6 Streaks

Streaks are defined as dark linear structures of variable thickness found at the periphery of a lesion (Stolz et al. 2002; Braun et al. 2005; Malvehy et al. 2007). Histologically they represent linear, heavily pigmented, junctional nests of atypical melanocytes (Ferrara et al. 2002; Soyer et al. 2000). Streaks can be found in both benign and malignant melanocytic lesions. They are specific for melanoma notably when they are unevenly distributed at the periphery of a lesion. Symmetrical arrangement of streaks around the entire lesion periphery is commonly found in Spitz nevi but can also be seen rarely in melanomas (Argenziano et al. 1999b).

4.1.7 Pseudopods/Radial Streaming

Pseudopods, also known as radial streaming, are defined as radially oriented or bulbous, fingerlike projections of pigment at the periphery of a lesion. They are either connected to the pigment network or directly connected to the tumor body (Soyer et al. 2012; Malvehy et al. 2007; Johr 2002). They correspond to intraepidermal or junctional confluent radial nests of melanocytes. Asymmetric pseudopod arrangement is one of the most specific features of superficial spreading melanoma subtype (Menzies 2001).

4.1.8 Blotches

Blotches, also known as black lamella, are defined as large concentrations of melanin pigment that obscure the visualization of other dermoscopic features of a given lesion. Blotches with irregular borders, sharp demarcation, and peripheral arrangement in a melanocytic lesion are very suggestive of a melanoma (Soyer et al. 2012; Malvehy et al. 2007; Massi et al. 2001a).

4.1.9 Blue-White Veil/Structures

Blue-white veil/structures is defined as an irregular, indistinct, confluent blue pigmentation with an overlying white, ground-glass haze that does not occupy the entire lesion (Soyer et al. 2012; Menzies et al. 2003; Braun et al. 2005; Reisfeld 2000; Malvehy et al. 2007; Argenziano et al. 2011b). It corresponds histopathologically to an aggregation of heavily pigmented cells or melanin in the dermis in combination with compact orthokeratosis (Massi et al. 2001b).

4.1.10 Regression

Regression is defined as a white scar-like depigmentation, lighter than the surrounding skin, or peppering (Braun et al. 2005; Malvehy et al. 2007). Histologically regression correlates to fibrosis, loss of pigmentation, and numerous melanophages in the papillary dermis (Ferrara et al. 2002). Regression is commonly found in melanoma, but also nevi can show a variable amount of regression although a different

distribution of regression and the variably association with white color helps in differentiating between the two entities (Zalaudek et al. 2004).

4.1.11 Atypical Vascular Pattern

An atypical vascular pattern is described as linear-irregular and/or dotted red vessels that are not seen in areas of regression. Moreover, the presence of polymorphous vessels is referred as atypical vascular pattern, and this can be found in malignant lesions either melanoma or squamous cell carcinoma. (Zalaudek et al. 2010a, b).

5 Special Site

5.1 Acral Lesions

Melanocytic acral lesions have specific patterns because of the presence of particular anatomic structures inherent to these locations on the palms and soles. The four main patterns of acral lesions are parallel furrow, lattice-like, fibrillar, and parallel ridge (Soyer et al. 2012; Malvehy et al. 2007). The parallel furrow presents with multiple parallel linear pigmentation in the sulci, or furrows, of glabrous skin. The lattice-like pattern presents with linear pigmentation that follow and cross the sulci, demonstrating a rectangular network of brownish lines punctuated by several whitish dots, similar in appearance to a string of pearls. The fibrillar pattern is characterized by numerous short and thin brown lines that are parallely arranged and run oblique to the ridges and furrows. The parallel ridge pattern, pathognomonic for acral melanoma, presents as pigmented bands on the ridges that are broader than the whitish lines in between. In addition to the four main patterns, a combination of globular, nontypical, transition, and globulostreak-like patterns can be observed less frequently (Kokgil et al. 2012; Miyazaki et al. 2005).

5.2 Facial Lesions

Melanocytic facial lesions present with difficult evaluation for naked eye examination and benefit from the use of dermoscopy. Because of the specific anatomy of facial skin characterized by numerous folliculo-sebaceous units and an effaced epidermis, lesions on facial skin reveal specific dermoscopic features (Soyer et al. 2012). Benign lesions typically present with pigmented follicles and pseudonetwork that is light brown to dark brown in color with symmetrical arrangement and absence of gray color that usually typify lentigo maligna, although it can be found also in non-melanocytic lesions. Specific melanoma criteria include annular-granular structures, asymmetrically pigmented follicles, rhomboidal structures, and gray pseudonetwork (Stante et al. 2005).

5.3 Non-melanocytic Lesions (Criteria)

5.3.1 Blue-Gray Ovoidal Structures

Blue-gray ovoidal structures are round to oval and often irregular in shape. Color ranges from brownish-gray to blue-gray (Soyer et al. 2012; Braun et al. 2005). They correlate histopathologically to heavily pigmented, solid aggregations of basaloid cells in the papillary dermis of superficial or nodular basal cell carcinoma, especially when found in the absence of melanocytic lesion criteria. This feature can also be found in melanocytic lesions (Ferrara et al. 2002).

5.3.2 Arborizing Vessels

Arborizing vessels are thickened, in-focus, branched red vessels that are highly specific for basal cell carcinoma. Typically, the caliber of the vessels decreases regularly from the origin toward the branching, arborizing thinner vessels (Soyer et al. 2012; Zalaudek et al. 2010a, b).

5.3.3 Milia-Like Cysts

Milia-like cysts are white or yellowish round structures that histologically represent intraepidermal horn globules or horn pseudocysts. Multiple milia-like cysts are a common finding in seborrheic keratosis. They can be observed in dermal nevi and melanoma, but usually they are

fewer in number (Soyer et al. 2012; Braun et al. 2005).

5.3.4 Comedo-Like Openings

Comedo-like openings are irregularly shaped, sharply well-circumscribed structures that can be brownish-yellow or brown-black that correlate histopathologically to keratin plugs within dilated follicular openings. They are commonly found in seborrheic keratoses (Braun et al. 2005; Ferrara et al. 2002).

5.3.5 Red Lacunae

Red lacunae are well-demarcated, round to oval structures that can be red, red-blue, dark-red, white, or black. They correlate histopathologically to dilated vascular spaces located in the upper dermis. Lacunae are commonly found in hemangiomas and angiokeratomas (Soyer et al. 2012; Braun et al. 2005).

5.3.6 Central White Patch

The central white patch is a well-circumscribed, round to oval, white area usually in the center of a firm lesion. It is highly diagnostic of dermatofibroma although it can be found in a wide range of lesions (Ferrara et al. 2002; Zaballos et al. 2008).

5.4 Diagnostic Algorithms

Since the inception and popularization of dermoscopy in clinical practice, many authors have published various methods to perform organized differential diagnosis of pigmented skin lesions. The most commonly used algorithms will be discussed below.

5.4.1 Pattern Analysis

Pattern Analysis is based on a two-step process, first to recognize whether a lesion is melanocytic or non-melanocytic and second to evaluate the lesion for specific criteria. This method requires much experience and hence led to the development of other methods that require less training and experience to diagnose skin lesions (Braun et al. 2005; Johr 2002).

5.4.2 ABCD Rule of Dermatoscopy

The ABCD rule of dermatoscopy was developed in an effort to simplify the process of lesion analysis. Four criteria are used for diagnosing melanoma, asymmetry (A), borders (B), colors (C), and different structural components (D). It is a semiquantitative, mathematical approach that awards points for the criteria identified in a lesion and a formula to determine a total dermatoscopy score (TDS) that is suggestive of diagnosis of benign, high-risk, or high diagnostic sensitivity for a melanoma (Johr 2002; Argenziano et al. 1998). To determine the asymmetry (A) score, the lesion is visually divided into two 90° right-angle axes and assigned a score ranging from 0 to 2. A lesion that is completely symmetrical in shape, color, and structure receives a score of 0. A lesion that is asymmetric in one axis is given a score of 1 and a lesion that is asymmetric in both axes is given a score of 2. The weight factor for asymmetry is 1.3 and subscores range from 0 to 2.6. To determine border (B) score, the lesion is visually divided into eight pie-shaped segments, and then the number of segments that contain an abrupt cutoff at the margins or the peripheral pigment pattern is noted, and each segment with an abrupt cutoff is given a score of 1. The weight factor for border score is 0.1 and subscores range from 0 to 0.8. Colors (C) evaluated include white, red, light brown, dark brown, black, and blue gray. It should be noted that white should only be counted if it is lighter than the surrounding skin and not confused with hypopigmentation. Each color is assigned one point, a weight factor of 0.5, and subscores range from 0.5 to 3.0. Different structural components (D) include pigment network, structureless areas, dots, globules, and streaks. Structureless or homogeneous areas should be greater than 10 % of the lesion, and branched streaks and dots are only counted when more than two are clearly seen. Each component is assigned one point, a weight factor of 0.5, and subscores range from 0.5 to 2.5. TDS is calculated by multiplying the total points in each category by their weight

factors: (A × 1.3) + (B × 0.1) + (C × 0.5) + (D × 0.5) = TDS. A TDS score <4.75 is suggestive of a benign lesion, 4.8–5.45 suggestive of suspicious for melanoma, and >5.45 highly suspicious for melanoma (Stolz et al. 1994).

5.4.3 Menzies Scoring Method

The Menzies method scores 11 different criteria as either present or absent which aims to reduce the intra and interobserver errors seen when criteria are graded numerically. The method has two categories: negative and positive features, with two and nine features, respectively, for each category. For melanoma diagnosis both of the negative features must not be found, and in addition at least one positive feature must be present. Negative features include point and axial symmetry of pigmentation and presence of a single color. Positive features include blue-white veil, multiple brown dots, peripheral black dots and globules, radial streaming and pseudopods, scar-like depigmentation (regression), multiple colors (five or six), multiple blue/gray dots, and broadened network. It should be noted that peripheral dots and globules must be black, and pseudopods/radial streaming should not be scored if they are regularly symmetrically arranged around the lesion periphery. Colors to be scored include black, tan, dark brown, red, gray, and blue. White is not counted as a color (Menzies et al. 1996, 2003; Johr 2002; Argenziano et al. 2011a).

5.4.4 7-Point Checklist

The 7-Point checklist is a newer method described by Argenziano and colleagues to analyze lesions that has fewer criteria than pattern analysis and is less complicated than the ABCD rule of dermatoscopy. It works on a point system that is divided into major and minor criteria found in a skin lesion. Major criteria receive two points each, and minor criteria receive one point each. Major criteria include atypical pigment network, blue-whitish veil, and an atypical vascular pattern. Minor criteria include irregular streaks, irregular pigmentation, irregular dots/globules, and regression structures. Irregular pigmentation is defined as black, brown, or gray featureless areas with irregular shape and/or distribution. A total score of 3 or greater has a 95% sensitivity of being a melanoma, and excision is recommended. This system is limited to aiding melanoma diagnosis and does not include criteria that aid in differentiating pigmented skin lesions that are non-melanocytic, such as seborrheic keratosis or basal cell carcinoma (Johr 2002; Argenziano et al. 1998). Under the revised 7-Point algorithm proposed by Argenziano and colleagues in 2011, excision is recommended if the total score is greater than 1 (Argenziano et al. 2011a).

5.4.5 3-Point Checklist

The 3-Point checklist is a recently proposed method that improves the diagnostic accuracy when screening for melanoma in nonexperts and encourages clinicians in specialties other than dermatology to use dermoscopy in general practice. The checklist is based on a simplified dermoscopic pattern analysis and consists of three criteria: asymmetry, atypical pigment network, and blue-white structures (Soyer et al. 2012). The definition of asymmetry is of color and structure in one or two perpendicular axes, and an atypical network is defined as pigment network with irregular holes and thick lines. The 3-Point checklist enables a clinician to have a sensitivity and specificity result comparable with the other algorithms that require much more training. In the original study the sensitivity of some of the nonexperts reached up to 96.3 %, and statistical analysis showed that the presence of any two of these criteria indicates a high likelihood of melanoma (Soyer et al. 2004; Zalaudek et al. 2006).

6 Applications

6.1 Skin Cancer

6.1.1 Melanoma

Melanoma-specific dermoscopic criteria include atypical network, irregular streaks, irregular dots/globules, irregular blotches, and blue-white structures. Specifically an atypical network with sharp cutoff at the lesion periphery, irregular dots

and globules that are unevenly distributed, irregular blotches that are well demarcated with irregular borders at the periphery of the lesion, and blue-white structures that either encompass the majority of the lesion or present with asymmetrical organization are all very suggestive of melanoma diagnosis (Soyer et al. 2012). Other dermoscopic criteria found in melanoma include crystalline structures (fine shiny white streaks visible under polarized light dermoscopy), atypical vascular structures, and negative pigment network (hypopigmented lines make up the grid and dark areas fill up the holes) (Haliasos et al. 2010; Balagula et al. 2012).

6.1.2 Lentigo Maligna

Lentigo maligna presents with specific dermoscopic features due to the presence of specific anatomy of the facial skin (Soyer et al. 2012). These criteria are not found in non-facial melanomas: annular-granular structures, asymmetrically pigmented follicles, rhomboidal structures, and gray pseudonetwork. Annular-granular structures are multiple brown or blue-gray dots surrounding the follicular adnexa with an annular-granular appearance. Asymmetrically pigmented follicles are gray circles/rings of pigmentation distributed asymmetrically around follicular adnexa. Sometimes, the gray circles may contain an inner gray dot or circle. Rhomboid structures are thickened areas of pigmentation surrounding the follicles with a rhomboidal appearance (a rhomboid is a parallelogram with unequal angles and sides). Gray pseudonetwork is gray pigmentation surrounding the follicular ostia formed by the confluence of annular-granular structures. Early lentigo maligna can be challenging and may reveal as the only clue to the presence of gray color predominantly surrounding the follicles. For this reason, any flat lesion arising on the face and presenting gray color should be carefully analyzed and either biopsied or monitored. It is imperative not to perform any treatment before obtaining a clear-cut diagnosis (Stante et al. 2005).

6.1.3 Basal Cell Carcinoma

Basal cell carcinoma dermoscopic features include arborizing vessels (telangiectasias), blue-gray blotches or ovoid nests, multiple blue-gray globules, leaf-like areas, spoke-wheel areas, and ulceration or multiple erosion (Soyer et al. 2012; Braun et al. 2005; Tiodorovic-Zivkovic et al. 2010; Sanchez-Martin et al. 2012).

6.1.4 Squamous Cell Carcinoma

Squamous cell carcinoma dermoscopic features include glomerular vessels, hairpin vessels, linear-irregular vessels, targetoid hair follicles, white structureless areas, a central mass of keratin, and ulceration (Soyer et al. 2012; Zalaudek et al. 2012; Rosendahl et al. 2012) (Fig. 1).

6.1.5 Merkel Cell Carcinoma

This rare aggressive cutaneous tumor usually presents as a nonspecific pink to red nodule, and due to its absence of characteristic clinical features, diagnosis is often delayed. Although there are no specific dermoscopic patterns for MCC, recent studies have shown that the majority of lesions present with a dermoscopic polymorphic vascular pattern composed of milky-red clods/areas in association with one or more additional vascular structures suggestive of malignancy such as arborizing, linear-irregular, dotted, and glomerular vessels (Dalle et al. 2012; Harting et al. 2012).

6.2 Melanocytic Lesions

6.2.1 Spitz/Reed Nevi

Spitz/Reed nevi present dermoscopically with a globular, starburst, or homogenous pattern before the lesion begins to involute. Lesions may present with central black homogeneous pigment network or blue-white structures (Argenziano et al. 1999a; Soyer et al. 2012). The globular pattern presents with numerous globules of various shape and size

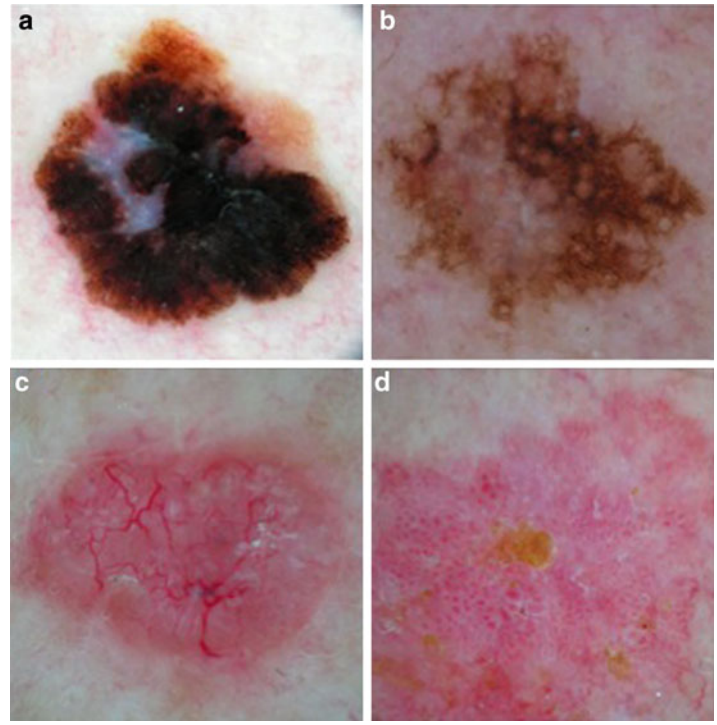

Fig. 1 Malignant tumors. (**a**) Melanoma; dermoscopic features: asymmetry, atypical network, irregular streaks, irregular dots/globules, irregular blotches, blue-white structures, sharply demarcated border. (**b**) Lentigo maligna; dermoscopic features: annular-granular structures, asymmetrically pigmented follicles, rhomboidal structures, gray pseudonetwork. (**c**) Basal cell carcinoma; dermoscopic features: clearly defined thick caliber arborizing vessels. (**d**) Squamous cell carcinoma; dermoscopic features: glomerular vessels, linear-irregular vessels, white structureless areas, a central mass of keratin

that are evenly distributed with color varying from light to dark brown, black, and blue. The starburst pattern presents with symmetrically arranged streaks and/or pseudopods at the lesion periphery. Differential diagnosis includes malignant melanoma, which in comparison may present with asymmetrical arrangement of pseudopods and/or streaks (Braun et al. 2005; Ferrara et al. 2002).

6.2.2 Clark Nevi

Cark nevi have an infinite variety of dermoscopic presentations and benefit from computer-aided digital dermoscopy, which provides rapid and exact digitized recording of skin lesions so that minor structural changes can be sensitively monitored and followed over time. In patients who present with many atypical nevi, the use of dermoscopy allows for the detection of the ugly duckling sign, a nevus or nevi that stand out from the rest of the patients' lesions, and helps guide the clinician to biopsy appropriate lesions for histopathologic analysis (Soyer et al. 2012; Argenziano et al. 2011c). In patients with multiple nevi, the application of the comparative approach can result in a better management of the patient and less surgical excisions of benign lesions. The comparative approach is the evaluation of all nevi in a given patient and the comparison between them in order to grade the ugliest ones (Roesch et al. 2006).

6.2.3 Congenital Nevi

Congenital nevi are defined as lesions that originate in utero. They typically present with reticular pattern which are commonly found on the lower extremities and the globular pattern which occurs more frequently on the head, neck, and torso. The size of these lesions permits to distinguish them as small (<1.5 cm), medium (1.5–19.9 cm), and large (>20 cm). Small- and medium-sized congenital nevi are fairly homogeneous in appearance, whereas large congenital nevi are often

heterogeneous, having multiple uniform islands of color and an irregular topography (Haliasos et al. 2010; Changchien et al. 2007).

6.2.4 Ink Spot Lentigo

Ink spot lentigo has a characteristic dermoscopic pattern. It presents as a bizarre-looking pigment network that is usually black in color, sharply demarcated, and in the absence of other criteria (Soyer et al. 2012).

6.2.5 Dermal Nevi

Dermal nevi dermoscopic features include papillomatous comedo-like openings and comma-like vessels. Manual compressibility and easy movement from side to side are clinical and dermoscopic features in favor of benign nature (Soyer et al. 2012).

6.2.6 Blue Nevi

Blue nevi dermoscopic features include a global pattern characterized by homogeneous pigmentation that is blue, blue-gray, blue-brown, or blue-black in the absence of pigment network (Soyer et al. 2012). Whitish scar-like depigmentation, which correlates histopathologically to fibrosis, can also be found (Ferrara et al. 2002). Differential diagnosis include nodular melanoma, cutaneous melanoma metastasis, pigmented BCC, Spitz/Reed nevi, hemangioma, dermatofibroma, and dermal nevus (Di Cesare et al. 2012; Ferrara et al. 2007).

6.3 Non-melanocytic Lesions and Others

6.3.1 Seborrheic Keratosis

Seborrheic keratosis dermoscopic specific features include milia-like cysts, comedo-like openings, and brown pseudonetwork (Soyer et al. 2012; Braun et al. 2005).

6.3.2 Actinic Keratosis

Actinic keratosis nonspecific criteria/patterns include red or brown pseudonetwork on a background of sun-damaged skin (Soyer et al. 2012; Zalaudek et al. 2012).

6.3.3 Keratoacanthoma

Keratoacanthoma nonspecific criteria/patterns include central keratotic plug, diffuse whitish coloration surrounding polymorphous vessels, and red to black streaks that represent hemorrhage (Soyer et al. 2012; Rosendahl et al. 2012).

6.3.4 Hemangioma

Hemangioma dermoscopic features include red lacunae that are in close proximity, without the presence of melanocytic lesion criteria (Ghibaudo et al. 2009).

6.3.5 Angiokeratoma

Angiokeratoma common dermoscopic findings include dark or red lacunae, whitish veil, and peripheral erythema with a hemorrhagic crust (Kim et al. 2012; Zaballos et al. 2007).

6.3.6 Pyogenic Granuloma

Pyogenic granuloma dermoscopic features include reddish homogeneous area, white collarette, white rail lines, and vascular structures such as red lacunae and telangiectasias. Unfortunately dermoscopy does not substitute histologic examination in this common benign, vascular lesion due to its difficult differentiation from amelanotic melanoma (Zaballos et al. 2010).

6.3.7 Dermatofibroma

Dermatofibromas have a wide range of presentation, but the most common dermoscopic specific pattern is a central white patch surrounded by a light pigmentation or delicate pigment network (Soyer et al. 2012; Zaballos et al. 2008).

6.3.8 Lichen Planus-Like Keratosis (LPLK)

Dermoscopic features of LPLK include diffuse and localized granular pattern composed of multiple blue-gray dots (regression), areas of uniform tan pigmentation, absence of brown globules, and

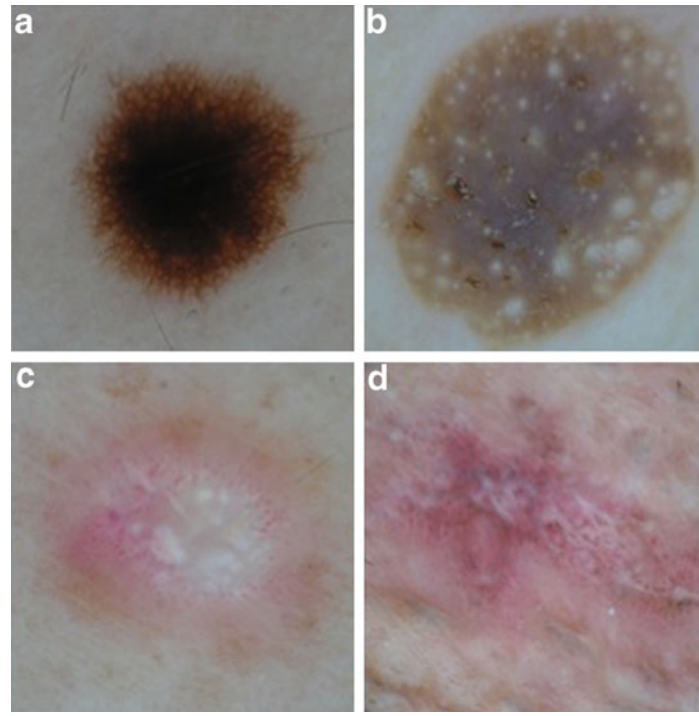

Fig. 2 Benign lesions. (**a**) Benign nevus; dermoscopic features: symmetrical/typical reticular network, central black lamella. (**b**) Seborrheic keratosis; dermoscopic features: milia-like cysts, comedo-like openings, brown pseudonetwork, hairpin vessels. (**c**) Dermatofibroma; dermoscopic features: central white patch, *dotted* vessels. (**d**) Lichen planus-like keratosis; dermoscopic features: diffuse granular pattern composed of multiple blue-gray dots (regression), areas of uniform tan pigmentation, absence of brown globules

areas of pigmented lesions such as seborrheic keratosis or solar lentigo. LPLK differential diagnoses include erythematous type mimicking an actinic keratosis, the papulo-keratotic type simulating a seborrheic keratosis, and the plaque-like type with clinical features of Bowen's disease or pagetoid basal cell carcinoma. The prominent regression structures may make it indistinguishable from lentigo maligna although the distinction between the two is not always reliable on a clinical-dermoscopic basis (Bugatti and Filosa 2007; Panizzon and Skaria 1990; Zaballos et al. 2005, 2006; Crotty and Menzies 2004) (Fig. 2).

6.3.9 Kaposi Sarcoma

Kaposi sarcoma dermoscopic features include bluish-reddish coloration, "rainbow pattern," and scaly surface. The patient's history is an important factor when considering such vascular-appearing lesions (Bugatti and Filosa 2007; Hu et al. 2009).

6.3.10 Eccrine Poroma

Eccrine poroma dermoscopic features include polymorphous irregular vessels, creamy-red areas, and multiple red lacunes. The polymorphic vascular pattern can be composed of irregular linear vessels, glomerular vessels, hairpin vessels, and newly described arborizing vessels combining with small circular endings with flowery appearance (Altamura et al. 2005; Aviles-Izquierdo et al. 2009; Aydingoz 2009).

6.3.11 Trichoscopy

Clinical diagnosis of hair and scalp disorders is not always straightforward, and traditionally a scalp biopsy is warranted in certain conditions that are deemed difficult to assess with the naked eye. Dermoscopy, particularly videodermoscopy, has been shown to improve the evaluation of these disorders and allows for the easy visualization of hair shafts of different types, hair follicles, cutaneous microvessels, and abnormalities of scalp color and structure (Ross et al. 2006a, b; Rudnicka et al. 2011; Mathew 2012).

6.3.12 Alopecia Areata

Alopecia areata trichoscopy features include yellow dots, black dots, micro-exclamation mark hairs, tapered hairs, upright regrowing hairs,

pigtail regrowing hairs, vellus hairs, and broken hairs. Yellow dots are predominant in long-lasting alopecia and are characterized by distention of the affected follicular infundibulum with keratinous material and sebum. Black dots and micro-exclamation mark hairs are markers of high disease activity (Ross et al. 2006b; Kowalska-Oledzka et al. 2012).

6.3.13 Cicatricial Alopecia

Cicatricial alopecia trichoscopy features include white and milky-red areas lacking follicular openings (Rakowska et al. 2012).

6.3.14 Androgenic Alopecia

Trichoscopy features include predominance of abnormalities in the frontal area, compared to the occipital area, which include increase proportion of thin and vellus hairs, hair shaft thickness heterogeneity, perifollicular discoloration (hyperpigmentation), and presence of a variable number of yellow dots (Rudnicka et al. 2011).

6.3.15 Tinea Capitis

Tinea capitis trichoscopy features include corkscrew hairs, comma hairs, and recently zigzag-shaped hairs with transverse structure gaps (Ross et al. 2006b).

6.3.16 Trichotillomania

Trichotillomania trichoscopy features include decreased hair density, short vellus hairs, broken hairs with different shaft lengths, coiled hairs, sparse yellow dots, and no exclamation mark hairs. Specifically in the differentiation of patchy alopecia, the absence of exclamation mark hairs suggests a diagnosis of trichotillomania (Ross et al. 2006b; Mathew 2012).

6.4 Inflammatory and Infectious Diseases

Dermoscopy is a useful tool in diagnosing inflammatory skin disorders and infectious diseases where unusual presentations precipitate difficult differentiation. Particularly the improved visualization of vessels and color variegations and other structures that are difficult to recognize with the naked eye allow for improved clinical judgment. Dermoscopy can also be applied to entomology, termed entomodermoscopy, where such a modality can magnify structures not easily visible with the naked eye (Lallas et al. 2012a, 2013; Zalaudek and Argenziano 2006; Tschandl et al. 2009).

6.4.1 Discoid Lupus Erythematosus

Discoid lupus erythematosus represents the most common subtype of cutaneous lupus erythematosus, and the use of dermoscopy aids in the differential diagnosis of other scarring alopecia etiologies. The most commonly found dermoscopic criteria are perifollicular whitish halo, follicular keratotic plugs, and telangiectasias. In scalp lesions, follicular red dots are specific for active lupus erythematosus (Lallas et al. 2013; Tosti et al. 2009).

6.4.2 Lichen Planus

Lichen planus presents with the pathognomonic pattern of white-crossing lines (Wickham striae) surrounded by dotted or linear vessels (Lallas et al. 2012a; Zalaudek and Argenziano 2006; Tiodorovic-Zivkovic et al. 2012).

6.4.3 Reticulohistiocytosis

Reticulohistiocytosis dermoscopic features include homogeneous pattern with various shades of yellow (setting-sun pattern), brown reticular structures, and central white scar-like patches and streaks. The most commonly found pattern is the homogeneous sun-setting pattern with various shades of yellow in combination with brown reticular structures. Dermoscopic differential diagnosis includes dermatofibroma (Kacar et al. 2010).

6.4.4 Granuloma Faciale

Granuloma faciale is a rare benign form of chronic leukocytoclastic vasculitis that can have serious cosmetic implications due to difficult treatment. While there are no specific criteria for this disease, dermoscopic features include focused elongated

vessels (telangiectasias) associated with a translucent white-gray background intermingled with whitish streaks (Caldarola et al. 2011).

6.4.5 Psoriasis

Psoriasis, especially when it presents with isolated lesions, renders diagnostic challenge when differentiating other dermatoses, namely, seborrheic dermatitis. Dermoscopic patterns of psoriasis include red dots or globules arranged in a homogeneous, regular, or ringlike fashion, twisted red loops, glomerular vessels, and an association with diffuse white scales (Ross et al. 2006a, b; Lallas et al. 2012a; Zalaudek and Argenziano 2006; Vázquez-López et al. 2007; Kim et al. 2011).

6.4.6 Seborrheic Dermatitis

Seborrheic dermatitis dermoscopic features include arborizing vessels, atypical red vessels with the absence of red dots and globules, and featureless areas devoid of any particular vascular patterns (Ross et al. 2006b; Lallas et al. 2012a; Kim et al. 2011).

6.4.7 Pityriasis Rosea

Pityriasis rosea dermoscopic features include yellowish background, structureless center, dotted vessels, and peripheral scales (collarette scaling) (Lallas et al. 2012a; Chuh 2001).

6.4.8 Lupus Vulgaris

Lupus vulgaris dermoscopic features include orange to golden pigmentation with sharply circumscribed linear telangiectases and white, net-like lines (Tschandl et al. 2009; Brasiello et al. 2009).

6.4.9 Mycosis Fungoides

Mycosis fungoides dermoscopic features include short, linear vessels, orange-yellowish patchy areas, and a characteristic vascular pattern composed of a dotted and a short, curved linear vessel. Differential diagnosis includes chronic dermatitis, where dermoscopy shows the absence of orange-yellowish patchy areas and instead the presence of white or yellow surface scales (Lallas et al. 2012b).

6.4.10 Molluscum Contagiosum

Molluscum contagiosum may present as a single or several small, inflamed difficult to diagnose lesions. Dermoscopic features that may aid in its diagnosis are presence of orifices, vessel subtypes (crown, radial, and punctiform), and the newly described vascular flower pattern (Tschandl et al. 2009; Ianhez et al. 2011; Vázquez-López et al. 2004).

6.4.11 Tinea Nigra

Tinea nigra dermoscopic features include fine light brown in part clustered lines suggestive of a reticular pattern. Differential diagnosis includes acral melanoma (Ross et al. 2006a; Tschandl et al. 2009).

6.4.12 Tunga Penetrans

Tunga penetrans dermoscopic features include a white to light brown nodule with a black pore surrounded in a targetoid fashion by a brown ring. The central pore corresponds to the posterior part of the exoskeleton of the sand fly (Tschandl et al. 2009).

6.4.13 Trichomycosis Palmellina

Trichomycosis palmellina dermoscopic features include yellowish translucent granuloma-like crusts that are found around the hair shaft. Differential diagnoses include lice infestation and deodorant debris or scales on axillary or pubic hair (Tschandl et al. 2009).

6.4.14 Furuncular Myiasis

Furuncular myiasis, caused by *D. hominis*, is a disease inherent to South America that has a difficult clinical differential diagnosis of boils, epidermoid cysts, and abscesses (Tschandl et al. 2009). Dermoscopy can help to confirm the suspected diagnosis in such lesions by providing clearer visualization of the parasite. Dermoscopic features include visualization of the posterior segment of the larva with its breathing spiracles looking like birds feet, seen in the center of a creamy-white body surrounded by black dots shaped as a thorn crown, which represents small spines in a circular row (Abraham et al. 2011; Llamas-Velasco et al. 2010; Bakos and Bakos 2007).

6.4.15 Scabies

Scabies dermoscopic features include small, dark, triangular structures and a subtle linear segment that can be seen below the base of the triangle. In combination both structures resemble a jet with contrail. The triangular structure corresponds to the pigmented anterior section of the mite (Tschandl et al. 2009; Argenziano et al. 1997).

6.4.16 Ticks

Dermoscopy provides a convenient magnification and allows for confirmation of the diagnosis in cases of a doubtable situation due to the small size of ticks. It is also useful to find out whether the tick has been completely removed from the skin, specifically to assess whether the tick has lost its hypostomes (Tschandl et al. 2009; Oiso et al. 2010).

6.4.17 Nits and Pseudonits

Vital nits are seen dermoscopically as brown, ovoid structures with a convex end. Empty or hatched nits are translucent with a planar end. Pseudonits are visualized dermoscopically as white bizarrely shaped, amorphous structures that may represent peripilar keratin casts due to dandruff (Zalaudek and Argenziano 2012).

6.4.18 Viral Warts

Dermoscopic features of plantar warts include red or black dots on a white-yellow base detected in the dermis that correspond to capillary loops in the papillary dermis that supply the wart (Tschandl et al. 2009; Lee et al. 2009).

7 Conclusion

Dermoscopy, also called dermatoscopy, opened a new era for dermatologists and general practitioners actively working in skin oncology aiming to diagnose theoretically all melanomas and trying to avoid the surgical excisions of nevi looking as melanoma. Several publications, over 2,000 in the last 20 years, discovered the morphologic universe of skin tumors, defining the specific dermoscopic features that help to correctly identify them while reaching a high diagnostic accuracy. Dermoscopy has also found its application in inflammatory skin diseases and infectious diseases, demonstrating that all histologic substrates render a specific dermoscopic pattern. Future directions imply the combination of dermoscopy with devices that may offer a deeper evaluation of skin architecture, and in this scenario, confocal microscopy may represent the perfect link between dermoscopy and histopathology (Longo et al. 2012).

References

Abraham LS, Azulay-Abulafia L, Aguiar Dde P, Torres F, Argenziano G. Dermoscopy features for the diagnosis of furuncular myiasis. An Bras Dermatol. 2011;86:160–2.

Alexandrescu DT. Melanoma costs: a dynamic model comparing estimated overall costs of various clinical stages. Dermatol Online J. 2009;15:1.

Altamura D, Piccolo D, Lozzi GP, Peris K. Eccrine poroma in an unusual site: a clinical and dermoscopic simulator of amelanotic melanoma. J Am Acad Dermatol. 2005;53:539–41.

Argenziano G, Fabbrocini G, Delfino M. Epiluminescence microscopy. A new approach to in vivo detection of *Sarcoptes scabiei*. Arch Dermatol. 1997;133:751–3.

Argenziano G, Fabbrocini G, Carli P, De Giorgi V, Sammarco E, Delfino M. Epiluminescence microscopy for the diagnosis of doubtful melanocytic skin lesions. Comparison of the ABCD rule of dermatoscopy and a new 7-point checklist based on pattern analysis. Arch Dermatol. 1998;134:1563–70.

Argenziano G, Scalvenzi M, Staibano S, Brunetti B, Piccolo D, Delfino M, De Rosa G, Soyer HP. Dermatoscopic pitfalls in differentiating pigmented Spitz nevi from cutaneous melanomas. Br J Dermatol. 1999;141:788–93.

Argenziano G, Soyer HP, Chimenti S, Argenziano G, Ruocco V. Impact of dermoscopy on the clinical management of pigmented skin lesions. Clin Dermatol. 2002;20:200–2.

Argenziano G, Soyer HP, Chimenti S, Talamini R, Corona R, Sera F, et al. Dermoscopy of pigmented skin lesions: results of a consensus meeting via the internet. J Am Acad Dermatol. 2003;48:679–93.

Argenziano G, Ferrara G, Francione S, Di Nola K, Martino A, Zalaudek I. Dermoscopy – the ultimate tool for melanoma diagnosis. Sem Cutan Med Surg. 2009;28:142–8.

Argenziano G, Catricalà C, Ardigo M, Buccini P, De Simone P, Eibenschutz L, Ferrari A, Mariani G, Silipo V, Sperduti I, Zalaudek I. Seven-point checklist of dermoscopy revisited. Br J Dermatol. 2011a;164:785–90.

Argenziano G, Longo C, Cameron A, Cavicchini S, Gourhant JY, Lallas A, McColl I, Rosendahl C, Thomas L, Tiodorovic-Zivkovic D, Zaballos P, Zalaudek I. Blue-black rule: a simple dermoscopic clue to recognize pigmented nodular melanoma. Br J Dermatol. 2011b;165:1251–5.

Argenziano G, Catricalà C, Ardigo M, Buccini P, De Simone P, Eibenschutz L, Ferrari A, Mariani G, Silipo V, Zalaudek I. Dermoscopy of patients with multiple nevi: improved management recommendations using a comparative diagnostic approach. Arch Dermatol. 2011c;147:46–9.

Aviles-Izquierdo JA, Velazquez-Tarjuelo D, Lecona-Echevarría M, Lázaro-Ochaita P. Dermoscopic features of eccrine poroma. Actas Dermo-Sifiliográficas. 2009;100:133–6.

Aydingoz IE. New dermoscopic vascular patterns in a case of eccrine poroma. J Eur Acad Dermatol Venereol. 2009;23:725–6.

Bakos RM, Bakos L. Dermoscopic diagnosis of furuncular myiasis. Arch Dermatol. 2007;143:123–4.

Balagula Y, Braun RP, Rabinovitz HS, Dusza SW, Scope A, Liebman TN, Mordente I, Siamas K, Marghoob AA. The significance of crystalline/chrysalis structures in the diagnosis of melanocytic and nonmelanocytic lesions. J Am Acad Dermatol. 2012;67:194.

Bassoli S, Seidenari S, Pellacani G, Longo C, Cesinaro AM. Reflectance confocal microscopy as an aid to dermoscopy to improve diagnosis on equivocal lesions: evaluation of three bluish nodules. Dermatol Res Pract. 2010;2010:168248.

Brasiello M, Zalaudek I, Ferrara G, Gourhant JY, Capoluongo P, Roma P, Argenziano G. Lupus vulgaris: a new look at an old symptom – the lupoma observed by dermoscopy. Dermatology. 2009;218:172–4.

Braun RP, Rabinovitz HS, Oliviero M, Kopf AW, Saurat JH. Dermoscopy of pigmented skin lesions. J Am Acad Dermatol. 2005;52:109–21.

Bugatti L, Filosa G. Dermoscopy of lichen planus-like keratosis: a model of inflammatory regression. J Eur Acad Dermatol Venereol. 2007;21:1392–7.

Caldarola G, Zalaudek I, Argenziano G, Bisceglia M, Pellicano R. Granuloma faciale: a case report on long-term treatment with topical tacrolimus and dermoscopic aspects. Dermatol Ther. 2011;24:508–11.

Changchien L, Dusza SW, Agero AL, et al. Age- and site-specific variation in the dermoscopic patterns of congenital melanocytic nevi: an aid to accurate classification and assessment of melanocytic nevi. Arch Dermatol. 2007 Aug;143(8):1007–14.

Chuh AA. Collarette scaling in pityriasis rosea demonstrated by digital epiluminescence dermatoscopy. Australas J Dermatol. 2001;42:288–90.

Crotty KA, Menzies SW. Dermoscopy and its role in diagnosing melanocytic lesions: a guide for pathologists. Pathology. 2004 Oct;36(5):470–7.

Dalle S, Parmentier L, Moscarella E, Phan A, Argenziano G, Thomas L. Dermoscopy of Merkel cell carcinoma. Dermatology. 2012;224:140–4.

Di Cesare A, Sera F, Gulia A, Coletti G, Micantonio T, Fargnoli MC, Peris K. The spectrum of dermatoscopic patterns in blue nevi. J Am Acad Dermatol. 2012;67:199–205.

Ferrara G, Argenziano G, Soyer HP, Staibano S, Ruocco E, De Rosa G. Dermoscopic-pathologic correlation: an atlas of 15 cases. Clin Dermatol. 2002;20:228–35.

Ferrara G, Soyer HP, Malvehy J, Piccolo D, Puig S, Sopena J, Zalaudek I, Argenziano G. The many faces of blue nevus: a clinicopathologic study. J Cutan Pathol. 2007;34:543–51.

Ghibaudo N, Lacour JP, Argenziano G, Ortonne JP, Bahadoran P. Fully regressive targetoid haemosiderotic haemangioma. J Eur Acad Dermatol Venereol. 2009;23:722–3.

Haliasos HC, Zalaudek I, Malvehy J, Lanschuetzer C, Hinter H, Hofmann-Wellenhof R, Braun R, Marghoob AA. Dermoscopy of benign and malignant neoplasms in the pediatric population. Sem Cutan Med Surg. 2010;29:218–31.

Harting MS, Ludgate MW, Fullen DR, Johnson TM, Bichakjian CK. Dermatoscopic vascular patterns in cutaneous Merkel cell carcinoma. J Am Acad Dermatol. 2012;66:923–7.

Hu SC, Ke CL, Lee CH, Wu CS, Chen GS, Cheng ST. Dermoscopy of Kaposi's sarcoma: areas exhibiting the multicoloured 'rainbow pattern'. J Eur Acad Dermatol Venereol. 2009;23:1128–32.

Ianhez M, Cestari Sda C, Enokihara MY, Seize MB. Dermoscopic patterns of molluscum contagiosum: a study of 211 lesions confirmed by histopathology. An Bras Dermatol. 2011;86:74–9.

Johr RH. Dermoscopy: alternative melanocytic algorithms – the ABCD rule of dermatoscopy, menzies scoring method, and 7-point checklist. Clin Dermatol. 2002;203:240–7.

Kacar N, Tasli L, Argenziano G, Demirkan N. Reticulohistiocytosis: different dermatoscopic faces and a good response to methotrexate treatment. Clin Exp Dermatol. 2010;35:e120–2.

Kim GW, Jung HJ, Ko HC, Kim MB, Lee WJ, Lee SJ, Kim DW, Kim BS. Dermoscopy can be useful in differentiating scalp psoriasis from seborrhoeic dermatitis. Br J Dermatol. 2011;164:652–6.

Kim JH, Kim MR, Lee SH, Lee SE, Lee SH. Dermoscopy: a useful tool for the diagnosis of angiokeratoma. Ann Dermatol. 2012;24:468–71.

Kittler H, Seltenheim M, Dawid M, Pehamberger H, Wolff K, Binder M. Frequency and characteristics of enlarging common melanocytic nevi. Arch Dermatol. 2000;136:316–20.

Kokgil TD, Ekmekci TR, Yasar S. Videodermoscopic pattern analysis of acral melanocytic nevi. J Dermatol. 2012;39:290–4.

Kowalska-Oledzka E, Slowinska M, Rakowska A, Czuwara J, Sicinska J, Olszewska M, Rudnicka L. 'Black dots' seen under trichoscopy are not specific for alopecia areata. Clin Exp Dermatol. 2012;37:615–9.

Lallas A, Kyrgidis A, Tzellos TG, Apalla Z, Karakyrious E, Karatolias A, Lefaki I, Sotiriou E, Loannides D, Argenziano G, Zalaudek I. Accuracy of dermoscopic criteria for the diagnosis of psoriasis, dermatitis, lichen planus and pityriasis rosea. Br J Dermatol. 2012a;166:1198–205.

Lallas A, Apalla Z, Lefaki I, Tzellos T, Karatolias A, Sotiriou E, Lazaridou E, Ioannides D, Zalaudek I, Argenziano G. Dermoscopy of early stage mycosis fungoides. J Eur Acad Dermatol Venereol. 2013 May;27(5):617–21.

Lallas A, Apalla Z, Lefaki I, Sotiriou E, Lazaridou E, Loannides D, Tiodorovic-Zivkovic D, Sidiropoulos T, Konstantinou D, Di Lernia V, Argenziano G, Zalaudek I. Dermoscopy of discoid lupus erythematosus. Br J Dermatol. 2013;168:284–8.

Lee DY, Park JH, Lee JH, Yang JM, Lee ES. The use of dermoscopy for the diagnosis of plantar wart. J Eur Acad Dermatol Venereol. 2009;23:726–7.

Liebman TN, Rabinovitz HS, Dusza SW, Marghoob AA. White shiny structures: dermoscopic features revealed under polarized light. J Eur Acad Dermatol Venereol. 2012;26:1493–7.

Llamas-Velasco M, Navarro R, Santiago Sánchez-Mateos D, De Argila D. Dermoscopy in furuncular myiasis. Actas Dermo-Sifiliográficas. 2010;101:894–6.

Longo C, Zalaudek I, Argenziano G, Pellacani G. New directions in dermatopathology: in vivo confocal microscopy in clinical practice. Dermatol Clin. 2012;30:799–814.

Malvehy J, Puig S. Follow-up of melanocytic skin lesions with digital total-body photography and digital dermoscopy: a two-step method. Clin Dermatol. 2002;20:297–304.

Malvehy J, Puig S, Argenziano G, Marghoob AA, Soyer HP, International Dermoscopy Society Board members. Dermoscopy report: proposal for standardization. Results of a consensus meeting of the International Dermoscopy Society. J Am Acad Dermatol. 2007;57:84–95.

Massi D, De Giorgi V, Soyer HP. Histopathologic correlates of dermoscopic criteria. Dermatol Clin. 2001a;19:259–68.

Massi D, De Giorgi V, Carli P, Santucci M. Diagnostic significance of the blue hue in dermoscopy of melanocytic lesions: a dermoscopic-pathologic study. Am J Dermatopathol. 2001b;23:463–9.

Mathew J. Trichoscopy as an aid in the diagnosis of trichotillomania. Int J Trichology. 2012;4:101–2.

Menzies SW. A method for the diagnosis of primary cutaneous melanoma using surface microscopy. Dermatol Clin. 2001;19:299–305.

Menzies SW, Ingvar C, McCarthy WH. A sensitivity and specificity analysis of the surface microscopy features of invasive melanoma. Melanoma Res. 1996;6:55–62.

Menzies SW, Crotty KA, Ingwar C, McCarthy WH. An atlas of surface microscopy of pigmented skin lesions: dermoscopy. 2nd ed. Roseville: McGraw Hill Australia; 2003.

Miyazaki A, Saida T, Koga H, Oguchi S, Suzuki T, Tsuchida T. Anatomical and histopathological correlates of the dermoscopic patterns seen in melanocytic nevi on the sole: a retrospective study. J Am Acad Dermatol. 2005;53:230–6.

Niederkorn A, Gabler G, Argenziano G, Muir J, Zalaudek I, Soyer HP, Hofmann-Wellenhof R. The user-generated web-based dermoscopy image archive of the international dermoscopy society: a contribution to E-learning and exchange of knowledge. Dermatology. 2011;222:131–7.

Oiso N, Nakano A, Yano Y, Kawada A. The diagnostic usefulness of dermoscopy for identifying six-legged larval ticks. Ticks Tick-Borne Dis. 2010;1:197–8.

Panizzon R, Skaria A. Solitary lichenoid benign keratosis: a clinicopathological investigation and comparison to lichen planus. Dermatologica. 1990;181:284–8.

Rakowska A, Slowinska M, Kowalska-Oledzka E, Warszawik O, Czuwara J, Olszewska M, Rudnicka L. Trichoscopy of cicatricial alopecia. J Drugs Dermatol. 2012;11:753–8.

Reisfeld PL. Blue in the skin. J Am Acad Dermatol. 2000;42:597–605.

Roesch A, Burgdorf W, Stolz W, Landthaler M, Vogt T. Dermatoscopy of "dysplastic nevi": a beacon in diagnostic darkness. Eur J Dermatol. 2006 Sep-Oct;16 (5):479–93.

Rosendahl C, Cameron A, Argenziano G, Zalaudek I, Tschandl P, Kittler H. Dermoscopy of squamous cell carcinoma and keratoacanthoma. Arch Dermatol. 2012;148:1386–92.

Ross EK, Vincenzi C, Tosti A. Videodermoscopy in the evaluation of hair and scalp disorders. J Am Acad Dermatol. 2006;55:799–806.

Rudnicka L, Olszewska M, Rakowska A, Slowinska M. Trichoscopy update 2011. J Dermatol Case Rep. 2011;5:82–8.

Salerni G, Terán T, Puig S, Malvehy J, Zalaudek I, Argenziano G, Kittler H. Meta-analysis of digital dermoscopy follow-up of melanocytic skin lesions: a study on behalf of the International Dermoscopy

Society. J Eur Acad Dermatol Venereol. 2012. doi:10.1111/jdv.12032 [Epub ahead of print].

Sanchez-Martin J, Vazquez-Lopez F, Perez-Oliva N, Argenziano G. Dermoscopy of small basal cell carcinoma: study of 100 lesions 5 mm or less in diameter. Dermatol Surg. 2012;38:947–50.

Soyer HP, Kenet RO, Wolf IH, Kenet BJ, Cerroni L. Clinicopathological correlation of pigmented skin lesions using dermoscopy. Eur J Dermatol. 2000;10:22–8.

Soyer HP, Argenziano G, Chimenti S, Ruocco V. Dermoscopy of pigmented skin lesions. Eur J Dermatol. 2001;11:270–6.

Soyer HP, Argenziano G, Zalaudek I, Corona R, Sera F, Talamini R, Barbato F, Baroni A, Cicale L, Di Stefani A, Farro P, Rossiello L, Ruocco E, Chimenti S. Three-point checklist of dermoscopy. A new screening method for early detection of melanoma. Dermatology. 2004;208:27–31.

Soyer P, Argenziano G, Hofmann-Wellenhof R, Zalaudek I. Dermoscopy the essentials. 2nd ed. Philadelphia: Elsevier/1296 Saunders; 2012.

Stante M, Giorgi V, Stanganelli I, Alfaioli B, Carli P. Dermoscopy for early detection of facial lentigo maligna. Br J Dermatol. 2005;152:361–4.

Stoecker WV, Wronkiewiecz M, Chowdhury R, Stanley RJ, Xu J, Bangert A, Shrestha B, Calcara DA, Rabinovitz HS, Oliviero M, Ahmed F, Perry LA, Drugge R. Detection of granularity in dermoscopy images of malignant melanoma using color and texture features. Comput Med Imaging Graph. 2011;35:144–7.

Stolz W, Riemann A, Cognetta AB, et al. ABCD rule of dermatoscopy: a new practical method for early recognition of malignant melanoma. Eur J Dermatol. 1994;4:521–7.

Stolz W, Brawm Falco O, Bilek P, Landthaler M, Burgforf WHC, Cognetta AB. Color atlas of dermatoscopy. 2nd ed. Oxford: Blackwell; 2002.

Tiodorovic-Zivkovic D, Zalaudek I, Ferrara G, Giorgio CM, Di Nola K, Procaccini EM, Argenziano G. Clinical and dermatoscopic findings in Bazex-Dupre-Christol and Gorlin-Goltz syndromes. J Am Acad Dermatol. 2010;63:722–4.

Tiodorovic-Zivkovic D, Argenziano G, Popovic D, Zalaudek I. Clinical and dermoscopic findings of a patient with co-existing lichen planus, lichen sclerosus and morphea. Eur J Dermatol. 2012;22:143–4.

Tosti A, Torres F, Misciali C, Vincenzi C, Starace M, Miteva M, Romanelli P. Follicular red dots: a novel dermoscopic pattern observed in scalp discoid lupus erythematosus. Arch Dermatol. 2009;145:1406–9.

Tschandl P, Argenziano G, Bakos R, Gourhant JY, Hofmann-Wellenhof R, Kittler H, Rosendahl C, Minas S, Zalaudek I. Dermoscopy and entomology (entomodermoscopy). J Dtsch Dermatol Ges. 2009;7:589–96.

Vázquez-López F, Kreusch J, Marghoob AA. Dermoscopic semiology: further insights into vascular features by screening a large spectrum of nontumoral skin lesions. Br J Dermatol. 2004;150:226–31.

Vázquez-López F, Zaballos P, Fueyo-Casado A, Sánchez-Martín J. A dermoscopy subpattern of plaque-type psoriasis: red globular rings. Arch Dermatol. 2007;143:1612.

Wang SQ, Dusza SW, Scope A, Braun RP, Kopf AW, Marghoob AA. Differences in dermoscopic images from nonpolarized dermoscope and polarized dermoscope influence the diagnostic accuracy and confidence level: a pilot study. Dermatol Surg. 2008;34:1389–95.

Zaballos P, Ara M, Puig S, Malvhey J. Clinical and dermoscopic image of an intermediate stage of regressing seborrheic keratosis in a lichenoid keratosis. Dermatol Surg. 2005;31:102–3.

Zaballos P, Martí E, Cuéllar F, Puig S, Malvehy J. Dermoscopy of lichenoid regressing seborrheic keratosis. Arch Dermatol. 2006;142:410.

Zaballos P, Daufi C, Puig S, Argenziano G, Moreno-Ramirez D, Cabo H, et al. Dermoscopy of solitary angiokeratomas: a morphological study. Arch Dermatol. 2007;143:318–25.

Zaballos P, Puig S, Llambrich A, Malvehy J. Dermoscopy of dermatofibromas: a prospective morphological study of 412 cases. Arch Dermatol. 2008;144:75–83.

Zaballos P, Carulla M, Ozdemir F, Zalaudek I, Bañuls J, Llambrich A, Puig S, Argenziano G, Malvehy J. Dermoscopy of pyogenic granuloma: a morphological study. Br J Dermatol. 2010;163:1229–37.

Zalaudek I, Argenziano G. Dermoscopy subpatterns of inflammatory skin disorders. Arch Dermatol. 2006;142:808.

Zalaudek I, Argenziano G. Dermoscopy of nits and pseudonits. N Engl J Med. 2012;367:1741.

Zalaudek I, Argenziano G, Ferrara G, et al. Clinically equivocal melanocytic skin lesions with features of regression: a dermoscopic-pathological study. Br J Dermatol. 2004;150:64–71.

Zalaudek I, Argenziano G, Soyer HP, Corona R, Sera F, Blum A, Braun RP, Cabo H, Ferrara G, Kopf AW, Langford D, Menzies SW, Pellacani G, Peris K, Seidenari S, Dermoscopy Working Group. Three-point checklist of dermoscopy: an open internet study. Br J Dermatol. 2006;154:431–7.

Zalaudek I, Docimo G, Argenziano G. Using dermoscopic criteria and patient-related factors for the management of pigmented melanocytic nevi. Arch Dermatol. 2009;145:816–26.

Zalaudek I, Kreusch J, Giacomel J. How to diagnose nonpigmented skin tumors: a review of vascular structures seen with dermoscopy: part I Melanocytic skin tumors. J Am Acad Dermatol. 2010a;63:361–74.

Zalaudek I, Kresuch J, Giacomel J, Ferrara G, et al. How to diagnose nonpigmented skin tumors: a review of vascular structures seen with dermoscopy: part II. Nonmelanocytic skin tumors. J Am Acad Dermatol. 2010b;63:377–86.

Zalaudek I, Giacomel J, Schmid K, Bondino S, Rosendahl C, Cavicchini S, Tourlaki A, Gasparini S, Bourne P, Keir J, Kittler H, Eibenschutz L, Catricalà C, Argenziano G. Dermatoscopy of facial actinic keratosis, intraepidermal carcinoma, and invasive squamous cell carcinoma: a progression model. J Am Acad Dermatol. 2012;66:589–97.

Digital Photography in Aesthetic Dermatology

22

Jean-Marie Sainthillier, Sophie Mac-Mary, and Philippe Humbert

Contents

J.-M. Sainthillier (✉)
Skinexigence, Besançon, France
e-mail: jmsainthillier@skinexigence.com

S. Mac-Mary
Skinexigence SAS, Bioparc, Besançon, France
e-mail: smac@skinexigence.com

P. Humbert
Department of Dermatology, University Hospital of Besançon, Besançon, France
e-mail: philippe.humbert@univ-fcomte.fr

P. Humbert et al. (eds.), *Agache's Measuring the Skin*,
DOI 10.1007/978-3-319-32383-1_22

Keywords
Digital photography • Aesthetic dermatology

1 Introduction

Digital photography offers interesting opportunities to dermatologists involved in aesthetic dermatology: low cost, flexibility, easiness and speediness of use, and possibility of computerized record keeping (Ali 2002; Becker 1999). A considerable number of applications have been developed to meet the needs of users and to automatize the most frequently used functions (image cropping or renaming, conversion into a different format, inclusion in a database, etc.), and most of these applications are free. The digital environment of photography has never been so performing and ergonomic.

However, a digital camera, regardless of its capacities, remains a camera with its own limits and constraints. Users should not ignore the basic rules of photography: exposure, aperture, shutter speed, and depth of field. These notions have always been and are still essential.

2 Fundamentals

In a digital camera (DC), as opposed to a classic camera (Daniel 2000), the film is replaced by a CCD (charge-coupled device) sensor composed of a multitude of photo sites (4–10 μm) sensitive to light (Bouillot 2005). These sites or photodetectors convert the photons that they receive into electrons by photoelectric effect, and these electrons will accumulate like in a basin. The number of electrons stored in each photo site is proportional to the intensity of light received. All detectors deliver an electric tension which can be converted and analyzed by the electronics and the software of the device. The CCD sensor is at the heart of the DC; its manufacturing quality and electronics determine the quality of the photograph which depends on the number of photo sites, therefore on the available points or pixels. Current devices have more than 10 million pixels, and cameras with 16 million pixels are now commercially available (Canon Eos Mark II has a 24 × 36 mm CMOS sensor of 21 million pixels and achieves 5,616 × 3,744 pixel images). Photographs taken with such a resolution are of great definition, as beautiful on the panoramic monitor of a computer as on a large paper print (140 × 120 cm minimum).

This CCD sensor can be fit into three main types of casing corresponding to three categories of DC: compact, bridge, and reflex. Compact cameras were originally entry-level digital cameras, but this is not the case any longer. As its name obviously reveals, it is made of a thin and light box (some models are waterproof and shockproof) including a built-in motorized objective lens, and sometimes a ×4 to ×7 zoom lens. It is usually preset and automated so that the user has almost nothing to do to take a satisfactory photograph (Canon Powershot, Panasonic Lumix, Nikon Coolpix).

In a bridge camera with electronic viewfinder, an LCD (liquid crystal display) screen is fit behind the ocular like on a video camera (it is called digital back). The viewfinder is therefore not optical and is cheaper to manufacture than the actual reflex finder. A more powerful zoom lens (×30) is attached to the camera body which often includes a stabilized optical system. Like a compact camera, this type of DC can record a video or even a high-definition film (Fujifilm FinePix, Olympus SP100, Pentax X90). Finally, in a reflex camera, the image formed by the objective is sent back toward the viewfinder and its ocular system. The image seen in the finder and by the CCD sensor is therefore the same. The body of this type of camera is usually larger and more cumbersome, but all its objectives and flashes are interchangeable, and any framing or angle is therefore possible. Reflex cameras are beyond any doubt the preferred option to take photographs on a professional level (Canon Eos, Nikon, Sony Alpha). Their technological superiority over the other categories of DC in terms of sensitivity, color reproduction, and reactivity is unquestionable.

3 Settings and Basics of Photography

Basic principles are similar in digital photography and in film photography for the process before the CCD sensor (Bouillot 2003). The following optical and photographical notions are presented in the specific context of photography of the skin in medical practice.

3.1 Light and Exposure

To take a good photograph, one condition is crucial: the right amount of light is necessary, no more no less (Sainthillier et al. 2009, 2012). In this context, exposure is defined as the exposure to light of the sensitive surface that will record the image. It corresponds therefore to the amount of light transmitted to the CCD sensor or to the film. If there is too much light, the photograph is "burnt" or overexposed; details disappear and are replaced by white saturated surfaces. If there is not enough light, the photograph is too dark or underexposed; details disappear in black zones. In both cases and in spite of the possibilities given by photo editing software programs, missing information is definitively lost.

3.2 Shutter Speed

The shutter is an electronic system designed to control the time of exposure, i.e., the period during which the light penetrates the camera and reaches the sensor. It may be compared to an opaque curtain which makes the chamber where the CCD is located completely dark. When the photograph is taken, the shutter opens (lifts up) for a certain time to let in an amount of light through the aperture of the diaphragm. The shutter speed is composed of seconds and fractions of seconds. High shutter speeds (above 1/250 = 1/250th of second) are interesting for photographs of moving subjects. In static photography, the speed is usually set up at 1/60. To avoid a blurry image, settings under 1/60 are not recommended (or the camera should be placed on a tripod to ensure stabilization).

3.3 Aperture of Diaphragm and Objective Lens

The lens of the device uses a diaphragm to dose the light entering the camera body. The aperture is between f/1 (wide aperture) and f/32 (small aperture). The letter f designates the quotient resulting from the division of the focal length by the aperture diameter of the diaphragm. For a given shutter speed, the amount of light penetrating the camera is multiplied by 2 when diaphragm settings are higher. A large aperture will let more light in, but it will also reduce the depth of field, i.e., the space between the foreground and the background where the photograph remains clear (Taheri et al. 2013). This can have a perturbing effect on the face, for example, because of its relief. If the focus is on the cheekbone, the nose and the forehead are blurry. A small aperture gives a large depth of field, but the flow of light reaching the CCD sensor is lower (Fig. 1).

The larger the aperture, the more luminous the viewfinder, and therefore, the more the lens can be used in difficult conditions, in poor light, or associated to higher shutter speeds. Manual and autofocus are also facilitated. The optical quality of a lens is globally based on its maximal aperture: 50 mm f/1.8

Fig. 1 In this extreme example (F/4, 1/60, ISO 400), the effect of the wide aperture on the depth of field is visible. The lips are clear, but most of the image in the background is blurred (not retouched image)

is common (130 €), 50 mm f/1.2 is excellent (600 €), and 50 mm f/1 is superior (3,000 €).

Shutter speed and aperture are therefore closely associated. It is possible to maintain the same quality of global exposure by using various combinations of aperture and speed. This is called the law of reciprocity. For one photographed scene, there are several possible combinations to achieve the adequate exposure of the sensor. It is therefore possible to let the light in for a long time (e.g., 1/30) with a small aperture (f/11 for instance) or let the light in for a very short time (1/500) with a large aperture (f/2.8). In both cases, the CCD sensor will receive exactly the same amount of light; exposure is the same.

3.4 Focal Length and Zoom

The focal length expressed in millimeters designates the distance separating the photosensitive surface of the sensor from the optical center of the lens. The focal length of the lens allows to frame the photographed subject more or less accurately and is broadly defined according to three categories:

- Wide angles (28–35 mm), i.e., short lengths, tend to distort perspective with an angle of vision that is more important than the human eye angle of vision.
- Standard focal lengths (38–70 mm) are close to the angle of vision of the human eye and are the most widely used.
- Long focal lengths (80–200 mm) and teleobjectives with very long focal lengths (over 200 mm).

A zoom lens or lens with variable focal length is able to vary the focal length within specific limits and therefore to reframe the image without changing position and without altering resolution.

Some cameras have a function called "digital zoom." It is in fact a software program; it increases the size of the digital image, not the actual image, through an interpolation method. This zoom lens is not relevant for photography in aesthetic dermatology and must be avoided.

3.5 Focus

In most cameras, it is an autofocus system triggered by gently pressing the push button. To get optimal focus, the contrast must be sufficient (it is difficult to operate the autofocus on a very homogeneous skin surface) or lighting must be adequate. In autofocus mode, detection points will not be found if the skin is not sufficiently exposed to light. In addition, the autofocus can be released and the focus can be activated manually in some circumstances.

3.6 Lighting and Flashlights

As indicated previously, light is the fundamental element in photography. In aesthetic dermatology, lighting must be sufficient to ensure adequate sharpness, without flattening the relief or erasing imperfections and without creating shadows on the face (Meneguini 2001). It also has to be constant in between camera shots to ensure that comparison before and after treatment is possible, for example.

A flash is a source of artificial light synchronized with the shutter and has a powerful but very short duration of lighting. Its power theoretically protects the DC from the influence of the changing character of ambient light. Its range is 0.5–3 m approximately. The built-in flash unit is usually not sufficient, and an additional flash unit can generally be mounted on an accessory shoe on top of the camera body. The additional flash unit is either more powerful (Canon Speedlite range) or not synchronized. Circular, annular, or twin flashes (Canon MT-24EX or METZ Mecablitz) are also very interesting. They ensure powerful, diffuse, and homogeneous lighting.

For entry-level models, it is also possible to adapt a flash diffuser (Delamax). It is a more or less rigid and transparent white case that is placed on top of the flash unit. Reflecting kits (Lumiquest Soft Screen) are also available at reasonable prices.

3.7 ISO Sensitivity

Photography requires light and a photosensitive surface. In traditional photography, this surface

is a film; in digital photography, it is an electronic sensor. The sensitivity of the support can be changed to adapt it to various lighting conditions.

The ISO speed (International Standards Organisation) replaces the old measuring systems (DIN, ASA) and identifies the sensitivity of a support. In normal conditions of daylight, the standard is set at 100 ISO. The higher the ISO speed (200, 400, 800, etc.), the more sensitive the support is to light, but the more the texture of the image is visible. A key point to remember is that the quality of the image is inversely proportional to the sensitivity of the sensor.

3.8 Polarization Filters

Some polarization filters are of interest to dermatologists because they break down the reflection of the light on the skin according to its diffuse or specular component (brightness) (Bargo and Kollias 2010; Matsubara 2011). These filters are fixed on the flash units and on the lenses (HOYA circular filters). Depending on the orientation of the filter, parallel or cross polarization is obtained (Fig. 2).

- Parallel polarized light reveals and accentuates the skin irregularities and microrelief. Brightness and contrast are increased, whereas colorimetric data are lost. This type of lighting is used in the study of acne or to follow up scars or lesions that become more visible (Rizoca and Kligman 2001).
- In contrast, cross polarized light accentuates the color and saturation of the skin. Reflection and brightness of the skin are completely eliminated. This type of polarization is very useful in studies on vascular pathologies such as rosacea (Miyamoto et al. 2002) or on the effects of a whitening product.

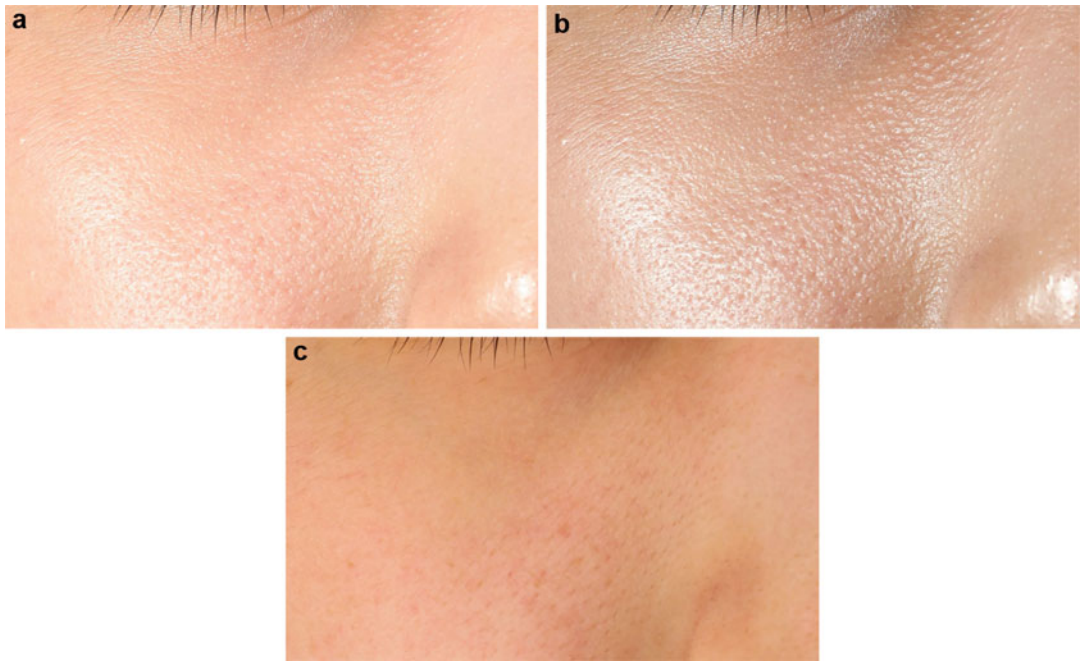

Fig. 2 Photographs (details) in normal light (*top*), parallel polarized light (*centre*) and cross polarized light (*bottom*). In light, reflection is eliminated and vascularization is revealed. In contrast, parallel polarization light accentuates reflection and brightness and gives the skin a metallic aspect

3.9 Reflection of UV Light

This type of lighting derives from Wood's work based on radiations found at the beginning and at the end of the visible spectrum (<450 nm) (Lucchina et al. 1996; Draelos et al. 2008). The flash unit produces UV-A without harming the volunteer. The resulting image provides visual evidence of the trace left by UV exposure. Several systems are commercially available (Canfield®, Faraghan®). They operate with a DC set at maximum sensitivity (1600 ISO) in order to detect the very limited part of visible light emitted by the flash unit. This explains why these images are usually very dark (Fig. 3).

3.10 LCD Monitor

Color rendering by a DC depends mostly on the monitor used to visualize the photograph. LCD flat screens have now completely replaced previous cathode ray screens. The screens are now very reactive with remanence under 5 ms, they are luminous, but they still present restricted angles of vision. Only panoramic screens are currently available (the ratio height/width, i.e., the format of the screen, is 16/9 or 16/10). A wide screen is recommended (24 or 26 in.), in 16/10, equipped with High-Definition Multimedia Interface (HDMI), allowing for an entirely digital audio/video interface (this implies to have also a graphic card with this interface). Asus, LG, and Iiyama provide very good quality monitors, and high-end screens can be found at Eizo (colorEdge) and NEC (SpectraView).

Calibration probes (Spyder3Pro of DataColor, i1Display LT of X-Rite) are used to ensure correct settings and adequate color rendering on a monitor. These probes of small size are fixed to the screen with suction pads and are directed by a software program that displays a series of known colors on the screen. The probe reads these colors and corrects the display deviations with a calibration profile or ICC (International Color Consortium) profile. This digital file

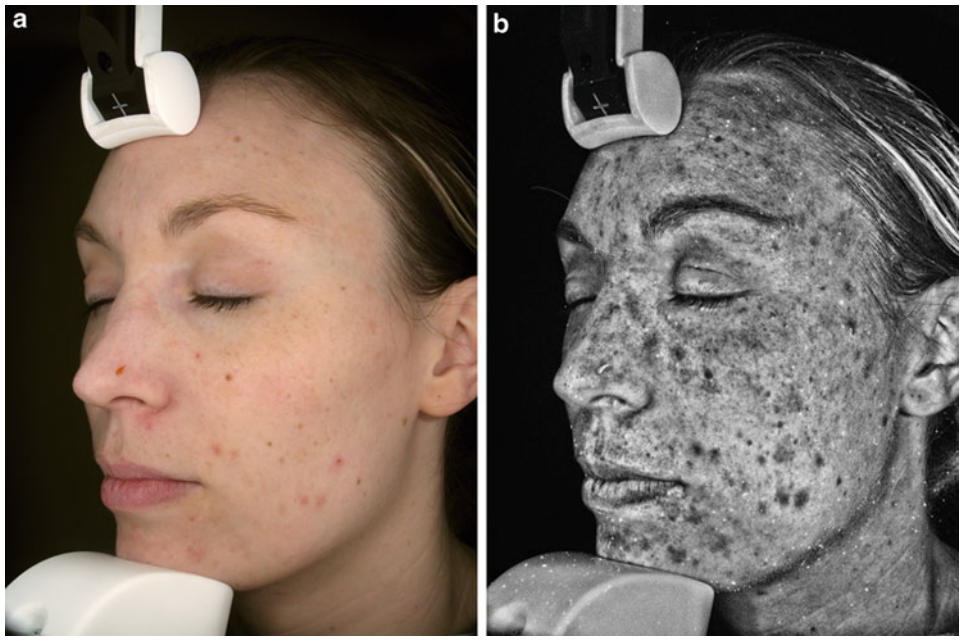

Fig. 3 Photographs in cross polarized light (*left*) and in UV light (*right*) taken with Visia® (Canfield) system. UV light reveals spots which are barely or not visible in normal light. UV photography is difficult to use because of its sensitivity to environmental conditions. Images must be taken while lighting is neutralized (either in total darkness or in an integrated system like in this example). A piece of garment or a jewel may perturb the image contrast

describes how the screen reproduces colors; it is directly controlled by the operating system. The ICC profile can characterize a monitor, a scanner, or a printer.

Color rendering in video projection is more complex (Delmas 2005). Depending on the quality of the projector, the rendering of some colors (especially magenta) may be surprising. The same difficulties arise when images are printed. The quality of printer and paper has a considerable influence on color reproduction.

3.11 Integrated Devices or "Lighting Boxes"

In recent years, we have seen the arrival of integrated photographic systems to study the face, composed of the most recent camera inserted into a "box" with a lighting system, a support to maintain the chin and the forehead and a software program for image capture. The volunteer places his/her face inside the device (which is similar to an integration sphere) where it is lit in homogeneous and reproducible conditions. The aim of these systems (Visioface®, Courage et Khazaka; Visia, Canfield®) is to obtain data for diagnostic purposes easily and speedily. They are of interest to dermatologists because they are comprehensive systems to take standardized photographs (Fig. 4).

Fig. 4 Example of integrated system "light box" (Visioface®, C&K). This independent comprehensive system consists of a box fitted with a camera, white light LEOs, chin and forehead rests to position the face, and image capture software. Homogeneous illumination is given by mirrors (visible inside the box) which distribute the light evenly on the face

4 Use of Digital Photography in Clinical Practice

The DC is set in "automatic mode," usually indicated on the mode control scroll wheel by a specific color. It calculates the aperture and shutter speed in relation to light exposure determined by a built-in exposure meter to find the ideal conditions. These constants are displayed in real time on the control monitor of the camera and in the viewfinder.

– If ambient light is adequate, the shutter speed will be between 1/60 and 1/125, the corresponding aperture of the diaphragm being f/5.6 and f/2.8, respectively. This is the best compromise to take a photograph with satisfactory exposure. The settings are then adjusted automatically by the autofocus system, and the photograph is of good quality.
– If ambient light is low, the shutter speed is automatically set between 1/15 and 1/30 with identical apertures (f/5.6 and f/2.8). The risk of motion blur is in this case very high, and it is likely that the autofocus will not stabilize during settings.

What are the options?

- First solution: use manual settings and increase sensitivity (ISO) of the CCD sensor (e.g., set at ISO 200 instead of 100). Adjusting settings manually can also allow the user to take photographs with a shutter priority, by fixing the speed at 1/60 as a precaution to avoid motion blur. The camera will select the maximal adapted aperture to ensure correct exposure. The depth of field may then be seriously compromised.

- Second solution: add or increase the power of the flash unit (increase of power can be adjusted on high-end flash units). It is however essential to not overexpose the central part of the photograph. This option is rarely appropriate.
- Third solution: to mount the DC on a tripod (Manfrotto type). All DCs have an accessory shoe to fix or remove them very quickly. It is then possible to increase the shutter speed without risk and let the light in for a longer period of time.
- Fourth solution: to increase the lighting of the room, either with additional neon lights or studio flashlights (Multiblitz Profilux). This is an ideal choice for the intensive practice of photography in a clinical environment because it ensures identical lighting for each photographic shot, thus reproducibility.

5 Computer Management of Images

Before addressing this subject, it may be useful to review a few fundamentals of digital photography (Russ 2007; Gonzalez and Woods 2008). Basic rules of photography are of considerable importance in the treatments and corrections that will be carried out on the images at a later stage.

5.1 Coding and Color

A pixel is the smallest element constituting an image. It has a coded value which defines its color (chrominance) and its intensity (luminance). This code is quantified on a number of bits which is the smallest unit that can be processed by a computer: 8 bits = 1 octet. The amount of data on each pixel depends on the number of bits on which coding or quantification is performed.

For example, coding on 1 bit (0 or 1) defines only two possible colors for each pixel, without any tone, which corresponds to a black and white image. 8-bit coding is equivalent to 2^8 different intensities per pixel, i.e., 256 colors or levels of gray per pixel. 24-bit coding corresponds to present standards which attribute to each pixel three primary color components (red, green, blue, or RGB coding), coded individually on 2^8 bits, giving a total of 2^{24}, equivalent to 16.7 million colors. In practice, the number of restituted colors depends on the quality of the screen and the graphic card. 32-bit coding has been available for a few years, but it requires computers at the highest end of the market.

5.2 White Balance

A new concept appears with the use of artificial lighting: color temperature. Each type of light includes a specific dominant color feature: rather orange for indoor lights (tungsten), bluish for daylight, whitish under overcast sky, or greenish under neon lights. Default automatic setting of color temperature for each photograph is done by the DC by trying to assess the lighting conditions; it is the auto white balance. If the adjustment is unsuitable, white, or neutral gray, look yellow or blue. It is possible to select the source of light in advance, so that it corrects the tone of the image. For these settings, a predetermined white balance adapted to the context of the shot is selected: incandescent light (halogen bulb), fluorescent tubes, sun (daylight), cloudy sky, and shadows. Reflex DCs can define a "personalized" white balance. For this adjustment, a white sheet (or a calibration gray card such as Kodak R27) is placed at the center of the scene. The camera is then set to adjust its balance from this photograph; these settings are saved in its internal memory.

5.3 Definition and Resolution

Definition and resolution are often confounded, but they refer to different features of an image. **Definition** expresses the number of pixels or elementary points of an image in height (lines) and in width (columns). It is calculated by multiplying the number of lines and columns. An image of 3,000 lines and 4,000 columns has a definition of 12 million pixels.

Resolution defines the fineness of display or reproduction of the details of the image and

expresses the number of pixels that compose it by unit of length. Depending on the system of measurement used (either metric or customary), resolution is expressed in points per centimeter (ppc) and points per inch (ppp or dpi), respectively. One inch is equivalent to 2.54 cm; it is therefore easy to go from one system to the other. As a rule, the larger the number of pixels in a measurement unit, the higher the resolution. 300 ppp resolution provides a level of details much higher than 72 ppp resolution.

It is possible to adjust specifically the quality of image of a DC with internal settings (usually three levels of quality: fine, normal, and basic) that reduce the definition of the image gradually. This function was useful in the past when memory cards were very expensive and their capacity limited (high-definition images are very large and require a lot of space in cards). However, the latest flash cards (Compact Flash or SDHC Cards [Secure Digital High Capacity] of 16 or 32 Go) are affordable and can store several thousands high-definition photographs easily.

5.4 Main Image Formats

Among all the formats available in a DC, three are specifically designed for photography: JPEG, TIFF, and RAW. They are very different and require specific procedures.

JPEG (Joint Photographic Expert Group) format is the most widely used in DCs. Only reflex cameras and a few high-end compact cameras offer other saving formats. Its huge success lies mainly on its excellent compromise between storage size and image quality (the size of a noncompressed image is often divided by 10, or even more). JPEG has a lossy compression mode (i.e., with loss of data, which accounts for the efficacy of its compression algorithm) based on the perception properties of the eye and whose rate can be set by the user. The higher the rate or inversely the lower the quality of compression, the more important is the loss of data, hence the degradation of the captured image. Loss of data is mainly visible in variations of tones, on contours, but does not alter the rendering of the variations of light. This degradation is cumulative (at each saving of the same JPEG file). Working on a JPEG file is therefore not recommended; it should be converted first into a format file of larger size, without altering data (TIFF files).

The **TIFF** (Tagged Image File Format) is an earlier graphic format which tends to disappear. It is able to store large size images (over 4 Go after compression) without impairing quality. It is independent from the operating system – which is an asset – and it can be found in PC, Mac, and Unix systems.

The **RAW** format is used in reflex cameras and high-end compact cameras (Canon PowerShot). Before creating the definitive file, the DC processes raw data issued from the sensor in order to correct some parameters such as the white balance. Then the data are converted into standard formats (TIFF or JPEG) and saved. In the RAW format, such preliminary treatments do not exist: the device creates a file with the raw data directly issued from the sensor. The captured photograph does not undergo any processing and has no compression-induced artifacts unlike with the JPEG format. In counterpart, this format has not really been standardized by the manufacturers (each new DC model induces a slight modification of the format and imposes an updating system), and it requires postproduction work with dedicated software (Adobe Lightroom, Photoshop CS6, or free software DC Raw). Finally, a RAW image has clearly a larger size than its copy in JPEG format.

As a reference, the size of a 3,504 × 2,336 image is approximately 2.23 Mo in JPEG (in fine mode), 23.4 Mo in TIFF, and 6.8 Mo in RAW.

EXIF (Exchangeable Image File Format) is a specification of file format incorporating metadata (data on data) for images in JPEG and TIFF formats. Metadata are tags embedded in the image file. They record the date and hour of the photographic shot, the settings (brand and model of DC, aperture, shutter, sensitivity, etc.), as well as GPS data if the camera has a geolocation system (Fig. 5). The latest image editing programs recognize these EXIF data and store them when the file is modified. It is directly accessible under Windows (XP, 7, or 8) in the menu “Properties of the image file” in the tab “Summary” and under Mac

Camera	
Fabricant	FUJIFILM
Modèle	FinePixS1Pro
Orientation	haut-gauche (1)
Résolution en X	72
Résolution en Y	72
Unité pour la résolution	Pouce
Logiciel	Digital Camera FinePixS1Pro Ver1.00
Date de modification	2004:02:23 11:48:58
Positionnement YCbCr	accollé (2)
Image	
Nombre-F	22.6
Programme d'exposition	Manuel (1)
Sensibilité équivalente ISO	400
Version EXIF	02.10
Date¦heure d'origine	2004:02:23 11:48:58
Date¦heure numérisées	2004:02:23 11:48:58
Configuration des composantes	YCbCr
Bits par pixel compressé	3/2
Vitesse d'obturation [s]	1/108
Indice d'ouverture	F22.6
Luminosité	35/4
Valeur compensation exposition	2/1
Mode calcul exposition	Moyenne pondérée au centre (2)
Flash	Flash allumé
Longueur de focale [mm]	59
Version FlashPix	01.00
Mode de couleur (BPP)	sRGB
Largeur de l'image	3040

Fig. 5 Example of EXIF data. The list includes the name of the manufacturer, the DC model, the date of creation, and the photographic settings (aperture, shutter, sensitivity). These data are helpful to adjust settings and find the best implementation in terms of equipment and environment to ensure optimal conditions of photography

OS X in the menu "Read data." These data are very useful to find lost photographic settings or to fix them manually when they are deemed satisfactory. They can be used as criteria to find photographs taken with specific settings (e.g., all the images taken with f/5.6 aperture).

5.5 Software Programs

Many dedicated software programs are available and adapted to the photographers' requirements. The following selection (Table 1) presents the leading freewares or inexpensive tools available in both Windows and Mac environments.

5.6 How to Rename and Identify Images

The names of all the files saved in the memory card of the DC are not very explicit. The root or prefix of the names is always invariant (DSC, IMG, IMAGE, etc., depending on the manufacturers). It is followed by a four-digit incremental order number and an extension (e.g., JPEG). It is therefore necessary to rename without delay the images according to the photographed area of the body, the subject's name, or pathology. This process can rarely be automated because of the variety of data that the user wants to highlight. It is possible to use FastStone Photo Resizer that has advanced functions to rename quickly and automatically a set of images. It can define all types of fields and rules to create prefixes or suffixes indexed on the number of selected files.

Once the images have been renamed satisfactorily, it is recommended to take time to add comments or key words, with the help of tools such as XnView or ThumbsPlus. The additional information is included in the image or the associated database.

Table 1 List of a few major software programs for the management of digital images and morphing (update in June 2013). Trial versions of all these programs are available

Software	Editor	Website	Functions	Price
ThumbsPlus 9.0	Cerious Software Inc	www.cerious.com	Visualization, localization and organization	99 USD
FastStone Image Viewer 4.8	FastStone Soft	www.faststone.org	Advanced visualization and organization	Freeware
FastStone Photo Resizer 3.1	FastStone Soft	www.faststone.org	Processing and conversion	Freeware
XNView 2.03	XnSoft	www.xnview.com	Visualization, Processing and conversion	Freeware
Picasa 3.9	Google	picasa.google.com	Visualization, creation of online albums	Freeware
IrfanView 4.35	Irfan Skiljan	www.irfanview.com	Visualization and conversion	Freeware
Photoshop CS6	Adobe	www.adobe.com	Creation, retouch and management	900 Euros
Photoshop Element 11	Adobe	www.adobe.com	Creation, retouch and management	80 Euros
GIMP 2.8	The GIMP Team	www.gimp.org	Creation, retouch and management	Freeware
PhotoFiltre 10.7.3	Antonio Da Cruz	www.photofiltregraphic.com	Creation, retouch and management	Freeware
FantaMorph 5	Abrosoft	www.fantamorph.com	Morphing	30 Euros
Popims Animator 4.01	Popims	www.popims.com	Morphing	Freeware

5.7 How to Visualize and Load Images

Intuitive and simultaneous visualization of several images is absolutely essential when their number is important. One must be able to quickly compare several photographs, select the best images, erase the blurry or missed shots, and remove doubles. To navigate easily among large numbers of images, recent software programs offer a visualization mode through tags similar to the miniatures used under Windows, i.e., shortcuts represented by small icons generated by and linked to original photographs. These icons can be manipulated, moved, or displayed in large numbers on contacts sheets. Most programs, such as IrfanView, ThumbsPlus, FastStone Image Viewer, Picasa (Windows), I photo, and Aperture (Mac OS X), also highlight with a color-coding system the files where images are stored. It is then easy to localize data quickly on the hard drive.

Another interesting ability of these programs is the possibility of a quick multicriteria research in a large database (ThumbsPlus manages databases of tens of thousands images). However, the efficacy of this type of research is based on the correct tagging of the images at the time of saving with a clear definition of key words. It is also possible to select images by similarity, by instructing the software program to find all the images resembling a reference image more or less exactly (a similarity threshold is defined).

Finally, these programs include simultaneous visualization of several images (FastStone Image Viewer is particularly efficient at this level). Before/after images can be synchronized and displayed side by side on the computer screen. All the moves inside an image (e.g., reframing or zooming) are instantly reproduced on the second image. The comparison of several images is therefore considerably facilitated (Fig. 6).

Fig. 6 Example of synchronization (with ThumbsPlus) between 3 photographs. All the operations (zooming, movements) on an image are reproduced on the other images, thus ensuring optimum comparison

5.8 How to Crop and Reframe Images

In view of their maximal definition, images from a DC cannot be used directly in good conditions. For example, the size of a slightly compressed 6 million pixel image in JPEG file format is 2.3 Mo.

The abovementioned systems are able to crop a series of images easily (for instance, all the images stored in a file) by batch processing (automated treatment) where the desired size or reduction percentage is indicated. Images can also be reframed by eliminating their edges systematically. Cropped or reframed images do not erase original images which remain available for future use.

Photographs used in PowerPoint presentations can be cropped in a definition not exceeding 800 × 600 pixels (even 640 × 480 pixels), quite sufficient for a computer monitor or a video projector. The presentation will be smooth even if it is used with a basic laptop.

In contrast, maximal definition is recommended for images used to illustrate articles since printing is usually carried out in high resolution. To obtain satisfactory printing results, the resolution of the document must be approximately 600 points per inch (dpi). With a size of printed image of 10 cm in width, it corresponds therefore to a definition in column of the image of at least 2,500 pixels. Publishers also prefer to work with noncompressed images.

Other treatments can be automated by batch processing, such as global modification of contrast, increase of luminosity, conversion into levels of gray or another format (JPEG to TIFF, for instance), rotation, addition of a text or a logo inside the image, etc.

5.9 Photo Editing Software

Besides these very specific tools, more ambitious software programs can operate the complete centralized management of images. These creation and retouch programs have filters to correct and improve photographs.

For 20 years, Adobe Photoshop has been the imaging and retouch program par excellence and the most widely used by photographers. It is a complex program (in particular in the management of layers), powerful to work on, retouch, or

export images with a complete and accurate control on compression and the possibility to import and process RAW format files. An affordable version of this exceptional software is available to the general public (Photoshop Elements).

Freewares and comprehensive programs have also been available for a few years (GIMP and PhotoFiltre). They are continuously improved and perfected, and their users form a very active community on the Internet (online assistance, tips, advice, etc.).

6 Practice of Photography in Aesthetic Dermatology

In the field of aesthetic medicine, photography must satisfy two requirements: to be as close as possible to reality and to be comparative, i.e., to ensure that photographing is reproducible (Canfield 2002; Halpern et al. 2003; Galdino et al. 2001).

Alterations on the surface of the epidermis (erythrosis, rosacea, pigmented spots, atrophy) are sometimes not very spectacular. Photography must neither enhance them by accentuating them with cross lighting, nor diminish them with flashlight.

To assess the improvement induced by a treatment on the surface of the epidermis (such as chemical peel, laser rejuvenation), images must be comparative. It is therefore crucial that the technique ensures the reproducible character of the shots which must be performed in similar rigorous conditions.

How to ensure reproducibility?

– The subject/patient must have a neutral appearance.
  The object of the photograph is the skin. All useless elements must be removed: necklace, earrings, scarf, etc. If the photograph is taken in a wider field, clothes must be covered with neutral material.
  Anything that is likely to hide the lesions must be removed, especially makeup. Makeup should be removed at least 10 mn before the photograph is taken, or ideally no makeup should be applied on the day. Even a basic skincare cream can cause alteration of the reflection of the light on the skin. Hair often hides or covers part of the forehead or sides of the face: it must be pulled back.
  The face must show no expression: the subject must refrain from smiling which emphasizes expression wrinkles, in particular near the eyes.
  The eyes must fix a point on a wall (either a clearly visible mark or a mirror). The subjects may also be asked to close their eyes quickly before the photograph is taken. Some authors recommend that the eyes be closed briefly to relax expression lines on the face (Tsukahara et al. 2009).
  Photographs must be taken in controlled environmental conditions: they depend of course on the availability of each clinic. Ideally a room or part of a room with neutral walls and no visible object should be dedicated to photography.

To obtain comparative shots, all the photographs of a series (before/after) must be taken in the same conditions.

- The patient must be advised not to change his/her appearance between shots. After aesthetic treatment, one may be tempted to modify other features such as hair color, new haircut, etc. It is not always easy to convince the subject to refrain from changing until the comparative photograph has been taken. It is however a primary requirement because the objective judgment of improvement can be influenced by alterations.
- Constancy of angle of shot: the same protocol must be followed to take each photograph. The DC must always be placed at the same distance from the subject to have the same focus. Ideally it should be possible to move around the subject seated in a predetermined place in the room. The subject must always look in the same direction. The various angles of shot can be marked on the floor to ensure reproducibility.

- Height must be adjustable so that the axis of the objective lens is horizontal, using a tripod or an adjustable stool.
- Stable lighting conditions: an artificial source of light (flash unit or light projector) ensures that the operation takes place in the same conditions and facilitates reproducibility.
- Reproducibility of colors: color stability in reflex DCs is generally very good as long as the device is not changed during the protocol. Colors can be corrected after the photograph has been taken if a color chart has been placed in the scene (Mini Colorchecker color chart, X-Rite). The reference colors of the chart are then available to document and guide future corrections of colors (Grana et al. 2005; Vander Haeghen et al. 2001).

It is essential to do preliminary tests with the equipment and to determine the optimal settings. Once adequate settings are identified, it is important to respect them. EXIF data associated to the photographs will be loaded to document imaging. These data will help the operator to refine settings and to set up the best possible working conditions in terms of equipment and environment.

7 Digital Photography in Dermatology

Digital photography provides the opportunity to set up easily an iconographic database of the main techniques used by dermatologists in their practice. The before/after photographs will be easily accessible and available to the dermatologist. It is recommended to anonymize them by adding a black strip on the patient's eyes or by blurring them.

A dermatologist with intense aesthetic practice can have a database of samples (in PowerPoint format) to show technical gestures to the patients prior to treatment: wrinkle filling, chemical peel, resurfacing, etc., and the expected results. These images can be put on line very easily (with Picasa in particular), or a dedicated website can be created. In this hypothesis, ethic regulations set by the medical authorities have to be respected.

Morphed images give the patient an idea of the results after treatment. Morphed images are produced with special effects used to create animated images that transform gradually and naturally an initial image into a final image. Professional software programs, such as Mirror Aesthetic Simulation, calculate a deformation of the image from the initial photograph, simulating the results after surgical treatment. This process is used mainly in plastic surgery. It is also interesting in aesthetic dermatology, for example, it can help illustrate changes in color to simulate postlaser erythema so that the patient is aware of the treatment side effects. Softwares such as Fantamorph or Popims Animator are easily accessible to dermatologists interested in this technique.

Although very attractive, these methods must not hide some negative effects. It is easy to make idealized simulations on the screen and to propose to the patients changes that will be difficult to achieve. The patients may be very disappointed.

Finally, it is essential to mention the existence of photographic scales (Bazin and Doublet 2007) which list in a book the criteria of cutaneous aging of female or male (Caucasian) faces. They are used to rate an area of the face with accuracy: glabella wrinkle, crow's foot wrinkles, wrinkles under the eyes, etc. The scales can also be used altogether to assess global aging of the face.

8 Conclusion

Digital photography does not simply imply a change of camera; it is a total change in the management of imaging, and it requires efficient mastering of information technology.

With this technique, working habits must be modified. One must keep in mind that digital photographs are saved and stored in a PC or laptop. They can be displayed on a monitor, projected, or printed with a color

printer or in a scientific article. However, in daily practice, digital imaging is used on the computer screen.

Computer science is not 100 % reliable, and it is essential to save data regularly. The widespread use of USB flash drives and external hard disks simplifies this process which was fastidious not so long ago. It is crucial that original photographs must be saved simultaneously on a high capacity hard drive and on CD-ROM or DVD.

The flexibility of the system, its reproducibility, and the possibility to classify and save images and to display several images on one screen to compare them make digital photography an ideal tool in aesthetic dermatology.

References

Ali MZ. Advantages of digital photography records keeping in plastic surgery. L Coli Phys Surg Pakistan. 2002;12:613–7.

Bargo PR, Kollias N. Measurement of skin texture through polarization imaging. Br J Dermatol. 2010;162:724–31.

Bazin R, Doublet E. Atlas du vieillissement cutané. Editions Med'Com 2007. Paris.

Becker DG. Standardized photography in facial plastic surgery: pearls and pitfalls. Facial Plast Surg. 1999;15:93–9.

Bouillot R. Cours de photographie numérique. Principes, acquisition et stockage. Paris: Dunod; 2003.

Bouillot R. Cours de traitement numérique de l'image. Paris: Dunod; 2005.

Canfield D. Reproductible photography for the aging face. Textbook of facial rejuvenation. London: Martin Dunitz; 2002.

Daniel F. Photographie argentique en dermatologie esthétique. Encycl Méd Chir (Editions Scientifiques et Médicales, Elsevier SAS, Paris), 50-275-A-10, Cosmétologie, 2000; 1–6.

Delmas J. La gestion des couleurs pour les photographes. Paris: Eyrolles; 2005.

Draelos ZD, Klein G, Biancone G. A novel ultraviolet photography technique for assessing photodamage. J Cosmet Dermatol. 2008;7:205–9.

Galdino GM, Vogel JE, Vander Kolk CA. Standardizing digital photography: it's not all in the eye of the beholder. Plast Reconstr Surg. 2001;108:1334–44.

Gonzalez RC, Woods RE. Digital image processing. New Jersey: Prentice Hall; 2008.

Grana C, Pellacani G, Seidenari S. Practical color calibration for dermoscopy, applied to a digital epiluminescence microscope. Skin Res Technol. 2005;11:242–7.

Halpern AC, Marghoob AA, Bialoglow TW, Witmer W, Slue W. Standardized positioning of patients (poses) for whole body cutaneous photography. J Am Acad Dermatol. 2003;49:593–8.

Lucchina LC, Kollias N, Gillies R, et al. Fluorescence photography in the evaluation of acne. J Am Acad Dermatol. 1996;35:58–63.

Matsubara A. Differences in the surface and subsurface reflection characteristics of facial skin by age group. Skin Res Technol. 2011;0:1–7.

Meneguini F. Clinical facial photography in a small office: lighting equipment and technique. Aesthet Plast Surg. 2001;25:299–306.

Miyamoto K, Takiwaki H, Hillebrand GC, Arase S. Utilization of a high-resolution digital imaging system for the objective and quantitative assessment of hyperpigmented spots on the face. Skin Res Technol. 2002;8:73–7.

Rizoca E, Kligman A. New photographic techniques for clinical evaluation of acne. JEADV. 2001;15 Suppl 3:13–8.

Russ JC. The image processing handbook. Boca Raton: CRC Press; 2007.

Sainthillier JM, Mac-Mary S, Humbert P. La photographie numérique: un outil scientifique. Ann Dermatol Venereol. 2009;136 suppl 6:S280–6.

Sainthillier J-M, Le Maitre M, Humbert P. Photographie numérique en dermatologie esthétique. EMC – Cosmétol Dermatol Esthét 2012;0(0):1–7.

Taheri A, Yentzer BA, Feldman SR. Focusing and depth of field in photography: application in dermatology practice. Skin Res Technol 2013;0:1–4.

Tsukahara K, Hotta M, Osanai O, et al. The effect of eye opening and closing on the result of facial wrinkle assessment. Skin Res Technol. 2009;15:384–91.

Vander Haeghen Y, Lemahieu I, Naeyaert JM. A calibrated color imaging system for use in Dermatology. In: Proceedings ProRISC/IEEE Benelux Workshop on Circuits, Systems and Signal Processing. Nederland, 2001.

Additional Information

Adobe TV: http://tv.adobe.com/fr/
Christophe Métairie Photographie: http://www.cmp-color.fr
Elephorm: http://www.elephorm.com
FOCUS Numérique: http://www.focus-numerique.com
Video2Brain: http://www.video2brain.com/
Volker Gilbert Photographie: http://www.volkergilbertphoto.com
X-RITE Photo: http://www.xritephoto.com

Stratum Corneum Histopathology

23

Marek Haftek

Contents

Keywords

Ultrastructure • Morphology • Stratum corneum • Epidermal barrier • Permeability

1 Under the Surface

Stratum corneum (SC) is the final product of the terminal differentiation of epidermal keratinocytes. It is elaborated on purpose and fulfills essential roles in terms of protection of the organism's living tissues. These functions encompass barrier functions against penetration of foreign molecules and pathogens, significant limitation of the transepidermal water loss, filtration of approximately 70 % of the deleterious UVB radiation, and mechanical resilience to other physical and chemical aggressions. Thanks to the continuous mitotic activity of the mother tissue, the epidermis, SC is continuously renewed. The cornified keratinocytes, corneocytes, are progressively shed from the skin surface, and their loss is adequately compensated through the keratinization of the most superficial living cells from the underlying *stratum granulosum*. This highly coordinated process ensures maintenance of the SC barrier and its adaptation to the environmental changes.

M. Haftek (✉)
Laboratoire de Recherche Dermatologique, EA 4169, Faculté de Médecine et de Pharmacie, Université Claude Bernard Lyon 1, Lyon, France
e-mail: marek.haftek@univ-lyon1.fr

P. Humbert et al. (eds.), *Agache's Measuring the Skin*,
DOI 10.1007/978-3-319-32383-1_23

2 Formation of the SC: Process of Cornification

Formation of the SC is a very rapid and, thus, very interactive process. Transformation of the most superficial living keratinocytes in the *stratum granulosum* into the cornified cells takes only 1–1.5 days (Baker and Blair 1968). During this short period, the granular layer cell massively releases its secretory contents into the apical intercellular space and efficiently degrades all its cytoplasmic organelles, beginning with the nucleus and mitochondria. The process is initiated and regulated by changes in the extracellular calcium gradient (Menon et al. 1994; Elias et al. 2002) and is mediated by caspase 14 (Eckhart et al. 2000; Denecker et al. 2008). Structural and bioactive proteins, hydrolytic enzymes, enzyme inhibitors, and lipids synthesized in the granular layer are all delivered into the extracellular space via the complex vesiculo-tubular system originating in the *trans*-Golgi: the so-called lamellar granules (Serre et al. 1991; Rassner et al. 1999; Ishida-Yamamoto et al. 2005). Within the SC, all these elements self-organize at the molecular level and perform their respective roles in a manner no more dependent on the cellular activity but largely influenced by the physical and chemical factors, e.g., temperature, humidity/hydration, and pH (Bouwstra et al. 2003a; Haftek et al. 1998; Rawlings and Harding 2004). Upon the process of cornification, important changes occur within the cytosol. Degradation of organelles is paralleled by dispersion of the keratohyalin granules containing profilaggrin. Dephosphorylation of profilaggrin is the first step permitting its processing to filaggrin, the protein involved in aggregation of intermediate filaments of keratin and consolidation of the corneocyte interior into a relatively homogeneous composite structure (Harding and Scott 1983; Markova et al. 1993). Later in the process, the arginine residues of filaggrin shall be converted to citrulline, and this loss of charge shall lead to the protein dissociation from keratins and its further degradation to amino acids (Kamata et al. 2009; Méchin et al. 2010). These hydrophilic final products of filaggrin processing largely influence water holding capacity of the SC and contribute to its acid pH. Histidine, one of the major components of filaggrin, is converted to urocanic acid, the latter being involved in protection against UV radiation (de Fine Olivarius et al. 1996; Mildner et al. 2010). At the keratinocyte periphery, various proteins become cross-linked by the cell membrane-bound transglutaminases, essentially TG1, TG3, and TG5, to form a cornified envelope (Kalinin et al. 2002; Candi et al. 2005). Several cytosolic proteins, including filaggrin and hornerin, are thus integrated into the highly insoluble peripheral structure principally composed of involucrin, loricrin, and small proline-rich proteins (Michel et al. 1988; Haftek et al. 1991; Steinert and Marekov 1999; Simon et al. 1996; Henry et al. 2011). Simultaneously, the plasma membrane phospholipids become replaced by the lamellar granule-derived sphingolipids (ceramides) (Elias et al. 2000). These latter molecules become also cross-linked by TG1 to the nascent cornified envelopes (Nemes et al. 1999). Thus, formed lipid envelopes constitute a matrix for alignment of the extracellular lipids and for formation of the intercorneocyte lipid bilayers (Wertz et al. 1989; Marekov and Steinert 1998). Together, the cornified cellular bricks and the self-organized lipid mortar form an efficient permeability barrier at the top of the skin (Elias 2006).

3 Structure of the SC

Cornified keratinocytes have the form of polygonal flat tiles. They are strikingly thinner than the underlying nucleated cells (1–2 μm thick) and about two times wider than the stratum spinosum keratinocytes (30–35 μm in diameter). This significant change in proportions comes with extensive cell overlapping and convolution of the lateral cell walls. In this setting, extracellular lipids structured in lamellae and filling intercorneocyte spaces are the principal factors limiting SC permeation either way:

outside in and inside out (Elias and Menon 1991). X-ray diffraction studies allow overall appreciation of the lipid lamellar phases present in the SC and indicate that SC lipids are organized in bilayers presenting two major periodicities (12–13 nm and 5–6 nm spacing between the polar head groups of lipid molecules within the bilayers). These studies reveal also the lateral packing pattern of molecules within the bilayer sheets (Bouwstra et al. 2003b). Long periodicity phase and orthorhombic lateral packing are predominant in normal SC, whereas a switch to the short periodicity phase and hexagonal lateral arrangement characterize functional states with increased SC permeability. Recently, ultrastructural studies of vitrified skin sections, in which the molecular arrangement has been preserved by ultra-rapid freezing of the tissue, have led to slightly different conclusions (Iwai et al. 2012; see also ▶ Chap. 33, "Cyanoacrylate Method"). Using this morphological approach, the authors propose that SC lipids are organized in homogeneous phases with 10–12 nm spacing of the repeating unit, corresponding to the length of a fully extended ceramide molecule. In the proposed model, one ceramide molecule would be associated with one fatty acid and one cholesterol molecule, consistent with our knowledge about the equimolar proportions between these major components of the SC lipid matrix (Bouwstra et al. 2003b). The spliced arrangement of ceramides would confer to the lipid bilayers more suppleness, compatible with the everyday physical requirements. However, the model does not integrate the variable length and nature of the hydrophobic carbon chains belonging to the different lipid species found in the SC. Also, it admits no space for water molecules within the SC extracellular spaces. Yet, water is necessary for functioning of the non-lipid components in the SC and notably those involved in the processing and rearrangement of the intercellular matrix. Lipid bilayers can be visualized with conventional electron microscopy using highly oxidizing reagents, such as osmium and ruthenium tetroxides. Although this classical approach induces notable artifacts related to the chemical fixation, dehydration with solvents, and tissue contrasting methods, the structural modifications are reproducible and well defined. Using this technique, it is possible to observe hydrophilic "faults" in the semicrystalline structure of the intercorneocyte spaces (Haftek et al. 1998). Such hydrophilic lacunae increase in size and change emplacement upon SC hydration obtained with simple occlusion (Fig. 1). They also swell after SC treatment with agents disorganizing lamellar lipids and thus constitute the primary permeation pathways. Extensive exposure to water makes SC more voluminous, as corneocytes absorb and retain humidity. Water binding capacity varies with the SC depth and depends largely on the presence of the so-called natural moisturizing factor resulting from the processing of filaggrin to free amino acids. As a consequence, three zones showing different compactness and hydration may be distinguished (Bouwstra et al. 2003a; Richter et al. 2004). Cohesion within the SC is provided by corneodesmosomes, which are structurally modified desmosomes having incorporated corneodesmosin (Serre et al. 1991; Haftek et al. 2006). Lipids, initially proposed to participate in the SC cohesion, do not show adhesive proprieties and rather behave as a spacer (Chapman et al. 1991). In the lower portion of SC, called SC *compactum*, corneodesmosomes are distributed all around the cells. In this highly cohesive part, the intercorneocyte spaces are almost entirely filled with lamellar lipids, and, therefore, this is where the permeability barrier is mainly located. Subsequently, corneodesmosomes attaching the stacked consecutive corneocyte layers are progressively degraded by serine proteases, principally kallikreins 5 and 7 (Voegli and Rawlings 2012). This introduces horizontal dissociation in the upper portion of SC, therefrom named SC *disjunctum* (Fig. 2). Interestingly, lateral connections between the corneocytes do persist also at this level. As a result, the so-called "basket-weave" pattern of the SC is frequently observed in standard histological skin samples, after tissue delipidation during dehydration procedures. It can be further enhanced by the application of permeabilizing agents, which facilitate mobility

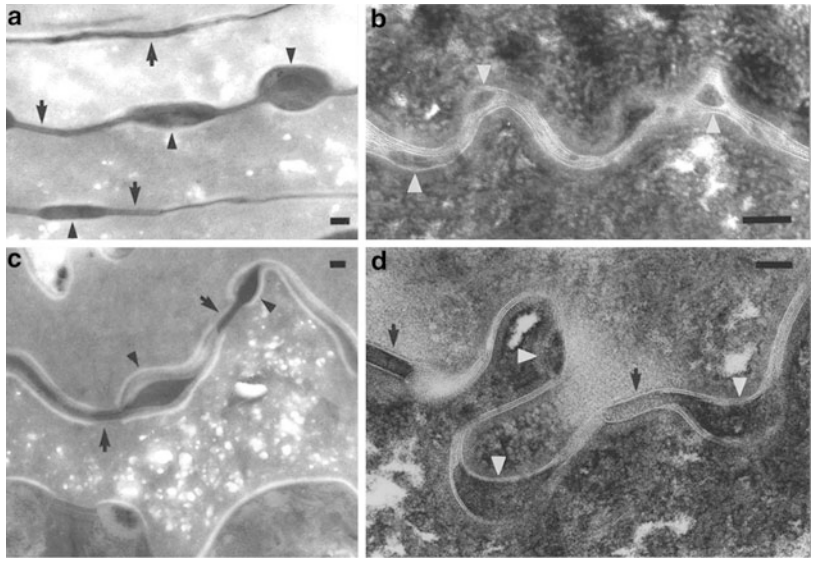

Fig. 1 Ultrastructure of intercorneocyte spaces in the SC *compactum* upon mild hydration. Normal human skin explants were examined with transmission electron microscopy using post-fixation with either osmium tetroxide (**a**, **c**) or with ruthenium tetroxide (**b**, **d**). Nonoccluded skin samples (**a**, **b**) showed rather narrow intercellular spaces containing focally hydrophilic (electron-dense) inclusions (*arrowheads*). Upon hydration, obtained by 6-h occlusion (**c**, **d**), the hydrophilic lacunae swelled, split the intercellular lipid lamellae, and were often encountered next to corneodesmosomes (*arrows*). This illustrates how the SC hydration results in the focal increase of the extracellular hydrophilic compartment, likely containing protein components issued from the lamellar granule extrusion, and facilitates interaction between these elements and the corneodesmosome substrate proteins. Bars = 100 nm (Micrographs adapted from Haftek et al. 1998, with permission from Microscopy Research and Techniques, John Wiley and Sons)

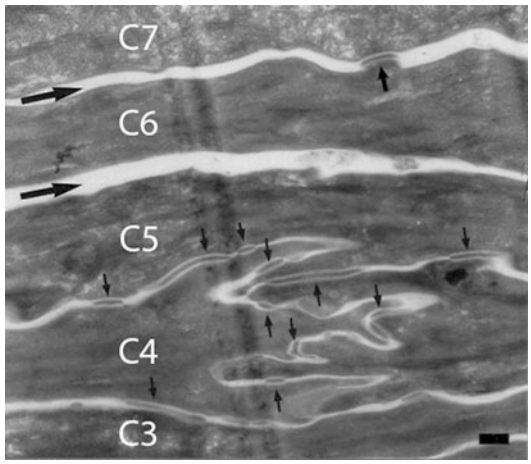

Fig. 2 Ultrastructure of normal human SC at the interface between SC *compactum* and SC *disjunctum*. Corneodesmosomes (*small arrows*) that join SC *compactum* cells (C3–C5) are numerous and distributed both between the lateral cell-cell contacts and between the successive cell layers. The latter localization is the primary target of proteolytic enzymes resulting in virtual disappearance of the interlayer corneodesmosomes (*big arrows*) and creation of the SC *disjunctum* (C6–7). Bar = 200 nm

of the endogenous intercellular enzymes (Fig. 3). Better resistance of the lateral corneodesmosomes has long been unexplained, since these structures do not differ biochemically and mechanically from the junctions situated between the successive corneocyte layers. Recent visualization of the tight junction remnants cross-linked to the corneocyte envelopes and situated in the lateral portions of the cells solves the puzzle (Haftek et al. 2011). Indeed, lateral corneodesmosomes appear to be less accessible to the catabolic enzymes because of the presence of tight junction – like fusion spots between the cell envelopes at this localization.

4 Desquamation

Transition from the SC *compactum* to *disjunctum* indicates the beginning of the desquamation process. Proteolytic enzymes and their natural inhibitors secreted into the intercellular spaces interact

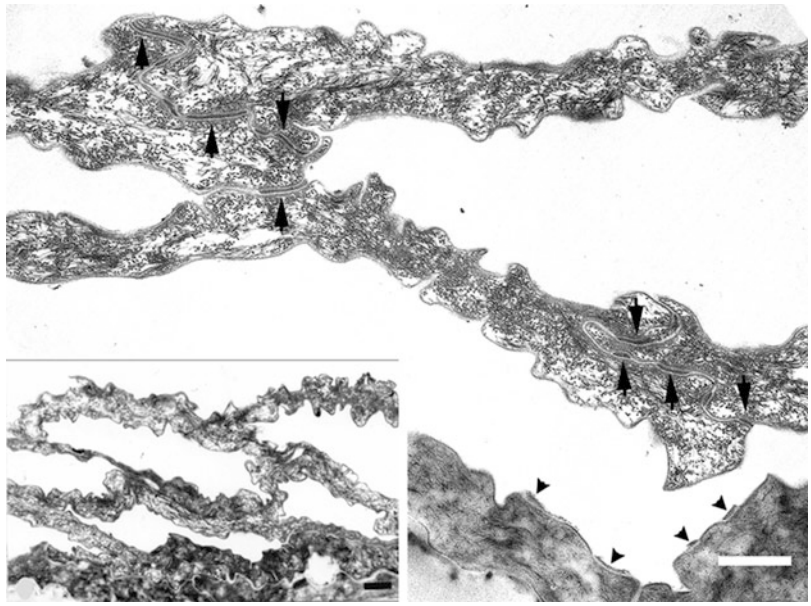

Fig. 3 Normal human SC dissociation induced by exposure to propylene glycol spares the lateral corneodesmosomes. The entire SC undergoes *disjunctum*-like transformation after 6-h topical application of the permeation agent, producing so-called basket-weave pattern (*inset*). Corneocytes maintain their lateral attachment, but lose corneodesmosomes providing interlayer contact (*arrowheads*). Intact lateral corneodesmosomes (*arrows*) are sealed within the portions of fused cornified lipid envelopes. Such intercorneocyte fusions have been demonstrated to correspond to cross-linked tight junction – like structures issued from the underlying living epidermal layers. Bars = 500 nm

with their respective substrates in a manner depending on the structural constraints, i.e., mobility within the hydrophobic intercellular matrix, shape of the extracellular space, and presence of tight junction-derived fusion points between cell envelopes, and on the physicochemical operating conditions, i.e., pH, hydration, and temperature. It has been proposed that self-organization of the lipids in continuous multilayered sheets could contribute to the lateral displacement of intercellular hydrophilic lacunae containing hydrolytic enzymes toward the immobile corneodesmosome structures, the latter representing enzyme substrates (Haftek et al. 1998). Corneodesmosomes attaching successive cell layers are cleaved first. Corneocytes remain in layers attached at the cell periphery to the neighboring cells. This situation persists up to the SC surface, where individual cells chip off due to the mechanical stress brought by drying and abrasion (Haftek et al. 1997). In normal human skin, the desquamation rate is approximately one cell layer in 21 h (Hoath and Leahy 2002), so that an adult loses about 2.5 million corneocytes every day.

5 Maintenance of the SC Homeostasis

Thickness of the SC varies between the anatomical sites from 5 to 20 corneocyte layers: an average of 16 layers (Grove and Kligman 1983). It takes in average 14 days to a corneocyte to evolve through the normal SC and to desquame at its surface (Johannesson and Hammar 1978). Because changes in the shedding rate influence the SC barrier quality, they constitute signals to the living layers, and notably to the proliferative compartment, to adapt accordingly (Proksch et al. 1993). This interactivity is necessary to maintain the epidermal homeostasis, and thus adequate barrier function, in changing environmental conditions.

In physiological conditions, thickening of the SC may be observed during the winter period and

is related to a slowdown in corneodesmosome degradation (Simon et al. 2001). A similar mechanism could also be evoked in the case of age-related skin dryness. Compensatory thickening of the palmar or plantar SC is constantly observed upon recurrent mechanical stimulation leading to the occurrence of calluses.

Skin pathology abounds in the manifestations involving SC appearance and function. They may involve SC overproduction, retention, or premature shedding. Excessive retention of otherwise normally keratinized SC is called hyperkeratosis, e.g., accumulation of cholesterol sulfate – a powerful inhibitor of serine proteases in SC – occurs in recessive X-linked ichthyosis. In this case, deficit in steroid sulfatase leads to improper degradation of corneodesmosomes and SC retention (Zettersten et al. 1998; see Oji et al. 2010a for a recent consensus overview of inherited defects of keratinization). Parakeratosis, a situation where non-degraded nuclei stay in the SC, results from imperfect keratinization and is most often due to epidermal hyperproliferation and inflammation. A typical example of such condition is psoriasis, where skin inflammatory reaction induces the epidermal response with prominent parakeratotic scale production and proinflammatory cytokine secretion, thus entertaining the disease's vicious circle (Krengel et al. 1998). Among the ichthyoses (non-bullous), congenital ichthyosiform erythroderma is also characterized by the presence of parakeratotic SC. Mutations of the transglutaminase-1 gene have been demonstrated in one of its clinical subsets (Huber et al. 1995). Here, leaky corneocytes and imperfectly organized SC promote reactive inflammation, epidermal hyperproliferation, and compensatory overproduction of the SC, still invalid but thicker. A localized loss of the SC (Kanitakis et al. 2010) or its diffuse shedding (Komatsu et al. 2006) constitutes another family of the anomalies of keratinization.

Epidermal response to the impaired barrier function of any origin is, most often, a compensatory increase in the SC thickness. Several and various causes are related to the structural fragility and/or increased permeability of the SC components. Here are some examples:

In various hereditary conditions, problems of epidermal differentiation may result from a deficient expression of one of the cell-cell junction proteins that is insufficiently compensated by similar members of the same family. Palmo-plantar keratoderma in Vohvinkel syndrome is linked to a deficient intercellular communication due to a particular mutation in the gene coding for connexin 26 (Maestrini et al. 1999), whereas erythrokeratodermia variabilis is caused by mutations in the genes of connexins 31 or 30.3 (Richard et al. 2003). The clinical manifestation of this ailment is thickening of the epidermis (acanthosis) with hyperkeratosis.

In the Ichthyosis, Hypotrychosis and Sclerosing Cholangitis (IHSC) syndrome, claudin-1 – deficient epidermis develops leaky tight junctions (Hadj-Rabia et al. 2004). In this case, ichthyosis appears to be due to the compensatory overexpression of tight junction -like structures in the SC (Haftek et al. 2013).

Mutations in genes coding for epidermal differentiation – associated keratins (K10, K1, K2e) lead to the mechanical fragility of the upper layers of keratinocytes in keratinopathic ichthyoses (epidermolytic types). Collapse of the keratinocyte cytoskeletons may provoke formation of superficial blisters; however, the typical tissue response is hyperkeratosis (Oji et al. 2010a; Osawa et al. 2011). In the Netherton's syndrome, it is the loss of intercorneocyte cohesion that underlies the appearance of festooned inflammatory and desquamating skin lesions. Premature corneodesmosome breakdown observed in this disease is caused by the absence of serine protease inhibitor LEKTI-1 encoded by Spink 5 gene (Chavanas et al. 2000). Clinical manifestations of peeling skin disease, provoked by the absence of corneodesmosin, concern exclusively the interface between the *stratum granulosum* and SC (Oji et al. 2010b). Cell-cell junctions lacking corneodesmosin are still present in the patients' SC and are protected by overexpressed tight junction – derived structures (Haftek et al. 2012). The resulting SC is quite resistant and functional. However, it can be easily peeled off as a whole sheet because the underlying desmosomes at the top of the living layers are fragile: not yet

consolidated by cross-linking to the cornified envelopes and not reinforced by the deficient corneodesmosin.

Permeability of the SC is largely dependent on its lipid content. Insufficient delivery of the intercellular lipids occurs in the skin of harlequin ichthyosis patients with a mutated ABCA12 lipid transporter gene (Akiyama et al. 2005). Retention of the lamellar granules results also in abnormally low levels of the extracellular proteolytic enzymes and, thus, decreased desquamation. Extensive hyperkeratosis occurs already *in utero* and, if the baby survives, evolves towards ichthyotic erythroderma (Haftek et al. 1996).

Imperfect lamellar lipid composition and, thus, deficient SC barrier function are encountered in patients with various dyslipidemias of dietary or metabolic origin (Elias et al. 2011). These clinical situations are also associated with abnormal keratinization.

Permeable cornified envelopes constitute another important factor influencing SC barrier function. Apart the previously mentioned case of transglutaminase 1 deficiency leading to non-bullous congenital ichthyotic erythroderma, mutations of genes coding various envelope components may result in a similar or related phenotype. Well-known examples include filaggrin mutations causing ichthyosis vulgaris and underlying some forms of atopic dermatitis (McLean and Irvine 2012) and Vohwinkel syndromic ichthyosis due to mutations in the loricrin gene (Schmuth et al. 2004).

6 Conclusion

SC formation is controlled by the underlying viable epidermal layers. Once secreted into the SC intercellular spaces, various components self-organize and interact in a highly ordered manner, in order to preserve the unique and functional architecture. Environmental conditions and pathological situations influence the structure and function of SC, resulting in compensatory responses. They lead, in vast majority of the cases, to the buildup of the SC barrier.

References

Akiyama M, Sugiyama-Nakagiri Y, Sakai K, McMillan JR, Goto M, Arita K, Tsuji-Abe Y, Tabata N, Matsuoka K, Sasaki R, Sawamura D, Shimizu H. Mutations in lipid transporter ABCA12 in harlequin ichthyosis and functional recovery by corrective gene transfer. J Clin Invest. 2005;115(7):1777–84.

Baker H, Blair CP. Cell replacement in the human stratum corneum in old age. Br J Dermatol. 1968;80:367–72.

Bouwstra JA, de Graaff A, Gooris GS, Nijsse J, Wiechers J, van Aelst AC. Water distribution and related morphology in human stratum corneum at different hydration levels. J Invest Dermatol. 2003a;120:750–8.

Bouwstra JA, Honeywell-Nguyen PL, Gooris GS, Ponec M. Structure of the skin barrier and its modulation by vesicular formulations. Prog Lipid Res. 2003b;42:1–36.

Candi E, Schmidt R, Melino G. The cornified envelope: a model of cell death in the skin. Nat Rev Mol Cell Biol. 2005;6:328–40.

Chapman SJ, Walsh A, Jackson SM, Friedmann PS. Lipids, proteins and corneocyte adhesion. Arch Dermatol Res. 1991;283:167–73.

Chavanas S, Bodemer C, Rochat A, Hamel-Teillac D, Ali M, Irvine AD, Bonafé JL, Wilkinson J, Taïeb A, Barrandon Y, Harper JI, de Prost Y, Hovnanian A. Mutations in SPINK5, encoding a serine protease inhibitor, cause Netherton syndrome. Nat Genet. 2000;25(2):141–2.

de Fine Olivarius F, Wulf HC, Crosby J, Norval M. The sunscreening effect of urocanic acid. Photodermatol Photoimmunol Photomed. 1996;12(3):95–9.

Denecker G, Ovaere P, Vandenabeele P, Declercq W. Caspase-14 reveals its secrets. J Cell Biol. 2008;180(3):451–8. doi:10.1083/jcb.200709098.

Eckhart L, Declercq W, Ban J, Rendl M, Lengauer B, Mayer C, Lippens S, Vandenabeele P, Tschachler E. Terminal differentiation of human keratinocytes and stratum corneum formation is associated with caspase-14 activation. J Invest Dermatol. 2000;115(6):1148–51.

Elias PM. Defensive functions of the stratum corneum: integrative aspects. In: Elias PM, Feingold KR, editors. Skin barrier. New York: Taylor & Francis; 2006. p. 5–14.

Elias PM, Menon GK. Structural and lipid biochemical correlates of the epidermal permeability barrier. Adv Lipid Res. 1991;24:1–26.

Elias PM, Fartasch M, Crumrine D, Behne M, Uchida Y, Holleran WM. Origin of the corneocyte lipid envelope (CLE): observations in harlequin ichthyosis and cultured human keratinocytes. J Invest Dermatol. 2000;115(4):765–9.

Elias PM, Ahn SK, Denda M, Brown BE, Crumrine D, Kimutai LK, Kömüves L, Lee SH, Feingold KR. Modulations in epidermal calcium regulate the expression of differentiation-specific markers. J Invest Dermatol. 2002;119(5):1128–36.

Elias PM, Crumrine D, Paller A, Rodriguez-Martin-M, Williams ML. Pathogenesis of the cutaneous phenotype in inherited disorders of cholesterol metabolism: therapeutic implications for topical treatment of these disorders. Dermatoendocrinology. 2011;3(2):100–6. doi:10.4161/derm.3.2.14831.

Grove G, Kligman A. Age-associated changes in human epidermal cell renewal. J Gerontol. 1983;38:137–42.

Hadj-Rabia S, Baala L, Vabres P, Hamel-Teillac D, Jacquemin E, Fabre M, Lyonnet S, De Prost Y, Munnich A, Hadchouel M, Smahi A. Claudin-1 gene mutations in neonatal sclerosing cholangitis associated with ichthyosis: a tight junction disease. Gastroenterology. 2004;127(5):1386–90. Erratum in: Gastroenterology. 2005;128(2):524.

Haftek M, Serre G, Mils V, Thivolet J. Immunocytochemical evidence for a possible role of cross-linked keratinocyte envelopes in stratum corneum cohesion. J Histochem Cytochem. 1991;39 (11):1531–8.

Haftek M, Cambazard F, Dhouailly D, Réano A, Lachaux A, Simon M, Serre G, Claudy A, Schmitt D. A longitudinal study of an harlequin infant evolving clinically towards non-bullous congenital ichthyotic erythroderma. Br J Dermatol. 1996;135: 448–53.

Haftek M, Simon M, Kanitakis J, Maréchal S, Claudy A, Serre G, Schmitt D. Expression of corneodesmosin in the granular layer and stratum corneum of normal and diseased epidermis. Br J Dermatol. 1997;137: 864–73.

Haftek M, Teillon MH, Schmitt D. Stratum corneum, corneodesmosomes and ex vivo percutaneous penetration. Microsc Res Tech. 1998;43(3):242–9. doi:10.1002/(SICI)1097029(19981101)43:3<242::AID-JEMT6>3.0.CO;2-G.

Haftek M, Simon M, Serre G. Corneodesmosomes: pivotal actors in the stratum corneum cohesion and desquamation. In: Elias PM, Feingold KR, editors. Skin barrier. New York: Taylor & Francis; 2006. p. 171–90.

Haftek M, Callejon S, Sandjeu Y, Padois K, Falson F, Pirot F, Portes P, Demarne F, Jannin V. Compartmentalization of the human stratum corneum by persistent tight junction -like structures. Exp Dermatol. 2011;20:617–21. doi:10.1111/j.1600-0625.2011.01315.x.

Haftek M, Callejon S, Pirot F, Traupe H, Oji V. Ultrastructural evaluation of the stratum corneum in peeling skin disease suggests a compensatory tight junction upregulation. J Invest Dermatol. 2012;132: S75–88. doi:10.1038/jid.2012.301 (abstract).

Haftek M, Abdayem R, Colomb E, Hadj-Rabia S. Tight junction (TJ)-like structures contribute to the compensatory hyperkeratosis in claudin-1 –deficient patient with Ichthyosis, Hypotrychosis and Sclerosing Cholangitis (IHSC) syndrome (Abstr.). J Invest Dermatol. 2013;134(4):1172–5.

Harding CR, Scott IR. Histidine-rich proteins (filaggrins). Structural and functional heterogeneity during epidermal differentiation. J Mol Biol. 1983;170:651–73.

Henry J, Hsu CY, Haftek M, Nachat R, de Koning HD, Gardinal-Galera I, Hitomi K, Balica S, Jean-Decoster C, Schmitt AM, Paul C, Serre G, Simon M. Hornerin is a component of the epidermal cornified cell envelopes. FASEB J. 2011;25(5):1567–76. doi:10.1096/fj.10-168658.

Hoath SB, Leahy DG. Formation and function of the stratum corneum. In: Marks R, editor. The essential stratum corneum. London: Martin Dunitz; 2002. p. 31–40.

Huber M, Rettler I, Bernasconi K, Frenk E, Lavrijsen SP, Ponec M, Bon A, Lautenschlager S, Schorderet DF, Hohl D. Mutations of keratinocyte transglutaminase in lamellar ichthyosis. Science. 1995;267 (5197):525–8.

Ishida-Yamamoto A, Deraison C, Bonnart C, Bitoun E, Robinson R, O'Brien TJ, Wakamatsu K, Ohtsubo S, Takahashi H, Hashimoto Y, Dopping-Hepenstal PJ, McGrath JA, Iizuka H, Richard G, Hovnanian A. LEKTI is localized in lamellar granules, separated from KLK5 and KLK7, and is secreted in the extracellular spaces of the superficial stratum granulosum. J Invest Dermatol. 2005;124(2):360–6.

Iwai I, Han H, den Hollander L, Svensson S, Ofverstedt LG, Anwar J, Brewer J, Bloksgaard M, Laloeuf A, Nosek D, Masich S, Bagatolli LA, Skoglund U, Norlén L. The human skin barrier is organized as stacked bilayers of fully extended ceramides with cholesterol molecules associated with the ceramide sphingoid moiety. J Invest Dermatol. 2012;132(9):2215–25. doi:10.1038/jid.2012.43.

Johannesson A, Hammar H. Measurement of the horny layer turnover after staining with dansyl chloride: description of a new method. Acta Derm Venereol. 1978;58:76–9.

Kalinin AE, Kajava AV, Steinert PM. Epithelial barrier function: assembly and structural features of the cornified cell envelope. Bioessays. 2002;24 (9):789–800.

Kamata Y, Taniguchi A, Yamamoto M, Nomura J, Ishihara K, Takahara H, Hibino T, Takeda A. Neutral cysteine protease bleomycin hydrolase is essential for the breakdown of deiminated filaggrin into amino acids. J Biol Chem. 2009;284(19):12829–36. doi:10.1074/jbc.M807908200.

Kanitakis J, Lora V, Chouvet B, Zambruno G, Haftek M, Faure M. Circumscribed palmo-plantar hypokeratosis: a disease of desquamation? Immunohistological study of five cases and literature review. J Eur Acad Dermatol Venereol. 2011;25(3):296–301. doi:10.1111/j.1468-3083.2010.03784.x.

Komatsu N, Suga Y, Saijoh K, Liu AC, Khan S, Mizuno Y, et al. Elevated human tissue kallikrein levels in the stratum corneum and serum of peeling skin syndrome-type B patients suggests an over-

desquamation of corneocytes. J Invest Dermatol. 2006; 126:2338–42.

Krengel S, Geilen CC, Orfanos CE, Schaumburg-Lever GM. Histopathology and electron microscopy of psoriasis. In: Roenigk HH, Maibach HI, editors. Psoriasis. New York: Marcel Dekker; 1998. p. 409–17.

Maestrini E, Korge BP, Ocana-Sierra J, Calzolari E, Cambiaghi S, Scudder PM, et al. A missense mutation in connexin26, D66H, causes mutilating keratoderma with sensorineural deafness (Vohwinkel's syndrome) in three unrelated families. Hum Mol Genet. 1999;8:1237–43.

Marekov LN, Steinert PM. Ceramides are bound to structural proteins of the human foreskin epidermal cornified cell envelope. J Biol Chem. 1998;273 (28):17763–70.

Markova NG, Marekov LN, Chipev CC, Gan SQ, Idler WW, Steinert PM. Profilaggrin is a major epidermal calcium-binding protein. Mol Cell Biol. 1993;13(1): 613–25.

McLean WH, Irvine AD. Heritable filaggrin disorders: the paradigm of atopic dermatitis. J Invest Dermatol. 2012;132(E1):E20–1. doi:10.1038/skinbio.2012.6.

Méchin MC, Coudane F, Adoue V, Arnaud J, Duplan H, Charveron M, Schmitt AM, Takahara H, Serre G, Simon M. Deimination is regulated at multiple levels including auto-deimination of peptidylarginine deiminases. Cell Mol Life Sci. 2010;67(9):1491–503. doi:10.1007/s00018-010-0262-5.

Menon GK, Price LF, Bommannan B, Elias PM, Feingold KR. Selective obliteration of the epidermal calcium gradient leads to enhanced lamellar body secretion. J Invest Dermatol. 1994;102(5):789–95.

Michel S, Schmidt R, Shroot B, Reichert U. Morphological and biochemical characterization of the cornified envelopes from human epidermal keratinocytes of different origin. J Invest Dermatol. 1988;91(1):11–5.

Mildner M, Jin J, Eckhart L, Kezic S, Gruber F, Barresi C, Stremnitzer C, Buchberger M, Mlitz V, Ballaun C, Sterniczky B, Födinger D, Tschachler E. Knockdown of filaggrin impairs diffusion barrier function and increases UV sensitivity in a human skin model. J Invest Dermatol. 2010;130(9):2286–94. doi:10.1038/jid.2010.115.

Nemes Z, Marekov LN, Fésüs L, Steinert PM. A novel function for transglutaminase 1: attachment of long-chain omega-hydroxyceramides to involucrin by ester bond formation. Proc Natl Acad Sci U S A. 1999;96 (15):8402–7.

Oji V, Tadini G, Akiyama M, Blanchet Bardon C, Bodemer C, Bourrat E, et al. Revised nomenclature and classification of inherited ichthyoses: results of the First Ichthyosis Consensus Conference in Sorèze. J Am Acad Dermatol. 2010a;63:607–41. doi:10.1016/j.jaad.2009.11.020.

Oji V, Eckl KM, Aufenvenne K, Nätebus M, Tarinski T, Ackermann K, Seller N, Metze D, Nürnberg G, Fölster-Holst R, Schäfer-Korting M, Hausser I, Traupe H, Hennies HC. Loss of corneodesmosin leads to severe skin barrier defect, pruritus, and atopy: unraveling the peeling skin disease. Am J Hum Genet. 2010b;87 (2):274–81. doi:10.1016/j.ajhg.2010.07.005.

Osawa R, Akiyama M, Izumi K, Ujiie H, Sakai K, Nemoto-Hasebe I, Yanagi T, Koizumi H, Shimizu H. Extremely severe palmoplantar hyperkeratosis in a generalized epidermolytic hyperkeratosis patient with a keratin 1 gene mutation. J Am Acad Dermatol. 2011;64(5):991–3. doi:10.1016/j.jaad.2009.04.019.

Proksch E, Holleran WM, Menon GK, Elias PM, Feingold KR. Barrier function regulates epidermal lipid and DNA synthesis. Br J Dermatol. 1993;128(5):473–82.

Rassner U, Feingold KR, Crumrine DA, Elias PM. Coordinate assembly of lipids and enzyme proteins into epidermal lamellar bodies. Tissue Cell. 1999;31(5):489–98.

Rawlings AV, Harding CR. Moisturization and skin barrier function. Dermatol Ther. 2004;17 Suppl 1:43–8.

Richard G, Brown N, Rouan F, Van der Schroeff JG, Bijlsma E, Eichenfield LF, et al. Genetic heterogeneity in erythrokeratodermia variabilis: novel mutations in the connexin gene GJB4 (Cx30.3) and genotype-phenotype correlations. J Invest Dermatol. 2003;120:601–9.

Richter T, Peuckert C, Sattler M, Koenig K, Riemann I, Hintze U, Wittern KP, Wiesendanger R, Wepf R. Dead but highly dynamic – the stratum corneum is divided into three hydration zones. Skin Pharmacol Physiol. 2004;17(5):246–57.

Schmuth M, Fluhr JW, Crumrine DC, Uchida Y, Hachem JP, Behne M, Moskowitz DG, Christiano AM, Feingold KR, Elias PM. Structural and functional consequences of loricrin mutations in human loricrin keratoderma (Vohwinkel syndrome with ichthyosis). J Invest Dermatol. 2004;122(4):909–22.

Serre G, Mils V, Haftek M, Vincent C, Croute F, Réano A, Ouhayoun JP, Bettinger S, Soleilhavoup JP. Identification of late differentiation antigens of human cornified epithelia, expressed in re-organized desmosomes and bound to cross-linked envelope. J Invest Dermatol. 1991;97(6):1061–72.

Simon M, Haftek M, Sebbag M, Montézin M, Girbal-Neuhauser E, Schmitt D, Serre G. Evidence that filaggrin is a component of cornified cell envelopes in human plantar epidermis. Biochem J. 1996;317 (Pt 1):173–7.

Simon M, Bernard D, Minondo AM, Camus C, Fiat F, Corcuff P, Schmidt R, Serre G. Persistence of both peripheral and non-peripheral corneodesmosomes in the upper stratum corneum of winter xerosis skin versus only peripheral in normal skin. J Invest Dermatol. 2001;116(1):23–30. doi:10.1046/j.1523-1747.2001.00208.x.

Steinert PM, Marekov LN. Initiation of assembly of the cell envelope barrier structure of stratified squamous epithelia. Mol Biol Cell. 1999;10(12):4247–61.

Voegli R, Rawlings AV. Desquamation: it is almost all about proteases. In: Lodén M, Maibach HI, editors. Treatment of dry skin syndrome. Berlin: Springer-Verlag; 2012. p. 149–78. doi:10.1007/978-3-642-27606-4_11.

Wertz PW, Swartzendruber DC, Kitko DJ, Madison KC, Downing DT. The role of the corneocyte lipid envelopes in cohesion of the stratum corneum. J Invest Dermatol. 1989;93:169–72.

Zettersten E, Man MQ, Sato J, Denda M, Farrell A, Ghadially R, Williams ML, Feingold KR, Elias PM. Recessive X-linked ichthyosis: role of cholesterol-sulfate accumulation in the barrier abnormality. J Invest Dermatol. 1998;111:784–90.

Molecular Organization of the Skin Barrier

24

Lars Norlén

Contents

Keywords

Cryo-electron microscopy of vitreous tissue section (CEMOVIS) • Skin • Lipid composition • Skin barrier • Molecular arrangement • Research • Skin lipid • Function • Structure

1 Introduction

The basic function of skin is to constitute a waterproof barrier between the body and the environment. In human, like in other land-living higher vertebrates, this barrier is essentially composed of uniquely organized lipids situated in the skin's horny layer.

The lack of knowledge about the molecular organization of the horny layer's lipid material has limited our understanding of the skin both in healthy and disease states. However, a recent breakthrough has come from the use of very high magnification cryo-electron microscopy of vitreous skin section (CEMOVIS) combined with electron microscopy (EM) simulation. This has allowed for molecular structure determination of the lipid material directly in situ and in its *near native state* (Iwai et al. 2012). The lipid material is organized in an arrangement not previously described in a biological system – stacked bilayers of fully extended ceramides with cholesterol molecules associated with the ceramide sphingoid moiety (Iwai et al. 2012).

L. Norlén (✉)
Department of Cell and Molecular Biology (CMB), Karolinska Institutet, and Dermatology Clinic, Karolinska University Hospital, Stockholm, Sweden
e-mail: lars.norlen@ki.se

P. Humbert et al. (eds.), *Agache's Measuring the Skin*,
DOI 10.1007/978-3-319-32383-1_24

Fig. 1 Historical time-line of skin barrier research (Adapted from Norlén (2013), with permission)

Below follows a brief account of current knowledge about the molecular organization of the horny layer's lipid material.

2 Brief History of Skin Barrier Research

Ever since it became clear that the skin's barrier function essentially is located to the epidermis (Homolle 1853; Duriau 1856), the molecular structure and function of the skin barrier have intrigued researchers (Fig. 1).

By sandpapering the skin surface, Winsor and Burch (1944) showed in the 1940s that the skin's barrier actually resides in the epidermal horny layer. In the 1950s–1960s, Berenson and Burch (Burch and Berenson 1951) and Onken and Moyer (1963) showed that horny layer impermeability essentially was a function of its lipid content. Brody (1966) then managed to locate the horny layer lipids to the extracellular space.

The first electron microscopy visualizations of the lipid material's stacked lamellar morphology came with Breathnach et al. (1973) and Elias and Friend (1975) in the early 1970s.

In the 1980s, the lipid material's basic composition was determined. A heterogeneous mixture of saturated, long-chain ceramides, free fatty acids, and cholesterol in a roughly 1:1:1 molar ratio (Wertz and Downing 1983; Wertz et al. 1987, 2003). Another important step was the introduction of ruthenium tetroxide staining, which revealed the lipid material's characteristic broad:narrow:broad electron lucent band staining pattern (Madison et al. 1987).

Soon afterwards, using small-angle X-ray diffraction on isolated horny layer, White et al. (1988), Garson et al. (1991), and Bouwstra et al. (1991) reported the presence of one shorter (ca 4.5 nm) and one longer (ca 6.5 nm) diffraction peak related to lipids. Also, McIntosh 2003) observed an asymmetric distribution of cholesterol molecules within model systems composed of extracted horny layer lipids.

In the early 1990s, the importance of the lipid material's phase state for its barrier properties began to be stressed (Forslind 1994). In 2001, Norlén proposed that the lipid material exists as a single and coherent gel phase (Norlén 2001), which was later supported by the experimental work of Iwai et al. (2012).

In 2012, Iwai et al. showed that the horny layer's lipid material is organized as stacked bilayers of fully extended ceramides with cholesterol molecules associated with the ceramide sphingoid moiety (Figs. 2 and 3; Iwai et al. 2012).

3 Skin Lipid Composition and Phase State

The most characteristic features of the lipid composition (Wertz et al. 2003) are (i) extensive compositional heterogeneity with broad, but invariable, chain length distributions (20–32C; peaking at 24C) in the ceramide fatty acid and free fatty acid fractions, (ii) almost complete dominance of saturated very long hydrocarbon chains (C20:0–C32:0), and (iii) large relative amounts of cholesterol (about 30 mol%).

These are the same as the factors that typically stabilize lipid gel phases. It was therefore proposed that the horny layer's lipid material exists as a single and coherent gel phase (Norlén 2001). The viscous gel-like behavior of the lipid material was recently demonstrated experimentally by its remarkable malleability in situ (Fig. 4; Iwai et al. 2012).

4 Molecular Structure Determination Directly In Situ

Cryo-electron microscopy of vitreous tissue section (CEMOVIS) yields high-resolution images of the horny layer's lipid material in situ and in its *near native state*. When combined with molecular modeling and electron microscopy (EM) simulation, CEMOVIS has proved to be remarkably effective in identifying the molecular organization of the horny layer lipids (Iwai et al. 2012).

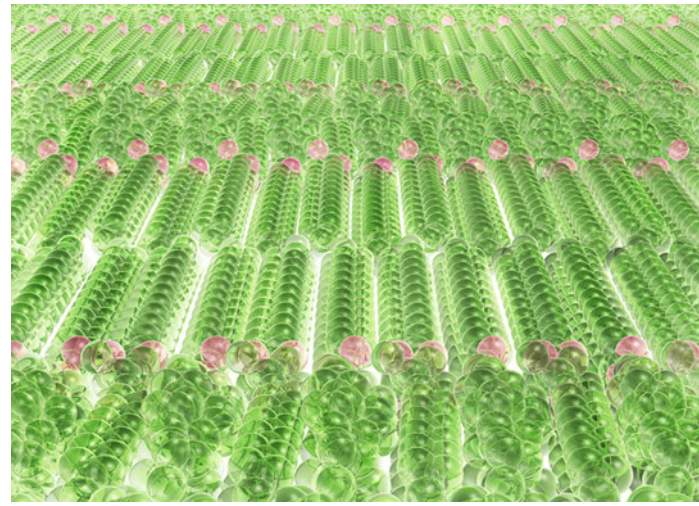

Fig. 2 Molecular arrangement of the skin barrier. The horny layer's lipid material is organized as stacked bilayers of fully extended ceramides with cholesterol molecules associated with the ceramide sphingoid moiety (Iwai et al. 2012). *Green spheres* represent hydrogen and carbon atoms in ceramides, cholesterol, and free fatty acids. *Red spheres* represent oxygen atoms (Adapted from Norlén (2013), with permission)

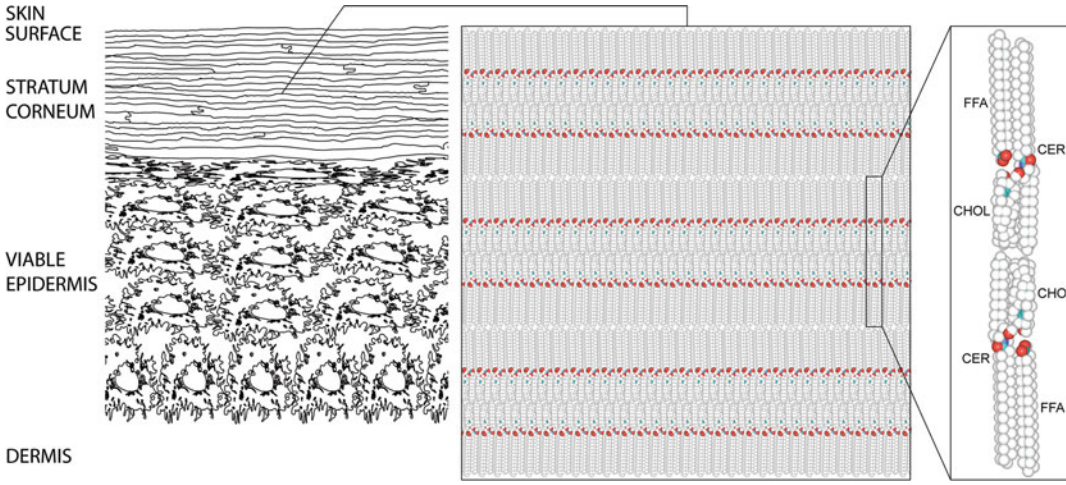

Fig. 3 Schematic drawing of skin. *Left part*: schematic cellular-scale drawing of epidermis. *Midpart*: molecular-scale drawing of the lamellar lipid material occupying the space between the cells of the horny layer. *Right part*: atomic model of the lipid material's repeating unit, composed of two mirrored subunits, each composed of one fully extended ceramide (*CER*) molecule, one cholesterol (*CHOL*) molecule, and one free fatty acid (*FFA*) molecule (Adapted from Norlén (2012), with permission)

The CEMOVIS-based structure determination procedure involves four stages (Norlén et al. 2013): cryo-electron microscopy of vitreous skin section (CEMOVIS) to yield high-resolution (∼1 nm) images of the lipid material (Fig. 5), construction of candidate molecular models for the lipid material (Fig. 6), simulation of electron micrographs resulting from the proposed molecular models (Fig. 6), and confrontation of the simulated micrographs with those observed experimentally to identify a molecular organization that is consistent with the observed CEMOVIS data (Fig. 7).

For a detailed description of the experimental procedure, see Norlén et al. (2013).

5 Skin Lipid Structure

The lipid organization that emerged from the high-resolution CEMOVIS data analysis of the horny layer's lipid material is a bilayer

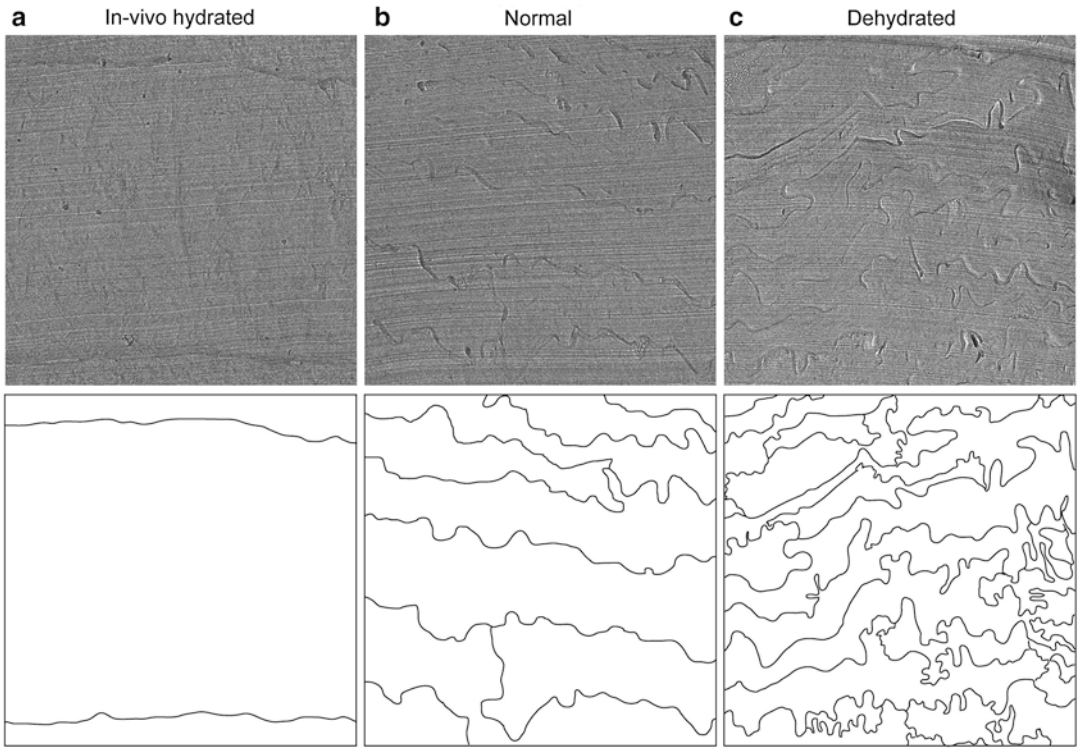

Fig. 4 The horny layer's lipid material is, despite its crystalline-like character, malleable. The horny layer's extracellular lipid material is folded locally. The folding decreases on hydration and increases on dehydration. Low magnification CEMOVIS micrographs of the horny layer after hydration in vivo (**a**), at normal in vivo conditions (**b**), and after hydration in vivo followed by dehydration ex vivo (**c**). The *lower panel* illustrates the folded pattern of the extracellular space. Image side lengths: 5 μm (Adapted from Iwai et al. (2012) (online supplementary material), with permission)

structure of fully extended (splayed chain) ceramides with the sphingoid moieties interfacing. Both cholesterol and the free fatty acid are distributed selectively: cholesterol at the ceramide sphingoid end and the free fatty acid at the ceramide fatty acid end (Iwai et al. 2012; Figs. 2 and 3).

6 Skin Lipid Function

A stacked, fully extended (splayed chain) ceramide bilayer arrangement (Figs. 2 and 3) with high cholesterol content (~30 mol%) and a highly heterogeneous but characteristic, lipid composition of saturated, long-chain ceramides and free fatty acids may represent an ideal barrier material for skin. This is because it may be largely impermeable to water as well as to both hydrophilic and lipophilic substances, because of its condensed chain packing and its alternating lipophilic (alkyl chain) and hydrophilic (headgroup) regions. Likewise, it may be resistant to both hydration and dehydration because of its lack of exchangeable water between lipid leaflets. It may also be resistant towards other kinds of environmental stress, such as temperature and pressure changes, because of its heterogeneous lipid composition and high cholesterol content, which stabilize gel-like chain packing and thereby prevent both lateral domain formation and induction of "pores" or nonlamellar morphologies. Further, this bilayer arrangement

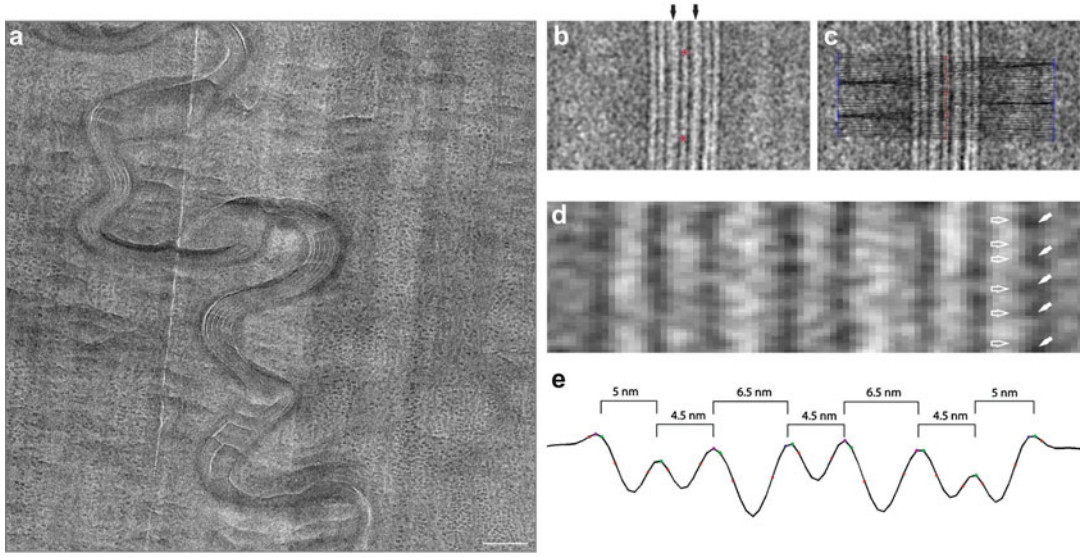

Fig. 5 The CEMOVIS intensity pattern of the horny layer's extracellular lipid material consists of folded stacked layers. (**a**) Medium magnification CEMOVIS micrograph of the interface between two cells in the midpart of the horny layer. Note that in CEMOVIS the tissue is unstained and that the pixel intensity is directly related to the local electron density of the sample. The stacked lamellar pattern represents the extracellular lipid material. Dark ~10 nm dots represent keratin intermediate filaments filling out the intracellular space. (**b**) High-magnification CEMOVIS micrograph of the extracellular space in the midpart of the horny layer. The averaged intensity profile of the lipid material was obtained by fuzzy distance-based image analysis. The *red stars* in (**b**) represent the manually chosen start and end points for fuzzy distance based path growing. (**c**) The *red line* represents the traced out path. *Stacked lines* mark extracted intensity profiles. (**d**) Enlarged area of the central part of (**b**). (**e**) Reversed averaged pixel intensity profile obtained from the extracted area in (**c**). Peaks in (**e**) correspond to dark bands and valleys to lucent bands in (**d**). *Black arrows* in (**b**) denote electron lucent narrow bands at the center of the 6.5 nm bands. Section thickness ~50 nm (**a**–**d**). Scale bar (**a**): 100 nm. Pixel size in (**a**–**d**): 6.02 Å (Adapted from Iwai et al. (2012), with permission)

may account for horny layer cell cohesion without advocating specialized intercellular adhesion structures such as desmosomes. The absence of desmosomes in the horny layer (above the fourth to fifth layers) may hence allow for sliding of horny layer cells to accommodate skin bending. Finally, as the interaction between the individual layers of the lipid material involves only hydrocarbons, the layers may be relatively free to slide with respect to one another, making the lipid material pliable. The fully extended ceramide bilayer arrangement, with high cholesterol content and heterogeneous saturated long-chain lipid composition, may thus meet the barrier needs of skin by being simultaneously impermeable and robust (Iwai et al. 2012).

7 Future Perspective

The elucidation of the basic molecular organization of the skin lipids is a first step towards building a complete molecular model for the stratum corneum that also includes the corneocytes. Outstanding questions in this respect are the nature of the molecular-level structure of the corneocyte keratin filament network and the interfacial corneocyte cell envelope. The potential application and further development of the combined approach of cryo-electron microscopy coupled with simulation is presently explored to elucidate the molecular organization of these remaining stratum corneum key components (Norlén et al. 2013; Figs. 8, 9, and 10).

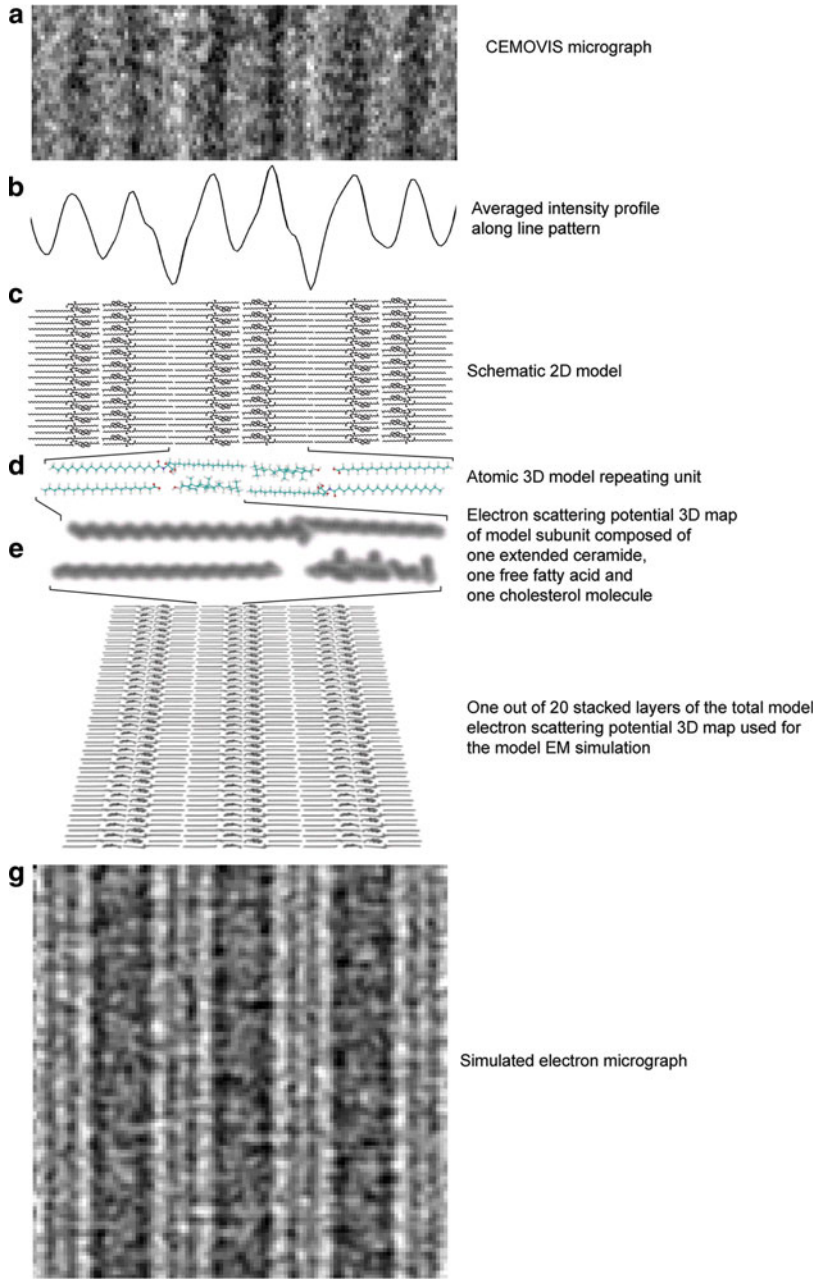

Fig. 6 Electron microscopy simulation of the horny layer's extracellular lipid material. (**a**) High-magnification CEMOVIS micrograph of the extracellular space in the midpart of the horny layer. (**b**) Corresponding averaged intensity profile obtained by fuzzy distance-based path growing. (**c**) Schematic 2D illustration of ceramides (tetracosanylphytosphingosine (C24:0)) in fully extended conformation with cholesterol associated with the ceramide sphingoid part and free fatty acids (lignoceric acid (C24:0)) associated with the ceramide fatty acid part. (**d**) Atomic 3D model of the repeating unit composed of two mirrored subunits, each composed of one fully extended ceramide molecule, one cholesterol molecule, and one free fatty acid molecule. (**e**) Calculated electron scattering potential of one model subunit. (**f**) Calculated electron scattering potential 3D maps of the topmost layer out of 20 superimposed layers used to generate the simulated electron micrograph (**g**). Defocus (**a**, **g**): −2.5 μm. Pixel size in (**a**, **g**): 3.31 Å (Adapted from Iwai et al. (2012), with permission)

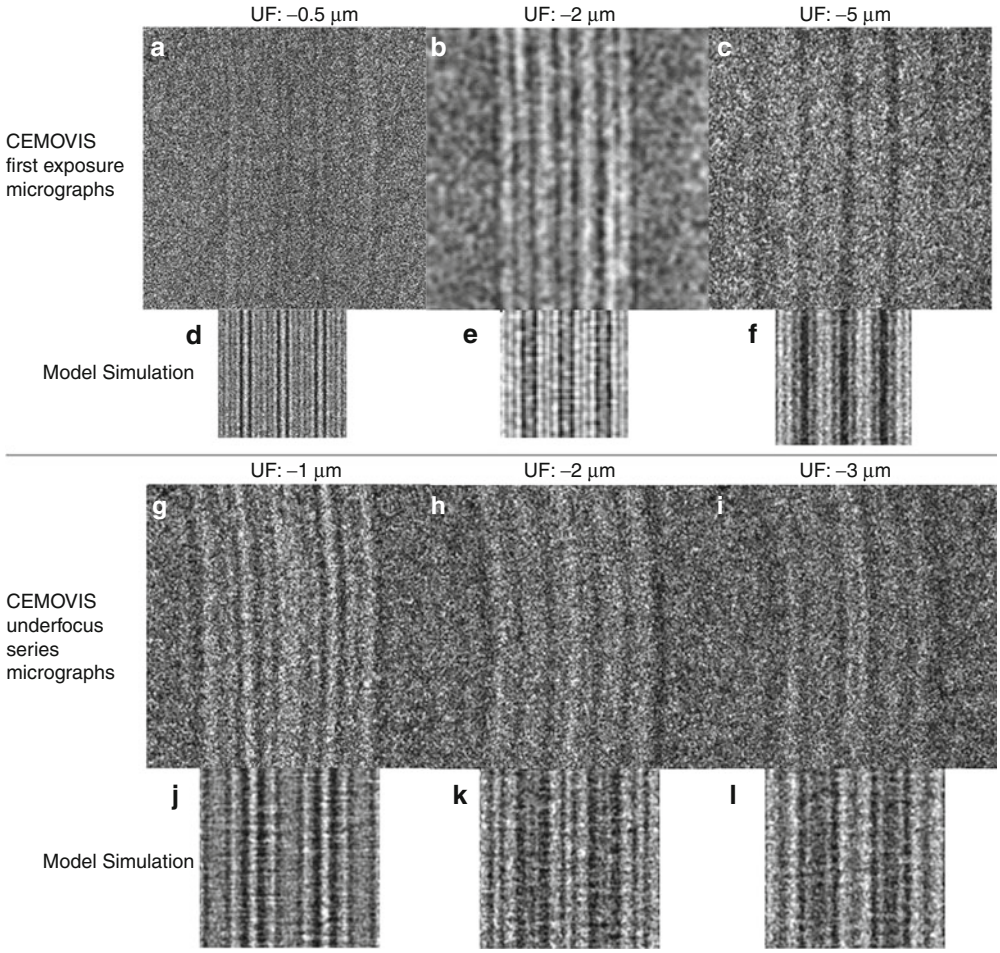

Fig. 7 Electron microscopy simulation of alternating fully extended ceramides with selective localization of cholesterol to the ceramide sphingoid part accurately accounts for the observed CEMOVIS intensity patterns as well as for the interference pattern changes observed in sequential CEMOVIS micrograph defocus-series obtained at very high magnification (≤1.88 Å pixel size). (**a**–**c**) High-magnification CEMOVIS micrographs (first exposition images) of the extracellular space in the midpart of the horny layer obtained at −0.5 µm (**a**), −2 µm (**b**), and −5 µm (**c**) defocus. At very low defocuses (−0.5 µm), (**a**) CEMOVIS intensity patterns can only be observed at very high magnification (≤1.88 Å pixel size). At very high defocuses (−5 µm), (**c**) image resolution is low but still allows for resolution of the ~11 nm repeating unit. The slightly larger lamellar repeat distance in (**b**) (~12 nm) compared to (**a**) and (**c**) (~11 nm) may be due to more pronounced compression of the vitreous skin section during cryo-sectioning along the lamellar plane in (**b**) compared to (**a**) and (**c**). (**d**–**f**) represents corresponding atomic 3D model (cf. Fig. 3 right part; Fig. 6d) electron microscopy simulation images recorded at −0.5 µm (**d**), −2 µm (**e**) and −5 µm (**f**) defocus. (**g**–**i**) Sequential CEMOVIS micrograph defocus-series obtained at very high magnification (1.88 Å pixel size). Note the fine changes in interference patterns caused by gradually increasing the microscope's defocus during repeated image acquisition at a fixed position. Due to electron beam damage after repeated electron exposure, the image contrast is lower in micrographs (**h**–**i**) compared to micrograph (**g**), which was acquired first. In micrograph (**i**) some shrinkage can be observed. This is probably due to mass loss during repeated electron exposure. Also, the curvature of the lamellar pattern is slightly increased in micrographs (**h**–**i**) compared to micrograph (**g**), which likewise may be caused by nonhomogeneous mass loss during repeated electron exposure. (**j**–**l**) represents corresponding atomic 3D model (cf. Fig. 3 right part; Fig. 6d) electron microscopy simulation images recorded at −1 µm (**j**), −2 µm (**k**), and −3 µm (**l**) defocus. It is shown that the atomic 3D model in Fig. 5 accurately accounts not only for the major features of the CEMOVIS micrographs (**a**–**f**) but also for the interference intensity pattern changes observed upon varying the microscope's defocus during image acquisition at very high magnification (**g**–**l**). Pixel size in (**c**, **f**): 3.31 Å, in (**b**, **e**): 6.02 Å, and in (**a**, **d** and **g**–**l**): 1.88 Å (Adapted from Iwai et al. (2012), with permission)

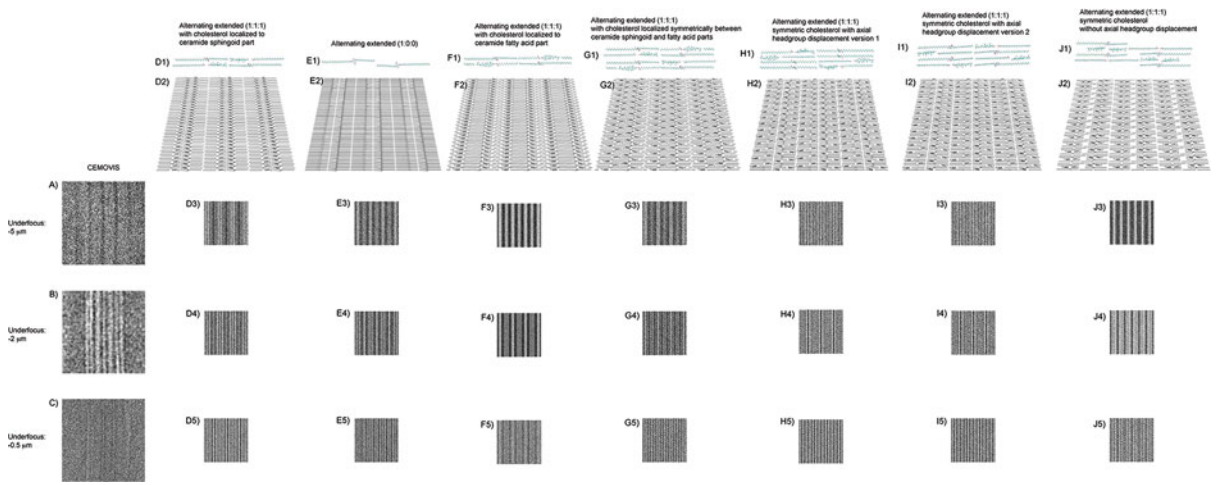

Fig. 8 Electron microscopy simulation results from seven fully extended ceramide bilayer models with varying cholesterol distribution. (**a**–**c**) CEMOVIS micrographs of the horny layer's extracellular lipid material acquired at −5 µm (**a**), −2 µm (**b**), and −0.5 µm (**c**) defocus. (*D3–J5*) Corresponding simulated electron micrographs obtained from seven fully extended ceramide models. (*D1–J1*) Repeating units for each simulated model. (*D2–J2*) Calculated electron scattering potential 3D maps of the topmost layer out of 20 superimposed layers used to generate each individual simulated micrograph (*D3–J5*). In model (**d**), cholesterol is selectively localized to the ceramide sphingoid part. In model (**e**), cholesterol has been removed to evaluate whether the simulation method could discriminate the presence (**d**) or absence (**e**) of cholesterol. In model (**f**), cholesterol is selectively localized to the ceramide fatty acid part. In models (**g**–**j**), cholesterol is homogenously distributed between the ceramide sphingoid and fatty acid parts. Contrary to models (**g**, **j**), models (**h**, **i**) express axial headgroup displacement of cholesterol and free fatty acids. Models (**h**, **i**) differ in that model (**h**) expresses a pairwise lateral distribution of ceramides while model (**i**) expresses a homogeneous lateral distribution of ceramides. Note that except for the position of the lipid headgroups, the localization of cholesterol within the fully extended ceramide structure largely determines the electron scattering properties of the models (Adapted from Iwai et al. (2012) (online supplementary material), with permission)

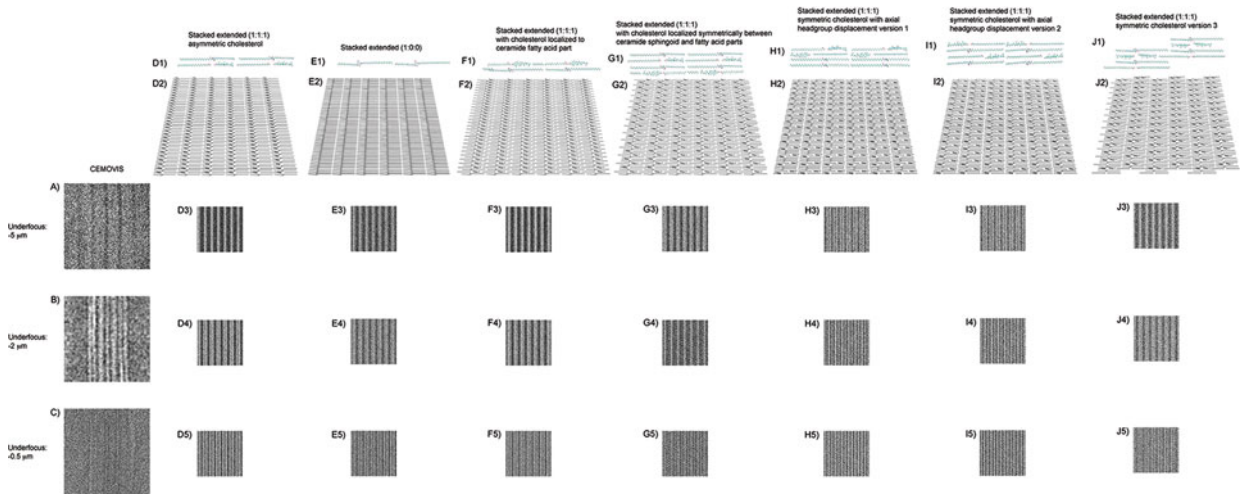

Fig. 9 Electron microscopy simulation results from seven fully extended ceramide stacked monolayer models with varying cholesterol distribution. (**a**–**c**) CEMOVIS micrographs of the horny layer's extracellular lipid material acquired at −5 µm (**a**), −2 µm (**b**), and −0.5 µm (**c**) defocus. (*D3–J5*) Corresponding simulated electron micrographs obtained from seven stacked fully extended ceramide models. (*D1–J1*) Two repeating units for each simulated model. (*D2–J2*) Calculated electron scattering potential 3D maps of the topmost layer out of 20 superimposed layers used to generate each individual simulated micrograph (*D3–J5*). In model (d), cholesterol is selectively localized to the ceramide sphingoid part. In model (**e**), cholesterol has been removed to evaluate whether the simulation method could discriminate the presence (**d**) or absence (**e**) of cholesterol. In model (**f**), cholesterol is selectively localized to the ceramide fatty acid part. In models (**g**–**j**), cholesterol is distributed homogenously between the ceramide sphingoid and fatty acid parts. Contrary to models (**g**, **j**), models (**h**, **i**) express axial headgroup displacement of cholesterol and free fatty acids. Models (**h**, **i**) differ in that model (**h**) expresses a pairwise lateral distribution of ceramides, while model (**i**) expresses a homogeneous lateral distribution of ceramides. Note that except for the position of the lipid headgroups, the localization of cholesterol within the fully extended ceramide structure largely determines the electron scattering properties of the models (Adapted from Iwai et al. (2012) (online supplementary material), with permission)

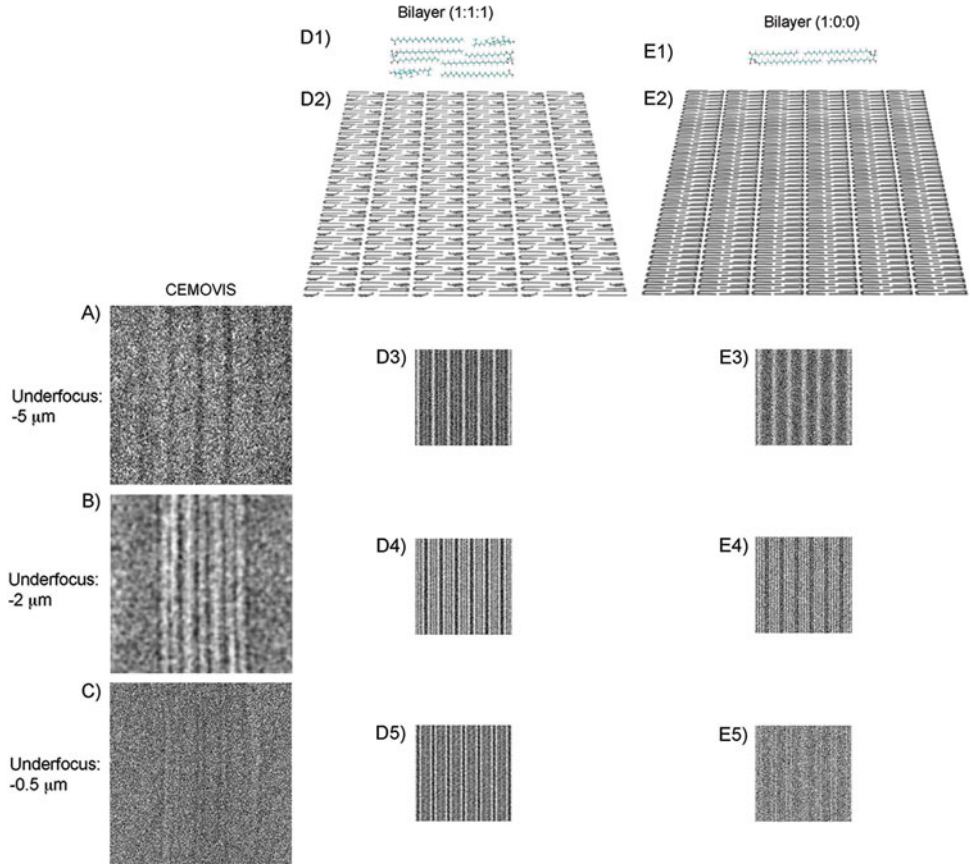

Fig. 10 Electron microscopy simulation results from two-folded ceramide bilayer models with and without the presence of cholesterol. (**a**–**c**) CEMOVIS micrographs of the horny layer's extracellular lipid material acquired at −5 μm (**a**), −2 μm (**b**), and −0.5 μm (**c**) defocus. (*D3–E5*) Corresponding simulated electron micrographs obtained from two-folded ceramide models. (*D1–E1*) Repeating units for each simulated model. (*D2–E2*) Calculated electron scattering potential 3D maps of the topmost layer out of 20 superimposed layers used to generate each individual simulated micrograph (*D3–E5*). In model (**d**), cholesterol is present. In model (**e**), cholesterol has been removed to ascertain if the simulation method could distinguish the presence (**d**) or absence (**e**) of cholesterol. Note that the presence of cholesterol within the folded ceramide structure largely determines the electron scattering properties of the models (Adapted from Iwai et al. (2012) (online supplementary material), with permission)

8 Summary

The skin barrier is essentially constituted by a uniquely organized lipid material situated between the cells of the horny layer of skin. This lipid material is organized as stacked bilayers of fully extended ceramides.

The physical state of the skin's lipid material is gel like.

The skin's lipid material is responsible for both the skin barrier's low permeability and its robustness towards environmental stress.

References

Bouwstra JA, Gooris GS, Van der Spek JA, Bras W. Structural investigations of human stratum corneum by small-angle X-ray scattering. J Invest Dermatol. 1991;97:1005–12.

Breathnach AS, Goodman T, Stolinski C, Gross M. Freeze fracture replication of cells of stratum corneum of human epidermis. J Anat. 1973;114:65–81.

Brody I. Intercellular space in normal human stratum corneum. Nature. 1966;209:472–6.

Burch GS, Berenson GE. Studies of diffusion of water through dead human skin: the effect of different environmental states and of chemical alterations of the epidermis. Am J Trop Med. 1951;31:842–53.

Duriau F. Recherches expérimentales sur l'absorption et l'exhalation par le tégument externe. Arch Gen Med T. 1856;7:161–73.

Elias PM, Friend DS. The permeability barrier in mammalian epidermis. J Cell Biol. 1975;65:180–91.

Forslind B. A domain mosaic model of the skin barrier. Acta Derm Venereol (Stockh). 1994;74:1–6.

Garson JC, Doucet J, Leveque J-L, Tsoucaris G. Oriented structure in human stratum corneum revealed by X-ray diffraction. J Invest Dermatol. 1991;96:43–9.

Homolle A. Expériences physiologiques sur l'absorption par la tégument externe chez l'homme dans le bain. Union Med. 1853;7:462.

Iwai I, Han H, den Hollander L, Svensson S, Öfverstedt L-G, Anwar J, Brewer J, Bloksgaard Mølgaard M, Laloeuf A, Nosek D, Masich S, Bagatolli L, Skoglund U, Norlén L. The human skin barrier is organized as stacked bilayers of fully-extended ceramides with cholesterol molecules associated with the ceramide sphingoid moiety. J Invest Dermatol. 2012;132:2215–25.

Madison KC, Swartzendruber DC, Wertz PW, Downing DT. Presence of intact intercellular lamellae in the upper layers of the stratum corneum. J Invest Dermatol. 1987;88:714–8.

McIntosh TJ. Organization of skin stratum corneum extracellular lamellae: diffraction evidence for asymmetric distribution of cholesterol. Biophys J. 2003;85:1675–81.

Norlén L. Skin barrier structure and function: the single gel-phase model. J Invest Dermatol. 2001;117(4):830–6.

Norlén L. Skin lipids. In: Roberts GCK, editor. Encyclopedia of biophysics. Springer; 2012.

Norlén L. Current understanding of skin barrier morphology. Skin Pharm Phys. 2013;26:213–6.

Norlén L, Anwar J, Öktem O. Chapter 10. Accessing the molecular organization of the stratum corneum using high resolution electron microscopy and computer simulation. In: Querleux B, editor. Computational biophysics of the skin. Pan Stanford Publishing; 2013. In press.

Onken HD, Moyer CA. The water barrier in human epidermis. Arch Dermatol. 1963;87:584–90.

Wertz PW, Downing DT. Ceramides of pig epidermis: structure determination. J Lipid Res. 1983;24:759–65.

Wertz PW, Swartzendruber DC, Madison KC, Downing DT. Composition and morphology of epidermal cyst lipids. J Invest Dermatol. 1987;89:419–24.

Wertz P, Norlén L. "Confidence Intervals" for the "true"lipid compositions of the human skin barrier? In: Forslind B, Lindberg M, editors. Skin, hair, and nails. Structure and function. Marcel Dekker; 2003. pp 85–106. Biochim Biophys Acta 304:265–275.

White SH, Mirejovsky D, King GI. Structure of lamellar lipid domains and corneocyte envelopes of murine stratum corneum. An x-ray diffraction study. Biochemsitry. 1988;27:3725–32.

Winsor T, Burch GE. Differential roles of layers of human epigastric skin on diffusion of water. Arch Intern Med. 1944;74:428–44.

Stratum Corneum Desquamation

25

Gérald E. Piérard, Trinh Hermanns-Lê, and Claudine Piérard-Franchimont

Contents

Keywords

Stratum corneum • Corneocyte • Corneodesmosome • Xerosis • Scaling • Squamometry

Abbreviations

ACD	Adhesive-coated disk
CSSS	Cyanoacrylate skin surface stripping
DC	Dansyl chloride
DHA	Dihydroxyacetone
ETT	Epidermal turnover time
NMF	Natural moisturizing factor
SC	Stratum corneum
SCMI	Skin capacitance mapping/imaging

1 Introduction

The epidermis is the continuous stratified squamous epithelium covering the skin. Both the physiologic cohesion and exfoliation are balanced functions of the stratum corneum (SC) integrity (Mohammed et al. 2011). Corneocyte desquamation is a complex multistep process that is globally related to the long-term keratinocyte renewal, but disconnected from the epidermal maturation (Piérard et al. 2000; Chu and Kollias 2011; Ishida-Yamamoto et al. 2011; Lin et al. 2012). By a matter of fact, the imperceptibly corneocyte casting off from the skin surface can be properly

G.E. Piérard (✉)
Laboratory of Skin Bioengineering and Imaging (LABIC), Liège University, Liège, Belgium

Service de Dermatopathologie, CHU du Sart Tilman, Liège, Belgium
e-mail: Gerald.pierard@ulg.ac.be

T. Hermanns-Lê
Laboratory of Skin Bioengineering and Imaging (LABIC), Liège University, Liège, Belgium

Service de Dermatopathologie, CHU du Sart Tilman, Liège, Belgium

Department of Dermatopathology, Unilab Lg, University Hospital of Liège, Liège, Belgium
e-mail: Trinh.hermanns@chu.ulg.ac.be; Trinh.le@ulg.ac.be

C. Piérard-Franchimont
Laboratory of Skin Bioengineering and Imaging (LABIC), Department of Clinical Sciences, Liège University, Liège, Belgium
e-mail: Claudine.franchimont@ulg.ac.be

P. Humbert et al. (eds.), *Agache's Measuring the Skin*,
DOI 10.1007/978-3-319-32383-1_25

appreciated only after considering the whole physiology of keratinocytes. In addition, it is essential to consider the molecular structures involved in the regular corneocyte adhesion and cohesion in order to perceive the intercellular binding defects present in the rough/dry skin condition, xerosis, and ichthyoses. Indeed, the SC is not simply an assembly of dead cells, but it represents a dynamic and metabolically interactive tissue.

Cell surface glycoproteins, specialized intercellular junctions such as (corneo)-desmosomes, focal adherens contacts, tight junctions, gap junctions, and keratinosomes play major roles in keratinocyte communications and adhesion (Haftek et al. 2011; Igawa et al. 2011). Desmosomes represent specific cell membrane contacts between adjacent keratinocytes forming well-circumscribed symmetrical intercellular junctions exhibiting specific ultrastructural features. They correspond to electron-dense plaques apposed along the cell membrane. They are composed of three parallel bands. The inner fibrillar band is the area where intracellular keratin filaments loop. Traversing filaments extend between intermediate filaments and globular structures located in the cell membrane. The intercellular space encased between the desmosomal plaques is about 30 nm thick and is centered by a dense line.

Plaque components were identified as desmoplakin I in simple epithelia, desmoplakin II in squamous epithelia, desmoplakin III or plakoglobin, desmoplakin IV in stratified epithelia, and desmocalmin which is a calmodulin-binding protein and D1 antigen. Desmoplakins are related to the cadherin family. Desmoglein and desmocollins I and II are transmembrane glycoproteins present in the intercellular area inside desmosomes.

The number of desmosomes globally increases with the maturation of the stratum spinosum. During the upward migration of keratinocytes, desmosomes are subject to endocytosis and are degraded inside the cells. Formation of new desmosomes probably occurs where cells are pushed in close contact to each other. During epidermal cornification in humans, desmosomal structures become asymmetrical. At the level of the first layer of corneocytes, plasma membrane thickening occurs in areas outside desmosomes. In upper layers, the characteristic trilaminar structure of desmosomes is altered into an electron-dense plug referred to as corneodesmosome. Strength of corneocyte attachment correlates with the number and distribution of corneodesmosomes. These structures are evenly distributed in the deep SC compactum and only present to corneocyte edges in the uppermost SC disjunctum. Intercorneocyte adhesion has a tongue-and-groove appearance with corneodesmosomes riveting corneocyte peripheries into a lipped groove on adjoining cells.

2 Disorders of Cornification and of Intercorneocyte Cohesion

As described above, the molecular structure of the normal SC is complex. Therefore, a broad scope of defects commonly underlies a variety of scaling disorders. Changes in the SC cohesion and renewal are then commonly uneven, and clumps of corneocytes are released from the skin surface instead of the normal single cell shedding. This phenomenon is defined as scaliness.

The epidermal turnover time (ETT) of the epidermis is the amount of time for the self-renewal of the whole keratinocyte population. It applies for the transit time of cells in the whole epidermis or in the SC alone. ETT represents the time needed for a given cell to pass from the basal layer to the outer surface of the skin. It represents about 52–75 days in the normal epidermis. ETT is typically reduced in most hyperproliferative conditions. The SC turnover time is about 2 weeks. It is evaluated by the dansyl chloride (DC) (Takahashi et al. 1987; Piérard 1992) or dihydroxyacetone (DHA) (Piérard and Piérard-Franchimont 1993; Uhoda et al. 2004) tests. In regular proliferative conditions, a xerotic SC is produced at a normal rate, but fails to desquamate due to persistent corneocyte cohesion. The relationship between disorders of cornification and hyperproliferative disorders encompasses two distinct conditions. In the first group, scaling commonly results from the flooding

of the SC with immature or incompletely mature cells (parakeratotic cells). In the second group, any altered barrier function drives epidermal hyperproliferation and in some instances tissue hyperplasia. The most common conditions where abnormal desquamation occurs are known to the layman as dandruff (12) and the so-called dry skin (Piérard 1989).

A key aspect of the orthokeratotic xerosis resides in a relative lack of the intracellular natural moisturizing factor (NMF) which maintains the corneocyte hydration as they move toward the skin surface. The osmotically active NMF results from the degradation of filaggrin. It represents the primary moisturization process of the SC. It fails due to interindividual variations, old age, and various other factors. Another unrelated reason for orthokeratotic xerosis is a defect in the breakdown of corneodesmosomes. Such process is normally due to enzymatic action released by keratinosomes (Egelrud and Lundstrom 1991). Changes in epidermal lipids, especially in ceramides and cholesterol sulfate, are commonly linked to changes in protease activity or access to corneodesmosomes. Failure to degrade corneodesmosomes correctly is a fundamental factor in many or most skin conditions where flaking occurs.

3 Treatments Affecting Desquamation

Retinoids are important regulators of terminal differentiation of the epidermis (Piérard-Franchimont et al. 1998; Kim et al. 2011). They are used as potent drugs to treat a series of hyperkeratotic disorders. The so-called keratolytics such as the a- and b-hydroxy acids are in fact desquamating agents probably acting on corneodesmosomal proteins, but leaving keratin molecules intact (Piérard-Franchimont et al. 1998; Lévêque et al. 1995). Both the emollients and moisturizers modify in an indirect way the corneocyte-to-corneocyte adhesion. Both cause a buildup of water in the SC. They lead to greater flexibility and extensibility of the SC.

4 Methods for Determining the Desquamation Rate

Various methods for evaluating the cohesion and exfoliation of the SC have been designed over the past decades (Roberts and Marks 1980; Piérard 1996; Piérard et al. 1992). They are associated with possible specific drawbacks in the sampling procedure and/or in the quantification process.

4.1 Quasi-Passive Collection Methods

Dandruff is probably the only skin condition allowing the collection of desquamating products in a really passive way (Piérard et al. 2006). A specific adhesive-coated disk (ACD) (D-Squame, CuDerm Corp., Dallas, TX, USA, or Corneodisc, C+K Electronic, Cologne, Germany) is applied under moderate pressure and for a few seconds on the target area of the scalp. On removal, dandruff remains stuck to the ACD. After deposition onto a dedicated background, the material is ready for the assessment. A crude method compares the aspect of the samples using a visual grading reference card. Such data are only provided on an ordinal scale. Another procedure relies on recording the specular light reflectance of the samples using adequate Charge coupled advice (CCD) cameras such as the Visiopor® PP34 (C+K Electronic). Image analysis provides quantitative data (Piérard-Franchimont et al. 2011). Still another procedure uses a staining step of the squames by a toluidine blue-basic fuchsin stain followed by the global assessment of the color. The chroma C value is used in reflectance colorimetry (Piérard et al.. 2006, 2015).

In other circumstances, when the spontaneous desquamation is not accessible by direct sampling, visualization of corneocytes remaining in the SC after a defined period of time is possible. The procedure begins by staining the SC with the fluorescent DC or the self-tanning DHA dye. Two ways of assessment are possible. The first assessment means consists of in vivo fluoro- or photometric measurements performed at regular

intervals. A kinetics of the dye fading can be performed (Takahashi et al. 1987; Uhoda et al. 2004). The procedure is affected by external factors altering desquamation, such as the mechanical effects of clothing, toiletries (Paye et al. 1994), and social contacts. The second assessment means consists of collecting the superficial part of the SC after a defined period of time (about 10 days). The harvesting methods are ACD and the cyanoacrylate skin surface stripping (CSSS). The material is examined under a fluorescence or white light microscope (Piérard 1992; Piérard and Piérard-Franchimont 1993; Piérard et al. 2014). Image analysis allows the quantification and localization of the stained and unstained corneocytes.

Still another cumbersome approach is the older chamber technique collecting all shedding corneocytes and squames from a defined skin area for a given time (Corcuff et al. 1987). A nonionic surfactant added in the chamber somewhat interferes with the natural spontaneous process of desquamation.

4.2 Mechanically Forced Collection Methods

The procedure of forced desquamation results from the application of some forces overcoming the intercorneocyte binding forces. This is achieved by rubbing or scratching the SC or following application of some adhesive-coated material. Early methods used various mechanical scrubbing devices. The access to such approaches was limited to a few laboratories. Tape strippings were not frequently used because the binding strength of the adhesive to the SC was heterogeneous between tapes.

Currently, the most common method for assessing scaliness and desquamation relies on controlled squamometry involving the commercially available ACD (Piérard et al. 1992; Paye et al. 1999; Shimizu and Maibach 1999; Piérard-Franchimont et al. 2000). The application pressure must be controlled by a dynamometer. It usually ranges between 10 and 25 kPa. The set time of ACD application must be defined. It is commonly limited to 5, 10, or 30 s, but possibly extended to 60 s when some effects of the transepidermal water loss are scrutinized. The assessments are similar to the abovementioned procedures in dandruff assessments. A high-resolution fluorescent visualization of corneocytes is provided by the combination of complimentary dyes (Guz et al. 2009).

Corneocyte quantification is possible using densitometry and spectroscopy methods (Schwarz et al. 2012). A gravimetric approach is also possible by carefully weighing the ACD before and immediately after sampling. This procedure requires much expertise to avoid any desiccation effect.

CSSS can be used for descriptive reports about the topography of hyperkeratosis in order to show the uneven pattern of scaliness over the skin surface (Piérard-Franchimont and Piérard 1985). Such evaluation is possibly combined to the recording of the skin capacitance mapping/imaging (SCMI) (Bazin et al. 2010).

References

Bazin R, Laquièze S, Rosillo A, Lévêque JL. Photoaging of the chest analyzed by capacitance imaging. Skin Res Technol. 2010;16:23–9.

Chu M, Kollias N. Documentation of normal stratum corneum scaling in an average population: features of differences among age, ethnicity and body site. Br J Dermatol. 2011;164:497–507.

Corcuff P, Chatenay F, Lévêque JL. Desquamation of the stratum corneum: kinetics following UV-induced injury. Acta Derm Venereol. 1987;134:S35–8.

Egelrud T, Lundstrom A. A chymotrypsin-like proteinase that may be involved in desquamation in plantar stratum corneum. Arch Dermatol Res. 1991;283:108–12.

Guz NV, Gaikwad RM, Dokukun ME, Sokolov I. A novel in vitro stripping method to study geometry of corneocytes with fluorescent microscopy: example of aging skin. Skin Res Technol. 2009;15:379–83.

Haftek M, Callejon S, Sandjeu Y, Padois K, Falson F, Pirot F, Portes P, Demarne F, Jannin V. Compartmentalization of the human stratum corneum by persistent tight junction-like structures. Exp Dermatol. 2011;20:617–21.

Igawa S, Kishibe M, Murakami M, Honma M, Takahashi H, Iizuka H, Ishida-Yamamoto A. Tight junctions in the stratum corneum explain spatial differences in corneodesmosome degradation. Exp Dermatol. 2011;20:53–7.

Ishida-Yamamoto A, Igawa S, Kishibe M. Order and disorder in corneocyte adhesion. J Dermatol. 2011;38:645–54.

Kim MY, Lee SE, Chang JY, Kim SC. Retinoid induces the degradation of corneodesmosomes and downregulation of corneodesmosomal cadherins: implications on the mechanism of retinoid-induced desquamation. Ann Dermatol. 2011;23:439–47.

Lévêque JL, Corcuff P, Gonnord G, Montastier C, Renault B, Bazin R, Piérard GE, Poelman MC. Mechanism of action of a lipophilic derivative of salicylic acid on normal skin. Skin Res Technol. 1995;1:115–22.

Lin TK, Crumrine D, Ackerman LD, Santiago JL, Roelandt T, Uchida Y, Hupe M, Fabrias G, Abad JL, Rice RH, Elias PM. Cellular changes that accompany shedding of human corneocytes. J Invest Dermatol. 2012;132:2430–9.

Mohammed D, Matts PJ, Hadgraft J, Lane ME. Depth profiling of stratum corneum biophysical and molecular properties. Br J Dermatol. 2011;164:957–65.

Paye M, Simion A, Piérard GE. Dansyl chloride labelling of stratum corneum: its rapid extraction from skin can predict skin irritation due to surfactants and cleansing products. Contact Dermatitis. 1994;30:91–6.

Paye M, Gomes G, Zerweg C, Piérard GE, Grove GG. A hand immersion test under laboratory-controlled usage conditions: a need for sensitive and controlled assessment methods. Contact Dermatitis. 1999;40:133–8.

Piérard GE. What do you mean by dry skin? Dermatologica. 1989;179:1–2.

Piérard GE. Microscopic evaluation of the dansyl chloride test. Dermatology. 1992;185:37–40.

Piérard GE. EEMCO guidance for the assessment of dry skin (xerosis) and ichthyosis: evaluation by stratum corneum strippings. Skin Res Technol. 1996;2:3–11.

Piérard GE, Piérard-Franchimont C. Dihydroxyacetone test as a substitute for the dansyl chloride test. Dermatology. 1993;186:133–7.

Piérard GE, Piérard-Franchimont C, Saint Léger D, Kligman AM. Squamometry: the assessment of xerosis by colorimetry of D-Squame adhesive discs. J Soc Cosmet Chem. 1992;47:297–305.

Piérard GE, Goffin V, Hermanns-Lê T, Piérard-Franchimont C. Corneocyte desquamation. Int J Mol Med. 2000;6:217–21.

Piérard GE, Xhauflaire-Uhoda E, Piérard-Franchimont C. The key role of corneocytes in pityrosporoses. Dermatology. 2006;212:23–6.

Piérard-Franchimont C, Piérard GE. Skin surface stripping in diagnosing and monitoring inflammatory, xerotic and neoplastic diseases. Pediatr Dermatol. 1985;2:180–4.

Piérard-Franchimont C, Goffin V, Piérard GE. Modulation of human stratum corneum properties by salicylic acid and all-trans-retinoic acid. Skin Pharmacol Appl Skin Physiol. 1998;11:266–72.

Piérard-Franchimont C, Henry F, Piérard GE. The SACD method and the XLRS squamometry test revisited. Int J Cosmet Sci. 2000;22:437–46.

Piérard-Franchimont C, Quatresooz P, Piérard GE. Specular light reflectance of flakes in seborrheic dermatitis of the scalp. A pilot study. Clin Exp Dermatol. 2011;36:793–6.

Piérard GE, Pierard-Franchimont C, Paquet P. Hermanns-Le T, Radermacher J, Delvenne P. Cyanoacrylate skin surface strippings and the 3S-Biokit advent in tropical dermatology. A look from Liège. The Scientific World Journal, 2014;214:462634.

Piérard GE, Courtois J, Ritacco C, Humbert P, Fanian F. Pierard-Franchimont C. From observational to analytical morphology of the stratum corneum : progress avoiding hazardous animal and human testings. Clinical, Cosmetic and Investigational Dermatology, 2015;8:113–125.

Roberts D, Marks R. The determination of regional and age variations in the rate of desquamation: a comparison of four techniques. J Invest Dermatol. 1980;74:13–6.

Schwarz JC, Klang V, Hoppel M, Wolzt M, Valenta C. Corneocyte quantification by NIR densitometry and UV/Vis spectroscopy for human and porcine skin and the role of skin cleaning procedures. Skin Pharmacol Physiol. 2012;25:142–9.

Shimizu T, Maibach HI. Squamometry: an evaluation method for a barrier protectant (tannic acid). Contact Dermatitis. 1999;40:189–91.

Takahashi M, Machida Y, Marks R. A new apparatus to measure rate of desquamation using dansyl chloride fluorescence. Arch Dermatol Res. 1987;279:281–2.

Uhoda E, Piérard-Franchimont C, Debatisse B, Wang X, Piérard GE. Repair kinetics of stratum corneum under repeated insults. Exog Dermatol. 2004;3:7–11.

Near-Infrared Densitometry for Improved Standardization of Tape Stripping and In Situ Determination of the Total Stratum Corneum Thickness

26

Steffi Hansen

Contents

Keywords

Near-infrared densitometry • Tape stripping • Skin • Stratum corneum thickness • Percutaneous absorption • Squame Scan

List of Abbreviations

API	Pharmacologically active ingredient
ATR-FTIR	Attenuated total reflectance Fourier transform infrared spectroscopy
AUC	Area under the SC concentration versus time curve
BE	Bioequivalence
BSA	Bovine serum albumin
c_{max}	Maximum concentration
DPK	Dermatopharmacokinetics
FDA	Food and Drug Administration
NIR	Near-infrared densitometry
SC	Stratum corneum
t_{max}	Time of maximum concentration
XlogP3	Octanol-water partition coefficient

1 Introduction

Tape stripping is a technique which is widely used for investigating skin absorption of topically applied products. Adhesive tapes are repeatedly applied to the same skin area treated with a cosmetic or pharmaceutical product to remove thin layers of stratum corneum (SC). The amount, of, for example, a pharmacologically active ingredient (API), can be determined directly by

S. Hansen (✉)
Department Drug Delivery, Helmholtz Institute for Pharmaceutical Research Saarland (HIPS), Helmholtz Center for Infection Research, Saarbruecken, Germany
e-mail: steffihansen@web.de

P. Humbert et al. (eds.), *Agache's Measuring the Skin*, DOI 10.1007/978-3-319-32383-1_26

spectroscopic methods (e.g., by performing Attenuated total reflectance Fourier transform infrared spectroscopy (ATR-FTIR) on the tapes or on the stripped skin surface) or after extracting the tape strips with a suitable solvent which dissolves the API.

Tape stripping is particularly useful for evaluating topical bioavailability of locally acting drugs for which systemic levels (in the blood or urine) are either not measurable or, except for estimating systemic side effects, have little meaning for their actual pharmacological efficacy. The data that is obtained is either reported as cumulative amount of API absorbed into the SC after a certain time (by summing up the amount of API extracted from all tapes, Fig. 1a) or as API concentration versus SC depth profiles (Fig. 1b). In order to determine API concentration at a certain SC depth, the amount of SC on each tape strip must be known. This amount is necessary to first of all determine the relative position within the SC and to calculate the volume of SC removed by the tape and thus determine the API concentration in this SC volume.

By performing tape stripping after different incubation times, the dermatopharmacokinetics (DPK) can be evaluated. This includes the maximum concentration (c_{max}), the time of maximum concentration (t_{max}), and the area under the SC concentration versus time curve (Fig. 1b). The tape stripping method has great potential as an alternative method for testing bioequivalence (BE) of topically applied generics in comparison to a reference product. Unfortunately, an FDA draft guideline recommending tape stripping for this purpose was withdrawn in 2002, after issues arose due to poorly defined experimental standardization. Currently, tape stripping is only recommended by the FDA for BE testing of drug classes which target the SC, such as antifungals (Narkar 2010). Furthermore for corticosteroids the in vivo skin blanching or vasoconstriction assay is recommended by the FDA for demonstrating BE, while any other topical generics have to be evaluated clinically.

In an effort to reestablish acceptance of tape stripping as a method for BE testing which is not limited to certain drug classes, standardization of the procedure is imperative. In this regard, methods to quantify the amount of SC removed by each tape strip have become the focus of research. Especially in the older literature, it is commonly assumed that one tape strip uniformly removes a single layer of corneocytes. Assuming a total SC thickness of, for example, 20 µm in humans, with each layer having a thickness of ca. 1 µm, this leads to the conclusion that a total number of 20 tapes will remove

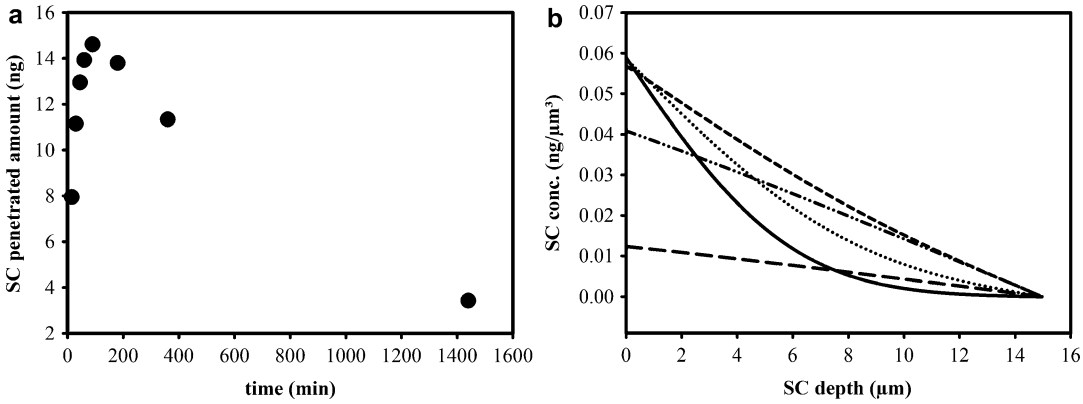

Fig. 1 Example: skin absorption of an API with MW 300 Da, XlogP3, finite dose 15 mg/15 µl in aqueous medium applied to an area of 1.767 cm^2 full thickness human skin in a Franz diffusion cell with acceptor volume of 3.5 ml; the data were simulated with DSkin Software Version 1.2.2, Scientific Consilience, Saarbrücken, Germany. (**a**) Cumulative amount of API penetrated into the SC after a certain time; (**b**) API concentration versus SC depth profiles (*black solid line* 15 min, *black dotted line* 30 min, *black short-dashed line* 1 h, *black dash-dotted line* 6 h, *black long-dashed line* 24 h)

the SC down to the viable epidermis. Meanwhile it is widely accepted that these assumptions may be misleading. First of all the SC thickness clearly differs between individuals and body regions and may also be influenced by the applied formulation. The most important parameter influencing tape stripping is intercorneocyte cohesion. Corneocyte cohesion decreases from the inside to the outside of the SC and is minimal in the stratum disjunctum which is ready to being desquamated. Consequently, usually the first two tapes remove considerably larger portions of SC than later tapes, while the last tapes usually remove very little amount of SC. Corneocyte cohesion further depends on skin hydration and is less in dry skin. Also, the stickiness of different adhesive tapes varies and will influence the amount of SC removed. In the event, for example, the number of tapes required to reach a certain depth within the SC or the total number of tapes to remove the SC quantitatively may differ between persons, test groups, and body sites. Thus it is necessary to employ a method to accurately determine the amount of SC on each tape strip. NIR densitometry is aptly suited for this purpose.

2 Near-Infrared (NIR) Densitometry for Standardizing Tape Stripping

NIR densitometry relies on measuring pseudo-absorption in the infrared range generated by a partially transparent obstacle obstructing the light path. For this purpose a circular infrared beam (wavelength 850 nm, 13 mm diameter) is directed onto a photodiode. A sample holder which takes up the tape strips is inserted into the beam path, and the intensity reduction in comparison to a blank reference tape (i.e., a tape strip which had not been in contact with the skin surface) is measured. Assuming homogeneous removal of the SC and thus homogeneous coverage density of the SC across the tape area, the corrected NIR pseudo-absorption ((abs. 850 nm) – (abs. 850 nm blank)) in % can be related to the average amount of SC removed per area (wt_{SC}/A):

$$wt_{SC}/A = ((\text{abs. 850 nm}) - (\text{abs. 850 nm blank}))/a \quad (1)$$

In Eq. 1 a is a constant obtained from linear regression analysis of the corrected NIR pseudo-absorption versus the amount of SC per area measured, for example, by protein quantification (Voegeli et al. 2007; Klang et al. 2011; Franzen et al. 2012). The constant may depend on the species and body region which is used, as well as on the adhesive tape brand. It has to be determined for the specific requirements of the experiment. SC from human or animal skin can be obtained for this purpose by trypsinization followed by freeze drying or desiccation (Kligman and Christophers 1963; Hansen et al. 2008). A calibration curve of accurately weighed amounts of dry SC is prepared, the protein is extracted by combined treatment with alkaline solution and shear stress, and the solution is neutralized and buffered if necessary. Tissue debris is removed by centrifugation, and the protein content in the so-prepared standards is determined by a custom protein quantification kit with adequate sensitivity. For further instructions see also the following references: Hahn et al. (2010) and Franzen et al. (2012). It should be kept in mind that if a protein assay is used as a reference method to compare against the NIR densitometry, this assay needs to be calibrated with SC protein from the same species that is later used in the experiments. This is necessary as the reaction efficiency of many assays strongly depends on the protein used (Klang et al. 2011). For example, our experience shows that 1 g of bovine serum albumin (BSA) corresponds to 4.27 g of human SC but only 1.84 g of SC from pig ears when analyzed under identical conditions (micro-BCA assay, see also Franzen et al. (2012)).

NIR densitometry has considerable advantages over other established methods which quantify the amount of SC removed by tape stripping, such as through quantifying the amount of protein on each tape, through gravimetric or other optical methods (Dreher et al. 1998, 2005; Weigmann et al. 1999; Jacobi et al. 2005). Voegeli et al. could demonstrate that NIR densitometry is robust with respect

to factors such as gender, age, body site, pH, and skin hydration (Voegeli et al. 2007). Most importantly, the result is available without delay, and tape and API are not destroyed by the measurement so that they are available for further analysis. Thus the amount of SC and the amount of API can be determined on exactly the same tape strip.

To obtain the SC thickness l_{SC} on each tape, both sides of Eq. 1 are divided by protein density ρ_{SC}. A reasonable estimate would be $\rho_{SC} = 1$ g/cm^3 (Hansen et al. 2009):

$$\begin{aligned} l_{SC}[\mu m] &= wt_{SC}/A/\rho_{SC} \\ &= ((\text{abs. } 850 \text{ nm}) - (\text{abs. } 850 \text{ nm blank}))/a' \end{aligned} \quad (2)$$

For tape stripping of pig ear skin in vitro, Franzen et al. determined a value of $a' = 23.9\ \mu m^{-1}$. They found no significant differences between D-Squame tape and tesafilm kristall-klar which can both be used with this constant (Franzen et al. 2012). In the literature only this value for pig ear skin in vitro is available. No values for human skin in vitro or in vivo have been published although several publications report correlations between NIR densitometry and protein quantification data; however in all cases, other proteins than SC protein were used for the calibration so that *a'* cannot easily be calculated.

Figure 2 and Table 1 show NIR pseudo-absorption data obtained for tape stripping of fresh and frozen human skin in vitro (Fig. 2a) and human skin in vivo (Fig. 2b) correlated with the respective SC weight per area data determined by a micro-protein assay. A linear regression analysis was performed, and the results are presented in Table 1. Tape stripping in vitro was performed on excised abdominal skin from three female Caucasian donors undergoing abdominal reduction surgery which was either used "fresh" on the day of surgery or after storing "frozen" at −26 °C for not longer than 3 months, taking care that the skin underwent no repeated freeze-thaw cycles. Tape stripping in vivo was performed on the inner forearm of two volunteers who had signed informed consent forms. Ethical agreement by the ethical committee of "Arztekammer des Saarlandes" was available. The tape stripping, NIR densitometry, and protein quantification procedures that were used have already been described by Franzen et al. (2012). Tape stripping was

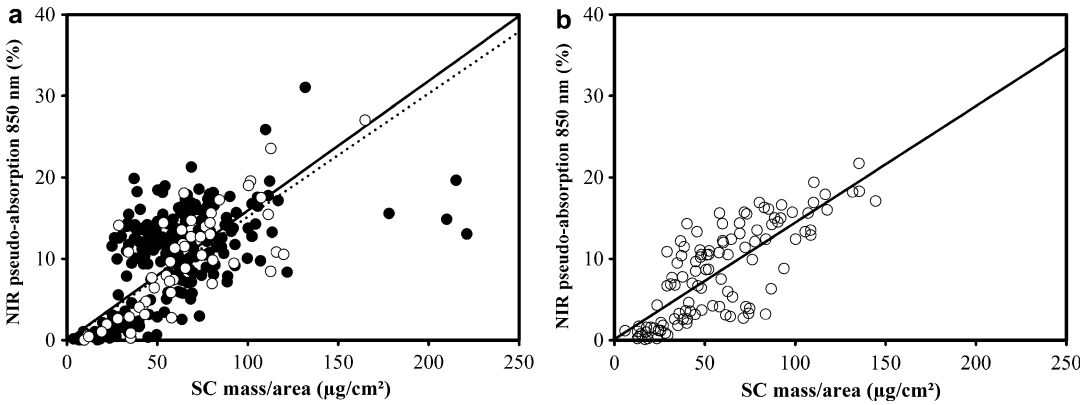

Fig. 2 (**a**) In vitro, human skin, *filled circle*/*solid line* = frozen skin, linear regression analysis: $n = 344$, slope = 0.159, $r^2 = 0.340$. *Open circle*/*dotted line* = fresh skin, linear regression analysis: $n = 52$, slope = 0.152, $r^2 = 0.619$. Overall fit, $n = 396$, linear regression analysis: $n = 52$, slope = 0.158, $r^2 = 0.387$. (**b**) In vivo, human skin; linear regression analysis: $n = 110$, slope = 0.145, $r^2 = 0.612$

Table 1 Conversion factor *a'* for different species, applicable to D-Squame tape and tesafilm kristall-klar

	a' (μm^{-1})
Pig ear skin in vitro	23.9
Human skin in vitro	15.8
Human skin in vivo	14.5

continued until the lower limit of quantification of the NIR densitometry was reached which indicates the complete removal of the SC (Hahn et al. 2010; Franzen et al. 2012).

The data in Fig. 2/Table 1 indicate that the constant *a'* obviously depends on species. It is higher for pig ear skin than human skin. Between *a'* for human skin in vitro and in vivo, there is only a small difference; differences between frozen and fresh skin in vitro are marginal. A higher value of *a'* indicates a steeper slope of the graph in Fig. 2, i.e., a lower SC mass per area generates a higher NIR pseudo-absorption. This difference is at least partially due to the different reaction efficiencies of human and porcine SC extract in the protein assay, as already mentioned. To check the accuracy of the obtained results for *a'* for both species, in a following section *a'* will be used to calculate the total SC thickness, and the results will be compared to a reference value determined by histological analysis.

3 Influence of Storage Time

For human skin the data in Fig. 2 shows that for the in vitro data storage over some limited time in the freezer at −26 °C considerably increases variability (compare $r^2 = 0.340$ and 0.619 for frozen and fresh skin in vitro, although *a'* is not influenced). The general recommendation based on this data is that NIR densitometry is suitable for analyzing the SC amount on tape strips obtained in vivo in human volunteers and in vitro only on fresh, non-frozen skin. This is different from excised pig ears in vitro where Franzen et al. reported that storage over 3 months (at 4 °C for up to 24 h and at −21 °C for up to 3 months) did not significantly influence the results (Franzen et al. 2012).

4 In Situ Determination of Total Stratum Corneum Thickness

It has now been established that NIR densitometry accurately determines the thickness of SC removed by each tape (Hahn et al. 2010), as well as the number of tapes required to remove the SC quantitatively (for in vitro human SC and stripping with tesafilm kristall-klar, the efficiency was 97 %; for excised pig ear skin with the same tape, the efficiency was 83 %; with D-Squame tape, it was 92 %) (Voegeli et al. 2007; Hahn et al. 2010; Klang et al. 2011; Franzen et al. 2012). Consequently, by continuing tape stripping down to the viable epidermis and by calculating the cumulative amount of SC removed, the result should equal the total SC thickness $l_{SC\text{-}tot}$:

$$l_{sc-tot} = \sum_{n=1}^{\infty} l_{SC-n} \tag{3}$$

Franzen et al. have demonstrated for tape stripping on excised pig ears that the total SC thickness can indeed be accurately determined based on Eq. 3 (Franzen et al. 2012). For eight different pig ears, they found no significant differences between the average thickness determined by NIR densitometry and the common histological method based on skin biopsies (Franzen et al. 2012). The data is reproduced in Table 2 and augmented by a value for fresh human skin in vitro. There were no significant differences between the NIR- and histology-based values for fresh human skin. It was interesting to observe that although the total SC thickness was very similar between human abdominal and pig ear skin, it took ca. 50 or even more tape strips to quantitatively remove the porcine SC, while ca. 20 tapes sufficed for human SC (tesafilm kristall-klar or D-Squame in both cases). This demonstrates once again the greater cohesion of porcine SC which had already been mentioned by, e.g., Klang et al. (2011).

Compared to histology NIR densitometry is quicker and averages the SC thickness over a

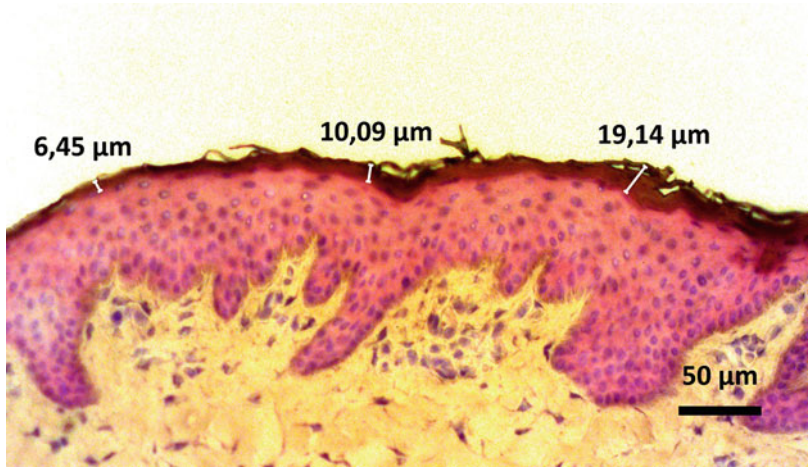

Fig. 3 Cross section (6 µm thickness) through frozen pig ear skin obtained using a cryomicrotome (MEV Cryostat, SLEE, Mainz, Germany) and stained using Mayer's hematoxylin and eosin. The optical microscope images were taken using a Zeiss Axio Scope A1 light microscope (Carl Zeiss Microscopy GmbH, Oberkochen, Germany) equipped with a digital camera (AxioCam ERc 5 s). Images were edited and labeled using the software ZEN lite 2011 (Carl Zeiss Microscopy GmbH, Oberkochen, Germany)

Table 2 SC thickness calculated according to Eq. 3 from NIR densitometry and histology

		NIR densitometry [µm]	Histology [µm]
Pig ear skin in vitro[a]	#1	14.9 ± 3.9	9.5 ± 2.2
	#2	10.9 ± 0.7	14.5 ± 5.2
	#3	9.0 ± 0.9	14.3 ± 4.7
	#4	8.6 ± 1.6	11.1 ± 3.3
	#5	9.9 ± 2.6	13.4 ± 4.8
	#6	13.1 ± 2.0	12.8 ± 3.7
	#7	12.7 ± 3.6	14.7 ± 6.7
	#8	12.6 ± 1.2	11.4 ± 2.4
Fresh human skin in vitro		10.0 ± 1.4	10.5 ± 2.9

[a]Data was reproduced from Franzen et al. (2012) (mean ± sd)

larger area (1.327 cm^2). In contrast the histological method requires an enormous amount of repeat measurements based on light microscopy images of cryosections from different skin biopsies to get a reasonable average of the total SC thickness, as the thickness varies visibly over a stretch of SC (Fig. 3).

In summary, NIR densitometry is a nondestructive, quick, and reliable method which can be a valuable alternative for determining the amount of SC on tape strips and the total SC thickness in situ.

References

Dreher F, Arens A, Hostynek JJ, Mudumba S, Ademola J, Maibach HI. Colorimetric method for quantifying human Stratum corneum removed by adhesive-tape stripping. Acta Derm-Venereol. 1998;78(3):186–9.

Dreher F, Modjtahedi BS, Modjtahedi SP, Maibach HI. Quantification of stratum corneum removal by adhesive tape stripping by total protein assay in 96-well microplates. Skin Res Technol. 2005;11(2):97–101.

Franzen L, Windbergs M, Hansen S. Assessment of near-infrared densitometry for in situ determination of the total stratum corneum thickness on pig skin: influence of storage time. Skin Pharmacol Physiol. 2012;25:249–56. doi:10.1159/000339905.

Hahn T, Hansen S, Neumann D, et al. Infrared densitometry: a fast and non-destructive method for exact stratum corneum depth calculation for in vitro tape-stripping. Skin Pharmacol Physiol. 2010;23:183–92. doi:10.1159/000288165.

Hansen S, Henning A, Naegel A, et al. In-silico model of skin penetration based on experimentally determined input parameters. Part I: experimental determination of partition and diffusion coefficients. Eur J Pharm Biopharm. 2008;68:352–67. doi:10.1016/j.ejpb.2007.05.012.

Hansen S, Naegel A, Heisig M, et al. The role of corneocytes in skin transport revised – a combined

computational and experimental approach. Pharm Res. 2009;26:1379–97.

Jacobi U, Ulrich J, Sterry W, Lademann J, Weigmann HJ. Estimation of the relative stratum corneum amount removed by tape stripping. Skin Res Technol. 2005;11(2):91–6.

Klang V, Schwarz JC, Hartl A, Valenta C. Facilitating in vitro tape stripping: application of infrared densitometry for quantification of porcine stratum corneum proteins. Skin Pharmacol Physiol. 2011;24:256–68. doi:10.1159/000326072. 000326072 [pii].

Kligman AM, Christophers E. Preparation of isolated sheets of human stratum corneum. Arch Dermatol Res. 1963;88:702–5.

Narkar Y. Bioequivalence for topical products – an update. Pharm Res. 2010;27:2590–601. doi:10.1007/s11095-010-0250-3.

Voegeli R, Heiland J, Doppler S, et al. Efficient and simple quantification of stratum corneum proteins on tape strippings by infrared densitometry. Skin Res Technol. 2007;13:242–51.

Weigmann H-JJ, Lademann J, Meffert H, Schaefer H, Sterry W. Determination of the horny layer profile by tape stripping in combination with optical spectroscopy in the visible range as a prerequisite to quantify percutaneous absorption. Skin Pharmacol Physiol. 1999;12 (1–2):34–45.

Infrared Densitometry for In Vitro Tape Stripping: Quantification of Porcine Corneocytes

27

Victoria Klang, Magdalena Hoppel, and Claudia Valenta

Contents

Keywords

Infrared densitometry • Stratum corneum • Porcine ear skin • Tape stripping • In vitro

Abbreviations

IR-D Infrared densitometry
SC Stratum corneum

1 Introduction: The Tape Stripping Method

The tape stripping method, where SC proteins are removed from the skin surface by means of standardized adhesive tapes, is a well-established method to obtain skin penetration data. The common experimental setup involves in vivo tape stripping on human forearm skin after application of a penetrant of interest. The parameters of application, such as the amount of formulation per cm^2, the location of the treated area, and the application time, have to be defined precisely. In this fashion, the skin penetration potential of penetrants such as drugs from newly developed vehicles can be evaluated.

The nature of the adhesive tapes employed for such experiments has to be defined as well. In order to ensure constant adhesive power of the tapes and better comparability between experiments, it is recommended to use a constant tape brand, e.g., Tesa®, D-Squame®, or Corneofix®, in all studies. The experimenter should be aware of

V. Klang (✉) • M. Hoppel (✉) • C. Valenta (✉)
Department of Pharmaceutical Technology and Biopharmaceutics, Faculty of Life Sciences, University of Vienna, Vienna, Austria
e-mail: victoria.klang@univie.ac.at; magdalena.hoppel@univie.ac.at; claudia.valenta@univie.ac.at

P. Humbert et al. (eds.), *Agache's Measuring the Skin*,
DOI 10.1007/978-3-319-32383-1_27

his role in ensuring constant application time and pressure as well as a rapid tape removal.

Having removed the adhesive tapes from the skin, the latter must be analyzed for two aspects. Firstly, the amount of penetrated drug has to be determined for each individual tape. In order to obtain an accurate penetration profile of an applied drug, it is not sufficient to merely correlate the recovered drug amounts to the tape number. So, secondly, the exact amount of SC thickness, i.e., the mass of corneocytes removed with each tape, has to be determined and correlated to the amount of drug recovered from the respective tape. By analyzing both drug content and amount of corneocyte aggregates on each tape, the accurate penetration depth of applied drugs can be determined (Weigmann et al. 1999).

For the quantification of SC proteins in vivo, different analytical methods have been proposed, such as differential weighing (Bommannan et al. 1996; Kalia et al. 1996, 2000; Weigmann et al. 2003; Marttin et al. 1996; Herkenne et al. 2006), microscopic techniques (Lindemann et al. 2003), and protein assays (Dreher et al. 1998, 2005). These techniques are comparatively time-consuming and may exhibit drawbacks in terms of accuracy, e.g., the gravimetric analysis is affected by residual moisture on the tapes. Recently, a new imaging method based on the analysis of pixel grayscale values and distribution has been introduced for quantification of SC proteins (Russell and Guy 2012). This technique is more accurate than differential weighing and has an acceptable signal-to-noise ratio.

A different approach is optical spectroscopy in the visible range, where the pseudo-absorption of the SC proteins serves to indirectly quantify the mass of corneocytes on the tapes (Weigmann et al. 1999, 2003). The pseudo-absorption is composed of reflection, scattering, and diffraction of the light by corneocytes and is not disturbed by the presence of other skin components (Weigmann et al. 1999, 2003, 2005, 2009; Lademann et al. 2009). The only drawback of this well-established method is the need for manual preparation of the sample tapes in order to analyze them with a specifically modified UV/Vis spectrophotometer with a larger measurement area.

Following these strategies developed by Lademann and co-workers, the use of IR-D represents a rapid and convenient approach to determine the optical pseudo-absorption of the proteins (Voegeli et al. 2007). In the past years, this technique has been found to be both practical and accurate for quantification of human corneocytes during tape stripping experiments on the human skin in vivo (Voegeli et al. 2007) and in vitro (Hahn et al. 2010). A particular advantage of IR-D is its nondestructive nature: after analysis of the tapes, the latter can be further analyzed, e.g., for their drug content. Recently, the technique of IR-D has been validated against gravimetric analysis for SC quantification of the human skin in vivo (Mohammed et al. 2012). Likewise, recent studies validating IR-D against the well-established method of UV/Vis spectroscopy were conducted by our group for both the human skin in vivo and porcine skin in vitro (Schwarz et al. 2012).

In summary, the discussed techniques for SC quantification have been mostly employed for the human skin in vivo or sometimes in vitro. Since the use of the human skin is not always an option due to legislative and organizational issues, efforts have been made to establish an in vitro substitute model for tape stripping experiments using the porcine ear (Schwarz et al. 2012; Klang et al. 2011, 2012). Porcine ear skin is generally accepted as a suitable in vitro substitute for the human skin (Herkenne et al. 2006) and particularly so regarding in vitro tape stripping (Sekkat et al. 2002; Jacobi et al. 2007). Porcine ears can be obtained from local farmers or slaughterhouses after clarifying that removal of the ears prior to sanitation processes such as high steam cleaning is essential.

2 Particularities of the Porcine Skin in Tape Stripping Experiments

Porcine ear skin requires preparation before starting tape stripping experiments. Firstly, it must be clarified whether fresh, refrigerated, or defrosted ears will be employed. Although differences have been shown to be small or negligible

for both the human skin in vitro (Hahn et al. 2010) and porcine skin in vitro (Klang et al. 2011; Franzen et al. 2012), it is recommended to choose one of the above options to obtain maximum reproducibility and comparability between results. In case of porcine ear skin, higher amounts of SC remained after tape stripping up to the IR-densitometric detection limit after 3 months of storage when compared to fresh porcine ear skin, i.e., the cohesion between the lower layers of corneocytes appeared to be increased. As a result, the calculated SC thickness might be systematically underestimated. Since the remaining SC, however, is frequently located within wrinkles, no errors in the calculated SC thickness will occur in such cases (Franzen et al. 2012).

For both fresh and defrosted ears, the subsequent preparation steps include cleaning of the ears, freeing them from hair, and confirming the intactness of the skin barrier function, e.g., by measuring the transepidermal water loss (Klang et al. 2011; Sekkat et al. 2002).

General aspects to keep in mind for in vitro tape stripping include exact marking of the stripping area, constant intensity and duration of pressure application, constant velocity of tape removal (Weigmann et al. 2003; Breternitz et al. 2007), and reduction of the influence of wrinkles by stretching and fixing of the ears and applying pressure with a rolling movement (Lademann et al. 2009; Breternitz et al. 2007; Dickel et al. 2010). Further aspects to be considered are the role of skin-cleaning procedures (Schwarz et al. 2012) and the possible interaction between the tapes and the applied formulations (Klang et al. 2012; Nagelreiter et al. 2013). For in vitro tape stripping, higher pressure may be required to obtain reproducible amounts of SC proteins (Hahn et al. 2010; Klang et al. 2011; Wagner et al. 2000).

When conducting the tape stripping process, porcine skin shows a different corneocyte distribution on the adhesive tapes than the human skin (Fig. 1). This is due to structural differences: the porcine skin cells throughout the epidermis are organized in polygonal clusters or columns that are separated by "canyons" (Carrer et al. 2008). These structures cause a distinct pattern of large corneocyte aggregates and intercluster regions that can be observed particularly on the first adhesive tapes removed from the skin surface. No such patterns are observed during tape stripping on the human skin.

The intercluster regions of porcine skin, which start as wrinkles on the skin surface, will exhibit lower corneocyte density on the tapes throughout the tape stripping process. Since the first few tapes generally exhibit the highest protein density due to the lower cohesion between corneocytes within the upper layers, comparatively inhomogeneous protein coverage of the tapes is obtained. As the tape stripping process proceeds, more homogeneous protein coverage is observed.

The type of tape plays a role in this context as well. Higher adhesive power will lead to a more irregular pattern of protein removal due to overall higher corneocyte content of the tapes. Consequently, D-Squame® tapes showed a more irregular protein removal due to their higher adhesive power than Corneofix® tapes, which was reflected in a lower coefficient of determination R^2 in our studies ($R^2 = 0.812$ for Corneofix®, $R^2 = 0.732$ for D-Squame® (Klang et al. 2011)). In independent studies using porcine ear skin, only slightly different values were obtained when comparing D-Squame® ($R^2 = 0.761$) and tesafilm® kristall-klar ($R^2 = 0.704$) (Franzen et al. 2012). In case of the human skin in vitro, better correlations were generally found using D-Squame® when compared to tesafilm® kristall-klar (Hahn et al. 2010).

Due to the canyon-like structures and the resulting inhomogeneous protein coverage of the tapes, it is all the more important to follow an exact working protocol including a highly reproducible way of pressure application and tape removal. Keeping these aspects in mind, accurate data can nevertheless be obtained with tape stripping on porcine skin and subsequent analysis of the pseudo-absorption, e.g., by UV/VIS spectroscopy (Weigmann et al. 2009). Despite the potential role of the "canyons" as shunt pathways through the epidermis, nearly identical penetration behavior was found for different sunscreens after tape stripping of the human skin in vivo and porcine skin in vitro (Weigmann et al. 2009). In general, a slightly higher permeability for porcine

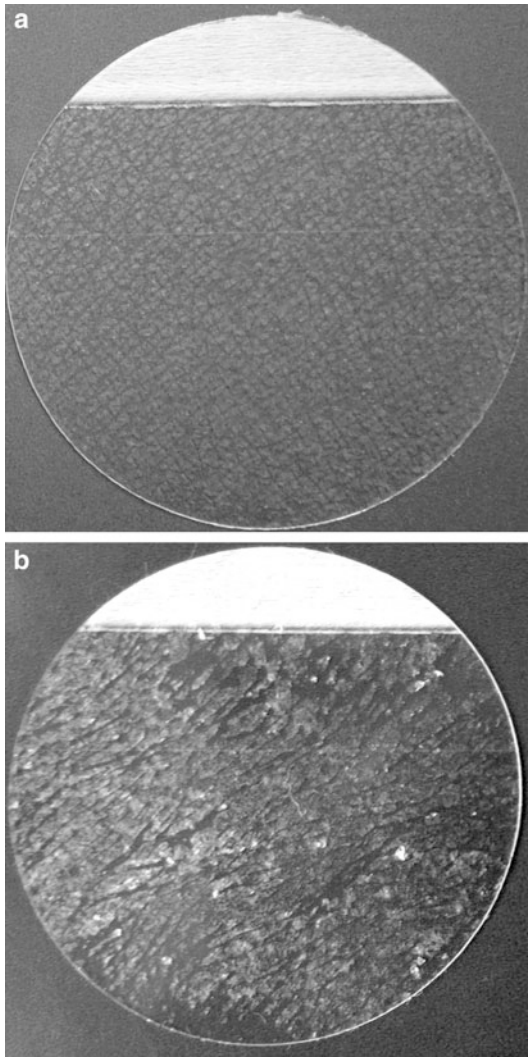

Fig. 1 Adhesive films removed from the skin surface of the human skin (**a**) and porcine ear skin (**b**) in the course of a tape stripping experiment. The shown adhesive tapes represent the respective first tapes to be removed from the skin surface, hence the large amount of adherent corneocytes (Figure 1a reprinted from Klang et al. (2011), Copyright © 2011, Karger Publishers)

skin has been reported (Singh et al. 2002; Godin and Touitou 2007), which may however also be related to the larger dimension of porcine hair follicles (Weigmann et al. 2009). Despite certain challenges regarding tape stripping on porcine skin, representative results can be obtained when keeping to an accurate working protocol. For in vitro experiments, porcine ear skin might be even more suitable than excised human skin since the porcine ear remains intact and the skin is still stretched out on the cartilage when the experiment is started; thus, contraction of elastic fibers and the resulting decrease of follicular penetration are avoided (Patzelt et al. 2008).

3 IR-Densitometry for the Quantification of Porcine Stratum Corneum Proteins

The IR-densitometer SquameScan™ 850A (Heiland electronic GmbH, Germany) was shown to be an efficient tool for quantification of SC proteins not only for the human skin in vivo (Voegeli et al. 2007) and in vitro (Hahn et al. 2010) but also for excised porcine ear skin (Klang et al. 2011; Franzen et al. 2012).

The device is used to determine the decrease in light intensity of a circular infrared laser beam at a wavelength of 850 nm (Fig. 2). This so-called pseudo-absorption value is then corrected against the pseudo-absorption measured for a blank adhesive tape within the same sample holder. The resulting pseudo-absorption value in % has then to be converted into the corresponding amount of protein per tape in μg/cm^2. This amount of SC proteins can furthermore be converted into the SC thickness removed with each tape.

To achieve these goals, validation of the IR densitometer for the quantification of porcine SC proteins was performed as follows: having conducted a set of tape stripping experiments, the amount of SC proteins on the tapes was subsequently determined by both IR-densitometry and the Micro BCA™ protein assay. The latter is a colorimetric assay based on the formation of a chelate complex that can be quantified by UV/Vis spectroscopy at $\lambda = 550$ nm. Methodological details can be found in the literature (Voegeli et al. 2007; Franzen et al. 2012). In order to calculate the SC mass removed with each tape, an estimated calibration curve based on the use of bovine serum albumin for calibration of the

Fig. 2 The IR-densitometer SquameScan™ 850A (Heiland electronic GmbH, Germany) for analysis of SC proteins on adhesive tapes. The sample holders provide space for a blank adhesive tape for correction against the background, followed by the sample tapes

protein assay was proposed (Klang et al. 2011). Taking into account the higher reaction efficiency of bovine serum albumin when compared to extracted porcine SC (Franzen et al. 2012), a more accurate calibration is obtained. The subsequent linear regression analysis between protein mass per tape and pseudo-absorption was performed for different standardized tape brands. Figure 3 shows the overall linear regression taking into account all tapes irrespective of obviously inhomogeneous protein coverage and tape brand. The resulting coefficient of determination R^2 of 0.729 is only slightly lower than that obtained when evaluating the samples of the two tape brands separately (Corneofix® with $R^2 = 0.812$ and D-Squame® with $R^2 = 0.732$ (Klang et al. 2011)) and is in good agreement with data from other working groups (D-Squame® with $R^2 = 0.761$, tesafilm® kristall-klar with $R^2 = 0.704$ (Franzen et al. 2012)).

In order to facilitate protein quantification by IR-D, a more restrictive evaluation was applied (Weigmann et al. 2003; Klang et al. 2011). Individual calibration curves for each experiment were calculated and extrapolated to the total SC depth, as represented by additional zero values. Taking into account all individual curves, a mean factor of proportionality $k = 0.224$ was obtained. The mass of SC proteins (m) on a normalized tape area of 1 cm^2 can be calculated using this value after IR-densitometric analysis of the respective pseudo-absorption at 850 nm (A_{corr}, after correction against a blank tape) by using the equation

$$m = \frac{A_{corr}}{0.224} \qquad \left(\text{in}\,\mu g/cm^2\right). \tag{1}$$

The obtained corneocyte mass on each tape can then be transformed into the corresponding SC thickness assuming a mean protein density (ρ_{sc}) of 1 g/cm^3 within the tissue (Sekkat et al. 2002). In accordance with the proposition of Franzen et al. (2012), this can be expressed as

$$t_{sc} = \frac{A_{corr}}{0.224 \cdot \rho_{sc}} = \frac{A_{corr}}{22.4} \qquad (\text{in } \mu m). \tag{2}$$

The accuracy of the proposed calculations and the resulting factor of proportionality k can be visualized by correlating the SC thickness determined by the two methods, i.e., the protein assay and IR-D, against the respective tape number (Klang et al. 2011). For Corneofix® tapes, the calculated SC thickness is highly comparable for the two methods (Fig. 4). In case of D-Squame®

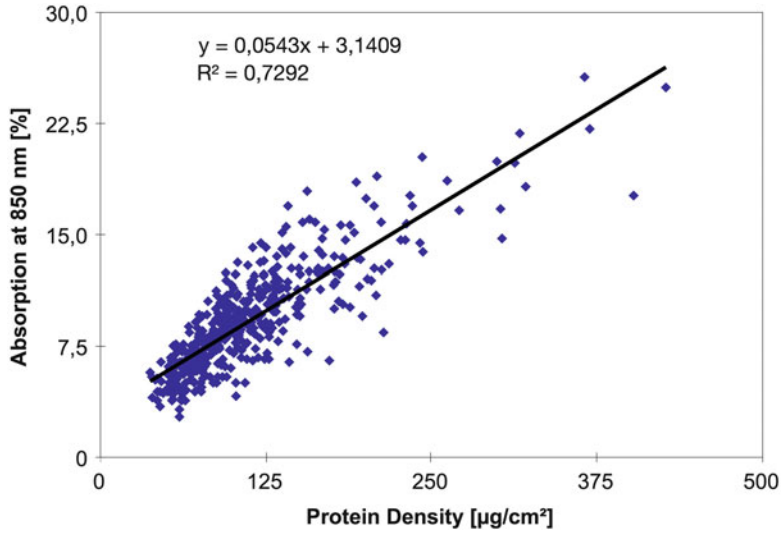

Fig. 3 Linear regression analysis of SC protein samples after sequential tape stripping on porcine ear skin (n = 480, all samples included irrespective of tape brand). For two types of adhesive film, Corneofix® and DSquame®, 12 experiments were, respectively, conducted during each of which 20 adhesive films were removed (n = 240 for each type of adhesive tape). The protein content of each tape was determined by IR-D at 850 nm and with the Micro BCA™ protein assay; the resulting data were plotted against each other

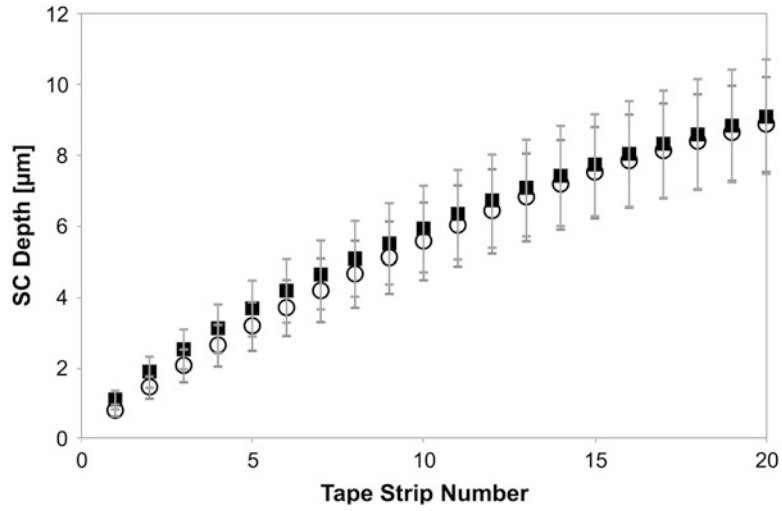

Fig. 4 Calculated SC depth reached after removal of 20 sequential Corneofix® adhesive tapes. The SC depth as determined after analysis of the tapes with the Micro BCA™ protein assay, taking into account a correction factor for bovine serum albumin versus SC protein (Franzen et al. 2012), is indicated by *black squares*. The corresponding values obtained after indirect protein quantification by IR-D at 850 nm using the proposed conversion factor of 0.224 are indicated by *white circles*. Values are means ± SD of n = 12 experiments

tapes, which possess higher adhesive power, a slight discrepancy between the values indicates that inhomogeneous protein coverage occurs more frequently.

The total SC thickness of the employed porcine skin in vitro can likewise be determined using IR-D. To this end, quantitative tape stripping experiments are performed until the detection limit of the IR densitometer is reached (Klang et al. 2011; Franzen et al. 2012). By summarizing the calculated amounts of SC on each tape, the entire thickness of removed SC can be calculated. Histological studies showed that the SC thickness as obtained by IR-D is highly comparable to that observed under the microscope (Franzen et al. 2012). The calculations of Franzen and colleagues and the above-presented equations deliver highly comparable results in terms of protein content per tape and corresponding SC thickness. Slightly different values in numerical outcome are obtained, but do not reach statistical significance ($p > 0.05$ for representative data sets); the method of IR-D has thus been validated in independent studies of different laboratories.

As opposed to the human skin, porcine corneocytes are removed in large clusters, which may lead to a more frequent occurrence of the stack effect and thus skewed IR-densitometric values of SC mass (Weigmann et al. 2003). Likewise, the relative amount of SC remaining after tape stripping was found to be higher for porcine skin in vitro than for the human skin in vitro (Franzen et al. 2012). Since the majority of the remaining corneocytes was however located within wrinkles, it can generally be assumed that the calculated SC thickness is sufficiently accurate.

In summary, IR-D is thus a convenient and nondestructive method for quantification of porcine SC proteins in tape stripping experiments using porcine ear skin. Despite the particularities of porcine SC when compared to its human counterpart, reproducible results can be obtained if a strict working protocol is maintained throughout all experiments.

References

Bommannan I, Potts RO, Guy RH. Examination of stratum corneum barrier function in vivo by infrared spectroscopy. J Invest Dermatol. 1996;95:403–8.

Breternitz M, Flach M, Prassler J, Elsner P, Fluhr JW. Acute barrier disruption by adhesive tapes is influenced by pressure, time and anatomical location: integrity and cohesion assessed by sequential tape stripping. A randomized, controlled study. Br J Dermatol. 2007;156:231–40.

Carrer DC, Vermehren C, Bagatolli LA. Pig skin structure and transdermal delivery of liposomes: a two photon microscopy study. J Control Release. 2008;132:12–20.

Dickel H, Goulioumis A, Gambichler T, Fluhr JW, Kamphowe J, Altmeyer P, Kuss O. Standardized tape stripping. A practical and reproducible protocol to uniformly reduce the stratum corneum. Skin Pharmacol Physiol. 2010;23:259–65.

Dreher F, Arens A, Hostynek JJ, Mudumba S, Ademola J, Maibach HI. Colorimetric method for quantifying human stratum corneum removed by adhesive-tape stripping. Acta Derm Venereol. 1998;78:186–9.

Dreher F, Modjtahedi BS, Modjtahedi SP, Maibach HI. Quantification of stratum corneum removal by adhesive tape stripping by total protein assay in 96-well microplates. Skin Res Technol. 2005;11:97–101.

Franzen L, Windbergs M, Hansen S. Assessment of near-infrared densitometry for in situ determination of the total stratum corneum thickness on pig skin: influence of storage time. Skin Pharmacol Physiol. 2012;25:249–56.

Godin B, Touitou E. Transdermal skin delivery: predictions for humans from in vivo, ex vivo and animal models. Adv Drug Deliv Rev. 2007;59:1152–61.

Hahn T, Hansen S, Neumann D, Kostka KH, Lehr CM, Muys L, Schaefer UF. Infrared densitometry: a fast and non-destructive method for exact stratum corneum depth calculation for in vitro tape-stripping. Skin Pharmacol Physiol. 2010;23:183–92.

Herkenne C, Naik A, Kalia YN, Hadgraft J, Guy RH. Pig ear skin ex vivo as a model for in vivo dermatopharmacokinetic studies in man. Pharm Res. 2006;23:1850–6.

Jacobi U, Kaiser M, Toll R, Mangelsdorf S, Audring H, Otberg N, Sterry W, Lademann J. Porcine ear skin: an in vitro model for human skin. Skin Res Technol. 2007;13:19–24.

Kalia YN, Pirot F, Guy RH. Homogeneous transport in a heterogeneous membrane: water diffusion across human stratum corneum in vivo. Biophys J. 1996;71:2692–700.

Kalia YN, Alberti I, Sekkat N, Curdy C, Naik A, Guy RH. Normalization of stratum corneum barrier function and transepidermal water loss in vivo. Pharm Res. 2000;17:1148–50.

Klang V, Schwarz JC, Hartl A, Valenta C. Facilitating in vitro tape stripping: application of infrared densitometry for quantification of porcine stratum corneum proteins. Skin Pharmacol Physiol. 2011;24: 256–68.

Klang V, Schwarz JC, Lenobel B, Nadj M, Auböck J, Wolzt M, Valenta C. In vitro vs in vivo tape stripping: validation of the porcine ear model and penetration assessment of novel sucrose stearate emulsions. Eur J Pharm Biopharm. 2012;80:604–14.

Lademann J, Jacobi U, Surber C, Weigmann HJ, Fluhr JW. The tape stripping procedure – evaluation of some critical parameters. Eur J Pharm Biopharm. 2009;72:317–23.

Lindemann U, Wilken K, Weigmann HJ, Schaefer H, Sterry W, Lademann J. Quantification of the horny layer using tape stripping and microscopic techniques. J Biomed Opt. 2003;8:601–7.

Marttin E, Neelissen-Subnel MT, De Haan FH, Bodde HE. A critical comparison of methods to quantify stratum corneum removed by tape stripping. Skin Pharmacol. 1996;9:69–77.

Mohammed D, Yang Q, Guy RH, Matts PJ, Hadgraft J, Lane ME. Comparison of gravimetric and spectroscopic approaches to quantify stratum corneum removed by tape-stripping. Eur J Pharm Biopharm. 2012;82:171–4.

Nagelreiter C, Raffeiner S, Geyerhofer C, Klang V, Valenta C. Influence of drug content, type of semi-solid vehicle and rheological properties on the skin penetration of the model drug fludrocortisone acetate. Int J Pharm. 2013;448:305–12.

Patzelt A, Richter H, Buettemeyer R, Roewert Huber HJ, Blume-Peytavi U, Sterry W, Lademann J. Differential stripping demonstrates a significant reduction of the hair follicle reservoir in vitro compared to in vivo. Eur J Pharm Biopharm. 2008;70: 234–8.

Russell LM, Guy RH. Novel imaging method to quantify stratum corneum in dermatopharmacokinetic studies. Pharm Res. 2012;29:2389–97.

Schwarz JC, Klang V, Hoppel M, Wolzt M, Valenta C. Corneocyte quantification by NIR densitometry and UV/Vis spectroscopy for human and porcine skin and the role of skin cleaning procedures. Skin Pharmacol Physiol. 2012;25:142–9.

Sekkat N, Kalia YN, Guy RH. Biophysical study of porcine ear skin in vitro and its comparison to human skin in vivo. J Pharm Sci. 2002;91:2376–81.

Singh S, Zhao K, Singh J. In vitro permeability and binding of hydrocarbons in pig ear and human abdominal skin. Drug Chem Toxicol. 2002;25:83–92.

Voegeli R, Heiland J, Doppler S, Rawlings AV, Schreier T. Efficient and simple quantification of stratum corneum proteins on tape strippings by infrared densitometry. Skin Res Technol. 2007;13:242–51.

Wagner H, Kostka KH, Lehr CM, Schaefer UF. Drug distribution in human skin using two different in vitro test systems: comparison with in vivo data. Pharm Res. 2000;17:1475–81.

Weigmann HJ, Lademann J, Meffert H, Schaefer H, Sterry W. Determination of the horny layer profile by tape stripping in combination with optical spectroscopy in the visible range as a prerequisite to quantify percutaneous absorption. Skin Pharmacol Appl Skin Physiol. 1999;12:34–45.

Weigmann HJ, Lindemann U, Antoniou C, Tsikrikas GN, Stratigos AI, Katsambas A, Sterry W, Lademann J. Uv/vis absorbance allows rapid, accurate, and reproducible mass determination of corneocytes removed by tape stripping. Skin Pharmacol Appl Skin Physiol. 2003;16:217–27.

Weigmann HJ, Jacobi U, Antoniou C, Tsikrikas GN, Wendel V, Rapp C, Gers-Barlag H, Sterry W, Lademann J. Determination of penetration profiles of topically applied substances by means of tape stripping and optical spectroscopy: UV filter substance in sunscreens. J Biomed Opt. 2005;10:14009.

Weigmann HJ, Schanzer S, Patzelt A, Bahaban V, Durat F, Sterry W, Lademann J. Comparison of human and porcine skin for characterization of sunscreens. J Biomed Opt. 2009;14:24–7.

Standardized Tape Stripping: A Practical and Reproducible Protocol to Reduce Uniformly the Stratum Corneum

28

Heinrich Dickel, Alexandros Goulioumis, Thilo Gambichler, Joachim W. Fluhr, Jeanette Kamphowe, Peter Altmeyer, and Oliver Kuss

Contents

A similar version of this contribution was published earlier in Dickel H, Goulioumis A, Gambichler T, Fluhr JW, Kamphowe J, Altmeyer P, Kuss O. Skin Pharmacol Physiol. 2010;23(5):259–65. S. Karger AG, Basel.

H. Dickel (✉) • T. Gambichler • J. Kamphowe • P. Altmeyer
Department of Dermatology and Allergology, Ruhr University Bochum, Bochum, Germany
e-mail: h.dickel@klinikum-bochum.de

A. Goulioumis
Department of Anesthesiology, Intensive Care and Pain Therapy, The Knappschaftskrankenhaus Dortmund, Dortmund, Germany

J.W. Fluhr
Department of Dermatology, Charité – Universitätsmedizin Berlin, Berlin, Germany
e-mail: Joachim.Fluhr@charite.de

O. Kuss
Institute for Biometry and Epidemiology, German Diabetes Center, Leibniz Institute for Diabetes Research at Heinrich Heine University Düsseldorf, Düsseldorf, Germany

P. Humbert et al. (eds.), *Agache's Measuring the Skin*,
DOI 10.1007/978-3-319-32383-1_28

Keywords
Tape stripping • Strip patch test • Stratum corneum • In vivo confocal laser scanning microscopy • Variability • Inter-rater agreement

Abbreviations

CI	Confidence interval
CLSM	Confocal laser scanning microscopy
PT	Patch test
Q1	25th Percentile
Q3	75th Percentile
SC	Stratum corneum
SD	Standard deviation
SL	Stratum lucidum
SPT	Strip patch test

1 Introduction

The epidermis consists of the physical, biochemical, and immunological barriers. The stratum corneum (SC) with its outermost layers serves as the principal physical barrier primarily against percutaneous penetration of various substances (Berrutti et al. 2000; Proksch et al. 2008; Zhang and Monteiro-Riviere 2008).

In 1939, Wolf (1939) introduced the tape-stripping method, whereby successive layers of the SC are removed by repeated strippings with adhesive cellophane tape, thus enabling to study morphologic details of human SC cells. In 1953, Spier and Natzel (1953) were the first to use this technique prior to patch testing, thus thinning the SC of the test area by mechanical reduction of corneocyte layers. Since then, the so-called strip patch test (SPT) is used as a modification of conventional patch testing (PT) to increase the bioavailability of test substances in the deeper epidermal cell layers, with the aim of lowering the minimum triggering level for positive test reactions in sensitized patients (Dickel et al. 2009b; Fernandes et al. 2007; Frosch et al. 1988; Oldhoff et al. 2004; Spier and Sixt 1955).

We proposed a first standardized protocol for performing uniformly the SPT (Dickel et al. 2004) and subsequently proved a significant increase of test sensitivity of SPT versus PT (Dickel et al. 2009a). It is still an open question, however, whether the considerable interindividual variation of tape strips for the SPT as derived from our protocol (Dickel et al. 2008) results in an interindividual similarity, i.e., reproducibility, of SC reduction. The latter would make SPT reactions comparable and further qualify the SPT procedure for practical use. Here, we report a clinical study which is aimed to investigate the variability and inter-rater agreement of our standardized SC reduction by the use of in vivo confocal laser scanning microscopy (CLSM).

2 Materials and Methods

This prospective, investigator-blinded clinical study was approved by the ethics committee of the Medical Faculty of Ruhr University Bochum (registration no. 2881, date of vote 2009-03-03). Procedures were explained in detail to all subjects, who signed informed consent forms prior to participation. The study was performed in September 2009 at the Department of Dermatology and Allergology, Ruhr University Bochum, Germany. Subjects received a small allowance for their voluntary study participation.

2.1 Study Population

For inclusion, subjects had to be at least 18 years old and had to have clinically normal skin on the back. Exclusion criteria were pregnancy and lactation.

2.2 Tape Stripping

Tape stripping was performed according to our formerly proposed protocol for performing the SPT (Dickel et al. 2004). Tape strips were carried out with a 3M™ Blenderm™ surgical tape (3M™ Medica, 3M Deutschland GmbH, Neuss, Germany; metric 25 mm × 4.5 m; CE no. 0493–BSI 0086–class I; batch no. 201407, exp. date 2014-07-01); any body hair was

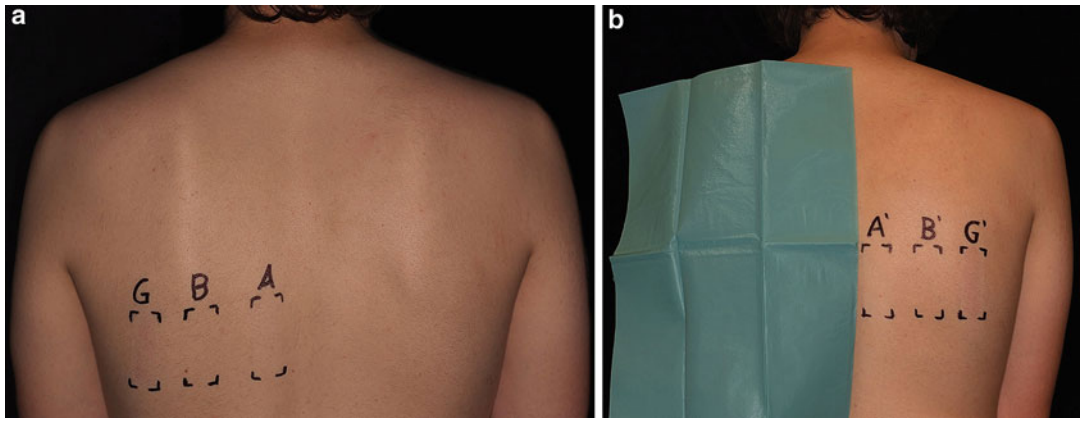

Fig. 1 Randomly chosen assembly of test areas on the back of one subject for rater 1 (**a**) and rater 2 (**b**) with no tape strips (B, B′), tape strips down to the stratum lucidum (G, G′), and calculated tape strips (tape strips down to the stratum lucidum × 11/26) for the SPT (A, A′)

removed before with a 3M™ clipper. In derogation from the original protocol, patch test substances were not applied.

All subjects were tested on one randomly chosen side of the back by rater 1 (A.G.; Fig. 1a). Three test areas were randomly marked with A, B, and G receiving the following treatments: B = no tape strips (baseline value of SC thickness measurement), G = strips down to the stratum lucidum (SL: reference value for calculating tape strips for the SPT), and A = calculated tape strips for the SPT (formula: tape strips down to the SL × 11/26 (Dickel et al. 2004); target value of SC thickness measurement). Randomization of test side and test areas was conducted according to a randomization list in the total of 75 subjects (supervised by O.K.). A subgroup of 18 subjects was additionally tested on the contralateral side of the back by rater 2 (H.D.) in a blinded manner (Fig. 1b). The three test areas receiving the same treatments were mirrored.

2.3 In Vivo Confocal Laser Scanning Microscopy

Confocal images of all test areas were obtained noninvasively using a VivaScope® 1500 (Lucid® Inc., Rochester, NY, USA) with VivaScan® Version 7 software. The technique applied with a laser wavelength of 830 nm gave confocal images with a lateral resolution of 0.5 μm and the ability to section SC to papillary dermis (penetration depth of imaging) in 0.94 μm vertical layers. For each test area, a stack consisting of such 140 vertical layers was captured. Quantitative image analysis was then performed with the public domain, Java-based image processing program ImageJ (National Institutes of Health, USA). For SC thickness measurements, vertical sections were reconstructed from the native stacks (Fig. 2a). The appearance of the densely packed keratin bundles in the SC reflecting the white rooflight produced by the CLSM was used to calculate SC thickness (Lucid® Inc. 2005). This reflection makes the SC appear more bright, while the other cell layers of the epidermis and papillary dermis appear darker. Per vertical section the mean out of five measured points put at random was defined as the SC thickness of the corresponding test area (performed by T.G.; Fig. 2a, b).

By using CLSM, we avoided biopsies from each of the test areas on the one hand and artifacts in SC thickness measurements in vitro by histological preparation on the other hand.

2.4 Blinding

Rater 2 was blinded with respect to (i) the number of tape strips performed in the test areas A and G and (ii) the skin reactions in these test areas treated

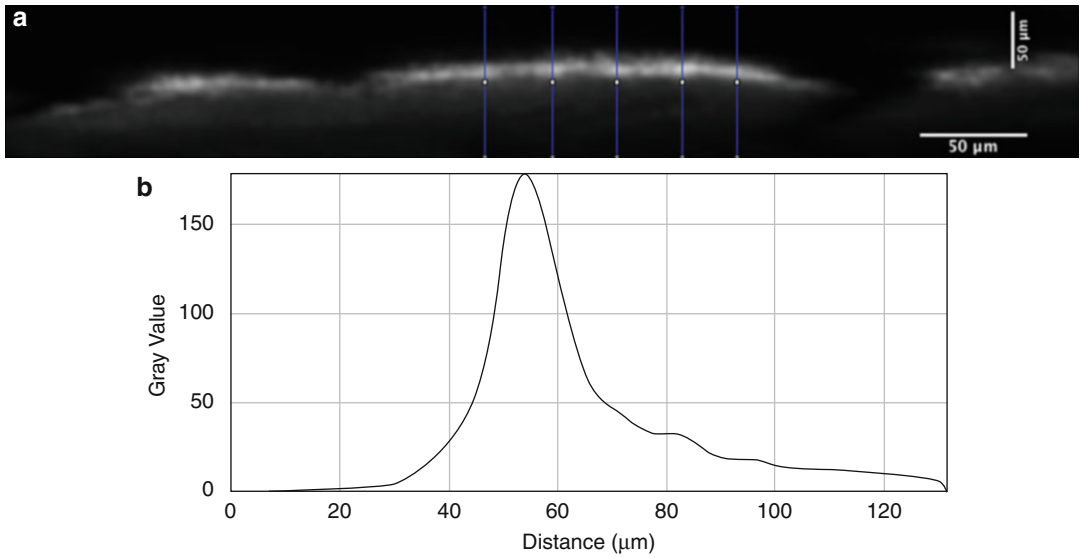

Fig. 2 Reconstructed vertical section (low-pass filter: Gaussian blur with $\sigma = 3$) of an in vivo confocal image stack of a test area (**a**). The *white* rooflights represent the stratum corneum (SC). Plotted in the image are the five measured points (*blue*) for calculating the mean of SC thickness. An exemplary intensity curve of the third measuring point is displayed (**b**); SC thickness is the distance between maximum and minimum of the first derivative of the function to the curve

accordingly by rater 1; the latter is depicted in Fig. 1b. The physician performing SC thickness measurements was blinded with respect to the kind of treatment of the respective test area.

2.5 Statistical Analysis

For sample size calculation, we assumed the values of SC reduction (relative to baseline before tape stripping) being normally distributed with a mean μ of 50 % (Frosch et al. 1988; Spier and Sixt 1955) and a standard deviation σ of 5 %. According to the 2σ-rule, this would mean that roughly 95 % of all relative SC reduction values would lie between 40 % and 60 %. We defined a length of 20 % points for this 4σ-interval as indicating clinical similarity of SC reduction across subjects, i.e., good reproducibility of our proposed protocol for performing the SPT (Dickel et al. 2004). As σ is the central parameter for this 4σ-interval, we planned this study based on a 95 % confidence interval (CI) for σ. By using a small simulation program (SAS code is available from O.K. on request), we found that 60 subjects would be enough to ensure that the length of this CI would not be larger than two units σ with an 80 % probability.

For descriptive purposes we report categorical variables as absolute (relative) frequencies and continuous variable as median (min-max, Q1, Q3). For the variable of central interest of the SC reduction (in %), we additionally give a histogram and report its standard deviation s together with the corresponding 4s-interval. All statistics are given with the respective 95 % CIs. As a sensitivity analysis, we also calculated the 4s-interval from a nonparametric bootstrap experiment (Haukoos and Lewis 2005) not using the assumption of normally distributed SC reduction values. We additionally checked (by Pearson correlation and differences in means) if subjects' age, sex, and Fitzpatrick skin phototype change the observed SC reduction of rater 1.

To assess inter-rater agreement, we drew a Bland-Altman plot (Bland and Altman 1986). This is defined as a scatterplot plotting, for all subjects, rater difference against the mean value of raters. Good agreement is indicated by (1) a random scatter of points in the plot and (2) most of the points

lying within the limits of agreement (mean rater difference ± 2 standard deviations (SD) of rater differences). Statistical analyses were conducted with SAS® (SAS Institute, Cary, NC, USA), version 9.2.

3 Results

Demographic and clinical characteristics of the 75 subjects tape stripped by rater 1 are summarized in Table 1. The complete distribution of relative SC reduction values is given in Fig. 3. As can be seen from the fitted normal density curve ($\mu = 31.3$ % and $\sigma = 4.4$ %), the values can safely be assumed as normally distributed. The estimated standard deviation s of 4.4 % (95 % CI, 3.8 %; 5.2 %) results in a 4s-interval from 22.5 % to 40.0 % with a length of 17.5 % (95 % CI, 15.1 %; 20.9 %). We therefore conclude that 95 % of all SC reduction values lie within an interval of length 17.5 % (95 % CI, 15.1 %; 20.9 %). As can be seen, the upper bound of the confidence is slightly larger than our prespecified critical value of clinical similarity of SC reduction of 20 %. The 4s-interval from the bootstrap experiment had a length of 19.3 % (95 % CI, 14.0 %; 20.5 %).

SC reduction by rater 1 was statistically significant but not clinically relevant changed by Fitzpatrick skin phototype ($P = 0.04$, F-test) because the subject with Fitzpatrick skin phototype V showed an outlying SC reduction value of 19.4 % (data not shown). However, no difference was seen for age (Pearson correlation −0.16 (95 % CI, −0.38; 0.07), $P = 0.16$) or sex (difference in means 0.5 % (95 % CI, −1.6 %; 2.5 %), $P = 0.66$, *t*-test).

Clinical characteristics of the subgroup of 18 subjects tape stripped independently by rater 1 and 2 are summarized in Table 2. In Fig. 4 we give the Bland-Altman plot to assess agreement in the subgroup of subjects that were rated by the two independent raters. We observe good agreement between the two raters, indicated by a decent random scatter of points and only a single value lying outside the limits of agreement.

Table 1 Demographic and clinical subject characteristics ($N = 75$; rater 1)

Characteristic	Value
Age (years), median (min-max, Q1, Q3)	25 (18–59, 23, 29)
Sex, n (%)	
Female	42 (56.0)
Male	33 (44.0)
Fitzpatrick skin phototype, n (%)	
I	4 (5.3)
II	26 (34.7)
III	35 (46.7)
IV	9 (12.0)
V	1 (1.3)
VI	0 (0.0)
Tape strips down to the SL, median (min-max, Q1, Q3)	38 (14–75, 30, 46)
Tape strips for the SPT,* median (min-max, Q1, Q3)	16 (6–32, 13, 19)
SC thickness (μm), median (min-max, Q1, Q3)	
Before tape stripping	13.0 (10.0–19.0, 11.6, 14.3)
After tape stripping	8.8 (6.9–12.8, 8.1, 9.6)
SC reduction (%), median (min-max, Q1, Q3)	31.6 (19.3–39.8, 28.6, 34.6)

Q1 25th percentile, *Q3* 75th percentile, *SL* stratum lucidum, *SPT* strip patch test; * = tape strips down to the SL × 11/26, *SC* stratum corneum

4 Discussion

In the present study, our proposed SPT protocol (Dickel et al. 2004) proved to be reproducible with respect to different patients or users. In daily clinical routine, we can therefore expect to receive a uniform SC reduction of approximately 30 % by this SPT protocol without any accessory equipment except for the 3M™ Blenderm™ surgical tape. Our in vivo SC thickness measurements on the upper back in the range from 10.0 to 19.0 μm with a median SC thickness of 13.0 μm (Table 1) coincide well with the literature reporting a range from 10.0 to 20.0 μm (Breternitz et al. 2007; Pirot et al. 1997; Scheuplein and Blank 1971) and a mean SC thickness of 11.0 μm and 9.4 μm, respectively (Holbrook and Odland 1974; Sandby-Møller et al. 2003).

Our results demonstrate further that the number of tape strippings performed for the SPT needs

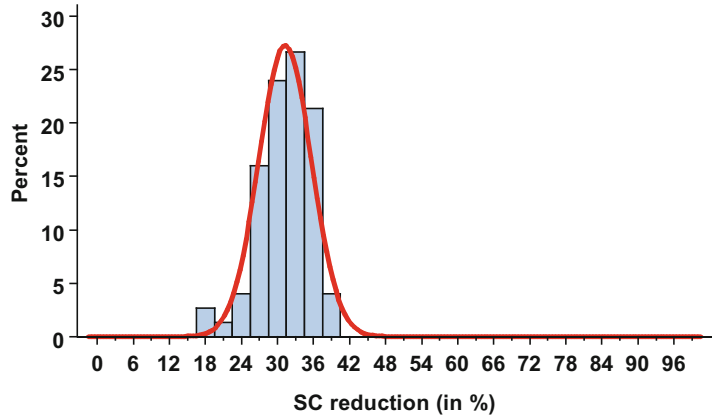

Fig. 3 Histogram for the stratum corneum (SC) reduction (in %) in the total of subjects ($N = 75$) by rater 1. Given is also fitted normal density curve with parameters $\mu = 31.3$ and $\sigma = 4.4$

Table 2 Clinical subject characteristics of subgroup ($n = 18$; rater 1 and 2)

Characteristic	Value
Tape strips down to the SL, median (min-max, Q1, Q3)	
Rater 1	28 (15–49, 26, 31)
Rater 2	29 (22–45, 27, 37)
Tape strips for the SPT,* median (min-max, Q1, Q3)	
Rater 1	12 (6–21, 11, 13)
Rater 2	12 (9–19, 11, 16)
SC thickness (μm), median (min-max, Q1, Q3)	
Before tape stripping	
Rater 1	13.2 (10.7–19.0, 12.0, 14.3)
Rater 2	12.3 (10.7–16.9, 11.8, 12.8)
After tape stripping	
Rater 1	9.0 (7.5–11.5, 8.4, 9.6)
Rater 2	8.6 (7.9–10.3, 8.1, 9.0)
SC reduction (%), median (min-max, Q1, Q3)	
Rater 1	31.5 (24.6–39.8, 29.7, 34.6)
Rater 2	31.0 (26.2–38.9, 27.3, 32.8)

Q1 25th percentile, *Q3* 75th percentile, *SL* stratum lucidum, *SPT* strip patch test; * = tape strips down to the SL × 11/26, *SC* stratum corneum

to be individualized (Table 1 and 2) (Dickel et al. 2008; Dickel et al. 2009a) and that a fixed, patient-independent number of tape strips for the SPT (cf. Lachapelle and Maibach 2009) is not appropriate. While a certain number of tape strippings may be sufficient to enhance absorption and permeability in one individual, it may be insufficient in another mainly due to interindividual differences in the SC structure (Berrutti et al. 2000; Jacobi et al. 2003; Weigmann et al. 2005). Thus, the variability in the amount of corneocyte layers removed between individual patients seems to be satisfactorily considered by our SPT protocol.

Although tape stripping increases considerably the absorption and penetration of applied substances to the skin (Choi et al. 2003), the reported effect is substantially dependent on the extent of SC removal (Kezic and Nielsen 2009). In pigskin it could be demonstrated that the outermost four or five corneocyte layers contain 40 % of the lipid and constitute most of the barrier function limiting cutaneous water loss and absorption or penetration of substances (Berrutti et al. 2000). Transferred to the human skin by assuming approximately 16 corneocyte layers of equal thickness on the back of Caucasian skin (Holbrook and Odland 1974; Rawlings 2006), reducing the SC by 30 % would hypothetically result in removing the same number of outermost corneocyte layers. However, our observed SC reduction value of 31 % by the SPT protocol (Fig. 3) contrasts with previous reports. To date, a fixed, patient-independent number of tape strips for the SPT – between 9 and 15 depending on source – was claimed to reduce the SC at about 50 % (Frosch et al. 1988; Müller 1980; Spier and Sixt 1955), but systematic investigations on this are not published yet. By drawing an analogy to biopharmaceutical data, Jacobi et al. (2005) described an equation of nonlinear correlation for estimating the relative amount of SC removed by sequential tape strips. For mathematical deduction, they studied the amount of SC removed by each tape strip in 11 subjects on the flexor

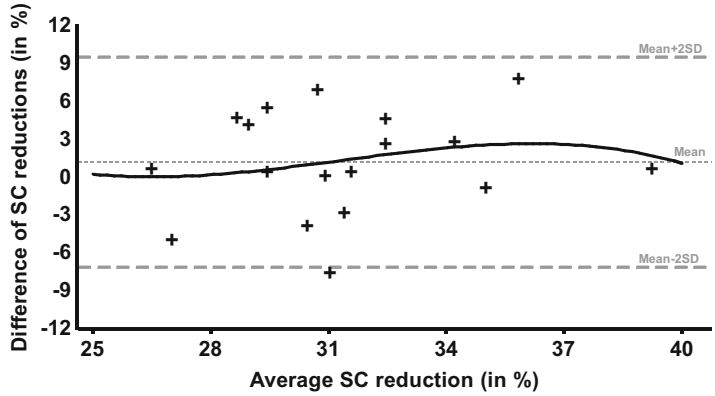

Fig. 4 Bland-Altman plot for measuring agreement between rater 1 and 2 in the subgroup of subjects ($n = 18$). Given is also a cubic polynomial fit for the data (*black line*) and lines indicating the mean difference of stratum corneum (SC) reductions (mean = 1.21 %) together with the limits of agreement (mean difference of SC reduction ± 2 SD (SD = 4.18 %), gray lines). *SD* standard deviation

forearms by pseudoabsorption using a UV/Vis spectrometer. According to their equation, a SC reduction of 31 % and 50 %, respectively, would be achieved by 8 and 14 tape strips. However, a direct transferability to our results is somewhat hampered most likely because of a differently chosen skin site and type of adhesive tape (Weigmann et al. 2005).

We understand that our SPT protocol (Dickel et al. 2004) may serve as a clinically useful guide for a uniform SPT procedure, not aiming at a general guideline for the tape-stripping procedure (Breternitz et al. 2007; Lindemann et al. 2003; Löffler et al. 2004). When SPT is employed according to our protocol, three crucial factors remain for improved standardization: (1) the exact pressure applied to the tape strip prior to stripping (default: "gently pressed downward by fingertips" Dickel et al. 2004), (2) the exact contact time of the tape strip to the skin (default: "2 seconds" Dickel et al. 2004), and (3) the exact tape strip removal rate (default: "one quick movement" Dickel et al. 2004; Breternitz et al. 2007; Choi et al. 2003; Lademann et al. 2009; Löffler et al. 2004). Achieving these factors, one might expect that the SC reduction values would lie closer together, i.e., within a smaller range than the found 22.5 % to 40.0 % in this study. However, we have to consider that the more technical demands are specified, the less frequently the SPT may be used in daily clinical routine (Lachapelle and Maibach 2009).

While it is the main objective of the SPT to reduce the SC penetration-limiting layer by defined and reproducible tape stripping prior to patch testing, there seems to be additional effects with at least partially overlapping pathophysiology which may explain the presence of contact dermatitis in patients with negative PT (Dickel et al. 2008). It is well known that in allergic contact dermatitis inflammation is a basic prerequisite for the adaptive immune system to respond (Bianchi and Manfredi 2009; Grabbe and Schwarz 1998; Martin and Jakob 2008). On the one side, repeated tape stripping itself is capable of evoking a mild and transient inflammation of the skin, thus leading to an immediate release of pro-inflammatory cytokines and chemokines and subsequently the accumulation of antigen-specific cells at the site of inflammation (Fluhr et al. 2008; Holzmann et al. 2004; Nickoloff and Naidu 1994; Onoue et al. 2009). The SPT might be therefore additionally understood as a combined diagnostic tool applying test substances with an irritant which gives the "danger signal" (Friedmann 2007) and hence maximizes the chance of the immune system to respond, i.e., augments allergic responses to the test substances. On the other side, enhanced penetration of a test substance into the living epidermis may increase the degree of skin

trauma by the test substance itself and thus increase the production of localized immunological trauma signals initiating an allergic response to the test substance (Basketter et al. 2008). However, parts of these defined multistage processes need to be further scrutinized.

In the present study, our proposed SPT protocol (Dickel et al. 2004) showed a good reproducibility with a SC reduction of 31 % and a good inter-rater agreement yielding a clinically adequate standardization. Uniformly performing the SPT is thus realizable in clinical practice with minimal effort and appears safe for clinical use because it is inexpensive and minimally invasive.

References

Basketter D, Darlenski R, Fluhr JW. Skin irritation and sensitization: mechanisms and new approaches for risk assessment. 2. Skin sensitization. Skin Pharmacol Physiol. 2008;21(4):191–202.

Berrutti LE, Singer AJ, McClain SA. Histopathologic effects of cutaneous tape stripping in pigs. Acad Emerg Med. 2000;7(12):1349–53. PubMed.

Bianchi ME, Manfredi AA. Immunology. Dangers in and out. Science. 2009;323(5922):1683–4. PubMed.

Bland JM, Altman DG. Statistical methods for assessing agreement between two methods of clinical measurement. Lancet. 1986;1(8476):307–10. PubMed.

Breternitz M, Flach M, Präßler J, Elsner P, Fluhr JW. Acute barrier disruption by adhesive tapes is influenced by pressure, time and anatomical location: integrity and cohesion assessed by sequential tape stripping; a randomized, controlled study. Br J Dermatol. 2007;156 (2):231–40.

Choi MJ, Zhai H, Löffler H, Dreher F, Maibach HI. Effect of tape stripping on percutaneous penetration and topical vaccination. Exog Dermatol. 2003;2(5):262–9.

Dickel H, Bruckner TM, Erdmann SM, Fluhr JW, Frosch PJ, Grabbe J, et al. The "strip" patch test: results of a multicentre study towards a standardization. Arch Dermatol Res. 2004;296(5):212–9.

Dickel H, Geier J, Kuss O, Altmeyer P. Strip patch test vs. conventional patch test to detect type IV sensitization in patients with allergic contact dermatitis. J Eur Acad Dermatol Venereol. 2008;22(12):1516–7. PubMed.

Dickel H, Kamphowe J, Geier J, Altmeyer P, Kuss O. Strip patch test vs. conventional patch test: investigation of dose-dependent test sensitivities in nickel- and chromium-sensitive subjects. J Eur Acad Dermatol Venereol. 2009a;23(9):1018–25.

Dickel H, Scola N, Altmeyer P. The strip patch test – indication in occupational dermatology demonstrated with a case history. J Dtsch Dermatol Ges. 2009b;11 (7):965–7.

Fernandes MFM, de Mello JF, Pires MC, Vizeu MCM. Comparative study of patch test using traditional method vs. prior skin abrading. J Eur Acad Dermatol Venereol. 2007;21(10):1351–9.

Fluhr JW, Darlenski R, Angelova-Fischer I, Tsankov N, Basketter D. Skin irritation and sensitization: mechanisms and new approaches for risk assessment. 1. Skin irritation. Skin Pharmacol Physiol. 2008;21(3):124–35. PubMed.

Friedmann PS. The relationships between exposure dose and response in induction and elicitation of contact hypersensitivity in humans. Br J Dermatol. 2007;157 (6):1093–102. PubMed.

Frosch PJ, Weickel R, Schmitt T, Krastel H. Nebenwirkungen von ophthalmologischen Externa. Z Hautkr. 1988;63(2):126–36.

Grabbe S, Schwarz T. Immunoregulatory mechanisms involved in elicitation of allergic contact hypersensitivity. Immunol Today. 1998;19(1):37–44. PubMed.

Haukoos JS, Lewis RJ. Advanced statistics: bootstrapping confidence intervals for statistics with "difficult" distributions. Acad Emerg Med. 2005;12(4):360–5. PubMed.

Holbrook KA, Odland GF. Regional differences in the thickness (cell layers) of the human stratum corneum: an ultrastructural analysis. J Invest Dermatol. 1974;62 (4):415–22. PubMed.

Holzmann S, Tripp CH, Schmuth M, Janke K, Koch F, Saeland S, et al. A model system using tape stripping for characterization of Langerhans cell-precursors in vivo. J Invest Dermatol. 2004;122(5):1165–74.

Jacobi U, Meykadeh N, Sterry W, Lademann J. Effect of the vehicle on the amount of stratum corneum removed by tape stripping. J Dtsch Dermatol Ges. 2003;1 (11):884–9.

Jacobi U, Weigmann HJ, Ulrich J, Sterry W, Lademann J. Estimation of the relative stratum corneum amount removed by tape stripping. Skin Res Technol. 2005;11 (2):91–6. PubMed.

Kezic S, Nielsen JB. Absorption of chemicals through compromised skin. Int Arch Occup Environ Health. 2009;82(6):677–88.

Lachapelle JM, Maibach HI. Patch testing and prick testing – a practical guide (official publication of the ICDRG). 2nd ed. Berlin: Springer; 2009. 195 p.

Lademann J, Jacobi U, Surber C, Weigmann H-J, Fluhr JW. The tape stripping procedure – evaluation of some critical parameters. Eur J Pharm Biopharm. 2009;72 (2):317–23. PubMed.

Lindemann U, Wilken K, Weigmann HJ, Schaefer H, Sterry W, Lademann J. Quantification of the horny layer using tape stripping and microscopic techniques. J Biomed Opt. 2003;8(4):601–7. PubMed.

Löffler H, Dreher F, Maibach HI. Stratum corneum adhesive tape stripping: influence of anatomical site, application pressure, duration and removal. Br J Dermatol. 2004;151(4):746–52.

Lucid® Inc. ImageJ applications for vivascopy: stratum corneum thickness analysis. Manual. Rochester, NY: 2005.

Martin SF, Jakob T. From innate to adaptive immune responses in contact hypersensitivity. Curr Opin Allergy Clin Immunol. 2008;8(4):289–93. PubMed.

Müller W. Das Berufsekzem. Berlin: Acron Verlag; 1980. 235 p.

Nickoloff BJ, Naidu Y. Perturbation of epidermal barrier function correlates with initiation of cytokine cascade in human skin. J Am Acad Dermatol. 1994;30 (4):535–46.

Oldhoff JM, Bihari IC, Knol EF, Bruijnzeel-Koomen CAFM, de Bruin-Weller MS. Atopy patch test in patients with atopic eczema/dermatitis syndrome: comparison of petrolatum and aqueous solution as a vehicle. Allergy. 2004;59(4):451–6.

Onoue A, Kabashima K, Kobayashi M, Mori T, Tokura Y. Induction of eosinophil- and Th2-attracting epidermal chemokines and cutaneous late-phase reaction in tape-stripped skin. Exp Dermatol. 2009;18(12):1036–43.

Pirot F, Kalia YN, Stinchcomb AL, Keating G, Bunge A, Guy RH. Characterization of the permeability barrier of human skin in vivo. Proc Natl Acad Sci U S A. 1997;94 (4):1562–7. PubMed.

Proksch E, Brandner JM, Jensen JM. The skin: an indispensable barrier. Exp Dermatol. 2008;17(12):1063–72. PubMed.

Rawlings AV. Ethnic skin types: are there differences in skin structure and function? Int J Cosmet Sci. 2006;28:79–93.

Sandby-Møller J, Poulsen T, Wulf HC. Epidermal thickness at different body sites: relationship to age, gender, pigmentation, blood content, skin type and smoking habits. Acta Dermatol Venereol (Stockh). 2003;83(6):410–3.

Scheuplein RJ, Blank IH. Permeability of the skin. Physiol Rev. 1971;51(4):702–47. PubMed.

Spier HW, Natzel R. Chromatallergie und Zementekzem. Gewerbedermatologischer und analytischer Beitrag. Hautarzt. 1953;4(2):63–5.

Spier HW, Sixt I. Untersuchungen über die Abhängigkeit des Ausfalles der Ekzem-Läppchenproben von der Hornschichtdicke. Quantitativer Abriß-Epikutantest Hautarzt. 1955;6(4):152–9.

Weigmann HJ, Ulrich J, Schanzer S, Jacobi U, Schaefer H, Sterry W, et al. Comparison of transepidermal water loss and spectroscopic absorbance to quantify changes of the stratum corneum after tape stripping. Skin Pharmacol Physiol. 2005;18(4):180–5.

Wolf J. Die innere Struktur der Zellen des Stratum desquamans der menschlichen Epidermis. Z Mikrosk Anat Forsch. 1939;46:170–202.

Zhang LW, Monteiro-Riviere NA. Assessment of quantum dot penetration into intact, tape-stripped, abraded and flexed rat skin. Skin Pharmacol Physiol. 2008;21 (3):166–80. PubMed.

Physical Methods to Measure *Stratum Corneum* Water Content In Vivo

29

Jean-claude Bernengo and Jean de Rigal

Contents

J.-c. Bernengo (✉)
Non Invasive Technologies, Paris, France
e-mail: bernjc@free.fr

J. de Rigal
L'Oréal Recherche, Chevilly Larue, France
e-mail: jderigal@rd.loreal.com; jderigal@bbox.fr

P. Humbert et al. (eds.), *Agache's Measuring the Skin*,
DOI 10.1007/978-3-319-32383-1_29

Keywords
Skin hydration • Water content • Calorimetry • Skin mechanics • Electrical measurements • Reflectometry • Infra-red • Raman

1 Introduction

The determination of *stratum corneum* (SC) water content has now become a widespread if not systematic practice in the assessment of cosmetics efficacy. It is also of importance in dermatology, allergology, and occupational medicine. The results are of special interest due to the multiple effects of hydration, in particular:

- On the suppleness of the *stratum corneum* and, hence, of all the skin
- On the decrease in the barrier function of the *stratum corneum* and, hence, on the modification of the physiology of cutaneous absorption
- On the activation of enzymatic processes in the intercorneocytic spaces and, hence, on the process of desquamation
- On the acceleration of bacterial proliferation in the *stratum disjunctum* and, hence, on the modification of the ecosystem of the skin surface

Numerous methods are available, and a considerable number of studies have been undertaken to find a simple, practical, and, above all, direct method. The difficulty resides precisely in the latter point. This chapter is a presentation of the methods currently available, in order to assist in selecting a technique, but also a presentation of some methods still confined to research laboratories, with the aim of showing the impressive range of possibilities and inciting development of devices that we would like to see appear on the market. This chapter exclusively addresses the determination of the water content of the *stratum corneum*.

1.1 Physicochemical Aspects of *Stratum Corneum* Water Content

The influence of the water content of the *stratum corneum* (SC) on its mechanical properties has long been known. In 1952, Blank (1952) described the changes in plasticity and flexibility of the SC related to its ability to retain exogenous water. In addition, the barrier property of the SC against transdermal water loss and the influence of water content on the cutaneous permeation of exogenous molecules are of primary importance in physiology and pharmacology.

1.1.1 State of the Water in the *Stratum Corneum*

In the SC, water exists in two thermodynamically very different states, mainly evidenced by thermal methods (differential scanning calorimetry (DSC), thermogravimetry):

- Free water, which can be frozen very close to 0 °C, in which numerous ionized and nonionized molecules are dissolved (metal salts, amino acids, urea)
- Bound water, which cannot be frozen at 0 °C but at much lower temperatures, in interaction with the proteins and lipids of the SC, and which accounts for 20–30 % of the total volume of water contained in the water-saturated layer (e.g., Walkley (1972), Inoue et al. (1986))

Bound water has mainly been studied by thermal methods (DSC, thermogravimetry) and by various vibration-based techniques (IR spectroscopy, NMR) (Hansen and Yellin 1972; Barry 1987). These two authors have shown that very strongly bound water (up to 7 % by weight) exists. The remainder is moderately strongly bound. The binding energies (15 and 18 kcal/mol, respectively) determined by Lévéque et al. (1987a) are of the same order as those of the hydrogen bonds between proteins and water known as "structural" bonds. Water-lipid interactions have been pointed out: modifications in structure occur in the

organization of the lipids of the SC when the water content increases. Water is mainly confined to the polar regions, for which it has a great affinity (ion dipole interactions). The insertion of water between these regions induces a decrease in the attractive forces of aliphatic chains and hence greater lipid fluidity (Barry 1987; Golden et al. 1986). The same mechanism is reported to underlie the increase in the cutaneous penetration (Behl and Barret 1981) of numerous drugs and vehicles (organic molecules).

1.1.2 Water Content Gradient

The water content of the SC is not uniformly distributed through its thickness: the more superficial layers are in equilibrium with the ambient water content, while the deeper layers exchange their free water with the epidermis and are close to saturation. It is not easy to demonstrate the gradient in vivo, but Warner et al. (1988) have confirmed it in skin biopsy specimens using electronic diffraction. In their results, water concentrations falls off regularly from 70 % at *stratum granulosum* level to 25 % superficially, which means that the water is entirely present in bound form even for moderately high water content values.

In vivo, Salter et al. (1992) attempted to study skin moisturization through nuclear magnetic resonance (NMR). Querleux et al. (1994) with the same technique confirmed the existence of a water gradient in the SC of the plantar area and observed the modifications induced by a hydrating cream or a detergent (see ▶ Chap. 44, "In Vivo Magnetic Resonance Imaging of the Skin"). Recent developments in confocal Raman spectroscopy (Caspers et al. 2001) have asserted the existence of this gradient and have enabled its quantification through a direct measure of the water content of the SC layers. More details are presented in Sect. 6.4.

1.1.3 Water Uptake by the *Stratum Corneum*

An isothermal SC water absorption curve is given in Fig. 1. This curve was plotted by pooling the results obtained by Blank (1952) with those of Lévéque et al. (1992). When the water content units are standardized, the results match perfectly. It is clearly shown that water content varies little between 30 % and 60 % relative humidity (RH), then increases considerably. The value extrapolated to 100 % RH is, according to Blank et al. (1984), of the order of 0.8 g/cm^3 (weight of water expressed relative to the total volume), i.e., a weight of water that is about threefold superior to that of the SC. Under those conditions, the thickness of the SC is also three times greater than that of the dry SC (Blank et al. 1984). In practice, the mass of water rarely exceeds that of the dry weight, equivalent to about 99 % relative humidity.

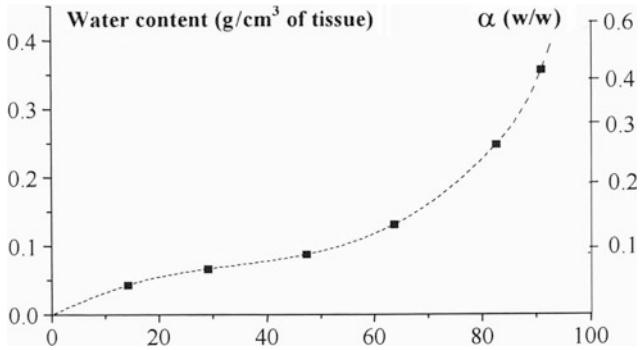

Fig. 1 Plot of the water absorption by the *Stratum Corneum* as a function of the relative humidity of the ambient air. Cv is expressed as the weight of water per volume of hydrated SC, while α is the ratio of the weight of water to the weight of dry SC. The Cv value extrapolated to saturation is about 0.8 g/cm^3, i.e., $\alpha = 3$ g/g (Blank et al. 1984)

1.1.4 Dermatological and Cosmetic Aspects

For a physicist or a chemist in charge of developing tests and methods to evaluate skin moisturization, this concept is mainly expressed in terms of the variation in the water content of the SC (most frequently measured by the variations in physical properties). For the dermatologist or cosmetics expert, cutaneous hydration is frequently a psychosensory phenomenon: a well moisturized skin is soft, smooth and, in other words, "in good condition." In contrast, a "dry skin" has special characteristics (desquamation, white and scaly plaques, irritation). It has been stated that this type of skin frequently lacks water (de Rigal et al. 1993) but that opinion remains controversial. Apart from the special unattractive appearance, dry skin has characteristics which, in an extreme form, may induce dermatological problems. The SC of a dry skin is twofold less flexible or deformable (Fig. 2) than that of a normal skin (Lévéque et al. 1987b). Repeatedly stressed during movements, the SC will tend to "fracture" constituting an open portal for infectious phenomena. On the legs, this is one of the characteristics of "scaly" skin, in which the margins of hard and smooth plaques are frequently surrounded by a red border, reflecting inflammation (de Rigal et al. 1993). A study of the variation in corneocyte size depending on the degree of dryness had previously pointed out the inflammatory characteristic of dry skin (Lévéque et al. 1987b).

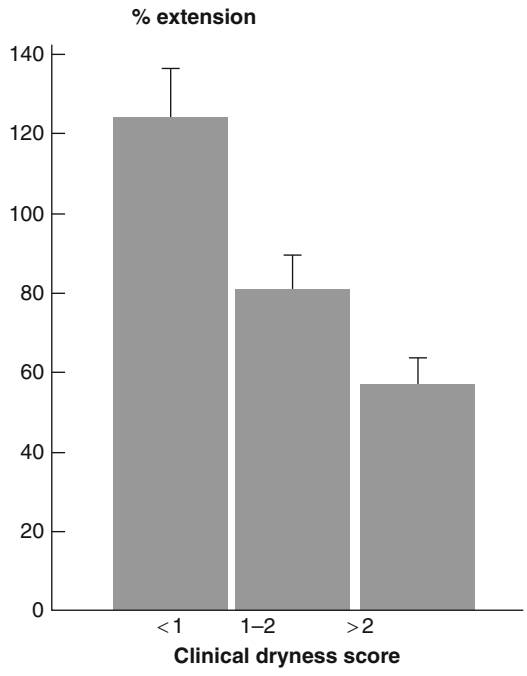

Fig. 2 Relationship between extensibility and clinical dry skin score (After Lévéque et al. (1987b))

The common concept of "dry skin" cannot, however, be considered equivalent to dehydration since it covers several states of miscellaneous etiologies the pathogenesis of which is not always clear. Such states may be induced by various agents (sun, surfactants), be of natural origin (aging), or result from climatic conditions (winter xerosis). It is, however, difficult to characterize these skin types in a rational manner (Piérard 1997). Each of the states, deriving from different mechanisms, has specific histological or biochemical characteristics (e.g., composition of the SC), although the clinical presentations may be the same. Some such states are indeed accompanied by dehydration of the SC.

Since Irvin Blank's work (Blank 1952) in the 1950s, it is now fully accepted that water plays a preponderant role in the physical properties of the SC. More recently, in the case of dry skin due to retention, corneosomes (the main agents responsible for the cohesion of corneocytes) are disturbed, as are the structures of the intercorneocyte lipid bilayers. In contrast to what is observed in moisturized skin, the corneosomes undergo less enzymatic degradation and thus remain present in high numbers in the more superficial layers of the SC (Piérard 1997). Since these results, several teams have demonstrated that hydration is an important factor in the mechanism of SC desquamation and that a proper water content promotes enzymatic function and regulates desquamation in isolated cells. The role of moisturizing agents (glycerol, urea, lactic acid, etc.) has been demonstrated and their beneficial influence clearly shown (Koyama et al. 1996; Rawling et al. 1992, 1995).

1.2 Presentation of the Methods Developed to Determine the Water Content of the SC

The early physical methods were based on the consequences of the presence of water in tissues. It is well known that a wet tissue is more supple (more deformable) and conducts electricity and heat better. Indirect methodologies were thus initially developed (measurement of electrical or thermal conductivity and mechanical measurements). However, the main disadvantage of those methods stays in the complexity of the relationship between the variation in water content and the changes in the measured physical property. In most cases, other factors are obviously involved in this relationship, in particular all the problems related to the contact between electrodes and skin and the influence of relief and mechanical properties on electrical and thermal properties (increased suppleness of the SC induces improved contact). Direct methods such as thermal analysis of the SC by DSC are not concerned by such questions and offer monitoring of the energy transitions of water molecules in the SC. Unfortunately, these techniques cannot be applied in vivo in humans.

This presentation will begin with thermal techniques, followed by techniques based on mechanical properties of the skin. Electrical measurements will take a major place, since they form the most popular group of techniques to evaluate skin hydration. Very clever methods combining optics and heat, so-called photothermal and photoacoustics will then be presented.

Techniques targeting directly the water molecule, and suitable for use in vivo, are still in development:

They concern essentially spectroscopy (near and middle infrared, Raman scattering) and will be exposed at the end of the chapter.

2 Thermal Techniques

2.1 Measurement of the Thermal Conductivity of the SC

2.1.1 Principle

The general law which governs the transport of energy or matter under the action of a potential F (thermal, mechanical, electrical, or chemical) states that the flux Φ of the quantity transported (heat, quantity of movement, electrical charge, number of molecules) is proportional and opposite to the gradient of the potential which creates the movement $\nabla \mathbf{F}$:

$$\Phi = -\mathrm{k} \cdot \nabla \mathbf{F} (\text{bold characters represent three-dimensional vectors}) \quad (1)$$

In the case of heat transport, Φ is the directional flow of heat (W/m^2) and $\nabla \mathbf{F}$ is replaced by the temperature gradient $\nabla \mathbf{T}$ present in the medium. The constant k is then the thermal conductivity, expressed in W/m/°.

A complex medium like the skin may be considered as a set of parallel thermal conductors. Hence, its average thermal conductivity is equal to the sum of the products of the elementary conductivities by the relative volume of each component, divided by the total volume. For the SC, two components are distinguished: free water ($\mathrm{k} = 0.6\ \mathrm{W/m/°}$) and the bound water-protein-lipid set ($\mathrm{k} = 0.18\ \mathrm{W/m/°}$). The overall thermal conductivity may then be approximated by Poppendieck et al. (1966):

$$\mathbf{k}(\mathrm{W/m/°}) = \text{Fraction of free water per unit volume} \times 0.6 + \text{Fraction of the set (protein + lipids + bound water) per unit volume} \times 0.18$$

Note that the fraction of free water per unit volume is identical to the free water content, expressed in g/cm^3. The latter can thus be calculated from the determination of thermal conductivity, k, if the second fraction per unit volume is known.

Thermal conductivity determinations on human skin have become a well-established practice since Lefevre (1901) conducted the first experiment in 1901. The first transducers for cutaneous use became available much more recently (Challoner 1975; Hensel and Brandt 1977). They functioned by dissipating a constant heating power and measuring the resulting heating effect. This "isocaloric" mode has several disadvantages, in particular the nonlinearity of the response which is, moreover, very slow. Since then, the principle of transducers operating in isothermal mode has been definitively adopted. The transducer maintains the tissue at a constant heat relative to the baseline temperature. The power dissipated by the transducer to maintain that heating effect is proportional to the thermal conductivity of the tissue. A continuous feedback loop permanently regulates heating with great precision. Thanks to this control loop, a rapid response time can be reached (time constant of about 0.1 s). (Note that the time constant is the time required for the phenomenon to fall to 37 % of its initial value).

2.1.2 Continuous-Heating Method: Hematron®

The continuous-heating method provides permanent monitoring of the variations in the thermal conductivity of the skin, but the corresponding probes must use two temperature transducers in order to measure the temperature difference between the heated and unheated medium at all times. Moreover, the determination of the water content of the SC requires using a special probe generating very superficial "microthermal" flux lines that do not reach the vascularized layer of the skin. The measurement probe shown in Fig. 3 is rectangular, and the two cavities are open so as to prevent occlusion of the skin and to ensure enhanced thermal insulation between the measurement and reference transducers. The flux lines are on the surface of the skin, particularly since their density falls off with the sqare of the depth considered.

2.1.3 Pulse-Heating Method

The probe is much simplified since it is merely a thermistor, which both generates the heat and determines temperature (Dittmar et al. 1988). The measurement is based on a two-phase cycle:

1. Passive phase of duration 24 s, during which the temperature of the skin at rest is determined
2. Active phase of duration 6 s, during which the temperature of the probe is stabilized at +6 °C above the previous value by a proportional, integral, and derivative regulator (PID)

The heating power necessary to maintain the temperature difference depends on the water content of the superficial layers (SC and living epidermis) but also on microcirculation in the dermis because of the propagation of the heat field in the skin. The power falls off very quickly with time, reaching a value that is almost constant (asymptotic P_{SS}) after 2 s. In a homogeneous material, the power obeys a law of the type:

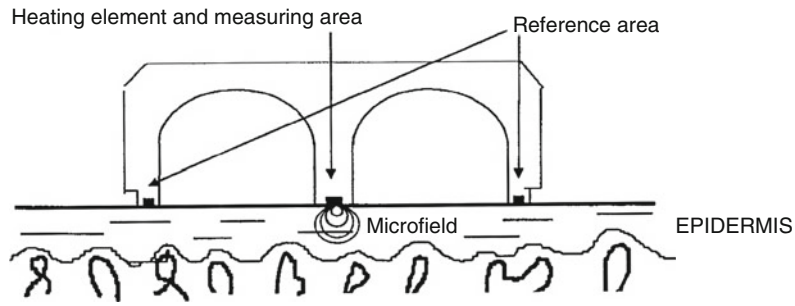

Fig. 3 Example of a thermal probe used to determine the superficial thermal conductivity of the skin: the Hematron of A. Dittmar (1988) has been marketed by the DERMSCAN company (France). Dimensions of the heating element: 1 mm × 15 mm

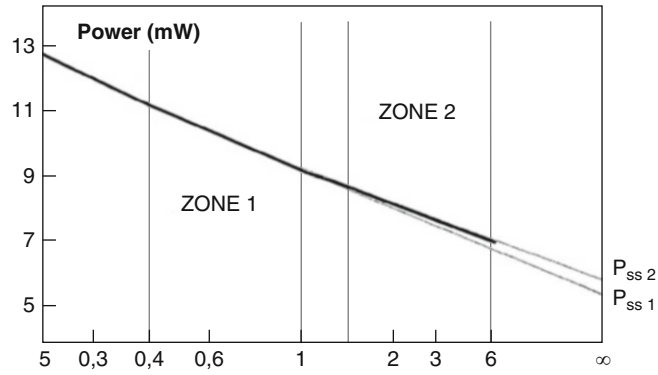

Fig. 4 The power dissipated by the probe on the skin of the cheek. Zone 1 corresponds to the *stratum corneum*: $P_{ss1} = 5.8$ mW, i.e., $k = 0.25$ W/m/° (After Arnaud et al. (1994)

$$P = \beta/\sqrt{t} + P_{SS} \qquad (2)$$

the plot of which is shown in Fig. 4, in which the time scale is in $1/\sqrt{t}$. The asymptotic power, P_{SS}, depends on the thermal conductivity of the medium and the thermal characteristics of the probe. Given P and t, P_{SS} may be determined by Eq. 2, by extrapolating to infinite time. In addition, calibration with various homogeneous materials (gels containing variable amounts of glycol, petrolatum, polystyrene foam) has confirmed the linear relationship below (Eq. 3), between $1/P_{SS}$ and 1/k, as indicated by the theory:

$$1/P_{SS}\left(mW^{-1}\right) = 0.11 + 0.014 \times 1/k\left(m.^{\circ}.W^{-1}\right) \qquad (3)$$

Given that relationship, the determination of k only requires determination of P_{SS} by extrapolation from the linear regression conducted on the experimental plot.

Figure 4 is an example obtained on the skin. It will be observed that the heating power does not obey the function (1) over the entire time interval. Power has to be adjusted by two functions of type (1), equivalent to two different β and P_{SS}. The value of P_{SS} for zone 1 of the graph enables calculation of the thermal conductivity of the superficial layer while that of zone 2 is related to the deeper layers and microcirculation. Figure 5 shows a typical result obtained with the device described above, used to determine the hydration of the skin on the forearm before and after application of an occlusion patch for 4 h. The increase in thermal conductivity reflects a marked variation in hydration (40–72 % of water volume relative to total volume). During the study, the authors showed that the occlusive patch did not markedly modify the cutaneous microcirculation (P_{SS2} of Fig. 4).

2.2 Determination of Thermal Effusivity

The water content of the SC may also be determined using the thermal effusivity, e, whose square is equal to the product of the thermal conductivity, k, the thermal capacity per unit volume, c, and the density, ρ, $\left(\mathbf{e^2} = \mathbf{k}.\boldsymbol{\rho}.\mathbf{c}\right)$. (The thermal capacity per unit volume of a body is the quantity of heat necessary to raise the temperature of a unit volume of the body from 24.5 to 25.5 °C. Thermal capacity is expressed in $cal.m^{-3}.°C^{-1}$ or in $J.m^{-3}.°C^{-1}$.) Thermal effusivity characterizes the aptitude of a medium to exchange heat with another medium. In the case of the water content of the SC, free water acts, in the same direction, on k and c, and hence the effusivity is particularly sensitive to water content.

In 1958, Hendler (Hendler et al. 1958) conducted in Hardy team initial determinations of skin effusivity using the method of photothermal radiometry described further in this chapter (§ 5.1). Balageas (1986) worked on the skin and modeled the heat transfers between the various layers. He demonstrated the feasibility of determining hydration by that method, with or without contact, which is of particular interest. A

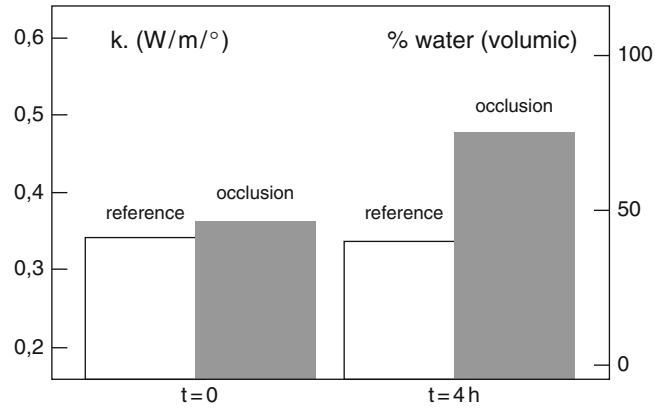

Fig. 5 The water content of the skin of the forearm pre- and post-occlusion for 4 h (% water = 100 × k − 18) / 0.42) (After Dittmar (1988))

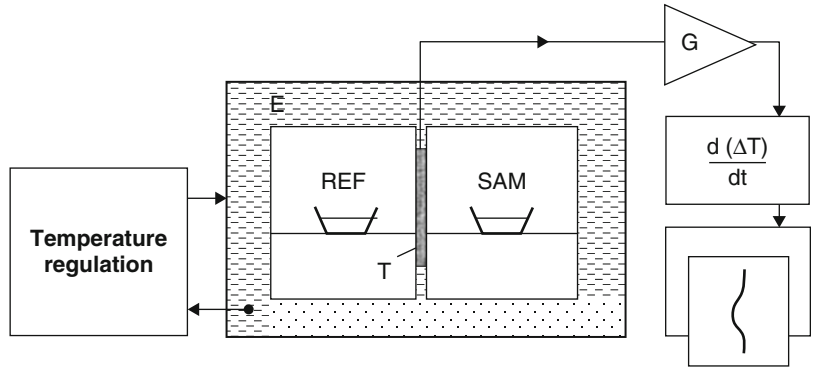

Fig. 6 Principle of differential scanning calorimetry
T thermocouples, *G* voltage amplifier, *E* isolated chamber

review of the various methods used by that team was published in 1990 (Balageas 1991).

2.3 Differential Scanning Calorimetry (DSC)

Differential scanning calorimetry (DSC) remains the reference method for characterizing the type of water contained in the SC since it enables direct measurement of the energies of interaction and phase changes of the various constituents of the SC. The method is therefore highly appropriate for the determination of the free and bound water contents of SC samples. Combined with physicochemical methods (cutaneous permeation) and structural methods (electron microscopy), DSC has also elucidated the influence of hydration on the molecular organization of the SC and explained the water retention and chemical barrier mechanisms cited above.

As indicated in Fig. 6, an SC sample (10 mg) is placed in one of the holders of the measurement chamber, while the reference holder contains a weight of distilled water with a thermal capacity as close as possible to that of the reference. The temperature of the measurement holder is then slowly and linearly increased (e.g., 1 °C/min) and the temperature difference, ΔT between the two chambers, is permanently measured by the thermocouples T. For as long as no energy absorption occurs in the SC, the quantity of heat required to heat the two chambers is identical (at least theoretically, because in practice a slight disequilibrium may occur) and hence ΔT is nil. However, if heat absorption occurs, this will no longer be the case. After calibrating the instrument, the electrical output signal of the apparatus (proportional to ΔT) can be directly related to the heat energy absorbed. The temperature at which heat absorption occurs and the intensity of that absorption are highly influenced by the water content of the

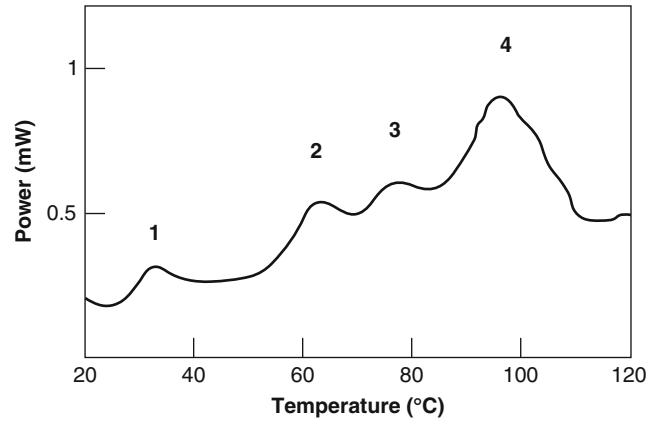

Fig. 7 Thermogram of human SC with 25 % (w/w) water content (After Goodman and Barry (1989))

SC. Determination of the transition temperatures and heat energy absorbed is thus a means of measuring the water content of the SC sample. In modern systems, ΔT is permanently nil since energy is supplied in an amount equal to that absorbed at all times. A DSC thermogram (Fig. 7) thus shows the instantly supplied power (negative) or, in the present case, the absorbed power (positive) related to the transition phenomenon observed. The area under each of the peaks is equivalent to the enthalpy of the corresponding transition. (Note that the variation in enthalpy, at constant pressure and in absence of work exchanges, as in the present case, is equivalent to the variation in the internal energy of the system.)

2.3.1 Application to Skin

Figure 7 shows an example of a thermogram obtained on human SC containing 25 % (w/w) of water. Each peak reflects a transition phenomenon directly related to the conformation of the SC:

- Peak 1: This peak is not systematically observed, even on healthy SC. If a sample is rendered lipid-free using an organic solvent, the peak disappears. The peak is therefore considered due to the melting of sebaceous lipids located at the surface of the skin (Golden et al. 1986).
- Peak 2: This peak reflects the melting of intracellular lipids (Golden et al. 1986). It is considered to reflect melting of the hydrophobic chains inserted into the lipid bilayers, similar to membranes (Barry 1987; Goodman and Barry 1989).

Table 1 Variations in the transition temperatures of each of the peaks for several SC water contents (After Goodman and Barry (1989))

	Transition temperature (°C)			
Water content	Peak 1	Peak 2	Peak 3	Peak 4
Dry	42 ± 1	77 ± 1	91 ± 22	not measured
10–20 %	41 ± 3	73 ± 1	86 ± 2	113 ± 5
30–40 %	39 ± 3	72 ± 1	85 ± 2	99 ± 3
50–60 %	37 ± 2	71 ± 1	83 ± 1	98 ± 5
>60 %	38 ± 2	70 ± 1	83 ± 2	95 ± 2

- Peak 3: This peak is very sensitive to hydration. Its transition temperature decreases, as does the area, when the water content of the SC increases (Golden et al. 1986, 1987). This peak is not easy to interpret, and one hypothesis is that it is associated with the changes induced by heat (thermal transition) in the lipid-protein complex between the intercellular lipids and corneocyte membrane (Golden et al. 1986, 1987; Khan and Kellaway 1989).
- Peak 4: This peak is considered, by many authors, to be due to thermal denaturation of intracellular keratin (α-keratin transformed into β-keratin). The denaturation is irreversible and observed even with lipid-free SC (Barry 1987; Golden et al. 1986; Knutson et al. 1985; Christensen et al. 1977).

The Table 1, after Goodman and Barry (1989), displays the variations in the transition

temperatures of each of the peaks for several SC water contents.

The decrease in the temperatures of the peak apices (transition temperatures) when hydration increases is accompanied by a decrease in the corresponding areas under the curve (enthalpies). Hydration introduces a change in the structure of the SC, which is located in the polar regions of the lipids (peaks 1, 2, and 3) and the intracellular keratin molecules (peak 4) (Barry 1987; Golden et al. 1986; Goodman and Barry 1989; van Duzec 1975). The greater fluidity of intercellular lipids is also considered to facilitate the transcutaneous absorption of polar or nonpolar drugs (Behl and Barret 1981). The position and enthalpy of peak 3 may be an indicator of the SC water content.

However, *use of DSC around the freezing temperature of free water* is a preferable technique, since it directly determines the weight of the free water contained in the sample. The sample is taken out after equilibration at ambient humidity (in general by stripping), then frozen as rapidly as possibly to keep the water in the sample. Figure 8 shows the thermograms obtained at about 0 °C for SC samples with different water contents: at 18 % no transition occurs, but at 33 % a small peak becomes visible. The peak continues to grow with higher water contents. The latent heat of melting of ice at atmospheric pressure is 80 cal/g (332 J/g) at 0 °C. Determining the transition enthalpy at about 0 °C enables direct calculation of the free water content of the sample. A further 30 % of bound water (not freezable) must be added to yield the total hydration of the SC. For water contents of less than 30 %, the method cannot be used directly, since Walkey (1972) has shown that the water of the SC was then mainly in bound form (in fact, the relationship between total water and bound water is linear, with an almost constant shift of 5 % by weight).

Differential scanning calorimetry thus enables the state of the water in the SC to be studied in thermodynamic terms. While not feasible in vivo, the method is readily used on ex vivo SC, i.e., immediately after stripping. Moreover, the method has the considerable advantage of avoiding complex and uncertain calibration (as is required, for example, with optical or electrical methods). Numerous systems are available commercially (Perkin-Elmer, etc.) for other industrial uses but may be directly used on SC samples.

3 Methods Based on Mechanical Properties

The mechanical properties of the skin reflect the behavior of its constituents, their organization, and their respective modifications. In consequence, mechanical methods of measurement enable rapid and simple determination of the variations in SC water content. The methods currently used are noninvasive and allow successive determinations on a given site in order to monitor the kinetics of a treatment and its carry-over effects.

The methods developed in the last 20 years may be divided into two main categories:

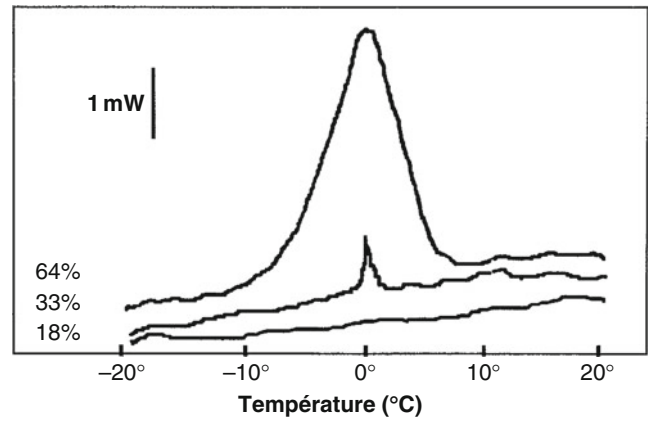

Fig. 8 Thermograms of skin with different water contents showing only freezable water. Bound water is not visible since it does not undergo a phase change at about 0 °C (After Walkey (1972))

- Those using deformation perpendicular to the plane of the skin (indentation, suction, levarometry, ballistometry)
- Those applying deformation in the plane of the skin (uniaxial extensibility, torsion, vibration, gas bearing electrodynamometer)

The latter methods are advantageous in that they measure the properties of the most superficial tissues, independent of the deep (adipose) tissues, providing the geometric dimensions of the assay and the imposed deformations are small (Vlashloom 1967; Christensen et al. 1977).

In recent years, methods based on the propagation of sound waves in tissues have emerged. Determination of the attenuation coefficients of the ultrasound waves leads to the intrinsic mechanical characteristics of the material under test by means of calculation and modeling (Bamber and Tristam 1990). These methods have encountered some success with respect to bulky organs like the liver but, for the time being, are not widespread and not routinely used on the skin.

3.1 Deformation in the Plane of the Skin

3.1.1 Torsion Method: Twistometer® or Dermal Torque Meter®

The first studies with this type of apparatus were conducted by Vlasbloom (1967). The system developed at that time had no ring to limit the geometry of the measurement zone. Following numerous improvements, a system was later marketed under the proprietary name of "Dermal Torque Meter" by the Diastron company (Andover, Surrey, UK). The stress is applied in the plane of the skin using a disk stuck onto it (double-sided adhesive). An angular displacement transducer measures the resultant deformation (it is in fact a method based on the measure of creep or deformation under a constant applied torque). A concentric guard ring (stuck also onto the skin) restricts the zone subject to the stress. The geometry and a few simplifying approximations enable calculation and generation of Young's modulus for the tissue under study (Agache et al. 1980).

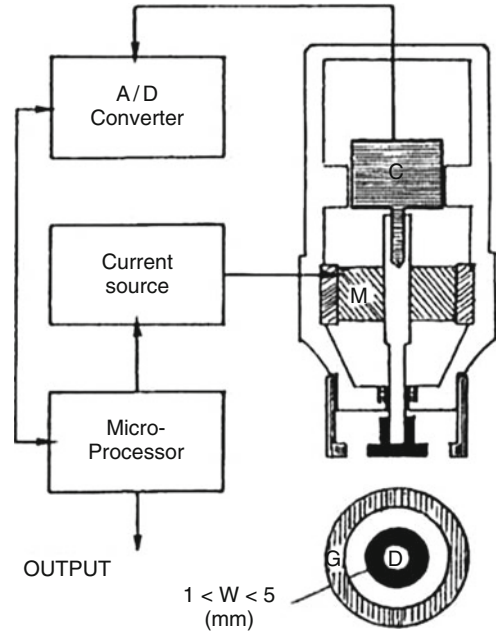

Fig. 9 Diagram of the Twistometer (After Lévéque and de Rigal (1985)) *M* torque motor, *C* angular displacement transducer, *G* guard ring, *W* gap width

Figure 9 shows the apparatus, and Fig. 10 displays the profile of the skin response curve.

The response diagrams are modeled by an equation of the following type:

$$U(t) = U_e + U_V(1 - \mathrm{Exp}(-t/c)) + A \cdot t^m \quad (4)$$

On the response, the profile of which is the same no matter the method, several parameters may be determined:

- U_e: immediate extensibility
- U_r: immediate recovery
- U_V: viscous deformation amplitude
- U_r/U_e: elasticity

On the basis of these parameters, the coefficients of Burger's rheological model, combining a Maxwell and a Kelvin-Voigt model in series as shown on Fig. 11 (the simplest for modeling the skin (Pichon et al. 1990)), can be calculated:

$$K_0 = C/U_e \; K_1 = C/U_v$$
$$\eta 0 = C/A \; \eta 1 = \tau.K1 = \tau.C/Uv$$

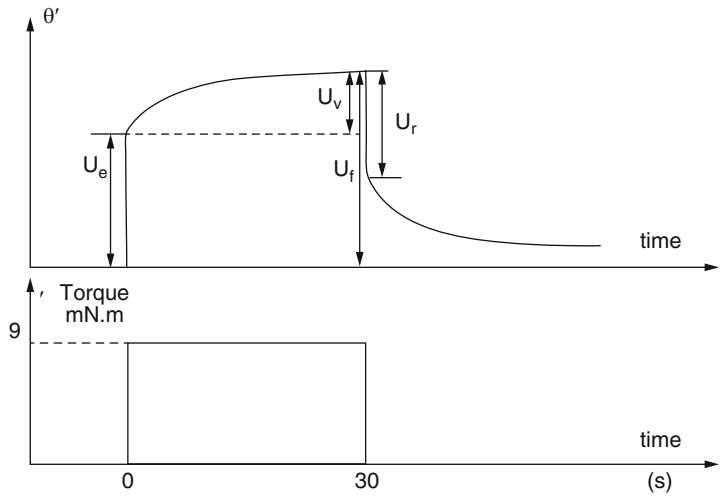

Fig. 10 General profile of the response curves of skin to stress and the main extensibility parameters determined from these curves (After Lévéque and de Rigal (1985))

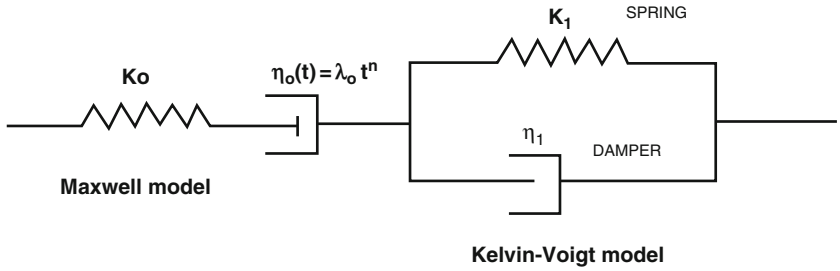

Fig. 11 Skin mechanical model for torsion measurements

where C is the value of the torque applied, K_0 and K_1 are the stiffness parameters and η_0 and η_1 are the viscosity parameters.

The value of **m** in Eq. 4 varies, depending on the author. Pichon et al. (1990) studied the recorded deformation using the finite element method (De Rigal 1996) and confirmed a value of $\mathbf{m} = 1/3$. In the same publication, the hydration phenomenon is shown to be measured mainly by the variations in parameter U_e (or K_0) and, to a lesser extent, K_1 and η_1. The latter parameter, η_0, is more clearly related to deeper structures (superficial dermis) (De Rigal 1996), as was to be clearly shown subsequently. Some authors use a value of **m** equal to 1 (Salter et al. 1992). Other rheological, and non-rheological, models have also been put forward (Salter 1993).

In 1985, Lévéque and de Rigal (1985) showed that the contribution of the SC to the measurement was of the order of 60–80 % for a gap width of 1 mm (Fig. 12a). The contribution decreased when this width increased (20 % for a width of 5 mm). The "immediate" moisturizing efficacy of a cosmetic formulation is shown in Fig. 12b. Figure 13 shows an example of the long-term effect of treatment. References Aubert et al. (1985a) and Randall Wicket et al. (1997) cite probative examples of the possibilities of the method with regard to evidencing short- and long-term moisturizing effects. It is clear that the apparatus measures deformations and that the parameters thus determined depend on any variations in the thickness of the *stratum corneum*. In the event of repeated determinations over several weeks or, more definitely, in the event of exposure to the sun, those variations must be taken into account in the interpretation. Moreover, caution is required in using

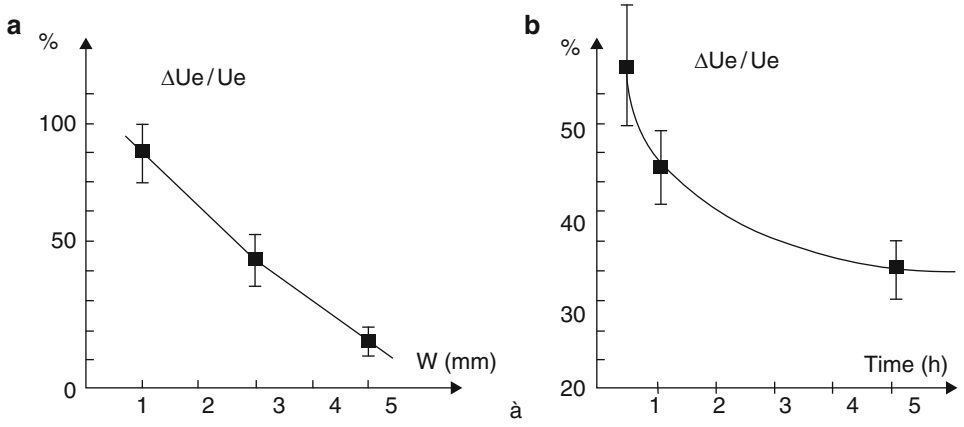

Fig. 12 (**a**) Influence of the geometry of the skin area under stress on the contribution of the *stratum corneum* to the determination (After Lévéque and de Rigal (1985)). **w** gap width. (**b**) Variation in the moisturizing efficacy of an emulsion following a single application (After Aubert et al. (1985a))

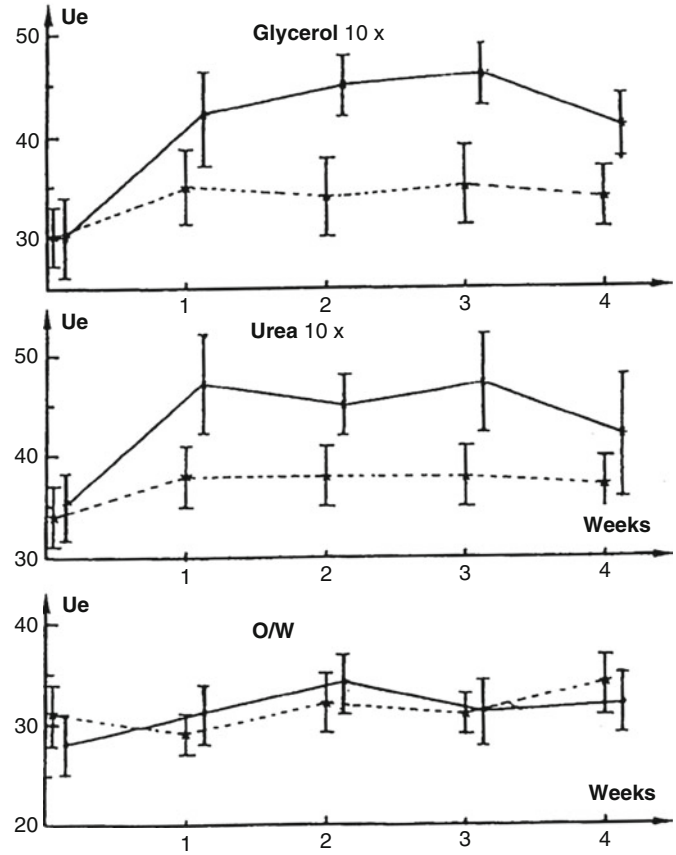

Fig. 13 Comparison of the moisturizing efficacy of three emulsions (same vehicle), treatment for 3 weeks and carry-over for 1 week, on the legs of 15 people per group. It will be observed that only the emulsion containing glycerol had a carry-over effect (After Levêque and de Rigal (1985))

dimensionless quantities: the ratio between two deformations obviously eliminates the dependency on thickness, which is true for some of them (e.g., U_e/U_r), while others remain time-dependent, such as U_f/U_e and U_V/U_e (through the exponential term).

3.1.2 Uniaxial Extension

Several authors have addressed this uniaxial extension method (Wijn 1980; Gunner et al. 1979). Two pads are stuck to the surface of the skin at a distance that varies as a function of the skin area subject to the stress. Either a force is generated by an electromagnet and the induced displacement measured as a function of time (the principle is identical to that of the Twistometer) or the displacement is imposed by a motor and the force recorded (relaxation phenomenon). These methods, while potentially interesting, have been little used in the study of hydration phenomena. In addition, they have the disadvantage of being sensitive to the orientation of the axis of the stress relative to the natural tension lines of the skin (Langer's lines) and that the area submitted to stress is not well defined.

3.1.3 Gas Bearing Electrodynamometer®

A little used but potentially very promising method has been developed by Christensen et al. (1977) and Hargens (1981), and used in cosmetic applications by Mass et al. (1983) and Cooper et al. (1985). The apparatus consists in the gas bearing electrodynamometer. It measures the displacement (3–4 mm) of a sensor stuck to the skin using a small disk and 2-sided adhesive. The sensor is alternately actuated by a sinusoidal electromagnetic field (1–2 Hz) generating a force of less than 10^{-3} N (Fig. 14). An oscilloscope displays the skin response (force-displacement plot) which is in the form of a hysteresis loop, characteristic of viscoelastic materials. The loop figure is used to calculate the following parameters:

- The slope of the main axis of the loop (or DSR, dynamic spring rate), comparable to Young's modulus
- The ratio between loop opening and displacement, or loss angle (for a purely elastic material, that angle is equal to 0)

The authors (Christensen et al. 1977, Hargens 1981) showed that the more the skin is hydrated, the more the angle of loss increases and the more the hysteresis loop is inclined on the displacement axis (same force but greater displacement) (Fig. 15). The effect of various formulations containing moisturizing active substances has been clearly shown (Schade 1912). According to the designers, this method has the major advantage of making it possible to record immediately after formulation application and thus studying the immediate moisturizing effects (in the very first few minutes).

3.1.4 Determination by Acoustic Wave Propagation

The principle is described in detail in reference (Potts et al. 1980). Broadly speaking, a vibrating

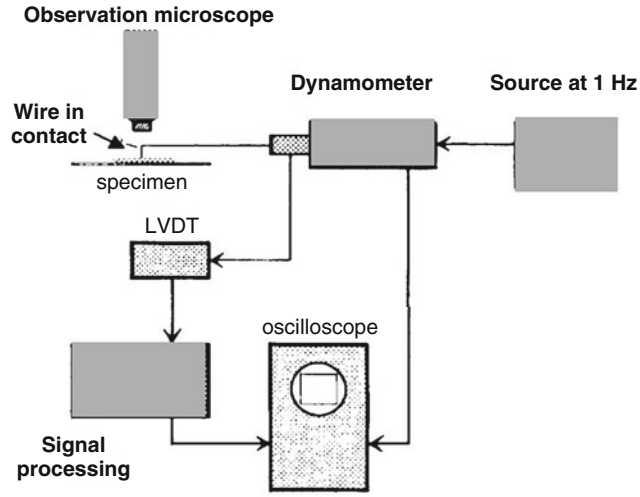

Fig. 14 Diagram of the gas bearing electrodynamometer (After Christensen et al. 1977). *LVDT* linear variable differential transformer

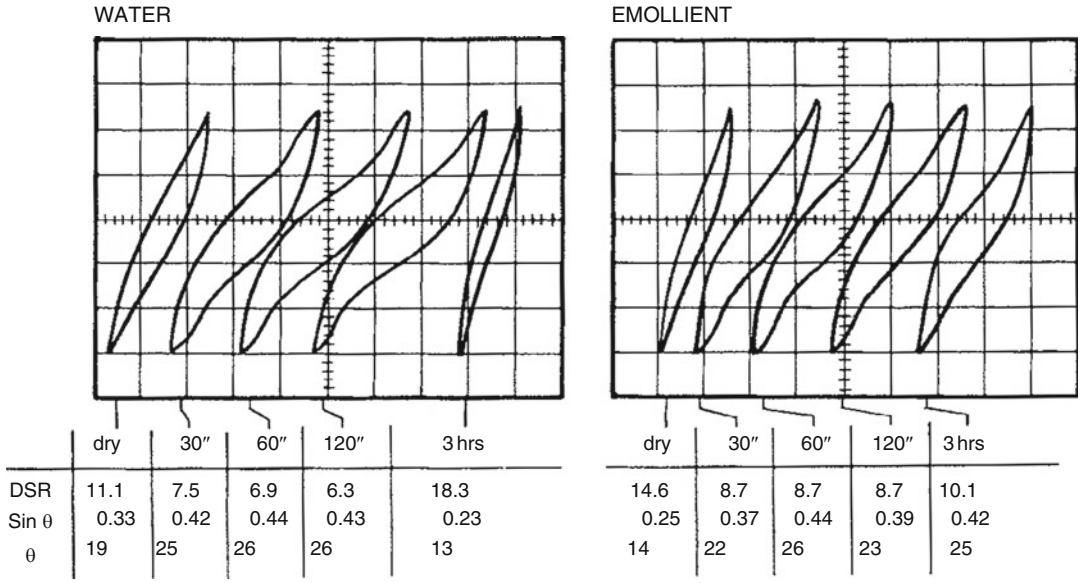

	dry	30″	60″	120″	3 hrs
DSR	11.1	7.5	6.9	6.3	18.3
Sin θ	0.33	0.42	0.44	0.43	0.23
θ	19	25	26	26	13

	dry	30″	60″	120″	3 hrs
DSR	14.6	8.7	8.7	8.7	10.1
Sin θ	0.25	0.37	0.44	0.39	0.42
θ	14	22	26	23	25

Fig. 15 Profile of the traction elongation curves obtained with the GBE, for water (*figure on left*) and an emulsion (*figure on right*). Note the differences in kinetics and efficacy (After Christensen et al. (1977))

source is placed on the zone under study and two vibration transducers in the axis of propagation determine the propagation velocity of the wave and the amplitude of the vibrations. The propagation velocity and damping coefficient are studied over a frequency band from 8 to 1016 Hz. The same authors (Potts and Buras 1985) showed that those parameters have a minimum for a frequency, F_{min}, whose values are 400 and 700 Hz for hydrated and dry skin, respectively. It should be noted that the F_{min} value increases with age, reflecting the dryness of the skin in the elderly.

This method does not seem to have undergone marked development in cosmetic or dermatological applications. It should be taken again into consideration for a new development with modern technologies.

3.2 Stress Perpendicular to the Plane of the Skin

Several methods stressing the skin perpendicular to its plane have been developed. The first studies were carried out by Grahame (1970). The best known and most widely used instrument is the Cutometer® which belongs to the suction group. Other methods include indentation, levarometry, and ballistometry.

3.2.1 Suction: Dermaflex®, Cutometer®

The Cutometer is by far the most widely used of this type of apparatus and is the only apparatus enabling determination of the mechanical properties of the SC using a probe of diameter 2 mm. The record profile is the same as that recorded using the Twistometer, and the parameters measured are identified using the same symbols.

3.2.2 Indentation or Levarometry

Since Schade's work (Schade 1912), several authors (review in Aframian and Dikstein (1995a)) have developed levarometric methods (traction perpendicular to the plane of the skin). The authors having attempted to determine hydration by indentation are equally numerous (Aframian and Dikstein 1995b). However, no moisturizing effect has been demonstrated even with very low pressures (Dikstein and Hartzshtark 1983) because the SC is very rigid and transmits stress to tissues with much lower stiffness.

3.2.3 Ballistometry

The principle of this system was developed by Tosti and is described in detail in reference (Tosti et al. 1977). The initial developments date back to the 1930s when an apparatus intended for ophthalmology, to determine ocular pressure, was used. That apparatus has no application in the determination of moisturizing effects.

3.3 Comparison of Method Sensitivities

Among the numerous mechanical methods, and apart from the problems related to the interpretation of the results, it is important to determine which method is the most pertinent or the most sensitive in order to quantify the moisturizing properties of cosmetic formulations. Several authors have studied the correlations, relative to moisturizing efficacy, of the various methods. Wickett's study (Wickett et al. 1996) showed that the parameters determined by the Twistometer or Dermal Torque Meter are more sensitive to hydration than those measured with the Cutometer. The sensitivity to variations in water content of the parameters determined with the Cutometer was compared to that of the determinations using the Dermal Phase Impedance Meter (NOVA) (Murray and Wickett 1996). This study showed that several parameters may vary under the influence of the water content of the SC, but no general rule could be given. Several reasons can be suggested:

- The absence of correlation between parameters assumed to measure the same effects may be due to different depths of investigation.
- The differences in sensitivity of the Cutometer parameters to water content may be due to effects of treatment with different formulations, since Aubert et al. (1985b) did show that some formulations respond more from a mechanical point of view, while others respond more from a dielectric point of view.

Various comparative studies have pointed out the difficulty to interpret the results of mechanical determinations in terms of water content and showed that the protocol and/or formulation (vehicle) of the moisturizing active substances can markedly affect the validity of the determinations.

4 Methods Based on Electrical Measurements

4.1 Definitions

As is the case for heat energy transport, electrical energy transport obeys the Eq. 1 but here the function, F, is the electric potential and $\nabla\mathbf{F}$ the electric field. The flux, Φ, is the flux of the electrical charges. The constant k becomes the electrical conductivity, σ.

The relationship of Eq. 1, in its electrical form, leads, in an homogeneous conductor, to Ohm's classic law:

$$\mathbf{I} = \mathbf{G} \,.\, \mathbf{V} \tag{5}$$

where **I** is the current, **V** the potential difference, **G** the conductance of the conductor through which the current is running and R its resistance. $R = 1/G$. G or R are the magnitudes measured in practice with our instruments. They enable the electrical conductivity, σ, to be determined. The latter is strongly dependent on the water content of the skin.

For an homogeneous conductor, $\mathbf{G} = \mathbf{a} \,.\, \sigma$ where **a** is a purely geometric factor of the medium measured. The conductance (or its reciprocal, the resistance) thus depends on the electrical conductivity but also the geometry of the conductor. This is the main problem encountered in interpreting the determinations on skin since it is difficult to accurately determine the geometry of the "conductor" in the skin. Moreover, since the skin is far to be homogeneous, σ will also depend on the path of the field lines in the "conductor."

Conductivity determinations on skin are rarely carried out using DC current since phenomena of

charge accumulation at the electrodes (polarization) and migration of ions and molecules (electrophoresis) occur. Moreover, the determination of potential differences using direct current is subject to interference from galvanic effects. It is therefore necessary to use alternating potentials and currents to obtain usable cutaneous conductivity determinations.

Let us see what happens to Eq. 5 (Ohm's law) if a sinusoidal alternating potential difference of frequency **f** and pulsation $\omega = 2\pi f$ is applied to a slab of conducting material such as skin.

$$V = V_0 \sin(\omega.t)$$

The corresponding current flowing through the slab will generally not be in phase with the potential difference and will thus be expressed as follows:

$$I = I_0 \sin(\omega.t + \phi)$$

ϕ is known as the phase shift or, more improperly, the "phase" of the potential relative to the current.

To take into account the phase shift, we must use the concept of admittance Y (and its reciprocal named impedance Z), Eq. 5 becoming:

$$I(\omega) = Y(\omega).V(\omega)$$

The admittance Y depends on frequency and consists in a conductive term G (in phase with the potential) and a capacitive term C (90° phase shift), frequently known, respectively, as real and imaginary terms, with reference to the complex notation used to handle admittances and impedances. Measuring Y at a given frequency requires the determination of the ratio I_0/V_0 called its modulus |Y| and that of its phase ϕ. From these two values, G and C can be computed using an electrical model.

Let's take a simple example of a circuit consisting of a conductance G and capacitance C in parallel (this circuit is the simplest to be proposed to reflect the electrical behavior of the skin (Schwan 1957), although very imperfect). The Y modulus is given by:

$$|Y| = \sqrt{G^2 + (C.\omega)^2} \quad (6)$$

and the phase shift ϕ between V and I is such that: $tg\ \phi = C.\omega / G = R.C.\omega$. To simplify the explanation of the conductive and capacitive terms, it should be remembered that the first is proportional to σ ($G = a.\sigma$, a being a geometric factor), hence to the number and mobility of the free charges in the medium, while the second depends on its polarizability measured by its dielectric constant ε ($C = a.\varepsilon$). (Note that a perfect dielectric is an insulator of electrical DC current). A dielectric is characterized by its relative dielectric constant, ε. In vacuum, $\varepsilon = 1$. For air, $\varepsilon = 1$. For distilled water, $\varepsilon = 80$.) In consequence, we frequently separate the current circulating in a complex medium such as the skin into conduction current (term in phase with the potential difference) and out-of-phase current (term in quadrature).

4.2 Dielectric Properties of the Skin

Schwan (1957) was the first to show that living tissues and, in particular, the skin have, like all materials, domains of dielectric relaxation. In other words, the dielectric constant and hence the material's property to polarize decrease for given frequencies of the applied alternating current. Three relaxation domains have been identified:

- Relaxation α at low frequencies (0.1–1000 Hz) mainly related to the *stratum corneum* since they almost entirely disappear following stripping
- Relaxation β between 100 kHz and 500 MHz related to the polarizability (permanent and induced) of macromolecules and the water associated with them ("structural" water)
- Relaxation γ at hyperfrequencies (3–30 GHz) reflecting vibration of water molecules that are free, to some extent, in the tissue

These relaxation mechanisms are far from being fully elucidated despite numerous modeling

attempts: in addition to the structural complexity of the layers of the skin, our knowledge of the local electric field and the elementary currents induced by that field is imperfect. If we restrict ourselves to the problem of the water content of the SC, there are at least two possible effects of water content on its electrical properties:

- An increase in conductivity, σ, due to the ions dissolved in extra- and intracellular water
- An increase in the dielectric constant, ε, due either to a change in the structure of the lipid and protein layers (plasticizing effects (Barry 1987)) or an increase in the free water content

The methods used to measure the water content of the SC thus attempt to exploit those three effects, depending on the frequency used and the quantity measured (G, C or complex admittance Y). An excellent review of the various electrical methods applied to the determination of cutaneous hydration was published in 1983 by Lévéque and de Rigal (1983). Since that date, a rather high number of instruments have been launched on the market, each manufacturer claiming to offer the best. To get a more precise idea on these devices from an experimental point of view, many authors have published comparison studies. As a good introduction, we suggest the work of Fluhr et al. (1999) in which five instruments based on electric measurements (among the most popular) are tested and compared.

4.3 Low-Frequency Instruments

The frequency range of the relaxation α, mainly being due to the SC, may seem the most appropriate for determination of water content. However, electrode polarization phenomena are very important: the electrode-skin contact may be considered (as a first approximation) as a capacitor in series with the impedance to be determined. The influence will be all the stronger, the lower the frequency. As an indication, with an electrode capacitance of 1 μF/cm^2 (usual value), an electrode of area 1 cm^2 will have a complex impedance of modulus $|Z| = 1600\Omega$ at 100 Hz. This impedance will be in series with the skin and will modify both the determination of the modulus and the phase of the signal.

Several solutions have been suggested to overcome that difficulty:

- A conducting gel containing a mixture of polyethylene glycol and saline, in adequate proportions to define a given relative humidity (RH). Clar et al. (1975) were thus able to demonstrate, on the forearm, the efficacy of several moisturizing creams using a measurement electrode of diameter 1.7 cm filled with the gel. The reference electrode was a large-area silver/silver chloride electrode placed on the same arm. Their results show that the conductance G and capacitance C both increase when the water content of the skin increases. This is logical since both the conductivity (because of dissolved ions) and the dielectric constant (due to the high dielectric constant of free water) increase.

  By way of an example, the conductance and capacitance of the skin of the forearm nearly double when the ambient relative humidity (RH) increases from 66 to 86 %, and this remains valid over the frequency range from 10 Hz to 10 kHz (relaxation α). Figure 16 shows the relaxation for the two relative humidity levels defined above.
- Electrodes which undergo little polarization (e.g., a combined Ag/AgCl electrode) and have a small area (<1 cm^2) are used. Once again, the density of the current flowing through the skin must remain low (<1 μA/cm^2) to minimize the electrolytic effects at the electrodes and the electrophoretic effect in the skin. Kalia et al. (1996) have studied the relaxation of arm skin by measuring the modulus and the phase of the impedance of a small surface of the skin, from 1 to 1000 Hz, before and after several stripping procedures.
- A four electrode assembly can be used. In this case, two electrodes of relatively large area supply the current to the medium, while two thin electrodes measure the potential difference at the terminals, under a very high impedance, on part of the medium in which the electric field is uniform. The polarization of the voltage

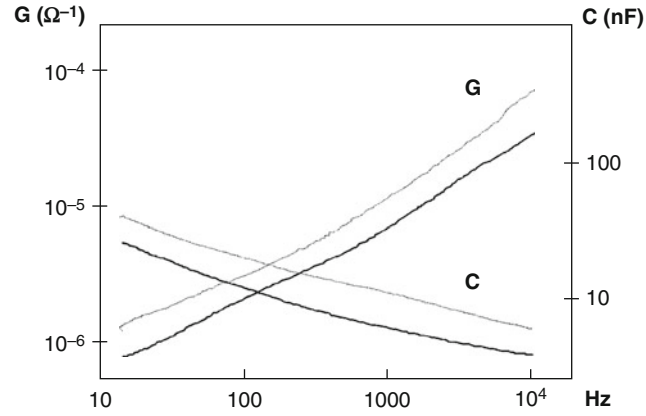

Fig. 16 Variations in conductance G and capacitance C at low frequency for two relative humidity levels *solid line* RH = 66 %, *dotted line* RH = 86 %

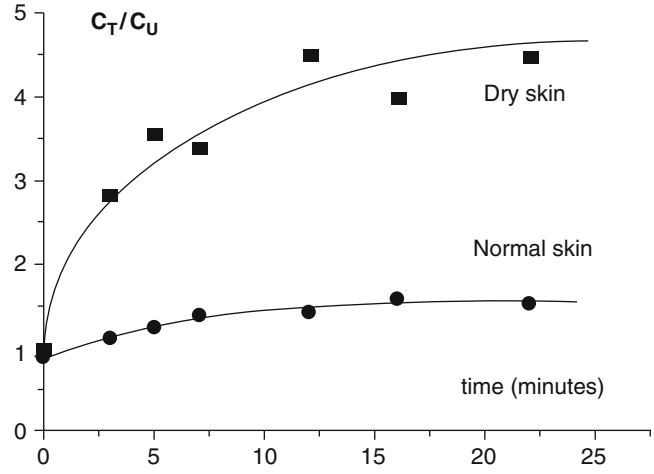

Fig. 17 Example of low-frequency capacitance determination (100 Hz) using the method by Serban et al. (1983). C_U and C_T are the capacitances measured on the skin pre- and post-occlusion using a film of liquid paraffin (Water diffusion index, $WDI = C_T/C_U - 1$)

electrodes has then no importance with respect to the determination. This principle has long been used for determinations on solutions (Ferris 1963; Bernengo and Hanss 1976) but is more difficult to use on the skin in vivo. Campbell et al. (1977) have succeeded in obtaining results which appeared promising.

– Several investigators decided to work with electrodes applied dry to the skin, a solution which presents the obvious advantage of enabling fast determination in equilibrium with the ambient relative humidity. In that case, the impedance of the contact at the electrode-skin interface is very sensitive to the pressure exerted on the electrode, and it is necessary to exert a slight, controlled overpressure to obtain reproducible results. As an illustration, Dikstein and Bercovici (1985) worked with gold-coated electrodes specially designed to apply constant pressure and obtained good results on water content by determining capacitance at 16 Hz.

Serban et al. (1983) used an innovative electrode (Serban et al. 1981) consisting of a grid closing a chamber in which a slight negative pressure was maintained in order to ensure that the electrode was applied to the skin with constant pressure (this electrode is marketed by Bor-Tru Inc., W. Redding, CT, USA). The reference electrode was an aluminum foil placed under the tongue. The capacitance of the skin under the electrode was measured, using an impedance meter, at 100 Hz. The values ranged from 0.5 to 25 nF, depending on the area and degree of hydration. Figure 17 shows the sensitivity of the

method, at occlusion, on two skin types subjectively rated dry and normal. The plot clearly shows that a stable capacitance value is obtained after 10 min of occlusion. This value is taken as the reference for maximum water content in order to calculate a "water diffusion index" (WDI) as follows:

$$\mathrm{WDI} = (C_{10} - C_0)/C_0$$

The index was well correlated with the subjective evaluation of skin dryness and with ambient relative humidity, after sufficiently long equilibration.

4.4 High-Frequency Instruments

Over the β relaxation frequency range, the electrode polarization interferes much less with the measurements than at low frequencies. Similarly, the ionic conductivity of any interfacial fluid or the variation in electrolyte concentration in the SC tends to be negligible at high frequencies. The investigator must nonetheless be conscious that the measurements are also related to the deep layers of the skin (the water content of which is fixed and high). Almost all commercially available instruments for determining cutaneous hydration operate at high frequency and are based on the following principle (Fig. 18):

A sinusoidal current generator I (ω) is connected to the measurement electrodes (generally concentric) either directly or through a matching coaxial cable. The external electrode acts as a guard ring to prevent dispersion of the flux lines (compulsory at high frequencies). A selective AC voltmeter tuned on the frequency of the generator or an instrument fulfilling that function such as a synchronous detector is used for measuring the amplitude and phase of the potential difference across the electrode terminals.

Although both admittance terms may be determined, only conductance G is generally used. Barel et al. (1991) have rigorously compared the respective advantages of conductance and capacitance determination in the evaluation of the water content of the SC. Tagami (1995), on the basis of in vivo and in vitro studies, reached the conclusion that, except for certain particularly thick areas of the SC, conductance provided a better feature of the water content of the SC than capacitance and yielded more reproducible results. It is nonetheless true that the calibration of a conductance determination in terms of the water content of the SC is highly delicate and will depend on the electrode-skin contact, the thickness of the SC, and the electrical properties of the deeper tissues.

4.4.1 Main Achievements

Lévêque and de Rigal (1983) have designed a portable instrument based on the principle described above and known as the Dermodiag®. The instrument uses a 10 MHz generator and determines the conductance between two concentric electrodes of external diameter 10 mm and interelectrode gap of about 1–4 mm. A constant pressure on the skin is ensured by a spring system. The instrument is routinely used in L'Oréal research laboratories to evaluate the action of moisturizing products and, more generally, the water content of the SC but is not commercially available.

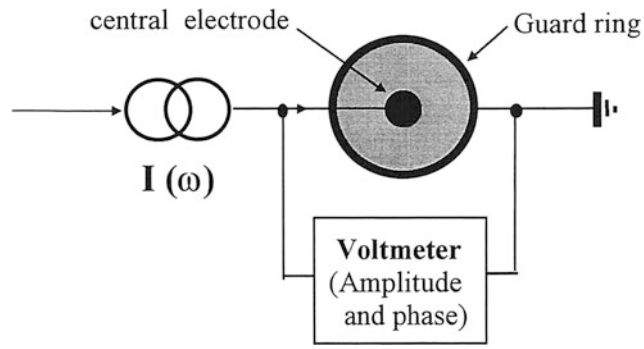

Fig. 18 Schematics of a concentric two electrodes high frequency device

Based on the same principle but fitted with a set of six variable diameter rings and a multifrequency generator, the SCIM® developed by S. Ollmar (Copenhagen, Denmark) (Emtestam and Ollmar 1993) is marketed by its designer. The apparatus uses a set of gaps to evaluate the impact of deeper tissues on the impedance determination of superficial layers and better elucidate the trajectory of the flux lines. A computer program uses five determinations at different gaps and different frequencies (between 1 kHz and 1 MHz) to calculate the water content of the epidermis and superficial dermis. In its current state, the instrument is not suitable for determining the water content of the SC since the range of impedances for which it has been designed is not compatible with the impedances of the dry SC (even in equilibrium with normal ambient relative humidity). The determinations are made by moisturizing the skin as much as possible using a compress soaked in normal saline, before positioning the apparatus, procedure which particularly addresses the changes in deep water contents observed in the course of irritant or inflammatory processes. The principle could nonetheless be advantageously applied to the determination of superficial water content.

Since 1980, Tagami et al. (1980) have been using a device developed by Masuda et al. (1980) to determine the amplitude and phase of the admittance of the skin at 3.5 MHz. Measurement electrode coupling is ensured by a matching circuit followed by a coaxial cable, thus providing great flexibility in use. The electrodes are concentric and have diameters from 1 to 4 mm. However, a 2-mm central electrode may also be used to enhance sensitivity. When the electrodes are applied to the skin, an initial fast rise in conductance and capacitance values is observed, followed by a slow drift due to the transepidermal water loss. Contact is thus maintained for a minimum time of 3 s to carry out the determination.

The apparatus, marketed under the proprietary name Skicon-200® by IBS Ltd. (Japan), has been thoroughly tested by Moseley et al. (1985) and calibration conducted on models consisting in SC placed on water-saturated filter paper (Tagami 1995). The authors admit that, since the determination is conducted on a small area, marked geographic variability is observed even between neighboring sites, due, for instance, to the density of the sweat glands and variations in SC thickness. As was the case with the previously considered instruments, a pressure control system is provided. A set of results is given indicatively in Fig. 19. The figure shows the time course of cutaneous conductance, as a function of the number of stripping procedures, on a healthy adult forearm. Numerous other results concerning the relationship between water content and transepidermal water loss in healthy and pathological skin are also available (Tagami 1988, 1995; Tagami and Yoshikuni 1985; Horii et al. 1989). A new concentric ring probe has been recently launched under the reference 200EX® announced to present a much smaller depth of measurement.

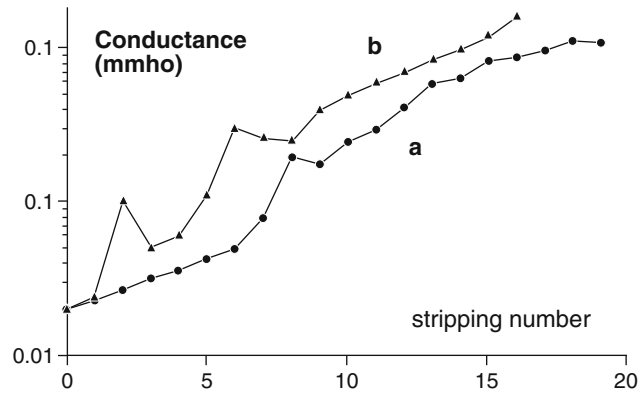

Fig. 19 Conductance of the skin after stripping showing the resultant increase in water content determined with the Skicon-200 (After Tagami (1988)). (**a**) 34-year-old woman, (**b**) 58-year-old man

An apparatus based on a very similar principle to that used in the previous device, and measuring high-frequency conductance changes, is manufactured by Nova Technologies, Gloucester (UK): the Nova DPM 9003®.

Martinsen et al. (1993) have presented a 3-electrode measurement system. The skin is included in the negative feedback loop of an operational amplifier. Since this circuit achieves a virtual ground, a unipolar determination is carried out, irrespective of electrode impedances, at least in theory. The current crossing the measurement electrode is determined by a current-tension converter, and since the alternating potential is imposed by a voltage generator, the admittance thus determined is exactly related to the volume of skin under the electrode. A frequency of 100 kHz was selected as a good compromise between electrode polarization and high capacitance leakages that occur at high frequency. The authors show that significant variations in admittance are measured with progressive moisturization of the skin but also report electrode-related reproducibility problems. While the 3-electrode system is based on an elegant principle, it is not certain that it contributes any marked improvement compared to existing high-frequency instruments.

The Corneometer® CM 825 from Courage and Khazaka (Cologne, Germany) has been described in detail by Barel and Clarys (1995) and has also been tested by Moseley et al. (1985) and Blichman and Serup (1988). The capacitance variations of the electrode-skin assembly $(C_0 + C_{skin})$ are measured by the displacement of the resonance frequency of the oscillating circuit connected to the oscillator. If the conductance G in parallel with the capacitance C is low, the oscillation frequency of an oscillating circuit containing an inductance L and a capacitance C in parallel is given by:

$$f_0 = 1 / \left(2\pi . \sqrt{L.C}\right) \text{ where } C = C_0 + C_{skin} \quad (7)$$

The early models of this type operated between 75 kHz empty and 40 kHz when moisturization is at a maximum, equivalent to a 3.5-fold variation in capacitance C. Since the dielectric constant of the SC ranges from 8 (dry SC) to 80 (pure water), the capacitance of the skin should also vary in the same ratio, if the determination only addresses the SC and not the deeper tissues. New models are supposed to operate at higher frequencies around 1 MHz.

The electrodes are innovative. They are comb shaped interdigitated on a grid, as shown in the Fig. 21 below, and gold coated. The electrodes are not in ohmic contact with the skin, since they are coated with a thin layer of vitrified insulating material (thickness 20 μ) with a low dielectric constant. The dimensions of the network are as follows: line width 50 μ, between-line space 75 μ, and size of the active part 7 × 7 mm. Former probes versions were analogic, while a digital version is now proposed, announced to be more stable (in frequency and amplitude). The comb shape has been kept unchanged.

An example of results obtained with this instrument on the forearm skin at several RH is given on Fig. 20. The correlation between readings and ambient humidity is quite satisfactory.

Since knowledge of the penetration depth of the electric field is essential for the interpretation of the results obtained by this method, layers of polyester film were inserted between the electrodes and the skin (Barel and Clarys 1995). This approach showed that the measurement depth was up to 100 μm, but the contribution of the total capacitance of a layer at that depth did not exceed one tenth of what it would have been at the surface. On the basis of these results, it is clear that the influence of the epidermis on the determination can be neglected. We may also suspect that the low water content values obtained in "dry skin" phenomenon and in other states of abnormal rugosity of the skin are only due to the persistence of imperfect contact with the skin surface. According to computations based on recent publications dealing with open comb capacitance modeling (Starzyk 2008), the presence of a layer of air of a few μm thickness under the sensor should not, theoretically, influence the measurements. These publications, together with well-known methods such as finite elements approach, might be used to better investigate the electric

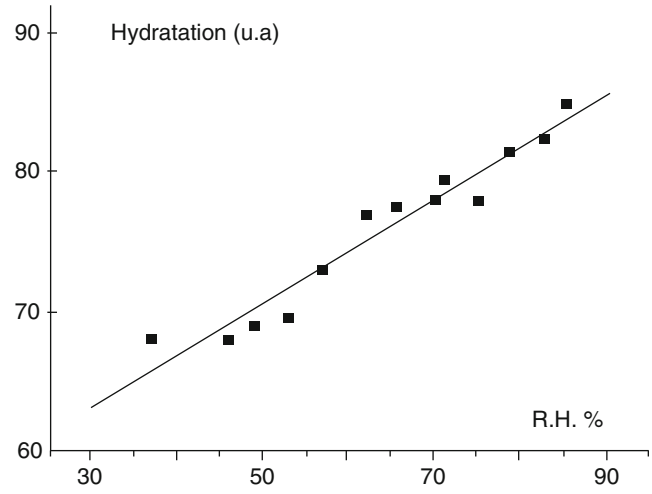

Fig. 20 Relationship between the corneometer reading and ambient relative humidity determined on the forearm at 22 C. Values obtained on 15 subjects aged 18–30 years. Correlation coefficient r = 0.98 (After Barel and Clarys (1995))

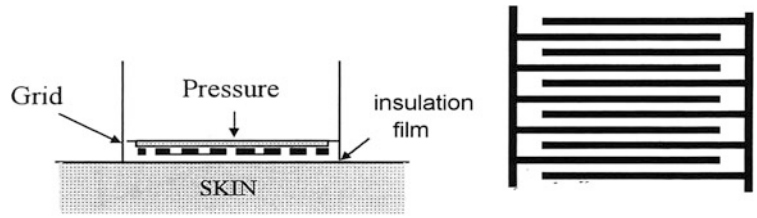

Fig. 21 Comb interdigitated electrodes for surface dielectric measurements

field strength inside the skin, considered as a multilayer dielectrics.

To conclude this chapter, let us have a look on Clarys et al. publication (Clarys et al. 2012). Recently, the authors have extensively compared two modern instruments: the Corneometer CM825® (C & K), which measures a capacitance, and the Skicon-200EX® (IDS), measuring a conductance. Due to their different principle, the devices calibration is very different: the value recorded on a filter patch saturated with a physiological solution is set to 120 arbitrary units (Corneometer), while a standard precision resistor is proposed for the Skicon. In vitro penetration depth evaluations led to values about 45 μm for the Corneometer and 20 μm for the Skicon.

In vivo hydration measurements were carried out on healthy male and female volunteers ($n = 20$) varying from 20 to 71 years of age. Several skin sites were examined to get hydration values from very dry to well hydrated. Correlations between the instruments were all highly significant (all $P < 0.001$). The mean intraperson variability, calculated over the total range of hydration measurements, is improved in the new version of both instruments, with a coefficient of variation (CV) figure around 7 % for the Corneometer and 10 % for the Skicon. The authors conclude that both devices are reliable and able to measure skin hydration, though presenting specificities: capacitance measurements being more sensitive on dry skins and conductance better suited for high hydration levels.

4.5 Hyperfrequency Measurements

Water is a polar liquid, in other words, composed of molecules bearing a permanent electric charge and, in consequence, oriented under the action of an external electric field. The relaxation frequency of this phenomenon is centered on 18 GHz at 20 °C and thus can be observed at hyperfrequencies. The water molecules bound to proteins relax at lower frequencies of the order of the GHz or even lower (according to the nature of

bound water, as already mentioned at the beginning of this chapter). Schwan (1957) was the first to carry out dielectric measurements on skin at hyperfrequencies with coaxial lines supplied by a klystron (A klystron is a very high-frequency generator (>1 GHz)). The γ relaxation described by this author being obviously related to water, it seemed obvious to try and exploit that phenomenon to determine the water content of the SC, particularly since hyperfrequencies propagate essentially at the surface of conductors ("skin" effect).

The development, in the 1970s, of coaxial cable testing, lead to the production of hyperfrequency equipment operating with pulses in the time domain (measure over time of the response to a pulse, time domain reflectometry, TDR). This technique opened the way for a new type of studies on living tissues, which were then directly placed at the end of the coaxial measurement line.

Moreover, as the theoretical studies progressed, the method proved to ensure concomitant monitoring of the relaxation of bound water and free water. The complexity of the required hyperfrequency instrumentation and the difficult interpretation of the results have not allowed a widespread use of these determinations on skin, despite the considerable potential. Following a doctoral dissertation on the subject (Djeldjellani 1989), investigations on skin water content were conducted by the L'Oréal research laboratories (Diakate et al. 1994). The major difficulty in the technique is associated with the applicator which ensures the transition between the coaxial line carrying the electromagnetic field and the skin. A "ground plane" antenna was developed (Djeldjellani 1989), but we consider that the future of the technique resides in the use of "strip lines" which can be placed in direct contact with the skin.

Using conventional instrumentation employing 1-GHz sinusoidal waves, Jacques (1979) determined the water content of the SC using an innovative interdigitated applicator which ensures extremely superficial flux lines (penetration depth: 3 μm). A linear relationship between the conduction current due to the free charges of the dielectric medium and the water content of the most superficial part of the SC was thus established. Hyperfrequency techniques, although very promising, have not yet been extensively used in dermatological and cosmetic metrology.

5 Photothermal and Photoacoustic Techniques

These techniques are based on the conversion of light energy into heat energy in the skin. This heat energy can then be directly detected by IR radiometry or be converted into pressure variations in an adiabatic chamber. The incident energy may be modulated periodically at a frequency, f (frequency mode or CW), or delivered in pulses (temporal or pulse mode). The collected signal will depend on the optical properties (absorption, diffusion) and thermal properties (diffusivity, effusivity) of the skin.

5.1 Pulse Radiometry

The principle is simple: a powerful pulse source (flashlight or laser) is targeted on a small surface area and the transient increase in temperature that occurs during beam absorption is monitored by infrared radiometry. The wavelength of the source depends on the application. This wavelength must match one absorption band of the tissue to ensure that optimal heat transfer takes place (Fig. 22).

Balageas et al. (1986) in their studies used a ruby laser emitting in the red range, a pulse duration of 350 μs, and an energy of 0.2 J/cm^2. They blackened the skin with carbon black to ensure the required heat transfer (of the order of 20 °C). Detection was conducted using an HgCdTe element cooled with liquid nitrogen and sensitive over the range $7-12\,\mu$. The temperature was monitored from 2 ms to 100 s after the light pulse. In a thermally uniform medium, the temperature variation, ΔT, due to the energy Q impinging on a unit area of the medium falls off as a function of time in accordance with the following relationship:

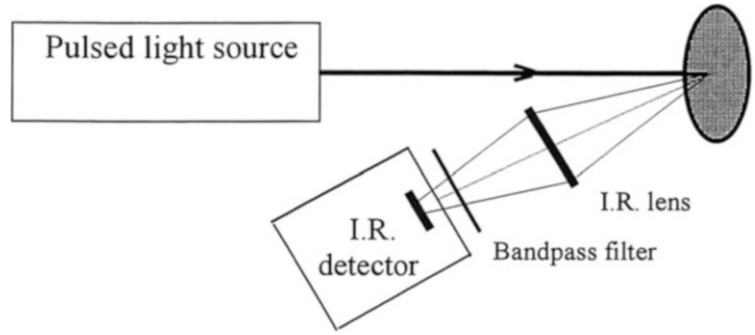

Fig. 22 Principle of pulsed photothermal measurements with infra-red detection

$$\Delta T = Q / \left(e.\sqrt{\pi}.\sqrt{t}\right) \quad (8)$$

e (t) is the medium effusivity (cf. Sect. 2.2)

If the medium is not homogeneous (as is the case with the SC), e (t) may be calculated at any time during the return to thermal equilibrium. For short times (<0.1 s), the measured effusivity is that of the SC (of the order of 1000 $J/m^2/s^{1/2}/K$). Since the square of the effusivity is proportional to the product of the thermal conductivity and the thermal capacity (cf. Sect. 2.1.5), the effusivity is very sensitive to the quantity of free water and, moreover, a contact-free measurement of water content is perfectly feasible. The authors observed that effusivity is not constant over time from 2 ms to 100 ms (as might have been expected with a homogeneous layer model (Stolwijk and Hardy 1965)) but regularly increased. The authors deduced that there is a variation in the thermal properties of the SC from the surface to its deep boundary. This variation may be explained by the gradient in water content. The free water concentration gradient in the SC may therefore be explored.

A related photothermal approach known as optothermal transient emission radiometry (OTTER) has been developed by Imhof et al. (1990). The authors used a cryogenic detector identical to that used above but their source was a Yag-Neodyme laser, 1.06 μ, delivering very short pulses (15 ns) with a repetition frequency of 20 Hz and fit with a harmonic generator so that the working wavelength be divided by 2, 3, or 4. The area illuminated by an optical fiber has a diameter of 6 mm, while the infrared beam is collected by an ellipsoidal mirror with a high numerical aperture focused on the detector. The signals received by the detector at each laser pulse are accumulated in a digital memory in order to enhance the signal/noise ratio. Filters are used to restrict the optical pass band of the detector so as to characterize (at least by a few points) the emission spectrum of the skin. In the study presented in Imhof et al. (1990), a wavelength of 355 nm was used and the temperature profiles were determined over a very short time, less than 10 ms. Under those conditions, only the SC is concerned by the thermal signal, as expected. Contact-free SC water content studies were conducted by the same team (Bindra et al. 1994) using this method. Currently, the method is among the most promising, although the instrumentation required is complex and expensive.

Using this technique, the Imhof team (Guo et al. 2001) has published results concerning the water content of SC samples, in terms of free and bound water (interacting with keratin). These samples were of the same kind as for Levèque et al. study (Lévéque et al. 1987a), i.e., normal, delipidized, and delipidized + water rinsed SC. A tunable laser source allowed to investigate water absorption around the 2.94 μ band, while the light emission is recorded at 13 μ. The authors observed that the absorption band of bound water at low humidity was neatly shifted towards high wavelengths, and was also narrower, compared to the bulk water band. The position of the peak envelope was shifted of about 30 nm downwards when the relative humidity rises from 3 % to 100 %. This shift showed a plateau between 10 % and 40 % RH on delipidized samples, while the decay was regular on normal SC. These results are in accordance

with previous data (Lévéque et al. 1987a) and show the powerful potentialities of OTTER techniques.

Recently, the same authors' team compared its OTTER technique with four popular instruments devoted to skin hydration measurements: Corneometer (C & K), NOVA DPM (DermLab), Moisture Checker (Scalar), and Fingerprint sensor (Fujitsu FBS200) (Xiao et al. 2010). Except for the last one, they all rely on some kind of impedance (capacitance or conductance) determination. OTTER showed a repeatability at least as good as the others, and a good correlation was found between the whole set of measurements, regarding several hydration conditions, from dry to wet skin.

5.2 Photoacoustic Spectrometry

The absorption of a light beam by the skin results in a localized temperature increase. The photoacoustic effect consists in transforming those temperature variations into gas pressure variations and the latter into an acoustic signal. The studies on skin were essentially carried out with an amplitude-modulated light beam at low frequency. We shall therefore restrict ourselves to this approach, which is more appropriate to the thickness of the SC, although techniques using pulsed rather than modulated light exposures have been developed (Patel and Tam 1981).

The theory of the photoacoustic effect is rather complex (e.g., Rosencwaig and Gersho 1976). Two aspects have to be looked for: From an optical point of view, the diffusion and absorption properties of the skin (absorption spectrum, optical penetration depth $\boldsymbol{\mu_0}$) are essential. Obviously, when working with the SC, UV radiation is preferable because it is particularly absorbed by that layer. Moreover, the technique is frequently used since Rosencwaig and Pines early wors (1977) to study sunscreens. On the other hand, the production of thermal waves is bound to the thermal diffusion length $\boldsymbol{\mu_T}$, inside the skin layers, which is an important factor to determine the depth at which the signal detected at the surface is generated. It is given by the relationship:

$$\mu_T = \sqrt{\alpha/(\pi.f)} \tag{9}$$

in which α is the thermal diffusivity and f the frequency of light beam modulation. For example, if the thermal diffusivity of the tissue is taken to be equal to that of pure water, $\boldsymbol{\mu T}$ is equal to 6.8 μm at 1000 Hz while $\mu T = 215\,\mu m$ at 1 Hz. It is thus clear that rather high frequencies are to be used for the SC and very low frequencies for studies of intracutaneous penetration (Bernengo et al. 1998).

The main limitation in the method in "in vivo" determinations is that the surface of the skin to be studied must be placed in a closed chamber to ensure adiabatic conversion of heat waves to sound waves and detection of the latter using a microphone. The measurements require a relatively long integration time due to the weakness of the electrical signal from the microphone. Hence, an increase in water content due to occlusion is inevitable.

The measuring cell has to be carefully designed to enable strong illumination of the skin and to feed the weak acoustic signal to the detection microphone. Several open models have been designed for in vivo work. Figure 23 shows three different cells that have been successfully used. Though synchronous detection is used, the signal at low frequency is greatly disturbed in vivo by body sounds (heart beat, muscles, blood circulation). For that reason, differential cells have been developed (Poulet and Chambron 1982; Guy and Bemengo 1986) with an at least tenfold improvement in the signal/noise ratio compared to the simple chamber cell.

Since the first UV spectra of the skin in vitro published by Pines and Cunningham (1981), numerous researchers have conducted studies of SC water content in vitro and in vivo (Campbell et al. 1979; Poulet and Chambron 1983; Giese and Kolmel 1983; Poulet 1985). Simon et al. in 1981 (Simon et al. 1981), working with the absorption band of water at 1.9 μm, determined the water content profile of the SC in vivo. While the free water contents obtained in this study were not accurate, since the bilayer model used at this time was not suitable (as showed later by Poulet (1985)), the concept nonetheless remains seductive. More recently, Takamoto et al. (1994)

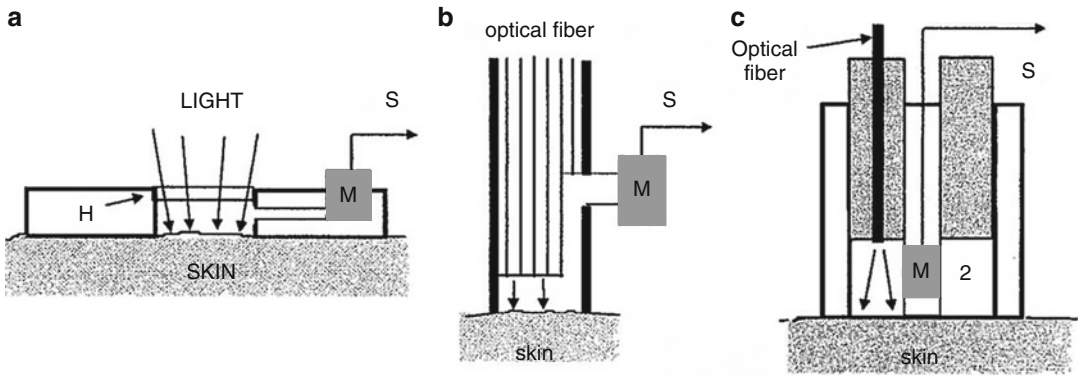

Fig. 23 Three types of cell used for photoacoustic measurements on skin. (**a**) direct illumination through the cell by Simon et al. (1981) (**b**) resonant cell by Takamoto et al. (1994) (**c**) low-frequency differential cell by Guy and Bernengo (1986) **S**: output of the electrical signal from the microphone, M

developed a very small volume (40 µL) resonance cell matched on 2.2 kHz . After optimizing the device, they obtained a fivefold gain in sensitivity compared to a conventional open cell. This gain led them to markedly lower the integration time, therefore reducing the passive hydration by occlusion and the dose of UV radiation received by the skin. Working with hairless mice, the authors were able to measure the variations in the photoacoustic signal induced by percutaneous absorption of an ointment (1 % IDM in PEG). Their results relate to the very superficial layers of the SC, since they were generated using a doubled argon laser at a wavelength of 257 nm, absorbed in the first few microns of the SC. The authors argue that the use of their device on man is problem-free since the energy received by the skin is low, less than 40 mJ for the study described above.

Lastly, it should be noted that some signal processing techniques used by photoacoustic scientists working on plastic and ceramic materials have been borrowed by researchers in the skin field: Baesso et al. (1994a) conducted phase measurements on the photoacoustic signal with a modulation frequency from 18 Hz to 62 Hz. The authors confirmed the SC diffusivity values obtained through photothermal determinations. The same authors studied the penetration of products into the skin using Fourier transform photoacoustic spectroscopy (Baesso et al. 1994b), thus adopting a pulsed technique that is in widespread use for powders and sintered materials (Patel et al. 1981).

Rompe et al. (2005) in 2005 have studied SC properties through photoacoustic technique, using a powerful xenon lamp and a monochromator in the range 240–400 nm. Frequency modulation was 17 and 70 Hz. They claimed a thermal diffusion length of 15 µ at the latter frequency and displayed a set of PA spectra of SC, showing clearly the influence of hydration on the spectral shape.

6 Optical Techniques in the Near and Middle Infrared

These optical methods target directly the water molecule, insofar as they quantify the amplitude variations of the reflected light inside and outside the absorbance peaks of that molecule. While calibration can be easily carried out in vitro, the transposition in vivo is not easy, and it is therefore frequently not possible to directly quantify water content. For the methods using the near IR (as for nearly all others), the calibration relationships determined in vitro (usually on multilayer phantoms) do not obviously apply in vivo since the light penetration conditions cannot be exactly compared and present a much higher variability (skin localization, SC thickness, molecular absorbers such as melanin, etc.). The influence of the surface state of the skin (diffusion, variation

in refractive index, etc.) may be very strong and lead to tricky interpretations of the results in terms of variation in water content.

6.1 Attenuated Total Reflection (ATR) Infrared Spectroscopy

Used both in the intermediate IR field (by chemists) and in the near-IR (NIR) range, ATR methods rely on the phenomena of multiple attenuated reflection to enhance determination sensitivity (Gloor et al. 1981a). The principle is shown on Fig. 24:

The optically perfect surface of a zinc or germanium selenide crystal (transparent in the IR) is applied to the skin. The incident beam is propagated by multiple reflections within the crystal. Following each reflection by the surface of the crystal in contact with the skin, a part of the energy is absorbed by the skin because of the evanescent wave phenomenon, related to the electromagnetic nature of light. When the beam leaves the crystal, the skin's absorption spectrum is recorded by an appropriate IR detector (thermal or semiconductors). Because of the submicronic penetration of evanescent waves, this method has the major advantage of only analyzing the first micron of SC thickness or even less. Schneider and Hansen (1997) have confirmed that the choice of crystal and angle of incidence enable analysis of the skin at depths ranging from 0.3 to 0.9 μ, i.e., of the order of the thickness of 1–2 layers of corneocytes. In consequence, the measures are strongly dependent on variations in ambient air humidity and therefore require rigorous equilibrium of the patients in laboratory ambient air. In addition, such measurements are also strongly dependent on the thickness of the sebum film (or residual cosmetic cream) on the skin surface. Some results supposedly related to SC had in fact to be partly or even totally attributed by such film effects.

In the homogeneous medium external to the prism, of refractive index n_2 (here the SC), the wave theory of light shows that the intensity of the evanescent wave decays exponentially from the surface of the prism (index n_1). The depth of penetration z (defined as the value for which the light intensity is divided by $e = 2.7$) is proportional to the wavelength, λ, and inversely proportional to a term including the sine of the angle of incidence. It depends on the refractive index n_2 of the SC and, hence, on its water content.

As an example, the values of z in a totally hydrated SC of index 1.33 are given below, for the four angles available on the Skin Analyzer (which description follows):

Angle	40°	45°	52°	60°
Depth z	0.3 λ	0.18 λ	0.14 λ	0.11 λ

It should be carefully noted that the parameter z does not define an abrupt penetration limit and that a noteworthy quantity of energy is absorbed at deeper levels. Those levels nonetheless remain much smaller than the thickness of the SC.

Several methods of quantifying water content on the basis of the ATR spectral data have been applied. They mainly refer to the middle IR absorption bands, though near IR can also be successfully used.

Middle IR techniques:

- The ratio between the absorbances of the amide I and II bands (6.06 and 6.45 μm, i.e., 1649 and 1540 cm^{-1}). This is a measurement of the water content (Gloor et al. 1980, 1981a), since the 6.06 μm band interferes with the 6.1 μm water band, the 6.45 μm band being independent.
- Measurement of the area of the water absorbance peak at 4.76 μm (2100 cm^{-1}) (Potts et al. 1985; Potts 1985) on the basis of calibration conducted in vitro, without using an internal standard.

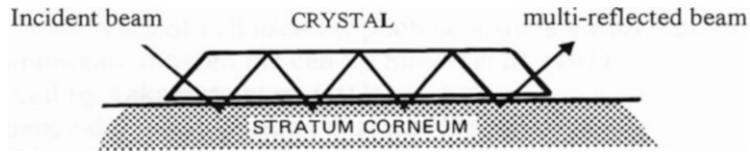

Fig. 24 The attenuated total reflexion (ATR) applicator

– Measurement of the absorbance at 8.94 μm (1118 cm^{-1}) and 9.65 μm (1036 cm^{-1}) (Comaish 1968).

Near IR experiment:

– The ratio between the absorbances at two wavelengths, 1.95 and 1.8 μm. The peak at 1.95 is specific of water (Koelmel and Mercer 1980), which does not absorb at the reference wavelength of 1.8 μm (Comaish 1968).

In order to enhance the resolution and quality of the results, the spectral determinations were analyzed using a Fourier transform IR spectrometer (Klimisch and Chandrag 1986). An ATR adapter is commercially available under the proprietary name Skin Analyzer from Perkin-Elmer, France. Three total reflection prisms providing different angles of incidence (between 40° and 60°) and hence different penetration depths are supplied. Zinc selenide is the most widely used prism material. The surface of the prism in contact with the skin is horizontal, and outside of the apparatus, so that the forearm can be layed on it. Zn-Se crystals mounted at the end of an optical fiber are now commercially available and allow measurements everywhere on the body, even on lips.

Unfortunately, the spectral acquisition duration, which is relatively long, induces a marked occlusion, which affects the measurements. Moreover, application of a cosmetic formulation, enhancing the quality of skin contact with the sensor, is liable to induce an artefactual increase in water content. The opposite effect occurs following serial treatment with surfactants. The influence of posttreatment modifications of the skin refractive index has not been evaluated, particularly in the presence of oil residues. It is true that the influence of the latter two sources of artifacts may be reduced by data processing methods (use of a ratio or an absorbance difference between two wavelengths, one being taken as the reference). Several authors have studied the influence of cosmetic formulations using this technique (Gloor et al. 1981b; Wirchrowski et al. 1985).

6.2 Near Infrared Spectroscopy (0.7–2.3 μ)

We are dealing in this chapter with direct reflection near infrared spectroscopy, as opposed to multiple reflexion ATR spectroscopy. This technique is employed in the analysis of the composition of materials and in the food industry for many years (Norris and Hart 1965). The method has been applied on skin to determine SC water content (Walling and Dabney 1989; Martin 1993) and cutaneous lipid content. It has a certain number of advantages compared to middle IR spectrophotometry:

– Greater sensitivity to water molecules, the absorbance peaks being well defined and rather isolated.
– Providing the signal is specifically processed, it is possible to extract information on bound and free water from the spectra.
– The analysis of surface diffusion enables characterization of the squamous conditions of the skin (in principle).
– The measurement time is sufficiently short for occlusion phenomena not to occur and for the water content to remain undisturbed.

In contrast, the technique has a marked disadvantage on ATR, related to variations in wave penetration into the skin. The volume under analyze varies with the wavelength in a complex manner, as is the photon path inside the skin multiple layers. Multiple scattering and nonradiative energy loss (absorption) occur simultaneously, and numerous models have been studied to work out quantitatively the light penetration in tissues (see for example (Kenji Iino et al. 2003)). As a rule, while scattering decreases when λ increases (whatever scattering model is considered), the mean absorption increases (without even considering lipid or water peaks). Skin transparency shows a maximum around 1.2 μm, at which the subcutaneous lipid peak is clearly visible, while it disappears at higher wavelengths.

In order to optimize exploitation of all the information contained in near IR spectra, many methods

of calculation have been developed. The simplest method consists in determining the ratio of reflected intensities or the difference between absorbances at two wavelengths selected as a function of the problem under study. In principle, the absorbance at the characteristic wavelength of the constituent is weighted by the absorbance at a wavelength at which the constituent does not absorb. An example is given for water in reference (de Rigal et al. 1993). With regard to the correction of the effects related to surface scattering, the multiple scattering correction (MSC) method makes it possible to recalculate an ideal spectrum (Isaksson and Mass 1988; Osborne and Fearn 1986; Geladi and MacDougall 1985). Other methods based on multivariate analysis or multiple regression are applied to spectral study, in which first or second derivatives calculus delivers enhanced information (Maes and Martens 1988). Methods based on partial least square (PLS) regression seem to be increasingly used. Those methods limit the information loss induced by a necessarily limited selection of wavelengths, when modeling the phenomenon under study (Wold et al. 1998). The various data processing methods were applied and compared in a single moisturizing efficacy study (Martin 1992).

Several basic research studies on the characterization of dry skin and the efficacy of moisturizing formulations have been published. They attempt to answer one frequently raised question, particularly by Kligman: "Is dry skin dry?" (de Rigal et al. 1993; Walling and Dabney 1989). A convincing study was carried out by de Rigal et al. (1993) using the Infra-Analyzer 500 from the Bran & Lubbe Company. The analyzer was modified in order to take "in vivo" determinations on all body areas. Its modification is shown in Fig. 25. The modified device, while maintaining basic performances and an integration sphere, made acquisition and processing of data in real time possible, which was not yet the case elsewhere (Wirchrowski et al. 1985). Working with isolated SC maintained under increasing controlled humidity conditions, the absorbance at 1.94 μm, expressed relative to that of a reference at 1.1 μm, was shown to be linearly correlated with water content. These results confirm those in reference (Walling and Dabney 1989), expressed as the absorbance at 1.94 μm, relative to a reference at 1.85 μm, although the data were acquired and processed by two different equipments.

Typical spectra recorded on the skin in vitro are shown in Fig. 26. The absorbance of the dermis alone is greater than that of the whole skin. This is due both to the increase in the analyzed volume (related to the greater penetration of the IR radiation), the absence of the less hydrated layer, and a reduced surface scattering. However, all the spectra show the peaks characteristic of water at 1.94 and 1.45 μm.

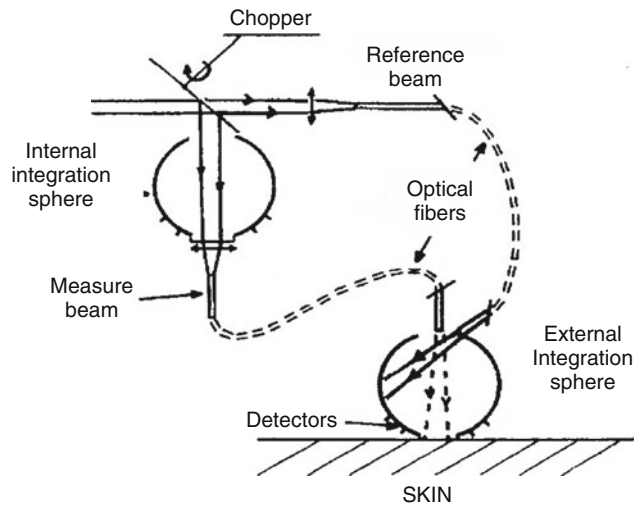

Fig. 25 Schematic representation of the modifications made to the Infra-Analyzer 500 (After de Rigal et al. (1993))

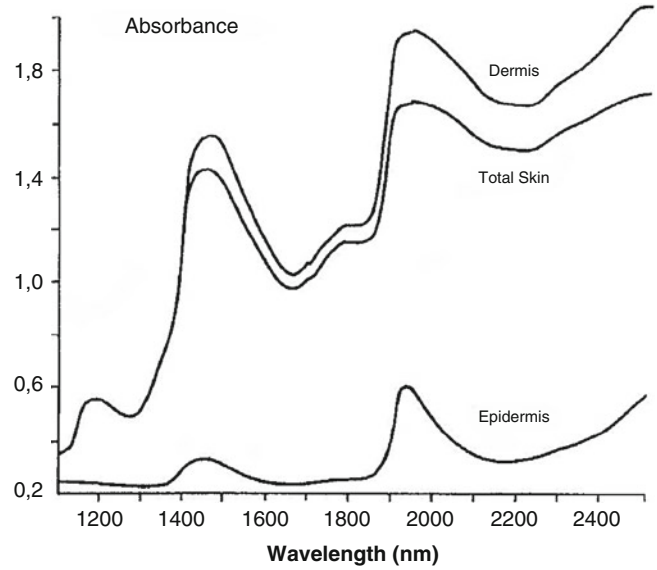

Fig. 26 Near-infrared absorbance spectra of the whole skin, epidermis, and dermis (After de Rigal et al. (1993))

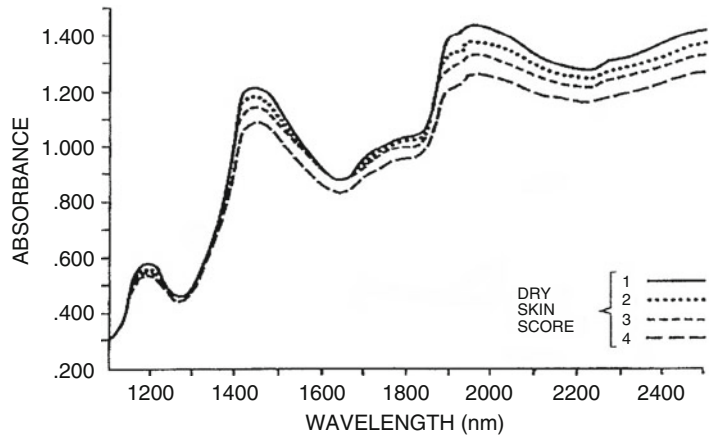

Fig. 27 Near-IR spectra of the skin at various dry skin scores. Intermediate scores are not shown. Each spectrum is a mean of the individual spectra for the same score (After de Rigal et al. (1993))

The study of skin hydration was carried out on the legs of a population of 159 women, following a clinical analysis of the skin condition using the following criteria: parchment-like, rugosity, presence of squamae, presence of scales ("snake skin"), and irritation (subclinical inflammation). Each of the criteria was scored 1 to 5 and the scores summed. The spectra obtained on Fig. 27 are related to the mean score, and the correlation with the set of clinical data is given on Fig. 28a. It is clear that the absorbance decreases when the dry skin condition becomes increasingly severe. This work also showed that the conductance method employed in parallel was not correlated with IR for high scores, since it appeared to saturate (Fig. 28b). This fact confirms and illustrates what has been frequently emphasized in this chapter: the artefactual influence of contact impedance when using dielectric methods (cf. Lévéque and de Rigal 1983).

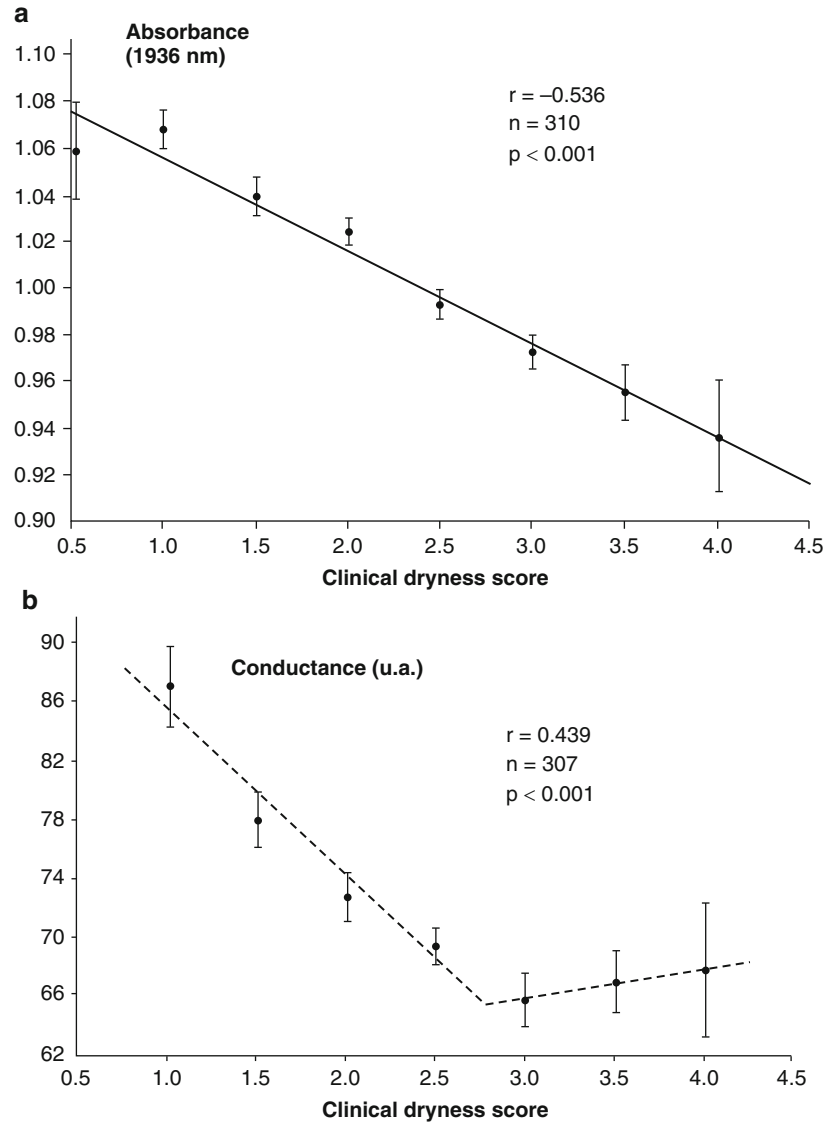

Fig. 28 (**a**) Linear correlation between near-IR absorbance (determined at 1936 nm) and overall clinical score for dry skin (After de Rigal et al. (1993)). (**b**) Relation between overall dry skin score and conductance. The correlation coefficients are for the entire data set (de Rigal et al. 1993)

In the same study, the efficacy of the five daily cosmetic treatments over a duration of 4 weeks has been sought for. The comparison between the clinical dry skin score and conductance and IR measurements illustrates their complementarity and evidences the difficulties of interpretation encountered with contact methods. The near-infrared analysis indubitably yields the classification that is the closest to reality in physical terms of water content, while the impedance determination was disturbed by the presence of squamae or scales.

Near-infrared spectroscopy affords also the possibility, after calibration, of predicting dry skin score, as shown by Walling and Dabney (1989). The conclusion of those two studies is that near-infrared spectroscopy is undoubtedly the reference method for skin moisturization measurements.

More recently, similar studies have been carried out with modern equipments (Kilpatrick-Liverman et al. 2006): A NIR5000 spectrometer (Cary/Agilent) equipped with a fiber optics probe ("Smartprobe") attachment delivered IR spectra, while conductivity measurements were completed using the Skicon 200 (lBS), which measures conductance at a frequency of 3.5 MHz. Clinical scores were performed either. Comparable NIR, Skicon, and visual dryness results were obtained for most of the experiments. However, the NIR was more effective to detect skin water content variations as a function of external humidity changes. As a matter of fact, the authors observed a direct correlation between the NIR readings and the relative humidity percentage (RH) unlike what was observed for the Skicon measurements. This last point confirms what was already noticed (Lévéque and de Rigal 1983; Rawling et al. 1992).

6.2.1 Near-Infrared Spectroscopic Imaging

Instruments have been designed to image the skin at NIR wavelengths. Apart from the well-known capillary observation, imaging devices working at 1450 nm or 1950 nm have appeared on the market and are now used to get images of water into the SC. Several groups are specialized on this subject. See for instance Wichrowski et al. (1995), Attas et al. (2001), and Zhang et al. (2005). Though skin hydration seems to be efficiently measured through that technique, it seems more adapted to precise molecular imaging of hemoglobin, lipids, and proteins in deeper skin layers.

6.3 Near-Infrared Ratiometry at Two Wavelengths

The analysis of near-infrared spectra of skin shows clearly the presence of two water absorption bands around 1450 and 1950 nm. Devices measuring simultaneously the reflectance at one wavelength outside and one inside absorption bands have been build and offered on the market. They have become recently light and affordable, due to the apparition of IR emitting diodes and detectors at the convenient wavelengths. Though very simple on the principle, care has to be taken to interpret the results on skin, since the two wavelengths penetration is very different if one is absorbed and the other is not. The same remark applies for the optical path of an outgoing ray. To get accurate measurements, a complex modelisation has to be carried out to take into account this optical path difference.

Random Monte Carlo-based calculations are widely used for this purpose (Kenji Iino et al. 2003), but practical application to skin relies on the knowledge of parameters which are all but well determined.

It appears liable in the first approach to bypass this question as long as variations on the same skin area are recorded, the technique being reliable and easy to perform. Nevertheless should beam penetration always be kept on mind.

Small devices have been widely marketed for the packaging and food industries, and chinese manufacturers have designed pen-sized skin moisturization measuring instruments (Konmision SC069 and other models). After a long validation period, a ratiometric NIR device working at 1950 and 1450 nm should be soon on the market (Non Invasive Technologies, Paris). These two wavelengths were selected because the penetration depths have been found (through computation and in vitro measurements) about identical, hence discarding the abovementioned drawback.

6.4 Confocal Raman Microspectroscopy

Raman spectroscopy is a vibrational spectroscopy, similar to IR spectroscopy but based on inelastic light scattering rather than absorption of light. It is out of this chapter's scope to expose the theory of Raman effect, which can be found in many textbooks. Let us recall that, in contrary to Rayleigh scattering, the scattered beam contains a small fraction at wavelengths longer than that of the incident light. This withdrawn energy has been gained by molecules to excite vibrations and depends on the structure, the interactions, and the chemical environment of these molecules.

As for IR spectra, Raman spectra are labeled in wave numbers (usually cm^{-1}), i.e., the reciprocal of the corresponding IR absorption wavelength. This scale is generalized because it is linear in energy: higher the wavenumber, higher is the vibrational energy involved in the wavelength shift.

Confocal Raman microspectroscopy brings the potential of Raman analysis to the field of confocal microscopy, its main feature being the aptitude to record Raman spectra of very thin optical slices. Casper and coworkers have pioneered the adaptation of the technique to skin observation (Caspers et al. 2001). Several instruments (more or less dedicated to dermo-cosmetology) are now on the market: **River Diagnostics** (3510 model), **B & W tek** (i-Raman model), and **Horiba** (LabRam-inv model).

Major applications of the technique in Dermatology are found in the characterization of intrinsic or extrinsic skin molecules under normal or pathological situations. For instance, Chrit et al. (2005) designed a very efficient and practical microprobe for "in vivo" chemical analysis. Recently, Zhao et al. (2010) compared melanin and protein spectra of normal skin and benign and malign diseases in the range 600–1700 cm^{-1}, pointing out the potentialities of Raman microscopy for skin disease diagnostic.

As long as SC hydration is concerned, the water band around 3400 cm^{-1} (O-H stretching) is generally compared to a protein peak around 2920 cm^{-1} (C-H^3 stretching). The excitation wavelength is in near IR, at 671, 730, or 850 nm, in order to minimize spurious fluorescence emission. At these wavelengths, the resolution in depth is about 5 μm. Since averaging is compulsory to make signal getting out of noise, exposure times might be rather long (1 min or more for Casper study (Caspers et al. 2001)), but the quality of modern equipments have shortened the measurement duration down to seconds.

The first water profiles published by Casper et al. on several locations of the arm (volar forearm, thenar) (Caspers et al. 2001) have been reproduced on Fig. 29, together with the Raman spectra from which they were computed. Ordinates have been directly labeled in %water weight/100 g of wet tissue, after conversion from the ratio of the two peak areas $(I_{3350–3550})/(I_{2910–2965})$.

These striking results have been later confirmed by other works, such as Chrit et al. (2005), already mentioned, working on a HORIBA microspectroscopic instrument, and Nakagawa et al. (2010) on a River Diagnostics model 3510. This latter publication shows SC water profiles obtained in a very short time (1–5 s), with a depth resolution of 2 μm, which emphasize the quality of the results obtained through the Raman microscopy technique.

Though optical coherence spectroscopy (Knuttel and Boehlau-Godau 2000) and nuclear magnetic resonance (Querleux et al. 1994) did show promising potentialities to give images of water inside SC, confocal Raman scattering appears as one of the best techniques to measure in depth the water content with a rather good resolution (2 μm). Since the acquisition times have been drastically lowered, its major drawback has to be found in the complexity and cost of the equipment. The assignation of bands might not be obvious, mainly on noisy spectra, but dedicated softwares and peak libraries are helpful in such conditions. These last years, manufacturers made efforts to deliver on the market portable and light Raman instruments (palm-hand devices), fiber coupled to an applicator (B & W tek). Such devices are macroscopic, and can only deliver an average SC water content, but offer plenty of capabilities to follow chemical events inside the skin.

7 Conclusion

To bring a conclusion to this long chapter, we hope to have shown the importance of the technical resources committed by public and private laboratories in an attempt to quantify the water content of the S*tratum Corneum*. The importance of those resources is justified by the considerable importance of this determination in dermatology and cosmetics.

Table 2 shows a summary of the main characteristics of the methods presented in this chapter,

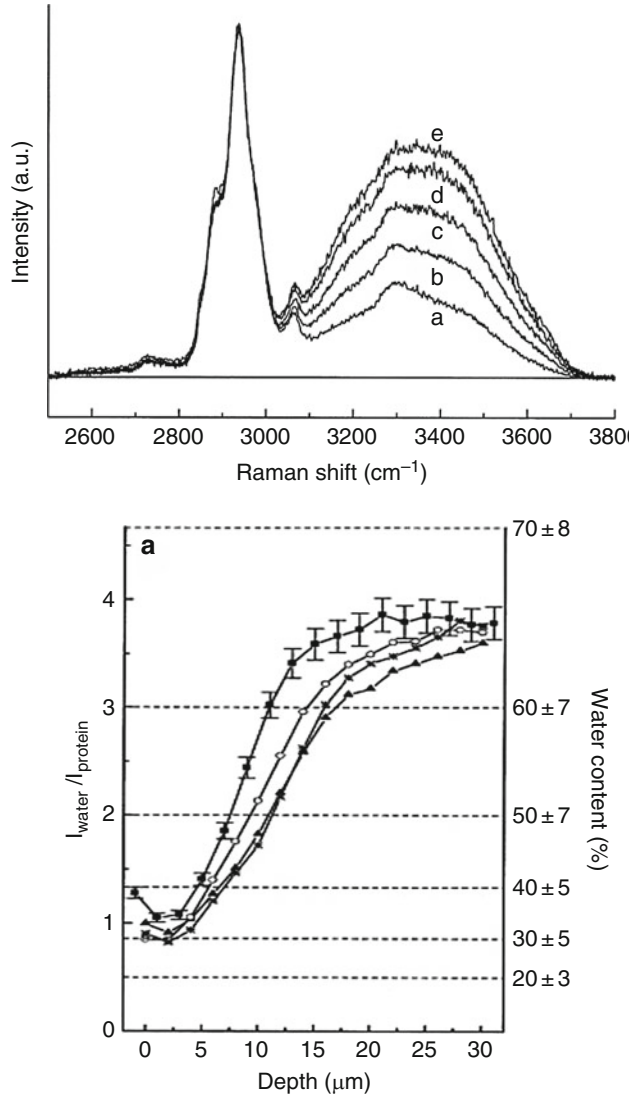

Fig. 29 Confocal Raman microspectroscopy of forearm skin at several depths and corresponding water content profile. Excitation in the near IR. The depth resolution is around 5 μm (From Casper et al. (2001))

in order to facilitate a selection by potential users. Many of them make use of equipment that is difficult to use for nonphysicists and which is, in addition, very expensive, making marketing them as integrated systems a poor profitability proposition, both for the manufacturer and the user. *The thermal and optical methods* warrant detailed discussion since they have given us precise determinations and thus *act as references for the calibration of devices which are more simple* with regard to their principles (but not with regard to result interpretation). The latter devices (mainly mechanical and electrical), which are essentially those marketed, supply reproducible and exploitable indications, if the user remains permanently aware of the variability of the physical and physicochemical parameters of the skin, as a function of site, age, environment and even, for moisturization, the subject's emotional status. The user must also bear in mind the physical properties of the various products and emulsions applied to the skin before or during moisturization

Table 2 Main characteristics of the in vivo SC water content measurement techniques

Principle	Instruments available	Contact with the skin	Potential interference with	Recommended use	Critical use
Electrical impedance methods	Skicon 200 XM[a] Corneometer CM825[b] Nova DPM9103[c] Moisturemeter SC4[d] Dermalab[e]	In vivo Yes	Surface variations (weak). Plasticity variations. Influence of ions on conductance	Short-term moisturizing efficacy. Comparative studies on contralateral zones.	Inter-individual comparisons
Thermal conductance methods	Hématron	In vivo Yes	Relief variations (weak). Plasticity variations	Short-term moisturizing efficacy. Comparative studies on contralateral zones.	
Mechanical methods	Cutometer Dermal Torque Meter Gas Bearing Electrodynamometer	In vivo Yes	Variations in *stratum corneum* thickness	Short-term moisturizing efficacy. Comparative studies on contralateral zones. Long-term moisturizing efficacy with associated thickness determinations.	Inter-individual comparisons with or without thickness determinations.
Calorimetric methods	DSC (many commercial instruments)	In vitro	Complex involvement of water molecules in the skin structures	Understanding of moisturization mechanisms and Lipid/water structural relationships	
Photothermal methods	OTTER	In vivo No contact	Presence of molecules absorbing light in the water bands	All types of study (nearly independent of surface state)	
	Photoacoustic (visible or IR)	No (not at the measurement site)	Presence of molecules absorbing light at the working wavelength. Variations in excitation. signal penetration (refractive index, surface state).	Short- and long-term moisturizing efficacy. Intra-individual comparative studies. Actinic effects on water content	Very colored or scattering formulations (locate the absorption window)

Spectroscopic methods: Near IR ATR IR FT IR	Many IR spectrographs are adaptable: Infra-Analyzer, Agilent "Smartprobe"	In vivo, might be avoided at the measurement site	Variations in surface back scattering. Modification in analysed volume (depth of penetration)	Short- and long-term moisturizing efficacy. Intra-individual comparative studies. Inter-individual comparisons.	Studies in the (residual) presence of formulations
Microspectroscopy RAMAN (confocal or conventional)	River Diagnostics 3510[f] Horiba LabRam inv[g] B&W tek i-Raman[h]	In vivo	Body movements occlusion for long exposures	In depth visualization of water in SC Short-term effects on molecular content are visible	Formulations may interfere (lipids)

[a]IBS Co. Hamamatsu, Japan
[b]Courage and Khazaka Electronic GmbH, 50829 Köln, Germany
[c]Nova Technology Corporation, Gloucester, MA 01930, USA
[d]Delfin Technologies Limited, 70211 Kuopio, Finland
[e]Cortex Technology, 9560 Hadsund, Denmark
[f]River Diagnostics B.V., 3029 AK Rotterdam, The Netherlands
[g]Horiba-Jobin-Yvon SAS, 91160 Longjumeau, France
[h]B&Wtek inc, 19 Shea Way, Newark, DE19713, USA

tests and particularly since they can themselves modify the signal detected by the sensor in addition to the required effect on the skin.

Finally, we would like to emphasize that only close cooperation between physicists, physicochemists, and biologists of the skin (including, of course, cosmetics specialists and dermatologists) was able to increase our basic knowledge and understanding of such a complex material as living skin and to allow the development of the very sophisticated methods described in this chapter.

References

Aframian VM, Dikstein S. Levarometry. In: Serup J, Jemec GBE, editors. Handbook of non-invasive methods and the skin. London: CRC Press; 1995a.

Aframian VM, Dikstein S. Indentometry. In: Serup J, Jemec GBE, editors. Handbook of non-invasive methods and the skin. London: CRC Press; 1995b.

Agache P, Monneur C, Léveque JL, de Rigal J. Mechanical properties and Young modulus of human skin in vivo. Arch Dcrmat Res. 1980;269:221–32.

Arnaud et al. A micro-thermal diffusion sensor for non invasive skin characterization. Sensors and Actuators. 1994;41-42:240–3.

Attas M, Hewko M, Payette J, Posthumus T, Sowa M, Mantsch H. Visualization of cutaneous Hemoglobin oxygenation and skin hydration using near-infrared spectroscopic imaging. Skin Res Technol. 2001;7(4):238–45.

Aubert L, Anthoine P, de Rigal J, Lévéque JL. An in vivo assessment of the biomechanical properties of human skin modifications under cosmetic product. Int J Cosmet Sci. 1985a;7:51–9.

Aubert L, Anthoine P, de Rigal J, Lévéque JL. An in vivo assessment of the biomechanical properties of human skin modifications under the influence of cosmetic products. Int J Cosmet Sci. 1985b;7:51–9.

Baesso ML, Shen J, Snook RD. Laser-induced photoacoustic signal phase study of stratum comeum and epidermis. Analyst. 1994a;119:561–2.

Baesso ML, Snook RD, Andrew JJ. Fourier transform IR photoacoustic spectroscopy to study the penetration of substances through skin. J Phys. 1994b;4:449–51.

Balageas DL. Characterization of living tissues from the measurement of thermal effusivity. Innov Tech Biol Med. 1991;12:145–53.

Balageas DL, Krapez JC, Cielo P. Pulsed photothermal modeling of layered materials. J Appl Phys. 1986;59:348–57.

Bamber JC, Tristam M. Diagnostic ultrasound. In: Webb S, editor. The physics of medical imaging. Bristol: Adam Hilger; 1990.

Barel AO, Clarys P. Measurement of epidermal capacitance. In: Serup J, editor. Handbook of non-invasive methods and the skin. London: CRC Press; 1995. p. 165–70.

Barel AO, Clarys P, Wessels B, de Romsee A. Noninvasive electrical measurement for evaluating the water content of the horny layer: comparison between the capacitance and the conductance measurements. In: Scott RC, Guy RH, Hadgraft J, editors. Prediction of percutaneous penetration – methods, measurements, modelling. London: IBC Technical Services; 1991. p. 238.

Barry BW. Mode of action of penetration enhancers in human skin. J Control Release. 1987;6:85–97.

Behl CR, Barret M. Hydration and percutaneous absorption. II: influence of hydration on water and alcanol permeation through Swiss mouse skin., comparison with hairless mouse. J Pharm Sci. 1981;70:l212–5.

Bernengo JC, Hanss M. Four electrode, very low frequency impedance comparator for ionic solutions. Rev Sci Instr. 1976;47:505–8.

Bernengo JC, Gasquez A, Falson-Rieg F. Photoacoustics as a tool for cutaneous permeation studies. High Temp High Pres. 1998;30:619–24.

Bindra RMS, Imhof, J Andrew J, Eclcston GM, Cummins PG (1994) Opto thermal measurements for non-invasive, non-occlusive monitoring of in vivo skin condition. IF SCC International Congress, Venice; 1994 Sept

Blank IH. Factors which influence the water content of the S.C. J Invest Dermatol. 1952;181:433–40.

Blank IH, Moloney J, Emslie AG, Simon I, Apt C. The diffusion of water across the stratum comeum as a function of its water content. J Invest Dermatol. 1984;82:l88–94.

Blichman CW, Serup J. Assessment of skin moisture. Acta Dermatol Venereol (Stockholm). 1988;68:284–90.

Campbell SD, Kraing KK, Schibli EG, Momii ST. Hydratation characteristics and electrical resistivity of *stratum corneum* using a noninvasive four-point electrode method. J Invest Dermatol. 1977;69:290–5.

Campbell SD, Yee SS, Afromowitz MA. Applications of photoacoustic spectroscopy to problems in dermatology research. IEEE Trans Biomed Eng. 1979;26:220–7.

Caspers PJ, Lucassen GV, Carter EA, Bruining HA, Puppels GW. In vivo confocal Raman microspectroscopy of the skin: noninvasive determination of molecular concentration profiles. J Invest Dermatol. 2001;1l6:434–42.

Challoner AVJ. Accurate measurement of skin blood flow by a thermal conductance method. Med Biol Eng. 1975;13:196–201.

Christensen MS, Hargens CW, Nacht S, Gaus EH. Viseoelastic properties of intact humanskin, instrumentation, hydration effect and the contribution of the stratum comeum. J Invest Dermatol. 1977;69:282–6.

Chrit L, Hadjur C, Morel S, Sockalingum G, Lebourdon G, Leroy F, Manfait M. In vivo chemical Investigation of human skin using a confocal Raman fiber optic microprobe. J Biomed Opt. 2005;10:44007.

Clar EJ, Her CP, Sturelle CG. Skin impedance and moisturization. J Soc Cosmet Chem. 1975;26:337–53.

Clarys P, Clijsen R, Taeymans J, Barel AO. Hydration measurements of the S.C.: comparison between the capacitance method (digital version of The Corneometer CM825) and the impedance method (Skicon-200EX). Skin Res Technol. 2012;18(3):316–23.

Comaish S. Infrared studies of human skin in vivo by multiple internal reflection. Br J Dermatol. 1968;80:522–8.

Cooper EP, Missel PJ, Hannon DP, Albright GB. Mechanical properties of dry, normal and glycerol-treated skin as measured by gas bearing electrodynamometer. J Soc Cosmet Chem. 1985;36:335.

De Rigal J. In vivo assessment of skin ageing and photoaging. A multiparametric approach. 20th anniversary symposium, International society for bioengineering and the skin. Miami; 1996 Feb 15–17.

de Rigal J, Losch M, Bazin R, Camus C, Sturelle C, Descamp V, Leveque JL. Near infra red spectroscopy: a new approach to the characterisation of dry skin. J Soc Cosmet Chem. 1993;44:197–209.

Diakate L, de Rigal J, Bemengo JC, Lévéque JL. Dielectric properties of skin at high frequencies by means of time domain reflectometry: a new approach to hydratation process. 10th international symposium on bioengineering and the skin. Cincinnati, Ohio; 1994 June.

Dikstein S, Bercovici PG. Measurement of skin surface capacitance at 16 Hz and at other frequencies. Bioeng Skin. 1985;1:357.

Dikstein S, Hartzshtark A. What does low pressure indentometry measure? Arztliche Cosmetol. 1983;13:327.

Dittmar A. Skin thermal conductivity: a reliable index of skin blood flow and hydratation. In: Lévéqne JL, editor. Cutaneous investigation in health and disease. New York: Marcel Dekker; 1988. p. 323–58.

Djeldjellani M. Mise au point d'un applicateur destiné a la mesure des propriétés diélectriques de la peau par TDR. Ph.D. dissertation, Université de Besancon; 1989.

Emtestam L, Ollmar S. Electric impedance index in human skin: measurement after occlusion in five anatomical regions and in mild irritant dermatitis. Contact Dermatitis. 1993;28:104–8.

Ferris CD. Four electrode null techniques for biological impedance work. Rev Sci Instrum. 1963;23:109–15.

Fluhr JW, Gloor M, Lazzerini S, Kleesz P, Grieshaber P, Berardesca E. Comparative study of five instruments measuring *stratum corneum* hydration (Corneometer CM 820 and CM 825, Skicon 200, Nova DPM 9003, DermaLab). Part II In vivo. Skin Res Technol. 1999;5(3):171–8.

Geladi P, MacDougall P. Linearization and scatter correction for NIR spectra of meat. Appl Spectrosc. 1985;39(3):491–500.

Giese K, Kolmel K. A photoacoustic hydration study of human *stratum corneum*. J Phys (Paris). 1983;44(C6-373):C6–378.

Gloor M, Willebrandt U, Thomer G, Kupferschmid W. Water content of the horny layer and skin surface lipids. Arch Dermatol Res. 1980;268:221–3.

Gloor M, Hirch G, Willebrandt U. On the use of infrared spectroscopy for in vivo measurement of water content of the horny layer after application of dermatological ointments. Arch Dermatol Res. 1981a;271:296–302.

Gloor M, Hirch G, Willebrandt U. On the use of infrared spectroscopy for in vivo measurement of water content of the homy layer after application of dennatological ointments. Arch Dermatol Res. 1981b;271:305–13.

Golden GM, Guzek DB, Harris RR, Mackie JE, Potts RO. Lipid thermotropic transitions in human *stratum corneum*. J Invest Dermatol. 1986;86:255–9.

Golden GM, Guzek DB, Kennedy AH, Mackie JE, Potts RO. Stratum comeum lipid phase transitions and water barrier properties. Biochemistry. 1987;26:2382–8.

Goodman M, Barry BW. Action of penetration enhancers on human stratum comeum as assessed by Differential scanning calorimetry. In: Bronaugh RL, Maibach HI, editors. Percutaneous absorption. New York: Marcel Dekker; 1989. p. 567–93.

Grahame R. A method for measuring human skin elasticity in vivo with observation of the effects of age, sex, and pregnancy. Clin Sci. 1970;39:223–38.

Gunner CW, Hutton WC, Burlin TE. The mechanical properties of skin in vivo. A portable hand held extensometer. Br J Dermatol. 1979;100:161–3.

Guo X, ImhofRE, de Rigal J (2001) Spectroscopic study of water-keratin interactions in *Stratum Corneum*. In: Proceedings of 11th international conference of photothermal and photoacoustic phenomena, Kyoto, Japan; 2000 June 25–29.

Guy M, Bemengo JC. Designing a differential cell for in vivo photoacoustic measurements of skin absorbance. Can J Phys. 1986;64:1142–5.

Hansen JR, Yellin W. NMR and Infra-red spectroscopic studies of stratum comeum hydration. In: Jellinek E, editor. Water structure and the water polymer interface. New York: Plenum Press; 1972.

Hargens CW. The gas bearing electrodynarnometer applied to measuring mechanical changes in skin and other tissues. In: Marks R, Payne P, editors. Bioengineering and the skin. Lancaster: MTP Press; 1981. p. 113–22.

Hendler E, Crosbie R, Hardy JD. Measurement of heating of the skin during exposure to infrared radiation. J Appl Physiol. 1958;12:177.

Hensel H, Brandt S. Plate element for recording of cutaneous blood flow. Pfliigers Archiv Eur J Phys. 1977;368: l65–7.

Horii I, Nakayama Y, Obata M, Tagami H. *Stratum corneum* hydratation and amino acid content in Xerotic skin. Br J Dermatol. 1989;121:587.

Imhof RE, Whitters CJ, Birch DJS. Opto-thermal in vivo monitoring of structural breakdown of an emulsion sunscreen on skin. Clin Mater. 1990;5:271–8.

Inoue T, Tsujii K, Okamoto K, Toda K. Differential scanning calorimetric studies on the melting behaviour of

water in stratum comeum. J Invest Dermatol. 1986;86:689–93.
Isaksson T, Mass T. The effect of multiplicative scatter correction and linearity improvement in NIR spectroscopy. Appl Spectrosc. 1988;42:1273–84.
Jacques SL. A linear measurement of the water content of the stratum comeum of human skin using a microwave probe. IEEE Eng Med Biol Soc Conf 180;1979.
Kalia YN, Pirot F, Guy RH. Homogeneous transport in a heterogeneous membrane: water diffusion across human stratum comeum in vivo. Biophys J. 1996;71:2692–700.
Kenji Iino K, Maruo K, Arimoto M, Hyodo K, Nakatani T, Yamada Y. Monte Carlo simulation of near infrared reflectance spectroscopy in the wavelength range from 1000 nm to 1900 nm. Opt Rev. 2003;10(6):600–6.
Khan ZU, Kellaway IW. Differential scanning calorimetry of DMSO treated human stratum comeum. Int J Pharm. 1989;55:129–34.
Kilpatrick-Liverman L, Kazmi P, Wolff E, Polefka TG. The use of near-infrared spectroscopy in skin care applications. Skin Res Technol. 2006;12(3):162–9.
Klimisch HM, Chandrag G. Use of Fourier transform infrared spectroscopy with attenuated total reflectance for in vivo quantification of polydimethylsiloxanes on human skin. J Soc Cosmet Chem. 1986;37:73–87.
Knutson K, Potts RO, Guzek DB, Golden GM, Mackie JE, Lambert WJ, Higuchi W. Macro- and molecular physical-chemical considerations in understanding drug transport in the *Stratum Corneum*. J Controll Release. 1985;2:67–87.
Knuttel A, Boehlau-Godau M. Spatially confined and temporally resolved refractive index and scattering evaluation in human skin performed with optical coherence tomography. J Biomed Opt. 2000;5:83–9.
Koelmel K, Mercer P. Determination of the moisture of the horny layer by means of infrared reflection at three different wavelengths. Arch Dermatol Res. 1980;268:206.
Koyama J, Nakanishi J, Masuda Y, Sato J, Nomura J, Suzuki, Y, Nakayama Y. The mechanism of desquamation in the stratum comeum and its relevance to skin care. IFSCC Congress, Sydney; 1996 Oct.
Lefevre J. Recherches sur la conductibilité de la peau de 1'organisme vivant et sur ses variations en fonction de la temperature extérieure. J Phys Theor Appl, Paris. 1901;3:380–8.
Lévéque JL, de Rigal J. Impedance methods for studying skin moisturisation. J Soc Cosmet Chem. 1983;34:419.
Lévéque JL, de Rigal J. In vivo measurement of the *stratum corneum* elasticity. Bioeng Skin. 1985;1:13–23.
Lévéque JL, Escoubez M, Rasseneur L. Water-keratin interaction in human stratum comeum. Bioeng Skin. 1987a;3:227–42.
Lévéque JL, Grove G, de Rigal J, Corcuff P, Kligman AM, St Leger D. Biophysical characterisation of dry facial skin. J Soc Cosmet Chem. 1987b;82:171–7.
Leveque JL, Ribaud C, Garson JC. Caractérisation biophysique du stratum coméum. Relation entre sa structure et ses propriétés. Path Biol. 1992;40:95–108.
Maes T, Martens H. Principal components regression in NIR analysis: viewpoints, background details and selection of components. J Chemom. 1988;2:155–67.
Martin KA. Qualitative interpretation of NIR reflectance measurements to determine moisturisation in skin. In: Making light work. Advances in NIR spectroscopy. Weinheim: VCH; 1992. p. 627–32.
Martin KA. Direct measurement of moisture in skin by NIR spectroscopy. J Soc Cosmet Chem. 1993;44:249–61.
Martinsen OG, Grimnes S, Karlsen I. An instrument for the evaluation of skin hydration by 100 kHz electrical admittance measurements. Innov Tech Biol Med. 1993;14:588–96.
Mass D, Short J, Turek A, Reinstein JA. In vivo measuring of skin softness using the gas bearing electrodynamometer. Int J Cosmet Sci. 1983;5:189–200.
Masuda K, Nishikawa M, Ichijo B. New methods of measuring capacitance and resistance of very high loss materials at high frequencies. IEEE Trans Instrum Meas. 1980;29:28.
Moseley H, English JSC, Coghill GM, Mackie RM. Assessment and use of a new skin hygrometer. Bioeng Skin. 1985;1:177.
Murray BC, Wickett RR. Sensitivity of cutometer data to *stratum corneum* hydration level. A preliminary study. Skin Res Technol. 1996;2:167–72.
Nakagawa N, Matsumoto M, Singo S. *In vivo* measurement of the water content in the dermis by confocal Raman spectroscopy. Skin Res Technol. 2010;16:137–41.
Norris KH, Hart JR. Direct spectrometric determination of moisture in seeds. Proceedings of the 1963 international symposium on humidity and moisture, principles and methods of measuring moisture. In: Liquids and solids. 4th ed. New York: Reinhold; 1965. p. 19–25.
Osborne KA, Fearn T. Near infrared spectroscopy. In: Food analysis. New York: Longman Scientific and Technology; 1986. p. 49–51.
Patel CKN, Tam AC. Pulsed optoacoustic spectroscopy of condensed matter. Rev Mod Phys. 1981;53:517–49.
Pichon E, de Rigal J, Lévéque JL. In vivo rheological study of the torsional characteristics of the skin. 8th international symposium on bioengineering and the skin, STRESA, Italy; 1990 June 13–16.
Piérard GE. Caractérisation des peaux seches, la biométrologie complète la clinique. Cosmétologie. 1997;14:48–51.
Pines E, Cunningham T. Dermatological photoacoustic spectroscopy. In: Marks R, Paynes PA, editors. Bioengineering and the skin. Lancaster: MTP Press; 1981. p. 283–90.
Poppendieck HF, Randall R, Breeden JA, Chambers JE, Murphy JR. Thermal conductivity measurements and predictions for biological fluids and tissues. Cryobiology. 1966;3:3l8–27.
Potts RO. In vivo measurement of water content of the stratum comeum using infrared spectroscopy: a review. Cosmet Toiletries. 1985;100:27–31.

Potts RO, Buras EM. In vivo changes in the dynamic viscosity of human stratum comeum as a function of age and ambient moisture. J Soc Cosmet Chem. 1985;136:169–76.

Potts RO, Buras EM, Chrisman DA. The dynamic mechanical properties of human skin in vivo. J Biomech. 1980;16:365–72.

Potts RO, Guzek DB, Harris RR, Mackie JE. A noninvasive in vivo technique to quantitatively measure water concentration of the *stratum corneum*, using attenuated total-reflectance infrared spectroscopy. Arch Dennatol Res. 1985;277:489–95.

Poulet P. Spectroscopie photoacoustique et sciences biomedicales. Ph.D. disseration, University of Strasbourg, France; 1985.

Poulet P, Chambron J. Conception and realisation of a photoacoustic detector for "in situ" spectroscopy. J Photoacoustics. 1982;1:329–46.

Poulet P, Chambron J. In vivo photoacoustic spectroscopy of the skin. J Phys (Paris). 1983;44:C6–413.

Querleux B, Richard S, Bittoun J, Jolivet J, Idy-Peretti I, Bazin R, de Lachariere O, Lévéque JL. In vivo hydration profile in skin layer by high resolution magnetic resonance imaging. Skin Pharmacol. 1994;7:2l0–6.

Randall Wicket R, Murray BC. Comparison of cutometer and DTM for skin elasticity measurements. 20th anniversary symposium, International society for bioengineering and the skin, Miami; 1997 Feb 15–17.

Rawling AV, Hope J, Rogers J, Mayo AM, Scott l. Mechanism of desquamation: new insights into dry flaky skin conditions. 17th IFSCC international congress, Yokohama; 1992 Oct 13–16.

Rawling A, Harding C, Wakinson A, Bank J, Ackerman C, Sabin R. The effect of glycerol and humidity on desmosome degradation in stratum comeum. Arch Dermatol Res. 1995;287:457–64.

Rompe PCB, dos Anjos FH, Mansanares AM, da Silva EC, Acosta-Avalos D, Barja PR. Characterization of human skin through photoacoustic spectroscopy. J Phys IV (Paris). 2005;125:785–7.

Rosencwaig A, Gersho A. Theory of the photoacoustic effect with solids. J Appl Phys. 1976;47:64–9.

Rosencweig A, Pines E. Stratum comeum studies with photoacoustie spectroscopy. J Invest Dermatol. 1977;75:500–7.

Salter DC. Skin mechanics measured in vivo using torsion, a new and accurate model more sensitive to age, sex and moisturising treatment. J Soc Cosmet Chem. 1993;44:197–209.

Salter DC, Hodgson RJ, Hall LD, Carpenter TA, Ablett S. Moisturisation processes in living human skin studied by magnetic resonance imaging. 17th IFSCC lntemational Congress, Yokohama, 1992 Oct 13–16.

Schade H. Die Elasticitatsfunktion des Bindegewebes und die Intravitale Messung ihrer Storungen. Z Exp Pathol Ther. 1912;11:369–99.

Schneider M, Hansen WG. Crystal effect on penetration depth in attenuated total reflectance Fourier transform infra-red study on human skin. Microchim Acta [Suppl]. 1997;14:677–8.

Schwan HP. Dielectric properties of living tissues. Adv Biol Med Phys. 1957;5:147–63.

Serban GP, Henry SM, Cotty VF, Marcus AD. In vivo evaluation of skin lotions by electrical capacitance and conductance. J Soc Cosmet Chem. 1981;32:421–35.

Serban GP, Henry SM, Cotty VF, Cohen GL, Riveley JA. Electrometric technique for the in vivo assessment of skin dryness, and the effect of chronic treatment with a lotion on the water barrier function of dry skin. J Soc Cosmet Chem. 1983;34:383–93.

Simon I, Emslie AG, Apt CM, Blank IH, Anderson RR. Determination in vivo of water concentration profile in human *stratum corneum* by a photoacoustic method. In: Marks R, Paynes PA, editors. Bioengineering and the skin. Lancaster: MTP Press; 1981. p. 187–95.

Starzyk F. Parametrisation of interdigit comb capacitor for dielectric impedance spectroscopy. Arch Mater Sci Eng. 2008;34(1):31–4.

Stolwijk JA, Hardy J. Skin and subcutaneous temperature changes during exposure to intense thermal radiation. J Appl Physiol. 1965;20:1006–13.

Tagami H. Impedance measurements. In: Lévéque JL, editor. Cutaneous investigation in health and disease. New York: Marcel Dekker; 1988. p. 79–111.

Tagami H. Measurements of electrical conductance and impedance. In: Serup J, editor. Handbook of non-invasive methods and the skin. London: CRC Press; 1995. p. 159–64.

Tagami H, Yoshikuni K. Interrelationship between water barrier and reservoir functions of pathologic stratum comeum. Arch Dermatol. 1985;121:642–5.

Tagami H, Oki M, Iwatsuki K, Kanamaru Y, Yamada M, Ichijo B. Evaluation of skin surface hydration in vivo by electrical measurement. J Invest Dermatol. 1980;75(500–5):07.

Takamoto R, Yamamoto S, Namba R, Takamatsu T, Matsuoka M, Sawada T. In vivo percutaneous absorptiometry by a laser photoacoustic method using a novel open-ended cell, combined with light guide. Anal Chem. 1994;66:2267–71.

Tosti A, Giovanni C, Fazzini ML, Villardita S. A ballistometer for the study of the plasto-elastic properties of the skin. J Invest Dermatol. 1977;69:282–6.

van Duzec BF. Thermal analysis of human *Stratum Corneum*. J Invest Dermatol. 1975;65:404–8.

Vlashloom DC. Skin elasticity. Ph.D. thesis. Holland: University of Utrech; 1967.

Walkley K. Bound water in stratum comeum measured by differential scanning calorimetry. J Invest Dermatol. 1972;59:225–7.

Walling PL, Dabney JM. Moisture in skin by NIR spectroscopy. J Soc Cosmet Chem. 1989;40:151–75.

Warner RR, Myers MC, Taylor DA. Electron probe analysis of human skin: determination of the water concentration profile. J Invest Dermatol. 1988;90:218–24.

Wichkowski K, Sore G, Khaïat K. Use of infrared spectroscopy for in vivo measurement of the *stratum corneum* moisturization after application of costmetic preparations. Int J Cosmet Sci. 1995;17(1):1–11.

Wickett RR, Murray BC. Comparison of cutometer and DTM for elasticity measurements. 20th Anniversary Symposium, Intemational Society for Bioengineering and the Skin. Miami; 1996 Feb 15–17.

Wijn P. The alinear viscoelastic properties of human skin in vivo for small deformations. Ph.D. dissertation, Catholic University, Nijmegen; 1980.

Wirchrowski K, Sore G, Khaiat A. Use of infrared spectroscopy for in vivo measurement of the *stratum corneum* moisturization after application of cosmetics preparations. Int J Cosmet Sci. 1985;17:1–11.

Wold S, Antti H, Qhman J. Orthogonal signal correction of NIR spectra. Chemometr Intell Lab Syst. 1998;44:175–85.

Xiao P, Ciortea LI, Singh H, Cui Y, Berg EP, Imhof RE. Opto-thermal in-vivo skin hydration measurements: – a comparison study of different measurement techniques. 15th International conference on photoacoustic and photothermal phenomena. J Phys Conf Ser. 2010; 214:012026.

Zhang SL, Meyers CL, Subramanyan K, Hancewicz TM. Near infrared imaging for measuring and visualizing skin hydration. A comparison with visual assessment and electrical methods. J Biomed Opt. 2005;10(3):031107.

Zhao JL, McLean DI, Zeng H. Recent advances in biomedical engineering. Vienna: IN-TECH; 2010. p. 455–74.

Stratum Corneum Dynamic Hydration Test

30

Katsuko Kikuchi and Hachiro Tagami

Contents

Keywords

Moisture accumulation test (MAT) • Anatomical locations • Skin moisturizers • Water accumulation velocity • Plastic occlusion stress test (POST) • Skin surface water loss (SSWL) • Sodium lauryl sulfate (SLS) • Sorption-desorption test (SDT) • Hypertrophic scars and keloids • Modified procedure and functional parameters • Normal skin water kinetics • Scaly skin • Test procedure • Topical steroids/calcineurin inhibitor • Stratum corneum (SC) • Endogenous hydration • Exogenous hydration • Simulation model • Transepidermal water loss (TEWL) • Van't Hoff's law • Impedance meter • Hydration state of the SC

Abbreviations

AD	Atopic dermatitis
AUC	Area under the curve
MAT	Moisture accumulation test
NMF	Natural moisturizing factor
POST	Plastic occlusion stress test
SC	Stratum corneum
SDT	Sorption-desorption test
SSWL	Skin surface water loss
TEWL	Transepidermal water loss
WA	Water accumulation
WAV	Water accumulation velocity
WHC	Water-holding capacity

K. Kikuchi (✉) • H. Tagami
Department of Dermatology, Tohoku University Graduate School of Medicine, Sendai, Japan
e-mail: kkikuchi@med.tohoku.ac.jp; hachitagami@ybb.ne.jp

P. Humbert et al. (eds.), *Agache's Measuring the Skin*,
DOI 10.1007/978-3-319-32383-1_30

1 Introduction

The surface of normal healthy skin is covered by an extremely thin and soft, but highly efficient, barrier membrane, i.e., the stratum corneum (SC), so that any substance from the environment with a molecular weight greater than 500 Da can hardly penetrate through it. Thus, even a small molecule such as water cannot easily penetrate it from the underlying wet, viable epidermis to the surrounding dry environment. Therefore, we can evaluate the barrier function of the SC in vivo instrumentally by measuring the amount of water evaporating from the skin surface as transepidermal water loss (TEWL) in a cool and dry environmental condition where no sweating takes place. In such a way, we can demonstrate that, clinically, even the merely pruritic dry skin surface found in atopic dermatitis (AD), i.e., atopic xerosis, shows slight but significantly higher TEWL than the normal skin of healthy individuals (Watanabe et al. 1991).

Moreover, the SC of a healthy skin surface maintains soft and smooth properties by binding water efficiently. In contrast, the SC produced in pathologic skin cannot effectively bind water, producing a dry, scaly skin surface due to the decrease in the SC hydration state, as noted in atopic xerosis or ichthyosis vulgaris. In such patients, even large protein molecules such as environmental allergens can penetrate into viable cutaneous tissue through finely cracked areas of the SC and induce hypersensitivity reactions. We can evaluate this hydration state of the superficial part of the SC that is under direct environmental influence by conducting instrumental measurements of the high-frequency conductance or capacitance of the skin in vivo (Tagami et al. 1980).

The SC is produced by the epidermis whose keratinocytes slowly differentiate into flat corneocytes, which overlap and tightly bind to each other with their corneodesmosomes to construct an extremely thin and flexible, but efficient, membranous barrier covering the normal skin. Although it is only 15 μm thick at most portions of our body surface, the SC of healthy skin enables us to live even in a very dry atmosphere. To construct an SC equipped with such an efficient barrier function, the narrow spaces between each overlapped, flattened corneocyte are tightly packed with unique intercellular lipids that are produced and excreted by the most differentiated keratinocytes present in the uppermost portion of the epidermis, the stratum granulosum. These lipids, which are uniquely composed of ceramides, cholesterol, and fatty acids, not only provide the SC an efficient barrier function but also exert a water-holding capacity to maintain the soft and flexible properties of the SC with the so-called natural moisturizing factor (NMF), which is mainly composed of amino acids derived from filaggrin after intracellular enzymatic proteolysis within the corneocytes, in addition to sweat-derived lactate and urea and sebum secreted from sebaceous glands of the adult face and scalp skin. Thus, the thin membranous SC covering healthy skin remains soft and smooth to the touch, in contrast to the rough and dry pathologic SC that is produced under diseased conditions. Because the latter is unable to bind water efficiently, firm, but fragile, dry SC is produced, which is clinically observable as a scaly, finely fissured skin surface even under normal ambient environmental conditions.

The hydration state of the SC is determined in a dynamic equilibrium between the water supply to the SC from the underlying wet epidermis and its loss from the skin surface, which is dependent on the ability of the SC to absorb water and to retain it. The water is supplied to the SC not only from the underlying living skin tissues but also from the outside, such as the atmospheric moisture, sweat, bath, shower, and topically applied hydrating agents.

As mentioned above, the water-binding capacity of the SC depends mainly on the presence of highly hygroscopic molecules, NMF, as well as polar lipids such as the ceramides present in the intercellular spaces (Yamamura and Tezuka 1989)

and even structural proteins. A small amount of water supplied from the outer layers of the SC also contributes to the maintenance of its flexibility as well as to facilitating the enzymatic reactions that drive the maturation of the SC (Rawlings et al. 1994; Rawlings and Harding 2004). The dynamic hydration tests of the SC described below give us much more information about the physiological or pathological properties of the SC than the simple, routinely conducted instrumental evaluations.

In this chapter, we describe three representative in vivo functional tests of the SC, i.e., SC dynamic hydration tests, the sorption-desorption test (SDT), moisture accumulation test (MAT), and plastic occlusion stress test (POST), to obtain detailed information noninvasively about the functional properties of the SC.

2 Stratum Corneum Hydration

2.1 Endogenous Hydration

The SC is the extremely thin and soft biological barrier membrane that protects the body from desiccation as well as from the invasion of various external, injurious agents. The deepest layer of the SC contacts with the wet living epidermal tissue, whereas the outermost layer of the SC is directly exposed to the dry environment. Thus, the SC constitutes a thin, but vital, membranous structure covering the whole body surface as a water permeation barrier, together with the tight junction of the granular layer of the epidermis. Moreover, there exists a decreasing water gradient from the deeper SC layers (70 %) toward the outermost SC ones (30 %) (Warner et al. 1988; Caspers et al. 2001; Egawa and Tagami 2008) in this extremely thin membranous structure. A steep water gradient is present from the superficial to a mid part of the SC, followed by a rather gradual gradient ranging from the mid to the deep part of the SC, as clearly demonstrable by in vivo Raman spectroscopy (Egawa and Kajikawa 2009).

The water within the SC exists as bound water and free water. The former is either tightly bound primary water or weakly bound secondary water. The secondary bound water, whose amount depends on the amounts of NMFs and extracellular polar lipids (Yamamura and Tezuka 1989), is decreased in the pathologic SC such as found in various dermatitic skin lesions or in clinically non-inflamed dry skin such as ichthyosis and senile xerosis, whereas the primary water does not show any great change even in pathologic, scaly skin (Takenouchi et al. 1986). The water present in the intercellular spaces is attracted toward the skin surface, due to the lower humidity of the atmosphere compared to that of the living skin tissue, where it is continuously evaporated from the skin surface as TEWL. Thus, the so-called TEWL consists of the water diffusing through the SC from the viable epidermis (true TEWL) and that lost from the physiological dehydration of corneocytes. Water from these two sources permeates the intercellular spaces of the SC that are also the routes for percutaneous absorption of various small molecular substances from the environment (Agache and Black 2004).

When the water evaporation is inhibited for a long period of time by covering the skin with an occlusive film, excessive water accumulates in the SC. If more than 50 % w/w hydration occurs, the corneocytes are observed to swell with the water behaving like bulk liquid water, i.e., free water. In the case of a hydration level of >300 % w/w, even extracellular pools of water become observable, making the SC fragile, and clinically noted as maceration.

2.2 Exogenous Hydration

When water contacts the skin surface, it so quickly permeates through the intercellular spaces of the SC and later crosses the cell membranes to swell the corneocytes, depending on the length of contact time (Tagami et al. 1980). Even with a short external water application, the

water content in the superficial part of the SC is increased rapidly, while that observed in the mid and lower part of the SC occurs more slowly (Egawa and Kajikawa 2009). This quick water uptake into the SC is thought to be the result of three physical phenomena, i.e., the first one is simple adhesion via surface tension forces, the second is diffusion (Fick's law) due to the lower water content of the cells and hydrophilic domains of the intercellular spaces, whereas the third one is absorbed possibly by an osmotic process via the semipermeable corneocyte cell wall due to the presence of intracellular NMF (van't Hoff's law). In this way, the water penetrates into the corneocytes, eventually causing their swelling. The resultant cell distension and intensity of the osmotic pressure may alter the property of the cell membranes, which accounts for the partial loss of small molecular NMF that takes place after prolonged water immersion. According to van't Hoff's law, the osmotic pressure, p, can be shown as $p = RTC$, where R is the perfect gas constant, T the absolute temperature, and C the concentration of hygroscopic substances, i.e., their number per unit volume is independent of their size or nature. Osmotic pressure increases considerably in the suprabasal portion of the SC where filaggrin disintegrates enzymatically into numerous molecules of NMF, releasing its strongly bound water. At the superficial SC layers, this pressure is much less since the NMF concentration is decreased (Agache and Black 2004).

When the applied exogenous water is removed, a drying process takes place rapidly at first and then more slowly afterward. This desorption is called skin surface water loss (SSWL), which is, however, different from TEWL (true TEWL). Both SSWL and TEWL can be measured by evaporimetry.

2.3 Instruments to Measure the Hydration State of the SC

As mentioned above, the hydration state of the SC, especially the hydration state of the skin surface, can be evaluated noninvasively by measuring the components of high-frequency impedance, i.e., conductance or capacitance, by simply applying the electrodes to the skin surface (Tagami et al. 1980). These instruments can also be employed in SC dynamic hydration tests. The skin surface hygrometers Skicon 200 EX (IBS Ltd., Hamamatsu, Japan) and Nova DPM 9003 (NOVA Technology Corporation, USA) are available for measurement of the high-frequency conductance. By contrast, Corneometer CM 825 (Courage and Khazaka, Köln, Germany) measures the high-frequency capacitance of the skin. Usually, the recordings of conductance or capacitance with these devices are made within 3 s to avoid the accumulation of evaporating water from the skin surface beneath the electrodes.

Since these instruments measure the skin hydration based on their own unique parameters, it is difficult to compare data inter-instrumentally. They also cannot provide the depth profile of water in the SC. However, as shown by Hashimoto-Kumasaka et al. (1993), the conductance measurement is more suitable for the evaluation of the hydration change taking place in the superficial portion of the SC, while the capacitance measurements assess the hydration state including much deeper portions of the SC. Namely, the former is more sensitive for assessing the hydration changes caused by the application of moisturizers or to conduct a water sorption-desorption test, whereas the latter is suited for evaluating even dry pathologic SC, such as a scaly skin surface (Fig. 1). Thus, in a simulation model of in vivo SC, the high-frequency conductance device shows a much closer correlation with the hydration state of the surface SC ($r = 0.99$) than the capacitance device ($r = 0.79$), suggesting that the former can more accurately assess the hydration dynamics of the superficial portion of the normal healthy SC, particularly that due to the accumulation of easily releasable secondary bound water (Hashimoto-Kumasaka et al. 1991). These characteristics can also be shown more clearly by comparing the obtained values after serial tape stripping of the SC (Hashimoto-Kumasaka et al. 1993) (Fig. 2).

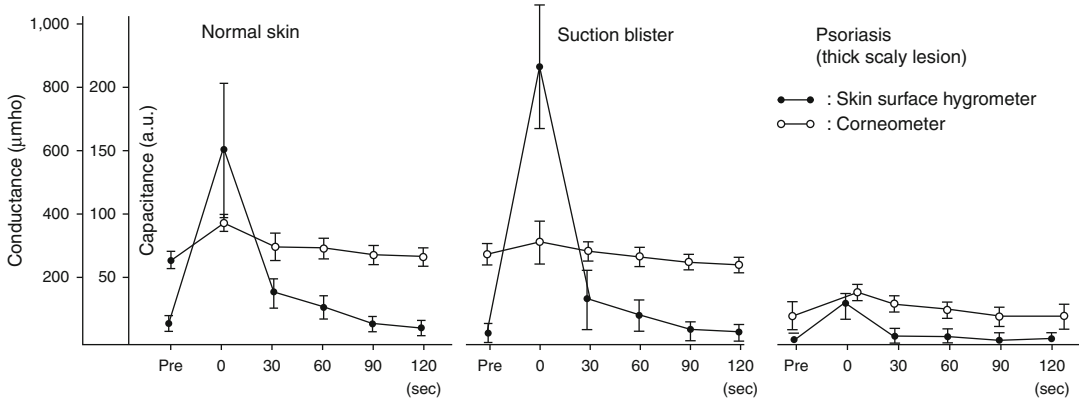

Fig. 1 In vivo water sorption-desorption test measured with the high-frequency conductance with Skicon 200 and the capacitance with Corneometer CM420, CM820 (From reference Hashimoto-Kumasaka et al. 1993). Skicon more clearly shows the increase in the SC hydration state compared with Corneometer after water application when comparing between the normal skin, the skin of suction blister, and scaly skin of a psoriasis patient

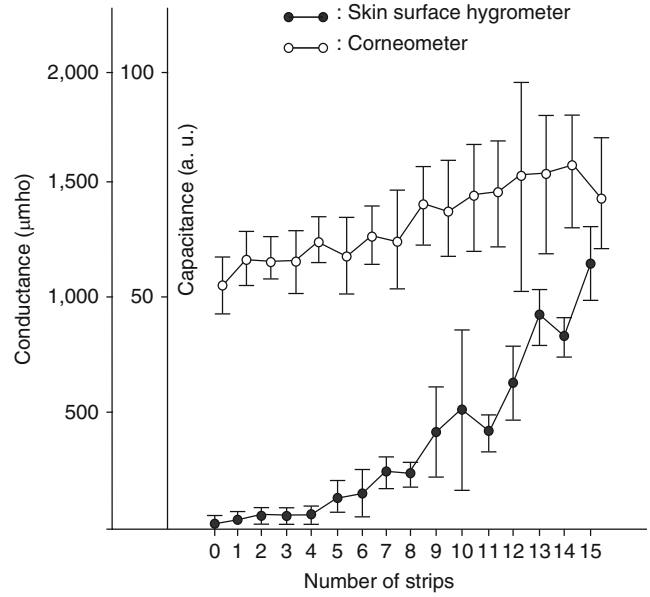

Fig. 2 Influence of serial tape stripping of SC on the electrical parameters in vivo

3 Stratum Corneum Dynamic Hydration Tests

3.1 Sorption-Desorption Test

The sorption-desorption test (SDT), a synonym of water sorption-desorption test, was originally proposed by Tagami et al. (1982) as a simple and practical method to assess the functional properties of the skin surface, i.e., the uppermost portion of the SC, in vivo in a short period of time. The test procedure consists of electromeasurements before and after the application of a droplet of water on the skin surface for 10 s to obtain data on the hygroscopic property of the skin surface and later serial measurements at intervals of 30 s for 2 min to evaluate the water-holding capacity of the skin surface (Tagami et al. 1982). The time course of water desorption

assessed by high-frequency conductance approximates the exponential curve, $W = W_{max} \cdot e^{-\lambda t}$, since the measured values can be plotted in a straight line on a semilogarithmic graph. λ indicates desorption rate constant (Tagami and Yoshikuni 1985).

3.2 Test Procedure Originally Described by Tagami et al.

The original authors utilized a high-frequency electric current of 3.5 MHz with a skin surface hygrometer that measures high-frequency conductance, Skicon, to follow the changes in the hydration state of the SC. First, a test area at least 1 cm in diameter is marked on the skin surface and the conductance value is measured with Skicon to obtain a prehydration level. Then, a drop of distilled water is placed over the test area for 10 s. Immediately after blotting the site with a pad of gauze or tissue paper, the measurement is made and repeated at intervals of 30 s for 2 min. Instead of distilled water, saline or PBS can also be used since the results are not greatly affected by the presence of electrolytes but only by the exogenous supply of water in vivo. They showed that the longer the water application time, the higher the hygroscopicity and water-holding capacity. Thus, they utilized 10 s for the water application time for the practical reason finishing this whole procedure in 2 min.

3.3 Normal Skin Water Kinetics

Under usual ambient conditions, normal skin surface shows a high rise in conductance just after the application of water, which is followed by a rapid falloff within 30 s, and thereafter by a gradual return to the prehydration levels within 2 min. By performing SDT before and after serial tape stripping, it is clearly demonstrable that a deeper portion of the SC is more hygroscopic than the superficial part (Tagami et al. 1982) (Fig. 3). Interestingly, the SDT with an in vivo

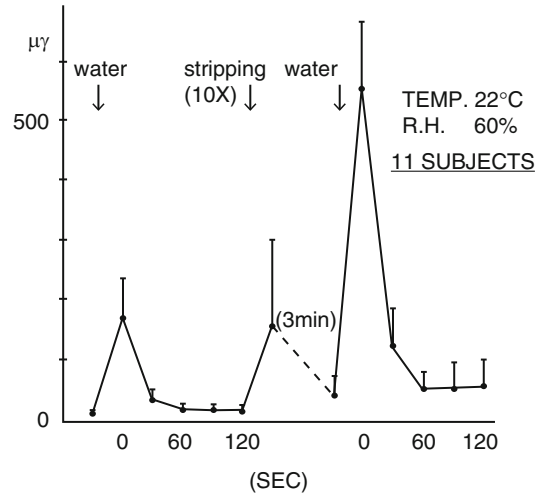

Fig. 3 Water sorption-desorption test on normal skin surface and that repeated 3 min after adhesive tape stripping of the SC 10 times (From reference Tagami et al. 1982)

simulation model by using a sheet of SC showed that the lowermost surface of the SC, which consists of only newly formed immature SC, exhibits much less water-holding capacity than the upper surface, because of the lower concentrations of NMF in the freshly produced corneocytes than those covering the skin surface (Hashimoto-Kumasaka et al. 1991). The finding that the largest amount of free amino acids is in the midportion indicates that the midportion has the greatest water-holding capacity (Hashimoto-Kumasaka et al. 1991). Therefore, by introducing a procedure of partial stripping of the SC before SDT, we can evaluate the functional properties at various levels of the midportion of the SC.

3.4 Modified Procedure of SDT and Definition of Functional Parameters

Modified procedures using other instruments and/or with longer water application time have been reported after the initial proposal of SDT by Tagami et al. (1982). Instead of skin hygrometer, Skicon, other measuring instruments such as

Corneometer (Agache et al. 2001; Pellacani and Seidenari 2001) or Nova DPM (Treffel and Gabard 1995) have been used to assess the hydration state of the SC.

The water application time of 10 s can also be elongated, which, however, requires a much longer follow-up time. Agache et al. (2001) reported such a modified methodology in which water was applied for 60 s then removed with soft paper towel. Thereafter, skin capacitance and TEWL were measured together there by employing Corneometer CM 820 and Evaporimeter EP1, respectively, after every 90 s up to 630 s. The areas under the TEWL-versus-time curve provide the absolute amounts of residual absorbed water. They were similarly bi-exponential, i.e., an initial rapid then a subsequent slower curve in the decrease kinetics measured with both instruments. The Corneometer values were found to change monoexponentially, reflecting the influence of the water content that is present even in the deeper portion of the SC.

The WHC, which is defined as the area under the curve (AUC) plotted by capacitance measurements, can be calculated by assuming that the prehydration value is equal to 0. The difference between the capacitance value measured immediately after water removal and that of the prehydration state can be defined as the water-sorption capacity (hygroscopicity) (Pellacani and Seidenari 2001).

3.5 SDT on Various Skin Conditions

3.5.1 Scaly Skin

The SDT can be performed on pathologically scaly skin due to various inflammatory dermatoses such as psoriasis, eczematous dermatitis, tinea corporis, and pityriasis alba, all of which demonstrated lower hygroscopicity and WHC values than those measured on the adjacent normal skin areas (Fig. 4) (Tagami et al. 1982; Urano-Suehisa and Tagami 1985). It is also possible to increase the sensitivity of the probe by using an MCC probe (Measurement Technologies Cincinnati, USA), whose skin-attaching portion is studded with 8 needle-like electrodes instead of an ordinary flat surface for the measurement of dry skin (Sasai et al. 1996). The sensitivity of the probe from the manufacturer (IBS Ltd., Hamamatsu, Japan) can also be increased with Skicon 200 EX as compared with Skicon 200.

3.5.2 Hypertrophic Scars and Keloids

Unique functional changes are found in the clinically smooth skin surfaces of hypertrophic scars and keloids. They show elevated values in both TEWL and high-frequency conductance compared to those obtained at the skin surface of mature atrophic scars (Suetake et al. 1996). These unique functional changes are much more clearly demonstrable with SDT, which shows both elevated hygroscopicity and WHC in fresh scar lesions, distinct from what is ordinarily observed in chronically inflamed lesions. These functional characteristics of hypertrophic scars have been noted to gradually return to those of normal skin levels when the scar characteristics later change into those of mature, flat, atrophic scars.

3.5.3 Functional Changes After Repeated Applications of Topical Steroids or Calcineurin Inhibitor

The SDT can detect even slight functional SC abnormalities of the skin, even when the static functional parameters do not show much change. It is known that repeated topical applications of high-potency glucocorticoid such as clobetasol propionate for a few weeks on normal skin produce not only a decreased barrier function that is demonstrable as enhanced TEWL but also a decreased hydration state of the SC (Kolbe et al. 2001). Topical ointment containing 0.12 % betamethasone-17-valerate, which is a less potent steroid than clobetasol propionate, did not induce these functional changes in TEWL or the hydration state in the normal skin surface even after twice-daily applications for 3 weeks. In this case, however, a decrease in both hygroscopicity and in WHC on the skin treated with this potent steroid ointment was clearly revealed by the SDT. In contrast, no such changes were observed on the

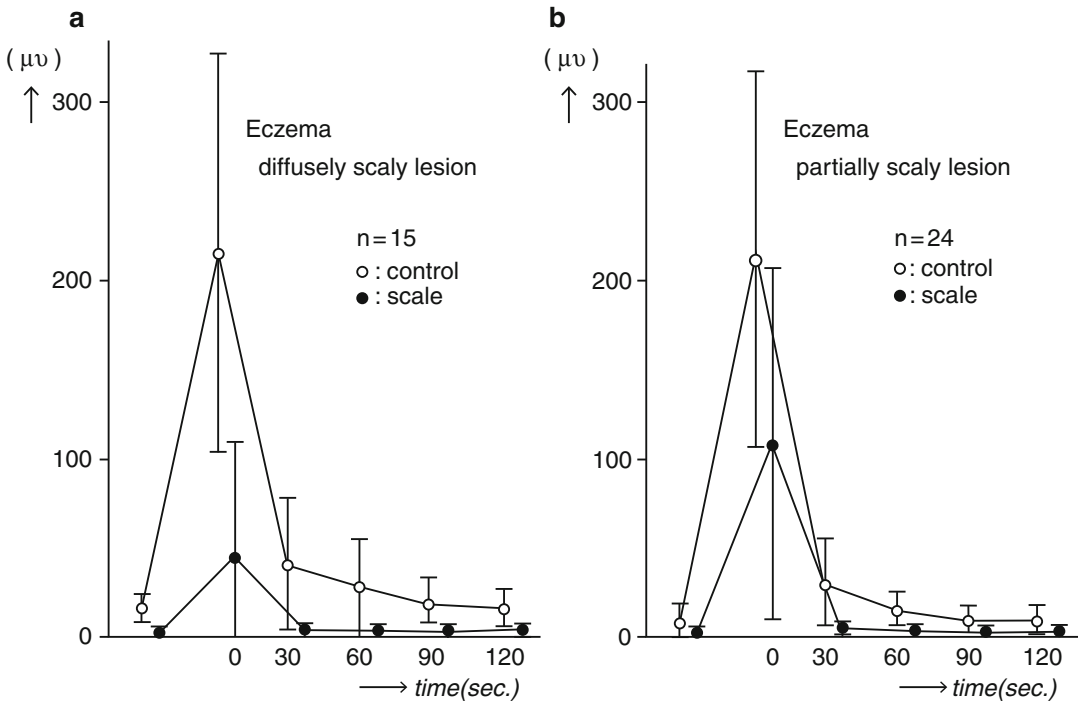

Fig. 4 Water sorption-desorption test carried out on eczematous lesions. As compared to diffusely scaly lesions (**a**), thin scaly ones (**b**) show more hygroscopicity, but water-holding capacity is still low (From reference Tagami et al. 1982)

skin after such repeated applications with either petrolatum or a calcineurin inhibitor, tacrolimus ointment for 3 weeks (Kikuchi and Tagami 2002).

3.5.4 The Skin Changes After Topical Application of Skin Moisturizers

Topical application of skin moisturizers obviously affects the hydration state of the SC, especially on its outer surface, immediately after their application. Such induced differences in the dynamic hydration state can be observed at certain periods of time after starting the application of various kinds of emollients by conducting the SDT. After 15 min acclimatization in an environmental chamber whose room temperature and relative humidity are maintained at 21 ± 1 °C and 50 ± 3 %, respectively, baseline measurements of the hydration state of the SC at the test area on the lower leg were performed with Skicon 200 EX (IBS Ltd., Hamamatsu, Japan). Then petrolatum, Hirudoid® Soft Ointment (W/O), and Hirudoid® Lotion (O/W) were applied on each test area. Both Hirudoid® Soft Ointment and Hirudoid® Lotion are popularly prescribed moisturizers in Japan that contain a heparinoid substance and glycerol as the main humectants. Two hours after the application of these moisturizers, the SDT was conducted with a slight modification of the original method described by Tagami et al. (1982). Namely, instead of applying a droplet of distilled water on the skin surface, cotton soaked with distilled water was applied on the skin surface for 10 s to avoid spilling of the water from the test area. The obtained hygroscopicity was highest on the area treated with Hirudoid® Lotion (O/W), followed by treated with Hirudoid® Soft Ointment (W/O), whereas it was lowest after the application of petrolatum. Judging from the most gradual logarithmic decay curve of water desorption, the WHC after the application of Hirudoid® Soft Ointment

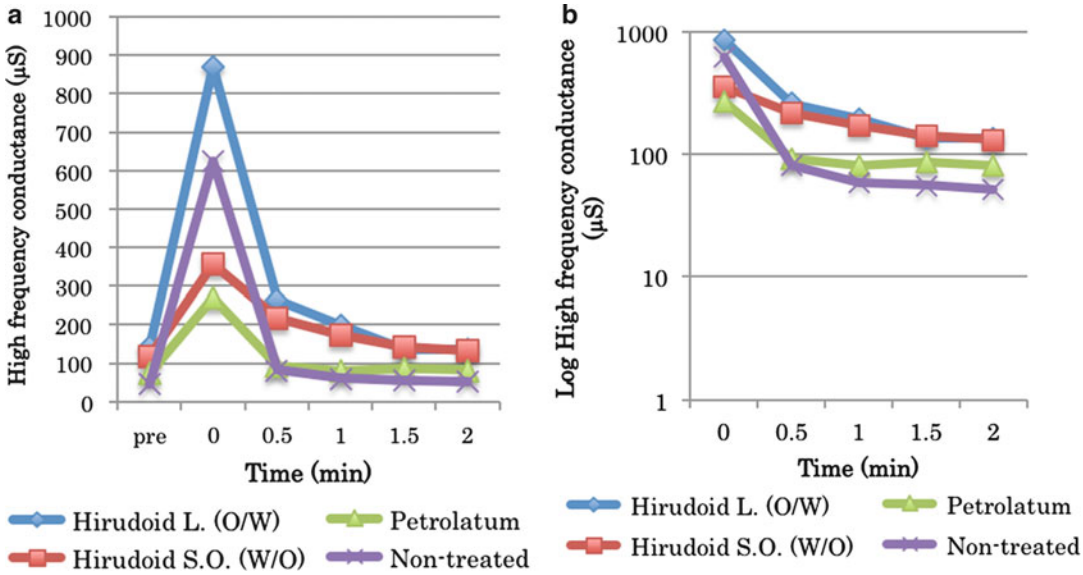

Fig. 5 The SDT on the skin after the application of various topical lubricants. Hygroscopicity was the highest after the application of Hirudoid® Lotion (O/W) (**a**), whereas the water-holding capacity (WHC) was better after the application of Hirudoid® Soft Ointment (W/O) (**b**)

(W/O) was found to be superior, although Hirudoid® Lotion was better than the other moisturizers considering the largest AUC due to its immediate effect (Fig. 5a, b). In contrast, it was difficult to find any increase in high-frequency conductance just after the application of oily lubricants such as petrolatum because they exert an occlusive effect at first that lowers the obtained hydration values just after the application.

3.5.5 Differences Among Different Anatomical Locations

Using the SDT, differences in the hydration functions of the SC were compared between the skin of the flexor forearm, flexor lower leg, and hyperkeratotic heel skin with fissures, after 15 min acclimatization in an environmental chamber whose room temperature and relative humidity were maintained at 21 ± 1 °C and 50 ± 3 %, respectively. The value of TEWL was highest on the heel, followed by the forearm, then the leg (29.5, 3.4, and 1.5 $gm^{-2}h^{-1}$, respectively). Baseline high-frequency conductance values on the heel, the forearm, and the leg were 7, 21, and 45 μS, respectively. Hygroscopicity was lowest on the heel and its WHC was also lowest, thus reflecting the uniquely firm skin surface characteristics of the plantar skin (Fig. 6a, b).

3.6 Moisture Accumulation Test (MAT)

As described above, the electrical parameters commonly used for evaluation of the hydration state of the SC, i.e., high-frequency conductance and capacitance, are usually obtained several seconds after application of the electrode to the skin surface in order to avoid the influence of accumulating water between the electrode and the skin surface that is induced by prolonging the electrode application time. In contrast, the MAT is devised to measure the pattern of this increase in the water content taking place in the upper portion of the SC due to the occlusive application of the electrodes.

Van Neste (1990) described the procedure of the MAT as follows. The Corneometer probe is applied continuously to the skin surface with

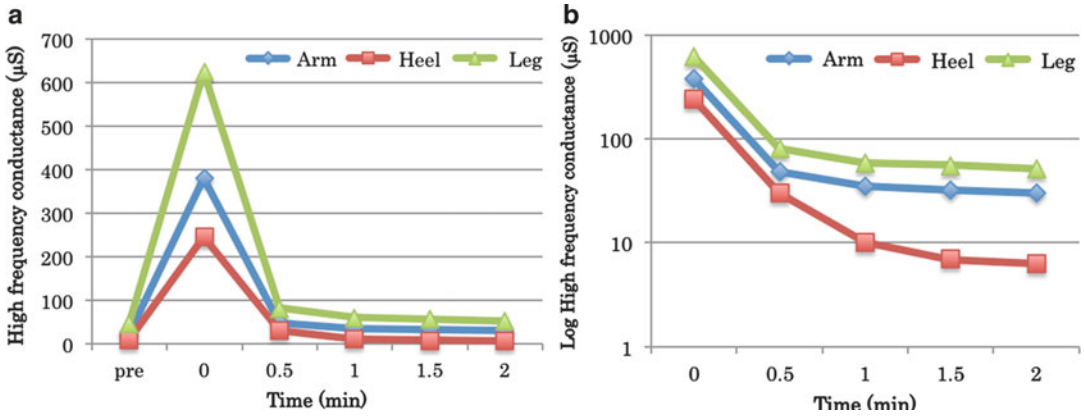

Fig. 6 The SDT on the skin of volar forearm, flexor lower leg, and hyperkeratotic heel associated with fissures. The hygroscopicity (**a**) as well as the WHC (**b**) on the heel was lowest among the test areas

moderate pressure. The obtained values of capacitance are then recorded every 3 s for up to 45 s. It initially increases rapidly, then more slowly afterward. Thus, the water accumulation velocity (WAV) is observed as a biphasic slope of increase in capacitance, consisting of an initial steep one that is followed by a gradual decrease afterward. This probably reflects the rapid hydrating process of the intercellular spaces of the corneocytes induced by the interruption of TEWL (initial phase), subsequently followed by the cellular hydration of the SC. The latter may arise from osmotic hydration, simple diffusion, or both. Thus, it is useful to assess these two parameters separately (Agache and Black 2004).

This MAT can also be performed using conductance-measuring instruments, i.e., Skicon or Nova DPM. Instead of those measurements at every 3 s up to 45 s as reported by van Neste, the hydration value can be read every 30 s for up to 3 (Treffel and Gabard 1995) or 5 min (Pellacani and Seidenari 2001), as modified by other researchers according to their respective purposes. The WAV during the first 30 s is calculated from the obtained readings (the reading made at 30 s – baseline value)/30, and the water accumulation (WA) is represented by the area under the curve (AUC) between the values of the baseline and those at the end of the measurements.

3.7 MAT Conducted Under Various Skin Conditions

The MAT and the abovementioned SDT clearly show differences in the dynamic parameters of the SC hydration function after the application of moisturizers or after irritation with sodium lauryl sulfate (SLS). The WAV was shown to be higher after the application of cream W/O than after that of cream O/W (Treffel and Gabard 1995).

3.7.1 Differences Among Anatomical Locations

We conducted the MAT on the skin of the flexor lower leg with or without partial tape stripping and on the hyperkeratotic heel by measuring the high-frequency conductance with Skicon 200 EX every 30 s up to 3 min in an environmental chamber whose room temperature and relative humidity were maintained at 21 ± 1 °C and 50 ± 3 %, respectively. The obtained values of TEWL on the flexor leg, heel, and 15 times' tape-stripped leg skin were 2.1, 18.9, and 16.8 $gm^{-2}h^{-1}$, respectively. The WA and the WAV were remarkably high on the skin after partial tape stripping as compared to those of the untreated heel or the leg skin (Fig. 7a). Moreover, the WA and the WAV were higher on the leg than on the heel (Fig. 7b), clearly indicating the poor water-holding capacity of the plantar SC despite the

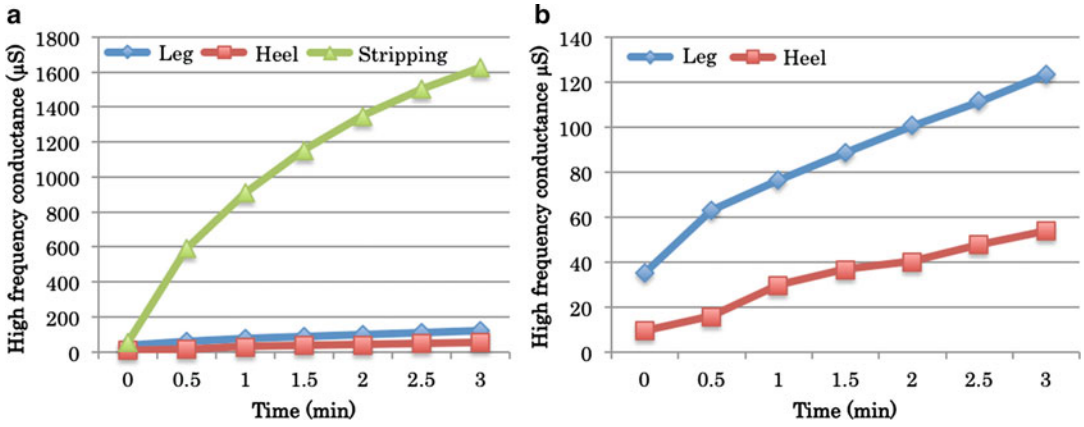

Fig. 7 The moisture accumulation test (*MAT*) on the skin of the flexor lower leg, with or without serial tape stripping, and a hyperkeratotic heel showing fissures. The water accumulation velocity (*WAV*) and the water accumulation (*WA*) were much higher on the skin after partial tape stripping of the SC (**a**). The WAV and WA were higher on the flexor leg than on the heel (**b**)

fact that its TEWL level was higher than that of the leg. This probably reflects the unique functional properties of the plantar SC, which is extremely thick as compared to the SC of other body locations (Ya-Xian et al. 1999). It is necessary to be firm enough to support the body weight without causing any damage to the underlying living skin tissues. In addition, it is also necessary for the plantar SC to maintain a certain level of flexibility, which can be attained with an adequate hydration state, in order to avoid painful cracking in such extremely thick SC. Therefore, the water barrier function of the plantar SC does not need to be so efficient as compared to that of the SC of other body locations, because of its rather massive water supply from the underlying wet epidermal tissue, helping the thick planter to maintain a certain level of flexibility.

3.7.2 After the Application of Skin Moisturizers

We also assessed the hydration state of the SC with the MAT after the application of various moisturizers. The same moisturizers employed in the SDT section were applied on the test areas of the lower legs. Two hours after the application of the moisturizers, the MAT was conducted together with measurement of the high-frequency conductance by Skicon 200 EX in the same environment as described above. The WA on the skin after the application of Hirudoid® Lotion (O/W) was the highest, but those after the application of Hirudoid® Soft Ointment or that of petrolatum were not higher than that of the non-treated control, indicating that the medium consisting of lotion has greater water-binding ability than W/O cream or petrolatum (Fig. 8).

3.8 Plastic Occlusion Stress Test (POST)

The POST involves measurement of the skin surface water loss (SSWL) by evaporimetry on a previously occluded skin site for an abnormally long period of time. It was first proposed by Berardesca and Maibach in 1988 (Berardesca and Maibach 1988, 1990). After abnormally long occlusion of the skin surface with an impermeable plastic film, the SC becomes overhydrated due to the permeation of water from the viable skin tissue. As described previously, with more than 50 % w/w hydration, the corneocytes become swollen where the accumulated water behaves like bulk liquid water. At hydration levels of >300 % w/w, extracellular pools of water become

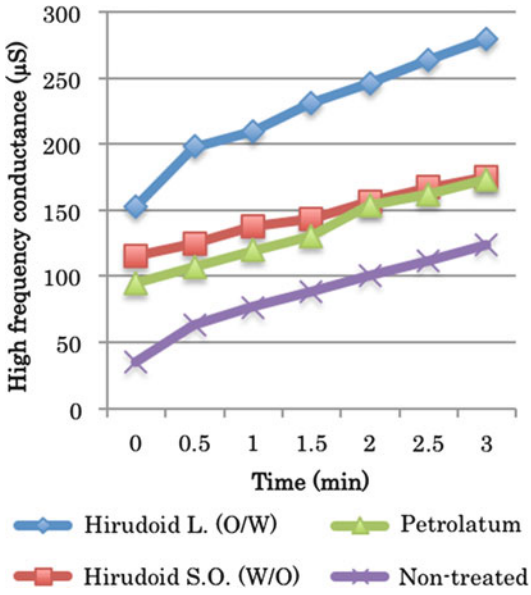

Fig. 8 The MAT conducted on the skin after the application of various moisturizers. The WA on the skin after Hirudoid® Lotion application was the highest among these topical agents

observable morphologically. Thus, SSWL is highest immediately after removal of the occlusion due to the excessive water evaporation from the SC. Then, the SSWL decreases together with water vaporization from the SC.

The practical procedure of the POST is as follows: first, an initial SSWL value (so-called TEWL) is measured on the test site with evaporimetry using Evaporimeter EP1 (SeroMed AB, Stockholm, Sweden), Tewameter (Courage and Khazaka, Köln, Germany), or DermaLab (Cortex Technologies, Denmark). Then, the test site is occluded with a water-impermeable film for 24 h. Immediately after removal of the film, the visible excess water on the skin surface is quickly wiped off with tissue paper and the SSWL is monitored every minute (or every 5 min) for 25–30 min (Berardesca and Maibach 1990).

The obtained SSWL decay curve appears to be bi-exponential, which can be easily quantified through logarithmic transformation. The second slope that appears after 10 min is subtracted from the overall log curve, allowing the initial decay curve to be obtained (0–9 min). The parameters obtained are the slope and the y-intercept of the SSWL/time log regression lines. The slopes (SSWL decrease rate constant) are expressed as a percentage of the SSWL decrease per unit time. The intercept of the initial slope is the log of the initial SSWL (it should not to be mistaken for the total desorbed water). This parameter is of less value than the SSWL rate constant (Agache and Black 2004).

The POST may also be performed using impedance meters, but in this case the measurement would be that of SC hydration and not that of SSWL.

3.9 POST Conducted in Various Skin Conditions

The POST was utilized to demonstrate non-visible skin damage such as that produced by a 3-day open application of 7 % sodium lauryl sulfate (SLS). SSWL decay curves are reported to show significant differences between control and SLS-treated skin (Berardesca and Maibach 1990). By performing the POST on the skin where different types of skin damage were elicited by tape stripping, lipid extraction, or skin surface biopsy, different parameters could be obtained as compared to non-treated control skin (Rosado et al. 2005). Furthermore, there was also a significant difference in the parameters obtained from the wrist and the volar forearm (Rosado et al. 2005), indicating the unique functional characteristics of the SC covering an area frequently placed under flexion and extension.

4 Discussion

The three representative in vivo tests, the SDT, MAT, and POST, described above demonstrate the dynamic hydration changes, induced either exogenously or endogenously in the SC, using different artificial hydration procedures. These hydration changes are followed by instrumental measurements. The SDT employs only exogenous water applied on the skin surface, whereas the MAT and the POST utilize water endogenously

accumulated by preventing water evaporation from the skin surface. When such excessive water accumulation is induced in the SC experimentally, it first quickly permeates into the intercellular spaces and thereafter even into the corneocytes where the water exists as secondary bound water and, much later, even as free water in the SC. Thus, the dynamic hydration of the SC depends on the ability of water-binding substances such as NMF as well as the function of the intercellular lipids. Namely, these tests can evaluate the ability of the SC to absorb water quickly and to hold it as long as possible. These dynamic changes in the hydration state of the SC are monitored by measuring the components of high-frequency impedance, i.e., conductance or capacitance, by simply applying an electrode to the skin surface of the test area. High-frequency conductance measured with the skin surface hygrometer, Skicon, most closely reflects the changes in the amount of water in the uppermost portion of the SC. Thus, this instrument appears to be the most practical and useful for conducting the SC dynamic hydration tests for evaluating the hydrating properties of the skin surface. The POST is rather time-consuming and complicated as compared to the SDT or the MAT, because the overhydration induced by the long-time occlusion may produce even structural damage in the SC such as maceration.

From a practical point of view, the SDT and MAT appear to be superior to the POST because of the ease of use even at outpatient clinics or at the bedside. Additionally, they can be finished within 5 min, whereas the latter requires a more than 24 h occlusion procedure before conducting the instrumental measurements.

5 Conclusion

The SDT and MAT conducted using high-frequency conductance may be the most practical and useful tests for assessing the dynamic hydration in the SC. By conducting these tests, we can demonstrate even slight changes in the SC moisturizing function, as observed in various skin conditions, as well as those changes occurring in the skin surface induced by the application of various skin care products and topical pharmacological agents. Despite various modifications proposed for conducting these tests as well as for evaluating the obtained functional parameters, further investigations are needed to standardize these practical tests to characterize further the local differences in the body surface, which will provide us better information for producing new skin care products appropriate to each body site.

References

Agache P, Black D. Stratum corneum dynamic hydration tests. In: Agache P, Humbert P, editors. Measuring the skin. Berlin Heidelberg: Springer-Verlag ; 2004.

Agache P, et al. Assessment of the water content of the stratum corneum using a sorption-desorption test. Dermatology. 2001;202(4):308–13.

Berardesca E, Maibach HI. Monitoring the water-holding capacity in visually non-irritated skin by plastic occlusion stress test (POST). Clin Exp Dermatol. 1990;15 (2):107–10.

Berardesca E, Maibach HI. The effect of non visible damage on the water holding capacity of the stratum corneum utilizing the plastic occlusion stress test (POST) (Preliminary report). In: First European Symposium on Contact Dermatitis. Heidelberg; 1988.

Caspers PJ, et al. In vivo confocal Raman microspectroscopy of the skin: noninvasive determination of molecular concentration profiles. J Invest Dermatol. 2001;116(3):434–42.

Egawa M, Kajikawa T. Changes in the depth profile of water in the stratum corneum treated with water. Skin Res Technol. 2009;15(2):242–9.

Egawa M, Tagami H. Comparison of the depth profiles of water and water-binding substances in the stratum corneum determined in vivo by Raman spectroscopy between the cheek and volar forearm skin: effects of age, seasonal changes and artificial forced hydration. Br J Dermatol. 2008;158(2):251–60.

Hashimoto-Kumasaka K, Horii I, Tagami H. In vitro comparison of water-holding capacity of the superficial and deeper layers of the stratum corneum. Arch Dermatol Res. 1991;283(5):342–6.

Hashimoto-Kumasaka K, Takahashi K, Tagami H. Electrical measurement of the water content of the stratum corneum in vivo and in vitro under various conditions: comparison between skin surface hygrometer and corneometer in evaluation of the skin surface hydration state. Acta Derm Venereol. 1993;73 (5):335–9.

Kikuchi K, Tagami H. Comparison of the effects of daily applications between topical corticosteroid and tacrolimus ointments on normal skin: evaluation with

noninvasive methods. Dermatology. 2002;205 (4):378–82.
Kolbe L, et al. Corticosteroid-induced atrophy and barrier impairment measured by non-invasive methods in human skin. Skin Res Technol. 2001;7(2):73–7.
Pellacani G, Seidenari S. Water sorption-desorption test and moisture accumulation test for functional assessment of atopic skin in children. Acta Derm Venereol. 2001;81(2):100–3.
Rawlings AV, Harding CR. Moisturization and skin barrier function. Dermatol Ther. 2004;17 Suppl 1:43–8.
Rawlings AV, et al. Stratum corneum moisturization at the molecular level. J Invest Dermatol. 1994;103(5):731–41.
Rosado C, Pinto P, Rodrigues LM. Modeling TEWL-desorption curves: a new practical approach for the quantitative in vivo assessment of skin barrier. Exp Dermatol. 2005;14(5):386–90.
Sasai S, Zhen YX, Tagami H. High-frequency conductance measurement of the skin surface hydration state of dry skin using a new probe studded with needle-form electrodes (MT-8C). Skin Res Technol. 1996;2(4):173–6.
Suetake T, et al. Functional analyses of the stratum corneum in scars – sequential studies after injury and comparison among keloids, hypertrophic scars, and atrophic scars. Arch Dermatol. 1996;132(12):1453–8.
Tagami H, Yoshikuni K. Interrelationship between water-barrier and reservoir functions of pathologic stratum corneum. Arch Dermatol. 1985;121(5):642–5.
Tagami H, et al. Evaluation of the skin surface hydration in vivo by electrical measurement. J Invest Dermatol. 1980;75(6):500–7.
Tagami H, et al. Water sorption-desorption test of the skin in vivo for functional assessment of the stratum corneum. J Invest Dermatol. 1982;78(5):425–8.
Takenouchi M, Suzuki H, Tagami H. Hydration characteristics of pathologic stratum corneum – evaluation of bound water. J Invest Dermatol. 1986;87 (5):574–6.
Treffel P, Gabard B. Stratum corneum dynamic function measurements after moisturizer or irritant application. Arch Dermatol Res. 1995;287(5):474–9.
Urano-Suehisa S, Tagami H. Functional and morphological analysis of the horny layer of pityriasis alba. Acta Derm Venereol. 1985;65(2):164–7.
van Neste D. In vivo evaluation of unbound water accumulation in stratum corneum. The influence of acute skin irritation induced by sodium laurylsulfate. Dermatologica. 1990;181(3):197–201.
Warner RR, Myers MC, Taylor DA. Electron probe analysis of human skin: determination of the water concentration profile. J Invest Dermatol. 1988;90(2):218–24.
Watanabe M, et al. Functional analyses of the superficial stratum corneum in atopic xerosis. Arch Dermatol. 1991;127(11):1689–92.
Yamamura T, Tezuka T. The water-holding capacity of the stratum corneum measured by 1H-NMR. J Invest Dermatol. 1989;93(1):160–4.
Ya-Xian Z, Suetake T, Tagami H. Number of cell layers of the stratum corneum in normal skin – relationship to the anatomical location on the body, age, sex and physical parameters. Arch Dermatol Res. 1999;291 (10):555–9.

Optothermal Measurement of Water Distribution Within Stratum Corneum

31

Perry Xiao

Contents

Keywords

Optothermal radiometry • Stratum corneum • Hydration and hydration gradient • Transdermal water loss • Water diffusion coefficient

1 Introduction

Stratum corneum (SC) is the outmost skin layer, which is about 15–20 layers and about 20 μm in thickness. Stratum corneum is dry outside and wet inside; there must be a water concentration gradient. The water exists in stratum corneum also in different status, i.e., free water and bound water. The water content in stratum corneum plays a key role in skin's barrier function as well as skin's cosmetic properties. However, to measure the water content within stratum corneum, especially the water distribution and/or status of water, is very difficult. Optothermal transient emission radiometry (OTTER) (Imhof et al. 1984, 1994, 1995) is an infrared remote sensing technology that can be used for such measurements. OTTER is a form of photothermal radiometry (PTR) or optothermal radiometry (OTR), which can be used for different purposes depending on the laser sources used and detection wavelengths selected. By using Nd:YAG laser (532 nm) or tunable OPO laser (400–590 nm) with broadband detection wavelength (5–13 μm), OTTER can be used for measuring skin pigments, e.g., melanin and hemoglobin, and epidermal thickness (Bindra et al. 1994a; Xiao et al. 1999, 2001a; Xiao and

P. Xiao (✉)
School of Engineering, London South Bank University, London, UK
e-mail: xiaop@lsbu.ac.uk

P. Humbert et al. (eds.), *Agache's Measuring the Skin*,
DOI 10.1007/978-3-319-32383-1_31

Imhof 1999a). By using Er:YAG laser (2.94 μm) with 13.1 μm detection wavelength, OTTER can be used for measuring stratum corneum hydration, i.e., water concentration (Bindra et al. 1994b), stratum corneum surface hydration and hydration gradient (Xiao and Imhof 1996, 1998), stratum corneum thickness (Xiao and Imhof 1997; Xiao et al. 2007), water diffusion within stratum corneum (Xiao and Imhof 1999b), and stratum corneum hydration depth profiles, as well as topically applied solvent concentration depth profiles (Xiao et al. 2001b, 2012a). OTTER can also be used for skin damage assessment (Bindra et al. 1996) and nail water content measurements (Xiao et al. 2009, 2011). By using a tunable OPO laser near 3 μm wavelength, OTTER can be used for studying stratum corneum water binding energy (Guo et al. 1999). Combined with transepidermal water loss (TEWL) measurements, OTTER can also be used for studying stratum corneum water diffusion coefficient, the status of water, and stratum corneum water-holding capability (Xiao et al. 2007, 2012b). By using Er:YAG laser (2.94 μm) with 9.5 μm detection wavelength, OTTER can also be used for topically applied solvent penetration measurements through the skin or nail (Xiao et al. 2001a, 2009, 2011).

2 Experimental Apparatus and Procedures

2.1 Apparatus

The water distribution within stratum corneum measurements was performed on traditional OTTER apparatus (see Fig. 1), which uses a pulsed laser (Q-switched Er:YAG, 2.94 μm wavelength, 100 ns pulse duration, 5 Hz repetition rate, 3–4 mJ/pulse, ~1 mm diameter laser spot size) as heat source to heat up the sample and a fast infrared detector (mercury cadmium telluride, or MCT) to pick up the consequent blackbody radiation increase from the sample surface.

By analyzing the shape of the signal, we can get information on the optical properties, thermal properties, and layered structure of the sample. Depending on the detection wavelength, the OTTER signals can either reflect the water concentration information in the skin (13.1 μm wavelength) or solvent concentration information within the skin (9.5 μm wavelength). With the detection depth less than 20 μm, OTTER is the only technology that can confine measurements within the stratum corneum.

2.2 Samples and Experimental Procedures

All the optothermal measurements were performed in an air condition-controlled standard laboratory environment (21 ± 1 °C and 40 ± 5 % relative humidity). For the in vivo measurements, skin sites of healthy volunteers were chosen. The volunteers were acclimatized for 20 min, and each skin site was wiped clean with EtOH/water (95 %) solution, prior to measurements.

3 Results and Discussions

3.1 In Vitro Skin Immersive Hydration

Skin immersive hydration was performed on a piece of skin sample from the sole of a volunteer's foot. It was fully hydrated by soaking in water overnight. Figure 2 shows the drying curves of the sample in the laboratory ambient environment (Xiao and Imhof 1999b). We can divide the drying process into three periods, A to B, B to C, and C to D. In the first period, the skin surface hydration, i.e., surface water content, is decreasing rapidly while the hydration gradient remains close to zero. The low hydration gradient indicates that the skin sample is and remains uniformly hydrated, and only surface water, i.e. free water, is lost during this period. In the second period, the skin sample begins to lose near-surface water, i.e., bound water, causing the surface hydration to decrease rapidly. This also causes the hydration gradient to increase rapidly, as a diffusion gradient is established close to the

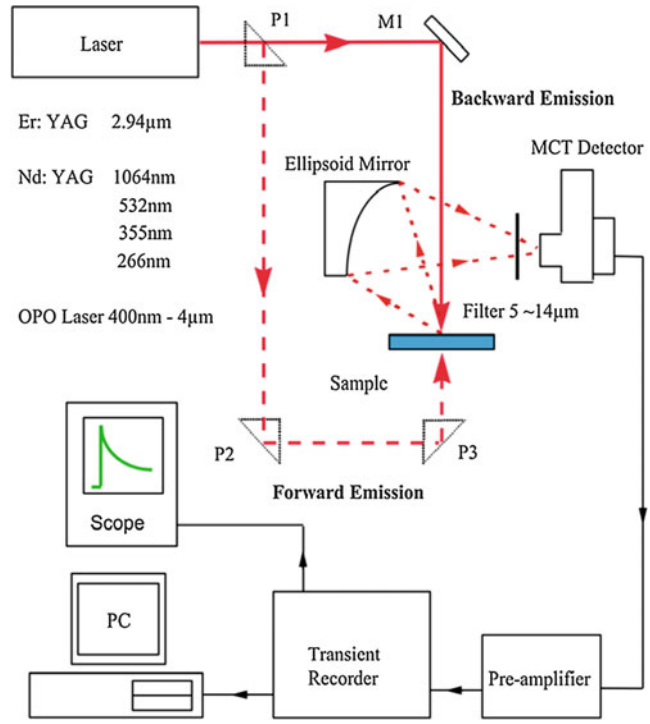

Fig. 1 Schematic diagram of optothermal transient emission radiometry (OTTER)

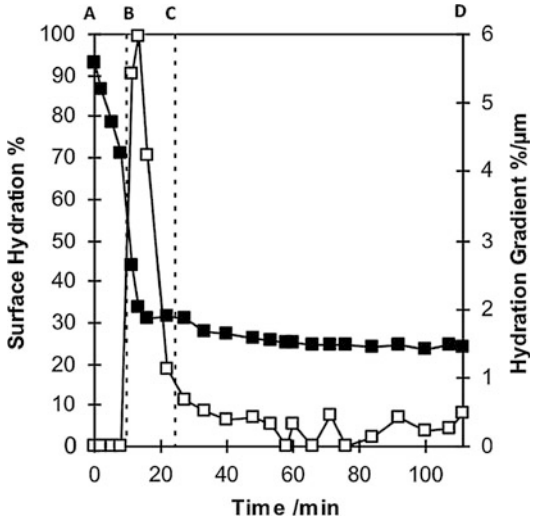

Fig. 2 Surface hydration (*solid squares*) and hydration gradient (*open squares*) measured on excised SC during a drying experiment

surface. This gradient peaks sharply during this period, as the diffusion region spreads inward from the surface. In the last period, steady conditions of water loss from the surface and diffusion of water within the whole of the sample are established. Surface hydration and hydration gradients are decreasing slowly during this period, as the sample approaches equilibrium with the moisture in the surrounding air.

3.2 In Vivo Volar Forearm Stratum Corneum Thickness Map

By combining the stratum corneum surface hydration and hydration gradient information, it is possible to calculate an estimated stratum corneum thickness. Figure 3 shows the stratum corneum thickness map of the volar forearm of a healthy male volunteer aged 20–30 (Xiao and Imhof 1997). The results show that stratum corneum is relatively thin and uniform for most part of the volar forearm; it thickens rapidly near the wrist. Such information could be very useful for transdermal drug delivery studies.

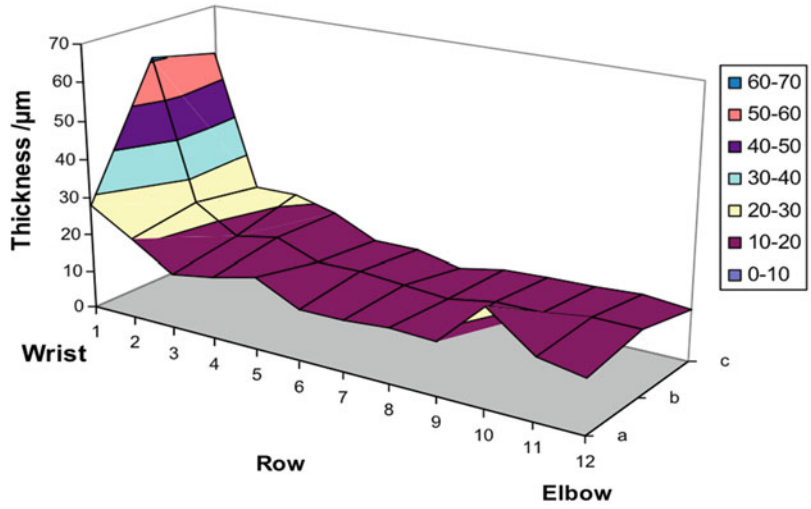

Fig. 3 Map of in vivo stratum corneum thickness of the left forearm

3.3 In Vivo Different Skin Site Measurements

Figure 4 shows the measurement results of different skin sites of four healthy volunteers, both male and female, aged 20–40. Figure 4a shows the stratum corneum surface hydration and hydration gradient results.

The results show that the stratum corneum surface hydration is high on the face, and low on the palm and finger, while, the hydration gradient is high on the arm and low on the palm and finger. Figure 4b shows the stratum corneum thickness results, which shows that it is thicker on the palm and finger and thinner on the arm. By combining the stratum corneum surface hydration and hydration gradient results (Fig. 4a) and TEWL results (Fig. 4c), we can also calculate the stratum corneum water diffusion coefficients of the different skin sites using Fick's first law (see Fig. 4d). The arm has lowest water diffusion coefficient and the palm has highest water diffusion coefficient. Water diffusion coefficient is also very useful for understanding the skin properties as well as in transdermal drug delivery studies.

3.4 In Vivo Stratum Corneum Hydration Depth Profiles

By analyzing the OTTER signal using segmented-least squares fitting, it is also possible to perform depth profiling of stratum corneum hydration, or topically applied solvent (Xiao et al. 2001b). Figure 5a shows the results of depth profiles at different skin sites, plus the nail and hair.

The results show that the face and forearm have the highest water hydration and hydration gradient, while the nail and hair have much lower hydration and hydration gradient. The curved structure of hair water hydration depth profile is likely to reflect the layered structure of the hair which holds different amounts of water. Figure 5b shows the stratum corneum hydration depth profiles on a volar forearm skin site during tape stripping using Scotch 3M tape. Each tape removes about 1 µm thickness of the stratum corneum. As tape strip number increases, the stratum corneum hydration depth profile also increases.

By scanning the skin surface, it is also possible to create a 3D hydration depth profile map. Figure 6 shows a 3D stratum corneum hydration depth profiles of a skin area from the wrist to the palm of a healthy male volunteer aged 20–30 (Pascut

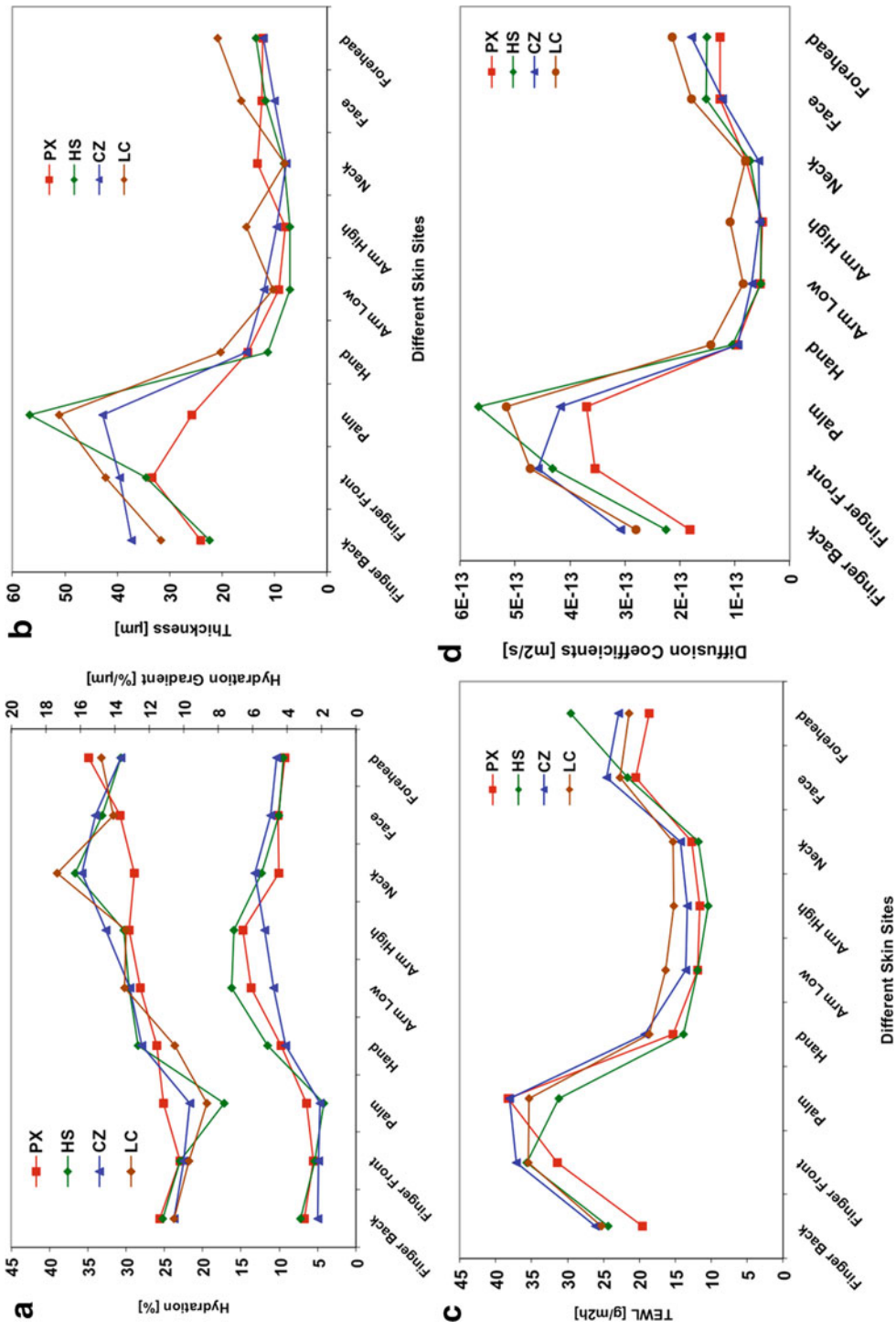

Fig. 4 (**a**) Stratum corneum surface hydration (*top* series) and hydration gradient (*bottom* series) at different skin sites; (**b**) Stratum corneum thickness at different skin sites; (**c**) TEWL at different skin sites; (**d**) Stratum corneum water diffusion coefficients at different skin sites

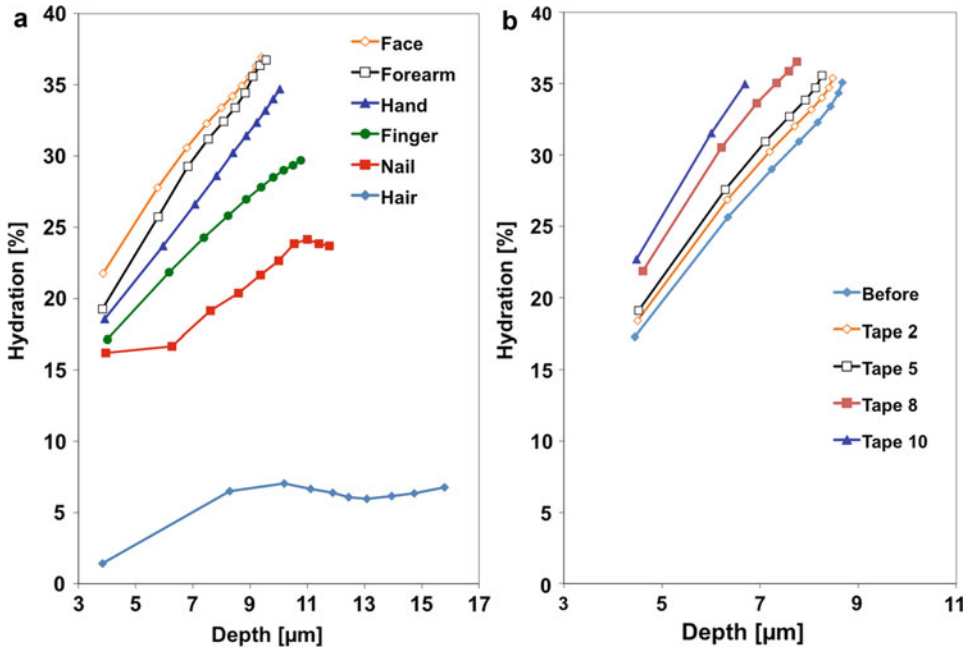

Fig. 5 (**a**) The stratum corneum hydration depth profiles of different skin sites (from *top* to *bottom*): the face, forearm, hand, finger, nail, and hair; (**b**) The stratum corneum hydration depth profiles during tape stripping

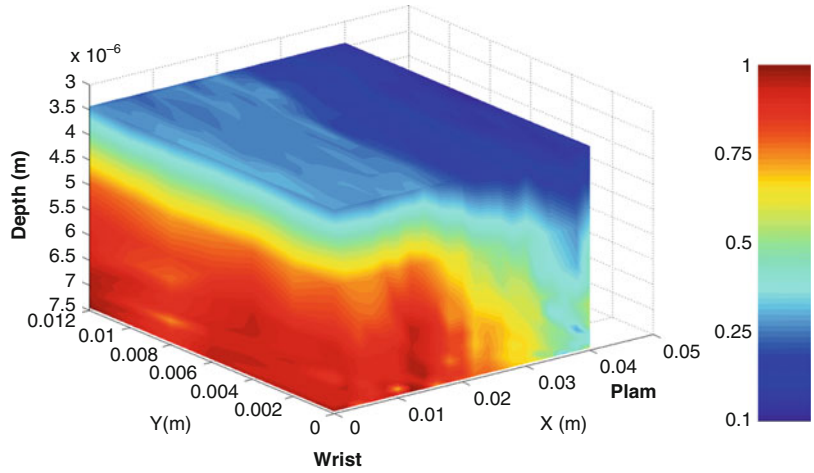

Fig. 6 3-D water hydration profile within SC on an area from the wrist to palm (*X* represents wrist-palm direction). The *color-coded* legend represents the normalized optical absorption coefficients

et al. 2003). The results show that from the wrist toward the palm, stratum corneum is getting dryer and thicker.

4 Conclusions

The results show that OTTER is a promising technology that can be used for stratum corneum hydration measurements, stratum corneum surface hydration and hydration gradient measurements, stratum corneum thickness measurements, stratum corneum hydration depth profiling, and topically applied solvent penetration depth profiling. By combining with TEWL measurements, it is also possible to measure stratum corneum water diffusion coefficient and stratum corneum water-holding capabilities.

Acknowledgments We thank EPSRC and London South Bank University for the financial support.

References

Bindra RMS, Imhof RE, Eccleston GM. In-vivo opto-thermal measurement of epidermal thickness. J Phys. 1994a;4(C7):445–8.

Bindra RMS, Imhof RE, Mochan A, Eccleston GM. Opto-thermal technique for in-vivo stratum corneum hydration measurement. J Phys. 1994b;4(C7):465–8.

Bindra RMS, Imhof RE, Xiao P, Andrew JJ, Wong J, Zhang B. Skin condition assessment: a comparative study of techniques. SPIE Proc. 1996;2681:17–30.

Guo X, Xiao P, Imhof RE. Photothermal excitation spectra using tunable OPO. In: 4th Gordon research conference on photoacoustic and photothermal phenomena, Colby-Sawyer College (North), New London, 28 June–2 July 1999.

Imhof RE, Birch DJS, Thornley FR, Gilchrist JR, Strivens TA. Opto-thermal transient emission radiometry. J Phys E: Sci Instrum. 1984;17:521–5.

Imhof RE, Zhang B, Birch DJS. Photothermal radiometry for NDE. In: Mandelis A, editor. Progress in photothermal and photoacoustic science and technology, vol. II. Englewood Cliffs: PTR Prentice Hall; 1994. p. 185–236.

Imhof RE, McKendrick AD, Xiao P. Thermal emission decay Fourier transform infrared spectroscopy. Rev Sci Instrum. 1995;66(11):5203–13.

Pascut FC, Xiao P, Imhof RE. In-vivo hydration profile mapping of human stratum corneum using fibre-optic opto-thermal radiometry. Rev Sci Instrum. 2003;74(1):770–2.

Xiao P, Imhof RE. Opto-thermal skin water concentration gradient measurement. SPIE Proc. 1996;2681:31–41.

Xiao P, Imhof RE. Optothermal measurement of stratum corneum thickness and hydration depth profile. SPIE Proc. 1997;2970D:50.

Xiao P, Imhof RE. Opto-thermal measurement of water distribution within the stratum corneum. In: Elsner P, Barel AO, Beraresca B, Serup J, editors. Skin bioengineering techniques and applications in dermatology and cosmetology, Current Problems in Dermatology, vol. 26. Basel: Karger; 1998. p. 48–60.

Xiao P, Imhof RE. Inverse method analysis in opto-thermal skin measurements. SPIE Proc. 1999a;3601:340–7.

Xiao P, Imhof RE. Water diffusion within stratum corneum, In: Scudieri F, Bertolotti M, editors. Photoacoustic and photothermal phenomena: 10 the international conference, Rome, Italy, 1999b. p. 573–5.

Xiao P, Guo X, Notingher I, Cowen JA, O'Driscoll D, Imhof RE. Opto- thermal skin pigment spectral depth profiling using an OPO laser. SPIE Proc. 1999;3601:348–54.

Xiao P, Gull SF, Imhof RE. Opto-thermal inverse modelling using a maximum entropy approach. Anal Sci. 2001a;17(Special Issue):394–7.

Xiao P, Cowen JA, Imhof RE. In-vivo transdermal drug diffusion depth profiling – a new approach to opto-thermal signal analysis. Anal Sci. 2001b;17(Special Issue):349–52.

Xiao P, Packham H, Zheng X, Singh H, Elliott C, Berg EP, Imhof RE. Opto- thermal radiometry and condenser-chamber method for stratum corneum water concentration measurements. Appl Phys B. 2007;86:715–9.

Xiao P, Ciorte LI, Singh H, Berg EP, Imhof RE. Opto-thermal radiometry for in-vivo nail measurements. J Phys: Conf Ser. 2009;214(1):012008.

Xiao P, Zheng X, Imhof RE, Hirata K, McAuley WJ, Mateus R, Hadgraft J, Lane ME. Opto-thermal transient emission radiometry (OTTER) to image diffusion in nails in vivo. Int J Pharm. 2011;406:111–3.

Xiao P, Ou X, Ciortea LI, Berg EP, Imhof RE. In-vivo skin solvent penetration measurements using opto-thermal radiometry and fingerprint sensor. Int J Thermophys. 2012a;33:1787–94. doi:10.1007/s10765-012-1318-6.

Xiao P, Wong W, Cottenden A, Imhof RE. In-vivo stratum corneum over-hydration and water diffusion coefficient measurements using opto-thermal radiometry and TEWL instruments. Int J Cosmet Sci. 2012b;34(4):328–31.

Cyanoacrylate Skin Surface Stripping for Visualizing the Stratum Corneum Structures and Dynamics

32

Gérald E. Piérard and Claudine Piérard-Franchimont

Contents

Keywords
Skin surface stripping • Stratum corneum • Corneosurfametry • Dansyl chloride • Microrelief • Corneoxenometry

Abbreviations

CSM	Corneosurfametry
CSSS	Cyanoacrylate skin surface stripping
CXM	Corneoxenometry
DHA	Dihydroxyacetone
SC	Stratum corneum

1 Introduction

The human stratum corneum (SC) is composed of keratin-enriched corneocytes embedded in a lipid-enriched intercellular matrix homing specific proteases and glycosidases. The SC represents a water-tight barrier controlling the internal aqueous balance of the body. It normally consists of about 20 tightly stacked layers of corneocytes that are renewed on a regular basis. This process is regulated by the progressive inconspicuous shedding of single corneocytes at the skin surface. Regional variations exist in the SC structure, and the palmoplantar epidermis strongly differs from all other body surfaces.

G.E. Piérard (✉)
Laboratory of Skin Bioengineering and Imaging (LABIC), Liège University, Liège, Belgium

Service de Dermatopathologie, CHU du Sart Tilman, Liège, Belgium
e-mail: Gerald.pierard@ulg.ac.be

C. Piérard-Franchimont
Laboratory of Skin Bioengineering and Imaging (LABIC), Department of Clinical Sciences, Liège University, Liège, Belgium
e-mail: Claudine.franchimont@ulg.ac.be

P. Humbert et al. (eds.), *Agache's Measuring the Skin*,
DOI 10.1007/978-3-319-32383-1_32

2 Sampling Procedure

Cyanoacrylate skin surface stripping (CSSS), formerly named skin surface biopsy, was designed when high-bond clear glues became available (Marks and Dawber 1971; Agache et al. 1972). Using a polyethylene slide as the sampling support was a further decisive step in the development of this technique (Lachapelle et al. 1977). At the dawn of the 1980s, CSSS entered the diagnostic world of dermatopathology (Piérard-Franchimont and Piérard 1985, 1987). The material is currently available as the 3S-Biokit (Courage +Khazaka Electronic, Cologne, Germany) (Piérard et al. 2014).

CSSS relies on collecting a thin layer from the outermost part of the healthy or diseased SC. Its thickness is uniform when collected from normal skin. This material is examined under the microscope looking for the presence of serum, parakeratosis, bacteria, fungi, parasites, neoplastic cells, and any other unusual structures. To perform a CSSS, a drop of cyanoacrylate is deposited off-center onto the polyester slide so as to leave an area free of glue for further handling in the laboratory and sampling identification. The part of the slide coated with cyanoacrylate is applied firmly to the skin and held in place for about 15–30 s. Harvesting the upper portion of the SC is obtained following a gentle traction exerted in parallel to the skin surface while the polyester slide is gently lifted up.

CSSS is conveniently collected from any glabrous area of the body, with two provisos. First, sampling from a hairy area is typically painful because of the hair tearing off, and the sampling quality is inadequate owing to the partial contact of the glue with the SC. It is therefore useful to shave these skin areas before harvesting a CSSS. Second, intracorneal cohesion on the palms and soles is such that it is difficult to collect a uniform continuous sheet of corneocytes. However, on these sites, sampling is commonly easier in conditions when the SC texture is compromised.

3 Microrelief Network of the Normal Stratum Corneum

Clinical examination of the normal skin surface commonly reveals the ordered network of microdepressions corresponding to first- and second-order lines (Piérard-Franchimont and Piérard 1987). Each pattern of line orientation is typical for each specific part of the body, but varies in appearance from one location to another. A correlation exists between the pattern of primary lines of the skin and grooves in the latticework papillary relief at the dermoepidermal interface (Piérard et al. 1974). The skin of youngers is characterized by the patterned intersections between the primary and secondary lines creating regular polyhedric plateaus. With aging, such a network alters its shape, aligning itself preferentially along major skin tension lines (Piérard-Franchimont and Piérard 1987; Makki et al. 1979). This process ends with the innate microrelief network disappearing among another configuration of wrinkles (Piérard-Franchimont and Piérard 1987). It is therefore possible to assess the texture of the superficial dermis indirectly on CSSS (Piérard-Franchimont and Piérard 1987). As a result, the skin microtopography, the dermal aging, as well as corticosteroid-induced atrophy, sclerosis, striae distensae, and many other changes in the connective tissue are conveniently assessed noninvasively on CSSS (Piérard-Franchimont and Piérard 1987). Such a microtopographic assessment is possibly highlighted using computerized image analysis (Arrese et al. 2004; Corcuff et al. 1989).

CSSS also collects some cornified material present in the pilosebaceous follicles at their openings (acrotrichium) at the skin surface. It is therefore possible to assess both the follicular density per surface area and the presence of any follicular

hyperkeratosis (Kerosis), comedones, trichostasis spinulosa, sebum, and some intrafollicular bacteria and mites (Mills and Kligman 1983; Piérard 1987; Groh et al. 1992; Pagnoni et al. 1994; Piérard et al. 1995; Uhoda et al. 2003a; Gerber et al. 2011).

4 CSSS Structural Changes of the Stratum Corneum

Noninfectious erythemato-squamous disorders conveniently assessed by CSSS include xeroses, as well as various spongiotic and parakeratotic dermatoses. Xeroses correspond to various forms of orthokeratotic and parakeratotic hyperkeratosis. This condition encompasses the presentation commonly referred to as "dry skin." This is similar to ichthyoses although at a different level of severity (Piérard-Franchimont and Piérard 1984, 1985, 1987; Franchimont 1980; Piérard 1996). Spongiotic conditions encompass superficial inflammatory reactions resulting in spongiosis and microvesiculation. Allergic contact dermatitis, atopic dermatitis, and pityriasis rosea belong to this group. Parakeratotic dermatoses commonly correspond to eczematids (ids) and stable psoriasis. Seborrheic dermatitis comes within this category when Pityrosporum yeasts are rare.

Contrasting with the uniformity of a normal SC in young people, xerosis is usually variable over the SC. A motley collection of corneocytes is responsible for a skin surface harshness. Parakeratotic corneocytes commonly keep tight intercellular connection. They form clumps and flakes.

Some structural changes alter the shape of individual corneocytes. Some environmental variations (temperature, moisture, dew point, etc.) influence the cohesion of the upmost SC. The effect of some chemicals (acids, bases, surfactants, penetration enhancers, etc.) significantly alters the protein composition of the corneocyte membrane or the nature of the intercellular lipids.

Many of the above-mentioned changes are discernible on CSSS using morphological or molecular techniques.

5 CSSS in Clinical Pharmacology Related to Epithelial Renewal

Some pharmacological agents and cosmetics attempt at improving the epidermal renewal rate. In fact, the keratinocyte proliferation is retarded in certain xeroses and during most aging types. Thus, it is wise to assess noninvasively the SC renewal in order to support any relevant therapeutic efficacy (Piérard 1996). One of these procedures involves application of dansyl chloride (DC) as a fluorescent dye to the skin (Takahashi et al. 1986; Piérard 1992). The progressive desquamation of the SC is responsible for a fluorescence decrease in proportion to the increased epidermal renewal by the test product. Harvesting a CSSS on the tenth day of this test reveals the area of renewed SC under a fluorescence microscope (Piérard 1992). The extent of persisting DC fluorescent areas is conveniently quantified by photodensitometry and morphometric analyses. The relationship between the DC fluorescence fading and the keratinocyte renewal depends on the experimental design. For instance, surfactants remove DC from the SC (Paye et al. 1994).

Due to the induction of contact dermatitis induced by DC, dihydroxyacetone (DHA) was introduced as a substitute (Piérard and Piérard-Franchimont 1993; Uhoda et al. 2004).

The various aspects of the acrotrichium help in making objective evaluations of comedogenesis induction and, conversely, some comedolytic effect of dedicated cosmetic products (Piérard et al. 1995; Mills and Kligman 1982a, b). The same samples, observed under fluorescence microscopy, possibly reveal the accumulation of certain anti-acne drugs, such as fluorescent tetracyclines, or again the presence of intrafollicular

fluorescent porphyrins focally secreted by bacteria of the genus *Propionibacterium acnes*.

6 Corneosurfametry and Corneoxenometry

CSSS is the substrate used for the corneosurfametry (CSM) bioassay predicting the irritant potential of cleansing products, such as surfactants present in personal care and household detergents (Piérard et al. 1994; Goffin et al. 1997; Henry et al. 1997; Uhoda et al. 2003b; Xhauflaire-Uhoda et al. 2006). Corneoxenometry (CXM) is a variant bioassay suitable for various other xenobiotics (Goffin et al. 2000; Xhauflaire-Uhoda et al. 2008a, b). The samples are sprinkled with a dilute solution of the test product (soap, shampoo, washing-up liquid, etc.). After a 2-h contact time, samples are stained with a toluidine blue-basic fuchsin solution. The intensity of the color is proportional to the degradation of the corneocyte wall (proteins and lipids) induced by the surfactant.

References

Agache P, Mairey J, Boyer JP. Le stripping du stratum corneum au cyanoacrylate. Intérêt en physiologie et en pathologie cutanées. J Med Lyon. 1972;53:1017–22.

Arrese JE, Quatresooz P, Piérard-Franchimont C, Piérard GE. Indications diagnostiques de la biopsie de surface au cyanoacrylate. L'avènement du 3S-Biokit. Dermatol Actual. 2004;83:5–13.

Corcuff P, Gracia AM, De Lacharrière O, Lévêque JL. Image analysis of the skin microrelief as a non invasive method to approach the dermal architecture. In: Piérard GE, Piérard-Franchimont C, editors. The dermis, from biology to diseases. Publ Monographies Dermatopathologiques Liégeoises; Liège, Belgium, 1989. p. 102–13.

Franchimont C. The stratum corneum xerotic from aging and photochemotherapy (PUVA). Am J Dermatopathol. 1980;4:295–304.

Gerber PA, Kukova G, Buhren B, et al. Density of Demodex folliculorum in patients receiving epidermal growth factor receptor inhibitors. Dermatology. 2011;222:144–7.

Goffin V, Piérard-Franchimont C, Piérard GE. Microwave corneosurfametry. A minute assessment of the skin compatibility of skin cleansing products. Skin Res Technol. 1997;3:242–4.

Goffin V, Henry F, Piérard-Franchimont C, Piérard GE. Penetration enhancers assessed by corneoxenometry. Skin Pharmacol Appl Skin Physiol. 2000;13:280–4.

Groh DG, Mills OH, Kligman AM. Quantitative assessment of cyanoacrylate follicular biopsies by image analysis. J Soc Cosmet Chem. 1992;43:101–12.

Henry F, Goffin V, Maibach HI, Piérard GE. Regional differences in stratum corneum reactivity to surfactants: quantitative assessment using the corneosurfametry bioassay. Contact Dermatitis. 1997;37:271–5.

Lachapelle JM, Gouverneur JC, Boulet M, Tennstedt D. A modified technique (using polyester tape) of skin surface biopsy. Br Dermatol. 1977;97:49–52.

Makki S, Barbenel JC, Agache P. A quantitative method for the assessment of the microtopography of human skin. Acta Dermatol. 1979;59:285–91.

Marks R, Dawber RPR. Skin surface biopsy: an improved technique for the examination of the horny layer. Br J Dermatol. 1971;84:117–23.

Mills OH, Kligman AM. A human model for assaying comedolytic substances. Br J Dermatol. 1982a;1982 (107):543–8.

Mills OH, Kligman AM. A human model for assessing comedogenic substances. Arch Dermatol. 1982b;118:903–5.

Mills OH, Kligman AM. The follicular biopsy. Dermatologica. 1983;167:57–63.

Pagnoni A, Kligman AM, El Gammal S, Stoudemayer T. Determination of density of follicles on various regions of the face by cyanoacrylate biopsy: correlation with sebum output. Br J Dermatol. 1994;132:862–5.

Paye M, Simion A, Piérard GE. Dansyl chloride labelling of stratum corneum: its rapid extraction from skin can predict skin irritation due to surfactants and cleansing products. Contact Dermatitis. 1994;30:91–6.

Piérard GE. Rate and topography of follicular sebum excretion. Dermatologica. 1987;175:280–3.

Piérard GE. Microscopy evaluation of the dansyl chloride test. Dermatology. 1992;185:37–40.

Piérard GE. EEMCO guidance for the assessment of dry skin (xerosis) and ichthyosis: evaluation by stratum corneum strippings. Skin Res Technol. 1996;2:3–11.

Piérard GE, Piérard-Franchimont C. Dihydroxyacetone test as a substitute for the dansyl chloride test. Dermatology. 1993;186:133–7.

Piérard GE, Hermanns JF, Lapière CM. Stereology of the dermo-epidermal junction. Dermatologica. 1974;149:266–73.

Piérard GE, Goffin V, Piérard-Franchimont C. Corneosurfametry: a predictive assessment of the interaction of personal care cleansing products with human stratum corneum. Dermatology. 1994;189:152–6.

Piérard GE, Piérard-Franchimont C, Goffin V. Digital image analysis of microcomedones. Dermatology. 1995;190:99–103.

Piérard-Franchimont C, Piérard GE. Xerosis: structure of rough skin. Int J Cosmet Sci. 1984;6:47–54.

Piérard-Franchimont C, Piérard GE. Skin surface stripping in diagnosing and monitoring inflammatory, xerotic and neoplastic diseases. Pediatr Dermatol. 1985;2:180–4.

Piérard-Franchimont C, Piérard GE. Assessment of aging and actinic damages by cyanoacrylate skin surface stripping. Am J Dermatopathol. 1987;9:500–9.

Piérard GE, Pierard-franchimont C, Paquet P, Hermanns-le T, Radermacher J, Delvenne P. Cyanoacrylate skin surface strippings and the 3S-Biokit advent in tropical dermatology. A look from Liège. The Scientific World Journal 2014;462634.

Takahashi M, Black D, Hughes B, Marks R. Exploration of a quantitative dansyl chloride technique for measurement of the rate of desquamation. Clin Exp Dermatol. 1986;12:246–9.

Uhoda E, Piérard-Franchimont C, Piérard GE. Comedolysis by a lipohydroxyacid formulation in acne prone subjects. Eur J Dermatol. 2003a;13:65–8.

Uhoda E, Goffin V, Piérard GE. Responsive corneosurfametry following in vivo preconditioning. Contact Dermatitis. 2003b;49:292–6.

Uhoda E, Piérard-Franchimont C, Debatisse B, et al. Repair kinetics of stratum corneum under repeated insults. Exog Dermatol. 2004;3:7–11.

Xhauflaire-Uhoda E, Loussouarn G, Haubrechts C, Saint-Léger D, Piérard GE. Skin capacitance imaging and corneosurfametry. A comparative assessment of the impact of surfactants on stratum corneum. Contact Dermatitis. 2006;54:249–53.

Xhauflaire-Uhoda E, Macarenko O, Denooz R, Charlier C, Piérard GE. Skin protection creams in medical settings: successful or evil? J Occup Med Toxicol. 2008a;3:15–20.

Xhauflaire-Uhoda E, Piérard-Franchimont C, Piérard GE. Effect of various concentrations of glycolic acid at the corneoxenometry and collaxenometry bioassays. J Cosmet Dermatol. 2008b;7:194–8.

Cyanoacrylate Method

33

Jakob Mutanu Jungersted

Contents

Keywords

Stratum corneum collection • Cyanoacrylate method • Stratum corneum lipids • Ceramides

Different methods have been used for the collection of stratum corneum for lipid analysis, all with different advantages and disadvantages (Table 1). We used the cyanoacrylate method, because of its simplicity and ability to produce low intraindividual differences (Jungersted et al. 2010).

The area of interest (the forearm) is wiped with acetone to eliminate contamination from surface lipids. A rinsed glass slide with a droplet of LiquiBand® (MedLogic, Plymouth, UK) cyanoacrylate glue is placed in one end, and held unto the skin for 1 min, and then slowly removed (Fig. 1). Hereby, a sample of the SC is attached to the glass slide, and the sample is then kept frozen until further analysis with high-performance thin-layer chromatography (HPTLC).

1 Critical Approach/Limitations

One concern could be that if the acetone used would change the lipid profile, however in a study on mouse skin, it has been shown that the SC lipids are not affected by the wiping with acetone (Rissmann et al. 2009).

The cyanoacrylate method does not give information on how deep into the stratum corneum the

J.M. Jungersted (✉)
Department of Dermatology, University of Copenhagen, Copenhagen, NV, Denmark
e-mail: jungersted@gmail.com

P. Humbert et al. (eds.), *Agache's Measuring the Skin*,
DOI 10.1007/978-3-319-32383-1_33

Table 1 SC collection methods

Method	Procedure	Advantages	Disadvantages
Biopsy	Punch or skin biopsies obtained from excess of skin from patients undergoing cosmetic surgery	Large amounts of SC	Risk of contamination from other lipids of epidermis when separating SC from rest of biopsy
Tape stripping	Tape stripping followed by analysis of SC attached to tape	Easily performed; no contamination from other layers of SC	Amount of SC obtained is limited; contamination from tape material
Cyanoacrylate stripping	Drop of cyanoacrylate resin on glass slide, pressed onto skin and then removed	Easily performed; no contamination from other layers of SC	Amount of SC obtained is limited
Organic solvents	Extraction chamber with organic solvents placed directly on skin, solvent stirred and then collected using pipette	Extracted lipids ready for further analysis	Method is inconvenient; measures have to be taken to avoid inhaling organic solvent; impossible to estimate from how deep in SC lipids are obtained
Azerbaijani scrub	Scrubbing of skin with moist crepe mitten	Simply performed; produces large amounts of SC	Must include large areas of skin to obtain enough SC, therefore method cannot be applied on localized anatomical sites; risk of contamination from surface lipids
Mechanically removed by scraping	Scraping of skin with scalpel	Large amounts of SC	Time-consuming

Reprint from Jungersted et al. (2010) (see article for references)

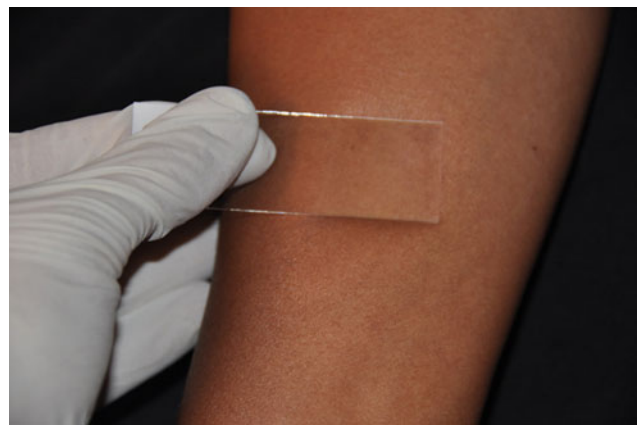

Fig. 1 Photo of the cyanoacrylate method

sample is obtained. The importance of this was investigated in a study where the cyanoacrylate method was compared to a method, where most of the SC was scraped off using a scalpel, and comparable results were achieved (Jungersted et al. 2010). The same is evident for the ceramide distribution at different depths of SC (Jungersted et al. 2010; Weerheim and Ponec 2001; Norlén et al. 1999). One should also note that compared to other methods used, it is fast and easy to handle, which is an important aspect when used in vivo on humans in an experimental setting (Jungersted et al. 2010).

Since all the samples from AD patients were taken from non-lesional skin, one could argue on the relevance of examining lesional skin as well.

However, before interpreting data of SC lipids from lesional skin, one would need to address confounding aspects, such as the difference in precise location of the lesion, as well as the unknown effect of superinfection and the degree and age of the lesion, which are why non-lesional skin was chosen.

References

Jungersted JM, Hellgren LI, Drachmann T, Jemec GBE, Agner T. Validation of cyanoacrylate method for collection of stratum corneum in human skin for lipid analysis. Skin Pharmacol Physiol. 2010;23:62–7.

Norlén L, Nicander I, Rozell BL, Ollmar S, Foerslind B. Inter- and intra-individual differences in human stratum corneum lipid content related to physical parameters of skin barrier function in vivo. J Invest Dermatol. 1999;112:72–7.

Rissmann R, Oudshoorn MHM, Hennink WE, Ponec M, Bouwstra JA. Skin barrier disruption by acetone: observations in hairless mouse skin model. Arch Dermatol Res. 2009;301:609–13.

Weerheim A, Ponec M. Determination of stratum corneum lipid profile by tape stripping in combination with high-performance-thin-layer chromatography. Arch Dermatol Res. 2001;293:191–9.

Stratum Corneum Biomechanics (Mechanics and Friction): Influence of Lipids and Moisturizers

34

Gustavo S. Luengo, Anne Potter, Marion Ghibaudo, Nawel Baghdadli, Ramona Enea, and Zhenhhua Song

Contents

Keywords
Stratum mechanics friction

1 Key Messages

- The stratum corneum layer has a net contribution to the skin's mechanical properties.
- The different constituents of SC (i.e., lipids, NMF, etc.) have a key role in maintaining these mechanical properties.
- In particular lipids seem to prevent the plastification of SC in presence of water. The absence of lipids and NMF rigidify the SC structure.
- SC flexibility would mainly be related to corneocyte connections and the macromolecular mobility and plasticization of intercellular spaces.
- Moisturizers can work efficiently by par example creating mechanically resistant surface films on the surfaces.
- The SC contributes to the friction properties of skin, in particular at low pressures.
- Lipids contribute to maintain the intrinsic friction of SC. Its absence diminishes the friction coefficient.
- The presence of water and humidity increases the friction of SC by its plastifying effect.
- Moisturizer's action on friction is dependent on the absence or presence of thin films at the surface of SC either decreasing or increasing it, respectively.

G.S. Luengo (✉) • A. Potter • M. Ghibaudo • N. Baghdadli • R. Enea • Z. Song
L'Oréal Research and Innovation, Aulnay-Sous- Bois, France
e-mail: gluengo@rd.loreal.com

P. Humbert et al. (eds.), *Agache's Measuring the Skin*,
DOI 10.1007/978-3-319-32383-1_34

2 Importance of the Stratum Corneum and Skin Physical Properties

The stratum corneum (SC) participates in the functional properties of the skin (Elias 2005). It protects our body from harsh environmental factors and mechanical insults. In the meantime, its ability to distort and its softness are responsible for the comfort of the skin. Most of the cosmetic treatments try to improve or repair the intrinsic properties of skin with SC as a prime target which eventually reflects in enhanced mechanical and tribological behavior.

3 The Structure of SC

The stratum corneum could be considered as a composite material mainly made of corneocytes embedded in intercellular cement containing lipids, water-soluble materials, and proteoglycans. Corneocytes are linked by glycoprotein junctions called corneodesmosomes. They form the elemental bricks of the brick/mortar pattern proposed to describe stratum corneum structure. Corneocytes are produced from living epidermal cells, the keratinocytes which undergo considerable structural and biochemical and mechanical changes eventually leading to fully keratinized, hard corneocytes (Elias 2005; Agache and Varchon 2004). Cell membrane and structure dramatically change along the process to ultimately take the well-known penta- or hexagonal flat shape ca. 200 nm thick and 40 μm wide.

4 Mechanical Properties

The influence of SC layer on the overall mechanical properties of the skin is recognized (Agache and Varchon 2004; Batisse et al. 2002). The stratum corneum can be isolated from skin and its robustness allows it to be tested using common mechanical traction tests. So, stress relaxation tests can been performed on human SC (Park and Baddiel 1972a, b; Wildnauer et al. 1970; Koutroupi and Barbenel 1990; Druot et al. 1985; Rochefort et al. 1986). A typical stress-strain (load-elongation) curve for human SC conditioned in water at 25 °C for one hour reveals three distinct regions separated by inflections at approximately 25 % and 125 % elongation. Using pure shear specimen geometry, SC showed nonlinear load-elongation behavior and stress relaxation, although the extensibility and rate of stress relaxation was considerably lower than that shown by other soft connective tissues (Koutroupi and Barbenel 1990). Rheological models have also been used to explain the results of tensile tests at constant strain rate (Druot et al. 1985). Finally, several mechanical instruments are used to measure the elastic modulus E and the effect of water or cosmetic ingredients as a function of application time (Lévêque et al. 1987; Takahashi et al. 1984, 1985; Rasseneur et al. 1982).

Ultrastructural changes in the SC were examined by Rawlings et al. (1995) using electron microscopy. The lipid layers progressively become disorganized soon after 5 % extension unlike desmosomes that resist until just before fracture of the tissue. Lévêque et al. (2002) combined transmission electron microscopy and X-ray diffraction. At 60 % extension, and although the detachment of lipid layers from one of the adjacent corneocytes was observed, X-ray analysis data showed that intercellular lipid organization kept unaltered.

Other experiments have explored the mechanical properties in the direction normal to the skin surface by fracture techniques. They allowed, for example, the fracture surface energy between two layers of SC (delamination energy) to be assessed. It has been estimated to be 3.6 kJ/m^2 which is comparable to that of tougher synthetic polymers (Koutroupi and Barbenel 1990). Delamination energy seems to be governed by cohesive properties of the intercellular boundaries of SC (Wu et al. 2002, 2006a, b) as it decreases when temperature and hydration level increase. On the other hand, it increases when lipids are extracted due to the interaction between remaining components that are less affected by hydration. Finally it is believed that delamination energy is not strongly correlated with expected corneosome cohesive contribution (Chapman et al. 1991; Wu et al. 2006b).

The SC stiffness in the direction normal to the skin surface is much lower than that reported in-plane. The mechanisms involved in this heterogeneousness may be related to additional SC microstructure (Wu et al. 2006b). Keratin intermediate filaments (IF) are linked to corneodesmosomes that build a bridge through the intercellular space to connect adjacent cells. The structural orientation and possible alignment of these keratin fibers, still controversial, might have a strong impact on mechanical anisotropy. Corneodesmosomes may facilitate the transmission of tensile forces between cells leading to greater stiffness and higher fracture energy observed in the in-plane orientation (Wu et al. 2002).

Another approach, reported (Richter et al. 2001) is based on the physical isolation of the individual components. Corneocyte is likely to be the most studied component. Although several studies have looked into the ultrastructure of corneocytes using optical and electron microscopes, few give insights into mechanical properties. Much work done in this field used "indirect" observations based on morphological changes of isolated corneocytes as a function of RH, for example. Richter et al. (2001) investigated and quantified the swelling of corneocytes in water using atomic force microscopy (AFM). They mainly observed change in thickness with no significant lateral alteration. A more direct approach was resorted to by Lévêque et al. (1988). The authors recorded the force needed to elongate isolated corneocytes immersed in water using a micro-handling technique. The calculated Young's elastic modulus was $E \sim 4.5 \times 10^8$ Pa although it was considered by the authors to be underestimated due to technical difficulties. Other teams like Yuan and Verma (2006) used atomic force microscope (AFM) together with a Triboscope nanoindenter and a nano-DMA (Hysitron, Minneapolis, MN, USA) to measure viscoelastic moduli (E' and E'') at the microscale. Measurements were made on isolated dry and wet stratum corneum at varying depths. Elastic moduli values obtained with a pure elastic model were of the order of 100 and 10 MPa for dry and wet SC, respectively. Tan δ increased from approximately 0.1–0.25. An apparent modulus variation with indentation depth was noticed. The origin of this behavior is not understood.

In our laboratories, we have focused on measuring mechanical properties of the stratum corneum at a submicron length scale in order to investigate the effect of SC components, humidity, and cosmetic treatments.

Here we report nanoindentation tests (Pavan et al. 2005; Potter et al. 2007) at controlled temperature and humidity that were performed with an MTS Nanoindenter XP using the continuous stiffness measurement method to assess SC viscoelastoplastic properties. The method consisted in superimposing a small shifting oscillation at a given frequency (a = 5 nm) during the indentation test. The frequency of added harmonic vibration was 32 Hz. The device was placed within a climatic chamber. Reduced Young's modulus and loss factor as a function of penetration depth were continuously recorded by simultaneous measurement of normal load and contact stiffness.

4.1 Influence of Humidity

The flexibility of the stratum corneum depends on its water content (Wildnauer et al. 1970; Druot et al. 1985; Lévêque et al. 1987; Takahashi et al. 1984). The effect of relative humidity on elastic modulus over the range 30–100 % is reflected, for example, by E value changing from 2 GPa at 30 %RH to 3 MPa at 100 % RH (Park and Baddiel 1972a).

Lévêque et al. studied water-keratin interactions in human SC (Lévêque et al. 1987). They recorded elastic modulus of human SC as well as water content and water interaction energy at various rates of relative humidity (RH). The important changes in the elastic modulus at RH lower than 60 % would be related to the condensation of a single layer of water molecules on active hydrophilic sites with a high interaction energy suggesting that the binding state of water molecules with keratin is an important factor in skin mechanics.

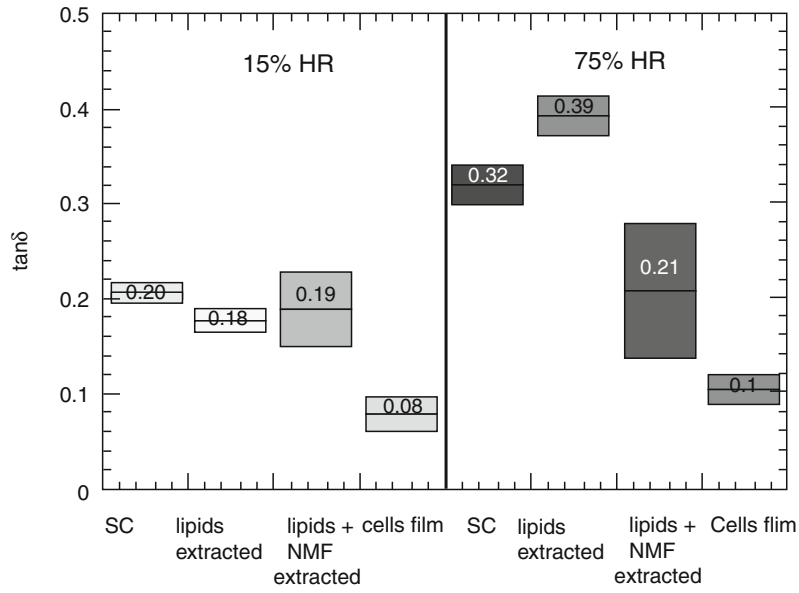

Fig. 1 Change in loss factor as a function of SC treatments at two humidity rates

In our experiments SC was used at 25 %, 50 %, and 70 % RH rates and then immersed in distilled water. The results are reported in Fig. 1.

Reduced Young's modulus was found to decrease and loss factor increased with increasing HR rate. Our hypothesis is that loss factor (tan δ) is closely related to macromolecular mobility and viscosity of lipid intercellular spaces.

A gradient of mechanical properties according to indentation plastic depth was noticed.

4.2 Influence of Lipids

Lipids are key SC structural elements which can be easily extracted. Intercellular lipids appear to play an important role in protecting the hydrosoluble substances (Park and Baddiel 1972a, b; Lévêque et al. 1987). It has however been fully recognized now that corneodesmosome complexes are key components in tissue cohesion and desquamation process (a role usually assigned to lipids).

The precise relationship between lipids and stratum corneum elasticity remains controversial. According to Middleton (1968), lipid removal has no consistent effect on SC extensibility, while Park and Baddiel (1972a, b) stated it did not influence SC elastic properties. In contrast, Leveque et al. (1987) suggested that lipids slightly contributed to plasticization of the stratum corneum.

Our results (Fig. 1) bring out:

- The role of intercellular lipids: At 70 % RH, loss factor is slightly higher with lipid-extracted SC than with untreated stratum corneum. In the former, water would easily reach hydrophilic intercellular spaces and plastification would be more significant. Viscosity of intercellular macromolecules (corneodesmosomes or other proteoglycans) is increased.
- The role of NMF: At 70 % RH, if in addition to lipids, NMF and other soluble intra- and extracellular proteins are extracted, the SC becomes stiffer and less dissipative. Water diffusion toward intracellular keratin sites is most likely restricted.
- The role of corneodesmosomes: At 15 and 70 % RH, the elastic modulus of the "corneocyte" film is much higher than that of natural stratum corneum. Loss factor is much smaller. "Corneocyte" film is stiffer. Macromolecular mobility of the junctions between constitutive elements (corneocytes) is very difficult.

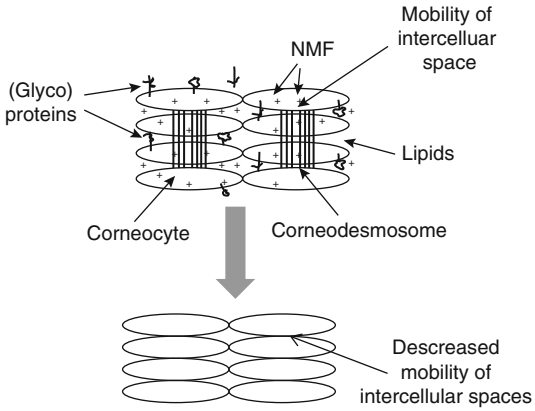

Fig. 2 Different elements of stratum corneum structure

These results demonstrate the importance of intercellular spaces in mechanical behavior of the stratum corneum. SC flexibility would mainly be related to corneocyte connections and the macromolecular mobility and plasticization of these junctions (Fig. 2).

4.3 Effect of Moisturizers

The effect of a cosmetic agent has been traditionally studied through the influence on stress-strain curve of a traction experiment. For example, the softening effect of emollients on stratum corneum is clearly seen and bigger than that of water alone (Rochefort et al. 1986). Water is unable to durably soften the stratum corneum whereas emollients are able to act in vitro, where the large pool of water in the deeper tissue layers is missing.

Takahashi et al. (1984, 1985) assessed the change in skin-softening effect of moisturizers and hydroxy acids with time following topical application thereby distinguishing the influence of typical formula components.

In our experiments we studied the effects of glycerol and a polymer (Aristoflex LNC). Loss factor values at 1 μm depth are reported in Fig. 3. After applying the moisturizing polymer, SC elastic modulus is reduced and loss factor is increased. This well-known plasticizing effect is induced by an increase in water retention within the stratum corneum.

The surface mechanical properties can also be measured. The mechanical values are reported at 100 nm depth (Fig. 8). The surface modulus was decreased after applying glycerol or urea solution. Amphiphilic polymer Aristoflex LNC increased the surface modulus as a result of surface polymer film formation.

With the nanoindentation technique, it is possible to measure both mass and surface mechanical properties of the stratum corneum. It allows us to investigate the effect of humidity or moisturizers and to identify the role of the various SC components.

The proposed hypothesis is that softness and flexibility of the stratum corneum are mainly related to corneocyte connections and to the viscosity and macromolecular mobility of intercellular space components. The strong effect of urea treatment on loss factor value supports this hypothesis. Further studies using specific treatments and different RH rates have to be conducted to substantiate this hypothesis.

The results contribute also to distinguishing the way different types of moisturizer work: hydrating effect of glycerol, plasticizing effect of urea associated with a strong interaction with protein components, and a new moisturizing mechanism by surface structuration with an amphiphilic polymer.

5 Friction Properties

To better understand the skin surface behavior and particularly the contribution of stratum corneum to general physical behavior of the skin, research based on tribological methods was developed. Needless to say, tribological data alone cannot explain the sensorial properties of the skin, but they can emphasize relevant physical parameters which allow skin condition and behavior to be more clearly described and understood. Together with other physical methods, tribology can help build a table of physical parameters useful to explore and decipher skin biophysics. As shown in the previous section, local experimental approaches involving instruments like tribometers and indenters are helpful to analyze skin, in vitro

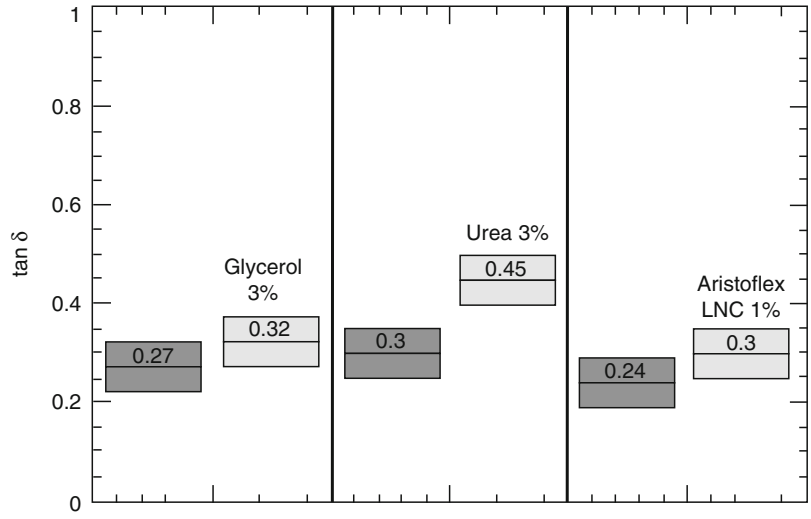

Fig. 3 Loss factor tanδ (1 μm depth) at 50 % HR of SC treated with aqueous solution of glycerol 3 %, aqueous solution of urea 3 %, and aqueous solution of polymer Aristoflex LNC 1 % (Clariant), respectively

and/or in vivo, to optimize critical parameters, and to advance reliable explanations.

While morphological deformation of the whole skin has been discussed in many papers as being at the origin of the observed friction in vivo (Johnson et al. 1993; Adams et al. 1999, 2007; Derler and Gerhardt 2012), it is worth noticing that few studies have been devoted to tribological properties of the stratum corneum itself (Johnson et al. 1993; Adams et al. 2007; Pailler-Mattei et al. 2007b).

To check whether skin physical properties change in relation to external conditions, scientists have performed in vivo experiments varying normal force (F_n), tangential force (F_t), and other physical parameters and analyzing friction coefficient (μ). Comaish and Bottom (1971) already noticed the problems associated with measure reproducibility when the load was not controlled. Much work has been done to describe the tribological properties of the skin (Gitis and Sivamani 2004; Johnson et al. 1993; Adams et al. 1999, 2007; Pailler-Mattei et al. 2007b; Comaish and Bottoms 1971; Sivamani and Maibach 2006; Sivamani et al. 2003a, b).

Friction force is known to follow Amonton's law in many systems. This basic law states that friction is simply linearly proportional to the applied load:

$$F = \mu L \tag{1}$$

From classical tribology (Bowden and Tabor 1954), friction force is known to have two contributing factors: an adhesion related term F_{adh} and another one related to deformation F_{def}. The adhesion term is linked to the surface energy (i.e., electrostatic, van der Waals, capillary forces) and to the contact area (Adams et al. 2007):

$$F = F_s + F_d \tag{2}$$

In general the deformation part can be ignored in non-dissipative contact as it may happen in elastic surfaces or low loads. The interfacial component is then mostly controlled by adhesion phenomena and is defined as:

$$F_s = \tau A \tag{3}$$

where A is the area of contact and τ the interfacial shear strength.

A general observation is the complexity of measurements and data interpretation. The differences originate from the complexity of the substrate, the explored zone, the geometry of the probe used, and the variety of experimental conditions (applied force, temperature, etc.).

In general we observe that friction coefficient depends on:

- Hygrometry (increase with it)
- Anatomical site
- Use of emollients and creams
- Applied load

In relation to the load, it is clear that Amonton's law ($F = \mu F_n$) is not always followed by skin friction. Derler et al. (2007) found that friction coefficient μ measured at the finger surface as a function of load (F_n ~ 0.2–15 N) was constant ca. (0.3–0.4) for dried skin. For hydrated skin, the friction coefficient was higher (~0.6) and decreased with load presumably due to adhesion. Fn decreases, just as Young's modulus. Consequently, the Amonton's law was not applicable to such surfaces (flexible).

Skin viscoelasticity can be in part responsible for the deviations from Amonton's law (Comaish and Bottoms 1971). El-Shimi et al. (1977) found that friction coefficient decreased with load (F_n ~ 0.25–1.8 N), while it became constant ($\mu = 0.5$) at higher forces (>7 N) also attributing this decrease to the viscoelastic properties of the skin, entailing the nonlinear deformation. Wolfram et al. (1983) suggested that at small forces (0.1–0.9 N), μ increased with F_n due to adhesion and softening of skin. Dowson et al. (1997) also suggested that adhesion influenced friction coefficient by increasing the surface of contact, adhesion increases, and μ value as well. It is likely that adhesion and surface deformation due to the applied force together influence friction coefficient value (μ) and the Amonton's law illegibility for such specific case is related to skin viscoelasticity.

Skin has a complex multilayer structure. Most of in vivo studies try to understand the sensorial perception in conditions where skin deformation is important. But when the charge is minimized, the influence of the deeper layers of skin is also minimized and the deformation term F_d decreases as the dissipative or viscoelastic contribution decreases (Bowden and Tabor 1954). In these conditions the SC characteristics and effect are maximized and may control the delicate texture observed at the surface of the skin. It is worth mentioning that most of in vivo studies are done with applied loads from 0.5 to 15 N.

Consequently, to understand the intrinsic properties of the stratum corneum (SC), several questions might be asked, such as:

- Does the physico-chemistry of SC play a key role in skin health and appearance?
- Does SC contribute to the general physical behavior of the skin tissue?
- How the tribological parameters are influenced by a cosmetic product?
- Do the interactions between water/moisturizer and SC influence consumer perception?

As we have previously mentioned, few studies have focused on the tribology of the stratum corneum ex vivo, isolated from the other layers. The advantage of isolating SC is the considerable potential for finding correlations with the dermatological efficacy of a treatment or product on this outermost layer of skin, before clinical studies.

It is worth mentioning here the work by Paillet-Mattei et al. (2007b) who used tape stripping to analyze the effect of SC ex vivo. By stripping successive layers of forearm skin in vivo, the authors did not observe much effect on friction behavior but an increase in adhesion. They concluded that there is not much effect on the bulk skin properties. In parallel, using an XP Nanoindenter (MTS) and a spherical diamond indenter of ~7 μm radius, they made some first measurements on isolated stratum corneum at low loads (0.1–1.0 mN) and at ~1 μm/s speed. After a transition zone (first 100 μm move), they measured a surprisingly high friction coefficient (~20), then decreasing to ~2 after sliding for 500 μm. These values are much higher than what is known for skin in vivo.

It is most likely that a steady state was not achieved in these experiments. In addition using a nanoindenter on SC makes the approach less direct than with a tribometer.

To assess specific answers with a view to explain the physical behavior of SC and the influence of SC surface topology, several aspects will be described: a short description of tribological

Fig. 4 Nanotribometer

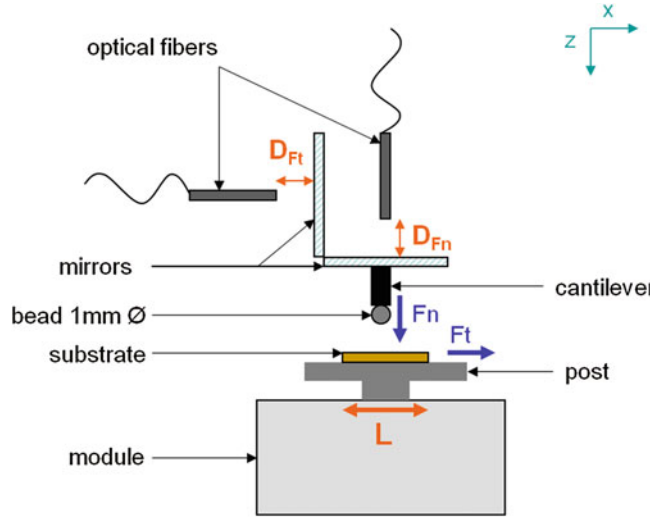

parameters that enhance sensorial behavior, the effect of hydration, the role of intracellular lipids in SC physical integrity, and the effect of cosmetic ingredients on SC tribological properties. These effects are illustrated with some examples of experiment carried out in our laboratories.

5.1 Friction Properties of SC In Vitro

We used a nanotribometer from ©CSM Instruments (Neuchâtel, Switzerland). A brief description of the device is shown in Fig. 4.

- **Module**: can change the tribometer from the straight mode to the circular mode.
- **Post**: it is a 12 mm diameter metallic disk on which we glue the substrate. In straight mode, its goes back and forth with an amplitude L.
- **Substrate**: fixed to the post to measure its friction factor. Here the substrate is *stratum corneum*, the upper layer of the skin from samples from abdominal plastic surgery.
- **Bead**: 1 mm in diameter, can be in steel, glass, and polymer. We chose stainless steel.
- **Cantilever**: it acts as a finite spring modulus and maintains the bead at one end.
- **Mirrors**: they are perpendicular to each other and linked to the cantilever. Their angle varies when the cantilever moves.
- **Optical fibers**: they send a light signal on the mirrors and detect variations of the reflected light signal, thanks to the mirrors' deflection when the cantilever moves.

Here are the characteristics of the cantilever used (Table 1):

We have focused on small normal loads Fn (2–20 mN) where few data is reported in the literature. It is important to note that for the consumer perception, the in vivo pressure can be between 5 and 10 kPa. For the 1 mm radius sphere of our tribometer, we have estimated it to be in the same range (6.4 kPa at 10 mN load).

We used isolated human stratum corneum whose thickness was 10–15 µm. Special care was taken on using clean samples. The stratum corneum was stuck with double glue line adhesive tape on 2 cm radius disks on the post. Finally, the experiments were performed at ambient temperature (25–30 °C) and controlled fixed humidity. Fig. 5 shows an example of the friction coefficient µ raw traces during each subsequent back and forth sliding cycle. Negative values represent an opposite sliding direction. It is worth noticing the friction behavior reproducibility after up to the 5 cycles used in these experiments.

Friction coefficient on the nude stratum corneum was measured on two or three positions, in order to have baseline value. Figure 5 shows an

Table 1 Tribomechanical parameters used in the friction tests

Cantilever	
Bead characteristics	
Bead diameter (mm)	1
Material	Stainless steel (other materials possible)
Normal force F_n	
Theoretical force range (mN)	2 – 150
Used force range (mN)	2 – 100
Force sensitivity (mN)	About 0.1*
Force feedback	Yes
Horizontal speed V_x	
Theoretical speed range (μm/s)	10 – 10,000
Used speed range (μm/s)	50 – 1000
Speed sensitivity (μm/s)	?
Vertical speed V_z (μm/s)	
Vertical speed range (μm/s)	Tunable
Indenter displacement L (mm)	
Maximum of amplitude (mm)	0.67
Displacement sensitivity (mm)	About $\pm 10^{-3}$ *
Cyclic mode	
Max cycles numbers	Up to 100

*Experimentally Measured

example of the friction coefficient μ raw traces during each subsequent back and forth sliding cycle. Negative values represent an opposite sliding direction. It is worth noticing the friction behavior reproducibility after up to the 5 cycles used in these experiments.

Several other materials were measured for comparison. It is of interest to notice that, in the same type of experiment, the SC friction coefficient is in the same range (0.2–0.4) as that measured for elastomeric silicone surfaces (See Fig. 6). As expected, Teflon showed a lower value.

Friction coefficient of human SC (see Fig. 7) did not change much according to load thus approaching an Amonton's behavior (friction force proportional to load) although we found a tendency to decrease at higher loads (~50 mN). As mentioned previously we have maintained in our trials 10 mN load as being close to in vivo applications.

In addition other experiments (not shown) have been done including a rubberlike layer below the stratum corneum. No alteration was observed in the results which confirm that the experimental conditions are appropriate for testing the stratum corneum without any concern about possible effect of the substrate underneath.

These results are of interest when compared with data reported in the literature for skin. In general, as discussed previously, the friction coefficient tends to decrease with load in in vivo experiment on skin (Wolfram 1983; Koudine et al. 2000). On the other hand, El-Shimi et al. (1977) observed an increase in the range of 0.2–1.8 N. In contrast, in our experiments, it seems that the stratum corneum deformations have not been big enough for this effect to be observed. It is most likely that the use of low loads and the mechanical properties of the stratum corneum itself make it more stable in terms of friction coefficient.

Another observation is that the traces observed at low loads are much richer in their shape, a phenomenon like stick-slip is enhanced, and the variability of friction coefficient during sliding is not stochastic. The traces are more sensible to the topography and micro relief of the stratum corneum. It is in these low load conditions where skin texture is most influencing sensorial touch, as suggested by some authors (Gitis and Sivamani 2004).

5.2 Influence of Humidity

Several experiments have been carried out at different humidity levels (25 %, 50 %, and 80 %).

In general we can observe an increase in friction coefficient with humidity level. The difference is more notable at 80 % where we observe a higher influence of load. If we add a water layer on the stratum corneum (by applying a drop, ~100 % relative humidity), there is a clear increase in friction coefficient (Fig. 8).

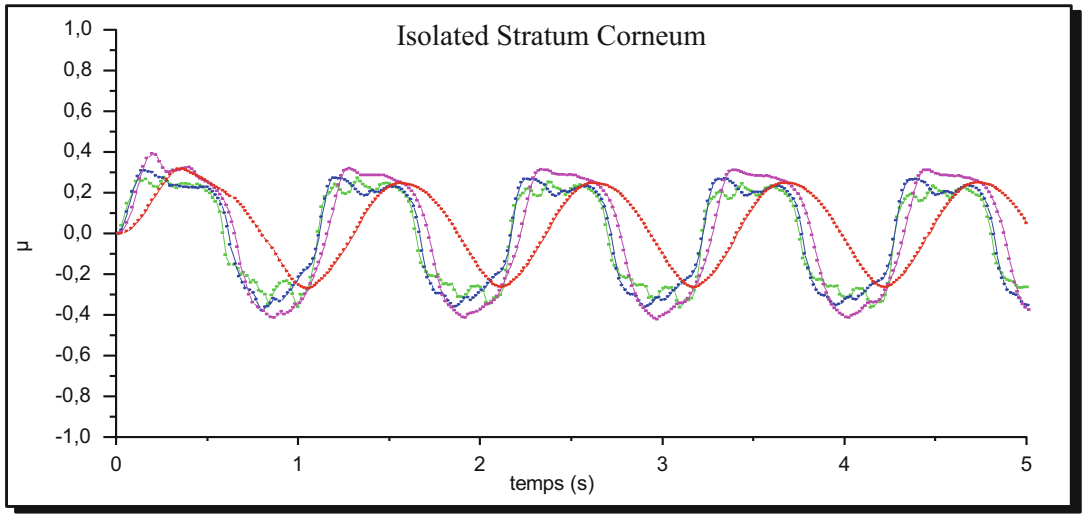

Fig. 5 Aspect of friction traces obtained on human stratum corneum during different back and forth sliding cycles (the red sinusoidal curve represents the mouvement of the slider). Notice the reproducibility of traces after each cycle

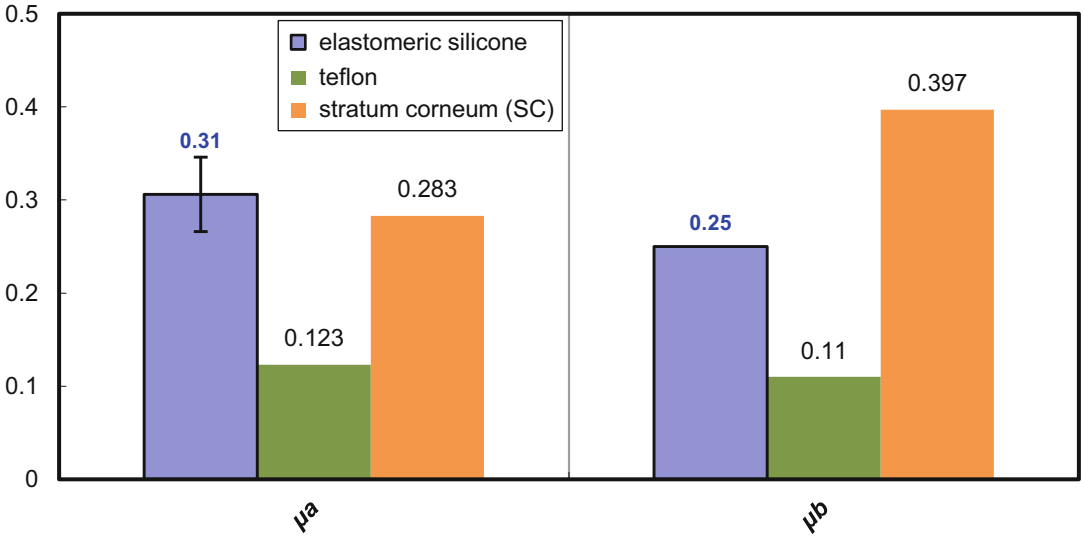

Fig. 6 Comparison of measured friction coefficients one way (μ_a) and return (μ_b) for stratum corneum and other reference materials. Conditions of measurement: Fn = 2 mN, v = 0,2 cm/s, L = 400 nm

It is most likely that in these conditions, the changes in mechanical properties (reduced modulus and increasing dissipation) seen in the previous section play an important role through altering the properties of the stratum corneum and through an increased influence of deformation on friction. In addition, the presence of a water layer further increases adhesion due to capillary forces. Both effects could be at the origin of the observed increase.

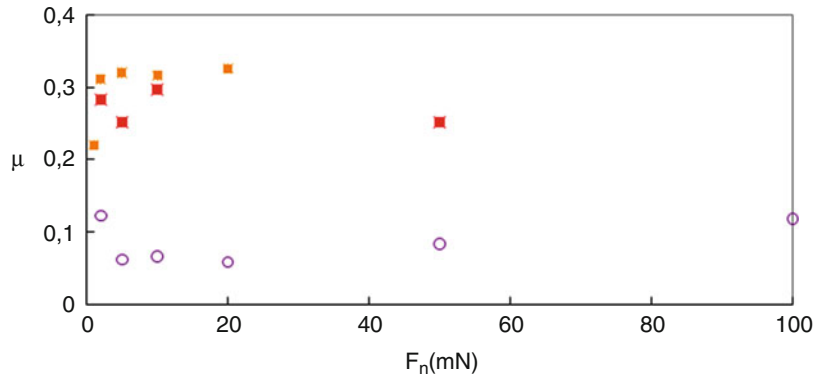

Fig. 7 Values of friction coefficient for human stratum corneum (*filled symbols*) and Teflon (*empty circles*) surfaces

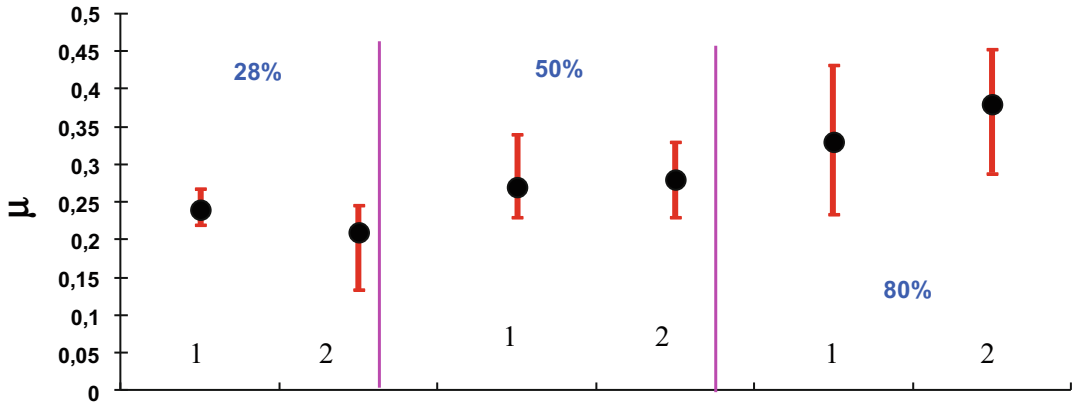

Fig. 8 Values of friction coefficient as a function of ambient humidity for two independent sources of stratum corneum samples (1 and 2 in the Figure)

5.3 Influence of Lipids

As discussed in the section on mechanical properties, the lipids form a barrier whose effect is clearly seen when they are removed. Water is lost faster and the stratum becomes less hydrated.

Our first experiments (Fig. 9) show that friction coefficient is indeed smaller when lipids are extracted from the stratum corneum. To our knowledge these measurements have been performed for the first time. We believe that the absence of lipids and the dryness of the stratum in such conditions diminish the influence of the deformation term on friction properties therefore decreasing friction coefficient.

5.4 Influence of Moisturizers

We deposited a cosmetic formulation containing a polymer of interest and glycerol (always the same amount of formulation). We measured it at different time points over 2 h post drying (2, 5, 10, 15, 20, 30, 60, and 120 min). Between two measurements, the bead was cleaned, to remove the formulation deposit.

5.4.1 Tested Formulas

Glycerol (7 %), or a polymer (Artistoflex LNC), was added to simplex formulation (*placebo*) belonging to moisturizer technology and containing Arlacel® (mannide monooleate) and Myrij® fatty alcohol, which is a neutral

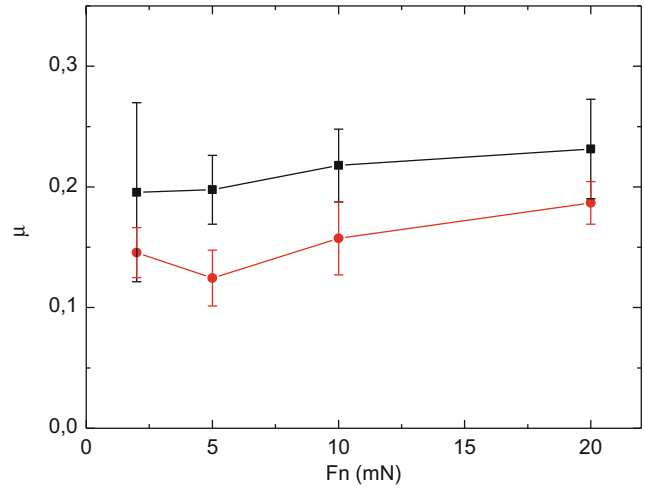

Fig. 9 Friction coefficient observed for stratum corneum before (*squares*) and after (*circles*) lipid extraction. Measurement conditions HR = 45 %, Fn = 2, 5, 10, 20 mN

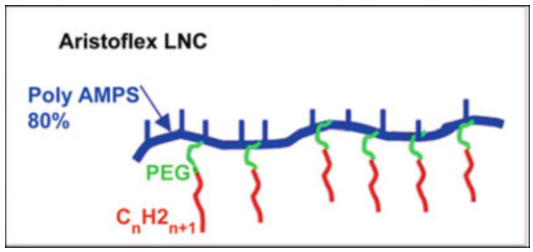

Fig. 10 Diagram showing the structure of copolymer Aristoflex LNC (Clariant)

formulation from a sensory point of view. We compared the properties of both formulas versus simplex formulation on isolated human stratum corneum, prepared from skin samples from abdominal plastic surgery.

In cosmetics, glycerol is often used as a moisturizing agent, solvent, and lubricant. Aristoflex LNC is a brush polymer with a PolyAMPS (2-acryloylamido-2-methylpropane-sulphonic acid) backbone, where polyethylene glycol (PEG) and polyethylene (PE) have been grafted (Fig. 10).

The friction measurements were performed according to the following conditions:

- Normal force: $F_n = 20$ mN
- Friction speed: $V_x = 400$ μm/s
- Measurement length: L = 670 μm
- Number of cycles: 1

Each formula was studied many times over a 2 h drying. Measurements were done before formula application ($t = 0$) and at different time points up to 120 min after application.

The results were compared with those from untreated stratum corneum. Figure 11 shows friction coefficient modulations after normalization with the stratum corneum friction coefficient:

$$\Delta\mu_d(\%) = 100\frac{\mu_d(\text{formula}) - \mu_d(\text{SC})}{\mu_d(\text{SC})}$$

Observations

- The placebo lowers μ_d.
- Aristoflex LNC increases μ_d.
- Glycerol lowers μ_d more than placebo.

We can thus rank the different formulas as follows:

$$\mu_d(\text{glycerol}) < \mu_d(\text{placebo}) < \mu_d(\text{SC}) < \mu_d(\text{Aristoflex})$$

Once again we observe a completely different pattern with film-forming polymers.

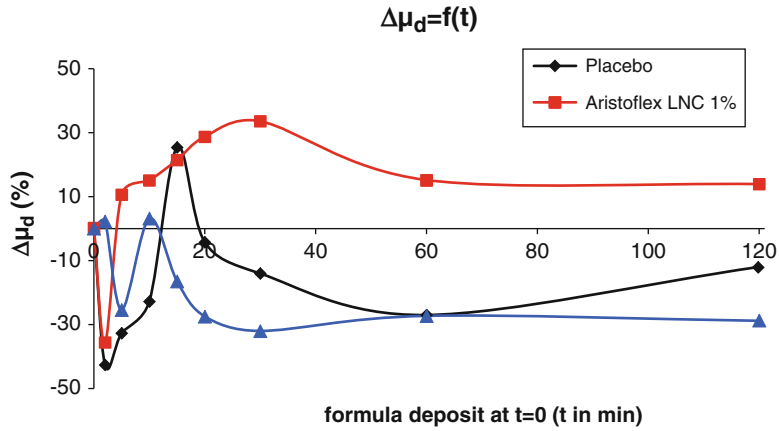

Fig. 11 Relative friction coefficient modulation during formula drying

Glycerol slightly decreases the friction coefficient of placebo formula that penetrates well into the stratum corneum. The decrease in friction coefficient can be related to the effect of glycerol still present at the surface with placebo formulation.

The polymer, which acts more as an occlusive moisturizer, hardens during the first 2–3 h following application but then softens slightly as seen in the mechanical tests. The higher friction is most likely related to the increase in effective viscosity of the film. Further penetration of the polymer film in the upper layers of SC makes film thinner, reducing its contribution in terms of viscous drag to the coefficient of friction.

6 Conclusion

We have reviewed recent knowledge on the mechanical and tribological properties of the outermost surface of the skin, the stratum corneum. While SC contribution in skin is considered to be important, few studies have allowed its role in vivo to be quantified.

New tests are now available that can help us to explore these properties in vitro. In particular we have shown the complex mechanical and frictional behavior of the stratum corneum can now be studied using nanoindentation technique and nano-tribometers. By selectively removing certain stratum corneum components (i.e., lipids), we can have more insight about their physical role. Finally some examples are given on the effect of glycerol and a common polymer on moisturizing formulations, emphasizing the important role of the absence or presence of thin coating films at the skin surface.

Further studies are needed to explore the properties of this outermost layer of the skin, especially to understand the effect of topography on skin friction particularly in those conditions where the deformations are minimized in vivo and where surface texture prevails. The effect of surface properties is not negligible and has been explored in other areas like packaging or textiles (Shao et al. 2010). Such experiments bring about the importance not only of roughness but also of spatial ordering of the surface pattern in the sensory perception.

References

Adams MJ, Gorman DM, Johnson SA, Briscoe BJ. The friction and lubrication of keratinous biosubstrates. In: Lal M, Lillford PJ, Naik VM, Prakash V, editors. Supramolecular and colloidal structures in biomaterials and biosubstrates. Singapore: Imperial College Press; 1999. p. 277–94.

Adams M, Briscoe B, Johnson S. Friction and lubrication of human skin. Tribology Letters. 2007;26(3):239–53.

Agache P, Varchon D. Skin mechanical function. In: Agache P, Humbert P, editors. Measuring the skin. Berlin: Springer; 2004. p. 429–45.

Barel AO, Courage W, Clarys P. Suction method for measurement of skin. In: Serup J, Jemec GBE, editors. Handbook of non-invasive methods and the skin. Boca Raton: CRC Press; 1995. p. 335.

Batisse D, Bazin R, Baldeweck T, Querleux B, Lévêque JL. Influence of age on the wrinkling capacities of skin. Skin Res Technol. 2002;8(3):148–54.

Bowden FP, Tabor D, editors. Friction and lubrication of solids. London: Oxford University Press; 1954.

Chapman SJ, Walsh A, Jackson SM, et al. Lipids, proteins and corneocytes adhesion. Arch Dermatol Res. 1991;283(3):167–73.

Comaish S, Bottoms E. The skin and friction: deviations from Amonton's laws, and the effects of hydration and lubrication. Br J Dermatol. 1971;84(1):37–43.

De Rigal J, Lévêque JL. Titre? Bioeng Skin. 1985;1:13.

Derler S, Gerhardt LC. Tribology of skin: review and analysis of experimental results for the friction coefficient of human skin. Tribol Lett. 2012;45:1–27.

Derler S, Schrade U, Gerhardt LC. Tribology of human skin and mechanical skin equivalents in contact with textiles. Wear. 2007;263(7–12):1112–6.

Dowson D, editor. Tribology and the skin surface. Boca Raton: CRC Press; 1997.

Druot P, Rochefort A, Agache P, et al. In vitro stress relaxation tests of human stratum corneum. Bioeng Skin. 1985;1:141–56.

Elias PM. Stratum corneum defensive functions: an integrated view. J Invest Dermatol. 2005;125(2):183–200.

El-Shimi AF. In vivo skin friction measurements. J Soc Cosmet Chem. 1977;28:37–51.

Gitis N, Sivamani R. Tribometrology of skin. Tribol Trans. 2004;47:461–9.

Grahame R, Holt PJL. The influence of ageing on the in vivo elasticity of human skin. Gerontologia. 1969;15 (2–3):121–39.

Johnson SA, Gorman DM, Adams MJ, Briscoe BJ. The friction and lubrication of human stratum corneum. In: Dowson D, editor. Thin films in tribology. London: Elsevier; 1993.

Koudine AA, Barquins M, Anthoine PH, Aubert L, Lévêque J-L. Frictional properties of skin: proposal of a new approach. Int J Cosmet Sci. 2000;22 (1):11–20.

Koutroupi KS, Barbenel JC. Mechanical and failure behaviour of the stratum corneum. J Biomech. 1990;23:281–7.

Lévêque JL, Escoubez M, Rasseneur L. Water-keratin interaction in human stratum corneum. Bioeng Skin. 1987;3:227–42.

Lévêque JL, Poelman MC, De Rigal J, Kligman AM. Are corneocytes elastic ? Dermatologica. 1988;176:65–9.

Lévêque JL, Hallegot P, Doucet J, et al. Structure and function of human stratum corneum under deformation. Dermatology. 2002;205:353–7.

Middelton JD. The mechanism of water binding in the stratum corneum. Br J Dermatol. 1968;80:437.

Pailler-Mattei C, Pavan S, Vargiolu R, Pirot F, Falson F, Zahouani H. Contribution of stratum corneum in determining bio-tribological properties of the human skin. Wear. 2007;263(7):1038–43.

Park AC, Baddiel CB. Rheology of stratum corneum – I: a molecular interpretation of the stress-strain curve. J Soc Cosmet Chem. 1972a;23:3–12.

Park AC, Baddiel CB. Rheology of stratum corneum – II: a physico-chemical investigation of factors influencing the water content of the stratum corneum. J Soc Cosmet Chem. 1972b;23:13–21.

Pavan S, Loubet JL, Potter A, et al. Nanoindentation of natural hair and stratum corneum as a function of humidity. Poster session, Instrumented Indentation Techniques, 28th annual meeting of The Adhesion Society, 13–16 Feb 2005, Mobile.

Potter A, Luengo G, Baltenneck C, et al. Measuring mechanical properties of stratum corneum and isolated corneocytes at sub-micron length scale. Poster session. Stratum Corneum V conference, 11–13 July 2007, Cardiff.

Rasseneur L, de Rigal J, Lévêque JL. Influence of the different constituents of horny layer on elasticity measurements. Int J Cosmet Sci. 1982;4:247–60.

Rawlings AV, Watkinson A, Harding CR, et al. Changes in stratum corneum lipid and desmosome structure together with water barrier function during mechanical stress. J Soc Cosmet Chem. 1995;46:141–51.

Richter T, Muller JH, Schwarz UD, Wepf R, Wiesendanger R. Investigation of the swelling of human skin cells in liquid media by tapping mode scanning force microscopy. Appl Phys A. 2001;72 (Suppl):S125–8.

Rochefort A, Druot P, Agache P, et al. A new technique for the evaluation of cosmetics effect on mechanical properties of stratum corneum and epidermis *in vitro*. Int J Cosmet Sci. 1986;8:27–36.

Shao F, Chen XJ, Barnes CJ, Henson B. A novel tactile sensation measurement system for qualifying touch perception. Proc Instn Mech Eng. 2010;224 (1):97–105.

Sivamani RK, Maibach HI. Tribology of skin. J Eng Tribol. 2006;220(J8):729–37.

Sivamani RK, Goodman J, Gitis NV, Maibach HI. Titre? Skin Res Technol. 2003a;9(3):235–9.

Sivamani RK, Goodman J, Gitis NV, Maibach HI. Titre? Skin Res Technol. 2003b;9(3):227–34.

Takahashi M, Yamada M, Machida Y. A new method to evaluate the softening effect of cosmetic ingredients on the skin. J Soc Cosmet Chem. 1984;35:171–81.

Takahashi M, Machida Y, Tsuda Y. The influence of hydroxyl acids on the rheological properties of stratum corneum. J Soc Cosmet Chem. 1985;36:177–87.

Wildnauer RH, Bothwell JW, Douglass AB. Stratum corneum biomechanical properties, influence of relative humidity on normal and extracted human stratum corneum. J Invest Dermatol. 1970;56 (1):72–8.

Wolfram EJ. Friction of skin. J Soc Cosmet Chem. 1983;34:465–76.

Wu KS, Van Osdol WW, Dauskardt RH. Mechanical and microstructural properties of stratum corneum. Mat Res Soc Symp Proc. 2002;724:N2.7.1–7.

Wu KS, Stefik MM, Dauskardt RH, et al. Graded delamination behavior of human stratum corneum. Biomaterials. 2006a;27:5861–70.

Wu KS, Van Osdol WW, Dauskardt RH. Mechanical properties of stratum corneum: effects of temperature, hydration and chemical treatment. Biomaterials. 2006b;27:785–95.

Yuan Y, Verma R. Measuring microelastic properties of stratum corneum. Colloids Surf B: Biointerfaces. 2006;48:6–12.

Effects of Sebum on Drug Transport Across the Human Stratum Corneum

35

Jui-Chen Tsai, Cheng-Che Eric Lan, and Hamm-Ming Sheu

Contents

Keywords

Sebum • Stratum corneum • Skin barrier function • Drug transport • Human in vivo • Lipid morphology

The differentiation process of sebocyte, the most active lipid-producing cell in the human beings, results in formation of sebum. As the sebum leaves from the sebocytes, it contains triglycerides, squalene, wax esters, and small amount of cholesterol esters. The bacterial enzymes along the follicular canal partially hydrolyzed the triglycerides of the sebum during the passage through follicular canal, so that the sebum content reaching the skin surface contained about 15–40 % free fatty acids, with the unsaturated fatty acid being more irritating than the saturated fatty acid. The sebum mixed with the deranged lamellar lipids from the keratinizing epithelium and formed the skin surface lipid film (SSLF) as it arrived at the skin surface. SSLF is a mixture of large amount of sebum combined with small portion of epidermal lipids. Occasionally, detached corneocytes are also present as demonstrated from the ultrastructural observations made by ruthenium tetroxide staining (Fig. 1). Our observation also demonstrated presence of sebum between the layers of desquamating corneocytes from the outermost several layers of the stratum corneum (SC) (Sheu et al. 1999). Previous infrared spectroscopic study demonstrated greater quantities and more disordered lipids in the outer layer of SC, an observation that is consistent with our morphological observation. These observations suggest a

J.-C. Tsai
Institute of Clinical Pharmacy and Pharmaceutical Sciences, National Cheng Kung University, College of Medicine, Tainan, Taiwan

C.-C.E. Lan
Department of Dermatology, Kaohsiung Medical University, Kaohsiung, Taiwan

H.-M. Sheu (✉)
Department of Dermatology, National Cheng Kung University College of Medicine and Hospital, Tainan, Taiwan
e-mail: hmsheu@mail.ncku.edu.tw

P. Humbert et al. (eds.), *Agache's Measuring the Skin*,
DOI 10.1007/978-3-319-32383-1_35

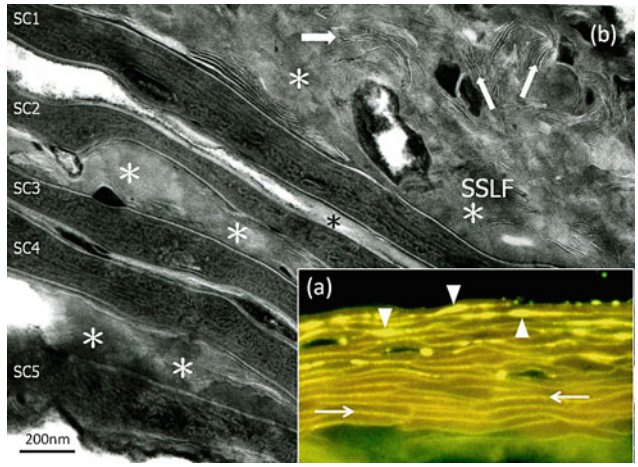

Fig. 1 Interaction of sebum with corneocytes. **a** Nile red staining of human forehead skin. Discrete irregularly stained particles and plaques are noted in the uppermost several layers of stratum corneum (*arrowheads*). In contrast, regular linear yellow-gold fluorescence (*arrows*) through the intercellular membrane regions of the stratum corneum is noted. **b** Using ruthenium tetroxide stain to observe the stratum corneum lipid structure under the electronic microscope. Note that the amorphous lipid granules (*) were observed in the skin surface lipid film (SSLF) and within the intercellular space of the uppermost several layers of the stratum corneum (SC1-SC5). Deranged lipid lamellae (*arrows*) within the SSLF are observed

possible interaction of SSLF with the corneocytes in the outermost layers of the SC (Bommannan et al. 1990).

1 Effects of Sebum on Epidermal Barrier Function and Stratum Corneum Lipid Morphology

The effects of sebum on skin barrier function have not been thoroughly investigated. Several in vitro studies suggested that sebum has negative effects on the skin permeability barrier. Functional study by electron diffraction demonstrated that human SC lipids were arranged in an orthorhombic packing pattern (crystalline phase). Upon mixing with sebaceous lipids, the presence of the hexagonal lattice (gel phase) increased (Pilgram et al. 2001). Therefore, the interaction between lipids from sebocytes with human SC lipids increased the fluidity of SC lipids, and it might also increase the SC permeability. Squire et al. demonstrated that sebum increases the permeability of the skin. They suggested that the damage to corny layer by the unsaturated fatty acid such as C16:1△6 may be involved in the process (Squier et al. 1994). The orderly structure of SC lipids is disrupted resulting in the change of drug permeability through the corneum layer when unsaturated fatty acid interacts with the corneum layer (Aungst et al. 1986). As shown in Fig. 2, sebum supplement on the human forearm in vivo produced a significant shift (3.8 ± 0.8 cm^{-1}, $p < 0.001$) of CH_2 asymmetric stretching frequency in the attenuated total reflectance-Fourier transform infrared (ATR-FTIR) spectra of the SC in comparison to the untreated site. Additionally, sebum removal from the forehead in vivo decreased the frequency of the CH_2 asymmetric stretching (1.2 ± 0.6 cm^{-1}, $p = 0.001$). As demonstrated in Fig. 2b, the results of the CH_2 symmetric stretching frequency shift paralleled that of CH_2 asymmetric stretching frequencies ($p < 0.001$) (Tsai et al. 2012). These frequencies have been demonstrated to correlate with the SC water permeability. More specifically, a shift to higher frequency in this region reflected an increased number of gauche conformers of the CH_2 groups along the alkyl chain, and these events resulted in more disorderly arrangement of SC lipid and increased membrane fluidity (Potts and Francoeur 1990). Taken together,

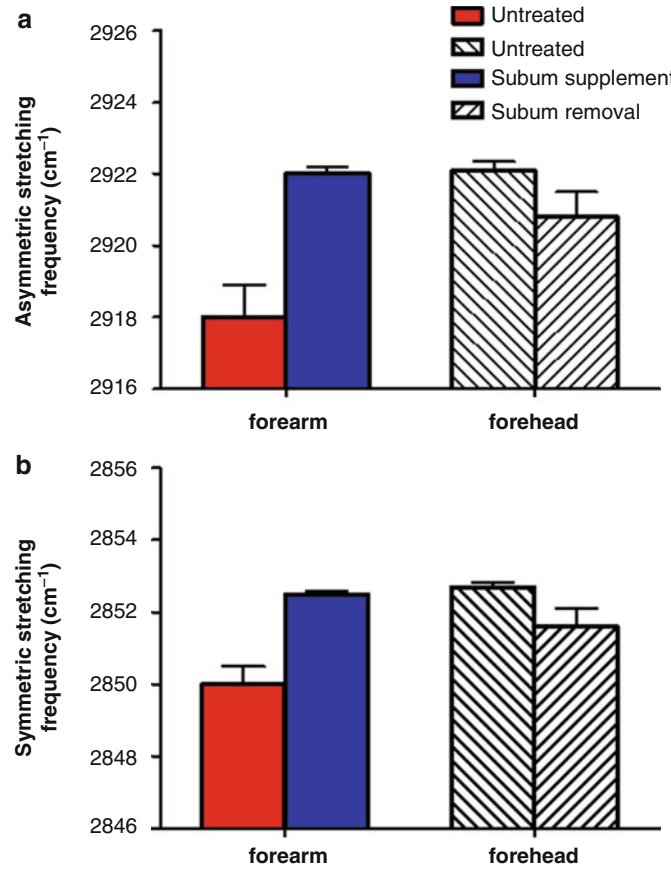

Fig. 2 Frequencies of CH_2 asymmetric and symmetric stretching bands in the ATR-FTIR spectra on the forearm and forehead by sebum treatments ($n = 8$). Sebum supplement increased, while sebum removal decreased the frequency of the CH_2 asymmetric and symmetric stretching strength

these results indicated that sebum per se has a detrimental effect on the structural and functional properties of skin barrier (Guo et al. 2015).

2 In Vivo Drug Permeation Protocol and Data Analysis

As shown in Fig. 3, by applying an aqueous gel containing 15 % bentonite clay and 0.2 % carboxymethyl cellulose to one side of each subject's forehead for 10 min and then washed with water, the sebum removal from the subject was achieved (Downing et al. 1982). On the other hand, sebum supplementation was achieved by treating the subject's forearm with 1 μl/cm^2 sebum (0.56 ± 0.04 mg/μl total lipids) for 1 h, and the unabsorbed sebum on the skin surface was removed using Kimwipes® at the end of the application period. After sebum removal or sebum supplementation as described above, saturated aqueous solutions of CP (4-cyanophenol) and CM (cimetidine) were applied to the skin of the forearm for 15 min and 5 h, respectively. For forehead, CM was applied for 0.5 h, using a patch. The skin surface was gently cleaned and dried with gauze pad after the indicated treatment period. Subsequently, repetitive adhesive-tape stripping for up to 10–15 times over 2–3 min was performed to quickly and progressively remove SC. The amount of CP and CM contained in the tape strips were determined with either ATR-FTIR spectroscopy or high-performance liquid chromatography. A balance with sensitivity of 10 μg was used to determine the mass of SC on each tape strip. Drug concentration (C(x)) was then expressed as a function of depth into the SC (Tsai et al. 2003).

The human SC thickness (L) during the in vivo studies was estimated by the two-point analysis in

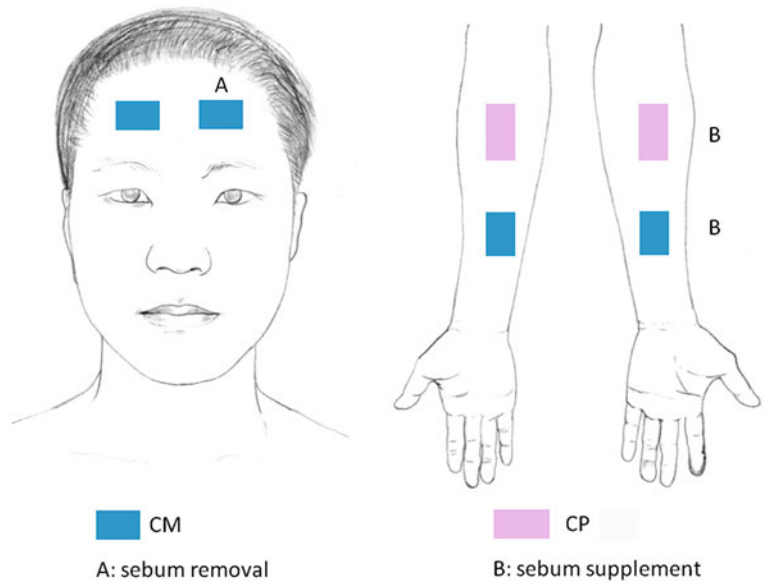

Fig. 3 Drug application scheme. *CM* cimetidine, *CP* 4-cyanophenol

accordance with the equation described by Pirot et al. (1998):

$$\mathrm{L} = x \cdot \mathrm{TEWL}_x / (\mathrm{TEWL}_x - \mathrm{TEWL}_0) \qquad (1)$$

where x represents the cumulative SC thickness removed by all the tape stripping, TEWL_0 (TWEL: transepidermal water loss) represents the average initial TEWL measured, and TEWL_x represents the average value of TEWL measured when xμm of SC have been removed.

With the SC thickness estimated from the equations described above, the data were then fitted into the following equation according to the Fick's second law of diffusion:

$$C(x) = KCveh\left\{1 - \frac{x}{L}\right\} - \sum_{n=1}^{\infty} \frac{2}{n\pi} KCveh * \sin\left(\frac{n\pi x}{L}\right) \exp\left(\frac{-Dn^2\pi^2 t}{L^2}\right) \qquad (2)$$

under the following boundary and initial conditions: (1) $C = C_0 = KC_{veh}$, at $x = 0$, $t \geqq 0$; (2) $C = 0$, at $x = L$, $t \geqq 0$; (3) $C = 0$, at $0 < x < L$, $t = 0$, where C_0 is the drug concentration at the skin surface (i.e., $x = 0$), D is the drug's diffusivity, and K is the SC/water partition coefficient of the drug, to yield values of K and D. The drug permeability ($P = KD/L$) into the SC was then deduced (Pirot et al. 1997).

3 Effects of Sebum on Drug Transport Across Human SC

The concentration profiles of CM in the SC on the subject No. 7's forehead were demonstrated in Fig. 4a. Figure 4b demonstrated the CM profile for the untreated and sebum-treated forearm from subject No. 8 after 5-h exposures to CM solution. The CP profiles for the forearm of subject No. 7 after 15-min exposure to CP solution are shown in Fig. 4c. The SC transport parameters K, D, and P of CM and CP for the nine subjects on the forehead with and without sebum removal, and on the forearm with and without sebum supplementation, are summarized in Table 1. Sebum content of the forehead reduced from 159.7 ± 36.7 to 6.5 ± 5.2 μg/cm^2 after the sebum removal process. Sebum content of the forearm increased from 1.0 ± 1.2 to 140.9 ± 33.4 μg/cm^2 after human sebum supplementation derived from washing the subjects' hair with alcohol.

These results demonstrated that in high sebum-containing areas including forehead, the SC permeability of CM ($\mathrm{P_{CM}}$), a hydrophilic molecule,

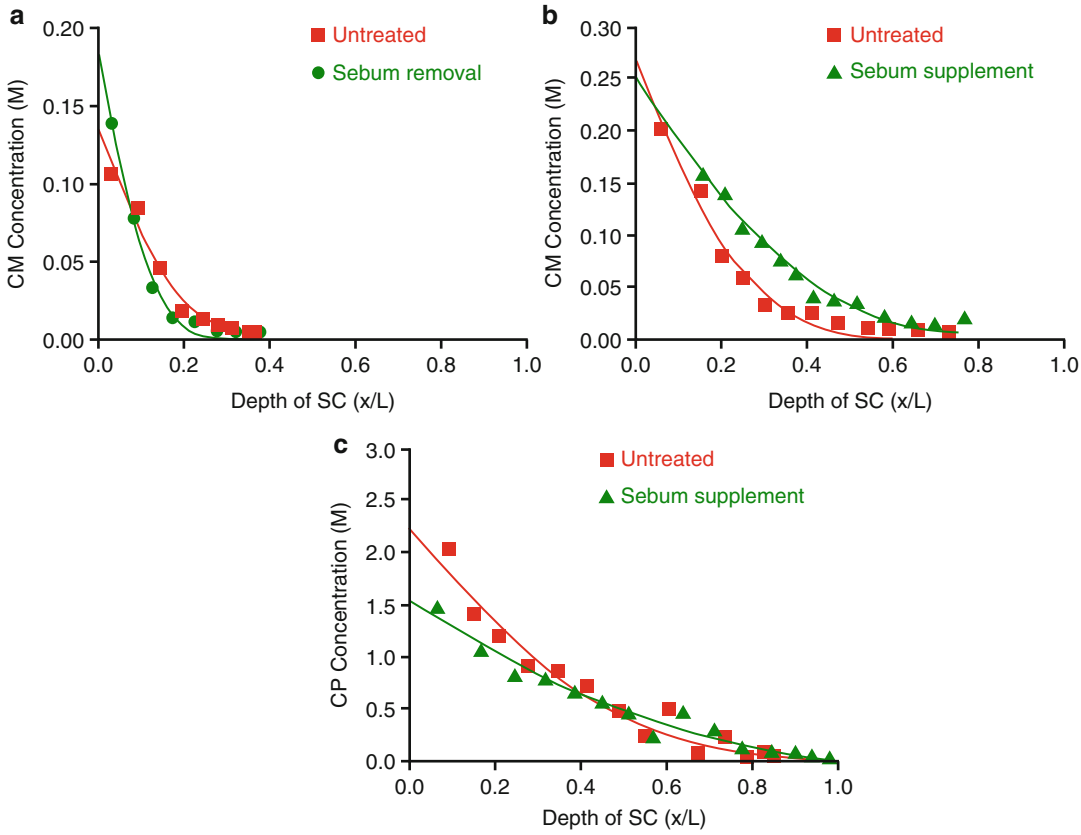

Fig. 4 Representative drug concentration profiles as a function of normalized depth (x/L) into the SC. The data points were experimentally determined. The *lines* through the results represent the best fits of Eq. 2. (**a**) CM on forehead of subject No. 7; (**b**) CM on forearm of subject No. 8; (**c**) CP on forearm of subject No. 7

may be four times higher than that for the forearm (39.2 ± 13.6 versus $10.3 \pm 5.5 \times 10^{-5}$ cm/h). In addition, the SC diffusivity 0f CM (D_{CM}) of the forehead may be eightfold of that in the forearm (61.7 ± 15.5 vs. $7.3 \pm 3.4 \times 10^{-9}$ cm^2/h). On the other hand, the drug partition into the SC (K_{CM}) of the forehead was only 43 % of the forearm (7.6 ± 1.4 vs. 17.6 ± 5.1). The differences in K_{CM}, D_{CM}, and P_{CM} between forehead and forearms were statistically significant ($p < 0.001$). The variations in SC permeability of CM between the forehead and forearm may be contributed by differences in thermodynamic and kinetic components. In support of our finding, similar results were previously shown for the regional variation of P_{CM} of other skin sites (Tsai et al. 2003). In murine skin model, chronic application of sebum induced structural changes in the SC (Guo et al. 2015), which could account for the eightfold differences in D_{CM} between the two untreated sites. Taken together, these results suggest that in clinical situations such as seborrheic dermatitis, a condition that involves excess sebum secretion and barrier disruption, the permeability barrier to hydrophilic molecules might be further aggravated.

As a result of sebum removal from the forehead, the partition K_{CM} increased 1.39-fold (9.8 ± 1.8 vs. 7.6 ± 1.4), and D_{CM} decreased 0.61-fold in comparison to the untreated site (37.9 ± 14.3 vs. $61.7 \pm 15.5 \times 10^{-9}$ cm^2/h). Subsequently, P_{CM} was decreased to 0.78-fold of control (30.8 ± 13.4 vs. $39.2 \pm 13.6 \times 10^{-5}$ cm/h). In the group which receive sebum supplementation to the forearm, D_{CM} increased 3.52-fold (23.7 ± 8.3 vs. $7.3 \pm 3.4 \times 10^{-9}$ cm^2/h) while the K_{CM} remained unchanged, such that P_{CM} at the

Table 1 Effects of sebum treatment on SC transport parameters of cimetidine and 4-cyanophenol for the forehead and forearm ($n = 9$)

Site	Forehead				Forearm			
Parameter	Untreated		Sebum removal		Untreated		Sebum supplement	
Cimetidine								
Sebum content (μg/cm^2)	159.7	±36.7	6.5	±5.2	1.0	±1.2	140.9	±33.4
$K_{SC/W}$	7.6	±1.4	9.8	±1.8	17.6	±5.1	17.7	±2.4
D_{CM} ($\times 10^9$ cm^2/h)	61.7	±15.5	37.9	±14.3	7.3	±3.4	23.7	±8.3
P_{CM} ($\times 10^5$ cm/h)	39.2	±13.6	30.8	±13.4	10.3	±5.5	34.2	±11.3
4-cyanophenol								
Sebum content (μg/cm^2)					1.5	±2.1	140.7	±36.9
$K_{SC/W}$					23.0	±2.9	15.4	±3.2
D_{CP} ($\times 10^7$ cm^2/h)					5.8	±2.2	8.5	±2.6
P_{CP} ($\times 10^3$ cm/h)					11.3	±4.9	11.0	±4.0

forearm supplemented with sebum was 3.25-fold of that of the control (34.2 ± 11.3 vs. $10.3 \pm 5.5 \times 10^{-5}$ cm/h). The permeability of CP (P_{CP}) was almost constant regardless of sebum supplementation to the forearm, which was the result of a 0.67-fold decrease in K_{CP} (15.4 ± 3.2 vs. 23.0 ± 2.9) and a 1.46-fold increase in D_{CP} (8.5 ± 2.6 vs. $5.8 \pm 2.2 \times 10^{-7}$ cm^2/h). All the transport parameters between the untreated and treated subject at the same site were significantly different ($p < 0.05$) for the same drug except for the $K_{SC/W}$ of CM and P_{CP} on the forearm. These results demonstrated that the magnitude of decrease in D_{CM} for the forehead by sebum removal (0.78-fold) to be less than the magnitude of increase for the forearm by sebum supplementation (3.52-fold). It is also likely that the presence of sebum in the forehead or forearm increased the diffusion of lipophilic and hydrophilic molecules, while the effect on partition is dependent on sites and drugs selected. These results were in accordance with previous report from Valiveti et al. (2008) and Valiveti and Lu (2007) using artificial sebum. More specifically, they suggested that there is no correlation between log K_{sebum} versus log K_{SC} for compounds with different chemical structures, and maximal flux observed through sebum was found to be higher than their corresponding skin fluxes for a homologous series of 4-hydroxybenzoic acid esters.

Finally, the observed CH_2 stretching frequency shift resulting from sebum treatment as demonstrated in Fig. 2 also reflected the alterations of SC permeability on CM. Therefore, the increased SC permeability of hydrophilic drug and altered barrier function of SC was achieved by sebum supplementation through disordering the structures of the intercellular lipid molecules.

4 Conclusions

For the first time in vivo, the effect of sebum on drug transport across human SC was demonstrated. For hydrophilic molecules, such as CM, the SC permeability on the forehead may be as much as four times the permeability on the forearm. Sebum supplement on the forearm, while has little effect on CP, increased the SC permeability of CM more than threefold. The SC permeability of the CM has a small but significant alteration (−22 %) after removal of sebum from the forehead. Although the sebum supplementation in both the forehead and forearm increased the diffusion of both lipophilic and hydrophilic molecules, the effect of sebum supplementation on partition is site and drug dependent. The alteration of SC permeability by sebum supplementation to hydrophilic drug may be attributable to the barrier function changes of SC induced by disordering structures of the intercellular lipid molecules. It is likely that removing the sebum from the face will reduce the absorption of hydrophilic compounds

contained in the formulations that were topically applied.

References

Aungst BJ, Rogers NJ, Shefter E. Enhancement of naloxone penetration through human skin in vitro using fatty acids, fatty alcohols, surfactants, sulfoxides, and amides. Int J Pharm. 1986;33(1−3):225–34.

Bommannan D, Potts RO, Guy RH. Examination of stratum corneum barrier function in vivo by infrared spectroscopy. J Invest Dermatol. 1990;95(4):403–8.

Downing DT, Stranieri AM, Strauss JS. The effect of accumulated lipids on measurements of sebum secretion in human skin. J Invest Dermatol. 1982;79(4):226–8.

Guo JW, Lin TK, Wu CH, Wei KC, Lan CCE, Peng ACY, Tsai JC, Sheu HM. Human sebum extract induces barrier disruption and cytokine expression in murine epidermis. J Dermatoll Sci 2015; 78:34–43.

Pilgram GS, van der Meulen J, Gooris GS, Koerten HK, Bouwstra JA. The influence of two azones and sebaceous lipids on the lateral organization of lipids isolated from human stratum corneum. Biochim Biophys Acta. 2001;1511(2):244–54.

Pirot F, Kalia YN, Stinchcomb AL, Keating G, Bunge A, Guy RH. Characterization of the permeability barrier of human skin *in vivo*. Proc Natl Acad Sci. 1997;94(4):1562–7.

Pirot F, Berardesca E, Kalia YN, Singh M, Maibach HI, Guy RH. Stratum corneum thickness and apparent water diffusivity: facile and noninvasive quantitation *in vivo*. Pharm Res. 1998;15(3):492–4.

Potts RO, Francoeur ML. Lipid biophysics of water loss through the skin. Proc Natl Acad Sci. 1990;87(10):3871–3.

Sheu HM, Chao SC, Wong TW, Lee JYY, Tsai JC. Human skin surface lipid film: an ultrastructural study and interaction with corneocytes and intercellular lipid lamellas of the stratum corneum. Br J Dermatol. 1999;140(3):385–91.

Squier CA, Wertz PW, Williams DM, Cruchley AT. Permeability of oral mucosa and skin with age. In: Squier CA, Hill MW, editors. The effect of aging in oral mucosa and skin. Boca Raton: CRC Press; 1994. p. 91–8.

Tsai JC, Lin CY, Sheu HM, Lo YL, Huang YH. Noninvasive characterization of regional variation in drug transport into human stratum corneum *in vivo*. Pharm Res. 2003;20(3):632–8.

Tsai JC, Lu CC, Lin MK, Guo JW, Sheu HM. Effects of sebum on drug transport across human stratum corneum *in vivo*. Skin Pharmacol Physiol. 2012;25(3):124–32.

Valiveti S, Lu GW. Diffusion properties of model compounds in artificial sebum. Int J Pharm. 2007;345(1–2):88–94.

Valiveti S, Wesley J, Lu GW. Investigation of drug partition property in artificial sebum. Int J Pharm. 2008;346(1–2):10–6.

Epidermal Physiology

36

Patricia Rousselle, Edgar Gentilhomme, and Yves Neveux

Contents

Keywords

Anti-bacterial peptide • Cytocrine secretion • Endocrine secretion • Epidermis • Epidermal barrier • Cytocrine secretion • Endocrine secretion • Proliferation and differentiation • Growth fraction, epidermis • hCAP-18 • Human keratinocytes • Melanocytes • Papillas

This chapter describes the epidermis, formerly called the Malpighi's layer. As the skin's outer layer, the epidermis provides the barrier function protecting mammals from environmental influences such as physical, chemical, or thermal stress and also against dehydration. The epidermis is a multilayered epithelium consisting of the interfollicular epidermis and associated hair follicles, sebaceous glands, and eccrine sweat glands. Although keratinocytes are the main epidermal cell type (95 % of the total cells), other cells are found in mammalian epidermis, such as melanocytes and Merkel and Langerhans cells. Merkel cells are neuroendocrine cells responsible for the touch sensory function of the skin. Melanocytes are specialized pigment cells producing melanin granules, which are transferred to keratinocytes for their protection against UV-induced DNA damage. Langerhans cells are epidermal dendritic cells involved in the adaptive immune

P. Rousselle (✉)
Tissue Biology and Therapeutic Engineering Unit, Institute of Protein Biology and Chemistry, UMR 5305 – CNRS, University of Lyon, Lyon, France
e-mail: patricia.rousselle@ibcp.fr

E. Gentilhomme
French Army Health Research Department, La tronche, France
e-mail: edgargentilhomme@crssa.net

Y. Neveux
Livernon, France
e-mail: yves.neveux@free.fr

P. Humbert et al. (eds.), *Agache's Measuring the Skin*,
DOI 10.1007/978-3-319-32383-1_36

response, playing a critical role in the barrier function of the skin. The epidermis itself is divided into five layers which are, from the inner to the outer most, the stratum germinativum (basal), stratum spinosum (spinous), stratum granulosum (granular), stratum lucidum (only found in thickened areas of the epidermis), and the stratum corneum (cornified). The epidermis consists in approximately ten layers of keratinocytes piled up from the basal layer to the cornified layer. In contrast with the stratum corneum that features a horizontal plane, the basal layer juxtaposes the dermis with the dermal-epidermal junction in a corrugated outline manner, alternating in-depth epidermal cones and dermal expansions named "papillas" (Fig. 1). The thickness of the viable epidermis lies from 75 to 150 μm according to anatomical site to reach 0.8 mm on the palms of the hands and 1.4 mm on the soles of the feet. Its metabolism seems close to 0.4 ml min^{-1}/100 g tissue (Krueger et al. 1994) (resting muscle, <0.2; muscle on exercise, 13–15; brain, 3–4 (Holtz 1996)).

Its fundamental and first known function is to generate the stratum corneum, the dead but vital barrier that separates our body from the environment. It is accomplished through its perpetual renewal from the division of basal cells and keratinization of uppermost layers: the total turnover takes about 15 days, the same as that of the stratum corneum. Other fundamental functions are extracellular matrix component production; hormone secretion; cytokine production ruling angiogenesis and vasomotricity in the papillary dermis; homing and maturation of cells responsible for the immune barrier (Aubin 2004) protection against ultraviolet light and homing of melanocytes (▶ Chap. 101, "Skin Photoprotection Function"); participation to the skin neurosensorial function and homing of Merkel cells (see dedicated chapters); participation in the skin mechanical protective function, thanks to its cellular abundant keratin filaments (see the dedicated chapter); and finally the capacity of self-repair (see the ▶ Chap. 47, "Skin Wound Healing Assessment").

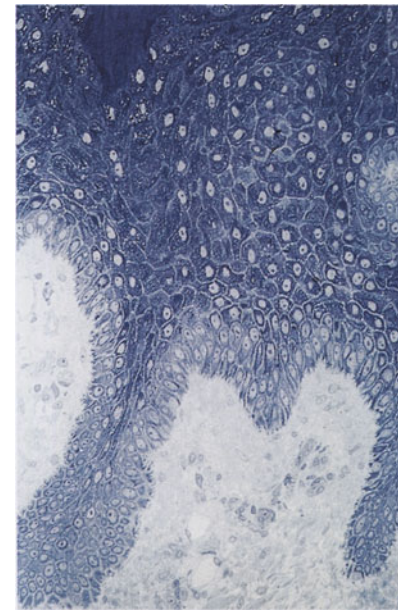

Fig. 1 Dermis and epidermis. Dermal papillae with a basal layer and numerous suprabasal differentiated layers. Resin semithin section. Toluidin blue staining. Objective ×100

1 Epidermal Proliferation and Differentiation

The epidermis is continuously renewed by the proliferation of stem cells and the differentiation of their progeny, which undergo terminal differentiation as they leave the basal layer and move upward toward the surface, where they die and slough off. As for most epithelial tissues, proliferation and differentiation occur in two juxtaposed compartments, represented by the basal layer and the numerous suprabasal layers. The keratinocyte population can be divided into at least three functional types, keratinocyte stem cells, transit amplifying cells, and postmitotic differentiating cells. Stem cells, responsible for tissue renewal, have a high mitotic potential but are rarely dividing. They give birth to transit amplifying cells, which after a finite number of division, are committed to differentiate. By this way, a high output of differentiated cells can be issued from a small number of infrequently solicited stem cells. The **growth fraction**

of human epidermis has been estimated to 10 % of stem cells and 50 % of transit amplifying cells versus 40 % of differentiated cells (Heenen and Galand 1997). On the basis of their morphological and functional characteristics, the proliferating cells have also been described as clonogenic keratinocytes: holoclones, meroclones, and paraclones (Barrandon and Green 1987). Located in the basal layer and in the bulge of hair follicles, stem cells can be characterized by their size (Barrandon and Green 1985), their high adhesive properties (Kaur and Li 2000), their high level of β1 integrin (Zhu et al. 1999), their expression of keratin K19 (Michel et al. 1996), and their high content in cytoplasmic β-catenin (Zhu and Watt 1999). Their spatial distribution in the basal layer is not randomly disposed, showing clusters of stem cells from which migrate transit amplifying cells (Jensen et al. 1999). Generation of differentiated progeny from stem cell is regulated by internal mechanisms such as transcription factors and by external controls in the cellular microenvironment such as secreted mediators, cellular interactions, integrins, or other elements (Watt and Hogan 2000). In this system, β1 integrin is particularly involved and induce, depending on the signaling pathway involved, either cellular adhesion or differentiation (Levy et al. 2000). Decrease of adhesion related to modifications of integrins (Kaur and Li 2000) and reduction in mitogen-activated protein (MAP) kinase activation (Zhu et al. 1999) induce this cellular exit from the stem cell compartment. After a finite number of divisions, the transit amplifying cells undergo an irreversible multistage process of differentiation. Keratinocytes committed to the differentiation program downregulate integrins to become less adhesive, move to the suprabasal compartment, and continue their upward movement until they are terminally differentiated and shed off. This produces several layers of keratinocytes, at different stages of differentiation that can be identified by the expression of keratins. Basal keratinocytes express keratins K5, K14, and K15, whereas differentiating keratinocytes express keratins K1 and K10. Integrins β1 and hemidesmosomal components (integrin α6β4 and BP180) decrease by transcriptional decrease of mRNA and by a post-translational mechanism of ineffective subunits. Some intracellular organelles disappear (mitochondria, nucleus, etc.) when other elements (keratohyalin granules, filaggrin, etc.) appear, leading to the future horny layer cells. During this cellular differentiation, modifications of receptors' expression are observed, either decreasing (receptors for TGFβ1, PDGF A, etc.) or increasing (receptors for acid FGF, basic FGF, PDGFβr, IL-1ra, etc.). Modulation of transmembrane ion transport is also noted with upregulation of sodium channels (Brouard et al. 1999; Deliconstantinos et al. 1995; Eming et al. 1998; Fenjves et al. 1989; Heenen and Galand 1997; Holick 1988; Insogna et al. 1988; Jensen et al. 1999; Kaplan et al. 1988; Katz and Taichman 1994, 1999; Kaur and Li 2000; Krueger et al. 1994; Kupper 1990; Levy et al. 2000; Malaviya et al. 1996; Martinez et al. 1997; Maruyama et al. 1995; Mazereeuw Hautier et al. 2000; Michel et al. 1996; Nathan and Sporn 1991; Oda et al. 1999).

2 Epidermal Secretions

Beside a function of protective barrier, epidermis has also a secretory activity (Boyce 1994), estimated in vitro to a rate of 0,67 µg protein/h/10^6 cells (Katz and Taichman 1994).

2.1 Cytocrine Secretion

Non-lesional epidermis is in a low steady state of secretion and keratinocytes seem quiescent. After endogenous or exogenous (physical, chemical, biological, or immunological) stimulation, the keratinocyte is "activated" and secretes various peptides. These peptides are represented by cytokines (IL-1α, IL-1β, IL-6), tumor necrosis factor (TNFα), growth factors (GMCSF, GCSF, MCSF, TGFα, acid and basic FGF, KGF, PDGF A, PDGF B, NGF), chemokines (IL-8, IFNγ-IL10, huGRO of G-X-C family, or MCAF of G-C family), or suppressor factors/anticytokines (TGFβ, K

LIF, Contra IL-1) (Stoof et al. 1994). Cytokines are small protein hormones primarily secreted by immune cells and are important mediators of host defense, post-injury repair, cell growth, and maturation. This secretion shows particular characteristics (Kupper 1990), such as the release of secondary cytokines after stimulation by primary cytokines. The activated keratinocyte is modulated through the action of specific receptors present on the cell membrane (IL-1 receptors, IFNγ receptors, etc.) and induced by stimulation. Species of activated keratinocytes and secretion types would differ depending on the nature of the signal. All these pleiotropic or specific peptides act by autocrine or paracrine mechanisms (Schröder 1995). Their action must be evaluated, considering numerous mechanisms of amplifying or inhibitory regulation (Nathan and Sporn 1991) such as action of anticytokines, direct antagonism between several cytokines (Reinartz et al. 1996), or specific action of the cytokine on the same keratinocyte (Maruyama et al. 1995). Structural proteins (heparin, decorin, etc.) or cellular environment such as interaction with fibroblastic cells (Boxman et al. 1996) or with a structure like the skin immune system (Bos and Kapsenberg 1993) modulates the effect of these factors (Figs. 2, 3, and 4).

Other proteins secreted by the epidermis are regularly identified. Katz and Taichman (Katz and Taichman 1999) listed a catalogue of twenty proteins released by keratinocytes in culture, suggesting new physiological functions to be identified. These proteins may induce various cellular responses. Among these, the phospholipase A2 was suggested to play a role in the maintenance of tissue integrity (Mazereeuw Hautier et al. 2000) and regeneration (Rys-Sikora et al. 2000). The multifunctional peptide adrenomedullin is involved in epithelial homeostasis or even in epidermal protection (Martinez et al. 1997). Many proteins, such as proteases (Katz and Taichman 1999) or antileukoproteinases (Wiedow et al. 1998), have been shown to be involved in matrix remodeling. Keratinocytes produce the basement membrane laminin 332 and modulate fibroblast behavior through the secretion of β1G-H3 (Katz and Taichman 1999).

2.2 Endocrine Secretion

In normal conditions, epidermis can also be a source of circulating compounds that have effects at distant sites in the body. The role of epidermis

Fig. 2 Stratum basale protrusions into the dermis. Thick keratin filaments bundles separate into small bundles which attach to hemidesmosomes at cell periphery (Small *arrow head*). Large arrowheads point at dermis reticulum fibers that are attached to the basement membrane perpendicularly. Fixation by glutaraldehyde and osmic acid. Uranyl acetate and lead citrate staining. × 29,000

Fig. 3 Stratum spinosum. Section though the periphery of a keratinocyte. Fixation by glutaraldehyde and osmic acid. Uranyl acetate and lead citrate staining. × 25,000

in vitamin D synthesis has been early shown (Holick 1988). Keratinocytes also release chemicals like triiodothyronine (Kaplan et al. 1988) or parathyroid hormone-related proteins (Insogna et al. 1988; Jensen et al. 1999; Kaplan et al. 1988; Katz and Taichman 1994, 1999; Kaur and Li 2000; Krueger et al. 1994; Kupper 1990; Levy et al. 2000; Malaviya et al. 1996; Martinez et al. 1997; Maruyama et al. 1995; Mazereeuw Hautier et al. 2000; Michel et al. 1996; Nathan and Sporn 1991; Oda et al. 1999; Reinartz et al. 1996; Rys-Sikora et al. 2000; Schauer et al. 1994; Shimizu et al. 1997; Schröder 1995; Stoof et al. 1994; Watt and Hogan 2000; Wiedow et al. 1998; Wysolmerski and Stewart 1998), endothelin, and the C3 complement component. Neuropeptides such as substance P (Bae et al. 1999) and neurohormones such as proopiomelanocortin and derived peptides αMSH and ACTH (Schauer et al. 1994) are produced by epidermal cells. The generation of nitric oxide (Deliconstantinos et al. 1995; Eming et al. 1998; Fenjves et al. 1989; Heenen and Galand 1997; Holick 1988; Insogna et al. 1988; Jensen et al. 1999; Kaplan et al. 1988; Katz and Taichman 1994, 1999; Kaur and Li 2000; Krueger et al. 1994; Kupper 1990; Levy et al. 2000; Malaviya et al. 1996; Martinez et al. 1997; Maruyama et al. 1995; Mazereeuw Hautier et al. 2000; Michel et al. 1996; Nathan and Sporn 1991; Oda et al. 1999; Reinartz et al. 1996; Rys-Sikora et al. 2000; Schauer et al. 1994; Shimizu et al. 1997) or histamine (Malaviya et al. 1996) has been also confirmed, showing the role of stimulated epidermis in inflammatory reactions. The systemic distribution of naturally produced protein has been found even after epidermal transplantation, as proved for apolipoprotein E (Fenjves et al. 1989). These results may permit the use of keratinocytes for gene therapy (Eming et al. 1998; Fenjves et al. 1989; Heenen and Galand 1997; Holick 1988; Insogna et al. 1988; Jensen et al. 1999; Kaplan et al. 1988; Katz and Taichman 1994; Katz and Taichman 1999; Kaur and Li 2000; Krueger et al. 1994).

Keratinocytes can synthesize acetylcholine and its receptors and thereby generate an autocrine system, which has been shown to regulate cell motility. Besides, the epidermis has the ability to generate catecholamine mediators including epinephrine. These catecholamines can activate adrenergic receptors present on keratinocytes to modulate their migratory behavior.

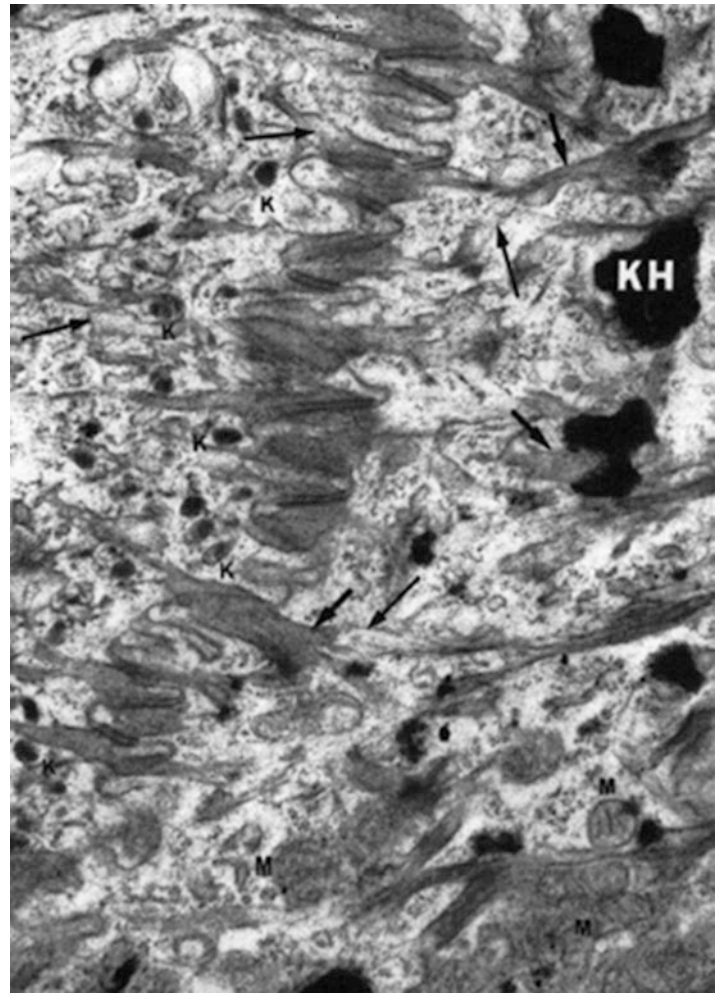

Fig. 4 Stratum granulosum: section through the boundary between two keratinocytes. *K* keratinosomes (Odland's bodies). *KH* keratohyalin. *M* mitochondria, *thick arrow* tonofilaments bundle, *thin arrow* single tonofilament. As in the whole epidermis, desmosomes bind cells at their tonofilaments bundles. Phosphate buffered glutaraldehyde and osmium after fixation. Uranyl acetate and lead citrate staining. × 30,000

2.3 Other Roles

A fine balance between cell proliferation and differentiation maintains the barrier function of the epidermis. In quiescent tissue, homeostasis is regulated by both autocrine and paracrine secretions. After stimulation, these secretions are amplified, and the epidermis acts as a transducer, transforming exogenous stimulations into specific immune or inflammatory responses.

Human keratinocytes play an important role in the innate immune response and produce several antibacterial peptides that are important for both homeostatic and wound healing purposes. Human keratinocytes are known to produce four such peptides: human beta defensin 1 (hBD-1), hBD-2, hBD-3, and hCAP-18 (as well as its biologic active proteolytic product LL-37) (Harder et al. 1997; Nizet et al. 2001). hCAP-18 is a member of the cathelicidin family of antimicrobials. Both hCAP-18 and LL-37 are expressed and released in response to an inflammatory stimulus (Ong et al. 2002). The cathelicidin hCAP-18 is normally processed and stored in the lamellar bodies of the keratinocytes and may be released as a result of injury or exposure to microbial components. After secretion, hCAP-18 is processed into LL-37 and various other peptides, which are important in killing the skin pathogens *S. aureus* and *C. albicans*. They might have a

major role in epithelium protection during wound healing (Dorschner et al. 2001) and psoriasis (Ong et al. 2002). In atopic dermatitis, the heavy carriage of *S. aureus* and the increased sensitivity to herpes and *M. contagiosum* infection may be related to a lower expression of both peptides, due to the production of IL-4 and IL-13 cytokines by Th2-T4 lymphocytes (Ong et al. 2002). Epidermis is also active by an intensive release of other peptides during wound healing. Beta-defensin-2 and LL-37 are upregulated in the epidermis of wounded human skin within 24 h of wounding, reaching highest levels at 48 h post-wounding and returning to basal levels when the wound is re-epithelialized.

Glossary

ACTH Adrenocorticotrophic hormone

Autocrine Peptides (cytokine, extracellular matrix components, epidermal proteins etc.) are released but bind immediately to receptors and act on the cell that produced them.

Contra IL-1 Contra interleukin 1

Endocrine Peptides, synthesized by the keratinocytes, enter the circulation and induce specific biologic responses in distant target tissues.

Exocrine Release of secretion toward the external part of the body. Glandular epithelia (sebaceous and sweat) of the skin are specialized for this function.

FGF Fibroblast growth factor. Either acid FGF or basic FGF

GCSF Granulocyte colony-stimulating factor

GMCSF Granulocyte-/macrophage-stimulating factor

Homeostasis Maintenance of the organism's physiological parameters at their normal value

huGRO Human growth factor

IL Interleukin: IL-1α, interleukin 1α; IL-1β, interleukin 1 β; IL-1ra, interleukin 1 receptor antagonist; IL-6, interleukin 6

IFNγ-IP10 Interferon gamma-induced protein

Juxtacrine Peptides are released and will act on cells in contact with the producing cell.

KGF Keratinocyte growth factor

K LIF Keratinocyte-derived lymphocyte inhibitory factor

MCAF Monocyte chemotactic and activating factor

MCSF Macrophage colony-stimulating factor

MSH Melanocyte-stimulating hormone

NGF Nerve growth factor

Paracrine Peptides are released by a cell and will act on cells immediately surrounding the producing cell.

PDGF Platelet-derived growth factor

TGFα Transforming growth factor alpha

TGFβ1 Transforming growth factor beta1

TNFα Tumor necrosis factor alpha

References

Aubin F. Skin immune system. In: Handbook of Measuring the skin. 1st edn. Berlin: Springer; 2004.

Bae S, Matsunaga Y, Tanaka Y, Katayama I. Autocrine induction of substance P mRNA and peptide in cultured normal human keratinocytes. Biochem Biophys Res Commun. 1999;263:327–33.

Barrandon Y, Green H. Cell size as a determinant of the clone-forming ability of human keratinocytes. Proc Natl Acad Sci U S A. 1985;82:5390–4.

Barrandon Y, Green H. Three clonal types of keratinocyte with different capacities for multiplication. Proc Natl Acad Sci U S A. 1987;84:2302–6.

Bos JD, Kapsenberg ML. The skin immune system: progress in cutaneous biology. Immun Today. 1993;14:75–8.

Boxman IL, Ruwhof C, Boerman OC, Lowik CW, Ponec M. Role of fibroblasts in the regulation of proinflammatory interleukin IL-1, IL-6 and IL-8 levels induced by keratinocyte derived IL-1. Arch Dermatol Res. 1996;288:391–8.

Boyce ST. Epidermis as a secretory tissue. J Invest Dermatol. 1994;102:8–10.

Brouard M, Casado M, Djelidi S, Barrandon Y, Farman N. Epithelial sodium channel in human epidermal keratinocytes: expression of its subunits and relation to sodium transport and differentiation. J Cell Sci. 1999;112:3343–52.

Deliconstantinos G, Villiotou V, Stravrides JC. Release by ultraviolet B (u.v.B) radiation of nitric oxide (NO) from human keratinocytes: a potential role for nitric oxide in erythema production. Br J Pharmacol. 1995;114:1257–65.

Dorschner RA, Pestonjamasp VK, Tamakuwala S, Ohtake T, Rudisill J, Nizet V, Agerberth B, Gudmundsson GH, Gallo RL. Cutaneous injury induces the release of cathelicidin anti-microbial

peptides active against group A Streptococcus. J Invest Dermatol. 2001;117:91–7.
Eming SA, Medalie DA, Tompkins RG, Yarmush ML, Morgan JR. Genetically modified human keratinocytes overexpressing PDGF-A enhance the performance of a composite skin graft. Hum Gene Ther. 1998;9:529–39.
Fenjves ES, Gordon DA, Pershing LK, Williams DL, Taichman LB. Systemic distribution of apolipoprotein E secreted by grafts of epidermal keratinocytes: implications for epidermal function and gene therapy. Proc Natl Acad Sci U S A. 1989;86:8803–7.
Harder J, Bartels J, Christophers E, Schroder J-M. A peptide antibiotic from human skin. Nature. 1997;6636:387–861.
Heenen M, Galand P. The growth fraction of normal human epidermis. Dermatology. 1997;194:313–7.
Holick MF. Skin: site of the synthesis of vitamin D and a target tissue for the active form, 1,25-Dihydroxyvitamin D3. In: Milestone LM, Edelson RL, editors. Endocrine, metabolic and immunologic functions of keratinocytes, vol. 548. New York: Annals of the New York Academy of Sciences; 1988. p. 14–26.
Holtz J. Hemodynamics in regional circulatory beds and local vascular reactivity. In: Greger R, Windhorst U, editors. Comprehensive human physiology. From cellular mechanisms to integration, vol. 2. Berlin: Springer; 1996. p. 1917–40.
Insogna KL, Stewart AF, Ikeda K, Centrella M, Milestone LM. Characterization of a parathyroid hormone-like peptide secreted by human keratinocytes. In: Milestone LM, Edelson RL, editors. Endocrine, metabolic and immunologic functions of keratinocytes, vol. 548. Ney York: Annals of the New York Academy of Sciences; 1988. p. 146–59.
Jensen UB, Lowel S, Watt FM. The spatial relationship between stem cells and their progeny in the basal layer of human epidermis: a new view based on whole-mount labelling and lineage analysis. Development. 1999;126:2409–18.
Kaplan MM, Gordon PR, Pan C, Lee JK, Gilchrest BA. Keratinocytes convert thyroxine to triiodothyronine. In: Milestone LM, Edelson RL, editors. Endocrine, metabolic and immunologic functions of keratinocytes, vol. 548. New York: Annals of the New York Academy of Sciences; 1988. p. 56–65.
Katz AB, Taichman LB. Epidermis as a secretory tissue: an in vitro model to study keratinocyte secretion. J Invest Dermatol. 1994;102:55–60.
Katz AB, Taichman LB. A partial catalog of proteins secreted by epidermal keratinocytes in culture. J Invest Dermatol. 1999;112:818–21.
Kaur P, Li A. Adhesive properties of human basal epidermal cells: an analysis of keratinocyte stem cells, transit amplifying cells and postmitotic differentiating cells. J Invest Dermatol. 2000;114:413–20.
Krueger GG, Morgan JR, Jorgensen CM, Schmidt L, Li HL, Kwan MK, Boyce ST, Wiley HS, Kaplan J, Petersen MJ. Genetically modified skin to treat disease: potential and limitations. J Invest Dermatol. 1994;103:76S–84.
Kupper TS. The activated keratinocyte: a model for inducible cytokine production by none-bone marrow-derived cells in cutaneous inflammatory and immune responses. J Invest Dermatol. 1990;94:146S–50.
Levy L, Broad S, Diekmann D, Evans RD, Watt FM. Beta 1 integrins regulate keratinocyte adhesion and differentiation. Mol Biol Cell. 2000;11:453–66.
Malaviya R, Morrisson AR, Pentland AP. Histamine in human epidermal cells is induced by ultraviolet light injury. J Invest Dermatol. 1996;106:785–9.
Martinez A, Elsasser TH, Muro-Cacho C, Moody TW, Miller MJ, Macri CJ, Cuttitta F. Expression of adrenomedullin and its receptor in normal and malignant human skin: a potential pluripotent role in the integument. Endocrinology. 1997;138:5597–604.
Maruyama K, Zhang JZ, Nihei Y, Ono I, Kaneko F. Regulatory effects of gamma interferon on IL-6 and IL-8 secretion by cultured human keratinocytes and dermal fibroblasts. J Dermatol. 1995;22:901–6.
Mazereeuw Hautier J, Redoules D, Tarroux R, Charveron M, Salles JP, Simon MF, Cerutti I, Assalit MF, Gall Y, Bonafe JL, Chap H. Identification of pancreatic type I secreted phospholipase A2 in human epidermis and its determination by tape striping. Br J Dermatol. 2000;142:424–31.
Michel M, Torok N, Godbout MJ, Luissier M, Gaudreau P, Royal A, Germain L. Keratin 19 as a biochemical marker of skin stem cells in vivo and in vitro: keratin 19 expressing cells are differentially localized in function of anatomic sites, and their number varies with donor age and culture stage. J Cell Sci. 1996;109:1017–28.
Nathan C, Sporn M. Cytokines in context. J Cell Biol. 1991;113:981–6.
Nizet V, Ohtake T, Lauth X, Trowbridge J, Rudisill J, Dorschner RA, Pestonjamasp V, Piraino J, Huttner K, Gallo RL. Innate antimicrobial peptide protects the skin from invasive bacterial infection. Nature. 2001;414:454–7.
Oda Y, Imanzahrai A, Kwong A, Komuves L, Elias PM, Largman C, Mauro T. Epithelial sodium channels are upregulated during epidermal differentiation. J Invest Dermatol. 1999;113:796–801.
Ong PY, Ohtake T, Brandt C, Strickland I, Boguniewicz M, Ganz T, Gallo RL, Leung DYM. Endogenous antimicrobial peptides and skin infections in atopic dermatitis. N Engl J Med. 2002;347:1151–60.
Reinartz J, Bechtel MJ, Kramer MD. Tumor necrosis factor alpha induced apoptosis in a human keratinocyte cell line (HaCat) is counteracted by transforming growth factor alpha. Exp Cell Res. 1996;228:334–40.
Rys-Sikora KE, Konger RL, Schoggins JW, Malaviya R, Pentland AP. Coordinate expression of secretory phospholipase A(2) and cyclooxygenase-2 in activated human keratinocytes. Am J Physiol Cell Physiol. 2000;278:C822–33.
Schauer E, Trautinger F, Köck A, Schwarz A, Bhardwaj R, Simon M, Ansel JC, Schwarz T, Luger TA.

Proopiomelanocortin derived peptides are synthesized and released by human keratinocytes. J Clin Invest. 1994;93:2258–62.

Schröder JM. Cytokine networks in the skin. J Invest Dermatol. 1995;105:20S–4.

Shimizu Y, Sakai M, Umemura Y, Ueda H. Immunohistochemical localization of nitric oxide synthase in normal human skin: expression of endothelial-type and inducible-type nitric oxide synthase in keratinocytes. J Dermatol. 1997;24:80–7.

Stoof TJ, Boorsma DM, Nickoloff BJ. Keratinocyte and immunological cytokines. In: Leigh IM, Lane EB, Watt FM, editors. The keratinocyte handbook. Cambridge: Cambridge University Press; 1994. p. 235–42.

Watt FM, Hogan BLM. Out of Eden: stem cells and their niches. Science. 2000;287:1427–30.

Wiedow O, Harder J, Bartels J, Streit V, Christopher E. Antileukoprotease in human skin: an antibiotic peptide constitutively produced by keratinocytes. Biochem Biophys Res Commun. 1998;248:904–9.

Wysolmerski JJ, Stewart AF. The physiology of parathyroid hormone-related protein: an emerging role as a developmental factor. Annu Rev Physiol. 1998;60:431–60.

Zhu AJ, Watt FM. Beta-catenin signalling modulates proliferative potential of human epidermal keratinocytes independently of intercellular adhesion. Development. 1999;126:2285–98.

Zhu AJ, Haase I, Watt FM. Signaling via beta1 integrins and mitogen-activated protein kinase determines human epidermal stem cell fate in vitro. Proc Natl Acad Sci U S A. 1999;96:6728–33.

Markers of Epidermal Proliferation and Differentiation

37

Patricia Rousselle, Edgar Gentilhomme, and Yves Neveux

Contents

Keywords

Anti 5-bromo-2-deoxyuridine (BrdU) antibody • Cytoplasmic proliferation markers • Epidermis • Cellular differentiation • Cytoplasmic proliferation markers • epidermal differentiation markers • Nuclear proliferation markers • Histidine-rich proteins • Involucrin • Keratins • Ki67 • Nuclear proliferation markers • Dynamic method • Static methods • Profilaggrin • Proliferating cell nuclear antigen (PCNA) • Proliferation indexes

The epidermis is characterized by its capacity to maintain homeostasis through a balanced equilibrium between proliferation and differentiation. It may also respond by a rapid and temporary amplification of cell turnover when a sudden tissue renewal is needed in wounds. Study and control of mechanisms involved in this response are of great interest.

They may be studied in vitro with carefully chosen experimental models (Dover 1994; Prignano et al. 1999) since the culture conditions often modify the homeostasis observed in vivo. Primary keratinocytes provide ideal experimental systems (Dotto 1999), and epidermal growth on dermal equivalents (Sanquer et al. 1990) and reepithelialization of partial thickness wounds (Jansson et al. 1996) have been studied for periods of 7–15 days. The expression of proliferation- and differentiation-specific markers enables to discriminate between epidermal growth and maturation.

P. Rousselle (✉)
Tissue Biology and Therapeutic Engineering Unit, Institute of Protein Biology and Chemistry, UMR 5305 – CNRS, University of Lyon, Lyon, France
e-mail: patricia.rousselle@ibcp.fr

E. Gentilhomme
French Army Health Research Department, La tronche, France
e-mail: edgargentilhomme@crssa.net

Y. Neveux
Livernon, France
e-mail: yves.neveux@free.fr

P. Humbert et al. (eds.), *Agache's Measuring the Skin*,
DOI 10.1007/978-3-319-32383-1_37

1 Epidermal Proliferation

Proliferating keratinocytes display specific morphological characteristics, at both nuclear and cytoplasmic levels.

1.1 Nuclear Proliferation Markers

Proliferation-specific markers are numerous and the most frequently used will be listed below. Static data such as relative length of cell cycle phases, or dynamic measurements such as cell cycle kinetics, can be obtained with these markers (Figs. 1, 2, 3, 4, and 5).

1.1.1 Static Methods

Methods with Prior Incubation

While nucleotides like adenine and guanine are incorporated into both DNA and RNA, thymidine is incorporated only in DNA. Incubation of a tissue or a biopsy with radiolabeled thymidine diluted in culture medium highlights the cellular fraction engaged in DNA synthesis during the incubation period. The development of anti 5-bromo-2-deoxyuridine (BrdU) antibody has provided an excellent thymidine analogue for a similar use. If both tritiated thymidine and BrdU are specifically incorporated during the cellular S-phase, the use of BrdU is easier to perform. However, experimental conditions influence the cellular responses to this labeling. The use of occlusive dressing enhances in vivo cutaneous penetration of BrdU. Labeling may be increased when endogenous synthesis of thymidine monophosphate is previously blocked (Wolff and Gnas 1989). Variable marker's distribution to the central cells of the biopsy, a possible toxicity induced by a prolonged incubation (Dover 1994), and different rates of incorporation into DNA (Hume and Saffhill 1986) must be also considered during the experimentation (Tables 1, 2, 3, 4, and 5).

Methods Without Prior Incubation

Unlike the precedent methods, these markers can be analyzed directly without pretreatment of samples. The proliferating cell nuclear antigen (PCNA) is a 36 kDa protein, cofactor of the DNA polymerase-δ necessary to the DNA replication (Celis et al. 1987). Expressed at low level in quiescent cells, PCNA is most abundant in late G1-phase and during the S-phase (Stewart and Dell'Orco 1992). The proportion of PCNA-positive cells exceeds that of tritiated thymidine-positive (Galand and Degraef 1989) or BrdU-positive cells (Jones et al. 1993) because some cells in the G0-phase are also weakly labeled. In a quiescent epidermis, the expression of PCNA is limited to rare cells in the basal layer (Furukawa et al. 1992), while in vitro, its expression is modulated by the culture conditions (Miyagawa et al. 1989). Its expression is enhanced by EGF (Jaskulski et al. 1988) and inhibited by rapamycin (Javier et al. 1997).

Ki67 is a nuclear protein expressed in cycling cells (G1-, S-, G2-, and M-phase) and absent in

Fig. 1 Epidermal biopsy on dermal equivalent. Progressive epithelial outgrowth by synergetic mechanisms of keratinocytes migration and proliferation. Inverted microscopy. Magnification ×100

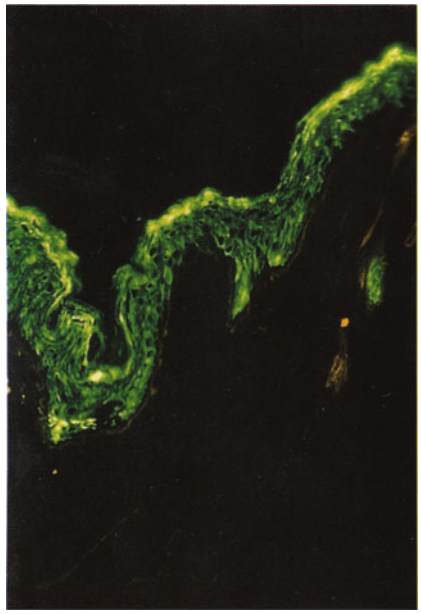

Fig. 2 Epidermal differentiation. In vivo human skin. Filaggrin in upper granular layers. Anti-filaggrin antibody revealed by immunoperoxidase. Magnification ×1000

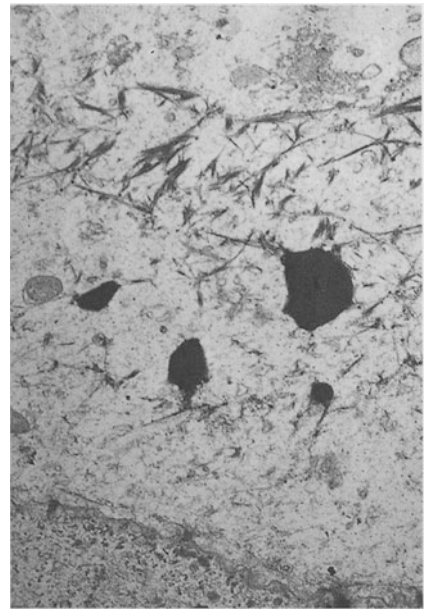

Fig. 3 In vitro epidermal differentiation. Expression of keratohyalin granules in the upper epidermis and profilaggrin in desquamating cells. Antiprofilaggrin antibody revealed by immunofluorescence. Magnification ×200

quiescent cells in G0-phase (Knaggs et al. 1994). Even if the nuclear labeling is restricted to proliferating cells of the basal layer, the index obtained with Ki67 is similar to that given by PCNA and exceeds the value obtained with BrdU. To allow antigen retrieval, labeling of paraffin-embedded tissue slices by immunohistochemistry requires a pretreatment prior to incubation with the antibody (Szekeres and de Giacomoni 1994); however, direct immunostaining is also possible on frozen tissue sections.

Histone genes are tightly coupled to the replicative stages of the cell cycle. The messenger RNAs (mRNAs) encoding these proteins are synthesized during the replication of DNA and are rapidly destabilized at the end of the S-phase of the cycle. Histone mRNAs may be detected by a classical in situ hybridization method. Unlike PCNA or Ki67, labeling with histone mRNAs is strictly similar to the value obtained with BrdU (Smith et al. 1995).

1.1.2 Dynamic Methods

Sequential labeling with two proliferation markers specific for the S-phase (tritiated thymidine and BrdU or BrdU and IodoUdR) enables to discriminate the different populations entering this phase. The measure of the different cellular fractions provides dynamic parameters such as the S-phase duration and total cell cycle times (Hyatt and Beebe 1992; Yanik et al. 1992). By this double-label technique, the determination of the cell cycle times may be correlated with the localization of a cytokine (Miller et al. 1992) or the measurement of the DNA content (Lin and Allison 1993; Van Erp et al. 1996).

1.2 Cytoplasmic Proliferation Markers

The transition from basal cell to corneocyte is a complex process that requires the simultaneous activation and inactivation of a wide variety of proteins and genes. In order for differentiation to produce a normal epidermal surface, these genes must be expressed at the correct time and location. The members of the keratin family are expressed

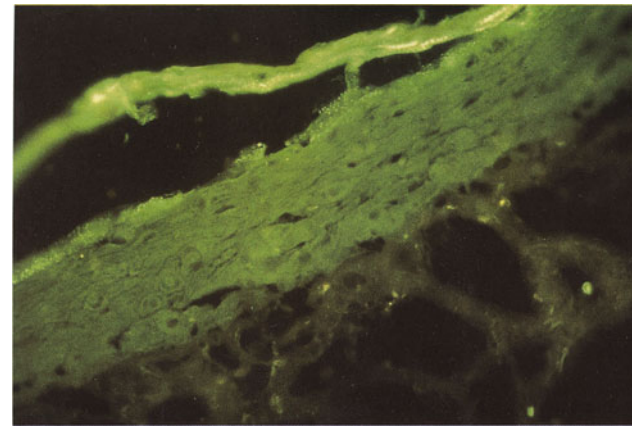

Fig. 4 In vitro epidermal differentiation. Expression of keratohyalin granules in superficial layers. Transmission electronic microscopy. Magnification ×6000

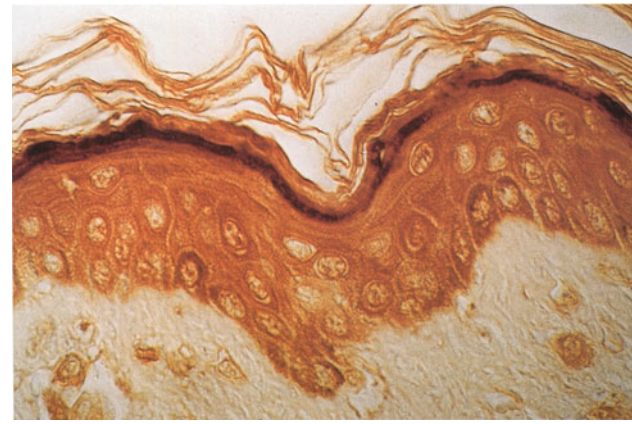

Fig. 5 In vivo epidermal differentiation. Detection of suprabasal cytokeratins by immunofluorescence (antiKL1 antibody). The subepidermal orange line highlights the dermo-epidermal junction. The basal epidermal layer is located in the non-labeled zone between this orange line and the fluorescent of KL1 cytokeratins. Magnification ×100

in a tightly regulated manner. The cytokeratins are a family of over 30 proteins that are assembled to form the intermediate filaments in epithelial cells. Based on sequence homology and expression pattern, the keratins can be divided into acidic and neutral-basic families. Keratins are expressed in pairs to assure the presence of a neutral-basic and acidic partner to permit filament assembly. Some data suggests that, reciprocally, some of these keratins influence cell proliferation and differentiation (Paramio et al. 1999). In quiescent epidermis, basal proliferative keratinocytes express cytokeratins K5 and K14. During hyperproliferative cellular responses in culture or during wound healing, keratinocytes express keratins K6, K16, and K17. Labeling of keratins alone or coupled with the measure of DNA content may be used to characterize epidermal proliferation (Mommers et al. 2000).

2 Cellular Differentiation

Biochemical and morphological modifications are observed during epidermal differentiation, leading to the appearance of specific cellular organelles, used as differentiation markers. The most frequently used are the keratins, the histidine-rich proteins (filaggrin/keratohyalin granules), the transglutaminases, and the cornified envelope precursors such as involucrin, loricrin, and small proline-rich proteins (Lee et al. 1999; Seishima et al. 1999). Numerous antibodies have been developed against these proteins during the recent years, enabling us to evaluate the degree of epidermal maturation.

When they differentiate, keratinocytes switch off keratins K5 and K14 and start K1 and K10 expression (Moll et al. 1982) in suprabasal layers.

Table 1 Proliferation indexes given by different authors. References correspond to authors cited in the text. The type of proliferation index used is specified before each result

Healthy skin	Active psoriasis	Acne	Irritation	Neoplasm	Ref.
BrdU: 5–6 %[a] Histone mRNAs: 5–6 %[a] Ki67: 46 %[b]	–	–	Histone mRNAs: 4 × healthy skin Ki67: 2 × healthy skin	–	Stewart and Dell'Orco (1992)
Ki67[c] Interfollicular skin: 5 % Follicles: 11 %	–	Ki67[c] Interfollicular: 25 % Follicles: 17 %	–	–	Knaggs et al. (1994)
PCNA: Undetectable	PCNA: I: 10 %	–	–	–	Miyagawa et al. (1989)
BrdU[d] Indice: 1,7–2,4 %	BrdU[d] I: 12,6 %	–	–	BrdU[d] I: 8–9,5 %	Van Erp et al. (1996)

PCNA proliferating cell nuclear antigen, *BrdU* bromodeoxyuridine
[a]Labeling limited to the basal layer. Suprabasal epidermis is not labeled
[b]Labeling noted in the basal and the three first suprabasal layers
[a, b]I = number of positive cells/ total number of basal and suprabasal cells X 100 %
[c]I = number of positive cells/total number of basal cells × 100 %
[d]Incubation with BrdU for 1–24 h prior to labeling. Index = fraction of positive cells reported to 1000 cells in the basal layer of healthy skin or in the basal and the two first suprabasal layers of psoriatic skin

Table 2 Compared proliferative indexes between human skin in vivo and in vitro cultured keratinocytes. References correspond to authors cited in the text. The type of proliferation index used is specified before each result

In vivo human skin	In vitro normal human keratinocytes	In vitro transfected keratinocytes	Ref.
PCNA[a] Rare basal keratinocytes Ki67[a] Nearly all the basal cells	PCNA[a] I: 15–30 % Ki67[a] I: 40–60 %	–	Furukawa et al. (1992)
PCNA: Undetectable	PCNA: 0,05 mM Ca++: 20–30 % 1,1 mM Ca++: 10 %	PCNA: SV40: 40 %	Miyagawa et al. (1989)

PCNA proliferating cell nuclear antigen
[a]I = fraction of positive cells **reported** to 500 or more cells counted at 400 magnification, with three separate counts for each determination

Keratins K2, K11, and K9 are also present in cornified epidermis.

Histidine-rich proteins aggregate with keratin filaments in cornified layers and represent an important source of amino acids necessary to the stratum corneum hydric balance. Profilaggrin, the precursor of filaggrin, is expressed in some populations of keratohyalin granules of suprabasal layers and is converted to filaggrin, which packages the keratin filaments into fibrils. Profilaggrin, filaggrin, and keratohyalin granules are indistinctly revealed by the same immunological labeling. Keratohyalin granules and filaggrin represent excellent markers of terminal differentiation, since their expression is noted from the granular layer (Bernerd and Asselineau 1997; Gerritsen et al. 1997) and is absent in nonkeratinized epidermis. Their expression in vitro is considered as a proof of a differentiated culture (Jansson et al. 1996).

Table 3 Published values of different cell cycle parameters for in vivo human skin (normal or diseased skin) and ex vivo cultures

	Ts	Tm	Tc	Tt	[ADN]	Ref.
Healthy skin	5,3 à 10,3	1,5	50 à 282	154 à 641	–	Dover (1994)
Psoriasis	6 à 16	1	163 à 326	308 à 457	–	Dover (1994)
Organ culture	11,5	1,5	59	–	–	Dover (1994)
Mammary carcinoma (MCa-11)	–	–	–	–	10–12 pg (a) 15–18 pg (b) 21–24 pg (c)	Lin and Allison (1993)

Ts, DNA synthesis time (corresponding to S-phase duration); Tm: mitosis time; Tc, cycling time; Tt, transit time for a keratinocyte to migrate from the basal to the horny layers. Ts, Tm, Tc, and Tt values are given in hours
[DNA]: DNA content at the middle of S-phase. DNA content is expressed in picograms. (a) Mean DNA content in G0-/G1-phase cells. (b) Mean DNA content in middle S-phase cells. (c) Mean DNA content in G2-/M-phase cells
References correspond to authors cited in the text. Each value is the highest given by the authors

Table 4 Values of keratinocyte cell cycle parameters (Van Erp et al. 1996). Cell suspensions are studied by flow cytometry. Ts, S-phase duration; TG1, G1-phase duration; TG2/M, G2-/M-phase duration; Tc, cell cycle duration. Durations are given in hours

% G0 cells	% cycle cells	% S-phase cells	% suprabasal cells	Ds	D(G1)	D(G2/M)	Dc
30 %	10 %	3,5 %	59,6 % +/– 4	9,7 h	7,6 h	11 h	28 h

Involucrin and loricrin are envelope precursor proteins that are expressed in the epidermal suprabasal layers. These proteins are cross-linked to form the cornified envelope by the enzyme transglutaminase which catalyzes the formation of inter-protein ε-(γ-glutamyl)lysine bonds. These transglutaminases are membrane-associated proteins, expressed in upper spinous and granular layers of the epidermis (Kim et al. 1995). Involucrin, rich in glutamine content, is the major cornified envelope precursor protein. Increasing calcium concentration stimulates the promoter activity of the gene encoding for involucrin (Ng et al. 2000; Tu et al. 1999). The expression of involucrin begins in high spinous and granular layers of the epidermis, distant from the proliferative layers. During wound healing, this expression may be found in all the suprabasal layers (Jansson et al. 1996; Mansbridge and Knapp 1987). In cellular culture or in psoriasis, involucrin is also expressed by S-phase keratinocytes (Dover and Watt 1987). Due to its expression in nonkeratinized corneal epithelium, involucrin is considered as an intermediate differentiation marker. Small proline-rich (SPR) proteins are synthesized sequentially after involucrin during differentiation (Ishida et al. 1997). Other cornified envelope precursors may be used, cornifin expressed in spinous or granular layers and loricrin in corneocytes (Bernerd and Asselineau 1997).

Epidermal homeostasis is maintained through a fine balance between cellular proliferation and differentiation. In normal epidermis, many factors (Schoop et al. 1999; Tu et al. 1999) control this cellular transition occurring in specific compartments. These signals include the activation of an extracellular Ca^{2+} receptor mechanism, the increase in cell-cell adhesions, and the detachment from the substratum. During wound healing, under the action of exogenous factors, this control may be less strictly determined, inducing defects in the balance between proliferation and differentiation. Specific markers allow to study each event, of which dysfunction may induce a pathological status.

Table 5 Main epidermal proliferation and differentiation markers. Specific localization and meanings

Marker	Localization	Signification	Technical conditions
BrdU	Basal layer First suprabasal layer Nuclear labeling	Proliferative cell S-Phase	C, Pa, Pn[a]
Histone mRNAs	Basal layer First suprabasal layer Cytoplasmic labeling	Proliferative cell S-Phase	Pa[a]
PCNA	Basal layer Nuclear labeling	Proliferative cell S- and G1-phase	Pa, Pn, IB, Cy[a]
Ki67	Basal layer First three suprabasal layers	Cycling cell G1-, S-, G2-, M-phase	C, Pa, IB, Ag, Cy[a]
Cytokeratins K6, K16, K17.	Cytoplasmic labeling	Cellular proliferation (fast "turnover")	C[a]
Cytokeratins K5, K14	Basal layer Cytoplasmic labeling	Non-differentiated cells	C, Pa, Ag[a]
Cytokeratin K19	Basal layers	Stem cell	C, Pa, Ag[a]
Cytokeratins K1, K10, K2, K11	Suprabasal layers Cytoplasmic labeling	Epidermal differentiation	C[a]
Involucrin	Upper spinous layers Granular layer Cytoplasmic labeling	Intermediate differentiation	C, Pa[a]
Cornifin	Spinous layer Granular layer	Epidermal differentiation	C
Transglutaminases	Granular layers Membrane labeling	Epidermal differentiation	C, IB[a]
Profilaggrin (KHG)	Granular layer and upper Cytoplasmic labeling	Terminal differentiation	C, Pa[a]
Loricrin	Horny layer	Terminal differentiation	C

[a]Commercially available to this day. Possible use of these antibodies in C, cryosections; P, paraffin; Cy, cytometry; IB, immunoblot; Ag, treatment prior to label (heating, digestion, unmasking solution, etc.); NP, nuclear permeabilization

Annex

There are many suppliers of antibodies, and the number of available antibodies (immunohistology, cytometry, etc.) regularly increases. Some suppliers seek worldwide for a specific product if wanted by the customer.

Ask for the technical bulletin of each product. This indicates the recommended method (histology, electrophoresis, cytometry, etc.) and conditions of use (fixation, congelation, treatment, etc.). Dilutions are just indicative and must be evaluated for each tissue and protocol.

Immunohistological studies are performed according to standard methodologies, with or without amplification or treatment. Many kits are actually available.

Some addresses of suppliers or distributors are given below. This list is far from being complete.

Biomedical Technologies, Inc., 378 Page Street. Stoughton. MA 02072 USA

Phone: 617-344-9942

Biosource International (Tagoimmunologicals°) 820 Flynn Road Camarillo CA 93012 USA

Phone: 1-805-987-0086

Dako Corporation. 6392 Via Real. Carpinteria CA 93013 USA

Phone: 1-805-566-6655

Pierce P.O Box 117. Rockford Illinois 61105 USA

Phone: 1-800-842-5007

Roche Diagnostics Corporation. 9115 Hague Road. P.O Box 50414. Indianapolis IN 46250-0414 USA

Phone: 800-428-5433

Sigma P.O Box 14508 St Louis Missouri 63178 USA

Phone: 800-325-3010

Southern Biotechnology Associates, Inc., P.O Box 26221. Birmingham. Alabama 35260 USA

Phone: 205-945-1774

Zymed Laboratories, Inc., 458 Carlton Court. South San Francisco CA 940 80–2012 USA

Phone: 800- 874–4494

References

Bernerd F, Asselineau D. Successive alteration and recovery of epidermal differentiation and morphogenesis after specific UVB-damages in skin reconstructed in vitro. Dev Biol. 1997;183:123–38.

Celis JE, Madsen P, Celis A, Nielsen HV, Gesser B. Cyclin (PCNA, auxiliary protein of DNA polymerase delta) is a central component of the pathway(s) leading to DNA replication and cell division. FEBS Lett. 1987;220:1–7.

Dotto GP. Signal transduction pathways controlling the switch between keratinocyte growth and differentiation. Crit Rev Oral Biol Med. 1999;10:442–57.

Dover R. Cell kinetics of keratinocytes. In: Leigh I, Lane B, Watt F, editors. The keratinocyte handbook. Cambridge: Cambridge University Press; 1994. p. 203–34.

Dover R, Watt FM. Measurement of the rate of epidermal terminal differentiation: expression of involucrin by S-phase keratinocytes in culture and in psoriatic plaques. J Invest Dermatol. 1987;89:349–52.

Furukawa F, Imamura S, Fujita M, Yoshitake K, Brown WR, Norris DA. Immunohistochemical localization of proliferating cell nuclear antigen/cyclin in human skin. Arch Dermatol Res. 1992;284:86–91.

Galand P, Degraef C. Cyclin/PCNA immunostaining as an alternative to tritiated thymidine pulse labeling for marking S phase cells in paraffin sections from animal and human tissues. Cell Tissue Kinet. 1989;22:383–92.

Gerritsen MJ, Elbers ME, de Jong EM, van de Kerkhof PC. Recruitment of cycling epidermal cells and expression of filaggrin, involucrin and tenascin in the margin of the active psoriatic plaque, in the uninvolved skin of psoriatic patients and in the normal healthy skin. J Dermatol Sci. 1997;14:179–88.

Hume WJ, Saffhill R. Iodo- and bromodeoxyuridine are excised at different rates from DNA of mouse tongue keratinocytes in vitro. Chem Biol Interact. 1986;60:227–32.

Hyatt GA, Beebe DC. Use of a double-label method to detect rapid changes in the rate of cell proliferation. J Histochem Cytochem. 1992;40:619–27.

Ishida YA, Kartasova T, Matsuo S, Kuroki T, Iizuka H. Involucrin and SPRR are synthesized sequentially in differentiating cultured epidermal cells. J Invest Dermatol. 1997;108:12–6.

Jansson K, Kratz G, Haegerstrand A. Characterization of a new in vitro model for studies of reepithelialization in human partial thickness wounds. In Vitro Cell Dev Biol Animal. 1996;32:534–40.

Jaskulski D, Gatti C, Travali S, Calabretta B, Baserga R. Regulation of the proliferating cell nuclear antigen cyclin and thymidine kinase mRNA levels by growth factors. J Biol Chem. 1988;263:10175–9.

Javier AF, Bata-Csorgo Z, Ellis CN, Kang S, Voorhees JJ, Cooper KD. Rapamycin (sirolimus) inhibits proliferating cell nuclear antigen expression and blocks cell cycle in the G1 phase in human keratinocyte stem cells. J Clin Invest. 1997;99:2094–9.

Jones HB, Clarke NAB, Barrass NC. Phenobarbital-induced hepatocellular proliferation: anti-bromodeoxyuridine and anti-proliferating cell nuclear antigen immunocytochemistry. J Histochem Cytochem. 1993;41:21–7.

Kim SY, Chung SI, Yoneda K, Steinert PM. Expression of transglutaminase 1 in human epidermis. J Invest Dermatol. 1995;104:211–7.

Knaggs HE, Holland DB, Morris C, Wood EJ, Cunliffe WJ. Quantification of cellular proliferation in acne using the monoclonal antibody Ki67. J Invest Dermatol. 1994;102:89–92.

Lee SC, Lee JB, Kook JP, Seo JJ, Nam KI, Park SS, Kim YP. Expression of differentiation markers during fetal skin development in humans: immunohistochemical studies on the precursor proteins forming the cornified envelope. J Invest Dermatol. 1999;112:882–6.

Lin P, Allison DC. Measurement of DNA content and of tritiated thymidine and bromodeoxyuridine incorporation by the same cells. J Histochem Cytochem. 1993;41:1435–6.

Mansbridge JN, Knapp AM. Changes in keratinocyte maturation during wound healing. J Invest Dermatol. 1987;89:253–63.

Miller MA, Bokhari SAJ, Qadir K, Raza A. Simultaneous assessment of TGFB and cell cycle kinetics using IUdR/BrdU infusions in human neoplasms from plastic-embedded tissue. J Histochem Cytochem. 1992;40:427–30.

Miyagawa S, Okada N, Takasaki Y, Iida T, Kitano Y, Yoshikawa K, Sakamoto K, Steinberg ML. Expression of proliferating cell nuclear antigen/cyclin in human keratinocytes. J Invest Dermatol. 1989;93:678–81.

Moll R, Franke WW, Schiller DL, Geiger B, Krepler R. The catalog of human cytokeratins: patterns of expression in normal epithelia, tumors and cultured cells. Cell. 1982;31:11–24.

Mommers JM, Goossen JW, van De Kerkhof PC, van Erp. Novel functional multiparameter flow cytometric assay to characterize proliferation in skin. Cytometry. 2000; 42:43–9.

Ng DC, Shafaee S, Lee D, Bikle DD. Requirement of an AP-1 site in the calcium response region of the involucrin promoter. J Biol Chem. 2000;275:24080–8.

Paramio JM, Casanova ML, Segrelles C, Mittnacht S, Lane EB, Jorcano JL. Modulation of cell proliferation by cytokeratins K10 and K16. Mol Cell Biol. 1999;19:3086–94.

Prignano F, Domenici L, Gerlini G, Pimpinelli N, Romagnoli P. Human keratinocytes cultured without a feeder layer undergo progressive loss of differentiation markers. Histol Histopathol. 1999;14:797–803.

Sanquer S, Coulomb B, Lebreton C, Dubertret L. Human dermal fibroblasts modulate the effects of retinoids on epidermal growth. J Invest Dermatol. 1990;95:700–4.

Schoop VM, Mirancea N, Fusenig NE. Epidermal organization and differentiation of HaCat keratinocytes in organotypic coculture with human dermal fibroblasts. J Invest Dermatol. 1999;112:343–53.

Seishima M, Nojiri M, Esaki C, Yoneda K, Eto Y, Kiajima Y. Activin A induces terminal differentiation of cultured human keratinocytes. J Invest Dermatol. 1999;112:432–6.

Smith MD, Healy E, Thompson V, Morley A, Rees JL. Use of in situ detection of histone mRNA in the assessment of epidermal proliferation: comparison with the Ki67 antigen and BrdU incorporation. Br J Dermatol. 1995;132:359–66.

Stewart CA, Dell'Orco RT. Expression of proliferating cell nuclear antigen during the cell cycle of human diploid fibroblasts. In Vitro Cell Dev Biol. 1992;28A:211–4.

Szekeres G, de Giacomoni P. Ki67 and p53 expression in cutaneous Bowen's disease: an immunohistochemical study of fixed-embedded tissue sections. Acta Derm Venereol. 1994;74:95–7.

Tu CL, Oda Y, Bikle DD. Effects of a calcium receptor activator on the cellular response to calcium in human keratinocytes. J Invest Dermatol. 1999;113:340–5.

Van Erp PE, Boezeman JB, Brons PP. Cell cycle kinetics in normal human skin by in vivo administration of iododeoxyuridine and application of a differentiation marker – implications for cell cycle kinetics in psoriatic skin. Anal Cell Pathol. 1996;11:43–54.

Wolff HH, Gnas W. Immunocytochemical detection of in vitro incorporated 5-bromodeoxyuridine in paraffin section of human skin. Arch Dermatol Res. 1989;281:209–12.

Yanik G, Youssuf N, Miller MA, Swerdlow SH, Lampkin B, Raza A. In vivo determination of cell cycle kinetics of non-hodgkin's lymphomas using iododeoxyuridine and bromodeoxyuridine. J Histochem Cytochem. 1992;40:723–8.

In Vivo Confocal Microscopy in Clinical Dermatology

38

Caterina Longo, Giovanni Pellacani, and Salvador Gonzalez

Contents

Keywords

Confocal microscopy • Melanoma • Nevi • Basal cell carcinoma • Inflammatory skin disease

Abbreviations

AK	Actinic keratosis
BCC	Basal cell carcinoma
DEJ	Dermo-epidermal junction
MM	Melanoma
RCM	Reflectance confocal microscopy
SCC	Squamous cell carcinoma
SSM	Superficial spreading melanomas

1 Introduction

Reflectance confocal microscopy (RCM) is a new noninvasive tool that enables the analysis of skin morphology at nearly histologic resolution (Rajadhyaksha et al. 1995, 1999; Gonzalez et al. 2001). Among the plethora of noninvasive tools applied in the clinical field for skin cancer diagnosis, RCM has emerged as a unique method for its capability to visualize the skin tissue with a resolution that is comparable to conventional histopathology. It allows a horizontal scanning of the imaged tissue with the great advantage of exploring a larger field of view compared to vertical sectioning obtained with conventional histopathology. Additionally, the horizontal plane offers a perfect overlap with clinical and dermoscopic image, and this is crucial to obtain a correct

C. Longo (✉)
Dermatology and Skin cancer Unit, Arcispedale Santa Maria Nuova-IRCCS, Reggio Emilia, Italy
e-mail: longo.caterina@gmail.com

G. Pellacani
Dermatology Unit, University of Modena and Reggio Emilia, Modena, Italy

S. Gonzalez
Dermatology Service, Memorial Sloan-Kettering Cancer Center, New York, NY, USA

Medicine Department, Alcalá University, Madrid, Spain

P. Humbert et al. (eds.), *Agache's Measuring the Skin*, DOI 10.1007/978-3-319-32383-1_38

diagnosis rendered by putting together all lesion's aspects. In this chapter we aim to report the main confocal applications in clinical practice.

1.1 Instruments

Currently, there are basically two types of confocal microscopes commercially available, which are fundamentally distinct in their approach: one is a full-scale microscope constituted by a large scanning head and the other is a handheld device.

The former confocal microscope (VivaScope® 1500, Lucid Inc., Rochester NY, USA) contains a probe (the head of the microscope) that is attached to the skin by using a disposable plastic window that is in turn taped to a metal ring. A confocal microscope consists of a point source of light, condenser, objective lenses, and a point detector (Rajadhyaksha et al. 1995, 1999). The pinhole collects light emanating only from the in-focus plane. The mechanism of bright contrast in reflectance confocal microscopy is backscattering. In gray-scale confocal images, structures that appear bright (white) have components with high refractive index compared with their surroundings and are similar in size to the wavelength of light. Backscattering is primarily governed by the structures' refractive index compared to surrounding medium. Highly reflective skin components include melanin, collagen, and keratin. The confocal scanning produces high-resolution black and white horizontal images (0.5 × 0.5 mm) with a lateral resolution of 1.0 μm and axial resolution of 3–5 μm. A sequence of full-resolution individual images at a given depth is acquired and "stitched" together to create a mosaic ranging in size from 2 × 2 to 8 × 8 mm. A vertical VivaStack® can be imaged. It consists of single high-resolution images acquired from the top skin surface up to 200 μm, corresponding to the papillary dermis, to obtain a sort of "optic biopsy."

The handheld RCM has been recently introduced on the market (VivaScope® 3000). This version is a smaller, flexible device that is quite useful in difficult to access areas (skin folds, ears). Unlike the 1500 version, it has a manual control for laser power on the probe, imaging depth, and capture, but it does not allow scanning of a large field of view needed, for example, to analyze the architecture of tumors. However, it is a promising tool that found its application in surgical pre-mapping or when multiple site imaging is requested.

2 Confocal Criteria for Melanocytic Lesions

2.1 Melanocytic Tumors

The major issue in skin oncology is to detect all tumors while reducing the number of unnecessary biopsies of benign lesions. To accomplish this goal, several instruments are being applied in clinical practice although the current gold standard relies on the combination of clinical inspection and dermoscopy. Dermoscopy is a noninvasive and cost-effective technique that has proven to be an essential tool in skin oncology (Argenziano et al. 2006, 2012) and general dermatology (Zalaudek et al. 2006) since it allows to check all lesions in a given patients in few minutes. RCM is currently considered a second-level examination in clinical practice with specific application in challenging cases or in special instances. In addition to dermoscopy, RCM is capable of delivering single-cell resolution in a few minutes at the patient's bedside (Pellacani et al. 2005a, 2007; Guitera et al. 2010).

2.2 Melanocytic Tumors

2.2.1 Nevi

Different patterns of melanocytic proliferation can be easily and reliably detected upon RCM (Pellacani et al. 2009a). Junctional nevi show a predominance of single-cell proliferation at DEJ that results in the presence of single small bright polygonal cells outlining the dermal papillae, generating the so-called ringed pattern on RCM (Pellacani et al. 2005b; Fig. 1). Some junctional nevi also display few nests located at the tip of the cristae, and this aspect shows up as a "meshwork" pattern on RCM that is made by the junctional

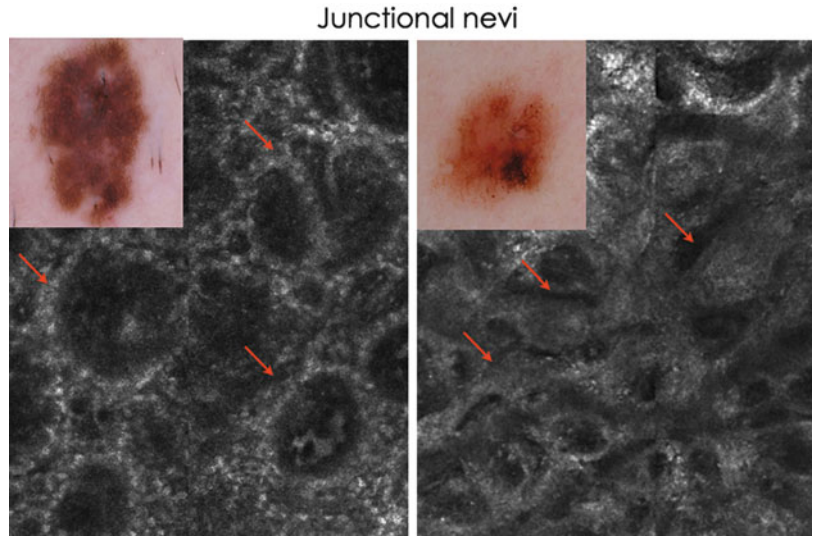

Fig. 1 Junctional nevi: they can show a ringed pattern showing bright rings surrounding hyporefractive dermal papillae or a meshwork pattern due to the presence of enlarging junctional nests (*arrows*)

enlargement between the papillae (Fig. 2). In these lesions, the presence of cytologic atypia is uncommon. Intradermal nevi reveal the presence of the so-called "clod" pattern where several nests fulfill completely the dermal compartment. Nests into the dermis can show up as compact dense or as "dense&sparse" nests (Pellacani et al. 2005c, d) where the aggregates are large and made by large roundish cells outlined by epidermal strands (Fig. 3).

Moreover, a combination of meshwork pattern + ringed or clod + meshwork + ringed can be found (Fig. 4). Usually the presence of clod pattern is apparent in the center of the lesion corresponding to the clinical palpable area and to the presence of variable sized dermal nests.

RCM is particularly useful in discriminating these lesions from melanoma since dermoscopy can be not enough specific, thus leading to the overlooking of these nevi.

This nevus type with combination of more than one RCM pattern is comprised also of the so-called atypical or dysplastic nevi. These nevi represent a puzzling picture that is shared by both RCM and histopathology. Upon RCM, it is possible to detect some morphologic aspects (Pellacani et al. 2012) such as bridging of the nests or the presence of atypical cells, but it is not always feasible to draw a line between a severe dysplastic nevus and an incipient melanoma. This challenge relies on the clinician's ability to "read" the confocal image or on his or her belief in the existence of a precursor lesion. The same scenario is present also in dermatopathology and accounts for the low interobserver agreement found when analyzing these kinds of pigmented lesions (Shoo et al. 2010; Weyers 2012).

Spitz/Reed nevi are a family of lesions that vary in terms of clinical-dermoscopic aspect, histologic features, and biologic attitudes. Confocal microscopy allows the analysis of the superficial dermis, and, thus, the exploration of the deeper part is not possible, hampering the evaluation of some relevant aspects such as maturation (Pellacani et al. 2004, 2009b).

Although the confocal features of Spitz nevi are partially characteristic, they remain in most cases, indistinguishable from melanoma. A good correlation was found for some histopathologic aspects and RCM features (Fig. 4), some of which are considered characteristic of Spitz nevi, such as sharp lateral demarcation and the presence of spindled cells. Other correlates that are not very specific include pagetoid infiltration, junctional and dermal nests, parakeratosis, trans-epidermal melanin elimination, and inflammatory infiltrate rich in melanophages. The frequent presence of features suggestive of malignancy in Spitz nevi, such as pagetoid and atypical cells, non-edged papillae, and dishomogeneous nests, and the

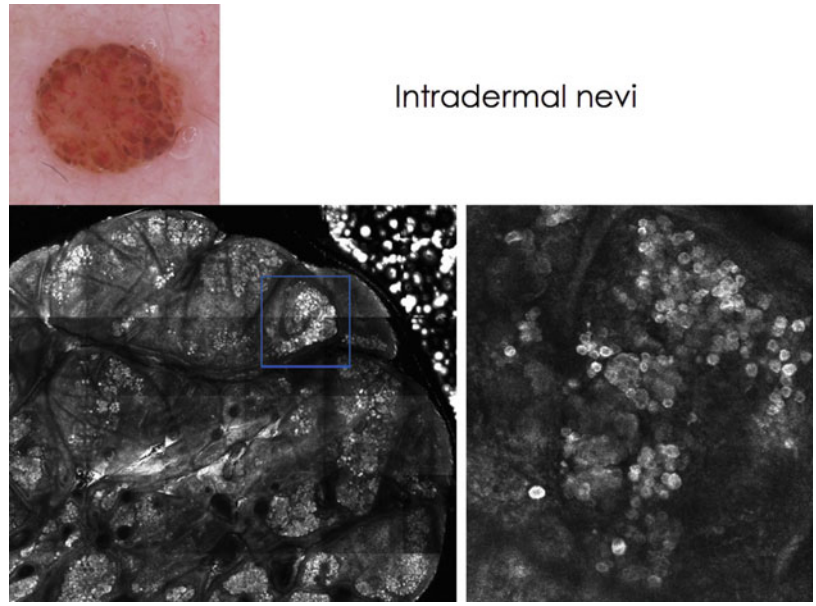

Fig. 2 Intradermal nevi are characterized by the presence of an overall clod pattern constituted by dense and sparse nests

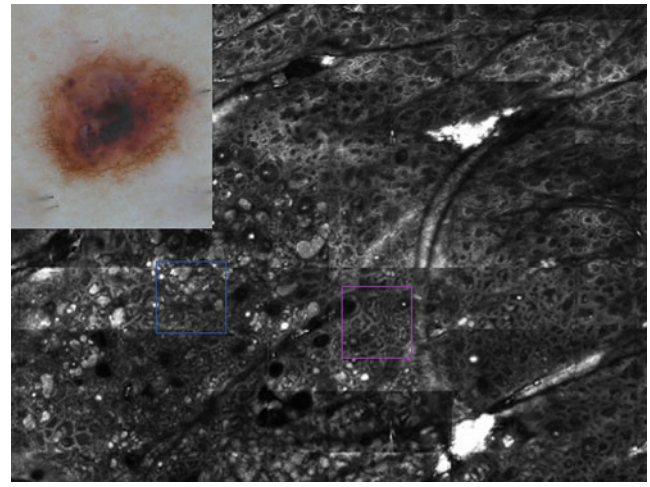

Fig. 3 Nevus showing a complex pattern with clod pattern in the center of the lesion (*blue square*) and ringed ones at the periphery (*purple square*)

impossibility to explore the deeper parts of a given lesion hamper a reliable diagnosis with RCM.

Blue nevi appear as a consequence of dermal proliferation of melanocytes. Since the RCM allows the visualization only of the upper dermis, these nevi do not represent the best candidate for confocal imaging. However, a few case reports describe the presence of spindled/dendritic melanocytes as a confocal clue that may be useful for the diagnosis of blue nevi (Puig et al. 2012).

2.2.2 Melanoma

Currently, melanoma (MM) is thought to be not a single entity but a family of diseases that includes distinct subtypes typified by peculiar morphologic and biologic aspects (Langley et al. 2001; Zalaudek et al. 2008; Segura et al. 2008; Longo et al. 2011). RCM diagnosis is based on major and minor criteria that have been extensively identified and tested for diagnostic accuracy (Pellacani et al. 2005a; Segura et al. 2009). To sum up, the most relevant criteria include the presence of

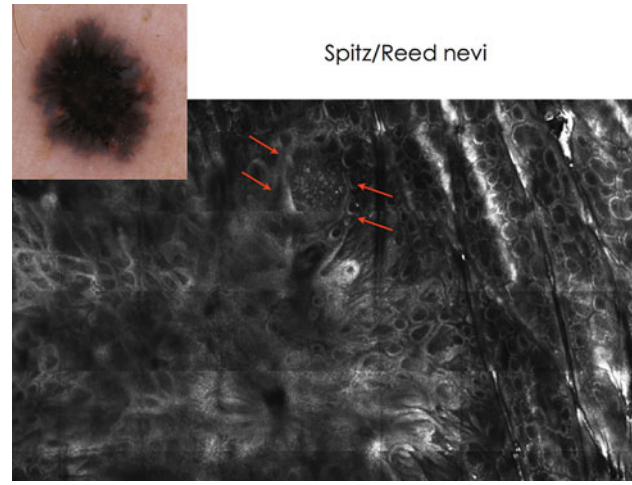

Fig. 4 A typical Spitz/Reed nevus showing a sharp lateral demarcation with large peripheral nests (*arrows*)

pagetoid spread, cytologic atypia at the DEJ, nonspecific architecture (non-edged papillae) (Fig. 5), melanocytes infiltrating dermal papillae, and atypical nesting including several nest type in particular sheetlike structures and cerebriform nests (Fig. 6). Pagetoid spread is one of the most striking criteria (Pellacani et al. 2005e; Longo et al. 2007), and it refers to the presence of melanocytes, round or dendritic shaped, arranged as single cells or small nests, within the epidermis. The presence of cytologic atypia is defined by the occurrence of atypical melanocytes at the DEJ. When evaluating the architecture, MMs typically show the absence of either a "regular" ringed clods or meshwork pattern as usually seen in nevi. Instead, they display an obvious interruption of the architecture with the onset of the so-called non-edged papillae (Pellacani et al. 2005b) when the contour of the papillae is not readily detectable, and it is often associated to the presence of atypical cells. In MMs, the junctional and dermal nesting is usually typified by the presence of atypical melanocytes and different degree of discohesion within the nests (dense&sparse nests and sheetlike structures).

2.2.3 Melanoma Subtypes

In superficial spreading melanomas (SSM), pagetoid spread is a hallmark, and it is characterized by the presence of variably shaped bright melanocytes with focal or widespread distribution. Pagetoid spread is also commonly observed in lentigo maligna type (Tannous et al. 2002; Guitera et al. 2010), especially around the hair follicles. Conversely, pagetoid cells are quite rare in "pure" nodular melanoma, whereas ulceration is a common finding at the epidermal level (Segura et al. 2008).

RCM highlights different shapes of melanocytes scattered throughout the epidermis at various levels in melanoma. Pagetoid cells usually have a round shape with bright granular cytoplasm and hyporefractive nucleus but can display a dendritic shape with a barely visible body and variably long branching terminal structures. A clear-cut distinction between dendritic-shaped melanocytes and Langerhans cells has not yet been established (Hashemi et al. 2012).

In MMs, especially in superficial spreading and lentigo maligna, the DEJ is characterized by ringed and/or meshwork architecture with large and bright pleomorphic ("atypical") cells in early MMs (Pellacani et al. 2005a). The cells can show the tendency to form nests that can still be compact or can be loosely arranged, depending on tumor progression. In early lesions it is a common finding to observe alteration or abrupt interruption of the normal DEJ architecture due to flattening of rete ridges resulting in irregularly shaped and not well-defined papillae (non-edged papillae) (Pellacani et al. 2005b) or disappearance of dermal papillae substituted by strands of atypical cells. In advanced stage of SSM, the massive tumor proliferation occupies the entire junction

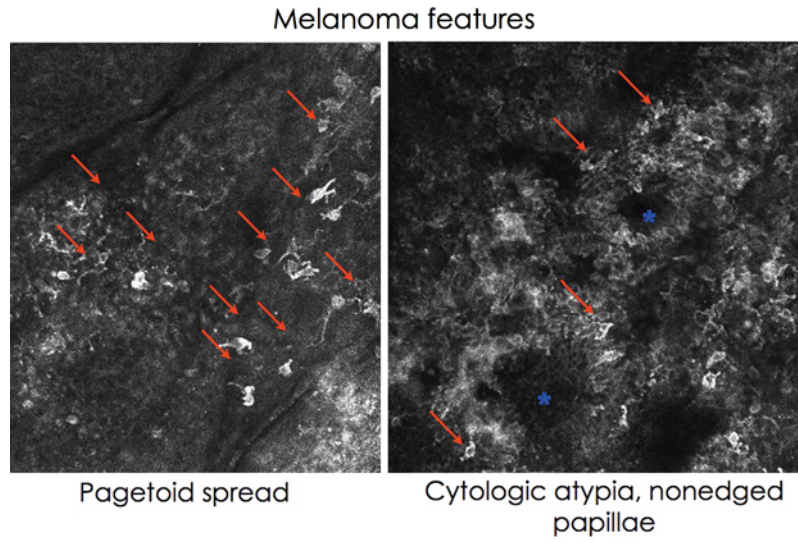

Fig. 5 Confocal criteria for melanoma diagnosis: large pagetoid cells with branching structures (*arrows*) and cytologic atypia typified by the presence of atypical melanocytes (*arrows*) outlining non-edged papillae

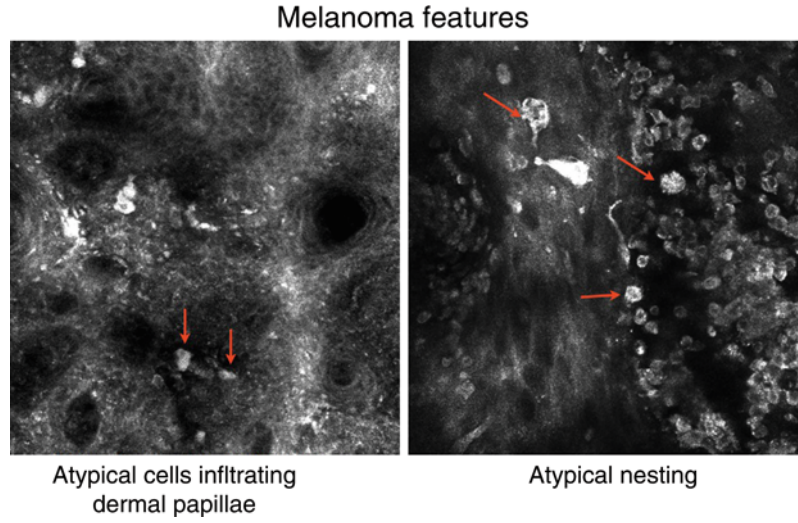

Fig. 6 Confocal criteria for melanoma diagnosis: atypical melanocytes infiltrating non-edged dermal papilla (*arrows*) and atypical nesting with loosely aggregates of large and bizarre-shaped melanocytes (*arrows*)

and can push up into the epidermal layers as loose aggregates of bright, large, and pleomorphic melanocytes. In nodular melanomas, RCM shows the presence of so-called "cerebriform" nests (Pellacani et al. 2005c, d) that consist of small and hyporefractive cells forming a large tumor mass separated by dark thin fissures and bright collagen septae.

Lesions with regression represent an important indication for RCM. When we deal with lesions that are exclusively characterized by bluish to grayish granules, the differential diagnosis includes lichenoid keratosis or a regressive melanoma. RCM is a powerful tool since it permits to discriminate between the former, showing only a florid inflammatory infiltrate, and the latter constituted by atypical melanocytes.

3 Malignant Non-melanoma Skin Tumors

Non-melanocytic tumors include basal cell carcinoma (BCC), actinic keratosis (AK), and squamous cell carcinoma (SCC), just to include the most common tumors.

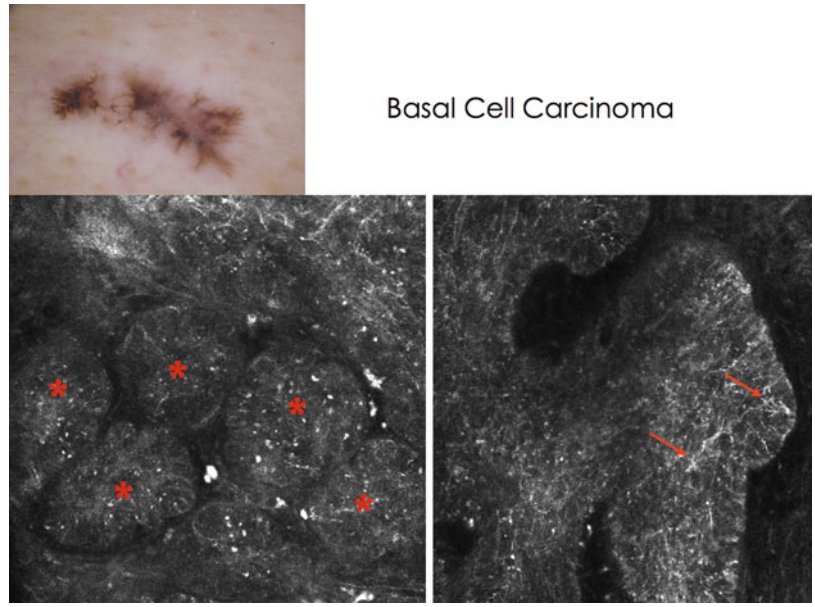

Fig. 7 Basal cell carcinoma showing solid and well-outlined basaloid islands (*asterisks*) and peripheral palisading (*arrows*)

3.1 Basal Cell Carcinoma

The main confocal features of BCC list the presence of tightly packed aggregates with peripheral palisading and lobulated shape (González and Tannous 2002; Ulrich et al. 2011; Nori et al. 2004; Agero et al. 2006), epidermal polarization, and the presence of blood vessels (Fig. 7). Basaloid aggregates are outlined by dark spaces that correspond to mucin and often are surrounded by a prominent vascularity. Histopathologically, the aggregates correspond to the basaloid islands. Interestingly, RCM highlights very well the presence of dendritic melanocytes entrapped within the basaloid islands observable in heavily pigmented BCC. RCM is particularly useful in pink flat BCCs not showing all dermoscopic criteria and in heavily pigmented BCCs that simulate MM.

3.2 Actinic Keratosis and Squamous Cell Carcinoma

AK and SCC display the presence of variable KC atypia. At the stratum corneum, superficial disruption with single detached keratinocytes seen as bright, polygonal cells of high reflectance can be observed (Aghassi et al. 2000; Ulrich et al. 2007). Furthermore, nucleated, highly reflective cells with dark center and sharp demarcation appear within the stratum corneum corresponding to parakeratosis. Atypical honeycomb pattern and architectural disarray of variable degree are seen at the level of the stratum granulosum and stratum spinosum corresponding to different degrees of keratinocyte dysplasia on histopathological exam. In SCC an atypical honeycomb or disarranged pattern of the spinous-granular layer is found along with round nucleated cells corresponding to pleomorphic keratinocytes (Fig. 8). Round blood vessels traversing through the dermal papillae perpendicular to the skin surface and scale crust appearing as brightly reflective amorphous islands on the surface of the skin are common findings in SCC (Rishpon et al. 2009). In cases with marked hyperkeratosis or abundant scale covering the entire lesion, in-depth imaging is limited by the keratin scattering, limiting exploration of the DEJ, which is fundamental for complete diagnosis.

4 Inflammatory Skin Diseases

Inflammatory skin diseases include spongiotic dermatitis, psoriasiform diseases, diseases with interface involvement, and pigmentary

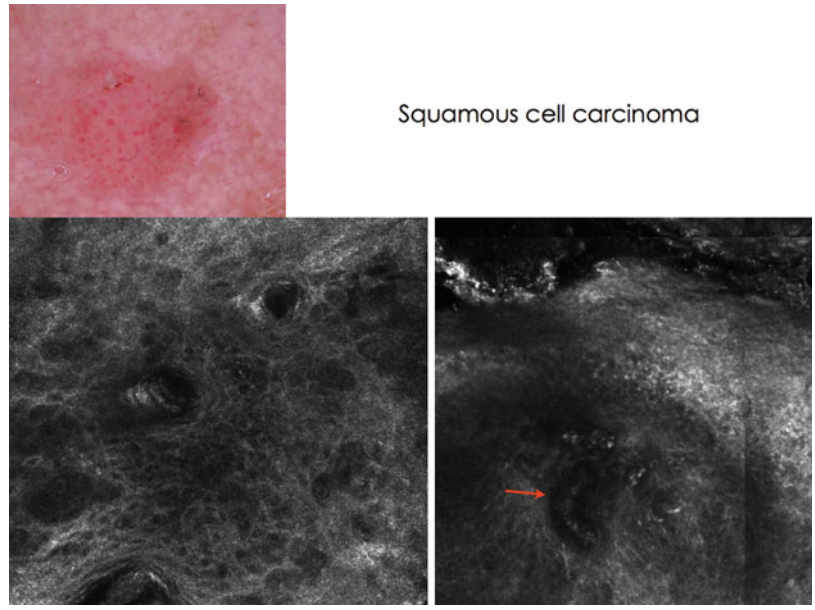

Fig. 8 Squamous cell carcinoma reveals the presence of atypical honeycombed pattern with variably shaped keratinocytes and S-shaped vessels (*arrow*)

non-tumoral skin disorders (i.e., vitiligo, melasma).

The main feature of spongiotic dermatitis on RCM is the presence of inter- or intracellular spongiosis. This corresponds to an increased intercellular brightness due to inter- or intracellular fluid accumulation that leads to the appearance of a regular honeycombed morphology (González et al. 1999; Astner et al. 2005). When spongiosis is more pronounced, it is possible to detect vesicle formation that appears as well-demarcated, dark hollow spaces between granular and spinous layer KCs. Commonly, exocytosis is associated with spongiosis, whereby the inflammatory cells are seen on RCM as bright, round highly refractive structures of about 8–10 μm, interspersed between keratinocytes. Inflammatory cells may also be observed to various extents in a perifollicular, perivascular, or interstitial dermal distribution.

Psoriasiform disease is distinguished by the presence of an increased number of non-rimmed papillae at the dermo-epidermal junction, resulting in a junctional profile similar to that of normal skin but with papillae surrounded by faint rings of basal KCs, instead of the typical bright rings (Gonzalez et al. 1999). Interestingly, S-shaped blood vessels are seen within the papillae, and they resemble the pattern observed in SCC in situ.

The hallmark in interface dermatitis is the inflammatory involvement of the dermo-epidermal junction. The inflammatory cells tend to obscure the junction profile and the dermal papillae with a more diffuse involvement in lichen planus and a focal distribution in lupus erythematosus (Moscarella et al. 2012). In the latter, the presence of inflammatory infiltrate can be seen in proximity of the adnexa that usually appear dilated (larger than 80–100 μm) and filled by highly refractive material in the lumen (hyperkeratotic infundibula).

Among the acquired pigmented disorders, RCM has been used to study vitiligo. Vitiligo lesional skin shows disappearance of the normal brightness at the dermo-epidermal junction where the edged papillae appear as a remnant of the pre-existing papillary ring (Ardigo et al. 2007).

5 Infectious Diseases

RCM has been applied in some infectious diseases although studies based on large cases are still lacking. Superficial mycosis can be easily

detected by RCM since it has a high-level resolution for the upper epidermis. Dermatophyte hyphae appear as bright linear branching structures within the epidermis with an excellent correlation with the ones seen upon light microscopy (Markus et al. 2001). With the same high resolution, it is possible to detect the presence of *Demodex folliculorum* within the hair follicles (Longo et al. 2012a). *Demodex* usually show up as multiple roundish well-outlined structures corresponding to the head-down mites living in the hair follicles. *Sarcoptes scabiei* is readily observed using RCM, including its feces and eggs within the burrow (Longo et al. 2005).

6 Monitoring of Nonsurgical Therapies

Due to its noninvasiveness and high resolution, RCM is a suitable candidate for treatment monitoring. Its role has been investigated for monitoring treatment efficacy of imiquimod in AK (Ulrich et al. 2010). RCM was able to visualize the inflammatory response induced by imiquimod and photodynamic therapy (Longo et al. 2012b) in clinically visible as well as in subclinical lesions within the cancerization field. Another study evaluated the efficacy of cryotherapy for superficial BCC (Ahlgrimm-Siess et al. 2009), showing early cell necrosis at the basal layer and within the superficial dermis 5 h after application of liquid nitrogen indicating effective cryotherapy. In this regard, RCM may allow the immediate evaluation of treatment efficacy after cryotherapy and may indicate if a second cryotherapy session is needed. RCM has also been employed in lentigo maligna treated with imiquimod (Nadiminti et al. 2010). RCM has also found application for the efficacy assessment of laser therapy for solar lentigines, vascular lesions, skin rejuvenation (Longo et al. 2013), and acne scars demonstrating the skin changes occurring after treatment and in long-term follow-up. The possibility to closely monitor the morphologic changes over time and gain new insight into the mechanism of action of laser devices could be useful in understanding side effects.

7 Conclusions

The introduction of RCM in clinical practice opened for the first time the possibility to obtain a histologic view of the skin in a noninvasive way with the main advantage of being painless, not scarring, and repeatable over time. The possibility to monitor lesions over time implies the opportunity to gain new insight into nevus development, melanoma biology, and therapy monitoring. However, the correct interpretation of RCM images requires an adequate training and of the main histopathologic aspects of each particular lesion.

References

Agero AL, Busam KJ, Benvenuto-Andrade C, Scope A, Gill M, Marghoob AA, González S, Halpern AC. Reflectance confocal microscopy of pigmented basal cell carcinoma. J Am Acad Dermatol. 2006;54:638–43.

Aghassi D, Anderson R, Gonzalez S. Confocal laser microscopic imaging of actinic keratosis in vivo: a preliminary report. J Am Acad Dermatol. 2000;43:42–8.

Ahlgrimm-Siess V, Horn M, Koller S, Ludwig R, Gerger A, Hofmann-Wellenhof R. Monitoring efficacy of cryotherapy for superficial basal cell carcinomas with in vivo reflectance confocal microscopy: a preliminary study. J Dermatol Sci. 2009;53(1):60–4.

Ardigo M, Malizewsky I, Dell'anna ML, Berardesca E, Picardo M. Preliminary evaluation of vitiligo using in vivo reflectance confocal microscopy. J Eur Acad Dermatol Venereol. 2007;21(10):1344–50.

Argenziano G, Puig S, Zalaudek I, Sera F, Corona R, et al. Dermoscopy improves accuracy of primary care physicians to triage lesions suggestive of skin cancer. J Clin Oncol. 2006;24(12):1877–82.

Argenziano G, Cerroni L, Zalaudek I, Staibano S, Hofmann-Wellenhof R, Arpaia N, et al. Accuracy in melanoma detection: a 10-year multicenter survey. J Am Acad Dermatol. 2012;67(1):54–9.

Astner S, González E, Cheung AC, Rius-Díaz F, Doukas AG, William F, González S. Non-invasive evaluation of the kinetics of allergic and irritant contact dermatitis. J Invest Dermatol. 2005;124(2):351–9.

González S, Tannous Z. Real-time, in vivo confocal reflectance microscopy of basal cell carcinoma. J Am Acad Dermatol. 2002;47:869–74.

González S, González E, White WM, Rajadhyaksha M, Anderson RR. Allergic contact dermatitis: correlation of in vivo confocal imaging to routine histology. J Am Acad Dermatol. 1999;40(5 Pt 1):708–13.

Gonzalez S, Rajadhyaksha M, Rubenstein G, Anderson R. Characterization of psoriasis in vivo by reflectance confocal microscopy. J Med. 1999;30:337–56.

Gonzalez S, Sackstein R, Anderson RR, Rajadhyaksha M. Real-time evidence of in vivo leukocyte trafficking in human skin by reflectance confocal microscopy. J Invest Dermatol. 2001;117:384–6.

Guitera P, Pellacani G, Crotty KA, Scolyer RA, Li LX, Bassoli S, Vinceti M, Rabinovitz H, Longo C, Menzies SW. The impact of in vivo reflectance confocal microscopy on the diagnostic accuracy of lentigo maligna and equivocal pigmented and nonpigmented macules of the face. J Invest Dermatol. 2010;130(8):2080–91.

Hashemi P, Pulitzer MP, Scope A, Kovalyshyn I, Halpern AC, Marghoob AA. Langerhans cells and melanocytes share similar morphologic features under in vivo reflectance confocal microscopy: a challenge for melanoma diagnosis. J Am Acad Dermatol. 2012;66(3):452–62.

Langley RGB, Rajadhyaksha M, Dwyer PJ, Sober AJ, Flotte TJ, Andersson RR. Confocal scanning laser microscopy of benign and malignant melanocytic skin lesions in vivo. J Am Acad Dermatol. 2001;45:365–76.

Longo C, Bassoli S, Monari P, Seidenari S, Pellacani G. Reflectance-mode confocal microscopy for the in vivo detection of *Sarcoptes scabiei*. Arch Dermatol. 2005;141(10):1336.

Longo C, Fantini F, Cesinaro AM, Bassoli S, Seidenari S, Pellacani G. Pigmented mammary Paget disease: dermoscopic, in vivo reflectance-mode confocal microscopic, and immunohistochemical study of a case. Arch Dermatol. 2007;143(6):752–4.

Longo C, Rito C, Beretti F, Cesinaro AM, Pieiro-Maceira J, Seidenari S, Pellacani G. De novo melanoma and melanoma arising from pre-existing nevus: in vivo morphologic differences as evaluated by confocal microscopy. J Am Acad Dermatol. 2011;65(3):604–14.

Longo C, Pellacani G, Ricci C, De Pace B, Argenziano G, Zalaudek I. In vivo detection of Demodex folliculorum by means of confocal microscopy. Br J Dermatol. 2012a;166(3):690–2.

Longo C, Casari A, Pepe P, Moscarella E, Zalaudek I, Argenziano G, Pellacani G. Confocal microscopy insights into the treatment and cellular immune response of basal cell carcinoma to photodynamic therapy. Dermatol. 2012b;225(3):264–70.

Longo C, Galimberti M, De Pace B, Pellacani G, Bencini PL. Laser skin rejuvenation: epidermal changes and collagen remodeling evaluated by in vivo confocal microscopy. Lasers Med Sci. 2013; 28(3):769–6.

Markus R, Huzaira M, Anderson RR, González S. A better potassium hydroxide preparation? In vivo diagnosis of tinea with confocal microscopy. Arch Dermatol. 2001;137(8):1076–8.

Moscarella E, González S, Agozzino M, Sánchez-Mateos JL, Panetta C, Contaldo M, Ardigò M. Pilot study on reflectance confocal microscopy imaging of lichen planus: a real-time, non-invasive aid for clinical diagnosis. J Eur Acad Dermatol Venereol. 2012;26(11):1258–65.

Nadiminti H, Scope A, Marghoob AA, Busam K, Nehal KS. Use of reflectance confocal microscopy to monitor response of lentigo maligna to nonsurgical treatment. Dermatol Surg. 2010;36(2):177–84.

Nori S, Rius-Díaz F, Cuevas J, Goldgeier M, Jaen P, Torres A, González S. Sensitivity and specificity of reflectance-mode confocal microscopy for in vivo diagnosis of basal cell carcinoma: a multicenter study. J Am Acad Dermatol. 2004;51:923–30.

Pellacani G, Cesinaro AM, Grana C, Seidenari S. In-vivo confocal scanning laser microscopy of pigmented Spitz nevi. Comparison of in-vivo confocal images with dermoscopy and routine histopathology. J Am Acad Dermatol. 2004;51:371–6.

Pellacani G, Cesinaro AM, Seidenari S. Reflectance-mode confocal microscopy of pigmented skin lesions – improvement in melanoma diagnostic specificity. J Am Acad Dermatol. 2005a;53:979–85.

Pellacani G, Cesinaro AM, Longo C, Grana C, Seidenari S. Microscopic in vivo description of cellular architecture of dermoscopic pigment network in nevi and melanomas. Arch Dermatol. 2005b;141:147–54.

Pellacani G, Cesinaro AM, Seidenari S. In vivo confocal reflectance microscopy for the characterization of melanocytic nests and correlation with dermoscopy and histology. Br J Dermatol. 2005c;152:384–6.

Pellacani G, Cesinaro AM, Seidenari S. In vivo assessment of melanocytic nests in nevi and melanomas by reflectance confocal microscopy. Mod Pathol. 2005d;18:469–74.

Pellacani G, Cesinaro AM, Seidenari S. Reflectance-mode confocal microscopy for the in vivo characterization of pagetoid melanocytosis in melanomas and nevi. J Invest Dermatol. 2005e;125:532–7.

Pellacani G, Guitera P, Longo C, Avramidis M, Seidenari S, Menzies S. The impact of in vivo reflectance confocal microscopy for the diagnostic accuracy of melanoma and equivocal melanocytic lesions. J Invest Dermatol. 2007;127:2759–65.

Pellacani G, Scope A, Ferrari B, Pupelli G, Bassoli S, Longo C, Cesinaro AM, Argenziano G, Hofmann-Wellenhof R, Malvehy J, Marghoob AA, Puig S, Seidenari S, Soyer HP, Zalaudek I. New insights into nevogenesis: in vivo characterization and follow-up of melanocytic nevi by reflectance confocal microscopy. J Am Acad Dermatol. 2009a;61(6):1001–13.

Pellacani G, Longo C, Ferrara G, Cesinaro AM, Bassoli S, Guitera P, Menzies SW, Seidenari S. Spitz nevi: in vivo confocal microscopic features, dermatoscopic aspects, histopathologic correlates, and diagnostic significance. J Am Acad Dermatol. 2009b;60(2):236–47.

Pellacani G, Farnetani F, Gonzalez S, Longo C, Cesinaro AM, Casari A, Beretti F, Seidenari S, Gill M. In vivo confocal microscopy for detection and grading of dysplastic nevi: a pilot study. J Am Acad Dermatol. 2012;66(3):e109–21.

Puig S, Di Giacomo TB, Serra D, Cabrini F, Alos L, Palou J, Malvehy J. Reflectance confocal microscopy of blue nevus. Eur J Dermatol. 2012;22(4):552–3.

Rajadhyaksha M, Grossman M, Esterowitz D, Webb RH, Anderson RR. In vivo confocal scanning laser microscopy of human skin: melanin provides strong contrast. J Invest Dermatol. 1995;104:946–52.

Rajadhyaksha M, Gonzalez S, Zavislan JM, Anderson RR, Web RH. In vivo confocal laser microscopy of human skin II: advances in instrumentation and comparison with histology. J Invest Dermatol. 1999;113:293–303.

Rishpon A, Kim N, Scope A, Porges L, Oliviero MC, Braun RP, Marghoob AA, Fox CA, Rabinovitz HS. Reflectance confocal microscopy criteria for squamous cell carcinomas and actinic keratoses. Arch Dermatol. 2009;145(7):766–72.

Segura S, Pellacani G, Puig S, Longo C, Bassoli S, Guitera P, Palou J, Menzies S, Seidenari S, Malvehy J. In vivo microscopic features of nodular melanomas: dermoscopy, confocal microscopy, and histopathologic correlates. Arch Dermatol. 2008;144(10):1311–20.

Segura S, Puig S, Carrera C, Palou J, Malvehy J. Development of a two-step method for the diagnosis of melanoma by reflectance confocal microscopy. J Am Acad Dermatol. 2009;61(2):216–29.

Shoo BA, Sagebiel RW, Kashani-Sabet M. Discordance in the histopathologic diagnosis of melanoma at a melanoma referral center. J Am Acad Dermatol. 2010;62(5):751–6.

Tannous ZS, Mihm MC, Flotte TJ, Gonzalez S. In vivo examination of lentigo maligna and malignant melanoma in situ, lentigo maligna type by near-infrared reflectance confocal microscopy: comparison of in vivo confocal images with histologic sections. J Am Acad Dermatol. 2002;46:260–3.

Ulrich M, Forschner T, Röwert-Huber J, González S, Stockfleth E, Sterry W, Astner S. Differentiation between actinic keratoses and disseminated superficial actinic porokeratoses with reflectance confocal microscopy. Br J Dermatol. 2007;156 Suppl 3:47–52.

Ulrich M, Krueger-Corcoran D, Roewert-Huber J, Sterry W, Stockfleth E, Astner S. Reflectance confocal microscopy for noninvasive monitoring of therapy and detection of subclinical actinic keratoses. Dermatology. 2010;220(1):15–24.

Ulrich M, Roewert-Huber J, González S, Rius-Diaz F, Stockfleth E, Kanitakis J. Peritumoral clefting in basal cell carcinoma: correlation of in vivo reflectance confocal microscopy and routine histology. J Cutan Pathol. 2011;38(2):190–5.

Weyers W. The 'epidemic' of melanoma between under- and overdiagnosis. J Cutan Pathol. 2012; 39(1):9–16.

Zalaudek I, Argenziano G, Di Stefani A, Ferrara G, Marghoob AA, Hofmann-Wellenhof R, Soyer HP, Braun R, Kerl H. Dermoscopy in general dermatology. Dermatology. 2006;212(1):7–18.

Zalaudek I, Marghoob AA, Scope A, Leinweber B, Ferrara G, Hofmann-Wellenhof R, Pellacani G, Soyer HP, Argenziano G. Three roots of melanoma. Arch Dermatol. 2008;144(10):1375–9.

Ex Vivo Confocal Microscopy in Clinical Dermatology

39

Julia Welzel, Raphaela Kästle, and Elke Sattler

Contents

Keywords
Reflectance confocal microscopy • Fluorescence confocal microscopy • Ex vivo • Mohs micrographic surgery • Rapid surgical pathology • Skin • Basal cell carcinoma

1 Introduction

Reflectance confocal microscopy is established as a valuable tool for in vivo non-invasive diagnosis of skin tumors and other skin conditions. The same technique can be used also for microscopic imaging of freshly excised tissue. After application of fluorescent dyes and by using lasers with different wavelengths for excitation, a staining of nuclei is possible in the fluorescence mode. The gray-scale images in the reflectance and the fluorescence mode can be combined and converted digitally into pseudo-color images looking like an H&E (hematoxylin/eosin) staining. Ex vivo confocal microscopy is a promising tool for rapid pathology of fresh tissue, especially for Mohs micrographic surgery of basal cell carcinoma.

2 Technique

The ex vivo confocal microscopy device VivaScope 2500 (Mavig, Germany) is a multiwave system. Three lasers with different

J. Welzel (✉) • R. Kästle
Department of Dermatology and Allergology, General Hospital Augsburg, Augsburg, Germany
e-mail: julia.welzel@klinikum-augsburg.de

E. Sattler
Department of Dermatology, Ludwig Maximilian University Munich, Munich, Germany

P. Humbert et al. (eds.), *Agache's Measuring the Skin*,
DOI 10.1007/978-3-319-32383-1_39

wavelengths at 488 nm, 658 nm, and 830 nm are installed. The laser at 830 nm is used for reflectance imaging. The first two lasers at 488 nm and 658 nm are combined with filters for elimination of the reflection, allowing only the fluorescence at longer wavelength to pass through. The fresh tissue is placed on a glass slide above the lens system and fixed by another plate to ensure a flat surface. The surface is scanned by imaging single square spots of 750 μm × 750 μm, composed to maps of up to 12 mm × 12 mm by lateral scanning, which takes some minutes.

3 Fluorescent Dyes

The first step of fresh tissue preparation is the application of 10 % acetic acid for 60 s to increase the contrast ("acetowhitening"). After rinsing with buffer solution, fluorescent dyes can be applied.

At 488 nm, acridine orange and sodium fluorescein are dyes, which are excited by illumination, leading to fluorescence at longer wavelength.

At 658 nm, methylene blue, toluidine blue, patent blue, and nile blue can be used for fluorescent staining.

The concentrations of the dyes are crucial to achieve optimal results. If the concentration is too low, the fluorescence signal is weak. If it is too high, quenching may occur, resulting in dark images. The effect of photo bleaching should also be considered, especially when using methylene blue. To avoid bleaching, the measurement time and scanning should be fast. Some dyes like nile blue are susceptible to changes of the pH value which might lead to a shift of the excitation and emission wavelength.

Our recommendations regarding the concentrations of the different dyes are:

- Acridine orange 0.6 mM, 1.2 mg/ml
- Sodium fluorescein 0.2–0.4 %
- Patent blue V 0.25 mg/ml (<6.25 mg/ml)
- Methylene blue 2 mg/ml
- Nile blue 0.2 mg/ml in 70 % ethanol

In our experience, the fluorescence dyes acridine orange and nile blue provide the best and most stable results.

4 Digital Staining

In the reflectance mode, collagen fibers and cytoplasm are the main sources of contrast, whereas in the fluorescence mode, the collagen is nearly invisible and the nuclei are stained strongly. By combining both images and by digital transformation of the grayscale into pseudo-colors, the images mimic the conventional H&E (hematoxylin/eosin) staining of histology (Bini et al. 2011). This may further facilitate the detection of small strands of epithelium within connective tissue and increase the sensitivity and specificity of ex vivo confocal microscopy.

5 Results

Confocal microscopy is meanwhile well established for the noninvasive in vivo imaging in dermatology, but just as long it has been successfully applied to image freshly excised tissue

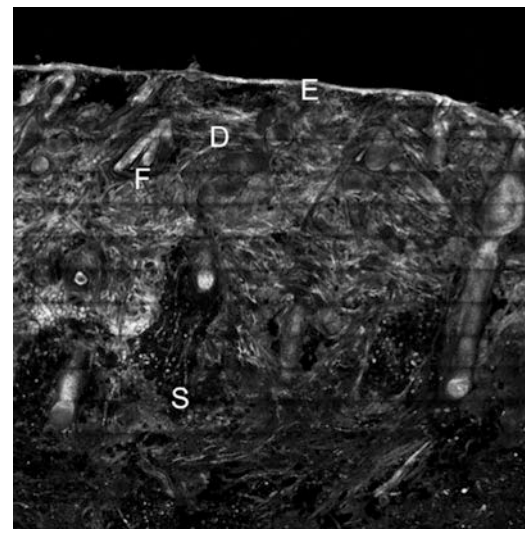

Fig. 1 Ex vivo confocal microscopy of normal skin in the reflectance mode. The epidermis (*E*), the dermis (*D*), glands and hair follicles (*F*), and subcutaneous fat (*S*) are displayed

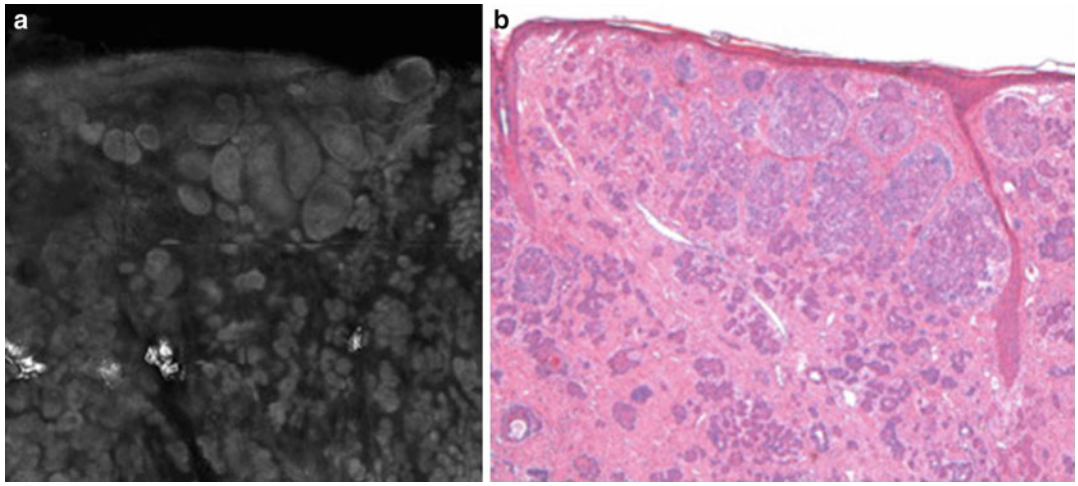

Fig. 2 Ex vivo confocal image of a basal cell carcinoma in the reflectance mode (*left*) compared to corresponding histology of the same tumor (*right*). The appearance of the small tumor nests is similar

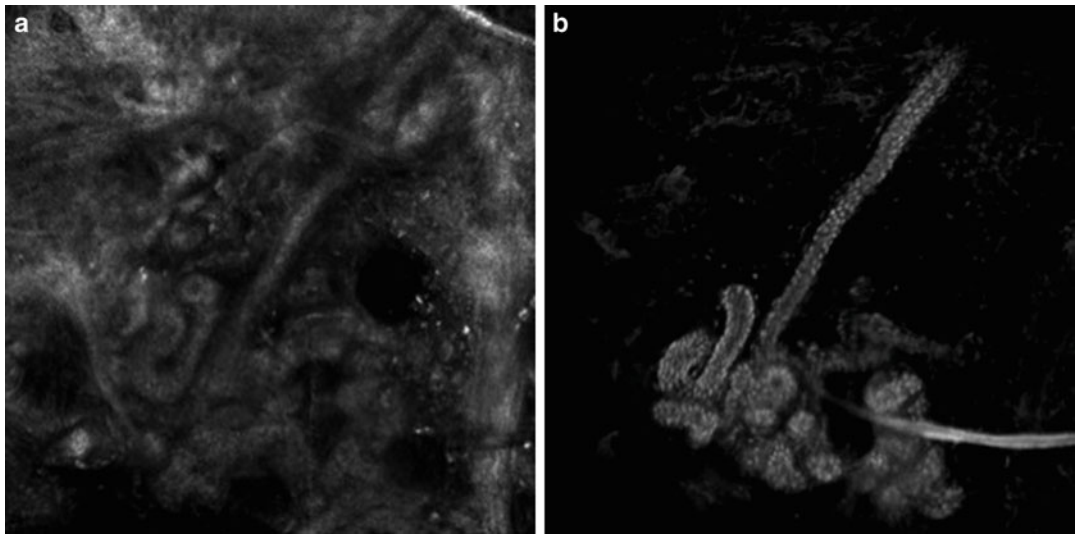

Fig. 3 Sweat gland with surrounding connective tissue in the reflectance mode (*left*) and fluorescence mode (*right*) after staining with patent blue. The dye stains the nuclei, whereas the connective tissue is left unstained (*right*), but shows a bright signal in the reflectance mode (*left*)

ex vivo. The first studies were performed using the reflectance mode. The normal skin architecture and basal cell carcinomas are clearly visible (Figs. 1 and 2). Typical histologic features were described, corresponding to conventional histology (Gareau et al. 2009b). Also squamous cell carcinomas were imaged and showed characteristic features like densely packed atypical nuclei (Horn et al. 2007). However, the contrast of reflectance confocal microscopy especially for detection of small residues of fibrotic basal cell carcinomas with dense, bright stroma was limited (Chung et al. 2004). Confocal and light microscopy findings were consistent in 84.6 % (Kaeb et al. 2009). The sensitivity to detect basal cell carcinomas in tissue margins was limited to 73.7 % resp. 80 % depending on the technique (Ziefle et al. 2010).

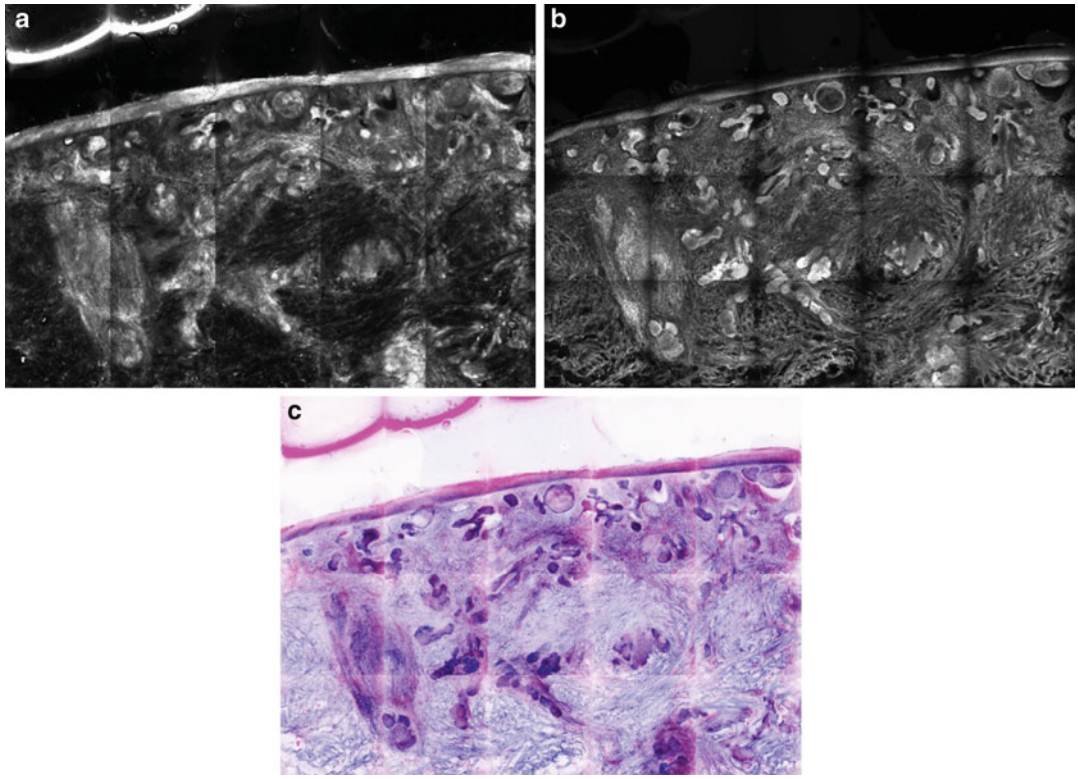

Fig. 4 Basal cell carcinoma in the reflectance mode (**a**), in the fluorescence mode after staining with acridine orange (**b**) and after combination of both images and digital staining (**c**). The latter image simulates the H&E staining of conventional histology. The tumor is easily detectable. Digital staining software by Dan Gareau and Milind Rajadhyaksha, Memorial Sloan-Kettering Cancer Center, New York

The development of multiwave systems for fluorescence confocal microscopy enhanced the diagnostic capability for examination of freshly excised tissue (Bennàssar et al. 2013a). The first step was to develop and evaluate staining protocols of fluorescent dyes. Several different dyes were investigated. Acridine orange was the most commonly used fluorescent dye, which gave stable and reproducible results (Gareau et al. 2008). Fluorescence confocal microscopy is demonstrated to be advantageous to the reflectance mode because epithelium shows more contrast to the stroma after fluorescence staining of the nuclei (Fig. 3). Therefore, it is easier to detect small tumors within a fibrotic connective tissue. This led to a high sensitivity of 96.6 % and specificity of 89.2 % in basal cell carcinomas (Gareau et al. 2009a; Karen et al. 2009).

Fluorescence confocal microscopy is not only used for diagnosing skin tumors but also for rapid surgical pathology because the staining and imaging take only a few minutes compared to fresh frozen tissue microscopy (Gareau et al. 2008). Case reports demonstrated its feasibility for bedside pathology (Bennàssar et al. 2012; Longo et al. 2013). Especially for histologic examination of tumor margins, the so-called Mohs micrographic surgery, ex vivo fluorescence confocal microscopy has demonstrated its value. The sensitivity for detection of basal cell carcinoma residues in the borders is 88 % and the specificity 99 % (Bennàssar et al. 2013b). Digital staining may further facilitate the interpretation of the confocal images (Fig. 4) (Bini et al. 2011; Gareau et al. 2012). First studies in general pathology demonstrated that the technique could also be used for

microscopy of other tissues than the skin like the breast, colon, and thyroid gland (Ragazzi et al. 2013).

The VivaScope 2500 is further improved. In the latest upgrade, the optical lens system is optimized for better image matching, and the measuring field is enlarged up to 20 mm × 20 mm.

6 Conclusion

Fluorescence confocal microscopy is a fast and reliable method for diagnosis of skin tumors and other pathologies in freshly excised tissue. It may represent an alternative to frozen sections for rapid surgical pathology and is of special interest for Mohs micrographic surgery to investigate tumor margins of basal cell carcinomas.

References

Bennàssar A, Vilalta A, Carrera C, Puig S, Malvehy J. Rapid diagnosis of two facial papules using ex vivo fluorescence confocal microscopy: toward a rapid bedside pathology. Dermatol Surg. 2012;38:1548–51.

Bennàssar A, Carrera C, Puig S, Vilalta A, Malvehy J. Fast evaluation of 69 basal cell carcinomas with ex vivo fluorescence confocal microscopy: criteria description, histopathological correlation, and interobserver agreement. JAMA Dermatol. 2013a;149:839–47.

Bennàssar A, Vilata A, Puig S, Malvehy J. Ex vivo fluorescence confocal microscopy for fast evaluation of tumour margins during mohs surgery. Br J Dermatol. 2013b. doi:10.1111/bjd.12671 [Epub ahead of print].

Bini J, Spain J, Nehal K, Hazelwood V, DiMarzio C, Rajadhyaksha M. Confocal mosaicing microscopy of human skin ex vivo: spectral analysis for digital staining to simulate histology-like appearance. J Biomed Opt. 2011;16:076008.

Chung VQ, Dwyer PJ, Nehal KS, Rajadhyaksha M, Menaker GM, Charles C, Jiang SB. Use of ex vivo confocal scanning laser microscopy during mohs surgery for nonmelanoma skin cancers. Dermatol Surg. 2004;30:1470–8.

Gareau DS, Li Y, Huang B, Eastman Z, Nehal KS, Rajadhyaksha M. Confocal mosaicing microscopy in mohs skin excisions: feasibility of rapid surgical pathology. J Biomed Opt. 2008;13:054001.

Gareau DS, Karen JK, Dusza SW, Tudisco M, Nehal KS, Rajadhyaksha M. Sensitivity and specificity for detecting basal cell carcinomas in mohs excisions with confocal fluorescence mosaicing microscopy. J Biomed Opt. 2009a;14:034012.

Gareau DS, Patel YG, Li Y, Aranda I, Halpern AC, Nehal KS, Rajadhyaksha M. Confocal mosaicing microscopy in skin excisions: a demonstration of rapid surgical pathology. J Microsc. 2009b;233:149–59.

Gareau DS, Jeon H, Nehal KS, Rajadhyaksha M. Rapid screening of cancer margins in tissue with multimodal confocal microscopy. J Surg Res. 2012;178:533–8.

Horn M, Gerger A, Koller S, Weger W, Langsenlehner U, Krippl P, Kerl H, Samonigg H, Smolle J. The use of confocal laser-scanning microscopy in microsurgery for invasive squamous cell carcinoma. Br J Dermatol. 2007;156:81–4.

Kaeb S, Landthaler M, Hohenleutner U. Confocal laser scanning microscopy – evaluation of native tissue sections in micrographic surgery. Lasers Med Sci. 2009;24:819–23.

Karen JK, Gareau DS, Dusza SW, Tudisco M, Rajadhyaksha M, Nehal KS. Detection of basal cell carcinomas in mohs excisions with fluorescence confocal mosaicing microscopy. Br J Dermatol. 2009;160:1242–50.

Longo C, Ragazzi M, Castagnetti F, Gardini S, Palmieri T, Lallas A, Moscarella E, Piana S, Pellacani G, Zalaudek I, Argenziano G. Inserting ex vivo fluorescence confocal microscopy perioperatively in mohs micrographic surgery expedites bedside assessment of excision margins in recurrent basal cell carcinoma. Dermatology. 2013;227:89–92.

Ragazzi M, Piana S, Longo C, Castagnetti F, Foroni M, Ferrari G, Gardini G, Pellacani G. Fluorescence confocal microscopy for pathologists. Mod Pathol. 2014; 27:460–71.

Ziefle S, Schüle D, Breuninger H, Schippert W, Moehrle M. Confocal laser scanning microscopy vs 3-dimensional histologic imaging in basal cell carcinoma. Arch Dermatol. 2010;146:843–7.

A Pharmaceutical Approach of Transcutaneous Oxygen Therapies

40

D. Salmon, S. Boutefnouchet, E. Gilbert, L. Roussel, and Fabrice Pirot

Contents

D. Salmon (✉) • F. Pirot
EA 4169 "Aspects Fondamentaux, Cliniques et Thérapeutiques de la Fonction Barrière Cutanée", Laboratoire de Pharmacie Galénique Industrielle – Faculté de Pharmacie., Université Claude Bernard Lyon 1, Lyon cedex 08, France

Unité de Préparation et de Contrôles des Médicaments, Service Pharmaceutique – Groupement Hospitalier Edouard Herriot-Hospices Civils de Lyon, Lyon cedex 03, France
e-mail: damien.salmon01@chu-lyon.fr; fabrice.pirot@univ-lyon1.fr

S. Boutefnouchet
Unité de Préparation et de Contrôles des Médicaments, Service Pharmaceutique – Groupement Hospitalier Edouard Herriot-Hospices Civils de Lyon, Lyon cedex 03, France

E. Gilbert • L. Roussel
EA 4169 "Aspects Fondamentaux, Cliniques et Thérapeutiques de la Fonction Barrière Cutanée", Laboratoire de Pharmacie Galénique Industrielle – Faculté de Pharmacie., Université Claude Bernard Lyon 1, Lyon cedex 08, France

P. Humbert et al. (eds.), *Agache's Measuring the Skin*,
DOI 10.1007/978-3-319-32383-1_40

Keywords
Oxygen • Skin • Permeability • Biopharmacy • Compounding

1 Introduction

Oxygen is an essential fuel and also a poison for living organisms. On the one hand, it can violently oxidize vital macromolecules (e.g., proteins and nucleic acids), and on the other hand, some of these macromolecules are specially designed to capture, transport, and use oxygen in many cascades of chemical reactions. These paradoxal properties have led, through adaptive evolution, organisms to develop strategies to precisely control and adapt the absorption of oxygen from the environment. Mammals mainly use their lungs through breathing and have developed their interfacial surface to meet their body's requirements in oxygen. The second interfacial surface of body in direct contact with environmental oxygen is human skin. Very naturally, an intimate relation emerged between the skin and oxygen homeostasis. And although the skin cannot anymore be considered as a "breathing organ" in humans, it has deep implications in oxygen supply management.

Nowadays, medical attention has been driven toward body supply in oxygen due to its wide impact on various physiopathological processes such as wound healing, skin aging, and immune reactions. Beyond hyperbaric oxygen therapy, innovative formulation technologies are being developed to enable oxygen delivery in a handy and efficient manner.

2 General Aspects on Oxygen and Skin

2.1 Physicochemistry of Oxygen

Atomic oxygen is a highly electronegative chemical element (symbol "O"; atomic number, 8) that forms compounds with most elements in often highly exothermic reactions. It is the most abundant element on earth surface. Furthermore, it represents 62 % (m/m) of the human body. Under normal conditions of temperature and pressure, atomic oxygen binds to form a diatomic colorless, odorless gas called oxygen (O_2). Oxygen is a small molecule with a molecular weight of 31.999 g/mol that exhibits a pressure and reverse-temperature-dependent solubility in water (i.e., 8.3 mg/L at 25 °C under atmospheric pressure).

2.2 Oxygen Physiology

Oxygen acts toward the human body at the same time (i) as a major metabolic substrate for cellular chemistry and (ii) as a signal in multiple metabolic pathways with a remnant effect after return to normal oxygen levels (Ladizinsky and Roe 2010).

Many essential physiological reactions require the presence of oxygen. Most importantly, oxygen is the terminal electron acceptor in mitochondrial respiration and it also plays a central role in many other metabolic processes. For instance, oxygen is required (i) for the production of nitric oxide by NO synthases, (ii) for the hydroxylation of the collagen, and (iii) for cholesterol synthesis.

Furthermore, oxygen levels are monitored at different points within the human body (e.g., the carotid, liver, and kidney) to induce homeostatic response to hypoxia (i.e., differential vasoconstriction/dilatation, erythropoietin, and red blood cell production). In case of acute environmental hypoxia, concomitant pulmonary vasoconstriction and systemic vasodilatation occur to ensure correct oxygenation of vital organs. Surprisingly, unlike the rest of systemic vasculature, skin vasculature undergoes vasoconstriction in response to acute environmental hypoxia. If hypoxia is prolonged, a hypoxia-inducible transcription factor (HIF)-mediated response progressively restores the cutaneous blood flow in the skin, leading to liver and kidney hypoxia and subsequent erythropoietin synthesis to enhance blood's oxygen-carrying capacity. Thus, the skin is the central actor of a bimodal response to acute/chronic environmental hypoxia in mammals (Boutin et al. 2008; Semenza 2008).

Eventually, oxygen supply is intimately intricate in skin aging processes as a cause (i.e., production of reactive oxygen species or ROS) and a potential treatment for a variety of skin discomforts; therefore, the development of oxygen therapies is a major interest of cosmetic companies with important economic and sanitary outcomes (Asadamongkol and Zhang 2014).

2.3 Oxygen Supply

Oxygen supply to human body's organs and tissues is mainly ensured by pulmonary absorption. In the lungs, gaseous oxygen needs to become dissolved in a fluid state to cross alveolar membrane. Once dissolved, oxygen diffuses within the body from areas of high concentration to areas of low concentration. Hemoglobin within red blood cells acts as a reservoir ensuring that plasmatic dissolved oxygen level is sufficiently maintained to ensure delivery to organs and tissues via capillary perfusion (Ladizinsky and Roe 2010).

Although transcutaneous absorption of oxygen is now known to occur in human, the ratio of the absorption surface between the skin and lungs (1–2 m^2 and 70 m^2, respectively) limits its impact as a source of systemic oxygenation. Overall, apart in premature infants, atmospheric oxygen transported through the human skin contributes in a negligible way (i.e., 2 %) to body oxygenation (Roe et al. 2010). As dermal vasculature does not cross its basal membrane, the epidermis can be considered as a physiologically hypoxic tissue where anaerobic glycolysis is likely to be important to sustain its high metabolic activity due to constant renewal (Boutin et al. 2008; Straseski et al. 2009). Moreover, due to its highly organized structure, skin barrier function further limits the extent of transcutaneous absorption of oxygen. However, considering local skin oxygen supply, transcutaneous absorption is (i) a physiologically relevant oxygen source down to the superficial dermis and (ii) the major source of oxygen for the outermost layers of unperfused epidermis (Ladizinsky and Roe 2010).

In human, skin's partial pressure in oxygen levels (pO_2) is highly correlated to the physiopathological state of the skin (Reading et al. 2013). For instance, wound repair outcome may be estimated regarding local oxygen tension. Non-hypoxic wounds (i.e., pO_2 >30 mmHg) will heal rapidly with no complications such as infection oppositely to hypoxic wounds (i.e., pO_2 between 13 and 30 mmHg). When pO_2 drops under 13 mmHg, basal metabolic activity cannot be sustained which leads to gangrenization (Roe et al. 2010).

2.4 Oxygen Skin Permeability

Due to its small molecular size, permeation of oxygen through the skin is likely to occur massively through porous structures such as skin appendages (e.g., eccrine glands). Permeation of oxygen through nonporous regions of the skin could also follow the transcellular pathway via transmembrane proteins such as aquaporins that exhibit gas transport capacities (Roe et al. 2010; Wang and Tajkhorshid 2007). Data is scarce on oxygen skin permeability but suggests it relies mostly on passive physicochemical-mediated transport and not active cellular mechanisms (Roe et al. 2010). Oxygen delivery from a saturated aqueous vehicle was assessed *ex vivo* using porcine skin. Exogenous (i.e., via the *stratum corneum*) and endogenous (i.e., via the dermis) administrations were simulated and revealed a higher permeation for endogenous delivery and a better skin penetration supposedly due to reservoir effect of *stratum corneum* lipid matrix with exogenous administration. However, some studies suggest tape stripping of the epidermis leads to enhanced oxygen penetration into the skin from an aqueous formulation (Ladizinsky and Roe 2010; Atrux-Tallau et al. 2009). Therefore, it is not clear if skin stratified structure and more specifically the *stratum corneum* can be considered as a major barrier to transcutaneous penetration of oxygen. Overall, oxygen absorption in the epidermis from the environment can be described using a Fickian model where a pO_2 gradient governs oxygen penetration. This theoretically enables local therapeutic approaches based on topical application of oxygen-loaded formulations (Reading et al. 2013).

3 Compounding Strategies for Oxygen

3.1 Gaseous Formulations of Oxygen

Oxygen therapy in the context of wound healing should be able to deliver sufficient oxygen to reach pO_2 found in healthy well-perfused tissues (i.e., >30 mmHg). Hyperbaric oxygen therapy is known to have significant impact on wound healing processes as long as blood perfusion is effective in the targeted tissue. Concerning the skin, hyperbaric oxygen therapy raises subcutaneous oxygen tension for several hours after return to normobaric conditions (Ladizinsky and Roe 2010). However, gaseous formulations of oxygen require that gaseous oxygen overcomes the gas/liquid phase boundary before it becomes bioavailable (Roe et al. 2010). Furthermore, high-pressure gaseous oxygen administration is limited as it will mechanically cause microvascular occlusion at administration site (Reading et al. 2013).

3.2 Liquid Formulations of Oxygen

3.2.1 Aqueous Formulations

As oxygen is bioavailable if dissolved in a fluid state, liquid formulations of oxygen might provide better biopharmaceutical capacity to deliver oxygen to the skin. Dissolved oxygen applied topically shows (i) faster rate and (ii) deeper depth of penetration in human skin than gaseous oxygen formulations applied topically (Roe et al. 2010).

Water shows higher penetration capacities through the skin than molecular oxygen and is capable of retaining up to 50 mg of oxygen per liter using simple enriching techniques. Therefore, water may be an interesting and inexpensive vehicle for a liquid formulation of oxygen. Furthermore, an aqueous-based formulation is likely to be supplemented with a large variety of compounds meant to support wound healing process in addition to oxygen (Reading et al. 2013).

Recent reports have shown the absorption of oxygen through the plantar surface of the foot and palmar surface of the hand, when immersed in water that contains high levels of dissolved oxygen. Moreover, age and patient's condition (e.g., diabetes) influence oxygen absorption and/or retention (Reading et al. 2013).

3.2.2 Fluorocarbons

Fluorocarbons are inert synthetic linear of cyclic hydrocarbons ranging from C8 to C10, wherein all or part of the hydrogen atoms have been replaced by fluorine or bromine. They exhibit low molecular weights (i.e., 450–500 Da) and are immiscible with both hydrophobic and aqueous solutions. They are used in industry as a refrigerant and propellant in aerosol canisters but also show a high capacity to dissolve and release oxygen and carbon dioxide. With their oxygen-carrying capacity being 50 times greater than that of water, fluorocarbons feature a better liquid vehicle than water for oxygen transport through the skin (Isaacs et al. 2011). Although nearly twice as dense, most have a similar kinematic viscosity as water.

The solubilization and release of oxygen by fluorocarbon are a physical entirely passive process, unlike the bonding and release of oxygen from hemoglobin in the blood. The amount of dissolved gas is (i) proportional to the partial pressure of the gas in the liquid which is in equilibrium, (ii) inversely proportional to the molecular weight of the fluorocarbons, and (iii) directly related to the number of fluorine atoms present. Physicochemical properties of selected fluorocarbons are given in Table 1 (Kaisers et al. 2003).

Linear fluorocarbons are better oxygen carriers. They are biologically and chemically inert and non-metabolized, and, being volatile, they are excreted through the lungs within a week. However, they accumulate in the reticuloendothelial system where their long-term effects are not yet established (Krafft 2001).

A major drawback consists in their immiscibility to water. Therefore, they must be administered either (i) as an emulsion, to be carried in the vasculature, or (ii) as a dispersion of fine particles of 0.1–0.2 mm in suspension in isotonic saline electrolyte. To obtain stable emulsions at ambient temperature, emulsifiers are necessary. Emulsifiers commonly used, such as egg yolk

Table 1 Physicochemical properties of selected PFCs

	FC-77	FC-75	FC-3280	Rimar 101	Perfluorodecalin	Perflubron
Chemical formula	50/50 mix of two isomers of $C_8F_{16}O$	40/40/20 mix of two isomers of $C_8F_{16}O$ and C_8F_{18}	C_8F_{18}	$C_8F_{16}o$	$C_{10}F_{18}$	$C_8F_{17}Br$
Molecular weight (Daltons)	Approx. 416	Approx. 420	438	416	462	499
Boiling point (°C)	97	102	102	101	142	143
Density at 25 °C (g ml^{-1})	1.78	1.78	1.76	1.77	1.95	1.93
Kinematic viscosity at 25 °C (Pa.s)	0.80	0.82	0.80	0.82	2.90	1.1
Vapor pressure at 37 °C (mmHg)	85	63	Approx. 51	64	14	11
Surface tension at 25 °C (dyne. cm^{-1})	15	15	15	15	15	18
Oxygen solubility at 25 °C (ml gas per 100 ml PFC)	50	52	Approx. 48	52	49	53
Carbon dioxide solubility at 25 °C (ml gas per 100 ml PFC)	198	160	Approx. 176	160	140	210

phospholipids, provide stable emulsions and can be sterilized without degradation. The ability to transport oxygen of these emulsions is dependent on the concentration of fluorocarbon. The emulsions that contain 45–60 % of fluorocarbon (w/v) seem optimal to transport oxygen, but their high viscosity limits the concentrations used.

3.3 Colloidal Formulations

3.3.1 Micro- and Nanosponges

Nanosponge and microsponge delivery systems were originally developed for topical delivery of drugs. This controlled release technology for topical agents consist of nano- or microporous beads loaded with active agent obtained by cross-linking of cyclodextrin. The average diameter of a nanosponge is below one micrometer, whereas for microsponges it ranges from 10 to 25 μm. These vehicles are designed to deliver efficiently a pharmaceutical active ingredient at minimum dose and to enhance stability. Nanosponge formulations might be potential gas delivery systems showing the ability to store and to release oxygen slowly over time. Furthermore, nanosponges exhibit high loading capacity for other gases (e.g., carbon dioxide and methylcyclopropene) (Cavalli et al. 2010; Patel and Oswal 2012).

3.3.2 Micro- and Nanobubbles

Microbubbles and nanobubbles are spherical gas-filled low-density structures with a mean diameter of 1–8 μm and >1 μm, respectively. They comprise a spherical cavity containing gas (e.g., oxygen) and gas-loading agents such as fluorocarbons. They are stabilized by a lipidic or polymeric coating. When introduced in an oxygen-deprived environment, oxygen-containing fluorocarbon microbubble will deflate, liberating their oxygen content. Subsequently, if the environment is reoxygenated, microbubbles will reload oxygen and recover a spherical shape. This property has important medical applications, for instance, in the development of synthetic blood substitutes. Furthermore, micro- and nanobubbles respond to ultrasonic stimulation by liberating their gaseous content, enabling to develop ultrasonic-driven targeting therapeutic strategies (Unger et al. 2004). For instance, gene transfection in reconstructed human skin was achieved by ultrasonic-enhanced microbubble delivery (Yang et al. 2005), and micro-/nanobubbles are presented as ultrasound-targeting oxygen delivery systems as adjuvant to antibiotics in anaerobic infections. Furthermore, many medical conditions, such as diabetes, burns, bedsores, and wounds, are possible fields of application of oxygen-filled micro-/nanobubbles besides other oxygenation approaches (Cavalli et al. 2009).

4 Clinical Applications

4.1 Interest of Oxygen Therapies

Numerous diseases are caused by tissular ischemia or hypoxia. Under some conditions, the HIF-mediated homeostatic response is not sufficient, and the use of hyperbaric oxygen therapy is required. Hyperbaric oxygen therapy has been shown to enhance bone, muscle, and skin healing, particularly in conditions of ischemia and low oxygen tension. In the skin, it is proved that hyperbaric oxygen has positive treatment effect on promoting wound healing of, e.g., chronic ulcers and diabetic foot (Thackham et al. 2008; Eskes et al. 2010). Moreover, hyperbaric oxygen increases levels of growth factors, such as vascular endothelial growth factor, and stimulates vasculogenic stem cell mobilization from the bone marrow in response to oxidative stress.

The goal of an oxygen therapy for wound care is to transfer sufficient oxygen to interstitial tissues to maintain a concentration above 30 mmHg found in healthy, well-perfused tissues. Oxygen concentration is paramount to the proliferation and differentiation of a variety of cell types. Various mechanisms have been proposed to explain positive effects of oxygen therapies on injured tissues. Indeed, high levels of oxygen stimulate the proliferation of fibroblasts and endothelial cells, differentiation and migration of keratinocytes, and angiogenesis and decrease edema in the periwound skin, through a vasoconstrictive effect. The functioning of several enzymes needed for the correct synthesis of collagen requires oxygen as a cofactor (Zgonis et al. 2005). Furthermore, hyperoxia facilitates the elimination of anaerobic bacteria by leukocytes through activation of the oxygen-dependent peroxidase system and promotes the production of ROS that attack bacterial structures (Fife et al. 2002).

4.2 Drawback of Oxygen Therapies

The use of oxygen therapy in hypoxic conditions is promising; however, abusive use poses risks, notably oxidative stress. This is especially true in the context of widespread oxygen therapies for cosmetic and esthetic means.

One potential danger is that ROS produced from oxygen are highly reactive and therefore exhibit potent toxicity, which often occurs under hyperbaric conditions. When oxygen exposure overpowers the tolerance of tissues, further exposure may eventually result in toxicity or oxidative injury. Oxygen toxicity occurs after extended periods of hyperbaric oxygen exposure and/or at high pressure.

It has also been reported that hyperbaric oxygen therapy increases the production of ROS within the tissue (Matsunami et al. 2009), thereby mobilizing cellular antioxidant responses (Godman et al. 2010). ROS can oxidize proteins and lipids and

Table 2 Contrasting hyperbaric oxygen therapy with topical oxygen delivery modalities for wound care

Systemic hyperbaric oxygenation	Topical delivery of oxygen
Systematically oxygenated blood at 2–3 atm	Topically oxygenated wound tissue at 1 atm
Requires specialized facilities and personnel	Portable device
Relatively expensive	Inexpensive
Relies on vascular system to deliver oxygen in wounds	Delivers oxygen to superficial wounded tissues severed from circulation
Poor vascularity of wound tissue limits oxygen diffusion	Oxygenation is independent of vascular bed
Risk of multiorgan oxygen toxicity	Limited and localized risk of toxicity

react with DNA to cause single-strand breaks and base modifications. This process imparts a number of molecular changes to skin tissue and an overwhelming of cellular protective responses, ultimately leading to increased levels of cell death (Pustisek and Situm 2012).

4.3 Topical Oxygen Delivery Strategies

As we have seen, different formulations exist that enable oxygen loading and dermal application in chronic wounds and to address the lack of oxygen due to low perfusion in certain skin diseases. As oxygen was found to better penetrate skin layers from exogenous supply than from endogenous supply, local topical delivery of oxygen appears a rational approach to enhance pO_2 in the skin (Atrux-Tallau et al. 2009).

Gas formulations are readily developed and available such as hyperbaric oxygen therapy; however, they remain inconvenient in terms of administration (Table 2). Liquid formulations in aqueous media or enhanced loading capacity media such as fluorocarbons appear handier, but drawbacks in compounding and delivery control have led to develop more complex formulations with targeting and controlled release characteristics. Colloidal formulations able to entrap oxygen show promising aptitudes and best meet these criteria. Other strategies such as incorporation of a vasodilating agent (e.g., nicotinate esters) may be interestingly combined to oxygen delivery systems to improve skin oxygen content by exogenous and endogenous supply (Krzic et al. 2001).

5 Conclusion

The perceived health and physiologic functioning of the skin depend on adequate oxygen availability, both oxygen present in the body and oxygen contributed by the external environment. The capacity of the skin to absorb oxygen from air has often been overlooked but can account for up to 2 % of the total oxygen consumed by the body and is especially important to the epidermis.

Formulations have been developed to overcome skin hypoxia. Complex colloidal formulations are not yet used at their full potential in the skin care area, however in rapid progress. Nevertheless, vigilance is required about frequent and or abusive use as high amounts of oxygen can cause oxidative stress resulting in the exact opposite of therapeutically expected effect.

References

Asadamongkol B, Zhang JH. The development of hyperbaric oxygen therapy for skin rejuvenation and treatment of photoaging. Med Gas Res. 2014;4:7.

Atrux-Tallau N, Le TH, Denis A, Padois K, Zahouani H, Haftek M, Falson F, Pirot F. Simultaneous characterization of oxygen transport into and through porcine skin exposed to oxygen-saturated water. Skin Pharmacol Physiol. 2009;22(4):210–7.

Boutin AT, Weidemann A, Fu Z, Mesropian L, Gradin K, Jamora C, Wiesener M, Eckardt KU, Koch CJ, Ellies LG, Haddad G, Haase VH, Simon MC, Poellinger L, Powell FL, Johnson RS. Epidermal sensing of oxygen is essential for systemic hypoxic response. Cell. 2008;133(2):223–34.

Cavalli R, Bisazza A, Giustetto P, Civra A, Lembo D, Trotta G, Guiot C, Trotta M. Preparation and characterization of dextran nanobubbles for oxygen delivery. Int J Pharm. 2009;381(2):160–5.

Cavalli R, Akhter AK, Bisazza A, Giustetto P, Trotta F, Vavia P. Nanosponge formulations as oxygen delivery systems. Int J Pharm. 2010;402(1–2):254–7.

Eskes A, Ubbink DT, Lubbers M, Lucas C, Vermeulen H. Hyperbaric oxygen therapy for treating acute surgical and traumatic wounds. Cochrane Database Syst Rev. 2010;(10):CD008059.

Fife CE, Buyukcakir C, Otto GH, Sheffield PJ, Warriner RA, Love TL, Mader J. The predictive value of transcutaneous oxygen tension measurement in diabetic lower extremity ulcers treated with hyperbaric oxygen therapy: a retrospective analysis of 1,144 patients. Wound Repair Regen. 2002;10(4):198–207.

Godman CA, Joshi R, Giardina C, Perdrizet G, Hightower LE. Hyperbaric oxygen treatment induces antioxidant gene expression. Ann N Y Acad Sci. 2010;1197:178–83.

Jonathan Isaacs, Ilvy Friebe, Satya Mallu, and Keith Bachman. Neurotrophic effects of perfluorocarbon emulsion gel: a pilot study. J Brachial Plex Peripher Nerve Inj. 2011;6:11.

Kaisers U, Kelly KP, Busch T. Liquid ventilation. Br J Anaesth. 2003;91(1):143–51.

Krafft MP. Fluorocarbons and fluorinated amphiphiles in drug delivery and biomedical research. Adv Drug Deliv Rev. 2001;47(2–3):209–28.

Krzic M, Sentjurc M, Kristl J. Improved skin oxygenation after benzyl nicotinate application in different carriers as measured by EPR oximetry in vivo. J Control Release. 2001;70(1–2):203–11.

Ladizinsky D, Roe D. New insights into oxygen therapy for wound healing. Wounds. 2010;22(12):294–300.

Matsunami T, Sato Y, Sato T, Ariga S, Shimomura T, Yukawa M. Oxidative stress and gene expression of antioxidant enzymes in the streptozotocin-induced diabetic rats under hyperbaric oxygen exposure. Int J Clin Exp Pathol. 2009;3(2):177–88.

Patel EK, Oswal RJ. Nanosponge and microsponges: a novel drug delivery system. Int J Res Pharm Chem. 2012;2(2):237–43.

Pustisek N, Situm M. UV-radiation, apoptosis and skin. Coll Antropol. 2012;35 Suppl 2:339–41.

Reading SA, Yeomans M, Levesque C. Skin oxygen tension is improved by immersion in oxygen-enriched water. Int J Cosmet Sci. 2013;35(6):600–7.

Roe DF, Gibbins BL, Ladizinsky DA. Topical dissolved oxygen penetrates skin: model and method. J Surg Res. 2010;159(1):e29–36.

Semenza GL. O2 sensing: only skin deep? Cell. 2008; 133(2):206–8.

Straseski JA, Gibson AL, Thomas-Virnig CL, Allen-Hoffmann BL. Oxygen deprivation inhibits basal keratinocyte proliferation in a model of human skin and induces regio-specific changes in the distribution of epidermal adherens junction proteins, aquaporin-3, and glycogen. Wound Repair Regen. 2009;17(4):606–16.

Thackham JA, McElwain DL, Long RJ. The use of hyperbaric oxygen therapy to treat chronic wounds: a review. Wound Repair Regen. 2008;16(3):321–30.

Unger EC, Porter T, Culp W, Labell R, Matsunaga T, Zutshi R. Therapeutic applications of lipid-coated microbubbles. Adv Drug Deliv Rev. 2004;56(9): 1291–314.

Wang Y, Tajkhorshid E. Molecular mechanisms of conduction and selectivity in aquaporin water channels. J Nutr. 2007;137(6 Suppl 1):1509S–15. discussion 1516S-1517S.

Yang L, Shirakata Y, Tamai K, Dai X, Hanakawa Y, Tokumaru S, Yahata Y, Tohyama M, Shiraishi K, Nagai H, Wang X, Murakami S, Sayama K, Kaneda Y, Hashimoto K. Microbubble-enhanced ultrasound for gene transfer into living skin equivalents. J Dermatol Sci. 2005;40(2):105–14.

Zgonis T, Garbalosa JC, Burns P, Vidt L, Lowery C. A retrospective study of patients with diabetes mellitus after partial foot amputation and hyperbaric oxygen treatment. J Foot Ankle Surg. 2005;44(4): 276–80.

Dermis Connective Tissue Histopathology

41

Pierre Agache

Contents

Keywords

Dermis • Elaunin fibers • Glycosaminoglycans (GAGs) • Lymphocytes • Microfibril-associated glycoproteins (MAGP) • Papillary/adventitial dermis • Reticular dermis • Skin appendages

The dermis (also called the cutis) is by far the thickest skin layer and amounts to about 7 % of the body weight. Its connective tissue is special because of its structure and because it holds many independent small organs, the hairs, and the sweat glands, together called skin appendages. Like other connective tissues, the dermis appears at first as a mesh of interconnected collagen fibers, elastic fibers and an interstitial ground substance rich in proteins and glycosaminoglycans (GAGs) (Fig. 1). Most of the collagen is formed by the assembly at regular intervals of strong fibrils (thickness: 20–100 nm) (Breathnagh 1971) (Fig. 2) separated by proteoglycans, arranged in interconnected bundles forming a network without detectable free extremities. The elastic fibers have a fibrillar skeleton composed of fibrillin (type 1 and 2) (thickness: 1.0–1.3 nm) and other fibrillar proteins (fibulin, microfibril-associated fibrillar protein, MAFP), at the center of which an amorphous substance, elastin, is deposited. They are interwoven with collagen fibers (Fig. 3). The fibrillar collagens and the elastic fibers are embedded in a viscous gel (so-called ground substance) made of nonfibrillar collagens,

This chapter was originally published under the ISBN 978-3-540-01771-4 with the following book title Measuring the Skin. The content has not been changed.

Pierre Agache: deceased.

P. Agache (✉)
Department of Dermatology, University Hospital of Besançon, Besançon, France
e-mail: aude.agache@free.fr; ferial.fanian@chu-besancon.fr; ferial.fanian@cert-besancon.com

P. Humbert et al. (eds.), *Agache's Measuring the Skin*, DOI 10.1007/978-3-319-32383-1_164

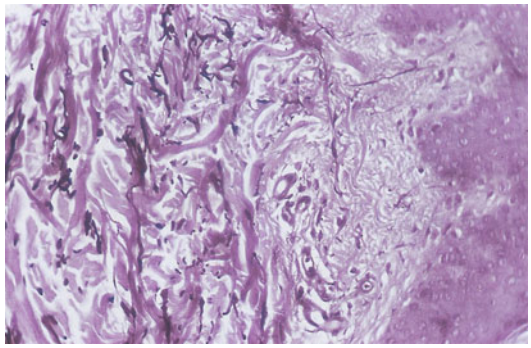

Fig. 1 Vertical section of the subpapillary and mid-dermis (optical microscope). Collagen bundles are colored in *pink* and elastic fibers in *violet*. Orcein. ×600 (Courtesy of Prof. Laurent, Department of Dermatology, University of Besançon, France)

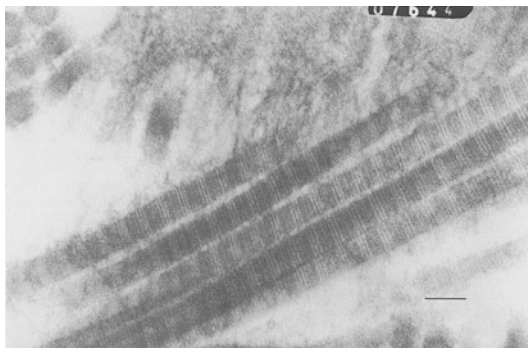

Fig. 2 Collagen fiber (transmission electron microscope). Note the transverse striation at every 60 nm, which is due to a gap in the relative positioning of the fibrils. Bar = 0.1 µm (Courtesy of Prof. Laurent, Department of Dermatology, University of Besançon, France)

proteoglycans (association of proteins and glycosaminoglycans), and microfibril-associated glycoproteins (MAGP) (Pope 1998). All these components of the dermis are synthesized by the fibrocytes (also called fibroblasts, although they are mature cells) that are abundant in young tissue but rare in older ones. Finally, a substantial amount of water is retained because of the high hygroscopic power of the MAGP. Microscope or ultrasound examination reveals two types of dermal connective tissue depending on the structure and location: the papillary/subpapillary and adventitial dermis, 20–100 µm wide, and the reticular dermis (or chorion) 10–20 times thicker.

1 Subpapillary and Adventitial Dermis

1.1 Structure

The subpapillary (subepidermal) or adventitial (around the pilosebaceous or sudoral appendages) dermis holds a thin fibrillar network mainly composed of type I and III collagen, type VII collagen, thin elastic fibers (type 2 fibrillin) and fibrillin 2 without elastin (oxytalan fibers) (Pope 1998). In the deeper part of the subepidermal dermis, collagen and elastic fibers are horizontally oriented, whereas in the upper part they are mostly vertical and connect the horizontal network to the dermoepidermal junction. This type of dermis looks clear under optical microscope because the ground substance (MAFP, MAGP) and the water it retains constitute the major part of its volume. Cohesion to epidermis is ensured by a basal membrane (a mesh of collagen IV, fibronectin, other fibrillar proteins, and globular collagens) connected to the epidermal keratinocytes by hemidesmosomes and to the collagen network by anchoring fibers (collagen VII) and a ramification of oxytalan fibers (see ▶ Chap. 36, "Epidermal Physiology," Fig. 2).

1.2 Function

The papillary/adventitial dermis functions are numerous:

1. It ensures the nutrition of the overlying layers of epithelium and their hormonal and paracrine exchanges thanks to the numerous vessels (arterioles, venules, blood and lymphatic capillaries) that it contains. As such, its thickness varies in relation to the activity of the overlying epithelium layers, and it must be regenerated before the healing of a wound begins. However, in this case, the papillary dermis reconstituted from inflammatory granulation tissue is generally more fibrous than normal, with few elastic fibers, and the dermoepidermal junction is devoid of papillary relief.
2. It partly controls percutaneous absorption thanks to its blood and lymphatic vessels. The lower the

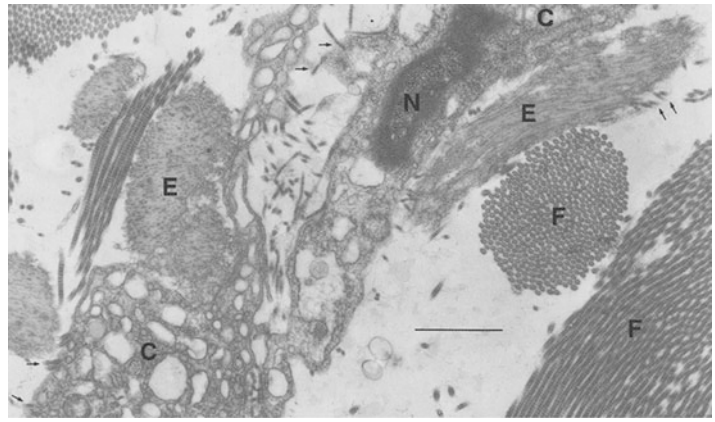

Fig. 3 Reticular dermis (transmission electron microscope). Two fibrocytes are seen in the center. Their cytoplasm (*C*) is rich in cistemae. *N* nucleus, *F* collagen fibrils perpendicularly oriented. *E* elastic fibers containing both elastin and fibrillin. Some collagen fibrils seem to stick to fibrocytes, others to elastic fibers (*arrows*). Bar = 1 μm (Courtesy of Prof. Laurent, Department of Dermatology, University of Besançon, France)

blood or lymph flow, the slower the decrease in the permeant concentration in the epidermis intercellular spaces; this process may explain the lower percutaneous absorption in the aged, in spite of the reduced thickness of the epidermis.

3. It has an architectural function: the collagen, fibrillin, and elastic fiber framework contributes to the protection of vessels and cells against mechanical aggressions (the reticular dermis fulfills this function more efficiently). The elastic fiber network ensures full recovery of shape after deformation. Elaunin fibers (elastic fibers with very little elastin) may be responsible for the maintenance of the dermoepidermal papillary relief; they disappear during actinic aging. Both synthesis and degradation of collagen, elastin, and fundamental substance by fibrocytes are possible, but what triggers the production of proteolytic enzymes is mainly inflammatory cells. It contains most of the nerve endings responsible for the tactile function of the hair (see ▶ Chaps. 76, "Scalp Sebaceous Function Assessment," and ▶ 99, "Skin Tensile Strength in Scleroderma").
4. In addition, adventitial/subepidermal dermis contains inflammation inducers, among them type C and Aδ nerve fibers providing proinflammatory neuropeptides, and (for the most part perivascularly located) mast cells, which are a source of potentially highly inflammatory substances. Accordingly, this type of dermis is mainly responsible for the strong reactivity of the skin. Around sweat gland secretory coils, abundant cholinergic nerves provide the acetylcholine responsible for sweat secretion when excited.
5. The papillary dermis contributes, together with the epidermis, to the immunological function of the skin by ensuring the transit of the immunocompetent cells (Langerhans cells, lymphocytes) toward the lymph nodes, directly or through its lymphatic vessels. Dendrocytes (Riley 1974), lymphocytes, and histiocytes also play a part in the SALT (skin-associated lymphoid tissue), which is of paramount importance in delayed hypersensitivity phenomena. Mast cells are also a major step in immediate hypersensitivity reactions.
6. An important quota of macrophages and histiocytes aid the dermis to remove the barely soluble waste of cellular or metabolic origin (e.g., extravasated red blood cells).

2 Reticular Dermis

The reticular dermis is very different, over 500 μm thick and subdivided sometimes into mid-dermis and deeper dermis. Under the optical microscope,

only a thick mesh of collagen bundles orientated in all directions in a plane parallel to the surface is detected. Vessel sections are rare. In most anatomical areas, they are only transfer arterioles and venules. In the palms and soles, numerous arteriolovenular shunts can also be found, which are involved in the thermal regulation of the extremities. The mid-dermis contains the pilosebaceous appendages (downy or vellus hairs) and the deep dermis contains the coiled part of the sweat glands and their excretory ducts. Apart from these epithelial structures (surrounded by adventitial dermis), there are few cells, almost only fibrocytes. The collagen bundles of the reticular dermis are formed by type 1 collagen (Fig. 2) coated with MAGP and MAFP, which maintain the fibers separated from one another (Scott 1992) and contribute to the water binding onto their surface, thus making the tissue swell. Scanning electron microscopy shows that these bundles appear curved and stretched in the direction of the highest tension of the skin as a result of thick elastic fibers (Piérard and Lapière 1987) (Fig. 4). They are made of type 1 fibrillin and elastin. The deep dermis is a little more dense than the mid-dermis but has a similar structure.

The reticular dermis function is mainly mechanical. It forms a solid structure, although distensible (up to about 25 %) as well as compressible, and protects the adnexal epithelia against mechanical aggressions. Because of its elasticity, it is responsible for the maintenance of the tissue shape and architecture. A partial failure of this function is found in hypertrophic scars, keloids, and stretch marks (striae gravidarum, striae distensae). Finally, the permanent tension of the reticular dermis, due to the traction exerted by elastic fibers, generates the folding of nonelastic overlying structures (viable epidermis and stratum corneum). This is the origin of the skin surface relief, which appears first at the deeper level of subpapillary dermis.

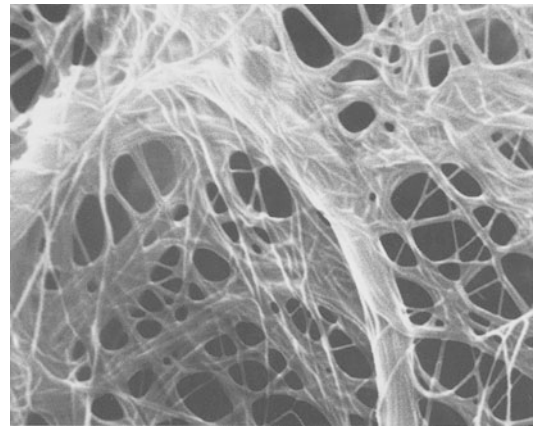

Fig. 4 Reticular dermis (scanning electron microscope). The spontaneous skin tension has been preserved and the ground substance discarded. Elastic fibers form a tense network attached to a curved collagen bundle. ×100,000 (Courtesy of Prof. Piérard, Department of Dermatopathology, University of Liège, Belgium)

References

Breathnagh AS. Atlas of the ultrastructure of human skin. Development, differentiation and post-natal features. London: Churchill; 1971.

Piérard GE, Lapière CM. Microanatomy of the dermis in relation to relaxed skin tension lines and Langer's lines. Am J Dermatopathol. 1987;9:219–24.

Pope FM. Dermis. In: Champion RH, Burton JL, Burns DA, Breathnagh SM, editors. Textbook of dermatology. 6th ed. Oxford: Blackwell; 1998. p. 59–92.

Riley PA. Dendrocytes. In: Jarrett A et al., editors. The physiology and pathophysiology of the skin, vol. 3. London: Academic; 1974.

Scott JE. Supramolecular organisation in the extracellular matrix. FASEB J. 1992;6:2639–45.

Evaluation of the Cutis by High-Resolution Sonography

42

Stephan El Gammal, Claudia El Gammal, Peter Altmeyer, and Michael Vogt

Contents

S. El Gammal (✉)
Dermatological Clinic, Diakonie Klinikum Bethesda, Freudenberg, Germany
e-mail: stephan@ElGammal.de

C. El Gammal
Dermatology, Medical Care Center, Diakonie Klinikum Jung-Stilling, Siegen, Germany

P. Altmeyer
Department of Dermatology and Allergology, Ruhr University Bochum, Bochum, Germany

M. Vogt
Institute for High Frequency Techniques of the Ruhr-University, Bochum, Germany

P. Humbert et al. (eds.), *Agache's Measuring the Skin*,
DOI 10.1007/978-3-319-32383-1_42

Keywords
Sonography • 22–100 MHz • Stratum corneum • Viable epidermis • Dermis • Subcutis • Inflammatory skin diseases • Skin tumors

1 Introduction

Clinical examination of skin pathology by inspection and palpation delivers crucial hints to determine the correct dermatological diagnosis. When examining tumorous or inflammatory diseases – apart from the involved skin area – the registration of in-depth expansion of the process is a further important clinical parameter. Sonography is an interesting tool to collect this missing information.

It has already conquered many specialities in medicine. Until 1975 ultrasound transducers with a center frequency and bandwidth of maximal 7.5 MHz were available. Attempts to evaluate inflammatory and tumorous processes in the skin using 1,5–5 MHz transducers delivered very unsatisfactory results (Rukinava and Mohar 1979). The pioneers Alexander and Miller (1979) were the first scientists measuring skin thickness using 15 MHz pulsed ultrasound.

Subsequently in the 1980s and 1990s specific 15 – 20 MHz ultrasound imaging systems were developed.

Figure 1 visualizes the number of Medline publications focusing on different *noninvasive skin imaging* methods over the past 30 years.

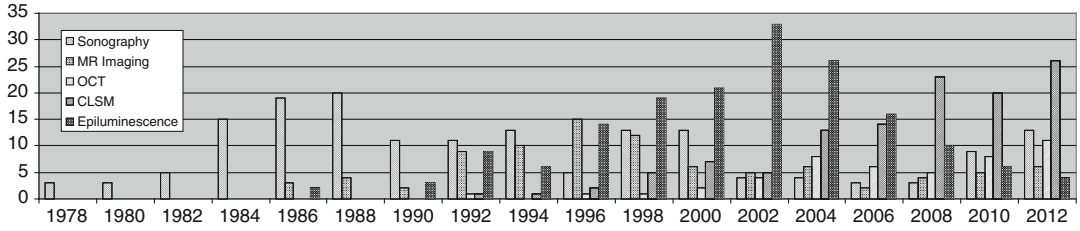

Fig. 1 Medline publications on noninvasive skin imaging methods. *MRI* magnetic resonance imaging, *OCT* optical coherence tomography, *CLSM* confocal laser scanning microscopy

Sonography is the oldest method to look at skin layers *beneath* the skin surface and was widely introduced to clinical dermatology in the 1990s. As the above chart (Fig. 1) displays, scientific research focused on epiluminescence microscopy ten years ago. The latter delivers additional information allowing one to differentiate between malignant and benign pigmented skin tumors, wherefore it was highly targeted by researchers during this period of time. Recent research deals with "subsurface" methods – e.g., confocal laser scanning microscopy and multiphoton microscopy – as they enable the evaluation of skin diseases and tumors at a cellular level, thus reducing skin biopsies. Many of these new exciting methods are presented elsewhere in this book.

During the past 25 years, 25 MHz sonography of the skin has become an accepted noninvasive imaging method in dermatology. Clinical applications are the preoperative determination of the extension of skin tumors (Hoffmann et al. 1992b; Fornage et al. 1993; Gropper et al. 1993; Harland et al. 1993; El Gammal et al. 1993; Gupta et al. 1996a; Desai et al. 2007), the monitoring of inflammatory lesions (Di Nardo et al. 1992; Stiller et al. 1994; Vaillant et al. 1994; Hoffmann et al. 1995; Gupta et al. 1996b) and sclerotic processes (Cole et al. 1981; Serup 1984; Myers et al. 1986; Akesson et al. 1986; Hoffmann et al. 1992a; Lévy et al. 1993; Ihn et al. 1995), and the objective judgment of skin tests, such as patch test reactions (Serup and Staberg 1987; Seidenari and di Nardo 1992; Seidenari 1995) and tuberculin test reaction (Beck et al. 1986), to name just a few.

Sonograms of the normal skin show, at their upper border, a thin, very echorich line, the so-called *skin entry echo*. Beneath, a broad, echorich band with scattered reflexes is seen, which corresponds to the dermis (Fig. 2). The subcutaneous fatty tissue is echolucent and traversed by obliquely oriented echorich connective tissue septae. As the epidermis is echopoor it cannot be visualized, and certainly structures within the epidermis cannot be differentiated (El Gammal et al. 1993; Fornage et al. 1993) due to the lack of resolution of transducers with center frequencies below 20 MHz.

To investigate the epidermis, the resolution must be improved. The axial resolution is mainly influenced by the bandwidth (Fig. 3). The lateral resolution is proportional to the center frequency and indirectly proportional to the focal length (El Gammal et al. 1993, 1995, 1999, 2007). By raising the center frequency and in consequence the bandwidth of the ultrasound transducer, the resolution increases.

At the same time signal penetration depth into the skin is reduced (Fig. 4); a burden one has to accept in order to receive more detailed sonograms.

The 100 MHz transducer technology was modified in such a way that skin structures up to 2 mm depth can be visualized (Paßmann et al. 1989; Ermert et al. 1997; El Gammal et al. 1999) at a very high resolution (Fig. 2 inset).

Considering that dermatology includes *all structures* from the skin surface to the muscle fascia, lower frequencies are necessary to study deep skin structures.

Today 10–18 MHz sonography is used to evaluate the peripheral lymph nodes of patients with skin tumors (Beyer et al. 1982; Brockmann et al. 1985; Blum and Dill-Müller 1998, 1999; Dill-Müller and Maschke 2007).

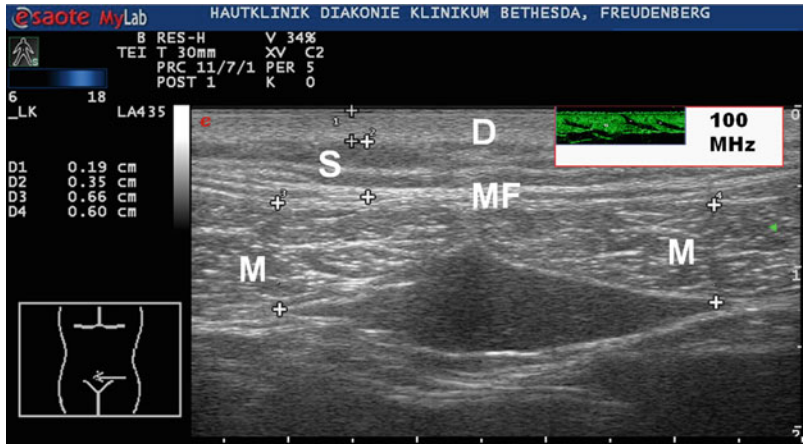

Fig. 2 Comparison of 15 MHz and 100 MHz sonography (*inset*). At 15 MHz the dermis is an ill-defined line at the upper part of sonogram due to insufficient resolution; at 100 MHz structures within the dermis are visualized (e.g., obliquely oriented hair follicles). *D* dermis, *S* subcutis, *MF* muscle fascia, *M* musculus rectus abdominis. The distance between two neighboring lines (*right* border of 15 MHz picture) is 5 mm

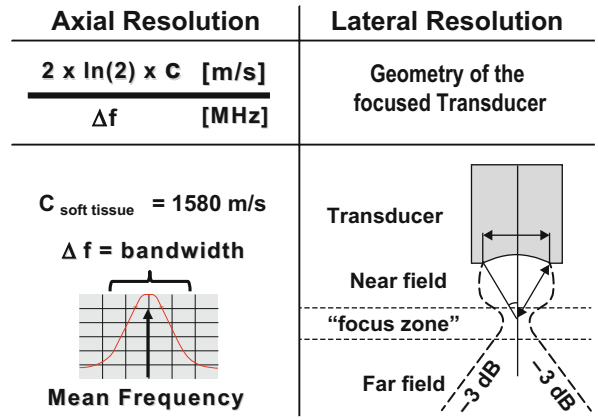

Fig. 3 Physical parameters influencing the axial and lateral resolution. The axial resolution is mainly influenced by the bandwidth of the transducer, the lateral resolution by the geometry of the transducer in the focus zone. The near and far field of the transducer bear multiple artifacts

Since 1995 "Sonography of the skin and subcutis (including the peripheral lymph nodes)" is part of the educational curriculum for dermatologists in Germany, a testimony that this method has become a routine diagnostic tool in dermatology.

2 Methods and Patients

To study the subcutis, an Esaote MyLaB60 ultrasound unit equipped with a 9–18 MHz linear array applicator was used. Ultrasound gel was used as coupling medium.

Examination of the dermis, epidermis, and stratum corneum was done with an experimental ultrasound imaging unit which can be operated with different transducers ranging from 20 to 250 MHz. Technical details have been published elsewhere (Ermert et al. 1997; Paßmann et al. 1989; El Gammal et al. 1995, 1999; Vogt et al. 2001; for transducer details see El Gammal et al. 2007).

A highly focused 100 MHz ceramic transducer (with a short depth in the focus zone of only 400 µm) with an excellent lateral resolution (Fig. 5b) was utilized. In order to obtain sharp sonograms not only from a stripe of 400 µm, but

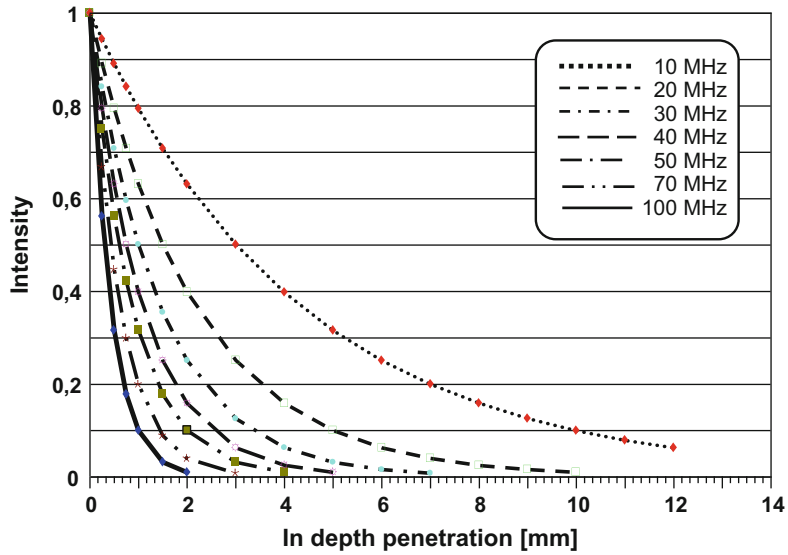

Fig. 4 Center frequency and in-depth penetration of the ultrasound beam. The curves have been plotted down to 0.01 (1–40 dB) of the initial energy I_0 (100 %, 1.00). When the center frequency is raised (and thereby the axial resolution is improved), the in-depth penetration of the ultrasound beam decreases significantly

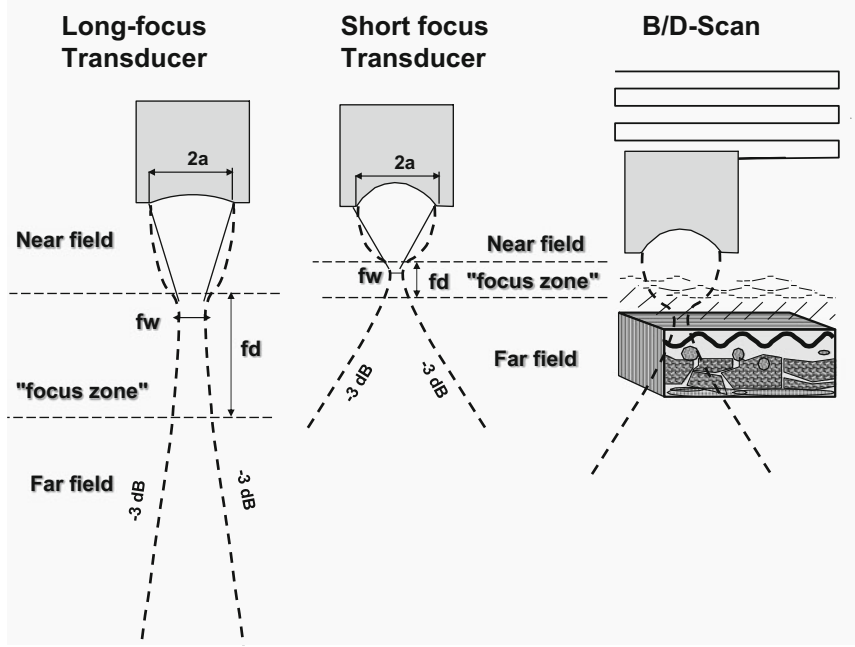

Fig. 5 (**a**) Usually long-focused transducer is used in mechanical scanners. The focal zone is defined by the focal width ***Fw*** and focal depth ***Fd***. (**b**) To improve lateral resolution (***Fw***), we used a short-focused transducer. The focal depth ***Fd*** is reduced to 400 µm. ***Fw*** = 30 µm. (**c**) B/D-Scan. The final sonogram is composed of several 400 µm wide image stripes, which are recorded one after the other, each in the focus zone of the transducer

from a wider part of the skin, we developed a mechanical focusing procedure, called Brightness/Depth-Scan (B/D-Scan; Fig. 5c). The principle of this method is to compose the sonogram of several 400 µm wide image stripes, which are recorded one after the other, each in the focus zone of the transducer (Ermert et al. 1997; Paßmann et al. 1989). After the uppermost stripe is recorded by lateral movement of the transducer over the selected area, the transducer is moved

vertically 400 μm toward the skin surface before the next image stripe is recorded. To eliminate movement artifacts between adjacent stripes, the overlapping parts (near field and far field) are used for adjustment by the computer program, which puts together the final image.

Before we put the image stripes together, every single stripe was processed in two steps. First, the internal echoes of the 100 MHz transducer were eliminated. The oscillation curves of all neighboring A-scans of the image were averaged, and the mean oscillation curve was then subtracted from every single A-scan. Secondly, the A-scans were demodulated. The envelope curve was determined by two complex fast Fourier transformations for every A-scan. This procedure provides optimal results, but does not allow to promptly view the recorded data. For this purpose a fast method of demodulation consisting of a digital rectification of the high-frequency A-scan combined with a non-recursive digital filter of the order of ten was additionally implemented. This linear-phase filter has a passband cutoff frequency of 150 MHz.

2.1 Patients and Volunteers

All volunteers and patients gave informed consent for all examinations.

Healthy Palmar Skin: ten right-handed volunteers with healthy skin (five men and five women, age 29–76, mean 56.4) were investigated. The index fingertip of the left hand was occluded for 30 min with an emulsion using a Finn chamber.

Healthy Glabrous Skin: Sonograms were taken from volunteers with healthy skin (age 20–32, mean 24.1) on the abdomen about 3 cm lateral the umbilicus ($n = 8$), the upper back over the scapula ($n = 11$), the dorsal forearm ($n = 9$), and the calf ($n = 14$). Sonograms of the volar wrist at the transition from palmar to glabrous skin were recorded ($n > 4$).

Psoriasis Vulgaris and Lichen Planus: 35 untreated, infiltrated, and slightly scaly psoriatic lesions on the extremities of 18 patients with chronic plaque-type psoriasis vulgaris and ten lichen planus papules of six patients were investigated. Sonograms were taken in the center and the margin of the lesions and in the surrounding normal skin.

Skin Tumors: Sonograms were taken from skin tumors (basal cell carcinoma, malignant melanoma, seborrheic keratosis, nevocellular nevi) and normal adjacent or contralateral skin. Then the tumors were excised for histology (see below). Only skin tumors with a poor subtumoral infiltrate in histology were included in our study: a total of 27 superficial basal cell carcinomas, 13 malignant melanomas, 16 nevocellular nevi, and 11 seborrheic keratoses were evaluated using statistical methods.

2.2 Image Processing and Statistical Evaluation

Image analysis was performed using the program AnalySIS® (Soft Imaging Software GmbH, Münster, Germany). Structures of interest within the sonographic image (e.g., entry echo or echopoor band) were manually delimited by a polygon, using a position cursor. The mean diameter in y-axis (average length of all A-scans in the polygon) and the mean gray level of the polygon area (value between 0 (black) and 255 (white)) were calculated.

In every sonogram all structures of interest (thickness of the skin entry echo, echodensity of the skin entry echo, echodensity of the echopoor tumor area, echodensity of the subtumoral region) were measured in the skin tumor region *and* in the adjacent or contralateral normal skin. Values were calculated as an index (% of the normal skin).

Finally, the *U*-test (Mann-Whitney-Wilcoxon) for unpaired observations was used to compare the parameters mentioned above. *P*-values of <0.05 were considered significant.

2.3 Correlation with Histology

From 79 patients (psoriasis plaques: $n = 11$, lichen planus papules: $n = 6$, basal cell carcinoma: $n = 27$, malignant melanoma: $n = 13$, nevocellular

nevi: $n = 16$, seborrheic keratoses: $n = 6$) a biopsy was taken after sonography. In order to obtain exactly correlating sonographic and histological images, a 10 mm long line was painted on the skin in the plane of the B-scan. After local anesthesia of the area, the skin was cut along this line down to the subcutis. Then a spindle-shaped excision was performed with this cut in the center. The two halves of the tissue spindle were separated and their central cutting planes placed on cardboard, to prevent distortion of the tissue during formalin fixation.

In all histological sections, the thickness of the epidermis (from the stratum granulosum to the lowest points of the rete pegs) and the thickness of the inflammatory infiltrate (from the uppermost parts of the dermal papillae downward) were measured. Furthermore it was checked whether there is a significant correlation between the thickness measurements in sonographic images and the corresponding histologic sections by using linear regression analysis.

3 Results

3.1 Normal Glabrous Skin

Sonograms of normal skin show at their upper border a thin, very echorich line, the so-called *skin entry echo*. The skin entry echo emerges due to an impedance jump at the intersection between the water (water is used as the coupling medium) and the waterpoor stratum corneum. The thin stratum corneum of glabrous skin obviously cannot be differentiated in 100 MHz sonograms. There is a tiny echopoor band (EPB) between the entry echo and the dermal reflexes. Below, a broad, echorich band with scattered reflexes is seen, which corresponds to the dermis (Fig. 6). The subcutaneous fatty tissue is echolucent with obliquely oriented echorich connective tissue septae.

The reticular dermis is visible as an echorich zone with densely scattered, confluent echo reflexes. It is sharply demarcated from the very echopoor subcutaneous fat. Within the dermis, hair follicle complexes are visible as homogeneous echopoor structures (Fig. 6). To find out which structures of the hair follicle complex can be visualized sonographically, "noninvasive" three-dimensional reconstructions were performed. The principles of three-dimensional reconstruction have extensively been discussed elsewhere (El Gammal et al. 1992, 1993). In Fig. 7a the sonograms of the left column are oriented perpendicular to the sonograms of the right column. The upper left sonogram shows a sharply delineated trifoliate echopoor structure at the dermis-subcutis interface. The middle left sonogram shows the hair follicle canal. The lower left sonogram exhibits an ill-defined structure in the dermis corresponding to the lobular structure of the sebaceous gland. The three-dimensional reconstruction (Fig. 7b) exhibits that the hair canal has an angle of 30° to the skin surface. The lobular structure of the sebaceous gland can be visualized. Using three-dimensional reconstructions, anagen follicles can be differentiated from telogen follicles (El Gammal et al. 1992).

3.2 Normal Palmar Skin

In 100 MHz sonograms of palmar skin, an echorich entry echo is seen at the upper border (Fig. 8). Where the dermatoglyphics are crossly cut (which is mostly the case), the entry echo is wavy; in parts with longitudinally cut dermatoglyphics, it appears as a straight line. Below the entry echo, there is an echopoor band, which will be referred to as EPB 1 (echopoor band 1) in the following. Next comes an echorich line, which runs parallel to the entry echo but is less intense (Figs. 8, 9, and 10). El Gammal et al. (1999) were able to show that the EPB 1 truly represents the stratum corneum by removing (tape stripping) and swelling (occlusion with petrolatum) of the horny layer.

Below the EPB 1, a second echopoor band is seen, which will be referred to as EPB 2 (echopoor band 2). Neither removal nor swelling of the horny layer changes its thickness significantly

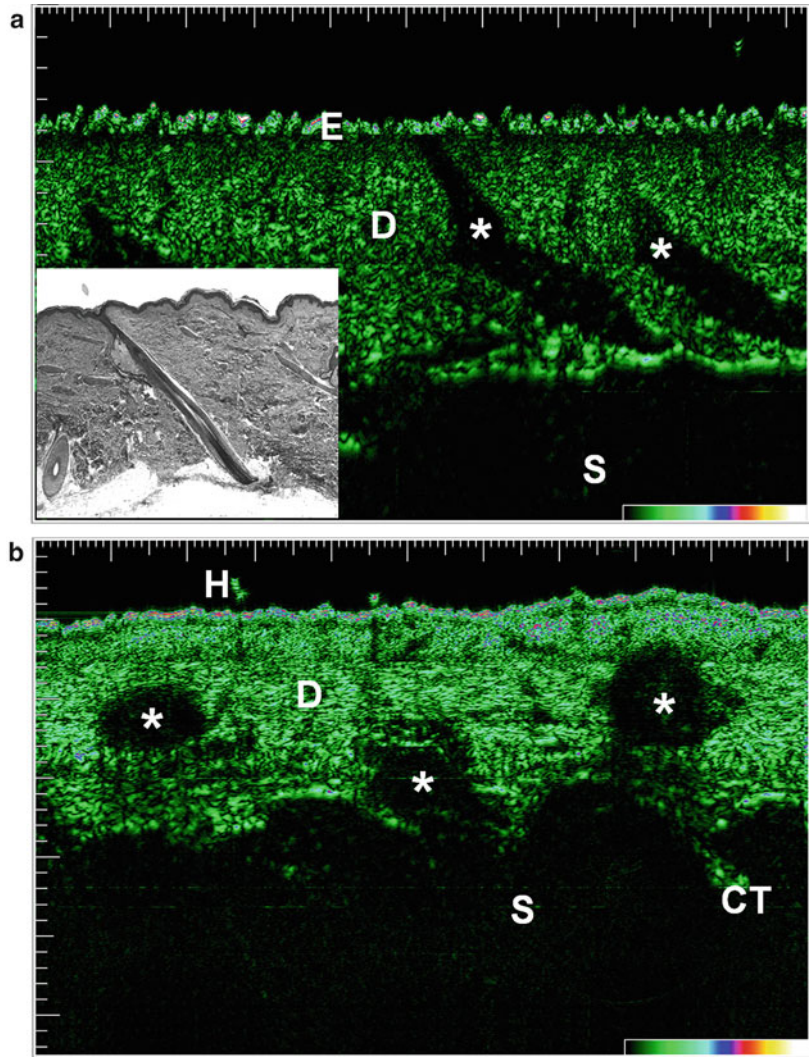

Fig. 6 Hair follicles are represented as echopoor structures in the echorich dermis. (**a**) Thigh; * longitudinal section of hair follicles; *Inset*: correlating histology. (**b**) Thigh; * cross sections of hair follicles. *E* Skin entry echo, *D* dermis, *S* subcutaneous fatty tissue, *CT* connective tissue septae in the subcutis, *H* hair (cross sectioned). Distance between two graduation marks = 100 µm

(El Gammal et al. 1999). The EPB 2 is separated from the EPB 1 by an echorich line. This line represents the interface between the waterpoor stratum corneum and the moist, living part of the epidermis. The lower border of the EPB 2 is defined by the scattered reflexes of the dermis (Figs. 8 and 9). This border is too straight to correspond to the undulating dermo-epidermal junction; it rather represents the interface between the papillary and reticular dermis.

In the EPB 1, twisted, echorich, about 100 µm wide structures are seen, which cross the EPB 1 vertically. The distance between the two of them is 800–950 µm or a multiple. Each of them ends in a small dip on top of a dermatoglyphic crest (Fig. 9). These structures represent eccrine sweat gland ducts. In the EPB 2 they are rarely visible; in the echorich dermis, they cannot be detected either.

Figure 10 shows the transition from palmar to glabrous skin on the wrist: The upper and lower border of the EPB 1 (skin entry echo and echorich line below) merge into one echorich line in glabrous skin, so that the EPB 1 disappears. The thin stratum corneum of glabrous skin cannot be differentiated in 100 MHz sonograms. The EPB

2 remains as the only echopoor band between the entry echo and the dermal reflexes. While the thickness of the entry echo is similar to the one in palmar skin, the echopoor band (EPB) of glabrous skin is markedly thinner than on the palms. On the lower extremities, it is thicker than on the trunk (El Gammal et al. 1999).

Concurrent with the sudden appearance of EPB 1, when moving from glabrous to ridged skin (palmar and plantar), the echogenicity of the

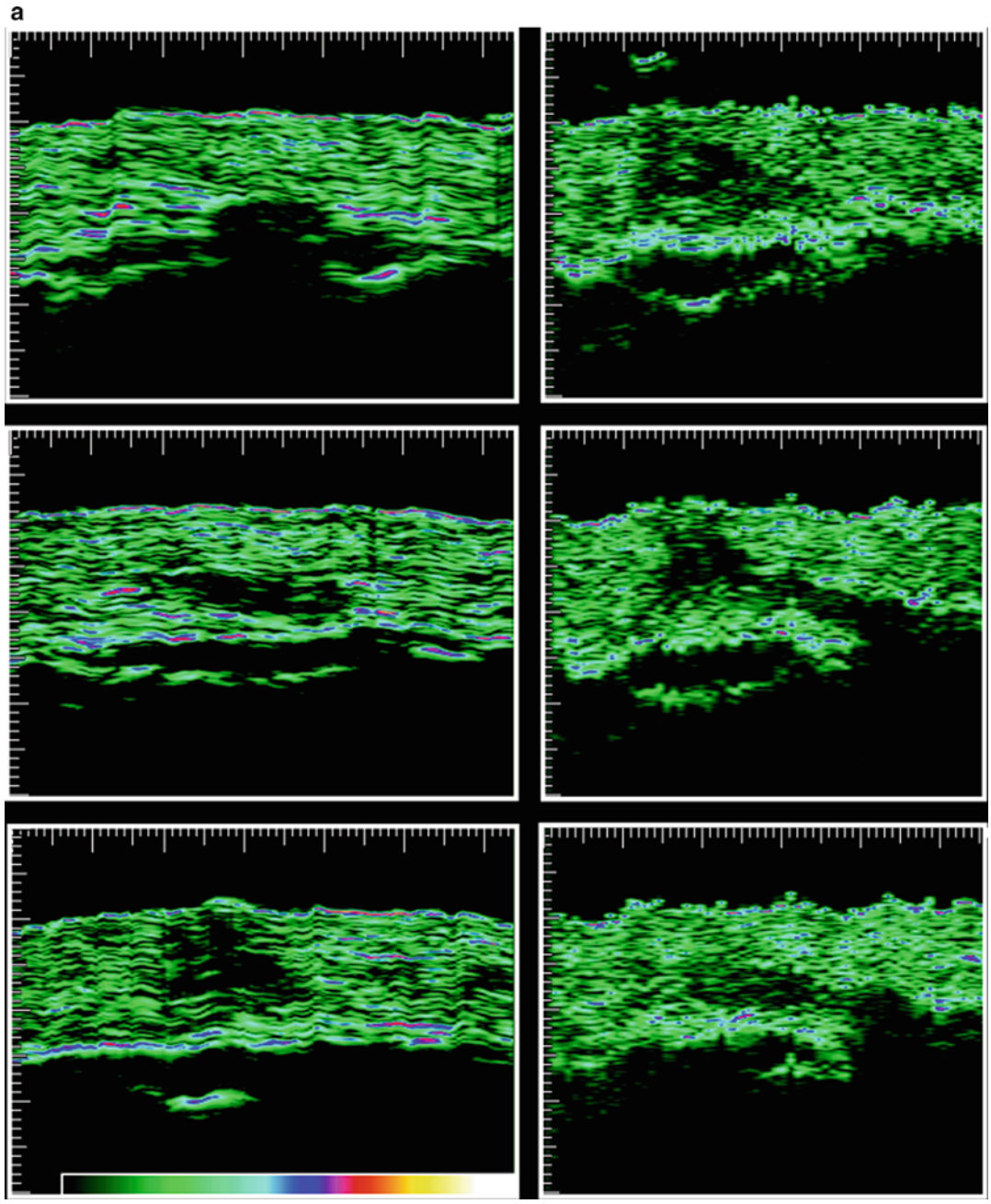

Fig. 7 (continued)

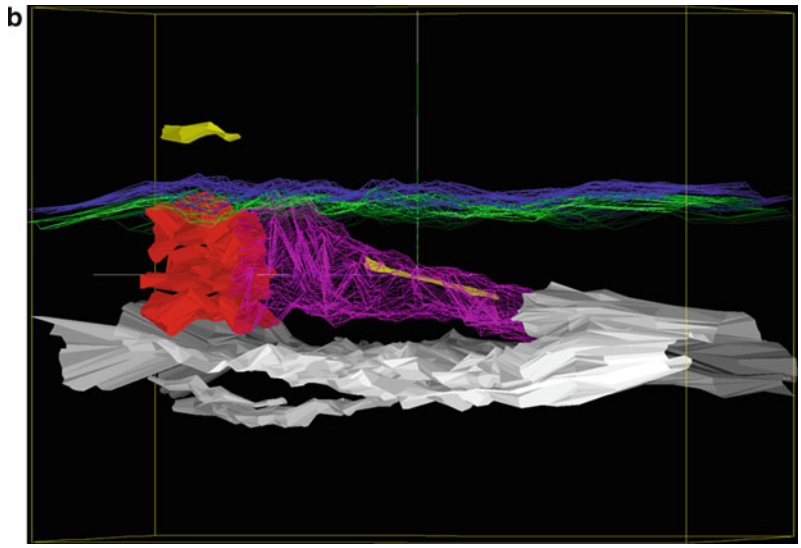

Fig. 7 Serial sections (**a**) and three-dimensional reconstruction of the hair follicle complex on the calf of a 23-year-old woman at 50 MHz. Voxel cube of 3,2 mm (thickness) × 6 × 6 mm. Sections were taken at 50 µm intervals. (**a**) The sonograms of the left column are perpendicular to the sonograms of the *right. Left upper* sonogram: sharply delimited trifoliate echopoor structure at the dermis-subcutis interface. *Left middle* sonogram: hair follicle canal. *Left lower* sonogram: ill-defined lobular structure of the sebaceous gland. *Right* sonograms: longitudinal section of the hair follicle. Note that the hair is slightly bent. (**b**) Three-dimensional reconstruction. The hair is oriented 30° to the skin surface. The hair can be seen in the middle of the hair canal (line reconstruction) and is invisible where it is more obliquely oriented (echo reflexes do not return to the transducer). The hair becomes visible again when it is oriented parallel to the skin surface. *Red* = lobular structure of the sebaceous gland. Distance between two graduation marks = 100 µm (with permission from El Gammal et al. 1992)

dermis is reduced compared to the glabrous skin. This can be explained by the strong absorption of the ultrasound energy in the upper layers of the stratum corneum.

3.3 Inflammatory Skin Diseases

Psoriasis vulgaris: Compared to normal skin, lesions of psoriasis vulgaris exhibit distinct alterations of the upper dermis.

At the border of a psoriatic lesion, the echopoor band (EPB) of normal skin widens into a broad echopoor band. The thickness of this band correlates very well with the thickness of the acanthotic epidermis plus the dermis with the inflammatory infiltrate in the corresponding histology (r = 0,94). No significant correlation was observed between the thickness of the echopoor band and the epidermis respectively the infiltrated dermis alone (El Gammal et al. 1999). The lower, quite straight border of EPB 2 is defined by the scattered reflexes of the dermis.

Furthermore, compared to normal skin distinct alterations of the entry echo are observed in psoriasis lesions. In untreated scaly plaques, several parallel, echorich lines are seen directly below the entry echo. They melt with the entry echo into an echorich band, which is significantly thicker than the entry echo in normal skin (111 ± 16 µm, n = 35, $p < 0{,}001$) and has a much more irregular surface.

The following observations show that the described band with varying echodensities represents the hyperkeratotic horny layer: After the application of petrolatum under occlusion for 60 min on a hyperkeratotic psoriatic plaque, the thickness of the echopoor band (EPB) increases, and its echodensity markedly decreases. Repeated tape stripping of the scaly surface results in a gradual decrease of the thickness of the echorich

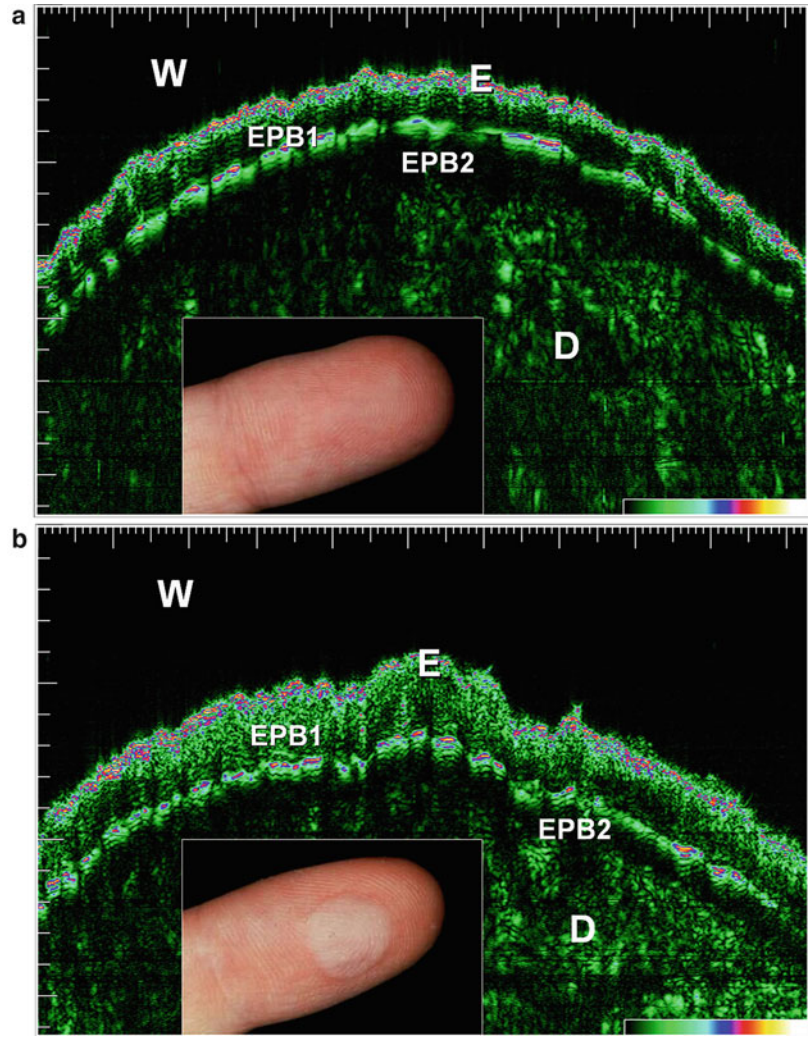

Fig. 8 Palmar side of the left index finger of a 30-year-old woman (distal phalanx) before (**c**) and after (**d**) 30 min occlusion of an emulsion. *W* water (coupling medium), *E* entry echo, *EPB 1* echopoor band 1, *EPB 2* echopoor band 2, *D* dermis. Distance between two graduation marks = 100 µm. *Insets*: photos of the finger before and after occlusion

band. When the scales are removed entirely, only a single echorich line remains.

In conclusion, the horny layer is echorich in untreated scaly psoriatic plaques; after treatment with petrolatum, its echodensity decreases. Furthermore the acanthotic epidermis and the dermis with the inflammatory infiltrate are represented as one single echopoor band (El Gammal et al. 1999, 2007).

Lichen planus: In lichen planus papules, the echopoor band (EPB) of normal glabrous skin focally widens into a spindle-shaped echopoor area. The maximal thickness of this band correlates well with the maximal thickness of the acanthotic epidermis and the dermal inflammatory infiltrate in the corresponding histology (r = 0,86). Thick lichen planus papules (Fig. 11) often exhibit an echopoor line (EPB 1) beneath the skin entry echo (El Gammal et al. 1999).

3.4 Skin Tumors

To study whether the improved resolution at 100 MHz has an impact on visualization of skin tumor details, thin basal cell carcinoma were evaluated using image analysis. The correlation of sonograms and histology reveals that the tumor parenchyma and stroma seen histologically as separate structures (inset, Fig. 12) are summed

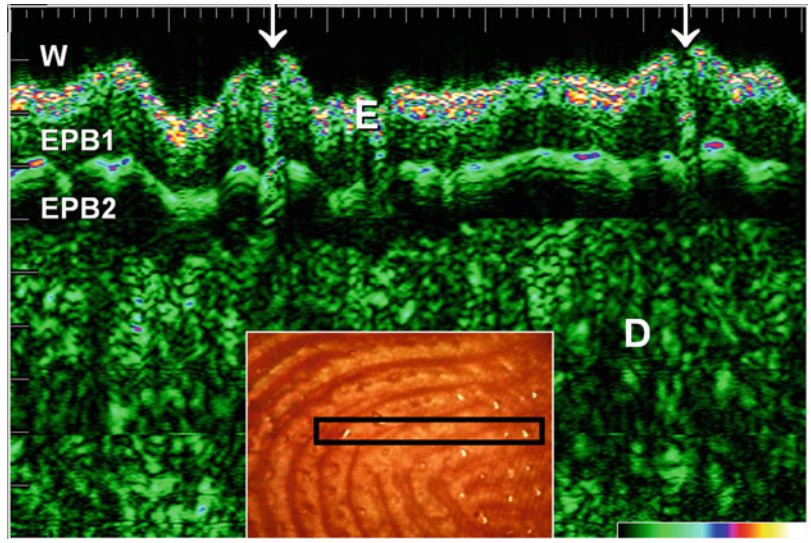

Fig. 9 Palmar side of the right index finger of a 39-year-old man at high magnification. *W* water (coupling medium), *E* entry echo, *D* dermis, *arrows* sweat gland duct orifices. Distance between two gradation marks = 100 µm. *Inset*: epiluminescence microscopic picture of the left index finger. On the crests of the dermatoglyphics, *white* points in a row are seen, which represent sweat gland ducts

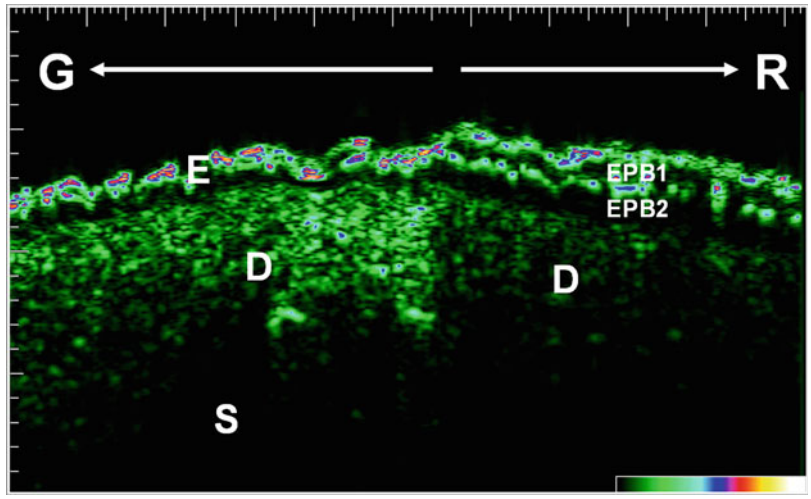

Fig. 10 At the transition from glabrous to the palmar skin, a second echorich line separates the EPB 1 (*upper* echopoor band) from the EPB 2 (*lower* echopoor band). The wrist of a 33-year-old woman. *E* skin entry echo, *G* glabrous skin, *R* ridged (palmar) skin, *D* dermis, *S* subcutis. Distance between two graduation marks = 100 µm

up to a uniform spindle-shaped echopoor area in the upper dermis in sonograms (Fig. 12). Tumor parenchyma and stroma are represented as one single echopoor area.

We further studied thin skin tumors (basal cell carcinoma, malignant melanoma, seborrheic keratosis, nevocellular nevi) using sonography and histology. Sonograms were evaluated by comparing the skin tumor region with the adjacent or contralateral normal skin (% change of the normal skin). Most parameters were not significant (Table 1). In seborrheic keratosis, the thickness of the skin entry echo was significantly increased. Furthermore in seborrheic keratosis, the mean echo intensity of the subtumoral region correlated with the thickness of the skin entry echo ($r = 0.92$).

In all tumors, the echodensity of the echopoor tumor region (Table 2a) did not vary in a statistically significant way, save seborrheic keratosis versus nevocellular nevus ($p = 0.05$). The echodensity of the subtumoral area was significantly ($p < 0.01$) different for all tumors (Table 2b), save for malignant melanoma versus nevocellular nevus ($p < 0.05$).

It can be concluded that differentiation between skin tumors is not possible by studying the echodensity of the echopoor tumor region. On the other hand, the echodensity of the subtumoral

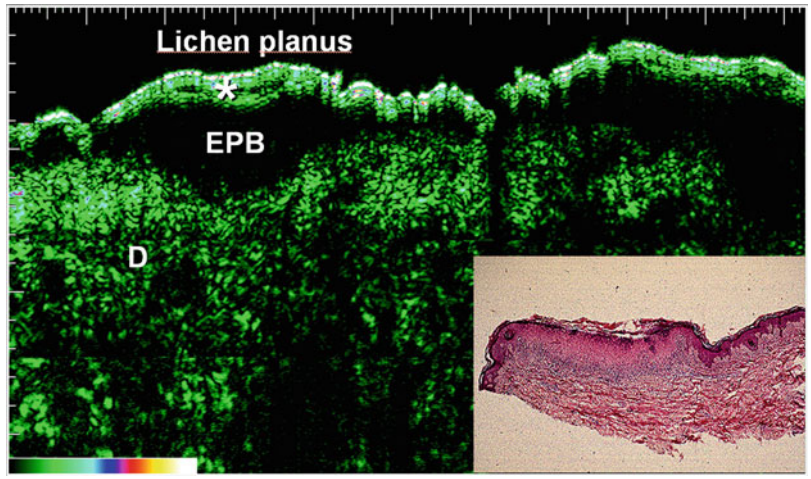

Fig. 11 Lichen planus papule on the thigh of a 65-year-old woman. In the middle of papule, an echopoor line (*) is seen between the skin entry echo and the echorich line beneath. Corresponding histology (*inset*) exhibits that this region has a significant hyperkeratosis. The histology exhibits furthermore that the EPB 2 corresponds to the str. Malpighii and the inflammatory infiltrate in the upper dermis. *EPB 2* echopoor band 2, *D* dermis. Distance between two graduation marks = 100 µm

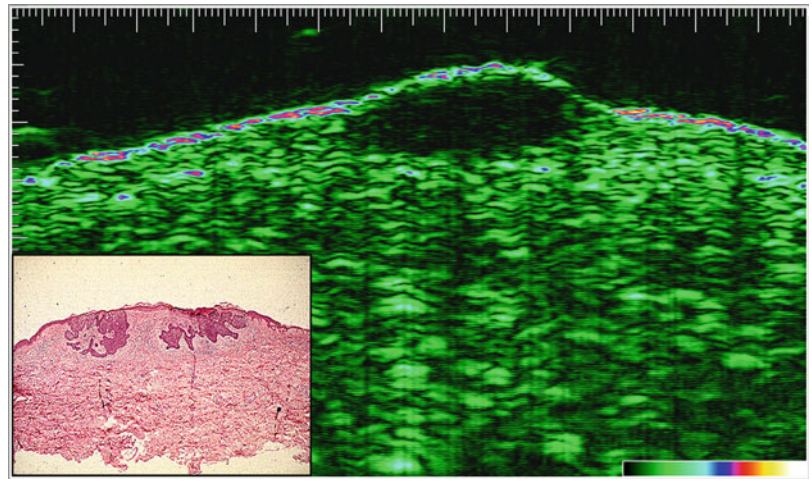

Fig. 12 Basal cell carcinoma on the back of a 78-year-old woman. Corresponding histology (*inset*) reveals that tumor parenchyma and stroma (together 912 µm thick) are summed up to a spindle-shaped echopoor area (maximal thickness 770 µm) in the upper dermis of the sonogram. Distance between two graduation marks = 100 µm

Table 1 Statistical analysis of different regions of interest in pigmented skin tumors

		NCN	MM	SebK	Bas
Skin entry echo	Thickness	n.s.	n.s.	$p = 0.02$	n.s.
	Mean echo intensity of the neighboring normal epidermis [%]	n.s.	n.s.	n.s.	n.s.
Echopoor tumor area	Mean echo intensity of the neighboring normal dermis [%]	33 % ± 9 %	16 % ± 6 %	13 % ± 6 %	25 % ± 9 %
Subtumoral Region	Mean echo intensity of the neighboring normal dermis [%]	71 % ± 23 %	50 % ± 15 %	25 % ± 3 %	86 % ± 24 %

n.s nonsignificant, *NCN* nevocellular nevus, *MM* malignant melanoma, *SebK* seborrheic keratosis, *Bas* basal cell carcinoma

Table 2 Evaluation of skin tumors, focusing on (a) the tumoral echopoor area and (b) the subtumoral region. (a) In all tumors, the echodensity of the echopoor tumor region does not vary in a statistically significant way, save SebK versus NCN ($p = 0.05$). (b) The subtumoral area is significantly ($p < 0.01$) different for all tumors, save for MM versus NCN ($p < 0.05$). *SebK* seborrheic keratosis, *MM* malignant melanoma, *Bas* basal cell carcinoma, *NCN* nevocellular nevus

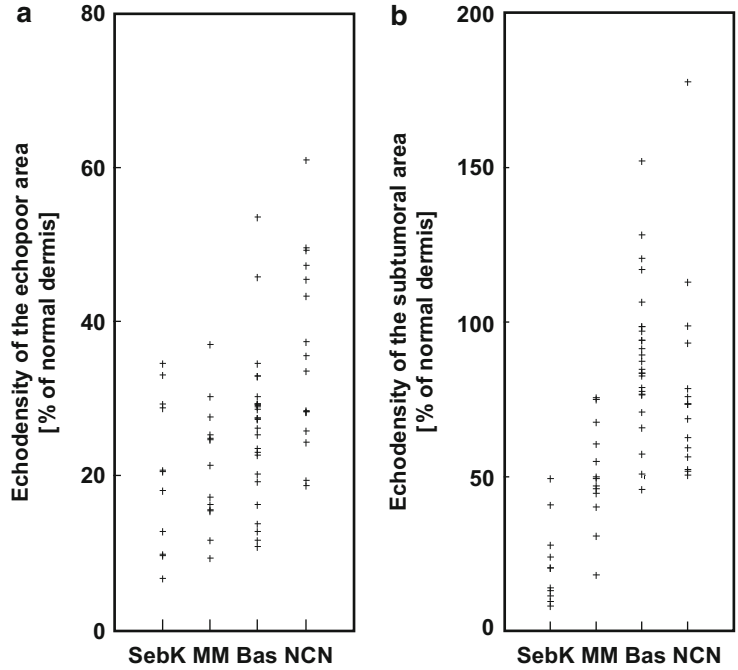

(normal) dermis gives an *indirect hint* about the absorption characteristics of the tumor region: these findings suggest that the absorption of echo reflexes is significantly different for all examined pigmented skin tumors, save malignant melanoma versus nevocellular nevus.

4 Discussion

Dermatology deals with all skin structures from the skin surface to the muscle fascia. Therefore imaging tools to look beneath the skin are required. Sonography is a particularly interesting method, because it is noninvasive and harmless (no radiation) and can be repeated if necessary.

7,5–15 MHz sonography has become a common tool to study the subcutis and subcutaneous pathologies. Typical examples are connective tissue diseases, cellulite, blood vessel diseases, soft tissue tumors, and lymph node pathology (Blum and Dill-Müller 1998, 1999; Dill-Müller and Maschke 2007; El Gammal et al. 2007).

20 MHz sonography is used to study the dermis. Different pathological processes (virtually all skin tumors, inflammatory infiltrates, edema, scar tissue, elastosis) as well as skin appendages and large blood vessels are represented as echopoor areas (Altmeyer et al. 1992; El Gammal et al. 1993; Fornage et al. 1993) within the echorich dermis.

Our 100 MHz experimental sonography unit allows a far more detailed visualization of the upper skin layers as compared to 20 MHz sonography. Especially with regard to the in vivo assessment of the horny layer, 100 MHz sonography is a valuable tool. Whereas in normal glabrous skin the stratum corneum is too thin (Kligman 1964, about 12–15 µm; Idson 1978, mean thickness of 15 µm for dry stratum corneum and 48 µm after hydration) to be separated from the entry echo, in the palmar skin and hyperkeratotic states, it is represented as a distinct band and its thickness can be easily determined. The results suggest that the echodensity of the horny layer depends on its water content: psoriatic scales,

appearing silvery because of the included air, are, for example, much more echorich than the moist stratum corneum of the palms. The significant impedance gap between the stratum corneum and the Malpighian layer – visible as an echorich line – can be explained by the different hydration states of these layers (El Gammal et al. 1999).

Today most authors agree that the skin entry echo is an artifact caused by the change in impedance between the coupling water and the horny layer (Querleux et al. 1988; Gniadecka et al. 1994; Hoffmann et al. 1994; Seidenari 1995). This hypothesis is confirmed by the presented results: the thickness and echodensity of the entry echo remain constant, no matter whether the horny layer is stripped, occluded with topical agents, or entirely removed (El Gammal et al. 1999). In most 20 MHz studies, the echo signal was strongly amplified to reach a high signal depth penetration. This however leads to a significant blurring of the entry echo. This effect as well as the low lateral resolution of only 200 µm entails that the entry echo is represented as a 100–250 µm thick, relatively homogeneous band at 20 MHz (Hoffmann et al. 1994). During image acquisition of the 100 MHz sonograms, the B/D-scan technology, which allows to select a specific amplification for each of the four to eight horizontal stripes, that compose the sonographic image was applied. An overamplification of the entry echo is thus avoided. Its thickness is about 80 µm and due to the excellent lateral resolution of 27 µm, it reflects even fine irregularities of the skin surface like the dermatoglyphics or the rough surface of psoriatic lesions.

In 20 MHz sonograms of normal glabrous skin, the dermal reflexes are directly adjacent to the entry echo; the viable epidermis, which is about 80 µm thick, cannot be visualized. At 100 MHz, the resolution is sufficient to show a thin echopoor band above the dermal reflexes in normal skin. Its thickness and its straight lower border suggest that it represents the viable epidermis together with the papillary dermis. At the transition from normal skin to a psoriatic plaque, this band widens into a 400–500 µm thick echolucent band. An echolucent band of comparable thickness has also been observed in 20 MHz sonograms of psoriatic lesions (Di Nardo et al. 1992; Fornage et al. 1993; Hoffmann et al. 1995; Seidenari 1995; Stiller et al. 1994; Vaillant et al. 1994). Conflicting theories have been proposed regarding its nature. While some authors equate it with the sum of acanthosis and the upper dermis with the inflammatory infiltrate (Fornage et al. 1993; Murakami and Miki 1989; Hoffmann et al. 1995), others interpret it as a correlate of the papillary dermis (Di Nardo et al. 1992; Stiller et al. 1994; Vaillant et al. 1994). Our results favor the first hypothesis: comparison with the corresponding histology revealed an excellent correlation between the thickness of this band and the histometric thickness of the Malpighian layer plus the inflammatory infiltrate. Moreover, in 100 MHz sonograms, this echopoor band always shows fairly straight borders. If it represented the viable epidermis only, we would expect an undulating lower border; if it was the correlate of the papillary dermis, the upper border would be wavy, especially in psoriatic lesions where there are prominent rete pegs. The lateral resolution of the 100 MHz transducer is high enough to depict structures of this dimension, as the cross sections of the dermatoglyphics in the palmar skin demonstrate. We can conclude that both the viable epidermis and the infiltrated dermis are echopoor and cannot be differentiated from each other.

These reflections illustrate that it is not only a question of resolution, whether a structure is visualized sonographically. As the study shows, the resolution of 100 MHz sonography allows to detect structures as small as a sweat gland duct in the horny layer. On the other hand, the viable epidermis cannot be distinguished from the papillary dermis, and, as one has learnt by studying skin tumors, the stroma of basal cell carcinoma cannot be distinguished from the tumor cell nests (Fig. 12), and inflammatory infiltrate cannot be distinguished from the papillary dermis (Fig. 11).

How can this be explained? According to Fields and Dunn (1973), echoes are only reflected from the border between two tissues, when they have a different acoustic impedance at the applied frequency. Obviously, there is no difference in

impedance between the viable epidermis, fine fibrillary connective tissue of the papillary dermis, compact tumor masses and dense lymphocytic infiltrate at 100 MHz but only between these structures and the reticular dermis. These acoustic tissue properties basically remain similar at 20 MHz and higher frequencies.

An entirely exact correlation of histometry and sonometry cannot be expected as various artifacts influence the measurements in both methods:

- Histological processing leads to tissue shrinkage and fat dissolution. The originally compact stratum corneum is transformed into the characteristic basket-weave structure which does not correspond to in vivo anatomy.
- Sonographic examination requires water as the coupling medium which itself may lead to swelling of the horny layer. To be able to calculate distances, the tissue-specific ultrasound speed has to be known. In dermatological sonography, distance calculations from the echo signal time-lapse are usually based on the sound speed of the dermis (1580 m/s) (Alexander and Miller 1979; Beck et al. 1986). In the nail plate however, Finlay et al. (1987) found a sound speed of 2,140 m/s comparing 20 MHz sonography and thickness measurements by a micrometer screw. Jemec and Serup (1989) divided the nail into two compartments with different speeds, an upper dry one (3,103 m/s) and a lower humid inner one (2,125 m/s). A similar situation must be postulated for the stratum corneum which consists of keratin and has a low content of water thereby having similar properties to the upper nail compartment.

Inflammatory Processes. Inflammatory dermatoses such as psoriasis vulgaris, lichen planus, and acute or chronic dermatitis show a characteristic echolucent band beneath the skin entry echo. It represents the acanthosis of the epidermis and the dermal infiltrate. In other words, the sonography does not discriminate between the acanthotic epithelium and subepidermal inflammatory infiltrate (Table 3). Despite this problem, high-resolution sonography has proven to be an excellent non-invasive method to study and follow-up progression and regression of cutaneous inflammation during the treatment of inflammatory skin diseases.

Table 3 Echopoor and echorich structures in high-resolution sonography

Echopoor	Echorich
Stratum corneum	Hairs (in the water coupling medium)
Stratum Malpighii (living epidermis layer)	Skin entry echo[a]
Hair follicle canal	Sweat gland duct (ridged skin)
Actinic elastosis	Reticular dermis (speckle texture)
Papillary dermis	Keratin inclusions
Solid tumor masses	Calcifications
Inflammatory (e.g., lymphocytic) infiltrate	
Blood vessel lumen	Blood vessel wall[a]

[a]Artifact due to the impedance jump between neighboring structures

Skin Tumors. Skin tumors can be well delineated, as long as they are confined to the echorich dermis. Nearly all skin tumors (of epithelial, melanocytic, angiomatous, or connective tissue origin) are echopoor. Exceptions are strong reflecting keratin inclusions, e.g., seborrheic keratosis and calcifications (calcinosis cutis).

Concerning skin tumor characterization, 50–100 MHz sonography was of little advantage in comparison to 20 MHz sonography: inflammatory infiltrate, tumor parenchyma, and stroma – they all were echopoor and looked alike (Table 3). As expected, the sonographic vertical thickness (the echopoor region comprises tumor *and* inflammatory infiltrate) of malignant melanoma was overestimated using 20 MHz (and to a lesser extent using 100 MHz) in comparison to histology (Gamblicher et al. 2007).

Differentiation between skin tumors was not possible when focusing on the echopoor tumor region (see Results). On the other hand, the echodensity of the subtumoral (normal) dermis gave an *indirect hint* about the absorption characteristics of the tumor region. This interesting finding has been confirmed by Harland et al. (2000).

Alterations of the dermal connective tissue. Both, the fibrosing of the dermis, e.g., in scars or in scleroderma, and the augmentation of elastotic material with simultaneous rarefaction of collagen in actinic elastosis lead to reduced echodensity sonographically; the dermis is represented darker. Since the tissue depth penetration at 20 MHz is up to 7 mm, thickened connective tissue structures in the dermis and the sclerosing process in the fatty tissue can be visualized in scleroderma. In different studies, it has been shown that progression and regression of scleroderma plaques can be quantitatively evaluated using sonography (Cole et al. 1981; Serup 1984; Akesson et al. 1986; Myers et al. 1986; Levy et al. 1993). Hoffmann et al. (1992b) found in 63 patients with morphea (circumscribed scleroderma) a mean increase of the thickness of the dermis of over 60 % in comparison to the contralateral healthy body side. In the inguinal region, where the healthy dermis is particularly thin, the dermal thickness increased significantly during the sclerosing phase (Hoffmann et al. 1992b).

References

Akesson A, Forsberg L, Hederström E, Wollheim E. Ultrasound examination of skin thickness in patients with progressive systemic sclerosis (scleroderma). Acta Radiol Diagn. 1986;27:91–4.

Alexander H, Miller DL. Determining skin thickness with pulsed ultrasound. J Invest Dermatol. 1979;72:17–9.

Altmeyer P, Hoffmann K, Stücker M, Goertz S, el-Gammal S, Altmeyer P, Hoffmann K, Stücker M, Goertz S, el-Gammal S, et al. General phenomena of ultrasound in dermatology. In: Altmeyer P, Altmeyer P, el-Gammal S, Hoffmann K, editors. Ultrasound in dermatology. Berlin/Heidelberg/New York: Springer; 1992. p. 55–79.

Beck JS, Speace VA, Lowe JG, Gibbs JH. Measurement of skin swelling in the tuberculin test by ultrasonography. J Immunol Methods. 1986;86:125–30.

Beyer D, Peters PE, Friedmann G. Leistungsbreite der Real-time-Sonographie bei Lymphknotenerkrankungen. Rontgenpraxis. 1982;35:393–402.

Blum A, Dill-Müller D. Sonographie der Lymphknoten und der Subkutis in der Dermatologie; Teil 1. Hautarzt. 1998;49:942–9.

Blum A, Dill-Müller D. Sonographie der Lymphknoten und der Subkutis in der Dermatologie; Teil 2. Hautarzt. 1999;50:62–73.

Brockmann WP, Maas R, Voigt H, Thoma G, Schweer S. Veränderungen peripherer Lymphknoten im Ultraschall. Ultraschall. 1985;6:164–9.

Cole CW, Handler SJ, Burnett K. The ultrasonic evaluation of skin thickness in sclerederma. J Clin Ultrasound (NY). 1981;9:501–3.

Desai TD, Desai AD, Horowitz DC, Kartono F, Wahl T. The use of high-frequency ultrasound in the evaluation of superficial and nodular basal cell carcinomas. Dermatol Surg. 2007;33:1220–7.

Di Nardo A, Seidenari S, Giannetti A. B-scanning evaluation with image analysis of psoriatic skin. Exp Dermatol. 1992;1:121–5.

Dill-Müller D, Maschke J. Ultraschalldiagnositk in der Dermatologie. JDDG. 2007;5:689–708.

El Gammal S, Hoffmann K, Kenkmann J, Altmeyer P, Höss A, Ermert H. Principles of three-dimensional reconstructions from high resolution ultrasound in dermatology. In: Altmeyer P, el-Gammal S, Hoffmann K, editors. Ultrasound in dermatology. Heidelberg/New York: Springer; 1992. p. 355–87.

El Gammal S, Auer T, Hoffmann K, Matthes U, Hammentgen R, Altmeyer P, Ermert H. High-frequency ultrasound: a non-invasive method for use in dermatology. In: Frosch P, Kligman AM, editors. Non-invasive methods in dermatology. Heidelberg/New York: Springer; 1993. p. 104–29.

El Gammal S, Auer T, Hoffmann K, Paßmann C, Ermert H. High resolution ultrasound of the human epidermis. In: Serup J, Jemec GBE, editors. In vivo examination of the skin: a handbook of non-invasive methods. Ann Arbor/London/Tokyo: CRC Press; 1995. p. 125.

El Gammal S, El Gammal C, Kaspar K, Pieck C, Altmeyer P, Vogt M, Ermert H. Sonography of the skin at 100 MHz enables in-vivo-visualization of stratum corneum and viable epidermis in palmar skin and psoriatic plaques. J Invest Dermatol. 1999;113:821–9.

El Gammal S, El Gammal C, Altmeyer P, Vogt M, Ermert H. Sonography of the skin in health and disease. In: Wilhelm KP, Elsner P, Berardesca E, Maibach HI, editors. Bioengineering of the skin – skin imaging and analysis. New York: Informa Healthcare; 2007. p. 353–75.

Ermert H, Vogt M, Paßmann C, El Gammal S, Kaspar K, Hoffmann K, Altmeyer P. High frequency ultrasound (50–150 MHz) in dermatology. In: Altmeyer P, Hoffmann K, Stücker M, editors. Skin cancer and UV radiation. Berlin: Springer; 1997. p. 1023–51.

Fields S, Dunn F. Correlation of echographic visualizability of tissue with biological composition and physiological state. J Acoust Soc Am. 1973;54:809–12.

Finlay AY, Moseley H, Duggan TC. Ultrasound transmission time: an in vivo guide to nail thickness. Br J Dermatol. 1987;117:765–70.

Fornage BD, McGavran MH, Duvic M, Waldron CA. Imaging of the skin with 20-MHz US. Radiology. 1993;189:69–76.

Gambichler T, Moussa G, Bahrenberg K, Vogt M, Ermert H, Weyhe D, Altmeyer P, Hoffmann K. Preoperative ultrasonic assessment of thin melanocytic skin lesions using a 100-MHz ultrasound transducer: a comparative study. Dermatol Surg. 2007;33:818–24.

Gniadecka M, Gniadecki R, Serup J, Søndergaard J. Ultrasound structure and digital image analysis of the subepidermal low echogenic band in aged human skin: diurnal changes and interindividual variability. J Invest Dermatol. 1994;102:362–5.

Gropper CA, Stiller MJ, Shupack JL, Driller J, Rorke M, Lizzi F. Diagnostic high-resolution ultrasound in dermatology. Int J Dermatol. 1993;32:243–50.

Gupta AK, Turnbull DH, Harasiewicz KA, Shum DT, Watteel GN, Fister FS, Sauder DN. The use of high-frequency ultrasound as a method of assessing the severity of a plaque of psoriasis. Arch Dermatol. 1996;132:658–62.

Harland CC, Bamber JC, Gusterson BA, Mortimer PS. High frequency, high resolution B-scan ultrasound in the assessment of skin tumours. Br J Dermatol. 1993;128:525–32.

Harland CC, Kale, Jackson P, Mortimer PS, Bamber JC. Differentiation of common pigmented skin lesions from melanoma by high resolution ultrasound. Br J Dermatol. 2000;143:281–9.

Hoffmann K, el-Gammal S, Gerbaulet U, Schatz H, Altmeyer P. Examination of circumscribed scleroderma using 20 MHz B-scan ultrasound. In: Altmeyer P, el-Gammal S, Hoffmann K, editors. Ultrasound in dermatology. Heidelberg/New York: Springer; 1992a. p. 231–43.

Hoffmann K, el-Gammal S, Winkler K, Jung J, Pistorius K, Altmeyer P. Skin tumours in high-frequency ultrasound. In: Altmeyer P, el-Gammal S, Hoffmann K, editors. Ultrasound in dermatology. Heidelberg/New York: Springer; 1992b. p. 181–201.

Hoffmann K, Stücker M, Dirschka T, Görtz S, el-Gammal S, Dirting K, Hoffmann A, Altmeyer P. Twenty MHz B-scan sonography for visualization and skin thickness measurement of human skin. J Eur Acad Dermatol. 1994;3:302–13.

Hoffmann K, Dirschka T, Schwarze H, el-Gammal S, Matthes U, Hoffmann A, Altmeyer P. 20 MHz sonography, colorimetry and image analysis in the evaluation of psoriasis vulgaris. J Dermatol Sci. 1995;9:103–10.

Idson B. Hydration and percutaneous absorption. Curr Probl Dermatol. 1978;7:132–4.

Ihn H, Shimozuma M, Fujimoto M, Sato S, Kikuchi K, Igarashi A, Soma Y, Tamaki K, Takehara K. Ultrasound measurement of skin thickness in systemic sclerosis. Br J Rheumatol. 1995;24:535–8.

Jemec GB, Serup J. Ultrasound structure of the human nail plate. Arch Dermatol. 1989;125:643–6.

Kligman AM. The biology of the stratum corneum. In: Montagna W, Lobitz WC, editors. The epidermis. New York: Academic; 1964. p. 387.

Lévy J, Gassmüller J, Audring H, Brenke A, Albrecht-Nebe H. Darstellung der subkutanen Atrophie bei der zirkumskripten Sklerodermie im 20 MHz-B-scan Ultraschall. Hautarzt. 1993;44:446–51.

Murakami S, Miki Y. Human skin histology using high-resolution echography. J Clin Ultrasound. 1989;17:77–82.

Myers SL, Cohen JS, Sheets PW, Bies JR. B-mode ultrasound evaluation of skin thickness in progressive systemic sclerosis. J Rheumatol. 1986;13:577–80.

Paßmann C, Ermert H, Auer T, Kaspar K, el-Gammal S, Altmeyer P. In vivo ultrasound biomicroscopy. Proceedings of IEEE ultrasonics symposium 1989, p. 1015–8.

Querleux B, Lévêque JL, de Rigal J. In vivo cross-sectional ultrasonic imaging of the skin. Dermatologica. 1988;177:332–7.

Rukinava B, Mohar N. An approach of ultrasound diagnostic techniques of the skin and subcutaneous tissue. Dermatologica. 1979;158:81–92.

Seidenari S. High-frequency sonography combined with image analysis: a non-invasive objective method for skin evaluation and description. Clin Dermatol. 1995;13:349–59.

Seidenari S, Di Nardo A. B scanning evaluation of irritant reactions with binary transformation and image analysis. Acta Dermatol Venereol Suppl (Stockh). 1992;175:9–13.

Serup J. Decreased skin thickness of pigmented spots appearing in localized scleroderma (morphoea) – measurement of skin thickness by 15 MHz pulsed ultrasound. Arch Dermatol Res. 1984;276:135–7.

Serup J, Staberg B. Ultrasound for assessment of allergic and irritant patch test reactions. Contact Dermatitis. 1987;17:80–4.

Stiller MJ, Gropper CA, Shupack JL, Lizzi F, Driller J, Rorke M. Diagnostic ultrasound in dermatology: current uses and future potential. Cutis. 1994;53:44–8.

Vaillant L, Berson M, Machet L, Callens A, Pourcelot L, Lorette G. Ultrasound imaging of psoriatic skin: a non-invasive technique to evaluate treatment of psoriasis. Int J Dermatol. 1994;33:786–90.

Vogt M, Kaspar K, Altmeyer P, Hoffmann K, El Gammal S. High frequency ultrasound for high resolution imaging. Frequenz. 2001;55:12–20.

Ex Vivo High-Frequency Ultrasound Imaging of the Skin

43

Paola Pasquali

Contents

Keywords

High-frequency ultrasound • High-resolution ultrasound • Skin echography • Skin ultrasound • Echography • Ultrasonography • Noninvasive imaging • Basal cell carcinoma • Treatment modality • High-frequency sonography • HFUS evaluation • Length • Shape • Tumor depth • Volume • Ex vivo • High-resolution echography • Noninvasive image • Noninvasive imaging techniques (NIIT)

Abbreviations

BCC	Basal cell carcinoma
HFUS	High-frequency ultrasound
HFUS/HRUS	High-frequency ultrasound/high-resolution ultrasound
NIIT	Noninvasive imaging techniques
PDT	Photodynamic therapy
SCC	Squamous cell carcinoma

1 Introduction

In daily dermatologic practice, skin tumors are a common cause of consultation. They are brought to the physician's attention by the patient, family members, friends, care takers, or other physicians. The appropriate therapeutic decision will have to be taken in each case: some tumors will be left untreated, some will be removed for cosmetic reasons, and others to relieve symptoms, and finally and most importantly, tumors will need to be treated for oncological reasons.

P. Pasquali (✉)
Dermatology Department, Pius Hospital de Valls, Valls, Spain
e-mail: pasqualipaola@gmail.com

P. Humbert et al. (eds.), *Agache's Measuring the Skin*,
DOI 10.1007/978-3-319-32383-1_50

For those tumors in which an intervention decision has been taken, one will need to obtain as much information as possible. The more one knows about the tumor, the better the choice of a therapeutic method. The best treatment is the one done right from the beginning, avoiding recurrences and additional interventions.

A complete clinical and dermoscopic evaluation by a dermatologist can raise the sensitivity for diagnosis of malignant tumors as high as 98 % (Ahnlide and Bjellerup 2013); however, the clinical/dermoscopic diagnosis will benefit from the use of noninvasive imaging techniques (NIIT) which add, complement, change, or confirm the original diagnosis.

High-frequency ultrasound (HFUS/HRUS, high-resolution ultrasound, high-resolution echography) is one of such techniques (Wortsman 2012; Wortsman and Wortsman 2010). It allows for a noninvasive evaluation of hidden parts of the tumor for further assessment and measurement (Pasquali et al. 2014; Hoffmann et al. 1989; Desai et al. 2007).

Some tumor characteristics that can be visualized by HFUS evaluation are the following:

- **Volume**/**Shape**.The knowledge of the volume of tumors can provide information on the nature of the tumor; for instance, most nodular basal cell carcinomas are roughly elliptical; invasive tumors show irregular shapes with indentations at the bottom; superficial basal cells are flat and elongated (Fig. 1). This knowledge helps in choosing the proper site for biopsy or helps in deciding the best tumor removal method.
- **Depth**. The knowledge of the depth of tumors helps decide the correct surgical technique. For

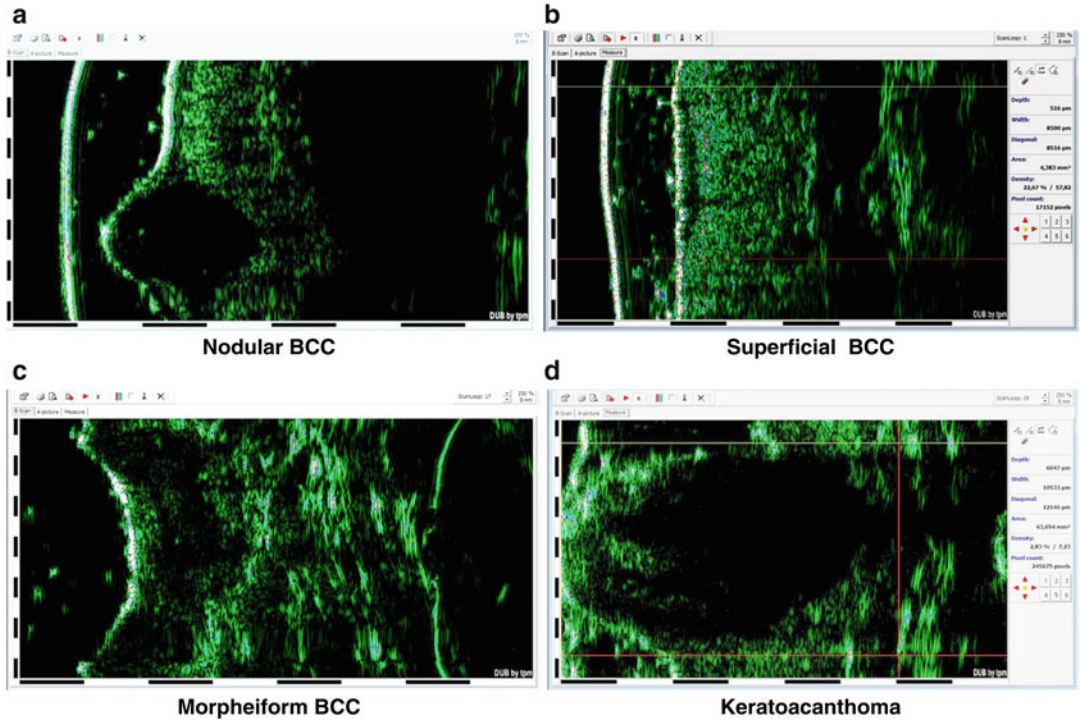

Fig. 1 Four tumors with different biological behavior and recognizable by HFUS. (**a**) Nodular BCC, tend to be elliptical; (**b**) superficial BCC, usually shallow lesions that can present themselves as isolated tumor islands, "pearl collar" array, or a thin and large tumor; (**c**) morpheaform BCC, tend to show their expansive and invasive nature in the form of indentations visible at the bottom or sides; they tend to have irregular shapes; and (**d**) keratoacanthoma, round, elliptical, and very large tumors with a protruding (external) part

example, superficial BCC lesions can be diagnosed by clinical/dermoscopic (Argenziano et al. 2013) examination. Treatment options include cryosurgery, topical immunomodulators like imiquimod, photodynamic therapy (PDT), and curettage/electrocoagulation, among others. There is no need for costly or invasive techniques like Mohs micrographic surgery. The HFUS image of a superficial BCC shows a hypoechoic elliptical area(s) of less than 1 mm in depth. They can be an elongated and shallow, single small oval, or multiple pebble-like lesions (Fig. 2) connected by a shallow hypoechoic stream that reminds of a collar necklace. Individually, each island of tumor is less than a millimeter in depth. Lengthwise, they can be small (1–2 mm) but can also be quite big, requiring a segmental HFUS evaluation in order to cover the whole area. In general, the length/depth ratio is 6 to 1 (Pasquali et al. 2012a). HFUS allows determining if BCC is only superficial or if the apparently looking "superficial BCC" is in reality an admixture tumor, as it is the case of roughly one-third of all BCC (Sexton et al. 1990; Crowson 2006) (Fig. 3). The latter is a common cause for treatment failure and recurrence that occur years later (Fig. 4). HFUS should be used to evaluate the entire tumor to note its depth in every point. The information obtained with the help of the HFUS technique is superior to a skin biopsy alone done "blindly" on the tumor (Kamyab-Hesari et al. 2012). Tumor visualization will be limited to certain dimension; for instance, with a 22 MHz TPM® equipment, depth determination is limited to 8 mm.

- **Length**. Some tumors have iceberg shape: they look small at the surface while the length underneath the surface is larger. This could be the cause of positive margins after surgery. Tumor visualization will be limited to certain dimension; for instance, with a 22 MHz TPM® equipment, length determination is limited to 13 mm.

A further use of HFUS is in an ex vivo setting (Petrella et al. 2010, 2012). Tumors are scanned once excised (surgery, shaving, or saucerization) in order to confirm total excision before sending the specimen to the pathologist. It is a noninvasive image that provides reassurance to the surgeon of having removed the tumor completely or

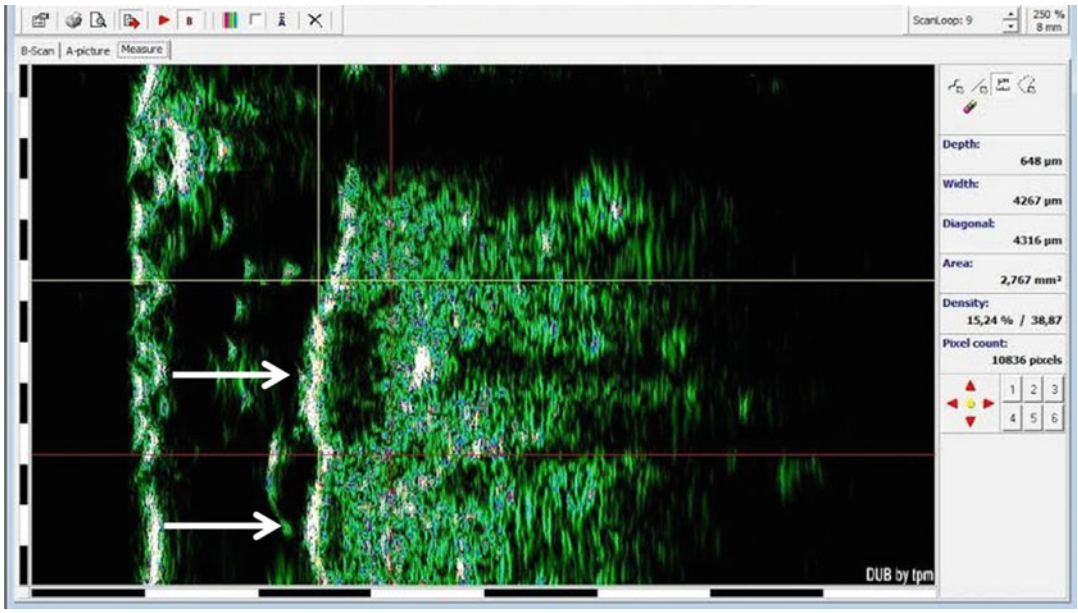

Fig. 2 The typical "pearl collar" image of a superficial BCC

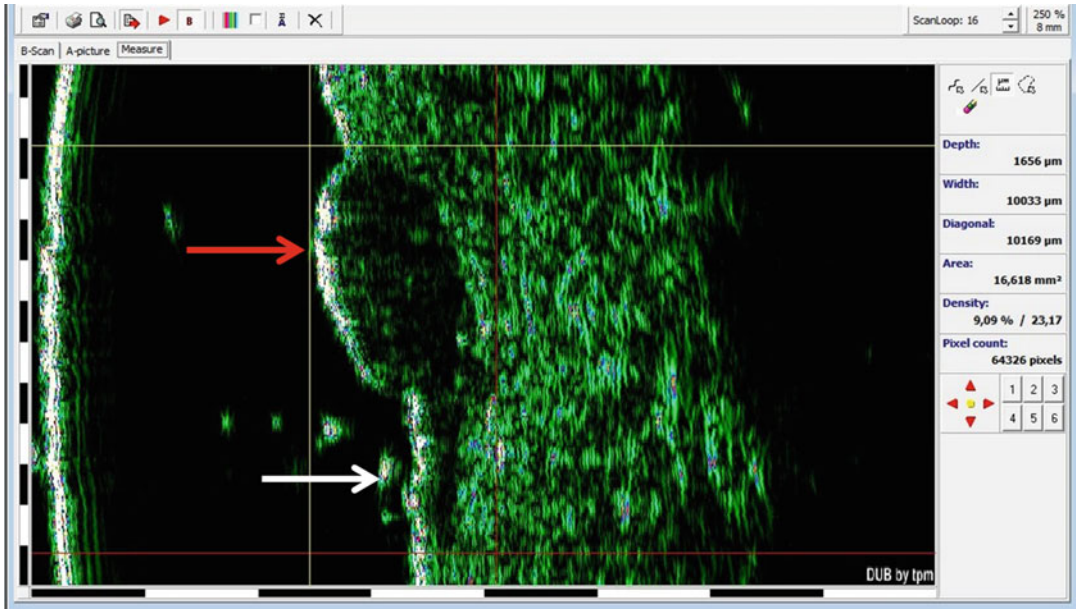

Fig. 3 An admixture tumor showing one part nodular BCC (*red arrow*) and one part superficial BCC (*white arrow*)

Fig. 4 Patient with a recurrence of a BCC that had been treated 15 years before with E&C (electrocoagulation with curettage). The tumoral mass underneath the skin mimicked an infected cyst

the need to extend the surgical margins. This "pre-path" surgical margin analysis does not substitute the need for histological evaluation nor pretend to correspond to Mohs surgery margin evaluation. It does however reassure the surgeon in requiring a minimum extra effort that translates in a better management of tumors.

Cases in the present chapter come from a public hospital practice and therefore are mostly skin malignancies.

2 High-Frequency Ultrasound Versus Pathology Versus Dermoscopy: From Bidimensional to Tridimensional Imaging

For tumors with visible margins, clinical and dermoscopic evaluations give bidimensional information (length and width) of the lesion. Dermoscopy will further confirm or even allow making a diagnosis, better define tumor boundaries, and determine in many cases

histopathologic subtype (Lallas et al. 2014). With this information (bidimensional, coplanar), the area of the tumor (on the surface) can be obtained.

HFUS gives length, width, and depth (tridimensional information) as well as area and density. With a 22 MHz ultrasound equipment from TPM®, one can reach up to 8 mm in depth with a bandwidth that goes up to 28 MHz, enabling to see the epidermis and dermis with a resolution of over 72 μm. The maximum length/width is 12.8 mm lineal.

A correlation between ultrasound (HFUS), histologic, and dermoscopic (DMS) measurements has been determined by several authors

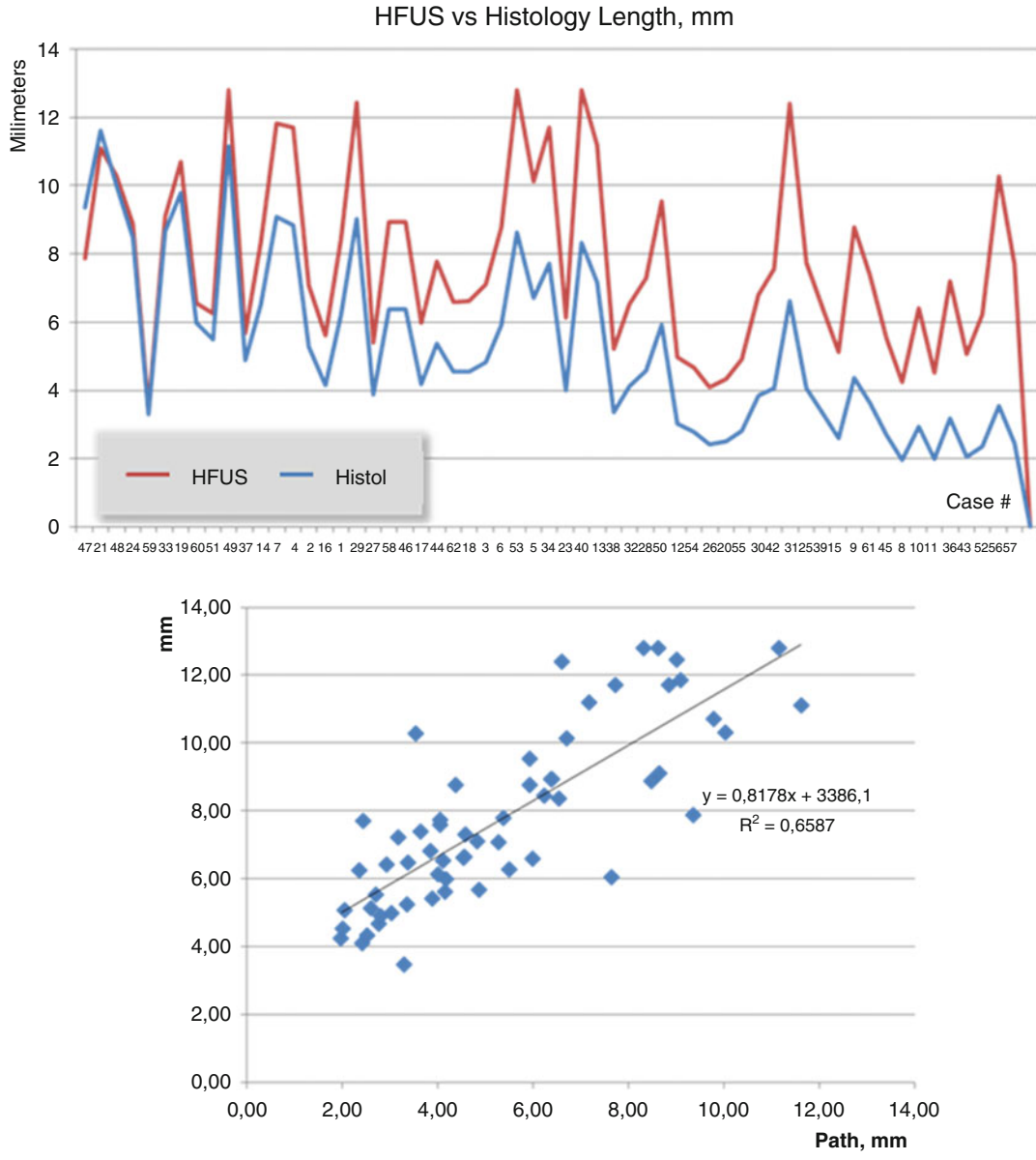

Fig. 5 Correlation of HFUS versus histology length (mm). The average length obtained from HFUS is greater than the histologic length

(Jovanovic and Pesic 2013; Crisan et al. 2013; Hinz et al. 2012; Nassiri-Kashani et al. 2013). In our personal series of BCCs, tumors' length was obtained from dermoscopy (superficial length), HFUS, and histology. We confirmed other author's observations that showed a correlation between HFUS length in relation to the one obtained on histopathologic specimen. We found a strong correlation between the HFUS and histologic lengths (Fig. 5). In addition, in 58/60 of cases, the average length obtained from the HFUS was greater than the histologic length (mean = 60.1 %, $r^2 = 0.66$).

As far as depth, measurement obtained by HFUS/HRUS in 49/61 cases was larger than the one obtained by histology, showing an average increase of 27 % and a moderately strong correlation ($r^2 = 0.65$). For larger tumors the percentage increase of HFUS/HRUS versus histology was smaller, but with a weak correlation ($r^2 = 0.29$).

A series of 24 BCCs dermoscopic, HFUS, and histologic lengths were compared, finding a clear relationship between them. Dermoscopic length was closer to HFUS and always larger than histology (Fig. 6). These results show that HFUS dimensions are closer to in situ tumor dimension.

3 Ex Vivo High-Frequency Ultrasound

Ex vivo HFUS is a simple and fast procedure where an ultrasound exam is performed on a surgical skin specimen removed by excision, shaving, or saucerization. The specimen is placed on gauze and covered with ultrasound gel. This evaluation helps visualize the whole tumor to confirm its complete removal. The HFUS probe should be placed over the specimen, maintaining the same position as in the presurgical HFUS. A previous mark in the skin along the longitudinal axis of tumor will help identify the correct position, especially for larger tumors.

In our series (Pasquali et al. 2012b) Pasquali et al. (In Press) of 62 patients, 74 tumors were measured both presurgically and ex vivo by HFUS before sending specimens for histologic examination (Fig. 7). In this group of tumors, only 12 were benign (1 foreign body, 2 dermatofibromas, 1 hamartoma, 5 intradermic nevi, 2 cysts, and 1 keloid) and the rest were malignant (58 BCC, 2 SCC, 1 atypical fibroxanthoma, and 1 hypertrophic actinic keratosis).

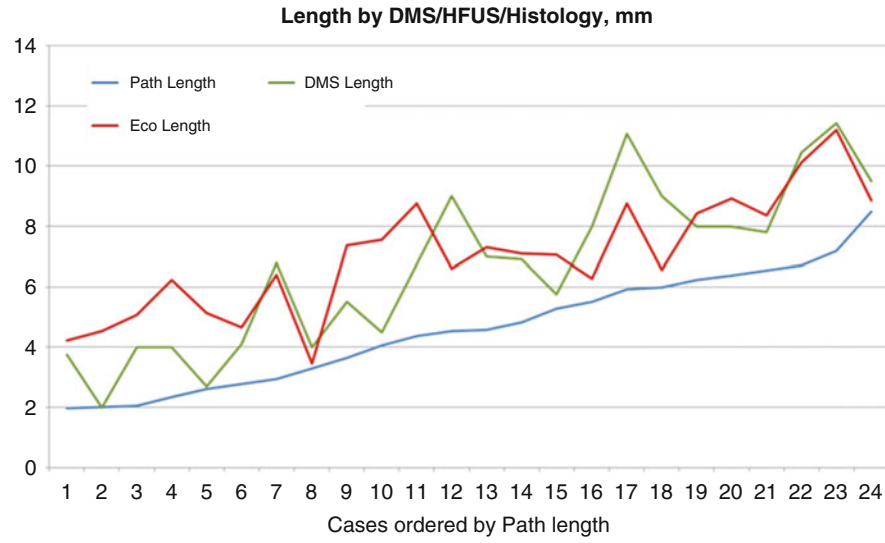

Fig. 6 Correlation between the dermoscopic, HFUS, and histologic length. The dermoscopic length was closer to the HFUS and always larger than the histologic length

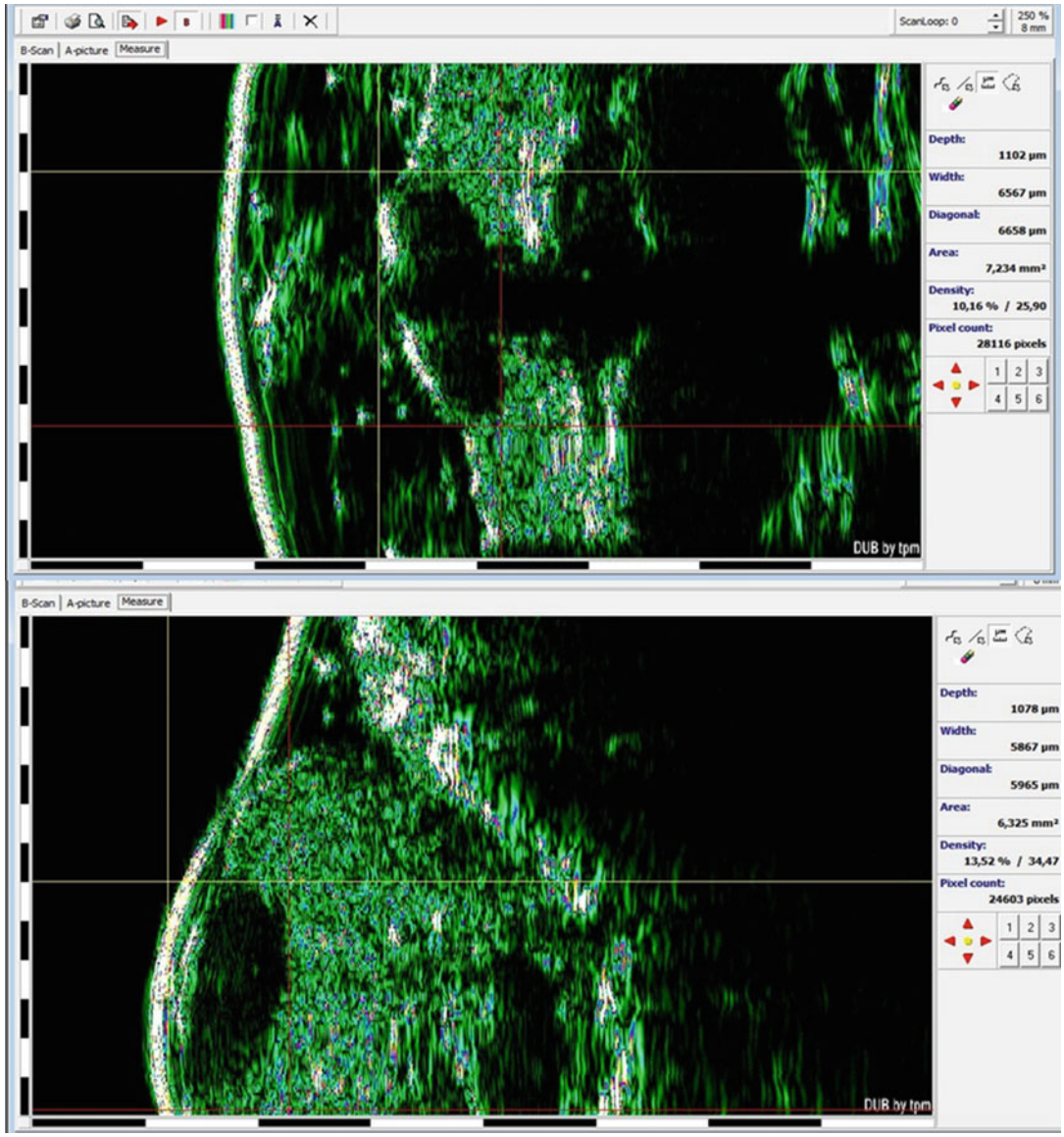

Fig. 7 Presurgical HFUS (*top image*) and ex vivo HFUS (*bottom image*) of a nodular BCC on the shoulder

As far as the anatomical location, 47 cases (63.5 %) were in the head/neck, 14 (18.9 %) were located in the posterior thorax, 4 in the chest/abdomen (5.4 %), 3 in upper extremities (4.1 %), and 6 in lower extremities (8.1 %).

A positive correlation was found between the ex vivo versus presurgical HFUS measurements both in length and depth. This correlation was moderately strong ($r^2 = 0.681$) for length while strong ($r^2 = 0.876$) for depth.

Although with some volatility, both length measurements by HFUS (presurgical and ex vivo) are not very far apart from each other (5 % average difference), but when compared to histology, they are always larger (36.1 % average difference between histology and ex vivo HFUS). The relationship between the length measurements can be seen in Fig. 8.

As far as the depth, the average difference between histology and ex vivo is 21.7 %. The

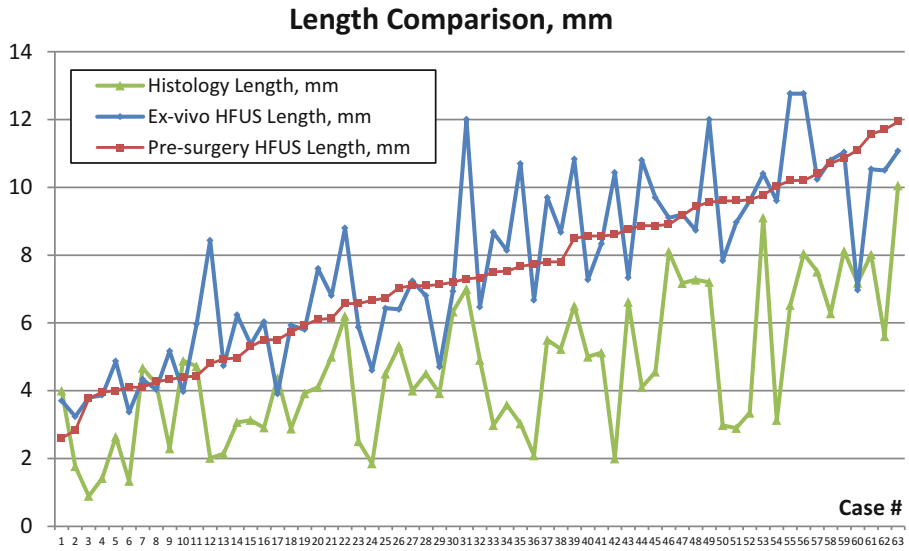

Fig. 8 Comparison of lengths obtained from presurgical (*red line*) and ex vivo (*blue line*) HFUS and histology (*green line*). Histologic length is smaller than both HFUS readings

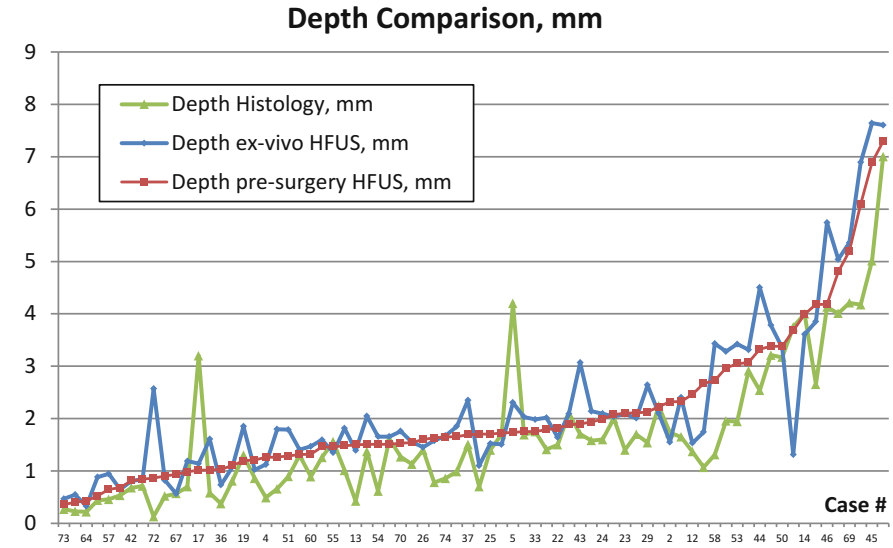

Fig. 9 Comparison of depths obtained from presurgical (*red line*) and ex vivo (*blue line*) HFUS and histology (*green line*)

relationship between the depth measurements can be seen in (Fig. 9).

The purpose of doing an ex vivo measurement is to visualize the total volume of tumor/margin. In addition to tumor's surface area information, HFUS evaluation can add value by providing the area of a longitudinal section. This can be obtained from HFUS by delimiting manually the tumor area (Figs. 10 and 11). The comparison of the areas obtained by presurgical and ex vivo

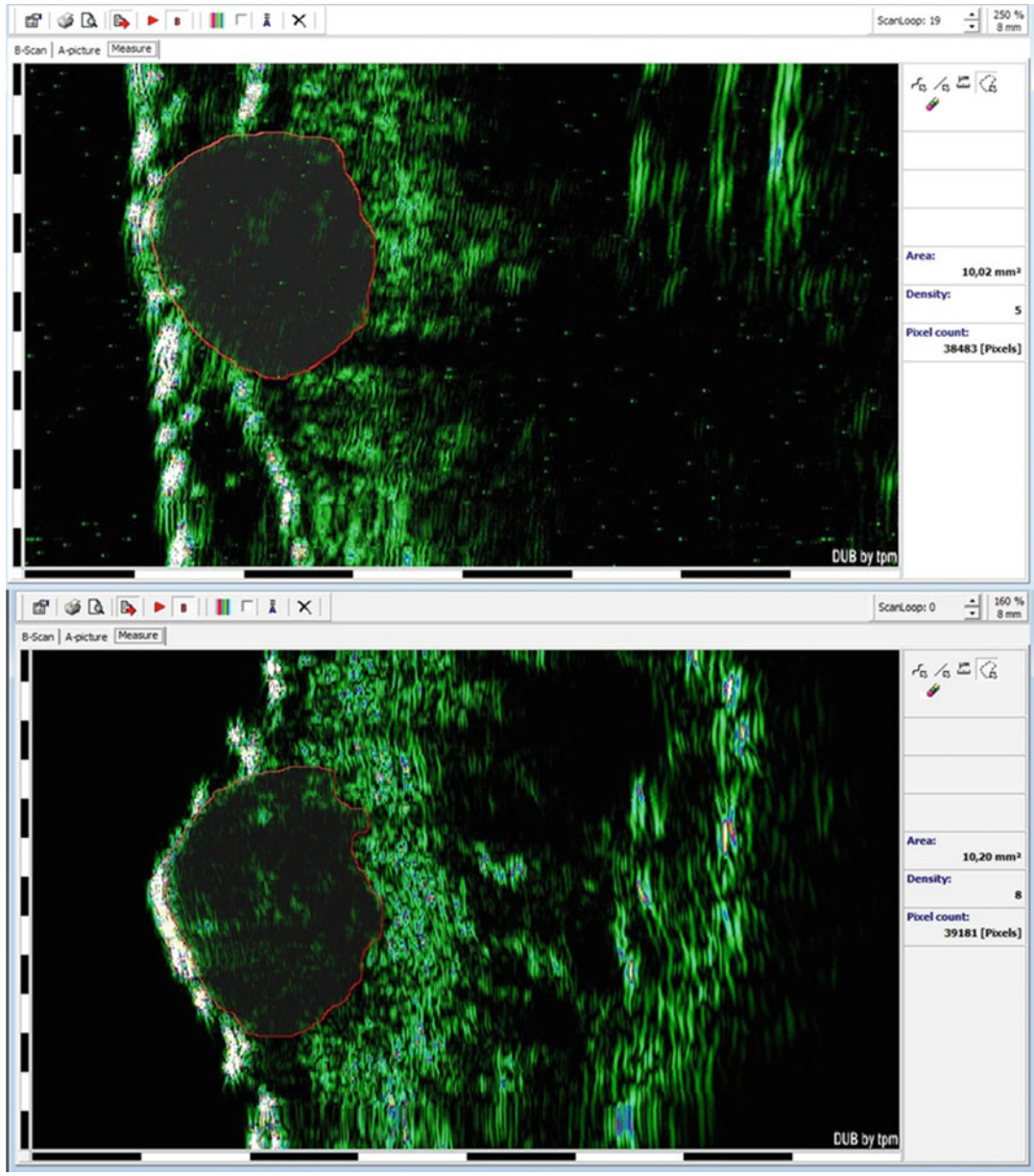

Fig. 10 Presurgical HFUS (*top image*) (area, 10.02 mm^2) and ex vivo HFUS (*bottom image*) (area, 10.20 mm^2) of a nodular BCC on the face

HFUS could give a better indication on the wholeness of removal. In the case of histology, an approximation can be done by using the area of an ellipse (area $= \pi * l * d$; l is length/2 and d is depth/2) and selecting those tumors of such shape such as nodular BCCs.

The correlation between both presurgical versus ex vivo HFUS areas and presurgical versus histology was strong ($r^2 = 0.794$ and $r^2 = 0.766$). The comparison between areas is shown in Fig. 12. On average, histology area is 32.9 % smaller than presurgical HFUS and 34.4 %

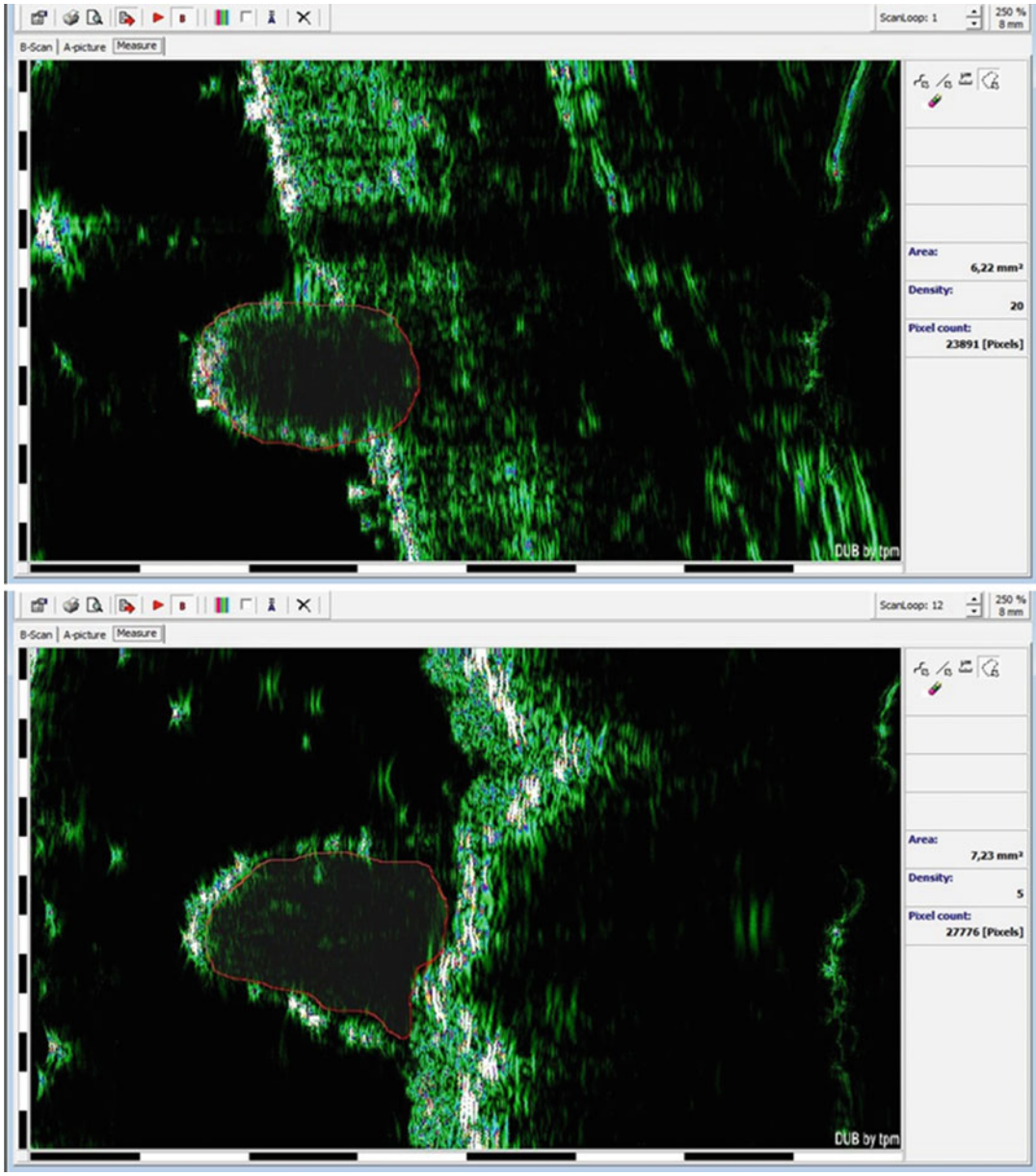

Fig. 11 Presurgical HFUS (*top image*) (area, 6.22 mm^2) and ex vivo HFUS (*bottom image*) (area, 7.23 mm^2) of an intradermal nevus on the face

smaller that ex vivo HFUS area. Ex vivo HFUS is 5 % larger than presurgery.

In 10/74 cases, the histology reported positive margins (3 benign lesions, 7 malignant lesions). Five out of seven malignant tumors were larger than 12 mm or deeper than 5 mm, leaving only 2/74 (2.7 %) tumors with positive histologic margins nonidentifiable by HFUS.

4 Conclusion

HFUS is a noninvasive technique that is affordable, versatile, and simple to utilize and learn. It is not time consuming in comparison to other NIIT and is readily accepted by patients. New generations of equipment are getting smaller to the point

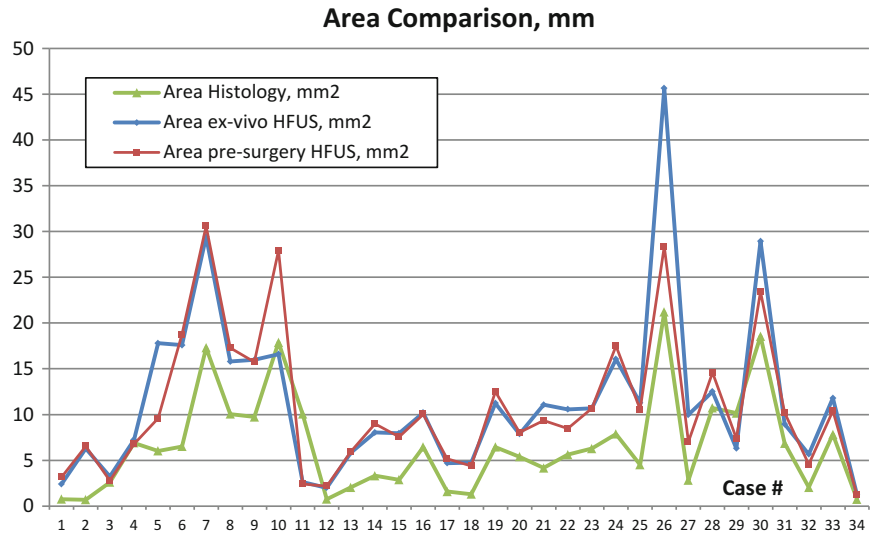

Fig. 12 Comparison of the areas obtained from presurgical (*red line*) and ex vivo (*blue line*) HFUS and histology (*green line*). Histologic tumor areas tend to be smaller than both presurgical and ex vivo HFUS

of fitting in the palm of a hand, can be transported from one operating room to another, and costwise are less expensive than most NIIT. In spite of this, HFUS is still not as popular as other NIITs.

The information obtained from a HFUS of a tumor is extremely useful for therapeutic planning or as a follow-up method for nonsurgical treatment. Many errors that occur when managing skin tumors could be reduced if surgeons had more information on them. Undertreating tumors has oncological, cosmetic, and economic consequences; in overtreatment cosmetic and economic consequences can be an issue.

HFUS/HRUS on skin tumors helps evaluate size, shape, and volume. It is a technique that is simple to learn, versatile with low cost, and available. However, it does not give information at cellular level like confocal microcopy does.

As far as volume, HFUS measurements give a discrete overestimation of tumor's size probably due to the presence of inflammatory infiltrates in the area immediately surrounding the tumor. On the other end, there is always an underestimation on histology which is probably due to the retraction of the tissue/loss of skin tightness/dehydration due to fixation of preparation.

The ex vivo HFUS overestimation is probably due to infiltration of local anesthesia and fluids from the surgical manipulation. Another consideration is specimen's orientation which can further introduce variations in measurements between HFUS and histology.

Comparison of HFUS/HRUS to histology dimensions gives valuable information to the surgeon. Histology reports do not reveal real tumor size and/or margins by underestimation. For a benign nevus excision, this is surely unimportant; however, in malignant tumors where margin excision has to follow specific guidelines, underestimation of tumor and free margins could appear as an incomplete excision and result in legal problems. Dermoscopy and HFUS give more accurate information on tumor dimension.

Ex vivo tumor measurements give surgeons reassurance of complete excision. Small tumors can just be saucerized or shaved, avoiding unnecessary surgery. Large admixture tumors can be removed surgically only on the deep parts, leaving the shallow areas for other less invasive forms of therapy.

HFUS/HRUS can be used to evaluate presurgical margins (Marmur et al. 2010). Ex vivo HFUS/HRUS could also be used to evaluate tumoral margins as well as to keep a record on the amount of the normal skin removed.

Additional clinical studies aimed to establish morphological differences between BCC subtypes and ex vivo margin correlation versus recurrences and broaden the spectrum to other malignant tumors are warranted.

References

Ahnlide I, Bjellerup M. Accuracy of clinical skin tumour diagnosis in a dermatological setting. Acta Derm Venereol. 2013;93(3):305–8.

Argenziano G, Giacomel J, Zalaudek I, et al. A clinico-dermoscopic approach for skin cancer screening: recommendations involving a survey of the International Dermoscopy Society. Dermatol Clin. 2013;31 (4):525–34.

Crisan M, Crisan D, Sannino G, Lupsor M, Badea R, Amzica F. Ultrasonographic staging of cutaneous malignant tumors: an ultrasonographic depth index. Arch Dermatol Res. 2013;305(4):305–13.

Crowson AN. Basal cell carcinoma: biology, morphology and clinical implications. Mod Pathol. 2006;19: S127–47.

Desai TD, Desai AD, Horowitz DC, Kartono F, Wahl T. The use of high-frequency ultrasound in the evaluation of superficial and nodular basal cell carcinomas. Dermatol Surg. 2007;33:1220–7.

Hinz T, Ehler LK, Hornung T, Voth H, Fortmeier I, Maier T, Höller T, Schmid-Wendtner MH. Preoperative characterization of basal cell carcinoma comparing tumour thickness measurement by optical coherence tomography, 20-MHz ultrasound and histopathology. Acta Derm Venereol. 2012;92 (2):132–7.

Hoffmann K, el Gammal S, Matthes U, Altmeyer P. Digital 20 MHz sonography of the skin in preoperative diagnosis. Z Hautkr. 1989;64(10):851–2, 855–8.

Jovanovic DL, Pesic ZU. Preoperative skin tumours thickness determination by high-frequency ultrasound on head and neck region. J Eur Acad Dermatol Venereol. 2013;27(2):251–3.

Kamyab-Hesari K, Seirafi H, Naraghi ZS, Shahshahani MM, Rahbar Z, Damavandi MR, Naraghi MM, Rezvani M, Aghazadeh N. Diagnostic accuracy of punch biopsy in subtyping basal cell carcinoma. J Eur Acad Dermatol Venereol. 2014 Feb;28(2):250–3. Epub 2012 Sep 18.

Lallas A, Apalla Z, Argenziano G, Longo C, Moscarella E, Specchio F, Raucci M, Zalaudek I. The dermatoscopic universe of basal cell carcinoma. Dermatol Pract Concept. 2014;4(3):11–24. doi:10.5826/dpc.0403a02. eCollection 2014.

Marmur ES, Berkowitz EZ, Fuchs BS, Singer GK, Yoo JY. Use of high-frequency, high-resolution ultrasound before Mohs surgery. Dermatol Surg. 2010;36 (6):841–7.

Nassiri-Kashani M, Sadr B, Fanian F, Kamyab K, Noormohammadpour P, Shahshahani MM, Zartab H, Naghizadeh MM, Sarraf-Yazdy M, Firooz A. Pre-operative assessment of basal cell carcinoma dimensions using high frequency ultrasonography and its correlation with histopathology. Skin Res Technol. 2013;19(1):e132–8.

Pasquali P, Camacho E, Fortuño A. Basal cell carcinomas measured with high frequency ultrasound (22 MHz, TPM®). Correlation between dermoscopy, histology and Ultrasound. 6th World Congress Meeting of Interdisciplinary Melanoma Skin Cancer Centres/8th EADO Congress. Poster. 14–17 Nov 2012.

Pasquali P, Camacho E, Fortuño A. Ex vivo measurement of skin tumors using 22 MHz high resolution ultrasound (TPM®). 6th World Congress Meeting of Interdisciplinary Melanoma Skin Cancer Centres/8th EADO Congress. Poster. 14–17 Nov 2012.

Pasquali P, Freites-Martinez A, Fortuño-Mar A. Ex vivo high frequency ultrasound: a novel proposal for management of surgical margins in patients with non-melanoma skin cáncer. J Am Acad Dermatol. (In Press) 10.1016/j.jaad.2016.01.006.

Pasquali P, Camacho E, Fortuño-Mar A. Use of 22 MHz high-frequency ultrasound in the management of skin cancer. In: Baldi A, Pasquali P, Spugnini EP, editors. Skin cancer a practical approach. New York: Humana Press Springer; 2014. p. 245–56.

Petrella LI, Valle HA, Issa PR, Martins CJ, Pereira WC, Machado JC. Study of cutaneous cell carcinomas ex vivo using ultrasound biomicroscopic images. Skin Res Technol. 2010;16(4):422–7.

Petrella LI, de Azevedo Valle H, Issa PR, Martins CJ, Machado JC, Pereira WC. Statistical analysis of high frequency ultrasonic backscattered signals from basal cell carcinomas. Ultrasound Med Biol. 2012;38 (10):1811–9. Epub 2012 Aug 21.

Sexton M, Jones DB, Maloney ME. Histologic pattern analysis of basal cell carcinoma. J Am Acad Dermatol. 1990;23:1118–26.

Wortsman X. Common applications of dermatologic sonography. J Ultrasound Med. 2012;31:97–111.

Wortsman X, Wortsman J. Clinical usefulness of variable-frequency ultrasound in localized lesions of the skin. J Am Acad Dermatol. 2010;62:247–56.

In Vivo Magnetic Resonance Imaging of the Skin

44

Rachid Kechidi and Sébastien Aubry

Contents

Keywords

Skin • MRI • Normal • Tumor • Physiology • Absorption

Abbreviations

BCC	Basal cell carcinoma
FIESTA	Fast imaging employing steady-state acquisition
MRI	Magnetic resonance imaging
SCC	Squamous cell carcinoma
$T1_w$	T1 weighted
$T2_W$	T2 weighted
US	Ultrasound

1 Introduction

As skin is an external human body wrap, it is usually examined by the clinical senses of sight and touch. Its composition and structure were first analyzed using optical microscopy and then electron microscopy from biopsy samples. Noninvasive imaging techniques of the skin have been first developed to improve the diagnostic accuracy of skin tumors (Smith and Macneil 2011).

The thickness of the skin and its heterogeneity require a submillimetric spatial resolution. Actual noninvasive imaging techniques are high-resolution ultrasound (US), confocal microscopy, optical coherence tomography, and magnetic resonance imaging (MRI). High-frequency ultrasound (20–100 MHz) is easy to use, is cheap, and provides an excellent axial and lateral

R. Kechidi
University Hospital of Besançon, Besançon, France
e-mail: r.kechidi@live.fr

S. Aubry (✉)
University Hospital of Besançon, Besançon, France

Department of Radiology, I4S Laboratory, INSERM EA4268, University of Franche-Comte, Besançon, France
e-mail: radio.aubry@free.fr

P. Humbert et al. (eds.), *Agache's Measuring the Skin*,
DOI 10.1007/978-3-319-32383-1_51

resolution (Lassau et al. 2007; Querleux et al. 1988; Fornage et al. 1993). Its correlation coefficient with histology for thickness analysis of tumors is superior or equal to 0.95 (Fornage et al. 1993; Harland et al. 1993). But its field of view, focused on the epidermis and dermis, is smaller than MRI. Confocal microscopy and optical coherence tomography appear complementary rather rivals to MRI because their field of examination concern in particular the superficial layers of the skin: confocal microscopy solely allows the study of the epidermis (Corcuff et al. 1993; Rajadhyaksha et al. 1995; Masters et al. 1997), and coherence tomography does not allow in-depth exploration beyond the papillary dermis (Mordon 2002; Welzel 2004).

MRI of the skin is a recent imaging technique: Bittoun et al. (1990) and Richard et al. (1991, 1993) were the first to carry out MRI of the skin in the early 1990s. Although it is expensive, it offers many advantages. Because of its wider field of view than US, its spatial resolution under 100 μm, and its excellent contrast, MRI allows high-quality imaging of every skin layers.

In addition to morphological analysis, it is also able to study some physical and biochemical properties of the skin. The objectives of this article are to remind technical aspect of MRI of the skin, to describe the normal features of the skin, to discuss challenges in diagnosis of skin disorders, and to present the principal applications of MRI for the in vivo characterization of its biochemical properties.

2 Technical Constraints

The order of magnitude of the thickness of the hypodermis is centimeter. That of the dermis is millimeter, and that of the epidermis and stratum corneum is 100 μm. Hence, compared to other applications of MRI, spatial resolution must reach 100 μm in order to analyze skin layers. The quality of any examination is the result of a compromise between acquisition time, signal-to-noise ratio, and spatial resolution. In daily practice, the length of each sequence is limited to 6 min in order to avoid motion artifacts. The design of small receive-only surface coils (Denis et al. 2008; Hyde et al. 1987; Kwon Song et al. 1997) has enabled to increase spatial resolution thanks to small field of views (2–6 cm) (Fig. 1). Higher magnetic fields (Bittoun et al. 1990; Aubry et al. 2009; Barral et al. 2010) increase signal-to-noise ratio, thus improving contrast and spatial resolution. However, even if the power of magnetic field may be correlated with some technical artifacts, it has been shown that, although visible, they do not hinder the interpretation of the images (Aubry et al. 2009). In vivo using high-field MRI and small dedicated coils, Aubry et al. (2009) demonstrated the good quality of normal skin images with resolution of 87 μm on spin-echo T1-weighted images corresponding to a field of view that is less than 3 cm. Basic sequences are T1 weighted ($T1_W$) and T2 weighted ($T2_W$). Contrast-enhanced $T1_W$ images may also be realized to study tumors (Pennasilico et al. 2002).

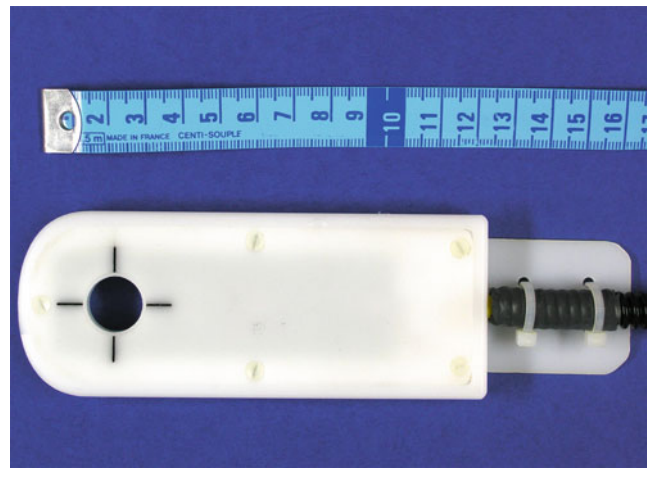

Fig. 1 Dedicated receive-only MRI coil. Its small diameter enables skin imaging with small field of view, aiming at increasing spatial resolution of images

3 Morphological Analysis of Normal Skin

The skin is composed of four main layers. Their MRI appearance is, from the surface to the deepest layer, as follows (Bittoun et al. 1990, 2006; Denis et al. 2008; Aubry et al. 2009) (Fig. 2):

- **The stratum corneum**
  The outermost protective layer, the stratum corneum is mainly composed of dead keratinocytes. It is visualized only at the heel (Denis et al. 2008) and the fingertips (Mirrashed and Sharp 2004a; Stefanowska 2010) as a high-signal band separated from the living epidermis by a low-signal band.
- **The epidermis**
  This layer is composed of keratinized stratified squamous epithelium. It appears as a thin superficial layer of high signal on $T1_W$ and $T2_W$ images.
- **The dermis**
  Fibrous tissue rich in collagen, the dermis is subdivided into papillary and reticular dermis. It contains cutaneous appendages including the hair follicles, sweat glands, and pilosebaceous follicles. The dermis has a low signal, visible deep within the epidermis. Pilosebaceous follicles appear as fine oblique lines running parallel, seen as high-signal intensity structures. These lines come from the hypodermis, passing through the dermis and the epidermis.

  In the face, on 3D fast imaging employing steady-state acquisition (FIESTA) images and on $T1_W$ images, the dermis can be subdivided into a superficial layer with higher-signal intensity and a deeper layer of lower signal (9) (Fig. 3). Richard (Richard et al. 1993) highlighted an increase in protonic density in the superficial dermis which is more significant among elderly people and could explain this MRI appearance. This may also correspond to the subepidermic hypoechoic band described on US images (Sandby-Moller and Wulf 2004), but its exact meaning remains to be found.
- **The hypodermis**
  The hypodermis is mainly composed of fat. It is sometimes considered part of the skin and sometimes as subcutaneous tissue (Bittoun et al. 2006; James 2006; Kim et al. 2008). This deepest layer of the skin is easily identified on MRI because of its considerably high signal on $T1_W$ and $T2_W$ images with fatty expansions in the deeper part of the dermis. The interlobular septum and its vessels determine the lobules and are characteristically low-signal intensity structures within the hypodermis.

Variations of normal MRI appearance of the skin depending on studied localization have to be known in order not to be misdiagnosed as abnormal: normal visualization of thick stratum corneum of the heel (Denis et al. 2008) and normal visualization of two sublayers within the dermis of the face (Aubry et al. 2009) (Fig. 3). Variations of the thickness of the dermis and epidermis depending on localization are also known (Fig. 4).

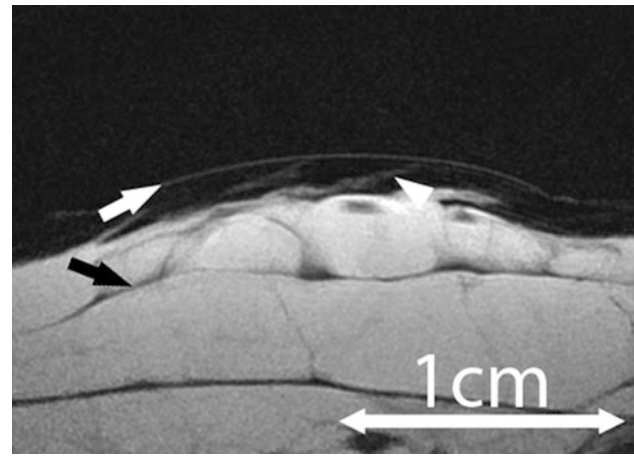

Fig. 2 $T1_W$ image of normal skin of the calf. The epidermis (*white arrow*) is a thin superficial line of high signal. The underlying dermis has a low signal, crossed by thin lines corresponding to pilosebaceous follicles (*white arrowhead*). The hypodermis has a high signal due to its high amount of fat. Within the hypodermis, *thin* low-signal lines correspond to interlobar septa (*black arrow*)

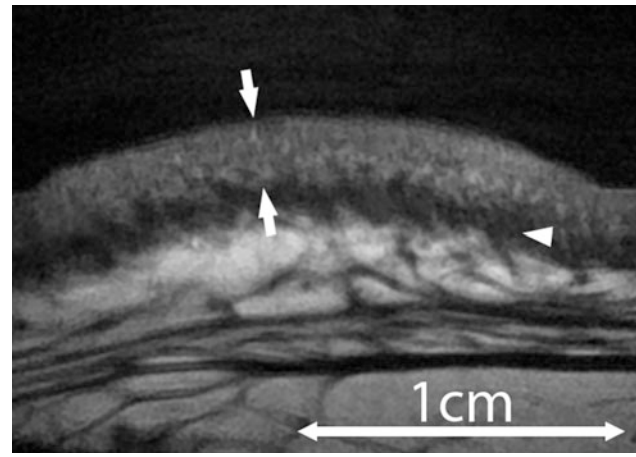

Fig. 3 At the face, on this $T1_W$ image, a superficial band of high-signal (*white arrows*) contrasts with a low-signal band at the deep aspect of the dermis (*white arrowhead*)

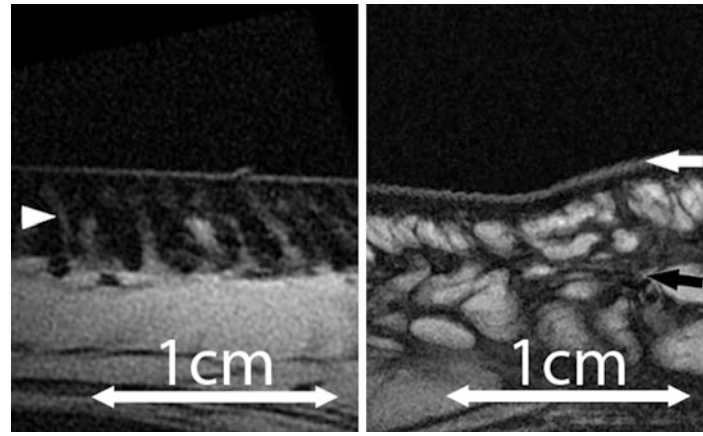

Fig. 4 The dermis of the back (*left*, *white arrowhead*) is *thicker* than that of the foot (*right*). On the other hand, at the sole, the epidermis (*white arrow*) appears to be *thicker*. We can also notice the extremely dense connective tissue within the hypodermis of the soles (*black arrow*)

4 MRI of Skin Disorders

Among all noninvasive skin imaging methods, ultrasound was the first to demonstrate an excellent correlation between image-derived skin thickness and histological measurements (Edwards et al. 1989); in fact the usefulness of US was demonstrated in the preoperative prediction of melanocytic tumor thickness and its effectiveness in differentiating between tumors $\leq$1 mm and those >1 mm (Hayashi et al. 2009; Vilana et al. 2009).

The remarkable anatomic detail and contrast obtained on MRI images has been used to generate in vivo 3D representations of skin pathologies such as nevi, acne, psoriasis, scleroderma, etc. (Sans et al.), although such images are not required for the diagnosis of these pathologies. In most clinical applications, the aim of MRI is to differentiate the different kinds of skin tumor and to estimate their extent before surgery in the case where surgical resection should be minimized in the example of facial tumor. It is also a help to diagnosis, localization, and delineation of some tumors that may be difficult to detect because of their topography, such as subungual glomus tumors. It also allows determining the degree of invasion of malignant tumors within deeper soft tissues and to measure their size and thickness. A review published in 2008 (Kim et al. 2008) aimed at listing the MRI features of most common aspects of several benign and malignant skin tumors.

4.1 Dermatofibrosarcoma Protuberans

This uncommon spindle cell tumor that typically develops in the dermis as an outward protruding mass is considered to be an intermediate-grade lesion. These lesions are typically within the dermis but can extend freely over the hypodermis and deeper, so leading sometimes to confusions with higher-grade sarcomas. Its most frequent localization is the trunk, accounting for almost half of all cases. Dermatofibrosarcoma protuberans has an excellent prognosis after complete resection but has a marked tendency to recur locally if inadequate surgical resection margins are obtained, which underlines the interest of MRI to delineate it.

On MR imaging the tumor appears as a well-defined lesion with a low signal on $T1_W$ images and a high signal on $T2_W$ images and usually is enhanced more strongly than other skin tumors on contrast-enhanced $T1_W$ images (Fig. 5). Occasionally hemorrhages occur in this tumor which results in a heterogeneous appearance on MR images (Torreggiani et al. 2002; Kransdorf and Meis-Kindblom 1994).

4.2 Glomus Tumor

Glomus tumor is a rare benign tumor that develops from neuromyoarterial glomus body which consists of an afferent arteriole, a tortuous arteriovenous, a system of collecting veins, and a neurovascular reticulum that regulates the flow of blood through the anastomosis. Glomus bodies are present in the stratum reticularis of the dermis throughout the body, but they are highly concentrated in the digits, palms, and soles of the feet. They may be difficult to detect when subungueal hence the interest of MRI (Bittoun et al. 2006; Goettmann et al. 1994; Drape et al. 1996).

MR imaging features that are considered diagnostic for glomus tumors include intermediate- or low-signal intensity on $T1_W$ images, marked high signal on $T2_W$ images, and strong enhancement after IV gadolinium infusion. Typical MR angiographic findings include areas of strong enhancement in the arterial phase and tumor blush, which increases in size in the delayed phase (Baek et al. 2010) (Fig. 6).

4.3 Malignant Melanoma

Most melanomas apparently arise de novo, but some develop in association with a preexisting nevus. Melanoma and pigmented tumors were first explored because the melanin pigments are paramagnetic and induce a shortening of T1 and T2 relaxation times (Zemtsov et al. 1989). Therefore, the expected signal for melanotic melanoma is high signal on $T1_W$ images and low signal on $T2_W$ images (Hawnaur et al. 1996; Marghoob et al. 2003). MRI may be used to measure the thickness and depth extension of melanomas and their volume and vascularization (Marghoob et al. 2003; Psaty and Halpern 2009). In a small

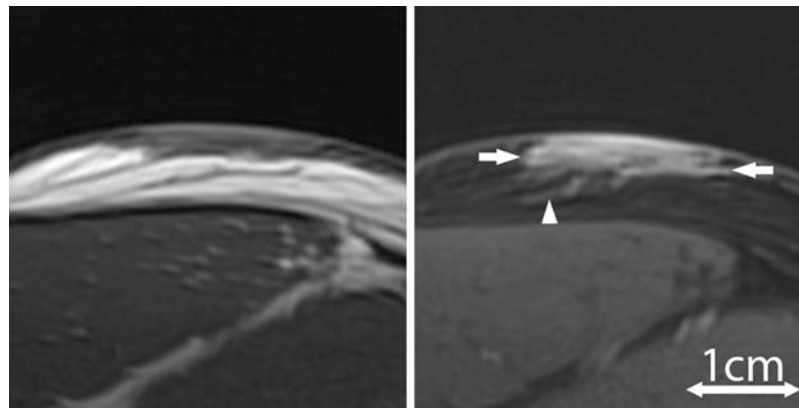

Fig. 5 MRI of a dermatofibrosarcoma. It has a slightly higher signal than the normal dermis on $T1_W$ image (*left*). On fat-saturated contrast-enhanced $T1_W$ image (*right*), this epidermal and dermal lesion (*between white arrows*) presents a strong enhancement and invades the hypodermis (*white arrowhead*) to a depth of 6 mm

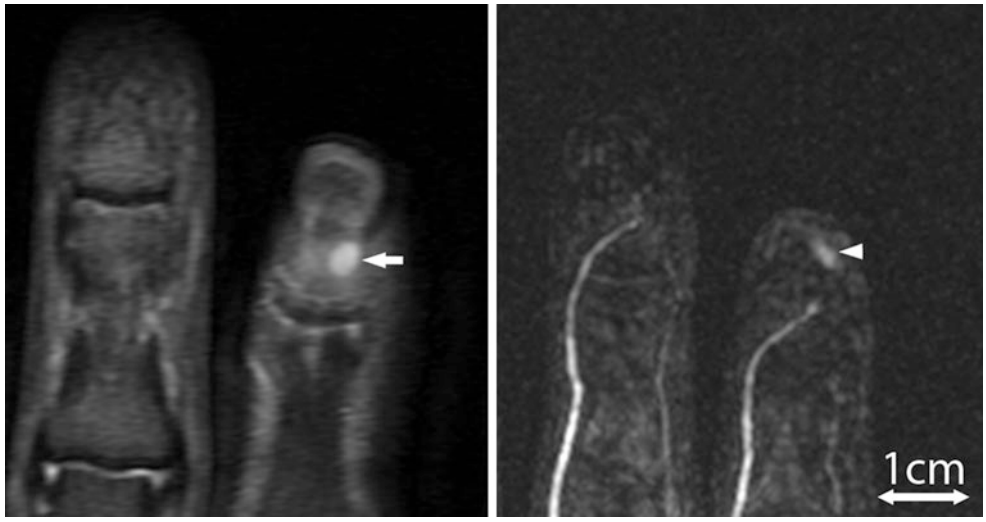

Fig. 6 This glomus tumor of the fourth finger appears as high-signal ovoid image of 3 mm diameter on proton density fat-saturated coronal image (*left*, *white arrow*). It is strongly enhanced on angiographic contrast-enhanced sequence (*right*, *white arrowhead*)

sample containing two melanomas, Ono et al. (Ono and Kaneko 1995) found a good correlation between the morphology and in-depth invasion of skin tumors in MRI with histological data.

4.4 Keratinocytic Skin Tumors

Keratinocytic skin tumors are derived from epidermal and keratinocytes of appendages, mainly including basal cell carcinoma (BCC) and squamous cell carcinoma (SCC). They account for approximately 90 % of all skin malignancies, and their incidence has increased rapidly in the past few years (Miller 2000). In vitro, using 7 Tesla MRI, (Aubry et al. 2012) have shown a good correlation between MRI and histologic measurements of nonmelanoma skin cancer (Fig. 7), but these results remain difficult to transpose to clinical routine because of time of acquisition and cost problems. Basal cell carcinoma, the most frequent, is a slow-growing tumor, mostly local, which rarely metastasize. Gufler et al. (2007) on seven cases of basal cell carcinoma of the face in 1.5 T MRI confirmed the usefulness of MRI to determine the extent of these tumors compared to adjacent soft tissues and the level in depth of tumor infiltration and to exclude a possible bone involvement.

Keratinocytic skin tumors have nonspecific signal intensity patterns, with high-signal intensity on $T2_W$ images, with relatively homogeneous enhancement after IV gadolinium chelates infusion. SCC may also be heterogeneous and include unenhanced region on the contrast-enhanced $T1_W$ images (Kim et al. 2008).

4.5 Benign Fibrous Histiocytoma

This is a very frequent tumor, located preferentially in the dermis where it is called histiocytoma cutis or dermatofibroma. These tumors arise most frequently between the second and the fourth decade and are mainly located at the extremities (Gonzalez and Duarte 1982).

On MR imaging the tumor appears as low to intermediate signal on T1w images and low- to high-signal intensity on fluid-sensitive MR sequences (Fig. 8). Occasionally hemorrhages occur in this tumor which results in an heterogeneous appearance on MR images (Kransdorf 2006).

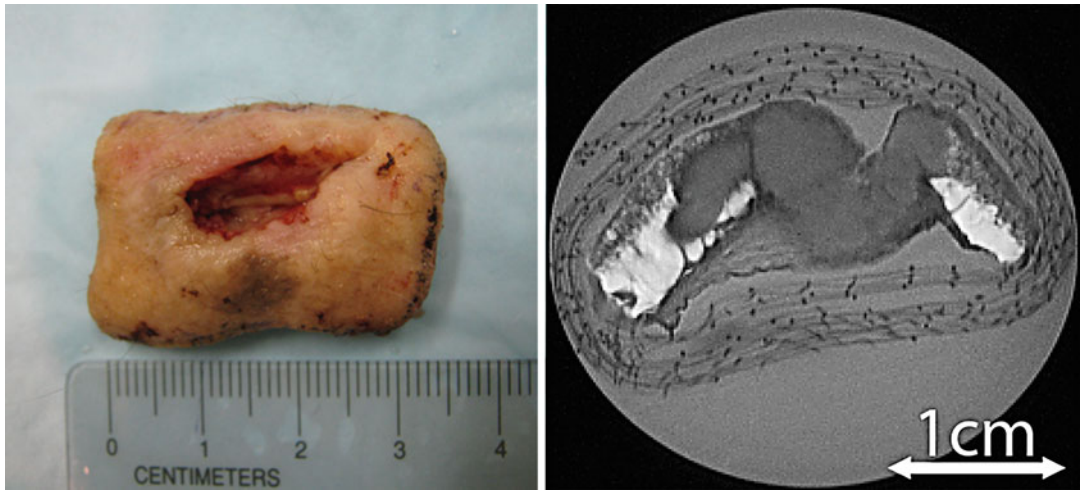

Fig. 7 Postoperative photograph of an ulcerated squamous cell carcinoma of the scalp (*left*). In vitro 7 Tesla $T2_W$ image through short axis of the tumor reveals that it invades the whole thickness of the sample: surgical margins were confirmed by pathologist to be positive. Contrast between the tumor and the skin is good enough to measure it accurately

5 Parametric Analysis of Biochemical Parameters of the Skin

5.1 T1 and T2 Relaxation Time and Proton Density

Compared to other imaging modalities, MRI has the particularity to capture a signal depending on the intrinsic parameters of the tissue: it provides information on the characteristics of water in the skin, through measurements of the relaxation times T1, T2, and proton density which reflect mobile water and lipid levels in the different skin layers (Richard et al. 1991; Querleux 2001). At the calf, T2 relaxation times have been estimated to 22.3 ± 7 ms for the epidermis, 13 ± 2.4 ms for the dermis, and 35.4 ± 3.6 ms for the hypodermis (Richard et al. 1991). Richard et al. (1993) demonstrated that the level of mobile water is twice as high in the epidermis than in the dermis, whatever the age of the subject. This quantitative measurement of the level of mobile water has also been used to calculate the hydration in the field of cosmetology. Recent changes in European directives require manufacturers to prove the effectiveness of cosmetics leading to researches in this field of skin hydration. Querleux et al. (1994) studied the hydration of the stratum corneum at the heel. Aubry et al. (Calzolari 2013) recently tried to estimate the T2 relaxation time and proton density of the dermis before and after applying moisturizer using the T2-mapping sequence (Fig. 9). Researchers also tried to distinguish benign versus malignant-pigmented skin cancer by measuring the relaxation times and T2 signal of lesions (Takahashi and Kohda 1992) (Fig. 8).

5.2 Magnetization Transfer

This property can be used in MRI to quantify mobile water of the different skin layers (Bittoun et al. 2006; Mirrashed and Sharp 2004a). A study published in 2004 showed a percentage of magnetization transfer activity in the dermis lower than the epidermis. Authors also observed a higher percentage of magnetization transfer activity in the papillary dermis compared to the reticular dermis (Mirrashed and Sharp 2004b).

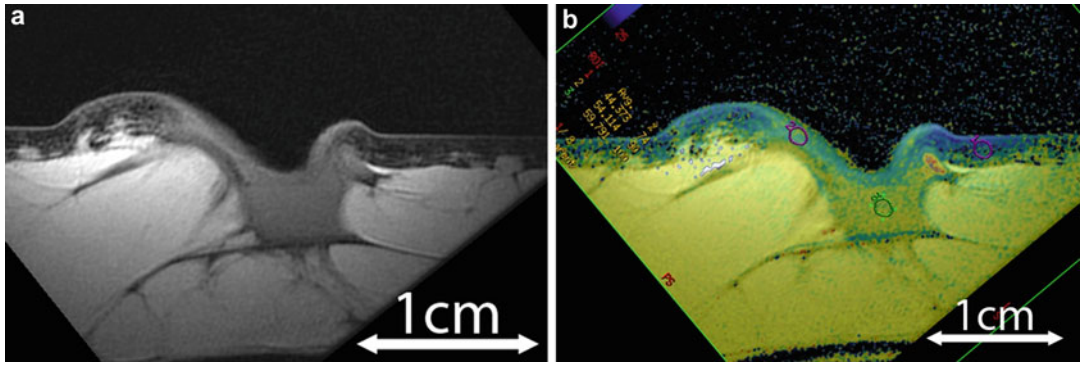

Fig. 8 $T1_W$ image of a histiocytofibroma. It has a slightly higher signal than the normal dermis (**a**). It invades the hypodermis to a depth of 7.8 mm. On T2 mapping (**b**), its T2 relaxation time is longer than the normal dermis (54–59 ms vs. 44 ms)

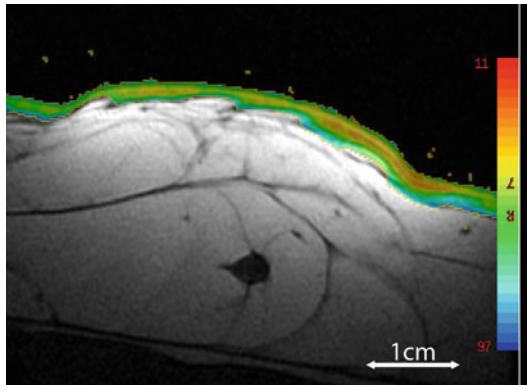

Fig. 9 T2-mapping image of a normal dermis of the calf. The T2 relaxation time of the dermis may be calculated with this sequence. This parameter may be useful for quantitative evaluation of cosmetics or for characterization of skin lesions

5.3 Water Diffusion Coefficient

Diffusion-weighted images give information on the microscopic movements of water in the skin. It is widely used in neuroradiology to detect early signs of ischemic stroke. Several studies have been conducted reporting a possible use of this sequence to quantify the mobility of free water in the skin with possible applications in the future to study the mechanisms of skin barrier function of the living epidermis healthy and pathological (Bittoun et al. 2006; Kinsey et al. 1997; McDonald et al. 2005; Lee et al. 1998).

5.4 Spectroscopy

MR spectroscopy of the skin is recent and remains a research activity. Studies conducted have focused on normal skin and hydration profile and feasibility of this technique (Querleux 2004; Weis et al. 2001). Several methods aim to obtain separate images and information of different molecules (water, lipids). The majority of researches have been done with phosphorous spectroscopy (Chen et al. 1992; Zemtsov et al. 1994; Collier et al. 1994) and very few with proton spectroscopy (Kim et al. 1989).

6 Conclusion

MRI is a noninvasive, non-radiating imaging modality that is also reproducible and non-operator dependent. Its good spatial resolution and contrast allow imaging of the different skin layers. Even if in clinical daily practice its spatial resolution is not sufficient for optimal analysis of the epidermis and very thin lesions, this imaging technique is distinguished from others by its holistic approach of the skin. Numerous studies have validated its feasibility and its interest to study the normal and pathologic skin. MRI seems able to play a useful role in the diagnosis and surgical assessment of particular cases of tumors. In addition, biochemical parameters evaluated by MRI are also promising to evaluate skin physiology, skin hydration, and effects of cosmetic products.

References

Aubry S, Leclerc O, Tremblay L, Rizcallah E, Croteau F, Orfali C, et al. 7-tesla MR imaging of non-melanoma skin cancer samples: correlation with histopathology. Skin Res Technol. 2012;18(4):413–20.

Aubry S, Casile C, Humbert P, Jehl J, Vidal C, Kastler B. Feasibility study of 3-T MR imaging of the skin. Eur Radiol. 2009;19(7):1595–603.

Baek HJ, Lee SJ, Cho KH, Choo HJ, Lee SM, Lee YH, et al. Subungual tumors: clinicopathologic correlation with US and MR imaging findings. Radiographics. 2010; 30(6):1621–36.

Barral JK, Bangerter NK, Hu BS, Nishimura DG. In vivo high-resolution magnetic resonance skin imaging at 1.5 T and 3 T. Magn Reson Med. 2010;63(3):790–6.

Bittoun J, Saint-Jalmes H, Querleux BG, Darrasse L, Jolivet O, Idy-Peretti I, et al. In vivo high-resolution MR imaging of the skin in a whole-body system at 1.5 T. Radiology. 1990;176(2):457–60.

Bittoun J, Querleux B, Darrasse L. Advances in MR imaging of the skin. NMR Biomed. 2006;19(7):723–30.

Chen Y, Richards TL, Izenberg S, Golden RN, Williams DL, Nelson JA, et al. In vivo phosphorus NMR spectroscopy of skin using a crossover surface coil. Magn Reson Med. 1992;23(1):46–54.

Collier SW, Sardon S, Ruiz-Cabello J, Johnson WA, Cohen JS, Schwartz SL. Measurement of pharmacodynamic effects of dexamethasone on epidermis by phosphorus nuclear magnetic resonance spectroscopy in vitro. J Pharm Sci. 1994;83(9):1339–44.

Corcuff P, Bertrand C, Leveque JL. Morphometry of human epidermis in vivo by real-time confocal microscopy. Arch Dermatol Res. 1993;285(8):475–81.

Denis A, Loustau O, Chiavassa-Gandois H, Vial J, Lalande Champetier de Ribes C, Railhac JJ, et al. High resolution MR imaging of the skin: normal imaging features. J Radiol. 2008;89(7–8 Pt 1):873–9.

Drape JL, Wolfram-Gabel W, Idy-Peretti I, Baran R, Goettmann S, Sick H, et al. The lunula: a magnetic resonance imagining approach to the subnail matrix area. J Invest Dermatol. 1996;106(5):1081–5.

Edwards C, Al-Aboosi MM, Marks R. The use of A-scan ultrasound in the assessment of small skin tumours. Br J Dermatol. 1989;121(3):297–304.

Fornage BD, McGavran MH, Duvic M, Waldron CA. Imaging of the skin with 20-MHz US. Radiology. 1993;189(1):69–76.

Goettmann S, Drape JL, Idy-Peretti I, Bittoun J, Thelen P, Arrive L, et al. Magnetic resonance imaging: a new tool in the diagnosis of tumours of the nail apparatus. Br J Dermatol. 1994;130(6):701–10.

Gonzalez S, Duarte I. Benign fibrous histiocytoma of the skin. A morphologic study of 290 cases. Pathol Res Pract. 1982;174(4):379–91.

Gufler H, Franke FE, Rau WS. High-resolution MRI of basal cell carcinomas of the face using a microscopy coil. AJR Am J Roentgenol. 2007;188 (5):W480–4.

Harland CC, Bamber JC, Gusterson BA, Mortimer PS. High frequency, high resolution B-scan ultrasound in the assessment of skin tumours. Br J Dermatol. 1993;128(5):525–32.

Hawnaur JM, Dobson MJ, Zhu XP, Watson Y. Skin: MR imaging findings at middle field strength. Radiology. 1996;201(3):868–72.

Hayashi K, Koga H, Uhara H, Saida T. High-frequency 30-MHz sonography in preoperative assessment of tumor thickness of primary melanoma: usefulness in determination of surgical margin and indication for sentinel lymph node biopsy. Int J Clin Oncol. 2009; 14(5):426–30.

Hyde JS, Jesmanowicz A, Kneeland JB. Surface coil for MR imaging of the skin. Magn Reson Med. 1987; 5(5):456–61.

James W. Andrews' diseases of the skin: clinical dermatology. 10th ed. Philadelphia: Saunders Elsevier; 2006.

Kim YH, Orenberg EK, Faull KF, Wade-Jardetzky NG, Jardetzky O. 1H NMR spectroscopy: an approach to evaluation of diseased skin in vivo. J Invest Dermatol. 1989;92(2):210–6.

Kim JH, Kim JY, Chun KA, Jee WH, Sung MS. MR imaging manifestations of skin tumors. Eur Radiol. 2008;18(11):2652–61.

Kinsey ST, Moerland TS, McFadden L, Locke BR. Spatial resolution of transdermal water mobility using NMR microscopy. Magn Reson Imaging. 1997;15(8): 939–47.

Kransdorf MJ. Benign fibrous and fibrohistiocytic tumors. In: Kransdorf MJ et al., editors. Imaging of soft tissue tumors. 2nd ed. Philadelphia: Lippincott Williams & Wilkins; 2006. p. 195–6.

Kransdorf MJ, Meis-Kindblom JM. Dermatofibrosarcoma protuberans: radiologic appearance. AJR Am J Roentgenol. 1994;163(2):391–4.

Kwon Song H, Wehrli FW, Ma J. In vivo MR microscopy of the human skin. Magn Reson Med. 1997;37:185–91.

Lassau N, Chami L, Peronneau P. Imaging of melanoma: accuracy of ultrasonography before and after contrast injection for diagnostic and early evaluation of treatments. Bull Cancer. 2007;94(1):93–8.

Calzolari L, Kastler A, Mac-Mary S, Humbert P, Kastler B, Aubry S.3T-MRI analysis of epidermis and dermis moisturizing using the T2-mapping sequence. Skin Res Technol. 2013 May;19(2):152-4

Lee D, Kim J, Lee H. Investigation of biochemical changes in skin layers by NMR microscopy. Skin Res Technol. 1998;4:142–6.

Marghoob AA, Swindle LD, Moricz CZ, Sanchez Negron FA, Slue B, Halpern AC, et al. Instruments and new technologies for the in vivo diagnosis of melanoma. J Am Acad Dermatol. 2003;49(5): 777–97; quiz 98–9.

Masters BR, Gonnord G, Corcuff P. Three-dimensional microscopic biopsy of in vivo human skin: a new technique based on a flexible confocal microscope. J Microsc. 1997;185(Pt 3):329–38.

McDonald PJ, Akhmerov A, Backhouse LJ, Pitts S. Magnetic resonance profiling of human skin in vivo using GARField magnets. J Pharm Sci. 2005;94(8):1850–60.

Miller S. The National Comprehensive Cancer Network (NCCN) guidelines of care for nonmelanoma skin cancers. Dermatol Surg. 2000;26:289–92.

Mirrashed F, Sharp JC. In vivo quantitative analysis of the effect of hydration (immersion and Vaseline treatment) in skin layers using high-resolution MRI and magnetisation transfer contrast. Skin Res Technol. 2004a;10(1):14–22.

Mirrashed F, Sharp JC. In vivo morphological characterisation of skin by MRI micro-imaging methods. Skin Res Technol. 2004b;10(3):149–60.

Mordon S. les techniques photoniques de l'UV aux IR. [cited 17/12/07]; Available from: e2phyin2p3fr/2002/actes/mordondoc. 2002.

Ono I, Kaneko F. Magnetic resonance imaging for diagnosing skin tumors. Clin Dermatol. 1995;13(4):393–9.

Pennasilico GM, Arcuri PP, Laschena F, Potenza C, Ruatti P, Bono R, et al. Magnetic resonance imaging in the diagnosis of melanoma: in vivo preliminary studies with dynamic contrast-enhanced subtraction. Melanoma Res. 2002;12(4):365–71.

Psaty EL, Halpern AC. Current and emerging technologies in melanoma diagnosis: the state of the art. Clin Dermatol. 2009;27(1):35–45.

Querleux B. Caractérisation de la peau humaine in vivo par imagerie et spectroscopie par résonance magnétique. In: Humbert P, Zaouani H, editors. Actualités en Ingénierie Cutanée. Paris: ESKA; 2001. p. 11–9.

Querleux B. Magnetic resonance imaging and spectroscopy of skin and subcutis. J Cosmet Dermatol. 2004;3(3):156–61.

Querleux B, Leveque JL, de Rigal J. In vivo cross-sectional ultrasonic imaging of human skin. Dermatologica. 1988;177(6):332–7.

Querleux B, Richard S, Bittoun J, Jolivet O, Idy-Peretti I, Bazin R, et al. In vivo hydration profile in skin layers by high-resolution magnetic resonance imaging. Skin Pharmacol. 1994;7(4):210–6.

Rajadhyaksha M, Grossman M, Esterowitz D, Webb RH, Anderson RR. In vivo confocal scanning laser microscopy of human skin: melanin provides strong contrast. J Invest Dermatol. 1995;104(6):946–52.

Richard S, Querleux B, Bittoun J, Idy-Peretti I, Jolivet O, Cermakova E, et al. In vivo proton relaxation times analysis of the skin layers by magnetic resonance imaging. J Invest Dermatol. 1991;97(1):120–5.

Richard S, Querleux B, Bittoun J, Jolivet O, Idy-Peretti I, de Lacharriere O, et al. Characterization of the skin in vivo by high resolution magnetic resonance imaging: water behavior and age-related effects. J Invest Dermatol. 1993;100(5):705–9.

Sandby-Moller J, Wulf HC. Ultrasonographic subepidermal low-echogenic band, dependence of age and body site. Skin Res Technol. 2004;10(1):57–63.

Sans N, Faruch M, Chiavassa-Gandois H, de Ribes CL, Paul C, Railhac JJ. High-resolution magnetic resonance imaging in study of the skin: normal patterns. Eur J Radiol. 2011;80(2):e176–81.

Smith L, Macneil S. State of the art in non-invasive imaging of cutaneous melanoma. Skin Res Technol. 2011;17(3):257-69.

Stefanowska J, Zakowiecki D, Cal K. Magnetic resonance imaging of the skin. J Eur Acad Dermatol Venereol. 2010; 24(8):875–80.

Takahashi M, Kohda H. Diagnostic utility of magnetic resonance imaging in malignant melanoma. J Am Acad Dermatol. 1992;27(1):51–4.

Torreggiani WC, Al-Ismail K, Munk PL, Nicolaou S, O'Connell JX, Knowling MA. Dermatofibrosarcoma protuberans: MR imaging features. AJR Am J Roentgenol. 2002;178(4):989–93.

Vilana R, Puig S, Sanchez M, Squarcia M, Lopez A, Castel T, et al. Preoperative assessment of cutaneous melanoma thickness using 10-MHz sonography. AJR Am J Roentgenol. 2009;193(3):639–43.

Weis J, Ericsson A, Astrom G, Szomolanyi P, Hemmingsson A. High-resolution spectroscopic imaging of the human skin. Magn Reson Imaging. 2001; 19(2):275–8.

Welzel J. Optical coherence tomography. In: Agache P, Humbert P, editors. Measuring the skin. Berlin: Springer; 2004. p. 222–9.

Zemtsov A, Lorig R, Bergfield WF, Bailin PL, Ng TC. Magnetic resonance imaging of cutaneous melanocytic lesions. J Dermatol Surg Oncol. 1989; 15(8):854–8.

Zemtsov A, Dixon L, Cameron G. Human in vivo phosphorus 31 magnetic resonance spectroscopy of psoriasis. A noninvasive tool to monitor response to treatment and to study pathophysiology of the disease. J Am Acad Dermatol. 1994;30(6):959–65.

Quantification of the Inhomogeneous Distribution of Topically Applied Substances on the Human Skin by Optical Spectroscopy: Definition of a Factor of Inhomogeneity

45

Hans-Jürgen Weigmann, Sabine Schanzer, Martina C. Meinke, Fanny Knorr, and Jürgen Lademann

Contents

H.-J. Weigmann • S. Schanzer • M.C. Meinke • F. Knorr • J. Lademann (✉)
Department of Dermatology, Venereology and Allergology, Center of Experimental and Applied Cutaneous Physiology, Charité - Universitätsmedizin Berlin, Berlin, Germany
e-mail: hweinet@alice-dsl.net; sabine.schanzer@charite.de; martina.meinke@charite.de; fanny.knorr@charite.de; juergen.lademann@charite.de

P. Humbert et al. (eds.), *Agache's Measuring the Skin*,
DOI 10.1007/978-3-319-32383-1_52

Keywords
Human skin profile • Topically applied formulations • Inhomogeneous distribution • Tape stripping • Optical spectroscopy

1 Introduction

The most common use of optical absorption spectroscopy is the quantification of substances in chemical systems. This application requires a homogeneous distribution of the absorbing substances, which results in a linear correlation between the spectroscopic data and the amount of the absorber under discussion (Beer-Lambert law). The measured overall signal is reduced if there are areas of different concentration or areas that are not covered with absorbing substances inside the examined area. For this reason, spectroscopy is suitable for determining the degree of inhomogeneity in the distribution of absorbers.

The surface of the human skin is characterized by specific structures, which differ individually. As furrows, wrinkles, hair follicles, sweat glands, dermal lesions, and the corneocytes (Schaefer and Redelmeier 1996; Fritsch 2004) form a typical surface character (Helfrich et al. 2008; Krutmann et al. 2008), topically applied formulations are distributed inhomogeneously. This

refers to cosmetic products generally and is of special interest considering in terms of sunscreens.

The protection efficacy of sunscreens is primarily determined by specific filter substances, which are included in these products. A given filter concentration results in a defined lowering of the radiation intensity by the absorbing species. This effect is reduced if the homogenous distribution is disturbed by the typical surface relief that reduces the protection efficacy of sunscreens (Jain et al. 2010; Rohr et al. 2010; Schroeder et al. 2010). A characterization of these changes can be achieved to determine a spectroscopically measured factor of inhomogeneity by comparing the absorbance measured for the applied sunscreen with the value of the identical amount of absorbers spread homogeneously. This value is well suited to quantify the filter distribution of topically applied substances on the surface of the human skin and to investigate the influence of different parameters (Weigmann et al. 2012a).

2 Materials and Methods

2.1 Volunteers

The study was conducted with 18 healthy volunteers (skin phototypes II and III (Fitzpatrick et al. 1993)), which were aged between 20 and 35 years. The volunteers had provided their written informed consent in agreement with the ethical approval obtained from the Ethics Committee of the Charité – Universitätsmedizin Berlin.

2.2 Applied Formulations

The investigation was realized using five different sunscreen formulations, COLIPA low standard product P1 (SPF 4), CTFA high standard product P2 (SPF 12), high standard product P3 (SPF 15.5) (COLIPA 1994), and commercial products, NIVEA Sun Sonnenmilch, SPF 8 and NIVEA Sun Feuchtigkeits-Sonnenmilch, SPF 26, which were applied onto the flexor forearm (2.0 mg/cm^2) (COLIPA 1994).

2.3 Tape Stripping

Tape stripping was performed 30 min after application using the standard protocol (Lademann et al. 2009; Weigmann et al. 1999). The adhesive film (*tesa* film No. 5529; Beiersdorf, Hamburg, Germany) was pressed onto the skin with a stamp for 5 s (pressure: 15 kp/cm^2) and then removed in one rapid movement.

2.4 UV/Visible Spectroscopic Measurements

The spectra were recorded in a range from 240 to 500 nm, using the UV/visible spectrometer (Lambda 5, PerkinElmer, Frankfurt/Main, Germany) with an integrating sphere. The extinction in the maximum of the UVB absorption bands was used as reference quantity.

2.4.1 Tape Strips

The original spectra measured with an empty tape as a reference were corrected by the spectra obtained from an untreated skin site using the software UV WinLab Version 2.70.01 (PerkinElmer), in order to eliminate the influence of the individual horny layer particles. Foregoing investigations (data not shown) indicated that the first tape strips reflect the degree of inhomogeneity most effectively.

2.4.2 Solutions

The absorbance values, characterizing the homogenous distribution of the absorbers, were determined after solving a definite part of the immediately measured tape strips in an adequate amount of ethanol (UVASOL; Merck, Darmstadt, Germany) and a subsequent separation from the horny layer particles by centrifugation (centrifuge MR 1812; Jouan GmbH, Unterhaching, Germany).

2.5 In Vivo Laser Scanning Microscopy

Laser scanning microscopy (VivaScope 1500 Multilaser, MAVIG GmbH München) with sodium fluorescein as marker substance was used to compare the distribution of topically applied substances on the human skin and on the tape strips immediately after stripping.

3 Results and Discussion

3.1 Illustration of the Distribution of Topically Applied Absorbers

The results obtained regarding the local distribution of topically applied substances using laser scanning microscopy are shown in Fig. 1.

The in vivo distribution of the fluorescent dye fluorescein on the skin (image a) is compared with the distribution found on tape strips immediately after their removal (image b). In both cases, the dye is concentrated around the corneocytes in the inter-lipid phase of the skin, illustrating one type of an inhomogeneous distribution pattern. The agreement found for the distribution in both samples verifies that the situation on the skin surface is correctly transferred to the tape strips. Therefore, the spectroscopic data determined after tape stripping should be suitable to quantify the degree of the inhomogeneity of topically applied substances on the skin.

3.2 Definition of a Factor of Inhomogeneity

The homogeneity of the distribution of topically applied formulations on the skin is not only influenced by the individual surface profile but additionally by the composition of the specific sunscreen.

3.2.1 Variation of the Volunteer-Specific Absorbance Values

The homogeneous absorbance in solution (A_{hom}) is compared with the absorbance found for the tape strips, reflecting the in vivo efficacy of the absorber in the investigated skin area (A_{inhom}). The results obtained for one model formulation (COLIPA P1) for six volunteers are shown in Fig. 2.

The actual absorbance measured in solution (A_{hom}) was determined by the concrete amount of

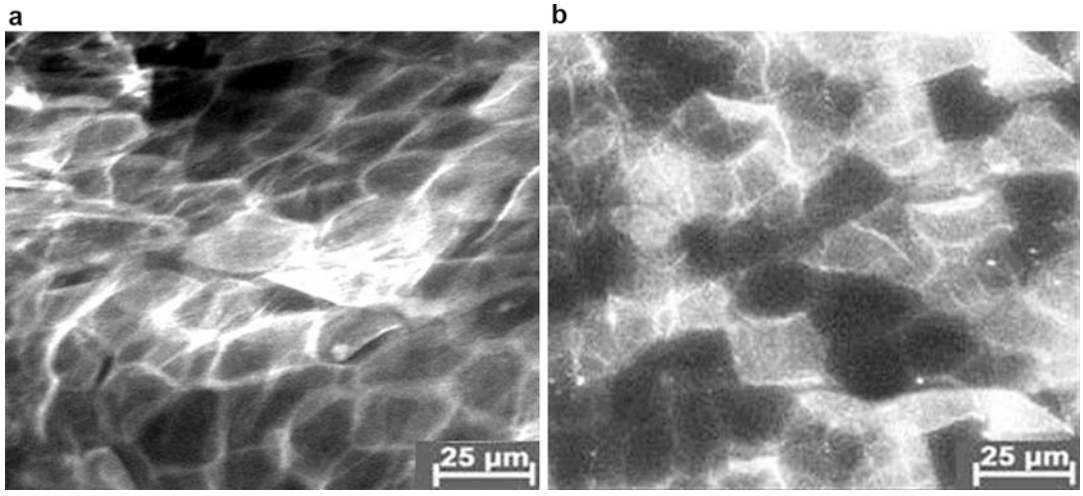

Fig. 1 Distribution of a fluorescent substance (sodium fluorescein) added to a topically applied sunscreen on the human skin. (**a**) Measured in vivo. (**b**) Measured in vitro on a tape strip that was removed from a corresponding skin site

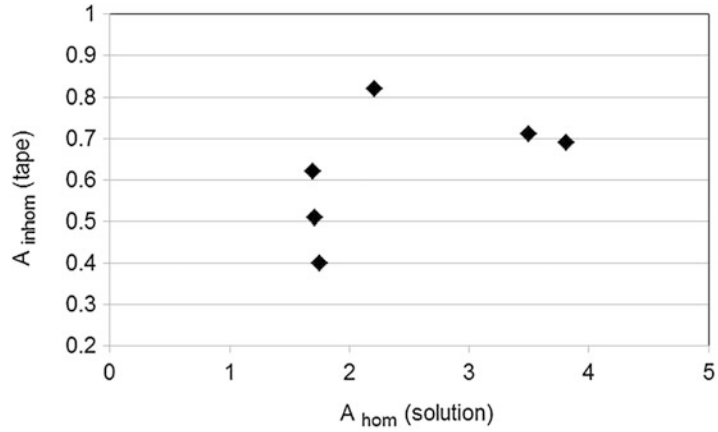

Fig. 2 Comparison of the absorbance measured for the model sunscreen COLIPA P1 (first tape strips of six volunteers). A_{inhom} absorbance on tape strips immediately after removal. A_{hom} absorbance in solution obtained after extraction of the tape strips

absorbing substances present in the investigated skin area. In three experiments, the corresponding value was nearly constant ($A_{hom} = 1.7$), according to identical amounts. Moreover, two data points were clearly different, verifying the well-known situation that the distribution inside the skin area under investigation is nonuniform.

The broad variation of the absorbance (A_{inhom} = 0.4–0.62) measured for the corresponding tape strips reflected the individual differences in the individual skin profiles of the three volunteers with nearly constant $A_{hom} = 1.7$. Both results illustrated the information provided by the spectroscopic data. Similar results were obtained for the other sunscreens under investigation.

3.2.2 Determination of the Factor of Inhomogeneity

The difference of the discussed spectroscopic values, i.e., the absorbance measured for the absolute amount of absorber, A_{hom}, and the profile-correlated spectroscopic data obtained from the tape strips, A_{inhom}, reflects the skin-specific distribution of the absorbers. Calculating the quotient between both values enables the definition of a factor of inhomogeneity:

$$F_{inhom} = A_{hom}/A_{inhom}.$$

In order to test the applicability of the obtained factors, the parameter influences must be considered.

3.3 Parameters Influencing the Factor of Inhomogeneity

3.3.1 Influence of Different Volunteers and Formulations

Discussing the parameter dependence of the proposed measured value, the range of variation found for the different volunteers and formulations must be considered. In Table 1, the obtained results are summarized.

The formulation-correlated mean values of the factors of inhomogeneity were the basis for obtaining information regarding the sunscreen-related changes in the distribution and the influences of the different volunteers.

The sunscreen-correlated values varied from $F_{inhom} = 3.9$ to 11.9. The mean value of all sunscreens amounted to $F_{inhom} = 8.3$, which corresponded to a standard deviation of 40 % for these data. This value described to what extent the investigated sunscreens change the inhomogeneity of the distribution. The reference to the mean values eliminated the influences of the different skin profiles of the volunteers.

The variation found for the individual volunteers is provided by the factors of inhomogeneity, which are summarized in the upper part of column 2–6. Considering the mean value of these standard deviations in percent amounted to 1.9, which corresponded to an overall value of 23 %.

The comparison of the two percentage values, 40 % and 23 %, indicated that the factors of

Table 1 Variation of the factor of inhomogeneity found for different volunteers and different formulations

	Factor of inhomogeneity				
	individual values for the different volunteers				
Volunteer	COLIPA P1 SPF 4	COLIPA P2 SPF 12	COLIPA P3 SPF 15.5	Sunscreen SPF 8	Sunscreen SPF 26
1	2.7	8.8	8.0	4.4	13.8
2	5.5	14.5	8.7	7.6	14.6
3	4.3	8.9	7.5	7.9	7.9
4	4.6	10.7	9.3	6.0	9.4
5	3.4	16.2	10.4	5.2	9.3
6	2.8	12.2	9.3	4.8	10.0
F_{inhom} mean value ± standard deviation (in percent)	3.9 ± 1.0 (26 %)	11.9 ± 3.0 (25 %)	9.0 ± 1.5 (15 %)	6.0 ± 1.5 (25 %)	10.8 ± 2.7 (25 %)

Overall mean value for the five formulations (3.9–11.9): $F_{inhom} = 8.3$, corresponding to a standard deviation of 40 %
Mean value of the standard deviations of the six volunteers (1.0–3.0) = 1.9 corresponding to a standard deviation of 23 %

inhomogeneity were influenced more strongly by the investigated formulations than by the individual skin structures of the volunteers.

3.3.2 Influence of Skin Pretreatment

An essential aspect for studying the distribution of absorbers on the skin surface was the correlation to the efficacy of sunscreens. From earlier investigations it is known that the inhomogeneous distribution reduced the protection by a factor of 10 (Lademann et al. 2004). On the contrary, a higher homogeneity enhances the protection. In a previously published study (Weigmann et al. 2012b), the influence of a pretreatment of the skin with a body lotion on the distribution of a sunscreen with SPF 8 was investigated. In the considered system, the factor of inhomogeneity evidently reflected the upgrade achieved by the pretreatment. The value $A_{inhom} = 11.5$ had dropped to $A_{inhom} = 6.5$ after pretreatment. Conformity was obtained, taking into account the enhancement of another spectroscopic value that characterizes the increased absorption of the incident sun radiation, the sum absorbance. This value increases after body lotion application.

Nevertheless, another study showed that a pretreatment led to a faster removal of the applied sunscreens from the skin during contact with water (Kluschke et al. 2014).

3.3.3 Comparison of the Factor of Inhomogeneity with the Optically Determined Volume of Furrows Characterizing the Skin Profile

The importance of the proposed factor of inhomogeneity was evaluated by comparing the results obtained by spectroscopy with data measured by another optical method (Gebauer et al. 2012). Using this technique, the skin profile was characterized directly by a specific optical three-dimensional measuring system that determines the characteristics of surfaces, taking into account the volume between the highest and the lowest points of the skin relief.

When these data were compared to the spectroscopic values, taking into account the three sunscreens, linear correlations were obtained at a statistical significance of $p \leq 0.01$ and a correlation coefficient of 0.98, 0.67, and 0.66, respectively. The reduced coefficients reflect different changes that were due to an individual modification of the skin surface following topical application of the sunscreen.

This compilation shows that the factor of inhomogeneity is not only well suited to recognize and to optimize the distribution of topically applied substances but also reflects correctly differences in the surface profile of the human skin.

4 Conclusion

The typical structure of the human skin influences the distribution of topically applied sunscreens characteristically. The resulting inhomogeneity determines the spectroscopic absorbance measured for tape strips after removal, A_{inhom}. The calculation of a quotient, taking into account the corresponding absorbance values obtained after extraction of the removed tape strips (A_{hom}), resulted in a factor of inhomogeneity: $F_{inhom} = A_{hom}/A_{inhom}$. Comparing the variation of the results obtained for different volunteers and sunscreens, it was found that the influence of the different formulations was higher than the volunteer-correlated data. The relevance of the factor of inhomogeneity was verified by results which were obtained by considering the influence a pretreatment of the skin before sunscreen application and by the good correlation found to the volume of furrows and wrinkles obtained by an independent method.

Acknowledgments The authors would like to thank the foundation "Skin Physiology" of the Donor Association for German Science and Humanities for their financial support. We thank Sabine Grenz for active linguistic and Heike Richter for technical assistance.

References

Fitzpatrick TB, Eisen AZ, Wolff K, Freedberg IM, Austen KF. Dermatology in general medicine. 4th ed. - New York: Mc Graw-Hill; 1993.

Fritsch P. Dermatologie Venerologie. 2nd ed. Berlin/Heidelberg: Springer; 2004. p. 19–24.

Gebauer V, Weigmann HJ, Schanzer S, Meinke MC, Vergou T, Sterry W, et al. Influence of skin aging effects on the skin surface profile and the correlated distribution of topically applied sunscreens. J Biophotonics. 2012;5(3):274–82.

Helfrich YR, Sachs DL, Voorhees JJ. Overview of skin aging and photoaging. Dermatol Nurs Dermatol Nurs Assoc. 2008;20(3):177–83.

Jain A, Rieger I, Rohr M, Schrader A. Antioxidant efficacy on human skin in vivo investigated by UVA-induced chemiluminescence decay analysis via induced chemiluminescence of human skin. Skin Pharmacol Physiol. 2010;23(5):266–72.

Kluschke F, Weigmann HJ, Schanzer S, Meinke M, Vergou T, Sterry W, et al. Gain or loss? Sunscreen efficiency after cosmetic pretreatment of the skin. Skin Pharmacol Physiol. 2014;27(2):82–9.

Krutmann J, Diepgen DL, Krutmann-Billmann C. Hautalterung. 2nd ed. Berlin/Heidelberg: Springer; 2008. p. 13–122.

Lademann J, Rudolph A, Jacobi U, Weigmann HJ, Schaefer H, Sterry W, et al. Influence of nonhomogeneous distribution of topically applied UV filters on sun protection factors. J Biomed Opt. 2004; 9(6):1358–62.

Lademann J, Jacobi U, Surber C, Weigmann HJ, Fluhr JW. The tape stripping procedure – evaluation of some critical parameters. Eur J Pharm Biopharm. 2009; 72(2):317–23.

Rohr M, Klette E, Ruppert S, Bimzcok R, Klebon B, Heinrich U, et al. In vitro sun protection factor: still a challenge with no final answer. Skin Pharmacol Physiol. 2010;23(4):201–12.

Schaefer H, Redelmeier TE. Skin barrier: principles of percutaneous absorption. Basel: Karger AG; 1996. p. 2.

Schroeder P, Calles C, Benesova T, Macaluso F, Krutmann J. Photoprotection beyond ultraviolet radiation – effective sun protection has to include protection against infrared A radiation-induced skin damage. Skin Pharmacol Physiol. 2010;23(1):15–7.

COLIPA. International sun protection factor (SPF) test method. Bruxelles: The European Cosmetic, Toiletry and Perfumery Association; 1994.

Weigmann HJ, Lademann J, Meffert H, Schaefer H, Sterry W. Determination of the horny layer profile by tape stripping in combination with optical spectroscopy in the visible range as a prerequisite to quantify percutaneous absorption. Skin Pharmacol Appl. 1999;12(1–2):34–45.

Weigmann HJ, Schanzer S, Vergou T, Antoniou C, Sterry W, Lademann J. Quantification of the inhomogeneous distribution of topically applied substances by optical spectroscopy: definition of a factor of inhomogeneity. Skin Pharmacol Physiol. 2012a;25(3):118–23.

Weigmann HJ, de Sainte Claire MS, Schanzer S, Patzelt A, Meinke M, Antoniou C, et al. Determination of the protection efficacy and homogeneity of the distribution of sunscreens applied onto skin pre-treated with cosmetic products. Skin Res Technol. 2012b;18 (2):245–50.

Optical Coherence Tomography Imaging of the Skin

46

Alia Arif Hussain, Lotte Themstrup, Mette Mogensen, and Gregor B. E. Jemec

Contents

Keywords

Actinic keratosis (AK) • Basal cell carcinomas (BCCs) • Bullous pemphigoid • Contact dermatitis • High-definition OCT (HD-OCT) • Imiquimod • Methyl aminolevulinate photodynamic therapy (MAL-PDT) • Non-melanoma skin cancer (NMSC) • Optical coherence tomography (OCT) • Dermatology • Fibrotic diseases • High definition • Interferometric technique • Porphyria cutanea tarda (PCT) • Psoriasis • Scleroderma • Wound healing

1 Background

Optical coherence tomography (OCT) is a noninvasive optical imaging technology routinely used in ophthalmology for retinal imaging. OCT has gained a prominent position in ophthalmological routine imaging since the 1990s (Huang et al. 1991; Swanson et al. 1993). The technology also has the potential to provide high-resolution images of other tissues such as the skin where it not only allows bedside in vivo diagnosis but also the noninvasive monitoring of lesional evolution or treatment. The OCT images are primarily displayed in a vertical view similar to ultrasound imaging. Compared to ultrasound, OCT images have a higher resolution albeit a lower penetration depth. Horizontal OCT

A.A. Hussain (✉) • L. Themstrup • G.B.E. Jemec
Department of Dermatology, Roskilde Hospital, University of Copenhagen, Roskilde, Denmark
e-mail: alia.arif.hussain@gmail.com; lotte.themstrup@gmail.com; gbj@regionsjaelland.dk

M. Mogensen
Department of Dermatology and Venereology, Bispebjerg Hospital, University of Copenhagen, Copenhagen, Denmark
e-mail: mogensen.mette@gmail.com

P. Humbert et al. (eds.), *Agache's Measuring the Skin*,
DOI 10.1007/978-3-319-32383-1_53

imaging akin to in vivo confocal microscopy is also possible. During the last 10–15 years, the OCT technique has been improved for skin imaging, reflecting both development in data processing and in optics.

2 Method and Basic Principles

OCT is an interferometric imaging technique that enables noninvasive, real-time, high-resolution, cross-sectional imaging in vivo. It works by detecting reflected and backscattered light from the tissue.

The images can either be two- or three-dimensional with a lateral resolution of <7.5 μm and axial resolution of <5 μm. The images can roughly be compared to histological morphology at a low resolution, but imaging of individual cells is not possible. The one-dimensional depth scan is called an A-scan, and many adjacent A-scans can be combined to thereby create a 2D or 3D image that provides more information about the specific sample.

When analyzing OCT images qualitatively, several types of reflectivity and scattering are relevant. Areas appearing white appear so due to reflection, whereas areas appearing black are sites of absorbing tissue. In normal skin, fluid and air are hyporeflective/absorbing media and therefore appear dark or even completely black. Areas with dense keratin or collagen are hyperreflective areas appearing bright.

High-definition OCT (HD-OCT) is a novel technique based on the principle of conventional OCT. During the past 2 years, several conducted studies have reported HD-OCT to have an improved resolution and with the possibility of imaging single cells which however comes with a diminished penetration depth. HD-OCT has been compared to reflectance confocal microscopy (RCM) (Boone et al. 2012a) in normal skin reporting that RCM offers the best lateral resolution, whereas HD-OCT provides the best penetration depth suggesting that HD-OCT fills the imaging gap between RCM and conventional OCT.

3 How to Use the OCT

OCT imaging is generally straightforward. All the commercial OCT systems come with a handheld probe. Most of the probes are in the size range of a standard cordless phone. This sometimes makes OCT imaging inside the ear and around the medial canthus difficult. The recording of an image ranging 6 mm takes a few seconds. Hundreds of images can be saved during a single OCT scan.

4 Applications in Dermatology

OCT imaging in dermatology has significantly advanced during the last decade (Gambichler et al. 2005; Olsen et al. 2015). Several clinical studies have found advantageous use of OCT in diagnosis of inflammatory skin conditions, wound healing, non-melanoma skin tumors, and blistering diseases, among others.

Skin biopsies are currently the gold standard for diagnosing a large number of dermatological diseases especially the non-melanoma skin cancers. Since biopsies are easily acquired, precise, and low cost, they constitute a tough competition to the introduction of any new imaging technologies in dermatology. However, in relation to non-melanoma skin cancer, there are several factors speaking in favor of noninvasive diagnosing.

First and foremost, noninvasive techniques, such as OCT, provide a nontraumatic and non-scarring aid to diagnosis which can be performed bedside and be repeated over time to monitor potential recurrence of an already diagnosed disease. Secondly, with the increase in noninvasive treatments, the need for rapid diagnosis and noninvasive monitoring is increased as well. Lastly, immunosuppressed patients have a higher incidence of non-melanoma skin cancer (Kempf et al. 2013; Jemec and Holm 2003), and OCT imaging could potentially save these patients from excessive biopsies and excisions of tumor-suspicious lesions.

OCT images of healthy skin present skin fluid and air as hyporeflective/absorbing areas, and

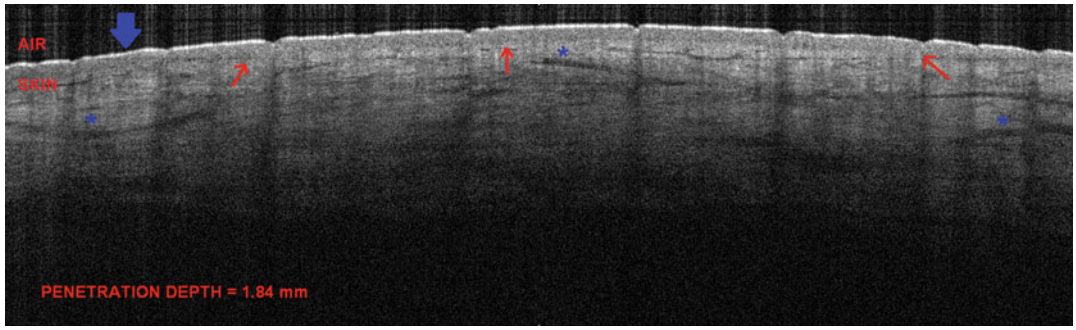

Fig. 1 Healthy skin. Healthy skin of the lower leg of a 28-year-old female. The penetration depth depends on the specific tissue, and in this OCT image of the skin, a penetration depth of 1.84 mm has been obtained. The *thin white* hyperreflective line (*thick blue arrow*) is not part of the skin but represents the entrance signal due to the shift from one medium (air) to another (skin). *Thin red arrows*: intact dermoepidermal junction. *Asterisks*: vessels

they appear dark/completely black, while hyperreflective areas appear bright. The penetration depth depends on the specific tissue. The abrupt change in refractive index from air to skin can result in a large entrance signal (Fig. 1) which can be reduced by using contact or coupling media on the part of the probe that is in contact with the skin. The media reduce the refractive index at the surface of the stratum corneum. In this way, glycerol absorbed into the skin seems to increase penetration depth by decreasing scattering and thus improving the OCT image (Serup et al. 2006). It has been suggested that speckle reduction by the appliance of the so-called spatial diversity compounding scheme (Mogensen et al. 2010) also has an improving effect on the imaging quality leading to better defined delineations of, e.g., skin tumors.

4.1 Basal Cell Carcinomas

Basal cell carcinomas (BCCs) have successfully been diagnosed with OCT in several clinical studies (Mogensen et al. 2009a). The clinical characteristics of BCC lesions in OCT images are alteration of the dermoepidermal junction (DEJ) and dark ovoid basaloid cell islands, and sometimes a dark, hyporeflective peripheral boundary (halo) can be identified. Secondary features include absence of normal hair follicles and glands and altered dermal capillaries directed toward the basaloid cell islands (Fig. 2; Hussain et al. 2015).

Studies have shown that certain histological features influence the quality of OCT images of BCC (Mogensen et al. 2011). The presence of inflammatory infiltrate significantly impairs the quality of images, while elastosis is associated with improved quality. Meanwhile, neither ulceration nor hyperkeratosis seemed to impair the quality of OCT images of BCC significantly which is of great importance as most BCC lesions have a hyperkeratotic surface.

The increasing incidence of BCC, making it the most common form of cancer in many countries (Madan et al. 2010), has given rise to extensive research to etiology, pathogenesis, and treatment. Skin biopsies and curettage or excision are currently the gold standard for diagnosis and treatment of non-melanoma skin cancer (NMSC). Taken into account that biopsies and excisions are invasive, are scarring, and have the potential of leading to infection, the noninvasive treatment options have been well received in dermatology. Imiquimod is a cream which can be used to treat superficial BCC. A recent study (Banzhaf et al. 2014) has shown that OCT can be used in the whole process of treating a superficial BCC – from the primary diagnosis to monitoring treatment effect and follow-up of potential residual tumor tissue. Photodynamic therapy with methyl aminolevulinate (MAL-PDT) is another noninvasive type of treatment. In a study (Themstrup et al. 2014) where OCT was performed

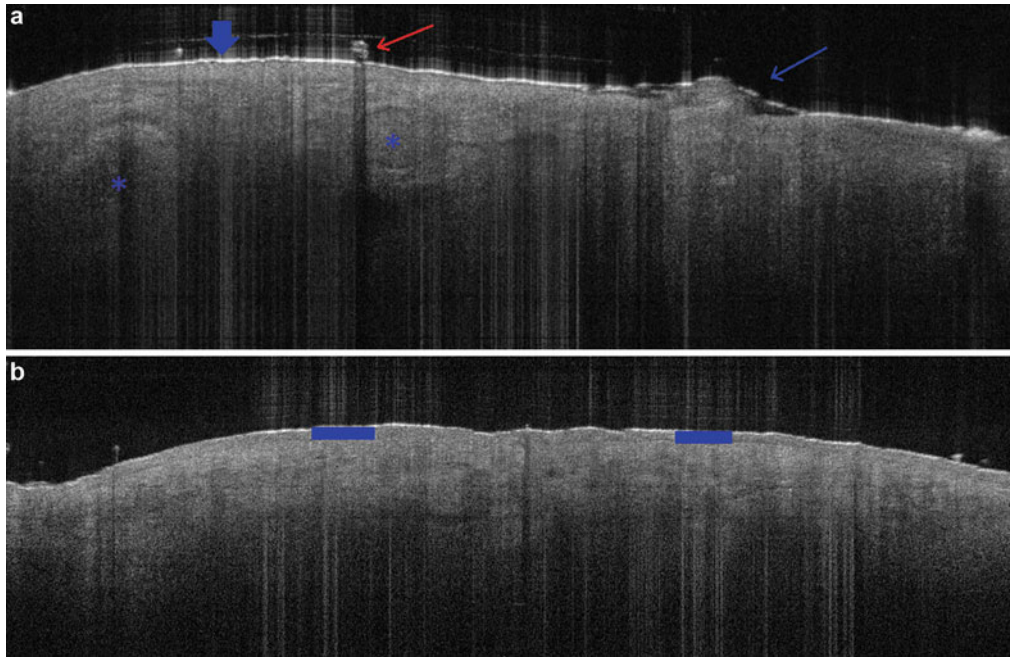

Fig. 2 (**a**) **Basal cell carcinoma**. OCT image of a 77-year-old man with a basal cell carcinoma lesion above the eyebrow. The OCT image shows disruption of the dermoepidermal junction (*thick blue arrow*) and an elevated darker area right at the skin surface corresponding to a small ulceration/crust (*thin blue arrow*). In the dermis, there are two rounded structures surrounded by a dark rim (*asterisk*). These structures correspond to basal cell tumor islands. The vertical hyporeflective streak stretching from the surface is a hair casting a shadow (*red arrow*). (**b**) Healthy skin adjacent to basal cell carcinoma lesion with the epidermis (*blue bars*), intact dermoepidermal junction and an underlying homogenous dermis

before MAL-PDT treatment and at a 3-month follow-up on 18 cases (14 BCC lesions and 4 actinic keratosis), the results showed that immediately after the MAL-PDT, it was not possible to monitor the treatment due to blurring and crust formation. At the follow-up, recurrence was suspected clinically in 5/18 cases and with OCT in 7/18 cases suggesting that OCT is able to identify 29 % more recurrences than clinical examinations alone which was subsequently confirmed by histology. This study implies that OCT is most suitable in the diagnosis and follow-up of treatment. A study on OCT monitoring of BCC treated with ingenol mebutate is being conducted at the moment.

Surgeons performing Mohs surgery (Wang et al. 2013; Alawi et al. 2013; Chan and Rohrer 2012) can use OCT to reduce the excised area without compromising the integrity of tumor-free borders. This reduces the number of invasive procedures needed. One study (Alawi et al. 2013) showed that in 84 % of cases, the OCT-defined lateral margins correctly indicated complete removal of the tumor. Furthermore, the surgical margins outlined by the surgeon never fell below the OCT-defined margin suggesting that OCT may be helpful.

OCT imaging of cutaneous lymphomas is also an area of development. A case report (Christian Ring et al. 2012) visualizing cutaneous T-cell lymphoma has illustrated a thickened and hyperreflective stratum corneum and several elongated hyporeflective structures (interpreted as lymphomatous infiltrates) in the dermis. There was a good immediate correlation between histology and OCT imaging of the sample. Similar findings in the dermis have been described in ocular lymphoma and may therefore be of importance in cutaneous lymphomas as well.

A pilot study regarding basal cell carcinoma (BCC) lesions (Boone et al. 2012b) visualized by

HD-OCT implied that HD-OCT facilitated in vivo diagnosis of BCC and even allowed the distinction between different BCC subtypes which is something that has not been possible with conventional OCT.

4.2 Actinic Keratosis

The OCT morphology of actinic keratosis (AK) is somewhat similar to that of a superficial squamous cell carcinoma (SCC). The AK lesions have the potential to regress spontaneously. However, a substantial proportion of AK lesions can progress to SCC. Unlike BCC lesions, SCC carries a risk of metastasizing (Schmitt and Bordeaux 2013).

It is a possibility to treat AK lesions noninvasively with, e.g., MAL-PDT, imiquimod, or cryosurgery. Cryotherapy is a commonly used lesionally directed therapy in which the tissue is frozen, and the tissue destruction occurs due to cellular damage incurred during the freeze-thaw cycles. Liquid nitrogen (−196 °C) is the most commonly used coolant, but solid carbon dioxide (−78.5 °C) and liquid CO_2 (−56.6 °C) have also been used. When AKs are treated by cryotherapy, tissue destruction is frequently preceded by clinical blistering. When the skin starts healing, the lesion tissue will peel off and thereby allow the appearance of new skin.

Due to the noninvasive treatment, it is quite relevant to have a noninvasive and non-scarring way of monitoring the treatment. Several conducted studies (Mogensen and Jemec 2007; Mogensen et al. 2009b, c) have implied that OCT can be beneficially used in AK diagnosis, treatment, and monitoring. The OCT characteristics of an AK include atypical thickening of the epidermis, especially the stratum corneum. Lymphocytic infiltrate from inflammation can at times be seen in the underlying area of the AK.

A recent study (Themstrup et al. 2012) indicates that OCT has the potential of monitoring cryotherapy in AK lesions. It was demonstrated that OCT can visualize and delineate the AK lesion with high accuracy. When cryotherapy is applied, an opaque iceball is imaged followed by vesicle formation shortly after the treatment. It was not possible to detect the freezing depth during the cryotherapy.

It has been reported that the in vivo diagnosis and grading of different actinic keratoses were possible using HD-OCT (Maier et al. 2013).

4.3 Inflammatory Skin Diseases

Another use for OCT is the visualization of common inflammatory diseases such as psoriasis and contact dermatitis. In the majority of cases, the diagnosis can be made by the naked eye, but in cases of doubt, skin biopsies and histology are performed for confirmation.

Psoriasis is a disease affecting a high number of patients. OCT can monitor the severity of the disease and monitor specific treatments by measuring structural changes such as epidermal thickness and optical density of the dermis (Gambichler et al. 2005; Morsy et al. 2010). In a recent study, the thickness of skin with psoriatic plaques was compared to healthy skin with a difference of 30–40 μm.

Furthermore, a study looked at psoriasis arthritis and nail abnormalities with OCT (Aydin et al. 2011, 2013). Eighteen patients with nail abnormalities were scanned with OCT and ultrasound, and the study implies that among the 180 nails, 67.8 % had clinical findings, whereas 33.9 % were abnormal with ultrasound and 44.4 % with OCT. OCT was reported to detect subtle abnormalities in 12 clinically normal nails and in 41 nails with normal ultrasound findings. The study found that a positive OCT had a sensitivity of 44.4 % and specificity of 95.8 % suggesting that OCT has a potential for detecting nail abnormalities. Regarding nail abnormalities, a study (Grover and Khurana 2012) focusing on onychomycosis reported OCT's ability to screen several areas within a nail plate and hence detect persisting fungal elements during local or systemic therapy.

Contact dermatitis (Morsy et al. 2010) is another common inflammatory skin disease. The OCT scanning visualized a higher and enlarged

entrance signal corresponding with the changes in stratum corneum with hyperkeratosis and parakeratosis.

A recent study applying Ackerman's algorithmic method of pattern recognition (Boone et al. 2013) indicated that HD-OCT is a promising method for noninvasive diagnosis, evaluation, and management of common inflammatory skin diseases by the visualization of individual cells in the epidermis and dermis and morphology of the DEJ, papillary dermis, and reticular dermis.

A case study (Banzhaf and Jemec 2012) showing OCT imaging of granulomatous lesions of the skin reported the visualization of a new shape, resembling a wing. Further studies on granulomatous skin diseases are required.

4.4 Fibrotic Diseases

Scleroderma and other fibrotic diseases, e.g., morphea (localized scleroderma), lichen sclerosus et atrophicus (LSA), keloids, and scars, are all characterized by fibrosis of the skin. Preliminary data suggest that OCT imaging of fibrotic diseases are characterized by a disarray of layering with a rather effaced DEJ. The dermis itself has been visualized as very homogenous and hyperreflective due to extensive fibrosis. The dermis may also display an intricate hyporeflective pattern. A characterization of the unique morphological differences may aid the understanding of lesional evolution and assessment of possible treatments. This is particularly important for scleroderma.

Systemic scleroderma is characterized by deposition of collagen, fibrointimal proliferation of small vessels, and vasospastic episodes. Over time, it may lead to tissue ischemia and extensive fibrosis of the skin and other organs. Due to the lack of curative treatment, the treatment goal is the prevention of disease progression by the use of, e.g., anti-fibrosing agents, topical emollients, and PUVA. With the rise of novel anti-fibrosing

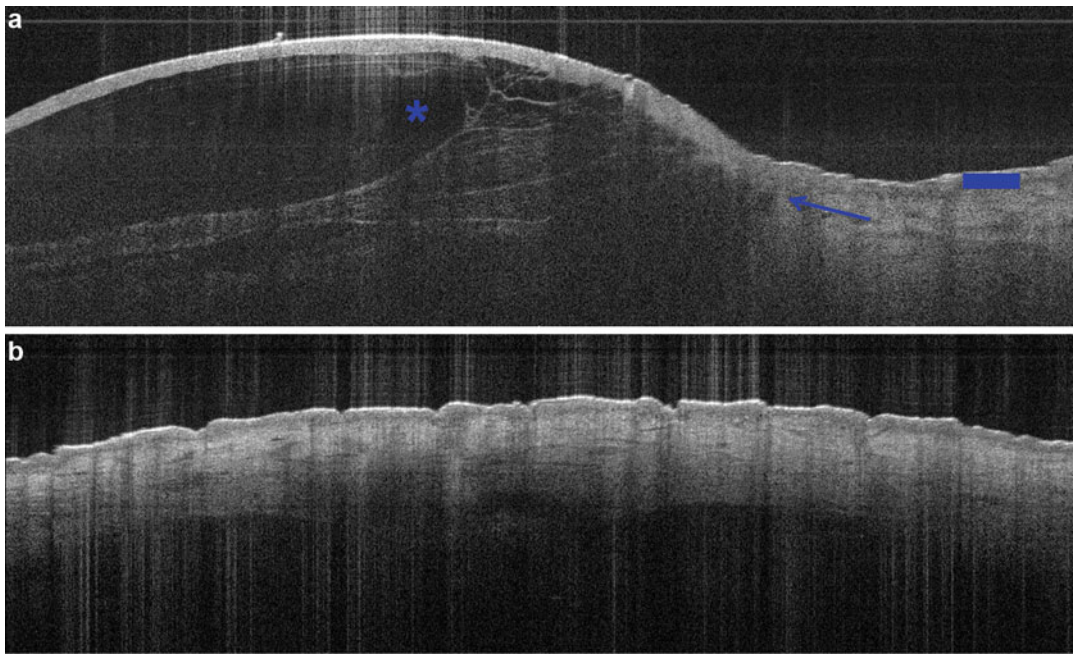

Fig. 3 (**a**) **Bullous pemphigoid**. OCT image of an 81-year-old woman with a bulla on the right thigh. The *blue bar* marks the intact dermoepidermal junction distinguishing the epidermis from the dermis. Notice the split in the skin (*blue arrow*) and the subepidermal location of the bulla. The actual bulla (*blue asterisk*) is hyporeflective due to the liquid content. The hyperreflective strokes inside the bulla may be the visualization of polymorphous inflammatory infiltrate. (**b**) OCT image showing healthy skin adjacent to the bulla

agents, the noninvasive monitoring of dermal collagen morphology becomes relevant in treatment trials (Abignano et al. 2013; Ring et al. 2015).

4.5 Bullous Diseases

Skin conditions involving bullae have been the subject of very few OCT studies and are still an area of interest with ongoing research. Fluid is an absorbing media and therefore appears dark (hyporeflective) or completely black (reflective).

It has been demonstrated that it is possible to differentiate between certain forms of bullous diseases. Overall bullae appear as dark, ovoid to round well-demarcated structures. It is possible to differentiate between intraepidermal and subepidermal bullae and thereby between blistering diseases such as bullous pemphigoid, burns, and pemphigus (Mogensen et al. 2008). However, the difference between bullous pemphigoid and pemphigus was too subtle to differentiate between the two diseases in the published series. Burn blisters were significantly different. These challenges may be met by future enhancement of the resolution of the OCT images (Fig. 3).

Porphyria cutanea tarda (PCT) blisters usually appear on sun-exposed areas of the body blisters especially on the dorsum of the hands. The bullae contain porphyrin-rich serous fluid and can be painful. Figure 4 depicts the difference between PCT on a hand and adjacent normal skin.

4.6 Wound Healing

Well-known complications subsequent to surgery and laser treatment, such as infection or prolonged wound healing, are challenging tasks in dermatology.

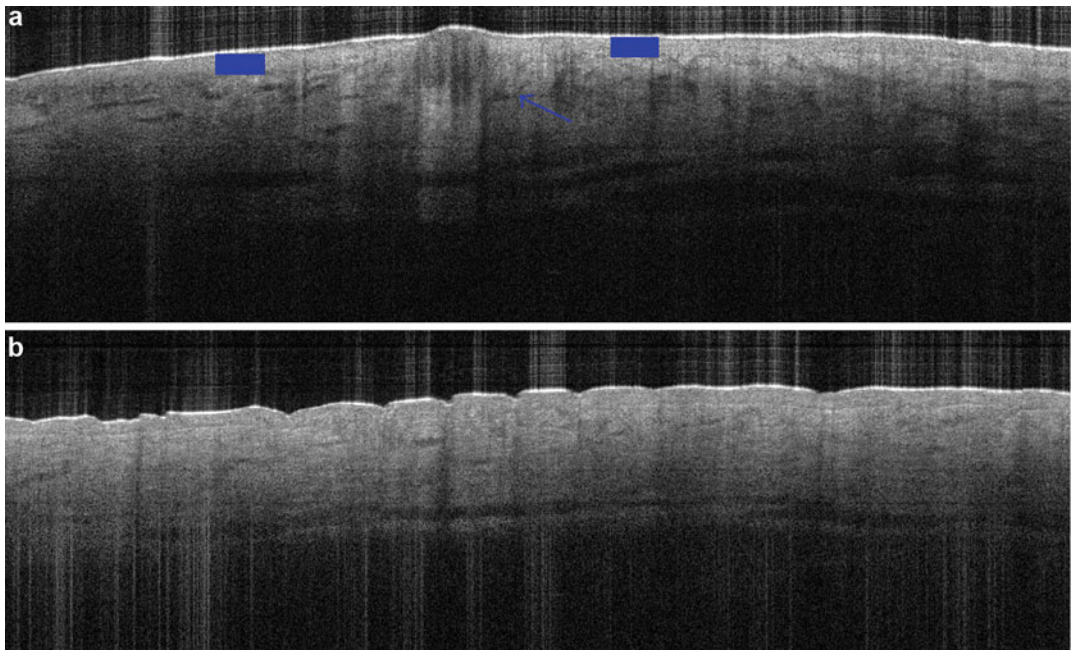

Fig. 4 (**a**) **Porphyria cutanea tarda**. Dorsum manus dexter of a 67-year-old female patient with porphyria cutanea tarda (PCT). The dermoepidermal junction is intact (*blue bars*), and the remains of a bulla (*thin blue arrow*) can be seen reaching down through the epidermis and into the dermis. The rounded structure (*blue arrow*) is the remainder of a bulla. The *blue bars* mark the dermoepidermal junction showing how the bulla extends into the dermis explaining why PCT heals with scarring. (**b**) Healthy skin adjacent to porphyria cutanea tarda

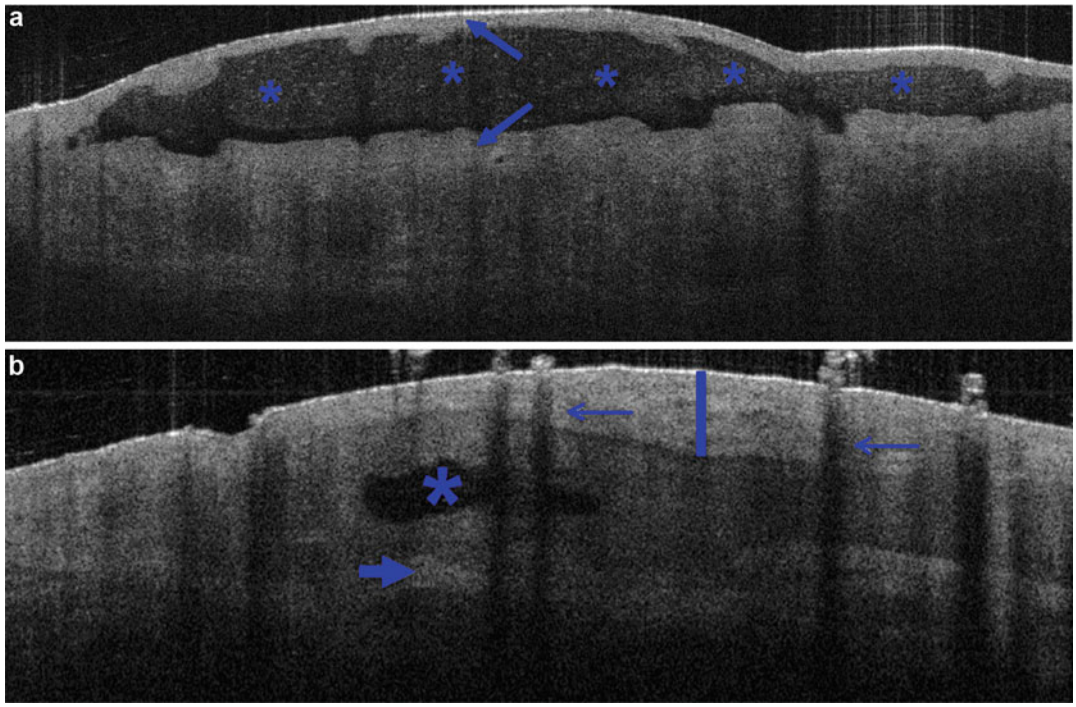

Fig. 5 (**a**) **Actinic keratosis**. OCT image of actinic keratosis lesion located on the back 20 min after 10 s of cryosurgery. *Asterisks*: a reflective bullae located along the dermoepidermal junction. *Upper blue arrow*: epidermis. *Lower blue arrow*: dermis. (**b**) **Residual basal cell carcinoma lesion**. OCT image showing residual basal cell carcinoma lesion at 3-month follow-up after photodynamic therapy. The lesion was located on the temple. *Blue vertical line*: disruption of normal layering. *Asterisk*: hyporeflective, necrotic center. *Thick blue arrow*: tumor stroma. *Thin blue arrows*: artifacts from hairs casting shadows

An animal study (Wang et al. 2008) tracking and monitoring morphological transformation during wound healing and tissue regeneration, after a collagen implant, indicated the possibility to detect reepithelialization, granulation tissue formation, and inflammatory response. Furthermore, it was reported that when longitudinal OCT was coupled with ultrahigh-resolution Doppler, it was possible to enhance the image fidelity and track neovascularization which is a common feature associated with tissue regeneration and cell/tissue differentiation. Another study (Kuck et al. 2014) concluded that there are comparable results between histological findings and OCT reporting that OCT allowed the detection of partial loss of the epidermis, vasoconstriction, vasodilatation, and epithelialization.

It has also been reported (Sattler et al. 2013) that confocal laser scanning microscopy (CLSM) and OCT can be used to quantify the kinetics of the dynamic wound healing process. Even though the wound healing seemed to be clinically complete after day 7 and 14 following fractional laser therapy, the majority of treated areas imaged by CLSM and OCT detected subepidermal defect even after 21 days (Fig. 5).

Banzhaf et al. (2016) recently investigated the closure of in vivo ablative fractional laser (AFXL)-channels using OCT and RCM. AFXL disrupts the skin barrier by creating microscopic vertical channels, inducing a wound healing response to moderate skin appearance. Depending on the applied energy level, the AFXL-channels appeared to remain open during

the first 24 hours, which may raise perspectives for optimal timing of laser-assisted drug delivery.

5 Conclusion

OCT imaging in dermatology is a diverse imaging tool easy and fast to apply at the bedside – and the images are relatively easy to interpret because of their similarity to more conventional imaging such as ultrasound and to histology. In general, the OCT imaging technique can supplement ultrasound imaging of the skin by performing high-resolution imaging of the epidermis and upper dermis. Because OCT imaging is easy to use and provides high-resolution skin images, the obstacle for clinical use is not the equipment itself – but rather the need for proper diagnostic research trials. It is imperative that OCT images of skin diseases, be it skin cancer, actinic keratosis, wounds, or blistering diseases, are correlated to different degrees or severities of the disease and non-diseased skin but also that inter- and intraobserver agreement is assessed in trials. At the current stage of OCT research in dermatology, most trials are still case reports and preliminary trials – but the future looks promising in many ways.

6 Future Development

Considering the fact that OCT in dermatology is still a novel technique, there are a number of dermatological diseases that still have not been investigated or investigated sufficiently using OCT. For NMSC and other diseases that have already been the subject of some studies, the future development involves validation of the diagnostic method including optimized definitions, sensitivity, specificity, inter- and intraobserver variation, and the development of diagnostic algorithms for the assessment of OCT images.

References

Abignano G, Aydin SZ, Castillo-Gallego C, Liakouli V, Woods D, Meekings A, Wakefield RJ, McGonagle DG, Emery P, Del Galdo F. Virtual skin biopsy by optical coherence tomography: the first quantitative imaging biomarker for scleroderma.Ann Rheum Dis. 2013; 72(11):1845–51.

Alawi SA, Kuck M, Wahrlich C, Batz S, McKenzie G, Fluhr JW, et al. Optical coherence tomography for presurgical margin assessment of non-melanoma skin cancer – a practical approach. Exp Dermatol. 2013;22(8):547–51.

Aydin SZ, Ash Z, Del Galdo F, Marzo-Ortega H, Wakefield RJ, Emery P, et al. Optical coherence tomography: a new tool to assess nail disease in psoriasis? Dermatology (Basel). 2011;222(4):311–3.

Aydin SZ, Castillo-Gallego C, Ash ZR, Abignano G, Marzo-Ortega H, Wittmann M, et al. Potential use of optical coherence tomography and high-frequency ultrasound for the assessment of nail disease in psoriasis and psoriatic arthritis. Dermatology (Basel). 2013;227(1):45–51.

Banzhaf C, Jemec GB. Imaging granulomatous lesions with optical coherence tomography. Case Rep Dermatol. 2012;4(1):14–8.

Banzhaf CA, Themstrup L, Ring HC, Mogensen M, Jemec GB. Optical coherence tomography imaging of non-melanoma skin cancer undergoing imiquimod therapy. Skin Res Technol. 2014;20(2):170–6.

Banzhaf CA, et al. Spatiotemporal closure of fractional laser-ablated channels imaged by optical coherence tomography and reflectance confocal microscopy. Lasers Surg Med. 2016;48(2):157–165.

Boone M, Jemec GB, Del Marmol V. High-definition optical coherence tomography enables visualization of individual cells in healthy skin: comparison to reflectance confocal microscopy. Exp Dermatol. 2012a; 21(10):740–4.

Boone MA, Norrenberg S, Jemec GB, Del Marmol V. Imaging of basal cell carcinoma by high-definition optical coherence tomography: histomorphological correlation. A pilot study. Br J Dermatol. 2012b; 167(4):856–64.

Boone M, Norrenberg S, Jemec G, Del Marmol V. High-definition optical coherence tomography: adapted algorithmic method for pattern analysis of inflammatory skin diseases: a pilot study. Arch Dermatol Res. 2013;305(4):283–97.

Chan CS, Rohrer TE. Optical coherence tomography and its role in mohs micrographic surgery: a case report. Case Rep Dermatol. 2012;4(3):269–74.

Christian Ring H, Hansen I, Stamp M, Jemec GB. Imaging cutaneous T-cell lymphoma with optical coherence tomography. Case Rep Dermatol. 2012;4(2):139–43.

Gambichler T, Moussa G, Sand M, Sand D, Altmeyer P, Hoffmann K. Applications of optical coherence tomography in dermatology. J Dermatol Sci. 2005;40(2):85–94.

Grover C, Khurana A. Onychomycosis: newer insights in pathogenesis and diagnosis. Indian J Dermatol Venereol Leprol. 2012;78(3):263–70.

Huang D, Swanson EA, Lin CP, Schuman JS, Stinson WG, Chang W, et al. Optical coherence tomography. Science (New York). 1991;254(5035):1178–81.

Hussain AA, Themstrup L, Jemec GB. Optical coherence tomography in the diagnosis of basal cell carcinoma. Arch Dermatol Res. 2015;307(1):1–10.

Jemec GB, Holm EA. Nonmelanoma skin cancer in organ transplant patients. Transplantation. 2003;75(3):253–7.

Kempf W, Mertz KD, Hofbauer GF, Tinguely M. Skin cancer in organ transplant recipients. Pathobiology. 2013;80(6):302–9.

Kuck M, Strese H, Alawi SA, Meinke MC, Fluhr JW, Burbach GJ, et al. Evaluation of optical coherence tomography as a non-invasive diagnostic tool in cutaneous wound healing. Skin Res Technol. 2014; 20(1):1–7.

Madan V, Lear JT, Szeimies RM. Non-melanoma skin cancer. Lancet. 2010;375(9715):673–85.

Maier T, Braun-Falco M, Laubender RP, Ruzicka T, Berking C. Actinic keratosis in the en-face and slice imaging mode of high-definition optical coherence tomography and comparison with histology. Br J Dermatol. 2013;168(1):120–8.

Mogensen M, Jemec GB. Diagnosis of nonmelanoma skin cancer/keratinocyte carcinoma: a review of diagnostic accuracy of nonmelanoma skin cancer diagnostic tests and technologies. Dermatol Surg. 2007;33(10): 1158–74.

Mogensen M, Morsy HA, Nurnberg BM, Jemec GB. Optical coherence tomography imaging of bullous diseases. J Eur Acad Dermatol Venereol. 2008;22(12): 1458–64.

Mogensen M, Thrane L, Jorgensen TM, Andersen PE, Jemec GB. OCT imaging of skin cancer and other dermatological diseases. J Biophotonics. 2009a; 2(6–7):442–51.

Mogensen M, Joergensen TM, Nurnberg BM, Morsy HA, Thomsen JB, Thrane L, et al. Assessment of optical coherence tomography imaging in the diagnosis of non-melanoma skin cancer and benign lesions versus normal skin: observer-blinded evaluation by dermatologists and pathologists. Dermatol Surg. 2009b;35(6): 965–72.

Mogensen M, Nurnberg BM, Forman JL, Thomsen JB, Thrane L, Jemec GB. In vivo thickness measurement of basal cell carcinoma and actinic keratosis with optical coherence tomography and 20-MHz ultrasound. Br J Dermatol. 2009c;160(5):1026–33.

Mogensen M, Jorgensen TM, Thrane L, Nurnberg BM, Jemec GB. Improved quality of optical coherence tomography imaging of basal cell carcinomas using speckle reduction. Exp Dermatol. 2010;19(8):e293–5.

Mogensen M, Nurnberg BM, Thrane L, Jorgensen TM, Andersen PE, Jemec GB. How histological features of basal cell carcinomas influence image quality in optical coherence tomography. J Biophotonics. 2011; 4(7–8):544–51.

Morsy H, Kamp S, Thrane L, Behrendt N, Saunder B, Zayan H, et al. Optical coherence tomography imaging of psoriasis vulgaris: correlation with histology and disease severity. Arch Dermatol Res. 2010;302(2): 105–11.

Olsen J, Themstrup L, Jemec GB. Optical coherence tomography in dermatology. G Ital Dermatol Venereol. 2015;150(5):603–15.

Ring HC, Mogensen M, Hussain AA, Steadman N, Banzhaf C, Themstrup L, Jemec GB. Imaging of collagen deposition disorders using optical coherence tomography. J Eur Acad Dermatol Venereol. 2015; 29(5):890–8.

Sattler EC, Poloczek K, Kastle R, Welzel J. Confocal laser scanning microscopy and optical coherence tomography for the evaluation of the kinetics and quantification of wound healing after fractional laser therapy. J Am Acad Dermatol. 2013;69(4):e165–73.

Schmitt AR, Bordeaux JS. Solar keratoses: photodynamic therapy, cryotherapy, 5-fluorouracil, imiquimod, diclofenac, or what? Facts and controversies. Clin Dermatol. 2013;31(6):712–7.

Serup J, Jemec GBE, Grove GL, editors. Handbook of non-invasive methods and the skin. 2nd ed. Boca Raton: Taylor and Francis Group; 2006.

Swanson EA, Izatt JA, Hee MR, Huang D, Lin CP, Schuman JS, et al. In vivo retinal imaging by optical coherence tomography. Opt Lett. 1993;18(21):1864–6.

Themstrup L, Banzhaf C, Mogensen M, Jemec GB. Cryosurgery treatment of actinic keratoses monitored by optical coherence tomography: a pilot study. Dermatology (Basel). 2012;225(3):242–7.

Themstrup L, Banzhaf CA, Mogensen M, Jemec GB. Optical coherence tomography imaging of non-melanoma skin cancer undergoing photodynamic therapy reveals subclinical residual lesions. Photodiagnosis Photodyn Ther. 2014;11(1):7–12.

Wang Z, Pan H, Yuan Z, Liu J, Chen W, Pan Y. Assessment of dermal wound repair after collagen implantation with optical coherence tomography. Tissue Eng Part C Methods. 2008;14(1):35–45.

Wang KX, Meekings A, Fluhr JW, McKenzie G, Lee DA, Fisher J, et al. Optical coherence tomography-based optimization of mohs micrographic surgery of Basal cell carcinoma: a pilot study. Dermatol Surg. 2013; 39(4):627–33.

Skin Wound Healing Assessment

47

Sylvie Meaume and Philippe Humbert

Contents

This chapter was originally published under the ISBN 978-3-540-01771-4 with the following book title Measuring the Skin. The content has not been changed.

S. Meaume (✉)
Department of Geriatrics, Wound Care Unit, Rothschild Hospital, Paris, France
e-mail: sylvie.meaume@rth.aphp.fr

P. Humbert
Department of Dermatology, University Hospital of Besançon, Besançon, France
e-mail: philippe.humbert@univ-fcomte.fr

P. Humbert et al. (eds.), *Agache's Measuring the Skin*,
DOI 10.1007/978-3-319-32383-1_54

Keywords
Alginate molds • Flexigrid® opsite • Graduated instrument • Interferometry • Planimetric Measurement • Polyurethane film • Scale paper • Silicon rubber • Standardized photograph • Stereophotogrammetry • Transparent tracings • Ultrasound • Video image analysis • Wound dimention • Wound healing assessment

The measurement of surface area, volume, and color of a chronic wound is an important step in its follow-up over time. Numerous techniques are available, ranging from the simple use of tracings to more sophisticated methods requiring the use of cameras, videos, and computers. When they exist, the techniques usually employed in outpatient care units to record the wound state over various time points are often inaccurate. Furthermore, studies of wound healing are often complicated by the few objective measurement methods that can be used in a noninvasive and ethical way in humans (Ahroni et al. 1992). However, quantitative methods that assess the wound healing rate are essential for checking the response to treatments, either drug-containing dressings or systemic therapies.

Briefly, wound measurements are of value for three main reasons:

- To monitor the time course of the wound (this is a part of patient assessment)
- To assess the efficacy of topical and/or systemic therapies
- To attempt to forecast the time required for healing

The degree of precision required is related to the purpose of the measurement as well as the technique to be used.

Wound assessment encounters three main difficulties:

- The definition of the wound perimeter. This is an entirely subjective estimate that depends on the observer, who decides what forms part of a wound or not. The most frequent source of error comes from the difficult delineation of the epidermis edge, owing to its thinness and translucency.
- The variable aspect of large, deep wounds, which depends on the position of the patient. Such wounds are capable of marked changes in appearance that render measurements unreliable if the patient is not placed in exactly the same position each time the wound is measured.
- The convex shape of human limbs. Measurements frequently do not take into account possible errors due to this factor.

Despite such problems, several measurement techniques can be employed to assess the surface or volume of wounds. Table 1 lists the principal ones.

1 Wound Parameters: Perimeter and Surface Area

The parameters most frequently used to measure a wound are the length of the principal axes (length and width of the wound), the projected surface area, and the perimeter. Different mathematical calculations can establish a relationship between the surface area of a wound, its perimeter, length, and width.

1.1 Direct Measurement of Wound Dimensions with a Ruler

Historically, the first parameters used were the outer dimensions of the wound: length (along the longest axis, L) and width (smaller axis perpendicular to the first, W). These parameters are measured directly on the wound using a graduated instrument. The same instrument must always be used if the aim is to compare dimensions, and strict conditions of asepsis must prevail to prevent the transmission of micro-organisms between patients. Although imprecise, this technique is the first objective approach to a wound (Fig. 1).

Table 1 Wound measurement techniques

In contact with the wound	Tracing: dimensions, surface area and contours
	Measurement of depth
	Volume: liquid or molding
Not in contact with the wound	Photography
	Video film
	Stereophotogrammetry
	Analysis of structured light

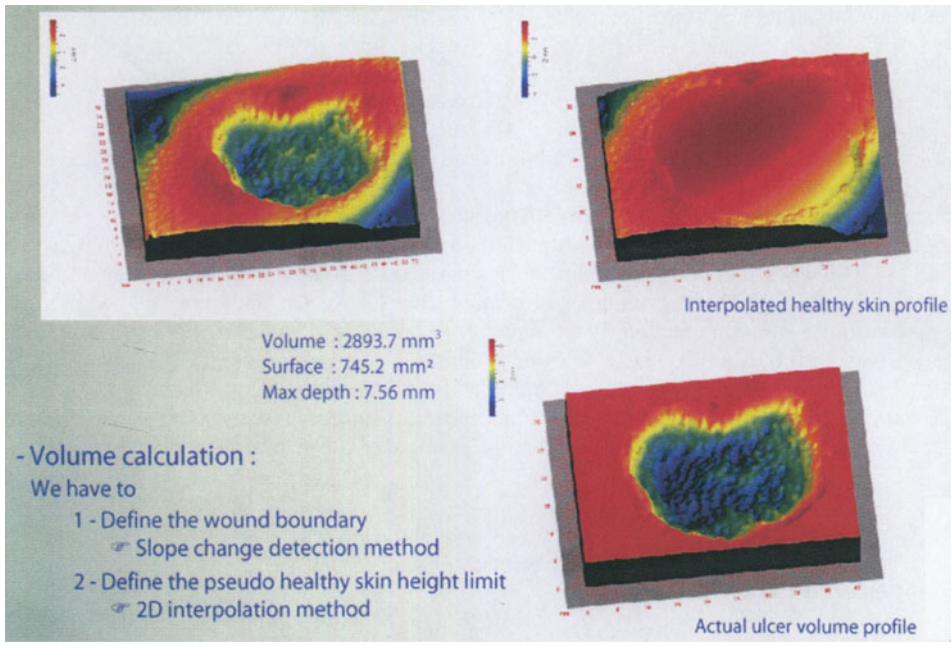

Fig. 1 Direct measurement of the length and width of a wound. Length 6.7 cm, width 4.8 cm. Calculation of surface area: A = 6.7 cm × 4.8 cm = 32.16 cm^2. Corrected surface area: A' = 32.16 × π/4 = 25.26 cm^2. By counting the number of 1 × 1 mm squares, A = 25 m^2. By using computerized digital image analysis, A = 26.28 cm^2

It calculates the surface area (A), which of course is subject to some error, but these can be partly circumvented through the application of formulae for corrected surface area (Vowden 1995; Mayrovitz 1997). Thus, according to Mayrovitz (1997), $A = 0.73 \times L \times W$ for a rectangular wound. The area of an elliptic wound may be calculated as follows: $A = 0.763 \times L \times W$ (Schubert 1997) or $A = 0.785 \times L \times W$ (Kundin 1989). This technique is principally applicable when wounds are rather shallow and regularly shaped. Good training in such measurements improves their sensitivity.

1.2 Transparent Tracings

1.2.1 Delineation of Perimeter on Transparent Material

The most commonly employed technique is that which uses an acetate film to obtain a tracing of the wound perimeter, drawn using a fine marker pen. The paper may be a plain transparent film or may be already calibrated in millimeters. As a general rule, it is better to use a double sheet of transparent material; the tracing is drawn on the upper sheet and the lower sheet, which is in direct contact with the wound and may be soiled by exudate, can be

discarded. Flexigrid OpSite (Smith and Nephew) is an adhesive, polyurethane film, which comprises a protective, cross-ruled film that can serve as a tracing to follow-up the treatment of superficial wounds. The principal limitation to this technique is the difficulty encountered by the observer in determining the perimeter of the wound with enough precision (Bohannon and Pfaller 1983). An overly thick line is also a source of error.

This is a rapid method (less than 1 min is required to complete the tracing of a wound), which is inexpensive and requires minimal training.

1.2.2 Use of Scale Paper

The next stage consists in analyzing the tracing. As above, the two main diameters, the perimeter, and the surface area can be measured. It is simplest to measure the surface area by placing the tracing on a sheet of graph paper and counting the number of 1-mm squares within the area (Gowland Hopkins and Jamieson 1983; Majeske 1992). This is a tiresome and lengthy method (10 min for a 70-cm^2 wound). When the wound outline does not perfectly meet the cross-ruling, the area can be deduced using the formula: $(N + N_C/2) \times$ surface of a square, where N is the number of squares fully contained and N_C the number of those that cross the outline. A more rapid method consists in cutting out the tracing or its copy on a card with a regular thickness, then weighing it on a high-precision scale (Bohannon and Pfaller 1983). Additional errors are possible when the drawing is reproduced and the card or film cut out.

The use of a scanner that copies the shape of the tracing and enters the data into a computer, or the use of a flat or camera scanner, obviates such drawbacks. A program then provides a rapid and accurate analysis of the tracings, calculating the area and the area of islands of newly formed epidermis that might have been recognized within the wound and traced (Coleridge Smith and Scurr 1989). This technique is the most widely employed in clinical studies aimed at validating products for wound treatment.

1.3 Computer-Assisted Planimetric Measurement

Computer-assisted planimetry is a wound measurement method often used in clinical studies. The perimeter of the wound is delineated by the clinician using a pen linked to a computer. There is a close correlation between the surface area of a wound measured by planimetry and the following parameters: length, width, perimeter, and the product of length by width (Kantor and Margolis 1998a, b). However, this correlation diminishes in the case of very large wounds. In addition, these parameters would be predictive of healing after 24 weeks. They may be taken either directly on the wound or indirectly from a tracing made on a transparent substrate (tracing paper, plastic film, or mylar) (Liskay et al. 1993), or from a standardized photograph.

All such measurements can calculate the healing rate, and more particularly the epithelialization. The latter appeared to be constant in certain studies (Redden et al. 1998), reaching about 1–2 mm per week. Furthermore, this rate would be independent of the size of the wound.

1.4 Photography

It is possible to measure a wound's parameters from a standardized photograph. The method has been compared with the conventional tracing method in certain studies, and the results obtained did not differ significantly (Griffin et al. 1993). This procedure by-passes an important disadvantage in the above-mentioned methods: direct contact with the wound, which may be painful and a source of contamination. However, note that, as an indirect procedure, it has a certain number of drawbacks. In order to know the scale of the image, a graduated ruler must be placed alongside the wound. It is often difficult to compensate for the concave or convex nature of the wound. The photograph must be taken exactly perpendicular to the wound. A deviation of only 20° from the perpendicular axis will cause a reduction in the

wound surface area of about 10 % (Palmer et al. 1989). Indeed, photography must take place under clearly defined placement and lighting conditions, and these conditions must be reproducible (Teot et al. 1996).

Different options are available when analyzing a photograph: computer-assisted image analysis is highly preferable to the old-fashioned projection of the photo onto a paper and the secondary tracing of wound contours. Interestingly, the information obtained from photographs can assess wound parameters other than dimensional ones: aspect of the wound bed, changes in color, as well as presence of necrosis, fibrin, granulation tissue, epithelialization. Standardization of the technique is essential: choice of focal distance, adjustment of speed and diaphragm, lighting, distance from the wound, and angle of shot. One group of authors (Minns and Whittle 1992) used a Polaroid camera with accessories, which allowed them to take photos at a constant angle and distance from the wound; photos could thus be compared. New Polaroid systems are particularly well-suited to the measurement of wounds. The Health Cam System allows the alignment of two lights, so that photographs are taken in a reproducible and comparable manner. Gridfilm allows for the superimposition of a grid over the wound for direct measurement. In most cases, a graduated scale is placed alongside the wound for easy measurement of its dimensions, whatever the magnification of the photo. In the semimanual recording technique, the contour of the wound is followed by a digital pen. The signal thus emitted, whose motion has previously been calibrated, is processed by microcomputer. Another technique consists in superimposing the contour traced by the operator using a mouse over the digital image of the wound, and visualizing it directly on the computer screen (image patterning process) (Mignot 1996).

In practice, a direct data recording from a photograph is difficult to obtain, except in the case of a wound with a simple, geometric shape and a well-defined perimeter. The use of calibrated photographs may be of value when studies are made in a single center, because the reproducibility required with respect to the conditions of photography at different stages of a treatment can be satisfactory. The current need for multicentre studies to assess wounds limits this method of evaluation, and tracings should be preferred. Techniques involving photographs appear to benefit from a certain degree of reliability and reproducibility, only if strict rules are respected (Etris et al. 1994; Griffin et al. 1993).

1.5 Video Image Analysis

Video image analysis employs a video camera to film a wound (Solomon et al. 1995). The recording of the image is then analyzed by computer using special software that corrects the figures obtained for wound dimensions to compensate for the concave or convex nature of the wound. The technique is more accurate than the analysis of photographs, and is simple, rapid, and inexpensive.

A comparison of measurements using rulers, tracings, or photographs is shown in Table 2.

Table 2 Comparison of three techniques to measure the surface area of a wound (From (Plassman 1995), with permission)

	Ruler (length, width)	Tracing of wound	Photograph
Ease of use	Easy	Easy	Moderately easy
Time required for recording	1 min	A few minutes	A few minutes
Cost	Very low	Low	Moderate
Use	Common	Common	Common
Type of record	Numbers	Tracing and numbers	Image and numbers
Contact with wound	Yes	Yes	No
Learning	Little	Moderate	Moderate
Percentage error[a]	20–25 %	8–10 %	10–12 %

[a]The lowest percentage corresponds to large wounds and the highest percentage to small wounds

2 Wound Volume

2.1 Graduated Ruler

The depth of a wound is not accessible to the measurement systems we have described above, because most wounds are three-dimensional, and therefore special techniques are necessary. The simplest consists in using a sterile blunt-tipped rod to assess the maximum depth of the wound (Covington et al. 1989; Thomas and Wysocki 1990). The technique involving the use of a cotton tip is easier in practice. However, such measurements are often inaccurate, and determination of the deepest point of the wound is subjective.

In 1989, Kundin (1989, 1985) developed a mathematical formula to assess the volume (V) of a wound through its surface area (A), using the two largest diameters (length, L, and width, W) and the depth (D): $V = A \times D \times 0.327$, where $A = L \times W \times 0.785$. Thomas (Thomas and Wysocki 1990) showed that these measurements were comparable to those obtained with tracings and photographs in the case of small wounds, and were consistently underestimated in the event of large or irregular wounds (particularly those with a sinuous shape). Variation in the measurement of the same wound, with the patient in the same position, nevertheless demonstrated standard deviations of 40 % regarding wound volume when using these methods (Plassmann et al. 1994).

2.2 Wound Molds Using Silicone Rubber

Since silicon rubber can harden and be stored, this high-precision and simple method uses profilometric analysis followed by computerized volume assessment (Zahouani et al. 1992; Humbert et al. 1998). The first stage consists in making a negative imprint of the wound using silicone rubber of a type frequently used in dentistry for its safety. Two products are commonly used: Silflo and Xantopren. The mixture obtained by mixing the silicone rubber with its catalyst has a viscous consistency and is applied into the wound using a spatula. It will shape all the wound contours to a very fine extent, penetrating into the smallest crevices. After 2–3 min to polymerize, and thus harden, it is easy to remove as a single piece corresponding to the negative shape of the wound. It is possible to store and archive this mould, as it would be unaffected by time. It is then scanned by a laser beam, which recognizes the location of each point using a positional detector. The vertical position of the laser spot (about 30 μm in diameter) can be deduced using double triangulation (Stil, Marseille, France and Digital Surf, Besançon, France) or after refocalization of the beam (Optilas, Evry, France). Parallel linear scannings of the mold surface create a certain number of profiles, the sum of which calculates wound volume. When assessing the volume of a leg ulcer, it is recommended that laser scanning be done along the axis of the leg, so as to cancel out the usual concave shape of the wound in this site. In some cases, this method also provides a precise definition of wound contours by automatic detection, which is achieved by comparing the altitude at each point with that of adjacent healthy skin.

The time course of a wound, or its healing, is a dynamic process. Monitoring thus requires repeated measurements over time. This method makes such measurements possible, particularly because of the safety of the silicone rubber used and the painless and nontraumatic nature of its application.

2.3 Weighing Alginate Molds

The use of an alginate mould makes it possible to measure wound volume by weighing or water displacement (Stotts et al. 1996). However, this method has certain limitations, particularly because of possible alterations in the alginate mold depending on its water content, conditions of storage, and on wound volume.

2.4 Stereophotogrammetry

Stereophotogrammetry (Bulstrode et al. 1986) measures the contours, surface area, and volume of a wound. It is based on determining the depth of

the wound viewing it from two different angles. The first models of this device were difficult to manipulate (Erikson et al. 1979), but new, simpler models are now available (Bulstrode et al. 1986). This method provides an accuracy of roughly 3.5 % for measurement of the surface area and 5 % for volume. This method, developed by Bulstrode in 1986 (Bulstrode et al. 1986), is not widely used. The time necessary for each evaluation is a further limitation to its everyday use.

2.5 Direct Measurement of Volume Using Physiological Saline and Polyurethane Film

Berg et al. (1990) reiterated the value of this simple method, which consists in placing a transparent adhesive film over a wound, and then injecting physiological saline below the film. The quantity of saline corresponds to the wound volume.

In practice, the wound is covered with a sterile polyurethane film and then filled with physiological saline solution, which is injected using a needle piercing the film. Evaluation of this method has shown that accuracy of more than 20 % is rarely possible (Plassmann et al. 1994), principally because some amount of liquid is absorbed by the wound, and losses by leakage occur around the adhesive through detachment of the film from the wound perimeter. Furthermore, it is sometimes impossible to place the patient in a satisfactory position to fill the wound with a liquid. Tissue detachment also constitutes a limitation to this technique, as does the potential risk of infection, discomfort for the patient, and the risk of trauma to the wound, which is inherent in any technique involving direct contact.

2.6 Analysis of Structured Light

Analyzing structured light measures the surface area and volume of a wound without direct physical contact. Parallel lines of colored light are projected onto the wound surface area. A video camera connected to a computer records any distortion to the light beams. The dimensions of the wound are then calculated by triangulation. The accuracy of this method is similar to the previous one, but its implementation is simpler (Plassman and Jones 1992).

2.7 Ultrasound

Ultrasound takes advantage of the difference in path length of an ultrasound wave reflecting at the bottom of the wound as compared with the adjacent normal skin. Healing may be assessed using this technique (Pugliese et al. 1992), as was demonstrated in a clinical study of wounds caused by punch biopsies in volunteer subjects. In this study, the depth and internal diameter of the wound were assessed by ultrasound at intervals while its outer surface area was measured by planimetry after first taking a tracing. This technique appears to be of value only if the wound is small in size, because it is necessary for the wound edges to lie within the field of the ultrasound beam, as they serve as a reference to measure wound depth. Application of the probe must not flatten these edges; appropriate precautions must be taken to avoid this. Several ultrasound scans should be taken (usually three), from which mean values of the parameters are determined. Ultrasound may also be useful to monitor wound dimensions following cryosurgery, or to better assess the quality of perilesional tissue (Rippon et al. 1998; Wertheim et al. 1999).

2.8 In Vivo Measurement Using Interferometry and Fringe Projection

A new technology based on the interferometry principle has been developed in the Besançon Laboratory of Engineering (France) (P. Humbert, unpublished data) in order to quantify the volume of ulcers in vivo. The three-dimensional reconstruction of wound profiles is based on the Fourier transform method of fringe pattern analysis (Fig. 1).

The system is composed of CCD camera and a projection module. The resolution of the system depends on the fringe width and on the angle

Table 3 Comparison of five methods to measure wound volume (From Plassmann et al. (1994), with permission)

	Ruler and cotton tip	Mold	Saline	Stereophotogrammetry	Structured light
Ease of use	Easy	Moderately easy	Moderately easy	Difficult	Difficult
Time required for recording	1 min	A few minutes	A few minutes	20–30 min	4–5 min
Cost	Very low	Low	Low	Very high	High
Use	Common	Common	Common	Research	Prototype
Type of record	Numbers	Mold and numbers	numbers	3D reconstitution	Image and numbers
Contact with wound	Yes	Yes	Yes	No	No
Training	A few hours	Less than 1 h	1 h	A few hours	A few hours
Percentage error[a]	10–40 %	5–15 %	8–25 %	0–3 %	3–5 %

[a]The lowest percentage corresponds to large wounds and the highest percentage to small wounds

between the optical axis of the camera and the optical axis of the projector. The deformation of the fringes over the reference plane is proportional to the height separating the object and the reference plane. Thus, an appropriate algorithm reconstructs the 3D profile from the projected fringes on the object, in this case the wound.

This system has a z-resolution of 10 μm for a 5 × 5-cm^2 area. The search for the perimeter and the volume of the wound is based on the previously described method by Zahouani et al. (1992).

A comparison between the above-mentioned measurement techniques is shown in Table 3.

3 Colorimetry or the Red-Yellow-Black Concept

The technology for colorimetry was developed by Hellgren and Vincent (1993; Vincent et al. 1994) and consists in taking account of the color characteristics of an ulcer, which are a function of its clinical stage. Necrotic lesions are black, a fibrinous surface looks yellow, and granulation tissue is red. This clinical description has been accepted worldwide as an indication of the stage and prognosis of an ulceration (Stotts 1990; Thomas 1990). Thus computerized colorimetry analysis (CWA, computerized wound analysis) was developed to ensure more objective measurements (Engström et al. 1990). A photograph of the wound is taken, together with a grey scale placed alongside the lesion to control the quality of the photograph. Photographic data are transmitted to a computer. The image is digitalized and reconstituted in the form of colored pixels. The color of each pixel is expressed in red, blue, and green values of intensity (each from 0 to 255). This method has been the subject of validation studies. In practice, the clinician takes the photographs using a camera recommended by the CWA Institute in Sweden, the promoter of the technique. Images are then sent to this center, where they are processed blind. The results are returned within 6 weeks. A detailed guide is provided regarding the best way to take the photo, as the reliability of the results depends upon its quality.

- CWA Institute, Box 8064, 42108 Via Frölunda, Sweden;
  Fax: +46-31-476803; Tel.: +46-18-183467
- Supplier of the camera:
  Mr. U. Nishimura
  Asanuma & Co. Ltd., Import–export Division, 7,3-2 chome,
  Hirakawa-cho, Chiyoda-ku, 102 Tokyo, Japan;
  Fax: +81-33-2397230

4 Conclusion

The clinical follow-up of wound healing requires data on the geometry of the lesion. This quantification is necessary to ensure an objective

assessment. The techniques most widely employed in clinical studies involve the tracing of wound contours using transparent film. Only rigorous training in this technique can lend credence to the results obtained. More sophisticated techniques that increase the accuracy of wound volume measurements are currently available, but are at present only employed in the research setting.

References

Ahroni JK, Boyko EJ, Pecoraro R. Reliability of computerised wound surface area determinations. Wounds. 1992;4:133–7.

Berg W, Traneroth C, Gunnarson A. A method for measuring pressure sores. Lancet. 1990;335:1445–6.

Bohannon RW, Pfaller BA. Documentation of wound surface area from tracings of wound perimeters. Phys Ther. 1983;63:1622–4.

Bulstrode CJK, Goode AW, Scott PJ. Stereophotogrammetry for measuring rates of cutaneous healing: a comparison with conventional techniques. Clin Sci. 1986;71:437–43.

Coleridge Smith PD, Scurr JH. Direct method for measuring venous ulcers. Br J Surg. 1989;76:689.

Covington JS, Griffin JW, Mendiius RK, Tooms RE, Clifft JK. Measurement of pressure ulcer volume using dental impression materials: suggestions from the field. Phys Ther. 1989;69:690–3.

Engström N, Hansson F, Hellgren L, Johansson T, Nordin B, Vincent J, Wahlberg A. Computerized wound image analysis. In: Wadström T, Eliasson I, Holder I, Ljung A, editors. Pathogenesis of wound and biomaterial-associated infections. London: Springer; 1990. p. 189–92.

Erikson G, Eklund AE, Tolergard K. Evaluation of leg ulcer treatment with stereophotogrammetry. Br J Dermatol. 1979;101:123–31.

Etris MB, Pribbles J, LaBrecque J. Evaluation of two wound measurement methods in multicenter, controlled study. Wounds. 1994;6:107–11.

Gowland Hopkins NF, Jamieson CW. Antibiotic concentration in the exudate of venous ulcers: the prediction of ulcer healing rate. Br J Surg. 1983;70:532–4.

Griffin JW, Tolley EA, Tooms RE, Reyes RA, Clifft JK. A comparison of photographic and transparency-based methods for measuring wound surface area: research report. Phys Ther. 1993;73:117–22.

Hellgren L, Vincent J. Evaluation techniques for the assessment of wound healing. In: Westerhof W, editor. Leg ulcers: diagnosis and treatment. Amsterdam: Elsevier Science Publishers; 1993. p. 381–4.

Humbert P, Assoul M, Mignot J. Technique volumétrique des plaies. J Plaies Cicatris. 1998;12:53–4.

Kantor J, Margolis DJ. Efficacy and prognostic value of simple wound measurements. Arch Dermatol. 1998a;134:1571–4.

Kantor J, Margolis DJ. Is planimetric wound measurement really necessary? The efficacy and prognostic value of simple wound measurements. Wound Repair Regen. 1998b;6:A245.

Kundin JI. Designing and developing a new measuring instrument. Preoperative Nurse Q. 1985;1:40–5.

Kundin JI. A new way to size up wounds. Am J Nurs. 1989;89:206–7.

Liskay AM, Mion LC, Davis BR. Comparison of two devices for wound measurement. Dermatol Nurs. 1993;5:437–41.

Majeske C. Reliability of wound surface measurements. Phys Ther. 1992;72:138–41.

Mayrovitz HN. Shape and area measurement considerations in the assessment of diabetic plantar ulcers. Wounds. 1997;9:21–8.

Mignot J. Techniques morphométriques d'évaluation de la cicatrisation d'un ulcère. Rev Prat. 1996;46:S18–22.

Minns J, Whittle D. A simple photographic recording system for pressure sore assessment. J Tissue Viability. 1992;2:126.

Palmer RM, Ring EFJ, Ledgard L. A digital video technique for audiographs and monitoring ulcers. J Photogr Sci. 1989;37:65–7.

Plassman P. Measuring wounds. J Wound Care. 1995;4:269–2720,0.

Plassman P, Jones BF. Measuring leg ulcers by color-coded structured light. J Wound Care. 1992;1:35–8.

Plassmann P, Melhuish JM, Harding KG. Methods of measuring wound size: a comparative study. Wounds. 1994;6:54–61.

Pugliese PT, Moncloa F, McFadden RT. Ultrasound evaluation of wound volume as a measure of wound healing rate. In: Altmeyer P, Le-Gammal S, Hoffmann K, editors. Ultrasound in dermatology. Berlin/Heidelberg/New York: Springer; 1992. p. 267–72.

Redden RA, Blum B, Kilpadi D, Feldman D. Quantitative assessment of wound healing rate. Wound Repair Regen. 1998;6:A246.

Rippon MG, Springett K, Walmsley R, Patrick K, Millson S. Ultrasound assessment of skin and wound tissue: comparison with histology. Skin Res Technol. 1998;4:147–54.

Schubert V. Measuring the area of chronic ulcers for consistent documentation in clinical practice. Wounds. 1997;9:153–9.

Solomon C, Munro AR, Van Rij AM, Christie R. The use of video image analysis for the measurement of veinous ulcers. Br J Dermatol. 1995;133:565–70.

Stotts NA. Seeing red and yellow and black. The three-color concept of wound care. Nursing. 1990;20:59–61.

Stotts NA, Salazar MJ, Wipke-Tevis D, McAdoo E. Accuracy of alginate molds for measuring wound volumes when prepared and stored under varying conditions. Wounds. 1996;8:158–64.

Teot L, Griffe O, Cherenfant E, Breuer JL. Photographie des plaies: standardisation, stockage, pièges à éviter. J Plaies Cicatris. 1996;4:25–30.

Thomas S. Wound management and dressings. London: Pharmaceutic Press; 1990. p. 81.

Thomas AC, Wysocki AB. The healing wound: a comparison of three clinically useful methods of measurement. Decubitus. 1990;3:18–25.

Vincent J, Bengtsson U, Engström N, Hansson F, Hellgren L, Johansson T, Lunnergard J, Moberg S. Computerized wound analysis. In: Wadström T, Holder IA, editors. Molecular pathogenesis of surgical infections. Int J Med Microbiol [Suppl]. 1994;27:499–507.

Vowden K. Common problems in wound care: wound and ulcer measurement. Br J Nurs. 1995;4:775–9.

Wertheim D, Malhuish J, Williams R, Harding K. Ultrasound imaging of the leg in patients with chronic wounds. Skin Res Technol. 1999;5:53–5.

Zahouani H, Assoul M, Janod P, Mignot J. Theoretical and experimental study of wound healing: application to leg ulcers. Med Biol Eng Comput. 1992;30:234–9.

Skin Blood Flow: Histophysiology

48

Pierre Agache

Contents

Keywords

Capacitive vessels • Hunting • Microvasculature • Perfusion pressure • Perifollicular networks • Perisudoral networks • Resistive vessels • Skin blood flow • Subepithelial networks • Vasoconstriction • Vasodilatation • Vasomotion

Like any other organ, the skin has a vascular system. Because of its dimensions (1 mm thickness), this system belongs to microcirculation only. Like all epithelia epidermis, pilosebaceous follicles, sweat glands, and their excretory ducts do not contain vessels and need a close nutritive network. Furthermore, this network must be able to develop angiogenesis, even in adults, in order to repair wounds. But the role of skin microcirculation goes beyond organ nutrition alone. Its involvement is essential in the thermal regulation of the organism and plays an important role in hemodynamics since it represents at least 9 % of the blood mass, with important variations up to 50 % (Martineaud and Seroussi 1977).

1 Microvasculature

The nutritive vessels consist of subepithelial dense capillary networks where exchanges with the extravascular elements take place (Fig. 1). There are three kinds of networks. The subepidermal network is the easiest to study. It

This chapter was originally published under the ISBN 978-3-540-01771-4 with the following book title Measuring the Skin. The content has not been changed.

Pierre Agache: deceased.

P. Agache (✉)
Department of Dermatology, University Hospital of Besançon, Besançon, France
e-mail: aude.agache@free.fr; ferial.fanian@chu-besancon.fr; ferial.fanian@cert-besancon.com

P. Humbert et al. (eds.), *Agache's Measuring the Skin*, DOI 10.1007/978-3-319-32383-1_55

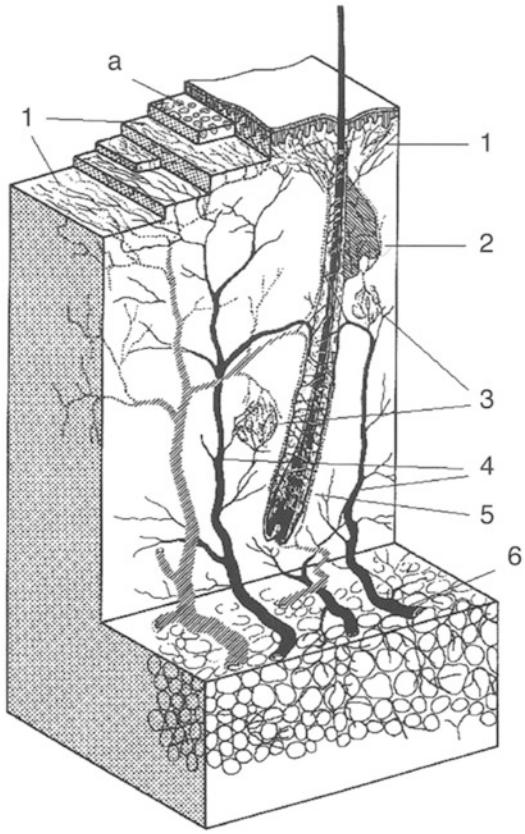

Fig. 1 A diagram of the skin microvasculature. *1* Subepidermal plexus, *2* perisudoral plexus, *3* perisebaceous plexus, *4* ascending arteriole, *5* perifollicular plexus; *6* cutaneous artery and subcutaneous plexus, a epidermal ridges horizontally cut (Modified from Stüttgen and Forssman (1981))

consists of the papillary loops (visible in capillaroscopy) and the horizontal plexus of the superficial dermis in which the loops emerge (Fig. 2). The second type consists of the perifollicular networks which nourish the pilosebaceous follicles: each has a well-developed papillary loop and a vascular netting around the external epithelial sheath, i.e., the outside part of the hair. There are as many networks as hairs, and their development follows the hair growth, which explains why a scalp wound causes substantial bleeding. The perisudoral networks form the third type of network. They are dense and placed around each sweat gland and the excretory duct until its emergence into the epidermis; there are between 10 and 700 eccrine glands per square centimeter of skin, depending on the area. The development of the perifollicular and perisudoral networks is at its maximum in the medium and deep dermis.

In addition, the dermis vascularization seems sparse, sometimes almost absent, showing transfer, not exchange, vessels. The supply of the subepidermal loops is ensured by progressive arterioles divided like the arms of a candelabrum in the upper part of the medium dermis (Spalteholz 1927) (Fig. 3). The deep dermis directly irrigates the progressive arterioles and the periadnexal networks; it receives its vessels from a large peri-fascia hypodermic plexus, which

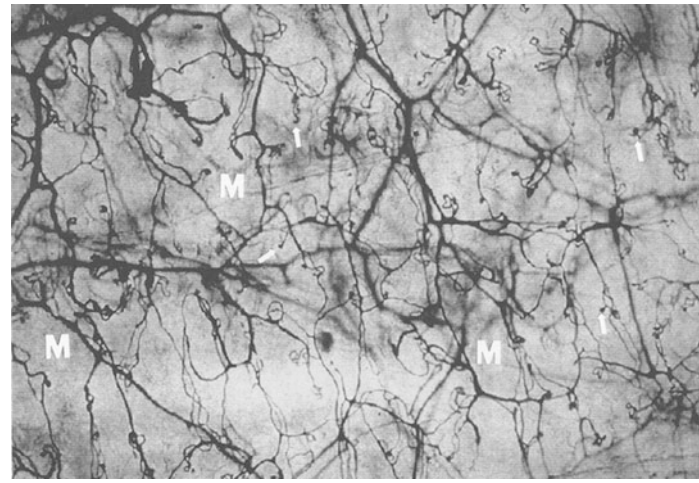

Fig. 2 Subepidermal plexus in the supramalleolar area, injected with Indian ink and viewed from above the skin. *Arrows* papillary loops. *M* A mesh of the subepidermal network (Laboratoire de Biophysique cutanée, Besançon, France and Revier (1981), with permission)

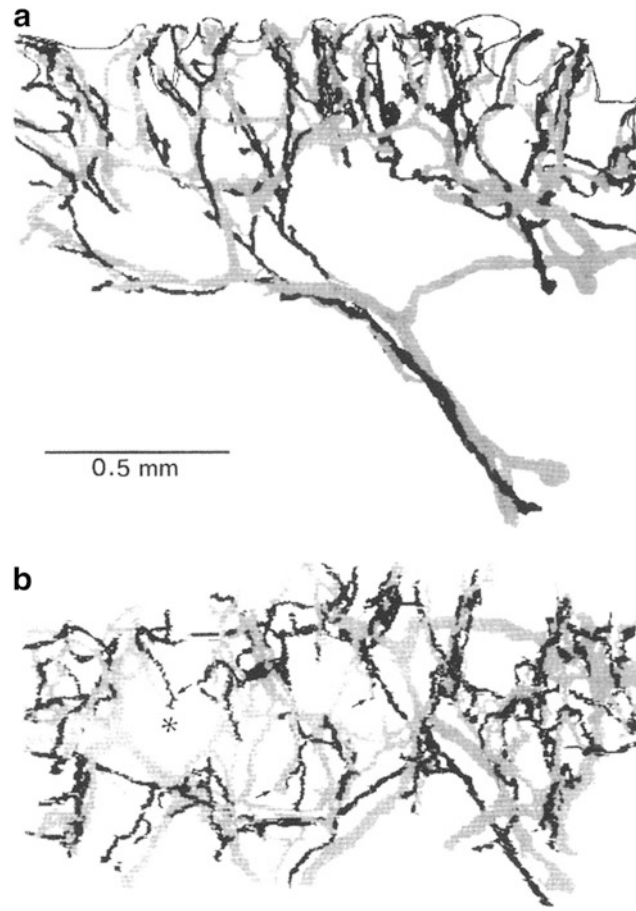

Fig. 3 (**a**, **b**) Candelabrum-like arborescence of a terminal arteriole. Three-dimensional reconstruction from histological slides. (**b**) The same arborescence as seen from above (after 70° rotation). Note the peripheral collection of blood. Arterioles are in *black*, venules in *gray* (From Braverman et al. (1990), with permission)

is supplied by the arteries intended for the integument (Casey 1990).

The subepithelial networks have an embryological origin in situ from mesenchymatous buds differentiating under the influence of epithelial stimuli (Ryan 1973). Inversely, the subcutaneous and deep dermal vessels are branches of the embryonic metameric vessels (Ryan 1973). In addition to these embryological differences, the subepidermal circulation (observed in capillaroscopy) is relatively autonomous compared to the deep circulation (observed with laser Doppler) (Fagrell et al. 1986). Is this fact sufficient to suggest there are two different systems? From an anatomical point of view, the answer is negative.

The cutaneous vessels are very anastomosed between themselves at all levels, from the hypodermis to the epidermis. The occurrence of a cutaneous infarction following a localized arteriole obliteration is therefore impossible. Some anastomoses such as the Masson glomus have a nerve command; they are especially numerous at the extremities where their role in the thermal exchanges with the environment is essential.

2 Metabolic and Thermoregulatory Needs

Two peculiar features characterize cutaneous vessels. First, their low differentiation in arterioles or venules, reflecting a reversible functional specialization in relation to the metabolic needs of the adjacent epithelium: the latter control both the morphology and the development level of the subepithelial capillary networks. For example, the microcirculation evolves in parallel with the

cycle of hair growth or the proliferation stage of the psoriatic epidermis (Braverman and Sibley 1982). Second, the deepest vessels are surrounded by smooth muscle fibers and the more superficial ones by pericytes (Higgins and Eady 1981). These cells give a better contractility and mechanical resistance to the cutaneous vessels than to the visceral capillary vessels. These two properties may be related to the sudden compression of the skin when it has to support the weight of the body changing position. In such cases, the blood is expelled in all directions, even against the flow, and still isolated blood pockets may form and persist as long as the position remains unchanged (In some circumstances, it may be useful to determine the pressure exerted by the body on a skin area (e.g., on the soles when standing, on the coccyx or scapulae when lying down, etc.). The firm RS Scan International (Belgium-RSscan INTERNATIONAL, Lammerdries 27, B-2250 Olen) provides tools for such measurements over solid surfaces: 60 × 50-cm measuring plates, with possible pressure averaging or mapping.)

The skin must be self-sufficient during these long perfusion breaks and, when there is no compression, the blood flow has to be higher than apparently needed by the metabolism. This factor is usually overlooked and adds to the requirements of the skin thermoregulation function: to eliminate excess calories, the superficial networks must behave like a radiator. The skin blood flow (Martineaud and Seroussi 1977) is approximately 0.5 l/min (heart, 5.5), reaching 0.9 l min^{-1} during moderate exercise (heart, 9.7) and up to 7 l min^{-1} during strenuous exercise in hot conditions. Inversely, the minimum blood flow is about 0.02 l min^{-1}. The range of flows is therefore wide, by a factor of 1 to 350. Since one of the major functions of the skin is to eliminate heat, its temperature is generally under 37 °C, even under clothes (Agache 2004).

As a consequence, in comfortable thermal conditions, i.e., the skin is not compressed, the blood flow exceeds actual needs and the blood composition is very close to arterial blood. This means that arterial blood gas can be measured by sampling cutaneous blood from the ear lobe.

3 Variations with Body Site and Age

The study of blood flow in resting conditions shows considerable differences between body areas (Tur et al. 1983), variations in both density and architecture of the vascular network. The head and extremities are particularly notable for their high vascular density. Age is another variation factor (Ryan 1993). In newborn babies, microcirculation is rich and homogenous, then vascular regression appears, especially on the surface (hence a less fresh complexion) followed by progressive specialization ending in a less good complexion and telangiectasias in older people. However, the global flow decreases little. Vasoconstriction induced by smoking has the same effect and contributes to premature vascular aging.

4 Resistive Vessels

The cutaneous blood flow, as in the rest of the body, is operated by two physical quantities: perfusion pressure and resistance to this perfusion. An Ohm law equivalent describes the relationship between the three quantities: flow is perfusion pressure/peripheral resistance. Perfusion pressure depends on the heart ejection and the condition of the proximal arteries. It is impaired in heart deficiency and arterial obstruction. On the other hand, peripheral resistance is controlled by the arterioles. These are numerous in the skin and have a strong tone. Consequently, they play an essential role in regulating blood pressure and protecting the capillary bed against endovascular pressure. In forehead arterioles, especially in dorsal recumbency, the systolic pressure varies with age (from 40 to 80 torr), in parallel with the systolic blood pressure, whereas the diastolic pressure remains constant: 15–20 torr whatever the age (Agache et al. 1993). Because of the tone of their wall, the cutaneous venules also take part in this resistive power but in a minor way.

5 Vasoconstriction

The permanent vasoconstriction of arterioles and venules comes from vasoconstrictor tone, which has a mixed origin: orthosympathetic (local release of noradrenaline) and myogenic (autonomous but permanent and powerful local response of the vascular wall to distension by blood pressure) (Holtz 1996). The orthosympathetic system is also responsible for the venoarteriolar reflex: arteriolar constriction in response to a distension of the venous walls. Its most noticeable effect is the considerable reduction in blood flow in the lower limbs, which prevents blood pressure from falling when one goes from a lying to a standing position.

The main vasoconstriction stimuli of central origin (Martineaud and Seroussi 1977) are inhalation, attempting to exhale with the glottis closed (Valsalva's maneuver), mental arithmetic, concentration, and psychological stresses. The main circulating substances having a vasoconstriction effect in the skin are corticoids (by inhibition of the NO vasodilator), adrenaline (action on the arteriole and venule α receptors, as it seems that there are no β receptors in the cutaneous vessels), and noradrenaline. Cold is a powerful cutaneous vasoconstrictor; most of the blood stored in the veins and venules (capacitive system) is shifted to the viscera, and the blood reaching the hypodermal plexus is shunted through the opening of the arteriovenous shunts. The skin becomes colder (outside cold and reduction in indoor heating). However, when the skin temperature decreases below 12 °C, vasoconstriction and vasodilatation take place alternately, probably to avoid the excessive cooling of the tissues (phenomenon called hunting).

Vasoconstriction can also be induced by the endothelial secretion of thromboxane A2, prostaglandin H2, angiotensin II, and endothelin, toward the parietal smooth muscle. Endothelin-1 is perhaps the most powerful vasoconstrictor peptide via its ETA receptor on vascular smooth muscle cell, while via its ETB receptor on endothelial cells it mediates vasodilatation.

6 Capacitive Vessels

The venules, because of their distensibility and volume and because they outnumber the arterioles, make up the capacitive vasculature. This accounts for the sudden reduction in blood flow velocity in these vessels, which favors transparietal exchanges. The venules of the subepithelial plexus, because of their good parietal permeability, are exchange vessels and are identified with what is usually called cutaneous capillaries. If the reduction in the blood flow velocity at their level is intensified by an added vasodilatation, as in inflammation, for example, stasis develops with possible leukocyte adherence, activation and diapedesis, and immune complex deposits. Cutaneous vasculitis is, in fact, venulitis. For the entire integument, the storage capacity of the skin is estimated at 600 ml, or 12 % of the blood volume (Martineaud and Seroussi 1977). Vascular congestion and increased permeability associated with erythrodermia lead to a reduction in plasmatic volume (Worm and Nielsen 1981). Strenuous exercise in very hot conditions (for example, running a marathon) can overdilate the capacitive skin vasculature, which can induce heart deficiency (Martineaud and Seroussi 1977). The same observation was made concerning generalized telangiectasias (Agache et al. 1973).

7 Vasodilatation

In cold or temperate climates, the skin temperature remains permanently below the central temperature: 95 °F (35 °C) on the face, 89.6 °F (32 °C) at the extremities. Vasodilatation takes place in case of heating of internal origin (muscular effort, digestion) or external origin (sun exposure), even without visible erythema. Beyond 107.6 °F (43 °C) vasoconstrictor orthosympathetic reflexes are annihilated. There is, therefore, a risk of orthostatic hypotension in someone suddenly standing up after sunbathing. Generalized cutaneous vasodilatation occurs during

Fig. 4 Vasomotion as observed with laser Doppler

pregnancy and postpartum, as well as in the luteal phase of the menstrual cycle. It is also observed in the evening and the early hours of the night (Martineaud and Seroussi 1977). Emotional or reflex (spicy food) vasodilatation is well known. Finally, any cutaneous ischemia (sustained local pressure, limb tourniquet) is followed by an apparently compensatory phase of reactive hyperemia.

The mechanism of vasodilatation is double: inhibition of the vasoconstrictor tone and local relaxation of the vessels under the influence of the reduced blood flow (pendent foot erythrosis in arterial insufficiency), local reflexes (NO-ergic), endothelial secretions (e.g., NO via activation of NO synthase by endothelial endothelin-1 ETB receptor (Tsukahara et al. 1994) and local vasodilators such as histamine, eicosanoids, PAF, kinins, etc.) (Worm and Nielsen 1981) and even secretions from the adjacent epithelium: when irritated the epidermis secretes NO (Palacio et al. 1997).

8 The Skin Blood Flow

Because of the numerous and continuous vasoconstrictive and vasodilative stimuli, the skin blood flow is permanently changing. Furthermore, some arterioles seem to function only sporadically: no explanation has been found for this phenomenon (Braverman et al. 1990). In addition, the vessels show local and autonomous variations in their diameter. The laser Doppler shows a rhythmic contraction of the skin vessels called vasomotion, superimposed on the heartbeat (60–80 min^{-1}) and the inspiratory vasoconstriction (18–24 min^{-1}). These variations in diameter have a low frequency: neurogenous β waves (6–10 min^{-1}) (they are eliminated by anesthetics), and myogenous α waves (1–2 min^{-1}) (they are generated by the smooth muscle coat of the vessel) (Kastrup et al. 1989) (Fig. 4). They are spontaneous, autonomous, and often not synchronous with those of the adjacent areas. Vasomotion facilitates the blood flow (Wilkin 1989) and is triggered or amplified after periods of relative ischemia and in arterial insufficiency of the lower limbs (Bollinger et al. 1991).

9 Conclusion

The skin microcirculation is an anastomotic system of vessels which are barely differentiated and have rather resistant walls; only near the epithelium is their structure well defined. This network has four major functions:

(a) A role in peripheral resistance,
(b) Nutrition of the epidermis and its annexes, and in particular resistance of the skin in long periods of compressive ischemia,
(c) Considerable vasomotion reactivity necessary for thermoregulation, and
(d) A major part in inflammation and skin reactivity.

Functions (b) and (c) reveal that at resting periods the blood flow is much higher than necessary for nutritional purposes. Finally, the skin microcirculation regulates transcutaneous absorption, ensures the nutrition of the interstitial dermal structures and neurosensorial elements, restorative angiogenesis, as well as classic endothelial functions, especially coagulation, fibrinolysis, and possibly fixation and elimination of the immune complexes.

References

Agache P, Maurat JP, Laurent R, Risold JC, Bidard de la Noe AM. Telangiectasies diffuses essentielles et insuffiance cardiaque d'origine cutanée. Bull Soc Fr Dermatol Syphiligr. 1973;80:511–3.

Agache PG, De Rigal J, Lévêque JL. Influence of an external pressure on skin microcirculation. In: Boccalon H, editor. Vascular medicine. Amsterdam: Excerpta Medica; 1993. p. 527–32.

Agache P. Thermometry and remote thermography. In: Handbook of Measuring the skin. 1st edn. Berlin: Springer; 2004. p. 354–62.

Bollinger A, Hoffinann U, Franzeck UK. Evaluation of flux motion in man by the laser Doppler technique. Blood Vessels. 1991;28:21–6.

Braverman IM, Sibley J. Role of the microcirculation in the treatment and pathogenesis of psoriasis. J Invest Dermatol. 1982;78:12–7.

Braverman IM, Keh A, Goldminz D. Correlation of laser Doppler wave patterns with underlying microvascular anatomy. J Invest Dermatol. 1990;95:283–6.

Casey R. Angio-architecture fascio-cutanée: une nouvelle approche de la vascularisation. Nouv Dermatol. 1990;9:763–9.

Fagrell B, Intaglietta M, Tsai AG, Ostergren J. Combination of laser Doppler flowmetry and capillary microscopy for evaluating the dynamics of skin microcirculation. In: Mahler F, Messmer K, Hammersen F, editors. Techniques in clinical capillary microscopy. Basel: Karger; 1986. p. 125–38.

Higgins JC, Eady RAJ. Human dermal microvasculature: I. Its segmental differentiation. Light and electron microscopic study. Br J Dermatol. 1981;104:117–29.

Holtz J. Hemodynamics in regional circulatory beds and local vascular reactivity. In: Greger R, Windhorst U, editors. Comprehensive human physiology. From cellular mechanisms to integration, vol. 2. Berlin/Heidelberg/New York: Springer; 1996. p. 1917–40.

Kastrup J, Bulow J, Lassen NA. Vasomotion in human skin before and after local heating recorded with laser Doppler flowmetry. Int J Microcirc Clin Exp. 1989;8:205–15.

Martineaud JJ, Seroussi R. Physiologie de la circulation cutantée. Paris: Masson; 1977.

Palacio S, Schmitt S, Viac J. Contact allergens and sodium lauryl sulphate upregulate vascular endothelial growth factor in normal keratinocytes. Br J Dermatol. 1997;137:540–5.

Revier J. Etude descriptive de la vascularisation dermique superficielle au niveau de la malléole interne. PhD in medicine, no. 69. France: Université de Besançon; 1981.

Ryan TJ. Structure, pattern and shape of the blood vessels of the skin. In: Jarrett A, editor. The physiology and pathophysiology of the skin, vol. 2. London: Academic; 1973. p. 577–652.

Ryan TJ. Direct observation of capillary modifications in the aged. In: Lévêque JL, Agache PG, editors. Aging skin: properties and functional changes. New York: Marcel Dekker; 1993. p. 87–104.

Spalteholz W. Blutgefässe der Haut. In: Jadassohn J, editor. Handbuch der Haut- und Geschlechtskrankheiten, vol. 1, part 1. Berlin/Heidelberg/New York: Springer; 1927.

Stüttgen G, Forssman WG. Pharmacology of the microvasculature of the skin. In: Stüttgen G, Spier H, Schwarz E, editors. Handbuch der Haut und Geschlechts krankheiten, Normal and pathologic physiology of the skin, III Erganzungswerk, vol. 1/4B. Berlin/Heidelberg/New York: Springer; 1981. p. 379–540.

Tsukahara H, Ende H, Magarinie HI, et al. Molecular and functional characterization of the nonisopeptide-selective ETB receptor in endothelial cells: receptor coupling to nitric oxide synthase. J Biol Chem. 1994;269:21778–85.

Tur E, Tur M, Maibach HI, Guy RH. Basal perfusion of the cutaneous microcirculation: measurements as a function of anatomic position. J Invest Dermatol. 1983;81:442–6.

Wilkin JK. Poiseuille, periodicity, and perfusion: rhythmic oscillatory vasomotion in the skin. J Invest Dermatol. 1989;93:1135–85.

Worm AM, Nielsen SL. Increased microvascular water filtration and blood flow in extensive skin disease. J Invest Dermatol. 1981;76:110–2.

Photoplethysmography in the Evaluation of Skin Conditions

49

Pierre Agache

Contents

Keywords

Finger arterial compliance • Light reflection rheography • Photoelectric cell • Photoplethysmography • Sphygmic photoplethysmography • Systolic photoplethysmography • Strain gauge plethysmography • Volume photoplethysmography

1 Indications

Peripheral arterial occlusive disease, vascular diseases of the extremities, arterial hypertension, lipodermatosclerosis and leg ulcers, stasis dermatitis, measurement of local vasoconstriction or vasodilatation.

2 Principle

Photoplethysmography (PPG) is an early technique (Hertzman 1937) based on the relative transparency of the human skin for red or near-infrared light (700–1000 nm), and on the diffusing effect of red blood cells (RBCs) which reduces these wavelengths retrodiffusion (Weinman 1967). The variation in the quantity of RBCs within the skin induces an inverse variations of the retrodiffused light detected on the surface

This chapter was originally published under the ISBN 978-3-540-01771-4 with the following book title Measuring the Skin. The content has not been changed.

Pierre Agache: deceased

P. Agache (✉)
Department of Dermatology, University Hospital of Besançon, Besançon, France
e-mail: aude.agache@free.fr; ferial.fanian@chu-besancon.fr; ferial.fanian@cert-besancon.com

P. Humbert et al. (eds.), *Agache's Measuring the Skin*, DOI 10.1007/978-3-319-32383-1_56

(about 1 % of incident light). Therefore, PPG (from the Greek words πλεθνσμοξ "increase" and Γραφη "writing") provides a measurement of any type (active or passive) blood volume *variation* at the tested site.

In practice, the source of light is placed against the skin (obviously the output will be better with red light rather than white light) and the retrodiffused light is detected by a photoelectric cell located in the same place. Two types of signals can be used: either the retrodiffused light systolic-diastolic variation, or through systolic-diastolic variation damping, the variation of the retrodiffused light baseline. In the first case, one deals with sphygmic or arterial PPG, in the second case with volumic or venous PPG. As a matter of fact the first type records the behaviour of the resistive vessels, whereas the second one is mainly influenced by the capacitive vessels. Historically the sphygmic PPG was the first method available but it was replaced in clinical practice by laser-doppler in the Seventies. However it provides irreplaceable data, but today, since the sphygmic PPG is rarely used, the term PPG usually applies to the volumic PPG.

As the amount of incident light remains constant, that of the retrodiffused light depends only on the variation of the quantity of RBCs within the illuminated volume, i.e., the skin vascular volume. The larger is this volume, and the lower is the retrodiffused light. The cutis deeper vessels and those of the subcutaneous plexus (small cutaneous arteries and veins) will mostly be responsible since they are larger than the superficial vessels. The PPG signal can be obtained only in arbitrary units (volts) because neither the volume of diffusion of the incident light, nor its absorption rate by tissues are known. PPG may be used on any part of the body, including the mouth and vagina.

3 Sphygmic (or systolic) PPG

In the devices, the signal is acquired at a frequency of about 20 Hz and always inverted in order to vary parallel to vascular volume. Therefore it is a pulse wave.

3.1 Morphology and Normal Values

The shape of the PPG pulse wave (Fig. 1) is similar to that of arteries, however it often shows in its descending part a shouldering and even an actual dicrotic wave occasionally. In the case of very elastic arterioles several rebound waves of decreasing amplitude may be observed (polycrotism). Quantification of the various parts of the curve has been carried out: total area of the sphygmic wave, ascending slope, descending slope, maximal amplitude, total duration of the wave, number and areas of the dicrotic waves. Comparative measurements require the stability of the device physical sensitivity with time (it has to be calibrated at regular intervals, gain should always be recorded, etc.) and of the similar physiological and environmental conditions (room temperature, subject acclimatisation, position, etc.). Unfortunately owing to the large variety of devices, no absolute value (in volts) can be proposed. Standardisation should be done.

In recumbent subjects at rest, on most areas of the body normal values are low and barely fluctuate (Fig. 2) (Tur et al. 1983). Head and neck on the one hand, and limb extremities on the other hand, are salient exceptions because the signal (systolic-diastolic variation) is both considerably higher and subject to great variation. This demonstrate

Fig. 1 Pulse waves obtained using sphygmic PPG (Laboratory of Skin Biophysics, Besançon)

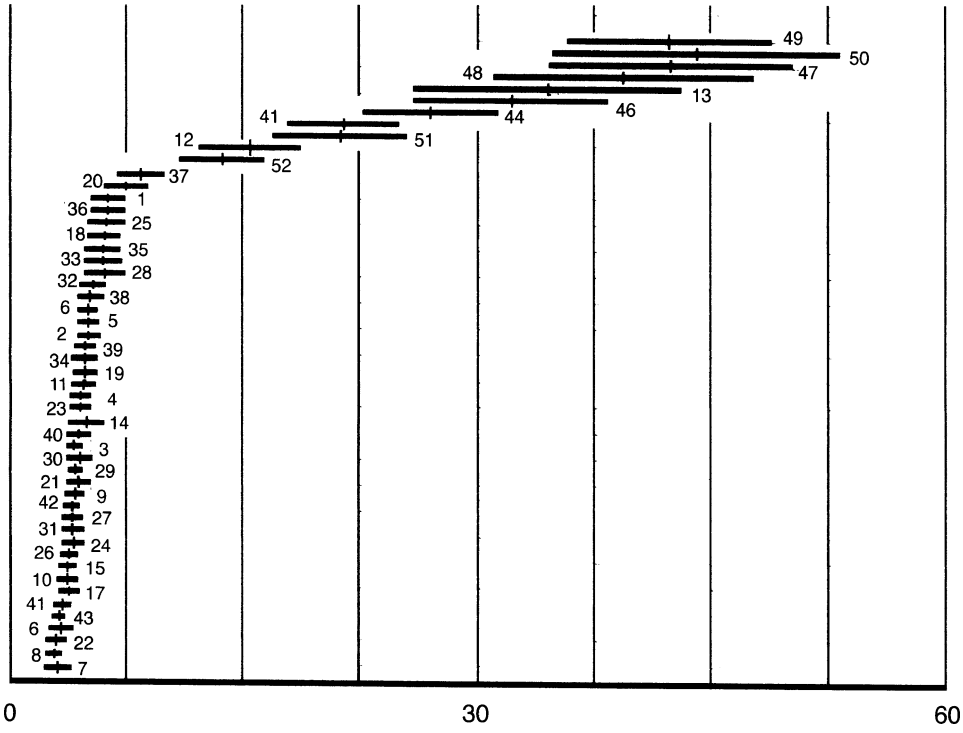

Fig. 2 Sphygmic PPG pulse waves amplitude distribution (in 10 naked recumbent subjects; room at 20–22 °C) (Tur et al. 1983). Mean and standard deviation (arbitrary units). Sites numbers: *1* supra-scapular, *2* infra-scapular, *3* infra-costal posterior, *4* upper buttock, *5* lower buttock, *6* thorax lateral, *7* infra-costal laterale, *8* hip, *9* below trochanter, *10* arm posterior, *11* forearm posterior, *12* palm, *13* forefinger pad, 14 upper thigh posterior, *15* lower thigh posterior, *16* popliteal area, *17* calf, *18* heel, *19* sole, *20* great toe pad, *21* upper thigh lateral, *22* lower thigh lateral, *23* popliteal lateral, *24* calf lateral, *25* sub-claviar, *26* infra-mammary, *27* para-umbilical, *28* iliac fossa, *30* arm anterior, *31* fore-arm anterior, *32* dorsal hand, *33* dorsal forefinger, *34* upper thigh anterior, *35* lower thigh anterior *36* knee anterior, *37* upper leg anterior, *38* lower leg anterior, *39* dorsum foot, *40* medial upper thigh, *41* medial lower thigh, *42* medial knee, *43* medial calf, *44* middle forehead, *45* upper fore-head lateral, *46* forehead lateral, *47* zygomatic area, *48* lowwer cheek, *49* ear lobe, *50* ear back, *51* mastoid area, *52* neck lateral

huge differences in the skin vasculature volume volume as well as in the vasomotor capacity: a phenomenon that the rather low room temperature in Fig. 2 experiment has helped revealing, given that the subjects ware naked at 23 ± 2 °C, which is well below the thermal neutrality temperature (30 °C); indeed one could be surprised by the very low values found for the soles and the toe pads, since it is well known that in these sites blood flow is considerably increased in warm conditions (Agache 2004). The PPG signal amplitude is greater in men than women and increases with age. After 60, this amplitude is on average more than double the amplitude found between the age of 20 and 57 (Lévêque et al. 1993), and parallels the elevation of blood pressure and the decrease of the microvasculature compliance. The PPG also reveals the vasomotion waves which, with a frequency of 6–8 per minute, shift up and down the baseline without modifying the pulse wave morphology.

3.2 Morphogenesis of the Microvasculature Pulse Wave

The shape of the PPG pulse wave depicts the systolic-diastolic variation of the vascular volume which itself depends on the transmural pressure. The latter results from two factors: the

perfusion pressure and the compliance (elasticity) of the vessel wall. The perfusion pressure depends on the arterial pressure upstream and on the resistance downstream. The latter is ruled by the vasoconstrictive tone of the skin vessels and the filling of the veins downstream. A reduced compliance makes the changes of vascular volume more sudden (steeper ascending and descending slopes) and precludes rebounds. Lifting the limb up, which reduces the perfusion pressure and therefore the transmural pressure, increases the amplitude, and inversely lowering the limb or standing up reduce the amplitude because the transmural pressure is increased due to the addition of the hydrostatic pressure. The same effect is observed in venous stasis and venous thrombosis.

3.3 Use in Disease

In the lower limbs an arterial occlusion upstream causes a reduction of the maximal amplitude, decreased slopes and makes the descending phase rigid. Should there be any doubt in the diagnosis, the latter would be confirmed by observing the reactive hyperaemia following 3 min proximal occlusion. While the norm is 3.4 ± 0.8 s to reach half the amplitude before occlusion, it would take over 10 s in case or peripheral occlusive arterial disease (Fronek et al. 1977). The venous hemodynamic troubles also reduce amplitude, weaken the slopes and mostly generate an important dicrotic wave (typical in acrocyanosis). If there was any ambiguity, the venous origin of troubles would be confirmed by their alleviation when the limb is lifted up (Rettori 1998).

3.4 Other Uses of the Sphygmic PPG

3.4.1 Measurement of the Distal Systolic Arterial Pressure

This can be achieved in a limb only. A tourniquet is placed proximal to the PPG sensor and the compression elevated so as to completely suppress the pulse waves; then the compression is gradually released. The systolic pressure is attained when pulse appears again.

3.4.2 Systolic Pressure, Diastolic Pressure and Compliance of the Skin Microvasculature

This important measurement can be achieved via vertical compression of the applied sensor (Agache et al. 1993). At first an increase of the wave amplitude is observed, then its decrease and finally its suppression when the compression equals the systolic pressure. At peak amplitude, the compression equals the diastolic pressure. This technical device thus provides the absolute value of the so-called "peripheral resistances" at the tested area. It is currently the only non invasive method allowing to obtain these parameters. Its rationale is the same as in the measurement of the blood pressure by the oscillometric method (Geddes 1970; Raines et al. 1973). Furthermore, the ratio peak amplitude/initial amplitude is a compliance index of the microvasculature. In a study carried out on 16 children, 18 adults and 25 subjects over 60, the systolic pressure was found 25 ± 4, 65 ± 8 and 150 ± 10 torr (1 torr = 1 mm Hg (in Torricelli's honour)), respectively; these values are 42 %, 42 % and 54 % respectively of the arm blood pressure in the same subjects. The diastolic pressures were 15, 18 and 16 torr, respectively, thus about the same in the three age groups. These figures match those in the nail capillaries as found using catheters (Mahler et al. 1979; Shore et al. 1993). The average compliance index decreased regularly with age, respectively at 6.0, 3.5 and 1.8 (Agache et al. 1993). PPG parameters characterise the deep vessels, as alluded to earlier. However the skin whitening pressure, which matches the sub-epidermal plexus vessels transmural pressure, remained stable, 30 torr, in the three age groups (Agache et al. 1993).

4 Volume (Diastolic) PPG

This type of PPG, also called light reflection rheography has met with considerable success when its utility was shown in venous stasis syndromes of the lower limbs. It records the baseline

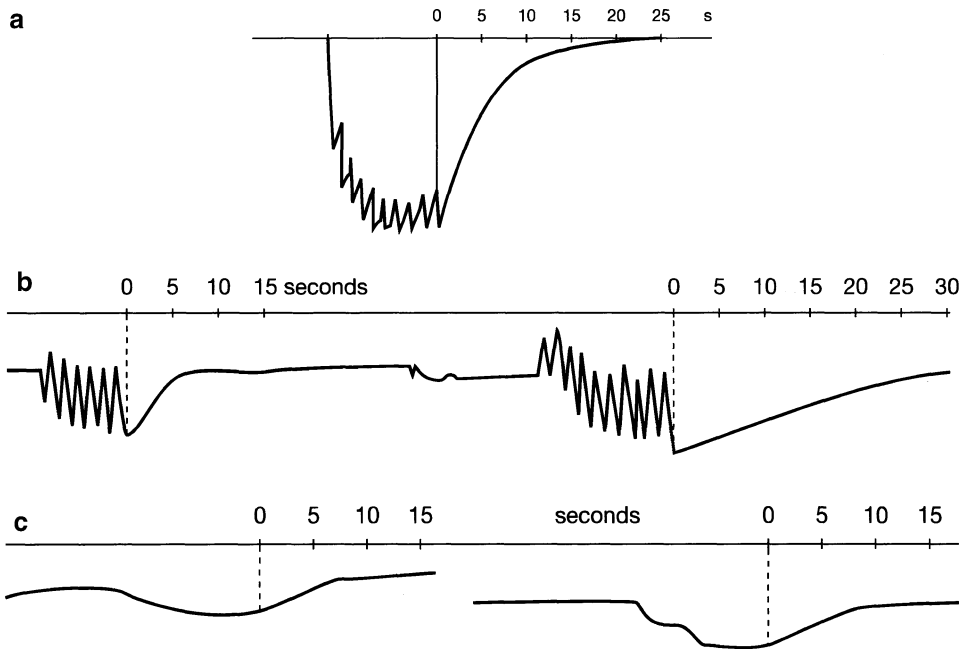

Fig. 3 Volumic PPG record in lower limb. lors d'un test de reflux veineux sous-cutané dans le membre inférieur. (**a**) normal (skin filling time: 25 s). (**b**) great saphene incompetence (skin filling time: 9 s), return to normal following great saphena compression above knee. (**c**) leg perforating veins incompetence (skin filling time: 7 s), no change following great saphena compression above knee; note the low calf pump efficacy (Laboratory of Skin Biophysics, Besançon)

signal through its systolic-diastolic variation damping. The sensor is that of pulse PPG but recording use direct current. The *difference* in the baseline level following its raise or decrease is a way to assess the skin blood volume *variation* (in volts) at the tested site. As for the pulse PPG it is mandatory to have external or internal calibration in order to be able to compare different subjects and confirm that the detector sensitivity has not shifted. The temperature of the test room should be between 20 °C and 25 °C, otherwise important vasomotor changes might occur. The subject, in resting position, must have been acclimated to the room temperature for 15 min at least.

To check the blood flow in a lower limb in case of lipodermatosclerosis with or without leg ulcer, the subject keep standing immobile (or if this is not possible, seated with his foot resting on a support). The probe is attached with double sided adhesive tape. When a stable value is obtained, the subject is asked to lift his heels regularly keeping the forefoot on the ground (for example every second for 10 s); the help of a metronome is useful. Another manoeuver consists in doing ten maximal forefoot lifting while keeping the heel on the ground (Belcaro et al. 1995). A decrease of the skin blood volume is observed during the first contractions (Fig. 3). While the foot is kept on the ground the recording is continued for the following 60 s. As soon as the movements stop, the skin starts to refill: the time required to reach the initial level (or so that 90 % of the emptying is corrected) is measured. It is important that the patient keeps immobile and relaxed until the end of the examination (without speaking, breathing normally).

The normal refilling time is usually 35 ± 12 s (Belcaro et al. 1995). When found shorter by more than two standard deviations (i.e., less than 11 s) it indicates deep intra-cutaneous or sub-cutaneous abnormal venous reflux. The emptying rate is another parameter which is related to the skin

blood content under a known hydrostatic pressure and consequently depends on the vertical distance between the PPG probe and the right auricle. The blood volume after the test is not always the same as the initial volume.

Note that the techniques of air or strain gauge plethysmography, when applied on the lower limb, measure the venous calf muscle pump efficacy, but not the possible venular refluxes, whereas the latter may be associated with a disturbed or apparently normal calf pump. The resolution of the imaging-doppler is too low to detect less than 1 mm diameter venules. The volumic PPG is therefore currently the only technique allowing to pinpoint venular backflow into the dermis or subcutis. Its suppression or reduction following application of a venous proximal tourniquet, suggests the responsibility of the saphenous system. If the tourniquet has no effect the backflow is either of local or of deep origin.

In other areas, the volumic PPG provides a measurement of the skin blood volume variation with changes of the perfusion pressure, or the venous pressure or the hydrostatic pressure. For a given pressure variation, the measurement of the skin blood volume variation allows to assess the tone (elasticity) of the capacity vessels. In cold environment the vasoconstriction is transcribed as a lowered baseline, with opposite results when the temperature rises. The volumic PPG also shows the vasomotion waves.

5 Precautions

- To ensure the good reproducibility, it is essential that the detector (which consists of a source of light and a photoelectric cell) is positioned parallel to the skin surface and with a constant and stable pressure. The latter must be as light as possible or it will alter the signal. It is even possible to avoid contact with the skin. It is convenient to use a ring of double sided adhesive paper, which should be preferred to the traditional pliers used on the fingertips.
- If the skin is wet or oily, the light penetration and outflow can be facilitated because the stratum corneum is more transparent; this induces an increase of the signal.
- The room temperature must be set between 20 °C and 25 °C for a subject dressed normally, otherwise important vasomotor changes will occur. The subject should be in resting position and acclimated to the temperature for 15 min.
- At present the voltage given by each type of device is different, since no external standard is available. Users should therefore have their own norm for each body site, age and skin temperature.

6 Commercialised Devices

- Medasonics (USA)
- Hemodynamics AV 1000 (Laumann Medizintechnik Gmbh, Germany) is developed especially for the supramalleolar volumic PPG and has a metronome, a temperature detector and a standard test for the foot movements.

References

Agache P, De Rigal J, Leveque JL. Influence of an external pressure on skin microcirculation. In: Boccalon H, editor. Vascular medicine. Amsterdam: Excerpta Medica; 1993. p. 527–33.

Agache P. Thermometry and remote thermography. In: Handbook of Measuring the skin. 1st edn. Berlin: Springer; 2004. p. 354–62.

Belcaro G, Christopoulos D, Nicolaides AN. Photoplethysmography and light reflection rheography: clinical applications in venous insufficiency. In: Serup J, Jemec GBE, editors. Non-invasive methods and the skin. Boca Raton: CRC Press; 1995. p. 443–8.

Fronek A, Coel M, Bernstein EF. The pulse-reappearance time: an index of overall blood flow impairment in the ischemic extremity. Surgery. 1977;81:376–81.

Geddes LA. The direct and indirect measurements of blood pressure. Chicago: Year Book Medical Publishers; 1970.

Hertzman AB. Photoelectric plethysmography of the fingers and toes in man. Proc Soc Exp Biol Med. 1937;37:529–34.

Lévêque JL, de Rigal J, Agache P. Indirect assessment of changes in skin microcirculation with age. In: Leveque

JL, Agache P, editors. Aging skin: properties and functional changes. New York: Marcel Dekker; 1993.

Mahler F, Muheim MH, Intaglietta M, Bollinger A, Anliker M. Blood pressure fluctuations in human nailfold capillaries. Am J Physiol. 1979;236(Heart Circ. PhysioL 5):H888–93.

Raines JK, Jaffrin MY, Rao S. A noninvasive pressure-pulse recorder: development and rationale. J Assoc Adv Med Instrum. 1973;7:245–50.

Rettori R. La pléthysmographie électronique dans les séquelles des phlébites et dans les artérites oblitérantes des membres inférieurs. In Cours dc perfectionnement de la Faculté de Médecine de Paris sur les maladies des vaisseaux périphériques. Ier Congrès de pathologie Vasculaire. Paris: L'Expansion Scientifique; 1998. p. 397–408.

Shore AC, Sandeman DD, Tooke JE. Effect of an increase in systemic blood pressure on nailfold capillary pressure in humans. Am J Physiol. 1993;265(or Heart Circ. Physiol. 34):H820–3.

Tur E, Tur M, Maibach HI, Guy RH. Basal perfusion of the cutaneous microcirculation: measurements as a function of anatomic position. J Invest Dermatol. 1983;81:442–6.

Weinman JA. Chapter 6:photoplethysmography. In: Manual of psychophysiological methods. Amsterdam: North Holland Publishing; 1967. p. 185–217.

Skin Microcirculation: Choosing the Appropriate Method

50

Pierre Agache

Contents

Keywords

Subepidermal plexus • Green laser doppler • Reflectometry • Clearance methods • Nutitive capillaries • arterioles • venules • Fingers and toes blood flow

Previous chapters witness the numerous methods available to measure skin blood flow. Each of them characterizes specific parameters. Consequently, it is necessary to compare these methods and replace them in the anatomical and physiological context. Thereupon can be examined their potential contribution in various situations: healthy skin or pathological conditions, skin pharmacology, skin metrology, etc. This chapter first examines at which depth the signal comes from, therefore the type of blood flow investigated, either deep or superficial. Secondly it will tentatively help select the most appropriate methods to investigate principally either the resistive or capacitive domain of the skin vascular network.

1 Selection from Anatomical Considerations

1.1 Measurement of Subepidermal Blood Flow

Two methods are specific and exclusive to the most superficial part of the subepidermal plexus and the papillary loops: transcutaneous oxygen

This chapter was originally published under the ISBN 978-3-540-01771-4 with the following book title Measuring the Skin. The content has not been changed.

Pierre Agache: deceased.

P. Agache (✉)
Department of Dermatology, University Hospital of Besançon, Besançon, France
e-mail: aude.agache@free.fr; ferial.fanian@chu-besancon.fr; ferial.fanian@cert-besancon.com

P. Humbert et al. (eds.), *Agache's Measuring the Skin*, DOI 10.1007/978-3-319-32383-1_57

pressure ($tcPO_2$) and capillaroscopy. Their meaning and parameters are very different.

- The $tcPO_2$ at 37 °C is theoretically able to measure the blood flow in the papillary loops in absolute units, and therefore is potentially a very useful method. However, the signal is so low and variable that the measurement is often not reliable; thus additional studies are required before using it for this purpose.

Usually the $tcPO_2$ is measured on the skin heated to 44 °C, a temperature which suppresses the vasoconstrictive tone. Its value is thus related to the capacity of the outermost part of the subepidermal vascular network to vasodilate (for example, $tcPO_2$ is reduced in lipodermatosclerosis and venous leg ulcers, and in lower limb arteriosclerosis). It also appears that the skin blood flow could be measured in specific units from the rate of the $tcPO_2$ reappearance after proximal occlusion release, but clinical confirmation is still lacking. On the other hand, the $tcPO_2$ falling rate during proximal occlusion is a way to measure oxygen consumption by the epidermis, and thus its metabolism. Although few studies have been carried out, this technique seems promising in skin disease.

Capillaroscopy has become feasible at any site of the skin. The extent of the superficial part of the subepidermal plexus and papillary loops can be quantified by image analysis. It is also possible to measure (in specific units) the dimensions of the vessels and the speed of the red blood cells. Both figures, once combined, can give access to blood flow in specific units, an uncommon and invaluable parameter. Few studies are available, but a priori the method could be used in diseased as well as in healthy skin, or to assess small variations of inflammatory origin.

1.2 The Subepidermal Plexus as a Whole

Several methods appear to be ideal for measuring the subepidermal plexus because of their operating mode: green laser Doppler, reflectometry, and colorimetry on the one hand, based on the absorption of a wavelength by hemoglobin, and thermal and epicutaneous xenon clearances on the other hand.

- Green laser Doppler uses a wavelength (543 nm) specifically absorbed by oxyhemoglobin. Its penetration depth probably goes beyond the most superficial parts of the subepidermal plexus, which provides a thorough investigation. However, it does not penetrate beyond that point, as indicated by its very weak signal. It is therefore an interesting means of measuring the average flux (amount of moving red blood cells multiplied by their average speed), probably in the entire plexus. Since it is given in arbitrary units, this value cannot be compared with the absolute values provided by the previous methods.
- Reflectometrydetects the absorption of green light by hemoglobin and its signal is made up exclusively of the 546- and 568-nm wavelength retrodiffusion following absorption. The mid-dermis (cutis) acts as a partial reflecting screen. This method therefore provides the measurement of the amount of blood almost exclusively present in the superficial dermis, i.e., the subepidermal plexus, unfortunately in arbitrary units. Easy-to-use devices are on the market. The same technique can be improved by the use of a spectrophotometer, which scans the skin surface at 5-nm intervals and selects the wavelengths specific to oxyhemoglobin and reduced hemoglobin, in order to measure the variations in the skin content in arteriolar (active vasodilatation) and venous (stasis, passive vasodilatation) blood separately.
- Colorimetry measures the retrodiffusion of a red-green-blue light tristimulus. The device transforms the intensity of the retrodiffused RGB spectrum into skin color expressed by the parameters $L^*a^*b^*$. In principle, blue is immediately and totally absorbed by hemoglobin. So is green, although to a lesser degree, as it goes down to the mid-dermis; its reflectance should therefore involve the entire superficial

dermal plexus. Red reaches the hypodermis; it is not absorbed but diffused by the red blood cells; therefore the amount of retrodiffused red decreases in relation to the deeper blood volume. Colorimetry could therefore explore all the skin vessels, whatever their depth, and assess the retrodiffused spectrum resulting from the whole skin blood. This spectrum is unknown and only its coordinates L^*a^*b are available. However, since the absorption of blue and green are predominant, it is probable that the signal is mainly influenced by the blood in the superficial dermis. Spectrocolorimeters operate according to the same principle, but they scan the skin surface over the entire visible spectrum. They are in principle more accurate.

– Clearance methods are obviously based on the washing out of a marker (xenon-133 or heat) that has diffused in the skin from the surface: hence a concentration gradient decreasing with penetration. The elimination process implies first the penetration of the vascular walls, which depends on their cumulated surface and the difference in concentration on each side of the wall. From skin biopsy autoradiography, it is known that the xenon gas capture by the vessels occurs entirely in the superficial dermis, therefore in the subepidermal plexus. The advantage of this method relies on the flow rate absolute value given in milliliters per minute per 100 g tissue, equivalent to milliliters per minute per square meter, assuming that the density and average thickness of the superficial dermis are 1 and 0.1 mm. Unfortunately, this method is cumbersome and available only in nuclear medicine units.

In contrast, thermal clearance implementation is easy and results are displayed immediately. It is based on is the same principle. The heat wash-out depends on the cumulated surface of the vascular walls and the temperature difference between the interstitial ground substance and blood. On the one hand, it is more important in the relatively cool superficial blood than in the deeper blood, and on the other hand, according to the author, the thermal gradient decreases steeply and concerns almost exclusively the first 100 μm, i.e., the superficial dermis. Thus, the signal reflects mainly the blood flow variation in the subepidermal plexus, expressed in skin thermal conductivity units. However, it appears that further investigations could lead to flow rate units since the thermal conductivity is given in absolute units. This promising method is no longer available, but a new device is said to be under development.

1.3 Measurement of the Whole Skin Blood Flow

The whole skin blood flow is given by methods using red or near-infrared light, since its penetration reaches the hypodermis. The vascular volume and the flow rate at this level are considerably higher than in the superficial dermis; consequently, these methods measure mainly the blood flow in the deep dermis and the superficial hypodermis (excluding adipose tissue).

– Laser Doppler devices indicate the number of moving red blood cells, their average speed, and the product of both measurements, giving the flow rate, all in arbitrary units. New technologies present two considerable advantages since they avoid contact between the transmitter and the skin and allow skin scanning. Therefore, blood flow is not altered by the measurement, and blood flow mapping is made possible. As a consequence, the measurement of vasomotor reactions in healthy or diseased skin is more accurate than with telethermography and can be done whatever the condition of the skin surface (wet, ulcerated, etc.), provided, obviously, that there is no ointment acting as a screen. In many experiments, the laser Doppler imager supersedes traditional laser Doppler because it also makes it possible to observe and record the flow on a fairly large area over a long period of time. However, one must be aware that flow changes restricted to the subepidermal plexus may go unnoticed with this method: a typical example is vasoconstriction from topical corticosteroids.

– Photoplethysmography (PPG) measures the blood volume variation within the constant skin illuminated volume. Each red blood cell diffuses light and reduces retrodiffusion proportionally. This method provides either the diastolic blood volume in the deeper part of the skin or its systolic increase. Its advantages are simplicity and low cost, and above all its capacity to separately analyze the resistive and capacitive sectors of skin microcirculation.

2 Selecting a Method Based on the Vessel Type to be Studied

2.1 Nutritive Capillaries

These vessels are located near the epidermis and appendage epithelia. Only the former are specifically accessible, using $tcPO_2$ and capillaroscopy. It seems that the papillary loops are not the only nutritive vessels of the epidermis: the more superficial venules also take part in this process, as well as in anatomical sites without papillary design. This underlines the advantage of newer capillaroscopy techniques, which make it possible to visualize the superficial part of the subepidermal plexus. The green laser Doppler is a technique that can also be considered as a means to measure the nutritive sector, although it also applies to vessels located deeper in this plexus. The nutritive capillaries of the pilosebaceous follicles and the sweat glands participate in the vascularization of the mid- and deep dermis and the global measurement of their volume or flow rate is a part of the PPG or laser Doppler signal.

2.2 Arterioles

The arteriolar, or upstream portion of the skin vascular system is specifically analyzed by thermal methods. Except for the extremities, the skin's spontaneous warm temperature indicates the arrival of a flow coming from the core, therefore from some skin arterioles being open. The available methods are punctual or liquid crystal thermometry, which gives an approximate mapping, and telethermography. The latter bears two salient advantages: it is a non-contact technique, allows sustained measurements, and provides skin temperature mapping. Active arteriolar vasodilatation (as in inflammation) and arteriolar spasm (as in hypersensitivity to cold or arterial hypertension) will therefore theoretically be investigated thoroughly by these methods. Skin surface thermometry is not sufficiently reliable, as it is influenced by external temperature. This is not the case for thermography, which measures IR light emission. Unfortunately, telethermography devices are very expensive.

The laser Doppler imager is currently challenging thermography in this field of investigation. In mid- or deep dermis or hypodermis, the flow is controlled by arterioles, which are not dilated during stasis or passive vasodilatation (also characterized by a stable or reduced flow). The topographical resolution (0.5 mm, sometimes 0.2 mm) is higher than that of thermography (5 mm). A 0.2-mm resolution even detects continuously perfused areas, each probably corresponding to a single arteriole. But on thin-skinned sites, venous blood is also recorded. Finally, the laser Doppler imager, as opposed to thermography, is not sensitive to wetness and is able to measure the flow on a de-epidermized area.

Systolic PPG is the oldest method to have been used in the study of skin microcirculation. The signal is a sphygmic wave, the morphology of which varies according to local hemodynamic conditions. It indicates the systolic-diastolic blood volume variation with time in the deep dermis. Arterioles are mainly concerned since they are the most pulsatile vessels.The PPG pulse wave morphological parameters have been used qualitatively to try and identify circulatory alterations downstream (e.g., stasis or increase in resistance) or upstream (e.g., arterial stricture or occlusion. This method was abandoned when laser Doppler was developed. However, the data provided by the systolic PPG are quite different and remain irreplaceable. A quantitative analysis

Table 1 The summary of the available methods for measuring the skin microcirculation and their characteristics.

Anatomical level	High pressure sector (arterioles, small arteries) Small total volume	Subepidermal nutritive vessels (capillaries, venules) Very small total volume	Low-pressure sector (venules, small veins) Large total volume
Subepidermal		$TcPO_2$ Capillaroscopy Green laser Doppler	Reflectometry Colorimetry Thermal clearance Xenon-133 clearance
Dermis and upper subcutis	Systolic PPG Red laser Doppler Thermometry Telethermography		Diastolic PPG

of morphological parameters would also be very useful: further physical and physiological studies are required.

2.3 Venules

The diastolic PPG signal expresses the sum of the arteriolar and venular volumes of the deep dermis and near hypodermis. As such, it can be a measure (in arbitrary units) of the skin passive blood supply during variations in the hydrostatic pressure or during a venular backflow from the subcutaneous veins in lower-limb venous insufficiency. It is obviously a useful method, which is irreplaceable in such diseases.

Clearance methods give greater importance to the capacitive sector of the subepidermal plexus because their walls are more permeable than those of the arterioles and the number of venules and the cumulated surface of their walls are much larger. The blood flow rate measured by xenon-133 clearance is probably closer to the venular than the arteriolar flow rate. The same holds true for the flow rate measured by thermal clearance.

3 Fingers and Toes

The examination of the extremities, in particular the fingertips and toes, is particular because of the large number of intradermal arteriovenous anastomoses, the interference of intense vasomotricity in relation to thermoregulation, and the thickness of the stratum corneum on the palmar aspects. As a result, the above-mentioned methods measuring the subepidermal nutritive blood flow cannot be used, and measurements with other methods are subject to error. Another old method, strain gauge plethysmography, can be used. Its principle is the measurement of the stretching of a strain gauge placed around a finger, resulting from the passage of the pulse or the position of the limb. The gauge is usually a thin rubber tube filled with mercury, the electric resistance of which, measured by a Wheatstone bridge, increases from its elongation and narrowing. The signal is similar to that of the PPG: a pulse wave or a horizontal straight line representing the limb or finger diastolic perimeter. If the gauge is calibrated, the measured difference in perimeter (i.e., in

volume) is given in absolute units: milliliters per minute for 100 ml soft tissue. The latter consists of the dermis with its numerous microvessels (arterioles, venules, capillaries, arteriovenous anastomoses), the hypodermis including fat, but also the laterodigital small arteries, the flow rate of which is impossible to evaluate separately.

4 Conclusion

The choice of one or several methods to measure skin microcirculation must therefore be determined according to specific needs, for example in phlebology: $tcPO_2$, PPG, and epicutaneous xenon-133 clearance are informative. Using several techniques for a single purpose is often rewarding because the meaning of experimental data is more easily understood. If a single device is to be used to measure an erythema or a pigmentation, colorimetry or reflectometry are particularly recommended. The choice of the device should also be made in relation with the request of a quantitative or semiquantitative type of measurement. Finally, whenever possible, measurements in absolute and specific units are always preferable. The table below summarizes the characteristics of available methods.

Lymphatic Microcirculation of the Skin 51

Pascale Quatresooz

Contents

Keywords
Lymphatic endothelial cells • Identification • Immunohistochemistry

Abbreviations
BECs Blood endothelial cells
LECs Lymphatic endothelial cells

1 Structure and Function

The lymphatic system is an open-ended network that returns lymph back to blood circulation. Microcirculation is the site where exchanges between blood or lymphatic vessels and tissues occur. Interstitial fluid that does not return to the blood by venules is collected by lymphatic capillaries and constitutes the lymph, a protein-rich exudate containing cells and macromolecules (Cueni and Detmar 2006; Parsi et al. 2011). Therefore, the lymph system plays an important role in homeostasis by this reabsorption of extracellular fluid (Van der Auwera et al. 2006). Lymphatic capillaries appear in the papillary dermis and drain into precollector vessels that link them to collector vessels. Lymph returns to the blood by large lymphatic trunks. Lymph vessels go through lymph nodes and constitute the way for immune circulating cells. The lymphatic system also plays an immune role that is particularly important in the skin as Langerhans cells pass by these vessels to reach lymph nodes (Bruyère and Noël 2010; Parsi et al. 2011). The lymphatic system originates

P. Quatresooz (✉)
Laboratory of Skin Bioengineering and Imaging, Department of Dermatopathology, University Hospital of Liège, Liège, Belgium

Department Histology, University of Liège, Liège, Belgium
e-mail: Pascale.quatresooz@chu.ulg.ac.be

P. Humbert et al. (eds.), *Agache's Measuring the Skin*,
DOI 10.1007/978-3-319-32383-1_58

from embryonic veins, and the development of lymphatic system begins when the cardiovascular system is already functioning (Cueni and Detmar 2006).

Lymphatic capillaries are blind-ended vessels that arise in the interstitial spaces of the dermal papillae. They are much larger than blood capillaries and stay away from epidermis, while blood capillary loops are close to the epidermis. These microvessels are lined by a single, nonfenestrated layer of endothelial cells that overlap but lack a basement membrane and pericytes (Parsi et al. 2011). These cells are linked to the extracellular dermal matrice by anchoring filaments. When interstitial pressure increases, LECs are pulled allowing capillary lumen to widen and excess fluid to be taken up.

Lymphatic vessels are particularly numerous in the dermis but are absent in the epidermis (Cueni and Detmar 2006). Lymphatic vessel density shows some anatomic variability that may contribute to the metastatic potential of primary cutaneous tumors (Duffy et al. 2010). However, body repartition of lymphatic vessels appears symmetric on both sides of a middle vertical line (Reynolds et al. 2010).

2 Identification of Initial Lymphatic Vessels

In spite of their high number, lymphatic vessels are difficult to distinguish in routine histological sections (Wu et al. 2012). BECs and LECs share many structural and molecular characteristics and are difficult to differentiate by histological morphology alone (Cueni and Detmar 2008; Oliver and Detmar 2002; Van der Auwera et al. 2006).

Little attention was paid to the lymphatic system until this century and most of the knowledge result from research performed during these last 10 years (Lee et al. 2010). Assessment of skin lymphatic microcirculation is of great importance in lymphedema, psoriasis, and systemic sclerosis pathogenesis as well as in tumor metastasis and wound healing. Some methods such as microlymphangiography via intradermal injections of fluorescein or dye allow to study the functional aspect of this microcirculation but do not really quantify it (Wu et al. 2012).

Immunohistochemical labeling is still the most common method to identify LECs. Lymphatic vascular endothelial hyaluronan receptor-1 (Lyve-1), Prox-1, podoplanin, VEGF-receptor-3 (VEGFR-3), and desmoplakin are the most frequent specific lymphatic markers studied (Bruyère and Noël 2010). Lyve-1 is highly expressed in lymphatic capillaries and at a lesser degree in larger vessels. Prox-1 is considered to be the most specific marker (Cueni and Detmar 2006), but its nuclear immunohistochemistry localization is not suitable for microscopic quantification. Therefore, for this purpose, it should be preferably used in double staining with others markers. Podoplanin is recognized by the D2-40 antibody. Several non-endothelial cells (basal keratinocytes by example) and some malignant tumors can also be labeled by this antibody. Despite the fact that VEGFR-3 is expressed by LECs in adult tissues, it can also be expressed by BECs in fenestrated capillaries and in pathological conditions (tumoral angiogenesis) (Cueni and Detmar 2006; Van der Auwera et al. 2006). Desmoplakin, a cytoplasmic protein, enters in the composition of junctions between LCE and extracellular matrix (Cueni and Detmar 2006). To obtain a reliable differentiation between BECs and LECs, several markers should be associated.

Currently, immunohistochemistry allows the assessment of important parameters such as structural characteristics, density, diameter, perimeter, surface area, and absolute c-vascular volume by using imaging quantification (Lokmic and Mitchell 2011; Wu et al. 2012). Confocal microscopy of whole-mount preparations and computer graphic three-dimensional reconstruction provide three-dimensional images and permit the quantification of lymphatic capillaries by imaging software (Cui 2006; Wu et al. 2012). However, these techniques are expensive, complex, and subject to artifacts. Further studies are necessary to determine the best method for studying lymphatic microcirculation (Wu et al. 2012).

References

Bruyère F, Noël A. Lymphangiogenesis: in vitro and in vivo models. FASEB J. 2010;24(1):8–21.

Cueni LN, Detmar M. New insights into the molecular control of the lymphatic vascular system and its role in disease. J Invest Dermatol. 2006;126(10):2167–77.

Cueni LN, Detmar M. The lymphatic system in health and disease. Lymphat Res Biol. 2008;6(3–4):109–22.

Cui Y. Confocal imaging: blood and lymphatic capillaries. Sci World J. 2006;6:12–5.

Duffy K, Hyde MA, Tanner B, Goldgar D, Bowen AR, Florell SR, et al. Anatomic variability in superficial blood vessel and lymphatic vessel density. J Cutan Pathol. 2010;37(10):1108–9.

Lee S, Choi I, Hong YK. Heterogeneity and plasticity of lymphatic endothelial cells. Semin Thromb Hemost. 2010;36(3):352–61.

Lokmic Z, Mitchell GM. Visualisation and stereological assessment of blood and lymphatic vessels. Histol Histopathol. 2011;26(6):781–96.

Oliver G, Detmar M. The rediscovery of the lymphatic system: old and new insights into the development and biological function of the lymphatic vasculature. Genes Dev. 2002;16(7):773–83.

Parsi K, Partsch H, Rabe E, Ramelet AA. Reticulate eruptions. Part 1: vascular networks and physiology. Australas J Dermatol. 2011;52(3):159–66.

Reynolds HM, Walker CG, Dunbar PR, O'Sullivan MJ, Uren RF, Thompson JF, et al. Functional anatomy of the lymphatics draining the skin: a detailed statistical analysis. J Anat. 2010;216 (3):344–55.

Van der Auwera I, Cao Y, Tille JC, Pepper MS, Jackson DG, Fox SB, et al. First international consensus on the methodology of lymphangiogenesis quantification in solid human tumours. Br J Cancer. 2006;95 (12):1611–25.

Wu X, Yu Z, Liu N. Comparison of approaches for microscopic imaging of skin lymphatic vessels. Scanning. 2012;34(3):174–80.

Assessment of Cutaneous Microvascular Function Using Laser Doppler Flowmetry and Acetylcholine Iontophoresis

52

Peter D. Drummond

Contents

Keywords

Cutaneous microvascular function • Intradermal delivery • Laser Doppler flowmetry • Transdermal iontophoresis • Serum glucose • Skin blood flow • Vascular smooth muscle relaxation • microdialysis • cardiovascular disease • diabetes • small fiber peripheral neuropathy

1 Introduction

Laser Doppler flowmetry has been employed for many years to assess cutaneous microvascular function in health and disease. It is often used in conjunction with transdermal iontophoresis of acetylcholine, as this provides information about the integrity both of the microvascular endothelium and the cutaneous sensory nerve supply. The reproducibility of this approach is reviewed below, and alternatives are discussed. In addition, some clinical applications are described.

2 Laser Doppler Flowmetry

This involves projection of a laser beam (typically 780 nm) into the skin and measurement of intensity and Doppler shifts in frequency in the near-infrared range of the backscattered light. The intensity of the reflected light is proportional to the concentration of red blood cells illuminated by the laser beam, and the shift in frequency is proportional to the

P.D. Drummond (✉)
School of Psychology and Exercise Science, Murdoch University, Perth, WA, Australia
e-mail: p.drummond@murdoch.edu.au

P. Humbert et al. (eds.), *Agache's Measuring the Skin*,
DOI 10.1007/978-3-319-32383-1_43

velocity of red blood cells moving through the illuminated tissue. When combined, these two values provide a measure of perfusion that varies in a linear fashion with microvascular blood flow (Ahn et al. 1987). The depth of measured flow (in the order of 1–1.5 mm) depends on the wavelength of the laser source (penetration is greater with longer wavelengths) (Berardesca et al. 2002). Thus, in the skin, the laser Doppler signal represents net flow through cutaneous arterioles, venous plexuses, and arteriovenous anastomoses.

Although laser Doppler flowmetry can be used to measure relative changes in skin blood flow, the signal cannot be calibrated in absolute units because of the complex nature of light scattering and site-to-site differences in the density and structure of the cutaneous microvasculature (Berardesca et al. 2002). Preferably, then, microvascular reactivity (e.g., to a drug or thermal challenge) should be expressed in perfusion units, normalized to measures taken at the same site under standard conditions (e.g., at rest or in response to a standard provocation).

Flow is sometimes expressed in relation to near-maximal flow at the site of interest. Heating the skin to 42 °C induces an axon reflex that peaks within a few minutes (Minson et al. 2001). Blood flow drops briefly then continues to rise gradually over the next 30–40 min, due to nonneural influences on the local microvasculature that involve nitric oxide (Kellogg et al. 2008). This approach evokes near-maximal increases in flow but can be cumbersome and time-consuming and controls only for the upper limit of nonneural influences on flow. Flow may also be expressed in response to vasodilatation evoked by administration of the nitric oxide donor sodium nitroprusside. However, the reproducibility of this response is extremely poor when assessed by laser Doppler flowmetry (Roustit and Cracowski 2012) and does not control for other influences on blood flow (e.g., the capacity of the sensory and autonomic nerve supply, vascular smooth muscle and endothelium, infiltrating immune cells and resident mast cells, fibroblasts and keratinocytes to release vasoactive substances). Another option is to express flow in relation to the peak of the axon reflex induced by 5–6 min of local heating (Brocx and Drummond 2009). This controls for spatial microvascular variations and sensory neural influences on blood flow, but may not account for nonneural influences on flow.

Perhaps the most commonly used approach is to express flow as a proportion of levels recorded during the baseline period before stimulus onset. Although this controls for site-to-site variation in cutaneous vascular and neural architecture, the response depends critically on the conditions under which baseline measures are obtained. Thus, it is important to standardize ambient temperature, time of day, prior levels of muscular activity, prior ingestion of substances that might influence flow (e.g., caffeine, nicotine, and alcohol), and, as much as possible, the participant's psychological state.

Flow is sometimes normalized in relation to mean blood pressure (i.e., so that flow is expressed in units of cutaneous vascular conductance), to control for effects of pressure on perfusion. However, the assumption that systemic pressure reflects perfusion pressure in the local microvasculature might not always hold true (e.g., when vasoactive drugs are administered locally or when the site of interest is heated or cooled).

3 Iontophoresis

Transdermal iontophoresis involves the use of an electric current to transfer charged or polarized molecules through the skin barrier. This typically involves passing a weak direct current through a drug solution contained in a capsule attached to the skin, to assist penetration of the drug through the stratum corneum. In this way, positively charged ions are repelled from the anode, and negatively charged ions are repelled from the cathode. Charged molecules enter primarily through hair follicles and sweat ducts and then diffuse through the extracellular space to the cutaneous microvasculature where they are dispersed through the circulating blood supply (Tesselaar and Sjoberg 2011). The dose delivered by this method is proportional to the current strength (measured in amperes) and duration (seconds)

and can be expressed as the iontophoretic charge (in Coulombs). However, the physiologically active component of the dose cannot be measured accurately because some of the electric current is carried by nondrug ions (e.g., in the solution vehicle or which originate in the skin). Furthermore, the relationship between dose and response is complex because some of the infused drug may bind nonselectively to cells in the stratum corneum or deeper within the skin or is cleared rapidly through the microvascular bed (particularly vasodilator drugs).

In addition, the electric current employed in iontophoresis can induce nonspecific vasodilator responses that alter local blood flow (Grossmann et al. 1995). This nonspecific response is stronger at the cathode than the anode and may involve several mechanisms. During iontophoresis, the electrolysis of water into hydrogen and oxygen results in an accumulation of hydrogen ions under the anode (Sato et al. 1993). Together with direct effects of the electric current on the resting potential of neural membranes, local changes in pH in the skin may depolarize sensory nerve fibers and trigger the antidromic release of vasoactive neuropeptides such as substance P and calcitonin gene-related peptide (CGRP) from the dermal network of nerve terminals (a process known as axon reflex vasodilatation). Thus, skin blood flow may increase within the receptive field of stimulated nerves up to several cm from the stimulated site. This component of the response can be blocked by prior treatment with capsaicin cream to desensitize C-nociceptive fibers and with local anesthetic agents such as EMLA cream that prevent depolarization (Durand et al. 2002). In addition to these mechanisms, local heating and other changes evoked by the movement of charged molecules through the skin may induce the production of prostaglandins which, in turn, trigger vasodilatation. For instance, the cyclooxygenase inhibitor indomethacin blocks anodal current-induced vasodilatation (Tartas et al. 2005). Curiously, pretreatment with celecoxib (which inhibits the formation of an inducible isoform of cyclooxygenase produced during inflammation) has no effect on anodal current-induced vasodilatation (Tartas et al. 2005), suggesting that the response is driven by the constitutive rather than the inducible cyclooxygenase isoform.

4 Measuring Microvascular Responses During Iontophoresis

Changes in blood flow during iontophoresis are often measured via a Laser Doppler flow probe inserted in the roof of the drug chamber directly over the site of drug infusion. This provides continuous measurement of blood flow from a single spot 2–3 mm in diameter at the site where the drug enters the skin. Unfortunately, microvascular responses vary considerably from one spot to another due to anatomical variation in the microvasculature (Braverman et al. 1990). For example, in a study in our laboratory, the reproducibility of the microvascular response to transdermal iontophoresis of acetylcholine was greater when the iontophoresis was repeated at the same site after a 50 min interval than when the iontophoresis was carried out at sites 10 cm apart on the volar forearm (Brocx and Drummond 2009). Responses were greater at proximal than distal sites in the forearm, possibly due to differences in thickness of the stratum corneum or in sweat gland or microvascular density. Thus, it is important to standardize the test site when making comparisons within individuals or between groups of patients and controls.

One solution to this problem is to measure changes in flow over a large surface area. Laser Doppler imaging achieves this by moving a laser beam across the region of interest to create a map of local blood flow. Although this minimizes the effect of structural variations on blood flow, it is difficult to capture rapid changes in flow because of the time required to scan the region of interest. An alternative is to use laser speckle contrast imaging, which employs a camera to generate a perfusion map of illuminated tissue based on the motion of particles in the region of interest. As perfusion maps can be generated quickly, rapid responses can be tracked with this approach (Mahe et al. 2012). In contrast to laser Doppler techniques, which detect flow to a depth of around

1 mm with a 780 nm laser beam, flow is detected to a depth of approximately 0.3 mm with laser speckle contrast imaging (corresponding to nutritional rather than arterial flow) (Mahe et al. 2012). The reproducibility of measures of blood flow is greater with laser Doppler imaging and laser speckle contrast imaging than with spot measures of laser Doppler flow (Mahe et al. 2012; Roustit and Cracowski 2012).

5 Reproducibility of the Cutaneous Vascular Response to Acetylcholine

Acetylcholine induces endothelium-dependent vasodilatation via stimulation of muscarinic receptors on the vascular endothelial surface (Cracowski et al. 2006). This releases nitric oxide, which induces vascular smooth muscle relaxation and, hence, vasodilatation. In addition, a flare surrounding the site of acetylcholine iontophoresis is mediated by an axon reflex that involves production of prostanoids (Berghoff et al. 2002).

The reproducibility of cutaneous microvascular responses to acetylcholine iontophoresis has not been firmly established due, in part, to the variety of doses, data expression methods, and protocols that have been employed (Agarwal et al. 2010; Klonizakis et al. 2011; Puissant et al. 2013; Tibirica et al. 2011). However, we recently used this technique to examine the reproducibility of vascular responses to stepped increases in acetylcholine delivered transdermally by iontophoresis (Brocx and Drummond 2009). One probe was positioned inside the iontophoresis chamber (to measure the direct endothelium-dependent component of the response), and another probe was positioned 5–8 mm outside the iontophoresis chamber (to measure the axon reflex) (Brocx and Drummond 2009). At the site of acetylcholine iontophoresis, laser Doppler flux data were expressed as a proportion of baseline and a proportion of the response to heating for 5–6 min. The reproducibility of each form of data expression was investigated within and across different forearm sites.

The direct response to acetylcholine was most reproducible when expressed in proportion to levels recorded after 5–6 min of local heating to 42 °C (the percentage of shared variance was 55 % when the iontophoresis was repeated at the same site on the volar forearm, and mean increases in flow were similar on both occasions) (Fig. 1). The association was also strong when expressed in proportion to levels recorded at baseline – the percentage of shared variance was 74 % when the acetylcholine iontophoresis was repeated at the same site. However, when data were expressed in this way, responses were consistently smaller during the second than first iontophoresis, in part because of a residual elevation of the baseline from the first iontophoresis (cumulative increases in flow across all doses were 68 times greater than baseline during the first iontophoresis compared with only 30 times greater than baseline during the second iontophoresis) (Fig. 2). Similarly, for axon reflex vasodilatation, 38 % of variance was shared between responses at times 1 and 2 when the iontophoresis was repeated at the same site on the volar forearm; however, responses were greater on the first than second occasion (cumulative increases in flow were 22 vs. 14 times greater than baseline, respectively) (Fig. 2). This illustrates the importance of minimizing nonspecific influences on basal flow if this form of data expression is used. We also attempted to identify the optimal current strength and duration for the iontophoresis of acetylcholine. The "dose-response" curve peaked at the site of iontophoresis but the axon reflex failed to plateau (Fig. 2), suggesting that a higher dose might be required to fully capture this response.

Additional variables that might influence the reproducibility of the vasodilator response to acetylcholine have been investigated recently. For example, microvascular responses in the legs to iontophoretic administration of acetylcholine were found to be lower in the standing than supine positions, presumably due to postural vasoconstrictor reflexes (Klonizakis et al. 2011). Nevertheless, responses were reproducible over a 2-week interval when measured with a laser

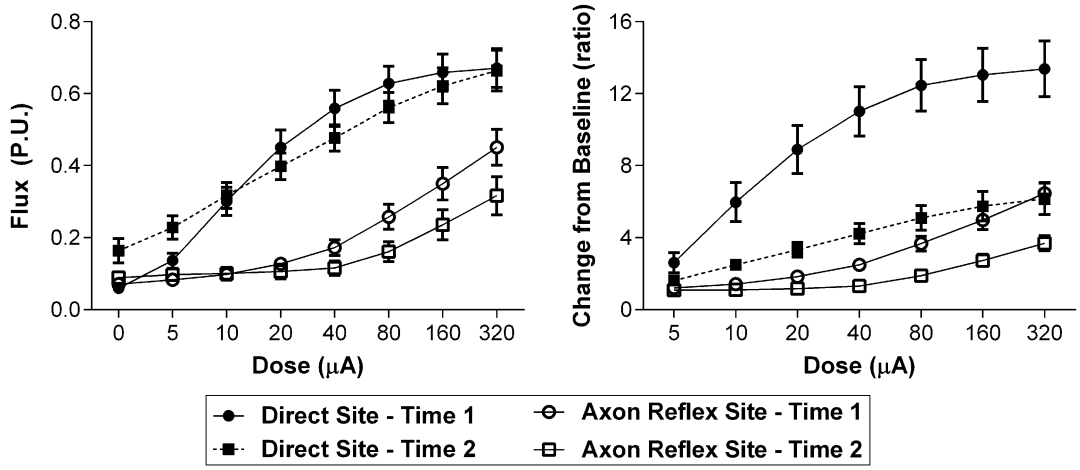

Fig. 1 Changes in blood flow (± standard error) during the transdermal iontophoresis of acetylcholine in the volar forearm 5 cm below the elbow, expressed as a proportion of the peak in blood flow when the forearm was heated to 42–43 °C for 5–6 min. For each dose of acetylcholine, an anodal current was supplied for 60 s in a drug chamber (internal diameter, 10 mm), and blood flow was monitored for a further 2 min at the site of drug administration. The entire procedure was repeated at the same site after an interval of 50 min. When expressed as a proportion of the peak in blood flow during forearm heating, peak and overall increases in blood flow were similar during both series of iontophoreses (Based on data presented by Brocx and Drummond (2009))

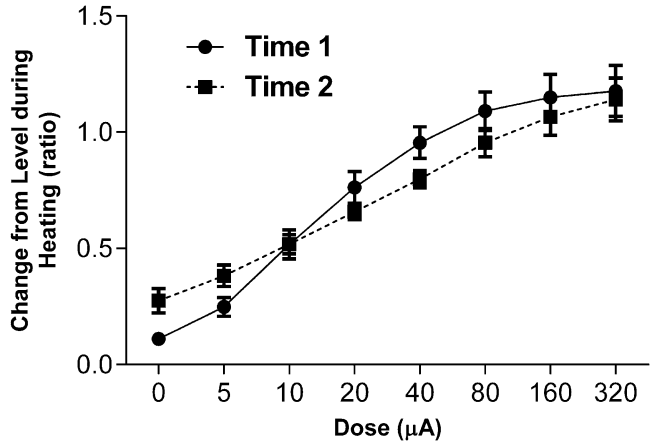

Fig. 2 Changes in blood flow (± standard error) during the transdermal iontophoresis of acetylcholine at the direct site (expressing endothelium-dependent vasodilatation) and 5–8 mm away (a site of axon reflex vasodilatation). Changes in blood flow (flux) are presented in arbitrary perfusion units (*PU*) and as a proportion of levels recorded for 2 min before the current was applied (baseline). When expressed as a proportion of baseline, increases in flow were greater during the first than second series of iontophoreses, due to residual basal vasodilatation after the first series (Based on data presented by Brocx and Drummond (2009))

Doppler imager and expressed in arbitrary perfusion units. In addition, the reproducibility of the peak response to acetylcholine iontophoresis was similar during single and incremental doses, despite concerns that axon reflex vasodilatation might mask endothelium-dependent vasodilatation to acetylcholine with incremental doses (Puissant et al. 2013).

6 Intradermal Delivery of Acetylcholine by Microdialysis

As an alternative to transdermal iontophoresis, drugs can be delivered intradermally through microdialysis fibers. This involves the insertion of porous catheters 0.5–1 mm under the skin surface for distances of several cm so that drugs can be delivered directly to the dermis, bypassing the skin barrier. An additional advantage of this technique is that biomarkers that diffuse from the extracellular fluid into the microdialysis fibers can be measured in the dialyzate, thereby providing an estimate of their local concentration.

One difficulty with microdialysis is that insertion of the fibers into the skin provokes an inflammatory reaction that might alter responses to the drug being delivered and/or the concentration of biomarkers of interest (Stenken et al. 2010). However, this inflammatory reaction appears to produce effects that differ from those provoked by axon reflexes during iontophoresis. For example, we found that iontophoresis of α_1-adrenoceptor agonists such as methoxamine and phenylephrine provoked an axon reflex when delivered transdermally by iontophoresis (Drummond 2009, 2011). The axon reflex could be blocked by prior application of local anesthetic agent (EMLA cream) to the skin surface and by α_1-adrenoceptor blockade and was inhibited by topical application of ibuprofen gel. In contrast, direct intradermal delivery of phenylephrine through microdialysis fibers did not provoke an axon reflex (Zahn et al. 2004). One interpretation of these findings is that phenylephrine amplifies an axon reflex initiated by the iontophoretic current, perhaps by stimulating α_1-adrenoceptors on keratinocytes or cutaneous nociceptors (Dawson et al. 2011).

When delivered through microdialysis fibers, acetylcholine triggers a flare in the surrounding skin that is mediated by antidromic release of neuropeptides such as CGRP from sensory nerve fibers (Schlereth et al. 2013). In addition, acetylcholine delivered intradermally through microdialysis fibers induces endothelium-dependent vasodilatation via nitric oxide and prostaglandins release (Medow et al. 2008). Thus, although intradermal delivery of acetylcholine by microdialysis may avoid some of the nonspecific effects evoked by current-assisted transdermal delivery, responses seem to be broadly similar in both modes of delivery.

7 Clinical Findings

Efficient regulation of local blood flow is crucial for optimal tissue functioning. Hence, many diseases are associated with vascular endothelial dysfunction and disruption of neurogenic inflammatory responses (Steinhoff et al. 2003; Widlansky et al. 2003). The integrity of these responses can be investigated clinically using acetylcholine to provoke endothelium-dependent and neurogenic vasodilatation.

Serum glucose has a strong inhibitory effect on endothelium-dependent vasodilatation via oxidative stress and low-grade inflammation and contributes to endothelial dysfunction in diabetes (Sena et al. 2013). This ultimately results in atherosclerosis, coronary artery disease, and widespread tissue destruction and organ failure (e.g., in diabetic neuropathy and retinopathy) (Gilbert 2013). In contrast, insulin augments endothelium-dependent vasodilatation in the skin (de Jongh et al. 2004). Thus, transdermal iontophoresis of acetylcholine is useful for detecting the extent of microvascular disturbances in patients with cardiovascular disease. For example, in patients with diabetic retinopathy, vasodilator responses to acetylcholine iontophoresis were smaller than in diabetic patients without retinopathy (Nguyen et al. 2011; Sasongko et al. 2012). The compromised vasodilator response was associated with low serum levels of high-density lipoprotein (HDL) cholesterol and apolipoprotein A1, a major component of HDL cholesterol (Sasongko et al. 2012). Similarly, the microvascular reaction to transdermal iontophoresis of acetylcholine was lower in patients with peripheral diabetic neuropathy than in diabetic patients without neuropathy (Tomesova et al. 2013). The microvascular disturbances associated with diabetic neuropathy

increase the likelihood of impaired wound healing, ulceration, and subsequent amputation of affected limbs (Chao and Cheing 2009).

Microvascular reactivity to transdermal acetylcholine is also impaired in obese individuals (Al-Tahami et al. 2011; de Jongh et al. 2004; Jonk et al. 2011). For example, acetylcholine-mediated vasodilatation was found to be smaller in obese insulin-resistant but nondiabetic individuals after ingesting a liquid mixed meal than in lean individuals (Jonk et al. 2011). However, deficits may depend on developmental factors or disease chronicity, as endothelium-dependent vasodilatation evoked by transdermal iontophoresis of acetylcholine was similar to responses in normotensive controls in lean, overweight, and obese hypertensive adolescents (Monostori et al. 2010).

Microvascular disturbances in patients with cardiovascular disease may be reversed by certain dietary substances and exercise. For example, the flavonoids in cocoa and dark chocolate appear to increase endothelium-dependent vasodilatation and counteract insulin resistance by increasing nitric oxide bioavailability (Grassi et al. 2013). Similar effects are associated with dietary supplementation with tuna fish oil (Khan et al. 2003). In addition, vitamin C may counteract the inhibitory influence of reactive oxygen species on endothelium-dependent vasodilatation (Rousseau et al. 2010). Acetylcholine-evoked vasodilatation is greater in active than sedentary individuals (Demiot et al. 2007) and increases after exercise training (Hodges et al. 2010). This may be particularly important for maintaining increased skin blood flow during exercise in older people, as microvascular disturbances increase with aging (Simmons et al. 2011).

Increases in skin blood flow can be detected up to 1 cm away from the site of acetylcholine iontophoresis; as these increases can be blocked by prior treatment of the skin with a topical anesthetic agent, they appear to result from axon reflexes mediated by C-fiber nociceptors (Caselli et al. 2003). This response was impaired in patients with peripheral diabetic neuropathy (Caselli et al. 2003, 2006), and deficits were associated with deficits in other indices of sensory and autonomic nerve function. As neurogenic vasodilatation to acetylcholine is attenuated in patients with mild symptoms of diabetic neuropathy (Caselli et al. 2006), loss of the neurogenic vasodilator response may represent an early marker of nerve dysfunction in patients with subclinical neuropathy.

Conversely, neurogenic vasodilatation to acetylcholine may be augmented in patients with inflammatory dermatological disorders such as rosacea. This condition generally affects the cheeks, nose, chin, or forehead and is characterized by flushing and acne-like facial papules or pustules (Elewski et al. 2011). We recently investigated endothelium-dependent and neurogenic vasodilator responses to transdermal iontophoresis of acetylcholine in patients with mild or severe rosacea and compared these responses to those in age- and sex-matched controls (Drummond and Su 2012). The intensity of stinging sensations provoked by the iontophoresis was greater in patients than controls. In addition, neurogenic vasodilatation was greater in patients with severe than mild symptoms, suggesting that axon reflexes augment flushing. If so, agents that decrease neurovascular reactivity (e.g., capsaicin cream) may alleviate symptoms in patients with severe rosacea.

8 Conclusions

Using laser Doppler flowmetry to monitor changes in blood flow during transdermal iontophoresis of acetylcholine has provided insights into microvascular function both in health and disease. Unfortunately, however, progress has been impeded by methodological difficulties – particularly concerning errors introduced by nonspecific responses to iontophoresis and the relatively poor reproducibility of spot measures of flow. In addition, the technique has suffered from a lack of standardization both in the form of delivery and the expression of data. Nevertheless, recent advances have partly overcome these problems. In particular, the reproducibility of responses is greater with laser Doppler imaging and laser speckle contrast imaging than with laser

Doppler flowmetry (Roustit and Cracowski 2012), as spatial variability in the microvascular architecture is minimized by averaging across a large region of interest. In addition, large chamber sizes (Ferrell et al. 2002) and low-density currents help to minimize the nonspecific component of response in iontophoresis (Droog et al. 2004). As these techniques are safe and noninvasive, they hold great promise as a window for assessing microvascular responses that reflect important elements of cardiovascular health.

References

Agarwal SC, Allen J, Murray A, Purcell IF. Comparative reproducibility of dermal microvascular blood flow changes in response to acetylcholine iontophoresis, hyperthermia and reactive hyperaemia. Physiol Meas. 2010;31:1–11.

Ahn H, Johansson K, Lundgren O, Nilsson GE. In vivo evaluation of signal processors for laser Doppler tissue flowmeters. Med Biol Eng Comput. 1987;25:207–11.

Al-Tahami BA, Bee YT, Ismail AA, Rasool AH. Impaired microvascular endothelial function in relatively young obese humans is associated with altered metabolic and inflammatory markers. Clin Hemorheol Microcirc. 2011;47:87–97.

Berardesca E, Leveque JL, Masson P, European Group for Efficacy Measurements on C, Other Topical P. EEMCO guidance for the measurement of skin microcirculation. Skin Pharmacol Appl Skin Physiol. 2002;15:442–56.

Berghoff M, Kathpal M, Kilo S, Hilz MJ, Freeman R. Vascular and neural mechanisms of ACh-mediated vasodilation in the forearm cutaneous microcirculation. J Appl Physiol. 2002;92:780–8.

Braverman IM, Keh A, Goldminz D. Correlation of laser Doppler wave patterns with underlying microvascular anatomy. J Invest Dermatol. 1990;95:283–6.

Brocx KA, Drummond PD. Reproducibility of cutaneous microvascular function assessment using laser Doppler flowmetry and acetylcholine iontophoresis. Skin Pharmacol Physiol. 2009;22:313–21.

Caselli A, Rich J, Hanane T, Uccioli L, Veves A. Role of C-nociceptive fibers in the nerve axon reflex-related vasodilation in diabetes. Neurology. 2003;60:297–300.

Caselli A, Spallone V, Marfia GA, Battista C, Pachatz C, Veves A, Uccioli L. Validation of the nerve axon reflex for the assessment of small nerve fibre dysfunction. J Neurol Neurosurg Psychiatry. 2006;77:927–32.

Chao CY, Cheing GL. Microvascular dysfunction in diabetic foot disease and ulceration. Diabetes Metab Res Rev. 2009;25:604–14.

Cracowski JL, Minson CT, Salvat-Melis M, Halliwill JR. Methodological issues in the assessment of skin microvascular endothelial function in humans. Trends Pharmacol Sci. 2006;27:503–8.

Dawson LF, Phillips JK, Finch PM, Inglis JJ, Drummond PD. Expression of alpha1-adrenoceptors on peripheral nociceptive neurons. Neuroscience. 2011;175:300–14.

de Jongh RT, Serne EH, RG IJ, de Vries G, Stehouwer CD. Impaired microvascular function in obesity: implications for obesity-associated microangiopathy, hypertension, and insulin resistance. Circulation. 2004;109:2529–35.

Demiot C, Dignat-George F, Fortrat JO, Sabatier F, Gharib C, Larina I, Gauquelin-Koch G, Hughson R, Custaud MA. WISE 2005: chronic bed rest impairs microcirculatory endothelium in women. Am J Physiol Heart Circ Physiol. 2007;293:H3159–64.

Droog EJ, Henricson J, Nilsson GE, Sjoberg F. A protocol for iontophoresis of acetylcholine and sodium nitroprusside that minimises nonspecific vasodilatory effects. Microvasc Res. 2004;67:197–202.

Drummond PD. Alpha-1 adrenoceptor stimulation triggers axon-reflex vasodilatation in human skin. Auton Neurosci: Basic Clin. 2009;151:159–63.

Drummond PD. Inflammation contributes to axon reflex vasodilatation evoked by iontophoresis of an alpha-1 adrenoceptor agonist. Auton Neurosci: Basic Clin. 2011;159:90–7.

Drummond PD, Su D. Endothelial and axon reflex vasodilatation to acetylcholine in rosacea-affected skin. Arch Dermatol Res. 2012;304:133–7.

Durand S, Fromy B, Bouye P, Saumet JL, Abraham P. Current-induced vasodilation during water iontophoresis (5 min, 0.10 mA) is delayed from current onset and involves aspirin sensitive mechanisms. J Vasc Res. 2002;39:59–71.

Elewski BE, Draelos Z, Dreno B, Jansen T, Layton A, Picardo M. Rosacea – global diversity and optimized outcome: proposed international consensus from the Rosacea International Expert Group. J Eur Acad Dermatol Venereol. 2011;25:188–200.

Ferrell WR, Ramsay JE, Brooks N, Lockhart JC, Dickson S, McNeece GM, Greer IA, Sattar N. Elimination of electrically induced iontophoretic artefacts: implications for non-invasive assessment of peripheral microvascular function. J Vasc Res. 2002;39:447–55.

Gilbert RE. Endothelial loss and repair in the vascular complications of diabetes. Circ J. 2013;77:849–56.

Grassi D, Desideri G, Ferri C. Protective effects of dark chocolate on endothelial function and diabetes. Curr Opin Clin Nutr Metab Care. 2013;16:662–8.

Grossmann M, Jamieson MJ, Kellogg Jr DL, Kosiba WA, Pergola PE, Crandall CG, Shepherd AM. The effect of iontophoresis on the cutaneous vasculature: evidence for current-induced hyperemia. Microvasc Res. 1995;50:444–52.

Hodges GJ, Sharp L, Stephenson C, Patwala AY, George KP, Goldspink DF, Tim Cable N. The effect of 48 weeks of aerobic exercise training on cutaneous

vasodilator function in post-menopausal females. Eur J Appl Physiol. 2010;108:1259–67.

Jonk AM, Houben AJ, Schaper NC, de Leeuw PW, Serne EH, Smulders YM, Stehouwer CD. Obesity is associated with impaired endothelial function in the postprandial state. Microvasc Res. 2011;82:423–9.

Kellogg Jr DL, Zhao JL, Wu Y. Endothelial nitric oxide synthase control mechanisms in the cutaneous vasculature of humans in vivo. Am J Physiol Heart Circ Physiol. 2008;295:H123–9.

Khan F, Elherik K, Bolton-Smith C, Barr R, Hill A, Murrie I, Belch JJ. The effects of dietary fatty acid supplementation on endothelial function and vascular tone in healthy subjects. Cardiovasc Res. 2003;59:955–62.

Klonizakis M, Manning G, Donnelly R. Assessment of lower limb microcirculation: exploring the reproducibility and clinical application of laser Doppler techniques. Skin Pharmacol Physiol. 2011;24:136–43.

Mahe G, Humeau-Heurtier A, Durand S, Leftheriotis G, Abraham P. Assessment of skin microvascular function and dysfunction with laser speckle contrast imaging. Circ Cardiovasc Imaging. 2012;5:155–63.

Medow MS, Glover JL, Stewart JM. Nitric oxide and prostaglandin inhibition during acetylcholine-mediated cutaneous vasodilation in humans. Microcirculation. 2008;15:569–79.

Minson CT, Berry LT, Joyner MJ. Nitric oxide and neurally mediated regulation of skin blood flow during local heating. J Appl Physiol. 2001;91:1619–26.

Monostori P, Barath A, Fazekas I, Hodi E, Mate A, Farkas I, Hracsko Z, Varga IS, Sumegi V, Gellen B, Bereczki C, Turi S. Microvascular reactivity in lean, overweight, and obese hypertensive adolescents. Eur J Pediatr. 2010;169:1369–74.

Nguyen TT, Shaw JE, Robinson C, Kawasaki R, Wang JJ, Kreis AJ, Wong TY. Diabetic retinopathy is related to both endothelium-dependent and -independent responses of skin microvascular flow. Diabetes Care. 2011;34:1389–93.

Puissant C, Abraham P, Durand S, Humeau-Heurtier A, Faure S, Leftheriotis G, Rousseau P, Mahe G. Reproducibility of non-invasive assessment of skin endothelial function using laser Doppler flowmetry and laser speckle contrast imaging. PLoS One. 2013;8:e61320.

Rousseau A, Tesselaar E, Henricson J, Sjoberg F. Prostaglandins and radical oxygen species are involved in microvascular effects of hyperoxia. J Vasc Res. 2010;47:441–50.

Roustit M, Cracowski JL. Non-invasive assessment of skin microvascular function in humans: an insight into methods. Microcirculation. 2012;19:47–64.

Sasongko MB, Wong TY, Nguyen TT, Kawasaki R, Jenkins AJ, Shaw J, Robinson C, Wang JJ. Serum apolipoproteins are associated with systemic and retinal microvascular function in people with diabetes. Diabetes. 2012;61:1785–92.

Sato K, Timm DE, Sato F, Templeton EA, Meletiou DS, Toyomoto T, Soos G, Sato SK. Generation and transit pathway of H+ is critical for inhibition of palmar sweating by iontophoresis in water. J Appl Physiol. 1993;75:2258–64.

Schlereth T, Breimhorst M, Werner N, Pottschmidt K, Drummond PD, Birklein F. Inhibition of neuropeptide degradation suppresses sweating but increases the area of the axon reflex flare. Exp Dermatol. 2013;22:299–301.

Sena CM, Pereira AM, Seica R. Endothelial dysfunction – a major mediator of diabetic vascular disease. Biochim Biophys Acta. 2013;1832:2216–31.

Simmons GH, Wong BJ, Holowatz LA, Kenney WL. Changes in the control of skin blood flow with exercise training: where do cutaneous vascular adaptations fit in? Exp Physiol. 2011;96:822–8.

Steinhoff M, Stander S, Seeliger S, Ansel JC, Schmelz M, Luger T. Modern aspects of cutaneous neurogenic inflammation. Arch Dermatol. 2003;139:1479–88.

Stenken JA, Church MK, Gill CA, Clough GF. How minimally invasive is microdialysis sampling? A cautionary note for cytokine collection in human skin and other clinical studies. AAPS J. 2010;12:73–8.

Tartas M, Bouye P, Koitka A, Durand S, Gallois Y, Saumet JL, Abraham P. Early vasodilator response to anodal current application in human is not impaired by cyclooxygenase-2 blockade. Am J Physiol Heart Circ Physiol. 2005;288:H1668–73.

Tesselaar E, Sjoberg F. Transdermal iontophoresis as an in-vivo technique for studying microvascular physiology. Microvasc Res. 2011;81:88–96.

Tibirica E, Matheus AS, Nunes B, Sperandei S, Gomes MB. Repeatability of the evaluation of systemic microvascular endothelial function using laser Doppler perfusion monitoring: clinical and statistical implications. Clinics (Sao Paulo). 2011;66:599–605.

Tomesova J, Gruberova J, Lacigova S, Cechurova D, Jankovec Z, Rusavy Z. Differences in skin microcirculation on the upper and lower extremities in patients with diabetes mellitus: relationship of diabetic neuropathy and skin microcirculation. Diabetes Technol Ther. 2013;15:968–75.

Widlansky ME, Gokce N, Keaney JF, Vita JA. The clinical implications of endothelial dysfunction. J Am Coll Cardiol. 2003;42:1149–60.

Zahn S, Leis S, Schick C, Schmelz M, Birklein F. No alpha-adrenoreceptor-induced C-fiber activation in healthy human skin. J Appl Physiol. 2004;96:1380–4.

Skin Capillaroscopy

53

Philippe Humbert, Jean-Marie Sainthillier, Sophie Mac-Mary, Thomas Lihoreau, Ferial Fanian, Adeline Jeudy, and Li Li

Contents

P. Humbert (✉)
Department of Dermatology, University Hospital of Besançon, Besançon, France
e-mail: philippe.humbert@univ-fcomte.fr

J.-M. Sainthillier
Skinexigence, Besançon, France
e-mail: jmsainthillier@skinexigence.com

S. Mac-Mary
Skinexigence SAS, Bioparc, Besançon, France
e-mail: smac@skinexigence.com

T. Lihoreau
Center for Research and Studies on the Integument (CERT), Department of Dermatology, Clinical Investigation Center (CIC INSERM 1431), Besançon University Hospital; INSERM UMR1098, FED4234 IBCT, University of Franche-Comté, Besançon, France
e-mail: tlihoreau@chu-besancon.fr

F. Fanian
Center for Study and Research on the Integuments, Department of Dermatology, University Hospital of Besançon, Besançon, France
e-mail: ferial.fanian@chu-besancon.fr; ferial.fanian@cert-besancon.com; fanian@gmail.com

P. Humbert et al. (eds.), *Agache's Measuring the Skin*,
DOI 10.1007/978-3-319-32383-1_60

A. Jeudy
Research and Studies Center on the Integument (CERT); Clinical Investigation Center (CIC BT506), Department of Dermatology, Besançon University Hospital, Besançon, France
e-mail: ajeudy@chu-besancon.fr

L. Li
Department of Dermatology, West China Hospital, Sichuan University, Chengdu, China

Keywords
Skin microcirculation • Capillaroscopy • Nailfold capillaroscopy

1 Introduction

Capillaroscopy is based on optical microscopy in vivo and designed to visualize superficial microvessels, i.e., arterioles (<300 μm), capillaries, and venules (Rhodin 1981). Although used in the study of the connective tissue, the retina, and the lingual and labial mucosae (Davis and Landau 1966; Merlen 1980), the main application fields of capillaroscopy are the skin and the nails. Skin capillaroscopy can be associated with sophisticated methods to analyze the blood flow speed, the capillary pressure, and the concentration of a fluorescent tracer, thus allowing accurate physiological and pharmacological investigations in humans (Table 1). However the straightforward morphological analysis of the superficial dermal capillary network provides a precise and non-traumatic assessment of various diseases involving microvessels; it is therefore nowadays the most widely used technique to study microcirculation in human clinics.

Table 1 Noninvasive bioengineering techniques used to study skin microcirculation

Skin temperature measurements
Capillaroscopy
Dynamic capillaroscopy
Dynamic capillaroscopy with dye
Laser Doppler flowmetry
Isotope techniques (^{133}Xenon)
Transcutaneous measurement of partial oxygen pressure
Capillary pressure
Photo pulse plethysmography
Infrared thermography
Colorimetry
Photoacoustic tomography
Optical coherence tomography
Laser Speckle contrast imaging
Tissue viability imaging
Hyperspectral imaging

Its principle is easy. After skin transparency has been enhanced, an optical magnifying system allows to visualize directly through the epidermis, the skin subepidermal microvasculature.

2 The Skin Subepidermal Microvasculature

The skin microvasculature comprises two horizontal plexuses, one located 1–1.5 mm below the skin surface and the other at the dermal-subcutaneous junction that mostly comprises collecting veins. Only the first one can be looked at using capillaroscopy. Arterioles rise from the deeper layers and divide into many capillary loops at the subepidermal level (Rhodin 1981; Braverman 2000). Then, the loops converge into collecting venules of the subepidermal plexus. The vascular network of the skin varies considerably from one area to another (Bongard and Bounameaux 1993; Miniati et al. 2001) (see ▶ Chap. 48, "Skin Blood Flow: Histophysiology").

Different functions are devolved to microcirculation in general and to the skin microcirculation particularly (Table 2). Tissue nutrition is its main function, besides metabolic exchanges, homeostasis of the interstitial fluid, blood pressure regulation, and thermoregulation. Thus, it may be considered that the skin microcirculation is composed of two functionally vascular beds: the thermoregulatory one which contributes 85 % of the total blood flow in the skin and the nutritive one contributing up to 15 % of the total blood flow, and that is mainly represented by the capillaries (see ▶ Chap. 48, "Skin Blood Flow: Histophysiology"). Both functional domains at their subepidermal level can be investigated by capillaroscopy.

Table 2 Main functions of the skin microcirculation

Metabolic exchanges and nutrition
Homeostasis of the interstitial fluid
Regulation of blood pressure
Thermoregulation

3 Biomicroscopes and Binocular Magnifying Glasses

The optical devices used are mainly stereomicroscopes (Carpentier 1999) or binocular magnifying glasses with the following requirements (Maricq 1981):

- Lighting is incident (epi-illumination), as powerful as possible for improved visualization, lateral because low-angled incidence increases contrast, and in cold light to avoid vasodilatation artifacts.
- The magnification varies from ×15 to ×100, but the features of diagnostic interest, especially the capillary network distribution, are easier to analyze using a low magnification; its panoramic vision also allows comprehensive and faster examination.
- The field depth is important, because it controls the sharpness of the capillary images since they are never exactly on a same plane.
- Several-centimeter frontal distance (objective-object) enables to examine uncooperative subjects or subjects with palmar retractions (for nail capillaroscopy) or with protruding lesions.
- The skin is prepared with the application of a drop of immersion oil. Sometimes, when its thickness remains a problem, the horny layer may be slightly stripped using adhesive tape.
- Microscope images can be collected by a camera or video camera.

4 Capillaroscopy (Humbert et al. 2006)

Among the different techniques available (Carpentier 1999; Allen et al. 2014) to study skin microcirculation, human skin capillaroscopy, a specialized form of intravital microscopy, is a method that allows direct visualization of the capillary network in vivo. Its principle is easy. After skin transparency has been enhanced by a drop of oil, an optical magnifying system allows visualization of its vascular network directly through the skin.

The optical devices used to examine the cutaneous capillaries in vivo are most of the time the light microscope and stereomicroscope (Carpentier 1999) but also the videocapillaroscope.

4.1 Contact Videomicroscopy

Videocapillaroscopy (Fig. 1) tends to replace the more conventional capillaroscopy. Contact videomicroscopy devices, appeared initially in the industry for nondestructive control processes, are now commercially available for skin

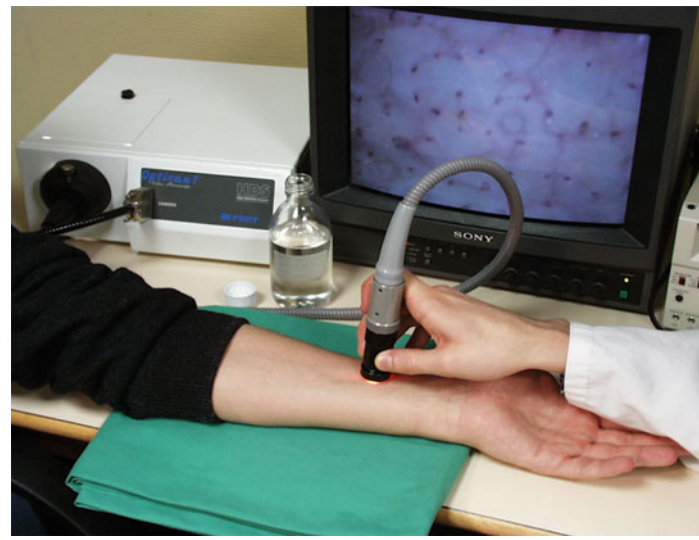

Fig. 1 Contact videocapillaroscopy with monitoring on TV. Videomicroscope Optican high-definition system (FORT ZI de la Gaudrée, 91415 Dourdan, France). Videotape recorder: SVO 9500 MDP Sony (Shinagawa, Ko Tokyo sp, Japan). Monitor: Sony PVM 1440 QM Japan. The ×200 magnification displays a 1.73 mm^2 area (Laboratory of Engineering and Cutaneous Biology, Besançon)

examination. They require epi-illumination of the skin surface (Jairo and Monari 2000) and image transmission to a video camera via the optics of a microscope. Their main characteristics are:

- The sensor is located at one end of a flexible cord which easily allows investigation of any skin site.
- The sensor is in contact with the skin, optical fibers conveying illuminating light.
- Lighting is provided by the handheld probe; it can therefore be accurately positioned in order to avoid specular reflection.
- The oil can be replaced by a thin layer of ultrasound gel.
- Images are displayed on a screen.
- Image computerization can be done during the examination; therefore the data quality can be controlled at once – the cost is currently equivalent to that of traditional microscopes.

The video imaging systems (Scopeman®, Microvision®, Microwatcher Model VS-10® (**commercially available equipment**: CapiFlow®, CapiFlow AB, Kista, Sweden; OP-120, Optilia Instruments AB, Sollentuna, Sweden; CapXview HD, Xport technologies, Craponne, France ; VideoCap, DS Medica, Milan, Italie ; CapiScope, KK Technology, Honiton, England; Scopeman Microtech, Mendota, UK; Microwatcher Model VS10, Mitsubishi Kasei Corp, Tokyo, Japan)) consist of a video signal control unit and a mini CCD camera. Flexible optical fibers convey an intense illuminating light to the dome cap of the camera head. A manually adjusted focusing system coupled with the camera head allows to obtain a sharp image of the capillary network. Magnification ranges from $\times 100$ to $\times 1000$. A magnification higher than $\times 600$ enables visualizing blood cells into the capillary. Venous congestion increases the number of capillaries detected. The video signal is then transformed into RGB images or recorded on videotape. Every picture can then be saved in a standardized image file format.

4.2 Periungual Capillaroscopy

Nailfold capillaroscopy (Figs. 2 and 3) is usually performed in order to search for capillary deformations, characterizing a pathological situation. In this area, capillaries lie in a horizontal plane, so that a large part of their loops can be observed. They have a special feature: loops are parallel and oriented toward the extremity of the finger. They look like hairpin bends with a diameter of 6–15 μm, and they flow in a more or less straight line. They are lined up in several rows. Capillaroscopy does not provide observation of the walls of the capillary, but of the erythrocytes column. Therefore only the capillaries which are functional during the study are visible. Some particular aspects of the capillary loops allow to

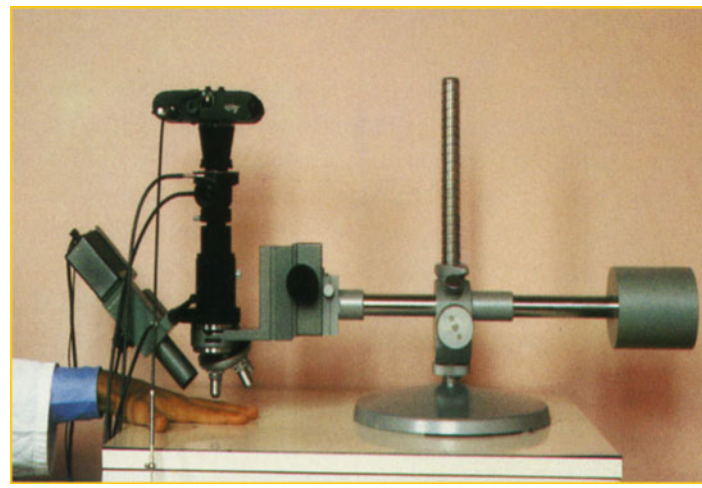

Fig. 2 Capillaroscopy equipment for the nailfold area analysis. Nikon SMZ system (Laboratory of Engineering and Cutaneous Biology, Besançon)

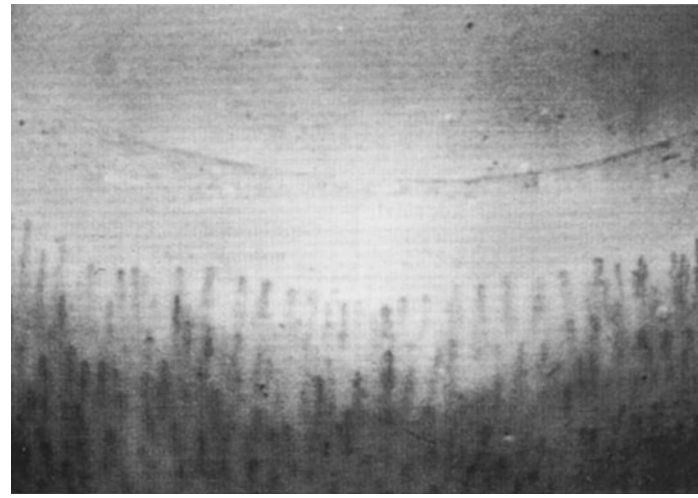

Fig. 3 Nailfold capillaroscopy: normal subject

detect some systemic conditions such as progressive systemic sclerosis and lupus erythematosus. Raynaud's phenomenon is the typical condition where capillaroscopy is of paramount importance because the capillary loop feature is often specific or predictive for a systemic disease. Thus, morphological abnormalities must systematically be looked for on all accessible fingers.

- Red blood cell extravasations produce brown deposits which move toward the epidermal edge in successive waves; these microhemorrhages show capillary malfunction which may be connected with microangiopathy or intense vasomotor storms or traumas.
- Meandering or little ramified capillaries (minor dystrophies) have no precise pathological significance, whereas the existence of many richly ramifying loops (like ferns or bushes) indicates capillary neogenesis suggesting vasculitis or connective tissue disease without pointing to more accurate diagnosis.
- An interesting feature is the existence of giant capillaries (over 50 μm diameter, five times the normal size), associated with heterogeneous decrease in capillary density and disorganization of the loop distribution. Such image is the hallmark of the so-called connective tissue diseases, evoking especially systemic sclerosis (Table 3), dermatomyositis, and conditions evolving into a scleroderma (Sharp and CREST syndromes) (Table 4). This feature, which occurs early in the course of the diseases, can be used in decision making (Carpentier and Maricq 1990; Maricq et al. 1980, 1982) (Fig. 4) and justifies periungual capillaroscopy in all cases of Raynaud's phenomenon (Maricq et al. 1982; Blockmans et al. 1996; Priollet et al. 1987).
- Moderate dilatations without rarefaction may hint to a moderate acrocyanosis which further on may typically show an important stasis in the venous limb inducing its sausage-like dilatation (monitoring may be needed while warming).
- Less frequent morphological variants may be of prognosis value. In systemic sclerosis with bad prognosis, capillaroscopy may show capillary destruction, rarefaction, and disorganization, but sometimes reactive

Table 3 Sensitivity and specificity of periungual capillaroscopy in the diagnosis of systemic scleroderma (From Carpentier and Maricq 1990)

	Sensitivity (%)	Specificity (%)
Maricq	84	98
Vayssairat	95	92
Carpentier	97	89
Houtman	–	92
Joyal	83	97
Jouany	97	83
Blockmans	85	93

Table 4 Prognostic value of the periungual capillaroscopy in an apparently isolated Raynaud's phenomenon (From Carpentier and Maricq 1990)

	Number of patients	Follow-up (years)	Incidence percentage of scleroderma	
			Normal capillaroscopy	Scleroderma pattern
Maricq (1983)	51	2.8	4.0	57
Priollet (1987)	73	4.7	1.9	65
Fitzgerald (1988)	58	2.7	4.8	60
Weiner (1991)	77	4.0	7.9	76

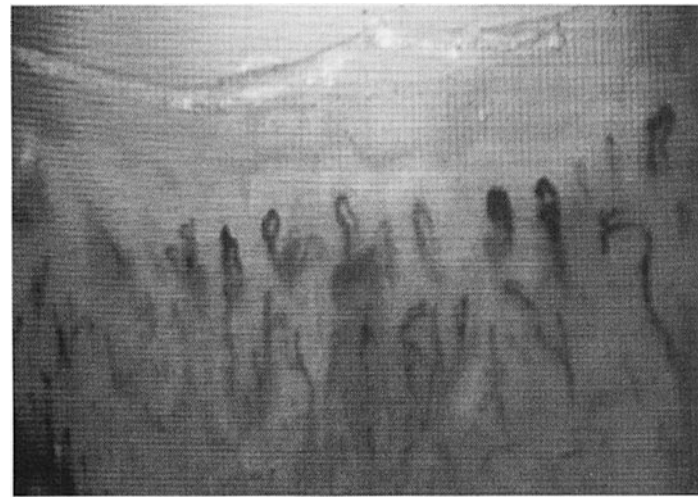

Fig. 4 Nailfold capillaroscopy: dilated capillaries with heterogeneous distribution

neogenesis with ramifications prevails over dilatation. Numerous megacapillaries are often found in limited and less progressive forms (Maricq et al. 1983; Lamboba et al. 2010).

4.3 "Any Site" Capillaroscopy

The availability of videomicroscopes together with advances in our knowledge about the importance of microcirculation in the pathogenesis of trophic complications of arterial and venous insufficiencies explains the present development of capillaroscopy on the skin.

4.3.1 Qualitative Capillaroscopy

Different architectural frameworks are found in the various skin body areas (Table 5). They might be related to the different epidermal thickness and microvasculature arrangements (Miniati et al. 2001). Parallel arrangement is observed in areas where the skin is thinner. On the opposite, perpendicular arrangement is observed on thicker skin areas.

Normal architectural framework shows two main patterns, a parallel and a perpendicular arrangement of capillary loops with respect to the skin surface. Capillaries with a parallel arrangement constitute the vascular network with meshes. These meshes can be regular or not. In most of skin body areas, loops are perpendicular to the skin surface, so that only the top can be seen. It looks like a point or a comma (Fig. 5). Capillary diameters vary from 15 to 20 μm in regions with parallel arrangement. The density ranges from 14 to 30 capillary loops per mm^2 in skin regions where loops are arranged perpendicular to the skin surface (Miniati et al. 2001). Both diameter and density variations are important in assessing the severity of arterial and venous diseases. Capillaroscopy possible clinical application seems therefore to increase considerably (Prasad et al. 1995).

Table 5 Different architectural frameworks of skin capillary network (Miniati et al. 2001)

Parallel arrangement and regular meshes network	Parallel arrangement with irregular meshes network	Perpendicular arrangement and regular dot line	Perpendicular arrangement and irregular dot line	Special pattern with parallel arrangement
Forehead	Trunk (anterior and posterior aspects)	Fingertip	Palm of hands	Fingernail fold
Cheekbone region		Eminencia tenar	Back of the hand and the foot	Labial mucosa
Cheek	Breast	Eminencia hipotenar		
Chin	Arms (external surface)	Tip of toes	Nipple	
Internal surface of arms	Legs (internal and external surfaces)			

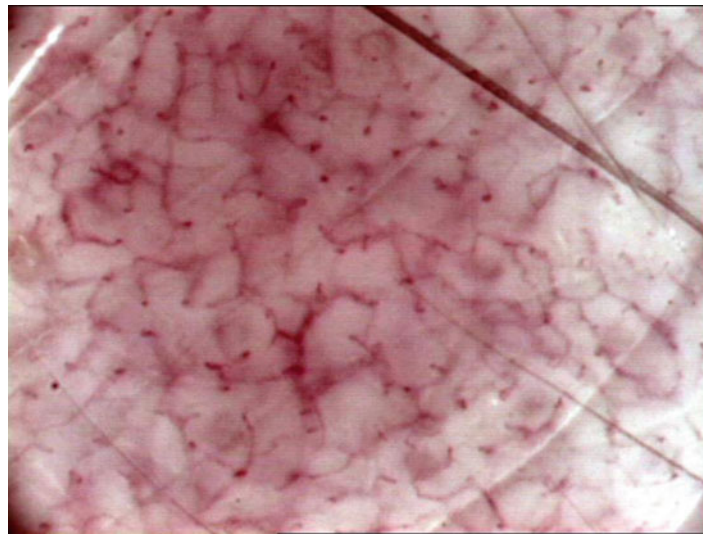

Fig. 5 Capillary network observed by videocapillaroscopy (volar forearm). *Dark red dots* are the tops of papillary loops. Below them, out of focus, the superficial part of the subepidermal vascular plexus is seen, where loops are inserted (magnification ×100)

5 Capillaroscopy and Systemic Diseases

Capillary network analysis in the volar aspect of the forearm, or in the fingers, could be of interest in **arterial hypertension**. It has been suggested that capillary rarefaction may be associated with the genesis of primary hypertension as it has been described in various tissues from patients with essential hypertension. A 15–20 % reduction in capillary density was found in nailfold capillaroscopy, and intravital fluorescein angiography found a 20 % reduction in capillary density in the forearm skin of hypertensive subjects compared with normotensive subjects (Prasad et al. 1995). Several other conditions such as peripheral arterial occlusion disease, lower limb venous insufficiency, diabetes mellitus, and psoriasis (Table 6) are serious candidates for subepidermal microcirculatory evaluation. Videocapillaroscopy is mainly performed on the instep in venous insufficiency and on the dorsum foot (first inter-metatarsal space and toes) in arterial insufficiency. **Venous insufficiency** is characterized by a decrease in capillary density, widening of dermal papillae the size of which becomes heterogeneous, and the contours marked by

dermite ocre hemosiderin deposits. The decrease in the capillary density is partially compensated for by their increased length, inducing an increased number of meanders, which can even take the shape of a glomerular cluster in the most severe forms (lipodermatosclerosis, white atrophy). As soon as the first trophic troubles occur, the venules are not visible any longer (Fig. 6) (Fagrell 1995a; Franzeck et al. 1984; Stucker et al. 1995).

In **arterial insufficiency**, Fagrell has described three classes of increasing severity and validated their discriminating value for the local trophic prognosis (Fagrell et al. 1984; Bollinger and Fagrell 1990):

(A) Capillary dilatation
(B) Edema impairing capillary visualization
(C) Absence of visible capillary (pre-necrosis stage)

Qualitative capillaroscopy is mainly used for the morphological information it provides, and it is superior to indirect techniques (laser Doppler, transcutaneous PO_2) because it is free from interpretation artifacts, a considerable advantage in a field as complex as microcirculation. However the absence of quantification and the subjective and operator-dependent character of capillaroscopy show its limitations, but they are about to be overcome with image analysis techniques which currently allow the development of quantitative capillaroscopy.

Table 6 Pathological or cosmetic usefulness of videocapillaroscopy

Peripheral arterial obliterative disorders (Fagrell 1995b)	Specific morphological changes
Venous insufficiency (Fagrell 1995b)	Rarefaction and dilatation of the capillary loops
Diabetes mellitus (Chang et al. 1997)	Tortuous and dilated capillaries
Hypertension (Serne et al. 2001)	Capillary rarefaction
Psoriasis (Bull et al. 1992)	Grossly dilated and tortuous capillaries
	Many more perfused capillaries
Aging (Priollet et al. 1987; Kelly et al. 1995)	Reduced dermal papillary loops
Effects of topical cosmetics or chemical agents	

6 Capillaroscopy and Smoke

Smoking induces morphological changes of capillary loops which become more tortuous but also loads to a decrease in capillary loop number in the face (Petitjean et al. 2006a). It has to be related to a decrease of the radiance in smokers (Petitjean et al. 2006b).

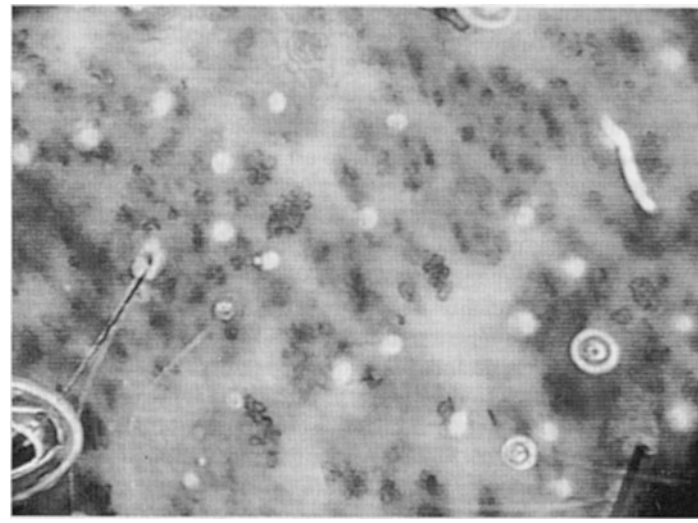

Fig. 6 Lower limb venous insufficiency: dilated loops and heterogeneous distribution

7 Age-Related Changes of the Cutaneous Microcirculation

A significant decrease in cutaneous capillary loop density is observed with age. The microvasculature is regularly formed in young skin, with many orderly arranged capillary loops (dots) and some horizontal vessels (lines) (Li et al. 2004). It becomes thicker, twisted, and irregular in older skins, with horizontal vessels that appear tortuous, elongated, disorganized, and dilated (Zhu V. Assessment of cutaneous microvasculature in aging and photoaging: a videocapillaroscopic study on Caucasian women. Personal data). Thus, the parallel vasculature can be more easily observed with aging. The result accords with that of biopsy specimens observed by light or electric microscope. As the epidermis becomes thinner, the transparency of the skin increases, facilitating the observation of the papillary vascular plexus. And as the vasculature expands and thickens, some of the microvasculature usually difficult to observe and the deeper vasculature can also be examined.

The capillary loops in the dermal papillae decrease but the subpapillary plexus increase with age (Li et al. 2006a). A marked site and age effect on the skin microcirculation has been demonstrated (Li et al. 2006b). The density of capillary loops in old people decrease by 40–70 % compared with young, whereas the vascular length increases by 35–150 %. Besides the capillary density in the back of the hand is four times higher than in the crow's feet. The vascular length in the crow's feet is three times longer than in the back of the hand.

8 Pharmacological Inhibition of the Dermal Microcirculation

A pharmacological agent such as Neo-Synephrine is able to induce dermal capillary density reduction after topical application (Degouy et al. 2002; Sainthillier et al. 2002). In this case, videocapillaroscopy is a reliable tool to quantify in vivo the capillary loop density in the dermis before and after the application of the solution. This pharmacological model could be useful to evaluate the effects of different cosmetic or drug agents able to inhibit the dermal adrenergic response in dermis.

9 Morphometry and Capillary Densitometry In Vivo

9.1 Imaging and Pattern Analysis

Automated morphometry in nailfold capillaroscopy is now available, based on the association of numerical image analysis with videomicroscopy (Michoud et al. 1994). The technique is quickly progressing in its processing capacities while its cost is reducing. The systems currently developed for skin microcirculation allow the automatic quantification of diameters, lengths, areas, and capillary densities; it is therefore possible to obtain very discriminating parameters for the diagnosis of connective tissue diseases while comparative follow-up is facilitated (Michoud et al. 1994).

9.2 Geometrical Capillary Network Analysis (Humbert et al. 2006)

In any body site quantitative capillaroscopy is made possible due to the development of computerized systems. Capillary position, size distribution and density, intercapillary distance, and volume fraction can be extracted from the images (Hern and Mortimer 1999; Sainthillier et al. 2003) (Figs. 7 and 8). An automated counting of capillaries is also available. Zhong et al. described a method to describe the capillary network by using image processing and Delaunay triangulation (Fig. 9) (Zhong et al. 2000). Since recent years have witnessed a strong resurgence of interest in the field on neural networks, we can imagine neural architectures for treating capillary distribution in the skin. Accordingly the efficiency of using auto-associative memory to detect and store quantitative capillary features is under investigation in some laboratories, while capillary networks are tentatively built up using capillary coordinates computed by the neural system (Sainthillier et al. 2005).

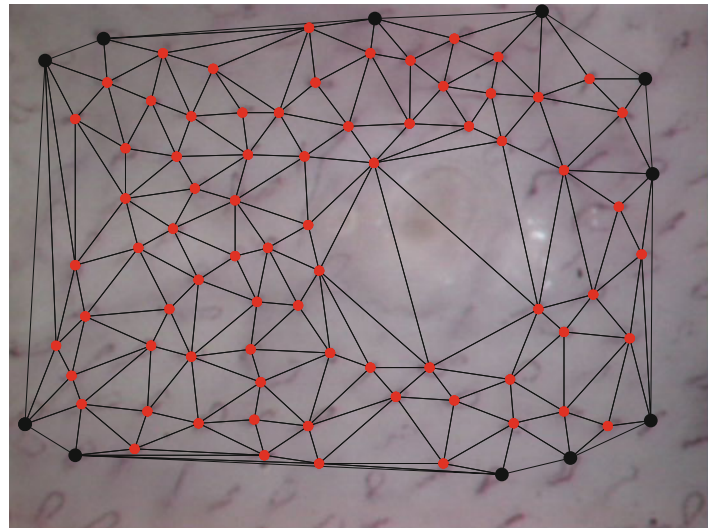

Fig. 7 Example of Delaunay triangulation applied to an image with noise (scalp, 1.52 × 1.14 mm^2, objective × 200). The red dots mark the detected capillaries, the black dots the capillaries located on the convex envelop. An artefact without capilliaries is visible at the centre, it loosens the structure of the network in this area

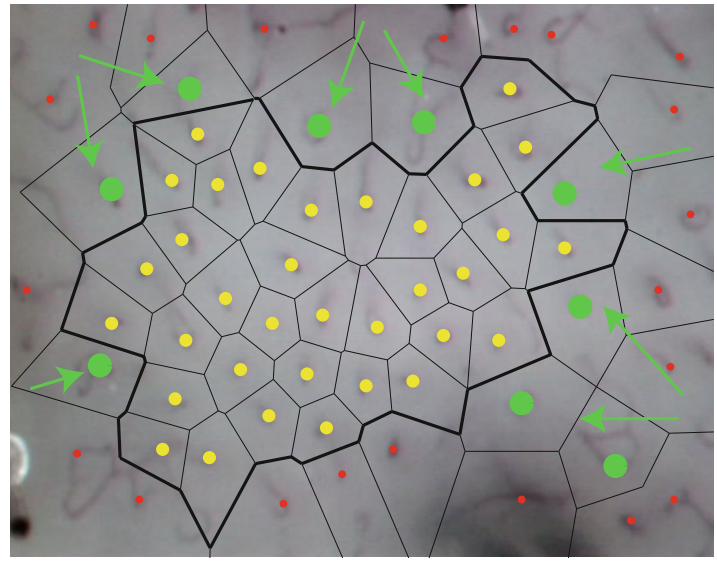

Fig. 8 Example of Voronoi diagram (scalp, 1.524 × 1.14 mm^2, objective × 200). Each polygonal cell is defined by a set of dots that are closer to the centre of the cell than any other dot in the diagram. The green arrows indicate the polygons eliminated from the calculation of surface (after normalisation of the distribution of the surfaces)

10 Capillary Hemodynamics

As far as clinical research is concerned, some capillaroscopy techniques have dealt with a quantitative approach of capillary hemodynamics.

10.1 Capillary Pressure Measurement

The direct measurement of the capillary pressure is possible with a micropipette controlled by a micro-manipulating device; the examined finger is carefully attached in order to avoid any movement. The measured pressure is that of the counterpressure that has to be exerted to avoid the return of the capillary red blood cells toward the micropipette. Instantaneous pressure can therefore be recorded on a simple water column, but a device has been developed which allows the recording of the pressure variations according to the weather using a servo control system based on the electrical resistance

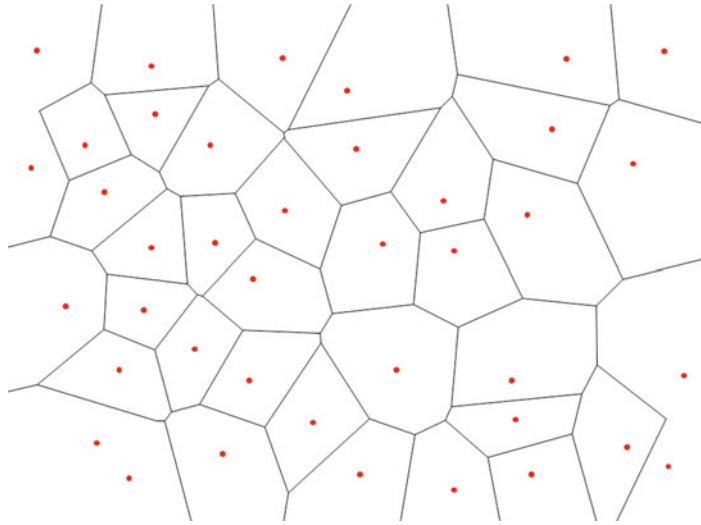

Fig. 9 The Voronoi diagram is a partition of the space into polyhedrons. Each polyhedron, called the Voronoi cell, is defined as the set of points which are closer to the center of the cell than to any other point in the diagram. The set of all Voronoi cells and their faces forms a cell complex. The verticals of this complex are called the Voronoi verticals, and the peripheral unbounded edges are the Voronoi rays. In this two-dimensional image each capillary barycenter is considered as the center of a polygon (Laboratory of Engineering and Cutaneous Biology, Besançon)

variations of the micropipette associated with blood inflow. This "servo-nulling system" (IPM®) enabled Mahler to show persistent synchronous oscillations of the arterial pulses at capillary level (Bollinger and Fagrell 1990). These techniques have been applied by Tooke's team also; they studied the influence of the skin temperature and position on the capillary pressure (Bollinger and Fagrell 1990). They have also shown the existence of a dysregulation of the skin capillary pressure in diabetic patients (Tooke 1995). The use of these techniques is rare because they require a sophisticated equipment, a great skill, a lot of experience, and the subjects' full cooperation.

10.2 Red Blood Cell Speed Assessment

Videocapillaroscopy (such as IPM®) has shown the heterogeneity of the capillary content (red blood cell aggregates, leukocytes, and plasmatic gaps and their moves along the blood flow). The optical density variations with time can be recorded in different points of the capillary loop, and by image cross correlation it has been possible to calculate the time necessary for the red blood cells to go from one point to the other and deduce their average speed.

CapiFlow® is a software permitting a direct and noninvasive assessment of blood cell velocity in single capillaries. The microscope is coupled with a television set up and a higher magnification (250–1000×) is needed than for videocapillaroscopy. So, one can easily observe blood cell aggregates in the lumen of the capillary loops. These aggregates are separated by plasma gaps. Obtaining a good, sharp, and contrasted picture is needed, and a relatively long straight portion (>40 μm) of the capillary loop has to be observed. The method requires very good optical quality images obtained with high magnification and without interfering movements and seemingly can only be used on periungual areas. It has allowed Fagrell's group to study vasomotion and post-ischemic reactive hyperemia at capillary level, in healthy subjects and in various diseases: arteritis, diabetes, and myeloproliferative syndromes (Bollinger and Fagrell 1990; Fagrell 1985; Hahn et al. 1998).

The technique called "flying spot" is simpler and consists in generating a virtual image moving

parallel to a capillary and controlling its speed while recording a capillary flow sequence. The red blood cell speed is then that of the virtual object; it is therefore an operator-dependent technique; however it can be used with average quality images (Boss et al. 1987).

11 Capillaroscopy and Fluorescent Tracers

Common capillaroscopy methods use the natural contrast produced by hemoglobin. As seen earlier, they do not visualize the capillary wall, but only the red blood cells that cast the vessel. Thus, only functional capillaries can be detected. But the column of red blood cells is most of the time separated from the vessel wall by a non-negligible plasma layer, even in periungual capillaries. Some capillaries may even be filled with plasma only, as in cases of hyperviscosity syndromes or vasoconstrictive episodes. The use of fluorescent products with plasmatic diffusion has permitted to visualize and measure the actual vessel diameter (Lamah et al. 1996). Furthermore the transcapillary diffusion of fluorescent tracers could also be quantified by videodensitometry. These techniques have mainly been developed, in humans, by Bollinger's group in Zurich. They used fluorescent tracers, mainly Na-fluorescein, which require a fluorescence microscope, that is to say with a system of mercury vapor illumination and a system of appropriate excitation and absorption filters (Bollinger and Fagrell 1990; Bollinger et al. 1982).

The more usual method uses intravenous injection of 0.02 ml/kg 20 % sodium fluoresceinate, a compound widely used in ophthalmology. The compound diffuses more or less quickly through the skin capillary wall. The technique has been used to quantify the transcapillary exchanges of small molecules. Plasma-perfused capillaries are delineated allowing the calculation of several perfusion indices (Carpentier and Maricq 1990). More invasive, because of the necessity to perform an intravenous injection, this technique improves greatly the detection of pathological abnormalities of the nutritional network. Diffusion was found increased in diabetes and systemic sclerosis (Fig. 10) (Bollinger and Fagrell 1990; Bollinger et al. 1982, 1986). Troubles resulting from endothelial damage have also been evidenced in lower limb chronic ischemia of arterial origin and in vasculitis.

The dextran FITC of molecular weight 150,000, injected intradermally, is resorbed by the lymphatic system and can therefore visualize its more superficial elements. The visualization of the small lymphatic canals has given information about their hydrodynamics (pressure, speed) with the

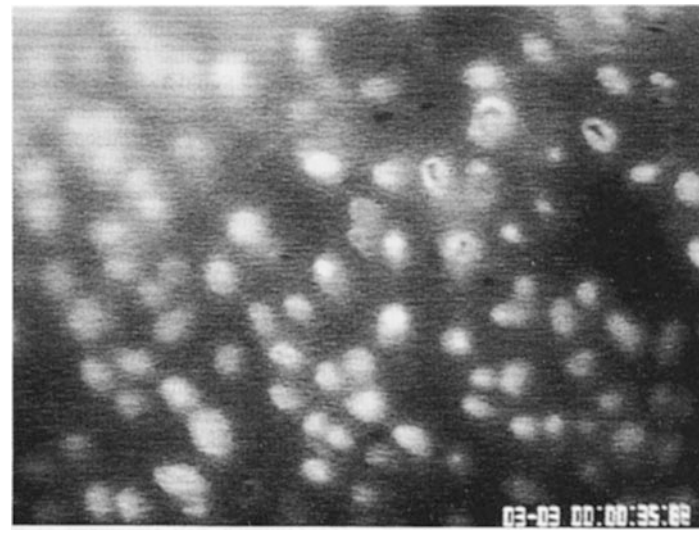

Fig. 10 Fluorescence capillaroscopy in a patient with systemic sclerosis. Large perivascular halo

abovementioned techniques used in blood capillaries (Bollinger et al. 1989; Franzeck et al. 1993; Mellor and Mortimer 2004).

The use of indocyanine green, which binds to albumin, explores the permeability to macromolecules. It has allowed to measure the capillary dimensions with accuracy and showed the existence of microaneurysms undetected by classic capillaroscopy. This technique requires infrared videomicroscopy. All these techniques remain in the field of research, as the innocuousness of compound injection has not been proved yet.

12 Conclusion

The determination of morphological or dynamic changes in the cutaneous microcirculation is one of the main objectives of the noninvasive biometrology techniques. As far as subepidermal microvasculature is concerned, capillaroscopy is both the oldest and the simplest one, while also the soundest as it is based on a visual and direct observation. Recent progress has made it available for any skin site, which is of major importance in dermatology and cosmetology. Thus, every capillary modification due to topical cosmetic products or chemical agents can be observed from now. In pathology, numerous are the conditions that can be examined with this new system. Hence, it is now being used routinely in most hospitals and companies. Furthermore capillaroscopy is becoming a quantitative tool, which will enhance its potential and foster its use both in research and clinical practice. Accordingly it is in the verge to serve as an irreplaceable way of studying the physiology and pathophysiology of the skin capillary circulation in health and disease.

References

Allen J, Howell K. Microvascular imaging: techniques and opportunities for clinical physiological measurements. Physiol Meas. 2014;35:R91–R141.

Blockmans D, Beyens G, Verhaeghe R. Predictive value of nailfold capillaroscopy in the diagnosis of connective tissue diseases. Clin Rheumatol. 1996;15:148–53.

Bollinger A, Fagrell B. Clinical capillaroscopy. Toronto: Hogrefe et Huber Ed; 1990.

Bollinger A, Jager K, Geser A, Sgier F, Seglias J. Transcapillary and interstitial diffusion of Na-fluorescein in chronic venous insufficiency with white atrophy. Int J Microcirc Clin Exp. 1982;1:5–17.

Bollinger A, Jager K, Siegenthaler W. Microangiopathy of progressive systemic sclerosis: evaluation by dynamic fluorescence videomicroscopy. Arch Intern Med. 1986;146:1541–5.

Bollinger A, Pfister G, Hoffmann U, Franzeck UK. Fluorescence microlymphography in chronic venous incompetence. Int Angiol. 1989;8:23–6.

Bongard O, Bounameaux H. Clinical investigation of skin microcirculation. Dermatology. 1993;186:6–11.

Boss C, Schneuwly P, Mahler F. Evaluation and clinical application of the flying spot method in clinical nailfold capillary TV-microscopy. Int J Microcirc Clin Exp. 1987;6:15–23.

Braverman IM. The cutaneous microcirculation. J Invest Dermatol. 2000;5:3–9.

Bull RH, Bates DO, Mortimer PS. Intravital video-capillaroscopy for the study of the microcirculation in psoriasis. Br J Dermatol. 1992;126:436–45.

Carpentier PH. Méthodes d'exploration vasculaire chez l'homme : microcirculation et veines. Therapie. 1999;54:369–74.

Carpentier PH, Maricq HR. Microvasculature in systemic sclerosis. Rheum Dis Clin N Am. 1990;16:75–91.

Chang CH, Tsai RK, Wu WC, Kuo SL, Yu HS. Use of dynamic capillaroscopy for studying cutaneous microcirculation in patients with diabetes mellitus. Microvasc Res. 1997;53:121–7.

Davis E, Landau J. Clinical capillary microscopy. Springfield: Thomas Ed; 1966.

Degouy A, Creidi P, Sainthillier JM, Marsault D, Muret P, Montastier C, Hirt JP, Besne I, Breton JL, Gharbi T, Humbert P. *In vivo* transcutaneous capillaroscopy: assessment of dermal capillary density decrease after topical pharmacological agent applications. Ann Dermatol Venereol. 2002;129:1S451–2 (Abstract).

Fagrell B. Dynamics of skin microcirculation in humans. J Cardiovasc Pharmacol. 1985;7 Suppl 3:S53–8.

Fagrell B. Vital microscopy and the pathophysiology of deep venous insufficiency. Int Angiol. 1995a;14:18–22.

Fagrell B. Advances in microcirculation network evaluation: an update. Int J Microcirc. 1995b;15 Suppl 1:34–40.

Fagrell B, Hermansson IL, Karlander SG, Ostergren J. Vital capillary microscopy for assessment of skin viability and microangiopathy in patients with diabetes mellitus. Acta Med Scand Suppl. 1984;687:25–8.

Franzeck UK, Bollinger A, Huch R, Huch A. Transcutaneous oxygen tension and capillary morphologic characteristics and density in patients with chronic venous incompetence. Circulation. 1984;70:806–11.

Franzeck UK, Haselbach P, Speiser D, Bollinger A. Microangiopathy of cutaneous blood and lymphatic capillaries in chronic venous insufficiency (CVI). Yale J Biol Med. 1993;66:37–46.

Hahn M, Heubach T, Steins A, Junger M. Hemodynamics in nailfold capillaries of patients with systemic scleroderma: synchronous measurements of capillary blood pressure and red blood cell velocity. J Invest Dermatol. 1998;110:982–5.

Hern S, Mortimer PS. Visualization of dermal blood vessels: capillaroscopy. Clin Exp Dermatol. 1999;24:473–8.

Humbert P, Sainthillier JM, Mac-Mary S, Petitjean A, Creidi P, Gharbi T. Capillaroscopy and videocapillaroscopy assessment of skin microcirculation: dermatological and cosmetic approaches. In: Serup J, Jemec GBE, Grove GL, editors. Handbook of non-invasive methods and the skin. 2nd ed. Boca Raton: Taylor & Francis; 2006. p. 679–87.

Jairo J, Monari M. Human capillaroscopy by light emitting diode epi-illumination. Microvasc Res. 2000;59:172–5.

Kelly RI, Pearse R, Bull RH, Leveque JL, de Rigal J, Mortimer PS. The effects of aging on the cutaneous microvasculature. J Am Acad Dermatol. 1995;33:749–56.

Lamah M, Chaudhry H, Mortimer PS, Dormandy JA. Repeatability of intravital capillaroscopic measurement of capillary density. Int J Microcirc Clin Exp. 1996;16:23–9.

Lamboba S, Muller-Ladner U. Capillaroscopic pattern in systemic sclerosis - an association with dynamics of processes of angio- and vasculogenesis. Microvascular Res. 2010;80:534–9.

Li L, Mary S, Sainthillier JM, Degouy A, Gharbi T, De Lacharriere O, Humbert P. Changes of cutaneous microcirculation in the different anatomic sites with aging in women. Chin J Microcirc. 2004;2:43–5.

Li L, Mac-Mary S, Marsaut D, Sainthillier JM, Nouveau S, Gharbi T, de Lacharrière O, Humbert P. Age-related changes in skin topography and microcirculation. Arch Dermatol Res. 2006a;297:412–6.

Li L, Mac-Mary S, Sainthillier JM, Nouveau S, de Lacharrière O, Humbert P. Age-related changes of the cutaneous microcirculation *in vivo*. Gerontology. 2006b;52:142–53.

Maricq HR. Wide-field capillary microscopy. Arthritis Rheum. 1981;24:1159–65.

Maricq HR, LeRoy EC, D'Angelo WA, Medsger Jr TA, Rodnan GP, Sharp GC, Wolfe JF. Diagnostic potential of *in vivo* capillary microscopy in scleroderma and related disorders. Arthritis Rheum. 1980;23:183–9.

Maricq HR, Weinberger AB, LeRoy EC. Early detection of scleroderma-spectrum disorders by *in vivo* capillary microscopy: a prospective study of patients with Raynaud's phenomenon. J Rheumatol. 1982;9:289–91.

Maricq HR, Harper FE, Khan MM, Tan EM, LeRoy EC. Microvascular abnormalities as possible predictors of disease subsets in Raynaud phenomenon and early connective tissue disease. Clin Exp Rheumatol. 1983;1:195–205.

Mellor R, Mortimer PS. Dermal lymphatics. In: Handbook of Measuring the skin. 1st edn. Berlin: Springer; 2004. p. 392–9.

Merlen JF. La capillaroscopie, moyen d'exploration fonctionnelle. Ann Med Nancy. 1980;19:189–95.

Michoud E, Poensin D, Carpentier PH. Digitized nailfold capillaroscopy. VASA. 1994;23:35–42.

Miniati B, Macchi C, Molino Lova R, Catini C, Gulisano M, Contini M, Conti AA, Gensini GF. Descriptive and morphometric anatomy of the architectural framework of microcirculation: a videocapillaroscopic study on healthy adult subjects. Ital J Anat Embryol. 2001;106:233–8.

Petitjean A, Mac-Mary S, Sainthillier JM, Muret P, Closs B, Humbert P. Effects of cigarette smoking on the skin of women. J Dermatol Sci. 2006a;42:259–61.

Petitjean A, Sainthillier JM, Muret P, Closs B, Gharbi T, Mac-Mary S, Humbert P. Effet du tabagisme chronique sur la microcirculation: étude par vidéocapillaroscopie. In: Uhoda E, Paye M, Piérard GE, editors. Actualités en ingénierie cutanée, vol. 4. Paris: ESKA; 2006b. p. 167–72.

Prasad A, Dunnill GS, Mortimer PS, MacGregor GA. Capillary rarefaction in the forearm skin in essential hypertension. J Hypertens. 1995;13:265–8.

Priollet P, Vayssairat M, Housset E. How to classify Raynaud phenomenon: long term follow-up study of 73 cases. Am J Med. 1987;83:494–8.

Rhodin JAG. Anatomy of the microcirculation. In: Effros RM, Schmid-Schöbein H, Ditzel J, editors. Microcirculation: current physiologic, medical and surgical concepts. New York: Academic; 1981. p. 11–7.

Sainthillier JM, Creidi P, Degouy A, Muret P, Montastier C, Hirt JP, Besne I, Breton L, Gharbi T, Humbert P. Topical application of a manganese gluconate preparation inhibits the effects of neosynephrin on the cutaneous microcirculation. Ann Dermatol Venereol. 2002;129:460. abstr.

Sainthillier JM, Degouy A, Gharbi T, Pieralli C, Humbert Ph. Geometrical capillary network analysis. Skin Res Technol. 2003;9:312–20.

Sainthillier JM, Gharbi T, Muret P, Humbert P. Skin capillary network recognition and analysis by means of neural algorithms. Skin Res Technol. 2005;11:9–16.

Serne EH, Gans RO, ter Maaten JC, Tangelder GJ, Donker AJ, Stehouwer CD. Impaired skin capillary recruitment in essential hypertension is caused by both functional and structural capillary rarefaction. Hypertension. 2001;38:238–42.

Shih TC, Zhang G, Wu CC, Hsiao HD, Wu TH, Lin KP, Huang TC. Hemodynamic analysis of capillary in finger nail-fold using computational fluid dynamics and image estimation. Microvascular Res. 2011;81:68–72.

Stucker M, Schobe MC, Hoffmann K, Schultz-Ehrenburg U. Cutaneous microcirculation in skin lesions associated with chronic venous insufficiency. Dermatol Surg. 1995;21:877–82.

Tooke JE. Microvascular function in human diabetes: a physiological perspective. Diabetes. 1995;44:721–6.

Zhong J, Asker CL, Salerud EG. Imaging, image processing and pattern analysis of skin capillary ensembles. Skin Res Technol. 2000;6:45–57.

Assessing Cutaneous Sensory Function and Vasomotor Responses

54

Parisa Gazerani, Thomas A. Nielsen, and Lars Arendt-Nielsen

Contents

Keywords
Skin • Sensory • Vasomotor • Cutaneous • Quantitative

1 Assessing Cutaneous Sensory Function

Noninvasive assessment of cutaneous sensory can be divided into three main categories:

- Quantitative assessment of ongoing clinical sensory abnormalities (e.g., itch, pain)
- Quantitative assessment of experimentally evoked cutaneous sensory responses for diagnosis and monitoring in the clinic
- Quantitative assessment of experimentally evoked cutaneous sensation for basic studies in healthy volunteers under normal conditions and conditions with experimentally induced cutaneous hyperexcitability (e.g., allokinesis, allodynia)

Quantitative sensory testing (QST) involves a large variety of stimulus modalities (thermal, mechanical, chemical, electrical) and assessment methods (psychophysics, electrophysiology, imaging, microdialysis). QST can provide an understanding of the mechanisms involved in sensory transduction, transmission, and perception under normal and pathophysiological conditions and hopefully provide mechanism-based diagnosis, prevention, and management of skin-related

P. Gazerani (✉) • T.A. Nielsen • L. Arendt-Nielsen
Department of Health Science and Technology, Faculty of Medicine, Center for Sensory-Motor Interaction (SMI), Aalborg University, Aalborg, Denmark
e-mail: gazerani@hst.aau.dk

P. Humbert et al. (eds.), *Agache's Measuring the Skin*,
DOI 10.1007/978-3-319-32383-1_61

disorders. Different QST protocols have been suggested for profiling patients (particularly in the area of pain), and the QST battery developed by the German Research Network on Neuropathic Pain is the one applied in most studies (Geber et al. 2011; Magerl et al. 2010; Maier et al. 2010). Briefly, the protocol assesses the function of small (thermal thresholds) and large (tactile and vibration thresholds) nerve fiber pathways and increased/decreased pain sensitivity (hyperalgesia, allodynia, hyperpathia, windup-like pain). The battery consists predominantly of cutaneous stimulus modalities but not including, e.g., itch and associated aspects such as allokinesis. The challenges for the future are to develop QST platforms adequate for children or elderly possible demented patients.

In QST studies, the focus and mind-set is often toward hyperexcitable responses, but it is important to focus both on "gain-of-sensory-function" and on "loss-of-sensory-function" as, e.g., hyperalgesia, analgesia, allodynia, and allokinesis.

Individual QST technologies for assessing sensory function can furthermore be used for drug profiling and for development of new therapies for, e.g., itch or pain.

A number of fundamental sensory mechanisms observed in animals have important implications, for which QST techniques should be developed and how they can be applied in human basic, clinical, and drug screening studies.

A variety of the sensory stimulation procedures may cause additional responses in association with the sensory responses. One such additional response is provocation of vasomotor reactions.

2 Assessing Provoked Vasomotor Reactions

Under physiological conditions, skin blood flow plays an essential role in thermoregulation. Proper and timely responses to heating and cooling due to, e.g., environmental changes control and maintain the body homeostasis. Cutaneous vasodilatation and vasoconstriction are the two key components of this thermoregulatory system. In humans, cutaneous circulation is under control of several systems including endothelial, adrenergic, and sensory systems. Several factors have been identified that alter function of these systems and malfunctioning result in different skin circulation disorders.

Application of direct local controlled heat on the skin promotes a transient vasodilation through an axon reflex that reaches to a plateau status. This phase is thought to be nitric oxide dependent and is followed by the die-away phenomenon, which is a slow reversal and has been shown to rely on intact sympathetic vasoconstrictor nerves. Barcroft and Edholm (1943) were first to test the effects of warming and cooling using a wide range of temperatures in human forearm skin. They found that blood flow reached its highest level at 42 °C, which was the maximum applied heat. They also reported a pattern following local heating that is mainly characterized by an early transient peak in skin blood flow, followed by a prolonged plateau phase and a return to blood flow levels of baseline over time. Their investigations provided a basis for later studies looking into possible involved mechanisms, e.g., how direct skin warming causes vasodilation. It has been known that direct warming of the skin causes a vasodilation that depends on several parameters, for instance, the degree of applied heat and that how fast the heat is being delivered (Hodges et al. 2009; Minson et al. 2001). Rapid application of local heat to 42 °C increases the skin blood flow to its maximum in the applied area (Minson et al. 2001; Johnson et al. 1986). This unique characteristic is perhaps due to the fact that at this temperature, cutaneous vascular smooth muscle is fully relaxed, and local warming to 42 °C is often used in experiment comparing blood flow measurement at different sites or different subjects (Kellogg et al. 1993). Several systems have an influence on the response pattern: the NO system, adrenergic nerves, and sensory nerves. Mechanisms underlying changes due to local warming have been reviewed elsewhere (Johnson and Kellogg 2010; Charkoudian 2010).

Based on the fact that local heat enhances blood flow in regional microcirculation and to some extent blood vessel permeability, this technique can be

used to facilitate drug transfer to the systemic circulation. Controlled heat application is a simple and noninvasive method that may improve transcutaneous drug delivery most likely through the enhancement of skin penetration of a topically applied medication or increasing of drug absorption.

Below, we highlight cutaneous vasomotor reactions in response to direct local controlled heat based on our findings through series of experiments in healthy humans. Although glabrous skin in the forearm has been the most commonly used site, various body regions have been tested in line with any potential sex-related difference that can alter response to direct local heating.

2.1 Paradigms of Direct Local Controlled Heat Application

Skin vasomotor responses in several different body regions of healthy men and women were recorded after application of direct local controlled heat (Gazerani and Arendt-Nielsen 2011). Different paradigms were applied (38, 41, and 43 °C, each for 15, 30, and 60 s) in forehead, forearm, dorsal hand, dorsal foot, and abdomen. Skin blood flow and skin temperature are measured by sophisticated techniques of laser Doppler imaging (MoorLDI), speckle contrast imaging (MoorFLPI), and thermography. Figures 1 and 2 show representative images taken by MoorFLPI and FLIR thermal camera following the application of transient direct local controlled heat (43°/60 s). One should consider that a linear association between surface temperature and blood flow has not always been shown (Vuksanovic et al. 2008). This study aimed at finding a standard basis to produce a stable and significant potentiating of skin perfusion that might be applicable for drug delivery purposes. Findings indicated that a transient direct local controlled heat application at 43 °C for 60 s can significantly elevate skin blood

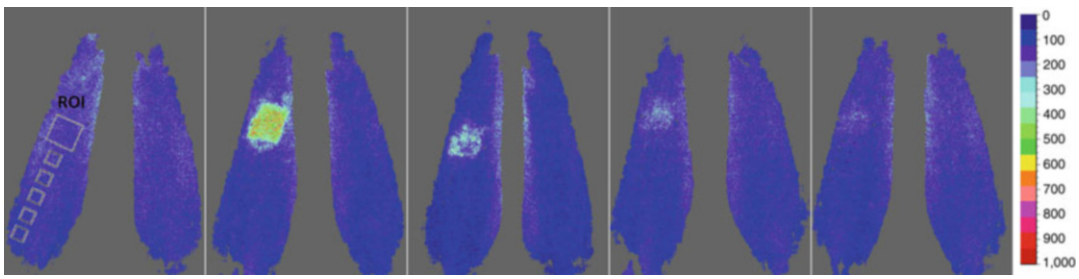

Fig. 1 Speckle contrast images taken by FLPI (Moor Instruments, Devon, UK). Recordings made from forearms at baseline, 1 min, 5 min, 10 min, and 15 min (left to right in the row) following the application of transient direct local controlled heat (43°/60 s). *Red* color represents high flow rates and *blue* color represents low flow rates. *ROI* region of interest 3 × 3 cm

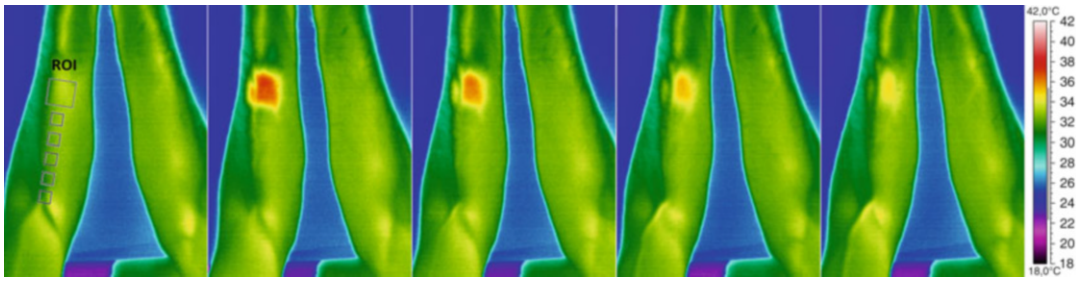

Fig. 2 Thermographic images taken by FLIR (ThermoVision A40M, Sweden). Recordings made from forearms at baseline, 1 min, 5 min, 10 min, and 15 min (left to right in the row) following the application of transient direct local controlled heat (43°/60 s). *Red* color represents higher temperatures and *blue* color represents lower temperatures. *ROI* region of interest 3 × 3 cm

flow and skin temperature with a peak at 5 min and maintenance above baseline for up to 15 min after termination of heat application (60 s). Interestingly, the various body regions did not show any difference, and the phenomenon of enhanced vasomotor responses was sex independent, pain-free, and well tolerated. In addition, the effect is retainable by repeated application of the same paradigm at 10 min intervals (Gazerani and Arendt-Nielsen 2011).

Enhancement of drug absorption from transdermal or subcutaneous delivery systems has been shown during a heat exposure (Shomaker et al. 2000; Klemsdal et al. 1992). This technique leads to elevated absorption rate and the total amount of the absorbed drug (plasma concentration) (Barry 2001). Enhanced drug absorption, through increased tissue perfusion, depends on several factors including the ability of a drug to diffuse across the membrane of the vessels, permeability of blood vessels within that region, and to some extent surface area available for drug diffusion (Song 1984). The anatomy of the vessel plexus in the skin and also the duration of vasodilatory response are important factors (Braverman 2000). Local controlled heat most likely enhances drug delivery by influencing the upper horizontal plexus which is located in the papillary dermis just below the epidermis. However, prolonged application of heat might also affect the lower horizontal plexus located in the deep dermis at the border of the underlying subcutaneous tissue. Results from the chosen paradigm in our study were not site or sex dependent, which reflect the general application of such technique to enhance vasomotor responses in human skin.

2.2 Application of the Selected Paradigm of Local Controlled Heat for Drug Delivery

Following setting up of the parameters, in two subsequent studies, we have tried to utilize the local controlled heat-evoked vasomotor response to investigate whether this technique can enhance the absorption of nicotine from a patch (Petersen et al. 2011) or insulin following subcutaneous injection (Jakobsen et al. 2011).

The nicotine patch study was based on previous reports on elevated drug uptake in subjects wearing a nicotine patch in a sauna (Vanakoski and Seppala 1998). Similar cases have been reported on elevated absorption of nitroglycerine from patches during exposure to high ambient temperature (Barkve et al. 1986).

2.2.1 Nicotine

For nicotine, we investigated whether the application of controlled local heat would result in elevated transdermal delivery from the nicotine patch mounted on the upper arm of healthy nonsmoking male Caucasian subjects. In addition to monitoring the vasomotor responses to heat by LDI and thermography, the residue of the nicotine patches was determined by high-performance liquid chromatography (HPLC) to have a measure of nicotine uptake from the patch. This study revealed a positive correlation between nicotine absorption and vasomotor response (Petersen et al. 2011). However, individual variation in responses was a limiting factor. Theoretically, following application of controlled local heat, drug uptake would increase from patches, and it may give a possibility for drug absorption at higher level or quickly when it is needed. It is valuable to note that drug concentration following heat application should still remain within the therapeutic range to avoid any safety issue and toxicity. To achieve this, different drugs should be tested in order to validate controlled local heat application as a method in cutaneous drug delivery.

2.2.2 Insulin

For insulin, we aimed to investigate whether local controlled heat application can enhance the absorption of drug from a reservoir in the subcutaneous tissue and elevate the insulin level or reduce the blood glucose (Jakobsen et al. 2011). The study was designed in a pharmacokinetic-type study to follow up changes over time with repeated blood sampling. This strategy allowed us to study the rate and amount of absorption of subcutaneously injected insulin (short-acting insulin: Actrapid®, 100 IU/ml). Controlled heat

application at the site of insulin injection significantly enhanced tissue perfusion. However, no correlation was found between insulin absorption and tissue perfusion. This finding suggests that tissue perfusion is not the rate-limiting factor in the absorption of high-concentration short-acting insulin from a subcutaneous depot. This is most likely due to the fact that dissociation of insulin hexamers into dimers and monomers is a major rate-limiting factor in this case. Therefore, insulin analogues can be better choices as these types are only present on absorbable forms, whereby dissociation should not constitute a limiting factor.

Insulin absorption rate from an injection site has been shown that it is related to ambient temperature (Vanakoski and Seppala 1998; Guerci and Sauvanet 2005; Koivisto et al. 1981). Warm environment has been associated for up to fivefold higher insulin absorption most likely due to elevated skin temperature and blood flow (Koivisto et al. 1981). The effect of sauna on insulin absorption from a subcutaneous injection site has also been investigated (Koivisto 1980; Cuppers et al. 1980).

3 Application of the Local Controlled Heat in Sensitized Skin

In a recent study (Nielsen et al. 2013), the magnitude, temporal and spatial pattern, and sex differences of the vasomotor responses to local controlled heat (43 °C for 60 s) before and after topical capsaicin (cream, 1 %) were assessed. This study aimed at finding the effect of controlled local heat on a pre-sensitized skin. Regions of interests were defined and monitored thoroughly by thermography and speckle contrast imager. The latter novel technique is highly sensitive with higher temporal resolution that can take blood flow images of large areas in different skin regions at the same time. Priming of skin sensitivity by topical capsaicin in this study significantly enhanced skin vasomotor responses for up to 30 min. The response was with a greater magnitude in females but longer and well spread in males. This prolonged and spatially expanded vasomotor response to the standardized local heat application was limited due to ceiling effect of the vascular network responses to capsaicin-induced neurogenic inflammation, which highlights the point that using controlled heat technique for drug delivery purposes might not yield the same results under normal intact skin in comparison with primed sensitized skin.

4 Conclusion

In summary, application of heat (43 °C) for a short duration of time (60 s) can enhance the local vasomotor responses with no associated short- or long-term side effect. Under normal condition, it lasts for 15 min, while the response is twice longer in a sensitized skin. The applied paradigm (43 °C for 60 s) was independent of body region or sex under normal condition; however, in a sensitized skin, females respond with a greater magnitude and males with longer lasting and more spread. Testing the method for two different drugs administered by two different routes showed that both routes of administration and drug itself are important factors to find a correlation (nicotine) or not to find a correlation (insulin).

References

Barcroft H, Edholm OG. The effect of temperature on blood flow and deep temperature in the human forearm. J Physiol. 1943;102(1):5–20.

Barkve TF, Langseth-Manrique K, Bredesen JE, Gjesdal K. Increased uptake of transdermal glyceryl trinitrate during physical exercise and during high ambient temperature. Am Heart J. 1986;112(3):537–41.

Barry BW. Novel mechanisms and devices to enable successful transdermal drug delivery. Eur J Pharmaceut Sci: Off J Eur Fed Pharmaceut Sci. 2001;14(2):101–14.

Braverman IM. The cutaneous microcirculation. J Invest Dermatol Symp Proc Soc Invest Dermatol Eur Soc Dermatol Res. 2000;5(1):3–9.

Charkoudian N. Mechanisms and modifiers of reflex induced cutaneous vasodilation and vasoconstriction in humans. J Appl Physiol. 2010;109(4):1221–8.

Cuppers HJ, Berchtold P, Berger M. Sauna-induced acceleration in insulin absorption. Br Med J. 1980; 281(6235):307.

Gazerani P, Arendt-Nielsen L. Cutaneous vasomotor reactions in response to controlled heat applied on various

body regions of healthy humans: evaluation of time course and application parameters. Int J Physiol Pathophysiol Pharmacol. 2011;3(3):202–9.

Geber C, Klein T, Azad S, et al. Test-retest and interobserver reliability of quantitative sensory testing according to the protocol of the German Research Network on Neuropathic Pain (DFNS): a multi-centre study. Pain. 2011;152(3):548–56.

Guerci B, Sauvanet JP. Subcutaneous insulin: pharmacokinetic variability and glycemic variability. Diabet Metab. 2005;31(4 Pt 2):4S7–24.

Hodges GJ, Kosiba WA, Zhao K, Johnson JM. The involvement of heating rate and vasoconstrictor nerves in the cutaneous vasodilator response to skin warming. Am J Physiol Heart Circ Physiol. 2009;296(1):H51–6.

Jakobsen LA, Jensen A, Larsen LE, et al. Effect of cutaneous blood flow on absorption of insulin: a methodological study in healthy male volunteers. Int J Physiol Pathophysiol Pharmacol. 2011;3(4):257–65.

Johnson JM, Kellogg Jr DL. Local thermal control of the human cutaneous circulation. J Appl Physiol. 2010;109(4):1229–38.

Johnson JM, O'leary DS, Taylor WF, Kosiba W. Effect of local warming on forearm reactive hyperaemia. Clin Physiol. 1986;6(4):337–46.

Kellogg Jr DL, Johnson JM, Kenney WL, Pergola PE, Kosiba WA. Mechanisms of control of skin blood flow during prolonged exercise in humans. Am J Physiol. 1993;265(2 Pt 2):H562–8.

Klemsdal TO, Gjesdal K, Bredesen JE. Heating and cooling of the nitroglycerin patch application area modify the plasma level of nitroglycerin. Eur J Clin Pharmacol. 1992;43(6):625–8.

Koivisto VA. Sauna-induced acceleration in insulin absorption. Br Med J. 1980;281(6240):621–2.

Koivisto VA, Fortney S, Hendler R, Felig P. A rise in ambient temperature augments insulin absorption in diabetic patients. Metab Clin Exp. 1981;30(4):402–5.

Magerl W, Krumova EK, Baron R, Tolle T, Treede RD, Maier C. Reference data for quantitative sensory testing (QST): refined stratification for age and a novel method for statistical comparison of group data. Pain. 2010;151(3):598–605.

Maier C, Baron R, Tolle TR, et al. Quantitative sensory testing in the German Research Network on Neuropathic Pain (DFNS): somatosensory abnormalities in 1236 patients with different neuropathic pain syndromes. Pain. 2010;150(3):439–50.

Minson CT, Berry LT, Joyner MJ. Nitric oxide and neurally mediated regulation of skin blood flow during local heating. J Appl Physiol. 2001;91(4):1619–26.

Nielsen TA, Da Silva LB, Arendt-Nielsen L, Gazerani P. The effect of topical capsaicin-induced sensitization on heat-evoked cutaneous vasomotor responses. Int J Physiol Pathophysiol Pharmacol. 2013;5(3):148–60.

Petersen KK, Rousing ML, Jensen C, Arendt-Nielsen L, Gazerani P. Effect of local controlled heat on transdermal delivery of nicotine. Int J Physiol Pathophysiol Pharmacol. 2011;3(3):236–42.

Shomaker TS, Zhang J, Ashburn MA. Assessing the impact of heat on the systemic delivery of fentanyl through the transdermal fentanyl delivery system. Pain Med. 2000;1(3):225–30.

Song CW. Effect of local hyperthermia on blood flow and microenvironment: a review. Cancer Res. 1984;44(10 Suppl):4721s–30s.

Vanakoski J, Seppala T. Heat exposure and drugs. A review of the effects of hyperthermia on pharmacokinetics. Clin Pharmacokinet. 1998;34(4):311–22.

Vuksanovic V, Sheppard LW, Stefanovska A. Nonlinear relationship between level of blood flow and skin temperature for different dynamics of temperature change. Biophys J. 2008;94(10):L78–80.

Studying the Oscillatory Components of Human Skin Microcirculation

55

Henrique Silva, Hugo Ferreira, and Luís Monteiro Rodrigues

Contents

H. Silva
CBIOS – Research Center for Biosciences and Health Technologies, Universidade Lusófona, Lisboa, Portugal

Department of Pharmacological Sciences, Universidade de Lisboa – School of Pharmacy, Lisbon, Portugal

H. Ferreira
Faculty of Sciences, Institute of Biophysics and Biomedical Engineering, Universidade de Lisboa, Lisboa, Portugal

L.M. Rodrigues (✉)
CBIOS – Research Center for Health Science and Technologies, Universidade Lusófona, Lisbon, Portugal

Department of Pharmacological Sciences, Universidade de Lisboa – School of Pharmacy, Lisbon, Portugal
e-mail: monteiro.rodrigues@ulusofona.pt; monteirorodrigues@sapo.pt

P. Humbert et al. (eds.), *Agache's Measuring the Skin*,
DOI 10.1007/978-3-319-32383-1_62

Keywords
LDF • Components analysis • Wavelet transform • DFA • Entropy analysis

1 Introduction

The term "microcirculation" refers to the blood vessels with a diameter plantar to 150 μm, which encompasses arterioles, capillaries, and venules. Recently, a physiology-based definition was proposed, according to which microcirculation refers to all vessels responding to an increase of internal pressure by a myogenic reduction in lumen diameter. This definition also includes small arteries (Levy et al. 2001). Microcirculation vessels provide a large surface area which is needed for blood-tissue exchange (Verdant and De Backer 2005), while avoiding large fluctuations in capillary hydrostatic pressure and determining the overall peripheral resistance (Levy et al. 2001).

1.1 Skin Microcirculation

The cutaneous vessels are present in the dermis and, according to their dimension, belong to the microcirculation. They are responsible for three main functions – skin tissue nutrition, thermoregulation heat exchange, and blood flow redistribution during stress (Roddie 1983). The skin vasculature has a peculiar organization, consisting of two horizontal arterial plexuses in the dermis –

an upper (superficial) horizontal plexus in the papillary dermis, involved in the skin nutrition, and a lower (deep) horizontal plexus at the dermal-subcutaneous border, involved in thermoregulation (Braverman 1997). A special feature of human skin microcirculation is arteriovenous anastomoses (AVAs), which are direct connections between arterioles and venules at the deep plexus. These are mainly found in the apical regions of the skin and are particularly numerous in the nail beds, digital tips and palmar surfaces, and soles and are practically absent in these areas dorsum (Braverman 1997).

Skin blood flow is regulated by both neural and local mechanisms. Neural mechanisms consist of sympathetic vasoconstrictor fibers that supply all skin areas, both glabrous and non-glabrous, and sympathetic vasodilator fibers that supply only the latter (Lenasi 2011). These neural-mediated mechanisms are modulated by diurnal rhythms (Aoki et al. 2003), physical exercise (Johnson et al. 1996), and menstrual cycle (Charkoudian and Johnson 2000).

The local mechanisms that control skin blood flow include factors released by the vascular endothelium and by local nerve endings. The endothelium responds to physical and chemical stimuli via production of a wide range of vasoconstrictor and vasodilator substances, which regulate vascular tone, cellular adhesion, thromboresistance, smooth muscle cell proliferation, and vessel wall inflammation (Deanfield et al. 2007; Minson 2010).

The skin is a favorable site for microvascular investigation because it is readily accessible and it allows the application of stimuli with noninvasive or minimally invasive procedures (Minson 2010). Furthermore, it has been suggested that the cutaneous microcirculation can serve as potentially representative of vasculature for the study of physiological regulation and systemic dysfunction mechanisms (Holowatz et al. 2008). Since microvascular dysfunction is a systemic process that occurs in a similar way in multiple tissue beds throughout the body (Sax et al. 1987), the skin can likely be used as a surrogate marker of systemic microvascular function in various diseases (Holowatz et al. 2008). It has been used as a research model for hypercholesterolemia (Khan et al. 1999), hypertension (Rizzoni et al. 2003), renal disease (Stewart et al. 2004), type II diabetes (Sokolnicki et al. 2006), peripheral vascular disease (Rossi and Carpi 2004), atherosclerotic coronary artery disease (Shamim-Uzzaman et al. 2002), heart failure (Cui et al. 2005), and primary aging (Thompson-torgerson et al. 2007).

Laser Doppler flowmetry (LDF) is definitely one of the most popular assessment techniques, although its use is not very common in the clinical setting. LDF is based upon measurement of the Doppler frequency shift in monochromatic laser light which is backscattered from cutaneous tissue. The frequency shift is associated with velocity of moving particles within the tissue, primarily red blood cells (Sacks et al. 1988). Moreover, it can be continuously measured when coupled to provocation tests which can change the resting flow conditions, allowing to assess the mechanisms involved (Holowatz et al. 2008; Rossi and Carpi 2004; Thompson-torgerson et al. 2007; Cracowski et al. 2006). The most commonly employed tests include postural changes (Abu-Own et al. 1994; Husmann et al. 2008; Silva et al. 2013a), limb occlusion (Silva et al. 2013a; Berry et al. 2000; Morales et al. 2005), drug application (Morris and Shore 1996), heating the skin (Minson et al. 1985; Schubert 2000), and oxygen breathing (Silva et al. 2013b; Crawford et al. 1985; Harward et al. 1985).

LDF provides a sensitive, continuous, noninvasive, and real-time assessment of blood flow, uninfluenced by the underlying skeletal muscle blood flow (Saumet et al. 1988). The considerably complex nature of the signal variability (Srinivasa and Sujatha 2011), however, can make LDF difficult to understand, justifying the use of several strategies to look further to its components, as follows:

1.2 Wavelet Transform

The oscillatory components of LDF signal have been investigated with linear methods, such as the

Fourier transform (Rossi et al. 2006) and the wavelet analysis (Bernjak et al. 2008).

A wavelet is defined as a small wave or oscillation that decays quickly. Morlet considered wavelets as a family of functions constructed from translations and dilations of a single function called the "mother wavelet" $\Psi(t)$ defined as (Sifuzzaman et al. 2009)

$$\Psi_{a,b}(t) = \frac{1}{\sqrt{|a|}}\Psi\left(\frac{t-b}{a}\right), a, b \in R, a \neq 0 \quad (1)$$

The parameter a is the scaling parameter or scale, and it measures the degree of compression. The parameter b is the translation parameter which determines the time location of the wavelet. If $|a| < 1$, then the wavelet in the above equation is the compressed version (smaller support in time domain) of the mother wavelet and corresponds mainly to higher frequencies. On the other hand, when $|a| > 1$, then $\Psi_{a,b}(t)$ has a larger time-width than $\Psi(t)$ and corresponds to lower frequencies. Thus, wavelets have time-widths adapted to their frequencies (Sifuzzaman et al. 2009).

These spectral analyses have shown several components, or oscillators, that regulate local blood flow and which are well-defined in their own frequency interval:

- Heart (0.6–2 Hz)
- Respiration (0.15–0.6 Hz)
- Myogenic activity at vessel wall (0.052–0.15 Hz)
- Sympathetic activity (0.021–0.052 Hz)
- NO-dependent metabolic activity (0.095–0.021 Hz) (Landsverk et al. 2007)

However, there is a complex interaction between these components, making the isolation of individual signals a difficult task.

1.3 Detrended Fluctuation Analysis

The detrended fluctuation analysis (DFA), a method developed by Peng et al. (1994), provides a quantitative parameter, the scaling exponent α that represents the correlation properties of nonstationary, noisy time series. The following procedure is used to calculate the scaling exponent α (Peng et al. 1995):

First, given a time series x_i, i = 1 , . . . ,N, is obtained:

$$y(k) = \sum_{i=1}^{k} [x_i - \overline{x}], \quad (2)$$

where

$$\overline{x} = \frac{1}{N}\sum_{i=1}^{N} x_i \quad (3)$$

Then, the cumulative summed series *y(k)* is divided into nonoverlapping boxes of equal length, *n*. In each box, we fit *y(k)*, using a least-square line fit, which represent the local trend in that box. The y-coordinate of the fit line in each box is denoted by $y_n(k)$. The cumulatively summed signal, *y(k)*, is detrended by subtracting the local trend, $y_n(k)$, in each box of length *n*. For a given box size *n*, the root-mean-square (rms) fluctuation for this cumulatively summed and detrended signal is calculated:

$$F(n) = \sqrt{\frac{1}{N}\sum_{k=1}^{N}\left[y(k) - y_n(k)^2\right]} \quad (4)$$

Repeating this calculation over all box sizes, we obtain a relationship between *F(n)* and the box size *n*. For fractal, self-similar, signals, *F(n)* behaves as a power-law function of *n*, and the data can be described by

$$F(n) \overset{d}{\equiv} Cn^{\alpha} \quad (5)$$

where *C* is a constant of proportionality and the ≡ symbol represents that the statistical properties of both sides of the previous equation are identical only in distribution. The scaling exponent α represents the correlation properties of the signal and e [F(*n*)] to log *n*, log[F(*n*)] = log C + α log *n*.

The classification of a fractal signal by DFA is possible based on the value of α (Eke et al. 2002): for the $0 < \alpha \leq 1$ corresponds to the fractional Gaussian noise (fGn). A value of $\alpha = 0.5$ indicates that the signal is completely uncorrelated

(white noise). When $\alpha < 0.5$ the signal indicates short-range correlation. Long-range correlations are present when $0.5 < \alpha \leq 1$. In the case of $\alpha > 1$, the time series is analogous to another class of fractal time signal, fractional Brownian motion (fBm). The value of $\alpha = 1.5$ corresponds to long-range correlations that are not necessarily related to stochastic processes and may be reflecting deterministic correlations.

The advantage of DFA over conventional methods is that it permits the detection of long-range correlations embedded in a seemingly nonstationary time series, while avoiding the spurious detection of apparent long-range correlations that are an artifact of nonstationarity (Peng et al. 1995). The DFA scaling exponents have been used to distinguish signals obtained from physiologic and pathophysiological conditions and have shown some utility as a diagnostic tool (Esen and Esen 2006).

1.4 Multiscale Entropy Analysis

Costa et al. (2002, 2012) proposed the multiscale entropy (MSE) concept, which allows the analyst to approach short and noisy physiological time series; MSE consists of obtaining the entropy values, which are a measure of uncertainty, through several scales. For this purpose, given a time series x_i, i = 1, . . . ,N, a consecutive coarse-grained time series $y^{(\tau)}$ is constructed:

$$y_j^{(\tau)} = \frac{1}{\tau} \sum_{i=(j-1)\tau+1}^{j\tau} x_i \qquad (6)$$

where τ represents the scale factor and $1 \leq j \leq {}^{N}/_{\tau}$. The sample entropy (SampEn) of each coarse-grained is then computed. *SampEn*(*m*,*r*,*N*) is the negative natural logarithm of the conditional probability that a dataset of length *N*, having repeated itself with a tolerance *r* for *m* points, will also repeat itself for *m* + *1* points, without allowing self-matches:

$$\mathrm{SampEn}(m, r, N) = -ln \frac{A^m(r)}{B^m(r)} \qquad (7)$$

where $A^m(r)$ is the probability that two sequences will match for m + 1 points and $B^m(r)$ is the probability that two sequences will match for *m* points. The more regular and predictable a time series, the lower the value of SampEn. The more random a time series, the higher the value of SampEn.

This chapter aims to discuss how the LDF signal obtained from a healthy group of volunteers performing a classic tourniquet-cuff occlusion in the lower limb can be obtained and characterized, having in mind its potential application as a powerful quantitative indicator of in vivo vascular function.

2 Materials and Methods

2.1 Subjects

A group of 30 subjects (15 males and 15 females), aged between 18 and 26 (22.3 ± 3.1) years old, was studied after informed written consent. The subjects had no known cardiovascular or metabolic disease, were nonsmokers, and were not taking any kind of medication, with the exception of four women who were taking oral contraceptives. Restrictions included caffeine and alcohol consumption as well as any topical products application 24 h before the test.

The experimental protocols conformed to standards set in the latest revision of the Declaration of Helsinki (*World Medical Association Declaration of Helsinki: ethical principles for medical research involving human subjects* 2013) and was approved by the Institutional Ethics Committee.

2.2 Instrument

Microcirculatory blood flow, expressed in arbitrary units (AU), was assessed by LDF (PeriFlux PF 5010 system, Perimed, Sweden), whose probe was applied on the plantar aspect of the second toe. A total of 23 min of LDF signal was recorded for each subject, with a sampling rate of 32 Hz.

2.3 Experimental Design

All measurements were performed with controlled room conditions (temperature: 21–23 °C; humidity: 40–60 %, with minimal air movement over the subject). Volunteers were lightly clothed and acclimatized for 30 min prior to any procedure, sitting upright with their feet exposed. The ankle-brachial index (ABI) was determined in all patients to exclude peripheral arterial disease. ABI is obtained by dividing the systolic blood pressure (SBP) measured at ankle level by the systolic blood pressure measured at arm level (Anderson et al. 2013). The suprasystolic occlusion maneuver, a perfusion-reducing protocol, was performed at the ankle level. With the subject seated in the upright position, a pneumatic cuff (PF 5051 Pressure Accessory Kit) was applied approximately 1 cm above the ankle for 10 min (phase I). Then, the cuff was manually inflated to 200 mmHg for 3 min (phase II). After this period the cuff was quickly deflated, allowing recovery (phase III). The experimental setting is illustrated in Fig. 1.

Fig. 1 Illustrative scheme of the experimental procedure

2.4 Data Analysis

The LDF signal was partitioned using a Morlet wavelet transform and subsequently selected based on the limits of the determined cone of influence. The subsequent analyses were performed on the LDF data excluding the segments inside the cone of influence. The amplitude ratio of each frequency component was determined by dividing the area under the curve of each component sine wave by the area under the curve of all components' sine waves.

The DFA α coefficient and MSE complexity index (CI), which corresponds to the area under the MSE curve, were determined for each segment of the LDF signal and for each component of the wavelet transform using MATLAB toolboxes. The DFA algorithm was implemented in which the LDF signal was divided into 100 boxes of 5,000 samples each. The MSE algorithm was implemented with $\tau = 36, m = 2$, and $r = 0.15\,x\,SD$, where SD is the standard deviation of the original time series.

Three periods, one of each phase of the protocol, were selected for statistical analysis: resting phase was considered between 6:30 and 9:30 min, the provocation phase was considered between 10:00 and 13:00 min, and the recovery phase was considered between 18:00 and 21:00 min. All statistical analyses were made with *IBM Corp. Released 2012. IBM SPSS Statistics for Windows*, *Version 21.0. Armonk*, *NY: IBM Corp*. The LDF signal component amplitude ratios, α exponents, and complexity indexes were compared for each phase of the protocol by the Wilcoxon matched-pairs signed-rank test. Gender contributions were compared with the Mann-Whitney *U* test for independent samples. A 95 % confidence interval was adopted.

3 Results and Discussion

Sample characteristics are displayed in Table 1. ABI values were normal in the two aged-matched groups, thus excluding peripheral arterial disease from our sample. The resting blood flow showed a wide variability, which could be attributed to the fact that all variables that influence it could not be controlled. These variables may include normal levels of physical activity, food intake before the procedure, phases of menstrual cycle (for women), and/or the different timings for measurements in different days (Tables 2 and 3).

The LDF signal for a representative volunteer is depicted in Fig. 2. The suprasystolic occlusion provokes a significant reduction in blood flow to the foot, due to the mechanical compression. As expected, when the occlusion was terminated, a reactive hyperemia was observed – a physiological response elicited in order to restore the tissue's viability and enable its recovery. After this period, the resting perfusion value is reestablished, suggesting recovery. Males were found to have a higher blood flow in the resting and recovery phases, and to suffer a lower perfusion reduction during occlusion, although none of these differences were found to be statistically significant.

3.1 Wavelet Transform Analysis

The wavelet transform has a finite resolution, resulting in broadened frequency peaks. The same was observed for the LDF signal. We observed that the lower frequency components displayed broader waves and higher frequency components displayed narrower waves, as displayed in Fig. 3. The LDF signal was found to be mainly of sympathetic and endothelial origin, owing to the large amplitude of these components' amplitude ratios. During limb occlusion there was a significant decrease in the cardiac, respiration, myogenic, and sympathetic amplitude ratios. However, the metabolic amplitude ratio increased significantly, suggesting that during occlusion there is an endothelium-dependent NO production increase. This supports known data (Dakak et al. 1998), since an important contributing stimulus for the development of the said hyperemia is the relaxation of vascular smooth muscle due to NO production. During the recovery period, all components' amplitudes returned to baseline, further suggesting a full recovery of the resting conditions.

Table 1 Sample characteristics (*SBP* systolic blood pressure, *ABI* ankle-brachial index, *sd* standard deviation)

Characteristic	Males ($n = 15$)	Females ($n = 15$)
Age (mean ± sd)	22.6 ± 3.1	22.0 ± 4.4
Ankle SBP (mmHg)	146.9 ± 11.7	132.6 ± 13,6
Arm SBP (mmHg)	125.6 ± 5.3	116.6 ± 11.5
ABI	1.2 ± 0.1	1.2 ± 0.1

3.2 DFA Analysis

The unpartitioned LDF signal showed $\alpha \sim 1.0$ during the resting phase, suggesting a 1/f noise-like behavior. The α exponent increased, although nonsignificantly, during the provocation phase. In addition, no significant differences were found between the resting and recovery phases. Figure 4 displays the DFA analysis of the LDF signal, suggesting different scaling regions for each segment. No gender differences were found in the α exponent for any of the phases of the procedure, suggesting a similar behavior of the LDF signal in males and females.

Regarding the partitioned LDF signal, all wavelet components showed $\alpha > 0.5$, translating positive self-correlated signals. However, different α exponents were observed for different components, as shown in Fig. 5. In the resting period, heart and respiration activity components showed $\alpha \sim 1.0$, suggesting that these phenomena have a 1/f noise-like behavior. However, myogenic ($\alpha \sim 1.42$), sympathetic ($\alpha \sim 1.55$), and metabolic ($\alpha \sim 1.50$) activity components could reflect physiological processes with characteristics closer to Brownian noise ($\alpha = 1.5$). The α exponents of the heart, respiration, myogenic, and sympathetic components significantly increased during occlusion and decreased for the metabolic activity component. During the recovery period, all activity

Table 2 Average and standard deviation values of LDF, alpha exponent, and CI for each phase of the protocol. Statistical comparison for phase I (* – $p < 0.05$)

	LDF			DFA α coefficient			MSE complexity index		
	Baseline	Provocation	Recovery	Baseline	Provocation	Recovery	Baseline	Provocation	Recovery
Males	46.51 ± 37.42	16.62 ± 20.30	39.07 ± 31.33	1.01 ± 0.24	1.16 ± 0.21	0.89 ± 0.39	36.61 ± 12.49	16.39 ± 15.46	33.57 ± 15.71
Females	48.19 ± 66.99	9.89 ± 7.34	46.40 ± 72.48	1.03 ± 0.22	1.11 ± 0.3	0.97 ± 0.27	35.84 ± 12.20	13 ± 11.64	38.25 ± 15.44
Total	47.35 ± 53.32	13.25 ± 15.38	42.73 ± 54.99	1.02 ± 0.23	1.13 ± 0.26	0.93 ± 0.33	36.22 ± 12.14	14.69 ± 13.55	35.91 ± 15.49
p-value	–	<0.001*	0.254	–	0.086	0.405	–	<0.001*	0.813

Table 3 Average and standard deviation values of the amplitude ratio of each component for each phase of the protocol. Statistical comparison for phase I (* – significant; $p < 0.05$)

	Wavelet amplitude ratios (%)			DFA α exponent			MSE complexity index		
Component	Baseline	Provocation	Recovery	Baseline	Provocation	Recovery	Baseline	Provocation	Recovery
Heart	3,90 ± 2,31	1,20 ± 0,72	4,18 ± 2,86	0,91 ± 0,21	1,04 ± 0,18	0,96 ± 0,16	38,95 ± 7,16	14,79 ± 9,83	35,91 ± 15,49
	–	<0.001*	0.441	–	0.023*	0.254	–	<0.001*	0.393
Respiration	6,20 ± 3,96	2,79 ± 1,69	6,82 ± 5,20	1,12 ± 0,23	1,24 ± 0,18	1,03 ± 0,16	14,12 ± 3,47	5,49 ± 4,11	15,03 ± 4,66
	–	<0.001*	0.382	–	0.020*	0.080	–	<0.001*	0.221
Myogenic	18,28 ± 6,98	7,40 ± 3,41	19,18 ± 7,55	1,42 ± 0,19	1,65 ± 0,18	1,42 ± 0,19	8,35 ± 2,84	1,98 ± 1,78	8,27 ± 3,45
	–	<0.001*	0.491	–	<0.001*	0.813	–	<0.001*	0.845
Sympathetic	28,91 ± 6,88	20,25 ± 4,72	27,19 ± 7,02	1,55 ± 0,21	1,81 ± 0,13	1,54 ± 0,22	6,81 ± 3,24	3,44 ± 1,17	7,16 ± 4,33
	–	<0.001*	0.309	–	<0.001*	0.704	–	<0.001*	0.750
metabolic	42,71 ± 9,17	68,36 ± 8,63	42,64 ± 13,32	1,50 ± 0,23	1,86 ± 0,14	1,48 ± 0,23	7,77 ± 4,66	3,23 ± 1,85	8,33 ± 3,85
	–	<0.001*	0.926	–	<0.001*	0.544	–	<0.001*	0.544

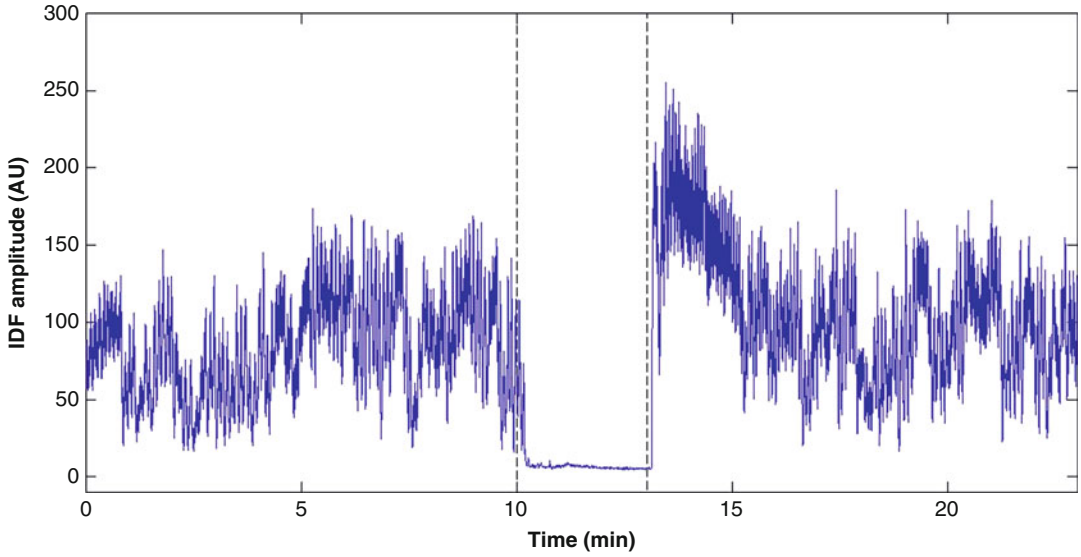

Fig. 2 Laser Doppler flowmetry (*LDF*) signal amplitude in time, showing the three experimental phases: resting, provocation, and recovery. Data is from a representative subject. The *vertical dotted lines* mark the beginning and end of the provocation phase (*AU* arbitrary units)

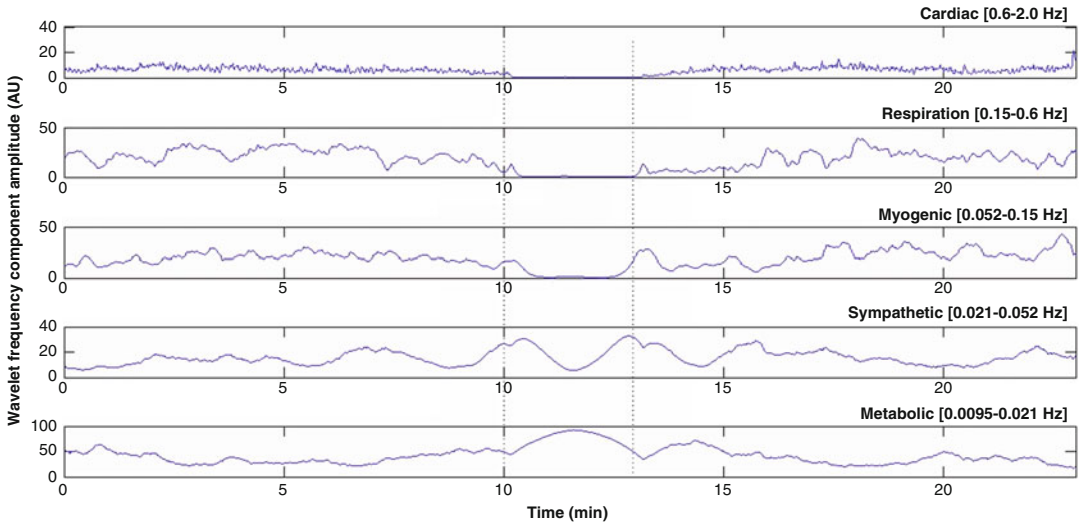

Fig. 3 Amplitude over time of each wavelet frequency component obtained for each experimental condition. Data is from a representative subject (*AU* arbitrary units). The *vertical dotted lines* mark the beginning and end of the provocation phase

components, α exponents, and complexity indexes return to baseline, suggesting a full perfusion recovery under the present experimental conditions. Our results are consistent with previously published studies (Ferreira et al. 2011), demonstrating that DFA is a sensitive method for assessing microvascular dynamics with corresponding changes in the scaling regions.

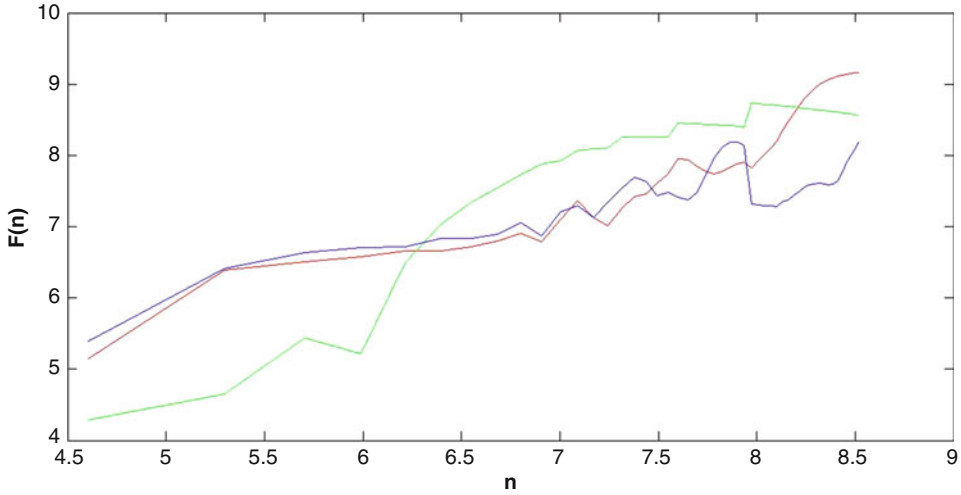

Fig. 4 Detrended fluctuation analysis of the LDF time series (one representative subject) shown in Fig. 2: resting (*red*), provocation (*green*), and recovery (*blue*)

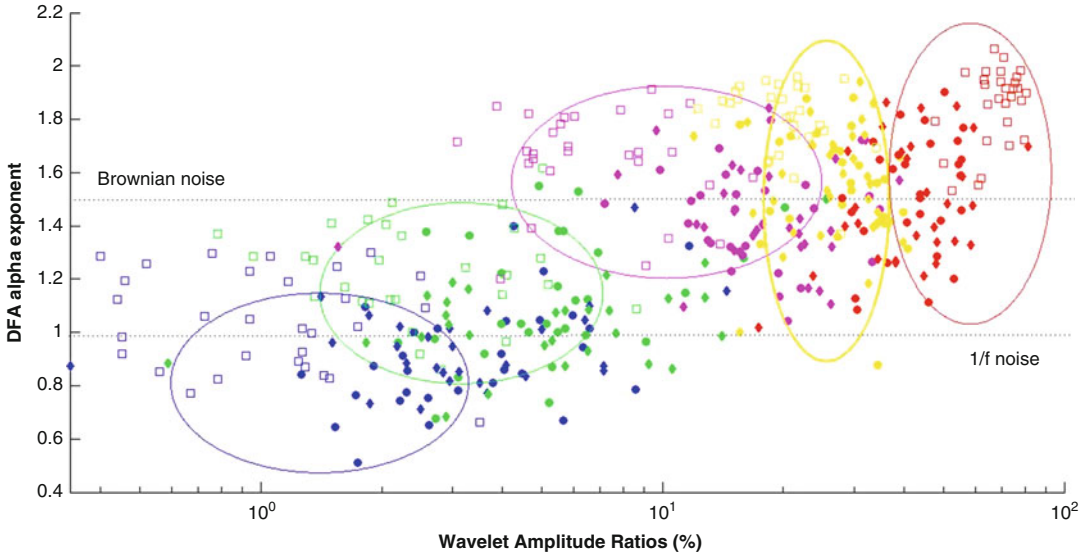

Fig. 5 Plot showing detrended fluctuation analysis (*DFA*) α exponents versus wavelet amplitude ratios (abscissa axis in log10 scale). The different frequency components are indicated by colors (heart, *blue*; respiration, *green*; myogenic, *pink*; sympathetic, *yellow*; and metabolic, *red*), and the different segments are indicated by symbols (baseline, *filled circles*; provocation, *open squares*; recovery, *filled diamonds*). *Dashed lines* for alpha=1 (1/f noise) and alpha=1.5 (Brownian noise) are shown for reference

3.3 MSE Analysis

The entropy of the unfractionated LDF signal in the resting phase decreased significantly during occlusion, likely due to its decrease in variability. The entropy value returned to baseline during recovery. No gender differences were determined for any of the phases of the procedure.

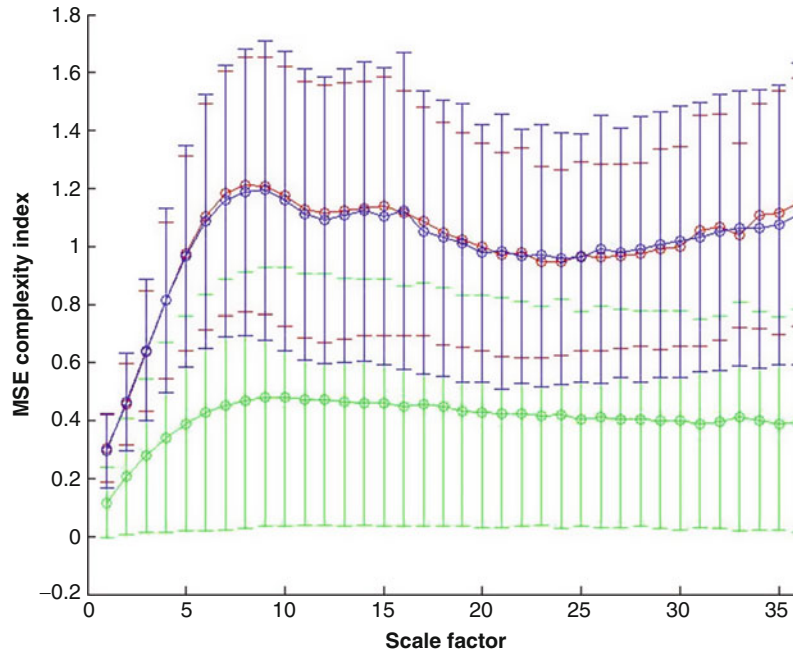

Fig. 6 Sample entropy versus scale factor of the different LDF signal segments (*red*, baseline; *green,* provocation; *blue,* recovery). *Vertical bars* represent the standard deviation

A plot of the scale factor versus CI for the different phases of the protocol is shown in Fig. 6. Our results have shown that MSE profiles for the three phases of the protocol were nonmonotonic, as previously observed (Guerreschi et al. 2012). In the resting and recovery phases, CI values increased to reach a maximum on $\tau = 8$ and $\tau = 9$. After reaching this maximum, CI values decreased until reaching $\tau = 12$, where they increased upon reaching $\tau = 15$ and $\tau = 16$ in the resting and recovery phases, respectively. From these time scales, the CI values decreased again until reaching a minimum on $\tau = 26$ and $\tau = 24$ for the resting and recovery phases, respectively. For the provocation phase, the MSE profile was also nonmonotonic, although less variable. CI values increased to a maximum for $\tau = 9$ and then decreased. For all phases, the processes occurring around the time scales corresponding to these maximum values had the highest irregularity, after which the processes become more regular and predictable.

Figure 7 shows a plot of alpha exponent of three LDF signal segments versus CI. It shows that the dispersion clouds related to resting and recovery are practically superimposed, further suggesting recovery of the LDF signal. The dispersion cloud related to the occlusion period, although partially detached from the other two, cannot be clearly isolated.

As observed in Fig. 8, the heart component exhibited the highest entropy value, suggesting a more random-like signal. Myogenic, sympathetic, and endothelial components were present with lower entropy values, suggesting a more regular and predictable signal. The entropy of the frequency components was significantly reduced during occlusion and returned to baseline during recovery.

4 Conclusions

The combined use of wavelet transform, DFA, and MSE appears to have interesting potential to become a complementary analysis tool for laser Doppler flowmetry. A deeper look into the oscillatory components of this complex measurement results, not only in a better view over the phenomena regulating skin microcirculation, but also contributes to expand the practical usefulness of LDF in clinical, diagnostic, or research settings.

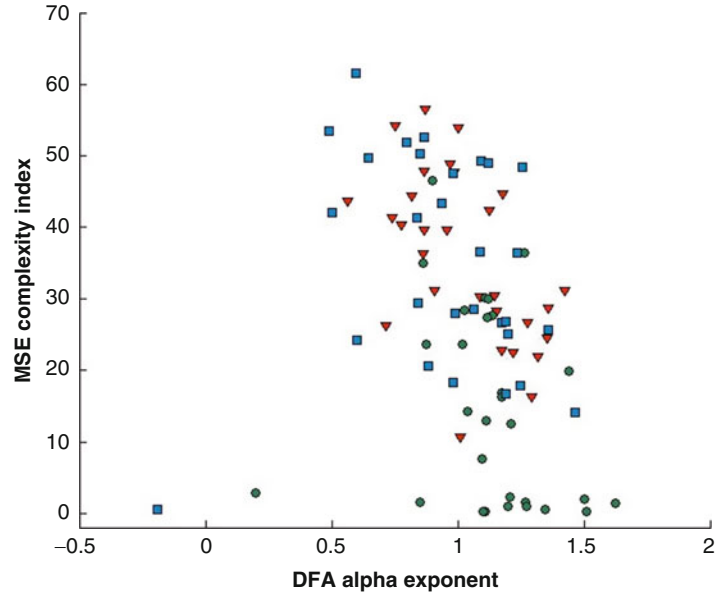

Fig. 7 DFA alpha exponent versus MSE complexity index (*CI*) of the three segments of the laser Doppler flowmetry (*LDF*) signal (*triangles,* baseline; *circles,* provocation; *squares,* recovery)

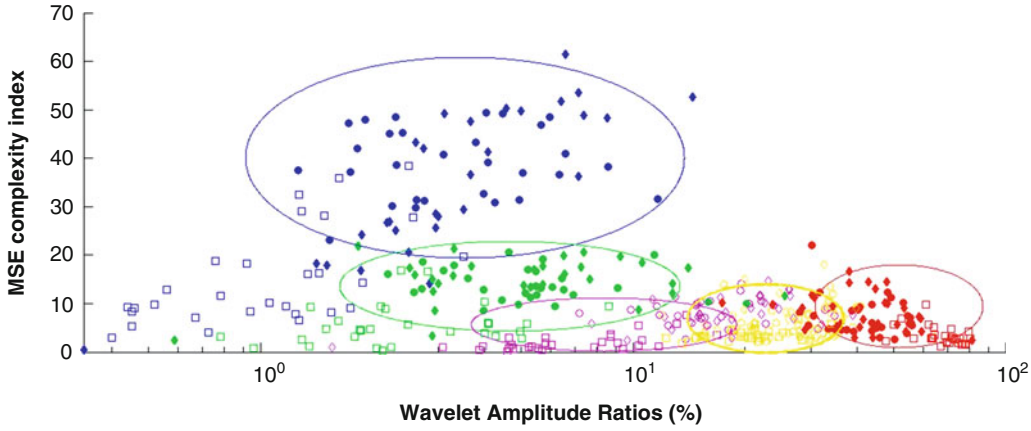

Fig. 8 Plot showing MSE complexity index (*CI*) versus wavelet amplitude ratios (abscissa axis in log10 scale). Different frequency components are indicated by colors (heart, *blue*; respiration, *green*; myogenic, *pink*; sympathetic, *yellow*; and metabolic, *red*), and different segments are indicated by symbols (baseline, *filled circles*; provocation, *open squares*; recovery, *filled diamonds*)

References

Abu-Own A, Scurr JH, Coleridge Smith PD. Effect of leg elevation on the skin microcirculation in chronic venous insufficiency. J Vasc Surg Off Publ Soc Vasc Surg Int Soc Cardiovasc Surg N Am Chapter. 1994;20(5):705–10.

Anderson JL, Halperin JL, Albert N, Bozkurt B, Brindis RG, Curtis LH, et al. Management of patients with peripheral artery disease (compilation of 2005 and 2011 ACCF/AHA guideline recommendations): a report of the American College of Cardiology Foundation/American Heart Association Task Force on Practice Guidelines. J Am Coll Cardiol. 2013;61(14):1555–70.

Aoki K, Stephens DP, Saad AR, Johnson JM. Cutaneous vasoconstrictor response to whole body skin cooling is altered by time of day. J Appl Physiol. 2003;94:930–4.

Bernjak A, Clarkson PB, McClintock PV, Stefanovska A. Microvasc Res. 2008;76(3):224–32.

Berry KL, Skyrme-Jones RA, Meredith IT. Occlusion cuff position is an important determinant of the time course

and magnitude of human brachial artery flow-mediated dilation. Clin Sci Lond Engl 1979. 2000;99(4):261–7.
Braverman I. REVIEW the cutaneous microcirculation: ultrastructure and microanatomical organization. Microcirculation. 1997;4(3):329–40.
Charkoudian N, Johnson JM. Female reproductive hormones and thermoregulatory control of skin blood flow. Exerc Sport Sci Ver. 2000;28:108–12.
Costa M, Goldberger AL, Peng CK. Multiscale entropy analysis of complex physiologic time series. Phys Rev Lett. 2002;89:062102.
Cracowski JL, Minson CT, Salvat-Melis M, Halliwill JR. Methodological issues in the assessment of skin microvascular endothelial function in humans. Trends Pharmacol Sci. 2006;27(9):503–8.
Crawford P, Good PA, Gutierrez E, Feinberg JH, Boehmer JP, Silber DH, Sinoway LI. Effects of supplemental oxygen on forearm vasodilation in humans. J Appl Physiol (Bethesda Md). 1985;82(5):1601–6.
Cui J, Arbab-Zadeh A, Prasad A, Durand S, Levine BD, Crandall CG. Effects of heat stress on thermoregulatory responses in congestive heart failure patients. Circulation. 2005;112:2286–92.
Dakak N, Husain S, Mulcahy D, Andrews NP, Panza JA, Waclawiw M, Schenke W, Quyyumi AA. Contribution of nitric oxide to reactive hyperemia: impact of endothelial dysfunction. Hypertension. 1998;32(1):9–15.
Deanfield JE, Halcox JP, Rabelink TJ. Endothelial function and dysfunction: testing and clinical relevance. Circulation. 2007;115(10):1285–95.
Eke A, Herman P, Kocsis L, Kozak L. Fractal characterization of complexity in temporal physiological signals. Physiol Meas. 2002;23(1):R1–38.
Esen F, Esen H. Detrended fluctuation analysis of laser Doppler flowmetry time series: the effect of extrinsic and intrinsic factors on the fractal scaling of microvascular blood flow. Physiol Meas. 2006;27(11):1241–53.
Ferreira HA, Fernandes CD, Pinto PC, Rodrigues LM. Use of wavelet transforms and detrended fluctuation analysis in the evaluation of human skin microcirculation. Biomed Biopharm Res. 2011;1(9):79–86.
Guerreschi E, Humeau-Heurtier A, Bricq S, Mahe G, Lefheriotis G. Proceedings of the 20th European Signal Processing Conference (EUSIPCO). 2012.
Harward TR, Volny J, Golbranson, Bernstein EF, Fronek A. Oxygen inhalation-induced transcutaneous. J Vasc Surg. 1985;2:220–7.
Holowatz LA, Thompson-Torgerson CS, Kenney WL. The human cutaneous circulation as a model of generalized microvascular function. J Appl Physiol. 2008;105(1):370–2.
Husmann M, Willenberg T, Keo HH, Spring S, Kalodiki E, Delis KT. Integrity of venoarteriolar reflex determines level of microvascular skin flow enhancement with intermittent pneumatic compression. J Vasc Surg. 2008;48(6):1509–13.
Johnson JM, Proppe DW. Cardiovascular adjustments to heat stress. In: Handbook of physiology. Environ Physiol. 1996;215–43, Am Physiol Soc, Bethesda.
Khan F, Litchfield SJ, Stonebridge PA, Belch JJ. Lipid-lowering and skin vascular responses in patients with hypercholesterolaemia and peripheral arterial obstructive disease. Vasc Med. 1999;4:233–8.
Landsverk SV, Kvandal P, Bernjak A, Ste- fanovska A, Kirkeboen KA. The effects of general anesthesia on human skin microcirculation evaluated by wavelet transform. Anesth Analg. 2007;105:1012–9.
Lenasi H. Assessment of human skin microcirculation and its endothelial function using laser Doppler flowmetry. In: Erondu OF, editor. Medical imaging. Rijeka: InTech; 2011. p. 271–96.
Levy BI, Ambrosio G, Pries AR, Struijker-Boudier HA. Microcirculation in hypertension: a new target for treatment? Circulation. 2001;104(6):735–40.
Minson CT. Thermal provocation to evaluate microvascular reactivity in human skin. J Appl Physiol. 2010;109:1239–46.
Minson CT, Holowatz LA, Wong BJ, Kenney WL, Wilkins BW. Decreased nitric oxide- and axon reflex-mediated cutaneous vasodilation with age during local heating. J Appl Physiol (Bethesda Md). 1985;93(5):1644–9.
Morales F, Graaff R, Smit AJ, Bertuglia S, Petoukhova AL, Steenbergen W, Rakhorst G. How to assess post-occlusive reactive hyperaemia by means of laser Doppler perfusion monitoring: application of a standardised protocol to patients with peripheral arterial obstructive disease. Microvasc Res. 2005;69(1–2):17–23.
Morris SJ, Shore AC. Skin blood flow responses to the iontophoresis of acetylcholine and sodium nitroprusside in man: possible mechanisms. J Physiol. 1996;496(Pt 2):531–42.
Peng CK, Buldyrev SV, Havlin S, Simons M, Stanley HE, Goldberger AL. Mosaic organization of DNA nucleotides. Phys Rev E Stat Phys Plasmas Fluids Relat Interdiscip Topics. 1994;49(2):1685–9.
Peng CK, Havlin S, Stanley HE, Goldberger AL. Quantification of scaling exponents and crossover phenomena in nonstationary heartbeat time series. Chaos. 1995;5(1):82–90.
Rizzoni D, Porteri E, Boari GE, DeCiuceis C, Sleiman I, Muiesan ML, et al. Prognostic significance of small-artery structure in hypertension. Circulation. 2003;108:2230–5.
Roddie IC. Circulation to skin and adipose tissue. In: Geiger S, editor. The cardiovascular system. Am Physiol Soc. 1983;285–317.
Rossi M, Carpi A. Skin microcirculation in peripheral arterial obliterative disease. Biomed Pharmacother. 2004;58(8):427–31.
Rossi M, Carpi A, Di Maria C, Galetta F, Santoro G. Spectral analysis of laser Doppler skin blood flow oscillations in human essential hypertension. Microvasc Res. 2006;72(1–2):34–41.
Sacks AH, Ksander G, O'Neill H, Perkash I. Difficulties in laser Doppler measurement of skin blood flow under applied external pressure. J Rehabil Res Dev. 1988;25(3):19–24.

Saumet JL, Kellogg Jr DL, Taylor WF, Johnson JM. Cutaneous laser-Doppler flowmetry: influence of underlying muscle blood flow. J App Physiol. 1988;65(1):478–81.

Sax FL, Cannon RO, Hanson C, Epstein SE. Impaired forearm vasodilator reserve in patients with microvascular angina. Evidence of a generalized disorder of vascular function? N Engl J Med. 1987;317: 1366–70.

Schubert V. The influence of local heating on skin microcirculation in pressure ulcers, monitored by a combined laser Doppler and transcutaneous oxygen tension probe. Clin Physiol (Oxford England). 2000;20(6):413–21.

Shamim-Uzzaman QA, Pfenninger D, Kehrer C, Chakrabarti A, Kacirotti N, Rubenfire M, et al. Altered cutaneous microvascular responses to reactive hyperaemia in coronary artery disease: a comparative study with conduit vessel responses. Clin Sci. 2002;103(3):267–73.

Sifuzzaman M, Islam MR, Ali MZ. Application of wavelet transform and its advantages compared to Fourier transform. J Phys Sci. 2009;13:121–34.

Silva H, Ferreira H, Tavares L, Bujan J, Rod-rigues LM. Exploring in vivo models to characterize peripheral microcirculation – a pilot study. Biomed Biopharm Res. 2013a;10(1):65–72.

Silva H, Ferreira H, Bujan J, Rodrigues LM. Exploring the oxygen challenge test as a microcirculation evaluation model. Biomed Biopharm Res. 2013b;10(2):209–15.

Sokolnicki LA, Roberts SK, Wilkins BW, Basu A, Charkoudian N, et al. Contribution of nitric oxide to cutaneous microvascular dilation in individuals with type 2 diabetes mellitus. Am J Physiol Endocrinol Metab. 2006;292:E314–8.

Srinivasa G, Sujatha N. Fractal dimension characterization of in-vivo laser Doppler flowmetry signals. Phys Procedia. 2011;19:49–54.

Stewart J, Kohen A, Brouder D, Rahim F, Adler S, Garrick R, Goligorsky MS. Noninvasive interrogation of microvasculature for signs of endothelial dysfunction in patients with chronic renal failure. Am J Physiol Heart Circ Physiol. 2004;287:H2687–E2696.

Thompson-torgerson CS, Holowatz LA, Flavahan NA, Kenney WL. Rho kinase-mediated local cold-induced cutaneous vasoconstriction is augmented in aged human skin. Am J Physiol Heart Circ Physiol. 2007;293(1):H30–6.

Verdant C, De Backer D. How monitoring of the microcirculation may help us at the bedside. Curr Opin Crit Care. 2005;11:240–4.

World Medical Association Declaration of Helsinki: ethical principles for medical research involving human subjects. JAMA : J Am Med Assoc. 2013;310(20):2191–4.

Epicutaneous 133-Xenon Clearance

56

Pierre Agache

Contents

Keywords
Epicutaneous xenon-133 clearance • Skin blood flow

Developed in the late 1960s (Sejrsen 1969), epicutaneous xenon-133 clearance was a considerable step forward: for the first time, an absolute measurement of the skin blood flow was possible. As such, it is still unchallenged and valid today. Although noninvasive, it requires complex and expensive equipment that can be used only in nuclear medicine units. For that reason, it has been supplanted by less reliable methods that are more accessible.

1 Principle

The principle of epicutaneous xenon-133 clearance is simple. A chemically inert although radioactive gas, xenon-133, is applied on the skin only for the time necessary for a small amount to penetrate. Then its gradual disappearance from the injection site is measured, since it is washed out depending on the blood flow. Once in the dermis, the xenon is extracted from the tissues by the blood capillaries, then evacuated by the collecting venules. However, the gas tissue/blood partition coefficients (ratio of the solubilities in both) are 0.7 and 10 for the dermis and adipose tissue, respectively. Such high liposolubility makes the whole process complicated. When going through

This chapter was originally published under the ISBN 978-3-540-01771-4 with the following book title Measuring the Skin. The content has not been changed.

Pierre Agache: deceased.

P. Agache (✉)
Department of Dermatology, University Hospital of Besançon, Besançon, France
e-mail: aude.agache@free.fr; ferial.fanian@chu-besancon.fr; ferial.fanian@cert-besancon.com

P. Humbert et al. (eds.), *Agache's Measuring the Skin*,
DOI 10.1007/978-3-319-32383-1_63

the hypodermis dissolved in the venous blood, a fraction of the gas leaves the veins toward the adipose tissue, but it is extracted from the adipose tissue after a short time by the xenon-deprived venous blood originating from the completely purified dermis. Furthermore, another fraction of the gas is dissolved in the stratum corneum, a structure rich in lipids, thus introducing a third source of elimination directly into the air at the skin surface. Monitoring the decreasing amount of xenon-133 vs time at the injection site is made possible with the γ rays (Xenon-133 also emits X-rays and β-rays (electrons). It is 50 available at CIS-BIO International, 91400 Saclay, 51 France) it sends out. The detector is a simple γ probe with a meter, set on 80-keV radiation; a gamma camera is not necessary. Xenon-133's physical half-life is 5.27 days; therefore its disintegration is next to zero following an examination lasting 1.5 h maximum.

2 Technique

Sweating must be avoided because stratum corneum hyperhydration and the presence of sweat in the sweat ducts and on the skin surface could facilitate a retrograde flow of xenon toward the surface. On dry skin free of any ointment, carefully degreased with ether and shaved if necessary, a plastic gas-proof chamber is attached to the skin with double-sided adhesive tape (No chamber is on the market and consequently it must be custom made, for example from the cast of a mylar sheet.). The air of the chamber is removed with a syringe and replaced by xenon-133 (specific activity, 10 mCi/cm^3) injected with another syringe. It is left in place for 3 min, then all the xenon is aspirated. The perfect adherence of the chamber to the skin must be checked during both aspirations. The chamber is then carefully removed (avoid a shock that might induce vasodilatation) and radioactivity is measured immediately at short intervals at first (for example every 10 s), then less often (for example every minute). Because of the relatively slow elimination, the test must last at least 1 h. These operations are performed under an extractor, and both operator and patient wear a lead protective apron, following the usual safety procedures against ionizing rays. The risk of radiodermatitis is insignificant. The chamber holds 1 cm^3 of xenon-133 gas, hence 10 mCi (370 mBq), and the recuperated volume is identical. The amount absorbed cannot be measured accurately, but from the number of counts found per minute (2,000–5,000); it is approximately 160 kBq, an insignificant amount because it represents roughly 10^{-4} times the dose of radiation generally used for diagnosis in thyroid gland diseases. Furthermore, in these diseases, the radioactive product (iodine-131) remains concentrated in a limited volume of tissue, whereas xenon is eliminated quickly by the respiratory system.

After test completion, the radioactivity vs time curve is smoothed and then mathematically processed using a two-compartment model that takes into account the anatomical xenon path and its two tissue/blood partition coefficients (Sejrsen 1969, 1995; Cardot et al. 1977). Its breakdown into two exponential curves (Fig. 1) provides the dermis and hypodermis wash-out time constants. These constants, multiplied by the respective partition coefficients, give the blood flows for 100 ml tissue, according to the

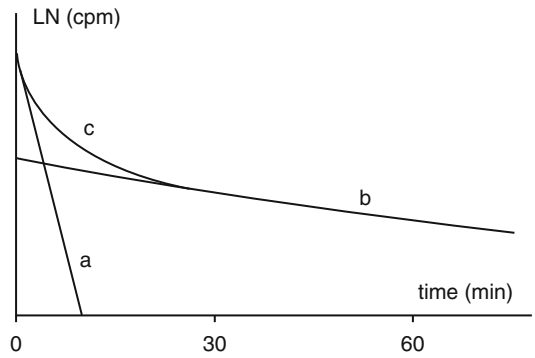

Fig. 1 Epicutaneous 133-xenon clearance. Schematic treatment of the signal vs time curve. Ordinate: counts/min natural logarithm. *a* Slope of the initial exponential curve (from the first 3 or 4 counts) describing the washing-out from the stratum corneum toward outside. *b* Slope of the final exponential curve (during the second half-hour) describing the washing-out from fat tissue toward venous blood. *c* Slope of the middle exponential curve (during the first half-hour) describing the washing-out from the dermis toward venous blood

formula: flow rate $= 0.693\lambda/t_{1/2}$ where λ is the partition coefficient and $t_{1/2}$ the time necessary for the xenon wash-out to reach 50 %. The calculation of the fraction of xenon that penetrates the subcutaneous tissue (slow exponential) is noticeably influenced by diffusion time; therefore the total length of the latter should be at least 30 min and if possible 1 h (Cardot et al. 1977).

A third exponential, which decreases very rapidly, sometimes interferes with the beginning of the curves. It corresponds to xenon's direct passage to the outside, probably picked up by the stratum corneum, which can be calculated by the slope of the first three or four points on the curve. The value obtained can be verified by applying a tourniquet that cuts off the blood flow proximally; a very slow decreasing curve is then observed, representing about 1 % of the wash-out (Sejrsen 1969; Greeson et al. 1973). Some authors ignore these first three or four points of the curve (Nyfors and Rothenborg 1970; Greeson et al. 1973; Kristensen and Wadskov 1977). Their elimination is better achieved by using the so-called peeling method (Baud et al. 1981), which also cancels out the artifacts due to subject movement during data recording.

3 Skin Blood Flow Values

Normal values (milliliters per minute for 100 g tissue) in recumbency, are displayed in Table 1. In psoriasis plaques (Bazin et al. 1981), the cutaneous and subcutaneous blood flows were 2.0 and 2.1 times as high as those of healthy skin, respectively. When healed following PUVA therapy, the same plaque values both drop to 1.3 times the values of healthy skin.

In systemic scleroderma (LeRoy et al. 1971), the blood flow in fingers collapses: 18 % of the normal flow usually found in this body site.

4 Comments

The pulse frequency is too high to be visible on the wash-out curve. But the additional low-frequency oscillations (6–8/min) corresponding to vasomotion may be visible if recording is done less than every 5 s.

An interesting comparative study (Cardot et al. 1979) of blood flow in the rabbit ear (rich in venoarterial shunts) and back (absence of shunts) shows that the ear subcutaneous flow is 25 % higher than skin blood flow at 18 °C, and only 7 % higher at 25 °C ($p < 0.01$). In the back, the opposite is observed: +26 % at 25 °C and −3 % at 18 °C. It is reasonable to think that the method could provide a means to assess venoarterial shunts, which in this example would represent about one-fourth of the global skin blood flow.

Flow measurement is based on the xenon diffusion from the tissues toward the vessels, which depends on the exchange area, i.e., the cumulated areas of the capillary walls. Therefore, the

Table 1 Normal skin blood flow (ml/100 g tissue). Epicutaneous 133-xenon technique

Site	Dermis	Hypodermis	Total	Author
First finger web	3.0 ± 1.0	5.7 ± 1.2		Sejrsen (1971)
Dorsum middle finger	6.4 ± 10.6			LeRoy (Cardot et al. 1979)
1st phalanx at 18 °C				
Idem after warming	28.0 ± 6.3			LeRoy (Cardot et al. 1979)
Forearm	5.1 ± 1.7			Sejrsen (1969)
Forearm	6.2 ± 0.8			Greeson et al. (1973)
Abdomen	4.5			Sejrsen (1969)
Beardless cheek	9.0			Sejrsen (1969)
Bearded cheek	15.2 ± 3.0			Sejrsen (1969)
Dorsum hand	6.9 ± 1.3		8.9 ± 0.9	Kristensen and Wadskov (1977)
Above lateral malleolus	6.2 ± 1.1	3.8 ± 1.6		Cardot et al. (1977)
Leg, lateral aspect	5.7 ± 1.2			Sejrsen (1969)

difference in blood flow measured using this method should be lower than the systolic-diastolic volume variations measured by photoplethysmography (PPG). Using PPG, the plaque/healthy skin ratios in psoriasis were 3.7 ± 1.6 ($n = 29$) and 1.2 ± 1.3 ($n = 18$) before and after treatment, respectively (Bazin et al. 1981). Using the xenon method, in the same patients, the ratios were 2.0 ± 1.5 ($n = 18$) and 1.3 ± 1.5 ($n = 10$) before and after treatment, respectively. In the same plaque, after healing by PUVA therapy ($n = 10$), the two methods reached the same proportion, 1.3 ± 1.4 and 1.3 ± 1.5 times that of the healthy skin.

References

Baud M, Cardot JC, Bazin R, Verdenet J, Bidet R. Comparaison de deux méthodes de détermination de la cinétique d'un système bicompartimental Application à la mesure des débits sanguins cutanés. CR Soc Biol (Paris). 1981;175(77025):215–778.

Bazin R, Cardot JC, Noyon G, Baud M, Blanc D, Agache P. Corrélation de deux méthodes de mesure du débit sanguin cutané : photopléthysmographie et xénon 133. CR Soc Biol (Paris). 1981;175(77925):215–785.

Cardot JC, Bazin R, Baud M, Agache P, Bidet R. Etude de la microcirculation cutanée par diffusion épicutanée du xénon 133. CR Soc Biol (Paris). 1977;171 (34025):215–344.

Cardot JC, Bazin R, Baud M, Verdenet J, Parmentier M. Mesure des débits sanguins cutanés et sous-cutanés au niveau de l'oreille de lapin par diffusion epicutanée de xénon 133. Influence des anastomoses artérioveineuses. CR Soc Biol (Paris). 1979;173 (74125):215–745.

Greeson TP, Levan NE, Freedman RI, Wong WH. Corticosteroid-induced vasoconstriction studied by xenon 133 clearance. J Invest Dermatol. 1973;61 (24225):215–44.

Kristensen JP, Wadskov S. Studies on 133xe wash-out from human skin: quantitative measurements of blood flow in normal and corticosteroid-treated skin. J Invest Dermatol. 1977;68:19625:215–200.

LeRoy EC, Downey J, Cannon PJ. Skin capillary blood flow in scleroderma. J Clin Invest. 1971;50: 930–9.

Nyfors A, Rothenborg HW. Cutaneous blood flow in psoriasis measured by 133xenon clearance. J Invest Dermatol. 1970;54(38125):215–385.

Sejrsen P. Blood flow in cutaneous tissue in man studied by washout of xenon-133. Circ Res. 1969;25:215–29.

Sejrsen P. Measurement of cutaneous blood flow by freely diffusible radioactive isotopes. Dan Med Bull. 1971;18 Suppl 3:1–40.

Sejrsen P. The 133Xenon wash-out technique for quantitative measurement of cutaneous and subcutaneous blood flow rates. In: Serup J, Jemec GBE, editors. Non-invasive methods and the skin. Boca Raton: CRC Press; 1995. p. 42925:215–435.

Carbon Dioxide Transcutaneous Pressure

57

Pierre Agache

Contents

Keywords

Bullous lesions • Carbone Dioxide • Fick's first law • Polarographic method • Severinghaus's electrode • Transcutaneous CO_2 pressure (tcPCO2)

Usefulness: Blood CO_2 monitoring in anesthesiology and intensive care medicine, evaluation of skin respiration, and skin blood flow measurement (incidentally).

1 Physiology

There is a small but continuous carbon dioxide (CO_2) release from the skin surface (Abernethy 1793). The gas originates both from the vascular subepidermal plexus and from an epidermal metabolic production. The transfer is a passive process of diffusion obeying Fick's first law. Accordingly, at a given temperature, the $tcPCO_2$ value depends on CO_2 concentration in the blood perfusing the skin, subepidermal skin blood flow, CO_2 epidermal production, CO_2 concentration in the ambient air, and CO_2 diffusion resistance across superficial skin tissues, especially the stratum corneum. The CO_2 partial pressure in the atmosphere is very low (less than 0.4 torr). On the other hand, the CO_2 diffusional resistance across superficial skin tissues is weak (1/28.5 times that of oxygen) and may be considered as constant in normal skin. Consequently, the main

This chapter was originally published under the ISBN 978-3-540-01771-4 with the following book title Measuring the Skin. The content has not been changed.

Pierre Agache: deceased.

P. Agache (✉)
Department of Dermatology, University Hospital of Besançon, Besançon, France
e-mail: aude.agache@free.fr; ferial.fanian@chu-besancon.fr; ferial.fanian@cert-besancon.com

P. Humbert et al. (eds.), *Agache's Measuring the Skin*, DOI 10.1007/978-3-319-32383-1_41

factors of $tcPCO_2$ variation are the CO_2 concentration in the blood perfusing the skin, the subepidermal skin blood flow, and the CO_2 epidermal metabolic production. All these factors are temperature dependent.

In normal conditions, the cutaneous blood PCO_2 is close or identical to arterial PCO_2 because of the low skin metabolism and the great excess of blood as compared to the needs for skin nutrition. This is the reason why blood gases in the past were measured by puncturing the ear lobe. The usual value is 40 torr. In case of impaired pulmonary function and defective oxygen uptake, hypercapnia occurs, which leads to an increased $tcPCO_2$. Conversely in acidosis, for example in uremia, there is a reduction in the blood CO_2 and a concomitant drop in $tcPCO_2$.

Carbon dioxide emission increases with the skin temperature above a 34 °C threshold (Shaw et al. 1929). Variation was found identical to that of transepidermal water loss (Thiele and Van Kempen 1972), probably through increased skin blood flow and diffusion coefficient across stratum corneum. Sweating, either spontaneous or pharmacologically induced (Thiele and Van Kempen 1972), also augments $tcPCO_2$, most probably through the increased blood flow associated with sweat gland activation. Occlusion of the skin surface increases $tcPCO_2$ (King et al. 1978), possibly by increasing stratum corneum permeability through its hydration, as simply applying water on the skin surface also raises the CO_2 emission (Frame et al. 1972). Direct exposure of the head and neck to sunlight induced an increased CO_2 loss at the volar forearm, although the skin temperature remained constant (Thiele and Van Kempen 1972); one can assume that subclinical sweating may have occurred. On the other hand, venous stasis with greatly increased CO_2 content in the blood did not increase transepidermal CO_2 loss (Ernstene and Volk 1932; Rothman 1957). During occlusion, forearm $tcPCO_2$ increases, possibly through anaerobic metabolic generation of lactic acid and titration of skin HCO_3– (Severinghaus et al. 1978). Upon occlusion release, $tcPCO_2$ shows a quasi-exponential return to control values, with a time constant depending on the skin blood flow.

2 Measurement

Several methods have been used for the measurement of cutaneous CO_2 release, including spectrophotometry by infrared analysis (CO_2 absorbs light at a 4.3-μm wavelength) (Thiele and Van Kempen 1972) and mass spectrometry (Christensen et al. 1991). They have been replaced by a polarographic method, which uses a contact electrode (Severinghaus'electrode) whose output is called the transcutaneous CO_2 pressure ($tcPCO_2$), although a fraction of the gas originates from the epidermis. As the CO_2 diffusion resistance is low and the electrode consumes no CO_2, the $tcPCO_2$ casual level and variation can be easily monitored when the skin is at 33 °C, the usual forearm temperature. Detailed measurement procedures can be found in Winberley et al. (1990) and Nickelsen (1995).

Current devices permit the simultaneous measurements of $tcPCO_2$ and $tcPO_2$, and the latter demands the skin to be heated to 44 °C. Consequently, $tcPCO_2$ is usually measured at 43–44 °C. A reasonable correction for temperature of about 4 % per degree Celsius has been proposed (Thiele and Van Kempen 1972) and supported by the data obtained by Christensen et al. (1991). Accordingly, the $tcPCO_2$ at 33 °C should be approximately 0.56 $tcPCO_2$ at 44 °C. On the other hand, the CO_2 arterial partial pressure ($PaCO_2$) can be deduced from $tcPCO_2$ using the following formula: at 43 °C $tcPCO_2$ (torr) = 1.245 $PaCO_2$ (torr) − 0.8 ($p = 0.98$) (Goldman et al. 1982). Subsequent correction for temperature should be made as stated above.

3 Normal Figures

3.1 $tcPCO_2$

In ten healthy males aged 24–36, regional variations were found (Takiwaki et al. 1991).

Forehead	67.2 ± 2.4 torr
Cheek	69.2 ± 2.8
Volar forearm	62.6 ± 3.3
Abdomen	63.7 ± 2.4
Back	63.9 ± 3.1
Leg, anterior aspect	61.1 ± 4.1
Leg, posterior aspect	62.8 ± 2.9
Palm	60.5 ± 3.1
Earlobe	315.7 ± 42.0 (42.1 ± 5.6 kPa) ($n = 7$) (Christensen et al. 1991)

The surprisingly high earlobe figure may originate from higher blood flow and/or lower resistance of a thinner stratum corneum, or a different method (mass spectrometry). The figures on the face are significantly higher ($p < 0.01$) than on the volar forearm. The difference may stem from either inconspicuous sweating or higher metabolism on the face.

3.2 Transcutaneous CO_2 loss (nl cm^{-2} min^{-1})

Site	$tcPCO_2$ (nl cm^{-2} min^{-1})	Reference
Hand	46	(Frame et al. 1972)
Forearm	18	(Frame et al. 1972)
Forearm[a]	77.3 ± 47.2 ($n = 7$)	(Thiele and Van Kempen 1972)
Forearm	23.1 ± 6.8 ($n = 30$)	(Wilson and Maibach 1982)
Upper back	28.1 ± 5.4 ($n = 21$ neonates)	(Wilson and Maibach 1982)

[a]As calculated for 32 °C (the usual skin temperature)

Earlier studies found figures roughly ten times higher (as quoted in Frame et al. (1972)), which may be due to different methodologies.

4 $TcPCO_2$ and Skin Diseases

In various skin lesions, whether sclerotic, inflammatory, acanthotic, or hyperkeratotic, in leg ulcers and in skin neoplasms, $tcPCO_2$ remained stable (Takiwaki et al. 1991). It was substantially elevated over prenecrotic tissues such as bullous lesions (pemphigoid) and ischemic lesions (necrotizing fasciitis, arterial insufficiency) "An extraordinarily high $tcPCO_2$ with low $tcPO_2$ may be regarded as a marker of prenecrotic epidermis and/or dermis caused by the severe disturbance of blood-gas exchange in the skin" (Takiwaki et al. 1991). Very high values probably indicate anaerobic tissue metabolism secondary to skin ischemia. Following skin damage by application of diluted NaOH solutions, the $tcCO_2$ loss increased in parallel with the transcutaneous water loss (Malten and Thiele 1973).

Conclusions can be drawn from Takiwaki's opinion (Takiwaki et al. 1991): "Unlike $tcPO_2$, $tcPCO_2$ is less influenced by cutaneous factors," and Bourgain and Grenouillet (1985) "The reasons why $tcPCO_2$ is less sensitive to circulatory variation (than $tcPO_2$) remain poorly understood." Accordingly, $tcPCO_2$ measurement may be useful, especially when done in association with $tcPO_2$ measurement, for investigating either lung or skin respiration.

References

Abernethy J. An essay of the nature of the matter perspired and absorbed from the skin. Surgical and physiological essays, part 2. London; 1793. pp. 107–140. (reference from Hansen TN, Sonoda Y, McIlroy MB (1980) Transfer of oxygen, nitrogen, and carbon dioxide through normal adult human skin. J Appl Physiol 49:438–443).

Bourgain JL, Grenouillet MC. Mesure transcutanée de la PO_2 et de la PCO_2. Agressologie (Paris). 1985;26:997–1003.

Christensen P, Hjarbaek J, Jensen B, Groenlund J. Measurement of transcutaneous PO_2, PCO_2 and skin blood flow at different probe temperatures using mass spectrometry. Acta Anaesthesiol Scand. 1991;35:631–4.

Ernstene AC, Volk MC. Cutaneous respiration in man, V. The rate of carbon dioxide elimination and oxygen absorption in subjects with diseases of the skin. J Clin Invest. 1932;11:377.

Frame GW, Strauss WG, Maibach HI. Carbon dioxide emission of the human arm and hand. J Invest Dermatol. 1972;59:155–9.

Goldman MD, Gribbin HR, Martin J. Transcutaneous PCO_2 in adults. Anaesthesia. 1982;37:944–6.

King RD, Cunico RL, Maibach H, Greenberg JH, West ML, Jeppsen JC. The effect of occlusion on carbon dioxide emission from human skin. Acta Derm Venereol (Stockh). 1978;58:135–8.

Malten KE, Thiele FAJ. Evaluation of skin damage. II Water loss and carbon dioxide measurements related to skin resistance measurements. Br J Dermatol. 1973;89:565–9.

Nickelsen CN. Measurement of transcutaneous PCO_2. In: Serup J, Jemec GBE, editors. Handbook of non-invasive methods and the skin. Boca Raton: CRC Press; 1995. p. 197–200.

Rothman S. Carbon dioxide delivery. In: Rothman S, editor. Physiology and biochemistry of human skin. Chicago: University of Chicago Press; 1957. p. 580.

Severinghaus JW, Stafford M, Thunstrom AM. Estimation of skin metabolism and blood flow with $tcPO_2$ and $tcPCO_2$ electrodes by cuff occlusion. Acta Anaesthesiol Scand Suppl. 1978;68:9–15.

Shaw LA, Messer AC, Weiss S. Cutaneous respiration in man. I. Factors affecting the rate of carbon dioxide elimination and oxygen absorption. Am J Physiol. 1929;90:107.

Takiwaki H, Nakanisi H, Shono Y, Arase S. The influence of cutaneous factors on the transcutaneous $tcPO_2$ and $tcPCO_2$ at various body sites. Br J Dermatol. 1991;125:243–7.

Thiele FAJ, Van Kempen LHJ. A micro method for measuring the carbon dioxide release by small skin areas. Br J Dermatol. 1972;86:463–71.

Wilson DR, Maibach HI. Carbon dioxide emission rate in the newborn. In: Maibach HI, Boisits EK, editors. Neonatal skin: structure and function. New York: Marcel Dekker; 1982. p. 111–3.

Winberley PD, Burnett RW, Covington AK, et al. Guidelines for transcutaneous PO_2 and PCO_2 measurement. International federation of clinical chemistry, scientific division: committee on pH, blood gases and electrolytes. Clin Chim Acta. 1990;190:S41–50.

Transcutaneous Oxygen Pressure

58

Pierre Agache

Contents

This chapter was originally published under the ISBN 978-3-540-01771-4 with the following book title Measuring the Skin. The content has not been changed.

Pierre Agache: deceased.

P. Agache (✉)
Department of Dermatology, University Hospital of Besançon, Besançon, France
e-mail: aude.agache@free.fr; ferial.fanian@chu-besancon.fr; ferial.fanian@cert-besancon.com

P. Humbert et al. (eds.), *Agache's Measuring the Skin*, DOI 10.1007/978-3-319-32383-1_64

Keywords
Anesthesiology • Child resuscitation • Dermatology • Heart surgery • Reactive hyperemia test • tcPO2 with kinetic tests • tcPO2 dynamic tests • Transcutaneous oxygen index • Transcutaneous oxygen pressure

In normal circulatory conditions, a fraction of the oxygen dissolved in plasma crosses the capillary wall and reaches the tissues, thus providing for their metabolic needs. This occurs in the skin subepithelial plexuses, in particular the subepidermal plexus. When the oxygen supply exceeds metabolic needs, the gas reaches the skin surface where it can be detected by a polarographic electrode and its partial pressure measured (It can also be detected by a mass spectrometer, but this technique is not as widely used.). The transcutaneous oxygen pressure ($tcPO_2$) depends on the O_2 plasmatic saturation level and local factors such as epidermal metabolic activity, the oxygen diffusion rate through superficial layers, oxyhemoglobin (HbO_2) supply, blood flow, and HbO_2 dissociation. When pulmonary function is normal, with no sign of anemia or proximal arterial insufficiency, only local factors are involved. Among them, blood flow is essential because it regulates the local oxygen supply. When the skin temperature is below 37 °C, the $tcPO_2$ is often low, barely measurable, and furthermore the diameter of the skin vessels varies continuously. For this reason, the $tcPO_2$ is usually measured after bringing the skin temperature up to 44 °C, which induces maximal vasodilation and skin blood flow while the skin temperature remains constant. As a consequence, the $tcPO_2$ is strongly increased and becomes easy to measure.

1 Consequences of Heating the Skin to 44 °C

There are a number of consequences when the skin is heated to 44 °C (Lübbers 1981).

- The O_2 diffusion through the stratum corneum is facilitated because of the increased fluidity of the intercellular lipid.
- The O_2 epidermal consumption is increased for some (Severinghaus 1979), reduced for others (Christensen et al. 1991).
- The HbO_2 dissociation curve is shifted to the right, which facilitates the release of oxygen from the red blood cells.
- Vasoconstriction due to the sympathetic tone is suppressed, inducing major arteriolar and capillary vasodilation: hence the skin blood is arterialized, with a PO_2 similar to the arterial PaO_2.
- The venoarteriolar reflex is suppressed; consequently, a venous distension (for example, by increased hydrostatic pressure) will no longer generate arterial and arteriolar vasoconstriction, but only passive vasodilation.

This shows that such a strong heating induces a nonphysiological state, which must not be overlooked for $tcPO_2$ interpretation.

2 Basal 44 °C $tcPO_2$, with Patient Supine

2.1 Regional Variations

The $tcPO_2$ measured on the chest (second intercostal space on the mid-clavicular line) is considered as the nearest to the PaO_2. In young adults, it is nearly 80 torr (1 torr = 1 mmHg (in honor of Torricelli)). On the thigh, it is 6 % lower, on the foot or the leg, 10 % lower (Hauser and Shoemaker 1983). There is no significant difference between the foot and the leg in healthy subjects (Hauser and Shoemaker 1983; Agache et al. 1992). The table below (Takiwaki 1994), although it provides slightly low figures, is of interest since it shows surprising regional variations that have yet to be explained.

Anatomical site	$tcPO_2$ (torr)	References (probands)
Ear lobe	49.2 ± 8.3	(Christensen et al. 1991) (7 young adults)
Forehead	26.6 ± 21.0	(Takiwaki 1994) (10 men aged 20–36 years)
Cheek	29.6 ± 9.8	(Takiwaki 1994)
Volar forearm	69.6 ± 5.3	(Takiwaki 1994)
Abdomen	63.8 ± 6.4	(Takiwaki 1994)
Back	60.6 ± 12.2	(Takiwaki 1994)
Over the shin	66.6 ± 6.1	(Takiwaki 1994)
Calf	67.3 ± 6.8	(Takiwaki 1994)
Palm	26.4 ± 6.6	(Takiwaki 1994)

When the stratum corneum is removed, the $tcPO_2$ on the palms rises to forearm values; however, on the forehead it remains low (Takiwaki 1994), perhaps due to higher epidermal metabolism. In children (10 subjects aged 3–9 years), the figures on the face (71.6 ± 7.9 torr) were similar to those of the forearm (76.3 ± 5.5 torr). This might indicate a change in facial vascular subepidermal network anatomy from childhood to adulthood (Takiwaki 1994).

2.2 Physiological Variations

The ratio $tcPO_2/PaO_2$ (transcutaneous index, TCI) is close to 1 in premature babies, exceeds 0.9 in children, and is approximately 0.8 in adults. In premature babies, the diffusion of oxygen is inversely proportional to the birth weight (Versmold et al. 1979).

In a single individual, the variability from 1 day to the next is nearly 10 % (Coleman et al. 1986). In a study on 75 healthy subjects, $tcPO_2$ was found higher in women by about 10 torr than in men (Agache et al. 1992), with a steady decrease with age: the regression lines were as follows (Agache et al. 1992):

- Women: $tcPO_2$ (torr) = 92.6 torr −0.37 age (years)
- Men: $tcPO_2$ (torr) = 83.6 torr −0.31 age (years).

The difference between sexes was highly significant for absolute values but regression slopes were identical. Reasons for lower values in men are not known, but can perhaps be explained by the thicker stratum corneum or higher epidermal metabolism.

2.3 Guidelines for $tcPO_2$ Interpretation

The basal $tcPO_2$ value at 44 °C, patient supine, depends on numerous factors that differ with pathology. Their identification is essential for a precise interpretation. The influence of each factor, the others being supposedly normal, is as follows:

- Respiratory factors: in premature and newborn babies, the $tcPO_2$ at 44 °C equals the oxygen partial pressure (PaO_2) of the arterial blood; hence the first use of this technique was in monitoring premature babies and in child anesthesia. In adults, $tcPO_2 \approx 0.8$ PaO_2 (Dautzenberg et al. 1981). Any abnormality in pulmonary ventilation or gas exchange alters the $tcPO_2$ (e.g., in diffuse scleroderma).
- General hemodynamic and hematological factors: shock (when the cardiac index is below 2.2 $dm^3\ min^{-1}\ m^{-2}$, the $tcPO_2$ decreases and does not reflect PaO_2 accurately (Bourgain and Grenouillet 1985)), HbO_2 saturation (smoking increases HbCO and reduces HbO_2, therefore the $tcPO_2$ as well), and hematocrit (its increase raises the $tcPO_2$).
- Local hemodynamic and hematological factors: volume of the capillaries per cubic centimeter of skin (in healthy subjects the $tcPO_2$ increases parallel to the density of papillary loops (Huch et al. 1983; Ryan 1992)), perfusion pressure ($tcPO_2$ decreases proportionally

with lowering of perfusion pressure (Eickhoff et al. 1980), but it does not increase in subjects with high blood pressure; hence the routine use of this technique in arterial insufficiency), and venous pressure (the $tcPO_2$ increases in parallel (Eickhoff et al. 1980)).
- Local tissue factor: O_2 diffusion through viable skin tissues, epidermal metabolism (the application of eugenol, which slows down the epidermal metabolism, increases $tcPO_2$ (Patel et al. 1989)), and O_2 diffusion within the stratum corneum. In case of very low $tcPO_2$, it is possible to obtain a measurable $tcPO_2$ by stripping the stratum corneum with 15 successive applications of adhesive tape, thus partially removing an obstacle to diffusion.

When the results indicate reduced $tcPO_2$, it is essential to be aware of technical errors such as erroneous calibration, alteration of the electrode membrane, lack of electrolyte, equilibration time too short, etc.

3 Basal $tcPO_2$ at 37 °C, Patient Supine

The basal $tcPO_2$ at 37 °C reflects the superficial blood flow in casual (physiological) conditions. At 37 °C, the superficial skin flow is irregular and much lower than at 44 °C. As a consequence, the basal $tcPO_2$ shows low and changing values (in the earlobe, 18.2 ± 16 torr (Christensen et al. 1991)). Furthermore, since physiological conditions are respected, the venoarteriolar reflex is maintained, thus the passage from lying position to standing or sitting position generally brings the $tcPO_2$ down to zero.

In psoriasis, its value is increased parallel to that of the laser Doppler because the vasodilatation is both superficial and deep sited (Duteil et al. 1993). In lipodermatosclerosis, the $tcPO_2$ at 37 °C is increased, indicating a high superficial flow rate (Dodd et al. 1985), while at 44 °C it drops, showing a drastic reduction of the vasodilatation reserve of superficial vessels.

Therefore, the 37 °C $tcPO_2$ is useful because it reflects exclusively the casual subepidermal blood flow, as opposed to the 44 °C $tcPO_2$, which reflects the subepidermal flow under maximal vasodilatation (i.e., the vasodilatation reserve), and the laser Doppler, which measures the flow in the deeper skin layers. As normal values are very low, stripping the stratum corneum may be of some interest in this case.

4 44 °C $tcPO_2$: Dynamic Tests

4.1 Reactive Hyperemia

The reactive hyperemia test can be done on limbs using a proximal (arterial) tourniquet for 3 min, or on another site by strong compression for the same length of time. The peak/basal ratio value is measured, together with the peak surface and the time necessary to reach this peak. It is a measure of the capacity of the local blood flow to increase from either a rise in perfusion pressure (from the reactive vasodilatation upstream) or an augmentation of the in situ vascular volume (number and diameter of the superficial capillaries), or both.

4.2 Switching the Subject from Lying to Sitting or Standing Position

Both the capillary volume and the intracapillary pressure change with the effect of the hydrostatic pressure (the perfusion pressure does not change): an increase in pressure in body sites below the heart, a decrease in pressure in sites located above the heart level.

4.3 Exercising

The $tcPO_2$ increases from the vasodilatation of the arteries upstream. The tests generally used are standardized "exercises" (walking on a treadmill, standing about, or tiptoeing in rhythm with a metronome). For information on these tests, see (Agache et al. 1993).

4.4 Oxygen Inhalation

The $tcPO_2$ increases in oxygen inhalation (5–10 dm^3/min) and may exceed the PaO_2 physiological values. In patients with arterial insufficiency, the extent of the increase is of value for prognosis (Bongard et al. 1992).

4.5 Partial Venous Occlusion

Partial venous occlusion (generally a 50-torr pressure through a tourniquet) is equivalent to a passage from a lying to a standing position.

5 $tcPO_2$ with Kinetic Tests

5.1 $tcPO_2$ Reduction Rate from Occlusion During O_2 Inhalation

This maneuver makes it possible to calculate the tissue consumption of O_2 using the formula: consumption $= \alpha(\Delta tcPO_2/\Delta t)$ (Severinghaus et al. 1978), where $\Delta tcPO_2$ is the difference before and after occlusion, Δt the reduction time, and α the solubility of O_2 ($\alpha = 28.8\ 10^{-6}$ ml g^{-1} $torr^{-1}$ at 44 °C, and 31.3 10–6 ml g^{-1} $torr^{-1}$ at 37 °C). The $tcPO_2$ reduction rate in healthy subjects' forearms is approximately 130 torr min^{-1} at 44 °C and 90 torr min^{-1} at 37 °C. This consumption is about $3.7\ 10^{-3}$ ml g^{-1} min^{-1} at 44 °C and $2.7\ 10^{-3}$ ml g^{-1} min^{-1} at 37 °C (Severinghaus et al. 1978). It is related to the epidermal metabolism.

5.2 $tcPO_2$ Recovery Rate After Suppression of the Occlusion

The $tcPO_2$ recovery rate after removing the occlusion (O_2 recovery index, ORI) reflects the superficial capillary blood flow, which depends on the available capillary volume and the perfusion pressure (Severinghaus et al. 1978). The same holds true for the basal $tcPO_2$ recovery time (O_2 reappearance time, ORT).

5.3 The $tcPO_2$ Recovery Rate

The use of Eugenol as a contact medium in the measurement of transcutaneous oxygen ($tcPO_2$) partially inhibits the metabolism in the underlying tissue, thereby reducing oxygen consumption and increasing $tcPO_2$ (Patel et al. 1989). Oxygen consumption in the tissue can be estimated from the rate at which $tcPO_2$ falls when blood flow is occluded, and blood flow in the tissue can be estimated from the rate at which $tcPO_2$ increases when the subject changes from breathing air to pure oxygen. Both these measurements have been made with Eugenol and distilled water as contact media. From these measurements it has proved possible to estimate the arterial oxygen tension (aPO_2) of healthy adults at a relatively low sensor temperature (43 °C). This method permits measuring the superficial blood flow when the subject starts inhaling pure oxygen.

6 Applications

6.1 Child Resuscitation

Basal $tcPO_2$ at 44 °C is used routinely in PaO_2 monitoring. It is the only means of detecting excessive PaO_2 (risk of retrolental fibroplasia) in premature babies in incubator. The probe must be moved every 4 h to avoid local burns.

6.2 Anesthesiology, Heart Surgery, Angiology

Basal $tcPO_2$ at 44 °C is a valuable means of measuring the tissue perfusion level distal to an arterial occlusion, and therefore to grade it (Agache et al. 1993). The basal $tcPO_2$ (foot, pretibial area, calf, thigh) in a supine subject both locates the vessel narrowing and assesses its severity. The latter can be improved by various maneuvers: reactive hyperemia, O_2 inhalation, standard exercise, passage from lying to standing position to evaluate the prognosis at stage IV (no increase indicates poor prognosis). When the $tcPO_2$ is low, in order to rule out a

respiratory cause, a concomitant measurement of the chest or arm $tcPO_2$ is recommended, in order to use the distal/chest or distal/brachial $tcPO_2$ ratio (Hauser and Shoemaker 1983). A basal $tcPO_2$ below 20 torr and a ratio below 0.2 would be incompatible with stump healing if amputation were carried out at the site of measurement (Kram et al. 1989).

Continuous $tcPO_2$ monitoring during a surgical operation helps detect bursts of hypoxia and pulmonary embolism (Bourgain and Grenouillet 1985). Under artificial breathing during anesthesia, it is an indicator of efficacy and a means of early detection of respiratory failure (Bourgain and Grenouillet 1985). In vascular surgery, it provides a continuous follow-up of the downstream blood flow and accordingly of the success of the operation (Neidhardt et al. 1987).

6.3 Dermatology

Basal 44 °C $tcPO_2$ was found reduced in all conditions investigated to date (Takiwaki 1994): lipodermatosclerosis with or without leg ulcer (Agache 1998) (perhaps due to perivascular sclerosis), morphea (perhaps from vascular atrophy), malignancies, inflammatory disorders, and diseases with acanthosis. Accordingly, the reduction was found even in conditions showing an expansion of the superficial vascular plexus. In psoriasis, $tcPO_2$ was found reduced by about 40 % (Patel et al. 1989; Duteil et al. 1993; Dodd et al. 1985; Agache et al. 1993; Bongard et al. 1992; Severinghaus et al. 1978; Kram et al. 1989; Neidhardt et al. 1987; Agache 1998; Kalis et al. 1990; Tronnier et al. 1979; Ott and Stüttgen 1984; Schalla 1986) and this reduction was alleviated along the improvement of the plaque (Duteil et al. 1993; Ott and Stüttgen 1984). To interpret these data, it is essential to point out what applies to the three main factors involved with the skin $tcPO_2$: superficial blood flow, epidermal metabolism, and O_2 diffusion rate through the epidermis.

Using $tcPO_2$ the measurement of the epidermal consumption of O_2, a well as the epidermal metabolism, is made possible by the combination of simple operations: measurement of the $tcPO_2$ reduction rate under occlusion and oxygen inhalation, with or without tape stripping. Seemingly this has been tried only in psoriasis, where an abnormally fast $tcPO_2$ decrease has been observed following vascular occlusion (187 torr min^{-1} in diseased skin and 111 torr min^{-1} in normal skin), suggesting an increase in the epidermal consumption of O_2 (the calculation gives 5.39 10–3 ml g^{-1} min^{-1} in diseased skin and 3.2 10^{-3} ml g^{-1} min^{-1} in normal skin), and thus of the epidermal metabolism (Ott and Stüttgen 1984). (P. Agache: it is obtained by multiplying the O_2 consumption by the thermal coefficient of O_2, evaluated at 20.27 kJ/l for a usual respiratory quotient (0.84) (Houdas and Guieu 1977). Using the above-mentioned figures, the results are 0.91 10^{-3} W cm^{-2} for healthy skin at 44 °C and 1.08 10^{-3} W cm^{-2} for lessions at 44 °C. Assuming that the cellular metabolism increases by 4 % per degree (Severinghaus et al. 1978), at 37 °C for psoriasis it is 0.71 10^{-3} W cm^{-2} in healthy skin and 0.87 10^{-3} W cm^{-2} in pathalogical skin (warmer by 1 °C) (healthy skin at 37 °C, 0.65 10^{-3} W cm^{-2} (Houdas and Guieu 1977)). The basal metabolic rate in young adults is approximately 4.3 10^{-3} W cm^{-2}.)

The absolute measurement of the subepidermal blood flow is also made possible using two methods, as suggested by Severinghaus et al. (Severinghaus et al. 1978). This is of great interest a priori, because the only other absolute measurement method of cutaneous blood flow, namely by epicutaneous xenon clearance, involves the whole skin. But further theoretical as well as experimental studies are needed before advising routine use.

In the first method, the flow is estimated from the equation: $\text{Flux} = E_{O2}/(aO_2 - vO_2)$, where E_{O2} is the epidermal O_2 consumption and $(aO_2 - vO_2)$ the difference of O_2 concentration in arterioles and venules. EO_2 is calculated as described in the paragraph above. Assuming that the capillary PO_2 is midway between arteriolar and venular PO_2 and considering that arteriolar and arterial PO_2 are identical (600 torr), venular PO_2 is calculated, hence its difference (PO_2 with arteriolar PO_2). The difference is converted into difference in concentrations, using the hemoglobin dissociation

curve at 44 °C and Hb = 14 g/dl. With this method, the authors found subepidermal blood flow at 44 °C to be 0.475 ml g^{-1} min^{-1}, a figure nine times higher than using xenon-133 clearance at the same site (volar forearm) at current skin temperature, showing how much the blood flow can be increased when the skin temperature is raised.

The second method is a blood flow measurement during reactive hyperemia, from the $tcPO_2$ recovery rate at 44 °C after occlusion, during pure oxygen inhalation. The $tcPO_2$ recovery rate fits an ascending exponential curve of formula $y = A(1 - \exp^{-t/\tau})$ where y is the $tcPO_2$ on each point of the curve, A is the final $tcPO_2$ and τ the time constant. The logarithmic transformation makes it possible to obtain τ (seconds). Then the blood flow rate Q is obtained by the formula $Q = 60\lambda/\tau$ where $\lambda = 0.9$ is the O_2 skin/blood partition coefficient, supposedly identical to the O_2 water/blood partition coefficient at the same temperature and with the same pressure. The authors found 1.2 ml g^{-1} min^{-1} for the skin blood flow at 44 °C during reactive hyperemia: a very high figure that should be confirmed.

According to the same authors, the measurement of the blood flow rate at 37 °C from the $tcPCO_2$ decreasing rate following occlusion release at 37 °C might also be performed using this method.

6.4 Toxicology

The 44 °C $tcPO_2$ has been shown to be significantly reduced in smokers, as a consequence of the reduced oxygen supply to the tissues in relation to the blood higher HbCO level (Lucas et al. 1989).

7 Practical Advice for Using $tcPO_2$

Calibration in relation to the atmospheric oxygen pressure must be carried out once or twice a day, depending on frequency, because there is a risk of the probe shifting (Winberley et al. 1990).

Theoretically, $PO_{2atm} = 0.2093\ P_{atm} - PH_2O_{atm}$, where 0.2093 is the O_2 fraction in the air. PH_2O_{atm} is obtained by multiplying the relative humidity by the absolute pressure of water vapor at room temperature (provided by tables). In practice, it is only necessary to check that the oxygen atmospheric pressure used by the device is 159 torr. Variations in barometric pressure within the interval 760 ± 15 torr can be ignored.

If a gas control is used for calibration, its value displayed by the device should vary from the standard value by less than 0.5 %.

Before measuring, any trace of ointment or cream must be removed (it would hamper the oxygen passage). Hairy skin should be shaved. A thin layer of electrolytic solution (usually provided by the manufacturer) is applied in order to ensure maximum contact between the electrode and the skin, to facilitate the oxygen transfer and to avoid any air intrusion. When the sensor is placed, 15–20 min are necessary until a stable value is obtained.

A number of concerns should be heeded:

- Heating to 44 °C is harmful for the tissues; therefore use of $tcPO_2$ at a same site must not exceed 4 or 5 h to avoid burns.
- When a $tcPO_2$ decrease is expected because of a PaO_2 decrease, the latter must be measured either through blood sampling or noninvasively by pulse oximetry. However, this technique is approximate, as it indicates only the Hb saturation level.
- Results are different depending on the probes.

8 Commercially Available Devices

- TCM3 Radiometer, Copenhagen, Denmark
- Cutaneous PO_2 monitor 632, Roche-Kontron, Basel, Switzerland

References

Agache P. Pathogénie des ulcères de jambe d'origine veineuse. Angeiologie. 1998;50:11–27.

Agache P-G, Lucas A, Agache A. Influence of age on transcutaneous oxygen pressure. In: Lévêque JL, Agache P, editors. Aging skin properties and functional changes. New York: Marcel Dekker; 1992. p. 125–32.

Agache P, Agache A, Lucas A. Transcutaneous oxygen pressure measurement: usefulness and limitations. In: Boccalon H, editor. Vascular medicine. Amsterdam: Excerpta Medica; 1993. p. 527–31.

Bongard O, Bounameaux H, Fagrell B. Effects of oxygen inhalation on skin microcirculation in patients with peripheral arterial occlusive disease. Circulation. 1992;86:878–86.

Bourgain JL, Grenouillet MC. Mesure transcutanée de la PO_2 et de la PCO_2. Agressologie (Paris). 1985;26:997–1003.

Christensen P, Hjarbaek J, Jensen B, Groenlund J. Measurement of transcutaneous PO_2, PCO_2 and skin blood flow at different probe temperatures using mass spectrometry. Acta Anaesthesiol Scand. 1991;35:631–4.

Coleman LS, Dowd GSE, Bentley G. Reproducibility of $tcPO_2$ measurements in normal volunteers. Clin Phys Physiol Meas. 1986;7:259–63.

Dautzenberg B, Carter H, Sors C. Mesure de la PO_2 par voie transcutanée ($tcPO_2$). Rev Fr Mal Respir. 1981;9:327–35.

Dodd HJ, Gaylarde PM, Sarkany I. Skin oxygen tension in venous insufficiency of the lower leg. J R Soc Med. 1985;78:373–6.

Duteil L, Queille-Roussel C, Czernielewski J. Assessing treatment of psoriasis and eczema by noninvasive methods. In: Frosch PJ, Kligman AM, editors. Noninvasive methods for the quantification of skin functions. Berlin/Heidelberg/New York: Springer; 1993. p. 223–40.

Eickhoff JH, Ishihara S, Jacobsen E. Effect of arterial and venous pressures on transcutaneous oxygen tension. Scand J Clin Lab Invest. 1980;40:755–60.

Hauser CJ, Shoemaker WC. Use of a transcutaneous regional perfusion index to quantify tissue perfusion in peripheral vascular disease. Ann Surg. 1983;197:337–43.

Houdas Y, Guieu JD. La fonction thermique. Villeurbanne: Simep-Editions; 1977.

Huch A, Franzeck UK, Huch R, Bollinger A. A transparent transcutaneous oxygen electrode for simultaneous studies of skin capillary morphology, flow dynamics and oxygenation. Int J Microcirc Clin Exp. 1983;2:103–8.

International Federation of Clinical Chemistry (IFCC) Scientific Division Committee on pH, blood gas and electrolytes. Guidelines for transcutaneous PO_2 and PCO_2 measurement. Ann Biol Clin. 1990;48:39–43.

Kalis B, de Rigal J, Léonard F, Lévêque JL, Riche O, Le Corre Y, de Lacharrière O. In vivo study of scleroderma by non-invasive techniques. Br J Dermatol. 1990;122:785–91.

Kram HB, Appel PL, Shoemaker WL. Multisensor transcutaneous oxymetric mapping to predict below-knee amputation wound healing: use of a critical PO_2. J Vasc Surg. 1989;9:796–800.

Lübbers DW. Theoretical basis of the transcutaneous blood gas measurement. Crit Care Med. 1981;9:721–33.

Lucas A, Agache P, Risold JC, Cuenot C. Variations de la $tcPO_2$ en fonction de la consommation du tabac chez le sujet sain. J Mal Vasc. 1989;14:363–4.

Neidhardt A, Costes Y, Sava P, Roullier M, Christophe JL, Bachour K. Apport en chirurgie vasculaire du monitorage per-opératoire de la circulation périphérique par la pression transcutanée d'oxygène ($tcPO_2$). Conv Méd. 1987;6:1–5.

Ott A, Stüttgen G. Microcirculation in psoriasis. Acta Derm Venereol. 1984;1135:90–102.

Patel BT, Delpy DT, Hillson PJ, Parker D. A topical metabolic inhibitor to improve transcutaneous estimation of arterial oxygen tension in adults. J Biomed Eng. 1989;11:381–3.

Ryan TJ. Direct observation of capillary modifications in the aged. In: Lévêque JL, Agache P, editors. Aging skin: properties and functional changes. New York: Marcel Dekker; 1992. p. 87–104.

Schalla W. The transcutaneous oxygen pressure ($tcPO_2$) as a non-invasive measurement of aerobic skin metabolism and skin permeability in psoriasis. In: Marks R, Plewing G, editors. Skin models. Models to study function and disease of skin. Berlin/Heidelberg/New York: Springer; 1986. p. 136–9.

Severinghaus JW. Current trends in continuous blood gas monitoring. Biotelem Patient Monit. 1979;6:9–15.

Severinghaus JW, Stafford M, Thunstrom AM. Estimation of skin metabolism and blood flow with $tcpO_2$ and $tcpCO_2$ electrodes by cuff occlusion. Acta Anaesthesiol Scand Suppl. 1978;68:9–15.

Takiwaki H. Transcutaneous PO_2 and PCO_2 measurement in dermatology. Acta Derm Venereol Suppl. 1994;185:21–5.

Tronnier H, Böttger EM, Hoffmann E. Transcutane PO_2-Messung unter UV-Therapie von Psoriasis und Akne (Vorläufige Mitteilung). Z Hautkr. 1979;54:546–50.

Versmold HT, Tooley WH, Severinghaus JW. Increase of skin O_2 diffusion resistance with birthweight. Birth Defects Orig Artic Ser. 1979;15:271–2.

Winberley PD, Burnett RW, Covington AK. International Federation of Clinical Chemistry (IFCC) Scientific Division Committee on pH, blood gase and electrolytes. Guidelines for transcutaneous PO_2 and PCO_2 measurement. Ann Biol Clin 1990;48: 39–43.

Skin Blood Flow in Systemic Sclerosis 59

Alessandra Della Rossa, Chiara Baldini, Massimiliano Cazzato, Marta Mosca, and Stefano Bombardieri

Contents

Keywords

Systemic sclerosis (SSc) • Skin • Microvascular involvement • Laser Doppler flowmetry (LDF) • Laser Doppler imaging (LDI) • Laser speckle contrast analysis (LASCA)

1 Introduction

Systemic sclerosis (SSc) is a rare and progressive connective tissue disease of multifactorial origin, characterized by vascular abnormalities and diffuse fibrosis in the skin and internal organs. The pathogenetic cornerstones of the disease are the activation of the immune system, vascular involvement, and increase of extracellular matrix deposition (Black et al. 2009).

Vasculopathy is a central feature of the disease, and structural abnormalities of the microvascular lining are evident in visceral organs as well as in the skin in the earliest stages of the disease (Kahaleh 2004).

Clinical and histologic findings suggest a key role for these alterations especially at the outset of the disease. Both permeability and vasomotility alterations might be due to an imbalance consisting of an increase of vasoconstricting factors (thromboxane, endothelin) associated to a relative decrease of vasodilator substances (prostacyclin and nitric oxide) (Flavahan 2008). The innate and adaptive immune system is activated in the perivascular areas and releases cytokines and growth factors (transforming growth factor beta

A. Della Rossa (✉) • C. Baldini • M. Cazzato • M. Mosca • S. Bombardieri
Dipartimento di malattie muscolo-scheletriche e cutanee, U.O. Reumatologia, Pisa, Italy
e-mail: a.dellarossa@ao-pisa.toscana.it; c.baldini@med.unipi.it; m_cazzato@virgilio.it; marta.mosca@med.unipi.it; s.bombardieri@int.med.unipi.it

P. Humbert et al. (eds.), *Agache's Measuring the Skin*,
DOI 10.1007/978-3-319-32383-1_65

(TGF-β), platelet-derived growth factor (PDGF)), and extensive fibrosis of the dermal and subcutaneous layers develops (Abraham et al. 2009).

The progressive losses of capillaries on one hand, and the vascular remodeling of arteriolar vessels on the other, result in insufficient blood flow, causing severe and chronic tissue hypoxia. Hypoxia is one of the most important stimuli of angiogenesis, leading to the expression of pro-angiogenic molecules, mainly of vascular endothelial growth factor (VEGF), which fosters the angiogenic process. Nevertheless, in SSc patients, there is evidence for defective adaptive angiogenesis. Failure of the angiogenic process in this disease largely depends on alteration in the balance between pro- and anti-angiogenic factors as well as on functional alterations of the molecular and cellular players involved in the angiogenic and vasculogenic program (Cipriani et al. 2011; Manetti et al. 2011).

Given these observations, it stands clear that microvascular involvement has a pivotal importance for the clinician involved in the management of SSc.

Peripheral microvascular damage in this disease is characterized by dynamic alteration of the capillaries that carries a progressive decrease in their density. Microvascular changes are typically observed in the nailfold bed by capillary microscopy and are in fact exploited for the early diagnosis of SSc and prognostication of disease evolution (Cutolo et al. 2010a).

However, capillaroscopy provides mostly static information, and no or few data on the dynamic of microvessels are given by this technique. On the other hand, a number of efforts have been made in the last few years, to explore the dynamic variations of skin blood flow in SSc-related disorders, in order to unveil the earliest alteration of the disease and to provide useful information on the variation of vascular response according to the stage of the disease and to treatment.

In this chapter we will review data about skin blood flow measurement in systemic sclerosis, with particular reference to laser techniques.

2 Techniques for Evaluating Skin Blood Flow

2.1 Clinimetric Methods

2.1.1 Thermometry and Thermal Imaging

Thermometry was introduced for the first time by T. Lewis as a quantitative index of skin blood flow. The measurements are obtained with or without skin contact. The surface temperature can be mapped with infrared cameras or through contact with crystal liquid. Skin temperature is representative of underlying blood flow, with both muscle and skin perfusion believed to contribute to the signal. These methods are seldom used nowadays, due to a number of limitations, such as the lack of discrimination between nutritional and thermoregulatory blood flow, the poor sensitivity for important variation of blood flow and the slow reactivity, and the poor spatial resolution (Imbert et al. 2010).

In clinical practice, thermal imaging is mainly used for the evaluation of Raynaud's phenomenon (Fig. 1). It has been shown that local cold exposure of the hand inhibits the postischemic hyperemic response in patients but not in normal controls; thermal imaging can detect this difference with a fair sensitivity, but it does not seem to discriminate between primary and secondary Raynaud's phenomenon (Imbert et al. 2010; Murray et al. 2009).

3 Global Microvascular Measurements

Different physical sensors are able to evaluate the microcirculation in superficial tissues. They can do this directly, such as the laser techniques, indirectly through nutritional efficacy with transcutaneous oxygen pressure (pO2) measurements, or globally as volume flow in plethysmographic methods (Imbert et al. 2010; Cracowski et al. 2006).

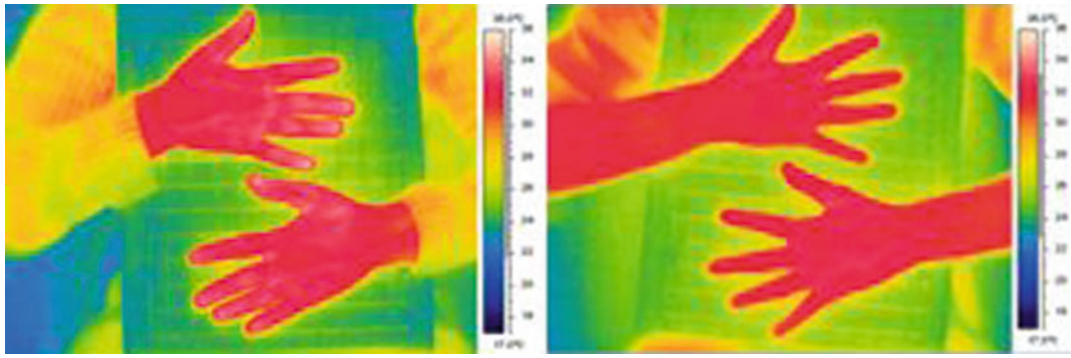

Fig. 1 Thermography images after cold challenge: healthy subject(*left side*) vs. Raynaud's phenomenon(*right side*)

4 Photoplethysmography

Photoplethysmography is an optical measurement technique that can be used to detect changes in blood volume in the microvascular bed of superficial tissues. Up to date photoplethysmography sensors are based on semiconductor technology with LED and matched photodetector devices working at the red or near-infrared wavelengths (Imbert et al. 2010; Allen 2007). Blood test vasoreactivity during cold challenge has been explored in Raynaud's phenomenon; the loss of dicrotic notch has been claimed as a typical sign of Raynaud's phenomenon secondary to systemic sclerosis, due to the reduction of vascular wall compliance (Cooke et al. 1993).

5 LDF and LDI

5.1 LDF

LDF is based on Doppler effect produced by red blood cells as they flow through superficial microvessels, when they reflect laser illumination. Low-power lasers are utilized with a probe able to detect and elaborate Doppler signal (Imbert et al. 2010; Rajan et al. 2009). It is a one-point measurement method, which records the integrated perfusion in a sampling volume in real time. It needs contact of the skin surface to explore by a sensor, fixed to the skin by a double-adhesive transparent tape. The depth of the measurement depends on the laser wavelength and the fiber separation. With standard fiber separation (0,25 mm), a wavelength of 780 nm has a measuring depth of 0,5–1 mm and an approximate volume of 1 mm^3.

In early studies HeNe lasers (632,8 nm) dominated; however, longer wavelengths (780–810 nm) are now preferred due to increased penetration depth and lower absorption by melanin, which shows less dependence on skin color and also a more efficient and stable process in the industrial production, using solid-state laser sources. Moreover, with these wavelengths, any dependence on oxygen saturation is eliminated. The signal captured is proportional to the mean velocity and to the number of red blood cells moving through the sampled tissue volume. Since the volume explored is not precisely determined, the measure is semiquantitative. Moreover, the vessels explored are not only the superficial skin capillaries but also the arterial and venous vessels of superficial and mid-dermis; other "parasite" movements can also influence the measurements. The physiological interpretation of the measurements obtained is thus not always univocal (Imbert et al. 2010; Li et al. 2006).

A number of refinements have improved this type of physiological signal, such as special software to analyze the velocimetric and volumetric

components of the signal or dual wavelength sensors that provide simultaneous measurements at two different depths (Imbert et al. 2010).

The main advantage of this method is its high sensitivity, which allows the recording of perfusion changes over time induced by spontaneous arteriolar vasomotion, as well as those occurring during the influence of physiological stimuli, such as post-occlusive reactive hyperemia (PORH), the venoarteriolar reflex, the reactivity to the administration by iontophoresis of vasoactive substances, or the systemic administration of medications (Fig. 2) (Salvat Melis et al. 2006; Rossi et al. 2012; Fries et al. 2005). Patients with SSc are characterized by either lower or normal peripheral blood perfusion as compared to healthy subjects (Correa et al. 2010; Cracowsky et al. 2002; Cutolo et al. 2010). Finger blood perfusion correlates negatively with the extent of nailfold microvascular damage evaluated by capillaroscopy and improves with i.v. iloprost treatment (Cutolo et al. 2010b; Sulli et al. 2014, 2013).

Moreover, SSc patients have impaired microvascular responses as compared with controls. Ischemic challenge and cold test have yielded similar results, where some studies reported no consistent differences in these tests between primary and secondary RP, while others contradicted these results (Cracowsky et al. 2002; Correa et al. 2010; Rajagopalan et al. 2003). A different kinetic of response to ischemic challenge and cold stimulus has been claimed within SSc cutaneous subsets, diffuse disease showing a distinct alteration of ischemic test and limited disease with a prevalent modification of the response to cold (Grattagliano et al. 2010).

SSc shows abnormal neurovascular response to local heating that is not related to the severity of skin involvement (Salvat Melis et al. 2006; Roustit et al. 2008; Boignard et al. 2005). Local release of vasodilator substances has yielded contradictory results; some authors claimed an alteration of endothelial dependent but not endothelial independent vasodilatation (Anderson et al. 1999), whereas others have reported an impairment of both responses (Rossi et al. 2008).

Fig. 2 Laser flow measurement: a probe detects Doppler shift of a low power laser beam as red blood cells flow through microcirculation. Iontophoresis allows local application of vasodilator substances. Tracings of blood flow are depicted on the screen (Courtesy of A. Moneta, Perimed Italia srl)

6 Laser Doppler Perfusion Imaging

Laser Doppler imaging (LDI) is a relatively new method that allows an objective assessment of skin perfusion over a wide skin surface. This is currently performed by a scanning beam and point by point perfusion measurements, which consequently lead to imaging times of several minutes. The measurement is noncontact and can register chronic changes or measure repetitively in quick succession. The LDI uses normally a low-power laser beam (1 mW) with a wavelength of 633 nm. Perfusion signals are combined to form a color-coded map, with a color scale ranging from dark blue (lowest value) to red (highest value) (Fig. 3). The size of the scanned area may range from 5×5 to 50×50 cm, depending on the distance of the scanner. The blood flow is expressed in arbitrary perfusion unit, since also in this case the volume sampled is not accurately determined. This technique, although limited by the slowness of imaging acquisition, has the advantage of conjugating the possibility of scanning a large surface area and evaluating dynamic changes over time (Imbert et al. 2010).

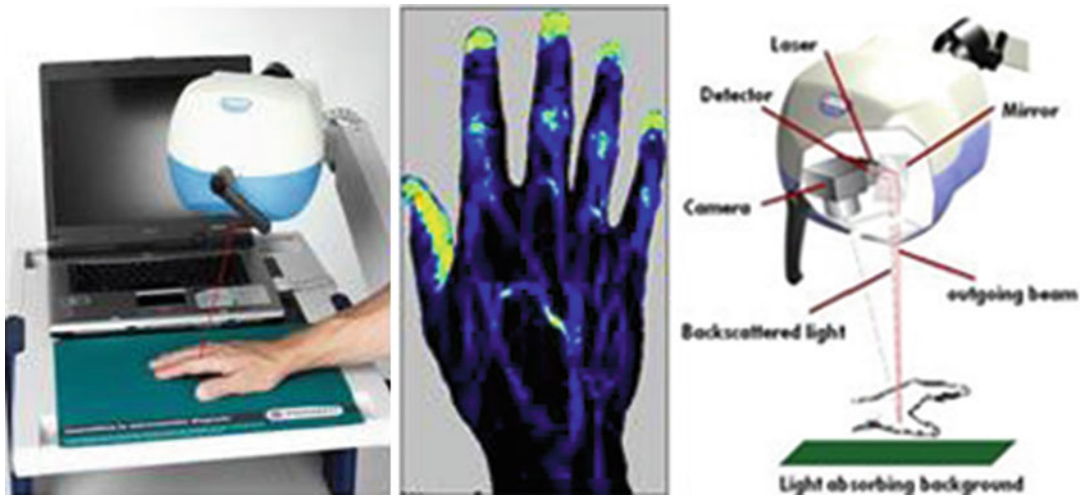

Fig. 3 Laser Doppler perfusion imager. Intensity signal from a color-coded scale ranging from *dark blue* (lowest value) to *red* (highest value) (Courtesy of A. Moneta, Perimed Italia srl)

It is a valuable tool for refining the differential diagnosis of Raynaud's phenomenon (Szabo et al. 2008; Rosato et al. 2009a) and for the evaluation of the dynamic changes of microcirculation after the local administration of vasoactive substances by iontophoresis or the systemic administration of drugs (Anderson et al. 2004; Rosato et al. 2010; Shah et al. 2013). Through intensity imaging and colorimetric scale, it is possible to evaluate the distribution and homogeneity of flux and regional differences between different skin areas; an association of dyshomogeneous perfusion and lack of proximal distal perfusion gradient was observed in SSc patients. This contrasts with healthy subject, where the gradient was maintained and the flux was homogeneous, and primary Raynaud's subjects, where lack of proximal distal gradient was combined with homogeneity of flux (Rosato et al. 2009a). Moreover, laser imaging alone can provide an indirect provisional estimate of possible digital artery obstruction (Rosato et al. 2009b).

7 Laser Speckle Contrast Imaging

A newer method to dynamically explore a relatively large skin area is laser speckle contrast imaging (LASCA). Like LDI, LASCA (or Perfusion Speckle Imager, PSI) is a noncontact method and can register blood flow over an area that may range from a few millimeters to several centimeters depending on the type of scanner and the distance of the head of the scanner from the skin surface. A laser-diffused light, with a wavelength of 785 nm, illuminates the area of interest, producing a speckle pattern of the whole scanned skin area, without the need of a point-to-point scanning, like in LDI described above. When a surface is illuminated by laser light, the backscattered light will generate a random interference pattern, consisting of dark and bright "dots." This pattern is called a speckle pattern. If the illuminated surface is static, the speckle pattern is stationary, and dots have a high contrast between each other. When there are moving particles, such as red blood cells in the living tissue, the speckle pattern will change over time, since the contrast between dots decreases inversely to the speed of the moving objects. These dynamic changes in the contrast are instantaneously recorded by a special camera positioned in the scanner head, with a high spatial resolution. Therefore, the PSI system presents the same advantages of LDI, with a higher speed of imaging acquisition and a better resolution. It is therefore possible to produce colored maps representing the blood flow distribution and also

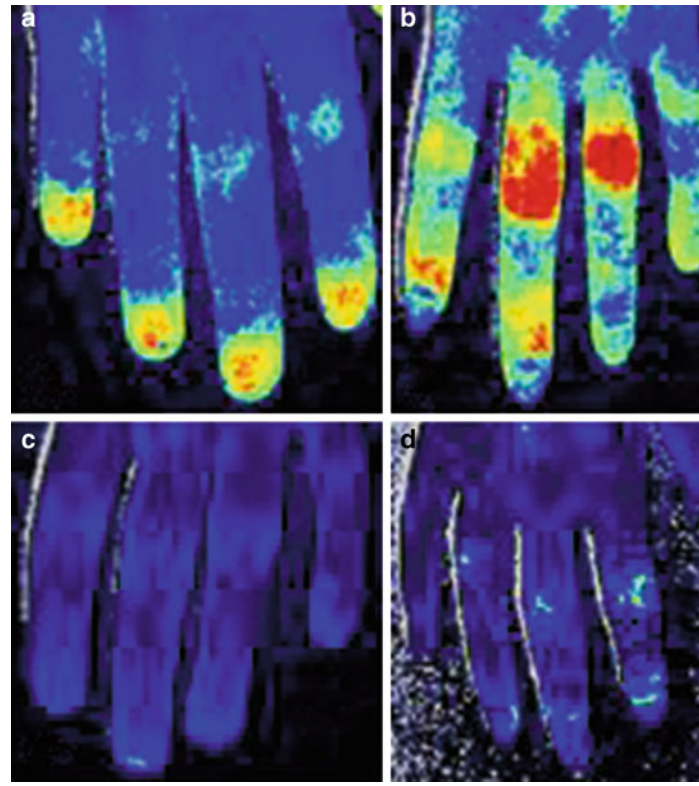

Fig. 4 Perfusion images are useful to detect regional differences in perfusion distribution and homogeneity of flux: i.e., presence of proximal distal gradient(**a**, **b**) with homogenous (**a**) vs. inhomogenous flux distribution (**b**), absence of proximal distal gradient (**c**, **d**) with homogenous (**c**) vs. inhomogenous flux distribution (**d**) (Pericam PSI, Perimed, Jarfalla)

to record continuously the blood flow changes, with movies owing a frame rate up to 90 frames per second (depending on the size of the scanned area) (Imbert et al. 2010; Briers 2006). In analogy with laser Doppler imaging, it is possible to evaluate the distribution and homogeneity of flux and regional differences between different skin areas (Fig. 4) (Della Rossa et al. 2013; Ruaro et al. 2013); at the same time, it is possible to explore the dynamic of microcirculation after physiological stimuli (Fig. 5), as well as the response to topical application of vasodilator substances by iontophoresis (Ruaro et al. 2013; Roustit et al. 2010).

Within SSc patients, difference in the ischemic challenge may help to better refine disease sub-setting, as early disease seems to show exaggerated POHR as compared to established disease. Peripheral blood perfusion is lower in SSc patients as compared to healthy subjects; moreover, skin blood flow linearly decreases with the increase of severity of microangiopathy assessed by capillaroscopy (Ruaro et al. 2013). When measuring basal skin blood flow, LASCA was found significantly less time-consuming than LDF; LASCA and LDF are highly correlated (Ruaro et al. 2013; Roustit et al. 2010), but LASCA shows lower intraoperator variability versus LDF analysis and is much better accepted by patients (Roustit et al. 2010).

8 Summary

Laser techniques have gained a growing attention as reliable and noninvasive methods to assess vascular reactivity in SSc patients.

LDF is a contact laser with single-point sampling; it is very sensitive and allows reliably to assess in real time small and rapid variation in skin blood flow, in response to physiological stimuli or to the application of vasodilator substances by iontophoresis or the administration of systemic drugs. The disadvantages of this technique are

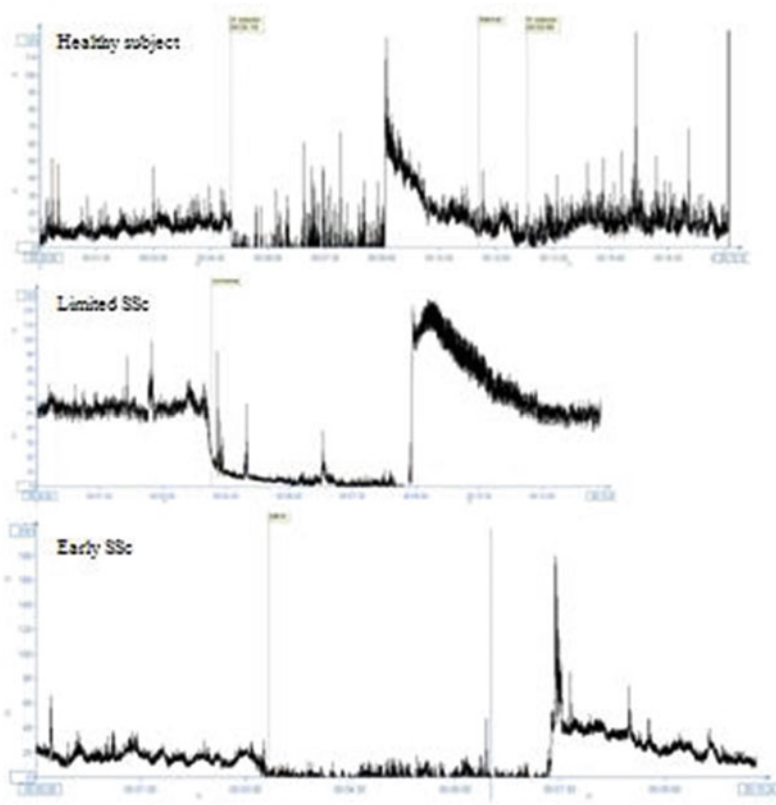

Fig. 5 Tracings of the postocclusive hyperemic response in a healthy subject as compared to limited SSc and early SSc (36) (Pericam PSI, Perimed, Jarfalla)

related to the need of contact with the skin (needs skin integrity) and the study of a single point that does not enable to explore larger areas.

LDI permits the mapping of a larger area and does not need contact, allowing the evaluation also of areas of injured skin. Through intensity color scales, it enables the assessment of regional differences in flow distribution, and it can consent the dynamic evaluation of flow after different kinds of stimuli (physical, pharmacological, local, or systemic). The main disadvantage is related to the relatively high scanning time that might not enable to detect shorter variations of flux.

LASCA is a newer whole field imaging tool that combines the rapidity of acquisition to the possibility of mapping a relatively large skin area without contact. It allows both qualitative evaluation of skin blood flow and assessment of flux distribution according to different areas. Dynamic variation after physiological or pharmacological stimuli can be assessed as well. It is reproducible, rapid, and much better accepted by patients than LDF.

Acknowledgment We are grateful to Dr Achille Moneta, Perimed Italia srl, for the revision of the technical sections of the manuscript and for supplying pictures.

References

Abraham DJ, Krieg T, Distler J, Distler O. Overview of pathogenesis of systemic sclerosis. Rheumatology (Oxford). 2009;48 suppl 3:iii3–7.

Allen J. Photoplethysmography and its application in clinical physiological measurement. Physiol Meas. 2007;28:R1–39.

Anderson ME, Moore RL, Hollis S, Clark S, Jayson MIV, Herrick AL. Endothelial dependent vasodilatation is impaired in patients with systemic sclerosis, as assessed by low dose iontophoresis. Clin Exp Rheumatol. 1999;17:49–54.

Anderson ME, Moore TL, Hollis S, Jayson MIV, King TA, Herrick AL. Digital vascular response to topical

glyceryl trinitrate, as measured by laser Doppler imaging, in primary Raynaud's phenomenon and systemic sclerosis. Rheumatology. 2004;41:324–8.

Black CM, Matucci-Cerinic M, Guillevin L. Progress in systemic sclerosis: a 10 year perspective. Rheumatology (Oxford). 2009;48(Suppl3):iii1–2.

Boignard A, Salvat Melis M, Carpentier PH, Minson CT, Grange L, Duc C, Darrot-Reynauld F, Cracowski JL. Local hyperemia to heating is impaired in secondary Raynaud's phenomenon. Artrhitis Res Ther. 2005;7:R1103–12.

Briers JD. Laser speckle contrast imaging for measuring blood flow. Proceedings of the symposium on photonics technologies for 7th framework program. Wroclaw 12–14 Oct 2006: 328–332.

Cipriani P, Marrelli A, Liakouli V, Di Benedetto P, Giacomelli R. Cellular players in angiogenesis during the course of systemic sclerosis. Autoimmun Rev. 2011;10(10):641–6.

Cooke ED, Steinberg MD, Pearson RM, et al. Reflex sympathetic dystrophy and repetitive strain injury: temperature and microcirculatory changes following mild cold stress. J R Soc Med. 1993;86:690–3.

Correa MJU, Andrade LEC, Kayser C. Comparison of laser doppler imaging, fingertip lacticemy test and nailfold capillaroscopy for assessment of digital microcirculation in systemic sclerosis. Arthritis Res Ther. 2010;12(4):R157.

Cracowski JL, Minson CT, Salvat-Melis M, Halliwill JR. Methodological issues in the assessment of skin microvascular endothelial function in humans. Trends Pharmacol Sci. 2006;27:503–8.

Cracowsky JL, Carpentier PH, Imbert B, Cachot S, Labesque FS, Bessard J, Bessard G. Increased urinary F2-isoprostanes in systemic sclerosis, but not in primary Raynaud's phenomenon. Arthritis Rheum. 2002;46:1319–23.

Cutolo M, Sulli A, Smith V. Assessing of microvascular changes in systemic sclerosis. Diagnosis and management. Nat Rev Rheumatol. 2010a;6:578–87.

Cutolo M, Ferrone C, Pizzorni C, Soldano S, Seriolo B, Sulli A. Peripheral blood perfusion correlates with microvascular abnormalities in Systemic sclerosis: a laser Doppler and nailfold videocapillaroscopy study. J Rheum. 2010b;37:1174–80.

Della Rossa A, Cazzato M, d'Ascanio A, Tavoni A, Bencivelli W, Pepe P, Mosca M, Baldini C, Rossi M, Bombardieri S. Alteration of microcirculation is a hallmark of very early systemic sclerosis patients: a laser speckle contrast analysis. Clin Exp Rheumatol. 2013;31(2 Suppl 76):109–14.

Flavahan NA. Regulation of vascular reactivity in scleroderma: new insights into Raynaud's phenomenon. Rheum Dis Clin N Am. 2008;34(1):81–7.

Fries R, Kaveh S, Wilmowsky H, Bohm M. Sildenafil in the treatment of Raynaud's phenomenon resistant to vasodilator therapy. Circulation. 2005;112:2980–5.

Grattagliano V, Iannone F, Praino E, De Zio A, Riccardi MT, Carrozzo N, et al. Digital laser doppler flowmetry may discriminate "limited" from "diffuse" systemic sclerosis. Microvasc Res. 2010;80(2):221–6.

Imbert B, Carpentier P. Techniques for evaluating the microcirculation. In: Cutolo M, Smith V, Sulli A, editors. Atlas of capillaroscopy in rheumatic diseases. Milano: Elsevier; 2010. p. 17–24. Chapter 3.

Kahaleh MB. Raynaud's phenomenon and the vascular disease in scleroderma. Curr Opin Rheumatol. 2004;16:718–22.

Li L, Mac-Mary S, Marsaut D, et al. Age related changes in skin topography and microcirculation. Arch Dermatol Res. 2006;297:412–6.

Manetti M, Guiducci S, Ibba-Manneschi L, Matucci-Cerinic M. Impaired angiogenesis in systemic sclerosis: the emerging role of the antiangiogenic VEGF(165) b splice variant. Trends Cardiovasc Med. 2011;21(7):204–10.

Murray AK, Moore TL, Manning JB, et al. Non invasive imaging techniques in the assessment of scleroderma spectrum disorders. Arthritis Rheum. 2009;61:103–11.

Rajagopalan S, Pfenninger D, Kehrer C, Chakrabarti A, Somers E, Pavlic R, et al. Increased asymmetric dimethylarginine and endothelin 1 levels in secondary Raynaud's phenomenon implications for vascular dysfunction and progression of disease. Arthritis Rheum. 2003;48(7):1992–2000.

Rajan V, Varghese B, Van Leeuwen TG, Steenbergen W. Review of methodological developments in laser Doppler flowmetry. Lasers Med Sci. 2009;24:269–83.

Rosato E, Borghese F, Pisarri S, Salsano F. Laser Doppler perfusion imaging is useful in the study of Raynaud's phenomenon and improves capillaroscopic diagnosis. J Rheumatol. 2009a;36:2257–63.

Rosato E, Roumpedaki E, Pisarri S, Salsano F. Digital ischemic necrosis in a patient with systemic sclerosis: the role of laser Doppler perfusion imaging. VASA. 2009b;38(4):390–3.

Rosato E, Molinaro I, Borghese F, Rossi C, Pisarri S, Salsano F. Bosentan improves skin perfusion of hands of patients with systemic sclerosis with pulmonary artery hypertension. J Rheumatol. 2010;37(12):2531–9.

Rossi M, Bazzichi L, Di Maria C, Franzoni F, Raimo K, Della Rossa A, Santoro G, Bombardieri S. Blunted increase of digital skin vasomotion following acetylcholine and sodium nitroprusside iontophoresis in systemic sclerosis patients. Rheumatology (Oxford). 2008;47(7):1012–7.

Rossi M, Bazzichi L, Ghiadoni L, Mencaroni I, Franzoni F, Bombardieri S. Increased skin vasoreactivity and stimulated vasomotion associated with simvastatin therapy in systemic sclerosis hypercholesterolemic patients. Rheumatol Int. 2012;32:3715–21.

Roustit M, Simmons GH, Carpentier P, Cracowski JL. Abnormal digital neurovascular response to local heating in systemic sclerosis. Rheumatology. 2008;47:860–4.

Roustit M, Millet C, Blaise S, Dofournet B, Cracowsky JL. Excellent reproducibility of laser speckle contrast imaging to assess skin microvascular reactivity. Microvasc Res. 2010;80:505–11.

Ruaro B, Sulli A, Alessandri E, Pizzorni C, Ferrari G, Cutolo M. Laser speckle contrast analysis: a new method to evaluate peripheral blood perfusion in systemic sclerosis patients. Ann Rheum Dis. 2013. doi:10.1136/annrheumdis-2013-203514. [Epub ahead of print] PubMed.

Salvat Melis M, Carpentier PH, Minson CT, Boignard A, Mc Cord GR, Paris A, Moreau-Gaudry A, Cracowski JL. Digital thermal hyperaemia impairment does not relate to skin fibrosis or macrovascular disease in Systemic sclerosis. Rheumatology. 2006;45:1490–6.

Shah AA, Schiopu E, Hummers LK, Wade M et al. Open label study of escalating doses of oral treprostinil diethanolamine in patients with systemic sclerosis and digital ischemia: pharmacokinetics and correlation with digital perfusion. Arthritis Res Ther. 2013;15(2):R54.

Sulli A, Ruaro B, Smith V, Pizzorni C, Zampogna G, Gallo M, Cutolo M. Progression of nailfold microvascular damage and antinuclear antibody pattern in systemic sclerosis. J Rheumatol. 2013;40(5):634–9.

Sulli A, Ruaro B, Alessandri E, Pizzorni C, Cimmino MA, Zampogna G, Gallo M, Cutolo M. Correlations between nailfold microangiopathy severity, finger dermal thickness and fingertip blood perfusion in systemic sclerosis patients. Ann Rheum Dis. 2014;73 (1):247–51.

Szabo N, Csijki Z, Szanto A, et al. Functional and morphological evaluation of hand microcirculation with nailfold capillaroscopy and laser Doppler imaging in Raynaud's and Sjogren's syndrome and poly/dermatomyositis. J Rheumatol. 2008;37:23–9.

Evaluation of Port-Wine Stains and Its Treatment

60

Yuanhong Li

Contents

Port-wine stains (PWSs) are cosmetically disfiguring, congenital capillary and venular malformations that affect 0.3–0.5 % of newborns (Jacobs and Walton 1976; Lorenz et al. 2000). The lesions are most frequently located on the face (often in a trigeminal dermatomal distribution) and the neck, which cannot disappear spontaneously. At birth, lesions are first noted as subtle, light pink patches. Delayed or inadequate treatment may result in nodularity, hypertrophy, and soft tissue overgrowth, causing dysmorphism, asymmetry, and occasional spontaneous bleeding (Kira et al. 2009). These changes in color and contour are attributed to progressive ectasia of the abnormal dermal vascular plexus. So it is essential to treat PWS as early as possible and maintain treatment to prevent the development of vascular nodules and hypertrophy in later years.

There appears to be no hereditary predilection for PWS within families and no certain risk factors for PWSs as well as no known ways to prevent them. The development of PWS is hypothesized that the deficiency or absence of surrounding neurons regulating blood flow through the ectatic postcapillary venules. The blood vessels are unable to constrict normally and remain permanently dilated. It is believed that PWSs develop within the first 2–8 weeks of gestations (Schneider et al. 1988). In addition, PWSs may occasionally develop progressive lymphangiectasia, soft tissue hypertrophy (Klippel-Trenaunay-Weber syndrome), Cobb syndrome, and Proteus syndrome (PS).

Y. Li (✉)
Department of Dermatology, No.1 Hospital of China Medical University, Shenyang, People's Republic of China
e-mail: liyuanhong@vip.sina.com

P. Humbert et al. (eds.), *Agache's Measuring the Skin*,
DOI 10.1007/978-3-319-32383-1_83

On histopathology, PWSs consist of dilated, ectatic capillary, and venule-sized vessels in both papillary and reticular dermis. These vessels, unlike capillary hemangiomas, are not proliferative and therefore only grow proportionally with the individual. While hemangiomas tend to spontaneous regression, PWS vessels become progressively tortuous and dilated over time. The pathogenesis is still not fully understood. One hypothesis is a lost capacity of vessel constriction and thus an abnormal regulation of blood flow. Recent studies indicate that RASA1 mutations cause capillary and arteriovenous malformations and hereditary capillary malformations and limb enlargement without arteriovenous malformation (Revencu et al. 2008; Boon et al. 2005; Hershkovitz et al. 2008). Vascular endothelial growth factor (VEGF) and VEGF-receptor 2 expression are significantly increased in PWS compared to controls, indicating that VEGF and VEGF-R2 may contribute to vessel proliferation and vasodilatation (Vural et al. 2008).

Traditional therapies including excision, cryotherapy, skin grafting, dermabrasion, and radiation therapy were reported to be inefficient and had many unacceptable side effects. In recent decades, laser therapies such as pulsed dye laser (PDL) have gained great popularity for PWS (Landthaler and Hohenleutner 2006). Other light-based devices, including alexandrite lasers, intense pulsed light (IPL), and combined 585/1064-nm devices, are also used to achieve desired lesion lightening. The basic principle is selective photothermolysis (SP). The preferential absorption of laser light is absorbed by hemoglobin and the subsequent conversion of the absorbed light into thermal energy that leads to the coagulation of blood vessels.

1 Treatment

1.1 PDL

PDL devices (577 nm, 585 nm, or 595 nm) are the most frequently used lasers to treat PWSs. Yellow light produced by PDL is preferentially absorbed by hemoglobin in the PWS blood vessels where, after being converted to heat, it causes thermal damage and thrombosis. Furthermore, the thermal relaxation time (Tr) for skin blood vessels 50–150 um in diameter is between 1.4 and 12.8 ms, so the 0.45–50 ms pulse duration produced by these lasers matches the Tr for dermal blood vessels, which confine the laser energy to the targeted vessel before much heat is lost by thermal diffusion out of the exposure field (Nelson et al. 1995).

It was shown that the penetration depth of 585-nm PDL is 1.2 mm, comparing to 0.5 mm at 577-nm PDL, below the basal membrane while retaining vascular selectivity (Tan et al. 1989). Histological studies (Fiskerstrand et al. 1996; Hohenleutner et al. 1995) showed that using 585-nm PDL treatment at 0.45-ms pulse duration, 5-mm spot size, and 6–8 J/cm^2 radiant exposure, the photocoagulation occurred at a depth of approximately 0.65 mm. Moreover, complete photocoagulation of the vessel lumen occurs in superficial vessels up to approximately 150 μm in diameter. However, larger and deeper vessels, owing to both shielding by superficial vessels and inadequate penetration depth, remain resistant (Lucassen et al. 1996), so longer PDL wavelengths are needed to further enhance the depth of photocoagulation and clearance (Geronemus et al. 2000). New-generation of long-pulsed tunable dye lasers (LPTDLs) offer potential advantages over conventional PDL. The LPTDL offers a pulse length of 1.5 ms and tunable wavelengths from 585 to 600 nm. These parameters are more useful in PWS that consist of more ectatic and deeper located vessels. The absorption coefficient of oxygenated hemoglobin is substantially lower at 595 nm than at 585 nm (Greve and Raulin 2004; Chang et al. 2002; Prahl 1999). Therefore, higher fluence and longer pulse durations are necessary when using a wavelength of 595 nm.

1.2 Pulsed Nd:YAG Laser (1,064 nm)

The penetration depth of 1,064 nm Nd:YAG laser pulses is deeper than PDL. Theoretically, it can be used to impact thicker and deep-lying blood vessels, which have particularly advantage in matured or hypertrophic PWSs. However, thermal injury of deeper blood vessels may lead to necrosis of

surrounding dermis and increase the risk of scarring compared to PDL. Yang et al. (2005) reported that 1,064 nm Nd:YAG laser was as effective as the PDL in the treatment of PWSs with the minimum purpuric dose. The 1,064-nm Nd:YAG laser also showed to be safe and effective for treating hypertrophic PWS of the lip (Kono et al. 2009).

In conclusion, the 1,064-nm Nd:YAG laser is an important device in the armamentarium of treatment options for PWS, particularly in the case of nodularity and hypertrophy.

1.3 A Dual-Wavelength Laser System (595-nm PDL and 1,064-nm Nd:YAG Laser)

The exact nature of the synergy for vascular lesions between PDL and Nd:YAG lasers remains unclear. One possible explanation is the shift in the light-absorption properties of blood during coagulation. The dual-wavelength laser system targets oxyhemoglobin by the 595-nm wavelength and then targets the methemoglobin (converted from oxyhemoglobin) by the latter 1,064-nm wavelength, because methemoglobin has a significant absorption peak near 1064 nm (Alves and Wajnberg 1993; Randeberg et al. 2004). In 2009, Alster and Tanzi (2009) reported that the dual-wavelength laser system was superior to PDL alone in the treatment of recalcitrant and hypertrophic PWS. Side effects were limited to mild purpura and vesicle formation in one patient that resolved without sequelae in 6 days. The synergies between PDL and 1064-nm Nd:YAG laser have also been evaluated by other authors and proved to be effective (Borges da Costa et al. 2009).

1.4 IPL

IPL devices emit polychromatic incoherent high-intensity pulsed light with an emission spectrum ranging from 500 to 1,400 nm, and pulse durations are in millisecond range. Therefore, IPL systems have a potential advantage over other laser systems because they incorporate the highly oxyhemoglobin selective wavelengths around 577–600 nm and also emit longer wavelengths allowing deeper penetration into the dermis and deeper capillary destruction (McGill et al. 2008).

IPL provides an alternative choice for PWS, owing to its broad-spectrum, lesser frequency of complications, and economic consideration. In some cases, fresh or laser-resistant PWS was effectively treated by IPL sources (Raulin et al. 1999; Bjerring et al. 2003; Ozdemir et al. 2008). Recently, Wang et al. (2013) have reported that 29 Chinese neck PWS patients (without any treatments before) received IPL therapy for five times at intervals of 4–5 weeks. Over 60 % patients achieved more than 50 % improvement.

1.5 Alexandrite Laser

The 755-nm alexandrite laser has been proven particularly useful in the treatment of hypertrophic and PDL-resistant PWS (Li et al. 2008; Izikson et al. 2009), especially when used in combination with PDL. The alexandrite laser has selective absorption of deoxyhemoglobin over oxyhemoglobin, so in theory it should preferentially damage venules (i.e., PWS vasculature) over arterioles and has 50–70 % deeper tissue penetration than PDL. We also need to tell patients that permanent hair reduction may occur with the alexandrite laser. Owing to the deeper tissue penetration and decreased absorption by hemoglobin of longer wavelength lasers, the alexandrite laser are associated with elevated risk of adverse effects such as pigmentary changes and scarring.

1.6 Photodynamic Therapy (PDT)

The basic principle of PDT is the intralesional or intracirculatory addition of an exogenous chromophore into the ectatic capillaries, serving as a photosensitizing drug. The tissue-localized drug is irradiated at an appropriate wavelength for selective absorption by the photosensitizer. This leads to the generation of reactive oxygen species, inducing intracapillary photothermal and photochemical effects and the destruction of the

vascular lesions in the dermis without damage to the normal overlying epidermis.

In 2013, Gao et al. (2013) reported a side-by-side comparison of PDT and PDL in the treatment of PWS birthmarks. 585-nm pulsed PDT was carried out with a combination of hematoporphyrin monomethyl (HMME) and a low-power copper vapor laser (510.6 and 578.2 nm). For red PWS, the blanching rates of PDL and PDT at 2 months ranged from 11–24 % to 22–55 %, respectively. For purple PWS, blanching rates of PDL and PDT ranged from 8–33 % to 30–45 %, respectively, which meant PDT is at least as effective as PDL and, in some cases, superior. Other authors did not find any significant benefit in combining PDT with PDL compared to PDL alone (Evans et al. 2005). However, other authors found a beneficial effect in combining benzoporphyrin derivative monoacid ring PDT with PDL in contrast to PDL alone [34].

In conclusion, PDT might offer additional therapeutic benefits in the treatment of PWS, but sometimes prolonged systemic visible light sensitivity after intravenous administration of porphyrin derivatives et al. practical problems limit its clinical application.

1.7 Dye Pulsed Light (Dye-PL)

Very recently, dye-PL has been introduced to treat PWS. The wavelength of dye-PL is from 500 to 600 nm, which incorporate the highly oxyhemoglobin selective wavelengths at 542 nm and 577 nm. The wavelength of dye-PL is close to 585/595-nm PDL. Theoretically, it is supposed to be suitable for the treatment of PWS. Further clinical and basic researches are needed to evaluate its efficacy.

2 Conclusion

Many different laser/light systems, as well as alternative treatment strategies, have been used to treat PWS. The 585–600 nm PDL with variable pulse widths (ranging from 0.45 to 10 ms) in combination with epidermal cooling modality proved to be safe and effective. However, blood vessel size and depth of PWS as well as revascularization make it difficult to completely eradicate lesions with current laser/light technology. Newer approaches and further randomized controlled trials are needed to establish the role of incoherent light sources and lasers other than the PDL.

References

Alster TS, Tanzi EL. Combined 595-nm and 1,064-nm laser irradiation of recalcitrant and hypertrophic port-wine stains in children and adults. Dermatol Surg. 2009;35:914–9.

Alves OC, Wajnberg E. Heat denaturation of metHb and HbNO: e.p.r. evidence for the existence of a new hemichrome. Int J Biol Macromol. 1993;15:273–9.

Bjerring P, Christiansen K, Troilius A. Intense pulsed light source for the treatment of dye laser resistant port-wine stain. J Cosmet Laser Ther. 2003;5:7–13.

Boon LM, Mulliken JB, Vikkula M. RASA1: variable phenotype with capillary and arteriovenous malformations. Curr Opin Genet Dev. 2005;15(3):265–9.

Borges da Costa J, Boixeda P, Moreno C, Santiago J. Treatment of resistant port-wine stains with a pulsed dual-wavelength 595- and 1064-nm laser: a histochemical evaluation of the vessel wall destruction and selectivity. Photomed Laser Surg. 2009;27(4):599–605.

Chang CJ, Kelly KM, Van Gemert MJ, Nelson JS. Comparing the effectiveness of 585-nm vs 595-nm wavelength pulsed dye laser treatment of port-wine stains in conjunction with cryogen spray cooling. Lasers Surg Med. 2002;31(5):352–8.

Evans AV, Robson A, Barlow RJ, Kurwa HA. Treatment of port-wine stains with photodynamic therapy, using pulsed dye laser as a light source, compared with pulsed dye laser alone: a pilot study. Lasers Surg Med. 2005;36(4):266–9.

Fiskerstrand EJ, Svaasand LO, Kopstad G, Ryggen K, Aase S. Photothermally induced vessel-wall necrosis after pulsed dye laser treatment: lack of response in port-wine stains with small sized or deeply located vessels. J Invest Dermatol. 1996;107:671–5.

Gao K, Huang Z, Yuan KH, Zhang B, Hu ZQ. Side-by-side comparison of photodynamic therapy and pulsed-dye laser treatment of port-wine stain birthmarks. Br J Dermatol. 2013;168(5):1040–6.

Geronemus RG, Quintana AT, Lou WW, Kauvar AN. High-fluence modified pulsed dye laser photocoagulation with dynamic cooling of port-wine stains in infancy. Arch Dermatol. 2000;136:942–3.

Greve B, Raulin C. Prospective study of port-wine stain treatment with dye laser: comparison of two wavelengths (585 nm vs. 595 nm) and two pulse durations

(0.5 milliseconds vs. 20 milliseconds). Lasers Surg Med. 2004;34(2):168–73.
Hershkovitz D, Bercovich D, Sprecher E, Lapidoth M. RASA1 mutations may cause hereditary capillary malformations without arteriovenous malformations. Br J Dermatol. 2008;158(5):1035–40.
Hohenleutner U, Hilbert M, Wlotzke U, Landthaler M. Epidermal damage and limited coagulation depth with the flashlamp-pumped pulsed dye laser: a histochemical study. J Invest Dermatol. 1995;104:798–802.
Izikson L, Nelson JS, Anderson RR. Treatment of hypertrophic and resistant port wine stains with a 755 nm laser: a case series of 20 patients. Lasers Surg Med. 2009;41:427–32.
Jacobs AH, Walton RG. The incidence of birthmarks in the neonate. Pediatrics. 1976;58:218–22.
Kira M, Roy GG, Hale EK. Port wine stain progression: a potential consequence of delayed and inadequate treatment? Lasers Sur Med. 2009;41:423–6.
Kono T, Frederick Groff W, Chan HH, Sakurai H, Yamaki T. Long-pulsed neodymium:yttrium-aluminum-garnet laser treatment for hypertrophic port-wine stains on the lips. J Cosmet Laser Ther. 2009;11(1):11–3.
Landthaler M, Hohenleutner U. Laser therapy of vascular lesions. Photodermatol Photoimmunol Photomed. 2006;22:324–32.
Li L, Kono T, Groff WF, Chan HH, Kitazawa Y, Nozaki M. Comparison study of a long-pulse pulsed dye laser and a long-pulse pulsed alexandrite laser in the treatment of port wine stains. J Cosmet Laser Ther. 2008;10:12–5.
Lorenz S, Maier C, Segerer H, et al. Skin changes in newborn infants in the first 5 days of life. Hautarzt. 2000;51:396–400.
Lucassen GW, Verkruysse W, Keijzer M, van Gemert MJ. Light distributions in a port wine stain model containing multiple cylindrical and curved blood vessels. Lasers Surg Med. 1996;18:345–57.
McGill DJ, MacLaren W, Mackay IR. A direct comparison of pulsed dye, alexandrite, KTP and Nd:YAG lasers and IPL in patients with previously treated capillary malformations. Lasers Surg Med. 2008;40(6):390–8.
Nelson JS, Milner TE, Svaasand LO, Kimel S. Laser pulse duration must match the estimated thermal relaxation time for successful photothermolysis of blood vessels. Lasers Med Sci. 1995;10:9–12.
Ozdemir M, Engin B, Mevlito lu I. Treatment of facial port-wine stains with intense pulsed light: a prospective study. J Cosmet Dermatol. 2008;7:127–31.
Prahl, S. (1999). Optical absorption of hemoglobin. http://omlc.ogi.edu/spectra/hemoglobin/. Accessed 12 Dec 2010.
Randeberg LL, Bonesronning JH, Dalaker M, et al. Methemoglobin formation during laser induced photothermolysis of vascular skin lesions. Lasers Surg Med. 2004;34:414–9.
Raulin C, Schroeter C, Weiss RA, et al. Treatment of port-wine stain with a noncoherent pulsed light source: a retrospective study. Arch Dermatol. 1999;135:679–83.
Revencu N, Boon LM, Mulliken JB, Enjolras O, Cordisco MR, Burrows PE, Clapuyt P, Hammer F, Dubois J, Baselga E, Brancati F, Carder R, Quintal JM, Dallapiccola B, Fischer G, Frieden IJ, Garzon M, Harper J, Johnson-Patel J, Labreze C, Martorell L, Paltiel HJ, Pohl A, Prendiville J, Quere I, Siegel DH, Valente EM, Van Hagen A, Van Hest L, Vaux KK, Vicente A, Weibel L, Chitayat D, Vikkula M. Parkes Weber syndrome, vein of Galen aneurysmal malformation, and other fast-flow vascular anomalies are caused by RASA1 mutations. Hum Mutat. 2008;29(7):959–65.
Schneider BV, Mitsuhashi Y, Schnyder UW. Ultrastructural observations in port wine stains. Arch Dermatol Res. 1988;280:338–45.
Tan OT, Murray S, Kurban AK. Action spectrum of vascular specific injury using pulsed irradiation. J Invest Dermatol. 1989;92:868–71.
Vural E, Ramakrishnan J, Cetin N, Buckmiller L, Suen JY, Fan CY. The expression of vascular endothelial growth factor and its receptors in port-wine stains. Otolaryngol Head Neck Surg. 2008;139(4):560–4.
Wang B, Wu Y, et al. Treatment of neck port-wine stain with intense pulsed light in Chinese population. J Cosmet Laser Ther. 2013;15(2):85–90.
Yang MU, Yaroslavsky AN, Farinelli WA, et al. Long-pulsed neodymium:yttrium-aluminum-garnet laser treatment for port-wine stains. J Am Acad Dermatol. 2005;52:480–90.

Rating Port-Wine Stains

61

Pierre Agache, Yasser Afifi, and Philippe Humbert

Contents

Keywords

Port-wine stains • Rating

1 Rating Port-Wine Stains

- Color (hue and lightness)
  1. Normal skin
  2. Pale pink
  3. Pale red or bright pink
  4. Pale purple or dark pink
  5. Dark red
  6. Bright purple or dark red
  7. Dark purple
- Patchiness
  1. Not at all patchy
  2. A little patchy
  3. Rather patchy
  4. Very patchy
- Boundary
  1. Vague
  2. Fairly sharp
  3. Very sharp
- Size
  1. Nonexistent
  2. Very small
  3. Small
  4. Medium
  5. Large
  6. Very large
- Shape
  1. Regular
  2. Somewhat irregular

This chapter was originally published under the ISBN 978-3-540-01771-4 with the following book title Measuring the Skin. The content has not been changed.

Pierre Agache: deceased.

P. Agache • P. Humbert
Department of Dermatology, University Hospital of Besançon, Besançon, France
e-mail: aude.agache@free.fr; ferial.fanian@chu-besancon.fr; ferial.fanian@cert-besancon.com; philippe.humbert@univ-fcomte.fr

Y. Afifi (✉)
Private Clinic, Rabat, Morocco
e-mail: yaafifi@yahoo.fr

P. Humbert et al. (eds.), *Agache's Measuring the Skin*,
DOI 10.1007/978-3-319-32383-1_100

   3. Very irregular
- Surface
   1. Smooth
   2. A little uneven
   3. Rather uneven
- Hypertrophy
   1. Not hypertrophic
   2. A little hypertrophic
   3. Rather hypertrophic
   4. Very hypertrophic

This rating was evaluated on 90 patients. Color and boundary were correlated as well as size and hypertrophy. Shape and patchiness were found to be difficult to distinguish (irregular shaped port-wine stains were often judged as patchy) (Koster et al. 1998).

Using morphometry, size, contour length, and shape regularity are easily and quickly assessed without a device. Accordingly, this classification might be easily replaced by a measurement.

References

Koster PHL, Bossuyt PMM, van der Horst CMAM, Gijsbers GHM, van Gemert MJC. Characterization of port-wine stain disfigurement. Plast Reconstr Surg. 1998;102:1210–6.

Sweat Gland Histophysiology

62

Claudine Piérard-Franchimont, Gérald E. Piérard, and Trinh Hermanns-Lê

Contents

Keywords

Apocrine sweat gland • Eccrine sweat gland • Apoeccrine sweat gland • Immunohistochemistry

List of Abbreviations

AESG	Apoeccrine sweat gland
ASG	Apocrine sweat gland
CEA	Carcinoembryonic antigen
CK	Cytokeratin
EMA	Epithelial membrane antigen
ESG	Eccrine sweat gland
SC	Stratum corneum
UEA	Ulex europaeus agglutinin

1 Introduction

In the human skin, sweat is produced by specialized glands. In the sweat apparatus, the constitutive cells are not destroyed in the secretion process. Cutaneous sweat glands correspond to two main types, namely, the eccrine (ESG) and apocrine (ASG) sweat glands. They are commonly distinguished by histomorphology (Saga 2001; Noël et al. 2013). The presence of putative apoeccrine sweat glands (AESG) has been further suggested (Sato et al. 1987). The sweat secretion is altered in both its amount and composition by various physiological and pathological events. The densities in ESG, ASG, and putative AESG differ over different body regions. In addition,

C. Piérard-Franchimont (✉)
Laboratory of Skin Bioengineering and Imaging (LABIC), Department of Clinical Sciences, Liège University, Liège, Belgium
e-mail: Claudine.franchimont@ulg.ac.be

G.E. Piérard
Laboratory of Skin Bioengineering and Imaging (LABIC), Liège University, Liège, Belgium

Service de Dermatopathologie, CHU du Sart Tilman, Liège, Belgium
e-mail: Gerald.pierard@ulg.ac.be

T. Hermanns-Lê
Laboratory of Skin Bioengineering and Imaging (LABIC), Liège University, Liège, Belgium

Service de Dermatopathologie, CHU du Sart Tilman, Liège, Belgium

Department of Dermatopathology, Unilab Lg, University Hospital of Liège, Liège, Belgium
e-mail: Trinh.hermanns@chu.ulg.ac.be; Trinh.le@ulg.ac.be

P. Humbert et al. (eds.), *Agache's Measuring the Skin*,
DOI 10.1007/978-3-319-32383-1_84

morphological and functional variations exist according to age and nature of specific stimuli. The skin surface bacterial microflora (biocene) plays a major role in causing sweat malodor.

Despite social and cultural differences among the world populations, excessive sweating and body malodors are usually perceived as unpleasant conditions (Sato et al. 1989). By contrast, regional hypohidrosis and anhidrosis appear less disturbing, although they impair the thermoregulation and commonly represent warning signs for several systemic diseases.

Although the morphologic microanatomy remains the basis of sweat gland classification, molecular phenotyping and functional characteristics should be combined when possible. In some conditions in humans, it is uncertain whether some glands are ESG or ASG depending on the selected criteria. Various immunohistochemical markers including cytokeratin (CK) phenotyping, as well as the epithelial membrane antigen (EMA), the carcinoembryonic antigen (CEA), and others, were introduced for this purpose (Noël et al. 2013; Wollina 1991; Saga 2002; Wilke et al. 2004). In addition, the identification of glycoconjugates was used to characterize sweat glands in health and disease (Wollina et al. 1989; Sames et al. 1999; Li et al. 2009).

2 Sweat Gland Structure

2.1 Eccrine Sweat Glands

Each ESG is composed of a deep coiled portion in continuation with a straight excreting intradermal duct ending as a spiral intraepidermal acrosyringium. The secretory portion represents about two-thirds of the coiled structure. It consists of an epithelial layer composed of large clear (secretory) cells admixed with smaller granular dark (mucoid) cells, and they are cuffed by spindle-shaped myoepithelial (contractile) cells. Clear cells contain glycogen and mitochondria in abundance. They produce the eccrine sweat. Fine canaliculi collecting the secreted sweat are squeezed between adjacent clear cells. Each of the canaliculi represents a pouch extending from the luminal space. The granular dark cells exhibit pyramidal conformation with a narrow base near the peripheral basement membrane. The intraepidermal acrosyringium is lined by epithelial cells similar to those of the straight intradermal duct.

The two to four million ESG are distributed over the human body reaching in average 60–200 per cm^2. They reach higher densities (about $600/cm^2$) on the palms and soles (Xhauflaire-Uhoda et al. 2010a). Every single ESG opens directly at the skin surface through an individual acrosyringium. ESG are absent from the lips, nail bed, and some portions of the genitalia. ESG activity is controlled by a unique cholinergic orthosympathetic innervation. Various thermal, emotional, intellectual, and gustatory stimuli activate dedicated centers of the brain controlling the ESG production. In addition, hypoglycemia, hyperthyroidism, and hypercapnia represent other stimuli for ESG production (Xhauflaire-Uhoda et al. 2010a). The global excretory ESG activity is low compared with that of the kidneys.

Eccrine sweat is the exocrine product of the deep coiled segment of the gland. The secretory sweat coils produce an isotonic ultrafiltrate of plasma. It corresponds to a clear, colorless, and odorless watery fluid enriched in organic and inorganic electrolytes. The eccrine sweat composition varies according to the secretion rate, the transit time inside the excretory duct, the aldosterone activity, the physical training, and the acclimatization to the environmental moisture and temperature. Indeed, during the eccrine sweat migration inside the intradermal duct, partial selective resorption of ions, particularly Na^+ and Cl^-, takes place. Other electrolytes are also reabsorbed, particularly in extreme sweating conditions. Eccrine sweat becomes hypotonic and contains much less electrolytes and minute amounts of glucose. By contrast, lactate increases in abundance. In the distal duct portion, sweat evaporates partially inside the acrosyringium, producing a mixture of vapor and liquid at the stratum corneum (SC) surface depending upon the rate of sweat production (Sato et al. 1989). The amount and composition of eccrine sweat at the SC surface show interindividual variations

modulated over time by the body site (Sato et al. 1989). Of note, eccrine sweat contains compounds of clinical importance, including heavy metals, some drugs, other organic compounds, and (photo-) allergens.

In regular conditions, the ESG activity appears intermittent over a large part of the body. Apparently, cyclic periodic outputs alternate with pauses. The pulsating rhythm is about 0.3–12 sweat outputs per minute. Such a rhythmic activity shows interindividual variations according to circumstances and body sites. It possibly results from spasmodic contractions of periluminal myoepithelial cells once distended by the sweat flow. In general, contiguous ESG appear active alternately. Even in case of profuse sweating, it is assumed that only about 50 % of the ESG release sweat simultaneously. Such functional feature is not present on the palmoplantar sites where sweat production is largely synchronized involving the vast majority of ESG (Sato et al. 1989; Xhauflaire-Uhoda et al. 2010a).

Sweating evaporation from ESG pores (Uhoda et al. 2005; Xhauflaire-Uhoda et al. 2010b) is a mechanism involved in body thermoregulation during exposure to either warm environment or body hyperthermia. By contrast, running sweat droplets over the skin surface has little or no thermoregulatory effect. Blood flow regulation and vasodilation of the superficial vasculature largely contribute to the homeothermic control. At rest, discrete water evaporation from each single sweat pore at the SC surface is added to the actual transepidermal water loss (TEWL) to form the global insensible perspiration reaching about 600 g daily for the whole body.

2.2 Apocrine Sweat Glands

Most ASG are located in the armpits and groins. They are fewer around the umbilicus, in the perineal region, and in the mammary areola. Each ASG consists of a deep coiled secretory portion connected to a duct. The glandular portion is formed by cuboidal or columnar cells containing granules and vacuoles in part pigmented. The apocrine excretory duct closely resembles the eccrine duct. It consists of a double or triple layer of rather similar cuboidal cells. Those forming the inner layer exhibit a faint luminal fringe. The peripheral basal layer contains numerous mitochondria and microvilli. The apocrine sweat is scanty and sticky in consistency.

ASG remain quiescent during childhood, and they become functionally mature under androgen stimulation at puberty. Afterward, the hormonal control is apparently no more operative, being replaced by both adrenergic and cholinergic stimuli.

Apocrine sweat consists of a lipid-rich liquid produced inside large ASG acini located deep in the dermis and hypodermis. It is released into apo-pilosebaceous ducts of adjacent hair canals before reaching the SC surface. Apocrine sweat is slightly viscous and milky, enriched in lipids, nitrogen, lactates, and various other ions including Na^+, K^+, Ca^{2+}, Mg^{2+}, Cl^-, and HCO^{3-}. The apocrine secretion appears to be derived from pinching off the apical cytoplasm of the secretory cells. Moll's glands on the lids, ceruminous glands in the ear canal, and pseudomammary anogenital glands are specially adapted ASG (Van Der Putte 1994).

2.3 Apoeccrine Sweat Glands

AESG were tentatively identified in the armpits where they were estimated to outnumber 25,000. It was assumed that the axillary skin contained approximately equal numbers of ESG, ASG, and AESG. The AESG were described to share some features in common with both the ESG and ASG (Sato et al. 1987). Their presence remains however a controversial issue (Sato et al. 1987; Hermanns-Lê et al. 2004). The distinction between AESG and both the ESG and ASG was mainly assessed on gross morphology (Uhoda et al. 2005). Their physiologic and pharmacologic stimulation appeared to be distinct from those controlling ASG. They possibly open directly onto the skin surface. They seemingly respond quickly to psychological stress, and they were considered to largely contribute to the abundant sweat produced in the armpit.

3 Sweat Gland Immunohistochemistry

A multipronged immunohistochemical approach is helpful in the study of human sweat glands. Although the excretory ducts appear phenotypically similar in the distinct sweat glands, the deep secretory coils show distinctive differentiation patterns.

The secretory coil and at a lesser extent the ductal cells of the ESG were identified by the CAM 5.2 antibody. All segments of the ASG including secretory and ductal cells were decorated by this antibody. The monoclonal CAM 5.2 CK antibody strongly reacts with CK 8 and at a lower extent with CK 7 (Noël et al. 2013). No reactivity has been disclosed with CK 18. The different ESG portions contain a cytoskeleton made of several distinct CK (Metze and Luger 1996; Metzler et al. 1990). They include CK 7, CK 8, CK 14, CK 18, and CK 19, as well as EMA and CEA (Li et al. 2009). It was reported that the expression intensity of CK 7, CK 18, and CK 19 was stronger than that of CK 8 and CK 14 (Li et al. 2009). A controversy exists about the presence of CK 10 (Li et al. 2009; Demirkesen et al. 1995).

The polyclonal S100-B protein antibody detects one of the 19 Ca^{2+}-binding proteins of the S100 family. The S100-B protein predominates inside the cytoplasm of ESG secretory cells. The monoclonal antihuman EMA antibody (Li et al. 2009; Metze and Luger 1996) and the polyclonal antihuman CEA antibody (Li et al. 2009) typically label sweat glands (Noël et al. 2013). EMA is located in the luminal coating of the eccrine secretory segment and in the dark cells as well. The ASG contain EMA in different segments including the glomerular structure and the excretory duct (Noël et al. 2013). CEA is present at all levels of the ESG. The ASG showed a heterogeneous CEA labeling on the luminal coating of the duct. UEA-1 is a lectin specifically binding to α-L fucosyl moieties. The anti-UEA-1 antibody reveals the lectin-binding sites corresponding to oligosaccharides with terminal α-fucose, some of which are present in sweat glands (Noël et al. 2013; Metzler et al. 1990). In the ESG secretory segments, clear cells exhibit strong cytoplasmic UEA-1 staining. ASG globally appear intensely labeled. A variable number of cells of the secretory ESG segment were strongly positive. The monoclonal antihuman CD138 detects the transmembrane syndecan-1 proteoglycan (Noël et al. 2013). A variable number of ESG secretory cells are strongly positive for this antibody. The monoclonal antibody to CD63 (NKI-C3) detects various proteins whose molecular weights range 25–100 kd. They are probably part of some lysosomal antigens located in cytoplasmic vacuoles (Noël et al. 2013). In ESG, CD63 immunostaining is present in the apical part of secretory cells. A positivity for the gross cystic disease fluid protein-15 appears typical for the ASG (Uhoda et al. 2005).

So far, AESG were not clearly and specifically distinguished using immunohistochemistry, and publications about this topic remain scanty and controversial (Sato et al. 1987; Hermanns-Lê et al. 2004). However, recent findings suggest that the immunoreactivity to the S100-B protein, CEA, and CD63 possibly helps identifying some AESG (Noël et al. 2013).

References

Demirkesen C, Hoede N, Moll R. Epithelial markers and differentiation in adnexal neoplasms of the skin: an immunohistochemical study including individual cytokeratins. J Cutan Pathol. 1995;22:518–35.

Hermanns-Lê T, Garcia R, Arrese JE, Piérard GE. Pitted keratolysis: new ultrastructural insight in keratohyalin granule and corneodesmosome alterations. Exog Dermatol. 2004;3:107–11.

Li HH, Zhou G, Fu XB, et al. Antigen expression of human eccrine sweat glands. J Cutan Pathol. 2009;36:318–24.

Metze D, Luger TA. Ultrastructural localization of carcinoembryonic antigen (CEA) glycoproteins and epithelial membrane antigen (EMA) in normal and neoplastic sweat glands. J Cutan Pathol. 1996;23:518–29.

Metzler G, Schaumburg-Lever G, Liebig K. Ultrastructural localization of keratin and alpha-L-fucose in human eccrine sweat glands. Arch Dermatol Res. 1990;282:12–6.

Noël F, Piérard GE, Delvenne P, et al. Immunohistochemical sweat gland profiles. J Cosmet Dermatol. 2013;12:179–86.

Saga K. Histochemical and immunohistochemical markers for human eccrine and apocrine sweat glands: an aid for

histopathologic differentiation of sweat gland tumors. J Invest Dermatol Symp Proc. 2001;6:49–53.
Saga K. Structure and function of human sweat glands studied with histochemistry and cytochemistry. Prog Histochem Cytochem. 2002;37:323–86.
Sames K, Moll I, van Damme EJ, et al. Lectin binding pattern and proteoglycan distribution in human eccrine sweat glands. Histochem J. 1999;31:739–46.
Sato K, Leidal R, Sato F. Morphology and development of an apoeccrine sweat gland in human axillae. Am J Physiol. 1987;252:166–80.
Sato K, Kang WH, Saga K, Sato KT. Biology of sweat glands and their disorders. I. Normal sweat gland function. J Am Acad Dermatol. 1989;20:537–63.
Uhoda E, Piérard-Franchimont C, Petit L, Piérard GE. The conundrum of skin pores in dermocosmetology. Dermatology. 2005;210:3–7.
Van Der Putte SC. Mammary-like glands of the vulva and their disorders. Int J Gynecol Pathol. 1994;13:150–60.
Wilke K, Keil FJ, Wittern KP, et al. Immunolabelling is essential for the differentiation of human axillary apoeccrine glands. J Invest Dermatol. 2004;123: A93.
Wollina U. Human eccrine sweat gland. Expression of neuroglandular antigens and coexpression of intermediate filaments. Histol Histopathol. 1991;6: 191–8.
Wollina U, Schaarschmidt HH, Hipler C, et al. Distribution of glycoconjugates in human skin appendages. Acta Histochem. 1989;87:87–93.
Xhauflaire-Uhoda E, Paquet P, Quatresooz P, Piérard GE. Characterization of the skin using capacitance imaging. Expert Rev Dermatol. 2010a;5:149–58.
Xhauflaire-Uhoda E, Piérard-Franchimont C, Piérard GE, et al. Weathering of the hairless scalp: a study using skin capacitance imaging and ultraviolet light-enhanced visualization. Clin Exp Dermatol. 2010b;35:83–5.

Sweat Gland Methods of Assessment

63

Claudine Piérard-Franchimont and Gérald E. Piérard

Contents

Keywords

Eccrine sweat gland • Apocrine sweat gland • Imperceptible perspiration • Skin capacitance mapping/imaging

Abbreviations

ASG	Apocrine sweat gland
ESG	Eccrine sweat gland
SC	Stratum corneum
SCMI	Skin capacitance mapping/imaging
SSWL	Skin surface water loss
TEWL	Transepidermal water loss

The functional activities of the eccrine sweat glands (ESG) and apocrine sweat glands (ASG) are clearly distinct in humans. The appropriate noninvasive methods assessing their excretion activities at the skin surface are distinct.

1 Biometrology of Eccrine Sweat Excretion

Eccrine sweating is the response to thermal, emotional, and gustatory stresses. It is under the control of acetylcholine from the cholinergic sympathetic innervation. ESG activity plays an essential role in regulating body temperature in physiological conditions. Such a function is altered by a series of systemic diseases. For instance, diabetic neuropathy frequently involves the distal sensorimotor innervation. The resulting

C. Piérard-Franchimont (✉)
Laboratory of Skin Bioengineering and Imaging (LABIC), Department of Clinical Sciences, Liège University, Liège, Belgium
e-mail: Claudine.franchimont@ulg.ac.be

G.E. Piérard
Laboratory of Skin Bioengineering and Imaging (LABIC), Liège University, Liège, Belgium

Service de Dermatopathologie, CHU du Sart Tilman, Liège, Belgium
e-mail: Gerald.pierard@ulg.ac.be

P. Humbert et al. (eds.), *Agache's Measuring the Skin*, DOI 10.1007/978-3-319-32383-1_85

peripheral sweating deficit is commonly responsible for unequivocal alterations in the length-dependent thermoregulatory sweating (Piérard 2003). Hence, legs affected by diabetic neuropathy are commonly hypohidrotic with a "compensatory" hyperhidrosis over the upper body regions (Xhauflaire-Uhoda et al. 2011). Other possible sweating alterations in diabetes include segmental hypohidrosis and more rarely isolated dermatome involvement. Some patients suffer from a combination of two or more of these patterns and even from global anhidrosis (Piérard 2003). The extent in body surface anhidrosis was reported to be correlated with the severity of clinical dysautonomia (Piérard 2003). Fine-tuning objective assessments of discrete aspects of the sweat gland dysfunction have been rarely explored so far using recent sensitive biometrological methods (Xhauflaire-Uhoda et al. 2011). However, considering the impact of ESG activities in a variety of physiopathological conditions, diverse methods are available for recording the ESG numbers and assessing their functional status (Piérard 2003). The in vivo tests belong to two major categories (Noël et al. 2012).

The first group of methods provides an overall information about the amount of excreted sweat, irrespective of the number of active ESG. Such assessments include the gravimetric method of collecting and weighing sweat at the skin surface. The global decrease in body weight over a couple of hours was used as an indication of the amount in sweat output over the selected period of time. Microcannulation of individual sweat ducts represented an ancillary cumbersome method. Global assessments of water evaporation from the skin surface were advocated using a variant of transepidermal water loss (TEWL) measurement. Electrometric procedures quantifying the stratum corneum (SC) moisture was expected to represent an indirect indication of the ESG production.

The second group of methods assesses the density of active ESG over a given skin surface area (Noël et al. 2012; Hermanns-Lê et al. 2004). In particular, skin capacitance mapping/imaging (SCMI) visualizing any tiny individual sweat output conveniently provides a real-time noninvasive information.

1.1 Gravimetric Method

The gravimetric method was formerly developed for quantifying the actual amount of eccrine sweat produced in excess under controlled conditions (duration, temperature, site, etc.) during defined time intervals. Thermal sweating was thus explored on absorbent filter papers or pads of defined dimensions placed under occlusion (Leyden et al. 1981). Any pharmacological stimulation or inhibition of ESG was possibly performed. In these procedures, the sampling material was weighed before and immediately after the collection period of sweat. A minimum amount of about 100 mg of sweat was necessary for reliable quantifications. A well-acclimatized person can produce up to 10 l of eccrine sweat over a single day.

1.2 Water Evaporation Quantification

Regular TEWL measurements are typically used for testing the SC barrier function. Such evaluations are performed in the absence of active sweating. However, such expectation proves to remain invalid in some circumstances. Indeed, the same devices designed for TEWL measurements in resting conditions are alternatively used for assessing the insensible perspiration with contribution of the discrete eccrine sweat evaporation at rest. The quantification of minute amounts of sweat vapor production in the instrumentally measured TEWL values has rarely been identified in the literature (Rennie et al. 1991) and remains commonly neglected in the interpretation of TEWL data. However, it is acknowledged that any physical, thermal, and emotional stress influences the regular TEWL through sweat production.

TEWL measurements are time consuming and typically confined to small skin areas. However, it is possible to perform continuous recordings, particularly with the open chamber method. This method is suitable for detecting moderate physiological changes in sweat evaporation. Of note, it is not convenient when sweat in excess is running at the skin surface without complete evaporation.

1.3 Sweat Visualization by Staining Procedures

Several simple methods advocated for sweat detection used specific dyes in vivo. The skin had first to be wiped for removing any residual sweat before performing the test procedure. The skin was then painted with the reactive dye or covered by a sweat-absorbing material soaked with the reagent. According to the dyes applied either singly or in combination, detection of sweat was rendered possible. The painting method conveniently allowed serial image recordings and image analysis of spontaneous sweating.

One procedure relied on filter paper impregnated with a 1 % bromophenol blue alcoholic solution. The material was deposited onto the sweating SC surface for a few seconds. The gray powder turned blue following contact with watery fluid at a pH above 4.6 which is consistent with sweat. After removal, a series of blue spots appeared at the site of sweat droplets. Alternatively, the skin was powdered with bromophenol blue, or the dye was dispersed in an oily vehicle to be applied as a thin film to the SC surface.

By far, the most simple and safe staining method relied on the iodine starch reaction. A 2 % iodine ethanol solution was painted on the skin. After spontaneous evaporation of the solvent, sheets of starch-enriched filter paper were held against the skin surface for a few seconds. Upon removal of the material, a dark blue imprint became apparent wherever sweating was active. As a variant method, a filter paper was dipped into ethanol solution of iodine and castor oil. After air drying, the paper was placed for 1 min onto the skin, lifted off, and powdered by starch in order to reveal blue dots. Another variant consisted in the application of starch dispersed in castor oil onto the iodine-painted skin. Active sweat pores appeared as dark blue spots at the skin surface. Image analysis allowed the assessment of the ESG numbers and activities.

The simplest and most versatile iodine starch method consisted of a single step procedure based on iodinated starch sprayed onto the SC. Sweat drops were visualized directly at the skin surface as dark blue/purple spots. This method was possibly repeated on the same site after wiping the iodinated starch from the skin surface. Safety procedures had to be guaranteed because inhalation of iodinated starch is hazardous. Several other dyes such as rhodamine were possibly used as well as Prussian blue powdered on a self-adhesive transparent tape turning blue after contact with sweat.

The sweat droplets were assumed to be hemispheric ($2/3\ \pi.r^3$) or almost a sphere ($\pi.r^3$) upon dripping. Calculating the sweat excretion rate over given skin areas was attempted by adding the estimated volume of each sweat droplet.

The aforementioned staining methods were probably prone to various flaws. A pitfall occurred with residual surfactants on SC altering sweat rheology. Dot merging resulted from sideways movement during the imprint stage or due to intense sweating, causing droplet running at the skin surface prior to imprint. In some circumstances it remained difficult to accurately delimit the area of skin from which the print was taken.

1.4 Staining Methods for Specific Organic Sweat Compounds

Some powder or liquid dyes applied onto the skin allowed detecting specific organic sweat compounds. For instance, astra blue revealed various organic ions. Quinizarin turned black in the presence of carbonates. Painting the skin with 5 % orthophthalaldialdehyde in xylene revealed within 2–3 min a black reaction product following contact with ammonia at the ESG pores.

Ninhydrin turned purple-blue in contact with amino acids. This chemical proved to be irritant for skin and was forbidden for local applications. A safer procedure used a filter paper dipped in 1 % ninhydrin acetone and heated for a few minutes at 120 °C in an incubator before application to the skin. A violet stain appeared at the site of sweat deposits.

1.5 Casting Methods

Silicone rubber methods relied on the hydrophobicity of the material. It was assumed that after application of the casting material to the skin

surface, any sweat droplets released from ESG pores would prevent deposition of the hydrophobic material, leading to imprints at the surface of the casting material.

The silicone rubber material is readily available, simple, and safe to be applied to any part of the body surface. This material admixed to the polymerizing agent forms a cast that is peeled off carefully from the skin surface before visualization under the microscope. A possible flaw with the replica technique is the inclusion of air bubbles under the casting material.

When the silicone rubber material is thin, sweat droplets appear as holes in a membrane. The number of ESG over the defined skin surface area is conveniently counted. A variant of the casting method relies on the application of a thin layer of petrolatum jelly to the skin surface. Beading of sweat droplets is recorded and image analysis determines the ESG density per SC unit area (Piérard 2003).

1.6 Electrometric Methods

Skin electric properties are altered by the SC moisture. Hence, skin capacitance and conductance are increased in the presence of sweat (Piérard 2003). These methods represent screening tools. However, they are infrequently used in functional assessments of sweat production because measures are only relative and indirect. In addition, a saturation effect of the SC rapidly occurs when sweating is abundant.

1.7 Skin Capacitance Mapping/Imaging

In physiological conditions, water is distinctly lost by minimal evaporation through the interadnexal epidermis and sweat glands. Basically, three distinct conditions are encountered regarding skin capacitance mapping/imaging (SCMI) aspects of the sweat gland activity (Xhauflaire-Uhoda et al. 2010a, b, 2011; Noël et al. 2012; Batisse et al. 2006; Lévêque et al. 2006; Piérard-Franchimont, Piérard 2015; Piérard-Franchimont et al. 2016). The SkinChip® and Sweatchip® devices as well as the Moisture Map HM100 device (CK Technology, Vise, openate…) (L'Oréal, Paris) operates though a multisensor probe generating detailed capacitance measurements at 50 μm resolution over the SC. The SCMI picture is displayed in a range of gray levels according to each capacitance value. Thus, a nonoptical capacitance map of the skin surface is created. The darker pixels represent high capacitance spots, while the clear ones correspond to lower capacitance values. Skin capacitance is considerably influenced by sweat. Any prolonged contact time over 5 s between SC and the SCMI probe increases the density in darker pixels, owing to accumulation of sweat, TEWL, and water saturation of the SC.

First, the sweat quiescent stage does not show any obvious SCMI manifestation. Second, sweat glands become discretely active even in the absence of visible sweating, in which case they emit only discrete amounts of water vapor. Such aspect of the imperceptible (insensible) perspiration through sweat pores is conveniently observed using SCMI when the subject is in a quiet condition without any overheating. Tiny black dots mark the joining up of each discretely active ESG at the SC surface. The tiny black dots correspond either to open ESG ducts or to soft cornified and moisturized caps of SC cuffing the sweat pores. Such structures probably exhibit a sweat-holding capacity capturing the sweat vapor. There is no running sweat at that stage of the ESG activity. In such a condition, sweat vapor is apparently emitted in minimal amounts and the casual TEWL nearly remains unaffected. However, this condition is also present in association with an overall increase in interadnexal SC moisturization (Noël et al. 2012). In such instance, TEWL is commonly increased (Noël et al. 2012). Third, watery sweat is poured out through active ESG, implying that the skin surface water loss (SSWL) reaches much higher values than the regular TEWL. When sweating is more active, SCMI black dots enlarge and some of them merge to form irregular black "puddles." This aspect is more closely related to SSWL than to TEWL. Because sweat appears as black dots, it is possible

to measure its contribution to the mean SCMI-derived gray level by thresholding the values under consideration (Noël et al. 2012).

SCMI after exercise shows the combination of two major changes affecting the sweat gland activity and the SC hydration (Xhauflaire-Uhoda et al. 2011). On the one hand, a large number of tiny black dots reveal the presence of boosted ESG. Their size and distribution over the skin surface are relatively uniform. Some larger dark spots result from both the enlargement and merging of the tiny black dots. On the other hand, the SCMI background appears darker than before exercise, indicating an increased SC moisture. These features were reported to be particularly obvious at completion and during about 1 min after exercise, and they faded after about 5 min.

Thus, SCMI represents a convenient way for studying the versatile ESG activity. The method is sensitive enough for detecting early signs of ESG activity under various stimulations. The influence of autonomic neuropathies on ESG, including the diabetic type (Xhauflaire-Uhoda et al. 2011; Noël et al. 2012), is possibly measured using the SCMI method. It must be stressed that some hyperkeratotic disorders interfere with sweat excretion. Tinea (pityriasis) versicolor and psoriasis represent such conditions where the sweat output is largely curbed (Uhoda et al. 2005; Xhauflaire-Uhoda et al. 2006).

2 Biometrology of Apocrine Sweat Excretion

Human ASG is confined to the regions of armpits, perineum, umbilicus, and breast areolae. They become functional at puberty. Some ASG functions include an odoriferous role, a sexual attractant, a territorial marker, and warning signals. The ASG production of pheromones is established in many species.

2.1 Apocrine Sweat Cannulation

Apocrine sweat present inside the collecting intradermal apo-pilosebaceous duct is possibly squeezed out in part at the skin surface by contracting smooth muscle cells with adrenaline 1:2,000 in physiologic saline. Such a procedure is painful. It is possibly performed after collecting apocrine sweat by capillary tubes from the apo-pilosebaceous duct. Approximately 1 µl of milky apocrine fluid is obtained from each ASG pore. However, only a limited number of apo-pilosebaceous ducts within the visibly adrenaline-blanched area actually release sweat.

2.2 Axillary Malodor Assessment

Studying axillary malodor requires controls of local shaving, previous applications of cleansing agents, deodorants, perfumes, and frequency of their respective applications in the armpits (Piérard 2003). In a common procedure, cotton gauze pads thoroughly cleaned and autoclaved are held in place in the target armpit for 6–9 h. Chromatographic analytic analysis allows detection of various chemicals responsible for malodor. However, there are limitations because of the complex nature and variable individual composition of axillary malodor chemistry. In addition, the analysis does not yield a quantitative malodor assessment.

In vitro microbiological evaluations demonstrate the efficacy of any compound curbing the microorganism growth involved in malodor. Thus, these techniques represent an indirect assessment of the potential deodorant activity. The in vivo microbiological evaluation relies on the microflora collection from the SC. Counting colonies after culture or performing a viability test under flow cytometry is possible. The most difficult aspect of the quantitative methods resides in the rigorous controlled collection of the bacterial bioscene from the skin surface.

References

Batisse D, Giron F, Lévêque JL. Capacitance imaging of the skin surface. Skin Res Technol. 2006;12:99–104.

Hermanns-Lê T, Garcia R, Arrese JE, Piérard GE. Pitted keratolysis: new ultrastructural insight in keratohyalin

granule and corneodesmosome alterations. Exog Dermatol. 2004;3:107–11.
Lévêque JL, Xhauflaire-Uhoda E, Piérard GE. Skin capacitance imaging, a new technique for investigating skin surface properties. Eur J Dermatol. 2006;16:500–6.
Leyden JJ, McGinley KJ, Hölzle E, et al. The microbiology of the human axilla and its relationship to axillary odor. J Invest Dermatol. 1981;77:413–6.
Noël F, Piérard-Franchimont C, Piérard GE, Quatresooz P. Sweaty skin, background and assessments. Int J Dermatol. 2012;51:647–55.
Piérard GE, the EEMCO group. EEMCO guidance for the efficacy assessment of antiperspirants and deodorants. Skin Pharmacol Appl Skin Physiol. 2003;16:324–42.
Piérard-Franchimont C., Piérard G.E. Sweat gland awakening on physical training. A skin capacitance mapping observation. Clin Res Dermatol. 2015;2:1–4.
Piérard-Franchimont, C., Hermanns-Lê T., Piérard G.E. Skin capacitance mapping of eccrine sweat gland activity during pregnancy. Open Access. J Science Technol. Vol. 4 (2016), Article ID 101187, 4 p.
Rennie PJ, Gower DB, Holland KT. In vitro and in vivo studies of human axillary odour and cutaneous microflora. Br J Dermatol. 1991;124:596–602.
Uhoda E, Piérard-Franchimont C, Piérard GE. Anhidrotic pityriasis versicolor. Dermatol Actual. 2005;89:16–7.
Xhauflaire-Uhoda E, Piérard-Franchimont C, Piérard GE. Skin capacitance mapping of psoriasis. J Eur Acad Dermatol Venereol. 2006;20:1261–5.
Xhauflaire-Uhoda E, Piérard GE, Quatresooz P. The skin landscape following nonoptical capacitance imaging. Am J Clin Dermatol. 2010a;11:89–94.
Xhauflaire-Uhoda E, Piérard-Franchimont C, Piérard GE, et al. Weathering of the hairless scalp: a study using skin capacitance imaging and ultraviolet light-enhanced visualization. Clin Exp Dermatol. 2010b;35:83–5.
Xhauflaire-Uhoda E, Mayeux G, Quatresooz P, et al. Facing up to the imperceptible perspiration modulation. Influence of diabetic neuropathy, physical exercise and antiperspirants. Skin Res Technol. 2011;17:487–93.

The Neurophysiology and Assessment of Human Skin Wetness Perception

64

Davide Filingeri, Simon Hodder, and George Havenith

Contents

D. Filingeri (✉) • S. Hodder • G. Havenith
Environmental Ergonomics Research Centre, Loughborough Design School, Loughborough University, Loughborough, UK
e-mail: davidefilingeri@hotmail.it; S.Hodder@lboro.ac.uk; G.Havenith@lboro.ac.uk

P. Humbert et al. (eds.), *Agache's Measuring the Skin*,
DOI 10.1007/978-3-319-32383-1_86

Keywords
Skin • Wetness • Skin receptors • Moisture • Sweat • Temperature • Tactile • Quantitative sensory testing • Psychometric scales • Perception

1 Introduction

Since the seminal work of Pharo Gagge at the John B. Pierce Foundation Laboratory (Gagge 1937), the measurement of skin wetness as a physical variable has received great attention, particularly for its role in the estimation of the body's heat balance under conditions of increased metabolic heat production (e.g., resulting from exercising muscles) and decreased gradient for heat loss to the environment (e.g., resulting from high ambient temperatures) (Nadel and Stolwijk 1973; Candas et al. 1979; Havenith 2001; Havenith et al. 2013). However, although much is known on the biophysical role of skin wetness in contributing to thermal homeostasis, surprisingly little has been done to elucidate how humans sense wetness on their skin and how the level of *physical* skin wetness relates to the level of *perceived* skin wetness.

Expanding the knowledge on how humans perceive skin wetness has both a fundamental and an applied significance. On the fundamental side, this could contribute to a better understanding of how the peripheral and central nervous systems interact to generate complex

somatic perceptions (Craig 2003). On the applied side, this could be useful for its potential clinical as well as industrial implications. Within the clinical context, this knowledge could contribute to the development of diagnostic tests for patients with somatosensory disorders (e.g., multiple sclerosis and diabetic neuropathy) (Gin et al. 2011) as well as skin conditions (Mayrovitz and Sims 2001). Within the industrial context, this knowledge could contribute to the development of new strategies in clothing design aiming to improve thermal comfort as well as to the design and optimization sanitary products for personal and patient care. Indeed, local skin wetness has been repeatedly shown to play a critical role in the onset of thermal and clothing discomfort (Fukazawa and Havenith 2009) as well as to be a risk factor for pressure ulcers when individuals are bed rested and wear sanitary products (e.g., diapers) (Mayrovitz and Sims 2001).

This chapter will present the state of the current knowledge about the neurophysiological and psychophysical bases of humans' ability to perceive skin wetness, along with an overview of the most recent methods used to asses this sensory feature of the human skin.

1.1 Skin Wetness as a Physical Variable

As a physical variable, skin wetness was first introduced by Gagge (1937) who recognized its critical role in the heat balance of the body. Whether due to increases in metabolic heat production (e.g., as a result of exercise) or exposure to hot environments, body core overheating is prevented, and heat balance maintained, by means of sweating (Candas et al. 1979). Evaporative heat loss through sweating plays a critical role in cooling the skin, thus maintaining a favorable core to skin gradient for heat losses from the body to the environment (Kondo et al. 1997). Therefore, within environmental conditions that allow full evaporation, the level of physical skin wetness represents an important parameter to ensure the evaporative efficiency of sweating (Candas et al. 1979). As such, skin wetness is defined as the fraction of the body covered by liquid at skin temperature (e.g., sweat), and it represents a physical measure of the degree of wetness involved in the process of evaporation (Gagge 1937). Skin wetness is usually expressed as a decimal fraction, with 1 representing the upper limit for a fully wet skin and 0.06 representing the minimal value due to insensible perspiration through the skin (Nishi and Gagge 1977).

Since Gagge's seminal work, the measurement of skin wetness as a physical variable has received great attention, particularly in the context of predicting the body's heat balance during conditions of increased metabolic heat production and decreased gradient for heat loss to the environment (Nadel and Stolwijk 1973; Candas et al. 1979; Havenith 2001; Havenith et al. 2013). However, although much is known on the biophysical role of skin wetness in contributing to thermal homeostasis, surprisingly little has been done to elucidate how humans sense wetness on their skin and how the level of *physical* skin wetness relates to the level of *perceived* skin wetness.

1.2 Skin Wetness as a Perceptual Variable

In contrast with insects, in which humidity receptors subserving *hygrosensation* have been identified and widely described (Tichy and Kallina 2010), humans' largest sensory organ, i.e., the skin, seems not to be provided with specific receptors for the sensation of wetness (Clark and Edholm 1985). Thus, as human beings, we seem to *learn* to perceive the wetness experienced when the skin is in contact with a wet surface or when sweat is produced (Bergmann Tiest et al. 2012a) through a complex multisensory integration (Driver and Spence 2000) of thermal (i.e., heat transfer) and tactile (i.e., mechanical pressure and skin friction) inputs generated by the interaction

between skin, moisture, and (if donned) clothing (Fukazawa and Havenith 2009). However, until very recently, what was still unclear was the individual role of thermal and tactile cues and how these are integrated peripherally as well as centrally by our nervous system when experiencing the perception of skin wetness.

Investigating the neurophysiological and psychophysical bases of human skin wetness perception has represented a challenge which has attracted the interest of many scientists since the early days of the twentieth century. To our knowledge, the first scientist who has attempted to explain the sensory basis of this skin perception was Bentley, who in 1900, with his famous "synthetic experiment," tested the perception of dipping a sheath-covered finger into a liquid; the results showed that the participants at first refused to believe that the finger was not actually wet (Bentley 1900). Based on these early observations, Bentley proposed a sensory-blending hypothesis which suggests the blend of pressure and coldness as responsible for evoking the perception of wetness.

Following this early work on the psychophysical bases of skin wetness perception, a number of studies have investigated the perception of skin wetness. By investigating the perceptual responses to either skin's contact with external wet and dry stimuli (Sweeney and Branson 1990a, b; Li 2005; Daanen 2009; Niedermann and Rossi 2012; Bergmann Tiest et al. 2012a, b; Ackerley et al. 2012; Filingeri et al. 2013, 2014a, b, c, 2015) or to the active production of sweat (Fukazawa and Havenith 2009; Lee et al. 2011; Gerrett et al. 2013), these studies have provided insights about the potential mechanisms for which skin wetness is sensed in humans.

The majority of these studies have endorsed the use of quantitative sensory testing as the preferred methodology to measure human skin wetness perception. Therefore, before reviewing the main findings of the abovementioned studies and before providing practical examples of how QST is performed in the context of measuring skin wetness perception, an overview of the characteristics of these tests will be provided.

2 Quantitative Sensory Testing

Quantitative sensory testing (QST) represents a noninvasive sensory examination of somatosensory modalities such as light touch, vibration, thermal, and pain sensation (Chong and Cros 2004). The basic psychophysical paradigm on which this test is based is that of *stimulus-response*: by exposing the participant to a stimulus with prespecified physical properties (e.g., temperature), the resulting sensory response (i.e., the presence/absence of any perception of the stimulus; estimation of the intensity of the stimulus) is measured in order to investigate the target somatosensory function (e.g., thermal sensitivity) (Walk et al. 2009).

QST can be divided into threshold detection tests and stimulus intensity ratings. Threshold detection tests use a graded series of stimuli of increasing and decreasing intensities in order to determine the sensory threshold at which the participant detects or no longer detects a particular somatosensory stimulus. Stimulus intensity tests use a fixed standard stimulus of known properties in order to determine the participant's ability to provide a quantitative rating of the stimulus' intensity (Chong and Cros 2004; Walk et al. 2009).

During a QST, and in response to the stimuli, participants are usually instructed to either report the presence or absence of a particular sensation with a *Yes-No* method (Chong and Cros 2004) or to report the intensity of the perceived stimulus on psychometric scales.

2.1 Psychometric Scales

Two main types of psychometric scales are commonly used when QST is administered with a stimulus intensity paradigm: Likert scales and visual analogue scales.

Likert scales (or categorical scales) are psychometric scales which are characterized by 4–11 points with designated verbal descriptors and anchor points at the extremes of the scale which define the range of sensations/perceptions

specifically tested within the construct of the scale (Likert 1932). Visual analogue scales are psychometric scales which are characterized by a straight line whose extreme points represent the anchor points for the sensation/perception specifically tested (Scott and Huskisson 1976).

With regard to the specificity of each type of scale, and how appropriate their use is according to the experimental conditions designed, it is generally accepted that Likert scales are preferable for the benefits that the presence of verbal descriptors provides in helping individuals to describe their sensations. This is particularly true when external noise or other distracters can influence the subjective ability to define one's own sensations (Lee et al. 2010). With regard to visual analogue scales, these are generally considered as preferable when a higher sensitivity in the measurement of a particular sensation is needed. Also, by not restricting individuals' ability to rate their sensation based on specific verbal descriptors, these scales are thought to provide individuals with a greater flexibility and thus accuracy in their sensation discrimination (Lee et al. 2010).

With regard to the use of QST in the investigation of skin wetness perception, this method has been widely used in the context of testing skin wetness perception as a result of the contact with an external wet or a dry stimulus. In light of this, the following paragraphs present an overview of the most representative studies which have endorsed the use of QST when investigating skin wetness perception.

3 Assessing Skin Wetness Perception: Overview of the Literature

Most of the literature on skin wetness perception has focused on investigating the minimum amounts of wetness that individuals are able to discriminate between (i.e., *discrimination of skin wetness*) and whether individuals are able to characterize the level of skin wetness they experience during the skin's contact with external (wet or dry) stimuli (i.e., *magnitude estimation of skin wetness*).

3.1 Discrimination Studies

During a discrimination experiment, Sweeney and Branson (1990b) showed that, when cotton test fabrics (25 cm^2) with different water content were applied to the upper back of 13 blindfolded female participants, these discriminated between moisture content with a discrimination threshold of 1.6 $\mu l \cdot cm^{-2}$ against a reference stimulus of 3.6 $\mu l \cdot cm^{-2}$ (Sweeney and Branson 1990b).

In line with this approach, Jeon et al. (2011) applied four 100 cm^2 specimens of different types of fabric (i.e., cotton, regular polyester, and two types of the so-called high-performance polyester) with a range of moisture contents (1–21 $\mu l \cdot cm^{-2}$) to the right and left inner forearm of ten blindfolded female participants (duration: 5 s). Test fabrics were applied simultaneously to two reference fabrics (with amounts of water of 5 and 15 $\mu l \cdot cm^{-2}$) and participants judged which stimulus caused greater wetness perception. This study found average discrimination thresholds which differed between the different materials (higher for, e.g., high-performance polyester) in the range of 1.9–2.6 $\mu l \cdot cm^{-2}$ against the 5 $\mu l \cdot cm^{-2}$ reference stimulus and from 3.6 to 5.4 ml against the 15 $ml \cdot cm^{-2}$ reference stimulus.

Similarly, in a study in which six males and six females (blindfolded) interacted with three different types of wet materials (i.e., 19.6 cm^2 thin and thick viscose and cotton wool), in two ways of exploring (i.e., the samples were either touched statically, flat on the table, in which case only thermal cues were available, or they were touched dynamically, picked up, and manipulated, in which case both thermal and mechanical cues were available), Bergmann Tiest et al. (2012a) found that discrimination thresholds ranged from ~25 to ~400 $\mu l \cdot cm^{-2}$ according to the type of contact with the stimuli (static vs. dynamic).

Overall, the abovementioned studies provided evidence in support of the individual ability to readily discriminate between higher and lower wetness levels. However, although endorsing the use of QST, by approaching the assessment of skin wetness perception with a *discrimination paradigm* (i.e., a forced choice between two options), these studies have provided limited

evidence on the potential sensory mechanisms involved in the subjects' ability to sense and discriminate skin wetness. In this respect, the studies which have approached the assessment of skin wetness with a *magnitude estimation paradigm* have provided more detailed insights on the potential sensory inputs underlying the human's ability to sense wetness on the skin, thus indicating this approach (i.e., QST with a magnitude estimation paradigm) as a potentially more effective method to assess skin wetness perception.

3.2 Magnitude Estimation Studies

The experimental studies that have investigated what sensory inputs contribute to skin wetness perception as a result of the contact with an external wet or dry stimulus have indicated that the thermal sense (and specifically cold sensations) could be the key player in driving the perception of wetness (Daanen 2009; Bergmann Tiest et al. 2012b; Ackerley et al. 2012). In support of this hypothesis, it has been proposed that, as we *learn* to perceive skin wetness, we tend to associate the cold sensations evoked by the drop in skin temperature occurring during the evaporation of moisture from the skin as a signal of the presence of moisture, and thus wetness, on the skin surface (Daanen 2009). Therefore, cold stimuli able to reproduce such skin cooling rates are suggested to suffice in evoking the perception of wetness (Bergmann Tiest et al. 2012b). In this respect, Daanen (2009) measured the temperature course of the skin (i.e., temperature's drop of 1–5 °C with a 0.05–0.2 $°C \cdot s^{-1}$ cooling rate) when this was wetted with drops of water with volumes in a range of 10–100 μl. The author suggested that the cold sensations experienced when such skin cooling occurs can contribute to the perception of skin wetness. Therefore, exposing the skin to a cold-dry stimulus producing such skin cooling was hypothesized and tested effective in evoking an illusory perception of skin wetness (Daanen 2009).

The critical role of cold sensations in inducing the perception of wetness had been previously observed by Yamakawa and Isaji (1987) during a magnitude estimation experiment performed with six different textiles in three wetness conditions and at three different temperatures (Yamakawa and Setsuku 1987). In this study the authors found that subjects' ratings in terms of perceived wetness correlated to the initial cooling rates occurring during the contact between the subjects' fingers and the test fabrics: a greater initial temperature drop was linked to a greater perception of wetness. In line with this, the role of coldness in sensing skin wetness has been further confirmed by Bergmann Tiest et al. (2012b), who showed that, when manipulating dry phase-change materials which induced cool sensations, participants perceived these as being wetter than non-treated dry fabrics.

Finally, Ackerley et al. (2012) have recently shown that nine blindfolded females readily discriminated between very small amounts of moisture (in the range of 1.6 $\mu l \cdot cm^{-2}$) applied with a tactile stimulator over different regions of the body. Although in the mentioned study no recordings of local skin temperature and thermal sensations were performed, the authors hypothesized that participants distinguished the greater from the smaller levels of moisture due to the resulting greater evaporative cooling which induced colder thermal sensations and thus wetter perceptions.

With regard to the potential contribution of other sensory modalities (than thermal) to the perception of skin wetness, Bergmann Tiest et al. (2012a) have recently provided evidence for the role of tactile inputs in the haptic perception of wetness. In their study, the authors observed that, during the interaction with wet materials (i.e., 19.6 cm^2 thin and thick viscose and cotton wool), wetness discrimination thresholds decreased significantly when individuals were allowed dynamic as opposed to the static touching. This indicated that individuals' skin wetness perception was increased by a higher availability of tactile information, as occurring during the dynamic exploration (as opposed to the static contact) of the wet materials. The authors concluded that, when thermal cues (e.g., thermal conductance of a wet material) provide insufficient sensory inputs, individuals seem to

use mechanical cues (e.g., stickiness resulting from the adhesion of a wet material to the skin) to aid them in the perception of wetness.

Overall, these magnitude estimation studies have provided more detailed insights on the sensory inputs which could significantly contribute to driving the perception of skin wetness during the contact with wet stimuli (e.g., thermal cold sensations). Furthermore, these studies have demonstrated that assessing the psychophysical processes involved in the perception of skin wetness by using QST with a magnitude estimation paradigm can provide reliable quantitative data about the neurophysiological mechanisms underlying this complex somatosensory experience. However, despite these studies having provided psychophysical evidence on the role of the different sensory cues involved in the perception of skin wetness during the skin's contact with external (dry or wet) stimuli, until very recently, still little was known on how this sensory information was then centrally integrated by the nervous system. Furthermore, the absence of a specific reference sensory model for the perception of skin wetness contributed to a lack of standardized procedures in the assessment of skin wetness perception.

In this respect, our group has recently performed a systematic experimental analysis of the neurophysiological and psychophysical factors which underpin human skin wetness perception, with the aim of developing a neurophysiological model which could be used as a frame of reference in the assessment of the perception of skin wetness (Filingeri et al. 2013, 2014a, b, c, 2015). In order to achieve this aim, we developed a structured and systematic methodology for the assessment of skin wetness perception. In light of this, and due to the practical implications that this systematic methodology might have in the context of standardizing the assessment of human skin wetness perception, an overview of this experimental work as well as of the sensory model for skin wetness perception, along with detailed information and practical examples of the methods and setups we used in these studies, will be presented below.

4 Quantitative Sensory Testing of Skin Wetness Perception: Empirical Framework

The aim of the experimental work performed by our group was to investigate the neurophysiological and psychophysical bases of humans' ability to perceive wetness on the skin (Filingeri et al. 2013, 2014a, b, c, 2015). The contact with an external wet or dry stimulus was considered as the scenario in which the perception of skin wetness can be experienced and assessed. Specifically, it was aimed to elucidate, from a mechanistic standpoint, the individual contribution as well as the interaction between the sensory cues which seem to drive the perception of skin wetness (i.e., cutaneous thermal and tactile inputs).

A QST with a magnitude estimation paradigm was used to investigate skin wetness perception as a result of the contact with an external stimulus. This approach has been previously shown to be more appropriate than a discrimination paradigm when investigating the sensory cues involved in the perception of skin wetness. A number of external stimuli, with different properties (i.e., temperature, pressure, level of wetness), were applied to different body regions (i.e., hairy and glabrous skin sites), during different activities (i.e., rest and exercise), during different environmental conditions (i.e., thermoneutral and warm), and during different sensory states (i.e., the presence/absence of a selective reduction in the activity of specific cutaneous nerve fibers). These studies provided evidence for and support to the development of a specific neurophysiological model for human skin wetness perception. As results of these studies, the following findings were obtained:

1. When the application of cold-dry stimuli on participants' hairy skin produced a drop in skin temperature ranging between 1.4 and 4.1 °C with a cooling rate of 0.14–0.41 $°C \cdot s^{-1}$ (a similar cooling rate as the one induced by the evaporation of water from the skin), an illusion of skin wetness perception was evoked; when cold-dry stimulations produced a drop in skin temperature of 0.2–0.7 °C with a cooling rate of 0.02–0.07 $°C \cdot s^{-1}$, skin wetness perception

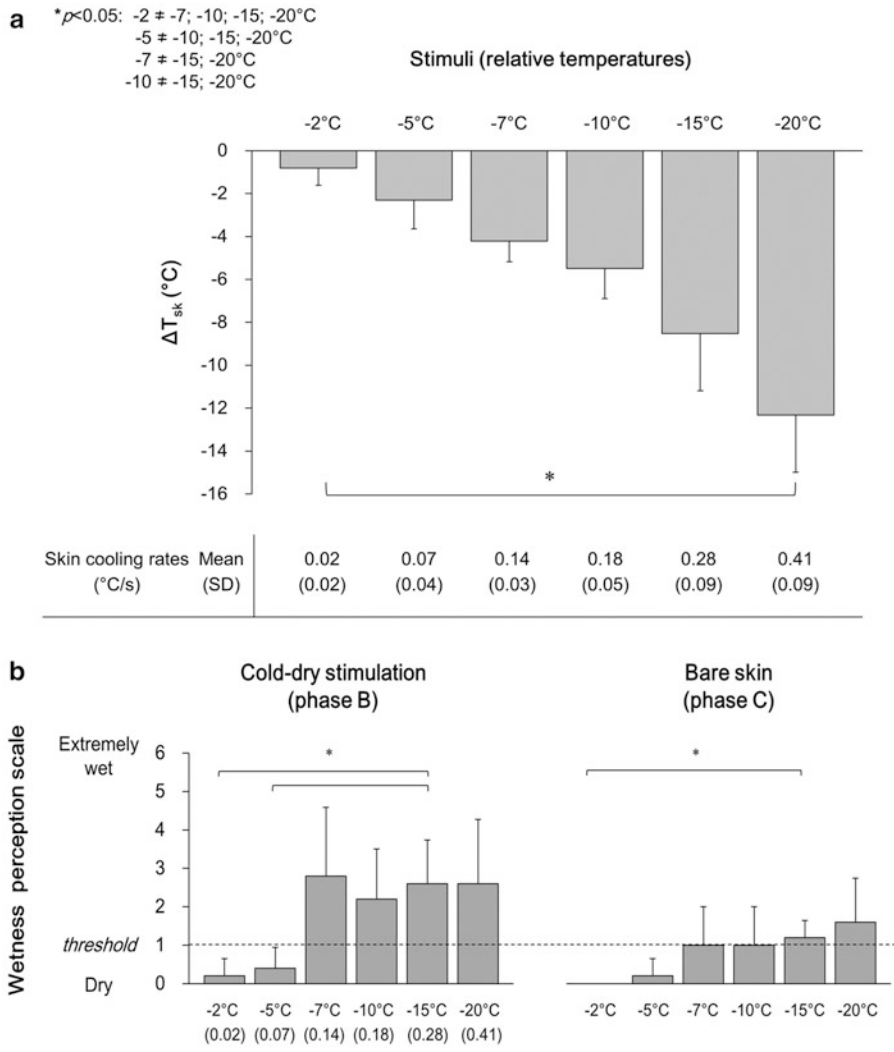

Fig. 1 (**a**) Relative variations in skin temperature drop from baseline (ΔT_{sk}) and corresponding cooling rates as a result of six cold-dry stimuli with decreasing contact temperatures. (**b**) Wetness perception scores recorded as a result of each of the six cold-dry stimuli (phase B) and during the following bare skin phase (**c**) (*$p < 0.05$). Skin cooling rates corresponding to each stimulus are reported between brackets. The point "1" of the wetness perception scale corresponds to the threshold set to identify perceived skin wetness (Reprinted from Neuroscience Letters, 551, Filingeri D, Redortier B, Hodder S, Havenith G, The role of decreasing contact temperatures and skin cooling in the perception of skin wetness, 65–69, Copyright (2013), with permission from Elsevier)

was little evoked and decreasing thermal sensations prevailed (Filingeri et al. 2013) (Fig. 1).

2. Cold-dry stimulations inducing skin cooling rates of 0.06–0.4 °C·s^{-1} were shown to evoke artificial skin wetness perceptions, with colder stimuli resulting in a higher frequency and magnitude of wetness perception. However, it was observed that the application of stimuli with a higher mechanical pressure on the skin (10 vs. 7 kPa) reduced the frequency of the times artificial wetness perceptions were evoked. Also, it was found that cold-dry stimuli were perceived as being wetter during exercise performed in a warm environment than during rest in the same environment, as well as than during exercise in the thermoneutral one (Filingeri et al. 2014c) (Fig. 2).

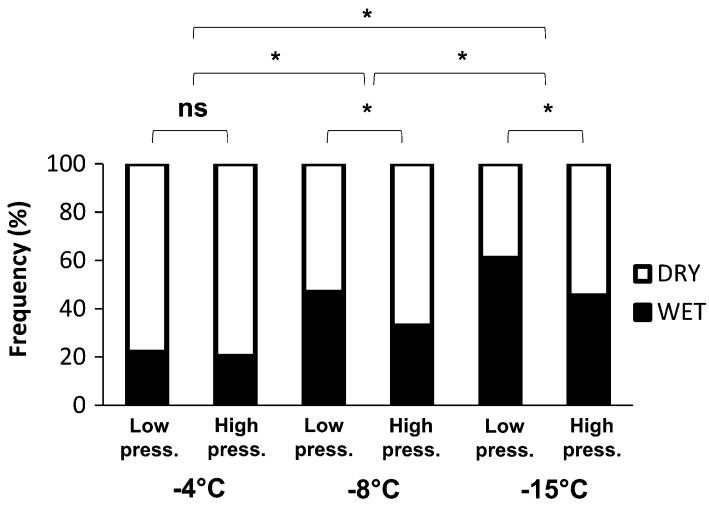

Fig. 2 Frequency distribution of local wetness perception scores as a result of three cold-dry stimuli (i.e., 4, 8, and 15 °C below local skin temperature) applied with low and high pressure. The frequency of times the same cold-dry stimulus was perceived as "dry" or as "wet" is indicated as a fraction (%) of the total responses recorded for each stimulus. Differences are indicated as statistically (*$p <$ 0.05) or as not statistically significant (i.e., ns) (Reprinted from Neuroscience, 258, Filingeri D, Redortier B, Hodder S, Havenith G, Thermal and tactile interactions in the perception of local skin wetness at rest and during exercise in thermo-neutral and warm environments, 121–-130, Copyright (2014), with permission from Elsevier)

3. The existence of regional differences in cutaneous thermosensitivity to cold has been shown to translate into significant regional differences in cutaneous wetness perception across the human torso. Interestingly, these regional sensory patterns were observed to be independent from the magnitude of local skin cooling caused by the stimulus. In other words, the regions in which the stimulus resulted in greater skin cooling (i.e., lateral chest) were not necessarily the ones in which the stimulus was perceived as colder, wetter, and more unpleasant (Filingeri et al. 2014a) (Fig. 3).
4. Warm temperature stimuli were shown to suppress the perception of skin wetness during initial static contact with a wet surface (Filingeri et al. 2015) (Fig. 4).
5. It was found that individuals perceived warm-wet and neutral-wet stimuli as significantly less wet than cold-wet ones, even when these were characterized by the same moisture content. Also, it was shown that when cutaneous cold and tactile sensitivity was diminished by a selective reduction in the activity of A-nerve afferents (subserving cold and light touch cutaneous sensitivity), wetness perception was significantly reduced. Finally, a trend was observed with the extent of perceived wetness being higher on the hairy than on the glabrous skin. This seems to be due to the structural (i.e., glabrous skin presents thicker stratum corneum and higher thermal insulation) and functional differences (i.e., glabrous skin presents higher density of mechanoreceptors, while hairy skin has a higher density of thermoreceptors) between hairy (more of a thermosensory organ) and glabrous skin (more of an organ for heat exchange) (Filingeri et al. 2014b) (Fig. 5).
6. Based on a concept of perceptual learning and Bayesian perceptual inference, the first neurophysiological model of cutaneous wetness sensitivity centered on the multisensory integration of cold and mechanosensitive skin afferents was developed in order to explain how humans sense warm, neutral, and cold skin wetness (Filingeri et al. 2014b) (Fig. 6).

The above-listed findings were obtained during five experimental studies which were conducted to

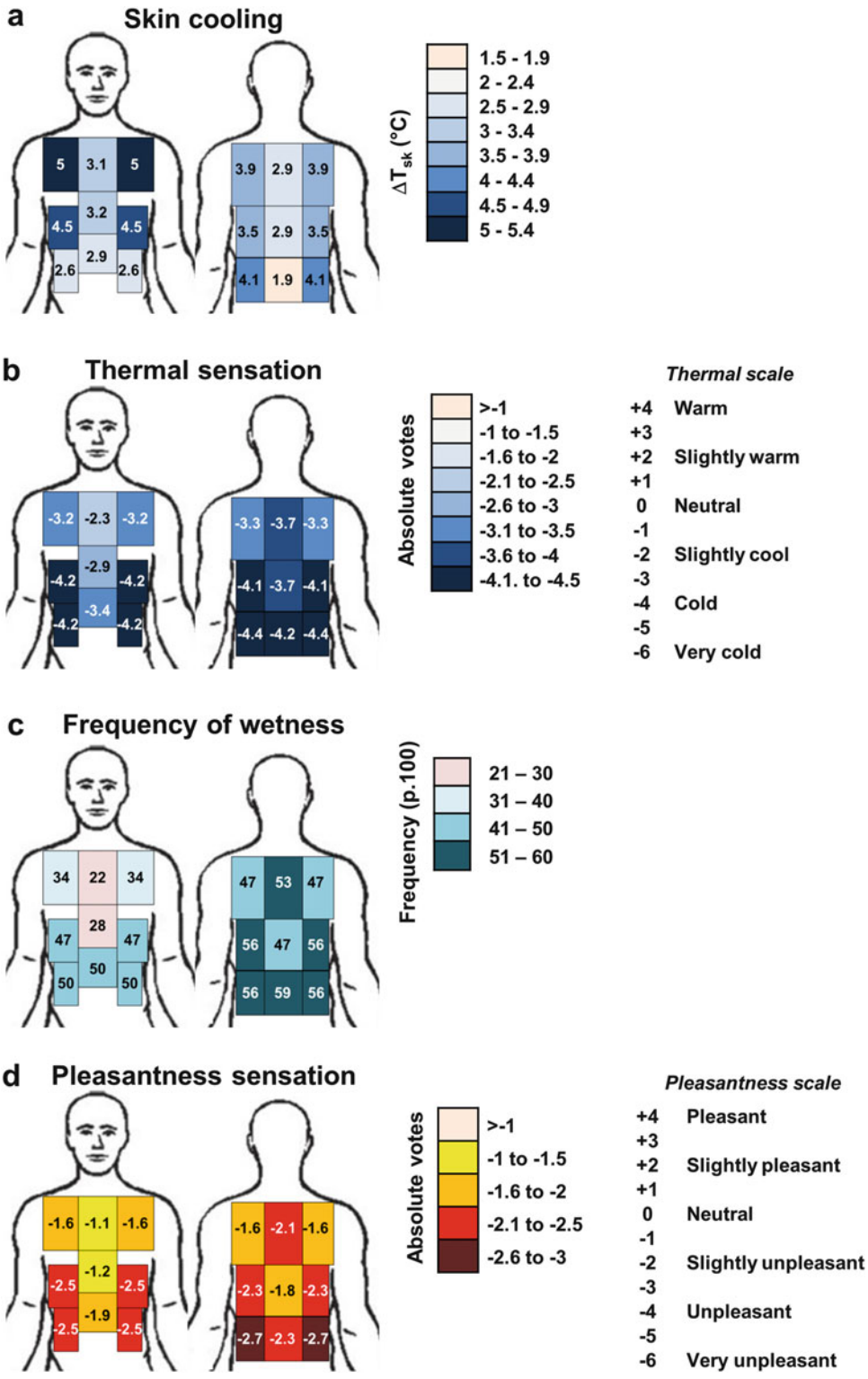

Fig. 3 (continued)

investigate skin wetness perception as resulting from the contact with an external (dry or wet) stimulus. These outcomes provided evidence for the primary role of cold thermal cues as well as mechanical cues in the form of pressure and stickiness in driving the perception of skin wetness.

In this respect, it deserves mention that, as an alternative way of experiencing skin wetness perception, the active production of sweat (either as resulting from exposures to warm environments or from exercise) represents a condition in which this sensory experience can also be assessed. Although in this context, the possibility to implement a quantitative approach and to use QST to isolate the individual contribution of the different sensory cues (i.e., thermal and tactile) is limited by the difficulties in strictly controlling the characteristics of the stimulus used (i.e., the amount and location of sweat-induced skin wetness), in order to provide the reader with a more comprehensive picture of the theoretical framework behind the perception of skin wetness; the findings of the most representative studies which have assessed skin wetness perception as resulting from active sweating are summarized below.

4.1 Skin Wetness Perception: Sweat Production

In a study in which thermal comfort sensitivity was investigated in relation to locally manipulated skin wetness (as resulting from exercise-induced sweat production), Fukazawa and Havenith (2009) found that the torso seems to have a lower sensitivity to wetness than the limbs. Similar findings were also reported by Gerrett et al. (2013) in a non-manipulated condition (natural sweat distribution across the torso during exercise). However, as sweat rates across the torso are much higher than on the limbs (Havenith et al. 2008; Smith and Havenith 2011, 2012), the skin wetness experienced in a non-manipulated condition is nevertheless higher for the torso (Gerrett et al. 2013). This is supported by Lee et al. (2011), who showed that individuals reported the torso (i.e., chest and back) to be the region more often perceived as wet during rest and moderate exercise in 25 °C and 32 °C ambient temperature and 50 % humidity.

Interestingly, in all these studies, skin temperature was always observed to increase significantly during the exercise protocols, suggesting that participants were able to both sense and regionally discriminate sweat-induced skin wetness, despite not experiencing any cold sensation, one of the main sensory cues which has been suggested to drive the perception of skin wetness (Filingeri et al. 2013, 2014a, b, c, 2015). It could therefore be suggested that in conditions of sweat-induced skin wetness, individuals rely more on tactile (e.g., stickiness of their clothing) than on thermal inputs (i.e., thermal cold sensations) to characterize their wetness perception. This

Fig. 3 Body maps showing the regional distribution of (**a**) local skin cooling (°C) caused by the application of the stimulus, (**b**) absolute mean votes for thermal sensation, (**c**) frequency of wetness perception, and (**d**) absolute mean votes for pleasantness sensation, as a result of the 10 s application of the relative cold-dry stimulus (15 °C lower than local T_{sk}) to each skin site, averaged over all conditions. Data were collected on the left side of the body and the body maps presented were developed assuming left-right symmetry (*see* Ouzzahra et al. 2012). Regions showing greater skin cooling, colder sensations, more frequent wetness perceptions, and more unpleasant sensations are represented in darker colors. Part of the rating scales used by the participants to score their absolute thermal and pleasantness sensations is reported next to the respective body maps. Two main tendencies are shown. First, the regional differences in thermal, wetness, and pleasantness sensation present a similar pattern across the torso (e.g., as opposed to the chest, the lateral and lower back appears more sensitive to cold, wetness, and thermal displeasure). Second, these sensory patterns seem independent from the regional variations in skin cooling (i.e., regions which show greater skin cooling, such as the lateral chest, are not necessarily the ones in which the stimulus was perceived as colder, more often wet, or more unpleasant) (Reprinted from Journal of Applied Physiology, doi: 10.1152/japplphysiol.00535.2014, Filingeri D, Fournet D, Hodder S, Havenith G, Body mapping of cutaneous wetness perception across the human torso during thermo-neutral and warm environmental exposures, Copyright (2014))

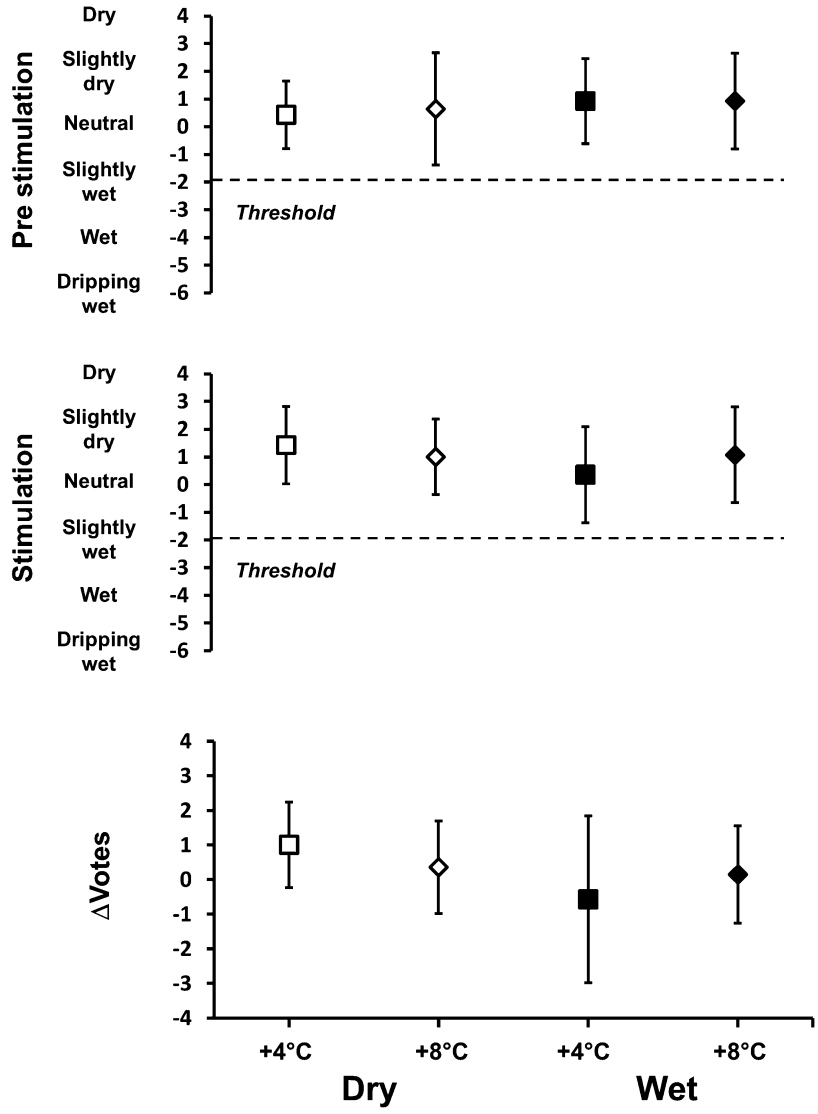

Fig. 4 Wetness perception scores recorded before (pre-stimulation) and during (stimulation) the application of the warm-dry and warm-wet stimuli. Average changes in vote (ΔVotes) from pre- to poststimulation are also reported (Filingeri et al. 2015) (Reprinted from Skin Research and Technology, doi: 10.1111/srt.12148, Filingeri D, Redortier B, Hodder S, Havenith G, Warm temperature stimulus suppresses the perception of skin wetness during initial contact with a wet surface, Copyright (2014), with permission from John Wiley and Sons)

hypothesis could be supported by the fact that a swelling state of the skin (due to sweat production) has been previously suggested as to potentially affect the regional perception of skin wetness by increasing the skin's sensitivity to tactile stimulation (Gerrett et al. 2013).

The possibility that, in conditions of sweat-induced skin wetness, individuals rely more on tactile than on thermal inputs to characterize their wetness perception could be also in line with what previously shown for the skin's contact with an external stimulus (i.e., manual exploration of a wet material) by Bergmann Tiest et al. (2012a), who reported that, when thermal cues (e.g., thermal conductance of a wet material) provide insufficient sensory inputs, individuals seem to use mechanical cues (e.g., stickiness resulting from the adhesion of a wet material to the skin) to aid them in the perception of wetness (Bergmann Tiest et al. 2012a). However, as in the abovementioned studies (Fukazawa and Havenith 2009; Lee et al. 2011; Gerrett et al. 2013), the mechanical interaction at the skin was neither manipulated nor controlled; these studies did not provide conclusive evidence on the potential link between the thermal and tactile changes occurring

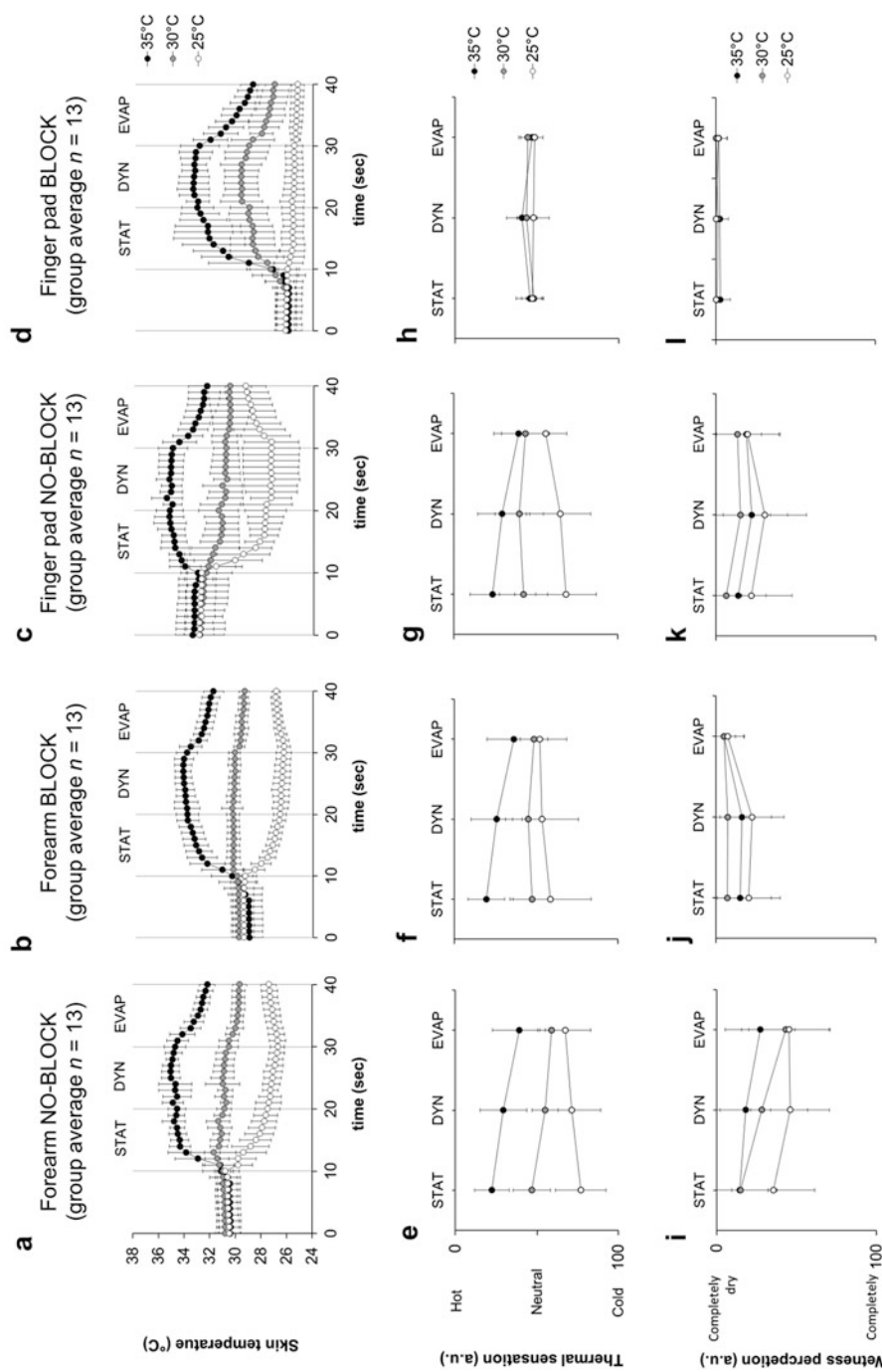

Fig. 5 (continued)

locally at the skin's surface when this was wet due to sweating and the resulting sensory inputs used by the participants to characterize their perception of skin wetness.

In this respect, the studies performed by our group (Filingeri et al. 2013, 2014a, b, c, 2015), which focused on assessing skin wetness perception during the contact with an external dry and/or wet stimulus, were conducted with the aim of isolating the individual contribution of thermal and tactile cues to the perception of wetness, so that a sensory model for wetness could be developed and thus used as a frame of reference also in those studies in which skin wetness is induced by the active production of sweat. In doing so, we developed a structured and systematic methodology for the assessment of skin wetness perception. The following paragraph summarizes the methodology developed (including all the relevant equipment used) and provides a practical outline of a typical experimental protocol as used in the assessment of skin wetness perception.

5 Quantitative Sensory Testing of Skin Wetness Perception: Practical Framework

When investigating the perception of skin wetness, one of the aims of the sensory testing is to isolate the individual contribution of cutaneous thermal and tactile cues to the perception of wetness so that the participant's somatosensory ability to perceive skin wetness can be assessed.

In this respect, as other sensory modalities than thermal and tactile (e.g., vision) can represent a potential confounding factor in the assessment of skin wetness perception, specific setups are needed. For example, as in the abovementioned studies, we wanted to limit the contribution of vision to the perceptual experience of skin wetness (thus focusing on the somatosensory components of this perception); we therefore did not provide participants with any specific information about the type of stimuli we used. Furthermore, during the assessment of skin wetness perception, participants were blind to the site of stimulation. This approach was considered necessary to reduce the contribution of any expectation effect as well as of any confounding factor in the assessment of skin wetness perception. Hence, specific setups were designed. An overview of their characteristics is presented below.

5.1 Experimental Setup

For the first study investigating skin wetness during the contact with an external stimulus, the forearm was chosen as preferred site for stimulation (Filingeri et al. 2013). In this respect, participants were informed only about the body region subjected to the stimulation. No information was provided on the type and magnitude of the stimulation to limit any expectation effects.

To blind the participants to the site of stimulation, an S-shaped wooden panel (width, 81 cm; length, 74 cm; height, 60 cm) was placed on a

Fig. 5 Forearm and finger pad skin temperature (°C) and corresponding ratings for thermal sensation and wetness perception (arbitrary units, a.u.) during the static (STAT), dynamic (DYN), and evaporation (EVAP) phases of contact with the warm-wet (35 °C), neutral-wet (30 °C), and cold-wet (25 °C) stimuli. Panels **a** and **b**, panels **e** and **g**, and panels **i** and **k** show skin temperature, thermal sensation, and wetness perception data, respectively, as recorded during the NO-BLOCK trial for the forearm and finger pad. Panels **b** and **d**, panels **f** and **h**, and panels **j** and **l** show skin temperature, thermal sensation, and wetness perception data, respectively, as recorded during the BLOCK trial for the forearm and finger pad. Two tendencies are illustrated. In the NO-BLOCK trials, thermal sensations matched the variation in skin temperature, and wetness perceptions increased with decreasing contact temperatures (static phase) and from static to dynamic to post contact (evaporation). In the BLOCK trials, cold sensitivity was reduced in the forearm, and both warmth and cold sensitivity were reduced on the finger pad. This resulted in a significant decrease in wetness perceptions during all temperature stimulations (and particularly during the cold one) and during all phases of interaction. Data are reported as mean (group average $n = 13$) and SD (*vertical lines*) (Reprinted from Journal of Neurophysiology, doi: 10.1152/jn.00120.2014, Filingeri D, Fournet D, Hodder S, Havenith G, Why wet feels wet? A neurophysiological model of human cutaneous wetness sensitivity, Copyright (2014))

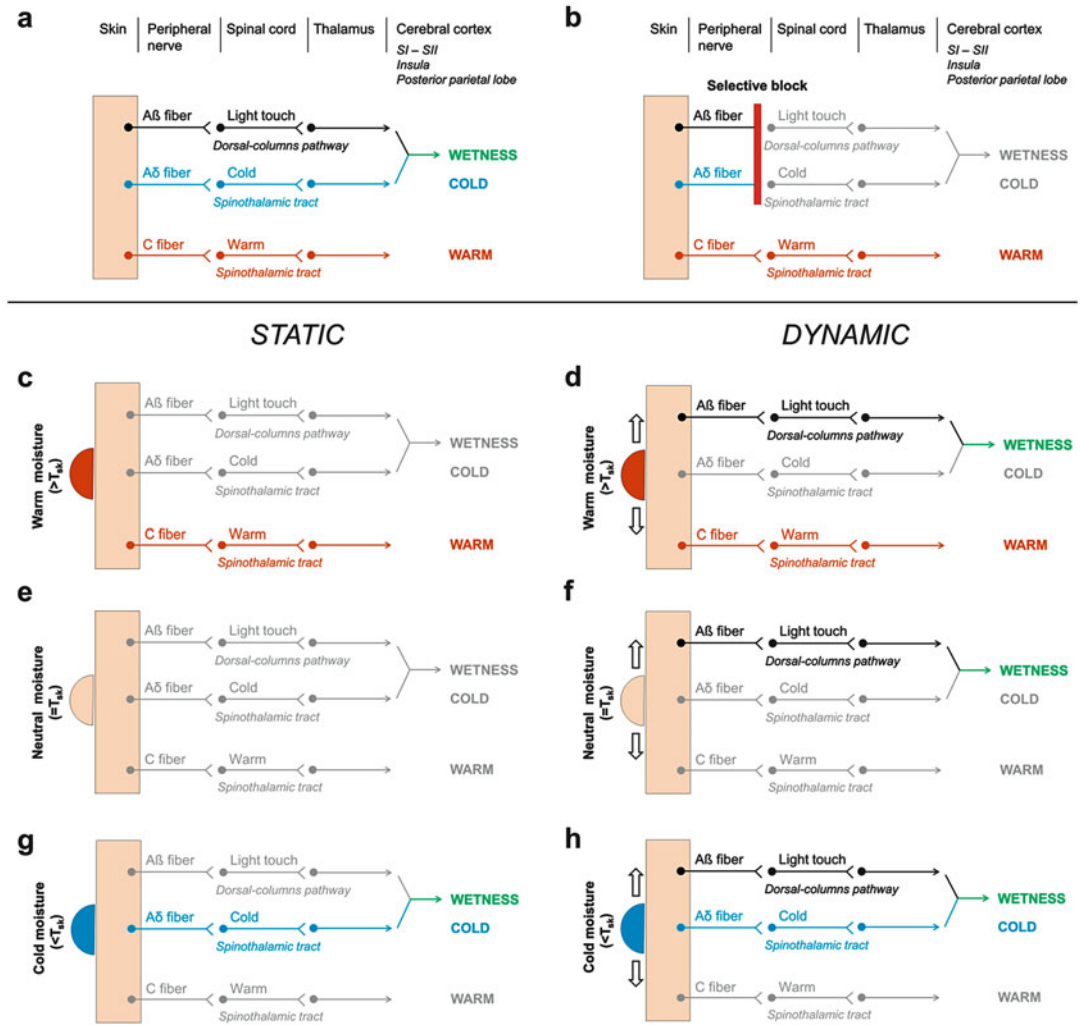

Fig. 6 Neurophysiological model of cutaneous wetness sensitivity. Mechano Aß, cold Aδ, and warm C-sensitive nerve fibers and their projections from the skin, through the peripheral nerve, spinal cord (via the dorsal column-medial lemniscal pathway and the spinothalamic tract), thalamus, and somatosensory cerebral cortex (including the primary and secondary somatosensory cortices SI and SII, the insular cortex, and the posterior parietal lobe), are shown. Panels **a** and **b** show the neural model of wetness sensitivity (consisting of Aδ and Aß afferents) under normal and under selective reduction in the activity of A-nerve fibers, respectively. Panels **c**, **e**, and **g** show the pathways for wetness sensitivity during static contact with warm, neutral, and cold moisture. Panels **d**, **f**, and **h** show the pathways for wetness sensitivity during dynamic contact with moisture (Reprinted from Journal of Neurophysiology, doi: 10.1152/jn.00120.2014, Filingeri D, Fournet D, Hodder S, Havenith G, Why wet feels wet? A neurophysiological model of human cutaneous wetness sensitivity, Copyright (2014))

table. A hole (width, 12 cm; height, 13 cm) in the panel allowed participants to enter their left forearm and lay it down with the palm facing upward. This setup did not allow the participants to see the stimuli that were applied on their forearm (Fig. 7).

For the second and third studies investigating skin wetness during the contact with an external stimulus, the upper and lower back were chosen as preferred sites for stimulation, as participants were tested either resting or exercising (cycling) (Filingeri et al. 2014c, 2015). In this respect,

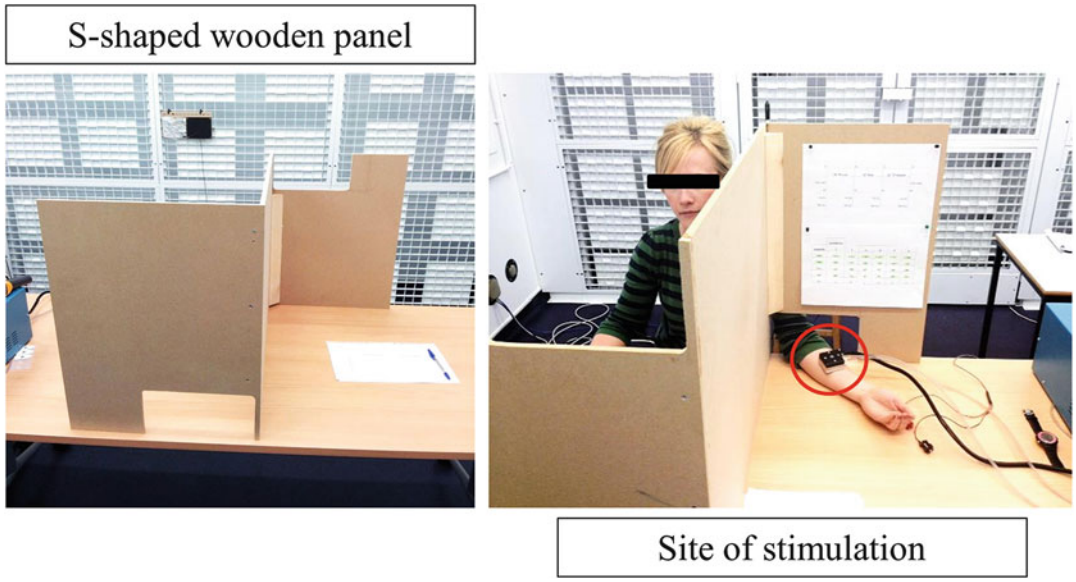

Fig. 7 The S-shaped wooden panel used to blind the participants to the site of stimulation

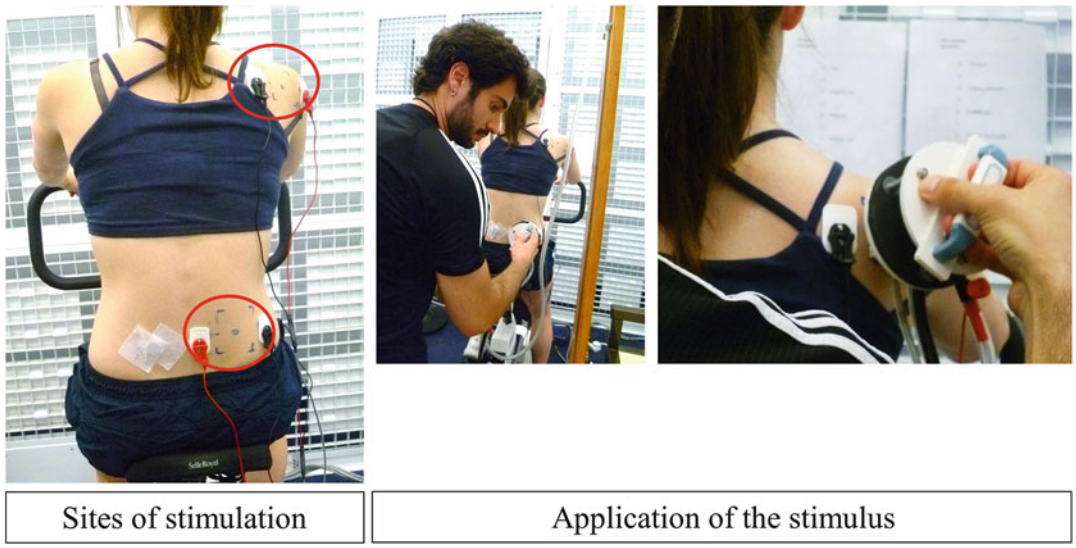

Fig. 8 The experimental setup adopted by Filingeri et al. (2014c, 2015)

participants were informed only about the body region subjected to the stimulation. No information was provided on the type and magnitude of the stimulation to limit any expectation effects. Being this their back, participants were naturally blind to the site of stimulation (Fig. 8).

For the fourth study investigating skin wetness during the contact with an external stimulus, as the regional sensitivity to skin wetness perception was investigated, 12 regions of the front and back of the torso were chosen as preferred sites for stimulation (Fig. 9) (Filingeri et al. 2014a). In this respect, participants were informed only about the body region subjected to the stimulation. No information was provided on the type and magnitude of the stimulation to limit any expectation effects.

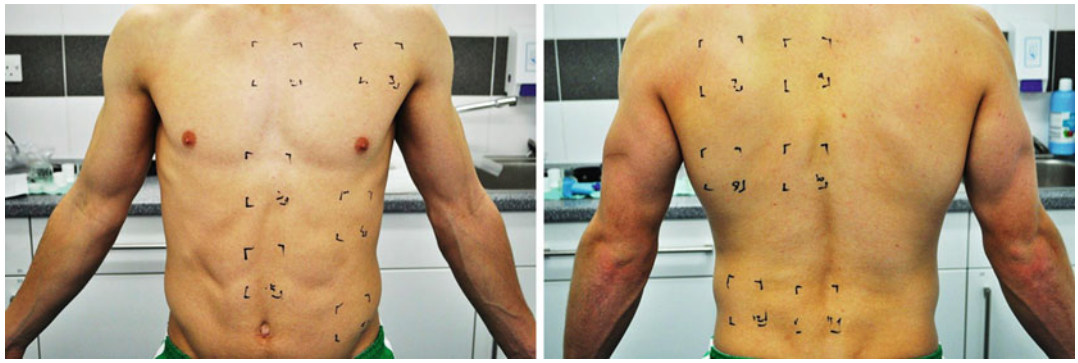

Fig. 9 The 12 skin sites of the front and back of the torso chosen for stimulation

Fig. 10 The experimental setup adopted by Filingeri et al. (2014a)

To blind the participants to the sites of stimulation, the following setup was designed (Fig. 10). When the front torso was stimulated, participants were asked to lie on a bench on their back, with their arms alongside the body and a rectangular-shaped textile screen (length, 81 cm; height, 67 cm) was placed above the participants' neck. The screen was adjusted until each participant confirmed that they could not see either their front torso or the investigator. When the back torso was stimulated, participants were asked to lie on their front, with their arms alongside the body, and to face toward the left, while the investigator was standing on their right-hand side (Filingeri et al. 2014a).

For the fifth and last study investigating skin wetness during the contact with an external stimulus, the forearm and index finger pad were chosen as preferred sites for stimulation (Fig. 11) (Filingeri et al. 2014b). In this respect, participants were informed only about the body region subjected to the stimulation. No information was provided on the type and magnitude of the stimulation to limit any expectation effects.

To blind the participants to the site of stimulation, an S-shaped wooden panel (width, 81 cm; length, 74 cm; height, 60 cm) was placed on a table. A hole (width, 12 cm; height, 13 cm) in the panel allowed participants to enter their left forearm so that they could interact with the stimuli.

Fig. 11 The two skin sites chosen for stimulation

This setup did not allow the participants to see the stimuli that were applied on their forearm. Furthermore, as in this study a compression ischemia protocol was used to selectively reduce cutaneous cold and tactile sensitivity; during the experimental tests in which this protocol was performed, a blood pressure cuff was applied on the participants' forearm (Fig. 12).

In summary, the experimental setups presented above provide practical examples on how to meet the conditions required for the assessment of skin wetness perception across different regions of the body as well as during different experimental conditions.

Meeting these experimental conditions with the appropriate setup is just one of the steps which are required when performing a QST of the perception of skin wetness. Indeed, the choice of the appropriate stimulator for delivering the specific stimuli required, as well as the choice of the appropriate physiological and psychometric measurements, and finally the design of an appropriate experimental protocol all represent factors which are essential to effectively assess this perception. An overview of these factors is presented below.

5.2 Stimulator

With regard to the type stimulator to be used to assess the perception of skin wetness, this has to satisfy specific criteria which are essential to effectively investigate the thermal and tactile components involved in the perception of skin wetness. The stimulator has to be:

- Controllable in terms of its temperature, in terms of the mechanical pressure this can generate on the skin, and in terms of its wetness level
- Relatively small and easily applicable to different parts of the body, during different conditions (e.g., rest and exercise)

In our studies, these criteria were found to be satisfied by the Physitemp thermal probe (Physitemp Instruments, Inc., USA). This thermal stimulator presents a thermal probe with a contact metallic surface of 25 cm^2 and a weight of 269 g (Fig. 13a). The thermal probe is driven by a thermoelectric (Peltier effect) module. The system is composed of a controller (readout unit) to which the thermal probe is connected. For stable operation, the thermoelectric module requires a trickle of cooling water. This is supplied by a pump and tank unit connected to the controller (Fig. 13b).

The thermal probe we used had a base adjustable temperature range of 20–30 °C. According to the base temperature, a temperature control range of ±20.5 °C is allowed. The thermal probe has a response time of <4 s in heating and cooling.

As it stood, the thermal probe assured that some of the requirements needed (i.e., having a controllable temperature as well as being relatively small and easily applicable to different parts of the body) were met. However, specific modifications were needed to assure that the same stimulator could allow the application of stimuli with different levels of wetness, as well as to control the mechanical pressure applied to the skin.

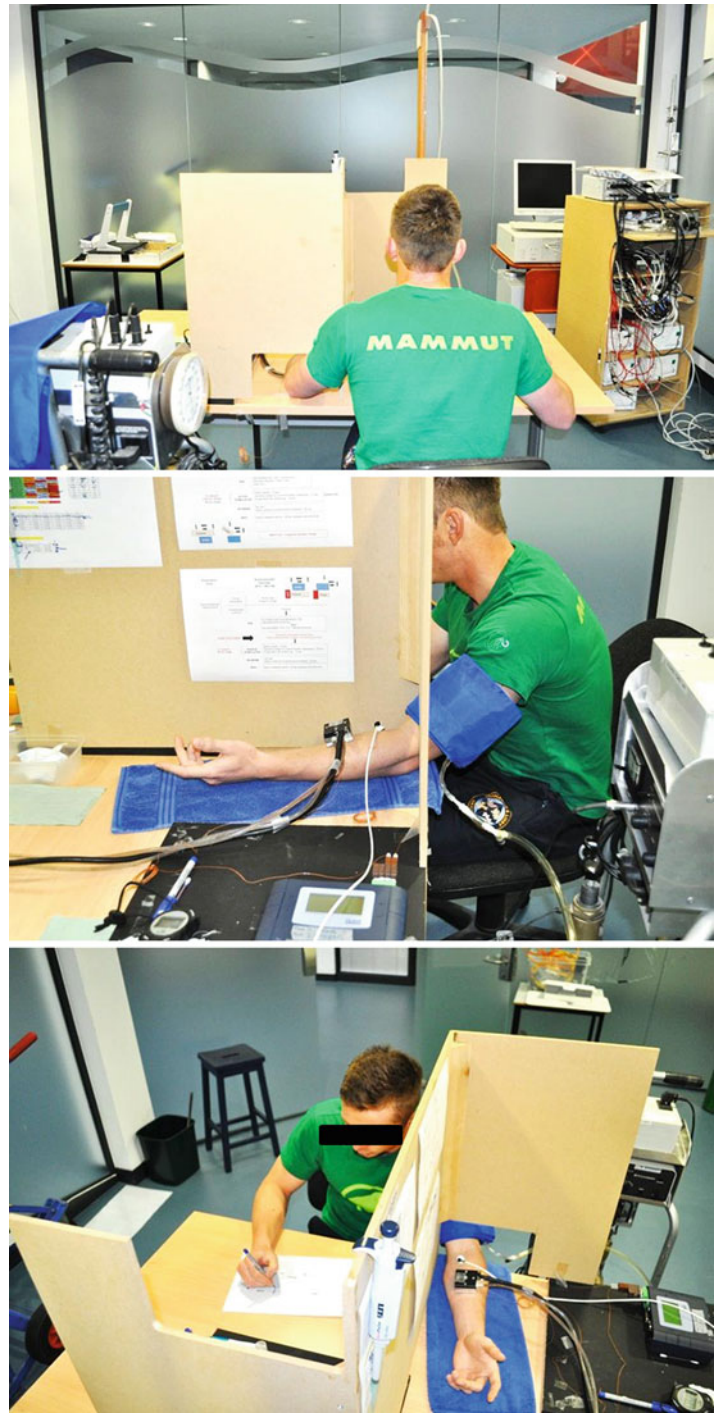

Fig. 12 The S-shaped wooden panel used to blind the participants to the site of stimulation

With regard to the first requirement, to make the contact with the probe's surface either dry or wet, test fabrics (100 % cotton) with a surface of 100 cm^2 were placed on the thermal probe and fixed by an elastic band (Fig. 14). According to the test, these were wetted with water at ambient temperature (~23 °C), using a variable volume pipettor (SciQuip Ltd., Newtown, UK).

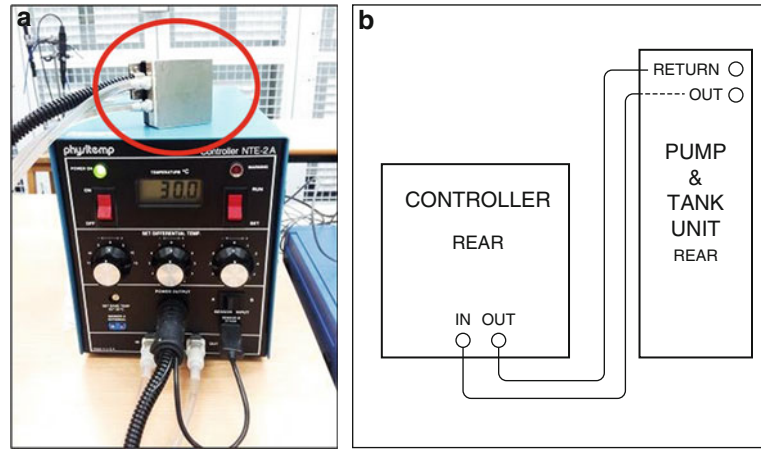

Fig. 13 The thermal probe used for the application of the external stimuli. Panel **a** shows the control unit with the three dials allowing control of the probe's temperature (step changes of ±5 °C, ±1 °C, or ±0.1 °C) and the thermal probe with the contact metallic surface of 25 cm^2 (in the *red circle*). Panel **b** shows a schematic diagram of how the control unit was connected to the pump and tank unit

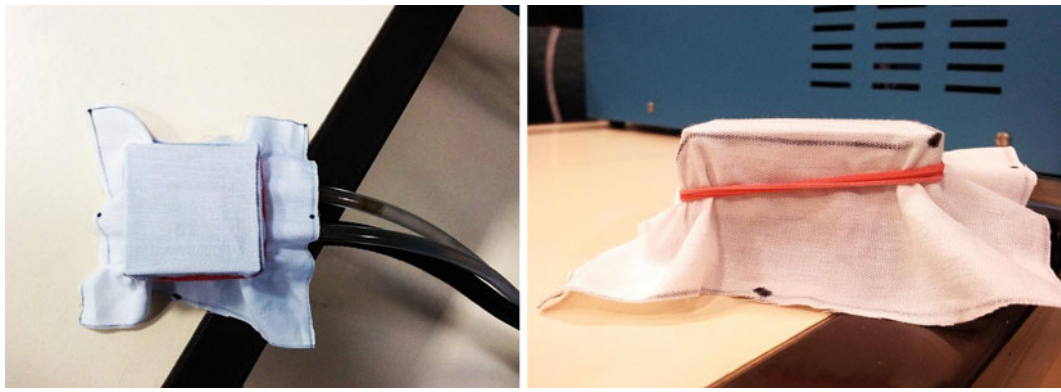

Fig. 14 The test fabrics used to make the probe's contact surface either dry or wet

To ensure that the wet fabric would reach the required probe's temperature, the contact temperature between the probe and the test fabric was monitored with a thin thermocouple (0.08 mm wire diameter, 40 gauge; 5SRTC-TT-TI-40-2M, Omega, Manchester, UK) placed on the thermal probe's surface. Probe-fabric temperature was then monitored online using a Grant Squirrel SQ2010 data logger (Grant Instruments Ltd., Cambridge, UK).

With regard to the second requirement, to manipulate and control the mechanical pressures applied by the thermal probe, we designed and developed a pressure control system (Fig. 15). The system consisted of an air bladder, inserted into a frame attached to the thermal probe, which was connected to a manometer (containing water) throughout a silicon tube. The frame consisted of two wooden disks laid one upon the other and coupled by three springs which allowed the top disk to scroll down freely. A handle was attached to the top disk so that the probe could be applied to the skin. When this happened, the air bladder deformed, producing a pressure change in the system which resulted in displacing the water in the manometer from its set "null" point (no pressure applied). The point reached by the water in the tube as a result of the pressure change was used as an indicator to control the mechanical pressure. To calibrate and standardize this last one, a digital scale (Mettler Toledo, Inc., USA) was used to measure the force resulting from the application of the probe.

The range between the lowest and the highest pressure applicable and measurable by the system resulted in 7–55 kPa. Tests were performed during

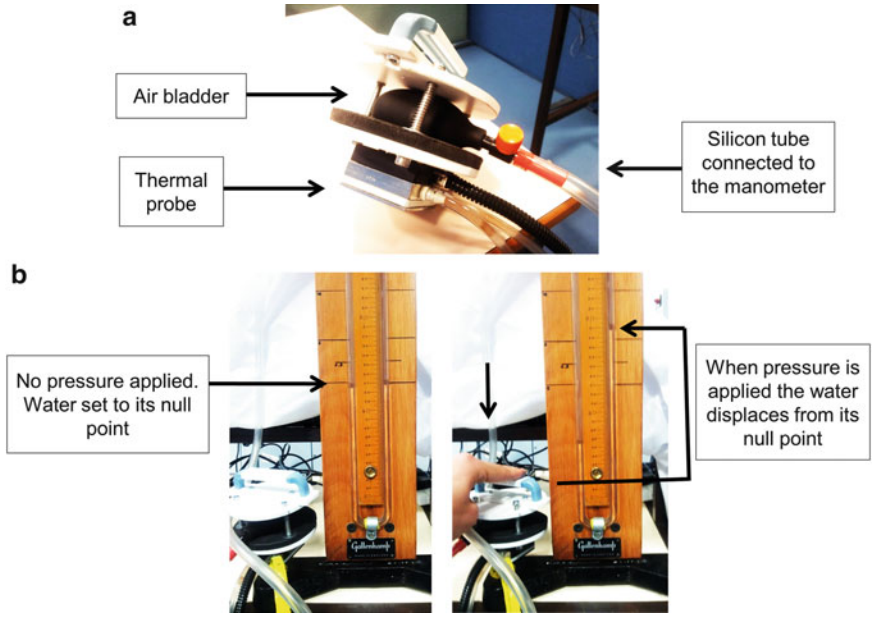

Fig. 15 The pressure control system developed to manipulate and control the mechanical pressures applied by the thermal probe. The system consists of an air bladder, inserted into a frame and attached to the thermal probe. The air bladder is connected to a manometer (containing water) throughout a silicon tube (**a**). When no pressure is applied to the system, the water in the manometer sets to its "null" point (**b**). When pressure is applied, the air bladder deforms, producing a pressure change in the system which displaces the water in the manometer from its set "null" point (**c**). The point reached by the water in the tube, as a result of the pressure change, is used as an indicator to control the mechanical pressure applied to the skin (Reprinted from Neuroscience, 258, Filingeri D, Redortier B, Hodder S, Havenith G, Thermal and tactile interactions in the perception of local skin wetness at rest and during exercise in thermo-neutral and warm environments, 121–130, Copyright (2014), with permission from Elsevier)

the development of the prototype to check the accuracy and repeatability of the nominal pressures applied with the pressure control system. One hundred trials were conducted. These consisted of measuring the force resulting from the application of the probe on a digital scale (Mettler Toledo, Inc., USA) while controlling that the water displacement on the manometer was the one required for the pressures selected. Ninety-five percent confidence interval values were calculated for the two reference pressures (i.e., 7 and 10 kPa) and resulted as follows: 7 kPa = 7.1 kPa (lower bound), 7.2 kPa (upper bound); 10 kPa = 10.4 kPa (lower bound), 10.6 kPa (upper bound).

It deserves mention that, although the stimulator described above was found to satisfy the criteria required for the assessment of skin wetness perception, alternative options to this device are available and have previously found to be effective in delivering controlled local dry and/or wet stimuli to the skin. An example of such devices is represented by the automated rotary tactile stimulator (Dancer Design, Wirral, UK) used by Ackerley et al. (2012) in their investigation of skin wetness sensitivity across different body sites.

The rotary tactile stimulator has four radial arms with a smooth, slightly rounded plastic surface at each end (length, 6 cm; width, 3 cm), on which test fabrics can be applied, e.g., by means of pieces of VELCRO®. The authors used this automated rotary tactile stimulator to deliver controlled moving stimuli at a predetermined force, direction, and speed to the skin sites, using custom-written scripts in LabVIEW (National Instruments, Austin, USA).

5.3 Measurement of Skin Temperature

In order to overcome previous limitations observed in the literature (i.e., the absence of specific physiological measurements of local changes at the skin during application of the external stimuli), for the assessment of skin wetness perception as performed in our recent studies, it was decided to monitor: (1) the local changes in skin temperature when the skin was stimulated with the probe and (2) the whole-body changes in mean skin temperature when participants were exposed to different environmental and exercising conditions.

Local skin temperature before or after the contact with the stimuli was measured by using a single-spot infrared thermometer (Fluke 566, Fluke Corporation, USA) with a temperature range of −40 °C to 800 °C and an accuracy of ±1 °C (Fig. 16). In order to maximize the accuracy of the temperature reading, during all testing the infrared thermometer was calibrated against a matte black plate whose temperature was monitored with a thermistor (Grant Instruments, Cambridge, UK).

Local skin temperature during the contact with the stimuli was measured by using a thin thermocouple (0.08 mm wire diameter, 40 gauge; 5SRTC-TT-TI-40-2M, Omega, Manchester, UK). This was applied either on the ventral side of the forearm or index finger pad using Transpore tape (3M, Loughborough, UK), with the sensor tip touching the skin, but not covered by tape (Fig. 17). To monitor (online) and record contact temperatures, the thermocouple was plugged in

Fig. 16 The infrared thermometer used to measure local skin temperature before or after the contact with the stimuli

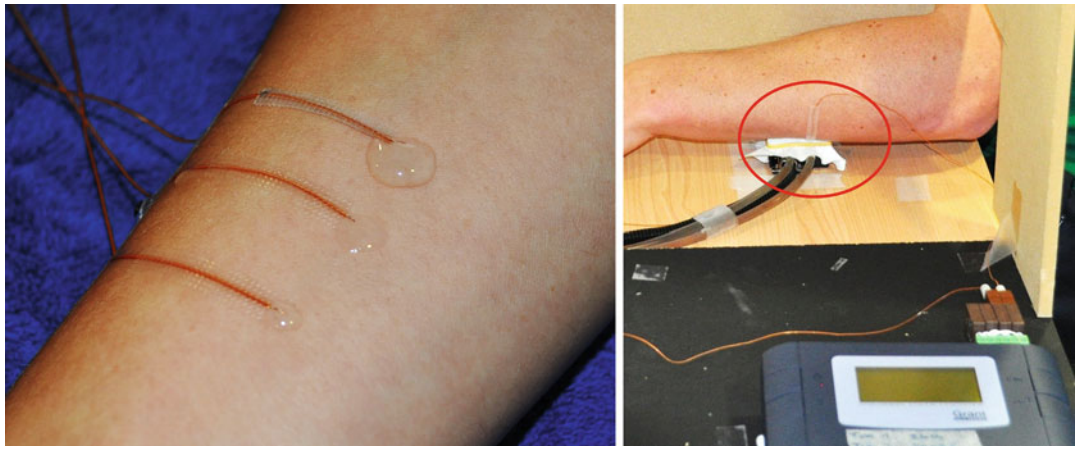

Fig. 17 The thin thermocouples used to measure local skin temperature during the contact with the stimuli

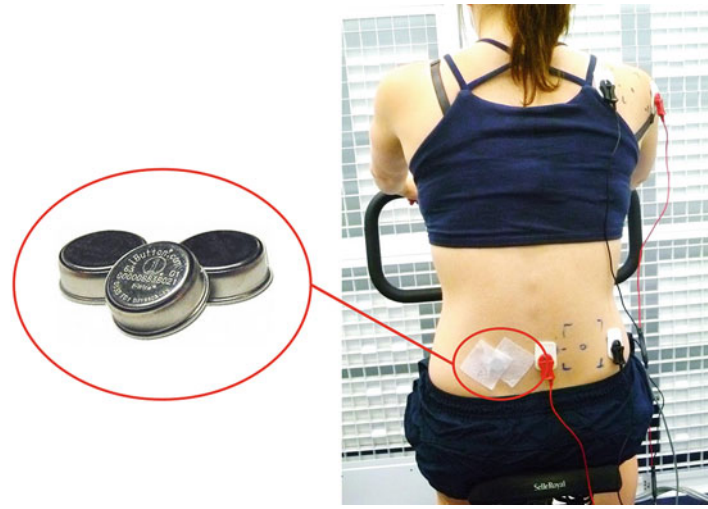

Fig. 18 The iButton (wireless temperature loggers) used to measure local skin temperature to be used for the estimation of mean skin temperature

Grant Squirrel SQ2010 data logger (Grant Instruments Ltd., Cambridge, UK).

Finally, to estimate mean skin temperature, iButton wireless temperature loggers (Maxim, San Jose, USA) with a temperature range of −55 to 100 °C, resolution of 0.5 °C, and response time of 2 s were used. These were taped to five skin sites on the left side of the body (i.e., cheek, abdomen, upper arm, lower back, and back lower thigh) to record local skin temperature (Fig. 18). Mean skin temperature (T_{sk}) was calculated according to the work of Houdas and Ring (1982) as follows:

$$\begin{aligned}\text{Mean } T_{sk} = {} & (\text{cheek} \times 0.07) \\ & + (\text{abdomen} \times 0.175) \\ & + (\text{upper arm} \times 0.19) \\ & + (\text{lower back} \times 0.175) \\ & + (\text{back lower thigh} \times 0.39)\end{aligned}$$

5.4 Measurement of Skin Wetness Perception

In order to measure skin wetness perception, two main types of psychometric scales were used within the experimental work we performed:

LIKERT SCALES

Thermal sensation	
+4	Warm
+3	
+2	Slighlty warm
+1	
0	Neutral
-1	
-2	Slighlty cool
-3	
-4	Cold
-5	
-6	Very cold

Wetness perception	
+4	Dry
+3	
+2	Slighlty dry
+1	
0	Neutral
-1	
-2	Slighlty wet
-3	
-4	Wet
-5	
-6	Dripping wet

VISUAL ANALOGUE SCALES

Thermal sensation	
0	Not cold at all
1	
2	
3	
4	
5	
6	Extremely cold
>6	Painfully cold

Wetness perception	
0	Dry
1	
2	
3	
4	
5	
6	Extremely wet

Thermal sensation

Hot _____ Cold

Wetness perception

Completeley dry _____ Completely wet

Fig. 19 Overview of the Likert scales and visual analogue scales used by Filingeri et al. (2013, 2014a, b, c, 2015) for the assessment of thermal sensation and skin wetness perception

Likert scales and visual analogue scales. These were used in conjunction with similar scales for the assessment of thermal sensation (Fig. 19).

With regard to the specificity of each type of scale, and how appropriate their use is according to the experimental conditions designed, it is generally accepted that Likert scales are preferable for the benefits that the presence of verbal descriptors provides in helping individuals to describe their sensations. This is particularly true when external noise or distracters can influence the subjective ability to define one's own sensations (Lee et al. 2010). In line with this point, and with regard to our experimental work, Likert scales were mainly used for those conditions in which skin wetness perception was assessed while participants were exercising or when they could not mark their sensation by handwriting due to a particular experimental setup.

With regard to visual analogue scales, these are generally considered as preferable when a higher sensitivity in the measurement of a particular sensation is needed. Also, by not restricting individuals' ability to rate their sensation based on specific verbal descriptors, these scales are thought to provide individuals with a greater flexibility and thus accuracy in their sensation discrimination (Lee et al. 2010). In line with this point, we primarily used visual analogue scales for those conditions in which skin wetness perception was assessed and a greater accuracy in wetness discrimination was needed by the participants, due to the large number of different stimuli these were exposed to (e.g., stimuli characterized by a wide range of temperatures).

6 Protocol for the Assessment of Skin Wetness Perception

Once the necessary requirements for the assessment of skin wetness perception are met (i.e., appropriate experimental setup, stimulator, physiological and psychometric measurements) the QST can be performed. However, in order to assure an effective and reliable assessment, a standardized experimental protocol must be performed. In this respect, and based on the experimental studies we have performed (Filingeri et al. 2013, 2014a, b, c, 2015), here we present

an example of a generic protocol to be used in the assessment of skin wetness perception:

1. The participant arrives to the laboratory or testing site 30 min before the time scheduled for the test to allow preparation procedures. Anthropometric parameters (i.e., seminude body mass, height, and skinfold thickness for body composition calculation) can be recorded to help characterize the participant.
2. The participant changes into comfortable clothing appropriate for the type of assessment. For example, if the participant is required to exercise during the assessment of skin wetness perception, clothing such as t-shirt, running shorts, socks, and running shoes will be required.
3. At this point, five iButton (Maxim, USA) are taped to five left skin sites (cheek, abdomen, upper arm, lower back, and back lower thigh) to record local skin temperature. The five temperature measurements can be recorded at 1 min intervals throughout the tests; these can then be averaged every 5 min and weighted according to the work of Houdas and Ring (1982), to give an estimate of mean skin temperature for the entire body. This approach is particularly useful when the assessment of skin wetness perception is performed in relation to the exposure to different ambient conditions which could potentially change the thermal state of the body.
4. The skin sites targeted for stimulation are then marked with a washable marker to assure consistency in the location of stimulation. These can be on any site of the body (examples from our experimental work include forearm, front and back of the torso, and index fingertip).
5. After preparation, the participant enters the testing room (or environmental chamber if the test is performed in different ambient conditions), and 10 min is allowed for stabilization and acclimation to the new environment. During this period, the participants familiarize with the psychometric rating scale designed to record individual thermal sensations and wetness perceptions. Specific instructions are provided on how to interpret and use the scale. For example, when using Likert scales (see Fig. 19), the following can be said to the participant:

During the test, I will ask you to rate your local thermal sensation and wetness perception. As soon as I apply the stimulus on your skin, try to report your local and very first sensation / perception using whatever number in the scales seems more appropriate to you

Also, when using visual analogue scales (see Fig. 19), the following instructions can be provided:

When reporting thermal sensations, I would like you to associate the anchor point "Hot" (on the left of the scale) to the idea of a burning hot pan, and the anchor point "Cold" (on the right of the scale) to the idea of an ice cube, and to mark a point on the scale which corresponds to the level of warmness or coldness you experience when the stimulus will be applied on your skin. Please consider the midpoint of the scale as a neutral point (to be marked if neither hot nor cold sensations are experienced). When reporting wetness perceptions, I would like you to associate the anchor point "Completely dry" (on the left of the scale) to the absence of any wetness. Thus, any marked point which is not on the left edge of the scale is considered to correspond to the perception of skin wetness, with the closer this is to the anchor point "Completely wet" (on the right of the scale), the greater the level of wetness you are experiencing during the application of the stimulus on your skin

6. After the stabilization and acclimation period, and according to the conditions (e.g., resting or exercising), the participant is asked to maintain a seated position or to move to an electromagnetically braked cycle ergometer (e.g., Lode Excalibur, the Netherlands) and start cycling at any required exercise intensity.
7. At this point the QST of the perception of skin wetness can be initiated. First, the participant is asked to rate thermal sensation and skin wetness perception just before the application of the stimulus in order to provide an indicator of baseline sensation for the skin site targeted for stimulation. At the same time, local skin temperature of the skin site targeted for stimulation is either measured with the infrared

thermometer or continuously monitored with a thermocouple at the contact site.

Secondly, the thermal probe is set with the required level of wetness (i.e., a fabric with known moisture content is applied on the probe as described in the *Stimulator* paragraph), set to the required temperature, and then applied by hand to the skin site with the set pressure. To avoid an effect of surprise on the transient sensations, a verbal warning is given prior to stimulation. The application of the probe can vary from a short (e.g., 10 s) to a longer contact (e.g., 30 s) according to whether an initial and transient sensation or a steady-state sensation is assessed.

During the stimulation, the probe is not moved and (according to the specific experimental setup) the participant cannot see the stimulated area.

At the end of the stimulation, the participant is instructed and encouraged to verbally report his/her local sensation and perception using whatever number in the Likert scale seems appropriate (integers only) or to mark a point on the visual analogue scale. Immediately after this, the probe is removed and, if skin temperature is measured with an infrared thermometer, the temperature of the stimulated area is recorded. This method allows perceptual rating to be made consistently close to the time when poststimulation skin temperature is recorded.

8. The above-outlined protocol can be then repeated if more than one stimulus is tested, allowing at least 1 min in between them. In case of multiple stimuli, and multiple tests, endorsing a balanced order of application will be useful in reducing to a minimum any learning and expectation effect.

As a potential alternative to the above-outlined protocol, the same procedure can be performed and skin wetness perception assessed, by having the participant actively interacting with stimuli instead of being passively exposed to it. The benefit of this approach is in the possibility of asking the participant to interact dynamically (as opposed to statically) with the stimulus, thus enabling the assessment of the tactile component (i.e., skin friction) of skin wetness perception.

In this respect, an example of this protocol, involving the use of the same experimental setup as shown in Figs. 7 and 11 (i.e., stimulation of the forearm or index finger pad), is presented below:

1. The thermal probe is secured with surgical tape on the side of the table which is not visible to the participant, with the thermally controlled surface facing upward.
2. Prior to interacting with the stimulus, and in order to set a specific baseline skin temperature, the participant is asked to insert their arm through the hole in the panel and place the forearm or index finger pad for at least 30 s on the thermal probe.
3. The participant then removes the arm from the thermal probe, places it on the side of the table visible to him/her, and waits 1 min for the stimulus to be prepared.
4. During this time, the probe is set to the required temperature, and the test fabric is secured to the probe and then wetted with the required amount of moisture with a pipettor. An average time of 1 min is usually required for the wet test fabric to reach the selected temperature.
5. Once the stimulus preparation is completed, the interaction with the wet stimulus is initiated. If both thermal and tactile cues are assessed, this interaction can consist of two phases: static and dynamic.
6. First, the participant is instructed to insert his/her left arm through the hole in the panel and to lower it until the forearm or index finger pad is in full contact with the thermal probe. As soon as in static contact, the participant is encouraged to rate his/her local thermal and wetness perceptions, e.g., by marking a point on the thermal and wetness scales he/she is provided with on the side of the table which is visible to him/her (response time ∼5 s).
7. Secondly, the participant is asked to move the forearm or index finger pad forward (∼2.5 cm) and backward (∼2.5 cm) twice while maintaining full contact with the thermal probe. At the end of this dynamic interaction, he/she is asked again to rate his/her local

thermal and wetness perceptions (response time ~5 s).
8. This sequence (i.e., setting the baseline skin temperature, preparing, and then interacting with the wet stimulus) can be repeated for each stimulus intended to be assessed, however assuring a balanced order in the administration, with at least 1 min in between successive applications.

Note: As no visual feedback is available during the stimulation, to assure consistency in the interaction with the stimuli (i.e., pressure applied to the probe and horizontal displacement during the dynamic phase), the investigator is supposed to gently guide the participants' arm throughout the interaction with each stimulus and to provide verbal instructions on when to change the interaction (e.g., from static to dynamic). Also, assure participants are familiarized with the experimental protocol prior to testing.

7 Conclusion and Recommendations

This chapter has presented the state of the current knowledge about the neurophysiological and psychophysical bases of humans' ability to perceive skin wetness, along with an overview of the most recent methods used to assess this sensory feature of the human skin.

The ability to perceive skin wetness represents one of the numerous somatosensory features of the skin. As humans seem not to be provided with specific humidity receptors on their skin, the ability to sense skin wetness has been shown to rely on a complex multisensory integration of thermal (i.e., heat transfer) and tactile (i.e., mechanical pressure and skin friction) inputs generated by the interaction between skin, moisture, and (if donned) clothing. Therefore, when assessing skin wetness as a perception, these parameters (i.e., cutaneous thermal and tactile sensitivity) should be measured and controlled within specific testing conditions.

Quantitative sensory testing has been shown to be a reliable method to assess the perception of skin wetness. However, this method has to be implemented within a specific experimental setup and performed according to a standardized protocol. In this respect, this chapter has provided an empirical framework for the perception of skin wetness as well as the first available sensory model which can be used as a frame of reference in the assessment of this perception. Furthermore, and in light of the latter, a practical framework for the assessment of this perception has been provided in order to standardize the procedure and assure consistency in the evaluation of skin wetness perception.

Still little is known on the complex sensory integration underpinning skin wetness perception as a somatosensory feature of the skin. However, due to the fundamental as well as practical implications that the ability to sense skin wetness has on everyday life, the possibility to develop and standardize specific testing procedures (as proposed in this chapter) is critical, not only to further the understanding of this sensory experience but also to design specific diagnostic tests which can be confidently and widely used within industrial as well as clinical contexts.

References

Ackerley R, Olausson H, Wessberg J, McGlone F. Wetness perception across body sites. Neurosci Lett. 2012;522(1):73–7.

Bentley I. The synthetic experiment. Am J Psychol. 1900;11(3):405–25.

Bergmann Tiest WM, Kosters ND, Kappers AM, Daanen HAM. Haptic perception of wetness. Acta Psychol (Amst). 2012a;141(2):159–63.

Bergmann Tiest WM, Kosters ND, Kappers AML, Daanen HAM. Phase change materials and the perception of wetness. Ergonomics. 2012b;55(4):508–12.

Candas V, Libert J, Vogt J. Human skin wettedness and evaporative efficiency of sweating. J Appl Physiol Respir Environ Exerc Physiol. 1979;46 (3):522–8.

Chong PST, Cros DP. Technology literature review: quantitative sensory testing. Muscle Nerve. 2004;29(5): 734–47.

Clark R, Edholm O. Man and his thermal environment. London: E. Arnold; 1985.

Craig A. Interoception: the sense of the physiological condition of the body. Curr Opin Neurobiol. 2003;13:500–505.

Daanen HAM. Method and system for alerting the occurrence of wetness. EP Patent. 2009;2:110–08.

Driver J, Spence C. Multisensory perception: beyond modularity and convergence. Curr Biol. 2000;10(20):R731–5.
Filingeri D, Redortier B, Hodder S, Havenith G. The role of decreasing contact temperatures and skin cooling in the perception of skin wetness. Neurosci Lett. 2013;551:65–9.
Filingeri D, Fournet D, Hodder S, Havenith G. Body mapping of cutaneous wetness perception across the human torso during thermo-neutral and warm environmental exposures. J Appl Physiol (1985). 2014a. 117:887–97.
Filingeri D, Fournet D, Hodder S, Havenith G. Why wet feels wet? A neurophysiological model of human cutaneous wetness sensitivity. J Neurophysiol. 2014b. 112:1457–69.
Filingeri D, Redortier B, Hodder S, Havenith G. Thermal and tactile interactions in the perception of local skin wetness at rest and during exercise in thermo-neutral and warm environments. Neuroscience. 2014c;258:121–30.
Filingeri D, Redortier B, Hodder S, Havenith G. Warm temperature stimulus suppresses the perception of skin wetness during initial contact with a wet surface. Skin Res Technol. 2015. 21:9–14.
Fukazawa T, Havenith G. Differences in comfort perception in relation to local and whole body skin wettedness. Eur J Appl Physiol. 2009;106(1):15–24.
Gagge A. A new physiological variable associated with sensible and insensible perspiration. Am J Physiol. 1937;120:277–87.
Gerrett N, Redortier B, Voelcker T, Havenith G. A comparison of galvanic skin conductance and skin wettedness as indicators of thermal discomfort during moderate and high metabolic rates. J Therm Biol. 2013;38(8):530–8.
Havenith G. Individualized model of human thermoregulation for the simulation of heat stress response. J Appl Physiol (1985). 2001;90(5):1943–54.
Havenith G, Fogarty A, Bartlett R, Smith CJ, Ventenat V. Male and female upper body sweat distribution during running measured with technical absorbents. Eur J Appl Physiol. 2008;104(2):245–55.
Havenith G, Bröde P, den Hartog E, Kuklane K, Holmer I, Rossi RM, Richards M, Farnworth B, Wang X. Evaporative cooling: effective latent heat of evaporation in relation to evaporation distance from the skin. J Appl Physiol (1985). 2013;114(6):778–85.
Houdas Y, Ring E. Human body temperature-Its measurement and regulation. Plenum Press, New York, NY, 1982.
Jeon E, Yoo S, Kim E. Psychophysical determination of moisture perception in high-performance shirt fabrics in relation to sweating level. Ergonomics. 2011;54(6):576–86.
Kondo N, Nakadome M, Zhang K, Shiojiri T, Shibasaki M, Hirata K, Iwata A. The effect of change in skin temperature due to evaporative cooling on sweating response during exercise. Int J Biometeorol. 1997;40(2):99–102.
Lee JY, Stone EA, Wakabayashi H, Tochihara Y. Issues in combining the categorical and visual analog scale for the assessment of perceived thermal sensation: methodological and conceptual considerations. Appl Ergon. 2010;41(2):282–90.
Lee J, Nakao K, Tochihara Y. Validity of perceived skin wettedness mapping to evaluate heat strain. Eur J Appl Physiol. 2011;111(10):2581–91.
Li Y. Perceptions of temperature, moisture and comfort in clothing during environmental transients. Ergonomics. 2005;48(3):234–48.
Likert R. A technique for the measurement of attitudes. Arch Psychol. 1932;22:5–55.
Mayrovitz HN, Sims N. Biophysical effects of water and synthetic urine on skin. Adv Skin Wound Care. 2001;14(6):302–8.
Nadel ER, Stolwijk JA. Effect of skin wettedness on sweat gland response. J Appl Physiol. 1973;35(5):689–94.
Niedermann R, Rossi R. Objective and subjective evaluation of the human thermal sensation of wet fabrics. Text Res J. 2012;82(4):374–84.
Nishi Y, Gagge A. Effective temperature scale useful for hypo-and hyperbaric environments. Aviat Space Environ Med. 1977;48(2):97–107.
Ouzzahra Y, Havenith G, Redortier B. Regional distribution of thermal sensitivity to cold at rest and during mild exercise in males. J Therm Biol. 2012;37:517–523.
Scott J, Huskisson EC. Graphic representation of pain. Pain. 1976;2(2):175–84.
Smith CJ, Havenith G. Body mapping of sweating patterns in male athletes in mild exercise-induced hyperthermia. Eur J Appl Physiol. 2011;111(7):1391–404.
Smith CJ, Havenith G. Body mapping of sweating patterns in athletes: a sex comparison. Med Sci Sports Exerc. 2012;44(12):2350–61.
Sweeney MM, Branson DH. Sensorial comfort: part I: a psychophysical method for assessing moisture sensation in clothing. Text Res J. 1990a;60(7):371–7.
Sweeney MM, Branson DH. Sensorial comfort: part II: a magnitude estimation approach for assessing moisture sensation 1. Text Res J. 1990b;60(8):447–52.
Tichy H, Kallina W. Insect hygroreceptor responses to continuous changes in humidity and air pressure. J Neurophysiol. 2010;103(6):3274–86.
Walk D, Sehgal N, Moeller-Bertram T, Edwards RR, Wasan A, Wallace M, Irving G, Argoff C, Backonja MM. Quantitative sensory testing and mapping: a review of nonautomated quantitative methods for examination of the patient with neuropathic pain. Clin J Pain. 2009;25(7):632–40.
Yamakawa M, Isaji S. Factors affecting the clamminess. J Text Mach Soc Jpn. 1987;33:9–15.
Yamakawa M, Setsuku I. Factors affecting the clamminess. J Text Mach Soc Jpn. 1987;33:9–15.

Gravimetry in Sweating Assessment in Primary Hyperhidrosis and Healthy Individuals

65

Tomasz J. Stefaniak

Contents

Keywords
Hyperhidrosis (HH) • Gravimetry • Objective evaluation

1 Background

Though hyperhidrosis is generally considered a subjectively perceived disease, it seems more and more doubtful that merely subjective evaluation is sufficient to qualify the patient to surgery (Haider and Solish 2005). Vapometry provides valuable and reliable method of assessment; nevertheless, it is not possible to be performed in multiple localizations (face, hands, armpits, trunk, feet) in more than one patient at the same time (Larson 2011). Moreover, the equipment for this assay is rather expensive and cannot be considered a standard instrument for a surgical clinic. In contrary, gravimetry is a simple, cheap, and fast method of objective evaluation of sweating (Heckmann et al. 2001; Hund et al. 2002; Stefaniak et al. 2011). Gravimetry is a short and easy method of objective measurement of sweating. It is performed by 1 min collection of sweat with 3-weighted cotton swab. Net weight is calculated as the difference between brutto and tara weights. To include individual differences determined by the area in which the sweating is preferred, the net weight is divided by the total body surface and therefore standardized. Adequate and objective evaluation of intensity of sweating plays an essential role in proper qualification to surgery and,

T.J. Stefaniak (✉)
Department of General, Endocrine and Transplant Surgery, Medical University of Gdansk, Gdansk, Poland
e-mail: wujstef@gumed.edu.pl

P. Humbert et al. (eds.), *Agache's Measuring the Skin*,
DOI 10.1007/978-3-319-32383-1_87

further, for reliable assessment of the results of intervention. In some anecdotal cases, despite obvious anhidrosis, the patients may still demand further treatment (Kreyden et al. 2002), which may arise from psychiatric conditions, such as body dysmorphic syndrome. In those patients, invasive treatment may lead not only to dissatisfaction but also to severe psychiatric disturbances or even suicide. Thanks to regular introduction of the quantitative evaluation of sweating prior and after surgery, it is possible to provide the patients with information on their sweating compared to the reference values.

Epidemiological studies concerning HH are based solely on subjective data gathered from questionnaires. Based on such data, Strutton et al. (2004) have shown that HH affects approximately 2.8 % of the population and that palmar HH occurs most often at approximately 13 years of age. Large Chinese studies (Tu et al. 2007), again solely based on subjective questionnaires and conducted in a group of 33,000 people, between the age of 11 and 22 years, have shown that HH occurs in 4.36 % of the general Chinese population. A similar questionnaire-based study has been conducted in the USA, finding HH in 1.4 % of the respondents (Adar et al. 1977). Another questionnaire-based study by Westphal et al. (2011) has shown a high HH prevalence, of up to 5.5 %, among the Brazilian population.

In most studies presented in the literature, the authors concentrate on relative impact of different forms of treatment on gravimetrically measured sweating (Heckmann et al. 2001; Hund et al. 2002; Hong et al. 2012; Lowe et al. 2007; Proebstle et al. 2002). Mostly, such measurements were performed in dermatological settings and concerned the results of local methods of treatment such as Botox treatment or iontophoresis. In those methods of treatment, associated with low level of transient complications or side effects, even less stringent approach to qualification will not cause long-term harm to the patients. Thanks to regular introduction of the quantitative evaluation of sweating prior and after surgery, it is possible to provide the patients with information on their sweating compared to the reference values. Due to that it was possible to confirm that the preoperative values of abdomino-lumbar sweating in the PHH patients are very low. The increase in sweating in this area is very often subjectively experienced by the patients. Nevertheless, in our experience the post-op abdomino-lumbar sweat rate remains low and not above the reference value found in our control subjects (Stefaniak 2013).

2 Technique to the Evaluation

Gravimetric assays have been performed similarly to the procedure described by Heckmann et al. (2001) and Hund et al. (2002). In short, after 15 min rest in sitting position, the patients were invited into the air-conditioned measure room in standardized temperature (24–25 °C) and humidity 15–17 %. The subjects were not allowed to consume alcohol 48 h prior to the assessment and had their last meal at least 6–8 h prior to testing. All tests were performed in disposable gloves.

A standard small cotton gauze pad has been weighted on a precise (d = 0.5 mg) weight scale (Radwag, Poland – scale type WPS 110/C/S, Poland). Then the pad was given to the participant who was asked to wipe carefully the area under evaluation. The procedure in each localization lasted 1 min. Then the pad was weighted again and a difference was calculated. To avoid a bias associated with different body areas of participants, the difference was standardized by division by body area calculated with the height of the participant (according to Mosteller, body area [m^2] = 0.01667 × height [cm]0.5 × mass [kg] 0.5) (Verbraecken et al. 2006). An Internet tool has been developed in order to simplify transcoding raw data into results adjusted to body surface of the patients (www.chirurgiapomorska.edu.pl/gravimetrictool).

Mean gravimetric intensity of sweating in PHH patients prior to surgery was 24.49 ± 45.64 mg/min/m^2 for facial, 153.37 ± 160.39 mg/min/m^2 for palmar, 66.23 ± 56.18 mg/min/m^2 for axillary, and 31.24 ± 72.97 mg/min/m^2 for abdomino-lumbar localizations (Stefaniak 2013). After surgery it was 14.48 ± 11.64 mg/min/m^2

for palmar, 23.63 ± 24.56 mg/min/m^2 for axillary, and 28.86 ± 56.05 mg/min/m^2 for abdomino-lumbar localizations (Stefaniak 2013). In another study by our team (Stefaniak et al. 2013) performed on healthy volunteers, mean value of gravimetrically evaluated intensity of sweating was, respectively, 19.15 ± 14.97, 18.49 ± 14.06, 42.39 ± 47.08, and 15.77 ± 16.87 mg/min/m^2.

The overall test–retest correlation was 0.71 (Stefaniak et al. 2013). Test–retest values measured in volunteers for different localizations were facial 0.64, palmar 0.54, axillary 0.84, and abdomino-lumbar 0.70. In follow-up patients it was, respectively, 0.82, 0.81, 0.79, and 0.66 (only follow-up results were included in test–retest evaluation).

As mentioned in the background of this chapter, the epidemiology of HH identifies about 1–4 % of population to suffer from intractable symptoms that should be considered a qualification to surgery. In normal distribution, it is calculated that 95.5 % of observations are within mean ±2 SD. Considering that only the upper limit of normative value is important for diagnosing hyperhidrosis, it can be calculated that 2.25 % of cases will be within the range higher than mean ±2 SD. This percentage is in accordance with epidemiological data on predominance of PHH in population, which has been reported to reach 2.8 % (Haider and Solish 2005; Strutton et al. 2004). Therefore, in order to obtain threshold for diagnosis of hyperhidrosis, double standard deviation was added to the mean from general population. Those thresholds are presented in the table below (Table 1).

3 Comment

It has to be underlined that gravimetric assessment, as a qualification standard, allows minimization of the risk of qualifying people for surgery who have a psychological problem with HH rather than a biological one. It is often that subjective HH assessment does not match the results of objective tests. This is usually so because patients tend to compare themselves to their peers, rather than looking upon themselves objectively. Another reason for "subjective–objective" discrepancies is through comparing the "ideal me" with the "real me." Bearing those discrepancies in mind, when assessing patients, we can often see that he or she has an overestimated subjective HH assessment, even though the objective test shows otherwise. On the other hand, patients that often meet the criteria for surgical treatment of HH tend not to see the real problem.

Considering what has been written above, the more important it seems to conduct additional objective assessments, which are characterized by high sensitivity, and allow screening for patients who actually suffer from intensive HH. Performing objective HH assessment also allows avoiding qualifying patients for surgery who, in fact, have mild HH and could benefit from other types of treatment such as iontophoresis or botulinum toxin therapy. It should also be mentioned that gravimetry can additionally add to qualitative evaluation of hyperhidrosis. This can be achieved by five-point evaluation (face, hands, armpits, abdomino-lumbar area, and feet). In primary hyperhidrosis, two out of five localizations will be increased (hands and feet), while the others

Table 1 Reference values of sweating in different areas of the body measured by gravimetry and suggested thresholds for qualification for sympathectomy (Stefaniak and Proczko 2013)

Threshold for qualification for sympathectomy (mg/min/m^2)	Mean value in 1-min gravimetric test divided by body surface (mg/min/m^2)	Localization
49	19	Face
46	18	Hands
136	42	Armpits
Not applicable[a]	16	Abdomino-lumbar
46	18	Feet

[a]Hyperhidrosis in this localization is not a qualification to sympathectomy

will be low, especially in abdomino-lumbar area. Increased values in all five areas will rather point to generalized hyperhidrosis due to endocrine problems, such as menopause, obesity, or sexual hormone disturbances (Stefaniak et al. 2012).

To sum up, basing ETS qualification solely on subjectively reported intensity of sweating may create the risk of qualifying for surgery patients in whom sweating does not exceed the normative value for the specific population or is a symptom of other underlying diseases. Taking into account the occurrence of post-ETS compensatory sweating (Lyra et al. 2008), as well as its unpredictable intensity (Lyra et al. 2008), qualifying patients that do not meet the objective HH criteria should be considered a mistake. The key message of this study is that when assessing patients suffering from HH, it is necessary to use both objective and subjective methods of evaluation.

4 Conclusion

Gravimetry is an easy, reproducible, cheap, and fast method of evaluation of sweating. The reference values are stable and can serve as a qualifying and follow-up tool for evaluation of the patients with PHH in any localization.

References

Adar R, Kurchin A, Zweig A, Mozes M. Palmar hyperhidrosis and its surgical treatment: a report of 100 cases. Ann Surg. 1977;186:34–41.

Haider A, Solish N. Focal hyperhidrosis: diagnosis and management. Can Med Assoc J. 2005;172(1):69–75.

Heckmann M, Ceballos-Baumann AO, Plewig G. Hyperhidrosis study group. Botulinum toxin a for axillary hyperhidrosis (excessive sweating). N Engl J Med. 2001;344(7):93–488.

Hong HC, Lupin M, O'Shaughnessy KF. Clinical evaluation of a microwave device for treating axillary hyperhidrosis. Dermatol Surg. 2012;38(5):35–728.

Hund M, Kinkelin I, Naumann M, Hamm H. Definition of axillary hyperhidrosis by gravimetric assessment. Arch Dermatol. 2002;138(4):41–539.

Kreyden OP, Heckmann M, Peschen M. Delusional hyperhidrosis as a risk for medical overtreatment: a case of botulinophilia. Arch Dermatol. 2002;138(4):9–538.

Larson DL. Definitive diagnosis and management of axillary hyperhidrosis: the VapoMeter and suction-assisted arthroscopic shaving. Aesthet Surg J. 2011;31(5): 9–552.

Lowe NJ, Glaser DA, Eadie N, Daggett S, et al. North American botox in primary axillary hyperhidrosis clinical study group. Botulinum toxin type A in the treatment of primary axillary hyperhidrosis: a 52-week multicenter double-blind, randomized, placebo-controlled study of efficacy and safety. J Am Acad Dermatol. 2007;56(4):11–604.

Lyra RM, Campos JR, Kang DW, et al. Guidelines for the prevention, diagnosis and treatment of compensatory hyperhidrosis. J Bras Pneumol. 2008;34:967–77.

Proebstle TM, Schneiders V, Knop J. Gravimetrically controlled efficacy of subcorial curettage: a prospective study for treatment of axillary hyperhidrosis. Dermatol Surg. 2002;28(11):6–1022.

Stefaniak TJ. Gravimetry in sweating assessment in primary hyperhidrosis and healthy individuals. Clin Auton Res. 2013;23(4):197–200.

Stefaniak T, Proczko-Markuszewska M, Royton A, Idestal A, et al. Importance of objective evaluation of sweating in qualification and follow-up of primary hyperhidrosis patients undergoing sympathectomy. In: International Symposium on Sympathetic Surgery, Abs. p 5, 2011 June 17–19; Odense, Final program; 2011.

Stefaniak T, Cwigon M, Łaski D. In the search for the treatment of compensatory sweating. Sci World J. 2012;2012:134547.

Stefaniak T, Tomaszewski KA, Proczko-Markuszewska M, Idestal A, Royton A, Abi-Khalil C. Is subjective hyperhidrosis assessment sufficient enough? Prevalence of hyperhidrosis among young Polish adults. J Dermatol. 2013;40(10):819–23.

Strutton DR, Kowalski JW, Glaser DA, Stang PE. US prevalence of hyperhidrosis and impact on individuals with axillary hyperhidrosis: results from a national survey. J Am Acad Dermatol. 2004;51(2):8–241.

Tu YR, Li X, Lin M, et al. Epidemiological survey of primary palmar hyperhidrosis in adolescent in Fuzhou of People's Republic of China. Eur J Cardiothorac Surg. 2007;31:737–9.

Verbraecken J, Van de Heyning P, De Backer W, Van Gaal L. Body surface area in normal-weight, overweight, and obese adults. A comparison study. Metabolism. 2006;55(4):24–515.

Westphal FL, de Carvalho MA, Lima LC, de Carvalho BC, Padilla R, Araujo KK. Prevalence of hyperhidrosis among medical students. Rev Col Bras Cir. 2011;38:392–7.

Subcutaneous Tissue Histophysiology 66

Helene M. Langevin and Pierre Agache

Contents

Keywords
subcutaneous tissue • adipose tissue • subcutis connective tissue

Between the dermis (syn: cutis) and the underlying bones, muscles, or fasciae lies a tissue of uneven thickness according to body sites and individuals, called subcutaneous tissue or subcutis (syn: hypodermis). The term "subcutaneous fascia" is sometimes used as a synonym for subcutaneous tissue, although this definition is the subject of current debate as outlined below. From an anatomical and physiological viewpoint, subcutaneous tissue contains two components which, although intricate, have different functions: the interstitial tissue and the adipose tissue.

1 The Interstitial Connective Tissue

1.1 Histomorphology

Subcutaneous interstitial connective resembles dermis in structure but is much looser. As such, it is a network of collagen and elastic fibers embedded in a ground substance made of a mucopolysaccharide gel sequestering a large amount of water and an additional small amount of "free" interstitial liquid (Brace and Guyton 1979). On its outer side, subcutaneous tissue is in direct contact with the dermis. The dermo-hypodermal junction is irregular, the dermis being attached to

Pierre Agache: deceased.

H.M. Langevin (✉)
Department of Neurological Sciences, University of Vermont, College of Medicine, Burlington, VT, USA
e-mail: helene.langevin@med.uvm.edu

P. Agache
Department of Dermatology, University Hospital of Besançon, Besançon, France
e-mail: aude.agache@free.fr; ferial.fanian@chu-besancon.fr; ferial.fanian@cert-besancon.com

P. Humbert et al. (eds.), *Agache's Measuring the Skin*,
DOI 10.1007/978-3-319-32383-1_88

subcutaneous tissue by extensions (retinacula cutis). The deepest sweat coils (▶ Chaps. 27, "Infrared Densitometry for In Vitro Tape Stripping: Quantification of Porcine Corneocytes," and ▶ 1, "The Human Skin: An Overview") and the bulbs of the terminal hairs in anagen phase are located in subcutaneous protrusions into the dermis. In some parts of the body, the subcutaneous tissue contains a thin layer of muscle, the subcutaneous muscle or panniculus carnosus. In humans, this muscle is only present in the neck and testis, while in most mammals this subcutaneous muscle covers most of the trunk. In humans (and also in pigs), there is one of more thin membranous layers (stratum membranosum) within the subcutaneous tissue that in some parts of the body separates subcutaneous tissue into two distinct zones: a fatty superficial layer (Camper's fascia) and a thinner, more membranous deeper layer (Scarpa's fascia).

There is some debate on the correct nomenclature of the membranous layers within subcutaneous tissue, with some referring to it as "subcutaneous fascia," while others have argued that this term should be used to designate the entire subcutaneous tissue and the membranous layer (s) designated as a "membranous layer(s) within the subcutaneous fascia" (Abu-Hijleh et al. 2006; Benjamin 2009; Lancerotto et al. 2011).

The loose structure of subcutaneous tissue makes it a path for blood and lymphatic vessels and nerves going to or coming from distant body sites; their course is short on the trunk and the cephalic areas and long on the limbs because of the elongation and deformation of the metameres during intrauterine limb growth. Additionally, the subcutaneous tissue holds a specific nervous structure, the Pacinian corpuscle, which acts as a mechanical pressure detector, as well as free nerve ending, especially in the part of subcutaneous tissue adjacent to perimuscular fasciae (Corey et al. 2011; Hoheisel et al. 2011; Tesarz et al. 2011). Finally it contains the subcutaneous adipose tissue which is an organ in itself.

Subcutaneous tissue is much more compliant than both dermis and perimuscular fasciae (Iatridis et al. 2003). Since it is situated between these less compliant structures, subcutaneous tissue is responsible for much of the deformation, or strain, that develops within non-muscle soft tissues as a result of externally or internally generated mechanical forces.

1.2 Interstitial Pressure

The interstitial pressure in the absence of mechanical stress has been studied in animals using a capsule with holes which has been inserted in the subcutaneous tissue and left in place until the end of the traumatic inflammation. Within the capsule, the pressure is negative and approximates 6 Torr (1 Torr = 1 mmHg (in honor of Torricelli)) (Brace and Guyton 1979). There is recent evidence that connective tissue fibroblasts actively participate in regulating interstitial fluid pressure and transcapillary fluid flow. A defining characteristic of areolar connective tissue is its loose collagen mesh filled with polyanionic glycosaminoglycans that bind large quantities of water. Reed et al. demonstrated that tension exerted by fibroblasts via integrins onto the collagen network restrains the loose matrix from excessively swelling by preventing osmotically active glycosaminoglycans from becoming maximally hydrated. One can thus think of areolar connective tissue as a meshwork with pores partially occupied by cells (fibroblasts) that hold on to the sides of the pores, keeping the mesh within a certain average pore size that prevents swelling (Reed and Rubin 2010; Wiig et al. 2003). During acute inflammation, loss of integrin-mediated cell-matrix tension results in a rapid drop in interstitial fluid pressure (becoming much more negative), causing a large rise in transcapillary fluid flux and the formation of edema.

1.3 Molecular Transfer Function

Insofar as blood capillaries run through the subcutaneous interstitium, exchanges and molecular transfers can occur. They are passive and regulated by the diffusion laws (Fick's laws). The

following formula applies to the passage from the blood capillaries toward the interstitial tissue:

$$J = K_f(P - p) - (\pi_d - \pi)$$

where J (moles $cm^{-2}\ h^{-1}$) is the flow, P and p are the perfusion and oncotic pressures in the capillary, and π_d and π the electrostatic and osmotic pressures in the ground substance. These exchanges apply especially to water and small molecules. However the capillary wall is not completely impermeable to proteins, resulting in a slow and continuous flow of large molecules into the interstitial tissue where the concentration in proteins reaches a quarter to three quarters of the plasmatic concentration (Renkin and Crone 1996). These proteins are first captured by the lymphatic capillaries and then drained toward the central veins (40–72-h cycle) (Renkin and Crone 1996). In case of edema, the distance over which metabolic exchanges have to be made is increased, which favors the occurrence of decubitus ulcers.

1.4 Shape Preservation

One of the major functions of the connective tissues is to preserve the overall shape of soft tissues (Scott 1975). The same applies to the subcutaneous connective tissue, which keeps the skin closely round the relief of the muscles and underlying bones. This function is secured by the gel nature of the ground substance and its hydration. In case of extracellular dehydration, the subcutis turgor decreases and loses its elasticity: the lower recovery of skin when it is raised is a sign frequently used in medicine. During aging the GAGs content decreases, inducing the laxity of the tissue.

1.5 Mechanical Function

The "looseness" of subcutaneous tissue allows the skin to be lifted up and moved laterally. Where the subcutis is absent (e.g., in a grafted area), the skin cannot be moved and is very fragile on friction. Limb movements also need skin sliding over joints and consequently subcutaneous shear. The looseness of areolar connective tissue layers within subcutaneous tissue also allows for some amount of "internal" gliding relative to stiffer adjacent membranous fascia layers (such as the subcutaneous membranous fascia layer mentioned above and perimuscular fasciae). In humans and animals, shear strain between subcutaneous connective tissue layers can be measured with ultrasound elastography.

Until recently, the stiffness of connective tissue was thought to be determined by the material properties of the extracellular matrix. It is now apparent that, at least in rodents, fibroblasts within "loose" areolar connective tissue play an active role in regulating the tension of the tissue. When the tissue is stretched, fibroblasts expand by actively remodeling their cytoskeleton (Langevin et al. 2005). This change in fibroblast shape is accompanied by the extracellular release of ATP and results in a drop in tissue tension (Langevin et al. 2011, 2013b). Whether similar tension regulation also occurs in humans remains unknown but could be important for adjusting interstitial fluid pressure and transcapillary fluid flow and prevent swelling when the tissue is stretched during body movements (Langevin et al. 2013a).

The deformability of subcutaneous tissue is anisotropic as moving the skin is easier in a specific direction. On the other hand, the filling of the subcutis by adipose tissue contributes to skin being permanently stretched. On the body sites subjected to high or prolonged external pressures, the adipose tissue forms a cushion which distributes the force on a larger area. Physiological body pressure sites (soles, buttocks) are provided with a thick fat (or muscular) mattress. The loss of adipose layer on the metatarsal heads is associated with thickened stratum corneum and callus formation. Subcutaneous fat-deprived people are prone to decubitus ulcers and pressure sores (type 1 pressure sore). However overweight people also are likely to develop such wounds. A lower mechanical resistance of subcutaneous tissue to shearing forces facilitates excessive sliding

of skin over bones when in semirecumbent position and results in endothelial damage of vessels crossing the fascia and their further occlusion and thrombosis. This is the most current mechanism of type 2 decubitus ulcers (Exton-Smith 1983).

2 The Subcutaneous Adipose Tissue

Humans, as aquatic mammals, are endowed with a subcutaneous adipose layer over their whole body (Vague et al. 1974), even in conditions of great thinness. Subcutaneous fat is absent on a few areas only: the eyelids, nose, ear pinna, and male genitalia. This adipose layer is in general thicker in females. It is one of the two components of the total fat mass, the other one being the deep adipose tissue. In addition to the well-developed cells, both contain a fraction of immature adipocytes that may grow upon endocrine stimuli and lead to obesity. The subsequent metabolic problems apply especially to deep adipose tissue.

2.1 White Adipose Tissue: Morphology

Adipocytes are voluminous cells (Table 1) compacted in lobules separated by thin connective tissue septa where run vessels and nerves. Each lobule has its own arteriole (Sudan and Payan 1974). The cells, round or deformed by mutual pressure, have a more or less regular diameter (about 50 μm). They harbor an enormous single lipidic vesicle devoid of membrane (Sudan and Payan 1974) and on the periphery a pushed away thin ring of 0.2–0.3-μm-thick cytoplasm containing a flattened nucleus. The adipocyte is surrounded by a regular and continuous basal membrane and a loose connective tissue (interstitium). The latter is made not of bundles but of isolated collagen fibers. It contains, very close to the cells, vessels without pericytes and an amyelinic nerve network. Neither naked axons nor contact with adipocyte membrane is found. Some fibroblasts, mast cells, and macrophages are visible (Sudan and Payan 1974), as well as a few adipoblasts, which are oblong cells with abundant cytoplasm and one or several small lipidic vacuoles. Adipogenesis is still possible in adults (Sudan and Payan 1974).

Adipocyte volume, as measured with Sjostrom and Bjorntrop's technique (Sjostrom et al. 1971), is usually larger in the subcutaneous tissue than around internal organs. It also shows a great variation according to body sites and sex (Fried and Kral 1987), being larger on the hips than on the shoulders in females and children and generally smaller in males (Table 1). Weight loss induced by sport reduces the adipocytes size, not their number.

2.2 Body Fat Mass and Subcutaneous Fat

Body fat mass decreases in males after the age of 13, whereas in females it still increases until adulthood (Table 2) and then keeps higher than in males over the whole life span (Table 3). In both

Table 1 Adipocytes mean volume (nl) (mean ± 2 sem) (Vague et al. 1984)

	Males			Females		
	Shoulder	Hip	n	Shoulder	Hip	n
5–9	046 ± 0.05	0.66 ± 0.07	17	0.50 ± 0.07	0.59 ± 0.07	9
10–14	0.42 ± 0.06	0.42 ± 0.06	24	0.48 ± 0.05	0.67 ± 0.09	17
15–19	0.37 ± 0.05	0.37 ± 0.05	22	0.50 ± 0.06	0.75 ± 0.09	25
20–29	0.39 ± 0.04	0.39 ± 0.04	42	0.49 ± 0.04	0.81 ± 0.05	53
30–39	0.39 ± 0.05	0.39 ± 0.05	22	0.47 ± 0.06	0.76 ± 0.08	21
40–49	0.42 ± 0.05	0.42 ± 0.05	27	0.47 ± 0.06	0.71 ± 0.07	20
50–69	0.42 ± 0.06	0.42 ± 0.06	13	0.51 ± 0.07	0.71 ± 0.08	14
70–91	0.46 ± 0.09	0.46 ± 0.09	13	0.53 ± 0.06	0.59 ± 0.06	22

sexes, it increases with age up to the 60s. Until the age of 15, in both sexes, fat is predominant on the lower part of the body. The same applies in women until the age of 50, at which time the fat increases in the upper part of the body, together with the body fat mass. In males, from puberty to old age, the fat is mostly located in the upper part of the body (Rebuffé-Scrive 1988; Vague et al. 1984; Table 4). This distribution is also found in obese subjects who are classified in two main categories: gynoid type if the subcutaneous fat accumulation is found mainly on the hips and thighs and android type if it is located preferentially on the upper part of the trunk and the abdomen. Android type obesity is associated with visceral deposits and an increased risk of arterial occlusive disease. Chubby cheeks are positively correlated with visceral obesity (Levine et al. 1998), as shown by computed tomography, but not with the subcutaneous fat thickness.

Table 2 Fraction of fat tissue in body weight (%), as measured from content in triglycerides (France 1970–1980) (mean ± 2 sem) (Vague et al. 1984)

Age group	Male	n	Female	n
5–9	14.0 ± 1.8	17	17.8 ± 2.2	9
10–14	13.3 ± 1.8	24	19.5 ± 2.0	17
15–19	11.4 ± 1.2	22	25.0 ± 1.8	25
20–29	11.0 ± 1.2	42	26.3 ± 1.9	53
30–39	11.1 ± 1.2	22	26.8 ± 2.2	21
40–49	12.0 ± 1.3	27	27.7 ± 2.4	20
50–69	12.2 ± 1.6	13	27.0 ± 3.2	14
70–91	10.8 ± 1.6	13	16.6 ± 2.3	22

2.3 Energetic Function

The adipose tissue's main function is to serve as the most important energy store of the organism. In normal conditions, it represents 10 % of the body weight or 40 days of energy expenditures, stored in the lipidic vesicle in the form of triglycerides (Black and Cunliffe 1998). In spite of histological appearance, the adipose tissue is very active: its metabolic rate is identical to that of the kidney, half that of the liver (Jungermann and Barth 1996).

After a meal, the chylomicrons of the circulating VLDL are hydrolyzed by the lipoprotein-lipase at the endothelial surface of the capillaries, and their fatty acids are captured by adipocytes, where, in the endoplasmic reticulum, they are transformed into triglyceride. Insulin stimulates fatty acids and glucose capture, together with fatty acids and triglyceride synthesis within the cell.

Releasing energy from adipose tissue consists in triglyceride hydrolysis into fatty acids by triglyceride-lipase (within the adipocyte endoplasmic reticulum), an event triggered by

Table 3 Body composition data pooled from studies in the USA and in the UK, obtained by DEXA. BMC: Body Mineral Mass (Wahner and Fogelman 1994)

Age group (years)	BMC (g)		Fat mass (g)	Lean mass (g)
	n	Mean ± sd	Mean ± sd	Mean ± sd
Females				
20–29	111	2,537 ± 424	19,556 ± 7,836	39,506 ± 4,787
30–39	94	2,580 ± 428	18,270 ± 7,951	39,538 ± 4,385
40–49	60	2,639 ± 353	23,284 ± 9,353	40,120 ± 3,976
50–59	143	2,400 ± 352	22,373 ± 6,932	38,057 ± 4,861
60–69	52	2,240 ± 350	23,124 ± 6,581	38,549 ± 4,063
70–79	25	2,256 ± 374	24,162 ± 7,369	38,082 ± 4,691
Males				
20–29	6	2,827 ± 747	14,757 ± 6,986	56,954 ± 5,069
30–39	33	3,078 ± 441	15,273 ± 3,755	56,036 ± 5,263
40–49	53	3,199 ± 459	16,790 ± 4,516	57,007 ± 6,101
50–59	59	3,265 ± 449	18,894 ± 5,011	58,150 ± 6,276
60–69	42	3,158 ± 383	18,079 ± 4,849	57,473 ± 5,484
70–79	24	3,144 ± 358	17,538 ± 5,310	55,255 ± 4,527

Table 4 Arm/thigh ratio of subcutaneous fat. Arm as well as thigh fat were assessed by a fat/muscle ratio: mean skin fold thickness from four circumferential sites (anterior, posterior, medial, lateral) divided by limb perimeter at the same level Lever and Schaumburg-Lever (1983)

Age group	Males	n	Females	n
5–9	0.84 ± 0.06	17	0.78 ± 0.04	9
10–14	0.85 ± 0.06	24	0.70 ± 0.05	17
15–19	1.04 ± 0.08	22	0.70 ± 0.06	25
20–29	1.16 ± 0.09	42	0.76 ± 0.05	53
30–39	1.19 ± 0.07	22	0.78 ± 0.08	21
40–49	1.16 ± 0.04	27	0.78 ± 0.08	20
50–69	1.14 ± 0.08	13	0.72 ± 0.08	14
70–91	1.09 ± 0.04	13	0.90 ± 0.10	22

glucagon and catecholamines. Oxidation by the peripheral tissues of these fatty acids may represent 80 % of the basal consumption of oxygen. Inside the adipocyte, lipolysis is facilitated by activation of β receptors (formation of cyclic AMP) (Mauriege et al. 1988), the contrary occurring when α receptors are activated. Cyclic AMP is destroyed by phosphodiesterase, but the latter is inhibited by theophylline (1.3 dimethylxanthine), hence the use of this product and caffeine (1.3,7 trimethylxanthine) as lipolytic. However the intensity of the response varies with body sites and sex; it depends on the relative proportion of β and α receptors. α2 receptors outnumber β receptors in the subcutaneous adipocytes, whereas they are found in similar quantities in the omental adipocytes (Mauriege et al. 1987). In females, the subcutaneous adipocytes of the gluteal and femoral areas have more α than β receptors and are larger than in males (Richelsen 1986). The lipoprotein-lipase activity is also higher (Fried and Kral 1987). It would be increased in situ by estrogen or progesterone injection (Rebuffé-Scrive 1987; Rebuffé-Scrive et al. 1985).

In addition to the release of fatty acids, other lipids, and metabolites, adipose tissue secretes several hundreds of identified bioactive factors (adipokines) including leptin, adiponectin, aplin, and vaspin that influence local adipogenesis, immune cell migration into adipose tissue, and adipocyte metabolism and function, as well as regulate metabolic processes in the brain, liver, muscle, vasculature, heart, and pancreatic β-cells (Cao 2014). Leptin (LPT), a 167-amino-acid protein, is secreted by adipocytes as soon as the lipid supply is sufficient. LPT inhibits the hypothalamic center for hunger and reduces the synthesis and release of the neuropeptide Y, which increases food intake, reduces thermogenesis, and increases insulin blood level. In short, LPT regulates the feeding habits, the metabolic level, the autonomous nervous system control, and the energetic equilibrium. LPT blood level is a reflection of body fat mass. For a similar BMI, it is much higher in women (testosterone would inhibit LPT synthesis and secretion). In obese subjects, the efficiency of the LPT is reduced and hyperleptinemia is observed. A lipid-rich diet would facilitate the resistance to LPT (Friedman 2000).

Adipoblasts can differentiate into adipocytes and therefore increase the fat mass when they mature. This transformation would require the action of plasminogen, after the fibronectin matrix which surrounds the adipoblast has been degraded by the plasma kallikrein (Selvarajan et al. 2001).

Although visceral adipose tissue was for decades considered a major culprit in development of the metabolic syndrome, recent evidence indicates that subcutaneous adipose tissue, especially on the trunk, also can be involved in the development of insulin resistance. Decreased adipocyte differentiation leading to adipocyte hypertrophy and spillover of free fatty acids can lead to local inflammation as well as ectopic fat deposition in other tissues such as liver and pancreas (Patel and Abate 2013).

2.4 Thermal Function

The subcutaneous adipose tissue contributes to the thermal insulation of the organism. The fatty areas (gluteus, outer sides of the arms, and thighs in children and women) are usually the coldest ones. The thermal inertia of fat is low: $22–32.10^{-5}$ $cal^2.cm^{-4}.°C^{-2}.s^{-1}$, whereas that of the skin without subcutis is higher than 90 $cal^2.cm^{-4}.°C^{-2}.s^{-1}$ (Houdas and Guieu 1977). This property is most useful to protect the inner organs (the core) in hot as well as cold environment, a

situation that should have been endured by many primitive humans.

2.5 Aesthetic Function

The body distribution of the subcutaneous adipose tissue is an essential component of the male and female morphology: predominance on shoulders and thorax in males and hips and buttocks in females. In the latter, the relief of the limb muscles is lightly marked, as it is masked by the adipose tissue. On the face, adipose tissue reduction preceding skin hyperlaxity is often the first sign of aging: in cases of obesity, the chubby cheeks maintain a barely wrinkled aspect on the face longer. Filling is a technique used in cosmetic surgery to compensate for a reduced adipose tissue. In infants under a year, the subcutaneous adipose tissue thickness, especially in the face and limbs, gives the child a typical morphology. It is likely to be an energy reserve before the start of a period where growth, standing, and exercise will be simultaneously acted.

2.6 Brown Fat

Brown fat has long been known for its thermogenic functions in hibernating animals. The morphology of their adipocytes is very specific because of the multilocular distribution of the adipose vesicles (Lever and Schaumburg-Lever 1983). It was, until recently, thought to be vestigial in humans and present mainly in fetus and newborns. However, the role of brown and "beige" fat is now being reexamined with the new understanding and knowledge that adipocytes within white adipose tissue can be induced to become thermogenic, especially after cold exposure (Lee et al. 2014; Peirce et al. 2014).

2.7 Conclusion

The subcutis is an area of the body that has received comparatively little attention, compared with the skin and underlying muscles. The anatomical continuity between the subcutaneous connective tissues, especially the membranous layers, and the fasciae enveloping muscles, is recently being appreciated from the points of view of biomechanics and sensory perception. There is no doubt that further incorporation of subcutaneous tissue into our understanding of the cutaneous, adipose, and musculoskeletal systems will inform our understanding of whole-body physiology.

References

Abu-Hijleh MF, Roshier AL, Al-Shboul Q, Dharap AS, Harris PF. The membranous layer of superficial fascia: evidence for its widespread distribution in the body. Surg Radiol Anat. 2006;28(6):606–19.

Benjamin M. The fascia of the limbs and back – a review. J Anat. 2009;214(1):1–18.

Black MM, Cunliffe WJ. Subcutaneous fat. In: Champion RH, Burton JL, Burns DA, Breathnagh SM, editors. Textbook of dermatology. 6th ed. Oxford: Blackwell; 1998. p. 2403–7.

Brace RA, Guyton AC. Interstitial fluid pressure: capsule, free fluid, gel fluid, and gel absorption pressure in subcutaneous tissue. Microvasc Res. 1979;18:217–28.

Cao H. Adipocytokines in obesity and metabolic disease. J Endocrinol. 2014;220(2):T47–59. doi:10.1530/JOE-13-0339. Print 2014 Feb.

Corey SM, Vizzard MA, Badger GJ, Langevin HM. Sensory innervation of the nonspecialized connective tissues in the low back of the rat. Cells Tissues Organs. 2011;194(6):521–30.

Exton-Smith AN. Pressure problems in the elderly. In: Barbenel JC, Forbes CD, Lowe GDO, editors. Pressure sores. Bath: The Pitman Press; 1983. p. 81–90.

Fried SK, Kral JG. Sex differences in regional distribution of fat cell size and lipoprotein lipase activity in morbidly obese patients. Int J Obes. 1987;11:129–40.

Friedman JM. Obesity in the new millennium. Nature. 2000;404:632–4.

Hoheisel U, Taguchi T, Treede RD, Mense S. Nociceptive input from the rat thoracolumbar fascia to lumbar dorsal horn neurons. Eur J Pain. 2011;15(8):810–5.

Houdas Y, Guieu JD. Physiologie humaine: la fonction thermique. Villeurbanne: Simep-editions; 1977.

Iatridis JC, Wu J, Yandow JA, Langevin HM. Subcutaneous tissue mechanical behavior is linear and viscoelastic under uniaxial tension. Connect Tissue Res. 2003;44(5):208–17.

Jungermann K, Barth CA. Energy metabolism and nutrition. In: Greger R, Windhorst U, editors. Comprehensive human physiology, vol. 2. Berlin: Springer; 1996. p. 1425–57.

Lancerotto L, Stecco C, Macchi V, Porzionato A, Stecco A, De Caro R. Layers of the abdominal wall: anatomical investigation of subcutaneous tissue and superficial fascia. Surg Radiol Anat. 2011;33(10):835–42.

Langevin HM, Bouffard NA, Badger GJ, Iatridis JC, Howe AK. Dynamic fibroblast cytoskeletal response to subcutaneous tissue stretch ex vivo and in vivo. Am J Physiol Cell Physiol. 2005;288(3):C747–56.

Langevin HM, Bouffard NA, Fox JR, Palmer BM, Wu J, Iatridis JC, Barnes WD, Badger GJ, Howe AK. Fibroblast cytoskeletal remodeling contributes to connective tissue tension. J Cell Physiol. 2011;226(5): 1166–75.

Langevin HM, Nedergaard M, Hhowe AK. Cellular control of connective tissue matrix tension. J Cell Biochem. 2013a;114:1714–9.

Langevin HM, Fujita T, Bouffard NA, Takano T, Koptiuch C, Badger GJ, Nedergaard M. Fibroblast cytoskeletal remodeling induced by tissue stretch involves ATP signaling. J Cell Physiol. 2013b;228(9): 1922–6.

Lee YH, Mottillo EP, Granneman JG. Adipose tissue plasticity from WAT to BAT and in between. Biochim Biophys Acta. 2014;1842(3):358–69.

Lever WF, Schaumburg-Lever G, editors. Histopathology of the skin. 6th ed. Philadelphia: Lippincott; 1983. p. 655.

Levine JA, Ray A, Jensen MD. Relation between chubby cheeks and visceral fat. N Engl J Med. 1998;339:1946–7.

Mauriege P, Galitzky J, Berlan M, Lafontan M. Heterogeneous distribution of bet and alpha-2 adrenoceptor binding sites in human fat cells from various fat deposits: functional consequences. Eur J Clin Invest. 1987;17:156–65.

Mauriege P, De Pergola G, Berlan M, Lafontan M. Human fat cell beta-adrenergic receptors: beta-agonist-dependent lipolytic responses and characterization of beta-adrenergic binding sites on human fat cell membranes with highly selective beta 1-antagonists. J Lipid Res. 1988;29:587–601.

Patel P, Abate N. Role of subcutaneous adipose tissue in the pathogenesis of insulin resistance. J Obes. 2013;2013:489187.

Peirce V, Carobbio S, Vidal-Puig A. The different shades of fat. Nature. 2014;510(7503):76–83.

Rebuffé-Scrive M. Regional adipose tissue metabolism in women during and after reproductive life and in men. In: Berry EM, Blondheim SH, Eliahou HE, Shafrir E, editors. Recent advances in obesity research: proc. 5th international congress on obesity, 14–19 September 1986. Jerusalem: Westport, Food & Nutrition Press; 1987. p. 82–91.

Rebuffé-Scrive M. Stéroid hormones and distribution of adipose tissue. Acta Med Scand. 1988;723 (Suppl):143–6.

Rebuffé-Scrive M, Enk L, Crona N, Lonnroth P, Abrahamssor L, Smith U, Bjorntop P. Fat cell metabolism in different regions in women: effect of menstrual cycle, pregnancy and lactation. J Clin Invest. 1985;75:1973–6.

Reed RK, Rubin K. Transcapillary exchange: role and importance of the interstitial fluid pressure and the extracellular matrix. Cardiovasc Res. 2010;87(2): 211–7.

Renkin EM, Crone C. Microcirculation and capillary exchange. In: Greger R, Windhorst U, editors. Comprehensive human physiology. From cellular mechanisms to integration, vol. 2. Berlin: Springer; 1996. p. 1965–79.

Richelsen B. Increased alpha 2- but similar beta-adrenergic receptor activities in subcutaneous gluteal adipocytes from females compared with males. Eur J Clin Invest. 1986;16:302–9.

Scott JE. Physiological function and chemical composition of pericellular proteoglycan (an evolutionary view). Proc R Soc Lond Ser B. 1975;271:235–42.

Selvarajan S, Lund LR, Takeuchi T, Craik CS, Werb Z. A plasma kallikrein-dependent plasminogen cascade required for adipocyte differentiation. Nat Cell Biol. 2001;3:267–75.

Sjostrom L, Björntorp P, Vrana J. Microscopic fat cell size measurements on frozen-cut adipose tissue in comparison with automatic determinations of osmium fixed fat cells. J Lipid Res. 1971;12:521.

Sudan N, Payan H. Ultrastructure du tissu adipeux blanc. Vie Med (Paris). 1974;37:4533–44.

Tesarz J, Hoheisel U, Wiedenhöfer B, Mense S. Sensory innervation of the thoracolumbar fascia in rats and humans. Neuroscience. 2011;194:302–8.

Vague J, Rubin P, Jubelin J, Vague P. Topographie des adipocytes chez l'homme. Vie Med (Paris). 1974;37:4547–58.

Vague J, Meignen JM, Negrin JF, Thomas M, Tramoni M, Jubelin J. Androgènes, oestrogènes et cortisol dans la physiopathologie du tissu adipeux. Sem Hôp Paris. 1984;60:1465–76.

Wahner HW, Fogelman I. Total body mineral and body composition by absorbtiometry. In Wahner HW, Fogelman I, (eds). The evaluation of osteoporosis: Dual energy X-ray absortiometry in clinical practice. Martin-Dunitz, London, 1994, 196–218.

Wiig H, Rubin K, Reed RK. New and active role of the interstitium in control of interstitial fluid pressure: potential therapeutic consequences. Acta Anaesthesiol Scand. 2003;47(2):111–21. Review.

Subcutis Metrology

67

Pierre Agache and Stéphane Diridollou

Contents

Keywords

Adipomuscular ratio • Adipose tissue • Bioelectrical impedance analysis (BIA) • Body mass index (BMI) • Connective subcutaneous tissue • Dual X-ray absorptiometry (DXA) • Fat Mass Distribution • Guyton's technique • Subcutis oxygen partial pressure • Skinfold thickness • Waist circumference • Waist–hip ratio

The subcutis (or hypodermis) harbors two types of tissue: the loose connective tissue, where blood, lymphatic vessels, and nerves find a path to muscles, bones, and skin (often at a distance as far as limbs are concerned); and the subcutaneous adipose tissue. Their physiology is different (see ▶ Chap. 41, "Dermis Connective tissue histopathology") but their metrology often uses the same techniques.

1 Metrology of the Adipose Tissue

1.1 Global Assessment

Adipose tissue is the energy reservoir of the organism. It provides for the basal metabolic rate and the additional energy needs whenever they are not entirely fulfilled by the diet. Hence the importance of its measurement or even approximate assessment.

In healthy adults, the fat mass amounts to 10–15 % of the body weight in men, 15–25 %

This chapter was originally published under the ISBN 978-3-540-01771-4 with the following book title Measuring the Skin. The content has not been changed.

Pierre Agache: deceased.

P. Agache (✉)
Department of Dermatology, University Hospital of Besançon, Besançon, France
e-mail: aude.agache@free.fr; ferial.fanian@chu-besancon.fr; ferial.fanian@cert-besancon.com

S. Diridollou
L'Oreal Research and Innovation, Chevilly, Larue, France
e-mail: sdiridollou@rd.loreal.com

P. Humbert et al. (eds.), *Agache's Measuring the Skin*,
DOI 10.1007/978-3-319-32383-1_91

in women. In both sexes it increases with age. This tissue is distributed in two distinct areas: the deep or visceral fat and the subcutaneous fat. Although there are many differences according to ethnic types, the visceral fat is especially developed within the mesentery, retroperitoneal area, and intermuscular spaces. The subcutaneous fat is present at all body sites (see ▶ Chap. 41, "Dermis Connective tissue histopathology"), although it is mostly developed in specific areas that vary with age and sex. Its development is not necessarily connected with that of the visceral fat, even in obese patients. Accordingly, obesity cannot be assessed by subcutaneous fat only (Rudolf et al. 2001). However, it seems that the buccal adipose tissue (buccal fat pad) may be a marker of visceral fat (Levine et al. 1996).

For the last 60 years, several methods have been devised to assess body fat. The first uses the difference in density between fat (0.90 g/cm^3) and nonfat tissue (1.10 g/cm^3) to calculate the proportion of the body weight that is lean mass and fat mass by underwater weighing (hydrodensitometry) (Behnke et al. 1942). Two other methods are based on calculating the lean mass and deducing the fat mass by subtraction from the body weight (Wahner and Fogelman 1994). Lean mass is assessed either through measurement of total body potassium counting (by ^{40}K low-level counting) assumed to be a body weight constant fraction (60 mmol/kg in females, 66 mmol/kg in males), or through total body water measurement by heavy water (a nonradioactive isotope) dilution, also assumed to be a body weight constant fraction (73.2 %). These methods are now used only by research laboratories and will not be described here.

Today two techniques are widely used for assessing the global fat mass: a simple and rather inexpensive one, the bioelectrical impedance assessment, and a more sophisticated and expensive one, dual X-ray absorptiometry (DXA).

1.1.1 Dual X-Ray Absorptiometry

Dual X-ray absorptiometry (DXA) is mainly used to quantify bone density, especially in osteoporosis, and has superseded dual photon absorptiometry (DPA) using the ^{153}Gd radionuclide source, but based on the same rationale. It uses X-ray with two energy levels (either 38 and 67 keV, or 40 and 100 keV). While propagating, the X-ray energy decreases depending on its initial level and on the composition of the traversed tissues. It is thus possible first to assess body mineral content (BMC) from the calcium-rich (bone) mass assumed to be a constant fraction (approximately 37 %) of the mineral component. Further on, the (non-mineral) soft tissue mass is partitioned into fat and (water-equivalent) lean body mass by a calibration procedure based on the attenuation of the soft tissue outside the bone (Wahner and Fogelman 1994). The composition of soft tissue is given by the R value, which is the ratio of beam attenuation at the lower energy relative to that at the higher energy. However, the raw data must be adjusted for body size. Accordingly, the following equation has been proposed for Caucasian females (based on n=203, aged 47.7±12.9 years):

$$\begin{aligned}\text{Total body fat (kg)} = {} & 25.25 - 0.35\,\text{height (cm)} \\ & + 0.84\,\text{weight (kg)} \\ & + 0.056\,\text{age (y)}\end{aligned}$$

In the same paper, other equations are proposed for lean mass, muscle mass, bone mineral content, for trunk, leg fat, etc. and also for black females (Aloia et al. 1999).

The technique comprises a series of transverse (front-to-back) scans made from head to toe at 1-cm intervals, the total scan time lying between 10 and 20 min. The intraindividual variation coefficient is below 5 %, even in obese subjects. The radiation dose is 12 μSv (sievert) for a spine investigation, and 0.6 μSv for total body scan (for a simple chest roentgenogram irradiation is 2–5 μSv) (The International Committee for Radiation Protection maximum authorized dose is 50,000 μSv/year. It will be lowered to 100,000 μSv over 5 years.).

It is possible to divide the total body scan into regional measurements (e.g., arms, legs, trunk, and head) and calculate the fat mass in each of these areas (Aloia et al. 1999; Mazess et al. 1990) (Table 1). Accordingly, the method can be used

Table 1 Fat and nonfat components in soft tissue of three body regions as found by DXA. Mean±SD; $n = 6$ males and 6 females. (Modified from Mazess et al. 1990)

Region	Fat tissue (g) males	Females	Lean tissue (g) males	Females
Arms	887±138	1,566±142	6,595±253	3,665±169
Legs	4,118±430	7,791±374	22,181±360	15,887±428
Trunk	4,274±459	7,072±436	26,237±530	17,504±499

for assessing the fat mass distribution (see Sect. 1.2) or the degree of fatness of a lower limb (e.g., in the follow-up of thigh cellulitis). However, it cannot give the tissue composition of a single transverse scan because X-scanning is only anterior-posterior.

Commercial instruments have their own software and calibration system and usually give slightly different results:

- Hologic QDR-2000/W, Hologic INC-35 crosby drive-Bedford MA 01730-USA
- Lunar DPX IQ #5226, Lunar Radiation Inc., Madison, WI, USA
- Norland Medical Systems-106 Corporate Park Drive. White plains. New York 10604-USA

1.1.2 Bioelectrical Impedance Analysis

Bioelectrical impedance analysis (BIA), a recently renewed method, is currently used by practitioners and nutritionists. It is a measurement of body water through its ability to conduct electric current. Impedance is extrapolated through a circular regression between reactance and resistance, the former being related to cell membranes and the latter to water conductivity. Total water (about two-thirds of body weight) is assessed by impedance at 1 MHz, and extracellular water by impedance at 5 kHz (Boulier et al. 1992). Water is located only within the lean mass, and its part depends on body size, sex, and age. From measurements in healthy subjects, predictive equations have been devised using height, weight, and age in various combinations (Hendel et al. 1996; Stolarczvk et al. 1997; Segal et al. 1988), which can compute the lean mass from the assessed total body impedance (Segal et al. (1988) have proposed four equations, each of them specific to a group: obese women (>30 % body fat), nonobese women (<30 % body fat), obese men (>20 % body fat), and nonobese men (<20 % body fat). For obviously nonobese female and male subjects, the Segal BIA average method can be used safely for their classification in low-fatness groups, thus avoiding lengthy measurements (Stolarczvk et al. 1997)). Finally, the fat mass is obtained by subtracting lean mass from body weight.

Most current devices use only 50 kHz and leg-to-leg BIA (Utter et al. 1999) (Biometer, Spengler Electronic, 94230 Cachan, France; TBF 521, Tanita Corporation of America, Inc, Arlington Heights, IL, USA). The battery-operated device resembles a portable scale where anterior feet and heel sites are separated and make up both scales and electrodes. The patient stands immobile on the device, and the weight first, then the fat mass are displayed on the connected computer. Other devices use several frequencies (5, 50, 100, 1000 kHz) and in addition assess total intracellular and extracellular body water (Analycor XF, Spengler Electronic, 94230 Cachan, France). The 1-MHz electrodes should by-pass the stratum corneum and consequently are thin needles to be inserted into the dermis or subcutis. In both cases, a chart is provided by the manufacturer, which makes it possible to position the obtained value relative to the normal range.

BIA has several advantages: low cost and portable devices, short duration of the assessment (less than 5 min), noninvasiveness (0.5 mA), and safety (battery operated). Like DXA, it estimates the total body fat and fat-free mass, and regional parameters. However, the measurement is indirect, based on assumptions relative to the body and lean mass water contents. It may not be valid for edematous or dehydrated people. In obese

patients, BIA is said to overestimate the lean mass relative to hydrodensitometry or DXA, mostly in tall people (Hendel et al. 1996; Carella et al. 1997).

1.1.3 Assessment of Fat Mass Normality: Body Mass Index

The body mass index (BMI) characterizes the body fatness, hence it is not the measurement of the body fat mass but an estimate of its normality. It is widely used in spite of being an approximation. BMI = weight (kg)/(body height)^2 (m^2)

Thinness	<18.5
Normal	18.5–24.9

The World Health Organization classification of the BMI (kg/m^2) for adults under 60 years is the following (World Health Organization 1997):

Overweight	25.0–29.9
Obesity	≥30.0
Class I	30.0–34.9: moderate or common obesity
Class II	35.0–39.5: severe obesity
Class III	≥40.0: massive obesity

In men and women over the age of 35, the normal BMI is between 21 and 25. After the age of 65 it goes up to 29 in women (Jungermann and Barth 1996). The higher musculoskeletal mass in black women may lead to misclassification as obese if their BMI lies between 18 and 30. In such cases, composition values for mineral, fat, and muscle mass should preferably be obtained from DXA and adjusted for ethnic background. In children, obesity is stated if the weight exceeds 20 % of the ideal weight in relation to size, but a more precise normal range often depends on the country and nutritional habits. In France, BMI tables from birth to 87 years have been constructed (Rolland-Cachera et al. 1991). For children in the USA, the Center for Disease Control (Centre for Disease Control 2000) published BMI curves in June 2000, which apply to age brackets between 2 and 20. The same year, the International Obesity Task Force (IOTF) (Cole et al. 2000) established a new definition for obesity for worldwide use: children having a BMI above the centile 1 (25 kg/m^2) are considered obese.

1.2 Fat Mass Distribution

The DXA method is quite appropriate for the assessment of fat distribution over the body through quantification of regional fat masses, especially trunk and upper or lower limbs. Again, the raw values should be adjusted for height and race (see Sect. 1.1.1). However, easier to handle and inexpensive measurements are also available in clinical practice.

1.2.1 Waist–Hip Ratio

The waist–hip ratio (WHR) is the ratio between the waist circumference (at umbilical level) and the hip circumference (the largest one). It is of great value in case of obesity. Android obesity cut-offs for males are, WHR >1.0, and for females, WHR >0.85 (Black and Cunliffe 1998), and for the 40–49-year age group, >0.95 and >0.80, respectively (Bray 1990). Android distribution is associated with a metabolic and cardiovascular risk associated with excess visceral fat.

1.2.2 Waist Circumference

According to some (Despres et al. 1991), waist circumference is more highly correlated with visceral abdominal fat than WHR. But its normal range varies with geographical regions and countries. For Caucasians, the upper limit of normality is 100 cm in men, 88 cm in women.

1.2.3 Adipomuscular Ratio

The adipomuscular ratio (AMR) is obtained by measuring, either at the upper arm or the thigh, the ratio of mean skinfold thickness (from four circumferential points: medial, lateral, anterior, posterior) to the limb perimeter (at the same site) (Vague et al. 1969, 1984). In females and males before the age of 15, this ratio is always higher in the thigh than in the upper arm. Normal values in a Caucasian population (France, 1960–1970) are quoted in ▶ Chap. 53, "Skin Capillaroscopy,"

Table 53.4. Using the ARM is somewhat outdated because DXA, impedance measurement, and computed tomography provide the same type of information with much better precision. Nevertheless, it can be still useful when modern equipment is not available.

1.3 Subcutaneous Fat Layer Thickness

1.3.1 Skinfold Thickness

The advantage of this old method is that it requires only a small and portable device, modified pinchers exerting constant pressure (Harpenden Skinfold Caliper, Holtain Skinfold Caliper, Lange Caliper, etc.). The measurement must be done quickly (1–2 s) because under sustained pressure the fold thickness gradually decreases.

The measurement should be taken at four different sites, then calculate the sum (Σ4SKF) (Lohman et al. 1988) ((1) triceps: a vertical fold measured on the midline of the posterior aspect of the upper arm, over the triceps muscle, at a point midway between the acromion and olecranon processes (elbow extended and relaxed); (2) biceps: a vertical fold on the anterior midline of the upper arm over the belly of the biceps muscle at the level of the triceps site; (3) subscapular: a diagonal fold just inferior to the inferior angle of the scapula; (4) suprailiac: a diagonal fold measured on the midaxillary line, immediately superior to the iliac crest (Lohman et al. 1988)).

To measure the subcutis thickness, it is essential to take two measurements on the same area: first that of the big fold including both skin and subcutis, then that of the skin alone (a very thin superficial fold); the latter value is then deducted from the former. This precaution is not mentioned in most published results: it was probably considered that the skin thickness was negligible compared to that of the adipose panicle, or that this measurement was of no use for the comparative studies of several anatomical sites. However, the skin thickness measured in this way can exceed 2 mm. Comparisons with ultrasound measurement have confirmed that the dermis thickness cannot be disregarded. Accordingly, ultrasound measurements are preferable whenever possible.

Normal values in shoulders and hips (reference sites to measure obesity) are between 5 and 10 mm (Table 2). Great variation is observed with body sites. The tricipital skinfold (upper arm) alone would seem less sensitive than BMI to detect overweight (Rudolf et al. 2001).

1.3.2 Photograding of Mechanically Accentuated Macrorelief

In order to assess the efficiency of anticellulite treatments quantitatively, a skinfold-derived measurement technique of the subcutis has recently been developed (Perin et al. 2000). In this condition, subcutaneous nodules are found under palpation. The proposed technique consists in lifting the area of interest (about 20 cm^2) using springs deeply pinching the skin on each side, and thus making the nodules bulge. A photograph under oblique light (30°) is then taken. It is quantified by comparison with a seven-degree photographic scale.

Table 2 Subcutaneous fat thickness (mm): mean ± 2 SEM of skinfold (averaged circumferential measures at the same level: lateral, anterior, medial, posterior) (From Vague et al. 1984)

Age group (years)	Males upper arm	Hip	*n*	Females upper arm	Hip	*n*
5–9	5.4±0.7	14.8±1.8	17	6.7±0.8	18.4±2.2	9
10–14	5.5±0.6	16.3±1.9	24	8.3±1.0	26.4±3.2	17
15–19	5.8±0.6	10.0±1.2	22	10.9±1.2	30.5±3.8	25
20–29	6.3±0.7	9.7±1.1	42	10.9±1.3	31.3±3.5	53
30–39	6.2±0.7	8.6±1.0	22	10.4±1.2	31.5±3.9	21
40–49	6.3±0.7	9.1±1.1	27	10.6±1.2	31.6±4.0	20
50–69	6.4±0.9	9.4±1.0	13	11.1±1.4	29.1±4.1	14
70–91	5.8±0.8	8.3±1.0	13	9.1±1.1	13.3±1.8	22

1.3.3 Ultrasound Imaging

For subcutis imaging, the devices should use ultrasound frequencies between 2 and 10 MHz, which give resolutions of a few hundred micrometers and investigate depths over several millimeters. These frequencies achieve the best compromise between spatial resolution, which increases with frequency, and focusing depth, which decreases with frequency. To study adipose tissue, linear scanning probes are generally used. In practice, 7.5-, 10-, and 13-MHz frequencies give axial resolutions at best of 300, 150, and 120 mm, respectively, for exploration depths of 110, 50, and 20 mm, respectively (Fig. 1). The probe contact area is 3–5 cm^2, the image displaying rate 10–50 images/s, and 128–512 echo lines on the image.

Adipose tissue imaging is easy and fast. Marked contrasts at the cutis-subcutis and subcutis-muscle interfaces allow easy observation and measure of tissue thickness (Fig. 2). The thigh subcutis thickness in normal women is between 20 mm and 60 mm, but may reach several hundred millimeters in obese subjects (Perin et al. 2000; Diridollou 2000; Schnebert et al. 1999; Pittet et al. 1996). Accordingly, on this particular site, 7.5–10-MHz frequencies provide the best compromise between a good axial resolution (150–300 μm) and an exploration depth up to 11 cm. Images of the same thigh area obtained at 7.5, 10, 13, and 20 MHz in the same subject (Fig. 3a–d) illustrate the choice of frequency in relation to the requested information (cutis or subcutis thickness, observation of retinacula cutis or of connective bundles). Ultrasound imaging is sensitive enough to measure the fat tissue thickness variation in relation to the menstrual cycle (Perin et al. 2000; Pittet et al. 1996, 1997) and to assess the efficiency of anticellulite products (Schnebert et al. 1999; Armengol et al. 1992). The methodology must be rigorous, paying particular attention to subject's position, probe position, control of probe pressure on the skin, site marking. Several measurements should be taken per image.

A study on 20 women aged 18–35 years (weight 58.2±6 kg) carried out by two operators (only one was experienced) showed that: (a) the subcutis thickness was 37.2±7.2 mm, (b) the reproducibility was 1–5 % depending on the operator's expertise, and (c) the correlation coefficient between operators was 0.985 (Diridollou 2000).

The subcutaneous fat thickness on the abdomen (in front of the rectus muscle) and on the back (infrascapular region) in seven newborn babies (Petersen et al. 1995) measured using a 15-MHz A-mode ultrasound device is presented in Table 3.

A technique commonly used to measure skin thickness (Einsenheiss et al. 1998), 20-MHz B-mode imaging, rarely visualizes the deeper part of the subcutis owing to ultrasound

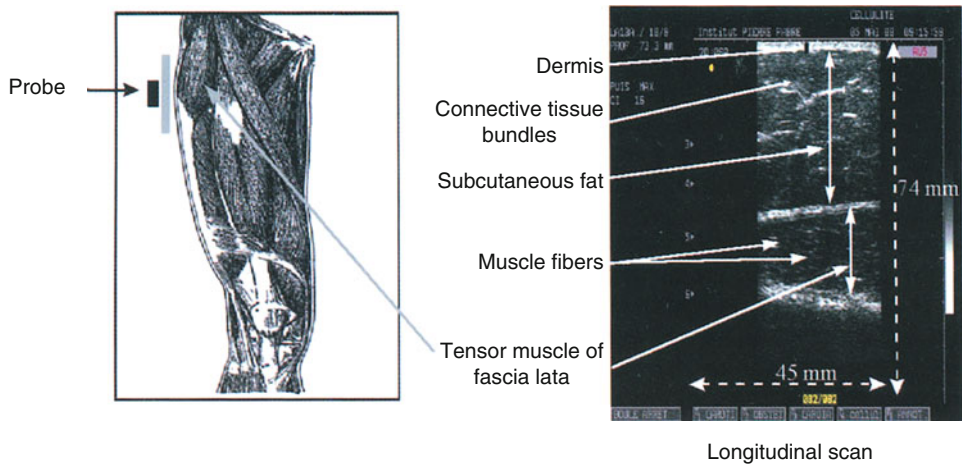

Fig. 1 A 7.5–10-MHz B-scan of the thigh, upper part lateral aspect. AU 5 (Esaote, Genoa, Italy) with a linear applicator

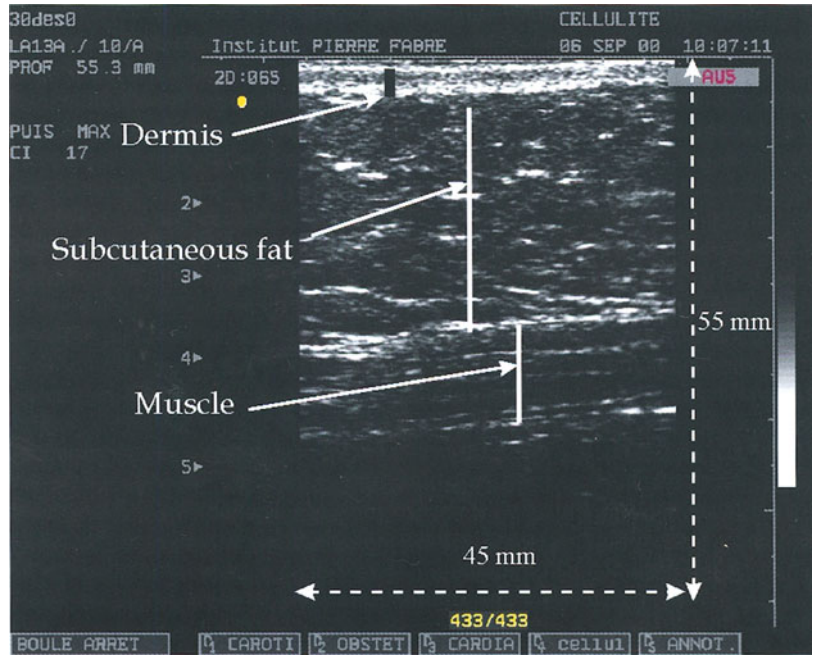

Fig. 2 A 10-MHz B-scan of the abdomen. Subcutis thickness: 26 mm. AU 5 (Esaote, Genoa, Italy) with a linear applicator

attenuation. However, it can be used to study the dermis-hypodermis interface, which is marked by anchoring dermal extensions within the hypodermis (retinacula cutis). Through summation of 28 images taken on a 482-mm^2 skin surface area (ultrasound C-mode imaging), the decrease in the actual-to-plane ratio interface area following treatment by massage in a case of cellulitis was demonstrated (Lucassen et al. 1997).

In conclusion, ultrasound imaging has the advantages of simplicity, rapidity, non-invasiveness, reliability, and reproducibility when associated with sound methodology. Its limitation is the substantial role of the operator's experience. The operator must pay particular attention to precise selection and marking out the investigated site, which is essential in repeat investigations.

1.3.4 Computed Tomography

Computed tomography (CT), an X-ray investigation method based on the analysis of reconstituted cross-sectional images, provides direct visualization and measurement of deep organs or structures. Its principle is X-ray differential transmission depending on the density, atomic composition, and thickness of the tissues they pass through. Serial measurements of absorption density, through various angles of incidence, provide a set of profiles from which a cross-sectional image is reconstituted. Equipment is available mainly in hospitals. Measurements more and more sensitive with time: helix scanner scans are 0.5 mm apart. From several cross-sections, images in any other incident angle can be computed. A CT single cross-section at umbilical level irradiates 1 μSv, but usually several adjacent cross-sections are necessary, and there is always substantial overlap between cross-sections, so that the total irradiation can come close to 100 μSv.

Although CT is not perfectly adapted to the study of soft tissues, the subcutis fat can, nevertheless, be studied because its density is lower than that of the skin and muscle (Enzi et al. 1986). Both cutis–subcutis and subcutis–muscle interfaces can easily be visualized and the subcutis thickness measured (Figs. 4 and 5). Computed tomography also provides a reliable measurement of the oral adipose tissue (Levine et al. 1996) and, at the lumbar level (L2–L3 interval), of the abdominal and subcutaneous fat (Jensen

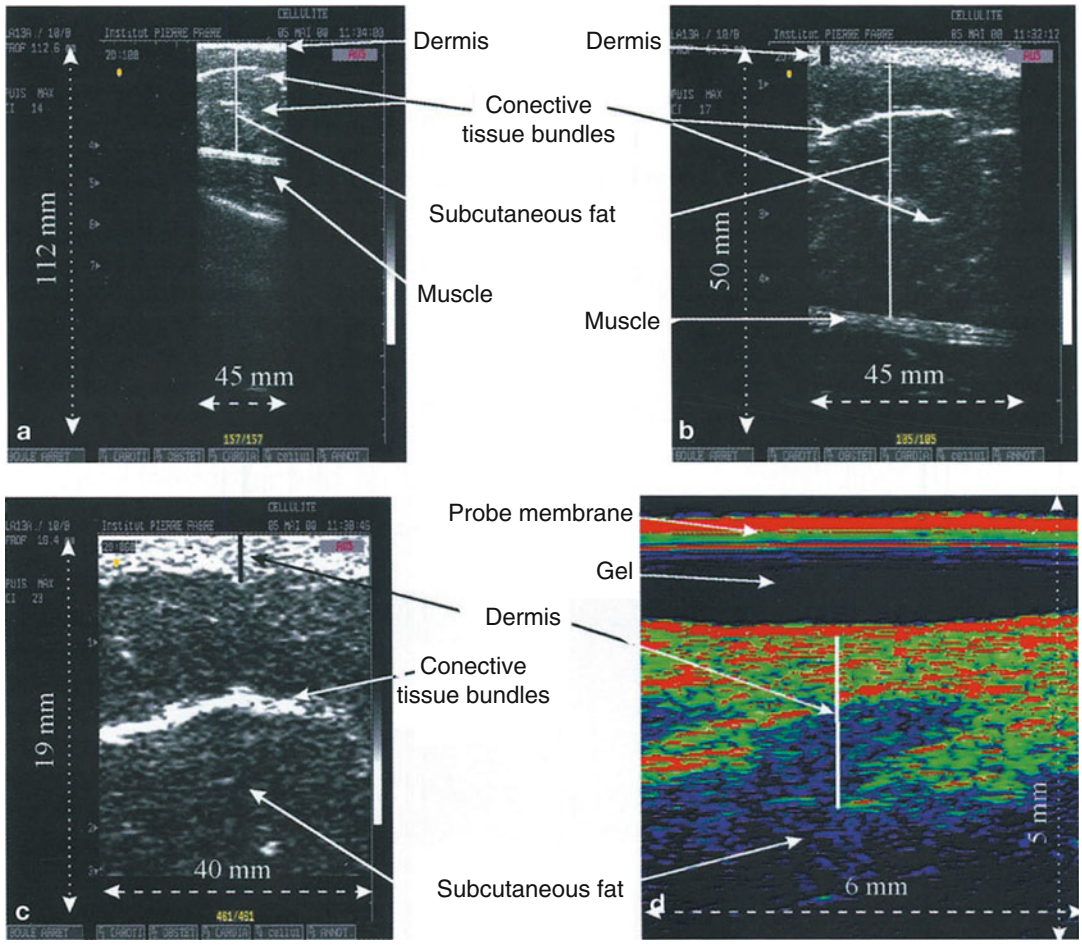

Fig. 3 (**a**–**d**) B-scan of the same area of the thigh, upper part lateral aspect. (**a**) 7.5 MHz. (**b**) 10 MHz. (**c**) 13 MHz. AU 5 (Esaote, Genoa, Italy). (**d**) 20 MHz Dermcup 2020 (2 MT, Labège, France)

Table 3 Neonate subcutis thickness (mm) (n=7), ultrasound A mode (From Petersen et al. 1995)

Body weight (g)	Abdomen	Back
1,095	0.65±0.07	0.77±0.10
1,810	0.78±0.13	0.95±0 13
1,940	1.52±0.20	1.53±0.16
2,900	1.67±0.17	1.87±0.19
3,390	1.80±0.16	1.74±0.23
3,890	1.95±0.31	1.84±0.27
4,750	2.90±0.22	2.45±0.24

et al. 1995). In a study of healthy subjects, the adipose tissue cross-sectional area was 8–20 cm^2 (cheeks), 16–100 cm^2 (visceral fat), and 20–150 cm^2 (subcutaneous fat).

The main advantage of CT is to provide cross-sectional images of any part of the body, thereby visualization and measurement of the subcutaneous fat thickness or amount at any site. The spatial resolution is about 1 mm. Rapidity and independence from the operator are clear advantages. Drawbacks include the use of X-ray (for a single cross-section at umbilical level irradiation is 0.01 Gy) and the expensive equipment available only in hospitals.

1.3.5 Nuclear Magnetic Resonance Imaging

Magnetic resonance imaging (MRI) comes from nuclear magnetic resonance (NMR), which was developed in 1946 by Bloch and Purcell and was

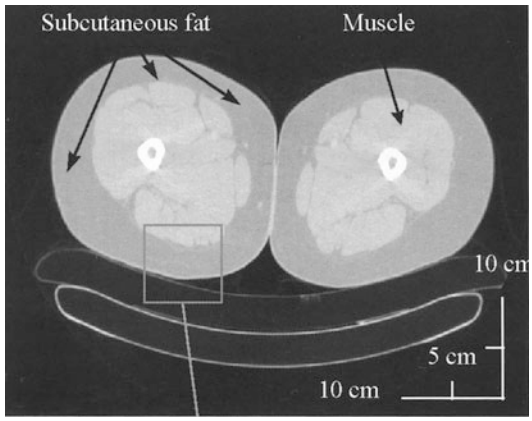

Fig. 4 Computed tomography cross-section of both thighs (Courtesy of Prof. Joffre, Radiology Department, Rangueil University Hospital, Toulouse, France)

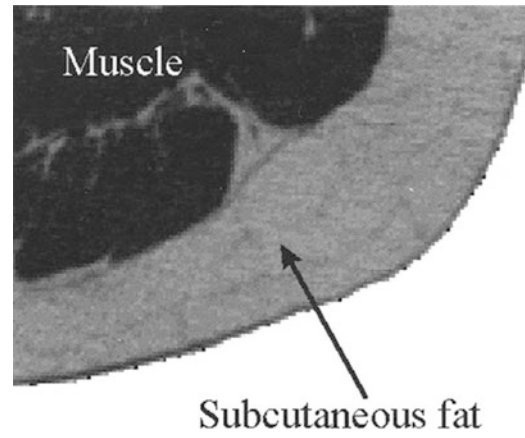

Fig. 5 Computed tomography of the thigh. Part of cross-section with fat enhancement (Courtesy of Prof. Joffre, Radiology Department, Rangueil University Hospital, Toulouse, France)

first used in chemistry. In the early 1980s, a major step forward was made in medical imaging with two types of investigation: magnetic resonance imaging (MRI), which shows body cross-sectional images, and magnetic resonance spectrometry (MRS). Both applications are based on the tissue atom nucleus magnetic moments interacting with magnetic fields. Hydrogen atom nuclei are concerned in imaging, those of hydrogen and phosphor-31 in spectroscopy. The nuclear spins, when placed in an intense magnetic field, divert and line up with the field axis. They are then excited by a radio-frequency wave, which turns them perpendicularly to this axis (through a resonance phenomenon). When excitation stops, the spins gradually recover their basal position (nuclear relaxation). Two types of magnetic interaction are described, characterized by the longitudinal (T1) and transverse (T2) relaxation times. After treatment of this basic signal, information is given either as a spectrum (MRS) or an image (MRI).

From the MRI-generated signals, it is possible to reconstitute a cross-sectional image of any part of the body. Hydrogen is a major component of water and lipids. This accounts for the better performance of MRI as compared to CT in visualizing soft tissues and mostly adipose tissue. Fat is easily detected through its intense T1 signal, giving a bright area on the image. This makes it possible to directly measure the thickness of the adipose layer (Figs. 6 and 7) and even to distinguish the connective tissue septa (Fig. 8). Nonfat nonbone tissues give a mid-intensity T1 or T2 signal and appear as grey areas (Fig. 8). Resolution is in the range of 70 μm to 1 mm, for investigation depths of a few millimeters to several centimeters, respectively. High resolutions are obtained by adding a special coil (see ▶ Chap. 41, "Dermis Connective Tissue Histopathology"). Furthermore, from the measurement of the relaxation times, MRI obtains data on lipid and water content of adipose tissue (Brix et al. 1993; Saiag et al. 1994; Krug et al. 1998; Richard et al. 1991, 1993; Lopez et al. 1997; Idy Peretti et al. 1998; Querleux et al. 1994, 1998, 2000; Franconi et al. 1995; Wright et al. 1998; Harada et al. 1994; Fowler et al. 1990; Schreiner et al. 1996).

The advantage of the method is the high-resolution images that give a precise measurement of adipose tissue thickness and distribution on cross-sections, without an operator's direct intervention. Providing an image of tissue composition is a specific output, particularly useful for the determination of subcutis water and lipid contents.

Querleux et al. (2002) studied the anatomy and physiology of subcutaneous adipose tissue

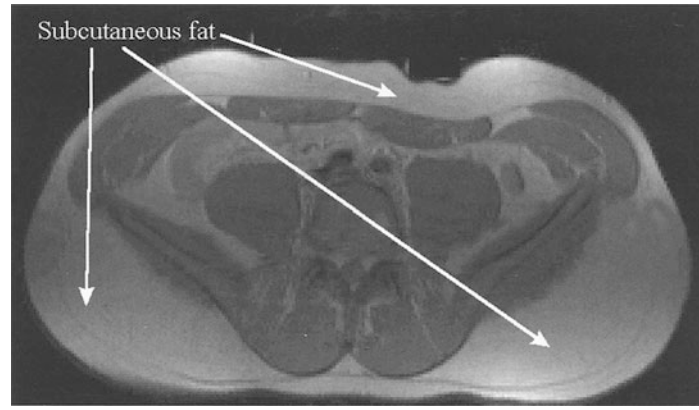

Fig. 6 MRI cross-section of lower abdomen. T1 relaxation (Courtesy of Prof. Joffre, Radiology Department, Rangueil University Hospital, Toulouse, France)

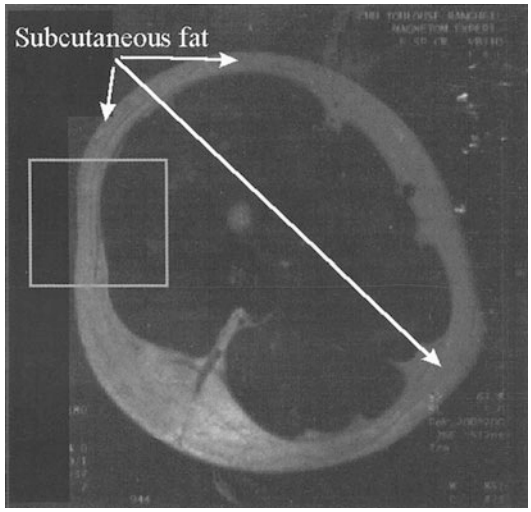

Fig. 7 MRI cross-section of the thigh. T1 relaxation (Courtesy of Prof. Joffre, Radiology Department, Rangueil University Hospital, Toulouse, France)

in relation to sex and the presence of cellulite. The topography of the dermal-hypodermal junction and the three-dimensional architecture of the subcutaneous fibrous septae were investigated using high spatial resolution. In addition, water and lipid fractions within fat lobules were quantified using proton spectroscopy. A study involving 21 women with cellulite was undertaken, and the results compared to 20 women with no cellulite and 23 men. The data showed deeper indentations of adipose tissue into the dermis, increased dermal thickness, and an increase in thickness of the deeper layer of subcutaneous adipose tissue. However, no change in water content or modification of unsaturated and saturated lipid fractions on a dipose tissue were observed in women with cellulite.

In conclusion, MRI is the most powerful tool for soft tissue imaging and quantification, especially fat tissue. It also provides cross-sections of any part of the body and from any angle. These advantages make it unique and irreplaceable. The drawback is the technical expense and complexity: MRI is meant for medical purposes and is available only in large hospitals (Fig. 9). It requires specifically trained staff and implies a long and stressful examination for volunteers. It is therefore a method reserved for research or exceptional circumstances.

2 Conclusion

Many methods are available today to investigate body fat. Choosing the appropriate ones depends on the objective of the measurement.

To demonstrate overweight or obesity and its type, BMI followed by WC and WHR are helpful and in current use. Quantification is provided by either DXA or BIA. For patient follow-up, the latter is preferable to DXA because of the risks associated with repeat X-ray irradiation. In children, the use of the CDC chart in the USA and the IOTF chart in

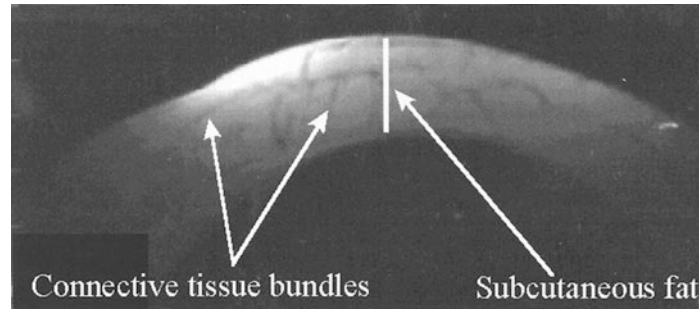

Fig. 8 MRI with additional surface coil. Cross-section of the thigh. T1 relaxation (Courtesy of Prof. Joffre, Radiology Department, Rangueil University Hospital, Toulouse, France)

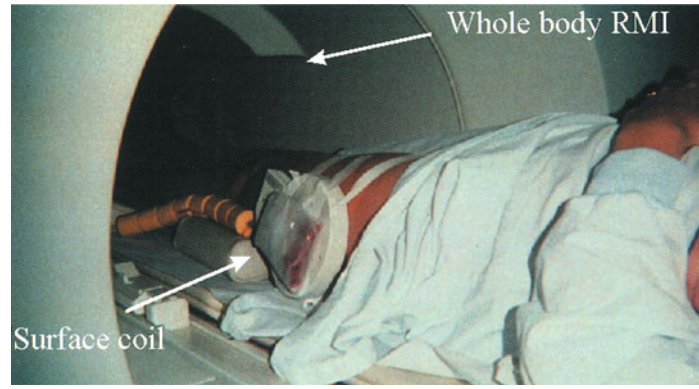

Fig. 9 MRI total body device with additional surface coil for skin and subcutis imaging (Courtesy of Prof. Joffre, Radiology Department, Rangueil University Hospital, Toulouse, France)

other countries should be associated with BMI. BIA is easy to handle and safe, but is an indirect method based on prediction equations and consequently bears some risk of uncertainty. DXA cannot be used repeatedly.

To measure the subcutaneous adipose tissue thickness on a particular site, ultrasound imaging at 10 MHz is the best technique. The measure of skinfold thickness, or its pinching variant is a good substitute when ultrasound equipment is lacking. CT and MRI should be only used for research.

3 Special Parameters of Connective Subcutaneous Tissue

3.1 Tissue Internal Pressure

With a simple experimental device, Merlen (1967) found that the pressure required to introduce a liquid into the forearm subcutis was between 1 and 15 Torr. The device consisted of a needle sealed at its extremity, with several holes bored on its sides, that is connected to a syringe via a glass container (whose purpose is to attenuate the increasing pressure rate from syringe action). Between the needle and the container (tap 1) and between the container and the syringe (tap 2), two 3-outlet taps are inserted to communicate with atmospheric pressure. A manometer is placed in a by-pass between tap 1 and the container. Measurement follows several sequential steps. (1) The syringe is filled with saline in slight excess and the liquid level on the tube is marked with ink. (2) Tap 1 is turned off and the needle is introduced into the subcutis. (3) Taps 1 and 2 are opened to the outside: the manometer shows zero (the saline is at atmospheric pressure). (4) Tap 2 is turned off and the minimum amount of air necessary to push the saline level in the tube is injected (i.e., to inject a small amount of saline into the subcutis). (5) Tap 1 is turned off and the pressure indicated on the manometer is noted.

In Guyton's technique (Brace and Guyton 1979), a capsule connected to a venous pressure transducer

is inserted into the subcutis for several days. The experiment was made in animals. In contrast with Merlen's data, a negative pressure was recorded. Its possible meaning is discussed in ▶ Chap. 66, "Subcutaneous Tissue Histophysiology," Sect. 1.2.

3.2 Subcutis Oxygen Partial Pressure

Subcutis oxygen partial pressure can be useful in diseases involving the subcutis, especially leg ulcers whatever their etiology, as well as in cosmetic and reconstructive surgery. However, it does not seem to be widely used.

The oxygen pressure in the subcutis can be monitored by introducing a microcatheter containing a Clark-type polarographic electrode (Revoxode) and a pH 7.4 electrolyte solution. The measurement is automated (LICOX cmp, GMS 24247 Kiel-Mielkendorf Germany, email: gmsmb@aol.com). In situ temperature and blood flow (laser Doppler) can be simultaneously recorded.

Another technique uses the oxygen-induced fluorescence extinction (Oxylite). It also provides subcutis oxygen partial pressure monitoring and simultaneous blood flow and temperature measurement (Oxford Optronix Ltd, Oxford, UK, e-mail: sales@oxford-optronix.com).

3.3 Mechanical Behavior

Subcutis mechanical function has a double purpose: first to allow the overlying skin to move as a whole, both horizontally and vertically, and second to attenuate and/or disperse the spells of external pressure. Although sound devices are commercially available that can apply forces able to make the skin move in every direction, and measure the displacement, apparently no data are available on the subcutis elastic or viscous resistance. However, some studies have investigated the subcutis behavior under compression, mainly aimed at assessing edema: the magnitude of mechanical impedance decreased with increased frequency (maximum at low frequencies of 10–30 Hz). It decreased with the degree of pitting edema but increased in case of hard, nonpitting edema. These variations in the subcutis water content paralleled those of in vitro water content of gels (Mridha and Ödman 1985). The same authors proposed a method to assess both the degree of edema and the edematous fluid viscosity. Using a disc 17 mm in diameter, the skin is depressed abruptly (26 mm s^{-1}) down to 4 mm, and the exerted force versus time is recorded for 30 s while the depression is maintained (Mridha and Ödman 1986). As the liquid flows out of the compressed area the force decreases. Using the curve of per cent decrease versus time assesses the volume of expelled liquid, according to the formula:

$$V_t = 0.9\,(1 - F_t/F_{t=0})$$

where V_t is the volume (ml) expelled at time t, F_t and $F_{t=0}$ are the forces at times t and zero, and 0.9 is the pressure head area multiplied by the indentation depth.

In normal tissue, two force decreasing rates were observed, a high, then a lower one, as in current relaxation experiments, indicating two types of viscosity. In pitting edema, a third and higher decreasing rate was found initially, due to the edematous fluid outflow. This simple method has the advantage of obviating the measurement of the tissue's elastic resistance.

References

Aloia JF, Vaswani A, Mikhail M, Raster ER. Body composition by dual-energy X-ray absorptiometry in black compared with white women. Osteoporos Int. 1999;10:114–9.

Armengol R, Girones E, Bellés A, Polo C, Pepio M, Gisbert JM, Garrofé C, Roldos F, Sanmarti E. Quantitative evaluation of the anti-cellulite efficacy by scan-ultrasound and its relation with traditional clinic studies. IFSCC. 1992;3:1218–39.

Behnke AR, Feen BG, Welham WC. Specific gravity of healthy men. JAMA. 1942;118:495–8.

Black MM, Cunliffe WJ. Subcutaneous fat. In: Rook A, Wilkinson DS, Ebling FJG, Champion RH, Burton JL, Burns DA, Breathnagh SM, editors. Textbook of dermatology. 6th ed. Oxford: Blackwell; 1998. p. 2403–7.

Boulier A, Thomasset AL, Apfelbaum M. Bioelectrical-impedance measurement of body water. Am J Clin Nutr. 1992;55:761–2.

Brace RA, Guyton AC. Interstitial fluid pressure: capsule, free fluid, gel fluid, and gel absorption pressure in subcutaneous tissue. Microvasc Res. 1979;18:217–28.

Bray GA. Obesity. In: Brown ML, editor. Present knowledge in nutrition. 6th ed. Washington: International Life Sciences Institute, Nutrition Foundation; 1990. p. 23–8.

Brix G, Heiland S, Bellemann ME, Koch T, Lorenz WL. MR imaging of fat-containing tissues: evaluation of two quantitative imaging techniques in comparison with localized proton spectroscopy. Magn Reson Imaging. 1993;11:977–91.

Carella MJ, Rodgers CD, Anderson D, Gossain VV. Serial measurements of body composition in obese subjects during a very low energy diet comparing bioelectrical impedance with hydrodensitometry. Obes Res. 1997;5:250–6.

Centre for Disease Control. Vital and health statistics of the Centre for Disease Control and Prevention/National Centre for Health Statistics (NCHS) growth charts: United States, No. 314; 2000.

Cole TJ, Bellizi MC, Flegal KM, Dietz WH. Establishing a standard definition for child overweight and obesity worldwide: international survey. BMJ. 2000;320:1240–3.

Despres JP, Prudhomme D, Pouliot MC, Tremhlay A, Bouchard C. Estimation of deep abdominal adipose-tissue accumulation from simple anthropometric measurements in men. Am J Clin Nutr. 1991;54:471–7.

Diridollou S. Echographie – Intérêt en dermatologie et dermo-cosmétologie. 2nd Colloque National d'Ingénierie Cutanée (Soc Fr Ing Cut); 2000 June 22–23, Toulouse; 2000.

Einsenheiss C, Welzel J, Schmeller W. The influence of female sex hormones on skin thickness: evaluation using 20 MHz sonography. Br J Dermatol. 1998;139:462–7.

Enzi G, Gasparo M, Biodetti PR, Fiore D, Semisa M, Zurlo F. Subcutaneous and visceral fat distribution according to sex, age and overweight, evaluated by computed tomography. Am J Clin Nutr. 1986;44:39–746.

Fowler PA, Casey CE, Cameron GG, Ester MA, Knight CH. Cyclic changes in composition and volume of the breast during the menstrual cycle, measured by magnetic resonance imaging. Br J Obstet Gynaecol. 1990;97:595–602.

Franconi F, Akoka S, Guesnet J, et al. Measurement of epidermal moisture content by magnetic resonance imaging: assessment of hydration cream. Br J Dermatol. 1995;132:913–7.

Harada M, Amano Y, Matsuzaki K, Hayashi Y, Nishitani H, Yoshizumi M, Yoshida O, Katoh I. Quantitative evaluation of intraarterial lymphocyte injection therapy for lymph edema using MR imaging. Acta Radiol. 1994;35:405–8.

Hendel HW, Gotfredsen A, Hoejgaard L, Andersen T, Hilsted J. Change in fat-free mass assessed by bioelectrical impedance, total body potassium and dual energy X-ray absorptiometry during prolonged weight loss. Scand J Lab Invest. 1996;56:671–9.

Idy Peretti I, Bittoun J, Alliot F, et al. Lymphedematous skin and subcutis: in vivo high resolution magnetic resonance imaging evaluation. J Invest Dermatol. 1998;110:782–7.

Jensen MD, Kanaley JA, Reed JE, Sheedy PE. Measurement of abdominal and visceral fat with computed tomography and dual-energy x-ray absorptiometry. Am J Clin Nutr. 1995;61:274–8.

Jungermann K, Barth CA. Energy metabolism and nutrition. In: Greger G, Windhorst U, editors. Comprehensive human physiology. Berlin/Heidelberg/New York: Springer; 1996. p. 1425–57.

Krug B, Kugel H, Schulze HJ, Krahe T, Gieseke J, Lackner K. High- resolution MR imaging of the cutis and subcutis. Acta Radiol. 1998;39:547–53.

Levine JA, Ray A, Jensen MD. Relation between chubby cheeks and visceral fat. N Engl J Med. 1996;339:1946–7.

Lohman TG, Roche AF, Martorell R, editors. Anthropometric standardization reference manual. Champaign: Human Kinetics Books; 1988.

Lopez JA, Saez F, Larena JA, Capelastegui A, Martin JI, Canteli B. MRI diagnosis and follow-up of subcutaneous fat necrosis. J MRI. 1997;7:929–32.

Lucassen GW, van der Sluys WLN, van Herk JJ, Nuijs AM, Wierenga PE, Barel AO, Lambrecht R. The effectiveness of massage treatment on cellulite as monitored by ultrasound imaging. Skin Res Technol. 1997;3:154–60.

Mazess RB, Baraen HS, Bisek JP, Hanson J. Dual-energy X-ray absorptiometry for total body and regional bone-mineral and soft-tissue composition. Am J Clin Nutr. 1990;51:1106–12.

Merlen JF. La pression tissulaire sous-cutanée: résistance élastique des tissus. Rev Med. 1967;24:1195–200.

Mridha M, Ödman S. Characterization of subcutaneous edema by mechanical impedance measurements. J Invest Dermatol. 1985;85:575–8.

Mridha M, Ödman S. Noninvasive method for the assessment of subcutaneous oedema. Med Biol Eng Comput. 1986;24:393–8.

Perin F, Pittet JC, Schnebert S, Perrier P, Tranquart F, Beau P. Ultrasonic assessment of variations in thickness of subcutaneous fat during normal menstrual cycle. Eur J Ultrasound. 2000;11:7–14.

Petersen JS, Petersen S, Serup J. High-frequency ultrasound measurement of dermis and subcutaneous fat in the newborn infant. Skin Res Technol. 1995; 1:86–9.

Pittet JC, Schnebert S, Perrier P, Beau P. Follow of the thickness evolution of the adipose tissue of the external face of thigh in woman by ultrasound. Skin Res Technol. 1996;12:223.

Pittet JC, Perrier C, Schnebert S, Perrier P, Tranquart F, Beau P. Variability of fatty tissue thickness measurement using ultrasonography (US). Skin Res Technol. 1997;3:205.

Querleux B, Richard S, Bittoun J, et al. In vivo hydration profile in skin layers by high resolution magnetic resonance imaging. Skin Pharmacol. 1994;7:210–6.

Querleux B, Jolivet O, Bittoun J et al. In vivo proton magnetic resonance spectroscopy in human skin. In Elsner P, Barel AO, Berardesca E, Gabard B, Serup J (eds): Skin bioengineering techniques and applications in dermatology and cosmetology. Curr Probl Dermatol. Basel, Karger. 1998;26:12–19.

Querleux B, Cornillon C, Alonso-Ricarte A, Jolivet O, Bittoun J. Do gender and cellulite grade induce modifications in the morphology and physiology of the subcutaneous adipose tissue? An in vivo MR imaging and spectroscopy study. Skin Res Technol. 2000;6:174.

Querleux B, Cornillon C, Jolivet O, Bittoun J. Anatomy and physiology of subcutaneous adipose tissue by in vivo magnetic resonance imaging and spectroscopy: relationships with sex and presence of cellulite. Skin Res Technol. 2002;8:118–24.

Richard S, Querleux B, Bittoun J, Jolivet O, Idy-Peretti I, Jolivet O, Cermakova E, Lévêque JL. In vivo proton relaxation times analysis of the skin layers by magnetic resonance imaging. J Invest Dermatol. 1991;97:120–5.

Richard S, Querleux B, Bittoun J, Jolivet O, Idy-Peretti I, De Lacharriere O, Leveque JL. Characterization of the skin in vivo by high resolution magnetic resonance imaging: water behavior and age related effects. J Invest Dermatol. 1993;100:705–9.

Rolland-Cachera MF, Cole TJ, Sempe M, Tichet J, Rossignol C, Charraud A. Body mass index variations: centiles from birth to 87 years. Eur J Clin Nutr. 1991;45:13–21.

Rudolf MC, Sahota P, Barth JH, Walker J. Increasing prevalence of obesity in primary school children: cohort study. Br Med J. 2001;322:1094–5.

Saiag P, Le Breton C, Pavlovic M, Fouchard N, Delzant G, Bigot JM. Magnetic resonance imaging in adults presenting with severe acute infectious cellulitis. Arch Dermatol. 1994;130:1150–8.

Schnebert S, Perin F, Pittet JC, Beau P, Perrier P, Pourcelot L. Echographie, une technique accessible et fiable pour mesurer l'efficacité des produits amincissants. Cosmétologie. 1999;22:35–8.

Schreiner PJ, Terry JG, Evans GW, Hinson WH, Crouse JR, Haiss G. Sex-specific associations of magnetic resonance imaging-derived intra-abdominal and subcutaneous fat areas with conventional anthropometric indices. Am J Epidemiol. 1996; 4:335–45.

Segal KR, Van Loan M, Fitzgerald PL, Hodgdon JA, Van Itallie TB. Lean body mass estimation by bioelectrical impedance analysis: a four-site cross-validation study. Am J Clin Nutr. 1988;47:7–14.

Stolarczvk LM, Heyward VH, Van Loan MD, Hicks VL, Wilson WL, Reano LM. The fatness-specific bioelectrical impedance analysis equations of Segal et al.: are they generalizable and practical? Am J Clin Nutr. 1997;66:8–17.

Utter AC, Nieman DC, Ward AN, Butterworth DE. Use of the leg-to-leg bioelectrical impedance method in assessing body-composition change in obese women. Am J Clin Nutr. 1999;69:603–7.

Vague J, Boyer J, Jubelin J, Nicolino J, Pinto C. Adipomuscular ratio in human subjects. In: Vague J, Denton RM, editors. Physiopathology of adipose tissue. Amsterdam: Excepta Med; 1969. p. 360–86.

Vague J, Meignen JM, Negrin JF, Thomas M, Tramoni M, Jubelin J. Androgènes, oestrogènes et cortisol dans la physiopathologie du tissu adipeux. Sem Hôpitaux Paris. 1984;60:1465–76.

Wahner HW, Fogelman I. Total body bone mineral and body composition by absorptiometry. In: Wahner HW, Fogelman I, editors. The evaluation of osteoporosis: dual energy X-ray absorptiometry in clinical practice. London: Martin Dunitz; 1994. p. 196–218.

World Health Organization. Obesity: preventing and managing the global epidemic. Report of a WHO consultation on obesity; 1997 June 3–5; Geneva; 1998 (WHO/NUT/NCD/98.1).

Wright AC, Bohning DE, Pecheny AP, Spicer KM. Magnetic resonance chemical shift microimaging of aging human skin in vivo: initial findings. Skin Res Technol. 1998;4:55–62.

Ultrasound of the Subcutaneous Tissue

68

Ximena Wortsman

Contents

Keywords

Subcutaneous tissue ultrasound • Skin ultrasound • Dermatologic ultrasound • Hypodermis ultrasound • Subcutaneous tissue • Hypodermis

1 Introduction

The subcutaneous tissue, also called hypodermis, is composed of an extensive network of fatty lobules separated by thin fibrovascular septa. It helps with thermoregulation, provides an energy store, and serves as a cushion to protect internal organs (Ebling et al. 1992). This mesodermic layer presents its own pathology and also may be affected by abnormalities that lie in the neighboring layers or structures.

The use of sonography for studying subcutaneous tissue has been growing in the last few decades due to the development of multichannel machines with high and variable frequency probes that currently range from 7 to 22 MHz (Wortsman 2012a). Importantly, these probes present high definition for studying both superficial and deep structures and can unveil both morphology and blood flow in real time.

X. Wortsman (✉)
Department of Radiology and Department of Dermatology, Institute for Diagnostic Imaging and Research of the Skin and Soft Tissues, Clinica Servet, Faculty of Medicine, University of Chile, Santiago, Chile
e-mail: xworts@yahoo.com

P. Humbert et al. (eds.), *Agache's Measuring the Skin*,
DOI 10.1007/978-3-319-32383-1_92

2 Technical Considerations

The requisites for observing subcutaneous tissue ideally are an adequate equipment (ideally, multichannel high-definition ultrasound machine with variable frequency probes that go from 7 to 22 MHz) and a trained sonographer with knowledge of both dermatologic pathology and ultrasound imaging (Wortsman 2012b).

The sonographic technique for exploring subcutaneous tissue is the same as was described for examining localized lesions of the skin (Wortsman and Wortsman 2010). A copious amount of gel is applied over the skin surface, and the probe is gently located on the lesional area. Virtually no compression of the subcutaneous tissue is performed, and the tissue is explored in its most natural form, preventing the collapse of slow flow vessels. Grayscale, color, and/or power Doppler images of the lesional area in at least two perpendicular axes are made. These color and power Doppler sequences allow the detection of the blood flow patterns. Then, 3D reconstructions of grayscale and/or power Doppler images can be performed to improve presentation and understanding of the pathology. These reconstructions are performed by doing a 5–8 s sweep in the region of interest.

3 Normal Anatomy

Subcutaneous tissue appears on sonography as a hypoechoic layer mostly composed of hypoechoic fatty lobules separated by hyperechoic linear fibrous septa (Wortsman et al. 2006; Fig. 1). Slow flow thin arterial and venous vessels are detected within this layer. The thickness of the subcutaneous tissue varies according to the corporal region. Thus, it may easily reach $\geq$1 cm in the abdominal wall or hips; however, it may be thin and measure $<$0.1 cm in the dorsum of the hands of a child.

On top of the subcutaneous tissue, there is a hyperechoic band that corresponds to the dermis. Beneath the subcutaneous tissue, other layers such as the hypoechoic fibrillar structure of the muscle layer or the hyperechoic fibrillar pattern of the tendons are detected.

4 Sonographic Measurements in the Subcutaneous Tissue

The current equipment allows us to measure directly from the machine the distance in all axes (cm), the area (cm^2) or volume (cm^3), and the peak systolic velocity of the vessels (cm/s). It is also possible to measure the resistive index of the arterial vessels (i.e., peak velocity systole – end velocity diastole/peak velocity systole), although this latter vascularity data is rarely used in the subcutaneous tissue, being more frequently used for assessing stenosis in the large arteries.

It is also possible to qualify the changes in the echotexture patterns in case of abnormalities. For example, under inflammatory conditions, the echogenicity of the fatty lobules in the

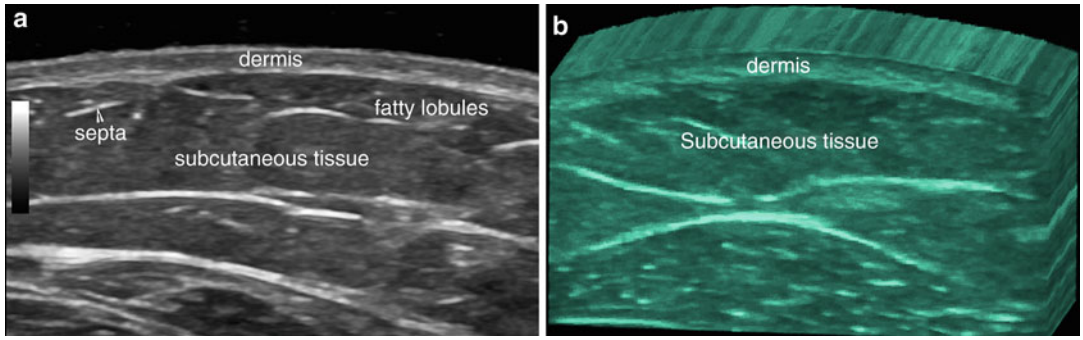

Fig. 1 Normal sonographic appearance of the subcutaneous tissue (transverse views). (**a**) Grayscale ultrasound shows the hypoechoic fatty lobules and the hyperechoic fibrous septa of the subcutaneous tissue. (**b**) 3D reconstruction (5–8 s sweep)

subcutaneous tissue usually increases (hyperechogenicity-white), and there may be anechoic fluid (black) within the septa. In the case of tumors, hypoechoic (gray) nodules that frequently show less echogenicity (dark) compared with the surrounding subcutaneous tissue can be found.

Vascularity patterns can also be qualified and compared with the non-lesional region. These can be defined as hypervascular or hypovascular areas.

5 Pathology

5.1 Inflammatory Conditions

5.1.1 Edema and Fluid Collections

The presence of interstitial edema in the subcutaneous tissue diffusely increases the echogenicity of the fatty lobules, and they also show blurry borders. Fluid collections such as seromas or hematomas appear as anechoic or hypoechoic commonly compressible structures that sometimes can show echoes (debris) or septa and usually decrease in size over time (Ryu et al. 2011).

5.1.2 Panniculitis

This condition implies the presence of inflammatory cellular infiltrates that usually involve both the fatty lobules and the septa. According to the main affected component, panniculitides can be separated in septal or lobular (Requena and Yus 2001; Requena and Sánchez 2001). On sonography the involvement of the lobules shows as hyperechogenicity in the fatty tissue, and the effects on the septa present as hypoechogenicity and thickening of the septal structures. Moreover, increased regional blood flow may be detected with color or power Doppler (Fig. 2). Inflammatory subcutaneous conditions with fat necrosis show as hyperechoic areas with anechoic pseudocystic structures that correspond to liquefaction sites in the fatty tissue (Ester et al. 2009).

5.1.3 Lymph Nodes

These are oval-shaped solid structures that belong to the immune system. They are composed of an outer capsule, mainly cellular, and an inner medulla with prominent ducts and sinuses. An external fibrous capsule surrounds the cellular capsule with the exception of the vascular hilum region. They are distributed in well-known anatomical regions, and they usually can become palpable under inflammatory or tumoral conditions. They show on sonography as oval-shaped structures with hypoechoic rim (cortex) and hyperechoic center (medulla). On color Doppler the vascular hilum is usually detected in one of the aspects containing

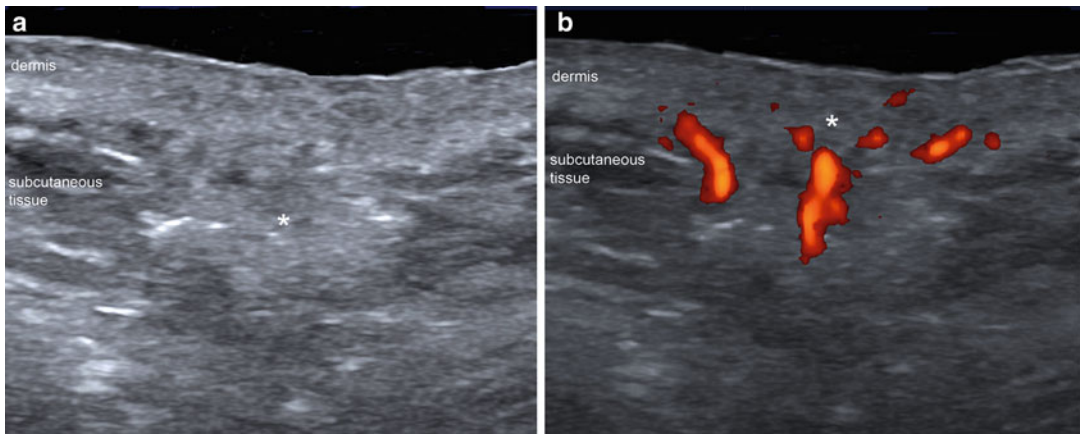

Fig. 2 Lobular panniculitis (transverse views, right cheek). (**a**) Grayscale ultrasound shows hyperechoic focal area (*) that involves the fatty lobules of the subcutaneous tissue. (**b**) Power Doppler ultrasound demonstrates increased vascularity within the affected subcutaneous region

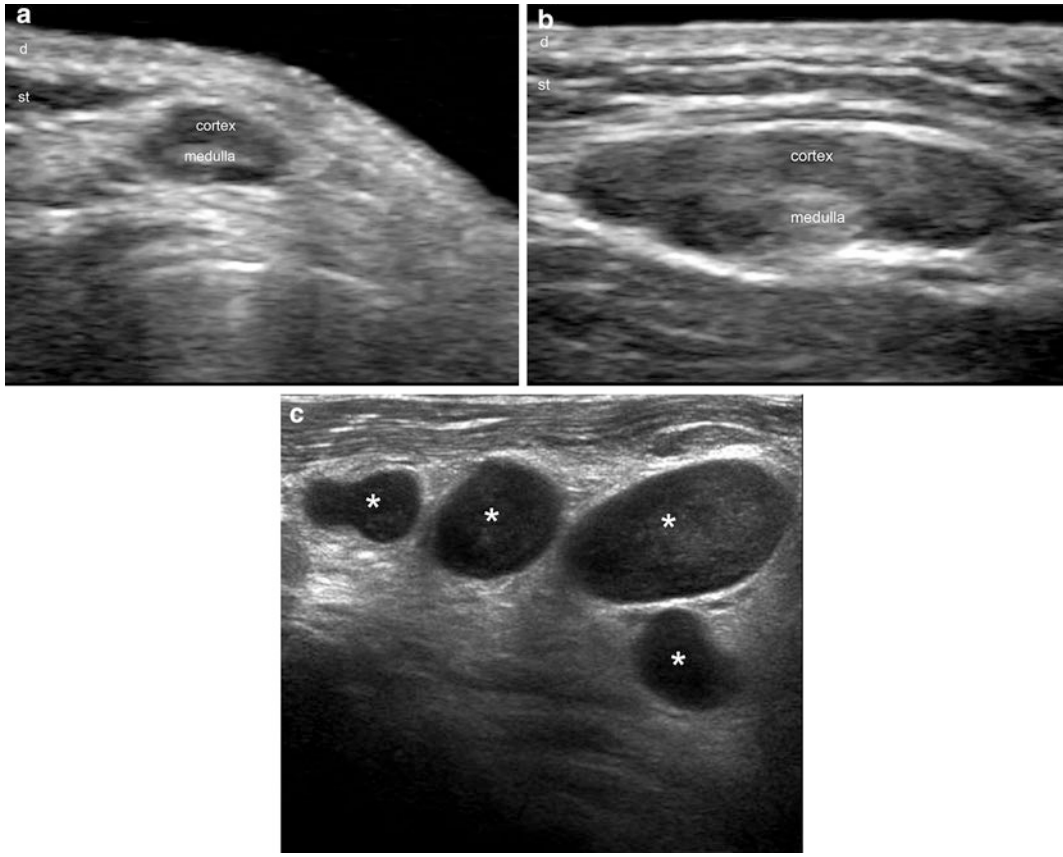

Fig. 3 Lymph nodes (grayscale ultrasounds; (**a**) and (**b**): transverse views; (**c**): longitudinal view). (**a**) Normal lymph node: well-defined, oval-shaped structure with hypoechoic cortex and hyperechoic medulla. (**b**) Inflammatory lymph node: enlarged oval-shaped structure that conserves the cortex-medulla echostructure. Notice the increased thickness of the cortex. (**c**) Metastatic lymph nodes: oval and round-shaped structures (*) that lose the hyperechoic medulla

low-flow arterial and venous vessels. Benign lymph nodes frequently conserve their oval shape and cortical and medullar echostructure. In contrast, malignant lymph nodes tend to show an oval or rounded shape and lose their hyperechoic center, therefore appearing as fully hypoechoic and sometimes with anechoic regions (Dudea et al. 2012; Fig. 3).

5.2 Tumors

There are multiple types of tumors that primarily or secondarily can affect the subcutaneous tissue. We will focus on causes of involvement that may be part of the common differential diagnoses in daily dermatological practice.

5.2.1 Benign

Cystic

Epidermal Cysts

These frequent dermatologic lesions are composed of stratified squamous epithelium with a granular layer and are commonly located in both the dermis and subcutaneous tissue. On sonography, they show up differently according to the

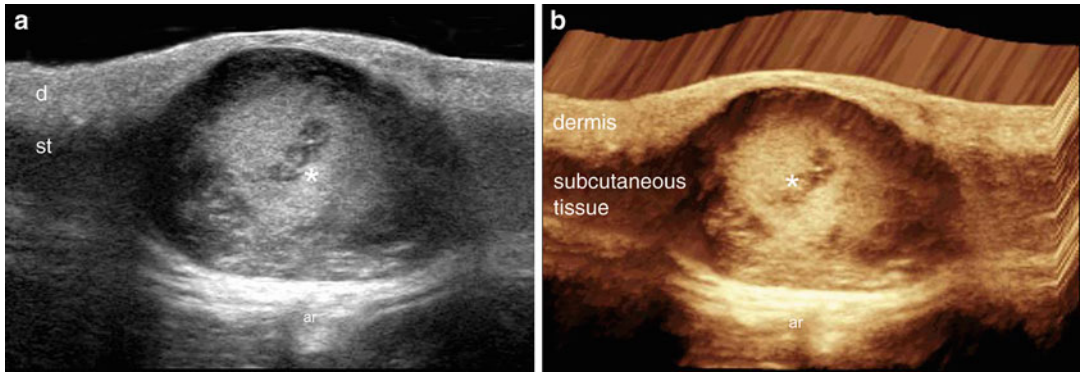

Fig. 4 Epidermal cyst (longitudinal views, lumbar region). (**a**) Grayscale ultrasound shows a well-defined, oval-shaped hypoechoic structure (*) with posterior acoustic reinforcement artifact. (**b**) 3D reconstruction of the lesion (5–8 s sweep). Abbreviations: *d* dermis, *st* subcutaneous tissue, *ar* posterior acoustic reinforcement artifact

integrity of their walls and the presence of inflammation. Intact cysts present as well-defined, oval- or round-shaped, anechoic or hypoechoic structures that elicit a posterior reinforcement artifact typically seen in fluid-filled lesions (Fig. 4). Under inflammation the cysts become enlarged, and the keratinous material is mixed with inflammatory components which increase the echogenicity of the content and the peripheral blood flow. When the cysts are completely ruptured, they tend to show as an ill-defined, irregular, and hypoechoic structure that usually conserves the posterior reinforcement artifact and can show prominent peripheral vascularity. Occasionally, an anechoic connecting tract is observed between the cyst and the subepidermal region (Wortsman 2012a, b; Yuan et al. 2012).

Pilonidal Cysts

These are pseudocystic lesions commonly founded in the intergluteal area and composed of a nest of keratin and hair tract fragments. On sonography they appear as oval-shaped hypoechoic structures located in the dermis and subcutaneous tissue. Frequently, hyperechoic linear hair fragments are detected within the cysts (Fig. 5). Under inflammation pilonidal cysts may show increased peripheral vascularity with low-flow arterial and venous vessels. Hypoechoic tracts connecting to the base of the hair follicles are common findings. Sonography may also demonstrate the axis and branches of the cyst which may support surgical planning (Wortsman 2012a, b; Solivetti et al. 2012; Mentes et al. 2009).

Vascular Tumors

Hemangiomas

These are the most common soft tissue tumors in infancy. They present an abnormal growth of endothelial cells. Commonly they involve the dermis and subcutaneous tissue. Hemangiomas tend to show a fast postnatal growth, followed by a slow involution period. On sonography, the appearance varies according to the phase of the hemangioma. In the initial proliferative phase, they present as hypoechoic hypervascular solid masses with prominent arterial and venous vessels and occasionally arteriovenous shunts. During the partial involution phase, hemangiomas show mixed echogenicity with hypoechoic and hyperechoic areas (Fig. 6). The blood flow tends to sequentially decrease over time. In the total involution phase, hemangiomas show as hyperechoic and hypovascular masses. Sonography can detect both subcutaneous and deeper layers or organ involvement (Wortsman 2012a, b; Dubois et al. 1998; Paltiel et al. 2000).

Vascular Malformations

These are errors of morphogenesis and are composed by an abnormal amount of vascular

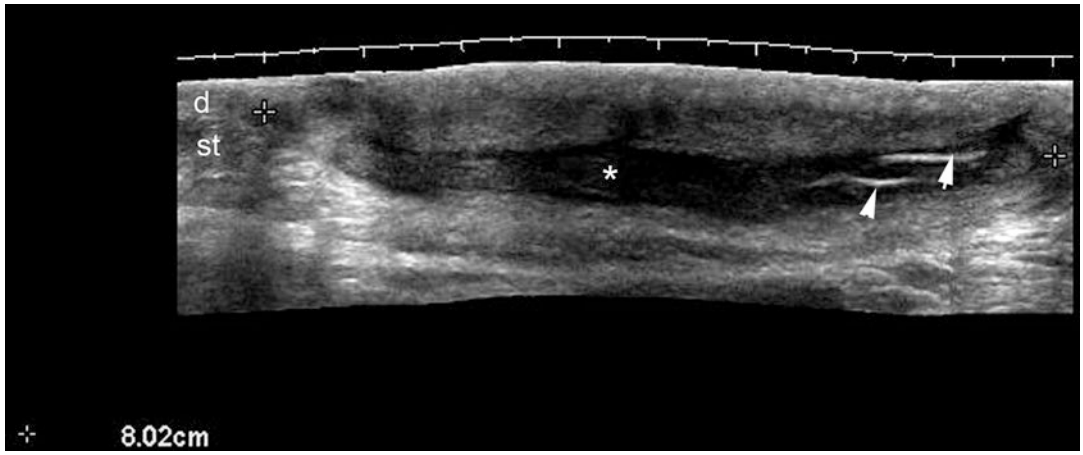

Fig. 5 Pilonidal cyst. Grayscale ultrasound (longitudinal view, intergluteal region) demonstrates 8.02 cm long dermal and subcutaneous hypoechoic structure (*, between markers) with hyperechoic lines that correspond to hair fragments (*arrows*). Abbreviations: *d* dermis, *st* subcutaneous tissue

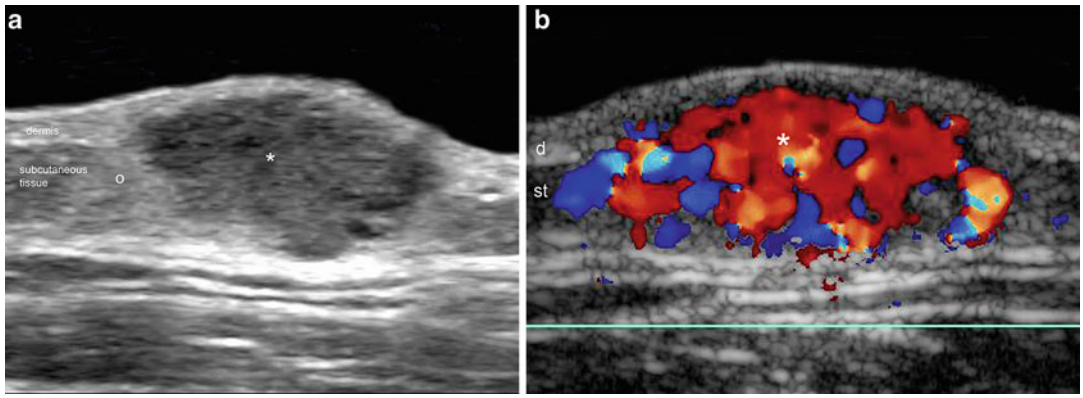

Fig. 6 Hemangioma (dorsal region). (**a**) Grayscale ultrasound (transverse view) shows an ill-defined, mixed echogenicity structure with hypoechoic (*) and hyperechoic (o) areas that involves the dermis and subcutaneous tissue. (**b**) Color Doppler ultrasound (longitudinal view) demonstrates prominent vascularity (colors) within the lesion

channels with normal endothelium. Usually they tend to grow in proportion with the child's growth. According to the type of channel, they can be classified into arterial, venous, lymphatic, or capillary. Also they can be separated according to the degree of vascularity into high (arterial or arteriovenous) or low (venous, lymphatic, or capillary) blood flow. There are also some mixed forms of vascular malformations. On sonography, they appear as nests of anechoic tubular or tortuous channels, hyperechoic islets, or anechoic pseudocystic structures. Spectral curve analysis can show the type of blood flow within the vascular tracts (arterial or venous) (Fig. 7). Additionally, sonography can rule out the presence of thrombus within the vessels which appears as hypoechoic content within these channels. In venous vascular malformations, hyperechoic calcium deposits, also called phleboliths, may be found (Wortsman 2012a, b; Paltiel et al. 2000).

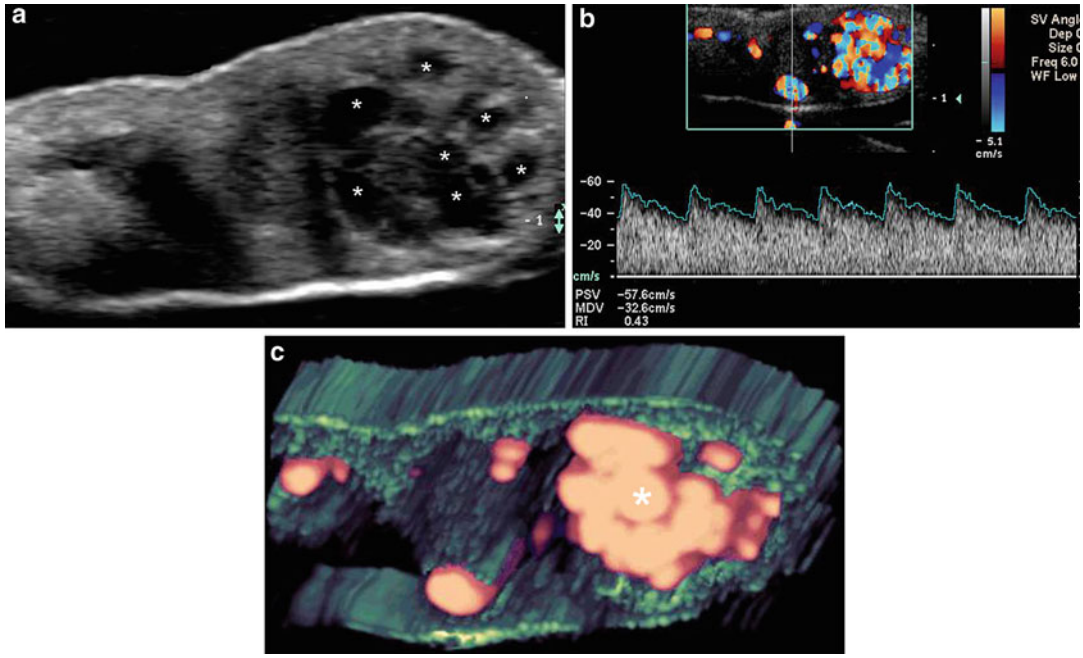

Fig. 7 High-flow arterial vascular malformation (transverse views, lobe of the left ear pinna). (**a**) Grayscale ultrasound demonstrates several anechoic tubular ducts and pseudocystic structures (*) in the subcutaneous tissue. (**b**) Color Doppler with spectral curve analysis shows high arterial flow (peak systolic velocity: 57.6 cm/s). (**c**) 3D power Doppler reconstruction demonstrates increased vascularity within the lesion (*)

Solid

Lipomatous Tumors

These are the most common soft tissue tumors and present as a proliferation of adipose cells that may be mixed with fibrous (fibrolipoma) or vascular (angiolipoma) tissue. Lipomas show a variable appearance on ultrasound according to the proportion of the histological components. Thus, fibrolipomas or simple lipomas tend to present as well-defined, oval-shaped hypoechoic solid subcutaneous masses that follow the axis of the skin layers (Fig. 8). Hyperechoic fibrous septa are commonly detected within the structure. In contrast angiolipomas tend to show as well-defined, round or oval-shaped hyperechoic structures in the subcutaneous tissue. Lipomas are usually hypovascular, and the finding of prominent vascularity within these lesions may give rise to the suspicion of atypical or malignant transformation (Wortsman 2012a, b; Fornage and Tassin 1991; Kuwano et al. 2009; Lee et al. 2011).

Hair Matrix-Derived Tumors

Pilomatrixomas

These hair matrix-derived tumors, also called epitheliomas of Malherbe, are most common in children and young adults. They are composed of a nest of lobules with basaloid and ghost cells, eosinophilic keratinous debris, and calcifications. Pilomatrixomas are surrounded by a fibrous pseudocapsule of connective tissue, and these tumors commonly involve the dermis and subcutaneous tissue. On sonography they show a wide range of appearances, the most common being the target type (hypoechoic rim and hyperechoic center) (Fig. 9). Other forms of presentation include the cystic type (anechoic and hypoechoic areas) and the completely calcified type (hyperechoic with posterior acoustic shadowing). In up to 80 % of the cases, hyperechoic calcium deposits are detectable within the tumors. Occasionally, pilomatrixomas can show prominent vascularity on color Doppler ultrasound (Hwang et al. 2005; Choo et al. 2010; Wortsman et al. 2010).

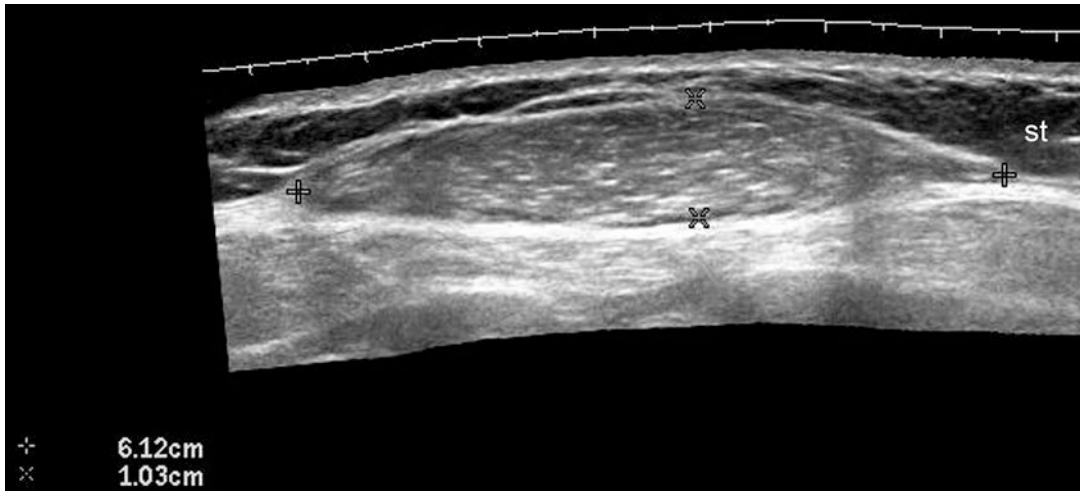

Fig. 8 Lipoma. Grayscale ultrasound (transverse view, right flank of the abdominal wall) shows 6.12 cm long × 1.03 cm wide, well-defined, oval-shaped hypoechoic mass (*) in the subcutaneous tissue

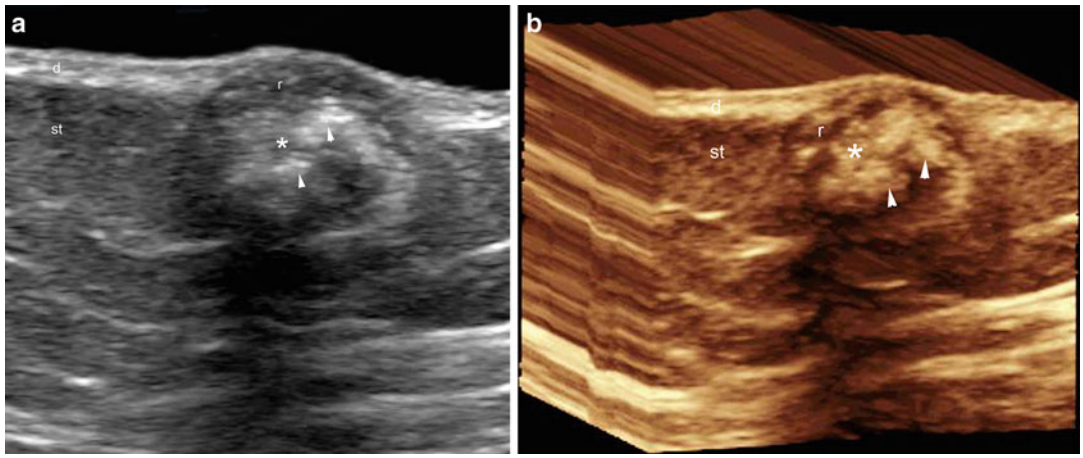

Fig. 9 Pilomatrixoma (longitudinal views, anterior aspect of the left leg). (**a**) Grayscale and (**b**) 3D reconstruction ultrasounds show dermal and subcutaneous, target-type structure with an hypoechoic rim (r) and hyperechoic center (*). Notice the hyperechoic spots (*arrowheads*) that correspond to calcium deposits. Abbreviations: *d* dermis, *st* subcutaneous tissue

5.2.2 Malignant

Melanoma Metastasis

On sonography, a locoregional staging of melanoma can be performed. Thus, secondary satellite (<2 cm from the primary lesion), in-transit metastasis (≥2 cm from the primary lesion), and lymph node metastasis can be detected. These metastases commonly involve the subcutaneous tissue and show as hypoechoic solid nodules that may present prominent vascularity (Fig. 10). Metastatic lymph nodes lose their hyperechoic center and show as round or oval-shaped hypoechoic structures. Commonly, anechoic areas due to hypercellularity (not necrosis) and tortuous and irregular vessels within the lymph nodes are observed (Gupta et al. 2011; Catalano et al. 2011).

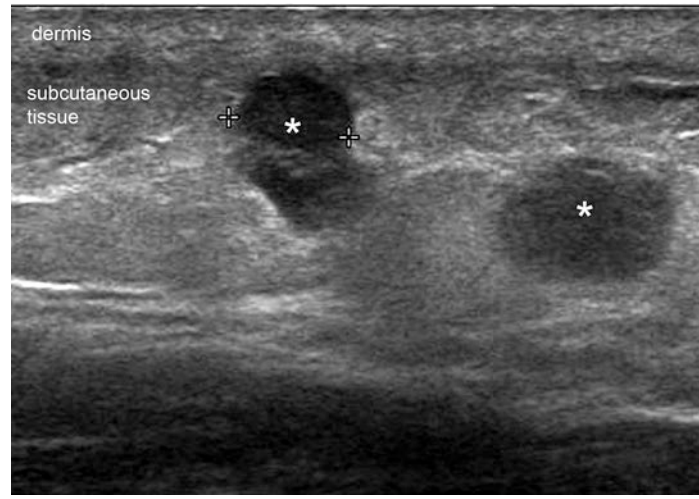

Fig. 10 In-transit metastasis of melanoma. Grayscale ultrasound (longitudinal view, posteromedial aspect of the left thigh) shows two well-defined, oval-shaped hypoechoic structures (*) in the subcutaneous tissue. Notice the increased echogenicity of the surrounding subcutaneous tissue secondary to regional edema

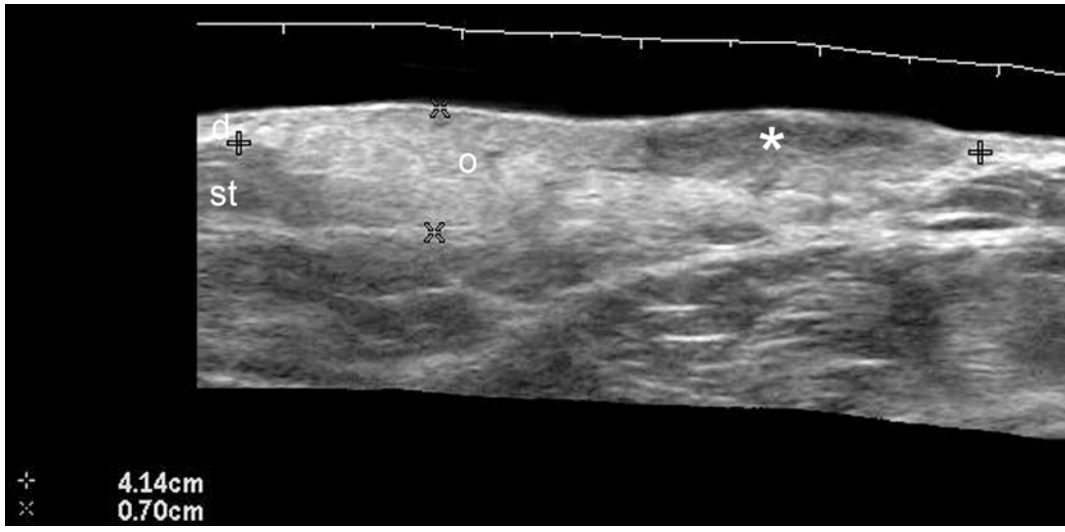

Fig. 11 Dermatofibrosarcoma protuberans. Grayscale ultrasound (longitudinal view, *left* arm) shows a 4.14 cm long × 0.7 cm depth, mixed echogenicity lesion (between markers) with hypoechoic (*) and hyperechoic pseudopodia-like (o) projections. Abbreviations: *d* dermis, *st* subcutaneous tissue

Dermatofibrosarcoma Protuberans

This locally aggressive cutaneous fibroblastic tumor mainly involves the trunk and proximal extremities of young and middle-aged adults. On histology, it shows a proliferation of spindle cells with elongated nuclei, with little or no pleomorphism. This malignant tumor commonly affects the dermis and subcutaneous tissue; however, it may also involve deeper layers. On sonography, the most common form of presentation is an ill-defined heterogeneous solid tumor with hypoechoic and hyperechoic areas that present lobulated borders with pseudopodia-like projections following a horizontal axis (Fig. 11). Slow flow vessels are frequently detected within the tumor (Oliveira-Soares et al. 2002; Shin et al. 2008).

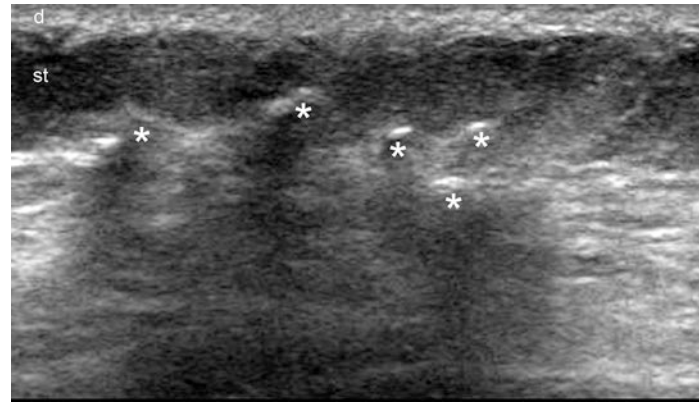

Fig. 12 Calcinosis. Grayscale ultrasound (longitudinal view, left flank of the abdominal wall) demonstrates hyperechoic spots (*) with posterior acoustic shadowing artifact. Abbreviations: *d* dermis, *st* subcutaneous tissue

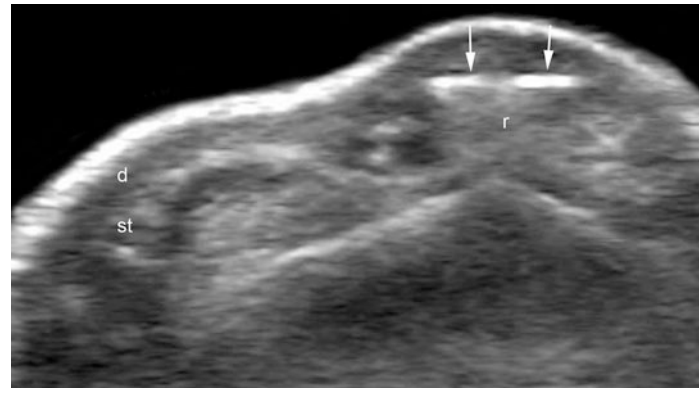

Fig. 13 Foreign body. Grayscale ultrasound (transverse view, dorsum of the right index finger) shows two hyperechoic linear fragments (*arrows*) that correspond to glass fragments and elicit posterior reverberation artifact (r). Abbreviations: *d* dermis, *st* subcutaneous tissue

5.3 Endogenous Material

5.3.1 Calcifications

Subcutaneous calcium deposits can be detected in several conditions such as inflammatory connective tissue diseases (e.g., secondary calcinosis) or associated with vascular malformations (phleboliths). The presence of gross heterotopic mature lamellar bone deposits in the subcutaneous tissue is named panniculitis ossificans (Wollina et al. 2009; Müller et al. 2010). The differentiation between isolated immature and mature lamellar bone is usually performed on histology. On sonography, calcium deposits appear as hyperechoic spots, and large-size calcium deposits commonly present a posterior acoustic shadowing artifact (Fig. 12).

5.4 Exogenous Material

5.4.1 Foreign Bodies

These are exogenous components usually accidentally embedded in the subcutaneous tissue. They can be separated according to their nature in organic (e.g., splinters of wood or thorns) or inert (e.g., fragments of glass and metal). On sonography they show as well-defined laminar or bilaminar hyperechoic structures surrounded by hypoechoic granulomatous tissue. Glass or metal fragments commonly produce a posterior reverberation artifact (Fig. 13). Ultrasound may support both the diagnosis and percutaneous extraction of the foreign structure (Wortsman 2012a; Bradley 2012).

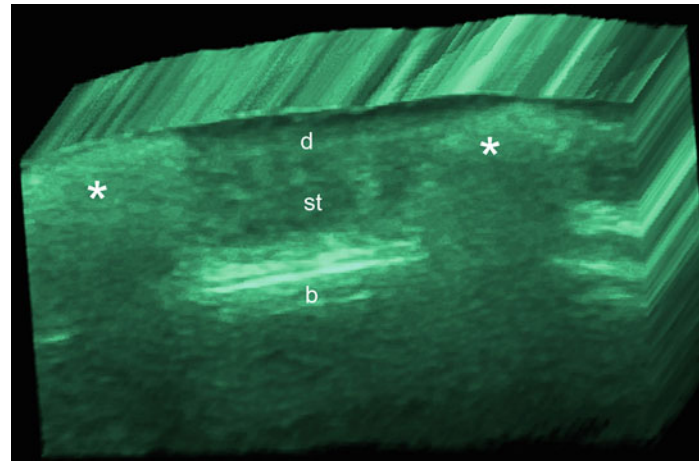

Fig. 14 Silicone oil. 3D reconstruction (transverse view, glabellar area, 5–8 s sweep) shows two hyperechoic deposits (*) in the dermis and subcutaneous tissue with posterior reverberation artifact. Abbreviations: *d* dermis, *st* subcutaneous tissue, *b* bony margin of the skull

5.4.2 Fillers

These compounds are used for cosmetic purposes and can be separated according to their characteristics into degradable, such as hyaluronic acid, and nondegradable, such as silicone oil, polymethyl methacrylate, calcium hydroxyapatite, and polyacrylamide. On sonography, these deposits are commonly found in the subcutaneous tissue and show different sonographic appearances. Thus, hyaluronic acid presents as small round or oval-shaped anechoic pseudocysts that decrease in size over time (3–6 months), usually becoming undetectable or barely detectable after 6 months. Silicone oil is not FDA approved but may be used off-label in some countries. It shows as hyperechoic deposits with posterior acoustic reverberation artifacts (Fig. 14). Polymethyl methacrylate appears as multiple bright hyperechoic dots that elicit a mini comet-tail artifact (small posterior reverberation artifact). Calcium hydroxyapatite presents as hyperechoic deposits with posterior acoustic shadowing artifacts. Polyacrylamide shows as well-defined medium- or large-size anechoic pseudocystic structures with increased echogenicity of the surrounding subcutaneous tissue. The latter polyacrylamide deposits have been reported to not modify their appearance for at least 18 months (Wortsman et al. 2012; Wortsman and Wortsman 2011, 2012).

6 Conclusion

Sonography can show with high definition the anatomical characteristics of a wide range of dermatologic and non-dermatologic conditions that affect the subcutaneous tissue. It allows measurement of the abnormalities in all axes in real time, demonstrating their vascularity patterns and giving a noninvasive insight into the pathophysiology of the subcutaneous entities.

References

Bradley M. Image-guided soft-tissue foreign body extraction – success and pitfalls. Clin Radiol. 2012;67:531–4.

Catalano O, Voit C, Sandomenico F, Mandato Y, Petrillo M, Franco R, Botti G, Caracò C, Mozzillo N, D'Errico AG. Previously reported sonographic appearances of regional melanoma metastases are not likely due to necrosis. J Ultrasound Med. 2011;30:1041–9.

Choo HJ, Lee SJ, Lee YH, Lee JH, Oh M, Kim MH, Lee EJ, Song JW, Kim SJ, Kim DW. Pilomatricomas: the diagnostic value of ultrasound. Skeletal Radiol. 2010;39:243–50.

Dubois J, Patriquin HB, Garel L, et al. Soft tissue hemangiomas in infants and children: diagnosis using Doppler sonography. Am J Roentgenol. 1998;171:247–52.

Dudea SM, Lenghel M, Botar-Jid C, Vasilescu D, Duma M. Ultrasonography of superficial lymph nodes: benign vs. malignant. Med Ultrason. 2012;14:294–306.

Ebling FJG, Eady RAJ, Leigh IM. Anatomy and organization of human skin. In: Rook AJ, Wilkinson DS, Ebling

FJG, editors. Textbook of dermatology. Oxford: Blackwell Scientific Publications; 1992. p. 49.
Ester AH, Carolyn RA, Ximena WC, Yamile CS, Dafne SV, Gabriela SB, et al. Newborn fat necrosis: case-report. Rev Chil Pediatria. 2009;80:60–4.
Fornage BD, Tassin GB. Sonographic appearances of superficial soft tissue lipomas. J Clin Ultrasound. 1991;19:215–20.
Gupta A, Rahman K, Shahid M, Kumar A, Qaseem SM, Hassan SA, Siddiqui FA. Sonographic assessment of cervical lymphadenopathy: role of high-resolution and color Doppler imaging. Head Neck. 2011;33:297–302.
Hwang JY, Lee SW, Lee SM. The common ultrasonographic features of pilomatricoma. J Ultrasound Med. 2005;24:1397–402.
Kuwano Y, Ishizaki K, Watanabe R, Nanko H. Efficacy of diagnostic ultrasonography of lipomas, epidermal cysts, and ganglions. Arch Dermatol. 2009;145:761–4.
Lee JY, Kim SM, Fessell DP, Jacobson JA. Sonography of benign palpable masses of the elbow. J Ultrasound Med. 2011;30:1113–9.
Mentes O, Oysul A, Harlak A, Zeybek N, Kozak O, Tufan T. Ultrasonography accurately evaluates the dimension and shape of the pilonidal sinus. Clinics (Sao Paulo). 2009;64(3):189–92.
Müller CS, Rass K, Tilgen W. Panniculitis ossificans non-traumatica of the scalp. J Cutan Pathol. 2010;37:703–4.
Oliveira-Soares R, Viana I, Vale E, Soares-Almeida LM, Picoto A. Dermatofibrosarcoma protuberans: a clinicopathological study of 20 cases. J Eur Acad Dermatol Venereol. 2002;16:441–6.
Paltiel HJ, Burrows PE, Kozakewich HPW, Zurakowski D, Mulliken JB. Soft tissue vascular anomalies: utility of US for diagnosis. Radiology. 2000;214:747–54.
Requena L, Sánchez YE. Panniculitis. Part II. Mostly lobular panniculitis. J Am Acad Dermatol. 2001;45:325–61.
Requena L, Yus ES. Panniculitis. Part I. Mostly septal panniculitis. J Am Acad Dermatol. 2001;45:163–83.
Ryu JK, Jin W, Kim GY. Sonographic appearances of small organizing hematomas and thrombi mimicking superficial soft tissue tumors. J Ultrasound Med. 2011;30(10):1431–6.
Shin YR, Kim JY, Sung MS, Jung JH. Sonographic findings of dermatofibrosarcoma protuberans with pathologic correlation. J Ultrasound Med. 2008;27:269–74.
Solivetti FM, Elia F, Panetta C, Teoli M, Bucher S, Di Carlo A. Preoperative advantages of HF sonography of pilonidal sinus. G Ital Dermatol Venereol. 2012;147:407–11.
Wollina U, Koch A, Schönlebe J, Witzigmann H, Kittner T. Panniculitis ossificans of the lower leg. Int J Low Extrem Wounds. 2009;8:165–8.
Wortsman X. Common applications of dermatologic sonography. J Ultrasound Med. 2012a;31:97–111.
Wortsman X. Sonography of cutaneous and ungual lumps and bumps. Ultrasound Clin. 2012b. doi:10.1016/j.cult.2012.08.006.
Wortsman X, Wortsman J. Clinical usefulness of variable frequency ultrasound in localized lesions of the skin. J Am Acad Dermatol. 2010;62:247–56.
Wortsman X, Wortsman J. Sonographic outcomes of cosmetic procedures. AJR Am J Roentgenol. 2011;197:W910–8.
Wortsman X, Wortsman J. Polyacrylamide fillers on skin ultrasound. J Eur Acad Dermatol Venereol. 2012;26:660–1.
Wortsman X., Holm EA, Jemec GBE. Ultrasound imaging of the subcutaneous tissue and adjacent structures, Chapter 2.9.11, In: Wortsman X, Holm EA, Jemec GBE, editors. Handbook of non-invasive methods and the skin, 2nd ed. Boca Raton, Taylor and Francis 2nd Ed, 2006. p. 515–30.
Wortsman X, Wortsman J, Arellano J, Oroz J, Giugliano C, Benavides MI, Bordon C. Pilomatrixomas presenting as vascular tumors on color Doppler ultrasound. J Pediatr Surg. 2010;45:2094–8.
Wortsman X, Wortsman J, Orlandi C, Cardenas G, Sazunic I, Jemec GBE. Ultrasound detection and identification of cosmetic fillers in the skin. J Eur Acad Dermatol Venereol. 2012;26:292–301.
Yuan WH, Hsu HC, Lai YC, Chou YH, Li AF. Differences in sonographic features of ruptured and unruptured epidermal cysts. J Ultrasound Med. 2012;31:265–72.

Cellulite: Definition and Evaluation

69

Doris Hexsel and Mariana Soirefmann

Contents

Keywords
Cellulite • Camera settings • Classification of Cellulite • Definition of Cellulite • Photografic documentation • Ultrasound • Magnetic resonance imaging (MRI) • Laser Doppler Flowmetry (LDF) • Pinch test • Thermography

1 Introduction

Cellulite is characterized by dimpled or puckered skin of the buttocks and posterior and lateral thighs. This condition has also been described as resembling an orange peel and cottage cheese or as having mattress-like appearance (Hexsel et al. 2010a; Hexsel and Soirefmann 2011) (Fig. 1).

Published studies suggest that approximately 85 % of postadolescent women have some degree of cellulite (Draelos and Marenus 1997; Harvard Women's Health Watch Cellulite meltdown 1998). In men, this condition is very rare as the result of differences in the connective tissue (Hexsel et al. 2010a).

According to Scherwitz and Braun-Falco (Khan et al. 2010), it was Alquier and Paviot who first described cellulite, in 1920, as a noninflammatory, complex cellular dystrophy of the mesenchymal tissue, where defects in water

D. Hexsel (✉)
Brazilian Center for Studies in Dermatology, Department of Dermatology, Pontificia Universidade Catolica do Rio Grande do Sul (PUC-RS), Porto Alegre, RS, Brazil
e-mail: doris@hexsel.com.br

M. Soirefmann
Dermatology Department, Pontificia Universidade Catolica do Rio Grande do Sul (PUC-RS), Porto Alegre, Brazil

P. Humbert et al. (eds.), *Agache's Measuring the Skin*,
DOI 10.1007/978-3-319-32383-1_97

Fig. 1 Depressed lesions of cellulite on the buttocks and upper thighs, with mattress-like appearance

metabolism led to saturation of adjacent tissues by interstitial liquids as a result of traumatic, topical infectious, or glandular stimuli.

Synonyms of cellulite include adiposis edematosa, incipient cellulite or status protusus cutis, full-blown cellulite or dermopanniculosis deformans, nodular liposclerosis, gynoid lipodystrophy, and edematofibrosclerotic panniculopathy (Khan et al. 2010).

2 Definition

Cellulite is defined as a localized metabolic disorder of subcutaneous tissue that provokes an alteration in the female body shape. It presents as a modification of skin topography evident by skin dimpling and nodularity. This condition occurs mainly in women on the pelvic region, lower limbs, and abdomen (Khan et al. 2010).

Cellulite usually presents after puberty and tends to be chronic (Hexsel et al. 2009a). While it is a common clinical condition affecting the majority of women of all countries and cultures, it is thought of as a female secondary sex characteristic (Khan et al. 2010; Hexsel et al. 2009a). Cellulite is rarely found in men (Hexsel et al. 2009a).

Differences in subcutaneous tissue architecture between men and women may explain the female sex predominance of this condition (Nürnberger and Müller 1978). Cellulite appears to be the result of localized adipose deposits and edema within the subcutaneous tissue. In women, bands of connective tissue are oriented longitudinally, from deep fascia to the dermis. These bands are the fibrous septae that segregate fat into channels. As the fat layer expands, it occurs herniation of subcutaneous fat within fibrous connective tissue, leading to a puckered appearance of the skin (Khan et al. 2010; Querleux et al. 2002; Piérard et al. 2000). The criss-crossing pattern of the connective tissue in the thighs and buttocks of men, which holds the fat layer, prevents the projection of the adipose tissue on the skin surface (Querleux et al. 2002; Piérard et al. 2000).

Different morphological patterns may be seen in cellulite patients. The skin surface alterations are mainly lower than the normal adjacent skin, but raised areas can also be seen. Depressed lesions occur because of the presence of fibrous septa that pull the skin surface down, and raised areas are the projection of underlying fat to the skin surface (Hexsel 2001).

Results of the magnetic resonance imaging analysis showed that cellulite depressions on the buttocks were significantly associated with the presence of underlying thick fibrous septa. It was found that all fibrous septa in the examined areas were perpendicular to the skin surface, and most of them were ramified (Hexsel and Soirefmann 2011; Hexsel et al. 2009b).

With aging and consequent increased laxity of the skin, the depressed lesions became more evident, as well as more linear or oval, following the skin lines and giving the skin a draped appearance (Hexsel et al. 2009b).

Regarding the importance of body weight, cellulite is not specific to overweight females, but added weight may cause enlargement of the fat lobules, further protrusion into the dermis, and exacerbation of this condition (Smalls et al. 2005).

3 Evaluation

The evaluation of a patient with cellulite may be done most of the times on clinical examination and sometimes using image exams.

Patients with cellulite should be evaluated in standing position with relaxed muscles, in order to correctly identify depressions of cellulite that are clearly apparent, independently of pinch test or muscular contraction (Hexsel and Mazzuco 2000). A pinch test can be done to make the lesions more evident (Fig. 2).

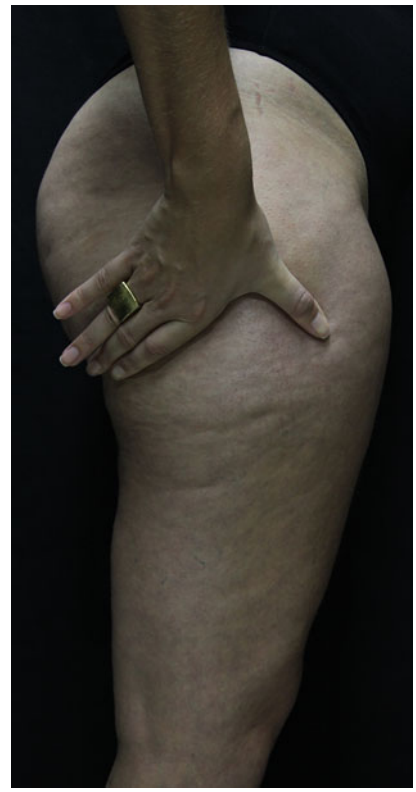

Fig. 2 Pinching the skin or pressing the affected areas can make cellulite lesions more evident

Digital photographs should always be taken before and after treatments. It is very important that these photographs follow the same standards, including light patterns, position, and camera settings (Figs. 3a-d) (Hexsel et al. 2001).

Gherardini et al. published a study that described the proper lighting, equipment, and backgrounds necessary to achieve standardization in photography for body contour surgery. General principles for clinical photography were reviewed, and the authors presented some consistent recommendations for photographic documentation of skin "textural" changes and "cellulite," allowing comparison of results and techniques (Gherardini et al. 1997). Khavkin et al. also highlighted the fact that standardized, high-quality images can be achieved by using proper equipment, lighting, and patient positioning (Khavkin and Ellis 2011). Persichetti et al. defined guidelines for accurate image capture in different anatomic areas, in order to obtain reasonable standardization, consistency, and reproducibility. The authors highlighted some important items (Persichetti et al. 2007), such as the following:

1. Background: The background must be an even, nonreflecting, monochromatic surface. A white or light blue drape can be held behind the patient by an assistant. Patient must be positioned 50–90 cm from the background.
2. Camera Settings: Single-lens reflex camera (SLR) digital camera is excellent for photographing, and it has a fixed focal length of 35–70 mm that guarantees an undistorted image, considering that the focal length of the human eye is 50 mm.
3. Position: The patient must be positioned at a distance from the camera, which varies the extent of the anatomic site to be included in

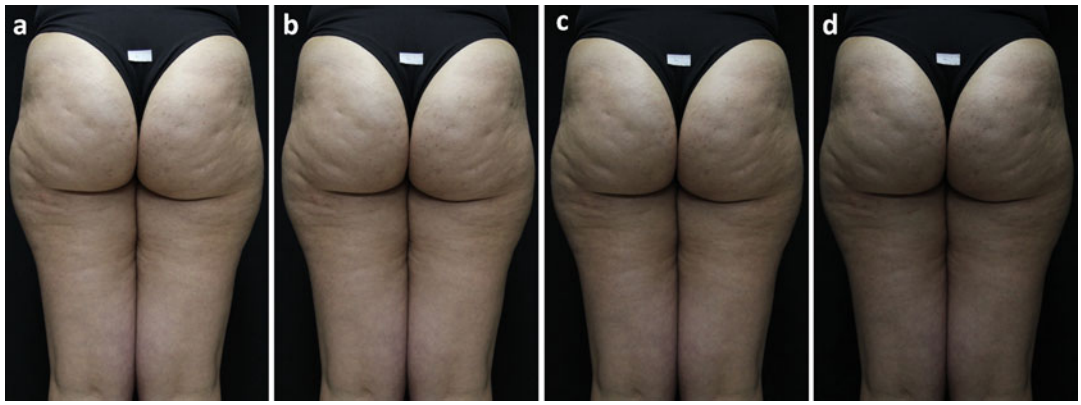

Fig. 3a-d A series of pictures of the same patient, in the same studio with the same lightning, but different camera settings

the picture. Generally, it is advisable to maintain the camera more than 1 m away from the patient, taking advantage of the zoom. The zoom is a type of lens that allows the operator to vary the focus, and only the optical zoom should be used when it is necessary to capture details (Persichetti et al. 2007).

4. Illumination: An adequate illumination must guarantee optimal definition of anatomic details and must be reproducible. In a photograph studio, lights are fixed which is certainly advantageous. Therefore, it is important to follow these items: two lamps at 45° with respect to the patient on a plane parallel to the frontal one. One of these lights should be in a sagittal plane, perpendicular to the frontal one, aiming downward. The other light should be behind the patient, on a plane parallel to the frontal one, aiming forward. This second lamp is placed at a distance 30–60 cm from the background. A "cold light" is always preferable (Persichetti et al. 2007). Other authors also highlight that an adequate illumination of the exam room with a light source in a downward position is helpful to visualize cellulite depressed lesions (Hexsel and Mazzuco 2000; Hexsel et al. 2010b).

There are a few devices in the market that were designed for photographic documentation of cellulite. These include the Vectra XT1® and IntelliStudio® systems, both from Canfield Scientific, Inc (USA). The Vectra XT1 is a three-dimensional camera system, with ultra high-resolution color image capture to produce a razor sharp definition of the smallest details. IntelliStudio® is a photo studio that makes consistent clinical quality photography, with fast and easy positioning to get the right view pre-op, and again to match it in the post-op session.

Recently, image exams may be indicated for cellulite adjunctive evaluation. The image exams may be used for research purposes or for special study of an individual case.

Ultrasound can be used to study the thickness and the quality of the connective tissue. This device may also be used to visualize the edematous component of cellulite (Biefeldt et al. 2008). Ultrasound imaging of the skin affected by cellulite reveals thinning of the dermis with subcutaneous fat pushing upward, which translates into the rumpled skin known as cellulite (Draelos 2005). Another study using a 20 MHz ultrasound shows that the frequency

of adipose protrusions into the dermis correlates with visual cellulite severity (Biefeldt et al. 2008).

Magnetic resonance imaging (MRI) allows visualization of specific changes in subcutaneous architecture caused by cellulite. This technique is able to show clearly images of the skin fat layers beneath the dermis and down to the level of muscles as well as to quantify herniations of adipose tissue into the dermis. Therefore, it is a good method to evaluate cellulite in clinical trials (Biefeldt et al. 2008) and also to determine anatomical features of cellulite (Hexsel et al. 2009b) (Fig. 4).

Laser Doppler flowmetry (LDF) is an optical technique used to evaluate the skin microcirculation which provides information on blood flow and erythema. The radiation is reflected by the skin and converted to electrical signal, which is proportional to the flux of erythrocytes of the blood flow. Therefore, it consists in a reliable method to estimate cutaneous microcirculation (Biefeldt et al. 2008).

Thermography is an effective technique to evaluate local skin temperature, and it is based on the detection of infrared radiation emitted by skin. Areas affected by cellulite present less local skin blood flow, consequently presenting lower temperatures (Biefeldt et al. 2008).

Newly, a thermal infrared camera was proposed as a reproducible method to assess the severity of cellulite. The conclusion of the study pointed out that the thermal camera can be used to reliably document the changes in the skin temperature that are related to the presence and the severity of cellulite (Nkengne et al. 2013). Further studies using image and thermal devices are necessary in order to improve the complementary evaluating and knowledge of this condition.

Patients should be classified regarding their degree of cellulite. This is important to determine the more appropriate treatment and to monitor treatment improvement. Two classifications of cellulite are currently used. The first is made on clinical basis (Table 1) (Hexsel and Mazzuco 2000).

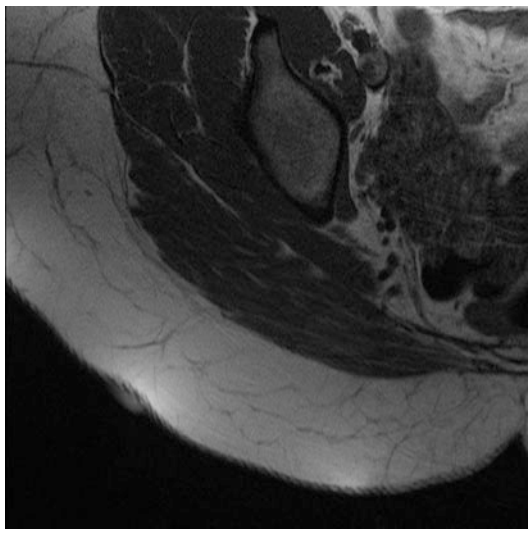

Fig. 4 MRI image of the buttock showing a skin marker on a depressed lesion of cellulite and its correspondent fibrous septa. MRI can be also used to study fat tissue in areas with cellulite

Table 1 Classification of cellulite based on clinical criteria (Nürnberger and Müller 1978)

Grade or stage	Clinical characteristics
0 (zero)	There is no alteration to the skin surface
I	The skin of the affected area is smooth while the subject is standing or lying, but the alterations to the skin surface can be seen by pinching the skin or with muscle contraction
II	The orange skin or mattress appearance is evident when standing, without the use of any manipulation (skin pinching or muscle contraction)
III	The alterations described in grade or stage II are present together with raised areas and nodules

Table 2 Hexsel and Dal'Forno and Hexsel e Cellulite Severity Scale (CSS) (Hexsel et al. 2009a)

(A) Number of evident depressions
This item refers to the total number of evident depressions by visual inspection in the area to be examined. The scores are expressed as:
ZERO = None/no depressions
1. A small amount: 1–4 depressions are visible
2. A moderate amount: 5–9 depressions are visible
3. A large amount: 10 or more depressions are visible
(B) Depth of depressions
This item evaluates the depth of depressions by visual inspection of the affected areas; comparison to the pictures of CSS is recommended
ZERO = No depressions
1. Superficial depressions
2. Medium depth depressions
3. Deep depressions
(C) Morphological appearance of skin surface alterations
Item C assesses the different morphological patterns of skin surface alterations; comparison with the pictures of CSS is recommended
ZERO = No raised areas
1. "Orange peel" appearance
2. "Cottage cheese" appearance
3. "Mattress" appearance
(D) Grade of laxity, flaccidity, or sagging skin
Laxity, flaccidity, or sagging skin confers the affected skin a draped appearance. This effect aggravates the appearance of cellulite. Item D assesses the grade of flaccidity, and comparison to the pictures of CSS is recommended
ZERO = Absence of laxity, flaccidity, or sagging skin
1. Slight draped appearance
2. Moderate draped appearance
3. Severe draped appearance
(E) First cellulite classification described by Nürnberger and Müller (1978)
This item incorporates the first classification of cellulite, shown in Table 1. Patients should be evaluated in the standing position with relaxed gluteus muscles. However, if the patient has no evident depressions, they should be asked to contract their gluteus muscles or the *pinch test* should be applied (by pinching the skin between the thumb and index finger) in order to differentiate between scores zero and 1
ZERO = Zero grade
1. First grade
2. Second grade
3. Third grade

Table 3 New classification of cellulite based on the results of scores of Cellulite Severity Scale

Points	New classification of cellulite
1–5	Mild
6–10	Moderate
11–15	Severe

Although this classification is useful, it does not attend to important additional morphologic aspects of cellulite (i.e., laxity) and is not the ideal for assessing treatment response. Hexsel, Dal'Forno, and Hexsel published a new cellulite classification (Hexsel et al. 2009a), based on a new scale in which important clinical and morphological aspects of cellulite are assessed. The scale is called *Hexsel* and *Dal'Forno* and Cellulite Severity Scale (Hexsel et al. 2009a) and is shown in Table 2. It is an alpha-photonumeric scale that grades cellulite on basis of five items: (A) number of evident depressed lesions, (B) depth of depressions, (C) morphologic appearance of skin surface alterations, (D) grade of flaccidity or sagging skin, and (E) cellulite classification by Nürnberger and Müller. Each of these items is graded from zero to three. The sum of these scores will lead to a new classification of the cellulite as mild, moderate, or severe, as shown in Table 3.

The publication of *Hexsel* and *Dal'Forno* and *Hexsel* Cellulite Severity Scale (Hexsel et al. 2009a) was of great value in the evaluation of cellulite patients, since this new classification included different aspects of cellulite lesions and additional morphologic characteristics (i.e., laxity) (Fig. 5).

References

Biefeldt S, Buttgereit P, Brandt M, et al. Non-invasive evaluation techniques to quantify the efficacy of cosmetic anti-cellulite products. Skin Res Technol. 2008;14(3):336–46.

Draelos DZ. The disease of cellulite. J Cosmet Dermatol. 2005;4:221–2.

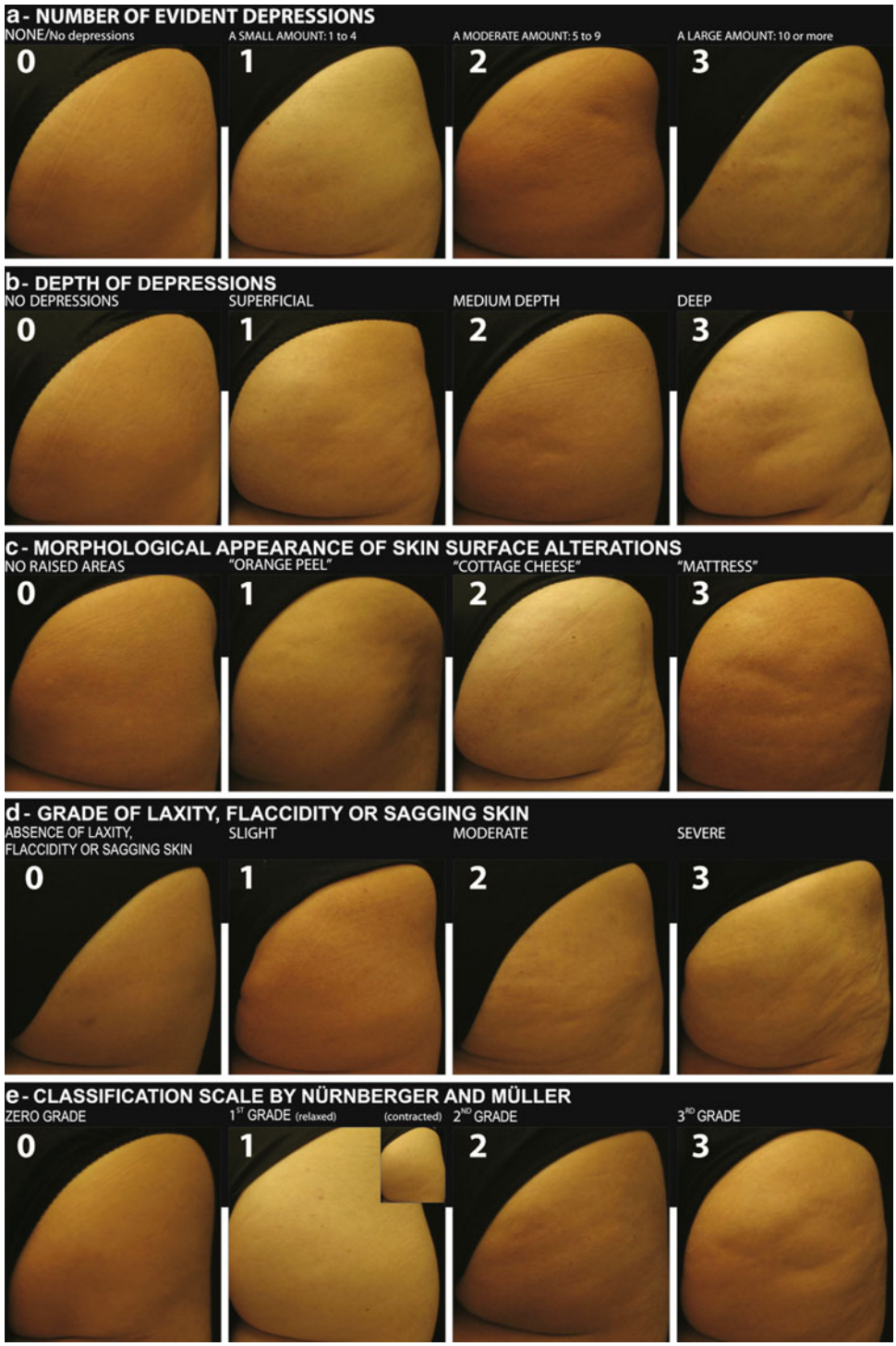

Fig. 5 Hexsel and Dal'Forno and Hexsel Cellulite Severity Scale (*CSS*) (Hexsel et al. 2009a)

Draelos ZD, Marenus KD. Cellulite. Etiology and purported treatment. Dermatol Surg. 1997;23(12):1177–81.

Gherardini G, Matarasso A, Serure AS, et al. Standardization in photography for body contour surgery and suction-assisted lipectomy. Plast Reconstr Surg. 1997;100(1):227–37.

Harvard Women's Health Watch Cellulite meltdown. Harv Health Pub Group. 1998;5:7.

Hexsel DM. Body repair. In: Parish LC, Brenner S, Ramos-e-Silva M, editors. Women's dermatology from infancy to maturity. New York: Parthenon Publishing; 2001. p. 586–95.

Hexsel DM, Mazzuco R. Subcision: a treatment for cellulite. Int J Dermatol. 2000;39(7):539–44.

Hexsel D, Soirefmann M. Cosmeceuticals for cellulite. Semin Cutan Med Surg. 2011;30(3):167–70.

Hexsel DM, Siega C, Schilling-Souza J, et al. A bipolar radiofrequency, infrared, vacuum and mechanical massage device for treatment of cellulite: a pilot study. J Cosmet Laser Therapy. 2001;13(6):297–302.

Hexsel DM, Dal'Forno T, Hexsel CL. A validated photonumeric cellulite severity scale. J Eur Acad Dermatol Venereol. 2009a;23(5):523–8.

Hexsel DM, Abreu M, Rodrigues T, et al. Side-by-side comparison of areas with and without cellulite depressions using magnetic resonance imaging. Dermatol Surg. 2009b;35:1–7.

Hexsel D, Zechemeister do Prado D, Goldman MP. Topical management of cellulite. In: Goldman M, Hexsel D, editors. Cellulite: pathophysiology and treatment. London: Informa Health Care; 2010a. p. 62–8.

Hexsel D, Dal'Forno T, Soirefmann M, Hexsel C. Reduction of cellulite with subcision. In: Murad A, Pongprutthipan M, editors. Body rejuvenation. New York: Taylor and Francis; 2010b. p. 167–72.

Khan MH, Victor F, Rao B, et al. Treatment of cellulite Part I. Pathophysiology. J Am Acad Dermatol. 2010;62(3):361–70.

Khavkin J, Ellis DAF. Standardized photography for skin surface. Facial Plast Surg N Am. 2011;19(2):241–6.

Nkengne A, Papillon A, Bertin C. Evaluation of the cellulite using a thermal infra-red camera. Skin Res Technol. 2013;19(1):231–7.

Nürnberger F, Müller G. So-called cellulite: an invented disease. J Dermatol Surg Oncol. 1978;4(3):221–9.

Persichetti P, Simone P, Langella M, Marangi GF, Carusi C. Digital photography in plastic surgery: how to achieve reasonable standardization outside a photographic studio. Aesth Plast Surg. 2007;31(2):194–200.

Piérard GE, Nizet JL, Piérard-Franchimont C. Cellulite: from standing fat herniation to hypodermal stretch marks. Am J Dermatopathol. 2000;22(1):34–7.

Querleux B, Cornillon C, Jolivet O, et al. Anatomy and physiology of subcutaneous adipose tissue by in vivo magnetic resonance imaging and spectroscopy: relationships with sex and presence of cellulite. Skin Res Technol. 2002;8:118–24.

Smalls LK, Lee CY, Whitestone J, et al. Quantitative model of cellulite: three dimensional skin surface topography, biophysical characterization and relationship to human perception. J Cosmet Sci. 2005;56:105–20.

Practical Surface Anthropometry

70

Shahram F. Mevaloo

Contents

Keywords

Surface anthropometry • Skinfold • Girth • Breadth • Body mass index (BMI) • Waist-to-hip ratio (WHR) • Percent of body Fat (PBF) • Body frame size

1 Basic Concepts

Anthropometry is defined as "measurement of the human body and its dimensions." Surface anthropometry involves measurements of body mass, stature, skeletal breadths, limb lengths, circumferences and skinfold thicknesses that are used, either as raw data or predicted values, to describe concepts such as absolute and body frame size, body composition, and body surface area (Stewart and Eston 2007). Anthropometry is a multidisciplinary science and has revelations with other sciences such as anatomy, physiology, medicine, and nutrition. Historically, the main concern in surface anthropometry has been the standardization of measurements. During the past 50 years, several researchers and organizations attempt to achieve universal recognition and provide international standards in anthropometry (Lohman et al. 1988; Norton and Olds 1996). This chapter is based on the latest standards of the International Society for the Advancement of Kinanthropometry (ISAK) (ISAK 2011), and its purpose is to present key principles, methods, and equipment for measuring the most commonly used anthropometric variables.

S.F. Mevaloo (✉)
Health Studies Group, Center for Strategic Research, I.R.I Ministry of Sport and Youth, Tehran, Iran
e-mail: sfaradjzadeh@yahoo.com

P. Humbert et al. (eds.), *Agache's Measuring the Skin*,
DOI 10.1007/978-3-319-32383-1_155

2 Standard Equipment

Stadiometer: (e.g., Holtain, SECA) mounted on wall or stand with sliding headboard and accurate to 1 mm. The stadiometer should be checked every month or after measuring 30 subjects, against a standard height.

Weighing scales: portable beam balance machine, calibrated in kilograms and tenths of kilograms (150 kg) (e.g., SECA). The electronic digital scales is becoming more general and is of the same accuracy.

Skinfold calipers: Harpenden or Slim Guide Skinfold Calipers calibrated to 10 $g \cdot mm^{-2}$, scale to 80 mm, which can be read to 0.1 mm and 0.5 mm, respectively. Holtain calipers have similar quality and can be used with equal precision.

Anthropometric tape: metal, with a stub extending 6–10 cm beyond the zero line (blank area). The Lufkin W606PM and its modified version Rosscraft anthropometric tape and CESCORF anthropometric tape are the preferred instrument for performing girth techniques. All can be read to 0.1 cm.

Segmometer: a flexible metal tape with rigid sliding branches for identifying lengths and landmark locations (Rosscraft), read to 1 mm.

Bone calipers: Tommy 2, Tommy 3, and Bonimeter 1 are good examples of bone calipers with extended branches and round pressure plates 15 mm in diameter.

3 Standard Methodology

3.1 Common Prerequisites

There are some important considerations for surface anthropometry measurements:

- Subjects require appropriate information in advance, and informed written consent should be obtained.
- Ensure that the physical space is large enough (3 × 3 m) and illuminated to allow the measurer moving freely, considering personal space (front space of the body of subject) and privacy of the subject.
- Subjects should be recovered from previous exercise, fully hydrated, and voided.
- Subjects should be asked to present themselves in minimal clothing. Swimsuits (two-piece suits for female subjects) are recommended.
- Cultural differences may preclude the acquisition of some or all measurements in some subjects. Measurement of females or children by male measures requires particular sensitivity and the individual's entitlement to a chaperone. It is always advisable to have another adult (preferably female) present in such circumstances.

3.2 Stature

Stature is measured to 1 mm without any footwear. The subject stands with head level, looking straight ahead, and the heels together. The subject inspires for measurement, and the recorder brings down the headboard to compress the hair.

3.3 Body Mass

Body mass is measured to 100 g. Clothing is also an issue, and the type and amount of clothing must be standardized. Body mass changes at various times of the day as a result of meal and beverage consumption, urination, defecation, and dehydration, or water loss. Therefore, a standard time (e.g., early in the morning, 12 h after any food and after voiding) is recommended.

3.4 Skinfolds

Skinfolds are the most commonly measured anthropometric sites in surface anthropometry. They are very good representative of level of fatness and subcutaneous fat storage in the body. To measure them, measurer needs to landmark at first. In fact, accurately landmarking is one of the vital aspects of good anthropometric measurement. A sound knowledge of surface anatomy is essential. Skeletal landmarks are the reference

points and must be located in the same procedure to guarantee reproducible measurements. Skinfold locations are marked with across, with two lines intersecting at right angles. A longer line shows the orientation of the skinfold, and the shorter one defines the finger and thumb placement. Bony edges are commonly marked with a short (0.5 cm) line, while points (e.g., the inferior tip of the scapula) are marked with a dot, from which linear measurements are made. A description of very common landmarks is summarized in Table 1.

Measurements of skinfold thicknesses should be made on the *right* side of the body. Skin of the subject should be dry, nongreasy, and healthy. The skinfold is raised by the left hand, which is positioned so that the thumb points downward and the back of the hand is in full view of the measurer. The fold is grasped firmly in the appropriate orientation, following the natural lines of the skin (*Langer's lines*), and raised far enough (but no further) so the fold has parallel sides. The measurer should use the thumb and index finger of the left hand to raise a fold that contains a double layer of both adipose tissue and skin. In order to eliminate muscle, good palpation technique guarantees a double layer of both adipose tissue and skin. The caliper jaws are applied 1 cm away from the thumb and index finger (fold), at a depth of mid-fingernail. It is important to hold the fold throughout the measurement procedure (Fig. 1).

The calipers are held perpendicular to the skinfold, the spring pressure is released, and the measurement value recorded after 2 s. The calipers are removed before the skinfold is released. Common skinfold sites are described in Table 2.

Table 1 Skeletal landmarks and the related skinfolds

Landmarks	Description
Mid-acromiale-radiale	*Midpoint level between the most lateral point in the superior border of the acromion process in the midway between the anterior and posterior border of the deltoid muscle (acromiale) and the point at the most upper and lateral border of the head of the radius bone (radiale) (triceps skinfold and biceps skinfold)*
Subscapularis	*The bottom tip the inferior angle of the scapula bone (subscapular skinfold)*
Iliocristale	*The most lateral point on the iliac crest on the ilioaxilla line (iliac crest Skinfold)*
Iliospinale	*The most inferior point or bottom tip of the anterior superior iliac spine (ASIS) (supraspinale skinfold)*
Omphalion	*The midpoint of the navel or umbilicus (abdominal skinfold)*

3.5 Girths

A cross-handed technique is the standard procedure with the stub held in the left hand and the housing in the right hand. The girth measurements are measured with tape at right angles to the long axis of a bone or body segment. The measurer, from the right side of the subject, passes the stub around the body segment, grasped by the right hand, and then passed back to the left hand which pulls it to the appropriate tension. The cross-handed technique is simply a matter of reaching across with the left hand and gripping the stub with the thumb and index finger while the right hand holds the housing. There should be no visible indentation of the skin at the measurement.

Fig. 1 A triceps skinfold measurement illustrating appropriate technique

Description of some common girth measurements are summarized in Table 3.

3.6 Breadth

Bony breadths are very important variables in surface anthropometry. They have been used in estimation of body size, body shape, and growth studies. For measurement purposes, the bone calipers lie on the backs of the hand while the thumbs rest against the inside edge of the caliper jaws and the extended index fingers positioned along the outer surface of the jaws. After finding the correct bony landmarks, the measurement is made with the calipers in place, with the pressure maintained along the index fingers. Description of some common girth measurements are summarized in Table 4.

Table 2 Skinfold measurements (location and orientation)

Skinfold	Location and orientation
Triceps	On the posterior aspect of the upper arm in the level of mid-acromiale-radiale (vertical)
Subscapular	Two cm lateral and inferior to the subscapulare (oblique)
Biceps	On the anterior aspect of the upper arm in the level of mid-acromiale-radiale (vertical)
Iliac crest	Immediately superior to iliospinale (horizontal)
Supraspinale	The intersection of iliocristale and iliospinale landmarks (oblique)
Abdominal	5 cm at right lateral of the omphalion (umbilicus) (vertical)
Front thigh	Midpoint of the perpendicular distance between the inguinal crease at the midline of the thigh and the midpoint of the posterior border of the patella when seated with the knee flexed to 90° (vertical)
Medial calf	The most medial aspect of the calf, at the level of maximum girth, with subject standing and weight evenly distributed (vertical)

4 Practical Usage

4.1 Body Mass Index (BMI)

The body mass index (BMI) is the ratio of body mass to stature squared: $\mathrm{BMI(kg/m2)} = \mathrm{BM(kg)/stature\ (m)2}$. In epidemiological studies, body mass index (BMI) is used as a crude index of overweight and obesity. ACSM (2014) recommends using BMI to evaluate obesity (BMI $\geq$30 kg/m^2) as a risk factor for coronary heart disease. Table 5 describes the classification of BMI.

4.2 Waist-to-Hip Ratio (WHR)

The waist-to-hip ratio (WHR) compares the girths of the waist to that of the hip. It is an indicator of body fat distribution (i.e., the apple or pear shape of body) or as a measure of general health. A high WHR has been recognized as a risk factor for chronic disease. This technique is simple to administer and requires only an anthropometric tape. In some cases, WHR may be a better

Table 3 Girth measurements (location and subject position)

Girth	Location	Subject position
Waist	Narrowest circumference between lowest rib border and pelvis	Arms folded **or** abducted
Hip	Greatest posterior protuberance of buttocks	Relaxed, feet together
Upper arm – relaxed	Mid-acromiale-radiale	Arm abducted slightly, elbow extended
Upper arm – flexed and tensed	Maximum in tensed state	Arm raised, elbow flexed at 45°
Calf	Maximum	Weight equally distributed

predictor of mortality than BMI. However, because it is a circumference ratio, it does not provide an indication of percent body fat. Standards for WHR values are shown in Table 6.

4.3 Percent of Body Fat (PBF)

The skinfold thicknesses have good correlation ($r = 0.7–0.9$) with the results of criterion techniques such as hydrodensitometry. The principle behind skinfold measurements is that the amount of subcutaneous fat is proportional to the total amount of body fat. It is assumed that nearly one-third of the total fat is located subcutaneously. This led to the proliferation of hundreds of regression equations to predict body fat. A list of the famous regression equations estimating percent of body fat is described by various resources (Norton and Olds 1996; Lohman et al. 1988). These equations can typically be divided into generalized equations and specific equations. Regression equations used to convert sum of skinfolds to percent body fat should consider some variables such as gender, age, and race for greatest accuracy. Norms of PBF values for women and men by age are summarized in Tables 7 and 8, respectively.

Table 4 Breadth measurements (location and subject position)

Breadth	Location	Subject position
Humerus	The distance between the medial and lateral epicondyles of the humerus	Subject in standing position, right arm raised horizontally, and elbow flexed at right angle to the upper arm
Femur	The distance between the medial and lateral epicondyles of the femur	Subject seated and knee is bent at right angle

Table 5 Classification of body mass index (BMI)

Classification	BMI value
Underweight	<18.5
Normal weight	18.5–24.9
Overweight	25–29.9
Obesity	30–39.9
Morbid obesity	>40

American College of Sports Medicine (2014)

4.4 Body Frame Size

Measures of frame size are supplemental to height and help to have a better estimation of the bone or body width. Body frame size as an important concept in the assessment and evaluation of body weight can increase the validation of the height-weight tables. Direct measurement of frame size is not possible. There is general agreement that measures used as substitutes for frame size should be distributed normally within a population, be highly correlated with lean body mass, and not be correlated with fat. Many sites have been proposed for the estimate of frame size:

Table 6 Norms of waist-to-hip ratio (WHR)

	Age	Low risk	Moderate risk	High risk	Very high risk
Male	20–29	<0.83	0.83–0.88	0.89–0.94	>0.94
	30–39	<0.84	0.84–0.91	0.92–0.96	>0.96
	40–49	<0.88	0.88–0.95	0.96–1.00	>1.00
	50–59	<0.90	0.90–0.96	0.97–1.02	>1.02
	60–69	<0.91	0.91–0.98	0.99–1.03	>1.03
Female	20–29	<0.71	0.71–0.77	0.78–0.82	>0.82
	30–39	<0.72	0.72–0.78	0.79–0.84	>0.84
	40–49	<0.73	0.73–0.79	0.80–0.87	>0.87
	50–59	<0.74	0.74–0.81	0.82–0.88	>0.88
	60–69	<0.76	0.76–0.83	0.84–0.90	>0.90

Heyward and Gibson (2014)

Table 7 Norms of percent of body fat (PBF) for women

	Age					
	20–29	30–39	40–49	50–59	60–69	70–79
Very lean	11.0–14.0	11.2–14.3	12.1–15.2	13.9–16.9	13.9–17.7	11.7–16.4
Excellent	15.0–17.0	15.5–17.5	16.8–19.5	19.1–22.3	20.2–23.3	18.3–22.5
Good	17.5–20.0	18.3–21.2	20.6–23.7	23.6–26.7	24.6–27.5	23.7–26.6
Fair	20.5–23.5	22.0–24.8	24.6–27.5	27.6–30.1	28.3–30.8	27.6–30.5
Poor	24.0–28.5	25.8–29.6	28.4–31.9	30.8–33.9	31.5–34.4	31.0–34.0
Very poor	30.5–38.5	31.5–39.0	33.4–39.1	35.0–39.8	35.6–40.3	35.3–40.2

ACSM (2014)

Table 8 Norms of percent of body fat (PBF) for men

	Age					
	20–29	30–39	40–49	50–59	60–69	70–79
Very lean	4.2–6.4	7.3–10.3	9.5–12.9	11.0–14.8	11.9–16.2	13.6–15.5
Excellent	7.9–10.5	12.4–14.9	15.0–17.5	17.0–19.4	18.1–20.2	17.5–20.1
Good	11.5–14.8	15.9–18.4	18.5–20.8	20.2–22.3	21.0–23.0	21.0–22.9
Fair	15.8–18.6	19.2–21.6	21.4–23.5	23.0–24.9	23.6–25.6	23.7–25.3
Poor	19.7–23.3	22.4–25.1	24.2–26.6	25.6–28.1	26.4–28.8	25.8–28.4
Very poor	24.9–33.4	26.4–34.4	27.8–35.2	29.2–36.4	29.8–36.8	29.4–37.2

ACSM (2014)

Table 9 Humerus (elbow) breadth norms (in cm) for men and women

	Age (years)	Small size	Medium size	Large size
Men	18–24	≤6.6	6.6–7.7	≥7.7
	25–34	≤6.7	6.7–7.9	≥7.9
	35–44	≤6.7	6.7–8.0	≥8.0
	45–54	≤6.7	6.7–8.1	≥8.1
	55–64	≤6.7	6.7–8.1	≥8.1
	65–74	≤6.7	6.7–8.1	≥8.1
Women	18–24	≤5.6	5.6–6.5	≥6.5
	25–34	≤5.7	5.7–6.8	≥6.8
	35–44	≤5.7	5.7–7.1	≥7.1
	45–54	≤5.7	5.7–7.2	≥7.2
	55–64	≤5.8	5.8–7.2	≥7.2
	65–74	≤5.8	5.8–7.2	≥7.2

Heyward and Gibson (2014)

- Humerus (elbow) breadth
- Bi-stylion (wrist) breadth
- Ankle breadth
- Femur (knee) breadth
- Biacromial (shoulder) breadth
- Bi-iliocristale (hip) breadth
- Bi-trochanteric breadth
- Ratio of height to wrist girth

Comparison and evaluation of these methods are hindered by differences in the study samples of factors that are potentially related to frame size and may confound the data. These include age, gender, and ethnicity. There are no reference standards for any of these measures except elbow breadth. In fact, the elbow breadth is currently the best measure for frame size for most applications because it has been validated, has reference values, and is relatively simple and practical to measure. Reference data for humerus breadth is described in Table 9.

References

Heyward V, Gibson A. Advanced fitness assessment and exercise prescription. 7th ed. Champaign: Human Kinetics; 2014.

International Society for the Advancement of Kinanthropometry. International standards for anthropometric assessment. Potchefstroom: North West University (Potchefstroom Campus); 2011.

Lohman TG, Roche AF, Martorell R, editors. Anthropometric standardization reference manual. Champaign: Human Kinetics; 1988.

Norton K, Olds T, editors. Anthropometrica. Sydney: University of New South Wales Press; 1996.

Pescatello LS. ACSM's guidelines for exercise testing and prescription. Baltimore: Lippincott, Williams and Wilkins; 2014.

Stewart A, Eston R. Surface anthropometry. In: Winter EM et al., editors. Sport and exercise physiology testing. London: Routledge; 2007. p. 76–83.

Dr. Shahram F. Mevaloo is a criterion anthropometrist, criterion photoscopic somatotype rater, and executive council member of the International Society for the Advancement of Kinanthropometry (ISAK). He is currently Head of Sport Nutrition and Anthropometry Committee of Iran Sport Medicine Federation.

Hair Histophysiology

71

Francisco M. Camacho

Contents

F.M. Camacho (✉)
School of Medicine, Medical-Surgical Dermatology Department, Hospital Universitario Virgen Macarena, University of Seville, Seville, Spain
e-mail: fmcamacho@us.es; camachodp@medynet.com

P. Humbert et al. (eds.), *Agache's Measuring the Skin*,
DOI 10.1007/978-3-319-32383-1_99

Keywords
Follicular stem cells • Hair shaft • Inner root sheath (IRS) • Outer root sheath (ORS) • Companion layer (CL) • Hair growth cycles • Thickness • Diameter • Length • Density • Growth

1 Introduction

The follicle is composed in its distal part by the bulb, which is formed by the hair matrix and papilla, and in its side wall, from the bottom up, by the bulge, which contains "follicular germ cells" and is the insertion site of the smooth erector muscle of the hair, the sebaceous glands, and the apocrine sweat gland. In the germinal compartment, bulb matrix cells are found and multiply due to the activation by the bulge cells, forming well-differentiated structures that correspond to the hair shaft and inner root sheath. Between the undifferentiated matrix cells and the differentiated cells, there is a limit, which is known as "Auber's line." The central part corresponds to the hair shaft and has three concentric layers from inside to outside: cortex, medulla, and hair cuticle or "epidermicule." The inner root sheath (IRS) also has three vertical layers known as the sheath's cuticle, Huxley's layer, and Henle's layer (outward, respectively). Between the IRS and outer root sheath (ORS), there is a single-cell layer known as the "companion layer" (CL). The ORS comes from the epithelium and, together with bulge stem cells, has great value in the

epithelialization of wounds. The ORS accompanies the hair follicle to the area between the erector muscle insertion and sebaceous gland, known as "Straile's area," where the temporary structures disintegrate (Fig. 1). Outside the ORS, there is a fibrous connective tissue sheath which forms the basal follicular membrane called "vitreous membrane" and a conjunctive sac in which the neurovascular structures are located. There are two follicle matrix areas: the hair bulb, with matrix cells around the dermal papilla, and the bulge matrix cells in the lower part of this structure. Follicular cycles are initiated by the "activation of the cells of the bulge."

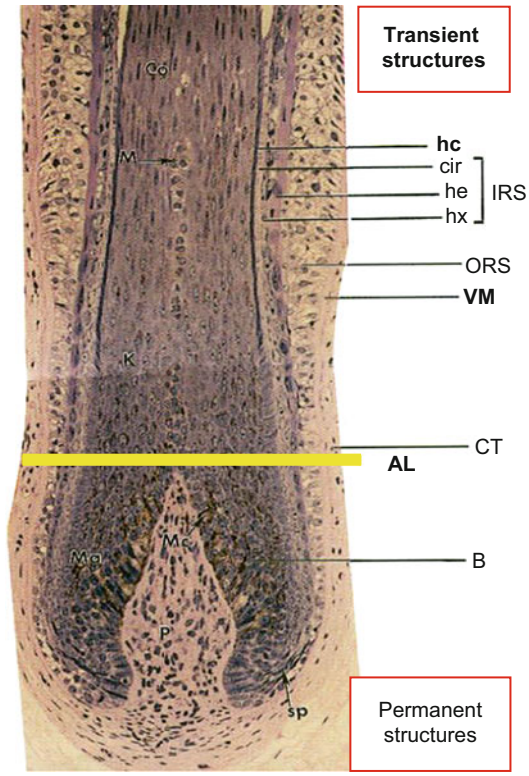

Fig. 1 Lower part of the follicle. In the bulb (*B*), the undifferentiated matrix cells (*Ma*) are arranged in a line as they ascend toward the keratogenous area (*K*) where the cortical cells (*Co*) are keratinized. The bulb contains the dermal papilla (*P*). Immediately above the matrix cells, a line known as Auber's line (*AL*) separates the permanent structures of transitory structures. The melanocytes (*Mc*) are arranged on the roof of the dermal papilla. Hair is composed by medullar cells located in the center. Note that the medulla is discontinuous. Surrounded the medulla are the hair cortex and epidermicule or hair cuticle (*hc*). The outer (*ORS*) and inner root sheath (*IRS*) with their three different layers (Henle's layer (*he*), Huxley's layer (*hx*), and the cuticle of the inner root sheath (*cir*)) can be followed easily until the level of the bulb, where they are separated by dark spinous cells (*sp*) that are the cells of the companion's layer. The connective tissue sheath (*CT*) is continued with the dermal papilla and is separated by a thick vitreous membrane (*VM*) which in its internal part can be confused with the basal membrane

The "hair growth cycles" are established from the time the child is born. While growing, the hair follicles are in the *anagen phase*, and when they are resting, they are in the *telogen phase*. The transition between these two states is the catagen phase. We call the stage in which the hair follicles eliminate the hair shaft in the telogen phase from its interior, remaining empty, the exogen phase. And the kenogen phase is the presence of "empty follicles" as a result of failure in telogen hair replacement by anagen hairs in early-onset alopecia. Anagen follicles are surrounded by dense plexus of arterioles and capillaries originating from the branches of the dermal plexus or directly from musculocutaneous arteries. Follicular innervation is different depending on whether it deals with terminal hair follicles or vellus hairs. Some myelinated nerves run parallel to the permanent part of the follicle, and other finer nerves form a network as a sock or bag surrounding the rest of the follicle. A cluster of parallel myelinated nerve fibers forming a stockade or "palisade" can be seen near the follicle canal and some of these nerves branch in the vicinity of their distal terminals, resulting in bulging, reminiscent of tines of a fork. The nerves are better organized around vellus hair follicles (Fig. 2a, 2b) than in the large terminal hair follicles, allowing their consideration as a "follicular tactile organ" (Holbrook 1983).

2 Follicular Formation: Embryology

Hair grows early and vigorously in the skin of human fetus. The hair follicle is differentiated toward the end of the second month (Holbrook 1983; Billingham 1958), first in the eyebrows, upper lip and chin, and then on the scalp and face. Around the fourth and fifth month, follicles

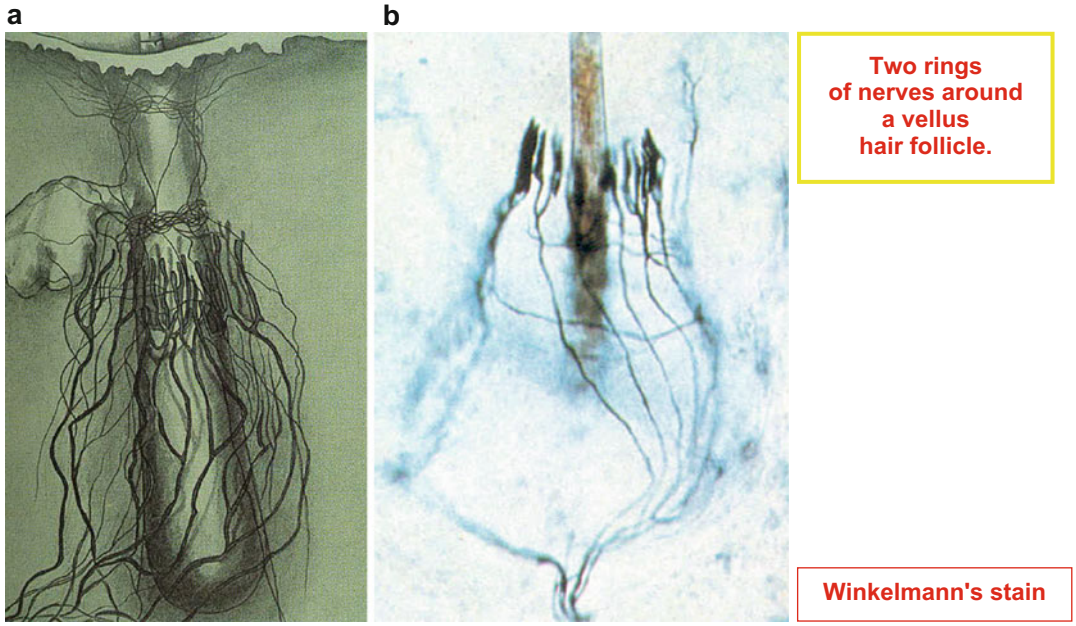

Fig. 2 (**a**) Nerves well organized around a vellus hair follicle. Schedule of the two rings of nerves around a vellus hair follicle forming a well-structured sensory nerve ending. (**b**) Myelinized nerves around a vellus hair follicle. Stained with Winkelmann's silver technique

are formed by the rest of the body and continue to form until the end of the pregnancy. Hair follicles are initiated along the hairlines, with a distribution that is generally similar in all people, and later, they are developed in the spaces between these lines, as the fetal body surface expands. According to available data, no new hair follicles are formed after birth because when we are born, we have all the hair follicles of the future (Billingham 1958).

During fetal life, the hairs grow to a certain length in the anagen phase, and then the follicles enter catagen and telogen phases. After a short rest period, the hair grows again, entering the anagen phase and substituting the telogen hair by a new hair (Montagna et al. 1992). In the embryonary life, this process may occur two or more times on the head and face and less frequently elsewhere (Montagna et al. 1992).

Differentiation of hair follicles in the human fetus begins by the presence of a cluster of cells. These cell aggregates, known as "primitive hair germ," cause a small bulging on the underside of the epidermis. As soon as the cells of the primitive hair germ become recognizable, mesenchymal cells in the dermis crowd underneath, they are signaling the appearance of the dermal papilla of that hair follicle. Both clusters penetrate obliquely in the dermis and result in the lower portion of the bulb, follicular papilla, and temporary structures and in the upper portion, the bulge where erector muscle is inserted, and sebaceous gland and apocrine gland.

2.1 Advances in Knowledge of the Differentiation of the Follicles in the Fetus

2.1.1 Knowledge Up to 1980

As Montagna and Camacho (2013) pointed out, the differentiation of hair follicles in the human fetus begins by the presence of a cell cluster in the basal layer of the still relatively undifferentiated, bilayered periderm which is the future epidermis. These cells of the epidermis basal layer are condensed and their small and basophilic nuclei are elongated and arranged perpendicular to the skin (Fig. 3a). These cell clusters, known as "primitive

hair germ," "bud," or "placode," produce a small bulge in the lower surface of the periderm and one may observe how below of this "bud" the mesenchymal cells of the dermis are accumulated, indicating the appearance of the dermal papilla of each hair follicle. The two cell groups, the basal cells of the hair germ and the mesenchymal cells of the papilla future, become more apparent, and begin to penetrate obliquely in the dermis pushed by a column of epithelial cells adopting a "club-shaped structure" (Fig. 3b).

The "club-shaped" column is claviform and has an anteroposterior tilt. This structure shows large columnar cells arranged radially in the periphery, while the central cells are aligned longitudinally. This is the "primordial follicle" completely constituted. The distal portion of the primordial follicle adopts a truncated appearance with which it pushes toward the interior of the dermis to the papillary mesenchymal cells (Fig. 3c). The claviform column begins to split their distal portion where they will collect the papillary mesenchymal cells. On the back side of the epithelial column, two protuberances grow: the lower one, at first the larger one although later it is reduced, corresponds to the insertion area of the erector muscle which corresponds to the bulge, and the upper one corresponds to the primordial sebaceous glands (Fig. 3d). At this early stage, it can be determined that cells of the middle of the sebaceous protuberance have a foamy cytoplasm, thus constituting the earliest synthesis and lipid accumulation. Also in this phase, the presence of the connective tissue is verified, and some mesenchymal cells that are grouped linearly under the sebaceous gland and positioned toward the bulge consisting of the outline of the future erector muscle. The follicle begins to split its truncated distal portion in order to grow around the dermal papillary cells, although it remains attached by a narrow pedicle to a group of cells that continues with the conjunctive peribulbar sheath. At first, pigmented melanocytes can be observed around the bulb, but, later, only in the upper portion above the dermal papilla. Most cells in the lower portion of the bulb are not differentiated and constitute the proliferating follicular matrix. The first follicle differentiation occurs in the inner root sheath, whose cells, which surround the dermal papilla, are longitudinally aligned, acquire trichohyalin granules, and later form the lining of the hair. When the primordial follicle is almost formed, it is found that the bulb has included the papilla and also undifferentiated matrix cells are observed on the basal membrane of the bulb, and the two side swellings which are the adhesion area of the erector muscle and sebaceous gland (Fig. 3d). Between 15 and 20 weeks above both swellings, a third protuberance or bulge to be the rudiment of apocrine sweat gland begins to be observed. And when the primordial follicle is already fully formed, on the inclined side portion, from bottom to top, the three swellings are observed, and in the center, one may observe how cortical cells begin to be differentiated, reaching the isthmus and infundibulum and constituting, along with the cells of the inner root sheath, the intraepidermal follicular canal. There will also appear the first hair shafts that will only possess cortical cells but will not have medulla or pigment (Fig. 4; Holbrook 1983; Montagna 1981; Hashimoto 1978; Montagna et al. 1985a).

2.1.2 Recent Knowledge on the Differentiation of the Follicles in Fetuses

As mentioned above, at the end of the second and beginning of the third month, primordial hair follicles, also called primitive hair follicles, may already be seen on the head, specifically in the area of the eyebrows or ciliary regions, interciliary upper lip, and chin. Shortly afterward, follicles appear on the forehead and scalp, and in the fourth to fifth month, they appear in the rest of the integument (Billingham 1958; Montagna et al. 1992; Pinkus 1910; Pinkus 1927; Koelliker 1850; Pinkus 1958; Montagna et al. 1967, 1974; Camacho et al. 2013).

The development of follicles is dyssynchronous in the body, being able to find fully formed follicles and others in various stages of differentiation in the same corporal regions. As the skin expands, primary or "secondary" follicles emerge among those already existing, and it is even possible to observe how other secondary or "tertiary" follicles

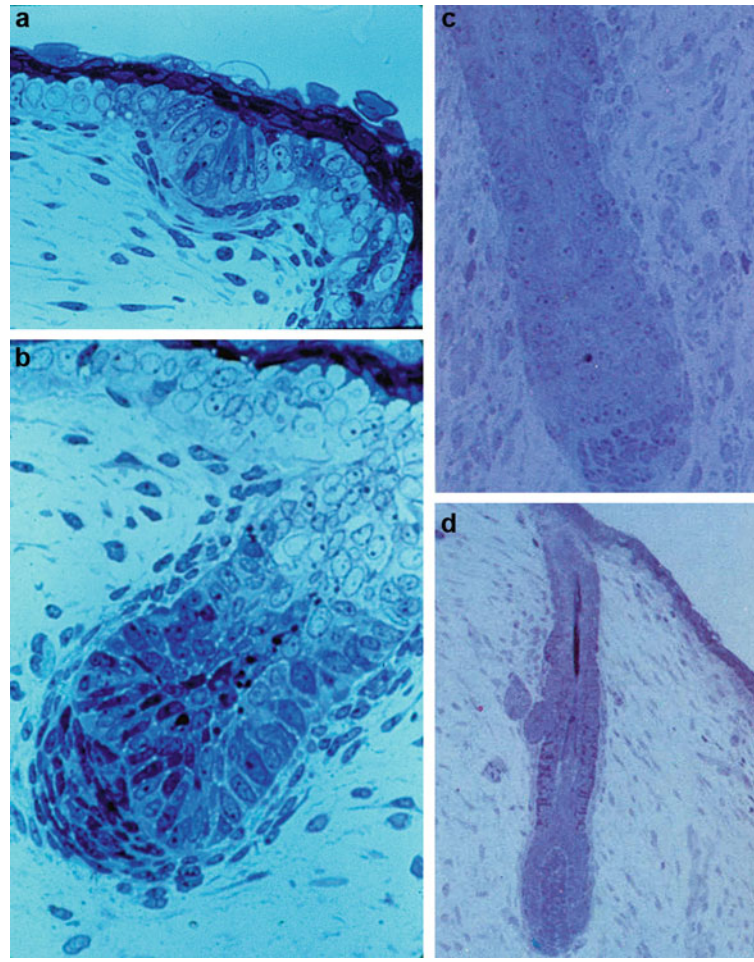

Fig. 3 (**a**) Placode. Basal epithelial cells with vertical alignment to the surface. Mesenchymal cells, the forerunner of the dermal papilla, are beginning to gather at the base of the bud. (**b**) The hair germ is well defined, and the dermal papilla cells are more clearly delineated at the base of the dimpled column of cells. (**c**) Primordial follicle. The cells in the core of the epithelial column are aligned perpendicularly and have begun to manufacture the keratin of the inner sheath. On the lateral wall, a primordial sebaceous gland is developing. (**d**) Primordial follicle is well developed. The bulb has included the dermal papilla. The follicular layers are well differentiated, and a hair is being formed in the center. In the lateral wall, two swelling are demonstrated, lower the bulge and upper the anlagen on a sebaceous gland. The erector muscle can be seen on the bulge

immediately emerge adjacent to those already formed to constitute groups of three or more follicles that are known today as "follicular units." Next to them, eccrine sweat glands can be observed. To observe the arrangement of the primary, secondary, or even tertiary follicles, "separate skin preparations" are used between the epidermis and dermis. If we destroy the dermis and hypodermis, the bulbs and follicles are observed heading to the epidermis, and when the epidermis is destroyed, one may observe the follicular ostium of these groups of follicles coming from the dermis.

Holbrook (1983) reminded us in his magnificent work, and in the photos presented in the second edition of Montagna and Camacho (2013; Fig. 5a–5d), that the small swelling on the lower surface of the epidermis, called "primitive hair germs," is CD10 positive (Poblet and Jiménez 2008) and the mesenchymal cells of the dermis accumulating underneath, indicating the appearance of the dermal papilla of each hair follicle, are CD34 positive (Poblet and Jiménez 2008).

The fact that both CD10 and CD34 are observed in the placode and in the accumulation of matrix cells of the papilla, respectively, of follicles in the anagen phase suggests that these proteins have a role in the initial stages of follicular formation. This is confirmed by the fact that CD10 is also expressed in the matrix cells, inner root sheath, and conjunctive sheath of the follicles in the anagen phase but disappears in catagen and is impossible to detect in telogen follicles. Through immunostaining with CD34, it is possible to verify it in the outer root sheath of the follicles in the

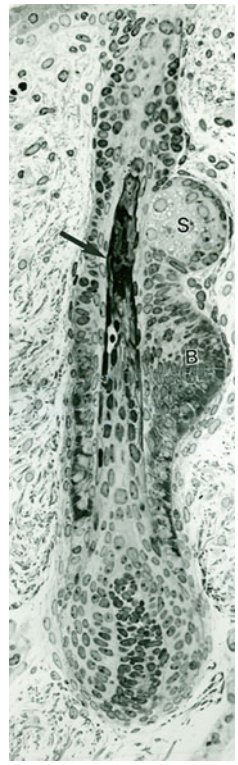

Fig. 4 Completely formed embryonic follicle. In the posterior part, one can see a superior bulge which corresponds to the outline of the sebaceous gland (*S*) and a lower protuberance which is the bulge (*B*). The arrow is pointing to the "hair cone" in whose tip only the inner root sheath is seen (Courtesy Dr. K. Holbrook. From Montagna and Camacho 1997)

anagen phase but not in fetal follicles which, we recall, is where it is expressed in the papillary cells, or in the catagen or telogen stages.

When the rudiment of the sebaceous gland becomes visible (Montagna et al. 2013), mesenchymal cells near the follicle are extended and aligned toward the posterior edge of the follicle. These primitive erector muscles extend toward the "bulge." At this time, the primary follicle is a keratinized solid epithelial structure (Langbein and Schweizer 2005; Schweizer et al. 2007; Langbein et al. 2013) surrounded by a mesenchymal sheath. Later, the smooth and primitive muscle cells are extended and their thickness increased.

2.1.3 Molecular Mechanisms Regulating Hair Follicle Development

Although it is not the purpose of this chapter to address all of the molecular mechanisms required for hair follicle formation, we will refer to the magnificent paper of Sarah E. Millar (2002), published in 2002 in the Journal of Investigative Dermatology, in which she commented on the "signals," known up to that time, that are emitted into the skin of mice and chicks during the embryogenesis phase between skin cells and the overlying epidermal cells that, although not completely superimposing the human cells, explain how the placode and hair germ formation begins, passing through the "club-shaped column" stage until the final formation. Without a doubt, today we know of many more "signals" of inhibition or promotion.

The first signal that the dermal cells are being accumulated under the epithelial cells in order to form the "primitive hair germ" (Figs. 3a and 5a) is induced by β-catenin, although the fibroblasts could also influence, at least it happens this way in the follicular neogenesis in adult skin (Collins et al. 2012). In any case, it is not clear that a key molecule for transferring the power of a signal (in this case, β-catenin would be a transducer of the Wnt signal) is going to be acting in this phase alone (Collins et al. 2012). What is clear is that in the initial development phase of the hair follicle, the first epidermal signals, located in the placode, can be promoters (Wnt, β-catenin (Myung et al. 2013; Ahn et al. 2013), factor linked to the increase in lymphocytes-1 [LEF1] (Wang et al. 2012), fibroblasts growth factor and FGF receptor genes [FGF/FGFR2-IIIB], MSX1, MSX2, ectodysplasin/ectodysplasin receptor [EDA/EDAR], NOGGIN, and DELTA-1/NOTCH) as well as inhibitors-repressors acting on cells that surround the placode (BMP2, BMP4, DELTA-1/NOTCH1). However, knowing that Wnt/β-catenin activation is required for the anagen phase (Myung et al. 2013), we still do not know what the source of production is. Therefore, from all of the above, it should be highlighted that it is certain that the first signal that initiates follicle development is Wnt, but it is not yet known if it comes from the epithelium or from the dermis (Fu and Hsu 2012). It has also been recently shown that the neurotrophin receptor p75 (p75NTR) is expressed in fibroblasts that later develop the dermal papilla and, although its role is not known, the authors suggest that it would act

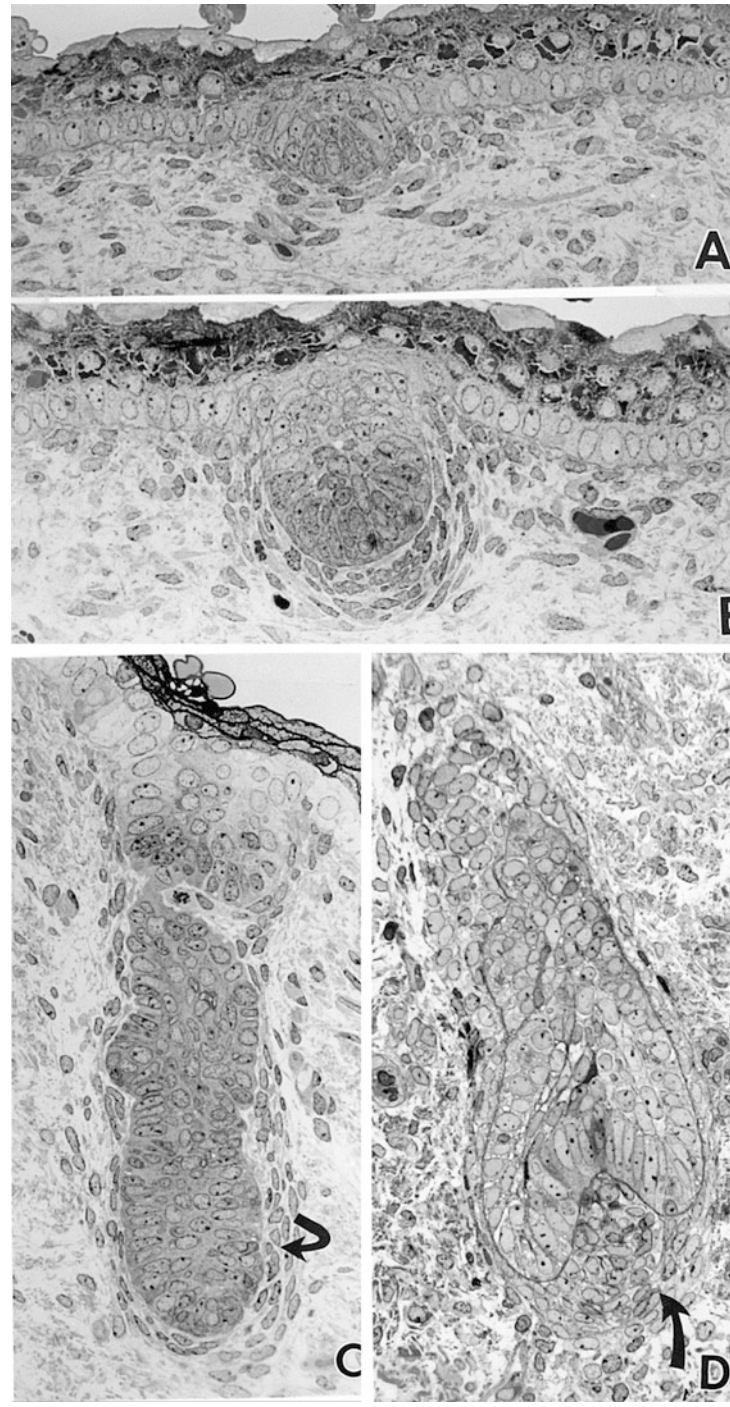

Fig. 5 Primitive hair germ developing in the basal layer of the periderm. Mesenchymal cells are gathering in the base of the germ (**a**). More advanced stage of the hair germ development in which one can clearly see the mesenchymal cells which make up the beginning of dermal papilla (**b**). Primitive elongated hair germ growing perpendicularly to periderm. On the *left* hand side, a protuberance can be observed. The base of the germ has a "clavate" shape. The arrow is signaling a condensation of mesenchymatous cells which represent the cells of the early dermal papilla (**c**). The primitive hair follicle growing around the future dermal papilla (**d**) (Courtesy Dr. K.Holbrook. From Montagna and Camacho 1997)

as a receptor which would negatively control the hair follicle through various routes.

Later, when the epithelial germ begins to be constituted, with the presence of the placode that pushes the papillary cells, Wnt would act as an epithelial signal and PDGF-A and Shh (Sonic hedgehog) as signals for the formation of the dermal papilla (Cui et al. 2011; Figs. 3b and 5b). Later on, in the club-shaped column phase, when the column increases and pushes the papillary cells, there is a second dermal signal caused by HGF/MET (Lindner et al. 2000), probably by ACTβA/FS and SOX18, and three signals for the proliferation of follicular epithelium (SHH), for polarity of the cells in the follicle (probably Wnt and Shh), and for the follicle (TGFα/EGFR and ETS2). Finally, the differentiation of the root sheaths begins. Until 2002, it was not known which was the signal for the differentiation of the inner sheath. The differentiation of the outer sheath is done by external NOTCH1, BMP2, BMP4, Wnt3, LEF1, NOVO1, HOXC13, and WHN and probably by MSX1 and MSG2.

Woo et al. (2012) reported that Shh regulates growth dermal follicular maturation maintaining the dermal papilla and also leads Noggin follicle morphogenesis. Finally, once the follicle is formed, the hair needs to come out. The matrix metalloproteinases are involved in the creation of the ductus from which the hair will protrude, especially metalloproteinase 9 (MMP-9); however, it is still unclear if other MMPs such as MMP-2 may modulate the effects of MMP-9, nor is it clear whether, as occurs with other cell types, the expression of MMP-9 is regulated by the Wnt, TGF-β/BMP, HGF, and EGF signaling pathway (Sharov et al. 2011). Recently, Cadau et al. (2013) have identified four new Wnt-related genes which could be involved in hair follicle initiation, two activators Wnt-2 and Zic-1, and two inhibitors, Dkk-2 and Dact-1. Nevertheless, this chapter does not attempt in any way to clarify each and every one of the signals the follicle receives for its formation; we only want to state that its development has a molecular mechanism which is increasingly better known, from which we will probably obtain therapies for the future (Li et al. 2013).

3 Hair Follicle Anatomy

As noted in the introduction, the follicle has in its distal portion the bulb which is composed by the hair matrix and the papilla. Downward on the lateral wall of the follicle, we have the sebaceous gland, the apocrine sweat gland, and the insertion of the smooth erector muscle by the Nagel elastic tendon. This tendon is comprised of elauninic and oxytalanic elastic fibers. The "bulge" is located in the area of insertion of the erector muscle, which forms an obtuse angle and contains "follicular germ cells" that will result in a new follicle after each catagen period (Lavker and Sun 1983; Cotsarelis et al. 1990).

The bulb matrix cells, which are found in the germinal compartment, multiply forming well-differentiated structures that correspond to the hair, inner root sheath (IRS), and another single-cell layer known as the companion layer. Among the not differentiated and the differentiated matrices, there is a limit, which was known as "critical level of Auber" and today is simply referred as "Auber's line" (Fig. 1).

The central part, which corresponds to the hair, has three concentric layers from inside outward: medulla, cortex, and hair cuticle or "epidermicule." The inner root sheath (IRS) consists of three vertical layers: cuticle of the sheath, which adheres like a zipper to the hair cuticle, Huxley's layer, and Henle's layer. Huxley's and Henle's layers are rich in trichohyalin granules, similar to the keratohyalin of the epidermis, but not in melanin (Langbein and Schweizer 2005; Schweizer et al. 2007; Langbein and Schweizer 2013). Huxley's layer has some cells with lateral projections of a "wing" type, for which reason they have been called "winged cells", which cross Henle's layer to reach the companion layer (CL) which is a single-cell layer that lies between the IRS and the ORS (Camacho Martínez 2009).

The outer root sheath (ORS) or "trichilemmal" is the outer epithelial layer of the follicle. It proliferates downward from the epithelium to the bulb and surrounds the two structures derived from the matrix cells. The ORS consists of a single-cell layer when it is around the hair bulb, but above the bulb, it gradually stratifies, and

farther above, it shows a seamless transition with the protuberance and the isthmus. This complete stratified ORS has an outer layer of palisade cells (ORSe) and two other layers, medium and internal (ORSm, ORSi), of the same cobblestone morphology or shape differences without signs of differentiation or keratinization (Fig. 6).

The ORS accompanies the hair to the follicle area between the insertion of the erector muscle and sebaceous gland, known as "Straile's area," where it disintegrates.

From this area, there only remains outside the ORS, which accompanies the follicle to the epidermis from which it comes, and while the follicle is in the dermis, it is also surrounded by a fibrous sheath of connective tissue that forms the basal follicular membrane, called "vitreous membrane," and by a conjunctive sac in which is found neurovascular structures (Rothnagel and Roop 1995).

In between the ORS and the IRS, there is a vertical structure of a single-cell layer called "companion layer" (CL) which accompanies the ORSi from the lower portion of the bulb to the upper part of the isthmus. The CL cells contain a clearly asymmetric cluster of bundles of intermediate filaments of compact keratin toward the center of the hair follicle known as "Hoepke circular filaments." The CL was considered by Pinkus (1910) as the innermost layer of the ORS but today is known to be an independent follicular structure (Montagna and Camacho 2013; Langbein and Schweizer 2013; Camacho Martínez 2009). In the edition of the book by Montagna and Camacho (1997), Montagna pointed out in reference to the 6D figure "Observe the large melanocytes and prickly dark cells (Sp), described for the first time, that separate the inner root sheath (IRS) from the external (ORS)" (Fig. 7; Montagna and Camacho 1997). He was describing the development of companion layer from the matrix cells of the bulb (Camacho Martínez 2009). In 1995, Rothnagel and Roop reminded the existence of companion layer between Hurler layer and ORS (Rothnagel and Roop 1995), and Winter et al. in 1998 the novel human type II cytokeratin, K6hf, specifically expressed in the companion layer (Winter et al. 1998).

When the follicle enters catagen phase, the bulb matrix cells together with the matrix cells of the papilla form the "secondary germ" and ascend until being situated near germ cells of the bulge.

After passing the resting phase, immediate physical interaction or "activation of bulge cells" occurs, thus beginning a new cycle of follicular growth. When the secondary germ moves toward the bulge, it leaves behind him, in the form of a tail or "serpentine" shape, a fibrous structure filled with remnants of fibrous connective sheaths of the follicle, vessels, and nerves (Forslind 2000; Fig. 8).

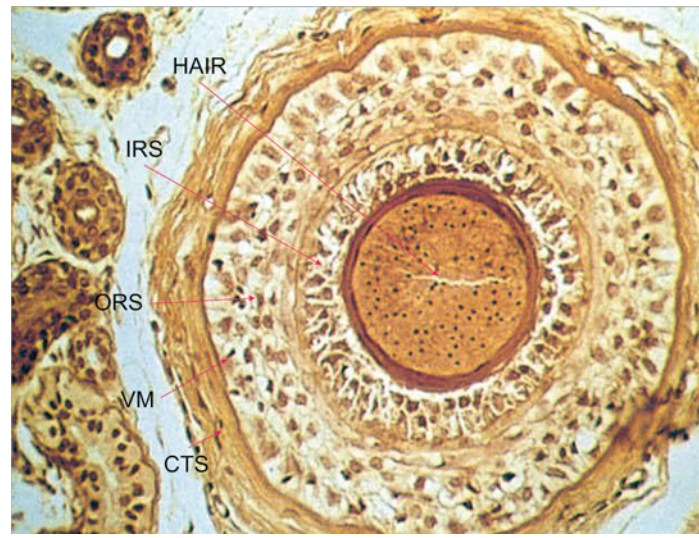

Fig. 6 Follicular transversal section. In the center, the hair with the medulla, cortex, and epidermicule. Surrounding the hair, the inner root sheath (*IRS*), the outer root sheath (*ORS*), the vitreous membrane (*VM*), and the connective tissue sheath (*CTS*)

3.1 The Importance of the Companion Layer

Having described in the introduction the general structure of the pilosebaceous follicle, we need to make a few comments on the most recently known follicular layer. I refer to the companion layer (CL).

Today, there is no doubt that the CL is a single-cell layer, very fragile, ranging from the germ cells of the bulb (Fig. 7) to the isthmus and just below the entrance of the sebaceous gland duct in the follicle canal. The fragility of the CL is what justifies that the pulling of the hairs breaks this layer in the lower portion of the follicle. This happens because the CL cells are asymmetrical and have few desmosomal connections with ORS cells, although, as noted above, they are closely related to the cells of Henle's layer by means of desmosomes and a circular network of intermediate filaments, called "belt or circular fibril."

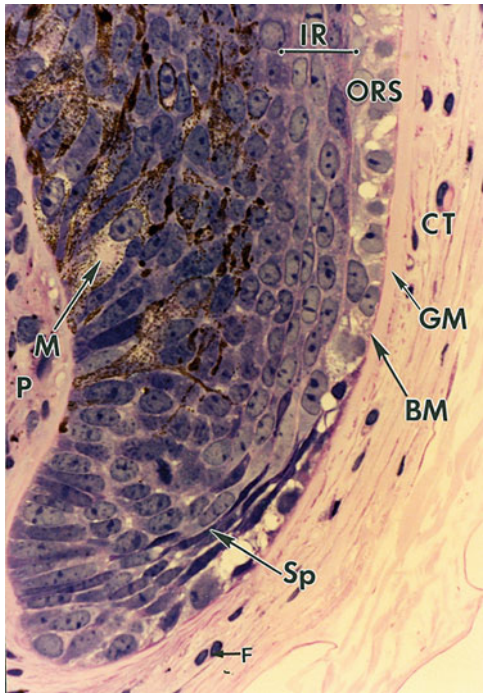

Fig. 7 The cells of the matrix and of the outer root sheath (*ORS*) are aimed upward. Note the large melanocytes (*M*) and also some dark spinous cells (*Sp*), which separate the inner root sheath (*IR*) from the outer root sheath (*ORS*). These dark cells are the companion layer's cells that are produced in the bulb. One can also see the dermal papilla (*P*), the connective tissue sheath (*CT*), and a thin basal membrane (*BM*) inside the vitreous membrane (*GM*). Fibroblasts (*F*) can be seen in the connective tissue sheath

The importance of the CL is that this single-cell layer next to the inner root sheath guides and holds the hair toward its outlet. In order to perform its function, it forms a block with the outer part of the inner root sheath cells, thanks to the winged cells coming from Huxley's layer. These cells, upon being introduced between the cells of Henle's layer and coming into contact with the companion layer by means of projections of intermediate filaments and/or desmosomes, form an IRS-CL block which will subsequently join the ORS, possibly allowing intercommunication of all the follicular layers. This phenomenon will ensure greater rigidity of all follicular layers, especially Henle's layer, and even the exchange of nutrients (Lindberg and Forslind 2004). The end of the companion layer occurs within the isthmus, slightly below the inlet of the sebaceous duct in the hair channel (Montagna and Camacho 2013).

4 Hairs

"Hairs" are keratinized skin elements with structural, mechanical, and physicochemical properties that are out of the ordinary. The cells that constitute them trap air bubbles, for which reason they float on water. It consists of three strata that, from the inside outward, are the medulla, cortex, and cuticle of the hair.

The hairs are produced in the follicles and each follicle can be influenced by endocrine-metabolic factors, especially hormones, being responsible of the changes from the puberty that justify the hair differences with the age. For example, in the scalp or in the face of a man, the hairs are transformed into vellus hair during senescence (Fig. 9) and the vellus hairs of areas hormone dependent are transformed into terminal hair during puberty. What really happens in these cycles is that the follicles "miniaturize" or increase in thickness, respectively. The follicles of the terminal hair penetrate the dermis to a depth of 3.6 mm, while the follicles of the vellus

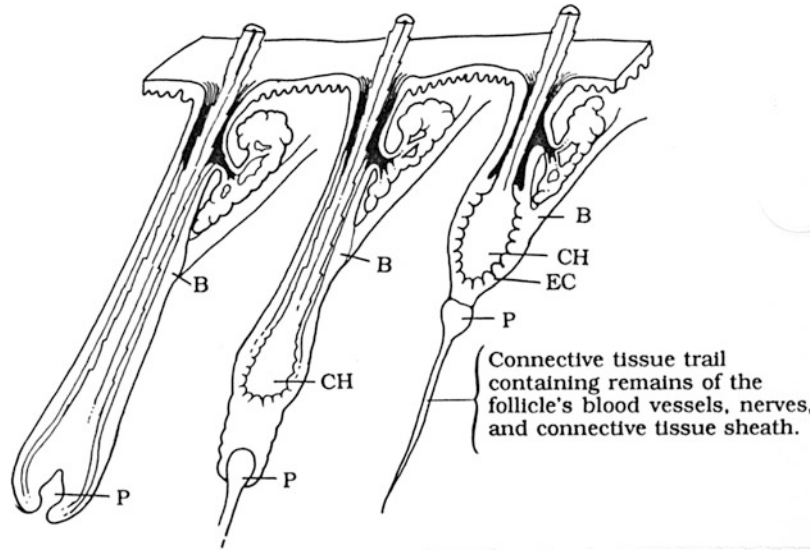

Fig. 8 Hair growth stages. Each stage is shown in cross section. On the left, there is an follicle "in anagen"; in the middle, there is a follicle "in catagen"; and on the right, there is a follicle "in telogen." This diagram notes the different parts of the follicle: dermal papilla (*P*), bulge (*B*), club hair (*CH*), and epithelial capsule (*EC*). In the figure, we can see the fibrous structure filled with remnants of fibrous connective sheaths of the follicle, vessels, and nerves

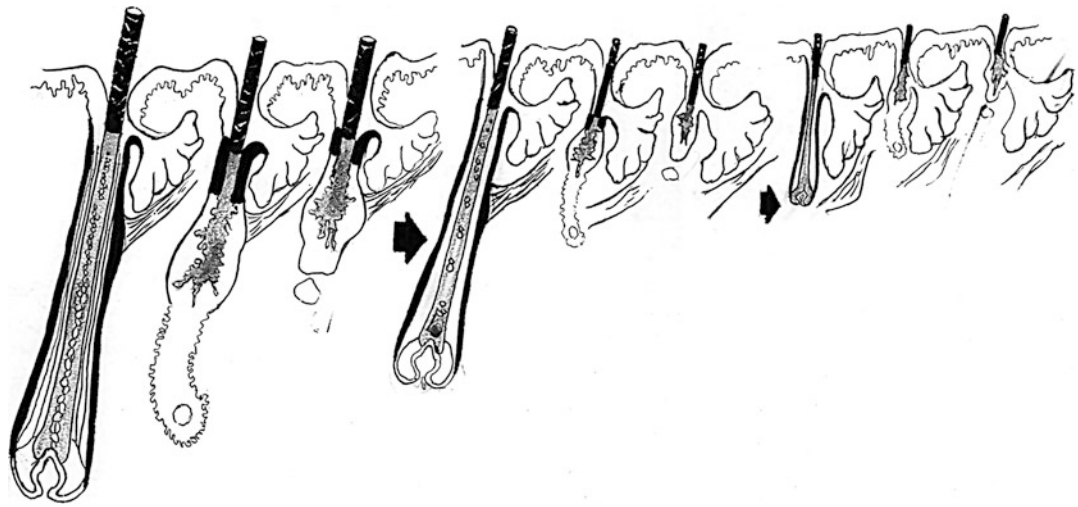

Fig. 9 In successive growth cycles, a transformation occurs on the scalp, from hair to vellus hair. Really, what happens in these cycles is that follicles "miniaturize"

hairs only penetrate the dermis to a depth of approximately 0.5 mm.

In the center of the hair shaft is the *medulla*, which in humans may be continuous, discontinuous, fragmented, or even nonexistent. The medulla is formed from a hemispherical structure, called pre-medulla, which is formed by the cells around the papilla above Auber's line (Fig. 1). In humans, the medulla is only found, consistently, in the pubic hair since in the scalp hair, its presence depends on population factors (Forslind 2000; Lindberg and Forslind 2004) and the body hair does not have medulla. However, the hair of the beard of males has a medulla composed of irregularly arranged but horizontal cells that are full of multiple keratohyalin granules and tend to form vesicles and air-filled spaces that act as insulators.

Surrounding the medulla is the *cortex*, comprised by elongated and keratinized cells containing varying amounts of pigment. It is the more compact structure of the hair shaft

composed of elongated, spindle-shaped cells loaded with bundles of intermediate keratin filaments. It originates in the matrix of the hair next to the cell compartment of the lower germ cells, below Auber's line, and extends from the upper portion of the bulb to the keratogenous zone which is the area where their cells are keratinized and no longer present nuclei, an area known as "Adamson's fringe" (Montagna 1981).

At the outermost portion of each hair is the *cuticle*, which is the protective layer of the hair shaft and which is formed by cells that are very large, thin, flat, scalelike, pigmented, intertwined, and oriented obliquely like shingles on a roof, with the free ends facing upward toward the end of the hair. The cells of the cuticle hold the hair and anchor it into the follicle, fixing it to the corresponding cuticular cells of the inner root sheath, which are directed downward (Fig. 10). Cuticle cells, of the hair as well as of the inner root sheath, are differentiated immediately above the bulb of hair follicles, where the cells of the cuticle begin to be keratinized in the pre-keratogenous area while the cells of the outer root sheath are keratinized at a higher level.

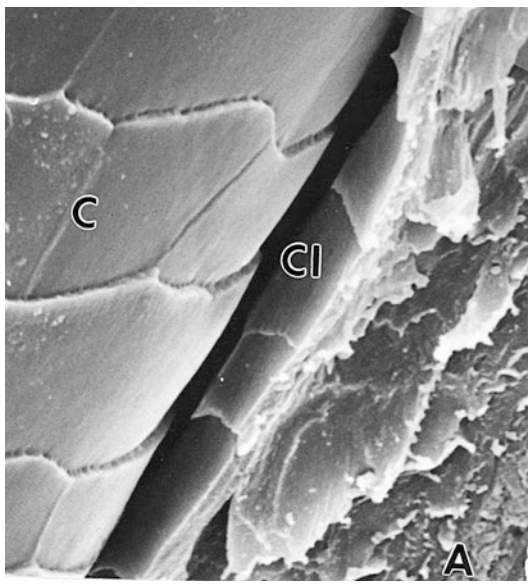

Fig. 10 SEM of a hair follicle. The edges of the cuticular cells of the hair (*C*) are smooth and aimed upward. The smaller cells aimed downward (*CI*) are cuticular cells of the inner root sheath. The cuticle cells attach the hair to the inside of the follicle (Courtesy Dr. D.Knutson. From Montagna and Camacho 1997 (Montagna and Camacho 1967))

Each hair is unique in that its "structure" is different from one segment to another (Fig. 11). Even the hairs formed in the "same" follicle may have very different structures. One must bear in mind that the hairs that emerge subsequently are not formed by the same follicle since each follicle is destroyed during the catagen phase.

The *hair* has an intrafollicular portion known as the "root" and an outer portion, the "shaft." The keratinoblasts of the matrix, among which are found melanocytes, multiply rapidly and are keratinized, but, contrary to what takes place in the surface epidermis, there is no granular stratum, for which reason this abrupt keratinization is complete within 1 mm above the apex of the papilla. From the inside out, the hair is composed of the medulla, cortex, and cuticle or epidermicule, with only the first two being melanized.

Despite observations to the contrary, there exists the same amount of hair on the body of a woman as on that of a man, with the difference being that the body hairs of women are smaller. Among the many factors responsible for the growth of hair on the human body are specific body areas, heredity, hormones, sex, race (Hamilton 1958), and age. The hairs are keratinous fibers and can be thick or thin, long or short, and straight, wavy, or curly. In cross section, curly hair looks like ribbons; the rest are mostly oval or ovoid.

The hairs are generated in the follicles. The two major categories of hair, "terminal hair" and "vellus hair", refer to its size. Felix Pinkus (Pinkus 1927) included the "intermediate-sized" hair which is between the cited two. Although there is the idea that all the hairs are the same among the different living species, one must remember that other mammals have other types of hair; this does not merit further comment.

The majority of the "terminal hairs" and "intermediate hairs" are thick, rigid, usually pigmented, and medullated; those on the scalp, eyebrows, eyelashes, beard, mustache, and axilla and pubic areas and on the limbs are terminal hairs.

The "vellus hairs" are generally without pigmentation and/or invisible. Those that can be seen are, in principle, short, without pigmentation, soft,

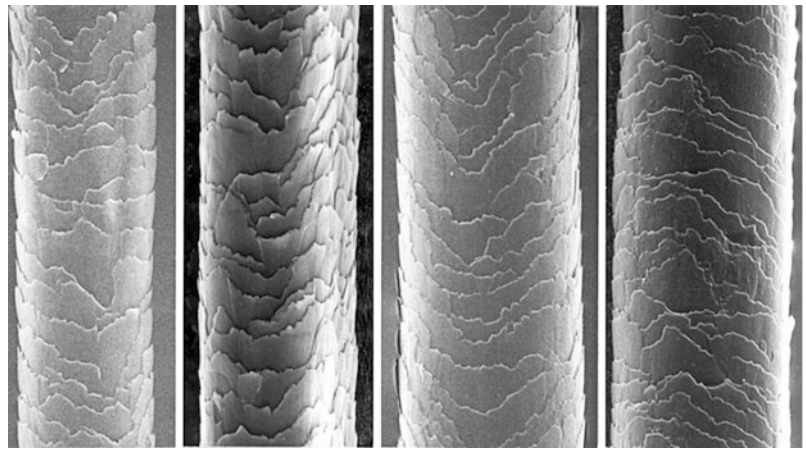

Fig. 11 SEM of hairs from the surface of chest of four men. It is impossible to differentiate these hairs only on the basis of their aspect (From Montagna and Camacho 1997)

Fig. 12 SEM image of the surface of the tragus of a male patient. One can see numerous vellus hairs which are not visible to the naked eye, rounding one terminal hair

and very thin; however, blond hairs that grow on the forearms, cheeks, and around the periphery of the areola of the breast can be short or very long. The majority of the areas of the human body apparently devoid of hairs, such as the forehead, eyelids, "prematurely" bald scalp, ears, and other areas erroneously called hairless (*hairless = skin without hair*), have numerous vellus hairs that can be seen very well with scanning electron microscopy (SEM) (Fig. 12) with follicles that are visible on histological skin preparations of "separated skin" when viewed with low-intensity light microscopy.

The "intermediate-sized hairs" may be 1 cm, more or less, and are found mostly on the limbs, abdomen, and thorax of hirsute Caucasian men. The intermediate hairs are not as large and long as terminal hairs, and most remain at the same size and appearance throughout the lifetime. Actually, in the elderly, intermediate-sized hairs of the beard, mustache, and other body areas tend to become thicker.

Human hair color goes from black to white, including red. This different color possibility is due to the variable number and distribution of melanosomes which produce melanin. The melanosomes are distributed in the form of rounded black points on cortical cells (Fig. 13). Most hairs contain eumelanin, a pigment that depending on its quantity produces black, dark brown, brown, light brown, blond hair color, in that order, while red hairs contain the same amount of eumelanin and pheomelanin (Ito and Wakamutsu 2011). The configuration of the hair surface can cause light to be scattered in different directions, which contributes to color and gloss.

As for hair growth, all body hair grows to the envisaged "length" that is characteristic of each area of the body and each individual. All hairs are replaced periodically by others of the same size and length. This means that the hair follicles have controlled growth and rest periods known as *hair growth cycles*. We are not immediately aware of these growth cycles because human hair growth is asynchronous, while it is synchronous (synchronous growth means that every hair on any skin area is in the same growth phase) in mice, lagomorphs, and others. Thus, in humans, neighboring hairs, even those that emerge through the same

Fig. 13 Melanosomes like *rounded black dots*, distributed over the cortical cells

orifice, may be in different phases of the cycle. Growth periods become less frequent in the elderly in which the periods of inactivity (*telogen*) are longer.

Most hairs "emerge" on the skin surface following characteristic patterns (Perkins et al. 1967) according to the body area and species. In human skin, particularly in older people, the patterns are difficult to identify. Hairs grow inclined from the head to the distal portions of the limbs, that is, arms and legs, but on the face, crown, dorsal-sacral region, abdomen, and certain areas, hairs grow following a spiral pattern.

The number of hairs, the patterns that emerge, the "density of distribution" on the body, and their growth rates (Saitoh et al. 1967) are similar in men and women, with the size of each hair that each follicle produces being the only real difference between the sexes. After the age of 50, the hair density generally decreases in both sexes, even in adults who show no signs of baldness on the scalp.

The "growth" of the majority of the hairs is approximately 0.4 mm per day (Saitoh et al. 1967). Barman et al. (1965) believe that in both sexes, the hair grows faster between 16 and 46 years of age. Puche et al. (1971) have observed that the density decreases in the axilla hair at a rate of about 0.31 hairs per year and Pecoraro believed that the rate of hair growth in humans is characteristic for each zone (Orentreich 1967). Some authors have calculated the percentage of terminal hair in respect to the vellus hair on each sex and in different parts of the adult human body; however, these data have no real value, as most of vellus hairs are not visible to the simple visual inspection, only being visible with SEM. Even so, of the 100,000–150,000 terminal hairs that are said to be growing on the scalp, around 10,000–15,000 are renewed every year, or what is the same, 35 per day (Randall 2004; Bradfield 1974). Although we know all these details, we must remember that the growth rate of other follicles varies depending on the age, health, and internal and external environmental conditions (Montagna et al. 1992).

In general, it is said that hair grows faster in women than in men (Orentreich 1967). Leaving apart the diurnal variations, and sex and age of individuals, Japanese researchers have estimated that human hair grows about 0.5 mm per day in the region of the crown of the head and 0.4 mm in the temples. The "lashes" that emerge in the anterior edge of the ciliary portion of the eyelid margin are more numerous and longer in the upper eyelid since in it, there are about 100–150 eyelashes, while on the lower eyelid, there are 70–75, and they are arranged in a single row but at different levels, so if any of the adjacent eyelashes, one or two, are lost, it will not leave a visible space (Cotsarelis et al. 1990). They grow for 30–45 days, after which they rest for 105 days. At the base of the eyelashes, there are modified sweat glands known as Moll glands and other sebaceous glands known as ciliary glands that secrete a sebaceous material like the Meibomian glands, which are about 20–30 sebaceous glands which are found in the posterior lip. This sebaceous material of the ciliary glands along with the Meibomian glands constitutes the rheum. The "eyebrow hairs," structures that measure about 5.5 cm and which are located between the forehead and eyelid, separated by the glabellar area, have a follicular cycle of 112 days and there are typically about 600 per eyebrow, approximately

100 per cm^2. The "beard hairs," the coarsest of the body, grow about 0.3 mm per day, and if they are not cut, they can grow up to 30 cm or more. With age, many unpigmented vellus hairs growing on the pinna, tragus, and antitragus, inside and around the external auricular orifice, on the surface of the nose, and into the nostrils of men can become intermediate or terminal hairs (Puche et al. 1971). Postmenopausal women often have visible hair in any place, but especially in the mustache area, along the side of the upper lip, on the chin area and jaw regions. The "*pubic hair*" usually, but not always, is curled or twisted on its axis and can reach 16 cm although it will be shorter or longer in some individuals; pubic hair coarseness is also an individual characteristic. In older people, pubic hair is usually almost straight, thinner, and longer than in young people. The pubic hair grows primarily in an area that outlines an inverted triangle in both men and women. Many people wrongly believe that pubic hair of men grows in a rhomboid shape, with the vertex of the major axis directed toward the navel. In reality, some Caucasian men have coarse hair that grows on the abdomen, tending to accumulate in the midline, but these hairs should not be confused with pubic hair. The "axillary hair," like the pubic hair, is also curly on its axis in young people, and it is said to be coarser in men than in women. As with the pubic hair, the axillary hairs become straight and thin with increasing age. Axillary hairs almost disappear in many older people both men and women.

5 Some Physiological Aspects of Hair

Human fetuses begin to show primordial follicles on the eyebrows, upper lip, and chin at the end of the second and beginning of the third month. These areas are the "hairlines" that have a similar distribution in each person. Later, follicles appear on the forehead and scalp, and from the 4th–5th month in the rest of the body. As the skin expands, primary and secondary follicles emerge between those already existing, forming groups of three or more.

The hair follicles of human scalp have completed two or more cycles of growth in utero whose sequences are the same as in postnatal life. Therefore, hairs are observed in *vernix caseosa*.

5.1 Hair Growth

Although the hair growth will be explained in another later chapter, it is necessary to describe the "follicular cycle" with three stages, the growth or "anagen" stage, the quiescent or rest or "telogen" stage, and the transition stage from anagen to telogen or "catagen." We adopt the term "anagen," and consequently "catagen" and "telogen," because the basic term is "anagenesis," which means "regeneration of destroyed parts from those conserved" (Fig. 14).

In the introduction, we noted that after the three stages of the cycle, there is an early anagen stage. This mechanism is not so simple since there are six stages of anagen (anagens I–VI) and two large parts in the cycle: proanagen and metanagen (Camacho et al. 2013).

5.1.1 Proanagen

This includes the first five stages of the anagen. In anagen I, cells of the papilla increase in size and increase RNA synthesis (Fig. 15a). At the same time, the secondary germ cells, probably induced by the cells of the bulge, were in turn activated or stimulated by the dermal papilla ("activation swelling" hypothesis) (Cotsarelis et al. 1990), beginning in depth growth (Figs. 15b). In anagen II, the secondary germ grows into the depths adopting a truncated pyramidal form that pitches toward the interior of the dermis to the papillary mesenchymal cells (Fig. 15c) and immediately after surrounds the papilla (Fig. 15d), starting the formation of hair and inner root sheath. In anagen III, the maximum follicular length is reached. At this stage, the bulb increases in size and tends to include all of the papilla, the dendritic melanocytes begin the formation of melanin, and hair may already be observed, although it is still short and surrounded by the inner root sheath (Fig. 15e). The anagen IV stage is characterized

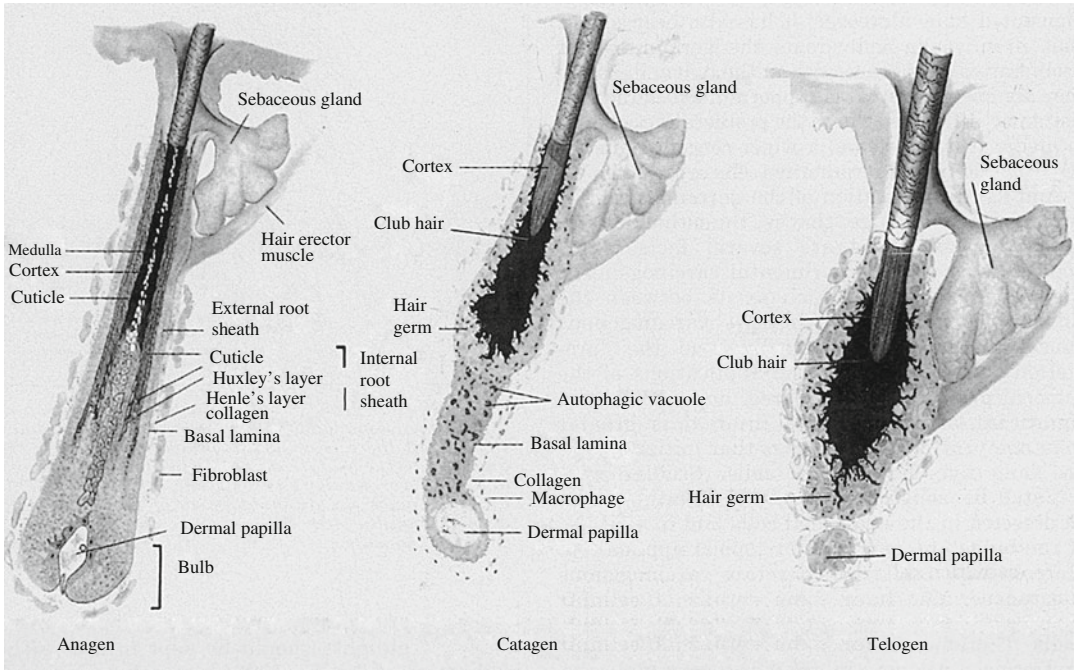

Fig. 14 Hair growth cycles. On the *left*, there is an active follicle "in anagen"; in the *middle*, there is a follicle "in catagen"; and on the *right*, there is a follicle "in telogen." Only the *lower* part labeled as transient is reabsorbed during catagen

by evident hair growth with the distal end at the level of the sebaceous gland. Furthermore, dermal papilla cells undergo proliferation and temporary decondensation, probably in response to a signal from the matrix. In anagen V, the distal end of the hair is at the level of the follicular ostium.

5.1.2 Metanagen

This encompasses from anagen VI, the stage in which the hair emerges in the skin surface, to the next rest stage, naturally including the catagen stage.

5.1.3 New Terms That Are Part of the Follicular Cycle

The terms "exogen" or "teloptosis" and "ketogen" have been introduced recently. We are going to explain them. When hair is in the telogen phase, it is eliminated constituting the "teloptosis" or "exogen" phase and the one that is inside the follicle in anagen should appear, corresponding to the final phase of anagen V, even within the proanagen stage and a prior step to metanagen. If there is hair in anagen inside, then the follicle is empty or in the "kenogen" phase, which is the true resting phase when the follicle is inactive. It is also known as "latent phase." Reduction in the duration of anagen with the extension of the ketogen occurs primarily in males with androgenetic alopecia.

5.2 Cyclic Follicular Activity

The activity varies according by the region and even in the same area. The cycle is typical of each follicle and is independent of the others. The anagen/telogen relationship expresses the cycle of each hair (Montagna et al. 1967; Camacho et al. 2013; Montagna 1988). The total number of hair follicles on the human body is estimated at about five million.

Hair follicles have a rate of mitotic activity in 12 h, usually during the night and during sleep.

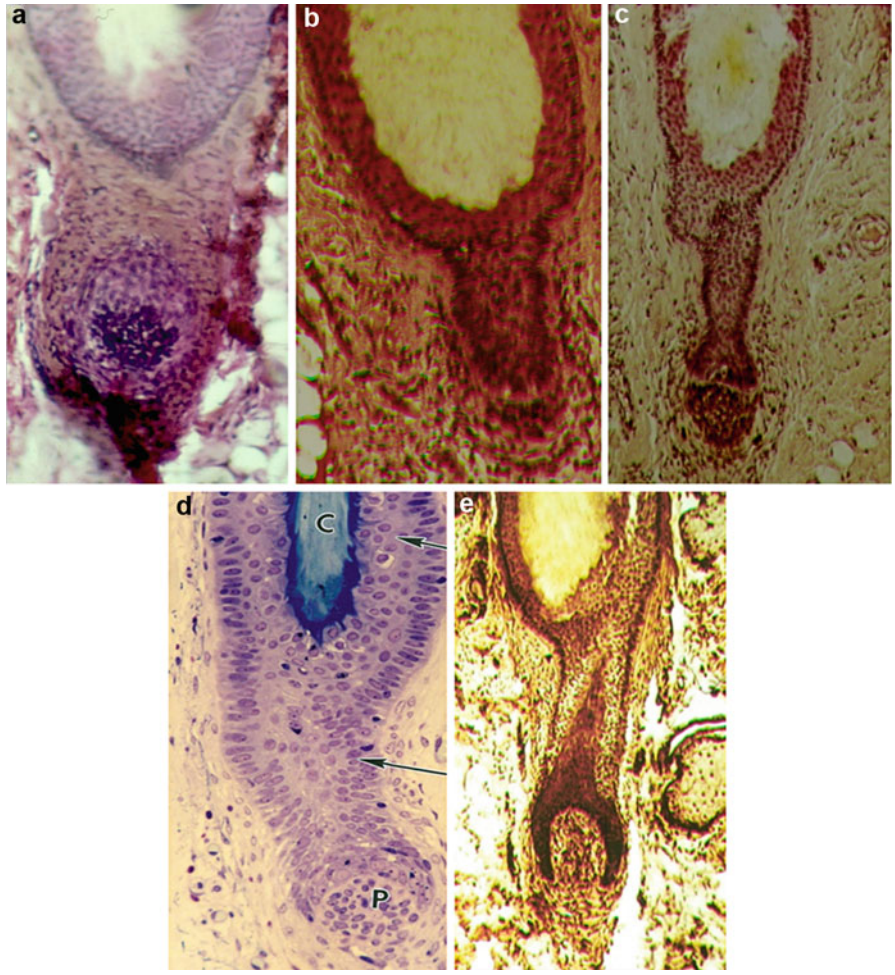

Fig. 15 Proanagen. (**a**) Finishes the telogen phase, the papilla cells of the secondary germ begin to increase in size and increase RNA synthesis. (**b**) At the same time, the matricial bulb cells of secondary germ also begin in depth growth. (**c**) In anagen II, the secondary germ grows into the depths adopting a truncated form that pushes toward the interior of the dermis to the papillary mesenchymal cells. (**d**) Immediately after surrounds the papilla, beginning the formation of hair and inner root sheath. (**e**) In anagen III, the maximum follicular length is reached. At this stage, the bulb increases in size and tends to include all of the papilla, the dendritic melanocytes begin the formation of melanin, and hair may already be observed, although still short and surrounded by the inner root sheath

Only the hair of the beard and forearms has a higher growth rate during the day.

The anagen phase is different depending on the hair type. Thus, the hair has an anagen phase of 2–6 years, that is, 3 years on average. As the telogen lasts 3–6 months and the catagen around 3 weeks, the "rule of three" (3 years-3 weeks-3 months) is used to define the duration of a follicular cycle of the scalp. However, the anagen stage is shorter in terminal hair of other regions; for example, the body has stages with periods of similar duration that reach a maximum of 6 months: that of the arms, 13 weeks of anagen and another period of telogen; and that of the legs, 20 weeks for both phases (Sayag and Aquilina 1989). Others have chronological differences in their cycles such as the beard, which has a 1-year anagen stage and a telogen stage of 10 weeks: that of the hands, a 10-week anagen stage and 7-week telogen stage (Camacho 1987); the pubic region with an anagen stage of 45 weeks and a telogen stage of 50 weeks; and the upper lip with an anagen stage of 12 weeks and a telogen stage of

6 weeks (Sayag and Aquilina 1989). Eyelashes have an anagen stage of 30 days, catagen stage of 15 days, and a telogen stage of 106 days (De Villez 1986).

In a normal scalp, one will observe 85–80 % of follicles in anagen, 13 % in telogen, and 1 % in catagen, which signifies that, since there are around 100,000–150,000 hairs, daily it has to shed 35–100 hairs, being this number higher after washing because this eliminates some that would not have been removed spontaneously (Camacho 1987). Without considering washing, the amount of hair left every day on the pillow, clothing, or combing varies between 31.9 and 37.6, considering that whenever more than 50 hairs are shed each day, the possible pathological cause should be investigated (Stroud 1987).

The percentages of cycle stage are different depending on the area; therefore, the number of telogen hairs is lower, in both sexes, in parietal and occipital regions than in frontal and crown areas. In the latest two regions, the telogen percentage is 17 %, being different in men and women because in the men, it is 18.22 %, while in women, it is 16.48 %, which explains the differences of frontal hair growth which is denser and lower in women than in men.

And to end this section, we must recall that the cycle of each follicle varies according to the region and even in the same area, with even the way of appearing is different since some come out surrounded by debris and others clean. In summary, each hair has its own characteristics that differentiate them from the adjacent hairs and, furthermore, there may be hair in different body areas with identical morphology (Montagna et al. 1967; Camacho et al. 2013; Montagna 1988; Uno and Montagna 1988).

These differences, or characteristics of each hair, have been studied closely in the areas with terminal hairs or unwanted vellus that are desired to be eliminated, especially in women. For that reason, we will not comment here the percentage in the anagen phase or the duration of the telogen phase of the vellus of the chest and abdomen that many men, called "metrosexuals," remove. In the beard area, 70 % of the hairs are in the anagen phase and the telogen phase lasts 10 weeks; the mustache area has 65 % of hairs in anagen and the telogen phase lasts 6 weeks; in the axilla, 30 % of the vellus are in anagen and the telogen usually lasts about 3 months; on the arms 20 % of hairs are in the anagen phase and telogen phase lasts about 18 weeks, and on the legs and thighs, there are also 20 % of the hairs in the anagen phase with the telogen phase lasting 24 weeks (Wanitphakdeedecha and Alster 2008; Table 1).

One datum that is known all over the world but until now no one knew why it occurs is that "the growth rate of gray-white hair is significantly higher than the black hair." In the study of the expression of genes of keratins and their associated proteins, it has been demonstrated that they are overstimulated to twice their activity in active growth of white-gray hair, compared with black-pigmented hair (Choi et al. 2011). The structure, follicular cycle, and pigmentation of eyelashes have been well studied by Bernard's team (Thibaut et al. 2010).

5.3 Hair Growth Pace After Being Pulled Out

This is a question asked by many patients after trichogram and after shaving the scalp. The new hair takes about 129 days to appear in the vertex, about 117 in the temporal regions, and about 92 days on the cheeks.

5.4 Hair Thickness

The volume or diameter of the hairs is related to the matrix/bulb. To check the hair diameter, one observes under graduated microscope 0.025 mm divisions. The diameter of the hair increases in the first 3 or 4 years of life, and it is somewhat less over the next 6 years and increases little from 12 years. The diameter of a *terminal hair* of the scalp of an adult is about 70 μm (60–84 μm) (Fig. 16). We speak of thick hair when its diameter is 0.1 mm, of an *intermediate hair* when it is about 0.05 mm, and thin hair when the diameter is approximately 0.025 mm (Olsen 1999). In older people, hair diameter is reduced, while in a young adult (21 years old) the percentage of hairs

Table 1 Hair growth cycle in different areas of the body

	% Telogen	% Anagen	Telogen duration	Follicular density (No. fol./cm^2)	Follicular depth
Scalp	10–15	85	3 months	350	3–5 mm
Eyebrows	85–95	5–15	3–4 months	100	1.1–1.4 mm.
Eyelashes	60–70	0–40	3.5 months	[a]	1.9–2.2 mm
Mustache	35	65	6 weeks	500	1–2.5 mm
Beard	30	70	10 weeks	500	2–4 mm
Axilla	70	30	3 months	65	3.5–4.5 mm
Trunk	[b]	[b]	10 weeks	70	2–4.5 mm
Pubic area	65–81	19–35	12 weeks	70	3.5–4.5 mm
Arms	72–86	14–28	2–4 months	80	[c]
Legs	62–88	12–38	3–6 months	60	2.5–4 mm
Thighs	64–83	17–36	2–3 months	60	2.5–4 mm

[a]There are 420 eyelashes between the two lids: on the upper lid, 100–150 measuring 8–10 mm and on the lower lid, 70–75 measuring 6–8 mm
[b]Differences between chest, abdomen, back, and lumbar regions
[c]No studies were found, probably due to lack of interest. It seems that the depth of the follicles in the dermis is different between males and females

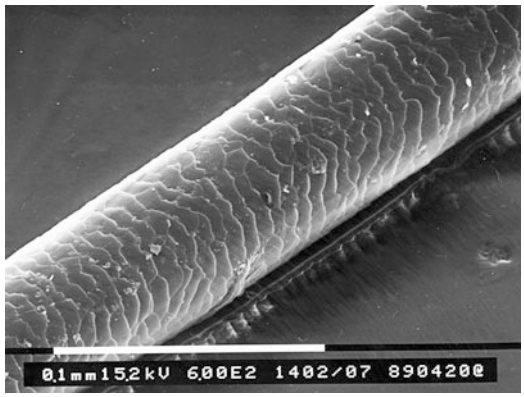

Fig. 16 SEM micrograph of a normal hair fiber. Note the increasing irregularity of the free cuticular edges (*left* to *right*). *White bar* 1 mm

according to thickness is 72.1 % thick, 18.8 % intermediate, and 10 % thin. This phenomenon occurs in all regions and is independent of follicular density. It is important, however, to remember that there is a direct relationship between the growth phase and thickness of the hair; therefore, 84 % of thick hairs are in the anagen phase, only 4 % in catagen and 12 % in the telogen phase.

Apart from the terminal hairs, there are vellus and intermediate hairs. The *vellus* are short, thin, and hypopigmented and have a diameter less than 0.03 mm, that is, like the thin terminal hairs. And before, we indicated that *intermediate hairs* have a thickness of about 0.05 mm (Sperling 1991). Besides this difference in thickness between vellus, terminal hairs, and intermediate hairs, there is also a difference between pigmented and nonpigmented terminal hairs, because the white or gray hair has greater thickness than the pigmented hair (Gayoso et al. 1982).

As about the "shape," the cross section of the hair during the first 2 years of life is round, later becoming oval. By about age 3, it has an oval surface area of about 0.25 mm^2 and gradually widens to reach 0.40 mm^2 at 17 years of age (Fig. 17). Therefore, from that moment, the terminal hair has a major axis and a minor axis (Hutchinson and Thompson 1997). Eyebrows and eyelashes are flat and curved. Follicular depth of the eyebrows in the dermis is from 1.02 to 1.20, and the eyelashes of 1.8–2.2 mm (Thibaut et al. 2010). The pubic vellus are twisted on their axis.

As we have indicated, the hair has an elliptical shape, but as it grows, that is to say, become separated from the scalp, it presents variations. Thus, it has been observed that the hair in full anagen phase, which is usually about 6–8 cm from the scalp, is when it presents its larger diameter but from that point, there are variations of the major transverse axis which is reduced by up to

Fig. 17 Cross section of normal Caucasian hair with a discontinuous medulla (*center*). The cut through the fiber caused a disorder of the cortex material when the compression forces of the cutting edges were released (*bottom* of fiber). *White bar* 0.1 mm

20 %, and its elliptical shape is reduced by approximately 13 %, while the minor transverse axis is unchanged. These changes, which are due to intrafollicular mechanisms, are responsible for the fact that as the hair grows in the anagen phase, it becomes thinner and round (Messenger 2011; Montagna et al. 1985b).

5.5 Hair Length or "Linear Growth"

This is related to the duration of the anagen phase. The *scalp hairs* grow from 0.37 to 0.50 mm per day, specifically about 0.5 mm per day in the region of the crown and 0.4 mm in the temporal region. The growth of hairs from other areas is different: the hairs of the *beard* grow about 0.27 mm per day; those of the *chest*, 0.44 mm; those of the *axilla*, 0.36 mm; those of the *thighs*, 0.29 mm; those of the *pubic area*, 0.40 mm; those of the *eyebrows*, 0.16 mm; those of the *back*, 0.13 mm; and those of the *forehead*, 0.03 mm.

The daily growth of hair in children has not been studied in depth. It is known that while the vertex is around 0.05 mm/day in the occipital and parietal regions, it is 0.30–0.35 mm/day in the parietal region. The hair growth on the thighs is 0.13–0.20 mm/day, a proportion that is usually maintained in adults.

With regard to the maximum hair growth, we know that the eyebrows measure about 1 cm (Montagna et al. 1985b) and the hair on the forehead varies between 1.5 and 2.2 mm, that of the chest between 3.4 and 5.1 mm, and that of the back between 4.9 and 6.4 mm. The beard hair in males can reach up to 30 cm, the pubic vellus up to 6 cm, and that of the axilla varies between 1 and 6 cm. We also know that the axillary and pubic vellus begins at puberty and has its greatest diameter around age 25 and declined thereafter (Messenger 2011).

5.6 Gender Differences

And in relation with gender differences, we know that the scalp hair diameter of the women increases from the age of 22 having its point of greatest diameter at 30 years of age and decreasing from that time (Messenger 2011). The eyebrows and nose hairs, those of the ears and even the beard, in women begin to grow later and also increase later remaining the same throughout their life except for the beard which grows in the elderly (Messenger 2011). For the other types of hair, we already accepted that there is the same amount of follicles and hair on the body of women as on men despite the appearance of "hairy" skin in males.

The implantation of frontal hairline is different in men and in women. In women, the hairline is more anterior (Fig. 18a), sometimes occupying almost the entire forehead and occasionally adopting a pyramidal form (Fig. 18b). Although there are differences between the values of the frontal hairline of Spanish and American women (Ceballos et al. 2013; Nusbaum and Fuentefria 2009) and the shape of the foreheads of Korean women (Jung et al. 2011), we cannot fail to mention that the measurements are made taking into account the average distances between a center front point known as "widow's peak" two "lateral protrusions" at about 4 cm and two other points at the temples at 4 cm too (Fig. 19, red line). The widow's peak measures 1.83 in width and 0.80 in height (Fig. 19, angulated red line). The forehead height is measured between the lowest point of the

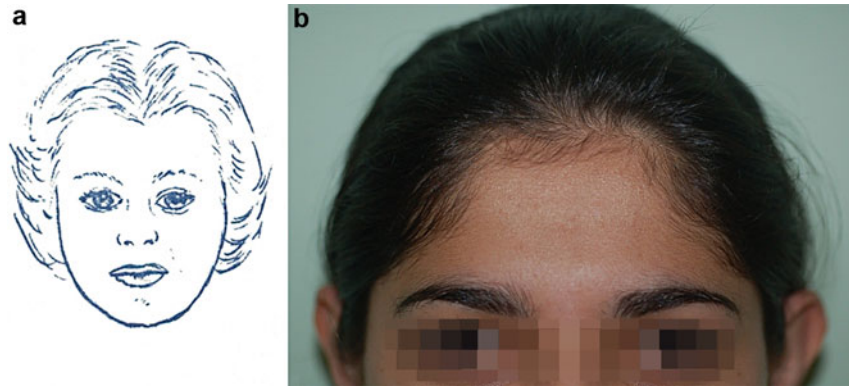

Fig. 18 (**a**) Normal frontal implantation hairline in woman. (**b**) Although it is lower than in men, occasionally, it can be very low occupying almost the entire forehead, at time adopting pyramidal form

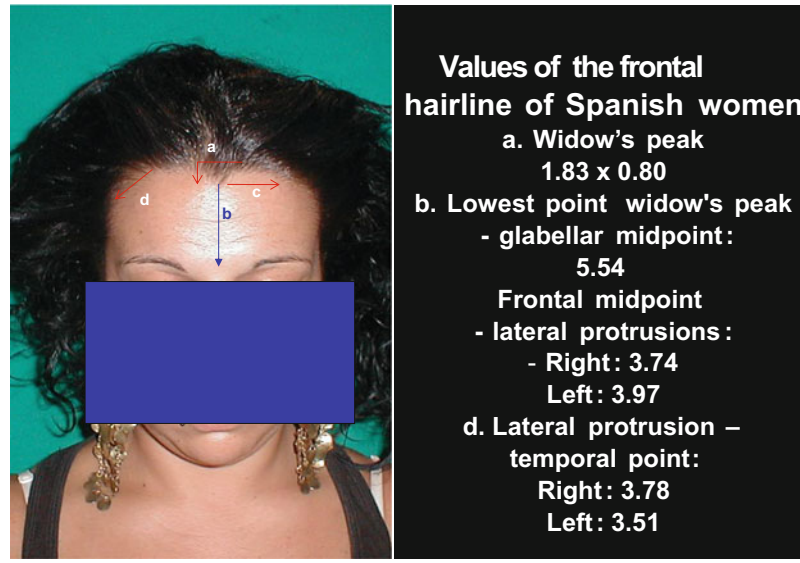

Fig. 19 Values of the frontal hairline of Spanish women. ***a*** Measures of the widow's peak: 1.83 wide – 0.80 high. ***b*** *blue* Measure from lowest point widow's peak to the glabellar midpoint: 5.54 cm. ***c*** Measure from the frontal midpoint to the lateral protrusions: *right*, 3.74 cm; *left*, 3.97 cm. ***d*** Distance between lateral protrusion and temporal points: *right*, 3.78 cm; *left*, 3.51 cm

widow's peak and glabellar midpoint, that in Spanish women, the middle is of 5.54 cm (Fig. 19, blue line). In addition, the outline of the temporal regions or receding hairlines must be assessed as triangular, concave (which are the known triangular or concave "receding hairlines," respectively), convex, or straight. The five forehead patterns of the Korean surgeons are round, M-shaped, rectangular, bell shaped, and triangular (Jung et al. 2011). In woman, the density of the mid-forehead line decreases with age from 293 ± 61.3 hairs per cm^2 at age 35 to 211 ± 55.1 hairs per cm^2 when she is 70 years old (Olsen 1999; Messenger 2011).

The rhythm and manner of growth are also different according to sex and area. Thus, the beard hair only tends to grow in the male with the exception of some individuals in whom it reaches a considerable length; in general, it only grows to 30 cm. Pubic vellus, which is curved and twisted around its axis and measures approximately 60 mm in length, is thinner, hypopigmented, and longer in the elderly. Also, pubic vellus grows differently in men than in women, considering it a secondary sexual characteristic because while in women it should be distributed in the shape of an inverted triangle on the

mons Venus, in the male, the distribution is rhomboidal with the greatest axis over the linea alba (Montagna et al. 1985b).

Even the scalp hair has a different growth rhythm for men and women, as in 10 days the average growth in males is 3.70 mm while in females it is 3.39 mm.

5.7 Racial Variations

There are also racial variations. For example, the black and oriental races have less body hair than whites. Moreover, the growth of the beard in Caucasian males is also much greater than in the Japanese. The only places lacking hairs are the palms, soles, dorsal surface of the last phalanx of the fingers, nipples, penis, clitoris, and inner surface of the vulva (Gayoso et al. 1982).

There are also variations regarding the direction of the hair: (a) Mongoloid and Caucasian hairs (Fig. 20a) are straight because the follicles are oriented vertically to the skin surface; (b) the hair of blacks are spirals, like wool, although with greater texture (Fig. 20b) because the follicles are curved and the lower portion is placed in an almost horizontal position to the skin surface (Blume et al. 1991); (c) the hair of Australasian aboriginals is wavy; and (d) the hair of white Caucasians can be of any shape, like above, including wooly hair spiral or, more commonly, straight hairs which tend to bend as the follicle makes an acute angle with the skin surface.

And writing about racial variations, there is a subject which is worth considering here. Caucasians may have straight or curly hair (Fig. 21a, 21b), and it may be blond (Fig. 22a), red (Fig. 22b), or black (Fig. 22c). Straight hairs are produced by follicles with a round lumen, while the curly hair come from follicles with an elliptical or oval lumen (Lindelöf et al. 1988). Moreover, both Caucasian males as well as females show a tendency to have body hair, which makes this one of the major racial differences since while Caucasian women may be hirsute, those of other races do not tend to be so (Montagna et al. 1985b).

5.8 Variations Chronological

With respect to the age, hair grows faster between 16 and 46 years, clearly decreasing after 50 years of age.

The percentages in anagen, catagen, and telogen hairs during fetal life and in the first

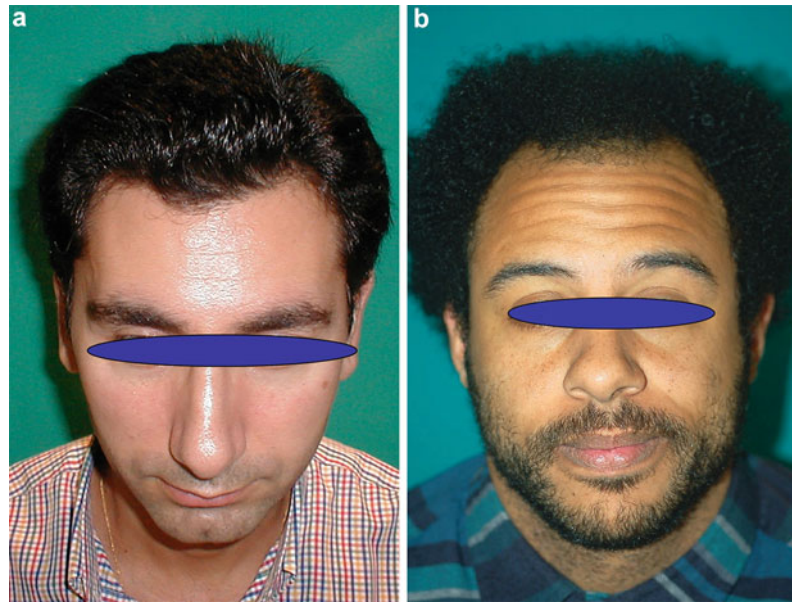

Fig. 20 *Variations regarding the direction of the hairs:* (**a**) *Mongoloid and Caucasian hair is straight whereas* (**b**) *Negroid hair is spiral shaped*

Fig. 21 *Caucasian can present straight or curly hair.* (**a**) *Caucasian boy with straight blonde hair.* (**b**) *Caucasian girl with fine curly hair*

Fig. 22 *Hair color* (**a**) A woman with straight blonde hair. (**b**) A woman with red curly hair (**c**) A woman with straight black hair

weeks after birth are totally different from those of adults because the cycles in the fetus are very short. Around the fifth month of intrauterine life, all the hairs are in anagen phase, although the follicles are small and produce very thin hairs. In another 8–10 weeks, that is, at about the seventh month of prenatal life, the majority of the follicles of the frontal and parietal regions pass to the telogen phase, beginning in the frontal region, and a week later in the parietal area. These cycles are very short, lasting about 8 weeks, beginning a new anagen cycle in these two regions about 5–6 weeks before birth. For this reason, at the moment of birth, there is a superposition of cycles according to areas because while the scalp hairs of the frontal and parietal areas are already in a new follicular anagen cycle, those of the occipital area are still in the first. The percentages of scalp hairs in catagen and telogen phases at the time of birth are 31.6 % of the frontal region, 26.1 % of the parietal region, and 16.1 % of the occipital region. After birth, the follicles of the temporal and occipital areas quickly become telogenic, with approximately 100 % of them being in this phase between the 10th and 16th weeks while only 50 % of those on the frontal region are telogenic. Around the

32nd to 40th weeks, the percentage of anagen hairs stabilize throughout the scalp. This percentage of 100 % of scalp hair in the telogen phase in the occipital region toward the tenth week justifies the presence of occipital alopecia in children who sleep in the supine position due to the friction with the pillow (Janniger and Bryngil 1993).

Children between 3 and 11 years of age have 90 % of their hairs in the anagen phase, with this percentage being higher in the occipital region, and in the crown than in the frontal, and parietal areas.

Research has been carried out in American children between 14 and 18 years of age on the hair density in different parts of the body, observing that the vellus that first appears is the pubic hair which is complete at age 16. Next emerges axillary vellus which at 14 years it is 40 %, at 16 years it is 97 %, and it is complete at 18 years of age. This is followed by the anterior surface of the legs, anterior surface of the thighs, forehead, abdomen, buttocks, cheeks, lumbar region, and arms (Table 2).

In adults over 50 years of age, a number of variations can be observed: (a) there is a lower hair density and a greater range of dispersion; (b) the hair density of women is less than that of men; (c) the growth rhythm is also less at this age; (d) both on the scalp and in other body regions the number of thick hairs is higher in older people than in those under 46 years of age; and (e) the proportion of scalp hairs in the telogen phase is greater, although there are differences according to age, such as males between 60 and 83 years show a lower proportion of scalp hairs in the telogen phase than those between 50 and 59 years (Barman et al. 1969).

Table 2 Percentage of hair growth in three ages of American children

Area	14 years	16 years	18 years
Pubic region	97	100	100
Axilla region	40	97	100
Anterior leg region	46	90	100
Anterior thigh region	30	67	95
Forehead	14	37	80
Abdomen	14	37	75
Buttocks	14	33	50
Cheeks	3	7	40
Lumbar region	3	7	20
Arms	0	0	10
Shoulders	0	0	0
Thorax	0	0	0
Ear canal	0	0	0

5.9 Follicular Density

"Follicular density on the scalp" refers to the "number of follicles per cm^2 of surface," which varies clearly according to the age (Table 3). In newborns, there is nearly almost double the number of follicles than between the ages of 20 and 30 years and about three times more than in 80–90 years. In addition, one must remember that bald people undergo a "miniaturization" of the follicles, which is because they also have a lower follicular density. The follicular density is not very different in both sexes.

An important aspect to note is that "speaking of follicular density is not the same as speaking of hair density" because, usually, the number of hairs that emerges is much smaller than the number of "follicular units" existing in the area. The follicular unit usually consists of four to five follicles, sometimes more, but with a common erector muscle. There are follicular units with low hair density that produce only one or two scalp hairs and others of high hair density containing three to five hairs (Messenger 2011). Prepubertal children,

Table 3 Follicular density in scalp by age

Age	cm^2
R. N.	1,135
3 m–1 year	795
20–30 years	615
30–50 years	485
50–70 years	465
70–80 years	465
80–90 years	435
Bald	
45–70 years	330
70–85 years	280

i.e., 3–9 years, have crown hair density of 250 hairs/cm^2 and 170–205 hairs/cm^2 in the parietal and occipital areas. Boys have a slightly higher scalp hair density than girls.

Studying scalp hair density in the parietal region of a group of women and two subgroups of men with a mean age of 60.5 years for men and 63.4 for women, it was found that the average density was 163.8 ± 12.6 (87–330) hairs/cm^2, with the group of women being 147 ± 10.4 (87–215) hairs/cm^2, the subgroup of men between the ages of 54 and 59 years being 178 ± 13,4 (104–330) hairs/cm^2, and the subgroup of men between ages of 60 and 83 years being 161 ± 13.6 (90–270) hairs/cm^2, with the density in the total groups of males being 168.5 ± 13 4 hairs/cm^2 (Messenger 2011).

In a recent study, it was shown that the hair density decreases with age (Barman et al. 1969), but another more current study, in which a group of males with or without androgenetic alopecia, aged between 25 and 32 years, except one who was 49, were followed up for 8–14 years, showed a reduction not only of hair density but also of the follicular activity. This is due to the fact that aging causes the growth cycles to be shorter, while the quiescent periods are lengthened, which leads to there being fewer active follicles and thus fewer and thinner hairs per unit area (Courtois et al. 1995).

For the study of follicular density on the scalp, the use of TrichoScan has been evaluated positively, among other reasons because it always is done in the same area and at the same distance. However, in order to know the hair density in other areas, such as the beard, the measurements of follicular density must be based on other measures. Wan et al. (2011) used transparent templates with a diameter of 2.5 cm which were placed on four or five areas of the treated beard, observing that the hair density grew in each of them after having been 2 days without shaving the area. Controls were performed in 2–4 weeks with a Nikon D70S machine at a distance of 30 cm. The overall assessment that resulted depended on a previously created scale in which areas with complete alopecia were evaluated as 0, while a score of 1 had very little repopulation, 2 had little repopulation, 3 moderately dense, 4 dense, and 5 very dense. An area with a count of 195.0 hairs was considered as moderately dense and with 237.2 hairs as dense ($P = 0.003$). While this type of counting may be valid, it has the limitations of not being able to get a tattoo in the area to take samples always in the same area and not using devices capable of taking the picture in the same projection and distance, so the results may be variable. However, it is an inexpensive method that uses an inexpensive material.

5.10 Seasonal Changes in Hair Growth

In many mammals, hair growth throughout the year is related to the length of daylight and to a lesser proportion to the existing temperature. The follicle interprets these environmental changes as if they were consequence of alterations of the pituitary and hypothalamic hormones, which in turn regulate the levels of many circulating hormones including the gonadal, thyroid, and corticosteroid hormones, which are well known that alter the mammalian follicular activity. Prolactin is involved in the seasonal changes of red deer, mink, and goat (Randall 2004).

Although the human hair growth is different from mammals, it also undergoes changes with the seasons. The scalp hair of Caucasians, both men and women, have an annual cycle with the highest loss in the autumn, while the percentage of scalp hairs in anagen at the beginning of spring is 90 % and in the summer 80 %; therefore, there are also people who notice the beginning of the falling hair season in summer.

And just as in mammals, there is greater hair loss in relation to the amount of daylight; it was found that men who work in closed places have increased hair loss when they are exposed to the sun for a much time in the long days of summer.

Hair growth of the beard and thighs has also been associated with winter or summer seasons. It has been observed that, while in winter it grows much slower, in summer it may even increase by 50 % in the beard and, although the percentage is not known, thigh hair grows faster in men than in women. These changes seem to be related with an

increase in the androgens that is found in the summer.

References

Ahn Y, Sims C, Logue JM, Weatherbee SD, Krumlauf R. Lrp4 and Wise interplay controls the formation and patterning of mammary and other skin appendage placodes by modulating Wnt signaling. Development. 2013;140:583–93.

Barman JM, Astore I, Pecoraro V. The normal trichogram of the adult. J Invest Dermatol. 1965;44:233–6.

Barman JM, Astore IPL, Pecoraro V. The normal trichogram of people over 50 years but apparently not bald. In: Montagna W, Dobson RL, editors. Advances in biology of the skin, Hair Growth, vol. 9. Oxford: Pergamon Ed; 1969. p. 211–20.

Billingham RE. A reconsideration of the phenomenon of hair neogenesis with particular reference to the healing of cutaneous wounds in adult mammals. In: Montagna W, Ellis RA, editors. The biology of hair growth. New York: Academic; 1958. p. 41–6.

Blume U, Ferracin J, Verschoore M, Czernielewski JM, Schaefer H. Physiology of the vellus hair follicle: hair growth and sebum excretion. Br J Dermatol. 1991;124:21–8.

Bradfield RB. The effects of malnutrition on the morphology of hair roots. In: Montagna W, Parakkal PF, editors. The structure and function of skin. San Francisco: Academic, A Subsidiary of Harcourt Brace Jovanovich, Pub; 1974.

Cadau S, Rosignoli C, Rhetore S, Voegel JJ, Parenteau-Bareil R, Berthod F. Early stages of hair follicle development: a step by step microarray identity. Eur J Dermatol. 2013;22 Suppl 2:4–10.

Camacho F. Anatomía y fisiología del folículo piloso. Piel. 1987;3:156–68.

Camacho Martínez FM. Aspectos anatomofisiológicos del cuero cabelludo. Monogr Dermatol. 2009;22:3–9.

Camacho FM, Montagna W. Algunos aspectos de la fisiología del folículo piloso. In: Camacho FM, Tosti A, Randall VA, Price V, editors. Montagna's trichology. Diseases of pilosebaceous follicle. 3rd ed. Madrid: Aula Médica Ed; 2013. p. 43–60.

Ceballos C, Priego C, Méndez C, Hoffnerr MV, García-Hernández MJ, Camacho FM. Study of frontal hairline patterns in Spanish caucasian women. Actas Dermosifiliogr. 2013;104:311–5.

Choi HI, Choi GI, Kim EK, et al. Hair graying is associated with active hair growth. Br J Dermatol. 2011;165:1183–9.

Collins CA, Jensen KB, MacRae EJ, Mansfield W, Watt FM. Polyclonal origin and hair induction ability of dermal papillae in neonatal and adult mouse back skin. Dev Biol. 2012;366:290–7.

Cotsarelis G, Sun TT, Lavker RM. Label-retailing cells reside in the bulge area of pilosebaceous unit: implications for follicular stem cells, hair cycle and skin carcinogenesis. Cell. 1990;61:1329–37.

Courtois M, Loussouarn G, Hourseau C, Grollier JF. Ageing and hair cycles. Br J Dermatol. 1995;132:86–93.

Cui CY, Kunisada M, Childress V, Michel M, Schlessinger D. Shh is required for Tabby hair follicle development. Cell Cycle. 2011;10:3379–86.

De Villez RL. The growth and loss of hair. Current Concepts. Upjohn Co. Kalamazoo, Michigan; 1986.

Forslind B. Structure and function of the hair follicle. In: Camacho FM, Randall VA, Price VH, editors. Hair and its disorders. Biology, pathology and management. London: Martin Dunitz; 2000. p. 3–15.

Fu J, Hsu W. Epidermal Wnt controls hair follicle induction by orchestrating dynamic signaling crosstalk between the epidermis and dermis. J Invest Dermatol. 2012. doi:10.1038/jid.2012.407.

Gayoso MJ, Camacho F, Diaz-Flores L, Dulanto F, Montagna W. Aspectos anatomofisiológicos de interés en tricología. In: Camacho F, Montagna W, editors. Tricología. Madrid: Garsi Ed; 1982. p. 39–69.

Hamilton JB. Age, sex and genetic factors in the regulation of hair growth in man: a comparison of Caucasian and Japanese populations. In: Montagna W, Ellis RA, editors. The biology of hair growth. New York: Academic; 1958. p. 451–68.

Hashimoto K. The apocrine gland. In: Jarrett A, editor. The physiology and pathophysiology of the skin. London: Academic; 1978. p. 1575–89.

Holbrook K. Structure and function of the developing human skin. In: Goldsmith LA, editor. Biochemistry and physiology of the skin, vol. 1. New York: Oxford University Press; 1983. p. 64–101.

Hutchinson PE, Thompson JR. The cross-sectional size and shape of human terminal scalp hair. Br J Dermatol. 1997;136:159–65.

Ito S, Wakamutsu K. Diversity of human hair pigmentation as studied by chemical analysis of eumelanin and pheomelanin. J Eur Acad Dermatol Venereol. 2011;25:1369–80.

Janniger CK, Bryngil JM. Hair in infancy and childhood. Cutis. 1993;51:336–8.

Jung JH, Rah DK, Yun IS. Classification of the female hairline and refined hairline correction techniques for Asian women. Dermatol Surg. 2011;37:495–500.

Koelliker A. Zur Entwicklungs Geschichte der ausseren Haut. Z Wiss Zool. 1850;2:67–92.

Langbein L, Schweizer J. The Keratins of the human hair follicle. Int Rev Cytol. 2005;243:1–78.

Langbein L, Schweizer J. Hair keratin and keratinization. Biochemical and physiological aspects. In: Camacho FM, Tosti A, Randall VA, Price V, editors. Madrid: Aula Médica Ed.; 2013.

Lavker RM, Sun TT. Epidermal stem cells. J Invest Dermatol. 1983;81:121S–7.
Li Y-H, Zhang K, Yang K, et al. Adenovirus-mediated Wnt10b overexpression induces hair follicle regeneration. J Invest Dermatol. 2013;133:42–8.
Lindberg M, Forslind B. Formation and structure: an introduction to hair. In: Forslind B, Lindberg M, editors. Skin, hair, and nails. London: Marcel Dekker; 2004. p. 273–84.
Lindelöf B, Forslind B, Hedblad M-A, Kaveus U. Human hair form. Morphology revealed by light and scanning electron microscopy and computer aided three-dimensional reconstruction. Arch Dermatol. 1988;124:1359–63.
Lindner G, Menrad A, Gherardi E, Merlino G, Welker P, Handjiski B, Roloff B, Paus R. Involvement of hepatocyte growth factor/scatter factor and met receptor signaling in hair follicle morphogenesis and cycling. FASEB J. 2000;14:319–32.
Messenger AG. Hair through the female life cycle. Br J Dermatol. 2011;165 Suppl 3:2–6.
Millar SE. Molecular mechanisms regulating hair follicle development. J Invest Dermatol. 2002;118:216–25.
Montagna W. El pelo y su crecimiento. In: Camacho F, Montagna W, editors. A review on hair and hair growth. Madrid: EGRAF-Garsy Ed; 1981. p. 15–38.
Montagna W. The hair growth cycle revised. An historical perspective. Jpn J Dermatol. 1988;98:1376–8.
Montagna W, Camacho F. The anatomy and development of hair, hair follicles, and the hair growth cycles. In: Camacho F, Montagna W, editors. Trichology. Diseases of pilosebaceous follicle. 2nd ed. Madrid: Aula Médica Ed; 1997. p. 1–27.
Montagna W, Camacho FM. Embriología y anatomía del folículo piloso. Ciclos de crecimiento del pelo. Desarrollo de los folículos pilosos humanos. Anatomía de la glándula sebácea, glándula apocrina, músculo erector. Vascularización e inervación. In: Camacho FM, Tosti A, Randall VA, Price V, editors. Madrid: Aula Médica Ed; 2013. p. 3–37.
Montagna W, Parakkal PF. The structure and function of skin. 3rd ed. London: Academic, A Subsidiary of Harcourt Brace Janovich Pub; 1974. p. 221–2.
Montagna W, Parker F, Tosti A. IX. Axillary gland. Your personal odors. In: Montagna W, Parker F, Tosti A, editors. Skin. Your owner's manual. Rome: Antonio Delfino Ed; 1985a. p. 86–94.
Montagna W, Parker F, Tosti A. The paradox of human hair. In: Montagna W, Parker F, Tosti A, editors. Skin your owner's manual. Rome: Antonio Delfino Ed; 1985b. p. 117–39.
Montagna W, Kligman AM, Carlisle KS. Atlas of normal human skin. Berlin: Springer; 1992.
Myung PS, Takeo M, Ito M, Atit RP. Epithelial Wnt ligand secretion is required for adult hair follicle growth and regeneration. J Invest Dermatiol. 2013;133:31–41.
Nusbaum BP, Fuentefria S. Naturally occurring female hairline patterns. Dermatol Surg. 2009;35:907–13.
Olsen EA. The midline part: an important physical clue to the clinical diagnosis of androgenetic alopecia in women. J Am Acad Dermatol. 1999;40:106–9.
Orentreich N. Scalp hair replacement in man. In: Montagna W, Dobson R, editors. The biology of skin, Hair Growth, vol. IX. Oxford: Pergamon Press Ed; 1967. p. 99–108.
Perkins EM, Smith AA, Ford DM. A study of hair groupings in primates. In: Montagna W, Robson RL, editors. Advances in biology of skin, Hair Growth, vol. IX. Oxford: Pergamon Press Ed; 1967. p. 357–67.
Pinkus F. The development of the integument. In: Keibel and Mall, editors. Manual of human embryology. J.B. Lippincott Co. Ed. Philadelphia; 1910; p. 243-91.
Pinkus F. Jadassohn's Handbuch der Haut u. In: Bloch B, Pinkus F, Spalteholz W, editors. Geschlechts Krankheiten. Berlin: Springer; 1927. p. 1–378.
Pinkus H. Embryology of hair. In: Montagna W, Ellis RA, editors. The biology of hair growth. New York: Academic; 1958. p. 1–32.
Poblet E, Jiménez F. CD10 and CD34 in fetal and adult human hair follicles; dynamic changes in their immunohistochemical expression during embryogenesis and hair cycling. Br J Dermatol. 2008;159:646–52.
Puche RC, Pecoraro V, Astore I, Barman JM. Relationships between the urinary 17-ketosteroids and some characteristics of the human scalp hair. Steroidologia. 1971;2:121–7.
Randall VA. Androgen influence on hair growth. In: Forslind B, Lindberg M, editors. Skin, hair, and nails. Structure and function. New York: Marcel Dekker; 2004. p. 365–89.
Rothnagel JA, Roop DR. Hair follicle companion layer: reacquainting an old friend. J Invest Dermatol. 1995;104 Suppl 5:42S–3.
Saitoh M, Uzuka M, Sakamoto M, Kobori T. The age of hair growth. In: Montagna W, Dobson RL, editors. Advances in biology of skin, Hair Growth, vol. IX. Oxford: Pergamon Press Ed; 1967. p. 183–201.
Sayag J, Aquilina C. Hirsutismes. Marsella, SOLAL Ed. 1989.
Schweizer J, Langbein L, Rogers MA, Winter H. Hair follicle-specific keratins and their diseases. Exp Cell Res. 2007;313:2010–20.
Sharov AA, Schroeder M, Sharova TY, et al. Matrix metalloproteinase-9 is involved in the regulation of hair canal formation. J Invest Dermatol. 2011;131:257–60.
Sperling LC. Hair anatomy for the clinician. J Am Acad Dermatol. 1991;25:1–17.
Stroud JD. Diagnosis and management of the hair loss patient. Cutis. 1987;40:272–6.
Thibaut S, De Becker E, Calsey L, Baras D, Karatas S, Jammayrac O, Pisella PJ, Bernard BA. Human eyelash characterization. Br J Dermatol. 2010;62:304–10.
Uno H, Montagna W. Anatomía del folículo piloso. Monogr Dermatol. 1988;1:3–32.

Wan J, Abuabara K, Kurd SK, et al. Reliability and validity of a photographic method for measuring facial hair density in man. Arch Dermatol. 2011; 147:1328–9.

Wang HD, Yang L, Yu XJ, He JP, Fan LH, Dong YJ, Dong CS, Liu TF. Immunolocalization of β-catenin and Lef-1 during postnatal hair follicle development in mice. Acta Histochem. 2012; 114:773–8.

Wanitphakdeedecha R, Alster TS. Physical means of treating unwanted hair. Dermatol Ther. 2008;21:392–401.

Winter H, Langbein L, Praetzel S, Jacobs M, Rogers MA, Schweizer J. A novel human type II cytokeratin, K6hf, specifically expressed in the companion layer of the hair follicle. J Invest Dermatol. 1998;111:955–62.

Woo WM, Zhen HH, Ae O. Shh maintains dermal papilla identify and morphogenesis via a Noggin-Shh regulatory loop. Genes Dev. 2012;26:1235–46.

Healthy Hair

72

Philippe Assouly

Contents

Keywords

Hair • Healthy • Scalp • Ethnic • Trichoglyphs • Whorl • Biofilm • Weathering

Even healthy hair seems easy to define, trying to state clearly frontiers between healthy and non-healthy remains more than difficult. This is notably because of variations between ethnical origins and modifications correlated to age or sex. For these reasons, specific parameters need to be well known before being categorized as *normal* (*healthy*) or *pathologic*.

1 Functions of Healthy Hairs

Hair functions are essential: as a protection barrier seems obvious (mechanical, thermal regulation, UV radiations), body hair loss along the evolution of the human race could have participated at human domination upon other animals. Hairs are of course also the reflection of customs and trends in societies, who now, can we say, roughly aspire to more scalp hair and less body hair. The role of the hair as a sexual differentiation (and dimorphism) – for animals and humans – and attraction, its meaning within religions, its significance in mythology, the symbolism related to shaving imposed as punishment or renunciation, and the psychological impact of losing loosing all the hair

P. Assouly (✉)
Centre Sabouraud, Saint-Louis Hospital, Paris, France
e-mail: philippe.assouly@orange.fr

P. Humbert et al. (eds.), *Agache's Measuring the Skin*,
DOI 10.1007/978-3-319-32383-1_102

due to chemotherapy or Alopecia Totalis testify to its importance.

2 The Healthy Hair Follicle

Each hair follicle on the body, according to each anatomical region, presents structure, shape, length, cycle, and orientation (angle implantation) specificities. As a common practical example, acquired kinky hair on the scalp can be a sign of becoming a "non-healthy" witness of androgenetic alopecia.

Three types of pilosebaceous follicles can be individualized: the "terminal follicle," on scalp and hairy areas, with voluminous hair and gland, the "vellus follicles" (on the limbs and lower part of the trunk) with both small components (hair length <1 cm, diameter <30 μm), and "sebaceous follicles" where the hair is of vellus type and the gland is voluminous found exclusively on the hairless seborrheic areas (head, shoulders, thorax).

Concerning the scalp, figures considered to be "normal" for healthy hairs are 100,000–150,000 hairs on the head (one-tenth of body hair), 200–300 per cm^2, which correspond for a hairstyle made of 20 cm length a total of 6 m^2 flat. The so-called *average* hair growth is 0.35–0.44 mm per day during the anagen phase which lasts from 1 to 7 years. We know the hair is divided into follicular units (FU): composed of three to five hairs, sebaceous glands, arrector muscles, and more often a single ostium. Terminal/vellus hair ratio is 7:1. The average diameter of a terminal hair varies from 0.07 to 0.09 mm and for a vellus, by definition, is less than 0.03 mm.

3 Healthy Hair Follicles: Differences and Limits

3.1 Ethnical Differences

In fact the number and the diameter of the hair are different according to the ethnic origin (Sperling 1999; Lee et al. 2002; Franbourg et al. 2003; Blume-Peytavi et al. 2008; Table 1, Fig. 1). The transversal section of the hair also varies: European hair appears elliptical, Asian (Mongoloid) circular, and African highly elliptical (sometimes "kidney-like" shape). These features lead to differences in form (straight, curly, kinky), in flexibility, but in this way make resistance differences (lowered on hair of black skin compared to the white skin and a fortiori from the Asian).

Sebum is most important in African subjects, so the flora of the scalp is hereby amended. The hair growth is reduced (256 ± 44 μm/day on black skin compared to 396 ± 55 μm/day on white skin). The average age of onset of hair whitening is different according to the ethnical origin (mid 30s for white skin, late 30s for Asian and medium quarantine for black skin). Whitening appears with a classical order: temples, vertex, rest of the scalp, beard, and body.

Table 1 Hair differences according to ethnic origins

Type	Average diameter (μm)	Number of hair
Blond (orig. European)	40–80	130,000
Brown hair to black (orig. European)	50–90	110,000
Red haired (orig. European)	50–90	90,000
African Americans	60–100	90,000
Asian (Korea)	80–120	90,000

Fig. 1 A healthy hair whorl

More details concerning ethnic hair, metrology, strength, and permeability of hairs will be presented in ▶ Chaps. 75, "Clinical Assessment of the Scalp and Hair," and ▶ 76, "Scalp Sebaceous Function Assessment").

3.2 Sexual Differences

In females hairs grow faster (Birch et al. 2001; Messenger 2011). During pregnancy the anagen stage is prolonged, but the menstrual cycle does not seem to affect the hair growth cycle.

3.3 Seasonal Influence

From the month of July, telogen counts are higher, inducing increased shedding in September-October.

3.4 Age-Related Differences

These modifications during life are also notable, for the size or the number of hair which changes. Concerning the scalp hair, reduction of the anagen phase, the diameter of hair however is increased in women between the ages of 22 and 30–35 to reduce then (Messenger 2011). Modification of body hair along life is evident: from the lanugo to the onset of puberty pilosity and later for men hair on trunk and later again increased thick hairs on eyebrows, ears, nostrils. The thickness of the scalp also changes (Garn et al. 1954) (4.8 mm at the age of, 5.6 mm at 40–69 years, and probably more for black people), but also the arrangement of the hair (including the loss of the temporal line during puberty). The amount of sebum is lower in the second childhood before puberty and also in women after age 60 or 70. If the involution of the hair or hair senescence (reduction of phase anagen, increase of the lag phase, decrease in density, and moderate reduction in size) is to be regarded as a natural phenomenon, it remains difficult to define precisely the limits from androgenetic alopecia.

4 Organization of Scalp Hair

The pattern of hair disposition on the scalp is divided into trichoglyphs, with a whorl, leant clockwise in 88.9% of the cases. Difficult to see on black skin, this whorl is unique in 95 % of cases, and in the remaining 5 %, there are two, or even three, very rarely more (a publication (Ruiz-Maldonado 2002) lists 14 whorls on a child). The whorl is usually located in front of the posterior fontanelle. It was noted on the right side in 40.4 %, median in 44.3 %, and left in 15.3 % (Samlaska et al. 1989). Its mode of occurrence is still discussed.

5 Flora of Healthy Hair Follicles

A so-called "healthy scalp" contains, in addition to bacteria dominated by *Propionibacterium acnes* – which could be organized in biofilms in the under part of hair follicles (Matard et al. 2012) – fungi and especially *Malassezia*, but also viruses and parasites (*Demodex folliculorum*). This flora remains poorly known; it enters the constitution of the microbiome, of the virobiome, of the mycobiome, and what might be termed parasitobiome.

6 Healthy Appearance of the Hair

The cuticle gives the hair a smooth contact, and the hair's shiny appearance is also a witness of its health. It enables the hair to reach a substantial length in addition to the term of the anagen phase. Altered by external aggressions (sun exposure, inadequate care as repeated oxidation bleaching, exaggerated combing) responsible for what is named "weathering," the hair loses its shine especially on the distal part and tends to fracture.

References

Birch MP, Messenger JF, Messenger AG. Hair density, hair diameter and the prevalence of female pattern hair loss. Br J Dermatol. 2001;144:297–304.

Blume-Peytavi U, Tosti A, Whiting D, Trueb R, editors. Hair growth and disorders. Berlin: Springer; 2008.

Franbourg A, Hallegot P, Baltenneck F, Toutain C, Leroy F. Current research on ethnic hair. J Am Acad Dermatol. 2003;48:S115–9.

Garn SM, Selby S, Young R. Scalp thickness and the fat-loss theory of balding. AMA Arch Derm Syphilol. 1954;70:601–8.

Lee HJ, Ha SJ, Lee JH, Kim JW, Kim HO, Whiting DA. Hair counts from scalp biopsy specimens in Asians. J Am Acad Dermatol. 2002;46:218–21.

Matard B, Meylheuc T, Briandet R, Casin I, Assouly P, Cavelier-Balloy B, Reygagne P. First evidence of bacterial biofilms in the anaerobe part of scalp hair follicles: a pilot comparative study in folliculitis decalvans. J Eur Acad Dermatol Venereol. 2012 Jul 11. J Eur Acad Dermatol Venereol. 2013;27:853–60, doi:10.1111/j.1468-3083.2012.04591.x.

Messenger AG. Hair through the female life cycle. Br J Dermatol. 2011;165 Suppl 3:2–6.

Ruiz-Maldonado R. A previously unreported syndrome of multiple scalp whorls and associated anomalies. Clin Exp Dermatol. 2002;27:21–3.

Samlaska CP, James WD, Sperling LC. Scalp whorls. J Am Acad Dermatol. 1989;21:553–6.

Sperling LC. Hair density in African Americans. Arch Dermatol. 1999;135:656–8.

The Hair Growth Cycle

73

Bruno A. Bernard

Keywords
Growth Cycle • Human Hair Follicle • Hypoxia • Pigmentation Unit • Stem Cells

Human hair fiber is produced by a unique and complex organ, the hair follicle. Starting the third month of human embryogenesis, epithelio-mesenchymal interactions result in the formation of 100,000–150,000 follicles, whose spatial distribution at the surface of the scalp is controlled by a process called reaction-diffusion. The hair follicle adopts a concentrical structure, each compartment being characterized by distinct and specific differentiation programs.

One remarkable feature of human hair follicle stems from its dynamics, the hair growth cycle, which involves successive phases of growth (anagen), involution (catagen), and rest (telogen), with an average duration of 3 years, 3 weeks, and 3 months, respectively. A side phase, termed "exogen," has been described, independent of the rest of the hair cycle, and during which the club fiber is actively released (Stenn 2005; Higgins et al. 2009) without direct consequence on anagen initiation (Higgins et al. 2009). Following hair loss, a latency period is observed in 80 % of hair cycles (Courtois et al. 1994), between hair shedding in exogen (Higgins et al. 2009) and the onset of a new anagen hair. The duration of this period, called kenogen (Rebora and Guarrera 2002), varies from 2 to 5 months on average (Courtois et al. 1994). At the end of the telogen-kenogen phase, a neomorphogenetic process takes place which results in the formation of a new hair follicle. We recently named this transitory phase the neogen phase (Bernard 2012).

As described, the hair cycle looks as regular as a clock, and an oscillator control has been looked for, but without success (Paus et al. 1999). In fact, we have demonstrated that human hair follicles do not adopt such a regular cyclic behavior. Each follicle has an autonomous and independent behavior, the transition from one phase to the next occurring after time intervals given stochastically by a lognormal distribution characterized by a mean and a variance (Halloy et al. 2000, 2002). From this analysis, it can be concluded that instead of a cyclical behavior with an intrinsic automaton, a bistable steady state controls human hair follicle behavior, which under a stochastic

B.A. Bernard (✉)
L'Oréal Research and Innovation, Clichy, France
e-mail: bbernard@rd.loreal.com

P. Humbert et al. (eds.), *Agache's Measuring the Skin*,
DOI 10.1007/978-3-319-32383-1_103

way jumps from the dormant to the active steady state and vice versa (Bernard 2012) (Fig. 1). This autonomous switching between two quasi-steady states, involving bistability and excitability, was recently mathematically modeled (Al-Nuaimi et al. 2012). This unique behavior guarantees the permanence of hairs at the scalp surface.

A number of factors were reported to positively or negatively modulate hair growth (Paus and Foitzik 2004). The positive effects of IGF-1 on hair growth were described as early as 1994 (Philpott et al. 1994) and attributed to IGF-1 secretion by dermal papilla (Itami and Inui 2005). More recently, the beneficial effects of IGF-1 were linked to the induction of platelet-derived growth factors A and B and by an apoptosis-preventing increase in Bcl2/Bax ratio (Ahn et al. 2012). Of note, 1,763 MHz radio frequency induces an increased IGF-1 synthesis in dermal papilla and stimulates human hair growth in vitro (Yoon et al. 2011).

Although the molecular mechanisms and molecular actors controlling the phase transitions have been extensively studied and characterized (Sennett and Rendl 2012), telogen phase was considered as a quiescent phase until recently. New data demonstrate that it is not that quiescent. Indeed, during this phase, the follicle is under the influence of factors that would repress the onset of a new follicle and factors that would trigger it (Plikus 2012). A strong expression of "bone morphogenic protein" (BMP) (Botchkarev et al. 2001) and "fibroblast growth factor-18" (FGF-18) (Kimura-Ueki et al. 2012) defines a refractory period, during which the neogen onset is prevented. The progressive increase in the production of BMP antagonist noggin, Wnt/Fzz/b-catenin pathway activators, and TGF-b2 (Higgins et al. 2009; Oshimori and Fuchs 2012) will reach a critical threshold shifting the telogen follicle to a competency status, receptive to FGF-7, secreted by the nearby dermal papilla (Greco et al. 2009)

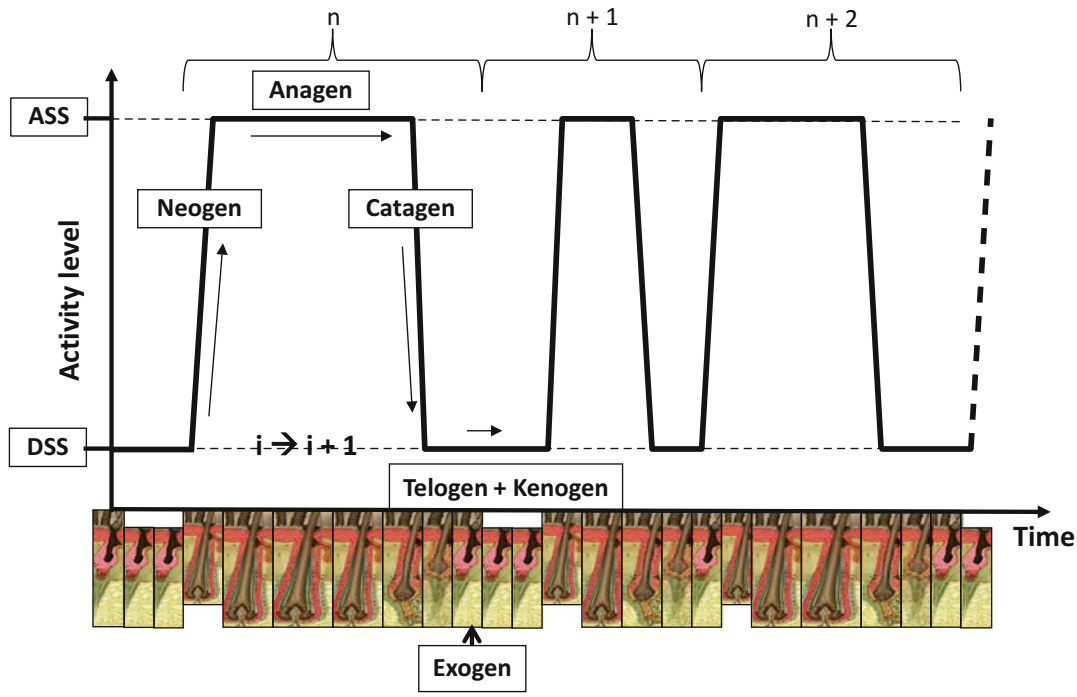

Fig. 1 New representation of the hair follicle behavior, with an active steady state (ASS) of fiber production (anagen) and a dormant steady state (DSS) (telogen/kenogen), interspaced by short-lasting phases of neomorphogenesis (neogen) and regression (catagen). Three successive periods (n, $n + 1$, $n + 2$) are represented

and ultimately triggering the onset of the neogen phase.

The hair follicle cycle is controlled by a number of factors (Paus and Foitzik 2004; Sennett and Rendl 2012), some of them stimulating anagen and others triggering catagen or maintaining telogen. For example, calcitonin gene-related peptide (CGRP) neuropeptide (Samuelov et al. 2012) and vanilloid-receptor-1 agonist capsaicin (Bodo et al. 2005) both induce premature catagen, while thymic peptides differentially modulate follicle growth. Indeed, if thymulin (TYL) increases hair growth rate, both thymosin α1 and thymosin β4 (TB4) slightly decrease hair shaft production. Moreover, TYL prolongs anagen while TB4 shortens it (Meier et al. 2012).

With regard to the hormonal control of hair growth, both androgens and estrogens modulate hair growth and cycling. It was already known that both TGF-β1 and TGF-β2 were androgen inducible in dermal papilla and behaved as anagen-to-catagen inducers (Inui and Itami 2011). Recent data have shown that dihydrotestosterone (DHT), the active form of testosterone, also induces IL-6 production by dermal papilla, which functions as an inhibitory paracrine mediator that inhibits hair shaft growth by suppressing matrix cell proliferation (Kwack et al. 2012a). DHT also induces DKK-1 production by dermal papilla cells, which in turn promotes catagen progression by suppressing Wnt/b-catenin signaling and inducing apoptosis in follicular keratinocytes (Kwack et al. 2012b). Altogether, these results position DHT as a major inducer of catagen. However, as androgens also inhibit the dermal papilla Wnt/β-catenin signaling pathway involved in hair follicle stem cell differentiation and onset of hair regeneration (Leiros et al. 2012), they must also be considered as neogen inhibitors. With respect to estrogens, they lead to reversible hair cycle retardation through inducing premature catagen by upregulating TGF-β2 and maintaining telogen by upregulating BMP4 (Hu et al. 2012).

Besides androgens and estrogens, prostaglandins now emerge as key modulators of hair growth. Human hair follicle is indeed endowed with a complete endogenous prostaglandin metabolism (Colombe et al. 2007; Michelet et al. 2008) and expresses an intricate network of prostaglandin receptors, including the GPR44 (PGD2) receptor (Colombe et al. 2008). While both latanoprost, a PGF2α analog, and bimatoprost, a prostamide-related F2α analog, stimulate hair growth (Khidhir et al. 2013), PGD2 was recently shown to inhibit hair growth through its binding to GPR44 receptor (Garza et al. 2012). Of note, PGD2 synthesis is increased in alopecic areas (Garza et al. 2012). These results suggest that hair growth is under a subtle balance between positive influence of PGE_2 et $PGF_2\alpha$ (Sasaki et al. 2005) and negative influence of PGD2.

Altogether, the above results demonstrate that hair growth is tightly regulated by growth factors, cytokines, neuropeptides, hormones, and environmental cues. However, the existence of anagen, catagen, telogen, and neogen phases underlines a unique feature of hair follicle that hair growth is not a continual process and hair follicle must be cyclically renewed. Hair follicle renewal requires transient activation of local reservoirs of stem cells. Seminal work in mice localized a reservoir of slow-cycling, epithelial stem cells in the bulge, a distinct segment of the outer root sheath (ORS) of mouse follicles (Cotsarelis et al. 1990). It is now known that the follicle is endowed with numerous stem cell reservoirs and that these reservoirs express different markers and seem to have different functions (Jaks et al. 2010). With respect to human hair follicles, early work suggested the existence of at least two pools of pluripotent cells (Lenoir et al. 1988). In accordance with these findings, high β1-integrin (CD29) expression was observed in sections of both the upper and lower ORS (Commo and Bernard 1997). In addition, K19 labeling clearly identified two groups of putative stem cells in the hair follicle (Commo et al. 2000). The upper and lower reservoirs of K19+ cells are not, however, identical and can be distinguished by differential expression of K15 and CD200, more highly expressed in the upper reservoir, and CD271, CD29, and CD34, more highly expressed in the lower reservoir (Inoue et al. 2009). This differential epitope mapping appears being not restricted to the ORS since the connective tissue sheath (CTS) in conjunction with these two reservoirs

also harbors distinct compartments. For example, one chondroitin sulfate epitope (4C3-CS) is specific for the upper CTS, while another chondroitin sulfate epitope (7D4-CS) and N-sulfated glucosamine-rich heparan sulfate epitope (HepSS-1) are only observed in the lower CTS (Malgouries et al. 2008). In summary, the human hair follicle can be characterized by the presence of at least two epithelial stem cell reservoirs that interact with specific microenvironments. Both reservoirs fuse during catagen and telogen phases and then separate again in early neogen and anagen (Commo et al. 2000). We recently demonstrated that the lower reservoir stem cells expressed hypoxia-specific markers, namely, carbonic anhydrase IX and GLUT-1 glucose transporter (Rathman-Josserand et al. 2013), highlighting the fact that the upper and lower stem cell reservoirs were subjected to very different microenvironments. As hypoxia is believed to promote an undifferentiated state in several stem and precursor cell populations (Mohyeldin et al. 2010), we propose that hypoxia signaling in suboptimal conditions would help maintain hair follicle stem cell functionality and hence prevent alopecia or at least favor neogenesis.

All above results underline the complexity of the regulatory networks which control human hair cycle and its successive phases of growth, involution, rest, and regeneration. Of note, the hair pigmentation unit responsible for hair pigmentation also undergoes cyclical alterations. In fact, a fully active follicle contains two melanocyte populations, one located on top of dermal papilla, the pigmentation unit, and one located in the basal layer of the upper outer root sheath, in the permanent part of the follicle (Commo and Bernard 2000). The former contains constitutively active melanocytes which produce melanin throughout anagen and transfer pigment-loaded melanosomes to the nearby cortical cells, whereas the latter is now considered as a reservoir for quiescent melanocyte progenitors/stem cells (Commo and Bernard 2000). During catagen, the pigmentation unit almost entirely disappears through a massive apoptotic process, whereas the melanocyte progenitors/stem cell reservoir remains unaffected and detectable during telogen (Commo and Bernard 2000). At the neogen onset, a subset of melanocyte progenitors is recruited, migrates down to the nascent bulb, and transiently amplifies to regenerate a fully functional pigmentation unit. This melanocyte behavior is another example of the unique cell dynamics and tissue choreography which characterize the human hair follicle growth cycle.

References

Ahn S-Y, Pi L-Q, Hwang ST, Lee W-S. Effect of IGF-I on hair growth is related to the anti-apoptotic effect of IGF-I and up-regulation of PDGF-a and PDGF-B. Ann Dermatol. 2012;24:26–31.

Al-Nuaimi Y, Goodfellow M, Paus R, Baier G. A prototypic mathematical model of the human hair cycle. J Theor Biol. 2012;310:143–59.

Bernard BA. The human hair follicle, a bistable organ? Exp Dermatol. 2012;21:401–3.

Bodo E, Bıro T, Telek A, Czifra G, Griger Z, Toth BI, et al. A hot new twist to hair biology: involvement of vanilloid receptor-1 (VR1/TRPV1) signaling in human hair growth control. Am J Pathol. 2005;166:985–98.

Botchkarev V, Botchkareva NV, Nakamura M, Huber O, Funa K, Lauster R, et al. Noggin is required for induction of the hair follicle growth phase in postnatal skin. FASEB J. 2001;15:2205–14.

Colombe L, Vindrios A, Michelet JF, Bernard BA. Prostaglandin metabolism in human hair follicle. Exp Dermatol. 2007;16:762–9.

Colombe L, Michelet JF, Bernard BA. Prostanoid receptors in anagen human hair follicles. Exp Dermatol. 2008;17:63–72.

Commo S, Bernard BA. The distribution of α2β1, α3β1 and α6β4 integrins identifies distinct subpopulations of basal keratinocytes in the outer root sheath of the human anagen hair follicle. Cell Mol Life Sci. 1997;53:466–71.

Commo S, Bernard BA. Melanocyte subpopulation turnover during the human hair cycle: an immunohistochemical study. Pigment Cell Res. 2000;13:253–9.

Commo S, Gaillard O, Bernard BA. The human hair follicle contains two distinct K19 positive compartments in the outer root sheath: a unifying hypothesis for stem cell reservoir? Differentiation. 2000;66:157–64.

Cotsarelis G, Sun TT, Lavker R. Label-retaining cells reside in the bulge area of pilosebaceous unit: implications for follicular stem cells, hair cycle, and skin carcinogenesis. Cell. 1990;61:1329–37.

Courtois M, Loussouarn G, Hourseau C, Grollier JF. Hair cycle and alopecia. Skin Pharmacol. 1994;7:84–9.

Garza LA, Liu Y, Yang Z, Alagesan B, Lawson JA, Norberg SM, et al. Prostaglandin D2 inhibits hair growth and is elevated in bald scalp of men with

androgenetic alopecia. Sci Transl Med. 2012;4: 126ra34.
Greco V, Chen T, Rendl M, Schober M, Pasolli HA, Stokes N, et al. A two-step mechanism for stem cell activation during hair regeneration. Cell Stem Cell. 2009;4:155–69.
Halloy J, Bernard BA, Loussouarn G, Goldbeter A. Modeling the dynamics of human hair cycles by a follicular automaton. Proc Natl Acad Sci U S A. 2000;97:8328–33.
Halloy J, Bernard BA, Loussouarn G, Goldbeter A. The follicular automaton model: effect of stochasticity and of synchronization of hair cycles. J Theor Biol. 2002;214:469–79.
Higgins CA, Westgate GE, Jahoda CAB. From telogen to exogen: mechanisms underlying formation and subsequent loss of the hair club fiber. J Invest Dermatol. 2009;129:2100–8.
Hu M, Zhang S, Lei X, Deng Z, Guo W, Qiu Z, et al. Estrogen leads to reversible hair cycle retardation through inducing premature catagen and maintaining telogen. PLoS ONE. 2012;7, e40124.
Inoue K, Aoi N, Sato T, Yamauchi Y, Suga H, Eto H, et al. Differential expression of stem-cell-associated markers in human hair follicle epithelial cells. Lab Invest. 2009;89:844–56.
Inui S, Itami S. Molecular basis of androgenetic alopecia: from androgen to paracrine mediators through dermal papilla. J Dermatol Sci. 2011;61:1–6.
Itami S, Inui S. Role of androgen in mesenchymal epithelial interactions in human hair follicle. J Invest Dermatol Symp Proc. 2005;10:209–11.
Jaks V, Kasper M, Tofftgard R. The hair follicle – a stem cell zoo. Exp Cell Res. 2010;316:1422–8.
Khidhir KG, Woodward DF, Farjo NP, Farjo BK, Tang ES, Wang JW, et al. The prostamide-related glaucoma therapy, bimatoprost, offers a novel approach for treating scalp alopecias. FASEB J. 2013;27:557–67.
Kimura-Ueki M, Oda Y, Oki J, Komi-Kuramochi A, Honda E, Asada M, et al. Hair cycle resting phase is regulated by cyclic epithelial FGF18 signaling. J Invest Dermatol. 2012;132:1338–45.
Kwack MH, Ahn JS, Kim MK, Kim JC, Sung YK. Dihydrotestosterone-inducible IL-6 inhibits elongation of human hair shafts by suppressing matrix cell proliferation and promotes regression of hair follicles in mice. J Invest Dermatol. 2012a; 132:43–9.
Kwack MH, Kim MK, Kim JC, Sung YK. Dikkopf-1 promotes regression of hair follicles. J Invest Dermatol. 2012b;132:1554–60.
Leiros GJ, Attorresi AI, Balana ME. Hair follicle stem cell differentiation is inhibited through cross-talk between Wnt/b-catenin and androgen signaling in dermal papilla cells from patients with androgenetic alopecia. Br J Dermatol. 2012;166:1035–42.
Lenoir MC, Bernard BA, Pautrat G, Darmon M, Shroot B. Outer root sheath cells of human hair follicle are able to regenerate a fully differentiated epidermis in vitro. Dev Biol. 1988;130:610–20.
Malgouries S, Thibaut S, Bernard BA. Proteoglycan expression patterns in human hair follicle. Br J Dermatol. 2008;158:234–42.
Meier N, Langan D, Hilbig H, Bodó E, Farjo NP, Farjo B, et al. Thymic peptides differentially modulate human hair follicle growth. J Invest Dermatol. 2012;132 (5):1516–9.
Michelet JF, Colombe L, Gautier B, Gaillard O, Benech F, Pereira R, et al. Expression of NAD+ dependent 15-hydroxyprostaglandin dehydrogenase and protection of prostaglandins in human hair follicle. Exp Dermatol. 2008;17:821–8.
Mohyeldin A, Garzon-Muvdi T, Quinones-Hinojosa A. Oxygen in stem cell biology: a critical component of the stem cell niche. Cell Stem Cell. 2010;7:150–61.
Oshimori N, Fuchs E. Paracrine TGF-b signaling counterbalances BMP-mediated repression in hair follicle stem cell activation. Cell Stem Cell. 2012;10:63–75.
Paus R, Foitzik K. In search of the "hair cycle clock": a guided tour. Differentiation. 2004;72:489–511.
Paus R, Müller-Röver S, Botchkarev VA. Chronobiology of the hair follicle: hunting the "hair cycle clock". J Invest Dermatol Symp Proc. 1999;4:338–45.
Philpott M, Sanders DA, Kealey T. Effects of insulin and insulin-like growth factors on cultured human hair follicles: IGF-I at physiologic concentrations is an important regulator of hair follicle growth in vitro. J Invest Dermatol. 1994;102:857–61.
Plikus MV. New activators and inhibitors in the hair cycle clock: targeting stem cells' state of competence. J Invest Dermatol. 2012;132:1321–4.
Rathman-Josserand M, Genty G, Lecardonnel J, Chabane S, Cousson A, Michelet JF, Bernard BA. Human hair follicle stem/progenitor cells express hypoxia markers. J Invest Dermatol. 2013;133: 2094–7.
Rebora A, Guarrera M. Kenogen. A new phase of the hair cycle? Dermatology. 2002;205:108–10.
Samuelov L, Kinori M, Bertolini M, Paus R. Neural controls of human hair growth: calcitonin gene-related peptide (CGRP) induces catagen. J Dermatol Sci. 2012;67:153–8.
Sasaki S, Hozumi Y, Kondo S. Influence of prostaglandin F2alpha and its analogues on hair regrowth and follicular melanogenesis in a murine model. Exp Dermatol. 2005;14:323–8.
Sennett R, Rendl M. Mesenchymal-epithelial interactions during hair follicle morphogenesis and cycling. Semin Cell Dev Biol. 2012;23:917–27.
Stenn K. Exogen is an active, separately controlled phase of the hair growth cycle. J Am Acad Dermatol. 2005;52:374–5.
Yoon SY, Kim KT, Jo SJ, Jeon SI, Choi HD, Kim KH, et al. Induction of hair growth by insulin-like growth factor-1 in 1,763 MHz radiofrequency-irradiated hair follicle cells. PLoS One. 2011;6(12), e28474.

Scalp Sebaceous Physiology

74

Yahya Dowlati, Alireza Firooz, and Hamed Zartab

Contents

Keywords
Scalp • Hair follicle • Sebum • Sebaceous

1 Sebaceous Glands

Sebaceous glands are multilobular structures which invaginate the dermis. At the periphery of glands, there are epithelial cells surrounded by a basement membrane. Generally, the duct of each gland is connected to a hair follicle and forms a pilosebaceous unit. The sebaceous glands may also exist without an apparent attachment to the hair follicle or, like on the forehead, may be connected to a vellus hair (Kligman and Shelley 1958).

Majority of sebaceous glands, together with hair itself, are a principal part of a pilosebaceous unit (Smith and Thiboutot 2008). Pilosebaceous unit differentiation occurs between months 2 and 4 of gestation. A complex signaling pathway between dermal mesenchymal cells and embryonic epidermis takes place and induces formation of dermal papilla which initiates the final differentiation of pilosebaceous unit (Tóth et al. 2011). Differentiation of pilosebaceous unit depends upon Sox9 signaling (Nowak et al. 2008). Differentiating toward hair follicle or toward sebaceous lineage depends on the presence or inhibition of β-catenin. Indian hedgehog signaling stimulates further sebaceous differentiation (Allen et al. 2003; Han et al. 2006; Niemann

Y. Dowlati (✉) • A. Firooz
Center for Research and Training in Skin Diseases and Leprosy, Tehran University of Medical Sciences, Tehran, Iran
e-mail: dowlatiy@yahoo.com; firozali@sina.tums.ac.ir

H. Zartab
Center for Research and Training in Skin Diseases and Leprosy, Tehran University of Medical Sciences, Tehran, Iran

Tissue Engineering and Wound Healing Lab, Department of Surgery, Division of Plastic Surgery, Brigham and Women's Hospital – Harvard Medical School, Boston, USA
e-mail: hzartabmd@yahoo.com; hzartab@partners.org; hzartabmd@gmail.com

P. Humbert et al. (eds.), *Agache's Measuring the Skin*,
DOI 10.1007/978-3-319-32383-1_104

et al. 2003). There are some other proteins/genes involved in embryonic development of sebaceous glands or their homeostasis. They include a protein expressed on stem cells called B lymphocyte-induced maturation protein 1 (Blimp 1) transcription factor and c-myc (Horsley et al. 2006; Schneider and Paus 2010; Schneider et al. 2009).

In the neonates, the cell organization of sebaceous acini consists of undifferentiated, differentiating, and differentiated, mature sebocytes (Tosti 1974). In adults, sebaceous glands can be divided into three zones: peripheral zone, maturation zone, and central necrosis zone of differentiated sebocytes (Schneider and Paus 2010; Thody and Shuster 1989). The number of glands is nearly constant throughout life, while their size can increase and their turnover speed slows down with aging (Fenske and Lober 1986; Zouboulis and Boschnakow 2001; Plewig and Kligman 1978).

Sebaceous glands are composed of sebocytes and sebum is the product of sebaceous glands. Sebocytes are formed from indifferent germinal cells in epithelium in the periphery of the glands. Newly formed cells migrate toward the center of the gland as the gland matures (Clarys and Barel 1995). Lipid synthesis and discharge in sebocytes last for more than a week (Plewig and Kligman 1978). Sebum is a species-specific mixture made of relatively nonpolar lipids (Nikkari 1974) including squalene, wax esters, cholesterol esters, triglycerides, and possibly some free cholesterols (Thody and Shuster 1989; Nikkari 1974; Ramasastry et al. 1970).

2 Sebaceous Glands and Hair Follicles

The hair follicle can be divided into various sections. The upper part of hair follicle up to the sebaceous duct is the infundibulum. In this region due to the absence of a tight attachment between hair shaft and the skin, the shaft can move. Sebaceous gland secretions fill the gap between the shaft and skin (Schaefer and Lademann 2001). Below the sebaceous duct is the isthmus. It continues up to the area of attachment of arrector pili muscle to the hair follicle. From the isthmus upward, the hair follicle does not disintegrate during follicle growth. At the location of attachment of arrector pili muscle, there is a bulge area which is a hair growth regulator (Viragh and Meuli 1995). The lower follicle starts below the bulge area, and here there is a keratogenous zone. Keratinization is an important process for hair growth and might be playing a role in the transporting processes. The sebaceous gland duct acts as a border in terms of keratinization: below the opening of sebaceous gland duct, the outer root sheath cells have little keratinization, if any, while above the sebaceous gland duct, outer root sheath cells are keratinized and are more similar to the cells of epidermis. Bulb is the lowest part of hair follicle and the location of matrix cells, the basement membrane, and the papilla. They are also hair growth regulators (Hashimoto and Shibazaki 1976). Below the bulge area and from outside to the center, the following layers can be observed: the outer root sheath, the inner root sheath and the Henle layer, the Huxley layer, and the cuticle (outermost layer of hair shaft). The hair shaft includes the cuticle, cortex, and medulla (Hashimoto and Shibazaki 1976; Bertolino et al. 1993).

Sebaceous glands can act as a target for topical application of drugs based on the fact that there is a direct connection between the follicular duct and the sebaceous gland (Agarwal et al. 2000).

Sebaceous glands of the scalp are important to maintain hair, and their absence can be associated with scarring alopecia (Schneider and Paus 2010; Sundberg et al. 2000). Hair follicles of pilosebaceous unit are categorized into vellus hair and terminal hair. Vellus hair reaches into the dermis, while the terminal hair goes deeper and into the subcutaneous fat layer. The highest density of hair follicles is on the scalp region (Sperling 1991). Sebaceous gland density is high on the scalp and the skin of the forehead. There are no sebaceous glands in the palms and soles; on the other body parts, they do exist more or less (Smith and Thiboutot 2008; Elias 1983).

3 Sebaceous Glands of the Scalp

Human scalp has the highest hair follicle density throughout the body (200 hairs per cm^2). It also has a dense and specific microflora. In addition, it produces a large amount of sebum (causal level of 150 $\mu g/cm^2$) (Pouradier et al. 2013). After using shampoo or local degreasing, scalp recoating restarts immediately and will complete within a couple of hours; proximal hair shafts on the scalp start recoating much later, and complete recoating can take 3 days (Pierard 1987). Sebum casual level is maximum on the forehead and on the scalp (Pierard 1987; Greene et al. 1970). A casual level of less than 50 $\mu g/cm^2$ is considered as hyperseborrhea. Hyperseborrhea (oily skin) refers to oversecretion of sebaceous glands in which the casual level can reach high levels of 500 $\mu g/cm^2$ and commonly affects areas rich in sebaceous glands such as the scalp. Both greater sebum production and a higher sebaceous gland density contribute to hyperseborrhea (Pierard 1987). It is a predisposing factor for seborrheic dermatitis (Smith and Thiboutot 2008).

A significant difference between the scalp and forehead in terms of sebum excretion was reported in early 1980s. This cannot be only justified by the density of sebaceous glands on the scalp and forehead because both have the same range of sebaceous gland density (400–900 per cm^2). The scalp has a slower refatting rate probably due to the fact that there are differences in follicular reservoir, the reservoir of lipid contained within the pilosebaceous unit (Kligman and Shelley 1958; Saint-Léger and Levegue 1982). The thin vellus hair on the scalp would increase the effective volume which is available for a lipid reservoir. The ratio between excretion and secretion kinetics differs between scalp and forehead regions due to the existence of hair follicles (Saint-Léger and Levegue 1982).

The scalp is a region with two characteristics: it is rich in sebum due to the abundance of sebaceous glands, and it is sensitive to androgens (Saint-Léger and Levegue 1982; Piérard-Franchimont and Piérard 1988). Each day, grams of sebum are delivered to the scalp and hair surfaces (Saint-Léger 2005). Sebaceous gland product is a nutrient for scalp biocenosis (Piérard-Franchimont et al. 2006). Sebum excretion rate in the scalps of people with androgenetic alopecia has been reported to be higher (Piérard-Franchimont and Piérard 1988) or equal (Maibach et al. 1968) than controls. Maibach et al. showed that the casual sebum level of the scalp in bald men is not higher than controls and suggested that the hairs normally act as a wick for disposing serum and in bald men this mechanism is not operative so sebum spreads on the skin and produces the oily appearance of bald scalp (Maibach et al. 1968). Sebaceous glands of bald scalp have been reported to have greater binding affinity for androgens compared to these glands in hairy scalp (Sawaya et al. 1989). Sebaceous glands of people suffering from androgenetic alopecia have shown increased levels of glutathione S-transferase activity and reactive oxygen species compared to normal hairy scalp sebaceous glands (Giralt et al. 1996).

Systemic hormonal status significantly affects the secretion of sebaceous glands, and therefore, the function of these glands changes with aging (Piérard-Franchimont and Piérard 2005). A recent study showed no significant difference in casual sebum level on the scalp with aging. On the forehead, on the other hand, the function of sebaceous glands showed a plateau phase at the 30s and then slowly decreased thereafter with a more prominent reduction from menopause (Nazzaro-Porro et al. 1979; Man et al. 2009).

It has been suggested that the scalp is not very reliable for assessment of sebaceous gland excretion due to the fact that sebaceous gland production and sebum behavior may be affected by several external factors such as scales, dandruff, migration along the hair shafts, etc. (Pouradier et al. 2013).

The biologic activity of sebaceous gland is regulated through interaction of different ligands with receptors on sebocyte surface such as androgen and estrogen receptors, PPARs and liver X

receptor (LXR) (Hong et al. 2008; Russel et al. 2007), neuropeptide receptors, and retinoid and vitamin D receptors (Schmuth et al. 2007; Zouboulis 2000, 2004). The interaction between the ligand and the receptor leads to activation of several pathways including differentiation, proliferation, lipogenesis, metabolism of hormones, and release of chemokines and cytokines (Zouboulis and Schagen 2008).

4 Factors Influencing the Functions of Sebocytes

- Bacterial stimuli such as *Propionibacterium acnes* and lipopolysaccharide (LPS) can affect Toll-like receptors 2, 4, and 6 and possibly increase β-defensins, cathelicidin, tumor necrosis factor-α (TNF-α), interleukin-8 (IL-8), and interleukin-1α (IL-1α) (Tóth et al. 2011; Lee et al. 2008a, 2009; Nagy et al. 2006; Oeff et al. 2006).
- Acid arachidonic might increase lipid synthesis, apoptosis, and differentiation and also increase interleukin-6 (IL-6), IL-8, leukotriene B4 (LTB4). Its potential target is not clearly known; it might be a protein kinase or peroxisome proliferator-activated receptors (PPARs) (Alestas et al. 2006; Tóth et al. 2009; Wrobel et al. 2003).
- Linoleic acid acts on PPARs and increases lipid synthesis, differentiation, and testosterone to 5-α-dihydrotestosterone (5-α-DHT) conversion (Chen et al. 2003; Rosenfield et al. 1998, 1999).
- Testosterone and 5-α-DHT act on androgen receptor and increase proliferation in the presence of cofactors such as PPAR agonists. They also increase lipid synthesis and differentiation (Rosenfield et al. 1998, 1999; Choudhry et al. 1992; Fritsch et al. 2001; Pelletier and Ren 2004).
- Estrogen binds to estrogen receptors α and β and might decrease sebogenesis, while progesterone binds to its receptor and its role is not well defined (Pelletier and Ren 2004; Deplewski and Rosenfield 2000; Guy et al. 1996).
- Corticosteroids have a permissive effect and also increase proliferation and decrease lipogenesis. Their receptor is not clear (Chen et al. 2006; Solminski et al. 1995; Zouboulis et al. 1998).
- Vitamin D3 binds to vitamin D receptor (VDR) and decreases IL-6 and IL-8 and also increases cathelicidin. It can increase or decrease proliferation based on the speed of proliferation and also can decrease lipid synthesis (Lee et al. 2008a; Kramer et al. 2009).
- Growth hormone binds to growth hormone receptor (GHR) and increases differentiation without having an effect on proliferation (Deplewski and Rosenfield 1999; Lobie et al. 1990).
- Insulin-like growth factor I (IGF-I) binds to IGF-I-1 receptor and increases proliferation and has a minor effect on differentiation. It also increases lipogenesis (Deplewski and Rosenfield 1999; Makrantonaki et al. 2008).
- Insulin binds to insulin receptor and increases proliferation and differentiation and also has a supportive role for 5α-DHT, GH, and IGF-I (Deplewski and Rosenfield 1999).
- Epidermal growth factor (EGF) binds to EGF receptor and increases proliferation while decreasing differentiation (Guy et al. 1996).
- Fibroblast growth factor 7 (FGF-7) binds to FGF receptor 2b and increases acne formation. Also knockout mice without the receptor undergo sebaceous gland atrophy (Grose et al. 2007; Zouboulis et al. 2002).
- IL-1β increases IL-8 while its receptor has not been described in sebocytes (Melnik et al. 2009).
- β-Endorphin binds μ opioid receptor and increases lipid synthesis, increases differentiation, and decreases proliferation (Melnik et al. 2009).
- Corticotropin-releasing hormone (CRH) binds to CRH receptors 1 and 2 and increases lipid synthesis, increases expression of 3-β-hydroxysteroid dehydrogenase/Δ5-4 isomerase, and increases differentiation while decreasing proliferation. It also increases IL-6 and IL-8 (Melnik et al. 2009; Krause et al. 2007; Slominski et al. 2004).

- α-Melanocyte-stimulating hormone (α-MSH or melanocortin) binds to melanocortin receptors 1 and 5 and increases differentiation and lipid synthesis while decreasing IL-8 (Bohm 2009; Bohm et al. 2002; Thiboutot et al. 2000).
- Adrenocorticotropin hormone (ACTH) binds to melanocortin receptor 2 and increases differentiation and lipid synthesis (Guo et al. 2010; Zhang et al. 2003).
- Substance P causes increase in IL-6, IL-8, TNF-α, and PPARγ lipid synthesis and also size of sebaceous glands and differentiation. Its receptor on sebocytes has not been described so far (Lee et al. 2008b; Toyoda and Morohashi 2001).
- Endocannabinoids bind to cannabinoid receptor 2 and increase differentiation, lipid synthesis, and apoptosis (Tóth et al. 2011; Dobrosi et al. 2008).
- Capsaicin binds to transient receptor potential vanilloid 1 (TRPV1) and retinoid X receptors (RXRs) and causes decrease in lipid synthesis and differentiation and also a decrease in IL-1β. It increases proliferation (TRPV1 specific) and necrosis (in large doses and is TRPV1 independent) (Tóth et al. 2009).

References

Agarwal R, Katare OP, Vyas SP. The pilosebaceous unit: a pivotal route for topical drug delivery. Methods Find Exp Clin Pharmacol. 2000;22:129–33.

Alestas T, Ganceviciene R, Fimmel S, Muller-Decker K, Zouboulis CC. Enzymes involved in the biosynthesis of leukotriene B4 and prostaglandin E2 are active in sebaceous glands. J Mol Med. 2006;84:75–87.

Allen M, Grachtchouk M, Sheng H, Grachtchouk V, Wang A, Wei LB, et al. Hedgehog signaling regulates sebaceous gland development. Am J Pathol. 2003;163:2173–8.

Bertolino AP, Klein LM, Freedberg IM. Biology of hair follicles. In: Fitzpatrick TB, Eisen AZ, Wolff K, Freedberg IM, Austen KF, editors. Dermatology in general medicine. New York: McGraw Hill; 1993. p. 289–93.

Bohm M. Neuroendocrine regulators: novel trends in sebaceous gland research with future perspectives for the treatment of acne and related disorders. Dermatoendocrinology. 2009;1:136–40.

Bohm M, Schiller M, Stander S, Seltmann H, Li Z, Brzoska T, et al. Evidence for expression of melanocortin-1 receptor in human sebocytes in vitro and in situ. J Invest Dermatol. 2002;118:533–9.

Chen W, Yang CC, Sheu HM, Seltmann H, Zouboulis CC. Expression of peroxisome proliferator-activated receptor and CCAAT/enhancer binding protein transcription factors in cultured human sebocytes. J Invest Dermatol. 2003;121:441–7.

Chen W, Liao CY, Hung CL, Lin TK, Sheu HM, Zouboulis CC. Potent corticosteroids inhibit lipogenesis in sebaceous glands. Dermatology. 2006;213:264–5.

Choudhry R, Hodgins MB, Van der Kwast TH, Brinkmann AO, Boersma WJ. Localization of androgen receptors in human skin by immunohistochemistry: implications for the hormonal regulation of hair growth, sebaceous glands and sweat glands. J Endocrinol. 1992;133:467–75.

Clarys P, Barel A. Quantitative evaluation of skin surface lipids. Clin Dermatol. 1995;13:307–21.

Deplewski D, Rosenfield RL. Growth hormone and insulin-like growth factors have different effects on sebaceous cell growth and differentiation. Endocrinology. 1999;140:4089–94.

Deplewski D, Rosenfield RL. Role of hormones in pilosebaceous unit development. Endocr Rev. 2000;21:363–92.

Dobrosi N, Tóth BI, Nagy G, Dozsa A, Geczy T, Nagy L, et al. Endocannabinoids enhance lipid synthesis and apoptosis of human sebocytes via cannabinoid receptor-2-mediated signaling. FASEB J. 2008;22:3685–95.

Elias PM. Epidermal lipids, barrier function and desquamation. J Invest Dermatol. 1983;80:44S–9.

Fenske NA, Lober CW. Structural and functional changes of normal aging skin. J Am Acad Dermatol. 1986;15:571–85.

Fritsch M, Orfanos CE, Zouboulis CC. Sebocytes are the key regulators of androgen homeostasis in human skin. J Invest Dermatol. 2001;116:793–800.

Giralt M, Cercello I, Nogues MR, Puerto AM, Ortin F, Argany N, et al. Glutathione, glutathione S-transferase and reactive oxygen species of human scalp sebaceous glands in male pattern baldness. J Invest Dermatol. 1996;107:154–8.

Greene RS, Downing DT, Pochi PE, Strauss JS. Anatomical variation in the amount and composition of human skin surface lipid. J Invest Dermatol. 1970;54:240–7.

Grose R, Fantl V, Werner S, Chioni AM, Jarosz M, Rudling R, et al. The role of fibroblast growth factor receptor 2b in skin homeostasis and cancer development. EMBO J. 2007;26:1268–78.

Guo HW, Deng J, Yang XC, Zhong BY, Shen Z, Yang SY, et al. Melanocortin receptor type 2 (MC2R, ACTH receptor) expression in patients with alopecia areata. Exp Dermatol. 2010;19:1020–2.

Guy R, Ridden C, Kealey T. The improved organ maintenance of human sebaceous gland: modeling in vitro the effects of epidermal growth factor, androgens, estrogens, 13-cis retinoic acid, and phenol red. J Invest Dermatol. 1996;106:454–60.

Han GW, Li AG, Liang YY, Owens P, He W, Lu SL, et al. Smad7-induced beta-catenin degradation alters epidermal appendage development. Dev Cell. 2006;11:301–12.

Hashimoto K, Shibazaki S. Ultrastructural study on differentiation and function of hair. In: Kobori T, Montagna W, Toda K, Ishibashi Y, Hori Y, Morikawa F, editors. Biology and disease of the hair. Tokyo: University of Tokyo Press; 1976. p. 23–57.

Hong I, Lee M, Na T, Zouboulis CC, Lee M. LXRα enhances lipid synthesis in SZ95 sebocytes. J Invest Dermatol. 2008;128:1266–72.

Horsley V, O'Carroll D, Tooze R, Ohinata Y, Saitou M, Obukhanych T, et al. Blimp1 defines a progenitor population that governs cellular input to the sebaceous gland. Cell. 2006;126:597–609.

Kligman AM, Shelley WB. An investigation of the biology of the human sebaceous gland. J Invest Dermatol. 1958;30:99–125.

Kramer C, Seltmann H, Seifert M, Tilgen W, Zouboulis CC, Reichrath J. Characterization of the vitamin D endocrine system in human sebocytes in vitro. J Steroid Biochem Mol Biol. 2009;113:9–16.

Krause K, Schnitger A, Fimmel S, Glass E, Zouboulis CC. Corticotropin-releasing hormone signaling is receptor-mediated and is predominant in the sebaceous glands. Horm Metab Res. 2007;39:166–70.

Lee DY, Yamasaki K, Rudsil J, Zouboulis CC, Park GT, Yang JM, et al. Sebocyte expression functional cathelicidin antimicrobial peptides and can act to kill propionibacterium acnes. J Invest Dermatol. 2008a;128:1863–6.

Lee WJ, Jung HD, Lee HJ, Kim BS, Lee SJ, do Kim W. Influence of substance-P on cultured sebocytes. Arch Dermatol Res. 2008b;300:311–6.

Lee DY, Huang CM, Nakatsuji T, Thiboutot D, Kang SA, Monestier M, et al. Histone H4 is a major component of the antimicrobial action of human sebocytes. J Invest Dermatol. 2009;129:2489–96.

Lobie PE, Breipohl W, Lincoln DT, Garcia-Aragon J, Waters MJ. Localization of the growth hormone receptor/binding protein in skin. J Endocrinol. 1990;126:467–71.

Maibach HI, Feldmann R, Payne B, Hutshell T. Scalp and forehead sebum production in male patterned alopecia. In: Biopathology of alopecia. Basel/New York: Karger; 1968, p. 171–6.

Makrantonaki E, Vogel K, Fimmel S, Oeff M, Seltmann H, Zouboulis CC. Interplay of IGF-I and 17 beta-estradiol at age-specific levels in human sebocytes and fibroblasts in vitro. Exp Gerontol. 2008;43:939–46.

Man MQ, Xin SJ, Song SP, Cho SY, Zhang XJ, Tu CX, et al. Variation of skin surface pH, sebum content and stratum corneum hydration with age and gender in a large Chinese population. Skin Pharmacol Physiol. 2009;22:190–9.

Melnik BC, Schmitz G, Zouboulis CC. Anti-acne agents attenuate FGFR2 signal transduction in acne. J Invest Dermatol. 2009;129:1868–77.

Nagy I, Pivarcsi A, Kis K, Koreck A, Bodai L, McDowell A, et al. Propionibacterium acnes and lipopolysaccharide induce the expression of antimicrobial peptides and proinflammatory cytokines/chemokines in human sebocytes. Microbes Infect. 2006;8:2195–205.

Nazzaro-Porro M, Passi S, Boniforti L, Belsito F. Effects of aging on fatty acids in skin surface lipids. J Invest Dermatol. 1979;73:112–7.

Niemann C, Unden AB, Lyle S, Zouboulis CC, Toftgard R, Watt FM. Indian hedgehog and beta-catenin signaling: role in the sebaceous lineage of normal and neoplastic mammalian epidermis. Proc Natl Acad Sci U S A. 2003;100:11873–80.

Nikkari T. Comparative chemistry of sebum. J Invest Dermatol. 1974;62:257–67.

Nowak JA, Polak L, Pasolli HA, Fuchs E. Hair follicle stem cells are specified and function in early skin morphogenesis. Cell Stem Cell. 2008;3:33–43.

Oeff MK, Seltmann H, Hiroi N, Nastos A, Makrantonaki E, Bornstein SR, et al. Differential regulation of Toll-like receptor and CD14 pathways by retinoids and corticosteroids in human sebocytes. Dermatology. 2006;213:266.

Pelletier G, Ren L. Localization of sex steroid receptors in human skin. Histol Histopathol. 2004;19:629–36.

Pierard GE. Rate and topography of follicular heterogeneity of sebum excretion. Dermatologica. 1987;175:280–3.

Piérard-Franchimont C, Piérard GE. Approche physiopathologique de la seborrhea du cuir chevelu. Ann Dermatol Vénér. 1988;115:451–3.

Piérard-Franchimont C, Piérard GE. Seborrhea. In: Bouillon C, Wilkinson J, editors. The science of hair care. 2nd ed. Boca Raton: Tailor and Francis; 2005. p. 583–607.

Piérard-Franchimont, Xhauflaire-Uhoda E, Piérard GE. Revisiting dandruff. Int J Cosmet Sci. 2006;28:311–8.

Plewig G, Kligman AM. Proliferative activity of the sebaceous glands of the aged. J Invest Dermatol. 1978;70:314–7.

Pouradier F, Céline C, D'arras MF, Flamant F, Panhard S, Diridollou S, et al. Functional and structural age-related changes in the scalp skin of Caucasian women. Skin Res Tech. 2013;0:1–10.

Ramasastry P, Downing DT, Pochi PE, Strauss JS. Chemical composition of human skin surface lipids from birth to puberty. J Invest Dermatol. 1970;54:139–44.

Rosenfield RL, Deplewski D, Kensis A, Ciletti N. Mechanisms of androgen induction of sebocyte differentiation. Dermatology. 1998;196:43–6.

Rosenfield RL, Kentsis A, Deplewski D, Ciletti N. Rat preputial sebocyte differentiation involves peroxisome proliferator-activated receptors. J Invest Dermatol. 1999;112:226–32.

Russel L, Harrison W, Bahta A, Zouboulis CC, Burrin J, Philpott M. Characterization of liver X receptor expression and function in human skin

and the pilosebaceous unit. Exp Dermatol. 2007;16: 844–52.
Saint-Léger D. Dandruff (pityriasis capitis simplex): of yeasts and men. In: Bouillon C, Wilkinson J, editors. The science of hair care. 2nd ed. Boca Raton: Tailor and Francis; 2005. p. 609–31.
Saint-Léger D, Levegue JL. A comparative study of refatting kinetics on the scalp and forehead. Br J Dermatol. 1982;106:669–75.
Sawaya ME, Hnig LS, Hsia SL. Increased androgen binding capacity in sebaceous glands in scalp of male-pattern baldness. J Invest Dermatol. 1989;92:91–5.
Schaefer H, Lademann J. The role of follicular penetration – a differential view. Skin Pharmacol Appl Skin Physiol. 2001;14 Suppl 1:23–7.
Schmuth M, Watson REB, Deplewski D, Durbac S, Zouboulis CC, Griffiths CEM. Nuclear hormone receptors in human skin. Horm Metab. 2007;39:96–105.
Schneider MR, Paus R. Sebocytes, multifaceted epithelial cells: lipid production and holocrine secretion. Int J Biochem Cell Biol. 2010;42:181–5.
Schneider MR, Schmidt-Ullrich R, Paus R. The hair follicle as a dynamic miniorgan. Curr Biol. 2009;19: R132–42.
Slominski A, Pisarchik A, Tobin DJ, Mazurkiewicz J. Differential expression of a cutaneous corticotropin-releasing hormone system. Endocrinology. 2004;145:941–50.
Smith KR, Thiboutot DM. Thematic review series: skin lipids. Sebaceous gland lipids: friend or foe? J Lipid Res. 2008;49:271–81.
Solminski A, Ermak G, Hwang J, Chakraborty A, Mazurkiewicz JE, Mihm M. Proopiomelanocortin, corticotrophin releasing hormone and corticotrophin releasing hormone receptor genes are expressed in human skin. FEBS Lett. 1995;374:113–6.
Sperling LC. Hair anatomy for the clinician. J Am Acad Dermatol. 1991;25:1–17.
Sundberg JP, Boggess D, Sundberg BA, Eilertsen K, Parimoo S, Filippi M, et al. Asebia-2J (Scd1(ab2J)): a new allele and a model for scarring alopecia. Am J Pathol. 2000;156:2067–75.
Thiboutot D, Sivarajah A, Gilliland K, Cong Z, Clawson G. The melanocortin 5 receptor is expressed in human sebaceous glands and rat preputial cells. J Invest Dermatol. 2000;115:614–9.
Thody AJ, Shuster S. Control and function of sebaceous glands. Physiol Rev. 1989;69:383–416.
Tosti A. A comparison of the histodynamics of sebaceous glands and epidermis in man: a microanatomic and morphometric study. J Invest Dermatol. 1974;62:147–52.
Tóth BI, Geczy T, Griger Z, Dozsa A, Seltmann H, Kovacs L, et al. Transient receptor potential vanilloid-1 signaling as a regulator of human sebocyte biology. J Invest Dermatol. 2009;129:329–39.
Tóth BI, Oláh A, Szöllősi AG, Czifra G, Bíró T. "Sebocytes' makeup" – novel mechanisms and concepts in the physiology of the human sebaceous glands. Pflugers Arch. 2011;416: 593–606.
Toyoda M, Morohashi M. Pathogenesis of acne. Med Electron Microsc. 2001;34:29–40.
Viragh PA, Meuli M. Human scalp hair follicle development from birth to adulthood: statistical study with special regard to putative stem cells in the bulge and proliferating cells in the matrix. Arch Dermatol Res. 1995;287:279–84.
Wrobel A, Seltmann H, Fimmel S, Muller-Decjer K, Tsukada M, Bogdanoff B, et al. Differentiation and apoptosis in human immortalized sebocytes. J Invest Dermatol. 2003;120:175–81.
Zhang L, Anthonavage M, Huang Q, Li WH, Eisinger M. Proopiomelanocortin peptides and sebogenesis. Ann N Y Acad Sci. 2003;994:154–61.
Zouboulis CC. Human skin: an independent peripheral endocrine organ. Horm Res. 2000;54:230–42.
Zouboulis CC. The human skin as a hormone target and an endocrine gland. Hormones. 2004;3:9–26.
Zouboulis CC, Boschnakow A. Chrono- and photoaging of the human sebaceous gland. Clin Exp Dermatol. 2001;26:600–7.
Zouboulis CC, Schagen S. The sebocyte culture: a model to study the pathophysiology of the sebaceous gland in sebostasis, seborrhea and acne. Arch Dermatol Res. 2008;300:397–413.
Zouboulis CC, Xia L, Akamatsu H, Seltmann H, Fritsch M, Hornemann S, et al. The human sebocyte culture model provides new insights into development and management of seborrhea and acne. Dermatology. 1998;196:21–31.
Zouboulis CC, Seltmann H, Hiroi N, Chen W, Young M, Oeff M, et al. Corticotropin-releasing hormone: an autocrine hormone that promotes lipogenesis in human sebocytes. Proc Natl Acad Sci U S A. 2002;99:7148–53.

Clinical Assessment of the Scalp and Hair

75

Won-Soo Lee

Keywords
Hair density • Pattern of hair loss • Hair-loss classification • Basic and specific classification (BASP) • Ethic differences • Familiar factors

The key factor of clinical assessment of scalp hair is to evaluate the density of hair and pattern of hair loss, if it exists. To achieve this goal, various classification methods have been proposed for describing hair density and pattern of hair loss. Pattern hair loss (PHL) typically present with the progressive thinning and shortening of hair in affected areas.

Various classification methods have been proposed for describing PHL. The first systematic classification of PHL was established by Hamilton (1951) in 1951. He sub-classified the patterns of baldness based on frontoparietal and frontal recession and vertex thinning and then evaluated a large group of men and women for the presence of specific patterns of hair loss from the prenatal period through the tenth decade of life. In 1975, Norwood (1975) refined Hamilton's classification by emphasizing temporofrontal or vertex-only subcategories of hair loss into seven types with a type A variant and reported the incidence of male pattern baldness at various ages in white adult male subjects. An additional pattern (type II vertex) to the Hamilton-Norwood classification system was introduced in the clinical trial of finasteride in male PHL (MPHL) (Kaufman et al. 1998). In 1992, Savin (1992) introduced a classification of MPHL based entirely on a pictorial depiction of hair density as derived from midline scalp part width. Olsen (2003) first proposed assigning separate designations (temporal, frontal, mid, and vertex) to the areas of the scalp that bald at different rates in different individuals with MPHL. Olsen (Olsen et al. 2003) also proposed an individualized classification system that assigned a density scale to each of these designated scalp areas in any given patient, which was further refined in a later publication. Subjects thus classified would have a TFMV classification (e.g., T3F2M0V3) (Olsen et al. 2003). In 1977, Ludwig (1977) presented quite a different picture of hair loss in women from that described by Hamilton (1951). He emphasized preservation of the frontal fringe despite progressive centrifugal loss over the top of the scalp and arbitrarily designated three gradations of hair loss. Olsen (1994) and Olsen et al. (2003) proposed that frontal

W.-S. Lee (✉)
Department of Dermatology, Institute of Hair and Cosmetic Medicine, Yonsei University Wonju College of Medicine, Wonju, Gangwon-Do, Republic of Korea
e-mail: leewonsoo@yonsei.ac.kr

P. Humbert et al. (eds.), *Agache's Measuring the Skin*,
DOI 10.1007/978-3-319-32383-1_105

accentuation (or the "Christmas tree" pattern) be considered another pattern of hair loss in women, which helps to distinguish PHL from other potential hair-loss mimicries in women.

Although the several aforementioned classification methods of PHL have been suggested, these classifications have some limitations (Lee et al. 2007). The Norwood-Hamilton classification is too detailed and is less stepwise in its description, making it difficult to memorize for common use. It also does not list some peculiar types of baldness, such as FPHL (Lee et al. 2007). Additionally, many women with MPHL cannot be classified using the Ludwig classification system (Olsen 2003; Olsen et al. 2003). In addition, for most of these classification systems, the clinicians must use distinct methodologies for each gender in order to correctly classify the pattern (Lee et al. 2007).

Lee et al. (2007) devised a new classification system named the basic and specific (BASP) classification, which is comprehensive and systematic regardless of race or gender.

This new classification of PHL was designed based on the pattern of hair loss, including the shape of the anterior hairline and the density of hair on the frontal and vertex areas. The basic types represent the shape of the anterior hairline, and the specific types represent the density of hair on specific areas, which are frontal and vertex. The shape of the anterior hairline is divided into four types: L, M, C, and U. In contrast to the basic types, the specific types may be selectively included when necessary. According to patterns observed at specific areas, there are two specific types: F and V. The final type is decided by the combination of the basic and specific type. One of the basic types must be selected, and the specific type may be selected if it exists. Each of the various types is subdivided into three or four subtypes, according to its severity (Lee et al. 2007).

During the balding process, the recession of the anterior hairline, represented with the basic type classification, relatively corresponds with the thinning of hair on the crown and vertex. However, because the degree of recession might be out of accordance with the density of hair in many individuals, the separation of both characteristics is important for proper classification. Furthermore, the combination of two features of PHL is better suited to more thorough description of the baldness phenotypes (Lee et al. 2007).

A total of 2,213 Korean subjects, comprised of 1,768 males and 445 females, were classified according to the BASP classification (Lee et al. 2007). For both sexes, the majority of patients enrolled in the study were in the third and fourth decades of life (65.1 % of males and 56.68 % of females). In males, the older as well as the younger group were more likely to have little recession of the frontal hairline (classified as type M1-2) and diffuse thinning over the top of the scalp (type F1-2). The women in the study developed typical female PHL. In men, regardless of age, 1,434 of the 1,768 males were classified as type M, accounting for 81.1 % of cases. Among the subtypes and according to the severity of baldness, the majority of subjects below 50 years of age were classified as type M1, whereas most subjects over the age of 50 were classified as type M2. The incidence of type L (9.3 %) tended to decrease with age, but those of types C (5.8 %) and U (3.8 %) tended to increase. In women, type L showed the highest frequency in all age groups, accounting for 210 (47.2 %) of 445 female subjects. Regardless of age, types M, C, and U were the next most common in order, observed in 121 women (27.2 %), 111 women (25.0 %), and 3 women (0.6 %) of the 445 subjects, respectively. Type C0 was the second most common subtype in female subjects between the second and fourth decade of life, and its incidence decreased with age. In men, type F, which is identical to FPHL in the Ludwig classification, was observed in 42.4 % (749/1,768) of male subjects, and type V was observed in 19.8 % (350/1,768). The grades of both types increased slightly with age. In women, type F was observed in 70.6 % (314/445) of female subjects with PHL (Lee et al. 2007).

Although the Norwood-Hamilton classification is the most commonly used classification worldwide, it can only be used in MPHL, and there are several types of male hair pattern that could not be described by this classification (Lee et al. 2007). Some previous studies were performed to estimate the reliability of the

Norwood-Hamilton classification and the result was unsatisfactory, even in the hands of expert appraisers (Taylor et al. 2004; Guarrera et al. 2009; Littman and White 2005). Hong et al. (2013) compared the reliability of the BASP and Norwood-Hamilton classifications. In terms of repeatability, the Norwood-Hamilton classification showed the lowest match rate in repeatability. Also, the intergroup reproducibility was higher with the BASP classification. In conclusion, the BASP classification not only classifies all kinds of hair-loss patterns regardless of sex or race, but also has better reproducibility and repeatability than the Norwood-Hamilton classification (Hong et al. 2013).

There are also racial differences in the density of hair and patterns of hair loss in different ethnic groups. In a previous study, FPHL was observed in 11.1 % of Korean males with PHL (Paik et al. 2001). In a Chinese study, MPHL was found in 13 of 108 (12 %) women with PHL, all of whom were over 50 years of age (Xu et al. 2009). In an Indian study, although it was possible to classify 80 % of cases of PHL and II (28 %) and III (15 %) were the most common types of PHL, 27 patients of 150 male subjects (18 %) did not fit into specific patterns according to the Norwood-Hamilton classification[16]. In addition, the type "a" variant was noted in 20 % of patients, clearly indicating the limitations of the existing classifications. There is considerable overlap in types IV, V, and VI in the Norwood classification, with the "a" variants further confusing the picture (Sehgal et al. 2007).

Family history plays an important role in the hair density and pattern of hair loss, which is believed to be influenced by genetic factors. However, the exact mode of inheritance has not been well characterized. A recent study by Lee et al. (2011) using the BASP classification revealed that familial factors affecting the morphology of PHL differ between males and females and for each BASP subtype. Parental influences on anterior hairline shape in men were predominantly from the paternal side, whereas these effects were less notable in women. In patients without family histories of PHL, a higher frequency of early-onset PHL than late-onset PHL was identified in men but not in women. Basic types of hair loss had a higher degree of heritability from the paternal side of the family, regardless of the specific type. This study provides detailed information indicating that each hair-loss pattern according to the BASP classification has different familial factors (Lee et al. 2011).

References

Guarrera M, Cardo P, Arrigo P, Rebora A. Reliability of Hamilton-Norwood classification. Int J Trichology. 2009;1:120–2.

Hamilton JB. Patterned loss of hair in man; types and incidence. Ann N Y Acad Sci. 1951;53:708–28.

Hong H, Ji JH, Lee YH, Kang H, Choi GS, Lee W-S. Reliability of the pattern hair loss classifications: a comparison of the basic and specific and Norwood-Hamilton classifications. J Dermatol. 2013;40:102–6.

Kaufman KD, Olsen EA, Whiting D, Savin R, DeVillez R, Bergfeld W, et al. Finasteride in the treatment of men with androgenetic alopecia. Finasteride Male Pattern Hair Loss Study Group. J Am Acad Dermatol. 1998;39:578–89.

Lee WS, Ro BI, Hong SP, Bak H, Sim WY, Kim DW, et al. A new classification of pattern hair loss that is universal for men and women: basic and specific (BASP) classification. J Am Acad Dermatol. 2007;57:37–46.

Lee WS, Oh Y, Ji JH, et al. Analysis of familial factors using the basic and specific (BASP) classification in Korean patients with androgenetic alopecia. J Am Acad Dermatol. 2011;65:40–7.

Littman AJ, White E. Reliability and validity of self-reported male balding patterns for use in epidemiologic studies. Ann Epidemiol. 2005;15:771–2.

Ludwig E. Classification of the types of androgenetic alopecia (common baldness) occurring in the female sex. Br J Dermatol. 1977;97:247–54.

Norwood OT. Male pattern baldness: classification and incidence. South Med J. 1975;68:1359–65.

Olsen EA. Androgenetic alopecia. In: Olsen EA, editor. Disorders of hair growth: diagnosis and treatment. New York: McGraw-Hill; 1994. p. 257–83.

Olsen EA. Current and novel methods for assessing efficacy of hair growth promoters in pattern hair loss. J Am Acad Dermatol. 2003;48:253–62.

Olsen EA, Canfield D, Canfield W, Budris K. A novel method for assessing regional scalp hair density in male pattern hair loss. In: Van Neste D, editor. Hair science and technology. New York: McGraw-Hill; 2003. p. 251–4.

Paik JH, Yoon JB, Sim WY, Kim BS, Kim NI. The prevalence and types of androgenetic alopecia in

Korean men and women. Br J Dermatol. 2001; 145:95–9.
Savin RC. A method for visually describing and quantitating hair loss in male pattern baldness. J Invest Dermatol. 1992;98:604.
Sehgal VN, Kak R, Aggarwal A, Srivastava G, Rajput P. Male pattern androgenetic alopecia in an Indian context: a perspective study. J Eur Acad Dermatol Venereol. 2007;21:473–9.
Taylor R, Matassa J, Leavy JE, Fritschi L. Validity of self reported male balding patterns in epidemiological studies. BMC Public Health. 2004;4:60.
Xu F, Sheng YY, Mu ZL, Lou W, Zhou J, Ren YT, et al. Prevalence and types of androgenetic alopecia in Shanghai, China: a community-based study. Br J Dermatol. 2009;160:629–32.

Scalp Sebaceous Function Assessment 76

Yahya Dowlati, Alireza Firooz, and Ali Rajabi-Estarabadi

Contents

Keywords
Scalp • Hair follicle • Sebum • Skin surface lipid • Measurement

Scalp has the highest density of hair follicles (200 hair/cm^2) and main sebum production (casual level of 150 μg/cm^2) (Agache 2000). The skin of the scalp is commonly exposed to many topical agents such as drugs, hair care, and cosmetic products. In normal conditions, numerous hairs make scalp an invisible region for instrumental measurements. Due to this limitation, there is a lack of information about the function of the stratum corneum (SC) of scalp skin including sebaceous gland function (O'goshi et al. 2000).

Three different types of pilosebaceous follicles are recognized which include terminal hair follicle, vellus hair follicle, and sebaceous follicle. This classification is based on the volume of the sebaceous glands and the size of the connected hairs. The largest sebaceous glands are present at the skin of scalp. Terminal hair follicles are present on the scalp and beard region in men where the hair shaft is thick, and the sebaceous gland size is medium to large (Uhoda et al. 2005; Pierard-Franchimont et al. 2010).

On the scalp, sebum appears partly as discrete droplets emerging from follicular outlets and partly as a surface coating. The droplets are unevenly spread on the hair (Pierard-Franchimont et al. 2010).

Y. Dowlati (✉) • A. Firooz • A. Rajabi-Estarabadi
Center for Research and Training in Skin Diseases and Leprosy, Tehran University of Medical Sciences, Tehran, Iran
e-mail: dowlatiy@yahoo.com; firozali@sina.tums.ac.ir; dralirajabi@yahoo.com

P. Humbert et al. (eds.), *Agache's Measuring the Skin*,
DOI 10.1007/978-3-319-32383-1_106

Scalp and skin sebum amounts must be distinguished. Estimating the amount of scalp sebum needs a miniature sampling method, and in some methods hair must be shaved 24–30 h before measurement. The amount of sebum is conveniently measured in vivo using photometric assessment and lipid-sensitive tapes (i.e., Sebumeter®) (Pierard-Franchimont et al. 2010; Pierard et al. 2000).

1 What Can Be Assessed?

Similar to the assessment of skin surface sebum (see ▶ Chap. 21, "Dermoscopy: Basic Knowledge of an Innovative Imaging Tool"), the composition of skin surface lipid (SSL), the quantitative parameters of sebum excretion, and glandular parameters (density and activity of sebaceous glands) can be measured on the skin surface of scalp. The only difference is in terms of sampling and preparing the scalp skin before beginning the assessments.

2 Methods of Collecting Scalp Sebum

2.1 Solvents

For collecting SSL from hairy skin (scalp and beard region in men), the best method is to rinse the hair with a solvent (e.g., ether). The rinse is filtered by using Whatman paper to separate the hairs and squames and then evaporated. The solvents most commonly used are shown in Table 21.1 of ▶ Chap. 21, "Dermoscopy: Basic Knowledge of an Innovative Imaging Tool." It seems that the most convenient and effective solvent is ether.

Unfortunately in this method, there is no control of the amount of sebum collected from follicular reservoirs which may have an influence on the results. On the other hand, the application of these solvents can alter the physiology and structure of the SC; hence this method is no more recommended for assessing the amount of SSLs (Pierard et al. 2000).

2.2 Photometric Methods and Lipid-Sensitive Tapes

2.2.1 Sebutape

The Sebutape© (CuDerm, Corp., Dallas, Texas) consists of a hydrophobic polymeric white film (Kligman et al. 1986) and is used to measure the sebum secretion (Dobrev 2007; Clarys and Barel 1996) and evaluate the distribution of skin pores (Pierard 1986; Nordstrom et al. 1986). There are innumerable, tiny air cavities, and the surface is coated with a lipid-porous adhesive which enables the tape to be sealed to the skin during the period of collection. The film absorbs the sebum originating from the follicular openings. As sebum reaches the skin surface, it is rapidly absorbed in to the film. As the air within the microcavities is displaced by sebum, the lipid-filled cavities become transparent to light. The output from each follicle forms a sharply defined spot; the size corresponds to the volume of the droplet. Sebum absorption by Sebutape is slow and perhaps incomplete because of the barrier of the glue (Saint-Leger and Cohen 1985).

For assessment of scalp sebaceous gland function, first the skin surface of scalp is ordinarily prepared by shaving 24–30 h in advance, and at the time of measurement, the surface is washed with soap and water to remove debris and lipids (Perkins et al. 2002). According to Beach et al., Sebutape samples can be collected before and 15 min after towel drying hair that is shampooed and conditioned (Beach et al. 2012). For greater accuracy, complete defatting can be obtained by wiping with a gauze pad soaked in hexane. The film is placed on the surface for 1–3 h and then a computer image analysis is conducted. In the places where the sebaceous secretion has been absorbed, the film becomes transparent. Thanks to the placing of the film on the dark background, we can receive the pore patterns (Clarys and Barel 1995). Lipids which are examined with this method can be also extracted and then analyzed with thin-layer chromatography (Nordstrom et al. 1986; Sisalli et al. 2006).

The self-adhesive application of the Sebutape omits the difficult procedures encountered in the other methods (▶ Chap. 21, "Dermoscopy: Basic

Knowledge of an Innovative Imaging Tool"). Moreover, the area under investigation is covered during the procedure, resulting in a more standardized collection. The Sebutape requires a shorter collection time, as most of the parameters can be determined after 1 h of collection and also, most of the evaluation methods can be carried out on the same principles as Sebutape: kinetic color measurement during the collection period, image analysis after the collection period, and quantitative and qualitative analysis after extraction of the lipids from the tape.

2.2.2 Sebufix F16

The Sebufix instrument is also commonly used. Here, similar to the Sebutape©, a polymer film is used to measure the activity of the sebaceous glands. For scalp application, the hairs in the area (1 cm^2) should be shaved before measurement. The film is image analyzed with a UV-light video camera (Visioscan VC 98®or Visioscope® PC 35, C + K Electronic, Cologne) device (Dobrev 2007). The Sebufix is thus very similar to the Sebutape; the only difference is the fact that in the case of the Sebutape, the film is placed on the selected area for 1–3 h and in the Sebufix for 30 s (Clarys and Barel 1996). Therefore, the Sebufix allows for measuring sebum secretion within a shorter period of time.

The method is not really quantitative because the relation between the surface of a spot and the quantity of sebum it contains is not known and several spots can rapidly coalesce. Accordingly, it cannot measure the CL, but it may provide an estimate of the refatting rate (▶ Chap. 21, "Dermoscopy: Basic Knowledge of an Innovative Imaging Tool"). It can display the distribution of the active sebaceous glands and the individual refatting rate of each gland (Saint-Leger and Cohen 1985).

2.2.3 Sebumeter SM 815 (Cassette)

This device facilitates objective measurement of sebum from the skin surface areas and can be used to determine the level of sebum on the skin surface or the rate of its secretion (Knaggs et al. n.d.; Tagami 2003; Schaefer and Kuhn-Bussius 1970; Bergler-Czop and Brzezińska-Wcisło 2010; Biro et al. 2003). It cannot, however, determine the state of the sebaceous glands (Son et al. 2008). The Sebumeter is a simple device, easy to operate, which can be used to make an objective classification of dry, normal, or oily skin (Nouveau-Richard et al. 2007; Youn et al. 2005; Kim et al. 2006) as well as to evaluate "the biological age" of the skin (Jacobsen et al. 1985; Marrakchi and Maibach 2007; Firooz et al. 2012). The measurement is based on grease-spot photometry. The Sebumeter cassette contains a mat synthetic tape, 0.1 mm thick. A special tape becomes transparent in contact with the sebum on the skin surface of scalp. For sebum determination, the measuring head of the cassette is inserted into the aperture of the device, where the transparency is measured by a light source sending light through the tape which is reflected by a little mirror behind the tape. A photocell measures the transparency. The light transmission represents the sebum content on the surface of the measuring area and is displayed in units from 0 to 350. The assessment should be measured 48 h after shampooing (Pouradier et al. 2013). The probe is applied once to the measuring area for 30 s which is controlled by a clock set in the device. The measuring head of the cassette exposes a 64 mm^2 measuring section of the tape. For a measurement, the tape is moved forward by a trigger at the side of the cassette to expose a new section of tape. The used tape is rewound inside the cassette. The accuracy of this device is about ±5 %. It would be the best choice for assessment of SSLs on hairy skin and scalp skin because there is no need to shave the hairs.

The applications of Sebumeter include (Firooz et al. 2007; Davari et al. 2008; Seirafi et al. 2009; Davoudi et al. 2010):

1. To study the effectiveness of hair and skin cosmetic products
2. To study sebaceous gland activity in different diseases
3. To assess the effectiveness of different kinds of treatment on skin diseases

Compared with Sebutape, the Sebumeter is more user friendly, and there is no need to clean the probe at each assessment and shave the scalp

hair before measurement for preparing. Thanks to its integrity, reproducibility, commercial availability, easy handling and operating, short measuring time, and numerical values, the Sebumeter is now used in most of the sebum evaluation studies (Yong et al. 2002; Ambroisine et al. 2007; Lee et al. 2006; Cheng et al. 2007, 2009; Stinco et al. 2007; Akhtar et al. 2010).

3 Commercialized Devices

- Sebumeter (SM 815): Courage+Khazaka electronic GmbH. Mathias-Brüggen-Str., Cologne, Germany. www.courage-khazaka.de
- Sebufix F16: Courage+Khazaka electronic GmbH. Mathias-Brüggen-Str., Cologne, Germany. www.courage-khazaka.de
- Visioscan VC98: Courage+Khazaka electronic GmbH. Mathias-Brüggen-Str., Cologne, Germany. www.courage-khazaka.de
- Visioscope® PC 35: Courage+Khazaka electronic GmbH. Mathias-Brüggen-Str., Cologne, Germany. www.courage-khazaka.de
- Sebutape: CUDERM Corp., Dallas, TX, USA. www.cuderm.com

References

Agache P. Physiologie de la peauet exploration fonctionnelles cutanees. Cachan: Editions Medicales Internationales; 2000.

Akhtar N, Khan BA, Mahmood T, et al. Formulation and evaluation of antisebum secretion effects of sea buckthorn w/o emulsion. J Pharm Bioallied Sci. 2010;2:13–7.

Ambroisine L, Ezzedine K, Elfakir A, et al. Relationships between visual and tactile features and biophysical parameters in human facial skin. Skin Res Technol. 2007;13:176–83.

Beach RA, Wilkinson KA, Gumedze F, Khumalo NPJ. Baseline sebum IL-1α is higher than expected in afro-textured hair: a risk factor for hair loss? J Cosmet Dermatol. 2012;11:9–16.

Bergler-Czop B, Brzezińska-Wcisło L. Assessment of the skin parameters – moisture, melanin content, pH and production of sebum in patients treated with oral isotretinoin: a preliminary report. Post Dermatol Alergol. 2010;27:83–9.

Biro K, Thaci D, Ochsendorf FR, et al. Efficacy of dexpanthenol in skin protection against irritation: a double-blind, placebo controlled study. Contact Dermatitis. 2003;49:80–4.

Cheng Y, Dong Y, Dong M, et al. Moisturizing and antisebum effect of cosmetic application on facial skin. J Cosmet Dermatol. 2007;6:172–7.

Cheng Y, Dong Y, Wang J, et al. Moisturizing and antisebum secretion effects of cosmetic application on human facial skin. J Cosmet Sci. 2009;60:7–14.

Clarys P, Barel A. Quantitative evaluation of skin surface lipids. Clin Dermatol. 1995;13:307–21.

Clarys PM, Barel AO. Sebumetry: a comparison between lipid collection techniques. Skin Res Technol. 1996;2:222.

Davari P, Gorouhi F, Jafarian S, Firooz A. A randomized investigator-blind trial of different passes of microdermabrasion therapy and their effects on skin biophysical characteristics. Int J Dermatol. 2008;47:508–13.

Davoudi SM, Sadr B, Hayatbakhsh MR, et al. Comparison of skin sebum and elasticity level in patients with sulfur mustard induced dermatitis and healthy controls. Skin Res Technol. 2010;16:237–42.

Dobrev H. Clinical and instrumental study of the efficacy of a new sebum control cream. J Cos Dermatol. 2007;6:113–8.

Firooz A, Gorouhi F, Davari P, et al. Comparison of hydration, sebum and pH values in clinically normal skin of patients with atopic dermatitis and healthy controls. Clin Exp Dermatol. 2007;32:321–2.

Firooz A, Sadr B, Babakoohi S, et al. Variation of biophysical parameters of the skin with age, gender and body region. Sci World J. 2012;2012:386936.

Jacobsen E, Billings JK, Frantz RA, et al. Age-related changes in sebaceous wax ester secretion rates in men and women. J Invest Dermatol. 1985;85:483–5.

Kim MK, Choi SY, Byun HJ, et al. Comparison of sebum secretion, skin type, pH in humans with and without acne. Arch Dermatol Res. 2006;298:113–9.

Kligman AM, Miller DL, Mcginley KJ. Sebutape: a device for visualizing and measuring human sebaceous secretion. J Soc Cosmet Chem. 1986;37:369–74.

Knaggs H, Bajor J, Becker W. The sebumeter and its use. Mediscript 12/88.

Lee SM, Huh CH, Park KC, Youn SW. Effects of repetitive superficial peels on facial sebum secretion in acne patients. J Eur Acad Dermatol Venereol. 2006; 20:964–8.

Marrakchi S, Maibach HI. Biophysical parameters of skin: map of human face, regional and age-related differences. Contact Dermatitis. 2007;57:28–34.

Nordstrom KM, Schmus HG, McGinley KJ, et al. Measurement of sebum output using a lipid adsorbent tape. J Invest Dermatol. 1986;87:260–3.

Nouveau-Richard S, Zhu W, Li YH, et al. Oily skin: specific features in Chinese women. Skin Res Tech. 2007;13:43–8.

O'goshi KI, Iguchi M, Tagami H. Functional analysis of the stratum corneum of scalp skin: studies in patients with alopecia areata and androgenetic alopecia. Arch Dermatol Res. 2000;292:605–11.

Perkins MA, Cardin CW, Osterhues MA, et al. A noninvasive tape absorption method for recovery of inflammatory mediators to differentiate normal from compromised scalp conditions. Skin Res Technol. 2002;8:187–93.

Pierard GE. Follicle to follicle heterogeneity of sebum excretion. Dermatologica. 1986;173:61–5.

Pierard GE, Pierard-Franchimont C, Marks R, et al. EEMCO guidance for the in vivo assessment of skin greasiness. Skin Pharmacol Appl Physiol. 2000;13:372–89.

Pierard-Franchimont C, Quatresooz P, Pierard GE. Sebum production. In: Farage MA, Miller KW, Maibach HI, editors. Textbook of aging skin. Berlin: Springer; 2010. p. 343–52.

Pouradier F, Céline C, Marie-Florence D, et al. Functional and structural age-related changes in the scalp skin of Caucasian women. Skin Res Technol. 2013. doi:10.1111/srt.12057 [Epub ahead of print].

Saint-Leger D, Cohen E. Practical study of qualitative and quantitative sebum excretion on the human forehead. Br J Dermatol. 1985;113:551–7.

Schaefer H, Kuhn-Bussius H. A method for the quantitative determination of human sebum secretion. Arch Klin Exp Dermatol. 1970;238:429–35.

Seirafi H, Farsinejad K, Firooz A, et al. Biophysical characteristics of skin in diabetes: a controlled study. J Eur Acad Dermatol Venereol. 2009;23:146–9.

Sisalli S, Adao A, Lebel M, et al. Sorptive tape extraction a novel sampling method for the in vivo study of skin. LC-GC Europe. 2006;19:33–9.

Son T, Han B, Jung B, Nelson JS. Fluorescent image analysis for evaluating the condition of facial sebaceous follicles. Skin Res Technol. 2008;14:201–7.

Stinco G, Bragadin G, Trotter D, et al. Relationship between sebostatic activity, tolerability and efficacy of three topical drugs to treat mild to moderate acne. J Eur Acad Dermatol Venereol. 2007;21:320–5.

Tagami H. Development of instruments for measuring the skin. J Jpn Med Assoc. 2003;129:1405–8.

Uhoda E, Pierard-Franchimont C, Petit L, Pierard GE. The conundrum of skin pores in dermocosmetology. Dermatology. 2005;210:3–7.

Yong SW, Kim SJ, Hwang IA, Park KC. Evaluation of facial skin type by sebumeter secretion: discrepancies between subjective descriptions and sebum secretion. Skin Res Technol. 2002;8:168–72.

Youn SW, Na JI, Choi SY, et al. Regional and seasonal variations in facial sebum secretions: a proposal for the definition of combination skin type. Skin Res Technol. 2005;11:189–95.

Photographic Techniques and Quantification of Hair Growth

77

Van Neste Dominique

Contents

Keywords

Hair measurement • Exogen • Hair loss • Hair growth • Hair shedding • Phototrichogram • Thickness • Hair cycle

Abbreviations

CCD	Charge-coupled devices
CE	Contrast enhancement
CE-	Contrast-enhanced
PTG-EC	phototrichogram with exogen collection
EC	Exogen collection
FDA	Food and Drug Administration
MPHL	Male pattern hair loss
PTG	Phototrichogram
SCS	Scalp coverage scoring

1 Introduction

This chapter will focus on the basic principles involved in human hair evaluation and more specifically in hair growth measurement. Historically, evaluation was rather subjective, and it took about 30,000 years before eventual categorical classification systems and clinical scoring together with objective follow-up methods became available (Fig. 1 adapted from Van Neste 2008). Although subjective approaches were classically considered to be sufficient to run the routine activities of a dermatology practice, more and more hair clinics were established, and these categorical classifications do not stand the process of scientific

V.N. Dominique (✉)
Skinterface Tournai and Brussels' Hair Clinic, Tournai, Belgium
e-mail: info@skinterface.be

P. Humbert et al. (eds.), *Agache's Measuring the Skin*,
DOI 10.1007/978-3-319-32383-1_107

investigation. There are some reports showing poor concordance and weak repeatability even with trained clinicians (personal unpublished observations and others; Guarrera et al. 2009).

During the last 25 years of the previous century, we thought that the time would come where more precise observation, understanding, and exchange of information between the practitioner and the patient could be required. In the early days of hair science (1960s and 1970s; reviewed in Van Neste 2002; Dawber and Van Neste 1995), all measurements were made in vivo (capillary tubes or stereomicroscopy observations), and numbers were published but no documentation allowed us to check a source file or an objective record. What was really observed and measured? How come institutions like the FDA (USA) ever accepted in vivo hair counts made by untrained and/or unexperienced investigators, whether doctors or nurses, and took those fancy numbers as evidence during hair regrowth trials in the 1980s and 1990s? As no images can be retrieved, no one will never be able to check, and this is but one of the weaker aspects of these observer-dependent methods.

Based on repeat close-up photography, the seminal work of Saitoh (Saitoh et al. 1970) opened up avenues for further technological progress after the 1970s. Photographic methods available until the late 1990s were gradually replaced in the early twenty-first century after the advent of microcomputers and charge-coupled devices (CCD) in digital cameras. These made imaging technology accessible to a larger community.

However, progress in hair clinics remains slow as it depends on a basic understanding of what is required to generate meaningful numbers as they relate to hair growth measurement. We refer the interested reader to other publications (Van Neste 2005, 2006a, 2013) where a number of basic points were illustrated and some prerequisites were proposed for this purpose.

Those who are acquainted with growth of hair and hair follicle cycling may easily skip the very short resume on basics and proceed to the next sections.

2 Basics About Hair Structure in Relation with Global and Analytical Imaging Procedures

Here, we shall briefly review some basics about hair follicle structure and function. Basics are necessary to understand why fine-tuning of technical aspects of hair imaging remains a prerequisite. Scalp hair is an appropriate example to introduce the concept of global and analytical methods while "zooming" into the field of hair (Fig. 2). Scalp hair appears as a stable mass of hair. It actually represents the cumulative end result of discrete changes of individual hair follicle dynamics: hair shedding and its continuous replacement by regrowing hair that results in global maintenance. The key to the appropriate assessment of a patient complaining about hair shedding or hair loss and recovering an appropriate amount of hair or achieving hair maintenance lays first in a thorough understanding of the hair cycle (for a review, see Stenn and Paus 2001).

In the past, we proposed a very simplified explanatory scheme for one single hair follicle (Fig. 3). On the scalp there are about over 100,000 follicles. Importantly, not all follicles are active at the same time: some produce hair while others are resting and clearly empty or dormant. After completion of this resting phase which includes telogen–exogen transition, the club hair is processed for its programmed release. Exogen phase resolves with the shedding of the old hair fibre. What is left over in the scalp is the old exogen follicle from where eventually a new hair follicle will derive and a new hair might become visible. Each follicle appears to function independently from its neighbours, i.e., the process of scalp hair growth is normally not synchronized. However, follicles in a certain field may express a common phenotype after exposure to some compounds, i.e., sex hormones or drug treatments. Some scalp areas, in genetically predisposed individuals, will show a phenotype of defective hair replacement, i.e., patterned balding (Figs. 1 and 2). In other areas (axillae, face, chest,

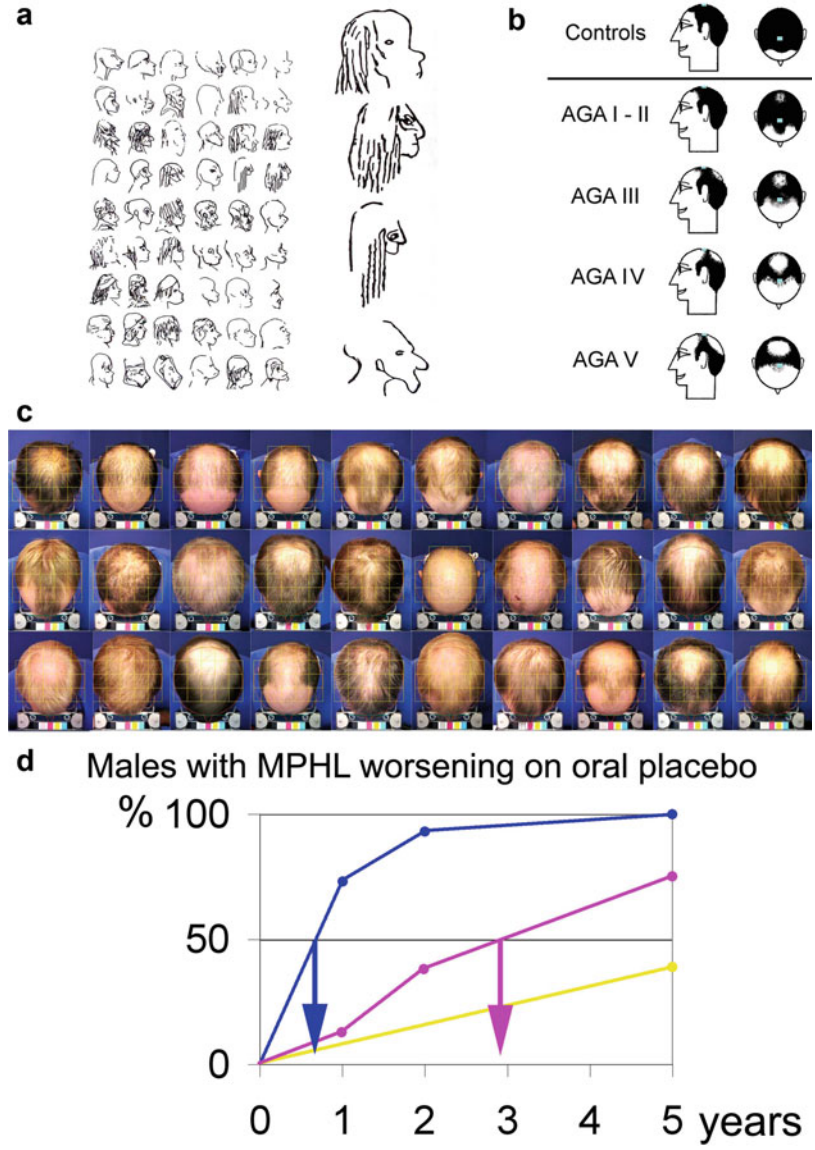

Fig. 1 Scalp hair patterning: 30,000 years from qualitative observation to quantitative dynamic measurements. Patterns of scalp hair in younger-looking and more aged subjects appeared already on the walls of caves in prehistorical times (**a**) (Modified after Van Neste 2008). They do not differ from the more recent cartoons inspired from the Hamilton–Norwood classification (**b**). A scientific observer will soon recognize that it is very difficult to squeeze the spectrum of patterns displayed by a group of 30 males, i.e., real patients (**c**), and ascribe the right man in the right place within these simplified classification schemes. In the *lower panel*, we show the results of a subgroup of patients who received placebo-containing pills during a 5-year period. We graphically estimated the time required for 50 % of the subjects to be considered as worsened compared to baseline (*arrow* derived from the intersection of regression *lines*). It would take about 9 months on placebo to have a reduced hair count (*blue line* and *arrow*) and 3 years with global imaging (*magenta line* and *arrow*), while a clinical investigator/observer (*yellow line*) would not detect worsening with progressive hair loss in 50 % of the subjects after 5 years on placebo!

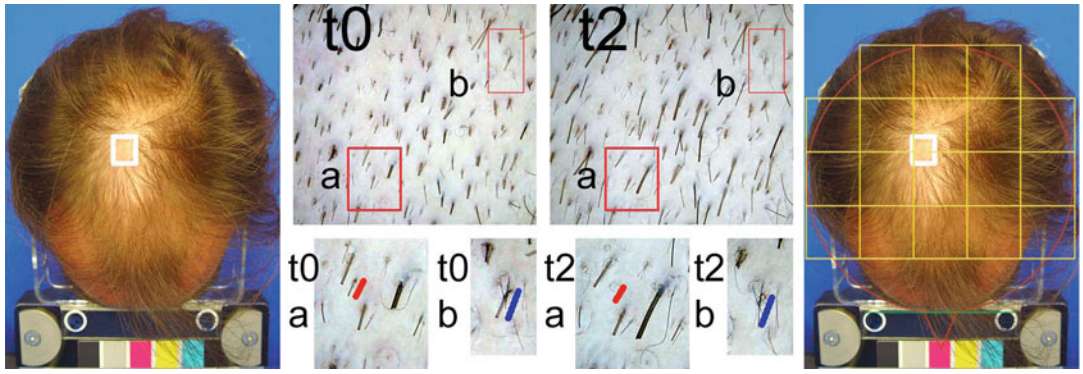

Fig. 2 Global imaging and CE-PTG-EC in Caucasian male pattern hair loss. On the global view (*left*), we show the region of interest (ROI; *white outline*) where we performed a contrast-enhanced phototrichogram with exogen collection (CE-PTG-EC). *Baseline* image (*t0*) shows that all hair is clipped very short in the ROI. All hair fibers are well contrasted against the background. Forty-eight hours later, a new image is taken (*t2*) after extracting the exogen hair. In the *lower panels*, two enlarged fields of t0 and t2 highlight the presence of exogen hair. These hairs are underscored as thin (*red* in *t0a*) and thick (*blue* in *t0b*) hair at t0. The underscored targets show that these exogen hairs are no longer visible in the images taken at t2 (*t2a* and *t2b*). Because exogen are entrapped in a matrix, the exogen hair can be examined under the stereomicroscope, and hair shedding of calibrated hair can be described as numbers per unit area. On the *right panel*, the same subject is shown with a grid superimposed on the image; each *square* can be rated individually for scalp coverage scoring (SCS) as will be detailed later

genital skin, etc.), other "patterns" will be expressed: the very thin hair follicles will now grow longer and coarser hair, and such hair usually grows during limited periods of time and is retained as telogen hair for prolonged periods of time as compared to the scalp hair. As such the clinical appearance of "hairiness" depends as much on the number of hair follicles as on systemic factors responsible for regional modulation of the hair follicle activity and duration of each of its cycle phases in particular.

3 From Global Photography to Analytical Evaluation of Hair Growth

There is not a single technical modality that will encompass with a sufficient degree of precision the many dimensions of hair (Sinclair et al. 2003; Van Neste et al. 2003a). At the one end of the spectrum is the clinical observation. Hair patterning has been classified but more recently documentation has been improved with global imaging. Such images document and illustrate files submitted to the health authorities or eventually to individual patients. At the other end one finds a number of more detailed imaging procedures and some of these will be reviewed.

3.1 Global Imaging

Standardization of global photography has been a significant step forward in scalp hair documentation not only by creating a permanent record but also more specifically by defining the conditions to prepare the scalp in order to prevent "photographic cures" for hair problems (Canfield 1996) as documented in Figs. 4 and 5.

Processing and rating of global images were initially intended to be performed as follows: the image taken before treatment is placed on the left while another image taken under similar conditions after the subject has taken or applied a drug for a given period of time is placed on the right. The expert views paired images and rate changes (right vs left or after vs before) on a seven-point scale ranging from greatly decreased (−3) to no change (0) and up to greatly increased (+3) (Kaufman 2002). Other techniques are based on scalp coverage scores (SCS; Van Neste et al. 2003b) where the observed scalp is divided into arbitrary subunit areas as shown in Figs. 1c, 2, 5, and 6.

Each field that is outlined can be scored individually (value of coverage between 0 and 5). Adjacent fields can be grouped and the mean value, i.e., a scalp coverage scoring (SCS), generates valuable quantification. This can be measured under randomization with blinding as to treatment and to time (Van Neste et al. 2003a, 2006). Trained experts' data can be traced in both the paired examination of global views (Google: FDA NDA 21-812/000, 2005) or with the SCS system (Van Neste et al. 2003b, 2006). The experience acquired during the last two decades clearly shows that analysis of standardized global images is more objective in the appreciation of hair growth effects after drug treatment as compared with subjective evaluations made by investigators or by patients. Nevertheless, global imaging requires a long period of time for detecting deterioration of the scalp condition (Fig. 1); this period of time may eventually result in the irreversible loss of a clinically significant number of follicular units (Van Neste 2008).

Global images require a high degree of standardization, and all the preparatory procedures remain key as the same holds true for its use in vivo. A simple "error in the lightning" or angle or distance between head and camera (Fig. 4) or even a different haircut or a hair dye session can have dramatic effects. As it modifies our interpretation in terms of therapeutic response, it potentially "ruins" a clinical file during a clinical study on a hair growth promoter!

Global viewing, even when highly standardized procedures are being used, does not resolve the question of hair cycling changes, but it remains clinically inspiring in terms of efficacy assessment. It is also an easy way to communicate between clinicians and patients. Stating it very simply: one is not in a position to infer from global imaging that hair grows faster or that hair fibers are thicker or that cycling is improved or a combination thereof!

Besides objective documentation and the risk of erroneous interpretation, we illustrate also the challenge faced by subjectivity: it is a daily experience that patients report their satisfaction or lack of it with our therapeutic proposals. In Fig. 5, we show two typical cases with a discrepancy between subjective and objective appreciation of efficacy. There was a great biological and clinically significant improvement in a pessimist patient as compared with a clear-cut biological and clinical worsening in an optimist patient! These psychological dimensions, i.e., satisfaction with oneself, are usually misinterpreted or underestimated during discussions with health authorities (FDA, EU or national health authorities). The wrong interpretation recurrently sounds like accurate technology is useless because the patient "can not appreciate the effect" or the consumer "can not perceive it." From a historical perspective, we evolved during the last 25 years from fancy in vivo hair counts to more precise noninvasive technologies that help us stay away from trichoquackery. In other words, one must be aware that subjective impressions of the patient and the clinician are influenced by far too many uncontrolled factors that are encompassed as "placebo" effect. We maintain that a combination of well-standardized global images together with a thoroughly validated analytical technology can get rid of all and any irrelevant or extraneous factors of variation, i.e., those influenced by subjectivity. The psychosocial aspects and influences on perception and satisfaction are usually put in the fore by companies, and these subjective, error-prone, aspects are not taken into account in this chapter.

3.2 Analytical Methods

3.2.1 A Brief Historical Review: What Did We Learn with the Conventional PTG?

The basic principle of the phototrichogram (PTG) consists of taking a close-up photograph of a certain area of the scalp. The hair is cut very close in preparation for the first photograph, followed by repeat photographic documentation after a certain period of time. This period of time should be long enough to allow the growth of a hair segment (time window which is usually between 24 and 72 h) but not too long in order to prevent outgrowth or too much overlapping of growing hair. The growth is then evaluated by comparing the two pictures. Hairs that have

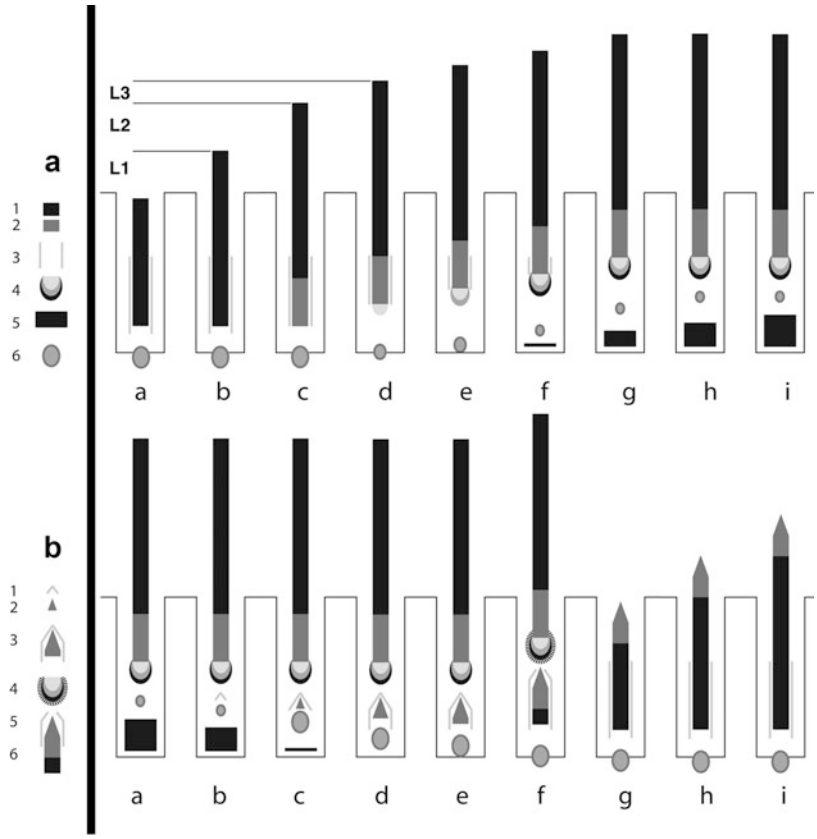

Fig. 3 Hair cycle. The hair growth phase (anagen) during which hair is visible at the skin surface and growing are shown in (**A**) while the apparent resting phase of the hair cycle (telogen) together with initiation of hair regrowth from the new follicle is shown in (**B**). (**A**) From growth to rest. The same hair follicle is represented at various times at the very end of the growth phase (day *a* to day *i*). At the skin surface, there is normal pigmented hair production with the constant daily hair production (measurable elongation *L1* and *L2* between days *a–b* and days *b–c*; notice that *L1* roughly equals *L2*). Then, in the depth of the hair follicle, the pigmentation of the newly synthesized hair shaft is gradually decreased (day *c*) as shown by the shaded area at the bottom of the hair fiber. This early event heralds the regression of the impermanent portion of the hair follicle and is followed by terminal differentiation of cells in the proliferation compartment (day *d*). This is associated with apoptosis and indicates the earliest morphological steps of the catagen phase. It will inevitably propel the follicle into telogen with the typical club hair formation. The shrinking dermal papilla (day *d*) begins an ascending movement together with the hair shaft (days *d–I*; estimated 21 days). This characterizes the catagen phase with an apparent elongation of the hair fiber (*I*) that reflects the outward migration of the hair shaft (*L3* is much smaller than the daily growth rate *L1* or *L2*). This can clearly be measured as slowing down of hair elongation rate and terminates with no growth during a while (see later). What is left after disappearance of the epithelial cells from the impermanent portion of the hair follicle are basement membranes followed by dermal connective tissue usually referred to as streamers or stelae shown as dark remnants at the bottom of the diagrams (days *f–i*). The true resting stage begins when catagen is completed, i.e., when the dermal papilla abuts to the bottom of the permanent portion of the hair follicle. Would there be no physical interaction between dermal papilla and the bulge, there would be no reactivation of stem cells now densely packed within this area. As a consequence, the next hair cycle (see **B**) would be definitely compromised. As of now no hair growth is observed at the surface (days *g–i*). (**B**) From rest to growth. During this stage, shown in the *lower panel*, one notices no elongation of hair fiber as it is seen at the skin surface (days *a–e*) but significant changes occur in the deeper parts of the hair follicle. The dermal papilla expands and attracts epithelial cells from the bulge (stem cell zone) in a downward movement (days *a–b*). To create space, previously deposited materials have to be digested (days *a–c*). The epithelial cells then start differentiation in an orderly fashion starting with the inner root sheath (forming the initial cone in *b* and then a funnel in *c*). The mirror image of the cuticle of the inner root sheath reflects on and contains the tip of the hair cuticle. In the very center of the newly formed hair shaft, one finds the tip of the newly

grown are in anagen phase and those, which have not, are in telogen phase.

In 1989, we devised scalp immersion photography (Van Neste et al. 1989) or proxigraphy (Van Neste et al. 1992) and listed a number of problems related to the fiber, its association with the follicular opening, and the scalp skin in the background and immediate surroundings. All these difficulties will be recapitulated at the end of the chapter, and one will be able to understand the progress made during the last 20 years. Then, the term "epiluminescence microscopy" took over. It is of note that image magnification (up to 200 times or more) does not correspond exactly to the optical equipment contained in instruments known as microscopes. In short, epiluminescence microscopy became the accepted denomination for examination under special lighting with high magnification.

The next step was to evaluate the limit of detection comparatively with another more invasive method (Rushton et al. 1993). As some uncertainties were detected, we considered with great care the discrepancies and devised contrast-enhanced (CE) phototrichogram (CE-PTG) as a further improvement (Blume et al. 1991; Van Neste 2001). The CE-PTG became almost equal in terms of resolution as transverse microscopy on serial sections made on scalp biopsies, while, at that time, only a few sections were considered as the gold standard (Headington 1982; Headington and Novak 1984; Whiting 1990, 1993, 1998; Headington 1993). So far, the CE-PTG remains the only noninvasive method that has documented all transitions of thick and thinning follicles from anagen to catagen to telogen phases on a follicular basis (Van Neste 2001).

3.2.2 What Can We Learn to Measure with the CE-PTG and Are There Possibly Further Improvements?

The assessment is made on one or a number of predefined scalp sites considered representative of the condition. After feeding the computer with source images and after a human intervention, preferably with the help of a trained and calibrated technician, the data that can be generated from a PTG are total number of hair present in a certain area (i.e. hair density (n/cm^2)), percentage of hair in the growth phase (anagen %), linear hair growth rate (LHGR; μm/day), and hair thickness (μm), and the latest developments added a split-up according to thickness of growing and resting hair together with the transition from telogen to exogen.

Thickness can be measured on hair clippings, on scalp biopsies, and on scalp hair photographs. It may seem trivial to state that the hair diameter evaluation is more precise with the microscope as the 3D movement allows measures to reflect diameter whenever the fiber section is not circular. Interestingly, the hair section remains almost

Fig. 3 (continued) formed less or yet unpigmented hair cortex (days *c*–*e*). The resting hair remains in the hair follicle for approximately 1–3 months (days *a*–*e*), and then a detachment process transforms the old telogen follicle into exogen where the release of the exogen hair can now take place either immediately (day *f*) or after a while during which it may stick in the follicle before being shed (days *f*–*g*). The shiny root end of the shed hair is the club. Before, during, or after hair shedding, there may be replacement by a new gradually thicker and more pigmented hair shaft (period *e*–*g*). Indeed, under physiological conditions, the follicle may proceed immediately or only after some lag time with new hair production (from *b* to *g*; up to 90 days). In conditions like androgenetic alopecia after shedding, the old follicle may remain empty for a longer period of time as a lag phase has been reported before the new regrowing hair follicle initiates a new hair cycle with a visible hair fiber at the scalp surface. Note that a prolonged adhesion to the epithelial structures may increase intrafollicular stasis of exogen hair: this turns into trichostasis due to abnormal accumulation of nonadherent or loosely attached elements. Also exogen does not always result in immediate recycling, and there may be a much longer interval before regrowth is recorded at the scalp surface. At the earliest visible stages, i.e., when the new anagen follicle is again deeply set into the dermis, one notices at the scalp surface a thin usually nonpigmented hair tip that is seen first (day *h*). This is soon followed by a thicker, more pigmented, and faster growing hair fiber (day *i*). All hair cycle transitions can now be recorded in vivo with noninvasive technologies. This sequence of course depends on the many systemic, regional, and local regulatory factors controlling the hair follicle activity during its replacement

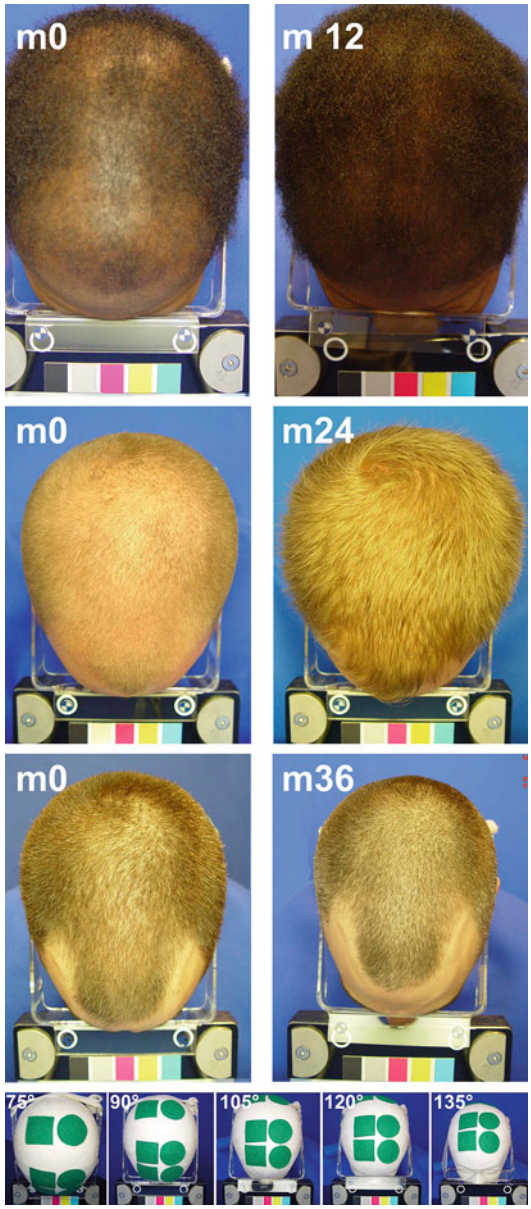

Fig. 4 Problems of standardization of global imaging in three subjects with male pattern hair loss (MPHL): Black African female (*upper panel*) and two Caucasian male (*middle* and *lower panels*) and in a series of images taken from an experimental model. In clinical cases, baseline view of the top of the head is shown on the *left panels* before treatment (*m0*). After 12, 24, or 36 months of treatment (*m12*, *m24*, and *m36*, respectively), images unravel some technical errors. These make interpretation hazardous in the absence of analytical data. The reader is invited to compare the color of the background (*left* and *right*) and the range of "objective" color patches (objective rulers included in the *lower* part of each image). These

circular when the fiber is thinner than or equal to 40 μm (Rushton 1988) independently of ethnic background.

Finally, the number of hair sprouting from one opening is another source of difficulty that has also been addressed recently. As the production of different hair follicles composing a single follicular unit is randomized, i.e., not synchronized, it may be difficult to formally trace "hair thinning" during the succession of individual hair follicle cycles! In addition, the complexity will even increase in scalp imaging in case an observer wishes to evaluate the susceptibility of each individual follicle to the follicular regression and eventually its progression towards organ deletion.

3.2.3 Technological Requirements

Before discussing in greater detail the practicalities for performing hair growth analysis and the data so generated, it is useful to recapitulate some difficulties that every investigator will encounter, sooner or later, as he becomes exposed to a new technology.

Fig. 4 (continued) objective color rulers are fixed onto the front panel fixed of the stereotactic device. These are recorded in all our pictures and clearly document differences in light exposure. One should now focus on hair length and style as well as on the position of the head in the stereotactic device: these are but a few of the many factors of variation such that improper (like in these three cases) or even appropriate global imaging documentation should in any case be supported by analytical data before interpretation is being provided in terms of improvement or worsening (see also Fig. 5). In the Caucasian proband, while changes in hair style suggest impressive differences, the same number of hair was present though growth fraction was improved after treatment. The influences of distance and angle on global perception were subject to image analysis in a model (shown in the *lowest panels*). Standardized pieces of green cloth with a known size were fixed in specific fields on a model. Those sites correspond to a number of anatomical fields known by clinicians as frontal, parietal, and vertex that are located, respectively, on anterior scalp, top of the head, and between top and posterior scalp. Images were taken with the model positioned at various angles (range from 75° to 135°). The measured surfaces in the two-dimensional images of the standard patches ranged from 6 % to 224 % of the value that was measured on the images taken at 90° (second image starting from the *left*)

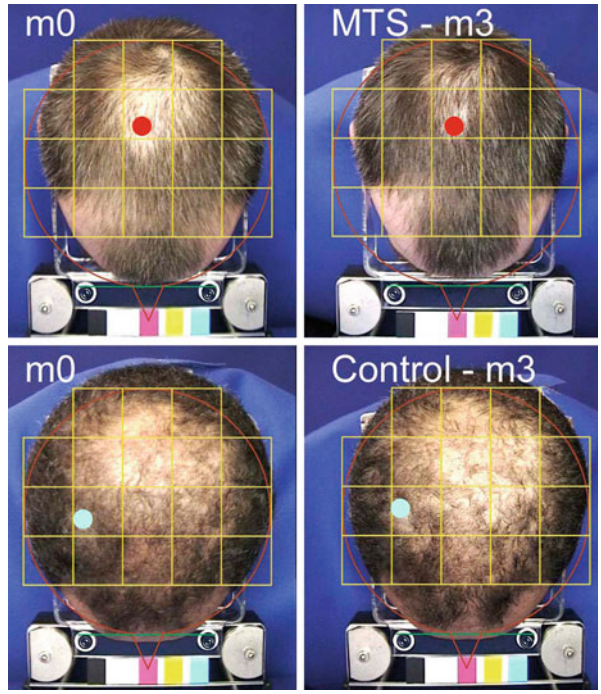

Fig. 5 Standardized global scalp imaging in male pattern hair loss testing topical treatment vs placebo, in combination with finasteride. In this study, a double-dummy placebo controlled protocol was used for the topical lotions while all subjects received an oral medication (finasteride 1 mg/day). They were assigned randomly to either minoxidil topical solution 5 % (MTS5%, once a day) or a control solution (containing ethanol–water and propylene glycol in the same proportions as the vehicle of the active MTS5%). The compliance was checked on counting the pills and weighing bottles containing lotion at monthly visits and with dairies. Compliance exceeded 98 %. Examine first the two images in the *top panel*. As compared with baseline (*m0*), changes in scalp coverage scoring (SCS) at month 3 were impressive in favor of MTS5%. The biological response of the scalp follicle target (*dot*) showed a 26 % increase of thick anagen hair per cm^2 (thick = hair fiber thickness over 40 μm). The scalp coverage scores (SCS) in the mid scalp and vertex area were 4.2 ± 0.8 at baseline and 4.7 ± 0.4 at m3. The mean difference 0.5 represents a 12 % increase in the SCS. Interestingly, we probed the level of subjective satisfaction in terms of change from baseline using a hair questionnaire exploring five items. In this individual, the rate of global satisfaction with changes from baseline was 56 %, which is rather low. Examine now the two images in the *lower panel*. In the subject treated with the control solution, the SCS (baseline 4.1 ± 0.7 vs m3: 3.8 ± 0.9) indicated objective worsening of the condition from the "blinded as to treatment" investigators' perspective who performed the SCS test in vivo. There was a 7.3 % global worsening (SCS method). This keeps in line with a 20 % decrease of the thick anagen hair count per cm^2 (growing hair with a thickness >40 μm in the target area, *dot*). This patient, using the same hair questionnaire, rated 72 % satisfaction in terms of global response of his scalp condition. Hence, we can mathematically estimate that the subject shown in the *top panels* is disappointed by an efficient treatment, who is considered as a pessimist, while the one shown in the *bottom panel* has a great degree of satisfaction while objectively worse and he could be considered as an optimist! The latter typifies the patient or consumer that makes trichoquakery "WORKS" supporting the useless hair procedures and hair restoration claims made by cosmetic products!

In order to keep analytical technology in the field of clinical relevance and within an acceptable range of variability, we suggested that a "clinically representative" field containing around 100 hair fibers would be acceptable (Van Neste 1993). There is no magic value to the number 100, but this means that a "5 hair detection error" still keeps variability lower than 5 %. We also stated that the analysis would be valuable only if "exhaustive" sampling took place. This means that all and any hair whatever its growth stage and whatever its thickness should be taken into account (Van Neste 1993, 2001). We would also like to add "whatever the nature of the

background skin" as a medical field technology should be compatible with all types of scalp encountered in the hair clinic. Since this was published, extensive quality control studies were conducted internally, and all criteria set forth in the context of validation (Bircher et al. 1994) were appropriately met by the CE-PTG technology including the collection of exogen hair (CE-PTG-EC) (Van Neste et al. 2007).

We can communicate the conclusion of this audit (Hugh Rushton, personal communication): "All files were revised independently by an external audit" who reported that "the Accuracy, Sensitivity, Reproducibility, Repeatability of the CE-PTG method including the results obtained with and without the exogen collection method were checked in detail and the methods for acquiring images through to editing the results were found to be appropriate and well documented." The variation for those parameters was found to be less than 3 % (Van Neste, 2015) and we realize that discussing all the statistical details is beyond the scope of this chapter.

Hence, we feel comfortable by the combination of a global and an analytical method to evaluate our patients (Fig. 6), while at the same time we keep in line with others (Pierard et al. 2004) and advise making a scalp biopsy for diagnostic purposes. Also making biopsies was a critical step to compare the invasive scalp biopsy approach with serial sectioning (i.e., exhaustive sampling) and performing the paired stereological analysis of individual hair follicles in order to validate the noninvasive procedures (Van Neste 2001). However, we think that making repeat scalp biopsies should be considered inappropriate for hair growth monitoring purposes. Indeed from a typical 4 mm diameter scalp biopsy specimen, one samples around 15 follicular units or less providing about 40 follicles (Headington 1982; Whiting 1990). This means that a one hair error represents a 2.5 % error, and as density decreases like in male pattern hair loss (MPHL), then the risk of variability increases. Also, it should be clear that one does not really measure the pharmacodynamic response of the individual hair follicles essentially because of the destructive nature of the sampling method. Hence, a statistical evaluation on different before and after samples is being made while even sampling itself may be subject to bias (personal communication at the Society for Investigative Dermatology, unpublished data).

Finally, the use of small destructive sampling methods and statistical evaluations led to the speculative interpretation that finasteride taken by man with MPHL would be able to revert affected

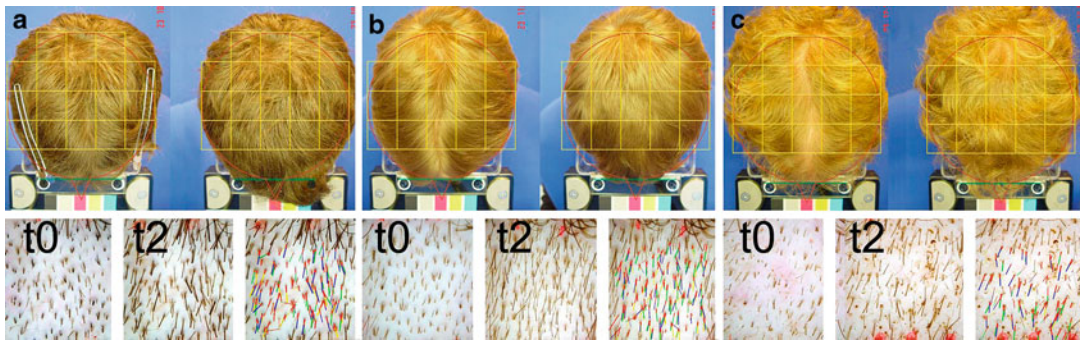

Fig. 6 Combined global viewing and CE-PTG-EC. The top of the head of three young male subjects complaining of hair shedding (**A**, **B**, **C**) is shown with a parting in the middle (*left panel*) and hair combed as spokes of a wheel (*right panel*). These views suggest an increasing visibility of scalp through the hair as one proceeds from subject **A** to **C**, especially when parting the scalp hair. However, there is no typical Hamilton–Norwood pattern. Therefore, we classify these subjects as preclinical and mild hair thinning. For each individual, phototrichograms are displayed. From *left* to *right* we show the baseline image (*t0*), 48 h later (*t2*), and the processed image ready for CE-PTG-EC analysis. The computer-assisted image analysis on the latter generates the detailed data shown in Table 1. These data confirm abnormal hair follicle performance as compared with male controls (data shown in Tables 2 and 3). Patients were diagnosed as preclinical or early stages of MPHL, and they were given medical treatment

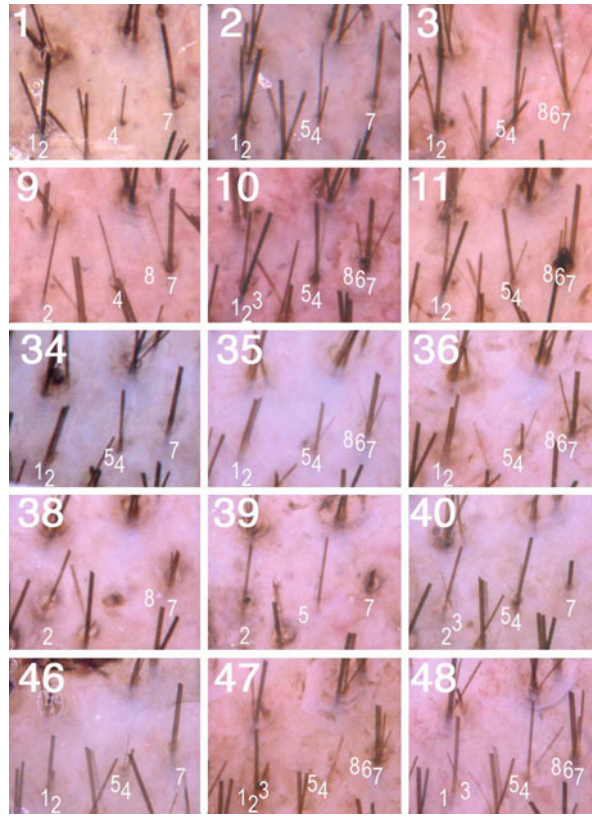

Fig. 7 Small fields of the scalp at selected time periods during the 48-month follow-up CE-PTG-EC study. The study of hair cycling with CE-PTG (we show only those images taken 48 h after clipping where the longer fibers represent anagen hair and the shorter ones telogen hair). While CE-PTG was made at monthly intervals, we do show only those months as numbered in the *upper left corner*. Months 1, 2, 3 (first *top panel*), 9, 10, and 11 (second row) belong to the "before treatment period." The *lower panels* (three bottom rows) show the same area from month 34 to 48 while volunteer was on oral finasteride treatment (1 mg/day from month 24–48). Individual hair fibers are numbered from 1 to 8, and their thickness and progression through the hair cycle can be appreciated objectively. The images point to the fact that more than one follicle opens into one orifice. When three or more hair fibers are creating a dynamic but complex field, it is almost impossible to secure a proper follow-up of individual hair follicle cycling

follicles producing vellus-like hair in one cycle into the production of terminal hair follicles (Whiting et al. 2003). However, direct evidence is lacking and this hypothesis remains unproven as reported elsewhere in detail (Van Neste 2006b; Van Neste et al. 2016), and source documentation is shown again herein (Fig. 7).

3.2.4 Advantages of Noninvasive Techniques over a Scalp Biopsy for the Study of Hair Cycling

While estimates of the cycling process as well as the duration of the lag phase remain a painstaking task, some effort has been made in this field (Courtois et al. 1994). The complexity of this investigative field has been somehow underestimated, and as more than one hair can grow from a single follicular opening and that hair cycles within a follicular unit are not synchronized, it is clear that accuracy cannot be certified, and it requires a great deal of caution to use the existing published figures without knowing all the uncertainties.

Biodynamics of the hair follicle is extremely active, and we now realize that some biological variability should appear when long-term studies

are launched. Furthermore, hair density or the number of hair per unit area is usually reported as number/cm^2 as it reflects the number of functionally active follicular units whether growing (anagen) or not (telogen). Because this is the highest number that can be generated, it will also probably vary the least. Under physiological conditions, i.e., the long duration of anagen phase, short telogen duration and exogen initiation will produce long and clearly visible hair at the scalp surface which may change dramatically in some hair disorders leading to hair loss and balding.

Under steady-state conditions, the percentage of anagen follicles properly reflects the time during which hair follicles are engaged in active growth. Now that we have some idea about the complexity of the field, let us review briefly how we got there starting with the classical phototrichogram and a number of variants where hair fiber thickness has been included either as it is measured under the microscope, on images, or with computer-assisted image analysis.

With a few notable exceptions, we may state that the thicker the fiber, the longer the duration of anagen. Hair has been classified into terminal, intermediate, and miniaturized, but there is no absolute consensus on the definition of the latter categories (sometimes less than 40 or less than 30 μm thickness). We suggest to pursue refined research work in that direction and to establish criteria for describing individual follicular performance rather than statistics such as average hair thicknesses or even worse cumulative hair thickness. The latter exposes the clinician to further confusion as it is a composite index of hair count + hair thickness. This means that it reflects the number of more or less frequently present hair shafts, i.e., duration of anagen combined with thickness. Besides other weaknesses of the system used for this particular composite index (see later), the cumulative hair thickness is often mistakenly translated by clinicians (Riedel-Baima and Riedel 2009) who subsequently interpret these data and use descriptive terms that are not relevant to the performance of individual hair follicles.

Many based their assumptions on the thickness of hair fibers, but we argue that there has not been enough attention in the past devoted to the combined analysis of variables such as growth rate, natural pigmentation (Van Neste 2004), and other factors such as scalp location in healthy controls and in functional disturbances.

Indeed in the earliest preclinical stages of MPHL in man, there was obvious shortening of the anagen phase detectable with this sensitive method (Van Neste 2013, 2006c) in the absence of clinically massive or obvious hair miniaturization. This preclinical stage evolves into patterning, i.e., the full-blown phenotype associated with a further shortening of the growth phase along with reduction in hair diameter (Van Neste et al. 2003a; Courtois et al. 1994, 1995, 1996; Tsuji et al. 1994; Ishino et al. 1997; Rushton 1999). The structural follicular regression process is associated with functional changes (shorter anagen duration, prolonged empty phase, and slower growth rates (Van Neste 2015 and Van Neste and Rushton 2015)) finally resulting in production of clinically non-visible hair (Van Neste 2002; Dawber and Van Neste 1995).

Similar findings from transversal studies were keeping in line with a gradual regression of follicular performances in males (Tsuji et al. 1994; Courtois et al. 1995, 1996; Ishino et al. 1997; Rushton 1999) while the process might follow a different pathway in females (Van Neste and Rushton 1997; Ueki et al. 2003; Van Neste 2006d).

Contrary to the thinnest hair with a circular section, thicker Caucasian hair may become elliptical. In Africans the hair flattens even more and some reports indicate differences in growth characteristics from Caucasians (Loussouarn 2001). However, data from patients and controls were not separated such that some confusion remains. As yet, we are not aware of any published data on the value of hair thickness evaluation on scalp photographs of properly selected Black African healthy controls and affected subjects. From the technological point of view, CE-PTG is again able to measure all and any hair including the nonpigmented and finest ones even against a pigmented skin background (Fig. 8). The same comment holds true for other body sites where curly and flattened hairs are the rule rather than the exception.

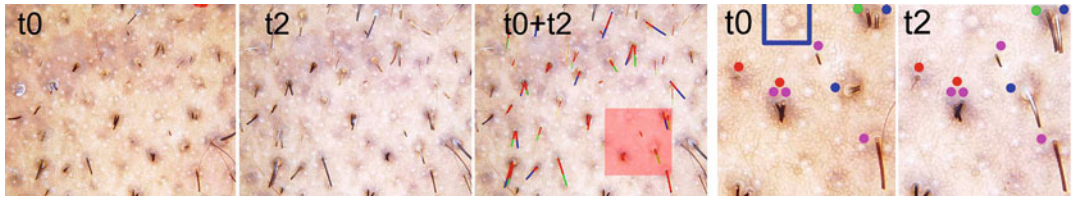

Fig. 8 Contrast-enhanced phototrichogram with exogen collection (CE-PTG-EC) in Black African scalp. The method we developed for Caucasian scalp performs exhaustive visualization and detects all and any hair even on Black African scalp, as shown here. A first image is taken immediately after clipping (*t0*) and a second one is made 48 h later (*t2*). There is a very low density of hair and very little growth as appears in the analysis of the combination t0 + t2. The region of interest (ROI) – as outlined in the latter panel – appears enlarged in the two views of t0 and t2 (two extreme *right panels*). Two distinct compartments can be analyzed in the enlarged ROI: the interfollicular epidermis and the hair follicle dynamics. The interfollicular epidermis shows the typical pigmented network in a honeycomb pattern with brighter spots. The pigment contained in the epithelium that outlines the acroinfundibulum of the hair follicle generates a slightly accentuated pigmented ring. The interfollicular scalp displays numerous small pale spots, usually less than 100 μm in diameter. These reflect acrosyringia or openings of sweat glands and should not be mistakenly interpreted as scarring alopecia. Besides the empty follicle (*blue* outline at t0), several hair types have been dot-mapped: nanohair that are not in the exogen stage (*red dots*) can either look isolated or appear amidst a follicular unit along with thicker hair. Cycling is easily observed on the thicker hair (*magenta dots*). These are split up into resting or telogen hair or anagen as they stay the same length or not at t0 and t2. The latter can be pigmented (*green dot*) or nonpigmented (*blue dots*). African scalp (and many other scalp conditions) cannot be analyzed by the commercially available automated hair analysis programs

Taken together, we found a significant correlation between paired microscopic measurements and thickness evaluation on Caucasian scalp hair photographs in the range of <20 μm to >100 μm thick hair fibers (less than 1–3 % variation depending on the parameters in a test using qualified technicians; Van Neste 2014) so reducing methodological errors of other approaches (Leroy and Van Neste 2002), and it would be worth some effort to pursue our research related to our earlier findings that there is a correlation between thickness and linear growth rates (Van Neste et al. 1991). We believe that there is still a lot to be learned like changes in the growth rate during aging (Ueki et al. 2003; Van Neste 2006d) and other phenomena associated with hair loss including but not limited to androgen-driven patterned hair loss, especially during clinical trials (Rushton et al. 2011). Once again, the human intervention and manual processing should be strictly controlled highlighting the difficulties encountered on the path of scientific and medical progress in the field of measuring hair follicle activity (Rushton et al. 2011).

When the photographic camera is replaced by a video or CCD camera equipped with specific lenses, other variants of PTG recording are obtained.

In fact, early reports in Orientals and Caucasians were published based on the assumption that the natural contrast between hair and scalp seems favorable enough for the application of any imaging method. While the low figures of hair density could possibly be in relation with ethnicity (Hayashi et al. 1991), more studies will be required after validation of these methods not using extra contrast enhancement (CE). As shown earlier (Blume et al. 1991; Leroy and Van Neste 2002) the use of CE is advisable in all cases and especially when balding is present or during aging. More recently, the use of epiluminescence and computer applications for textile fiber analysis was integrated into hair recognition. Such a system has been proposed (Hoffmann 2001) initially with a major source of variability (area less than 0.25 cm^2) because the number of hair so analyzed is definitely less than 100 and dropping below statistically acceptable population sample size (Van Neste 1993). The recent increased size of the scalp area has solved that very point, but others remain to be clarified as will be discussed later in this chapter. Furthermore, automated systems generate consistent

numbers without securing that all hairs in the field were detected. Various commercial brands have been proposed such as TrichoScan® (Hoffmann 2001), the French CapilliCARE (data in file), the Russian system by TrichoScience (V. Tkachev, personal communication), and the Korean system (Kang et al. 2009). The two latter brands announced a fully automated system in the early days of development. Soon, they had to realize that full automation is less reliable and decided to involve human observers during the image processing. So the dream of an easy and fast method vanishes as it was, is, and will probably remain for a period of time – a time-consuming procedure.

Because it seems so fast and user-friendly, some clinicians eventually labeled the CE-PTG as an "obsolete technique" (Camacho-Martinez 2009). While TrichoScan® might appear as the most convenient method, more and more in-depth investigations end up with a better identification of unidentified sources of discrepancies. While evidence about errors can be traced in the earliest publications (Hoffmann 2001; Hoffmann and Van Neste 2006) and is now well established by us and others in scalp hair (Van Neste and Trüeb 2006, 2008; Saraogi and Dhurat 2010; Tajima et al. 2007; Lopez et al. 2011), promoters and clinicians behave like believers and continue to advocate its use (Camacho and Montagna 2013) albeit more evidence has been published on discrepancies in the same textbooks (Van Neste 2013). More studies will be required in order to get a consensus about the evidence-based source studies. The fact that the TrichoScan® method has been noticed as acceptable by a committee of experts does not mean that those experts did some auditing or methodological evaluation in view of qualification or validation of this technique (Pierard et al. 2004). Accordingly the committee stated in the absence of experimental evidence that such imaging technologies "provide insight into the complexities of hair cycling and shedding." The non-substantiated comments by such committee should be considered as nonrelevant to the domain of sciences.

We advise everyone who uses the TrichoScan® method to search for a number of hair visible in the source images that could not be detected or were erroneously interpreted by the analyzer and ask themselves whether the discrepancies are of any clinical significance, because such errors cannot be rejected by those who developed the computerized automated system (Hoffmann and Van Neste 2006). Therefore, since convenience and speed of action have become a trendy way of considering progress in the field of science, some time should be spent at providing sound information about the limits of the automated method of hair measurement.

While the method analyzes only a limited number of clinical situations and even when all clinical conditions are suitable for the computer, it does not generate all data that may be of interest to the observer in terms of diagnosis, prognosis, progression from miniaturization, and reversible inhibition towards organ deletion or any other clinically relevant information.

In high-density hair like the scalp especially in the thinning process (Van Neste 2013) and low-density hair where good natural contrast between skin and hair is documented, the quantitative evaluation is likewise error-prone such as that of the TrichoScan®. As illustrated in Fig. 9, all sources of variation with CE-PTG-EC coupled with computer-assisted image analysis after manual processing (CAIAMP) can easily be traced vs "pseudo-counts" by the automated analysis.

Such scientific observations confirm an academic opinion expressed some years ago by independent clinical observers (Chamberlain and Dawber 2003): "the potential of computer-assisted technology in this field is yet to be maximized and the currently available tools are less than ideal."

3.2.5 Future Trends in Computerized Methods

More than two decades ago, we listed the different problems arising when automated computer-assisted image analysis (ACAIA) came into the scope of hair growth measurement and we would like to add an updated comment (Van Neste 1989). Some problems have been solved. Accurate

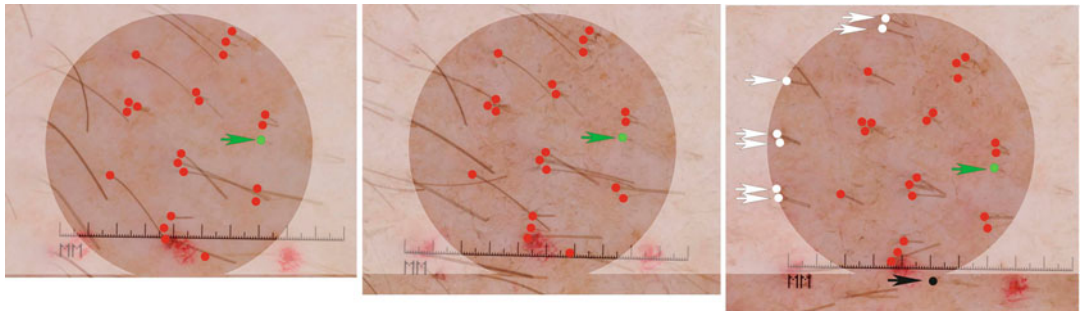

Fig. 9 Low density as a model to understand what is meant by "variability." In biological evaluation, there is always some degree of variability. For the sake of demonstration on very low density, we tested hair counting in body sites with good natural contrast between skin and hair (Van Neste, 2014). Images were obtained from the same site before hair dye (*left*), immediately after hair dye (*middle*), and after clipping (*right*). Thick hair (≥30 μm) and thin hair (<30 μm) counts were obtained with our CE-PTG-EC technique with computer-assisted analysis after manual processing. Dot mapping was color-coded in the image on the *left* (thick = *red dot*; thin = *green dot*), and topography of the dots was maintained from *left* to *right*. The thin hair on the *left* had a thickness of 25 μm. After the hair dye, the cuticula becomes visible and adds some μm to the detected width which becomes >30 μm (*middle* and *right panels*). Therefore, from *left* to *right*, we found 21, 22, and 28 thick hairs. The change from 21 to 22 is explained by the only thin hair that was found on the *left panel*. How to explain a shift from 22 to 28? Due to a small shift (*right panel*), one thick hair was found outside the target area (*black dot*). At the same time seven thick hairs entered into the field (*white dots* and *arrows*). In comparison, the same images were analyzed with TrichoScan®. From *left* to *right*, the automated software described 6.5, 7.5, and 4.5 thin hairs and 53, 78.5, and 103 thick hairs. These are major unexplained variations related to measurement errors that cannot be accepted as real hair counts!

analysis still requires expert human intervention during the sampling and processing of images (Figs. 6, 7, 8, 9, and 10). To date we are easily coping with the three dimensions involved in hair, and we are mastering the requirements in terms of enlargement factor or pixel size, immersion, and polarized light. We also wiped out the problem of backscattering of light and other problems linked to presence of sebum droplets, sweat, and scales. More recent developments helped us to clear the scene from any other loosely attached elements such as exogen hair. Increasing contrast between scalp and hair allow us to express data in a single-case observation or to perform accurate time-course studies of hair growth changes using highly standardized operating and monitoring procedures. As an example of the technological resolving power, we discussed recently on hair pigmentation during aging and how it might affect the outcome of a clinical trial. Initially non-visible hair under conventional PTG may become visible for drug effects such as increased pigmentation, initiation of short-lived but thick anagen hair, etc. The spectrum of follicular bio-responses is actually underestimated and requires sophisticated investigations.

As usual, when facing new technologies, clinicians occasionally express their fears about new information generated by these up-to-date technologies, for example, take into account the fact that thin hair is becoming visible (Olsen 2003) even though thinning remains underestimated with automated tools and remains hard to confess as illustrated elsewhere (see Fig. 2 in Hoffmann and Van Neste 2006). More recenty (Van Neste and Rushton 2013), we provided evidence from data appearing in published papers rated as "high quality" that FDA-approved technologies for hair counting might be confounded by topical agents: undetected hair present at baseline would become visible at later stages because of a modification of the biophysical properties of skin and hair by the vehicle, i.e., nondrug-related effects resulting in high increases of hair counts or not only thin hair that is becoming visible (Olsen 2003)!

This clearly illustrates that our message did not come completely through and we hope today's statement will become a landmark:

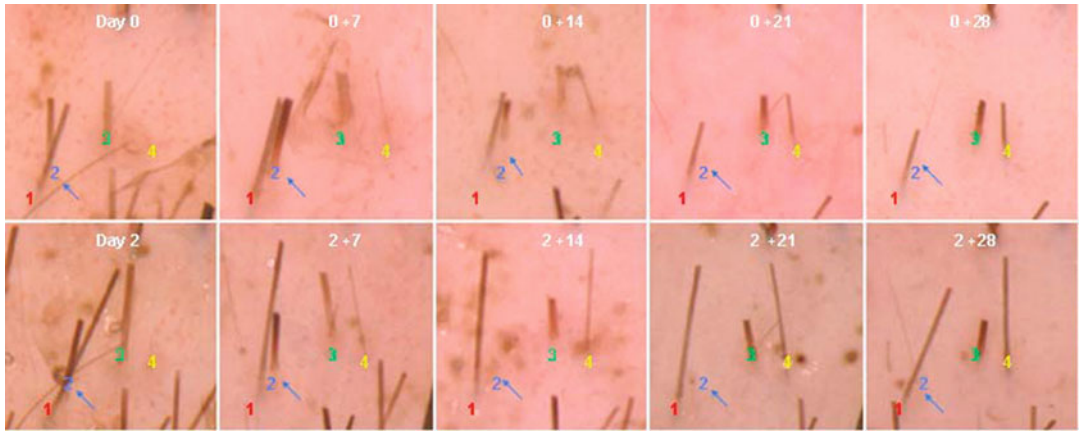

Fig. 10 Within 1 month, weekly follow-up of scalp with CE-PTG-EC showing all hair cycle transitions. Interestingly, a simple statement like "good natural contrast between skin and hair" can be measured as reflected by no change in hair counts after the hair dye (*left* and *middle panels*). A scalp field was monitored at weekly intervals during 1 month. Each week, there were duplicate visits for the CE-PTG-EC; top row shows image taken immediately after clipping (from *left* to *right*: day 0, 0+7, 0+14, 0+21, and 0+28) and bottom row shows the same 2 days later without clipping (0 + 2, etc.). Individually numbered hair fibers can easily be followed over time as images are compared *left top*, *left bottom*, and then *top* +7, which is again immediately after clipping and so on. Hair 1: Continuously growing anagen. Hair 2 (with *arrow*): The minimal elongation reflects no-growth stage, i.e., end catagen–telogen (day 0 up to day 0 + 14). Between day 14 and day 2 + 14, the fiber was collected as exogen. The tip of the very thin fiber shows up at day 0 + 28 indicating new anagen that grows further on day 2 + 28. Hair 3: Thick catagen hair (day 0–day 2 and probably day 0 + 7 and day 2 + 7) that stays in telogen all over time after day 9. Hair 4: Earliest stage of anagen showing up at the scalp surface at some time between day 0 and day 2. The thickness increases in a few weeks. Rapidly growing fine tips at the surface reflect intense proliferation in deeply seated root of a thick hair follicle (revisit images from *right* to *left*)

Table 1 Analytical data generated with computer-assisted image analysis of CE-PTG-EC

	A	B	C
Thick hair density	215*	274	167***
Thick anagen hair %	66**	75*	57***
Thin hair %	18	17	26***
Nanohair	41***	39***	86***
Exogen hair	3	2	11**

Whenever data from the three subjects shown in Fig. 6 reach the limits or differ slightly, moderately, or severely from controls (unpublished data; Tables 2 and 3), numbers are marked, respectively, as *, **, or ***

Thick hair displays a width over 40 μm and is shown as thick hair density (n/cm^2) with percent of growing hair (thick anagen %). The lower limit or reduced % of thick anagen as compared to controls indicates in all three cases a shortening of the duration of anagen

Thinner hair expressed as a proportion of the total (sum of thick and thin hair counts; data not shown) indicates that subject C is most severely affected. He may represent a later step in the process of decreased hair follicle performance as thick hair numbers and thick anagen % are already much lower than subjects A or B

In all three subjects, there is a tremendous increase of nanohair whose width is less than 20 μm. We consider this as an early marker of the preclinical stages of male pattern hair loss even when a "normal" number of thick hair is still present (subject B)

Taken together, lowered hair density and anagen % with increased % thinning and a high number of nanohair and exogen hair in subject C confirm that he is the worst affected one of the three. We speculate that irreversible functional damage or organ deletion might follow if the condition continues to progress without treatment

Table 2 Normal values in male and female controls with CE-PTG-EC (usual criteria)

♂♀	∂ nano	∂ total	∂ thick	∂ thin	∂ exogen
Mean	6	295	241	54	2
St. dev.	5	50	41	22	2
P5	0	211	171	22	0
P95	17	370	301	89	7
♂	∂ nano	∂ total	∂ thick	∂ thin	∂ exogen
Mean	6	285	240	44	3
St. dev.	5	59	47	20	3
P5	0	198	172	20	0
P95	18	389	323	83	9
♀	∂ nano	∂ total	∂ thick	∂ thin	∂ exogen
Mean	6	309	242	67	2
St. dev.	5	30	33	18	2
P5	1	256	189	44	0
P95	17	351	293	96	5

Normal hair values were evaluated on the top of the head during four repeat observations (two during summer and two during winter) in young volunteers (16–20 years) who did not complain of hair shedding or hair loss
The table details values of the more familiar criteria like density (n/cm^2) that we split up according to hair fiber thickness: total hair (Ø ≥20 μm), thin hair (20≤ Ø <40 μm), and thick hair (Ø ≥40 μm) as well as nanohair (Ø <20 μm) that were not included in the other hair counts due to uncertainties
The statistics like mean and standard deviation are shown together with "extreme normal limits" of CE-PTG-EC data (either P5 or P95) as a group and separately for male and female

Table 3 Normal values in male and female controls with CE-PTG-EC (less usual criteria)

♂♀	∂ anagen	% anagen	Thick as % of total	∂ thick anagen	Thick % anagen	Thin as % of total	∂ thin anagen	Thin % anagen
Mean	248	84 %	82 %	214	89 %	18 %	33	60 %
St. dev.	42	9 %	7 %	35	8 %	7 %	19	19 %
P5	174	68 %	73 %	151	75 %	9 %	9	32 %
P95	302	96 %	91 %	261	99 %	27 %	72	89 %
♂	∂ anagen	% anagen	Thick as % of total	∂ thick anagen	Thick % anagen	Thin as % of total	∂ thin anagen	Thin % anagen
Mean	230	82 %	85 %	207	87 %	15 %	23	54 %
St. dev.	44	9 %	5 %	38	8 %	5 %	11	17 %
P5	160	67 %	75 %	147	74 %	8 %	9	29 %
P95	296	95 %	92 %	265	98 %	25 %	42	83 %
♀	∂ anagen	% anagen	Thick as % of total	∂ thick anagen	Thick % anagen	Thin as % of total	∂ thin anagen	Thin % anagen
Mean	271	88 %	78 %	224	93 %	22 %	47	69 %
St. dev.	26	7 %	6 %	27	7 %	6 %	18	17 %
P5	230	73 %	67 %	182	78 %	15 %	25	43 %
P95	305	96 %	85 %	257	99 %	33 %	82	91 %

This table details more statistics on less usual criteria such as absolute densities (∂ = density; n/cm^2) of anagen hair and its %, the proportion of thick (% of total hair count shown in Table 1), density of thick anagen hair, and proportion of growing hair in the thick hair subpopulation (thick % anagen) and the proportion of thin (% of total hair count shown in Table 1), density of thin anagen hair, and proportion of growing hair in the thin hair subpopulation (thin % anagen)
The statistics like mean and standard deviation are shown together with "extreme normal limits" of CE-PTG-EC data (either P5 or P95) as a group and separately for male and female

1. Contrast enhancement makes not only thin hair more visible but also thick less pigmented hair more visible.
2. All and any hair in any patient whatever his/her genetic condition or background must be measured and taken into account.

Why is this necessary? This is necessary because of the following: first, in order to establish a proper description in the context of a diagnostic procedure; second, in order to know whether a miniaturized hair has any potential meaning or is just useless as a potential site for drug action; third in order to know what a normal scalp functioning program represents (data in Tables 2 and 3 help to clarify the status of patients shown in Fig. 5 and Table 1); and fourth, to get rid of nondrug-related effects. The illusion of efficacy must be tracked whatever the substrate of measurement (hair in our case!) with a scientific method! Anything else should be considered as dogmatic statements, erroneous interpretations, or speculative issues contributing to maintaining hair science and technology in the marshlands of trichoquackery.

The future will tell whether the work done during the last decade will definitely bring such systems closer to the status of medically acceptable as diagnostic, prognostic, and therapeutic monitoring tools.

4 Conclusion

A bold statement would be to say that the assessment of hair loss requires some experience and a lot of technological effort in order to grasp all the variables involved in hair measurement. There was a time when some colleagues argued that measurement methods were not necessary as the patient could tell when hair is growing or not. It is obvious that this is untrue as soon as one enters the continuum of the hair replacement process especially when some hair is still present. Such a statement also looks outdated when one acknowledges the importance of the placebo effect. Indeed, subjective evaluation may reach 60 % or more satisfaction while significantly decreased hair counts clearly document the natural worsening of the condition (Kaufman 2002). Our experience points to the fact that a combination of a highly sensitive and precise analytical approach together with a global calibrated method seems advisable in the context of kinetic monitoring of hair growth and hair loss in the hair clinic in general, and this is warmly recommended in the context of efficacy analysis of new (and recognized!) compounds in future clinical trials.

References

Bircher A, de Boer EM, Agner T, Wahlberg JE, Serup J. Guidelines for measurement of cutaneous blood flow by laser Doppler flowmetry. Contact Dermatitis. 1994;30:65–72.

Blume U, Ferracin I, Verschoore M, Czernielewski JM, Schaefer H. Physiology of the vellus hair follicle: hair growth and sebum excretion. Br J Dermatol. 1991;124:21–8.

Camacho FM, Tosti A (Editores), Randall VA, Price VH (Co-Editoras). Montagna – Tercera Edicion. Trichologia: Enfermedades del foliculo pilosebaceo, vols. I–II. Madrid: Aulamédica; 2013. p. 1–1297. ISBN978-84-7885-571-1.

Camacho-Martinez F. Hair loss in women. Semin Cutan Med Surg. 2009;28:19–32.

Canfield D. Photographic documentation of hair growth in androgenetic alopecia. Dermatol Clin. 1996;14:713–21.

Chamberlain AJ, Dawber RP. Methods of evaluating hair growth. Australas J Dermatol. 2003;44:10–8.

Courtois M, Loussouarn G, Hourseau C, Grollier JF. Hair cycle and alopecia. Skin Pharmacol. 1994;7:84–9.

Courtois M, Loussouarn G, Hourseau C, Grollier JF. Ageing and hair cycles. Br J Dermatol. 1995;132:86–93.

Courtois M, Loussouarn G, Hourseau S, Grollier JF. Periodicity in the growth and shedding of hair. Br J Dermatol. 1996;134:47–54.

Dawber R, Van Neste D. Hair and scalp disorders. Common presenting signs, differential diagnosis and treatment. 2nd ed. London: Martin Dunitz; 1995. Taylor & Francis group, 2004:1-294. ISBN 1 84 184 193 5.

Guarrera M, Cardo P, Arrigo P, Rebora A. Reliability of Hamilton-Norwood classification. Int J Trichology. 2009;1:120–2.

Hayashi S, Miyamoto I, Takeda K. Measurement of human hair growth by optical microscopy and image analysis. Br J Dermatol. 1991;125:123–9.

Headington JT. Histological findings in androgenic alopecia treated with topical minoxidil. Br J Dermatol. 1982;107 Suppl 22:20–1.

Headington JT. Telogen effluvium. New concepts and review. Arch Dermatol. 1993;129:356–63.
Headington JT, Novak E. Clinical and histologic studies of male pattern baldness treated with topical minoxidil. Curr Ther Res. 1984;36:1098–106.
Hoffmann R. TrichoScan: combining epiluminescence microscopy with digital image analysis for the measurement of hair growth in vivo. Eur J Dermatol. 2001;11:362–8.
Hoffmann R, Van Neste D. Recent findings with computerized methods for scalp hair growth measurements. J Investig Dermatol Symp Proc. 2006;10:285–8.
Ishino A, Uzuka M, Tsuji Y, Nakanishi J, Hanzawa N, Imamura S. Progressive decrease in hair diameter in japanese with male pattern baldness. J Dermatol. 1997;24:758–64.
Kang H, Kang TW, Lee SD, Park YM, Kim HO, Kim SY. The changing patterns of hair density and thickness in South Korean women with hair loss: clinical office-based phototrichogram analysis. Int J Dermatol. 2009;48:14–21.
Kaufman KD. Long-term (5-year) multinational experience with finasteride 1 mg in the treatment of men with androgenetic alopecia. Eur J Dermatol. 2002;12:38–49.
Leroy T, Van Neste D. Contrast enhanced phototrichogram pinpoints scalp hair changes in androgen sensitive areas of male androgenetic alopecia. Skin Res Technol. 2002;8:106–11.
Lopez V, Martin JM, Sanchez R, Ortega C, Ricart JM. Usefulness of Trichoscan professional in the evaluation of hair loss in females. Report of 180 cases. J Eur Acad Dermatol Venereol. 2011;25:1068–72.
Loussouarn G. African hair growth parameters. Br J Dermatol. 2001;145:294–7.
Olsen EA. Current and novel methods for assessing efficacy of hair growth promoters in pattern hair loss. J Am Acad Dermatol. 2003;48:253–62.
Pierard GE, Pierard-Franchimont C, Marks R, Elsner P. EEMCO guidance for the assessment of hair shedding and alopecia. Skin Pharmacol Physiol. 2004;17:98–110.
Riedel-Baima B, Riedel A. Use of the trichoscan to assess female pattern hair loss. Dermatol Surg. 2009;35:651–5.
Rushton DH. Chemical and morphological properties of scalp hair in normal and abnormal states. Cardiff: University of Wales; 1988. p. 1–247.
Rushton DH. Androgenetic alopecia in men: the scale of the problem and prospects for treatment. Int J Clin Pract. 1999;53:50–3.
Rushton DH, De Brouwer B, De Coster W, Van Neste D. Comparative evaluation of scalp hair by phototrichogram and unit area trichogram analysis within the same subjects. Acta Derm Venereol (Stockh). 1993;73:150–3.
Rushton DH, Gilkes JJH, Van Neste D. No improvement in male-pattern hair loss using LASER-hair-comb therapy: a 6-month, half-head, assessor-blinded investigation in two men. Clin Exp Dermatol. 2011;37:300–15. doi:10.1111/j.1365-2230.2011.04208.x.
Rushton DH, Norris M, Van Neste D. Hair regrowth in male and female pattern hair loss does not involve the conversion of vellus hair to terminal hair. Exp Dermatol. 2016. doi:10.1111/exd.12945.
Saitoh M, Uzuka M, Sakamoto M. Human hair cycle. J Invest Dermatol. 1970;54:65–81.
Saraogi PP, Dhurat RS. Automated digital image analysis (Trichoscan®) for human hair growth analysis; ease versus errors. Int J Trichology. 2010;2:5–13.
Sinclair R, Jolley D, Mallari R, Magee J, Tosti A, Piracinni BM, Vincenzi C, Happle R, Ferrando J, Grimalt R, Leroy T, Van Neste D, Zlotogorski A, Christiano AM, Whiting D. Morphological approach to hair disorders. J Investig Dermatol Symp Proc. 2003;8:56–64.
Stenn KS, Paus R. Controls of hair follicle cycling. Physiol Rev. 2001;81:449–94.
Tajima M, Hamada C, Arai T, Miyazawa M, Shibata R, Ishino A. Characteristic features of Japanese women's hair with aging and with progressing hair loss. J Dermatol Sci. 2007;45:93–103.
Tsuji Y, Ishino A, Hanzawa N, Uzaka M, Okazaki K, Adachi K, Imamura S. Quantitative evaluations of male pattern baldness. J Dermatol Sci. 1994;7:136–41.
Ueki R, Tsuboi R, Inaba Y, Ogawa H. Phototrichogram analysis of Japanese female subjects with chronic diffuse hair loss. J Investig Dermatol Symp Proc. 2003;8:116–20.
Van Neste D. Dynamic exploration of hair growth: critical review of methods available and their usefulness in the clinical trial protocol. In: Van Neste D, Lachapelle JM, Antoine JL, editors. Trends in human hair growth and alopecia research. Lancaster: Kluwer Academic Publishers; 1989. p. 143–54.
Van Neste DJJ. Hair growth evaluation in clinical dermatology. Dermatology. 1993;187:233–4.
Van Neste DJJ. Contrast enhanced phototrichogram (CE-PTG): an improved non-invasive technique for measurement of scalp hair dynamics in androgenetic alopecia – validation study with histology after transverse sectioning of scalp biopsies. Eur J Dermatol. 2001;4:326–31.
Van Neste D. Assessment of hair loss. Clinical relevance of hair growth evaluation methods. Clin Exp Dermatol. 2002;27:358–65.
Van Neste D. Thickness, medullation and growth rate of female scalp hair are subject to significant variation according to pigmentation and scalp location during ageing. Eur J Dermatol. 2004;14:28–32.
Van Neste D. Hair. In: Barel AO, Paye M, Maibach HI, editors. Handbook of cosmetic science and technology. 2nd ed. New York: Marcel Dekker; 2005. p. 61–87.
Van Neste D. Photographic and computerized techniques for quantification of hair growth. In: Serup J, Jemec GBE, Grove GL, editors. Handbook of non-invasive

methods and the skin. 2nd ed. Boca Raton: Taylor and Frances; 2006a. p. 883–94.
Van Neste D. Natural scalp hair regression in preclinical stages of male androgenetic alopecia and its reversal by finasteride. Skin Pharmacol Physiol. 2006b; 19:168–76.
Van Neste D. Hair. In: Paye M, Barel AO, Maibach HI, editors. Handbook of cosmetic science and technology. 2nd ed. Boca Raton: Taylor and Frances; 2006c. p. 61–87.
Van Neste D. Female patients complaining about hair loss: documentation of defective scalp hair dynamics with contrast-enhanced phototrichogram. Skin Res Technol. 2006d;12:83–8.
Van Neste D. Placebo pills, lotions or potions and the natural progression of patterned hair loss in males: another step away from "trichoquakery"? Eur J Dermatol. 2008;18:373–5.
Van Neste D. Obtencion de imagenes del cuero cabelludo: percepcion global y metodos analiticos. El fototrichograma y otros metodos alternativos para medir el crecimiento del cabello. In: Camacho FM, Tosti A, Editores, Randall VA, Price VH, Co-Editoras. Montagna – Tercera Edicion. Trichologia: Enfermedades del foliculo pilosebaceo, vol. I. 2013. p. 159–71. ISBN978-84-7885-572-8.
Van Neste D. Why care about Linear Hair Growth Rates (LHGR)? A study using in vivo imaging and computer assisted image analysis after manual processing (CAIAMP) in unaffected male controls and men with male pattern hair loss (MPHL). Eur J Dermatol. 2014;24:568–76.
Van Neste DJJ. Body hair counts during hair length reduction procedures: a comparative study between Computer Assisted Image Analysis after Manual Processing (CAIAMP) and Trichoscan. Skin Res Technol. 2015;21:373–9. doi: 10.1111/srt.12207.
Van Neste DJJ, Rushton DH. Hair problems in women. Clin Dermatol. 1997;15:113–25.
Van Neste DJJ, Rushton DH. Gender differences in scalp hair growth rates are maintained but reduced in pattern hair loss compared to controls. Skin Res Technol. 2015. doi: 10.1111/srt.12274.
Van Neste DJJ, Rushton HD. What is the meaning of the "visible pigmented non-vellus hair count" in FDA-approved clinical trial reports? Abstract. 7th World Congress for Hair Research, Edinburgh; 2013.
Van Neste D, Trüeb R. Critical study of hair growth analysis with computer-assisted methods. J Eur Acad Dermatol Venereol. 2006;20:578–85.
Van Neste D, Trüeb RM. An 'inconvenient truth' about Trichoscan claims? J Eur Acad Dermatol Venereol. 2008;22:101.
Van Neste D, Dumortier M, De Coster W. Phototrichogram analysis: technical aspects and problems in relation to automated quantitative evaluation of hair growth by computer-assisted image analysis. In: Van Neste D, Lachapelle JM, Antoine JL, editors. Trends in human hair growth an alopecia research. Lancaster: Kluwer Academic Publishers; 1989. p. 155–65.
Van Neste D, De Brouwer B, Dumortier M. Reduced linear hair growth rates of vellus and of terminal hairs produced by human balding scalp grafted onto nude mice. Ann N Y Acad Sci. 1991;642: 480–2.
Van Neste DJJ, Dumortier M, De Brouwer B, De Coster W. Scalp immersion proxigraphy (SIP): an improved imaging technique for phototrichogram analysis. J Eur Acad Dermatol Venereol. 1992; 1:187–91.
Van Neste D, Blume-Peytavi U, Grimalt R, Messenger A. Hair science and technology. Tournai: Skinterface; 2003a.
Van Neste D, Leroy T, Sandraps E. Validation and clinical relevance of a novel scalp coverage scoring method. Skin Res Technol. 2003b;9:64–72.
Van Neste D, Sandraps E, Herbaut D, Lelubre P, Leroy T. Validation of scalp coverage scoring methods for scalp hair loss in male pattern hair loss (androgenetic alopecia). Skin Res Technol. 2006; 12:89–93.
Van Neste D, Leroy T, Conil S. Exogen hair characterization in human scalp. Skin Res Technol. 2007;13:436–43.
Whiting DA. The value of horizontal sections of scalp biopsies. J Cutan Aging Cosm Dermatol. 1990; 1:165–73.
Whiting DA. Diagnostic and predictive value of horizontal sections of scalp biopsy specimens in male pattern androgenetic alopecia. J Am Acad Dermatol. 1993;28:755–63.
Whiting DA. Scalp biopsy as a diagnostic and prognostic tool in androgenetic alopecia. Dermatol Ther. 1998;8:24–33.
Whiting DA, Olsen EA, Savin R, Halper L, Rodgers A, Wang L, Hustad C, Palmisano J. Efficacy and tolerability of finasteride 1 mg in men aged 41 to 60 years with male pattern hair loss. Eur J Dermatol. 2003;13:150–60.

Scalp Confocal Microscopy

78

Marina Agozzino and Marco Ardigò

Contents

Keywords

In vivo reflectance confocal microscopy • Non-invasive diagnosis • Non-invasive therapeutical follow-up • Scalp • Alopecias • Inflammatory diseases • Skin tumors

1 Introduction

Scalp diseases frequently need microscopical support for diagnosis because of the peculiar anatomical site and the complexity of the differential diagnosis between different inflammatory skin disorders and tumors.

Skin biopsies of the scalp areas could be needed in order to select the appropriate therapeutical approach. However, histopathology confirmation is generally difficult because of inadequate sampling (too superficial, limited by the pain, bleeding and sometimes not detailed).

Optical histology of the scalp usually requires horizontal cut, especially for alopecia examination, in order to better evaluate the adnexal structures epithelium. Dermoscopy of the scalp is commonly used as a valid support to the clinical diagnosis and patient management, but presents several limits because it lacks microscopical detailed information needed especially for inflammatory diseases and therapeutical follow-up.

In order to solve the problem, in vivo reflectance confocal microscopy (RCM) is a noninvasive, high-resolution imaging technique that already demonstrated its usefulness for the

M. Agozzino (✉) • M. Ardigò
San Gallicano Dermatological Institute, Rome, Italy
e-mail: ardigo@ifo.it; ardigo@ifo.it

P. Humbert et al. (eds.), *Agache's Measuring the Skin*,
DOI 10.1007/978-3-319-32383-1_108

diagnosis, therapeutical follow-up, and management of inflammatory disorders and neoplastic lesions. RCM offers the clinicians the possibility of a real-time, noninvasive microscopical examination of the tissue with very high lateral resolution, giving cellular details.

2 The In Vivo Reflectance Confocal Microscopy Technique

RCM Vivascope 1500 (Lucid Technologies, Henrietta, NY, U.S.A.) and Vivascope 3000 are the commercially, in vivo confocal microscopes that can be used in the clinical routine. Both the systems operate with a diode Class 3A laser (European version), at a wavelength of 830 nm, with power <35 mW at tissue level. A 30 × 0.9 numerical aperture (NA) water immersion objective lens is used. Contrast is provided by differences in the refractive index due to molecule and organelle size present in the cell's cytoplasm as well as the extracellular microstructures within the tissue (Rajadhyaksha et al. 1995; Marghoob and Halpern 2005). Throughout RCM examination of pathological skin, single microscopic changes affecting the different skin layers are visualized with a new, direct point of view. Horizontal mosaics (VivaBlock), composed of a collection of single RCM frames, ranging from 2 to 8 mm can be performed with Vivascope 1500 version, and vertical "microtomographic" skin analyses (VivaStack) can be performed during examination in both versions of the system.

On the scalp, different from the Vivascope 1500, Vivascope 3000, thanks to its ergonomic design, doesn't need to be connected by an adhesive window to the skin avoiding hair cutting and reducing artifacts. Video series can be performed for analyzing and recording dynamic processes such as blood flow in dermal vessels. Vertical VivaStack software imaging (a sequence of images captured from the same area going down stepwise 5 ml for every image) is used for the evaluation of adnexal structures from the ostium to the maximum depth.

3 RCM of the Scalp

Using RCM on the scalp, all the different skin layers can be evaluated disclosing microscopical details as hair shafts, adnexal infundibular epithelium (focusing on the opening), and stroma.

In literature, RCM has been already demonstrated to be able to identify both microscopical features characterizing specific inflammatory process with high grade of correspondence and correlation to optical histology (Ardigò et al. 2011a, b). More recently in vivo RCM has been used for the evaluation and management of inflammatory skin diseases involving the scalp showing a high potential in the diagnosis (Rudnicka et al. 2008) as well as in therapeutical management (Agozzino et al. 2011).

As demonstrated for melanocytic and non-melanocytic tumors affecting the skin, RCM provides similar diagnostic information also for the lesions involving the scalp.

In inflammatory scalp diseases, RCM has been demonstrated to be useful for clinical-microscopical correlation supporting the diagnosis (Moscarella et al. 2012; Ardigò et al. 2007, 2009). Moreover, it can be of great value in choosing the best biopsy site in order to obtain microscopic diagnostic criteria. It can be considered as an intermediate step between trichoscopy and horizontal histology getting information about adnexal structure distribution and density, hair shaft integrity and size, localization and semi-quantification of inflammatory cells in different epidermal layers, dermal scarring, and vascularization.

A major limit of RCM of the scalp is the depth of imaging confined to the upper dermis without the possibility of visualizing the reticular dermis, hair follicle, glands, and distinguishing sub-type of leukocytes. Moreover, when the adhesive window of the Vivascope 1500 has to be connected to the scalp the presence of hair cause artifacts (hair bubble, obscuration of the tissue below, etc.); in this case the handheld confocal device named Vivascope 3000 is preferred as it doesn't need to be attacched to the skin for confocal imaging. Handheld version gives the possibility of a larger field of tissue visualization during the same

clinical session without hair cutting (Rajadhyaksha et al. 1999), but lacks the possibility of a total lesion mapping for an overview of the process.

3.1 RCM of the Normal Scalp

In non-affected scalp, RCM lets the visualization of the terminal hair shaft structures with high definition of the medulla, visible as a strongly bright structure, the shaft, and cuticle. Also the infundibular epithelium and the openings of the follicle and glands can be evaluated.

3.2 RCM of the Hair Shaft

Consequently, in cases of diseases affecting exclusively the hair shaft (i.e., uncombable hair syndrome, pili torti, trichothiodystrophy), RCM discloses diagnostic clues as the alteration of hair in terms of medulla thickness and uniformity of the cuticula (Rudnicka et al. 2008) or the involvement of the adnexal epithelium in case of exocentric inflammatory processes (LPP, LED, AGA, etc.) (Agozzino et al. 2011).

3.3 RCM of Nonscarring Alopecia

Throughout RCM of the scalp, it is possible to evaluate major and distinctive microscopic criteria as the presence of inflammatory cells with adnexotropism and presence or absence of the scar tissue (sclerosis of the upper dermis). In non-scarring alopecias (i.e., alopecia areata), those features are absent. In specific, in alopecia areata, dermoscopical structures as yellow dots can be observed with RCM and correlated with dermoscopy disclosing their microscopical correspondence (Ardigò et al. 2011b).

Similarly, in androgenetic alopecia, preliminary data confirms that a more detailed distribution and evaluation of the degree of the miniaturization of follicle can be seen using RCM. In particular RCM lets the visualization of miniaturized follicle differently nonvisible at dermoscopy. Moreover, RCM discloses the presence of inflammatory cell infiltration and dilated vessels involving epithelial structure where miniaturized hair follicle is present disclosing the inflammatory component of androgenetic alopecia with consequent therapeutical implications.

3.4 RCM of Scarring Alopecia

RCM for cicatricial alopecia has been tested prevalently in discoid lupus erythematosus (DLE), lichen planopilaris (LPP), and its variant defining the real power of this technique in differential diagnosis with noncicatricial alopecias. Biopsy sampling and therapeutical follow-up can be done with RCm in the case of the suspect of cicatricial alopecia.

The main confocal feature seen in scarring alopecias is represented by the dermal sclerosis of the upper dermis. The inflammatory process is focused around and inside the adnexal epithelium, in the epidermis, and inflammatory obscuration of the dermoepidermal junction (interface dermatitis) can be observed (Fig. 1). Throughout the RCM follow-up, useful microscopical criteria for the treatment management can be identified (Agozzino et al. 2011): in responsive cases, reduction of epidermal and dermal inflammation and disappearance of inflammatory cells around adnexal structures can easily observed with RCM.

3.5 RCM of Common Inflammatory Diseases

Starting from the previous experience on inflammatory conditions involving the skin, diseases like psoriasis (Ardigò et al. 2009), contact dermatitis (Ardigò et al. 2012), and other inflammatory processes, RCM can be applied on the scalp. In details, it has been demonstrated that RCM lets the identification of the most common and distinctive microscopical criteria useful for the differentiation between spongiotic dermatitis and

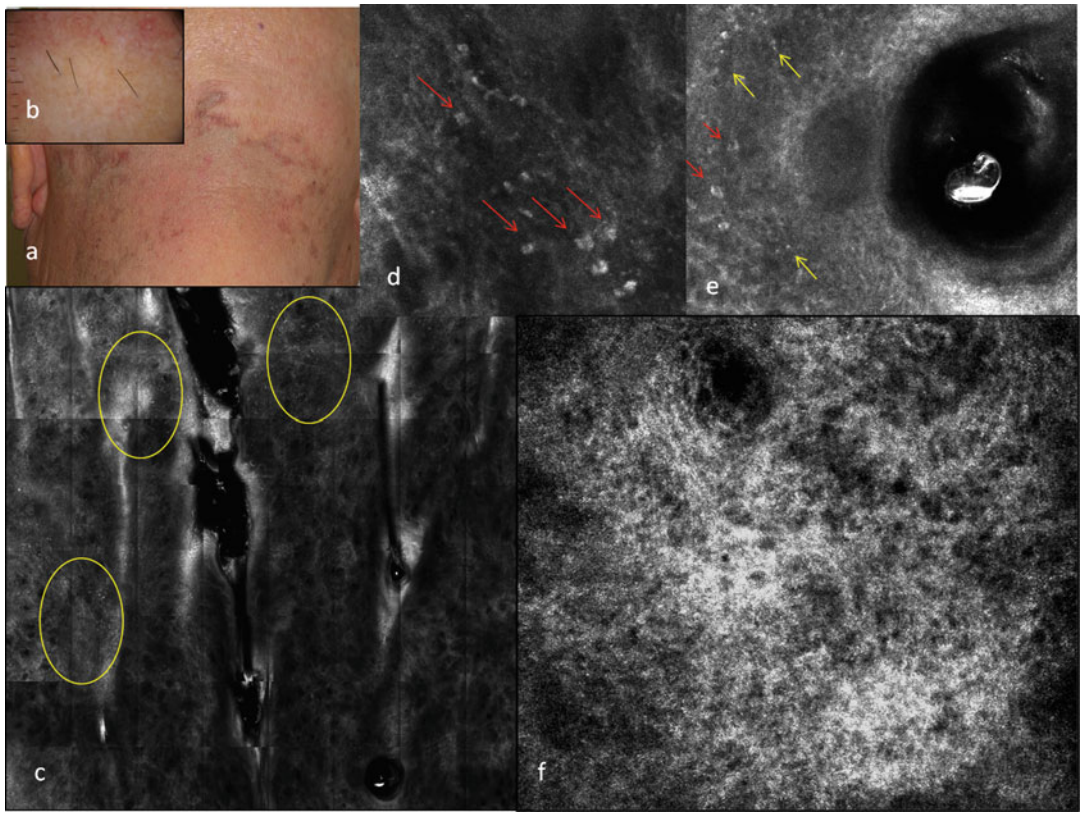

Fig. 1 (**a**, **b**) Clinical and dermoscopical pictures of LPP showing multiple violaceous papules located on the nuchal region; (**c**) RCM mosaic image at the level of DEJ. Papillary rims obscured by inflammatory cells infiltrate disclosing the focal interface changes (*yellow circles*) and inflammatory involvement of adnexal structures; (**d**) RCM single frame of inflammatory cells infiltrate, focused around adnexal structure, composed of numerous brightly refractile, plump, oval to polygonal cells corresponding to melanophages (*red arrows*); (**e**) RCM close-up around the adnexal epithelium showing inflammatory cell infiltrate composed of melanophages (*red arrows*) and small, less refractile, roundish cells corresponding probably to lymphocytes (*yellow arrows*); (**f**) RCM image at the level of the upper dermis showing dermal sclerosis associated with obscuration of follicular ostia for the increased and thickened number of dermal fibers

hyperkeratotic process. In this way, it is possible to discriminate allergic and irritant contact dermatitis, from psoriasis or seborrheic dermatitis involving the scalp areas.

In contact dermatitis, moderate to severe spongiosis reaching vesicle formation associated with dilated dermal vessels can be visualized by RCM as dark areas (due to the presence of nonretractile water into the tissue) in comparison to the surrounding epidermis associated with the presence of cellular bright elements corresponding to inflammatory cells. Differently, in psoriasis, using RCM, thickening of the stratum corneum with parakeratosis, thickening of the epidermis (evaluated using vertical tomographic analysis of the tissue – Vertical VivaStack) with papillomatosis, and presence of vertically oriented vessels filling the dermal papillae can be visualized (Ardigò et al. 2009) (Fig. 2). Thick and parakeratotic stratum corneum with thick epidermis is a microscopical feature common between psoriasis and seborrheic dermatitis, but the second is associated with medium to severe epidermal spongiosis and dermal inflammation. Moreover, in seborrheic dermatitis, inflammation is seen to be associated with the presence of horizontally orientated, enlarged vessels in the upper dermis (not published observation).

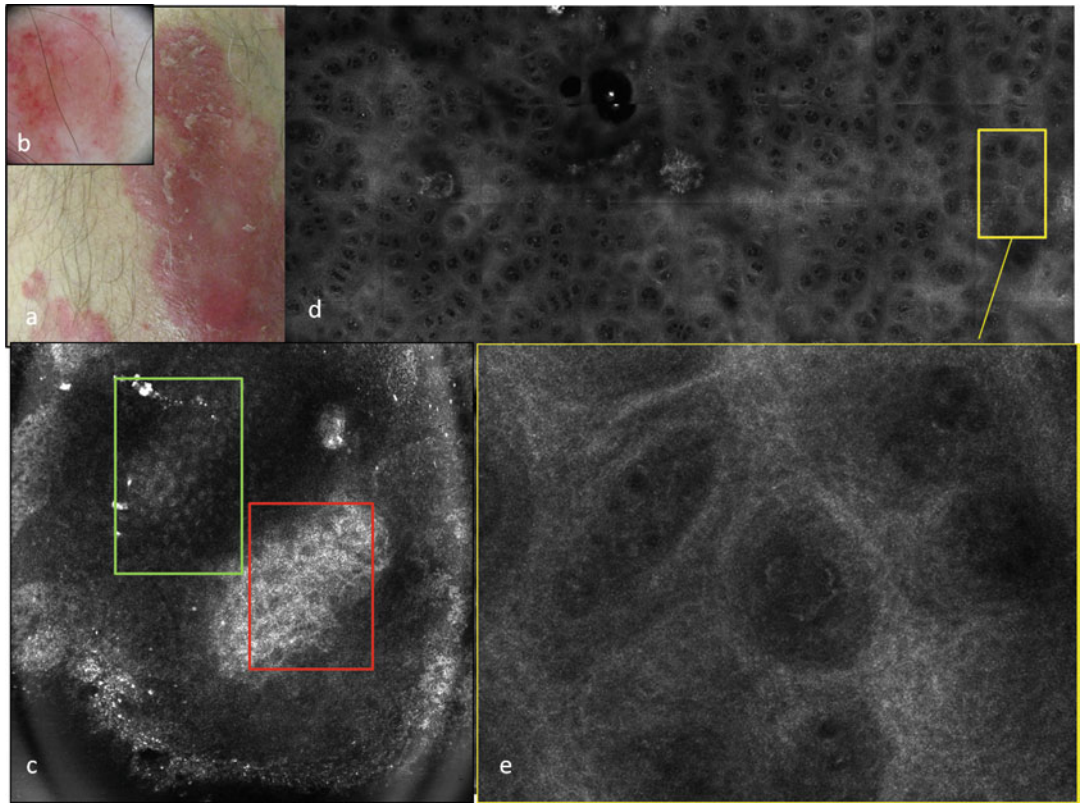

Fig. 2 (**a**, **b**) Clinical and dermoscopical images of psoriasis; (**c**) RCM single frame at the level of the stratum corneum showing presence of refractile nucleated structures corresponding to the paracornification (*red square*) and Munro abscesses (*green square*); (**d**) RCM Vivablock mosaic at the level of DEJ shows an increased number and density of dermal papillae (papillomatosis); (**e**) RCM close-up of papillomatosis shows dilated dermal papillae with thin interpapillary spaces, inside the papillae dilated vessels are visible

The possibility of real-time microscopical confirmation of the clinical diagnosis of inflammatory diseases ranging from contact dermatitis to psoriasis gives the clinician the possibility of a better selection of treatment and a more precise management of patient with scalp diseases.

3.6 RCM of Skin Tumors of the Scalp

The spread experience on RCM on both benign and malignant skin tumors can be easily transferred to the scalp trying to avoid or at least to limit the number of unnecessary biopsies of benign lesions in such a bleeding and painful anatomical area. Moreover, melanocytic and epithelial tumors can be mapped in order to define the extension of the lesion and limit the margins of the excision preserving healthy tissue in an area where reconstruction and/or flips are difficult procedures.

Confocal microscopy distinctive features of the nevi (i.e., preserved skin structure with junctional proliferation of normally structured melanocytes and/or regular nest size and distribution in the upper dermis) or melanoma (i.e., up migrated or round, dendritic atypical melanocytes, disarranged epidermis and dermis, inflammatory cells) involving the scalp are substantially the same as the once seen in lesions arising in other anatomical sites (Pellacani et al. 2012; Pupelli et al. 2013) (Fig. 3). Same happened for all the most common malignant epithelial tumors (i.e., basal cell carcinoma, squamous cell carcinoma) and for seborrheic keratosis (Guitera et al. 2012).

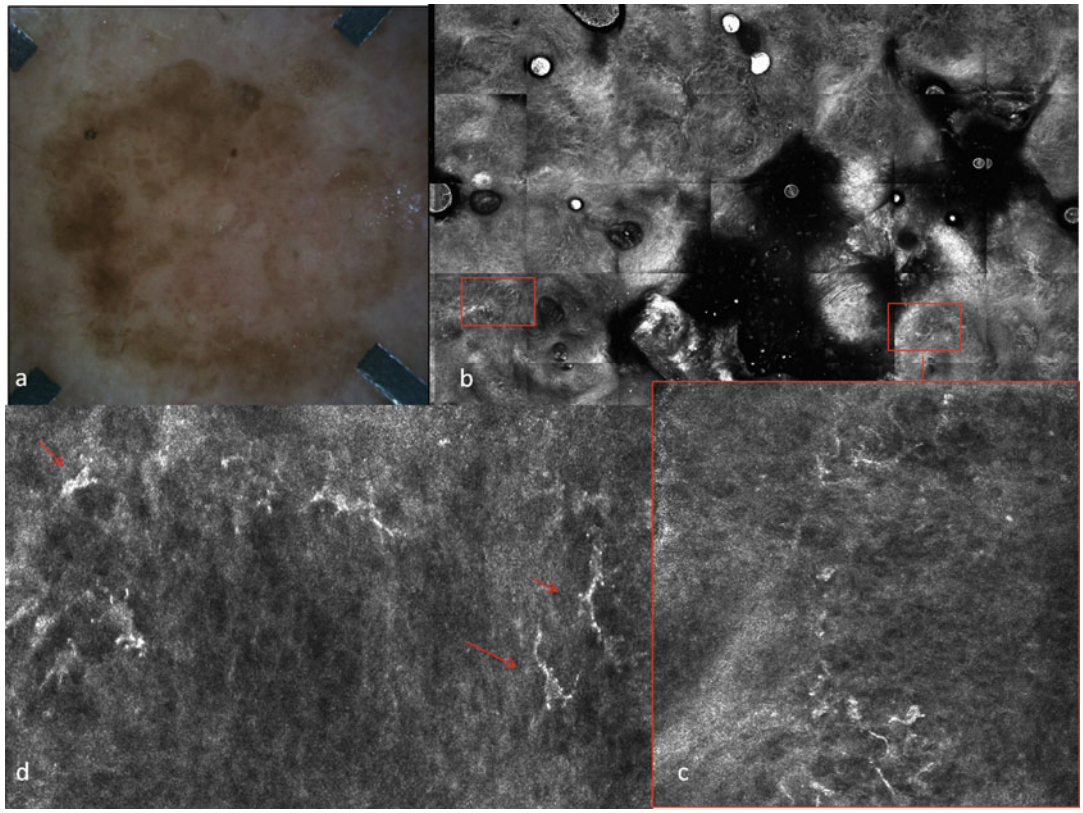

Fig. 3 (**a**) Dermoscopic image of a pigmented lesion located on the scalp and diagnosed as melanoma; (**b**) RCM mosaic at the level of granulosum spinosum layer shows at scanning, the presence of atypical cells, to note the presence of areas of artifacts due to the limit of the blocks on the scalp because of the presence of hairs; (**c**, **d**) RCM close-up of the previous Block disclose the presence of multiple large cells with bright cytoplasm and dark nucleus with clearly visible dendrites connected to the cells corresponding to dendritic pagetoid cells (*red arrows*)

The main limit for the RCM examination on the scalp is represented by the presence of hair and the convexity of the scalp limiting the attachment of the adhesive windows and determining artifacts. A valid solution is represented by the use of the handheld confocal microscope that lets the examination of 1 mm large spots and permits to scans handily all the "front" of the lesion.

4 Conclusions

In conclusion, in addition to the possibility of clinical-dermoscopical-confocal correlation for the diagnosis, mapping, and management of scalp melanocytic as well as non-melanocytic tumors, RCM seems to be particularly useful for inflammatory scalp diseases as already proven for the skin lesions. If RCM differentiation of psoriasis versus seborrheic dermatitis can be useful for a better management of patients, probably, the most interesting application of RCM on the scalp is alopecias due to its high sensitivity and sensibility in differential diagnosis between cicatricial and noncicatricial alopecias. Moreover, the therapeutical follow-up of scarring alopecias using dermoscopy in association with RCM has been demonstrated to be much more precise than using only dermoscopy, thanks to the possibility of a "quasi" histological examination of tissue.

References

Agozzino M, Tosti A, Barbieri L, Moscarella E, Cota C, Berardesca E, Ardigò M. Confocal microscopic features of scarring alopecia: preliminary report. Br J Dermatol. 2011;165(3):534–40.

Ardigò M, Maliszewski I, Cota C, Scope A, Sacerdoti G, Gonzalez S, Berardesca E. Preliminary evaluation of in vivo reflectance confocal microscopy features of Discoid lupus erythematosus. Br J Dermatol. 2007;156:1196–203.

Ardigò M, Cota C, Berardesca V, Gonzàles S. Concordance between in vivo reflectance confocal microscopy and histology in the evaluation of plaque psoriasis. J Am Acad Dermatol. 2009;23:660–7.

Ardigò M, Torres F, Abraham LS, Piñeiro-Maceira J, Cameli N, Berardesca E, Tosti A. Reflectance confocal microscopy can differentiate dermoscopic white dots of the scalp between sweat gland ducts or follicular infundibulum. Br J Dermatol. 2011a;164(5):1122–4.

Ardigò M, Tosti A, Cameli N, Vincenzi C, Misciali C, Berardesca E. Reflectance confocal microscopy of the yellow dot pattern in alopecia areata. Arch Dermatol. 2011b;147(1):61–4.

Ardigò M, Longo C, Cristaudo A, Berardesca E, Pellacani G. Evaluation of allergic vesicular reaction to patch test using in vivo confocal microscopy. Skin Res Technol. 2012;18(1):61–3.

Guitera P, Menzies SW, Longo C, Cesinaro AM, Scolyer RA, Pellacani G. In vivo confocal microscopy for diagnosis of melanoma and basal cell carcinoma using a two-step method: analysis of 710 consecutive clinically equivocal cases. J Invest Dermatol. 2012;132(10):2386–94.

Marghoob AA, Halpern A. Confocal scanning laser reflectance microscopy. Arch Dermatol. 2005;141:212–5.

Moscarella E, González S, Agozzino M, Sánchez-Mateos JL, Panetta C, Contaldo M, Ardigò M. Pilot study on reflectance confocal microscopy imaging of lichen planus: a real-time, non-invasive aid for clinical diagnosis. J Eur Acad Dermatol Venereol. 2012;26(10):1258–65.

Pellacani G, Farnetani F, Gonzalez S, Longo C, Cesinaro AM, Casari A, Beretti F, Seidenari S, Gill M. In vivo confocal microscopy for detection and grading of dysplastic nevi: a pilot study. J Am Acad Dermatol. 2012;66(3):e109–21.

Pupelli G, Longo C, Veneziano L, Cesinaro AM, Ferrara G, Piana S, Moscarella E, Ricci C, Zalaudek I, Seidenari S, Argenziano G, Pellacani G. Small diameter melanocytic lesions: morphological analysis by means of in vivo confocal microscopy. Br J Dermatol. 2013;168(5):1027–33.

Rajadhyaksha M, Grossmann M, Esterowitz D, et al. In vivo confocal scanning laser microscopy of human skin: melanin provides strong contrast. J Invest Dermatol. 1995;104:946–52.

Rajadhyaksha M, González S, Zavislan JM, et al. In vivo confocal scanning laser microscopy of human skin II: advances in instrumentation and comparison to histology. J Invest Dermatol. 1999;113:293–303.

Rudnicka L, Olszewska M, Rakowska A. In vivo reflectance confocal microscopy: usefulness for diagnosing hair diseases. J Dermatol Case Rep. 2008;2(4):55–9.

Trichoscopy

79

Lidia Rudnicka

Contents

Keywords

Alopecia areata • Androgenetic alopecia • Androgenic alopecia • Dermoscopy • Dermatoscopy • Female pattern hair loss • Follicular unit • Hair • Hair shaft thickness • Trichoscopy • Lupus • Telogen effluvium

The term "trichoscopy" refers to dermoscopy of hair and scalp (Rudnicka et al. 2008, 2012). The method allows to visualize growing hair shafts and scalp skin at multifold magnification (Fig. 1). The usual in-office working magnification of a handheld dermoscope is 10–20-fold, but a magnification of 70-fold or more may be achieved with a digital dermoscope (videodermoscope).

Among the dermoscopes, there are devices which require immersion fluid and dermoscopes which use polarized light to cancel out reflections from the stratum corneum. Polarized light dermoscopes may have a contact or noncontact lens. Devices, which combine contact and noncontact attributes (hybrid dermoscopes), are also available. The choice of a particular device is a matter of individual preference. They do not differ significantly by their usefulness for performing trichoscopy.

Trichoscopy is based on analysis of main structures, which may be visualized with a dermoscope. These structures may be divided into four big groups: (1) hair shafts, (2) hair follicle openings (dots), (3) perifollicular epidermis, and (4) blood vessels.

L. Rudnicka (✉)
Department of Dermatology, Medical University of Warsaw, Warsaw, Poland
e-mail: lidia.rudnicka@dermatolodzy.com.pl

P. Humbert et al. (eds.), *Agache's Measuring the Skin*,
DOI 10.1007/978-3-319-32383-1_109

Fig. 1 Performing trichoscopy with a handheld dermoscope

Measurement value

Objekt-Typ	Length	Area	Text	Angle	Coord.	MaxDist	MinDist	AvgDist	Up
Line1	,0979								
Line2	,0787								
Line3	,0825								
Line4	,1023								
Line5	,0779								
Line6	,0939								
Line7	,0855								
Line8	,0738								
Line9	,1107								
Line10	,0880								

Fig. 2 Measuring hair shaft thickness in trichoscopy performed with a digital dermoscope

1 Hair Shafts

Most hairs viewed by trichoscopy are normal terminal hairs. They are over 55 μm thick, uniform in thickness and color (Fig. 2) (Rakowska 2009; Vogt et al. 2008). Hair shaft thickness may be roughly estimated with a handheld dermoscope (thin, intermediate, thick). Many videodermoscopes possess software allowing detailed assessment of hair shaft thickness in micrometers. Precise measurement of hair shaft thickness is not essential for diagnosis, but may be useful for monitoring treatment efficacy and in clinical trials (Olszewska and Rudnicka 2005). In such cases hair may be measured according to the method by Rakowska et al. (Rakowska 2009), which is based on evaluation of average thickness of about 20 hair shafts, separately in the frontal area,

parietal area, and the occipital area. This distinction is of particular importance in evaluation of treatment efficacy in female and male androgenetic alopecia.

Up to about 10 % of normal human scalp hairs are vellus hairs, defined as hypopigmented, nonmedullated hairs which are less than 30 μm in thickness and less than 2–3 mm in length (Rakowska 2009; Vogt et al. 2008). An increased proportion of vellus hairs is characteristic for male and female androgenetic alopecia, where vellus hairs replace terminal hairs in the process of hair follicle miniaturization (Inui et al. 2009; Van Neste 2006). High percentage of vellus and intermediate hairs contributes to high hair shaft thickness heterogeneity, a hallmark of androgenetic alopecia (Inui et al. 2009; Rakowska et al. 2009). New, healthy, regrowing hairs are also short and thin, but they differ from vellus hairs by their upright position, firm appearance, and pointed end.

Various hair shaft structure defects may be identified by trichoscopy. A classification of hair shaft abnormalities observed in trichoscopy was recently suggested in a publication by Rudnicka et al. (2012). This classification distinguishes fractured hairs, narrowings, nodular structures, curls and twists, bands, and short hairs $\leq$1 cm.

An important measurable parameter in trichoscopy is the number of hairs emerging from one follicular unit (Fig. 3). Usually two to three hairs emerge from one follicular unit. Occasionally, four emerging hairs may be found, but this is more common in patients with dark skin phototypes, than in Caucasians. The percentage of follicular units with only one emerging hair shaft is usually less than 30 % in healthy individuals. The number of hair shafts emerging from one follicular unit is decreased in various types of hairs loss, especially in telogen effluvium and androgenetic alopecia. Successful therapy results in a significant increase of the percentage of follicular units with two or three hairs and in an increase of the average number of hairs per follicular unit. For monitoring treatment efficacy, it is advisable to calculate the average number of hairs per follicular unit separately for the frontal area, the parietal area, and the occipital area (Rakowska 2009). Usually, the average number is calculated based on results obtained in four fields of view of a dermoscope.

The number of hairs in one follicular unit is increased in tufted folliculitis. These may be small tufts, of five to seven hairs. Small tufts may be observed in inflammatory diseases, such tinea capitis or lichen planopilaris. Big tufts of ten or more hairs result from merging few follicular units and are characteristic of folliculitis decalvans. The big tufts are usually walled by a wide, hyperkeratotic, scaly hair follicle opening.

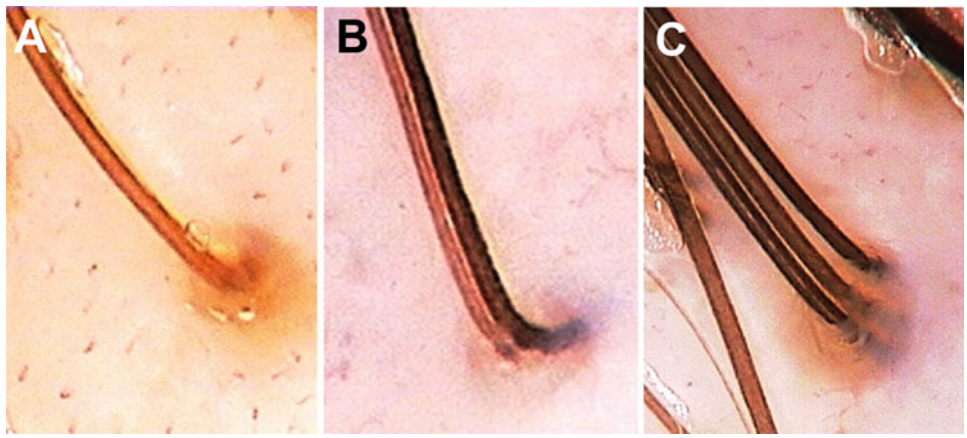

Fig. 3 A decreased number of hair shafts per follicular unit may be an indicator of hair loss. In such cases follicular units with one (**a**) and two hairs (**b**) predominate. In a healthy person, most units contain three hairs (**c**)

2 Hair Follicle Openings

The term "dots" refers to hair follicle openings seen from the perspective of a dermoscope. Black dots are residues of pigmented hairs broken or destroyed at scalp level. Yellow dots are follicular infundibula with keratotic material and/or sebum. Fibrotic white dots represent fibrosis in areas of selective follicular destruction. Pinpoint white dots are observed in patients with dark skin phototypes. They correspond to empty hair follicles or to the epidermal portion of eccrine sweat ducts. Red dots were described in discoid lupus erythematosus. Pink to pink-brown dots are a characteristic finding in the eyebrow area of patients with frontal fibrosing alopecia (Rudnicka et al. 2012; Ross et al. 2006).

The number of "dots" may be calculated per field of view of a dermoscope and used for monitoring treatment efficacy. For example, the average number of black dots per field of view is considered a marker of disease activity in alopecia areata (Inui et al. 2008).

3 Perifollicular Epidermis

Perifollicular and interfollicular skin surface provides significant information, which may facilitate diagnosis in hair and scalp diseases. It is one of the measurable parameters in the presence of perifollicular brown color ("peripilar sign"), which is believed to correspond to the presence of lymphocytic infiltrates (Deloche et al. 2004; Wallace and de Berker 2010). This finding is common in androgenic alopecia (Inui 2011) and telogen effluvium and may be seen in up to 10 % of hair follicle openings in healthy individuals (Rakowska 2009). The peripilar sign disappears with successful therapy of hair loss.

Epidermal scaling is a common finding in various inflammatory scalp diseases and in healthy individuals. The intensity of scaling may be assessed by trichoscopy and graded in a semiquantitative manner from 0 (for no scaling) to 4 (severe scaling).

In conclusion, trichoscopy is a novel method of noninvasive skin imaging that may be applied for diagnosing hair and scalp diseases as well as for quantitative evaluation and monitoring of hair loss.

4 Blood Vessels

Trichoscopy of normal scalp shows multiple thin arborizing vessels in the occipital area and pinpoint vessels in the frontal area (Rakowska 2009). Abnormalities in thickness and structure of blood vessels may provide clues for the diagnosis of several inflammatory scalp diseases, such as psoriasis, discoid lupus erythematosus, or dissecting cellulitis (Rudnicka et al. 2012).

References

Deloche C, de Lacharriere O, Misciali C, Piraccini BM, Vincenzi C, Bastien P, Tardy I, Bernard BA, Tosti A. Histological features of peripilar signs associated with androgenetic alopecia. Arch Dermatol Res. 2004;295(10):422–8.

Inui S. Trichoscopy for common hair loss diseases: algorithmic method for diagnosis. J Dermatol. 2011; 38(1):71–5.

Inui S, Nakajima T, Nakagawa K, Itami S. Clinical significance of dermoscopy in alopecia areata: analysis of 300 cases. Int J Dermatol. 2008;47(7):688–93.

Inui S, Nakajima T, Itami S. Scalp dermoscopy of androgenetic alopecia in Asian people. J Dermatol. 2009; 36(2):82–5.

Olszewska M, Rudnicka L. Effective treatment of female androgenic alopecia with dutasteride. J Drugs Dermatol. 2005;4(5):637–40.

Rakowska A. Trichoscopy (hair and scalp videodermoscopy) in the healthy female. Method standardization and norms for measurable parameters. J Dermatol Case Rep. 2009;3(1):14–9.

Rakowska A, Slowinska M, Kowalska-Oledzka E, Olszewska M, Rudnicka L. Dermoscopy in female androgenic alopecia: method standardization and diagnostic criteria. Int J Trichology. 2009;1(2):123–30.

Ross EK, Vincenzi C, Tosti A. Videodermoscopy in the evaluation of hair and scalp disorders. J Am Acad Dermatol. 2006;55(5):799–806.

Rudnicka L, Olszewska M, Rakowska A, Kowalska-Oledzka E, Slowinska M. Trichoscopy: a new method for diagnosing hair loss. J Drugs Dermatol. 2008; 7(7):651–4.

Rudnicka L, Olszewska M, Rakowska A. Atlas of trichoscopy: dermoscopy in hair and scalp disease. London: Springer; 2012.

Van Neste D. Natural scalp hair regression in preclinical stages of male androgenetic alopecia and its reversal by finasteride. Skin Pharmacol Physiol. 2006; 19(3):168–76.

Vogt A, McElwee K, Blume-Peytavi U. Biology of the hair follicle. In: Blume-Peytavi U, Tosti A, Whiting D, Trüeb R, editors. Hair; from basic science to clinical application. Berlin: Springer; 2008. p. 1–22. ISBN 3540469087.

Wallace MP, de Berker DA. Hair diagnoses and signs: the use of dermatoscopy. Clin Exp Dermatol. 2010;35(1):41–6.

Hair Trichogram

80

Alexandre Guichard and Ferial Fanian

Contents

Keywords

Trichogram • Hair pluck test • Alopecia • Anagen • Catagen • Telogen • Hair root • Hair shaft • Hair cycle

Abbreviations

AA	Alopecia areata
AGA	Androgenic alopecia
LAH	Loose anagen hair
N/A	Not available (Table 1) or not applicable (Table 2)

1 Introduction

Hair disorders are common diseases, frequently observed in dermatology. Alopecia has an important psychological impact on patients suffering from it. Therefore, the management of the patient must be complete and reassuring. The examination should be composed of a complete history taking, clinical and trichoscopic examinations, blood tests, trichogram, and sometimes biopsies.

The trichogram or hair pluck test is a semi-invasive, qualitative, and quantitative method which expresses the number and the proportion of hairs in the different phases of the hair cycle. The procedure is easy to perform and reliable and consists of a microscopic evaluation of plucked hairs in order to determine their cycle phases: anagen, catagen, or telogen and thus assess the dynamic phenomenon of hair cycle. Van Scott et al. introduced the trichogram in 1957, and in

A. Guichard (✉)
Center for Research and Studies on the Integument (CERT), Department of Dermatology, Clinical Investigation Center (CIC INSERM 1431), Besançon University Hospital; INSERM UMR1098, FED4234 IBCT, University of Franche-Comté, Besançon, France
e-mail: guichard.alexandre@gmail.com

F. Fanian
Center for Study and Research on the Integuments, Department of Dermatology, University Hospital of Besançon, Besançon, France
e-mail: ferial.fanian@chu-besancon.fr; ferial.fanian@cert-besancon.com; fanian@gmail.com

P. Humbert et al. (eds.), *Agache's Measuring the Skin*, DOI 10.1007/978-3-319-32383-1_110

the middle of 1960s, Barman and Pecoraro described several trichometric features and established normal values.

The sampling is already a part of the treatment, because the patient is less anxious and feels understood. Indeed, the sampling process is as important as the test result.

The trichogram allows also the assessment of hair shaft and diameter and also its anomalies.

This technique is employed for diagnosis, prognosis, and treatment monitoring of hair disorders but provides also the hair growth assessment in clinical trials in medical and cosmetic fields.

2 The Plucking Procedure

2.1 Material

The material is not expensive and easily available (Fig. 1):

- Forceps with rubber-protected jaws
- Adhesive tape or mounting medium, glass slides, and cover slips
- A pair of scissors
- Microscope (magnification 10×, 20×, and 40×) or microfilm reader (48×)

Fig. 1 Materials for the trichogram: microfilm reader, glass slides, cover slips, mounting medium, tape, scissors, forceps with rubber-protected jaws, and micrometric slide

2.2 Procedure

It is recommended to do the trichogram on an unwashed and untreated scalp for 5 days. In fact, no mechanical actions must be done: washing, brushing, and drying in a period of 5 days before the trichogram. Indeed, mechanical actions may eliminate telogen hairs and consequently reduce their number during the plucking which may lead to an artificial reduction of telogen rate leading to false results.

Selecting the plucking zone depends on the clinical status. In diffuse alopecia, a central part of the affected area and also non-affected area, as a control, should be sampled. For example, in androgenic alopecia (AGA), the first point is 2 cm behind the frontal line and 2 cm from the midline, and the second zone should be on the occipital region, 2 cm besides *protuberantia occipitalis externa*. In focal alopecia, the first point would be at the border of the lesion and the second on the contralateral, clinically unaffected side.

Trichoscopic examination may be, firstly, performed to determine the more relevant area to pluck.

- A bundle of about 30 hairs is carefully ranged. Plucking more hairs is frequently used, but it is difficult to pluck when it is painful and represents an important amount of hairs (Dhurat and Saraogi 2009). According to our experience, 30 hairs represent a reliable quantity to provide enough information.
- The lock of hairs is tightly plucked with the forceps as close as possible to the scalp, in order to avoid dystrophic and broken hairs and to pluck miniaturized hairs as well.
- One hand maintains the scalp stretched, while the other hand pulls rapidly with a unique ample movement in the direction of their emergence (Fig. 2). Plucking very curly, African, or short hairs is more difficult and may be done one by one with tweezers.
- A vigorous massage of the area, just after the sampling, relieves the discomfort caused by the sampling.

Fig. 2 Plucking procedure

- Hairs are arranged side by side on a glass slide and taped with transparent adhesive tape. It is also possible to use mounting medium used in microscopy like Eukitt® or Corbit-Balsam and cover slips. The mounting medium contains a preservative that is more expensive and may form air bubbles. It is permanent, and the procedure is longer because it needs a drying time. It is recommended not to cut taped hairs to assess their lengths and diameters in order to distinguish regrowing hairs from miniaturized hairs.
- Bulbs are examined at low magnification with a light microscope or on a screen of a microfilm reader. The latter allows an immediate global visualization of the entire sample on a wider screen and makes the count easier. Moreover, the screen is more useful to show and explain the shedding process to the patient.
- The sampling can be preserved and examined several weeks after sampling since the bulbs retain their morphology. Results and slides should be archived for patient follow-up.

3 Information Collected

The hair plucking procedure and analysis need a short training in order to obtain reliable and reproducible results. Indeed, if the trichogram is carried out inappropriately, many dystrophic and broken hairs are obtained and make the interpretation impossible.

The main objective of the trichogram is to evaluate hair roots, but the microscopic evaluation allows also the assessment of diameter and shaft morphology.

Cycle phasing and counting of the fair and white hairs (canities) are more difficult due to the absence of pigmentation.

3.1 Hair Root Assessment

3.1.1 Morphological Characteristics of Hair Roots During the Different Hair Cycle Phases

Anagen, the Growth Phase

The anagen root presents a darkish keratogenous zone, with the presence of melanin in matrix (Fig. 3a–c). A double translucent epithelial sheath can be presented and intact or partially present or sometimes absent (naked anagen).

Different patterns of anagen hair roots can be observed on the trichogram according to the different anagen stages. Trained examiner may be able to differentiate anagen stages; nevertheless, it needs a long training. However, the inter- and intraindividual variety of the time duration of these stages does not have a real clinical interest.

In early stage, hair roots are widest at their proximal end and narrow on the distal part (trapezoidal shape). In late stage, hair roots have a diameter more uniform throughout (rectangular shape).

Often an angulation of root and/or shaft can be observed.

The diameter of anagen hairs of children and fair or red-hair adults is lower, and the medulla is sometimes absent, making the distinction between hair cycle phase more complicated.

Catagen, the Regressing Phase Mediated by Apoptosis Phase

Catagen hairs are rare, less than 2 %, and sometimes difficult to distinguish from telogen (Fig. 4). The diameter of catagen hair root is smaller; sheaths persist but are shorter and narrower than those in anagen phase.

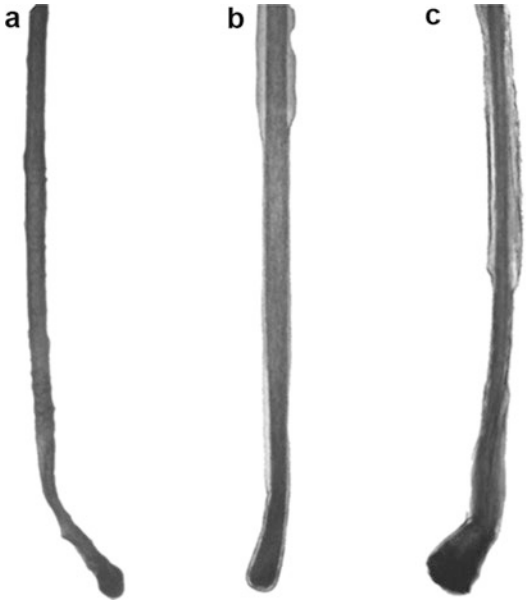

Fig. 3 Anagen hairs: (**a**) Anagen hair naked, (**b**) anagen hair with sheath and rectangle root, and (**c**) anagen hair with sheath and trapezoidal root

Early catagen hairs show an equal diameter throughout and a slight keratinized tip.

Late catagen hairs have a club-shaped tip, less keratinized (the future telogen), and ended by a "tail" corresponding to an epithelial cord remnant joining the papilla.

A high proportion of catagen hairs inform about the alopecia progress.

Telogen, the Quiescent Phase

Telogen hairs have a typical club-shaped root, have a thickening of the proximal end, and keratinized, mostly transparent but partly pigmented ("swab" shape) (Fig. 5). Although they have no internal or external root sheath, their club-shaped roots are surrounded by an epithelial sac, sometimes absent. The presence of this epithelial sheath indicate strong binding, suggesting early telogen, whereas the absence of an epithelial sheath indicates loose binding accompanied with hair shedding (Piérard-Franchimont and Piérard 2001).

Fig. 4 Catagen hairs

No angulations are observed on telogen hairs.

3.1.2 Other Morphological Features Observed

Dystrophic Hairs

In the literature, the terms "dystrophic" and "dysplastic" hair roots are rather confusing and sometimes be used in place of each other (Fig. 6). Basically, these two terms refer to an abnormal anagen hair with shaft and/or root defect. To avoid misunderstanding and confusion with other diseases, we suggest to use the unique term of "dystrophic hair."

This impairment may be an artifact due to the plucking procedure (too slow epilation) or a real disease such as keratinization impairment in "loose anagen hair syndrome" or the inflammatory aggression of bulb and papilla in "alopecia areata" and "psoriasis." However, dystrophic hairs can also be observed in healthy scalp (approximately less than 5 %).

A dystrophic hair may be characterized by several patterns:

- Absence of sheaths.
- Decreased matrix diameter; dystrophic hairs are thinner.

Fig. 5 (**a**) Telogen hair surrounded by an epithelial sac. (**b**) Telogen hair naked

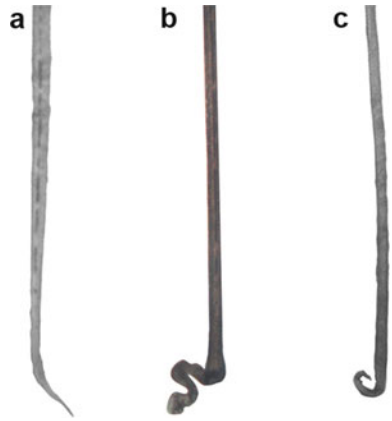

Fig. 6 Dsytrophic hairs: (**a**) Dystrophic naked hair with a tapered root, (**b**) dystrophic hair with "wavy" shaft, and (**c**) dystrophic naked hair with a hook-shaped root

- Marked hair shaft constriction.
- Rupture of the hair around the upper third of the papilla leading to a tapered root.
- Lower end of the hair shaft is usually wavy.

Fig. 7 Broken hair

- Deformation of the bulb which looks distended, stretched, and colorless.
- Often hair roots show >20° angulation: "hooked hair."

Broken Hairs

Usually they correspond to anagen hair shafts that break off due to the fragility of the hair or an inadequate plucking technique (Fig. 7). The shaft presents a cutoff section excluding the root.

It seems necessary to count them as the healthy anagen hairs because this indicates their strong adherence to the scalp. However, fragility may be the clue of a pathology or deficiency; therefore, a pull test should be associated. If the number of broken hairs is lower than 10 % and the pull test is negative, they will be counted as anagen hairs. Beyond 10 %, the trichogram is not interpretable.

Artifacts

- Pseudomonilethrix, described by Bentley-Phillips et al. in 1973 (Bentley-Phillips and Bayles 1973), corresponds to a hair shaft abnormality characterized by globular swelling ("nodes") or irregular flattened areas with a larger diameter than normal shaft (Fig. 8). These abnormalities occur in brittle or pathologic hairs but also in normal hairs. In fact, pseudomonilethrix represents an artifact

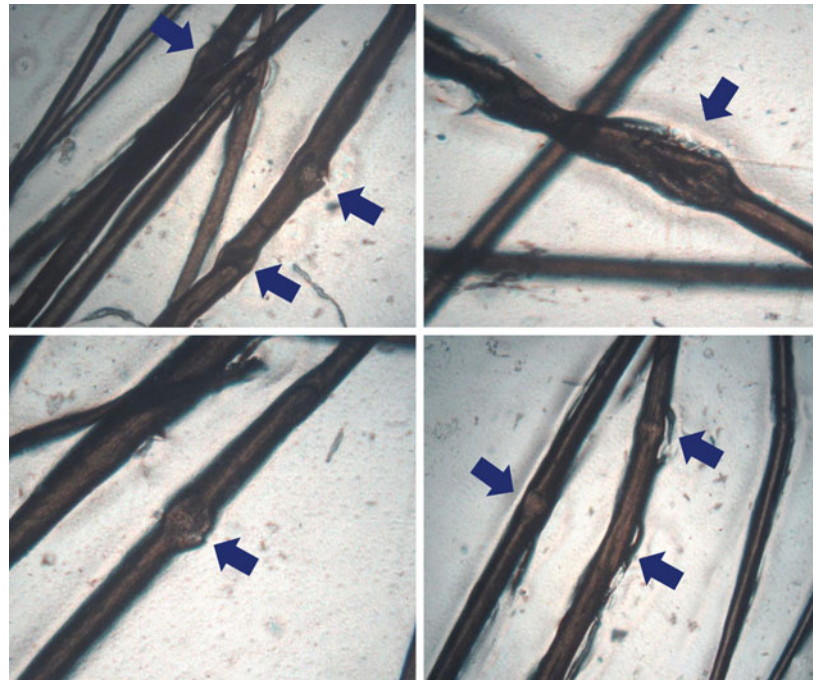

Fig. 8 Pseudomonilethrix induced manually by the plucking procedure. *Blue arrows* represent globular swelling ("nodes")

induced by a traumatic process of preparing the hair for microscopic examination (forceps or pressure on the glass slide or tape) rather than a pathologic hair shaft defect (Ferrando et al. 1990). This artifact could be misinterpreted and confused with congenital hair shaft defect including monilethrix, trichorrhexis nodosa, trichorrhexis invaginata, pili torti, or wooly hair. This artifact could be avoided by using rubber-armed forceps to gently plucked hairs and taping on the slide with low pressure.

- Impairments of the hair shaft can occur if the tweezers do not close tightly enough and slip along the shaft (Fig. 9).

3.2 Hair Diameter Assessment

3.2.1 Androgenic Alopecia

Besides the root assessment, the hair shaft diameter can be also evaluated with the trichogram. During hair growth, the new anagen hairs have their definitive diameter; thus, a thinner hair indicates an impact of androgens which reduce the cycle phase duration and consequently decrease the length and diameter of hairs. When the diversity of hair shaft diameter is high, this phenomenon, called miniaturization, is a hallmark of AGA. It has been suggested that if in trichoscopy miniaturization is more than 20 % of the entire scalp, it is highly diagnostic of AGA. In the other hand, the presence of more than 10 % in the frontal area by itself is also highly suggestive for this diagnosis (Miteva and Tosti 2012).

To measure the diameter of plucked hair shaft with precision, a micrometric scale like a micrometric calibration slide for microscope objective can be used.

A normal terminal hair is 50 μm (blond hairs) to 120 μm thick (Asiatic hairs). Miniaturized hair is defined as fine, short, and unpigmented hair with a diameter less than 40 μm (Rushton et al. 1983).

Although the trichogram allows a qualitative measurement of the miniaturization, it provides

Fig. 9 Impairment of the hair shaft induced by tweezers

only a semi-quantitative indication. Indeed, some miniaturized hairs are too thin to be plucked so the quantification will be neither exhaustive nor accurate. Nevertheless, if the number of miniaturized hair counted in the trichogram is higher than 20 %, it means that there are at least 20 % of miniaturized hairs on the scalp and makes the diagnosis of AGA.

3.2.2 Deficiency

The trichogram may also emphasize some severe nutritional deficiency. During severe diet, protein deficiency (kwashiorkor), or severe digestive diseases with malabsorption, the hair shaft diameter and melanin ratio may decrease brutally leading to thinner and brighter hairs. In the case of intermittent deficiency, the diameter may vary throughout the shaft with alteration from low to normal diameter. The clinical presentation, called flag sign, corresponds to a sequential band of light and dark color along individual hair fibers due to an intermittent protein deficiency.

3.3 Hair Shaft Assessment

The hair length may be correlated with the hair shaft diameter which is the reason that may distinguish the difference between regrowing hair and miniaturized hair. In the case of regrowing hairs after telogen effluvium, the short hair with normal diameter (50–120 μm) can be observed, while in miniaturized hairs, the short hair with poor diameter (<40 μm) and pigmentation can be observable which is a hallmark of AGA.

Moreover, hair length is a time indicator and it can be used as a witness for calculating the onset of pathology. Knowing the speed of hair growth, which is about 1.3 cm per month, it is possible to estimate the onset of a telogen effluvium and find the triggering factors by measuring the length of regrowth anagen hairs (2–4 months retrospectively).

Finally, trichogram is a microscopic examination which, accordingly, may detect shaft abnormalities and make the diagnosis of congenital hair shaft defect including monilethrix, trichorrhexis nodosa, trichorrhexis invaginata, pili torti, wooly hair, etc.

4 Results

1. An overview of trichogram resuts in normal condition (Hillmann and Blume-Peytavi 2009; Agache et al. 2004; Peereboom-Wynia et al. 1993; Martinez and Montagna 1997; Blume-Peytavi 2008) and in the context of common scalp diseases (Galliker and Trüeb 2012; Rakowska et al. 2009; Tosti et al. 1997; Trüeb 2009; Bleiker 2005; Paus et al. 2013; Cantatore-Francis and Orlow 2009; Dhurat and Deshpande 2010; Lachapelle and Pierard 1977; Oranje et al. 1986; Stanimirović et al. 1998) are presented in Table 1.

Table 1 Trichogram characteristics of different hair conditions of Caucasians' scalps taking into account inter- and intraindividual, seasons, gender, and phototype variations. In gray, normal values; −, lower than the normal value; =, equal to the normal value; +, higher than the normal value, a. In this study, Pecoraro et al. included catagen hairs in the telogen group

Conditions	Assessed sites	Anagen (%)	Telogen (%)	Catagen (%)	Broken (%)	Dystrophic (%)	Specific characteristics
Normal Adult (Hillmann and Blume-Peytavi 2009; Agache et al. 2004; Peereboom-Wynia et al. 1993; Martinez and Montagna 1997; Blume-Peytavi 2008)	The entire scalp	70–90	10–20	<2	<10	<5	The rate of dystrophic anagen can occasionally reach higher in children, adolescents and adults with thin hairs
Normal Newborn (Pecoraro et al. 1964a)	Frontal Parietal Occipital	65 75 90	32 8–9 2–3	2–3 16 6–7	N/A	N/A	
Normal Child (Pecoraro et al. 1964b)	Frontal Parietal Occipital	90 92 97	10 8 3	N/A	N/A	N/A	
Telogen effluvium	Entire scalp	−	++	= or +		= or +	Dystrophic hairs increase in acute metabolic disorders or failure
Androgenetic alopecia (Rushton et al. 1983; Galliker and Trüeb 2012; Rakowska et al. 2009)	Frontal	−	+	= or +		= or +	Miniaturized hairs (diameter <40μm)>20 %: AGA
							Miniaturized 10–20 %: highly suggestive of AGA
	Occipital	=	=	=	=	=	Miniaturized hairs <10 %: AGA not excluded. Make correlation with trichoscopy
Alopecia areata (Peereboom-Wynia et al. 1993; Tosti et al. 1997)	Margin of lesion	− −	+	= or +		++	Increase in dystrophic hairs is a sign of onset of AA
	Contralateral non-affected area	=	=	=		= or +	

Anagen effluvium (Trüeb 2009; Bleiker et al. 2005; Paus et al. 2013)	Entire scalp	− −	= or +	=	+	+	Mild to moderate chemotherapy-induced damage: dystrophic anagen
							Severe chemotherapy-induced damage: dystrophic catagen
							Hairs are more brittle: number of broken hairs increases
							Often a telogen effluvium is associated
Loose anagen hair syndrome (Tosti et al. 1997; Cantatore-Francis and Orlow 2009; Dhurat and Deshpande 2010)	Entire scalp	− −	= or −			++ (>70 % LAH)	Normal anagen hairs are transformed in loose anagen hair (LAH) (dystrophic hairs) which are naked anagen devoid of inner root sheath with misshapen bulbs and ruffled cuticles
Trichotillomania (Cantatore-Francis and Orlow 2009; Lachapelle and Pierard 1977; Oranje et al. 1986)	Frontotemporal or frontoparietal	=	−	= or +		+	Telogen hairs with fractured hair fibers
	Sometimes occipital region in younger children						Roots sheaths are preserved
	Non-affected area	=	=	=	=	=	
Psoriasis (Stanimirović et al. 1998)	Psoriatic plaque	−	= or +	=		+	Dystrophic hair shaft without root sheath
	Non-affected area	=	=	=	=	=	

Table 2 Collection sheet for adult's trichogram

Area sampled

✖: Affected area plucked

●: Non-affected area plucked

Patient's data :

Date :

Trichogram

	AFFECTED AREA Total:		NON-AFFECTED AREA Total:		NORMAL VALUES
	Number	%	Number	%	
Anagen hairs With sheath Without sheath (naked anagen)					**[>70 %]**
Dystrophi chairs					**[<5 %]**
Telogen hairs					**[10%-20%]**
Catagen hairs					**[<2 %]**
Broken hairs					**[<10 %]**
Miniaturized hairs					**[<10%]** *>20%: AGA* *[10-20%]: Abnormal*
Ratio Anagen/Telogen		N/A		N/A	**[>5]** *[4-5]: Dubious* *<4: Abnormal*

Conclusion:

2. Example of a collection sheet (Table 2)

On healthy scalp, the anagen/telogen ratio is stable and more than 5. An anagen/telogen ratio lower than 5 is abnormal but does not provide any additional data. For example, in telogen effluvium, the telogen percentage is not correlated with severity of hair loss (Guarrera et al. 1997).

3. Physiological variations

The distribution of cycle phases on the scalp is heterogeneous and depends on inter and intraindividual variations:

(a) *Scalp location*

In both genders, the number of telogen hairs is higher on frontal and vertex regions than on parietal and occipital regions.

(b) *Gender*
In the entire scalp, the number of hairs in a telogen phase is higher in males than in females (Barman et al. 1965).

(c) *Age* (Table 1)
Basically, on newborns' scalp, the anagen phase predominates (65–90 %), but catagen hairs are more frequently observed in newborns than in adults. The telogen phase is most predominant in the frontal region, and the catagen occurs most frequently in the parietal regions than others (Pecoraro et al. 1964a).

In childhood before puberty, generally 90 % or more of hairs are in the anagen phase. Moreover, the number of hairs in telogen phase is lower than in adults. Finally, the proportion of telogen hairs in the frontal and parietal regions is higher than in occipital region (Pecoraro et al. 1964b).

In adulthood, hairs are mostly in the anagen phase; nevertheless, the number of hairs in telogen phase increases with age in each scalp regions (Barman et al. 1965). Moreover, the number of miniaturized hairs increases with age due to the effects of androgens and the progressive physiological degeneration of the dermal papilla which accelerate the hair cycle.

(d) *Seasons*
During summer the percentage of telogen hairs increases, while the percentage of anagen decreases which explains the autumnal hair shedding. The same phenomenon occurs in spring but less remarkable. The telogen rate is the lowest in late winter (Kahn et al. 2009; Kunz et al. 2009).

5 Conclusion

Trichogram is an important tool in clinical practice and provides a good diagnostic and prognostic indicator for different etiologies of alopecia, and it can be also useful in treatment management. Thanks to its reproducibility, the trichogram is also used in the routine disease follow-up and in clinical trials as a primary endpoint as well.

This semi-invasive, rapid, objective, and inexpensive microscopic evaluation provides reliable information about hair root, hair shaft, and hair viability.

Although trichogram was widely used routinely for decades, nowadays many dermatologists discontinued this examination due to the lack of knowledge in the interpretation. Indeed, although the procedure is simple, it needs a short training and good experience in the plucking procedure as well as in interpretation to benefit the advantages of this technique.

References

Agache PG, Humbert P, Maibach HI. Measuring the skin. New York: Springer; 2004. 812 p.

Barman JM, Astore I, Pecoraro V. The normal trichogram of the adult. J Investig Dermatol. 1965;44(4):233–6.

Bentley-Phillips B, Bayles MA. A previously undescribed hereditary hair anomaly (pseudo-monilethrix). Br J Dermatol. 1973;89(2):159–67.

Bleiker TO, Nicolaou N, Traulsen J, Hutchinson PE. 'Atrophic telogen effluvium' from cytotoxic drugs and a randomized controlled trial to investigate the possible protective effect of pretreatment with a topical vitamin D3 analogue in humans. Br J Dermatol. 2005;153(1):103–12.

Blume-Peytavi U. Hair growth and disorders: with 85 tables. Berlin: Springer; 2008. 571 p.

Cantatore-Francis JL, Orlow SJ. Practical guidelines for evaluation of loose anagen hair syndrome. Arch Dermatol. 2009;145(10):1123–8.

Dhurat RP, Deshpande DJ. Loose anagen hair syndrome. Int J Trichol. 2010;2(2):96–100.

Dhurat R, Saraogi P. Hair evaluation methods: merits and demerits. Int J Trichol. 2009;1(2):108–19.

Ferrando J, Fontarnau R, Haussman G. Is pseudomonilethrix an artifact? Int J Dermatol. 1990;29(5):380–2.

Galliker NA, Trüeb RM. Value of trichoscopy versus trichogram for diagnosis of female androgenetic alopecia. Int J Trichol. 2012;4(1):19–22.

Guarrera M, Semino MT, Rebora A. Quantitating hair loss in women: a critical approach. Dermatology (Basel). 1997;194(1):12–6.

Hillmann K, Blume-Peytavi U. Diagnosis of hair disorders. Semin Cutan Med Surg. 2009;28(1):33–8.

Kahn CM, Guerrero AR, Césped MC. Seasonal variation of trichogram in Chilean subjects. Rev Med Chil. 2009;137(11):1437–40.

Kunz M, Seifert B, Trüeb RM. Seasonality of hair shedding in healthy women complaining of hair loss. Dermatology (Basel). 2009;219(2):105–10.

Lachapelle JM, Pierard GE. Traumatic alopecia in trichotillomania: a pathogenic interpretation of histologic lesions in the pilosebaceous unit. J Cutan Pathol. 1977;4(2):51–67.

Martinez FC, Montagna W. Trichologie: maladies du follicule pilosébacé. Madrid: Grupo Aula Medica; 1997. 767 p.

Miteva M, Tosti A. Hair and scalp dermatoscopy. J Am Acad Dermatol. 2012;67(5):1040–8.

Oranje AP, Peereboom-Wynia JD, De Raeymaecker DM. Trichotillomania in childhood. J Am Acad Dermatol. 1986;15(4 Pt 1):614–9.

Paus R, Haslam IS, Sharov AA, Botchkarev VA. Pathobiology of chemotherapy-induced hair loss. Lancet Oncol. 2013;14(2):e50–9.

Pecoraro V, Astore I, Barman JM. Cycle of the scalp hair of the new-born child1. J Investig Dermatol. 1964a;43(3):145–7.

Pecoraro V, Astore I, Barman J, Araujo CI. The normal trichogram in the child before the age of puberty1. J Investig Dermatol. 1964b;42(6):427–30.

Peereboom-Wynia JD, Beek CH, Mulder PG, Stolz E. The trichogram as a prognostic tool in alopecia areata. Acta Derm Venereol. 1993;73(4):280–2.

Piérard-Franchimont C, Piérard GE. Teloptosis, a turning point in hair shedding biorhythms. Dermatology (Basel). 2001;203(2):115–7.

Rakowska A, Slowinska M, Kowalska-Oledzka E, Olszewska M, Rudnicka L. Dermoscopy in female androgenic alopecia: method standardization and diagnostic criteria. Int J Trichol. 2009;1(2):123–30.

Rushton H, James KC, Mortimer CH. The unit area trichogram in the assessment of androgen-dependent alopecia. Br J Dermatol. 1983;109(4):429–37.

Stanimirović A, Skerlev M, Stipić T, Beck T, Basta-Juzbasić A, Ivanković D. Has psoriasis its own characteristic trichogram? J Dermatol Sci. 1998;17(2):156–9.

Tosti A, Peluso AM, Misciali C, Venturo N, Patrizi A, Fanti PA. Loose anagen hair. Arch Dermatol. 1997;133(9):1089–93.

Trüeb RM. Chemotherapy-induced alopecia. Semin Cutan Med Surg. 2009;28(1):11–4.

Phototrichogram

81

Pascal Reygagne

Contents

Keywords

Androgenetic alopecia (AGA) • Contrast-enhanced phototrichogram (CE-PTG) • Non-invasive methods • Phototrichogram (PTG) • Trichogram • Automated PTG • CE-PTG • Scalp biopsy • TrichoScan professional version 3 (TrichoScan 3)

1 Introduction

Various methods are available for evaluation of a patient complaining of hair loss. Those methods can be invasive, semi-invasive, or noninvasive (Dhurat and Saraogi 2009).

Scalp biopsy is an invasive method.

Semi-invasive methods are pull test, trichogram, or unit area trichogram.

Noninvasive methods include efficacy questionnaire, quality of life questionnaire, daily hair count, standardized wash test, 60 s hair comb test, hair weight, hair diameter measurement, global photographic assessment, dermoscopy, videomicroscopy, photographic hair count, and phototrichogram.

The phototrichogram (PTG) is a safe, noninvasive, and reproducible method that allows in vivo study of the hair cycle. PTG is able to quantify a lot of hair growth parameters including hair density. Hair loss and hair thinning are the main complaints in clinical hair diseases. Even if the diagnosis of androgenic alopecia is clinical, clinical assessment of the hair density is not easy

P. Reygagne (✉)
Centre de Santé Sabouraud, Hôpital Saint Louis, Paris, France
e-mail: p.reygagne@centresabouraud.fr

P. Humbert et al. (eds.), *Agache's Measuring the Skin*,
DOI 10.1007/978-3-319-32383-1_114

especially at the beginning when hair density is nearly normal, and we need a sensitive tool to measure hair loss and hair density and to monitor effect of treatments on alopecia. The phototrichogram is based on the following principle: after shaving a target area of the scalp, it's possible to distinguish growing hairs in anagen phase which lengthen by about 0.35 mm a day and the resting hairs in telogen phase. As a trichogram, PTG is able to quantify percentage of anagen and telogen hair. And as a macrophotography of a selected area (global hair count) (Canfield 1996), or as a unit area phototrichogram (Rushton et al. 1983), or as a scalp biopsy (Whiting et al. 1999), PTG is able to quantify density of hair. Furthermore PTG can measure hair growth speed and hair diameter, and it's possible to check carefully and to control all those values on stored photographies.

For those reasons PTG is nowadays the gold standard for noninvasive hair growth measurement in hair research and in clinical studies or for a patient's follow-up assessment during treatment of none scarring or scarring alopecia. Most of the time PTG is combined in clinical studies with a cosmetic assessment included a questionnaire and global photographs.

2 History

The PTG was described for the first time by Satoh in 1970, on scalp and body hair of three Japanese men studied over a period of 2 years (Saitoh et al. 1970). Fiquet and Courtois were the first to propose PTG to access hair growth, severity of alopecia, and evolution after anti-hair loss treatments (Fiquet and Courtois 1979; Courtois et al. 1982). Then Bouhanna and Guarrera improved the methodology (Bouhanna 1982, 1984; Guarrera and Ciulla 1986) and Bouhanna invented in 1988 a variant, the tractiophototrichogram (Bouhanna 1988). The advantage of the tractiophototrichogram is to avoid the second visit necessary for a classical PTG: you choose the area of interest; you pull all the hairs of this area firmly between thumb and forefinger to eliminate telogen hair. You count the number of eliminated telogen hair and after you take a picture to count the remaining anagen hair. The main problem is that the traction is not standardized and investigator dependent, and now the tractiophototrichogram is not in use anymore. In 1991 Blume used the PTG for visual and manual vellus hair count, and vellus hairs, generally colorless, were dyed (Table 1) (Blume et al. 1991). Classical PTG even on the scalp is limited by the contrast between hair and scalp color. This contrast is poor in the case of fair or white hair and in the case of AGA because of the miniaturization process: vellus hairs are thinner and lighter than terminal hair. In 1992 Van Neste introduced the application of an immersion oil (scalp immersion photographic method) (Van Neste et al. 1992); and in 2001 he added hair dye to proposed the contrast-enhanced PTG (CE-PTG) (Van Neste 2001). With an increase of contrast and resolution, thanks to the use of immersion oil and hair dyer, CE-PTG is nowadays the most sensitive methodology specially in case of fair hair or AGA. A comparative evaluation of scalp hair by PTG and unit area trichogram analysis showed comparable results in the same subjects for anagen hairs (Rushton et al. 1993), and CE-PTG is as sensitive as transverse sectioning of scalp biopsies for detecting hair and percentage of anagen and telogen hairs (Van Neste 2001).

Table 1 Phototrichogram results for vellus hair follicles in healthy subjects (Blume et al. 1991)

Localization	Density	% Anagen	Rate of growth
Facial hair females (forehead)	448/cm^2	48	0.037 mm/day
Thorax hair females (back)	93/cm^2	31	0.15 mm/day
Thorax hair females (chest)	53/cm^2	42	0.11 mm/day
Facial hair males (forehead)	429/cm^2	49	0.025 mm/day
Thorax hair males (back)	77/cm^2	32	0.12 mm/day
Thorax hair males (chest)	61/cm^2	35	0.11 mm/day

The CE-PTG is the best tool to access hair regrowth in clinical research, but CE-PTG without automatic analysis is time consuming and difficult to perform in clinical practice. For this reason some authors developed automatic hair counts and analysis, easier to use in clinical practice. First attempts to automate the process began in 1986 (Pelfini and Calligaro 1986; Hayashi et al. 1991) and then continued with Dominique Van Neste who was the most well-known pioneer of this new method (Van Neste et al. 1989, 1992).

3 Methodology: CE-PTG

We are going to describe the CE-PTG which is in 2014 the best method to access hair growth and hair loss. The CE-PTG is used to detect and quantify early changes of decreased hair density, diameter, or growth in diffuse alopecia or in androgenetic alopecia (AGA). This method is usually used for scalp hairs but analysis of body hairs is also possible.

First of all the area of interest must be chosen in an active area. In the case of AGA, it could be the vertex or an anterior or lateral area close to the vertex in a transitional area of hair loss. It's possible to choose an anterior area along the receding hairline but it's more visible. It's always better for cosmetic reason to avoid the parting. In the case of scarring alopecia, you must choose an area along the border of an inflammatory patch.

On day 0 a scalp area of interest of about 1 cm^2 is delineated with a standardized plastic template applied on the selected area. All hairs of this area are combed through this template with the help of a little curved hook or a pointed scissor and shaved with a surgical curved scissor or a hairliner or better a mini haircut (Wella® or Ermilia®) (Photo 1, 2, and 3). The length must be the same for all the hairs of the area, and short hair shafts should remain visible (about 0,5 mm), and that's difficult with a scissor and easier with a mini haircut. Adhesive tape can delimited the target area shaved to avoid the crossing of outside hair (Photo 4). It is very important to remove carefully all clipped hair with an adhesive strip or with pulsed hair to avoid their count in the target. A magnifying glass can help to check the area is definitely clean. A brown or best a black dyer is used to dye hairs of the target area to enhance the contrast between hair and scalp before the photography. This is always necessary in the case of blond, gray, or white hair; it is not essential in the case of very dark hair, but vellus hairs are always more visible if they are dying. After 10–15 min, the area is cleaned with an antiseptic alcoholic solution. You must choose a time of application, according to the hair and the used dyer, long enough to dye the hair but not too long to don't dye the scalp. Usually more than 15 min would unintentionally dye the scalp and less than 10 min resulted in uncompleted staining of hair.

Photo 1 Hair liner

The photography is taken with a macrocamera or a video camera (Photo 5) under fixed distance, fixed magnification, and fixed light conditions. It's possible to use different devices: Canfield camera (Photo 6) or medical Nikkor lenses, Canon or FotoFinder medicam (Photo 7), etc. Image quality is better with the scalp immersion proxigraphy method: the camera device includes a glass slide at fixed distance, and by pressing the glass slide on the scalp, you flatten the scalp and the hairs. The scalp is photographed under the glass slide with a drop of immersion oil between the glass slide and the scalp (Photo 8). This increases the resolution of the images. A hydroalcoholic antiseptic solution can also be used, and with a hydroalcoholic solution or with water, it's easier to avoid bullous formation around follicles between the glass and the scalp.

Photo 2 Mini hair cut

On day 2–3, the second photography is taken without shaving the hair but after hair dyer and with the same methodology. The most difficult is to photograph exactly the same area, and for that you can use semipermanent dot tattoo or a nevus or an angioma. In the case of tattoo, you can use one tattoo in the center of a circle if your target area is a circle. In this case it's better to don't use a black tattoo which could mask few hairs on the photographies. A red tattoo is better. If your target area is a square, you can use black or dark brown color at two opposite corners of the square just outside of the target for hair counting. In France the only brand of tattoo with a CE approvement for medical tattooing is Biochromaderm® (Laboratoires Biotic Phocea). If there is no nevus and no angioma and if the patient doesn't agree for a tattoo, you can exactly measure the distance between the

Photo 3 Shaving of the selected area

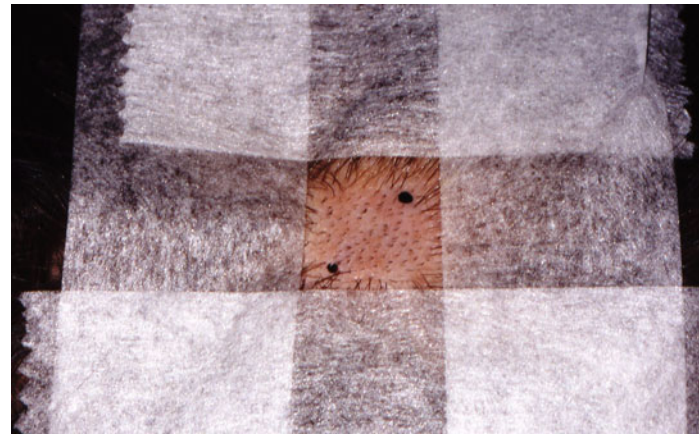

Photo 4 Adhesive tape delimite the target area

Photo 5 Achievement of the photo

area and the nose and between the area and left and right ears. After you must check exactly the follicular location of few typical follicular units on previous photography, but it's very difficult and time consuming and the use of a dot tattoo is easier and guaranties the analysis of the same area to insure reproducibility over a long period of time in clinical studies (Courtois et al. 1995).

An interval of 2 days between the first and the second photography of the PTG is enough to see and measure elongation of hair. It's important in case of linear hair growth hair measurement to respect the same hour in the day for both photographies. An interval of 3 days can measure a more precise elongation of hair but if interval is longer, hairs are too long, and because of many crossings or overlap of hairs, hair counts and interpretation of picture are more difficult. Some hair can be forgotten or otherwise counted twice.

Results (Photo 9): comparing the first and the second photographies with the help of manual marking of hairs on images allows to measure number of hair, anagen hair, telogen hair, hair elongation, hair diameter, terminal hair (with a diameter >40 μm), and vellus hair (with a diameter <40 μm). The detection limit is depending on the resolution, quality, and magnificence of the photographs. Usually hairs under 5 μm of diameter are not visible.

Photo 6 Candfield camera

Photo 7 Fotofinder medicam

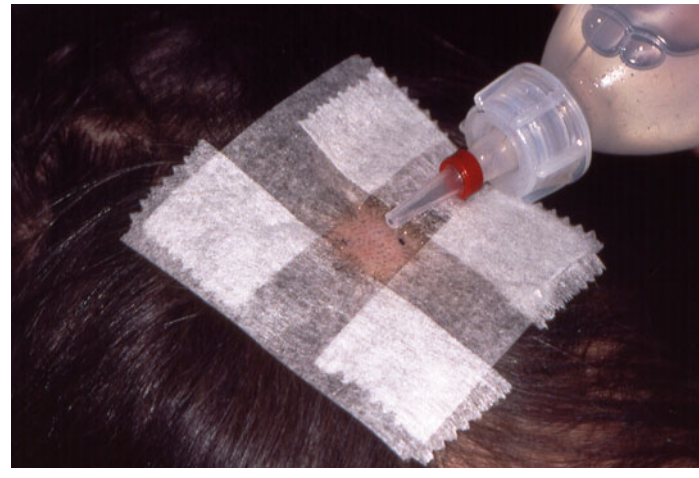

Photo 8 A drop of immersion oil

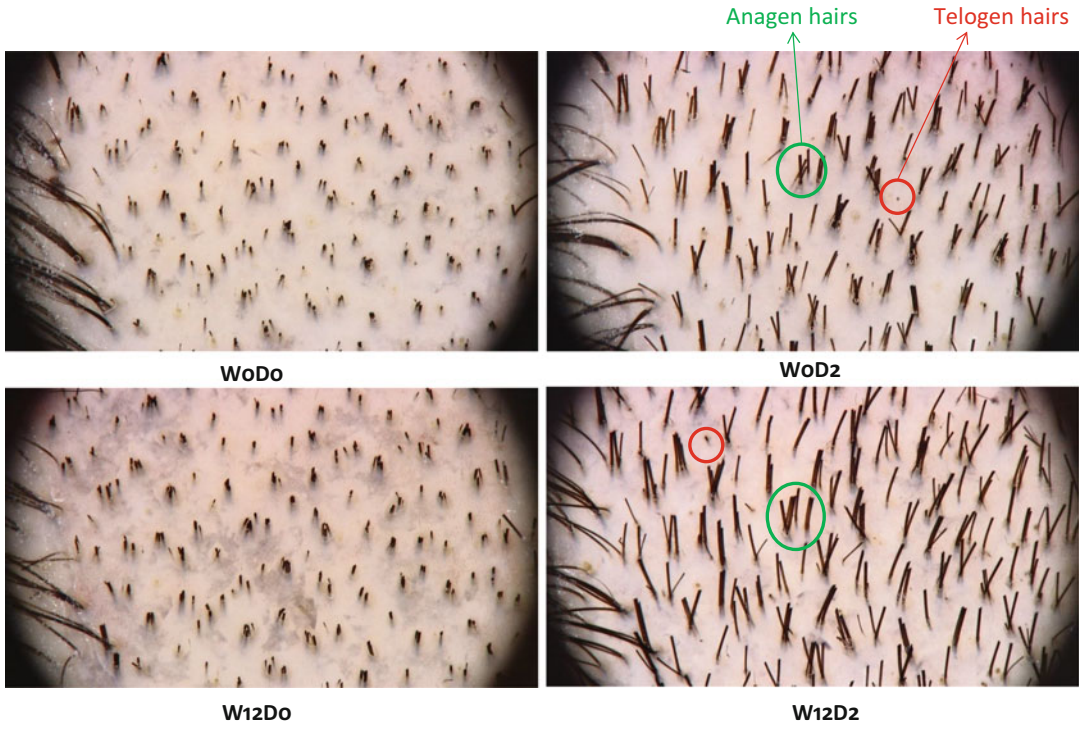

	Total Hair count	Hair Density (1/cm2)	Anagen hairs (%)	Telogen hairs (%)
Week 0	113	201	74,3 %	25,7 %
Week 12	123	218,8	85,5 %	14,5 %

Photo 9 Phototrichogram assessment before and after a topical treatment

- Elongation of hair indicates an anagen hair.
- No elongation or missing hair on the second photo indicates a telogen hair.

Evaluation parameters:

- Total number of hair in the target area (H)
- Total density of hair (H/cm^2)
- Number of terminal hair (TH)
- Density of terminal hair (TH/cm^2)
- Number of vellus hair (V)
- Density of vellus hair (V/cm^2)
- Percentage of terminal hair (TH/H) × 100 %
- Percentage of vellus hair (V/H) × 100 %
- Terminal-to-vellus ratio (H/V)
- Total number of anagen hair (A)
- Total anagen hair density (A/cm^2)
- Total number of telogen hair (T)
- Total telogen hair density (T/cm^2)
- Percentage of anagen hair (A/H) × 100 %
- Percentage of telogen hair (T/H) × 100 %
- Anagen-to-telogen ratio (A/T)
- Length (mm)
- Linear hair growth rate (LHGR; mm/day)

The LHGR is the length of hair on the second photo minus the length of hair on the first photo, divided by the interval of time between the two photos in days.

The best parameters correlated to the hair volume and the cosmetic improvement are:

- Total density of hair
- Total density of terminal hair

Percentage of anagen hair, percentage of terminal hair, and LHGR can be considered.

The worst parameter is the A/T ratio: variations are very important, and an increase of this parameter is possible without increase of anagen hair density, with a decrease of telogen hair density, and with a decrease of total density of hair, without cosmetic improvement and with a worsening of the alopecia.

3.1 Advantages of PTG

- Reproducible procedure
- No hair plucking and no painful, noninvasive method
- Information on density (as for macrophotography alone)
- Information on % of anagen and telogen hair (as for trichogram)
- Information on hair diameter
- Possibility to survey over many years the evolution of exactly the same groups of hair on the same precise area of the scalp (Courtois et al. 1995)
- Storing pictures to control results

3.2 Inconvenience of PTG

- No visualization of hair shafts.
- Need of two visit for the patient with 2 or 3 days of interval.
- Need to shave the target area.
- Manual hair count is time consuming.
- Manual count is investigator dependent.
- Automated PTG Is Expensive
- Detection of hair is dependent on the magnification and the sensibility of the photographic procedure.
- Tattoos (0.2–0.5 mm) can remain many years if red or brown and all the life if black.

In clinical studies CE-PTG is usually combined with a global photographic assessment for evaluating quantitative improvement with the CE-PTG and cosmetic improvement induced by treatment with the global photographic assessment.

4 Automated PTG

Conventional manual hair counts on photographs of CE-PTG are accurate but laborious and very time consuming, and results are investigator dependent even for the same photographs.

First attempts to automate the counts of PTG began in 1986 (Pelfini and Calligaro 1986; Hayashi et al. 1991; Van Neste et al. 1989, 1992).

In 1996, L'Oreal proposed an automatic system count, but this has not been available for the public (Chatenay et al. 1996).

The Folliscope™ version 2.8 (LeadM Corp, Seoul, South Korea) is a semiautomated tool using videodermoscopy of scalp and software to help the manual count (Photo 10). The Folliscope uses a light and small video camera, easily portable with a port-USB connection. The 100-fold lens magnification allows measuring easily hair thickness. Hair thickness is measured by mouse point dragging from one side to the other side of the hair shaft (Photo 11). The 50-fold lens is used to access hair density, but the hair count is not fully automated, so this count can change with different investigator and target area is too small for accurate PTG. Accurate results needs to analyze three locations in each chosen area for hair count and five to ten hairs for thickness or hair diameter (Lee et al. 2012).

In 2001 (Hoffman 2001) Hoffman described a fully automated method for the measurement of CE-PTG parameters, thanks to a new software named TrichoScan®. His method combines epiluminescence videomicroscopy with automatic digital analysis. The first version was able to count total number of hair, number of telogen and anagen hair, percentage of telogen or anagen hair, hair growth rate, and anagen/telogen ratio,

Photo 10 Folliscope screen folliscope

Frontal area

Density = 170/cm²

Vellus hair < 40 μm= 43%

Occipital area

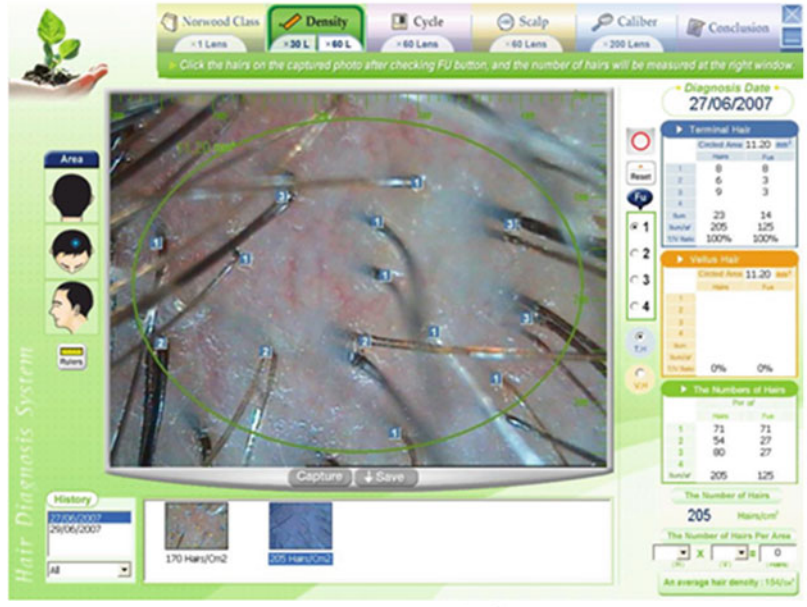

Density = 205/cm²

Vellus hair < 40 μm = 0%

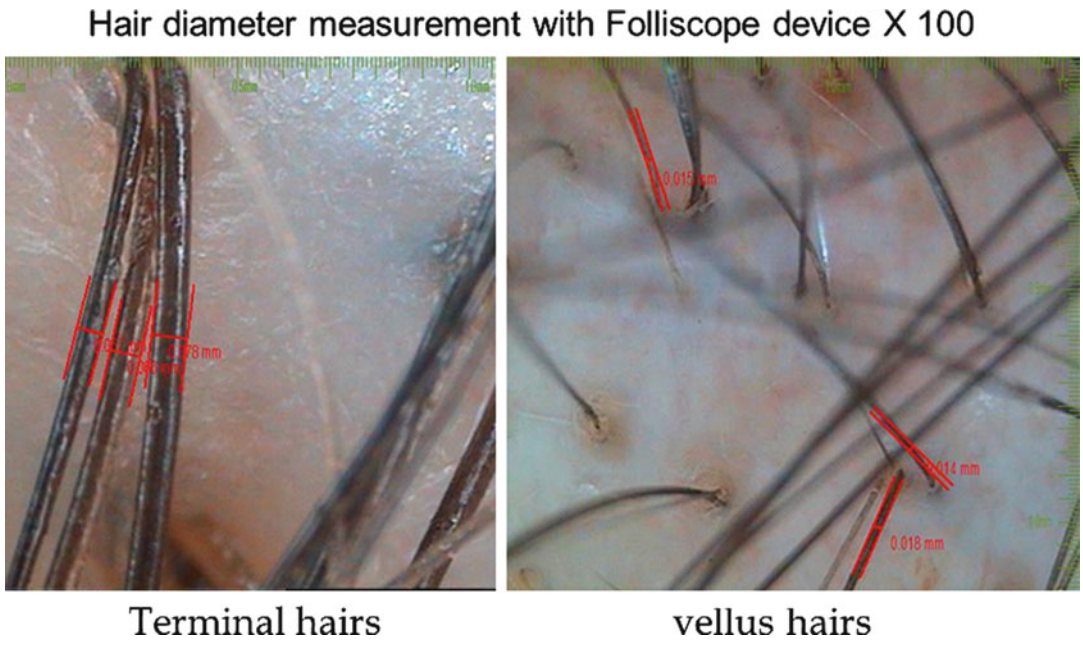

Photo 11 Hair diameter measurement with Folliscope

inside a circle target area of 0.642 cm^2, with a good intraclass correlation within the same TrichoScan operator and for different TrichoScan operator (Hoffman 2001).

TrichoScan is able to demonstrate in a small group of 12 men with AGA a significant increase in total number of hair after 3 and 6 months of treatment with finasteride 1 mg/day (+17 % at month 3, $p = 0.055$ and +20 % at month 6, $p = 0.021$) (Hoffman 2003). Furthermore in the same group, increase of hair thickness was +11 % at month 3 ($p = 0.034$) and +18 % at month 6 ($p = 0.006$) (Hoffman 2003). Also TrichoScan allows to demonstrate significant increase of hair density, cumulative hair thickness, and terminal hair count in a small group of 10 women and 21 men with AGA after 6 months of treatment with 5 % topical minoxidil (Hoffmann and Van Neste 2005).

For few authors TrichoScan seems no better than the clinical observation or no better than the modified wash test to diagnosis telogen effluvium (Guarrera et al. 2013). But it's difficult to conclude that without a gold standard assessment. The TrichoScan has been validated to measure severity and evolution of hair growth in androgenetic alopecia (Gassmueller et al. 2009). This new tool obtains quickly reproducible results with a smaller margin of operator error than the hair manual count (Gassmueller et al. 2009). TrichoScan is not a good tool for alopecia areata. Hair is a tricky material for automated computer-assisted analysis and in Indian population (Saraogi and Dhurat 2010), and in some other cases, TrichoScan can overestimate the number of telogen hair by erroneous fragmentation of hair stands and underestimate the vellus hair percentage specially vellus hair under 10 μm of diameter (Van Neste and Trüeb 2006), but those errors are reproducible and vellus hairs under 10 μm of diameter are with no cosmetic value. For those reason TrichoScan is a good tool for big clinical studies.

The last available version is TrichoScan Professional Version 3 (Photo 12). TrichoScan 3 is able to count total number of hair, vellus hair (<40 μm), terminal hair, anagen and telogen hair, and in a research version hair diameter and cumulative hair thickness. The detection limit of the software is between 5 and 10 μm. TrichoScan can quantify more important miniaturization of hair diameter in the crown area than in the

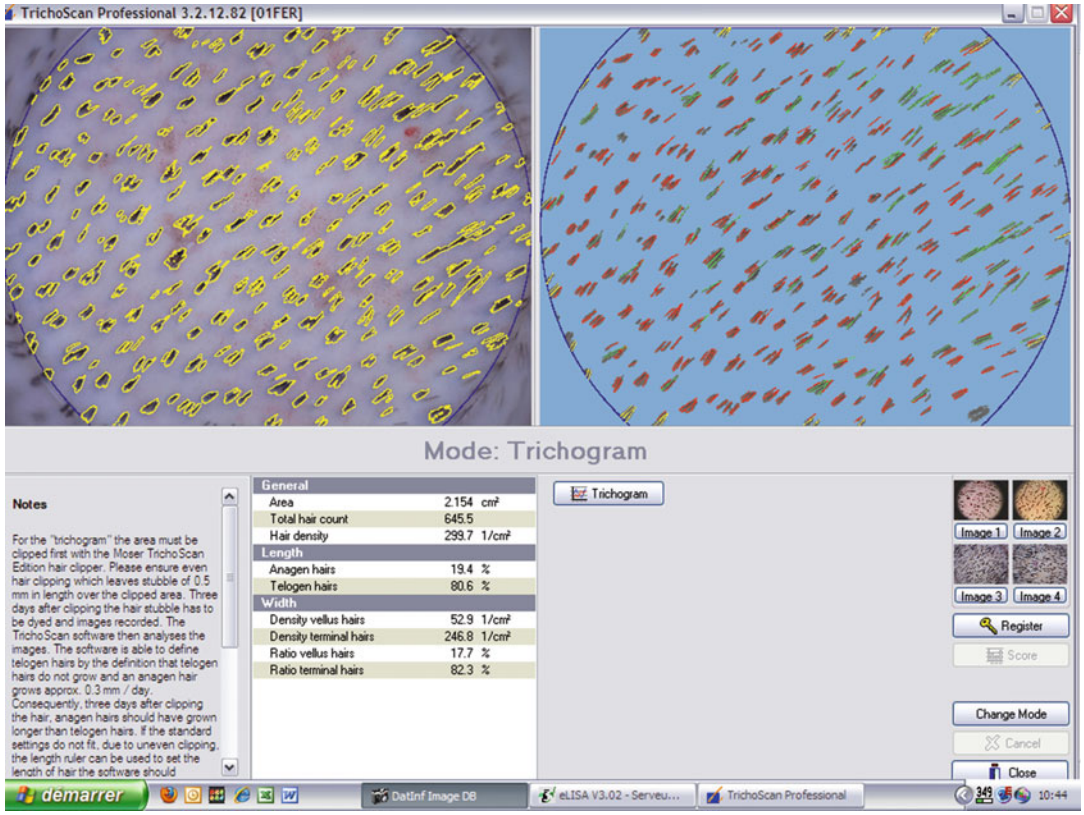

Photo 12 TrichoScan 3 Screenshot results

occipital one in women with AGA, and in this way it can help to make a good surgical decision for micrographs (Riedel-Baima and Riedel 2009).

TrichoScan is very popular in Germany and Italy and TrichoScan® is used for clinical practice and for clinical studies.

TrichoScan can access hair growth and length of the growing hairs after hair removal on the body (Kuck et al. 2012) or on the face (Hoffman 2008) or demonstrate an increased telogen/anagen ratio in patients with scalp psoriasis (Kasumagić-Halilović et al. 2010).

Technical procedures are the same than for classical CE-PTG, but accurate results need a better image quality than for a manual count. The software is able to count as hair dirty area, remnants of the hair dye, melanocytic nevi, or dark tattoo. It's very important to clean carefully the scalp to avoid remnant of coloration on the scalp and to avoid dot tattoo inside the target area, except if the tattoo is slightly red because the red color will not interfere with the automatic hair count. For a good quality image suitable for analysis and to avoid air bubbles between the scalp and the slide of the camera, it's important to use for immersion a hydroalcoholic lotion or water. It's better to avoid oil for this immersion. The software measures length of hairs on the second picture. There is a standard limit of 0.63 mm with the TrichoScan 3 and shorter hairs are counted as telogen and longer as anagen. The target area is a circle of 0.526 mm^2. The circle is the best figure to minimize the perimeter/surface ratio. This is important to reduce hair count errors along the limits of the target area. TrichoScan will analyze the same area before and after treatment. It is quicker than a visual count and this software allows different technicians without a great experience to get accurate and reproducible results. Fotofinder Trichoscale is a new software wich

Table 2 Hair density assessment with PTG in healthy population, depending on the methodology, age, sex, and ethnicity

Author	Methodology	Patients	Hair density/cm^2
Birch 2001 (UK)	Visual counting	Healthy women 35 years old	Mild scalp density 293
D'Amico 2001 (Italy)	Phototrichogram using videomicroscopy	20 healthy women	Vertex density 300 ± 20
Ueki 2003 (Japan)	Phototrichogram	31 healthy women	120
Nakazawa 2006 (Japan)	Phototrichogram	Healthy women 30 years old	230
		Healthy women 60 years old	199
Aktan 2007 (Turkish)	Visual counting	31 healthy women 35 years old	Mild scalp density 212.8 ± 32.9
	TrichoScan	31 healthy women 35 years old	Mild scalp density 141.7/cm^2 ± 21.6
Kim 2013 (Korea)	Folliscope PT 2.8	683 healthy women	123–165
		674 healthy men	126–171

alllows to determines follicular units, percentage of vellus hair, hair diameters and cumutative thicknes.

5 Normal Results

According to the ethnicity, the total number of scalp hair follicles varies from 150,000 to 90,000.

Results of phototrichogram are depending on the methodology, age, pathology, and origin of the studied population. For example, European scalp hair density is more important than Asian scalp hair density, but thicker hair is more important in Asian population with or without AGA (Lee et al. 2012). With PTG frontal and occipital density are lower in Asian women with untreated AGA (114 and 118 hair/cm^2) compared to European women (127 and 140 hairs/cm^2).

Hair density in healthy women ranges from 175 to 450 hairs/cm^2 (Aktan et al. 2007). Results of normal total hair density with PTG are reported in Table 2 (Birch et al. 2001; D'Amico et al. 2001; Ueki et al. 2003; Nakazawa et al. 2006, Aktan et al. 2007; Kim et al. 2013).

Due to individual differences, some overlap in hair density and in percentage of telogen hair exists between normal population and males or females with hair loss (Kim et al. 2013).

References

Aktan S, Akarsu S, Ilknur T, Demirtaşoğlu M, Ozkan S. Quantification of female pattern hair loss: a study in a Turkish population. Eur J Dermatol. 2007;17:321–4.

Birch MP, Messenger JF, Messenger AG. Hair density, hair diameter and the prevalence of female pattern hair loss. Br J Dermatol. 2001;144:297–304.

Blume U, Ferracin J, Verschoore M, Czernielewski JM, Schaefer H. Physiology of the vellus hair follicle: hair growth and sebum excretion. Br J Dermatol. 1991;124:21–8.

Bouhanna P. The advantage of phototrichogram in hair surgery. Communication at the international Advanced Hair Replacement symposium, Birmingham; 1982.

Bouhanna P. The phototrichogram; a technique for the objective evaluation of the diagnosis and course of diffuse alopecia. In: Montagna W et al., editors. Hair and aesthetic medicine. Roma: Salus internazionale; 1984. p. 277–80.

Bouhanna P. Le tractiophototrichogramme, méthode d'appréciation objective d'une chute de cheveux. Ann Dermatol Venereol. 1988;115:759–64.

Canfield D. Photographic documentation of hair growth in androgenetic alopecia. Dermatol Clin. 1996;14:713–21.

Chatenay F, Courtois M, Loussouarn G, Hourseau C. Phototrichogram: an entirely automated method of quantification by image analysis. In: Van Neste D, Randall VA, editors. Hair research for the next millennium. Amsterdam: Elsevier Science; 1996. p. 105–8.

Courtois M, Cesarini JP, Giland S, Grollier JF, Aron-Brunetière R. Etude de la formule pilaire: comparaison de deux méthodes: trichogramme et méthode photographique de Saitoh. Ann Dermatol Venereol. 1982;109:424.

Courtois M, Loussouarn G, Hourseau C, Grollier JF. Ageing and hair cycles. Br J Dermatol. 1995;132:86–93.

D'Amico D, Vaccaro M, Guarneri F, Borgia F, Cannavo S, Guarneri B. Phototrichogram using videomicroscopy: a useful technique in the evaluation of scalp hair. Eur J Dermatol. 2001;11:17–20.

Dhurat R, Saraogi P. Hair evaluation methods: merits and demerits. Int J Trichology. 2009;1:108–19.

Fiquet C, Courtois M. Une technique originale d'appréciation de la croissance et de la chute des cheveux. Cutis (Paris). 1979;3:975–83.

Gassmueller J, Rowold E, Frase T, Hughes-Formella B. Validation of TrichoScan technology as a fully-automated tool for evaluation of hair growth parameters. Eur J Dermatol. 2009;19:224–31.

Guarrera M, Ciulla MP. A quantitative evaluation of hair loss: the phototrichogram. J Appl Cosmetol. 1986;4:61–6.

Guarrera M, Fiorucci MC, Rebora A. Methods of hair loss evaluation: a comparison of TrichoScan(®) with the modified wash test. Exp Dermatol. 2013;22:482–4.

Hayashi S, Miyamoto I, Takeda K. Measurement of human hair growth by optical microscopy and image analysis. Br J Dermatol. 1991;125:123–9.

Hoffmann R. TrichoScan: combining epiluminescence microscopy with digital image analysis for the measurement of hair growth in vivo. Eur J Dermatol. 2001;11:362–8.

Hoffmann R. TrichoScan: a novel tool for the analysis of hair growth in vivo. J Investig Dermatol Symp Proc. 2003;8:109–15.

Hoffmann R. A 4-month, open-label study evaluating the efficacy of eflornithine 11.5% cream in the treatment of unwanted facial hair in women using TrichoScan. Eur J Dermatol. 2008;18:65–70.

Hoffmann R, Van Neste D. Recent findings with computerized methods for scalp hair growth measurements. J Investig Dermatol Symp Proc. 2005;10:285–8.

Kasumagić-Halilović E, Prohić A, Begović B. TrichoScan as a method to determine hair root pattern in patients with scalp psoriasis. Acta Dermatovenerol Croat. 2010;18:146–50.

Kim JE, Lee JH, Choi KH, Lee WS, Choi GS, Kwon OS, Kim MB, Huh CH, Ihm CW, Kye YC, Ro BI, Sim WY, Kim do W, HO K, Kang H. Phototrichogram analysis of normal scalp hair characteristics with aging. Eur J Dermatol. 2013;23:849–56.

Kuck M, Schanzer S, Ulrich M, Garcia Bartels N, Meinke MC, Fluhr J, Krah M, Blume-Peytavi U, Stockfleth E, Lademann J. Analysis of the efficiency of hair removal by different optical methods: comparison of Trichoscan, reflectance confocal microscopy, and optical coherence tomography. J Biomed Opt. 2012;17:101504.

Lee BS, Chan JY, Monselise A, McElwee K, Shapiro J. Assessment of hair density and caliber in Caucasian and Asian female subjects with female pattern hair loss by using the Folliscope. J Am Acad Dermatol. 2012;66:166–7.

Nakazawa Y, Komori Y, Kio K, Shimada Y, Tajima T, Murayama N, Tsuchida K, Lino M, Tajima M. Characterization of scalp and hair of the female with each period. J Dermatol Sci. 2006;42:187–8 (Abstract).

Pelfini C, Calligaro A. Evaluation of hair growth by means of morphometric computerized analysis. J Appl Cosmetol. 1986;4:67–76.

Riedel-Baima B, Riedel A. Use of the TrichoScan to assess female pattern hair loss. Dermatol Surg. 2009;35:651–5.

Rushton H, James KC, Mortimer CH. The unit area trichogram in the assessment of androgen-dependent alopecia. Br J Dermatol. 1983;109:429–37.

Rushton DH, de Brouwer B, de Coster W, van Neste DJ. Comparative evaluation of scalp hair by phototrichogram and unit area trichogram analysis within the same subjects. Acta Derm Venereol. 1993;73:150–3.

Saitoh M, Uzuka M, Sakamoto M. Human hair cycle. J Invest Dermatol. 1970;54:65–81.

Saraogi PP, Dhurat RS. Automated digital image analysis (TrichoScan®) for human hair growth analysis: ease versus errors. Int J Trichology. 2010;2:5–13.

Ueki R, Tsuboi R, Inaba Y, Ogawa H. Phototrichogram analysis of Japanese female subjects with chronic diffuse hair loss. J Investig Dermatol Symp Proc. 2003;8:116–20.

Van Neste DJ. Contrast enhanced phototrichogram (CE-PTG): an improved non-invasive technique for measurement of scalp hair dynamics in androgenetic alopecia – validation study with histology after transverse sectioning of scalp biopsies. Eur J Dermatol. 2001;11:326–31.

Van Neste D, Trüeb RM. Critical study of hair growth analysis with computer-assisted methods. J Eur Acad Dermatol Venereol. 2006;20:578–83.

Van Neste DJ, Dumroyier M, De Coster W. Phototrichogram analysis. Technical aspects and problems in relation with automated quantitative evaluation of hair growth by computer assisted image analysis. In: Van Neste DJ, Lacahpelle JM, Antoine JL, editors. Trends in human hair growth and alopecia research. Dordrecht: Kluwer; 1989. p. 155–65.

Van Neste DJ, Dumortier M, De Coster W. Scalp immersion proxigraphy (SIP): an improved imaging technique for phototrichogram analysis. J Eur Acad Dermatol Venereol. 1992;1:187–91.

Whiting DA, Waldstreicher J, Sanchez M, Kaufman KD. Measuring reversal of hair miniaturization in androgenetic alopecia by follicular counts in horizontal sections of serial scalp biopsies: results of finasteride 1 mg treatment of men and postmenopausal women. J Investig Dermatol Symp Proc. 1999;4:282–4.

Hair Evaluation Method: Pull Test and Wash Test

82

Marcella Guarrera and Alfredo Rebora

Contents

Keywords
Wash test • Pull test • Noninvasive methods

1 Introduction

Hair loss is a common complaint in both genders and often entails psychological distresses which may be severe. Hence, the problem needs to be approached thoroughly, and this requires using a quantitative, possibly noninvasive, assessment. Useful noninvasive methods are the pull test and the modified wash test (MWT).

2 The Pull Test

The pull test should be tried first in any patient complaining of hair loss. The method requires that the patient is examined when his/her hair has not been washed recently and, in fact, a 5-day abstention from the last shampooing is recommended. Unfortunately, the large majority of patients seeking advice in the office are so kind as to come with their hair shampooed the very same morning. In such a condition, the pull test is useless, unless the hair shedding is massive.

Two different procedures (Camacho and Montagna 1997) come under the same title: in the first one, a cluster of 40–50 hairs is grasped between two fingers, while two fingers of the other hand apply a steady traction (Figs. 1 and 2). This procedure serves essentially to test the fragility of the

M. Guarrera (✉) • A. Rebora
Department of Health Sciences-Section of Dermatology, University of Genoa, Genoa, Italy
e-mail: guarrera@unige.it

P. Humbert et al. (eds.), *Agache's Measuring the Skin*,
DOI 10.1007/978-3-319-32383-1_115

Fig. 1 Pull test. Two hands grasp a cluster of 40–50 hairs, while the other one applies a steady traction on the hair shafts

Fig. 2 Sabouraud's maneuver. Only one hand sinks into the hairs and applies a gentle traction

hair shaft. In the second procedure, once called *Sabouraud's maneuver*, the widen fingers of one hand are sunk into the hairs (if they are long enough) and apply a gentle traction. The hairs retained between the fingers are counted. In both procedures four different areas of the scalp should be tested: the right and left parietals and the frontal and occipital areas.

Normally, only telogen hairs are shed and, in the adults, their number does not exceed four to five for the whole scalp. Collecting more than eight to ten hairs suggests the diagnosis of telogen effluvium (TE). When the hands are full of hairs, the diagnosis of alopecia areata incognita (AAI) should be surmised. In androgenetic alopecia (AGA), the total hair number is in between four and ten. The presence of dystrophic hairs suggests active alopecia areata and AAI. In cicatricial alopecias and in pemphigus, some anagen hairs are extracted with their outer sheaths (Delmonte et al. 2000). In the loose anagen syndrome (LAS), many hairs are extracted and, if observed under a low magnification microscopy, lack the outer sheath and their cuticles are ruffled. To diagnose LAS at least 70 % of the hairs should show these features (Tosti and Piraccini 2002).

The pull test is a rough method and their reliability is low mainly because of the variable strength of traction, but, if performed correctly, is a good indicator of the severity of hair loss.

In physiology, the pull test performed on 60 healthy children (4–10 years old) established that the normal mean loss was 1.77 ± 1.57 (Rebora et al. 2016).

3 The Wash Test (Modified)

MWT is a simple noninvasive method, designed for the office, that permits the diagnosis and the assessment of the severity of hair loss (Rebora et al. 2005).

The method is based on the fact that in TE only terminal hairs are shed, while also miniaturized hairs or vellus hairs are lost in AGA. According to Rushton, vellus hairs are shorter than 3 cm and thinner than 40 μm (Rushton 1993). For sake of easiness, only the length of the shed hairs is measured.

After 5 days of abstention from shampooing, the patients wash and rinse their hair in a sink with the draining hole covered by a gauze and collect all hairs remaining in the gauze. The patients should not comb their hairs before or during the shampoo and should not use hair conditioner after the shampoo. The hairs shed when the patient,

after soaping and rinsing, brushes and dries the hair are not considered. The collected hairs are let dry and put in a paper envelop. The examiner counts the number of all collected hairs and the percentage of the vellus hairs. Studying the hair roots under a microscope may provide additional information, namely, the presence and the prevalence of exogen and/or dystrophic roots (Rebora et al. 2014; Quercetani et al. 2011). The latter, associated with a global number exceeding 350, is diagnostic of AAI.

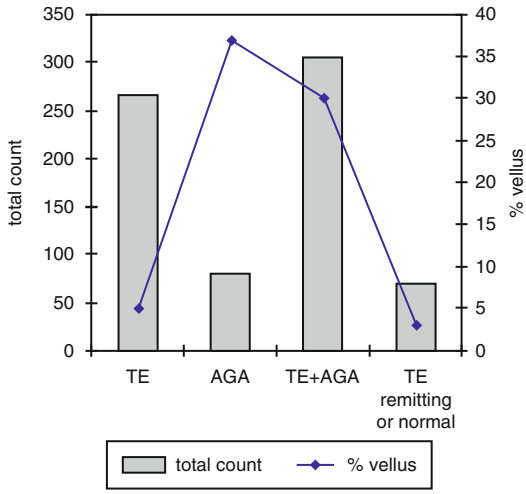

Fig. 3 Modified wash test. The four different results obtained with the modified wash test. AGA, TE, AGA +TE, and normality or remitting TE. The *columns* indicate the total number of shed hairs; the *line* indicates the percentages of vellus hairs collected with the shampooing

The results suggest four possible diagnoses (Fig. 3): more than 100 shed hairs with less than 10 % vellus indicates TE, less than 100 hairs with more than 10 % vellus suggests AGA, more than 100 hairs with more than 10 % vellus suggests the association of AGA+ TE, and less than 100 hairs with less than 10 % vellus reflects normality or a remitting TE. Actually, a statistical analysis suggested that the cutoff value is 91 instead of 100 (Guarrera et al. 2011).

In physiology, the wash test performed well in an attempt to establish the "normal" shedding (Rampini et al. 1999). In a group of prepubertal children of both genders, free from five alpha reductase and therefore of AGA, we were able to verify that "normally" they shed 10.68 ± 3.01 hairs, a number that steadily increases up to 11 years when puberty is approaching (Fig. 4). This finding ruled out the arbitrary figure of 100 hairs that would be allegedly shed daily in "normal" subjects.

MWT is a reliable and reproducible method. In a study of ours (Guarrera et al. 2011), the interclass correlation coefficient, which is a measure of the level of reproducibility among measures (reliability), proved to be almost perfect in a group of patients with AGA for both total hair count and vellus hairs percentage (0.96 and 0.85, respectively) and in normal and TE groups of patients for the vellus hair percentage (0.88 and 0.84, respectively). Good reliability was found in all other cases, but in the total hair count of normal subjects in which it was only moderate (0.43). In addition, sensitivity and specificity, as assessed using the receiver

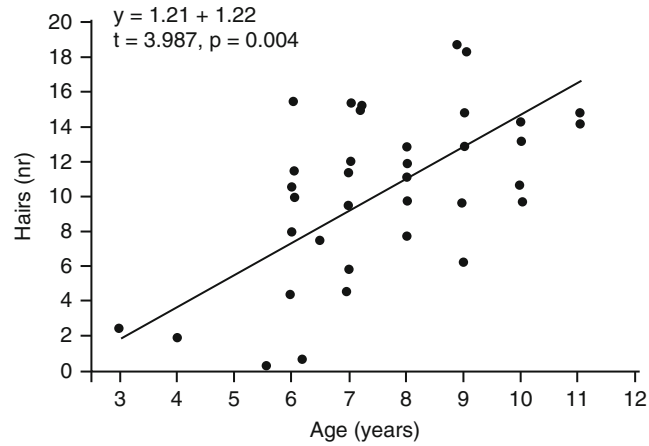

Fig. 4 The wash test in children. The "normal" shedding as found in a group of prepubertal children of both genders

operating characteristic (ROC) curves, ranged from 81 % to 100 % (p: 0.0045–0.001), except for the vellus hair percentage of TE patients in which they were low (64.3 % and 50 %, respectively) and for the total hair count of AGA patients in which sensitivity was low (50 %).

MWT has a number of advantages. First, it easily permits AGA and TE to be diagnosed precisely with a simple noninvasive and cheap procedure. Other methods, like phototrichogram or computer-aided dermoscopy, are either time-consuming or more expensive. In addition, they fail to detect dystrophic hairs whenever they are haphazardly scattered all over the scalp as in AAI. A comparison with TrichoScan® (Guarrera et al. 2013) revealed that MWT was better ($k = 0.32$ vs. 0.22) especially, as expected, at detecting TE. Second, it distinguishes the association AGA+TE which other methods cannot diagnose. Third, it permits to recognize people who claim to lose hairs but in fact do not. More important, it provides a quantitative assessment of the severity of both TE (the global number of the shed terminal hairs) and AGA (the percentage of vellus hairs) and to decide, in case of the association AGA+TE, which of the two disorders is the most important and should be treated first. Lastly, MWT consents patients in treatment to be followed-up and the efficacy of the treatment to be verified. If the patients with TE are instructed to count at least all shed hairs at home, they can perform the duty nicely over time providing invaluable information about the state of their disorder.

Drawbacks consist in the difficulty in convincing young patients to abstain from shampooing for 5 days, in testing people with curly hairs which entangle during shampooing yielding underestimated results and in testing young male patients with hairs shorter than 4 cm. A possible major source of bias is the risk that the patients comb their hair immediately before washing them or that they vary each time the modality of shampooing. It is sufficient, however, to recommend to collect their shampooed hairs in the morning before any other toilet care.

References

Camacho F, Montagna W. Trichologie. Madrid: Grupo Aula Médica; 1997. p. 101–2.

Delmonte S, Semino MT, Parodi A, Rebora A. Normal anagen effluvium: a sign of pemphigus vulgaris. Br J Dermatol. 2000;142:1244–5.

Guarrera M, Cardo PP, Rebora A. Assessing the reliability of the modified wash test. G Ital Dermatol Venereol. 2011;146:289–93.

Guarrera M, Fiorucci MC, Rebora A. Methods of hair loss evaluation: a comparison of TrichoScan(®) with the modified wash test. Exp Dermatol. 2013;22:482–4.

Quercetani R, Rebora AE, Fedi MC, Carelli G, Mei S, Chelli A, Poli E. Patients with profuse hair shedding may reveal anagen hair dystrophy: a diagnostic clue of alopecia areata incognita. J Eur Acad Dermatol Venereol. 2011;25:808–10.

Rampini P, Guarrera M, Rampini E, Rebora A. Assessing hair shedding in children. Dermatology. 1999;199:256–7.

Rebora A. Telogen effluvium revisited. G. Ital Dermatol Venereol, Venereol 2014;149:47–54.

Rebora A, Guarrera M, Baldari M, et al. Distinguishing androgenetic alopecia from chronic telogen effluvium when associated in the same patient. Arch Dermatol. 2005;143:1243–5.

Rebora A, Guarrera M, Drago F et al. Int J Dermatol 2016;55:e7–e10.

Rushton DH. Management of hair loss in women. Dermatol Clin. 1993;11:47–53.

Tosti A, Piraccini BM. Loose anagen hair syndrome and loose anagen hair. Arch Dermatol. 2002;138:521–2.

Hair Polarized Microscopy

83

Adriana Rakowska

Contents

Keywords

Hair cortex • Hair shaft • Hair shaft dystrophy • Light microscopy • Pili torti • Polarized light microscopy • Polarizer • Monilethrix • Pseudomonilethrix • Trichorrhexis nodosa • Trichothiodystrophy

1 Background

Polarized light microscopy is a contrast-enhancing technique that is designed to observe and photograph specimens that are visible primarily due to their optically anisotropic character (Weaver 2003). The technique is based on the rule of reflection and transmission which states that the angle of reflection is equal to the angle of incidence for any particular light ray irradiating a smooth, reflective surface. When the surface is irregular and a broad beam of light is used, then we get diffuse reflection. When the surface is polished and we use a narrow beam of light, then we get specular reflection, and this reflected light can be polarized (McCrone et al. 1978; Carlton 2011).

In a polarizing microscope, there are two polarizing filters known as polarizer and analyzer. Only light oscillating in one direction is allowed to pass through them. A polarizer is placed in the light path before the specimen; an analyzer is positioned in the optical pathway between the objective rear aperture and the observation tubes or camera port.

A. Rakowska (✉)
Department of Dermatology, Medical University of Warsaw, Warsaw, Poland
e-mail: adriana.rakowska@gmail.com

P. Humbert et al. (eds.), *Agache's Measuring the Skin*,
DOI 10.1007/978-3-319-32383-1_116

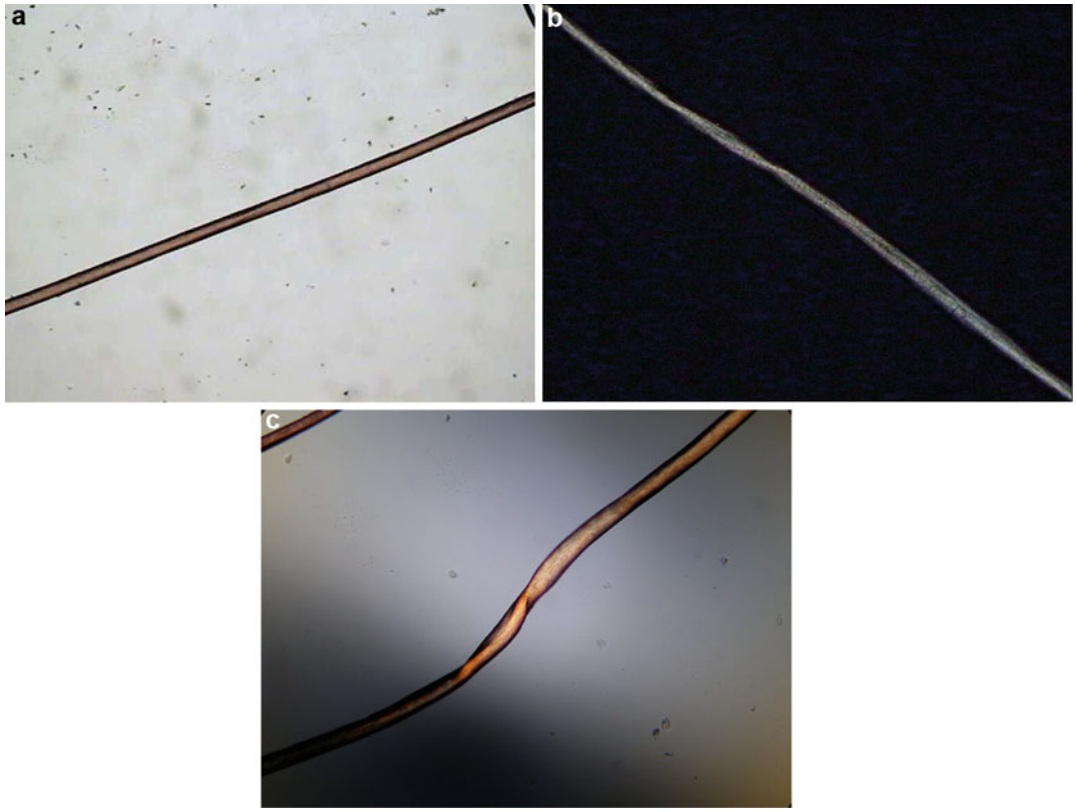

Fig. 1 Polarized light microscopy in differential diagnosis of hair shaft abnormalities. (**a**) This picture shows hair shaft with irregular contour, but it is difficult to differentiate if this is caused by hair shaft twist along the long axis or if this is nodosity (light microscopy, ×10); (**b**) polarized light microscopy shows that the hair shaft seen in picture **a** has few twists along the long axis, and the diagnosis in this case is pili torti (×10); (**c**) polarized light microscopy allows to observe details of the hair inner structures (×20)

When the vibration azimuths of both filters are positioned at right angles to each other, the polarizer and analyzer are said to be crossed, with no light passing through the system and a dark view field present in the eyepieces. When the filters are positioned perpendicularly to one another, the image contrast arose, and the specimen details can be observed on a dark background.

2 Polarized Light Microscopy in Hair Analysis

As compared to light microcopy, the examination of hair shafts under polarized light provides more varied and very bright hues to the hair inner structures. It is a result of cortex fibrillar nature and interference phenomenon.

The main indication for polarized light microscopy is congenital and acquired hair shaft abnormalities because differentiation between nodosities, narrowings, and twist (Fig. 1a, b, c) of hair shafts or even changes in hair color is easy in this technique (Valente et al. 2006; Itin and Fistarol 2005).

The role of polarized light microscopy is crucial in the diagnosis of trichothiodystrophy (Rakowska et al. 2008). Trichothiodystrophy, or sulfur-deficient brittle hair, identifies a group of rare and complex neuroectodermal disorders with remarkable clinical heterogeneity (Morice-Picard et al. 2009). Clinical features of patients

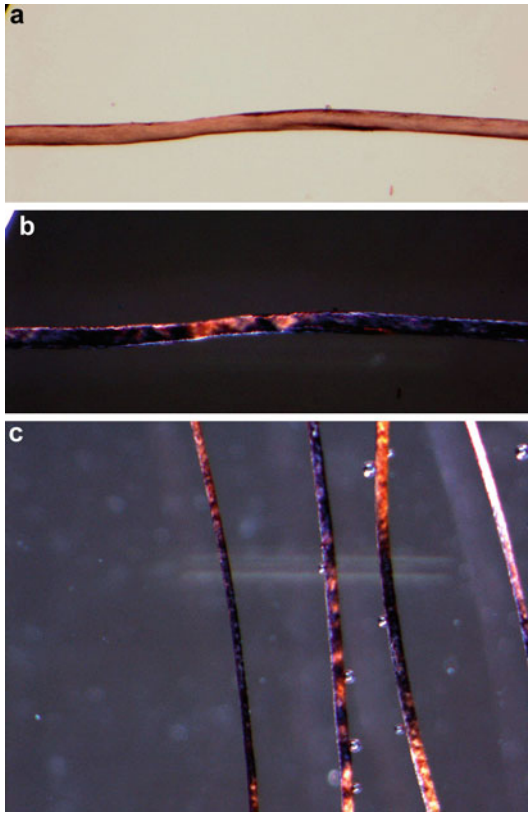

Fig. 2 Polarized light in trichothiodystrophy. (**a**) Light microscopy shows hair shaft with an irregular, undulating contour (×40); (**b**) the same hair shaft seen in polarized light shows striking alternating bright and dark bands referred to as "tiger tail" banding. This is crucial for diagnosis of trichothiodystrophy (×40); (**c**) the diagnosis of trichothiodystrophy can be set if almost all hairs seen under polarized light revealed tiger tail banding (×10)

with TTD vary widely in nature and severity, and the single common feature in all patients is the fragile hair (Liang et al. 2005). With polarizing microscopy, using crossed polarizers, hair shafts show a distinctive hair feature: striking alternating bright and dark bands, often referred to as "tiger tail" banding (Fig. 2b, c) (Itin and Pittelkow 1991). Light microscopy shows hair shafts with an irregular, undulating contour (Sperling and DiGiovanna 2003). The bright and dark bands seen with polarized light correspond to the undulating orientation of the cortical fibers in TTD patients (Fig. 2a). The diagnosis of TTD cannot be made on the basis of seeing a few hairs that appear to have alternating bright and dark bands; rather all hair should show the tiger tail pattern and all should have an undulating irregular contour (Fig. 2a, b).

The structural abnormality that causes the interrupted transverse bright lines along the hair shafts is not completely understood. An X- ray microanalysis revealed alternating content of sulfur along the long axis of the hair (Itin et al. 2001). The X-ray analysis results also showed that calcium was absent in tracts corresponding to dark bands, whereas it was normally present in light bands (Richetta et al. 2001). The amino acid analysis of the hair shows the notably low cysteine content (less than half of normal content because of major reduction in synthesis of high-sulfur matrix proteins) that parallels the low total sulfur content (Itin et al. 2001).

References

Carlton RA. Polarized light microscopy. In: Pharmaceutical microscopy. Springer New York: Springer; 2011. p. 7–64.

Itin PH, Fistarol SK. Hair shaft abnormalities – clues to diagnosis and treatment. Dermatology. 2005;211(1):63–71.

Itin PH, Pittelkow MR. Trichothiodystrophy with chronic neutropenia and mild mental retardation. J Am Acad Dermatol. 1991;24(2 Pt 2):356–8.

Itin PH, Sarasin A, Pittelkow MR. Trichothiodystrophy: update on the sulfur-deficient brittle hair syndromes. J Am Acad Dermatol. 2001;44(6):891–920; quiz 1–4.

Liang C, Kraemer KH, Morris A, Schiffmann R, Price VH, Menefee E, et al. Characterization of tiger-tail banding and hair shaft abnormalities in trichothiodystrophy. J Am Acad Dermatol. 2005;52(2):224–32.

McCrone WC, McCrone LB, Delly JG. Polarized light microscopy. Ann Arbor: Ann Arbor Science Publishers; 1978.

Morice-Picard F, Cario-Andre M, Rezvani H, Lacombe D, Sarasin A, Taieb A. New clinico-genetic classification of trichothiodystrophy. Am J Med Genet A. 2009;149A(9):2020–30.

Rakowska A, Slowinska M, Kowalska-Oledzka E, Rudnicka L. Trichoscopy in genetic hair shaft abnormalities. J Dermatol Case Rep. 2008;2(3):14–20.

Richetta A, Giustini S, Rossi A, Calvieri S. What's new in trichothiodystrophy. J Eur Acad Dermatol Venereol. 2001;15(1):1–4.

Sperling LC, DiGiovanna JJ. "Curly" wood and tiger tails: an explanation for light and dark banding with polarization in trichothiodystrophy. Arch Dermatol. 2003;139(9):1189–92.

Valente NY, Machado MC, Boggio P, Alves AC, Bergonse FN, Casella E, et al. Polarized light microscopy of hair shafts aids in the differential diagnosis of Chediak-Higashi and Griscelli-Prunieras syndromes. Clinics (Sao Paulo). 2006; 61(4):327–32.

Weaver R. Rediscovering polarized light. Am Lab. 2003;35:55–61.

Hair-Hair Contact Dynamics and Interactions Studied with Atomic Force Microscopy

84

Gustavo S. Luengo, Hiroyasu Mizuno, and Mark W. Rutland

Contents

Keywords
Hair • Surface chemistry

1 Introduction

The heterogeneous structure of the surface of hair, with its innate variability of morphology due to its biological origin, is at the base of the interaction with the external agents, from natural (UV, brushing) to cosmetic treatments (dyeing, bleaching, etc.). Consequently, the knowledge of the surface of hair (or skin and nails) is essential to develop innovative and functional cosmetic products (Zviak 1986).

The structure of the cosmetic substrate impairs its intrinsic mechanical and physicochemical properties that are manifested at the macroscale in many different ways. Hair fibers, for instance, although considered to have an exceptional resistance are affected by continuous exposure to sunlight, weathering its properties. In addition most of the cosmetic treatments try to improve or repair the intrinsic properties of hair which eventually reflects in enhanced mechanical and tribological behavior.

Hair is roughly a cylindrical fiber of ~50–100 μm diameter. The overall number of hairs covering a normal human head is comprised between 120,000–150,000, which leads to a significant surface area (typically ~6 m^2 for ~20 cm-long hairs).

G.S. Luengo (✉)
L'Oréal Research and Innovation, Aulnay-Sous- Bois, France
e-mail: gluengo@rd.loreal.com

H. Mizuno
L'OREAL, KSP Research and Innovation center, Kawasaki, Japan

M.W. Rutland
KTH, Royal Institute of Technology, Stockholm, Sweden
e-mail: mark@kth.se

P. Humbert et al. (eds.), *Agache's Measuring the Skin*,
DOI 10.1007/978-3-319-32383-1_118

In cosmetics, hairstyle, hair perception, and hair manageability depend on numerous parameters: geometry of the fibers (length, diameter, ellipticity, degree of curl), topography of the implantation, and in particular fiber-to-fiber interactions. The combinations of all these parameters result in extremely different cosmetic properties.

The cuticle forms the outer surface of hair. It has an overlapping scalelike (approximately 50 μm across by 0.5 μm thick) structure protecting the cortex and oriented from the root to the tip of the fiber to produce a series of scale edges on the outer surface of each hair. The final structure of the outermost layer of the cuticle (epicuticle) is of special interest: the surface properties of hair depend on the physicochemical properties of this layer.

The most recent findings have shown that the epicuticle membrane of hair fibers contains highly cross-linked protein (∼75 %) and fatty acids (∼25 %). Among these adsorbed fatty acids, the 18-methyleicosanoic acid (18-MEA) is the most abundant 50 % w/w (Yorimoto and Naito 1994), appears to be covalently grafted on the outer surface (constitutes the outer β-layer) via covalent thioester linkages to the protein (Wertz and Downings 1988; Evans and Lanczki 1997), and is considered to play an important role in the physicochemical and tribological properties of hair.

Based on these observations, a model is used to explain the fine molecular structure of the hair surface (Negri et al. 1996) depicting a highly ordered monolayer of 18-MEA grafted to the proteins of the epicuticle that would explain the excellent tribological properties of natural hair in ambient conditions (Breakspear et al. 2005; Huson et al. 2008).

It is not clear how these various chemical regions contribute to the overall interactions (noncontact forces like van der Waals and electrostatics and in contact as friction and adhesion) between the fibers, which determine the dynamic as well as the static behavior of the hair in both water and dry states. Inter-fiber interaction is the basis of an individual's everyday perception of the state of their hair, and it is therefore not unexpected that its comprehension is of interest to the hair care and cosmetic industry (Bouillon and Wilkinson 2005; Robbins 2001). Still, the means by which a complex multifiber system may adopt different three-dimensional shapes, or how a system of hundreds of thousands of fibers interact among each other while in motion, are questions for the physics community and go beyond a purely cosmetic interest and extend to other fields, ranging from textiles (Mizuno et al. 2006; Huang et al. 2009) to character animation in the cinema and entertainment industries (Ward et al. 2007).

The surface of hair consists of scales laid out like roof tiles. This structure results in anisotropy during interactions; hair fibers exhibit macroscopically what is known as "differential friction effect," i.e., friction is different when sliding "root to tip" versus "tip to root." The friction coefficient is higher when sliding takes place from the hair end to the root ("against the scales"). Generally, a relatively characteristic stick-slip phenomenon is also observed (LaTorre and Bhushan 2006).

Technologies like atomic force microscopy (AFM) can be of great importance for the development of cosmetic products, as well as for understanding their mode of action. These methods can provide essential information about the structure of the surface, its properties, and their evolution after an applied treatment due in particular at the possibility to interact with them locally, right at the structure of interest.

For example, by conventional AFM the properties of the outermost layers of hair, and in particular the effect of a (18-MEA), have been often studied. The presence of this layer can be easily detected by observing an increase of adhesion and friction of a SiN tip when this layer was not present (e.g., this may happen in certain pathologies or on bleached hair).

2 Crossed Fiber Atomic Force Microscopy

To have access to the interaction between fibers, we use the AFM in crossed fiber mode to measure both the forces in contact (friction and adhesion) and the noncontact forces in both air medium and

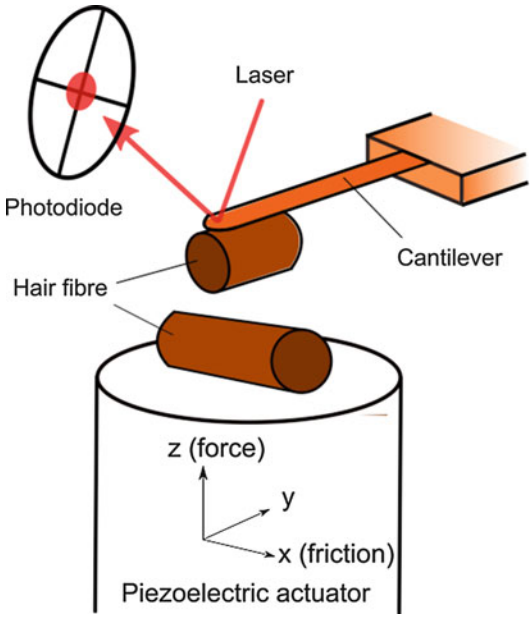

Fig. 1 A representation of the crossed human hair fiber system used in the AFM. The nominal lengths of the *upper* and *lower* hair segments are typically 60 and 500 μm, respectively. The hair diameter ranged from 53 to 94 μm

aqueous medium. These latter forces consist of the van der Waals interaction and charge interactions and in addition to providing fundamental information about the nature of the hair surface are also interactions that should be taken into account to understand and predict the behavior of any multifiber system especially in a humid or aqueous environment (Fig. 1).

The AFM cantilevers used were silicon and tipless (NSC12, MikroMasch, Estonia) with a specified normal spring constant of 0.65 N/m. Etched tungsten wires attached to a micromanipulator (Eppendorf) were used to position the glue and the fiber pieces, respectively, on an AFM cantilever under a stereomicroscope. Fig. 2a shows a scanning electron micrograph of a hair fiber which has been trimmed using a focused ion beam, FIB (Volkert and Minor 2007), to alleviate this issue. If the hair fiber on the AFM cantilever is long, then it will also bend and deform under normal and lateral forces, and there is no way of reliably obtaining the effective spring constant. Secondly the AFM cantilever actually sits at about 12° to the surface. Therefore, if the hair protrudes too far beyond the cantilever, it may potentially strike the substrate before the hair-hair contact is made and preclude force measurement. The outer (left hand) cut is that performed with the FIB, and it is apparent that this edge is finer than the inner cut which was performed with ordinary clippers.

The experimental technique allows the separation between the two fibers to be controlled with nm resolution and both the normal force and friction between hair fibers to be determined with a resolution of nN. The crossed cylindrical geometry is equivalent to that of a sphere interacting with a flat surface.

The force and friction experiments were performed using an atomic force microscope (Nanoscope IIIa, PicoForce, Veeco) according to protocols described in an IUPAC report (Ralston et al. 2005). Briefly, each AFM experiment started by acquiring two normal force curves at a constant scan rate of 400 nm/s. Afterwards, friction measurements were run at sliding velocities varying between 4 and 20 μm/s with scan size of 10 μm. These rates, relatively slow, represent well the random small dynamic deviations from a static equilibrium shape that occur in a hair assembly and are experimentally convenient. An initially low applied load was gradually increased to the maximum value (typically 100–120 nN) and then reduced again until the surfaces spontaneously separated. These latter experimental parameters *are* relevant for the interactions experienced by hair in daily life. The relatively large scan size was chosen to ensure that the probe would cross a cuticle edge at least once while sliding (the distance between cuticle edges is around 5 μm as can be seen in Fig. 2).

For the measurements performed in liquid, the hair fibers were exposed to each surfactant solution for approximately 15 min before force and friction measurements. The surfactant was tetradecyl trimethylammonium bromide (TTAB) (≥99 %, Sigma-Aldrich, Germany). A small amount of background electrolyte (1 mM NaCl, 99.99 %, Merck, Germany) was used for the aqueous systems, which is a standard practice in surface force measurement since it limits the thickness of any electrical double layer to a

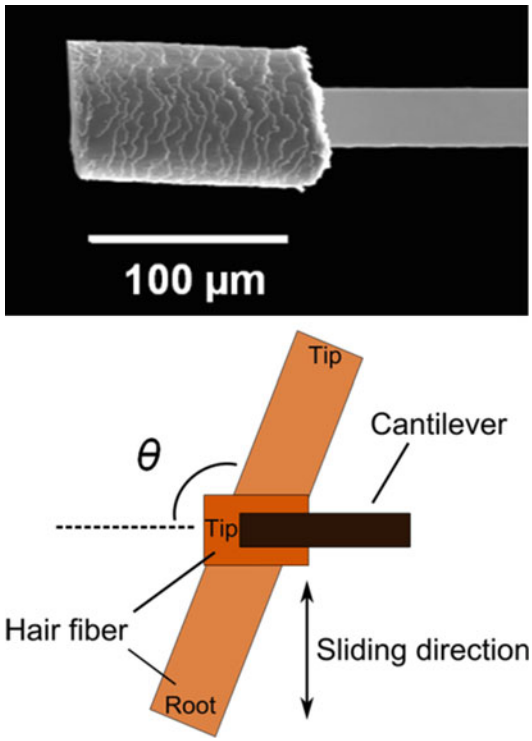

Fig. 2 (**a**) SEM image of the hair probe attached to a cantilever. The fiber has been truncated with an FIB to reduce overhang and minimize the effect of the fiber on the mechanical response of the FM cantilever. The FIB cut is considerably smoother than the conventional cut. In this example the "root" direction of the fiber is to the right. (**b**) Diagram of the crossed hair fiber system viewed from *above*. θ is the angle between tips of the two hair fiber cuts and defines the sliding angle. *Inset*: SEM image of hair probe attached to cantilever. The outer (*left-hand*) cut is that performed with the FIB and it is finer than the inner cut (*right hand*) performed with ordinary scissors

convenient experimental range and renders the fitting of the force curves much simpler (Ducker et al. 1991; Israelachvili and Adams 1978). To simplify, we refer to the solutions *not* containing surfactant as "water."

For studying the angle dependence of friction, the lower fiber was rotated relative to the hair probe manually to achieve different relative sliding angles. Irrespective of the angle of the lower fiber to the cantilever, the movement of the lower surface was normal to the long axis of the cantilever/upper fiber (see Fig. 2b). Measurements were performed at low humidity (25–30 %) and high humidity (70–75 %) levels, controlled by potassium chloride-saturated aqueous solution (Rockland 1960). The normal and torsional signal of the cantilever changed in response to the humid environment due to expansion of the hair arising from moisture gain (Robbins 2001). Hence experiments were not performed until after the signal had stabilized (typically 3 h).

If the shape of a probe is not perfectly cylindrical or if the probe is not precisely mounted at the center of the cantilever, the normal load applied to the probe in fact *twists* the cantilever *even in the absence of sliding*. For hair probes (which have a large diameter compared to the cantilever width), this induced torsion can be large. Thus, to be able to isolate directional effects in sliding friction and to get independent friction coefficients for the two sliding directions, we developed a method to accurately account for the asymmetry-induced twist (see reference Mizuno et al. 2010).

3 Interaction Forces Between Hair Fibers

Figure 3 shows the forces on approach and the effect of surfactant addition to the solution for the case of native hair. It is possible to observe a repulsive force at longer range from overlap of the electrical double layers (Verwey and Overbeek 1999) associated with a negative electrical charge at the surface (arising primarily from dissociation of polar proteinaceous moieties (Robbins 2001)). At shorter range, below about 15 nm, an attractive force component is observed before a final elastic/steric compression of the surfaces into a rigid compliance. This attractive component appears to be slightly too long ranged to be solely due to dispersion forces (van der Waals or Lifshitz interaction) and may also reflect the inherent hydrophobicity of the native hair caused by the palisade layer of fatty acids (see the inset in Fig. 3). A continuous, tightly packed lipid layer with the alkyl chains presented to the aqueous phase is expected to display hydrophobic behavior, and forces between such surfaces are known to be attractive

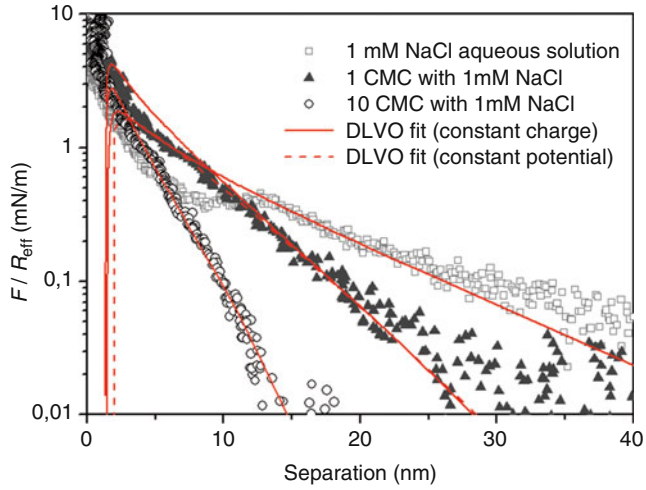

Fig. 3 Normal force curves for native hair measured in 1 mM NaCl in the presence of TTAB solutions. (□) no surfactant, (▲) 1 CMC, and (○) 10 CMC. The CMC of TTAB at 1 mM NaCl is 3.2 mM. κ^{-1} is 9.6 nm for the water, 4.7 nm for the 1 CMC solution, and 2.6 nm for the 10 CMC solution. The fitted surface potentials are −42 mV for water and +33 mV for 10 CMC. The surface potential for 1 cmc is constrained to a value of +50 mV, and the ensuing effective radius is 1.0 μm (see text). The Debye length has been constrained to the calculated value from the solution conditions, except for the 10 cmc case where the calculation is dependent on knowledge of the degree of dissociation of the micelles

(Carambassis et al. 1998; Tyrrell and Attard 2001; Stevens et al. 2005), though the range of this force is highly variable depending on the specific surface involved, and various mechanisms have been proposed (Christenson and Claesson 2001; Meyer et al. 2006; Eriksson and Henriksson 2007). There is however broad consensus (Eriksson et al. 1989) that at short range (of the order of that observed here), this force is related to the unfavorable water structure associated with the hydrocarbon-water interface (Tyrode et al. 2005; Hore et al. 2008).

From this force data, fitting of DLVO allows determination of both a surface potential and effective surface charge. For that we need to know the local effective radius of interaction (certainly considerably smaller than the mean of the fiber radii ∼40 μm). We used an internal reference based on the layer of surfactant that remains between the surfaces in contact (Atkin et al. 2003; Rutland and Parker 1994; Stiernstedt et al. 2005; Koopal et al. 2005). In effect, the surface potential of TTAB is well known between surfaces of well-characterized radius. Consequently the radius can be *estimated* by scaling the *measured force* to fit the *expected double-layer interaction*. The potential of a TTAB surface has previously been obtained (Stiernstedt et al. 2005) and is expected to be of the order of +50 mV. In each experiment employing a different pair of hairs, the double-layer force in 1 cmc solution was scaled to fit this value and resulted in effective radii of curvature between 1.0 and 1.5 μm. The surface potentials obtained from fitting the curves with DLVO theory (Chan et al. 1980) are thus −42 mV (native hair in solution), +50 mV at 1 cmc (constrained), and +33 mV at 10 cmc. The native hair surface is well known to be negatively charged, and the zeta potential of hair has been reported to be around −12 mV at pH 5.5 (Jachowicz and Berthiaume 1989). As expected zeta potential is lower because it is measured further from the charged surface (Giesbers et al. 2002) and averaged over the hair surface, rather than a local measurement at the cuticle edge. At 10 cmc the lower potential reflects the higher electrolyte concentration associated with the counterions and may well also reflect heterogeneity associated with a loss of hydrophobicity due to lipid removal.

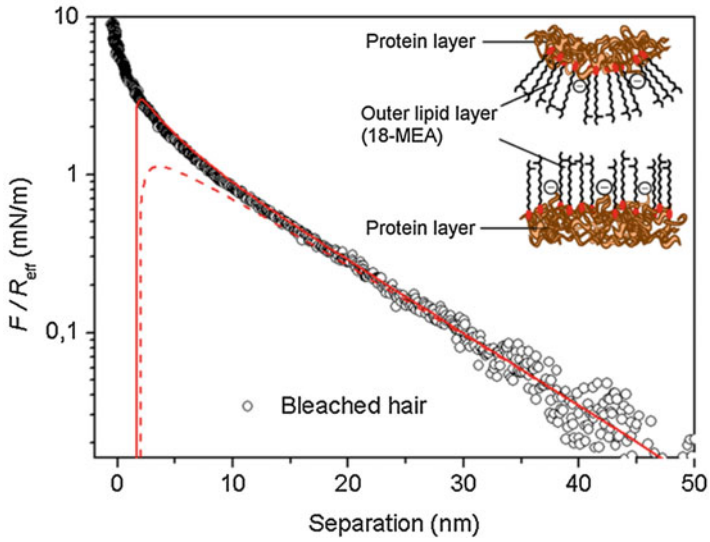

Fig. 4 Normal force curves of bleached hair measured in 1 mM NaCl aqueous solution with corresponding DLVO fits (*solid* and *dashed line*). The curve is the average of ten individual measurements and normalized by the effective radius, R_{eff}. The Debye length, κ^{-1}, was 9.6 nm and was not a fitting parameter. The *solid line* is the constant charge limit and the *dashed line* is the constant potential limit. A somewhat arbitrary Hamaker constant of 5×10^{-21} J was employed based on the Hamaker constant in air ($\sim 4.4 \times 10^{-20}$ J), calculated from the Lifshitz-van der Waals surface energy component of H_2O_2 treated hair fiber[51]. (No attractive component is visible in the interaction, and no adhesion was observed.) A surface potential of −55 mV was estimated from the DLVO fits. The *inset* is a schematic of the native hair surfaces facing each other in crossed fiber configuration. The outer surface consists predominantly of lipids, the majority of which are 18-methyleicosanoic acid (18-MEA) covalently bonded to the underlying protein

Figure 4 shows the forces in aqueous solution between two bleached hair fibers. The effect of this treatment is a reduction in the hydrophobicity of the protective outer layer which is provided by a palisade layer of lipid molecules, schematically shown in the inset (Huson et al. 2008; Breakspear et al. 2005; Jones and Rivett 1997; Swift 1999).

The double-layer potential obtained from fitting DLVO theory to the data returns a surface potential of −55 mV and surface charge 0.49 μC/cm^2 which is larger than for the case of native hair shown in Fig. 3. The larger value in the case of the bleached hair is consistent with the exposure of a larger amount of charge-bearing protein, ordinarily protected by the lipid layer. In addition the attractive force of 3.1 ± 1.1 mN/m observed in the native hair case and ascribed to the more hydrophobic nature of the surface is not observed in this case.

Force measurement is rendered more difficult in air because of the formation of static charges, and the curves reflect a long-ranged attraction characteristic of a Coulombic interaction which is illustrated in Fig. 5. This implies that after the initial contact, charge transfer occurs from one hair fiber to the other. In this case the force is negative, indicating a uniformly *attractive* force. As the solid line demonstrates, the form of the force is consistent with a Coulombic interaction. The force is so long ranged (in the Figure measured up to 800 nm long) that the cuticle height starts to influence the appearance of the force. The inset to the figure nonetheless shows that at very short separations, a steeply attractive van der Waals force takes over from the electrostatic force. Using a similar radius of ∼1–1.5 μm leads to a Hamaker constant for the system of 2×10^{-20} J. This value is slightly lower than that predicted from contact angles (Molina et al. 2001), but is of the right order of magnitude.

When two hair fibers interact in vivo, they do so in a much more humid environment which would discharge the static electricity. We note that in extremely dry conditions, where the

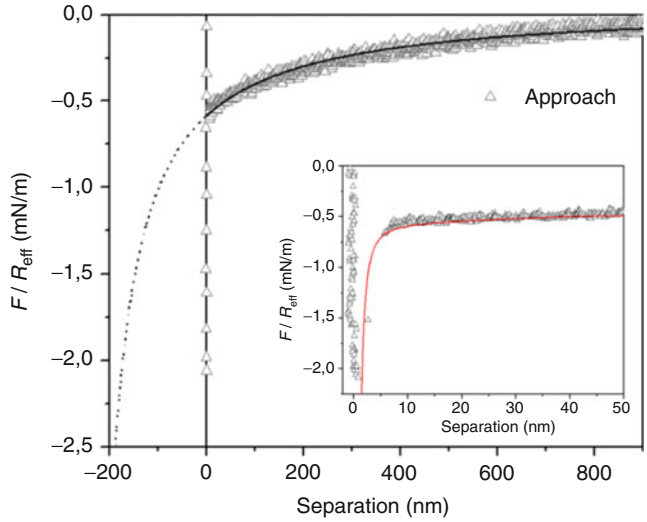

Fig. 5 The long-ranged attractive interaction in air. The effective radius is 1.0 μm obtained as described in text. The *solid line* fits the functional form of the Coulomb attraction to the data, and the apparent zero separation of the Coulomb interaction is offset by 250 nm to the apparent zero of separation for the force measurement. (This corresponds to about 50 % of the cuticle height.) *Inset*: the short-ranged part of the interaction where the van der Waals interaction dominates the interaction below approximately 7 nm and the surfaces jump into contact due to a spring instability. The *solid line* in the *inset* corresponds to the theoretical van der Waals interaction assuming a Hamaker constant of 2×10^{-20} J

humidity in the hair itself is also reduced, static electricity is commonly observed, for example, during brushing. (In this case of course, the interaction is repulsive between the hairs as the charge transfer occurs between the hair and the brush and the hairs have the same charge sign.) Opposite charging in a symmetric system is somewhat unexpected, but in fact this phenomenon is rather well documented for hair, where the heterogeneity of the surfaces renders this possible if the cuticle edges (which tend to have a higher density of polar, ionizable material) are implicated in the contact (Robbins 2001).

4 Friction of Natural Fibers: Effect of Sliding Angle

The friction force measured by AFM is obtained from the cantilever torsion and the ensuing lateral photodiode response as the hair probe slides over the lower haircut in a reciprocating way.

The friction coefficients obtained for both native and bleached hair (70 % RH) are shown in Figs. 6 and 7. In the case of native hair (Fig. 6), there appears to be only very slight, if any, dependence of $\mu_{against}$ and μ_{along} on the sliding angle. Figure 6b shows how $\Delta\mu$ ($\mu_{against} - \mu_{along}$) varies with sliding angle; for 74 % of the measurements, $\Delta\mu$ is within the range of ± 0.05. This indicates that while in most cases $\Delta\mu$ is positive (i.e., sliding against the cuticle direction involves higher friction), the directional effect is negligible for native hair at almost all angles. The apparent absence of directional effects, the large radius in comparison to cuticle height, means that mechanical interlock of the cuticles (the origin of directional effects) is only feasible for certain angles and conditions.

For bleached hair however, a very different behavior was observed. $\mu_{against}$ was systematically larger than μ_{along} (Fig. 7a) indicating that the directional effect and mechanical interlocking are significant with weathered hair. Furthermore, there appears to be a strong angular dependence of this effect (Fig. 7b). We thus speculate that two mechanisms are involved in this phenomenon: (a) at all sliding angles, $\Delta\mu$ is enhanced due to lifted, ragged cuticles (LaTorre and Bhushan

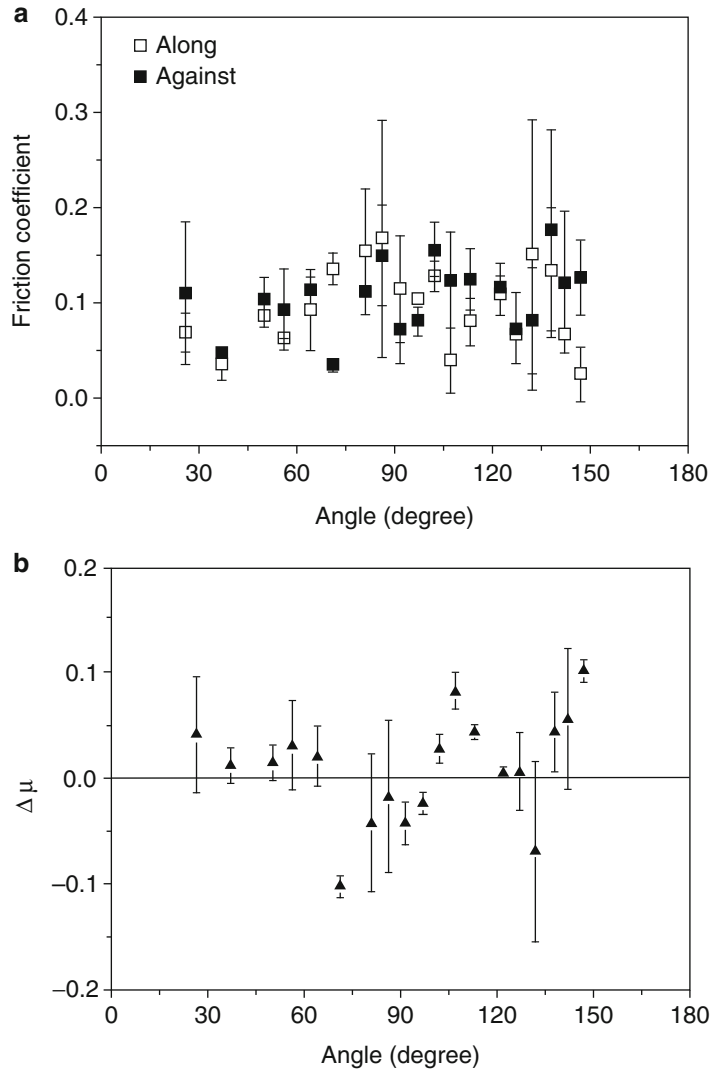

Fig. 6 Friction coefficient of native hair at different sliding angles at high RH (**a**) and difference in friction coefficients against versus along the cuticle (**b**). The average $\mu_{against}$ and μ_{along} are 0.11 and 0.10, respectively

2006), and (b) variation of Δμ with sliding angle is associated with the probability of antiparallel cuticle-cuticle interaction.

From geometrical considerations the highest probability that two cuticles both meet and interlock during sliding is at 45° and 135°, and the lowest probability is at 90°. In Figure 7b, which shows Δμ for bleached hair, it is possible to interpret two peaks on either side of a minimum as expected from the above treatment. The experimental maxima are found at roughly 70° and 130° and the minimum at around 100°. The angle of 130° is close to the predicted angle of the highest probability, but 70° is rather different from the other predicted maximum for reasons that remain unclear. We can only conclude from that particular result that mechanical interlocking is not the primary cause of directional hysteresis. Damaged/lifted cuticles merely have to be involved in the sliding contact, and the extra friction sliding against the cuticle direction may well be due to deformation ("bending back") of the cuticle. With undamaged hair the cuticle lies "flush" with the fiber so that bending back is unlikely.

Finally we reiterate that the AFM technique developed here for angular dependence measurement always provides movement at right angles to the cantilever mounted probe. Thus the movement

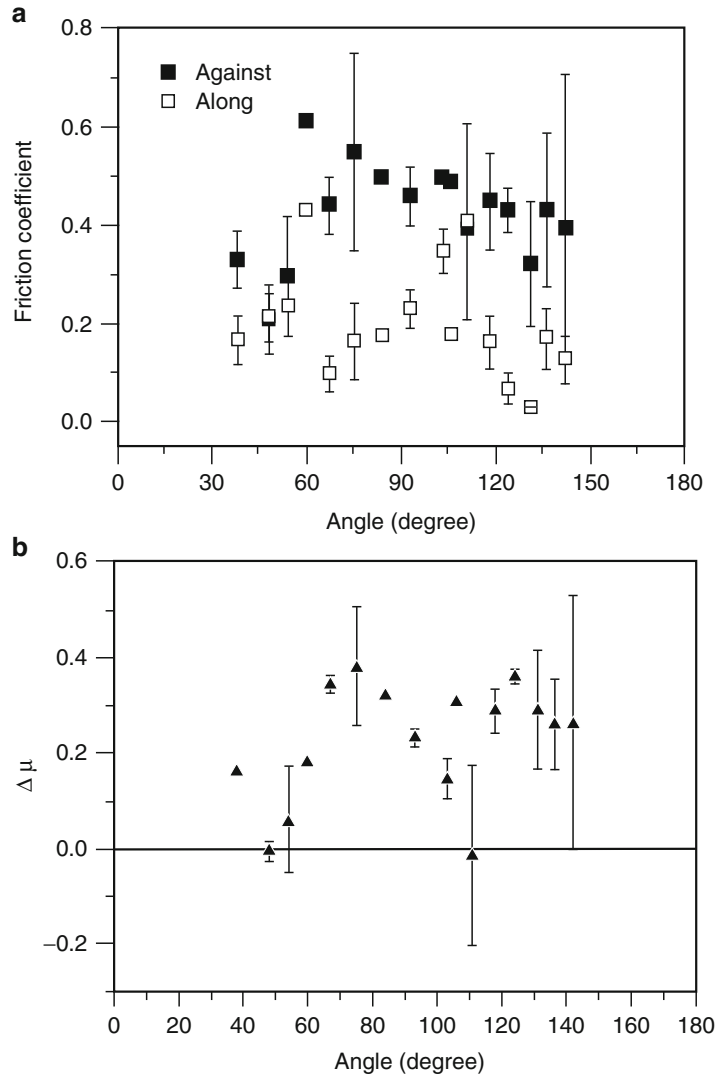

Fig. 7 Friction coefficient of treated hair at different sliding angles at high RH (**a**) and difference in friction coefficients when shearing against versus along the cuticle (**b**). The average $\mu_{against}$ and μ_{along} are 0.42 and 0.20, respectively, for bleached hair

is not axial with the lower fiber. This geometry is essentially a constraint of the AFM device, but in fact is more representative of the type of moving contact typically formed by two hair fibers. The antiparallel arrangement is an extremely unlikely conformation on, for example, a head of hair, but in the case of wool fibers in textiles, it is expected.

5 Conclusions

Both the contact and noncontact forces between hair fibers at nanoscale contacts, with high resolution of both the force and separation, can be measured. The action of well-characterized cationic surfactants alters the range and magnitude of these forces. Despite the relatively complex chemical structure of hair, the novel fiber-fiber probe technique shows the interactions to depend on the following classical forces – van der Waals and Poisson-Boltzmann in liquid and Coulombic and van der Waals attraction in air.

The friction coefficient of native hair is relatively independent of sliding angle and the directional effect is not clearly observed. On the other hand, bleached hair exhibits a clear directional effect at most sliding angles due to higher surface roughness, and this is a periodic function of the

angle. This finding is related to the likely cuticle-surface or cuticle-cuticle interaction between two hair fibers, and it is clear that cuticle lifting and serration (a result of oxidative damage) is a necessary requirement for directional effects between hair fibers to be observed. The directional effect has a symmetrical distribution with sliding angle, i.e., when sliding one cuticle against the other, it does not appear to matter whether cuticles are aligned parallel or antiparallel on the counter surface. This implies that frictional hysteresis may in fact be due to deformation (bending) of single lifted cuticle edges rather than mechanical interlocking of the cuticles as has previously been surmised.

Quantitative analysis of friction at various sliding angles can now be applied to other fiber systems. This is particularly useful to understand properties of fiber assemblies whose fibers interact at various angles, for example, polyester fibers, the inter-fiber friction of which determines mechanical strength of the array. Finally this kind of information will be essential for predicting the dynamic behavior of multifiber assemblies.

References

Atkin R, Craig VSJ, Wanless EJ, Biggs S. Mechanism of cationic surfactant adsorption at the solid-aqueous interface. Adv Colloid Interface Sci. 2003;103:219.

Bouillon C, Wilkinson J. The science of hair care. 2nd ed. New York: Informa Healthcare; 2005.

Breakspear S, Smith JR, Luengo GJ. Effect of the covalently linked fatty acid 18-MEA on the nanotribology of hair's outermost surface. Struct Biol. 2005;149:235–42.

Carambassis A, Jonker LC, Attard P, Rutland MW. Forces measured between hydrophobic surfaces due to a submicroscopic bridging bubble. Phys Rev Lett. 1998;80:5357.

Chan DYC, Pashley RM, White LR. A simple algorithm for the calculation of the electrostatic repulsion between identical charged surfaces in electrolyte. J Colloid Interface Sci. 1980;77:283.

Christenson HK, Claesson PM. Adv Colloid Interface Sci. 2001;91:391.

Ducker WA, Senden TJ, Pashley RM. Direct measurement of colloidal forces using an atomic force microscope. Nature. 1991;353:239.

Eriksson JC, Henriksson U. Langmuir. Bridging-cluster model for hydrophobic atraction. 2007;23:10026.

Eriksson JC, Ljunggren S, Claesson PM. A phenomenological theory of long-range hydrophobic attraction forces based on a square-gradient variational approach. J Chem Soc Faraday Trans. 1989;2:85–163.

Evans DJ, Lanczki M. Cleavage of integral surface lipids of wool by aminolysis. Text Res J. 1997;67:435–44.

Giesbers M, Kleijn JM, Cohen Stuart MA. J Colloid Interface Sci. 2002;248:88.

Hore DK, Walker DS, Richmond GL. Water at hydrophobic surfaces: When weaker is better. J Am Chem Soc. 2008;130:1800.

Huang F, Li KC, Kulachenko A. Measurement of interfiber friction force for pulp fibers by atomic force microscopy. J Mater Sci. 2009;44:3770.

Huson M, Evans D, Church J, Hutchinson S, Maxwell J, Corino GJ. New insights into the nature of the wool fibre surface. Struct Biol. 2008;163:127–36.

Israelachvili JN, Adams GE. Measurement of forces between two mica surfaces in aqueous electrolyte solutions in the range 0–100 nm. J Chem Soc Faraday Trans. 1978;1(74):975.

Jachowicz J, Berthiaume MD. Heterocoagulation of silicon emulsions on keratin fibers. J Colloid Interface Sci. 1989;133:118.

Jones LN, Rivett DE. The role of 18-methyleicosanoic acid in the structure and formation of mammalian hair fibres. Micron. 1997;28:469.

Koopal LK, Leermakers FAM, Lokar WJ, Ducker WA. Modeling of confinement-induced phase transitions for surfactant layers on amphiphilic surfaces. Langmuir. 2005;21:10089.

LaTorre C, Bhushan B. Nanotribological characterization of human hair and skin using atomic force microscopy. Ultramicroscopy. 2006;106:720.

Meyer EE, Rosenberg KJ, Israelachvili J. Recent progress in understanding hydrophobic interactions. Proc Natl Acad Sci U S A. 2006;103:15739.

Mizuno H, Kjellin M, Nordgren N, Pettersson T, Wallqvist V, Fielden M, Rutland MW. Friction measurement between polyester fibres using the fibre probe SPM. Aust J Chem. 2006;59:390.

Mizuno H, Luengo GS, Rutland MW. Interactions between crossed hair fibers at the nanoscale. Langmuir. 2010;26 (24):18909–15.

Molina R, Comelles F, Juliá MR, Erra P. Chemical modifications on human hair studied by means of contact angle determination. J Colloid Interface Sci. 2001;237:40.

Negri A, Rankin DA, Nelson WG, Rivett DE. A transmission electron microscope study of covalently bound fatty acids in the cell membranes of wool fibers. Text Res J. 1996;66:491.

Ralston J, Larson I, Rutland MW, Feiler AA, Kleijn M. Atomic force microscopy and direct surface force measurements (IUPAC technical report). Pure Appl Chem. 2005;77:2149.

Robbins CR. Chemical and physical behavior of human hair. 4th ed. New York: Springer; 2001.

Rockland LB. Anal Chem. Saturated salt solutions for static control of relative humidity between 5° and 40° C. 1960;32:1375.

Rutland MW, Parker JL. Surfaces forces between silica surfaces in cationic surfactant solutions: adsorption and bilayer formation at normal and high pH. Langmuir. 1994;10:1110.

Stevens H, Considine RF, Drummond CJ, Hayes RA, Attard P. Effects of degassing on the long-range attractive force between hydrophobic surfaces in water. Langmuir. 2005;21:6399.

Stiernstedt J, Fröberg JC, Tiberg F, Rutland MW. Forces between silica surfaces with adsorbed cationic surfactants: Influence of salt and added nonionic surfactants. Langmuir. 2005;21:1875.

Swift JA. Human hair cuticle: biologically conspired to the owner's advantage. J Cosmet Sci. 1999;50:23.

Tyrode E, Johnson CM, Kumpulainen A, Rutland MW, Claesson PM. Hydration state of nonionic surfactant monolayers at the liquid/vapor interface: Structure determination by vibrational sum frequency spectroscopy. J Am Chem Soc. 2005;127:16848.

Tyrrell JWG, Attard P. Images of nanobubbles on hydrophobic surfaces and their interactions. Phys Rev Lett. 2001;87:176104.

Verwey EJW, Overbeek JTG. Theory of the stability of lyophobic colloids. New York: Dover Publications; 1999.

Volkert CA, Minor AM. Focused ion beam microscopy and micromachinin. MRS Bull. 2007;32:389.

Ward K, Bertails F, Kim TY, Marschner SR, Cani MP, Lin MC. A survey on hair modeling: Styling, simulation, and rendering. IEEE Trans Vis Comput Graph. 2007;13:213.

Wertz PT, Downings DT. Integral lipids of human hair. Lipids. 1988;23:878–81.

Yorimoto N, Naito S. Physical and chemical properties of integral lipids in hair cell membrane complex. Proc Int Symp Fiber Sci Technol. Yokohama, 1994;215.

Zviak C. The science of hair care. New York: Marcel Dekker; 1986.

Nail Anatomy and Physiology

85

Robert Baran

Contents

Keywords

Bucky therapy • Cuticle • Entheses • Eponychium • Hardness of nails • Hyponychium • Nail biting • Onychodermal band • pH of nail plate • Simple gravimetric method • Soft keratin • Tactile discrimination

1 Anatomy

The nail which grows throughout the life is a transparent, semihard, oblong tablet with a long longitudinal axis in the hands, transverse in the feet (De Berker et al. 2007).

Its upper side is smooth and glossy. The nail plate sinks at an acute angle into a large deep groove, practically parallel to the cutaneous surface, the nail cul-de-sac (or posterior or proximal groove) (Fig. 1). The lateral nail grooves complete the bezel of the nail. They are lined by the lateral folds. The visible part of the nail ends with a free edge, which owes its whitish color to the underlying presence of air. The onychodermal (onychocorneal) band presents at the distal margin of the nail bed a contrasting hue in comparison with the rest of the nail bed. Normally, this a transverse band of 1–1.5 mm of a deeper pink (Caucasian) or brown (Afro-Caribbean). Its color or presence may vary with disease or pressure which influences the vascular supply. It represents the fast barrier to penetration of materials beyond the nail plate (Sonnex et al. 1991). The nail bed's dorsal surface is characterized by longitudinal

R. Baran (✉)
Nail Disease Center, Cannes, France
e-mail: baran.r@wanadoo.fr

P. Humbert et al. (eds.), *Agache's Measuring the Skin*,
DOI 10.1007/978-3-319-32383-1_119

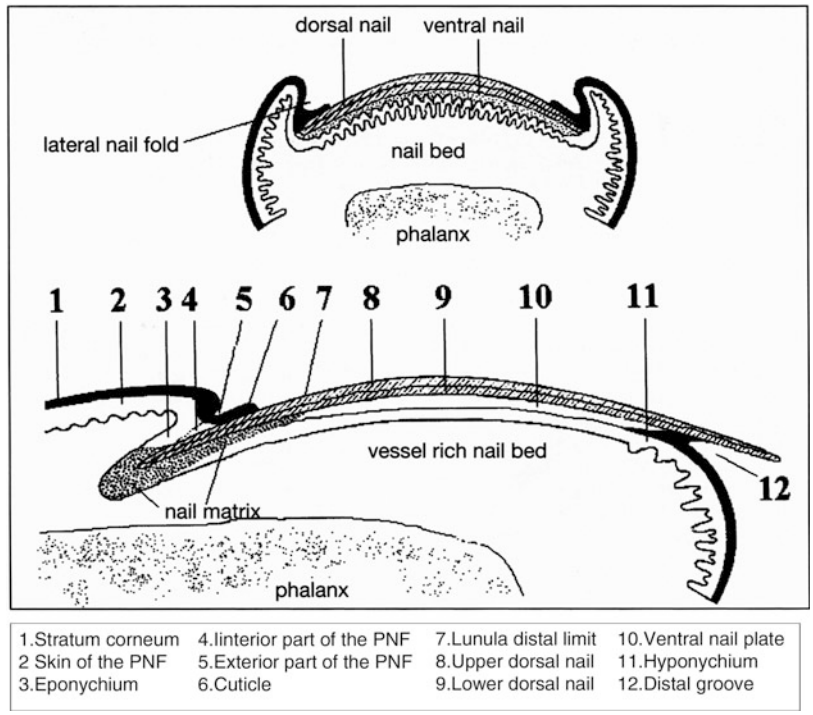

Fig. 1 Nail diagrams

ridges, and a complementary set of ridges is also found on the underside of the nail plate (though not at its free edge), which has led to the nail plate being described as led on rails as it grows out and to the suggestion that the ridges contribute to adhesion between the nail plate and the nail bed.

The proximal nail fold (or dorsal or PNF) is an expansion of the epidermis of the dorsal aspect of the distal phalanx. Its ventral part constitutes the roof of the proximal nail groove, which covers, on approximately 0.5 cm, the thinned base of the nail that is loosely stuck to the matrix. The cuticle, which ends the fold, adheres strongly to the upper side of the plate and seals the virtual space that opens onto the nail cul-de-sac. The inner side of the lateral folds is also lined with a stratified epithelium and produces a soft keratin that does not flake off but tends to persist as a thin and rough membrane overflowing on the neighboring surface of the nail. Because of the lateral folds that it connects, the proximal nail fold provides a continuous anatomical path for the spreading of pathological processes.

The nail matrix covers the floor of the cul-de-sac and rises on the posterior quarter of the roof of the proximal nail groove, the anterior three-quarters of which constitute the eponychium. The deep side of the matrix rests on the terminal osseous phalanx and forms a crescent with posteroinferior concavity. On the big toes, both ends of the crescent are located on a plane lower than that of the fingers. This anatomical layout explains the appearance of spicules when the matrix horns are incompletely excised in the radical treatment of a growing nail. The lunula, opaque white, with an anterior arc-shaped edge, corresponds to the distal and visible portion of the matrix. Particularly noticeable on the thumbs, it may be absent or covered by the cuticle on the other fingers. The proximal portion of the matrix produces the upper third of the nail plate, its distal part the lower two-thirds.

The thickness of the nail (0.50–0.75 mm in the fingers, up to 1 mm in the toes) is proportional to the length of the matrix. As a consequence, the thickness of the tablet depends on the global

number of germinative cells. However, the thickness seems to be increased in manual workers. Usually, the thinning of the nail plate can proceed from a diminution of the length of the matrix (transverse biopsy), a matrix compression, in which case this thinning will be limited to a nail segment, a stopping or a reduction of the cellular divisions of the matrix (responsible for Beau lines).

Ahead of the lunula, the pinkish area seen by transparency corresponds to the nail bed: the absence of fatty tissue puts the mesenchyme directly in contact with the bone. Contrary to the matrix epithelium, the epithelium of the bed adheres to the ventral part of the nail plate after a surgical nail avulsion. It shows the dermal papillae of the nail bed arranged in longitudinal parallel furrows resembling corrugated iron, in transverse section. They follow the longitudinal crests of the ventral aspect of the nail plate.

The hyponychium which contains the solenhorn corresponds to the area where the nail plate loosens from the underlying tissue. A condition where forward extension of the hyponychium anchoring to the undersurface of the nail plate and obliterating the distal groove is called ventral pterygium (collagenoses, causalgia, etc.). Its horny substance accumulates physiologically in the distal groove, an arc-shaped furrow with anterior convexity. The distal groove marks the most distal boundary between the nail unit and the fingertip.

Entheses are the sites of insertion of tendons ligaments or joint capsules to bone. Entheses consist of both soft tissue (tendon ligament and their fibrocartilages) and hard tissue (calcified fibrocartilage, adjacent bone, and trabecular network) components. In many sites, the enthesis is more than simply a focal attachment joint and it is intimately associated anatomically and functionally with the synovium forming a distinct organ referred to as the synovio-entheseal complex.

The circulation of the nail apparatus is supplied by two digital arteries that course along the digits and give off branches to the distal and proximal arches.

The sensory nerves to the dorsum of the distal phalanx of the three middle fingers are derived from fine, oblique, dorsal branches of the volar collateral nerves. Longitudinal branches of the dorsal collateral nerves supply the terminal phalanx of the fifth digit and the thumb.

Histology recognizes nail matrix and nail bed that have no granular layer in contrast to the upper ventral aspect of the proximal nail fold and the hyponychium.

The functions of the nail unit are manifold. Equivalent to claws and hooves in other mammals, the nail allows one to manipulate objects, enhances the sensation of fine touch, protects the delicate tips of fingers and toes against trauma, and is used for scratching and grooming. But among its multiple functions, the nail provides counter pressure to the pulp that is essential to the tactile sensation involving the fingers and to the prevention of hyperthrophy of the nail bed and the distal pulp.

Nail biting, which severely compromises the beauty of nails, is known to serve several needs, including providing a sense of relief as well as alleviating boredom (Williams et al. 2007). Finally, the nail unit is in some respects comparable to a hair follicle sectioned longitudinally and laid on its side.

2 Hardness

Excellent biophysical studies by Forslind et al. (1980) explain the hardness of the nails by the ultrastructural organization of the keratin fibrils, the main bulk of which are oriented perpendicular to the growth axes of the nail and parallel to its surface. They appear birefringent under polarized microscopy. The study of the diffraction of the nail fragments exposed to X-rays supports the concept of the fibril arrangement that provides for the torsional rigidity of the nail plate and a high breaking strength.

The keratin fibers are stabilized by the disulfur bridges of the cystine molecules and by the double

transverse and longitudinal convexity of the plate. This double curvature prevents lateral buckling. The transverse curvature is due to the shape of the terminal osseous phalanx and the existence of a dorsal strip of connective tissue, the bundles of which settle on its lateral edges. The longitudinal curvature could be due to a difference in growth rate between the cells in the nail plate and/or a pressure forming the curvature growing faster than the lower. Hardness is also due to the adherence of the cells to each other, their connection, and their typical architectural layout in two layers in the nail plate. The superficial layer is made of small cells (2.2 μm), a discreetly indented cellular membrane, and regular intercellular spaces presenting ampullar dilatations between cells. The lower part is made of larger cells (5.5 μm), the cellular membrane of which has an anfractuous contour and intercellular spaces containing anchoring knots. Finally, an intracellular envelope, the marginal strip, gradually forms on the internal part of the cellular membrane. The continuous intercellular junctions (tight junctions) explain the good quality of cell interaction and the rigidity of the dorsal nail. The cellular surface is proportionally greater than the volume because the edges of the cells of the underlying layer overlap each other. As a consequence, the properties of this area, stemming from the distal part of the matrix, are more plastic than those observed in the superficial part of the tablet, which is hard and breakable. Different aggressions (e.g., detergents) will contribute to its cleavage. The cutting capacity of the plate is also a result of these two layers.

3 Nail Plate pH

The pH of the nail plate surface was around 5, with toenails having a significantly higher pH than fingernails. Immediately after hand washing, the nail surface pH increased significantly, from pH 5.1 $\pm$ 0.4 to 5.3 $\pm$ 0.5. However, this was not sustained with time, and the pH returned to prewashing levels within 20 min. Gender had an influence on unwashed, but not washed, nail plate pH. The pH of the nail plate interior was lower than that of its surface (Murdan et al. 2011).

4 Penetration and Function as a Barrier

It seems obvious that the barrier function is of great practical interest when using medicine through the nails. Burch and Winsor (1946) used a simple gravimetric method to measure the diffusion of water through the nails postmortem and on various cutaneous areas. The rate of diffusion through the nails was similar to that observed in palms and soles.

Spruit (1971) measured out the nail loss in vapor in vivo by letting nitrogen pass through the tablet and measuring the water carried by the gas. There was a constant inversely proportional ratio in the nail between the vapor loss and the thickness of the nail.

Walters et al. (1983) brought forward information on the permeability coefficients in the nail for water, methanol, and ethanol in vitro. They also showed that the nail was less permeable to *n*-alkanols when hydrophobia was increased and that polar compounds could easily go through the nail keratin.

The penetration is increased even more when the solubility of the product in the carrier is improved, which is achieved by decreasing its pH. Baran (2000) showed that some antifungal products, in particular, could go through the nail barrier and act as transungual delivery systems. Hemidy et al.(1994) suggested a new simulation model, the sheep hoof, in order to study the topical penetration of antifungal products into hard keratin in vitro. A good work on drug delivery to the nail following topical application has been published (Murthy and Maibach 2013).

5 Transmission of Radiation

Nails can transmit light. In the study by Gammeltoft and Wulf (1980) nails of normal thickness transmit about 30 % of Bucky rays (12 kV) compared to 80 % of X-rays at 29 kV: Bucky therapy is therefore inefficient when pathological nails are thick, whereas 60 % of X-rays at 29 kV are likely to go through them.

Parker and Diffey (1983) showed that the nail plate acts like a sunscreen that imposes strong limits to the transmission of UVB (280–315 nm), but allows wavelengths over 330 nm only to go through. According to Baran and Juhlin (1987, 2002), 3–20 % of radiation between 313 and 500 nm pass through a normal nail, whereas their penetration through a psoriatic nail is lower than 4 %.

6 Tactile Sensibility on the Finger Nail

Tactile discrimination and threshold values over the nail plates and finger pulps were measured on 300 digits in 30 healthy subjects with a mean age of 23 years. Subjects with cosmetic nail modifications, injuries, neurological deficits, dermatological conditions, or history of upper limb surgery were excluded. Equivalence testing was conducted to look for clinical equivalence between values obtained at both sites.

The mean static 2-point discrimination, moving 2-point discrimination, and threshold value over the human nail were 6.7 mm, 2.4 mm, and 0.06 g, respectively. The corresponding values for the finger pulp were 2.4 mm, 2.2 mm, and 0.01 g, respectively. The static 2-point discrimination and threshold values were superior for the finger pulp, whereas moving 2-point discrimination values at both sites were clinically equivalent. This study suggests that tactile discrimination and threshold levels can be measured over the nail plate and that moving 2-point discrimination values are clinically equivalent to those obtained on the corresponding pulp. This highlights the importance of the nail plate in the sensory function of the fingertip. The normative data from this study may be useful in establishing the impact of nail injury and the contribution of the nail to the overall function of the hand (Seah et al. 2013).

References

Baran R. Nails. In: Gabard B, Surber C, Treffel P, Elsner P, editors. Dermatopharmacology of topical anti fungal preparations in nail tissue. Berlin/Heidelberg/New York: Springer; 2000.

Baran R, Juhlin L. Drug induced photo-onycholysis: three subtypes identified in a study of 50 cases. J Am Acad Dermatol. 1987;17:1012–6.

Baran R, Juhlin L. Photoonycholysis. Photodermatol Photoimmunol Photomed. 2002;18:202–7.

Burch GE, Winsor T. Diffusion of water through dead plantar, palmar and dorsal human skin and through toenails. Arch Derm Syphilol. 1946;53:39–41.

De Berker DAR, André J, Baran R. Nail biology and nail science. Int J Cosmet Sci. 2007;29:241–75.

Forslind B, Nordstrom G, Toijer D, et al. The rigidity of human fingernails: a biophysical investigation on influencing physical parameters. Acta Derm Venereol. 1980;60:217–22.

Gammeltoft M, Wulf HC. Transmission of 12 kV Grenz rays and 29 kV X rays through normal and diseased nails. Acta Derm Venereol. 1980;60:431–2.

Hemidy PY, Makki S, Muret P, Chaumont JP, Millet J. The use of sheep hoof plates for substituting human nails in transungual absorption studies. J Appl Cosmetol. 1994;12:73–84.

Murdan S, Milcovich G, Goriparthi GS. An assessment of the human nail plate pH. Skin Pharmacol Physiol. 2011;24:175–81.

Murthy SN, Maibach HI. Topical nail products and ungual drug delivery. Boca Raton: CRC Press; 2013.

Parker SG, Diffey BL. The transmission of optical radiation through human nails. Br J Dermatol. 1983;108:11–6.

Seah BZQ, Wu CCH, Sebastien SJ, Lahiri A. Tactile sensibility on the fingernail. J Hand Surg [Am]. 2013;38:2159–63.

Sonnex TS, Griffiths WAD, Nicole WJ. The nature and significance of transverse white band of human nails. Semin Dermatol. 1991;10:12–6.

Spruit D. Measurement of water vapor loss through human nail in vivo. J Invest Dermatol. 1971;56:359–61.

Walters KA, Flynn GL, Marvel JR. Physicochemical characterization of the human nail: permeation pattern for water and the homologous alcohols and differences with respect to the stratum corneum. J Pharm Pharmacol. 1983;35:28–33.

Williams TI, Rose R, Chisholm S. What is the function of nail biting: an analog assessment study. Behav Res Ther. 2007;45:989–95.

Nail Metrology

86

Robert Baran

Contents

R. Baran (✉)
Nail Disease Center, Cannes, France
e-mail: baran.r@wanadoo.fr

P. Humbert et al. (eds.), *Agache's Measuring the Skin*,
DOI 10.1007/978-3-319-32383-1_120

Keywords

Abrasion • Bone scintigraphy • Color of nail plate • Dawber's technique • Digital thermography • Dual flow cytometry • Indentation method • Knoop indenter • Linear nail growth • Magnetic resonance imaging (MRI) • Melanoma • Molecular and knock out studies • Nail flexometer • Nail thickness • Onychomycosis • Optical coherence tomography (OCT) • Optical profilometry • Proximal nail fold • Proximal nail fold capillaroscopy • Reflectance confocal microscopy (RCM) • Sclerometry • Synchrotron X-ray microdiffraction • Transillumination • Ultrasonography • Vasomotricity • Wood's light examination • Yellow-green nail fluorescence

1 Nail Plate

The metrology of the nail plate encompasses routine techniques as well as more sophisticated and even experimental ones. Often the examination of only a nail clipping may be of great interest.

1.1 Linear Nail Growth

Nail growth derives from the nail matrix and can be assessed at tissue level or macroscopically in terms of nail length, mass, or thickness (Moffitt and de Berker 2000). In Dawber's technique, (1970) a T-shaped scratch is made on the

fingernails at a distance X (approximately 3 mm) from the proximal nail fold (PNF). After a period of approximately 1 month, the scratch will have moved and its distance to the proximal nail fold will have grown to Y. Daily nail growth is calculated as (Y-X)/number of days. Measurement is made with a dermoscope with integral scale. All patients are asked not to push back their cuticles during the period of the study. Toenails are estimated to grow around 1 mm/month. Orentreich et al. (1979) measured the linear nail growth in dogs by cutting a shallow groove in the proximal nail with a piece of hacksaw blade. A screw set two-pointed caliper marked the distance from the groove to the proximal skin fold of the nail. The distance between the points of the caliper was then measured to the nearest 0.1 mm with a micrometer built into a magnifying glass. Measurements at 4-week intervals were made on nails 2, 3, and 4 of the right front paw. The average outgrowth was divided by the elapsed time in weeks for the rate of linear nail growth in millimeters per week. Orentreich measured circadian and temperature effects on the linear nail growth rate in humans with a split-image range finder adapted to a trinocular microscope. With this instrumentation, measurements of nail growth were made over intervals as short as 15 min. Heikkila et al. (1996) measured nail growth by making indentations on the nail surface and then measuring the change in the volume of these grooves as they reached the free edge. There was a reduction in volume of 30–50 %, which was taken as evidence of a contribution of the nail bed to the nail plate. However, this interpretation is less believable than the possibility that the nail is losing cells from the surface, and histology of grooves in a similar study shows that this is likely to be the case (de Berker and Forslind 2004). Yaemsiri et al. (2009) recorded distance and time between the two measurements. Average fingernail growth rate was faster than that of toenails (3.47 vs. 1.62 mm/month, $P < 0.01$). Nail growth rates have increased compared with previous estimates conducted decades ago. Toenail clippings may reflect a long exposure time frame given the relatively slow growth rate.

A transverse scratch at the convex apogee of the lunula is the easiest technique and subsequent measurements are made with reference to the lunula. The introduction of magnified photographs, before and after comparison of these photographs, has increased the precisions of these methods. As the lunula is not always visible in all digits (it becomes progressively more concealed beneath the PNF in the more lateral digits) and is rarely seen in toes (to measure growth in digits with no apparent lunula), the PNF must be used as a substitute. As a measure of total matrix activity, estimation of linear nail growth could be misleading. Hamilton et al. (1955) sought to measure volume by the following equation:

$$\begin{aligned}&\text{thickness(mm)} \times \text{breath(mm)}\\ &\quad \times \text{ length grown per day}\\ &\quad = \text{ volume.}\end{aligned}$$

In some diseases, this may alter the impression of reduced nail growth – where a nail that is thickened has a low longitudinal growth rate but is still producing the same mass of nail. For example, in yellow nail syndrome, "the nail that grows half as fast grows twice as thick" (Moffitt and de Berker 2000).

1.2 A Normal Nail Grows Out Straight

Kligman (1961) explains why a nail grows out instead of up, and this is because its base is covered by the proximal nail fold (PNF). This is wrong (Baran 1981). The so-called proof of Kligman explanting the nail matrix placed in the forearm and which grew a perpendicular pillar of keratin to the axis of the matrix explant ignores a rule empirically known in genetics: One cannot conceive a normal nail atop an anomalous ungual phalanx, because there is a "bone-dependent nail formation" (Baran and Juhlin 1986). Recent molecular and knockout studies support this theory showing that mesenchymal condensation forming the distal phalanx occurs at the time of

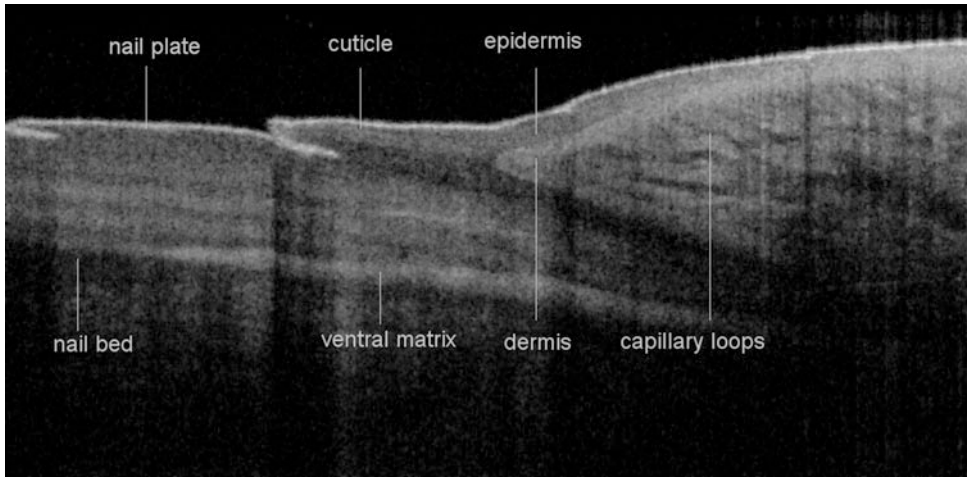

Fig. 1 Optical coherence tomography. Normal nail

the epidermal thickening and formation of the nail fold (Seitz and Hamm 2005). To provide additional support to the absence of the role of the PNF which has no effect on the direction of the nail growth, I have cut the PNF of several fingers presenting with recalcitrant chronic paronychia without any secondary change in the direction of the nail growth. Moreover Jamieson (1893) has reported on a patient with congenital aplasia of the PNF and the nail grew out instead of up. Finally, K. Hashimoto (Hashimoto et al. 1966) has clearly demonstrated that in early embryonic life, the nail was formed by the dorsal, apical, and ventral matrices and that all the matrix cells were oriented in a central-distal direction. The programmed process maintains itself throughout adult life.

1.3 Thickness

The simplest way to measure the nail thickness at its free border is to use a caliper.

Finlay et al. (Finlay 1988) used a handheld electronic micrometer (Moore and Wright Ltd, Sheffield, UK), which measures with an accuracy of +/−2 um.

For the other parts of the nail in vivo, the most readily available method is the 20/25-MHz ultrasound imaging, keeping in mind that the ultrasound speed in the nail plate is about 3,100 ms^{-1} (only 1,600 ms^{-1} in viable skin). Accordingly, nail thickness displayed by current skin imaging devices should be corrected.

In standard optical coherence tomography (OCT), the nail plate appears as a layered structure containing a varying number of horizontal homogenous bands of varying intensity and thickness (Fig. 1).

Polarization sensitive OCT (PS-OCT) images of the nail plate also show a layered structure. The refractive index of the nail was 1.47 ± 0.09; OCT and PS-OCT had low coefficients of variation, 6.31 and 6.53, respectively, compared with other methods: high-frequency ultrasound 12.70 and calipers 14.03 (Mogensen et al. 2007).

1.4 Roughness

Although the nail plate surface relief can be measured directly in vivo, replicas are useful, because they suppress the inevitable trembling due to heart beats and can be done in the doctor's office with further treatment in a specialized center. They may be analyzed by either computerized image analysis or optical profilometry and related techniques. Longitudinal ridges are made of small rectilinear projections extending from the PNF as far as the free edge of the nail or they may

stop short. They may be interrupted at regular intervals, giving rise to a beaded or sausages like appearance (For technical detail, see ▶ Chap. 5, "Skin Color and Pigmentation," 1st ed.).

Optical profilometry has permitted a study of acquired nail beading in patients receiving intermittent itraconazole and has shown that it could be an indicator of faster nail growth (De Doncker and Piérard 1994). In addition, optical profilometry and laser techniques can quantify other nail surface alterations such as trachyonychia, pitting, and grooves (Nikkels-Tassoudji et al. 1995; Piérard and Piérard-Franchimont 1996a).

Piérard et al. (Piérard and Piérard-Franchimont 1996b) have also measured the changes in nail surface contours during 3 mg/kg per day cyclosporin A therapy, a new objective technique used to assess the efficacy of a drug.

1.5 Color

Changes in the color of the nail plate are due to changes in the bulk or at the surface of the nail or in the underlying tissues, which are then seen through the translucent nail plate. Exogenous as well as endogenous factors can affect all or part of the nail plate. The pattern of discoloration can indicate the cause: If discoloration follows the shape of the proximal nail fold and grows out with the nail, it is caused by a topical application of agents. On the contrary, if discoloration corresponds to the shape of the lunula, its origin is systemic.

Nail pigmentation can be best measured by spectrophotometry, which determines whether the discoloration originates from melanin or not (for principle and technical details, see ▶ Chaps. 4, "The Skin Surface Ecosystem: A Presentation," and ▶ 44, "In Vivo Magnetic Resonance Imaging of the Skin," 1st ed.). The epithelium of the matrix contains melanocytes and Langerhans cells. Melanocytes are about 200/mm^2 in number (about 1150/mm^2 in the epidermis). Most of them are dormant and do not produce pigment. However, in dark-skinned subjects longitudinal melanonychia can be observed. Melanocytes are rare (47/mm^2) or may be absent (Perrin et al. 1997).

1.6 Physical Properties of Nails

The five important nail properties include (Schoon 2005):

1. Strength, the ability to resist breaking under a heavy load
2. Hardness measuring a surface's resistance to be scratching or denting
3. Flexibility which allows a substance to bend
4. Toughness, a balance of strength and flexibility
5. Wear resistance that is the ability to resist abrasion or rubbing

Numerous authors have devised more or less complicated machines in order to measure some of these properties. However, to our knowledge, there is at present no commercially available instrument able to perform these measurements. Accordingly, technical details can be found in the quoted articles. Before doing any experiment, it must be remembered that the main factor influencing these properties is the water content of the nail.

Young et al. (1965) used nail specimens of rectangular cross-section produced by gently sanding the edges of the fingernail clippings with fine emery paper. They were tested as simply supported beams of rectangular cross-section on a span of 0.33 cm. A testing machine devoid of inertia and equipped with a strain-gage-type dynamometer was used for loading the specimen. The full scale loading range was 2 kg or less, and the speed of moving gear was 0.05 cm/min. The load was supplied through a bar having a radius of 0.013 cm.

The Knoop indenter is an instrument that measures hardness by measuring depth of indentation of a fixed load on a constant area. Knoop hardness of fingernails requires specimens suitably prepared for testing if meaningful reproducible hardness numbers are to be obtained. The purpose of

the Newman and Young study was to establish the order of magnitude of the indentation hardness of fingernails. Human nail specimens were subjected to spherical ball indentation statically. The hardness number found was 9 kg/mm^2 (88.3 MPa). Interferometric studies have revealed that the indents are not spherical in shape: Their central portion is either flat or slightly elevated. These studies reveal that the human nail has a tremendous capacity of recovery when deformed by mechanical operation. The relaxation time of internal stress is quite long so that recovery continues for a long period, about 1 h.

Maloney and Paquette (Maloney et al. 1977) developed and tested a miniature apparatus for measuring the physical properties of fingernails. Included were a device for cutting test specimens; a template for preparing tensile bar samples; an apparatus for performing flexural, tensile, and tearing tests; and finally a device for determining impact absorption (ballistometry). The ranges of fingernail physical properties were as follows: flexural strength, 4,928 lb/in^2 (33,8 kPa) to 17,653 lb/in^2 (122 kPa); tensile strength, 4,464 lb/in^2 (30,8 kPa) to 17,081 lb/in^2 (118 kPa); tearing resistance 274.3–672.2 lb/in (48 10^3–118 10^3 N/m); and impact absorption (rebound ratio) 0.4632–0.7273. Maloney and Paquette demonstrated differences related to age, sex, and digit.

Finlay et al. (1980) developed the nail flexometer to determine the effect of various materials on nail flexibility. It repeatedly flexed longitudinal nail sections up to 90° and recorded the number of bendings required to fracture each section. Immersion in water or a phospholipid-water preparation greatly increased the flexibility of untreated and lipid extracted nails; immersion in mineral oil did not. Nail flexibility was directly related to the duration of immersion in water.

In an attempt to quantify the main physical properties of nails, Baden measured (Baden 1970) the velocity of sound in nail plate, for assessing elasticity, water-binding capacity, and the rate at which water diffuses through it. Interestingly, measurement of the modulus of nail elasticity gave values similar to those of hair and suggested that connections between cells contributed to the strength of nail tissue.

Nail exhibits viscous flow for the property of withstanding breaking and buckling, but rigidity or stiffness would be more appropriate. Measuring the effective elastic modulus of nail, they found E = 1.21+/−0.07 (SEM) GPa and stressed the importance of water content on nail physical properties.

The measurement of the physical properties of nails was addressed by Vargiolu et al. (1999) using an indentation method and the Vickers indentor (pyramidal in shape). Recording the plot of resisting force versus depth of indentation during loading (maximum applied: 0.12 N) and unloading phases made it possible to calculate nail hardness (ratio of force to imprint area) and Young's modulus E (initial tangent of the unloading phase). They found E = 1.6, 4.7, and 5.6 GPa at 20 months, 27 years, and 65 years of age, respectively.

1.7 Fluorescence of Nail Under Wood's Light

Wood's light examination can be rapidly and easily performed in vivo. Normal nails exhibit a whitish fluorescence. A yellow fluorescence of the lunulae (Hendricks 1980) and the nails (Dopuglas 1963; Zaun and Dill-Müller 1999) has been observed in patients taking oral tetracycline and a red fluorescence when taking demethylchlortetracycline (Kierland et al. 1946).

Interestingly, quinacrine hydrochloride also results in yellow-green nail fluorescence. This technique can be helpful in distinguishing these drug-induced nail pigmentations from other causes of yellow nails.

1.8 In Vitro Nail Examination with Polarized Light

Polarized light can be helpful in the examination of the underside of nails. A light microscope

identifies the longitudinal ridge plate (Apolinar and Rowe 1980).

In true leukonychia, the nail structure under polarized light appears disrupted due to disorganization of the keratin fibrils (Baran and Achten 1969).

2 Capillaroscopy of the Proximal Nail Fold

Proximal nail fold capillaroscopy is a simple, in vivo, noninvasive, and reliable technique used to evaluate superficial microvascular structures (Vaudaine 2012).

The capillaroscope is composed of an optical microscope with a ×50 to ×200 magnification and a cold light source in order to avoid vasodilation.

The microvascular structures of the proximal nail fold and the vessels are not seen from above and have a peculiar arrangement of vascular loops parallel to the skin surface.

Skin is "prepared" with an ointment of cedar oil or liquid petrolatum in order to obtain a better transparency of the epidermal structures. Second, third, fourth, and fifth fingernails of both hands are consecutively examined.

Some authors have suggested the use of a dermoscope (or an ophthalmoscope) to perform a capillaroscopic examination of the proximal nail fold. The lower magnification permits visualization of megacapillaries but is insufficient to explore other components of the bloodstream in detail.

Useful information can be obtained by an overall examination of the vascular structures. Capillary loops physiologically have a hairpin shape and are arranged in two parallel longitudinal rows in the proximal nail fold. Usually 12–18 loops are found per millimeter. Proximally, the subpapillary veins can be observed with a disposition perpendicular to the capillary loops.

Different patterns can also be observed in places without any pathological significance: glomerular aspect, elongated and tortuous loops. Pathological changes include ramified vessels, elongated loops, mega capillaries, parallelism disruption, and microaneurysms.

With the highest magnification, the bloodstream can be observed: a continuous stream or an intermittent one with flow stops, which irregularly occur over time.

Vasomotricity can be subjectively evaluated by detailed observation of a vascular field. It is found very active in idiopathic Raynaud phenomenon and decreased in acrocyanosis. In lupus erythematosus, vasomotricity rapidly and intensively changes over time and within the same capillary loop.

Examination of the background also yields useful information. Physiologically, the color of the background is pinkish but can be orange in cases of venous stasis. Dark epidermal pigmentation can impair the visibility of the capillaries.

A pericapillary halo can be observed in inflammatory conditions or in cases of vascular stasis.

Hazy aspects can be observed in scleroderma. Hemorrhages are observed in cases of evolutive microangiopathy. In this instance, the typical aspect of a pearl necklace permits the differential diagnosis with trauma-induced hemorrhages with a blotch aspect.

It is possible to measure capillary blood cell velocity, dynamic capillary blood pressure, and transcapillary diffusion of fluorescent tracers in human skin. Vital capillaroscopy is successfully used to study the microcirculation of human skin capillaries. Capillary videomicroscopy at the proximal nail fold in connection with a local cold exposure test is a method with clinical applicability in vasospastic disease (For details and technical information on capillaroscopy, see ▶ Chap. 40, "A Pharmaceutical Approach of Transcutaneous Oxygen Therapies," 1st ed.).

3 Nail Plate and Nail Bed

3.1 Transillumination

Transillumination is useful to distinguish between intrinsic nail plate chromonychia and surface changes (Goldman 1962; Ekin et al. 1997)

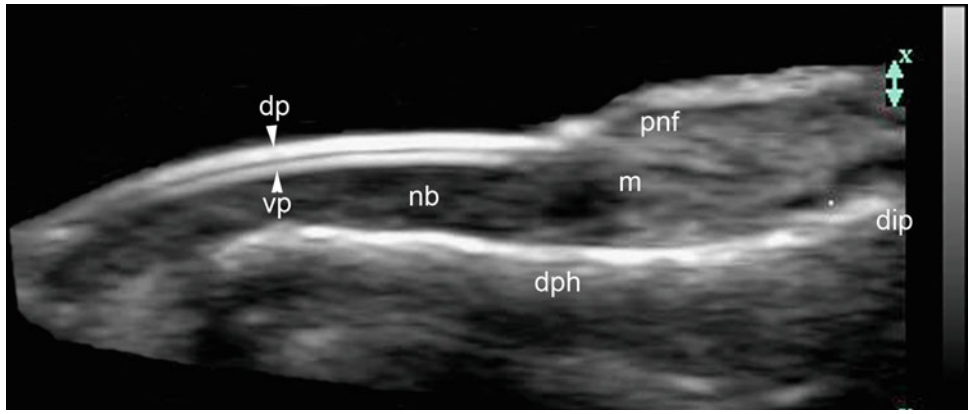

Fig. 2 Normal nail sonography (Courtesy of Ximena Wortsmann, Chile)

- Transillumination is the least expensive technique. The patient is taken into a dark room. It is possible to transilluminate a digit by shining a strong penlight beam upward through the pulp or to use a fiber-optic probe directed at the border adjacent to a cystic tumor, the light being directed into the dorsum of the distal interphalangeal joint.
- Transillumination is helpful in identifying the cystic nature of the lesions, especially when they are not characteristic locations or deep in the tissue. It also identifies multiple lobes when present.
- Transillumination may be used for diagnosis of subungual glomus tumors. Because it has a different color on the transillumination test, the tumor can be localized and its size easily estimated.

3.2 Digital Thermography

Digital thermography (Passareti et al. 1988) is highly sensitive in glomus tumors; it shows a light circumscribed circular zone in the digit (For technical and theoretical discussion, see ▶ Chap. 38, "In Vivo Confocal Microscopy in Clinical Dermatology," 1st ed.).

3.3 Ultrasonography

Ideally, a compact linear and variable-frequency probe that works in the range of frequencies from 7 to 18 Mhz is used for performing the examination. The nail unit comprises three main areas: the nail plate, the subungual, and the paronychial tissues. The dorsal and ventral plates present a bilaminar hyperechoic structure (two parallel lines) separated by an almost virtual hypoechoic tissue (interplate space) (Fig. 2). Low-velocity arterial and venous vessels are usually detectable within the nail bed (color Doppler with spectral curve analysis) (Fig. 3). The distal insertion of the lateral bands of the extensor tendon in the distal phalanx shows a fibrillar hyperechoic pattern, typical of the tendinous structures and lastly the bony margin of the distal phalanx shows a continuous hyperechoic line following the contour of the cortex of the bone that is only interrupted by the anechogenicity of the distal interphalangeal joint space that contains a virtual amount of fluid and cartilage.

Finlay et al. (1987) measured human fingernail thickness in vivo using an adapted electronic micrometer and ultrasound transmission time was measured both distally and proximally. Distal ultrasound nail transmission time correlated well with micrometer measurements. Distal nail transmission time was 8.8 % less than proximal transmission time (See also ▶ Chap. 20, "Skin Friction Coefficient").

Jemec and Gniadeska (1999) used high-frequency ultrasound to conduct longitudinal studies of psoriatic nail changes during therapy.

The exact location of a glomus tumor is easy to detect if there is discoloration of the nail.

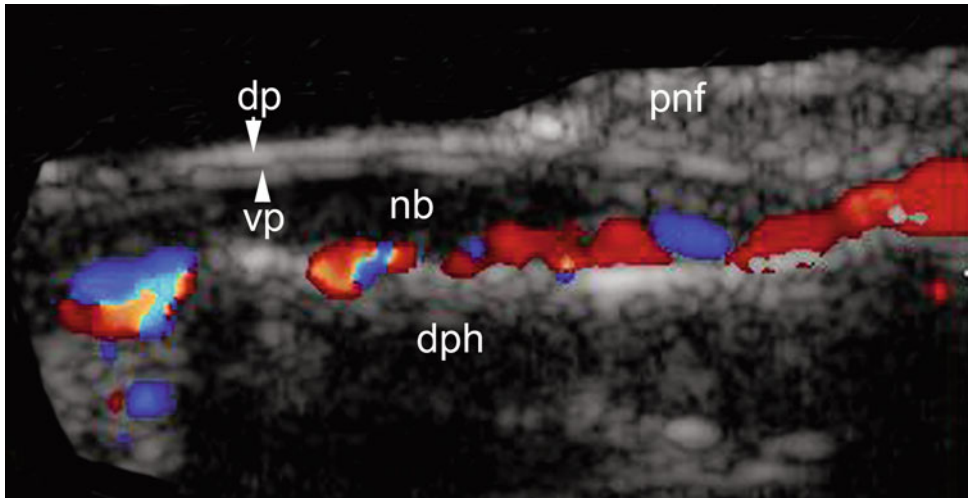

Fig. 3 Ultrasonography with color Doppler (Courtesy of Ximena Wortsmann, Chile)

However, there are cases in which the tumor is difficult to locate. Ultrasonography (US) might be useful for detecting glomus tumor before surgery. Echograms give clear echoic shadows of subungual tumors (Wortsman and Jemec 2013).

The sonographic aspect of mucoid pseudocyst includes a poorly echogenic round mass or simple thickening of the subungual space, and these features do not distinguish it from glomus tumors or angioma.

A 30-MHz frequency high-resolution B-mode was applied to normal and damaged nails, and the echograms confirmed the diagnostic value to the nail plate deformity (Hirai and Fumiiri 1995).

Ultrasonography imaging with high-frequency transducers is useful in both the diagnosis and the preoperative three-dimensional localization of glomus tumors. The diagnosis should be made on the combination of as appropriate clinical setting and the demonstration of a local, hypoechoic mass.

Differential sonographic diagnosis should include implantation, mucoid pseudocyst, and angiomas. Hematomas beneath the nail plate may be particularly misleading.

The sensitivity of this investigative method depends on the instrument used and on the experience of the operator. Limitations of detection with ultrasonography are related to the resolution of the sonographic transducer. Commercially available devices, working at 20 MHz, use an aqueous gel as a coupling milieu between probe and skin. This may hydrate the nail and make it swell. Accordingly, any examination should be of very short duration if aimed at dimensional or structural investigation. On the other hand, the nail thickness is calculated from the time the US beam goes down and returns, and current devices are set to the US speed in viable tissue ($=1{,}600$ m s^{-1}), whereas it is much higher in nails ($=3{,}100$ m s^{-1} in dorsal nail and $=2{,}100$ m s^{-1} in ventral nail). Therefore, a correct ultrasound measurement of nail thickness must take this into account; otherwise the nail would be found erroneously thin.

The specificity of sonography is low, so its diagnostic value is limited. However, it should be used as a first choice, because it is inexpensive and provides the possibility of defining the lesion in nearly 50 % of cases.

US and clinical findings show good correlation for the assessment of the nail in psoriatic disease. The demonstration of subungual extensor tendon enthesopathy in both psoriasis and psoriatic arthritis (PsA) supports the importance of enthesopathy in nail disease pathogenesis whether or not clinical arthritis is present (Aydin et al. 2012). In addition, Aydin et al. (2013a) used ultrasonography with power Doppler to test the hypothesis that subclinical enthesopathy in

PsA was associated with an inflammatory or vascular phenotype compared to that seen in psoriasis. Their study shows that the ultrasound appearances of subclinical enthesitis in psoriasis differ from the subclinical enthesitis in PsA, with PsA patients having more power Doppler. This is suggestive of a more inflammatory or vascular process in PsA and offers potentially novel insights into the progression from skin to joint disease in psoriasis.

3.4 Optical Coherence Tomography

Optical coherence tomography (OCT) is an optical analogue of US, using infrared light instead of acoustic waves. The reflection of the light waves (Piérard 1993; Corcuff and Levêque 1993; Kaufman et al. 1995; Hongcharu et al. 2000) from the tissue is measured and processed in order to improve the signal-to-noise ratio and transfer to a computer generating an OCT image. The axial resolution is determined by the bandwidth of the light source, which is 1–2 mm in general, limiting its use to very superficial tissues.

It has also been widely investigated in dermatology, particularly in nonmelanoma skin cancers. For nail disease, it was suggested to be useful as a diagnostic tool in onychomycosis. Additionally, comparison of high-resolution US and OCT indicated the benefits of OCT such as a better ability to differentiate morphological details and nail thickness. OCT may be regarded as an optical analogue of US providing of better resolution but inferior penetration (Fig. 1).

OCT is compatible with both physical findings and with US in patients with symptomatic nail disease in psoriasis. Surprisingly, the diffuse nail dystrophy shown on clinical photographs was associated with a relative normality of superficial nail but OCT abnormalities at the nail plate anchorage to the underlying skin. The validation of the use of OCT in measuring the thickness of the nail plate in comparison to US has already been demonstrated. This suggests that OCT may have the potential to provide quantitative data regarding psoriatic nails and may be a more accurate and objective outcome measure, potentially suitable as a surrogate outcome measure in interventional trials. OCT detected subtle abnormalities in 12 clinically normal nails and in 41 nails with normal US findings (Aydin et al. 2013b).

3.5 Reflectance Confocal Microscopy

Reflectance confocal microscopy (RCM) is an emerging technique which, by a real-time confocal microscope, uses reflected light to optically section living tissue at various depths, to examine and image layers of the nail unit without stains in vivo (Cinotti et al. 2014). Due to the fact that both the light and the microscope objective are focused at the same specific focal plane, objects and structures above and below this plane do not interfere with the formed image. RCM gives horizontal images of the analyzed tissue with resolution at a cellular level and without alteration of the tissue surface. Skin and nails are ideal locations to be explored by RCM because they are easily accessible sites. The depth to which the confocal microscope can optically penetrate is limited by the light penetration into the tissue and by the reflectivity of the observed structures and corresponds to 200–300 μm for skin tissue.

The unique properties of RCM make it possible to explore the capillary nailfold and the nails extending to the deeper layers of the nail plate and nail bed.

RCM is able to display single corneocytes and the integrity of their borders. The nail plate can be scanned from the surface to the lower part adjacent to the underlying nail bed. Three different layers can be differentiated by RCM, according to the intensity of the reflection. The superficial layer shows a brighter reflection, followed by a zone with a poorer signal, followed again by a brighter zone in the deepest part.

Two main applications interest the dermatologist:

1. **Confocal microscopy and onychomycosis**

   Hongcharu et al. (2000) first reported the possible application of in vivo RCM for the

diagnosis of onychomycosis. RCM produces high-resolution images and has the great advantage of being noninvasive. Nails can therefore be imaged in their native state at high resolution and contrast without fixing, sectioning, or staining. Hongcharu et al. correlated RCM findings with the results from routine KOH preparations. RCM is faster and more accurate than the conventional microscope used with KOH preparations in the diagnosis of onychomycosis.

As attempts to document fungal infection by KOH preparations and fungal culture are sometimes unsatisfactory, RCM is an additional tool that can be used in these cases.

2. **Confocal microscopy and melanonychia**

Recent studies showed that the proximal nail fold could be reclined during nail biopsy procedure in order to better visualize nail matrix pigmentation and to perform intraoperative dermoscopy and RCM.

In most cases, the images obtained both by ex vivo and in vivo RCM were reliable enough to make the diagnosis and the slight loss of quality, sometimes observed in vivo because of subtle movements, did not have any impact on the diagnostic value of the observed features. Intraoperative RCM revealed sufficiently atypical cytological and architectural features to accurately suggest the correct final diagnosis of melanoma. A good correlation between RCM and histopathology was found: Subungual melanoma was diagnosed intraoperatively in seven out of eight cases that proved to be melanomas by histological examination (Debarbieux et al. 2012).

The authors suggest that RCM is a promising tool for the intraoperative diagnosis of melanonychia because it combines the advantages of dermoscopy (noninvasive examination of the whole interested area without alteration of the epithelial surface) and histopathology (resolution at a cellular level). RCM offers a good contrast between melanocytes and adjacent structures. It permits the visualization of architectural and cytological features of the melanocytic proliferation. Ex vivo examination can be used either alone or as a complementary technique if the data provided by in vivo examination are not diagnostic.

3.6 In Vitro Dual Flow Cytometry

Dual flow cytometry after labeling fungal proteins with fluorescein isothiocyanate (FITC, Sigma Chemical Company) and fungal DNA with propidium iodide (PI, Sigma Chemical Company) was performed by Arrese et al. (1995) following a variant of Miller and Quarles' method. This technique was found between culture data, revealing a single fungus and positivity of fungal filaments with monoclonal antibodies. The dual dye combination of FITC and PI yielded strong detectable fluorescence of fungi.

3.7 Magnetic Resonance Imaging

Magnetic resonance imaging (MRI) is an effective method of locating tumors, particularly where there is diagnostic difficulty. It can be used in a range of periungual neoplasms, although it is most useful when the tumor contrasts with surrounding tissues with respect to density, fluid, or fat content (Drape et al. 1995; Goettmaann et al. 1994).

The most marked example of this is with mucoid cysts, but even normal soft tissues can be differentiated and an in vivo anatomical assessment made using MRI. This can be a useful means of identifying the inflammatory changes of psoriatic arthritis where it has consequences for the soft tissue element of the nail unit and consequently affects nail growth and appearance and remains the gold standard for glomus tumors of the nail unit.

MRI detects tumors only 1 mm wide; defines their tissue characteristics; determines their site, which facilitates surgical management.

T_1-weighted sequence allows morphological evaluation of lesional contour and anatomical extension.

T_2-weighted sequence defines tissue characterization from signal intensity emitted by the tumor.

Gadolinium assesses the vascularization of the tumors and may highlight the lesional contours.

The signals obtained in the various sequences are characteristic and can differentiate the most common tumors encountered in the nail region.

Drapé et al. have shown that high-resolution sagittal magnetic resonance images depict an oval area in the dermis beneath the nail matrix that gives a particular signal. This study defines the MRI characteristics of this area and examines its correlation with the lunula. A high-resolution surface gradient coil, especially designed for skin imaging was used on a 1.5 T magnetic resonance unit. The subnail matrix (SNM) areas of 12 subjects had a significantly longer T2 relaxation time and a higher enhancement ratio after injection of gadolinium than did the nail bed dermis. The length of the SNM area distal to the free edge of the proximal nail fold was highly correlated with the length of the lunula ($R = 0.98$) in 30 fingers and 10 toes. The total length of the SNM area was somewhat correlated with the nail thickness ($R = 0.86$) in 30 fingers. The histology and microvascularization of the subungual tissue in 21 fingers showed that this SNM area had specific features: The area was composed of loose connective tissue without bundles, and the reticular and subdermal vascular networks had large regular meshes in this oval area. The lunula is shown to be linked to a well-defined area in the underlying dermis with a specific histology and microvascularization (Drapé et al. 1996).

3.8 Synchrotron X-ray Microdiffraction Structure of Human Nail

Three layers from the outer to the inner side of the human nail were observed by synchrotron X-ray microdiffraction. These are associated with the histological dorsal, intermediate, and ventral plates. The hair-like type a-keratin filaments are only present in the intermediate layer and are perfectly oriented perpendicularly to the growth axis in the nail plate. Keratin filaments of stratum corneum type, found in the dorsal and ventral cells, are oriented in two privileged directions: parallel and perpendicular to the growth axis. This "sandwich" structure in the corneocytes and the strong intercellular junctions gives the nail high mechanical rigidity and hardness. Lipid bilayers parallel to the nail surface fill certain ampullar dilations of the dorsal plate and intercellular spaces in the ventral plate. The use of X-ray microdiffraction shows that onychomycosis disrupts the keratin structure, probably during the synthesis phase (Garson et al. 2000).

3.9 Tribological Characteristics of the Nail Surface

Abrasion, micro-induction, and sclerometry are used to investigate the reactions of the nail surface. In particular, sclerometry simulates, by a scraping technique, the effects of wear and tear on its surface. This later leads to deformities of the surface and to an appreciable removal of material. These insults produce deterioration in the morphological, mechanical, and optical properties and, thereby, the loss of the principal functions of the nail (Vargiolu et al. 1999). Simulation of the worn nail by abrasion or sclerometry facilitates the study of wear, which is the prime target of cosmetic application such as nail hardeners and surface striae and nail varnishes (resistance to wear).

3.10 Bone Scintigraphy

The value of bone scintigraphy in refining the diagnostic accuracy of enthesoarticular involvement was demonstrated in a study of patients with early psoriatic arthropathy (Namey and Rosenthall 1976).

High-resolution [^{18}F] fluoride position emission tomography of the distal interphalangeal joint in psoriatic arthritis is an exploratory study suggesting diffuse increased bone metabolism involving the entire distal phalanx periosteum and entheses (Tan et al. 2013).

4 Nail Clipping

Nail Clipping is a common procedure used in forensic analysis. However, it has been used to evaluate titanium which has been found in

patients affected by yellow nail syndrome and leading to the removal of dental implants followed by the cure of this condition (Berglund and Carlmark 2011).

References

Apolinar E, Rowe WF. Examination of human fingernail ridges by means of polarized light. J Forensic Sci. 1980;25:156–61.

Arrese JE, Piérard-Franchimont C, Greimers R, Piérard GE. Fungi in onychomycosis. A study by immunohistochemistry and dual flow cytometry. J Eur Acad Dermato Venereol. 1995;4:123–30.

Aydin SZ, Castillo-Gallego C, Ash ZR, Marzo-Ortega H, Emery P, Wakefield RJ, Wittmann M, McGonagle D. Ultrasonographic assessment of nail in psoriatic disease shows a link between onychopathy and distal interphalangeal joint extensor tendon enthesopathy. Dermatology. 2012;225:231–5.

Aydin SZ, Ash ZR, Tinazzi I, Castillo-Gallego C, Kwok C, Goodfield M, et al. The link between enthesitis and arthritis in psoriatic arthritis: a switch to a vascular phenotype at insertions may play a role in arthritis development. Ann Rheum Dis. 2013a;72:992–5.

Aydin SZ, Castillo-Gallego C, Ash ZR, Abignano G, Marzo-Ortega H, Wittman M, Del Galdo F, McGonagle D. Potential use of optical coherence tomography and high-frequency ultrasound for the assessment of nail disease in psoriasis and psoriatic arthritis. Dermatology. 2013b;227:45–51.

Baden HP. The physical properties of nail. J Invest Dermatol. 1970;55:116–22.

Baran R. Nail growth direction revisited. J Am Acad Dermatol. 1981;4:78–83.

Baran R, Achten G. Les associations congénitales de koïlonychie et de leuconychie totale. Arch Belg Dermatol Suppl. 1969;25:13–29.

Baran R, Juhlin L. Bone-dependant nail formation. Br J Dermatol. 1986;114:371–5.

Berglund F, Carlmark B. Titanium, sinusitis and the YNS. Biol Trace Elem Res. 2011;143:1–7.

Cinotti E, Fouilloux B, Perrot JL, Labeille B, Douchet C, Cambazard F. Confocal microscopy for healthy and pathological nail. J Eur Acad Dermatol Venererol. JEADV 2014;28:853–858.

Corcuff P, Levêque JL. In vivo vision of the human skin with the tandem scanning microscope. Dermatology. 1993;186:50–4.

Dawber RPR. Fingernail growth in normal and psoriatic subjects. Br J Dermatol. 1970;82:454.

de Berker DAR, Forslind B. The structure and properties of nails and periungual tissues. In: Forslind B, Linberg M, Norlen L, editors. Skin, hair and nails, structure and function. New-York: Marcel Dekker; 2004.

De Doncker P, Piérard G. Acquired nail beading in patients receiving itraconazole. An indicator of faster nail growth? A study using optical profilometry. Clin Exp Derm. 1994;19:404–6.

Debarbieux S, Hospod V, Depaepe L, Blame B, Poulalhon N, Thomas L. Perioperative confocal microscopy of the nail matrix in the management of in situ or minimally invasive subungual melanomas. Br J Dermatol. 2012;167:828–36.

Dopuglas AC. The deposition of tetracycline in human nails and teeth: a complication of long-term treatment. Br J Dis Chest. 1963;57:44–7.

Drape JL, Idy-Peretti I, Goettmann S, et al. Subungual glomus tumors: evaluation with MR imaging. Radiology. 1995;195:507–15.

Drapé JL, Wolfram-Gabel W, Idy-Peretti I, Baran R, Goettmann S, et al. The lunula: a magnetic resonance imagining approach to the subnail matrix area. J Invest Dermatol. 1996;106:1081–5.

Ekin A, Özkan M, Kabaklioglu T. Subungual glomus tumours: a different approach to diagnosis and treatment. J Hand Surg. 1997;2:228–9.

Finlay AY. The physical properties and function of nails. In: Marks R, Barton SP, Edwards C, editors. The physical nature of skin. Lancaster: MTP Press; 1988. p. 143–54.

Finlay AY, Frost P, Keith AD, et al. The rigidity of human fingernails: a biophysical investigation on influencing physical parameters. Acta Dermato Venerol. 1980;60:217–22.

Finlay AY, Moseley H, Duggan JC. Ultrasound transmission time. An in vivo guide to nail thickness. Br J Dermatol. 1987;117:765–70.

Garson JC, Baltenneck F, Leroy F, Riekel C, Muller M. Histological structure of human nail as studied by synchroton X-ray microdiffraction. Cell Mol Biol. 2000;46:1025–34.

Goettmaann S, Drape JL, Idy-Peretti I, et al. MRI: a new tool in the diagnosis of tumours of the nail apparatus. Br J Dermatol. 1994;130:701–10.

Goldman L. Transillumination of the fingertip as aid in examination of nail changes. Arch Dermatol. 1962;85:644.

Hamilton JB, Terada H, Mestler GE. Studies of growth throughout the lifespan in Japanese: growth and size of nail and their relationship to age, sex heredity and other factors. J Gerontol. 1955;10:401–15.

Hashimoto K, Gross BG, Nelson R, Lever WF. The ultrastructure of the skin of human embryos. III The formation of the nail in 16–18 week-old embryos. J Invest Dermatol. 1966;47:205–17.

Heikkila H, Stubb S, Kiistala U. Nail growth measurement employing nail indentation – an experimental follow-up study of nail growth in situ. Clin Exp Dermatol. 1996;21:96–9.

Hendricks AA. Yellow lunulae with fluorescence after tetracycline therapy. Arch Dermatol. 1980;116:438–40.

Hirai T, Fumiiri M. Ultrasonic observation of the nail matrix. Dermatol Surg. 1995;21:158–61.
Hongcharu W, Dwyer P, Gonzalez S, Anderson R. Confirmation of onychomycosis by in vivo confocal microscopy. J Am Acad Dermatol. 2000;42:214–6.
Jamieson A. Congenital malformation of the nails. Trans Med Soc Edinburgh. 1893;12:191–2.
Jemec GBE, Gniadeska M. In vivo studies of normal and psoriatic finger nails using high frequency ultrasound. Turk J Dermatopathol. 1999;8:1–5.
Kaufman SC, Beuerman RW, Greer DL. Confocal microscopy: a new tool for the study of the nail unit. J Am Acad Dermatol. 1995;32:668–70.
Kierland RR, Sheard C, Masson HL, Lobitz WC. Fluorescence of nails from quinacrine hydrochloride. JAMA. 1946;131:809–10.
Kligman AM. Why do nails grow out instead of up? Arch Dermatol. 1961;84:181–3.
Maloney MJ, Paquette EG, Shansky A. The physical properties of fingernails. Apparatus for physical measurements. J Soc Cosmet Chem. 1977;28:415–25.
Moffitt DL, de Berker DAR. Yellow nail syndrome: the nail that grows half as fast grows twice as think. Clin Exp Dermatol. 2000;25:21–3.
Mogensen M, Thomsen JB, Skovgaard LT, Jemec GB. Nail thickness measurements using optical coherence tomography and 20-MHz ultrasonography. Br J Dermatol. 2007;157:894–900.
Namey TC, Rosenthall L. Periarticular uptake of 99 mtechnicium diphosphanate in psoriatics: correlation with cutaneous activity. Arthritis Rheum. 1976;19:607–12.
Nikkels-Tassoudji N, Piérard-Franchimont C, De Doncker P, Piérard GE. Optical profilometry of nail dystrophies. Dermatology. 1995;190:301–4.
Orentreich N, Markofsky J, Vogelman JH. The effect of aging on the rate of linear nail growth. I Invest Dermatol. 1979;73:120–30.
Passareti U, Gigliotti S, Fusco M. Thermography and hand's glomus tumors. Chir Mano. 1988;25:163–6.
Perrin C, Michiels JF, Pisani A, Ortonne JP. Anatomic distribution of Melanocytes in normal nail unit "an immunohistochimical investigation". Am J Dermatopathol. 1997;19:462–7.
Piérard GE. In vivo confocal microscopy: a new paradigm in dermatology. Dermatology. 1993;186:4–5.
Piérard GE, Piérard-Franchimont C. Fractal microrelief of the skin and nail. J Internal Dermatol Pediatr. 1996a;8:75–9.
Piérard GE, Piérard-Franchimont C. Dynamics of psoriatic trachyonychia during low-dose cyclosporine A treatment: a pilot study onychochronobiology using optical profilometry. Dermatology. 1996b;192:116–9.
Schoon D. Nail structure and product chemistry. 2nd ed. Clifton Park: Thomson-Delmar Learning; 2005. p. 19–31.
Seitz CS, Hamm H. Congenital brachydactyly and nail hypoplasia: clue to bone-dependant nail formation. Br J Dermatol. 2005;152:1339–42.
Tan A, Tanner SF, Waller ML, Hensor EMA, Burns A, Jeavons AP, Bury RF, Emery P, McGonagle D. High-resolution [^{18}F] fluoride positron emission tomography of the distal interphalangeal joint in psoriatic arthritis – a bone-enthesis – nail complex. Rheumatology. 2013;52:898–904.
Vargiolu R, Zahouani H, Carpentier L. Caractérisation tribologique de la surface de l'ongle. 1er Colloque d'Ingénierie Cutanée, Arbois; 1999, 28–29 Mai
Vaudaine M. Proximal nail fold capillaroscopy. In: Baran R, editor. Dawber's nail diseases and their management. Oxford: Wiley-Blackwell; 2012. p. 125–32.
Wortsman X, Jemec G. Dermatologic ultrasound with clinical and histological correlations. New York: Springer; 2013.
Yaemsiri S, Hou N, Slining MM, et al. Growth rate of human fingernails and toenails in healthy American young adults. J Eur Acad Dermatol Venereol. 2009;24:420–3.
Young RW, Newman SB, Capott RJ. Strenght of fingernails. J Invest Dermatol. 1965;44:358–60.
Zaun H, Dill-Müller D. Kranthafte Verändermigen des Nagels. 7th ed. Balingen: Spitta Verlag; 1999. p. 60.

Nail Growth Evaluation and Factors Affecting Nail Growth

87

Shari R. Lipner and Richard K. Scher

Contents

Keywords
Nail growth • Nail measurement • Modulation of nail growth • Nail growth evaluation

1 Part I: Nail Growth Evaluation

Nail evaluations have been documented in the literature as early as 1684. However, the modern-day measuring technique dates back to 1939 by Gilchrist and Buxton in their pivotal study of nail growth. They utilized a fixed groove in the nail compared to another reference point and then measured the change over a set period of time. Subsequent studies remained similar to this original technique, although with some modifications to reference points and use of magnification and photography to increase accuracy. Figure 1 shows the reference points commonly used in nail measurements.

Robert Boyle, a physicist, was given credit for being the first to publish on nail growth in his paper that appeared in 1684 (Boyle 1684; Heller 1927). In 1871, Weir Mitchell published on the transverse serrations and the slow growth of the nails on the paralyzed hand of a 56-year-old woman under his care for a stroke. He then had the idea to stain the nails with nitric acid in men with hemiplegia to study the growth of their nails (Fritsch 1981). Nail growth has been quantitated in the literature as early as 1929, when Halban and Spitzer measured it by the distance a stain on the nail advanced from the cuticle (Halban 1928). In

S.R. Lipner (✉) • R.K. Scher
Department of Dermatology, Weill Cornell Medical College, New York, NY, USA
e-mail: shl9032@med.cornell.edu; scherri@med.cornell.edu

P. Humbert et al. (eds.), *Agache's Measuring the Skin*,
DOI 10.1007/978-3-319-32383-1_121

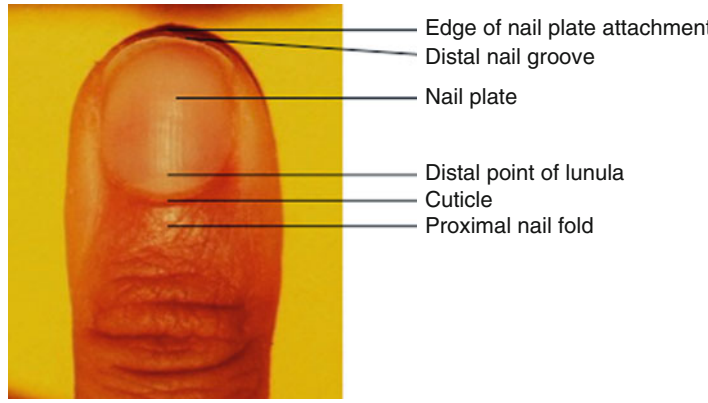

Fig. 1 Reference points for nail growth measurements

1930, Voit quantitated nail growth by measuring the weight of fingernail and toenail clippings of three subjects (Voit 1930). In 1937, Basler published on using a special "biomicrometer" to measure nail growth hourly. He measured the progression of a distance between two brass strips, one cemented to the nail and the other cemented to the skin and overlapping the nail. He also used a microscope to increase the accuracy of these measurements, but commented that this was difficult due to slight movements of the finger (Basler 1937).

The modern-day measuring technique dates back to 1939, when Gilchrist and Buxton studied nail growth in undergraduates and elementary school children in Oxford. Over the years, this method has been modified, but still remains similar to the original method described. These methods utilize an imprint of a fixed reference mark on the nail and then measuring the change in position compared to a fixed structure separate from the nail after a certain time period. Gilchrist and Buxton made a transverse scratch with a small file, described as that used for opening glass ampules, approximately 2 mm from the central point of the most distal margin of the lunula. Measurements were made with a magnifier fitted with a micrometer scale, and they were able to make measurements as small as 0.1 mm. They recorded measurements approximately once per month as the transverse scratch moved distally and thus calculated the daily growth rate of the nail. They commented that the margin of the lunula as a landmark was sharp enough for the thumb, the index, and middle fingernails, but the ring and fifth fingers were not as distinct. They also noted that the lunula might not be visible in all people, making measurements impossible. They advised that if the eponychium was obscuring the lunula, Vaseline could be rubbed over the nail (Gilchrist and Dudley Buxton 1939). While using the lunula as a fixed point has been used in many large-scale studies, one shortcoming of this reference point is that it may be blurred when using high magnification (Dawber and Baran 1987).

In 1953, Bean published on a 10-year study of the growth of his left thumbnail. He commented in this paper, referring to the previous work on the subject, that nail measurements could be made in three different ways: first, marking the nail with an indelible stain such as nitric acid; second, scoring the nail with a sharp instrument; and third, weighing or measuring clippings from the nail. He chose to make a transverse marking on the nail plate on the first of the month where the nail emerged from the cuticle and repeated this process every month. He then recorded the number of days needed for this mark to grow from this reference point to the site of separation of the nail plate from its bed. To make this mark, he first used a razor blade and later used a sharp file commonly employed to open small glass vials, as Gilchrist and Buxton described. The linear growth rate was then recalculated each year and assigned to the starting month. This technique gave average growth rates over periods of approximately 120 days. Therefore, it was appropriate for studies

lasting a few months, but not appropriate for measuring growth over periods of less than a month. It should be noted that the disadvantages of using the cuticle as reference point are that it may be damaged due to hydration, dehydration, friction, and manicuring. Furthermore, it may be hard to see or even absent in some individuals (Dawber and Baran 1987). He also showed that weights of fingernail clippings are subject to large errors because of wearing away of the nail. In addition, weight measurements are not considered accurate for short-term measurements of nail growth because it may take 5 months for changes in thickness to grow out to the point that they can be measured (Bean 1953).

Slight variations have been made to the original method described by Gilchrist and Buxton. In 1955, Hillman, like the previous authors, made the transverse mark at the convex margin of the lunula and made measurements using the lunula as a reference point. However, to increase the accuracy of the measurements, he also employed electrocardiogram-type calipers and a blocked steel ruler. He made measurements every 2–8 weeks, with an average interval of 46 days (Hillman 1955).

Later, Babcock improved nail growth measurements by taking magnified photographs over time and comparing the photographs. This allowed for optical enlargement of the distance to be measured, as well as the ability to thoroughly analyze permanent records at a later point in time. The author also commented on the difficulty of choosing a reference point for the measurements. He stated that the cuticle should not be used because it can easily be manipulated and moved. He said the same was true of the point of separation of the nail plate from its bed. He also believed that the lunula was not a good choice because as noted previously, it may not be visible on all digits. In addition, the lunula is not sharp when magnified and is blurred on photographs. Due to the shortcomings of the previous methods, he tested three reference points, namely, the phalanx bone, the skin near the nail, and the lunula. His methods were innovative, but would not pass the institutional review boards of today. He marked the nail with a deep scratch, which was then filled with bismuth amalgam. This made it radiopaque and allowed comparison with the underlying bony reference points on x-ray. A follow-up x-ray, after refilling the scratch with amalgam, allowed growth estimation. He also took enlarged photographs (6.4×) on the same day and took an average of five individual readings made with calipers. He concluded that using the lunula as a reference point along with positive transparencies was more precise for measuring growth of nails than lunula photograph or skin photograph methods. He concluded that there was no significant difference between the rate of nail growth measured by x-ray and photographs, the latter being easier to perform (Babcock 1955). This technique was modified only slightly by Sibinga who used a different optical system to magnify the photographs as high as 35-fold. This made it possible to measure nail growth daily and conduct studies of nail growth over a period as short as a month (Sibinga 1959).

In 1958, Geoghegan et al. published on nail growth in 49 naval personnel. The authors made a transverse mark at the margin of the lunula of the first and third fingernails of each hand and made weekly measurements over 2–6-week periods. They used a Beck Luminex magnifier with a scale calibrated to tenths of a millimeter (Geoghegan et al. 1958).

Four years later, Morton used a modified form of Babcock's technique to measure nail growth. He drilled small index holes (0.0135 in.) into the thumbnail using a twist drill in a thumb chuck. The holes were superficial and did not penetrate through the nail plate. These holes were then filled with black wax. The lens used to photograph the nails was 2.5× and the resulting negatives were then enlarged to a total magnification of 10×. Skin creases were used as references points. The nails were photographed once per week for a total of 12 weeks. Because Morton concluded that his technique was not sufficient to study the effects of therapy on onychomycosis, he performed a 5-month study using time-lapse cinematography. He required the patient to come to the hospital twice daily, every day, including holidays and weekends for 5 months. He used a plaster cast of the patient's hand for standardization and a

micrometer cursor that coincided with the spacing of two small holes drilled into the nail (Morton 1962).

In 1963, Bean published a 20-year study of his own nail growth, which was a continuation of his previous studies. He modified his original technique from the 10-year study with a tattoo on the proximal nail fold adjacent to the cuticle as a reference point. He tattooed his skin to make a permanent reference mark in the case that his cuticle advanced or receded (Bean 1963). He also started to use magnified photographs. He used the same technique as he continued the study as a 25-year study of his left thumbnail (Bean 1968).

In 1970, Dawber modified the original method used by Gilchrist and Buxton by using a different reference point (Dawber 1970a). He made a T-shaped scratch 3 mm from the cuticle and measured the change after a period of 27–35 days (mean 32 days) using the cuticle as the reference point. Measurements were made with an 8× magnifier calibrated with a linear scale accurate to 0.1 mm. All patients were asked to avoid pushing back their cuticles during the study. Measurement from the base of the nail to the lunula in the midline of the nail was made on the thumbs of all patients with visible lunulas.

In Bean's 30-year nail study, he continued to use a small file to make a transverse groove in the nail just at the edge of the free margin of the cuticle. He added to the measuring techniques he mentioned in his previous papers that the nail could be marked with the juice from the walnut hull or little holes could be punched or drilled into the nail. He also noted that during certain phases of the study, he took detailed photographs of the nail, in order to take measurements of the nail over short periods of time. The camera was fixed on a rack and the thumb was inserted into a wooden frame to make more precise measurements (Bean 1974).

Orentreich et al., in 1979, studied the effect of aging on linear growth. The authors used a glass slide to make a transverse groove just distal to the lunula of the nail plate. They used a glass reticule calibrated to 0.1 mm intervals, built into a magnifying glass, to measure the distances from the transverse groove proximally to the distal edge of the hyponychium and from the transverse groove distally to the distal emergence of the nail plate from the nail bed. To obtain linear growth in mm per week, these two measurements were obtained at set intervals, and their average was divided by time elapsed in weeks. To make measurements in intervals as short as 15 min, they used a split-image range finder adapted to a trinocular microscope and could make measurements with an accuracy of 0.01 um (Orentreich et al. 1979).

In Bean's 35-year study of nail growth, published in 1980, he noted that nail polish could also be used to mark the nail, but he still preferred to use a file to make a transverse groove in the nail because it was the most simple. He continued to use the same technique of making an indentation on the first of the month and measuring until the mark advanced to the free margin of the nail (Bean 1980).

A summary of nail growth measurement methods by date and with modifications is shown in Table 1. Figure 2 shows a schematic of the techniques commonly used to measure nail growth.

Nail growth measurements can also be utilized to determine drug effectiveness in onychomycosis with several variations from the methods described above. This is based upon the concept that antifungal drugs act clinically as barriers to the invasion of the fungus toward the proximal nail plate and that a normal nail plate should be produced after an effective dose of the antifungal medication is given. In addition, the nail grows out distally; however, the fungus grows in the opposite direction to nail growth. In one study, the authors marked the nail plate superficially with a scalpel parallel to the onychomycotic border, in the midline of the nail. The groove was filled with ink and distance measured from this point to the proximal nail fold. The barrier effect of the medication was then measured at monthly intervals. If the dose of the medication is effective, then the onychomycotic area will not invade proximal to the mark, and the amount of new nail plate will be reflective of normal nail plate production. If, however, the onychomycotic area invades

Table 1 Summary of nail growth measurement methods

Authors	Reference point	Notes
Gilchrist and Buxton (1939)	2 mm from distal point of lunula	Lunula not clear in 4th and 5th fingers, blurred with magnification
Bean (1953)	Cuticle	Cuticle may be damaged due to hydration, dehydration, friction, and manicuring. May be hard to see or absent in some individuals
Hillman (1955)	Convex margin of lunula	Used calipers to increase accuracy
Babcock (1955)	Lunula	Magnified photographs 6.4×
Sibinga (1959)	Lunula	Magnified photographs 35×
Geoghegan et al. (1958)	Lunula	Beck Luminex magnifier
Morton (1962)	Lunula	Drilled holes, magnified photographs
Bean (1963)	Tattoo on proximal nail fold adjacent to cuticle	Magnified photographs
Dawber (1970a)	3 mm from cuticle	8× magnifier
Orentreich et al. (1979)	Convex margin of lunula	Magnifier

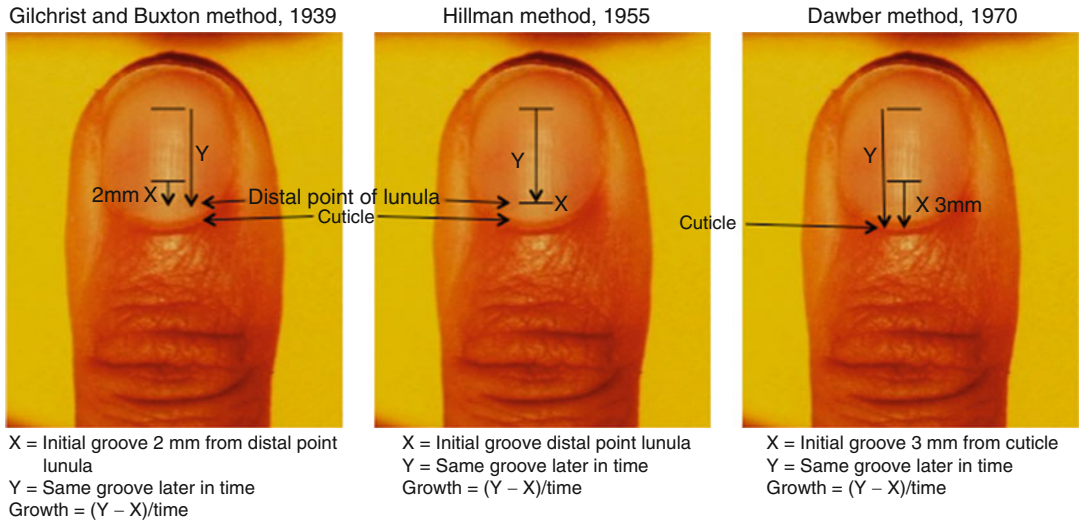

Fig. 2 Schematic for commonly used nail growth measurements

proximal to the transverse groove, then the medication is not effective at that dose. A new transverse groove can be made and evaluated monthly as the dose of the medication is increased (Zaias and Drachman 1983).

In 2002, Sawhney published a study on the effect of high altitude on nail growth, involving 22 healthy highlander troops and 6 lowlander troops. He employed the method described previously by Dawber, as he made a T-shaped cut on the nail plate of the right index finger in each subject with a blade, 3–4 mm away from the proximal nail fold. The baseline reading and the subsequent reading after 2–3 months were taken using a vernier caliper and the proximal nail fold as reference point (Sawhney 2002).

Some authors overcame the concern over variation in the non-nail plate reference point by using two reference points. This has been performed by making a scratch or a mark with a

CO_2 laser at the uppermost midpoint of the lunula and measuring the distance to the distal limit of the nail plate attachment, visible through the nail plate. Subsequent measurements are made from both the lunula and the edge of nail plate attachment. Their sum should always be equal as a way of verifying the method (Yu et al. 2004).

In 2010, Yaemsiri et al. published a study on the growth rate of fingernails and toenails in healthy American young adults. This study differed from previous studies in that measurements were made without the aid of photographs or magnification and were done by the patients. Twenty-two subjects marked their nails adjacent to the proximal nail fold with the 4-1/2 in. sapphire nail file provided. They recorded the date and the distance from the proximal nail fold to the mark using a 6-in. stainless steel ruler provided. One to 3 months later, participants repeated this measurement. Nail growth rate was calculated based on recorded distance and time between the two measurements. The standard error using this technique ranged from 0.07 to 0.12 mm per month (Yaemsiri et al. 2010).

Optical profilometry has been cited as an alternative way to study nail growth. This technique utilizes surface imaging of the nail to measure nail surface irregularities and does not require using marks or scratches on the nail plate. This technique has been reported by De Doncker and Piérard in a study of nail growth during itraconazole therapy. Nail beading was correlated with faster matrix turnover. It should be noted that only nail clippings and not entire in vivo nail plates were assessed (Doncker and Pierard 1994).

While the methods described all involve measurement of linear growth, Hamilton et al. attempted to measure volumetric growth using the equation, volume = thickness (mm) · breadth (mm) · length grown per day (mm). The authors measured thickness of the nail using micrometer calipers in the midline of clippings from the free edge of the nail. They specifically used the proximal portion of the clippings rather than the distal portion was since the latter is known to undergo crumbling or wearing away (Bean 1953). They repeated this measurement in three places, namely, the midline, the lateral edge, and the midway between the midline and the lateral edge. They noted that no significant error was introduced if the measurement was 1.0 mm from the midline in children or 3.0 mm in adults. They also noted that both humidity and dryness did not affect measurements of thickness. The calipers were fitted with a release mechanism to prevent compression of the nail. Prior to measurement, magnification of 5× was used and debris was scraped from the undersurface of the clippings using a sharp razor blade. Needlepoint calipers were used to measure the greatest breadth of the nail in the subjects. The authors noted that due to the mediolateral curvature of the nail, this value did not represent the true width of the nail. To measure length, they made an incision on the surface of the nail plate and recorded the distance it moved over a period of 6 weeks. They magnified the nail 2× and used needlepoint calipers. They used the cuticle as the reference point (Hamilton et al. 1955).

In an attempt to determine whether only the nail matrix forms the nail plate or whether there is also a contribution of the nail bed, Johnson et al. measured volumetric growth with respect to linear growth, irrespective of time. The authors used cadaveric avulsed nails and measured the thickness at three different points in the nail using either screw-gauge micrometer or vernier calipers. They calculated the thickness of each sample from the mean of three measurements. They also calculated the mass in three parts of the nail plate by calculating the surface area of each sample by tracing onto paper, weighing it on a balance, and then calculating mass as dry weight/unit area (Johnson et al. 1991).

2 Part II: Factors Affecting Nail Growth

2.1 Introduction

The nail unit is metabolically and mitotically active throughout life. The germinative layers of the nail matrix undergo DNA synthesis, divide, and differentiate to produce the nail plate without a quiescent phase. Normal growth arises from the

germinative nail matrix with a small contribution from its nail bed and proceeds linearly (Hillman 1955; Johnson et al. 1991; Baran 1981; Fleckman 1997; De Berker et al. 1996). Nail growth rates in the literature vary within a small range, and the average growth rate is 3 mm per month for fingernails and 1 mm per month for toenails (Hillman 1955; Geyer et al. 2004). Therefore, it typically takes 4–6 months for a fingernail to completely grow out and between 12 and 18 months for a toenail to completely grow out (Cohen and Scher 1992). A recent publication found a growth rate of 3.47 mm/month for fingernails and 1.62 mm/month for toenails in healthy young adults. The authors concluded that the longitudinal growth has increased over time. However, it should be noted that in this study, the subjects, rather than the physicians, took the measurements so the data may not be directly comparable to earlier studies (Yaemsiri et al. 2010).

The proliferative capacity of the nail matrix cells determines the nail growth rate. However the longitudinal growth rate can be affected by physiology, the environment, certain disease states, trauma, and treatments as shown in Table 2. It should be noted that detailed growth kinetics have been performed for some, but not all of these factors and variables. Some of the published work is based upon observations in one patient or small case series. In addition, some of the studies have shown conflicting data, which is indicated in the table and elaborated on in the text. The effect of these variables on nail growth is medically important, because some factors can be modified and medications prescribed to change the rate of nail growth. While altering the rate of nail growth by itself may not cure an abnormal nail, when used as an adjunct with other treatments, it may provide a more rapid and complete cure (Geyer et al. 2004). For instance, by decreasing the nail growth rate of psoriatic nails, which grow faster than normal, may lead to improvement in the abnormal nails in combination with psoriasis treatments (Dawber 1970b; Farber and Nall 1992). On the other hand, to treat nails affected by onychomycosis, which may grow more slowly than normal (Elewski 1998; Cohen et al. 1982; Tosti and Piraccini 2003), augmenting longitudinal nail growth in combination with antifungal drugs may lead to a better cure rate (Evans 2001; Baran and Hay 2001).

2.2 Physiology and Nail Growth

A decrease in nail growth with age was first suggested by Voit, who studied the nails of three subjects of different ages (Voit 1930). Bean studied his left thumbnail over a period of 35 years and observed a small but consistent decrease in nail growth rate as he became older. Notably, when he started the study at age 32, the nail growth rate was 3.69 mm per month, and at the end of the study at age 67, his nail growth rate was 2.85 mm/month (Bean 1953, 1963, 1968, 1974, 1980). Hillman and Hamilton et al. both confirmed the finding of decreased nail growth with age (Hillman 1955; Hamilton et al. 1955). Dawber found a decrease in nail growth with age both in normal subjects and in those with nail psoriasis (Dawber 1970a). It should be noted that Clark and Buxton and Gilchrist and Buxton in two different studies did not observe a variation in fingernail growth with age; however, they had a narrow span of younger years represented in their studies (Gilchrist and Dudley Buxton 1939; LeGros Clark and Buxton 1938). In addition, Edwards and Schott saw no effect of age on the growth of toenails (Edwards and Schott 1937).

The data on the difference in nail growth rates between men and women is controversial, but most studies have found that there is no statistically significant difference in rates between the sexes. For example, Clark and Buxton and Gilchrist and Buxton in two different reports did not observe any variation in nail growth with sex (Gilchrist and Dudley Buxton 1939; LeGros Clark and Buxton 1938). Similar results were seen by both Voit and Head and Sherren (Voit 1930; Head and Sherren 1908). In addition, Hamilton et al. found that nails in males grew faster than nails in females only in the 15–19-year-old age group. In other age groups, the results were not statistically significant (Hamilton et al. 1955). Dawber also did not observe any statistical significant difference in nail growth between men and

Table 2 Factors influencing longitudinal nail growth rates

Faster	Slower	No change	Notes
Physiology			
Younger individuals	Older individuals		A small number of conflicting studies show no difference
		Men and women	One conflicting report
Pregnancy	Postpartum	Maternal weight at conception, maternal weight gain during pregnancy, parity, duration of gestation, length of labor, maternal smoking habits	
		Birth order, age of mother at time of birth	
		Puberty	
		Within family	
Third fingernail	1st and 5th fingernails		
			Nutrition – conflicting reports, no consensus
			Right hand, left hand, handedness – conflicting reports, no consensus
		Height, weight	
		Nail thickness	
		Nail plate length	
Environment			
Day	Night		Season, weather – conflicting results, no consensus
Trauma			
Nail biting			
Nail avulsion			
		Smoking	
		Moderate stress	
	Paralysis, immobilization in splint or cast		Reversed with regaining of function in limb, massage
Disease states and nail conditions			
	Acute severe illnesses	Acute minor illnesses	Some conflicting data
A-V shunts	Cardiovascular disease		
Increased circulation	Decreased circulation		
Hyperthyroidism	Hypothyroidism		
		Family history cancer, hypertension, coronary artery disease, diabetes mellitus	
Psoriasis			
Onycholysis			
Pityriasis rubra pilaris			

(*continued*)

Table 2 (continued)

Faster	Slower	No change	Notes
Congenital bullous ichthyosiform erythroderma			
	Yellow nail syndrome		
	Brittle nail syndrome		
	Lichen planus		
	Onychomycosis		
Medications			
Fluconazole			
Terbinafine			
Itraconazole			One conflicting study
Levodopa			
Benoxaprofen			
Oral phosphate, calcitriol, calcium			
Oral contraceptives			
Biotin			
Cysteine			
	Methotrexate	Corticosteroids	
	Azathioprine		
	Psoralen with UVA therapy		
			Oral retinoids – conflicting results, no consensus
	Lithium		
	Sulfonamides		
	Gold		
	Zidovudine		
	Cyclosporine		
	Heparin		

women (Dawber 1970a). Hillman, on the other hand, found in his study that the mean nail growth rate for men was higher than that of women (Hillman 1955).

Halban and Spitzer showed that during pregnancy, nail growth rates are one fourth to one third higher than normal (Halban 1928). Hillman supported this earlier study by showing that during pregnancy, nails grow faster. He also showed that the nails grow even faster at later stages of pregnancy. Furthermore, he observed a decrease in nail growth rates postpartum. He found that nail growth rate was unaffected by maternal weight at conception, maternal weight gain during pregnancy, parity, duration of gestation, and length of labor. Maternal smoking habits had no effect on nail growth rates (Hillman 1960). In a separate study, he also found that birth order and age of the mother at time of birth had no effect on nail growth (Hillman 1955).

One study showed that there is also no change in nail growth rate with pubertal development. In this study, the authors took into account axillary hair, rate of growth of axillary hair or beard, and the incidence and severity of acne (Hamilton et al. 1955).

In a small number of subjects, in two independent studies, it was shown that there are familial patterns of nail growth. For example, Hamilton et al. found that both male and female siblings had growth rates that were similar to the rest of the family (Hamilton et al. 1955). Hillman also showed the rate of fingernail growth in a set of identical twins and a set of fraternal twins was similar between those siblings (Hillman 1955).

Clark and Buxton showed that nails on the longer fingers grew more rapidly than the shorter fingers (LeGros Clark and Buxton 1938). Hillman confirmed this finding, in that he observed the fingernail on the third fingernail grew faster than the others (Hillman 1955). This was confirmed once again by Hamilton et al., in their studies of Japanese subjects (Hamilton et al. 1955). Dawber also agreed that that middle fingernail grew more rapidly than the other nails (Dawber 1970a).

The connection between nutrition and nail growth is controversial. For example, more rapid growth of nails has been associated with better nutritional status in one study (Gilchrist and Dudley Buxton 1939). However, it should be noted that at the time the relevant study was performed, nutritional status was based on general physical appearance as opposed to clinical signs of specific nutrient deficiencies (Hillman 1960). Similarly, it was also observed that during periods of starvation, (Ivanowsky 1923) and malnutrition conditions, such as kwashiorkor and marasmus (Fitzpatrick et al. 1971), nail growth is slowed. Hamilton also mentions unpublished studies on rodents, in which nail growth is slowed with starvation (Hamilton et al. 1955). In contrast, in another study, nutritional status, as estimated by the thickness of skinfolds measured with calipers, had no effect on linear nail growth (Hamilton et al. 1955). In addition, a study was also done on ten newborn infants who were hospitalized, to evaluate the requirements of essential amino acids. For brief periods of time, single amino acids were removed from their diets, and weight gain either decreased or halted. It was found that omitting these amino acids from the diet had no effect on nail growth (Sibinga 1959). Finally, the effect of calorie restriction on nail growth was also studied in seven obese adults who were on 600/day calorie diets over 1–2 months. It was found that diet had no effect on nail growth rates (Sibinga 1959).

There is disagreement on the data for the influence of the right and left hands and handedness on nail growth rates. Some studies did not show consistent differences in growth between different hands and also showed that handedness had no effect on nail growth (Hillman 1955; LeGros Clark and Buxton 1938). However, Dawber found that on average the nails on the right hand grew faster than the nails on the left hand (Dawber 1970a).

Numerous studies have substantiated the finding that height has no effect on nail growth (Hillman 1955, 1960; Hamilton et al. 1955). Some studies have also shown that weight has no influence on nail growth rates (Hillman 1955; Hamilton et al. 1955; Hewitt and Hillman 1966). Weight gain or loss does not affect growth kinetics (Hillman 1955). Additionally, nail thickness and nail plate length do not affect the linear growth rate of the nail (Hamilton et al. 1955).

2.3 Environment and Nail Growth

Basler showed that nail growth was faster during the day than at night (Basler 1937). It has been hypothesized that this difference is due to diurnal variations in blood pressure, with lower blood pressure at night (Riddle 1908).

The effect of seasonal variation on nail growth rates is controversial. Some studies have emphasized that seasons affected the growth rate of nails, with nails growing faster in warmer weather and slower in colder weather (Gilchrist and Dudley Buxton 1939; LeGros Clark and Buxton 1938). Another report supported this association in a study of 49 sailors in the British navy in the temperate waters around Britain and on an Arctic cruise. The authors found that mean daily nail

growth in the Arctic environment was slower than in the temperate region (Geoghegan et al. 1958). Bier hypothesized that nails grow faster in warmer weather due to a relative hyperemia to the nail apparatus as opposed to slower growth in cooler weather with ischemia (Bier 1905). However, several other studies failed to demonstrate any variation of nail growth with season, and two of these studies included men exposed to varying temperatures in Antarctica (Hillman 1955; Bean 1974; Donovan 1977; Gormly and Ledingham 1983).

2.4 Trauma and Nail Growth

Trauma, such as nail biting, has been found to increase the rate of growth of nails in numerous studies (Hillman 1955; Hamilton et al. 1955; LeGros Clark and Buxton 1938). In addition, in patients with onychomycosis who failed traditional treatments, when the nails were avulsed, the fungal load was reduced, and while no formal studies were done, the trauma of the surgery may provide mechanical stimulation for faster regrowth (Zaias 1990).

One study showed that smoking has no effect on nail growth (Hillman 1955). In addition, moderate stress such as that experienced during final exam periods had no influence on nail growth rates (Hillman 1955).

Numerous studies have also shown that immobilization and paralysis cause a temporary slowing of nail growth. This was first reported as early as 1871, when Mitchell observed that the nails on the paralyzed hand of a 56-year-old woman under his care for a stroke grew more slowly than those of the unaffected hand. He subsequently studied the nails of two men with hemiplegia; he saw soon after the acute episode and found that the nails of the paralyzed hand ceased to grow. However, growth returned at its usual rate, abruptly in one man after 12 days and in the other man after 21 days, when they regained function in the limb (Mitchell 1871). This finding was confirmed by Blake, who also observed that nail growth was slowed in the paralyzed side in hemiplegia (Blake 1899). Head and Sherren also observed that nails grow slower in the paralyzed side. Interestingly, they showed similar results when there is immobilization with a limb or finger fixed in a splint or cast. They found that massage stimulated growth (Head and Sherren 1908).

2.5 Disease States and Nail Conditions and Nail Growth

While there is no change in nail growth with acute minor illnesses (Hillman 1955), most of the data support that acute severe illnesses are associated with a slowing of nail growth (Bean 1953, 1974; Sibinga 1959). Bean reported on two episodes of influenza like cold with severe respiratory infection that were associated with slowing of nail growth (Bean 1974). In addition, with the mumps, there was almost a complete cessation of nail growth (Bean 1953). Sibinga found that in all 23 patients that he studied with the measles, there was a slowing in the nail growth rate. He also found a cessation of nail growth in an adult patient with mumps complicated by orchitis and a premature infant with staphylococcus septicemia (Sibinga 1959). On the other hand, ten children with acute febrile tuberculosis did not have a slowing of nail growth (Sibinga 1959).

Chronic diseases and conditions can also affect nail growth. High-flow vascular states such as arteriovenous shunts, as well as hyperthyroidism, are associated with increased nail growth (Orentreich et al. 1979). Conversely, decreased circulation, congestive heart failure, and hypothyroidism have been reported to cause a decrease in nail growth (Orentreich et al. 1979).

Hillman noted that family history had no affect on nail growth, specifically cancer, hypertension, coronary artery disease, and diabetes mellitus (Hillman 1955).

Dawber reported that psoriatic nails affected by pitting grew faster than clinically normal nails from patients with psoriasis, which in turn grew faster than nails of healthy controls (Dawber 1970a). In addition, Dawber et al. found that nails affected by onycholysis, whether idiopathic or caused by psoriasis, grew faster than clinically unaffected nails in the same patient and faster than normal controls (Dawber et al. 1971).

Other diseases besides psoriasis, in which there is faster nail growth, are pityriasis rubra pilaris and congenital bullous ichthyosiform erythroderma (Samman 1978). It is believed that the nail matrix is hyperproliferative in these diseases (Dawber 1980).

Nail conditions may cause a deceleration or cessation of nail growth. One example is the yellow nail syndrome (YNS), which is characterized by the triad of yellow nails, lymphedema, and respiratory disease. Nail growth is significantly slowed with fingernails reported to grow 0.12–0.27 mm per week (Samman and White 1964), which is three to six times slower than the average nail growth rate (Hillman 1955; Geyer et al. 2004). The decrease in longitudinal growth is usually compensated by increased nail thickness, with the observation that "the nail that grows half as fast grows twice as thick" (Moffitt and de Berker 2000). Another nail condition in which there is slow nail growth is the brittle nail syndrome. It is characterized by dehydration of the nail plate, which may lead to breakage and splitting. Nail plates are often brittle, frayed at the distal edge, and have longitudinal ridging (Scher and Bodian 1991). In addition, lichen planus (LP) may involve nails about 10 % of the time (Samman 1961) and has been reported to result in slowed nail growth (Baran 2000; Tosti et al. 2000). There is inflammation of the nail matrix, which may lead to onychorrhexis, pterygium formation, and scarring. Inflammation of the nail bed may result in permanent dystrophy.

Nail infections can also cause a slowing of longitudinal nail growth. Onychomycosis is the fungal infection of the nails. One study showed that when onychomycosis affects more than half of the total nail plate, the growth rate of the nail is slower than the unaffected toenails (Yu et al. 2004).

2.6 Medications and Nail Growth

Many medications have been shown to accelerate the rate of nail growth. However, it should be noted that much of the data are not derived from double-blind, placebo controlled trials. In 1992, Shelley and Shelley showed that there was increased nail growth associated with fluconazole therapy (Shelley and Shelley 1992). There were also three independent studies comparing terbinafine with griseofulvin in patients with onychomycosis, all showing a higher overall growth rate with terbinafine as compared to griseofulvin therapy (Haneke et al. 1995; Faergemann et al. 1995; Baran et al. 1997). Two studies have shown increased nail growth rate with itraconazole. In one study, patients with onychomycosis were treated with a pulse regimen of 400 mg daily for 1 week per month, for a total of 3–4 months. The authors calculated an average growth rate was 2.4–2.7 mm per month in the patients treated with itraconazole, while in unaffected individuals the average growth rate was 1.1 mm per month (Doncker and Pierard 1994). There is also a published case report on a patient with YNS treated with pulse itraconazole therapy for 4 months, with an acceleration of growth (Luyten et al. 1996). However, it should be noted that in another report of eight patients with YNS treated with pulse itraconazole therapy for 6 months, there was no increase in nail growth (Tosti et al. 2002). In addition, since there were no control patients with onychomycosis or yellow nail syndromes in these studies, it is not clear whether these antifungals are accelerating nail growth or whether the nail is growing faster because the nail is cured.

There is an isolated case report of a woman treated for Parkinson's disease with levodopa for 12 months, who had an increase in nail growth on therapy (Miller 1973). There are two published studies on patients taking benoxaprofen who had an increase in nail growth rate (Fenton et al. 1982; Fenton and Wilkinson 1983). There is also an isolated case report of a patient being treated for hypophosphatemic osteomalacia with oral phosphate, calcitriol, and calcium during the time of increased bone turnover, who had increased nail growth (Hogan et al. 1984). Oral contraceptives have also been reported to increase the growth of

nails (Knight 1974). Biotin and cysteine have also been reported to increase nail growth (Piraccini and Tosti 1999). Notably, it has been shown that biotin may reduce nail fragility, while also increasing both the thickness and rate of longitudinal growth (Uyttendaele et al. 2003).

Medications can also decrease the rate of nail growth. The chemotherapeutics likely decrease the mitotic activity of the nail matrix keratinocytes. For example, methotrexate had a marked suppressive effect on nail growth in psoriatic patients (Dawber 1970b). In addition, azathioprine also decreased nail growth in patients with psoriasis, but less so than methotrexate. Interestingly, corticosteroids had no effect on nail growth in patients with psoriasis (Dawber 1970b). However, psoralen in combination with ultraviolet A therapy has been shown to slow nail growth in patients with psoriasis (Landherr et al. 1982).

The data on the effect of retinoids on nail growth is controversial, with some studies suggesting increased nail growth and others showing the opposite effect. For example, animal models show that retinoids increase nail growth (Baran 1986), and a similar finding was reported in humans in two separate studies (Fritsch 1981; Ott 1977). In addition, in a small study of 28 patients, the oral retinoid, etretinate, was shown to increase the nail growth rate in patients with psoriasis over their baseline. On the other hand, etretinate had no effect on nail growth in patients without psoriasis who were being treated with this drug for other reasons (basal cell carcinoma, basal cell nevus syndrome, lichen planus, actinic keratosis, and palmoplantar keratoderma) (Galosi et al. 1985). In other studies, there has been a slower growth of nails during oral retinoid treatment (Baran 1982). For example, in one study of 130 patients taking etretinate, linear nail growth was reduced in roughly half the patients treated (Baran 1986).

Other drugs that have been associated with a decreased nail growth rate are lithium, sulfonamides, gold, zidovudine, cyclosporine, and heparin (Piraccini and Tosti 1999). It should be noted that detailed growth kinetics were not performed.

References

Babcock MJ. Methods for measuring fingernail growth rates in nutritional studies. J Nutr. 1955;55(2):323–36.

Baran R. Nail growth direction revisited. Why do nails grow out instead of up? J Am Acad Dermatol. 1981;4(1):78–84.

Baran R. Therapeutic assessment and side-effects of the aromatic retinoid on the nail apparatus. Ann Dermatol Venereol. 1982;109(4):367–71.

Baran R. Etretinate and the nails (study of 130 cases). Possible mechanisms of some side-effects. Clin Exp Dermatol. 1986;11(2):148–52.

Baran R. Lichen planus of the nails mimicking the yellow nail syndrome. Br J Dermatol. 2000;143(5):1117–8.

Baran R, Hay RJ. New evidence for the efficacy of combination therapy in onychomycosis. Br J Dermatol. 2001;145 Suppl 60:1.

Baran R, Belaich S, Beylot C. Comparative multicenter double- blind study of terbinafine (250 mg per day) versus griseofulvin (1 g per day) in the treatment of dermatophyte onychomycosis. J Dermatol Treat. 1997;8:93–7.

Basler A. Growth processes in fully developed organisms. Med Klin 1937;1664–1666.

Bean WB. A note on fingernail growth. J Invest Dermatol. 1953;20(1):27–31.

Bean WB. Nail growth. A twenty-year study. Arch Intern Med. 1963;111:476–82.

Bean WB. Nail growth. Tweny-five years' observation. Arch Intern Med. 1968;122(4):359–61.

Bean WB. Nail growth: 30 years of observation. Arch Intern Med. 1974;134(3):497–502.

Bean WB. Nail growth. Thirty-five years of observation. Arch Intern Med. 1980;140(1):73–6.

Bier A. Hyperemia as a therapeutic agent. Chicago: Roberston; 1905.

Blake E. On the study of the hand: for indications of local and general disease. London/New York: H.J. Glaisher; Putnam's; 1899.

Boyle R. Experiments and considerations about the porosity of bodies. London: Sam Smith; 1684.

Cohen PR, Scher RK. Geriatric nail disorders: diagnosis and treatment. J Am Acad Dermatol. 1992;26(4):521–31.

Cohen JL, Scher RK, Pappert AS. The nail and fungus infections. In: Elewski BE, editor. Cutaneous fungal infections. New York: Igaku-Shoin; 1982. p. 106–22.

Dawber R. Fingernail growth in normal and psoriatic subjects. Br J Dermatol. 1970a;82(5):454–7.

Dawber RP. The effect of methotrexate, corticosteroids and azathioprine on fingernail growth in psoriasis. Br J Dermatol. 1970b;83(6):680–3.

Dawber RP. The ultrastructure and growth of human nails. Arch Dermatol Res. 1980;269(2):197–204.

Dawber R, Baran R. Nail growth. Cutis. 1987;39(2): 99–103.

Dawber RP, Samman PD, Bottoms E. Fingernail growth in idiopathic and psoriatic onycholysis. Br J Dermatol. 1971;85(6):558–60.

De Berker D, Mawhinney B, Sviland L. Quantification of regional matrix nail production. Br J Dermatol. 1996;134(6):1083–6.

Doncker PD, Pierard GE. Acquired nail beading in patients receiving itraconazole – an indicator of faster nail growth? A study using optical profilometry. Clin Exp Dermatol. 1994;19(5):404–6.

Donovan KM. Antarctic environment and nail growth. Br J Dermatol. 1977;96(5):507–10.

Edwards LP, Schott RG. The daily rate of growth of toe nails. Ohio J Sci. 1937;37:91–8.

Elewski BE. Onychomycosis: pathogenesis, diagnosis, and management. Clin Microbiol Rev. 1998;11(3): 415–29.

Evans EG. The rationale for combination therapy. Br J Dermatol. 2001;145 Suppl 60:9–13.

Faergemann J, Anderson C, Hersle K, Hradil E, Nordin P, Kaaman T, et al. Double-blind, parallel-group comparison of terbinafine and griseofulvin in the treatment of toenail onychomycosis. J Am Acad Dermatol. 1995;32(5 Pt 1):750–3.

Farber EM, Nall L. Nail psoriasis. Cutis. 1992;50(3): 174–8.

Fenton DA, Wilkinson JD. Milia, increased nail growth and hypertrichosis following treatment with benoxaprofen. J R Soc Med. 1983;76(6): 525–7.

Fenton DA, English JS, Wilkinson JD. Reversal of male-pattern baldness, hypertrichosis, and accelerated hair and nail growth in patients receiving benoxaprofen. Br Med J. 1982;284(6324):1228–9.

Fitzpatrick TB, Arndt KA, Clark WH, Eisen AZ, Van Scott EJ, Vaughan JH. Dermatology in general medicine. New York: McGraw-Hill; 1971. p. 1078.

Fleckman P. Basic science of the nail unit. In: Scher RK, Daniel CR, editors. Nails: therapy, diagnosis, surgery. 3rd ed. Philadelphia: Saunders; 1997. p. 37–54.

Fritsch P. Oral retinoids in dermatology. Int J Dermatol. 1981;20(5):314–29.

Galosi A, Plewig G, Braun-Falco O. The effect of aromatic retinoid Ro 10-9359 (etretinate). on fingernail growth. Arch Dermatol Res. 1985;277(2):138–40.

Geoghegan B, Roberts DF, Sampford MR. A possible climatic effect on nail growth. J Appl Physiol. 1958;13(1):135–8.

Geyer AS, Onumah N, Uyttendaele H, Scher RK. Modulation of linear nail growth to treat diseases of the nail. J Am Acad Dermatol. 2004;50(2):229–34.

Gilchrist ML, Dudley Buxton LH. The relation of fingernail growth to nutritional status. J Anat. 1939;73(4): 575–82.

Gormly PJ, Ledingham JE. Nail growth in Antarctic regions. Australas J Dermatol. 1983;24(2):86–9.

Halban JS, M.Z. On the increased growth of nails in pregnancy. Monatschr f Gerburtsh u Gyuak. 1928;82.

Hamilton JB, Terada H, Mestler GE. Studies of growth throughout the lifespan in Japanese: growth and size of nails and their relationship to age, sex, heredity, and other factors. J Gerontol. 1955;10(4):401–15.

Haneke E, Tausch I, Brautigam M, Weidinger G, Welzel D. Short-duration treatment of fingernail dermatophytosis: a randomized, double-blind study with terbinafine and griseofulvin. LAGOS III Study Group. J Am Acad Dermatol. 1995;32(1):72–7.

Head H, Sherren J. Injury to the peripheral nerves in man: changes in the nails associated with nerve injuries. Brain. 1908;28:263.

Heller J. Die Erkrankungen der Nagel, Jadassohn's Handbuch der Haut und Geschelechtskrankhetiten, vol. 13. Berlin: Springer; 1927. p. 34–40.

Hewitt D, Hillman RW. Relation between rate of nail growth in pregnant women and estimated previous general growth rate. Am J Clin Nutr. 1966;19(6): 436–9.

Hillman RW. Fingernail growth in the human subject; rates and variations in 300 individuals. Hum Biol. 1955;27 (4):274–83.

Hillman RW. Fingernail growth in pregnancy: relations to some common parameters of the reproductive process. Hum Biol. 1960;32:119–34.

Hogan DB, McNair S, Young J, Crilly RG. Nail growth, calcium, and vitamin D. Ann Intern Med. 1984;101(2):283.

Ivanowsky A. Physical modifications of the population of Russia under Famine. Am J Phys Anthropol. 1923;6:331–53.

Johnson M, Comaish JS, Shuster S. Nail is produced by the normal nail bed: a controversy resolved. Br J Dermatol. 1991;125(1):27–9.

Knight JF. Letter: side benefits of the pill. Med J Aust. 1974;2(18):680.

Landherr G, Braun-Falco O, Hofmann C, Plewig G, Galosi A. [Growth of finger nails in psoriasis patients undergoing PUVA therapy]. Der Hautarzt. Z Dermatol Venerol verwandte Geb. 1982;33(4):210–3.

LeGros Clark WE, Buxton LHD. Studies in nail growth. Br J Dermatol. 1938;50:221–9.

Luyten C, Andre J, Walraevens C, De Doncker P. Yellow nail syndrome and onychomycosis. Experience with itraconazole pulse therapy combined with vitamin E. Dermatology. 1996;192(4):406–8.

Miller E. Levodopa and nail growth. N Engl J Med. 1973;288(17):916.

Mitchell SW. On the growth of nails as a prognostic indication in cerebral paralysis. Am J Med Sci. 1871;61:420.

Moffitt DL, de Berker DA. Yellow nail syndrome: the nail that grows half as fast grows twice as thick. Clin Exp Dermatol. 2000;25(1):21–3.

Morton R. Visual assessment of nail growth. Med Biol Illus. 1962;12:26–30.

Orentreich N, Markofsky J, Vogelman JH. The effect of aging on the rate of linear nail growth. J Invest Dermatol. 1979;73(1):126–30.

Ott F. Treatment of psoriasis with an orally effective aromatic retinoid. Schweiz Med Wochenschr. 1977;107(5):144–7.

Piraccini BM, Tosti A. Drug-induced nail disorders: incidence, management and prognosis. Drug Saf Int J Med Toxicol Drug Exp. 1999;21(3):187–201.

Riddle O. The genesis of fault-bars in feathers and the cause of alternation of light and dark fundamental bars. Biol Bull. 1908;14:328–70.

Samman PD. The nails in lichen planus. Br J Dermatol. 1961;73:288–92.

Samman PD. The nails in disease. 3rd ed. London: Heinemann; 1978. p. 14.

Samman PD, White WF. The "Yellow Nail" syndrome. Br J Dermatol. 1964;76:153–7.

Sawhney MP. High altitude and nail growth. Indian J Dermatol Venereol Leprol. 2002;68(3):131–2.

Scher RK, Bodian AB. Brittle nails. Semin Dermatol. 1991;10(1):21–5.

Shelley WB, Shelley ED. A dermatologic diary. Portrait of a practice. Cutis. 1992;50(6):399–406.

Sibinga MS. Observations on growth of fingernails in health and disease. Pediatrics. 1959;24(2):225–33.

Tosti A, Piraccini BM. Biology of nails. In: Freedberg IM, Eisen AZ, Wolff K, Austen KF, Goldsmith LA, Katz SI, editors. Fitzpatrick's dermatology in general medicine 1. New York: McGraw- Hill; 2003. p. 159–63.

Tosti A, Piraccini BM, Cameli N. Nail changes in lichen planus may resemble those of yellow nail syndrome. Br J Dermatol. 2000;142(4):848–9.

Tosti A, Piraccini BM, Iorizzo M. Systemic itraconazole in the yellow nail syndrome. Br J Dermatol. 2002;146(6):1064–7.

Uyttendaele H, Geyer A, Scher RK. Brittle nails: pathogenesis and treatment. J Drugs Dermatol JDD. 2003;2(1):48–9.

Voit E. Uber die Grosse der Emeuerung der Homgebilde beim Menschen; die Nagel. Ztschr f Biol. 1930;90:509–24. 25–48, 49–56.

Yaemsiri S, Hou N, Slining MM, He K. Growth rate of human fingernails and toenails in healthy American young adults. J Eur Acad Dermatol Venereol JEADV. 2010;24(4):420–3.

Yu HJ, Kwon HM, Oh DH, Kim JS. Is slow nail growth a risk factor for onychomycosis? Clin Exp Dermatol. 2004;29(4):415–8.

Zaias N. The nail in health and disease. Norwalk: Appleton & Lange; 1990. p. 1–255.

Zaias N, Drachman D. A method for the determination of drug effectiveness in onychomycosis. Trials with ketoconazole and griseofulvin ultramicrosize. J Am Acad Dermatol. 1983;9(6):912–9.

The pH of the Human Nail Plate

88

S. Murdan, G. Milcovich, and G. S. Goriparthi

Contents

Keywords
Nail • pH • Surface • Tape stripping • Washing • Gender • Acidity

1 Introduction

In contrast to the large body of literature on skin pH and its alterations in certain skin disorders (Schmid-Wendtner and Korting 2006; Ali and Yosipovitch 2013; Stefaniak et al. 2013; Fluhr and Bankova 2006) and on nail properties (Gupchup and Zatz 1999; Murdan 2012), there is very little literature on the pH of the nail plate. An understanding of the nail plate pH is however extremely important. It is possible that nail plate pH has a role in the health and antimicrobial defense of the nail unit, in the same way that the acidic nature of the skin is vital to the latter's barrier properties and integrity. In this context, the pH of the nail plate was measured in our laboratory, in volunteers with healthy nails, to determine the baseline (i.e., in health) values (Murdan et al. 2011). The influences of gender, anatomical site (finger/toe), side (left/right), digit (1–5 of fingernails), and washing, on the nail plate pH, were explored. In addition, pH of the nail plate interior was measured.

The nail plate's surface pH was measured potentiometrically using an apparatus (skin pH

The work described in this chapter was supported by the School of Pharmacy, University of London (now UCL School of Pharmacy).

S. Murdan (✉) • G. Milcovich • G.S. Goriparthi
Department of Pharmaceutics, UCL School of Pharmacy, London, UK
e-mail: s.murdan@ucl.ac.uk

P. Humbert et al. (eds.), *Agache's Measuring the Skin*,
DOI 10.1007/978-3-319-32383-1_122

meter PH 905®, Courage and Khazaka GmbH, Germany) that is commonly used to measure skin pH. A hydrated planar glass electrode connected to a pH meter was placed on the nail plate. It is expected that water-soluble components of the nail plate would be extracted out of the nail plate and into the liquid interface between the nail and the pH-measuring probe. The pH of this solution would then be read by the glass electrode and would give an indication of the pH of the nail plate surface. The pH value thus obtained due to the extraction of only the water-soluble components out of the nail plate should be regarded as an apparent pH and interpreted with caution, as has been suggested for skin pH (Rieger 1989).

Measuring the pH of the nail plate surface using an apparatus originally designed for the skin presents a number of challenges. Unlike the skin, the nail plate is a hard surface, such that it is difficult to create a perfectly good interface between the nail plate and the flat glass probe. Certain nail plates, such as the little fingernails and all the toenails (except for digit 1), are too curved or have too small area, while others are too ridged, to allow measurement. Nevertheless, it was possible to measure the nail plate pH in many nail plates in 37 individuals (16 females and 21 males, aged 22–69 years old) recruited for the study.

2 Measurements

Measurements were performed in vivo following ethics approval, in an air-conditioned room where the temperature ranged from 20.1 °C to 25.2 °C (mean 22.8 ± 1.1 °C) and the relative humidity ranged from 22 % to 35 % (mean 28.0 ± 3.4 %). Volunteers rested in the room for 20 min prior to measurement to acclimatize. The pH probe was rinsed with distilled water and applied at right angle to the nail plate with gentle pressure for about 1 min before the pH was read. Multiple readings were taken to ensure the pH had stabilized and the stable pH value was then recorded. To determine the influence of washing, volunteers washed their hands with tap water and Cussons Carex® (sensitive) handwash (whose pH was 4.02) and blotted them dry using paper towels. The pH of the washed nail plates was measured immediately afterward and then at time intervals, to investigate for changes in pH with time. It was found that following washing, the nail plate pH stabilized within 20 min. Subsequently, a larger study was conducted to measure the pH of washed finger- and toenail plates, where the volunteers washed their hands and feet as described above and rested in the room for 20 min prior to measurement.

To determine the pH of the nail plate interior, the thumbnail plates were used. Following acclimatization and an initial pH measurement, the nail plates were tape stripped; an adhesive disk (D-Squame, Cuderm, Dallas, USA) was applied to the nail plate and firmly pressed by the operator for 30 s before being removed. This was repeated a number of times, and the pH of the newly exposed nail plate surface was measured after every ten strips and at the end of the experiment, when the volunteer felt tingling and discomfort at the nail and stripping was stopped. The different volunteers experienced discomfort following different extents of tape stripping. Thus, in the unwashed nails group, the volunteers received a total of either 15 (one volunteer), 20 (one volunteer), 30 (two volunteers), 40 (one volunteer), or 50 (one volunteer) strippings. In the washed nails group, the volunteers received a total of either 15 (one volunteer), 20 (five volunteers), 30 (one volunteer), and 40 (three volunteers) tape strippings. The different tolerances of the volunteers to tape stripping are likely due to interindividual variability in the mechanical properties of the nail plate, such that different amounts of nail cells/layers would be removed by each tape strip. Such interindividual variability reflects results by Tudela et al. who reported variable amounts of nail protein removed in different individuals following 20 tape strips in each volunteer (Tudela et al. 2008).

3 Results and Discussion

3.1 pH of Unwashed Nail Plate Surface

The pH of the nail plate surface was found to be acidic (Table 1). The mean (± SD) pH of the surface of unwashed nail plates was 5.0 ± 0.5, with a minimum of 3.4 and a maximum of 6.3 measured in 157 fingernails and 33 big toenails in 15 males and 13 females. These pH values are expected to be due to the extraction of water-soluble components of the nail plate into the liquid interface between the nail plate and the pH-measuring probe, as well as residual cosmetics such as hand creams and the presence of sweat (which has a pH of 5–7 (Agache and Candas 2004)) and sebum (a large proportion of which is made up of free fatty acids (Agache 2004)) on the nail plate. Low levels of sebum have been measured on the nail plates (Murdan et al. 2012); sweat and sebum may be present on the nails following contact between the skin and nail and/or their flow from the surrounding skin onto the nail plate.

General linear model statistical analysis showed an influence of gender and anatomical site (finger/toe), with nail plate pH being higher in males and in toenails ($p < 0.01$), while side (right/left) had no influence ($p = 0.2$). In addition, no significant differences were found among the pH of the ten fingernails ($p > 0.01$, repeated measures ANOVA using pH values from 15 volunteers where it had been possible to measure all ten fingernails). A lack of difference in nail plate pH between right and left sides and among the ten fingernails could be due to the similar environments experienced by the right and left hands or feet and by the digits.

It is not known why toenail pH was statistically higher than fingernail pH (Table 1). Toenail plates are thicker, grow at a slower rate compared to fingernails (Fleckman 2005), and allow a smaller transonychial water loss than the fingernails (Murdan et al. 2008). It is interesting, though, to note that the higher toenail pH (compared to fingernail pH) reflects the statistically higher foot skin pH compared to hand skin pH reported in a small cohort of Japanese men (Chikakane and Takahashi 1995). Although the reason for the higher toenail pH is unclear, it may have clinical significance. If the acidic nature of the nail plate does have a role in antimicrobial defense, the lower acidity of toenail plate (compared to the fingernails) might contribute to their greater susceptibility to onychomycosis (fungal infections of the nail). Indeed, a higher incidence of onychomycosis (Midgley et al. 1994), greater recalcitrance to treatment, and the need for longer treatment duration in toenails compared to fingernails are well known (BNF 2012). The higher toenail pH might also favor the production of fungal spores; the latter's production by *Trichophyton rubrum* – was shown in vitro to increase when the medium pH was increased from pH 4.5 to pH 7.5 and to decrease thereafter (Yazdanparast and Barton 2006). A higher toenail pH could favor the presence of fungal spores,

Table 1 Measured pH of unwashed and washed finger- and toenail plate surface in males and females (Reproduced with permission from Murdan et al. 2011)

	pH of the nail plate surface			
	mean ± SD			
	(Minimum-maximum; N = number of nails in n = number of volunteers)			
	Unwashed nails		Washed and rested nails	
Gender	Fingernails	Toenails	Fingernails	Toenails
Males	5.1 ± 0.5 (3.4–6.1; $N = 87$ in $n = 10$)	5.3 ± 0.4 (4.5–6.3; $N = 20$ in $n = 10$)	5.1 ± 0.5 (3.9–6.4; $N = 125$ in $n = 13$)	5.3 ± 0.7 (4.1–6.9; $N = 20$ in $n = 11$)
Females	4.8 ± 0.4 (3.8–5.7; $N = 70$ in $n = 7$)	5.4 ± 0.5 (4.4–5.8; $N =$ 13 in $n = 7$)	5.1 ± 0.6 (3.9–6.5; $N = 79$ in $n = 9$)	5.1 ± 0.6 (4.7–6.9; $N = 13$ in $n = 7$)

which provide a reservoir for fungal infection. The influence of gender on nail plate pH is discussed in the next section.

3.2 pH of Washed Nail Plate Surface

In order to remove the possible influence of extraneous substances such as residual cosmetics on the nail plate pH, nails were washed. Immediately after handwashing and drying, the pH of the fingernail surface increased, from a mean ± SD of 5.1 ± 0.4 to 5.3 ± 0.5 (paired *t*-test, $p < 0.01$, $N =$ 140 fingernails in 14 volunteers). This could be due to the nails being exposed to high pH during washing. Although the liquid cleanser had a pH of 4.02, the pH of the washing solution (cleanser + tap water) would have been much higher, the pH of a 2 %w/w aqueous solution of the cleanser in tap water being measured to be 7.90. The raised nail plate pH was however not sustained with time, as shown in Fig. 1. Within 20 min of washing, the pH had decreased to prewashing levels. The transient increase in the pH of the nail plate surface and subsequent return to prewashing levels reflect the profile of skin pH upon washing (Gfatter et al. 1997; Korting et al. 1987).

Subsequently, a larger study was conducted to measure the pH of washed, dried, and rested (for at least 20 min) finger- and toenail plates. The mean (± SD) pH of the surface of washed nail plates was found to be 5.1 ± 0.6, with a minimum of 3.9 and a maximum of 6.9 measured in 204 fingernails and 32 big toenails in 13 males and 9 females. The pH of toenail plates was higher than those of fingernail plates (Table 1, general linear model, $p = 0.01$), while right/left side and gender had no influence ($p > 0.2$). As for the unwashed nails, the pH of the ten fingernails did not differ significantly (repeated measures ANOVA, $p = 0.2$, pH of all ten fingernails measured in 15 volunteers).

When the pH of washed and unwashed nails were compared (Table 1), it was found that washing did not significantly influence finger- and toenail plate pH in males (independent t-tests ($p \geq 0.5$, Table 1)). In females, however, washed fingernails had a significantly higher pH than unwashed ones ($p < 0.01$), while there was no difference in the pH of their toenails ($p \geq 0.5$). This suggests that washing removed something from the fingernails, such as hand creams. The fact that gender influenced the pH of unwashed nails, but not that of washed ones, indicates that the lower pH in females' unwashed nails was due to an exogenous factor, such as residual hand creams. The use of cosmetics such as moisturizers has been suggested as a potential reason for reported differences in skin pH between males and females and for the conflicting reports on the influence of gender on skin pH (Burry et al. 2001), although a recent systematic study found consistently higher skin (forehead, cheek, neck,

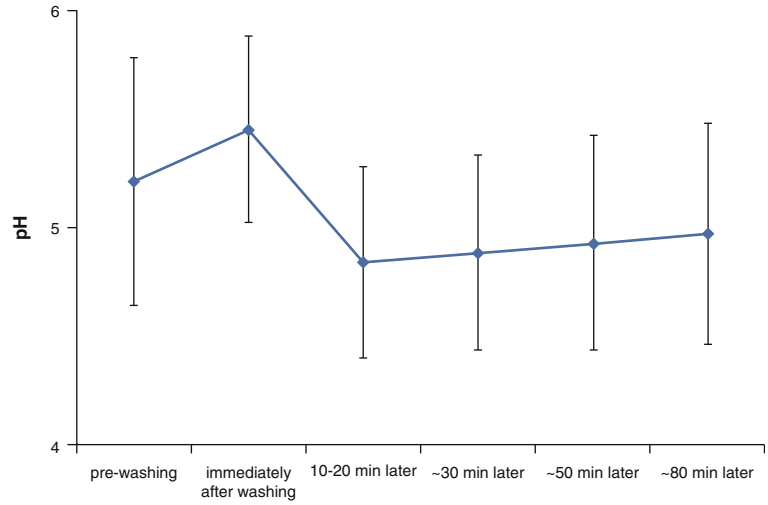

Fig. 1 Change in nail plate surface pH upon washing and subsequently with time. The latter is given as an approximation, rather than a definite value as the time varied slightly for each volunteer and for each nail, depending on the durations of pH measurements (Reproduced with permission from Murdan et al. 2011)

forearm, and hand) pH in females compared to males (Luebberding et al. 2013). Further studies where volunteers refrain from using topical products on the hands and feet and use the same cleansers for washing, for a run-in phase prior to measurement of nail plate pH, could shed more light on the influence of gender on nail plate pH.

3.3 pH of the Nail Plate interior

Tape stripping removes nail plate cells, and the newly exposed nail plate surface appears somewhat "flaky" (Fig. 2) with volunteers complaining of a tingling sensation at the nail once a certain number of strips had been removed. Different volunteers had different numbers of tape stripping performed before they complained of discomfort and before the experiment was stopped; hence, pre-stripping and post-stripping pH for each volunteer were compared to investigate for differences, if any, between the surface and interior nail plate pH. For unwashed nails, a statistically significant difference (paired *t*-test, $p < 0.05$; $N = 12$ thumbnails in six volunteers) was found, with the pH of the nail plate interior (4.1 ± 0.7) being lower than that of its surface (4.7 ± 0.7). For washed nails (20 thumbnails in ten volunteers), the pH of the nail plate interior was also slightly lower (4.8 ± 0.6) than that at its surface which were 5.1 ± 0.5 (before washing) and 5.2 ± 0.7 (after washing and resting).

Fig. 2 The "flaky" appearance of the nail plate surface after tape stripping. This volunteer received a total of 15 tape strips, at which point he felt discomfort and tingling (Reproduced with permission from Murdan et al. 2011)

The lower pH of the nail plate interior could be due to enhanced extraction of acidic, water-soluble nail components during the pH measurement, once the topmost nail layers had been removed by tape stripping. The topmost layer of the nail plate is known to be the least permeable part of the nail plate, and its removal results in increased permeation of chemicals into the nail plate (Kobayashi et al. 1999). Similarly, removal of the topmost nail layer is expected to increase the movement of molecules out of the bulk of the nail plate and into the liquid interface between the nail plate and the pH-measuring probe. A decrease in nail plate pH upon tape stripping reflects the **initial** reduction in skin pH upon tape stripping that has been observed prior to an increase in skin pH upon further tape stripping (Wilhelm et al. 1991; Berardesca et al. 1998; Wagner et al. 2003; Ohman and Vahlquist 1994).

4 Conclusions

The pH of the nail plate surface was measured to be around 5, with toenails having significantly higher pH than fingernails. There was no difference, however, among the ten fingernails or between the two great toenails. Gender influenced the pH of unwashed fingernails – with women having lower pH compared to men – but had no influence on the pH of washed ones, suggesting the influence of an exogenous factor on women's lower fingernail pH. Washing the nails with a liquid cleanser and tap water transiently increased pH, which subsequently returned to prewashing values within 20 min. Tape stripping the nail plates in order to measure the pH of the nail plate interior revealed a lower pH inside the nail plate compared to its surface.

This study has shown that it is possible to measure the surface pH of nail plates using the Courage and Khazaka skin pH meter, although a long stabilization time is needed, and the small area and high curvature of certain nail plates preclude their measurement.

5 Future Work

The study has established pH values of healthy finger- and toenail plates. Much more needs to be done, to understand the origin and significance of the nail plate acidity and any changes in the diseased state. The influence of factors such as aging, environment, and systemic disease, e.g., diabetes, on the nail plate pH could indicate how these factors predispose one to develop nail diseases such as onychomycosis. Changes, if any, in diseased nails should enable a greater understanding of these diseases and investigations into new prevention and treatment modalities. For example, changes in nail plate pH in onychomycosis, if any, could shed light on factors which influence fungal colonization and infections. Fungi are known to detect and respond to their environmental pH, secreting the appropriate proteolytic enzymes, which allows fungal invasion and subsequent infection (Martinez-Rossi et al. 2012). The dermatophyte, *T. rubrum*, has also been shown to alter the pH of the growth medium to pH values ranging from 8.3 to 8.9, irrespective of the initial medium pH (Ferreira-Nozawa et al. 2003). Whether such a change in nail plate pH occurs in vivo in onychomycotic nails remains to be seen. The difficulties of using the glass electrode of the pH meter were mentioned above. An electrode that is more flexible and smaller in area is needed to enable more accurate measurements on nail plates.

References

Agache P. Sebaceous physiology. In: Agache P, Humbert P, editors. Measuring the skin. Berlin: Springer; 2004. p. 271–80.

Agache P, Candas V. Eccrine sweat glands. In: Agache P, Humbert P, editors. Measuring the skin. Berlin: Springer; 2004. p. 302–9.

Ali SM, Yosipovitch G. Skin pH: from basic science to basic skin care. Acta Derm Venereol. 2013; 93(3):261–7.

Berardesca E, et al. Differences in stratum corneum pH gradient when comparing white Caucasian and black African-American skin. Br J Dermatol. 1998;139(5): 855–7.

BNF. British national formulary. 63rd ed. London: BMJ Group & RPS Publishing; 2012.

Burry JS, et al. Erroneous gender differences in axillary skin surface/sweat pH. Int J Cosmet Sci. 2001; 23(2):99–107.

Chikakane K, Takahashi H. Measurement of skin pH and its significance in cutaneous diseases. Clin Dermatol. 1995;13(4):299–306.

Ferreira-Nozawa MS, et al. The dermatophyte Trichophyton rubrum secretes an EDTA-sensitive alkaline phosphatase on high-phosphate medium. Braz J Microbiol. 2003;34(2):161–4.

Fleckman P. Structure and function of the nail unit. In: Scher R, Daniel III CR, editors. Nails. Diagnosis therapy surgery. Philadelphia: Elsevier Saunders; 2005. p. 13–25.

Fluhr J, Bankova L. Skin surface pH: mechanism, measurement, importance. In: Serup J, Jemec GBE, Grove GL, editors. Handbook of non-invasive methods and the skin. Boca Raton: Taylor & Francis; 2006. p. 411–20.

Gfatter R, Hackl P, Braun F. Effects of soap and detergents on skin surface pH, stratum corneum hydration and fat content in infants. Dermatology. 1997;195(3):258–62.

Gupchup GV, Zatz JL. Structural characteristics and permeability properties of the human nail: a review. J Cosmet Sci. 1999;50(6):363–85.

Kobayashi Y, et al. Drug permeation through the three layers of the human nail plate. J Pharm Pharmacol. 1999;51(3):271–8.

Korting HC, et al. Influence of repeated washings with soap and synthetic detergents on ph and resident flora of the skin of forehead and forearm – results of a crossover trial in healthy probationers. Acta Derm Venereol. 1987;67(1):41–7.

Luebberding S, Krueger N, Kerscher M. Skin physiology in men and women: in vivo evaluation of 300 people including TEWL, SC hydration, sebum content and skin surface pH. Int J Cosmet Sci. 2013;35(5): 477–83.

Martinez-Rossi NM, et al. Role of pH in the pathogenesis of dermatophytoses. Mycoses. 2012;55(5): 381–7.

Midgley G, Moore MK, Cook JC. Mycology of nail disorders. J Am Acad Dermatol. 1994;31:S68–74.

Murdan S. The nail: anatomy, physiology, diseases and treatment. In: Murthy SN, Maibach H, editors. Topical nail products and ungual drug delivery. Boca Raton: CRC Press, Taylor & Francis; 2012. p. 1–36.

Murdan S, Hinsu D, Guimier M. A few aspects of transonychial water loss (TOWL): inter-individual, and intra-individual inter-finger, inter-hand and inter-day variabilities, and the influence of nail plate hydration, filing and varnish. Eur J Pharm Biopharm. 2008;70(2):684–9.

Murdan S, Milcovich G, Goriparthi GS. An assessment of the human nail plate pH. Skin Pharmacol Physiol. 2011;24(4):175–81.

Murdan S, Milcovich G, Goriparthi G. Is there any sebum on the nail plate surface?. In: UK PharmSci conference. Nottingham; 2012.

Ohman H, Vahlquist A. In-vivo studies concerning a ph gradient in human stratum-corneum and upper epidermis. Acta Derm Venereol. 1994;74(5):375–9.

Rieger M. The apparent pH of the skin. Cosmet Toiletries. 1989;104:53–60.

Schmid-Wendtner MH, Korting HC. The pH of the skin surface and its impact on the barrier function. Skin Pharmacol Physiol. 2006;19(6):296–302.

Stefaniak AB, et al. International guidelines for the in vivo assessment of skin properties in non-clinical settings: part 1. pH. Skin Res Technol. 2013; 19(2):59–68.

Tudela E, et al. Tape stripping on a human nail: quantification of removal. Skin Res Technol. 2008; 14(4):472–7.

Wagner H, et al. pH profiles in human skin: influence of two in vitro test systems for drug delivery testing. Eur J Pharm Biopharm. 2003;55(1):57–65.

Wilhelm D, Elsner P, Maibach HI. Standardized trauma (tape stripping) in human vulvar and forearm skin – effects on transepidermal water-loss, capacitance and ph. Acta Derm Venereol. 1991;71(2):123–6.

Yazdanparast SA, Barton RC. Arthroconidia production in Trichophyton rubrum and a new ex vivo model of onychomycosis. J Med Microbiol. 2006;55(Pt 11): 1577–81.

High-Frequency Ultrasound of the Nail

89

Charles B. Kromann, Ximena Wortsman, and Gregor B. E. Jemec

Contents

Keywords

Imaging • Ultrasound • Skin • Nail • Anatomy

The nail is of functional and cosmetic importance and therefore constitutes a sensitive area for most patients. Clinical diagnosis may also pose a challenge, but the usual diagnostic recourse to biopsy is influenced by the risk of subsequent scarring and risk of lasting nail deformities. In addition patients would often prefer noninvasive diagnostics. High-frequency ultrasound imaging is therefore a suitable and generally available technique for nail studies.

1 About Ultrasound

Ultrasonography is real-time noninvasive diagnostic imaging based on a principle of inaudible sound waves that are transmitted through the material examined and the analysis, of the subsequent reflected echoes, which is converted to a two-dimensional visualization of the material. The sound waves are characterized by their amplitude, propagation speed, and frequency. Differences in the reflected sound waves are caused by the different acoustic impedances of different substances changing the amplitude or propagation speed of the sound waves. Generally hard or dry materials and air have higher impedance shown as (hyperechoic) bright areas, whereas fluids have low impedance and are shown as (hypoechoic) dark areas (Wortsman and Jemec 2006; Bitsch et al. 2011).

C.B. Kromann (✉)
Department of Dermatology, Roskilde, Zealand University Hospital, University of Copenhagen, Copenhagen, Denmark
e-mail: charles.kromann@gmail.com

X. Wortsman
Department of Radiology and Department of Dermatology, Institute for Diagnostic Imaging and Research of the Skin and Soft Tissues, Clinica Servet, Faculty of Medicine, University of Chile, Santiago, Chile

G.B.E. Jemec
Department of Dermatology, Roskilde Hospital, University of Copenhagen, Roskilde, Denmark
e-mail: gbj@regionsjaelland.dk

P. Humbert et al. (eds.), *Agache's Measuring the Skin*,
DOI 10.1007/978-3-319-32383-1_123

In standard grayscale mode (B-mode) ultrasound, the frequency is constant. High frequencies generally create high resolution and shallow penetration, whereas low frequencies yield low resolution but deeper penetration.

When analyzing changes in the frequencies of reflected echoes, it is possible to visualize movement of material, most often flow of liquids through Doppler ultrasound. This is often shown as a blue to red color overlay (color Doppler mode) or as monochrome overlay (power Doppler mode) on the B-mode ultrasound visualization. Flow in selected areas of the examined material can be further explored both visually and auditory by using spectral Doppler mode.

A static computer-assisted three-dimensional visualization is also a possibility in many ultrasonographic devices enabling an overview of complex lesions such as the nail apparatus (Bitsch et al. 2011).

2 Technical Features/Handling

Many different ultrasound devices are marketed, and modern equipment is readily available in many hospitals that provide a wide range of capabilities, which include the technical capability to image the skin and the nail. The quality of imaging equipment has generally improved, prices have decreased, and handheld devices are now widely available and affordable.

The ultrasound device is basically a computer connected to specialized transducer containing the piezoelectric crystals. As in personal computers, big processors and screens with high numbers of pixels provide better images. High-frequency transducers usually linear or compact linear probes (hockey stick shaped) are commonly used for studying the skin and nail (Bitsch et al. 2011).

These variable frequency probes range in their upper frequencies between 15 and 22 MHz; however the same probes may also work in lower frequencies that range from 7 to 8 MHz. Therefore the operator may set the parameters of the machine according to the depth of the anatomical structure under study. This range will suffice in both appropriate depth and high resolution, with higher frequencies being more suitable for the imaging of the nail apparatus.

An abundance of gel should be used to discriminate all the layers of the skin or nail from top to bottom. As opposed to internal organs, a minimum of pressure should be applied to avoid thinning out layers of the skin or closing vasculature.

The digit under examination should be as extended as possible to ensure recognizable landmarks during scanning. Longitudinal and transverse planes should be scanned through. B-mode (grayscale), Doppler color flow, Doppler power flow, and (rarely) Doppler spectral analyses can be relevant regarding the nail (Wortsman and Jemec 2006; Wortsman 2013).

3 Anatomy/Acoustic Properties of the Nail

3.1 Anatomy of the Nail

The anatomy of the nail unit is well described. The surface anatomy consists of the nail plate, the proximal and lateral nail folds, the lateral nail grooves, and the eponychium. The nail plate itself can be described as convex both longitudinally and transversely – with a distal free margin, a hyponychium, a central nail plate, and a proximal lunula. Changes in the nail plate are described in ▶ Chap. 92, "Gene Expression and Genetic Evaluation of the Skin."

Beneath the nail plate is the nail bed. Proximally, underlying the lunula is the nail matrix and nail sinus producing the keratinocytes of which the nail plate consists and further distally the nail bed consists of a thin epidermis overlying a collagenous dermis and the distal phalanx.

The most prominent nerves and vessels in the digits run on the palmar side. Both the neural and arterial supply to the distal phalanx is primarily provided by palmar conduits; however the nail matrix is supplied from the dorsal arterial arcade. Clusters of arteriovenous shunts, glomus bodies, are found in the nail bed (Fleckman 2005).

The entheses of extensor tendons are found adjacent to the nail matrix.

4 Normal Nail Sonography

The different tissues of the nail have different densities and thus different echogenicities. The nail plate has a characteristic bilamellar structure with a central hypoechoic interplate space (Jemec and Serup 1989). See Fig. 1. The speed of sound in the nail plate has been determined at 2459 m/s, compared to the 1580 m/s estimated speed of sound in the skin. It is thought that the bilamellar structure reflects the water (35 %) distribution in the nail plate, with a dry outer compartment in which the speed of sound is 3103 m/s and a deeper more humid compartment in which the speed of sound is 2125 m/s (Jemec and Serup 1989).

Under the nail bed, it is possible to detect the hyperechoic linear bony margin of the distal phalanx. Proximally to the nail plate and in close proximity to the mail matrix, the insertion of the extensor digitorum tendon on the phalanx can be visualized. Low-velocity blood flow can be detected in the nail bed, usually close to the bony margin of the distal phalanx (Fig. 2). The

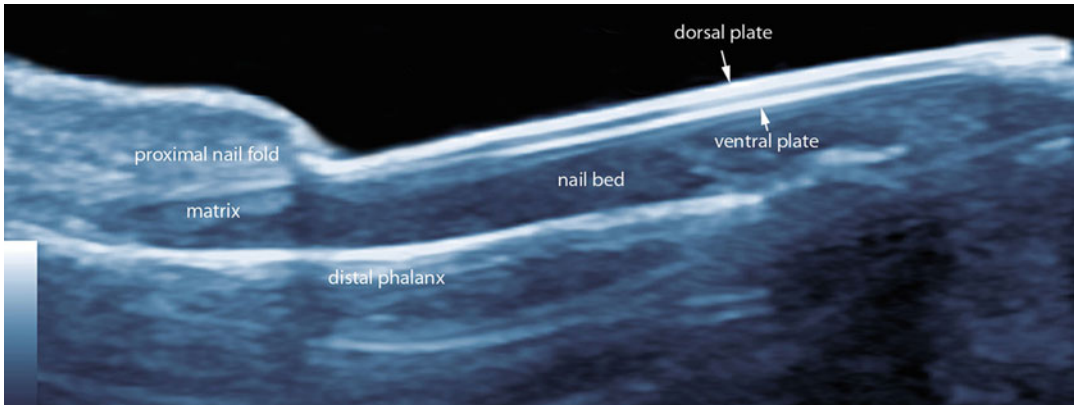

Fig. 1 Ultrasonography of normal nail plate (*grayscale*, longitudinal view) showing the different part of the nail unit

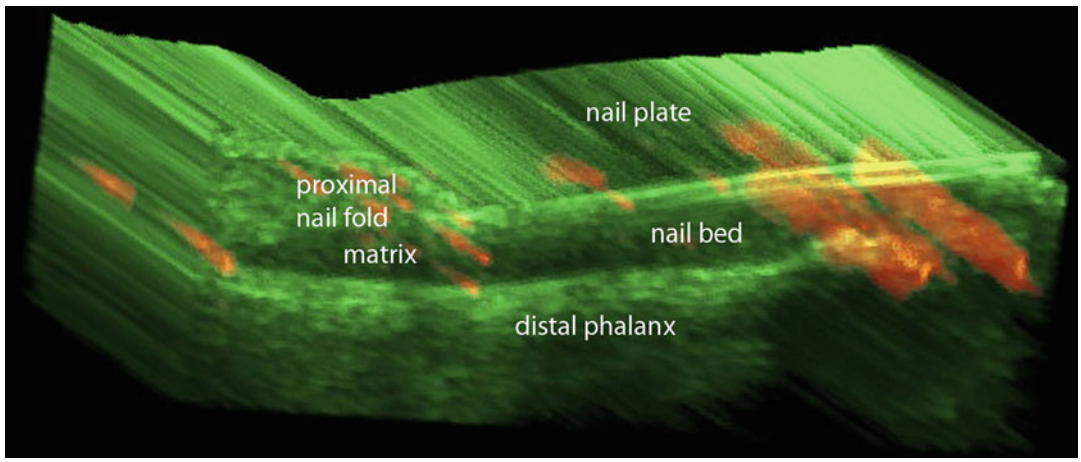

Fig. 2 3D power Doppler reconstruction of the nail unit (longitudinal view) demonstrates the vascularity (*red color*) within the nail bed

Table 1 Sonographic nail findings

Pathology	Typical findings
Alopecia areata	In alopecia areata, two thirds of patients have somewhat unspecific nail involvement, which however may precede scalp affection. Most often nail pitting and nail dystrophy are seen similar to nail changes in psoriasis. However, in contrast with psoriasis, usually the nail bed is hypovascular (Wortsman 2013)
Ichthyosis	Often nails are thickened and the hypoechoic thin layer between the dorsal and ventral plates is no longer discernible (Wortsman and Aranibar 2001)
Benign tumors	Glomus tumors – these benign vascular tumors are derived from the neuromyoarterial glomus and clinically present exquisite pain in the nail region. Sonographically, they appear as a hypoechoic well-defined nodule that commonly shows hypervascularity. Scalloping of the bony margin of the distal phalanx is a frequent associated finding (Wortsman and Jemec 2009)
	Onychomatricoma – seen as yellow bands along the nail. Sometimes added convexity can make the nail cone shaped. Often hypoechoic areas with hyperechoic spots or lines of the nail bed and interplate space are seen. The underlying bone is usually unremarkable (Soto et al. 2009)
	Keratoacanthoma – these squamocellular neoplasms can rarely occur in the nail bed. Appears as a well-defined solid mass with a central cystic/anechoic area surrounded by hypoechoic tissue and enhancement artifact. Can affect both nail plate and bony margin. With Doppler the tumor will show hypovascularity (Choi et al. 2007)
	Granuloma – a chronic proliferative inflammatory scarring reaction most often involving periungual tissue, but also nail bed or even matrix. Sonographically hypoechoic lesion without sharp demarcation. Increased nail bed thickness, corrugated upward skewed nail plates (Wortsman et al. 2010b)
	Verrucae – subungual warts are hypoechoic spindle-shaped elements resulting in thickened nail plates (Wortsman et al. 2010c)
Dermatomyositis	A telltale sign in prolonged disease is the calcinosis. Small epidermal fingertip calcium deposits visualized as hyperechoic deposits with pronounced posterior acoustic shadowing (Wortsman 2013)
Malignant tumors	Bowen disease – no early diagnosis is possible in Bowen disease; however in later stages an hypoechoic solid mass that erode the nail plate may be found (Wortsman 2013)
	Malignant melanoma – when arising from the nail matrix, it is typically seen as a dark-pigmented longitudinal stripe involving the lunula and the hyponychium. Early diagnosis by sonography is difficult, because pigments are currently not detected by ultrasound. Nevertheless, hypoechoic ill-defined areas and localized hypervascularity may be found. In later stages, a hypoechoic solid tumor can be seen (Wortsman 2013)
Onychomadesis	Onychomadesis is basically a Beau line with full separation, instead of an indentation. After nail growth arrest onychomadesis is seen. The nail plate separates from the matrix. Typically two unconnected hyperechoic nail plates are seen. Often the distal nail plate is somewhat thickened (Wortsman et al. 2010a)
Psoriasis	Psoriatic nail involvement is linked to psoriatic arthritis and severity of skin disease. Classic findings are thickened nail beds measured by the distance between the nail plate and the phalanx. Thickening of both plates and blurring of the ventral nail plate. In late disease even blurring of dorsal plate is seen as well. Corrugated nail plate can be seen
	Hypervascularity in the nail bed during active disease giving increased Doppler activity (Gutierrez et al. 2009)
Scleroderma	Vascular damage is in focus with nail pathology in scleroderma patients. Thickened nail beds with lower echogenicity and thickened nail plates with loss of interplate space. Commonly the nail bed shows hypovascularity (Wortsman et al. 2011)
SLE	Irregular nail beds and plates and hypovascularity are often seen (Wortsman et al. 2011)
Subungual abscess	Anechoic areas with acoustic enhancement and inflamed and thickened nail beds. Hyperechoic air bubbles may be present. Sinus tracts increasing the risk of joint affection or osteitis can be followed if present (Wortsman 2013)

skin surrounding the nail plate is almost devoid of fat, though in other ways no different from a normal skin sonography (Wortsman and Jemec 2006; Wortsman 2013).

5 Pathology/Applications

Diagnosing ungual, subungual, or periungual pathologies clinically is often difficult as the nail plate naturally prevents closer inspection. Similarly, the use of diagnostic biopsies through the nail or in the periungual area is often painful or unpleasant to the patient and potentially harmful as the nail matrix is easily damaged leaving the patient with a permanent defect in a cosmetically important area.

The convenience and the noninvasive dynamic nature of ultrasound enable the early diagnosis of common nail pathology. The use of this imaging method relies on an interpretation of basic sonographic tissue characteristics:

1. Inflammation: The inflammation causes dilatation of vessels and subsequent edema and possibly abscess formation. The vascular changes are best visualized using color Doppler or power Doppler, which shows hypervascularity and increased flow. Inflammation generally presents as associated hypoechoic areas. In older lesions a reactive thickening of the nail bed will often be seen.
2. Tumors: The sonographic image depends on the density of the tumor. When measuring tumors, using a standard procedure is therefore an advantage. Diagnostically, it is important to know the precise position of the tumor, size, composition, what structures are involved, and if it is hypo- or hypervascularized.
3. Abscess or cysts: Fluid-filled cavities with or without air appear anechoic and show no Doppler activity, but often enhancement artifacts, where underlying tissue appears hyperreflective.

A summarized review of nail pathologies as identified by ultrasound is given in Table 1.

6 Conclusion

High-frequency ultrasound of the nail can give valuable clues and support early diagnoses and is easy to use. Both rare and more frequent lesions can be diagnosed with ultrasound examination in context of the clinical work-up.

Sonography is not the same as, e.g., histology. It is not as detailed and does not allow the same detail of diagnosis, but it offers an important advantage over histology as it provides functional real-time information about the tissue as well. A prime example of this is the bilamellar images of the nail plate, where sonography reflects hydration which would otherwise not be seen. Similarly, the density and perfusion of tissue are readily available in ultrasound, but not in histology, making it an important imaging method for clinical manifestations in the skin.

The simple and dynamic nature of the sonographic examination and the ready accessibility compared to the, e.g., magnetic resonance imaging are important factors when choosing diagnostic methods. Lastly, sonography can offer a noninvasive window into the physiopathology of nail diseases.

References

Bitsch M, Bessmann EL, Jensen F. Hvad er ultralyd? In: Bitsch M, Jensen F, editors. Klinisk Ultralyd Skanning. Copenhagen: FADL; 2011.

Choi JH, Shin DH, Shin DS, Cho KH. Subungual keratoacanthoma: ultrasound and magnetic resonance imaging findings. Skeletal Radiol. 2007;36:769–72.

Fleckman P. Structure and function of the nail unit, Chapter 3. In: Scher RK, Daniel C, editors. Nails. 3rd ed. Philadelphia: Elsevier; 2005.

Gutierrez M, Wortsman X, Filippucci E, De Angelis R, Filosa G, Grassi W. High-frequency sonography in the evaluation of psoriasis: nail and skin involvement. J Ultrasound Med. 2009;28:1569–74.

Jemec GB, Serup J. Ultrasound structure of the human nail plate. Arch Dermatol. 1989;125:643–6.

Soto R, Wortsman X, Corredoira Y. Onychomatricoma: clinical and sonographic findings. Arch Dermatol. 2009;145:1461–2.

Wortsman X. Sonography of the nail, Chapter 18. In: Wortsman X, Jemec GBE, editors. Dermatologic ultrasound with clinical and histologic correlations. Heidelberg: Springer; 2013.

Wortsman X, Aranibar L. Postnatal 2-and 3-dimensional sonography of the skin and nail in congenital autosomal recessive ichthyosis correlated with cutaneous histologic findings. J Ultrasound Med. 2001;30:1437–9.

Wortsman X, Jemec GBE. Ultrasound imaging of nails. Dermatol Clin. 2006;24:323–8.

Wortsman X, Jemec G. Role of high-variable frequency ultrasound in preoperative diagnosis of glomus tumors. Am J Clin Dermatol. 2009;10:23–7.

Wortsman X, Wortsman J, Guerrero R. Anatomical changes in retronychia and onychomadesis detected using ultrasound. Dermatol Surg. 2010a;36:1615–20.

Wortsman X, Wortsman J, Soto R, Saavedra T, Honeyman J, Sazunic I, Corredoira Y. Benign tumors and pseudotumors of the nail: a novel application of sonography. J Ultrasound Med. 2010b; 29:803–16.

Wortsman X, Jemec GB, Sazunic I. Anatomical detection of inflammatory changes associated with plantar warts by ultrasound. Dermatology. 2010c;220:213–7.

Wortsman X, Gutierrez M, Saavedra T, Honeyman J. The role of ultrasound in rheumatic skin and nail lesions: a multi-specialist approach. Clin Rheumatol. 2011; 30:739–48.

Fibroblast Evaluation: Extracellular Matrix Synthesis

90

Céline Viennet and Patrice Muret

Contents

Keywords
Skin • Fibroblast • Culture • Extracellular matrix

1 ECM and Skin Culture Models

Much of knowledge on fibroblast physiology is based on monolayer culture studies. After few passages of cells grown from a skin biopsy, fibroblasts exhibit their phenotypic and metabolic characteristics. Thus, cultured papillary and reticular fibroblasts exhibit stable differences in the production of some, but not all, extracellular matrix molecules (Sorrell and Caplan 2004) (Table 1).

To study cell-cell and cell-matrix interactions, three-dimensional organotypic cultures are used. Bell et al. (1979) introduced equivalent dermis models, so-called lattices, in which fibroblasts are embedded into different collagen gel systems. Free-floating lattices retract over time as fibroblasts migrate and reorganize the collagenous matrix. Tense lattices develop internal tension as gel retraction is prevented by attachment of the matrix (Viennet et al. 2005). Such models have revealed the importance of fibroblast adherence to the matrix through mechano-sensing integrin signaling (Dallon and Ehrlich 2008). When integrins bind collagen, they transduce a signal which regulates cellular biological functions, such as proliferation, migration, and matrix metabolism. Intracellular signaling cascades such as

C. Viennet (✉)
Engineering and Cutaneous Biology Laboratory, UMR 1098, University of Franche-Comte, Besançon, France
e-mail: celine.viennet@univ-fcomte.fr

P. Muret
Engineering and Cutaneous Biology Laboratory, UMR 1098, University of Franche-Comte, Besançon, France

Clinical Pharmacology Department, University Hospital, Besançon, France
e-mail: patrice.muret@univ-fcomte.fr; p1muret@chu-besancon.fr

P. Humbert et al. (eds.), *Agache's Measuring the Skin*,
DOI 10.1007/978-3-319-32383-1_124

Table 1 Expression of extracellular matrix molecules by monolayer cultures of dermal fibroblasts (from Sorrell and Caplan 2004)

Matrix component	Papillary fibroblasts	Reticular fibroblasts
Collagens I and III	Produced – ratio same as for reticular cells	Produced – ratio same as for papillary cells
Collagens V and VI	Produced	Produced
Collagen XII	Produced	Produced
Collagen XIV	Not produced in monolayer culture	Not produced in monolayer culture
Collagen XVI	Produced at high levels	Produced at low levels
Tenascin-C	Produced	Produced
Tenascin-X	Not studied	Not studied
Versican	Produced at low levels	Produced at high levels
Decorin	Produced at high levels	Produced at low levels

transforming growth factor-β (TGF-β), extracellular signal-regulated kinases, p38 mitogen-activated protein kinase, and Wnt/β-catenin pathway have been implicated in the regulation of ECM production in fibroblasts.

Fibroblasts synthesize matrix metalloproteinases (MMPs), which are responsible for the turnover of collagen and elastic fibers. MMPs are zinc-dependent enzymes involved in the degradation of ECM and in the release and activation of growth factors and cytokines. Their activity is controlled by tissue inhibitors of metalloproteinases (TIMPs), and their production is regulated by a number of factors, including cell/ECM interaction, mechanical force, and the expression of cytokines/growth factors (TGF-β, IL-1, TNFα). According to the MMPs expression profile, it is possible to characterize different subtypes of fibroblasts: oral fibroblasts exhibit increased levels of the active form of MMP-2 as compared to dermal fibroblasts (Stephens et al. 2001). Expression or activation of MMPs differs if fibroblasts are cultured in monolayer or in three-dimensional collagen lattice. MMP activity is significantly induced when keratinocytes and fibroblasts were cocultured. Paracrine interaction between keratinocytes and fibroblasts appears to play an important role in the regulation of collagen metabolism (Tandara and Mustoe 2011).

Gene expression and synthesis of ECM molecules in biological models of the skin can be measured by PCR, zymography, and ELISA.

Due to diverse synthetic functions, fibroblast activities need control. Improper control results in synthesis of excessive or inadequate products that are reflected in disease processes such as scleroderma, systemic sclerosis, and keloids, but also in wrinkles and premature aging of the skin.

2 ECM in Skin Aging

With aging, fibroblasts lose their proliferative potential, and they show diminished ECM biosynthesis capacity, resulting in dermal atrophy and wrinkle formation. Compared to adjacent skin fibroblasts, wrinkle-cultured fibroblasts show decreased production of type I collagen and increased synthesis of MMP-1 (Fig. 1). In monolayer culture, fibroblasts from old donors, or even in vitro aged fibroblasts, have been shown to express age-specific features. Aged fibroblasts show a decrease in proliferation and type I collagen production and an increase in MMP-1 synthesis compared to young ones (Humbert et al. 2012).

One of the causes of aging is the appearance of the advanced glycosylation end products (AGEs) during life. The glycation reaction results from a nonenzymatic reaction between a sugar and a free amine group of Lys, Arg amino acids in proteins. Therefore, it seems that AGEs modify the expression and the synthesis of ECM molecules. They provoke the activation of fibroblasts; the increase of type III and IV collagens; MMP-1, MMP-2, and MMP-9 production; and the modification of α6 and β1 integrin patterns (Pageon et al. 2007; Pageon 2010) (Fig. 2).

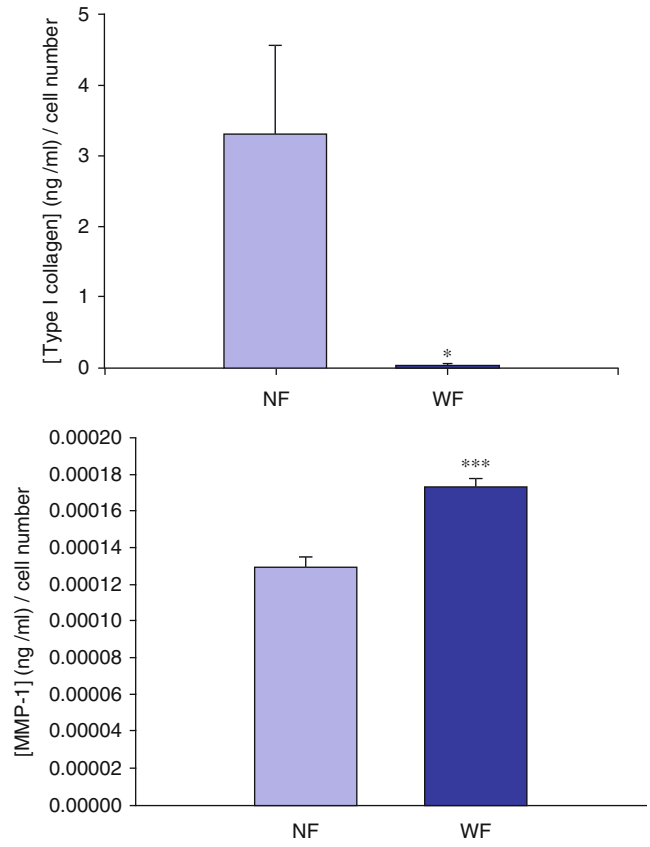

Fig. 1 Expression of type I collagen and MMP-1 molecules by monolayer cultures of adjacent skin (*NF*) and wrinkle fibroblasts (*WF*) (Unpublished data)

3 ECM in Wound Healing and Fibrosis

Wound healing is a complex process that involves inflammation, granulation tissue formation, and tissue remodeling, and this is all regulated by a number of cytokines and growth factors. Fibroblasts play a crucial role in wound healing. During this process, fibroblasts proliferate and produce many of the ECM molecules in a TGF-β-dependent manner, and this contributes to the recovery of connective tissue integrity.

The expression by dermal fibroblasts of several genes and the synthesis of proteins involved in skin wound healing were found to be tension inducible (Agha et al. 2011). This is the case of type I and III collagens and procollagen C-proteinase (enzyme required for the formation of insoluble collagen fibers) whose expression is increased by mechanical tension (Lambert et al. 2001; Kessler et al. 2001). Other ECM components are also induced by mechanical tension such as Tenascin-C, a modulator of cell adhesion, migration, and growth (Chiquet-Ehrismann and Chiquet 2003). As regards the remodeling of ECM, MMP-1, MMP-3, MMP-9, and MMP-13 are upregulated when tensile forces are dissipated (Lambert et al. 2001).

Disruption of either production or degradation of ECM and imbalances between MMPs and TIMPs production can lead to abnormal scarring. Both keloids and hypertrophic scars are cutaneous abnormalities that are characterized by excessive accumulation of connective tissue, especially collagen. When compared with normal fibroblasts, keloid fibroblasts exhibit an altered expression of several molecules implied in all wound healing phases. Cultured keloid fibroblasts showed increased production of type I collagen,

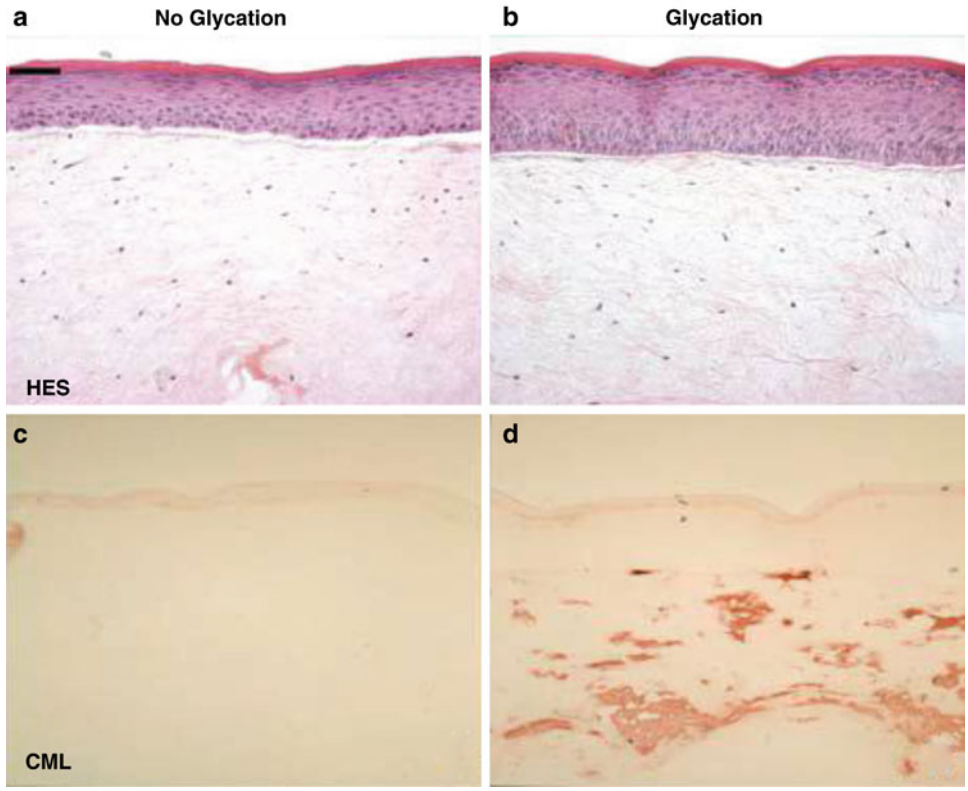

Fig. 2 HES histological staining (**a**, **b**) and AGE labeling (**c**, **d**) of skin reconstructed in vitro using untreated collagen (**a**, **c**) or preglycated collagen (**b**, **d**). The histological pictures look similar except that the dermal organization seems to be modified by glycation (bar = 100 μm) (From Pageon et al. 2007)

fibronectin, MMP-1, MMP-2, MMP-3, MMP-13, MMP-19, and TIMP-1. MMP-8 is decreased (Shih et al. 2010). In addition, increased production of MMPs had a role in the high migratory activity of cultured keloid fibroblasts (Fujiwara et al. 2005).

Systemic scleroderma is a generalized disorder characterized by excessive deposition of ECM. The overproduction of type I, III, and VI collagens by systemic and localized scleroderma fibroblasts has been demonstrated (Krieg et al. 1981). Increased matrix deposition has been shown to be due to enhanced gene transcription and stability of mRNA. In comparison with normal fibroblasts, systemic scleroderma fibroblasts respond differently to their extracellular environment, indicating an altered feedback (Herzhoff et al. 1999).

4 Conclusion

The extracellular matrix is one of the most important regulators of cellular and tissue function in the body. Tightly controlled ECM homeostasis is essential for development, wound healing, and normal organ homeostasis, and dysregulation can result in pathological conditions. Fibroblasts are the major cells in the dermis, and these cells provide tensile strength and elasticity through the production and secretion of various components of ECM, including collagens, elastin, glycoproteins, and proteoglycans. Thus enhancing the activity of fibroblasts, in the context of ECM production, may have beneficial effects on maintenance of skin texture.

References

Agha R, Ogawa R, Pietramaggiori G, Orgill DP. A review of the role of mechanical forces in cutaneous wound healing. J Surg Res. 2011;171(2):700–8.

Bell E, Ivarson B, Merrill C. Production of a tissue-like structure by contraction of collagen lattices by human fibroblasts of different proliferative potential in vitro. Proc Natl Acad Sci U S A. 1979;76: 1274–8.

Chiquet-Ehrismann R, Chiquet M. Tenascins: regulation and putative functions during pathological stress. J Pathol. 2003;200(4):488–99.

Dallon JC, Ehrlich HP. A review of fibroblast-populated collagen lattices. Wound Repair Regen. 2008;16(4): 472–9.

Fujiwara M, Muragaki Y, Ooshima A. A keloid-derived fibroblasts show increased secretion of factors involved in collagen turnover and depend on matrix metalloproteinase for migration. Br J Dermatol. 2005;153(2):295–300.

Herzhoff K, Sollberg S, Huerkamp C, Krieg T, Eckes B. Fibroblast expression of collagen integrin receptors alpha1beta1 and alpha2beta1 is not changed in systemic scleroderma. Br J Dermatol. 1999;141(2): 218–23.

Humbert P, Viennet C, Legagneux K, Grandmottet F, Robin S, Muret P. In the shadow of the wrinkle: experimental models. J Cosmet Dermatol. 2012;11(1): 79–83.

Kessler D, Dethlefsen S, Haase I, Plomann M, Hirche F, Krieg T, Eckes B. Fibroblasts in mechanically stressed collagen lattices assume a "synthetic" phenotype. J Biol Chem. 2001;276(39):36575–8.

Krieg T, Luderschmidt C, Weber L, Müller PK, Braun-Falco O. Scleroderma fibroblasts: some aspects of in vitro assessment of collagen synthesis. Arch Dermatol Res. 1981;270(3):263–72.

Lambert CA, Colige AC, Munaut C, Lapière CM, Nusgens BV. Distinct pathways in the over-expression of matrix metalloproteinases in human fibroblasts by relaxation of mechanical tension. Matrix Biol. 2001;20(7): 397–408.

Pageon H. Reaction of glycation and human skin: the effects on the skin and its components, reconstructed skin as a model. Pathol Biol. 2010;58(3):226–31.

Pageon H, Bakala H, Monnier VM, Asselineau D. Collagen glycation triggers the formation of aged skin in vitro. Eur J Dermatol. 2007;17(1):12–20.

Shih B, Garside E, McGrouther DA, Bayat A. Molecular dissection of abnormal wound healing processes resulting in keloid disease. Wound Repair Regen. 2010;18(2):139–53.

Sorrell JM, Caplan AI. Fibroblast heterogeneity: more than skin deep. J Cell Sci. 2004;117:667–75.

Stephens P, Davies KJ, Occleston N, Pleass RD, Kon C, Daniels J, Khaw PT, Thomas DW. Skin and oral fibroblasts exhibit phenotypic differences in extracellular matrix reorganization and matrix metalloproteinase activity. Br J Dermatol. 2001;114:229–37.

Tandara AA, Mustoe TA. MMP- and TIMP-secretion by human cutaneous keratinocytes and fibroblasts – impact of coculture and hydration. J Plast Reconstr Aesthet Surg. 2011;64:108–16.

Viennet C, Bride J, Armbruster V, Aubin F, Gabiot AC, Gharbi T, Humbert P. Contractile forces generated by striae distensae fibroblasts embedded in collagen lattices. Arch Dermatol Res. 2005;297(1):10–7.

Mechanical Properties of Fibroblasts

91

Carol Courderot-Masuyer

Keywords

Fibroblasts • Mechanical stress • Contractile forces • Dermis • Ulcer legs • Wrinkles • Stretch marks • Photoaging

As well as their primary role in extracellular matrix production, fibroblasts are capable of contraction (Gabbiani et al. 1971; Grinnell 1994; Ryan et al. 1974). The mechanical behavior of the skin in the rest state corresponds with the dermis. External forces applied on the skin are transmitted to the dermis, and internal forces of the dermis affect the epidermal surface. Internal forces are the result of the natural tension of the network of fibers of the dermis and the contractile activity-induced tension of the fibroblasts on fibers. External forces applied on the surface of the skin are the result of compression, tension, and friction forces. Mechanical stress stimulates the proliferation of fibroblasts and modulates their phenotype by inducing the expression of alpha-smooth muscle actin and differentiation into myofibroblasts. Mechanical compression induces apoptosis and regulates the release of cytokines. Previous studies have found that fibroblasts in granulation tissue are myofibroblasts and suggest that they might produce the force of wound contraction (Darby and Gabbiani 1990; Hirschel et al. 1971; Schurch et al. 1984). An in vitro model that is considered to be an equivalent of the process of wound contraction has already been established. Bell et al. reported that the incorporation of fibroblasts in a collagen gel induces a progressive contraction of the gel, resulting in the formation of a dense collagen disk, called retracted lattice (Fig. 1) (Bell et al. 1979). Fibroblasts reduce their proliferation potential, and three mechanisms seem to be responsible for lattice contraction: cell contraction, cell tractional force related to locomotion, and cell elongation (Dallon and Ehrlich 2008). Contraction is determined by measurements of gel diameter over a period of time. A new device, the Glasbox® (Fig. 2), has been developed by Professor Philippe Humbert (Besançon, France), which can measure directly the forces exerted by fibroblasts on the collagen gel (Viennet et al. 2004). The culture model used is a tense lattice in which cells are seeded within a collagen matrix immobilized at its extremities. Contraction is inhibited and lattice formation is associated with the production of internal tension. This model developed is based on a silicon slide, which is fine enough to be

C. Courderot-Masuyer (✉)
Bioexigence, Besançon, France
e-mail: bioexigence@wanadoo.fr

P. Humbert et al. (eds.), *Agache's Measuring the Skin*,
DOI 10.1007/978-3-319-32383-1_125

curved by even the weak forces involved in the tense collagen lattice. The slide deformation is measured by strain gauges deposited on its surface. The collagen lattice is attached to the sensor through a grid etched on the silicon stripe. Such tense lattices are more closely related to the skin than retracted lattices in terms of both internal structure and mechanical behavior, because the skin is also permanently under tension. Several force measurement devices are described in the literature (Campbell et al. 2003; Chapuis et al. 1996; Darby et al. 1991; Eastwood et al. 1994; Kasugai et al. 1990; Kolodney and Wysolmerski 1992). Different cell sources have been studied to test the idea that the ability of fibroblasts to generate contractile forces vary between populations (Delvoye et al. 1986; Gillery et al. 1991; Rayan and Tomasek 1994). Glasbox® makes it possible

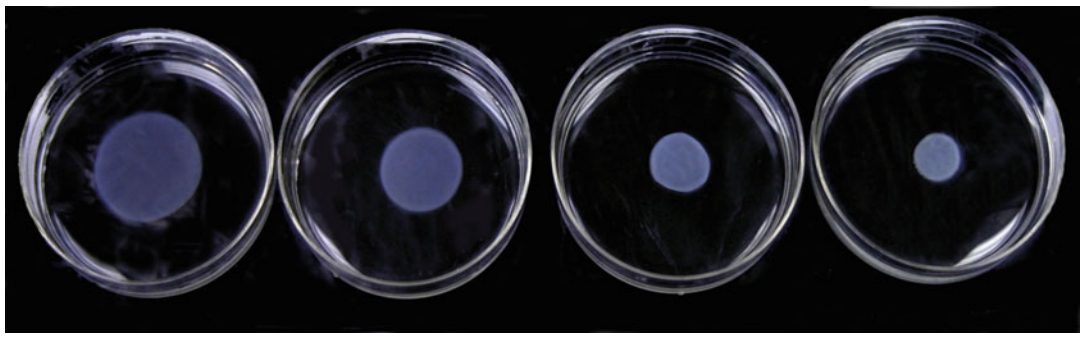

Fig. 1 Evolution of the diameter of collagen lattices over 10 days of culture

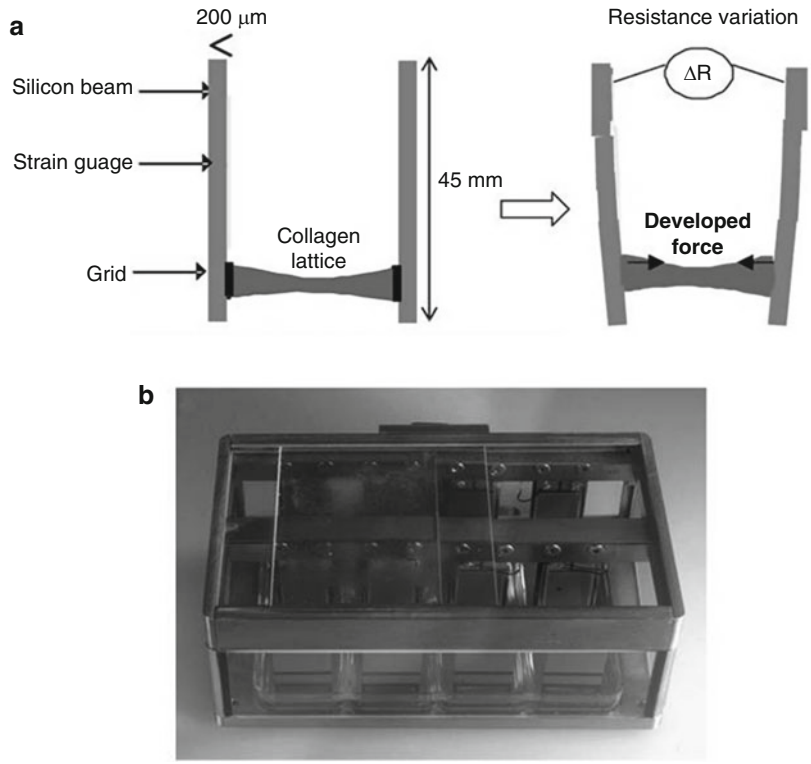

Fig. 2 (**a**) Schematic diagram of the Glasbox. (**b**) View of the Glasbox. The cell chamber was composed of eight rectangular culture wells in which lattices developed. Two opposite silicon beams hanged down into each well. The lattice was attached to this sensor through a grid directly etched on the lower part of the beams. A strain gauge was deposited at the beam surface and connected to form a Wheatstone bridge. The strain gauges signal output was amplified and then converted and collected by a computer, which included an acquisition card and a specific program for giving directly the forces in real time

to detect differences in contractile forces of fibroblasts from leg venous ulcers, stretch marks, irradiated fibroblasts, and wrinkles when those are compared to surrounding normal "healthy skin." Fibroblasts from early stretch marks were the richest cells in alpha-smooth muscle actin filaments and generated the highest contractile forces. Their peak contractile force was 26 % greater than normal fibroblasts. There was a 150 % higher level of alpha-smooth muscle actin content in fibroblasts from early stretch marks. On the contrary, there was no significant difference in contraction forces between old stretch mark fibroblasts and normal fibroblasts. Normal fibroblasts do not express alpha-smooth muscle actin. The contractile properties of fibroblasts vary depending of the stage of the disease (Viennet et al. 2005). The device Glasbox® makes it possible to know whether an active might have relaxing effects on contractile forces in order to prevent the formation of stretch marks. The evaluation of the mechanical activity of venous ulcer fibroblasts showed that, in comparison with ulcer-edge fibroblasts, the force generation with ulcer-centered fibroblasts was much enhanced, and this is also correlated to the presence of high levels of alpha-smooth muscle actin. So in chronic venous ulcer, the generation of contractile forces and the formation of cytoplasmic actin filaments are not affected (Viennet et al. 2004). The development of contractile forces by fibroblasts after UVA irradiation was also studied using the Glasbox device. Several studies have proven that UVA wavelengths by themselves participate in the long-term clinical effects of photoaging (Lavker et al. 1995). Only UVA reach dermal fibroblasts. In sun-exposed skin and during skin aging, the normal fibrillary pattern of dermal extracellular matrix (ECM) is replaced by nonfunctional ECM, in which the normally divalent collagen cross-links have been replaced by trivalent cross-links, causing thickening and tangling of collagen fibrils (Kligman and Kligman 1986). Advanced glycation end products (AGEs), the products of nonenzymatic glycation and oxidation of proteins and lipids, modify skin elastin especially during UV-induced photoaging (Mitzutari et al. 1997) and AGEs accumulate on skin elastin and collagen, interfering with normal skin function and structure (Wondrak et al. 2002). Okano et al. postulated that AGEs bind to fibroblast cell membranes, contributing to the progression of skin aging (Okano et al. 2002). The UVA-generated reactive oxygen species are also responsible for the cross-linking of proteins (such as collagen), oxidation of sulfhydryl groups causing disulfide cross-links, oxidative inactivation of certain enzymes causing functional impairment of cells (fibroblasts, keratinocytes, melanocytes, Langerhans cells), and liberation of proteases, collagenase, and elastase (Dalle Cabonare and Pathak 1992). Reduced synthesis of collagen I is a characteristic feature of chronologically aged skin and enhanced by photodamage (Varani et al. 2006). A recent study showed a decrease in contractile forces of fibroblasts after UVA irradiation and secondly the protective and restoring effects of a mixture of silanols on photoaging through the study of its effects on collagen I production and on the alterations of mechanical properties of fibroblasts provoked by UVA irradiation (Figs. 3, 4, and 5) (Robin et al. 2012). Differences in biomechanical behavior and synthesis between normal aged fibroblasts and fibroblasts from the base of wrinkles from the same patient have been shown. Fibroblasts from wrinkles synthesize lower levels of collagen I than normal aged fibroblasts (Jouandeaud et al. 2004). A recent study showed that L-poly lactic acid modified the metabolic state of wrinkle fibroblasts. A restoration of the production of collagen I and the cell migration was noted after 42 days of culture of wrinkle fibroblasts with L-poly lactic acid showing a direct effect of L-poly lactic acid on metabolic properties of wrinkle fibroblasts (Courderot-Masuyer et al. 2012). The device Glasbox also showed that wrinkle fibroblasts developed lower contractile forces than those of normal aged fibroblasts (Fig. 6). Glasbox allows a screening of actives in order to choose the best one used for its anti-wrinkle properties. In conclusion, the quantification of contractile forces of fibroblasts shows discrepancies between

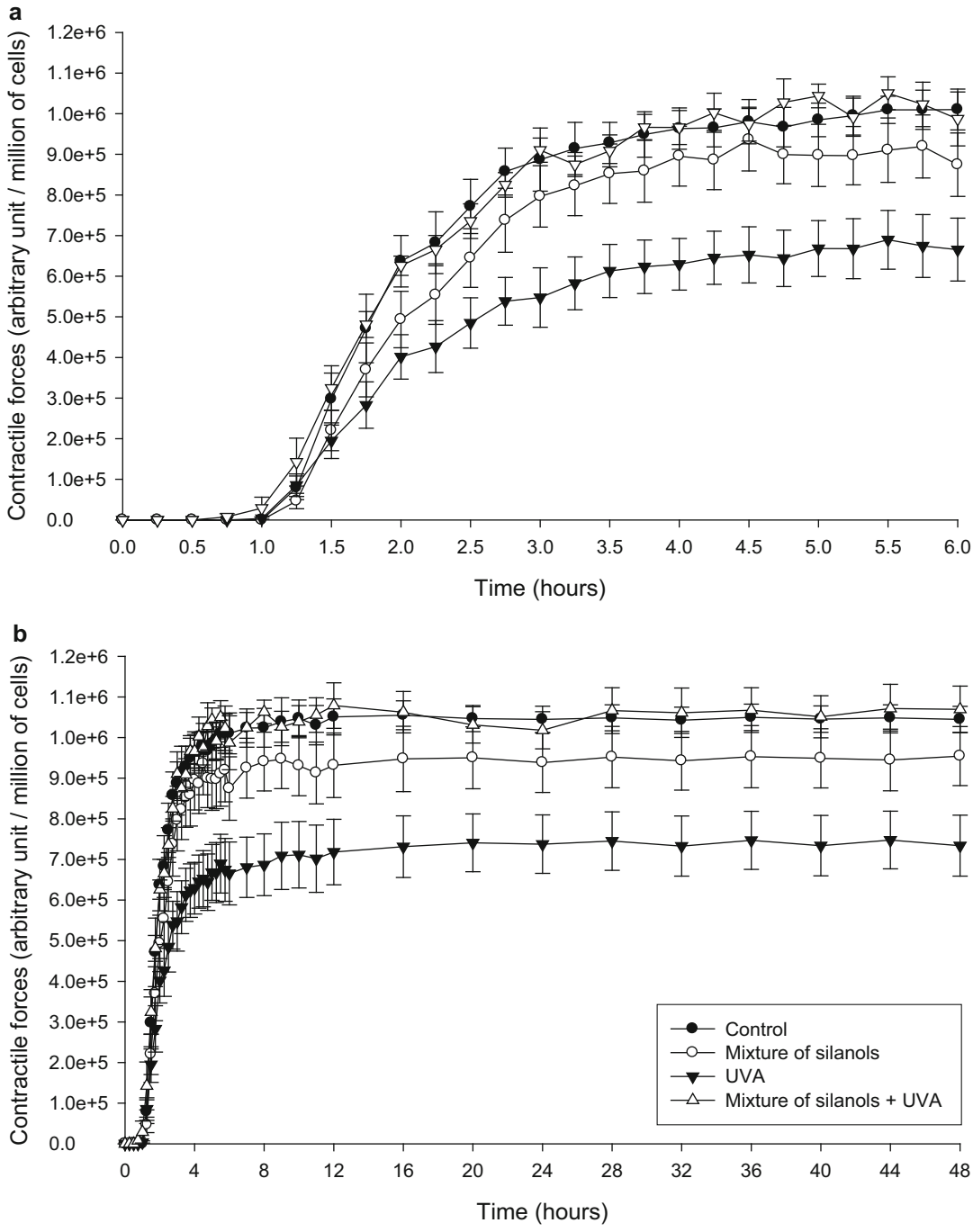

Fig. 3 Quantification of contractile forces developed by fibroblasts after UVA irradiation in the presence or not of the mixture of two silanols (monomethylsilanetriol mannuronate and dimethylsilanediol salicylate) according to the time. (**a**) Details of the measurements of contractile forces of fibroblasts for 6 h, (**b**) measurements of contractile forces for 48 h

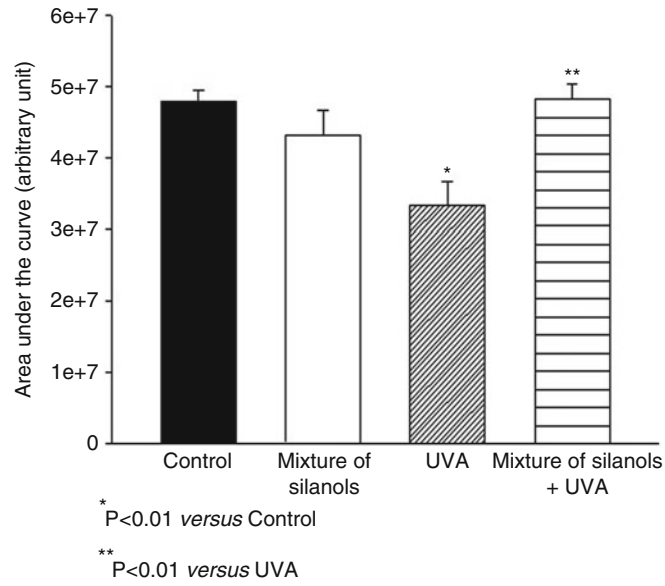

Fig. 4 Quantification of contractile forces developed by fibroblasts after UVA irradiation in the presence or not of the mixture of two silanols. Results were expressed as area under the curve (AUC).*$p < 0.05$, **$p < 0.01$ versus control

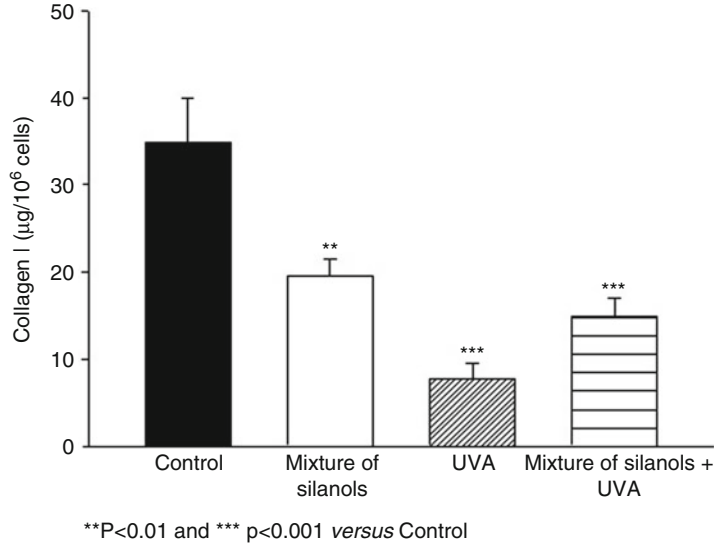

Fig. 5 Collagen I production by irradiated fibroblasts with and without the presence of the mixture of two silanols (monomethylsilanetriol mannuronate and dimethylsilanediol salicylate). Results were as expressed as µg/10^6 cells (mean ± sem). **$p < 0.01$, ***$p < 0.001$ versus control

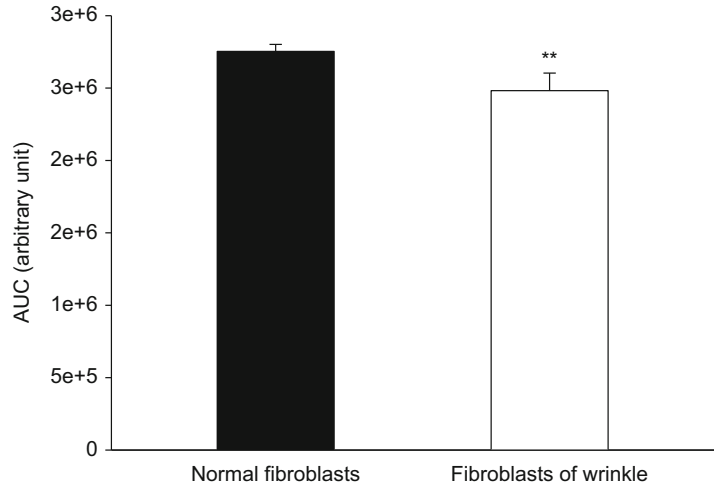

Fig. 6 Quantification of contractile forces developed by wrinkle fibroblasts and normal aged fibroblasts forms the same patient. Results were expressed as area under the curve (AUC). $^{**}p < 0.01$ versus normal fibroblasts

populations of fibroblasts. The contractile properties of fibroblasts also vary depending on the stage of the disease or the aging of the skin.

References

Bell E, Ivarsson B, Merril C. Production of a tissue-like structure by contraction of collagen lattices by human fibroblasts of different proliferative potential in vitro. Proc Natl Acad Sci U S A. 1979;3:1274–8.

Campbell BH, Clark WW, Wang J. A multi-station culture force monitor system to study cellular contractility. J Biomech. 2003;36:137–40.

Chapuis JF, Lucarz-Bietry A, Agache P, Humbert P. A mechanical study of tense collagen lattice. Eur J Dermatol. 1996;6:56–60.

Courderot-Masuyer C, Robin S, Tauzin H, Humbert P. Evaluation of the behaviour of wrinkles fibroblasts and normal aged fibroblasts in the presence of Poly-L-Lactic acid. J Cosmet Dermatol Sci Appl. 2012;2:20–7.

Dalle Cabonare M, Pathak MA. Skin photosensitizing agents and the role of reactive oxygen species in photoaging. J Photochem Photobiol B. 1992;14:105–24.

Dallon JC, Ehrlich HP. A review of fibroblast-populated collagen lattices. Wound Repair Regen. 2008;16:472–9.

Darby I, Gabbiani G. A-smooth muscle actin is transiently expressed by myofibroblasts during experimental wound healing. Lab Invest. 1990;63:21–9.

Darby I, Delvoye P, Wiliquet P, Leveque JL, Nusgens BV, Lapiere CM. Measurement of mechanical forces generated by skin fibroblasts embedded in a three-dimensional collagen gel. J Invest Dermatol. 1991;16:324–30.

Delvoye P, Mauch C, Krieg T, Lapiere CM. Contraction of collagen lattices by fibroblasts from patients and animals with heritable disorders of connective tissue. Br J Dermatol. 1986;115:139–46.

Eastwood M, MacGrouther A, Brown RA. A culture force monitor for measurement of contraction forces generated in human dermal fibroblast cultures: evidence of cell-matrix mechanical signalling. Biochim Biophys Acta. 1994;1201:186–92.

Gabbiani G, Ryan GB, Majno G. Presence of modified fibroblasts in granulation tissue and their possible role in wound contraction. Experientia. 1971;27(5):49–50.

Gillery P, Maquart FX, Le Corre Y, Kalis B, Borel JP. Variability in the retraction of collagen lattices by scleroderma fibroblasts – relationships to protein synthesis and clinical data. Clin Exp Dermatol. 1991;16:324–30.

Grinnell F. Fibroblasts, myofibroblasts, and wound contraction. J Cell Biol. 1994;124:401–4.

Hirschel BJ, Gabbiani G, Ryan GB, Majno G. Fibroblast of granulation tissue: immunofluorescent staining with antismooth muscle serum. Proc Exp Biol Med. 1971;138:466–9.

Jouandeaud M, Viennet C, Bordes S, Closs B, Humbert P. Comparison of the biomechanical and biosynthetic behavior of normal human fibroblasts and fibroblasts from forehead wrinkle. IFSCC Mag. 2004;7:2–6.

Kasugai S, Susuki S, Shibata S, Yasiu S, Amano H, Ogura H. Measurement of the isometric contractile forces generated by dog periodontal ligament fibroblasts *in vitro*. Arch Oral Biol. 1990;35:597–601.

Kligman LH, Kligman AM. The nature of photoaging: its prevention and repair. Photodermatology. 1986;3:215–27.

Kolodney MS, Wysolmerski RB. Isometric contraction by fibroblasts and endothelial cells in tissue culture: a quantitative study. J Cell Biol. 1992;117:73–82.

Lavker RM, Veres DA, Irwin CJ. Quantitative assessment of cumulative damage from repetitive exposures to

suberythemogenic doses of UVA in human skin. Photochem Photobiol. 1995;62:348–52.

Mitzutari K, Ono T, Ikeda K, Kayashima K, Horiuchi S. Photo-enhanced modification of human skin elastin in actinic elastosis by N(epsilon)-(carboxymethyl)lysine, one of the glycoxidation products of the Maillard reaction. J Invest Dermatol. 1997;108:797–802.

Okano Y, Masaki H, Sakuri H. Dysfunction of dermal fibroblasts induced by advanced glycation end products (AGEs) and the contribution of a nonspecific interaction with cell membrane and AGEs. J Dermatol Sci. 2002;29:171–80.

Rayan GM, Tomasek JJ. Generation of contractile force by cultured Dupuytren's disease and normal palmar fibroblasts. Tissue Cell. 1994;26:747–56.

Robin S, Courderot-Masuyer C, Tauzin H, Guillon S, Gaborit J, Harbon S, Humbert P. Evaluation of protective and restoring effects of a mixture of silanols on photoaging. Use of a device allowing the quantification of human fibroblasts after UVA irradiation. Int J Cosmet Sci. 2012;34:311–7.

Ryan GB, Cliff WJ, Gabbiani G, Irle C, Montandon D, Statkov PR, Majno G. Myofibroblasts in human granulation tissue. Hum Pathol. 1974;5:55–67.

Schurch W, Seemayer TA, Legace R, Gabbiani G. The intermediate filament cytoskeleton of myofibroblasts: an immunofluorescence and ultrastructural study. Virchows Arch A Pathol Anat Histopathol. 1984; 403:323–36.

Varani J, Dame MK, Rittie L, Fligiel SEG, Kanh S, Fisher Voorhees JJ. Decreased collagen production in chronologically aged skin. Am J Pathol. 2006;168: 1861–8.

Viennet C, Armbruster V, Gabiot AC, Gharbi T, Humbert P. Comparative contractile properties and alpha-smooth muscle actin filament distribution between cultured human fibroblasts from venous ulcers and normal skin. J Wound Care. 2004; 13(9):358–61.

Viennet C, Bride J, Armbruster V, Aubin F, Gabiot AC, Gharbi T, Humbert P. Contractile forces generated by striae distensae fibroblasts embedded in collagen lattices. Arch Dermatol Res. 2005;297:10–7.

Wondrak GT, Roberts MJ, Jacobson EL. Photosensitized growth inhibition of cultured human skin cells: mechanism and suppression of oxidative stress from solar irradiation of glycated proteins. J Invest Dermatol. 2002;119:489–98.

Gene Expression and Genetic Evaluation of the Skin

92

Philippe Benech

If our brains were simple enough for us to understand them, we'd be so simple that we couldn't. (Ian Stewart, The Collapse of Chaos: Discovering Simplicity in a Complex World)

Contents

Keywords

DNA microarray • Gene expression • Transcriptomics • Functional genomics • Genetic testing • Single nucleotide polymorphism

1 Introduction

Skin is the largest organ of the body and performs many functions that support its protective role and survival. It helps us sense our surroundings and provides a barrier to environmental insults. Greater understanding of the mechanisms of skin development and the molecular interactions, within and between skin cells, benefits from large-scale proteomic and genomic technologies. These technologies contribute to increase our knowledge of skin diseases and injuries as well as to evaluate/develop therapeutics to treat them.

For scientist, skin is a very exciting tissue eliciting specific features: its physiology requires constant cell renewal and the involvement of different cell types that ensure simultaneously distinct functions. One may imagine easily the

P. Benech (✉)
Faculté de Médecine Secteur Nord, UMR 7259 (NICN)
CNRS – Aix-Marseille Université, Marseille, France
e-mail: philippe.benech@univ-amu.fr

P. Humbert et al. (eds.), *Agache's Measuring the Skin*,
DOI 10.1007/978-3-319-32383-1_126

number of genes expressed to maintain the homeostasis of basic functions in each cell types and the other number of genes, which are involved to respond to injuries or external stimuli.

The difference between a skin cell and other cells is mainly a matter of gene expression. Whereas all cells have the same DNA, their behavior is determined by the proteins, which are synthesized. The instructions to produce those proteins are carried by RNA, and the value of probing RNAs is well recognized to gain insight into the expression differences that define tissues, developmental stages, and diseases.

Today, to get an overview of the transcriptional state of a cell, the so-called transcriptome or cellular RNA content, two options are available: DNA microarrays and RNA-seq.

The transcriptome is dynamic and changes under different circumstances due to different patterns of gene expression. The study of the transcriptome is termed transcriptomics and is based on the evaluation of a change in gene expression that is the translation of information encoded in a gene into protein or RNA structures that are present and operating in the cell. Expressed genes include genes that are transcribed into messenger RNA (mRNA), the key intermediary in gene expression, which translates the DNA's genetic code into the amino acids that make up proteins. Some genes are transcribed into RNAs that are not translated into protein. Among them, transfer and ribosomal RNAs contribute to protein synthesis, and microRNAs (miRNAs), more recently discovered, are small noncoding RNA molecules, which function in transcriptional and posttranscriptional regulation of gene expression. It is noteworthy that, due to other posttranscriptional gene regulation events, there is not necessarily always a strong correlation between the abundance of mRNA and the related proteins. However, RNA quantification is still a useful tool in determining how the transcriptional machinery of the cell is affected in the presence of external signals (e.g., drug treatment) or how cells differ between a healthy state and a diseased state.

2 Technological and Methodological Aspects

2.1 DNA Microarrays

DNA microarrays are a high-throughput screening system based on the properties of nucleic acids such as DNA to interact/hybridize with a complementary strand of either DNA or RNA (Schena et al. 1995). Microscopic DNA spots are attached to a small 2D surface, usually a glass slide, and each spot contains picomoles of a specific gene sequence. Thus, gene sequences of the whole genome can be represented on an array, and due to miniaturization of the processes, one slide can contain eight arrays allowing the quantification of RNAs issued from different biological samples at one time. Their density can reach roughly 60,000 DNA spots including, for each gene, similar sequences to evaluate the reproducibility as well as different sequences to detect alternative RNA species issued from a same gene (called splicing variants). Through the formation of hydrogen bonds between complementary nucleotide base pairs, each DNA sequence (known as probes) will hybridize a cDNA or cRNA (also called antisense RNA) sample (called target) under high-stringency conditions. This sample results from the processing of all RNAs extracted from cells into cDNAs or cRNAs labeled with a fluorophore. Using a laser scanner, the intensity of the emitted fluorescence after probe-target hybridization is detected and quantified to determine relative abundance of all RNAs between different experimental conditions (Fig. 1). Indeed, microarrays use relative quantification in which the intensity of one given DNA spot in one array is compared to the intensity of the same spot in another array. The identity of the DNA spot (the name of the gene from which the short spotted sequence is derived) is known by its position on the array. The process of measuring gene expression is called expression analysis or gene expression profiling.

The result from such analysis is typically a list of selected genes whose expression levels changed during the experiment. It is then up to

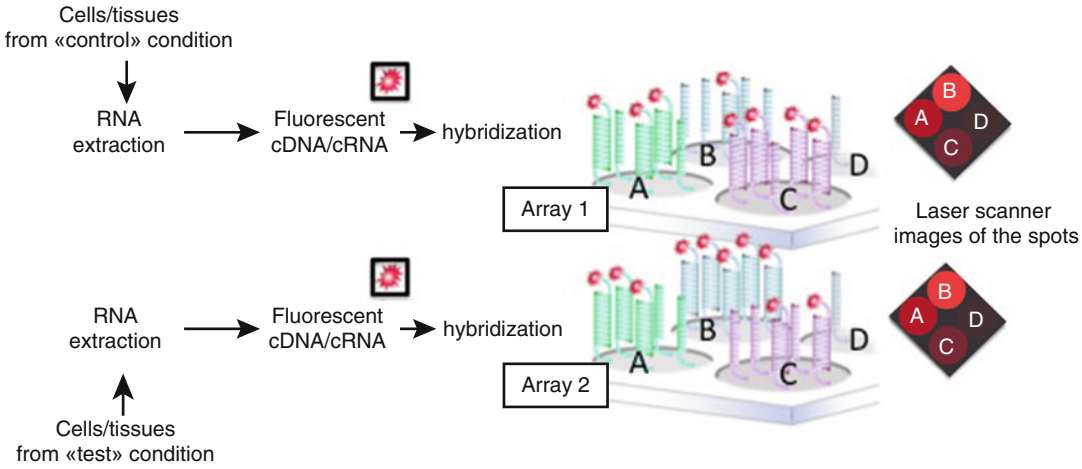

Fig. 1 Target generation for DNA microarray hybridization. RNAs are processed into cDNA or cRNA fluorescent molecules. These molecules issued from either "control condition" or "test condition" are then hybridized to spotted DNA/oligonucleotide arrays which are submitted to a laser scanner for quantification of the emitted fluorescence. Spot *A*: no modulation between the two conditions is detected; spot *B*: expression of the corresponding gene is upregulated in the test condition; spot *C*: expression is downregulated; spot *D*: the absence of signal means that the corresponding gene is not expressed in the cells/tissues

the user to make sense of this list that means to determine the affected biological processes in which the modulated genes are involved.

2.2 RNA-seq

Another kind of transcriptome analysis is performed using the next-generation DNA sequencing (NGS) technology called RNA-seq, in which total RNA is reverse-transcribed into cDNA, converted into a sequencing library, sequenced, and analyzed (reviewed in Wang et al. 2009). NGS is a very high-throughput technique for generating millions of sequences at one time in order to analyze organisms at a genomic level. This allows the researcher to sequence and compare data at a rate previously not possible. In contrast to DNA microarrays that required the knowledge of the genome sequence, NGS will read whatever cDNA is in the sample.

One advantage of RNA-seq over microarrays is that it offers a wider dynamic range than microarrays and generally can pick up less abundant transcripts. Unlike microarrays, which report relative expression values based on fluorescence intensity, RNA-seq can report those abundances absolutely, because it counts the transcripts that it reads. Finally, RNA-seq can reveal transcript structure and splicing and can even identify novel isoforms, gene fusions, and allele-specific variants. Indeed, the development of such high-throughput sequencing technology has increased the determination of single changes in gene sequences, termed single nucleotide polymorphism (SNP). For instance, SNPs were found to contribute to normal variation in physiological processes such as pigmentary phenotype (reviewed in Rees and Harding 2012) as well as to distinct susceptibilities to cancers such as melanoma (Kunz et al. 2013).

However, the cost of RNA-seq remains, presently, much higher than DNA microarrays and limits its use. In most cases, investigators are not interested in the absolute level of an expression but whether expression changes between two conditions. Thus, when sensitivity is not limiting, the low cost, short turn-around time, exceptional quantitative accuracy, and ease of data generation all make the glass slide microarray an acceptable choice (Peterson 2010).

2.3 Experimental Design

Since the starting biological material from which RNAs will be extracted to perform a gene expression analysis involves cells, it has to keep in mind that cell lines, primary cell cultures, 2D/3D epidermis model, or skin explants might not give similar answers. The absence of cross talks between cells, genetic backgrounds but also anatomical site differences, distinct areas of the same biopsy, and conditions of cultures have strong impacts on gene expression and, as a consequence, on protein contents.

Thus, due to the biological complexity of gene expression, the considerations of experimental design are preliminary of critical importance. It is currently admitted that replication of the biological samples, which includes independent RNA extractions, is essential for drawing conclusions. However, having in mind the cost of an array, the question is, how many replicates should be performed in order to generate statistically relevant data? Moreover, gene expression is a dynamic process, and the number of replicates will be multiplied according to different experimental conditions including kinetics and/or dose responses. In contrast to cells issued from a same batch (cells will be splitted accordingly to the number of experimental conditions required) that should provide similar data, significant differences might appear when using biopsies or cultured skin explants. As we mentioned, these differences are not artifacts and rely mainly on distinct genetic background and physiological status of skin areas among donors. Again, the number of arrays to be performed with RNAs extracted from a cohort (e.g., healthy donors and patients) should be high enough to provide statistical significance.

On the other hand, the use of commercial kits for RNA extraction and the design of commercial microarrays, which contain similar DNA spots all over the array to ensure the homogeneity of the hybridization, reduce considerably the need of technical replicates (two RNA samples obtained from each experimental unit). As reviewed by Lander (Lander 1999), good scientific questions and high quality of RNA have more impacts on the results than the technology itself.

2.4 Data Normalization

Following microarray hybridization, the resulting data are submitted to image analyses, and background corrections are performed to provide a final expression value for each RNA transcript. Microarray data sets are commonly very large, and analytical precision is influenced by a number of variables. Statistical challenges include taking into account effects of background noise and appropriate normalization of the data. Each commercial microarray platform provides their own tools for normalization based on specific algorithms for image analyses (gridding, spot recognition of the scanned image, removal, or marking of poor-quality and low-density features) and data processing (background subtraction, determination of spot intensities, and intensity ratios). Several consortiums such as the "Microarray Quality Control (MAQC) project" conducted by the US Food and Drug Administration (FDA) and the MGED Society have developed standards and quality control metrics which allow the use of microarray data in drug discovery, clinical practice, and regulatory decision-making.

2.5 Data Analyses

Once normalization is achieved, the question is then, how to extract useful information based on gene lists issued from test and control conditions? A basic tool is provided by clustering procedures, which rely on automatic classification of the data (Hand et al. 2001). One can distinguish between unsupervised and supervised procedures. The great majority of computational methods that have evolved for microarray data analyses can all be referred to three main approaches: "class discovery," "class comparison," and "class prediction." In class discovery,

the objects are not grouped into predefined classes; this approach is therefore "unsupervised." A clustering algorithm is applied and genes and/or samples are grouped on the basis of similarity across conditions. The method starts with the definition of a distance metric to represent the distance between the genes and the samples in terms of gene expression. The algorithm then groups the objects such that the distance between objects of the same group is minimized while the distance between objects of different groups is maximized. In class comparison studies the classes are defined on the basis of a prior knowledge, independently from the expression profiles. The method is therefore "supervised" and is used to determine if the expression profiles are different between the predefined classes. The typical output of this approach is a list of genes differentially expressed genes between the classes. Commonly used methods to assess the statistical significance of differential expression are *t*-test and ANOVA. The class prediction approach is also "supervised," as it starts from prior knowledge to group the objects of study (e.g., the biological samples) into different classes. These methods have great potentialities in clinical research, and applications have been described for risk assessment, diagnostic testing, prognostic stratification, and treatment selection (Golub et al. 1999).

Even though several strategies exist to identify genes whose expression is modulated, biologists are more confident with fold change and t-statistic, presumably because of their simplicity and interpretability. Obviously, identification of differentially expressed genes relies on fold changes based, for each gene, on a ratio of the intensity values of the "test" condition and those of the control (patients vs. healthy volunteers, treated patients or cells/biopsies vs. untreated controls). Several reports indicate that fold change results in more reproducible gene lists than the t-statistics (Witten and Tibshirani 2007) and the choice of the method used to identify modulated genes can greatly affect the set of genes that are identified (Jeffery et al. 2006).

2.6 Functional Interpretation of Microarray Experiments

In most of the cases, several hundreds of genes can be found either upregulated or downregulated. The biological interpretation of the results, which involves translating these data into useful biological knowledge, still remains a challenge. Methods leading to classify genes, according solely to their relationships with biologically relevant terms such as those defined by the Gene Ontology (GO) project, present low performances. Indeed, a classification of the genes based on the enrichment in significant biological terms fails to determine precisely how altogether gene products function within a particular biological process. Moreover, their activities, through posttranscriptional events or distinct interactions with other partners, can be different depending on cell types or tissues. It is therefore important to determine among the modulated genes those whose expression can be regulated by the same transcriptional factors or as products are involved within a given signaling pathway (Fig. 2). Several free or commercial software integrating a combination of interactive and visualization tools have been developed to identify the involvement of the gene products in molecular interactions, pathways, diseases, and processes (reviewed in Kelder et al. (2010), Hedegaard et al. (2009), Benech et al. (2007), Barrey et al. (2009, 2012), Mille-Hamard et al. (2012)). They are mainly based on text mining performed either on curated publications or on an exhaustive list of published abstracts issued from PubMed, a bibliographic database for the biomedical literature provided by the National Center for Biotechnology Information (NCBI). Their efficiency relies on the use of multidimensional correlation matrixes enabling, toward iterative queries, to integrate genes within functional networks in a specific physiologic/pathologic or tissue context (Fig. 3). Highlighting such functional networks issued from gene expression profiling leads to a better understanding of the molecular basis that sustained physiological processes, therapeutic responses, or diseases.

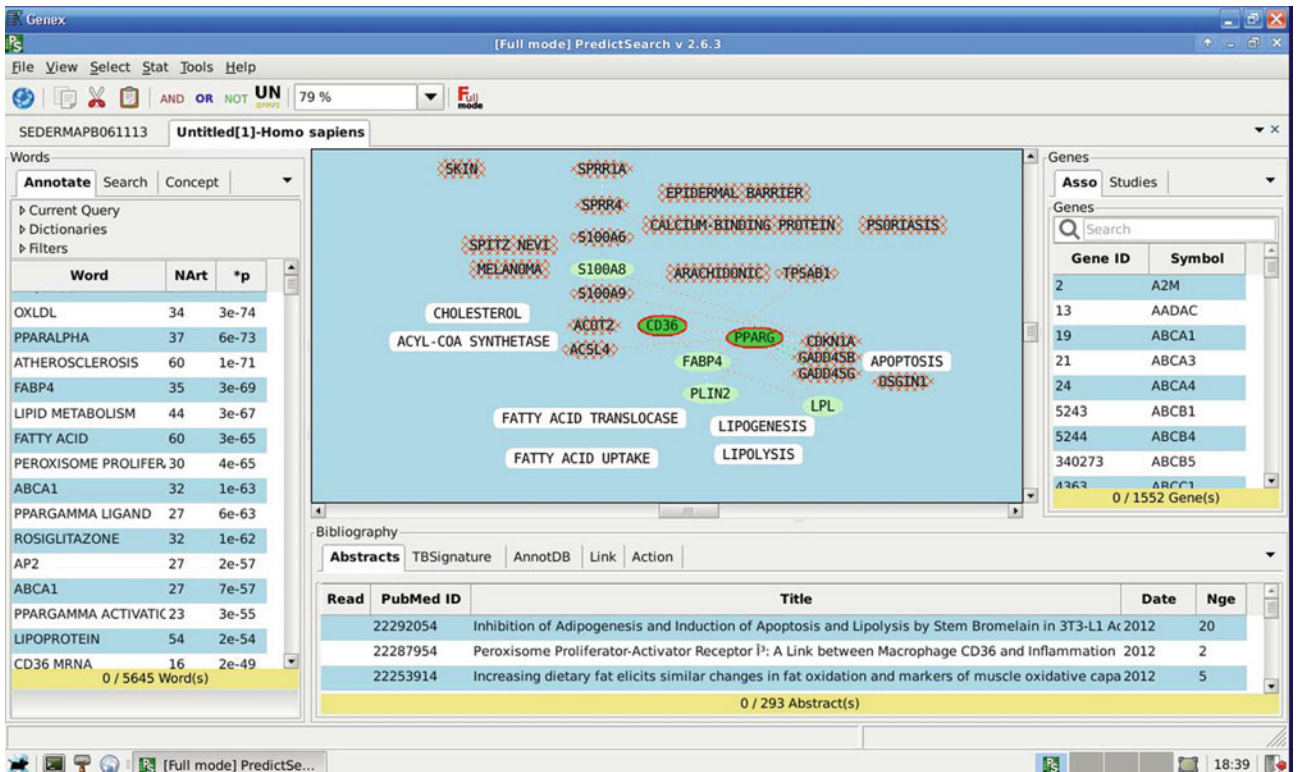

Fig. 2 Screenshot illustrating the correlations found between modulated genes. The software (PredictSearch™) allows the identification of biological terms co-cited with genes (*left* panel) that can be dropped into the working desktop. These terms can be selected according to p-values or the number of publications. Genes or terms, which do not present any relationships with the selected genes (*underlined in red*), are hachured. Abstracts can be retrieved to check the accuracy of the link between one or several genes and one or several terms (*bottom* panel). Additional genes related to the selected genes are listed in the right panel (e.g., 1552 genes are co-cited with CD36 and/or PPARG in the literature)

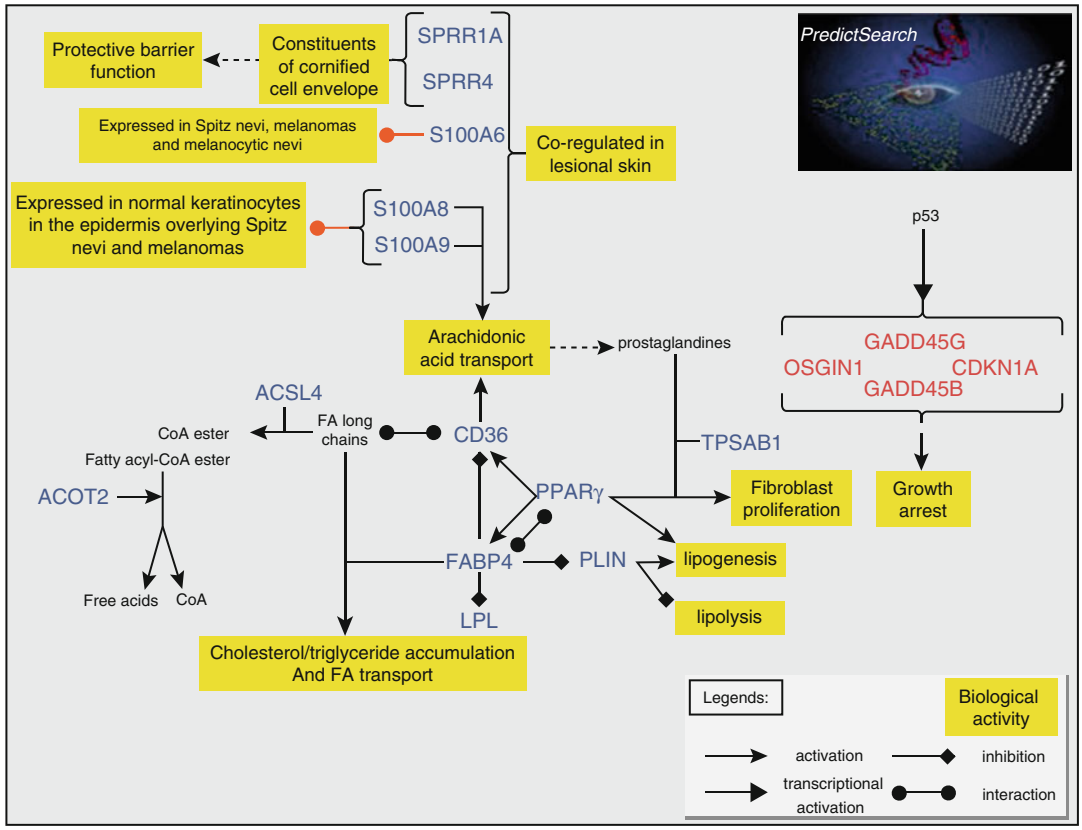

Fig. 3 Schematic representation of a genomic network. The correlation identified through the use of text mining-based computational tools is integrated into functional networks allowing to see how genes work together within defined biological processes. Genes whose expression is upregulated or downregulated are indicated in *blue* or in *red*, respectively

3 Gene Expression Profiling and Psoriasis: A Case Study

Psoriasis is an immune-mediated disease which is associated with a chronic inflammation leading to uncontrolled keratinocyte proliferation and altered differentiation. Several DNA microarray experiments were undertaken to gain a better knowledge of this pathology (Bowcock et al. 2001; Oestreicher et al. 2001; Zhou et al. 2003). For instance, one of these studies (Zhou et al. 2003) found that 1300 genes were differentially expressed between lesional and non-lesional skin. Among them, a significant number of genes were related to immune signaling cascades and some encode chemokines, which had not been described in psoriasis before. The functions of these chemokines, involved in the regulation of T lymphocyte and dendritic cell trafficking, support the local tissue invasion of inflammatory cells seen in psoriasis. More recently, comparison of different published lists of differentially expressed genes (DEG) has shown apparent inconsistencies based on the number of overlapping genes (Suarez-Farinas et al. 2010). Although all data were issued using the same DNA microarray platform, there are many reasons that could explain such discrepancies. Indeed, distinct array series and laboratory effects should account for the variability found among these studies. However, our own experience suggests that alternative statistical tests and choices of cutoffs contribute mainly for the low overlap between DEG. It is likely that the DEG found in common among the distinct analyses

(Suarez-Farinas et al. 2010) define the hallmarks of the pathology, keratinocyte proliferation, and inflammation. Inflammation is supported by the identification of DEG, known to be upregulated in psoriasis, such as IFNγ (interferon gamma)-regulated genes, genes encoding antimicrobial peptides, and proinflammatory proteins. Current statistical tools to analyze common features among patients lead to smooth the data and result in the loss of key elements, which account for individual differences illustrating the heterogeneity of the pathology. Thus, heterogeneous biological variations existing in psoriatic patients should explain the apparent low reproducibility of DEG detection. Several reports (Shi et al. 2008; Zhang et al. 2008) discussed these issues and concluded to the need of developing novel metrics, in particular for evaluating the reproducibility of data in terms of correlated molecular processes rather than simply counting the overlaps of genes. An intriguing possibility is that non-overlapping DEG would be more informative since they can be markers for patient stratification as well as disease severity.

Ainali et al. have recently investigated the involvement of molecular subtypes that might impact on prognosis or treatment outcomes (Ainali et al. 2012). Transcriptomic analyses of skin samples from inflamed/lesional type (PP) and non-inflamed/non-lesional tissue (PN) of 37 psoriatic patients as well as from 34 normal individuals (NN) were performed. Based on an unsupervised hierarchical clustering, they showed that as it can be expected, NN and PN co-clustered away from PP. Whereas under-expressed genes were related to immune responses and fibrotic processes, overexpressed genes encode proteins involved in keratinocyte proliferation and differentiation. Further analyses distinguished among PP two subgroups whose network clusters were enriched either in Wnt, Notch, TGF-beta, and ErbB signaling pathways or in metabolic and BMP pathways. This indicated that the two lesional psoriatic subgroups possess different functional properties, suggesting different underlying biological processes although they were clinically difficult to distinguish. The authors proposed that these differences might help explain why some patients have a different disease course and why some respond better to therapy. However, besides the link of each of these pathways with psoriasis, potential relationships among these pathways and their potential global impact in psoriasis were not discussed.

The Wnt signaling pathways are a group of signal transduction pathways, which act either in a paracrine or autocrine manner. The three best characterized Wnt signaling pathways are the canonical Wnt pathway, the noncanonical planar cell polarity pathway, and the noncanonical Wnt/calcium pathway. The difference between them is that a canonical pathway involves the β-catenin while a noncanonical pathway operates independently of it (Rao and Kühl 2010). Wnt signaling plays a critical role in different processes including embryonic development, axis patterning, cell fate specification, cell proliferation, cell migration, and insulin sensitivity (reviewed in Nusse and Varmus). An evidence for altered Wnt signaling in psoriatic skin came from a previous gene expression profiling study showing an overexpression of the RNA encoding Wnt-5a, one member of the Wnt protein family, in biopsies from lesional psoriatic skin (Gudjonsson et al. 2010). The results suggested a shift away from canonical Wnt signaling toward noncanonical pathways driven by interactions between Wnt-5a and its cognate receptors in psoriasis. This shift might be likely related to an impaired homeostatic inhibition of Wnt signaling. The authors proposed that Wnt-5a might have a role in inducing the marked vascular changes in lesional skin, influencing epidermal proliferation, and in the amplification of inflammatory responses.

Interestingly, an intricate functional relationship between Wnt and Notch signaling during the assignment of cells to particular fates has been proposed (Hayward et al. 2008). Both signaling belong to the six major and universal transduction cellular devices providing the basic machinery for cell fate transitions and assignments that underlie embryonic development (reviewed in Martinez Arias and Stewart 2002). It has been suggested that Wnt and Notch signaling could act on alternative pathways to determine

the effectiveness of other signaling pathways that drive the specific fates, with low Notch signaling favoring Wnt signaling and vice versa (Hayward et al. 2008). Taking into account the possible involvement of β-catenin in self-renewal of different types of stem cells (Lowry et al. 2005), a fine-tuning of Wnt and Notch signaling might have a crucial impact in the dysregulation of proliferation/differentiation. In line with this hypothesis, whereas in the skin, Wnt promotes the stem cell fate, Notch promotes the "transit-amplifying" (TA) cell compartment fate (Lowell et al. 2000).

Similarly, it has been shown that Wnt and ErbB signaling crosstalk and transactivate one another in development and cancer (reviewed in Hu and Li 2010). ErbB family, implicated in the development and progression of most common epithelial malignancies, is composed of four members, ErbB1 (also known as EGFR), ErbB2 (HER2), ErbB3 (HER3), and ErbB4 (HER4), which are involved in the autocrine growth pathway (Bièche et al. 2003). ErbB1/EGFR is a cell surface receptor that binds to epidermal growth factor (EGF), transforming growth factor-alpha (TGFA), amphiregulin (AREG), but also epiregulin (EREG), betacellulin (BTC), and heparin-binding EGF (HB-EGF). In addition to EGFR expression, EGFR ligands such as AREG, HB-EGF, and EREG are known to be overexpressed in psoriasis lesions, and EGFR binding induces receptor dimerization and tyrosine phosphorylation leading to cell proliferation. Recent advances in the knowledge of the EGFR pathway revealed its contribution to distinct immune/inflammatory functions in the epidermis. Indeed, EGFR ligands are involved in a number of immune protective mechanisms through the expression of several antimicrobial peptides (Sørensen et al. 2003), in the induction of leukocyte attractants (Miller et al. 2005), as well as in the regulation of chemokines implicated in the massive recruitment of T cells, monocytes, and immature dendritic cells (Mascia et al. 2003). It has been proposed that the ErbB signaling pathway has to be part of TGFA-ligand-driven amplification circuit during keratinocyte response to skin inflammation (Mascia et al. 2010). Although the most common adverse effect seen with EGFR inhibition therapy is a pronounced skin inflammatory response (Robert et al. 2005), blockers of the EGFR kinase have been suggested to be potent antipsoriasis agents (Ben-Bassat and Klein 2000). These apparent opposite observations might illustrate the ability of the EGFR-ligand system to act as a link between proliferation and innate and adaptive immune responses and support the two main hypotheses about the process that occurs in the development of the disease. Whereas the first hypothesis considers psoriasis as primarily an alteration leading to excessive growth and skin cell renewal, the second sees the disease as being an immune-mediated disorder. According to the second hypothesis, the excessive cell renewal is secondary to the production of cytokines by T cells, following their activation and migration to the dermis. The recent finding that Th17 cells carrying TCR recognizing epidermal autoantigen induce psoriasis-like inflammation (Nishimoto et al. 2013) together with the presence of different antigens possibly related to the various clinical subtypes of psoriasis (Hagforsen et al. 2007) supports the later hypothesis. It is noteworthy that disturbances in protein degradation processes in the skin can be attributed from the increased expression of genes encoding the components of the ATP/ubiquitin-dependent non-lysosomal proteolytic pathway involved in peptide processing and presentation to T cells (Bowcock et al. 2001).

If the different gene expression studies described here highlight the involvement of converging pathways (Wnt, Notch, and EGFR signaling) in psoriasis, the distinction among causes and consequences remains unclear. This is a recurrent criticism, which is made against DNA microarray technologies, generating somehow a sense of frustration. On one hand, deeper functional analyses should be systematically performed to precise the nature of the relationships existing between the differential expressed genes helping to propose a sequence of the events leading to the pathology. On the other hand, it is likely that performing gene expression comparison between skin biopsies and peripheral blood mononuclear cells from the same patients as well as between a variety of autoimmune diseases should be of particular importance. Indeed, the overall comparison, toward the

identification of correlations, might allow defining the respective contribution of the immune system, the inflammation, and the proliferation/differentiation processes.

4 SNP-Based Genetic Testing and Its Contribution in Dermatology

As mentioned previously, the RNA-seq technology provides not only a quantification of RNA molecules but allows also the sequencing of the RNA transcripts, which leads to the identification of RNA variants and in particular of SNPs. Whereas some SNPs are located in the gene sequence corresponding to the RNA transcripts, they are most commonly found in regions between genes, and therefore such SNPs can be detected only on genomic DNA. Occurring once in every 300 nucleotides on average, which means there are roughly ten million SNPs in a human genome, SNPs are the most common type of genetic variation among people.

Representing a single nucleotide difference, the presence of an SNP does not lead systematically to a change in the amino acid sequence of a protein. In contrast, missense (a change affecting the amino acid) or nonsense (introduction of a stop codon affecting the size of the protein) SNPs might have drastic consequences on the activity of a protein (gain or loss of functions). When SNPs are located within a regulatory region that controls the transcription of a gene, gene expression can be altered.

SNP detection, as part of genetic/DNA testing, is more and more used to predict individual's responses to drugs, susceptibility to environmental factors, and risks of developing particular diseases. However, without genetic consultation, the expanding use of direct-to-consumer (DTC) genetic testing by private companies to determine a person's chance of developing a disease is having an unforeseen consequence. Indeed, people, without showing any symptoms, are facing an exaggerated and inaccurate message about the connection between genetic information and disease risk. In many cases, DNA variants are only slightly associated with risk, or there is little good evidence to support any association. Moreover, as we have described in psoriasis, the risk to develop diseases depends on complex interactions between genes and lifestyle accounts for much of our susceptibility to diseases. Even diseases caused by a single gene, such as cystic fibrosis, are influenced by other genes that can affect the degree of severity.

In addition to RNA-seq, various analytical methods, including DNA sequencing, are available to discover or to detect SNPs. Several bioinformatics databases exist helping interpretation and analysis or describing associations between polymorphisms and diseases, and genome-wide association studies (GWASs) are commonly used for polygenic diseases such as type 2 diabetes, obesity, and Crohn's disease. GWASs scan DNA from a large panel of patients with a particular disease to look for SNPs. Databases resulting from the Human Genome Project and the International HapMap Project contain the reference human genome and maps of common genetic variation in large populations (National Institutes of Health; International HapMap Consortium 2003). Thus, the potential impact of SNPs can be deduced by determining whether homozygous or heterozygous SNPs are more frequent in the affected patients than in controls from an ethnically similar population.

Different approaches of genetic testing have been undertaken to study dermatological diseases (reviewed in Kwon et al. 2013). In addition to the characterization of several psoriatic susceptibility loci including human leukocyte antigens (HLA) and PSORS (Saneczko et al. 1997; Jullien and Barker 2006; Al Robaee 2010), large-scale GWASs have identified polymorphisms within genes encoding cytokines with functional relevance to psoriasis (Pietrzak et al. 2008). Even though some of these SNPs present a good discriminant power and thus can be used for psoriasis prediction (Fang et al. 2011), they are not necessarily causal markers for the disease.

As for gene expression, GWAS fails to distinguish among causes and effects, and there is a considerable interest in pathway analysis. Several approaches for testing associations with pathways

have been proposed (reviewed in Zhao et al. 2011). Furthermore, RNA-seq technology or combination of gene expression profiling and GWASs should reveal the biological impacts of particular SNPs within patient subgroups. It has been shown that the risk variant in IL12B associates with its increased expression and predisposes to stronger Th1 polarization (Johnston et al. 2013). These effects result from a deviation of the local inflammatory environment toward IL12/IFNγ at the expense of IL-23/IL-17 responses. In a recent report (Swindell et al. 2013), the same group, analyzing expression patterns in psoriatic lesions from 163 patients, has shown that most increased DEG can be explained by keratinocyte activity and inflammatory cell infiltration. They identified subgroups that differ depending on inflammatory cell infiltration and IFN-γ activity. Moreover, the differences allow differentiating between etanercept responders and nonresponders, providing a means to predict treatment outcomes with anti-TNF therapy. It has been proposed that the patient-specific differences rely, at least in part, on the developmental context for each psoriasis lesion, which is likely shaped by an integration of genetic and environmental signals.

5 Conclusion and Perspectives

The progress made in identifying the basic variation present in human brings a number of exciting opportunities and challenges. Gene expression, genotyping of SNPs, and copy number variations have become extremely important to researchers for understanding dermatological disorders and molecular mechanisms. These technologies highlight the variability occurring between individual patients, probably on the basis of their age, ethnicity, sex, genetics, skin types, and environmental influences. Undoubtedly, combined analysis of global gene expression, DNA variation, and functional approaches through the development of computational tools will take advantage of the increasing enrichment of bioinformatics databases. At a nexus in medical history, the challenge is to learn how to use the acquired repository of information to change the course of disease management. Dermatologists, which have an easy access to biological samples issued from their patients, have to be at the forefront of this history. Indeed, according to the dermatology advances toward personalized medicine, transcriptomic and genetic investigations will be part of the personalized dermatology practice of the near future. As qualified counselors, they would have to warn the public about the possible risks of direct-to-consumer genetic testing proposed on the Internet and the potentially misleading or oversimplified explanations of the results.

References

Ainali C, Valeyev N, Perera G, Williams A, Gudjonson JE, Ouzounis CA, Nestle FO, Tsoka S. Transcriptomic classification reveals molecular subtypes in psoriasis. BMC Genomics. 2012;13:472.

Al Robaee AA. Molecular genetics of psoriasis (principles, technology, gene location, genetic polymorphism and gene expression). Int J Health Sci (Qassim). 2010;4 (2):103–27.

Barrey E, Mucher E, Jeansoule N, Larcher T, Larcher T, Guigand L, Herszberg B, Chaffaux S, Guerin G, Mata X, Benech P, Canale M, Alibert O, Maltere P, Gidrol X, Barrey E, Mucher E, Jeansoule N, Larcher T. Gene expression profiling in equine polysaccharide storage myopathy revealed inflammation, glycogenesis inhibition, hypoxia and mitochondrial dysfunctions. BMC Vet Res. 2009;5(1):29.

Barrey E, Jayr VL, Mucher E, Gospodnetic S, Joly F, Benech P, Alibert O, Gidrol X, Mata X, Vaiman A, Guerin G. Transcriptomic analysis of muscle in horses suffering from recurrent exertional rhabdomyolysis revealed energetic pathway alterations and disruption in the cytosolic calcium regulation. Anim Genet. 2012;43(3):271–81.

Ben-Bassat H, Klein BY. Inhibitors of tyrosine kinases in the treatment of psoriasis. Curr Pharm Des. 2000;6 (9):933–42.

Benech P, Mas-Chamberlin C, Mondon P, Lintner K. PredictSearch: understanding biological activity of cosmetic ingredients. Personal Care Asia September. 2007:61(8):61–65.

Bièche I, Onody P, Tozlu S, Driouch K, Vidaud M, Lidereau R. Prognostic value of ERBB family mRNA expression in breast carcinomas. Int J Cancer. 2003;106 (5):758–65.

Bowcock AM, Shannon W, Du F, Duncan J, Cao K, Aftergut K, Catier J, Fernandez-Vina MA, Menter A. Insights into psoriasis and other inflammatory diseases

from large-scale gene expression studies. Hum Mol Genet. 2001; 10:1793–1805.
Fang S, Fang X, Xiong M. Psoriasis prediction from genome-wide SNP profiles. BMC Dermatol. 2011; 11:1.
Golub TR, Slonim DK, Tamayo P, Huard C, Gaasenbeek M, Mesirov JP, Coller H, Loh ML, Downing JR, Caligiuri MA, et al. Molecular classification of cancer: class discovery and class prediction by gene expression monitoring. Science. 1999; 286:531–7.
Gudjonsson JE, Johnston A, Stoll SW, Riblett MB, Xing X, Kochkodan JJ, Ding J, Nair RP, Aphale A, Voorhees JJ, Elder JT. Evidence for altered Wnt signaling in psoriatic skin. J Invest Dermatol. 2010;130 (7):1849–59.
Hagforsen E, Sunnerberg K, Michaëlsson G, Kämpe O, Hedstrand H. Psoriasis autoantigens in normal scalp skin – identification by expression cloning. J Invest Dermatol. 2007;127(9):2276–80.
Hand D, Mannila H, Smyth P. Principles of data-mining. Cambridge, MA: The MIT Press; 2001.
Hayward P, Kalmar T, Arias AM. Wnt/Notch signalling and information processing during development. Development. 2008;135(3):411–24.
Hedegaard J, Arce C, Bicciato S, Bonnet A, Buitenhuis B, Collado-Romero M, Conley LN, Sancristobal M, Ferrari F, Garrido JJ, Groenen MA, Hornshøj H, Hulsegge I, Jiang L, Jiménez-Marín A, Kommadath A, Lagarrigue S, Leunissen JA, Liaubet L, Neerincx PB, Nie H, van der Poel J, Prickett D, Ramirez-Boo M, Rebel JM, Robert-Granié C, Skarman A, Smits MA, Sørensen P, Tosser-Klopp G, Watson M. Methods for interpreting lists of affected genes obtained in a DNA microarray experiment. BMC Proc. 2009;3 Suppl 4:S5.
Hu T, Li C. Convergence between Wnt-β-catenin and EGFR signaling in cancer. Mol Cancer. 2010;9:236.
International HapMap Consortium. The International HapMap Project. Nature. 2003;426:789–96.
Jeffery IB, Higgins DG, Culhane AC. Comparison and evaluation of methods for generating differentially expressed gene lists from microarray data. BMC Bioinformatics. 2006;7:359.
Johnston A, Xing X, Swindell WR, Kochkodan J, Riblett M, Nair RP, Stuart PE, Ding J, Voorhees JJ, Elder JT, Gudjonsson JE. Susceptibility-associated genetic variation at IL12B enhances Th1 polarization in psoriasis. Hum Mol Genet. 2013;22(9):1807–15.
Jullien D, Barker JN. Genetics of psoriasis. J Eur Acad Dermatol Venereol. 2006;20 Suppl 2:42–51.
Kelder T, Conklin BR, Evelo CT, Pico AR. Finding the right questions: exploratory pathway analysis to enhance biological discovery in large datasets. PLoS Biol. 2010;31:8(8).
Kunz M, Dannemann M, Kelso J. High-throughput sequencing of the melanoma genome. Exp Dermatol. 2013;22(1):10–7.
Kwon EK, Basel D, Siegel D, Martin KL. A review of next-generation genetic testing for the dermatologist. Pediatr Dermatol. 2013;30(4):401–8.
Lander ES. Array of hope. Nat Genet. 1999;21(Suppl):3–4.
Lowell S, Jones P, Le Roux I, Dunne J, Watt FM. Stimulation of human epidermal differentiation by delta-notch signalling at the boundaries of stem-cell clusters. Curr Biol. 2000;10:491–500.
Lowry WE, Blanpain C, Nowak JA, Guasch G, Lewis L, Fuchs E. Defining the impact of beta-catenin/Tcf transactivation on epithelial stem cells. Genes Dev. 2005;19:1596–611.
Martinez Arias A, Stewart A. Molecular principles of animal development. New York: Oxford University Press; 2002.
Mascia F, Mariani V, Girolomoni G, Pastore S. Blockade of the EGF receptor induces a deranged chemokine expression in keratinocytes leading to enhanced skin inflammation. Am J Pathol. 2003;163:303–12.
Mascia F, Cataisson C, Lee TC, Threadgill D, Mariani V, Amerio P, Chandrasekhara C, Souto Adeva G, Girolomoni G, Yuspa SH, Pastore S. EGFR regulates the expression of keratinocyte-derived granulocyte/macrophage colony-stimulating factor in vitro and in vivo. J Invest Dermatol. 2010; 130(3):682–93.
Mille-Hamard L, Billat VL, Henry E, Bonnamy B, Joly F, Benech P, Barrey E. Skeletal muscle alterations and exercise performance decrease in erythropoietin-deficient mice: a comparative study. BMC Med Genomics. 2012;5(1):29.
Miller LS, Sørensen OE, Liu PT, Jalian HR, Eshttiaghpour D, Behmanesh BE, et al. TGF-α regulates TLR expression and function on epidermal keratinocytes. J Immunol. 2005;174:6137–43.
National Institutes of Health. All about the human genome project internet. Bethesda: National Institutes of Health (2012). http://www.genome.gov/10001772. Accessed 5 Jan 2012.
Nishimoto S, Kotani H, Tsuruta S, Shimizu N, Ito M, Shichita T, Morita R, Takahashi H, Amagai M, Yoshimura A. Th17 cells carrying TCR recognizing epidermal autoantigen induce psoriasis-like skin inflammation. J Immunol. 2013;191(6):3065–72.
Nusse R, Varmus H. Three decades of Wnts: a personal perspective on how a scientific field developed. EMBO J.2012;31(12):2670–84.
Oestreicher JL, Walters IB, Kikuchi T, et al. Molecular classification of psoriasis disease-associated DNA microarray technology in dermatology genes through pharmacogenomic expression profiling. Pharmacogenomics J. 2001;1:272–87.
Peterson S. DNA microarrays RNAseq-the winner and new heavyweight champion is?. . .It's a draw. Infect Dis Microb Environ Genomics Seq. http://blogs.jcvi.org/2010/02/dna-microarrays-vs-rnaseq-the-winner-and-new-heavyweight-champion-is-it's-a-draw/. Accessed on 3 Feb 2010.

Pietrzak A, Zalewska A, Chodorowska G, Nockowski P, Michalak-Stoma A, Osemlak P, Krasowska D. Genes and structure of selected cytokines involved in pathogenesis of psoriasis. Folia Histochem Cytobiol. 2008;46(1):11–21.

Rao T, Kühl M. An updated overview on Wnt signaling pathways: a prelude for more. Circ Res. 2010;106: 1798–806.

Rees JL, Harding RM. Understanding the evolution of human pigmentation: recent contributions from population genetics. J Invest Dermatol. 2012;132(3 Pt 2):846–53.

Robert C, Soria JC, Spatz A, Le Cesne A, Malka D, Pautier P, et al. Cutaneous side-effects of kinase inhibitors and blocking antibodies. Lancet Oncol. 2005;6:491–500.

Saneczko F, Kaszuba A, Trznadel-BudŸko E. Human leukocyte antigens (HLA) in psoriasis. (Polish). Pol Merk Lek. 1997;3:210–2.

Schena M, Shalon D, Davis RW, Brown PO. Quantitative monitoring of gene expression patterns with a complementary DNA microarray. Science. 1995;270 (5235):467–70.

Shi L, Jones WD, Jensen RV, Harris SC, Perkins RG, et al. The balance of reproducibility, sensitivity, and specificity of lists of differentially expressed genes in microarray studies. BMC Bioinformatics. 2008;9 Suppl 9:S10.

Sørensen OE, Cowland JB, Theilgaard-Mönch K, Liu L, Ganz T, Borrregaard N. Wound healing and expression of antimicrobial peptides/polypeptides in human keratinocytes, a consequence of common growth factors. J Immunol. 2003;170:5583–9.

Suarez-Farinas M, Lowes MA, Zaba LC, Krueger JG. Evaluation of the psoriasis transcriptome across different studies by gene set enrichment analyses (GSEA). PLoS One. 2010;5(4):e10247.

Swindell WR, Johnston A, Voorhees JJ, Elder JT, Gudjonsson JE. Dissecting the psoriasis transcriptome: inflammatory- and cytokine-driven gene expression in lesions from 163 patients. BMC Genomics. 2013; 14:527.

Wang Z, Gerstein M, Snyder M. RNA-Seq: a revolutionary tool for transcriptomics. Nat Rev Genet. 2009;10 (1):57–63.

Witten DM, Tibshirani R. A comparison of fold-change and the t-statistic for microarray data analyses. Stanford: Stanford University; 2007. p. 1–13.

Zhang M, Yao C, Guo Z, Zou J, Zhang L, et al. Apparently low reproducibility of true differential expression discoveries in microarray studies. Bioinformatics. 2008;24:2057–63.

Zhao J, Gupta S, Seielstad M, Liu J, Thalamuthu A. Pathway-based analysis using reduced gene subsets in genome-wide association studies. BMC Bioinformatics. 2011;12:17.

Zhou X, Krueger JG, Kao MC, et al. Novel mechanisms of T-cell and dendritic cell activation revealed by profiling of psoriasis on the 63,100-element oligonucleotide array. Physiol Genomics. 2003;13: 69–78.

Biometrology Guidelines for the In Vivo Assessment of Skin Surface pH in Nonclinical Settings

93

Aleksandr B. Stefaniak and Johan L. Du Plessis

Contents

Keywords

Skin surface pH • Glass planar electrode • Workplace measurement • Occupational skin diseases • Stratum corneum

The outer surface of the skin is coated with a co-mixture of aqueous sweat and oily sebum that together help to maintain skin surface pH. Among its functions, skin surface pH promotes maintenance of the skin barrier integrity, regulates epidermal barrier homeostasis, and maintains microbial flora balance (Ali and Yosipovitch 2013). In occupational settings, the skin is potentially exposed (sometimes simultaneously) to various chemical, physical, and mechanical stressors. These exposures may alter the skin surface pH which is problematic for several reasons. First, changes in skin surface pH can expedite the dissolution and/or partitioning of many chemicals thereby increasing their bioaccessibility on the skin (Collins 1957; Hemingway and Molokhia 1987). Secondly, skin surface pH will influence the formation of water soluble complexes between dissolved ions and sweat constituents, which, in turn, influences their interactions with skin proteins and cellular constituents (Stefaniak et al. 2014). Finally, alterations of skin surface pH can impair the barrier properties of the stratum

A.B. Stefaniak (✉)
Centers for Disease Control and Prevention, National Institute for Occupational Safety and Health, Morgantown, WV, USA
e-mail: AStefaniak@cdc.gov

J.L. Du Plessis
Occupational Hygiene and Health Research Initiative, North-West University, Potchefstroom, South Africa
e-mail: Johan.DuPlessis@nwu.ac.za

P. Humbert et al. (eds.), *Agache's Measuring the Skin*,
DOI 10.1007/978-3-319-32383-1_127

corneum, thereby making it easier for chemicals to penetrate and enter the body.

Measurement of skin surface pH is usually performed in highly controlled clinical settings (Parra and Paye 2003). However, the ability to measure skin surface pH in nonclinical settings such as the work environment offers many advantages. Importantly, both the amount of contaminant on the skin and the pH of the skin surface can be assessed almost simultaneously, thereby providing a more accurate characterization of the skin barrier condition at the time of exposure (Du Plessis et al. 2013). Knowledge of skin surface pH can also be used to identify opportunities for implementation of control strategies to protect workers, e.g., use of chemical-resistant gloves by workers with acidic skin pH to minimize contaminant dissolution/partitioning. Additionally, the influence of activities such as hand washing with an alkaline soap on skin surface pH can be documented to provide feedback to managers and workers on how specific tasks can change the skin barrier properties. In this chapter, practical guidance for measurement of skin surface pH in nonclinical settings is described. Details of the skin surface acidity and instruments for measurement of skin surface pH are described in ▶ Chap. 12, "Measurement of Skin Surface Acidity," respectively.

1 Apparent Skin Surface pH

The universal method for measuring skin surface pH is the glass planar electrode connected to a voltage meter. In chemistry, pH is defined as $-\log[H^+]$ concentration of a pure aqueous solution. However, the skin surface film is not pure water; rather, it is a mixture of aqueous sweat, sebum lipids, and cellular degradation products (Rippke et al. 2002). As such, the skin surface pH is not a measure of H^+ ion concentration, but is a measure of H^+ ion release from amphiphilic free fatty acid lipids into water that is applied to the skin with the glass planar electrode. More accurately, the pH measured on the skin surface should be referred to as the *apparent skin surface pH* (Parra and Paye 2003).

2 Factors Influencing Skin Surface pH

Several endogenous, exogenous, and environmental factors relevant to work environments may affect skin surface pH (Table 1). In general, values of skin surface pH vary among anatomical positions (e.g., forehead versus forearm) and within locations (e.g., T- and U-zones of the face) (Ehlers et al. 2001a; Kim et al. 2006; Kleesz et al. 2012; Kobayashi and Tagami 2004; Lee et al. 2013; Luebberding et al. 2013a, b, 2014; Marrakchi and Maibach 2007; Youn et al. 2013; Zlotogorski 1987) though not all investigators have observed differences (Pratchyapruit et al. 2007; Schreml et al. 2012; Treffel et al. 1994). Data on the influence of gender on skin surface pH are not fully understood; some studies report differences between sexes (Ehlers et al. 2001a; Kim et al. 2006; Luebberding et al. 2013a; Youn et al. 2013; Jacobi et al. 2005; Man et al. 2009; Ohman and Vahlquist 1994) but others do not (Zlotogorski 1987; Dikstein and Zlotogorski 1994; Wilhelm et al. 1991). Data are conflicting on the role of ethnicity in skin surface pH (Lee et al. 2013; Berardesca et al. 1998; Grimes et al. 2004; Warrier et al. 1996; Wesley and Maibach 2003). Skin diseases such as atopic dermatitis, urticaria, and irritant contact dermatitis may alter skin surface pH in adults (Cork et al. 2009; Jungersted et al. 2010; Kezic et al. 2012; Knor et al. 2011; Ohman and Vahlquist 1998; Schmid-Wendtner and Korting 2006; Ye et al. 2014). Some studies indicate that skin surface pH varies during the day, with minimal values often observed in the evening or early morning (Ehlers et al. 2001b; Latreille et al. 2004; Le Fur et al. 2001; Yosipovitch et al. 1998), which has implications for shift work. Age influences skin surface pH, with values becoming less acidic after ages 70–95 years (Luebberding et al. 2014; Marrakchi and Maibach 2007; Zlotogorski 1987; Schreml

Table 1 Factors that influence skin surface pH

Factor	References	Effect[a]
Endogenous		
Anatomical position	(Ehlers et al. 2001a; Kim et al. 2006; Kleesz et al. 2012; Kobayashi and Tagami 2004; Lee et al. 2013; Luebberding et al. 2013a, b, 2014; Marrakchi and Maibach 2007; Youn et al. 2013; Zlotogorski 1987)	+
Gender	(Ehlers et al. 2001a; Kim et al. 2006; Luebberding et al. 2013a; Youn et al. 2013; Zlotogorski 1987; Jacobi et al. 2005; Man et al. 2009; Ohman and Vahlquist 1994; Dikstein and Zlotogorski 1994; Wilhelm et al. 1991)	±
Ethnicity	(Lee et al. 2013; Berardesca et al. 1998; Grimes et al. 2004; Warrier et al. 1996; Wesley and Maibach 2003)	±
Skin health	(Cork et al. 2009; Jungersted et al. 2010; Kezic et al. 2012; Knor et al. 2011; Ohman and Vahlquist 1998; Schmid-Wendtner and Korting 2006; Ye et al. 2014)	+
Rhythmicity/ circadian rhythm	(Ehlers et al. 2001b; Latreille et al. 2004; Le Fur et al. 2001; Yosipovitch et al. 1998)	+
Exogenous		
Washing	(Duncan et al. 2013; Korting et al. 1987, 1990, 1991; Moldovan and Nanu 2010; Grunewald et al. 1995; Lambers et al. 2006)	+
Occlusion	(Rippke et al. 2002)	+
Exertion	(Luebberding et al. 2013c; Wang et al. 2013)	+
Environmental		
Seasonality	(Abe et al. 1980; De Paepe et al. 2009; Galzote et al. 2014)	±

Adapted from Stefaniak et al. (2013)
[a]+ = has an influence; ± = inconclusive data

et al. 2012; Man et al. 2009; Wilhelm et al. 1991; Dikstein et al. 1984; Sato et al. 2014); however, these ages are generally outside of normal working years.

Exogenous factors that influence skin surface pH and are frequently encountered in the workplace include hygiene practices (i.e., frequency, use of soaps and detergents), use of topical products (i.e., lotions, barrier creams, and cosmetics) and occlusion (e.g., from use of protective garments). Of high relevance is skin hygiene, which may involve harsh soaps, especially in dirty and greasy workplaces, or frequent hand washings among healthcare workers (Jungbauer et al. 2004; Keegel et al. 2012) and food preparers (Steiner et al. 2011). Alkaline soaps tend to raise skin surface pH, whereas acidic soaps tend to cause only a slight increase or even a lowering of skin surface pH (Duncan et al. 2013; Korting et al. 1987, 1990, 1991; Moldovan and Nanu 2010). The effects of soaps, synthetic detergents, and topical products is often transient with skin pH returning to baseline within 2 h (Duncan et al. 2013; Korting et al. 1987; Moldovan and Nanu 2010) though recovery may be incomplete up to 12 h after washing (Grunewald et al. 1995; Lambers et al. 2006). Alcohol-based hand rubs used by healthcare workers may lower skin surface pH, though results are inconsistent (Ahmed-Lecheheb et al. 2012). Use of occlusive disposable gloves for just 2 h can increase skin surface pH for up to 4 h after removal (Rippke et al. 2002). Exercise is known to increase skin pH which may be relevant for non-sedentary jobs such as landscapers and construction workers (Luebberding et al. 2013c; Wang et al. 2013).

The influence of season on skin surface pH is unclear (Abe et al. 1980; De Paepe et al. 2009; Galzote et al. 2014), but investigators should be aware of it as a factor, especially when studying outdoor workers.

3 Measurement Protocol for Nonclinical Settings

As described in Sect. 2, many factors encountered in workplace settings can influence skin surface pH. Hence, it is crucial that any protocol

for a workplace study is well designed to enable the specific research question to be answered. This protocol must include clear instructions to participants regarding behaviors that may influence measurement results. To facilitate the development of a study protocol, a checklist that captures many of the considerations for workplace measurement of skin surface pH is provided in ▶ Chap. 94, "Biometrology Guidelines for the In Vivo Assessment of Transepidermal Water Loss and Skin Hydration in Nonclinical Settings."

3.1 Workplace Measurement Considerations

When designing a study protocol, it is crucial to consider real-world limitations that can be encountered in workplace settings. For example, clinical guidelines recommend that skin surface pH measurements should be made 2–3 h after washing with tap water, 5 h after washing with synthetic detergents, and 10 h after washing with alkaline soaps (Parra and Paye 2003). If ointments, body lotions, and other topical products are applied to the measurement location, clinical guidance is to wait 12 h before measurement (John 2006). Realistically, such long lag times are generally not possible during a standard 8 h work shift, particularly among professions that engage in wet work such as healthcare workers and food handlers who frequently wash their hands or cosmetologists who frequently handle lotions, dyes, and other products (Jungbauer et al. 2004; Steiner et al. 2011; Lysdal et al. 2012). Hence, measurements in nonclinical settings should be made before washing or application of ointments and lotions if feasible (e.g., prior to the start of a work shift and before the end of a shift). If measurements cannot be made before washing or application of topical products, the researcher should be aware of the influence of water, soaps, etc. on skin surface pH (Table 1) in data interpretation. Finally, no measurements should be made on skin that is inflamed or adjacent to such areas (Stefaniak et al. 2013).

Use of personal protective garments such as coverall suits and gloves made of highly occlusive material is commonplace in work environments (Jungbauer et al. 2004; Lysdal et al. 2012). Even garments made from natural textiles (e.g., cotton) can be occlusive in work situations. Given that even short-term use of occlusive gloves can lead to elevated skin surface pH for hours after use (Rippke et al. 2002), researchers must observe whether a study participant wore protective garments (gloves, coveralls, elastomeric facepiece respirators, etc.) over an anatomical measurement position and document the event when reporting results.

3.2 Measurement Environment

Ideally, a study participant should be acclimated to the measurement environment for at least 20 min prior to determination of skin surface pH (Parra and Paye 2003). Workplace studies are challenging because measurements are usually made prior to, during, and/or after a worker's shift. Measurements performed before or after a work shift place a burden on the employee who must arrive at work early or stay later, but he or she may not be compensated for their time. Measurements made during a work shift place a burden on employers in terms of lost productivity, staffing reassignments, and paid wages. Hence, it may not be feasible for a worker to acclimate for 20 min plus time for measurements, especially if multiple measurements are to be made throughout a work shift.

In clinical settings, ambient conditions for measurement of skin surface pH are temperature of 20–22 °C and relative humidity of 40–60 % (Parra and Paye 2003). In workplace studies, researchers may not have full control over the ambient temperature and humidity levels where measurements are to be performed because doors and windows may be open (or closed) to cool (or heat) the workspace. As such, for workplace studies every effort should be made to perform measurements at 20–22 °C and relative humidity of 40–60 %; however, if these conditions are not possible, the investigator should control and

characterize the measurement atmosphere as far as reasonably practical and provide a detailed description of the conditions when reporting results.

3.3 Measurement of Skin Surface pH

It is important that the glass planar pH electrode is handled and used in accordance with the manufacturer's instructions. Prior to use, the electrode should be calibrated using at least a two-point calibration with buffers that span the expected skin surface pH values (e.g., pH 4–7) and recalibrated as specified by the manufacturer or verified periodically using standard buffers. The pH electrode and the meter should be equilibrated in the same environment in which measurements will be taken for at least 20 min prior to use (Parra and Paye 2003).

The skin surface at the measurement location should be clean and free of cosmetics and lotions or other topical products. If necessary, the skin can be cleaned using a clean, dry, oil- and lotion-free tissue paper. Water alone can alter pH and should not be used to clean the skin at the measurement location (Lambers et al. 2006). Typically, the electrode surface is moistened with 20 μL of distilled water prior to placing it on the skin (Parra and Paye 2003); however, Lambers et al. (2006) report that water volumes up to 100 μL do not influence measurement results. The pH electrode should be held at a right angle to the skin with gentle pressure to ensure optimal contact (Ehlers et al. 2001b); avoid applying excessive pressure which can affect the volume of liquid at the interface of the electrode and skin (Parra and Paye 2003). Measurements should be recorded when a stable signal (as defined by the instrument manufacturer) is achieved.

Three sequential measurements should be made at the same anatomical position, with a 5 s lag time between measurements, and the results averaged. To reduce any possible effect of electrode contamination on skin pH measurements, it should be rinsed with deionized water periodically (Ehlers et al. 2001b). All measurements at a given anatomical position should be made before moving to the next position (Stefaniak et al. 2013). If repeat measures of skin surface pH will be made at a given anatomical position (e.g., pre- and post-work shift), record both sets of measurements at the same position to reduce error. Digital photography is useful for documenting the anatomical positions to ensure consistency in measurements. If simultaneous assessment of skin exposure to a contaminant is also a study goal, the area of pH measurement should be as close as possible to the area monitored for skin exposure without confounding the respective measurements. Finally, if other biophysical skin measurements are to be made, Kottner et al. (2014) recommend determination of transepidermal water loss before determination of skin surface pH or stratum corneum hydration to avoid measurement bias.

Measurements obtained by different researchers may introduce variability to the results (because they might use different pressures or probe angles); therefore, the same person should perform all measurements. Report skin pH values with precision of ± 0.1 units. Between measurements, the electrode and meter should be stored in accordance with the manufacturer's instructions.

4 Data Interpretation and Reporting

The factors that influence skin surface pH (Table 1) illustrate the challenges associated with measurements in workplace settings with myriad exposures. Additionally, consensus is lacking in regard to reference values for skin surface pH of normal or diseased skin. As such, reporting absolute values of skin surface pH can be problematic, especially when comparing data among studies. Therefore, measurement results should be reported in relative terms, such as percent change over a work shift. All measurement results for a given set of conditions should be expressed with both a measure of central tendency (e.g., arithmetic mean of three repeat measurements) and variability (i.e., standard deviation or percentiles). If the aim of a study warrants use of a control

group, the volunteers should be matched to workers with respect to relevant endogenous, exogenous, and environmental factors and measurements made in a similar environment with the same instrumentation to ensure consistency in data collection.

A minimum data set should be reported with any study results, including: (1) relevant endogenous (anatomical site, skin health at time of measurement, date, time, etc.), exogenous (skin hygiene, use of topical products, use of occlusive garments at measurement locations, etc.), and environmental (season, geographical location) factors; (2) measurement conditions (acclimation time and conditions for equipment and participants, pH electrode calibration, number of measurements, etc.); (3) measurement results in relative terms (percent change) accompanied by a measure of central tendency and variability; and (4) pertinent deviations from the study protocol and the measurement guidance provided herein.

References

Abe T, Mayuzumi J, Kikuchi N, Arai S. Seasonal variations in skin temperature, skin pH, evaporative water loss and skin surface lipid values on human skin. Chem Pharm Bull (Tokyo). 1980;28(2):387–92.

Ahmed-Lecheheb D, Cunat L, Hartemann P, Hautemaniere A. Prospective observational study to assess hand skin condition after application of alcohol-based hand rub solutions. Am J Infect Control. 2012;40(2):160–4.

Ali SM, Yosipovitch G. Skin pH: from basic science to basic skin care. Acta Derm Venereol. 2013;93(3): 261–7.

Berardesca E, Pirot F, Singh M, Maibach H. Differences in stratum corneum pH gradient when comparing white Caucasian and black African-American skin. Br J Dermatol. 1998;139(5):855–7.

Collins KJ. The corrosion of metal by palmar sweat. Br J Ind Med. 1957;14(3):191–7.

Cork MJ, Danby SG, Vasilopoulos Y, Hadgraft J, Lane ME, Moustafa M, et al. Epidermal barrier dysfunction in atopic dermatitis. J Invest Dermatol. 2009;129(8):1892–908.

De Paepe K, Houben E, Adam R, Hachem JP, Roseeuw D, Rogiers V. Seasonal effects on the nasolabial skin condition. Skin Pharmacol Physiol. 2009;22(1):8–14.

Dikstein S, Zlotogorski A. Measurement of skin pH. Acta Derm Venereol Suppl (Stockh). 1994;185:18–20.

Dikstein S, Hartzshtark A, Bercovici P. The dependence of low-pressure indentation, slackness, and surface pH on age in forehead skin of women. J Soc Cosmet Chem. 1984;35:221–8.

Du Plessis JL, Eloff FC, Engelbrecht S, Laubscher PJ, van Aarde MN, Franken A. Dermal exposure and changes in skin barrier function of base metal refinery workers co-exposed to cobalt and nickel. Occup Health South Afr. 2013;19(1):6–12.

Duncan CN, Riley TV, Carson KC, Budgeon CA, Siffleet J. The effect of an acidic cleanser versus soap on the skin pH and micro-flora of adult patients: a non-randomised two group crossover study in an intensive care unit. Intensive Crit Care Nurs. 2013;29(5): 291–6.

Ehlers C, Ivens UI, Moller ML, Senderovitz T, Serup J. Females have lower skin surface pH than men. A study on the surface of gender, forearm site variation, right/left difference and time of the day on the skin surface pH. Skin Res Technol. 2001a;7 (2):90–4.

Ehlers C, Ivens UI, Moller ML, Senderovitz T, Serup J. Comparison of two pH meters used for skin surface pH measurement: the pH meter 'pH900' from Courage & Khazaka versus the pH meter '1140' from Mettler Toledo. Skin Res Technol. 2001b;7(2):84–9.

Galzote C, Estanislao R, Suero MO, Khaiat A, Mangubat MI, Moideen R, et al. Characterization of facial skin of various Asian populations through visual and non-invasive instrumental evaluations: influence of seasons. Skin Res Technol. 2014;20:453–62.

Grimes P, Edison BL, Green BA, Wildnauer RH. Evaluation of inherent differences between African American and white skin surface properties using subjective and objective measures. Cutis. 2004;73(6):392–6.

Grunewald AM, Gloor M, Gehring W, Kleesz P. Damage to the skin by repetitive washing. Contact Dermatitis. 1995;32(4):225–32.

Hemingway JD, Molokhia MM. The dissolution of metallic nickel in artificial sweat. Contact Dermatitis. 1987;16(2):99–105.

Jacobi U, Gautier J, Sterry W, Lademann J. Gender-related differences in the physiology of the stratum corneum. Dermatology. 2005;211(4):312–7.

John S. Primary and acquired sensitive skin. In: Berardesca E, Fluhr J, Maibach H, editors. The sensitive skin syndrome. New York: Taylor & Francis; 2006. p. 129–47.

Jungbauer FH, Lensen GJ, Groothoff JW, Coenraads PJ. Exposure of the hands to wet work in nurses. Contact Dermatitis. 2004;50(4):225–9.

Jungersted JM, Scheer H, Mempel M, Baurecht H, Cifuentes L, Hogh JK, et al. Stratum corneum lipids, skin barrier function and filaggrin mutations in patients with atopic eczema. Allergy. 2010;65(7):911–8.

Keegel TG, Nixon RL, LaMontagne AD. Exposure to wet work in working Australians. Contact Dermatitis. 2012;66(2):87–94.

Kezic S, O'Regan GM, Lutter R, Jakasa I, Koster ES, Saunders S, et al. Filaggrin loss-of-function mutations are associated with enhanced expression of IL-1 cytokines in the stratum corneum of patients with atopic dermatitis and in a murine model of filaggrin deficiency. J Allergy Clin Immunol. 2012;129(4):1031–9.

Kim MK, Patel RA, Shinn AH, Choi SY, Byun HJ, Huh CH, et al. Evaluation of gender difference in skin type and pH. J Dermatol Sci. 2006;41(2):153–6.

Kleesz P, Darlenski R, Fluhr JW. Full-body skin mapping for six biophysical parameters: baseline values at 16 anatomical sites in 125 human subjects. Skin Pharmacol Physiol. 2012;25(1):25–33.

Knor T, Meholjic-Fetahovic A, Mehmedagic A. Stratum corneum hydration and skin surface pH in patients with atopic dermatitis. Acta Dermatovenerol Croat. 2011; 19(4):242–7.

Kobayashi H, Tagami H. Distinct locational differences observable in biophysical functions of the facial skin: with special emphasis on the poor functional properties of the stratum corneum of the perioral region. Int J Cosmet Sci. 2004;26(2):91–101.

Korting HC, Kober M, Mueller M, Braun-Falco O. Influence of repeated washings with soap and synthetic detergents on pH and resident flora of the skin of forehead and forearm. Results of a cross-over trial in health probationers. Acta Derm Venereol. 1987; 67(1):41–7.

Korting HC, Hubner K, Greiner K, Hamm G, Braun-Falco O. Differences in the skin surface pH and bacterial microflora due to the long-term application of synthetic detergent preparations of pH 5.5 and pH 7.0. Results of a crossover trial in healthy volunteers. Acta Derm Venereol. 1990; 70(5):429–31.

Korting HC, Megele M, Mehringer L, Vieluf D, Zienicke H, Hamm G, et al. Influence of skin cleansing preparation acidity on skin surface properties. Int J Cosmet Sci. 1991;13(2):91–102.

Kottner J, Ludriksone L, Garcia Bartels N, Blume-Peytavi U. Do repeated skin barrier measurements influence each other's results? An explorative study. Skin Pharmacol Physiol. 2014;27(2):90–6.

Lambers H, Piessens S, Bloem A, Pronk H, Finkel P. Natural skin surface pH is on average below 5, which is beneficial for its resident flora. Int J Cosmet Sci. 2006;28(5):359–70.

Latreille J, Guinot C, Robert-Granie C, Le Fur I, Tenenhaus M, Foulley JL. Daily variations in skin surface properties using mixed model methodology. Skin Pharmacol Physiol. 2004;17(3):133–40.

Le Fur I, Reinberg A, Lopez S, Morizot F, Mechkouri M, Tschachler E. Analysis of circadian and ultradian rhythms of skin surface properties of face and forearm of healthy women. J Invest Dermatol. 2001; 117(3):718–24.

Lee MR, Nam GW, Jung YC, Park SY, Han JY, Cho JC, et al. Comparison of the skin biophysical parameters of Southeast Asia females: forehead-cheek and ethnic groups. J Eur Acad Dermatol Venereol. 2013; 27(12):1521–6.

Luebberding S, Krueger N, Kerscher M. Skin physiology in men and women: in vivo evaluation of 300 people including TEWL, SC hydration, sebum content and skin surface pH. Int J Cosmet Sci. 2013a; 35(5):477–83.

Luebberding S, Krueger N, Kerscher M. Age-related changes in skin barrier function – quantitative evaluation of 150 female subjects. Int J Cosmet Sci. 2013b; 35(2):183–90.

Luebberding S, Kolbe L, Kerscher M. Influence of sportive activity on skin barrier function: a quantitative evaluation of 60 athletes. Int J Dermatol. 2013c; 52(6):745–9.

Luebberding S, Krueger N, Kerscher M. Age-related changes in male skin: quantitative evaluation of one hundred and fifty male subjects. Skin Pharmacol Physiol. 2014;27(1):9–17.

Lysdal SH, Johansen JD, Flyvholm MA, Sosted H. A quantification of occupational skin exposures and the use of protective gloves among hairdressers in Denmark. Contact Dermatitis. 2012; 66(6):323–34.

Man MQ, Xin SJ, Song SP, Cho SY, Zhang XJ, Tu CX, et al. Variation of skin surface pH, sebum content and stratum corneum hydration with age and gender in a large Chinese population. Skin Pharmacol Physiol. 2009;22(4):190–9.

Marrakchi S, Maibach HI. Biophysical parameters of skin: map of human face, regional, and age-related differences. Contact Dermatitis. 2007;57(1):28–34.

Moldovan M, Nanu A. Influence of cleansing product type on several skin parameters after single use. Farmacia. 2010;58(1):29–37.

Ohman H, Vahlquist A. In vivo studies concerning a pH gradient in human stratum corneum and upper epidermis. Acta Derm Venereol. 1994;74(5):375–9.

Ohman H, Vahlquist A. The pH gradient over the stratum corneum differs in X-linked recessive and autosomal dominant ichthyosis: a clue to the molecular origin of the "acid skin mantle"? J Invest Dermatol. 1998; 111(4):674–7.

Parra JL, Paye M. EEMCO guidance for the in vivo assessment of skin surface pH. Skin Pharmacol Appl Ski Physiol. 2003;16(3):188–202.

Pratchyapruit W, Kikuchi K, Gritiyarangasan P, Aiba S, Tagami H. Functional analyses of the eyelid skin constituting the most soft and smooth area on the face: contribution of its remarkably large superficial corneocytes to effective water-holding capacity of the stratum corneum. Skin Res Technol. 2007;13 (2):169–75.

Rippke F, Schreiner V, Schwanitz HJ. The acidic milieu of the horny layer: new findings on the physiology and pathophysiology of skin pH. Am J Clin Dermatol. 2002;3(4):261–72.

Sato N, Kitahara T, Fujimura T. Age-related changes of stratum corneum functions of skin on the trunk and the limbs. Skin Pharmacol Physiol. 2014; 27(4):181.

Schmid-Wendtner MH, Korting HC. The pH of the skin surface and its impact on the barrier function. Skin Pharmacol Physiol. 2006;19(6):296–302.

Schreml S, Zeller V, Meier RJ, Korting HC, Behm B, Landthaler M, et al. Impact of age and body site on adult female skin surface pH. Dermatology. 2012; 224(1):66–71.

Stefaniak AB, Plessis J, John SM, Eloff F, Agner T, Chou TC, et al. International guidelines for the in vivo assessment of skin properties in non-clinical settings: part 1. pH. Skin Res Technol. 2013;19(2):59–68.

Stefaniak AB, Duling MG, Geer L, Virji MA. Dissolution of the metal sensitizers Ni, Be, Cr in artificial sweat to improve estimates of dermal bioaccessibility. Environ Sci Process Impact. 2014;16(2):341–51.

Steiner MF, Dick FD, Scaife AR, Semple S, Paudyal P, Ayres JG. High prevalence of skin symptoms among bakery workers. Occup Med (Lond). 2011; 61(4):280–2.

Treffel P, Panisset F, Faivre B, Agache P. Hydration, transepidermal water loss, pH and skin surface parameters: correlations and variations between dominant and non-dominant forearms. Br J Dermatol. 1994; 130(3):325–8.

Wang S, Zhang G, Meng H, Li L. Effect of exercise-induced sweating on facial sebum, stratum corneum hydration, and skin surface pH in normal population. Skin Res Technol. 2013;19(1):e312–7.

Warrier A, Kligman A, Harper R, Bowman J, Wickett R. A comparison of black and white skin using noninvasive methods. J Soc Cosmet Chem. 1996; 47:229–40.

Wesley NO, Maibach HI. Racial (ethnic) differences in skin properties: the objective data. Am J Clin Dermatol. 2003;4(12):843–60.

Wilhelm KP, Cua AB, Maibach HI. Skin aging. Effect on transepidermal water loss, stratum corneum hydration, skin surface pH, and casual sebum content. Arch Dermatol. 1991;127(12):1806–9.

Ye YM, Kim BE, Shin YS, Park HS, Leung DY. Increased epidermal filaggrin in chronic idiopathic urticaria is associated with severity of urticaria. Ann Allergy Asthma Immunol. 2014;112(6):533–8.

Yosipovitch G, Xiong GL, Haus E, Sackett-Lundeen L, Ashkenazi I, Maibach HI. Time-dependent variations of the skin barrier function in humans: transepidermal water loss, stratum corneum hydration, skin surface pH, and skin temperature. J Invest Dermatol. 1998;110(1):20–3.

Youn SH, Choi CW, Choi JW, Youn SW. The skin surface pH and its different influence on the development of acne lesion according to gender and age. Skin Res Technol. 2013;19(2):131–6.

Zlotogorski A. Distribution of skin surface pH on the forehead and cheek of adults. Arch Dermatol Res. 1987;279(6):398–401.

Biometrology Guidelines for the In Vivo Assessment of Transepidermal Water Loss and Skin Hydration in Nonclinical Settings

94

Johan L. Du Plessis and Aleksandr B. Stefaniak

Contents

J.L. Du Plessis (✉)
Occupational Hygiene and Health Research Initiative, North-West University, Potchefstroom, South Africa
e-mail: Johan.duPlessis@nwu.ac.za

A.B. Stefaniak
Centers for Disease Control and Prevention, National Institute for Occupational Safety and Health, Morgantown, WV, USA
e-mail: AStefaniak@cdc.gov

P. Humbert et al. (eds.), *Agache's Measuring the Skin*,
DOI 10.1007/978-3-319-32383-1_128

Keywords
Occupation • Skin hydration • Transepidermal water loss • Skin barrier • Guideline • Nonclinical • Measurement

Abbreviations

RH	Relative humidity
SC	Stratum corneum
TEWL	Transepidermal water loss

1 Introduction

The most important functions of the skin are to prevent loss of fluids from within the body to the environment and to prevent entry of xenobiotic substances and infectious agents into the body (Zhai and Maibach 2002; Agache 2004; Proksch et al. 2008). This barrier function resides primarily in the epidermis and consists of a physical and biochemical barrier (Proksch et al. 2008). Corneocytes and lipids of the stratum corneum (SC) form the physical barrier, while the slightly acidic hydro-lipid film on the skin surface serves as a complementary biochemical barrier (Korting et al. 1990; Ohman and Vahlquist 1998). Skin barrier functionality and skin appearance are maintained by the interaction between transepidermal water loss (TEWL), SC hydration, sebum levels on the skin, and skin surface pH (Roskos and Guy 1989; Wilhelm et al. 1991).

TEWL and skin hydration have been widely used as surrogate markers for assessing skin barrier function (Zhai and Maibach 2002; Pirot and Falson 2004; Rogiers 2001; Levin and Maibach 2005; Tupker and Pinnagoda 2006; Rawlings 2006; Darlenski et al. 2009). The most prominent finding is elevated TEWL in a number of skin diseases (e.g., atopic dermatitis, eczema, and psoriasis) and in experimental studies in which solvent and detergents are applied to the skin (Proksch et al. 2008; Darlenski et al. 2009). Furthermore, elevated TEWL values in a disturbed skin barrier are frequently correlated with low hydration of the SC (Proksch et al. 2008).

In occupational environments, damage to the skin and a compromised skin barrier, although not necessarily visible, commonly occur as a result of physical/mechanical and chemical damage. Evidence suggests that a compromised skin barrier may increase dermal penetration and absorption of chemicals and of larger substances (e.g., particulates and proteins), which normally cannot effectively penetrate intact skin (Kezic and Nielsen 2009). Scrubbing, friction, or abrasion may partially or completely remove the SC and thus disrupt the skin barrier by exposing the epidermis to the environment (Fluhr et al. 2008; Kezic and Nielsen 2009). Organic solvents increase skin permeability by extracting and altering the structure of intercellular lipids from the SC, while desmosomes may also be damaged (Kezic and Nielsen 2009). Surfactants (detergents) interact with skin lipids and proteins leading to disorganization of extracellular lipids, reducing corneocyte cohesion and decreasing skin hydration (Kezic and Nielsen 2009; Nielsen 2005). Occlusion created by prolonged wearing of protective clothing, in particular impervious gloves, prevents evaporation of water thereby leading to accumulation of water in intercellular spaces across the SC and swelling of corneocytes (Zhai and Maibach 2002). This swelling disrupts SC lipid bilayers leading to enhanced skin permeation of substances due to the lower diffusion resistance provided. Prolonged contact with water, i.e., wet work, has a similar effect as that of occlusion on the SC (Kezic and Nielsen 2009).

A number of studies have been published in which changes in skin barrier function in occupational settings have been investigated. The findings of these studies are beyond the scope of this chapter, yet the most notable occupational settings were (contaminants, where applicable, indicated in brackets) (*i*) metal industry (water-soluble oils and mineral oils) (Coenraads et al. 1986; Goh and Gan 1994; Berndt et al. 1999; Kütting et al. 2010); (*ii*) health care, in particular nurses (Smit et al. 1994; Hachem et al. 2002); (*iii*) hairdressers (wet work and chemicals in hair products) (Smit et al. 1994; John et al. 2000; Packham et al. 2005); (*iv*) rayon manufacturing (carbon disulfide and sulfuric acid) (Chou et al. 2004); (*v*) manufacturing industry (ultralow humidity) (Chou et al. 2005); (*vi*) food industry (wet work) (Packham et al. 2005; Bauer et al. 2007); (*vii*) daycare/nurseries (wet work) (Packham et al. 2005); (*viii*) construction industry (cement containing chromium) (Chou et al. 2008); and (*ix*) base metal refineries (sulfuric acid during refining of nickel and cobalt) (Du Plessis et al. 2010, 2013).

Guidelines for the in vivo measurement of TEWL and skin hydration in highly controlled clinical settings are well known and widely used (Rogiers 2001; Pinnagoda et al. 1990; Berardesca 1997), and guidelines for the measurement of TEWL, skin hydration, and skin surface pH in nonclinical settings were published recently (Du Plessis et al. 2013; Stefaniak et al. 2013). “Real-life” occupational environments may be more variable and difficult to control, as a result of numerous and often uncontrollable factors, which presents unique measurement challenges not encountered in clinical settings. This chapter presents these published guidelines, as well as amendments since publication thereof, for the in vivo measurement of TEWL and skin hydration in nonclinical settings such as the workplace.

2 Instrumentation for Measurement of TEWL and Skin Hydration

TEWL can be measured in vivo by using a closed-chamber or an open-chamber method. The measurement principles of these instruments are described in ▶ Chap. 108, "Transepidermal Water Loss", but the reader may also consult Pirot and Falson (2004), Tupker and Pinnagoda (2006), and Imhof et al. (2009, 2014).

The open-chamber measurement method is widely used in clinical and experimental research and is the standard against which newer closed-chamber methods are judged (Imhof et al. 2009; Fluhr and Darlenski 2014; Imhof et al. 2014). However, the open-chamber method has a number of limitations, such as being easily influenced by disturbances in ambient air movement, calibration inconsistencies, angular dependence, temperature dependence, contact pressure dependence, and relatively long measurement times of approximately 30 s (Imhof et al. 2014). In contrast, closed-chamber methods are not influenced by ambient air movements, and the overall measurement time of unventilated-closed chamber instruments is very short (<10 s) (Nuutinen 2006; Imhof et al. 2009), making them useful for measurements in nonclinical settings. Some manufacturers claim that measurement with closed-chamber-type instruments is not affected by the probe angle, but several studies reported an angular dependence (Raynor et al. 2004; Cohen et al. 2009).

The commercially available open-chamber instruments are the DermaLab (Cortex Technology, Hadsund, Denmark), Evaporimeter (ServoMed, Stockholm, Sweden), and Tewameter (Courage and Khazaka, Cologne, Germany). The AquaFlux (Biox Systems Ltd, London, United Kingdom) is a condenser-type closed-chamber instrument, while the AS-CT1 (Asahi Biomed Company Ltd, Yokohama, Japan) and the VapoMeter (Delfin Technologies, Kuopio, Finland) are unventilated closed-chamber instruments that are commercially available (Du Plessis et al. 2013).

Skin hydration can be measured based on three principles, namely, capacitance, conductance, and impedance (Barel and Clarys 2014). These principles are addressed in ▶ Chap. 15, "Measurement of Skin Surface Hydration". Commercially available instruments based on conductance as measurement principle are the Corneometer (Courage and Khazaka, Cologne, Germany) and the MoistureMeter SC (Delfin Technologies, Kuopio, Finland). The ASA-M2 (Asahi Biomed Company Ltd, Yokohama, Japan) and Skicon (ISBS Co Ltd, Hamamatsu, Japan) are based on capacitance as a measurement principle, while the DermaLab Moisture Unit (Cortex Technology, Hadsund, Denmark) and Nova Dermal Phase Meter (Nova Technology Corporation, Portsmouth, NH, USA) are based on impedance as a measurement principle (Du Plessis et al. 2013).

3 Guideline Protocol for Measurement of TEWL and Skin Hydration in Nonclinical Settings

The aim of this protocol is to provide guidelines and best practices for measurement of TEWL and skin hydration in nonclinical settings by recognizing and accounting for, and to the extent possible, eliminating, or minimizing the influences of endogenous-, exogenous-, environmental-, and measurement/instrumentation-related factors (Table 1).

3.1 Informed Consent

Informed consent must be obtained from each participant (worker) in accordance with the human subject policy of the institution(s) governing the study prior to performing any measurements. The informed consent must provide

Table 1 Influence of endogenous-, exogenous-, environmental-, and measurement/instrumentation-related factors on TEWL and skin hydration (Adapted from Du Plessis et al. 2013; Fluhr and Darlenski 2014)

	TEWL	Skin hydration
Endogenous factors		
Age	Yes[a]	Yes
Gender	No	No
Ethnicity	Controversial	Controversial
Anatomical position	Yes	Yes
Skin temperature	Yes	Yes
Sweating	Yes	Yes
Circadian rhythm	Yes	Controversial
Skin health	Yes	Yes
Exogenous factors		
Skin washing and wet work	Yes	Yes
Solvents/surfactants	Yes	Yes
Occlusion	Yes	Controversial
Skin damage	Yes	Yes
Intake of vasoactive substances (drugs, caffeine, nicotine)	Yes	Yes[b]
Environmental and measurement factors		
Air convection/movement	Yes/no[c]	Yes
Ambient temperature	Yes	Yes
Relative humidity	Yes	Yes
Direct light	Yes	
Season	Yes	Yes

[a]Baseline TEWL is independent of age among persons in their working years, slightly lower >60 years
[b]Smoking only
[c]Closed-chamber instruments are not influenced by air convection or movement, while open-chamber instruments are

precise information on the purpose(s) of the study, a description of the procedures to be performed, the participant's responsibilities, risks and benefits of participation, and any other pertinent information relevant to the study.

3.2 Instructions to Participants

After obtaining informed consent, precise instructions should be communicated to participants regarding acceptable and permissible hygiene practices (skin washing), the use of topical products (i.e., cosmetics, lotions, and barrier creams), and ingestion of potential vasoactive substances such as caffeine (including beverages), nicotine (smoking), and/or drugs (medicines) prior to measurements (Rogiers 2001; Brandner et al. 2006; Crowther et al. 2008; Fluhr and Darlenski 2014).

3.3 Instruments

For TEWL measurements in nonclinical settings, such as workplaces, it is highly recommended that a closed-chamber-type instrument be used because this design is not influenced by air movement and has short measuring times, and some are small battery-operated devices making them easily portable (Imhof et al. 2009, 2014). The two most prominent closed-chamber TEWL instruments in literature are the AquaFlux and VapoMeter. They differ in measurement principle, concept, and design with the aforementioned using a condenser-chamber method of measurement in a benchtop, mains-powered design. The VapoMeter uses an unventilated-chamber method of measurement in a small self-contained, battery-powered design. Their performance characteristics, described by Imhof et al. (2014), differ as

well with the AquaFlux having higher accuracy, sensitivity, and repeatability, with speed of measurement (short measurement time, i.e., 7–16 s) and mobility as the main features of the VapoMeter.

If, however, an open-chamber TEWL instrument is to be used in nonclinical settings, the use of a draft shield will help to minimize the effect of air movement on measurements to a great extent.

One manufacturer of an open-chamber-type TEWL instrument recommends measurement of skin temperature prior to measurements as Rogiers (2001) found that a difference between skin temperature and probe temperature influences TEWL values. The TEWL probe heater is set at the skin temperature measured, and the TEWL probe/instrument is heated to a temperature corresponding to that of the skin before making measurements.

In addition, an ambient thermometer and relative humidity (RH) meter are required to record ambient temperature and RH.

3.4 Preparation, Handling, and Storage of Instruments

The instrument should be turned on at least 15–30 min prior to taking measurements in the area in which actual measurements will be taken (Pinnagoda et al. 1990; Tupker and Pinnagoda 2006; Imhof et al. 2009, 2014). If the instruments are to be used intermittently during the day, it should not be switched off between measurements (Tupker and Pinnagoda 2006). However, battery-operated instruments are designed to switch-off automatically after a few minutes of nonuse to prolong battery life. Prior to and during measurements, the TEWL probe, in particular the VapoMeter, should always be handled with an insulated glove as holding the probe causes an increase in the temperature of the probe through heat transfer and subsequently influences TEWL readings (Rogiers 2001; Imhof et al. 2009, 2014; De Paepe et al. 2005).

For hygienic purposes, the probe head must be wiped with an alcohol-soaked tissue after completion of measurements on a study participant in order to prevent possible transfer of infections between participants. Another alternative is the use of single-use disposable shields, which are available from some manufacturers. It should be noted that the use of shields increases the distance between the skin and probe sensors and the use thereof should be reported.

Between uses, the instruments should be cleaned and stored in accordance with the manufacturer's instructions. In general, this implies cleaning of the instrument/probe with a soft tissue or an alcohol-soaked tissue to remove excessive dirt and storage in a clean dry place with temperature and RH resembling that of the usual environment when used (Du Plessis et al. 2013).

3.5 Calibration of Instruments

Only calibrated TEWL and hydration instruments should be used for measurements. Two types of calibration could possibly be performed, namely, manufacturer calibration and prior to use calibration (not applicable to all instruments). Manufacturer calibration requires that the instrument be sent to the manufacturer for calibration at specified predetermined intervals, usually once a year. Biannual or quarterly manufacturer calibration is recommended, if practicable, with very frequent use. Calibration prior to use should be performed at regular intervals as specified by the manufacturer. The procedures of prior to use calibration may vary between manufacturers and should also be done in accordance to the instructions provided by the manufacturer. Due to the simplicity of some calibration procedures, calibration could easily be performed daily. For further quality control purposes, and if practicable, prior to use calibrations could be verified after performing a set number of measurements on a specific day or in between prior to use calibrations (Du Plessis et al. 2013).

Two flux calibration methods, as described in detail by Imhof et al. (2009), are currently in use

for TEWL instruments, namely, the more commonly used wet-cup method (for open- and closed-chamber-type instruments) and a new droplet method (for instruments capable of recording continuous flux, but not unventilated closed-chamber-type instruments).

For skin hydration instruments, a two-point (low- and high-value) in vitro calibration check on cellulose and filter pads should be performed prior to use and during periodic verifications of calibration (Du Plessis et al. 2013; Barel and Clarys 2014).

3.6 Measurement of TEWL and/or Skin Hydration

Prior to measurement of TEWL and/or skin hydration, a participant should be acclimated to the measurement environment to avoid errors caused by environmental temperature or sweating. EEMCO's clinical study guidelines recommend an acclimation period of least 15–30 min at an ambient temperature (20–22 °C) and relative humidity (40–60 %) prior to measuring TEWL (Rogiers 2001; Pinnagoda et al. 1990) and at least 20 min for skin hydration (Berardesca 1997). More recently, Fluhr and Darlenski (2014) suggested ambient temperatures as low as 18 °C, but not exceeding 21 °C for TEWL measurements with an acclimation period of 20–30 min. Barel and Clarys (2014) state a constant ambient temperature of 20–21 °C as ideal for skin hydration measurements.

In the workplace, it may not always be possible for a worker to leave their shift long enough to acclimate for 20–30 min plus time for measurements. Workers may also be unwilling to have measurements performed in their own time (before, during, or after a shift) because of personal reasons. An acclimation period as long as practicably possible, but preferably at least 20 min, is recommended. In nonclinical settings, such as workplaces, the environmental conditions recommended for clinical studies may not be readily achievable. In experiences gained from past workplace assessments, researchers may be provided a space for testing where there is little control over the ambient temperature, humidity, and air movement. Hence, it is recommended that measurement conditions be controlled and characterized (reported) as far as reasonably practicable. Measurements during extreme conditions of cold, heat, or RH should be avoided (Du Plessis et al. 2013).

The anatomical position(s) to be measured should be exposed to ambient air for at least 10 min prior to measurement (Berardesca 1997), but ideally for a period corresponding to the acclimation period in the measurement environment.

Application of topical products, washing, occlusion, smoking, and ingestion of caffeinated beverages may influence TEWL and skin hydration values (Du Plessis et al. 2013). Ingestion of caffeinated beverages should be avoided at least 3 h prior to and during the work shift (Crowther et al. 2008). Topical products should not be applied to the intended measuring area and should be avoided for at least 12 h prior to participation/measurement (John 2006; Fluhr and Darlenski 2014). However, in occupational settings such as health care, the food industry, and cosmetology, where frequent (hand) washing or use of topical products and lotions occurs, it is not feasible. The same applies to the use of barrier creams in the workplace. Therefore, the use of any topical product or lotion should be noted according to the type used, frequency of application, and time of last application (Du Plessis et al. 2013). In workplace studies, acute changes in TEWL and skin hydration during or for the duration of a work shift while following normal working procedures are of interest. Because of the acute effects of washing on TEWL and skin hydration (Voegeli 2008), it is recommended that measurements be made before washing or application of topical products and lotions. Wearing of highly occlusive personal protective clothing such as gloves and coverall suits made of various types of textiles and materials is common practice in many work environments. As such, it is important to verify whether the worker (participant) wore protective clothing over an anatomical position and, if so, to record information regarding the type of protective clothing, frequency of use, duration of use, time between last use, and measurement.

No measurement should be made on clinically inflamed or diseased skin or in very close proximity to such a position. If the measurement position is compromised by disease or injury, a nearby position may be used, but should be recorded as such. If a nearby position cannot be identified, the participant should rather be excluded from the study (Du Plessis et al. 2013).

The recommended anatomical position for TEWL and skin hydration measurements in clinical studies is the volar forearm away from the wrist (Berardesca 1997; Rogiers 2001), even though other anatomical positions have also been measured. In the workplace TEWL and skin hydration measurements should be made on anatomical positions relevant to the activities and tasks of workers. Even if another anatomical position is of interest, it is still highly recommended to measure TEWL and skin hydration at the mid-volar forearm as a reference. A complicating factor in all likelihood will be the use of personal protective clothing and respirators, leaving in many instances the volar forearm occluded and only the neck and cheeks not occluded. In these instances, study goals must be considered to determine the most appropriate anatomical positions to be measured, and if measured, factors influencing measurement values should be noted and considered when data is interpreted (Du Plessis et al. 2013). For skin hydration measurements in particular, the presence of body hair may interfere with the sensor-skin contact interface, which may influence measured values (Berardesca 1997). Measurement on extremely hairy positions should be avoided, or, alternatively, hair should be removed, but the skin should be allowed to recover before measurements (Du Plessis et al. 2013).

A horizontal probe angle is of particular importance when using an open-chamber-type TEWL probe as not to disturb natural air convection. External air movements do not interfere with measurements of closed-chamber-type TEWL instruments, but natural convection can also occur inside their measurement chambers. Therefore, angular dependence may also be an issue (Imhof et al. 2014). It is suggested that all TEWL measurements be done on horizontal skin surfaces irrespective of the type of instrument used (Imhof et al. 2009, 2014). If measuring the cheek or neck, the study participant must lie down, if possible, or adjust his body position to ensure a horizontal measurement area.

Contact pressure between the probe head and skin influences measurements made using open-chamber-type TEWL probes (Gabard and Treffel 2004; Tupker and Pinnagoda 2006) which can be ascribed to probe head design (Imhof et al. 2014). Closed-chamber-type TEWL instruments have minimal sensitivity to contact pressure, but timing of skin contact is of more importance as ambient temperature and RH are measured shortly before skin contact is made. For both types of TEWL instruments, adequate (light) constant pressure should be applied on the probe to ensure leak-free contact between the probe and skin and that the probe does not slide over the skin (Imhof et al. 2009, 2014). Skin hydration probes are equipped with a spring mechanism, which ensures application of adequate contact pressure before a measurement can be made (Barel and Clarys 2006). It should be noted that it is possible to trigger a measurement at lower (incomplete compression of the spring mechanism) and higher pressure, with the latter leading to significantly higher measurement values (Barel and Clarys 2014). The user should develop a technique resulting in repeatable application of constant yet adequate pressure to trigger a measurement.

Measurements should be recorded when a stable signal is achieved. Because of differences in TEWL and skin hydration instruments, a measurement should be considered stable when it meets the criteria as defined by the manufacturer. It is also recommended that all TEWL and skin hydration measurements be made by the same person to reduce variability (Du Plessis et al. 2013). The number of measurements made on each anatomical position is highly variable in published clinical studies. It is recommended that three sequential measurements be made on the same anatomical position and the results averaged. A waiting time of 5 s between sequential skin hydration measurements on the same anatomical position is recommended by one manufacturer (C&K 2004), even though we have found

no statistical significant difference between values of measurements taken at intervals of 1, 5, and 10 s ($p > 0.74$, unpublished data). Furthermore, it is recommended that all measurements be made on a given anatomical position before moving to the next position. Kottner et al. (2014) recommend that if more than one biophysical parameter is measured on the same position, TEWL should be measured first, followed by other parameters. If repeat measurements are made on a specific anatomical position (e.g., before shift and after shift), both sets of measurements must be recorded at the exact same position to reduce errors. The exact same measurement position can be obtained by photographing the measurement position and using the photograph as a reference for future measurements, marking the skin adjacent to the measurement position with a nontoxic ink and/or using a template (Du Plessis et al. 2013).

3.7 Interpretation of Measurement Results

There is a lack of consensus regarding TEWL and skin hydration reference values for normal and/or diseased skin. As an example, there are differences between skin hydration reference values provided by the manufacturer (C&K 2004) and those reported by three independent studies using the same instrument (Barel and Clarys 2006; Heinrich et al. 2003; Packham et al. 2005). As such, it is recommended that results for a given anatomical position be reported and compared as a relative (or percentage) change in TEWL and/or skin hydration values. To illustrate, if the aim of a study is to assess acute changes in TEWL (Δ) caused by exposure to a contaminant, then quantifying the difference in TEWL relative to the before-shift values (baseline, t_0) for a worker or group of workers would be appropriate (Eq. 1):

$$\%\Delta\mathrm{TEWL} = [(\mathrm{TEWL}_{t_1} - \mathrm{TEWL}_{t_0})/\mathrm{TEWL}_{t_0}] \times 100 \quad (1)$$

where TEWLt_0 is TEWL value at baseline or time 0 (e.g., before shift) and TEWLt_1 is TEWL value at time interval (e.g., shift interval or end of shift).

If the aim of a study is to assess chronic changes caused by exposure or disease, then expressing the difference in TEWL and/or skin hydration between a worker (or group of workers) and control subject (control group) as a percentage is preferred over absolute values. When using a control group, the subjects in the control group should be matched to workers as reasonably as possible with respect to relevant endogenous, exogenous, and environmental factors, and measurements should be made in a similar environment with the same instruments (Du Plessis et al. 2013).

TEWL and skin hydration results at a given anatomical position should be expressed as the arithmetic mean ± standard deviation and graphically by bar graphs, but preferably box and whisker plots, displaying the mean, median, minimum, maximum, and percentiles (which may differ between software packages).

4 Data Reporting

To enable meaningful communication of results and possible comparison of results between studies, a basic data set should be collected and reported with study results. Apart from recording and reporting of notable deviations from the guidelines, the following information, as listed by Du Plessis et al. (2013), and amended below, must be reported (a checklist to facilitate collection of pertinent information is also provided in the same publication).

- Endogenous factors
  - (a) The anatomical position(s) and exact measurement site(s) of TEWL and/or skin hydration.
  - (b) Rationale for the choice of anatomical position(s) and site(s).
  - (c) Skin health at time of measurements. For measurements on hands and wrists, health can be documented and assessed using, for example, a validated teledermatology toolkit for standardized hand photographs in nonclinical settings (Steiner et al. 2011).
  - (d) A skin symptoms questionnaire for current symptoms is recommended.

(e) Date and time of day when measurements were performed. Note that if measurements are made on different days for the same study participant, to the extent feasible, measurements should be made at the same time of day to minimize any possible effects of circadian rhythms.

- Exogenous factors
  (a) Hygiene (washing) practices prior to measurement, including conformance, or deviations from instructions given to study participants.
  (b) Use of any topical products, including conformance or deviations from instructions given to study participants. Note also if skin was wiped dry before measurement because of use of topical products.
  (c) Exposure to chemicals or mechanical damage to the skin as a result of tasks performed.
  (d) Use of any personal protective clothing or other materials that might have caused occlusion of the skin, including the type of covering, frequency and duration of use, and time since last use.
  (e) Ingestion of medication, caffeinated beverages, or smoking prior to measurement.
- Environmental factors
  (a) Calendar date, season, and time of TEWL and skin hydration measurements
  (b) Average outdoor ambient temperature and RH
  (c) Ambient workplace temperature and RH
  (d) Ambient temperature and RH where measurements are made
- Experimental and measurement/instrumentation factors
  (a) The type of instrument/probe according to model and manufacturer
  (b) Equilibration time of TEWL instrument and/or hydration instrument in measurement environment
  (c) Calibration (manufacturer and prior to use, if applicable) of the TEWL instrument and/or skin hydration instrument
  (d) Frequency with which the calibration was verified during the study
  (e) Acclimation conditions of study participants prior to measurements, including duration, ambient temperature, and RH in measurement area
  (f) How the instrument was applied to the skin surface, including handling of the TEWL probe and time to achieve a stable measurement in accordance with the manufacturer instructions
  (g) The number of measurements per anatomical position and lag time between measurements

5 Summary

The skin is frequently and continuously exposed to a variety of physical stressors and chemical contaminants in the work environment with the potential to affect the skin barrier. Therefore, in addition to assessing exposure to a stressor or chemical contaminant, it is also of importance to characterize the condition of the skin, i.e., the barrier function, at the time of exposure. A consensus summary of guidelines and best practices for measurement of TEWL and skin hydration in nonclinical environments, with emphasis on occupational settings as a worst-case scenario, was developed. This chapter presents these guidelines as well as amendments since initial publication thereof. Key points of this guidelines are (*i*) recognition and minimization, to the extent feasible, of the influences of relevant endogenous-, exogenous-, environmental-, and measurement/instrumentation-related factors; (*ii*) recommendation of instruments to be used for measurement of in particular TEWL; (*iii*) recommendation of standardized reporting of measurement results; and (*iv*) accurate disclosure of notable deviations from the guidelines. The intention of these guidelines is to provide consistency in nonclinical measurement and reporting of TEWL and/or skin hydration results which is essential for comparison of different studies.

Acknowledgments Mention of a specific product or company does not constitute endorsement by the Centers for Disease Control and Prevention. The findings and

conclusions in this report are those of the authors and do not necessarily represent the views of NIOSH.

References

Agache P. Stratum corneum histophysiology. In: Agache P, Humbert P, editors. Measuring the skin. Germany: Springer; 2004. p. 95–100.

Barel AO, Clarys P. Measurement of epidermal capacitance. In: Serup J, Jemec GBE, Grove GL, editors. Handbook of non-invasive methods and the skin. 2nd ed. Boca Raton: CRC Press; 2006. p. 337–44.

Barel AO, Clarys P. Skin capacitance. In: Berardesca E et al., editors. Non invasive diagnostic techniques in clinical dermatology. Berlin: Springer; 2014. p. 357–65.

Bauer A, Kelterer D, Bartsch R, Stadeler M, Elsner P. Skin protection in the food industry. Curr Probl Dermatol. 2007;34:138–50.

Berardesca E. EEMCO guidance for the assessment of stratum corneum hydration: electrical methods. Skin Res Technol. 1997;3:126–32.

Berndt U, Hinnen U, Iliev D, Elsner P. Is occupational irritant contact dermatitis predictable by cutaneous bioengineering methods? Results of the Swiss metalworkers' eczema study (PROMETES). Dermatology. 1999;198:351–4.

Brandner JM, Behne MJ, Huesing B, Moll I. Caffeine improves barrier function in male skin. Int J Cosmet Sci. 2006;28:343–7.

C&K. Derma unit SSC3 information and operation instructions. Germany: CK Electronic GmbH; 2004.

Chou T-C, Shih T-S, Tsai J-C, Wu J-D, Sheu H-M, Chang H-Y. Effect of occupational exposure to rayon manufacturing chemicals on skin barrier to evaporative water loss. J Occup Health. 2004;46:410–7.

Chou T-C, Lin K-H, Wang S-M, Lee C-W, Su S-B, Shih T-S, Chang H-Y. Transepidermal water loss and skin capacitance alterations among workers in an ultra-low humidity environment. Arch Dermatol Res. 2005;196:489–95.

Chou T-C, Wang PC, Wu JD, Sheu SC, Wu TN, Chang HY, Shih TS. Skin barrier alteration associated with chromium exposure and smoking amongst cement workers. Epidemiology. 2008;19:S142–3.

Coenraads P-J, Lee J, Pinnagoda J. Changes in water vapor loss from the skin of metal industry workers monitored during exposure to oils. Scand J Work Environ Health. 1986;12:494–8.

Cohen JC, Hartman DG, Garofalo MJ, Basehoar A, Raynor B, Ashbrenner E, Akin FJ. Comparison of closed chamber and open chamber evaporimetry. Skin Res Technol. 2009;15:51–4.

Crowther JM, Sieg A, Blenkiron P, Marcott C, Matts PJ, Kaczvinsky JR, Rawlings AV. Measuring the effects of topical moisturizers on changes in stratum corneum thickness, water gradients and hydration in vivo. Br J Dermatol. 2008;159:567–77.

Darlenski R, Sassning S, Tsankov N, Fluhr JW. Non-invasive in vivo methods for investigation of the skin barrier. Eur J Pham Biopharm. 2009;72:295–303.

De Paepe K, Houben E, Adam R, Wiesemann F, Rogiers V. Validation of the VapoMeter, a closed unventilated chamber system to assess transepidermal water loss vs. the open chamber Tewameter®. Skin Res Technol. 2005;11:61–9.

Du Plessis JL, Eloff FC, Badenhorst CJ, Olivier J, Laubsher PJ, van Aarde MN, Franken A. Assessment of dermal exposure and skin condition of workers exposed to nickel at a South African base metal refinery. Ann Occup Hyg. 2010;54:23–30.

Du Plessis JL, Eloff FC, Engelbrecht S, Laubsher PJ, van Aarde MN, Franken A. Dermal exposure and changes in skin barrier function of base metal refinery workers co-exposed to cobalt and nickel. Occup Health South Afr. 2013a;19:6–12.

Du Plessis J, Stefaniak AB, Eloff FC, John SM, Agner T, Chou TC, Nixon R, Steiner MFC, Franken A, Kudla I, Holness DL. Guidelines for the in vivo assessment of skin properties in workplace settings: part 2. Transepidermal water loss and skin hydration. Skin Res Technol. 2013b;19:265–78.

Fluhr JW, Darlenski R. Transepidermal water loss (TEWL). In: Berardesca E et al., editors. Non invasive diagnostic techniques in clinical dermatology. Berlin: Springer; 2014. p. 353–6.

Fluhr JW, Darlenski R, Angelova-Fisher I, Tsankov N, Basketter D. Skin irritation and sensitisation: mechanisms and new approaches for risk assessment. Skin Pharmacol Physiol. 2008;21:124–35.

Gabard B, Treffel P. Transepidermal water loss. In: Agache P, Humbert P, editors. Measuring the skin. Germany: Springer; 2004. p. 553–64.

Goh CL, Gan SL. Efficacies of a barrier cream and an afterwork emollient cream against cutting fluid dermatitis in metalworkers: a prospective study. Contact Dermatitis. 1994;31:176–80.

Hachem JP, De Paepe K, Sterckx G, Kaufman L, Rogiers V, Roseeu D. Evaluation of biophysical and clinical parameters of skin barrier function among hospital workers. Contact Dermatitis. 2002;46:220–3.

Heinrich U, Koop U, Leneveu-Duchemin MC, Osterrieder S, Bielfeldt C. Multicentre comparison of skin hydration in terms of physical-, physiological- and product-dependent parameters by the capacitative method (Corneometer CM 825). Int J Cosmet Sci. 2003;25:45–53.

Imhof RE, De Jesus ME, Xiao P, Ciortea LI, Berg EP. Closed-chamber transepidermal water loss measurement: microclimate, calibration and performance. Int J Cosmet Sci. 2009;31:97–118.

Imhof B, Xiao P, Angelova-Fischer I. TEWL, closed chamber methods: aquaflux and vapometer. In: Berardesca E et al., editors. Non invasive diagnostic techniques in

clinical dermatology. Berlin: Springer; 2014. p. 345–52.
John SM. Primary and acquired sensitive skin. In: Berardesca E, Fluhr J, Maibach HI, editors. The sensitive skin syndrome. New York: Taylor & Francis; 2006. p. 129–47.
John SM, Uter W, Schwanitz HJ. Relevance of multiparametric skin bioengineering in a prospectively-followed cohort of junior hairdressers. Contact Dermatitis. 2000;43:161–168.
Kezic S, Nielsen JB. Absorption of chemicals through compromised skin. Int Arch Occup Environ Health. 2009;82:677–88.
Korting HC, Hübner K, Greiner K, Hamm G, Braun-Falco O. Differences in the skin surface pH and bacterial microflora due to long-term application of synthetic detergent preparations of pH 5.5 and pH 7.0. Results of a cross-over trial in healthy volunteers. Acta Derm Venereol. 1990;70:429–31.
Kottner J, Ludriksone L, Bartels NG, Blume-Peytavi U. Do repeated skin barrier measurements influence each other's results? An explorative study. Skin Pharmacol Physiol. 2014;27:90–6.
Kütting B, Uter W, Baumeister T, Schaller B, Weistenhöffer W, Drexler H. Non-invasive bioengineering methods in an intervention study in 1020 male metal workers: results and implications for occupational dermatology. Contact Dermatitis. 2010;62:272–8.
Levin J, Maibach H. The correlation between transepidermal water loss and percutaneous absorption: an overview. J Control Release. 2005;103:291–9.
Nielsen JB. Percutaneous penetration through slightly damaged skin. Arch Dermatol Res. 2005;296:560–7.
Nuutinen J. Mesurement of transepidermal water loss by closed-chamber systems. In: Serup J, Jemec GBE, Grove GL, editors. Handbook of non-invasive methods and the skin. 2nd ed. Boca Raton: CRC Press; 2006. p. 411–20.
Ohman H, Vahlquist A. The pH gradient over the stratum corneum differs in X-linked recessive and autosomal dominant ichthyosis. A clue to the molecular origin of the "acid skin mantle"? J Invest Dermatol. 1998;111:674–7.
Packham CL, Packham HE, Packham HM, Cherrington A. Investigation into different skin conditions in certain occupations. J R Soc Prom Health. 2005;125:181–5.
Pinnagoda J, Tupker RA, Agner T, Serup J. Guidelines for transepidermal water loss (TEWL) measurement. Contact Dermatitis. 1990;22:164–78.
Pirot F, Falson F. Skin barrier function. In: Agache P, Humbert P, editors. Measuring the skin. Germany: Springer; 2004. p. 513–24.
Proksch E, Brandner JM, Jensen J-M. The skin: an indispensable barrier. Exp Dermatol. 2008;17:1063–72.
Rawlings AV. Ethnic skin types: are there differences in skin structure and function? Int J Cosmet Sci. 2006;28:79–93.
Raynor B, Ashbrenner E, Garofalo M, Cohen J, Akin F. The practical dynamics of transepidermal water loss (TEWL): pharmacokinetic modeling and the limitations of closed-chamber evaporimetry. Skin Res Tech. 2004;10:3. Abstract.
Rogiers V. EEMCO guidance for the assessment of transepidermal water loss in cosmetic sciences. Skin Pharmacol Appl Skin Physiol. 2001;14:117–28.
Roskos KV, Guy RH. Assessment of skin barrier function using transepidermal water loss: effect of age. Pharmacol Res. 1989;6:949–53.
Smit HA, van Rijssen A, Vandenbroucke JP, Coenraads PJ. Susceptibility to and incidence of hand dermatitis in a cohort of apprentice hairdressers and nurses. Scand J Work Environ Health. 1994;20:113–21.
Stefaniak AB, Du Plessis JL, John SM, Eloff FC, Agner T, Chou TC, Nixon R, Steiner MFC, Kudla I, Holness DL. Guidelines for the in vivo assessment of skin properties in workplace settings: part 1. pH. Skin Res Technol. 2013;19:59–68.
Steiner M, Dick FD, Ormerod A, Semple SE, Murphy E, Ayres JG. Teledermatology in occupational skin health surveillance – diagnostic accuracy and reliability. Dermatitis. 2011;22:295.
Tupker RA, Pinnagoda J. Measurement of transepidermal water loss by semi open systems. In: Serup J, Jemec GBE, Grove GL, editors. Handbook of non-invasive methods and the skin. 2nd ed. Boca Raton: CRC Press; 2006. p. 383–92.
Voegeli D. The effect of washing and drying practices on skin barrier function. J Wound Ostomy Continence Nurs. 2008;35:84–90.
Wilhelm KP, Cua AB, Maibach HI. Skin aging. Effect on transpeidermal water loss, stratum corneum hydration, skin surface pH, and casual sebum content. Arch Dermatol. 1991;127:1806–9.
Zhai H, Maibach HI. Occlusion vs. skin barrier function. Skin Res Technol. 2002;8:1–6.

Skin Mechanical Function

95

Pierre Agache and Daniel Varchon

Contents

This chapter was originally published under the ISBN 978-3-540-01771-4 with the following book title Measuring the Skin. The content has not been changed.

Pierre Agache: deceased.

P. Agache (✉)
Department of Dermatology, University Hospital of Besançon, Besançon, France
e-mail: aude.agache@free.fr; ferial.fanian@chu-besancon.fr; ferial.fanian@cert-besancon.com

D. Varchon
Laboratoire de Mécanique Appliquée R. Chaléat, University of Franche-Comté, Besançon, France
e-mail: daniel.varchon@univ-fcomte.fr

P. Humbert et al. (eds.), *Agache's Measuring the Skin*, DOI 10.1007/978-3-319-32383-1_129

Keywords

Elastic deformation • Elastic modulus • In vitro mechanical behavior • Resistance to friction • Skin elastic behavior • Skin hardness • Skin mechanical anisotropy • Skin mechanical behavior • Skin viscosity

The skin has three main mechanical roles: (1) to instantly or permanently match the changes in shape and volume of the under-lying organs and the adipose tissue; (2) to protect them against mechanical external aggressions; and (3) to facilitate the gripping of objects and the ground by palms and soles.

1 A Mechanical View of Skin Anatomy

The skin is a composite material stratified in three layers of different mechanical properties. The superficial layer, the 15-µm-thick stratum corneum, is very firm but pliable and naturally wrinkled; underneath, the less rigid 50-µm-thick viable epidermis is also wrinkled; and the under-lying third layer, the 1-mm-thick dermis, is elastic and naturally contracted. These three layers lie on the hypodermis (or subcutis), whose thickness, often filled with adipose tissue, can range from 1 mm to more than 5 cm and behaves like a cushion. Various structures with specific mechanical roles are found in each layer. For example, in its upper half the dermis holds hairs inserted obliquely like posts. This complex structure

is, however, compensated by perfect anatomical adjustment and harmony of behaviors (e.g., the creasing of the first two layers corresponds to the contracted state of the dermis), so that in normal in vivo conditions each layer behaves mechanically like the whole in spite of very different intrinsic properties. This justifies the investigation of the global mechanical behavior of skin as though it was a homogenous material.

The major mechanical component is the dermis. Like all connective tissues, it is a felting of collagen fibers immersed in a viscous fluid called "ground substance," rich in glycoproteins. The dermis has two main functions: to maintain the spatial organization of underlying tissues and to resist external mechanical stresses. Anatomically and functionally two parts need to be considered. The thin superficial or subpapillary dermis thickness of 50–200 μm is proportional to the epidermal thickness (Frost and Van Scott 1966). It is made of a loose tissue, rich in glycoproteins, with thin elastic fibers and collagen bundles where the proportion of collagen III is higher than in the deeper reticular dermis (Lapière et al. 1988). It is rich in blood, lymph vessels, and nerves. Its content in water and vascular volume show physiological variations that can alter the mechanical behavior of the skin as a whole. Below this superficial dermis, the remaining dermis, chorion or reticular dermis (about 1 mm thick), is formed by thicker bundles of collagen (2–20 μm) close to one another and connected by large elastic fibers (0.1–0.4 μm). Fewer vessels and nerves are found, but they are bigger. The structure of the dermis under transmission and scanning electron microscopy is described in ▶ Chap. 41, "Dermis Connective Tissue Histopathology."

The dermo-epidermal junction is well defined, but both structures are interwoven. Dermal papillae penetrate the epidermis whose lower border shows roughly conical interpapillary rete pegs, thus increasing the interface. In a histological cross-section, the length of the latter can be longer than the straight line by 20 % (Frost and Van Scott 1966). The junctional structure has specific attachment devices whose dimensions and distribution are known (Barton 1988) (see ▶ Chap. 156, "Main Skin Biological Constants"), and its physical properties have been studied (Beerens 1977). The contour of the dermo-epidermal junction must not be mistaken for the skin surface relief, which also shapes it, but is more interspaced and has a different pattern.

The viable epidermis (30–80 μm thick) comprises five to ten layers of cells (keratinocytes) with an impressive keratin cytoskeleton (tonofilaments) communicating from one cell to the other by very strong keratin ties (desmosomes) (see ▶ Chap. 37, "Markers of Epidermal Proliferation and Differentiation"). This configuration makes it more rigid than the other soft tissues. Its mechanical properties are unknown, but when the whole epidermis, including the stratum corneum, is submitted to traction in vitro and compared to the stratum corneum alone from the same body site, the following observations are made: increased slopes of the elastic and plastic phases, a higher force, and less strain at rupture and a similar total spent energy (Ferguson J, Agache P, unpublished data). This indicates an increased rigidity due to the sole addition of the viable epidermis. Consequently, the part played by this layer in the skin's mechanical behavior must not be overlooked.

The limit between the reticular dermis and the hypodermis is irregular and poorly defined. To our knowledge the mechanical properties of the hypodermis, a loose conjunctive tissue often loaded with fat, have not been studied, but levarometry and suction methods would permit an in vivo, noninvasive investigation (see ▶ Chap. 95, "Skin Mechanical Function"). By allowing the skin to move as a whole on the underlying structures, this layer plays a major part in the absorption of external forces having a tangential component. In scars where the hypodermis has disappeared, the skin loses its mobility and sustains considerably higher stretching and friction constraints.

2 Total Skin Mechanical Behavior

When the skin is submitted to a sudden and sustained strain (a creep test), three successive behaviors are found (Fig. 1). Phase I is an immediate extension (Ue) which is considered to be purely elastic because it is too quick for a viscous phenomenon to appear. It is followed by two phases (Uv) in which viscosity plays a part:

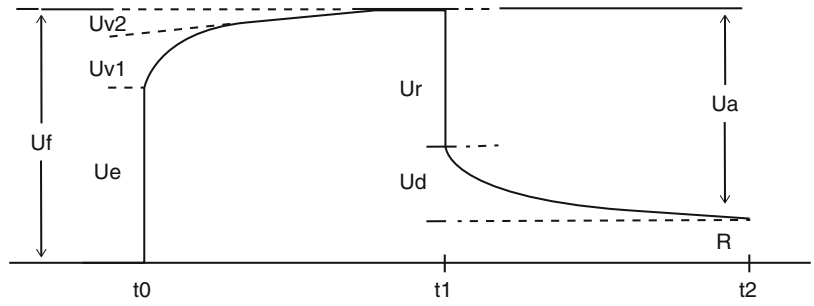

Fig. 1 Creep experiment: skin deformation versus time. Uf: deformation at the end of force application. Ue: immediate deformation (elastic). Uv1: viscoelastic deformation. Uv2: late deformation (entirely viscous). Ua: recovery at the end of the experiment. R: residual deformation at the end of the experiment. Ur: immediate recovery. Ud: late recovery

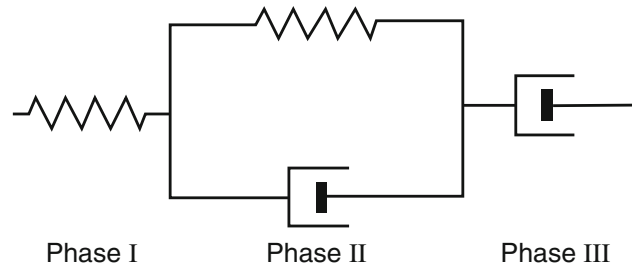

Fig. 2 A model of the skin mechanical components involved in a creep experiment (extension phase only)

phase II with variable creep (Uv1) and phase III with constant creep (Uv2). As the test is carried out in vivo, it implies that the strain keeps below 25 % and is reversible. A greater strain, not shown in Fig. 1, would cause irreversible deformation (plastic phase). Such deformations, which are painful, occur only from traumas.

Scientists have proposed an analog model of this behavior (Fig. 2) in which phase I is represented by a spring, phase II by a spring and a dashpot in parallel, and phase III by only a dashpot since it is a linear function of time. The limit between phases I and II is imprecise and depends on the balance between elastic and viscous resistance inside the tissue, which both vary with the body site, age and the individuals. The limit between phases II and III is also imprecise. When the strain suddenly disappears, the skin retracts immediately, but incompletely and goes back through similar phases, with the difference that full recovery requires a long time – from a few minutes to several hours, depending on the extent of the strain, its duration and the mechanical condition of the skin.

2.1 Elastic Behavior

Whatever the method used (uniaxial extensions (Wijn et al. 1978), torsion (Wijn et al. 1976) suction (Agache et al. 1995), or progressive extension at constant rate (Vasselet and Agache 1987) the skin's elastic tissue mechanical properties cannot be known from raw data (Ue, Uf, etc.) because the latter depend on both the device and the method. These can only be determined from intrinsic parameters: strain ε (relative deformation) and stress σ (force divided by its application area), which are computed from the raw data and the geometry of the deformation (see ▶ Chap. 95, "Skin Mechanical Function").

The stress/strain curves in vitro and in vivo are identical and of an exponential type (Fig. 3). The tangents to the curve are the elastic moduli

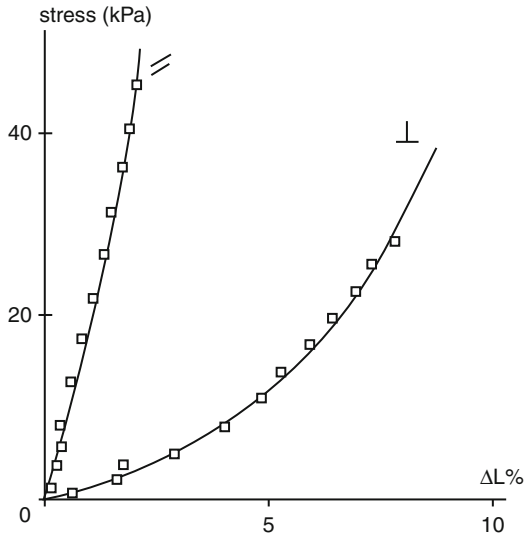

Fig. 3 Stress–strain curve of the skin (calf) parallel and perpendicular to Langer's lines (Modified from Wijn et al. (1981))

$E = d\sigma/d\varepsilon$ at different elongations. According to the Fung's formula (Fung 1972):

$$E = E_0 + k\sigma$$

where E_0 is the modulus for zero stress (Young's modulus). In some remarkable work conducted by the Nijmegen group in the early 1980s, this linear relation was verified in vivo by Wijn et al. (1981) on more than 50 subjects ($r > 0.998$). It implies the following relations:

$$E = E_0 e^{k\varepsilon} \quad \sigma = E_0/k\left(e^{k\varepsilon} - 1\right) \quad \text{and}$$
$$\varepsilon = 1/k \ \ln(1 + k\sigma/E_0)$$

They show that the elastic moduli during extension are the initial (Young's) modulus exponentially increased by elongation. The initial modulus E_0 and the multiplying factor k are the two fundamental parameters of the skin's mechanical behavior under low stress during the supposedly purely elastic phase (phase I of the Kelvin-Voigt analog model, Fig. 2). At the elastic limit, that is for elongation between 20 % and 30 % across and about 10 % along the limb axis, the stress/strain curve bends towards horizontal indicating plasticity (Manschot and Brakkee 1986). Torsion tests verify the same equations (Wijn et al. 1981), with a shear modulus $G = d\tau/d\gamma$, τ being the shear stress and γ the shear angle (different from the skin twisting angle). The equation $G = G_0 + k\tau$ is also verified. From a biological viewpoint, these equations mean that all the individual spring-like fibers responsible for the stress during this elastic phase have the same force (expressed by the value of k), but that they are exponentially engaged as elongation takes place.

Uniaxial extension elongates only the fibers oriented along the extension axis (Wijn et al. 1976; Piérard and Lapière 1987). At first (E_0), there are few of them, but when the elongation increases, more and more fibers become orientated along this axis and contribute to the resistance. At each value of strain, the elastic modulus E therefore expresses the number of fibers involved and the strength k of each fiber. Manschott and Brakkee (1986), of the Nijmeren group, also used a sinusoidal model of a collagen fiber derived from the anatomy of tendons. In a uniaxial extension experiment in 61 subjects, they were able to calculate the mean fibril diameter, the mean amplitude and slope of the fiber sinusoid, and the number of fibers that lie parallel and perpendicular to Langer's lines.

Ever since Dupuytren, it has been known that in resting conditions the skin is stretched preferentially in a particular direction, later described by Langer (1978), hence the term Langer's lines. In their experiments on the human calf, Wijn et al. (1978) observed that the linear relations $E = f(\sigma)$ parallel and perpendicular to the limb axis (at this site it makes a 30° angle with Langer's lines) were parallel, the only difference being the value of E_0 was higher in the direction of the limb axis (hence closer to Langer's lines). Accordingly, in resting conditions, there are more fibers orientated in the direction of the Langer's lines, and the mechanical anisotropy and the increase of the elastic modulus during extension are two independent phenomena. The ratio of the Young's moduli parallel (//) to and perpendicular ($\perp$) to the Langer's lines is the anisotropy parameter of the elastic fibers' distribution (named A), which is characteristic of each body area.

On the calf in vivo, the value of the Young's modulus (E_0//) as found by Wijn et al. (1981) from uniaxial extension (Wijn et al. 1981) was 1.714 MPa, with k = 0.244 (without units) and A = 16.0. The modulus at elastic limit was about 20 MPa along and 4 MPa across the limb axis (Manschot and Brakkee 1986).

On the volar forearm, the value differs depending on the method. From uniaxial extension at 1 % s^{-1} along the limb axis (up to 45° from Langer's lines), Vasselet et al. found E = 3 MPa (Vasselet and Agache 1987); Escoffier et al. found E = 1.12 MPa (Escoffier et al. 1989) with the torsion method; and using the suction method, the calculated values were lower (e.g., in young adults between 0.13 MPa (Diridollou et al. 2000) and 0.20 MPa (Khatyr F, Varchon D, Agache P, unpublished data), and in those over 50 years around 0.20 MPa (Diridollou et al. 2001)). Obviously, further work comparing the methods at the same place in the same person is needed.

The higher modulus in the calf as compared to the forearm may be related to the need to compensate for the increased hydrostatic pressure. Indeed, using a suction device, the Danish group showed that over the whole body there is a centrifugal decreasing gradient in skin extensibility (Ue parameter). In the evening, it tends to decrease (Gniadecka et al. 1994), suggesting fatigue of the elastic tissue. In the aged, the gradient loosening may be related to the well-known degradation of elastic tissue.

The calf skin's Young's modulus parallel to Langer's lines steadily decreases with age, going from 1 to 4 MPa at 20 years to below 2 MPa at 65 years of age (Wijn et al. 1981). Using a suction device on the volar forearm, Diridollou et al. (2001) found it to be stable until 50 years of age, then rising. The origin of the discrepancy remains obscure. The declined modulus matches the current observation of the lowered skin resiliency with aging.

It is usually thought that the skin's elastic behavior mainly relies upon the elastic fibers of the reticular dermis. However, the Young's modulus of the elastic fibers is close to 0.3 MPa (Burton 1968; Caro et al. 1978). Since elastin represents less than 4 % of the dry weight of the skin and collagen 80 %, it was speculated (Manschot and Brakkee 1986) that if the elastic fibers alone were responsible for the resistance to extension, the skin elastic modulus would not exceed 0.01 MPa. Consequently, collagen bundles may be deeply involved in the skin's elasticity via their resistance to partial flattening of their twists (Comninou and Yannas 1976). Manschott and Brakkee (1986), through modeling the collagen fibrils, showed that collagen alone could account for the experimental values of the Young's modulus at elastic limit, making the role of elastic fibers "insignificant." This result is not surprising as by this stage the collagen fibers are almost straightened and bear the bulk of the stress. Elastic fibers seem to play a role mostly in low stress. The role of the elastic tissue degradation has been advocated in the aging process and in diseases like *cutis laxa* (Grahame and Holt 1969; Fazio et al. 1989) and *pseudoxanthoma elasticum* (Wijn et al. 1981; Harvey et al. 1975) in which the skin loses its resiliency. In the above studies, the role of the epidermis has been overlooked. This layer follows the creases and plateaus of the skin surface relief. Upon stretching, it is not elongated but partially unfolded (Ferguson and Barbenel 1981). The resistance of the stratum corneum to unfolding in the elastic phase has a modulus (volar forearm, measurement by suction) ten times that of the whole skin on the same area (Panisset et al. 1993). Accordingly, the total skin Young's modulus should be partitioned into a stratum corneum fraction (about 11 %) and a dermis fraction (about 89 %) (Panisset et al. 1993).

2.2 Viscous Phases of Extension (Creep)

In creep tests, the phase II of the skin deformation versus time (Uv_1) is curvilinear and has been described by a decreasing exponential function according to the equation:

$$Uv_1 = Uv_1 max \left(1 - e^{-t/r}\right)$$

The phase III (Uv_2) is a straight line described as $Uv_2 = At$ (Vlasblom 1967). Some authors have also suggested $Uv_2 = At^{1/3}$ (Pichon et al. 1990). These equations are drawn from the analogue model of Fig. 2. The use of this model has been criticized because it is able to fit the experimental curve only if the elastic phase is considered below the elastic limit (Vasselet and Agache 1987), and because it has only two relaxation times (only two dashpots in the model); thus, it assumes that the skin has only two viscosity coefficients, which is evidently an oversimplified although useful approach. According to Vasselet (Vasselet and Agache 1987), the deformation angle θ in torsion tests would be better described in the viscous phase by the logarithmic equation: $\theta = b \cdot \ln(1 + nt)$, where b is the elongation rate and n the elongation before the viscous phase. Unfortunately, these theoretical considerations do not yet have a practical application. In clinical practice, only viscoelastic deformations (Uv, Fig. 1) are usually measured, without any assessment of the intrinsic mechanical parameters (i.e., stress, strain, viscosity coefficients). ▶ Chapter 96, "Mechanical Behaviour Assessmentof the Skin" (Sect. 11.1, "Searching for Intrinsic Mechanical Properties") shows a simple way to perform the calculation of the intrinsic viscosity parameters 0_1 and 0_2, with an example.

From a biological point of view, a viscous behavior may originate from both a collagen network deformation and a displacement of the ground substance within the network. The mobility of the latter depends on several factors: network toughness, ground substance viscosity, and perhaps its links to the network through proteoglycans.

The parameter Uv, corrected for skin thickness, remains stable with aging (Escoffier et al. 1989), which is known to be associated with the decrease of proteoglycans in the ground substance, thus lowering its viscosity. The latter assertion is supported by a small but steady decrease of the relaxation time using high torque (Escoffier et al. 1989). As Uv is both viscous and elastic, the lower ground substance viscosity in aged skin might be compensated for by a reduced ability of the collagen network to elongate (increased rigidity or toughness through molecular cross-linking), but increased strength of the elastic tissue is improbable. The skin extensibility (Ue) decreases only after 75 years (Escoffier et al. 1989).

Using the data analysis method described in ▶ Sect. 11.1 of the next chapter, the skin viscosity associated with phases II (0_1) and III (0_2) of a creep experiment on volar forearm were found to be around 0.4 MPa and 12 MPa, respectively in young adults (Khatyr F, Varchon D, Agache P, unpublished data). In phase II (viscoelastic), the corresponding elastic modulus was around 0.475 MPa in the same subjects. This shows the steep increase in viscous resistance with small strain increment.

2.3 Recovery Phase

In a creep test, when the stress is suddenly removed, the skin immediately starts to regain its original dimensions (this applies to physiological deformations less than 25 %). As during extension, the recovery goes through an immediate phase (Ur) supposedly only elastic, then a viscoelastic phase (Ud), and finally a long-lasting residual deformation (R) (Fig. 1). In clinical practice, the "skin elasticity" (i.e., its spring-like recoil capacity) is assessed by the ratio between immediate recovery and immediate deformation (Ur/Ue). Both Ue and Uv are always higher than Ur and Ud because to achieve straining the external force must always be higher than the associated internal skin recoiling force and tissue resistance to deformation (i.e., viscosity). During recovery, the viscous resistance is about the same as during extension; whereas, the skin recoiling force is always lower than the applied external force. The skin recoil is rapid in children and takes a long time in the elderly. Consequently, on the volar forearm, the ratio Ur/Ue decreases with aging-regularly from over 0.9 in childhood down to 0.7 after 65 years of age (Escoffier et al. 1989).

In a progressive loading-unloading experiment (see Fig. 47.2), the delayed recovery generates a hysteresis on the force/deformation curve – the

more "elastic" the skin, the smaller the hysteresis loop area. The latter has the dimension of work, as shown by its formula: 3[(loading minus unloading force) × deformation]. It represents the work of elastic fibers striving against the tissue viscosity. Aging increases viscosity (although that of the ground substance is decreased) as shown by the increased hysteresis area (Diridollou et al. 2001), but it also reduces the number of elastic fibers (the latter mostly in actinic aging), as shown by histological observations. Consequently, both the decreased recoiling force and increased resistance to deformation contribute to the delayed recovery in the elderly.

2.4 Other Characteristics of Mechanical Behavior

- The intracutaneous structures always retain part of the latest deformation they have sustained. This residual deformation is obviously corrected in the course of any subsequent deformation but is not specifically due to it. "Preconditioning" is used to circumvent it.
- If identical elongations are repeated, and the skin has time to recover between each elongation, the constraint increases (Vasselet and Agache 1987). This "hardening" of the skin, similar to that of many other materials ("strain hardening") is probably a physiological phenomenon, but its biological support remains conjectural-consolidation of the collagen network by new molecular cross-links?
- Like any material, skin shrinks when it is stretched. In mechanics, this phenomenon is described by the Poisson's ratio (ν) which is the ratio of the relative decreases in transverse dimensions to the relative increase in length. With skin, the Poisson's ratio probably varies during extension because the ground substance can be attracted into the collagen network at the beginning of the test (hence $\nu < 0.5$) as suggested by ultrasound examination (Diridollou et al. 1998), and then expelled when extension progresses (hence $\nu > 0.5$). As a matter of fact, to achieve tensed suction blisters, only a 400 mbar suction for 2–3 h is needed; the blister originates from a dermo-epidermal separation into which interstitial liquid flows. For small and short lasting deformations as used in skin tests, the skin does not swell, so the value $\nu = 0.4$ or 0.5 is generally used.
- Attempts to assess the skin's mechanical impedance have also been made by making its surface vibrate and measuring the parameters at phase II of the analogue model of Fig. 2. The contributing parameters are mainly elastic from 30 to 200 Hz and viscous from 300 to 1000 Hz. Both elasticity and viscosity parameters increase when the skin is compressed (Thompson et al. 1981).
- The skin's compressibility is a mechanical property of the same or even greater importance than extensibility. Most impacts we sustain are directed perpendicularly to our body's surface. Furthermore, the skin must bear the weight of the body for long periods of time in sitting or lying positions. Skin resistance to this compression is an essential component of its continuous blood perfusion and constitutes a protecting factor against decubitus ulcers. A 12 KPa pressure on the volar forearm with a 20 mm diameter disk, choosing arbitrarily a Poisson ratio $\nu = 0.3$ and using the formula (Hayes et al. 1972):

$$G = P(1 - v)/RKd^4$$

where P is the pressure applied, d the diameter of the disk and K a parameter without dimensions function of t/R, provided a shear modulus G between 1 and 2 kPa (Bader and Bowker 1983).

This modulus decreases in old people (Bader and Bowker 1983). Lanir has also studied the deformations produced by compression and has given their mathematical expression (Lanir 1981). The biological substrate of compressibility mainly consists in the capacity of the dermis ground substance to be ejected laterally, which involves its viscosity, the fiber network tightness and the interstitial pressure. The resistance of the few elastic fibers laid out parallel to the skin surface

and stretched by the compressive shift must also be considered.

2.5 Mechanical Anisotropy

Skin resistance to traction predominates in the Langer's lines direction and varies with body site. These lines have been detected on a corpse from the oval shape of an incision made with a round awl, and they correspond to the main axis of the oval (Fig. 4). Excised skin shrinks more and has minimum extensibility in that direction. It is therefore an anisotropy of the spontaneous skin tension "in resting conditions," which is distinct from the skin tension from positional, muscular or visceral origin. This phenomenon is the source of the Young's modulus (E_0) anisotropy (Wijn et al. 1981), whose distribution angle shows a maximum in the Langer's lines axis (Manschot et al. 1982) (Fig. 3). These data favor a similar orientation of the elastic fibers involved in the skin tone. Assuming that the fibers are independent, it has been calculated that, on the calf, 76 % were in the direction of the Langer lines and 5.1 % perpendicular (Manschot et al. 1982). Of course, this distribution concerns only the elastic fibers, which are parallel to the skin surface.

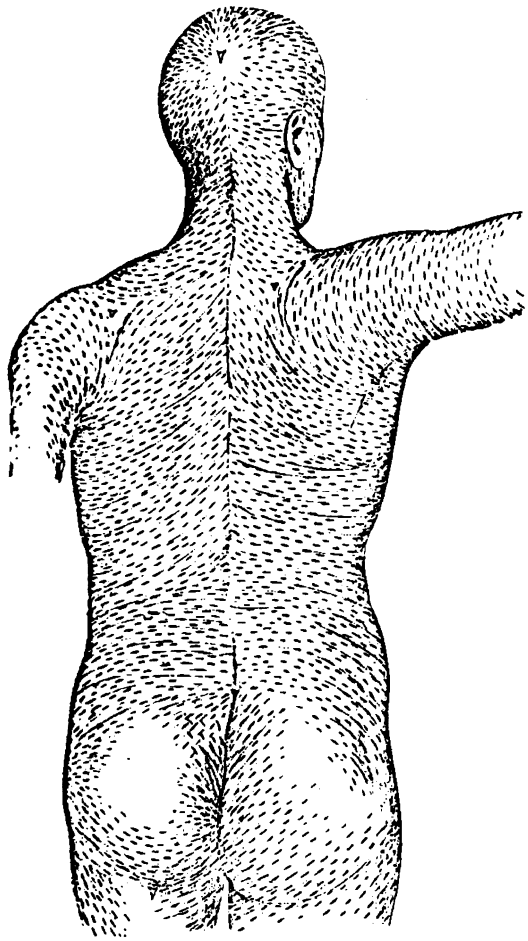

Fig. 4 Langer's lines (From the original article, 1861)

Observation of the dermis with scanning electron microscopy confirms this data (Piérard and Lapière 1987). In *retracted* skin the collagen bundles look tortuous, with no special direction, and sinuous elastic fibers are fixed to them in several places, especially in their concave portion. In *nonretracted* skin, the thinnest collagen bundles as well as the elastic fibers are straightened in the direction of the Langer's lines and almost parallel; the thickest bundles remain tortuous and oriented in all directions, but their shape seems to be modified by the traction from the orientated bundles and fibers (Piérard and Lapière 1987). Contrary to common belief in the past, Langer's lines do not reflect an anisotropy of the collagen density but an anisotropy of the reticular dermis collagen bundles' direction and elastic fibers' tension. The latter is quantified in vivo by mechanical exploration (Manschot et al. 1982).

The superficial (subpapillary) dermis collagen bundles are not linearly oriented and are not related to the cleavage line orientation (Namikawa et al. 1986). Thus, only the reticular dermis seemingly takes part in the anisotropic skin's mechanical properties.

2.6 In Vitro Mechanical Behavior

The in vitro stress–strain curve appears as exponential as in vivo. During extension at a constant rate until rupture of a completely relaxed skin sample immersed in an isotonic solution, three phases have been described, with concomitant examination of the tissue under scanning electron microscope (Brown 1973) (Samples were

8 mm wide and taken from the abdomen, where the skin thickness was found to be 1.8 mm by ultrasound (Tan et al. 1982)). The first one, stretching up to about 40 %, corresponded to physiological extensions and in vivo studies. It showed low resistance (the less than 10 g, hence $E < 7$ kPa), unfolding of the skin relief and partial alignment of some collagen bundles of the superficial dermis (Brown 1973). In the second phase (stretching from 40 to 70 %), the skin became stiff and the modulus was 510 kPa (assuming that the section remained unchanged), the keratinocytes became elongated, the collagen bundles of the superficial and deep dermis and the elastic fibers lined up in the direction of the traction, but the collagen of the mid-dermis remained sinuous. The next phase was a prerupture stage during which the modulus remained constant, and the bundles became compacted and often independent within the network; however, the latter persisted and no free extremities were seen Rupture occurred at 90 % elongation. This study characterizes the behavior of *immersed* skin, which accounts for the very low modulus and exceptional extensibility in phase I (in in vitro extension experiments made in open air the modulus of abdominal skin stretched at 0.7 % s^{-1} was 7–50 MPa (Kenedi et al. 1965; Daly and Odland 1973)). The author considers that the role of the stratum corneum resistance to the unfolding then extension was negligible; this is probable because of the immersion which might have considerably reduced its unfolding then elongation moduli (Agache et al. 1973; Wildnauer et al. 1971). Since the dermis is a physiologically immersed tissue, the conclusions of these in vitro immersion studies are likely to be applicable in vivo, but to the dermis only.

For extensions beyond physiological limits, the modulus increases regularly with age, going from 3 MPa in children to 20 MPa after the age of 50 (Rollhauser 1950). At this stage, the skin is barely more extensible than tendon. Plastic and pre-rupture phases may provide data on the structure of collagen, especially chain cross-linking, if the dimension of the fibers can be known through electron microscope examination. These data could be useful for better understanding acquired or congenital diseases involving the connective tissue. Scar tissue has a higher elastic modulus than the adjacent healthy skin, which implies that the collagen bundles are more tightly compacted and probably more frequently interconnected (Kenedi et al. 1965).

Beyond the phase of physiological extension, the sample is greatly shrunk transversely without becoming thin throughout (Kenedi et al. 1965), and the ratio between narrowing and stretching increases very quickly. This is related to the leak of interstitial fluid during the test, because the Poisson's ratio remains constant afterwards until rupture (i.e., the sample volume does not rise, contrary to nonorganic materials). In adults, its values vary from 0.5 to over 1.3, indicating a diminution of volume at the end of extension. With age, the squeeze of the ground substance occurs for moderate extensions and the loss of volume gets more probable. This corresponds with the decrease of the skin viscosity of the aged skin, and the fact that by this time the dermis holds more free water because of the loss of proteoglycans.

The Rheometer (Dia-Stron Ltd, Andover, Hampshire, UK) is a commercialised device allowing in vitro uniaxial extension or compression of skin samples, as well as the study of forced relaxation and shape recovery.

3 Mechanical Behavior of the Stratum Corneum

The stratum corneum (SC) is approximately 15 μm thick except in palms and soles where it reaches 1 mm (▶ Chap. 23, "Stratum Corneum Histopathology"). It is a dead structure formed by about 19 layers of piled keratinized cells (corneocytes). These are flat (0.3 μm), roughly pentagonal (diameter 30 μm) and separated by 0.07 μm wide intercellular spaces. Each cell has a thick membrane much more resistant than the heart of the cell. The intercellular spaces are filled with stratified lipids and proteinaceous enzymes, and traversed by keratinized cellular binding bridges (corneodesmosomes). The adherence between cells decreases towards the surface, but is always lower than the cell wall

solidity, so that spontaneous desquamation (one cell layer per day) or SC tape stripping only deals with intercellular spaces (details on desquamation are provided in ▶ Chap. 25, "Stratum Corneum Desquamation"). The structure and physical properties of the human and animal SC are similar. As a consequence, its mechanical properties have been investigated in pig, rat and humans.

3.1 In Vitro

- In 1956, Peck and Glick (1956), applying a durometer used in the leather industry, noticed that the hardness of dry human SC in vitro is comparable to glass and cannot be softened by mineral oil, lanolin, or glycerin. However, such behavior depends mostly on its hydration. The addition of 10 % of its water is sufficient to make it soft and pliable; the same can be obtained by a 60 % ambient relative humidity (RH) (Blank 1952), but its hardness is still 70 % that of glass, which is noticeable. Water uptake by the SC (Singer and Vinson 1966; Middleton 1968) varies exponentially with relative humidity (more details in ▶ Chap. 29, "Physical Methods to Measure Stratum Corneum Water Content In Vivo").
- The SC force/extension curve is that of a viscoelastic material strongly influenced by its hydration (Fig. 5). A RH shift from 0 % to 100 % is associated with an increase of the *maximum extension* and *rupture work*, and a reduction of the *force at rupture* (Wildnauer et al. 1971; Kligman 1964; Papir et al. 1975). The elastic modulus decreases drastically with a higher RH, and this effect is more marked beyond 60 % (Middleton 1968; Papir et al. 1975; Park and Baddiel 1972). Microruptures of the SC occur in vivo in some conditions (ichtyosis, hyperkeratosis, etc.) or even in healthy skin (subjective feeling of poor skin elasticity on the face, chapping and cracks on the hands of housemaids, cement workers, etc.). This situation is often due to the hardening of the stratum corneum caused by its dryness.
- The mechanical behaviour of the SC is also sensitive to temperature, and its rise has the same effect as an RH rise (Wilkes et al. 1973). Between 25 °C and 60 °C, for a 10 % water content, the change in the *force at rupture* and the *extension at rupture* is similar to a change of RH from 26 % to 100 % (Middleton 1969; Spencer 1976). The elastic modulus decreases exponentially, becoming 1000 times lower when the temperature changes from 25 °C to 60 °C. Temperature and water potentiate each other (Spencer 1976; Spencer et al. 1975). Consequently in constant RH conditions, the SC hydration increases by 50 % when the temperature rises from 20 °C to 30 °C, but the

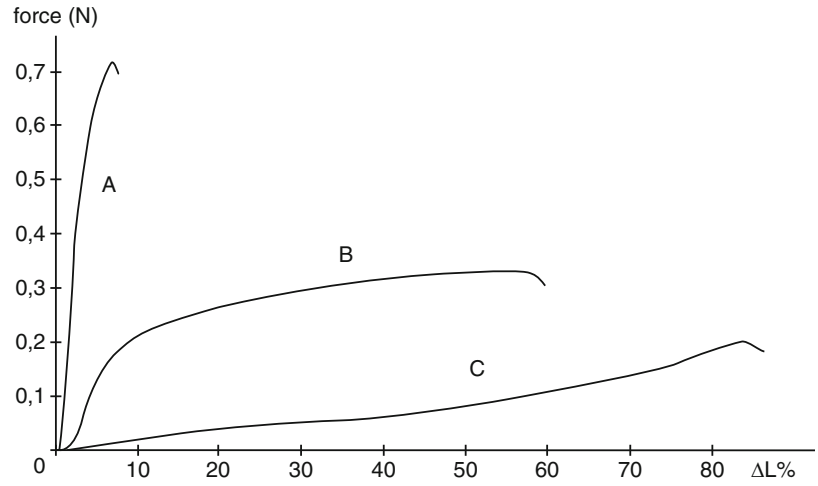

Fig. 5 Stratum corneum mechanical behavior under uniaxial elongation in vitro. Samples taken from the back. Traction at constant rate up to rupture. *A* RH = 50 %, *B* RH = 80 %, *C* RH = 90 % (From (Vasselet 1989), Laboratoire de Biophysique Cutanée, Besançon)

temperature dependence decreases at high RH and abates when RH reaches 90 %.

- The SC force/elongation curve at constant elongation rate shows one, two or three phases depending on the hydration level of the tissue (Fig. 5). The first one, up to a 10 % extension, is considered purely elastic. However, its slope increases if the extension rate rises (Wilkes et al. 1973), thus confirming the viscoelastic nature of the material. Phase II, absent in low RH, is an irreversible elongation with a low slope (so-called plastic phase). Only very hydrated SC shows a third phase, of a rather steep slope, before rupture. Preconditioning does not exist with SC, which is an important difference with the whole skin, indicating the absence of mobile components in the material (Koutroupi and Barbenel 1990). The two main intrinsic parameters of phase I are, therefore, the elastic modulus and the viscosity coefficient. The quasi-static elastic modulus of the back SC (9–10 μm thick (Holbrook and Odland 1974)) is as follows:

E (MPa)	T (°C)	RH (%)	Elongation rate (% s^{-1})	Reference
50	22	82	0.42	(Ferguson 1980)
10–200	22	60	0.22	(Vasselet 1989)
210	19	75	0.08	(Koutroupi and Barbenel 1990)

The dynamic modulus was found to be 600 MPa (Takahashi et al. 1981). A thorough investigation of the complex elastic modulus in relation to the stimulation frequency has been carried out (Rasseneur et al. 1982). The other parameters of the force/elongation curve at 25 % min^{-1} elongation rate in 82 % RH and at 22 °C (Ferguson J, Agache P, unpublished data) are:

Elastic limit	10 % elongation
Elongation at rupture	32–35 %
Force at rupture	15–19 g, hence a strain of 3.7–4.7 MPa
Rupture work	7.5–9.0 mJ, which is 1.9–2.3 kJm^{-2} (other authors have found 3.6 kJm^{-2} (Koutroupi and Barbenel 1990))

In an abdominal scar, a considerable increase of the elastic limit (over 4 times the standard deviation) and of the elastic modulus (Ferguson J, Agache P, unpublished data) were observed.

The in vitro behavior of the SC under traction probably reflects the intercellular ties (Frost and Van Scott 1966) because the final rupture is always extracellular, although the corneocytes are very elongated. The most resistant components are the corneodesmosomes which are, therefore, likely to be the structures involved. In the course of elongation, they bear both a direct and a shear force and their numbers fall (Agache et al. 1973). The rupture of a corneodesmosome placed in a drop of water, carried out with a micromanipulator, required a force of 0.19 10^{-3} N (Lévêque et al. 1988). Given that a section of corneodesmosomes is about 7250 nm^2 (25 nm × 290 nm (Barton 1988)), the stress is 26 GPa. The corneocyte membranes are also very resistant. The same authors observed that the corneocytes placed in a drop of water could be folded easily, but that their maximal extension was 30 % (without breaking) with an elongation modulus of 450 MPa (Lévêque et al. 1988). These figures are about two to eight times higher than those of the SC extended in vitro (see the table above). This suggests that the cumulated section areas of involved desmosomes represent only one eighth to one half of the SC section area. Measurements under electron microscopy could readily confirm this hypothesis.

- The viscous behavior and the constitutive equation of human SC have been studied by traction-relaxation tests and creep tests (Vasselet 1989). The relative relaxation versus Napierian logarithm of time is a straight line, which excludes a single viscosity coefficient. However, the standard viscoelastic model based on the existence of several viscosity coefficients does not permit reconstruction of

the complete traction-relaxation curve. On the other hand, the SC quickly hardens following repeated tractions (strain hardening). The constitutive equation of the elastic and viscoelastic phases of the SC should therefore include one elasticity parameter, two nonlinear viscosity parameters and one strain hardening parameter. Based on torsional creep experiments, Vasselet suggests the following equation which fits the experimental curves:

$$d\varepsilon/dt = (dF/dt)/E + Kf^{n}\ \varepsilon_{v}{}^{m}$$

where the elastic deformation is described by (dF/dt)/E and the viscous deformation by $Kf^{n}\ \varepsilon_{v}{}^{m}$ (E is the elastic modulus, F the force applied, K and n the intrinsic viscosity parameters, m the strain hardening parameter). The link between these parameters and the anatomical components of the SC are yet to be determined.

- Is the mechanical behavior of the SC directional? In the case of a 5 % extension, there does not appear to be any difference between elongations, either parallel or perpendicular to the skin furrows (Elfbaum and Wolfram 1970). Samples coming from the lower part of the back, where the Langer's lines are horizontal do not show significant differences either (Ferguson J, Agache P, unpublished data). This could be easily explained by the fact that the anisotropic physiological furrows of the SC in vivo are determined by the underlying layers, while the in vitro SC has been separated from them and has become lax in the course of manipulations and exposure to room conditions. As a matter of fact, no furrow was visible on its surface. These results show that the SC does not present any structural anisotropy.
- In vitro, the SC is in environmental conditions which are very different from the physiological situation. In vivo, it is closely associated with the underlying viable layer to which it is strongly attached. To separate them, it is necessary to use proteolytic enzymes, such as trypsin, which destroy the desmosomes of the viable tissue (trypsin above 0.125 % increases the elastic limit and the elasticity modulus in a dose-dependent way (Ferguson J, Agache P, unpublished data)). Owing to its location, the SC is subjected to humidity and temperature gradients, which decrease from the deepest layers toward the surface. Agache et al. (1973), using human SC sampled on the back (top of a cantharidin blister) with its upper part exposed to the air and its deep side moistened in order to be as close as possible to in vivo conditions, also found a fall in the rupture work when the RH shifted from 40 % to 88 %. However, they observed a decrease of the maximum extension, while the elasticity modulus remained unchanged. These discrepancies with the mechanical behavior under uniform conditions show that the deeper part of the SC has a major influence on its global mechanical behavior. The authors suggest that hyperhydration of the skin surface weakens the SC, thus providing an explanation for the toe web fissuring in "athlete's foot" (Agache et al. 1973).
- The full thickness of the SC matches the creases forming the skin relief. It partly unfolds when the skin is stretched, but does not extend. One can therefore wonder if the intrinsic properties of the SC characterized in vitro are relevant to the mechanical function of the skin in vivo. The answer is positive as far as its hardness and capacity to absorb mechanical shocks are concerned. However, its extensibility is involved only in critical, extra-physiological situations, during high shear strains. The latter can reach 33 % without apparent damage, an extension which would cause the rupture of flat SC (cf. *supra*).

The Rheometer commercialized by Dia-Stron Ltd, (Andover, Hampshire, UK) allows the mechanical study of the SC in vitro by uniaxial extension.

3.2 In Vivo

Hardness. To assess SC hardness in vivo, Peck and Glick (Peck and Glick 1956) measured the penetration depth of needles (0.8 mm, 1.5 mm and

2 mm diameter) according to the force applied (100 g, 200 g, and 400 g). They observed that penetration does not increase after a foot bath, although the SC should have become softer. These results cast some doubt about the soundness of the technique. The question has been resumed by the Cardiff's group (Nicholls et al. 1978; Graves and Edwards 2002), based on the rationale that the stratum corneum should be indented at a velocity greater than $5q10^3$ ms^{-1} and to a depth equivalent to its thickness. A new device, named Microindentometer, was constructed, which permits the skin resistance to indentation to be obtained in a reliable way. However, the authors believe further developments are needed before using it in practice (Graves and Edwards 2002).

Several studies were done using the same type of device to assess diseased skin's hardness in vivo (Falanga and Bucalo 1993; Romanelli and Falanga 1995). These are reviewed in reference (Romanelli and Falanga 2002). In fact, this is the only way to quantitatively rate the severity of the disease instead of a purely clinical rating by pinching or pressing the skin.

Elastic modulus. In vivo, the SC matches the furrows of the skin surface microrelief. The deeper the furrows (Rtm parameter) and the steeper their sides (Δq parameter), the higher their physiological limit of extension, as indicated by the beginning of whitening of the skin (Ferguson and Barbenel 1981). At this limit, the average roughness of the skin surface is reduced by half. The direction of the higher extensibility, examined on the thigh, chest, abdomen, forearm and foot, is perpendicular to the direction of the main furrows (extensibility on the forearm: 10 %//, 27 % ⊥). As a consequence, the SC in vivo does not sustain elongation stresses, but only unfolding stresses. However, its resistance to this unfolding is an important feature of the global skin resistance to stretching. The absolute value of its modulus, measured on the volar forearm by a suction method (described in ▶ Chap. 95, "Skin Mechanical Function"), was 57.8 MPa (Panisset et al. 1993). The extent of this contribution explains why the mechanical behavior of the whole skin can be altered by products that modify the suppleness of the SC, and why it is possible to assess the variation of the SC mechanical behavior by measuring that of the whole skin.

Resistance to Friction. This is an interesting property of the skin surface when one knows the importance of the friction coefficient in the prehensile function of palms and gripping of objects, as well as the traction of the foot on the ground in walking and running. In 1955, Naylor (Naylor 1955) monitored the friction coefficient (μ) of polyethylene moved at a constant speed and with a pre-determined pressure on the inner part of the tibia's bony area (a zone without fatty tissue) after shaving the hairs. From an initial value of 0.5 μ doubled after degreasing with ether, and peanut oil brought it down to 0.25, thus explaining its alleviation by the lipids of the skin surface. The action of water is more complex: μ is reduced on wet skin (hydrodynamic friction coefficient – water sliding on itself), but increased on moist skin (static friction coefficient). On thoroughly dried skin, the friction coefficient was 0.5 with wool material, and much lower with nylon material (Comaish and Bottoms 1971). The lowest value was found with non woven Teflon ($\mu = 0.2$). Dry talc is an excellent lubricant, but when it is damp its friction coefficient increases considerably.

The kinetics of the static friction coefficient following application of water is worth relating (Highley et al. 1977). As soon as the skin is moistened, a peak appears, in connection with the surface tension of water; it is of short duration because water mixes with the surface hydrophilic lipids which reduce this tension. Then a secondary peak occurs, and although the skin does not look humid any more, it seems to be associated with additional hydration of the skin surface. The formula $f = \mu P^n$, where P is the weight of the applied object and n an empirical number dependent on the tested surface ($n < 1$) (Comaish and Bottoms 1971), allows one to calculate μ from the friction force f. Following the time-course of the static friction coefficient also permits the substantivity of topical preparations to be assessed, especially emulsions.

The question has been revisited recently by Zahouani et al. (2002) who used a steel ball moving over the skin surface, and monitored the vertical load force F_z and the horizontal resisting friction force F_x. When the ball was moved over a distance

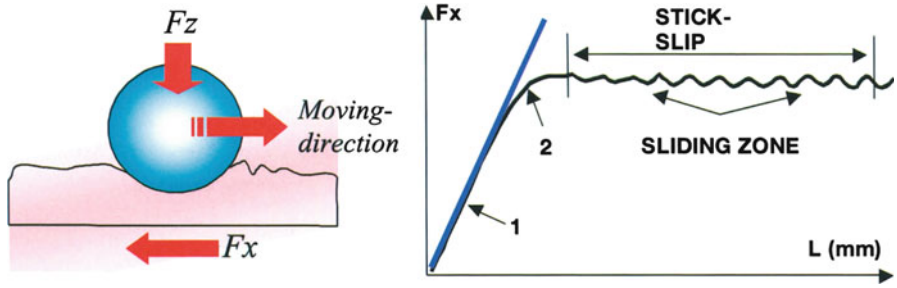

Fig. 6 The three phases of the skin friction

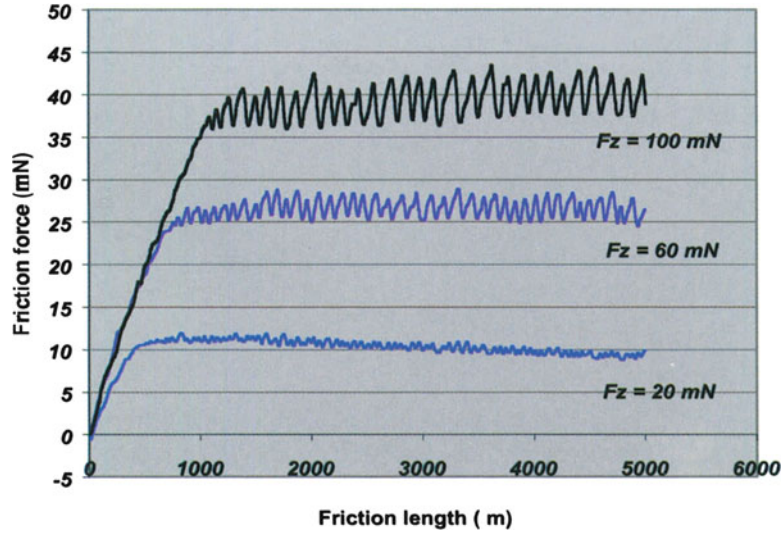

Fig. 7 Volar forearm friction force versus vertical load in a 40-year-old-woman

of about 5–15 mm with a velocity in the range of 0.3 to 2 mm/s, registration of the friction force F_x showed three distinct phases (Fig. 6). The first one is a linear increase up to a maximum which defines the static friction coefficient μ_s:

$$\mu_s = \frac{F_{x\,maz}}{F_z}$$

The slope of the linear curve corresponds to the horizontal stiffness of the skin, K_x (N/m).

Phase II is a transition regime between the static and dynamic friction. Phase III is the dynamic friction phase, which is generated by the unstable balance between the maximum friction stress and the creep of the skin relief. It shows an alternate "Stick–slip" motion depending on the local and environmental conditions. The slope of the "Stick" phases provide information about the horizontal stiffness of the skin. In this phase, the dynamic friction coefficient z is defined as the ratio: mean friction force/vertical load.

$$\mu_z = F_{x\,mean}/F_z$$

A test made on a 40-year-old woman (volar forearm) performed under three vertical loads and with a velocity of 600 μms-1 showed the dependence of the two skin friction coefficients on the vertical load (Fig. 7), which is in contradiction with Amonton's Law.

	Normal load F_z	Penetration depth:	Horizontal stiffness: K_x	Static friction coefficient:	Dynamic friction coefficient:
Before hydration	50 mN	1823 µm	51 N/m	1.35	1.12
5 min after hydration	50 mN	1929 µm	41 N/m	2.24	1.55
10 min after hydration	50 mN	1912 µm	51 N/m	0.69	0.65

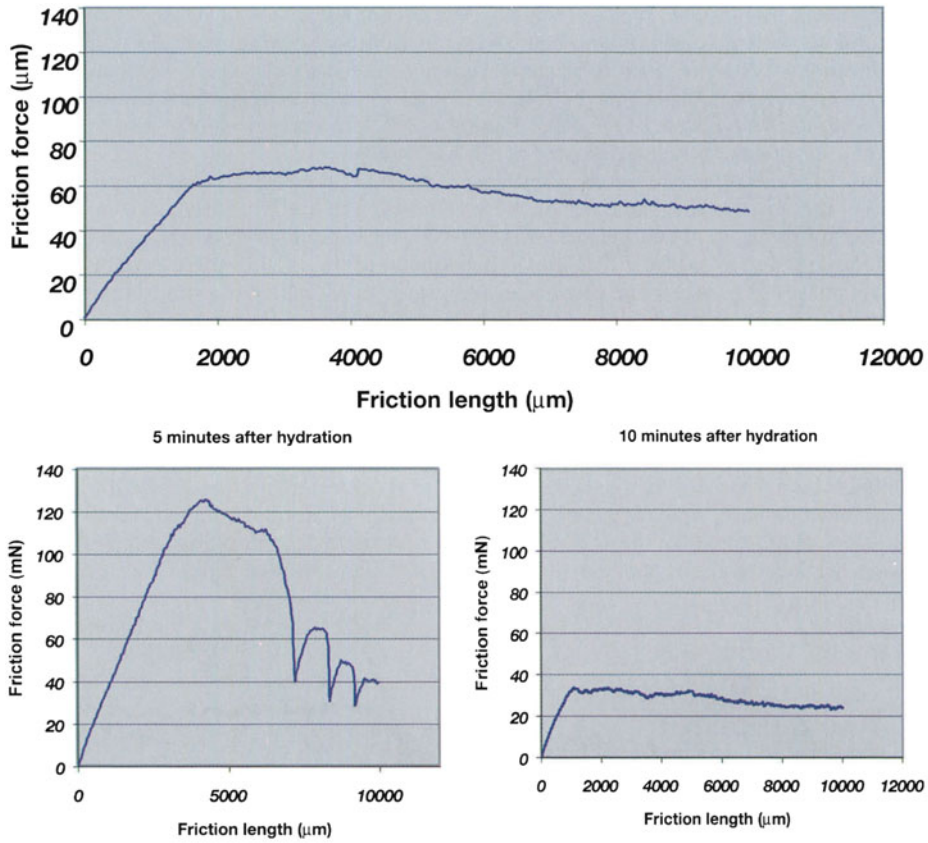

	Normal load F_z	Penetration depth:	Horizontal stiffness: K_x	Static friction coefficient:	Dynamic friction coefficient:
Before hydration	50 mN	1823 µm	51 N/m	1.35	1.12
5 min after hydration	50 mN	1929 µm	41 N/m	2.24	1.55
10 min after hydration	50 mN	1912 µm	51 N/m	0.69	0.65

Fig. 8 Volar forearm friction force versus skin hydration. *Table:* volar forearm friction parameters after hydration by water

Also of interest is the first increase and then decrease of the static and dynamic parameters after hydration by water (Fig. 8).

References

Agache P, Boyer JP, Laurent R. Biomechanical properties and microscopic morphology of human stratum corneum incubated on a wet pad in vitro. Arch Dermatol Forsch. 1973;246:271–83.

Agache P, Panisset F, Varchon D, Humbert PH. Mesure du module d'Young du stratum corneum et du derme humain in vivo. XXème Congrès Soc Biomécanique, Lausanne, 11–12 Sept 1995. Arch Physiol Biochem. 1995;C81 (Abstract).

Bader DL, Bowker P. Mechanical characteristics of skin and underlying tissue in vivo. Biomaterials. 1983;4:305–8.

Barton SP. Epidermal dimensions at the ultrastructural level. In: Marks R, Barton SP, Edwards C, editors. The physical nature of the skin. Lancaster: MTP Press; 1988. p. 13–22.

Beerens ECJ. Dermo-epidermal adherence. A study on repair after separation effected by suction blistering. Thesis, University of Utrecht; 1977.

Blank IH. Factors which influence the water content of the stratum corneum. J Invest Dermatol. 1952;18:433–40.

Brown IA. A scanning electron microscope study of the effects of uniaxial tension on human skin. Br J Dermatol. 1973;89:383–93.

Burton AC. Les parois des vaiseaux sanguins et leurs fonctions. In: Burton AC, editor. Physiologie et biophysique de la circulation. Masson: Paris; 1968. p. 63–75.

Caro C, Pedley T, Schroter R, Seed W. The mechanics of the circulation. Oxford: Oxford University Press; 1978.

Comaish S, Bottoms E. The skin and friction: deviation from Amonton's laws and the effect of hydration and lubrification. Br J Dermatol. 1971;84:37–43.

Comninou M, Yannas J. Dependence of stress strain nonlinearity of connective tissue on the geometry of collagen fibres. J Biomech. 1976;13:463–8.

Daly CH, Odland GF. Age-related changes in the mechanical properties of human skin. J Invest Dermatol. 1973;73:84–7.

Diridollou S, Bcrson M, Black D, Grcgoirc JM, Patat E, Gall Y. Subcutaneous fat involvement in skin deformation following suction. In: 12th International Symposium on Bioengineering and the Skin and Joint ISBS/DCES Poster Sessions; 1998 June 25–27; Boston; 1998.

Diridollou S, Black D, Lagarde JM, Gall Y, Berson M, Vabre V, Patat F, Vaillant L. Sex- and site-dependent variations in the thickness and mechanical properties of human skin in vivo. Int J Cosmet Sci. 2000;22:421–35.

Diridollou S, Vabre V, Berson M, Vaillant L, Black D, Lagarde JM, Grégoire JM, Gall Y, Patat F. Skin ageing: changes of physical properties of human skin in vivo. Int J Cosmet Sci. 2001;23:353–62.

Elfbaum SG, Wolfram MA. Effect of demethyl sulfoxide and other reagents upon mechanical properties of stratum comeum strips. J Soc Cosmet Chem. 1970;21:129–40.

Escoffier C, De Rigal J, Rochefort A, Vasselet R, Lévêque J-L, Agache P. Age-related mechanical properties of human skin: an in vivo study. J Invest Dermatol. 1989;93:353–7.

Falanga V, Bucalo B. Use of a durometer to assess skin hardness. J Am Acad Dermatol. 1993;29:47–51.

Fazio MJ, Olsen DR, Uitto JJ. Skin aging: lessons from cutis laxa and elastoderma. Cutis. 1989;43:437–44.

Ferguson J. The structural and mechanical properties of human stratum corneum. Thesis, University of Strathclyde; 1980.

Ferguson J, Barbenel JC. Skin surface patterns and the directional mechanical properties of the dermis. In: Marks R, Payne PA, editors. Bioengineering and the skin. Lancaster: MTP Press; 1981. p. 83–92.

Frost P, Van Scott EJ. Ichtyosiform dermatoses: classification based on anatomic and biometric observations. Arch Dermatol. 1966;94:113–26.

Fung YCB. Stress–strain-history relations of soft tissues in simple elongations. In: Fung YCB et al., editors. Biomechanics, its foundations and objectives. Englewood Cliffs: Prentice Hall; 1972. p. 181–208.

Gniadecka M, Gniadecki R, Serup J, Sondergaard J. Skin mechanical properties present adaptation to man's upright position. Acta Derm Venereol. 1994;74:188–90.

Grahame R, Holt PJL. The influence of ageing on the in vivo elasticity of human skin. Gerontologia. 1969;15:121–9.

Graves CJ, Edwards C. The microindentometer. In: Elsner P, Berardesca E, Wilhelm KP, Maibach HI, editors. Bioenginering of the skin: skin biomechanics. Boca Raton: CRC Press; 2002. p. 161–78.

Harvey W, Pope FM, Grahame R. Cutaneous extensibility in pseudoxanthoma elasticum (PXE). Br J Dermatol. 1975;92:679–83.

Hayes WC, Keer LM, Herrmann G, Mockross LF. A mathematical analysis for indentation tests of articular cartilage. J Biomech. 1972;6:541–51.

Highley DR, Coomey M, DenBeste M, Wolfram LJ. Frictional properties of skin. J Invest Dermatol. 1977;69:303–5.

Holbrook KA, Odland GF. Regional differences in the thickness (cell layers) of the human stratum corneum: an ultrastructural analysis. J Invest Dermatol. 1974;62:415–22.

Kenedi RM, Gibson T, Daly CH. Bio-engineering studies of the human skin. In: Kenedi RM, editor.

Biomechanics and related bioengineering topics. Oxford: Pergamon Press; 1965. p. 147–58.
Kligman AM. Biology of the stratum corneum. In: Montagna W, Lobitz WC, editors. The epidermis. London: Academic; 1964. p. 387–433.
Koutroupi KS, Barbenel JC. Mechanical and failure behaviour of the stratum corneum. J Biomech. 1990;23:281–7.
Langer K. On the anatomy and physiology of the skin. 1: The cleavability of the cutis (English translation by T Gibson). Br J Plast Surg. 1978;31:3–8.
Lanir Y. The fibrous structure of the skin and its relation to mechanical behaviour. In: Marks R, Payne PA, editors. Bioengineering and the skin. Lancaster: MTP Press; 1981. p. 93–5.
Lapière CM, Nusgens BV, Pierard GE. The architectural organization and function of the macromolecules in the dermis. In: Marks RM, Barton SP, Edwards C, editors. The physical nature of the skin. Lancaster/Boston: MTP Press; 1988. p. 163–76.
Lévêque JL, Poelman MC, de Rigal J, Kligman AM. Are comeocytes elastic? Dermatologica. 1988;76:65–9.
Manschot JFM, Brakkee AJM. The measurement and modelling of the mechanical properties of human skin in vivo: the model. J Biomech. 1986;19:517–21.
Manschot JFM, Wijn PFF, Brakkee AJM. The angular distribution function of the elastic fibres in the skin as estimated from in vivo measurements. In: Huiskes R, van Campen DH, de Wijn JR, editors. Biomechanics: principles and applications, Developments in biomechanics, vol. 1. The Hague: M. Nijhoff; 1982. p. 411–8.
Middleton JD. The mechanism of water binding in stratum corneum. Br J Dermatol. 1968;80:437–50.
Middleton JD. The effect of temperature on extensibility of isolated corneum and its relation to skin chapping. Br J Dermatol. 1969;81:717–21.
Namikawa A, Sakai H, Motegi K, Oka T. Cleavage lines of skin. In: Lierse W, editor. Bibliotheca Anatomica, vol. 27. Basel: Karger; 1986. p. 1–60.
Naylor PFD. The skin surface and friction. Br J Dermatol. 1955;67:239–48.
Nicholls S, King S, Guibarra E, Marks R. Measurement of point deformation of human skin in vivo: contribution of the stratum comeum. J Invest Dermatol. 1978;70:227 (Abstract).
Panisset F, Varchon D, Agache P. Non invasive assessment of stratum corneum Young's modulus in vivo. In: XIVth International Congress on Biomechanics; 1993 July 4–8; Paris, Congrès Annuel de Recherche Dermatologique; 1993 Oct 14–16; Nimes, and 10th International Symposium of Bioengineering and the Skin; 1994 June 13–15; Cincinnati; 1993.
Papir YS, Hsu KH, Wildnauer RH. The mechanical properties of stratum corneum. 1: The effect of water and ambient temperature on the tensile properties of newborn rat corneum. Biochim Biophys Acta. 1975;399:170–80.
Park AC, Baddiel CB. Rheology of stratum corneum. 2: a physico-chemical investigation of factors influencing the water content of the corneum. J Soc Cosmet Chem. 1972;23:13–21.
Peck S, Glick AW. A new method for measuring the hardness of keratin. J Soc Cosmet Chem. 1956;7:530–40.
Pichon E, De Rigal J, Lévêque J-L. In vivo rheological study of the torsional characteristics of the skin. In: 8th International Symposium on Bioengineering and the Skin; 1990 June 13–16; Stresa; 1990.
Piérard GE, Lapière CM. Microanatomy of the dermis in relation to relaxed skin tension lines and Langer's lines. Am J Dermatopathol. 1987;9:219–24.
Rasseneur L, de Rigal J, Lévêque JC. Simultaneous determination of the static and dynamic modulus of elasticity of stratum comeum. Bioeng Newls. 1982;1:52–64.
Rollhauser H. The tensile strength of human skin. Gegenbauers Morph Jb. 1950;90:249–61.
Romanelli M, Falanga V. Use of a durometer to measure the degree of skin induration in lipodermatosclerosis. J Am Acad Dermatol. 1995;32:188–91.
Romanelli M, Falanga V. The durometer. In: Elsner P, Berardesca E, Wilhelm KP, Maibach HI, editors. Bioenginering of the skin: skin biomechanics. Boca Raton: CRC Press; 2002. p. 139–45.
Singer ED, Vinson LJ. The water binding properties of skin. Proc Sci Section Toilet Goods Ass. 1966;46:29.
Spencer TS. Water and the horny layer. J Soc Cosmet Chem. 1976;27:63.
Spencer TS, Linamen CE, Akers WA, Jones HE. Temperature dependence of water content of stratum corneum. Br J Dermatol. 1975;93:159–64.
Takahashi M, Kawasaki K, Tanaka M, Ohta S, Tsuda Y. The mechanism of stratum corneum plasticization with water. In: Marks R, Payne PA, editors. Bioengineering and the skin. Lancaster: MTM Press; 1981. p. 67–76.
Tan CY, Statham B, Marks R, Payne PA. Skin thickness measurement by pulsed ultrasound: its reproducibility, validation and variability. Br J Dermatol. 1982;106:657–67.
Thompson DE, Husseln HMG, Perritt RQ. Point impedance characterization of soft tissues in vivo. In: Marks R, Payne PA, editors. Bioengineering and the skin. Lancaster: MTP Press; 1981. p. 103–11.
Vasselet R. Etude mécanique du stratum corneum humain in vitro. Thesis, University of Besançon; 1989.
Vasselet R, Agache P. Perspectives de modélisation des propriétés mécaniques de la peau humaine in vivo. In: Vasselet R, editor. Étude in vitro des propriétés mécaniques du stratum corneum humain à partir des essais de traction-relaxation et fluage: identification de son comportement viscoélastique à un modèle rhéologique non linéaire avec écrouissage. Thèse Sciences pour l'Ingénieur, Besançon; 1987. p. 213–33.
Vlasblom DC. Skin elasticity. PhD thesis, University of Utrecht; 1967.
Wijn PFF, Brakkee AJM, Stienen GJM, Vendrik AJH. Mechanical properties of human skin in vivo for small

deformations: a comparison of uniaxial strain and torsion measurements. In: Kenedi RM et al., editors. Bed sore biomechanics. London: Macmillan; 1976. p. 103–8.

Wijn PFF, Brakkee AJM, Vendrik AJH. The alinear viscoelastic properties of the human skin in vivo for small deformations. In: Reul H, editor. Conference Digest of the 1st ICMMB; 1978; Aachen. Baden-Baden: Witzstrock; 1978. p. 207–10.

Wijn PFF, Brakkee AJM, Kuiper JP, Vendrik AJH. The alinear viscoelastic properties of human skin in vivo related to sex and age. In: Marks R, Payne PA, editors. Bioengineering and the skin. Lancaster: MTP Press; 1981. p. 135–46.

Wildnauer RH, Bothwell JW, Douglass AB. Stratum corneum biomechanical properties. 1. Influence of relative humidity on normal and extracted human stratum corneum. J Invest Dermatol. 1971;56:72–8.

Wilkes GL, Brown IA, Wildnauer RH. The biomechanical properties of skin: a polymer composite. CRC Crit Rev Bioeng. 1973;1:453–95.

Zahouani H, Pailler-Mattei C, Vargiolu R, Abellan MA. Assessment of the elasticity and tactile properties of the human skin surface by tribological tests. In: 22nd IFSCC Congress, Proceedings' oral papers, vol 2; 2002 Sept; Edinburgh; 2002.

Mechanical Behaviour Assessment of the Skin

96

Pierre Agache and Daniel Varchon

Contents

This chapter was originally published under the ISBN 978-3-540-01771-4 with the following book title Measuring the Skin. The content has not been changed.

Pierre Agache: deceased.

P. Agache (✉)
Department of Dermatology, University Hospital of Besançon, Besançon, France
e-mail: aude.agache@free.fr; ferial.fanian@chu-besancon.fr; ferial.fanian@cert-besancon.com

D. Varchon
Laboratoire de Mécanique Appliquée R. Chaléat, University of Franche-Comté, Besançon, France
e-mail: daniel.varchon@univ-fcomte.fr

P. Humbert et al. (eds.), *Agache's Measuring the Skin*,
DOI 10.1007/978-3-319-32383-1_130

Keywords
Ballistometry • Barbenel's method • Borges method • Skin compressibility • Creep • Cutometer • Dermagraph • Dermal torque meter • Dynamic spring rate (DSR) • Extensometer • Gas-bearing electrodynamometer (GBE) • Indentometry • Kelvin-Voigt model • Levarometry • Linear skin rheometer • Skin mechanical behavior • Skin progressive deformation tests • Skin relaxation tests • Reviscometer • Skin microrelief • Stark's method • Strain in mechanics

Principle Current Uses. Efficacy tests of cosmetics and anti-aging products, measurement of UV impact, follow-up of skin sclerotic diseases (scleroderma, morphea, radiodermatitis, etc.), atrophies (from corticosteroids, in rheumatisms, striae distensae, etc.), diagnosis of connective tissue diseases (Ehlers-Danlos syndromes, elastic pseudoxanthoma, mid-dermis elastolysis, etc.), foresight tests in plastic and cosmetic surgery, characterization of elasticity and viscosity of healthy or pathological skin, and research in skin physiology.

1 Aims

The two main purposes of skin mechanical testing are:

- To follow up and record the mechanical behavior of the skin or one of its components in the course of a disease, a treatment, or following cosmetic application, etc.
- To access the intrinsic mechanical properties and functional condition of the main tissue or structures involved: either elastic components (elastic fibers, connective bundle weaving, stratum corneum pliability), or components with a viscous behavior (interstitial fluid mobility and viscosity, frictions within the tissues)

Since the shape of skin can be changed in different ways (stretching, torsion, compression, etc.) and to different degrees, it is possible to impose a constraint preferentially on a given component and so assess its behavior independently. As a consequence, the assessment of the mechanical behavior opens new fields of anatomical or functional investigation of theoretically all the various components of the skin, because every biological structure has a mechanical behavior and these play a part of the overall skin behavior.

2 Methodology in Biomechanics

The measurement of the skin's mechanical properties is restricted to noninvasive methods designed to be used on the skin in vivo and in everyday conditions. The study of its behavior when subjected to excessive, traumatic strains may be interesting in itself but can only be performed in vitro (see ▶ Sect. 2.6 in Chap. 95, "Skin Mechanical Function" and ▶ Sect. 3.1 in Chap. 95, "Skin Mechanical Function"). Several constraints can be used: stretching, torsion, suction, compression, percussion, elevation, etc. For each, the test can be performed in different ways: constant force applied suddenly and deformation measured versus time (creep test, Fig. 1); increasing force applied at a constant rate and measurement of deformation; increasing strain applied at a constant rate and measurement of the resisting force (traction test, Fig. 2); permanent deformation applied suddenly and measurement of the resisting force versus time (relaxation test, Fig. 3); and oscillating stress (dynamic test, for example by propagation of sound).

Although it may be an important step in the clinical evaluation of a skin lesion, the assessment of skin hardness has not yet gained general acceptance. The use of a durometer, an industrial device, needs a firm basis below the skin, which

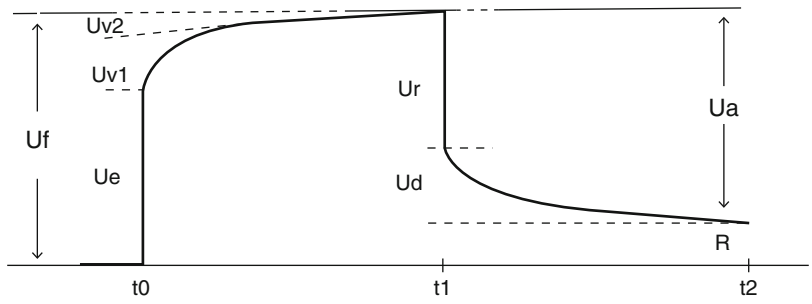

Fig. 1 Creep test. Deformation versus time. Uf maximum deformation, Ue immediate (elastic) deformation, Uv_1 viscoelastic deformation, Uv_2 viscous deformation, Ur immediate (elastic) recovery, Ud delayed (viscoelastic) recovery, Ua maximum recovery at the end of the test, R residual deformation at the end of the test

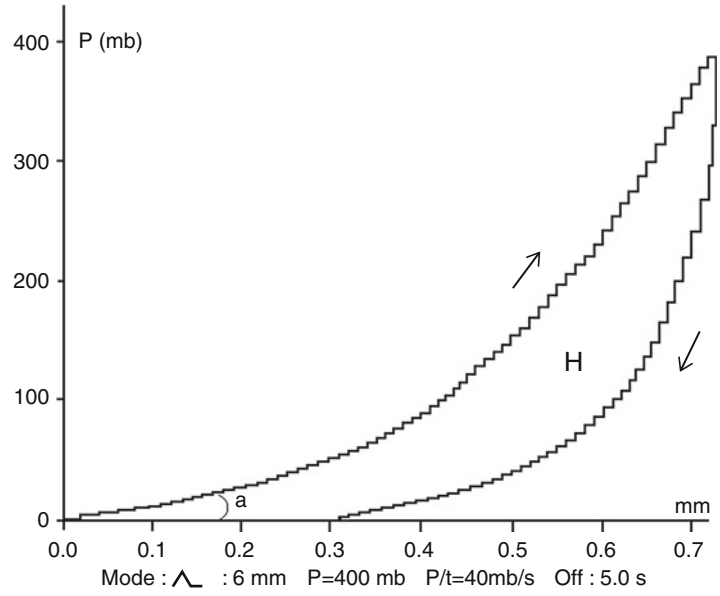

Fig. 2 Progressive deformation cycle by suction (Cutometer) on the volar forearm. Y-axis: pressure P (mbar). X-axis: skin bulging height (mm). *Arrows* indicate the progression of the graph over time. Angle a: slope of traction phase. H: hysteresis. The test characteristics are displayed under the x-axis (type of cycle, chamber diameter, maximum depression, pressure increasing rate, etc.)

is not available as some subcutis exists at all body sites. A tentative manual assessment using three standard hardness disks as controls gave satisfactory results with keloids (Flores et al. 1998). After a rapid training on three standard rubber disks of graded hardness, the interobserver variability (13 dermatologists) was 9.25 %. Although this was only a 3-point scale, the method may be useful in clinical practice.

2.1 Descriptive Versus Absolute Mechanical Parameters

Devices in mechanics record deformations or forces. These parameters are called descriptive or phenomenological because they depend on the applied stress (suction, torsion, etc.) and the device used. Such parameters, identifiable on Figs. 1, 2, and 3 (e.g., force F, deformation Ue), describe a behavior under

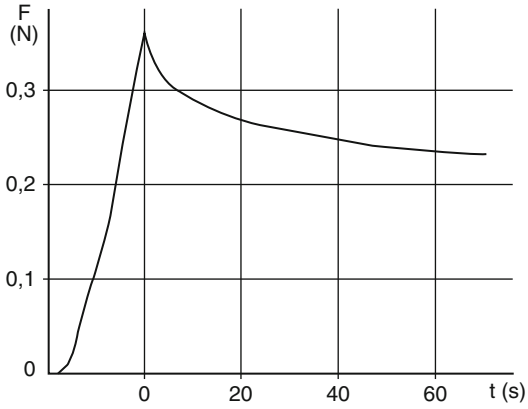

Fig. 3 Relaxation test. Force (skin resistance) versus time. The extension rate was 1 %/s for 10 s (the Extensometer could not move faster). Consequently, some relaxation took place before the measurement started (Vasselet and Agache 1987)

particular conditions, and comparison with other data is possible only if the latter have been obtained under the same conditions. However, this behavior reflects intrinsic properties of the material, which are of value and worth identifying. Intrinsic properties can be described by parameters of general mechanics, named intrinsic or absolute parameters. These permit comparisons between materials and experimental results whatever the type of test. Conversion of descriptive or phenomenological parameters into absolute parameters is thus highly desirable and scientifically profitable. The observed deformation (length, angle, etc.) should be converted into relative deformation (or strain) ε in %; the force F in newtons is converted into stress σ in pascals; and all of this is given in three dimensions of space. The relative deformation can be computed only if the limits of the area of deformed skin and the geometry of deformation are known with precision. The stress $\sigma = F/a$ is the force applied divided by the area a, in m^2, of the sample section. The skin thickness at the measurement site must be assessed (usually by ultrasound imaging) to calculate a. The ways to perform conversions will be examined with each method.

2.2 Creep

A creep test curve is depicted in Fig. 1. Deformation types are: immediate deformation *Ue* (*e* for "elastic"), delayed deformation *Uv* (*v* for "viscous") which tends towards an asymptotic limit, the final deformation $Uf = Ue + Uv$ (*f* for final), immediate recovery *Ur* (*r* for recovery), delayed recovery *Ud* (*d* for delayed), the total recovery $Ua = Ur + Ud$ (*a* for added), and the residual deformation *R*. The limit between *Ue* and *Uv* is imprecise. It is usually determined approximately with the naked eye, but there is a simple and accurate solution from the mathematical processing of the *Uv* curve, which is exponential: $Uv = Uvmax\,(1 - e^{-t/\tau})$, where $Uvmax = Uf - Ue$. Hence, $\ln(Uvmax - Uv) = Uvmax - t/\tau$ (This equation is valid only if $t \geq 3\tau$ is verified later.). Using this equation, the experimental measurement of some *Uv* values allows *Uvmax* to be determined and subsequently *Ue*. The calculation also gives the time constant τ which is the time it takes *Uv* to reach 63 % of *Uvmax*. It is a measurement of the viscous displacement rate, and $1/\tau$ is an index of the tissue fluidity.

The same holds true for the limit between *Ur* and *Ud*. The time constant of this recovery phase is another measurement of the viscous displacement rate of the same tissue. However, the latter depends on the force generating the movement. As a consequence, the comparison between both fluidity values would more or less be the comparison of the internal recovery force with the externally applied force.

How long does the force have to be applied to let the viscous movement have time to occur and be evaluated accurately? In the past (Sanders 1973; Agachel et al. 1980), a test duration of 2–120 s was used. However, *Uv* consists of a first short and curvilinear phase (Uv_1), then a second phase, comparable to a straight line (Uv_2), in accordance with the model of Fig. 1 of ▶ Chap. 95, "Skin Mechanical Function". The former describes the viscoelastic behavior, while the latter reflects a viscosity which is different (higher) from the first one and has less practical applications. For this reason, most creep tests last only 2–5 s because their main purpose is to assess the elastic resistance, a practical index of the skin tone. To measure the two types of viscosity, it would be necessary to extend the application of force by at least 10 s (see Sect. 11.1).

2.3 Progressive Deformation Tests

Progressive deformation tests provide a graph of force F (newtons) versus deformation U (meters) (Fig. 2). In a cycle comprising an increasing and then decreasing force at a constant pace, the deformation is always more pronounced when the force is decreasing then in the increasing phase at the same force. A hysteresis loop thus appears, whose area is relative to the viscous deformation (Diridollou et al. 2000a). In such tests, the descriptive parameters are the ascending slope (force/elongation), which expresses the skin's increasing stiffness (under these particular experimental conditions), and the hysteresis loop area, $j(F_1 - F_2) \times$ elongation, where F_1 and F_2 are the force during loading and unloading, respectively. In this test, like in the preceding one, the relative deformation must not exceed 15 %. This threshold is often detected by the initiation of pain.

2.4 Relaxation Tests

In relaxation tests, the skin resisting force F is measured continuously versus time (Fig. 3). The sudden stretching induces a resistance force F_0, whose nature is only elastic (equivalent to *Ue* in the creep test) because it occurs too fast for viscous movement to appear. The latter starts in the immediate aftermath and is detected by the progressive reduction of the resisting force (relaxation of the elastic structures). Consequently, not only does this test evaluate the immediate deformation *Ue*, but also the rate and extent of the viscous flow. Although it is a very informative test, none of the commercially available devices can do it and no prototype seems to be in progress. Consequently, it will not be described.

3 Suction

3.1 Implementation

1. To perform a *creep test*, the suction chamber is secured on the skin with double-sided adhesive tape to prevent any skin slippage during suction. When suction is applied, a roughly hemispherical elevation of the skin appears whose height is measured by the device at short time intervals (less than 1 s). The suction is maintained for a few seconds, then stopped, and then the measurement is continued for the same time length, which is usually not long enough for the skin to regain its initial condition (Fig. 1). The five descriptive parameters to be obtained are: *Ue, Uf, Ur, Ua*, and *R*. For a given suction, the elevation will be higher if the skin is more supple. The extent of recovery increases with the skin tone and decreases with its viscosity. Usually *Ue* decreases over the first four suctions and then remains stable. This is a typical preconditioning phenomenon and shows the capacity of the skin to orient its elastic structures in the direction of stretching.
2. For a progressive loading and unloading test, a stepwise increasing suction is applied and the graph of the suction force F versus deformation Uf is recorded (Fig. 2). The tangents to the ascending slope are the successive skin stiffness moduli in the experimental conditions, especially for a given increasing suction rate – as the higher the rate, the steeper the slope. As in creep tests, the first curve is different from the subsequent ones, up to the fourth (preconditioning phenomenon). If a cycle is carried out at the same rate, two other interesting parameters are obtained: the hysteresis loop area and the slope of the descending curve. The ascending slope increases with the skin tone and decreases with its viscosity. The opposite is true for the descending slope. The hysteresis area is related to the skin viscosity.

3.2 Devices

The two devices currently available on the market give the exact limits of the area submitted to suction; therefore, the conversion of the descriptive parameters into absolute parameters is possible. The obtained parameters are the mean of the two directional parameters in the horizontal plane, since the skin is mechanically anisotropic in this plane.

The Dermaflex A^2 (Gniadecka and Serup 1995) has a 10-mm diameter suction chamber and can achieve suctions up to 0.5 bar for 2–20 s. It is also possible with its software to program 1–30 successive cycles of suction-recovery and to record its graph. Directly available parameters are: (1) distensibility *Uf* after the first suction (called this as it is a distension), *Ue* is not provided; (2) the resilient distension $R = Uf - Ua$; (3) the relative elastic retraction (RER) or elasticity index *R/Uf* (a viscoelasticity index because both elements of the ratio have a viscous component); and finally, (4) the increase of *Uf* between the first and the last suction, which is a measurement of the preconditioning while the differential area between suction and recovery curves (the hysteresis loop) is an index of skin viscosity. On the adult volar forearm, the approximate values obtained by six cycles of suction at 0.3 bar for 4 s are (Overgaard Olsen and Jemec 1993):

Viscoelastic distensibility	$Uf = 0.65$ mm
Residual distension	$R = 0.60$ mm
Elasticity	$R/Uf = 65$ %
Hysteresis (preconditioning)	$Uf4 - Uf1 = 0.19$ mm

Considering the diameter of the suction chamber (10 mm), the above mentioned parameters are not sensitive to the variations of the stratum corneum's suppleness because this layer is barely involved in the bulging. However, they can be sensitive to the mechanical properties of the hypodermis (resistance of this layer to the upward movement of the skin), even in areas where it looks loose (Panisset 1992; Diridollou et al. 1998).

A simplified device aimed at roughly investigating the skin's softness, which utilizes probes for measuring transepidermal water loss and epidermal hydration in a global apparatus, the Dermalab (Cortex Technology, Hadsund, Denmark), has recently been put on the market (Serup 2002). Within a suction chamber of 10 mm in diameter, a suction is progressively applied until the skin bulging reaches 1.5 mm. A pretension suction and several extension–-recovery cycles can be done. The result is expressed as the necessary time and suction, a calculated parameter would be related to the elasticity modulus, and the time and suction necessary for raising the skin to an intermediary level. This poor scientific device is obviously intended for retail cosmetic traders.

The Cutometer SEM 474 (Courage-Khazaka, Cologne, Germany) has a cylindrical chamber in which a sudden suction of 0.1–0.5 bar (10–50 kPa) can be obtained. Four chambers of different diameters are available: 2, 4, 6 and 8 mm. In the creep mode, suction can be performed for 0.1–60 s. The program can produce successive suction-recovery cycles. The graph of deformation is recorded, and with a cursor system, all the required extension parameters are directly provided (*Ue*, etc.). The ratios (*Uv/Ue*, etc.) and preconditioning ought to be calculated. To have accurate values, the suction device has to be applied on the skin with a constant pressure which is ensured by a spring located in the probe (Asserin et al. 1994). On the volar forearm of young adults, the values of *Uf* for different diameters of chamber and different pressures are displayed in Fig. 4 (Panisset 1992). They indicate that skin resistance with the 8 mm chamber increased, a lower Uf, whereas a reduction was expected. This is the result of a beginning resistance by the hypodermis to the elevation of the skin. The Cutometer can also be used in a *progressive deformation test* mode. In this case, the suction is gradually increased. The device displays the graph of deformation versus the suction force (Fig. 2).

The 2-mm chamber is sensitive to the stratum corneum's mechanical behavior (for example, with a 0.4 bar suction). This is not the case for other diameters. On the volar forearm, using the 2-, 4- and 6-mm chambers even with a 0.5 bar suction does not seem to involve any resistance from the hypodermis, but this is likely with the 8-mm chamber, even for a 0.1-bar suction (Fig. 4) (Panisset 1992). On other sites, where the hypodermis is less loose or scanty, this is much more probable, even with the small chambers. Parameters *Ue, Uv, Ur, Uf* as well as *Uv/Ue* and *Ur/Uf* have been measured by Cua et al. (1990), in 20- to 30-year-old and 70- to 80- year-old subjects and on 11 body sites, using the 2-mm chamber with a 500-mbar pressure for 5 s. The ratios *Ur/Ue, Uv/Ue* and *Ur/Uf* in 20- to 30-year-old and 60-

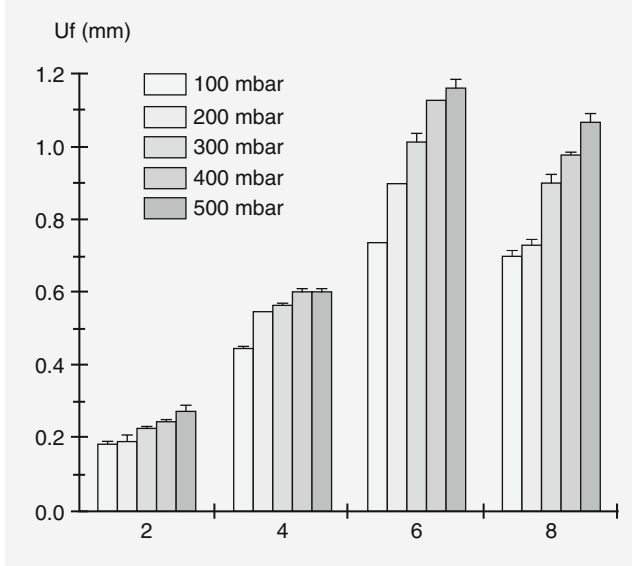

Fig. 4 *Uf* values (Cutometer) on the volar forearm of a 26-year-old subject (Panisset 1992). Five pressures (suction) for each chamber diameter (2, 4, 6, 8 mm). Mean and standard deviation (n = 10 tests per column). The steady *Uf* increase with pressure ceased to be observed with the 8 mm chamber, suggesting a reduced bulging due to hypodermis distension

to 70-year-old subjects, on four body sites, using different chambers and pressure values, and the influence of preconditioning have been investigated by Barel et al. (1998).

The Dermagraph (Rüetschi AG, Yverdon and Murten, Switzerland) uses a vacuum probe of 20 mm in diameter and 442 g in weight. The experiment is a 6-s creep followed by a 4-s recovery. The obtained parameters are the skin's immediate extensibility Ue, the final extensibility Uf, the immediate recovery Ur, and the ratio Uf/Ur. In a study of 22 body areas in 96 healthy volunteers and 10 patients with systemic sclerosis (Haüselman et al. 2002), it was found that in normal subjects Uf and Ur were higher in females, higher in torso, and lower in limb extremities. Surprisingly, no change with aging was found. The authors also concluded that "the Dermagraph can be used in longitudinal studies in patients with systemic sclerosis".

The large suction chamber aperture (20 mm) minimizes the stratum corneum's influence in the results, but enhances that of the subcutis. Resistance of the latter would decrease the extensibility and consequently skew skin data. Testing subcutis resistance needs comparison of data obtained with several suction forces (see Fig. 4). The assertion of Dermagraph utility in systemic sclerosis is obviously also valid for the Dermaflex A and the Cutometer SEM 474.

3.3 Conversion of Descriptive Parameters into Absolute Parameters

It is based upon the geometry of the deformation (Panisset 1992; Agache et al. 1992). In a creep experiment, considering that: (1) the skin is a homogeneous and isotropic material (a wrong but useful hypothesis), (2) the skin deformation in the suction chamber is a part of a sphere and its vertical section is the segment of a circle, then the formulas to calculate the strain a and the relative elongation e are as follows:

$$R = (U2 + r2)/2U \qquad \sin\theta/2 = r/R \qquad L = R\theta(\theta \text{ in radians})$$

$$\sigma = PR/2e(P \text{ expressed in kPa}) \qquad \varepsilon = (L/2 - r)/r$$

where P is the suction (pascals), U the elevation of the skin in the suction chamber (meters), r the radius of the suction chamber (meters), e the skin thickness (meters), L the length of the arc made by the stretched skin, R the radius of the

circle of this arc, and θ the angle that faces this arc. Depending on whether *Ue* or *Uf* is used, the strain, and as a consequence the modulus, will be slightly different. Both choices can be used, but must be indicated.

In a progressive loading-unloading test, using a prototype similar to the Cutometer, but a different model, the formula used to compute the initial stress F0, the stress F during loading, and the relative elongation during loading, proved to be more complicated (Diridollou et al. 2000a).

The analysis of the viscous behavior in a creep test (with the calculation of the viscosity coefficient) and in a progressive loading-unloading test (with the calculation of a non-restored energy ratio) are described in Sect. 11.1.

4 Torsion Method

4.1 Equipment

In this method, a ring of skin located between a central disk and a peripheral ring or plaque is submitted to a sudden torsion by application of a constant torque on the central disk (Agache 1995). The resulting rotation angle of the disk is the deformation measured. The Dermal Torque Meter (Dia-Stron Ltd, Andover, Hampshire, UK) is derived from the Twistometer (L'Oréal), which has not been commercialised. The disk and the ring should be glued firmly onto the skin with double-sided adhesive tape. The operator can program 1–20 torsion cycles, selecting their duration (1–99 s), their frequency (intervals from 1 s), the torque intensity ($0–30 \times 10^{-3}$ Nm with a 0.1×10^{-3} Nm resolution). The torsion angle can be measured from 0°–40° with a 0.02° resolution. The diameter of the central rotating disk is 20 mm, and the peripheral rings can test 1, 3 and 5 mm large skin rings.

In the creep mode, the device records the graph of the angle (in degrees) versus time (seconds) and the standard deformation parameters *Ue*, etc. A *progressive traction* mode is also available, by measuring the torsion angle at each step of the torque rise. The result is the graph of the torsion angle versus the applied torque. As in the suction method, the first curve is different from the others, with stability being reached by the fourth one (preconditioning).

A 1-mm skin ring is very sensitive to the stratum corneum's behavior changes (Agache 1995). To assess the whole skin behavior, it is preferable to use the 3-mm ring and a $2–10 \times 10^{-3}$ Nm torque (de Rigal and Lévêque 1985). On the volar forearm, a 0.028 Nm torque on a 5-mm wide skin ring makes the skin rotate (*Ue*) of 5.3° in children and 2.6° after the age of 70 (Agachel et al. 1980). Greater torques risk involving hypodermis resistance.

When one wants only the relative variation of the elastic modulus, that is ΔE/E, an approximation is given by the following formula: $\Delta E/E = -(\Delta Ue/Ue + \Delta e/e)$, where e and Δe are the skin thickness and its variation (Agache 1995). The measurement of the absolute value of E requires the additional calculations described below.

4.2 Conversion of Descriptive Parameters into Absolute Parameters

As in a suction test, the geometry of the skin deformation is known since the limits of this deformation are well-identified. It is therefore possible to get the absolute parameters of the deformation assuming that the skin is homogeneous and there is no shear gradient within the epidermis (which is wrong but useful). The formula describing the strain σ (N/m^2) and the relative elongation ε (%) on a point located at a distance d from the center of the disk are:

$$\sigma = -C/2\ \pi d^2 e \quad \varepsilon = -\sin\alpha/d^2\ \left(1/r^2 - 1/R^2\right)$$

where C (N · m) is the applied torque, R (meters) the radius of the plate, r (meters) the radius of the central disk, e (meters) the skin thickness, α (radians) the measured rotation angle (Courtesy of P. Vescovo, Laboratoire de Mécanique Appliquée, Besançon University, France).

Parameters are slightly different if the angle a is taken from *Ue* or *Uf*. Both choices are valid but must be indicated for obvious reasons.

The analysis of the viscous behavior and the description of the viscosity coefficient are described in Sect. 11.1.

5 Uniaxial Elongation

To interpret the results, it is necessary to consider the skin mechanical anisotropy and compare the direction of the elongation with Langer's lines. On the other hand, in this kind of test the limits of the stretched area are not known. Consequently, the calculation of the absolute parameters from raw data would be impossible. However, it has been shown that when the ratio width of jaws/sample length is equal or higher than four, the strained skin area is practically limited to the area in between the jaws (Stark 1980). Another way to work this problem out is to apply a finite elements model to the possibly stressed area (i.e., in between and beyond the jaws). This allows the deformation field to be computed over the whole deformed area for a given position and given dimensions of the jaws, whatever the mechanical properties of the tested material, and thus determining its absolute elastic parameters.

5.1 Repeat Creep Experiment

This technique uses the oldest commercialized device aimed at assessing the skin's mechanical behavior – the Gas-Bearing Electrodynamometer (GBE) (Gas-Bearing Electrodynamometer, manufactured on request by C.W. Hargens, registered professional engineer, 1006 Preston Road, Erdenheim, Pennsylvania 19038, USA). A small disk is glued to the skin and moved forward and backward with a periodicity of 1 Hz. The stretching of the skin is recorded on the abscissa and the applied force on the ordinate. Each cycle consists of extensions in opposite directions maintained for about 0.5 s each. Although the elongation is mostly elastic, a small viscoelastic deformation is generated during the cycle (hysteresis), and as a consequence the graphs of the cycles are superimposed ellipses (Fig. 5). The steepness of the slope of the ellipse is an indication of the skin stiffness, and the width of the ellipse indicates the capacity of the skin to undergo passive deformation. Both quantities were measured by their projection on the abscissa.

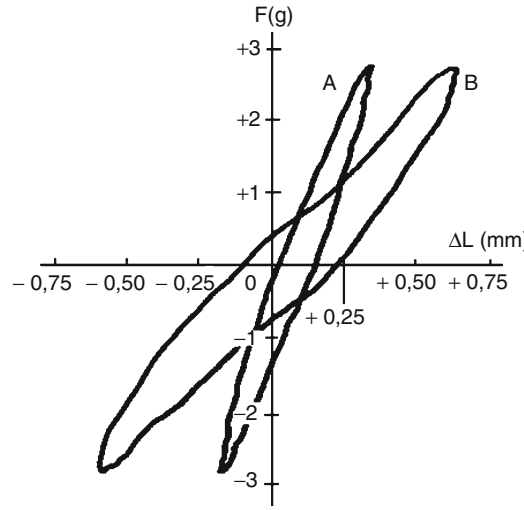

Fig. 5 Gas Bearing Extensometer. Dorsum of hand, RH 20 % ((Cooper et al. 1985), modified). F force (g), ΔL elongation (mm). *A* Before and *B* after water application. The decreasing overall slope together with the ellipse widening (hysteresis) stem from the stratum corneum's increased suppleness and decreased viscosity

The apparatus (Hargens 1981; Christensen et al. 1977) was made of two electromagnetic devices: one applies an intermittent traction force, and the other measures the movement back and forth. The shaft holding the disk at one extremity and placed on the skin is activated by a magnetic force and moves in a tube filled with air, without contact with its walls to avoid friction, hence the name of the apparatus. The disk is not glued directly on the skin, but is inserted into a small applicator that is attached to the skin by adhesive. It can be removed easily and used elsewhere. The applied forces keep the movement of the applicator to less than 1 mm in each direction. The stretched skin area is unknown. Parameters are therefore only descriptive.

Recently, the original device has been replaced by the newer Linear Skin Rheometer, which is based on the same principle but uses totally different equipment, both more sensitive and precise (Matts and Goodyer 1998; Matts 2002). The probe stuck to the skin transmits an oscillating force parallel to the surface at a frequency of about 0.33 Hz (each cycle lasts 3 s), and both the force and probe displacement (about 1 mm) are measured (3,000 pairs of points over each cycle). A connected computer controls the applied force through a feedback loop aimed at adjusting the force to the skin's response. The following equations are used to model the obtained loop:

$$F = F_{max} \sin \quad (t) \quad P = P_{max} \sin (t + T)$$

where F and P are the applied force and probe displacement, respectively, and T is the delayed displacement relative to force. It follows that the hysteresis area is obtained by the formula:

$$F_{max} \sin (t) P_{max} \cos (t + T)$$

The axis of the ellipse, indicating skin stiffness, is given by the ratio F_{max}/P_{max} and is called the *dynamic spring rate* (DSR) by the author. Conversely, P_{max}/F_{max} expresses skin softness.

Applied to ichthyotic skin, the GBE showed an increase of the slope of the ellipse and its narrowing, both phenomena revealing the dehydration of the stratum corneum. Inversely, the application of an emollient was followed by a lasting decrease of the slope and a widening of the ellipse. The same effect was even more marked when the stratum corneum was incised around the applicator, thus confirming the excellent sensitivity of the device to the behavior of this structure. However, different skin sites with identical stratum corneum did not yield the same results, which indicates that other layers of the skin are involved.

5.2 Acoustical Wave Propagation

Assuming that the skin is a thin membrane and the sound propagation is uniaxial, the dynamic Young's modulus is given by the formula $E = Dc^2$, where D is the density and c the sound propagation velocity.

The Reviscometer RVM 600 (Reviscometer RVM 600, *Courage & Khazaka*, Cologne, Germany) is a new device aimed at evaluating the mechanical behavior of the skin using ultrasound propagation. Two needle probes are placed on the skin 2 mm apart at a low and constant pressure. One emits an acoustic shock wave, the other is a receiver. The emitter-receiver traveling time of the signal is the measured parameter. The wave is acoustic in nature (not to be mistaken for a shear wave!), and is made of a series of unknown frequencies. As the sound propagation velocity remains independent of the frequency, the device should permit the calculation of the stratum corneum's dynamic Young's modulus rather than the overall skin modulus because of the higher velocity in the horny layer.

5.3 Progressive Extension

The Extensometer (The Extensometer, marketed by Cutech and the Stiefel Laboratories, is no longer available) had two pads that were fastened to the skin, one stayed fixed, and the other moved at a constant speed. The resisting force of the skin was measured versus time (Gunner et al. 1979). At first the 10 mm wide pads were 5 mm apart, the speed was 0.35 mm s^{-1} (3.5 % s^{-1}), and the maximum elongation was 4 mm. In uniaxial extension, the lateral limits of the stretched area are usually unknown, as seen earlier. However, the stretched skin area might lie exclusively between the pads if the ratio of pad width to sample length was greater than or equal to four (Stark 1980). With the Extensometer, this means that before extension the pads should have been separated by less than 2.5 mm. As that was not the case, it would have been impossible to have access to the elasticity fundamental parameters. Furthermore, since the extension is linear, a correct interpretation also needed to compare the direction of the traction with Langer's lines because the skin is mechanically anisotropic.

The actual deformation could nevertheless be known using the finite elements method. After having chosen a Poisson's ratio, the Young's modulus is calculated by the usual formula $E = F/e\,l^*\varepsilon$ where F is the force measured, ε the relative elongation measured, e the skin thickness, and l* the *equivalent width* of the sample measured by the finite elements method (Vescovo et al. 2000).

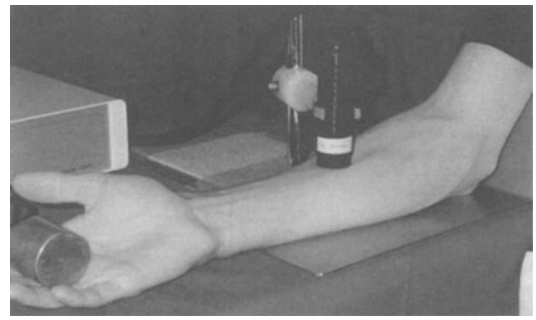

Fig. 6 Position of the forearm for a suction test

6 Skin Compressibility

6.1 Indentometry

Indentometry is the measurement of the depression caused in the skin by a small disk pushed down vertically. It can be performed only on body sites where the skin covers bones, or it would measure the compressibility of the underlying muscles (Piérard 1984). The graph of the deformation versus time is of creep type. Dikstein's prototype (Manny-Aframian and Dikstein 1995a) used a 10 g/cm^2 load (0.98 kPa) applied on the forehead for 10 s, resulting in a depression of about 0.5 mm. He found that between the ages of 20 and 70 the depression depth decreased but the difference was not significant. The same applied to Ur (80.5 % at the age of 20 compared to 65.5 % at 70). Edema reduced both parameters, while hydration of the stratum corneum had no effect.

Compressibility strongly differs from extensibility because the collagen bundles of the dermis are oriented structurally parallel to the surface and form a protective viscoelastic cushion against direct impacts. Consequently, indentometry mainly evaluates the capacity of the interstitial ground substance to be moved. This depends on its viscosity and the spaces available within the collagen network. To a lesser extent, the vertical stretching of the elastic fibers around the disk (Lanir et al. 1993) and the pressure in the interstitial tissue are also involved.

Lanir tried to define the geometry of the deformation and calculate the resistance resulting from the elastic structures and viscosity as well as the intrinsic parameters of compressibility (Lanir et al. 1990).

The technique was recently reexamined by Zahouani et al. (2002) through monitoring the penetration of a spherical indentor in the skin by means of a laser beam deflection measurement and recording the vertical force F_z. The maximum indentation depth during a loading–unloading cycle was 2,000 μm with a resolution of 0.07 μm, and the load range was 0.1–100 mN. The graph of the loading–unloading cycle at a constant velocity showed a hysteresis loop due to the viscoelastic nature of the skin.

Through the calculation of the radius a of the ball circle of contact with the skin at indentation depth * (Fig. 6), and considering that a is small comparatively to the radius R of the ball (very shallow indentation), the authors were able to compute the pressure on the ball along the radius a $(0 < r < a)$ and the absolute mechanical parameters: stress F and strain.

$$\sigma = \frac{3}{2\pi}\frac{F_z}{a^2}\left(1 - \frac{r^2}{a^2}\right) \text{ and } \varepsilon = 0,4\,\frac{a}{R}(\%)$$

Further treatment of the loading and unloading curves with the calculation of the strain velocity permitted the assessment of mechanical properties of the skin under compression and calculation of the elastic and viscous energy (Fig. 7).

An example of the mechanical response of the skin versus ageing is presented in Fig. 8 and Table 1. The table summarizes the parameters of two females (volar forearm) aged 27 and 51. The total energy dissipated over the cycle (W_T) was divided into its elastic (W_e/W_T) and viscous (W_v/W_T) fractions.

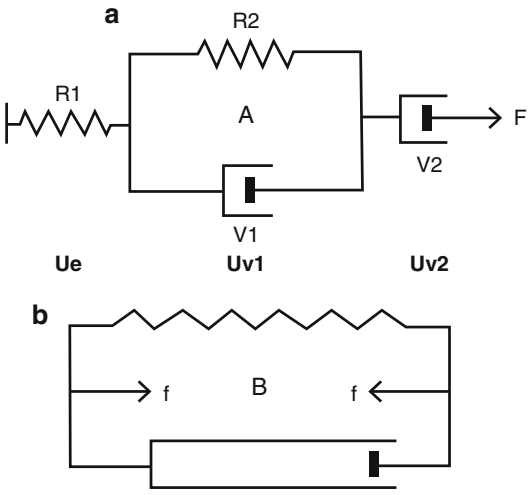

Fig. 7 Analogue models of the skin's mechanical behavior. A Kelvin-Voigt model of the extension process (situation before extension). Ue phase: R1 spring elongates alone. UV1 phase: R2 spring and V1 dashpot resist together. The V2 dashpot resists over the whole test duration. B Tentative model of the recovery process (situation before recovery). F external stretching force, f skin self-retraction force. During recovery the internal spring and dashpot oppose each other

Additionally, this indentation technique permitted the authors to describe the behavior of the skin surface adhesion force along the whole loading-unloading cycle, and to show the influence of this attractive force on the indentation parameters (Agache et al. 2004). It was also used to study the frictional properties of the skin surface (see ▶ Chap. 95, "Skin Mechanical Function").

6.2 Ballistometry

This technique (Ballistometer Dia-Stron Ltd, Unit 9, Focus 303, Business Centre, South Way, Andover, UK) records the successive rebounds of a light hammer falling with a given energy onto a surface (Adhoute et al. 1993; Hargens 1995). The kinetic energy can be transformed into rebound, deformation or heat. The more that is transformed into rebound, the more elastic the surface. Because of its kinetic energy, the hammer makes a small depression on the

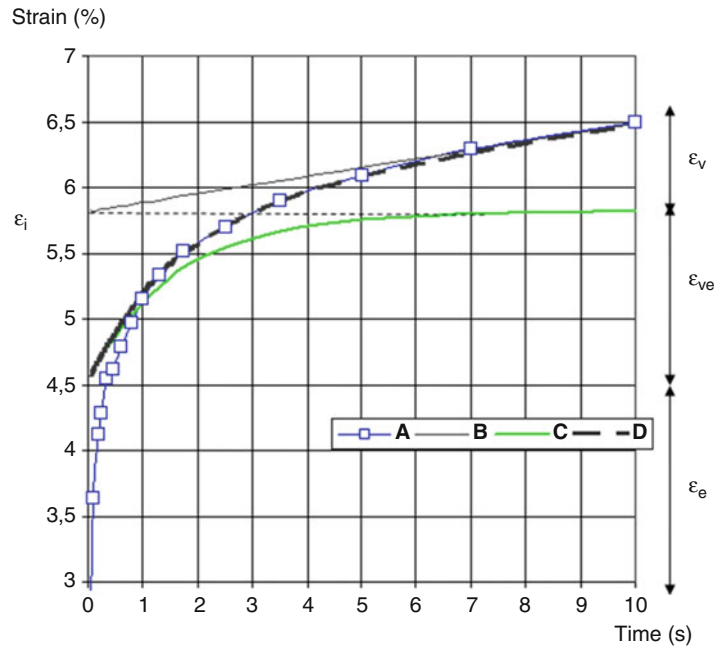

Fig. 8 Creep experiment data processing. Example of Sect. 11.1: each U has been replaced by its corresponding strain ε. *A* experimental curve, *B* straight line showing the purely viscous elongation over the whole experiment, *C* viscoelastic + viscous deformation over time curve: it exactly matches the A curve (except values before 1 s which are not valid: see text). *D* viscoelastic deformation over time curve, which equals the C curve after subtraction of the B line

Table 1 Influence of aging on indentation parameters (see Fig. 8)

Mechanical parameters	Subject A (27 years)	Subject B (51 Years)
Vertical load: F_z	60 mN	60 mN
Penetration depth: δ	2311 μm	1416 μm
Contact radius: a	3831 μm	2999 μm
Vertical stiffness: K_z	52 N/m	128 N/m
Compression Young's modulus E	7.1 kPa	21 kPa
Elastic fraction: W_e/W_T	90.7 %	81 %
Viscous fraction: W_v/W_T	9.3 %	19 %

skin (compression phase), but since the skin is elastic it sends the energy back to the hammer (restitution phase), hence the rebound. Obviously, the sent back energy is always lower than the initial one, because the deformation is associated with absorption of some energy due to skin viscosity. The height and duration of each rebound is therefore lower than the previous one.

The ballistometry's main parameter is the restitution coefficient $e = (h_2/h_1)^{0.5}$ where h_1 and h_2 are the first and second rebound heights. This ratio stays constant up to the last rebound: $dY/dn = -kY$. Hence, amplitudes of the rebounds are $Y = Y_0e^{-kn}$, where Y_0 is the height of the falling mass before the test, n the sequential rebound number, and k is the skin absorption coefficient (Adhoute et al. 1993).

The restitution coefficient depends on two factors: it is increased by the skin elasticity and decreased by the skin viscosity. The skin absorption coefficient *k* is closely related to the restitution coefficient *e*. Thus, only the first parameter is original, and since it does not depend on experimental conditions, it is more suitable for comparing the results from different laboratories. The hammer impact force on the skin is Moq/L, where Mo is "the hammer momentum", the angular displacement when the hammer reaches the skin surface level, and L is the hammer length. When it is plotted against the penetration depth of the hammer into the skin, a force-deformation curve equivalent to the ascendant part of Fig. 2 of this chapter is obtained (Pugliese and Potts 2002). It should not be mistaken for a stress–strain curve because neither stress (i.e., force divided by skin application area) nor strain (i.e., skin relative deformation) in the three coordinates is known. Consequently, intrinsic skin parameters cannot currently be calculated from ballistometry experiments.

The elastic response depends on the extent of the skin distension (the hammer penetration depth), and the viscous response is all the stronger when this distension is fast (Hargens 1995). From a practical viewpoint, it is advised to use low hammer falling speeds to reduce this viscous component and increase the amplitude of the rebounds, thus providing more accurate measurements. On the other hand, by modifying also the mass of the hammer it might be possible to dissociate and possibly measure the two components of the skin reactivity. Additional theoretical works are necessary to find out if this is possible (Hargens 1995).

In 1976, Tosti et al. (1977) were the first to evaluate the elasticity of the skin surface through its capacity to induce the rebound of a 0.5-g hammer falling from a 2-cm height. For a given body site, the restitution coefficient was found to be constant: 0.5 on the forehead, 0.6 on the dorsum hand, and 0.7 on the thigh. This ratio decreases noticeably with age (Tosti et al. 1977; Pugliese and Potts 2002). The same was observed with the amplitude of the first rebound (Fthenakis et al. 1991; Pugliese and Potts 2002). On the other hand, *k* ranged between 0.4 and 1.1 and increased with age (Adhoute et al. 1993).

7 Resistance to Skin Lifting

The technique, levarometry, measures the height of a lifted small disk affixed to the skin and pulled vertically. Dikstein's prototype (Manny-Aframian and Dikstein 1995b) measured the elevation of a 2.5-mm diameter disk with tractions between 5–40 g/cm^2 (0.5–3.9 pKa) for 10 s. The graph of the elevation versus time has a creep type. On the volar forearm, below 2.0 kPa, the elevation was lower in males, and on the forehead, it decreased with ageing regardless of the traction force. The Dikstein apparatus did not use any guard-ring, which allowed the adjacent skin to move up together with the disk.

Levarometry seems to be the simplest method to assess the mechanical behavior of the hypodermis because the skin sustains only a negligible stretch in the course of lifting. The limits of the area subjected to stress are not known; as a consequence, it is not possible to compute the absolute parameters. The device is not commercially available.

8 Identification of Langer's Lines

On all body sites, the skin tension is greater in the direction of Langer's lines (Langer 1978). These are responsible for the anisotropic deformation of incised or excised skin. An incision carried out along Langer's lines widens less and closing it requires less pull. This reflects the intrinsic tension of the skin, which is distinct from the additional tension induced by increases in volume of the underlying tissues, such as muscle contraction, edema, or a particular posture which stretches the skin. The identification of Langer's lines must, therefore, be made on relaxed skin.

8.1 Stark's Method

According to the definition, the direction of the maximum tension can be found by stretching the skin in several directions with an equal force – the direction of minimum elongation is that of Langer's lines. Stark developed a simple device comparable to a compass: two branches with claws at their extremities part spontaneously by 30 mm under the action of a 14.2 g/mm spring. He could measure the elongation of the skin into eight directions quickly, each measurement requiring only 1.5 s. This device is not commercially available (Stark 1977).

8.2 Borges' Method

This similar method is less accurate, but even quicker, and consists of creasing the skin between the thumb and the index in all directions until the furrows are regular and parallel. They follow Langer's lines. In the other directions, they are impeded by the skin tension that makes them irregular (Borges 1989).

8.3 Barbenel's Method

The measurement of the extensibility of the skin using the suction method is valid only if slippage of the skin into the suction chamber is prevented. If, inversely, this movement is facilitated, the most extensible direction of the skin will appear easily, that is to say perpendicularly to Langer's lines. If the contour of the chamber is drawn in during suction, when the chamber is removed, an oval outline is observed instead of a circle and its main axis corresponds to Langer's lines (Barbenel 1995).

8.4 Skin Microrelief

Apart from the palms and soles, the skin microrelief is made of plateaus separated by valleys. The latter are roughly parallel and orientated in two or three directions, and this layout is characteristic of each body area. The direction of the deepest valleys matches Langer's lines. There may be one or two other preferential

directions, indicating an ordered nonorthogonal mechanical anisotropy. This method has an advantage over the others as it is insensitive to extrinsic skin tensions. Its physiological interpretation is simple. The cutis is normally retracted (skin tension) and extensible, whereas the epidermis has none of these properties. Therefore, the epidermal creasing responsible for the microrelief appears to be a transformation of tension allowing the creases to be flattened by stretching them. The superficial dermis, an intermediary zone between epidermis and cutis, is precisely the place where the skin relief begins. This mechanical transduction is one of its functions (Pierard et al. 2003).

8.5 Acoustical Shockwave Propagation Velocity

As the propagation velocity of a shear stimulus within the skin is direction dependent (Vexler et al. 1999), one may assume that it also holds true for acoustic waves. Consequently, the skin mechanical anisotropy can be assessed using the Reviscometer (see Sect. 5.2), which measures the propagation velocity of an acoustic shockwave along 2 mm in four directions (Nizet et al. 2001).

9 Conditions for a Reliable Measurement

- In suction, torsion, and extension methods, it is necessary to take care that the skin does *not* slip at all into or under the device. Hairs should be shaved, sweating prevented, and any trace of ointment removed. Although the adherence of double-sided adhesive tapes is higher than the low forces exerted on the skin surface, it has to be checked. The use of cyanoacrylate glue ensures that the skin does not move. When publishing, it is recommended to mention with precision the type of adhesive used. Anyway, testing the adhesive device (Tokumura et al. 1999) is mandatory.
- The weight of the measuring apparatus may considerably alter the mechanical behavior of the skin. It should, therefore, be cancelled out, for example by a bracket holding the device so that it only touches the skin. If this is not the case, the pressure on the skin has to be indicated. The Cutometer must always be used exerting the pressure recommended by the manufacturer (Asserin et al. 1994).
- The part of the apparatus which is in contact with the skin must be parallel or perpendicular to the skin, according to the type of method. Any deviation introduces a significant error.
- The subject's posture is a possible factor of exogenous skin tension (adding to its endogenous tension). Unless it is intended to measure this additional tension, the mechanical test should be performed on relaxed skin (Fig. 6). However, the skin must not be crinkled as extension could then be mistaken for flattening out.
- The behavior of the skin is sensitive to the temperature and relative humidity of the test room. These must be indicated. Mechanical tests should be performed after a 20 min wait in the room or in similar conditions, so that the skin and the whole body have time to adapt their behavior to these conditions (for example, vasoconstriction induced by the cold may alter the test results' generalizability). The subject should be in comfortable thermal conditions.
- For repetitive tests at the same site, the tested area should be delineated with precision because the skin behavior may not be identical a few millimeters further away.

10 Conditions for a Correct Interpretation

Most devices measure deformation (Ue, etc.) versus force. Evidently *deformation* and *elongation* are not synonyms. However, deformation is sometimes mistaken for relative elongation, which is also called the strain in mechanics.

Relative elongation ε is measured as a percentage of the initial length. Stress σ, which is measured in pascals, is the force divided by the section of skin involved and requires the measurement of the skin thickness. Only these parameters describe the intrinsic mechanical behavior of the skin.

10.1 Definition of the Object of the Research

- If only comparisons are to be made, the measurement of the different deformations and their interrelations is sufficient (e.g., age-related evolution of Ur/Ue (Escoffier et al. 1989) or softening effect of a topical preparation on the stratum corneum (de Rigal and Lévêque 1985)).
- If the study of the change in skin intrinsic behavior (e.g., the elasticity modulus) is also the objective of the study, it is necessary to measure the skin thickness and use the formula: $\Delta E/E = -(\Delta Ue/Ue + \Delta e/e)$, where e and Δe are the skin thickness and variation. An example is the comparison of skin extensibility in Ehlers-Danlos and Marfan syndromes and healthy skin (Bramont et al. 1988).
- Finally, if intrinsic parameters are researched, several tests have to be performed with increasing forces. For each force it is necessary to calculate: the relative elongation, stress, and relaxation time; then, the elasticity modulus E (or shear modulus G); and the viscosity η versus stress. The help of an engineer or physicist may be useful.
- For uniaxial measurements, the skin mechanical anisotropy must be considered, and tests should preferably be performed parallel and perpendicular to Langer's lines. In any case, the direction of the extension in relation to these lines must be known.
- In a mechanical test, the first extension is more important than the following ones for an identical stress. The reason is a small residual deformation is caused by the previous mechanical constraint, even if it is not recent. Preconditioning the skin consists of repeating the test at least four times in a row so as to eliminate any trace of this unknown previous action and begin the mechanical study in reproducible conditions. Nevertheless, it is possible to study the skin without preconditioning since it is its spontaneous state, even though there is a risk of higher variability. However, mechanical tests should not be conducted in subjects who have exercised intensely in the previous 24 h because their skin may remain abnormally conditioned.
- Knowing the limits of the method is essential for accurate interpretation. For example, the use of an 8 mm diameter suction chamber is more likely to give the measurement of the mechanical resistance of the skin and hypodermis as a whole (Fig. 4) rather than the skin alone.

11 Skin Structure-Rheology Relationships

As mentioned in the introduction, one of the objectives of mechanical function investigations is to obtain data on the mechanical properties of the skin, and further, on the origin of the observed data in terms of intracutaneous structural behavior.

11.1 Searching for Intrinsic Mechanical Properties

11.1.1 Analysis of the Extension Phase

The extension phase is characterized by the opposition between an applied external force and the joint resistance of the elastic and viscous components of the tissue. The Fig. 7a analogue model is used for its analysis. Spring R1 is responsible for the resistance to the immediate deformation Ue (because of the suddenness of the force, no viscous deformation has time to occur); a second spring R2 is responsible, together with the viscosity, for the resistance to deformation in the course of the curvilinear

phase Uv1. Viscosity is represented by dashpots, the first one V1 is extended during Uv1; the second one V2 is deformed during the rectilinear phases Uv2.

Intrinsic Properties of Elastic Structures. The intrinsic properties of elastic structures are computed from the loading phase only. The elasticity modulus E (pascals) in extension experiments and the shear modulus G (pascals) in torsion experiments are the main parameters. In a suction test, E is obtained by the formula (Agache et al. 1992, 1995): $E = (1 - \nu)\sigma/\varepsilon$ where σ is the strain, ε the relative extension, ν the Poisson's ratio chosen arbitrarily at 0.4 (slight increase in volume) or 0.5 (no change in volume) (see ▶ Sect. 2.4 in Chap. 95, "Skin Mechanical Function"). The shear modulus G is obtained by the formula: $G = C(1/r^2 - 1/R^2)/4\pi e \sin\alpha$, where C(N · m) is the applied torque, e(m) the skin thickness, r and R(m) the radiuses of the disk and the guard ring, and α (radians) the rotation angle measured. The formula $E = 2G(1 + \nu)$ permits the shifting from one modulus to the other assuming that the skin is homogeneous and isotropic (an incorrect assumption although acceptable in this particular case).

In a creep experiment using a 0.4 bar suction maintained for 2 s, the average elasticity modulus on the forearm of 20 subjects aged 25.5 ± 2.1 was found to be 814 kPa (Agache et al. 1992). To find out Young's modulus E_0, which is the intrinsic stiffness of the skin if its natural tension was cancelled (i.e., its elastic structures fully recoiled), it is necessary to perform several creep tests with increasing forces and draw the curve of the elasticity moduli versus the stresses. An ascending straight line is then obtained: its intercept with the ordinate is E0; the negative intercept with the abscissa σ_0 is the natural tension of the skin in resting conditions; and the slope m (without dimensions) measures the intrinsic behavior of the elastic structures of the skin, that is to say their stiffening according to the stress they sustain.

In the course of a progressive traction test using the Kelvin-Voigt model, the deformation would stem almost exclusively from the extension of the spring R1, provided that each step of the increasing suction was short enough to give the dashpots V1 and V2 no time for stretching; making the final deformation similar to the added Ue of creep tests. Conversely, if the stepwise increasing suction is lengthy, then a viscous deformation has time to take place and the observed deformation would be similar to the added Uf of creep tests. For each stress σ and relative extension ε, E is calculated, then the graph of E versus σ is drawn – it is usually an ascending straight line. The extrapolation for $\sigma = 0$ gives the Young's modulus E_0. In a study on 24 subjects aged between 60 and 70, Barel et al. (1998) found that for a depression between 0.15 and 0.5 bar E stayed apparently constant ($E = E_0$) and was about 146 kPa in the volar forearm, 214 kPa in the forehead, and 272 kPa in the temporal areas. These figures seem rather low. This could be due to a low suction increasing rate which let a viscous deformation take place (through the dashpots) and so diminishes the contribution of the springs. Using another device and another analogue model, Diridollou et al. found E = 120 kPa in volar forearm and 230 kPa in forehead (Diridollou et al. 2000b). The forehead values, as found by Barel (Barel et al. 1998) and Diridollou (Diridollou et al. 2000b), although congruent, may be too high because at this location the subcutis is much less developed than in the forearm and might oppose some resistance to the skin bulging. This should be checked before accepting these results.

Intrinsic Properties of the Viscous Flow. The physical parameter is the viscosity coefficient η (in poise = $N \cdot s/m^2 = Pa \cdot s$), which increases with the viscosity of the material.

In the course of a protracted *creep test*, the total viscous deformation is expressed by the equation $Uf - Ue = Uv(1 - e^{-t/\tau}) + At$ (Vlasblom 1967), where $Uv(1 - e^{-t/\tau})$ corresponds to Uv_1 (the curved part of Uv), which represents the joint extensions of the spring R2 and the dashpot V1. While At corresponds to Uv_2 (the straight part of Uv) and the elongation of the dashpot V2 during the entire duration of the application of the force (Fig. 7a). Obviously this model is wrong if

$t = \infty$, but it is valid for mechanical tests of normal duration. There is no globally accepted criterion for defining the limit between Uv_1 and Uv_2. A priori, it may be assumed that in a creep test lasting at least 10 s, the last 5 s apply to the purely viscous phase and the first five to the viscoelastic phase.

For the calculation of the intrinsic properties, it is first necessary to convert the descriptive parameters (U and F) of each measurement point into absolute parameters (ε and σ) using the formulas mentioned in Sect. 3.3. One may assume that the skin does not become thinner significantly and thus that the stress σ remains constant over the whole test. As seen in Fig. 8, the total relative deformation ε_t (curve A) is the sum of the deformations ε_e (purely elastic, instantaneous), and ε_{ve} (viscoelastic, curve C), and ε_v (purely viscous, straight line B). Only ε_t is known.

First, ε_v is calculated (Fig. 8, straight line B). Using the ε values at the longest times (for example from 6 to 10 s) the slope of ε versus time (parameter A of the global equation), and intercept (ε_1) are determined. Dividing the stress σ by the slope gives the viscosity η_2 of the dashpot V2. On the other hand the intercept ε_i is the sum: $\varepsilon_e + \varepsilon_{ve}$. (Fig. 8).

The viscoelastic deformation ε_{ve} is then measured at shorter times (for example between 2 and 5 s). It is given by the formula: $\varepsilon_i - \varepsilon_{ve} = (\varepsilon_i - \varepsilon_e) \exp - t/\tau$, or: $\ln(\varepsilon_i - \varepsilon_{ve}) = \ln(\varepsilon_i - \varepsilon_e) - t/\tau$.

This function is a descending straight line whose slope is $1/\tau$ and intercept $\ln(\varepsilon_i - \varepsilon_e)$. As a result, ε_e is found, and also $E2/\eta 1 = t/\tau$. The elasticity moduli of the springs R1 (E_1) and R2 (E_2) are then calculated as follows: $E_1 = (1 - \nu)\sigma/\varepsilon_e$, and $E_2 = (1 - \nu)\sigma/\varepsilon_{ve}$. Since E_2 is known, η1 can be obtained.

By using a Cutometer with a 4-mm diameter probe and a 400-mbar suction on the volar forearm, and arbitrarily taking a 1-mm skin thickness and a Poisson's ratio $\nu = 0.4$, the following values are found: $E_1 = 1.09$ MPa, $E_2 = 3.40$ MPa, $\eta 1 = 4.5$ MPa · s, and $\eta 2 = 110$ MPa · s. With the Cutometer, deformation measurements must not be done before 1 s (suction loading time).

In a torsion creep test or in a progressive traction test, the calculations are much more complex. Using a progressive loading–unloading test, Diridollou et al. (2000b) have computed an "unrestored energy ratio" which reflects the extent of recovery at the end of the test.

11.1.2 Analysis of the Recovery Phase

To our knowledge, analysis of the recovery phase has not yet been done although it is rich in information. To begin with, modeling of the extension phase must be completed by a spring in parallel, which would be the responsible component of even delayed total recovery. The simplest model possible is shown in Fig. 7b. Additional studies seem therefore necessary before this phase can be used to investigate the intrinsic properties of the skin. Similar problems occur for torsional measurements and progressive extension tests.

11.2 Connections between Intrinsic Parameters and Biology

What is the biological counterpart of mechanical parameters? It looks as if skin elastic structural elements (springs) were interwoven with others slowing down their extension and recoil (dashpots).

- The *springs* include, among others:
- The dermal elastic network (number of fibres involved and their stiffness)
- The curvature of collagen bundles (number of curvatures involved and their stiffness)
- The skin relief (especially the folding of the stratum corneum)

These three types of springs are parallel. Current tests measure their behavior as a whole. However, it should soon be possible to measure them separately and to get access to their intrinsic parameters (see (Panisset 1992; Agache et al. 1995; Wijn et al. 1981)). In the example mentioned at the end of the preceding paragraph,

one may imagine that E_1 reflects the behavior (force × density) of the elastic network, and E_2 the much higher stiffness values of the woven collagen network together with the stratum corneum rigidity.

- The absorbing systems include, especially:
  - The viscosity of the interstitial ground substance (role of the proteoglycans)
  - The difficult flow of the liquids inside the fibre network (because of its tightness, for example)
  - The interstitial pressure (the interstitial liquids expelled in the course of torsion and especially compression must move against it)
  - Friction between proteins and other large molecules

In the example of Sect. 11.1, η1 likely represents the above mentioned absorbing systems, and η2 is 24 times more resistant to the gradual dissociation of the dermo-epidermal junction (a suction at this value induces a suction blister in 1 h). The measurement of the absolute parameters of these phenomena is thus of obvious interest.

- Examples of possible weakening of the springs (Ue would increase):
  - Softening effect of emollients on the stratum corneum (de Rigal and Lévêque 1985)
  - Lower quantity and stiffness of collagen (Ehlers Danlos type 2) (Bramont et al. 1988)
- Examples of possible strengthening of the springs (Ue would decrease):
  - Higher quantity and stiffness of collagen (systemic sclerodermia) (Agache and Humbert 1993)
  - Elastic fiber regeneration (effect of retinoids on corticosteroid atrophy) (de Lacharriere et al. 1990)
  - More numerous elastic fibers along Langer's lines (Wijn et al. 1981)
  - Global thickening of the skin (changes from childhood to adulthood) (Agachel et al. 1980)
  - After the age of 65, despite the thinned skin, Ue does not increase, revealing the increase of E (Escoffier et al. 1989)
- Examples of possible increase of viscosity (Uv would decrease):
  - Scleromyxoedema (Pierard 1993)
  - Tightening of the collagen network (change from childhood to adulthood) (Escoffier et al. 1989)
- Examples of possible decrease of viscosity (Uv would increase):
  - Decrease of glycosaminoglycans after the age of 60
  - Decrease of oedema (Piérard-Franchimont et al. 1998)

12 Selecting the Appropriate Method

- Use devices providing recognized variables for the deformations – for creep tests that is: *Ue, Uv, Uf, Ur* (Sanders 1973), *Ua* (Barel et al. 1998), *Ud* (proposed here), and *R*; and for ballistometry, the restitution coefficient.
- To guarantee reliance and absence of shift, devices should be checked and calibrated regularly.
- The variations of the mechanical behavior of the stratum corneum are more easily assessed by devices that include a probe attached to the skin because in such cases the force is maximal at the surface. Whatever the apparatus, it is necessary to utilize small probes (chamber of 2-mm diameter for the Cutometer, 1-mm wide skin ring for the Dermal Torque Meter). The smaller the surface involved, the more important the role of the stratum corneum in the deformation because the ratio of stratum corneum thickness to involved surface area increases. Owing to the large diameter of its probe (10 mm) the Dermaflex A is less sensitive to variations of the stratum corneum

rigidity. Ballistometry is barely capable of detecting them.
– The acquisition of a skin thickness measuring device depends on the objectives. It is needed if absolute parameters and intrinsic properties are wanted, but not for comparative studies in the same individual, when the skin thickness is supposed to stay constant.

13 Progress in Methodology

In conclusion, we mention technological development in skin biomechanics because it is a new and barely mature domain in dermatological science. Achieving a prototype that allows quantitative data to be gathered is a valuable first step, even if the parameters used are purely descriptive and exclusive to this device. It is then possible to carry out tests on products and follow the courses of some diseases. Many prototypes developed in laboratories had and still have this function. A second important stage is to put the device on the market, which is usually a guarantee of soundness and reliability. Compared to prototypes, commercialized equipment have the advantage of being tested and used by everybody, hence they facilitate comparisons between laboratories and the use of the same parameters by all the investigators. Up to now most published papers use purely descriptive (phenomenological) mechanical parameters which depend on the device. However, using skin thickness measurement and simple calculations, absolute and universal mechanical parameters, those of physics, can be obtained, which allows linking the mechanical *behavior* of the skin with its intrinsic *properties*. The latter depend neither on the measurement method, nor on the apparatus. This advance in methodology will contribute to the expansion of the skin mechanical functions assessment and foster its use in clinical medicine in the near future.

References

Adhoute H, Berbis E, Privat Y. Ballistometric properties of aged skin. In: Lévêque JL, Agache P, editors. Aging skin: properties and functional changes. New York: Marcel Dekker; 1993. p. 39–48.

Agache P. Twistometry measurement of skin elasticity. In: Serup J, Jemec GBE, editors. Handbook of non-invasive methods and the skin. Baca Raton: CRC Press; 1995. p. 319–28.

Agache P, Humbert P. Moyens objectifs d'évaluation de la sclérose cutanée. Objectif Peau. 1993;1:117–22.

Agache P, Varchon D, Humbert Ph, Rochefort A. Non invasive assessment of biaxial Young's modulus of human skin in vivo (Poster). In: 9th International Symposium on Bioengineering and the skin; 1992 Oct 19–20; Sendai; 1992.

Agache P, Panisset F, Varchon D, Humbert Ph. Mesure du module d'Young du stratum corneum et du derme humain in vivo. In: XXème Congrès Soc Biomécanique; 1995 Sept 11–12; Lausanne; 1995. Arch Physiol Biochem C81(Abstract).

Agachel P, Monneur C, Leveque JL, de Rigal J. Mechanical properties and Young's modulus of human skin in vivo. Arch Dermatol Res. 1980;269:221–32.

Agache P, Elkyhat A, Mavon A, Measurement of skin surface wettability. In: Handbook of Measuring the skin. 1st edn. Berlin: Springer; 2004. p. 87–94.

Asserin J, Agache P, Humbert Ph. Checking the mechanical performance of a skin suction meter: the Cutometer (Poster). In: 10th International Symposium of Bioengineering and the Skin; 1994 June 13–15; Cincinnati; 1995; Congrès Annuel de Recherche Dermatologique; 1994 Oct 27–29; Lyon; and J Invest Dermatol 104:165 (Abstract).

Barbenel JC. Identification of Langer's lines. In: Serup J, Jemec GBE, editors. Handbook of non-invasive methods and the skin. Boca Raton: CRC Press; 1995. p. 341–4.

Barel AO, Lambrecht R, Clarys P. Mechanical function of the skin: state of the art. In: Elsner P et al., editors. Skin bioengineering techniques and applications in dermatology and cosmetology. Basel: Karger; 1998. p. 69–83.

Borges AF. Relaxed skin tension lines. Dermatol Clin. 1989;7:169–77.

Bramont C, Vasselet R, Rochefort A, Agache P. Mechanical properties of the skin in Marfan syndrome and Ehlers-Danlos syndrome. Bioeng Skin. 1988;4:217–27.

Christensen MS, Hargens CW, Nacht S, Gans EH. Viscoelastic properties of intact human skin: instrumentation, hydration effects, and the contribution of the stratum corneum. J Invest Dermatol. 1977;69:282.

Cooper EP, Missel PJ, Hannon DP, Albright GB. Mechanical properties of dry, normal and glycerol-treated skin, as measured by gas bearing electrodynamometer. J Soc Cosmet Chem. 1985;36:335–47.

Cua AB, Wilhelm KP, Maibach HI. Elastic properties of human skin: relation to age, sex, and anatomical region. Arch Dermatol Res. 1990;282:283–8.

de Lacharriere O, Escoffier C, Gracia AM, Teillac D, Saint Léger D, Berrebi C, Debure A, Leveque JL,

Kreis H, De Prost Y. Reversal effects of topical retinoic acid on the skin of kidney transplant recipients under systemic corticotherapy. J Invest Dermatol. 1990;95:516–22.

de Rigal J, Lévêque JL. In vivo measurement of the stratum corneum elasticity. Bioeng Skin. 1985;1:13–23.

Diridollou S, Berson M, Black D, Gregoire JM, Patat E, Gall Y. Subcutaneous fat involvement in skin deformation following suction. In: 12th International Symposium on Bioengineering and the Skin and Joint ISBS/DCES Poster Sessions; 1998 June 25–27; Boston; 1998.

Diridollou S, Patat F, Gens F, Vaillant L, Black D, Lagarde JM, Gall Y, Berson M. In vivo model of the mechanical properties of the human skin under suction. Skin Res Technol. 2000a;6:214–21.

Diridollou S, Black D, Lagarde JM, Gall Y, Berson M, Vabre V, Patat F, Vaillant L. Sex- and site-dependent variations in the thickness and mechanical properties of human skin in vivo. Int J Cosmet Sci. 2000b;22:421–35.

Escoffier C, de Rigal J, Rochefort A, Vasselet R, Lévêque J-L, Agache P. Age-related mechanical properties of human skin: an in vivo study. J Invest Dermatol. 1989;93:353–7.

Flores J, Berman B, Burdick A, Jonusas AM. The effectiveness of a new method for assessing induration. J Am Acad Dermatol. 1998;39:1021–2.

Fthenakis CG, Maes DH, Smith WP. In vivo assessment of skin elasticity using ballistometry. J Soc Cosmet Chem. 1991;42:211–22.

Gniadecka M, Serup J. Suction chamber method for measurement of skin mechanical properties: the Dermaflex. In: Serup J, Jemec GBE, editors. Handbook of non-invasive methods and the skin. Boca Raton: CRC Press; 1995. p. 329–34.

Gunner CW, Hutton WC, Burlin TE. The mechanical properties of skin in vivo: a portable hand-held extensometer. Br J Dermatol. 1979;100:161–3.

Hargens CW. The gas bearing electrodynamometer (GBE) applied to measuring mechanical changes in skin and other tissues. In: Marks R, Payne PA, editors. Bioengineering and the skin. Lancaster: MTP-Press; 1981. p. 113–22.

Hargens CW. Ballistometry. In: Serup J, Jemec GBE, editors. Handbook of non-invasive methods and the skin. Boca Raton: CRC Press; 1995. p. 359–66.

Haüselman H, Huber K, Seifert B, Michel B. The Dermagraph in patients with systemic sclerosis and in healthy volunteers. In: Elsner P, Berardesca E, Wilhelm KP, Maibach HI, editors. Bioenginering of the skin: skin biomechanics. Boca Raton: CRC Press; 2002. p. 123–38.

Langer K. On the anatomy and physiology of the skin. 1: the cleavability of the cutis (English trans: Gibson T). Br J Plast Surg. 1978;31:3–8.

Lanir Y, Dikstein S, Hartzshtark A, Manny V. In vivo indentation of human skin. J Biomech Eng. 1990;112:63–9.

Lanir Y, Manny V, Zlotogorsky A, Shafran A, Dikstein S. Influence of ageing on the in vivo mechanics of the skin. Skin Pharmacol. 1993;6:223–30.

Manny-Aframian V, Dikstein S. Indentometry. In: Serup J, Jemec GBE, editors. Handbook of non-invasive methods and the skin. Boca Raton: CRC Press; 1995a. p. 349–52.

Manny-Aframian V, Dikstein S. Levarometry. In: Serup J, Jemec GBE, editors. Handbook of non-invasive methods and the skin. Boca Raton: CRC Press; 1995b. p. 345–8.

Matts PJ. The gas-bearing electrodynamometer and linear skin rheometer. In: Elsner P, Berardesca E, Wilhelm KP, Maibach HI, editors. Bioenginering of the skin: skin biomechanics. Boca Raton: CRC Press; 2002. p. 99–109.

Matts PJ, Goodyer E. A new instrument to measure the mechanical properties of human stratum corneum in vivo. J Cosmet Sci. 1998;49:321.

Nizet JL, Piérard-Franchimont C, Piérard GE. Influence of body posture and gravitational forces on shear wave propagation in the skin. Dermatology. 2001;202:177–80.

Overgaard Olsen L, Jemec GBE. The influence of water, glycerin, paraffin oil and ethanol on skin mechanics. Acta Derm Venereol. 1993;73:404–6.

Panisset F. Le stratum corneum: sa place dans la fonction mécanique de la peau humaine in vivo. Thèse de Pharmacie, Besançon, N°2592039; 1992.

Piérard GE. Évaluation des propriétés mécaniques de la peau par les méthodes d'indentation et de compression. Dermatologica. 1984;168:61–6.

Pierard GE. Mechanical properties of aged skin: indentation and elevation experiments. In: Lévêque JL, Agache P, editors. Aging skin: properties and functional changes. New York: Marcel Dekker; 1993. p. 49–56.

Piérard GE, Uhoda I, Piérard-Franchimont C. From skin microrelief to wrinkles: an area ripe for investigation. J Cosmet Dermatol. 2003;2(1):21–8.

Piérard-Franchimont C, Letawe C, Fumal I, Van Cromphaut I, Pierard GE. Gravitational syndrome and tensile properties of skin in the elderly. Dermatology. 1998;197:317–20.

Pugliese PT, Potts JR. The ballistometer. In: Elsner P, Berardesca E, Wilhelm KP, Maibach HI, editors. Bioenginering of the skin: skin biomechanics. Boca Raton: CRC Press; 2002. p. 147–59.

Sanders R. Torsional elasticity of human skin in vivo. Pflugers Arch. 1973;342:255–60.

Serup J. The Dermalab. In: Elsner P, Berardesca E, Wilhelm KP, Maibach HI, editors. Bioenginering of the skin: skin biomechanics. Boca Raton: CRC Press; 2002. p. 117–21.

Stark HL. Directional variations in the extensibility of human skin. Br J Plast Sur. 1977;30:105–14.

Stark HL. An interpretation of the initial low-stiffness phase of the in vivo load extension relationship for human skin. Eng Med. 1980;9:184–8.

Tokumura F, Ohyama K, Fujisawa H, Suzuki M, Nukatsuka H. Time-dependent changes in dermal peeling force of adhesive tapes. Skin Res Technol. 1999;5:33–6.

Tosti A, Compagno G, Fazzini ML, Villardita S. A ballistometer for the study of the plastoelastic properties of skin. J Invest Dermatol. 1977;69:315–7.

Vasselet R, Agache P. Perspectives de modélisation des propriétés mécaniques de la peau humaine in vivo. In: Vasselet R, editor. Étude in vitro des propriétés mécaniques du stratum corneum humain à partir des essais de traction–relaxation et fluage: identification de son comportement viscoélastique à un modèle rhéologique non linéaire avec écrouissage. Thèse Sciences pour l'Ingénieur, Besançon; 1987. pp 213–233.

Vescovo P, Jacquet E, Burtheret A, Varchon D, Coral H, Humbert PH. Méthodologie expérimentale sur matériaux biologiques: application à la peau humaine. In: Mécano-transduction, matériaux et structures des sciences de l'ingénieur et du vivant. Paris: Tec et Doc; 2000. pp. 317–24.

Vexler A, Polyansky I, Gorotletsky R. Evaluation of skin viscoelasticity and anisotropy by measurement of speed of shear wave propagation with viscoelasticity skin analyzer. J Invest Dermatol. 1999;113:732–9.

Vlasblom DC. Skin elasticity. PhD Thesis, University of Utrecht; 1967

Wijn PFF, Brakkee AJM, Kuiper JP, Vendrik AJH. The alinear viscoelastic properties of human skin in vivo related to sex and age. In: Marks R, Payne PA, editors. Bioengineering and the skin. Lancaster: MTP Press; 1981. p. 135–46.

Zahouani H, Pailler-Mattei C, Vargiolu R, Abellan MA. Assessment of the elasticity and tactile properties of the human skin surface by tribological tests. In: Proceedings oral papers. Vol. 2. 22nd IFSCC Congress; 2002 Sept; Edinburgh; 2002.

The Durometer Measurement of the Skin: Hardware and Measuring Principles

97

Salvatore Panduri, Valentina Dini, and Marco Romanelli

Contents

Keywords
Durometer • Skin hardness • Morphea • Lipodermatosclerosis • Venous disease • Neurophatic foot • Shore units (SU) scale

1 Introduction

1.1 The Measuring System

The first instrument used to assess skin hardness was a Rex® durometer (model 1700, Rex Gauge Company, Inc., Glenview, IL). This instrument is the international standard for measuring the hardness of rubber, plastic, nonmetallic materials, and soft tissue such as skin. The durometer is a portable hand-held device, which is provided with a calibrated gauge that registers linearly the relative degree of hardness on a scale of units divided from 0 to 100 shore units (SU) scale (Fig. 1). This feature is the result of a spring-loaded interior that senses hardness by applying an indentation load on the specimen. The bottom of the durometer has a small, dull indentor which is retractable and is responsible for the measurements registered on the gauge (Fig. 2). The instrument is rested by gravity against the skin and must be held in a vertical position. Initial hardness is defined as that recorded within 1 s of firm contact of the durometer with the skin. For many materials, this initial reading remains unaltered after the first second of measurement (near perfect elasticity). Imperfect elasticity is referred to as plasticity

S. Panduri • V. Dini • M. Romanelli (✉)
Department of Dermatology, University of Pisa, Pisa, Italy
e-mail: m.romanelli@med.unipi.it

P. Humbert et al. (eds.), *Agache's Measuring the Skin*,
DOI 10.1007/978-3-319-32383-1_131

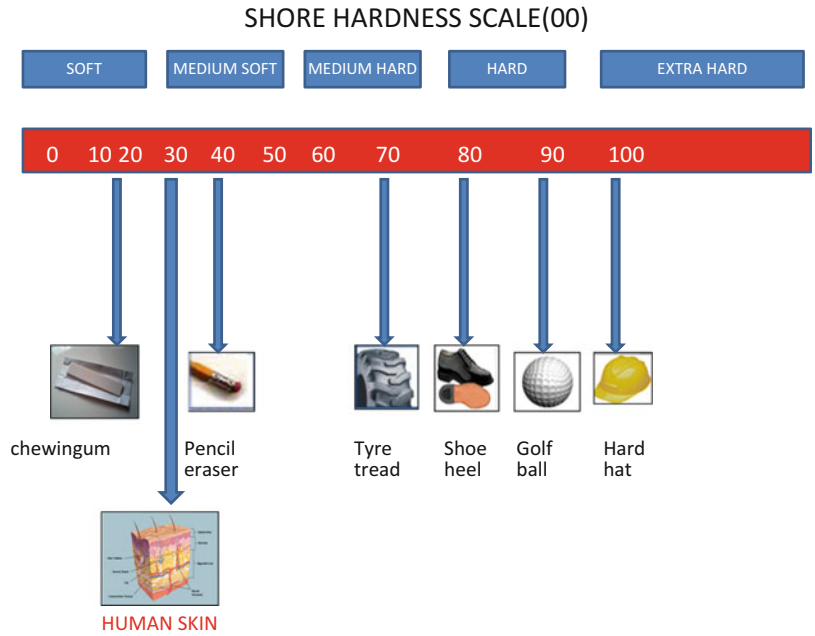

Fig. 1 shore hardness scale

Fig. 2 durometer

and is observed when continued contact of the durometer with the surface leads to a higher reading. The degree of this plasticity is referred to as "creep," and in animal tissue the amount of creep is minimal. The type of durometer used in dermatology to assess skin hardness is Model 0, which is provided with an 822 g springload. To eliminate operator error, the company has improved the first model with a specified amount of weight (400 g), located on top of the instrument, which is used to depress the indentor without any additional pressure. This constant load principle provides a more consistent reading to the operator every time the gauge is applied to the skin. For measurements on the skin, the durometer is used at 25 °C and four consecutive readings are usually taken at the same site. Between readings, the durometer is reset to 0 and measurements are made with the patient supine, thus avoiding muscle tension or contraction.

1.2 Accuracy and Reproducibility of the Measurements

Durometer readings obtained with four consecutive determinations at the same site in each subject and in different clinical conditions differed constantly by less than 5 % (Falanga and Bucalo 1993; Aghassi et al. 1995). The durometer was tested for interobserver and intraobserver

variability in a study (Seyger et al. 1997) where patients with morphea, a localized form of scleroderma, were investigated for skin induration. The durometer was used in combination with a skin scoring system called MSS (modified skin score) (Zachariae et al. 1994). The interobserver variability in the durometer score was only 0.5 % and was even lower than the interobserver variability of the MSS (0.5 vs. 2.2 %). The intraobserver variability, which is the variation in readings obtained by the same observer, was estimated as 0.5. Insensitive durometer readings were found in different areas of the skin, such as the forehead and dorsal digit, where subcutaneous tissue is less represented. The hypothesis of underlying bone or tendon structure giving higher readings at these sites was raised as a possible explanation for this failure to discriminate between normal and indurated skin (Falanga and Bucalo 1993).

2 Medical Applications

2.1 Scleroderma

Sclerodermatous skin is characterized by induration of the lower dermis and directly underlying tissue, which could be affected diffusely as in systemic sclerosis or in a more localized involvement as in morphea. The degree and extent of skin hardness in scleroderma are used as a prognostic value for the disease and generally assessed subjectively using a clinical skin scoring system. Objective measurements of skin involvement in scleroderma have included the use of ultrasonography, skin elastometers, transcutaneous oxygen tension measurements, and also much more sophisticated techniques such as magnetic resonance imaging. All these methods were able to provide useful information about the extent of skin involvement, but are generally considered not practical for sequential measurements in clinical practice. Falanga and Bucalo (1993) were the first to describe the use of a durometer in combination with systemic sclerosis. They investigated six anatomic sites in 12 patients and in 12 control individuals using the durometer in combination with skin severity score. A direct relationship between the skin severity score and durometer readings was present for all anatomic sites except the forehead: the higher the skin score, the greater the amount of deflection measured with the durometer ($p = 0.0032$, $p = 0.0002$, and $p = 0.005$ for skin score of 1, 2, and 3, respectively). Moreover, the durometer was able to differentiate between increased levels of skin hardness. In this study, no statistically significant relationships were found among body weight, skin score, diameter of anatomic site measured, and durometer readings. The use of the durometer was not associated with any pain or discomfort. Similar results of increased skin hardness in morphea were obtained by Aghassi et al. (1995) in a study where the durometer was also used in combination with a laser Doppler perfusion imager. In that study the authors found a relationship between age and durometer readings over the ventral aspect of the forearm, in normal controls. Skin hardness rises from birth, reaches a constant level by puberty, and then remains steady until age 65 years, when the skin progressively begins to lose its firm quality. Women had lower durometer readings compared with men, and the instrument was able to define contiguous areas in different degrees of sclerosis in morphea lesions. The efficacy of treatment has been investigated in patients with localized scleroderma by means of durometer readings in two different studies. Moon et al. (2012) investigated 31 patients with systemic sclerosis in order to evaluate the correlation between durometer score and Rodnan skin score (MRSS), scleroderma symptoms, and physical functions. Skin involvement was evaluated with the use of the durometer and MRSS. The other parameters that the authors considered were: health assessment questionnaire (HAQ), disability indices, Keitel function test (KTF) scores, grip strengths, and the scleroderma-visual analog scale (scleroderma-VAS). The total durometer score correlated well with MRSS ($r = 0.537$, $p = 0.002$) and KTF scores ($r = 0.608$, $p < 0.001$), but correlated poorly with HAQ disability indices ($r = 0.202$, $p = 0.276$) and individual scleroderma-VAS scores. Skin hardness measured with the durometer were found to

correlate well with the MRSS scores of fingers, hands, forearms, upper arms, thighs, and feet. This study suggests that these skin sites should be considered when skin hardness is measured with a durometer in patients with systemic sclerosis.

Seyger et al. (1998) evaluated the effect of low-dose methotrexate (15 mg/week) in nine patients with widespread morphea in a 24-week trial using the durometer and other clinical assessments to monitor the therapeutic regimen. A total of seven patients out of nine showed a decrease of durometer readings at the end of the trial, with mean values changing from 101 ± 13.9 before the treatment, to 89.7 ± 10.3 after treatment ($p = 0.07$). The greatest improvement in durometer score among the sites examined was the efficacy in the arm region ($p = 0.03$). In another study, Karrer et al. (2000) evaluated the efficacy of topical photodynamic therapy by means of durometer readings and clinical score in five patients with progressive localized scleroderma who had failed to respond to other therapies. In all patients, the therapy was highly effective as measured by durometer score, which showed a mean reduction of 20 % after a treatment period of 6 months. Kroft et al. (2009) used durometer score and other parameters (surface area measurements, photography, clinical features score) to evaluate the efficacy of treatment for morphea with topical tacrolimus 0.1 %. This study examined 10 patients with active plaque morphea treated with tacrolimus 0.1 % ointment and an emollient (petrolatum) on two selected morphea plaques, applied twice daily for 12 weeks. The results demonstrated an improvement in the scleroderma plaques treated with topical tacrolimus 0.1 %, resulting in a significant reduction in durometer and clinical feature scores.

2.2 Lipodermatosclerosis

Chronic lipodermatosclerosis is characterized by hyperpigmented indurated skin on the medial aspect of the leg and is common in patients with venous insufficiency. The severity of induration of lipodermatosclerosis has been associated with poor ulcer healing. Nemeth et al. (1989) reported a correlation between the degree of skin induration in lipodermatosclerosis and ulcer healing. They used a clinical score to assess skin induration and found that lipodermatosclerosis was less severe in patients who had ulcers that healed than in two who had ulcers that did not heal. Durometer testing of skin hardness was performed on a group of patients with lipodermatosclerosis with and without venous ulcers (Romanelli and Falanga 1995). A clinical scoring for hardness by a blinded observer was used in combination with durometer measurements at a skin site midway between the upper and lower margin of lipodermatosclerosis. Measurements of transcutaneous oxygen pressure ($TcpO_2$) at the same site were also performed. Compared with normal skin in control subjects, increased skin severity scores were associated with higher durometer readings ($p < 0.01$). This direct correlation between clinical scores and durometer readings was linear ($r = 0.9621$); the durometer was able to differentiate between increased levels of skin hardness. Thus, a skin severity score of two reflected a higher durometer reading than that of a skin score of 1 ($p = 0.0016$). An inverse and statistically significant relationship ($r = 0.431$; $p = 0.0079$) between $TcpO_2$ measurements and durometer readings was found in patients and control subjects (Table 1). The correlation between $TcpO_2$ measurements and durometer readings found in that study confirms the hypothesis of poor oxygen diffusion through dense and thickened skin, as occurs in lipodermatosclerosis. Le Blanc et al. (1997) used a durometer to assess the area of lipodermatosclerosis around venous ulcers and obtain a map of skin induration. Their hypothesis was that maximum skin induration correlated with the presence of ulcers. The authors found that venous ulcers were located in skin that was most affected by lipodermatosclerosis. Durometer measurements showed a progressive and linear decrease from the top of the ulcer edge to the knee ($r = 0.925$). In the same study, the authors tested 14 patients with pitting edema and eight controls without edema. There were no significant

Table 1 Relation between $TcpO_2$ measurements and durometer readings or clinical severity score (inset)

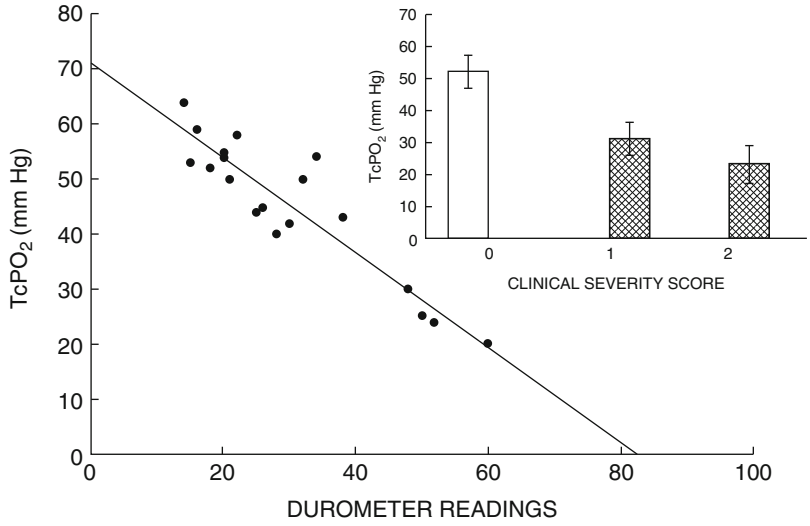

differences in durometer readings in patients with minimal or more severe edema ($p > 0.05$), regardless of anatomic location.

Choh et al. (2010) used a durometer for the assessment of venous disease. They investigated 107 patients with isolated venous disease and volunteers attending outpatient clinics; for all patients the CEAP classifications were assessed (clinical, aethiological, anatomical, and pathological). The measurement with a durometer was made on the skin 15 cm above the medial malleolus on nonulcerated tissue with patient and limb in recumbency. The authors considered the average of four measurements. The results of this study demonstrated that there is statistically significant evidence that age and CEAP classification correlated with durometry ($p < 0.0001$). Thus, durometry could help in monitoring pre-ulcerative venous disease and in identifying high risk patients.

2.3 Neuropathic Foot

Patients with diabetes with peripheral polyneuropathy are at increased risk of foot ulceration. One of the key events in the pathogenetic pathway to neuropathic ulceration is hyperkeratosis, which develops in areas of increased pressure. Nonenzymatic glycosylation and autonomic dyshidrosis have been implicated in the pathogenesis of skin hardening. Piaggesi et al. (1999) measured skin hardness at three different sites on foot of a selected group of patients with diabetes, avoiding areas with bony prominences. Skin hardness was more pronounced in neuropathic patients than in nonneuropathic patients and controls ($p < 0.01$.) Among neuropathic patients, those with metatarsal hyperkeratosis had significantly higher durometer readings compared with those without hyperkeratosis. Subjects were also evaluated for neuropathy by determining the vibration perception threshold (VPT) with a biothesiometer. This instrument is an electrical device provided with a vibrating probe, which is applied to the test site and to which an increasing vibrating intensity is applied. The lowest of three intensities of vibration defines the VPT. In that study, a significant positive correlation was found between durometer readings and VPT at the malleolus ($r = 0.516$) and the allux ($r = 0.624$) in neuropathic patients (Table 2). Cuaderes et al. (2009) have evaluated skin hardness and pressures of the foot in diabetes patients. Skin hardness was measured with a

Table 2 Correlation between vibration perception threshold at allux (VPT-A) and skin hardness measurements at medial (DMT-M) in neuropathic diabetic patients

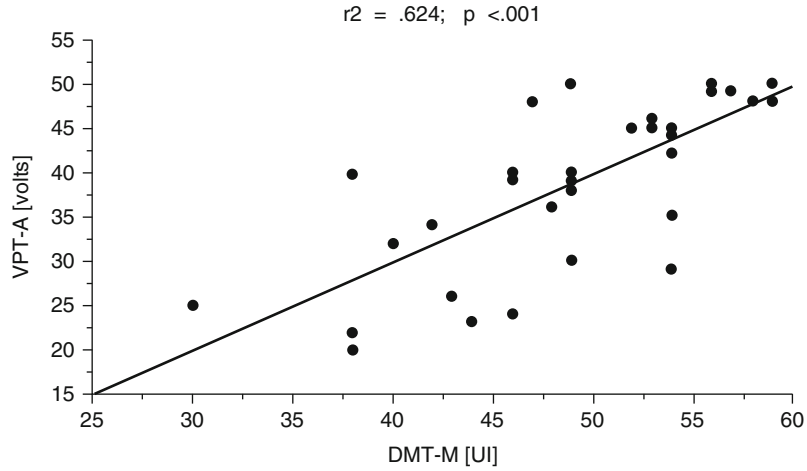

durometer applied at 10 sites(plantar side of the allux, third and fifth toes, first, third, and fifth metatarsal heads, medial and lateral midfoot, heel, and the dorsal aspect between the hallux and second toe). The readings of durometer and pressurestat have demonstrated a concordance that was acceptable at the hallux, the third toe, the first, third, and fifth metatarsal heads. Since most diabetic foot ulcers occur in these sites, both durometer and pressurestat may be useful screening tools to determine the degree of risk.

3 Conclusions

Durometry is a technique for measuring skin hardness. The methods takes advantage of the ability of the durometer to sense and record hardness on a linear scale, and it is unique in its simplicity and ease of use. Measurements with durometer are highly reproducible in the same subject and in persons with the same degree of skin induration. Data obtained indicate that the durometer may be insensitive when used in areas of skin where the subcutaneous tissue is not well represented. At this stage, the instrument is used as a standard noninvasive tool to measure skin hardness in systemic sclerosis. The authors believe that durometry could be applied in other dermatological diseases to assess skin involvement and to monitor the efficacy of treatment.

References

Aghassi D, Monoson T, Braverman I. Reproducible measurements to quantify cutaneous involvement in scleroderma. Arch Dermatol. 1995;131(10):1160–6.

Choh CT, Wall ML, Brown MD, et al. Use of durometry in assessment in venous disease. Phlebology. 2010;25(2): 94–9.

Cuaderes E, Khan MM, Azzarello MM. Reliability and limitations of the durometer and PressureStat to measure plantar foot characteristics in Native Americans with diabetes. J Nurs Meas. 2009;17(1):3–18.

Falanga V, Bucalo B. Use of durometer to assess skin hardness. J Am Acad Dermatol. 1993;29(1):47–51.

Karrer S, et al. Topical photodynamic therapy for localized scleroderma. Acta Derm Venereol (Stockh). 2000; 80(1):26–7.

Kroft EB, Groeneveld TJ, Seyger MM, et al. Efficacy of topical pacrolimus 0.1% in active plaque morphea: randomized, double-blind, emollient-controlled pilot study. Am J Clin Dermatol. 2009;10(3):181–7.

Le Blanc N, et al. Durometer measurements of skin induration in venous disease. Dermatol Surg. 1997;23(4): 285–7.

Moon KW, Song R, Kim JH, et al. The correlation between durometer score and modified Roadnan skin score in systemic sclerosis. Rheumatol Int. 2012;32(8):2465–70.

Nemeth AJ, Eaglestein WH, Falanga V. Clinical parameters and transcutaneous oxygen measurements for the

prognosis of venous ulcer. J Am Acad Dermatol. 1989;20(2 Pt 1):186–90.

Piaggesi A, Romanelli M, Schipani E, et al. Hardness of plantar skin in diabetic neuropathic feet. J Diabet Complications. 1999;13(3):129–34.

Romanelli M, Falanga V. Use of durometer to measure the degree of skin induration in lipodermatosclerosis. J Am Acad Dermatol. 1995;32(2 Pt 1):188–91.

Seyger MMB, et al. Reliability of two methods to assess morphea: skin scoring and the use of a durometer. J Am Acad Dermatol. 1997;37(5 Pt 1):793–6.

Seyger MMB, et al. Low-dose methotrexate in the treatments of widespread morphea. J Am Acad Dermatol. 1998;39(2 Pt 1):220–5.

Zachariae H, et al. Skin scoring in systemic sclerosis: a modification- relations to subtypes and the aminoterminal propeptide of type III procollagen (PIIINP). Acta Derm Venereol (Stockh). 1994;74(6): 444–6.

Skin Viscoelasticity by Acoustic Velocity and Dispersion: Effects of Tension in Stratum Corneum

98

Eduardo Ruvolo, Christina Lee, and Nikiforos Kollias

Contents

Keywords

Elasticity • Reviscometer • Aging • Skin moisturization • Skin viscoelasticity • Mechanical properties of the skin

1 Introduction

Reduction of skin elasticity with aging is attributed to skin thinning due to loss of elastin and collagen in the dermal matrix (Jansen and Rottier 1957; Lavker et al. 1987), as well as to loss of subcutaneous tissue mass (fat layers and muscle mass) and stiffening of collagen with increased cross-linking. Age is also expected to affect the directionality of the mechanical properties of the skin. During development, from infancy to adolescence, the skin is expected to respond to tension isotropically to accommodate for growth, while in adulthood this isotropic behavior is expected to regress due to site-specific habituation to tension.

The mechanical strength of the skin is primarily attributed to the dermal matrix, which consists predominantly of collagen and elastin. Collagen molecules form fibrils, fibers, and bundles, which are arranged in a basket-weave pattern. This allows the dermis to deform due to pressure and at the same time to minimize tears. The collagen bundles vary in size as we progress from the upper (papillary) to the deeper

Nikiforos Kollias has retired.

E. Ruvolo • C. Lee (✉) • N. Kollias
Johnson & Johnson Consumer and Personal Products Worldwide, Skillman, NJ, USA
e-mail: eruvolojr@gmail.com; CLee56@its.jnj.com

P. Humbert et al. (eds.), *Agache's Measuring the Skin*,
DOI 10.1007/978-3-319-32383-1_132

(reticular) layers of the dermis and are normally under tension that ranges from 0 to 20 N/m depending on the body site, direction, and posture (Skin Mechanics 1986; Nizet et al. 2001). Ever since the nineteenth century, surgeons have recognized the fact that this tension load is directional by observing that circular punctures in the skin produce elliptical holes (Nizet et al. 2001). These lines, termed "Langer's lines" (Langer 1861), represent the directions of skin's maximum tension and have been identified over the whole body (Cox 1942; Gibson et al. 1969). They are used as the preferred direction in which surgical incisions are made so that the tension across the wound is minimal. Furthermore, it is known that dermal fibroblasts generate tension and change their orientation along the tensile direction (Takakuda and Miyairi 1996). The mechanical properties of the skin are thus expected to follow the anisotropy in tension defined by the Langer's lines.

A number of techniques have been developed to study the mechanical properties of the skin and their dependence on aging (Elsner 1995; Rodrigues 2001). They are primarily based on the concept that assessing the applied force necessary to pull or push the skin gives an estimate of the elastic and plastic properties of the tissue, and they can be classified in the following categories: (a) instruments that generate a light vacuum on the skin surface and determine the height to which the skin may be pulled under constant suction and then the rate at which the skin returns to its original shape; b) instruments that use two concentric cylinders that are placed in contact with the skin and measure the angular displacement under torque and the rate at which the skin returns to equilibrium once the torque is removed; and (c) instruments that assess the firmness/elasticity of the skin by determining the height recovery of a small mass as it bounces after striking the skin from a predetermined height (Serup and Jemec 2006). All of the above types of instrumentation measure parameters that are affected by the mechanical properties of the skin surface as well as the deeper structures of the dermis and even the subcutaneous tissues. Therefore, the information we can get from them is not always limited to the skin. These methods do not offer any information on mechanical anisotropy.

Another type of instrument allows for the evaluation of the mechanical properties of a material by measuring of the propagation time of a shear wave between two sensors placed on the material surface. The distance between the sensors and the frequency of the shear wave determine the penetration depth of sampling. The commercial version of this method of accessing viscoelasticity of the skin is the Reviscometer® RVM 600. The Reviscometer® has been designed to sample up to a few tenths of microns in depth making it suitable for measurements of the mechanical parameters of the epidermis and the papillary layers of the dermis. The applied pulse frequency is in the audible range (4.5 KHz). The velocity of sound in a material depends on the density of the material and tension that is under. Mechanical vibrations propagate faster at the direction of higher tension, and as with a guitar string, the higher the tension, the higher the frequency of oscillation after plucking. As the preferred disposition of the collagen fibers corresponds to the skin's cleavage lines (Langer's lines), the speed of propagation of elastic disturbances on the skin will depend strongly on orientation.

Previous investigations have shown a weak dependence of the shear wave propagation time on the skin with aging (Nizet et al. 2001; Dahlgren and Elsnau 1986; Vexler et al. 1999). A common denominator of these studies was that the measurements were performed at a limited number of angular positions of the probe, typically at four positions at increments of 45°. Therefore, directional features with angular width less than 45° were ignored or averaged out. More recent studies have shown a strong correlation between shear wave propagation and age (Ruvolo et al. 2007).

In a previous chapter (Ruvolo Jr et al. 2014), the authors described experiments and studies using the same technique that document changes in density of the tissue and the effects on the speed of sound when active ingredients produced changes in the packing of the viable keratinocytes. In this chapter we demonstrate through a number of studies the sensitivity and utility of the measurement of the viscoelastic properties of the skin

by acoustic shear wave propagation (velocity and angular dispersion). In the studies presented in this chapter, the Reviscometer® RVM 600 was used, but other instruments using the same principle of actuation can be used. This technique provides unique information on the directional dependence of elastic parameters of the superficial layers and characterizes the tensile forces acting on the skin surface by measuring the anisotropy of the viscoelastic properties of the skin at different ages, correlating the changes in the anisotropy with structural features of the skin. Thus, we attempt to characterize the tensile forces acting on the skin surface by measuring the anisotropy of the viscoelastic properties of the skin before and after topical application of moisturizers. To this end, we established a new data acquisition methodology for the technique (via Reviscometer® RVM 600) with high angular resolution, and we defined a novel mechanical parameter that relates to the anisotropy and coherence of skin viscoelasticity.

2 The Technique-Hardware Description

In 1980 Prof. Hagen Tronnier (1980) developed a method to measure resonance frequencies in the skin. Later, in 1999 Vexler (Vexler et al. 1999) described a viscoelastic skin analyzer that resembles more the commercial instrument (Reviscometer® RVM 600, Courage + Khazaka Electronic GmbH, Cologne, Germany).

A noninvasive way to assess the mechanical properties of viscoelastic materials, such as the skin, is by investigating the propagation of a mechanical disturbance along their surface. The speed of propagation of a pulse or of a periodic (wave) mechanical disturbance depends on the tension in the material in the direction of propagation and on the density of the material (Doukas et al. 2001). The amplitude of such a stimulus should be small so that no permanent changes are produced in the material and the coupling between the device producing the perturbation and the medium under study, e.g., the skin, should be robust (Vexler et al. 1999; Potts et al. 1983; Dorogi et al. 1986; Mridha et al. 1992). The following description is based on the construction and use of the Reviscometer® RVM 600.

The probe that comes in contact with the skin includes two piezoelectric transducers spaced by approximately 2 mm and mounted on two independent supports. One transducer generates a small amplitude acoustic pulse, <0.2 mm, in the audible range 4.5 KHz, and the second acts as the receiver. The time it takes for the acoustic pulse to travel from the transmitter to the receiver is defined as the resonance running time (RRT value $\times 10^{-6}$ s). The values of the RRT may be used to calculate the velocity of propagation of the acoustic pulse. If we consider the one-dimensional longitudinal model for the sonic propagation from Dahlgren (Dahlgren and Elsnau 1986), Young's modulus of elasticity (E) of the material is directly related to the square of the sonic transmission velocity, c:

$$E = dc^{2} \cdot 10^{6} \quad (1)$$

where E is in N/m^2, d is the density of the skin in g/cm^3, and c is in m/s. Therefore, the modulus of elasticity may be determined once the velocity of propagation has been measured.

To ensure good contact (no slipping) between the transducers and the skin, a constant pressure is applied; the pressure that the probe exerts on the skin is regulated by a spring mechanism: a given amount of pressure is necessary for the measurement sequence to start. The probe is held perpendicular to the skin surface by a hollow cylindrical holder that is attached to the surface of the skin with double-sided adhesive tape. The manufacturer made marks on the holder along its periphery at angular intervals of 45°. In all the work presented in this chapter, we used a modified probe-holder assembly by placing a millimeter scale on the probe and another on the holder. We carried out measurements by rotating the probe within the holder so that the lines of the two scales would align with each other. This corresponds to making measurements every 3° for a total interval of 100–180°. Custom acquisition software was developed in LabVIEW 6.0 (National Instruments Corporation, Austin, TX).

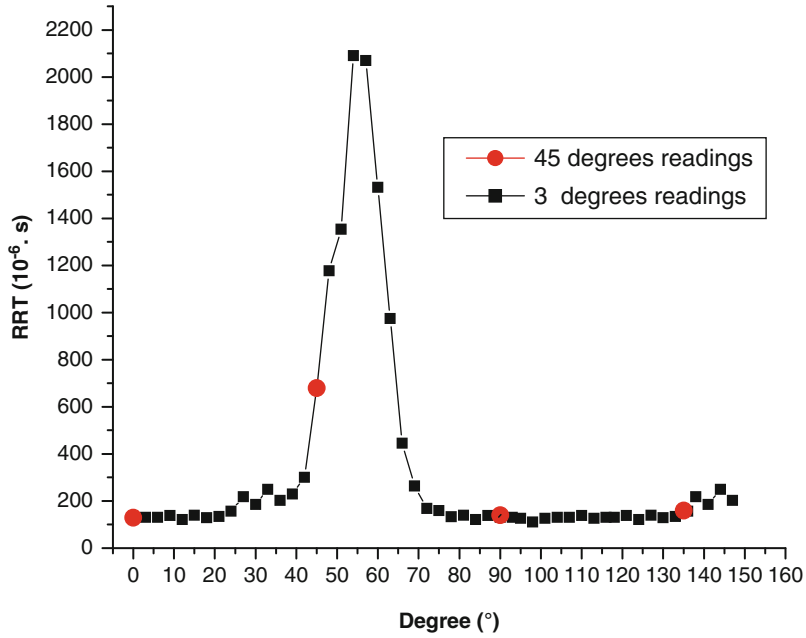

Fig. 1 Typical data obtained with a Reviscometer® from the upper inner arm of a 47-year-old subject. Data shows same location readings acquired in increments of 3° (*black squares*) and 45° (*red circles*)

To demonstrate the need of acquiring data at increased angular resolution, we recorded the Reviscometer readings from the same skin site (upper inner arm) of a volunteer of 47 years at intervals of 45° and of 3° (Fig. 1). It is evident that the features with width less than 45° may be missed. Following the Nyquist sampling criterion, using 3° intervals, we could accurately record features of at least 6° angular dispersion width. Typically for older individuals having narrower maxima, the angular dispersion width can be in the order of 10°. Taking measurements with high angular resolution increases the chances of recording the skin's radial anisotropy accurately. Increased angular resolution of viscoelasticity readings provides information that would be otherwise missed.

The dependence of the measured RRT values obtained from human skin on the angle of measurement may be described by a Gaussian curve, Fig. 2. Two parameters may be determined from the Gaussian fit function: the full width at half maximum (FWHM) and the amplitude of the curve, which corresponds to the angular anisotropy of the RRT. The anisotropy is defined as the ratio between the maximum and minimum RRT of the measurements on a given skin site:

$$\mathrm{A} = \frac{RRT_{\max}}{RRT_{\min}} \tag{2}$$

The definitions for minimum and maximum RRT values (RRT_{min} and RRT_{max}, correspondingly) as well as the full width at half maximum (FWHM) of the fitted curve are demonstrated in Fig. 2; these correspond to two new mechanical parameters that may be determined in the skin based on measurements with the Reviscometer®, and they are anisotropy and angular dispersion width (FWHM).

The Reviscometer® does not work equally well on all skin sites. Skin sites with high density of vellus hairs present difficulties in the interface between the transducers and the skin. Equally difficult has been to obtain good data from skin sites where the skin is tight such as the calves, the forehead, etc. The instrument gives very reliable and high-quality data from sites where the skin is particularly "soft" to the touch such as the upper inner arm, neck, abdomen, breast, thighs, and in particular the inner aspect and the sides of the torso. It is interesting to note that the sites where good measurements may be made with the Reviscometer® are also skin sites where "stretch" marks are likely to appear.

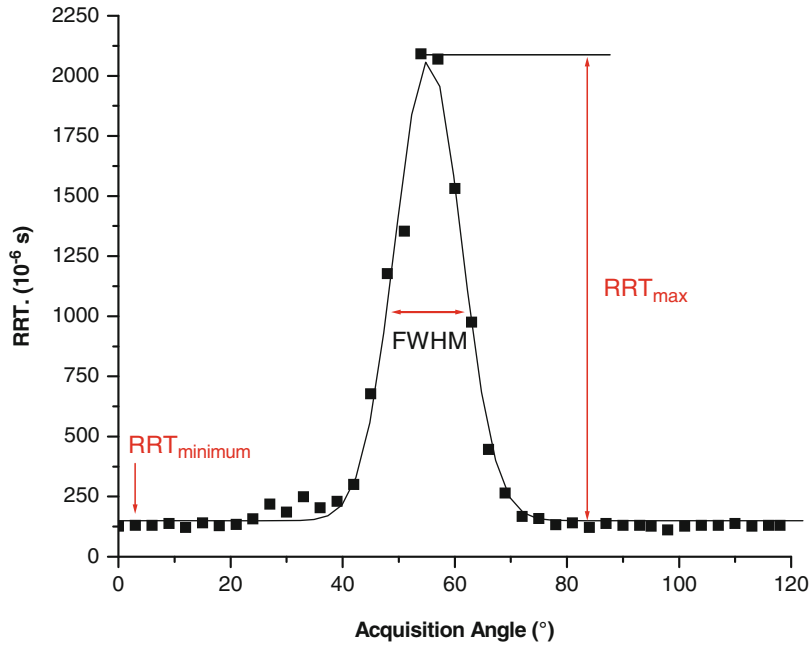

Fig. 2 Illustrates the RRT data obtained from the upper inner arm of the same subject as in Fig. 1. Data was obtained in increments of 3° over a range of 120°. A Gaussian curve was fitted. The relevant parameters obtained from such a fit are shown. These are the minimum RRT (*RRTmin*), maximum RRT (*RRTmax*), and the full width of half maximum (*FWHM*) of the curve

3 Instrument Calibration

Typical RRT reading from anatomical sites like dorsal and ventral forearm ranges from 100 to 450 × 10^{-6} s. The manufacturer supplies with the instrument an elastomer standard with an RRT = 230 ± 30 × 10^{-6} s. The RRT value for the standard is suitable for a great majority of the values obtained in different parts of the body.

When different Reviscometer® probes were used to measure skin viscoelasticity of the same skin site, we observed the readings to vary between probes, possibly due to differences in the distance between the transducers and differences in their sensitivities. Therefore, the probes were calibrated against a wider range of viscoelastic standards. To this end, we used the standard thermoplastic elastomers' durometer (Biscoe and Sebastian 1993) test block kits for Shore scale A (Rex Gauge Company Inc., Buffalo Grove, IL) and Shore scale 00 (Corporate Consulting, Service and Instruments, Inc., Akron, Ohio). These materials were chosen because of their wide response range of RRT readings (200–1,100 × 10^{-6} s). Measurements were repeated ten times in each sample and the data were averaged. The elastomers were isotropic in terms of RRT values. All measurements were taken at ambient conditions at a temperature of 18 °C and a relative humidity of 40–50 %. Table 1 shows the Shore type, the International Rubber Hardness Degree (IRHD) (ASTM 2003), and the density (g/cm^3) of the standard test blocks used in this study. Shore hardness is a measure of the resistance of material to indentation by a spring-loaded indenter. The hardness testing of plastic material is most commonly measured by the Shore (durometer) hardness test or Rockwell hardness test; the higher the number, the greater is the resistance to indentation. Using Eq. 1 we estimated the speed of sound in each elastomer as illustrated in Table 1. Figure 3a shows the RRT values versus the speed of sound (m/s) on the standards for two different probes, and Fig. 3b. illustrates the same elastomers as a function of Young's modulus (MPa). It can be observed from Fig. 3a, b that the probes have similar responses for elastomers with low RRTs but differ at high RRTs. For the elastomers, we can notice that RRTs presented a higher correlation (Fig. 3a, $R^2 = 0.92$ and $R^2 = 0.94$) with the speed of sound than with Young's modulus (Fig. 3b, $R^2 = 0.81$ and $R^2 = 0.83$). Since Young's modulus is defined as the ratio of the stress over the strain in the range of

stress that Hooke's law holds during tensile tests making linearizing assumptions, the shear wave propagation (RRTs or the speed of sound) on the elastomers can be a better measurement of the surface elastic properties.

The standard elastomer blocks can be used to correlate the readings from one probe to the other by plotting elastomers measurements as illustrated in Fig. 4. The correlation between the two testing probes can be described by a linear fit ($r^2 = 0.92$). As an example, Fig. 5 illustrates RRT readings, as a function of the angle, taken in the upper inner arm of a 41-year-old subject with two different probes. Taking the readings from the probe with lower sensitivity, Probe 02120709, and applying the linear correction obtained from the readings on the testing blocks (Y = 220.1 + 1.94 * xScale (X)), we can observe in Fig. 5 that the readings obtained with the probe with lower sensitivity are much closer to the probe with higher dynamic range.

Table 1 Physical Parameters of the Durometer Test Blocks used for calibration

Hardness Shore Type	IRDH	Young's Modulus (MPa)	Density (g/cm3)	Speed of Sound (m/s)
00	31	0.133	0.91	384
00	46.9	0.303	0.92	574
00	54.5	0.412	0.93	669
00	63.1	0.414	0.95	660
00	77.3	0.916	0.98	965
A	29	1.024	1.06	983
A	42.8	1.801	1.22	1215
A	50.2	2.367	1.31	1345

4 Viscoelastic Properties of the Skin at Different Ages and Different Anatomical Sites

It is well known that the human skin changes with age particularly in becoming more "loose" and less "elastic." This has been shown on the back of the hand as a "pinch" test where we observe the

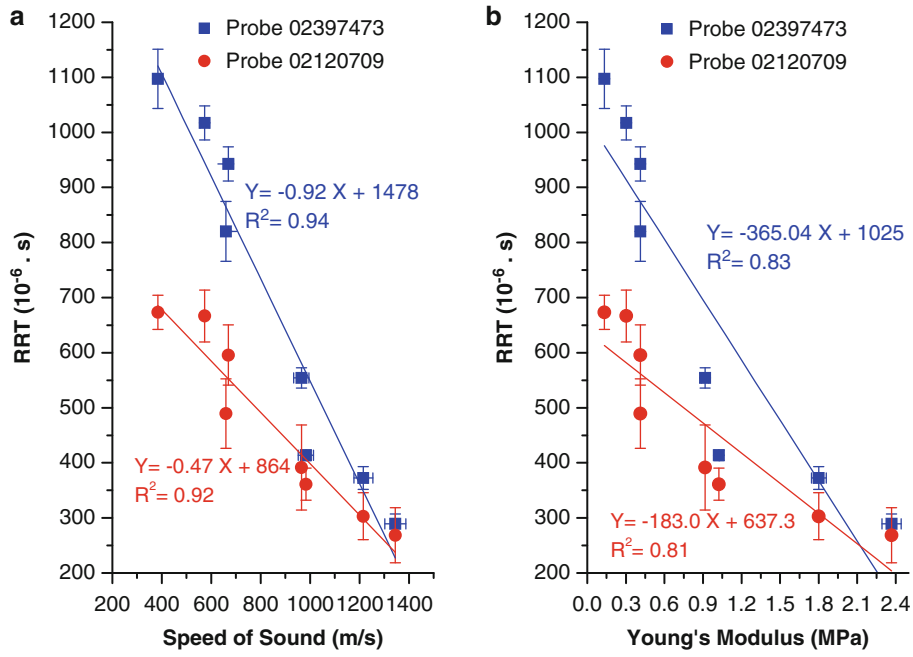

Fig. 3 The Reviscometer® data for two different probes as supplied by the manufacturer. (**a**) Illustrates the viscoelastic properties of the different elastomers as a function of the speed of sound (m/s). (**b**) The viscoelastic properties of the different elastomers as a function of Young's modulus (*MPa*). Data represents mean value and *error bars* are the standard deviation of the mean (mean + standard deviation)

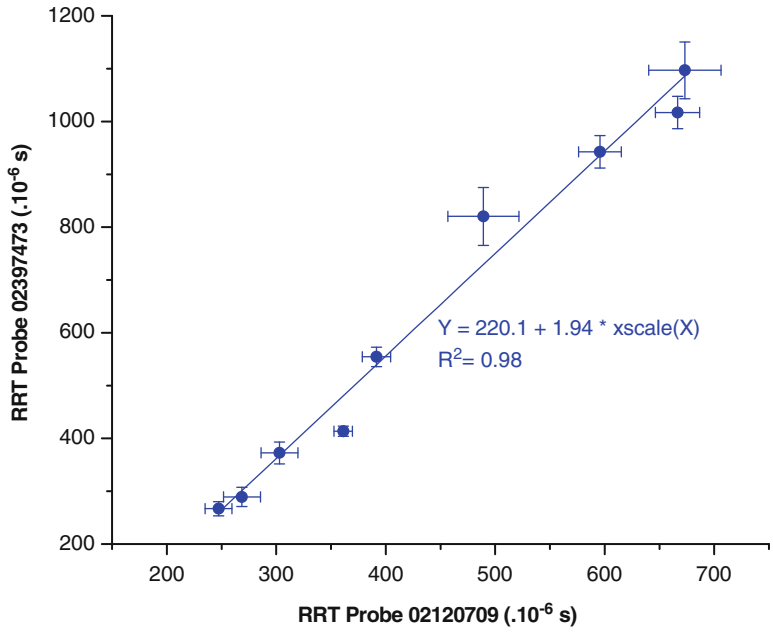

Fig. 4 The correlation of RRT probe values for elastomers with different hardness. The figure shows the linear correlation between the two probes. Data represents mean value and *error bars* are the standard deviation of the mean (mean ± standard deviation)

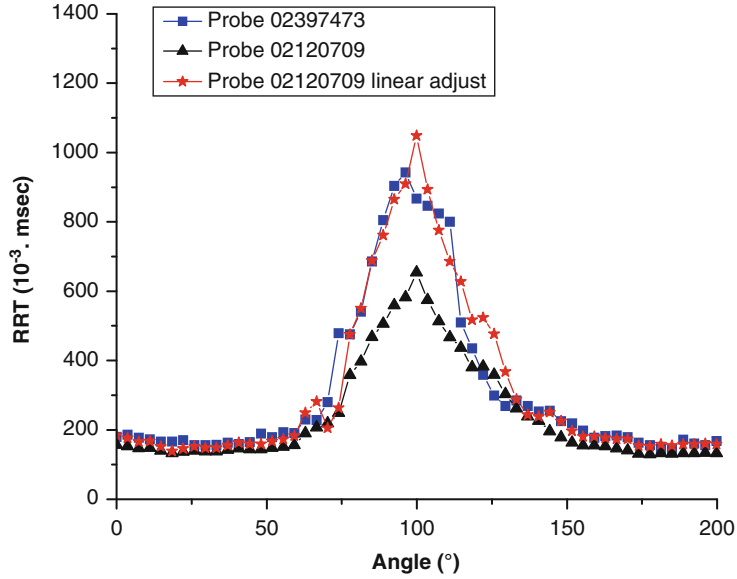

Fig. 5 Illustrates measurement at the upper inner arm performed with two different probes. A linear correction ($y = 220.1 + 1.94$*x) was applied to the probe 02120709 to obtain the adjusted reading (*red star*)

speed with which the skin returns to its original state after being pinched and in lateral compression between two fingers of the skin – in young skin, the skin surface produces a single "bulge," whereas old skin produces a multitude of wrinkle patterns. It has been concluded that the elastic properties of the skin must change for such pronounced changes to be observed. However, the changes documented in measurements using instruments that study the deformation of the surface of the skin when exposed to a negative pressure have been shown to be of the order of 33 % over 50 years age interval (from 10 to 60 years). This number does not provide adequate documentation of the observed changes with age because of the small dynamic range. As the Reviscometer®

assesses the superficial layers of the skin, it was felt that monitoring age-related changes in the mechanical properties of the superficial skin would provide a more accurate representation of the observed changes with age.

The study protocols were approved by an independent ethics committee, and subjects were in general good health and gave informed consent. RRT measurements were taken from 239 volunteers with skin types, from very light Caucasian (Types I and II) to African-Americans (Type VI). The volunteers were divided into five age groups: 0–2 years (1.8 ± 1.1, mean ± standard deviation), 14–20 years (17 ± 4.2), 24–40 years (32.5 ± 10.6), 55–60 years (57.5 ± 3.5), and 65–75 years (70 ± 7). Measurements with a Reviscometer® were taken on the upper inner arm at 15 cm above the elbow from 0° to 100° in 3° increments, where the initial orientation of the probe was chosen as the direction that gave the lowest RRT reading. Reviscometer® readings were also taken on the neck and dorsal and ventral forearm of 117 of the volunteers.

The mean value and standard deviation were calculated for each age group and the treated sites. JMP® statistical software (SAS Institute Inc., Cary, NC) was used to perform analysis of variance using a standard least squares analysis. Statistical significance was considered for $P < 0.05$.

In order to ensure the relation between visual appearance and mechanical properties, in vivo macroimaging was also performed on the upper inner arm and dorsal forearm of the 239 subjects. A video-microscope image system (HiScope®, Model KH-2400, Hirox Inc., Tokyo, Japan) was used to acquire close-up images (2.8 × 2.1 mm image size) of tested area using a 100× magnification lens (Model MX-100Z, Hirox Inc., Tokyo, Japan). This image system allows examination of the skin surface texture or of subsurface features depending on the illumination at a grazing angle. In this study, grazing angle illumination was used to enhance the contrast of skin texture.

Typical RRT profiles recorded from the upper inner arm for three different age groups are shown in Fig. 6. We observed that while the RRT_{min} values remained fairly constant for the age groups tested, the RRT_{max} values increased with age. Thus the anisotropy ratio given by Eq. 2 also increased with age (Fig. 7). Furthermore, the width of the RRT profiles becomes narrower, i.e., the angular dispersion width decreases, with age (Fig. 7). These changes are statistically significant ($P < 0.01$) between the age groups. Since RRT anisotropy increases while angular

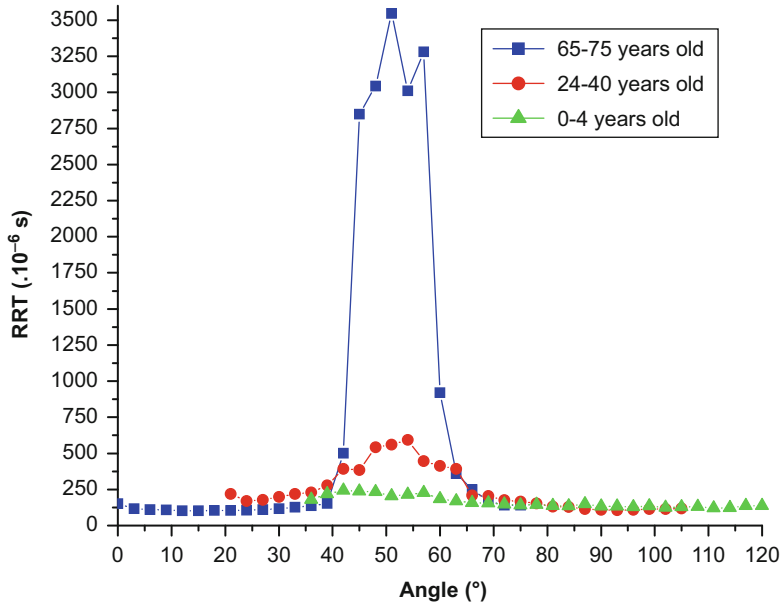

Fig. 6 Skin viscoelastic properties depend on aging. Representative resonance running time (*RRT*) profiles recorded from the upper inner arm for three age groups: 0–4 years (*green triangles*), 24–40 years (*red circles*), and 65–75 years (*blue squares*)

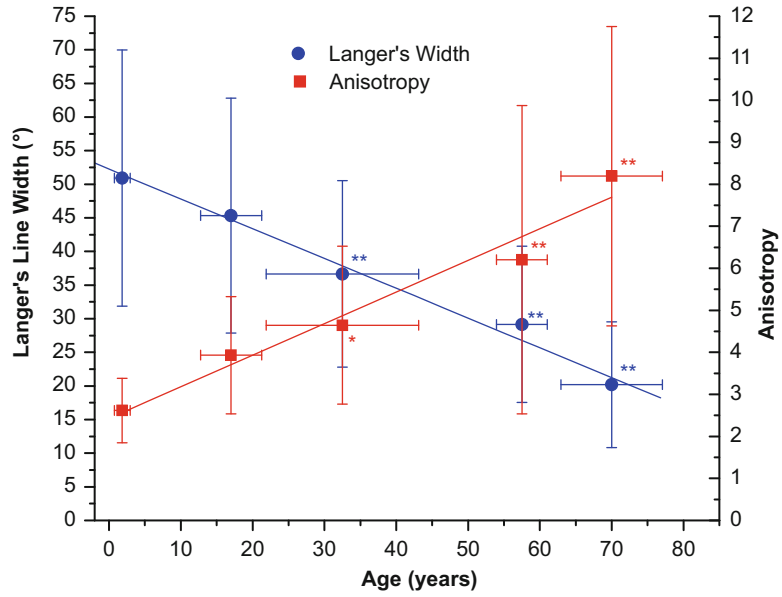

Fig. 7 Skin viscoelastic properties show strong age dependence. The anisotropy ratio (*red squares*) increases, while the angular dispersion width (*blue circles*) decreases with age. Measurements were taken on the upper inner arm: * $p < 0.01$, ** $p < 0.001$when compared with the youngest age group. Data represents mean value and *error bars* are the standard deviation of the mean (mean ± standard deviation)

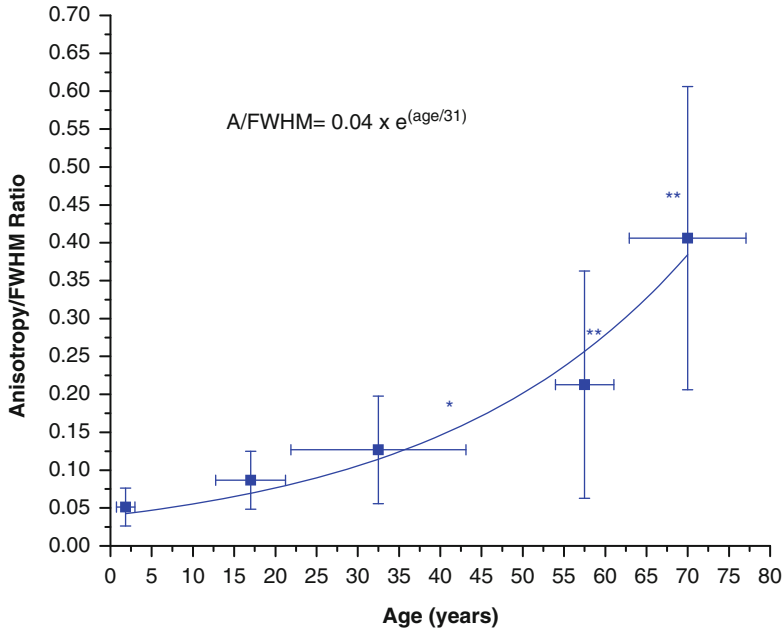

Fig. 8 The ratio of anisotropy to angular dispersion width provides a single viscoelasticity parameter that is age dependent that is characterized by a wider dynamic range than each of the two parameters individually: * $p < 0.03$, ** $p < 0.001$ compared with the youngest age group. Data represents mean value and *error bars* are the standard deviation of the mean (mean ± standard deviation)

dispersion width decreases with age, we can define the ratio of these two as a single viscoelastic parameter that documents the age-dependent changes in the skin and that provides a wider dynamic range than either (Fig. 8). The relationship of this parameter to age is best represented by an exponential equation, and the data may be fitted with the equation:

$$\text{Anisotropy ratio} = \frac{\text{Anisotropy}}{\text{FWHM}} = 0.04.e^{\frac{\text{age}}{31}} \quad (3)$$

The anisotropy ratio values for each of the older age groups are statistically different compared to those for the youngest group.

The mechanical and physical properties of the skin have been extensively studied (Skin

Mechanics 1986; Rodrigues 2001; Serup and Jemec 2006). These investigations describe the skin as being a viscoelastic medium and interpret the skin with homogeneous density and isotropic elastic moduli. The mechanical properties of the skin stem from contributions of its structural components such as collagen, elastin, keratin, and the purely viscous interstitial fluids (Dahlgren and Elsnau 1986). According to Eq. 1, the speed of shear wave propagation depends on the density of the medium in the direction of the sound propagation. Results presented in this chapter show that the shear wave propagation on the surface of the skin is anisotropic and thus the tissue density and tension that relates to the skin mechanical properties is also anisotropic. These two parameters are independent for non-compressible media, but in the skin or viscoelastic materials, they are probably not independent. We can make an analogy with the strings of a guitar; the sound produced by a string depends on its tension and also the density of the material (type and thickness).

The skin at the upper inner arm sites undergoes considerable changes with age in its structure and therefore its mechanical properties. It is evident in Fig. 6 that the RRT readings of young skin are more isotropic when compared with the other two age groups. For the 24–40 years group, there is a distinct increase in the anisotropy, and for the older group, a very well-defined RRT maximum.

This may also be observed in the skin microrelief imaged by the video-microscope imager. Skin microrelief involves patterns on the ventral forearm that is characteristic for different age groups. The in vivo microscopy images of Fig. 9 are representative for the age groups: 0–4 years, 14–24 years, 24–40 years, and 65–75 years. It is evident that the triangular and hexagonal patterns of the younger ages are replaced progressively with linear directional patterns presumably reflecting flattening of dermal papillae and stronger collagen fiber alignment in the papillary dermis. The change of these patterns is accompanied by decrease in viscoelastic anisotropy and increase in angular dispersion width that indicates a strong directional dependence. The anisotropy values for the four subjects imaged are 2.1 (16 months, Fig. 9a), 2.4 (14 years, Fig. 9b), 4.2 (39 years, Fig. 9c), and 15.6 (70 years, Fig. 9d), and the angular dispersion width values are correspondingly 108°, 84°, 40°, and 35°. The viscoelastic anisotropy relates to cutaneous structural feature changes as a function of age.

We can get a better idea of the co-localization of the directionality of skin microrelief and the angular distribution of the RRT values in Fig. 10. A video-microscope image of the upper inner arm of a 47-year-old subject was imaged using 100× magnification. The transmitter and receiver tips of the Reviscometer transducers are drawn, to scale, and the RRT readings from the same site are over-plotted in polar coordinates. Very importantly, the maximum of the RRT values co-localizes with the skin surface microrelief (Fig. 10). Skin microrelief on the upper inner arm develops with age (Fig. 9) in a fashion that parallels the development of RRT anisotropy. Tensions are progressively developed with age in preferential orientations producing changes in the distribution and shape of the dermatoglyphics. In young skin, the relief lines look more plump and rounded on the top and form star-like patterns. As individuals get older, the glyphic structures become flatter and anisotropic, i.e., not symmetric in all directions but elongated in the direction of permanent tension. The directionality is closely related to the tension. The elongation of the glyphics occurs along the direction of increased tension.

A video-microscope image (Hirox, Japan 100× lens) from the upper inner arm of a 70-year-old subject is illustrated in Fig. 11. This figure shows in scale the relation between the orientation of the probe (transducer tips) and the skin microrelief lines. When the transducer tips are oriented perpendicular to the relief lines as illustrated in Fig. 11a, the RRT value is at minimum, typically around 250×10^{-6} s, corresponding to 1,800 m/s for the speed of the sound (based on the probe calibration). The tension of the skin is at maximum and the shear waves propagate faster along this direction (along the relief lines). Conversely, a maximum of the RRT value is recorded when the transducer tips are placed parallel to the relief lines (Fig. 11b). An

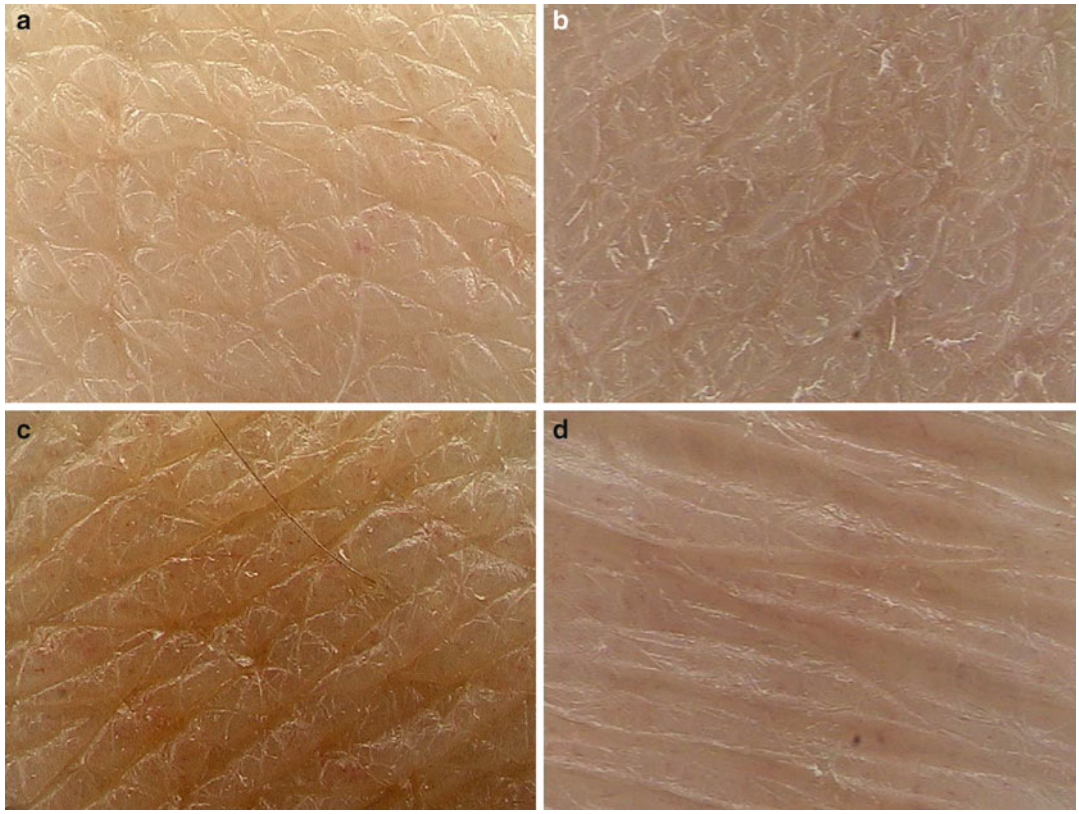

Fig. 9 Illustrates the cutaneous structural feature and viscoelastic changes at different ages. In vivo microscopy images from the upper inner arm representative for the age groups: (**a**) 0–4 years (Anisotropy = 2.1; FWHM = 108°), (**b**) 14–24 years (Anisotropy = 2.4; FWHM = 84°), (**c**) 24–40 years (Anisotropy = 4.2; FWHM = 40°), and (**d**) 65–75 years (Anisotropy = 15.6; FWHM = 35°)

RRT value of 1,100 × 10^{-6} s corresponds to a speed of sound of 390 m/s, a value close to that of the speed of sound in the air (340 m/s). This is the direction of lowest skin tension.

Measurements of the anisotropy ratio at different body sites (neck, upper inner arm, ventral forearm, and dorsal forearm) showed that the age dependence is not the same over the whole body (Fig. 12). The rate of change of viscoelastic properties depends on the anatomical site. The anisotropy increases with age and most notably at anatomical sites where the skin is considered to be "tender" or "soft," such as the upper inner arm and the neck. Interestingly, the most dramatic changes happen on body sites where the skin is considered to be "looser" or "softer" like the neck and the upper inner arm. The viscoelastic properties of the skin at the ventral and dorsal side of the forearm are not statistically different and do not show any significant change within the age range tested here.

4.1 The Effects of Moisturizers on the Resonance Running Time (RRT): A Better Tool for Assessing What Consumers Relate to as "Soft"

Many different approaches for the management of dry skin have been studied. They can be separated into emollients, humectants, and occlusive agents or a combination of them depending on the treatment approach. There

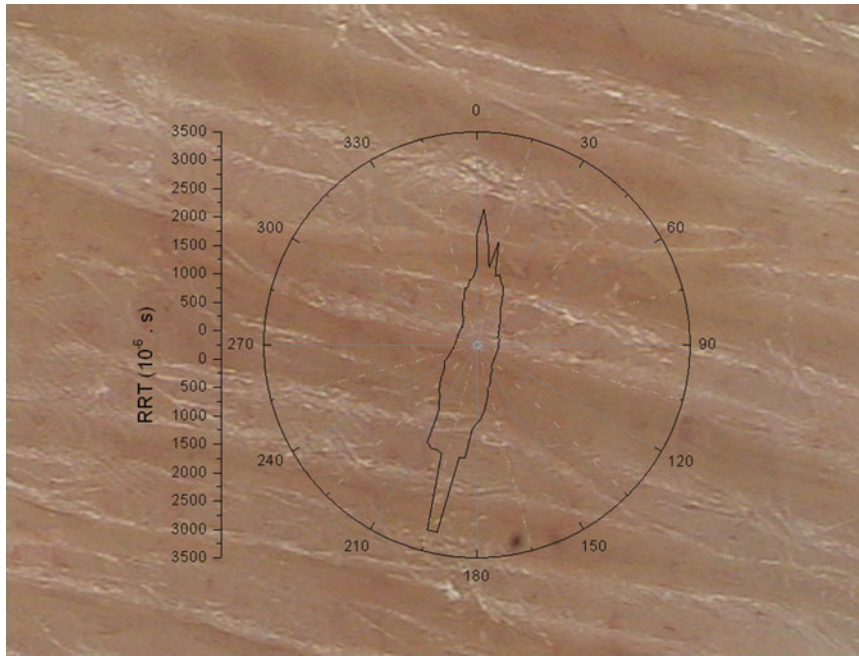

Fig. 10 The viscoelastic anisotropy of the skin follows the direction of microrelief lines with the line connecting the RRT maxima in a direction perpendicular to the microrelief (Langer's line). As an example, a video-microscope image (100×) of the skin is shown with a plot of the RRT values superimposed plotted as a function of the angle, i.e., in polar coordinates

are many different noninvasive instrumentation and clinical assessment to evaluate improvements and grade xerosis. In this study, we wanted to compare three ingredients commonly used in the cosmetic industry for the treatment of dry skin: glycerin, petrolatum, and dimethicone. Glycerin has been shown to have a wide range of benefits to the skin when topically applied. Glycerin acts as a humectant; one molecule of glycerin binds six molecules of water. Glycerin has also been shown to be a lipid-phase modulator, inhibiting the transition of stratum corneum lipids from liquid to solid crystals. Petrolatum and dimethicone act mostly as occlusive materials by helping reduce the amount of water loss to the environment. Dimethicone is an FDA-monographed ingredient as a skin protectant for concentration ranges from 1 % to 30 %.

This was a blinded clinical study, split lower leg, randomized 3 week study with noninvasive and self-assessment measurements at baseline and week 3 after 1 week washout period with a mild liquid cleanser. Ninety-eight women (48 Caucasian and 50 African-American) were recruited with self-identified dry skin and use of body moisturizer at least five times per week. $N = 11–13$/treatment cell/ethnic group. Tested products were applied twice daily on the lower leg. Tested products were divided in four different groups according to their main treatment approach: Product A (10 % glycerin), Product B (10 % petrolatum), Product C (5 % dimethicone), and Product D (12.5 % glycerin, 4 % petrolatum, and 1.25 % dimethicone). Products A, B, and C were formulated in the same simple emulsion base, and Product D was a more complex emulsion formulation.

The skin hydration properties were assessed by measuring skin conductance (Skicon® 200, I.B.S Co., Ltd., Japan), transepidermal water loss (VapoMeter®, Delfin Technologies, Finland), flaking (D-Squame®, CuDerm, USA), and 295 nm skin fluorescence (SkinScan®, Horiba Jobin Yvon Inc., Edison, NJ, USA) and skin viscoelasticity (Reviscometer®, Courage + Khazaka Electronic GmbH, Cologne, Germany).

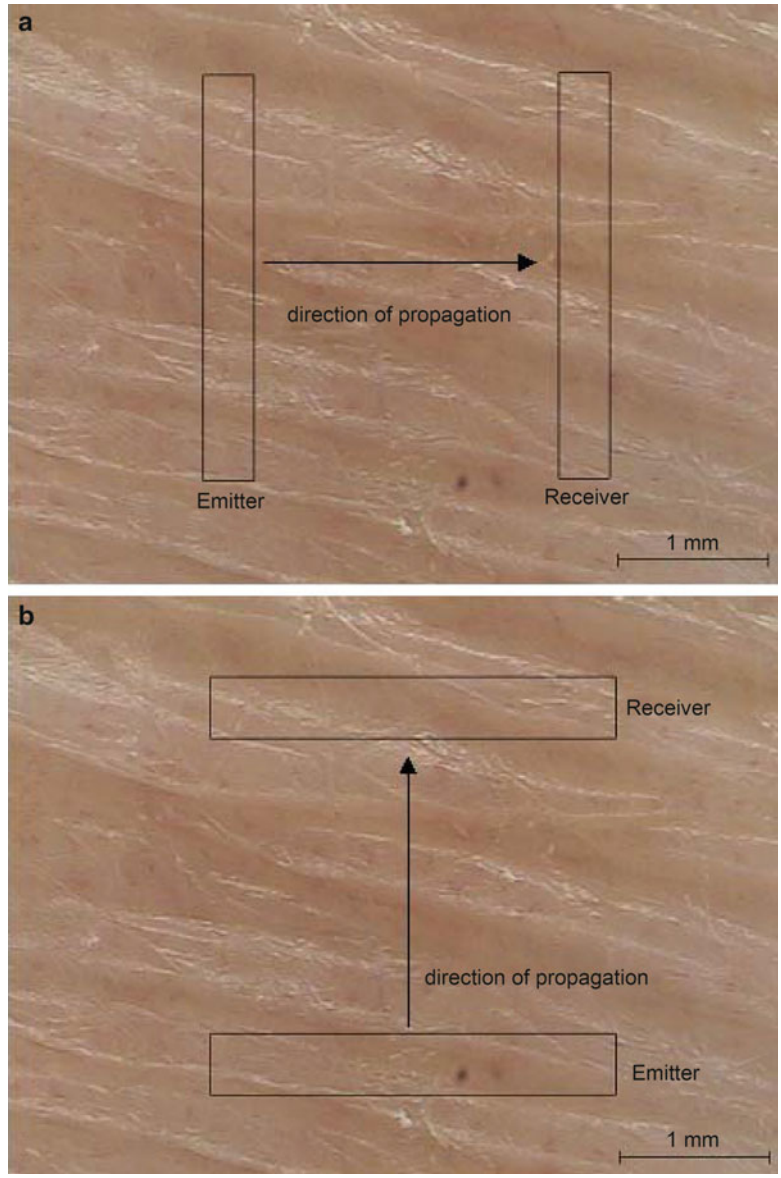

Fig. 11 An example of video-microscope image (HiScope, Hirox with 100× lens) of the upper inner arm from a 70-year-old subject. The figure shows in scale the Reviscometer® transducer tips in relation to skin dermatoglyphics. **a** The signal propagating in the direction of Langer's lines. Lower values in resonance running time; typical values are between 100 x 10^{-6} s and 300 x 10^{-6} s depending on probe response and tested site. b The signal propagating perpendicular to the direction of Langer's lines corresponding to high values in RRT. Typical values can reach up to 3,000 x 10^{-6} s depending on probe response and tested site

Glycerin significantly outperformed petrolatum and dimethicone in increasing skin conductance and reducing the desquamation index. Additionally, glycerin also significantly decreased 295 nm skin fluorescence (tryptophan fluorescence) when compared to baseline. Several studies (Kollias et al. 1998; Doukas et al. 2001; Stamatas et al. 2006) suggest that a hyperproliferation state had existed when the skin was dry at baseline and through the use of a humectant, the proliferation rate was returned to a normal healthy skin level (Russell et al. 2012).

Since there is no statistical difference in terms of ethnicity, we considered all different ethnical groups as one cohort for the viscoelastic assessment. The effects of the treatment over time were evaluated. An example of a viscoelastic measurement as a function of the probe angle for a baseline reading and after 3 weeks treating the lower legs with Product A is illustrated in Fig. 13. We observe a significant decrease in the angular

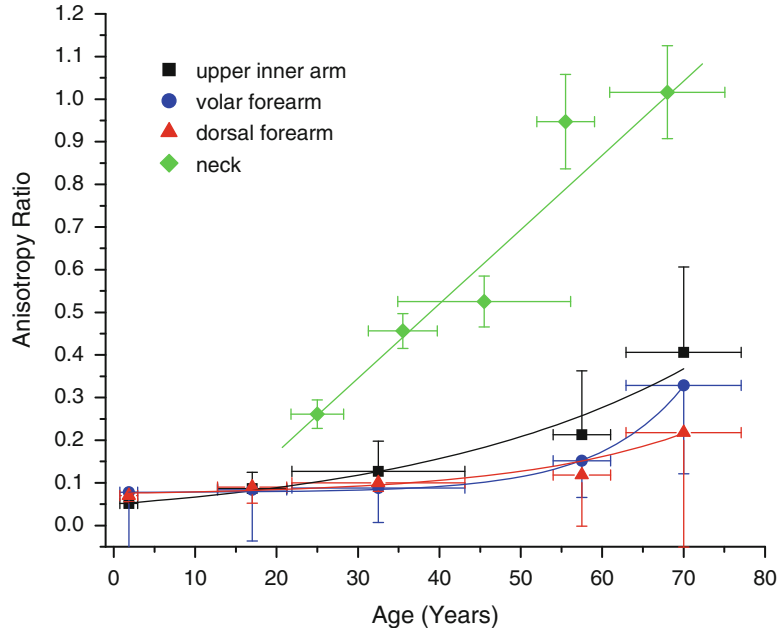

Fig. 12 The anisotropy ratio increases with age showing greater rate of increase for skin sites that are "softer." The anisotropy ratio is shown as a function of age for a number of anatomical sites: neck (*green diamonds*), upper inner arm (*black squares*), ventral forearm (*blue circles*), and dorsal forearm (*red triangles*). Data represents mean value and *error bars* are the standard deviation of the mean (mean ± standard deviation)

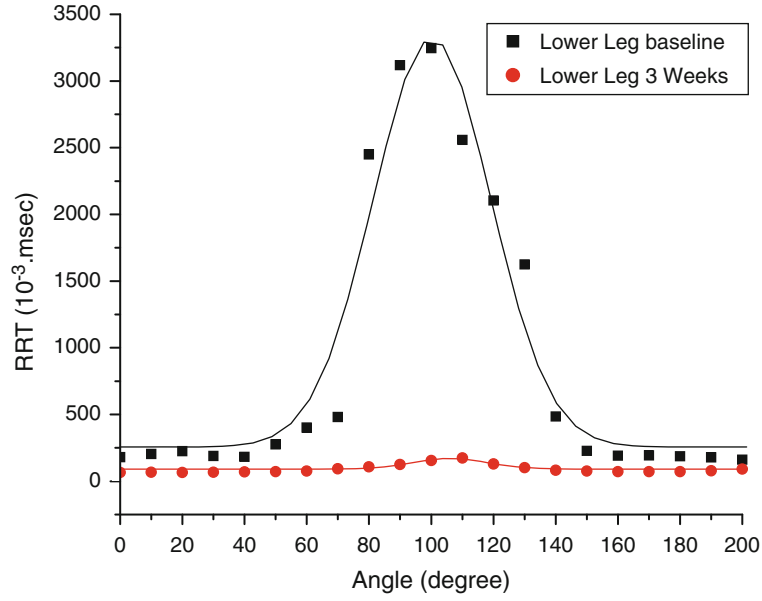

Fig. 13 Resonance running time in 10^{-3} ms as a function of the probe angle (degree) measured on the lower leg before and after 3 weeks of treatment with 10 % glycerin

values of the resonance running time with the treatment indicating significant increase in the local density (lower RRTs), decrease in anisotropy (tension), increase in moisturization, and significant changes in the viscoelasticity of the stratum corneum.

Figure 14 shows the lower leg skin anisotropy measurement before and after 3 weeks of treatment using 4 different moisturization products (mean values _ standard error). Note that the lower leg does not present a high anisotropy at baseline. Mean anisotropy for the lower leg in this study is around 2.5. For the same age group, the anisotropy of the upper inner arm is about three or four times higher. Product A shows significant decrease in anisotropy ($p < 0.5$)

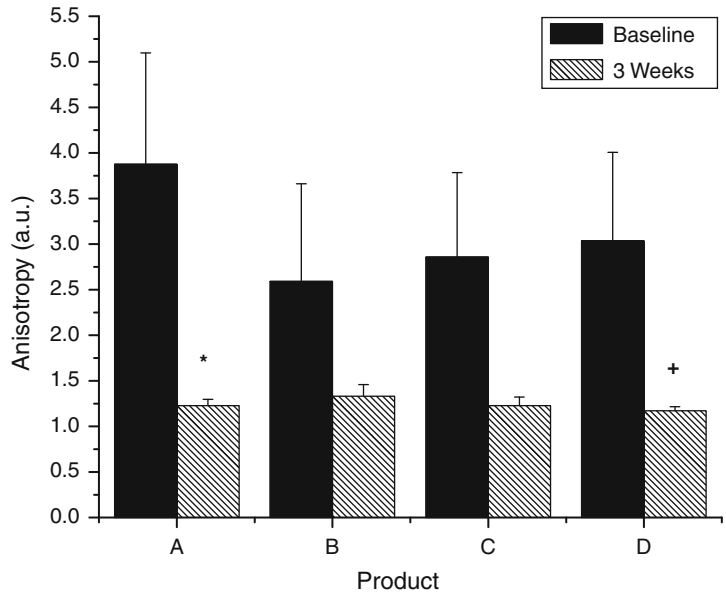

Fig. 14 Lower leg anisotropy measured with the Reviscometer® RVM 600 at baseline and after 3 weeks of treatment. *Error bars* represent the standard deviation (mean for three readings, mean values ± standard deviation)

when compared with baseline readings, and Product D presents a directional decrease in anisotropy ($p < 0.1$) when compared with baseline readings.

5 Discussion

In this chapter, we investigated the age dependence, site dependence, and the effect of moisturizers on skin viscoelastic properties. To this end, we employed a commercially available instrument (Reviscometer® RVM 600, Courage + Khazaka Electronic GmbH, Cologne, Germany), we improved on the acquisition method (measuring at narrow angle intervals), and we defined a parameter that relates the RRT anisotropy and angular dispersion. These parameters provide a wide dynamic range that reflects more accurately the age-dependent changes of skin mechanical properties than the methods proposed so far. Using the modified Reviscometer® method, we characterized the directional characteristics of cutaneous viscoelastic properties, and we provided evidence that the directionality relates to the direction of the microrelief lines on the skin surface. These lines develop as the skin ages and correspond to the tension lines described by the Langer's lines (Langer 1861). This method also can be used in surgeries showing the directions of lower tensions in the skin that can minimize scarring postoperatively.

As shown in Fig. 1, we can see that very important information is lost when we perform the Reviscometer® readings at 45° interval recommended by the manufacturer. The proposed 3° interval procedure allows us to resolve skin anisotropy and to define two novel skin mechanical parameters: anisotropy and the angular dispersion width (FWHM).

The mechanical properties of the skin are an important factor in the determination of the "quality" of the skin. They are as important as the visual appearance of the skin. Changes in the visual appearance include pigmented lesions and minor inflammatory lesions that render the skin nonuniform. Changes in the mechanical properties involve large areas of the skin and are believed to be expressions of aging. One of the dominant characteristics of skin aging is loss of elasticity. Although the changes in the mechanical properties of the skin over several decades of life are substantial, objective measurements have failed to capture their magnitude thus far. Moreover, the mechanical properties of the skin are not isotropic (uniform in all directions), and there is a

need to assess this angular anisotropy. During development, from infancy to adolescence, the skin is expected to respond to tension isotropically to accommodate for growth, while in adulthood this isotropic behavior regresses due to site-specific habituation to tension.

The mechanical and physical properties of the skin have been extensively studied (Skin Mechanics 1986; Rodrigues 2001; Serup and Jemec 2006). These investigations describe the skin as being a viscoelastic medium and interpret the skin with homogeneous density and isotropic elastic moduli. The mechanical properties of the skin stem from contributions of its structural components such as collagen, elastin, keratin, and the purely viscous interstitial fluids (Dahlgren and Elsnau 1986). According to Eq. 1, the speed of shear wave propagation depends on the density of the medium in the direction of the sound propagation. Results presented in this paper show that the shear wave propagation on the surface of the skin is anisotropic and thus the tissue density that relates to the skin mechanical properties is also anisotropic.

We report that this anisotropy increases with age and most notably at anatomical sites where the skin is considered to be "tender," such as the upper inner arm and the neck. Interestingly, the viscoelastic properties of the skin at the ventral and dorsal side of the forearm are not statistically different and do not show any significant change with age.

The skin at the upper inner arm sites changes considerably in structure and mechanical properties with age (Fig. 9). It is evident in Figs. 6 and 7 that the RRT readings of young skin are more isotropic compared with the other two age groups. For the 24–40 year group, there is a distinct increase in the anisotropy, and for the older group, a very well defined RRT maximum.

Very importantly, the maximum of the RRT values co-localizes with the skin surface microrelief (Fig. 10). Skin microrelief on the upper inner arm develops with age (Fig. 9) in a fashion that parallels the development of RRT anisotropy. Tensions are progressively developed with age in preferential orientations producing changes in the distribution and shape of the dermatoglyphics. In young skin, the relief lines look more plump and rounded on the top. The older we get, the glyphics tend to get flatter and less organized and surface lines are more pronounced.

The orientation of the probe (transducer tips) relative to the skin microrelief lines has a big influence in the measured RRT value. When the transducer tips are oriented perpendicular to the relief lines as illustrated in Fig. 11a, the RRT value is at minimum, typically around 250×10^{-6} s, corresponding to 1,800 m/s for the speed of the sound (based on the probe calibration). The tension of the skin is at maximum and the shear waves propagate faster along this direction (along the relief lines). Conversely, a maximum of the RRT value is recorded when the transducer tips are placed parallel to the relief lines (Fig. 11b). An RRT value of $1{,}100 \times 10^{-6}$ s corresponds to a speed of sound of 390 m/s, a value close to that of the speed of sound in the air (340 m/s). This is the direction of lowest skin tension. The speed of the sound in the skin depends on both density and direction.

The skin is inhomogeneous and all other mechanical probes produce measures of averages over the area sampled by the probe. Local inhomogeneities which may be thought of as early events in the development of any skin lesion would be missed because their effect would be minimized because of averaging. Although the local inhomogeneity shows uncertainties in the data, we placed the Reviscometer® probe on places avoiding vellus hair and erector pillow muscles to minimize the variability.

The 4.5 kHz frequency used in the probe makes the sound waves propagate across the surface of the skin, stratum corneum, epidermis, and the very superficial part of the dermis making it the ideal instrument to assess superficial changes in the tissue. When we apply moisturizers on the skin, we observed a significant reduction of the skin stiffness and tensions induced by dryness (Fig. 13) and arriving at a normal low base level of the natural skin tension.

The use of shear wave propagation may be capable of providing valuable information especially on the mechanical properties of the superficial layers of the skin than the suction probes which provide information that includes the bulk of the structural matrix. This is because it actually provides two measures: one depending on density of the skin and the other depending on the angular anisotropy (tension). In order to be able to capitalize on the use of such instrument, we are forced to work on skin sites that show marked changes in anisotropy with age. Even measuring in areas of the skin with low anisotropy, such as the lower leg, the technique proved to be very useful and sensitive in assessing the changes in mechanical properties of the skin with the use of moisturizers.

In summary, we present here a sensitive method of measuring the mechanical properties of the superficial layers of the skin. We demonstrate that the method can be used to document changes in the mechanical properties of the skin with age and the correlation of the angular anisotropy with these properties to the orientation of dermatoglyphics is also related to the orientation of Langer's lines. In a previous work (Ruvolo Jr et al. 2014), we demonstrated that the use of specific antiaging ingredient (2-(dimethylamino)ethanol) can contract keratinocytes in the viable epidermis, changing the tissue density, and this can be assessed by an increase in the velocity of the sound in the tissue. In this chapter, we demonstrated that the use of moisturizers can reduce skin tensions induced by "dryness" by decreasing skin anisotropy. Finally, the probe produces sound waves that propagate throughout the superficial layers of the skin allowing us to assess density and the tensions of the surface of the tissue.

References

ASTM. D2240-03 standard test method for rubber property – durometer hardness. West Conshohocken: ASTM International; 2003.

Biscoe B, Sebastian K. Analysis of the "durometer" indentation. Rubber Chem Technol. 1993;66:827–36.

Cox H. The cleavage lines of the skin. Br J Surg. 1942;29:234–40.

Dahlgren R, Elsnau W. Measurement of skin condition by sonic velocity. J Soc Cosmet Chem. 1986;35:1–9.

Dorogi PL, DeWitt GM, Stone BR, Buras Jr EM. Viscoelastometry of skin in vivo using shear wave propagation. Bioeng Skin. 1986;2:59–70.

Doukas AG, Soukos NS, Babusis S, Appa Y, Kollias N. Fluorescence excitation spectroscopy for the measurement of epidermal proliferation. Photochem Photobiol. 2001;74(1):96–102.

Elsner P. Skin elasticity. In: Bardesca E, Elsner P, Wilhelm K, Maibach H, editors. Bioengineering of the skin: methods and instrumentation. Boca Raton: CRC Press; 1995.

Gibson T, Stark H, Evans J. Directional variation in extensibility of human skin in vivo. J Biomech. 1969;2:201–4.

Jansen L, Rottier PB. Elasticity of human skin related to age. Dermatologica. 1957;115:106–11.

Kollias N, Gilles R, Moran M, Kochevar IE, Anderson RR. Endogenous skin fluorescence includes bands that may serve as quantitative markers of aging and photoaging. J Invest Dermatol. 1998;111(5):776–80.

Langer K. Zur Anatomie und Physiologie der Haut: I. Uber die Splatbarkeit der Cutis. Sitzungber Akad Wiss Wien. 1861;44:19–46.

Lavker RM, Zheng PS, Dong G. Aged skin: a study by light, transmission electron, and scanning electron microscopy. J Invest Dermatol. 1987;88:44s–51.

Mridha M, Odman S, Oberg PA. Mechanical pulse wave propagation in gel, normal and oedematous tissues. J Biomech. 1992;25:1213–8.

Nizet JL, Pierard-Franchimont C, Pierard GE. Influence of body posture and gravitational forces on shear wave propagation in the skin. Dermatology. 2001;202:177–80.

Potts RO, Chrisman DA, Burns EM. The dynamic mechanical properties of human skin in vivo. J Biomech. 1983;16:365–72.

Rodrigues L. EEMCO guidance to the in vivo assessment of tensile functional properties of the skin. Part 2: instrumentation and test modes. Skin Pharmacol Appl Skin Physiol. 2001;14:52–67.

Russell M, Lee C, Ruvolo E. Stratum corneum hydration and barrier benefits with glycerin on xerotic skin. Proceedings of Stratum Corneum VII. Cardiff, UK. 2012.

Ruvolo Jr E, Kollias N. Assessment of mechanical properties of skin by shear wave propagation and acoustic dispersion. In: Berardesca E, Maibach H, Wilhelm K, editors. Non invasive diagnostic techniques in clinical dermatology. Berlin: Springer; 2014. p. 233–50. DOI 10.1007/978-3-642-32109-2_21.

Ruvolo Jr EC, Stamatas GN, Kollias N. Skin viscoelasticity displays site- and age-dependent angular anisotropy. Skin Pharmacol Physiol. 2007;20:313–21.

Serup J, Jemec G, Grove G. Handbook of non-invasive methods and the skin. Boca Raton: CRC Press; 2006.

Lanir Y. Skin mechanics. In: Skalak R, Chien S, editors. Handbook of bioengineering. New York: MacGraw-Hill; 1986. p. 11.11–24.

Stamatas GN, Estanislao RB, Suero M, Rivera ZS, Li J, Khait A, Kollias N. Facial skin fluorescence as a marker of the skin's response to chronic environmental insults and its dependence on age. Br J Dermatol. 2006;154:25–132.

Takakuda K, Miyairi H. Tensile behaviour of fibroblasts cultured in collagen gel. Biomaterials. 1996;17:1393–7.

Tronnier H. Dermatologisch-phamakologische Methoden zur Prüfung kosmeticher Präparate und Grundstoffe. Ärzliche Kosmotogie. 1980;10:361–7.

Vexler A, Polyansky I, Gorodetsky R. Evaluation of skin viscoelasticity and anisotropy by measurement of speed of shear wave propagation with viscoelasticity skin analyzer. J Investig Dermatol. 1999;113:732–9.

Skin Tensile Strength in Scleroderma

99

Gérald E. Piérard, Trinh Hermanns-Lê, and Claudine Piérard-Franchimont

Contents

G.E. Piérard (✉)
Laboratory of Skin Bioengineering and Imaging (LABIC), Liège University, Liège, Belgium

Service de Dermatopathologie, CHU du Sart Tilman, Liège, Belgium
e-mail: Gerald.pierard@ulg.ac.be

T. Hermanns-Lê
Laboratory of Skin Bioengineering and Imaging (LABIC), Liège University, Liège, Belgium

Service de Dermatopathologie, CHU du Sart Tilman, Liège, Belgium

Department of Dermatopathology, Unilab Lg, University Hospital of Liège, Liège, Belgium
e-mail: Trinh.le@ulg.ac.be; Trinh.hermanns@chu.ulg.ac.be

C. Piérard-Franchimont
Laboratory of Skin Bioengineering and Imaging (LABIC), Department of Clinical Sciences, Liège University, Liège, Belgium
e-mail: Claudine.franchimont@ulg.ac.be

P. Humbert et al. (eds.), *Agache's Measuring the Skin*,
DOI 10.1007/978-3-319-32383-1_133

Keywords
Dermis • Connective tissue strength • Skin viscoelasticity • Biomechanics • Tensile strength • Scleroderma • Skin stiffness

1 Introduction

In recent decades, various instrumentations were developed for assessing the in vivo skin viscoelasticity (Piérard et al. 2013a; Rodrigues and EEMCO group 2001; Sandford et al. 2013; Shang et al. 2010). The methods relied on various approaches including uniaxial and biaxial stretching, suction, elevation, indentation, torsion, ballistometry, and vibration procedures (Murry and Wickett 1997; Rodrigues and EEMCO group 2001). The devices afford sound although some distinct or even contradictory information. The time-honored suction method aims at measuring the skin deformation caused by any decrease in external pressure exerted over a defined skin area (Cua et al. 1990; Diridollou et al. 2000a; Livarinen et al. 2013; Piérard et al. 1995, 2013a). In such a procedure, skin deformation occurs as a function of the suction force, its time of application, and the area of the stressed skin (Piérard 1999; Piérard et al. 1995; Schlangen et al. 2003). It corresponds to a specific in vivo expression of the overall skin viscoelasticity.

2 Skin Biomechanics

From a physiopathological standpoint, three clinically relevant physical characteristics of skin biomechanics are crucial, namely, (a) the skin stiffness corresponding to the resistance to any shape change, (b) the skin elasticity representing the ability to recover spontaneously the initial shape after deformation, and (c) the skin viscous deformation over time under constant force leading to the creep extension (Piérard et al. 2013a). Over a large part of the body, the overall skin viscoelasticity mainly depends on the extracellular matrix (ECM) of the cutaneous connective tissue forming the dermo-hypodermal layers. Only minimal contribution is expected from the epidermis (Piérard 1999).

The bulk of the regular dermis controlling skin viscoelasticity consists of a complex fibrous network forming the ECM scaffold. The major set of fibrous components corresponds to the collagen fibers determining both the mechanical stability of the tissue and its resistance to deformation. Such a structure fails in severe dermal atrophy or dermatoporosis (Kaya and Saurat 2007). A second set of components is formed by elastic fibers present in smaller amounts. They restore any bent collagen bundle to its relaxed standing position (Langton et al. 2012; Piérard and Lapière 1987). The loosely interconnected complex fiber scaffold is permeated by amorphous hydrated ECM compounds corresponding to proteoglycans, glycoproteins, and glycosaminoglycans. Dermal cells are responsible for maintaining and remodeling the macromolecular matrix. They correspond to several distinct cell types including among others fibroblasts, dermal dendrocytes, mast cells, and myofibroblasts. They potentially exert some contractile activity upon the fibrous networks through the intervention of adhesion molecules (Binai et al. 2012). Their tensegrity, adhesion properties to ECM fibers, and contractility are therefore important in the force transduction inside the dermis.

As a rule, the in vivo ECM viscoelasticity is quite difficult to assess with repeatability and confidence. The global response of skin to any mechanical stress depends on tensile biomechanical and rheological characteristics expressed by the composite nature of the skin and subcutaneous tissues (Piérard and Lapière 1987). In cutaneous scleroderma, the tissue remodeling affects indiscriminately all levels of the ECM, and the mechanical impact of the coarse collagen networks likely predominates over other structural changes.

In a series of connective tissue disorders including scleroderma, the assessment of the skin viscoelasticity is primordial for evaluating with confidence both the disease severity and any therapeutic response (Piérard et al. 2013b). In general, the overall tensile characteristics of the whole skin are representative of the properties of the dermis and subcutaneous tissues. Obviously, the tensile strength of normal skin contrasts with sclerotic conditions. Healthy skin exhibits both flexibility and relative resistance to deformation, allowing casual body movements and partial temporary reversible compression and distention. Once the forces responsible for skin deformation are released, elasticity allows the skin to return spontaneously and progressively to its initial shape. As such, progressive resistance to deformation, flexibility, and elasticity must be adequately balanced to govern the optimal skin tensile strength. The behavior of the three-dimensional ECM fibrous meshworks combines the response of its components to which the deformation is applied. Such properties represent the functional expression of the structural configuration of the ECM from the molecular level to the macromolecular organization and the microscopic configurations.

In any instances, the viscoelasticity variations of the skin owing to body region, age, and gender outweigh the discrete variations in the intrinsic molecular compositions (Piérard 1999; Piérard et al. 2013a). Due to the composite structure of the dermo-hypodermal tissues, the in vivo skin viscoelastic properties are notoriously complex to assess precisely and are difficult to interpret particularly in some pathological conditions (Piérard 1999). The typical mechanical response of each macromolecular component is variable

within the wide range of force intensities encountered in daily life and more exceptional conditions. This fact obviously adds to the difficulties encountered when interpreting experimental and observational data and unraveling the tensile strength complexity of the skin.

3 Connective Tissue Structure

A global interdependence links the structure and mechanical functions of the skin ECM. The basic properties of each fibrous component have been identified in vitro. However, the relationships between the structures and functions of skin ECM appear complexified and intricated in vivo. The multifaceted wavy to straight presentations of fibers at rest govern for a large part the ECM viscoelastic properties of the tissue. The variable looseness to compactness configurations of the ECM fibrous networks are determining. The situation is even more complex in presence of physical entanglements between the diverse fibrous structures and networks.

The bulk of the reticular ECM dermis in scleroderma consists of a dense accumulation of collagen fiber. The individual collagen fibrils are packed into fiber units and further in fiber bundles. The way by which fibrils are packed and held together is important with regard to the ECM mechanical properties. Cross-links between collagen molecules are not the primary cause for fibril aggregation in fibers and bundles. Rather, the interfibrillar matrix plays a major role. On a higher hierarchial level, the coarse collagen bundles are interconnected with each other. They are often closely packed and stretched in superimposed planes grossly oriented parallel to the skin surface. Elastic fibers present in smaller amounts normally serve to restore deformed collagen bundles to a relaxed and wavy position. This pattern is hardly possible in skin involved in scleroderma.

Both the thickness and intimate structure of the ECM play prominent and independent mechanical functions. For instance, a major role is occasionally ascribed to the structure, density, and location of the elastic fibers when tensile strength is involved in discrete skin deformations. In fact, although it is acknowledged that these fibers exhibit typical elastic properties, any change in the overall elastic functional properties of the skin cannot be ascribed solely to them. Many other structures participate in tissue elasticity, and it is practically impossible to disentangle their respective contributions in the tensile response of the skin (Piérard 1999).

The dermis is a heterogeneous structure because it exhibits tremendous differences between its different layers and with the variable extent in solar elastosis. In addition, the volume of the hypodermis and of the eventual sebaceous glands is of equal importance if not greater than the dermal thickness itself in their influence upon the overall tensile functional properties of the skin. In fact, the fat-enriched lobules made of either sebocytes or adipocytes put the dermis under tension, limiting the mobility of skin (Piérard 1999). As a consequence of these uncertainties, the calculation of ratios between in vivo tensile stress and tissue strain (Young's modulus, shear modulus, bulk modulus) is only viewed as theoretical concepts with probably little relevance when applied in vivo to the complex composite of structures making skin and its subcutaneous tissue.

4 Clinical Assessment of Scleroderma Involvement

Scleroderma represents a heterogeneous group of conditions with distinct clinical manifestations. The main clinical presentations are the localized forms (morphea, monomelic type) and the systemic forms (Walters et al. 2009). The classification of systemic scleroderma distinguishes three grades. Grade I corresponds to acroscleroderma including the Raynaud's syndrome subgroup. Grade II is acroscleroderma with progression of sclerosis from distal to proximal areas of the limbs. Grade III is diffuse scleroderma usually starting on the trunk with rapid progression to acral areas.

Skin involvement in scleroderma is characterized by hardness and hidebound resulting from

massive deposition and straightening of collagen bundles in the dermis and hypodermis. Temporary dermal edema is commonly present. Skin induration and tethering are commonly evaluated according to skin severity scoring extrapolated from clinical palpation (Clements et al. 1990, 1993; Pope et al. 1995). Some overlap exists between different skin scorings including the "skin thickness index" and the "skin tethering/hidebound index." The skin thickness/hidebinding is scored in a 4-point scale (0, normal; 1, mild; 2, moderate; 3, severe). It is acknowledged that sclerotic skin changes correlate with both the overall disease activity and prognosis of systemic sclerosis. Unfortunately, such assessments remain subjective with low intra- and interobserver reproducibility. In addition, they are not free of bias. According to studies, the modified Rodnan skin score has been calculated from observations gained on 17, 26, or 74 body areas.

5 Instrumental Assessment of the Skin Tensile Strength

Skin involvement in systemic sclerosis most often begins on the acral portion of the limbs, where it usually remains more prominent than on other body sites. It would be conceivable to choose other specific target sites for biomechanical assessments. However, the physical properties of normal skin vary greatly depending on the body site. In addition, computation of many measurements should be performed before recommending a specific body site other than the forearm for comparative assessments of acroscleroderma.

The understanding of skin viscoelasticity is so complex in scleroderma that it is difficult to obtain anything approaching clean results as obtained by scrutinizing the molecular structure of the dermis (Martin et al. 2012). A minimum functional workup is however recommended as early as in Raynaud's syndrome (Pistorius and Carpentier 2012). However, the correct interpretation of in vivo mechanical measurements requires the basic knowledge of the overall skin microstructure, including the arrangement of collagen and elastic fibers, and their relation to other ECM components.

In general, the tensile strength, temperature, and thickness of scleroderma skin have been studied noninvasively by a series of distinct methods (Aghassi et al. 1995; Enomoto et al. 1996; Hermanns-Lê et al. 2001; Pauling et al. 2012; Reisfeld 1994; Scheja and Akesson 1997; Seyger et al. 1997; Zhang et al. 2011). It is beyond doubt that the various tissue thicknesses affect the overall tensile strength of the skin in scleroderma. However, it is hazardous and probably misleading to use the dermal thickness measured using ultrasound methods as a major severity criterion for scleroderma. Indeed, although the dermis is often thickened, variations in time are usually large. When the collagen and elastic fibers are stretched at rest during the induration phase, cutaneous edema subsides and skin thickness commonly decreases.

The real value of measuring the skin tensile strength in vivo is occasionally uncertain because confounding factors are not always suspected clinically. These include regional differences in the tensile strength, variability due to body site, posture, and subject age, gender, and cumulative ultraviolet exposures (Diridollou et al. 2000b; Schlangen et al. 2003). Anyway, some measurements are very informative (Fett and Werth 2011; Hermanns-Lê et al. 2013; Piérard et al. 2013b).

Of note, tensile strength of the whole skin is time dependent. Indeed, when skin is stressed by a load, the overall response of the organ alters its shape in a nonlinear way. A rapid extension normally takes place at first to give way to a viscoelastic phase with lower extension. When the force is maintained at a particular level for a period, further extension, known as the creep or viscous extension, gradually takes place (Piérard et al. 2013a). Such phenomenon, resulting from the recent stress history, occurs when a series of stresses are consecutively applied and removed at the same site (Fig. 1). When the deformation (strain) is maintained for a while (days and weeks), tissue remodeling progressively takes place and is responsible for a biological creep corresponding to relaxation distinct from the mechanical creep. Because of the above

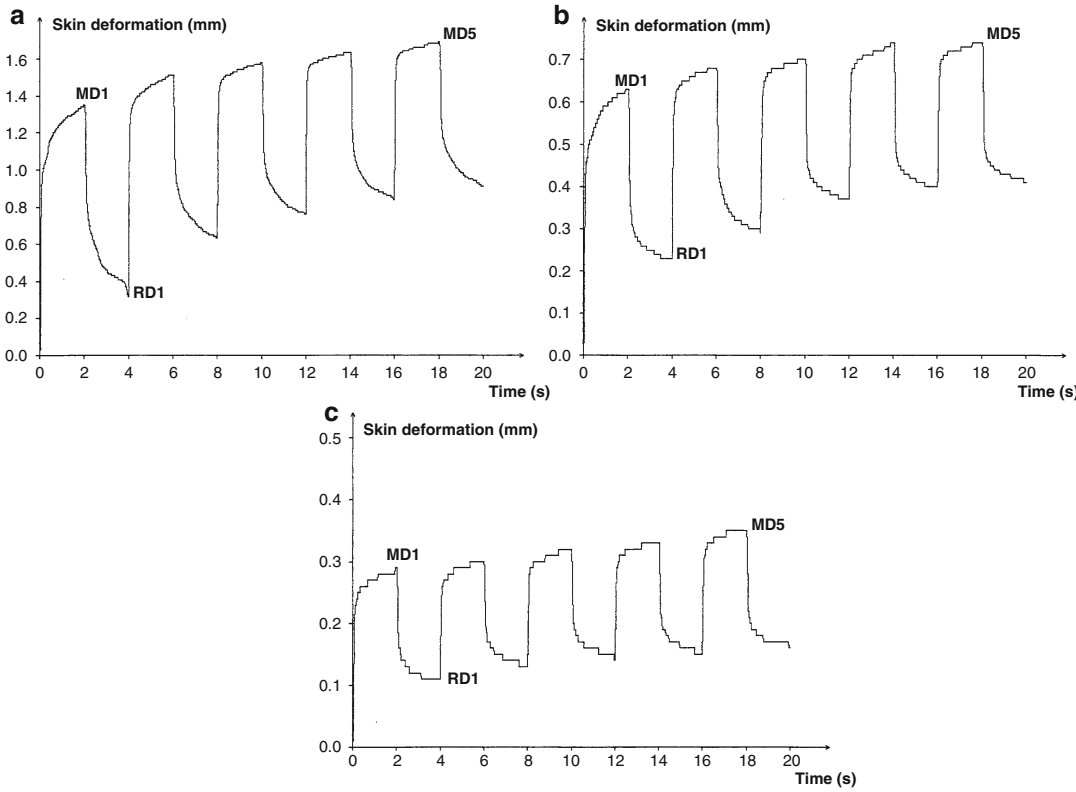

Fig. 1 Evaluation of the skin deformation over tissue during five successive cycles of 2 s suction and relaxation phases. (**a**) High skin deformation (MD1), biological elasticity (MD1-RD1/MD1^{-1}), and creep extension (MD5-MD1). (**b**) Moderate skin deformability. **c** Low skin deformability

considerations, the time-dependent tensile strength in part depends on the rate of load application, the duration for which it is sustained, the previous stress history, as well as the possible preconditioning of the site. In scleroderma, the biological creep and mechanical creep are reduced, particularly during the sclerotic stage (Fig. 1).

Hidebinding is the most impressive and typical change in scleroderma. This feature is not directly related to the dermal thickening. In fact, it is difficult to pinch sclerotic skin into a fold. Only a few noninvasive bioengineering methods adequately assess the deep fixation and induration of the skin. Among them, the suction method is a close imitation of lifting the skin between the fingers for assessing adequately hidebinding (Piérard et al. 2013b) (Fig. 2). Indeed, an important aspect of the global tensile skin functional properties is tethering of the ECM skin to the fat layer. In scleroderma it limits the free mobility of the dermis. The quantitative assessment of skin toughness in scleroderma using the suction method is of interest for monitoring both the progression of the disease and the therapeutic efficacy. A limited number of studies on skin viscoelasticity have been carried out until now in patients with scleroderma (Dobrev 1999, 2007; Fett and Werth 2011; Hermanns-Lê et al. 2013; Nikkels-Tassoudji et al. 1996; Piérard-Franchimont et al. 1998). They were performed in experimental designs using distinct devices in absence of any standardized protocol. Hence, results are difficult to compare, even if there is overall agreement concerning the basic and specific changes in the viscoelastic properties of skin.

The size of the test area influences the data (Piérard et al. 1995) which appear conflicting in

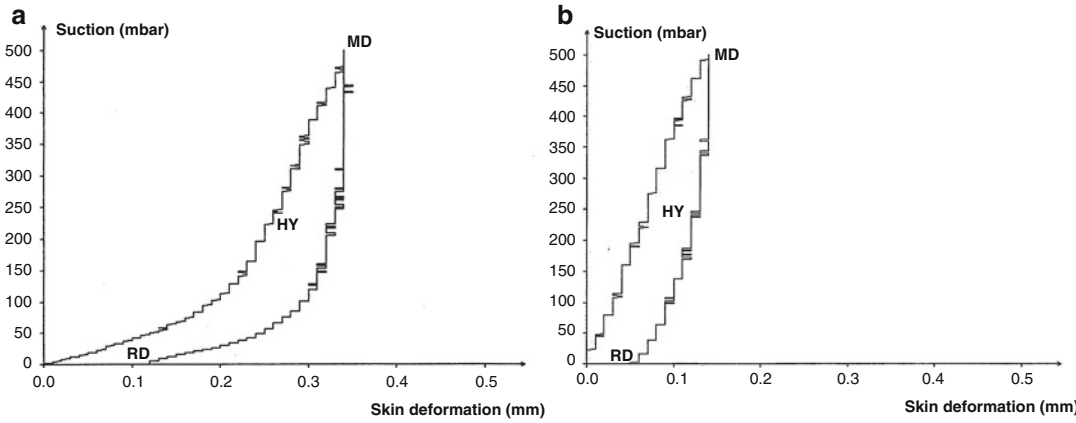

Fig. 2 One single cycle of progressive suction and relaxation. (**a**) High deformability (*MD*) and low residual deformation (*RD*) and hysteresis (*HY*). (**b**) Low deformability (*MD*), residual deformation (*RD*), and hysteresis (*HY*)

some instances. The superficial dermis of scleroderma can be atrophic, and skin distension measured on a small area (2-mm measuring probe) increases. By contrast, hidebinding the skin to underlying tissues is responsible for low distensibility when measured on a larger surface area. The resistance to vertical stress is essentially due to the dermis rather than the hypodermis, although the relative contribution of each is not easily distinguished. The subcutaneous fat compartment is likely more involved by high suction forces applied to large surface areas than by lower suction to smaller surface areas. The main alterations in scleroderma being localized in the reticular dermis and hypodermis, a large measuring probe and a high suction force might appear to yield more relevant information (Hermanns-Lê et al. 2013). At all stages of scleroderma, the overall skin distensibility decreases. This functional characteristic is linked to the stretching of the collagen fibers and reflects the skin induration and the deep tethering. The viscoelastic ratio is highly variable among patients and even in time in a given patient. This aspect is ascribed in part to fluctuations in dermal edema and ECM load in proteoglycans. The immediate retraction ability following the suction release is often decreased. The biological elasticity is either unmodified or increased, particularly during the terminal sclerotic phase of the disease.

Individual values in scleroderma can be compared to the 10th and 90th percentiles of the normal reference population. According to the evolution in time of the viscoelastic parameters relevant to the clinical presentation, four rheological stages of acroscleroderma were tentatively proposed. They corresponded to the incipient, progressive, overt, and regressive stages, respectively (Piérard et al. 2013b).

6 Assessment of Therapeutic Efficacy

Objective evaluations of skin stiffening have obvious advantages over subjective clinical rating. It is an adjunct to the range of biological and functional evaluations already in use for estimating internal organ involvement by scleroderma. The therapeutic efficacy is commonly different on the different organs affected by scleroderma. For instance, improvement in pulmonary function is not usually correlated with recovery of skin mobility.

Any decrease in skin stiffness in scleroderma does not occur spontaneously or under various ancillary treatments. Only a few clinical studies have reported therapeutic improvements of scleroderma Beyer et al. (2012). They await confirmation using criteria of evidence-based

medicine (Andres et al. 2010; Herrick et al. 1994; Humbert et al. 1990, 1993; Piérard et al. 2013c). Owing to the natural course of acroscleroderma, any therapy resulting in stabilization of the skin involvement should be regarded as beneficial. A drug yielding a prominent regression of cutaneous sclerosis is not yet available.

References

Aghassi D, Monoson T, Braverman I. Reproducible measurements to quantify cutaneous involvement in scleroderma. Arch Dermatol. 1995;131:1160–6.

Andres C, Kollmar A, Mempel M, Hein R, Ring J, Eberlein B. Successful ultraviolet A1 phototherapy in the treatment of localized scleroderma: a retrospective and prospective study. Br J Dermatol. 2010;162:445–7.

Beyer C, Distler O, Distler JH. Innovative antifibrotic therapies in systemic sclerosis. Curr Opin Rheumatol. 2012;24:274–80.

Binai N, O'Reilly S, Griffiths B, van Laar JM, Hügle T. Differentiation potential of $CD14^{+}$ monocytes into myofibroblasts in patients with systemic sclerosis. PLoS One. 2012;7:e33508.

Clements PJ, Lachenbruch PA, Ng SC, Simmons M, Sterz M, Furst DE. Skin score: a semi-quantitative measure of cutaneous involvement that improves prediction of prognosis in systemic sclerosis. Arthritis Rheum. 1990;33:1256–63.

Clements PJ, Lachenbruch PA, Seibold JR, Zee B, Steen VD, Brennan P, Silman AJ, Allegar N, Varga J, Massa M. Skin thickness score in systemic sclerosis: an assessment of interobserver variability in three independent studies. J Rheumatol. 1993;20:1892–6.

Cua AB, Wilhelm KP, Maibach HI. Elastic properties of human skin: relation to age, sex, and anatomical region. Arch Dermatol Res. 1990;282:283–8.

Diridollou S, Patat F, Gens F, Vaillant L, Black D, Lagard eJM, Gall Y, Berson M. In vivo model of the mechanical properties of the human skin under suction. Skin Res Technol. 2000a;6:214–21.

Diridollou S, Black D, Lagarde JM, Gall Y, Berson M, Vabre V, Patat F, Vaillant L. Sex- and site-dependent variations in the thickness and mechanical properties of human skin in vivo. Int J Cosmet Sci. 2000b;22:421–35.

Dobrev HP. In vivo study of skin mechanical properties in patients with systemic sclerosis. J Am Acad Dermatol. 1999;40:436–42.

Dobrev H. In vivo study of skin mechanical properties in Raynaud's phenomenon. Skin Res Technol. 2007;13:91–4.

Enomoto D, Mekkes NH, Bossuyt JR, Hoekzema R, Bos JD. Quantification of cutaneous sclerosis with a skin elasticity meter in patients with generalized scleroderma. J Am Acad Dermatol. 1996;35:381–7.

Fett N, Werth VP. Update on morphea: part II. Outcome measures and treatment. J Am Acad Dermatol. 2011;64:231–42.

Hermanns-Lê T, Jonlet F, Scheen A, Piérard GE. Age- and body mass index-related changes in cutaneous shear wave velocity. Exp Gerontol. 2001;36:363–72.

Hermanns-Lê T, Piérard-Franchimont C, Piérard GE, André B, de Roover C, Renwart L, et al. How I explore… the skin functional involvement in scleroderma. Rev Med Liege. 2013;68:141–7.

Herrick AL, Gush RJ, Tully M, Jayson MI. A controlled trial of the effect of topical glyceryl trinitrate on skin blood flow and skin elasticity in scleroderma. Ann Rheum Dis. 1994;53:212.

Humbert P, Dupond JL, Rochefort A, Vasselet R, Lucas A, Laurent R, Agache P. Localized scleroderma – response to 1,25-dihydroxyvitamin D3. Clin Exp Dermatol. 1990;15:396–8.

Humbert P, Dupond JL, Agache P, Laurent R, Rochefort A, Drobacheff C, de Wazieres B, Aubin F. Treatment of scleroderma with oral 1,25-dihydroxyvitamin D3: evaluation of skin involvement using non-invasive techniques. Results of an open prospective trial. Acta Derm Venereol. 1993;73:449–51.

Kaya G, Saurat JH. Dermatoporosis: a chronic cutaneous insufficiency/fragility syndrome. Clinicopathological features, mechanisms, prevention and potential treatments. Dermatology. 2007;215:284–94.

Langton AK, Sherratt MJ, Griffiths CE, Watson RE. Differential expression of elastic fibre components in intrinsically aged skin. Biogerontology. 2012;13:37–48.

Livarinen JT, Korhonen RK, Julkunen P, et al. Experimental and computational analysis of soft tissue mechanical response under negative pressure in forearm. Skin Res Technol. 2013;19:e356–65.

Martin P, Teodoro WR, Velosa AP, de Morais J, Carrasco S, Christmann RB, Goldenstein-Schainberg-C, Parra ER, Katayama ML, Sotto MN, Capelozzi VL, Yoshinari NH. Abnormal collagen V deposition in dermis correlates with skin thickening and disease activity in systemic sclerosis. Autoimmun Res. 2012;11:827–35.

Murry BC, Wickett RR. Correlations between Dermal torque meter®, Cutometer®, and Dermal phase meter® measurements of human skin. Skin Res Technol. 1997;3:101–6.

Nikkels-Tassoudji N, Henry F, Piérard-Franchimont C, Piérard GE. Computerized evaluation of skin stiffening in scleroderma. Eur J Clin Invest. 1996;26:457–60.

Pauling JD, Shipley JA, Harris ND, McHugh NJ. Use of infrared thermography as an endpoint in therapeutic trials of Raynaud's phenomenon and systemic sclerosis. Clin Exp Rheumatol. 2012;30:S103–15.

Piérard GE. EEMCO guidance to the in vivo assessment of tensile functional properties of the skin. Part 1: relevance to the structures and ageing of the skin and subcutaneous tissues. Skin Pharmacol Physiol. 1999;12:352–62.

Piérard GE, Lapière CM. Microanatomy of the dermis in relation to relaxed skin tension lines and Langer's lines. Am J Dermatopathol. 1987;9:219–24.

Piérard GE, Kort R, Letawe C, Olemans C, Piérard-Franchimont C. Biomechanical assessment of photodamage. Derivation of a cutaneous extrinsic ageing score. Skin Res Technol. 1995a;1:17–20.

Piérard GE, Nikkels-Tassoudji N, Piérard-Franchimont C. Influence of the test area on the mechanical properties of skin. Dermatology. 1995b;191:9–15.

Piérard GE, Piérard S, Delvenne P, Piérard-Franchimont C. In vivo evaluation of the skin tensile strength by the suction method. Coping with hysteresis and creep extension. Int Sch Res Netw Dermatol. 2013a;841217:2013.

Piérard GE, Hermanns-Lê T, Piérard-Franchimont C. Scleroderma: skin stiffness, assessment using the stress-strain relationship under progressive suction. Exp Opin Med Diagn. 2013b;7:119–25.

Piérard-Franchimont C, Nikkels-Tassoudji N, Lefèbvre P, Piérard GE. Subclinical skin stiffening in adults suffering from type 1 diabetes mellitus. A comparison with Raynaud's syndrome. J Med Eng Technol. 1998;22:206–10.

Pistorius MA, Carpentier PH. Minimal work-up for Raynaud syndrome: a consensus report. J Mal Vasc. 2012;37:207–12.

Pope JE, Baron M, Bellamy N, Campbell J, Carette S, Chalmers I, Dales P, Hanly J, Kaminska EA, Lee P, et al. Variability of skin scores and clinical measurements in scleroderma. J Rheumatol. 1995;22:1271–6.

Reisfeld PL. A hard subject: use of Durometer to assess skin hardness. J Am Acad Dermatol. 1994;31:515.

Rodrigues L, EEMCO group. EEMCO guidance to the in vivo assessment of tensile functional properties of the skin. Part 2: instrumentation and test modes. Skin Pharmacol Appl Skin Physiol. 2001;14:52–67.

Sandford EY, Chen YI, Hunter I, Hillebrand G, Jones L. Capturing skin properties from dynamic mechanical analyses. Skin Res Technol. 2013;19:e339–48.

Scheja A, Akesson A. Comparison of high frequency (20 MHz) ultrasound and palpation for the assessment of skin involvement in systemic sclerosis (scleroderma). Clin Exp Rheumatol. 1997;15:283–8.

Schlangen LJM, Brooken D, Van Kemenade PM. Correlations between small aperture skin suction parameters: statistical analysis and mechanical model. Skin Res Technol. 2003;9:122–30.

Seyger MM, van den Hoogen FH, de Boo T, de Jong EM. Reliability of two methods to assess morphea: skin scoring and the use of a Durometer. J Am Acad Dermatol. 1997;37:793–6.

Shang X, Yen MR, Gaber MW. Studies of biaxial mechanical properties and nonlinear finite element modeling of skin. Mol Cell Biomech. 2010;7:92–104.

Walters R, Pulitzer M, Kamino H. Elastic fiber pattern in scleroderma/morphea. J Cutan Pathol. 2009;36:952–7.

Zhang X, Osborn TG, Pittelkow MR, Qiang B, Kinnick RR, Greenleaf JF. Quantitative assessment of scleroderma by surface wave technique. Med Eng Phys. 2011;33:31–7.

Model-Based Interpretation of Skin Microstructural and Mechanical Measurements

100

Jessica W. Y. Jor, Matthew D. Parker, Martyn P. Nash, Andrew J. Taberner, and Poul M. F. Nielsen

Contents

Keywords

Structurally based constitutive modeling • Skin biomechanics • Collagen • Noninvasive imaging • Mechanical testing

1 Introduction

The skin is the largest organ in the human body and provides a number of protective, sensory, and regulatory functions (Kanitakis 2002). It is a composite tissue comprised of three main layers (Wilkes et al. 1973): (i) the *epidermis*, a thin layer of cells that undergo continuous renewal and migration toward the external surface; (ii) the *dermis*, comprising of collagen and elastin fibrous networks embedded within a proteoglycan matrix to provide the skin with its mechanical stability; and (iii) the *hypodermis*, the deepest layer composed mainly of adipose tissue, with the role of insulation, energy storage, and shock absorption.

Being a composite tissue, the human skin exhibits a complex, highly nonlinear, anisotropic, viscoelastic, and heterogeneous mechanical response. The overall mechanical behavior of the skin is largely dependent on the tissue composition and the properties of its individual constituents. The major load-bearing tissue component in the skin is collagen, making up 60 % to 80 % of dry tissue weight (Wilkes et al. 1973). In contrast, elastin fibers (1 % to 4 % of dry tissue weight) enable the skin to elastically recoil upon

J.W.Y. Jor (✉) • M.D. Parker
Auckland Bioengineering Institute, University of Auckland, Auckland, New Zealand
e-mail: j.jor@auckland.ac.nz

M.P. Nash • A.J. Taberner • P.M.F. Nielsen
Auckland Bioengineering Institute, University of Auckland, Auckland, New Zealand

Department of Engineering Science, University of Auckland, Auckland, New Zealand

P. Humbert et al. (eds.), *Agache's Measuring the Skin*,
DOI 10.1007/978-3-319-32383-1_134

stretching (Carton et al. 1962) and, together with the proteoglycan ground matrix, determine the overall mechanical response of the skin at low strains (Daly 1969; Harkness and Harkness 1959).

Some of the first measurements of skin properties were made as early as 1880. In his classical study using human cadavers, Langer measured the shape of elliptical wounds created from circular punctures of the skin (Langer 1861; for English translation refer to Langer 1978). The observation of such direction-dependent opening of wounds suggested that in vivo skin exists in a state of inherent nonuniform pretension. Histological studies later discovered that the directions of these tension lines are associated with the underlying collagen fiber arrangement (Ridge and Wright 1966; Cox 1941).

The typical stress-strain response of the skin, and how it relates to the geometric arrangement of the collagen network, have been well established in early histological studies (Craik and McNeil 1964; Daly 1966; Finlay 1969). As shown in Fig. 1, the stress-strain response consists of three main phases. In phase I, the majority of the collagen fibers are initially undulated. The gradual increase in stress with strain is thought to correspond to the reorientation of undulated fibers toward the axis of loading before straightening. The gradual stiffening observed in phase II is mainly due to an increasing number of realigned fibers beginning to bear load as they become straightened and stretched. Since there exists a varying degree of fiber undulation, the distinct nonlinear response of the skin is attributed to this gradual recruitment of fibers resisting tension at different stages of deformation. On the other hand, the anisotropic response is thought to be the result of the nonuniform distribution of fiber orientation. Phase III shows a linear stress response at higher strains. At this stage, the majority of fibers are stretched along the axis of loading; thus, the mechanical response is mostly dependent upon the intrinsic mechanical properties of the fibers.

Being the physical barrier between the body and the external environment, knowledge of the mechanical behavior of skin is relevant across many medical applications. Orientations of Langer's lines have become important considerations when planning surgical incisions to minimize scarring of the skin tissue (Borges and Alexander 1962). Recently, finite element (FE) models of the skin have been used to predict appearance outcome and stress distributions of surgical incisions (Yoshida et al. 2000, 2001; Buganza Tepole et al. 2014a; Flynn 2010; Lott-Crumpler and Chaudhry 2001) and facial surgery (Cavicchi et al. 2009; Koch et al. 1996; Keeve et al. 1998). Similarly, understanding skin friction mechanisms is important for the prevention, and design of treatment, for pressure ulcers (Derler and Gerhardt 2012).

Advances in tissue engineering have led to the development of biomaterials for the treatment of skin injuries such as severe burns and large nevi (Wood 2011). Successful outcomes of using skin

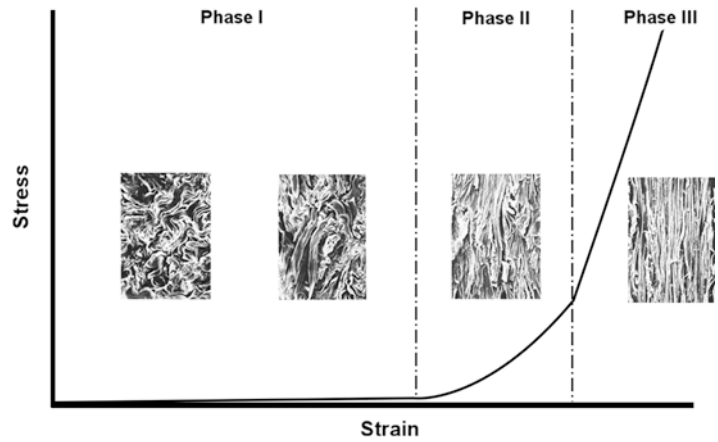

Fig. 1 A typical stress-strain response of human skin. Scanning electron microscope images of parallel sections of the dermis reveal the organization of collagen fibers corresponding to each loading phase (Reproduced from Brown (1973))

replacement rely critically on accurate knowledge of the mechanical properties of natural, healthy skin (MacNeil 2007). Together with mechanical testing of in vitro collagen scaffolds (Blackwood et al. 2008), accurate computational modeling of the skin can shed light on the mechanisms of wound healing, scar formation, and skin graft contraction (Harrison and MacNeil 2008). In addition, there has been growing interest in using skin measurements and modeling to inform the design of consumer products (Hendriks and Franklin 2009) and medical devices (Taberner et al. 2012; Groves et al. 2012) across the pharmaceutical, cosmetics (Paye et al. 2007; Sandford et al. 2013), and animation (Hung et al. 2009; Edward et al. 2012) industries.

Computational modeling is a powerful tool for developing a quantitative understanding of skin mechanics. Furthermore, accurate characterization of skin mechanics is important for modeling the mechanical behavior of other organs and tissues that are tightly tethered to the skin, such as the breast (Lee et al. 2013) and foot (Fontanella et al. 2014). Here, we present a summary of state-of-the-art biomechanical models of the skin, with an emphasis on structurally based constitutive models that can provide useful insights into the tissue structure-function relationship. The success of applying constitutive models often critically relies on accurate and quantitative measurements of skin tissue structural and mechanical properties. We review the current approaches in measuring skin properties and discuss the challenges associated with integrating computational modeling with experimental data measurements.

2 Constitutive Modeling of the Skin

Numerous constitutive models have been developed to describe the mechanical characteristics of the skin. These constitutive models have various functional forms due to specific assumptions related to skin properties (such as nonlinearity, anisotropy, viscoelasticity, and the deformation modes). Skin constitutive models can be divided into two main categories: (i) *phenomenological models* that use mathematical functions to provide best fits to measured experimental data and (ii) *structural models* that relate constitutive parameters directly to the underlying geometric and mechanical properties of individual tissue components.

2.1 Phenomenological Models

Early phenomenological models were derived from uniaxial tensile tests (Ridge and Wright 1966; Daly 1966; Tong and Fung 1976; Kenedi et al. 1965). Some phenomenological models describe the mechanical response of the skin by its Young's modulus using a linear elastic formulation (Manschot and Brakkee 1986; Agache et al. 1980; Bader and Bowker 1983; Diridollou et al. 2000; Delalleau et al. 2008a). A variety of experimental studies have demonstrated that the mechanical response of the skin is highly nonlinear (Lanir and Fung 1974; Flynn et al. 2011a; Meijer et al. 1999); therefore, the linear elastic approach is an oversimplified representation unless a narrow strain range is specified. More recent strain-invariant-based models have assumed nonlinear, isotropic mechanical properties in the form of Mooney-Rivlin (Hendriks et al. 2003; Shergold et al. 2006) and Ogden models (Shergold et al. 2006; Flynn et al. 2011b, c; Evans and Holt 2009).

The observed nonlinear stiffening with increasing strain in the skin was represented in the 13-parameter model proposed by Tong and Fung (1976), based upon their classical biaxial tensile experiments of rabbit skin. This model has also been used to characterize the mechanical response of in vivo human skin (Flynn et al. 2011b; Kvistedal and Nielsen 2009). Several other nonlinear phenomenological models have been proposed (Veronda and Westmann 1970; Bischoff et al. 2000), and although most are able to provide relatively good fits to the measured experimental skin data, their constitutive parameters generally do not represent any physical attributes of skin tissues. Thus, interpretation of these parameters and models provides limited predictive capability or insight into the relationship

between tissue microstructure and macroscopic mechanical properties of the skin.

2.2 Structural Models

The macroscopic mechanical response of the skin is determined by the organization of its structural constituents, and this has motivated the development of structurally based constitutive models of the skin (Manschot and Brakkee 1986; Decraemer et al. 1980; Diamant et al. 1972; Comninou and Yannas 1976). The pioneering studies of Lanir and colleagues were the first to comprehensively incorporate the geometric and mechanical properties of individual microstructural components into a constitutive model of the skin (Lanir 1979, 1983). Using this approach, the total strain energy of the tissue is assumed to equate to the sum of the strain energies of the collagen and elastin fiber networks embedded within a proteoglycan matrix. Individual fiber components are assumed to be initially undulating, and only begin to resist tension when completely straightened and stretched. Continuous statistical distributions are used to mathematically represent the variations in fiber orientation and undulation. This structural model has been used to characterize the uniaxial response of in vitro rat skin (Belkoff and Haut 1991), in vivo human skin (Meijer et al. 1999), and multiaxial experiments of in vitro pig skin (Jor et al. 2011a). The structural approach has been widely applied in modeling a range of other body organs and tissues, including the myocardium (Horowitz et al. 1988), heart valves (Billiar and Sacks 2000a; Sacks et al. 2006), and pericardium (Sacks 2003).

The use of statistical distributions to represent variations in fiber orientation and undulation is relatively complicated. To address this, invariant-based approaches to structural models have been developed to represent the straightening of collagen fibers using exponential functions instead of statistical distributions (Gasser et al. 2006; Holzapfel and Gasser 2000). The Gasser-Ogden-Holzapfel (GOH) model was initially applied to characterize the mechanics of arterial walls (Holzapfel et al. 2002), myocardium (Holzapfel and Ogden 2009a), aortic valves (Freed et al. 2005), in vitro human skin (Annaidh et al. 2012; Tonge et al. 2013), and skin flaps (Buganza Tepole et al. 2014b). In addition, closed-form analytic expressions have been proposed to describe fibers modeled with a von Mises orientation distribution and an exponential stress-strain function (Raghupathy and Barocas 2009). Such analytic solutions are only attainable for certain statistical distributions and cannot describe variations in fiber undulation (Fan and Sacks 2014). Flynn et al. developed a discrete six-fiber model that can be integrated to provide analytic formulations of the strain energy functions (Flynn et al. 2011d). In this model, six weighted collagen-elastin fiber bundles are oriented such that they pass through opposing vertices of an icosahedron. Collagen fiber undulation is described by a step function, while elastin fibers are modeled using a neo-Hookean constitutive relation. This model provided good fits to biaxial rabbit skin and uniaxial pig skin tensile measurements. However, one limitation of the model is that the weights of the fibers did not provide a pure representation of anisotropy (i.e., isotropy was not achieved when the weights of all fibers were equal). A generalized invariant model (Flynn and Rubin 2012) was later developed to overcome this limitation, although it led to larger errors compared with their earlier model when fitted to the same sets of data.

A transversely isotropic constitutive model (Groves et al. 2013), consisting of three fiber families embedded within an isotropic Veronda-Westmann ground matrix (Veronda and Westmann 1970), was recently used to simulate the uniaxial mechanical response of in vitro human and murine skin. The anisotropic nature of the model, initially proposed by Weiss et al. (1996), was described by three fiber families, and the straightening of fibers was represented by an exponential function. Like many other structurally based constitutive models that are able to provide good fits to experimental measurements, this model involves a large number of constitutive parameters (in this case, 14 parameters without considering viscoelasticity), which makes and typically non-unique identification of parameters difficult.

2.3 Time-Dependent Models

The skin is known to exhibit time-dependent mechanical properties, due to effects such as viscoelasticity and preconditioning (Lokshin and Lanir 2009a). Viscoelasticity is thought to be due to the shearing interaction between fibers and the ground matrix, dissipative friction of fibers, and displacement of the interstitial fluid (Wilkes et al. 1973; Oomens et al. 1987; Silver et al. 2001). Preconditioning describes the reduction in maximum stress with load cycling until a repeatable response is observed (Fung 1993). This phenomenon has been observed in both in vitro and in vivo skin (Lanir and Fung 1974).

Bischoff et al. modeled the force-stretch response of collagen in the skin using an invariant-based eight-chain model (Bischoff et al. 2000), initially proposed by Arruda and Boyce for simulating the response of elastomers (Arruda and Boyce 1993). Although being able to provide relatively good fits to uniaxial in vitro human and rat skin (Belkoff and Haut 1991; Gunner et al. 1979; Dunn et al. 1985), this model was not able to simulate the effects of the ground matrix and the anisotropic response caused by the collagen fibers. Instead, anisotropy was modeled by adding an anisotropic prestress state to an isotropic constitutive model. In more recent studies, anisotropic and time-dependent effects were introduced using a three-element rheological formulation (Bischoff et al. 2004) or by assuming quasi-linear viscoelasticity at the fiber level (Bischoff 2006).

Few models of skin mechanics have considered preconditioning effects. Rubin et al. used an empirical approach to model facial skin as a composite of elastic and dissipative components (Rubin and Bodner 2002; Rubin et al. 1998). Lokshin and Lanir proposed a comprehensive structural constitutive formulation that incorporates several characteristics of skin mechanics (including nonlinearity, anisotropy, viscoelasticity, and preconditioning effects) (Lokshin and Lanir 2009a, b). Building upon earlier models (Lanir 1983), this approach assumes quasi-linear viscoelasticity for both the collagen and elastin fiber networks. Preconditioning is accounted for using two approaches: for collagen fibers, it is assumed that preconditioning results in an increase in the fiber stress-free length while the slope of the stress-strain curve remains unchanged; for elastin fibers, preconditioning is suggested to occur via strain softening of the elastin fibers (i.e., the fiber stress-free length remains unchanged). This model was shown to provide good fits to in vitro uniaxial rat and biaxial rabbit skin data. Although the model requires 31 constitutive parameters for the biaxial case, inter-sample variance of the estimated parameters was small compared to other phenomenological models. Parametric analysis demonstrated that most parameters were significant contributors to the model, with the strongest being the fiber orientation and undulation distributions, the fiber stress-strain relationship, and the viscoelasticity and preconditioning effects.

3 Skin Measurements for Mechanics Characterization

Biomechanical modeling of the skin can be a useful technique for predicting the in vivo stress state, which is difficult to measure. The development of constitutive models that reflect the intrinsic complex mechanical properties of the skin is not a trivial task. Although state-of-the-art structural models are capable of representing a wide range of skin characteristics, reliable identification of the constitutive parameters remains a major challenge. This is because there are typically a large number of parameters that need to be determined, and these parameters are often correlated for any given set of experimental data. Furthermore, application of computational models is often hindered by the lack of quantitative and in vivo experimental data on skin mechanics.

Using numerical-experimental approaches (e.g., inverse FE analysis), identification of constitutive parameters is performed through minimizing the differences between experimental and model-predicted data. Nonunique estimates may arise due to correlation between constitutive parameters, resulting in multiple local minima with similar goodness of fit. In addition,

parameter estimates often exhibit large inter-specimen variation (Tonge et al. 2013), which is in part attributed to the large variability in structural characteristics across individuals or specimens. Since parameters of structural models typically have a physical interpretation (e.g., fiber orientation, undulation, density), measurements of skin microstructure can be directly incorporated into these models to reduce the number of unknown parameters requiring numerical estimation. However, surprisingly few studies have explored the full potential of integrating skin measurements into structural models, mainly due to the challenges associated with quantifying tissue structure in skin.

Accurate characterization of skin mechanics requires a model-based approach for the analyses and interpretation of skin measurements. For such investigations, it is important to consider (1) quantitative measurements of skin tissue structure, ideally performed using noninvasive in vivo imaging modalities, and (2) force and deformation measurements from in vivo skin subjected to rich sets of three-dimensional (3D) deformations. To obtain such skin measurements, there is a need to develop sophisticated imaging techniques and instrumentation and integrate these into a computational modeling framework.

3.1 Measurements of Skin Structure

3.1.1 Invasive Imaging

From early histological studies, the geometric arrangement of collagen fibers has been shown to play an important role in determining the mechanical response of soft tissues (Craik and McNeil 1964; Finlay 1969; Brown 1973). For this reason, knowledge of collagen orientation in soft tissues has been of great interest over the years.

A number of studies described the degree of collagen fiber anisotropy using a relative index of collagen alignment. Fiber anisotropy was quantified by either (1) fitting ovals to binary, cross-sectional images of the skin using polarized light and taking the major axes of the fitted ovals as the alignment index parameter (Melis et al. 2002), or (2) performing Fourier analysis and using the width-height ratio of the power spectrum as an estimate of the alignment index (Noorlander et al. 2002; van Zuijlen et al. 2002). An alignment index of zero (or one) represents an isotropic (or aligned) distribution of fibers, respectively. Although being a quantitative measure of fiber anisotropy, these techniques do not characterize the absolute fiber orientations with respect to the body axes, as required for use in structural constitutive modeling based on statistical distributions.

The well-known small angle light-scattering (SALS) imaging technique (Sacks et al. 1997) was developed by Sacks et al. to quantify collagen orientations in samples of soft connective tissues, such as the pericardium and heart valves. This technique uses a laser to illuminate the tissue, and the resulting scattering of light by the fibrous structures is measured. The angular distribution of collagen fibers is directly correlated to the angular distribution of the scattered light. Although the SALS technique can provide experimentally measured angular distributions of collagen fibers for direct incorporation into structural models of various thin soft tissues (Sacks et al. 2006; Sacks 2003; Sacks and Gloeckner 1999; Sacks and Sun 2003), it has been shown that this technique is not suitable for detecting scattered light from considerably thicker tissue such as the skin (Meijer et al. 1999). The SALS technique is also limited to quantification of fiber orientations in the plane of the membrane specimen.

Most conventional high-resolution imaging modalities are limited to relatively small spatial scales (i.e., in the order of hundreds of microns). For imaging tissue structures over larger spatial scales, additional issues associated with image registration and distortion must be addressed. To this end, Jor et al. used extended-volume confocal laser scanning microscopy (CLSM) to image collagen in porcine skin over a field of view of 3 mm by 2 mm (Jor et al. 2011b). Skin sections were stained with picrosirius red, which is a collagen-specific stain. An oblique arrangement of collagen fiber bundles between the epidermis and hypodermis was observed in transverse confocal images (see Fig. 2). To extract quantitative measurements of fiber orientation, a structure-tensor approach

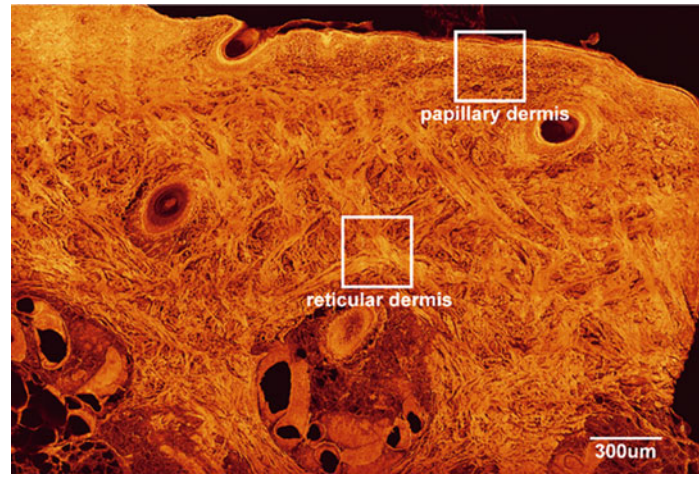

Fig. 2 High-resolution CLSM imaging of transverse sections of in vitro porcine skin, showing a distinct lattice organization of collagen fibers in the reticular dermis region (Reprinted with permission from Jor et al. (2011a))

(Jahne 2004) (based on first-order derivatives of the image) was implemented. Orientation data were subsequently fitted to a bimodal, von Mises distribution. Using this approach, fiber orientations could be directly incorporated into a structural constitutive modeling framework using a simple two-parameter mathematical representation. Ni Annaidh et al. performed bright-field microscopy imaging of excised human skin taken parallel to the epidermis, with the collagen fibers rendered visible using a van Gieson stain (Annaidh et al. 2012). Collagen orientation was quantified using automated imaging techniques, and similar to the work of Jor et al., the measured fiber orientations were fitted to von Mises distributions for use in a structurally based constitutive model of skin.

3.1.2 Noninvasive In Vivo Imaging

Conventional microscopy techniques involve excising tissues into thin sections, offering the ability to image tissues with high spatial resolution and to resolve structures deep in the tissues. Routine histology procedures involve tissue sectioning, fixation, and staining, all of which may cause undesirable changes in tissue morphology or its mechanical behavior. In addition, tissue biopsies required for clinical diagnosis are time-consuming and can be painful for the patient. For these reasons, major research efforts have recently been directed toward noninvasive imaging of the skin. Noninvasive imaging may improve diagnostic capabilities in clinical settings by providing real-time, patient-specific tissue structural information.

The common noninvasive high-resolution imaging modalities for skin tissues include confocal laser scanning microscopy (CLSM), optical coherence tomography (OCT), and two-photon microscopy (TPM). CLSM allows optical sectioning of the tissue by using point illumination and a pinhole to eliminate out-of-focus signal. High resolution in both the planes parallel (0.5 μm to 1.0 μm) and perpendicular (3 μm to 5 μm) with respect to the skin surface is usually achieved. However, penetration depth in the skin has been limited to ∼350 μm (i.e., the superficial papillary dermis region) (Rajadhyaksha et al. 1999). This is mainly due to increased scattering in deeper skin layers, resulting in a reduction of the signal-to-noise ratio with increasing imaging depth (Neerken et al. 2004). In vivo CLSM has been used for imaging different structures within both normal (Rajadhyaksha et al. 1995, 1999) and diseased (Scope et al. 2007; González et al. 2006) skin, including epidermal cells, collagen network in the papillary dermis, blood vessels, sebaceous glands, and hair follicles. However, analyses of CLSM images remain qualitative to date. There is no quantitative description of collagen geometric arrangement using in vivo CLSM.

OCT is a real-time imaging modality based upon measurements of reflected light as a function of depth (Schmitt 1999; Welzel 2008). Compared

with CLSM, OCT has a greater tissue penetration depth of up to 2 mm (Pierce et al. 2004a), with in-plane resolution in the order of 10 μm. OCT imaging has been extensively used to image tissue structures of in vivo human skin (Welzel 2008; Mogensen et al. 2009). In particular, polarization-sensitive OCT (PS-OCT) takes advantage of the intrinsic birefringent properties of collagen (De Boer et al. 1997, 1999; Pierce et al. 2004b; Saxer et al. 2000). Because collagen has the ability to alter the polarization state of light, PS-OCT can be used to quantify tissue damage by measuring changes in the polarization state of the reflected light. It has been shown that changes in birefringence occur with aging (Sakai et al. 2008), thermal denaturation of collagen fibers associated with burns (Pierce et al. 2004c; Park et al. 2001; Kaiser et al. 2011), and the development of basal skin carcinoma tumors (Strasswimmer et al. 2004). Thus, PS-OCT has the potential to reflect the state of health of the skin by providing additional information on the structural integrity of the collagen network.

On the other hand, TPM uses femtosecond, near-infrared (680 nm to 1,100 nm) lasers to enable high-resolution deep imaging of tissues without the need for staining or external markers (Perry et al. 2012; So et al. 2000; Helmchen and Denk 2005). The laser is focused through the objective lens to ensure that excitation of fluorescence is confined to the objective's focal volume. Penetration depth differs for various types of soft tissues. Imaging depth greater than 1 mm is attainable for highly transparent tissue such as the cornea, whereas penetration depth is limited to 200 μm to 300 μm for highly scattering tissues such as the skin (So et al. 2000). There are two types of TPM nonlinear signals: two-photon excitation fluorescence (TPEF) and second harmonic generation (SHG) (Masters et al. 1998; Baldewecka et al. 2012; Konig and Riemann 2003; Jiang et al. 2011; Raub et al. 2007). Since both techniques involve two photons interacting with the target material, TPEF and SHG signals are typically acquired simultaneously during imaging and later distinguished using spectral emission filters. The intrinsic fluorophores within both the epidermis (e.g., flavins, keratin, and melanin) and the elastin network contribute to the TPEF signal, while the collagen network is responsible for generating a strong SHG signal due to its non-centrosymmetric triple helix structure. It is thus possible to image both elastin and collagen networks simultaneously, by separating the TPEF and SHG signals, respectively. Upon heating, the structure of the collagen molecule changes to a centrosymmetric random coil, which leads to a reduction in SHG signal intensity. Thus, SHG microscopy has been used to qualitatively observe structural changes in collagen caused by thermal denaturation in various tissues, such as the dermis (Yasui et al. 2010; Lin et al. 2006), cornea (Lin et al. 2005), and tendons (Sun et al. 2006). Recently, in vivo SHG microscopy has been used for assessing burns by analyzing SHG vanishing patterns to quantify the extent of thermal denaturation of dermal collagen (Tanaka et al. 2013).

Since there are clear differences in both the penetration depth and the imaging resolution for CLSM, OCT, and TPM, each imaging modality reveals different information on tissue structure. While OCT imaging provides the greatest penetration depth, it can be difficult to distinguish individual tissue structures due to low in-plane resolution. Instead, OCT provides a measurement of the optical structural heterogeneities within the tissue (Neerken et al. 2004). In addition, CLSM and TPM provide images parallel to the skin surface, whereas OCT imaging typically results in transverse views through the depth of the skin. To provide a comprehensive understanding of skin structure, it is advantageous to develop multimodal imaging techniques to combine complementary measurements from various imaging modalities (Neerken et al. 2004; Masters and So 2001; Yeh et al. 2004).

Current in vivo imaging modalities provide promising means to visualize subsurface skin structures. However, there remains a need to develop techniques to enable imaging depth that spans the complete dermis layer, which is necessary for characterizing the collagen network. Recent developments in photoacoustic microscopy (PAM) have enabled high-resolution imaging deeper than 1 mm below the skin surface (Zhang et al. 2006).

PAM involves the detection of sound waves emitted by the vibration of objects when they reflect light energy. Although in vivo PAM has not been shown to reveal collagen structure, it provides additional functional information such as angiogenesis and oxygen saturation (Kaiser et al. 2011). Multimodal imaging that integrates PAM with OCT has been used to investigate the microanatomy and microvasculature in mouse ears (Jiao et al. 2009). In addition, techniques to integrate noninvasive imaging with mechanical testing of tissues have the potential to reveal important information about structural changes in the fibrous network during mechanical loading (Zoumi et al. 2004; Gusachenko et al. 2012). Image analyses techniques require further development in order to better correlate in vivo images with conventional histology and to quantify parameters from images for incorporation into structurally based constitutive models of the skin.

3.2 Measurements of Skin Mechanics

Precise mechanical experimentation is essential for the accurate parameterization of constitutive models. Such accuracy relies on tight control of a selected deformation protocol, its associated boundary conditions, and its replication in computational models. Traditional tissue characterization studies were performed in vitro. As discussed earlier, excision of tissue for in vitro experimentation can alter the structure, loading environment, and mechanical properties of the skin, such as prestress and humidification from underlying tissues. It is currently not possible to completely replicate in vivo boundary and environmental conditions; thus, we rely on in vivo experimentation for a complete characterization of the skin.

Choosing certain deformation modes can reduce the complexity of boundary conditions that must be recreated in computational models. For in vivo studies, relatively straightforward boundary conditions are provided by simple, controlled deformation modes such as extension and/or compression along one axis (Gunner et al. 1979; Coutts et al. 2013; Lim et al. 2008; Jacquet et al. 2008; Gahagnon et al. 2012) or two axes (Kvistedal and Nielsen 2009; WanAbas 1994), torsion (Escoffier et al. 1989; Leveque et al. 1984; Salter et al. 1993; Finlay 1970; Duggan 1967), suction (Delalleau et al. 2008a, 2009; Hendriks et al. 2003, 2006; Viatour et al. 1995; Krueger et al. 2011; Sutradhar and Miller 2013; Woo et al. 2014), indentation (Groves et al. 2012; Bader and Bowker 1983; Flynn et al. 2011d; Flynn and Rubin 2012; Bischoff et al. 2004; Boyer et al. 2009; Zahouani et al. 2009; Flynn and McCormack 2010; Tran et al. 2005; Moerman et al. 2009; Pailler-Mattei et al. 2008; Delalleau et al. 2006), ballistometry (Woo et al. 2014; Fthenakis et al. 1991), and shear wave propagation (Paye et al. 2007; Zhang and Greenleaf 2007; Zhang et al. 2008; Verhaegen et al. 2010). Each method identifies certain aspects of skin behavior, but development is still required to completely characterize the 3D mechanical properties of the skin. This section describes various deformation modes that have been reported in recent literature and identifies some possible improvements for experimental instrumentation.

Early experimental studies of in vivo skin adapted the extensometry tests developed for in vitro tissues (Lanir and Fung 1974) and elastomers (Rivlin et al. 1951; Treloar et al. 1976). Extensometry tests stretch the skin within the plane of the surface and can identify the stress-strain anisotropy within the surface plane. In vivo extensometry tests typically produce stiffer measures than their in vitro counterparts, primarily due to the pretension of the skin. Studies where the extensometer probe tips were shielded from the surrounding tissue have helped to reduce the disparity in such observations (Lim et al. 2008; Jacquet et al. 2008). Biaxial extensometry was thought to provide complete 3D stress-strain characterization, assuming the skin is incompressible. Lanir and Fung (1974) reported that the change in the third dimension of an incompressible material can be fully described by the deformations in the other two dimensions. This interpretation has been widely adopted in the literature (Gunner et al. 1979; Lim et al. 2008; Gahagnon et al. 2012; Delalleau et al. 2008b; Billiar and

Sacks 2000b; Bismuth et al. 2014). However, Holzapfel and Ogden (2009b) demonstrated, with the use of invariants, that biaxial testing alone is not enough to characterize the 3D response of an orthotropic material, regardless of incompressibility. While biaxial extensometry offers useful characterization within the surface plane, further deformation protocols are required for full 3D characterization of skin properties.

Suction devices are perhaps the most widely adopted tools quoted in the literature to date. A negative pressure is imparted on the skin surface and the resulting elevation is measured. These instruments are often used in clinical studies (Jachowicz et al. 2008; Piérard et al. 2013, 2014a, b; Boyer et al. 2012; Luebberding et al. 2014; Ohshima et al. 2013; Osmola-Mańkowska et al. 2013; Bonaparte and Ellis 2014) as they provide readily interpretable measures of the bulk properties of skin with good inter-operator repeatability. Typical clinical measures include viscous and elastic properties of bulk tissue. Although the design of suction devices offers some degree of boundary constraint, studies sometimes include additional guard rings (Piérard et al. 2014a). A useful feature of suction tests has been demonstrated by Hendriks et al. (2006), who showed that different skin layers could be recruited to the overall mechanical response by changing the diameter of the suction device. Ultrasound imaging through the skin layers demonstrated that probes of 2 mm diameter elicited a response only from the most superficial structures, while the dermis was gradually recruited with increasing suction diameter. Devices presented in the literature typically provide single-point measures of surface deflection, rather than making multiple measurements across the skin surface. As such, in the absence of deformation or shape information, suction methods are incapable of resolving anisotropy. Therefore, experimental data from suction devices are typically interpreted using simple models (Delalleau et al. 2008a, 2009; Hendriks et al. 2003, 2006; Viatour et al. 1995; Sutradhar and Miller 2013; Woo et al. 2014). The availability of commercial products such as the Cutometer® SEM 575® (Courage +Khazaka Electronic GmbH, Koln, Germany) and Dermaflex® (Cortex Technology, Hadsund, Denmark) has ensured that this mode of deformation remains popular in current research.

Indentation devices have also been used to extract material properties of individual layers (Jachowicz et al. 2007). In these experiments, the diameter of an indenter probe tip was varied. Typical indentation experiments are incapable of measuring anisotropy, due to limited deformation measurements and the use of symmetric heads. Anisotropy may be identified if multiple surface or volume measurements are made, or through the use of asymmetric heads. Bischoff et al. proposed the use of an asymmetric head to enable anisotropic characterization, whereby a series of indentations were performed at one site, with the head placed at different orientations (Bischoff et al. 2004). This method has not been demonstrated on the skin but has been successfully applied to anisotropic softgels (Namani et al. 2012). Flynn et al. presented an indentation robot that could perform complex 3D deformation profiles (Flynn et al. 2011a, c, 2013) (see Fig. 3). These tests demonstrated the nonlinear, viscoelastic, and anisotropic properties of the skin on the forearm, upper arm (Flynn et al. 2011a, c), and face (Flynn et al. 2013). Recent studies have focused at the tens of micron scale of epidermal cells (Crichton et al. 2013), which is important for characterization of the topmost cell layers of the skin (Boyer et al. 2009; Boyer and Zahouani 2007; Kendall et al. 2007). Further indentation studies have attempted to characterize the dynamic response of the skin, parameterizing skin into mass, stiffness, and damping terms using sinusoidal deformation perturbations (Boyer et al. 2009) as well as stochastic perturbations (Sandford et al. 2013; Chen and Hunter 2012, 2013). These models treat the skin as a single layer but may prove useful in applications such as microneedle and needle-free transdermal drug delivery (Sandford et al. 2013).

Studies spanning from the 1960s to the 1990s have used torsion tests to characterize the mechanical response of the skin (Escoffier et al. 1989; Salter et al. 1993; Finlay 1970; Duggan 1967). Several studies used the Dermal Torque Meter™ (Dia-Stron Ltd., Andover, UK), which includes a

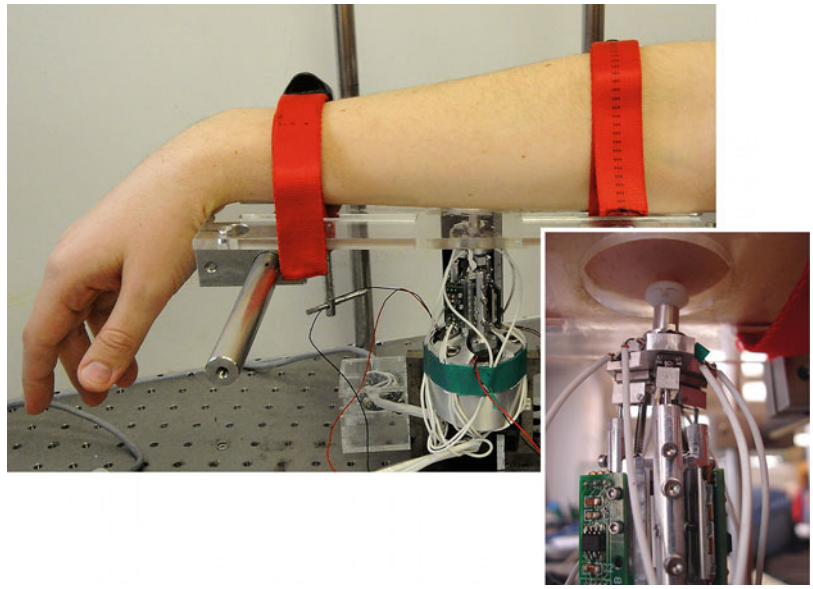

Fig. 3 Indentation tests on in vivo human skin using a force-sensitive microrobot, which consists of a probe that can be moved within a volume by actuating three parallel axes (Reprinted with permission from Flynn et al. (2011a))

nonmoving guard ring to separate a region of the skin from the surrounding tissues and a rotational probe to provide measures of elasticity. Torque meters are designed to preferentially assess the mechanical properties of the stratum corneum and remaining epidermal sub-layers by limiting deformations to above the dermis, in the plane parallel to the skin. De Rigal and Lévêque showed that by reducing the size of the torsional probe, the effect of epidermal hydration on the stress-strain response was increased, supporting the hypothesis that these devices preferentially measure the epidermal response (de Rigal and Leveque 1985). Torque meters have been shown to be more sensitive to epidermal hydration than the Cutometer® (Murray and Wickett 1997). However, torsion devices seem to have fallen out of favor, possibly due to their inability to measure anisotropy and their relatively isolated response limited to the epidermal layer.

An expanding field of work has started utilizing shear waves or surface acoustic waves for skin measurements. The Reviscometer® (Courage +Khazaka Electronic GmbH, Koln, Germany) is a product designed to characterize the anisotropy within the surface plane. This probe includes an emitter needle sensor that induces acoustic shear waves at the surface of the skin, and a receiver needle sensor that measures the time for the wave to propagate from the emitter to the receiver. This time delay is reported to be inversely proportional to tissue density and stiffness. From such measurements, the degree of fiber alignment, and thus anisotropy, can be interpreted. In vivo studies using this method tend to have been applied to clinical analyses (Paye et al. 2007; Verhaegen et al. 2010; Neto et al. 2014), rather than to constitutive models. However, Zhang et al. (2008) and Zhang and Greenleaf (2007) used their own surface wave tool to generate vibrations between 100 Hz and 400 Hz, and the resulting data were interpreted using a Voigt model, which produced estimates of shear elasticity and shear viscosity of the skin. Li et al. (2012a) presented a method that used a piezoceramic actuator to create impulses that were measured using OCT and interpreted the measurements using a linear constitutive model. Chen et al. (2014) suggested a laser-induced surface acoustic wave device, which was simulated in a FE model of skin containing a melanoma. Similar devices have been developed for other soft materials, such as an air-pulse-derived surface wave system used on corneal tissue-mimicking gel phantoms (Wang et al. 2013), ex vivo myxoma, and adipose tissue (Wang et al. 2012). The utility of these devices is limited in that they do not impose large strains on the tissue. Unless an external device imposes larger deformations, these devices are

restricted to measuring the linear mechanical properties of the skin under small strains.

Complete 3D characterization of in vivo skin cannot be achieved by any of the methods outlined above. Each technique lacks the control of boundary and environmental conditions in living subjects, and there is insufficient complexity of deformations to capture all aspects of skin mechanics. A notable confounding factor is the pretension inherent in vivo skin. Although this is well recognized in the literature, authors either tend to ignore it (Lim et al. 2008), account for uniaxial tension (Jacquet et al. 2008), or treat pretension as an unmeasured parameter that must be identified in an optimization process (Flynn et al. 2011c). Measuring pretension in vivo would provide significant improvement over current characterization methods. Kvistedal and Nielsen (2009) reported indirect estimates of skin pretension through use of a multi-motor biaxial extensometer. Control of individual motor pairs allowed the assessment and adjustment of biaxial tension in the skin in vitro. A similar problem exists with controlling boundary conditions in vivo. Techniques described in the literature often tether the skin to a rigid structure using compression and/or adhesives (Flynn et al. 2011a, 2013; Hendriks et al. 2003; Verhaegen et al. 2010; Bischoff et al. 2009). It is typically assumed (without validation) that compression and adhesives applied at the surface of the skin will provide sufficient constraint to the underlying dermis and subcutaneous tissues and that they do not disrupt the mechanical properties of the tissue being measured.

In future studies, skin characterization should aim to create richer data sets by combining multiple deformation and/or imaging modalities to enable more rigorous tests for determining model parameters. By subjecting skin to multiple modes of deformation, the constitutive parameters can be more reliably identified. For example, biaxial stretches coupled with indentation could provide measures in three dimensions while adjusting prestress. For example, Neto et al. suggested that by combining Cutometer® with Reviscometer® measurements, a more complete characterization of the skin could be achieved with a reduction in the number of parameters of interest from a single device (Neto et al. 2014). Recent studies have coupled deformation instrumentation with imaging devices. For example, ultrasound has been used to image the dermis under suction to measure and account for changes in dermal thickness.

In vivo CLSM (Rajadhyaksha et al. 1995, 1999) and OCT (Delalleau et al. 2006) are capable of tracking sub-layers within the dermis as it deforms during mechanical characterization studies. The combination of ultrasound (Coutts et al. 2013; Gahagnon et al. 2012; Iagnocco et al. 2010; Mofid et al. 2004; Sandrin et al. 2002) and magnetic resonance imaging (Sinkus et al. 2005) or OCT (Li et al. 2012a, b; Kennedy et al. 2009) with simple mechanical loading has led to a range of elastographic techniques. Elastography provides highly localized, depth-wise estimates of mechanical properties, such as Young's modulus, shear modulus, and shear viscosity. Such methods will inevitably incorporate more sophisticated constitutive models and enhance the cross-sectional characterization of the skin. Of particular significance, elastographic techniques may improve the characterization of the hypodermis (Gennisson and Baldeweck 2004; Van Houten et al. 2003), which has traditionally been neglected due to its inaccessibility.

Digital image correlation methods can be used to track surface deformation of in vivo skin (Groves et al. 2012; Evans and Holt 2009; Kvistedal and Nielsen 2009; Staloff and Rafailovitch 2008; Kacenjar et al. 2013) and other tissues (Bischoff et al. 2009; Ji et al. 2011). Malcolm et al. (2002) developed a system that captured heterogeneous two-dimensional strain fields with sub-pixel accuracy, and this technique was applied in vivo by Kvistedal and Nielsen (2009). This method has been extended to 3D (Azhar et al. 2011; Parker et al. 2012; HajiRassouliha et al. 2013) and promises to enhance 3D characterization of in vivo skin properties. There is no clear frontrunner amongst the various imaging modalities, as the methods have differing degrees of spatial resolution and penetration depth. From the limited overlap in both imaging and mechanical perturbation, it is

apparent that the combination of multiple testing protocols from the same in vivo sample provides the best way to comprehensively characterize the structure-function relationships of the skin.

4 Conclusions

Realizing the full potential of using computational modeling to characterize skin mechanics relies critically on the availability of quantitative skin measurements of both tissue structure and mechanical properties. Future scientific advancement should focus upon the development of instrumentation that is capable of measuring the mechanical properties of in vivo skin subjected to a comprehensive range of 3D deformations and the tightly integrated modeling techniques used to interpret these data. In order to translate research outcomes into the clinical setting, there is a need to further develop noninvasive, multimodal imaging capabilities for measuring individual-specific skin properties. The combination of noninvasive imaging with mechanical testing apparatus, and model-based interpretation of the combined datasets will greatly facilitate our understanding of changes in skin microstructure under mechanical loading.

References

Agache PG, Monneur C, Leveque JL, de Rigal J. Mechanical properties and Young's modulus of human skin in vivo. Arch Dermatol Res. 1980;269(3):221–32.

Annaidh AN, Bruyère K, Destrade M, Gilchrist MD, Maurini C, Otténio M, et al. Automated estimation of collagen fibre dispersion in the dermis and its contribution to the anisotropic behaviour of skin. Ann Biomed Eng. 2012;40(8):1666–78.

Arruda EM, Boyce MC. A three-dimensional constitutive model for the large stretch behavior of rubber elastic materials. J Mech Phys Solids. 1993;41(2):389–412.

Azhar M, Taberner A, Nash MP, Nielsen PMF. 3D material point tracking using phase based cross-correlation stereoscopy. 26th International Conference on Image and Vision Computing New Zealand IVCNZ; 2011.

Bader DL, Bowker P. Mechanical characteristics of skin and underlying tissues in vivo. Biomaterials. 1983;4(4):305–8.

Baldewecka T, Tancrèdeb E, Dokladalc P, Koudoroc S, Morardc V, Meyerc F, et al., editors. In vivo multiphoton microscopy associated to 3D image processing for human skin characterization. Proc of SPIE Vol; 2012.

Belkoff SM, Haut RC. A structural model used to evaluate the changing microstructure of maturing rat skin. J Biomech. 1991;24(8):711–20.

Billiar KL, Sacks MS. Biaxial mechanical properties of the native and glutaraldehyde-treated aortic valve cusp: part II – a structural constitutive model. J Biomech Eng. 2000a;122:327–35.

Billiar KL, Sacks MS. Biaxial mechanical properties of the natural and glutaraldehyde treated aortic valve cusp – part I: experimental results. J Biomech Eng. 2000b;122(1):23–30.

Bischoff JE. Reduced parameter formulation for incorporating fiber level viscoelasticity into tissue level biomechanical models. Ann Biomed Eng. 2006;34(7):1164–72.

Bischoff JE, Arruda EM, Grosh K. Finite element modeling of human skin using an isotropic, nonlinear elastic constitutive model. J Biomech. 2000;33(6):645–52.

Bischoff JE, Arruda EM, Grosh K. A rheological network model for the continuum anisotropic and viscoelastic behavior of soft tissue. Biomech Model Mechanobiol. 2004;3(1):56–65.

Bischoff JE, Drexler ES, Slifka AJ, McCowan CN. Quantifying nonlinear anisotropic elastic material properties of biological tissue by use of membrane inflation. Comput Methods Biomech Biomed Engin. 2009;12(3):353–69.

Bismuth C, Gerin C, Viguier E, Fau D, Dupasquier F, Cavetier L, et al. The biomechanical properties of canine skin measured in situ by uniaxial extension. J Biomech. 2014;47(5):1067–73.

Blackwood KA, McKean R, Canton I, Freeman CO, Franklin KL, Cole D, et al. Development of biodegradable electrospun scaffolds for dermal replacement. Biomaterials. 2008;29(21):3091–104.

Bonaparte JP, Ellis D. Skin biomechanical changes after injection of onabotulinum toxin A: prospective assessment of elasticity and pliability. Otolaryngol Head Neck Surg. 2014;150(6):949–55.

Borges AF, Alexander JE. Relaxed skin tension lines, z-plasties on scars, and fusiform excision of lesions. Br J Plast Surg. 1962;15:242–54.

Boyer G, Zahouani H, (eds). In vivo characterization of viscoelastic properties of human skin using dynamic micro-indentation. Conf Proc IEEE Eng Med Biol Soc 2007; pp 4584–4587. Lyon.

Boyer G, Laquièze L, Le Bot A, Laquièze S, Zahouani H. Dynamic indentation on human skin in vivo: ageing effects. Skin Res Technol. 2009;15(1):55–67.

Boyer G, Pailler Mattei C, Molimard J, Pericoi M, Laquieze S, Zahouani H. Non contact method for in vivo assessment of skin mechanical properties for assessing effect of ageing. Med Eng Phys. 2012;34(2):172–8.

Brown IA. A scanning electron microscope study of the effects of uniaxial tension on human skin. Br J Dermatol. 1973;89(4):383–93.

Buganza Tepole A, Gosain AK, Kuhl E. Computational modeling of skin: using stress profiles as predictor for tissue necrosis in reconstructive surgery. Comput Struct. 2014a;143:32–9.

Buganza Tepole A, Gart M, Gosain AK, Kuhl E. Characterization of living skin using multi-view stereo and isogeometric analysis. Acta Mater. 2014b;10(11):4822–31.

Carton RW, Dainauskas J, Clark JW. Elastic properties of single elastic fibers. J Appl Phycol. 1962;17(3):547–51.

Cavicchi A, Gambarotta L, Massabò R. Computational modeling of reconstructive surgery: the effects of the natural tension on skin wrinkling. Finite Elem Anal Des. 2009;45:519–29.

Chen Y, Hunter IW. Stochastic system identification of skin properties: linear and wiener static nonlinear methods. Ann Biomed Eng. 2012;40(10):2277–91.

Chen Y, Hunter IW. Nonlinear stochastic system identification of skin using volterra kernels. Ann Biomed Eng. 2013;41(4):847–62.

Chen K, Fu X, Dorantes-Gonzalez DJ, Lu Z, Li T, Li Y, et al. Simulation study of melanoma detection in human skin tissues by laser-generated surface acoustic waves. J Biomed Opt. 2014;19(7):077007.

Comninou M, Yannas IV. Dependence of stress-strain nonlinearity of connective tissues on the geometry of collagen fibers. J Biomech. 1976;9(7):427–33.

Coutts L, Bamber J, Miller N. Multi-directional in vivo tensile skin stiffness measurement for the design of a reproducible tensile strain elastography protocol. Skin Res Technol. 2013;19(1):e37–44.

Cox HT. The cleavage lines of the skin. Br J Surg. 1941; 29(114):234–40.

Craik JE, McNeil IRR. In: Kenedi RM, editor. Biomechanics and related bioengineering topics. Oxford: Pergamon Press; 1964. p. 159–64.

Crichton ML, Chen X, Huang H, Kendall MAF. Elastic modulus and viscoelastic properties of full thickness skin characterised at micro scales. Biomaterials. 2013;34(8):2087–97.

Daly CH. The biomechanical characteristics of human skin. Glasgow: University of Strathclyde; 1966.

Daly CH, editor. The role of elastin in the mechanical behavior of human skin. 8th Int Conf Med Biol Eng; Chicago. 1969.

De Boer JF, Milner TE, van Gemert MJC, Nelson JS. Two-dimensional birefringence imaging in biological tissue by polarization-sensitive optical coherence tomography. Opt Lett. 1997;22(12):934–6.

De Boer JF, Milner TE, Nelson JS. Determination of the depth-resolved Stokes parameters of light backscattered from turbid media by use of polarization-sensitive optical coherence tomography. Opt Lett. 1999;24(5):300–2.

de Rigal J, Leveque JL. In vivo measurement of the stratum corneum elasticity. Bioeng Skin. 1985;1:13–23.

Decraemer WF, Maes MA, Vanhuyse VJ, Vanpeperstraete P. A non-linear viscoelastic constitutive equation for soft biological tissues, based upon a structural model. J Biomech. 1980;13(7):559–64.

Delalleau A, Josse G, Lagarde JM, Zahouani H, Bergheau JM. Characterization of the mechanical properties of skin by inverse analysis combined with the indentation test. J Biomech. 2006;39(9):1603–10.

Delalleau A, Josse G, Lagarde JM, Zahouani H, Bergheau JM. A nonlinear elastic behavior to identify the mechanical parameters of human skin in vivo. Skin Res Technol. 2008a;14(2):152–64.

Delalleau A, Josse G, Lagarde J, Zahouani H, Bergheau J. Characterization of the mechanical properties of skin by inverse analysis combined with an extensometry test. Wear. 2008b;264(5):405–10.

Delalleau A, Josse G, George J, Mofid Y, Ossant F, Lagarde J-M. A human skin ultrasonic imaging to analyse its mechanical properties. Eur J Comput Mech. 2009;18(1):105–16.

Derler S, Gerhardt LC. Tribology of skin: review and analysis of experimental results for the friction coefficient of human skin. Tribol Lett. 2012;45:1–27.

Diamant J, Keller A, Baer E, Litt M, Arridge RG. Collagen; ultrastructure and its relation to mechanical properties as a function of ageing. Proc R Soc Lond B Biol Sci. 1972;180(60):293–315.

Diridollou S, Patat F, Gens F, Vaillant L, Black D, Lagarde JM, et al. In vivo model of the mechanical properties of the human skin under suction. Skin Res Technol. 2000;6(4):214–21.

Duggan TC. Dynamic mechanical testing of living tissue. 7 th international conference on medical and biological engineering, Stockholm. vol. 27, no. 1, 1967.

Dunn MG, Silver FH, Swann DA. Mechanical analysis of hypertrophic scar tissue: structural basis for apparent increased rigidity. J Invest Dermatol. 1985;84(1):9–13.

Edward L, Dakpe S, Feissel P, Devauchelle B, Marin F. Quantification of facial movements by motion capture. Comput Methods Biomech Biomed Engin. 2012;15 Suppl 1:259–60.

Escoffier C, de Rigal J, Rochefort A, Vasselet R, Leveque JL, Agache PG. Age-related mechanical properties of human skin: an in vivo study. J Invest Dermatol. 1989;93(3):353–7.

Evans SL, Holt CA. Measuring the mechanical properties of human skin in vivo using digital image correlation and finite element modelling. J Strain Anal Eng. 2009;44:337–45.

Fan R, Sacks MS. Simulation of planar soft tissues using a structural constitutive model: finite element implementation and validation. J Biomech. 2014;47(9):2043–54.

Finlay B. Scanning electron microscopy of the human dermis under uni-axial strain. Biomed Eng. 1969;4(7): 322–7.

Finlay B. Dynamic mechanical testing of human skin ‘in vivo’. J Biomech. 1970;3:557–68.

Flynn C. Finite element models of wound closure. J Tissue Viabil. 2010;19:137–49.

Flynn C, McCormack BA. Simulating the wrinkling and aging of skin with a multi-layer finite element model. J Biomech. 2010;43(3):442–8.

Flynn C, Rubin MB. An anisotropic discrete fibre model based on a generalised strain invariant with application to soft biological tissues. Int J Eng Sci. 2012;60:66–76.

Flynn C, Taberner A, Nielsen P. Measurement of the force-displacement response of in vivo human skin under a rich set of deformations. Med Eng Phys. 2011a;33(5): 610–9.

Flynn C, Taberner A, Nielsen P. Modeling the mechanical response of human skin under a rich set of deformations. Ann Biomed Eng. 2011b;39(7):1935–46.

Flynn C, Taberner A, Nielsen P. Mechanical characterisation of in vivo human skin using a 3D force-sensitive micro-robot and finite element analysis. Biomech Model Mechanobiol. 2011c;10(1):27–38.

Flynn C, Rubin MB, Nielsen P. A model for the anisotropic response of fibrous soft tissues using six discrete fibre bundles. Int J Numer Method Biomed Eng. 2011d; 27(11):1793–811.

Flynn C, Taberner AJT, Nielsen PMF, Fels S. Simulating the three-dimensional deformation of in vivo facial skin. J Mech Behav Biomed Mater. 2013;28:484–94.

Fontanella C, Carniel E, Forestiero A, Natali A. Investigation of the mechanical behaviour of the foot skin. Skin Res Technol. 2014;20(4):445–52.

Freed AD, Einstein DR, Vesely I. Invariant formulation for dispersed transverse isotropy in aortic heart valves: an efficient means for modeling fiber splay. Biomech Model Mechanobiol. 2005;4(2–3):100–17.

Fthenakis C, Maes D, Smith W. In vivo assessment of skin elasticity using ballistometry. J Soc Cosmet Chem. 1991;42:211–22.

Fung Y. Biomechanics: mechanical properties of living tissues. New York: Springer; 1993.

Gahagnon S, Mofid Y, Josse G, Ossant F. Skin anisotropy in vivo and initial natural stress effect: a quantitative study using high-frequency static elastography. J Biomech. 2012;45(16):2680–5.

Gasser TC, Ogden RW, Holzapfel GA. Hyperelastic modelling of arterial layers with distributed collagen fibre orientations. J R Soc Interface. 2006;3(6):15–35.

Gennisson J, Baldeweck T. Assessment of elastic parameters of human skin using dynamic elastography. IEEE Trans Ultrason Ferroelectr Freq Control. 2004;51:980–9.

González S, Gilaberte-Calzada Y, Jaén-Olasold P, Rajadhyaksha M, Torres A, Halpern A. In vivo reflectance mode confocal microscopy in clinical and surgical dermatology. In: Serup J, Jemec GBE, Grove GL, editors. Handbook of non-invasive methods and the skin. 2nd ed. Boca Raton: CRC Press; 2006.

Groves R, Coulman S, Birchall JC, Evans SL. Quantifying the mechanical properties of human skin to optimise future microneedle device design. Comput Methods Biomech Biomed Engin. 2012;15(1):73–82.

Groves RB, Coulman SA, Birchall JC, Evans SL. An anisotropic, hyperelastic model for skin: experimental measurements, finite element modelling and identification of parameters for human and murine skin. J Mech Behav Biomed Mater. 2013;18:167–80.

Gunner CW, Hutton WC, Burlin TE. The mechanical properties of skin in vivo – a portable hand-held extensometer. Br J Dermatol. 1979;100(2):161–3.

Gusachenko I, Tran V, Houssen YG, Allain JM, Schanne-Klein MC. Polarization-resolved second-harmonic generation in tendon upon mechanical stretching. Biophys J. 2012;102(9):2220–9.

HajiRassouliha A, Babarenda Gamage TP, Parker MD, Nash MP, Taberner AJ, Nielsen PM. FPGA implementation of 2D cross-correlation for real-time 3D tracking of deformable surfaces. Inimage and vision computing New Zealand (IVCNZ), 28th International Conference, 2013, pp. 352–357. IEEE.

Harkness ML, Harkness RD. Effect of enzymes on mechanical properties of tissues. Nature. 1959;183:1821–2.

Harrison CA, MacNeil S. The mechanism of skin graft contraction: an update on current research and potential future therapies. Burns. 2008;34:153–63.

Helmchen F, Denk W. Deep tissue two-photon microscopy. Nat Methods. 2005;2(12):932–40.

Hendriks CP, Franklin SE. Influence of surface roughness, material and climate conditions on the friction of human skin. Tribol Lett. 2009;37:361–73.

Hendriks FM, Brokken D, van Eemeren JTWM, Oomens CWJ, Baaijens FPT, Horsten JBAM. A numerical-experimental method to characterize the non-linear mechanical behaviour of human skin. Skin Res Technol. 2003;9(3):274–83.

Hendriks FM, Brokken D, Oomens CWJ, Bader DL, Baaijens FPT. The relative contributions of different skin layers to the mechanical behavior of human skin in vivo using suction experiments. Med Eng Phys. 2006;28(3):259–66.

Holzapfel GA, Gasser TC. A new constitutive framework for arterial wall mechanics and a comparative study of material model. J Elast. 2000;61:1–48.

Holzapfel GA, Ogden RW. Constitutive modelling of passive myocardium: a structurally based framework for material characterization. Philos Transact A Math Phys Eng Sci. 2009a;367(1902):3445–75.

Holzapfel GA, Ogden RW. On planar biaxial tests for anisotropic nonlinearly elastic solids. A continuum mechanical framework. Math Mech Solids. 2009b;14:474–89.

Holzapfel GA, Gasser TC, Stadler M. A structural model for the viscoelastic behavior of arterial walls: continuum formulation and finite element analysis. Eur J Mech A Solids. 2002;21:441–63.

Horowitz A, Lanir Y, Yin FCP, Perl M, Sheinman I, Strumpf RK. Structural three dimensional constitutive law for the passive myocardium. J Biomech Eng. 1988;110:200–7.

Hung A, Mithraratne K, Sagar M, Hunter P. Multilayer soft tissue continuum model: towards realistic simulation of facial expressions. Proc World Acad Sci Eng Technol. 2009;54:134–8.

Iagnocco A, Kaloudi O, Perella C, Bandinelli F, Riccieri V, Vasile M, et al. Ultrasound elastography assessment of skin involvement in systemic sclerosis: lights and shadows. J Rheumatol. 2010;37:1688–91.

Jachowicz J, McMullen R, Prettypaul D. Indentometric analysis of in vivo skin and comparison with artificial skin models. Skin Res Technol. 2007;13(3):299–309.

Jachowicz J, McMullen R, Prettypaul D. Alteration of skin mechanics by thin polymer films. Skin Res Technol. 2008;14(3):312–9.

Jacquet E, Josse G, Khatyr F, Garcin C. A new experimental method for measuring skin's natural tension. Skin Res Technol. 2008;14:1–7.

Jahne B. Practical handbook on image processing for scientific and technical applications. 2nd ed. Boca Raton: CRC Press; 2004. p. 419–42.

Ji S, Fan X, Roberts D, Paulsen K, editors. Cortical surface strain estimation using stereovision. Medical Image Computing and Computer-Assisted Intervention–MICCAI 2011; 2011.

Jiang X, Zhong J, Liu Y, Yu H, Zhuo S, Chen J. Two-photon fluorescence and second-harmonic generation imaging of collagen in human tissue based on multiphoton microscopy. Scanning. 2011;33(1):53–6.

Jiao S, Xie Z, Zhang HF, Puliafito CA. Simultaneous multimodal imaging with integrated photoacoustic microscopy and optical coherence tomography. Opt Lett. 2009;34(19):2961–3.

Jor JWY, Nash MP, Nielsen PMF, Hunter PJ. Estimating material parameters of a structurally based constitutive relation for skin mechanics. Biomech Model Mechanobiol. 2011a;10(5):767–78.

Jor JWY, Nielsen PMF, Nash MP, Hunter PJ. Modelling collagen fibre orientation in porcine skin based upon confocal laser scanning microscopy. Skin Res Technol. 2011b;17(2):149–59.

Kacenjar S, Chen S, Jafri M, Wall B, Pedersen R, Bezozo R. Near real-time skin deformation mapping. IS&T/SPIE electronic imaging: International Society for Optics and Photonics; 2013;86550G-G.

Kaiser M, Yafi A, Cinat M, Choi B, Durkin AJ. Noninvasive assessment of burn wound severity using optical technology: a review of current and future modalities. Burns. 2011;37:377–86.

Kanitakis J. Anatomy, histology and immunohistochemistry of normal human skin. Eur J Dermatol. 2002; 12(4):390–9.

Keeve E, Girod S, Kikinis R, Girod B. Deformable modeling of facial tissue for craniofacial surgery simulation. Comput Aided Surg. 1998;3(5):228–38.

Kendall MF, Chong Y-F, Cock A. The mechanical properties of the skin epidermis in relation to targeted gene and drug delivery. Biomaterials. 2007;28: 4968–77.

Kenedi RM, Gibson T, Daly CH. Bioengineering studies of the human skin. In: Jackson SF, Harkness RD, Partridge SM, Tristram GR, editors. Structure and function of connective and skeletal tissue. London: Butterworths; 1965. p. 388–95.

Kennedy BF, Hillman TR, McLaughlin RA, Quirk BC, Sampson DD. In vivo dynamic optical coherence elastography using a ring actuator. Opt Express. 2009;17:21762–72.

Koch RM, Gross MH, Carls FR, von Büren DF, Fankhauser G, Parish YIH, editors. Simulating facial surgery using finite element models. In: Proceedings of the 23rd Annual Conference on Computer Graphics and Interactive Techniques. New Orleans: ACM. 1996.

Konig K, Riemann I. High-resolution multiphoton tomography of human skin with subcellular spatial resolution and picosecond time resolution. J Biomed Opt. 2003; 8(3):432–9.

Krueger N, Luebberding S, Oltmer M, Streker M, Kerscher M. Age-related changes in skin mechanical properties: a quantitative evaluation of 120 female subjects. Skin Res Technol. 2011;17(2):141–8.

Kvistedal YA, Nielsen PMF. Estimating material parameters of human skin in vivo. Biomech Model Mechanobiol. 2009;8(1):1–8.

Langer K. Zur Anatomie und physiologie der haut 1. Uever der spaltbarkeit der cutis. Sitzungsber Akad Wiss Wien. 1861;44:19.

Langer K. On the anatomy and physiology of the skin. I. The cleavability of the cutis. Br J Plast Surg. 1978;31:3–8.

Lanir Y. A structural theory for the homogeneous biaxial stress-strain relationships in flat collagenous tissues. J Biomech. 1979;12(6):423–36.

Lanir Y. Constitutive equations for fibrous connective tissues. J Biomech. 1983;16(1):1–12.

Lanir Y, Fung YC. Two-dimensional mechanical properties of rabbit skin. II. Experimental results. J Biomech. 1974;7(2):171–82.

Lee AW, Rajagopal V, Babarenda Gamage TP, Doyle AJ, Nielsen PM, Nash MP. Breast lesion co-localisation between X-ray and MR images using finite element modelling. Med Image Anal. 2013;17(8): 1256–64.

Leveque JL, Corcuff P, de Rigal J, Agache P. In vivo studies of the evolution of physical properties of the human skin with age. Int J Dermatol. 1984;23(5): 322–9.

Li C, Guan G, Reif R, Huang Z, Wang RK. Determining elastic properties of skin by measuring surface waves from an impulse mechanical stimulus using phase-sensitive optical coherence tomography. J R Soc Interface. 2012a;9(70):831–41.

Li C, Guan G, Cheng X, Huang Z, Wang RK. Quantitative elastography provided by surface acoustic waves measured by phase-sensitive optical coherence tomography. Opt Lett. 2012b;37(4):722–4.

Lim K, Chew C, Chen P, Jeyapalina S, Ho H, Rappel J, et al. New extensometer to measure in vivo uniaxial mechanical properties of human skin. J Biomech. 2008;41(5):931–6.

Lin WC, Lin SJ, Jee SH, Dong CY, Tan HY, Teng SW, Lo W. Characterizing the thermally induced structural

changes to intact porcine eye, part 1: second harmonic generation imaging of cornea stroma. J Biomed Opt. 2005;10(5):054019.

Lin M-G, Jee S-H, Chen Y-F, Lin S-J, Dong C-Y, Yang T-L, et al. Evaluation of dermal thermal damage by multiphoton autofluorescence and second-harmonic-generation microscopy. J Biomed Opt. 2006;11(6): 064006.

Lokshin O, Lanir Y. Viscoelasticity and preconditioning of rat skin under uniaxial stretch: microstructural constitutive characterization. J Biomech Eng. 2009a;131(3): 31009.

Lokshin O, Lanir Y. Micro and macro rheology of planar tissues. Biomaterials. 2009b;30:3118–27.

Lott-Crumpler D, Chaudhry H. Optimal patterns for suturing wounds of complex shapes to foster healing. J Biomech. 2001;34(1):51–8.

Luebberding S, Krueger N, Kerscher M. Mechanical properties of human skin in vivo: a comparative evaluation in 300 men and women. Skin Res Technol. 2014;20(2): 127–35.

MacNeil S. Progress and opportunities for tissue-engineered skin. Nature. 2007;445(7130):874–80.

Malcolm DTK, Nielsen PMF, Hunter PJ, Charette PG. Strain measurement in biaxially loaded inhomogeneous, anisotropic elastic membranes. Biomech Model Mechanobiol. 2002;1:197–210.

Manschot JF, Brakkee AJ. The measurement and modelling of the mechanical properties of human skin in vivo – II. The model. J Biomech. 1986;19(7):517–21.

Masters BR, So PT. Confocal microscopy and multi-photon excitation microscopy of human skin in vivo. Opt Express. 2001;8(1):2–10.

Masters B, So P, Gratton E. Optical biopsy of in vivo human skin: multi-photon excitation microscopy. Laser Med Sci. 1998;13(3):196–203.

Meijer R, Douven LFA, Oomens CWJ. Characterisation of anisotropic and non-linear behaviour of human skin in vivo. Comput Methods Biomech Biomed Engin. 1999;2(1):13–27.

Melis P, Noorlander ML, van der Horst CMA, van Noorden CJF. Rapid alignment of collagen fibers in the dermis of undermined and not undermined skin stretched with a skin-stretching device. Plast Reconstr Surg. 2002;109(2):674–82.

Moerman KM, Holt CA, Evans SL, Simms CK. Digital image correlation and finite element modelling as a method to determine mechanical properties of human soft tissue in vivo. J Biomech. 2009;42(8):1150–3.

Mofid Y, Ossant F, Patat F, Imberdis C, Josse G, editors. High frequency elastography for in-vivo study of the mechanical behavior of skin. 2004 I.E. International Ultrasonics, Ferroelectrics, and Frequency Control Joint 50th Anniversary Conference; Montreal. 2004.

Mogensen M, Thrane L, Joergensen TM, Andersen PE, Jemec GBE. Optical coherence tomography for imaging of skin and skin diseases. Semin Cutan Med Surg. 2009;28(3):196–202.

Murray BC, Wickett RR. Correlations between dermal torque meter, cutometer, and dermal phase meter measurements of human skin. Skin Res Technol. 1997;3:101–6.

Namani R, Feng Y, Okamoto RJ, Jesuraj N, Sakiyama-Elbert SE, Genin GM, et al. Elastic characterization of transversely isotropic soft materials by dynamic shear and asymmetric indentation. J Biomech Eng. 2012;134:061004.

Neerken S, Lucassen GW, Bisschop MA, Lenderink E, Nuijs TA. Characterization of age-related effects in human skin: a comparative study that applies confocal laser scanning microscopy and optical coherence tomography. J Biomed Opt. 2004;9(2):274–81.

Neto P, Ferreira M, Bahia F, Costa P. Improvement of the methods for skin mechanical properties evaluation through correlation between different techniques and factor analysis. Skin Res Technol. 2014;19(4): 405–16.

Noorlander ML, Melis P, Jonker A, van Noorden CJF. A quantitative method to determine the orientation of collagen fibers in the dermis. J Histochem Cytochem. 2002;50(11):1469–74.

Ohshima H, Kinoshita S, Oyobikawa M, Futagawa M, Takiwaki H, Ishiko A, et al. Use of cutometer area parameters in evaluating age-related changes in the skin elasticity of the cheek. Skin Res Technol. 2013;19(1):e238–42.

Oomens CWJ, Van Campen DH, Grootenboer HJ. A mixture approach to the mechanics of skin. J Biomech. 1987;20(9):877–85.

Osmola-Mańkowska A, Silny W, Dańczak-Pazdrowska A, Polańska A, Olek-Hrab K, Sadowska-Przytocka A, et al. Assessment of chronic sclerodermoid Graft-versus-Host disease patients, using 20 MHz high-frequency ultrasonography and cutometer methods. Skin Res Technol. 2013;19(1):e417–22.

Pailler-Mattei C, Bec S, Zahouani H. In vivo measurements of the elastic mechanical properties of human skin by indentation tests. Med Eng Phys. 2008;30(5): 599–606.

Park BH, Saxer C, Srinivas SM, Nelson JS, de Boer JF. In vivo burn depth determination by high-speed fiber-based polarization sensitive optical coherence tomography. J Biomed Opt. 2001;6(4):474–9.

Parker MD, Azhar M, Babarenda Gamage TP, Alvares D, Taberner AJ, Nielsen PMF, editors. Surface deformation tracking of a silicone gel skin phantom in response to normal indentation. 34th Annual International Conference of the IEEE Engineering in Medicine and Biology Society (EMBC'12); 2012 2012-08-28 to 2012-09-01. San Diego: IEEE.

Paye M, Mac-Mary S, Elkhyat A, Tarrit C, Mermet P, Humbert P. Use of the Reviscometer® for measuring cosmetics-induced skin surface effects. Skin Res Technol. 2007;13(4):343–9.

Perry SW, Burke RM, Brown EB. Two-photon and second harmonic microscopy in clinical and translational cancer research. Ann Biomed Eng. 2012;40(2):277–91.

Piérard GE, Hermanns-Lê T, Piérard-Franchimont C. Scleroderma: skin stiffness assessment using the stress-strain relationship under progressive suction. Expert Opin Med Diagn. 2013;7(2):119–25.

Piérard GE, Hermanns-Lê T, Paquet P, Piérard-Franchimont C. Skin viscoelasticity during hormone replacement therapy for climacteric ageing. Int J Cosmet. 2014a;36(1):88–92.

Piérard GE, Paquet P, Piérard-Franchimont C. Skin viscoelasticity in incipient gravitational syndrome. J Cosmet Dermatol. 2014b;13(1):52–5.

Pierce MC, Strasswimmer J, Park BH, Cense B, de Boer JF. Birefringence measurements in human skin using polarization-sensitive optical coherence tomography. J Biomed Opt. 2004a;9(2):287–91.

Pierce MC, Strasswimmer J, Park BH, Cense B, de Boer JF. Advances in optical coherence tomography imaging for dermatology. J Invest Dermatol. 2004b;123(3): 458–63.

Pierce MC, Sheridan RL, Hyle Park B, Cense B, de Boer JF. Collagen denaturation can be quantified in burned human skin using polarization-sensitive optical coherence tomography. Burns. 2004c;30(6):511–7.

Raghupathy R, Barocas VH. A close-form structural model of planar fibrous tissue mechanics. J Biomech. 2009;42:1424–8.

Rajadhyaksha M, Grossman M, Esterowitz D, Webb RH, Anderson RR. In vivo confocal scanning laser microscopy of human skin: melanin provides strong contrast. J Invest Dermatol. 1995;104(6):946–52.

Rajadhyaksha M, González S, Zavislan JM, Anderson RR, Webb RH. In vivo confocal scanning laser microscopy of human skin II: advances in instrumentation and comparison with histology1. J Invest Dermatol. 1999;113(3):293–303.

Raub CB, Suresh V, Krasieva T, Lyubovitsky J, Mih JD, Putnam AJ, Tromberg BJ, George SC. Noninvasive assessment of collagen gel microstructure and mechanics using multiphoton microscopy. Biophys J. 2007; 92(6):2212–22.

Ridge MD, Wright V. The directional effects of skin. A bio-engineering study of skin with particular reference to Langer's lines. J Invest Dermatol. 1966;46(4):341–6.

Rivlin RS, Saunders D, Rivlin R, Saunders D. Large elastic deformations of isotropic materials. VII. Experiments on the deformation of rubber. Philos Transact A Math Phys Eng Sci. 1951;243(865):251–88.

Rubin M, Bodner S. A three-dimensional nonlinear model for dissipative response of soft tissue. Int J Solids Struct. 2002;39(19):5081–99.

Rubin MB, Bodner SR, Binur NS, et al. An elastic-viscoplastic model for excised facial tissues. J Biomech Eng. 1998;120(5):686.

Sacks MS. Incorporation of experimentally-derived fiber orientation into a structural constitutive model for planar collagenous tissues. J Biomech Eng. 2003;125(2): 280–7.

Sacks MS, Gloeckner DC. Quantification of the fiber architecture and biaxial mechanical behavior of porcine intestinal submucosa. J Biomed Mater Res A. 1999;46:1–10.

Sacks MS, Sun W. Multiaxial mechanical behavior of biological materials. Annu Rev Biomed Eng. 2003;5:251–84.

Sacks MS, Smith DB, Hiester ED. A small angle light scattering device for planar connective tissue microstructural analysis. Ann Biomed Eng. 1997;25:678–89.

Sacks MS, Mirnajafi A, Sun W, Schmidt P. Bioprosthetic heart valve heterograft biomaterials: structure, mechanical behavior and computational simulation. Expert Rev Med Devices. 2006;3(6):817–34.

Sakai S, Yamanari M, Miyazawa A, Matsumoto M, Nakagawa N, Sugawara T, et al. In vivo three-dimensional birefringence analysis shows collagen differences between young and old photo-aged human skin. J Invest Dermatol. 2008;128(7):1641–7.

Salter DC, McArthur HC, Crosse JE, Dickens AD. Skin mechanics measured in vivo using torsion: a new and accurate model more sensitive to age, sex and moisturizing treatment. Int J Cosmet. 1993;15(5):200–18.

Sandford E, Chen Y, Hunter I, Hillebrand G, Jones L. Capturing skin properties from dynamic mechanical analyses. Skin Res Technol. 2013;19(1):e339–48.

Sandrin L, Tanter M, Gennisson J-L, Catheline S, Fink M. Shear elasticity probe for soft tissues with 1-D transient elastography. IEEE Trans Ultrason Ferroelectr Freq Control. 2002;49:436–46.

Saxer CE, de Boer JF, Park BH, Zhao Y, Chen Z, Nelson JS. High-speed fiber based polarization-sensitive optical coherence tomography of in vivo human skin. Opt Lett. 2000;25(18):1355–7.

Schmitt JM. Optical coherence tomography (OCT): a review. IEEE J Sel Top Quantum Electron. 1999;5(4): 1205–15.

Scope A, Benvenuto-Andrade C, Agero A-LC, Malvehy J, Puig S, Rajadhyaksha M, et al. In vivo reflectance confocal microscopy imaging of melanocytic skin lesions: consensus terminology glossary and illustrative images. J Am Acad Dermatol. 2007;57(4):644–58.

Shergold OA, Fleck NA, Radford D. The uniaxial stress versus strain response of pig skin and silicone rubber at low and high strain rates. Int J Impact Eng. 2006;32:1384–402.

Silver FH, Freeman JW, DeVore D. Viscoelastic properties of human skin and processed dermis. Skin Res Technol. 2001;7(1):8–23.

Sinkus R, Tanter M, Catheline S, Lorenzen J, Kuhl C, Sondermann E, et al. Imaging anisotropic and viscous properties of breast tissue by magnetic resonance-elastography. Magn Reson Med. 2005;53:372–87.

So PT, Dong CY, Masters BR, Berland KM. Two-photon excitation fluorescence microscopy. Annu Rev Biomed Eng. 2000;2(1):399–429.

Staloff IA, Rafailovitch M. Measurement of skin stretch using digital image speckle correlation. Skin Res Technol. 2008;14(3):298–303.

Strasswimmer J, Pierce MC, Park BH, Neel V, Boer JFD. Polarization-sensitive optical coherence tomography of

invasive basal cell carcinoma. J Biomed Opt. 2004; 9(2):292–8.
Sun Y, Wei-Liang Chen, Sung-Jan Lin, Shiou-Hwa Jee, Yang-Fang Chen, Ling-Chih Lin, Peter TC So, Chen-Yuan Dong. Investigating mechanisms of collagen thermal denaturation by high resolution second-harmonic generation imaging. Biophys J. 2006;91(7): 2620–5.
Sutradhar A, Miller MJ. In vivo measurement of breast skin elasticity and breast skin thickness. Skin Res Technol. 2013;19(1):e191–9.
Taberner A, Hogan NC, Hunter IW. Needle-free jet injection using real-time controlled linear Lorentz-force actuators. Med Eng Phys. 2012;34(9):1228–35.
Tanaka R, Fukushima S-I, Sasaki K, Tanaka Y, Murota H, Matsumoto T, et al. In vivo visualization of dermal collagen fiber in skin burn by collagen-sensitive second-harmonic-generation microscopy. J Biomed Opt. 2013;18(6):61231.
Tong P, Fung YC. The stress-strain relationship for the skin. J Biomech. 1976;9(10):649–57.
Tonge TK, Voo LM, Nguyen TD. Full-field bulge test for planar anisotropic tissues: part II – a thin shell method for determining material parameters and comparison of two distributed fiber modeling approaches. Acta Mater. 2013;9:5926–42.
Tran H, Charleux F, Ehrlacher A, Ho Ba Tho M, editors. Propriétés mécaniques multi-couches de la peau humaine in vivo. Colloque National en Calcul des Structures. 2005.
Treloar L, Hopkins H, Rivlin R, Ball J. The mechanics of rubber elasticity [and discussions]. Proc R Soc Lond A Mat. 1976;351(1666):301–30.
Van Houten EEW, Doyley MM, Kennedy FE, Weaver JB, Paulsen KD. Initial in vivo experience with steady-state subzone-based MR elastography of the human breast. J Magn Reson Imaging. 2003;17:72–85.
van Zuijlen PPM, de Vries HJC, Lamme EN, Coppens JE, van Marle J, Kreis RW, et al. Morphometry of dermal collagen orientation by Fourier analysis is superior to multi-observer assessment. J Pathol. 2002;198:284–91.
Verhaegen PDHM, Res EM, Van Engelen A, Middelkoop E, Van Zuijlen PPM. A reliable, non-invasive measurement tool for anisotropy in normal skin and scar tissue. Skin Res Technol. 2010;16(3): 325–31.
Veronda DR, Westmann RA. Mechanical characterization of skin-finite deformations. J Biomech. 1970;3(1):111–24.
Viatour M, Henry F, Pierard GE. A computerized analysis of intrinsic forces in the skin. Clin Exp Dermatol. 1995;20(4):308–12.
WanAbas WA. Biaxial tension test of human skin in vivo. Biomed Mater Eng. 1994;4(7):473–86.
Wang S, Li J, Manapuram RK, Menodiado FM, Ingram DR, Twa MD, et al. Noncontact measurement of elasticity for the detection of soft-tissue tumors using phase-sensitive optical coherence tomography combined with a focused air-puff system. Opt Lett. 2012;37(24):5184–6.
Wang S, Larin KV, Li J, Vantipalli S, Manapuram RK, Aglyamov S, et al. A focused air-pulse system for optical-coherence-tomography-based measurements of tissue elasticity. Laser Phys Lett. 2013; 10(7):075605.
Weiss JA, Maker BN, Govindjee S. Finite element implementation of incompressible, transversely isotropic hyperelasticity. Comput Methods Appl Mech Eng. 1996;135(1–2):107–35.
Welzel J. Optical coherence tomography in dermatology: a review. Skin Res Technol. 2008;7(1):1–9.
Wilkes GL, Brown IA, Wildnauer RH. The biomechanical properties of skin. CRC Crit Rev Bioeng. 1973;1(4): 453–95.
Woo MS, Moon KJ, Jung HY, Park SR, Moon TK, Kim NS, et al. Comparison of skin elasticity test results from the Ballistometer® and Cutometer®. Skin Res Technol. 2014;20(4):422–8.
Wood F. Tissue engineering of skin. In: Atala A, Lanza R, Thomson JA, Nerem RM, editors. Principles of regenerative medicine. London: Academic/Elsevier; 2011. p. 1063–78.
Yasui T, Sasaki K, Tanaka R, Fukushima SI, Araki T. Determination of burn depth based on depth-resolved second-harmonic-generation imaging of dermal collagen. In: America TOSo, editor. Biomedical Optics. Miami; 2010. p. BSuD104.
Yeh AT, Kao B, Jung WG, Chen Z, Nelson JS, Tromberg BJ. Imaging wound healing using optical coherence tomography and multiphoton microscopy in an in vitro skin-equivalent tissue model. J Biomed Opt. 2004;9(2):248–53.
Yoshida H, Tsutsumi S, Mizunuma M, Yanai A. Three-dimensional finite element analysis of skin suture: part 1: spindle model and S-shaped modified model. Med Eng Phys. 2000;22(7):481–5.
Yoshida H, Tsutsumi S, Mizunuma M, Yanai A. A surgical simulation system of skin sutures using a three-dimensional finite element method. Clin Biomech. 2001;16(7):621–6.
Zahouani H, Pailler-Mattei C, Sohm B, Vargiolu R, Cenizo V, Debret R. Characterization of the mechanical properties of a dermal equivalent compared with human skin in vivo by indentation and static friction tests. Skin Res Technol. 2009;15(1):68–76.
Zhang X, Greenleaf JF. Estimation of tissue's elasticity with surface wave speed. J Acoust Soc Am. 2007;122:2522.
Zhang HF, Maslov K, Stoica G, Wang LV. Functional photoacoustic microscopy for high-resolution and non-invasive in vivo imaging. Nat Biotechnol. 2006;24(7):848–51.
Zhang X, Kinnick R, Pittelkow M, Greenleaf J, editors. Skin viscoelasticity with surface wave method. Ultrasonics Symposium, 2008 IUS 2008 IEEE. IEEE. 2008.
Zoumi A, Lu X, Kassab GS, Tromberg BJ. Imaging coronary artery microstructure using second-harmonic and two-photon fluorescence microscopy. Biophys J. 2004;87(4):2778.

Skin Photoprotection Function

101

Dominique Leroy

Contents

Keywords

Skin anti-radicals defense • Melanin • Melanin barrier • Minimum erythema dose (MED) • Nucleotids excision–resynthesis • Oxygenated free radicals • P53 gene • Photo-induced pigmentation • Phototype • Stratum corneum photo-barrier • Stress proteins • Tanning

Before entering the atmosphere, the sun's radiation spectrum ranges from 200 to 2600 nm. At approximately 20–30 km from the earth's surface, the first alteration occurs, due to the presence of ozone which absorbs ultraviolet C light (100–280 nm). While penetrating deeper into the atmosphere, solar radiation loses energy by molecular diffusion and absorption by water vapor. The types of optical radiation reaching the skin are ultraviolet light (UV), visible light, and infrared (IR). The shortest wavelengths, UVB (290–320 nm) and UVA (320–400 nm), are the most likely to generate biological effects. Some of them are beneficial such as the caloric effect of IR, the anti-rickets action of UVB which transforms 7-dehydrocholesterol into vitamin D, the anti-depressive effect of visible light and IR warmth, and the global anti-inflammatory and anti-allergic effects. Other impacts are harmful or even dangerous such as sunburning (UVB), skin photo-aging (UVA), and photo-cancerogenesis.

To counteract optical radiation, the skin has some adaptable and defensive mechanisms with

This chapter was originally published under the ISBN 978-3-540-01771-4 with the following book title Measuring the Skin. The content has not been changed.

D. Leroy (✉)
Dermatologist, Department of Dermatology, University Hospital centre, Caen, France
e-mail: dominique.leroy10@wanadoo.fr

P. Humbert et al. (eds.), *Agache's Measuring the Skin*,
DOI 10.1007/978-3-319-32383-1_135

individual variation. The main ways of defense are the thickening of the horny layer, the production of melanin, the activation of antioxidant molecules, the DNA repairing systems, and the secretion of cytokines.

1 Stratum Corneum Barrier

1.1 Pilosity

Humans have kept hair only on the scalp, thus indicating their adaptation to the standing position. The scalp is, therefore, well-protected except for young children and people with baldness.

1.2 The Horny Layer

The role of the horny layer as a photoprotector is demonstrated by the impossibility of getting sunburned on the palms and soles where the stratum corneum is thick. Photoprotection is first related to the optical properties of the skin which limit the penetration of radiation (Fig. 1). Less than 8 % of incident light is reflected at the air–skin interface, whatever the phototype. Over 92 % of the incident light therefore penetrates the skin and undergoes various optical paths through reflection, diffraction, and absorption (Anderson and Parrish 1981). Diffraction is important since the stratum corneum is made up of keratin filaments lined up parallel to the surface, in a pseudocrystalline structure. Absorption of light takes place in melanin, urocanic acid, and keratin, which is rich in polar amino acids. The penetration of optical radiation varies according to the wavelength – only 10 % of radiation under 320 nm (UVB) reaches the dermis (Everett et al. 1966). In contrast, UVA, visible light, and IR traverse the epidermis, the dermis, and partially the subcutis (Fig. 2). Water and liquids with refraction indices higher than water increase UV transmission through the stratum corneum (Solan and Laden 1977; Bruls et al. 1984).

The stratum corneum acts as a photoprotector mostly against UV light. UVB induces hyperkeratosis and stratum corneum thickening, thus reducing UV transmission (Epstein et al. 1970; Sterenborg et al. 1986). There are minor differences in stratum corneum thickening between

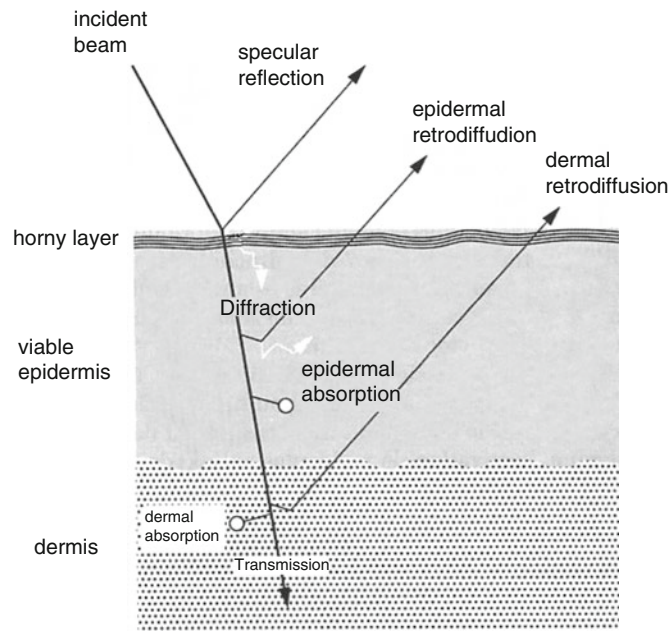

Fig. 1 Paths of optical radiation within the skin

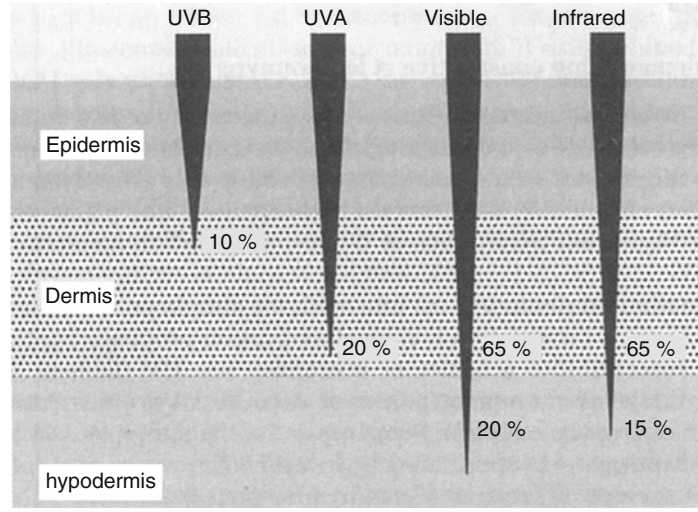

Fig. 2 Penetration depth of optical radiation

races, however photosensitivity varies extensively (Thomson 1955; Weigand et al. 1974). In black subjects, the great photoprotective capacity of the stratum corneum could be due mainly to the diffusion of light by melanin. However, in fair-skinned subjects, the stratum corneum thickness keeps an important role, as it appears that keratin is a better filter than melanin. Vitiligo is an interesting model to study photoprotection induced by epidermal hyperplasia. Skin affected by vitiligo is not pigmented because of the absence of melanin production, and consequently, photoprotection is provided only by the horny layer and the rest of the epidermis. The vitiligo skin compensates for the absence of melanin by epidermal hyperplasia and hyperkeratosis (Gniadecka et al. 1996). Furthermore, photoprotection by UVA alone is lower than by overall sun irradiation because UVA stimulates melanogenesis without causing a significant stratum corneum thickening. However, the relative importance of stratum corneum thickening versus development of pigmentation in photoprotection function is still debated (Westerhof and Uscanga 1998; Bech-Thomsen and Wulf 1995).

1.3 Urocanic Acid

Urocanic acid is produced by histidine deamination through UV activated histidinase (Morrison 1985). Under UVB absorption, it switches from trans- to cis-urocanic acid. This molecule acts as a UVB filter (de Fine Olivarius et al. 1996) and could be the photoreceptor responsible for UV-induced immunosuppression; however, the precise mechanism of this effect is not well understood (Redondo et al. 1996; Lappin et al. 1997).

1.4 Surface Lipids

UV irradiation has beneficial effects on the barrier function of the skin. As a matter of fact, skin irradiated with UVB or UVA appears more resistant to primary irritants, thus indicating the improvement of the barrier function (Lehmann et al. 1991). This improvement is not due to an epidermal hyperplasia which does not appear after UVA irradiation, but coincides with an increase in lipids in the stratum corneum, especially ceramides (Holleran et al. 1997).

2 Melanin Barrier

2.1 Constitutive Pigmentation and Phototype

The color of healthy skin results from the superposition of four colors: yellow from carotenoids in the epidermis, red from oxyhemoglobin in

capillaries, blue from reduced hemoglobin in venules, and yellow-brown from epidermal melanin. The skin color is the result of both a genetically predetermined constitutive pigmentation and an acquired pigmentation in relation to UV irradiation.

Knowing the phototype is a simple way to predict the reactions of the skin facing UV irradiation. The Fitzpatrick's classification (Fitzpatrick 1988) is based on the occurrence of sun-burning and sun-tanning (Table 1). The tanning action spectrum lies mainly in UVB, but at doses next to those triggering sunburn. For subjects with a phototype I or II (light skin), the UVB dose that induces tanning is higher than that causing sunburn; thus, these subjects burn before they tan. It is the opposite for subjects with phototype IV (dark skin) who tan before they burn.

Other classifications (Cesarini 1988) incorporate phenotypic characteristics such as complexion, hair color, and the presence of ephelides (Table 2). There are few papers about dark skin phototypes. At first, all dark skins had been classified in Fitzpatrick's type V (Fitzpatrick 1988). Later, a phototype was found for Asian type dark skin (Kawada 1986). In fact, dark skin is heterogeneous and includes Fitzpatrick's phototypes II, III, IV and V (Youn et al. 1997).

The minimum erythema dose (MED), which corresponds to the smallest quantity of UVB inducing an erythema, is also a simple method to measure photosensitivity. Several papers have shown that a good correlation existed between MED and phototype (Shono et al. 1986; Andreassi et al. 1987). A low MED is observed in subjects with red hair, blue eyes, and freckles. In contrast, other publications have not confirmed the correlation between MED and proneness to sunburn, neither in Caucasians (Westerhof et al. 1990), nor in Asians (Chung et al. 1994). The method involving a chromameter to measure the skin color is more objective than the assessment of the phototype and would provide a more accurate assessment of photosensitivity (Wee et al. 1997).

2.2 Melanin

In human skin, melanin is located in melanosomes, solid spherical particles 20–40 nm in diameter. It is also found as a soluble form in the vesicles of premelanosomes. The melanins are a heterogeneous group of pigments which can be separated into two families according to their chemical structure and color. Pheomelanins, rich

Table 1 Fitzpatrick's classification of phototypes (Fitzpatrick 1988)

Complexion	Phototype	Sunburn	Tan
White	I	Always burn	Do not tan
	II	Burn easily	Tan slightly
	III	Burn moderately	Tan progressively
	IV	Burn a little	Always tan
Dark (Mediterranean, Asian, Arabic)	V	Rarely burn	Tan intensely
Black	VI	Never burn	Tan very intensely

Table 2 Classification of phototypes including phenotypic characteristics

Phototype	Hair	Complexion	Ephelides	Sunburns	Tan
I	Red		+++	Constant ++	0
II	Blond	Fair	++	Constant +	Light tan
III	Blond	Fair	+	Frequent	Clear
	Brown	te	0	Frequent	Medium
IV	Brown	te	0	Rare	Dark
V (Mediterranean)	Brown	Brown	0	Uncommon	Very dark
VI (black)	Black	Black	0	None	Black

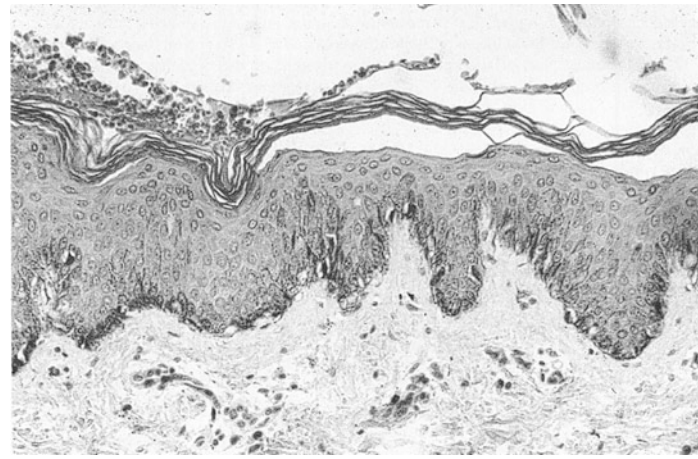

Fig. 3 Melanocytes in epidermis basal layer. Caucasian skin. Silver staining (Laboratory of Skin Biophysics, Besançon)

in sulfur, are associated with the yellow or red color predominant in red-haired subjects. Eumelanins, insoluble black or brown pigments, poor in sulfur, are found in brown or black subjects. Both categories are the terminal products of two divergent metabolic pathways after formation of an intermediate compound dopaquinone (Kollias et al. 1991).

The composition of melanin in a given individual depends on genetic and environmental factors. The photoprotection properties are maximal for eumelanins and much lower for pheomelanins. The excellent photoprotection of black skin is due to large amounts of melanin, predominantly eumelanin. The appearance of ephelides, or freckles, in red-haired subjects after exposure could be correlated to the making of eumelanins by melanocytes, which synthesized pheomelanins initially. As a matter of fact, pheomelanins seem to act as actual carcinogens, after phototoxic activation, by generating photoproducts which attack the cells (Menon et al. 1983).

Melanin is synthesized by melanocytes located in the basal layer of the epidermis (Fig. 3), interspersed with keratinocytes close to the basement membrane, where they are easily recognized because they are devoid of keratin tonofilaments (Fig. 4). They produce dendrites, which extend into the epidermal intercellular space of basal and suprabasal layers (Fig. 5). Melanin loaded melanosomes are carried in these dendrites and then eaten by the neighboring keratinocytes where they take on an umbrella-shaped distribution, which protects the cellular nucleus and DNA (Kaidbey et al. 1979) (Fig. 6). This functional cooperation between keratinocytes and melanocytes led to the concept of *epidermal melanin unit* (Fig. 5), which operates under genetic control and environmental factors.

In healthy skin, the distribution of melanin is different depending on whether a tan is induced by UVB, UVA, or PUVA (Psoralen + UVA). After exposure to UVB, the melanocytes are stimulated, hence both production of melanin and transfer into keratinocytes increase. The latter are also stimulated and proliferate resulting in an increased concentration of melanin in the epidermis. After UVA exposure, a large amount of melanin is found in melanocytes and keratinocytes of the basal layer, although in the rest of the epidermis the melanin concentration remains unchanged. As keratinocytes die to form the horny layer, melanosomes are destroyed and melanin is dispersed in the cytoplasm.

2.3 Photoprotection by Melanin

The photoprotective function of melanin is well established (Morison 1985). Exposed to the sun's rays, the skin darkens and is then less sensitive to ensuing exposures. People with teskin are less sensitive to sunlight than fair-skinned individuals. Vitiligo skin MED (no melanin) is lower than that

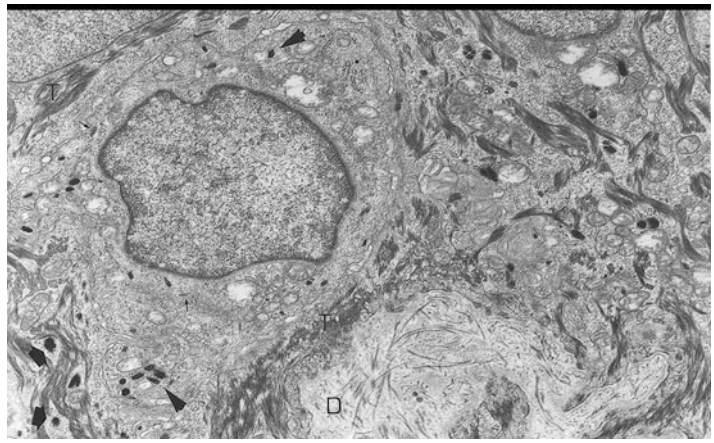

Fig. 4 Melanocyte in Caucasian skin. *Small arrows* immature melanosome in melanocyte, *arrowheads* mature melanosome in melanocyte, *thick arrows* mature melanosome in neighboring keratinocyte, *D* dermis, *T* keratin tonofilament bundle in neighboring keratinocyte. Glutaraldehyde and osmic acid post-fixation; uranyl acetate and lead citrate staining. Magnification × 3200 (Courtesy of professor René Laurent, department of Dermatology, Besançon)

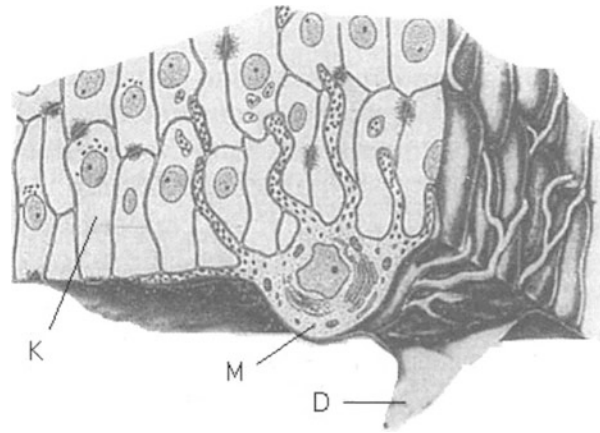

Fig. 5 A diagram of the epidermal melanin unit ((Quevedo 1969), modified)

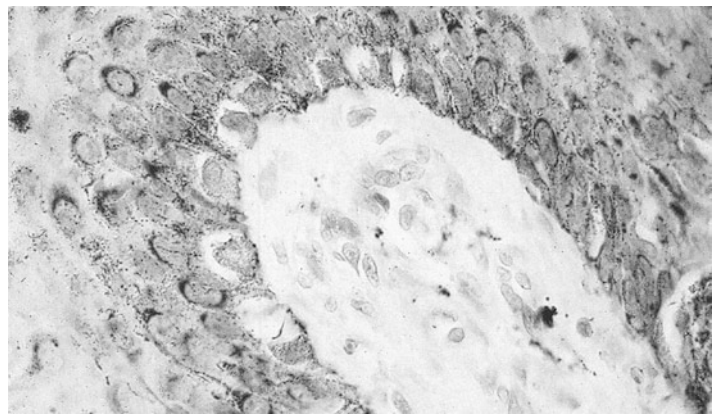

Fig. 6 "Umbrella" like topography of supra nuclear melanosomes within basal layer keratinocytes. Caucasian skin. Silver staining (Laboratory of Skin Biophysics, Besançon)

of healthy skin. The incidence of skin cancers on uncovered body areas is lower in individuals with pigmented skin compared to individuals with fair skin.

The photoprotection function of melanin is based essentially on UV light absorption capacity (Kollias 1995). It has been studied in vitro in cuttlefish (Zeise et al. 1992). In vivo, only the comparison of the reflection spectra of pigmented skins with those of nonpigmented skins, such as the skin of subjects suffering from vitiligo (Kollias and Baqer 1985) or albinism, can provide the absorption characteristics of melanin pigmentation. For both cuttlefish and human melanin, maximal absorption would take place at 335 nm. It is implied that melanin protection capacity would be more efficient against UVA than UVB (Kollias and Baqer 1988).

2.4 Photo-induced Pigmentation or Tan

The melanin concentration and distribution in the epidermis can be altered by exposure to radiation. The spectral profile of the pigment obtained varies according to the radiation received. There are two phases in photo-induced pigmentation.

- UVA induces an immediate pigmentation known as Meirowski's phenomenon or Immediate Pigment Darkening (IPD). This occurs within minutes following exposure and disappears in a few hours. However, when the dose received is high enough, the pigmentation is intense and persists several days. It is a grayish pigmentation due to photo oxidation of the existing melanin before melanocytic stimulation (Beitner and Wennersten 1985; Hönigsmann et al. 1986). This immediate pigmentation reflects the individual level of constitutive pigmentation because it is absent or minimal for phototypes I or II (Agin et al. 1985). The immediate pigmentation has no protecting effect against actinic erythema due to UVB. Conversely, in case of a subMED dose, it can facilitate the occurrence of an erythema by a photoaddition mechanism (Paul and Parrish 1982; Black et al. 1985).

Late UVA pigmentation (by 24–48 h) always precedes the inflammatory reaction, the pigmenting dose being lower than the erythema dose. UVA therefore induces a tan without sunburn. The pigment induced by UVA is characterized by the presence of a component which absorbs in the visible range

- UVB is responsible for late pigmentation or casual tan – the tan starts 2 days after exposure, reaches its maximum approximately on the 20th day and disappears gradually if there is no other exposure. With UVB, an inflammatory reaction or actinic erythema always precedes pigmentation, and there is no detectable pigmentation as long as the erythema is not sufficiently faded. Tanning results from new melanin synthesis as well as morphological and functional alterations of melanocytes and keratinocytes. The number of melanosomes and their transfer to the keratinocytes are strongly augmented. At 9–10 days following UVB exposure, the resulting pigment shows a maximum absorption at 300 nm.
- Visible light induces two types of hyperpigmentation, one is temporary, the other persistent (Kollias and Baqer 1984). The latter appears only after exposure to high radiance (>720 J/cm^2). Such a huge dose of visible light can be obtained in the same length of time as necessary for UVA persistent pigmentation to appear. With visible light, pigmentation occurs without the inflammatory reaction.
- With PUVA, the pigmentation and inflammatory responses are a sort of combination of those obtained after UVB on one hand and UVA on the other. A maximum absorption at 300 nm is observed for UVB, as well as two absorption bands at 542 and 571 nm due to oxyhemoglobin. This implies that there is a strong vascular component in the pigmentation induced by PUVA. The absorption bands due to oxyhemoglobin persist for several months.

The above discussion shows that the relation between melanocytic stimulation and skin inflammation varies depending on the wavelength. The pigment formed following exposure to UVB, UVA, or PUVA lasts several months, sometimes years, and does not extend beyond the irradiated areas, but remains well delineated. However, UV exposure can induce an increase in the number of melanocytes also in the protected skin, especially in subjects with phototype I or II (Stierner et al. 1989).

The protection provided by late pigmentation varies with the phototype. The darker the phototype, the more easily the subject becomes tanned; and tan is made easier when the subject is already tanned. This gradual natural photoprotection is most efficient against UVB, but paradoxically an effective tan permits longer sun exposures, hence an increase risk of harmful effects in the long term.

3 Anti-Radicals Defense

3.1 Oxygenated Free Radicals

UV induces damage through the endogenous chromophores normally present in the skin. UVB has a direct noxious effect on nucleic acids, urocanic acid, and some proteins. Conversely, UVA initiates photosensitization reactions, which lead to the production of oxygenated free radicals. The latter have a single electron on the outer layer which makes them unstable and very reactive. They will associate their free electron with another electron from an adjacent molecule which will in turn alters its structure. The targets of these oxygenated free radicals are numerous, especially nucleic acids and polyunsaturated fatty acids. Nucleic acids undergo a number of oxidative damages leading to strand breaks, which may disturb the expression of genetic material and cause mutation. The oxidative damages inflicted on the unsaturated fatty acids of the cellular membranes will induce membrane ruptures, inactivation of membrane receptors, and release cytotoxic substances and mediators of inflammation.

3.2 Antioxidants

To fight off the excessive formation of reactive oxygenated species and the consequences of their formation, the cells have a number of defense systems. The skin has enzymatic systems such as superoxide dismutases, catalases, and peroxidases, and also small antioxidant molecules or free radical scavengers, such as vitamins A, C, and E, β-carotene, glutathione, and trace elements like selenium, zinc, and copper.

Vitamin E, especially α-tocopherol, protects the membranes against oxidation, acts in synergy with other antioxidant systems and can be regenerated by vitamin C (Fryer 1993; Eberlein-König et al. 1998). Vitamin C is a strong antioxidant which could be effective in topical applications (Darr et al. 1992). Carotenoids are yellow, orange, or red pigments, and their role as photoprotectors has been known for a long time. β-carotene, the yellow–orange pigment of carrots, is a precursor of vitamin A. Even absorbed in large quantity, β-carotene does not generate toxicity by hypervitaminosis A. Its antioxidant properties, as well as its provitamin A activity, might be effective against cancer. Lycopene, a carotenoid nonprecursor of vitamin A, seems even more efficient at scavenging oxygen free radicals (Di Mascio et al. 1989). Selenium is a trace element essential for human health and as the active site of glutathione peroxydase, it is directly involved in the extinction of free radical (La Ruche and Césarini 1991). Other antioxidants exist such as zinc, which is one of the active sites of superoxide dismutase. Cysteine derivatives might play a photoprotective role by increasing the intracellular concentrations in glutathione (Steenvoorden and Beijersbergen van Henegouwen 1997).

These antioxidant molecules can prevent some of the damages caused by sun exposure. For example, dyskeratotic cells, or sunburnt cells,

observed in the epidermis 24 h after exposure, are significantly less numerous if superoxide dismutase is injected before or immediately after UV irradiation (Danno et al. 1984). In order to strengthen natural defenses, supplementation in carotenoids, vitamin E, vitamin C, and selenium seem justified, especially as the plasmatic ratio of some of them would decrease after sun exposure (White et al. 1988). The association of several antioxidant molecules would help the skin control the oxidative stress induced by UV light (La Ruche and Césarini 1991).

3.3 Stress Proteins

Any cellular attack results in increased synthesis of stress proteins which temporarily protect the sensitive molecules from a new onslaught (Applegate et al. 1997). Such proteins have been found in the skin following UV or IR exposure.

4 DNA Repair

When anti-free radical defenses are overwhelmed and damages are inflicted on the DNA, there are still some specific enzymatic repair systems. Damages essentially affect thymine, causing the formation of dimers between two adjacent thymines on the same DNA strand.

4.1 Nucleotids Excision–Resynthesis

The repair mechanism by excision-synthesis of nucleotides, which occurs at the start of UV irradiation, is able to discard the bulk of damaged DNA. The mechanism consists in four stages: recognition and incision of the DNA strand carrying the dimer, excision of the damaged DNA, synthesis of a new DNA from the opposite undamaged DNA, and rejoining the two ends of the repaired strand.

The fundamental role of this repair system is demonstrated in xeroderma pigmentosum. In the course of this genetic disease, characterized by a defective repair of UV-induced lesions, early occurrence of skin tumors on exposed skin is observed (Dumaz et al. 1995).

Other repair systems can also be altered, with risks of errors and therefore, of mutagenicity.

4.2 The P53 Gene

Following DNA damage by UV, a P53 gene is activated which increases the synthesis of the P53 protein (Krekels et al. 1997). This natural protein plays a major role in the preservation of the genome integrity – either it facilitates DNA repair by stopping or slowing down the cellular cycle which leaves time for the DNA to be repaired, or it induces cell apoptosis if the DNA lesions are too serious. When a P53 gene mutation occurs, the production of an abnormal P53 protein with altered functions is observed. It is no longer able to induce correct DNA repair, which can lead to the development of tumors.

5 Immune Response

Like numerous cells, keratinocytes secrete cytokines, in small quantities at basal state. Following UV exposure, the secretion increases, especially of IL_1, IL_6, IL_{10}, and TNF-α. Simultaneously, there is an increase of the secretion of prostaglandins, which are important mediators of inflammation (Schwarz and Luger 1989).

UV light is also involved in the skin's immune response by making the Langerhans cells unable to process and present antigens to lymphocytes. This photo-immunosuppression (which may be of interest in developing treatments for some skin allergy diseases) can favor the development of carcinomas (Morison 1989).

In conclusion, two major points should be kept in mind: (1) great individual variation exists in the effectiveness of natural photoprotection, and

(2) in subjects with type I and II phototypes, natural photoprotection is not safe enough, and demands additional artificial photoprotection such as clothing and sunscreens.

Acknowledgments Dr. Rik Roelandts (University of Leuven, Belgium) is warmly acknowledged for reviewing the manuscript.

References

Agin PP, Desrochers DL, Sayre RM. The relationship of immediate pigment darkening to minimal erythemal dose, skin type, and eye color. Photodermatology. 1985;2:288–94.

Anderson RR, Parrish JA. The optics of human skin. J Invest Dermatol. 1981;77:13–9.

Andreassi L, Simoni S, Fiorini P, Fimiani M. Phenotypic characters related to skin type and minimal erythemal dose. Photodermatology. 1987;4:43–6.

Applegate LA, Scaletta C, Fourtanier A, Mascotto RE, Seité S, Frenk E. Expression of DNA damage and stress proteins by UVA irradiation of human skin in vivo. Eur J Dermatol. 1997;7:215–9.

Bech-Thomsen N, Wulf HC. Photoprotection due to pigmentation and epidermal thickness after repeated exposure to ultraviolet light and psoralen plus ultraviolet A therapy. Photodermatol Photoimmunol Photomed. 1995;11:213–8.

Beitner H, Wennersten G. A qualitative and quantitative transmission electronmicroscopic study of the immediate pigment darkening reaction. Photodermatology. 1985;2:273–8.

Black G, Matzinger E, Gange RW. Lack of photoprotection against UVB-induced erythema by immediate pigmentation induced by 382 nm radiation. J Invest Dermatol. 1985;85:448–9.

Bruls WAG, Slaper H, van der Leun JC, Berrens L. Transmission of human epidermis and stratum corneum as a function of thickness in the ultraviolet and visible wavelengths. Photochem Photobiol. 1984;40:485–94.

Cesarini JP. Photo-induced events in the human melanocytic system: photoaggression and photoprotection. Pigment Cell Res. 1988;1:223–33.

Chung JH, Koh WS, Youn JI. Relevance of skin phototyping to a Korean population. Clin Exp Dermatol. 1994;19:476–8.

Danno K, Horio T, Takigawa M, Imamura S. Role of oxygen intermediates in UV-induced epidermal cell injury. J Invest Dermatol. 1984;83:166–8.

Darr D, Combs S, Dunston S, Manning T, Spinnell S. Topical vitamine C protects porcine skin from ultraviolet radiation-induced damage. Br J Dermatol. 1992;127:247–53.

de Fine Olivarius F, Wulf HC, Crosby J, Norval M. The sunscreening effect of urocanic acid. Photodermatol Photoimmunol Photomed. 1996;12:95–9.

Di Mascio P, Kaiser S, Sies H. Lycopene as the most efficient biological carotenoid singlet oxygen quencher. Arch Biochem Biophys. 1989;274:532–8.

Dumaz N, Marionnet C, Eveno E, Robert C, Vuillaume M, Stary A, et al. Photosensitivity and genetic diseases. In: Dubertret L, Santus R, Morlière P, editors. Ozone, sun, cancer, molecular and cellular mechanisms prevention. Paris: Editions Inserm; 1995. p. 140–4.

Eberlein-König B, Placzek M, Przybilla B. Protective effect against sunburn of combined systemic ascorbic acid (vitamin C) and d-α-tocopherol (vitamin E). J Am Acad Dermatol. 1998;38:45–8.

Epstein JH, Fukuyama K, Fye K. Effects of ultraviolet radiation on the mitotic cycle and DNA, RNA and protein synthesis in mammalian epidermis in vivo. Photochem Photobiol. 1970;12:57–65.

Everett MA, Yeargers E, Sayre RM, Olson RL. Penetration of epidermis by ultraviolet rays. Photochem Photobiol. 1966;5:533–42.

Fitzpatrick TB. The validity and practicality of sun-reactive skin types I through VI. Arch Dermatol. 1988;124:869–71.

Fryer MJ. Evidence for the photoprotective effects of vitamin E. Photochem Photobiol. 1993;58:304–12.

Gniadecka M, Wulf HC, Mortensen NN, Poulsen T. Photoprotection in vitiligo and normal skin. A quantitative assessment of the role of stratum corneum, viable epidermis and pigmentation. Acta Derm Venereol. 1996;76:429–32.

Holleran WM, Uchida Y, Halkier-Sorensen L, Haratake A, Hara M, Epstein JH, et al. Structural and biochemical basis for the UVB-induced alterations in epidermal barrier function. Photodermatol Photoimmunol Photomed. 1997;13:117–28.

Hönigsmann H, Schuler G, Aberer W, Romani N, Wolff K. Immediate pigment darkening phenomenon. A reevaluation of its mechanisms. J Invest Dermatol. 1986;87:648–52.

Kaidbey KH, Agin PP, Sayre RM, Kligman AM. Photoprotection by melanin – a comparison of black and Caucasian skin. J Am Acad Dermatol. 1979;1:249–60.

Kawada A. UVB-induced erythema, delayed tanning, and UVA-induced immediate tanning in Japanese skin. Photodermatology. 1986;3:327–33.

Kollias N. Aspects of photoprotection by epidermal melanin pigmentation at the molecular, cellular and organ levels: a review. In: Dubertret L, Santus R, Morlière P, editors. Ozone, sun, cancer, molecular and cellular mechanisms prevention. Paris: Editions Inserm; 1995. p. 187–98.

Kollias N, Baqer A. An experimental study of the changes in pigmentation in human skin in vivo with visible and near infrared light. Photochem Photobiol. 1984;39:651–9.

Kollias N, Baqer A. Spectroscopic characteristics of human melanin in vivo. J Invest Dermatol. 1985;85:38–42.

Kollias N, Baqer AH. The role of human melanin in providing photoprotection from solar mid-ultraviolet radiation (280–320 nm). J Soc Cosmet Chem. 1988;39:347–54.

Kollias N, Sayre RM, Zeise L, Chedekel MR. Photoprotection by melanin. J Photochem Photobiol B Biol. 1991;9:135–60.

Krekels G, Voorter C, Kuik F, Verhaegh M, Ramaekers F, Neumann M. DNA-protection by sunscreens: p53-immunostaining. Eur J Dermatol. 1997;7:259–62.

La Ruche G, Césarini JP. Protective effect of oral selenium plus copper associated with vitamin complex on sunburn cell formation in human skin. Photodermatol Photoimmunol Photomed. 1991;8:232–5.

Lappin MB, Weiss JM, Schöpf E, Norval M, Simon JC. Physiologic doses of urocanic acid do not alter the allostimulatory function or the development of murine dendritic cells in vitro. Photodermatol Photoimmunol Photomed. 1997;13:163–8.

Lehmann P, Hölzle E, Melnik B, Plewig G. Effects of ultraviolet A and B on the skin barrier: a functional, electron microscopic and lipid biochemical study. Photodermatol Photoimmunol Photomed. 1991;8:129–34.

Menon IA, Persad S, Haberman HF, Kurian CJ. A comparative study of the physical and chemical properties of melanins isolated from human black and red hair. J Invest Dermatol. 1983;80:202–6.

Morison WL. What is the function of melanin. Arch Dermatol. 1985;121:1160–3.

Morison WL. Effects of ultraviolet radiation on the immune system in humans. Photochem Photobiol. 1989;50:515–24.

Morrison H. Photochemistry and photobiology of urocanic acid. Photodermatology. 1985;2:158–65.

Paul BS, Parrish JA. The interaction of UVA and UVB in the production of threshold erythema. J Invest Dermatol. 1982;78:371–4.

Quevedo Jr WC. The control of color in mammals. Am Zool. 1969;9:531–40.

Redondo P, Garcia-Foncillas J, Cuevillas F, Espana A, Quintanilla E. Effects of low concentrations of cis-and trans-urocanic acid on cytokine elaboration by keratinocytes. Photodermatol Photoimmunol Photomed. 1996;12:237–43.

Schwarz T, Luger TA. Effect of UV irradiation on epidermal cell cytokine production. J Photochem Photobiol B Biol. 1989;4:1–13.

Shono S, Imura M, Ota M, Ono S, Toda K. The relationship of skin color, UVB-induced erythema, and melanogenesis. J Invest Dermatol. 1986;84:265–7.

Solan JL, Laden K. Factors affecting the penetration of light through stratum corneum. J Soc Cosmet Chem. 1977;28:125–37.

Steenvoorden DPT, Beijersbergen van Henegouwen GMJ. Cysteine derivatives protect against UV-induced reactive intermediates in human keratinocytes: the role of glutathione synthesis. Photochem Photobiol. 1997;66:665–71.

Sterenborg HJCM, de Gruijl FR, van der Leun JC. UV-induced epidermal hyperplasia in hairless mice. Photodermatology. 1986;3:206–14.

Stierner U, Rosdahl I, Augustsson A, Kagedal B. UVB irradiation induces melanocyte increase in both exposed and shielded human skin. J Invest Dermatol. 1989;92:561–4.

Thomson ML. Relative efficiency of pigment and horny layer thickness in protecting the skin of Europeans and Africans against solar ultraviolet radiation. J Physiol. 1955;127:236–46.

Wee LKS, Chong TK, Koh Soo Quee D. Assessment of skin types, skin colours and cutaneous responses to ultraviolet radiation in an Asian population. Photodermatol Photoimmunol Photomed. 1997;13:169–72.

Weigand DA, Haygood C, Gaylor JR. Cell layers and density of negro and caucasian stratum corneum. J Invest Dermatol. 1974;62:563–8.

Westerhof W, Uscanga OE. Photoprotection in vitiligo and normal skin. Acta Derm Venereol. 1998;78:149–50.

Westerhof W, Estevez-Uscanga O, Meens J, Kammeyer A, Durocq M, Cario I. The relation between constitutional skin color and photosensitivity estimated from UV-induced erythema and pigmentation dose–response curves. J Invest Dermatol. 1990;94:812–6.

White WS, Kim C-I, Kalkwarf HJ, Bustos P, Roe DA. Ultraviolet light-induced reductions in plasma carotenoid levels. Am J Clin Nutr. 1988; 47:879–83.

Youn JI, Oh JK, Kim BK, Suh DH, Chung JH, Oh SJ, et al. Relationship between skin phototype and MED in Korean, brown skin. Photodermatol Photoimmunol Photomed. 1997;13:208–11.

Zeise L, Addison RB, Chedekel MR. Bio-analytical studies of eumelanins. I. Characterization of melanin the particle. Pigment Cell Res. 1992;Suppl 2:48–53.

Radical Production by Infrared Irradiation in Human Skin

102

Maxim E. Darvin, Martina C. Meinke, and Jürgen Lademann

Contents

M.E. Darvin (✉) • M.C. Meinke • J. Lademann
Department of Dermatology, Venereology and Allergology, Center of Experimental and Applied Cutaneous Physiology, Charité – Universitätsmedizin Berlin, Berlin, Germany
e-mail: maxim.darvin@charite.de; martina.meinke@charite.de; juergen.lademann@charite.de

P. Humbert et al. (eds.), *Agache's Measuring the Skin*,
DOI 10.1007/978-3-319-32383-1_136

Keywords
Antioxidants • Carotenoids • Beta-carotene • Lycopene • Resonance Raman spectroscopy • Electron paramagnetic resonance spectroscopy • Reactive oxygen species • Heat shock radicals • Protection

1 Introduction

The negative effect of solar radiation is usually associated with ultraviolet (UV) radiation (Schade et al. 2005; Norval and Halliday 2011; Matthews et al. 2010a, b; Sklar et al. 2013-; Murphy 2009) due to its ability to generate free radicals in the skin (Zastrow et al. 2004; Darvin et al. 2006a; Halliwell 2007). The action of free radicals can result in oxidative cell damage (Taylor and Sober 1996; Dumay et al. 2001), the development of premature skin aging (Harman 1983; Biesalski and Obermueller-Jevic 2001; Alaluf et al. 2002; Sies and Stahl 2004), and even skin cancer (Krutmann 2001; Moon and Oh 2001). Taking this fact into consideration, different sunscreens are available on the market which provides an efficient defense against both UVB and UVA spectral ranges.

However, human skin is predominantly exposed to near-infrared radiation (NIR: 760–3,000 nm), which comprises approximately 54 % of the total solar radiation that reaches the surface of the earth (Kochevar et al. 1999). Many studies show that NIR could act both

therapeutically and pathologically depending on the applied doses (Bensadoun and Nair 2012; Akhalaya et al. in press). Both effects of solar IR on human skin are associated with the generation of ROS, whereby the applied dose plays a crucial role, acting therapeutically (low doses) or pathologically (high doses). This appears to be dependent on the corresponding signaling pathways: NF-kB for therapeutic effects and AP-1 for pathological effects (Akhalaya et al. in press).

The pathological effect of high-dose solar infrared (IR) radiation for human skin is a scientifically accepted phenomenon (Schieke et al. 2002; Schroeder et al. 2008a, b; Cho et al. 2009; Tanaka et al. 2011; Zastrow et al. 2009; Krutmann et al. 2012). Analysis of recent studies shows that IR radiation induces the generation of ROS in the skin (Zastrow et al. 2009; Darvin et al. 2010a, b). The generated free radicals (mostly ROS) underlie all infrared-affected cutaneous effects, such as increased proliferation of cells, gene expression of inflammatory cytokines, and suppression of the synthesis of proinflammatory mediators (Karu 2008; Galluzzi et al. 2012; Schieke et al. 2003; Calles et al. 2010). During NIR exposure, the skin surface temperature increases from 27.6–33.1 °C (Kleesz et al. 2012) to 41–45 °C, which can induce the generation of heat shock radicals (Cho et al. 2009; Shin et al. 2008). The different signaling pathways of NIR-induced ROS and NIR-induced heat shock ROS generation act independently, multiplying the influence on each other by increasing the doses of irradiation and/or increasing the temperature (Akhalaya et al. in press).

The defense mechanism of the human body against the action of the excess amount of free radicals is based on the synergistic action of different antioxidants including carotenoids, vitamins, enzymes, and others (Darvin et al. 2006b). In the skin, carotenoids ,beta-carotene, and lycopene are known to be powerful antioxidants that act effectively to neutralize ROS, including singlet oxygen (Palozza and Krinsky 1992; Krinsky 2001; Darvin et al. 2011a). The side effect of such interactions with high amounts of radicals can lead to the destruction of the carotenoids and, as a result, depletion of the antioxidant defense system of the organism (Ribaya-Mercado et al. 1995). The amount of destroyed cutaneous carotenoids can be well correlated with the amount of generated free radicals in the skin, which was confirmed by EPR measurements, showing that carotenoids could serve as marker substances for the entire antioxidant status of the human epidermis (Haag et al. 2011; Lauer et al. 2013). Recently it has become possible to measure the concentration of cutaneous carotenoids noninvasively by resonance Raman spectroscopy (Hata et al. 2000; Darvin et al. 2005a). This method was used in the present study to investigate the influence of IR irradiation on the antioxidant status of human skin.

The present chapter describes the results obtained by noninvasive methods to measure the generation of free radicals in the skin subsequent to NIR and IRA irradiations. In the first step of this study, the stability of the carotenoids in the human skin under exposure with IR irradiation was investigated in vivo using resonance Raman spectroscopy. In the second step of this study, EPR spectrometry was used under in vitro conditions to analyze whether the obtained changes in the carotenoid concentration during IR irradiation are in fact caused by the generation of free radicals in the skin. In the third step, the concentration of the carotenoids in the skin was varied by topical application of a single antioxidant component formulation containing beta-carotene in order to investigate a potential protective effect on the skin.

2 Materials and Methods

2.1 Resonance Raman Spectroscopy (RRS)

The concentration of carotenoids in human skin was determined quickly and noninvasively with a high sensitivity using resonance Raman spectroscopy. This in vivo method was chosen for the measurements because of the advantages in comparison to other methods (Darvin et al. 2013). The main measurement principle is based on the optimal combination of laser excitation wavelengths

and carotenoid absorption as well as the design solution of the setup. The resonance regime of excitation lies in the blue-green range of the spectra, where carotenoids have a maximal absorption, and gives rise to the strong enhancement of the Raman signal of carotenoids, making this method very well suited for measurements in the skin. The argon laser operated at 488 nm and 514.5 nm was used as a source of excitation. The carotenoid concentration was determined by the intensity of the carbon-carbon double bond stretching vibration of the carotenoid molecules line measured at 1,523 cm^{-1}. Other Raman lines of carotenoids measured at 1,005 cm^{-1} and 1,156 cm^{-1} were not taken into consideration.

A detailed technical description of resonance Raman spectroscopy of cutaneous carotenoids was previously provided by our group (Darvin et al. 2005a, b).

2.2 Electron Paramagnetic Resonance Spectroscopy (EPR)

The in vitro measurement of infrared light-induced free radicals was carried out by EPR spectroscopy using the stable long-lived free radical spin marker 3-carboxy-2,2,5,5-tetramethyl-pyrrolidine-1-oxyl (PCA) from Sigma (Steinheim, Germany) and a L-band EPR-spectrometer from Magnettech GmbH (Berlin, Germany). The PCA spin marker generates an EPR signal whose intensity corresponds to the PCA concentration.

Due to the interaction between PCA long-lived free radicals and the IR-induced short-lived free radicals, PCA is reduced to its corresponding hydroxylamine, which does not generate any EPR signal. As a result of this recombination, the concentration of PCA marker is decreased, thus providing information about the quantity of generated radicals (Herrling et al. 2003).

PCA was chosen for application on porcine skin samples for scavenging induced free radicals (Herrling et al. 2003) as it is stable in porcine ear skin without irradiation (Haag et al. 2010). A filter paper disc was placed on the punch biopsy and 50 µl PCA (10 mM in water/ethanol 50/50 v/v) was added. After a 30-min incubation time, the skin samples were washed with water and dried with soft tissue paper, and the initial EPR signals were recorded for each sample. The kinetics of the PCA degradation was measured every 10 min, subsequent to IR irradiation of the samples.

Taking the strong dependence between the intensity of EPR signals and the temperature (Rockenbauer et al. 2006) of the investigative samples into consideration, EPR measurements were performed on the samples after they had cooled down to room temperature (approximately 23 °C).

2.3 Sources of Infrared Irradiation

Two infrared sources were used in the study. The first source was a radiator illuminated in the NIR range of the spectra (Philips Infrared RI 1521, Nederland). The second source represented a radiator connected with a water filter in front of the radiation head, which emitted the IRA radiation (Hydrosun Medizintechnik GmbH, Germany).

Both radiators were used for in vivo irradiation of human skin at a power density of 170–190 mW/cm^2 for 30 min (doses 306–342 J/cm^2), which is recommended for therapeutic action, and at the power density 105–115 mW/cm^2 for 30 min (doses 189–207 J/cm^2) in case of in vitro measurements on porcine ear skin. The reduced power density was performed on the porcine skin samples in order to limit the skin surface temperature to a value of 42 °C.

2.4 Determination of the Skin Temperature

The temperature of the skin surface was measured noninvasively subsequent to the infrared irradiation using a noncontact thermometer (Rytek Schlender Messtechnik).

2.5 Experimental Design

The in vivo investigations were carried out on the flexor forearms of 12 healthy volunteers (3 males,

9 females) aged between 25 and 35 years. On each flexor forearm, two areas of 4 × 4 cm^2 were marked with a permanent marker. Before IR irradiation, one area of each arm was pretreated homogeneously with 2 mg/cm^2 of an o/w formulation containing 0.2 % beta-carotene. The other two skin areas remained untreated.

The pretreated and untreated skin areas were irradiated with two different IR radiators operating in NIR and IRA spectral ranges.

The same procedure was performed with the porcine ear skin used for in vitro measurements.

In order to examine the radical formation process in the formulation during IR irradiation, the o/w formulation containing 0.2 % of beta-carotene antioxidant was placed in a cuvette consisting of two glass plates with a 1.0-mm distance holder between them to exclude the insiccation and oxidation. Then IR irradiation emitted by the NIR was performed on 12 samples. The other 12 samples were irradiated with IRA. All measurements were performed at a power density of 170 mW/cm^2 for 30 min. Control measurements without IR irradiation were performed on six samples.

Approval for the in vivo study had been obtained from the Ethics Committee of the Charité – Universitätsmedizin Berlin.

3 Results and Discussion

3.1 Kinetic of Carotenoids Measured with RRS Subsequent to Infrared Irradiation

3.1.1 Beta-Carotene-Containing Formulation

The o/w formulation containing 0.2 % of beta-carotene was measured in vitro before and after IR irradiation with the use of resonance Raman spectroscopy. Control measurements without irradiation were performed at the same time.

The measurements showed no differences in the beta-carotene concentration in the irradiated samples for both NIR and IRA radiators before and after irradiation as well as in control samples.

This indicates that free radicals were not produced in the formulation itself subsequent to the IRA and NIR irradiations as well as during the IR-induced heating of the sample. Additionally, beta-carotene was not influenced directly by the applied infrared radiations.

3.1.2 Influence of the Infrared Irradiation on the Cutaneous Carotenoid Concentration In Vivo

To increase the level of cutaneous antioxidants artificially, the formulation containing beta-carotene was applied topically. This resulted in an increase of the absolute carotenoid concentration in the skin of volunteers to 1.75 ± 0.29 times on average for all volunteers (Darvin et al. 2011b). The obtained beta-carotene concentration is close to the physiological concentration, thus pro-oxidative effects can most likely be excluded (Darvin et al. 2011a).

The concentration of carotenoids in the skin of all volunteers before and after irradiation with IRA and NIR radiators is shown on Fig. 1a (non-pretreated skin) and 1b (pretreated skin). Obtained degradations were found to be statistically significant ($*p < 0.005$).

As can be seen from the figures, the carotenoid concentration is reduced after IRA and NIR irradiation. On average, the magnitude of the degradation of carotenoids in the skin after IR irradiation was determined at 23 % for IRA and 33 % for the NIR, independently of the pretreatment of the irradiated skin areas. The average destruction of carotenoids obtained after the application of NIR was 10 % higher than after the application of IRA, which was found to be statistically significant. Obtained results are in agreement with previously published results (Darvin et al. 2007, 2009).

The absolute amount of the carotenoids destroyed after IR irradiation on average was higher in the case of the pretreatment with the formulation containing beta-carotene than for the untreated skin (Fig. 1). The antioxidant stability of the formulation containing beta-carotene can be substantially increased if a mixture of different antioxidants at different concentrations is applied. This effect can be investigated using different methods (Darvin et al. 2010c; Meinke et al. 2013).

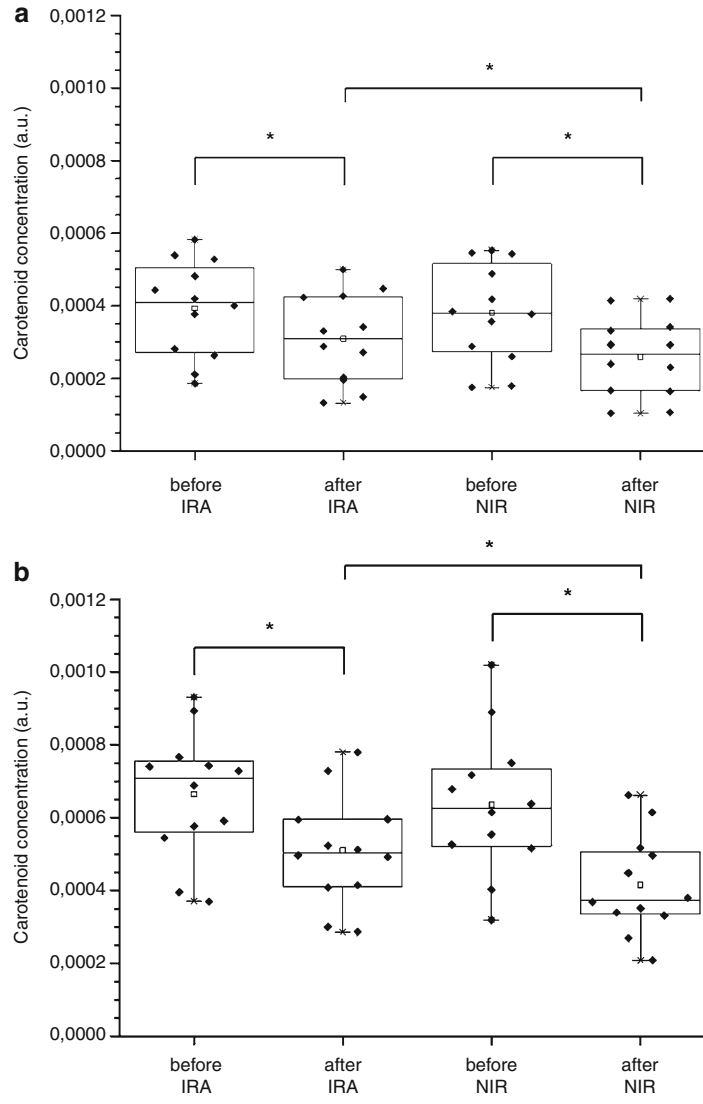

Fig. 1 Box plot of the carotenoid concentration in the non-pretreated skin area (**a**) and beta-carotene pretreated skin area (**b**) of all volunteers before and after irradiation with IRA and NIR radiators measured in different time points. *$p < 0.005$, pairwise comparison with Wilcoxon-signed test

Figure 2 shows the correlation between the individual level of carotenoids in the non-pretreated skin and the magnitude of carotenoids remaining after 30 min of IR irradiation with NIR (a) and IRA (b). As can be seen, correlations with correlation factors $R^2 = 0.60$ and $R^2 = 0.63$ were observed for the NIR and IRA irradiation, respectively. This correlation is not surprising and can be explained by the production of the specific amount of free radicals after IR exposure of the skin. In this case, all volunteers received approximately the same quantity of free radicals, which gave rise to carotenoid degradation. The volunteers, who had a low initial concentration of carotenoids in their skin, were found to have a higher magnitude of destruction. This means that the volunteers with a high individual level of carotenoid antioxidant substances in the skin had an additional defense potential against the influence of IR irradiation associated with the production of free radicals.

A comparison of the typical degradation dynamics of carotenoids in the untreated and pretreated skin areas in case of both IR radiators showed that a decrease of carotenoids in the skin

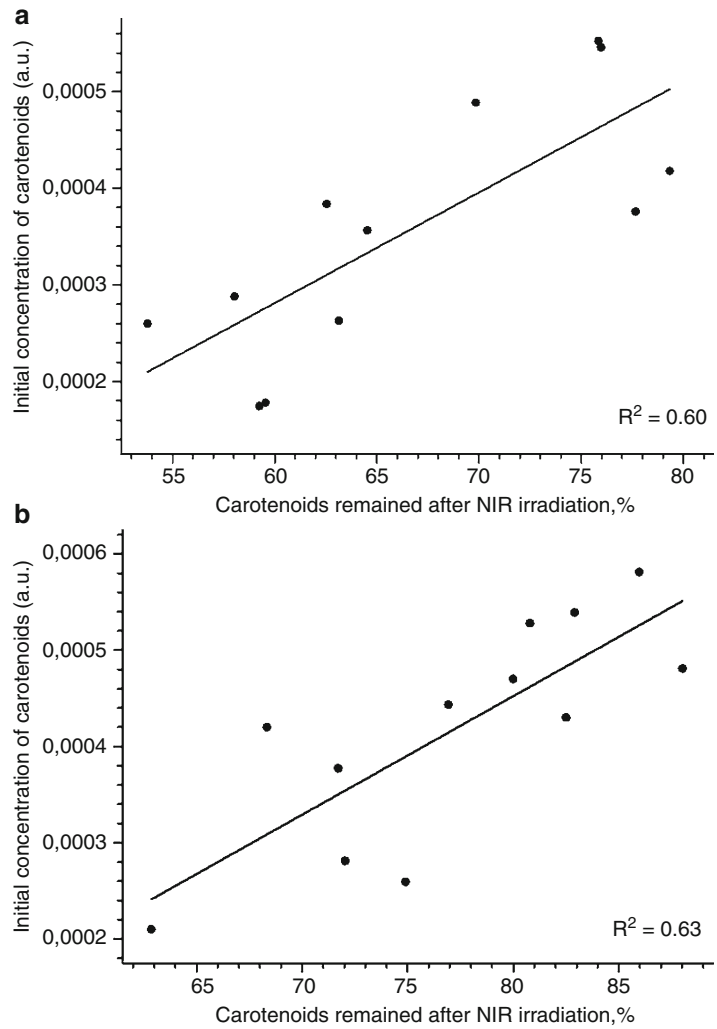

Fig. 2 Correlation between the individual level of carotenoids in the skin of 12 volunteers and the magnitude of carotenoids remaining after 30 min of IR irradiation with NIR (**a**) and IRA (**b**)

occurs constantly during IR irradiation (data not shown).

3.2 EPR Kinetics Subsequent to Infrared Irradiation In Vitro

Using EPR measurements, the radical formation process was investigated in vitro on porcine ear skin samples, which are considered to be a suitable model for human skin (Haag et al. 2010; Simon and Maibach 2000). Figure 3 shows the average value of the decrease of PCA spin marker in the skin without ("1"), subsequent to IRA ("2") and NIR ("3") irradiations. Most of the measured values were found to be statistically significant.

After the irradiation, the skin surface temperature was measured to be ~41.5 °C after the irradiation with NIR and ~39 °C with IRA, on average. Further investigations with PCA solutions have shown that PCA is not affected by IR irradiation nor by the resulting increased temperature due to its stability.

Thus, the obtained results showed that IR irradiation produced short-lived free radicals (mostly ROS (Zastrow et al. 2009)) in the skin, which were measured by the degradation of the PCA spin marker. The amount of generated free radicals is approximately 10 % higher for NIR in

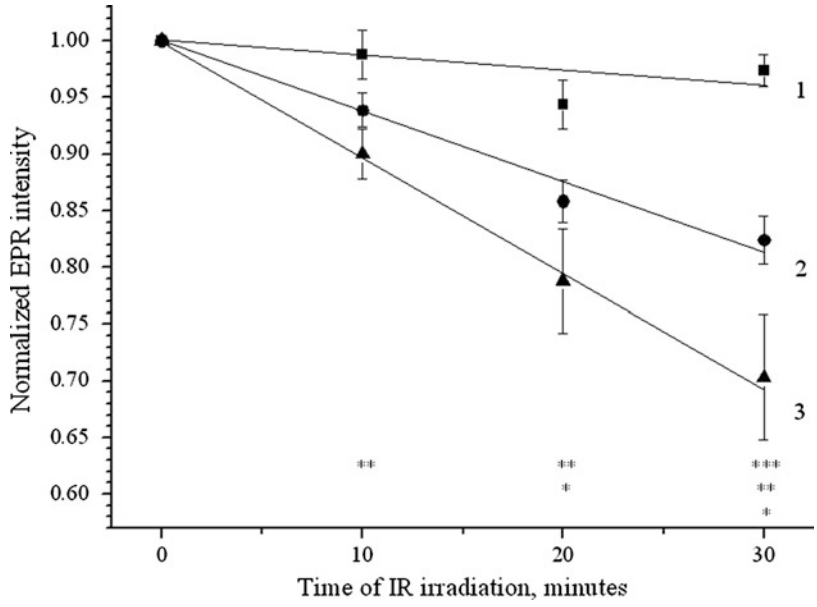

Fig. 3 Decay of the PCA in the porcine skin biopsies without ("1"), subsequent to IRA ("2") and NIR ("3") irradiation. "*," significance between "1" and "2"; "**," significance between "1" and "3"; "***," significance between "2" and "3" (Wilcoxon test, $p < 0.05$) (Taken from Darvin et al. (2011c))

comparison to the IRA, despite the applied same doses of irradiation.

3.3 Influence of Infrared Radiation-Induced Heat on the Skin

IR irradiation of human skin may increase the skin temperature due to the high absorption by cutaneous water. The pathological changes in human skin can be developed if the skin temperature exceeds 39 °C (Akhalaya et al. in press; Zastrow et al. 2009; Jung et al. 2010). Under these conditions, the heat shock-induced formation of ROS can be a consequence, which gives rise to the synthesis of MMPs as well as its subsequent pathological action on the skin tissue. However, in the skin, the formation of NIR radiation-induced ROS and heat shock-induced ROS occurs independently on each other by utilizing different pathways (Akhalaya et al. in press; Schieke et al. 2002; Lan et al. 2013). They potentiate the influence of each other only when skin temperature exceeds a value of 39 °C.

Results obtained in vivo show that during IR irradiation, the skin surface temperature increased continuously, reaching maximal values of 39.1 ± 0.7 °C subsequent to IRA radiation and 41.3 ± 0.6 °C subsequent to NIR radiation. Thus, it can be supposed that the difference between ROS production for IRA and NIR irradiations in the skin (see Fig. 3) is due to the formation of heat shock-induced ROS in the skin.

4 Conclusion

Free radicals (mostly ROS) are produced in human skin subsequent to IR irradiation, for which mainly the IRA range of the solar IR spectrum is responsible. The ROS generation is dependent of the applied IR doses. The IR radiation-induced heat can act pathologically through the formation of heat shock-induced ROS when the skin temperature exceeds 39 °C.

Consequently, during the NIR irradiation of the skin, ROS are produced, and their concentration is increased subsequent to the increase of the IR dose. When the skin temperature exceeds 39 °C, the heat shock-induced ROS are additionally produced in the skin, thereby multiplying the action of NIR radiation-induced ROS.

It was shown in the in vivo measurements that IR-induced free radicals can be effectively neutralized by cutaneous antioxidants and additionally by the topical application of antioxidant

substances including beta-carotene. The effectiveness of the neutralization of free radicals can be substantially increased if a mixture of different antioxidants at different concentrations is applied. The questions related to the optimization of the mixture of antioxidants used in cosmetic formulations should be investigated in the future, and the utilization of modern noninvasive techniques is expected to be indispensable in this undertaking.

The volunteers with a healthy lifestyle, characterized for instance by the consumption of high amounts of fruit and vegetables, accumulate more antioxidants in their skin and, thus, are better protected against IR-induced damage than other volunteers.

References

Akhalaya MJ, Maksimov GV, Rubin AB, Lademann J, Darvin ME. Molecular action mechanisms of solar infrared radiation and heat on human skin. Ageing Research Reviews 2014;16:1–11.

Alaluf S, Heinrich U, Stahl W, Tronnier H, Wiseman S. Dietary carotenoids contribute to normal human skin color and UV photosensitivity. J Nutr. 2002;132(3): 399–403.

Bensadoun RJ, Nair RG. Low-level laser therapy in the prevention and treatment of cancer therapy-induced mucositis: 2012 state of the art based on literature review and meta-analysis. Curr Opin Oncol. 2012; 24(4):363–70.

Biesalski HK, Obermueller-Jevic UC. UV light, beta-carotene and human skin – beneficial and potentially harmful effects. Arch Biochem Biophys. 2001;389(1): 1–6.

Calles C, Schneider M, Macaluso F, Benesova T, Krutmann J, Schroeder P. Infrared A radiation influences the skin fibroblast transcriptome: mechanisms and consequences. J Invest Dermatol. 2010;130(6): 1524–36.

Cho S, Shin MH, Kim YK, Seo JE, Lee YM, Park CH, et al. Effects of infrared radiation and heat on human skin aging in vivo. J Investig Dermatol Symp Proc. 2009;14(1):15–9.

Darvin ME, Gersonde I, Meinke M, Sterry W, Lademann J. Non-invasive in vivo determination of the carotenoids beta-carotene and lycopene concentrations in the human skin using the Raman spectroscopic method. J Phys D Appl Phys. 2005a;38(15):2696–700.

Darvin ME, Gersonde I, Albrecht H, Gonchukov SA, Sterry W, Lademann J. Determination of beta carotene and lycopene concentrations in human skin using resonance Raman spectroscopy. Laser Phys. 2005b; 15(2):295–9.

Darvin ME, Gersonde I, Albrecht H, Sterry W, Lademann J. In vivo Raman spectroscopic analysis of the influence of UV radiation on carotenoid antioxidant substance degradation of the human skin. Laser Phys. 2006a;16(5): 833–7.

Darvin M, Zastrow L, Sterry W, Lademann J. Effect of supplemented and topically applied antioxidant substances on human tissue. Skin Pharmacol Physiol. 2006b;19(5):238–47.

Darvin ME, Gersonde I, Albrecht H, Zastrow L, Sterry W, Lademann J. In vivo Raman spectroscopic analysis of the influence of IR radiation on the carotenoid antioxidant substances beta-carotene and lycopene in the human skin. Formation of free radicals. Laser Phys Lett. 2007;4(4):318–21.

Darvin ME, Zastrov L, Gonchukov SA, Lademann J. Influence of IR radiation on the carotenoid content in human skin. Opt Spectrosc. 2009;107(6):917–20.

Darvin ME, Haag S, Meinke M, Zastrow L, Sterry W, Lademann J. Radical production by infrared A irradiation in human tissue. Skin Pharmacol Physiol. 2010a;23(1):40–6.

Darvin ME, Haag SF, Lademann J, Zastrow L, Sterry W, Meinke MC. Formation of free radicals in human skin during irradiation with infrared light. J Invest Dermatol. 2010b;130(2):629–31.

Darvin ME, Sterry W, Lademann J. Resonance Raman spectroscopy as an effective tool for the determination of antioxidative stability of cosmetic formulations. J Biophotonics. 2010c;3(1–2):82–8.

Darvin ME, Sterry W, Lademann J, Vergou T. The role of carotenoids in human skin. Molecules. 2011a;16(12): 10491–506.

Darvin ME, Fluhr JW, Meinke MC, Zastrow L, Sterry W, Lademann J. Topical beta-carotene protects against infra-red-light-induced free radicals. Exp Dermatol. 2011b;20(2):125–9.

Darvin ME, Haag SF, Meinke MC, Sterry W, Lademann J. Determination of the influence of IR radiation on the antioxidative network of the human skin. J Biophotonics. 2011c;4(1–2):21–9.

Darvin ME, Meinke MC, Sterry W, Lademann J. Optical methods for noninvasive determination of carotenoids in human and animal skin. J Biomed Opt. 2013;18(6): 61230.

Dumay O, Karam A, Vian L, Moyal D, Hourseau C, Stoebner P, et al. Ultraviolet AI exposure of human skin results in Langerhans cell depletion and reduction of epidermal antigen-presenting cell function: partial protection by a broad-spectrum sunscreen. Br J Dermatol. 2001;144(6):1161–8.

Galluzzi L, Kepp O, Kroemer G. Mitochondria: master regulators of danger signalling. Nat Rev Mol Cell Biol. 2012;13(12):780–8.

Haag SF, Bechtel A, Darvin ME, Klein F, Groth N, Schafer-Korting M, et al. Comparative study of carotenoids, catalase and radical formation in human and

animal skin. Skin Pharmacol Physiol. 2010;23(6): 306–12.
Haag SF, Taskoparan B, Darvin ME, Groth N, Lademann J, Sterry W, et al. Determination of the antioxidative capacity of the skin in vivo using resonance Raman and electron paramagnetic resonance spectroscopy. Exp Dermatol. 2011;20(6):483–7.
Halliwell B. Biochemistry of oxidative stress. Biochem Soc Trans. 2007;35(Pt 5):1147–50.
Harman D. Free-radical theory of aging – consequences of mitochondrial aging. Age. 1983;6(3):86–94.
Hata TR, Scholz TA, Ermakov IV, McClane RW, Khachik F, Gellermann W, et al. Non-invasive raman spectroscopic detection of carotenoids in human skin. J Invest Dermatol. 2000;115(3):441–8.
Herrling T, Fuchs J, Rehberg J, Groth N. UV-induced free radicals in the skin detected by ESR spectroscopy and imaging using nitroxides. Free Radic Biol Med. 2003;35(1):59–67.
Jung T, Hohn A, Piazena H, Grune T. Effects of water-filtered infrared A irradiation on human fibroblasts. Free Radic Biol Med. 2010;48(1):153–60.
Karu TI. Mitochondrial signaling in mammalian cells activated by red and near-IR radiation. Photochem Photobiol. 2008;84(5):1091–9.
Kleesz P, Darlenski R, Fluhr JW. Full-body skin mapping for six biophysical parameters: baseline values at 16 anatomical sites in 125 human subjects. Skin Pharmacol Physiol. 2012;25(1):25–33.
Kochevar IE, Pathak MA, Parish AJ. Photophysics, photochemistry, and photobiology. In: Fitzpatrick A, editor. Dermatology in general medicine. New York: McGraw-Hill; 1999. p. 220–9.
Krinsky NI. Carotenoids as antioxidants. Nutrition. 2001;17(10):815–7.
Krutmann J. Inhibitory effects of sunscreens on the development of skin cancer. Hautarzt. 2001;52(1):62–3.
Krutmann J, Morita A, Chung JH. Sun exposure: what molecular photodermatology tells us about its good and bad sides. J Invest Dermatol. 2012;132(3 Pt 2):976–84.
Lan CC, Wu CS, Yu HS. Solar-simulated radiation and heat treatment induced metalloproteinase-1 expression in cultured dermal fibroblasts via distinct pathways: implications on reduction of sun-associated aging. J Dermatol Sci. 2013;72(3):290–5.
Lauer AC, Groth N, Haag SF, Darvin ME, Lademann J, Meinke MC. Radical scavenging capacity in human skin before and after vitamin C uptake: an in vivo feasibility study using electron paramagnetic resonance spectroscopy. J Invest Dermatol. 2013;133(4):1102–4.
Matthews YJ, Halliday GM, Phan TA, Damian DL. Wavelength dependency for UVA-induced suppression of recall immunity in humans. J Dermatol Sci. 2010a;59(3):192–7.
Matthews YJ, Halliday GM, Phan TA, Damian DL. A UVB wavelength dependency for local suppression of recall immunity in humans demonstrates a peak at 300 nm. J Invest Dermatol. 2010b;130(6): 1680–4.
Meinke MC, Syring F, Schanzer S, Haag SF, Graf R, Loch M, et al. Radical protection by differently composed creams in the UV/VIS and IR spectral ranges. Photochem Photobiol. 2013;89(5):1079–84.
Moon JS, Oh CH. Solar damage in skin tumors: quantification of elastotic material. Dermatology. 2001;202(4): 289–92.
Murphy GM. Ultraviolet radiation and immunosuppression. Br J Dermatol. 2009;161 Suppl 3:90–5.
Norval M, Halliday GM. The consequences of UV-induced immunosuppression for human health. Photochem Photobiol. 2011;87(5):965–77.
Palozza P, Krinsky NI. Antioxidant effects of carotenoids in vivo and in vitro: an overview. Methods Enzymol. 1992;213:403–20.
Ribaya-Mercado JD, Garmyn M, Gilchrest BA, Russell RM. Skin lycopene is destroyed preferentially over beta-carotene during ultraviolet irradiation in humans. J Nutr. 1995;125(7):1854–9.
Rockenbauer A, Nagy NV, Le Moigne F, Gigmes D, Tordo P. Thermodynamic analysis of the chemical exchange of beta-phosphorylated cyclic nitroxides by using two-dimensional (temperature versus magnetic field) simulation of ESR spectra: the impact of labile solvent-solute interactions on molecular dynamics. J Phys Chem A. 2006;110(31):9542–8.
Schade N, Esser C, Krutmann J. Ultraviolet B radiation-induced immunosuppression: molecular mechanisms and cellular alterations. Photochem Photobiol Sci. 2005;4(9):699–708.
Schieke S, Stege H, Kurten V, Grether-Beck S, Sies H, Krutmann J. Infrared-A radiation-induced matrix metalloproteinase 1 expression is mediated through extracellular signal-regulated kinase 1/2 activation in human dermal fibroblasts. J Invest Dermatol. 2002; 119(6):1323–9.
Schieke SM, Schroeder P, Krutmann J. Cutaneous effects of infrared radiation: from clinical observations to molecular response mechanisms. Photodermatol Photoimmunol Photomed. 2003;19(5):228–34.
Schroeder P, Haendeler J, Krutmann J. The role of near infrared radiation in photoaging of the skin. Exp Gerontol. 2008a;43(7):629–32.
Schroeder P, Lademann J, Darvin ME, Stege H, Marks C, Bruhnke S, et al. Infrared radiation-induced matrix metalloproteinase in human skin: implications for protection. J Invest Dermatol. 2008b;128(10):2491–7.
Shin MH, Moon YJ, Seo JE, Lee Y, Kim KH, Chung JH. Reactive oxygen species produced by NADPH oxidase, xanthine oxidase, and mitochondrial electron transport system mediate heat shock-induced MMP-1 and MMP-9 expression. Free Radic Biol Med. 2008;44(4):635–45.
Sies H, Stahl W. Nutritional protection against skin damage from sunlight. Annu Rev Nutr. 2004;24:173–200.
Simon GA, Maibach HI. The pig as an experimental animal model of percutaneous permeation in man: qualitative and quantitative observations – an overview. Skin Pharmacol Appl Skin Physiol. 2000;13(5):229–34.

Sklar LR, Almutawa F, Lim HW, Hamzavi I. Effects of ultraviolet radiation, visible light, and infrared radiation on erythema and pigmentation: a review. Photochem Photobiol Sci. 2013;12(1):54–64.

Tanaka Y, Matsuo K, Yuzuriha S. Near-infrared irradiation nonthermally induces long-lasting vasodilation by causing apoptosis of vascular smooth muscle cells. Eplasty. 2011;11:e22.

Taylor CR, Sober AJ. Sun exposure and skin disease. Annu Rev Med. 1996;47:181–91.

Zastrow L, Ferrero L, Herrling T, Groth N. Integrated sun protection factor: a new sun protection factor based on free radicals generated by UV irradiation. Skin Pharmacol Physiol. 2004;17(5):219–31.

Zastrow L, Groth N, Klein F, Kockott D, Lademann J, Renneberg R, et al. The missing link – light-induced (280–1,600 nm) free radical formation in human skin. Skin Pharmacol Physiol. 2009;22(1):31–44.

Phototoxicity, Photoirritation, and Photoallergy Detection and Assessment

103

Jean-Claude Beani

Contents

Keywords

Centra UV-Messgerat® • Crescendo reaction model • Decrescendo reaction model • Fluorescent light tubes • High pressure UVA lamps • Minimal erythema dose • Photoallergic potential • Photodermatosis • Photointradermal test • Photopatch test • Photoprick test • Phototoxic and photoallergic reactions • Phototoxicity • Plateauing reaction model • Prick-test method • Scarified photopatch test • Solar simulator • Systemic phototest

Photosensitization includes the events triggered within the skin by the interaction of a molecule (called photosensitizer or chromophore) and wavelengths usually located in the ultraviolet (UV) light. It may be related either to phototoxicity, an inflammatory reaction depending on UV light dose and chromophore concentration, or to photoallergy, a specific immune reaction requiring a primary sensitization phase.

The in vivo testing of a compound's photosensitizing potential is needed in two circumstances:

- To check in a patient a compound suspected to be at the origin of an exogenous photosensitization
- The prospective evaluation of the photosensitizing potential of a drug before its commercialization

J.-C. Beani (✉)
Clinique Universitaire de Dermato-Vénéréologie, Photobiologie et Allergologie, Pôle Pluridisciplinaire de Médecine, CHU de Grenoble, Grenoble, France
e-mail: jeanclaudebeani@gmail.com; jcbeani@chu-grenoble.fr

P. Humbert et al. (eds.), *Agache's Measuring the Skin*, DOI 10.1007/978-3-319-32383-1_137

Photosensitization tests combine compound introducing into the skin and further skin irradiation using an artificial light source. They are of three types: photopatch tests, photointradermal test, and systemic phototests. In photopatch tests, the compound is applied on the skin which eventually has been previously treated in order to increase penetration (abrasion of the horny layer or scarification). In photointradermal and photoprick test, the compound is intradermally injected in order to bypass the skin barrier. A prior measurement of the minimal erythema dose in UVB and UVA is necessary to help select the appropriate UV light doses. In photodermatoses exploration, one should also try to experimentally reproduce the light-induced eruption.

1 Material

1.1 Light Sources

Different types of sources are available (Anderson 1993; Beani 1987; Hölzle et al. 1987; Leroy et al. 1992).

- The *solar simulator* is the basic equipment. The Xenon arc lamp which emits a continuous spectrum, combined with a water filter to remove infrared ray and a WG305 Schott filter to eliminate shorter UV, is the common way to obtain a spectrum similar to that of solar light. Two devices are widely used in France: one from the CUNOW company, directly derived from equipment used in research and especially the Dermolum 3® (Müller, Moosining Germany). Interposition of cut-off filters or of a monochromator enables selecting the appropriate wavelengths.
- *High pressure UVA lamps* (UVAsun® 3000, Mutzhas, Munich RFA) are also essential; they emit very high UVA doses with a 330–460 nm spectrum (free from UVB), allowing in less than half an hour 100 J/cm^2 to be received by the skin placed at 30 cm of the lamp.
- *Fluorescent light tubes* emitting UVB (Philips TL12® or Sylvania F75®) or UVA (Philips TL09® OR Sylvania F85®); these tubes are either of small size for very localized irradiation or easily placed in a phototherapy cabin when bigger.
- *Slides projector with a Schott WG450 filter*: it is used for visible light irradiation, a rarely used test.

1.2 Diaphragms

Exposure time is set and irradiated area outlined through the interposition of a diaphragm between the light source and the skin.

Two types of diaphragm are necessary:

- A pierced plaque (usually 9 holes) 15–20 mm in diameter, covered by a second plaque which is moved manually or motorized. The movement of the front plaque uncovers the holes through which UVA or UVB light penetrates in preset geometrical or arithmetic progression doses. This computer-controlled device called sensitometer is integrated in the Müller solar simulator.
- A plaque with sufficient aperture to irradiate a large skin area, usually 5 × 10 cm^2.

1.3 Dosimeters

For better soundness, the measuring device should match the source spectrum. Two types of devices are widely used:

- The dosimeters Centra UV-Messgerat® (Osram, Munich) and IL9700® Research Radiometer (International Light, Newburyport, Massachusetts USA) which have two probes, one to measure UVB, the other UVA.
- Thermopiles (e.g., Kipp Zonen, 93270 Sevran France) which are connected to a voltmeter are sensitive to the whole spectrum (i.e., UV, visible, and infrared light). If they are calibrated for low energies, they can be connected to a monochromator.

1.4 Subject's Position

The selected skin area, usually the back, must be placed perpendicular to the light source and diaphragms; to facilitate positioning, a laterally and vertically motorized seat is helpful (Leroy and Dompmartin 1988).

2 Methodology

2.1 Minimal Erythema Dose (MED)

It is the lowest (A and/or B) UV dose which induces a visible erythema on the whole irradiated area. Its assessment uses a sensitometer. Irradiation by the solar simulator total spectrum results in the polychromatic (UVA and UVB) MED, also called MED_B, because the induced erythema is related almost exclusively to UVB. MED_A is provided either by a solar simulator-induced irradiation filtered by window glass or by a high pressure UVA source.

The tested area is the shoulder or the buttock. Reading is made 24 h after irradiation: MED_B in millijoule/cm^2 and MED_A in joule/cm^2. It should be made also immediately and 30 min after irradiation when early abnormal photosensitivity is suspected (e.g., solar urticaria).

The MED quantify the subject's actinic sensitivity which is related to his/her phototype. Accordingly, it is key parameter to select the UV light doses to be used in case of photosensitivity testing.

2.2 Photopatch Test (Syn: Photoepidermotest)

The investigated compound is applied as in any skin patch test, then the tested area is irradiated; the test is declared positive if a reaction appears only after irradiation. Until 1980, photopatch tests were not standardized, thus accounting for their poor reliability by these times (Hölzle et al. 1985). The first standardization attempts were proposed by the photopatch tests Scandinavian group (Thune 1988) followed by the German-Austrian-Swiss group (Hölzle et al. 1991) and the French group (Beani 1987; Jeanmougin M. et le Groupe de Recherche en Photobiologie Cutanée 1986). A consensus has finally been found although some points are debated.

- The *tested area* is usually the nontanned back skin.
- The *tested compound* (in petrolatum or alcohol) is applied in a Finn Chamber®, left in place for 24 h before irradiation and 48 h for the nonirradiated control.
- *Irradiation* takes place 24 h after application. However, this length of time may be inadequate, showing the difficulty of a fully standardized procedure because all photoallergens do not react in the same way. As example, for 6-methyl-coumarin the optimal time interval between application and irradiation is shorter, between 30 and 60 min (Jackson et al. 1980).

UVA irradiation is mandatory, as most photosensitizer's absorption spectrum is in UVA. The type of UVA source may affect the results; Przybilla et al. (1991) on a series of 27 compounds in 81 patients found a better efficiency with irradiation by TL09 type UVA fluorescent tubes than by high pressure UVA source. The UVA doses are chosen according to the expected type of reaction. Duguid et al. (1993) have shown, in patients with photoallergic positive patch tests obtained after 5 J/cm^2 irradiation, that irradiation between 0.7 and 1.9 J/cm^2 could elicit the same scores. Murphy (Murphy and White 1987), Cronin (1984), and English et al. (1987) have also shown that low doses (1–2 J/cm^2) are sufficient to elicit photoallergic reaction. In contrast, elicitation of a dose-dependent phototoxic reaction requires 10 or even 20 J/cm^2.

However, some molecules have their action spectrum in UVB. Consequently, to prevent any missing in detection, both UVA and UVB irradiation in parallel are now considered mandatory (Beani 1987; Jeanmougin M. et le Groupe de Recherche en Photobiologie Cutanée 1986; Jung 1981; Leroy et al. 1992; Przybilla et al. 1987). The UVB dose to be used is 0.75 MED_B, emitted by a solar simulator.

- Controls comprise skin irradiation without compound and skin irradiation with vehicle alone.
- *Photopatch tests interpretation*: reading is immediate following irradiation, then after 20 min, 24 h, 48 h, and 72 h and if possible later; in accordance with the international regulations regarding patch tests assessment, reactions are quantified:

+: erythema and flat papules or infiltration
++: erythema with papules and vesicles
+++: erythema with papules and blisters

A reaction limited to the irradiated area is universally considered positive (Gould et al. 1995). However, there is no consensus when both irradiated and nonirradiated areas are positive. The North American Contact Dermatitis group (Menz et al. 1988) and the Scandinavian group (Jansen et al. 1982) diagnose as photo-aggravated contact allergy a stronger reaction in irradiated area. Unless it is obvious, the "aggravation" assessment is subjective, however, and it seems difficult and unrealistic to grade the intensity of an erythema (The reader is advised to see ▶ Chap. 105, "Skin Barrier Function". The interpretation of these reactions is, therefore, uncertain.

- *Phototoxic and photoallergic reactions* must be distinguished: the former generates a well-defined erythema of early onset (24th hour) and straight of maximum intensity, sometimes associated with necrosis, whereas the latter evolves gradually and results in an eczema; biopsy may be useful to differentiate the reactions.

Hölzle et al. (1991) and Neuman et al. (1994) have refined the diagnosis through observation of intensity parameters over 4 days: erythema, infiltration, papules, vesicles, and blisters. Responses were classified into four types:

– The first type, called *decrescendo reaction model*, is similar to a contact toxic irritant reaction: a well-limited erythema, maximum on the first day, fading the following days. The absence of secondary inflammatory reaction suggests either a pharmacological effect of the compound or a phototoxic reaction. Further photo tests are needed before any conclusion is drawn. An example of this type of reaction is obtained with furosemide.
– The second type, named *combined reaction model*, shows an intense erythema on the first day which decreases the following days while on the second day an infiltration appears followed by papules and vesicles on the fourth day. It is interpreted as an initial phototoxic reaction followed by an allergic reaction. Examples of this type of reaction are found with tetrachlorosalicylamide, antiseptics, PABA, "*musk ambrette,*" or fragrance mixtures.
– The third type, the *plateauing reaction model,* shows a persistent erythema from the first up to the fourth day, often associated with an infiltration but rarely with vesicles or blisters. It is found preferentially with chlorpromazine and thioprofenic acid. Its meaning remains unknown.
– The fourth type, called *crescendo reaction model*, mimics an allergic reaction; erythema is not the prevailing sign, but papules and vesicles are present. Examples are given by fentichlor, 4-isopropyl-dibenzoyl-methane, 2-hydroxy-4-methoxy-benzophenone, and p-methoxyisoamylcinnamate.

This time-course based analysis aimed at differentiating pharmacological, phototoxic, and photoallergic reactions on clinical grounds, although potentially very useful, requires additional validation.

2.3 Scarified Photopatch Test

Before applying the tested molecule, control and irradiated areas are scarified diagonally with a small needle exerting a pressure strong enough to cut the epidermis without inducing bleeding (Kaidbey and Kligman 1978b; Kurumaji and Shono 1992). Then the irradiation and

interpretation procedures are not different from standard photopatch tests.

This method is interesting because it facilitates the penetration of compounds that have a low transcutaneous absorption capacity leading to false-negative reactions with standard photopatch tests (Kurumaji and Shono 1992). However, a recent study failed to show a better sensitivity in the diagnosis of drug-induced photosensitization (Conilleau et al. 2000).

2.4 Photointradermal Test

The epidermal barrier is bypassed in this technique. Epstein (1939) was the first to experiment it with sulfanilamide and obtained constant positive results. Schorr and Monash (1963) used it to confirm the phototoxic effect of dimethylchlotetracycline and tetracycline. Two key studies stand out in view of the number of tested drugs and the protocol used: the study by Kligman and Breit (1968), later improved by Kaidbey and Kligman (1978a), whose protocol is still the reference. It was recently used in a French study (Peyron and Pedailles 1986). Five intradermal injections, 0.1 ml of the compound diluted solution each, are carried out in the same subject; 15 min later, two sites are irradiated, one with 10 J/cm^2 UVA, the second one with 0.75 MED_B UVB. There are three controls: nonirradiated compound injected skin, UVA irradiated saline injected skin, and UVB irradiated saline injected skin. Reading takes place immediately, 6 h and 24 h later, as in common photopatch tests.

2.5 Photoprick Test

The prick-test method, widely used in IgE-mediated allergy testing for its low risk of systemic reaction, has recently been adapted to photobiological investigations under the name photoprick test (Bourrain et al. 1997).

The technique consists in three pricks made through a drop of the compound diluted in water covering 1 cm^2 skin (Stallerpoint®, Lab. Stallergène, Fresnes, France). The area is immediately irradiated 5 J/cm^2 UVA. A nonirradiated prick-test and a prick-test with the irradiated vehicle serve as controls. The same tests can be done in parallel with 0.75 MED_B UVB.

This method has the same purpose as photoscarification, but it is easy to implement and is safe as far as the risk of systemic reaction is concerned.

2.6 Systemic Phototest

It consists in performing photobiological tests after administration of a potential photosensitizer, usually a drug, by its usual oral or injected route (Beani 1987; Diffey and Langtry 1989; Emmett 1986; Ferguson 1995; Ferguson and Johnson 1990, 1993; Guidichi and Maguire 1985; Hölzle et al. 1987; Jonhson and Ferguson 1990; Leroy et al. 1992; Ljunggren and Bjellerup 1986; Meola et al. 1993; Schürer et al. 1992). It is imperative that the tested subject do not expose his (her) back to light over the whole test duration.

The two following methods are the most widely used:

- MED_A and MED_B assessment with immediate, early (5, 30, 30 min, and 4 h), and delayed (24, 48, and 72 h) reading: this is mainly used to identify phototoxicity (MEDs are lowered) although a protracted erythema may also (theoretically) indicate photoallergy.
- A phototest: a limited area (5 × 5 cm) on the back is irradiated with either infra-erythema UVB dose (0.5 or 0.75 MED_B) or 10 J/cm^2 UVA; immediate reading, then 30 min, 1 h, 4 h, 24 h, 48 h, and 72 h, and whenever possible one week after irradiation. Reactions may be phototoxic and/or photoallergic. They are differentiated on clinical grounds (aspect and time course), in some cases with the help of histological examination.

- The drug can be taken in a single dose, 2–3 times the therapeutic dose; because of frequent uncertainty regarding the drug pharmacokinetics, phototests are then repeated at different

times (1/2, 1, 2, 4, 6, and 8 h) after drug intake. Alternatively, the drug can be taken over a period of 5–7 days at usual doses before a single triggering irradiation is carried out when it is assumed that the skin is saturated with the substance.

- A last rarely used *variant* is to study a patient who still takes the drug: gradually increased UVB (5–100 mJ/cm^2) and UVA (1–15 J/cm^2) doses are given; an erythema arising at a dose lower than expected indicates phototoxicity. The test should be repeated 2 weeks or more after stopping the drug intake and by then the MED must have gone back to normal. The final proof will include a reintroduction test with an additional phototesting. This is often not possible in practice (Gould et al. 1995). In a recent optimization of this technique (Vousden et al. 1999), the MED was calculated before and after 5 days of drug intake, using several wavelengths delivered through a monochromator. A photosensitization index was defined as the ratio of MEDs before and after drug intake. This index would permit to compare the photosensitization potential of various compounds and to define their action spectrum.

3 Selection of the Appropriate Method

3.1 Detection and Quantification of a Compound Phototoxic or Photosensitizing Potential

The purpose of this type of study is to detect a phototoxic or photosensitizing potential of medicines before their commercialization. It is the natural complement of similar studies previously carried out *in vitro* or in animals. The test is performed in healthy phototype II to IV subjects. Exclusion criteria are those commonly used in research in man. In addition, any intake of potentially photosensitizing drug including oral contraceptive for the 3 months preceding the test must be avoided. The average number of volunteers is usually 30. The standard photobiological tests can only demonstrate a phototoxic potential. They are inappropriate for detecting a photoallergic potential since such reaction requires an earlier sensitization.

3.1.1 Detection of Phototoxic Power

Photopatch tests are the most widely used. Phototoxic reactions are dose dependent, therefore testing use increasing concentrations and progressive UV doses. However, in a prospective study, limitations of the method for compounds systemically taken have been shown (Jeanmougin M. et le Groupe de Recherche en Photobiologie Cutanée 1986). First, the responsible chromophore is often not the native drug but one of its metabolites. Second, the tested drug may not traverse the stratum corneum and thus fail to elicit a response of the viable tissue. Efficiency can be improved through additional procedures which facilitate the cutaneous penetration; however, such protocols are heavier and may raise ethical problems.

Detection is also possible through systemic administration of the drug. A comparison of both MED_A and MED_B before and after 5–7 days drug intake is a method usually preferred over the phototest kinetics observation following a single high dose. Drug administration is randomized between two groups, one taking the verum, the other one the placebo. In some studies additional subgroups are created in order to compare the photosensitizing potential of various drugs within each chemical class; this has been done within the fluoroquinolones (Ferguson and Johnson 1990, 1993) resulting in the following relative risk quantification (Scheife et al. 1993): Fleroxacin $\gg$ Lomefloxacin, Pefloxacin $\gg$ Ciprofloxacin $>$ Enoxicin, Norfloxacin, Floxacin.

For detection of phototoxic power, we lack comparative study of efficacy between systemic tests and photopatch tests.

3.1.2 Detection of a Photoallergic Potential: Photo-maximization Test

To detect a photoallergic potential, Kaidbey and Kligman (and 1980) proposed in 1980 a test in man adapted from the maximization test used for detection of potential contact sensitizers. They used a 150 W solar simulator polychromatic light for hypersensitivity induction and UVA light (solar simulator equipped with a WG345 filter) for elicitation .

The induction phase consists in six steps: (1) application of the compound under a 2.5 cm^2 patch kept for 24 h, (2) irradiation of a 0.8 cm diameter area of the patch with three MED polychromatic light as emitted by the solar simulator, (3) the test area is left uncovered for 48 h, (4) new patch application on the same area for 24 h, (5) the test area is left uncovered for 24 h, and (6) new irradiation as in step 1. This sequence was repeated six times. In fair skin subjects (phototype I and II), the second sensitizing irradiation is usually followed by an intense sometimes blistering inflammatory reaction.

The induced photosensitization is revealed 10–14 days after the last irradiation: a patch test is made on an area different from that used for sensitization and irradiated 4 J/cm^2 UVA (solar simulator with WG345 filter). Controls include a similar photopatch test with the vehicle only and a nonirradiated patch test. Readings are to be recorded 24 h and 48 h after irradiation. To differentiate phototoxic and photoallergic reactions, the authors recommend to reduce both the concentrations of the tested compound and the irradiation doses.

However interesting this method may be, it raises a major ethical issue, the risk of photosensitizing the volunteers.

3.2 Investigations in Photodermatoses

Obviously, the diagnosis of photodermatosis is established through the patient's interview and clinical examination but if there are no apparent lesions, the use of photobiological exploration becomes essential (Beani 1987; Emmett 1986; Epstein 1962; Goerz et al. 1995; Hölzle et al. 1987; Leroy et al. 1992; Meola et al. 1993; Selvaag and Thune 1996). Photopatch tests are commonly used but are weighty and time consuming when compared to the experimental reproduction of the lesions, which is the preferred test in the diagnosis. They should be used only if photosensitization is strongly suspected. It is necessary to use them appropriately as one cannot completely avoid the risk of inducing photosensitization by the tests themselves (Meola et al. 1993).

- Here the purpose of a photopatch tests is to look for a photoallergy to the compound, possibly at the origin of the disease, whereas identifying a phototoxic reaction would only suggest the compound is potentially photosensitizing without relation to the disease (the same remark applies to all the above mentioned photobiological tests). Making a difference between the two types of results requires low UV doses and low compound concentrations (British Photodermatology Group Workshop report 1997; Emmett 1986; Goerz et al. 1995; Jeanmougin M. et le Groupe de Recherche en Photobiologie Cutanée 1986; Menz et al. 1988; Schauder 1985) because photoallergic reactions are not dose dependent. Accordingly, the suggested UVA dose is only 5 J/cm^2; in case of doubtful reaction, the test should be made again but with still reduced UV doses. The tested compounds are selected according to the patient's history, and tests with standard compounds involving the most usual photosensitizers are also systematically carried out.
- Photopatch test's efficiency in finding the responsible agent is satisfactory in contact photoallergy but poor in systemic drug-induced photoallergy. For example, in the latter case a negative result does not mean nonresponsibility of the suspected drug and a positive result with a drug from the standard battery does not imply its involvement either.

The responsibility of the drug requires that the patient has been in contact with it and that in the patient's history photosensitization bursts match contacts with the drug. Illustration of the poor photopatch test's efficiency and how cautious should be the interpretation in case of suspected photoallergy is given by a recent paper (Conilleau et al. 2000) where among 15 patients suffering from drug photoallergy only three had photopatch tests positive to the suspected compound. This confirms a study from the German-Austrian-Swiss photopatch tests group (870 tested patients): 2,041 photopatch tests were positive but only 108 were considered as evidence of photoallergy with clinical relevance (Hölzle et al. 1991). This low specificity is also shown in a Mayo Clinic's study (Menz et al. 1988), in which only 14 out of 27 positive photopatch tests were confirmed as having clinical relevance.

While it is difficult to explain these false-positive photopatch tests of photoallergic type, possible explanations can be found to the false-negative results: compound low penetration capacity, unsuitable vehicle, inappropriate methodology (UV dose, irradiation time, etc.), and wrong interpretation. In fact, there is a lack of soundness in most investigations related to the diagnosis of drug-induced photoallergy. Especially, facilitated transcutaneous penetration in photopatch tests and the use of systemic tests should increase their reliability. But such tests cannot be used in routine and remain restricted to research laboratories.

References

Anderson TF. Light sources in photomedicine. In: Lim HW, Soter NA, editors. Clinical photomedicine. New York: Marcel Dekker; 1993. p. 37–58.

Beani JC. Interprétation des tests photobiologiques. Ann Dermatol Venereol. 1987;114(1):123–6.

Bourrain JL, Paillet C, Woodward C, Beani JC, Amblard P. Diagnosis of photosensitivity to flupenthixol by photoprick testing. Photodermatol Photoimmunol Photomed. 1997;13:159–61.

British Photodermatology Group Workshop report. Photopatch testing- methods and indications. Br J Dermatol. 1997;136:371–6.

Conilleau V, Dompmartin A, Michel M, Verneuil L, Leroy D. Photoscratch testing in systemic drug-induced photosensitivity. Photodermatol Photoimmunol Photomed. 2000;16:62–6.

Cronin E. Photosensitivity to musk ambrette. Contact Dermatitis. 1984;11:88–92.

Diffey BL, Langtry J. Phototoxic potential of thiazide diuretics in normal subjects. Arch Dermatol. 1989;125:1355–8.

Duguid C, O'Sullivan D, Murphy GM. Determination of threshold UV-A elicitation dose in photopatch testing. Contact Dermatitis. 1993;29:192–4.

Emmett EA. Evaluation of the photosensitive patient. In: De Leo VA, editor. Dermatologic clinics, photosensitivity diseases. Philadelphia: Saunders; 1986. p. 195–202.

English JS, White IR, Cronin E. Sensitivity to sunscreens. Contact Dermatitis. 1987;17:159–62.

Epstein S. Photoallergy and primary photosensitivity of sulfanilamide. J Invest Dermatol. 1939;2:43–51.

Epstein JH. Polymorphous light eruptions: phototest technique studies. Arch Dermatol. 1962;85:502–4.

Ferguson J. Fluoroquinolone photosensitization: a review of clinical and laboratory studies. Photochem Photobiol. 1995;62(6):954–8.

Ferguson J, Johnson BE. Ciprofloxacin-induced photosensitivity: in vitro and in vivo studies. Br J Dermatol. 1990;123:9–20.

Ferguson J, Johnson BE. Clinical and laboratory studies of the photosensitizing potential of norfloxacin, a 4-quinolone broad-spectrum antibiotic. Br J Dermatol. 1993;128:285–95.

General information will be found in Marzulli FN, Maibach HI (eds): Dermato-toxicology and Pharmacology. 6th edition, John Wiley and sons, New York, 2002.

Goerz G, Merk HF, Hölzle E. Photoallergy. In: Kruttmann J, Elmets CA, editors. Photoimmunology. Oxford: Blackwell Science; 1995. p. 176–86.

Gould JW, Mercurio MG, Elmets CA. Cutaneous photosensitivity diseases induced by exogenous agents. J Am Acad Dermatol. 1995;33(4):551–73.

Guidichi PA, Maguire HC. Experimental photoallergy to systemic drugs. J Invest Dermatol. 1985;85:207–17.

Hölzle E, Plewig G, Hoffman C, et al. Photopatch testing – result of a survey on test procedures and experimental findings. Z Hautkr. 1985;151:361–5.

Hölzle E, Plewig G, Lehmann P. Photodermatoses – diagnostic procedures and their interpretation. Photodermatol. 1987;4:109–11.

Hölzle E, Neumann N, Hausen B, Przybilla B, Schauder S, Hönigsmann H, Bircher A, Plewig G. Photopatch testing: the 5-year experience of the German, Austrian and Swiss photopatch group. J Am Acad Dermatol. 1991;25:59–68.

Jackson RT, Nesbitt LT, De Leo VA. 6-methylcoumarin photocontact dermatitis. J Am Acad Dermatol. 1980;2:124–7.

Jansen CT, Wennersten G, Rystedt I, Thune P, Brodthagen H. The Scandinavian standard photopatch test procedure. Contact Dermatitis. 1982;8:155–8.

Jeanmougin M. et le Groupe de Recherche en Photobiologie Cutanée. Détermination du pouvoir photosensibilisant d'un médicament par la méthode des photopatch-tests Nouv Dermatol. 1986; 50:204–8.

Jonhson BE, Ferguson J. Drug and chemical photosensitivity. Sem Dermatol. 1990;9:39–46.

Jung EG. Die belichtete epikutantestung. Akt Dermatol. 1981;7:163–5.

Kaidbey KH, Kligman AM. Identification of systemic phototoxic drugs by human intradermal assay. J Invest Dermatol. 1978a;70:272–4.

Kaidbey KH, Kligman A. Identification of topical photosensitizing agents in humans. J Invest Dermatol. 1978b;70:149–51.

Kaidbey H, Kligman A. Photomaximisation test for identifying photoallergic contact sensitizers. Contact Dermatitis. 1980;6:161–9.

Kligman AM, Breit R. The identification of phototoxic drugs by human assay. J Invest Dermatol. 1968;51:90–9.

Kurumaji Y, Shono M. Scarified photopatch testing in lomefloxacin photosensitivity. Contact Dermatitis. 1992;26:5–10.

Leroy D, Dompmartin A. A motorized chair for phototesting. Photodermatol. 1988;5:230–1.

Leroy D, Dompmartin A. Les moyens d'exploration des eczémas liés à la lumière. In: Lorette G, Vaillant L, editors. Les Eczémas. Paris: Doin; 1992. p. 104–11.

Ljunggren B, Bjellerup M. Systemic drug photosensitivity. Photodermatol. 1986;3:26–35.

Menz J, Muller SA, Connolly SM. Photopatch testing: a six year experience. J Am Acad Dermatol. 1988;18:1044–7.

Meola T, Lim HW, Soter NA. Evaluation of the photosensitive patient. In: Lim HW, Soter NA, editors. Clinical photomedicine. New York: Marcel Dekker; 1993. p. 153–66.

Murphy GM, White IR. Photoallergic contact dermatitis to 2-ethoxyethyl-p-methoxycinnamate. Contact Dermatitis. 1987;16:296.

Neumann JH, Hölzle E, Lehmann P, Benediter S, Tapernoux B, Plewig G. Pattern analysis of photopatch test reactions. Photodermatol Photoimmunol Photomed. 1994;10:65–73.

Peyron JL, Pedailles S. Etude in vivo de la phototoxicité chez l'homme par la technique des photointra dermoréactions (photo-IDR). Nouv Dermatol. 1986;5 (3):208–9.

Przybilla B, Ring J, Schwab U, et al. Photosensibilisierende eigenschafter nichtsteroidaler antirheumatika in photopatch-test. Hautarzt. 1987;38:18–25.

Przybilla B, Hölzle E, Enders F, Gollhausen R, Ring J. Photopatch testing with different ultraviolet A sources can yield discrepant test results. Photodermatol Photoimmunol Photomed. 1991;8:57–61.

Schauder S. How to avoid phototoxic reactions in photopatch testing with chlorpromazine. Photodermatol. 1985;2:95–100.

Scheife RT, Cramer WR, Decker EL. Photosensitizing potential of ofloxacin. Int J Dermatol. 1993;32:413–6.

Schorr WF, Monash S. Photoirradiation studies of two tetracyclines. Arch Dermatol. 1963;88:440–4.

Schürer NY, Hölzle E, Plewig G, Lehmann P. Photosensitivity induced by quinidine sulfate: experimental reproduction of skin lesions. Photodermatol Photoimmunol Photomed. 1992;9:78–82.

Selvaag E, Thune P. Drug photosensitivity in Norway. Acta Derm Venereol. 1996;76:405–6.

Thune P. The Scandinavian multicenter photopatch test study. Photodermatol. 1988;5:261–9.

Vousden M, Ferguson J, Richards J, Bird N, Allen A. Evaluation of phototoxic potential of gemifloxacin in healthy volunteers compared with ciprofloxacin. Chemotherapy. 1999;45:512–20.

Photobiological Assessment of Sunscreens

104

D. Moyal

Contents

Keywords

Sun protection factor (SPF) • UVA protection factor(UVAPF) • In vivo • In vitro • Critical wavelength • ISO • FDA USA • Waterresistance

There is a well-documented need for effective UVB and UVA photoprotection of the human skin by topically applied sunscreens. To evaluate and standardize the efficacy of the latter, the US FDA published in 1978 (Department of Health, Education, and Welfare and FDA USA 1978) the first method to determine the sun protection factor (SPF). In 1982, the German DIN also published a method (Deutsches Institut für Normung 1984), yet not harmonized with the US one, especially in terms of the amount of applied product (1.5 mg/cm^2 instead of 2 mg/cm^2). The US FDA revised the method in 1988, 1993, and 1999, and the last version was published in 2011 (Department of Health and Human Services and FDA USA 2011).

In 1994, the European Cosmetics Association (COLIPA) published the first European guidelines on the determination of SPF (The European Cosmetic Toiletry and Perfumery Association COLIPA 1994) and, later (2003), a revised version together with the Japanese Cosmetic Industry

D. Moyal (✉)
La Roche-Posay Laboratoire Dermatologique, Asnieres Sur Seine, France
e-mail: dominique.moyal@loreal.com

P. Humbert et al. (eds.), *Agache's Measuring the Skin*, DOI 10.1007/978-3-319-32383-1_138

Association (JCIA) and the Cosmetic Toiletries and Fragrances Association (CTFA) from South Africa (CTFA SA et al. 2003). This method, called the International SPF test method, was the first step of harmonization. The same method was published again in 2006 (CTFA SA et al. 2006) with the support of the US industry association CTFA (now called PCPC). Australia published an SPF test method in 1993 and revised it in 1998 (Australian/New Zealand Standards 1998). Since the International SPF test method, the US FDA and the Australian methods led to different results; the International Standardization Organization Technical Committee on Cosmetics Products (ISO TC217) decided, in 2006, to elaborate an ISO standard for the in vivo determination of the SPF.

In 2006, a request emerged from the European Commission (2006) to obtain standards for assessing both the UVB and the UVA protection afforded by sunscreen products. It was requested to develop in vitro methods giving equivalent results to the in vivo approach, the latter being the reference. The EU Commission also recommended that the methods used should take into account photo-instability of products to avoid an overestimation of protection factors. In vivo SPF and in vivo UVAPF (persistent pigment darkening) test methods take photodegradation into account since appropriate UV doses are used to induce erythema on the human skin for SPF determination or pigmentation for UVAPF determination.

When in vitro methods are used, they should also take into account this issue to provide relevant evaluation.

1 Determination of the Sun Protection Factor (SPF)

In 2010, the International Standardization Organization (ISO) working group n°7 in charge of the sun protection methods within the technical committee TC 217 on cosmetic products published the first ISO standard on the determination of the SPF (ISO 24444). This ISO standard (ISO 24444) is based upon the 2006 international test method for SPF determination (CTFA SA et al. 2006). In 2011, the US Food and Drug Agency (FDA) published a final monograph (Department of Health and Human Services and FDA USA 2011) that included an in vivo SPF test method also based upon the International SPF test method 2006 and similar to the ISO 24444. However, some differences still exist, as described in Table 1.

This ISO standard has been adopted by the EU and South Africa in 2010, by Australia, Mercosur, Japan, and Mexico in 2012, and Canada in 2013 (Table 2). However, there is no recognition of ISO 24444 by the US FDA. In addition, some countries do not recognize the US FDA method. Practically speaking, this situation implies retesting the same products when marketed in these countries and finally raises ethical and cost issues.

2 Determination of UVA Protection

In 2006, the European Commission recommended to use the persistent pigment darkening (PPD) as endpoint for determining UVA protection through a method similar to the JCIA method (Japan Cosmetic Industry Association (JCIA) 1995) or any in vitro method able to provide similar and reliable results. In addition, the critical wavelength, an evaluation of the width of the absorbance of the sunscreen product, should be determined and be at least equal to 370 nm.

2.1 In Vivo UVA Protection

Japan (JCIA) was first to publish (January 1996) an official in vivo method to determine the level of UVA protection, adopting the PPD method for assessment of the UVA efficacy of sunscreen products (Japan Cosmetic Industry Association (JCIA) 1995). Korea and China adopted this method in 2001 and 2007, respectively. Finally,

Table 1 Determination of in vivo SPF: main differences between the ISO 24444:2010 and FDA USA 2011 methods

Parameters	ISO 24444 2010	FDA USA 2011
Test subjects	Combination of phototypes I, II, and III and determination of ITA° (skin color) for selection	Phototypes I, II, and III
	(ITA° value >28° very fair, fair skin, and intermediate skin color)	10 subjects maximum, 3 subjects rejected for listed reason
	10–20 subjects according to the statistical criteria for test validation	
	Max 5 subjects rejected for listed reason	
Test conditions	Product application, UV exposure, and MED assessment should be carried out in stable conditions, with a room temperature from 18 to 26 °C	For the evaluation, the subjects should be in the same position as when the site is irradiated
	All steps of the procedure shall be performed in the same position: either an upright, seated, or prone position (excepted powders should be tested in prone position)	
Test sites	Application surface, between 30 and 60 cm^2	Application surface, minimum of 30 cm^2
Product quantity and application	(2.00 +/− 0.05) mg/cm^2; sensitivity of the balance at least 0.1 mg; method of weighing by loss	2 mg/cm^2
	Droplets on the whole test site, spreading time in the range of 20–50 s, low pressure of application	Spread the product as evenly as possible
	Powders, spatula, finger, applicator puff + water or other suitable solvent	Finger cot without pre-saturation
	Finger cot optional but recommended; when employed the finger cot should not be pre-saturated with the product	Drying time before UV exposure at least 15 min
	Drying time before UV exposure 15–30 min	
UV exposures	Pre-estimation of individual MEDu by experienced technician or by colorimetry (ITA°) or provisional MEDu up to 1 week before the test	Initial MEDu with 1.25 geometric progression
	UV dose progression for the protected and unprotected sites:	UV dose progression for unprotected site, 25 %
	For expected SPF ≤25, 25 % or less	UV dose progression for protected sites:
	For expected SPF >25, 15 % or less	For expected SPF <8, 25 %
		For expected SPF 8–15, 20 %
		For expected SPF >15, 15 %
Reference formulations for validation of the test	P2, P3, P7	P2
Statistical validation of the test	95 % confidence interval must be ≤17 % of the mean	No statistical criteria
	Add subjects from 10 to 20 to fulfill the criteria, if not reject the test	

the in vivo UVA method has been standardized by ISO TC217 and published in 2011 under the reference ISO 24442 (ISO 24442), now adopted or accepted in many countries (Table 2).

The PPD skin response has been selected for the development of a standardized protocol because it fulfills the different criteria needed to develop a relevant method to quantify the efficacy

Table 2 Adoption/recognition of ISO standards

	Europe	Australia 2012	South Africa 2013	USA 2011	Canada 2013	Mercosur 2012	Mexico 2012	Japan 2012
In vivo SPF	ISO 24444	ISO 24444	ISO 24444	FDA 2011	FDA 2011 ISO 24444	Interna2006 FDA 1999 or updates (ISO 24444; FDA 2011)	FDA 2011 ISO 24444	ISO 24444
In vivo UVA	ISO 24442	No	ISO 24442 JCIA 1995	No	ISO 24442	JCIA 1995 or updates (ISO 24442)	ISO 24442	ISO 24442
In vitro UVA	ISO 24443	ISO 24443	ISO 24443	FDA 2011	ISO 24443 COLIPA 2011 FDA 2011	COLIPA 2009 or all updates (COLIPA 2011, ISO 24443)	COLIPA 2011, ISO 24443, FDA 2011	No

of sunscreen products against UVAs such as (i) an action spectrum covering the entire UVA range and as flat as possible; (ii) independent of the fluence rate; (iii) a stable endpoint, the PPD reaction appearing stable over 240 min; and (iv) dependent on the UVA doses, classically from 10 to 25 J/cm^2 for an untreated skin site to allow the minimal pigmenting dose to be determined. Since the PPD response requires doses greater than 10 J.cm^{-2} (approximately 40 min of a midday summer sunlight), the photostability of sunscreens is also challenged during PPD test procedure.

The sunscreen-testing protocol developed using this endpoint is similar to the design of the SPF test. The major elements of the protocol include the exposure of skin phototypes II, III, and IV, i.e., subjects prone to elicit an induced pigmentation, a xenon arc solar simulator filtered with a WG335 filter 3 mm in thickness and UG11 filter 1 mm, multiple-incremental doses (25 % progression) of UVA with and without sunscreen protection, and observation of the pigment responses 2–24 h post UVA exposures. The protection index is determined as the ratio of the dose required for a minimally perceptible pigment response in sunscreen treated skin divided by the dose that induces the same response in unprotected skin. It has been demonstrated that using this protocol, the results are reproducible on a large range of products and various levels of UVA protection.

There are some minor differences between the JCIA protocol and the ISO 24442 standard, among which is the inclusion of a new reference formulation called S2 (mean UVAPF 12.7 with acceptance range [10.7–14.7]) that should be tested together with products of expected UVAPF >12 for validating the test (Moyal et al. 2007).

2.2 In Vitro UVA Protection

In 2007, the European Cosmetics Association (COLIPA, now Cosmetics Europe) published a guideline on the determination of UVA protection factor using an in vitro method (COLIPA 2007). This method has been developed to provide UVA protection factors correlated with in vivo UVA protection factors, i.e., an alternative to the in vivo method. This method was revised in 2011 (COLIPA 2011; Moyal et al. 2013) and published as an ISO standard (ISO 24443) in 2012 (ISO 24443). This method allows both the UVA protection factor and the critical wavelength value to be determined. The procedure comes as follows:

1.3 mg/cm^2 of sunscreen product is applied to polymethyl methacrylate (PMMA) plate with about 5 μm roughness. The transmission through the sunscreen coated sample is cross-multiplied by the UVA source emission spectrum and the PPD action spectrum. To reduce the operator influence, a calibration step is incorporated into the computations. The spectral absorbance is adjusted by a scalar multiplier so that the predicted SPF matches the clinically measured SPF, yielding an "absolute" absorbance curve from which UVA protection can be predicted using the following equations:

$$\mathrm{SPF}_{\text{in vitro}} = \frac{\int_{\lambda=290\mathrm{nm}}^{\lambda=400\mathrm{nm}} E(\lambda) * I(\lambda) * d\lambda}{\int_{\lambda=290\mathrm{nm}}^{\lambda=400\mathrm{nm}} E(\lambda) * I(\lambda) * 10^{-A_0(\lambda)} * d\lambda}$$

$$\mathrm{SPF}_{\text{in vitro, adj}} = \mathrm{SPF\,labelled} = \frac{\int_{\lambda=290\mathrm{nm}}^{\lambda=400\mathrm{nm}} E(\lambda) * I(\lambda) * d\lambda}{\int_{\lambda=290\mathrm{nm}}^{\lambda=400\mathrm{nm}} E(\lambda) * I(\lambda) * 10^{-A_0(\lambda)*C} * d\lambda}$$

$$\mathrm{UVAPF}_0 = \frac{\int_{\lambda=320\mathrm{nm}}^{\lambda=400\mathrm{nm}} P(\lambda) * I(\lambda) * d\lambda}{\int_{\lambda=320\mathrm{nm}}^{\lambda=400\mathrm{nm}} P(\lambda) * I(\lambda) * 10^{-A_0(\lambda)*C} * d\lambda}$$

The UVA dose to be delivered for taking into account the product photounstability if any is defined as the initial UVAPF0 obtained before UV exposure by calculations multiplied by 1.2 J/cm^2 (e.g., for a UVAPF0 = 10, the UVA dose will be 10 × 1.2 J/cm^2 = 12 J/cm^2).

$$\mathrm{D} = \mathrm{UVAPF}_0 \times 1.2\ \mathrm{J/cm^2}$$

Post exposure, the in vitro spectrum is measured again on the same plate and is transformed using the previously determined constant c. The UVAPF is recalculated using this transformed spectrum after the exposure step.

$$\mathrm{UVAPF} = \frac{\int_{\lambda=320\mathrm{nm}}^{\lambda=400\mathrm{nm}} P(\lambda) * I(\lambda) * d\lambda}{\int_{\lambda=320\mathrm{nm}}^{\lambda=400\mathrm{nm}} P(\lambda) * I(\lambda) * 10^{-A(\lambda)*C} * d\lambda}$$

Results from this in vitro UVA method have been compared to those from the in vivo PPD method for photostable and photounstable sunscreen products. Both a good reproducibility between laboratories and a significant correlation with the in vivo method were found.

2.3 Critical Wavelength

The absorption curve of most sunscreen agents presents a common feature, i.e., its absorption value is high wavelengths around 290 nm and decreases gradually with increasing wavelengths. The width of the curve represents the range of UV wavelengths where the sunscreen agent does absorb, that is to say, whether it has a wide range of absorption. The critical wavelength refers to the wavelength λc >290 nm where the area under the absorption curve accounts for 90 % of the total area of the entire absorption spectra (290–400 nm). It can be expressed by the formula

$$\int_{290}^{\lambda c} A\lambda.d\lambda = 0.9 \int_{290}^{400} A\lambda.d\lambda$$

A (λ), the absorbance of the sunscreen agent at the wavelength of λnm

dλ, the intervals between the wavelengths

Table 3 UVA in vitro: main differences between ISO 24443:2012 and FDA USA 2011

Parameters	ISO 24443:2012	FDA 2011
Substrate/plate	PMMA with 5 μm mean roughness	PMMA with roughness from 2 to 7 μm
	At least 4	At least 3
Application rate	1.3 mg/cm^2 without finger cot	0.75 mg/cm^2 with fingercot
Drying time and temperature	At least 30 min in the dark, temperature 25–35 °C	Not defined
UV source irradiance level	40–200 W/m^2	Up to 1500 W/m^2
Irradiation dose	1.2 J/cm^2 × UVAPF0	4 MEDs (8 J/cm^2)
Temperature during irradiation	25–35 °C	Not defined
Correction of the absorbance curve using in vivo SPF value	Yes	No
Reference formulation for test validation	S2 SPF 16 UVAPF acceptance range [10.7–14.7]	No
Statistical validation	95 % confidence interval must be ≤17 % of the mean UVAPF	No

In 2011, the US FDA published a final rule including a method to determine the critical wavelength (Department of Health and Human Services and FDA USA 2011). This method is however not harmonized with the ISO 24443 standard and can lead to different results. A summary of the main differences between the two methods is provided in Table 3.

2.4 UVA Protection Criteria

Combining both the determination of the level of UVA protection and the critical wavelength method to measure the broadness of UVA absorbance has been first proposed for assessing UVA protection of sunscreen products by the EU Commission (2006) and further adopted by other countries such as Australia, Mercosur, Mexico, and Canada. The value of the UVA protection factor (UVAPF) must be at least one-third that of the SPF.

The critical wavelength value must be ≥370 nm to qualify the product as "broad spectrum" in the USA and Canada.

3 Determination of Water Resistance

There are three main protocols for the measurement of water resistance of sunscreen products issued by COLIPA (2005), Australia (2012) (AS/NZS 2604), and the USA (2011) (Department of Health and Human Services and FDA USA 2011). These protocols differ by some technical aspects related to the water immersion procedure (Table 4).

The criteria and the labeling to support the claim water resistant are also different (Table 4).

ISO TC217 WG7 is working on a water resistance standard to harmonize the method.

4 Conclusion

The development of ISO standards and its worldwide adoption is paramount to avoid local retesting especially when only in vivo methods exist. These standards are precious references for both industry and legal authorities. A same method used by all allows better comparability between products and, ultimately, a better information toward consumers.

Table 4 Water resistance: comparison of the main parameters of three methods

	Europe	USA	Australia
Method	COLIPA guidelines for evaluating sun product WR, December 2005	FDA Final Monograph Sunscreen Drug Products for OTC Human Use, 2011	Australian/New Zealand Standard AS/NZS 2604:2012 Sunscreen Products – Evaluation and Classification
Recommended immersion devices	Spa pool, Jacuzzi, or bathtub with water circulation	Indoor fresh water pool, whirlpool or Jacuzzi	Indoor simulated swim test device (SSTD) approximately 1.8 m × 1.8 m
Water temperature	29 ± 2 °C	23–32 °C	33 ± 2 °C
Water agitation	Continuous circulation, no air agitation	Not specified	For each 20 min immersion period: water circulation for 16 min and air agitation for 4 min
Water quality	Drinking water meeting EC council directive 98/83/EC Mg and Ca (combined) content min. 50 mg/ml and max. 500 mg/ml; sanitized with bromide or chlorine or refilling for each volunteer	Drinking water meeting standard 40 CFR part 141	pH between 6.8 and 7.2
Recommended procedure	Measurement of a static SPF and the SPF after water immersion for 20 min, 15 min air-dry, 20 min immersion, air-dry ≥15 min until completely dry	Measurement of the SPF after immersion: 20 min moderate activity in water, 15 min rest, another 20 min moderate activity in water, air-dry period (duration not specified)	Measurement of the SPF after immersion: 20 min immersion in the water, 5 min rest period, another 20 min water immersion For WR claim >40 min the schedule of alternating 20 min immersion and 5 min rest to be continued. After the last immersion period air-dry ≥15 min
Number of subjects	Min. 10 to max. 20 valid values from max. 25 subjects, according to statistical compliance criteria on static SPF	At least 10 valid values from max. 13 subjects	Min. 10 to max. 20 valid values from max. 25 subjects, according to statistical compliance criteria on SPF after immersion
Reference WR product	Yes, P2, to be tested at least every 4 months WR for P2 >50 %	No	No
Calculation of mean WR	For each subject individually: %WRi = (SPFw-1)/(SPFs-1) * 100. The mean %WR is the arithmetic mean of n individual %WRi values	The WR SPF is the arithmetical mean of all individual SPFs measured after immersion minus A	The WR SPF is the arithmetical mean of all individual SPFs measured after immersion

(*continued*)

Table 4 (continued)

	Europe	USA	Australia
Statistical criteria	A product is water resistant, if the mean %WR – d is ≥50 % of the static SPF (d is the 90 % unilateral confidence value) and the 95 % bilateral confidence interval of mean static SPF lies within ±17 % of the static SPF	The mean WR SPF minus A ($A = t * s/\sqrt{n}$ with t being the Student's t value for 5 % error probability)	The 95 % bilateral confidence interval of mean post immersion SPF lies within ± 17 % of the static SPF
Labeling	Water resistant (if criteria are fulfilled after 40 min); very water resistant (if criteria are fulfilled after 80 min); SPF before immersion is labeled	Water resistant (40 min), water resistant (80 min) SPF –A determined after immersion is labeled	Water resistant 40 min, 2 h, 4 h SPF after immersion is labeled

References

AS/NZS 2604:2012 Australian/New Zealand Standard. Sunscreen products – evaluation and classification.

Australian/New-Zealand Standards. Australian/New-Zealand standard sunscreen products Evaluation and classification. [2604]. 1998.

COLIPA. Guidelines for evaluating sun product water resistance. 2005.

COLIPA. Method for in vitro determination of UVA protection provided by sunscreen products. 2007.

COLIPA. Guideline .In vitro Method for the determination of the UVA protection factor and "critical wavelength" values of sunscreen products. 2007.

Guideline.In vitro Method for the determination of the UVA protection factor and "critical wavelength" values of sunscreen products. 2009.

COLIPA. Method for in vitro determination of UVA protection. COLIPA guidelines. 2011.

CTFA SA, COLIPA, JCIA, CTFA. International sun protection factor (SPF) test method. 2006.

CTFA SA, COLIPA, JCIA. International sun protection factor (SPF) test method. 2003.

Department of Health and Human Services, FDA USA. Labeling and effectiveness testing: sunscreen drug products for over-the-counter human use. Final rule. [21 CFR Parts 201 and 310. 2011.

Department of Health, Education and Welfare, FDA USA. Sunscreen drug products for over-the-counter human use. Proposed safety, effective and labeling conditions. Federal Register CFR Part 352. 1978.

Deutsches Institut für Normung: Experimentelle dermatologische Bewertung des Erythemschutzes von externen Sonnenschutzmitteln für die menschliche Haut. DIN 67501. 1984.

European Commission. Recommendation on the efficacy of sunscreen products and the claims made relating thereto. OJL 265/39, 26.9.2006.

ISO 24442:2011. Cosmetics- sun protection test methods- in vivo determination of sunscreen UVA protection.

ISO 24443:2012. UVA in vitro cosmetics- sun protection test methods- determination of sunscreen UVA photoprotection *in vitro*.

ISO 24444:2010. Cosmetics- sun protection test methods- In vivo determination of the sun protection factor (SPF).

Japan Cosmetic Industry Association (JCIA). Japan Cosmetic Industry Association measurement standard for UVA protection efficacy. 15 Nov 1995.

Moyal D, Pissavini M, Boyer F, Perier V, Frêlon JH. In vivo persistent pigment darkening method: proposal for a new standard product for UVA protection factor determination. Int J Cosmet Sci. 2007;29:443–9.

Moyal D, Alard V, Bertin C, Boyer F, Brown MW, Kolbe L, Matts P, Pissavini M. The revised COLIPA *in vitro* UVA method. Int J Cosmet Sci. 2013;35:35–40.

The European Cosmetic Toiletry and Perfumery Association COLIPA. Colipa sun protection factor test method. Ref. 94/289-October. 1994.

Skin Barrier Function

105

Fabrice Pirot and Françoise Falson

Contents

This chapter was originally published under the ISBN 978-3-540-01771-4 with the following book title Measuring the Skin. The content has not been changed.

F. Pirot (✉)
EA 4169 “Aspects Fondamentaux, Cliniques et Thérapeutiques de la Fonction Barrière Cutanée”, Laboratoire de Pharmacie Galénique Industrielle – Faculté de Pharmacie., Université Claude Bernard Lyon 1, Lyon cedex 08, France

Unité de Préparation et de Contrôles des Médicaments, Service Pharmaceutique – Groupement Hospitalier Edouard Herriot-Hospices Civils de Lyon, Lyon cedex 03, France
e-mail: fabrice.pirot@univ-lyon1.fr

F. Falson
ISPB-Faculté de Pharmacie, University of Lyon, Lyon, France
e-mail: francoise.rieg-falson@univ-lyon1.fr

P. Humbert et al. (eds.), *Agache's Measuring the Skin*,
DOI 10.1007/978-3-319-32383-1_139

Keywords
Stratum corneum barrier function • skin lipids • Water transport in SC- Skin permeability • Transepidermal water loss (TEWL) • Skin hydrolipidic film

Adaptation to terrestrial life necessitates the presence of a highly impermeable epidermal membrane which restrains both insensible water loss from the body, transepidermal water loss (TEWL), and the entrance of exogenous substances into the body. This highly efficient barrier is already present in the newborn in whom the TEWL is close to normal adult values. On the other hand, in premature neonates (<33 weeks effective gestational age), an immature barrier function is manifested by an increased TEWL and percutaneous absorption of xenobiotics, which is well-correlated with the degree of prematurity (Hammarlund and Sedan 1979; Nachman and Esterly 1971; Rutter and Hull 1979). In the severely premature neonate (<28 weeks EGA), this compromised barrier function is an important cause of morbidity resulting from hypothermia, electrolyte imbalance, and cutaneous infections (Belgaumkar and Scott 1975; Lorenz et al. 1982; Maurer et al. 1984). The time required for the development of a fully functional skin barrier in this premature population is reported to be in the order of 2–4 weeks after birth (Evans and Rutter 1986).

The barrier function of the skin resides in the stratum corneum (SC). The permeability of the SC is dependent on the makeup of the intercellular spaces which consist of hydrophobic lipids arranged as lamellar bilayers (Elias and Menon 1991; Elias 1983). These lamellae are predominantly composed of three classes of lipids: ceramides, free fatty acids, and cholesterol (Schürer and Elias 1991). These lipids (or their precursors) are secreted into the intercellular spaces by epidermal lamellar bodies (Odland bodies) at the stratum granulosum–SC interface (Elias and Menon 1991). After secretion, the glucosylceramides and phospholipids are transformed, respectively, by glucosidases and lipases into ceramides and free fatty acids. The cholesterol in the SC is derived from the hydrolysis of cholesterol sulfate in the intercellular spaces, and by secretion from the lamellar bodies (Williams et al. 1998).

In this chapter, the molecular organization of the intercellular SC lipids is described (nature of lipid constituents, lipid conformation, compositional variation as a function of body site). A study of the skin barrier function correlating macroscopic biophysical measures with the functional status is presented. Finally, a noninvasive method for the determination of SC thickness, in vivo and in man, is described.

1 Molecular Organization of the SC

The SC lipids consist of cholesterol esters (15 %), cholesterol (32 %), saturated long-chain fatty acids (16 %), and ceramides (37 %) (Norlen et al. 1998).

The fatty acid composition of abdominal SC is presented in Table 1 (Elias 1990; Lampe et al. 1983). The endogenous free fatty acids are predominantly composed of long-chained

Table 1 Lipid composition of human abdominal SC (Adapted from Elias (1990) and Lampe et al. (1983))

Substances	mol %
Polar lipids	
Phosphatidylethanolamine	Trace
Cholesterol sulfate	2
Neutral lipids	
Free cholesterol	22
Free fatty acids	42
C14:0	3.8
C16:0	36.8
C18:0	9.9
C18:1	33.1
C18:2	12.5
C20:0	0.3
C20:1	Trace
C22:0	Trace
Triglycerides	Trace
Sterol/was esters	10
Sphingolipids	
Ceramides	24

saturated molecules (Norlen et al. 1998). The principal components, characterized by little interindividual variation, are lignoceric (C24:0) and hexacosanoic (C26:0) acids. In addition, traces of longer chain (C32-C36) saturated fatty acids have also been detected in the deeper regions of human forearm SC (Norlen et al. 1998). An analysis of the composition of free fatty acids as a function of SC depth demonstrates a decrease in the levels of C14:0, C16:0, C16:1, C18:0, and C18:1, but an increase in the amount of C24:1 (Bonte et al. 1997). The relative ratios of unsaturated/saturated free fatty acids, fatty acids/cholesterol and fatty acids/ceramides appear to decrease deeper in the SC.

Freeze fracture electron microscopy has shown that corneocytes in the SC are separated by multiple sheets of lipid lamellae (Elias and Friend 1975). These lamellae arise from stacks of lamellar disks that are extruded from the granular cells and then fused edge to edge to form sheets (Lavker 1976). Intercellular lamellae are composed of alternate hydrophobic (electron lucent) and hydrophilic (electron dense) lamellae (Landmann 1988). Each sheet therefore consists of two lipid bilayers, and there are one, two, or more such sheets in each intercellular space (Swartzendruber et al. 1987). A lucent band consisting of a monomolecular layer of N-(ω-hydroxyacyl)sphingosines is chemically bound to the horny cell envelope (Swartzendruber et al. 1987). The interaction between the ceramides and corneocyte protein envelopes probably occur via an ester linkage with glutamine or glutamate residues (Downing 1992). The β-sheet protein conformation of the corneocyte envelope is thought to permit a dense liaison with ceramide molecules thus creating a highly resistant and impermeable envelope (Lazo et al. 1995). As a result, the diffusion of water across the corneocyte is limited by virtue of the hydrophobic coating. Despite the rather low concentration of these covalently bound lipids (1.4 % of the SC mass and 53 % of protein bound lipids), they play a fundamental role in the mechanical and enzymatic resistance of the SC (Wertz and Downing 1987; Wertz et al. 1989). Therefore, Swartzendruber suggested that each corneocyte possesses a lipid envelope that may function both in corneocyte cohesion and in the barrier properties of the epidermis. A model of the linkage of ω-hydroxyacylsphingosines to the cornecoyte envelope (Swartzendruber et al. 1987) and the arrangement of double bilayers between corneocytes (Swartzendruber et al. 1989) are presented in Figs. 1 and 2.

2 SC Barrier Function and Skin Lipids

2.1 Barrier Function and Skin Lipid Extraction

Previous studies have demonstrated the essential role of the intercellular lipids in percutaneous absorption (Elias and Friend 1975; Nemanic and Elias 1980; Smith et al. 1982) and in the barrier function of the skin (Grubauer et al. 1989; Imokawa et al. 1986; Imokawa and Hattori 1985) showing (a) the importance of lipids in limiting water transport across hairless mouse skin, and (b) that extraction of sphingolipids and neutral lipids using a polar solvent (acetone) resulted in the greatest barrier disruption (Grubauer et al. 1989). The extraction of nonpolar lipids with petroleum ether provoked only a mild perturbation of the barrier (Grubauer et al. 1989). The sphingolipids, and particularly the ceramides, are considered to contribute to this barrier function by stabilizing the intercellular lipid lamellae (Ward and du Reau 1991).

2.2 Recovery of Barrier Function by Skin Lipids

In a similar study, Imokawa et al. (Imokawa et al. 1991) showed that the application of SC lipids to skin previously treated with organic solvents, restored the barrier function and was accompanied by the formation of intercellular lipid lamellae. An equimolar mixture of ceramides, cholesterol, and fatty acids (either essential fatty acids such as linoleic acid, or nonessential fatty acids as palmitic or stearic acids) was shown to accelerate recovery of

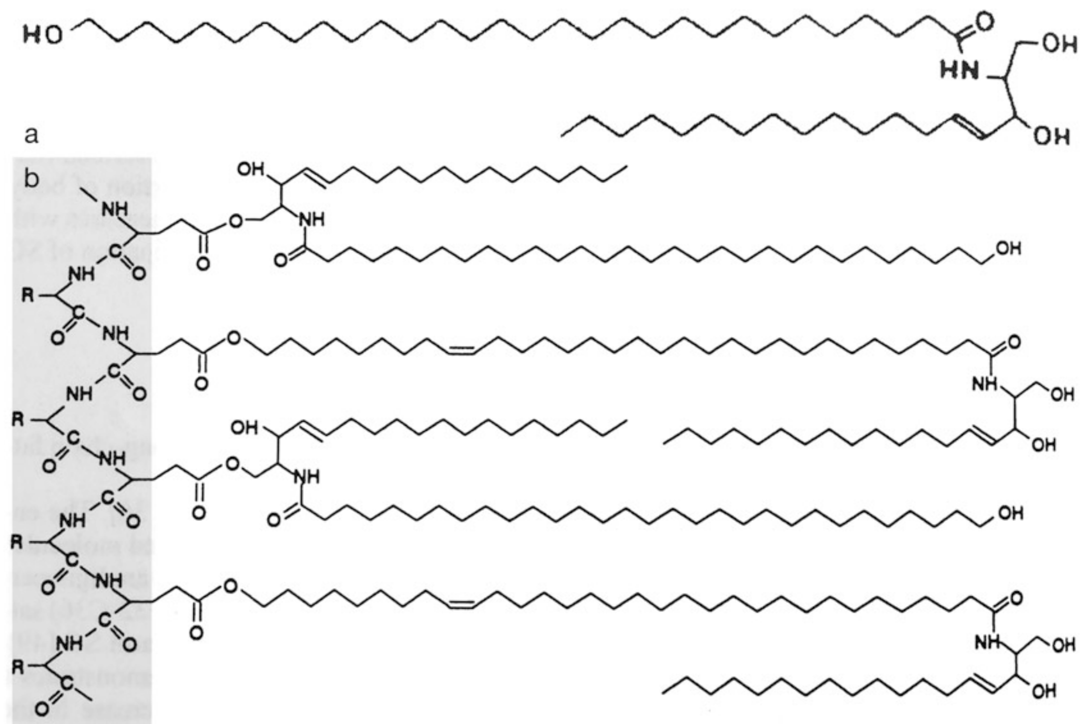

Fig. 1 (**a**) A representative structure of the ω-hydroxyacylsphingosines liberated from ester linkage with the horny cell envelope. (**b**) Postulated arrangement of ω-hydroxyacylsphingosines esterified with alterning γ-glutamyl groups in a β-pleated polypeptide chain (From Swartzendruber et al. 1987, with permission)

skin barrier function in mice and in humans, in vivo (Mao-Qiang et al. 1996). These lipids are incorporated rapidly (within approximately 2 h) into the cellular layers of the viable epidermis, then into the nascent, budding lamellar bodies, and finally within the intercellular lamellae. The diffusion within the viable epidermis of these endogenous lipids applied to intact human skin is thought to be equally rapid (Mao-Qiang et al. 1995). The application of an equimolar mixture of ceramides, cholesterol, and fatty acids was shown to accelerate barrier function recovery more rapidly than Vaseline (difference observed after 8 h) (Mao-Qiang et al. 1996).

2.3 Effect of Age and Seasonal Variation on SC Lipids

The biosynthesis of the majority of SC lipids, especially that of ceramides, decreases significantly with age (Rogers et al. 1996). Similarly, SC lipid synthesis decreases during the winter months regardless of the body site. The relative level of ceramide 1 linoleate declines during winter in older subjects, while the relative amount of ceramide 1 oleate increases. The levels of lignoceric and heptadecanoic acids decrease during winter while those of the other fatty acids remain almost constant. The decreased amount of SC lipids in older subjects contributes to their higher susceptibility to altered skin barrier function and skin dryness, particularly in winter.

3 SC Barrier Function and Hydration

The movement of water across the epidermis plays an important role in barrier repair (Grubauer et al. 1989) since the application of an impermeable covering over a damaged barrier

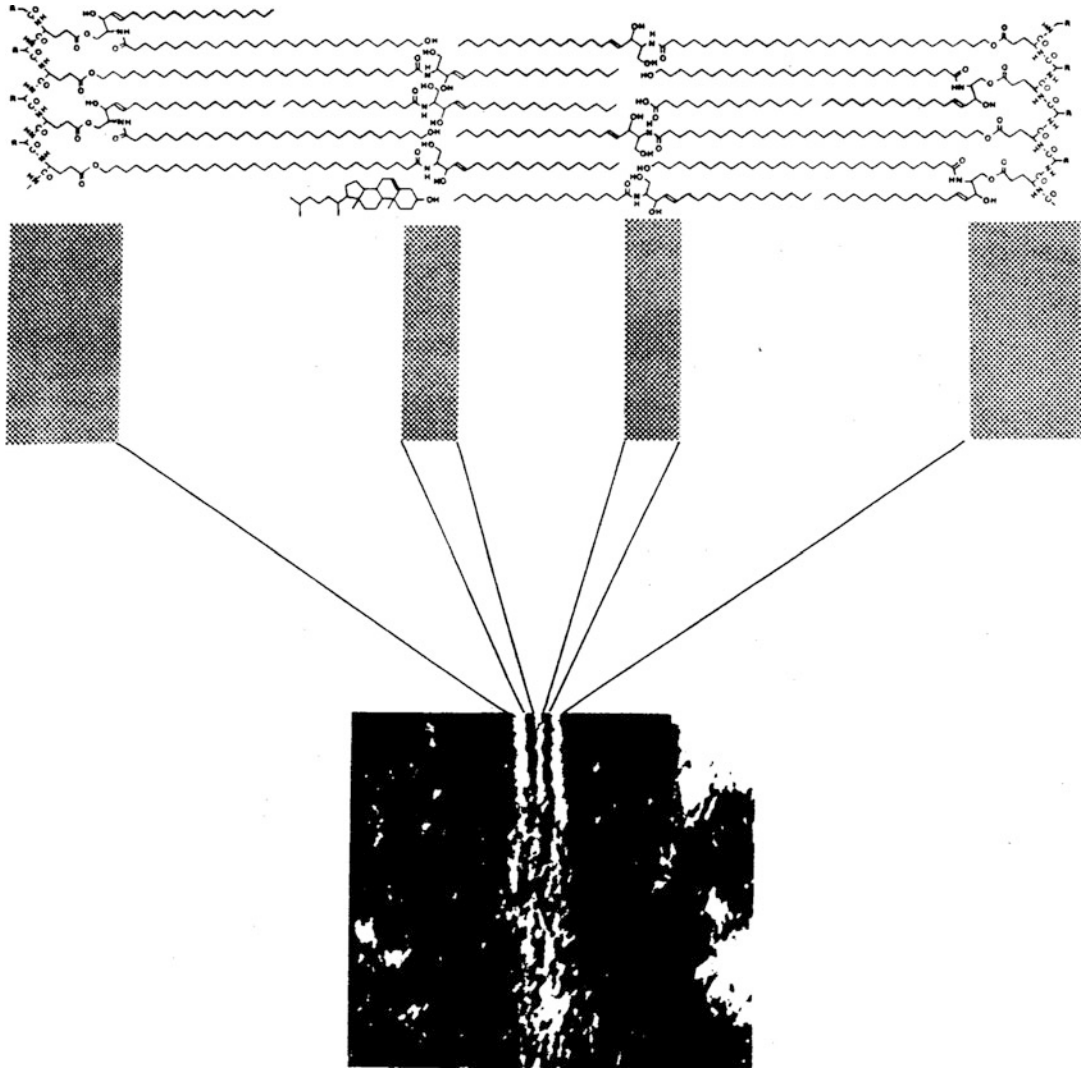

Fig. 2 Diagram of intercellular lipid lamellae based on studies by Swartzendruber et al. (From Swartzendruber et al. 1989, with permission). In *gray* on the chart (and *black* on the electron micrograph) are hydrophilic layers, whereas lipophilic layers are *white* both on the chart and the electron micrograph image

impedes recovery. Consequently, it is probable that the factors that regulate transcutaneous water transport are able to modulate skin barrier function. The ambient relative humidity also influences the transcutaneous diffusion of water. In a recent study, Denda et al. (1998a) demonstrated that the basal TEWL was reduced by almost 31 % from 19.9 ± 5.0 mg/m2/h to 13.8 ± 2.6 mg/m^2/h in animals maintained in a dry (RH < 10 %) versus humid (RH:80 %) environment. Furthermore, the number of lamellar bodies in the stratum granulosum cells (and their exocytosis) as well as the number of SC layers were elevated in animals maintained in a dry environment (RH < 10 %). Exposure to a low humidity for 48 h results in increased epidermal DNA synthesis (Denda et al. 1998b). The epidermal thickness and dry weight are also increased in a dry environment (Denda et al. 1998b). These changes may correspond to a homeostatic response to counter excessive TEWL in a dry environment (Denda

Table 2 Skin permeability coefficients for water as a function of relative humidity and treatment with hydrophilic/lipophilic agents

Relative humidity (%)	SC thickness (μm)	$10^8 \cdot P$ (cm s^{-1})
46[a]	11.6	3.9
62[a]	11.5	5.5
81[a]	12.4	17.9
93[a]	15.6	20.0
75[b]	15.0	11.0
60[c]	12.6	21.0
Formulation[d]	Water solubility in formulations	$10^8 \cdot P$ (cm s^{-1})
Diethyleneglycol monoethylic ether (I)	Miscible in all parts	65
Propyleneglycol dipelargonate (II)	<0.001	0.001
Mixture I + II (50/50. v/v)	0.04	0.04

[a]Through human skin (Blank et al. 1984)
[b]Through pig skin (Potts et al. 1991)
[c]In vivo in man (Pirot et al. 1998)
[d]Through hairless mouse skin treated with variable hydrophylic formulations (De Carvalho et al. 1996)

et al. 1998b). Water transport across the skin can be increased in the presence of hydrophilic excipients (e.g., diethyleneglycol monoethyl ether), which favors the partitioning of water towards the external surface in contrast to the presence of lipophilic substances (e.g., propylene glycol dipelargonate) (De Carvalho et al. 1993). Table 2 shows the variation in cutaneous water permeability coefficients as a function of relative humidity and treatment with lipophilic or hydrophilic formulations.

4 Characterization of SC Barrier Function

4.1 TEWL Measurement

The diffusion of water from the deeper layers of the epidermis towards the skin surface is an insensible phenomenon (distinct from perspiration), which is limited by the presence of the stratum corneum. Approximately 65 % of insensible water loss (TEWL) is attributed to evaporation from the skin surface. This diffusion depends not only on homeostatic mechanisms, but also on external factors such as humidity, temperature, and atmospheric pressure (Sato et al. 1998). In the absence of a convective current, the human body is surrounded by a layer of water vapor. TEWL measurements permit an evaluation of the skin barrier function (Elias and Menon 1991; Grubauer et al. 1989). The insensible water loss from the skin can be calculated from a measurement of the water vapor pressure gradient at the skin surface:

$$\frac{1}{A}\frac{dm}{dt} = -D'\frac{\Delta P}{\Delta x}$$

where *dm/(A dt)* is the quantity of evaporated water per unit time and surface area (g $m^{-2}h^{-1}$), D′ is a constant equal to 0.670×10^{-3} g mhPa^{-1} (at a temperature of 300 K and atmospheric pressure of 101 kPa), δP/δx is the water vapor pressure gradient (Pa m^{-1}) (Chapman and Cowling 1953; Eckert and Drake 1959). At the skin surface, the water vapor pressure gradient is relatively constant in the absence of external convection currents (Ueda 1956). Consequently, this gradient can be estimated by measuring the difference in water vapor pressure between two discrete points aligned perpendicularly to the skin surface. The vapor pressure is calculated as the product of the relative humidity and the saturated water vapor pressure, which is dependent on temperature. The relative humidity and temperature are measured

using a sensor (rh) and thermistor (th), respectively, which are coupled in a probe (Nilsson 1977). This method does not require regulation of the local water vapor pressure, as with hygrometric measures (which use circulating gas in a ventilated chamber) and gravimetric measures (which use saturated salt solutions in an unventilated chamber).

4.2 Measurement of Water Diffusivity and SC Thickness in Vivo

The diffusion of water in the SC is made complex by the heterogeneous structure of the membrane. El-Shime and Princen (El-Shime and Princen 1978) and Blank et al. (1984) demonstrated that SC water diffusivity increased with increasing membrane water content. The degree of SC hydration modifies its affinity for water (Hansen and Yelin 1972). Despite its heterogeneity, the SC has been regarded as a homogeneous membrane where each cellular layer contributes equally to the TEWL (Kligman 1964). The latter was recently demonstrated by Kalia et al. (1996) and Pirot et al. (1998), who have shown that SC water transport can be simply described in terms of Fick's first law of diffusion:

$$\mathrm{PIE_H} = \frac{\gamma \cdot \mathrm{D}}{\mathrm{H}}$$

where γ is the product of the SC lipid-viable epidermis partition coefficient K of water and ΔC (the water concentration difference across the membrane), and D is the average apparent diffusivity of water across the SC of thickness H. The total SC thickness can be calculated from the x-axis intercept of the function $y = 1/\mathrm{TEWL_{H-x}} = f(x)$ (Fig. 3). This methodology was recently used to determine the SC thickness from different body sites (Schwindt et al. 1998) (Fig. 4).

The self-diffusion coefficient of water is approximately 3×10^{-5} cm^2/s (Andrussow and Schramm 1969), and is about 100-fold and 10,000-fold smaller in a SC lipid model and SC, respectively (Schwindt et al. 1998).

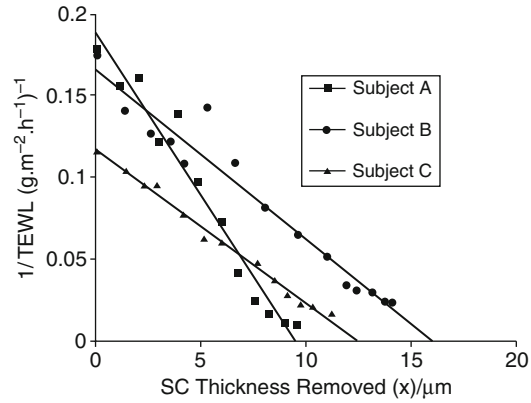

Fig. 3 Linear relationship between 1/TEWL and forearm SC thickness for three subjects (From Kalia et al. 1996, with permission)

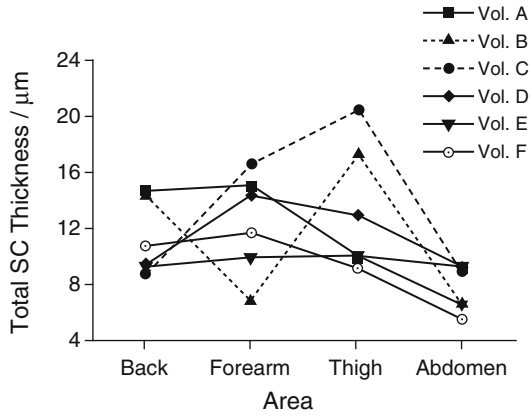

Fig. 4 Regional variations in SC thickness H for six subjects(From Schwindt et al. 1998, with permission)

4.3 TEWL and SC Morphology

Potts and Francoeur (1991) have shown that the intrinsic water diffusivity in the SC is comparable to that obtained in other lipidic membranes. However, the water diffusion pathway across the SC is 50 times greater than the absolute membrane thickness in which the lipids form a continuous, and tortuous, extracellular milieu.

4.4 Electrical Properties: Impedance and Conductance Measurements of the SC

The passage of an electrical current across the SC is dependent on the hydration state of the membrane. Measurements of electrical impedance or resistance have been frequently used to ascertain the SC hydration level. The passage of current across the SC is dependent on (1) the orientation of dipole moments of SC constituents such as keratin, (2) ionic motion within the SC, and (3) water mobility and proton exchange in the SC (Leveque and de Rigal 1983). The SC impedance, measured at high frequency, decreases (1) with increased hydration (Tagami et al. 1980), (2) following the removal of SC layers (i.e., after tape stripping), especially of the outermost layers 34], and (3) after treatment with hydrating agents (Clar et al. 1975). Tagami (Tagami et al. 1994) demonstrated, using measurements of cutaneous conductance at high frequency, that the capacity for water absorption and retention is markedly decreased in psoriatic lesions and in regions treated with Vaseline and a formulation containing urea (10 %). This technique has helped to highlight the correlation between the degree of hydration and the amino acid content in the SC of patients suffering from senile ichthyosis (Horii et al. 1989).

4.5 Infrared Spectroscopy

Water absorbs infrared radiation; this property has been exploited to quantify, noninvasively SC hydration using attenuated total reflectance infrared spectroscopy (ATR-IR). Accordingly, it has been shown that the absorbance at 3400 cm^{-1} (2.9 μm) characteristic of OH stretching vibrations increases in the deeper layers of the SC, suggesting a corresponding increase in water content as a function of SC depth (Baier 1978). Using Fourier transform infrared spectroscopy (FTIR), a water content of 0.12 ± 0.01 g cm-3 (mean ± SD; n = 6) was measured in six human subjects (Potts et al. 1985b). This value increased to 0.22 ± 0.02 g cm^{-3} after treatment with Vaseline for 5 h and returned to the initial value 30–45 min after removal of this occlusive layer.

5 Water Transport in the SC

Potts and Francoeur (1990) compared, using FTIR, the variation in SC water permeability and lipid conformation as a function of temperature. Their results demonstrated an important modification in the lipid hydrocarbon chains supporting Träuble's (1971) hypothesis that the diffusion of water occurred through free volume voids created in the lipid infrastructure. In an earlier study, the same group examined skin barrier function in vitro and the SC permeability to water using differential scanning calorimetry and infrared spectroscopy (Golden et al. 1987). At temperatures below 70 °C, the movement of water across the SC requires an activation energy of 17 kcal/mol, a value comparable with that obtained for a range of biomembranes. In addition, Golden et al. (1987) have shown that the flux of water is inversely related to the degree of conformational order of SC lipids. In a recent study, Gay et al. (1994) reported that a fraction of the intercellular SC lipids existed in an orthorhombic crystalline arrangement, implicating alkyl chains longer than 22 carbon atoms. Independent x-ray diffraction studies have demonstrated the presence of these structures in the SC of hairless mice (White et al. 1988), premature rats (Wilkes et al. 1973), and humans (Bouwstra et al. 1991; Garson et al. 1991). Such configurations, associated with nonlipid constituents, disappear between 45–65 °C. At physiological temperature, these orthorhombic lipids are thought to play an important role in the SC barrier function. Bouwstra et al. (1992) have shown, using x-ray diffraction, that the SC lipids from human skin are arranged as two types of lamellar structures with repeating distances of 6.4 and 13.4 nm. The introduction of molecules such as cholesterol destroys this configuration (Umemura et al. 1980). According to Gay et al. (1994) these orthorhombic lipids, associated with ceramides, could be located at the level of the corneocyte membranes, which could explain (in part) the poor permeability of these cells. Moreover, Gay et al. (1994) showed a

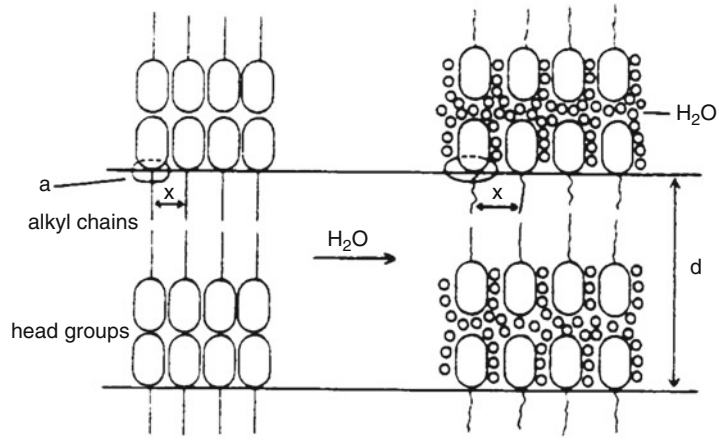

Fig. 5 Uptake of water in a bilayer: a possible mechanism, *a:* interfacial area per molecule. *d:* repeat distance. *x:* distance between two alkyl chains (From Bouwstra et al. 1991, with permission)

significant change in the infrared CH_2 stretching frequency of the SC lipid alkyl chains at relative humidities above 40 % w/w, suggesting a transition of the orthorhombic lipids and hence a change in barrier function.

Interestingly, no change in the X-ray diffraction pattern of SC lipids is observed as a function of hydration (Bouwstra et al. 1992). According to Bouwstra et al. (1992), water does not induce a swelling of the multilamellar lipid structure. Water can be incorporated into the lipid polar head regions (Fig. 5) and hence increase the interfacial area per lipid molecule without modifying the lamellar repeat distance (Bouwstra et al. 1991). This increase in interfacial area could thus be accompanied by a lateral swelling of alkyl chains and a decreased resistance in the interior of the membrane (Mak et al. 1991).

6 Conclusion

The physiology of the skin barrier function is a complex phenomenon that has only been partially elucidated. The key aspect of this function resides in the SC, at the skin-environment interface. The integrity of the skin barrier function may be evaluated by measurements of TEWL. While the measurement of water transport across the SC is now relatively straight-forward, the intimate understanding of this passive phenomenon is still the object of research and controversy, due in part to the remarkable anisotropic nature of the membrane.

In spite of this heterogeneous character, the diffusion of water across the SC appears to be a homogeneous process. If the thickness of the SC can be determined with some degree of accuracy, the route of water transport and hence, its diffusional pathway are still controversial. The intercellular lipid matrix is the only continuous structure of the SC (from the basal layers to the exterior). A number of different studies have shown that the intercellular lipids contribute to the skin barrier function. Water diffusion across this lipid matrix is considered to occur through the formation of free volume voids, created by thermal fluctuations, in the lipid hydrocarbon chains. Molecules of water can thus be transported across the SC thickness. This phenomenon is dependent on the temperature, the relative humidity, and the hydration state of the membrane. It is probable that an increase in water diffusivity subsequent to an increase in external temperature, relative humidity, and the level of membrane hydration reflects a modification of the orthorhombic configuration of certain intercellular lipids. The elevated SC water content (as a result of increased relative humidity) could subsequently lead to membrane fluidization (Alonso et al. 1996). This effect is probably predominant near the hydrophilic head groups of the fatty acid chains and may contribute to an increased water permeability across the SC. Further studies should help elucidate the level of these orthorhombic lipids and the influence of different treatments on their conformation and the reversibility of their phase

transitions. The study of water transport across the skin is of major interest as it also provides insight into the functional status of the barrier. However, conventional noninvasive methods based on electrical (Clar et al. 1975; Leveque and de Rigal 1983; Tagami et al. 1980), mechanical (de Rigal and Lévêque 1985; Potts et al. 1985a) and spectroscopic (de Rigal et al. 1992; Potts et al. 1985a) properties provide general information regarding bulk water transport across the skin, but do not provide a detailed picture of localized diffusion in the corneocytes and in the intercellular spaces.

Acknowledgements Dr Aarti Naik is acknowledged for the translation of this chapter.

References

Alonso A, Meirelles NC, Yushmanov VE, Tabak M. Water increases the fluidity of intercellular membranes of stratum corneum: correlation with water permeability, elastic, and electrical resistance properties. J Invest Dermatol. 1996;106:1058–63.

Andrussow L, Schramm B. Eigenschaften der Materie in ihren Aggregatszustanden. In: Schäfer K, editor. Transportphenomene I (Viskositdt und Diffusion). Berlin/Heidelberg/New York: Springer; 1969. p. 5.

Baier RE. Noninvasive, rapid characterization of human skin chemistry in situ. J Soc Cosmet Chem. 1978;29:283–306.

Belgaumkar JK, Scott KE. Effects of low humidity on small premature infants in servocontrol incubators. I. Decrease in rectal temperature. Bio Neonate. 1975;26:337–47.

Blank IH, Moloney J, Emslie AG, Simon I, Apt C. The diffusion of water across the stratum corneum as a function of its water content. J Invest Dermatol. 1984;82:188–94.

Bonte F, Saunois A, Pinguet P, Meybeck A. Existence of a lipid gradient in the upper stratum corneum and its possible biological significance. Arch Dermatol Res. 1997;289(2):78–82.

Bouwstra JA, Gooris GS, Van der Spek JA, Bras W. Structural investigations of human stratum corneum by small-angle X-ray scattering. J Invest Dermatol. 1991;97:1005–12.

Bouwstra JA, Gooris GS, Salomons-de Vries MA, Van der Spek JA, Bras W. Structure of human stratum corneum as a function of temperature and hydration: a wide-angle X-ray diffraction study. Int J Pharm. 1992;84:205–16.

Chapman S, Cowling TG. The mathematical theory of non-uniform gases. Cambridge: Cambridge Univ Press; 1953. p. 244.

Clar EJ, Her CP, Sturelle CG. Skin impedance and moisturization. J Soc Cosmet Chem. 1975;26:337–53.

De Carvalho M, Falson-Rieg F, Eynard I, Rojas J, Lafforgue L, Hadgraft J. Changes in vehicle composition during skin permeation studies. In: Brain KR, James VJ, Walters KA, editors. Prediction of Percutaneous Penetration, vol. 3B. Cardiff: STS Publishing; 1993. p. 251–4.

De Carvalho M, Charasse N, Falson-Rieg F, Had- graft J. Effect of water transport from the receptor compartment on the percutaneous in vitro absorption of estradiol. In Brain KR, James VJ, Walters KA, editors. Prediction g/ Percutaneous Penetration, Vol. 4b, STS Publishing, Cardiff, 1996, pp. 286–289

de Rigal J, Lévêque JL. In vivo measurement of the stratum corneum elasticity. Bioeng Skin. 1985;1:13.

de Rigal J, Losch MJ, Bazin R, Camus C, Sturelle C, Descamps V, Lévêque JL. Near infrared spectroscopy: a new approach to the characterization of dry skin. IFSCC. 1992;3:1131–46.

Denda M, Sato J, Masuda Y, Tsuchiya T, Koyama J, Kuramoto M, Elias PM, Feingold KR. Exposure to a dry environment enhances epidermal permeability barrier funnction. J Invest Dermatol. 1998a;111:858–63.

Denda M, Sato J, Tsuchiya T, Elias PM, Feingold KR. Low humidity stimulates epidermal DNA synthesis and amplifies the hyperproliferative response to barrier disruption: implication for seasonal exacerbations of inflammatory dermatoses. J Invest Dermatol. 1998b;111:873–8.

Downing DT. Lipid and protein structures in the permeability barrier of mammalian epidermis. J Lipid Res. 1992;33:301–13.

Eckert ERG, Drake RM. Heat and mass transfer. New York: Mc Graw-Hill; 1959. p. 449–56.

Elias PM. Epidermal lipids, barrier function, and desquamation. J Invest Dermatol. 1983;80:44s–9.

Elias PM. Chapter 2: The importance of epidermal lipids for the stratum corneum barrier. In: Osbourne D, Amann A, editors. Topical drug delivery formulations. New York: Marcel Dekker; 1990.

Elias PM, Friend DS. The permeability barrier in mammalian epidermis. J Cell Biol. 1975;65:180–91.

Elias PM, Menon GK. Structural and lipid biochemical correlates of the epidermal permeability barrier. Adv Lipid Res. 1991;24:1–26.

El-Shime AF, Princen HM. Diffusion characteristics of water vapor in some keratins. Colloid Polym Sci. 1978;256:209–17.

Evans NJ, Rutter NK. Development of the epidermis in the newborn. Biol Neonate. 1986;47:74–80.

Garson JC, Doucet J, Leveque JL, Tsoucaris G. Oriented structure in human stratum corneum revealed by X-ray diffraction. J Invest Dermatol. 1991;1991(96):43–9.

Gay CL, Guy RH, Golden GM, Mak VHW, Francoeur ML. Characterization of low-temperature (i.e., <65C) lipid transitions in human stratum corneum. J Invest Dermatol. 1994;103:233–9.

Golden GM, Gusek DB, Kennedy AH, Mckie JE, Potts RO. Stratum corneum lipid phase transitions and water barrier properties. Biochemistry. 1987;26: 2382–8.

Grubauer G, Feingold KR, Harris RM, Elias PM. Lipid content and lipid type as determinants of the epidermal permeability barrier. J Lipid Res. 1989;30:89–96.

Hammarlund K, Sedan G. Transepidermal water loss in newborn infants III. relation to gestational age. Acta Paediatr Scand. 1979;68:795–801.

Hansen JR, Yelin W. NMR and infrared spectroscopic studies of stratum corneum hydration. In: Jellinek HHG, editor. Water structure and the water-polymer interface. New York: Plenum Publishing; 1972. p. 19–28.

Horii I, Nakayama Y, Obota M, Tagami H. Stratum corneum hydration and aminoa acid content in xerotic skin. Br J Dermatol. 1989;121:587–92.

Imokawa G, Hattori M. A possible function of structural lipids in the water-holding properties of the stratum corneum. J Invest Dermatol. 1985;83:282–4.

Imokawa G, Akasaki S, Hattori M, Yoshizuka N. Selective recovery of deranged water-holding properties by stratum corneum lipids. J Invest Dermatol. 1986;87:758–61.

Imokawa G, Kuno H, Kawai M. Stratum corneum lipids serve as a bound-water modulator. J Invest Dermatol. 1991;96:845–51.

Kalia YN, Pirot F, Guy RH. Homogeneous transport in a heterogeneous membrane: water diffusion across human stratum corneum in vivo. Biophys J. 1996;71:2691–700.

Kligman AN. The biology of the stratum corneum. In: Montagna W, Lobitz WC, editors. The epidermis. New York: Academic; 1964. p. 387–433.

Lampe M, Burlingame A, Whitney J, Williams M, Brown B, Roitman E, Elias PM. Human stratum corneum lipids: characterisation and regional variations. J Lipid Res. 1983;24:120–30.

Landmann L. The epidermal permeability barrier. Anat Embryol. 1988;178:1–13.

Lavker RM. Membrane-coating granules: the fate of the discharged lamellae. J Ultrastruct Res. 1976;55:79–86.

Lazo ND, Meine JG, Downing DT. Lipids are covalently attached to rigid corneocyte protein envelopes existing predominantly as *B*-sheets: a solid-state nuclear magnetic resonance study. J Invest Dermatol. 1995;105:296–300.

Leveque JL, de Rigal J. Impedance methods for studying skin moisturization. J Soc Cosmet Chem. 1983;1983 (34):419–28.

Lorenz JM, Kleinman LI, Kotagal UR, Reller MD. Water balance in very-low-birth-weight infants. Relationship to water and sodium intake and effect on outcome. J Pediatr. 1982;101:423–32.

Mak VHW, Potts RO, Guy RH. Does hydration affect intercellular lipid organization in the stratum corneum. Pharm Res. 1991;8:1064–5.

Mao-Qiang M, Brown BE, Wu S, Feingold KR, Elias PM. Exogenous non-physiological versus physiological lipids: divergent mechanisms for correction of permeability barrier dysfunction. Arch Dermatol. 1995;131:809–76.

Mao-Qiang M, Feingold KR, Thomfeldt CR, Elias PM. Optimization of physiological lipid mixtures for barrier repair. J Invest Dermatol. 1996;106:1096–101.

Maurer A, Micheli JL, Schentz Y, et al. Transepidermal water loss and resting energy expenditure in preterm infants. Helv Paediatr Acta. 1984;39:405–18.

Nachman RL, Esterly NB. Increased skin permeability in preterm infants. J Pediatr. 1971;79:628–32.

Nemanic MK, Elias PM. In situ precipitation: a novel cytochemical technique for visualization of permeability pathways in mammalian stratum corneum. J Histochem Cytochem. 1980;28:573–80.

Nilsson GE. On the measurement of evaporative water loss. Methods and clinical applications. Linköping studies in science and technology Dissertations N11 [dissertation]. Linköping: Linköping University medical Dissertations N48; (1977). p. 9–42.

Norlen L, Nicander I, Lundh Rozell B, Ollmar S, Forslind B. Inter- and intra-individual differences in human stratum corneum lipid content related to physical parameters of skin barrier function in vivo. J Invest Dermatol. 1998;112(1):72–7.

Pirot F, Berardesca E, Kalia YN, Singh M, Maibach HI, Guy RH. Stratum corneum thickness and apparent water diffusivity: facile and noninvasive quantification in vivo. Pharm Res. 1998;15(3):492–4.

Potts RO, Francoeur ML. Lipids biophysics of water loss through the skin. Proc Natl Acad Sci U S A. 1990;87:3871–3.

Potts RO, Francoeur ML. The influence of stratum corneum morphology on water permeability. J Invest Dermatol. 1991;96:495–9.

Potts RO, Chrisman DA, Buras EM. The dynamic mechanical properties of human skin in vivo. Bioeng Skin. 1985a;1:13.

Potts RO, Gusek DB, Harris RR, Mckie JE. A noninvasive, in vivo technique to quantitatively measure water concentration of the stratum corneum using attenuated total-reflectance infrared spectroscopy. Arch Dermatol Res. 1985b;277:489–95.

Potts RO, Mak VH, Guy RH, Francoeur ML. Strategies to enhance permeability via stratum corneum lipid pathways. Adv Lipid Res. 1991;24:173–210.

Rogers J, Harding C, Mayo A, Banks J, Rawlings A. Stratum corneum lipids: the effect of ageing and the seasons. Arch Dermatol Res. 1996;288(12): 765–70.

Rutter N, Hull D. Water loss from the skin of term and preterm babies. Arch Dis Child. 1979;54:858–68.

Sato J, Denda M, Nakanishi J, Koyama J. Dry conditions affects desquamation of tratum corneum in vivo. J Dermatol Sci. 1998;18(3):163–9.

Schürer NY, Elias PM. The biochemistry and function of stratum corneum lipids. Adv Lipid Res. 1991;24:27–56.

Schwindt DA, Wilhelm KP, Maibach HI. Water diffusion characteristics of human stratum corneum at different anatomical sites in vivo. J Invest Dermatol. 1998;111:385–9.

Smith WP, Christenson MS, Nacht S, Gans EH. Effects of lipids on the aggregation and permeability of human stratum corneum. J Invest Dermatol. 1982;78:7–11.

Swartzendruber DC, Wertz PW, Madison KC, Downing DT. Evidence that the comeocyte has a chemically bound lipid envelope. J Invest Dermatol. 1987;88: 709–13.

Swartzendruber DC, Wertz PW, Kitko DJ, Madison KC, Downing DT. Molecular models of the intercellular lipid lamellae in mammalian stratum orneum. J Invest Dermatol. 1989;92:251–7.

Tagami H. Quantitative measurements of water concentration of thestratum corneum in vivo by high-frequency current. Acta Derm Venereol Suppl. 1994;185:29–33.

Tagami H, Ohi M, Iwatsuki K, Kanamaru Y, Yamada M, Ichijo B. Evaluation of the skin surface hydration in vivo by electrical measurement. J Invest Dermatol. 1980;75:500–7.

Traüble H. The movement of molecules across lipid membranes: a molecular theory. J Membr Bio. 1971;4: 193–208.

Ueda M. Measurements of the gradient of water vapour pressure and the diffusion coefficient. J Appl Phys Jap. 1956;25:144–9.

Umemura J, Cameron DG, Mantsch HH. A FTIR spectroscopic study of the molecular interaction of cholesterol with DPPC. Biochim Biophys Acta. 1980;602:32–44.

Ward AJI, du Reau C. The essential role of lipid bilayers in the determination of stratum corneum permeability. Int J Pharm. 1991;74:137–46.

Wertz PW, Downing DT. Covalently bound ω-hydroxyacylsphingosine in the stratum corneum. Biochim Biophys Acta. 1987;917:108–11.

Wertz PW, Madison KC, Downing DT. Covalently bound lipids of human stratum corneum. J Invest Dermatol. 1989;92:109–11.

White SH, Mirejovsky D, King GI. Structure of lamellar lipid domains and corneocyte envelopes of murine stratum corneum. An X-ray diffraction study. Biochem. 1988;27:3725–32.

Wilkes GL, Nguyen AL, Wildnauer RE. Thermal stability of the crystalline lipid structure as studied by X-ray diffraction and differential thermal analysis. Biochim Biophys Acta. 1973;304:267–75.

Williams ML, Hanley K, Elias PM, Feingold KR. Ontogeny of the epidermal permeability barrier. J Investig Dermatol Symp Proc. 1998;3(2):75–9.

In vivo Skin Absorption and Skin Pharmacology

106

Youssef Lboutounne and Patrice Muret

Contents

This chapter was initiated in the first edition of "Measuring the skin" book (2004) by Pr. Pierre Agache.

Y. Lboutounne (✉)
CIC-BT CHU, Besançon, France
e-mail: youssef-lboutounne@hotmail.fr

P. Muret
Engineering and Cutaneous Biology Laboratory, UMR 1098, University of Franche-Comte, Besançon, France

Clinical Pharmacology Department, University Hospital, Besançon, France
e-mail: patrice.muret@univ-fcomte.fr; p1muret@chu-besancon.fr

P. Humbert et al. (eds.), *Agache's Measuring the Skin*,
DOI 10.1007/978-3-319-32383-1_140

Keywords
Fick's laws • Diffusion coefficient • Lag time • Partition coefficient • Permeability coefficient • Microdialysis • Near-infrared spectroscopy • Physiologically based pharmacokinetic (PBPK) modeling • Plasma level method • Raman spectroscopy • Skin absorption • Cutaneous absorption, Pharmacokinetic parameters • Spectroscopic methods • Stratum corneum • Tape stripping

1 Definition

Skin absorption occurs from occupational, environmental, consumer skin exposure to chemicals, cosmetics, and pharmaceutical products. Skin absorption is a global term that describes the transport of chemicals from the outer surface of the skin to the systemic circulation (OECD 2004). This is often divided into:

- Penetration, which is the entry of a substance into a particular layer or structure, such as the entrance of a compound into the stratum corneum
- Permeation, which is the penetration through one layer into a second layer that is both functionally and structurally different from the first layer
- Resorption, which is the uptake of a substance into the skin lymph and local vascular system and in most cases will lead to entry into the systemic circulation (systemic absorption)

Skin absorption is a field of interest mainly to pharmacologists and toxicologists. The main purpose is obviously to know the amount of compound (solute) which has penetrated the organism, either its total amount or the amount per skin surface unit.

2 Topical Absorption Process

Skin absorption is related to a flow of matter diffusing through the stratum corneum, the outermost barrier, and subsequent layers. This process is illustrated in Fig. 1 (Lane 2013).

Three principal phases occur during skin absorption:

Phase 1: The solute leaves its vehicle and dissolves in the film coating the skin surface (lipids from the stratum corneum intercellular spaces, sebum, sweat, water, paraffin from the environment, etc.). This change of solvent is directed, and limited, by the solubility ratio, called partition coefficient (K).

Phase 2: The solute enters the stratum corneum intercellular spaces and is distributed according to a linearly decreasing concentration toward the deeper layers; its flow rate is determined by the diffusion coefficient (D). The filling of the stratum corneum is limited by its maximum storage capacity.

Phase 3: The solute penetrates the living tissue. This actual absorption phase begins before the second one has ended. It is controlled, and limited, by the solubility ratio in both tissues (which explains the very low passage of very lipophilic molecules). After a transient phase, this flow reaches a maximum which remains stable as long as the substance is in sufficient quantity on the skin surface. It is the phase of steady-state flux during which the amounts of compound going in and out of the stratum corneum are equal, while the amount stored inside this layer is continuously renewed but keeps identical and maximum. The amount absorbed during this phase is given by the first Fick's law:

$$Q = P \ Act \tag{1}$$

This formula expresses the fact that the quantity absorbed Q (g) is proportional to the application area A (cm^2), the application time t (hours), the applied concentration C (g/cm^3), and a particular factor P ($cm\ h^{-1}$) called permeability coefficient. It is important to highlight the fact that the exclusive "motor" of this molecular transfer is the concentration difference (C) on each side of the stratum corneum and that the absorbed quantity (Q) is at any time proportional to this difference. The applied quantity (the "dose") eventually plays a part only through the

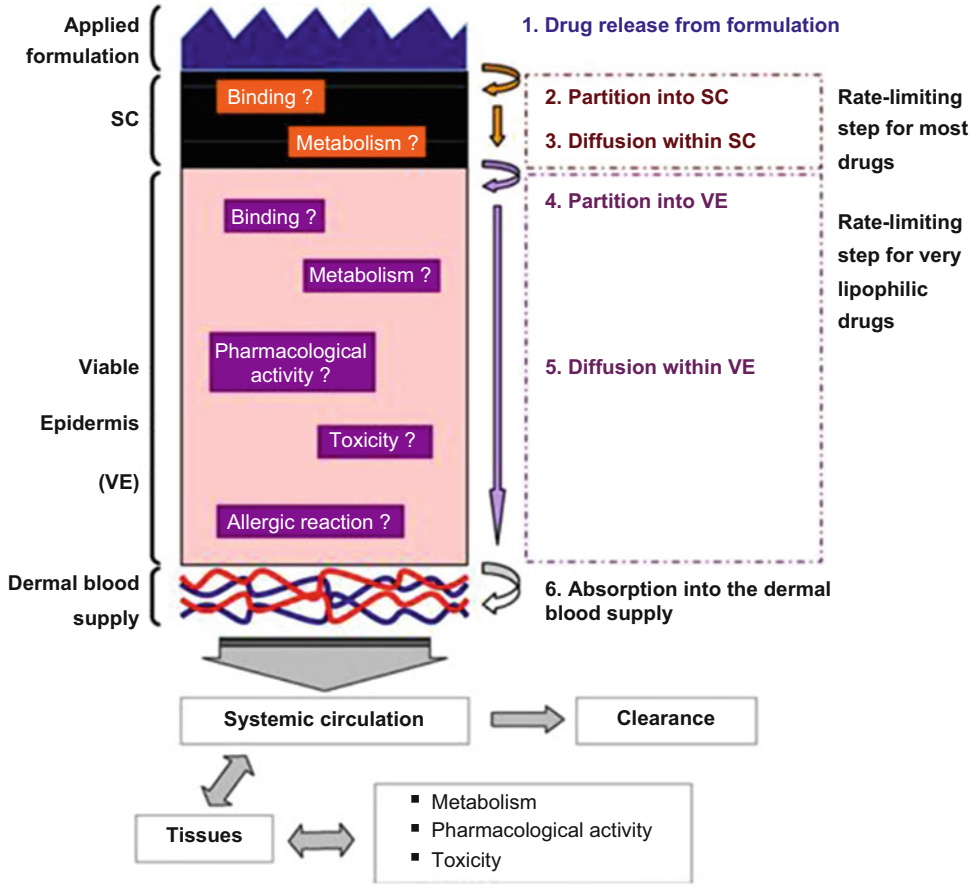

Fig. 1 Schematic representation of the processes involved in drug transport into and across the skin from any topical or transdermal applied formulation (Reported from Lane (2013))

application area or concentration, never through the thickness of the applied coat. This steady-state flux lasts as long as the solute concentration in the applied preparation remains unchanged. Without any new application, it will decrease, inducing the reduction then the end of the absorption.

Mention is made of "infinite dose" when the quantity applied is such that the concentration is not reduced before the steady-state flux has had time to be responsible for the almost entire absorbed quantity. This is usually the case when the quantity of cream applied is over 1 mg/cm^2, and the application is renewed every hour at least (the absence of visible cream on the skin should be avoided).

The experiment is called "finite dose" type if the amount of compound on the surface is not sufficient to reach the maximum flux. A typical example is when the molecule has a great affinity for the stratum corneum (it disappears quickly from the formulation and the partition coefficient comes down) or when the applied dose is very small (less than 0.5 mg/cm^2 cream).

3 Absorption Parameters

The cutaneous or percutaneous absorption is expressed differently depending on whether it refers to the transit through the stratum corneum only or the joint transit through other cutaneous tissues (epidermis, entire skin). The parameters of the flux across the stratum corneum (actual absorption) are those of

Fick's laws. The transepidermal or transcutaneous passage is described by pharmacokinetic parameters requiring compartment models based also on diffusion but not on Fick's laws. Finally, empirical or purely descriptive parameters are used sometimes, in particular when the former cannot be used. The choice of reliable parameters is very important as it guarantees the reliable reading and interpretation of the measures, especially their extrapolation to other situations.

3.1 Parameters Derived from Fick's Laws

J (g cm^{-2} h^{-1}): steady-state (maximum) absorption flux per unit skin area.
P (cm h^{-1}): permeability coefficient: it characterizes the absorption of a given compound in a given vehicle.
K (no dimensions): solubility of the solute in the stratum corneum divided by its solubility in its vehicle.
D (cm^{-2} h^{-1}): speed of transfer in the stratum corneum and capacity to penetrate the living tissue.
τ (hours): "lag time."

To use and calculate these parameters, different equations are available (Scheuplein 1978):

Q (g cm^{-2}) indicates a quantity per unit skin area.
C (g cm^{-3}) is the applied concentration.
t (hours) is the application time since the beginning.
e (cm) is the stratum corneum thickness.

Steady-state flux:

$$J = Q/t = PC \tag{2}$$

Permeability coefficient:

$$P = KD/e \text{ hence } J = KDC/e \tag{3}$$

Cumulated amount entered into the stratum corneum (Fig. 1, top curve):

$$Q_{in} = J(t + 2\tau) \tag{4}$$

Cumulated amount having left the stratum corneum (Fig. 1, bottom curve):

$$Q_{out} = J(t - \tau) \tag{5}$$

Maximum amount stored in the stratum corneum (Fig. 1, middle curve):

$$Q_m = KCe/2 \tag{6}$$

Lag time:

$$\tau = e^2/6D \tag{7}$$

The actual absorption corresponds to Q_{out} (lower curve). However, during this period of maximum flow, the quantity Q_m remains stored in the SC, the leaks toward the living tissue being compensated by an equivalent supply. It may be interesting to know this maximum storage capacity as it constitutes a reservoir (Mitragotri 2003) likely to empty quickly into the living tissue if the diffusion coefficient happens to increase; this occurs in case of hyperhydration of the SC, for example, under occlusion or during a contact allergy patch testing.

At the beginning of the application, before the flow is at its maximum, the second Fick's law is applicable as long as the solute concentration in its vehicle remains unchanged.

3.1.1 Partition Coefficient (K)

It is defined as the ratio "solubility in the stratum corneum/solubility in the applied formulation."

This ratio can be measured in vitro by using powdered stratum corneum from foot callus (Wester and Maibach 1995) or, preferably, stratum corneum from other body sites. The latter is obtained by immersion of an epidermis sample (isolated from dermis using the usual techniques) in 0.01 % trypsin in water (Kligman and Christophers 1964). Five milligrams of stratum corneum is immersed in 100 μl of the tested formulation and left until equilibrium (Scheuplein 1965).

It can be measured in vivo by three procedures. Firstly, by dosing the solute in the stratum

corneum at the stage of constant flow or in its vicinity (therefore after a half hour application at least). Assuming that the SC thickness is made up of 20 layers, and leaving aside the reduction of the weight of the strips with depth, the quantity found in the first 15 strips should represent about three fourths of the total. Knowing this, it is possible to obtain the partition coefficient with the abovementioned Eq. 6. Another method consists in dosing the solute in the first 5 strips, then in the 5 following ones, and so on until 20 strips are completed. The concentration close the surface, obtained through a linear regression, divided by the applied concentration, gives the partition coefficient. The principle of the last method is to measure the constant store during an absorption measurement by the "difference method" (Sect. 4.9) and then apply Eq. 6.

3.1.2 Diffusion Coefficient (D)

It corresponds to the diffusion speed inside the stratum corneum (and also the partition coefficient between living tissue and stratum corneum, although this is not taken into account in the theory). It is theoretically independent from the vehicle (but this is not always confirmed in practice). It can be calculated from J or P only if K is known. Tables of the diffusion coefficient have been drawn up (Table 1): as their use is in cm^{-2} h^{-1} (or cm^{-2} s^{-1}), concentration must be recorded in g cm^{-3} and skin thickness in cm^2.

3.1.3 Permeability Coefficient (P)

It characterizes the capacity of a solute to be absorbed from a given vehicle. It can be obtained directly by the "method of differences" (Sect. 4.9), by dividing the steady-state flux by the applied concentration. Other methods which indicate the flux entering not the stratum granulosum but more distal tissue only (dermis, blood, urine) can only give an estimate. The value of P for the same solute but with vehicle B instead of A can be obtained by multiplying P_A by the solubility in A to solubility in B ratio.

The values of P vary widely from one product to another, between 10^{-6} and 5 10^{-2} cm h^{-1} (Mitragotri 2003; Table 2). If *water is the vehicle*,

Table 1 Water diffusion coefficients (D (cm^2 h^{-1} × 10^6)) at 30 °C (Scheuplein and Bronaugh 1983)

Body site	e (μm)	D (cm^2 h^{-1} × 10^6)
Abdomen	15,0	2,16
Volar forearm	16,0	2,12
Back	10,5	3,24
Forehead	13,0	1,44
Scrotum	5,0	0,36
Dorsum hand	49,0	4,32
Palm	400	29,88
Sole	600	38,16

E (μm): stratum corneum thickness

Table 2 Permeability coefficients (P (cm/h) measured in human skin models (Reported and modified from Mitragotri (2003)

Solute	Molecular weight	Log $K_{o/w}$	Permeability (cm/h)
Skin permeability to hydrophobic solutes (*Ko*/w >1)			
Corticosterone	346	1.94	$1.0 \times 10^{-4} - 5.4 \times 10^{-4}$
Estradiol	272	3.86	$3.0 \times 10^{-3} - 6.1 \times 10^{-3}$
Hydrocortisone	362	1.53	$1.6 \times 10^{-5} - 2.3 \times 10^{-4}$
Progesterone	314	3.77	$1.3 \times 10^{-2} - 3.0 \times 10^{-2}$
Testosterone	288	3.31	$2.2 \times 10^{-3} - 5.3 \times 10^{-3}$
Skin permeability to hydrophilic solutes (*Ko*/w <1)			
Water	18	−1.38	$1.3 \times 10^{-3} - 1.7 \times 10^{-3}$
Ethanol	46	−0.31	8.0×10^{-4}
Urea	60	−2.11	1.5×10^{-4}
Caffeine	194	−0.02	1.0×10^{-4}
Scopolamine	303	−1.58	5.0×10^{-5}
Human serum albumin	65,000	–	1.4×10^{-6}
Dextran	70,000	–	8.0×10^{-6}

it is sometimes not necessary to perform absorption measurements to calculate P, because it can be estimated from the molecular weight (M) and the partition coefficient octanol-water (K_{ow} measurable in vitro), according to the following formula:

$$\log\ P\left(\mathrm{cm\,h^{-1}}\right) = 0.74\ \log\ K_{ow} - 6.0\ 10^{-3}\mathrm{M} - 6.36 \quad (8)$$

Knowing P will help predict the steady-state absorption flux, according to Eq. 2, and the quantity that would be absorbed during this time (Eq. 1). To investigate further and be able to draw the curves of Fig. 1, it is necessary to know K or D as well.

3.1.4 Lag Time (τ)

This time, which is the intercept of the steady-state absorption flux straight line with the time axis (Fig. 2), takes place after the absorption has started and reflects the delayed absorption into the viable tissue related to the penetration into the stratum corneum, because the lines of entry into the SC and of entry in the viable tissue are 3τ apart, that is, 0.5 on Fig. 2 normalized absorption curve.

Direct lag time measurement in vivo is not possible, but its calculation is easy with Eq. 7. Its variations are in a narrow range. Lag time depends directly on the diffusion coefficient (D) and also shows variations with the vehicle (therefore with coefficient K and the SC store).

3.2 Pharmacokinetic Parameters

After passing through the SC, compounds diffuse through the epidermis and then the dermis and finally enter the blood capillaries. Pharmacologists and toxicologists use compartment models to treat these successive transfers. For example, (Guy et al. 1982) to process the data yielded by the "excreta method" (Sect. 4.1), four successive transfers can be considered: skin surface-SC, SC-living part of the skin, skin-blood, and blood-urine. Knowing the concentrations in the latter compartments, and considering that the transfer flows vary exponentially with time with constant coefficients, all the percutaneous absorption phases can be processed. Furthermore, the fate of the absorbed amounts in deeper tissue, for example, hypodermis, fat, muscle, or joints, can be predicted (Marty 1976; Schaefer and Redelmeier 1996).

Physiologically based pharmacokinetic modeling (PBPK) takes into account the physiological, metabolic, and chemical-specific parameters to quantitatively simulate the absorption and elimination of a compound and determine the permeability constant (K_p). Although the technique can be elaborated only in animals, due to the necessity of organs sampling, it can be extrapolated to man. The formula to calculate K_p is the following (Thrall et al. 2002):

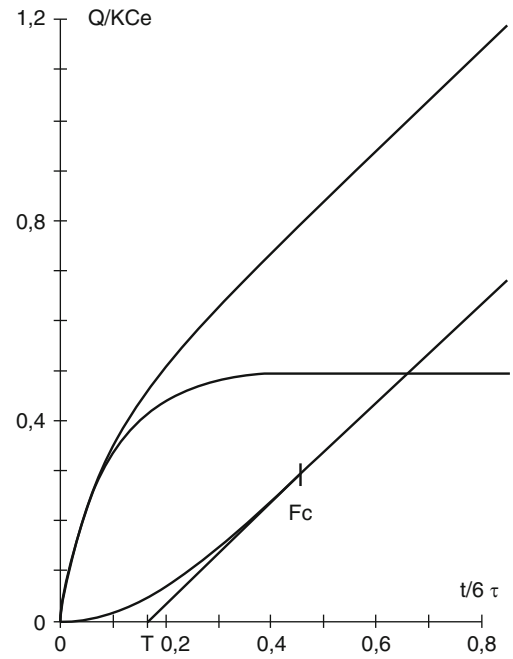

Fig. 2 Kinetics of skin absorption. The upper curve is the graph of amounts entering the stratum corneum. The lower curve is the graph of amounts entering the viable tissue. The curve in between (difference between the two curve ordinates) depicts the quantity within the stratum corneum. The three curves are normalized; thus, they are valid whatever the applied concentration (C) and the permeability coefficient (KD/e). In abscissa, application time divided by e^2/D (hence with 6 τ as the unit time). In ordinate Q/KCe: amounts normalized by the stratum corneum maximum storage capacity. K: partition coefficient; e: stratum corneum thickness; D: diffusion coefficient; Fc: starting of the steady-state flux; τ: lag time. The equations of the three curves are presented in Appendix 1

$$dQ_{sk}/dt = K_p A_s \left(C_{liq} - C_{sk}/P_{sk:liq}\right) + F_{sk}\left(C_a - C_{sk}/P_{sk:b}\right)$$

where Q_{sk} is the amount of compound in the skin compartment, A_s is the exposed surface area, C_{liq} is the liquid concentration, C_{sk} is the concentration of compound in the skin compartment, $P_{sk:liq}$ is the skin to saline partition coefficient, F_{sk} is the blood flow rate to the skin, C_a is the arterial concentration, and $P_{sk:b}$ is the skin to blood partition coefficient.

The calculation of the transfer coefficients is explained in specialized papers (Wépierre 1977). A brief description of their use is given in Sect. 4.2 regarding the "plasma level method."

3.3 Descriptive Parameters (Not Derived from Fick's Laws)

If, as the applied amount diminishes, the concentration in the vehicle decreases ("finite dose"), the profile of the absorption flux versus time or of the concentration time course in the target tissue is then an asymmetrical bell-shaped curve ending in asymptote, where three parameters can be found: the maximum flux per cm^2 skin area (J_{max}) and its appearance time (t_{max}) and the area under the curve (AUC) up to t time which indicates the total amount received over the interval t_0-t. If the flux is recorded until its ending (often several hours or days after exhaustion of the applied amount), the AUC reflects the *total absorbed amount*. The latter can be expressed in % of the applied amount, but this notation is ambiguous and confusing because this percentage would not be valid for another amount. In other words, the total absorbed amount obviously depends on the applied amount but is not proportional to it.

4 Absorption Measurement Methods in Man In Vivo

Several methods to measure cutaneous or percutaneous absorption in man in vivo have been used. An inventory has been made by Schaefer et al. in a book entitled "Skin Permeability" (Schaefer et al. 1982). These methods mainly concern the absorbed compound in its travel beyond the SC, which could be called the postabsorption. In the following paragraphs, only the leading methods still used today will be mentioned. Because of the small amounts absorbed (the skin is meant to be a barrier: it is only ten times more permeable than Teflon), all the methods require powerful dosage techniques, since the use of radioisotopes is strictly controlled.

4.1 The "Excreta Method"

This was the first method available to measure absorption in man in vivo (Feldmann and Maibach 1965, 1969), in particular for dermocorticosteroids with the use of radiolabeled isotopes. It was successful and is still considered as the reference method. Its principle is to apply on the skin a small quantity of compound in acetone and then collect all the urine over 120 h, thus covering the whole duration of the absorption. The time curve of amounts excreted into urine is drawn (in % of the applied dose). A proportion of the substance may have been captured or metabolized by cutaneous tissues before reaching the plasma; a correction factor is therefore applied. It is estimated by measuring the proportion of the same compound found in the urine during the 120-h period that follows its intravenous injection. The final result is expressed by the ratio *total radioactivity following topical administration*/*total radioactivity following parenteral administration*, the latter being considered as equivalent to a 100 % absorption. This ratio is named "absolute bioavailability by topical administration" (Maibach and Wester 1989): it varies from 63 % to 75 % for hydrocortisone (Maibach and Wester 1989). These data may be processed by pharmacokinetic modeling (Potts and Guy 1992). Pulmonary elimination can replace urinary elimination for volatile substances (Lauweris et al. 1978; Wester and Maibach 1999).

This method provides two pieces of information: *the percentage of the applied amount eliminated in the urine and the percentage of the applied amount retained and/or metabolized in*

the skin (i.e., *not penetrating blood vessels*). Both parameters depend on absorption (passage through the SC) but do not measure it. They measure the visceral availability of the absorbed amounts. The method is therefore more pharmacological than toxicological.

The complexity of this experimentation and the fact that the compound has to be intravenously injected are drawbacks which account for its rare use. Nevertheless, it has provided useful comparisons between products administered identically (Wester and Noonan 1978) or between different anatomic sites (Wester and Maibach 1989) or between man and different animal species.

4.2 Breath Analysis

When the tested permeant or its metabolites are excreted at least in part by the lungs, the analysis of exhaled breath can be a way to indirectly assess percutaneous skin absorption. Since the first attempts more than 10 years ago, technical progress has been made to detect and assess in real time minute amounts of volatile compounds, on the order of 1–10 parts-per-billion (10^{-9} concentration) (Thrall et al. 2002). Thus, monitoring percutaneous absorption is made possible (Thrall et al. 2002). Physiologically based pharmacokinetic modeling is usually associated with this technique which is still uncommon due to its complexity.

4.3 Plasma Level Method

The plasma concentration of a compound increases after its absorption by the skin. If the assessment method is very sensitive (e.g., using isotope labeling) or if the absorbed amounts are high, the blood concentration kinetics can be followed. The plasma level results from the difference between what penetrates the blood compartment and what goes out of it to tissues and through elimination especially in the urine. Plasma level versus time shows a bell-shaped asymmetrical curve ending in asymptote. Assuming that compound inflow and outflow are

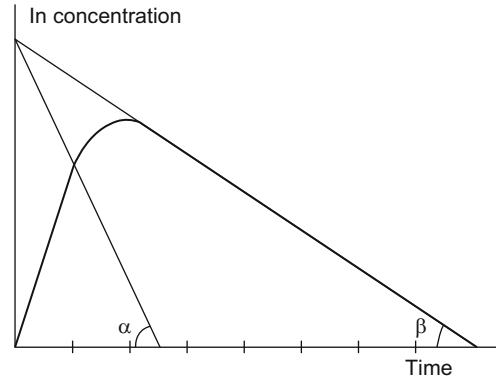

Fig. 3 Kinetics of plasma concentration following percutaneous absorption. Semi-logarithmic chart. The *straight line* by which angle α is defined is the graph of entries into plasma; it is the difference between the descending line and the experimental curve. $tg\alpha = k_e$ (observed) et $tg\beta = k_a$ (calculated)

exponential functions of time, whose rates are characterized by their transfer coefficient k_a and k_e, respectively, both coefficients can be obtained using the logarithm of the concentration versus time curve. This data processing, traditional in pharmacokinetics, uses a simple mathematical formulation (Schaefer et al. 1982; Fig. 3). It is not necessary to wait until the end of the absorption to process the data, but only to have an elimination phase long enough to permit a safe calculation. The parameter k_a describes the concentration raising rate, a consequence of the increased (supposedly exponential) flow of the compound into the plasma. This inflow rate (a quantity of matter per unit time) can be obtained by multiplying the observed concentration by the plasma volume or by using the following formula:

$$\text{Plasma concentration} = \text{inflow}/\text{clearance}.$$

This parameter concerns postabsorption. Assuming that it is proportional to what has penetrated the living epidermis (therefore assuming absence of retention within the skin), it is also, like the absorption rate, proportional to the application area, the applied concentration, the partition coefficient, and the diffusion coefficient of the compound. If these parameters are known for another vehicle or another compound, it is then possible to

anticipate absorption by a simple rule of three. Note that the amount lost either by tissue fixation or metabolism which might occur in the skin can be estimated by difference with the curve of plasma concentration following intravenous injection of the same compound.

In this type of method, only the nontoxic compounds can be studied. Because of the low plasma concentrations always observed (the amount absorbed is diluted in 5 l of blood), this method requires the use of radioactive isotopes or sensitive analytical methods and also a high absorption rate (i.e., on a relatively large skin area and at optimal concentration).

4.4 Absorption Measured by Local Biological Effects

Measurable effects are erythema or skin temperature rise (induced by nicotinic esters), blanching (induced by dermocorticoids), or reduced tactile sensitivity (induced by local anesthetics (Leopold and Maibach 1999). These are usually studied in "finite dose" situation. The usable parameters are the *appearance time* of the effect, its *maximal intensity* and *the length of time* to reach it, the *duration* of the effect, and the *area under the curve effect time* (Leopold 1999).

Recently the effects have been quantified using standard products, which yield a relative bioavailability, and associated with parameter P of Fick's laws. The concentration time course $C_d = f(t)$ of the compound in its diffusion zone, the dermis, is simulated by a classic open mono-compartment model where inflow depends on P (measured in an infinite dose experiment), the outflow constant k_e and the distribution volume V_d being, respectively, defined at 0.2 h^{-1} and 10 ml. If the efficient minimal concentration is known, traditional equations then provide the theoretical graph of the efficient concentration versus time; as a consequence, the dermal bioavailability is also given, although it is different from the actual absorption since the epidermis has been crossed and may have retained or altered the compound. A linear relationship has been found between P and the inverse of the appearance time of the effect (Leopold 1998). Knowing P, it is then possible to anticipate this appearance time which is often associated with C_{dmax} and t_{max} (the latter being the same for the concentration and the efficient concentration).

4.5 Disappearance of a Radioactive Isotope: "Surface Disappearance or Recovery Method"

The progressive reduction of the radiation emitted by a radiolabeled compound applied on the skin has been used to follow up the penetration of the compound and therefore measure its absorption time. The radioactivity versus time is measured using a Geiger-Müller device, placed at a (fixed) small distance from the skin (Wahlberg 1965).

With caffeine, estradiol, and aspirin, all applied in acetone, the radioactivity measured after a 24-h exposure (the skin has been protected to prevent desquamation) was found equal to the sum of the radioactive emissions of the 15–20 "strips" carried out at the same site later (Guy et al. 1987). This shows that the method is likely to measure the amounts stored in the stratum corneum rather than the actual absorption.

4.6 "Suction blister Method"

Since blisters appear at the dermoepidermal junction, this method is the in vivo equivalent of the in vitro absorption measurement by a static cell; however, it has the advantage of having a physiological collecting phase (Guy et al. 1987; Walker et al. 1993; Averbeck et al. 1989; Treffel et al. 1991a; Huuskonen et al. 1984). The blister forms a compartment distinct from the superficial dermis with which exchanges are somewhat reduced; as a consequence, the blister fluid is less subjected to blood convection than the interstitial fluid, hence the slowing down of the elimination of the absorbed compound and possible slowing down of the absorption.

The compound must be applied when the blister is completely formed to prevent the

intensification of the transfer by an aspiration mechanism (Agren 1990; Humbert et al. 1991). The blister fluid can be sampled only once; absorption can therefore be measured at one time only for each blister; however, it is possible to achieve simultaneously up to 21 blisters on each forearm (Treffel et al. 1991a). The measured result is a concentration in a relatively closed volume that is supposedly hemispherical, hence the possible approximate calculation of the amount which has reached the superficial dermis in a given time. In a study on acitretin absorption (Laugier et al. 1994), the concentrations of acitretin and its metabolites in the blister fluid were obviously lower than in plasma; this could be explained by the capture of the permeated compound by the living epidermis. This method therefore measures the subepidermal bioavailability rather than the actual absorption.

How can we use the parameter obtained, that is to say the *concentration time course in the blister*? Assuming a constant ratio between this concentration and the steady-state absorption flux (which is not always true), one could extrapolate to other situations by a simple rule of three. This would require a measurement in "infinite dose" situation. If it is not the case, the only possible extrapolation of the maximal concentration c_{max} is to another application area.

4.7 Microdialysis

Microdialysis is a continuous sampling technique in which a molecule of interest is collected under the skin. The method involves placing of a fiber (probe) in the dermis. The probe must be inserted under local anesthesia parallel to the skin surface and its insertion depth measured by ultrasound echography at 20 MHz, ensuring that it is not in the hypodermis. The probe is semipermeable and perfused with physiologically relevant media at a slow rate using a microdialysis pump. Compounds can diffuse into or out of the probe depending on the direction of the concentration gradient. Microdialysis gives only a concentration, not a flow, since the distribution volume in the dermis is unknown.

Microdialysis has been successfully used for demonstrating the bioequivalence of topical dosage forms (Narkar 2010a; Stenken et al. 2010) and can be used for monitoring intradermal and subcutaneous tissue drug concentrations after application of transdermal drug formulations (Katikaneni et al. 2011; Paturi et al. 2010; Siddoju et al. 2011).

Holmgaard et al. (2010) have listed 72 publications concerning a number of in vivo microdialysis studies of pharmacokinetics of topically applied drugs, pesticides, and other substances administered as creams, ointments, gels, or in transdermal therapeutic systems (patches). Table 3 reported from Holmgaard et al. (2010) lists the molecule that has been studied in these 72 publications.

4.8 Tape Stripping Method

Tape stripping consists in a sequential application and removal of adhesive tapes onto the skin surface, in order to collect layers of SC (Lademann et al. 2009; Herkenne et al. 2008a; Loffler et al. 2004). It is a minimally invasive method for the removal and sampling of stratum corneum (SC). The removed adhesive films are subsequently analyzed for their drug content and to determine the amount of penetrated and the penetration depth into the skin of topically applied drug. Tape stripping method is also known as the dermatopharmacokinetic (DPK).

To quantify the amount of stratum corneum removed on each tape stripping, different methods can be used:

- Gravimetric: The weight of the SC removed is calculated from the weight difference of the strip of tape prior to application and after removal.
- Spectroscopic: Aggregates of corneocytes reduce transmission of the light resulting in a linear increase of nonspecific absorption in correlation with the number of layers of cells collected SC, called pseudo-absorption (Jacobi et al. 2005; Lademann et al. 2006).

Table 3 Molecules studied by in vivo microdialysis listed studies of topical applications and dermal measurements (in vivo only) from 72 publication reported by Holmgaard et al. (2010)

Substance	MW, g/mol	Log pow	Object
2-Butoxy ethanol	118.18	0.83	Rat, human
2,4-Dichlorophenoxacetic acid	221.04	2.81	Mouse
5-Fluorouracil	130.08	−0.89	Rat
8-Methoxypsoralen	216.19	2.14	Human
Acetyl salicylate	180.16	1.19	Rat
Acyclovir	225.21	−1.8	Human, rabbit
Ascorbic acid	176.12	−1.88	Human
Aminolevulinic acid	131.13	−4.40	Human
Betamethasone 17-valerate	476.58	3.5	Rat, human
Betamethasone 21-dipropionate	504.60	3.24	Rat, human
Calcipotriol	412.61	4.40	Rat, human
Cyclosporine	1202.61	1.00	Rat
Diclofenac	296.15	4.51	Rat, human
Dipyrone	311.36	−4.76	Rat
Enoxacin	320.32	−0.20	Rat
Estradiol	272.39	4.01	Human
Esterom components	–	–	Rat
Ethanol	46.07	−0.31	Human
Felbinac	212.24	3.19	Rat
Fluconazole	306.27	0.5	Rat
Flurbiprofen	244.26	4.16	Pig, rat
Fusidic acid	516.71	6.75	Rat, human
Glucose	180.16	−3.24	Rat, human
Granisetron	348.9	−0.42	Rat
Ketoprofen	254.28	3.00	Rat, human
Lidocaine	234.34	2.44	Rat, pig, human
Malathion	330.36	2.75	Human
Methotrexate	454.44	−1.85	Rat, rabbit
Metronidazole	171.15	0.00	Human
Methyl nicotinate	137.14	0.64	Human
Methyl salicylate	151.14	2.99	Dogs
Nicotine	162.16	1.17	Human
Penciclovir	253.26	−2.12	Human
Prilocaine	220.31	−0.38	Rat, pig
Propanol	60.09	0.25	Human
Puerarin	416.38	0.5	Rat
Salicylate esters	250.33	5.97	Human
Salicylic acid	138.13	2.26	Rat, human
Toluene	92.14	2.73	Rat
Tranilast	327.33	3.62	Rat
Valproate	166.20	−0.85	Rat

- Microscopic techniques were used to determine the ratio covering density of the corneocytes adhering to the tape (Lindemann et al. 2003).

In order to remove the SC homogeneously, several parameters should be taken into consideration including application pressure, removal velocity, duration, and anatomical site.

In DPK study for bioequivalence, drug levels should be assessed in at least eight different sites (Fig. 3): at four of the sites, levels are measured during uptake (e.g., 0.25, 0.5, 1, and 3 h post-application), and then, after cleaning the drug from the remaining sites, levels are assessed during clearance (e.g., 4, 6, 8, and 24 h post-application).

4.9 Difference Method

It consists in measuring, at regular intervals, the amount of compound that disappears from the skin surface. The amount which has penetrated the SC, the upper curve of Fig. 2, is measured by deducting it from the amount applied. All the absorption parameters of Fick's laws can then be found.

It is necessary to operate in conditions of infinite dose. If the first samples are taken during the first 2 h, the curve of the total disappeared quantity is biphasic: first a fast penetration rate reflects the filling of the SC, and then a straight line of lower slope indicates the steady-state flux. If the first sampling is carried out after the first hour, it is unlikely that the first slope will be observed, but this is not important. As a matter of fact, the theory shows (Fig. 2) that the intercept of the line with the ordinate (axis of quantities) indicates two thirds of the amount stored in the SC in the steady-state flux phase, hence the possible calculation of this amount. It can then be subtracted from the disappeared quantities, providing the absorbed quantities. Fick's law parameters are obtained by the formulae mentioned in Sect. 3.1. Even the kinetics of the SC filling is accessible. The total absorbed quantities, taking into account the initial period of increasing flux, are given by Eqs. 4 and 5 and the store in the SC by Eq. 6.

Table 4 Absorption of caffeine (Chambin-Remoussenard et al. 1993), an amphiphilic easily absorbed compound

Vehicle	Applied concentration	Measured flux ($g\ cm^{-2}\ h^{-1}$)	SC store ($g\ cm^{-2}$)	P ($cm\ h^{-1}$)	K	D ($cm^2\ h^{-1}$)	τ
Acetone	250×10^{-6}	93×10^{-9}	645×10^{-9}	374×10^{-6}	3.43	163×10^{-9}	2 h 18
O/W cream	664×10^{-6}	87×10^{-9}	1400×10^{-9}	131×10^{-6}	2.81	70×10^{-9}	5 h 18

Table 5 Absorption of 5-methoxypsoralen (Treffel et al. 1991b), a very lipophilic poorly absorbed compound

Vehicle	Applied concentration	Measured flux ($g\ cm^{-2}\ h^{-1}$)	SC store ($g\ cm^{-2}$)	P ($cm\ h^{-1}$)	K	D ($cm^2\ h^{-1}$)	τ
O/W cream	29.2×10^{-6}	4.5×10^{-9}	3.6×10^{-9}	154×10^{-6}	0.167	1.38×10^{-6}	16 min

In the experiment shown in Table 4, computing the regression line of the disappeared amounts versus time gave through its slope the steady-state flux and through its intercept with ordinates two thirds of the store in the SC. This permitted the calculation of the other Fick's law parameters by using Eqs. 2 to 7. It was verified that the *disappeared* quantities (Q_{in}) calculated for 6 h (respectively, 985×10^{-9} g cm^{-2} from acetone and 1453×10^{-9} g cm^{-2} from the cream) corresponded to the recorded figures (respectively, 995×10^{-9} g cm^{-2} and 1443×10^{-9} g cm^{-2}). The SC store appeared to equal 7–16 h of steady-state flux from acetone and cream, respectively, and it doubled when the vehicle was an O/W cream rather than acetone, which induced a double lag time τ. On the other hand, D was 2.3 times higher with acetone than with cream, which indicates the (otherwise well-documented) alteration of the cutaneous barrier by the solvent. Over 6 h, the total *absorbed* amounts (Q_{out}) have therefore been 344 ng/cm^{-2} from acetone and only 61 ng/cm^{-2} from the cream.

In another experiment (Table 5), the total disappeared amount over 6 h was 29.6 ng/cm^{-2} (the calculation gave 28.2 ng/cm^{-2}) and the absorbed amounts 25.8 ng/cm^{-2}. The SC store and the partition coefficient were noticeably low, in contrast with the diffusion coefficient 20 times that of caffeine. However, by applying ten times higher concentrations, thereby close to those of caffeine, the absorption flux and the store, although ten times higher, would have remained much lower.

Therefore, the difference method permits measurement (and calculation) of the absorbed and stored amounts. Furthermore, by studying hourly fluxes, it is easy to verify whether the steady-state flux is reached or if the finite dose conditions still apply. The parameters obtained provide a maximum possibility of extrapolation (see Sect. 5). In case of a "finite dose" experiment, it is possible to estimate the time when the applied amount is exhausted and at that moment, to measure the maximal amount stored and absorbed. For products with a limited and known application time (e.g., rinsed products), it is easy to know the maximal stored and absorbed amounts (Fig. 4).

The difference method does not require the use radioisotope labeling if a sensitive assessment technique is available. The favored analytical methods are high-performance liquid chromatography (Chambin-Remoussenard et al. 1993; Treffel et al. 1991b), spectrophotometry (Treffel et al. 1991b), and gas chromatography. The main difficulty lies in sampling all the substance remaining on the skin surface; if some remains on the skin, the absorbed amount will be overestimated. Inversely, if the collection is aggressive and alters the SC, some of the compound might be removed, inducing an underestimate of the absorbed amount. Finally, as in the previous method, it is essential to ensure that the absorbed compound diffuses freely inside the SC and is neither adsorbed nor chemically linked with an SC constituent: this would increase the store without modifying the absorption flow rate (Mitragotri 2003).

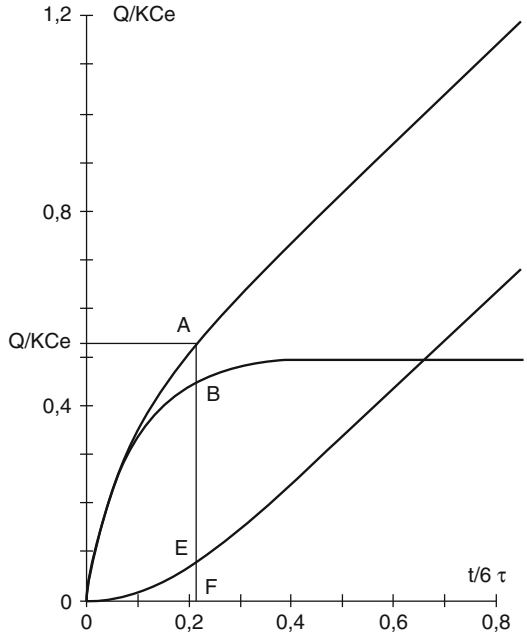

Fig. 4 Maximum amount that entered in the stratum corneum in case of finite dose. At point F, the applied dose is exhausted. Distance AF: maximum entered the stratum corneum. Distance EF: maximum absorbed. Distance BF: maximum stored. In abscissa, application time divided by e^2/D (hence with 6 τ as the unit time). In ordinate Q/KCe: amounts normalized by the stratum corneum maximum storage capacity. K: partition coefficient; e: stratum corneum thickness; D: diffusion coefficient. τ: lag time

If the vehicle is a volatile solvent or a cream, it should be applied in open cells, for example, 2.5-cm-diameter simple rings stuck on the skin (Chambin-Remoussenard et al. 1993; Rougier et al. 1990). The number of cells applied should be equal to the number of samplings (e.g., six cells if the purpose is to follow up the flow for 5 h, because the first sampling is made in part from the initial increasing flux and is used only as a reference for the following period of time). If the vehicle is a liquid or a gas, closed cells are necessary. The Düsseldorf group has developed plastic cells (inner diameter: 4 cm) designed to be applied on the external side of the arm and maintained by a copper ring and Velcro (Leopold and Lippold 1992). At the top is a hole for emptying and filling in without removing the cell. One cell can, therefore, be used to follow the same product for several hours (it is emptied and filled each hour). Thus, the simultaneous absorption of several products can be studied (Merfort et al. 1994). Thral et al. used nonoccluded cells covered with "a Muslim patch" containing activated charcoal to trap volatile compounds (Thrall et al. 2002).

4.10 The "Stratum Corneum Gradient Method"

After 15-min application, the skin is washed, 20 subsequent SC strippings are performed, and the compound concentration in each strip is measured (Pirot et al. 1997; Pirot 1996; Higo et al. 1993). The data are then introduced in the equation of the second Fick's law which describes the concentration gradient versus time, applied concentration and diffusion parameters K and D which can then be obtained, as well as the amount absorbed. If the method is used after the steady-state flux has settled, a rectilinear concentration gradient is found. Therefore, it is sufficient to sample four series of three successive strippings, first to check that the concentration decreases linearly with depth and then to access all Fick's laws parameters.

In this method, it is necessary to know the depth level and concentration for each strip. The depth level is not the strip number since the stripped amount depends on each subject, body site, and amount of SC already removed. It can be found by dividing the volume removed by the stripped skin surface area. The D-Squame (using a constant pressure maintained 5 s followed by a mild stripping (Dreher et al. 1998)) has the advantage of being easy to use and generates few adhesion changes for a given pressure. The removed volume is obtained by dividing the weight by the density (≈1.20). The weight of the SC removed by each strip (100–300 μg) is measured either by weighing the adhesive tape before and after stripping (Pirot et al. 1997) or by protein colorimetric assessment (Dreher et al. 1998). Strips must be immediately stored in a waterproof flask to prevent water loss. The weighing process is long and delicate because of the possible variation in the SC and the disk hydration during the operation.

The protein colorimetric assessment is quicker; it is based on the traditional method of Lowry followed by a spectrophotometric measurement at 750 nm (Dreher et al. 1998). The strips are placed in 1 ml NaOH 1 M and shaken for 2 h. Neutralization is obtained by adding 1 ml HCI 1M for 5–10 s, and then the colorimetric assessment is achieved.

This method also requires the absorbed compound to be assessed in very small SC samples. Photoacoustic spectroscopy, spectrophotometry in UV light, and infrared attenuated total reflectance associated with treatment by Fourier transform (ATR-FTIR) are fast methods. In the latter, with λ between 2250 and 2200 cm^{-1}, that, is 4–5 μm, and for a concentration of 196 nMole in water (saturation), the 4-cyanophenol sampled by stripping was 0.05–1.1 mol and the quantification limit 2.54 nMole/cm^2 (Pirot et al. 1997; Higo et al. 1993).

4.11 Spectroscopic Methods

A prerequisite for the spectroscopic technique is that the molecule of interest should possess distinct spectral features of sufficient intensity to be able to differentiate from the skin spectrum (Dreher et al. 1998; Kezic 2008). Raman spectroscopy and near-infrared spectroscopy are advanced noninvasive in vivo techniques for real-time determination of diffusion of drugs and chemicals into the human skin (Herkenne et al. 2008b; Zhao et al. 2008), Confocal Raman spectroscopy has been used in vivo to identify the molecular structure of the skin, level of skin hydration, and effect of moisturizing agents on skin hydration (Caussin et al. 2009; Darlenski et al. 2009) and to study the penetration of certain chemicals like urea and dimethylsulfoxide into the skin (Caspers et al. 2002; Wascotte et al. 2007). It has also been used to show relative effects of different classes of penetration enhancers on topical delivery of retinol (Pudney et al. 2007; Melot et al. 2009). Although its noninvasive nature and possibility of real-time profiling of drugs penetrating into the skin make this technique attractive, a major drawback of Raman spectroscopy is that it is semiquantitative. It allows relative measurements rather than absolute determination of drug concentration in the skin. Near IR is a noninvasive, quantitative technique which is still in development. Initially, attenuated total reflectance-Fourier transform infrared spectroscopy (ATR-FTIR) method was developed by Guy et al. (Stinchcomb et al. 1999; Reddy et al. 2002) to quantify the drug in tape strips in order to avoid drug extraction procedure; however, tape stripping was still required.

4.12 Confocal Laser Scanning Microscopy

Confocal laser scanning microscopy is another tool to quantify dermatopharmacokinetics parameters. The confocal images are possible for fluorescent drugs or probes and do not require to prepare the skin to make optical sections. This tool focuses a beam to a given depth within the tissue and measures the concentration of penetrant or drug molecule at the level of focus. Thus, this tool allows an investigator to generate a concentration profile following topical application of drug product (Mayee and Rawat 2010). The confocal images can be obtained in the plane parallel to sample surface or in the plane perpendicular (Wu et al. 2009). This method has been widely used in assessing drug penetration or distribution in the skin layers following topical application of microparticles, nanoparticles, and vesicular systems such as liposomes, niosomes, etc. (Desai et al. 2013; Khurana et al. 2013; Wang et al. 2013).

5 Prediction of Cutaneous Absorption

The objective of most absorption measurements in toxicology or therapeutics is to be able to predict how much compound will be absorbed in other situations, i.e., be found in the SC, the dermis, and the skin as a whole, or enter the bloodstream and be distributed to internal organs. Other situations means other application area, other body site, diseased skin, different application

times, concentrations, formulations, or other compounds whose parameters P (permeability coefficient), K (partition coefficient), or D (diffusion coefficient) are known. Prediction of absorption in the new situation is made by extrapolation from an experimental situation; it is achieved by simple multiplication by a rule of three of the experimentally found parameter values. For example, given the steady-state flux J of a compound in a previous experiment, what would be the steady-state flux J′ of the same compound in another vehicle and in another concentrations, all other things keeping unchanged (same body site, etc.). If the partition coefficients and applied concentrations were known (K and K′ and C and C′, respectively), the answer would be $J' = J\,K'C'/KC$. This important question deserves attention because of the numerous errors found, especially in toxicological practice. What are the conditions for a safe extrapolation? This depends on the parameter(s) used and the means by which the absorption has been expressed.

5.1 Extrapolation to Another Application Area

The *total absorbed quantity* (g) (in a given time in case of an infinite dose and after dose exhaustion in case of finite dose) depends on the application area because the absorption flux is defined per unit area (g cm^{-2} $h^{-}1$). Consequently the quantities which penetrate the SC, stay there, or pass through it are directly proportional to the application area. A double area absorbs a double quantity, whatever the experiment is in infinite or finite dose. This is also true for amounts received further down (dermis, plasma); hence, the extrapolation by a rule of three is possible for the plasma inflow rate coefficient (plasma entry fits an exponential function).

It is somehow different for *concentrations* in tissues or blood because they are a quantity per unit of distribution volume. The concentration in the first layers of the living epidermis is obviously independent from the application area. Inside the dermis, the same holds true except at the borders of the area, because of lateral diffusion within the interstitium. Therefore, in general, for a double application area, the *local* concentration would remain identical. A *local* biological effect, although identical theoretically, might be enhanced through lateral diffusion and reciprocal reinforcement. The *plasma* concentration (g cm^{-3}) is proportional to the ratio inflow/outflow rate coefficients, both rates being exponential. Whereas the inflow rate coefficient is proportional to the application area, the outflow rate coefficient depends on the plasma concentration and so keeps constant. It follows that in case of a doubled application area, the ratio will be double and also the plasma concentration. This is the case whatever the experiment is with infinite or finite dose.

5.2 Extrapolation to Another Application Duration

The cutaneous absorption depends on time and becomes proportional to it as soon as the steady-state flux begins. The rule of three is therefore theoretically possible only for the sampled quantities during this period. However, if it lasts several hours, the absorbed amount before the steady-state flux becomes negligible and one can consider that the steady-state flux has existed since the beginning. Amounts absorbed before the steady-state flux settlement in situation of "infinite dose" cannot be extrapolated by a simple rule of three to a different application duration; it is necessary to have recourse to the graphs of Fig. 2. On the other hand, the descriptive parameters and those of "finite dose" cannot be extrapolated to different times.

5.3 Extrapolation Using Fick's Laws Diffusion Parameters

It is valid only in case of infinite dose:

– From the parameters K (partition coefficient), C (applied concentration), e (SC thickness), or P (permeability coefficient), the extrapolation can be done by simple rule of three, using Eqs. 1 and 3.

– From D or t, it is necessary to use Eqs. 4 or 5 if the phase before the constant flow is to be taken into account. If it is considered negligible (e.g., if the steady-state flux has lasted several hours), D can be used by a simple rule of three; assuming that this steady-state flux has started at time zero, a slight error by excess is then made. To extrapolate to a period anterior to the steady-state flux, it is necessary to use the equations of Appendix 1 or their graphs.
– But D (and therefore P) depends also on the SC barrier condition. This may be known through the transepidermal water loss (TEWL), a parameter easily measured which, for a given atmospheric vapor pressure, reflects the water diffusion coefficient. Now, the diffusion coefficient of all other substances changes usually in parallel. A doubled TEWL would permit anticipating a doubling of any P or D coefficient, therefore of absorbed amount. The measurement of the TEWL is, therefore, worth using systematically for absorption studies in disease (Yosipovitch et al. 1998), in occupational medicine, and in safety testing of topical medicines, cosmetic, and hygiene products, in short, whenever alteration of the barrier function may be suspected (Aalto-Korte and Turpeinen 1996).

5.4 Extrapolation from Parameters

All *Fickian parameters* can serve to extrapolation, provided the experimental as well as the predicted situations are steady-state fluxes. An example is given in Sect. 5, first paragraph.

Pharmacokinetics parameters (i.e., transfer coefficients) deal with post-absorption. Entry coefficients (inflow rates) increase with the cutaneous absorption rate (the steady-state flux), whereas outflow coefficients are generally insensitive because they depend on the concentration within the compartment. Accordingly all events which increase the flux (such as increase of application area, applied concentration, contact duration, permeability or diffusion coefficient, or decreased skin thickness) will also increase proportionally the entry coefficients. However, all the quantity absorbed is not transmitted to the compartments owing to some retention in the epidermis and/or the dermis, but one may assume that the proportion keeps constant. For example, if the skin absorption flux is thought to have doubled, one can consider that the plasma inflow coefficient will also be doubled, assuming that the retention in the skin will remain a constant fraction of the absorbed amount (which is not always true because of a possible tissue saturation). The same holds true as far as the availability to the dermis is concerned (measured in suction blisters or by hemodialysis) because the compound fixation within the epidermis may not remain a constant fraction of the absorbed quantity. The concentrations in the compartments, especially the blood, are less correlated than the entry coefficients because of the damping effect of the concomitant outflow which depends on the concentration within the compartment only. Thus, if the skin absorption flux is doubled, one cannot consider that the urinary elimination will also be doubled. It should be stressed that only the pharmacokinetics parameters obtained during a steady-state flux can be used for extrapolation.

Descriptive parameters, J_{max}, t_{max}, AUC, and % of applied dose, are not liable to any extrapolation. Of course, J_{max} and AUC increase when the absorption flux increases, but no proportionality factor is then applicable. Unfortunately a number of toxicological data originated from finite dose experiments are wrongly produced in this way. One exception, however the compound and its derivatives *cumulated collection,* can be expected to be proportional to the application area. Finally, as mentioned above, the percentage of the applied dose can never be used to predict the absorbed quantity of another dose, whether the experiment was dose finite or infinite dose type, except though for very small doses.

6 New Devices for Ex Vivo Percutaneous Absorption Measurement

The most common technique for ex vivo measuring of percutaneous absorption is based on the use of excised skin mounted in a diffusion cell system.

The basic design of a diffusion cell consists of an upper donor compartment and a reservoir compartment separated by a skin sample (Organisation for economic cooperation and development test no. 428 2004; Fig. 5).

Usually, ex vivo percutaneous absorption experiments with diffusion cells like "Franz diffusion cell type" are often conducted in open conditions, in which the skin surface is in contact with ambient environment of each laboratory or in occluded condition with skin covering by impermeable membrane. These conditions of use either ambient laboratory or occlusion are peculiar and don't reflect all real skin exposure conditions.

Actually, the skin surface is subjected to daily gradients in external temperature and humidity which varies almost permanently in both the indoor and outdoor air according to the seasons, geographic regions, and in terms of lifestyle and daily movements of individuals (Zhang and Yoshino 2013; Rudd and Henderson 2007; Kalamees et al. 2009).

Contact between skin surface and our external environment directly, through clothing or transdermal drug delivery systems, induces a microclimate at the skin surface which arises from heat and material transfer between the skin and the external environment. That microclimate can impact skin properties (Singh and Maibach 2013) and then its interaction with xenobiotics substances that come in contact with the skin (Fritsch et al. 1963; Chang and Riviere 1991, 1993; Meuling et al. 1997). Therefore, variations in environmental parameters must be considered when assessing percutaneous absorption.

To study the influence of external temperature and humidity, a new apparatus has been developed by Lboutounne et al. (2014), (Fig. 6). This

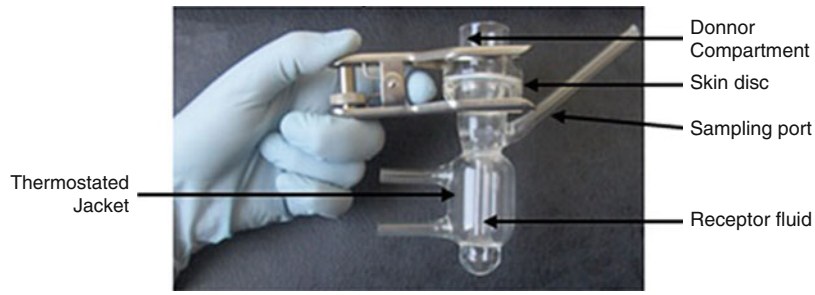

Fig. 5 Franz diffusion cell and its compartments

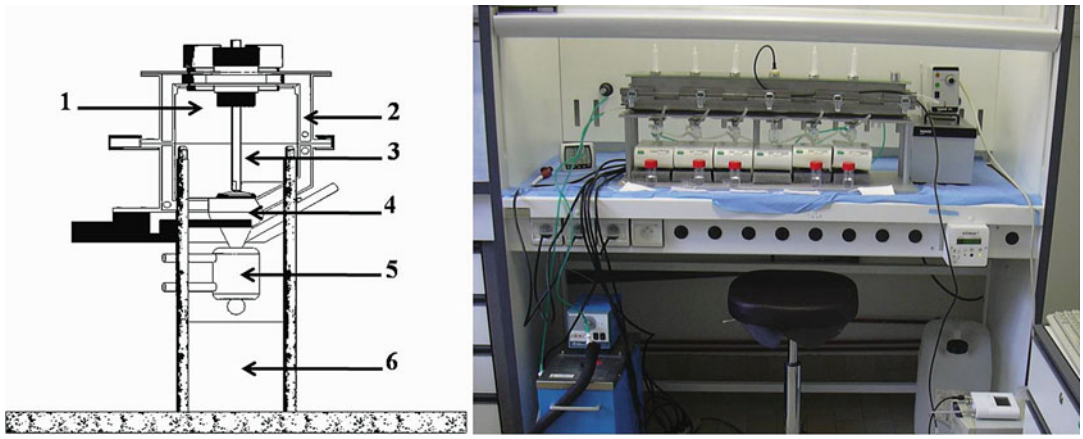

Fig. 6 Cumulative absorption (ng/cm^2) kinetics of caffeine during 24 h of skin exposure, at different environmental conditions. Values are mean ± SEM (n = 5): (**a**) 70 %–42 °C and 28 %–42 °C; (**b**) Open condition and occlusion; (**c**) 70 %–27 °C and 28 %–27 °C

apparatus was made up of an Inox chamber. The chamber is thermostated by a water bath. Six diffusion cell receiver compartments are fixed to the chamber. Relative humidity and temperature were controlled inside the chamber by a sensor. This sensor is connected to a computer which allowed a monitoring of the two parameters during experiments. Reservoirs are integrated in the chamber and filled with saturated salt solutions to create a precise relative humidity. A given saturated salt solution provides only one relative humidity (RH) at any desired temperature; a different relative humidity must be achieved by selecting another appropriate salt.

This apparatus has been used to study the influence of external temperature and humidity on percutaneous absorption of caffeine. Two different salts were used in this study: sodium chloride (NaCl) that provides 70 % RH and lithium chloride (LiCl) which provides 28 % RH.

The kinetic curve profile of percutaneous absorption of caffeine revealed different shape characteristics depending on environmental exposure conditions (Fig. 7). We observed at 27 °C/28 % RH and in unoccluded condition (27 °C/33 %) a kinetic profile that seems to be "like a finite dose," whereas at 27 °C/70 % RH or under occlusion, the profile curve went toward an "infinite dose profile." These kinetic profiles were related to evaporative process of the deposited preparation on skin surface combined with water uptake resulting from water flux through skin. This evaporative process leads to an increase of caffeine concentration in donor compartment, which went toward saturation then beginning of caffeine crystallization until its complete crystallization on the skin surface.

The cumulative amount of caffeine absorbed (ng/cm^2) after 24 h for all environmental conditions and compared with occlusion and open conditions was reported in Fig. 8: in unoccluded conditions and in occlusion, the cumulative amounts of caffeine after 24 h of skin exposure were, respectively, 2.73 ± 0.61 μg/ml and 9.35 ± 1.04 μg/ml ($p = 0.018$).

At 27 °C, increased humidity from 28 % RH to 70 % RH leads a significantly increase in percutaneous absorption by a factor 3 after 24 h of exposure with a cumulative amount of 11.87 ± 2.37 (μg/ml) at 70 % and 3.09 ± 0.37 (μg/ml) at 28 % ($p < 0.01$). However, at a temperature of 42 °C, there is less pronounced difference in percutaneous absorption of caffeine between 70 % (8.12 ± 2.43 (μg/ml)) and 28 % (6.5 ± 1.57 (μg/ml)) ($p > 0.05$).

Results of this study highlight a preponderant role of microclimate above the skin on percutaneous absorption of caffeine.

The device used in this study will be a useful tool to investigate ex vivo, the influence of microclimate above the skin on percutaneous absorption profile. Basing on the described concept, a new diffusion cell for percutaneous absorption studies under controlled environmental conditions was developed (Fig. 9).

7 Concluding Remarks

Below are some strengths and limitations of some major points in skin absorption.

- Before any measurement, one ought to remember that it is first and foremost a passage through the SC, a purely passive diffusion process obeying Fick's laws. Its kinetics should be remembered with its two phases, transient and steady-state maximum fluxes, and also the events taking place within the SC: entry, storage, going out into the viable epidermis, all depicted by the curves of Fig. 1. One should finally remember the physical variables which control the phenomenon: application area (A), duration of the application (t), partition coefficient (K), applied concentration (C), SC thickness (e), and diffusion coefficient (D).
- When performing a measurement, the "infinite dose" mode is preferable whenever possible because it is more profitable. It provides the maximal possibilities of extrapolation to other situations.
- A measurement of the TEWL before and immediately after a skin absorption measurement is advised, in order to detect a nonspecific modification of the SC barrier in the interval.
- The SC store is a reservoir for further leakage of the compound into the viable tissue. Its

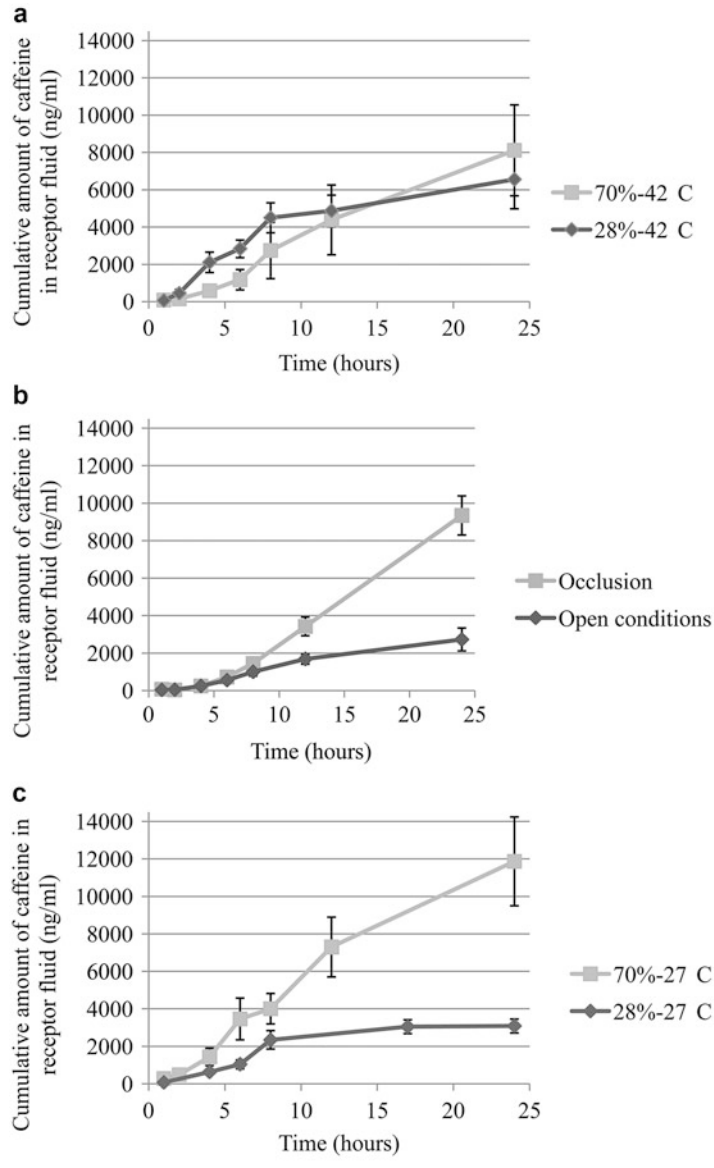

Fig. 7 Cumulative amount (ng/cm^2) of caffeine absorbed after 24 h at different environmental conditions. Values are means ± SEM ($n = 5$). † Significantly different compared to occlusion $P < 0.05$, *$P < 0.05$, **$P < 0.01$ significantly different compared to open conditions

assessment by SC stripping may be useful in any case, even after short applications, because it may contain large amounts of the compound, and is quickly constituted. After a 30-min application, using the stripping method constitutes a simple and fast way to assess the SC crossing capacity of a compound whatever the formulation.

– Percutaneous absorption (or skin post-absorption) parameters mainly deal with compartments (e.g., dermis or plasma) and concentration data. They can be connected to the absorption rate through their inflow rate coefficients if they have been measured during a period of constant flow or stable and maximal concentration. Concentrations also depend on outflow rates and thus are less sensitive to the absorption rate. Urine concentrations only depend on blood concentrations.
– The "% of the applied dose" parameter can be used for predicting another dose only if both doses are very small (less than 1 mg formulation per cm^2).

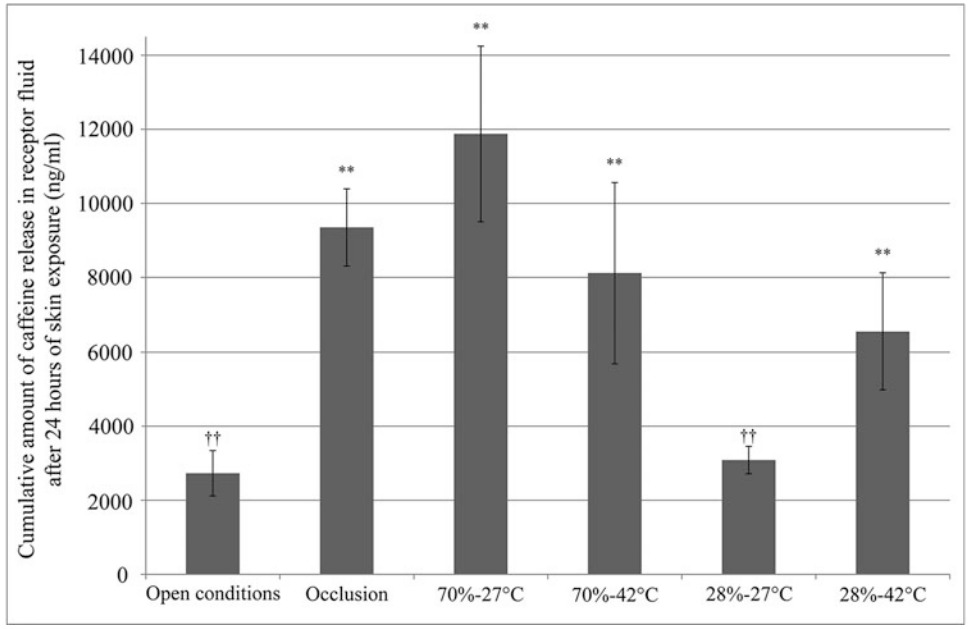

Fig. 8 The new ex vivo device. *1* Exposure chamber (donor compartment). *2* Thermostated jacketed. *3* Movable occlusion system. *4* Skin emplacement. *5* Diffusion cell (receiver compartment). *6* Magnetic stirrer

Fig. 9 Design of a new diffusion cells for percutaneous absorption studies under controlled environmental conditions

Appendix 1: Equations of Curves Graph in Fig. 1

$$y_1 = x + 1/3 - 2/\pi^2 \sum_{n=1}^{\infty} 1/n^2 \ \exp\left(-n^2\pi^2 x\right) \quad (9)$$

$$y_2 = x - 1/6 - 2/\pi^2 \sum_{n=1}^{\infty} 1/n^2 \exp\left(-n^2\pi^2 x\right) \quad (10)$$

$$y_2 = x - 1/6 - 2/\pi^2 \sum_{n=1}^{\infty} 1/n^2 \exp\left(-n^2\pi^2 x\right) \quad (11)$$

Equation 9: quantity entering the stratum corneum (Fig. 1, upper curve).

Equation 10: quantity entering the viable tissue (Fig. 1, lower curve).

Equation 11: quantity within the stratum corneum (Fig. 1, middle curve).

$x = Dt/e^2$, and $y = Q/KCe$ (i.e., quantity for any partition coefficient K, applied concentration C, and stratum corneum thickness e); KCe is also the maximum possible store within the stratum corneum (the actual store is always half of the maximum, as shown in Fig. 2). Quantities are per unit skin surface area (g/cm^2).

At any time $y_1 = y_2 + y_3$. As soon as the steady-state flux is reached, Eqs. 9, 10, and 11 transform into section "Parameters Derived from Fick's Laws" (Eqs. 4, 5, and 6, respectively).

References

Aalto-Korte K, Turpeinen M. Transepidermal water loss predicts systemic absorption of topical hydrocortisone in atopic dermatitis. Br J Dermatol. 1996;135:489–504.

Agren MS. Percutaneous absorption of zinc from zinc oxide applied topically to intact skin in man. Dermatologica. 1990;180:36–9.

Averbeck D, Averbeck S, Blais J, Moysan A, Huppe G, Morliere B, Prognon P, Vigny P, Dubertret L. Suction blister fluid: its use for pharmacodynamic and toxicological studies of drugs and metabolites in vivo in human skin after topical or systemic administration. In: Maibach HI, Lowe NJ, editors. Models in dermatology, vol. 4. Basel: Karger; 1989. p. 5–11.

Caspers PJ, Williams AC, Carter EA, Edwards HG, Barry BW, Bruining HA, et al. Monitoring the penetration enhancer dimethyl sulfoxide in human stratum corneum in vivo by confocal Raman spectroscopy. Pharm Res. 2002;19:1577–80.

Caussin J, Rozema E, Gooris GS, Wiechers JW, Pavel S, Bouwstra JA. Hydrophilic and lipophilic moisturizers have similar penetration profiles but different effects on SC water distribution in vivo. Exp Dermatol. 2009;18:954–61.

Chambin-Remoussenard O, Treffel P, Bechtel Y, Agache P. Surface recovery and stripping methods to quantify percutaneous absorption of caffeine in humans. J Pharm Sci. 1993;82:l099–1101.

Chang SK, Riviere JE. Percutaneous absorption of parathion in vitro in porcine skin: effects of dose, temperature, humidity, and perfusate composition on absorptive flux. Fundam Appl Toxicol. 1991;17:494–504.

Chang S-K, Riviere JE. Effect of humidity and occlusion on the percutaneous absorption of parathion in vitro. Pharm Res. 1993;10:152–5.

Darlenski R, Sassning S, Tsankov N, Fluhr JW. Non-invasive in vivo methods for investigation of the skin barrier physical properties. Eur J Pharm Biopharm. 2009;72:295–303.

Desai PR, Shah PP, Hayden P, Singh M. Investigation of follicular and non-follicular pathways for polyarginine and oleic acid-modified nanoparticles. Pharm Res. 2013;30:1037–49.

Dreher F, Arens A, Hostynek JJ, Mudumba S, Ademola J, Maibach HI. Colorimetric method for quantifying human stratum corneum removed by adhesive-tape-stripping. Acta Derm Venereol. 1998;78:186–9.

Feldmann RJ, Maibach HI. Penetration of C14C hydrocortisone through normal skin. Arch Dermatol. 1965;91:661–6.

Feldmann RJ, Maibach HI. Percutaneous penetration of steroids in man. J Invest Dermatol. 1969;52:89–94.

Fritsch WC, Stoughton RB, Stapelfeldt A. The effect of temperature and humidity on the penetration of c14 acetylsalicylic acid in excised human skin1. J Invest Dermatol. 1963;41:307–11.

Guy RH, Hadgraft J, Maibach HI. A pharmacokinetic model for percutaneous absorption. Int J Pharm. 1982;11:119–29.

Guy RH, Bucks DA, McMaster JR, Villaflor DA, Roskos KV, Hinz RS, Maibach HI. Kinetics of drug absorption across human skin in vivo. Developments in methodology. In: Pharmacology and the skin, vol. 1, 1987. p. 70–6.

Herkenne C, Alberti I, Naik A, Kalia YN, Mathy FX, Préat V, Guy RH. In vivo methods for the assessment of topical drug bioavailability. Pharm Res. 2008;25:87–103.

Higo N, Naik A, Bommi Bommannan D, Potts RO, Guy RH. Validation of reflectance infrared spectroscopy as a quantitative method to measure percutaneous absorption in vivo. Pharm Res. 1993;10:101500–6.

Holmgaard R, Nielsen JB, Benfeldt E. Microdialysis sampling for investigations of bioavailability and bioequivalence of topically administered drugs: current state and future perspectives. Skin Pharmacol Physiol. 2010;23:225–43.

Humbert P, Treffel P, Makki S, Millet J, Agache P. Peak blistering point: influence on fluid levels of 5-MOP in human skin in vivo after systemic administration. Arch Dermatol Res. 1991;283:297–9.

Huuskonen H, Koulu L, Wilen G. Quantitative determination of methoxsalen in human serum, suction blister fluid and epidermis, by gas chromatography mass spectrometry. Photodermatology. 1984;1:137–40.

Jacobi U, Kaiser M, Richter H, Audring H, Sterry W, Lademann J. The number of SC cell layers correlates with the pseudo-absorption of the corneocytes. Skin Pharmacol Physiol. 2005;18:175–9.

Kalamees T, Korpi M, Vinha J, Kurnitski J. The effects of ventilation systems and building fabric on the stability

of indoor temperature and humidity in Finnish detached houses. Build Environ. 2009;44:1643–50.
Katikaneni S, Kasha P, Badkar A, Banga A. Iontophoresis of a 13 kDa protein monitored by subcutaneous microdialysis in vivo. Bioanalysis. 2011;3(21): 2419–26.
Kezic S. Methods for measuring in-vivo percutaneous absorption in humans. Hum Exp Toxicol. 2008;27:289–95.
Khurana S, Jain NK, Bedi PM. Nanoemulsion based gel for transdermal delivery of meloxicam: physico-chemical, mechanistic investigation. Life Sci. 2013;92:383–92.
Kligman AM, Christophers E. Preparation of isolated sheets of human stratum corneum. Arch Dermatol. 1964;88:702–5.
Lademann J, Ilgevicius A, Zurbau O, Liess HD, Schanzer S, Weigmann HJ, Antoniou C, Pelchrzim RV, Sterry W. Penetration studies of topically applied substances: optical determination of the amount of stratum corneum removed by tape stripping. J Biomed Opt. 2006;11:054026.
Lademann J, Jacobi U, Surber C, Weigmann HJ, Fluhr JW. The tape stripping procedure: evaluation of some critical parameters. Eur J Pharm Biopharm. 2009;72:317–23.
Lane ME. Skin penetration enhancers. Int J Pharm. 2013;447:12.
Laugier JP, Surber C, Bun H, Geiger JM, Wilhelm KP, Durand A, Maibach HI. Determination of acitretin in the skin, in the suction blister, and in plasma of human volunteers after multiple oral dosing. J Pharm Sci. 1994;83:623–8.
Lauweris RR, Dath T, Lachapelle JM. The influence of two barrier creams on the percutaneous absorption of m-xylene in man. J Occup Med. 1978;20:17–20.
Lboutounne Y, Silva J, Pazart L, Bérard M, Muret P, Humbert P. Microclimate next to the skin: influence on percutaneous absorption of caffeine (*ex-vivo* study). Skin Res Technol. 2014;20:293–8. doi:10.1111/srt.12118.
Leopold CS. How accurate is the determination of the relative bioavailability of transdermal drug formulations from pharmacodynamic response data? Pharm Acta Helv. 1998;73:63–7.
Leopold CS. The maximum pharmacodynamic effect as a response parameter: pharmacokinetic considerations. J Pharm Pharmacol. 1999;51:1–11.
Leopold CS, Lippold BC. A new application chamber for skin penetration studies. Pharm Res. 1992;9:1215–8.
Leopold CS, Maibach HI. Percutaneous penetration of local anesthetic bases: pharmacodynamic measurements. J Invest Dermatol. 1999;113:101–4.
Lindemann U, Weigmann H-J, Schaefer H, Sterry W, Lademann J. Evaluation of the pseudo-absorption method to quantify human stratum corneum removed by tape stripping using the protein absorption. Skin Pharmacol Physiol. 2003;16:228–36.
Loffler H, Dreher F, Maibach HI. Stratum corneum adhesive tape stripping: influence of anatomical site, application pressure, duration and removal. Br J Dermatol. 2004;151:746–52.
Maibach HI, Wester RC. Percutaneous absorption: in vivo methods in humans and in animals. J Am Coll Toxicol. 1989;8:803–13.
Marty JP. Fixation des substances chimiques dans les structures superficielles de la peau: importance dans les problèmes de décontaminationet de biodisponibilité. Thèse, Université de Paris-Sud, 1976.
Mayee R, Rawat S. Pharmacokinetic studies of topical formulations-a review. Int J Pharm Clin Res. 2010;2:98–100.
Melot M, Pudney PD, Williamson AM, Caspers PJ, VanDerPol A, Puppels GJ. Studying the effectiveness of penetration enhancers to deliver retinol through the stratum corneum by in vivo confocal Raman spectroscopy. J Control Release. 2009;138:32–9.
Merfort I, Heilmann J, Hagedorn-Leweke U, Lippold BC. In vivo skin penetration studies of camomile flavones. Pharmazie. 1994;49:509–11.
Meuling WJA, Franssen AC, Brouwer DH, van Hemmen JJ. The influence of skin moisture on the dermal absorption of propoxur in human volunteers: a consideration for biological monitoring practices. Sci Total Environ. 1997;199:165–72.
Mitragotri S. Modeling skin permeability to hydrophilic and hydrophobic solutes based on four permeation pathways. J Control Release. 2003;86:69–92.
Narkar Y. Bioequivalence for topical products—an update. Pharm Res. 2010;27(12):2590–601.
OECD. Test guideline 427: skin absorption: in vivo method. Paris: Organisation for Economic Co-operation and Development; 2004.
OECD. Test No. 428: skin absorption: in vitro method, OECD guidelines for the testing of chemicals, section 4, OECD Publishing, Paris. DOI: http://dx.doi.org/10.1787/9789264071087-en.
Paturi J, Kim HD, Chakraborty B, Friden PM, Banga AK. Transdermal and intradermal iontophoretic delivery of dexamethasone sodium phosphate: quantification of the drug localized in skin. J Drug Target. 2010;18(2):134–40.
Pirot F. Analyse, mesure et prédiction de la diffusion dans le stratum corneum humain. Besançon: Thèse Sciences de la Vie et de la Santé; 1996.
Pirot F, Kalia YN, Stinchcomb AL, Keating G, Bunge A, Guy RH. Characterization of the permeability barrier of human skin in vivo. Proc Natl Acad Sci U S A. 1997;94:1562–7.
Potts RO, Guy RH. Predicting skin permeability. Pharm Res. 1992;9:663–9.
Pudney PD, Melot M, Caspers PJ, Van Der Pol A, Puppels GJ. An in vivo confocal Raman study of the delivery of trans retinol to the skin. Appl Spectrosc. 2007;61:804–11.
Reddy MB, Stinchcomb AL, Guy RH, Bunge AL. Determining dermal absorption parameters in vivo from tape strip data. Pharm Res. 2002;19:292–8.

Rougier A, Rallis M, Krien P, Lotte C. In vivo percutaneous absorption: a key role for stratum corneum/vehicle partitioning. Arch Dermatol Res. 1990;282:498–505.

Rudd A, Henderson HI. Monitored indoor moisture and temperature conditions in humid-climate US residences. ASHRAE Trans. 2007;113:435–49.

Schaefer H, Redelmeier TE, editors. Skin barrier. Principles of percutaneous absorption. Basel: Karger; 1996.

Schaefer H, Zesch A, Stüttgen G, editors. Skin permeability. Berlin: Springer; 1982.

Scheuplein RJ. Mechanism of percutaneous absorption. I. Routes of penetration and the influence of solubility. J Invest Dermatol. 1965;45:334–46.

Scheuplein RJ. Permeability of the skin: a review of major concepts. In: Simon GA et al., editors. Skin: drug application and evaluation of environmental hazards, Current problems in dermatology, vol. 7. Basel: Karger; 1978. p. 172–86.

Scheuplein RJ, Bronaugh RJ. Percutaneous absorption. In: Goldsmith LA, editor. Biochemistry and biology of the skin. Oxford: Oxford University Press; 1983. p. 1255–95.

Siddoju S, Sachdeva V, Friden PM, Banga AK. Iontophoretic delivery of acyclovir: intradermal drug monitoring using microdialysis and quantification by skin extraction. PDA J Pharm Sci Technol. 2011;65(5):432–44.

Singh B, Maibach H. Climate and skin function: an overview. Skin Res Technol. 2013;19:207–12.

Stenken JA, Church MK, Gill CA, Clough GF. How minimally invasive is microdialysis sampling? A cautionary note for cytokine collection in human skin and other clinical studies. AAPS J. 2010;12(1):73–8.

Stinchcomb AL, Pirot F, Touraille GD, Bunge AL, Guy RH. Chemical uptake into human stratum corneum in vivo from volatile and non-volatile solvents. Pharm Res. 1999;16:1288–93.

Thrall KD, Poet TS, Corley RA, Maibach HI, Wester RC. Innovative methods to determine percutaneous absorption in humans. In: Bronaugh RL, Maibach HI, editors. Topical absorption of dermatological products. New York: Marcel Dekker; 2002. p. 299–309.

Treffel P, Makki S, Faivre B, Humbert P, Blanc D, Agache P. Citropten and Bergapten suction blister fluid concentrations after solar product application in man. Skin Pharmacol. 1991a;4:100–8.

Treffel P, Humbert P, Makki S, Faivre B, Agache P. Use of a surface recovery technique to evaluate percutaneous absorption of 5-methoxypsoralen in humans. Arch Dermatol Res. 1991b;283:487–9.

Wahlberg GE. "Disappearance measurements". Method for studying percutaneous absorption of isotope-labeled compounds emitting gamma rays. Acta Derm Venereol. 1965;45:397–414.

Walker J, Romualda DK, Seideman P, Day RO. Pharmacokinetics of ibuprofen enantiomers in plasma and suction blister fluid in healthy volunteers. J Pharm Sci. 1993;82:787–90.

Wang Y, Su W, Li Q, Li C, Wang H, Li Y, Cao Y, Chang J, Zhang L. Preparation and evaluation of lidocaine hydrochloride-loaded TAT-conjugated polymeric liposomes for transdermal delivery. Int J Pharm. 2013;441:748–56.

Wascotte V, Caspers P, de Sterke J, Jadoul M, Guy RH, Preat V. Assessment of the "skin reservoir" of urea by confocal Raman microspectroscopy and reverse iontophoresis in vivo. Pharm Res. 2007;24:1897–901.

Wépierre J, editor. Abrégé de pharmacodynamie générale. Paris: Masson; 1977.

Wester RC, Maibach HI. Regional variation in percutaneous absorption. In: Bronaugh RL, Maibach HI, editors. Percutaneous absorption. 2nd ed. New York: Marcel Dekker; 1989. p. 111–9.

Wester RC, Maibach HI. Noninvasive techniques for assessment of skin penetration and bioavailability. In: Serup J, Jemec GBE, editors. Handbook of non-invasive methods and the skin. Boca Raton: CRC Press; 1995. p. 201–6.

Wester RC, Maibach HI. In vivo methods for percutaneous absorption measurements. In: Bronaugh RL, Maibach HI, editors. Percutaneous absorption. 3rd ed. New York: Marcel Dekker; 1999. p. 215–27.

Wester R, Noonan PK. Topical bioavailability of a potential anti-acne agent as determined by cumulative excretion and areas under plasma concentration-time curves. J Invest Dermatol. 1978;70:92–4.

Wu X, Price GJ, Guy RH. Disposition of nanoparticles and an associated lipophilic permeant following topical application to the skin. Mol Pharmacol. 2009;6:1441–8.

Yosipovitch G, Glen L, Xiong GL, Haus E, Sackett-Lundeen L, Ashkenazi I, Maibach HI. Time-dependent variations of the skin barrier function in humans: transepidermal water loss, stratum corneum hydration, skin surface ph, and skin temperature. J Invest Dermatol. 1998;110:20–3.

Zhang H, Yoshino H. An alysis of indoor humidity environment in Chinese residential buildings. Build Environ. 2013;45:2132–40.

Zhao J, Lui H, McLean DI, Zeng H. Integrated real-time Raman system for clinical in vivo skin analysis. Skin Res Technol. 2008;14:484–92.

Biological and Pharmacological Tests for the Exploration of Skin Barrier Function

107

Pierre Treffel and Bernard Gabard

Contents

Keywords
skin • cutaneous absorption • skin barrier • nicotinic acid esters • corticosteroids

An investigation of the skin barrier function may be conducted following different approaches in vitro (Franz 1975) or in vivo (Feldmann and Maibach 1965; Rougier et al. 1983) by measuring the amount of a given compound permeating the different skin layers. On the other hand, quantification of a cutaneous (Oestmann et al. 1993) or systemic biological reaction may also be used for studying the skin barrier function. We will only describe cutaneous biological reactions in man after application of pharmacologically active compounds.

1 Skin Barrier Function

1.1 Physiological Basis of Skin Barrier

Although the skin remains a very complex organ, two main layers are characterized from a macroscopic point of view: an external epithelium called epidermis, and a vascularized stroma, the dermis, physiologically supporting the epidermis. The genuine barrier against xenobiotics is located within the epidermis, which itself comprises two main layers, the viable epidermis and the horny layer. The biological reactions that will be

This chapter was originally published under the ISBN 978-3-540-01771-4 with the following book title Measuring the Skin. The content has not been changed.

P. Treffel (✉)
Pharmaceutical laboratory, Codexial Dermatologie, Vandœuvre-lès-Nancy, France
e-mail: Pierre.treffel@codexial-dermatologie.com

B. Gabard
Lörrach, Germany
e-mail: b.gabard@iderma.ch

P. Humbert et al. (eds.), *Agache's Measuring the Skin*,
DOI 10.1007/978-3-319-32383-1_141

measured are mainly vascular responses arising from the dermal microcirculation.

1.2 Pharmacologically Active Molecules

Numerous compounds affect the dermal microcirculation after topical application and influence skin color to be more white or red. For example, nicotinic acid esters are vasodilators inducing a clear erythema. Methyl- (NM, MW = 137.1), ethyl- (NE, MW = 151.2), butyl- (NB, MW = 179.2) and hexyl-nicotinate (NH, MW = 207.3), here quoted by increasing order of lipophilicity, are the most used. Usual concentrations amount to 0.5–10 mM after solubilization in appropriate solvents. These molecules, after crossing the epidermis more or less easily depending on the state of the cutaneous barrier, will dilate the capillary loops in the dermis, then the small arteries of the superficial vascular plexus, and finally the blood vessels of the lower dermal plexus. Thus, the measurement of skin blood flow or of skin color will allow an estimation of the skin barrier function. When considering nicotinic acid esters, the presence or the absence of an erythematous reaction may be an indication of skin barrier function.

Corticosteroids induce a decrease of dermal blood flow (a vasoconstriction). The mechanism (s) of this reaction are poorly understood. The resulting skin whitening, or blanching reaction, may be used for the investigation of skin penetration of the corresponding compounds (Mac Kenzie and Stoughton 1962; Mac Kenzie 1962). However, due to the great differences in pharmacological activity between different corticosteroid molecules (their anti-inflammatory potency is related to their corticosteroid classification), the whitening reaction often does not really reflect percutaneous absorption (also see ▶ Chap. 133, "Assessment of Erythema and Pallor" Sect. 10). Nevertheless, the measurement of skin color remains of value for cutaneous bioequivalence studies where the same molecule is applied onto the skin in different formulations (Caron et al. 1990; Pershing et al. 1991; Pershing et al. 1992).

2 Skin Color Changes after Nicotinic Acid Ester Application

2.1 Cutaneous Application

Methyl nicotinate is dissolved in water, while the other esters are solubilized using, among others, propylene glycol, isopropanol, or liquid paraffin (Treffel and Gabard 1993; Issachar et al. 1998). Small filter paper discs (diameter <1 cm) are soaked in these different solutions (an aqueous solution of NM 5 mM is often used) and brought into contact with the skin for a short time, usually 15–30 s. The internal (or ventral) side of the forearm is the place of choice for application in humans. Alternatively, the aqueous NM solution may be applied with a micropipette (10–50 µl).

The cutaneous reaction may be followed visually using color charts or precisely and reproducibly measured with a suitable instrument. The measurements are done every 10 min until 40 min, and then at 60 and 90 min. By that time, the vascular reaction generally has vanished and the reddening has disappeared.

2.2 Instruments

Two instruments are commonly used (see ▶ Chap. 133, "Assessment of Erythema and Pallor"). The Chromameter (Minolta, Japan) allows the precise evaluation of skin color (Wilhem and Maibach 1989) and the laser Doppler velocimeter (Perimed, Sweden and Moor, UK) is used for determination of cutaneous blood flow (Bircher et al. 1994).

2.3 Characteristic Parameters

After cutaneous application of a nicotinic acid ester, several parameters may be evaluated: latency or time lag before appearance of the erythemal reaction, time to peak or maximal value, duration of the erythemal reaction, and area under the erythemal intensity versus time curve. Although both measuring techniques (skin color and skin blood flow) seem

complementary, skin color is more appropriate for the evaluation of nicotinic acid ester penetration. Indeed, the superficial dermal plexus is responsible for the reddening of the skin measured by chromametry. The laser Doppler data also include values from the lower dermal plexus featuring a more important blood flow that may be modified by external factors such as temperature and stress.

2.4 Nicotinic Acid Esters for the Investigation of Skin Barrier Function

The vasodilator properties of NM had already been used by 1962 for the investigation of skin barrier function differences depending on the anatomical site (Cronin and Stoughton 1962). Areas showing a strong or weaker barrier were characterized. These results were later validated using other techniques (Feldmann and Maibach 1967).

Stripping of the horny layer or tearing away the stratum corneum with an adhesive tape diminishes latency and accelerates the appearance of skin reddening (Guessant et al. 1993). Using the same phenomena, racial differences between Caucasian, black and Asian subjects were shown (Guy et al. 1985; Kompaore and Tsuruta 1993). Age may also be a factor influencing the cutaneous response to nicotinic acid ester application (Roskos et al. 1990).

Elsner and Maibach (1991) have shown that the erythemal reaction to NM application was less intense and of shorter duration on vulval skin than on forearm skin. The lower sensitivity of this anatomical region compared to the forearm is one of the factors discussed by the authors to explain this surprising result. Indeed, in this particular case, a skin area with a known reduced barrier function shows a diminished erythemal reaction. The pharmacodynamic aspect of the reaction then becomes important, because percutaneous absorption is not the only factor determining the skin response. Also, circadian rhythms have been shown to influence the cutaneous nicotinic acid ester reaction (Reinberg et al. 1995). These results show that pharmacodynamics must be considered when evaluating skin changes.

3 Skin Color Changes after Corticosteroid Application

3.1 Cutaneous Application

The described method is based on the original work of Mac Kenzie (Mac Kenzie and Stoughton 1962). The different products to be tested (dermatological formulations containing corticosteroids) are applied under occlusion on the inner side of the forearm at the dose of 2–10 mg/cm^2. The duration of application may vary between 0.25 and 6 h. For each application time, the kinetics of the blanching reaction are followed at 0.25, 0.5, 1, 2, 4, 6, 8, and 24 h on each tested area after cleaning the skin and removing the unpenetrated product.

3.2 Instruments

Although some authors advocate the use of laser Doppler measurements (Anja et al. 1998), visual scoring of skin whitening or measurement of skin color using the Minolta Chromameter seems to be more sensitive and widely used (Mac Kenzie and Stoughton 1962; Mac Kenzie 1962; Caron et al. 1990; Pershing et al. 1991; Pershing et al. 1992; see ▶ Chap. 133, "Assessment of Erythema and Pallor").

3.3 Characteristic Parameters

For each application duration, the relevant parameters for quantifying the blanching reaction are: time to maximal value (reaction peak), maximal value, and the area under the time curve. These different parameters may be compared and used for the appreciation of cutaneous bioavailability of different products, but are less suitable for evaluation of percutaneous skin absorption.

4 Conclusion

Skin barrier function may be qualitatively appreciated by the evaluation of biological or pharmacological reactions using nicotinic acid esters or

corticosteroids. However, the skin response represents the sum of complex and intricate phenomena. Indeed, skin barrier state, cutaneous blood vessel sensitivity to the applied compound, corticosteroid potency class, and the level of blood flow in a given skin area, all these factors simultaneously contribute to the measured biological response. Therefore, the quantitative extrapolation of the obtained results as to percutaneous absorption must be done carefully.

References

Anja S, Joep V, Martino N, Alfons K. Evaluation of the vasoconstrictive effects of topical steroids by Laser-Doppler-Perfusion-Imaging. Acta Derm Venereol (Stockh). 1998;78:15–8.

Bircher A, De Boer EM, Agner T, Wahlberg JE, Serup J. Guidelines for measurement of cutaneous blood flow by laser Doppler flowmetry. Contact Dermatitis. 1994;30:65–72.

Caron D, Queille-Roussel C, Shah V, Schaefer H. Correlation between the drug penetration and the blanching effect of topically applied hydrocortisone creams in human beings. J Am Acad Dermatol. 1990;23:458–62.

Cronin E, Stoughton RB. Percutaneous absorption: regional variations and the effect of hydration and epidermal stripping. Br J Dermatol. 1962;74:265–72.

Elsner P, Maibach HI. Cutaneous responses to topical methyl nicotinate in human forearm and vulvar skin. J Dermatol Sci. 1991;2:341–5.

Feldmann RJ, Maibach HI. Penetration of 14 C hydrocortisone through normal skin. The effect of stripping and occlusion. Arch Dermatol. 1965;91:661–6.

Feldmann RJ, Maibach HI. Regional variation in percutaneous penetration of 14 C cortisol in man. J Invest Dermatol. 1967;48:181–3.

Franz TJ. Percutaneous absorption. On the relevance of the in vitro data. J Invest Dermatol. 1975;64:190–5.

Guessant C, Marty JP, Dupont C. Evaluation de la barrière cutanée chez l'homme par deux méthodes non-invasives (vélocimétrie laser Doppler et chromamétrie). Int J Cosmet. 1993;15:89–99.

Guy RH, Tur E, Bjerke S, Maibach HI. Are there age and racial differences to methyl nicotinate-induced vasodilatation in human skin? J Am Acad Dermatol. 1985;12:1001–6.

Issachar N, Gall Y, Borrel M, Poelman MC. Correlation between percutaneous penetration of methyl nicotinate and sensitive skin, using laser Doppler imaging. Contact Dermatitis. 1998;39:182–6.

Kompaore F, Tsuruta H. In vivo differences between Asian, Black and White in the stratum corneum barrier function. Int Arch Occup Environ Health. 1993;65: S223–5.

Mac Kenzie AW. Percutaneous absorption of steroids. Arch Dermatol. 1962;86:611–4.

Mac Kenzie AW, Stoughton RB. Method for comparing percutaneous absorption of steroids. Arch Dermatol. 1962;86:608–10.

Oestmann E, Lavrijsen APM, Hermans J, Ponec M. Skin barrier function in healthy volunteers as assessed by transepidermel water loss and vascular response to hexyl nicotinate: intra- and inter-individual variability. Br J Dermatol. 1993;128:130–6.

Pershing L, Silver B, Krueger G, Shah V, Skelley J. Feasibility of measuring the bioavailability of topical betamethasone dipropionate in commercial formulations using drug content in skin and a skin blanching bioassay. Pharm Res. 1991;9:45–51.

Pershing L, Lambert L, Shah V, Lam S. Variability and correlation of chromameter and tape-stripping methods with the visual skin blanching assay in the quantitative assessment of topical 0.05% betamethasone dipropionate bioavailability in humans. Int J Pharm. 1992;86:201–10.

Reinberg AE, Soudant E, Koulbanis C, Bazin R, Nicolaï A, Mechkouri M, Touitou Y. Circadian dosing time dependency in the forearm skin penetration of methyl and hexyl nicotinate. Life Sci. 1995;57:1507–13.

Roskos KV, Bircher AJ, Maibach HI, Guy RH. Pharmacodynamic measurements of methyl nicotinate percutaneous absorption: the effect of aging on microcirculation. Br J Dermatol. 1990;122:165–71.

Rougier A, Dupuis D, Lotte C, Roguet R, Schaefer H. In vivo correlation between stratum corneum function and percutaneous absorption. J Invest Dermatol. 1983;81:275–8.

Treffel P, Gabard B. Feasibility of measuring the bioavailability of topical ibuprofen in commercial formulations using drug content in epidermis and a methyl nicotinate skin inflammation assay. Skin Pharmacol. 1993;6:268–75.

Wilhem KP, Maibach HI. Skin color reflectance measurements for objective quantification of erythema in human beings. J Am Acad Dermatol. 1989;21:1306–8.

Transepidermal Water Loss

108

Bernard Gabard and Pierre Treffel

Contents

Keywords

Evaporimeter • Fick's law • Open cylinder method • Passive diffusion • Skin barrier function • Skin irritation • Transepidermal water loss (TEWL) • Clinical dermatology • Experimental dermatology • Instruments • Physiological principles • Practical recommendations • Precision • Reproducibility • Sources of error and variation factors • Theoretical principles

The use of noninvasive measurement methods for the examination of different physiological functions of the skin or for the characterization of pharmacological or pathological reactions is recent. Following the development of suitable techniques, instruments are now available for the evaluation of such different cutaneous parameters as color, elasticity, dermal blood flow, hydration of the horny layer, sebum excretion, and, of course, transepidermal water loss (TEWL). This equipment may replace the usual visual evaluation of skin state and are able to catch changes that otherwise would be not detected by the human eye.

Numerous advantages arise from using these techniques: independence toward investigator's subjectivity, numerical results and not ordered nominal data, better standardization of the experiments, better possibilities of interlaboratory comparisons, no requirement of highly specialized personnel, etc. For all these reasons, these new techniques are of growing interest for dermatological laboratories. Moreover, the increasing automation of data acquisition allows for the

This chapter was originally published under the ISBN 978-3-540-01771-4 with the following book title Measuring the Skin. The content has not been changed.

B. Gabard (✉)
Lörrach, Germany
e-mail: b.gabard@iderma.ch

P. Treffel
Pharmaceutical laboratory, Codexial Dermatologie, Vandœuvre-lès-Nancy, France
e-mail: Pierre.treffel@codexial-dermatologie.com

P. Humbert et al. (eds.), *Agache's Measuring the Skin*,
DOI 10.1007/978-3-319-32383-1_142

simultaneous evaluation of several parameters if necessary.

1 Transepidermal Water Loss

1.1 Basic Physiological Principles

Water has two possibilities in crossing the skin from the viable tissues toward the outer environment: active transport by sweating and passive diffusion through the horny layer. Sweating (*perspiratio sensibilis*) is one possibility for the body to control its temperature. It may also express psychic stress. Sweating may peak at maximal values of 2–4 l/h. On the contrary, transepidermal water loss (TEWL, *perspiratio insensibilis*) is not visible to the naked eye. Given no air turbulence, the skin is covered by a transition layer where moisture is transferred from the surface of the skin to the surrounding atmosphere, building up a protective sheet toward environment. The quantity of water crossing the stratum corneum on this way is estimated at 300–400 ml per day under normal conditions, that means 1/10th to 1/20th of sweating. Given this difference, it is mandatory to eliminate sweating during TEWL measurements. (Note: Water loss due to expired water vapor is also included in the term *perspiratio insensibilis*. But for the sake of clarity, only water loss through the horny layer will be considered here.)

1.2 Theoretical Principles

The diffusion barrier is situated entirely within the horny layer (Wilson and Maibach 1989; Lévêque 1989). The TEWL is a passive phenomenon due to the water vapor pressure gradient on both sides of the layer. Water concentration in the epidermis, which is well hydrated in contact with the dermis, is estimated to be 48–49 mol. This value is also found at the deeper side of the horny layer. On the other side, water concentration at skin surface, which is in contact with drier surroundings, is lower and was shown to be around 12 mol (ambient conditions: relative humidity 40 %, temperature 31 °C). The pressure gradient thus amounts to 37 mol (Wilson and Maibach 1989). Thus, if the relative humidity of the surrounding air is 100 %, the TEWL will decrease almost to zero, and inversely, if the relative humidity is 0 %, TEWL will be maximal (Fig. 1).

Passive diffusion of water through the horny layer is described by the 1st Fich's law (Schaefer and Redelmeier 1996). At equilibrium, the flux of water (J, mol cm^{-1} s^{-1}) travelling upon a given distance (δ, cm) is proportional to the concentration gradient (ΔC) and to the diffusion coefficient

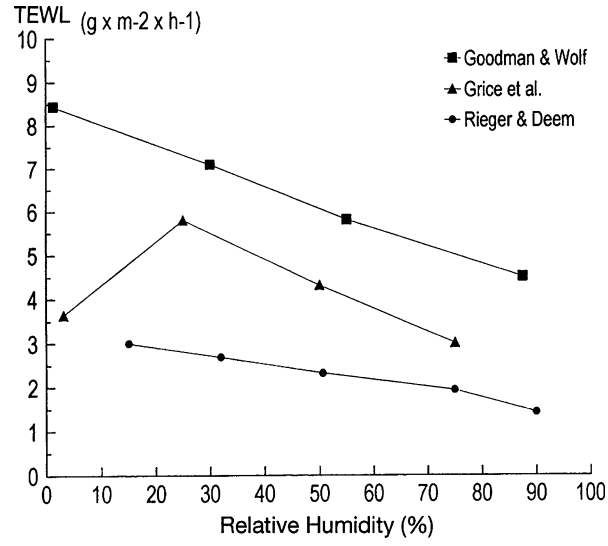

Fig. 1 Effect of relative humidity on TEWL: results of three studies

(D, cm^2/s). However, the horny layer is not an inert membrane, but shows some affinity to water and Fick's law needs to be modified by the introduction of a partition coefficient K_m (Wilson and Maibach 1989; Potts and Francoeur 1991):

$$K_m = \frac{\text{(Water concentration in the lower horny layer)}}{\text{(Water concentration in the intercellular space of living epidermis)}}$$

Fick's law thus writes $J = -K_m \times D\,(\Delta C/\Delta\delta)$

K_m amounts to 0.06 (Potts and Francoeur 1991). The negative symbol "−" shows that the flux is directed toward lower concentrations.

2 Methods and Measurement Devices

2.1 Introduction

Different measurement methods were described by Wilson and Maibach (1989). Briefly they list:

- Urine osmolarity
- Body weight
- Closed cylinder method: weight of an hygroscopic substance
- Ventilated chamber
- Electrohygrometer
- Thermal conductivity cell
- Dew-point hygrometer
- Electrolytic water vapor analyzer
- Open cylinder

This list is not exhaustive. The results obtained using these different methods are hardly comparable because of the difficulty in measuring TEWL under standardized conditions and the importance of several variation factors (see Sect. 3). A recently published review (Pinnagoda 1994a) shows that the measured values may depend, within certain limits, on the method employed. Wilson and Maibach (1989) described these different techniques with their advantages and drawbacks, but some of these are obsolete and/or not commercially available. For these reasons, only the last one, the most commonly used, will be described. Several instruments are commercialized using the open cylinder method for measurement, and recent reviews describe this method in detail (Pinnagoda 1994a; Pinnagoda and Tupker 1995).

2.2 The Open Cylinder Method

A probe is applied on the skin surface, built as a cylindrical chamber open to the surrounding air. A 0.8–1 cm^2 skin area (value depends on the instrument) is delimited by the probe and constitutes the bottom of the chamber. Two sensors (semiconductors) measuring relative humidity are situated at two different levels vertically in the chamber. Each is coupled to a thermistor (Fig. 2). The distance from the sensors to the skin surface is calculated for an optimal evaluation of the water vapor pressure gradient arising within the chamber between the skin and the surrounding air.

Water pressure at each level is calculated from the following equation:

$$P = RH \times p_{sat}$$

p_{sat} is pressure at water saturation. Relative humidity (RH: %) is measured by the semiconductors; p_{sat} is calculated by the instrument, given the air temperature at each sensor level. The vapor pressure difference between the two measurement levels determines the slope of the pressure gradient. The TEWL is directly expressed in $g\,m^{-2}\,h^{-1}$.

2.3 Instruments

Several instruments using the open cylinder method are available: the Evaporimeter, the

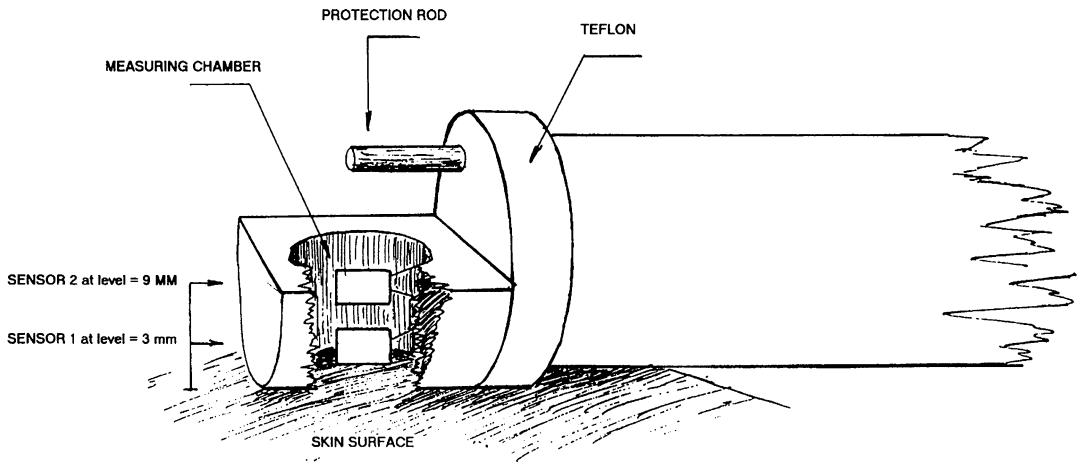

Fig. 2 Schema of the TEWL measuring head

Tewameter, and more recently the DermaLab (for manufacturer's location, see Evaporimètre®; Tewamètre®; DermaLab®). An evaluation of both the Evaporimeter and the Tewameter and a comparison of the results obtained with these machines were published by Barel and Clarys in 1995 (Barel and Clarys 1995a, b). A similar comparative evaluation of the DermaLab and of the Evaporimeter was recently published by Grove et al. (1999). This last publication also lists previous reports dealing with comparative performance studies of the Evaporimeter. The geometry of the measuring probe and possibly the manufacturer's calibration method vary slightly between the different instruments, as well as the electronic treatment of measured data. Although the values obtained with one instrument are highly correlated to the values obtained with the other, some differences may remain between the values and between their variations after a given challenge (Barel and Clarys 1995b; Grove et al. 1999).

A portable device has recently been put on the market: Model H4300 (Nikkiso YSI Company Ltd, Tokyo, Japan). Its principle is based on the progressive increase in relative humidity inside a closed chamber, due to continuous water evaporation from the skin surface on which the chamber is placed. A linear correlation was found with DermaLab ($R^2 = 0.917$), but the obtained values were much lower (Tagami et al. 2002).

3 Sources of Error, Standardization, and Practical Recommendations

3.1 Introduction

Because of the dependency of the TEWL on the water vapor pressure gradient on the skin surface, every intrinsic or extrinsic factor influencing either the thickness of the transition layer from skin surface to surrounding air or the slope of the gradient within the transition layer will modify the TEWL. Moreover, given the sensitivity of the measuring probes, any change in the environmental microclimate will be detected and will consequently modify the indicated values unless the measuring conditions have been rigorously standardized. Precise recommendations concerning this particular point have been published (Pinnagoda et al. 1990; Rogiers 1995; Pinnagoda 1994b).

3.2 Sources of Error and Variation Factors

Variation factors may be classified as follows:

- Instrumental factors
- Environmental factors
- Individual factors

These factors have already been extensively reviewed (Pinnagoda and Tupker 1995; Barel and Clarys 1995b; Grove et al. 1999; Pinnagoda et al. 1990; Rogiers 1995; Pinnagoda 1994b) and listed (Pinnagoda et al. 1990), and their relative influence has also been evaluated. For these reasons, the interested reader will consult the original publications for more details.

- Instrumental factors
  - Preheating of the instrument: at least 15 min for electronic circuit stabilization. It is not recommended to switch off the instrument between the measurements.
  - Instrument zeroing: After preheating, under measuring conditions (see Sect. 3.4).
  - Measurement technique (see Sect. 3.4 and Pinnagoda et al. (1990); Rogiers (1995)).
  - Variation of zero during the measurements: to be regularly controlled.
  - Humidity and temperature variations in the open chamber: the probe must not be left in place on the skin; avoid contact with sweat.
  - During measurements the probe should remain horizontal.
  - Use of a protecting grid to avoid contact with a test product applied on the skin.
  - Pressure of the probe onto the skin.
  - Regular calibration of the probe following the manufacturer's instructions and as requested by GLPs.
  - Inter-instrumental variations (see Grove et al. (1999); Pinnagoda et al. (1990)).
  - Precision of the measurements (see Sect. 3.3).
- Environmental factors
  - Air convection and turbulences during the measurements
  - Environmental temperature
  - Environmental humidity
- Individual factors
  - Sweating
  - Skin temperature
  - Anatomical location of the measurement
- Conclusions

  The relative importance of these factors is not the same. If a minimal standardization is assured, instrumental factors are less important. The greatest variations are then due to the environmental and individual factors. Figures 3, 4 (Barel and Clarys 1995b), and 5 (Van Kemenade 1998) illustrate, for example, the respective influences of the environmental temperature or relative humidity on measured values. Figure 5, showing recent data, is of particular interest: a sudden variation of the relative humidity from 53 % to 89 % provokes a fall of the TEWL, which thereafter slowly returns but stabilizes at a level lower than starting values. This last phenomenon is due to a change of the hydration of the horny layer, which also depends on the environmental

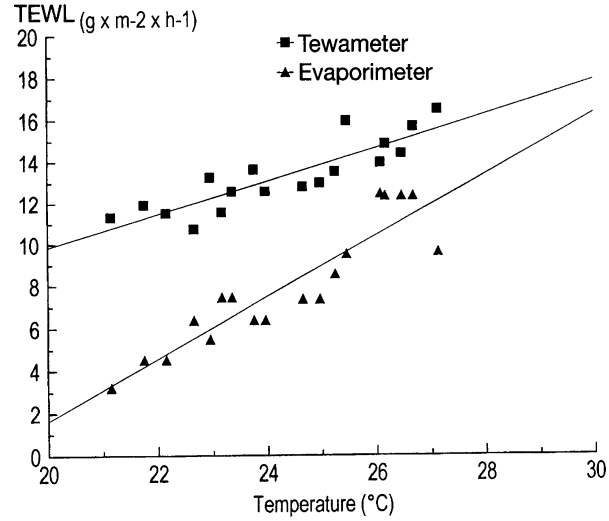

Fig. 3 Forearm TEWL versus ambient temperature, as measured with Evaporimeter and Tewameter

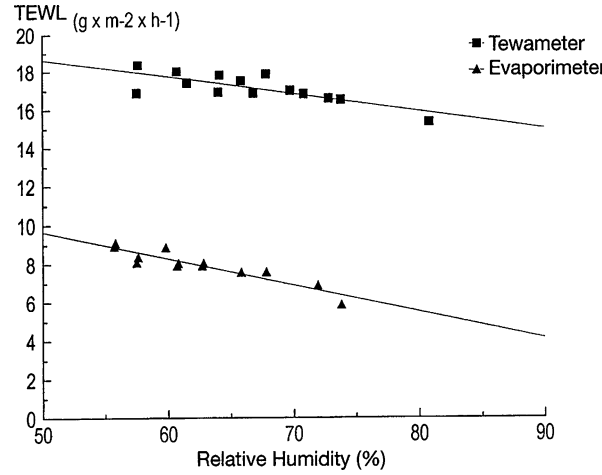

Fig. 4 Forearm TEWL versus ambient relative humidity, as measured with Evaporimeter and Tewameter

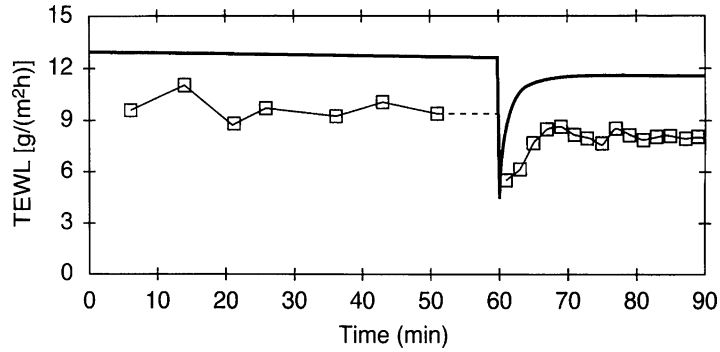

Fig. 5 TEWL versus sudden change in ambient relative humidity: within 1 h TEWL raised from 53% to 83%. Line with open squares measured TEWL, black unbroken line modelled TEWL

relative humidity. As to the individual factors, variations between to different anatomical are shown in Table 1 (Clarys et al. 1997).

3.3 Precision and Reproducibility of the Measurements

- Precision

  The following data are given by the manufacturers:
  - Evaporimeter: Precision ± 15 % (EP 1), ± 5 % (EP2)
  - Tewameter: Precision ± 15 % (±1.0 g m^{-2} h^{-1} if RH < 30 %), ± 10 % (±0.5 g m^{-2} h^{-1} if RH > 30 %)

The precision of the measurements is difficult to check, because the exact value of the TEWL must be measured using a gravimetric method (Wilson and Maibach 1989; Barel and Clarys 1995b). If such measurements are made, it appears that a correction is necessary to obtain absolute values (Petro and Komor 1987), particularly if these values are high and exceed 50 g m^{-2} h^{-1} (Pinnagoda and Tupker 1995; Petro and Komor 1987). This correction is given by the following equation:

$$TEWL_{corr} = Bx^{k}$$

where B is the measured TEWL value (g m^{-2} h^{-1}), x a constant (x = 0.025 cm),

Table 1 Table 1 Mean TEWL for various sites of the body measured with a Tewameter. Mean ±S.D for 16 volunteers

Body site	TEWL (g/m²h)
Forehead	20.1±4.8
Chest	10.7±1.3
Abdomen	9.9±1.8
Forearm (inner surface)	10.4±3.1
Calf	9.6±1.8

and k the slope of the line: [logTEWL = f (distance between the lower sensor and the skin surface)]. k has been determined for measurements on the volar forearm: k = −0.049 (Petro and Komor 1987).

- Reproducibility

  The reproducibility of the measurements is good if the measuring conditions have been standardized. Barel and Clarys (1995a, b) found variation coefficients between 3 and 8 %. Pinnagoda et al. published slightly higher values between 8 % and 15 % (Pinnagoda et al. 1989). Grove et al. (1999) published coefficient of variations of 4–47 % depending on the type of equipment used and on the level of the measured values (higher variations encountered if low values are measured).

3.4 Practical Recommendations

The control of environmental factors is only achieved by conducting the measurements in an air-conditioned room, featuring temperature, and relative humidity control. Turbulences and air convection in the near surroundings of the measuring probe are best eliminated by conducting the measurements inside a protecting box, e.g., an incubator with holes for the placement of the forearms (Pinnagoda et al. 1990). An open top should avoid buildup of temperature and water vapor inside the box. The measuring plane should remain horizontal, thus allowing the gradient to be built correctly in the measuring chamber. The pressure of the probe on the skin should remain low.

Control of individual factors is achieved by a strict selection of the study subjects, by allowing enough time for their relaxation before entering the experimental phase of the study ensuring their perfect adaptation to the controlled environmental conditions. For example, it is important to distinguish between atopic and non-atopic subjects, because the TEWL of atopic subjects is elevated in comparison to non-atopic ones, even if the skin of the atopics looks normal. Adaptation to the environmental conditions requires at least 20 min before measurements start. An experimental protocol should be available (Salter 1996), which excludes, for example, subjects having ingested spiced food that may provoke sweating. Stress also may provoke sweating; therefore, individuals should be thoroughly instructed and allowed to relax completely before starting with the study. These conditions ensure better reproducibility and precision of the measurements.

TEWL is tightly correlated to the barrier function of the horny layer. On the other hand, the barrier function also depends on the water content of the horny layer. The relationship between TEWL and the stratum corneum hydration must be considered in particular situations such as in newborn babies or old people or in measurements on a diseased skin (Berardesca and Maibach 1990).

Last but not least, some components of dermatological products may influence the measured values. Morrison (1992) showed that propylene glycol in a formulation could lead to an overestimation of the TEWL due to an interaction of this compound with the measuring probe. Dermatological or cosmetic products contain water that evaporates following application, and this evaporation adds to the underlying TEWL for a certain time. In this case, the measured value is known as skin surface water loss (SSWL). SSWL is also encountered during such particular experiments as the plastic occlusion stress test (POST) featuring a prolonged skin occlusion leading to water accumulation in the horny layer (Berardesca and Maibach 1990; Berardesca and Elsner 1994).

4 Practical Examples

Lastly, some practical examples of the use of TEWL are described in experimental and, more briefly, in clinical dermatology.

4.1 Experimental Dermatology

- Skin barrier function

  The results obtained by the group of A. Rougier (1994) or of M. Ponec (Oestmann et al. 1993) show a tight relationship between TEWL and the penetration of some chemicals through the skin, such as benzoic acid, acetylsalicylic acid, caffeine, or hexyl nicotinate. This relationship may still be valid in some pathological situations (Lavrijsen et al. 1993).
- Skin irritation

  TEWL is sensitive to skin irritation due to many different substances such as detergents or surfactants (Wilhelm et al. 1989; Effendy and Maibach 1995; Gabard 1991), all-trans retinoic acid (Gabard 1991; Effendy et al. 1996a), alpha-hydroxy acids such as glycolic acid (Effendy et al. 1995), newborn fecal enzymes (Andersen et al. 1994), or vitamin D derivatives (Effendy et al. 1996b; Fullerton and Serup 1997). Sodium lauryl sulfate is probably the most commonly used standard irritant in experimental dermatology. A recent guideline was published by the Standardization Group of the European Society of Contact Dermatitis about the standardization of experiments using this compound (Tupker et al. 1997). Measurement of TEWL may also be beneficial in experiments with animals or for comparison with human skin values (Fullerton and Serup 1997; Gendimenico et al. 1995; Gabard et al. 1995; Von Brenken et al. 1997). Differences may be encountered between various animal species as well as between animals and humans (Effendy et al. 1996b; Fullerton and Serup 1997; Von Brenken et al. 1997).
- Effects of UV irradiation

  Differences also are noticed between animals and humans considering the TEWL changes after an UV-B irradiation (Frödin et al. 1988; Haratake et al. 1997).
- Evaluation of topical products

  TEWL may be advantageously used for the investigation of some properties of topical products such as moisturizers (skin hydrating creams) after application on the skin. Measurement of the TEWL allows to characterize the changes of the product after application and the effect of different humectants contained in the product and also to precisely evaluate the occlusive properties of the formulation (Gabard 1994; Marti-Mestres et al. 1994).
- Therapeutic effects of topical products

  The TEWL also allows the evaluation of the therapeutic effect of topical products applied on diseased skin with a modified barrier function in animals and/or humans (Ghadially et al. 1992; Gabard et al. 1996; Lodén 1996, 1997; Mortz et al. 1997). The composition of the formulations may also be optimized with these experimental models (Zettersten et al. 1997). These experiments show on one side that contradictory results may be obtained if a diseased skin with modified barrier function is treated by a given formulation and on the other side that the obtained results on product efficacy may not be extrapolated in a straightforward manner from animals to humans.

4.2 Clinical Dermatology

Pinnagoda and Tupker (1995) published pertinent examples of improving medical care by the use of TEWL measurements in pathological situations:

- Various types of cutaneous inflammation.
- Follow-up of the course of atopic dermatitis (Aalto-Korte 1995; Seidenari and Giusti 1995): Aalto-Corte (1995) could show that the improvement of skin barrier function as measured by TEWL was accompanied by a decrease of the cutaneous absorption of hydrocortisone used for treatment.

- Psoriasis, different types of ichthyoses.
- Wound healing, regeneration of burned skin.
- Follow-up of newborn babies.
- Possibility of differentiating between an allergic or irritant reaction after patch testing (Giorgini et al. 1996).

This list remains succinct; the interested reader will report with benefit to the publication of Pinnagoda and Tupker (1995) where in-depth information are given about clinical applications of TEWL measurements. Obviously, some complications remain concerning a daily use of this technique in a hospital environment, the most important one being the necessity to conduct the measurements in a controlled and standardized environment.

5 Conclusions

The TEWL mirrors the integrity of the physiological barrier built up by the horny layer. Due to the availability of easy-to-use and precise equipments, the TEWL may now be easily measured. In that way, important information on skin water barrier may be gathered, concerning, for example, the behavior of topical products during development and use, differences between man and animals, etc. This information is pertinent, considering the fact that TEWL remains the most sensitive parameter for the detection of a cutaneous irritation. However, the obtained results are meaningful only if well-standardized measurement conditions are guaranteed. This remains an obstacle to an extended daily use.

References

Aalto-Korte K. Improvement of skin barrier function during treatment of atopic dermatitis. J Am Acad Dermatol. 1995;33:969–72.

Andersen PH, Bucher AP, Saeed I, Lee PC, Davis JA, Maibach HI. Faecal enzymes: in vivo human skin irritation. Contact Dermatitis. 1994;30:152–8.

Barel AO, Clarys P. Comparison of methods for measurement of transepidermal water loss. In: Serup J, Jemec JBE, editors. Handbook of non-invasive methods and the skin. Boca Raton: CRC Press; 1995a. p. 179–84.

Barel AO, Clarys P. Study of the stratum corneum barrier function by transepidermal water loss measurements: comparison between two commercial instruments: evaporimeter® and tewameter®. Skin Pharmacol. 1995b;8:186–95.

Berardesca E, Elsner P. Dynamic measurements: the plastic occlusion stress test (POST) and the moisture accumulation test (MAT). In: Elsner P, Berardesca E, Maibach HI, editors. Bioengineering of the skin: water and the stratum corneum. Boca Raton: CRC Press; 1994. p. 97–102.

Berardesca E, Maibach HI. Transepidermal water loss and skin surface hydration in the non invasive assessment of stratum corneum function. Dermatosen. 1990;38:50–3.

Clarys P, Manou I, Barel A. Relationship between anatomical site and response to halcinonide and methyl nicotinate studied by bioengineering techniques. Skin Res Technol. 1997;3:161–8.

DermaLab®: Cortex Technology, Smedevaenget 10, DK-9560 Hasund, Denmark. http://www.cortex.dk

Effendy I, Maibach HI. Surfactants and experimental irritant contact dermatitis. Contact Dermatitis. 1995;33:217–25.

Effendy I, Kwangsukstith C, Lee JY, Maibach HI. Functional changes in human stratum corneum induced by topical glycolic acid: comparison with all-trans retinoic acid. Acta Derm Venereol. 1995;75:455–8.

Effendy I, Weltfriend S, Patil S, Maibach HI. Differential irritant skin responses to topical retinoic acid and sodium lauryl sulphate: alone and in crossover design. Br J Dermatol. 1996a;134:424–30.

Effendy I, Kwangsukstith C, Chiappe M, Maibach HI. Effects of calcipotriol on stratum corneum barrier function, hydration and cell renewal in humans. Br J Dermatol. 1996b;135:545–9.

Evaporimètre®: Servo Med AB, P.O. Box 47, S-432 21 Varberg, Sweden. http://www.servomed.se

Frödin T, Molin L, Skogh M. Effects ofsingle doses of UVA, UVB, and UVC on skin blood flow, water content, and barrier function measured by laser-Doppler flowmetry, optothermal infrared spectrometry, and evaporimetry. Photodermatology. 1988;5:187–95.

Fullerton A, Serup J. Topical D-vitamins: multiparametric comparison of the irritant potential of calcipotriol, tacalcitol and calcitriol in a hairless guinea pig model. Contact Dermatitis. 1997;36:184–90.

Gabard B. Appearance and regression of a local skin irritation in two different models. Dermatosen. 1991;39:111–6.

Gabard B. Testing the efficacy of moisturizers. In: Elsner P, Berardesca E, Maibach HI, editors. Bioengineering of the skin: water and the stratum corneum. Boca Raton: CRC Press; 1994. p. 147–67.

Gabard B, Treffel P, Charton-Picard F, Eloy R. Irritant reactions on hairless micropig skin: a model for testing barrier creams? In: Elsner P, Maibach HI, editors. Irritant dermatitis: new clinical and experimental aspects, Current Problems in Dermatology, vol. 23. Basel: Karger; 1995. p. 275–87.

Gabard B, Elsner P, Treffel P. Barrier function of the skin in a repetitive irritation model and influence of 2 different treatments. Skin Res Technol. 1996;2:78–82.

Gendimenico GJ, Liebel FT, Fernandez JA, Mezick JA. Evaluation of topical retinoids for cutaneous pharmacological activity in Yucatan microswine. Arch Dermatol Res. 1995;287:675–9.

Ghadially R, Halkier-Sorensen L, Elias PM. Effects of petrolatum on stratum corneum structure and function. J Am Acad Dermatol. 1992;26:387–96.

Giorgini S, Brusi C, Sertoli A. Evaporimetry in the differentiation of allergic, irritant and doubtful patch test reactions. Skin Res Technol. 1996;2:49–51.

Grove GL, Grove MJ, Zerweck C, Pierce E. Comparative metrology of the evaporimeter and the DermaLab TEWL probe. Skin Res Technol. 1999;5:1–8.

Haratake A, Uchida Y, Schmuth M, Tanno O, Yasuda R, Epstein JH, Elias PM, Holleran WM. UVB-induced alterations in permeability barrier function: roles for epidermal hyperproliferation and thymocyte-mediated response. J Invest Dermatol. 1997;108: 769–75.

Lavrijsen APM, Oestmann E, Hermans J, Boddé HE, Vermeer BJ, Ponec M. Barrier function parameters in various keratinization disorders: transepidermal water loss and vascular response to hexyl nicotinate. Br J Dermatol. 1993;129:547–54.

Lévêque JL. Measurement of transepidermal water loss. In: Lévêque JL, editor. Cutaneous investigation in health and disease: noninvasive methods and instrumentation. New York: Marcel Dekker; 1989. p. 134–52. chap. 6.

Lodén M. Urea-containing moisturizers influence barrier properties of normal skin. Arch Dermatol Res. 1996;288:103–7.

Lodén M. Barrier recovery and influence of irritant stimuli in skin treated with a moisturizing cream. Contact Dermatitis. 1997;36:256–60.

Marti-Mestres G, Passet J, Maillols H, Van Sam V, Guilhou JJ, Mestres JP, Guillot B. Evaluation expérimentale de l'hydratation et du pouvoir occlusif in vivo et in vitro d'excipients lipophiles et de leur émulsions phase huile continue. Int J Cosmet Sci. 1994;16:161–70.

Morrison BM. ServoMed evaporimeter: precautions when evaluating the effect of skin care products on barrier function. J Soc Cosmet Chem. 1992;43:161–7.

Mortz CG, Andersen KE, Halkier-Sorensen L. The efficacy of different moisturizers on barrier recovery in hairless mice evaluated by non-invasive bioengineering methods. Contact Dermatitis. 1997;36: 297–301.

Oestmann E, Lavrijsen APM, Hermans J, Ponec M. Skin barrier function in healthy volunteers as assessed by transepidermal water loss and vascular response to hexyl nicotinate: intra- and inter-individual variability. Br J Dermatol. 1993;128:130–6.

Petro AJ, Komor JA. Correction to absolute values of evaporation rates measured by the ServoMed evaporimeter. Bioeng Skin. 1987;3:271–80.

Pinnagoda J. Hardware and measuring principles: evaporimeter. In: Elsner P, Berardesca E, Maibach HI, editors. Bioengineering of the skin: water and the stratum corneum. Boca Raton: CRC Press; 1994a. p. 51–8.

Pinnagoda J. Standardization of measurements. In: Elsner P, Berardesca E, Maibach HI, editors. Bioengineering of the skin: water and the stratum corneum. Boca Raton: CRC Press; 1994b. p. 59–65.

Pinnagoda J, Tupker RA. Measurement of transepidermal water loss. In: Serup J, Jemec JBE, editors. Handbook of non-invasive methods and the skin. Boca Raton: CRC Press; 1995. p. 173–8.

Pinnagoda J, Tupker RA, Smit JA, Coenraads PJ, Nater JP. The intra- and inter-individual variability and reliability of transepidermal water loss measurements. Contact Dermatitis. 1989;21:255–9.

Pinnagoda J, Tupker RA, Agner T, Serup J. Guidelines for transepidermal water loss (TEWL) measurement. Contact Dermatitis. 1990;22:164–78.

Potts RO, Francoeur ML. The influence of stratum corneum morphology on water permeability. J Invest Dermatol. 1991;96:495–9.

Rogiers V. Transepidermal water loss measurements in patch test assessment: the need for standardisation. In: Elsner P, Maibach HI, editors. Irritant dermatitis: new clinical and experimental aspects, Current Problems in Dermatology, vol. 23. Basel: Karger; 1995. p. 152–8.

Rougier A. TEWL and transcutaneous absorption. In: Elsner P, Berardesca E, Maibach HI, editors. Bioengineering of the skin: water and the stratum corneum. Boca Raton: CRC Press; 1994. p. 103–13.

Salter D. Non-invasive cosmetic efficacy testing in human volunteers: some general principles. Skin Res Technol. 1996;2:59–63.

Schaefer H, Redelmeier TE. Skin barrier; principles of percutaneous absorption. Bâle: Karger; 1996. p. 87–9.

Seidenari S, Giusti G. Objective assessment of the skin of children affected by atopic dermatitis: a study of pH, capacitance and TEWL in eczematous and clinically uninvolved skin. Acta Derm Venereol. 1995;73:429–33.

Tagami H, Kobayashi H, Kikuchi K. A portable device using a closed chamber system for measuring transepidermal water loss: comparison with the conventional method. Skin Res Technol. 2002;8:7–12.

Tewamètre®: Courage + Khazaka electronic GmbH, Mathias-Brüggen-Str. 91, D-50829 Cologne, Allemagne. http://www.courage-khazaka.de

Tupker RA, Willis C, Berardesca E, Lee CH, Fartasch M, Agner T, Serup J. Guidelines on sodium lauryl sulphate (SLS) exposure tests. Contact Dermatitis. 1997;37:53–69.

Van Kemenade P. Water and ion transport through intact and damaged skin. PhD Thesis, Technische Universiteit Eindhoven; 1998. ISBN 90-386-0760-1.

Von Brenken S, Jensen JM, Fartasch M, Procksch E. Topical vitamin D3 derivatives impair the epidermal permeability barrier in normal mouse skin. Dermatology. 1997;194:151–6.

Wilhelm KP, Surber C, Maibach HI. Quantification of sodium lauryl sulphate irritant dermatitis in man: comparison of four techniques: skin color reflectance, transepidermal water loss, laser Doppler flow measurement and visual scores. Arch Dermatol Res. 1989;281:293–5.

Wilson DR, Maibach HI. Transepidermal water loss: a review. In: Lévêque JL, editor. Cutaneous investigation in health and disease: noninvasive methods and instrumentation. New York: Marcel Dekker; 1989. p. 113–33. chap. 6.

Zettersten EM, Ghadially R, Feingold KR, Crumrine D, Elias PM. Optimal ratios of topical stratum corneum lipids improve barrier recovery in chronologically aged skin. J Am Acad Dermatol. 1997;37:403–8.

Suction Blisters and Microdialysis 109

Sophie Mac-Mary and Patrice Muret

Contents

Keywords
Microcollector • Microdialysis • Micropump • No net flux calibration • Relative recovery calibration • Retrodyalisis • Suction blisters

The extracellular space represents the junction point of nutriments, mediators, hormones, drugs, and metabolites as well as toxins with cutaneous cell targets. Few techniques nowadays allow the study of these compartments in vivo in the dermis. Scientists usually study plasmatic pharmacokinetics to solve the problems with drug dermal kinetics. However, two techniques allow pharmacokinetic or metabolism studies to be performed by studying endogenous or exogenous substance concentrations in extracellular fluids:

1. A relatively old technique, suction blisters (Kiistala 1967)
2. A more recent technique, at least for its cutaneous applications, microdialysis (Anderson et al. 1991)

1 Suction Blisters

1.1 History

The principle of suction blister formation is old, and scientists have continued to improve this technique and develop practical applications. In 1900, Weinfeld reported that subepidermal

This chapter was originally published under the ISBN 978-3-540-01771-4 with the following book title Measuring the Skin. The content has not been changed.

S. Mac-Mary (✉)
Skinexigence SAS, Bioparc, Besançon, France
e-mail: smac@skinexigence.com

P. Muret
Engineering and Cutaneous Biology Laboratory, UMR 1098, University of Franche-Comte, Besançon, France

Clinical Pharmacology Department, University Hospital, Besançon, France
e-mail: patrice.muret@univ-fcomte.fr; p1muret@chu-besancon.fr

P. Humbert et al. (eds.), *Agache's Measuring the Skin*, DOI 10.1007/978-3-319-32383-1_143

blisters could be obtained by using hydrostatical pressure on the epidermal face of human cadaver skin fragments. However, it was Kiistala, in 1967, who really developed the suction blistering technique (Kiistala 1967).

1.2 Principle

A steel cap, perforated by either one or several round holes of definite diameters (4–14 mm), and connected to a tube leading to an electric vacuum pump is applied on the volar forearm. A slight suction pressure (from 200 to 300 mmHg) is applied on the skin. After about 2 h (the length of time varies with each volunteer), the interstitial fluid has accumulated between the dermis and epidermis, which is progressively peeled off. This process involves the formation of a blister, called a suction blister (Fig. 1). The volume of the collected fluid varies from 50 to 150 µL per blister. Five to six chambers may be needed to perform a good pharmacokinetic analysis.

1.3 Applications

This technique permits pharmacokinetic analysis of drugs to be performed by measuring their concentrations in the liquid of the blisters, but also in the roof (composed of living epidermis) and the floor (composed of living dermis). It allows fundamental pharmacological or/and biochemical studies to be performed.

For example, histamine assays have allowed the characterization of urticarial reactions more accurately (Neittaanmaki et al. 1984) and interleukin assays to characterize some pathologies like psoriasis (Prens et al. 1990), bullous pemphigoïd (Schmidt et al. 1996), or mastocytosis (Brockow et al. 2002). Prostaglandin analyses have facilitated the comprehension of their dermal kinetics during sun exposure (Gilchrest et al. 1981). Jensen et al. (1995) have performed suction blisters in six diabetic patients in order to establish a correlation between plasmatic concentrations and extracellular levels of glucose.

The blister fluid is used in pharmacokinetics to assess drugs concentrations, administered topically as well as systemically, and eventually their metabolites (Averbeck et al. 1989). Such kinetics have been obtained with compounds like citroptene or bergaptene topically administered (Treffel et al. 1991), R and S forms of ibuprofen administered orally (Walker et al. 1993), and very lipophilic molecules like acitretin (Surber et al. 1993).

1.4 Limits

– Influence of the peak blistering point: a study performed with rats (Schäfer-Korting

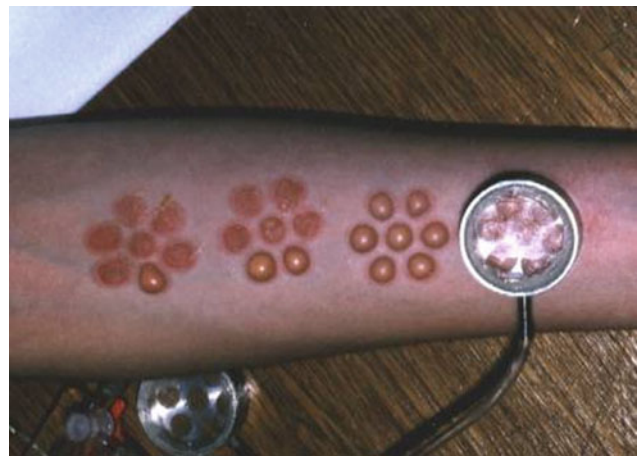

Fig. 1 Suction blisters: apparatus and blisters performed on the volar forearm of a volunteer

et al. 1985) has shown the influence of the peak blistering point on the drug levels as confirmed by other clinical studies with psoralen (Humbert et al. 1991). Drugs administered before the formation of the blister penetrate the skin by diffusion, whereas drugs penetrate the skin by convection if they are administered during the blister formation. This implies a better availability of drugs when they are administered simultaneously to the blister formation. Gupta and Kumar have also reviewed in 2000 the different factors which could influence the suction blister induction time (Gupta and Kumar 2000).

- Influence of age and site on the peak blistering point: Grove et al. showed in 1982 (Grove et al. 1982), with experiments performed after applications of ammonium hydroxide aqueous solution, that the peak blistering point is shorter in older people, whereas the blisters last longer.
- Number of bubbles and wound healing: this technique involves a scar which prevents reuse on the same site for several months. The dimensions of the steel capsule limit the number of points for pharmacokinetics.
- The liquid collected is proteic, which has to be extracted to be analyzed by High Performance Liquid Chromatography, for example.

2 Microdialysis

2.1 History

With microdialysis, it is possible to extract chemical substances contained in extracellular fluids without extracting liquids, and to introduce substances without injecting liquids. One major interest of microdialysis is the possibility to work in sterile conditions, the probe constituting a closed liquid system. This technique has been used for about 25 years in neuropharmacology. Ungerstedt (Ungerstedt and Pycock 1974) invented microdialysis by introducing a probe in a rat brain for the first time in 1974, and then improved the perfusing method in the 1980s.

For about 10 years, the number of applications and publications in relation to microdialysis has increased continuously. Microdialysis can be used for the study of many tissues such as eyes, muscles, lung, and heart (Elmquist and Sawchuk 1997). Its application in cutaneous biology is recent (Anderson et al. 1991), but rapidly expanding.

2.2 Principle

The principle is based on the use of probes, equipped at their extremities with semi-permeable membranes. This probe, once inserted into a tissue, can mimic the function of a capillary blood vessel. It is connected at one end to a micropump, which permits perfusing the system at constant flow with a physiological solution (Ringer, phosphate buffer, etc.), and at the other extremity, to a collector which allows collection of dialysates at regular intervals. Microdialysis is, therefore, based on a dynamic diffusion phenomenon. As the liquid reaches the membrane, a concentration gradient is established, and the studied substance goes from the most concentrated medium to the less concentrated one (Fig. 2).

As microdialysis implies a dynamic phenomenon, the concentration of the studied compound in dialysate is only a fraction of its real concentration in the medium where the membrane is located. The Relative Recovery represents the ratio between the concentrations of dialysate and tissue. The results can also be expressed as absolute recovery, which represents the cumulative quantity of recovered substances per time unit.

2.3 Calibration

2.3.1 Relative Recovery

As dialysate represents only a fraction of the quantity actually present in a tissue, it is necessary to estimate this Relative Recovery (R.R.) in vitro in order to use microdialysis in vivo quantitatively. This necessitates several experiments where several parameters will be changed: perfusion rate, nature of the membrane, concentration,

etc. in order to improve the relative recovery and the experimental conditions.

2.3.2 No Net Flux (Le Quellec et al. 1995; Lönnroth et al. 1987)

An in vitro calibration can be a source of mistakes as the diffusion in a tissue is not as simple as in a liquid. Several calibrations in vivo have been suggested, like the No Net Flux. The principle of No Net Flux is based on the fact that the flux direction of a molecule is only directed by the concentration gradient. This means that if the microdialysis probe is perfused with a lower concentration of substances than the dermis concentration, the flux will be from the tissue to the dialysate. If the probe is perfused with greater concentrations than the interstitial fluid, the substances will pass from the probe to the tissue. This technique also consists of perfusing the probe with different concentrations, which have already been chosen in order to be lower and greater than the dermis concentration expected. A line is drawn with the concentration of the perfusate (Cin) in abscissa and the difference between perfusate and dialysate in ordinate (DC = Cin -Cout) (Fig. 3). A linear regression allows the assessment of the point of No Net Flux (crossing with the abscissa scale), which represents the concentration of the compound in the tissue, and the slope of the line gives the Absolute Recovery.

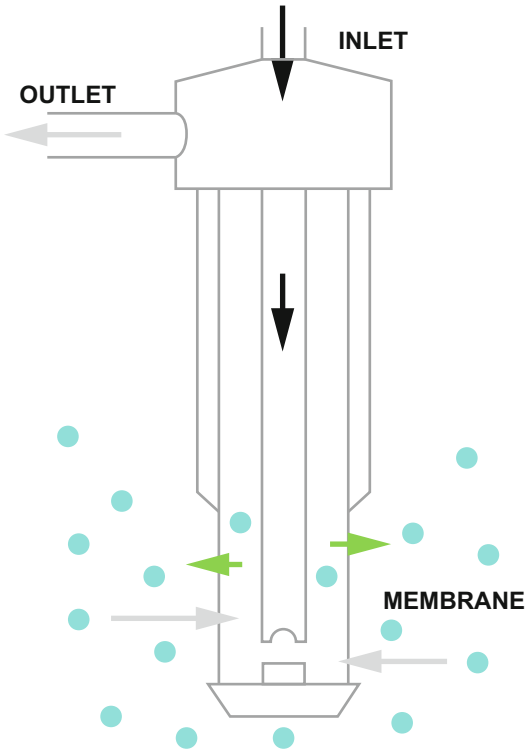

Fig. 2 Schema of a microdialysis probe

2.3.3 Retrodialysis

The concept of retrodialysis is based on the same idea as No Net Flux, only the concentration gradient determines the flux direction through the dialysis membrane. This technique is mainly used for exogenous substances. It assesses the relative decrease of perfused

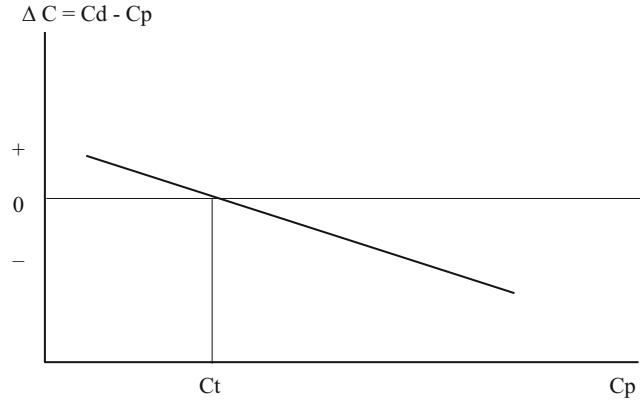

Fig. 3 Principle of the No Net Flux Method. *Ct* concentration in the tissue, *Cp* concentration in the perfusate, *Cd* concentration in the dialysate

concentration when the probe is placed in a medium where the substance concentration is zero or negligible.

$$R.R. = \Delta c / C_{in}$$

where

- Cin = concentration of compound in the perfusate
- Cout = concentration of compound in the dialysate
- Dc = Cin -Cout

2.4 Material

2.4.1 Micropump

Several types of pump have been customized, but the principle is always the same: perfusion of a very low volume of liquid at constant flow rate. CMA's pumps (CMA/Microdialysis, Solna, Sweden), allow perfusion at flow rates from 1 nL/min – 1 mL/min, 1–3 syringes simultaneously. The most frequently used perfusion rates vary from 1 to 5 μL/min. There is also now a portable, battery-operated, micro-processor controlled syringe pump which is very easy to use. The pump is small, with rounded corners and is lightweight. It can be fixed to a belt or carried in an ambulant patient's pocket.

2.4.2 Perfusion Fluid

This liquid has to act like a vehicle for the substances it has to extract. Its composition must be similar to the extracellular fluid composition in order to avoid interaction with biological phenomena which take place around the probe. They are usually perfused with a physiological fluid like Ringer or a phosphate buffer (pH 7.4). Some authors have proposed adding glucose in the dialysis buffer in order to avoid its draining from the extracellular medium and a possible alteration of the cellular metabolism. It can be useful sometimes to add albumin in the dialysate for the study of compounds with a high protein binding capacity in order to avoid the sticking of these compounds to the membrane and the tubing. The perfusion fluid must not contain any air bubbles or any particles to prevent any alteration of the perfusion speed or reduction of the membrane exchange area.

2.4.3 Probes

Probes can be customized in series or in parallel. The first ones are probes customized from dialysis fibers. The second ones are commercialized by CMA. In these probes, a semi-permeable membrane is glued between the tip of an inner steel cannula and the outer steel shaft. The perfusion fluid enters the membrane space through two holes in the inner cannula and flows into the shaft to the outlet. Different constructions and sizes of microdialysis probes are available for various organs and biological species. The CMA/20 Microdialysis Probe is designed for dialysis experiments in moving soft tissues such as skin and adipose tissue, as well as in blood, vitreous fluid of the eye, etc. As with the other models, the probe is of concentric construction, but is made completely from plastic materials. Due to its flexibility, the probe must be implanted into the tissue with the help of a steel needle and split tubing – the Introducer. The membrane is available in both 20- and 100-kDa cut-off. The CMA 60 Microdialysis Catheter is designed for microdialysis in adipose tissue and resting skeletal muscle. The CMA 60 Microdialysis Catheter has been especially developed to achieve excellent diffusion characteristics. This probe has the EC homologation. The dialyzing polyamide membrane is 30 mm long. Insertion into the tissue is easily achieved with the help of a unique slit cannula introducer that leaves the catheter in place when withdrawn.

2.4.4 Microcollector

An automatic system is used to collect dialysates. The collection can be powered by and controlled through the microinjection pump, which changes vial positions according to the volume preset on the pump. The CMA/140 Microfraction Collector can simultaneously collect fractions from up to

three probes in a range of between 1 to 50 μL with maximal precision. Some systems have a thermoelectric cooling system that cools down to +4 °C when the fractions can be collected in sealed vials. Both are important considerations for the prevention of evaporation and chemical degradation. A needle arm is equipped with a sensor mechanism which makes it possible to collect fractions as small as 1 μL at the bottom of each vial.

2.5 Application in Cutaneous Biology

Microdialysis allows monitoring of the extracellular fluid of a specific tissue continuously (from several hours to several days), as opposed to the suction blisters which allow concentrations to be obtained at specific times only.

2.5.1 Insertion of Probes

The probes are fragile and therefore cannot be inserted without having the recourse of a guide (catheter 20-gauge). The probe can be localized thanks to ultrasonography (Groth 1996; Hegemann et al. 1995) (Fig. 4).

Many studies assess the trauma involved from probe insertion in the skin. Anderson et al. in 1994 (Anderson et al. 1994) and then Groth in 1998 (Groth et al. 1998) have shown the effect of probe insertion, with or without local anesthetics. This insertion involves the secretion of endogenous substances like histamine. Linden et al. have also shown the interest of studying this reaction, which seems to be predictable of the skin's individual reactivity in general (Linden et al. 2000). The insertion also produces a significant increase of blood flux, as shown by laser Doppler, as well as the appearance of a small erythema (Groth 1998). These reactions tend to decrease and to disappear after 30–120 min. Krogstadt et al. performed a histological study on skin biopsies performed after probe insertion. They have found some slight bleeding but neither edema nor inflammatory reactions after 8–10 h of dialysis (Krogstad et al. 1996). Rapid changes in glucose levels have been detected, showing that the trauma hasn't altered the microdialysis results.

The experiment shows that after a local anesthesia (lidocaine injection or topical EMLA application), insertion is not painful. After 60–90 min, most of the reactions induced by the insertion are over.

The main advantage of microdialysis is that this technique leaves only small scars on the insertion site, and they disappear quickly (Fig. 5).

2.5.2 Monitoring of Endogenous Substances

Another advantage of microdialysis is to allow the continuous monitoring of the endogenous substances' concentration in the dermis compartment, like glucose, lactate, glycerol, and pyruvate. It

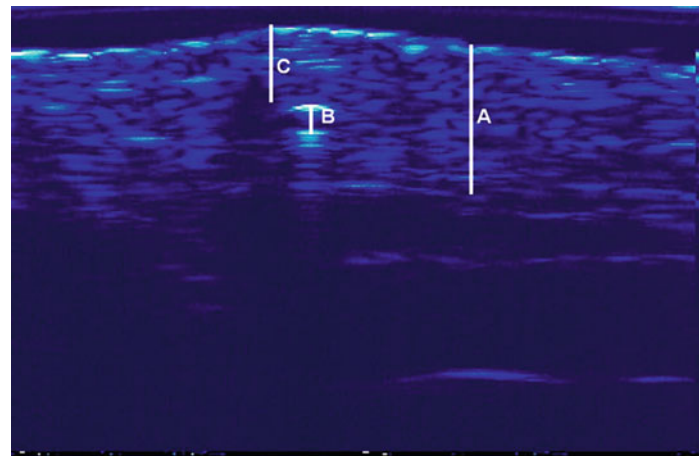

Fig. 4 Depth measurement of a microdialysis probe by ultrasound imaging (Dermcup). (*a*) dermis thickness, (*b*) probe inner diameter, (*c*) probe depth

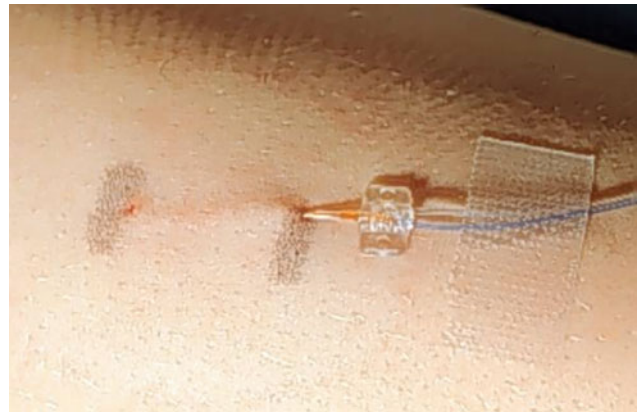

Fig. 5 A microdialysis probe inserted in the volar forearm of a volunteer

allows, for example, glucose and lactate concentrations to be followed in premature babies (De Boer et al. 1994a), lactate concentrations during physical exercises (De Boer et al. 1994b), or glucose concentrations in diabetic patients (Hoss et al. 2001). In 1996, Meyerhoff et al. developed a system combining microdialysis with a detector equipped with an amperometric glucose oxidase electrode (Meyerhoff et al. 1996). A microdialysis probe is inserted into the abdomen of diabetic patients, and their concentration in glucose is monitored by a watch. An alarm starts when concentrations reach critical values.

Microdialysis can be used also as a monitoring technique during a surgical intervention such as transfer flap tissue. It can be a useful tool in predicting flap viability: it has already been shown that the glucose concentration is reduced whereas the lactate and glycerol levels increase during flap ischemia (Röjdmark et al. 1997).

This technique allows the mechanism of reactions involved in contact dermatitis or different pathologies to be studied, as it has already been done for psoriasis (Krogstad et al. 1997), atopic dermatitis (Rukwied et al. 2000a), mastocytosis (Krogstad and Roupe 2001), with the study of histamine (Anderson et al. 1992; Rukwied et al. 2000b; Horsmanheimo et al. 1996; Petersen et al. 1992, 1997), interleukin concentrations (Anderson et al. 1995), nitric oxide (Katugampola et al. 2000), iron (Leveque et al. 2000), or ascorbic acid (Leveque et al. 2001).

2.5.3 Bioavailability of Exogeneous Substances

The first study on the application of microdialysis in cutaneous biology was published by Anderson in 1991, with a study on the absorption of ethanol (Anderson et al. 1991). Ault et al. have compared the results obtained with microdialysis and Franz Cells, by inserting one microdialysis probe into the receptor chamber of a Franz cell, and another into the dermis of a skin fragment, in order to study the pharmacokinetics of 5-fluorouracil (Ault et al. 1992). The results obtained from both techniques were well correlated.

Other kinds of pharmacokinetics have been performed. This technique is good for screening the bioavailability of different formulations. It has been used, for example, to study the effect of enhancers on the percutaneous absorption of methotrexate and cyclosporine (Matsuyama et al. 1994; Nakashima et al. 1996).

It can also be used to study the pharmacokinetics of transdermal drug delivery systems, as already performed for nicotine (Hegemann et al. 1995b; Müller et al. 1995).

At least one major interest of microdialysis is its use to compare the pharmacokinetics of a drug to its pharmacodynamic characteristics. Several studies have been performed in cancerology (Blöchl-Daum et al. 1996; Joukhadar et al. 2001) or to study the efficacy of antibiotics in bacterial infections (Brunner et al. 2000).

2.6 Limits

2.6.1 Low Volumes

The low perfusion speed used in microdialysis involves the collection of a small volume of fluid (from ca. 10 to 200 µL). It also requires very sensitive analysis techniques like High Performance Liquid Chromatography, Mass Spectrometry or immunology assays (ELISA, etc.). This technique is also interesting because the samples obtained are quite clean; large molecules such as albumin cannot be collected with the classical membranes and the analyses do not require any extraction step.

2.6.2 The Relative Recovery

The recovery depends on several parameters (like perfusion speed, physicochemical properties of the studied compound, etc.). It is therefore necessary to estimate the R.R. for each experiment. This can be possible thanks to some special calibration techniques (cf. Section 2.3, "Instruments" in ▶ Chap. 108, "Transepidermal Water Loss").

2.6.3 Lipophilic Compounds

The poor affinity of lipophilic compounds for the hydrophilic perfusate causes a very poor recovery for this kind of product. A study has been performed on transdermal drug delivery, with good results for nicotine (Hegemann et al. 1995b; Müller et al. 1995), but not for estradiol (Müller et al. 1995). Other studies have also shown this kind of problem with calcipotriol, fusidic acid, and betamethasone valerate, unless they are used at high concentrations or after systemic administration (Groth 1996). The best solution for these products would be to change the dialysate (Kreilgaard et al. 2001).

3 Conclusion

We have compared two techniques used in cutaneous pharmacological studies: suction blisters and microdialysis. Brunner et al. have found a close correlation between the pharmacokinetic of paracetamol obtained from these techniques and in plasma (Brunner et al. 1998). Benfeld et al. have also simultaneously investigated these techniques for in vivo sampling of peripheral compartment pharmacokinetics after systemic administration of acetylsalicylic acid (Benfeldt et al. 1999). Both techniques were in excellent concordance with even closer correlation between maximum concentrations obtained by microdialysis and suction blister fluid sampling.

In spite of these results, the concentrations of theophylline measured with suction blister seemed to be overestimated, whereas those measured in microdialysate were similar to those found in plasma (Muller et al. 1998). Another study has been conducted with the combination of these techniques to clarify the roles of nitric oxide and prostaglandin E2 in the generation of UVB-induced vasodilatation (Rhodes et al. 2001). The results from both techniques provided the involvement of prostaglandin E2 in the production of UV-induced erythema. However, nitric oxide was not detectable in suction blister fluid. This phenomenon could be explained by a protein contamination of the suction blister fluid.

These two techniques are interesting for obtaining pharmacokinetics of drugs or to study the secretion of endogenous substances. However, after comparing the tolerability of the sampling procedure, ease of analysis, and detail in chronology, microdialysis seems superior for sampling in vivo pharmacokinetics in the dermis.

Microdialysis promises to be a main technique in the future. We expect to find the best solution to study lipophilic compounds, in order to improve their recovery and to prevent them from sticking to the membrane and the tubing. This technique is non-invasive, requires only one probe to perform a complete pharmacokinetic analysis without any pain for the volunteer, and can be used ex vivo as well as in vivo, in animals as well as in humans.

References

Anderson C, Andersson T, Molander M. Ethanol absorption across human skin measured by in vivo microdialysis technique. Acta Derm Venereol (Stockh). 1991;71:389–93.

Anderson C, Andersson T, Andersson RGG. In vivo microdialysis estimation of histamine in human skin. Skin Pharmacol. 1992;5:177–83.

Anderson C, Andersson T, Wardell K. Changes in skin circulation after insertion of a microdialysis probe visualized by laser Doppler perfusion imaging. J Invest Dermatol. 1994;102:807–11.

Anderson C, Svensson C, Sjögren F, Andersson T, Wårdell K. Human in vivo microdialysis technique can be used to measure cytokines in contact reactions. Curr Prob Dermatol. 1995;23:121–30.

Ault JM, Lunte CE, Meltzer NM, Riley CM. Microdialysis sampling for the investigation of dermal drug transport. Pharm Res. 1992;9:1256–61.

Averbeck D, Averbeck S, Blais J, Moysan A, Huppe G, Morliere B, Prognon P, Vigny P, Dubertret L. Suction blister fluid: its use for pharmacodynamic and toxicological studies of drugs and metabolites in vivo in human skin after topical or systemic administration. In: Maibach HI, Lowe NJ, editors. Models in dermatology, vol. 4. Basel: Karger; 1989. p. 5–11.

Benfeldt E, Serup J, Menne T. Microdialysis vs. suction blister technique for in vivo sampling of pharmacokinetics in the human dermis. Acta Derm Venereol. 1999;79:338–42.

Blöchl-Daum B, Müller M, Meisinger V, Eichler HG, Fassolt A, Pehamberger H. Measurement pf extracellular fluid carboplatin kinetics in melanoma metastases with microdialysis. Br J Cancer. 1996;73:920–4.

Brockow K, Akin C, Huber M, Scott LM, Schwartz LB, Metcalfe DD. Levels of mast-cell growth factors in plasma and in suction skin blister fluid in adult with mastocytosis: correlation with dermal mast-cell numbers and mast-cell tryptase. J Allergy Clin Immunol. 2002;109:82–8.

Brunner M, Schmiedberger A, Schmid R, Jager D, Piegler E, Eichler HG, Muller M. Direct assessment of peripheral pharmacokinetics in humans: comparison between cantharides blister fluid sampling, in vivo microdialysis and saliva sampling. Br J Clin Pharmacol. 1998;46:425–31.

Brunner M, Pernerstorfer T, Mayer BX, Eichler HG, Muller M. Surgery and intensive care procedures affect the target site distribution of piperacillin. Crit Care Med. 2000;28:1754–9.

De Boer J, Baarsma R, Okken A, Plijter-Groendijk H, Korf J. Application of transcutaneous microdialysis and continuous flow analysis for on-line glucose monitoring in newborn infants. J Lab Clin Med. 1994a;124:210–7.

De Boer J, Plijter-Groendijk H, Visser KR, Mook GA, Korf J. Continuous monitoring of lactate during exercise in humans using subcutaneous and transcutaneous microdialysis. Eur J Appl Physiol. 1994b;69:281–6.

Elmquist WF, Sawchuk RJ. Application of microdialysis in pharmacodynamic studies. Pharm Res. 1997;14:267–88.

Gilchrest BA, Soter NA, Stoff JS, Mihm Jr MC. The human sunburn reaction: histologic and biochemical studies. J Am Acad Dermatol. 1981;5:411–22.

Groth L. Cutaneous microdialysis. Methodology and validation. Acta Derm Venereol (Stockh). 1996;76([Suppl 197]):1–61.

Groth L. Cutaneous microdialysis in man: effects of needle insertion trauma and anaesthesia on skin perfusion, erythema and skin thickness. Acta Derm Venereol (Stockh). 1998;78:5–9.

Groth L, Jørgensen A, Serup J. Cutaneous microdialysis in the rat: insertion trauma studied by ultrasound imaging. Acta Derm Venereol (Stockh). 1998;78:10–4.

Grove GL, Duncan S, Kligman AM. Effect of ageing on the blistering of human skin with ammonium hydroxide. Br J Dermatol. 1982;107:393–400.

Gupta S, Kumar B. Suction blister induction time: 15 minutes or 150 minutes? Dermatol Surg. 2000;26(8):754–6.

Hegemann L, Forstinger C, Partsch B, Lagler I, Krotz S, Wolff K. Microdialysis in cutaneous pharmacology: kinetic analysis of transdermally delivered nicotine. J Invest Dermatol. 1995;104:839–43.

Horsmanheimo L, Harvima IT, Harvima RJ, Ylönen J, Naukkarinen A, Horsmanheimo M. Histamine release in skin monitored with the microdialysis technique does not correlate with the weal size induced by cow allergen. Br J Dermatol. 1996;134:94–100.

Hoss U, Kalatz B, Gessler R, Pfleiderer HJ, Andreis E, Rutschmann M, Rinne H, Schoemaker M, Fussgaenger RD. A novel method for continuous online glucose monitoring in humans: the comparative microdialysis technique. Diabetes Technol Ther. 2001;3:237–43.

Humbert P, Treffel P, Makki S, Millet J, Agache P. Peak blistering point: influence on fluid levels of 5-MOP in human skin in vivo after systemic administration. Arch Dermatol Res. 1991;283:297–9.

Jensen BM, Bjerring P, Christiansen JS, Ørskov H. Glucose content in human skin: relationship with blood glucose levels. Scand J Clin Lab Invest. 1995;55:427–32.

Joukhadar C, Klein N, Mader RM, Schrolnberger C, Rizovski B, Heere-Ress E, Pehamberger H. Penetration of dacarbazine and its active metabolite 5-aminoimidazole-4-carboxamide into cutaneous metastases of human malignant melanoma. Cancer. 2001;92:2190–6.

Katugampola R, Church MK, Clough GF. The neurogenic vasodilator response to endothelin-1: a study in human skin in vivo. Exp Physiol. 2000;85:839–46.

Kiistala U. Suction blisters in the study of cellular dynamics of inflammation. Acta Derm Venereol. 1967;48:466–77.

Kreilgaard M, Kemme MJ, Burggraaf J, Schoemaker RC, Cohen AF. Influence of a microemulsion vehicle on cutaneous bioequivalence of a lipophilic model drug assessed by microdialysis and pharmacodynamics. Pharm Res. 2001;18:593–9.

Krogstad AL, Roupe G. Microdialysis of histamine from patients with mastocytosis. Exp Dermatol. 2001;10:118–23.

Krogstad AL, Jansson PA, Gisslen P, Lönnroth P. Microdialysis methodology for the measurement of dermal interstitial fluid in humans. Br J Dermatol. 1996;134:1005–12.

Krogstad AL, Lonnroth P, Larson G, Wallin BG. Increased interstitial histamine concentration in the psoriatic plaque. J Invest Dermatol. 1997;109:632–5.

Le Quellec A, Dupin S, Genissel P, Saivin S, Marchand B, Houin G. Microdialysis probes calibration: gradient and tissue dependent changes in no net flux and reverse dialysis methods. J Pharmacol Toxicol Meth. 1995;33:11–6.

Leveque N, Mary S, Humbert P, Makki S, Muret P, Kantelip JP. Ascorbic acid assessment in human dermis by a microdialysis technique associated with gas chromatography–mass spectrometry. Eur J Mass Spectrom. 2000;6:397–404.

Leveque N, Robin S, Makki S, Muret P, Mary S, Berthelot A, Humbert P. Iron concentrations in human skin dermis assessed by microdialysis associated with atomic absorption spectrometry. Biol Pharm Bull. 2001;24:10–3.

Linden M, Andersson T, Wardell K, Anderson C. Is vascular reactivity in skin predictable? Skin Res Technol. 2000;6:27–30.

Lönnroth P, Jansson PA, Smith U. A microdialysis method allowing characterization of intercellular water space in humans. Am J Physiol Endocrinol Metab. 1987;253: E228–31.

Matsuyama K, Nakashima M, Nakaboh Y, Ichikawa M, Yano T, Satoh S. Application of in vivo microdialysis to transdermal absorption of methotrexate in rats. Pharm Res. 1994;11:684–6.

Meyerhoff C, Mennel FJ, Stenberg F, Hoss U, Pfeiffer EF. Current status of the glucose sensor. Endrocrinologist. 1996;6:51–8.

Müller M, Schmid R, Wagner O, Osten BV, Shayganfar H, Heichler HG. In vivo characterization of transdermal drug transport by microdialysis. J Control Release. 1995;37:49–57.

Muller M, Brunner M, Schmid R, Putz EM, Schmiedberger A, Wallner I, Eichler HG. Comparison of three different experimental methods for the assessment of peripheral compartment pharmacokinetics in humans. Life Sci. 1998;62:PL227–34.

Nakashima M, Zhao MF, Ohya H, Sakurai M, Sasaki H, Matsuyama K, Ichikawa M. Evaluation of in-vivo transdermal absorption of cyclosporin with absorption enhancer using intradermal microdialysis in rats. J Pharm Pharmacol. 1996;48:1143–6.

Neittaanmaki H, Karjalainen S, Fraki JE, Kiistala U. Suction blister device with regulation of temperature: demonstration of histamine release and temperature change in cold urticaria. Arch Dermatol Res. 1984;276:317–21.

Petersen LJ, Skov PS, Bindslv-Jensen C, Søndergaard J. Histamine release in immediate-type hypersensitivity reactions in intact human skin measured by microdialysis. Allergy. 1992;47:635–7.

Petersen LJ, Winge K, Brodin E, SKOV PS. No release of histamine and substance P in capsaicin-induced neurogenic inflammation in intact human skin in vivo: a microdialysis study. Clin Exp Allergy. 1997;27:957–65.

Prens EP, Benne K, Van Damme J, Bakkus M, Brakel K, Benner R, Van Joost T. Interleukin-1 and interleukin-6 in psoriasis. J Invest Dermatol. 1990;95:121S–4.

Rhodes LE, Belgi G, Parslew R, McLoughlin L, Clough GF, Friedmann PS. Ultraviolet-B-induced erythema is mediated by nitric oxide and prostaglandin E2 in combination. J Invest Dermatol. 2001;117:880–5.

Röjdmark J, Blomqvist L, Malm M, Adams-Ray B, Ungerstedt U. Metabolism in myocutaneous flaps studied by in situ microdialysis. Scand J Plast Reconstr Hand Surg. 1997;31:1–8.

Rukwied R, Lischetzki G, McGlone F, Heyer G, Schmelz M. Mast cell mediators other than histamine induce pruritus in atopic dermatitis patients: a dermal microdialysis study. Br J Dermatol. 2000;142:1114–20.

Schäfer-Korting M, Grimm HV, Mutschler E. Morphologische, biochemische und pharmakokinetische Untersuchungen an Saugblasen in Abhängigkeit von der Art und dem Zeitpunkt ihrer Entstehung. Arch Pharm (Weinheim). 1985;318:711–20.

Schmidt E, Bastian B, Dummer R, Tony HP, Brocker EB, Zillikens D. Detection of elevated levels of IL-4, IL-6, and il-10 in blister fluid of bullous pemphigoid. Arch Dermatol Res. 1996;288:353–7.

Surber C, Wilhelm KP, Bermann D, Maibach HI. In vivo skin penetration of acitretin in volunteers using three sampling techniques. Pharm Res. 1993;10:1291–4.

Treffel P, Makki S, Faivre B, Humbert P, Blanc D, Agache P. Citropten and bergapten suction blister fluid concentrations after solar product application in man. Skin Pharmacol. 1991;4:100–8.

Ungerstedt U, Pycock CH. Functional correlate of dopamine neurotransmission. Bull Schweiz Akad Mad Wiss. 1974;30:44–55.

Walker J, Romualda DK, Seideman P, Day RO. Pharmacokinetics of ibuprofen enantiomers in plasma and suction blister fluid in healthy volunteers. J Pharmaceut Sci. 1993;82:787–90.

Measuring Silica Nanoparticles in the Skin

110

Shohreh Nafisi, Monika Schäfer-Korting, and Howard I. Maibach

Contents

Declaration of Interest: The authors report no conflicts of interest.

S. Nafisi (✉)
Department of Chemistry, Central Tehran Branch, IAU, Tehran, Iran

Department of Dermatology, University of California, San Francisco, CA, USA
e-mail: drshnafisi@gmail.com

M. Schäfer-Korting
Institute of Pharmacy, Pharmacology and Toxicology, FreieUniversität Berlin, Berlin, Germany

H.I. Maibach (✉)
Department of Dermatology, School of Medicine, University of California, San Francisco, CA, USA
e-mail: maibachh@derm.ucsf.edu

P. Humbert et al. (eds.), *Agache's Measuring the Skin*,
DOI 10.1007/978-3-319-32383-1_44

Keywords
Silica nanoparticles • Percutaneous penetration • Toxicity

Abbreviations

SC	Stratum corneum
SNPs	Silica nanoparticles

1 Introduction

Nanoparticles are commonly defined 1–100 nm objects or – at least – one dimension being less than 100 nm. The International Organization for Standardization defines the term "nanomaterial" as "material with any external dimensions in the nanoscale or having internal structure or surface structure in the nanoscale" (EU Commission Recommendation on the definition of nanomaterial 2011). Other definitions have been proposed. A recent proposal is based on surface area rather than size (a nanoparticle should have a specific surface area $>60\ m^2/cm^3$), thus reflecting the critical importance of this parameter in governing reactivity and toxicity of nanomaterials (Kreyling et al. 2010). Nanomaterials can be divided into two large groups: ultrafine nanosized particles not intentionally produced and engineered nanoparticles produced in a controlled, engineered way. Engineered nanoparticles, because of their large surface-to-volume ratios, exhibit chemical, physical, and biological properties distinctly different from the same materials in the bulk form, but such properties may lead to adverse effects on human health and environmental systems (Oberdörster et al. 2005).

Nanoparticles, novel carrier systems developed as an alternative to traditional vehicles show important advantages for dermal application of cosmetics and pharmaceuticals.

Nanoparticles are able to increase the penetration of active ingredients into the skin, allowing increased targeting to the epidermis and consequently improve treatment efficiency and reducing the systemic absorption of drugs and cosmetic agents. The biocompability of the nanoparticles and their biodegradation chemical nature has opened new advancements in cosmetic and pharmaceutical industries for effective topical delivery of drugs and active substances. Currently many substances are under investigation for topical drug delivery, however the toxicological investigations are of great importance (Firouz et al. 2016; Nassiri-Kashani et al. 2016; Behtash et al. 2016; Firooz et al. 2015; Nafisi and Maibach 2015; Agudelo et al. 2013a; Agudelo et al. 2013b; Tajmir-Riahi et al. 2014; Nafisi and Maibach 2016; Nafisi et al. 2016).

Nanoparticles can enter the body through inhalation, absorption through the skin or the digestive tract, voluntary injection, or implantation for drug delivery. The skin, the largest organ, is a primary barrier to nanoparticle exposure from naturally occurring and engineered nanomaterials found in the environment and workplace. Thus, the skin may be an unintended route for localized and possibly systemic exposure to nanoparticles released during manufacture, use, and disposal (Proksch et al. 2008; Prow et al. 2011; Labouta and Schneider 2013). Nanoparticles may induce a spectrum of adverse health effects ranging from localized damage (e.g., irritant contact dermatitis) to induction of immune-mediated responses (e.g., allergic contact dermatitis and pulmonary responses) or systemic toxicity (e.g., neurotoxicity and hepatotoxicity) (Poland et al. 2013).

Recently, silica nanoparticles (SNPs) have attracted significant interest because of their unique properties such as hydrophilic surface favoring protracted circulation, following i.v. administration, versatile silane chemistry for surface functionalization, ease of large-scale synthesis, and low cost of NP production (Slowing et al. 2008; Barbe et al. 2004). SNPs are widely applied in chemical industry, agriculture, and cosmetics (Willey 1982). In addition, they are being developed in medical uses including for diagnosis and therapy (Tang and Cheng 2013; Tang et al. 2012), probes for biomarkers for optical imaging (Lee et al. 2009), controlled release drug delivery, as well as gene transfection carriers (Slowing et al. 2008). Such medical approaches

have numerous applications including skin cancer therapy (Scodeller et al. 2013; Benezra et al. 2011; De Louise 2012), transdermal drug delivery (Prausnitz et al. 2012), transcutaneous vaccination, and gene delivery (Bharali et al. 2005). They can act as carrier for drugs with low solubility and might improve drug safety, stability, and performance (De Villiers et al. 2009). With the growing commercialization of silica nanoparticles, human exposure to these materials is increasing, and many aspects related to their toxicity should be studied.

The main goal of this review is to organize the current state of the art relating to skin absorption of silica nanoparticles based on the ten parameters of percutaneous penetration while raising awareness of silica nanomaterials' toxicity among scientists and manufacturers handling them. The importance of such overview stems from percutaneous penetration research tradition dating back to World War II military studies, focused on a one-step penetration model (Tregear 1996). Such work corrected misconceptions (i.e., skin being largely impermeable); subsequent chemical, in vivo and in vitro, experiments document a far more complex penetration model – whose steps may be highly clinically relevant to the nanotoxicity debate.

2 Silica

Silicon dioxide, also known as silica, an oxide of silicon with the chemical formula SiO_2 is the most common element found in nature and is widely distributed in dusts, sands, planetoids, and planets (Georgia State University, Hyperphysics). Silica can be classified into two main classes: crystalline and amorphous. Different forms of silica and their properties are in Table 1.

2.1 Crystalline Silica

Crystalline micron-sized silica is a basic component of soil, sand, granite, and many other minerals (Iier 1979; Unger 1979). Silica exposure is a serious threat to workers and has been classified as a human lung carcinogen (OSHA 2002).

2.2 Amorphous Silica

Amorphous silica is synthetic silica except biogenic diatomaceous earth, composed of ultimate particles or structural unit less than 1 μm in diameter. Synthetic and natural amorphous silica are important materials for their variety of technological applications due to their physicochemical properties such as surface area, pore properties, bulk density, etc. (Iier 1979; IMA Europe 2014).

2.2.1 Natural Amorphous Silica

Diatoms are microscopic, eukaryotic, unicellular algae ubiquitously present in almost every water habitat on earth. Diatom cell walls are composed of silica (hydrated silicon dioxide) (Iier 1979; IMA Europe 2014).

2.2.2 Synthetic Amorphous Silica (SAS)

Different synthetic amorphous (noncrystalline) silica particles (Table 1) have large specific to geometric surface ratio (Iier 1979). SAS particles are generally regarded to be safe, with no or minimal chronic effects. However, increasing use of various forms of noncrystalline silica particles, and in particular the nanosized, requires more thorough examination of their possible health effects (Choi et al. 2008; Fruijtier-Polloth 2012). They can be categorized as mesoporous and nonporous based on their biomedical applications (Tang and Cheng 2013).

Pyrogenic or Fumed Silica

Pyrogenic or fumed silica, an extremely low bulk density powder with high surface area and synthesized by thermal process, consists of amorphous silica particles fused into branched, chainlike, three-dimensional secondary particles and can agglomerate into tertiary particles (Iier 1979; Willey 1982). Fumed silica is not listed as a carcinogen by OSHA, ECETOC, or NTP (ECETOC 2006). Due to its fineness and thinness, it can easily become airborne, making it an

Table 1 Different forms of silica, including crystalline silica, natural amorphous silica, and synthetic amorphous silica

Silica forms			Synthesis method	Size	Surface area	Applications	Reference
1. Crystalline silica			–	0.5–3 μm	9.4 m^2/g	Manufacture of glass, abrasives, ceramics, enamels, scouring, castings in molds	Iler 1979; Unger 1979
2. Amorphous silica	2.1. Natural amorphous		–	0.5–2 μm	High porosity	Filtration agent, abrasive, absorbent, industrial filler	Iler 1979; ECETOC 2006; IMA Europe 2014
	2.2. Synthetic amorphous silica (SAS)	2.2.1. Pyrogenic or fumed silica	Thermal process	5–50 nm	50–600 m^2/g Nonporous Low bulk density	Counteracts oily or greasy skin feel, raising sun protection, improving storage, stabilize emulsions, temperature, and stability	Iler 1979; Willey 1982; ECETOC 2006
		2.2.2. Precipitated amorphous silica	Wet process	5–100 nm	30–500 m^2/g Porous	Rubber and plastics, cleaning, thickening, polishing agent in toothpastes, food processing, pharmaceuticals additive as anticaking, absorbent, antiblocking agent in polymer films	Iler 1979; ECETOC 2006
		2.2.3. Silica gel	Wet process	30–100 nm	800 m^2/g Porous	Abrasives in carbonless papers, fining agent and catalysis, desiccant, stationary phase in chromatography, anticaking agent, filter aid, emulsifying agent, viscosity control agent, anti-settling agent	Iler 1979; ECETOC 2006; IMA Europe 2014
		2.2.4. Nonporous silica nanoparticles	Different synthesis methods	50–2,000 nm Controllable sphere size	Nonporous and porous Controllable surface properties	Masks in lithography, optical sensor, drug delivery, gene delivery, molecular imaging	Stober and Fink 1968; Xia et al. 2000; Tang and Cheng 2013
		2.2.5. Mesoporous silica nanoparticles (MSNs)	Different synthesis methods	2–50 nm Controllable pore size, morphology	High surface area (>1,000 m^2/g) Porous, high pore volume (0.5–2.5 cm^3/g) High drug loading capability	Confined-space catalysis; acoustic, thermal, and electrical insulation; enzyme immobilization; drug delivery system; cell marker; gene transfection reagents Imaging modality, bone tissue regeneration	Tang et al. 2012; Slowing et al. 2010; Wan and Zhao 2007; Hoffman et al. 2006; Garcia-Bennett. 2011; Vallet-Regi et al. 2007; Lou et al. 2008; Liu et al. 2011
		2.2.6. Silica host for other NPs	–	–	–	Medical imaging, drug delivery	Piao et al. 2008

inhalation risk, capable of causing irritation (Otterstedt and Brandreth 1998).

Precipitated Amorphous Silica

Precipitated amorphous silica, consisting of a three-dimensional network of coagulated primary silica particles and prepared by wet process, is not classified as dangerous regarding physical and chemical hazards (Iier 1979; ECETOC 2006).

Silica Gel

Silica gel also referred to as silica aerogel or hydrated silica is a white, fluffy powder or milky suspension of fine amorphous spherical particles in a liquid phase. It is odorless, tasteless and nontoxic and can be prepared by wet process (Iier 1979; ECETOC 2006; IMA Europe 2014).

Nonporous Silica Nanoparticles

Nonporous silica nanoparticles or monodisperse silica spheres (diameters ranging from 50 to 2 μm) were firstly prepared by Stöber process (Stober and Fink 1968) in which tetraalkoxysilane was added to an excess amount of water containing a low molar-mass alcohol and ammonia. These particles are porous or nonporous. The pores are not some random accidents but an inherent property of them (Van Blaadern et al. 1992; Xia et al. 2000). Synthesis methods based on the type of silicate ester, alcohol, volume ratios, and reaction condition were developed in order to control the size, shape, and surface properties (Zhang et al. 2003; Xia et al. 2000; Tang and Cheng 2013). Biomedical applications of monodispersed silica spheres for therapy and diagnosis are categorized based on the different active cargoes delivered by silica NPs: drug delivery for small molecule drugs, proteins, or photosensitizers; gene delivery; and molecular imaging by incorporating different contrast agents. Nonporous silica NPs can deliver cargoes through encapsulation or conjugation (Tang and Cheng 2013).

Mesoporous Silica Nanoparticles (MSNs)

Mesoporous silica nanoparticles, characterized by their mesopores (2–50 nm pore size), are widely used for delivery of active payloads based on physical or chemical adsorption. They have been synthesized as ordered or hollow/rattle-type mesoporous silica structures. Ordered mesoporous silica nanoparticles with uniform pore size and a long-range ordered pore structure were first reported in the early 1990s using surfactants as structure-directing agents (SDAs) (Kresge et al. 1992). Size, morphology, pore size, and structure of MSNs can be rationally designed, and the synthesis process can be freely controlled (Wan and Zhao 2007; Hoffman et al. 2006; Slowing et al. 2010; Garcia-Bennett 2011; Tang et al. 2012). With the abundant availability of various surfactants and a deep understanding of sol–gel chemistry, ordered MSNs with different structures as MCM, SBA, MSU, KIT-1, and FSM have been developed. Until now most research on drug delivery and cancer therapy applications of ordered MSNs are based on MCM-41, MCM-48, and SBA-15 (Tang et al. 2012). Lack of toxicity of various ordered mesoporous silica has been deduced from both in vivo and in vitro studies (Garcia-Bennett 2011; Vallet-Regi et al. 2007; Chen et al. 2013). Hollow/rattle-type mesoporous silica with interstitial hollow space and mesoporous shell has low density and high specific area, which are ideal as new-generation drug delivery systems with extraordinarily high loading capacity. Different synthesis methods (by tuning the composition and concentration of surfactants during synthesis) for preparing hollow and rattle type with various sizes and particle morphology have been reported. Surface chemistry plays a key role in the cellular interactions and toxicity (Tang et al. 2012). They have been actively explored for enzyme immobilization, confined-space catalysis, and acoustic, thermal, and electrical insulation (Lou et al. 2008; Liu et al. 2011).

Silica Host for Other NPs

Silica can be used as a host material for other types of functional NPs (e.g., gold NPs, QDs, and iron oxide NPs) to form hybrid NPs. This important class of silica-based hybrid nanomedicines has been thoroughly reviewed by Piao group (2008). Ultrasmall multimodal silica nanoparticles

(Cornell dots, C dots) have been FDA approved for the first in-human clinical trial for targeted diagnostics of advanced melanoma (Benezra et al. 2011; Friedman 2011).

3 Percutaneous Penetration of Silica Nanoparticles

The skin, a unique barrier composed of several highly organized and heterogeneous layers, also includes a number of appendages such as hair follicles and sweat and sebaceous glands. It is composed of three layers from the outside to inside: epidermis, dermis, and hypodermis. However, from a penetration perspective, epidermis and dermis are the most important. The outermost layer of the epidermis is the *stratum corneum* (SC), to which the main barrier function of the skin is attributed (Bouwstraa et al. 2003; Prausnitz et al. 2012). Four pathways of penetration across the skin have been identified depending on physicochemical properties of the compound: intercellular, transcellular, and two transappendageal – through hair follicles and sweat glands (Scheuplein 1967). Simplified representation of the skin and routes of penetration are shown in Fig. 1. Percutaneous absorption, a dynamic process, has many components with which a penetrant interacts before possibly gaining systemic access. Accurate assessment of nanoparticle penetration is challenging, with results dependent on ten parameters of percutaneous penetration: (1) physiochemical properties of nanoparticle; (2) vehicle effects; (3) surface area, dose, duration, and frequency of exposure; (4) distribution; (5) sub-anatomical pathways (skin appendages); (6) skin surface conditions; (7) additional factors of skin penetration and permeation; (8) loss from skin surface, exfoliation, and wash effect; (9) elimination and photochemical transformation; and (10) the method of determining absorption and toxicity, which is of high relevance, too. These are issues considered from the perspective of nanoparticles and the potential risks of dermal exposure. Understanding the potential for silica nanoparticle dermal penetration and possible toxicological outcomes is of great importance (Ngo et al. 2012). The following passages overview experiments related to transcutaneously applied silica nanoparticles based on the relevant properties which affect percutaneous penetration. Summary of the literature data is in Table 2.

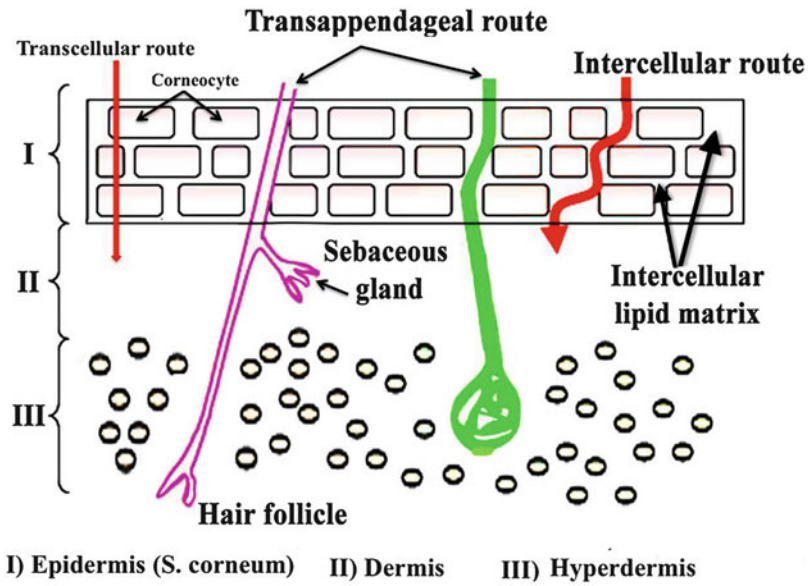

Fig. 1 Simplified representation of the skin and routes of penetration

Table 2 Summary of literature data on physicochemistry, toxicity, and the percutaneous penetration of silica nanoparticles (SNPs)

	Research question	Study type	Results	Author (year)
Physicochemical properties of penetrant	SNPs (7, 10–20 nm)	**In vitro:**	SNPs (7, 10–20 nm) reduced cell viabilities of CHKs in a dose-dependent manner	Park et al. 2010
	Cytotoxic effect	Human keratinocyte cell line HaCaT	No irritation (SNP; 500 μg/ml)	
	Acute cutaneous toxicity	Human skin equivalent model (HSEM)	No acute cutaneous irritation	
	Skin irritation	**In vivo:** rabbit; Draize test		
	SNPs (20, 100 nm); negatively charged (NC), weakly negatively charged (WNC)	**In vitro:**	NC-SNP (20 nm), more toxic than NC-SNP (100 nm)	Park et al. 2013
	Cytotoxicity	Human keratinocyte cell line HaCaT	NC-SNP (20 nm) more toxic than WNC-SNP (20 nm)	
	ROS generation	Intercellular ROS	No irritation	
	Skin irritation	EpiDerm skin irritation on human skin equivalent model	No phototoxicity	
	Skin phototoxicity	3T3 NRU phototoxicity test in murine 3T3 fibroblast cell	No sensitization	
	Skin sensitization	**In vivo:** mouse; local lymph node assay (LLNA)		
	SNPs (70, 300, 1,000 nm)	**In vitro:**	SNPs (70 nm); elevated level of ROS, DNA damage	Nabeshi et al. 2011a
	Zeta potentials:	LDH release assay	Endocytosis involved in SNP70-mediated cellular effects	
	SNP-70, −21.6 ± 4.5 mV	Human keratinocyte cell line HaCaT		
	SNP-300, −31.3 ± 6.5 mV			
	SNP-1,000, −37.7 ± 4.6 mV			
	ROS generation; DNA damage			
	SNPs (42 ± 3 nm to 291 ± 9); positive and negative surface charges	**In vitro:** human keratinocyte cell line HaCaT, dendritic cells	Positively charged functionalization of SNP enhanced in vitro cellular uptake	Rancan et al. 2012
	Zeta potentials:	**In vivo:** cyanoacrylate skin surface stripping (CSSS)	Particles taken up by skin cells in a size-dependent manner	
	SNP-42, −22 ± 3 mV		SNP (42 ± 3 nm) found in epidermal and dendritic cells	

(*continued*)

Table 2 (continued)

	Research question	Study type	Results	Author (year)
	SNP-75, -45 ± 4 mV		SNP (>75 nm) penetration blocked by human skin	
	SNP-200, -56 ± 5 mV			
	SNP-300, -48 ± 2 mV			
	Cellular uptake			
	Skin penetration			
	SNPs (30, 48, 118, 535 nm)	**In vitro:** mouse keratinocytes HEL-30	All SNP sizes were taken up into the cell, localized into the cytoplasm	Yu et al. 2009
	Cellular uptake, localization	LDH release assay	SNPs 30, 48 nm (100 μg/mL), more toxic than 118, 535 nm particles	
	ROS formation		ROS formation did not show any significant change between controls and the exposed cells	
	Cytotoxicity		LDH leakage was dose- and size-dependent with exposure to 30, 48 nm SNPs	
			No LDH leakage for either 118 or 535 nm SNPs	
	Fluorescent nonporous SiO_2 (10–200 nm); different charges	**In vitro:** normal human dermal fibroblasts	Smallest particles; high, fast cytotoxicity	Quignard et al. 2012
	Zeta potentials:		Genotoxic effects for negatively charged colloids (10 nm)	
	SNP-40, 56 ± 5 mV			
	SNP-200, 50 ± 4 mV			
	SNP- +10, 42 ± 4 mV			
	SNP- -10, -18 ± 4 mV			
	Cytotoxicity			
	Genotoxicity			
	Monodispersed SNPs (80, 500 nm)	**In vitro:** normal human dermal fibroblasts	SNP (80 nm) more strongly affects cell viability, mitochondrial membrane potential	Zhang et al. 2010
	Zeta potentials:		Both particles internalized into fibroblasts within a short time	
	SNP-80, -5.2 ± 0.2 mV		Cell adhesion, migration affected by uptake of SNPs regardless of size	
	SNP-500, -9.8 ± 1.2 mV			
	In culture medium with 10 % FBS			
	Cytotoxicity, cellular uptake			
	SNPs (30, 70, 100, 300, 1,000 nm)	**In vivo:** mouse	SNP (different sizes) penetrated skin barrier, induced various immunological effects, allergic diseases; AD	Hirai et al. 2012; Takahashi et al. 2013

(*continued*)

Table 2 (continued)

	Research question	Study type	Results	Author (year)
	Zeta potentials:	Ear thickness measurements	By decreasing SNP size, IL-18 and TSLP production increased, led to systemic Th2 response, aggravation of AD-like skin lesions as induced by Dp antigen treatment	
	SNP-30, −14.0 ± 0.3 mV	Histopathological analysis		
	SNP-70, −19.5 ± 1.0 mV			
	SNP-100, −24.3 ± 0.5 mV			
	SNP-300, −25.8 ± 0.7 mV			
	SNP-1,000, −33.2 ± 1.4 mV			
	Skin penetration			
	Skin allergic disease			
	SNP coated with bifunctional methoxy-terminated and PEG (7 nm)	**In vivo:** mouse, M21 melanoma xenograft mouse	Specific tumor targeting	Benezra et al. 2011
	Effect on tumor		High-affinity/avidity binding	
			Favorable tumor-to-blood residence time ratios	
			Enhanced tumor-selective	
			Longer-term pharmacokinetic clearance	
	Functionalized mesoporous silica (FMS; 30 nm) bound to monoclonal antibody (mAb) to CTLA4	**In vivo:** mouse established melanomas derived from SC injection of cells from the SW1 clone	More antitumor activity of FMS-anti-CTLA4 than that of anti-CTL4 alone	Lei et al. 2010
	Antitumor activity		No toxicity	
	Release kinetics			
Vehicle effect	Dermal delivery of silica microparticles (3 μm) in water and in 65 % ethanolic *Spilanthes* extract	**Ex vivo:** percutaneous absorption human skin	SNP (3 μm) penetrated living epidermis	Boonen et al. 2011
	Skin penetration		By formulating in 65 % ethanolic medium, reached dermis	
	Dermal delivery of lipophilic fluorescent probe: all-*trans*-retinol-acridine orange 10-nonyl bromide (AONB) using SNP coating of negatively charged lecithin and positively charged oleylamine	**Ex vivo:** percutaneous absorption porcine skin	Increased skin retention and depth of penetration to upper dermis for all-*trans*-retinol-AONB	Ghouchi-Eskandar et al. 2009a
	Dermal delivery of all-*trans*-retinol by SNP-coated submicron oil-in-water emulsions	**Ex vivo:** percutaneous absorption porcine skin	Sustained release, targeted dermal delivery of all-*trans*-retinol from oil-in-water emulsions	Ghouchi-Eskandar et al. 2009b

(*continued*)

Table 2 (continued)

	Research question	Study type	Results	Author (year)
	Dermal delivery of quercetin using lipid nanoparticles and colloidal silica	**In vivo:** percutaneous absorption human skin; tape stripping	Increased diffusion down to *stratum corneum*	Scalia et al. 2013
	Dermal delivery of quercetin using MCM-41 (plain or octyl-functionalized)	**In vitro:** DPPH assay	Increased efficiency of quercetin encapsulated by MCM-41	Berlier et al. 2013a
	Dermal delivery of rutin using NH_2-MCM-41	**In vitro:**	Greater accumulation in porcine skin	Berlier et al. 2013b
	Diffusion	DPPH assay	Maintained antioxidant properties	
	Antiradical activity	**Ex vivo:** percutaneous absorption porcine skin	Better activity and photostability	
	UV irradiation			
	Skin permeation			
	Dermal delivery of Trolox using MCM-41	**In vitro:**	Slower release of Trolox by inclusion in MCM-41	Gastaldi et al. 2012
	Photodegradation	Release	Increased photostability for complex particularly in O/W emulsion	
	Antiradical activity	DPPH assay	Maintained radical scavenging activity of Trolox	
	Dermal delivery of octyl methoxycinnamate (OMC) using MCM-41 formulated in Emulgel	**In vitro:** release	Increased release rate in Emulgel	Ambrogi et al. 2013
	Release		Broader photoprotection range, improvement of sunscreen photostability	
	Photostability			
	Hyaluronidase (Hyal) immobilized on SNP as adjuvants of carboplatin (CP)	**In vivo:** mouse bearing A375 human melanoma	Enhanced tumor volume reduction with SNP-Hyal compared to non-immobilized Hyal	Scodeller et al. 2013
	Antitumor			
	Dermal delivery of caffeine using silica nanocomposites	**Ex vivo:** percutaneous absorption of pig skin	Reduced, delayed permeation	Pilloni et al. 2013
	Skin permeation studies			
Surface area, dose, duration, and frequency of exposure	Skin penetration of consumers exposed to spray atmosphere of SAS nanoparticles	Modeling of consumer exposure	Skin penetration was unlikely	Michel et al. 2013
		Modeling of environmental exposure	Low toxicity	
			No systemic exposure	
Distribution	SNPs (70, 300, 1,000 nm)	**In vitro:**	Mutagenic activity in vitro	Nabeshi et al. 2011b
	Zeta potentials:	Human keratinocyte cell line HaCaT	SNPs (70 nm) penetrated *stratum corneum*, entered skin, lymph nodes, liver, cerebral cortex, and hippocampus	
	SNP-70, -21.6 ± 4.5 mV	DNA damage (Comet assay)		
	SNP-300, -31.3 ± 6.5 mV	Mutagenicity assay (Ames test)		

(*continued*)

Table 2 (continued)

	Research question	Study type	Results	Author (year)
	SNP-1,000, −37.7 ± 4.6 mV	**In vivo:** mice BALB/c		
	Cellular localization			
	Cytotoxicity			
	Skin penetration			
	Systemic effects			
	SNP (70 nm)	**In vivo:** mouse	SNPs (70 nm) observed in keratinocyte layer, Langerhans cells, and dermis of mouse	Tsunoda et al. 2011
	(No information for Zeta potential or charge)		After 3 days, SNP detected in cervical lymph node cells	
	Skin penetration			
	Systemic effect			
Sub-anatomical pathways (skin appendages)	Silica oxide (300–1,000 nm)	**In vitro:** human terminal and vellus hairs from Caucasian males, porcine hair follicle	Best follicle penetration of SNP 646 nm in size	Lademann et al. 2009
	(No information for Zeta potential or charge)		Optimal particle size corresponded to structure of hair and follicles	
	Influence of hair cuticula thickness on penetration into hair follicles			
Skin surface conditions	AHAPS-SiO_2 (55 ± 6 nm)	**In vivo:** SKH1 mouse	Penetration of AHAPS-SiO_2 through skin was not observed	Ostrowski et al. 2014
	(No information for Zeta potential or charge)		After subcutaneous injection, AHAPS-SiO_2 were incorporated by macrophages, transported to regional lymph node	
	Skin penetration on intact skin, tape-stripped, inflamed skin		No adverse effects on cells, tissues	
	Subcutaneous injection			
Additional factors of skin penetration and permeation	No research			
Loss from skin surface, exfoliation, and wash effect	No research			
Elimination and photochemical transformation	No research			
Method of determining absorption and toxicity	No research			

3.1 Physiochemical Properties of Silica Nanoparticles

Physiochemical properties of the penetrant may be the most pervasive factor influencing penetration since they influence interactions with the skin components (cell layers, cell membranes, lipids) and the extent to which nanoparticles penetrate or release associated ingredients into the skin. Physiochemical properties influencing nanoparticle penetration resemble the major factors influencing the penetration of chemicals across the skin. It is generally viewed that nanoparticle size, agglomeration/aggregation state, shape, crystal structure, chemical composition, surface chemistry, surface charge, porosity, dose, exposure time, and applied formulation are major factors which influence nanoparticle dermal penetration and toxicity (Poland et al. 2013; Thurn et al. 2007; Ngo et al. 2012).

There exist experiments which relate the physicochemical properties of silica nanoparticles to their percutaneous penetration (Table 2).

The relationship between different sizes of SNP ranging from 291 ± 9 to 42 ± 3 nm (single-unit size) with positive and negative surface charges and skin penetration has recently been examined.

Despite partial silica particle aggregation occurring after transfer in physiological media, particles were taken up by skin cells in a size-dependent manner, and SNPs above 75 nm in size did not penetrate human skin. Functionalization of the particle surface with positively charged groups enhanced in vitro cellular uptake, despite the fact that a large fraction of the positively charged particles were aggregated leading to lower internalization ratios especially by primary skin cells (Rancan et al. 2012).

Hair follicles represent important shunt routes into the skin for drugs and chemicals (Otberg et al. 2008). In vitro studies of nanoparticles sized from 122 to 1,000 nm suggested that particles in the size range of 400–700 nm had optimal penetration depth in porcine hair follicles compared to those smaller or larger. Depending on nanoparticle size, different depths and thereby different target structures within the hair follicle can be reached (Patzelt et al. 2011). For single silica oxide particles ranging in size from 300 to 1,000 nm, follicle penetration depth increased between 300 and 646 nm-sized particles and then decreased for particles larger than 646 nm (Lademann et al. 2009). It can be concluded that the optimal particle size for the deepest penetration corresponds approximately to the rough surface structure of the hair.

Having overcome the skin barrier, amorphous silica nanoparticles (SNPs) can induce various immunological effects and allergic diseases such as AD as intradermal injection of mite antigen (Dp) plus silica particles (diameter of single-unit size: 30–1,000 nm) into the ear of NC/Nga mice resulted in AD-like skin lesions. DP-induced sensitization and signs of AD were aggravated by SNP in a size-dependent manner compared to that of Dp alone. Clinical signs were correlated with excessive induction of total IgE and Dp-specific IgE and were associated with induction of IL-18 and thymic stromal lymphopoietin (TSLP) which led to systemic Th2 response in the skin lesions (Hirai et al. 2012; Takahashi et al. 2013; Table 2).

Park et al. (2013) studied cytotoxicity on keratinocytes and ROS generation by negatively charged NC and weakly negatively charged WNC-SNPs (20 and 100 nm in size). Smaller-sized NC-SNPs appeared more toxic than the larger sized (100 nm), and NC-SNPs (20 nm) showed more toxicity than the respective WNC-SNPs (20 nm). Skin irritation and contact sensitization were not detected (Park et al. 2013). Compared to larger SNPs (single unit 300, 1,000 nm), the SNPs of 70 nm diameter induced an elevated level of reactive oxygen species (ROS), leading to DNA damage of HaCaT cells, a spontaneously transformed human keratinocyte cell line (Nabeshi et al. 2011a). Proliferation of HaCaT cells was inhibited in a dose- and size-dependent manner (Nabeshi et al. 2011b). Viability and mitochondrial membrane potential of human dermal fibroblasts were more strongly affected by SNPs 80 nm in size, but adhesion and migration ability of the fibroblasts were impaired by SNPs, single units being 80 and

500 nm in diameter (Zhang et al. 2010). Moreover, cellular uptake and localization of amorphous SNPs (30, 48, 118, and 535 nm) in mouse keratinocytes (HEL-30) appeared to be independent of particle size. Dose-dependent LDH leakage and significant cytotoxicity at high concentrations (100 μg/mL), however, were seen with exposure to 30 and 48 nm nanoparticles. No LDH leakage was observed for the larger nanoparticles. Redox potential of cells (GSH level) was reduced significantly only with SNP 30 nm in size at concentrations of 50 μg/mL and higher (Yu et al. 2009). Fate of fluorescent nonporous SiO_2 nanoparticles (single-unit diameter: 10–200 nm) varying in charge (negative and positive) was studied in normal human dermal fibroblasts. Uptake of silica nanoparticles was determined by fluorescence spectroscopy and TEM. Largest particles did not impact on cellular function. Outside and inside the fibroblasts, extensive aggregation was seen with smaller SNPs, either negatively or positively charged. Small SNPs of either charge induced major detrimental effects on fibroblast viability, and exposure to negatively charged particles 10 nm in diameter resulted in genotoxic effects. Fluorescence reading revealed that positively charged silica nanoparticles (>40 nm) were taken as aggregates followed by a significant decrease in the size of the SNPs located in endocytic vesicles, and both colloidal and soluble species were released without impact on cellular function (Quignard et al. 2012). In summary, size and charge of amorphous silica nanoparticles are critical for biological effects, and particles below 100 nm in size are more toxic (Table 2).

In addition, particle surface area may play a crucial role in the toxicity of SNPs which can be related to their surface interfacing with the biological milieu (Elias et al. 2000; Waters et al. 2009; Napierska et al. 2010) and forming a protein corona. Even a minor surface modification can change biological effect, and surface functionalization, such as for binding of specific ligands, allow nanoparticle targeting of specific cell populations and subcellular components. Moreover, adsorbed proteins forming the corona can change the extent and depth of penetration as well as cytotoxicity (Oberdörster et al. 2005). In order to target M21 melanomas in a xenograft mouse model, multimodal silica nanoparticles were coated with bifunctional methoxy-terminated polyethylene glycol (PEG) chains (∼0.5 kDa; 7 nm). Neutral-charged PEG-functionalized SNPs were poorly uptaken by noncancer cells, and the bifunctional group enabled attachment of the integrin targeting RGDY peptide labeled with ^{124}I (Benezra et al. 2011). In another study, functionalized mesoporous silica (FMS) with a rigid, uniform, open nanopore geometry of tens of nanometers was used for loading of a monoclonal antibody (mAb) binding to CTLA4 – an immunoregulatory molecule overexpressed in melanoma (Leach et al. 1996). Protein spontaneously entrapped in FMS and release of the entrapped proteins from FMS were controlled based on the functional groups and pore sizes. This strategy enhanced inhibition of tumor growth compared to the free antibody given systemically (Lei et al. 2010; Table 2). Further study is needed to assess the effect of surface modification of nanoparticles on mAb penetration and toxicity following topical use as peptides which are rapidly degraded in human skin by proteinases (Do et al. 2014).

3.2 Vehicle Effects

One general approach to overcoming the barrier properties of the skin is to use penetration enhancers or nanoparticles that help promote drug diffusion through the *stratum corneum* to viable epidermis and dermis. Dermal absorption of a compound will be influenced by vehicle solubility and partitioning of the compound between vehicle and skin. Agents that are more soluble in an aqueous vehicle may tend towards limited absorption into the lipid-rich *SC*. Vehicle pH may influence the ionization state of the compound and the rate of partitioning into *stratum corneum* (Ngo et al. 2012). It also affects colloidal stability and agglomeration status which may alter penetration dynamics. Vehicle-dependent effects on penetration behavior of drugs following topical application have been widely

examined (Smith and Maibach 2006). There is also an increasing understanding of the effects of nanoparticles on penetration enhancement in general (Korting and Schäfer-Korting 2010; Alnasif et al. 2014).

Oil-based microemulsions, solvents or surfactants, referred to as penetration enhancers, accelerants, adjuvants, or absorption promoters, act by reducing drug binding and interactions with skin components (Ngo et al. 2012). For silica particles, skin penetration studies showed that silica microparticles (3 μm) could penetrate living epidermis and, when formulated in the 65 % ethanolic medium, even reach the dermis. This demonstrated the relevance of the vehicle in which silica microparticles were presented (Boonen et al. 2011).

Nanoemulsions are oil dispersed in water and have been used for penetration enhancement of hydrophilic and lipophilic substances. Nanoemulsions are transparent, and their small size and hydrophilic exterior may facilitate transport of active ingredients across the *stratum corneum* of the epidermis (Nohynek et al. 2007). Eskandar and coworkers investigated SNP-coated submicron oil-in-water emulsions for stabilization and skin penetration of lipophilic agents, retinol and a fluorescent dye, namely, acridine orange 10-nonyl bromide. Lecithin and oleylamine addition, respectively, were used for the induction of negative and positive charge to the emulsion. Both formulations improved retinol resistance towards UV-induced degradation, controlled release, and significantly enhanced the penetration of both agents into excised porcine skin compared to free agent used for control. With the positively charged formulation, penetration was even seen in the upper dermis without major penetration of the agents (Ghouchi-Eskandar et al. 2009a, b). Moreover, solid-state nanoparticle-coated emulsion prepared by freeze-drying significantly enhanced retinol stability (Ghouchi-Eskandar et al. 2012; Table 2).

Flavonoids such as quercetin and rutin are used in topical cosmetic and pharmaceutical products because of their antioxidant and radical scavenging properties, but their application is limited by their poor physicochemical stability. In human volunteers, addition of colloidal silica (average particle diameter: 486 nm) to an emulsion significantly increased the quercetin penetration into *stratum corneum* to 26.7 ± 4.1 % of the applied dose, the enhancement being more marked in the deep *stratum corneum* sampled by tape stripping. Silica particles were detectable in the intermediate region of human *stratum corneum* and hence could act as a carrier for quercetin (Scalia et al. 2013). Mesoporous silica (MCM-41) has widely been proposed as a vehicle able to improve the penetration and performance of drugs. Complexes of quercetin with plain or octyl-functionalized MCM-41 were formed based on host/guest interaction due to the formation of Si-OH/quercetin hydrogen-bonded adducts and strengthened by octyl functionalization. Immobilization of quercetin particularly on octyl-functionalized silica increased stability without undermining the antioxidant efficacy of quercetin opening the way for an innovative employment of mesoporous composite materials in the skin care field and topical products (Berlier et al. 2013a). Moreover, immobilization of rutin in the pores of in aminopropyl silica (NH_2-MCM-41) stabilized the agent against UV degradation and enhanced the accumulation in porcine skin ex vivo while maintaining rutin's antioxidant properties (Berlier et al. 2013b). Octyl methoxycinnamate is an efficient and widely used UV filter yet shows light susceptibility (photoinstability) and potential skin permeation which is not wanted with sunscreen products. For improvement of photostability and safety, octyl methoxycinnamate was entrapped in the pores of the mesoporous silicate MCM-41, pore openings were plugged, and the loaded nanoparticles incorporated into a lipid-based cosmetic formulation allowed a broader photoprotection range and remarkable improvement of sunscreen photostability (Ambrogi et al. 2013). In addition, inclusion of Trolox (a water-soluble analog of vitamin E) in the MCM-41 matrix retarded in vitro release and increased photostability for complexed agent particularly in O/W emulsion. Importantly, the radical scavenging activity of Trolox was maintained after immobilization (Gastaldi et al. 2012; Table 2).

Recently, hyaluronidase (degrading enzyme of hyaluronic acid) was immobilized on 250 nm SNPas adjuvants of carboplatin (CP) and peritumorally injected in A375 human melanoma-bearing mice. Enzyme activity was maintained, SNP-immobilized hyaluronidase cleaved hyaluronic acid overexpressed by the tumor cells, and tumor volume was significantly more declined compared to non-immobilized Hyal used for comparison (Scodeller et al. 2013; Table 2).

In cases where skin penetration is not desired, penetration reducers can inhibit the compound from entering the systemic circulation (Trommer and Neubert 2006). Barrier-enhancing emulsions have reduced the penetration of exogenous proteins into the hair follicles to varying degrees (Meinke et al. 2011). Caffeine loading to a silica nanocomposite resulting in the formulation of both core shell and multilayered caffeine–silica structures reduced and delayed caffeine permeation of pig skin in comparison with the reference gel, independently from the amount of the tested formulation (Pilloni et al. 2013; Table 2).

3.3 Surface Area, Dose, Duration, and Frequency of Exposure

Following skin contact, amount of chemical absorbed, which is often expressed as dose per area (cm^2), depends greatly on several conditions of exposure (Ngo et al. 2012). Increasing surface area over which a chemical is in contact will increase absorption. Percent absorption also depends upon the concentration and dose applied per unit area. For many compounds, percent absorption at relatively high concentrations is inversely related to applied dose (Wester et al. 1980). In other words, percent absorbed increases as skin loading decreases, and the function is nonlinear. This is attributed to saturation of the absorptive skin capacity. Despite a decrease in efficiency of absorption, in terms of percent absorption, a continued increase in total penetration, in mass, can be observed with increased dose. Similarly, with multiple applications and frequency of exposures, the skin may become saturated and resist penetration from subsequent doses (Wester et al. 1977; Wester et al. 1980). Moreover, dermal penetration tends to increase with duration of contact or exposure, and compounds retained in the skin layers may become released available after the contact material had been removed from the skin surface. Experimental protocols often set periods of exposure and sample collection that may not be relevant. It is often necessary to extrapolate long-term exposure from short-term data. In general, total absorption of a compound appears to be linearly correlated with the amount of penetration into the *stratum corneum* observed shortly after application (Rougier et al. 1987). While many studies investigate dermal absorption of a compound following a single dose, multiple or repeated exposures are more clinically relevant to real life (Ngo et al. 2012). Synthetic amorphous silicon dioxide (SiO_2) nanoparticles have been widely used in a glass cleaner formulation (spray application). Workers and consumers are frequently exposed to it during production and used as spray application. Percutaneous penetration of SiO_2 is unlikely as the hydrophilic character of uncoated SiO_2 does not favor skin penetration (Michel et al. 2013; Table 2). Engineered nanomaterials are incorporated into textile products; nanotextiles include nanosilica, nanolayered silica, nano-silver, nano-TiO_2, nano-ZnO, nano-alumina (Al_2O_3), carbon black, and carbon nanotubes (Som et al. 2011). These nanomaterials are used to improve textile properties such as wrinkle resistance, water repellency, antimicrobial and antistatic properties, and UV and flammability resistance. Since there is continuous and intimate contact between clothing and skin, transfer and absorption of nanomaterials under these conditions should be considered (Ngo et al. 2012).

3.4 Distribution

Once the *stratum corneum* has been breached, interactions with the deeper components of the permeability barrier and finally access to the vascular system and thus systemic availability will

again depend on the physiochemical properties of the penetrant in question (Menczel and Maibach 1970). Perfusion of the dermis promotes absorption and creates a sink for chemicals that have traversed the epidermis. Subsequent distribution of a chemical to target sites or organs within the body will also depend on blood flow. By reducing local blood flow, such as with the use of a vasoconstrictor, systemic absorption can be inhibited. At the same time, drug penetration into deeper tissue layers adjacent to the application site may be enhanced by reduced blood flow (Higaki et al. 2005). Local and systemic toxicity following dermal absorption of drugs or chemicals across the skin has been widely evaluated (Alikhan and Maibach 2011). Proposed toxic effects of nanoparticles entering the systemic circulation include perturbation of the immune system, as well as other organ systems.

Once more, size and surface physicochemical properties of silica nanoparticles contribute decisively to their biological effects. Following 3 days of topical application to mouse, SNPs (70 nm in size) were observed in keratinocyte layer including the Langerhans cells, dermis, and lymph node (Tsunoda 2011). Application of SNP (single-unit size) to the ears of mice (250 μg/ear/day) for 28 days resulted in particles being detected in the skin, regional lymph nodes, and parenchymal hepatocytes present in the liver, cerebral cortex, and hippocampus (Nabeshi et al. 2011b; Table 2).

Yet analysis was based upon murine skin and TEM analysis with no confirmation that the electron-dense regions were, in fact, particles of interest. More experimental data – including those generated in human skin – is needed to confirm the results.

3.5 Sub-anatomical Pathways (Skin Appendages)

Although the *stratum corneum* plays a critical role in the function of permeability barrier, there are many components with which a penetrant interacts before entering the body. In recent years, it has been suggested that skin appendages represent important shunt routes into skin for drugs and chemicals. Skin appendages include hair follicles, sebaceous glands, and sweat glands, which originate in the dermis (Ngo et al. 2012; Poland et al. 2013). Particle size influences the penetration depth, with different follicle structures interacting with particles of particular size (Patzelt et al. 2011; Toll et al. 2004; Vogt et al. 2006). For silica oxide particles ranging in size from 300 to 1,000 nm, follicle penetration depth increased up to about 650 nm-sized particles and then decreased for larger particles. It can be suggested that the optimal particle size for the deepest penetration corresponded approximately to the structure of hair and follicles (Lademann et al. 2009; Table 2).

3.6 Skin Surface Condition

Surface conditions including hydration, occlusion, pH, and temperature are the factors which affect skin absorption (Ngo et al. 2010). The degree of interactions with the different skin components determines the time and the chemical residues that persist or accumulate in the skin as well as the time required to traverse the different layers and enter the systemic circulation (Jacobi et al. 2007; Lademann et al. 2006).

Importantly, structure and integrity of skin will be compromised by damage or disease. Chemical or physical skin insults may cause change in the skin's barrier function, resulting in the increased permeability of numerous compounds (Ngo et al. 2010). However, a recent study on the penetration of *N*-(6-aminohexyl)-aminopropyltrimethoxysilane nanoparticles (55 ± 6 nm diameter) on intact, tape-stripped, or on inflamed skin of SKH1 mice with induced allergic contact dermatitis showed no penetration of the rigid particles through the skin regardless of the kind of barrier disruption. After subcutaneous injection, however, the nanoparticles were incorporated by macrophages and transported to the regional lymph node; adverse effects were not detected (Ostrowski et al. 2014).

3.7 Additional Factors of Skin Penetration and Permeation

The extent of dermal absorption varies from one body region to another and partially attributed to skin thickness and the number of cell layers in the *SC* (Ngo et al. 2010). Besides regional variation, population variability may be of relevance. Variability in skin properties reported for different groups in human population provides a potential basis for differences in the rate and extent of drug absorption between the various skin types (Mangelsdorf et al. 2006).

3.8 Loss from Skin Surface, Exfoliation, and Wash Effect

Persistence of a chemical on the skin will depend on its resistance to removal or inactivation which depends on the mechanisms of removal of nanoparticles from the skin surface including volatilization, sweating, washing, friction with or transfer to other surfaces, and exfoliation (Ngo et al. 2010). Washing influences the absorption of nanoparticles into the skin. Washing and rubbing an area of substance-treated skin can remove part of the dose. Washing the application site between doses, a common step in experimental protocols of dermal absorption studies, may enhance percutaneous absorption (Ngo et al. 2010).

3.9 Elimination and Photochemical Transformation

The skin is capable of a wide range of metabolic functions and is recognized as a significant site of biotransformation and photochemical transformation. Cutaneous metabolism and photochemical transformation play essential role in absorption of compounds by transforming them into metabolites (Götz et al. 2012; Jäckh et al. 2011; Bätz et al. 2013; Ngo et al. 2010). Depending on the compound, elimination may or may not be in proportion to the dose absorbed (Marzulli and Maibach 1975; Nigg and Stamper 1989).

3.10 Method of Determining Absorption and Toxicity

When evaluating dermal data, differences in experimental parameters such as animal species, anatomical site, skin sample preparation, skin disease presence, role of penetration enhancers, and exposure conditions affect the interpretation and comparisons between studies. It is important to control experimental condition in a systematic way (Ngo et al. 2012).

Only recently, a predictive mathematical approach has been described which allows to take formulation effects into consideration, too (Guth et al. 2014). Yet applicability for nanoparticle-based formulations requires evaluation.

For silica nanoparticles, present experimental data focus on physiochemical properties; vehicle effects; surface area, dose, duration, and frequency of exposure; distribution; and sub-anatomical pathways. Information regarding physicochemical properties of SNPs is not sufficient to draw a robust conclusion for their skin penetration; vehicle effects need more study; the experiments on dose relationships, exposure duration, surface area, frequency, and sub-anatomical pathways are minimal; and no information exists on the other parameters. More experimental data are needed to understand factors which affect the percutaneous penetration of silica nanoparticles. Research gaps in percutaneous penetration of silica nanoparticles (SNPs) are in Tables 2 and 3.

4 Skin Absorption and Toxicity of Silica Nanoparticles

Penetration of a material through the skin barrier can trigger numerous toxic effects, both local and systemic. Compounds that reach the *stratum granulosum*, for example, can interact with the viable keratinocytes and trigger an inflammatory reaction. Compounds that reach the *stratum spinosum* can interact with Langerhans cells (from the immune system) and initiate an allergic reaction responsible for phenomenon such as contact dermatitis. Skin cancer may also be induced

Table 3 Research gaps in percutaneous penetration of silica nanoparticles (SNPs)

10 Factors affecting percutaneous penetration of nanoparticles (Ngo et al. 2012)		Researches on silica nanoparticles (SNPs)
1	Physiochemical properties of the nanoparticle	+
2	Vehicle effects	+
3	Surface area, dose, duration, and frequency of exposure	Minimal research
4	Distribution	Minimal research
5	Sub-anatomical pathways (skin appendages)	Minimal research
6	Skin surface conditions	Minimal research
7	Additional factors of skin penetration and permeation	No research
8	Loss from skin surface, exfoliation, and wash effect	No research
9	Elimination and photochemical transformation	No research
10	Method of determining absorption and toxicity	No research

following dermal exposure depending on the chemical and its ability to penetrate skin and reach the viable layers, where it can potentially transform normal cells or enhance proliferation of transformed cells. All of these effects can be grouped as dermal toxicity. However, when a compound manages to cross the epidermis, it becomes accessible to dermis and potentially accessible to the systemic circulatory and lymphatic systems. As a result such compounds can cause damage in distal organs, by translocation through the circulatory system or by triggering systemic reactions. These can lead to a wide range of toxic effects and disease such as systemic inflammation, organ toxicity, and cancer (Poland et al. 2013; Raju and Rom 1998; Napierska et al. 2010; Crosera et al. 2009). Toxicity of NPs can depend on not only the material itself but also the administration route to the living body. In particular, intraperitoneal and intravenous injection may lead to fatal outcomes (Hudson et al. 2008). I

It is important to evaluate safety of nanoparticles using specific toxicological studies prior to a wider implementation. General toxicological principles of compounds are discussed by Hayes (Hayes and Kruger 2014). Regulatory aspects of exposure to toxic substances are specified by Wilhelm (Wilhelm et al. 2012). There remains the need to increase the predictability of current nanoparticle toxicity testing by transitioning from qualitative, descriptive animal testing to quantitative, mechanistic, and pathway-based toxicity testing in human cells or cell lines using high-throughput approaches. Standard methods and platform should be used to investigate the numerous biophysicochemical interactions at the nano-/bio-interface (Nel et al. 2013). Classical investigation protocols must be adapted and re-standardized to the new nanosized compounds. Cell cultures (Bernstein and Vaughan 1999), Franz diffusion cells (Franz 1975), tape stripping (Escobar-Chávez et al. 2008), and human skin implantations on animals are powerful tools to study particle interaction with human dermal tissue. However, new methods and new technique applications have to be developed (Monteiro-Riviere and Inman 2006; SCCP 2007). In particular microscopy techniques like coherent anti-Stokes Raman scattering (CARS), transmission electron microscopy (TEM), confocal laser scanning microscope (CLSM), fluorescence-lifetime imaging microscopy (FLIM), near-infrared II fluorescence, and other ion beam techniques are necessary to visualize nanoparticles into biological structures (Alnasif et al. 2014; Moger et al. 2008; Welsher et al. 2011).

Because silica nanoparticles are widely used nanomaterials, chances of being exposed to SNPs in daily life are high. There are major concerns about the biocompatibility, toxicity, in vivo biodistribution, and efficacy of SNPs of various particle sizes. While some data reports that silica particles are biocompatible, nontoxic, and stable (ECETOC 2006; OECD 2004; Butz 2009; Gamer et al. 2006; Mavon et al. 2007; Pfluecker et al. 2001; Fruijtier-Polloth et al. 2012; Low et al. 2009; Rosenholm et al. 2011; Michel et al. 2013), others show that the uptake of nanoparticles by cells may eventually lead to perturbation of cellular pathways and induce toxicity (Hirai et al. 2012;

Park et al. 2010, 2013; Quignard et al. 2012; Nabeshi et al. 2011a, b; Takahashi et al. 2013; Yu et al. 2009). Toxicity of silica NPs depends strongly on their physicochemical properties such as particle size, shape, porosity, chemical purity, and solubility (Yu et al. 2011, 2012; Waters et al. 2009). Particle surface area play a crucial role in the toxicity of silica (Elias et al. 2000; Zhang et al. 2010) which can be related to their surface interfacing with the biological milieu rather than to particle size or shape (Fenoglio et al. 2000). In vivo toxicology data associated with the nanoparticles has led to persistent and valid safety concerns prompting particle-design modifications including size, composition, and surface chemistry (Schipper et al. 2009) and need for rapid clearance from the body within a reasonable timescale (Choi et al. 2010).

5 Conclusions

Loading to SNPs can improve physicochemical stability of labile drugs and to adjust the release profile and skin penetration. Yet, the results of this literature survey show that the data related to toxicity of SNPs are few and are insufficient to clearly identify and characterize the health hazards SNPs may pose, and defining the appropriate conditions for safe use of these materials is currently not possible.

Accurate assessment of nanoparticle penetration depends on ten parameters of percutaneous penetration. For silica nanoparticles, experimental data are focused on six parameters, and there is no data on the other parameters (Tables 2 and 3). Moreover, only results from short-term in vivo studies of silica nanoparticles are available while data following chronic dermal effects are still to be awaited. In addition, relationships among SNPs, physicochemical properties, absorbency, localization, and biological responses are not well understood. Besides relative lack of information on the safety or hazards of SNPs, often conflicting evidence is emerging in the literature as a result of a general lack of standard procedures, as well as insufficient characterization of silica nanomaterials in biological systems. Information is insufficient to clearly identify and characterize the health hazards SNPs may pose, and defining the appropriate conditions for safe use of these materials is currently not possible.

There are gaps in understanding human and environmental risk that manufactured silica nanoparticles may pose for those occupationally exposed and for consumers. There is need for assessing the health and environmental impacts, the nanoparticle life cycle, the human exposure routes, the behavior of nanoparticles in the body, and the risk for workers. In particular, dermal absorption and skin penetration of nanoparticles need an evaluation by the most advanced analytical techniques. Understanding the behavior of NPs when they contact the skin surface and their interaction with the different skin layers would ultimately lead to the design of the "ideal" carrier or diagnostic agent in terms of the physicochemical parameters of the NPs, in addition to other factors (e.g., formulation and environmental factors) influencing skin penetration of NPs.

Acknowledgment The authors appreciate Central Tehran Branch, IAU, Tehran, Iran for support of this work.

References

Agudelo D, Nafisi S, Tajmir-Riahi HA. Encapsulation of milk-lactoglobulin by chitosan nanoparticles. J Phys Chem B. 2013a;117:6403–9.

Agudelo D, Sanyakamdhorn S, Nafisi S, Tajmir-Riahi HA. Transporting antitumor drug tamoxifen and its metabolites, 4-Hydroxytamoxifen and endoxifen by chitosan nanoparticles. PLoS One. 2013b;8:e60250.

Alikhan FS, Maibach HI. Topical absorption and systemic toxicity. Cutan Ocul Toxicol. 2011;30:175–86.

Alnasif N, Zoschke C, Fleige E, Brodwolf R, Boreham A, Rühl E, et al. Penetration of normal, damaged and diseased skin – an in vitro study on dendritic core-multishell nanotransporters. J Control Release. 2014;185C:45–50.

Ambrogi V, Latterini L, Marmottini F, Pagano C, Ricci M. Mesoporous silicate MCM-41 as a particulate carrier for octylmethoxycinnamate: sunscreen release and photostability. J Pharm Sci. 2013;102:1468–75.

Barbe C, Bartlett J, Kong LG, Finnie K, Lin HQ, Larkin M. Silica particles: a novel drug-delivery system. Adv Mater. 2004;16:1959–66.

Bätz F, Klipper W, Korting HC, Henkler F, Landsiedel R, Luch A, et al. Esterase activity in excised and

reconstructed human skin – biotransformation of prednicarbate and the model dye fluorescein diacetate. Eur J Pharm Biopharm. 2013;84:374–85.

Behtash A, Nafisi S, Maibach HI. New generation of fluconazole: a review on existing researches and technologies. Cur Drug Deliv. 2016, Manuscript in Publishing.

Benezra M, Penate-Medina O, Zanzonico PB, Schaer D, Ow H, Burns A, et al. Multimodal silica nanoparticles are effective cancer-targeted probes in a model of human melanoma. J Clin Invest. 2011;121:2768–80.

Berlier G, Gastaldi L, Ugazio E, Miletto I, Iliade P, Sapino S. Stabilization of quercetin flavonoid in MCM-41 mesoporous silica: positive effect of surface functionalization. J Colloid Interface Sci. 2013a;393:109–18.

Berlier G, Gastaldi L, Sapino S, Miletto I, Bottinelli E, Chirio D, et al. MCM-41 as a useful vector for rutin topical formulations: synthesis, characterization and testing. Int J Pharm. 2013b;457:177–86.

Bernstein IA, Vaughan FL. Cultured keratinocytes in in vitro dermatotoxicological investigation: a review. J Toxicol Environ Health B. 1999;2:1–30.

Bharali DJ, Klejbor I, Stachowiak EK, Dutta P, Roy I, Kaur N, et al. Organically modified silica nanoparticles: a nonviral vector for in vivo gene delivery and expression in the brain. Proc Natl Acad Sci U S A. 2005;102:11539–44.

Boonen J, Baert B, Lambert J, De Spiegeleer B. Skin penetration of silica microparticles. Pharmazie. 2011;66:463–4.

Bouwstra JA, Honeywell-Nguyen PL, Gooris GS, Ponec M. Structure of the skin barrier and its modulation by vesicular formulations. Prog Lipid Res. 2003;42:1–36.

Butz T. Dermal penetration of nanoparticles-what we know and what we don't. SöFW J10. 2009;135:30–4.

Chen Y, Chen H, Shi J. In vivo bio-safety evaluations and diagnostic/therapeutic applications of chemically designed mesoporous silica nanoparticles. Adv Mater. 2013;18:3144–76.

Choi M, Cho WS, Han BS, Cho M, Kim SY, Yi JY, et al. Transient pulmonary fibrogenic effect induced by intratracheal instillation of ultrafine amorphous silica in A/J mice. Toxicol Lett. 2008;182:97–101.

Choi HS, Liu W, Liu F, Nasr K, Misra P, Bawendi MG, et al. Design considerations for tumor-targeted nanoparticles. Nat Nanotechnol. 2010;5:42–7.

Crosera M, Bovenzi M, Maina G, Adami G, Zanette C, Florio C, et al. Nanoparticle dermal absorption and toxicity: a review of the literature. Int Arch Occup Environ Health. 2009;82:1043–55.

De Louise LA. Applications of nanotechnology in dermatology. J Invest Dermatol. 2012;132:964–75.

De Villiers MM, Aramwit P, Kwon GS. Nanotechnology in drug delivery. New York: Springer/AAPS Press; 2009.

Do N, Weindl G, Grohmann L, Salwiczek M, Koksch B, Korting HC, et al. Cationic membrane-active peptides – anticancer and antifungal activity as well as penetration into human skin. Exp Dermatol. 2014;23:326–31.

ECETOC. Synthetic amorphous silica (CAS No. 7631-86-9) – JACC REPORT No. 51. Brussels: European Centre for Ecotoxicology and Toxicology of Chemicals; 2006. p. 6339–51. ISSN-0773-2006.

Elias Z, Poirot O, Daniere MC, Terzetti F, Marande AM, Dzwigaj S, et al. Cytotoxic and transforming effects of silica particles with different surface properties in Syrian hamster embryo (SHE) cells. Toxicol In Vitro. 2000;14:409–22.

Escobar-Chávez JJ, Merino-Sanjuan V, Lopez-Cervantes-M, Urban-Morlan Z, Pinon-Segundo E, Quintanar-Guerrero D, et al. The tape stripping technique as a method for drug qualification in skin. J Pharm Pharmaceut Sci. 2008;11:104–30.

EU Commission Recommendation. Definition of nanomaterial. Available at http://eurlex.europa.eu/LexUriServ/LexUriServ.do?uri=OJ:L:2011:275:0038:0040:EN:PDF (2011).

Fenoglio I, Martra G, Coluccia S, Fubini B. Possible role of ascorbic acid in the oxidative damage induced by inhaled crystalline silica particles. Chem Res Toxicol. 2000;13:971–5.

Firooz A, Nafisi S, Maibach HI. Novel drug delivery strategies for improving econazole antifungal action. Int J Pharm. 2015;495:599–607.

Firouz A, Namdar R, Nafisi S, Maibach HI. Nano-sized technologies for miconazole skin delivery. Cur Pharm Biotech. 2016;17:524–31.

Franz J. Percutaneous absorption on the relevance of in-vitro data. J Invest Dermatol. 1975;67:190–5.

Friedman R. Nano dot technology enters clinical trials. J Natl Cancer Inst. 2011;103:1428–9.

Fruijtier-Polloth C. The toxicological mode of action and the safety of synthetic amorphous silica-A nanostructured material. Toxicol. 2012, 11;294(2–3):61–79.

Gamer AO, Leibold E, van Ravenzwaay B. The in vitro absorption of microfine zinc oxide and titanium dioxide through porcine skin. Toxicol In Vitro. 2006;20:301–7.

Garcia-Bennett AE. Synthesis, toxicology and potential of ordered mesoporous materials in nanomedicine. Nanomedicine. 2011;6:867–77.

Gastaldi L, Ugazio E, Sapino S, Iliade P, Miletto I, Berlier G. Mesoporous silica as a carrier for topical application: the Trolox case study. Phys Chem Chem Phys. 2012;14:11318–26.

Georgia State University. Hyperphysics. Abundances of the elements in the earth's crust. Available at http://hyperphysics.phy-astr.gsu.edu/hbase/tables/elabund.html

Ghouchi-Eskandar N, Simovic S, Prestidge CA. Chemical stability and phase distribution of all-trans-retinol in nanoparticle-coated emulsions. Int J Pharm. 2009a;376:186–94.

Ghouchi-Eskandar N, Simovic S, Prestidge CA. Nanoparticle coated emulsions as novel dermal delivery vehicles. Curr Drug Deliv. 2009b;6:367–73.

Ghouchi-Eskandar N, Simovic S, Prestidge CA. Solid-state nanoparticle coated emulsions for encapsulation and improving the chemical stability of all-trans-retinol. Int J Pharm. 2012;423:384–91.

Götz C, Pfeiffer R, Blatz V, Tigges J, Jäckh C, Freytag EM, et al. Xenobiotic metabolism capacities of human skin in comparison with a 3D epidermis model and keratinocyte-based cell culture as in vitro alternatives for chemical testing: activating enzymes (phase I). Exp Dermatol. 2012;1:358–63.

Guth K, Riviere JE, Brooks JD, Dammann M, Fabian E, van Ravenzwaay B, et al. In silico models to predict dermal absorption from complex agrochemical formulations. SAR QSAR Environ Res. 2014;25:565–88.

Hayes AW, Kruger CL. Hayes' principles and methods of toxicology. New York: CRC Press; 2014.

Higaki K, Nakayama K, Suyama T, Amnuaikit C, Ogawara K, Kimura T. Enhancement of topical delivery of drugs via direct penetration by reducing blood flow rate in skin. Int J Pharm. 2005;288:227–33.

Hirai T, Yoshikawa T, Nabeshi H, Yoshida T, Tochigi S, Ichihashi K, et al. Amorphous silica nanoparticles size-dependently aggravate atopic dermatitis-like skin lesions following an intradermal injection. Part Fibre Toxicol. 2012;9:3–14.

Hoffmann F, Cornelius M, Morell J, Fröba M. Silica-based mesoporous organic-inorganic hybrid materials. Angew Chem Int Edit. 2006;45:3216–51.

Hudson SP, Padera RF, Langer R, Kohane DS. The biocompatibility of mesoporous silicates. Biomaterials. 2008;29:4045–55.

Iier RK. The chemistry of silica. New York: Wiley; 1979.

IMA Europe. Crystalline silica and health from a European industry perspective. Available at www.crystallinesilica.eu (2014).

Jäckh C, Blatz V, Fabian E, Guth K, van Ravenzwaay B, Reisinger K, et al. Characterization of enzyme activities of Cytochrome P450 enzymes, Flavin-dependent monooxygenases, N-acetyltransferases and UDP-glucuronyltransferases in human reconstructed epidermis and full-thickness skin models. Toxicol In Vitro. 2011;25:1209–14.

Jacobi U, Engel K, Patzelt A, Worm M, Sterry W, Lademann J. Penetration of pollen proteins into the skin. Skin Pharmacol Physiol. 2007;20:297–304.

Korting HC, Schäfer–Korting M. Carriers in the topical treatment of skin disease. Handb Exp Pharmacol. 2010;197:435–68.

Kresge CT, Leonowicz ME, Roth WJ, Vartul JC, Beck JS. Ordered mesoporous molecular sieves synthesized by a liquid-crystal template mechanism. Nature. 1992;359:710–2.

Kreyling WG, Behnke MS, Chaudhry Q. A complementary, definition of nanomaterial. Nano Today. 2010;5:165–8.

Labouta HI, Schneider M. Interaction of inorganic nanoparticles with the skin barrier: current status and critical review. Nanomed Nanotechnol Biol Med. 2013;9:39–54.

Lademann J, Richter H, Schaefer UF, Blume-Peytavi U, Teichmann A, Otberg N, et al. Hair follicles – a long-term reservoir for drug delivery. Skin Pharmacol Physiol. 2006;19:232–6.

Lademann J, Patzelt A, Richter H, Antoniou C, Sterry W, Knorr F. Determination of the cuticula thickness of human and porcine hairs and their potential influence on the penetration of nanoparticles into the hair follicles. J Biomed Opt. 2009;14:021014-1–4.

Leach DR, Krummel MF, Allison JP. Enhancement of antitumor immunity by CTLA-4 blockade. Science. 1996;271:1734–6.

Lee CH, Cheng SH, Wang YJ, Chen YC, Chen NT, Souris J, et al. Near-infrared mesoporous silica nanoparticles for optical imaging: characterization and In vivo biodistribution. Adv Funct Mater. 2009;19:215–22.

Lei C, Liu P, Chen B, Mao Y, Engelmann H, Shin Y, et al. Local release of highly loaded antibodies from functionalized nanoporous support for cancer immunotherapy. J Am Chem Soc. 2010;132:6906–7.

Liu J, Qiao SZ, Chen JS, Lou XWD, Xing X, Lu GQM. Yolk/shell nanoparticles: new platforms for nanoreactors, drug delivery and lithium-ion batteries. Chem Commun. 2011;47:12578–91.

Lou XWD, Archer LA, Yang Z. Hollow micro-/nanostructures: synthesis and applications. Adv Mater. 2008;20:3987–4019.

Low SP, Voelcker NH, Canham LT, Williams KA. The biocompatibility of porous silicon in tissues of the eye. Biomaterials. 2009;30:2873–80.

Mangelsdorf S, Otberg N, Maibach HI, Sinkgraven R, Sterry W, Lademann J. Ethnic variation in vellus hair follicle size and distribution. Skin Pharmacol Physiol. 2006;19:159–67.

Marzulli FN, Maibach HI. Relevance of animal models-the hexachlorophene story. In: Maibach HI, editor. Animal models in dermatology. Edinburgh: Churchill Living Stone; 1975. p. 156–67.

Mavon A, Miquel C, Lejeune O, Payre B, Moretto P. In vitro percutaneous absorption and in vivo stratum corneum distribution of an organic and a mineral sunscreen. Skin Pharmacol Physiol. 2007;20:10–20.

Meinke MC, Patzelt A, Richter H, Schanzer S, Sterry W, Filbry A, et al. Prevention of follicular penetration: barrier-enhancing formulations against the penetration of pollen allergens into hair follicles. Skin Pharmacol Physiol. 2011;24:144–50.

Menczel E, Maibach HI. In vitro human percutaneous penetration of benzyl alcohol and testosterone: epidermal-dermal retention. J Invest Dermatol. 1970;54:386–94.

Michel K, Scheel J, Karsten S, Stelter N, Wind T. Risk assessment of amorphous silicon dioxide nanoparticles in a glass cleaner formulation. Nanotoxicology. 2013;7:974–88.

Moger J, Johnston BD, Tyler CR. Imaging metal oxide nanoparticles in biological structures with CARS microscopy. Opt Express. 2008;16:3408–19.

Monteiro-Riviere NA, Inman AO. Challenges for assessing carbon nanomaterial toxicity to the skin. Carbon. 2006;44:1070–8.

Nabeshi H, Yoshikawa T, Matsuyama K, Nakazato Y, Tochigi S, Kondoh S, et al. Amorphous nanosilica induce endocytosis-dependent ROS generation and DNA damage in human keratinocytes. Part Fibre Toxicol. 2011a;8:1–10.

Nabeshi H, Yoshikawa T, Matsuyama K, Nakazato Y, Matsuo K, Arimori A, et al. Systemic distribution, nuclear entry and cytotoxicity of amorphous nanosilica following topical application. Biomaterials. 2011b;32:2713–24.

Nafisi S, Maibach HI. Silica nanoparticles: promising nanoparticles for increasing cosmetic ingredients/drugs efficacy. Cosmet Toilet. 2015.

Nafisi S, Maibach HI. Skin penetration of nanoparticles. In: Souto EB, editor. Emerging nanotechnologies in immunology: the design, application and toxicology of nanopharmaceuticals and nanovaccines. Elsevier; 2016. In Publishing.

Nafisi S, Maibach HI. Nanotechnology in cosmetics. In: Yamashita Y, Lochhead RY, Maibach HI, editors. Cosmetics and nanotechnology in cosmetics science and technology: theoretical principles and applications. Elsevier; 2016. In Publishing.

Napierska D, Thomassen LC, Lison D, Martens JA, Hoet PH. The nanosilica hazard: another variable entity. Part Fibre Toxicol. 2010;7:39–71.

Nassiri-Kashani M, Namdar N, Nafisi S, Maibach HI. Improved voriconazole skin delivery by nanoparticles. Pharmaceut Chem J. 2016;50:76–79.

Nel A, Xia T, Meng H, Wang X, Lin S, JI Z, Zhang H. Nanomaterial toxicity testing in the 21st century: use of a predictive toxicological approach and high-throughput screening. Acc Chem Res. 2013;46:607–21.

Ngo MA, Malley MO, Maibach HI. Percutaneous absorption and exposure assessment of pesticides. J Appl Toxicol. 2010;30:91–114.

Ngo MA, Malley MO, Maibach HI. Perspectives on percutaneous penetration of nanomaterials. In: Nasir A, Friedman A, Wang S, editors. Nanotechnology in dermatology. New York: Springer; 2012. p. 63–86.

Nigg HN, Stamper JH. Biological monitoring for pesticide dose determination. In: Wang RGM, Wang CA, Franklin CA, Honeycutt RC, Reinert JC, editors. Biological monitoring for pesticide exposure: measurement, estimation, and risk reduction. Washington, DC: American Chemical Society; 1989. p. 6–27.

Nohynek GJ, Lademann J, Ribaud C, Roberts MS. Grey goo on the skin? Nanotechnology, cosmetic and sunscreen safety. Crit Rev Toxicol. 2007;37:251–77.

Oberdörster G, Maynard A, Donaldson K, Castranova V, Fitzpatrick J, Ausman K, et al. Principles for characterizing the potential human health effects from exposure to nanomaterials: elements of a screening strategy. Part Fibre Toxicol. 2005;2:8.

OECD SIDS. Synthetic amorphous silica and silicates. Available at http://www.chem.unep.ch/irptc/sids/oecdsids/Silicates.pdf (2004).

OSHA 3177. Occupational Safety and Health Administration. Crystalline silica exposure. Health hazard information for construction employees. Available at https://www.osha.gov/Publications/osha3177.pdf (2002>).

Ostrowski A, Nordmeyer D, Boreham A, Brodwolf R, Mundhenk L, Fluhr JW. Skin barrier disruptions in tape stripped and allergic dermatitis models have no effect on dermal penetration and systemic distribution of AHAPS-functionalized silica nanoparticles. Nanomedicine. 2014;10:1571–81.

Otberg N, Patzelt A, Rasulev U, Hagemeister T, Linscheid M, Sinkgraven R, et al. The role of hair follicles in the percutaneous absorption of caffeine. Br J Clin Pharmacol. 2008;65:488–92.

Otterstedt JE, Brandreth DA. Small particles technology. New York: Plenum Press; 1998.

Park YH, Kim JN, Jeong SH, Choi JE, Lee SH, Choi BH, et al. Assessment of dermal toxicity of nanosilica using cultured keratinocytes, a human skin equivalent model and an in vivo model. Toxicology. 2010;267:178–81.

Park YH, Bae HC, Jang Y, JeongSH LHN, Ryu WI, et al. Effect of the size and surface charge of silica nanoparticles on cutaneous toxicity. Mol Cell Toxicol. 2013;9:67–74.

Patzelt A, Richter H, Knorr F, Schafer U, Lehr CM, Dahne L, et al. Selective follicular targeting by modification of the particle sizes. J Control Release. 2011;150:45–8.

Pfluecker F, Wendel V, Hohenberg H, Gartner E, Will T, Pfeiffer S, et al. The human stratum corneum layer: an effective barrier against dermal uptake of different forms of topically applied micronised titanium dioxide. Skin Pharmacol Appl Skin Physiol. 2001;14 Suppl 1:92–7.

Piao Y, Burns A, Kim J, Wiesner U, Hyeon T. Designed fabrication of silica-based nanostructured particle systems for nanomedicine applications. Adv Funct Mater. 2008;18:3745–58.

Pilloni M, Ennas G, Casu M, Fadda AM, Frongia F, Marongiu F, et al. Drug silica nanocomposite: preparation, characterization and skin permeation studies. Pharm Dev Technol. 2013;18:626–33.

Poland CA, Read SAK, Varet J, Carse G, Christensen FM, Hankin SM. Dermal absorption of nanomaterials, Environmental Project No.1504. Denmark: The Danish Environmental Protection Agency; 2013.

Prausnitz MR, Elias PM, Franz TJ, Schmuth M, Tsai JC, Menon GK, et al. Skin barrier and transdermal drug delivery. In: Bolognia J, Jorizzo JL, Schaffer JV, editors. Dermatology. Philadelphia: Saunders; 2012. p. 2065–73.

Proksch E, Brandner JM, Jensen JM. The skin: an indispensable barrier. Exp Dermatol. 2008;17:1063–72.

Prow TW, Grice JE, Lin LL, Faye R, Butler M, Becker W, et al. Nanoparticles and microparticles for skin drug delivery. Adv Drug Deliv Rev. 2011;63:470–91.
Quignard S, Mosser G, Boissière M, Coradin T. Long-term fate of silica nanoparticles interacting with human dermal fibroblasts. Biomaterials. 2012;33:4431–42.
Rancan F, Gao Q, Graf C, Troppens S, Hadam S, Hackbarth S, et al. Skin penetration and cellular uptake of amorphous silica nanoparticles with variable size, surface functionalization, and colloidal stability. ACS Nano. 2012;6:6829–42.
Raju B, Rom WN. Silica, some silicates, coal dust and para-aramid fibrils. IARC monographs on the evaluation of carcinogenic risks to humans. Cancer Cause Control. 1998;68:351–3.
Rosenholm JM, Sahlgren C, Linden M. Multifunctional mesoporous silica nanoparticles for combined therapeutic, diagnostic and targeted action in cancer treatment. Curr Drug Targets. 2011;12:1166–86.
Rougier A, Lotte C, Maibach HI. In vivo percutaneous penetration of some organic compounds related to anatomic site in humans: predictive assessment by the stripping method. J Pharm Sci. 1987;76:451–4.
Scalia S, Franceschinis E, Bertelli D, Iannuccelli V. Comparative evaluation of the effect of permeation enhancers, lipid nanoparticles and colloidal silica on in vivo human skin penetration of quercetin. Skin Pharmacol Physiol. 2013;26:57–67.
SCCP – Scientific Committee on Consumer Products. Preliminary opinion on safety of nanomaterials in cosmetic products. Available at http://ec.europa.eu/health/ph_risk/committees/04_sccp/docs/sccp_o_099.pdf (2007).
Scheuplein RJ. Mechanism of percutaneous absorption. II. Transient diffusion and the relative importance of various routes of skin penetration. J Invest Dermatol. 1967;48:79–88.
Schipper ML, Iyer G, Koh AL, Cheng Z, Ebenstein Y, Aharoni A, et al. Particle size, surface coating, and PEGylation influence the biodistribution of quantum dots in living mice. Small. 2009;5:126–34.
Scodeller P, Catalano PN, Salguero N, Duran H, Wolosiuk A, Soler-Illia GJAA. Hyaluronan degrading silica nanoparticles for skin cancer therapy. Nanoscale. 2013;5:9690–8.
Slowing II, Vivero-Escoto JL, Wu CW, Lin VSY. Mesoporous silica nanoparticles as controlled release drug delivery and gene transfection carriers. Adv Drug Deliv Rev. 2008;60:1278–88.
Slowing II, Vivero-Escoto JL, Trewyn BG, Lin VSY. Mesoporous silica nanoparticles: structural design and applications. J Mater Chem. 2010;20:7924–37.
Smith EW, Maibach HI. Percutaneous penetration enhancers. Boca Raton: CRC Press; 2006.
Som C, Wick P, Krug H, Nowack B. Environmental and health effects of nanomaterials in nanotextiles and facade coatings. Environ Int. 2011;37:1131–42.
Stober W, Fink A. Controlled growth of monodisperse silica spheres in the micron size range. J Colloid Interface Sci. 1968;26:62–9.
Tajmir-Riahi HA, Nafisi S, Sanyakamdhorn S, Agudelo D, Chanphai P. Applications of chitosan nanoparticles in drug delivery. In: Jain KK, editor. Drug delivery systems. Springer; 2014. Chapter 11, p. 165–84.
Takahashi H, Yoshioka Y, Hirai T, Ichihashi KI, Nishijima N, Yoshida T, et al. The size effects of amorphous silica nanoparticles on atopic dermatitis-like skin lesion (P6259). J Immunol. 2013;190:181.12.
Tang L, Cheng J. Nonporous silica nanoparticles for nanomedicine application. Nano Today. 2013;8:290–312.
Tang F, Li L, Chen D. Mesoporous silica nanoparticles: synthesis, biocompatibility and drug delivery. Adv Mater. 2012;24:1504–34.
Thurn KT, Brown E, Wu A, Vogt S, Lai B, Maser J, et al. Nanoparticles for applications in cellular imaging. Nanoscale Res Lett. 2007;2:430–41.
Toll R, Jacobi U, Richter H, Lademann J, Schaefer H, Blume-Peytavi U. Penetration profile of microspheres in follicular targeting of terminal hair follicles. J Invest Dermatol. 2004;123:168–76.
Tregear RT. Physical functions of skin. London: Academic; 1996.
Trommer H, Neubert RH. Overcoming the stratum corneum: the modulation of skin penetration. A review. Skin Pharmacol Physiol. 2006;19:106–21.
Tsunoda S. Transdermal penetration and biodistribution of nanomaterials and their acute toxicity in vivo. Yakugaku Zasshi. 2011;131:203–7.
Unger KK. Porous silica. Amsterdam: Elsevier; 1979.
Vallet-Regi M, Balas F, Arcos D. Mesoporous materials for drug delivery. Angew Chem Int Ed. 2007;46:7548–58.
Van Blaadern A, Van Geest J, Vrij A. Monodisperse colloidal silica spheres from tetraalkoxysilanes: particle formation and growth mechanism. J Colloid Interface Sci. 1992;154:481–501.
Vogt A, Combadiere B, Hadam S, Stieler KM, Lademann J, Schaefer H, et al. 40 nm, but not 750 or 1,500 nm, nanoparticles enter epidermal CD1a+ cells after transcutaneous application on human skin. J Invest Dermatol. 2006;126:1316–22.
Wan Y, Zhao DY. On the controllable soft-templating approach to mesoporous silicates. Chem Rev. 2007;107:2821–60.
Waters KM, Masiello LM, Zangar RC, Tarasevich BJ, Karin NJ, Quesenberry RD, et al. Macrophage responses to silica nanoparticles are highly conserved across particle sizes. Toxicol Sci. 2009;107:553–69.
Welsher K, Sherlock SP, Dai H. Deep-tissue anatomical imaging of mice using carbon nanotube fluorophores in the second near-infrared window. Proc Natl Acad Sci U S A. 2011;108:8943–8.
Wester RC, Noonan PK, Maibach HI. Frequency of application on percutaneous absorption of hydrocortisone. Arch Dermatol. 1977;113:620–2.
Wester RC, Noonan PK, Maibach HI. Variations in percutaneous absorption of testosterone in the rhesus monkey due to anatomic site of application and

frequency of application. Arch Dermatol Res. 1980;267:229–35.

Wilhelm KP, Zhai H, Maibach HI. Dermatotoxicology. New York: CRC Press; 2012.

Willey JD. Amorphous silica. Kirk-Othmer encyclopedia of chemical technology. New York: Wiley; 1982. p. 766–81.

Xia Y, Gates B, Yin Y, Lu Y. Monodispersed colloidal spheres: old materials with new applications. Colloidal spheres. Adv Mater. 2000;12:693–713.

Yu KO, Grabinski CM, Schrand AM, Murdock RC, Wang W, Gu B, et al. Toxicity of amorphous silica nanoparticles in mouse keratinocytes. J Nanopart Res. 2009;11:15–24.

Yu T, Malugin A, Ghandehari H. Impact of silica nanoparticle design on cellular toxicity and hemolytic activity. ACS Nano. 2011;5:5717–28.

Yu T, Greish K, McGill LD, Ray A, Ghandehari H. Influence of geometry, porosity, and surface characteristics of silica nanoparticles on acute toxicity: their vasculature effect and tolerance threshold. ACS Nano. 2012;6:2289–301.

Zhang JH, Zhan P, Wang ZL, Zhang WY, Ming NB. Preparation of monodisperse silica particles with controllable size and shape. J Mater Res. 2003;18:649–53.

Zhang YY, Hu L, Yu DH, Gao CY. Influence of silica particle internalization on adhesion and migration of human dermal fibroblasts. Biomaterials. 2010;31:8465–74.

Predicting Hydration's Effects on Topical Delivery

111

Farhaan Hafeez and Howard I. Maibach

Contents

Keywords
Barrier function • Occlusion • Percutaneous absorption/penetration • Stratum corneum • Octanol-water partition coefficient • Hydrophilicity • Lipophilicity • In vitro • In vivo

1 Introduction

Hydration of the skin is often achieved through occlusion. Occlusion refers to the impervious-to-water covering of the skin directly or indirectly by various means, including tape, gloves, impermeable dressings, and even transdermal devices (Kligman 1996). Certain topical vehicles, e.g., petrolatum and paraffin, contain fats and/or polymer oils that may generate occlusive effects by reducing water loss (Berardesca and Maibach 1988). The epidermis of healthy skin provides an efficient barrier against the infiltration of exogenous and potentially harmful substances, and the stratum corneum typically has a water content of 10–20 % by weight. Skin occlusion increases the water content of the stratum corneum up to 50 %, and even a short time occlusion (30 min) results in significantly increased hydration (Bucks et al. 1991; Bucks and Maibach 1999a; Ryatt et al. 1986). By increasing stratum corneum hydration, occlusion influences percutaneous absorption by altering the partitioning between the chemical penetrant and the skin and swelling corneocytes and possibly altering the intercellular lipid phase organization, increasing skin surface

Modified with permission from: Hafeez F, Maibach HI. Occlusion's Effect on In Vivo Percutaneous Penetration of Chemicals in Man and Monkey: Partition Coefficient Effects. *Skin Pharmacology and Physiology* 2013; 26(2):85–91

Hafeez F, Maibach HI. Do Partition Coefficients (liphophilicity/hydrophilicity) Predict Effects of Occlusion on Percutaneous Penetration in Vitro: A Retrospective Review. *Cutaneous and Ocular Toxicology* (in press)

F. Hafeez (✉)
Department of Dermatology, University of California, San Francisco, San Francisco, CA, USA
e-mail: farhaanhafeez@gmail.com; farhaan.hafeez@yale.edu

H.I. Maibach
Department of Dermatology, School of Medicine, University of California, San Francisco, CA, USA
e-mail: maibachh@derm.ucsf.edu

P. Humbert et al. (eds.), *Agache's Measuring the Skin*,
DOI 10.1007/978-3-319-32383-1_45

temperature, and increasing blood flow (Bucks and Maibach 1999a; Ryatt et al. 1986; Haftek et al. 1998).

In general, occlusion is widely utilized to enhance the penetration of applied drugs in clinical practice; however, occlusion does not increase the percutaneous absorption of all chemicals (Bucks et al. 1991; Bucks and Maibach 1999a). In fact, evidence suggests skin occlusion is more complex than previously thought as it can induce changes in epidermal lipid content, DNA synthesis, epidermal turnover, skin pH, epidermal morphology, sweat glands, and Langerhans cell stresses (Aly et al. 1978; Rajka et al. 1981; Faergemann et al. 1983; Alvarez et al. 1983; Eaglstein 1984; Mertz and Eaglstein 1984; Silverman et al. 1989; Agner and Serup 1993; Matsumura et al. 1995; Berardesca and Maibach 1996; Leow and Maibach 1997; Denda et al. 1998; Kömüves et al. 1999; Fluhr et al. 1999; Warner et al. 1999). This overview focuses on what effect occlusion has on the in vitro and in vivo percutaneous absorption of compounds of varying lipophilicities/hydrophilicities. As few cosmetic ingredients have been studied, other chemical classes noted here may provide guidance for the formulator.

2 Results of In Vitro Experiments

After examining the research articles generated by the search results, five original research articles were obtained that used in vitro occlusion models and provided insight regarding the role of partition coefficients in predicting occlusion's effects on percutaneous penetration; articles that dealt with occlusion and percutaneous penetration but did not shed light on how the lipophilicity/hydrophilicity of a compound could affect occlusion efficacy were excluded. The log of the octanol-water partition coefficients (log Kow) reported here was taken from the publications cited, or they were taken from values obtained from The PubChem Project (http://pubchem.ncbi.nlm.nih.gov/) and LogKow, a databank of evaluated octanol-water partition coefficients (http://logkow.cisti.nrc.ca/logkow/).

Gummer investigated the in vitro percutaneous penetration of methanol and ethanol through full-thickness, excised guinea pig skin at varying volumes and under various occlusive conditions (Gummer and Maibach 1986). Though neither compound demonstrated an increase in penetration with increasing dose volume, they determined that occlusion significantly enhanced penetration ($p < 0.01$) when compared to nonocclusion (see Table 1). Also, the nature of the occlusive material greatly affected both the penetrated amounts of the compounds and the profiles of the amount penetrating per hour. Methanol showed both a greater penetration rate and a greater total penetration than ethanol even though both alcohols have similar octanol-water coefficients. The larger molecular size of ethanol may explain why it penetrated excised guinea pig skin more slowly.

Table 1 In vitro penetration of 14C-labeled methanol and ethanol through guinea pig skin. Occlusion-enhanced penetration of both chemicals compared to nonocclusion. *SD* standard deviation, *ER* enhancement ratio (penetration of occluded chemical divided by penetration of nonoccluded chemical under otherwise identical conditions including dosing) (Modified from Gummer and Maibach 1986)

		Penetration: % of applied dose ± SD	
Volume of alcohol (μL)	Occlusive device	Methanol	Ethanol
50	None	0.48 ± 0.09	0.94 ± 0.14
100	None	1.33 ± 0.30	0.38 ± 0.04
200	None	1.40 ± 0.07	0.29 ± 0.01
100	Parafilm	13.2 ± 2.7 (ER = 9.9 ± 3.0)	8.10 ± 0.43 (ER = 21 ± 2.5)
100	Gel bond	34.8 ± 1.8 (ER = 26 ± 6.1)	23.5 ± 1.6 (ER = 62 ± 7.8)
100	Hill Top chamber	44.2 ± 3.0 (ER = 33 ± 7.8)	27.10 ± 2.54 (ER = 71 ± 10)

Treffel et al. compared the in vitro permeation profiles of two compounds with different physiochemical properties, citropten (lipophilic) and caffeine (amphiphilic), under occluded versus nonoccluded conditions over a 24-hour period using an in vitro model involving human abdominal skin (Treffel et al. 1992). The data demonstrated that occlusion increased the permeation of citropten (partition coefficient = 2.17) 1.6 times over nonoccluded conditions ($p < 0.05$), but occlusion did not enhance the permeation of caffeine (partition coefficient = 0.02). Their results bolster the idea that occlusion does not enhance the percutaneous penetration of all compounds, especially hydrophilic compounds (Bucks et al. 1991).

Roper et al. determined the percutaneous absorption of 2-phenoxyethanol (lipophilic compound; log Kow = 1.16) applied in methanol through nonoccluded rat and human skin in vitro in two diffusion cell systems over 24 h (Roper et al. 1997; Pomona College Medicinal Chemistry Project et al. 1987). Under nonoccluded conditions, 2-phenoxyethanol was greatly lost by evaporation, but once occlusion was applied, evaporation was decreased and total absorption increased.

Taylor et al. studied the effect occlusion exerts upon the in vitro percutaneous penetration of the model penetrant linoleic acid (log Kow = 7.05) dissolved in solvents of two different volatilities, ethanol and cyclomethicone (Taylor et al. 2002; D'Amboise and Hanai 1982). Using porcine skin, nonocclusion resulted in a greater skin concentration of linoleic acid dissolved in an ethanolic vehicle when compared to occlusion ($p < 0.05$); similar statistically significant trends were observed when linoleic acid was dissolved in the less volatile organic solvent cyclomethicone, i.e., nonocclusion resulted in greater percutaneous absorption of linoleic acid in cyclomethicone than occlusion. Then, the authors compared these studies with the percutaneous penetration of glycerol, a hydrophilic molecule, dissolved in an aqueous solution. They did not find statistically significant differences in the concentrations of glycerol in the skin and the receptor cell when comparing the occluded and nonoccluded conditions. The authors attributed their results, which revealed that occlusion did not enhance the percutaneous penetration of the lipophilic compound linoleic acid, to the increase in the concentration gradient of linoleic acid enabled by nonocclusion due to the unimpeded evaporation of the volatile solvents, which provided a greater driving force for percutaneous absorption than occlusion, which prevented evaporation. They found these findings consistent with experiments conducted by Stinchomb et al. which revealed that by increasing the volatility of solvents, one can increase the concentration of the penetrant in the donor phase and enhance the deposition and delivery of the penetrant into the skin (Stinchomb et al. 1999).

Brooks and Riviere used isolated perfused porcine skin flap (IPPSF) topical experiments to study the percutaneous absorption of 14C-labeled phenol (log Kow = 1.50) versus para-nitrophenol (PNP) (log Kow = 1.91) at two concentrations (4 versus 40 μg/cm^2) in two vehicles (acetone versus ethanol) under occluded versus nonoccluded conditions for 8 h in order to determine if dose, vehicle, or occlusion had significant effects on percutaneous penetration (see Tables 2 and 3) (Brooks and Riviere 1996; Korenman and Gorokhov 1973; Brecken-Folse et al. 1994). For phenol, occlusion enhanced the absorption, penetration into tissues, and total recoveries when compared to nonoccluded conditions. Phenol's absorption and penetration into tissues was greater when dissolved in an ethanol vehicle compared to the acetone vehicle under nonocclusive conditions, but phenol's absorption and penetration under occlusive conditions was greater with acetone than with ethanol. Phenol in acetone had a greater percentage of applied dose penetration into tissues at a low dose rather than a high dose, which could suggest a fixed absorption rate for the penetrant (this was also seen for PNP, but only under occlusion). With regard to PNP, neither its dose, vehicle, nor occlusion had a significant effect on total recovery of labeled PNP. These findings led the authors to conclude that absorption of phenol and PNP are dependent upon the vehicle, occlusion, and penetrant.

Table 2 Effects of dose, vehicle, and occlusion on percutaneous penetration of phenol. *SD* standard deviation, *ER* enhancement ratio (penetration of occluded chemical divided by penetration of nonoccluded chemical under otherwise identical conditions including dosing) (Modified from Brooks and Riviere 1996)

	Dose (μg/cm^2)	Penetration (% dose)
Nonoccluded phenol in acetone, 40 μg/cm^2		
Mean ± SD	40.0 ± 0.00	2.60 ± 0.03
Nonoccluded phenol in EtOH, 40 μg/cm^2		
Mean± SD	40.0 ± 0.00	8.49 ± 3.80
Occluded phenol in acetone, 40 μg/cm^2		
Mean ± SD	39.50 ± 0.35	12.21 ± 2.06 (ER = 4.70 ± 0.794)
Occluded phenol in EtOH, 40 μg/cm^2		
Mean± SD	40.20 ± 0.35	8.42 ± 3.23 (ER = 0.99 ± 0.584)
Nonoccluded phenol in acetone, 4.0 μg/cm^2		
Mean ± SD	4.0 ± 0.00	3.88 ± 1.25
Nonoccluded phenol in EtOH, 4.0 μg/cm^2		
Mean ± SD	4.0 ± 0.00	6.24 ± 1.42
Occluded phenol in acetone, 4.0 μg/cm^2		
Mean ± SD	5.17 ± 0.53	17.06 ± 2.04 (ER = 4.40 ± 1.51)
Occluded phenol in EtOH, 4.0 μg/cm^2		
Mean ± SD	5.01 ± 0.62	10.09 ± 1.91 (ER = 1.62 ± 0.479)

Table 3 Effects of dose, vehicle, and occlusion on percutaneous penetration of para-nitrophenol (PNP). *SD* standard deviation, *ER* enhancement ratio (penetration of occluded chemical divided by penetration of nonoccluded chemical under otherwise identical conditions including dosing) (Modified from Brooks and Riviere 1996)

	Dose (μg/cm^2)	Penetration (% dose)
Nonoccluded PNP in acetone, 40 μg/cm^2		
Mean ± SD	43.43 ± 1.25	33.41 ± 3.82
Nonoccluded PNP in EtOH, 40 μg/cm^2		
Mean ± SD	40.93 ± 1.65	31.67 ± 4.19
Occluded PNP in acetone, 40 μg/cm^2		
Mean ± SD	45.13 ± 3.53	24.47 ± 5.08 (ER = 0.732 ± 0.174)
Occluded PNP in EtOH, 40 μg/cm^2		
Mean ± SD	43.28 ± 1.94	7.20 ± 1.58 (ER = 0.23 ± 0.058)
Nonoccluded PNP in acetone, 4.0 μg/cm^2		
Mean ± SD	3.28 ± 0.11	14.19 ± 0.94
Nonoccluded PNP in EtOH, 4.0 μg/cm^2		
Mean ± SD	4.38 ± 0.21	13.32 ± 3.10
Occluded PNP in acetone, 4.0 μg/cm^2		
Mean ± SD	4.433 ± 0.232	28.845 ± 5.171 (ER = 2.033 ± 0.388)
Occluded PNP in EtOH, 4.0 μg/cm^2		
Mean ± SD	3.95 ± 0.05	9.04 ± 2.59 (ER = 0.68 ± 0.25)

3 Results of In Vivo Experiments

Feldmann was the first to correlate the increased pharmacologic effect of hydrocortisone under occlusive conditions with the pharmacokinetics of the penetration of 14C hydrocortisone through normal skin (Feldmann and Maibach 1965). Following the topical application of 14C hydrocortisone to the ventral forearm of human volunteers, the rate and extent of 14C-labeled excretion was measured. The application site was either nonoccluded or occluded with plastic wrap. For the nonoccluded condition, the application site

Table 4 Total excretion data summary for topical application of 14C hydrocortisone to the ventral forearm of human volunteers. The total excretion is the total amount of 14C hydrocortisone excreted in urine after 10 days reported as the percentage of the dose applied (Modified from Feldmann and Maibach 1965)

Method of topical administration	Total excretion (% of dose)	Ratio to unmodified skin
Unmodified	0.46 %	1×
Occluded	4.48	10×
Stripped	0.91	2×
Stripped and occluded	14.91	32×

was washed 24 h post application, while for the occluded skin condition, the plastic wrap was left in place for 96 h post application before the site was washed. The urine for both conditions was collected for 10 days. The percent of the applied dose excreted into the urine after 10 days was 0.46 $\pm$ 0.2 (mean $\pm$ SD) for the nonoccluded condition and 4.48 $\pm$ 2.7 for the occluded condition (Table 4). The occlusive condition significantly increased (tenfold) the cumulative absorption of hydrocortisone compared to the nonoccluded condition ($p = 0.01$). The authors noted that the difference of application duration (24 h exposure for the nonoccluded site versus 96 h exposure for the occluded site) could affect absorption as measured by the cumulative amount of drug excreted into urine, but the significant difference observed in percent dose absorbed at 12 and 24 h between occluded and nonoccluded conditions could not be explained by differences in application duration.

Feldmann then later studied the effect of occlusion on the percutaneous penetration of pesticides (Maibach et al. 1974). They applied 14C-radiolabeled pesticides to the forearm of volunteers, and the rate and extent of 14C-labeled urinary excretion was determined using sensitive methods that allowed the doses to be in micrograms, far below the toxic range of any pesticide. From their experiments, it is evident occlusion has a variable effect on penetration; at a minimum, occlusion increased the penetration of azodrin approximately threefold while at the other extreme, it increased the penetration of malathion almost tenfold (Table 5 and Fig. 1). In general, as the octanol-water partition coefficients increased, occlusion had a greater effect on enhancing penetration, though enhancement by occlusion peaked for malathion and then decreased as the octanol-water partition coefficients further increased. In order to understand how occlusion duration affects penetration, the authors of the study then documented the effects of occluding malathion under variable amounts of time (Table 6). As the occlusion duration increased, the penetration of malathion increased as well, and that by 2 h of occlusion, the penetration had almost doubled, and that by 8 h, penetration almost increased by fourfold. There have been few, if any experiments, besides this one that have documented the effect of occlusion duration on percutaneous penetration.

Guy et al. studied how occlusion impacts the percutaneous absorption of a variety of steroids (progesterone, testosterone, estradiol, and hydrocortisone) in vivo (Guy et al. 1987). In the control studies, they applied the 14C-radiolabeled steroids dissolved in acetone to the ventral forearm of volunteers and then tracked the elimination of the compounds into urine. In the occlusive studies, after evaporation of the acetone vehicle, the site of application was covered with a plastic (Hill Top) chamber. In all cases, the application sites were washed after 24 h using a standardized procedure (Bucks et al. 1985). In the occlusive studies, the authors covered the administration site again with a new chamber after the washing. These studies reveal that occlusion significantly increased the percutaneous absorption of estradiol, testosterone, and progesterone but not that of hydrocortisone, which had the lowest octanol-water partition coefficient among the steroids used (Table 7 and Fig. 2). Moreover, under both occlusion and nonocclusion, percutaneous absorption increased with increasing octanol-water partition coefficient up to testosterone but declined for progesterone.

Table 5 Effect of occlusion on the penetration of pesticides. Kow =octanol-water partition coefficients. *ER* enhancement ratio (penetration of occluded chemical divided by penetration of nonoccluded chemical under otherwise identical conditions including dosing) (Modified from Maibach et al. 1974)

Compound	Log Kow	Control (nonocclusion)	Occlusion (24 h)	ER
Diquat	−3.05	0.4 %	1.4 %	3.5
Baygon	0.14	19.6	68.8	3.5
Azodrin	1.03	14.7	33.6	2.3
Guthion	2.75	15.9	56.1	3.5
Malathion	2.89	6.8	62.8	9.2
Lindane	3.55	9.3	82.1	8.8
Parathion	3.9	8.6	54.8	6.4
Dieldrin	5.4	7.7	65.5	8.5

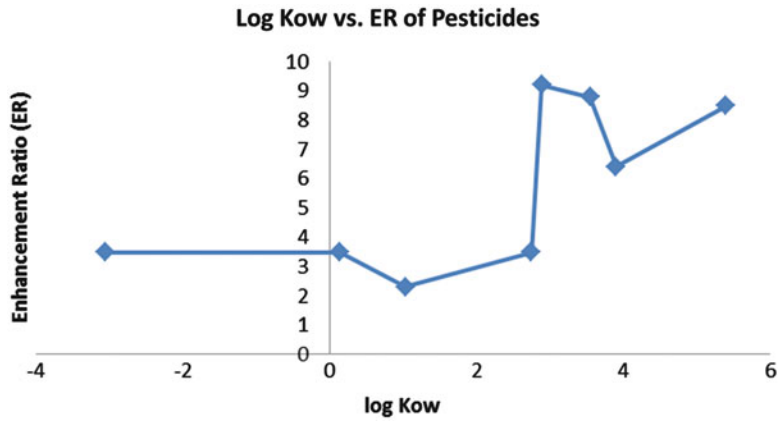

Fig. 1 Log Kow of enhancement ratio (ER) of pesticides. This figure plots the ER of the various pesticides as a function of their log Kows. Kow = octanol-water partition coefficient (Modified from Maibach et al. 1974)

Table 6 Effect of occlusion duration on penetration of malathion (Modified from Maibach et al. 1974)

Duration (hours)	Penetration (%)
0	9.6 %
0.5	7.3
1	12.7
2	16.6
4	24.2
8	38.8
24	62.8

Bucks et al. measured the percutaneous absorption of these same four steroids (hydrocortisone, estradiol, testosterone, and progesterone) in vivo in man under occluded and "protected" (i.e., covered but nonocclusive) conditions (Bucks et al. 1988). Using the same methodology as Guy et al., the 14C-labeled chemicals were applied in acetone to the ventral forearm of volunteers. After vehicle evaporation, the application sites were covered with a semirigid polypropylene chamber for 24 h; intact chambers were used as the occlusive condition, while the "protected" condition was created by boring several small holes through the chamber. Urine was then collected for 7 days post application. In excellent agreement with the previous study by Guy et al., steroid absorption increased with increasing lipophilicity up to a point, but the penetration of progesterone (the most hydrophobic of the steroids) did not continue the trend. With the exception of hydrocortisone, 24 h occlusion significantly increased ($p < 0.01$) percutaneous absorption of the steroids. From these studies, it seemed occlusion enhanced the percutaneous absorption of the more lipophilic steroids but not that of hydrocortisone, the most water-soluble steroid.

Bucks then investigated the effect of occlusion on the in vivo percutaneous absorption of phenols (Bucks et al. 1987, 1988). Nine 14C-ring-labeled

Table 7 Occlusion's effects on percutaneous absorption of steroids in man as a function of penetrant octanol-water partition coefficient. The exposure period was 24 h at 4 μg/cm^2 prior to washing with soap and water. Kow = octanol-water partition coefficient. *SD* standard deviation, *ER* enhancement ratio (penetration of occluded chemical divided by penetration of nonoccluded chemical under otherwise identical conditions including dosing) (Modified from Guy et al. 1987; Bucks and Maibach 1999b)

Compound	log Kow	% applied dose absorbed (mean ± SD)		ER
		Nonoccluded	Occluded	
Hydrocortisone	1.61	2 ± 2	4 ± 2	2 ± 2
Estradiol	3.15	11 ± 5	27 ± 6	2.5 ± 1
Testosterone	3.32	13 ± 3	46 ± 15	3.5 ± 1
Progesterone	3.87	11 ± 6	33 ± 9	3 ± 2

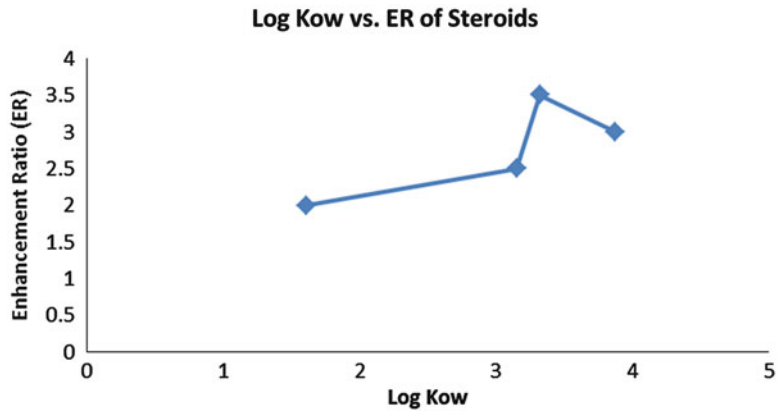

Fig. 2 Log Kow of enhancement ratio (ER) of steroids. This figure plots the ER of the various steroids as a function of their log Kows. Kow = octanol-water partition coefficient (Modified from Guy et al. 1987; Bucks and Maibach 1999b)

para-substituted phenols (4-aminophenol, 4-acetamidophenol, 4-propionylamidophenol, phenol, 4-cyanophenol, 4-nitrophenol, 4-iodophenol, 4-heptyloxyphenol, and 4-pentyloxyphenol) were applied in ethanol to the ventral forearm of male volunteers. After vehicle evaporation, the application site was covered with either an occlusive or protective chamber. After 24 h, the chamber was removed, and the site washed. The application site was then recovered with a new chamber of the same type. Urine was collected for 7 days. On the seventh day, the second chamber was removed, the application site washed, and the upper layers of stratum corneum removed from the application site by tape stripping. These studies indicate that occlusion significantly increased ($p < 0.05$) the absorption of phenol, heptyloxyphenol, and pentyloxyphenol, but occlusion did not significantly increase the absorption of aminophenol, acetaminophen, propionylamidophenol, cyanophenol, nitrophenol, and iodophenol (Table 8 and Fig. 3). The two compounds with the lowest octanol-water partition coefficient demonstrated the least enhancement in absorption under occlusion.

Afterwards Bronaugh et al. investigated the effect of occlusion on the percutaneous absorption of six additional volatile compounds (benzyl acetate, benzamide, benzoin, benzophenone, benzyl benzoate, and benzyl alcohol) in vivo in rhesus monkeys and humans for 24 h employing two occlusion methods, plastic wrap and glass chamber (Bronaugh et al. 1990). In general, occlusion enhanced the absorption of these compounds (Table 9). However, differences in absorption were observed between the plastic wrap and glass chamber occlusive conditions. Benzoin and benzyl acetate absorption were lower under the plastic wrap condition compared to the nonocclusive conditions; the authors conjectured that this discrepancy may be due to compound sequestration by the plastic. Glass chamber occlusion resulted in greater absorption than the

Table 8 Percutaneous absorption of phenols in humans under occluded and protected conditions. Compounds were applied topically in a single dose (2–4 μg/cm^2) from 95 % ethanol to the ventral forearm for 24 h. After 24 h, site was washed with soap and water

Compound	log Kow	% Dose absorbed (mean ± SD)		ER
		Protected[a]	Occluded[b]	
Aminophenol	0.04	6 ± 3	8 ± 3	1.3 ± 0.8
Acetaminophen	0.32	4 ± 3	3 ± 2	0.75 ± 0.8
Propionylamidophenol	0.86	11 ± 7	19 ± 9	1.7 ± 1.4
Phenol	1.46	24 ± 6	34 ± 4	1.4 ± 0.4[C]
Cyanophenol	1.60	31 ± 16	46 ± 6	1.5 ± 0.8
Nitrophenol	1.91	38 ± 11	37 ± 18	0.97 ± 0.6
Iodophenol	2.91	24 ± 6	28 ± 6	1.2 ± 0.4
Heptyloxyphenol	3.16	23 ± 10	36 ± 9	1.6 ± 0.8[d]
Pentyloxyphenol	3.51	13 ± 4	29 ± 8	2.2 ± 0.9[c]

Modified from Ref. (Bucks et al. 1987, 1988)
[a]Dose site covered with a ventilated plastic chamber
[b]Dose site was covered with an occlusive chamber
[c]Significant difference at $p < 0.01$
[d]Significant difference at $p < 0.05$

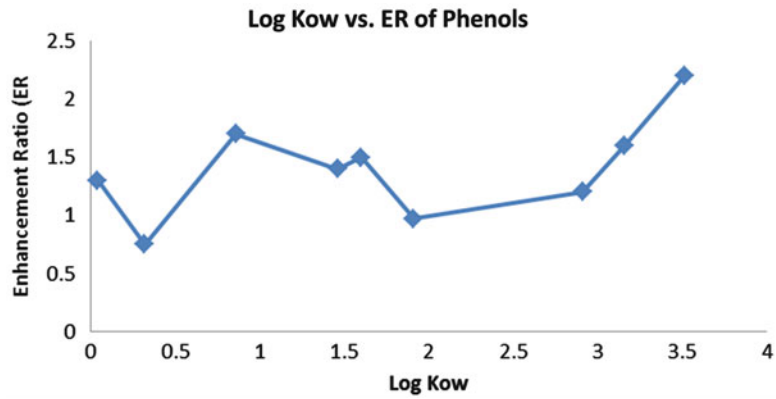

Fig. 3 Log Kow of enhancement ratio (ER) of phenols. This figure plots the ER of the various phenols as a function of their log Kows. Kow = octanol-water partition coefficient (Modified from (Bucks et al. 1987, 1988)

Table 9 Effect of occlusion on percutaneous absorption of benzyl derivatives in monkey. Kow =octanol-water partition coefficients. *ER* enhancement ratio (penetration of occluded chemical divided by penetration of nonoccluded chemical under otherwise identical conditions including dosing) (Modified from Bronaugh et al. 1990)

Compound	log Kow	% Dose absorbed		
		Nonoccluded	Plastic wrap occlusion	Glass chamber occlusion
Benzamide	0.64	47 ± 14	85 ± 8 (ER = 1.8 ± 0.6)	73 ± 20 (ER = 1.6 ± 0.6)
Benzyl alcohol	0.87	32 ± 9	56 ± 29 (ER = 1.8 + 1)	80 ± 15 (ER = 2.5 ± 0.8)
Benzoin	1.35	49 ± 6	43 ± 12 (ER = 0.9 ± 0.3)	77 ± 4 (ER = 1.6 ± 0.2)
Benzyl acetate	1.96	35 ± 19	17 ± 5 (ER = 0.5 ± 0.3)	79 ± 15 (ER = 2.3 ± 1.3)
Benzophenone	3.18	44 ± 15	69 ± 12 (ER = 1.6 ± 0.6)	69 ± 10 (ER = 1.6 ± 0.6)
Benzyl benzoate	3.97	57 ± 21	71 ± 9 (ER = 1.2 ± 0.5)	65 ± 20 (ER = 1.1 ± 0.5)

nonoccluded and plastic wrap occlusion conditions for all the compounds except benzyl benzoate and benzophenone (benzyl benzoate had greater absorption under plastic wrap occlusion than glass chamber occlusion while benzophenone had the same magnitude increase in percent dose absorbed for both occlusive conditions). The authors attempted to correlate the compounds' octanol-water partition coefficients with their occlusion-enhanced skin permeation, but surprisingly, no apparent trends were found. One explanation for this lack of correlation could be that the volatile chemicals evaporated prior to application of the occluding device, which can impact subsequent measures of penetration (Gilpin et al. 2009).

Pellanda et al. investigated the effect of pre- and post-occlusion on the permeation of triamcinolone acetonide (log Kow = 2.53) into the stratum corneum (Pellanda et al. 2007). Their two experiments involved the forearms of ten healthy volunteers. In experiment 1, they applied triamcinolone acetonide (TACA) in acetone to three sites per arm with one arm being pre-occluded for 16 h. In experiment 2, the same dose of TACA in acetone was applied on two sites per arm with one arm being occluded after application till skin sampling. Then, stratum corneum samples were removed by tape stripping at 0.5, 4, and 24 h for experiment 1 and at 4 and 24 h for experiment 2. The amount of corneocytes adhering to the tape strips were quantified directly using a spectrophotometer, and the amount of TACA adhering to each tape was quantified using high-performance liquid chromatography (HPLC). They found that pre-occlusion produced no significant effect on TACA penetration into the stratum corneum, while occlusion after application enhanced TACA penetration significantly by a factor of 2.

4 Discussion

In the nineteenth century, petrolatum was widely used, especially in extemporaneous pharmacist-produced prescriptions, and it remains in use in numerous cosmetic formulations, especially moisturizers, in the twenty-first century. In addition, cosmetic formulations often use oils, especially mineral oil, for their occlusive effects. The general availability of robust evaporimeters has allowed laboratories to readily quantify the degree of occlusion, i.e., inhibition of transepidermal water loss, produced by an ingredient being considered for final formulation.

The data presented here represents a first step in relating the effect of this occlusion on penetration. Note, however, that these studies summarized were performed with total occlusion; much work remains to be done in generating penetration data with the usually less occlusive cosmetic ingredients. Further, we have little data on the effect of occlusive ingredients on those anatomic sites that are partially occluded, such as the axilla, groin, inframammary folds, and toe webs. At least one of these sites – the axilla – demonstrates increased flux compared to the forearm (Feldmann and Maibach 1967).

Skin occlusion can increase the hydration of the stratum corneum up to 50 %, which can have substantial effects on the percutaneous absorption of penetrants by altering the partitioning between the chemical penetrant and the skin, swelling corneocytes, and promoting the uptake of water into the intercellular lipid domains (Bucks et al. 1991; Bucks and Maibach 1999a; Ryatt et al. 1986; Haftek et al. 1998). Though occlusion is widely utilized to enhance the penetration of applied drugs in clinical practice, occlusion does not increase the percutaneous absorption of all chemicals; it is not well understood which chemicals occlusion enhances the penetration through skin (Bucks et al. 1991; Bucks and Maibach 1999a). Here we focus on what effect occlusion has on the percutaneous absorption of compounds of varying lipophilicities/hydrophilicities.

First, occlusion enhances the percutaneous absorption of many but not all compounds. For example, Guy et al. and Bucks et al. found that when measuring occlusion's effects on the

penetration of steroids, the most hydrophilic steroid of the ones being tested, hydrocortisone, did not demonstrate statistically significant enhanced penetration under occlusion (Guy et al. 1987; Bucks et al. 1988). Moreover, Bucks et al. also demonstrated that occlusion did not significantly enhance the penetration of many phenols being tested (Bucks et al. 1987).

Second, occlusion seems to enhance the penetration of very lipophilic compounds more so than very hydrophilic compounds. Bucks et al. and Guy et al. showed that occlusion enhanced the penetration of the most lipophilic steroids (as measured by octanol-water partition coefficient) more so than the least lipophilic ones (Guy et al. 1987; Bucks and Maibach 1999b; Bucks et al. 1988). In addition, Bucks et al. demonstrated that the phenols with the lowest octanol-water partition coefficients had the least enhancement in penetration under occlusion (Bucks and Maibach 1999b; Bucks et al. 1987, 1988).

Thirdly, though occlusion enhances the penetration of the most lipophilic compounds and often fails to enhance the penetration of the least lipophilic steroids, a relationship between a compound's octanol-water partition coefficient and its occlusion-induced enhancement cannot be delineated. With regard to steroid penetration through skin, these studies showed that while a positive relationship exists between a penetrant's octanol-water partition coefficient and its occlusion-enhanced penetration, this relationship is not a linear one (Guy et al. 1987; Bucks et al. 1988). However, with regard to occlusion's effects on the penetration of phenols, no relationship was found between the octanol-water partition coefficient of the penetrant and the extent of its penetration under occlusion (Bucks and Maibach 1999b; Bucks et al. 1987). After investigating the effect of occlusion on the penetration of volatile compounds in vivo in rhesus monkeys, Bronaugh et al. failed to correlate the penetrant's octanol-water partition coefficients with occlusion-enhanced skin permeation (Bronaugh et al. 1990).

Finally, the general shape of the figures plotting the enhancement ratios (the ratio of occlusion-enhanced penetration over nonoccluded penetration) as a function of the logarithms of octanol-water partition coefficients suggests that the enhancement in penetration afforded by occlusion increases up to a point as the partition coefficients increase, but then this enhancement declines as the partition coefficients further rise (see Figs. 1, 2, and 3). Occlusion may enhance the penetration of lipophilic compounds more so than hydrophilic ones due to the rich lipid composition of the stratum corneum, but as the partition coefficients further increase, permeation may be hindered for these very lipophilic compounds as the water content present in the epidermis, which occlusion only increases, assumes a larger role in limiting the permeation of lipophilic compounds.

Moreover, though the data regarding the effect of time on occlusion's effect on penetration is limited, it seems penetration increases with increasing duration of occlusion. However, the study that was presented only documented the effect of occlusion duration for one chemical, the lipophilic compound malathion. More experiments investigating the effect of occlusion duration on a range of chemicals, both lipophilic and hydrophilic, are needed.

In conclusion, occlusion does not universally enhance percutaneous penetration. Occlusion may enhance the penetration of the most lipophilic compounds but often fails to increase the penetration of compounds that are relatively hydrophilic. The in vivo studies reinforce the conclusions drawn from in vitro studies that partition coefficients cannot reliably predict the effect of occlusion on percutaneous penetration. It seems the degree of penetration enhancement provided by occlusion is compound-specific and may be influenced by vehicle selection, temperature, humidity, and method of occlusion. As in many areas of skin biology, what seems to be a simple issue may, in fact, be complex – which seems to be the case for the effect of partition coefficient and occlusion on penetration. Taken together, this data provides some insights to aid the formulator especially interested in occlusive vehicles and should lead to experiments that will provide data on ingredients such as petrolatum, oils, etc., which are presumably not fully occlusive.

References

Agner T, Serup J. Time course of occlusive effects on skin evaluated by measurement of transepidermal water loss (TEWL): including patch tests with sodium lauryl sulphate and water. Contact Dermatitis. 1993;28:6–9.

Alvarez OM, Mertz PM, Eaglstein WH. The effect of occlusive dressings on collagen synthesis and re-epithelialization in superficial wounds. J Surg Res. 1983;35:142–8.

Aly R, Shirley C, Cunico B, Maibach HI. Effect of prolonged occlusion on the microbial flora, pH, carbon dioxide and transepidermal water loss on human skin. J Invest Dermatol. 1978;71:378–81.

Berardesca E, Maibach HI. Skin occlusion: treatment or drug-like device? Skin Pharmacol. 1988;1:207.

Berardesca E, Maibach HI. The plastic occlusion stress test (POST) as a model to investigate skin barrier function. In: Maibach HI, editor. Dermatologic research techniques. Boca Raton: CRC Press; 1996. p. 179–86.

Brecken-Folse JA, Mayer FL, Pedigo LE, Marking LL. Acute toxicity of 4-nitrophenol, 2,4-dinitrophenol, terbufos and trichlorfon to grass shrimp (Palaemonetes spp.) and sheepshead minnows (Cyprinodon variegatos) as affected by salinity and temperature. Environ Toxicol Chem. 1994;13(1):67–77.

Bronaugh RL, Wester RC, Bucks D, Maibach HI, Sarason R. In vivo percutaneous absorption of fragrance ingredients in rhesus monkeys and humans. Food Chem Toxicol. 1990;28:369–73.

Brooks JD, Riviere JE. Quantitative percutaneous absorption and cutaneous distribution of binary mixtures of phenol and paranitrophenol in isolated perfused porcine skin. Fundam Appl Toxicol. 1996;32:233–43.

Bucks D, Maibach HI. Occlusion does not uniformly enhance penetration in vivo. In: Bronaugh RL, Maibach HI, editors. Percutaneous absorption: drugs, cosmetics, mechanisms, methodology. 3rd ed. New York: Dekker; 1999a. p. 81–105.

Bucks D, Maibach HI. Occlusion does not uniformly enhance penetration in vivo. In: Bronaugh RL, Maibach HI, editors. Percutaneous absorption: drugs, cosmetics, mechanisms, methodology. 3rd ed. New York: Dekker; 1999b. p. 81–105.

Bucks DAW, Maibach HI, Guy RH. Percutaneous absorption of steroids: effect of repeated application. J Pharm Sci. 1985;74:1337–9.

Bucks DA, McMaster JR, Maibach HI, Guy RH. Percutaneous absorption of phenols in vivo. Clin Res. 1987;35:672A.

Bucks DA, McMaster JR, Maibach HI, Guy RH. Bioavailability of topically administered steroids: a 'mass balance' technique. J Invest Dermatol. 1988;91:29–33.

Bucks D, Guy R, Maibach HI. Effects of occlusion. In: Bronaugh RL, Maibach HI, editors. In vitro percutaneous absorption: principles, fundamentals, and applications. Boca Raton: CRC Press; 1991. p. 85–114.

D'Amboise M, Hanai T. Hydrophobicity and retention in reversed-phase liquid chromatography. J Liq Chromatogr. 1982;5(2):229–44.

Denda M, Sato J, Tsuchiya T, Elias PM, Feingold KR. Low humidity stimulates epidermal DNA synthesis and amplifies the hyperproliferative response to barrier disruption: implication for seasonal exacerbations of inflammatory dermatoses. J Invest Dermatol. 1998;111:873–8.

Eaglstein WH. Effect of occlusive dressings on wound healing. Clin Dermatol. 1984;2:107–11.

Faergemann J, Aly R, Wilson DR, Maibach HI. Skin occlusion: effect on Pityrosporum orbiculare, skin PCO2, pH, transepidermal water loss, and water content. Arch Dermatol Res. 1983;275:383–7.

Feldmann RJ, Maibach HI. Penetration of 14-C hydrocortisone through normal skin: the effect of stripping and occlusion. Arch Dermatol. 1965;91:661–6.

Feldmann RJ, Maibach HI. Regional variation in percutaneous penetration of 14C cortisol in man. J Invest Dermatol. 1967;48:181–3.

Fluhr JW, Lazzerini S, Distante F, Gloor M, Berardesca E. Effects of prolonged occlusion on stratum corneum barrier function and water holding capacity. Skin Pharmacol Appl Skin Physiol. 1999;12:193–8.

Gilpin SJ, Hui X, Maibach HI. Volatility of fragrance chemicals: patch testing implications. Dermatitis. 2009;20:200–7.

Gummer CL, Maibach HI. The penetration of [14C] ethanol and [14C] methanol through excised guinea pig skin in vitro. Food Chem Toxicol. 1986;24:305–9.

Guy RH, Bucks DAW, McMaster JR, Villaflor DA, Roskos KV, Hinz RS, Maibach HI. Kinetics of drug absorption across human skin in vivo. In: Shroot B, Schaefer H, editors. Skin pharmacokinetics. Basel: Karger; 1987. p. 70–6.

Haftek M, Teillon MH, Schmitt D. Stratum corneum, corneodesmosomes and ex vivo percutaneous penetration. Microsc Res Tech. 1998;43:242–9.

Kligman AM. Hydration injury to human skin. In: Van der Valk PGM, Maibach HI, editors. The irritant contact dermatitis syndrome. Boca Raton: CRC Press; 1996. p. 187–94.

Kömüves LG, Hanley K, Jiang Y, Katagiri C, Elias PM, Williams ML, Feingold KR. Induction of of selected lipid metabolic enzymes and differentiation-linked structural proteins by air exposure in fetal rat skin explants. J Invest Dermatol. 1999;112:303–9.

Korenman YI, Gorokhov AA. Distribution of diphenylolpropane between certain organic solvents and water. J Appl Chem. 1973;46(11):2751–3.

Leow YH, Maibach HI. Effect of occlusion on skin. J Dermatol Treat. 1997;8:139–42.

Maibach HI, Feldmann RJ. Systemic absorption of pesticides through the skin of man; in Task Group on Occupational Exposure to Pesticides, editors, Occupational exposure to pesticides. Report to the Federal Working Group on Pest Management from the Task Group on

Occupational Exposure to Pesticides. Washington, Federal Working Group on Pest Management; 1974. p. 120–127.

Matsumura H, Oka K, Umekage K, Akita H, Kawai J, Kitazawa Y, Suda S, Tsubota K, Ninomiya Y, Hirai H, Miyata K, Morikubo K, Nakagawa M, Okada T, Kawai K. Effect of occlusion on human skin. Contact Dermatitis. 1995;33:231–5.

Mertz PM, Eaglstein WH. The effect of a semiocclusive dressing on the microbial population in superficial wounds. Arch Surg. 1984;119:287–9.

Pellanda C, Strub B, Figuiredo V, Rufli T, Imanidis G, Surber C. Topical bioavailability of triamcinolone acetonide: effect of occlusion. Skin Pharmacol Physiol. 2007;20:50–6.

Pomona College Medicinal Chemistry Project, Claremont, CA 91711, Log P Database, (C. Hansch and A. Leo), July 1987 edition.

Rajka G, Aly R, Bayles C, Tang Y, Maibach HI. The effect of short term occlusion on the cutaneous flora in atopic dermatitis and psoriasis. Acta Derm Venereol. 1981;61:150–3.

Roper CS, Howes D, Blain PG, Williams FM. Percutaneous penetration of 2-phenoxyethanol through rat and human skin. Food Chem Toxicol. 1997;35:1009–16.

Ryatt KS, Stevenson JM, Maibach HI, Guy RH. Pharmacodynamic measurement of percutaneous penetration enhancement in vivo. J Pharm Sci. 1986;75:374–7.

Silverman RA, Lender J, Elmets CA. Effects of occlusive and semiocclusive dressings on the return of barrier function to transepidermal water loss in standardized human wounds. J Am Acad Dermatol. 1989;20:755–60.

Stinchomb AL, Pirot F, Touraille GD, Bunge AL, Guy RH. Chemical uptake into human stratum corneum in vivo from volatile and non-volatile solvents. Pharm Res. 1999;16:1288–93.

Taylor LJ, Robert SL, Long M, Rawlings AV, Tubek J, Whitehead L, Moss GP. Effect of occlusion on the percutaneous penetration of linoleic acid and glycerol. Int J Pharmaceut. 2002;249:157–64.

Treffel P, Muret P, Muret-D'Aniello P, Coumes-Marquet-S, Agache P. Effect of occlusion on in vitro percutaneous absorption of two compounds with different physicochemical properties. Skin Pharmacol. 1992;5:108–13.

Warner RR, Boissy YL, Lilly NA, Spears MJ, McKillop K, Marshall JL, Stone KJ. Water disrupts stratum corneum lipid lamellae: damage is similar to surfactants. J Invest Dermatol. 1999;113:960–6.

Multiphoton Tomography

112

Karsten König

Contents

Keywords

Multiphoton • Two-photon • Tomography • Autofluorescence • Elastin • Collagen • NAD(P)H • FLIM • SHG • THG • CARS • Optical biopsy • Functional imaging • Melanoma • Dermatitis • Cosmetics • Aging • Sunscreen • Basalioma • Nevi • Fluorescence lifetime imaging (FLIM) • Human pathological skin • Principle of • Second harmonic generation (SHG) • Third harmonic generation (THG)

1 Introduction

In the past decade, multiphoton tomography (MPT) has emerged as a powerful noninvasive label-free 3D-imaging technique for in vivo human skin characterization (König and Riemann 2003; König et al. 2007; König 2008, 2012). MPT has superior submicron spatial resolution, single-photon sensitivity, and functional imaging capability compared to other 3D tissue imaging techniques such as 20–100 MHz ultrasound (Korting et al. 1999, 2010a), optical coherence tomography (OCT) (Drexler and Fujimoto 2008; König et al. 2009; Annesh et al. 2011), and confocal reflectance microscopy (Rajadhyaksha 1999; Koehler et al. 2011, Table 1).

Furthermore, two-photon excited fluorescence elastin can be easily co-registered with collagen where the signal is based on second-harmonic generation (SHG) (König and Riemann 2003; Campagnola et al. 2001). This allows to

K. König (✉)
Department of Biophotonics and Laser Technology, Saarland University, Saarbruecken, Germany

JenLab GmbH, Jena, Germany
e-mail: k.koenig@blt.uni-saarland.de

P. Humbert et al. (eds.), *Agache's Measuring the Skin*,
DOI 10.1007/978-3-319-32383-1_46

Table 1 Comparison of 3D skin-imaging methods

Method	Intracellular imaging	Resolution (μm)	Functional imaging	Chemical information	Signal depth	FOV (mm^2)	Price
US	No	>10	No	No	>1 mm	5 × 5	€
OCT	No	>10	No	No	>0.5 mm	>5 × 5	€€
CRM	Yes	>1	No	No	<0.15 mm	0.3 × 0.3/4 × 4	€€€
MPT	Yes	<0.5	Yes	Yes	<0.3 μm	0.3 × 0.3/4 × 4	€€€€

US ultrasound, *OCT* optical coherence tomography, *CRM* confocal reflectance microscopy (confocal laser scanning microscopy), *MPT* multiphoton tomography

characterize the dermal fiber networks and to determine the skin age by the parameter *skin aging index SAAID* (Lin et al. 2005; Koehler et al. 2006). The physical taken tissue sample, the slicing, the staining, and the microscopic visualization are not required.

MPT opens the way to provide label-free optical biopsies with the best spatial resolution of all clinical tissue imaging methods. The biopsies can be obtained within seconds by femtosecond laser beam scanning in different skin depths (optical sectioning) with a typical section thickness of 2 μm. The lateral resolution is about 300–400 nm. This allows even the imaging of intratissue organelles, nuclei, and single dermal fibers.

2 Principle of Multiphoton Tomography

The tomographs are based on near-infrared (NIR) laser radiation in the spectral range of 700–1,000 nm which corresponds to the *optical window of cells and tissues*. This provides a high light penetration depth. However, laser class 1M clinical multiphoton tomographs have a signal depth limitation of 200–320 μm due to the working distance of the high-numerical-aperture focusing optics.

The MPT signals of the human skin are mainly based on two-photon autofluorescence (AF) and SHG. These signals provide sufficient information to image the morphological features of cells and the extracellular matrix (ECM) such as the cell nucleus, single mitochondria, dendrites, dermal papillae (DP), hair shafts, microvessels, elastin fibers, and collagen structures. The dermal-epidermal junction (DEJ) can be easily visualized in 3D.

Endogenous fluorophores include keratin, NAD(P)H, flavins, melanin, and a variety of porphyrins (König and Schneckenburger 1994; Breunig et al. 2010). SHG-active components include fibrillar collagens, muscle components (myosin rod domains), and nerves.

MPT provides not only morphological features. It can be used for functional imaging due to the detection of the biosensors NAD(P)H and flavins. Both types of coenzymes are involved in the respiratory chain activity and therefore in the cell's metabolism. The oxidized coenzyme NAD(P) does not fluoresce. Therefore, any oxidation by reactive oxygen species (ROS) results in a decrease of autofluorescence. The action of ROS scavengers results in an AF increase. The ratios of (i) NAD(P)H/flavins and (ii) free NAD(P)H/bound NAD(P)H are further parameters of cellular metabolism (Chance 1962; Schneckenburger and König 1992).

MPT provides information of the ratio of NAD(P)H-protein complexes (bound NAD(P)H) and free NAD(P)H (non-bound) by the method of fluorescence lifetime imaging (FLIM) (Bugiel et al. 1989; König and Wabnitz 1990; Becker 2005; König et al. 2010b). The fluorescence lifetime τ is a characteristic parameter of the fluorophore and its microenvironment and nearly independent on concentration. Free and bound NAD(P)H have typical fluorescence lifetimes of 0.3 ns and 2.2 ns, respectively. The porphyrin *protoporphyrin IX* that is produced by the skin bacterium *Propionibacterium acnes* has a typical τ value of 11 ns, whereas the flavin *flavomononucleotide* (FMN) has a lifetime of 5.3 ns (König and

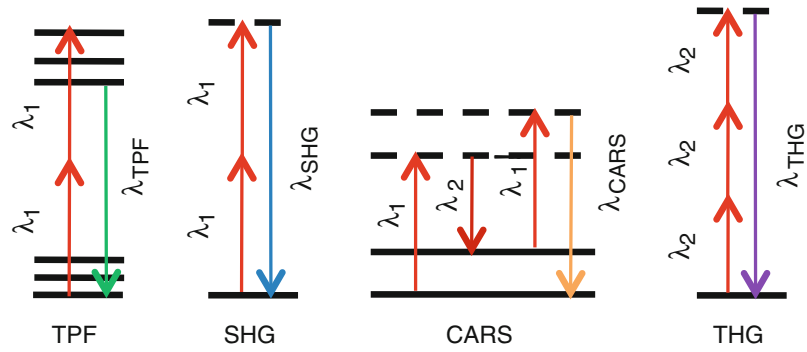

Signal	Signal Source
AF intensity	NAD(P)H, flavins, melanin, keratin, porphyrins, elastin
AF lifetime (FLIM)	NAD(P)H, flavins, melanin, keratin, porphyrins, elastin
SHG	collagen fibrils, muscels, nerves
THG	membranes, erythrocytes
CARS	lipids, water, chemicals

Fig. 1 Scheme of signal generation. Two-photon processes result in fluorescence and second-harmonic generation. Three-photon processes result in third-harmonic generation. CARS requires two laser beams

Schneckenburger 1994; König et al. 2010b). Therefore, FLIM provides a further contrast mechanism to image different types of fluorophores and their binding behavior.

Very recent MPT developments include also chemical fingerprint information based on an additional coherent anti-Stokes Raman scattering (CARS) module (König et al. 2011a; Breunig et al. 2012, 2013; Weinigel 2014). CARS provides similar information as Raman spectroscopy and depicts molecule vibration signals. However, CARS imaging has the advantage of being several orders faster than Raman imaging. MPT-CARS tomography provides an optical CARS section within 1 s without any averaging. In contrast to the one-beam multiphoton tomographs for AF, FLIM, and SHG, the add-on CARS module requires a second laser beam that has to overlap in time and space with the first beam within the target.

The certified multiphoton CARS tomograph MPTflex-CARS provides information on lipids based on the CH stretch vibration and on water. More chemical information can be obtained by tuning the laser wavelengths of the two-beam module to a specific spectral region of interest.

Figure 1 describes schematically the various nonlinear processes in multiphoton tomography and lists the sources of signals (AF, SHG, THG, CARS) generated in the non-labeled human skin. All processes require high transient light intensities that are provided by tight focusing of the femtosecond laser beams. Eighty million laser pulses per second at very low picojoule pulse energy and a mean power of 2–20 mW are applied. One optical section of 0.3 × 0.3 mm^2 that consists of 512 × 512 pixels can be acquired within 1 s.

Figure 2 shows the two types of certified flexible multiphoton tomographs. The tomograph MPTflex is for fluorescence and SHG imaging. The larger system MPTflex-CARS has an additional wavelength extension unit based on a

Fig. 2 The multiphoton tomographs MPTflex and MPTflex-CARS

photonic-crystal fiber (CARS module) to generate a second laser beam at the spectral range of 900–1,200 nm. This additional laser beam can be also used to realize third-harmonic generation (THG) (Débarre et al. 2006) in order to visualize membranes such as from erythrocytes. Both systems possess a flexible mechanical/optical arm with a patented 360° scan head as demonstrated in Fig. 3.

The older certified multiphoton tomographs of the first generation called *DermaInspect* (JenLab GmbH, Jena, Germany) are not flexible and require a vibration-controlled optical table.

Figure 4 shows a typical stack of horizontal multiphoton sections of the normal forearm skin. The major signal from the outermost layer *stratum corneum* originates from keratin-containing corneocytes. Going deeper into the living epidermis, the images are dominated by NAD(P)H-containing keratinocytes. Upon reaching the

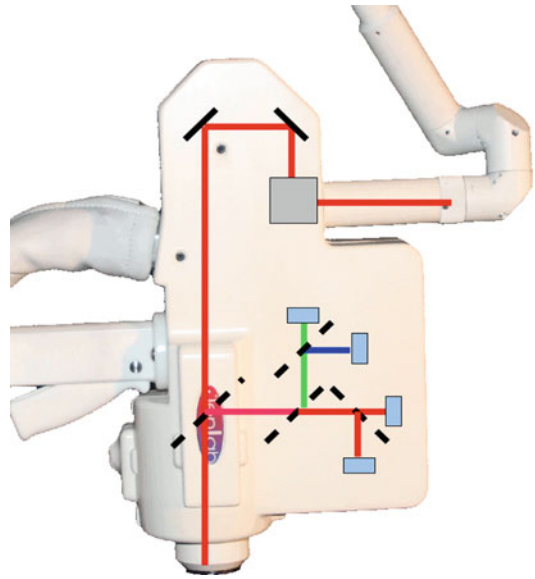

Fig. 3 The flexible scan head provides easy access to various skin regions

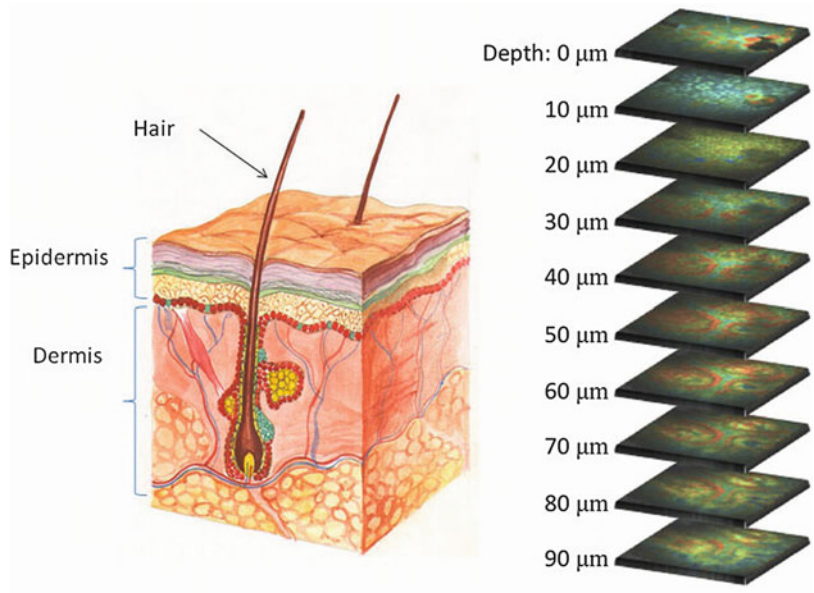

Fig. 4 Multiphoton tomographs provide stacks of optical sections within seconds

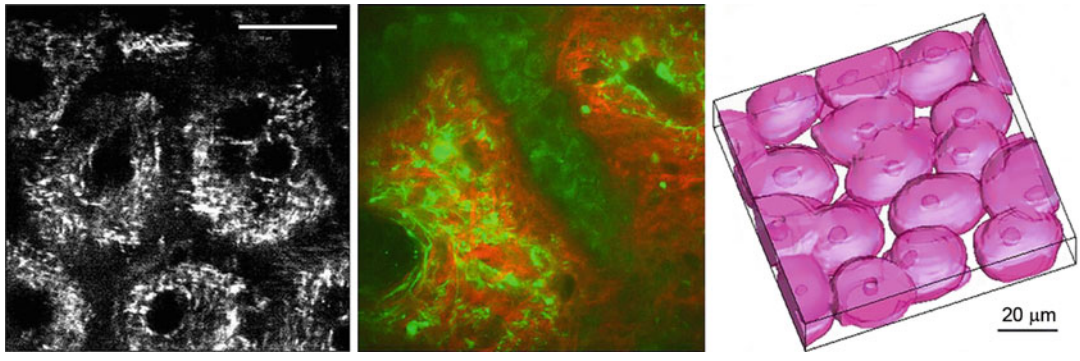

Fig. 5 Multiphoton tomography provides the best resolution of all tissue imaging techniques (0.3 µm lateral resolution). Even deep-tissue single-mitochondria and single-elastin fibers can be imaged noninvasively and label-free

stratum basale, the fluorophore melanin provides the highest fluorescence quantum yield. Therefore, keratinocytes with melanin tend to provide stronger signals than keratinocytes without melanin. At the DEJ, first SHG signals occur from the top of the dermal papillae.

Using the zoom function, the tomographs allow a very close look into single living cells deep into the epidermis. As depicted in Fig. 5, the extremely high submicron spatial resolution allows even the visualization of a single intracellular intratissue mitochondrion. The images in Fig. 6 demonstrate the corresponding FLIM image where the pseudo-color depicts the fluorescence lifetime.

Wide-field high-resolution images up to 3×3 mm^2 can be generated mosaic-like by the motorized scan head. Also vertical sections (x,z-scans) can also obtained (Fig. 7).

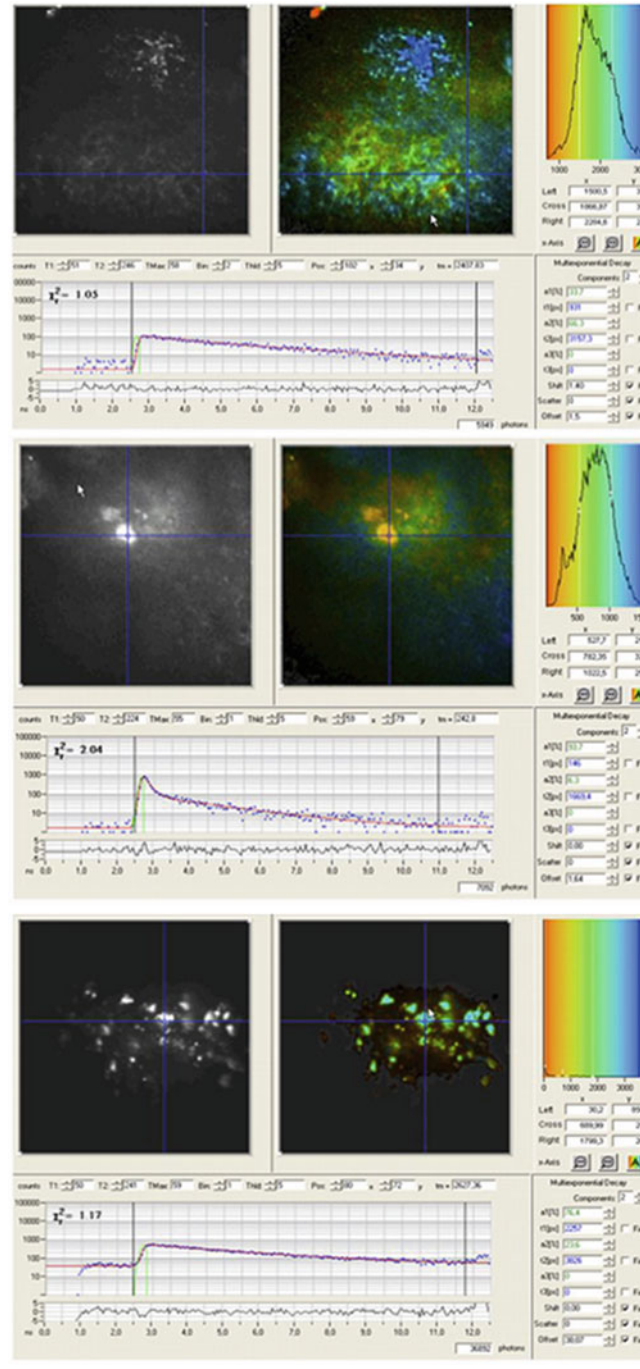

Fig. 6 The pseudocolor-coded FLIM image depicts the mean fluorescence lifetime per pixel as fourth dimension. The image shows the distribution of intradermal fluorescent tattoo nanoparticles and a typical fluorescence decay curve of a single particle

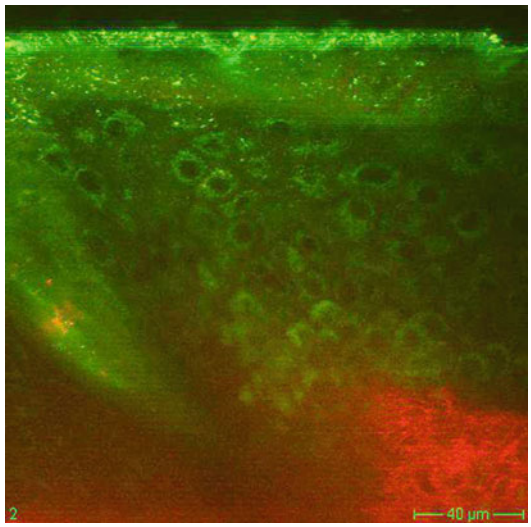

Fig. 7 Vertical section (x,z-scans) can also be generated with the multiphoton tomograph

3 Applications

Major applications of multiphoton tomography are the evaluation of human pathological skin as well as the in situ intradermal detection of pharmaceutics and cosmetics.

Medical investigations include:

i. The early diagnosis of *malignant melanoma* and other skin cancers (Dimitrow et al. 2009; Seidenari et al. 2012a; Patalay et al. 2012)
ii. Early diagnosis of *dermatitis* and monitoring of treatment effects (Huck et al. 2016)
iii. The optimization of chronic wound management and photodynamic therapy of *actinic keratosis*
iv. Intradermal lipid distribution of patients with *psoriasis* and skin cancer(Breunig et al. 2012, 2013; Weinigel) as well as
v. The evaluation of skin aging induced by UV exposure and smoking (Koehler et al. 2008, 2009)

Also the in situ distribution and characterization of tattoo nanoparticles in the skin has been studied (König).

Furthermore, multiphoton tomographs are involved in the astronaut's health program of the European Space Agency (ESA) to test preflight and post-flight skin conditions of the astronauts and to evaluate the effects of long-term (6 months) extraterrestrial work at the international space lab ISS.

The major cosmetic and pharmaceutical companies employ multiphoton tomographs to evaluate and study:

i. The biosafety of sunscreen nanoparticles (Zvyagin et al. 2008; Sanchez et al. 2010; Darvin et al. 2012)
ii. The skin age and the efficacy of antiaging products (Bazin et al. 2010; Decenciere et al. 2013; Puschmann et al. 2012; Miyamaoto and Kudoh 2013)
iii. Melanin types and dyes in hairs (Ehlers et al. 2007)
iv. The skin barrier function (Richter et al. 2004)
v. The effects of cosmetics on cellular metabolism
vi. Drug delivery (König et al. 2006, 2011b; Roberts et al. 2008; Prowv et al. 2011)
vii. The use of multiphoton tomography in tissue engineering (Roberts et al. 2011)

4 Skin Aging Index SAAID

Multiphoton tomography allows the accurate determination of the skin age by measuring age-associated alterations in the extracellular matrix, in particular the fiber network. The quantitative parameter SAAID characterizes the collagen-elastin ratio of the dermis. It is defined as

$$\mathrm{SAAID} = (\mathrm{SHG} - \mathrm{AF})/(\mathrm{SHG} + \mathrm{AF})$$

with values between −1 and 1. Negative values mean that the elastin autofluorescence is stronger than the SHG signal from collagen. A value of 0 means that both signals are similar. The parameter depends on the relative tissue position and requires statistical analysis. The SAAID correlates with the biological age of healthy

volunteers as shown by in vivo multiphoton tomography on healthy subjects. Smoking and tanning influence the SAAID values and show skin ages older than biological ages.

The multiphoton tomographs employ two or more photodetectors (photomultipliers). This allows the simultaneous imaging of the elastin fiber network by AF and the collagen network by SHG within one scan. The detectors can operate in the analogue mode (signal intensities) and in the single-photon counting (SPC) mode.

For quantitative imaging, two approaches are currently undertaken. The first one is based on the computation of the mean intensities or counts of AF and SHG signals. The second one is based on pixel densities.

The company L'Oreal developed an automatic 3D segmentation software to analyze the dermal-epidermal junction (DEJ), the skin surface, and the elastin-collagen networks (Decenciere et al. 2013). In particular, they calculated a 3D SAAID index where a huge number of voxels from the upper dermis was considered. A mean epidermal thickness of young vs. old European skin of 66 μm versus 59 μm was determined. The density of elastic fibers was found to be increased with age, whereas the density of collagen did not differ between young and old skin. The SAAID decreased with age.

The company Beiersdorf named the elastin-to-collagen ratio as the ELCOR parameter. ELCOR is indirectly proportional to the SAIID index. As expected, an increase of the ELCOR values with age was measured when studying the volar forearm skin of chronically sun-exposed with sun-protected skin (Puschmann et al. 2012).

The company Procter & Gamble studied cellular metabolism in dependence on age by measuring the NAD(P)H values in the *stratum granulosum* of 59 Japanese female indoor workers (Miyamaoto and Kudoh 2013). Interestingly, they found statistically different NAD(P)H levels of 38.8 vs. 32.7 in the young group (20s) compared with elderly women (60s), respectively. New cosmetic care products for aging skin focus.

5 FLIM Tomography to Study Dermatitis

In addition to the three spatial dimensions, a fourth dimension can be added based on fluorescence lifetime imaging (FLIM). In principle, the arrival times of the emitted photons with regard to the femtosecond excitation pulses are measured using time-correlated single-photon counting (TCSPC). The typical temporal resolution is 270 ps. The fourth dimension *fluorescence lifetime* can be depicted as color-coded signal per pixel where the color reflects, e.g., a mean fluorescence lifetime per pixel based on a bi-exponential deconvolution. SHG can be detected as component with a lifetime "zero."

The hospital at the University of Muenster, Germany, is using the FLIM module to measure the skin inflammation and to study the effects of cortisone treatment to patients suffering from severe dermatitis (Huck et al. 2016). The clinicians found a strong correlation between the strength of disease and the mean autofluorescence lifetime of the epidermis and observed a lifetime change as a result of treatment effects (Fig. 7).

Other groups work on multiphoton FLIM tomography to evaluate the clinical potential for early tumor diagnostics (Arginelli et al. 2013; Manfredini et al. 2013; Seidenari et al. 2012b, c; Koehler et al. 2012; Benati et al. 2011; Patalay et al. 2011).

The FLIM modality in the multiphoton tomographs is based on SPC. Typically, 100 photons are counted within 1 pixel for 12 μs beam dwell times. SPC provides therefore real photon numbers from region of interests that can be used for quantitative imaging and the generation of intratissue concentration maps.

6 CARS of Psoriasis

The multiphoton tomograph MPTflex-CARS is employed in clinical studies on the Charite, Berlin, on patients suffering from skin cancer, the head and feet syndrome, and psoriasis (König et al. 2011a, Breunig et al. 2012, 2013). The tomograph was employed to visualize the C=H

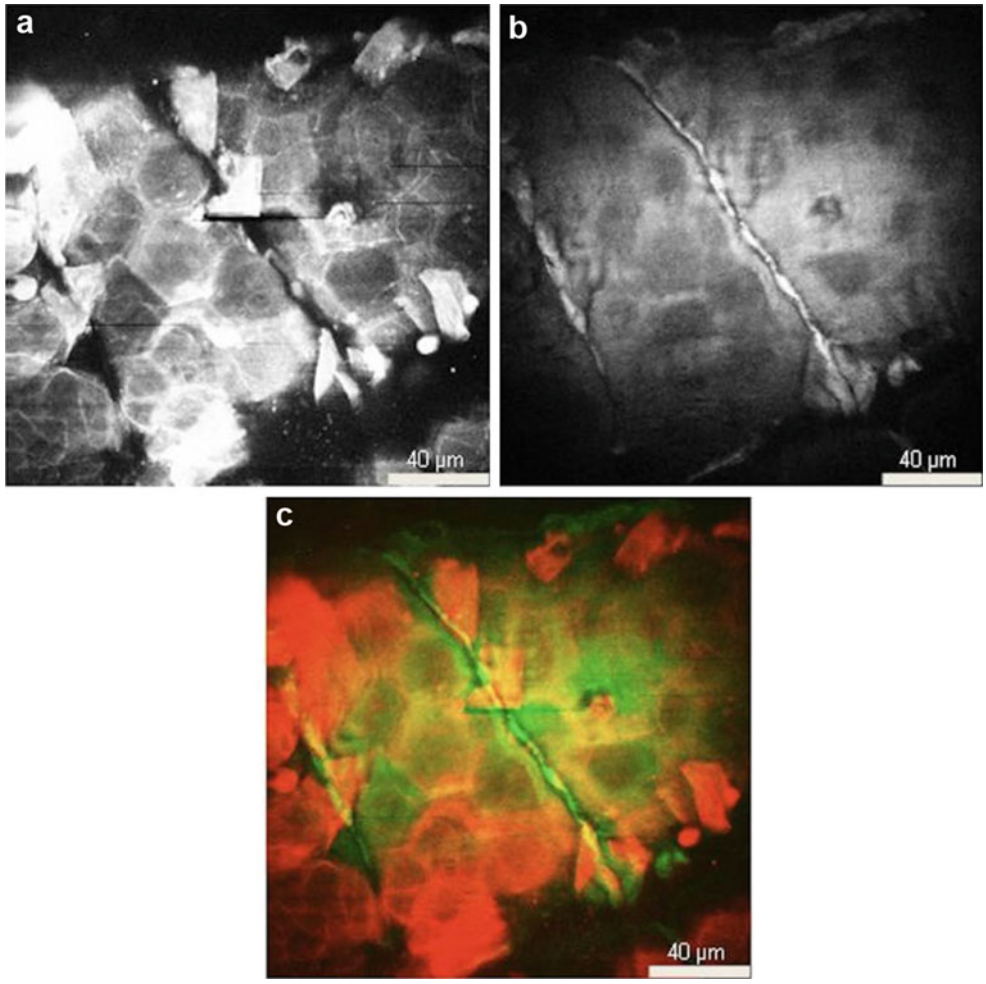

Fig. 8 Multiphoton CARS tomography. (**a**) Optical AF section showing NAD(P)H distribution. (**b**) Optical CARS section showing lipid distribution. (**c**) Overlay (König 2011a)

stretch vibration which mainly indicates lipids. Figure 8 demonstrates one section out of an optical biopsy that contained information on AF, and CARS. The autofluorescence image depicts mainly the distribution of the reduced coenzyme NAD(P)H, whereas the CARS image shows the lipid distribution of the exact same intratissue section. As seen, the CARS image provides additional information. In the study on patients suffering from psoriasis, significant modifications of the lipid distribution were found compared to healthy skin areas. Multiple clinical studies are currently going on trace chemotherapeutics in the sweat pores and their microenvironment of cancer patients as well as to study drug delivery.

7 Conclusion

Multiphoton tomography (MPT) is a novel, high-resolution, and safe (Fischer et al. 2008) high-tech skin imaging modality based on near-infrared femtosecond laser technology. MPT provides morphological and functional optical biopsies (e.g., Balu et al. 2013) within seconds and with submicron resolution without any labeling.

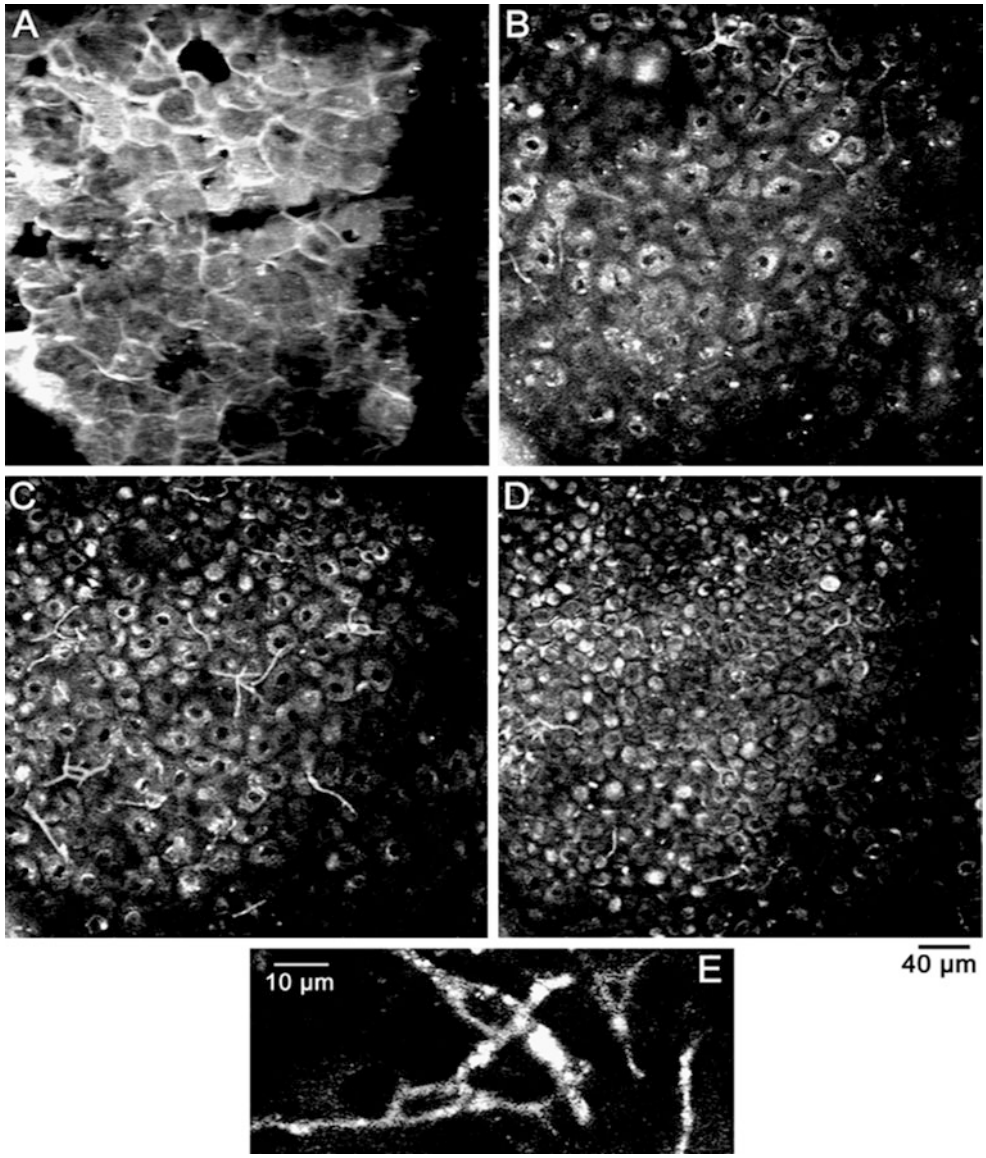

Fig. 9 Multiphoton tomography can be used in early detection of malignant melanoma. Melanocytes can be easily imaged as well as cell-cell distances, irregular morphology, and pleophorism

It has the potential to reduce significantly the number of physically taken skin biopsies, to support personalized medicine by evaluating therapeutic strategies and providing rapid diagnostic images, as well as to measure drug delivery. One major application is the early diagnosis of pigmented lesions. Fig. 9 shows typical optical sections of a patient suffering from malignant melanoma.

Multiphoton tomography is also employed in research and test centers of major cosmetic companies to prove the biosafety of sunscreen and make-up nanoparticles and the efficacy of antiaging products.

References

Annesh A, Weingast J, Weinigel M, Höfer M, Nemecek R, Binder M, König K, et al. 3D multiphoton/optical coherence tomography for clinical diagnosis of nonmelanoma skin cancers. J Biomed Opt. 2011;3:653–74.

Arginelli F, Manfredini M, Bassoli S, Dunsby C, French P, König K, Magnoni C, Ponti G, Talbot C, Seidenari S. High resolution diagnosis of common nevi by multiphoton laser tomography and fluorescence lifetime imaging. Skin Res Technol. 2013;19: 194–204.

Balu, Mazhar A, Hayakawa CK, Mittal R, Krasieva TB, König K, Venugopalan V, Tromberg BJ. In vivo multiphoton NADH fluorescence reveals depth-dependent keratinocyte metabolism in human skin. Biophys J. 2013;104:258–67.

Bazin R, Flament F, Colonna A, LeHarzic R, Bückle R, Piot B, et al. Clinical study on the effects of a cosmetic product on dermal extracellular matrix components using a high-resolution multiphoton tomograph. Skin Res Technol. 2010;16:305–10.

Becker W. Advanced time-correlated single photon counting techniques. Berlin: Springer; 2005.

Benati E, Bellini V, Borsari S, Dunsby C, Ferrari C, French P, Guanti M, Guardoli D, Koenig K, Pellacani G, Ponti G, Schianchi S, Talbot C, Seidenari S. Quantitative evaluation of healthy epidermis by means of multiphoton microscopy and fluorescence lifetime imaging microscopy. Skin Res Technol. 2011. doi:10.1111/j.1600-0846.2011.00496.x.

Breunig HG, Studier H, König K. Multiphoton excitation characteristics of cellular fluorophores of human skin in vivo. Opt Express. 2010;18:7857–7871.16.

Breunig HG, Bückle R, Kellner-Höfer M, Weinigel M, Lademann J, Sterry W, et al. Combined in vivo multiphoton and CARS imaging of healthy and disease-affected human skin. Microsc Res Tech. 2012;75:492–8.

Breunig HG, Weinigel M, Bückle R, Kellner-Höfer M, Lademann J, Darvin ME, Sterry W, König K. Clinical coherent anti-stokes Raman scattering and multiphoton tomography of human skin with femtosecond laser and photonic crystal fiber. Laser Phys Lett. 2013;10:025604.

Bugiel I, König K, Wabnitz H. Investigation of cells by fluorescence laser scanning microscopy with subnanosecond time resolution. Lasers Life Sci. 1989;3:1–7.

Campagnola PJ, Clark HA, Mohler WA, Lewis A, Loew LM. Second-harmonic imaging microscopy of living cells. J Biomed Opt. 2001;6:277–86.

Chance B. Science. 1962;137:499–508. or Chance, Jossis Nature 184(1959)195–196.

Darvin ME, König K, Kellner-Höfer M, Breunig HG, Werncke W, Meinke MC, Patzelt A, Sterry W, Lademann J. Safety assessment by multiphoton fluorescence/ second harmonic generation/hyper-Rayleigh scattering tomography of ZnO nanoparticles used in cosmetic products. Skin Pharmacol Physiol. 2012;25:219–26.

Débarre D, Supatto W, Pena AM, Fabre A, Tordjmann T, Combettes L, et al. Imaging lipid bodies in cells and tissues using third-harmonic generation microscopy. Nat Methods. 2006;3:47–53.

Decenciere E, et al. Automatic 3D segmentation of multiphoton images: a key step for the quantification of human skin. Skin Res Technol. 2013;19:115–24.

Dimitrow E, Ziemer M, Koehler MJ, Norgauer J, König K, Elsner P, et al. Sensitivity and specificity of multiphoton laser tomography for *in vivo* and *ex vivo* diagnosis of malignant melanoma. J Invest Dermatol. 2009;129:1752–8.

Drexler W, Fujimoto JG. Optical coherence tomography. Heidelberg: Springer; 2008.

Ehlers A, Riemann I, Stark M, König K. Multiphoton fluorescence lifetime imaging of human hair. Microsc Res Technol. 2007;70:154–61.

Fischer F, Volkmer B, Puschmann S, Greinert R, Breitbar E, Kiefer J, et al. Assessing the risk of skin damage due to femtosecond laser irradiation. J Biophoton. 2008;1:470–7.51. M.

Huck V, Gorzelanny C, Thomas K, Getova V, Niemeyer V, Zens K, Unnerstall TR, Feger JS, Fallah MA, Metze D, Ständer S, Luger TA, König K, Mess C, Schneider SW. From morphology to biochemical state-intravital multiphoton fluorescence lifetime imaging of inflamed human skin. Sci Rep. 2016;6:22789.

Koehler MJ, König K, Elsner P, Buckle R, Kaatz M. In vivo assessment of human skin aging by multiphoton laser scanning tomography. Opt Lett. 2006;31:2879–81.

Koehler MJ, Hahn S, Preller A, Elsner P, Ziemer M, Bauer A, et al. Morphological skin ageing criteria by multiphoton laser scanning tomography: non-invasive in vivo scoring of the dermal fibre network. Exp Dermatol. 2008;17:519–23.

Koehler MJ, Preller A, Kindler N, Elsner P, König K, Bückle R, et al. Intrinsic, solar and sunbed-induced skin aging measured *in vivo* by multiphoton laser tomography and biophysical methods. Skin Res Technol. 2009;15:357–63.

Koehler MJ, Speicher M, Lange-Asschenfeldt S, Stockfleth E, Metz S, Elsner P, et al. Clinical application of multiphoton tomography in combination with confocal laser scanning microscopy for in vivo evaluation of skin diseases. Exp Dermatol. 2011;20:589–94.

Koehler MJ, Preller A, Elsner P, König K, Hipler UC, Kaatz M. Non-invasive evaluation of dermal elastosis by in vivo multiphoton tomography with autofluorescence lifetime measurements. Exp Dermatol. 2012;21(1):48–51.

König K. Clinical multiphoton tomography. J Biophotonics. 2008;1:13–23.

König K. Hybrid multiphoton multimodal tomography of in vivo human skin. Intravital. 2012;1:8.

König K. Multiphoton tomography of intratissue tattoo nanoparticles. Proc SPIE 8207.

König K, Riemann I. High-resolution multiphoton tomography of human skin with spatial resolution and picosecond time resolution. J Biomed Opt. 2003;8:432–9.

König K, Schneckenburger H. Laser-induced autofluorescence for medical diagnosis. J Fluoresc. 1994;4(1):17–40.

König K, Wabnitz H. Fluoreszenzuntersuchungen rnit hoher zeitlicher, spektraler und raumlicher Auflösung. Labortechnik. 1990;23:26–31.

König K, Ehlers A, Stracke F, Reimann I. In vivo drug screening in human skin using femtosecond laser multiphoton tomography. Skin Pharmacol Physiol. 2006;19:78–88.

König K, Ehlers A, Riemann I, Schenkl S, Bückle R, Kaatz M. Clinical two-photon microendoscopy. MicroscRes Technol. 2007;70:398–402.

König K, Speicher M, Bückle R, Reckfort J, McKenzie G, Welzel J, et al. Clinical optical coherence tomography combined with multiphoton tomography of patients with skin diseases. J Biophoton. 2009;2:389–97.

König K, Speicher M, Köhler MJ, Scharenberg R, Kaatz M. Clinical application of multiphoton tomography in combination with high-frequency ultrasound for evaluation of skin diseases. J Biophoton. 2010a;3: 759–73.

König K, Uchugonova A, Gorjup E. Multiphoton fluorescence lifetime imaging of 3D-stem cell spheroids during differentiation. Microsc Res Tech. 2010b;74:9–17. doi:10.1002/jemt.20866.print. 7(2011)9-17.

König K, Breunig HG, Bückle R, Kellner-Höfer M, Weinigel M, Büttner E, et al. Optical skin biopsies by clinical CARS and multiphoton fluorescence/SHG tomography. Laser Phys Lett. 2011a;1:1–3.

König K, Raphael AP, Lin L, Grice JE, Soyer HP, Breunig HG, Roberts MS, Prow TW. Applications of multiphoton tomographs and femtosecond laser nanoprocessing microscopes in drug delivery research. Adv Drug Deliv Rev Res. 2011b;63:388–404.

Korting H-C, Gottlöber P, Schmid-Wendtner M-H, Peter R-U. Ultraschall in der Dermatologie – Ein Atlas. Berlin: Blackwell Wissenschafts-Verlag; 1999.

Lin SJ, Wu RJ, Tan HY, Lo W, Lin WC, Young TH, et al. Evaluating cutaneous photoaging by use of multiphoton fluorescence and second-harmonic generation microscopy. Opt Lett. 2005;30:2275–7.

Manfredini M, Arginelli F, Dunsby C, French P, Talbot C, König K, Ponti G, Pellacani G, Seidenari S. High-resolution imaging of basal cell carcinoma: a comparison between multiphoton microscopy with fluorescence lifetime imaging and reflectance confocal microscopy. Skin Res Technol. 2013;19:e433–43. doi:10.1111/j.1600-0846.2012.00661181.

Miyamaoto K, Kudoh H. Quantification and visualization of cellular NAD(P)H in young and aged female facial skin with in vivo two-photon tomography. Br J Dermatol. 2013;169:25–31.

Patalay R, Talbot C, Alexandrov Y, Munro I, Neil MAA, König K, French PMW, Chu A, Stamp GW, Dunsby C. Quantification of cellular autofluorescence of human skin using multiphoton tomography and fluorescence lifetime imaging in two spectral detection channels. Biomed Opt Express. 2011;2(12):3295. Published online 10 Nov 2011.

Prowv TW, Grice JE, Li L, Faye R, Butler MK, Becker W, König K, et al. Applications of multiphoton tomographs and femtosecond laser nanoprocessing microscopes in drug delivery research. Adv Drug Deliv Rev. 2011;63:388–404.

Puschmann S, Rahn CD, Wenck H, Gallinat S, Fischer F. Approach to quantify human dermal skin aging using multiphoton laser scanning microscopy. J Biomed Opt. 2012;17:036005.

Patalay R, Talbot C, Alexandrov Y, Lenz MO, Kumar S, Warren S, Munro I, Neil MAA, König K, French PMW, Chu A, Stamp GW, Dunsby C. Multispectral fluorescence lifetime imaging using multiphoton tomography for the evaluation of basal cell carcinomas. PloS ONE 7(9)2012:e43460. doi:10.1371/journal.pone.0043460.

Rajadhyaksha M. In vivo confocal scanning laser microscopy. J Invest Dermatol. 1999;13:293–303.

Richter T, Peuckert C, Sattler M, König K, Riemann I, Hintze U, et al. Dead but highly dynamic – the stratum corneum is divided into three hydration zones. Skin Pharmacol Physiol. 2004;17:246–57.

Roberts MS, Roberts MJ, Robertson TA, Sanchez W, Thorling C, Zou Y, et al. In vitr*o* and *in vivo* imaging of xenobiotic transport in human skin and in the rat liver. J Biophoton. 2008;1:478–93.

Roberts MS, Dancik Y, Thorling C, Prow TW, Li L, Grice JE, et al. Non-invasive imaging of skin physiology and percutaneous penetration using fluorescence spectral and lifetime imaging with multiphoton and confocal microscopy. Eur J Pharm Biopharm. 2011;77:469–88 [27].

Sanchez WY, Prow TW, Sanchez WH, Grice JE, Roberts MS. Time-correlated single photon counting for simultaneous monitoring of zinc oxide nanoparticles and NAD(P)H in intact and barrier-disrupted volunteer skin. J Biomed Optics. 2010;15, 046008.

Schenke-Layland K, Riemann I, Damour O, Stock UA, König K. Two-photon microscopes and in vivo multiphoton tomographs – novel diagnostic tools for tissue engineering and drug delivery. Adv Drug Deliv Rev: 2006;58(7):878–96. doi:10.1016/j.addr.2006.07.004.

Schneckenburger H, König K. Fluorescence decay kinetics and imaging of NAD(P)H and flavins as metabolic indicators. Opt Eng. 1992;31:1447–51.

Seidenari S, Arginelli F, Dunsby C, French PMW, König K, Magnoni C, Manfreddini M, Talbot C, Ponti G. Multiphoton laser tomography and fluorescence lifetime imaging of basal cell carcinoma: morphological features for non-invasive diagnostics. Exp Dermatol. 2012a;21:831–6.

Seidenari S, Arginelli F, Bassoli S, Cautela J, French PMW, Guanti M, Guardoli D, König K, Talbot C, Dunsby C. Multiphoton laser microscopy and fluorescence lifetime imaging for the evaluation of the skin. Dermatol Res Pract. 2012b;2012:810749. doi:10.1155/2012/810749.

Weinigel M, Breunig HG, Lademann J, König K. In vivo histology: optical biopsies with chemical contrast using multiphoton/CARS tomography. Laser Phys Lett. 2014;11:055601.

Zvyagin AV, Zhao X, Gierden A, Sanchez W, Ross JA, Roberts MS. Imaging of zinc oxide nanoparticle penetration in human skin in vitro and in vivo. J Biomed Opt. 2008;13, 064031.

Storage Conditions of the Skin Affect Tissue Structure and In Vitro Percutaneous Penetration

113

Jesper B. Nielsen and Luis Bagatolli

Keywords
Human skin • In vitro • Storage conditions • Skin structure • Percutaneous penetration • Two-photon excitation fluorescence microscopy

Humans are exposed dermally due to unintentional occupational skin exposure as well as following intentional use of cosmetics and topically applied pharmaceutical drugs. In all cases valid information on the potential for percutaneous penetration and temporary deposition of the relevant chemical or drug within the skin is needed to perform an initial and credible hazard assessment.

In vivo studies are often seen as the gold standard for this kind of assessments. However, for ethical, logistic, and cost-related reasons, we need alternative methods that can replace in vivo studies in humans as well as experimental animals. The implementation of more recent legislation in Europe banning the use of experimental animals in relation to testing of cosmetic products has further pushed forward the replacement of in vivo methods and refinement of experimental in vitro models to study skin penetration.

Different organizations have issued recommendations and guidelines for the study of in vitro percutaneous penetration. One of the most cited of these guidelines is the OECD guideline 428 (OECD 428 2004). As a guideline it does not describe a single ideal in vitro method, but rather outlines different options and choices to be made when doing this kind of experiments. The different decisions to be taken relate to using static or flow-through systems, using full-thickness skin or dermatomed skin, using animal or human skin, using one or the other donor and receptor fluids, and using fresh or frozen skin. Thus, several in vitro methodological procedures are acceptable as long as they are based on valid arguments – valid in the sense that the experimental model reflects the problem to be addressed and will allow a trustworthy answer to the research question.

As stratum corneum is seen as the main barrier for percutaneous penetration, especially for the vast majority of compounds dependent on passive diffusion, the status of the epidermal barrier is

J.B. Nielsen (✉)
Department of Public Health, University of Southern Denmark, Odense, Denmark
e-mail: jbnielsen@health.sdu.dk

L. Bagatolli
Membrane Biophysics and Biophotonics group/ MEMPHYS Center for Biomembrane Physics, Department of Biochemistry and Molecular Biology, University of Southern Denmark, Odense, Denmark

P. Humbert et al. (eds.), *Agache's Measuring the Skin*,
DOI 10.1007/978-3-319-32383-1_47

significant. Being composed of a stacked layer of dead cells, the storage by freezing of the skin for later in vitro experiments has long been accepted instead of using fresh skin, though it has more recently been questioned.

The problem is relevant, as it for logistic and other practical reasons is difficult to perform in vitro studies on percutaneous penetration on fresh human skin obtained directly from surgery. Skin samples are therefore stored until experimental procedures can be initiated. Skin samples may be kept viable at 4 °C for 2–4 weeks (DeBono et al. 1998), though gradually losing its metabolic capacity within days (Fahmy et al. 1993). The physical characteristics responsible for barrier properties and integrity in relation to passive diffusion across the skin are maintained for longer (Bronaugh et al. 1986). Storage at low temperatures may generate small ice crystals, which may potentially impair the structure and thereby the integrity of the skin depending on degree and length of freezing conditions. As a consequence, most guidelines for experimental studies on percutaneous penetration address this issue.

However, requirements stated in different guidelines are not all that specific as to storage conditions. Some recommend storage at −20 °C, whereas others also accept storage at lower temperatures. Recommendations from the European Centre for the Validation of Alternative Methods (ECVAM) and the International Programme on Chemical Safety (IPCS) state that storage of the skin at −20 °C for up to a year is acceptable (Howes et al. 1996; IPCS: Dermal absorption 2006), whereas the EU Scientific Committee on Consumer Products (SCCP) states that the skin can be stored at −20 °C or lower (SCCP/0970/06 2006). All recommendations appear to rely on a single paper published in 1986 stating that human skin can usually be stored at −20 °C for up to a year with no changes in water permeability, but in some cases with apparent deterioration of the barrier (Bronaugh et al. 1986). Moreover, this study from 1986 did not actually judge the influence of storage at −20 °C on a comparison with fresh skin, but based the evaluation on cadaver skin. Given that cadaver skin has most often been sampled following unknown conditions for an unspecified time period, this might not be the optimal skin source as a basis for all existing guidelines on storage of the skin before experimental studies. The present OECD guideline 428 for the testing of chemicals avoids this dilemma by not describing specific requirements concerning storage conditions, but instead requires that evidence should be presented that the barrier function of the skin is maintained (OECD 428 2004).

Recently, imaging techniques based on nonlinear optics have been developed to an extent that allows pictorial description of skin structures including visualization of the different skin strata and associated dynamical information (Masters and So 2001; Brewer et al. 2013; Bloksgaard et al. 2013). For example, the two-photon excitation fluorescence microscopy (TPEFM) technique is noninvasive and based on a nonlinear process in which a fluorophore absorbs two photons simultaneously. This mode of excitation offers advantages compared to traditional laser scanning confocal fluorescence microscopy (LSCM). As infrared light is utilized as excitation source, the penetration depth can be up to 900 μm, almost fivefold higher than regular confocal fluorescence microscopy, allowing in-depth, three-dimensional examination of relatively thick biological specimens (Bloksgaard et al. 2013).

Based on this technique, a recent image analysis of the skin stored at−20 °C and −80 °C (Nielsen et al. 2011) revealed clear discrepancies from the normal distribution of keratinocytes in fresh skin as well as extensive cell desquamation in stratum corneum and apparent swelling of cells causing a larger average cell size in the deeper layers of the skin and an induction of broader canyons between polygonal clusters of the epidermis (Fig. 1). The structural changes in upper as well as deeper regions of epidermis observed via imaging techniques demonstrate that storage of human skin at −80 °C induces significant structural changes in the skin that will potentially affect percutaneous penetration of chemicals (Nielsen et al. 2011). The structural effects on the skin stored at −20 °C were less prominent and appeared limited to the upper strata of stratum corneum (Nielsen et al. 2011).

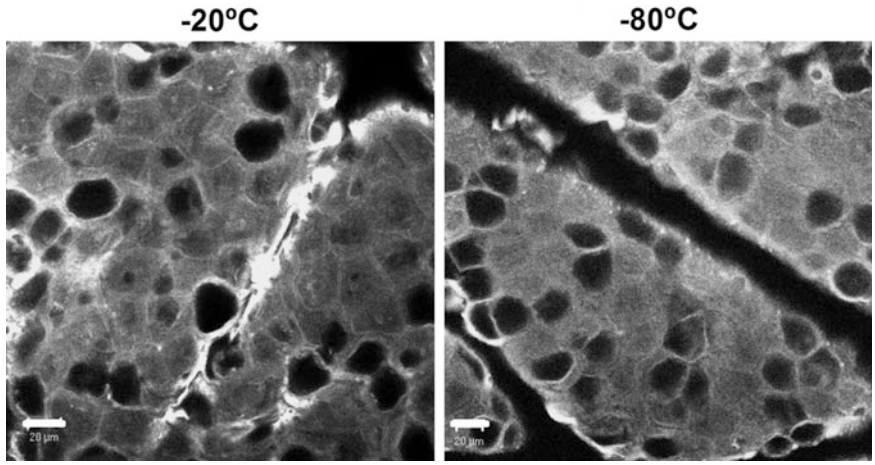

Fig. 1 Representative stratum corneum autofluorescence (TPEFM) images of human skin after storage at −20 °C and −80 °C. Scale bar is 20 µm (Reproduced from Nielsen et al. (2011) with permission from Karger Publishers)

Table 1 Summary of data available in the open literature on the influence of skin storage at −20 °C on percutaneous penetration rates (Flux).Flux through skin stored at −20 °C is given as the estimated percentage of flux through fresh skin from the same experiment

Skin source	Penetrant	Flux(%)	Reference
Rat, abdomen	Diclofenac	96	Sintov and Botner (2006)
Hairless Guinea pig, abdomen	Diclofenac	150[a]	Sintov and Botner (2006)
Pig, ear	Diclofenac	517[a]	Sintov and Botner (2006)
Pig, abdomen	^3H_2O	124[a]	Payne et al. (2013)
Human, abdomen	Caffeine	100–120	Nielsen et al. (2011)
Human, abdomen	Anisole	89	Dennerlein et al. (2013)
Human, abdomen	Cyclohexanone	146	Dennerlein et al. (2013)
Human, abdomen	1,4 dioxane	75	Dennerlein et al. (2013)

[a]Statistically increased compared to penetration rate through fresh skin

The limited more recently published data in the open literature on the influence of storage of the skin at −20 °C on the percutaneous penetration of topically applied chemicals is presented in Table 1. From each of the available studies, the ratio between the comparable groups with fresh skin and skin frozen at −20 °C is calculated. It should be noted that all numbers on flux come with significant standard deviations and together with an often limited group size, this causes the differences compared to fresh skin experiments to remain statistically insignificant for most cases including all cases with human skin. However, in those cases with statistical differences, the flux is always increased following freezing indicating a varying degree of damage to the skin barrier. It is perhaps also noteworthy that the one case deviating significantly from the other cases was performed on the skin from the ear (Sintov and Botner 2006), whereas the rest of the experiments were performed on abdominal skin (Sintov and Botner 2006; Payne et al. 2013; Nielsen et al. 2011; Dennerlein et al. 2013).

Only but a few studies have tested the influence of storage temperatures lower than −20 °C on the percutaneous penetration of different penetrants. These studies include testing the penetration of caffeine through human skin after storage at −80 °C, measuring penetration of the T-2 toxin (a mycotoxin) through human and monkey skin after storage at −60 °C, and evaluating the penetration of N,N-dietyl-*m*-toluamide through pig

skin stored at −80 °C (Nielsen et al. 2011; Kemppainen et al. 1986; Hawkins and Reifenrath 1984). These three studies all demonstrate significantly increased penetration rate through the skin stored at these low temperatures.

The image analysis demonstrates that storage of human skin at −20 °C causes visible structural changes in only but the upper epidermal strata of the skin. The upper strata will be expected to act as a stronger barrier to hydrophilic compounds as to lipophilic compounds due to its more lipophilic character. A structural damage to the upper layers could therefore be expected to have a more pronounced effect on the penetration of hydrophilic compounds as compared to lipophilic compounds. This suggestion fits well with observations demonstrating that applying hydrophilic compounds in a lipophilic microemulsion eliminates the influence of freezing on the percutaneous penetration (Sintov and Botner 2006). The suggestion that a specific stratum of the epidermal membrane acts as a stronger barrier toward hydrophilic compounds and another stratum for more lipophilic compounds requires, however, more supporting evidence from experimental studies.

The observed effect of storage at −20 °C on the percutaneous penetration through human skin is less than 50 % (Nielsen et al. 2011; Dennerlein et al. 2013). Considering the inherent variability in these studies related to interindividual variability between skin donors (50–60 %) and interlaboratory variability (up to ten times), the observed effects of skin storage at −20 °C are relatively limited. Instead of prescribing specific storage conditions, the more pragmatic and functional approach, until more documentation is available, is therefore to follow the recommendations given in the OECD guidelines that skin specimens used for in vitro studies on percutaneous penetration should have intact barrier integrity, which can be tested and reported based on different well-described methods.

Based on presently available data, it can be concluded:

1. Storage of human skin at −80 °C causes significant structural changes in upper as well as more deeper parts of stratum corneum. These more severe changes correspond to significantly increased percutaneous penetration of chemicals applied to skin specimens stored at very low temperatures. Storage of human skin for later use in in vitro studies on percutaneous penetration is therefore not recommended at these low temperatures.
2. Storage of human skin at −20 °C causes structural changes in the upper stratum corneum observable with image techniques such as TPEFM. The presently available literature does, however, not support that the observed structural damage to the integrity is sufficient to cause a general and significantly increased in vitro percutaneous penetration across human skin stored at −20 °C. The use of the skin stored at −20 °C for in vitro studies on percutaneous penetration therefore seems acceptable as long as the barrier integrity is documented.

Acknowledgments The Danish National Research Foundation is acknowledged for supporting MEMPHYS – Center for Biomembrane Physics.

References

Bloksgaard M, Brewer J, Bagatolli LA. Structural and dynamical aspects of skin studied by multiphoton excitation fluorescence microscopy-based methods. Eur J Pharm Sci. 2013;50:586–94.

Brewer J, Kubiak J, Bloksgaard M, Sørensen JA, Bagatolli LA. Spatially resolved two color diffusion measurements in human skin applied to transdermal liposome penetration. J Invest Dermatol. 2013;133:1260–8.

Bronaugh RL, Stewart RF, Simon M. Methods for in vitro percutaneous absorption studies. Vii: use of excised human skin. J Pharm Sci. 1986;75:1094–7.

DeBono R, Rao GS, Berry RB. The survival of human skin stored by refrigeration at 4 degrees C in McCoy's 5a medium: does oxygenation of the medium improve storage time? Plast Reconstr Surg. 1998;102:78–83.

Dennerlein K, Schneider D, Göen T, Schaller KH, Drexler H, Korinth G. Studies on percutaneous penetration of chemicals – impact of storage conditions for excised human skin. Toxicol In Vitro. 2013;27:708–13.

Fahmy FS, Navsaria HA, Frame JD, Jones CR, Leigh IM. Skin graft storage and keratinocyte viability. Br J Plast Surg. 1993;46:292–5.

Hawkins GSJ, Reifenrath WG. Development of an in vitro model for determining the fate of chemicals applied to skin. Fundam Appl Toxicol. 1984;4:S133–44.

Howes D, Guy R, Hadgraft J, Heylings J, Hoeck U, Kemper F, Maibach H, Marty J-P, Merk H, Parra J, Rekkas D, Rondelli I, Schaefer H, Täuber U, Verbiese N. Methods for assessing percutaneous absorption, ECVAM workshop report n. 13. Altern Lab Anim. 1996;24:81–106.

IPCS: Dermal absorption. Geneva, World Health Organisation, International Programme on Chemical safety (Environmental Health Criteria 235). 2006.

Kemppainen BW, Riley RT, Pace JG, Hoerr FJ. Effects of skin storage conditions and concentration of applied dose on [3h]t-2 toxin penetration through excised human and monkey skin. Food Chem Toxicol. 1986;24:221–7.

Masters BR, So PTC. Confocal microscopy and two-photon excitation microscopy of human skin in vivo. Opt Exp. 2001;8:2–10.

Nielsen JB, Plasencia L, Sørensen JA, Bagatolli LA. Storage conditions of skin affect tissue structure and subsequent in vitro percutaneous penetration. Skin Pharmacol Physiol. 2011;24:93–102.

OECD 428: OECD guideline for testing of chemicals, guideline 428: skin absorption: in vitro method., Organization for Economic Cooperation and Development, Paris, adopted 13 Apr 2004.

Payne OJ, Graham SJ, Dalton CH, Spencer PM, Mansson R, Jenner J, Azeke J, Braue E. The effects of sulfur mustard exposure and freezing on transdermal penetration of tritiated water through ex vivo pig skin. Toxicol In Vitro. 2013;27:79–83.

SCCP/0970/06.: Basic criteria for the in vitro assessment of dermal absorption of cosmetic ingredients, updated March 2006, adopted by the scientific committee on consumer products (SCCP) during the 7th plenary meeting of 28 March 2006.

Sintov AC, Botner S. Transdermal drug delivery using microemulsion and aqueous systems: influence of skin storage conditions on the in vitro permeability of diclofenac from aqueous vehicle systems. Int J Pharm. 2006;311:55–62.

Epidermal Barrier Treatments Based on Vernix Caseosa

114

Marty O. Visscher

Contents

Keywords

Vernix • Stratum corneum • Barrier • Wound • Hydration • Free amino acids • pH • Natural moisturizing factor

1 Introduction

Healthy full-term newborn skin is well developed and functional at birth, despite being exposed to water and amniotic fluid for 9 months. The epidermis is thick and the stratum corneum (SC) layers are well formed. Transepidermal water loss (TEWL) is very low at birth for full-term infants and equal to or lower than adults, indicating a highly effective skin barrier (Cunico et al. 1977; Yosipovitch et al. 2000). However, the question is, how does the full-term infant develop an excellent barrier while in water? Usually, continuous exposure to water causes significant skin damage, including maceration of the SC and disruption of its well-organized structure and injury to the epidermis. Typically, skin cultures have to be exposed to dry conditions for cornification to occur. If the epidermis is covered with water, the SC does not form (Supp et al. 1999). Yet, in utero, the SC forms to cover the epidermis in the high water environment.

Vernix caseosa is the mixture of sebaceous gland secretions, lanugo, and desquamated epithelial cells that covers the skin of the fetus during the last trimester of gestation and appears in varying amounts on newborn infants. Vernix from full-

M.O. Visscher (✉)
Skin Sciences Program, Division of Plastic Surgery, Cincinnati Children's Hospital Medical Center, Cincinnati, OH, USA

Department of Surgery, College of Medicine, University of Cincinnati, Cincinnati, OH, USA
e-mail: marty.visscher@gmail.com

P. Humbert et al. (eds.), *Agache's Measuring the Skin*, DOI 10.1007/978-3-319-32383-1_48

term infants is a remarkably consistent mixture of 80 % water, 10 % protein, and 10 % lipid fractions, consisting primarily of cornified cells embedded in an amorphous lipid matrix (Hoeger et al. 2002; Pickens et al. 2000; Rissmann et al. 2006). There are flat, differentiated corneocytes with cell envelopes are 1–2 μm thick. The cells lack distinct nuclei, corneodesmosomes, and organization. They have lower keratin levels than mature stratum corneum cells, varying in stage of keratinization (Pickens et al. 2000; Agorastos et al. 1988). Most of the water is localized to the intracorneocyte region, but small, round structures have been observed in the nonlamellar lipid matrix (Pickens et al. 2000; Rissmann et al. 2006). They are believed to be hydrated domains and pools of rapidly releasable extracorneocyte water (Tansirikongkol et al. 2008).

This chapter will address this question: based on the structure and composition, what could vernix do for the epidermal barrier?

2 Vernix Composition and Structure

2.1 Formation

Vernix begins to coat the fetal skin surface from head to toe and back to front during the last trimester, presumably under hormonal control (Hoath et al. 2006). Vernix includes lipids of the types made by sebaceous gland (Rissmann et al. 2006; Nicolaides et al. 1972), and the cornified cells may originate from hair follicles, analogous to the production of terminally differentiated infundibular keratinocytes in acne (Kurokawa et al. 2009). Vernix extrudes onto the interfollicular epidermis through the hair shaft, spreads over the surface throughout gestation (Hardman et al. 1998) and, presumably, protects the epidermis from exposure to amniotic fluid (Fig. 1; Youssef et al. 2001). It is likely that fetal epidermis has a high water flux potential driven by osmotic gradients since cornification is incomplete. Isolated vernix corneocytes can swell and contract as a function of a hypoosmotic or hyperosmotic environment (Hoath et al. 2006) supporting a potential role for vernix in osmoregulation intra-amniotically. Vernix may impose a semi-regulated barrier and/or physiological gradient for transepidermal water and nutrients in utero, facilitating cornification via increased DNA and lipid synthesis. The asymmetric submerged culture model is consistent with this hypothesis (Thakoersing et al. 2010).

2.2 Lipids

Vernix contains free lipids including sterol esters, wax esters, dihydroxy wax esters, squalene, triglycerides, diacylglycerol, monoacylglycerol, phospholipids, cholesterol, fatty acids, and ceramides (Rissmann et al. 2006; Tollin et al. 2005). The vernix lipids bound to the corneocytes include ω-hydroxy acids (bound to corneocyte envelope), fatty acids, ω-hydroxyceramides CerA (sphingosine), and CerB (6-hydroxysphingosine) (Rissmann et al. 2006). Unlike native SC where cholesterol, free fatty acids, and ceramides constitute 80 % of total lipids, these classes represent 10 % of vernix lipids, and nonpolar species are the major components. The free fatty acids are dominated by saturated chain lengths C16:0 (14 %) and C24:0 (24.5 %). C18:lin-9 (6.4 %) is the most abundant monounsaturated fatty acid, and C18:2n-6 (9.6 %) is the highest polyunsaturated fatty acid (Tollin et al. 2005). Branched chains are 29 % of the fatty acids and include 30 different chain lengths, from 11 to 26 carbons (Ran-Ressler et al. 2008). In contrast, SC fatty acids are straight chained and generally 22 or 24 carbons (Wertz 2006). The lower levels of long chain ceramides and high fraction of unsaturated or branched chains may lead to the more fluid, nonlamellar organization seen in vernix (Rissmann et al. 2006). Covalently bound lipids comprise about 1 % of vernix (Rissmann et al. 2006), generally the same as in SC, although vernix has higher levels of ω-hydroxeicosanoic acid and nearly absent levels of ω-hydroxyacid with 30 C-atoms (Rissmann et al. 2006).

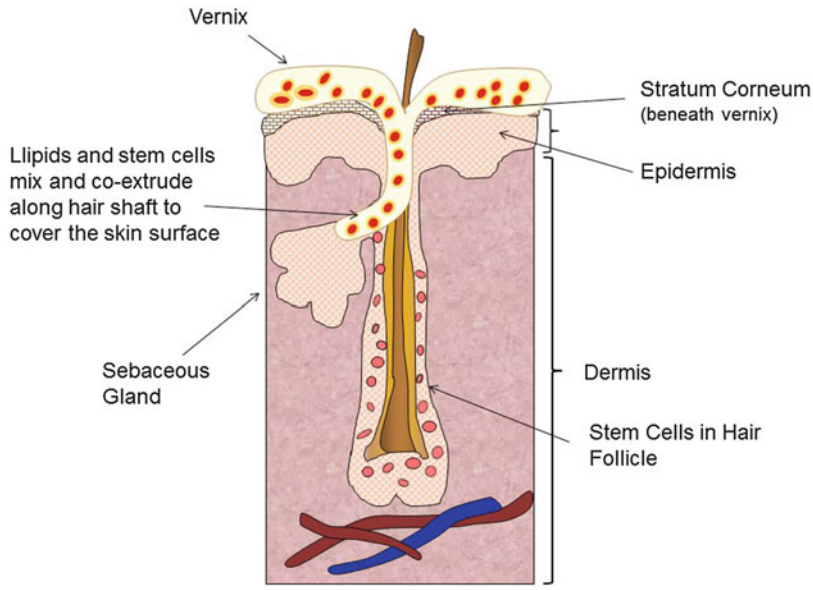

Fig. 1 Vernix formation. Vernix extrudes onto the interfollicular epidermis through the hair shaft and spreads over the surface throughout gestation and, presumably, protects the epidermis from exposure to amniotic fluid

Vernix from female and male newborns differed significantly in wax esters and triglycerides; two classes are believed to originate from the sebaceous glands. For both, the relative amounts of longer-chain-length lipids were greater in females versus males (Mikova et al. 2014). The shorter carbon chain species were higher in males versus females. Given that the composition of epidermal lipids changes during gestation, it is possible that the vernix composition changes throughout the last trimester. In infants of 31–40 weeks gestation, the cholesterol/squalene ratio decreased around 36 weeks, reflecting increased squalene and suggesting a surge in sebaceous gland function near birth (Wysocki et al. 1981). The variation as a function of gestational age and the implications for SC development is largely unexplored.

2.3 Proteins

An analysis of vernix ($n = 34$ infants) using liquid chromatography and tandem mass spectrometry identified 203 proteins and grouped them via protein analysis software (Holm et al. 2014). The major classes were hydrolases (14.4 %), proteases (10.8 %), enzyme modulators (10.8 %), cytoskeletal proteins (9.8), structural proteins (6.9 %), transfer/carrier proteins (5.6 %), calcium-binding proteins (5.6 %), immunity proteins (5.6 %), and signaling molecules (4.9 %) (Table 1). Polyubiquitin-C regulates innate and adaptive immunity and calmodulin-like protein 5 is associated with late keratinocyte differentiation and SC formation. Both were negatively associated with the development of atopic dermatitis by 24 months compared to infants without disease (Holm et al. 2014). The SC proteins keratins 1, 10, and 11, involucrin, and filaggrin are present in vernix (Narendran et al. 2010; Visscher et al. 2011a). Analysis of the free amino acid (FAA) component of natural moisturizing factor (NMF) revealed higher levels of glutamic acid and histidine and lower levels of glycine and serine compared to the amino acid profile of filaggrin (McKinley-Grant et al. 1989) ($p < 0.05$, Table 2).

2.4 Antimicrobial Activity

Vernix contains antimicrobial agents, including proteins and lipids, and exhibits a range of bioactivity against common fungal and bacterial pathogens (Tollin et al. 2005; Akinbi et al. 2004; Marchini et al. 2002; Yoshio et al. 2003). The innate immune proteins,

calgranulin A, B, and C, cystatin A, and UGRP-1 have been identified (Tollin et al. 2005). Lactoferrin, lysozyme, secretory leukocyte protease inhibitor, and human neutrophil peptides 1–3 were found in vernix from healthy full-term births (Akinbi et al. 2004). These antimicrobial peptides appear as hydrated inclusion bodies that may result from process-induced coalescence (Fig. 2). The presence of a quick release pool of soluble antimicrobials would be a major benefit for the fetus faced with chorioamnionitis or other intrauterine infection, although this hypothesis has not yet been tested. Vernix samples had muramidase activity and were active against the growth of group B *Streptococcus*, *L. monocytogenes*, and *K. pneumoniae*. The cathelicidin LL-37, known to protect keratinocytes from apoptosis (Bouzari et al. 2009), was found and demonstrated antimicrobial activity against *B. megaterium* Bm11 (gram positive) (Marchini et al. 2002). Combinations of vernix lipids and LL-37 in ratios of 3:1 and 7:1 displayed greater antimicrobial inhibition than LL-37 alone, indicating synergetic innate immunity. Vernix and amniotic fluid from healthy infants showed activity to Bm11 and *C. albicans* (Yoshio et al. 2003).

Table 1 Classes of proteins identified in vernix caseosa (Holm et al. 2014)

Class	Percent	Class	Percent
Hydrolase	14.4	Signaling molecule	4.9
Calcium binding	5.6	Enzyme modulator	10.8
Cytoskeletal	9.8	Defense/ immunity	5.6
Structural	6.9	Transfer/ carrier	5.6
Protease	10.8	Membrane traffic	0.3
Extracellular matrix	2.6	Transcription factor	0.7
Transporter	3.9	Chaperone	1.0
Transferase	2.3	Cell junction	0.3
Oxidoreductase	3.9	Surfactant	0.7
Lyase	1.3	Storage	0.3
Cell adhesion molecule	2.9	Isomerase	1.6
Ligase	1.0	Receptor	2.0
Nucleic acid binding	2.3		

3 Treatments

Epidermal barrier treatments based on vernix derive from the chemical composition, the physical structure, and the resulting properties that they confer (impart). The properties of vernix suggest several uses for treating the epidermal barrier for common skin maladies.

3.1 Hydration/Moisturization

Vernix has a higher than typical water content compared to conventional ointments. It loses

Table 2 Amino acid composition of vernix relative to fully hydrolyzed filaggrin (McKinley-Grant et al. 1989)

	Vernix (pmoles/μg soluble protein)	Indexed to glycine	Filaggrin (pmoles/μg filaggrin)	Indexed to glycine
Glycine	78.5 ± 19	1.0	2981	1.0
Serine	114.6 ± 13	1.4	2640	0.9
Glutamic acid	284.6 ± 27	3.6	1100	0.4
Histidine	459.4 ± 92	5.8	900	0.3
Arginine	151.4 ± 12	1.9	500	0.2
Citrulline	134.6 ± 13	1.7	70	0.02

The values are from the HPLC analysis as pmoles amino acid per μg soluble protein (extracted from tapes) for native vernix and adult skin. For comparison, the relative amino acids in filaggrin are given as pmoles per μg of protein based on the composition from full acid hydrolysis (McKinley-Grant et al. 1989). The FAAs for vernix, adult skin, and filaggrin are also shown as indices, i.e., normalized to glycine

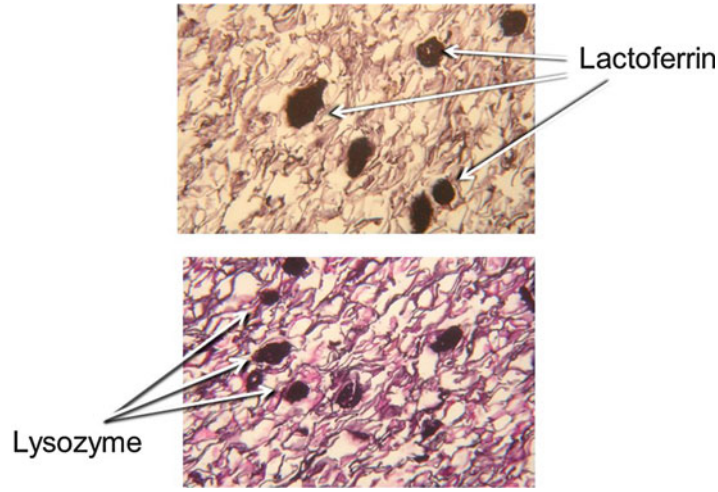

Fig. 2 Electron micrographs of vernix showing antimicrobial peptides. Lactoferrin, lysozyme, secretory leukocyte protease inhibitor, and human neutrophil peptides 1–3 were found in vernix from healthy full-term births. These antimicrobial peptides appear as hydrated inclusion bodies that may result from process-induced coalescence as shown in electron micrographs of vernix stained for lactoferrin and lysozyme

and resorbs water, indicating a use for SC hydration (Tansirikongkol et al. 2008). The free amino acid levels in vernix are about 0.3 μmol per cm^2 which may account in part for the slow water release and water resorption. The water holding capacity for vernix-treated adult volar forearm skin was higher than an untreated control ($p < 0.05$) (Bautista et al. 2000). The water holding capacity for skin treated with a water-in-oil cream (Eucerin©), an anhydrous barrier (petrolatum), and a low-water cream (Aquaphor©) did not differ from untreated skin (Fig. 3). The water-binding capacity (peak sorption following application of exogenous water) of vernix-treated skin was higher than the untreated control, while values for Eucerin, petrolatum, and Aquaphor were lower ($p < 0.05$).

Infant skin hydration decreases over the first day and then increases during the first 2 weeks, in contrast to mother's skin where hydration is relatively constant, suggesting adaptive changes to the postnatal environment (Visscher et al. 2000). Vernix was left on the skin in one group of newborns and wiped off for another group. Vernix-treated skin was significantly more hydrated and less erythematous at birth and 24 h later versus skin where vernix was removed ($p < 0.05$) (Visscher et al. 2005). Vernix-retained skin had higher levels of FAA 24 h after birth ($p < 0.05$), paralleling the higher hydration.

3.2 Skin Surface Acidity

An acidic skin surface is necessary for the effective functioning of enzymes in stratum corneum formation and integrity, i.e., lipid metabolism, bilayer structure, ceramide synthesis, processing of GlcCer precursors to form ceramide for SC lipids, and desquamation (Schmid-Wendtner and Korting 2006; Rippke et al. 2002; Holleran et al. 2006), for bacterial homeostasis, skin colonization, and inhibition of pathogenic bacteria (Aly et al. 1978; Puhvel et al. 1975; Fluhr et al. 2001). Acidification enhances SC integrity and cohesion in neonatal and aged skin (Hachem et al. 2010; Hatano et al. 2009). The apparent skin pH was lower for infants with vernix retained after birth and 24 h than when vernix was removed ($p < 0.05$) (Visscher et al. 2005). Vernix may facilitate colonization with commensal organisms.

3.3 Stratum Corneum Barrier Repair

Alteration of the skin environment after SC damage has profound effects on the rate and effectiveness of barrier repair. Damaged SC treated with semipermeable films recovers more quickly than under complete occlusion or no occlusion, as reported after tape stripping and in premature

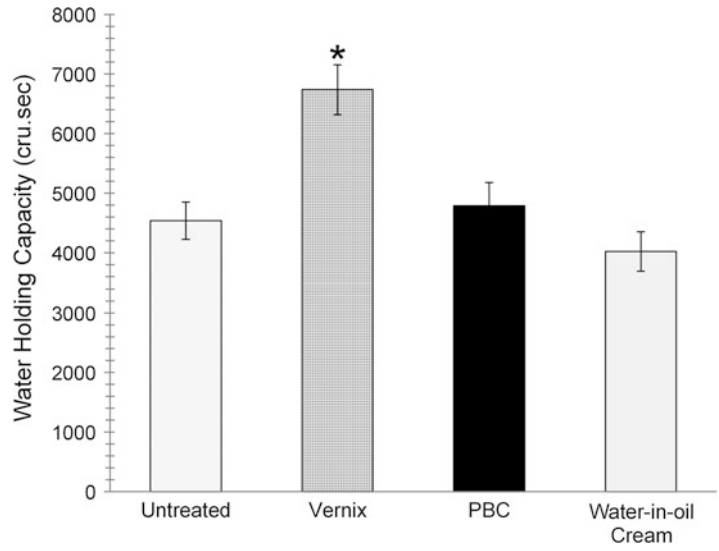

Fig. 3 Water holding capacity for vernix, PBC,, and a water-in-oil cream. The water holding capacity for vernix-treated adult volar forearm skin was higher than an untreated control ($p < 0.05$). The water holding capacity for skin treated with a water-in-oil cream (Eucerin©), an anhydrous barrier (PBC), and a low-water cream (Aquaphor©) did not differ from untreated skin. *Indicates significantly different from all other treatments ($p < 0.05$) (Adapted from Bautista et al. 2000)

infants (Schunck et al. 2005; Visscher et al. 2001; Bhandari et al. 2005; Mancini et al. 1994). This artificial barrier can be provided by creams, ointments, films, or dressings. Vernix films are semipermeable, with water vapor transmission rates of 19–70 g/m^2/h, depending upon thickness, while petrolatum-based films are in the occlusive range (Gunt 2002; Tansirikongkol et al. 2007a; Visscher et al. 2002).

The effects of twice-daily application of vernix and a petrolatum-based cream (PBC) (both 2.5 mg/cm^2) on early-stage SC repair were compared versus a fully occlusive film and untreated skin (tape stripped, no occlusion) in adult forearm skin tape stripped to achieve TEWL of 29–50 g/m^2/h, comparable to values for infants < 30 weeks gestation (Visscher et al. 2011a; Sedin et al. 1983). Vernix and PBC facilitated barrier repair with higher rates of recovery than full occlusion ($p < 0.05$) (Fig. 4a). Both were comparable to the recovery for untreated (stripped) skin. Skin hydration (immediate reading) was higher for PBC than vernix and untreated. Vernix-treated skin tended to be more hydrated than untreated ($p = 0.06$). Taken together, the data suggest that vernix treatment results in a more hydrated SC than without treatment (no occlusion). Visual erythema was higher for full occlusion than untreated (stripped, no occlusion) vernix and PBC ($p < 0.05$). Visual dryness was greater for full occlusion versus no occlusion and vernix ($p < 0.05$). PBC was drier than no occlusion ($p < 0.05$) and directionally drier than vernix ($p = 0.09$) (Fig. 5). Following complete SC removal via tape stripping in hairless mice, TEWL was 79 g/m^2/h. One application of vernix and PBC (both at 5 mg/cm^2) enhanced SC barrier repair versus no treatment, but recovery was more rapid with vernix than PBC (Fig. 4b). Skin treated with PBC was more erythematous than with vernix or untreated (Oudshoorn et al. 2009a).

3.4 Wound Healing

Wounds at the epidermal and superficial dermal level were created on a minipig with an erbium: YAG laser at ablation depths of 20 or 25 μm and treated twice daily with vernix, a PBC (both at 2.5 mg/cm^2), or left untreated (wounded, no occlusion) for 7 days (Visscher et al. 2011b). Wounds from 20 μm ablation recovered more quickly with vernix or PBC versus no treatment, and the recovery was greater on day 2 for PBS versus vernix. Repair rates were similar for all sites on day 7, although recovery was not complete, i.e., 76–88 % (Fig. 4c). Both vernix and PBC produced similar recovery for 25 μm ablation. Wound-healing effects of vernix on lower extremity ulcers have been reported (Zhukov et al. 1992).

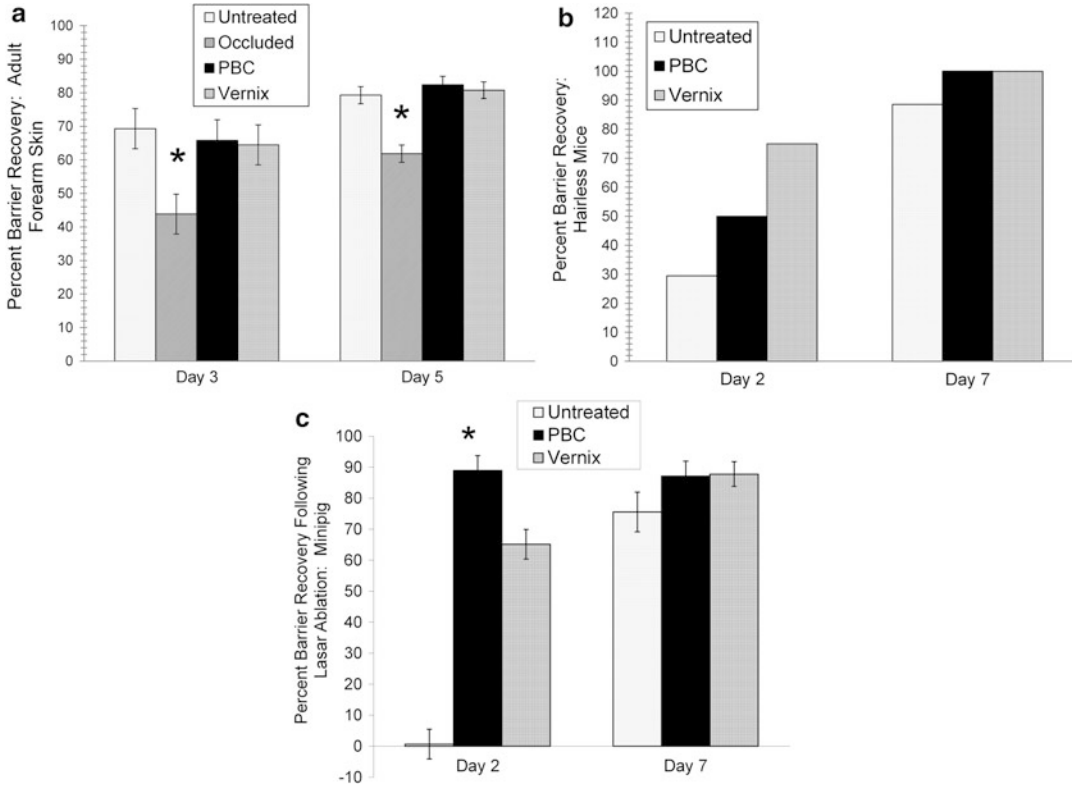

Fig. 4 (**a**, **b**, **c**) **Effect of vernix on barrier recovery**. The effect of vernix treatment on epidermal damage in three investigations is shown in **a**, **b**, and **c**. (**a**) The effects of twice-daily application of vernix and a petrolatum-based cream (*PBC*) (both 2.5 mg/cm^2) on early-stage SC repair were compared versus a fully occlusive film and untreated skin (tape stripped, no occlusion) in adult forearm tape-stripped skin. Vernix and PBC facilitated barrier repair with higher rates of recovery than full occlusion ($p < 0.05$). Both were comparable to the recovery for untreated (stripped) skin. *Indicates significant difference versus untreated, tape-stripped skin. (**b**) One application of vernix and PBC (both at 5 mg/cm^2) enhanced SC barrier repair in hairless mice versus no treatment, but recovery was more rapid with vernix than PBC. Skin treated with PBC was more erythematous than with vernix or untreated. (**c**) Wounds from 20 μm laser ablation in the minipig recovered more quickly with vernix or PBC versus no treatment, and the recovery was greater on day 2 for PBS versus vernix. Repair rates were similar for all sites on day 7, although recovery was not complete, i.e., 76–88 %. Both vernix and PBC produced similar recovery for 25 μm ablation. *Indicates significant difference from untreated (damaged) and vernix ($p < 0.05$) (a adapted from Visscher et al. 2011b; b adapted from Oudshoorn et al. 2009a; c used with permission from Visscher et al. 2011b)

The free amino acids in vernix may have a role in wound healing. Repair rates were increased, and infection was controlled for wounds, including burns and diabetic ulcers, when nutrients (amino acids, salts, ascorbic acid, D-glucose polysaccharide) were applied after daily debridement (Silvetti 1981). Sericin, a mixture of silk proteins, peptides, and amino acids, healed wounds more quickly than the PBC control in rats (Aramwit and Sangcakul 2007). Treatment with four amino acids (glycine, L-lysine, L-proline, L-leucine) and hyaluronic acid increased wound healing (Corsetti et al. 2009).

3.5 Synthetic Vernix

Topical creams based on native vernix caseosa as a prototype have been reported. Formulas with high water content and vernix-like lipids have water release profiles similar to native vernix and water vapor transport rates in the

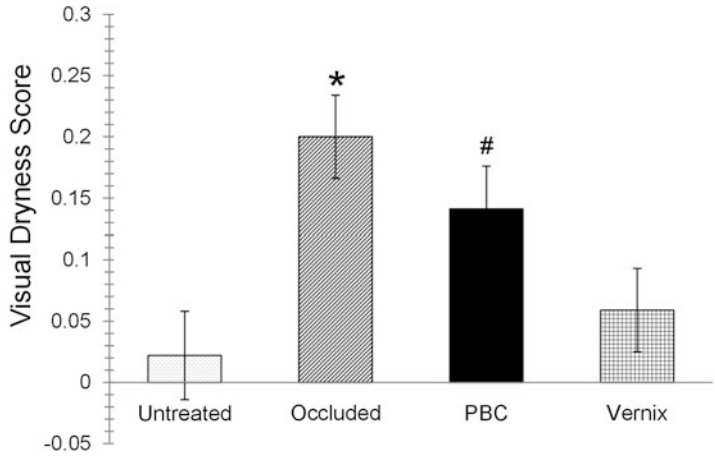

Fig. 5 Effect of vernix on skin dryness. The effects of twice-daily application of vernix and a petrolatum-based cream (*PBC*) (both 2.5 mg/cm^2) on early-stage SC repair were compared versus a fully occlusive film and untreated skin (tape stripped, no occlusion) in adult forearm tape-stripped skin. Visual dryness was greater for full occlusion versus no occlusion and vernix ($p < 0.05$). PBC was drier than no occlusion ($p < 0.05$) and directionally drier than vernix ($p = 0.09$). *Indicates significantly different from no occlusion and vernix. #Indicates directional difference versus vernix and a significant difference from no occlusion (Adapted from Visscher et al. 2011b)

"semipermeable" range (Tansirikongkol et al. 2007a). Synthetic lipid mixtures, based on the vernix lipid composition and formulated to match the thermal and structural properties, were comparable to native vernix and provided increased barrier repair versus a PBC in the hairless mouse (Rissmann et al. 2008). Formulas with lipid-coated microgel particles in a ratio of 2:1 particles/lipid most closely resembled the water release profile of native vernix (Rissmann et al. 2009). Synthetic formulations with hydrated moieties, a version with the physiological lipid mixture, and native vernix were more effective than PBC for SC barrier repair (Oudshoorn et al. 2009b).

4 Summary

Vernix has multiple physical and biological functions that are provided simultaneously, e.g., wound healing with antimicrobial activity, during gestation and immediately after birth. They are multifunctional compared to conventional creams. Vernix functions as a skin cleanser (Moraille et al. 2005). In vitro, it has a low surface energy, suggesting that it creates a protective hydrophobic layer around the fetus (Youssef et al. 2001). Vernix contains multiple cytokines, including IL1α, IL1β, TNFα, IL-6, IL-8, and MCP, although the role is the subject of future investigations (Narendran et al. 2010). Vernix contains the SC lipids, cholesterol, ceramides, and fatty acids (e.g., oleic, linoleic, and long chain species) and non-SC lipids, e.g., sterol esters, triglycerides, and squalene (Rissmann et al. 2006; Tollin et al. 2005). The ceramide component, e.g., type and ratio to other lipid classes, influences the barrier properties in SC model systems (Kessner et al. 2008). Vernix films impede penetration of the exogenous enzyme chymotrypsin (found in meconium) in vitro (Tansirikongkol et al. 2007b) and, hypothetically establish epidermal-amniotic fluid gradients of water, nutrients, and electrolytes necessary for normal architecture and barrier formation (Thakoersing et al. 2010). Vernix films are semipermeable, unlike those of petrolatum-based creams. Premature infants of 26.2 weeks GA (mean) were treated with PBC twice daily and compared to a cohort without daily application (PBC applied only to local dryness or compromise) (Edwards et al. 2004). Nosocomial infection rates were higher for the PBC infants of

501–750 g. Since PBC at levels> 1 g/cm^2 are occlusive to water vapor transport (Gunt 2002; Joseph 2002), the applied amount may be been sufficiently occlusive to delay SC barrier development and/or to permit growth of coagulase-negative *Staphylococcus* (Visscher 2003).

Overall, vernix facilitates development of the stratum corneum protective barrier in the normal, full-term infant through a variety of protective and adaptive mechanisms. Very premature infants are born before vernix is fully distributed on the skin in utero and, consequently, may be deprived of the benefits. Epidermal barrier treatments based on vernix may protect them from vulnerabilities including delayed barrier maturation, delayed acid mantle formation, infection, and water loss.

References

Agorastos T, Hollweg G, Grussendorf EI, Papaloucas A. Features of vernix caseosa cells. Am J Perinatol. 1988;5:253–9.

Akinbi HT, Narendran V, Pass AK, Markart P, Hoath SB. Host defense proteins in vernix caseosa and amniotic fluid. Am J Obstet Gynecol. 2004;191:2090–6.

Aly R, Shirley C, Cunico B, Maibach HI. Effect of prolonged occlusion on the microbial flora, ph, carbon dioxide and transepidermal water loss on human skin. J Invest Dermatol. 1978;71:378–81.

Aramwit P, Sangcakul A. The effects of sericin cream on wound healing in rats. Biosci Biotechnol Biochem. 2007;71:2473–7.

Bautista MI, Wickett RR, Visscher MO, Pickens WL, Hoath SB. Characterization of vernix caseosa as a natural biofilm: comparison to standard oil-based ointments. Pediatr Dermatol. 2000;17:253–60.

Bhandari V, Brodsky N, Porat R. Improved outcome of extremely low birth weight infants with tegaderm application to skin. J Perinatol. 2005;25:276–81.

Bouzari N, Kim N, Kirsner RS. Defense of the skin with LL-37. J Invest Dermatol. 2009;129:814.

Corsetti G, D'Antona G, Dioguardi FS, Rezzani R. Topical application of dressing with amino acids improves cutaneous wound healing in aged rats. Acta Histochem. 2009;112:497–507.

Cunico RL, Maibach HI, Khan H, Bloom E. Skin barrier properties in the newborn. Transepidermal water loss and carbon dioxide emission rates. Biol Neonate. 1977;32:177–82.

Edwards WH, Conner JM, Soll RF. The effect of prophylactic ointment therapy on nosocomial sepsis rates and skin integrity in infants with birth weights of 501 to 1000 g. Pediatrics. 2004;113:1195–203.

Fluhr JW, Kao J, Jain M, Ahn SK, Feingold KR, Elias PM. Generation of free fatty acids from phospholipids regulates stratum corneum acidification and integrity. J Invest Dermatol. 2001;117:44–51.

Gunt H. Water handling properties of vernix caseosa: pharmacy. Cincinnati: University of Cincinnati; 2002.

Hachem JP, Roelandt T, Schurer N, Pu X, Fluhr J, Giddelo C, Man MQ, Crumrine D, Roseeuw D, Feingold KR, Mauro T, Elias PM. Acute acidification of stratum corneum membrane domains using polyhydroxyl acids improves lipid processing and inhibits degradation of corneodesmosomes. J Invest Dermatol. 2010;130:500–10.

Hardman MJ, Sisi P, Banbury DN, Byrne C. Patterned acquisition of skin barrier function during development. Development. 1998;125:1541–52.

Hatano Y, Man MQ, Uchida Y, Crumrine D, Scharschmidt TC, Kim EG, Mauro TM, Feingold KR, Elias PM, Holleran WM. Maintenance of an acidic stratum corneum prevents emergence of murine atopic dermatitis. J Invest Dermatol. 2009;129:1824–35.

Hoath SB, Pickens WL, Visscher MO. The biology of vernix caseosa. Int J Cosmet Sci. 2006;28:319–33.

Hoeger PH, Schreiner V, Klaassen IA, Enzmann CC, Friedrichs K, Bleck O. Epidermal barrier lipids in human vernix caseosa: corresponding ceramide pattern in vernix and fetal skin. Br J Dermatol. 2002;146:194–201.

Holleran WM, Takagi Y, Uchida Y. Epidermal sphingolipids: metabolism, function, and roles in skin disorders. FEBS Lett. 2006;580:5456–66.

Holm T, Rutishauser D, Kai-Larsen Y, Lyutvinskiy Y, Stenius F, Zubarev RA, Agerberth B, Alm J, Scheynius A. Protein biomarkers in vernix with potential to predict the development of atopic eczema in early childhood. Allergy. 2014;69:104–12.

Joseph WR. Physical characterization of vernix caseosa: implications for biological function. Pharmacy. [Ph. D.]. Cincinnati: University of Cincinnati; 2002. p. 135.

Kessner D, Ruettinger A, Kiselev MA, Wartewig S, Neubert RH. Properties of ceramides and their impact on the stratum corneum structure, part 2: stratum corneum lipid model systems. Skin Pharmacol Physiol. 2008;21:58–74.

Kurokawa I, Danby FW, Ju Q, Wang X, Xiang LF, Xia L, Chen W, Nagy I, Picardo M, Suh DH, Ganceviciene R, Schagen S, Tsatsou F, Zouboulis CC. New developments in our understanding of acne pathogenesis and treatment. Exp Dermatol. 2009;18:821–32.

Mancini AJ, Sookdeo-Drost S, Madison KC, Smoller BR, Lane AT. Semipermeable dressings improve epidermal barrier function in premature infants. Pediatr Res. 1994;36:306–14.

Marchini G, Lindow S, Brismar H, Stabi B, Berggren V, Ulfgren AK, Lonne-Rahm S, Agerberth B, Gudmundsson GH. The newborn infant is protected

by an innate antimicrobial barrier: peptide antibiotics are present in the skin and vernix caseosa. Br J Dermatol. 2002;147:1127–34.

McKinley-Grant LJ, Idler WW, Bernstein IA, Parry DA, Cannizzaro L, Croce CM, Huebner K, Lessin SR, Steinert PM. Characterization of a cdna clone encoding human filaggrin and localization of the gene to chromosome region 1q21. Proc Natl Acad Sci U S A. 1989;86:4848–52.

Mikova R, Vrkoslav V, Hanus R, Hakova E, Habova Z, Dolezal A, Plavka R, Coufal P, Cvacka J. Newborn boys and girls differ in the lipid composition of vernix caseosa. PLoS One. 2014;9, e99173.

Moraille R, Pickens WL, Visscher MO, Hoath SB. A novel role for vernix caseosa as a skin cleanser. Biol Neonate. 2005;87:8–14.

Narendran V, Visscher MO, Abril I, Hendrix SW, Hoath SB. Biomarkers of epidermal innate immunity in premature and full-term infants. Pediatr Res. 2010;67:382–6.

Nicolaides N, Fu HC, Ansari MN, Rice GR. The fatty acids of wax esters and sterol esters from vernix caseosa and from human skin surface lipid. Lipids. 1972;7:506–17.

Oudshoorn MH, Rissmann R, van der Coelen D, Hennink WE, Ponec M, Bouwstra JA. Development of a murine model to evaluate the effect of vernix caseosa on skin barrier recovery. Exp Dermatol. 2009a;18:178–84.

Oudshoorn MH, Rissmann R, van der Coelen D, Hennink WE, Ponec M, Bouwstra JA. Effect of synthetic vernix biofilms on barrier recovery of damaged mouse skin. Exp Dermatol. 2009b;18:695–703.

Pickens WL, Warner RR, Boissy YL, Boissy RE, Hoath SB. Characterization of vernix caseosa: water content, morphology, and elemental analysis. J Invest Dermatol. 2000;115:875–81.

Puhvel SM, Reisner RM, Amirian DA. Quantification of bacteria in isolated pilosebaceous follicles in normal skin. J Invest Dermatol. 1975;65:525–31.

Ran-Ressler RR, Devapatla S, Lawrence P, Brenna JT. Branched chain fatty acids are constituents of the normal healthy newborn gastrointestinal tract. Pediatr Res. 2008;64:605–9.

Rippke F, Schreiner V, Schwanitz HJ. The acidic milieu of the horny layer: new findings on the physiology and pathophysiology of skin ph. Am J Clin Dermatol. 2002;3:261–72.

Rissmann R, Oudshoorn MH, Kocks E, Hennink WE, Ponec M, Bouwstra JA. Lanolin-derived lipid mixtures mimic closely the lipid composition and organization of vernix caseosa lipids. Biochim Biophys Acta. 2008;1778:2350–60.

Rissmann R, Groenink HW, Weerheim AM, Hoath SB, Ponec M, Bouwstra JA. New insights into ultrastructure, lipid composition and organization of vernix caseosa. J Invest Dermatol. 2006;126:1823–33.

Rissmann R, Oudshoorn MH, Zwier R, Ponec M, Bouwstra JA, Hennink WE. Mimicking vernix caseosa–preparation and characterization of synthetic biofilms. Int J Pharm. 2009;372:59–65.

Schmid-Wendtner MH, Korting HC. The ph of the skin surface and its impact on the barrier function. Skin Pharmacol Physiol. 2006;19:296–302.

Schunck M, Neumann C, Proksch E. Artificial barrier repair in wounds by semi-occlusive foils reduced wound contraction and enhanced cell migration and reepithelization in mouse skin. J Invest Dermatol. 2005;125:1063–71.

Sedin G, Hammarlund K, Stromberg B. Transepidermal water loss in full-term and pre-term infants. Acta Paediatr Scand Suppl. 1983;305:27–31.

Silvetti AN. An effective method of treating long-enduring wounds and ulcers by topical applications of solutions of nutrients. J Dermatol Surg Oncol. 1981;7:501–8.

Supp AP, Wickett RR, Swope VB, Harriger MD, Hoath SB, Boyce ST. Incubation of cultured skin substitutes in reduced humidity promotes cornification in vitro and stable engraftment in athymic mice. Wound Repair Regen. 1999;7:226–37.

Tansirikongkol A, Visscher MO, Wickett RR. Water-handling properties of vernix caseosa and a synthetic analogue. J Cosmet Sci. 2007a;58:651–62.

Tansirikongkol A, Wickett RR, Visscher MO, Hoath SB. Effect of vernix caseosa on the penetration of chymotryptic enzyme: potential role in epidermal barrier development. Pediatr Res. 2007b;62:49–53.

Tansirikongkol A, Hoath SB, Pickens WL, Visscher MO, Wickett RR. Equilibrium water content in native vernix and its cellular component. J Pharm Sci. 2008;97:985–94.

Thakoersing VS, Ponec M, Bouwstra JA. Generation of human skin equivalents under submerged conditions-mimicking the in utero environment. Tissue Eng Part A. 2010;16:1433–41.

Tollin M, Bergsson G, Kai-Larsen Y, Lengqvist J, Sjovall J, Griffiths W, Skuladottir GV, Haraldsson A, Jornvall H, Gudmundsson GH, Agerberth B. Vernix caseosa as a multi-component defence system based on polypeptides, lipids and their interactions. Cell Mol Life Sci. 2005;62:2390–9.

Visscher MO. Environmental interactions. In: Hoath SB, Maibach HI, editors. Neonatal skin structure and function. 2nd ed. New York: Marcel Dekker; 2003.

Visscher MO, Chatterjee R, Munson KA, Pickens WL, Hoath SB. Changes in diapered and nondiapered infant skin over the first month of life. Pediatr Dermatol. 2000;17:45–51.

Visscher M, Hoath SB, Conroy E, Wickett RR. Effect of semipermeable membranes on skin barrier repair following tape stripping. Arch Dermatol Res. 2001;293:491–9.

Visscher M, Narendran V, Joseph W, Gunt H, Hoath S. Development of topical epidermal barriers for preterm infant skin: comparison of aquaphor and vernix caseosa. Baltimore: Pediatric Academic Society Annual Meeting; 2002.

Visscher MO, Narendran V, Pickens WL, LaRuffa AA, Meinzen-Derr J, Allen K, Hoath SB. Vernix caseosa in neonatal adaptation. J Perinatol. 2005;25:440–6.

Visscher MO, Utturkar R, Pickens WL, LaRuffa AA, Robinson M, Wickett RR, Narendran V, Hoath SB. Neonatal skin maturation–vernix caseosa and free amino acids. Pediatr Dermatol. 2011a;28:122–32.

Visscher MO, Barai N, LaRuffa AA, Pickens WL, Narendran V, Hoath SB. Epidermal barrier treatments based on vernix caseosa. Skin Pharmacol Physiol. 2011b;24(6):322–9.

Wertz PW. Biochemistry of human stratum corneum lipids. In: Elias P, Feingold K, editors. Skin barrier. New York: Taylor & Francis; 2006. p. 33–42.

Wysocki SJ, Grauaug A, O'Neill G, Hahnel R. Lipids in forehead vernix from newborn infants. Biol Neonate. 1981;39:300–4.

Yoshio H, Tollin M, Gudmundsson GH, Lagercrantz H, Jornvall H, Marchini G, Agerberth B. Antimicrobial polypeptides of human vernix caseosa and amniotic fluid: implications for newborn innate defense. Pediatr Res. 2003;53:211–6.

Yosipovitch G, Maayan-Metzger A, Merlob P, Sirota L. Skin barrier properties in different body areas in neonates. Pediatrics. 2000;106:105–8.

Youssef W, Wickett RR, Hoath SB. Surface free energy characterization of vernix caseosa. Potential role in waterproofing the newborn infant. Skin Res Technol. 2001;7:10–7.

Zhukov BN, Neverova EI, Nikitin KE, Kostiaev VE, Myshentsev PN. A comparative evaluation of the use of vernix caseosa and solcoseryl in treating patients with trophic ulcers of the lower extremities. Vestn Khir Im I I Grek. 1992;148:339–41.

Assessing the Effects of Fiber-Based Materials on the Skin

115

Jackson Leong, Kathryn L. Hatch, and Howard I. Maibach

Contents

J. Leong (✉)
Dermatology Department, University of California, San Francisco, San Francisco, CA, USA
e-mail: jacksonleong@gmail.com

K.L. Hatch
Department of Agricultural and Biosystems Engineering, University of Arizona, Tucson, AZ, USA
e-mail: khatch@ag.arizona.edu

H.I. Maibach
Department of Dermatology, School of Medicine, University of California, San Francisco, CA, USA
e-mail: maibachh@derm.ucsf.edu

P. Humbert et al. (eds.), *Agache's Measuring the Skin*,
DOI 10.1007/978-3-319-32383-1_49

Keywords
ACD • Fabric • Fiber • Allergic • Contact • Dermatitis • Textile

Near the end of the 1980s, the first research results concerning skin property changes resulting from covering the skin with diapers and garment fabrics (fiber-based materials) appeared in the literature (Zimmerer et al. 1986; Hatch et al. 1987; Wester et al. 1985). The bioengineering instruments used were a focused microwave probe to determine the water content of the SC, an evaporimeter to assess the rate of evaporation of transepidermal water from the skin surface, and a laser Doppler velocimeter instrument to measure capillary blood. Low interest in using bioengineering instruments to study the effect of diapers (Campbell et al. 1987; Davis et al. 1989; Wilson and Dallas 1990; Berg et al. 1994; Akin et al. 1997; Grove et al. 1998, 2002; Odio et al. 2000a, b; Partsch et al. 2000; Zhai et al. 2002; Visscher et al. 2000) and garment fabrics (Hatch et al. 1990a, b, 1992a, 1997; Barker et al. 1990; Markee et al. 1990, 1991; Cameron et al. 1997) has continued. Research results about the effects of washing the skin with cloth towels (textile products) and baby wipes (paper products) using bioengineering instruments have become available (Priestley et al. 1996; Farage 2000; Odio and Friedlander; Odio et al. 2001).

This chapter reviews studies whose results have advanced our knowledge about the effects of fiber-based materials on the human skin with the use of bioengineering instrumentation. The emphasis is on how fiber-based materials change properties of the skin they cover and/or contact. Readers are referred to sources of information about the bioengineering instrumentation used (Berardesca et al. 1995; Elsner et al. 2002; Hatch et al. 1992b). Our purpose is to encourage further work in this area.

1 Diapers/Incontinence Products

1.1 Specifications and Aims

Cloth diapers and incontinence products may be a large rectangle piece of fabric which has to be folded by the caregiver, a large rectangle of cloth prefolded and sewn to create a multiple-layered product, or a form-fitted multilayer textile product. Cloth diapers are intended to be laundered after each use and reused. The fiber content of the fabric comprising cloth diaper is usually cotton because this fiber is absorbent, soft, and resistant enough to acids, alkalis, and abrasive action to make a satisfactory diaper. Some cloth diapers are made with a polypropylene section, a section that contacts the wearer's skin. Waterproof pants are usually put on over the cloth diaper to reduce contamination of the environment as the diaper becomes soiled. In contrast, disposable diapers and disposable incontinent products are one-time use products made entirely or partially of paper products. Minimally, they have a top (liner) sheet that contacts the skin when the diaper is worn, an absorbent core layer, and a bottom sheet (back or outer) that serves the same function as the waterproof pants in the cloth diaper ensemble. Disposable products may have six layers: top sheet, intake layer, secondary layer, absorbent core, tissue layer, and bottom sheet (Grove et al. 1998).

The engineering of a diaper/incontinence product system is based on keeping the diapered area of the skin as close to the hydration level as it would be if un-diapered. Keeping the diapered area as close to normal hydration as possible is of considerable interest because it has been shown that skin permeability, CO_2 emission, frictional trauma, and growth of pathogenic microorganisms are increased as skin hydration increases, and the skin's barrier properties are also compromised (Aly et al. 1978; Zhai and Maibach 2001a, b, 2002). The clinical consequence of such an environment under diapers is erythema, mild rash, and outright diaper dermatitis, conditions unpleasant to the wearer and care provider.

Wearing of cloth or disposable diapers by infants or the wearing of cloth or disposable incontinence products by incontinent individuals creates a fairly closed environment; how closed it is depends on the fit of the product, the specific materials used, and the specific layering system. Fit influences (1) the amount of air passing between the product and the skin surface and, therefore, the amount of water carried out of the system as vaporous water and (2) how close

moisture (urine) is to the skin surface when the diaper becomes wet. The type of materials influences moisture properties, softness, and the coefficient of friction. Which properties are needed depends on the location of the material in the assemblage (system). Desirable features of top sheet materials are low absorbency and high wickability, plus a low coefficient of friction because it is in direct contact with the skin. Properties for the absorbent layer's material are high absorbency and high water retention. Properties for the bottom sheet are high water vapor permeability (breathability) and high waterproofness (high resistance to the passage of liquid water).

This section reviews those studies in which bioengineering instrumentation was used to compare marketplace products, to develop improved diapering systems, and to enhance experimental produces for studying the effects of diapers/incontinence product on the skin. They are presented in chronological order that best reveals the advancement in diapers/incontinence product design and adjustment of methodologies to detect differences due to product design.

1.2 Evaluating Conventional Disposables and Cloth Diapers

Zimmerer et al. (1986), the first team to publish study results, were interested in the alteration in skin wetness due to covering the skin with wet and dry conventional disposable and cloth diapers. In addition to assessing skin wetness, they assessed changes in skin friction, the skin's susceptibility to abrasion damage, its permeability, and its support of microbial growth. Adults wore prepared diaper patches on their arms which had been preloaded with synthetic urine, a procedural method that the research team had established was as valid as placing the materials on infants in the diapered area. An evaporimeter was used to measure the rate of evaporative water loss off the skin surface following removal of the diaper materials from the subject's forearms. Evaporative water loss (EWL) rates were proportional to diaper wetness. The wetter the diaper patches, the greater the EWL rate. At equivalent water loadings, cloth diaper material produced greater EWL rates than the disposable diaper. Increased EWL rates were accompanied by undesirable increases in the coefficient of friction, abrasion damage, skin permeability, and microbial growth. An increase in the coefficient of friction results in the skin more easily damaged by abrasion and that exhibits a reduced barrier capacity.

1.3 Evaluating Absorbent Core Materials

Absorbent gel disposable diapers were compared to reusable cloth and conventional disposable diapers in a study by Campbell et al. (1987). Differences in skin health were expected because adding the gel material to the absorbent middle layer of the diaper would increase absorbent capacity and moisture holding/binding capability relative to the other two diaper designs. In this investigation, 1,614 infants were assigned to wear the three different diapers. Like Zimmerer et al. (1986), the main focus was studying the hydration state of the skirt. An evaporimeter was used to collect EWL rate data. The measurement sites were located in the suprapubic and buttock areas and assessment was done before and immediately after the diaper was removed. The skin under the absorbent gel disposable diapers was significantly less wet, closer to normal skin pH, and had a lower degree of diaper dermatitis than the skin under the conventional disposable or reusable cloth diapers. The results were consistent with the researchers' hypothesis that better control in the diaper area of skin wetness, skin pH, and prevention of the mixing of urine and feces produce a better diaper environment.

Fluff absorbent and fluff plus absorbent polymer diapers were used in a study by Davis et al. (1989). Differences were expected because the addition of absorbent polymers to the absorbent inner layer of the diaper should improve fluid binding and help control the pH in the diaper environment. Skin effects were assessed for the change in skin hydration, alteration of skin pH, and occurrence and severity of diaper dermatitis. The clinical study involved approximately

150 infants over 15 weeks, with each infant wearing fluff diapers and absorbent polymer diapers. Again, an evaporimeter was used as well as an electrical conductance instrument to assess water content. Urine loads in the diapers were determined gravimetrically. Expert graders also evaluated infants' diapered skin. Results showed that diapers with absorbent polymer provided a better skin environment than those with fluff because skin wetness was lower and pH control better compared to the fluff absorbent only diaper. In addition, the clinicians' grades indicated a directional reduction in diaper rash severity under the diaper with the absorbent polymer.

Five brands of superabsorbent (SA) diapers were compared to five brands of reusable cloth diapers and four brands of conventional disposables by Wilson and Dallas (1990). Using the Zimmerer et al. model, they asked 80 healthy volunteers to wear a 2 in. wet diaper patch on their volar forearms for 2 h. This team was interested in the relationship between diaper wetness (the amount of synthetic urine remaining in the patch at the end of 2 h of skirt contact) and skin wetness at that same time. The same amount of synthetic urine was placed in each patch (preloaded); the amount represented a moderate amount based on the previous work of Zimmerer et al. (1986). An evaporimeter was used to measure excess skin wetness attributed to the patches. The amount of moisture retained in the patches was determined at the time of removal. The SA disposable diapers kept the skin drier and retained more synthetic urine than cloth reusable and conventional disposable diapers. The SA brands evaluated did an equally adequate job in keeping the skin dry and in retaining moisture. Conventional disposable diapers were less able to keep the skin dry than SA diapers and were not superior to cloth products in most instances. Cloth diapers' ability to lower skin wetness depended on their construction: those with several layers of the same fabric were less successful in keeping the skin dry than ones that contained middle layers of unwoven components. Among these results, the most interesting one is that the diapers that retained the most preloaded moisture during the 2 h wearing period, the SA type, were also those where the skin was the least hydrated. So the amount of moisture in these diapers was not related to increased skin hydration. This result makes sense when one realizes that the underlying idea for the SA diaper design is to move moisture away from the skin and retain it at a distance from the skin surface so it is not available to hydrate the skin. Odio and Friedlander (Odio and Friedlander) suggested that the reason significant differences were not found among the SA brands was that the methodology was not designed to detect these differences.

Akin et al. (1997) worked to design a methodology to more reliably and realistically assess the effectiveness of absorbent articles in mitigating skin hydration. Changes made were to (1) cover a greater amount of skin surface, (2) measure the amount of water retained in the core (absorbent layer) and in the top sheet rather than total water retained, and (3) load the diaper with urine after its placement on the skin rather than preloading it.

They wrapped disposable diapers with different absorbent structures around the forearms of adult volunteers, then loaded the diaper with urine substitute, and held the wet diaper in place for l h. Then they measured the hydration of the volar region by evaporimeter and compared that data to data obtained by measuring skin hydration in the diaper region of children who had worn control-loaded diapers in the usual way. The amounts of fluid retained in various portions of the diaper were measured. One result was that evaporative water loss measurements on adult forearms were a reliable test for comparing the effectiveness of absorbent articles in preventing skin hydration provided that (1) the complete garment was used and (2) fluid was loaded into the garment in a manner that simulated normal urination. Other results were that (1) the skin on adult forearms and skin in the diaper region of children were concordant in their response to wet diapers, and (2) skin wetness was directly related to the amount of liquid retained in layers close to the skin. This methodology was used by subsequent researchers.

Also, highly important to note here is a study by Berg et al. (1994) which was conducted to evaluate the strength of the association of diaper dermatitis with skin wetness and pH. Data was

collected in four diaper clinical trials involving 1,601 infants and over 15,000 individual measurements of skin wetness, skin pH, and observations of diaper rash severity. The data was statistically analyzed. Subjects wore their own diaper product for 4 weeks to establish baseline data, then wore a test diaper product for 8 weeks, and then their own diaper again for 4 weeks. Berg et al. (1994) provide no description of the test diaper but it is likely it is a superabsorbent disposable given the year in which the study was conducted and the company that employed the authors. The skin of the diapered area was visually evaluated for evidence of diaper dermatitis by trained graders every 2 weeks of the l6-week trial. Skin wetness and skin pH measurements were taken at each grading session. Mean EWL values for each infant were calculated as the mean of front and back readings at all-time points, minus a control value obtained on undiapered skin of the thigh. Areas of dermatitis were avoided.

Diapered skin wetness was significantly elevated compared with that of adjacent undiapered skin. Therefore, both pH and skin wetness have an impact on diaper dermatitis. At each grading period, elevated physical measurements were associated with elevated diaper dermatitis grades. Skin wetness was more strongly associated with diaper dermatitis than pH at each grading period.

A retrospective evaluation of 12 clinical studies conducted before and after the introduction of absorbent gelling materials by Odioet al. (Odio and Friedlander) was undertaken to determine whether utilization of these absorbent materials was associated with a marked reduction in the severity of diaper dermatitis. Six of the clinical trials were conducted before the introduction of the new diapers and six following involving 4,000 children. The severity of diaper dermatitis was less after the new core material introduction.

1.4 Evaluating Bottom Shoot Materials

Superabsorbent diapers that differed in type of bottom (back) sheet material were studied by Grove et al. (1998). One diaper (E) had a waterproof breathable bottom sheet and two others (A and B) had a conventional waterproof bottom sheet. Except for the bottom sheet, diaper E was identical to B. In waterproof breathable bottom sheet diapers, the microporous membrane used for the back sheet is permeable to air and water vapor (is breathable) but impervious to liquid (waterproof). In the study, an intact diaper was attached to the adult forearm or a child wore the diaper. The diapers were loaded with liquid, simulating urination during actual use. After a 1 h exposure period, the hydration state of the underlying skin was evaluated using computerized evaporimetry as well as by using electrical conductance. Comparative studies were also run in the diaper region of children who wore both types of SA diapers. Test diapers were dissected and fluid distribution within various layers was measured gravimetrically.

Both the adult and child model methods gave identical evaporimeter readings of skin hydration for the three test diapers. In each case the diapers were shown to be significantly different from each other with $p < 0.001$. Commercial diaper A left the skin wetter while the experimental breathable diaper E kept the skin significantly dryer. The correlation coefficient of adult and child tests was 0.895. The adult EWL measurements were higher than children's due to differences in probe placement.

Conductance (skin hydration) data also showed the same differences as evaporimetry but there was more variability in the data. Although diapers A and B contained superabsorbent polymer (SAP) at about the same levels, diaper A caused significantly more skin hydration in all tests with all procedures. The apparent cause of this difference was thought to be due to differences in the liquid distribution in the diapers – in diaper A almost 12 % of the total fluid volume remained in the skin-accessible layers and was able to contact the epidermis. In diaper B, virtually all of the fluid was locked into the absorbent core and away from the skin surface. This difference in liquid distribution is consistent with the skin dryness performance of the two products. Diaper E caused the least amount of skin hydration. It had a breathable bottom sheet (outer layer).

Lane et al. (1990) confirmed that disposable diapers containing absorbent gelling material resulted in fewer occurrences and less severe diaper dermatitis after testing 140 infants diapered in either conventional cellulose core disposable diapers and diapers containing the cellulose core plus the gel material. Akin et al. (2001) later determined that children who wore gel diapers with a breathable outer layer had fewer occurrences of Candida and common diaper dermatitis than when wearing gel diaper without the breathable outer layer. They also provide a water vapor transmission rate for the breathable film as >3,000 g/m^2/day and for an occlusive bottom sheet film as zero.

1.5 Evaluating Top Layer Materials

A disposable diaper designed with a top (inner) layer supposedly capable of delivering to the skin a formulation intended to protect that skin from over-hydration, and irritation was studied by Odio et al. (2000a, b). The objectives of the first phase were to (1) determine the extent of the delivery of the formulation from the top sheet during normal use of the diaper and (2) whether the amount transferred was sufficient to have an impact on the skin surface microtopography. The objective of the second phase was to assess skin condition. The formulation incorporated into the top layer of the experimental diaper was petrolatum because this formulation has a history of promoting healthier skin in diapered areas by enhancing SC's barrier function and rendering it more resilient to hydrating, irritant, and mechanical insults.

To study the delivery of the petrolatum, 60 children, 16–24 months of age, were assigned randomly to one of two groups. Group one children had two tapes attached to their buttocks. After wearing the experimental diaper for 3 h, one tape was removed, and after a second experimental diaper was worn for 3 h, the other type was removed. Group 2 children also had two tapes affixed to their buttocks. These children wore experimental diapers for a 24 h period, times for diaper changes being done according to the parent's normal routine.

Parents were not to wipe the tapes. One tape was removed at 18 h. When these children returned to the laboratory at 24 h, the second tape was removed. Subsequently, the tapes were extracted and the amount of petrolatum transferred was calculated. Results were that during normal diaper use, formulation transfer from the diaper to the skin occurred in a cumulative, time-dependent manner.

To study the effect of the delivered petrolatum on skin microtopography, two independent, blinded, and randomized clinical trials were conducted on 110 children. In time period 1 at the first visit, a skin surface replica was taken on each buttock of each child in an area free of evidence of skin damage. Children were then assigned to a group in which they would only wear the control diaper for 9 days or to a group in which they would wear only the experimental diaper for 9 days. The control diaper was identical to the experimental diaper except for the absence of the petrolatum formulation. The control diaper was the superabsorbent type (the core being AGM/cellulose). Parents were given instructions about bathing and diapering the child. On day 10, a second skin replica was made. Children who wore the experimental diaper were dismissed from the study. Those who had worn the control diaper were then assigned randomly to a group to remain on the control diaper or to use the experimental diaper for l week. All children returned to the lab on day 18 and another skin replica was taken the same as for visits l and 2. The day 10 roughness measurement served as the baseline against which the day 18 roughness measurements could be compared. Importantly, one set of this comparison data (day 10–18) is for children who had worn a high-quality control diaper for an extended period of time before wearing the experimental diaper. Results were that the use of the formulation-treated diaper was associated with significant reduction in skin surface roughness compared to the control diaper.

In phase two, two studies were conducted. The first was designed to determine whether repeated use of the formulation-treated diaper would improve the erythema profile of diapered skin relative to that of infants wearing the control diaper. The second study determined the effect of the test diaper on the diaper rash profile of children during a 4-week period of use of the control and test products. A noticeable reduction in the severity of erythema occurred among the infants who used the test diaper compared to those who wore the control product. There was also a noticeable reduction in the severity of erythema for the infants wearing the control diaper, establishing that wearing a high-quality formulation-free diaper assists with diapered area skin health. Even though the rash scores varied markedly over time for both groups, results were that there was a consistent reduction in diaper dermatitis among children using the test product compared to the control product.

1.6 Other Investigations

Partsch et al. (2000) and Grove et al. (2002) evaluated change in the scrotal, skin, and/or core temperatures under the diapered area of young boys. The procedure used by Partsch et al. was to record scrotal temperatures over a 24 h period in the child's home using a Thermoport device which was designed for long-term monitoring in adult males. One series of temperatures was taken while the child wore a disposable diaper (German Pampers Premium, Proctor and Gamble) and while wearing a reusable diaper (whether a protective cover was worn or not is not known). They found that mean scrotal temperatures under the disposable diapers were significantly higher than under the reusable diapers. The procedure used by Grove et al. (2002) was to continuously monitor scrotal and skin surface temperatures under controlled laboratory conditions using temperature probes designed for pediatric studies. Temperature of the tympanic membrane was measured using an infrared thermometer as an estimate of core temperature for each individual at various times during the 2 h session. The subjects were 70 normal healthy boys, 3–25 months old. The diapering situations included reusable cloth diapers used with and without a protective cover and various disposable diapers. The findings were that scrotal temperatures were the same during the wearing of disposable diapers and reusable cloth diapers with protective cover. Scrotal temperature was lower when the reusable diaper was worn without the cover. On average scrotal temperature was significantly lower than core temperature. Skin surface temperatures increased when covered by a diaper.

Zhai et al. (2002) investigated the relationship of stratum corneum hydration and skin permeability as a result of covering adult skin with wet occlusive patches and wet diapers for 10 min, 30 min, and 3 h. Nine women wore the patches on their forearms after baseline values for water evaporation rate (WER), skin blood flow volume (BFV), capacitance (Cap), and redness (a*) were determined. Immediately after removal of the patches, either 20 μL of methyl or hexyl nicotinate was applied to various sites. WER and Cap readings were recorded at designated sites 0, 5, 10, 15, and 20 min after nicotinate application. The a* and BFV measurements were made on each nicotinate-challenged site 5, 10, 15, 20, 30, 40, and 60 min after the nicotinate application. Findings were that wet patches and diapers increased skin hyperhydration proportional to exposure time. Permeation of nicotinate increased for hydrated skin versus control, as soon as 10 min of patch exposure. There was no evidence of increased permeation rates with increased hyperhydration once a relatively low threshold of hyperhydration was achieved. The researchers concluded that there were no meaningful differences in permeation following either diapering simulation and suggested that the "WER-Area Under the Curve Method was superior to capacitance for measuring the absolute extent of hyperhydration."

Visscher et al. (2000) investigated (1) the normative features of newborn SC hydration and

barrier properties during the first month of life, (2) identified differences in skin hydration and barrier properties of diapered skin versus undiapered control sites, and (3) compared the barrier properties and hydration of infant skin with those of adult skin under similar environmental conditions. One purpose of the study was to determine whether newborn children's mothers' volar forearms might be used to learn about the hydration effects of diapering newborns. Thirty-one term infants were evaluated in the hospital on postnatal day l and at home on days 4, 7, 14, 21, and 28 for a total of six visits. Measurements included baseline skin hydration, continuous capacitive reactance, and environmental conditions. The skin sites were below the waistband of the diaper above the symphysis pubis and above the waistband. Measurements were taken 25 min after diaper removal to allow evaporation of surface moisture. Changes in epidermal barrier properties over the first 4 weeks of life included an increase in surface hydration, a decrease in transepidermal water movement under occlusion, a decrease in surface water desorption rate, and an increase in surface pH. Diapered and undiapered regions were indistinguishable at birth but exhibited differential behavior over the first 14 days, with the diapered region showing a higher pH and increased hydration. Maternal measurements remained constant throughout the period. They concluded that healthy newborn skin undergoes progressive changes in epidermal barrier properties over the first 28 days. Adult skin testing does not replicate newborn skin during the first month of life.

2 Garment Fabrics

2.1 Specifications

Fabric is a thin, planar material whose smallest material unit is a textile fiber, a unit of matter that is characterized by having a length at least 100 times its diameter or width and which can be spun into yarn or made into fabric. The diameter of textile fibers is small – generally, 0.0004–0.002 in. (10–50 μm). Their length varies from ∼7/8 in. (∼1.8 cm) to many miles. The other material component of fabrics is yarn, long thin structures composed of fibers. In addition to fiber content, a fabric may also have a colorant content (dyes and pigments) and a chemical finish content. Fabric is the most suitable material for covering the human body because it usually allows insensible perspiration (TEW) to pass through it and it moves as the body moves (bends, stretches, etc.).

Placing garment fabric over the skin does not usually create nearly the occlusive environment that results from the wearing of diapers/incontinence products. However, placing any garment fabric on the skin has the potential to change skin properties. Fabrics differ from each other in water vapor permeability (a property commonly called breathability), in absorbance of water vapor, in capability to absorb, adsorb, and imbibe liquid water, in wicking ability (the ability to move water from one surface to the other by capillarity), in softness (ease of bending), and in surface characteristics. Like diapers, garment fabrics may become saturated with water, the water in this case being most often perspiration or rainwater. Continuing to wear wet fabrics after swimming, snorkeling, and other water activities keeps a water supply near the skin surface. Wetted fabric may be a source of water to increase SC hydration. Wetted fabric may lie closer to the skin surface than dry fabric and may alter the degree of friction of the fabric on the skin.

The motivation for studying the effect of fabric on skin properties does not lie in the need to reduce a singular major skin health such as underlies the study of the effect of diapers on the skin they cover. Rather, the motivations have been to learn (1) under what wearing conditions can changes be detected and (2) what properties of the fabric may account for the differences in the magnitude of change. The long-term motivation is that test procedures might be developed that would aid in evaluating high-performance sports apparel and occupational protective garment systems (systems in which the outer layer of the system provides a barrier to wearer generated moisture dissipation).

In this section, we review a series of studies in which the effect of garment fabric on the skin was

studied. These studies are grouped by the type of fabric used in the experiment.

2.2 Triacetate and Polyester Fabrics Experiment

In the earliest study (Hatch et al. 1987), our objective was to (1) determine whether a change in SC hydration could be detected after being covered by a fabric swatch using available bioengineering instrumentation and (2) whether the fiber composition of the fabric made a difference in the hydration state of the skin lying under it. Two woven dress weight fabrics that were alike except in fiber composition were selected. The fiber composition of one was polyester (a manufactured synthetic fiber with poor moisture absorption) and the other triacetate (a manufactured cellulosic fiber with moisture absorption capacity about five times greater than polyester). Swatches of each of these fabrics were placed on a sedentary subject's forearms with and without a covering of occlusive plastic film. A focused microwave probe was used to assess SC water content and an evaporimeter measured rate of transepidermal water loss (TEWL) before and after removal of the fabric swatches.

Placement of either triacetate or polyester on the forearm without a covering of film did not cause detectable changes in water content or evaporation measured immediately after fabric removal even when the fabric had been in contact with the skin for 90 min. SC water content and evaporation increased as the fabric film remained on the forearm longer. SC water content was generally greater at polyester/film-covered forearm sites than at triacetate/film-covered sites, but there was not a significant statistical difference due to fabric type (fiber composition). Forearm water evaporation after fabric swatch removal was also greater for polyester/film sites than for triacetate/film sites; this difference was statistically significant. Occluded fabric placed on the skin, therefore, influenced SC water content and water evaporation rate. The data suggest that fiber absorption differences influenced the hydration of the covered skin. The triacetate fabric was absorbing more of the transepidermal water than the polyester fabric.

Encouraged by these results, our team decided to undertake a study in which we would investigate changes in skin hydration due to (1) activity level of subject (sedentary, vigorously active, and resting after activity), (2) the exercise environment (hot-humid and hot-dry), and (3) the moisture holding capacity of the fabric of the exercise garments. Another objective was to assess comfort sensations (wet sensation and skin contact comfort) of the fabric to confirm differences in the bioengineering instrumentation results. We also were interested in whether the stiffness of fibers might alter capillary blood flow and designed this experiment to include this objective.

2.3 Jersey Knit Garments Experiment

Three jersey knit fabrics were made. The fabric construction, jersey knit, is that one usually used for the manufacture of T-shirts. One fabric was made entirely from cotton fibers, one from l.5 denier polyester, and one from 3.5 denier polyester. Cotton fiber, known to be highly absorbent, and polyester fiber, known to absorb little or no moisture, were of interest because of the large difference in absorbent capacity. Two deniers (weight per unit length) of polyester fiber were used so that the stiffness of the fibers were be different. A 3.5 denier polyester is the maximum size polyester fiber used for garment fabrics. The fabric made from it was noticeable rougher than the fabric made from the 1.5 denier fiber. Each fabric was characterized instrumentally for its comfort properties (absorption, heat conductivity, etc.) (Hatch et al. 1990a) and its mechanical and surface properties related to wearing comfort (Barker et al. 1990).

The three jersey knit fabrics (100 % cotton, 100 % 1.5 denier polyester, 100 % 3.5 denier polyester) were made into long sleeve T-shirts and pants of various sizes. The upper back section was designed with a zippered section so that instrumental measurements could be taken on the upper back. Ten female subjects were enrolled

into the study alter it was ascertained that they were capable of doing the exercise routine in the experimental environments. For each session, they first acclimated in the exercise chamber, and baseline measurements were taken including rate of evaporative water loss using an evaporimeter, water content of the SC using a focused microwave probe, and capillary blood flow using laser Doppler velocimetry. In six sessions, each subject exercised and rested in a hot, humid environment wearing each of the three garments and then in a hot, dry environment wearing each of the three garments. Garments were laundered between sessions. Cutaneous assessments (rate of evaporative water loss, water content of the SC, and capillary blood flow) were made under the fabric 20 min following placement of the fabric on the skin, after 40 min of vigorous exercise, and 20 min after exercise ceased. Subjects we're asked for their perceptions of contact comfort using a standard contact comfort scale.

2.3.1 Skin Hydration Results

Rate of skin evaporative water loss from the skin surface was lower in the higher humidity environment at all TEWL measurement times (Hatch et al. 1990b). More water accumulated in the subjects' SC when they exercised in the humid environment. Capillary blood flow was not significantly influenced by environment. Skin temperature statistically differed in the two environments, but differences were negligible. Statistically significant differences in the physiological measurements did exist as a result of fabric type. The researchers speculated that the results might have been different with snugger garments.

There were no significant differences in water evaporation or SC water content due to the type of fabric (Markee et al. 1991). Calculation of thermophysiological comfort limits (Hatch et al. 1990a) for each of the fabrics based on heat and moisture measurements supported the nonsignificant results. The large differences in water absorption capability of the fabrics did not influence skin hydration state. This result probably reflects the fact that the fabrics did not lie on the skin surface. All three fabrics increased the level of SC water content and water evaporation due to placement on the skin surface. Exercise level (sedentary, vigorous, resting) significantly influenced skin wetness state. Further, subjects did not indicate differences between the fabrics for wetness or thermal sensations, a result explainable in terms of the extremely small differences in water and heat transport fabric data and the statistically insignificant differences in SC hydration and evaporative water loss from the skin surface (Hatch et al. 1990a). The regression model for wetness sensation showed that SC water content and evaporative water loss were statistically significant determinants.

2.3.2 Effect on Blood Flow

No statistically significant differences in capillary blood flow were detected at upper back measurement sites when ten female subjects exercised in garments made from the jersey knit fabrics of differing fiber contents (Markee et al. 1991). This occurred even though the characterization testing showed that the fabrics differed in fiber and fabric stiffness as well as in other low-stress mechanical properties (Barker et al. 1990). Unfortunately, we probably took the laser Doppler measurements on the wrong skin site. We had noted redness at the tops of the shoulders of the subjects with the fairest skin following 40 min of exercise when the 3.5 denier polyester garment was worn. However, no laser Doppler measurements were taken at these sites during the exercise protocol. We speculated that the stiffness of the polyester fiber was causing the redness, and the skin/fabric contact at the tops of the shoulders was greater enough in this region for the redness to develop.

The link between blood flow and perceived sensations was addressed by regression analysis (Markee et al. 1990). Skin temperature was a significant determinant of perceived thermal comfort in the regression model, but capillary blood flow was not. Capillary blood flow was the only physiological factor with a statistically significant effect on overall comfort. The researchers suspected a link between the mechanical and surface features of the fabric and capillary blood flow.

2.4 Jersey Knit Fabric Swatch Experiments

Further work was undertaken with the jersey knit fabrics because we were surprised to observe that our female subjects' upper back SC were as hydrated under their cotton exercise garments as under their polyester exercise garments (Hatch et al. 1992a). This was particularly noteworthy because the cotton T-shirts were wetted more with sweat over the measurement sites than the polyester T-shirts. We expected to find a significant difference in SC hydration, not only under the cotton and polyester garments but also under the two polyester fabrics that contained different denier fibers. The purpose of this study was to determine the effect of fiber type and fabric moisture content on SC hydration. The six combinations of treatments were cotton at regain, 38.6 %, and 75 % moisture content; 3.5 % polyester at regain and at saturation (38.6 %), and 1.5 denier polyester at saturation (38.6 %). Using an occluded plastic dome, fabric swatches were placed on both normal and hydrated volar forearm skin of subjects for a specified time period and then removed. Two minutes alter removal, evaporative water loss and skin temperatures were measured. The design of the study was a randomized complete block with all possible treatment combinations applied to each subject. Data were analyzed using analyses of variance on the linear and quadratic coefficients of best fit lines and Bonferroni t-tests.

For normal skin, SC hydration generally increased as fabric moisture content increased. The SC was significantly drier after being in contact with cotton fabric at regain than at the two moisture content levels above regain and also under polyester fabric. For hydrated skin, the hydration state was significantly lower under the cotton fabric at regain than at 38.6 % moisture content and at saturation, but was not significantly different under the polyester fabric at regain and at saturation.

Some of these results were not as expected and needed yet further examination. We wondered whether the observed decrease in evaporative water loss from time 30 to time 60 was statistically significant for the cotton/44 % and polyester/35 % treatments, and also if the observed increase in evaporative water loss from time 30 to time 60 was statistically significant, for the cotton/75 % treatment. Further, we wondered whether the explanation we offered in that paper about these results was correct. This was our first experiment in which the fabrics were wet prior to placement. We designed an experiment to monitor the amount of moisture in the fabric as well as the alteration in evaporative waterless from the SC. In the last of this sequence of studies (Hatch et al. 1997), the objective was to examine the relationship between fabric moisture content at the time of fabric removal and level of SC hydration so that the role of fabric moisture might be better understood.

Three fabric/moisture treatments were placed on the SC – 3.5 denier polyester fabric with an initial moisture content of 35 % and cotton fabrics with either 44 % or 75 % initial moisture content – then covered with an occlusive dome. SC evaporative water loss (EWL) is measured before treatment placement and after 30 and 60 min of contact. The amount of moisture in the fabric at time of removal was calculated in two different ways; the three analyses of variance were done using the evaporative water loss and the two fabric final moisture content data sets. The rate of TEWL is significantly higher alter 30 min of treatment contact with SC than alter 60 min of contact. The amount of moisture in the fabrics is significantly less at time 60 than at time 30, implying that the SC is more hydrated at 30 min than at 60 min. However, the fabrics contain less moisture when removed at 60 min than at 30 min. As fabric moisture content decreases, SC hydration decreases. The question we are not able to answer is "Where does the moisture go that is initially in the fabric?"

2.5 Wool Fabric

Wester et al. (1985) were interested in whether the insulating nature of certain fabrics altered human capillary blood flow. Capillary blood flow was measured using laser Doppler velocimetry, a

noninvasive low-power laser light optical technique. Two fabrics that differed significantly in thermal conductivity, a fourfold difference as determined by the guarded hot plate method, were placed on the upper arm often on female volunteers. Blood flow was significantly higher under the fabric with the lower thermal conductivity.

Wester et al. (1985) also investigated whether the abrasive nature and/or prickly nature of certain fabrics might alter capillary blood flow. Two wool fabrics were selected that differed substantially in contact sensation – one was soft, the other coarse. The thermal effect was controlled by layering the fabrics before they were worn under a tricot top on the upper back. On one side of the upper back, the coarse fabric contacted the skin, and on the other side, the soft fabric contacted the skin. Skin blood flow increased from 0 to 3 h, but there was no statistically significant difference between the fabrics. Six of the nine volunteers, however, showed higher blood flow when the coarse fabric was next to the skin than when the softer fabric was next to the skin. The researchers concluded that fabric influences skin blood flow but that it is not known whether the prickling or abrasive action of the fabric's fibers on the skin altered blood flow or whether any flow alteration was undetectable due to instrumentation and methodological limitations.

2.6 Multiple Fabric Skin Hydration Experiment

Cameron et al. (1997) investigated the effects of fabric made from natural and synthetic fibers and film on transepidermal water loss from the SC using an occluded system. Sixteen fabrics differing in fiber type and construction were placed on the volar forearm of 35 female subjects in a dry state (standard moisture regain) and a wetted state. Each fabric was in place for 40 min before TEWL was measured. There was no statistically significant difference in TEWL measurements on a control skin site from the beginning to the end of the 75-min test session in a controlled, conditioned environment. Placement of dry fabrics on the skin did not significantly affect the hydration level of the SC, though all dry fabrics did increase the hydration level slightly. Wetted wool and cotton fabrics significantly hydrated the SC when levels were compared to either normal skin or skin covered by dry fabrics. Of the seven synthetic fiber fabrics tested in the wetted state, three acrylic, PTFE, and spun nylon significantly increased the SC hydration level. These three fabrics and the natural fiber fabrics had comparable wetted moisture content.

In summary, much remains to be accomplished in studying the effect of garment fabrics on the skin. Using bioengineering instrumentation remains a viable avenue for the development of high-performance fabrics in which moisture management is a key issue.

3 Cleansing Cloths for Infants

Cleansing cloths to clean the diapered area of infants are of two major types: cotton wash cloths which are textile products and disposable wipes which are usually considered paper products. Disposable baby wipes have been used in North America for over 30 years and cotton wash cloths for even longer. Which of the two types of products and which type of disposable wipe is the safest to use have been recently investigated using bioengineering instrumentation.

3.1 Effect on Skin pH

Priestley et al. (1996) investigated changes in skin pH after the use of disposable baby wipes. They enrolled 317 babies with non-diseased skin ages 4–12 months of both genders into the study. They set up a double-blind safety in use comparison of four different brands of baby wipes over a 10-week period. For the first 2 weeks, the babies' skins were cleaned with only soap and water after each diaper change. Then, in the next 8-week

period, each baby was allocated one or other of the products for normal home use. The wipes differed in cleansing lotion formulation (emollients, preservative, pH) and fibrous composition.

Results were that there were no clinically detectable differences (erythema, frequency of rashes, edema, and desquamation) among the wipes. There were significant changes in the pH of pubic and buttock skin inside the diaper area. In particular, the brand of wipes with the lower pH (2.8) in the lotion reduced the mean skin pH from 5.6 to 5.0 ($p < 0.01$), and those with a pH of 5.5 had no significant effect. Wipes of pH 3.7 gave a final skin pH of 5.4, but the downward trend was not statistically significant. The authors note that skin pH was depressed by topical application of lotion in the wipes during the experimental period which was only a fraction of the total time wipes might be used on each infant. A longer time frame should be used to know the long-term effect.

3.2 Forearm Test Method Development

Farage (2000) developed a modified forearm-controlled application test method for evaluating the mildness of disposable wipe products on the skin. The procedure developed includes a semi-occlusive patch system, a system intended to mimic the hydrated conditions common to the skin in the diaper area, and repeated washing cycles. Visual scoring is done for erythema and dryness and instrumental scoring for redness (chromometer) and transepidermal water loss (evaporimeter). The procedure includes details for obtaining the hydration level recommended, applying the test products, and test duration to achieve significant endpoints for all product assessments.

Four baby wipe disposable products were selected once the protocol was established. Differences were found among the products on all assessments. The products were not described. What characteristics of the products accounted for the differences in skin state is therefore not available.

3.3 Suitability of Wipe Use on Dermatitis Skin

Odio et al. (Odio and Friedlander) investigated the suitability of using infant wipes on children with dermatitis skin. They looked for possible differences in rates of skin repair at a tape-stripped skin site that was not wiped and at a tape-stripped site that was wiped with a high-quality baby wipe. The tape stripping was done on the volar forearm of adults until a stable rate in transepidermal water loss was achieved at approximately 30 g/m^2/h above base rate (a condition thought to correspond with that observed on the skin of children who are experiencing a moderate to severe diaper dermatitis reaction). One tape-stripped site served as a control, and the other was rubbed with the wipe in a manner simulating the amount of wiping a child's skin might experience in a normal day. A single grader, who did not know which treatment was applied to each site, scored the sites for degree of erythema. Results were that erythema scores declined at a relatively uniform rate during the course of the 4 days of the study at both control and wipe-treated sites; importantly, scores remained comparable between sites through the entire study, and by day 4, erythema was almost completely gone at the control and test site. It was concluded that the use of a high-quality infant wipe does not interfere with the normal process of skin repair.

3.4 Cotton Washcloth and Water Versus Disposable Baby Wipes

Odio et al. (2001) designed four experiments to study the effects on skin cleansed with water and a high-quality cotton washcloth intended for hygiene care of children and with two different brands of high-quality disposable baby wipes.

Study 1 was an 8-day in-use skin mildness comparison of the products on 82 children. All children were in good health at the enrollment visit, weighing 16–28 lbs, were disposable diaper wearers, and had Fitzpatrick skin types I–III.

None had known contact allergies, presented with moderate or greater erythema or rash in the diaper area, or took medication that might influence skin condition or might increase stool frequency. They all wore the same disposable diaper immediately following enrollment in the study. Usual cleansing practices at diaper changes were done during the first week but no lotions, creams, or powders were used after cleansing. Half of the infant then cleansed with one of the wipe products for 8 days and the other half with the cotton washcloths and water. Again, no lotions, creams, or powders were used. No instructions were provided for cleansing. Assessments were visual skin erythema by an experienced grader, skin barrier status by evaporimetry, and skin surface microtopography.

Skin redness observed in the genital region of infants who were cleansed with the cloth and water was not different than that of infants who were cleansed with the disposable wipe. However, in the perianal area, where cleansing tends to be more vigorously done for hygiene reasons, skin redness scores were statistically higher for the children cleansed with cloth and water than for those cleansed with the disposable wipe. No significant changes occurred in TEWL as a result of cleaning with both products. Surface roughness of skin increased for infants cleansed with cloth plus water, but not for those cleansed with the disposable baby wipe, but the difference was not statistically significant.

Study 2 was a 2-week study to evaluate change in baseline transepidermal water loss due to controlled cleansing using (1) a washcloth with water, (2) a washcloth with soap and water, and (3) a baby wipe on degradation of skin barrier integrity using the Farage test procedure (Farage 2000) on 24 females 18–45 years old. They were in good health, had skin types I–III, and agreed to adhere to specific skin-cleansing routines and not use skin care products that might interfere with the study. They were not taking medication that would affect skin condition, nor were they pregnant or lactating.

Subjects suspended the use of all skin care products on forearms l week before the first clinic visit, a visit during which volar arm skin sites were demarcated and assigned a treatment. Cleansing was done at the clinic on days 1 through 5, spaced at 90 min intervals. There were three cleansing session of 30 s duration and one of 60 s duration. TEWL loss was assessed on day 1 prior to initial cleaning and on day 5, 90 min after the last cleansing.

Repeated, daily cleansing using disposable wipes yielded no detectable change in skin barrier integrity (elevated TEWL). However, cleansing with the washcloth (both with water and with water and soap) resulted in a statistically significant increase from the baseline indicating detectable degradation of the epidermis. The degradation was greater when soap was used.

Study 3 was a 5-day study to evaluate the rate of skin repair following controlled cleansing with two brands of disposable wipes and with the cloth plus water. On day 1, erythema scores and baseline TEWL measurements were taken at a control and two treatment volar forearm sites of 24 female subjects. Subjects met the same criteria for inclusion as in study 1. Sites were tape stripped until the rate was about 50 $g/m^2/h$. Cleansing of the treatment sites was done in the clinic on four consecutive days. Erythema scores and TEWL measurements were taken each day.

Skin repair, as evidenced by a return of TEWL measurements to the baseline measurement, and reduction of skin redness scores proceeded at comparable rates at sites cleansed with disposable wipes and the control site. In contrast, the sites cleansed with the washcloth and water showed a pronounced delay in the rate of barrier recovery.

Study 4 was designed to determine stinging sensation of wipe lotions on compromised skin, especially nasolabial folds. One side was exposed to wipe lotion and the other to water (negative control). Neurosensory response was scored from 0 (no sensation) to 5.0 (extreme stinging). Females eligible for this study had to have no evidence of epidermal damage in the study area and had a sting response to 10 % lactic acid. Facial skin care products were not used for 1 week except the use of soap for cleaning. TEWL measurements were taken on day 1 and 2, the days the subjects became familiar with the sting test. On day 3, TEWL is taken and then the skin tape

stripped. This was repeated on the afternoon of day 3, the morning and afternoon of day 4, and the morning of day 5. On the afternoon of day 5, a final TEWL measurement was taken at each nasolabial fold. Water was applied to onefold and lotion to the other. Two minutes later each subject graded the sensation. Fifteen minutes later, lactic acid was applied to both folds and the subjects rated the sensation to verily the sting sensitivity of the subjects.

Sting responses were not statistically different for water application and wipe lotion application to the compromised skin of the female subjects. The sensations evoked by both treatments were below the sting range of the scoring scale.

Overall, the results of the four studies showed that cleansing with high-quality baby wipes leads to less compromised skin. The results of this study should not be generalized to all wipe products as there are many brands available in the marketplace.

4 Disperse Dye Effects on the Skin

4.1 Evaluating Commercial and Pure Textile Dyes

Malinauskine (Malinauskiene et al. 2011) explored disperse dyes, D Orange 1 and D Yellow 3, and its sensitizers present in the commercial dye. Two disperse dye azo-dyes (D Orange 1 and D Yellow 3) were tested because they were found to most frequently result in a positive testing in their dermatitis department. The tests were carried out on ten patients who previously tested positive for reactions with D Orange 1 and D Yellow 3. The test was carried out using commercial dye and purified dye. Diluted purified dye, water-soluble residues of D Orange 1 and D Yellow 3 diluted to a concentration of 1.0 % w/v in distilled water, and naphthalene sulfonate 1.0 % aq w/v were used for the patch testing. The commercial dye was separated into its water-soluble and fat-soluble fractions where the samples were then diluted to a concentration of 1.0 % w/v using distilled water. The patch testing for the commercial dyes was done using thin-layer chromatography to separate the dye from any impurities. The separated spots are then cut from the TLC and placed on the back of the patients for 48 h using Scanpor tape. The pure dyes did not require any separation using TLC for patch testing. The test showed that there was some reactivity on different spots of the TLC which indicates that there are sensitizers present in commercial dyes DO1 and DY3 that are not present in purified DO1 and DY3.

4.2 Interaction Between Skin Bacteria and Textile Dyes

Malinauskine et al. (2012) further investigated the effects of human skin bacteria breaking down textile dyes into corresponding aromatic amines. Studies have also show that a cross-reactivity between disperse dyes and para-amino compounds could result in positive reactions or cross-sensitization. This test was carried out on ten patients who have previously tested positive for reactions with D Orange 1 and D Yellow 3. Possible azo degradation pathways for both D Orange 1 and D Yellow 3 were found to be p-aminodiphenylamine, 4-Nitroaniline, 4-Aminoacetanilide, and 2-Amino-p-cresol. Furthermore, the para-amino compounds, black rubber mix, and p-phenylenediamine (PPD) were also patch tested. Black rubber mix contains a mixture of *N*-cyclohexyl-*N*′-phenyl-4-phenylenediamine (CPPD), *N*,*N*′-Diphenyl-4-phenylenediamine (DPPD), and *N*-Isopropyl-*N*′-phenyl-4-phenylenediamine (IPPD). Pure samples of each of these chemicals were obtained for the test. High-performance liquid chromatography was done on the pure samples D Orange 1 and D Yellow 3 to confirm that none of the azo-degraded chemicals were present. The patch tested was done using purified DO1 and DY3, PPD, CPPD, DPPD, and IPPD all dissolved in acetone and prepared as 1.0 % wt/vol. The patients were also tested with different concentrations of the purified dyes; previous patients who reacted +++ to 1.0 % concentrations were tested with 0.01 %, while people who previously did not react to the dyes were tested with the highest concentration, 1.0 %. The patients were also tested with possible azo-dye

degradations, p-Aminodiphenylamine, 4-nitroaniline, 4-aminoacetanilide, and 2-amino-p-cresol, at concentrations equimolar to the dilution series of DO1 and DY3 starting at 1.0 % wt/vol. Patch testing were done using Finn chambers on Scanpor tape using 15 uL and left on the back for 48 h. Results showed that all patients who react positive to DO1 also react positive to p-aminodiphenylamine, a possible metabolite of the former. Also, patients who reacted positively to DY3 also reacted positive to 2-Amino-p-cresol, which is a precursor to DY3. The results of the test show that it is possible that major sensitizers in ACD from DO1 and DY3 can be due to their metabolites, p-aminodiphenylamine, and 2-Amino-p-cresol, respectively, which might be formed through the azoreductase pathway of skin bacteria.

5 Footwear Dermatitis

Svecova (Švecová et al. 2013) investigated contact dermatitis due to the mold inhibitor, dimethyl fumarate (DMF), found in footwear. DMF has been shown to be a potent sensitizer in very low concentrations and may acute dermatitis. Tests were carried out on nine female patients who were admitted to the University Hospital Department of Dermatology in Bratislava, Slovakia for footwear acute contact dermatitis associated with DMF. Patch testing was done using textile lining from the patients' boots that caused their contact dermatitis and 0.1 % of commercially prepared DMF. The patch testing was carried out on the patients using Curates patch test chambers which were left on for 2 days. Furthermore, chemical analysis was used on the footwear that caused the patients' skin reactions. The shoes were extracted for samples then tested using gas chromatography/mass spectrometry (GC/MS), atomic absorption spectroscopy (AAS), and UV-Vis. The results of the patch testing confirmed that the patients' ACD was caused by their footwear. Additionally, seven of the nine patients tested positive to the 0.1 % DMF patch test. Chemical analyses of the sample material from the patients' shoes detected DMF at concentrations of 25–80 mg/kg, much higher than the allowed concentration of 0.1 mg/kg in EU. The analysis of the textile lining confirmed that DMF is the only chemical that could cause ACD. The lining of the material could have also contributed to the development of ACD due to its insulating and chemical properties which results in warmth, humidity, and occlusive environment, conditions that would contribute to the leaching of any allergens. Skin penetration can also be enhanced by sweating which can result in an increased penetration of the allergen. The results of the tests confirm the presence of DMF and its contribution of causing ACD in the patients.

6 Conclusion

The use of bioengineering instruments has allowed the study of the effects of fiber-based materials on the skin they cover and/or contact. The development of diapers and incontinence products has been enhanced because the effects of changing components of the system on the skin environment can be assessed instrumentally as well as by trained clinicians. Additionally, the safety of using baby wipe products has been advanced because skin effects can be assessed instrumentally using adult subjects. Effects of garment fabrics on human skin are not as well studied, but promising outcomes can be achieved by the use of these instruments.

7 Interpretation: Skin Tolerance

As noted here, we have some information on how skin tolerates (or does not) fabric. Even though considerable progress has been made, the experimental data remains sparse – and would benefit from further in-depth data such as effects of ethnicity, age, gender, regional anatomic variation, and climate.

As to safety (dermatotoxicology and percutaneous absorption) of chemical transfer from fabric to skin, much remains to be done. At present, the safety of nano-silver is being investigated, yet this represents but one chemical class. Ngo details the 15 principles of percutaneous penetration

including transfer (from fabric) and a critique of knowledge of percutaneous penetration of nanos such as silver-treated fabric (Mai et al. 2012, 2013).

References

Akin FJ, Lemmen JT, Bozarth DL, Garafalo MJ, Grove GL. A refined method to evaluate diapers for effectiveness in reducing skin hydration using the adult forearm. Skin Res Technol. 1997;3:173–6.

Akin F, Spraker M, Aly R, Leyden J, Raynor W, Landin W. Effects of breathable disposable diapers: reduced prevalence of Candia and common diaper dermatitis. Pediatric. 2001;18(4):282–90.

Aly R, Shirley C, Cunico B, Maibach HI. Effect of prolonged occlusion on the microflora, pH, carbon dioxide and transepidermal water loss on human skin. J Invest Dermatol. 1978;7:378–81.

Barker RL, Randhakrishnaiah S, Woo SS, Hatch KL, Markee NL, Maibach HI. In vivo cutaneous and perceived comfort response to fabric. 2. Mechanical and surface related comfort property determinations for three experimental knit fabrics. Text Res J. 1990;60:490–4.

Berardesca E, Elsner P, Wilhelm K-P, Maibach HI. Bioengineering of the skin: methods and instrumentation. Boca Raton: CRC Press; 1995.

Berg RW, Milligan MC, Sarbaugh FC. Association of skin wetness and ph with diaper dermatitis. Pediatr Dermatol. 1994;11(1):18–20.

Cameron BA, Brown DM, Dallas MJ, Brandt B. Effect of natural and synthetic fibers and film and moisture content on stratum corneum hydration in an occlusive system. Text Res J. 1997;67(8):585–92.

Campbell RL, Seymour JL, Stone LC, Milligan MC. Clinical studies with disposable diapers containing absorbent gelling materials: evaluation of effects on infant skin condition. J Am Acad Dermatol. 1987;17:978–87.

Davis JA, Leyden JJ, Grove GL, Raynor WJ. Comparison of disposable diapers with fluff absorbent and fluff plus absorbent polymers: effects on skin hydration, skin ph, and diaper dermatitis. Pediatr Dermatol. 1989;6(2):102–8.

Elsner P, Berardesca E, Wilhelm K-P, Maibach HI. Bioengineering of the skin: skin biomechanics. Boca Raton: CRC Press; 2002.

Farage MA. Development of a modified forearm controlled application test method for evaluating the skin mildness of disposable wipe products. J Cosmet Sci. 2000;51(153–167):2000.

Grove GL, Lemmen JT, Garafalo M, Akin FJ. Assessment of skin hydration caused by diapers and incontinence articles. Curr Prob Dermatol. 1998;26:183–95.

Grove GL, Grove MJ, Bates NT, Wagman LM, Leyden JJ. Scrotal temperatures do not differ among young boys wearing disposable or reusable diapers. Skin Res Technol. 2002;8:260–70.

Hatch KL, Wilson D, Maibach HI. Fabric-caused changes in human skin: in vivo water content and water evaporation. Text Res J. 1987;57:583–91.

Hatch KL, Woo SS, Barker RL, Randhakrishnaiah S, Markee NL, Maibach HI. In vivo cutaneous and perceived comfort response to fabric. 1. Thermophysiological comfort determinations for three experimental knit fabrics. Text Res J. 1990a;60:406–12.

Hatch KL, Markee NL, Barker RL, Woo SS, Randhakrishnaiah P, Maibach HI. In vivo cutaneous and perceived comfort response to fabric. 3. Water content and blood flow in human skin under garments worn by exercising subjects in a hot, humid environment. Text Res J. 1990b;60:510–9.

Hatch KL, Markee NL, Prato H, Zeronian H, Maibach HI, Kuehl RO, Axelson RD. In vivo cutaneous and perceived comfort response to fabric. 5. The effect of fiber type and fabric moisture content on the hydration state of human stratum corneum. Text Res J. 1992a;66(11):638–47.

Hatch KL, Markee NL, Maibach HI. Skin response to fabric: a review of studies and assessment methods. Cloth Text Res J. 1992b;10(4):54–63.

Hatch KL, Prato HH, Zeronian SH, Maibach HI. In vivo cutaneous and perceived comfort response to fabric. 6. The effect of moist fabrics on stratum corneum hydration. Text Res J. 1997;67:926–31.

Lane AT, Rehder PA, Helm K. Evaluation of diapers containing absorbent gelling materials with conventional disposable diapers in newborn infants. Am J Dis Child. 1990;144:315–8.

Mai AN, Howard IM. 15 factors of percutaneous penetration of pesticides. Parameters for Pesticide QSAR and PBPK/PD Models for Human Risk Assessment. 2012;67–86. doi:10.1021/bk-2012-1099.ch006.

Mai AN, Michael O'Malley, Howard IM. Perspectives on percutaneous penetration of nanomaterials. Nanotechnol Dermatol. 2013;63–86. doi:10.1007/978-1-4614-5034-4_7.

Malinauskiene L, Zimerson E, Bruze M, Ryberg K, Isaksson M. Textile dyes disperse orange 1 and yellow 3 contain more than one allergen as shown by patch testing with thin-layer chromatograms. Dermatitis. 2011;22(6):335–43. doi:10.2310/6620.2011.11043.

Malinauskiene L, Zimerson E, Bruze M, Ryberg K, Isaksson M. Patch testing with the textile dyes disperse orange 1 and disperse yellow 3 and some of their potential metabolites, and simultaneous reactions to para-amino compounds. Contact Dermatitis. 2012;67(3):130–40. doi:10.1111/j.1600-0536.2012.02080.x.

Markee NL, Hatch KL, Maibach HI, Barker RL, Randhakrishnaiah P, Woo SS. In vivo cutaneous and perceived comfort response to fabric. 4. Perceived sensations to three experimental garments worn by subjects exercising in a hot, humid environment. Text Res J. 1990;60:561–8.

Markee NL, Hatch KL, French SN, Maibach HI, Wester R. Effect of exercise garment fabric and environment on cutaneous conditions of human subjects. Cloth Text Res. 1991;19(4):1–8.

Odio M, Friedlander SF. Diaper dermatitis and advances in diaper technology. Curr Opin Pediatr. 2000;12(4): 342–6.

Odio MR, O'Connor RJ,F, Baldwin S. Continuous topical administration of petrolatum formulation by a novel disposable diaper. 1. Effect on skin surface microtopography. Dermatology. 2000a;200:232–7.

Odio MR, O'Connor RJ, Sarbaugh F, Baldwin S. Continuous topical administration of a petrolatum formulation by a novel disposable diaper. 2. Effect on skin condition. Dermatology. 2000b;200(3):238–43.

Odio M, Streicher-Scott J, Hansen RC. Disposable baby wipes: efficacy and skin mildness. Dermatol Nurs. 2001;13(2):107–12, 117–8, 121.

Partsch CJ, Aukamp M, Sippell WG. Scrotal temperature is increased in disposable plastic lined nappies. Arch Dis Child. 2000;83:364–9.

Priestley GC, McVittie E, Aldridge RD. Changes in skin pH after the use of baby wipes. Pediatr Dermatol. 1996;13(4):14–7.

Švecová D, Šimaljakova M, Doležalová A. Footwear contact dermatitis from dimethyl fumarate. Int J Dermatol. 2013;52(7):803–7. doi:10.1111/j.1365-4632.2012.05512.x.

Visscher MO, Chatterjee R, Munson KA, Pickens WL, Hoath SB. Changes in diapered and nondiapered infant skin over the first month of life. Pediatr Dermatol. 2000;17(1):45–5I.

Wester RC, Hatch KL, Maibach HI. Blood flow changes in fabric-contacted human skin. Bioeng Skin. 1985; 3:276.

Wilson PA, Dallas MJ. Diaper performance: maintenance of healthy skin. Pediatr Dermatol. 1990;7(3):179–84.

Zhai H, Maibach HI. Effects of skin occlusion on percutaneous absorption: an overview. Skin Pharmacol Appl Skin Physiol. 2001a;14:1–10.

Zhai H, Maibach HI. Skin occlusion and irritant and allergic contact dermatitis: an overview. Contact Dermatol. 2001b;44:201–6.

Zhai H, Maibach HI. Occlusion vs. skin barrier function. Skin Res Technol. 2002;8:1–6.

Zhai H, Ebel JP, Chatterjee R, Stone KJ, Gartstein V, Juhlin KD, Pelosi A, Maibach HI. Hydration vs. skin permeability to nicotinates in man. Skin Res Technol. 2002;8:13–8.

Zimmerer RE, Lawson KD, Calvert CJ. The effects of wearing diapers on skin. Pediatr Dermatol. 1986;3(2):95–101.

Human Epidermal Barrier May Be Quantitatively Described by Compartmental Analysis of Water Dynamics

116

Luís Monteiro Rodrigues and Catarina Rosado

Contents

Keywords

TEWL • Dynamical measurement • POST • Epidermal desorption curve • Dynamical water mass(DWM) • Evaporation half-life time (t1/2 evap)

1 Modeling TEWL-Desorption Curves

1.1 Introduction

The accurate assessment of skin barrier function represents a challenge, one that has been undertaken by multiple approaches. TEWL is traditionally recognized to be indicative of this skin property (Lotte et al. 1987; Pinnagoda and Tupker 1995); however, several works have reported a poor correlation between damage inflicted to the skin and changes in TEWL values (Chilcott et al. 2002; Bashir et al. 2001). Additionally, the methodology is limited by providing only instantaneous data susceptible to great variability (anatomical, climatic, circadian, sweat gland activity).

Dynamic strategies have been developed to overcome the pitfalls of this variability. The skin response to determined stimuli can be evaluated, enabling a more thorough investigation of the factors that influence the skin water dynamics in the superficial and in the deeper layers. The plastic occlusion stress test (POST) is an example of this approach, based on a prolonged skin occlusion (usually 24 h). It aims to noninvasively quantify

L.M. Rodrigues (✉)
CBIOS – Research Center for Health Science and Technologies, Universidade Lusófona, Lisbon, Portugal

Department of Pharmacological Sciences, Universidade de Lisboa – School of Pharmacy, Lisbon, Portugal
e-mail: monteiro.rodrigues@ulusofona.pt; monteirorodrigues@sapo.pt

C. Rosado
Universidade Lusófona (CBIOS – Research Center for Health Science and Technologies), Lisbon, Portugal

P. Humbert et al. (eds.), *Agache's Measuring the Skin*,
DOI 10.1007/978-3-319-32383-1_66

functional parameters of the stratum corneum in order to better assess barrier function (Turek et al. 1982; Werner et al. 1982; Berardesca et al. 1990, 1993; Berardesca and Maibach 1990; Piérard-Franchimont et al. 1995). Initial protocols fitted the skin surface water loss (SSWL) curves obtained when occlusion was terminated, either using bi-exponential regression analysis or by transforming the data in log and then using simple regression analysis (Berardesca and Maibach 1990; Fluhr et al. 1999). It can be argued that these models are too simplistic to describe the complex water balance between the different layers of the skin.

Further developments on the mathematical modeling of the TEWL curves that result from a POST (Rodrigues et al. 1999; Rosado et al. 2005) have enabled a more detailed quantitative characterization of the dynamic water balance established between the deep and the superficial skin structures (Pinto et al. 2002). In this section, the discriminative capacity of the model to two different types of variation in the cutaneous barrier is presented – insults inflicted to the skin (tape stripping, skin surface biopsy, and lipid extraction with ether:acetone) or differences in two distinct anatomical regions.

1.2 Methods

Fourteen volunteers (mean age 27.2 ± 9.8) participated in this study after informed consent. A total of nine volunteers were tested in each type of study conducted: effect of tape stripping, effect of lipid extraction, effect of skin surface biopsy, and difference between wrist and mid volar forearm (Rosado et al. 2005). The procedures followed were in accordance with the ethical standards of the responsible committee on human experimentation and with the Helsinki Declaration.

One site was marked in each volar forearm of the volunteer. One arm was assigned as the untreated control, and on the other arm (treated site) one of three different insults to the skin barrier was performed: 20 tape strips, lipid extraction with a 1:1 mixture of ether:acetone, or four skinsurface biopsies (SSB) with cyanoacrylate (Marks and Dawber 1971). Both sites (control and treated) were then covered with an occlusive patch for 24 h, after which the desorption curves were recorded. The same procedure was applied to the study of anatomical differences. The occlusion and measurements were conducted in the same arm, on one site in the mid volar forearm and another in the wrist. After patch removal, TEWL measurements were continuously registered for 30 min. The mathematical model was adjusted to the data points using a specially modified simplex routine and the software ADAPT written in Fortran. Calculated parameters considered relevant to the study were $t_{1/2evap}$ (evaporation half-life) and DWM (dynamic water mass) (Rodrigues et al. 1999). Nonparametric comparative analysis (Wilcoxon sign-rank test) was used in this study. A 0.05 significance level was adopted.

1.3 Mathematical Model

A bi-compartmental model was employed to describe the in vivo mechanisms of water distribution (Rodrigues et al. 1999). There is no direct correspondence with the histological organization of the human skin: compartment 1 represents the skin barrier with poor water content and compartment 2 represents the fully hydrated deeper layers of the skin.

Occluding the skin with a patch dramatically changes the water balance between these two compartments. From the water flux established according to Fick's first law of diffusion and the compartmental model defined, the variable TEWL can be modulated by a set of two linear first order differential equations (Rodrigues et al. 1999). After solving, in order to compartment 1, the solution is in the form of an algebraic sum of two exponential terms (Eq. 1).

$$\mathrm{TEWL} = \mathrm{B} + \mathrm{I}\left(e^{-\mathrm{K_{evap}}\times \mathrm{t}} - e^{-\mathrm{K_{hydr}}\times \mathrm{t}}\right) \qquad (1)$$

where:

B – baseline effect
I – multiplicative parameter common to both exponentials

K_{evap} – evaporation rate constant (used to evaluate the barrier function)

K_{hydr} – hydration rate constant related to the distribution of the water through both compartments

The two exponentials are affected by the macroconstants K_{evap} and K_{hydr}. The latter represents the water initially eliminated and is related to the occlusion period and to the water retention capacity of the stratum corneum. K_{evap} describes the evaporation process to the exterior and is affected by changes to the barrier function. These are the most important parameters provided by the model. The baseline effect is also relevant and represents the basal finite amount of water continuously lost through the skin. The model describes this physiological process using the variable B, which at $t = 0$ is equal to TEWL.

A transformation of K_{evap} is suggested, to simplify data interpretation (Eq. 2)

$$t_{½evap} = \frac{Ln(2)}{K_{evap}} \tag{2}$$

where $t_{½evap}$ represents the evaporation half-life period – the time the system takes to reduce its water loss to half.

Dynamic water mass (DWM) represents the relevant water mass involved in the desorption process. The area under the curve from t_{max} obtains this parameter until the end of the process.

The final analysis of this work was performed adjusting the experimental data to the model to obtain the most important and relevant parameters, namely K_{evap}, $t_{½evap}$, t_{max}, and DWM.

1.4 Results

The different desorption curves obtained after a 24 h occlusion are represented in Fig. 1. It can be seen that in the site where fourskin surface biopsies (SSB) were performed (Fig. 1a), the decay in the curves is faster than that obtained in the untreated control site. This fact is reflected in $t_{1/2evap}$ (Table 1), which was lower in the SSB site ($p = 0.008$); however, DWM was not significantly different from the controls ($p = 0.735$). The difference between the parameters obtained in the tape stripped and lipid extraction sites and the controls is less marked and never reaches a statistical level of significance (Table 1).

The results reflecting anatomical differences are quite distinct. When a 24 h occlusion is performed in the wrist, the decay in the curves is slower than that occurring in the mid volar forearm (Fig. 1b). These results are expressed by an approximately twofold increase in the $t_{1/2evap}$ and in the DWM (Table 2). There are statistically significant differences between the parameters obtained in the two anatomical sites ($p = 0.018$ for $t_{1/2evap}$ and $p = 0.028$ for DWM).

1.5 Discussion

Dramatic differences in the hydric dynamics of the skin submitted to SSB, the most aggressive insult applied, are clearly revealed by the data obtained by this work. Additionally, well-defined anatomical differences were found between the skin of the wrist and the mid volar forearm.

The lower $t_{1/2evap}$ obtained in the site where SSB was performed can be attributed to reduced water accumulation in the stratum corneum, since this layer has been "thinned" by the procedure. Superficial water accumulates during the occlusion period, but because it is not bound, it is released immediately as soon as occlusion ceases. This is supported by the fact that DWM is not different to that of the control, since the faster decay rate observed in the SSB sites is then compensated by a faster decay to basal values. Interestingly, these results also indicate that even though many layers of corneocytes have been removed, no significant damage to skin barrier function is observed.

The results obtained in the wrist have a different interpretation. The corneocytes in this anatomical region have a smaller diameter than in the volar forearm (Rougier 1994), large blood vessels are closer to the surface, and basal TEWL is significantly higher (Rodrigues and Pereira 1998). These differences contribute to the higher

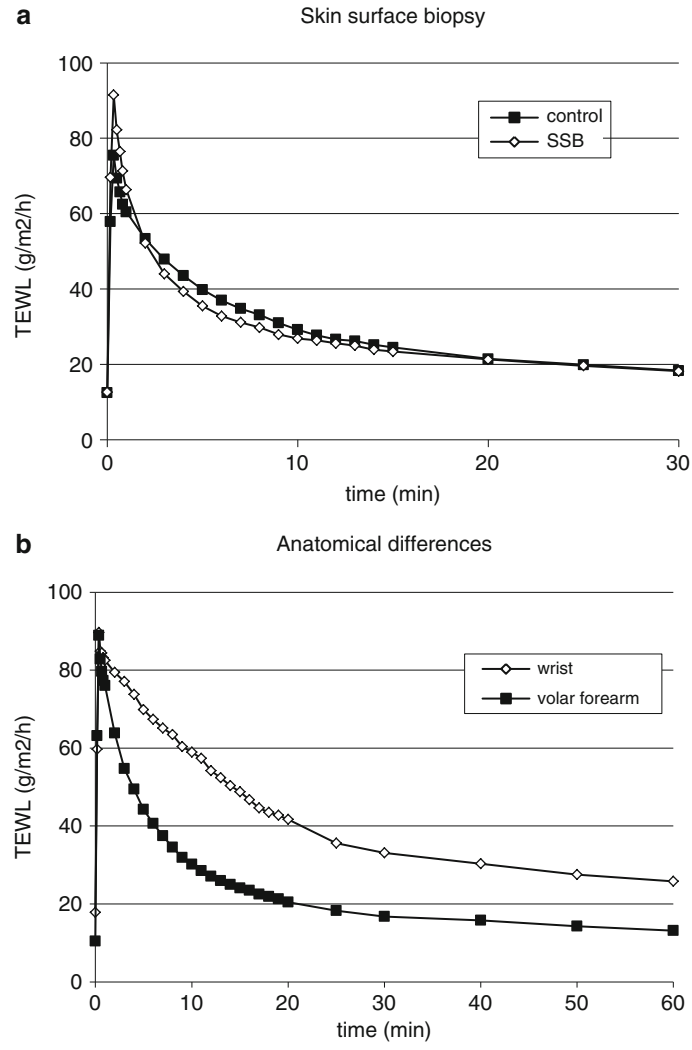

Fig. 1 POST desorption curves obtained after 24 h occlusion: (**a**) insults to the barrier – SSB (mean values, $n = 9$), (**b**) anatomical differences – mid volar forearm and wrist (mean values, $n = 9$)

Table 1 Parameters obtained in the study of the impact of different insults to the skin barrier (mean ± SD, $n = 9$)

Insult performed	$t_{1/2evap}$ (min)		DWM (g/m^2)	
Lipid extraction Control	3.03 ± 1.19 3.64 ± 0.52	$p > 0.05$	833.9 ± 138.8 722.4 ± 61.6	$p > 0.05$
Tape stripping Control	3.33 ± 2.04 3.60 ± 1.26	$p > 0.05$	727.4 ± 235.0 793.9 ± 153.0	$p > 0.05$
Skin surface biopsy Control	1.94 ± 0.85 4.30 ± 1.36	$p = 0.008$	833.2 ± 144.2 836.3 ± 226.0	$p > 0.05$

Table 2 Parameters obtained in the study of anatomical differences (mean ± SD, $n = 9$)

Anatomical site	$t_{1/2evap}$ (min)		DWM (g/m^2)	
Wrist	13.73 ± 5.49	$p = 0.018$	1513.7 ± 421.0	$p = 0.028$
Mid volar forearm	3.67 ± 1.13		875.3 ± 120.3	

values of $t_{1/2evap}$ and DWM. More water accumulates during the occlusion, and the different functionality of the barrier at this site slows down its release and allows more water to be lost.

The other perturbations of the skin barrier caused more subtle changes in the water dynamics which could not be so clearly assessed by this methodology, and the results likely reflect the "milder" impact of these procedures. Solvent mixtures are reported to extract primarily the superficial lipids, including sebaceous gland lipids, cholesterol, and free fatty acids. Work conducted by Jokura et al. (1995) showed that lipid extraction of intact stratum corneum with ether:acetone (1:1) did not induce any significant change in the nuclear magnetic resonance spectrum and did not significantly affect stratum corneum elasticity. Visscher et al. performed a similar study where the impact of ether:acetone in TEWL and Moisture Accumulation Test (MAT) was assessed (Visscher et al. 2003). This group observed significant increases in TEWL but no effects in MAT.

In contrast, there are conflicting reports in the literature regarding the extent of damage inflicted by tape stripping (Cernasov and Macchio 1997; Ohman and Vahlquist 1994; Rosado and Rodrigues 2003), and it is widely accepted that depending on the adhesive and pressure applied, differing amounts of cells are removed in each tape strip (Bashir et al. 2001).

In conclusion, the work shows that compartmental modeling of the TEWL desorption curves provides detailed information on the water retention capacity of the skin and on cutaneous water dynamics.

2 Applications of the Methodology

2.1 Assessment of Dry Skin

2.1.1 Introduction

One the most widely occurring skin disorders is dry skin, or xerosis. It is the result of a range of environmental and pathological factors that affect epidermal proliferation and differentiation (Engelke et al. 1997). The stratum corneum lipid bilayers and the epidermal components are altered, which results in a decrease in the water content and reduced barrier function (Rogers et al. 1996).

In the clinical practice, xerosis is commonly evaluated by subjective visual scoring systems (Kligman 1987; Serup 1995). The most commonly employed strategies to quantitatively assess xerosis have been measurements of skin capacitance and/or transepidermal water loss (TEWL), both with limitations that have been previously discussed.

In this section, the methodology of mathematical modeling of POST TEWL curves is applied to the quantitative assessment of differences between normal and dry skin.

2.1.2 Material and Methods

Twenty healthy female volunteers, aged between 20 and 55 (mean 30.4 $\pm$ 13.4 years old), participated in this study. Ten volunteers were classified with normal skin and ten with dry skin. The work was developed in accordance with the ethics requirements and following the relevant experimental guidelines. The skin type was evaluated by self-assessment and clinical scoring systems (Kligman 1987). Since xerosis is generally more severe in the frontal aspect of the leg, the entire study was conducted on this anatomical site. There was a 1 week pretrial period, during which volunteers were requested to refrain from applying any product containing moisturizing ingredients to the test sites, and bathing habits were standardized.

All volunteers were submitted to the POST methodology previously described (Rosado and Rodrigues 2006). The mathematical model was adjusted to the data points and relevant parameters were calculated.

Nonparametric comparative analysis (Wilcoxon sign-rank test) was used in this study. A 0.05 significance level was adopted.

2.1.3 Results

The desorption curves obtained after removal of the occlusive patch, applied for 24 h, are represented in Fig. 2. It can be readily appreciated that dry and normal skin present different profiles.

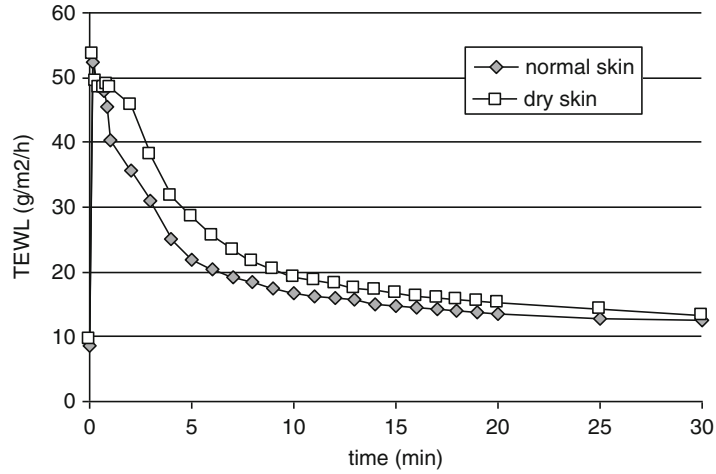

Fig. 2 Desorption profiles obtained after removal of the occlusive patch (mean, $n = 10$)

Table 3 Parameters obtained in the study (mean ± SD, $n = 10$)

	$t_{1/2evap}$ (min)		DWM (g/m^2)	
Normal skin	2.03 ± 0.91	$p = 0.018$	497.46 ± 80.87	$p = 0.059$
Dry skin	3.95 ± 1.90		613.58 ± 130.99	

In normal skin, the decrease in TEWL after occlusion is rapid and pronounced. Conversely, when dry skin is occluded, TEWL decreases at a slower pace. These results are translated in a higher $t_{1/2evap}$ for dry skin, almost double of that obtained in normal skin, and in a more elevated DWM (Table 3). There is a marked statistical difference between the $t_{1/2evap}$ results ($p = 0.018$) and a less pronounced difference for DWM ($p = 0.059$).

2.1.4 Discussion

The first attempts to quantify skin dryness were essentially based in the visual observation and grading of parameters such as flake size, roughness, and color (Kligman 1987; Serup 1995). This approach is subjective, but nevertheless, in the clinical perception of dry skin there is an evident need for the integration of different parameters which can only be perceived through the human intervention (Grove et al. 2002). Many noninvasive bioengineering devices using electrical properties or photothermal or acoustic techniques have been developed over the last three decades with applications in this area (Imhof et al. 1990; Pines and Cunningham 1981). These devices are very useful to study stratum corneum function and competence in moisture content and retention. However, dynamic tests are in general more informative, principally because they are not reliant on single measurements.

The marked differences observed in the results of this study confirm the applicability of the methodology. Subjects with dry skin presented a greater water accumulation capacity and different water dynamics. The higher DWM can be explained by two factors. First, the weakened barrier function causes a higher loss of water through the skin. Additionally, dry skin has an increased rate of proliferation of epidermal cells, but the desquamation of corneocytes is impaired, which contributes to epidermal thickening. This leads to a greater capacity to accumulate water and, therefore, to the higher amount of water released after occlusion. The $t_{1/2evap}$ is extended because the mass of water being released is greater.

These findings confirm that the modeling of the TEWL curves resulting from a POST is a sensitive methodology, able to detect differences in the water dynamics and barrier function of normal and dry skin. This advocates its potential application to efficacy testing of products that are used to reestablish skin hydration.

2.2 Assessment of Moisturizers and Barrier Function Restoration

2.2.1 Introduction

Moisturizers are among the most universally employed personal care products. Many formulations aim not only to increase skin hydration but also to treat the underlying causes of dryness and restore barrier function and have even been classified by some authors as "therapeutic moisturizers" (Kligman 1987).

One of the most consensually accepted approaches to the study of the efficacy of moisturizers is the regression method developed by Kligman (1987), where after application of the product for 2 weeks, the rate of regression to the original state is measured, usually using a visual scoring system. One of the main drawbacks of this methodology is the fact that it must be conducted for a period of a minimum of 5 weeks. Other strategies based in the measurement of skin capacitance or TEWL provide insufficient information.

In this section, the discriminative capacity of the mathematical modeling of POST TEWL curves is applied to the efficacy testing of moisturizing products.

2.2.2 Methods

Fifteen female volunteers with severe dry skin participated in this study, after informed consent (mean age 43.9 ± 11.6 years) (Rosado et al. 2009). The entire study was conducted on the lower leg. All volunteers exhibited marked xerosis, as well as uniform dryness across contralateral sites. The work was developed in accordance with the ethical requirements and following the relevant experimental guidelines.

There was a 1 week pretrial period, during which volunteers were requested to refrain from applying any product containing moisturizing ingredients to the test sites. Bathing habits were also standardized.

A moisturizing cream containing 15 % urea (Kératosane® 15, Uriage, France) was applied to the test areas twice daily by all volunteers for 2 weeks. At the end of the 2 week application period, all volunteers were submitted to the POST methodology previously described (Rogiers 2001; Pinnagoda et al. 1990). The mathematical model was adjusted to the data points and relevant parameters were calculated.

2.2.3 Results

The TEWL desorption curves obtained in the control and treated sites after removal of the occlusive patch are represented in Fig. 3. It can be seen that in the site that was treated for 2 weeks with cream, the decay in the curves is slower than that obtained in the untreated control site. Additionally, the area under the curve is lower in the control (untreated)

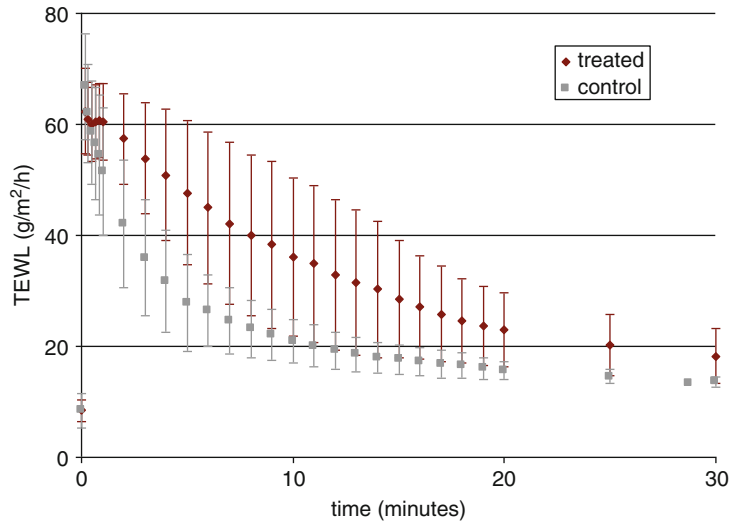

Fig. 3 TEWL decay profiles obtained in the study (mean ± SD, $n = 12$)

Table 4 Parameters obtained in the study of the efficacy of moisturizers (mean ± SD, $n = 12$)

	k_{evap}		$t_{1/2evap}$ (min)		DWM (g/m^2)	
Treated site	0.102 ± 0.083	$p = 0.002$	11.43 ± 8.42	$p = 0.005$	955.7 ± 266.6	$p = 0.010$
Control site	0.334 ± 0.170		2.54 ± 1.39		650.3 ± 104.8	

dry skin. The previously mentioned features have been transformed in quantitative parameters by the mathematical model adjusted to the TEWL data points (Table 4). The obtained parameters show statistically significant differences between the different kinetic parameters obtained in the control and treated sites (nonparametric Wilcoxon rank-sign test): a slower K_{evap} in the treated site, as well as a higher $t_{1/2evap}$ and DWM.

2.2.4 Discussion

Moisturizers are widely used, and almost every type of cosmetic incorporates moisturizing ingredients. Even though dry skin is far from being a life-threatening condition, the symptoms of severe xerosis are unpleasant, and for these patients the use of moisturizers is important to maintaining quality of life. Some formulations claim not only to improve barrier function but also to create an environment optimal to healing and prevention of recurrent damage (Yokota and Maibach 2006).

The regression method developed by Kligman (1987) measures the rate of regression to the original state using a visual scoring system after application of the product for 2 weeks. One significant drawback of this methodology is the fact that it must be conducted for a period of a minimum of 5 weeks.

The use of noninvasive bioengineering equipment has led to other strategies, such as measurements of electrical capacitance. Other methods use a model that examines regeneration of skin barrier function after aggression (usually with aqueous solutions of sodium lauryl sulfate), when compared to irritated untreated skin (Held et al. 2001). Another approach investigates the efficacy, the tolerance, and the effects of moisturizers on quality of life (Giordano-Labadie et al. 2006).

One of the earlier attempts to use TEWL measurements and occlusion (that is, inhibition of water evaporation from the skin surface) to assess moisturizers was performed by Rietschel (1978). The moisturizers were applied to a plastic film and the skin, and an objective rank ordering of moisturizers was achieved by monitoring moisture enhancement of applied substances.

Further developments on the mathematical modeling of the TEWL curves that result from a POST have contributed to a more accurate quantitative description of the cutaneous water mass balance over time (Rodrigues et al. 1999), and it is reasonable to assume that the method could be used in the study of moisturizing products.

The results obtained in this investigation established significant differences between the different kinetic parameters obtained in the control and treated sites. The data obtained in the site treated with cream exhibit a slower decay in the TEWL values and a higher water mass released after removal of the occlusion. This can be attributed to the presence of hygroscopic excipients (urea, glycerine, lactic acid, and pyrrolidone carboxylic acid sodium). The increase in the DWM and $t_{1/2evap}$ can be explained by two factors: the previously explained higher accumulation of water in the stratum corneum and the keratolytic action of urea that leads to a thinning of the stratum corneum, which in turn leads to a higher TEWL than that occurring through the thicker dry skin. Urea has been associated to improved epidermal lipid biosynthesis and improved barrier performance (Loden 2000). The alterations observed in the water dynamics indicate the previously mentioned effect and confirm the efficacy of the cosmetic formulation.

The efficacy testing approach developed in this study is compatible with home application of the product, which is an important factor to ensure compliance by the volunteers. When the methodology is compared to the regression test, its main benefit is that it can be completed in 3 weeks and, if the volunteers are experienced, it is possible to

reduce the number of visits to the research center to two.

2.3 Assessment of Barrier Impairment in Sensitive Skin

2.3.1 Introduction

Sensitive skin is a subjective and vague affliction that almost half of the world's population declares to suffer from, and the skincare market offers numerous products that claim to be particularly suitable for this type of consumer (Kligman et al. 2006; Willis et al. 2001). The characterization of sensitive skin is difficult, due to the wide variety of causes and symptoms that it may include (Pons-Guiraud 2004), ranging from obvious cutaneous alterations such as redness or dryness to complaints that are subjective and sensory, with signs such as stinging, burning, or itching (Frosch and Kligman 1982).

Skin sensitivity seems to be associated to an impaired skin barrier function (Kligman et al. 2006), enabling the penetration of substances that stimulate the keratinocytes and Langerhans cells to produce mediators that are involved in its characteristic inflammatory response (Willis et al. 2001; Frosch and Kligman 1982; Farage et al. 2006). Another factor that may equally contribute to a higher cutaneous susceptibility is a neurosensory hyperreactivity, causing the self-perceived sensations of discomfort when sensitive skin is exposed (Willis et al. 2001).

The lack of visible clinical signs and the high subjectivity associated to sensitive skin have hampered the development of a simple method to diagnose and quantitatively analyze this condition. The more common approaches are scoring of signs of irritation, assessment of the subjective (neurosensory) responses, and skin function tests (Primavera and Berardesca 2005; Issachar et al. 1997; Yosipovitch and Maibach 1998; Lee and Maibach 1995; Marriott et al. 2005; Gean et al. 1989; Seidenari et al. 1998; Bornkessel et al. 2005).

In this section, the mathematical modeling of POST TEWL curves is applied to the quantitative analysis of sensitive skin.

2.3.2 Methods

A total of 33 healthy female volunteers participated in the study (Pinto et al. 2011). Fifteen volunteers constituted the group of subjects with self-perceived sensitive skin (age range 23–64, mean age 54 $\pm$ 10 years). The remaining 18 volunteers formed the control group, with self-perceived normal skin (age range 20–58, mean age 34 $\pm$ 10 years). The work was developed in accordance with the ethical requirements and following the relevant experimental guidelines.

A site was selected in the back of the hand of each volunteer, between the thumb and the index finger, and the baseline TEWL values were registered with a Tewameter TM 300® (CK Electronics, GmbH, Germany), following published guidelines (Rogiers 2001). All subjects were then submitted to the POST methodology previously described (Rogiers 2001; Pinnagoda et al. 1990). The mathematical model was adjusted to the data points and relevant parameters were calculated.

Nonparametric comparative analysis (Wilcoxon sign-rank test) was used in this study. A 0.05 significance level was adopted.

2.3.3 Results

The mean basal TEWL values exhibited by the volunteers of the two groups (normal and sensitive skin) were compared, and no statistically significant differences were found ($p = 0.059$).

The desorption curves obtained after a 24 h occlusion, as well as the model fitting to the experimental data are represented in Fig. 4. It can be seen that the decay in the curves obtained in volunteers with normal skin is faster than that obtained in the sensitive skin subjects. Additionally, the area under the curve is smaller in the normal skin group.

Relevant quantitative parameters were determined by the mathematical model adjusted to the TEWL data points (Table 5). These results epitomize statistically significant differences between the different kinetic parameters obtained in the two groups, translated in higher $t_{1/2evap}$ and DWM in the sensitive skin volunteers.

The continuous lines observed in Fig. 4 represent the calculated data obtained by application of

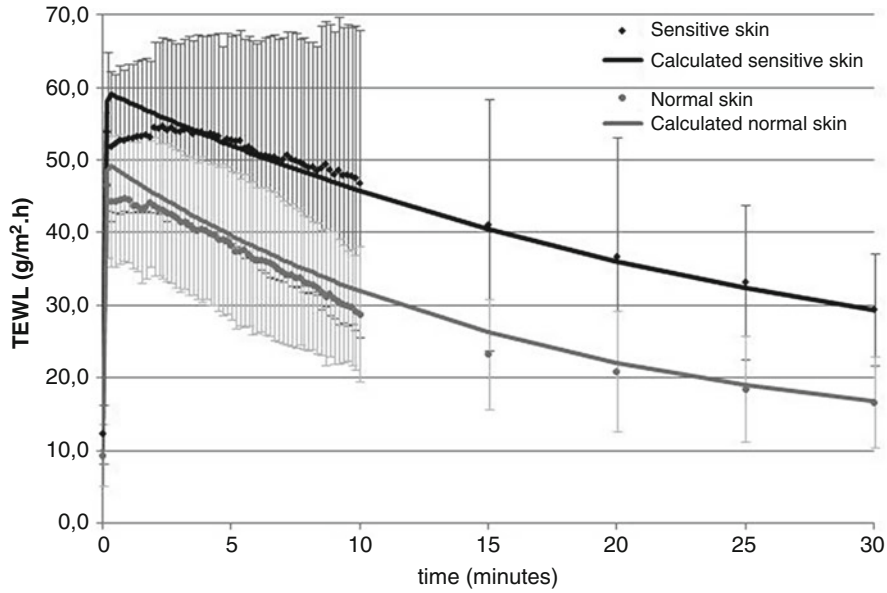

Fig. 4 POST desorption curves obtained after 24 h occlusion (mean ± SD); the continuous lines represent the calculated data obtained by application of the model to the median individual parameters

Table 5 Parameters obtained in the study (mean ± SD)

Group	$t_{1/2evap}$ (min)		DWM (g/m^2)	
Sensitive skin	33.81 ± 39.72	$p = 0.005$	1216.45 ± 299.83	$p = 0.0001$
Normal skin	10.15 ± 5.34		787.51 ± 196.98	

the model to the median individual parameters. These data points are within the range of standard deviation of the mean experimental results, indicating that a good fit was achieved between the data generated by the model and the experimental data.

2.3.4 Discussion

Multiple attempts have been made to find the ideal method to test sensitive skin. Irritant reactivity tests measure objective signs of irritation after long-term application of model substances under occlusion; however, this does not reflect the real-life situation. Sensory reactivity tests are based on the sensory information that is reported by the individuals, normally expressed in a subjective magnitude scale. Dermal function tests relying on bioengineering methodologies have had a limited application, since negligible differences were found in the baseline biophysical parameters of individuals with sensitive skin.

Sensitive skin is a multifactorial skin condition, attributed to neurosensory hyperreactivity, a lower discomfort threshold, and an incompetent cutaneous barrier. It is irrefutable that TEWL measurements constitute an essential tool to ascertain barrier function; however, its limitations have been described earlier and may explain the difficulties experienced by researchers attempting to detect differences in subjects with sensitive skin (Seidenari et al. 1998; Distante et al. 2002), as well as the results from this study that were described previously in the text.

This study aimed to identify unequivocal substantiation of barrier impairment via the modeling of the TEWL curves resulting from a POST. This methodology would then be used as the basis of a reproducible, noninvasive, and cost-effective test to assess sensitive skin.

The results obtained in the present work confirm the previous assumptions. Statistically significant differences were established between the

different kinetic parameters obtained in the normal and sensitive skin groups. The scrutiny of the kinetic data and desorption profiles obtained in the subjects with sensitive skin points to a slower decay in the TEWL values and a higher water mass released after removal of occlusion, which translate into higher values of $t_{1/2evap}$ and DWM. An increase in both parameters can be explained by an impaired barrier function. The impaired barrier causes more water accumulation during the occlusion. Thus, a higher mass of water is lost with a higher half-life time once the patch is removed.

In conclusion, this investigation successfully correlates the elusive sensory complaints with impairment in the cutaneous barrier. A new clinical relevance to this quantitative strategy has emerged, one that can be applied both in the early diagnosis and characterization of the skin sensitivity syndrome and in the efficacy assessment of topical products designed for individuals with this skin condition.

3 Conclusions

TEWL is one of the most popular noninvasive variables from skin bioengineering and has become the main indicator of in vivo epidermal barrier function. Differing measurement guidelines have been known for quite some time and have been progressively adopted, but only a few papers have focused on the need to assess such variables from a dynamic point of view. In 1982, Hachiro Tagami and coworkers (1982) did set a basis for the measurement of epidermal hygroscopicity, motivating the development of stress tests such as the POST (Berardesca et al. 1990; Berardesca and Maibach 1990; Jokura et al. 1995) to quantify skin water modifications following occlusion. Gioia and Celleno (2002) proposed an original physical model to simulate the dynamics of epidermal (free) water evaporation and TEWL in hydrated skin. The model was developed to study the behavior of hydrated skin when occluded by permeable/impermeable materials and was applied to the effect of diapers on normal and nonnormal skin. TEWL modeling was also applied to analyze the barrier and the driving force components of TEWL in irritancy testing (Endo et al. 2007).

To our knowledge, none of these approaches have been able to equate to other practical applications involving the quantification of the in vivo skin barrier. In contrast, our model was applied to different testing conditions and its discriminative capacity clearly proven. In fact, our model is inspired by the particular histological-functional organization of the human skin, justifying the compartmental analysis approach. This means a close relationship between the model and the in vivo physiology from the conceptual point of view, strengthening the value of the kinetic assumptions behind the simulation of the mechanisms of water distribution in vivo following occlusion (POST).

Thus, the compartmental modeling of the TEWL desorption curves clearly describes the cutaneous water dynamics in different conditions, providing a unique way to rigorously quantify this central characteristic of human in vivo skin. Furthermore, its conceptual frame and construction allows an easy access to common users, motivating the development of current easy-to-wear programs that will help to improve TEWL data quality and expand the utility of this variable.

References

Bashir SJ, Chew AL, Anigbogu A, Dreher F, Maibach HI. Physical and physiological effects of stratum corneum tape stripping. Skin Res Technol. 2001;7(1):40–8.

Berardesca E, Maibach HI. Monitoring the water-holding capacity in visually non-irritated skin by plastic occlusion stress test (POST). Clin Exp Dermatol. 1990;15(2):107–10.

Berardesca E, Fideli D, Gabba P, Cespa M, Raggiosi G, Maibach HI. Ranking of surfactant skin irritancy in vivo in man using the plastic occlusion stress test (POST). Contact Dermatitis. 1990;23(1):1–5.

Berardesca E, Herbst R, Maibach H. Plastic occlusion stress test as a model to investigate the effects of skin delipidization on the stratum corneum water holding capacity in vivo. Dermatology. 1993;187(2):91–4.

Bornkessel A, Flach M, Arens-Corell M, Elsner P, Fluhr JW. Functional assessment of a washing emulsion for sensitive skin: mild impairment of stratum corneum hydration, pH, barrier function, lipid content, integrity

and cohesion in a controlled washing test. Skin Res Technol. 2005;11(1):53–60.
Cernasov D, Macchio R. Octyldodecyl neopentanoate – its effect on the performance of sunscreen formulations. Cosmet Toilet. 1997;112:75–82.
Chilcott RP, Dalton CH, Emmanuel AJ, Allen CE, Bradley ST. Transepidermal water loss does not correlate with skin barrier function in vitro. J Invest Dermatol. 2002;118(5):871–5.
Distante F, Rigano L, D'Agostino R, Bonfigli A, Berardesca E. Intra- and inter-individual differences in sensitive skin. Cosmet Toilet. 2002;117:39–46.
Endo K, Suzuki N, Yoshida O, Sato H, Fujikura Y. The barrier component and the barrier force component and the driving force component of trans epidermal water loss and their application to skin irritant tests. Skin Res Technol. 2007;13:425–35.
Engelke M, Jensen JM, Ekanayake-Mudiyanselage S, Proksch E. Effects of xerosis and ageing on epidermal proliferation and differentiation. Br J Dermatol. 1997;137(2):219–25.
Farage MA, Katsarou A, Maibach HI. Sensory, clinical and physiological factors in sensitive skin: a review. Contact Dermatitis. 2006;55(1):1–14.
Fluhr JW, Lazzerini S, Distante F, Gloor M, Berardesca E. Effects of prolonged occlusion on stratum corneum barrier function and water holding capacity. Skin Pharmacol Physiol. 1999;12(4):193–8.
Frosch PJ, Kligman AM. Recognition of chemically vulnerable and delicate skin. In: Principles of cosmetics for the dermatologist. 1982. p. 287–96.
Gean CJ, Tur E, Maibach HI, Guy RH. Cutaneous responses to topical methyl nicotinate in black, oriental, and caucasian subjects. Arch Dermatol Res. 1989;281 (2):95–8.
Gioia F, Celleno L. The dynamics of trans epidermal water loss (TEWL) from hydrated skin. Skin Res Technol. 2002;8:178–86.
Giordano-Labadie F, Cambazard F, Guillet G, Combemale P, Mengeaud V. Evaluation of a new moisturizer (Exomega milk) in children with atopic dermatitis. J Dermatolog Treat. 2006;17(2):78–81.
Grove GL, Zerweck C, Pierce E. Noninvasive instrumental methods for assessing moisturizers. In: Skin moisturization. 2002. p. 499–528.
Held E, Lund H, Agner T. Effect of different moisturizers on SLS-irritated human skin. Contact Dermatitis. 2001;44(4):229–34.
Imhof RE, Whitters CJ, Birch DJS. Opto-thermal in-vivo monitoring of structural breakdown of an emulsion sunscreen on skin. Clin Mater. 1990;5(2–4):271–8.
Issachar N, Gall Y, Borell MT, Poelman MC. pH measurements during lactic acid stinging test in normal and sensitive skin. Contact Dermatitis. 1997;36(3):152–5.
Jokura Y, Ishikawa S, Tokuda H, Imokawa G. Molecular analysis of elastic properties of the stratum corneum by solid-state 13C-nuclear magnetic resonance spectroscopy. J Invest Dermatol. 1995;104(5):806–12.
Kligman AM. Regression method for assessing the efficacy of moisturizers. Cosmet Toilet. 1987;93:27–35.
Kligman AM, Sadiq I, Zhen Y, Crosby M. Experimental studies on the nature of sensitive skin. Skin Res Technol. 2006;12(4):217–22.
Lee CH, Maibach HI. The sodium lauryl sulfate model: an overview. Contact Dermatitis. 1995;33(1):1–7.
Loden M. Urea. In: Dry skin and moisturizers. 2000. p. 243–57.
Lotte C, Rougier A, Wilson D, Maibach HI. In vivo relationship between transepidermal water loss and percutaneous penetration of some organic compounds in man: effect of anatomic site. Arch Dermatol Res. 1987;279:351–6.
Marks R, Dawber RP. Skin surface biopsy: an improved technique for the examination of the horny layer. Br J Dermatol. 1971;84(2):117–23.
Marriott M, Holmes J, Peters L, Cooper K, Rowson M, Basketter DA. The complex problem of sensitive skin. Contact Dermatitis. 2005;53(2):93–9.
Ohman H, Vahlquist A. In vivo studies concerning a pH gradient in human stratum corneum and upper epidermis. Acta Derm Venereol. 1994;74(5):375–9.
Piérard-Franchimont C, Letawe C, Goffin V, Piérard GE. Skin water-holding capacity and transdermal estrogen therapy for menopause: a pilot study. Maturitas. 1995;22(2):151–4.
Pines E, Cunningham T. Dermatological photoacoustic spectroscopy. In: Bioengineering of the skin: water and the stratum corneum. 1981. p. 283–90.
Pinnagoda J, Tupker RA. Measurements of transepidermal water loss. In: Handbook of non-invasive methods and the skin. 1995. p. 173–9.
Pinnagoda J, Tupker RA, Agner T, Serup J. Guidelines for transepidermal water loss (TEWL) measurement: a report from the standardisation group of the European Society of Contact Dermatitis. Contact Dermatitis. 1990;22:164–72.
Pinto PC, Pereira LM, Minhós R, Rodrigues LM. Testing the discriminative capacity of compartmental modeling for the analysis of the in vivo epidermal water content changes following topical application under occlusion. IFSCC Mag. 2002;5:1–6.
Pinto P, Rosado C, Parreirão C, Rodrigues LM. Is there any barrier impairment in sensitive skin?: a quantitative analysis of sensitive skin by mathematical modeling of transepidermal water loss desorption curves. Skin Res Technol. 2011;17(2):181–5.
Pons-Guiraud A. Sensitive skin: a complex and multifactorial syndrome. J Cosmet Dermatol. 2004;3(3):145–8.
Primavera G, Berardesca E. Sensitive skin: mechanisms and diagnosis. Int J Cosmet Sci. 2005;27(1):1–10.
Rietschel RL. A method to evaluate skin moisturizers in vivo. J Invest Dermatol. 1978;70(3):152–5.
Rodrigues L, Pereira LM. Basal transepidermal water loss: right/left forearm difference and motoric dominance. Skin Res Technol. 1998;4(3):135–7.
Rodrigues L, Pinto P, Galego N, Silva PA, Pereira LM. Transepidermal water loss kinetic modeling

approach for the parameterization of skin water dynamics. Skin Res Technol. 1999;5(2):72–82.

Rogers J, Harding C, Mayo A, Banks J, Rawlings A. Stratum corneum lipids: the effect of ageing and the seasons. Arch Dermatol Res. 1996;288(12): 765–70.

Rogiers V. EEMCO guidance for the assessment of transepidermal water loss in cosmetic sciences. Skin Pharmacol Physiol. 2001;14(2):117–28.

Rosado C, Rodrigues LM. In vivo study of the physiological impact of stratum corneum sampling methods. Int J Cosmet Sci. 2003;25:1–8.

Rosado C, Rodrigues LM. Assessment of dry skin using dynamic methods. J Appl Cosmetol. 2006;24 (December):139–57.

Rosado C, Pinto P, Rodrigues LM. Modeling TEWL-desorption curves: a new practical approach for the quantitative in vivo assessment of skin barrier. Exp Dermatol. 2005;14(5):386–90.

Rosado C, Pinto P, Rodrigues LM. Assessment of moisturizers and barrier function restoration using dynamic methods. Skin Res Technol. 2009;15(1):77–83.

Rougier A. TEWL and transcutaneous absorption. In: Bioengineering of the skin: water and the stratum corneum. 1994. p. 103–13.

Seidenari S, Francomano M, Mantovani L. Baseline biophysical parameters in subjects with sensitive skin. Contact Dermatitis. 1998;38(6):311–5.

Serup J. EEMCO guidance for the assessment of dry skin (xerosis) and ichthyosis: clinical scoring systems. Skin Res Technol. 1995;1(3):109–14.

Tagami H, Kanamaru Y, Inoue K, Suehisa S, Inoue F, Iwatsuki K, Yoshikuni K, Yamada M. Water sorption-desorption test of the skin in vivo for functional assessment of the stratum corneum. J Invest Dermatol. 1982;78(5):425–8.

Turek BA, Vieu M, Leduc M, Nadvornik IM, Jedla E. Water content and moisture-binding capacity of some types of human soft and hard horn. Curr Med Res Opin. 1982;7 Suppl 2:87–90.

Visscher MO, Tolia GT, Wickett RR, Hoath SB. Effect of soaking and natural moisturizing factor on stratum corneum water-handling properties. J Cosmet Sci. 2003;54(3):289–300.

Werner E, Lindberg M, Forslind B. The water-binding capacity of the stratum corneum in dry noneczematous skin of atopic eczema. Acta Derm Venereol. 1982;62:334–7.

Willis CM, Shaw S, De Lacharrière O, et al. Sensitive skin: an epidemiological study. Br J Dermatol. 2001;145(2): 258–63.

Yokota M, Maibach HI. Moisturizer effect on irritant dermatitis: an overview. Contact Dermatitis. 2006;55(2):65–72.

Yosipovitch G, Maibach HI. Thermal sensory analyzer. Boon to the study of C and A delta fibers. Curr Probl Dermatol. 1998;26:84–9.

Skin Reactivity and Proneness to Irritation

117

Pierre Agache

Contents

Keywords

Burning test • Corneosurfametry • Dansyl chloride test • Histamine itching test • Irritants • Irritating effect • Kligman and Wooding test • Oclusive tests • Skin hypersensitivity reactions • Skin irritability testing • Skin irritation • Skin irritation proneness • Soap chamber test • Sting test

1 Applications

Cosmetology (tests of tolerance, selection of subjects for tolerance tests), Regulation acts fulfilment (identification of primary irritants), Occupational medicine (detection of subjects at risk and health-hazard products, measurement of skin alterations of occupational origin), Allergology (identification of irritants and orthoergic reactions).

2 Definition

The terms reactivity and irritation proneness, although close, are not synonyms. Reactivity implies the capacity to develop certain symptoms following an external stimulus, whatever the type of symptom induced (erythema, papule, pustule, visible desquamation, pigmentation. . .). Irritability on the other hand applies only to the capacity to produce an erythema or an unpleasant subjective feeling (tension, burning sensation, itch).

This chapter was originally published under the ISBN 978-3-540-01771-4 with the following book title Measuring the Skin. The content has not been changed.

Pierre Agache: deceased.

P. Agache (✉)
Department of Dermatology, University Hospital of Besançon, Besançon, France
e-mail: aude.agache@free.fr; ferial.fanian@chu-besancon.fr; ferial.fanian@cert-besancon.com

P. Humbert et al. (eds.), *Agache's Measuring the Skin*, DOI 10.1007/978-3-319-32383-1_67

However all these cutaneous signs are "intolerance reactions" of a so-called "orthoergic" mechanism, therefore implying no immunological factor; allergic reactivity is described in the following ▶ Chap. 118, "Cutaneous Testing: Detection and Assessment of Allergy."

Usually an acute (primary) "irritant" is a product which produces an intolerance reaction in more than 90 % (in fact, more than 50 %) of healthy subjects when it is applied on the skin in usual conditions (concentration, vehicle, mode of application) (Wahlberg and Maibach 1980). Such compounds are called "primary irritants" and a list of them has been established by the European Union (Annexe à la Directive 92/69 CEE du 31 juillet 1992). The interest of this list is twofold: (1) to entice manufacturers to find a substitute, (2) if this is not possible, to inform about possible health hazards and specific precautions to be taken. The legal obligation to evaluate the potential irritating effect of all the products that may be in contact with the human skin has led to perform a series of tests in healthy subjects.

This first selection is of little interest in cosmetology where the purpose is to detect in much less aggressive compounds, those who are susceptible to induce very moderately noxious or unpleasant side-effects in a minority of people. It is therefore necessary to seek subjects who may be intolerant to these products, subjects with "sensitive" skin, who make only a small portion of healthy population. It is difficult to identify them because of the variability of reactions and the dependence on both ambient conditions (temperature, wind, humidity, sun exposure) and physiological conditions (menstrual, circadian and annual cycle, etc.. . .). In this case, the measurement deals with the subject irritability rather than the product agressivity.

3 Detection of Acute (Primary) Irritants

Screening tests are used to determine if a product should be classified among primary irritants. This may be associated with the study the reactivity of subjects who professionally may come in contact with such products. This practice is considered non ethical in some countries, because it would lead to selection of workers on a basis of the possible occurrence of orthoergic dermatitis, which often is not severe enough to justify a ban. However it may be useful before job for people prone to contact allergy because the latter (which would justify a ban) is considerably activated by orthoergic dermatitis.

3.1 Lists of Primary Irritants

They indicate the concentration limit above which the product is considered irritant for healthy people. The lists below are not comprehensive.

European Union list (Annexe à la Directive 92/69 CEE du 31 juillet 1992)

Based on the Draize test in rabbits, it remains valid until it can be replaced by tests in humans.

Willis et al. list (Willis et al. 1988)

After a 48-h application in a small Finn chamber, the products listed below have been registered as irritants because about 75 % of the subjects studied have developed a 2 + erythema:

Benzalkonium chloride	0.5 % in water
Sodium lauryl sulfate	5 % in water
Croton oil	0.8 % yellow petrolatum
Dithranol	0.02 % yellow petrolatum
Nonanoic acid	80 % propane-1-ol
Propylene glycol	100 % in water
NaOH	2 % in water

Frosch and Kligman list (Frosch and Kligman 1976)

Ninety products are assessed by the chamber-scarification test.

York et al. list (York et al. 1996)

The irritant effect is evaluated compared to 20 % sodium lauryl sulphate (SLS), graded as "irritant" by the EU. SLS 20 % caused irritation in 45–50 % of the subjects after a 15-min to 4-h exposure in York et al.'s experiment. For example this test classifies NaOH 0.5 % as an "irritant" (60 % of the subjects were "irritated"

at 1 h, compared to 12 % by SLS 20 %). The list includes 27 products already registered by the EU and shows 8 points of discrepancy with the EU classification.

3.2 Assessment of the Irritating Effect

Not all products are irritating to the same extent and in the same way. In other words, the plot *irritation = f(concentration)* and *irritation = f(exposure duration)* are not identical, which complicates the implementation and interpretation of the tests. Furthermore, the type of irritation depends on the biological effect, which leads to the use of *specific tests* for tensioactives, organic solvents, acids, alkalis, pro-inflammatory substances, mechanical irritants, etc.. . . To compensate for the use of the product over a long time by the future consumer, *maximisation* is often necessary (e.g., by using concentrations beyond real life situations, or through preliminary skin damage). It is also possible to perform tests with *repeated exposure*. The possible part played by the vehicle must not be overlooked because it may have its own irritability and/or enhance the penetration of the active product. Irritation can be delayed; hence the necessity to read the test not only at the end of exposure but also up to 72 h later. Table 1 shows the most common problems and their answers.

It is essential to use an internationally admitted positive standard which plays two parts: validation of the test and classification in relation to other studies. It must have an accurate chemical definition, an average pH and should have been designed in order to meet three specific conditions regarding its innocuousness: absence of general toxicity, carcinogenicity, sensitiveness potential. As a *general standard* as well as a *detergents standard*, sodium lauryl sulfate (= sodium dodecylsulfate) (SLS) is widely accepted. Its properties and mode of use have been the subject of extensive general review (Tupker et al. 1997). Taking the European Union list as a reference, a 20 % concentration has been proposed (Basketter et al. 1994). This high concentration is valid only for the determination of primary irritants.

The selection of a *standard solvent* is more delicate because the irritation potency varies considerably from one solvent to another and raises steeply with concentration (Frosch and Kurte 1994). The mixture chloroform-methanol has been suggested (see Sect. 4.2, third item).

Various *standard vehicles* have been used: water, ethanol, petrolatum gelly, talc powder, vanishing cream USP, according to the vehicle chosen for the test, depending on anticipated contact conditions.

3.2.1 Open Tests

- Alkali resistance test (Burckhardt 1964; Locher 1962) (▶ Chap. 12, "Measurement of Skin Surface Acidity")
- Test of resistance to organic solvents (Leder 1943) and chloroform-methanol (Klaschka et al. 1972). The latter has been modified by Frosch and Kurte (1994) (cf Sect. 4.2 Burning test).
- Test with ammoniac, benzalkonium chloride, croton oil, kerosene, DMSO

Table 1 Ten main difficulties to overcome during primary irritants detection tests

Problem	Possible solution
1. Current use over a long time period	Maximisation
2. Repeated use	Repetitive tests (Cumulative Irritation Assay)
3. Variation in the time for reaction	Immediate reading by at 72 h
4. Various types of reaction	Use the reactivity limit or perform a specific test
5. Interindividual variability	Panel of very sensitive subjects
6. Need to avoid strong reactions	Stop application early enough
7. Intraindividual variability	Use positive (standard irritant) and negative control
8. Influence of the vehicle	Specific test with standard vehicle
9. Different investigators	Instrumental measurements
10. Quantification is of little use	Observe the irritation threshold only

These tests mainly apply to corrosive or very irritating substances, thus justifying very short exposure times (seconds or minutes). Their aggressiveness pose ethical problems. For this reason, most of them are abandoned, especially as alternative methods in vitro are available for most of them (Rougier et al. 1994; Whittle 1993).

3.2.2 Kligman and Wooding Test (Kligman and Wooding 1967)

The object of this test is to take into account the effect of repeated applications (from 10 to 20 days). It is based on the measurement in each subject of the onset time of the reaction, which is more easily detected than intensity. This eliminates almost completely the risk of over-reaction which is often unpredictable because of the very large variability of individual sensitivity. The objective was also to determine the irritation threshold according to the rules of toxicology and to have a unique test for all types of reaction.

The authors noticed that, for a given concentration, the % of irritated patients versus duration of application fits a sigmoid curve. Hence their idea to measure, for each concentration, the duration of application which induces a reaction in 50 % of studied subjects (Irritative Time IT50), and for a 24 h application, the minimal concentration inducing reaction in 50 % of subjects (Irritative Dose ID50). The first index is used for mild irritants, the second one for stronger irritants. A standard substance, used as a base to classify products, is introduced into the test. The test is performed on the back of the subject using occlusive patch-tests, (its sensitivity was found similar to that of the face). The authors indicate that the variability from one observer to the other is lower when assessing whether irritation does exist or not than the degree of irritation, because it is easier for the naked eye to detect the smallest erythema than to evaluate its intensity.

Bahmer and Feldmann (1995) updated this clever method by replacing patch-tests by applications in large Finn Chamber (diameter 12 mm, surface 113 mm^2); the studied areas (volar forearm) are examined every 24 h including a new application of the product exactly in the same place, the maximal application duration being 12 days. The proportion p(t) of patients showing irritation onset at time t is obtained by the formula $p(t) = 1/[1 + (\tau/t)^{\lambda}]$ where τ is IT50 and λ is the slope of the sigmoid curve at time τ, which indicates the rate of irritation increase when application is protracted (Fig. 1). This method becomes also applicable to moderately irritant products. The following table is an example (Bahmer and Feldmann 1995):

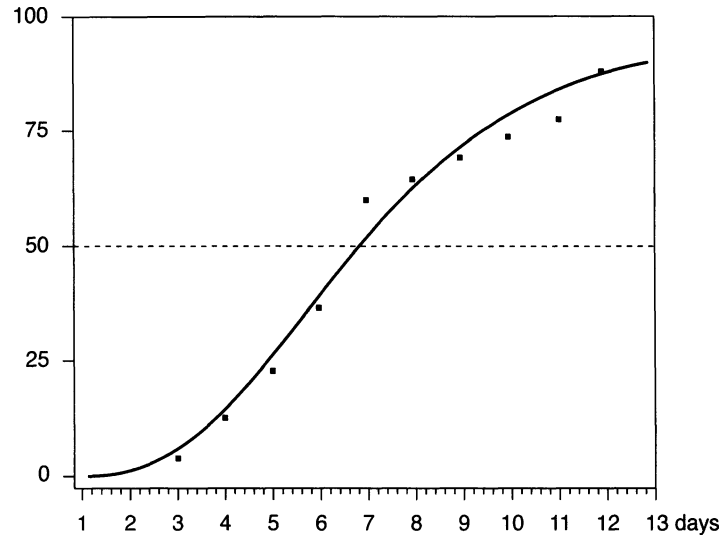

Fig. 1 Kligman and Wooding test as modified by Bahmer and Feldmann. Percent of irritated subjects versus 0.05 % SLS application time. The curve was drawn from experimental points and § 2.2.2 formula. Intersection with the horizontal dotted line corresponds to irritation occurring in 50 % of tested subjects (IT 50 % = 6,8 days)

SLS concentration	τ (days)	λ (% irritated subjects per application supplementary day)
0.05 %	6.8	12.5
0.10 %	5.2	22.7
0.25 %	3.6	29.4

3.2.3 Other Global Occlusive Tests (Non Comprehensive List)

- The classic occlusive patch test read at 24, 48 and 96 h should be abandoned because of the risk of false negatives (Frosch and Pilz 1995).
- The *Chamber Scarification Test* (Frosch and Kligman 1976) consists in making eight crossed scarifications (using a 30 gauge needle) on the tested area in order to increase the skin irritability. The product is then applied in a Dühring chamber (diameter 12 mm, 113 mm^2) once a day for 3 days. Reading takes place 30 min after the last application, grading intensity from 0 to 5. The "scarification index" (irritation threshold on healthy skin/threshold on irritated skin) expresses the capacity of the tested product to irritate the skin in these conditions. In this way the irritant potency of 70 substances has been classified in four categories: low 0–0.4; mild 0.5–1.4; moderate 1.5–2.4; strong 2.2–4.0.

On the other hand, the authors propose constituting very sensitive panels of "hyperirritable" subjects selected because they have shown a bright erythema with oedema and small vesicles following application of SLS at 5 % in water for 24 h on volar forearm. Because of its irritative potency 2–50 times higher than an ordinary patch, this test is rarely performed today.

- The *Basketter test* (Basketter et al. 1994) purpose is to classify primary irritants without causing severe lesions in volunteers. The irritant standard is 20 % SLS. To lessen variability between investigators, only the irritation threshold is considered. To obviate intense reaction, the successive exposure times are progressive: 1/4, 1/2, 1, 2, 3, 4 h (maximum) with interruption of the process as soon as intolerance appears (1/4 h and 1/2 are optional for a priori poorly irritant substances). A Plain Hill Top Chamber (diameter 25 mm, surface 490 mm^2) has been selected in order to increase the irritative effect. Out of 30 subjects, the number of subjects who have developed intolerance is counted for each concentration. The tested concentration is graded "irritant" if this number is not significantly lower than the number obtained with 20 % SLS.

4 Detection and Assessment of Hypersensitivity Reactions

These measurements have two objectives: to detect hypersensitive subjects and to assess tolerance of products which are not primary irritants. They involve mostly cosmetologists, but also allergologists who are interested in non allergic irritation.

4.1 Irritation Patterns

Intolerance to SLS, a standard compound of irritants and detergents, is manifested by erythema and desquamation which evolve in skin surface fissuring (Tupker et al. 1997). Irritation may also be only subjective: stinging, burning sensation, feeling skin tensed, itch. All these signs are never found in the same subject altogether and are not connected. Accordingly specific tests and selective subjects panels are needed to let them appear.

The most sensitive subjects are those in the course of an eczema or who in the past experienced eczema or orthoergic dermatitis. Otherwise they are women, children, subjects with very clear skin and I and II phototypes. The least sensitive subjects are men and subjects over 50.

Skin irritability increases in winter and when the absolute atmospheric humidity is low (Uter et al. 1998; Basketter et al. 1996). It increases also in the pre-menstrual phase (Agner et al. 1990), and if the skin is warm (Clarys et al. 1997). It intensifies with any other simultaneous aggression (sun, wind, mechanical factor…) (Frosch 1992).

Irritability depends on the *body site*: in decreasing order (Frosch 1992): face, back, elbow crease, forearm, leg, wrist. It increases in parallel to the *application area*. Prior application of W/O emulsion or urea cream decreases it (Loden and Andersson 1996).

It is essential to consider all these factors when implementing the test and reading the results. It is therefore mandatory to use a positive control (in addition to the negative control) so as not to be influenced by the possible variation of the overall panel sensitivity with time.

4.2 Irritability Testing

4.2.1 General Tests

For clinical assessment it is recommended to determine the *irritation threshold*, for which the eye or touch have a high discriminating power. Tests will assess either the irritant minimal concentration for a constant application time, or the minimal application time for a constant concentration. The Kligman & Wooding test modified by Bahmer and Feldmann (1995) may be used, as well as the Basketter's test (Basketter et al. 1994), but as a positive control, with substitution of 20 % SLS by a lower concentration for example 0.05 %, 0.10 % or 0.25 %.

4.2.2 Sting Test (Sensory Irritation) (Frosch and Kligman 1977)

Some people complain of a stinging sensation following application of certain creams. Typically the stinging feeling starts one or two minutes after application of the cosmetic, intensifies during the following 5–10 min when it becomes intense, then subsides and disappears in 15–20 min; it is rarely associated with an erythema. It must be differentiated from a burning sensation or itch, the latter being typically associated with the desire to scratch the skin.

The purpose of the Sting Test is to select a panel of subjects able to detect substances that could cause this type of reaction. Because of the rarity of the phenomenon, it has to be performed on women (size of the panel: 5–10) who have already developed similar episodes or believe they have a "sensitive skin" (Grove et al. 1984).

The typical protocol consists firstly in inducing a profuse (thermal) sweating of the face. A cotton bud impregnated with a water solution of lactic acid at 5 % is rubbed on the area between nose and cheek, with the symmetrical side as a control. The feeling is assessed as soon as the product is applied (immediate scoring), then at 2.5 min, 5 min and 8 min (retarded score = mean of the last 3 scores) by a scale from 0 to 3+. The "stinging potential" of a subject is evaluated as follows: light for a score between 0.4 and 1, moderate between 1 and 2, and important between 2 and 3. The test can be performed at ambient temperature and without sweating using 10 % lactic acid (Grove et al. 1984).

Only the face is responsive to this phenomenon, with the following decreasing sensitivity: paranasal creases > cheeks > chin > lower eyelid > retroauricular area.

Stinging is enhanced by actinic erythema, skin irritation, stripping of the stratum corneum.

The origin of the stinging phenomenon may be an abnormal sensitivity of the skin to acids or a particular reactivity of the acidic coat of the skin surface. The skin pH, which decreases immediately after application of lactic acid, is restored faster in "stingers" in the 15–30 min following application (Issachar et al. 1997).

4.2.3 Burning Test (Grove et al. 1984)

The object of this test is to identify (and possibly select for a specific panel) the subjects who have a propensity to burning sensation (often associated with propensity to stinging) following the application of some cosmetics.

A depression is produced in the skin using the greased extremity of a cylindrical metal bar (diameter 8 mm). Then 10 µl of a chloroform-methanol mixture (20:80) is poured into this hollow which is immediately sealed with a plastic film. The appearance time of an intense burning sensation is measured with a chronometer and the product immediately removed. On the face, where this test is usually performed, it varies from 3 to

30 s. The paranasal creases are the most sensitive site.

4.2.4 Histamine Itching Test (Grove et al. 1984)

This test has been developed to identify the (rare) people who often feel itchy after applying cosmetics. 10 µl of 4 % histamine are placed in a depression in the skin produced using the same procedure as in the burning test. The subject indicates the intensity of the pruritus on a scale from 0 to 3+, after 2.5 min, 5 min and 10 min. At the end of this process, the histamine papule which always appears even in the absence of pruritus (about 50 % of cases) is measured. Contrarily to the stinging and burning sensations which are easily identified, feeling itchy is more difficult to recognise and requires the training of the volunteers.

4.2.5 Soap Chamber Test

The objective is to assess the irritancy potential of soaps and detergents specifically. The typical test (Frosch and Kligman 1979) consists in applying 100 µl of a 8 % watery solution of the soap, heated at 40 °C, on the forearm, in a Dühring chamber. The application lasts 24 h the first day (on a Monday) and 6 h the 4 following days. Reading is done 3 days later (the next Monday), looking for erythema (4 grades), desquamation (3 grades) and fissuring (3 grades). The delay between the end of the test and the reading permits specific effects to appear. The final score is the sum of the means of the three parameters.

For the assessment of mild soaps which alter the stratum corneum barrier prior to induce an erythema, Simion et al. (1991) proposed the following modifications: first reading 3 h after the first application of 24 h (in order to stop the experiment for the 3+ reactive subjects); then renewed application for 21 h and final reading 3 h later. They also suggest to use water as a positive control. In order to increase the test efficacy, they recommend using a panel of volunteers selected from their being intolerant to detergents, and to reject subjects with TEWL $> 8\ gm^{-2}h^{-1}$. At each reading, the clinical score is completed by an instrumental erythema and TEWL measurement.

4.3 Clinical Assessment of Irritation

The eye is a remarkable detector of the erythema threshold. But it is less effective in evaluating intensity. The same applies to desquamation. Conversely the touch and eye are not reliable to evaluate the small alterations of the skin relief. Non instrumental erythema measurements are discussed in this book, ▶ Chap. 105, "Skin Barrier Function." As for the other signs, a few examples of structured scales which have already been used are listed below:

Clinical scoring of skin dryness (Paye et al. 1994)

0	No squames or dandruff: smooth relief
1	A few squames, or slightly irregular relief
2	Mild dandruff, squames, small wrinkles
3	Noticeable desquamation, evident wrinkles
4	Severe desquamation, very visible wrinkles

Clinical scoring of superficial fissuring (Frosch and Kligman 1979)

0	No change
1	Thin cracks
2	1 or several fissures
3	Large fissures with exsudation or haemorrhage

Clinical scoring of desquamation (sight and touch) (Frosch and Kligman 1979)

0	No visible desquamation
1	Mild
2	Moderate
3	Severe with large squames.

Purely subjective symptoms (dryness feeling, tense skin sensation, pruritus, stinging and/or burning) are better appreciated by their threshold (the symptom exists or not) than by their intensity. However it is sometimes useful to record intensity, even in a very approximate way (Finkey 1987), or to use a device designed for autoevaluation as in the measurement of pruritus (this book, ▶ Chap. 131, "Itch Metrology").

4.4 Sensitive Skin

Sensitive or reactive skin is a fairly common condition. Being still poorly defined and almost purely subjective, its definition, actual prevalence, recognition, testing and treatment make a challenge for both dermatologists and cosmetologists. A valuable attempt to answer most of these questions was made in a recent thesis from which were drawn the following data (De Lacharrière 2002).

The condition has been termed "status cosmeticus" in 1990 (Fisher 1990), but was first recognized as an entity in 1986 by Thiers who wrote (Thiers 1986) "Usually one deals with a woman aged about 30 years, often with a clear complexion. . . . From a short time, she complains that her face, seldom her hands too, badly react to every applied product, whether sophisticated or not. In a couple of seconds the patient feels a warm and burning sensation rather than itch. The treated skin at once strongly reddens, but without immediate weal neither late vesicle formation. Within a few hours, sometimes only the day after, all symptoms subside. When redness has faded out, one or two days later, a fine and transient desquamation appears. One is impressed by the intensity of the erythema, and of the burning sensation, the scanty desquamation, the absence of any sign of allergy such as urticaria, or eczema. Once the reaction has settled, any new attempt induces a relapse."

In a survey conducted in a randomly selected British population (2058 women and 260 men) (Willis et al. 2001), the incidence of the self-reported condition was 51.4 % for women and 38.2 % for men, and 10,0 % and 5.8 % respectively for a "very sensitive" skin. In another population in the USA (800 women) comprising Afro-Americans, Asians, Euro-Americans, and Hispanics, the prevalence was similar (52 %) (Jourdain 2002). Among 2000 Chinese women (Yang et al. 2002) the mean incidence was 36.1 % and showed a regular decreases with aging (e.g., 49.1 % and 20.1 % in the 18–20 y and 51–55 y groups, respectively).

The conditions (as found in 887 English women with sensitive skin (De Lacharrière 2002)) involves sensorial signs: itching, stinging, burning, and skin tightness sensation occurring on the face (nose paranasal, forehead, perioral area, cheekbone, chin). Erythema was absent or faint. "Dry skin" was often associated, but was not so dry as to induce increased roughness and desquamation (both assessed (De Lacharrière 2002)). In another survey (1037 randomly selected English women (De Lacharrière 2002)) the condition was found not associated with present or past allergy (atopic dermatitis, contact eczema). This was confirmed later (De Lacharrière et al. 2001). In Caucasians the symptoms are mostly triggered either by contact with hard water, soap, make-up removers, or by environmental factors (wind, cold or warm weather, fast temperature change), or by both. Spicy food may also generate skin reaction especially in the Asians (Jourdain 2002; Yang et al. 2002). In England proneness to blushing and seborrhea are also predisposing factors. The stinging test (10 % lactic acid cotton tip gently rubbed 10 times) showed positive in 48 out of 88 English subjects, that is only in "moderately" and "very" (not in "slightly") reactive skins (De Lacharrière 2002).

Neither an increased TEWL (De Lacharrière 2002) nor an increased sensitivity to SLS (0.5–3 %) (Reiche et al. 1998) implying an impaired skin barrier, were found associated with sensitive skin. The skin hydration (capacitance) was normal (De Lacharrière 2002). But the sebum excretion rate (as found with Sebutape) was significantly increased (De Lacharrière 2002).

All these data led the author to presumably rely the condition to an increased superficial skin vessels and/or sensorial nerves reactivity. Accordingly testing with capsaicin was undertaken: 0.05 ml of 0.075 % capsaicin in a cream (Zostrix®) over 4 cm^2 on the jaw angle, with scoring at 3, 5, 10, 20, and 30 min for stinging (0–3), burning (0–3), itching (0–3) (De Lacharrière et al. 1997). Both stinging and itching scores were significantly higher in sensitive skin, increasing in parallel with the severity of the condition. In contrast, no difference was observed in patients with and without contact allergy (De Lacharrière et al. 1997). Brain activated areas during a lactic acid stinging test were examined in nine women with sensitive skin as compared with nine control women, using

functional magnetic resonance imaging (Querleux et al. 2002). Whereas in controls only the opposite side Sylvian nose paranasal area was activated, in sensitive persons activation was bilateral and associated with that of the prefrontal (as in pain sensation) and cingular areas. This experiment suggests that sensitive skin may be a functional neurosensory condition close to hypersensitivity to pain (Querleux et al. 2002).

The conclusion of this set of experiments is that sensitive skin can be detected using an appropriate questionnaire and confirmed by testing with lactic acid and capsaicin. Owing to the lack of difference between the author's grade 1 (slight) sensitive skin and controls, "true" sensitive skin should perhaps be restricted to grade 2 (moderate) and 3 (very) sensitive skin, that is people experiencing.

4.5 Instrumental Assessment of Irritation

4.5.1 Invisible Erythema and Vasodilatation

Some devices are more sensitive than the eye and capable to detect "infra-clinical erythemas." Contrary to allergic or actinic reaction, these mild or minimal irritations are characterised by vasodilatation limited to the sub-epidermal vascular plexus, the deep blood flow keeping barely elevated or normal. They are therefore better assessed by the techniques specific to superficial skin blood flow (reflectometry or spectroreflectometry (Nangia et al. 1996), green laser-doppler, capillaroscopy) (see ▶ Chap. 133, "Assessment of Erythema and Pallor"). Laser-doppler may be useful to detect stingers, independently of an erythema (Lammintausta et al. 1992).

4.5.2 TEWL

In mild erythemas induced by irritation TEWL is increased in proportion to the severity of the irritation. Because this water flux reflects the permeability of the stratum corneum its intensification is observed following a barrier damage due to detergents and other substances aggressive to the horny layer. It is sensitive to SLS and reacts in a dose-dependent and linear way, which is not the case of the clinical response (Tupker et al. 1997). Following an occlusive test, TEWL must always be measured at least 1 h after the end of application, the skin being left uncovered (Tupker et al. 1997). Furthermore, a high basal TEWL has a prospective value (Murahata et al. 1986), indicating a more permeable stratum corneum and a resulting increased tendency to irritation.

4.5.3 Impedance

The measurement of conductance has given inconstant results. The quotient of the absolute impedance at 20 kHz by the impedance at 1 Mhz (irritation index) decreases when the irritation increases (Ollmar and Emtestam 1992). This would be an indirect measurement of the intercellular oedema of the viable epidermis.

Whilst TEWL and stratum corneum capacitance remain unchanged, the sorption–desorption test and moisture-accumulation test detected a barrier alteration one hour after a 15-min application of 0.1 % SLS, through significant reductions of hygroscopicity (water sorption), water holding capacity and moisture accumulation (Treffel and Gabard 1996).

4.5.4 Skin Relief (Using Silicon Polymer Replicas)

On the volar forearm, hyperhydration is associated with the narrowing of the furrows and the dilatation of the plateaus, the surface of which can become wrinkled. After application of an irritant for 24 h, the normal triangular pattern recedes, desquamation occurs, the crests crossing the plateaux become larger, and in particular the furrows become deeper. These alterations seem reproducible and related to the intensity of the irritation (Kawai et al. 1992; Sato et al. 1996). They are similar to what is observed when the stratum corneum is dehydrated.

4.5.5 Desquamation (Agache 2004)

A static quantification (D-Squames, turbine method) and a dynamic measurement (reduced stratum corneum renewal time) have been used to detect and assess some damage of the horny

layer and alteration of the viable epidermis behaviour, respectively.

4.5.6 Dansyl Chloride Test (Fluorescence Under Wood Light)

This test measures how the storage of dansyl chloride (DC) by the stratum corneum is reduced under the effect of the application of the tested product; it seems to be associated with its irritating effect (Paye et al. 1994). It is not known whether the DC is extracted by the detergent or whether its absorption by the living tissue is facilitated. The sensitivity of the test may be similar to that of TEWL.

On two areas on the volar forearm DC 5 % in petrolatum gelly (vaseline) is applied under semi-occlusive patch for 18 h later. After patch removal the skin is thoroughly rinsed with tap water and the homogeneity of the fluorescence under Wood light is checked. During the following 7 days, no soap or detergent is applied, therefore the test begins 8 days after DC application. In the morning, on one of the areas (the other serving as control) 0.15 ml of the tested preparation heated at 40 °C is applied in a Hill Top Chamber for 30 min and the skin is thoroughly rinsed. The same procedure (30 min application, ablation, rinsing) is renewed twice in the same day, with a minimum interval of 1 h 30. After the last operation, a visual measurement of the reduction of fluorescence compared to the control site is achieved, using a scale from 0 to 4. The authors found it to be correlated with the irritation grade (even in absence of erythema) (Paye et al. 1994).

4.5.7 Corneosurfametry (Stratum Corneum Alteration Test) (Piérard et al. 1994, 1995; Goffin et al. 1995)

As the stratum corneum acts as a barrier against penetration of foreign substances into the living tissue, its integrity is essential in the protection against irritation. Piérard et al. noticed that the first sign of alteration of the stratum corneum by detergents was an increase of its colorability by Polychrome Multiple Stain (a mixture of fuchsine and toluidine blue). Corneosurfametry consists in measuring this effect on the most superficial layers obtained by stripping with cyanoacrylate glue. It is, therefore, an in vitro test carried out on material that has been sampled in vivo.

Each sampling is put in contact with the tested product for 2 h at 20 °C. It is then rinsed with tap water and stained for 3 min. Its color is then measured with a Chromameter CR200 according to the system L*a*b*. It is also possible to observe the type of stratum corneum alteration using a microscope. The authors use 3 parameters: (i) the ratio luminance/chroma, named CIM (Colorimetric Index of Mildness), (ii) the global difference in colour with the effect of water application called CSMI (CorneoSurfaMetry Index), (iii) the added differences of both previous indices with water indices, called ODC (Overall Difference in Corneosurfametry)[1].

The CSMI after application of detergents differs significantly from the CSMI after application of water. This permits to classify the products in relation to water and a standard detergent, for example 1 % SLS. Furthermore the effect of water alone is a way to detect and assess the stratum corneum fragility and makes it possible to compare or rely this factor with the skin irritability. In this way the authors have found different proneness to irritation in six body sites, as well as a different stratum corneum stainability in subjects with dermatitis of the hands and forearms (Henry et al. 1997).

4.5.8 Mediators of Inflammation Assessment in Stratum Corneum (Perkins et al. 1999, 2001)

This method uses the ability of stratum corneum to store peptides up to its uppermost layers originating in the viable tissue. Consequently, inflammatory mediators such as Interleukin-1" (IL-1") can be collected at the skin surface to detect a

[1] $CIM = L^*-(a^{*2} + b^{*2})^{0.5}$; $CSMI = [\Delta L^{*2} + \Delta(a^{*2} + b^{*2})]^{0.5}$; $ODC = [(\Delta CIM)^2 + (\Delta CSMI)^2]^{0.5}$. However, CIM is redundant because L* and $(a^{*2} + b^{*2})^{0.5}$ are inversely correlated; furthermore it evolves parallel to CSMI. The ODC index is also redundant because it adds up the same variation expressed differently. Only the CSMI index has a clear significance: the colour difference in colour between treatment with water and with the tested product.

cutaneous inflammation even in the absence of clinical signs. The authors used Sebutape, applied for only 1 min, to collect a thin layer of stratum corneum in which human IL-1", its receptor antagonist IL-1RA, and IL-8 could be assessed using specific ELISA kits (R&D Systems, Minneapolis, MN, USA.). Total protein in the sample was also assessed, using the Pierce enhanced microtiter assay (Pierce, Rockford, IL, USA) with bovine serum albumin used as the standard, in order to calculate the ratio cytokine/protein which is independent of the amount of stratum corneum collected. IL-1" was recovered from all normal subjects, at a level depending on the body site, whereas IL-8 was absent. No age related differences were found. The ratio IL-1"/IL-1RA was higher in sun exposed areas (face, lower leg in females) as compared to covered sites (upper back, upper arm, under arm, upper leg), most probably signaling subliminal inflammation. Upon skin irritation (heat rash, erythema, diaper rash in infants) IL-1" levels were significantly elevated. In babies suffering of diaper dermatitis, a correlation was found between the rash grade and IL-1" level. In these infants, IL-8 was also found in the Sebutape samplings at measurable level. Skin application of 20 % SLS for 1 h was followed 24 h later by a strong increase of both IL-1" and IL-8, while water application only induced a smaller but clear cut augmentation. Consequently, the method seems promising for detection and monitoring sub-clinical skin irritation.

References

Agache P. Metrology of the stratum corneum. In: Handbook of Measuring the skin. 1st edn. Berlin: Springer; 2004. p. 101–10.

Agner T, Fullerton A, Brohy-Johansen U, Batsberg W. Irritant patch testing: penetration of SLS into human skin. Skin Pharmacol. 1990;3:213–7.

Annexe à la Directive 92/69 CEE du 31 juillet 1992: dixseptième adaptation au progrès technique de la Directive 67/548 CEE. Journal Officiel de l'Union Européenne L841992:36: 1

Bahmer FA, Feldmann U. Objective and reproducible assessment of irritants in vivo. A reappraisal of the IT50 in honour of Kligman and Wooding. In: Elsner P, Maibach HI, editors. Irritant dermatitis: new clinical and experimental aspects. Basel: Karger; 1995. p. 288–95.

Basketter PA, Whittle E, Griffiths HA, York M. The identification and classification of skin irritation hazard by a human patch test. Fd Chem Toxicol. 1994;32:769–75.

Basketter DA, Griffiths HA, Wang XM, Wilhelm KP, McFadden J. Individual, ethnic and seasonal variability in irritant susceptibility of skin: the implications for a predictive human patch test. Contact Dermatitis. 1996;35:208–13.

Burckhardt W. Praktische und theoretische Bedeutung der Alkalineutralisations- und Alkaliresistenzproben. Arch Klin Exp Dermatol. 1964;219:600–3.

Clarys P, Manou I, Barel AO. Influence of temperature on irritation in the hand/forearm immersion test. Contact Dermatitis. 1997;36:240–3.

De Lacharrière O. Contribution à l'étude des peaux sensibles et réactives. Aspects épidémiologiques,cliniques et physiopathologiques. Thesis, University of Besançon; Dec 9th; 2002.

De Lacharrière O, Reiche L, Montastier C, Nicholson M, Courbière C, Willis C, Wilkinson JD, Leclaire J. Skin reaction to capsaicin: a new way for the understanding of sensitive skin. Australas J Dermatol. 1997;38(S2):3–313.

De Lacharrière O, Jourdain R, Bastien P, Garrigue JL. Sensitive skin is not a subclinical expression of contact allergy. Contact Dermatitis. 2001;44:131–2.

Finkey J. Evaluation of subjective irritation induced by soap materials. J Soc Cosmet Chem. 1987;82:153–61.

Fisher AA. "Status cosmeticus": a cosmetic intolerance syndrome. Cutis. 1990;46:109–10.

Frosch PJ. Cutaneous irritation. In: Rycroft RJG, Menné T, Frosch PJ, Benezra C, editors. Textbook of contact dermatitis. Berlin: Springer; 1992. p. 28–61.

Frosch PJ, Kligman AM. The chamber-scarification test: a new method for assessing the irritancy of soap. Contact Dermatitis. 1976;2:314–24.

Frosch PJ, Kligman AM. A method for appraising the stinging capacity of topically applied substances. J Soc Cosmet Chem. 1977;28:197–209.

Frosch PJ, Kligman AM. The soap chamber test: a new method for assessing the irritancy of soaps. J Am Acad Dermatol. 1979;1:35–41.

Frosch PJ, Kurte A. Efficacy of skin barrier creams: (IV) The repetitive irritation test (RIT) with a set of 4 standard irritants. Contact Dermatitis. 1994;31:161–8.

Frosch PJ, Pilz B. Irritant patch test techniques. In: Serup J, Jemec GBE, editors. Handbook of non-invasive methods and the skin. Boca Raton: CRC Press; 1995. p. 587–91.

Goffin V, Paye M, Piérard GE. Comparison of in vitro predictive tests for irritation induced by anionic surfactants. Contact Dermatitis. 1995;33:38–41.

Grove GL, Soschin DM, Kligman AM. Adverse subjective reactions to topical agents. In: Drill VA, Lazar P, editors. Cutaneous toxicity. New York: Raven; 1984. p. 203–11.

Henry F, Goffin V, Maibach HI, Piérard GE. Regional differences in stratum corneum reactivity to surfactants. Quantitative assessment using the corneosurfametry bioassay. Contact Dermatitis. 1997;37:271–5.

Issachar N, Gall Y, Borrel MT, Poelman MC. pH measurements during lactic acid stinging test in normal and sensitive skin. Contact Dermatitis. 1997;36:152–5.

Jourdain R, de Lacharrière O, Bastien P, Maibach HI. Ethnic variations in self- perceived sensitive skin: epidemiological survey. Contact Dermatitis. 2002;46:162–9.

Kawai K, Nakagawa M, Kawai J, Kawai K. Evaluation of skin irritancy of sodium lauryl sulphate: a comparative study between the replica method and visual evaluation. Contact Dermatitis. 1992;27:174–81.

Klaschka F, Mengel G, Nörenberg M. Quantitative und qualitative Hornschicht-Diagnostik. Arch Dermatol Forsch. 1972;244:69–76.

Kligman AM, Wooding WM. A method for the measurement and evaluation of irritants on human skin. J Invest Dermatol. 1967;49:78–94.

Lammintausta K, cité par Frosch in Rycroft et al, 1992. (Ref 22).

Leder M. Die Benzintoleranz der Haut. Dermatologica. 1943;88:316–33.

Locher G. Permeabilitätsprüfung der Haut Ekzemkranker und Hautgesunder für der neuen Indikator Nitrazingelb "Geigy," Modifizierung der Alkalieresistenzprobe, pH Verlauf in der Tiefe des Stratum corneum. Dermatologica. 1962;124:159–82.

Loden W, Andersson AC. Effect of topically applied lipids on surfactant-irritated skin. Br J Dermatol. 1996;134:215–20.

Murahata R, Crove DM, Roheim JR. The use of transepidermal water loss to measure and predict the irritation response to surfactants. Int J Cosmet Sci. 1986;8:225–31.

Nangia A, Andersen PH, Berner B, Maibach HI. High dissociation constants (pKa) of basic permeants are associated with in vivo skin irritation in man. Contact Dermatitis. 1996;34:237–42.

Ollmar S, Emtestam L. Electrical impedance applied to non-invasive detection of irritation in skin. Contact Dermatitis. 1992;27:37–42.

Paye M, Simion FA, Piérard GE. Dansyl chloride labelling of stratum corneum: its rapid extraction from skin can predict skin irritation due to surfactants and cleansing products. Contact Dermatitis. 1994;30:91–6.

Piérard GE, Goffin V, Piérard-Franchimont C. Corneosurfametry: a predictive assessment of the interaction of personal care cleansing products with human stratum corneum. Dermatology. 1994;189:152–6.

Piérard GE, Goffin V, Hermanns-Lê T, Arrese JE, Piérard-Franchimont C. Surfactant induced dermatitis. A comparison of corneosurfametry with predictive testing on human and reconstructed skin. J Am Acad Dermatol. 1995;33:462–9.

Querleux B, Jourdain R, Dauchot K, Burnod Y, Bittoun J, Bastien P, de Lacharrière O. Sensitive skin: specific brain activation revealed by functional MRI. Ann Dermatol Venereol. 2002;129:1S11–77 (ICOl99) (abstract).

Perkins MA, Osterhues MA, Robinson MK (1999) Noninvasive method for assessing inflammatory changes in chemically treated skin. J Invest Dermatol 112:601.

Perkins MA, Osterhues MA, Farage MA, Robinson MK (2001) A noninvasive method to assess skin irritation and compromised skin conditions using simple tape adsorption of molecular using simple tape adsorption of molecular markers of inflammation. Skin Res Technol 7:227–237.

Reiche L, Willis C, Wilkinson J, Shaw S, de Lacharrière O. Clinical morphology of sodium lauryl sulfate (SLS) and nonanoic acid (NAA) irritant patch test reactions at 48h and 96h in 152 subjects. Contact Dermatitis. 1998;39:240–3.

Rougier A, Goldberg AM, Maibach HI, editors. In vitro skin toxicology. Irritation, phototoxicity, sensitization. New York: Mary Ann Liebert; 1994.

Sato A, Obata K, Ikeda Y, et al. Evaluation of human skin irritation by carboxylic acids, alcohols, esters and aldehydes, with nitrocellulose-replica method and closed patch testing. Contact Dermatitis. 1996;34:12–6.

Simion FA, Rhein LD, Grove GL, et al. Sequential order of skin responses to surfactants during a soap chamber test. Contact Dermatitis. 1991;25:242–9.

Thiers H. Peau sensible. In: Thiers H, editor. Les Cosmétiques. 2nd ed. Paris: Masson; 1986. p. 266–8.

Treffel P, Gabard B. Measurement of sodium lauryl sulfate-induced skin irritation. Acta Derm Venereol. 1996;76:341–3.

Tupker RA, Willis C, Berardesca E, Lee CH, Fartasch M, Agner T, Serup J. Guidelines on sodîum lauryl sulfate (SLS) exposure tests. A report from the standardization group* of the European Society of contact dermatitis. Contact Dermatitis. 1997;37:53–69.

Uter W, Gefeller O, Schwanitz HJ. An epidemiological study of the influence of season (cold and dry air) on the occurrence of irritant skin changes of the hands. Br J Dermatol. 1998;138:266–72.

Wahlberg JE, Maibach HI. Nonanoic acid irritation: a positive control at routine patch testing? Contact Dermatitis. 1980;6:128–30.

Whittle E, Basketter D. The in vitro skin corrosivity test. Development of method using human skin. Toxicol In Vitro. 1993;7:265–8.

Willis CM, Stephens CJM, Wilkinson JD. Experimentally-induced irritant contact dermatitis. Determination of optimum irritant concentrations. Contact Dermatitis. 1988;18:20–4.

Willis CM, Shaw S, de Lacharrière O, Baverel M, Reiche L, Jourdain R, Bastien P, Wilkinson JD. Sensitive skin: an epidemiological study. Br J Dermatol. 2001;145:258–63.

Yang FZ, de Lacharrière O, Lian S, Yang ZL, LI L, Zhou W, Nouveau S, Qian BY, Bouillon C, Ran YP. Sensitive skin: specific features in Chinese skin. A clinical study on 2000 Chinese women. Ann Dermatol Venereol. 2002;129:1S11–77 (IC0355) (abstract).

York M, Griffiths HA, Whittle E, Basketter DA. Eval ati on of a human patch test for the identification and classification of skin irritation potential. Contact Dermatitis. 1996;34:204–12.

Cutaneous Testing: Detection and Assessment of Allergy

118

Martine Vigan

Contents

Keywords

Prick testing • Patch testing • Open testing • Allergy • Cosmetovigilance

Patients often turn to dermatologists because of problems of skin allergy, either of an external origin (contact allergy) or associated with allergenic compounds intake (endogenous allergic reaction). Skin tests are also frequently used to confirm the allergic mechanism of noncutaneous diseases (asthma, conjunctivitis). Investigations apply mainly to either immediate IgE-mediated Gell and Coombs' type I allergy or delayed, cell-mediated type IV allergy. The reading is also immediate or delayed, depending on the mechanism involved.

1 Immediate Hypersensitivity (or Allergy) Testing

The principle of these tests is to reproduce the Lewis triad within 20 min by applying the allergen on or into the skin. (Hypersensitivity refers to a general mechanism, whereas allergy refers to its clinical manifestations.) Common uses of immediate hypersensitivity tests in dermatology are atopy, investigation about possible allergy to molds or foods, contact urticaria, reaction to

M. Vigan (✉)
Department of Dermatology, University Hospital of Besancon, Besançon, France
e-mail: martine.vigan@gmail.com

P. Humbert et al. (eds.), *Agache's Measuring the Skin*,
DOI 10.1007/978-3-319-32383-1_68

Table 1 Causes of false negative prick tests

Skin hyporeactivity (positive controls are negative): deficient mastocytes and/or neuromediators
Current 15 min is not the proper reading time: incorrect allergen formulation, very low allergen penetration
Medicine weakening effect: it can be detected through the controls H1 antihistamines, imipramine, phenothiazine, and dopamine induce constantly false negatives Hypnotics, theophylline, beta-mimetics, nonsteroidal anti-inflammatory drugs, and paracetamol may induce false negatives Long-term corticosteroid systemic or topical therapy can render prick tests difficult to interpret

medicine, oral syndrome, anaphylactic shock, and some visceral diseases (Castelain and Castelain 1992; Lachapelle and Maibach 2012). One should always keep in mind that hypersensitivity refers to a general mechanism, whereas allergy refers to its clinical manifestations.

In order to interpret the test, patients must meet some requirements. The skin must be able to develop a type I reaction; this response may be disturbed by drug intake (Table 1) or by aging (it decreases with age). The response may also be different with the tested body site.

1.1 Immediate Hypersensitivity

1.1.1 Intradermal Skin Tests

It was the first allergy test to be described (-Mantoux 1908; Lachapelle and Maibach 2012; Bernstein and Storms 1995a, b). A solution with the allergen is injected into the superficial dermis. Usually, 0.02–0.03 ml produces a 3–5 mm diameter papule. Reading is done by comparison with a negative control (the vehicle alone) (Fig. 1). The advantages of this method are good reproducibility, sensitivity, and the possibility to use a dilution series (the only method that can assess the threshold and intensity of the allergic reaction). Its drawbacks are the pain it may induce, the necessary use of injectable substances only (e.g., medicine, venom, airborne allergens prepared for such test), and mainly the risk to generate a systemic anaphylactic reaction. Some believe that the sensitivity of this test is too high and poses a risk of false positivity; the use of control "healthy subjects" may overcome this risk, but raises ethical questions. The risk of inducing a sensitization is also discussed.

1.1.2 Prick Test

Method

Described as early as 1924 by Lewis and Grant, this test became widely used only after its modification by Pepys in 1972 (Pepys 1975). A drop of the allergenic mixture is put on the skin, and then a puncture is made of the skin through the drop, avoiding bleeding; reading takes place after 15–20 min. For a well-trained operator, the puncture is practically standardized. The usually tested sites are the volar forearm and the back. A minimum distance of 4 cm between tests is essential to avoid reading problems in case of strong positivity. Disposable pins are mandatory. Common material is in plastic (Stallerpoint, Allerbiopoint). The prick through the allergen-containing drop should be done on the skin tensed between thumb and forefinger, without twisting the pin (Fig. 2). For the purpose of standardization, the Coated Phazest® which contains the allergen was tried.

The prick test differs from

- The open test: the product such as a cosmetic product is placed on the skin without epidermal wounding.
- The open patch test, such as SAFT (Skin Application Food Test), where the allergen is placed on the skin, and sometimes occluded for 15 min, but without epidermal wounding.
- The linear nonstandardized non-bloody epidermal scarification, on which the allergen is placed afterwards.
- The intradermal test.

These tests are read after 15–20 min, sometimes more.

Fig. 1 IDR, positive reaction at 20 min

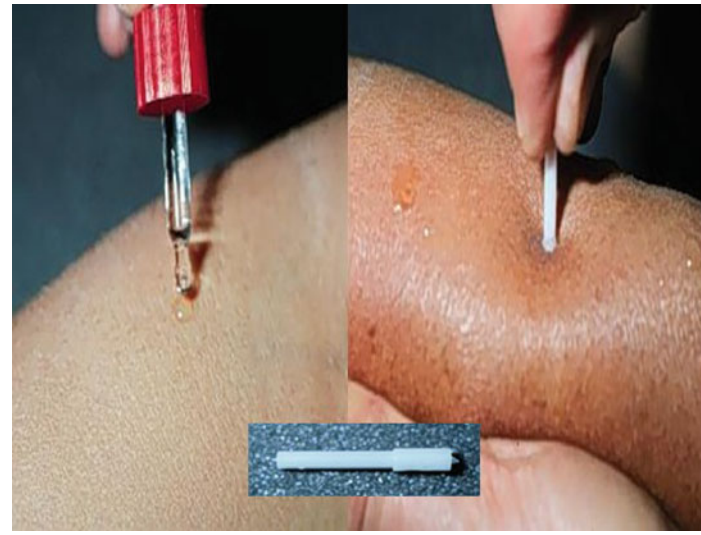

Fig. 2 Prick testing; a drop of allergen is put on the skin and then pricked through the stretched skin

Allergens

There is no "standard kit" of allergens. Samples are on the market, most of them in a phenyl-glycerol-saline solution. Some allergens (e.g., dermatophagoides, cat hairs) are standardized, and their dilution is expressed in reactivity index (IR) defined by the reaction of the prick carried out in specific conditions compared to the codeine control, but most of them are not, and variations are possible between kits. They must be refrigerated and shaken before use. Regarding food samples, the allergens on the market can be used, but in most cases crude or frozen pieces of food or more reactive freshly made mixtures are tested. Medicines are used at their usual concentration or with dilution depending on clinical history. The skin reactivity is tested by positive control (histamine 10 mg/ml) and a negative control (the allergen vehicle). The drop is wiped off at the time of the reading.

Reading

After 15/20 min, the whole tested area is patted dry with absorbing paper. When tests are patted dry one after the other, care should be taken not to carry the allergen from one prick to another. The Lewis triad pattern varies with age: vivid erythema in newborn babies and papule only in old subjects.

Negative criteria: A test is negative if comparable to the negative control, while the positive controls are clearly positive. A papular negative

control indicates dermographism; in that case a similar reaction with tested compounds should be considered as negative.

Positive criteria: The reading of the prick tests is not standardized. Pruritus, pseudopodia, and the comparison of the papule and erythema (flare) diameters with those of the positive controls attest a positive test. Reading is not quantitative; no dilution series is used. Pseudopods are interesting to be noted; they are seen mainly if the reaction is allergic (Fig. 3).

Dubious tests: The test cannot be interpreted if positive controls are negative or if the negative control produces a reaction (Fig. 4).

Late reaction: Some allergens induce a flare and papule reaction which appears within 12 h and may last up to 48 h (e.g., cockroach test). There is no explanation to these types of reaction which cannot be used in diagnosis, except in adverse drug reactions where they point to a possible delayed hypersensitivity.

Modulating Factors of Prick Tests

The skin reactivity is altered by strong pressure, thinness of the skin, mastocyte density, and substance P concentration. Treatment by beta blockers or IMAO does not seem to interfere with reactivity of prick tests; however the efficacy of adrenaline in case of anaphylactic reaction may be hindered. The prick tests' reproducibility is good only if the possible enhancing or attenuating factors have been eliminated at the time of the test.

Enhancing Factors and False Positive Tests

Tests performed while clinical signs of allergy are present (e.g., a seasonal rhinitis) will be more strongly positive. Some allergens (e.g., hymenoptera venom, Gruyère cheese) contain vasoactive substances and can produce positive tests by direct histamine release. A test may be considered as indicating a type I hypersensitivity only if at least ten healthy controls (a debated figure) tested

Fig. 3 Prick test: Lewis triad and pseudopods

Fig. 4 Prick testing, positive reaction at day 2 with drugs

in the same conditions remain negative or if IgE specific of the allergen are found in the patient's blood.

Attenuating Factors and False Negative Tests

Tests performed too near a severe allergic bout with total mastocytes degranulation can be false negative. Some medicines (e.g., corticosteroids, antihistamines) make the tests attenuated or negative. Desensitization weakens positive tests to the allergen. Some peripheral neuropathies might render prick tests negative, but children suffering from spinal dysraphism can be tested in the anesthetic zone without any problem.

Adverse Effects

Since 1987 no death has been attributed to prick tests, but nonstandardized allergens may generate anaphylactic reactions or delayed and persisting inflammatory reactions (e.g., plant sap). Focal reactions are possible; it is necessary to have at one's disposal corticosteroids, epinephrine/adrenalin, and injectable antihistamines as well as respiratory ventilation material.

Diagnostic Value of Prick Tests

The prick test is an easy to use method whatever the subject's age; several allergens can be tested in one consultation; the specificity of the method is good; however its sensitivity is poor (250 times less sensitive than the intradermal test) (Menardo et al. 1982). Faced with a suggestive clinical case and a negative prick, it is possible to repeat the test and maybe to complete it with an intradermal test. A prick test positive alone does not mean that the patient is allergic. Interpretation must always be connected to the clinical history, and if any doubt arises the prick test can be followed by provocation tests, but it raises ethical questions. The assumed mechanism of a positive reaction to an allergen may be confirmed by the specific IgE assessment; if its blood level is abnormally high, then the patient obviously presents a type I sensitization, but allergy is based on clinical signs only. The results of the prick test are not quantitative and cannot be used to quantify this allergy nor type I sensitization.

1.1.3 Other Tests

Other tests are used, but in a more unusual way: open test, scratch test, and prick test followed by occlusion. The principle is always the same: to reproduce the Lewis triad.

The most interesting test is the *open test.* The allergen is placed onto the skin, in conditions similar to when it induced reaction. The test is positive if the Lewis triad appears within 20 min or more. The test is indicated in case of anaphylactic reaction to an allergen for which there is no standardized extract (drugs, cosmetics); if it is negative, then a prick test can be carried out.

The *labial provocation test* can be used, with caution, especially for food (Menardo et al. 1982). The piece of food is held for 2 min by the hand inserted in a vinyl glove on the vermilion border of the lower lip. The test is positive if redness and pruritus appear within 20 min. As penetration through mucus membranes is fast and high, there may be in case of high hypersensitivity a risk of excessive lacrimation, nasal discharge, bronchial spasm, and shock.

Oral provocation tests are always thought over for awhile before implemented. Their main use is the detection of food allergy in atopic children (Rancé and Dutau 1997) when the labial provocation test is negative. For drugs, provocation tests are questionable.

Usage tests are contraindicated in case of contact urticaria as they bear a nonnegligible risk of anaphylactic shock.

Reintroduction tests are only aimed at confirming the innocuousness of a drug that was suspected in the first place then cleared, especially to make the patient feel secure. These tests must be carried out in a hospital ward because there is a nonnegligible vital risk (Bock 1991).

2 Delayed Hypersensitivity

The principle of these tests is to reproduce the lesion of delayed hypersensitivity (eczema in type) by the "mini-reintroduction" of the allergen into the target organ, namely, the skin. Indications are contact dermatitis, atopic dermatitis (Lachapelle et al. 1992; Giordano-Labadie

et al. 1999; Isolauri and Turjanmaa 1996), adverse drug reactions (Barbaud et al. 2001; Lachapelle and Tennstedt 1998), and atypical contact dermatitis.

The test can be interpreted correctly (Pons-Guiraud 1995) only if the patient is compliant and well informed.

He must have normal cellular immunity, and one should remember that the latter is reduced during pregnancy and is strongly weakened by cyclosporin, azathioprin, corticosteroid therapy, and ACTH and when CD4 lymphocytes are lower than 500/cm^3. Topical ultraviolet ray or immunodepressive drug on the tested zone in the preceding month should be banned.

2.1 Main Tests of Delayed Hypersensitivity

2.1.1 Epicutaneous Patch Testing

Material and Method

The main clinical sign of contact allergy is an eczema localized primarily at the site of contact with allergen (Lachapelle and Maibach 2012; Lachapelle et al. 1992). The patch test aims at reproducing the disease on a small area. It is usually achieved on the back by applying the allergen under occlusion, formerly under a gauze pad, today in a metal or plastic chamber (Finn Chamber, square chambers of Van der Bend, etc.) (Lachapelle 2010). Following removal of the chamber protecting lid, a minimal amount (from 15 µl in Fin Chambers to 20in Van der Bend of liquid or 20 mg allergen in petrolatum jelly deposited with a syringe (Bruze et al. 2007; Fig. 5)) is placed at its center. If necessary the surplus is wiped off, and then the preparation is attached to the patient's skin. The place and content of each chamber are carefully recorded in the patient's file, usually using a sketch. The material is maintained in place with Mefix ®. The chamber is removed after 48 h, and their positions are marked on the patient's back with a fluorescent-yellow pen (which will necessitate a wood lamp for detection 72 or 96 h later) or with a dermographic pen (marketed by companies selling equipment for patch testing). When positive, the test shows the typical eczematous lesions, namely, erythema, edema, and vesicles. A first reading is made immediately after the chamber is removed; the patient has to return 1 or 2 days later for a second reading. The patients should be informed before the tests so that they can make necessary arrangements.

The manual positioning of allergens in the chambers is a worrying source of variation. The TRUE Test® is a standardized patch test method where the chamber contains the allergen in an inert gel; it is found on the market at a free prize (more than € 15 or US $ 12 for a standard ICDRG series which contains allergens that are not updated).

Allergens

Those on the market have a definite concentration and a vehicle adapted to skin penetration (Lachapelle 1995; Fischer 1995). There is standard series (or baseline series) that contains allergens whose overall positivity rate is 1 % at least, when used systematically in people suffering from contact allergy. Its contents are updated at regular intervals. It palliates some failings in the patient history evaluation, and it can be complemented by an additional series also "routinely" used and set up from the physician's experience (Raison 2012). Baseline series vary according to geographical areas; the International Standard Series recommended by the ICDRG (International Contact Dermatitis Research Group) contains 21 allergens, and the European baseline series contains 28 allergens. Depending on the information provided by the patient, additional series can also be used (hairdressers, textiles, cosmetics, eyelids, feet, etc.), as well as the patient's own products (nonfoaming cosmetics and medical topics are tested under occlusion). For the emergent allergens, concentration is empirical or based on multicentric studies and subject to frequent revision (de Groot 2008).

Patch Test Reading

Reading takes place after 48 h, 72 h, or 96 h. *It should conform to a fixed standard.* The ICDRG

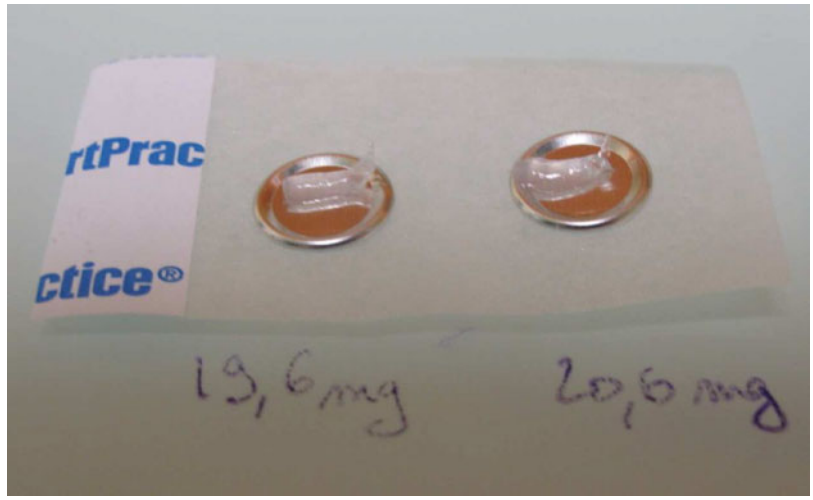

Fig. 5 20 mg of each allergen in petrolatum should be in the Finn Chambers

international score is used, based on the presence or absence of eczema basic lesions (Lachapelle and Maibach 2012; Vigan 1995).

A positive test of irritant type has no value as far as allergy is concerned. Such effects are the so-called soap effect, shampoo effect, follicular vesicles, croton effect, blistering effect, and necrosis.

If the positive test is of allergic type, it is then scored in cross (Table 2). The reading of epicutaneous patch tests is mainly clinical; the contribution of histology is limited because in case of doubt, it is also uncertain. TEWL measurement, colorimetry, and laser Doppler have been used, but the results were not convincing enough to be used in current practice.

The ICDRG grading records semiquantitatively the intensity of the allergic reaction. The appearance time (often the quicker is the appearance time, and the more sensitized is the patient) is also a way to assess this intensity. Pruritus is not considered in the score, whereas it is a typical symptom of eczema because it is too subjective. Calibration of this patch test reading is necessary (Svedman et al. 2012).

Table 2 Reading score of epicutaneous patch tests

Europe	USA	
NT	NT	Not tested
-	0	Negative reaction (but false negative are possible)
+?	1	Doubtful reaction = erythema only
+	2	Weak reaction = erythema and slight infiltration, possible small papule (no vesicle)
++	3	Strong reaction = erythema, infiltration, and vesicles
+++	4	Extreme reaction = erythema, infiltration, coalescent vesicles, and blister
IR	IR	Irritant reaction (false positive)

Unwanted Effects

They are rare (Castelain 1995; Inerot and Möller 2000; Kamphof et al. 2003; Vigan 1996) and take the following forms:

- False positive reactions: impurities contaminating the allergen, allergy to the support or the vehicle, angry back syndrome, irritation from too long application time, or too high concentration.
- Negative false reaction: too early reading, inappropriate testing, antigenic extinction phenomenon, too low concentration, too short occlusion, and photo allergy.
- Irritant reaction and atopic dermatitis outbreak on the tested area.
- Persistent depigmentation and complication special to some allergens (vegetables, *p*-amino compounds, acrylates, etc.).
- Keloid scars or persistent pigmentation, usually due to a technical error (Fig. 6).

Fig. 6 Patch testing, keloid scars due to a technical error

- Immediate-type reaction with a risk of anaphylaxis; this reaction is often revealed at first by the patient who complains about a pruritus during the test and confirmed when a urticarial papule is seen when the chamber is lifted. The allergen must then be removed immediately and the patient kept under observation and treated if necessary.
- Distant eczema outbreak or flare up: the area affected by eczema is reactivated although it has healed.
- Active sensitization: they should be considered when the test becomes positive beyond 1 week (Van Ketel 1973) and when the allergen is tested again, the new test reacts in usual reading. Active sensitization has to be differenced from booster effect (Vigan et al. 1997).

Interpretation of Positive Tests

A positive test is valid only when its relevance is established, that is: (i) when the allergen is found in products in contact with the patient, (ii) when the topography of the skin lesions is compatible with this contact, and (iii) when eviction induces recovery (Dooms-Goossens 1996). Contact may be direct, or by proxy, or airborne, or transmitted by the hands. Systemic contact ought to be considered sometimes. Relevance may be actual or past. Some tests are relevant only through crossed reactivity. The test is all the more relevant if its score is ++ or +++, but this varies according to the allergens.

A positive test is of diagnostic value for type IV allergy (late or delayed hypersensitivity) in the following conditions: (1) if the allergen is known and standardized or (2) if the allergen is unknown and the patient reacts to increasing dilutions, whereas control subjects remain negative.

2.1.2 Open Test

It is used to test foaming products or manufactured products of uncertain composition and pH $3 \ll 9$ (Dooms-Goossens 1990). A drop of the product investigated is placed on the skin of the patient's back. When dried, if there is no reaction, it is covered by a microporous adhesive. Reading takes place as for patch tests. If the application area becomes red or whitish before being covered, the product is immediately rinsed by an adapted solvent (petrolatum for a lipophilic product, water for a hydrophilic substance).

2.1.3 ROAT (Repeated Open Application Test)

It is used whenever the patch test is not possible, (in case of allergic reaction to some cosmetic allergens, the patient may try a ROAT for any new cosmetic; this obviates the absence of labeling) or if it is negative, while the clinical significance is obvious, or if a manufactured product has a weak (+?, +) positive reaction (Dooms-Goossens 1995). The patient applies the tested substance on the elbow crease, or the outer side of the arm, every morning and evening (Fig. 7). No reaction within 15 days implies that the test is negative.

2.1.4 Usage Test

If all the tests are negative in spite of their obvious pertinence, the product may be used

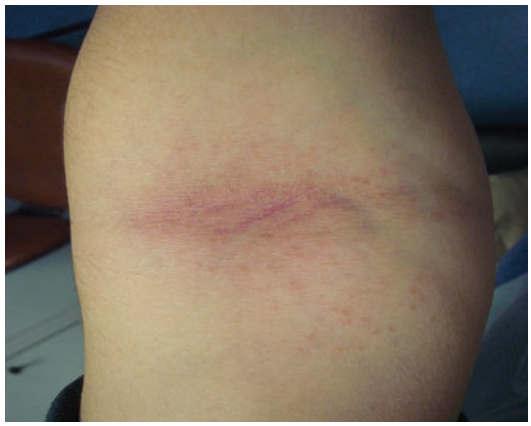

Fig. 7 ROAT, positive reaction to a cream at day 4

again in normal conditions, as a test for confirmation or denial of allergy. This test is rarely used. In case of positivity, it is often difficult to confirm the type IV hypersensitivity mechanism.

2.1.5 Intradermal Test

Its main use is to detect hypersensitivity to tuberculin, a particular type of cellular (= late = delayed) hypersensitivity. Reading takes place after 48 h and semiquantification indicates the degree of hypersensitivity. It is today largely replaced by multipuncture kits. Tests to microbial and fungal antigens have been gradually abandoned because of the difficulty in determining relevance. Tests to drugs may give delayed reactions even in the absence of immediate reactions; they are then often associated with positive patch tests to the drug (Fig. 8). These delayed reactions can evolve during weeks and result in residual atrophy. To avoid such a complication, it is preferable to start testing medicines with open tests or prick tests with immediate reading, to continue with epicutaneous tests with monitoring during 30 min to detect an immediate reaction under occlusion, and then perform the reading after 48/72 h; finally in the absence of delayed reaction terminate by an intradermal test. This attitude is not valid for all medicines and all type of reaction (e.g., curares, because curare allergy is always type 1).

3 Hypersensitivity to Cosmetics

3.1 Allergy to Cosmetics, Testing, and Risk Assessment

Immediate hypersensitivity reactions can be diagnosed by open immediate reading tests and if they are negative, immediate reading pricks tests; sometimes the test can turn positive in 1 h, so patients have to be survey longer than for other prick tests (Lauriere et al. 2006; Chinuki et al. 2011). These tests must be carried out in a hospital ward because there is a nonnegligible vital risk. Delayed hypersensitivity reactions can be diagnosed by adapted tests, with delayed reading. In the case of cosmetics, it is necessary to be aware of false positive tests, due to the presence of lauryl sulfate, for example, and false negative tests due to the low concentration of allergen in the finished product. To test some components of a finished product which has induced a positive reaction, it is essential to know their INCI name, concentration, vehicle, and pH. A too acidic or too alkaline pH precludes tests with the nonmodified compound.

3.2 Assessment of the Allergic Potential

It is not possible to assess the type I allergic potential of a new component of cosmetics in humans using a predictive test because of possible systemic unwanted effects (anaphylaxis); however, the allergic potential can be evaluated retrospectively through cosmetovigilance (Chinuki et al. 2011).

The various predictive methods of the type IV allergic potential are confronted with the fact that conditions in which the assessment takes place are different from the actual conditions of use (Kligman and Basketter 1995) and to the ban prohibiting the sale of cosmetic products tested on animals.

Epicutaneous patch testing achieved before marketing in (well informed) volunteers suffering of contact allergy to other products and thus more susceptible to develop allergy may be useful and,

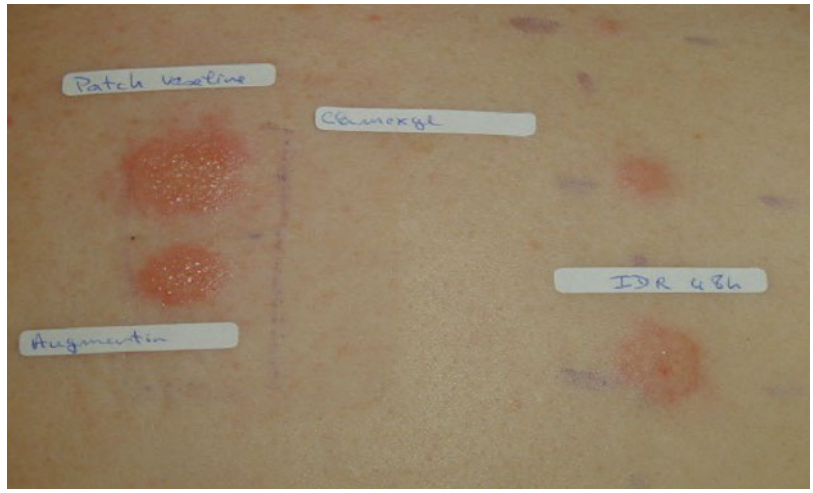

Fig. 8 IDR, positive reaction at D4, in the same time patch test are positive

in case of positivity, prevent the marketing, but the negativity of these tests does not provide any conclusion, and it raises ethical questions. Usage tests on control subjects and ROAT can have the same usefulness, but they raise epidemiological questions. So this kind of methods to predict the allergic potential tend to be given up and to be replaced by alternative method and Quantitative Structure Relationship method (Grace et al. 2004).

Active "cosmetosurveillance" (Vigan et al. 1996) implies the epicutaneous patch testing of all newly introduced products. This may be done in well-informed patients in addition to their being tested with the standard series. In this way an allergenic potential can be early detected. When negative, the test read at 48 and 72 or 96 h as usual, must be reevaluated after 15 days to detect a possible active sensitization. Some ethical questions have to be solved.

Cosmetovigilance can detect emergent allergen (Salverda et al. 2013).

4 Conclusion

Methods which assess allergy by skin tests require soundness and rigor to avert risks for the patient. Some of them are vital (anaphylaxis); others are irreversible (scars, depigmentation). The physician who performs these investigations is liable for them and must be in a position to foresee the risk in order to assume responsibility. Skin tests in humans are the only method to detect allergic reactions; they are more reliable than in vitro tests.

Skin tests are the only possible methods to detect allergens and set up actions for individual and collective prevention. However it is essential that test reading is done in sound conditions (good lighting, proper time) and by an experienced physician; a positive test may affect the patient's life (Frimat 1995).

Intensity of type I sensitization can be assessed only by intradermal tests, whereas epicutaneous testing is the best method to evidence type IV reactions. Patch testing implementation is optimized by standardization which permits semiquantification. For a well-known and standardized allergen, the ICDRG grading and the positivity appearance time are the two parameters of the intensity of the reaction. For an unknown allergen, an idea of this intensity will be given by the reactions with different dilutions. Finally, cutaneous tests cannot always be used to predict the allergic potential of a substance, but through active cosmetosurveillance and cosmetovigilance they can help to detect and assess it as soon as it appears.

Some patch testing device suppliers:

– Hermal, Kurt Herrmann AG, PO box 28, 2057 Reinbeck, Hamburg, Germany

– Chemotechnique Diagnostics, PO box 80, 230 42 Tygelsjö, Malmö, Sweden

References

Barbaud A, Gonçalo M, Bruynzeel D, Bircher A. Guidelines for performing skin tests with drugs in the investigation of cutaneous adverse drug reactions. Contact Dermatitis. 2001;45:321–8.

Bernstein IL, Storms WW. Summary statements of practice parameters for allergy diagnostic tests. Ann Allergy. 1995a;75:543–52.

Bernstein IL, Storms WW. Practice parameters for allergy diagnostic testing. Ann Allergy. 1995b;75:553–61.

Bock SA. Oral challenge procedures. In: Metcalfe DD, Sampson HA, Simon RA, editors. Food allergy. Boston: Blackwell; 1991. p. 81–95.

Bruze M, Isaksson M, Gruvberger B, et al. Recommendation of appropriate amounts of petrolatum preparation to be applied at patch testing. Contact Dermatitis. 2007;56:281–5.

Castelain M. Complications des tests épicutanés. In: Progrès en dermato-allergologie: 16e Cours d'actualisation en dermato-allergologie du GERDA, Arcachon. Paris: John Libbey Eurotext; 1995. p. 233–44.

Castelain PY, Castelain M. Qu'attendre des prick-tests en dermatoallergologie? In: 13e Cours d'actualisation en dermato-allergologie du GERDA. Nantes/Paris: John Libbey Eurotext; 1992. p. 24–31.

Chinuki Y, Kaneko S, Sakieda K, et al. A case of wheat-dependent exercise-induced anaphylaxis sensitized with hydrolysed wheat protein in a soap. Contact Dermatitis. 2011;65(1):55–7.

de Groot AC. Test concentrations and vehicles for 4350 chemicals. Patch testing. Wapserveen: Acdegroot Publishing; 2008.

Dooms-Goossens A. Comment tester les produits apportés ? In: 11ème Cours d'actualisa- tion en dermato-allergologie du GERDA, Genève. Paris: John Libbey Eurotext; 1990. p. 45–55.

Dooms-Goossens A. Tests semi-ouverts, ROAT. In: Progrès en dermatoallergologie: 16e Cours d'actualisation en dermato-allergologie du GERDA, Arcachon. Paris: John Libbey Eurotext; 1995. p. 257–60.

Dooms-Goossens A. Evaluation critique du test épicutané. In: Progrès en dermato- allergologie: 17ème Cours d'actualisation en dermato-allergologie du GERDA, Bâle. Paris: John Libbey Eurotext; 1996, p. 103–7.

Fischer T. Allergic patch test techniques. In: Serup J, Jemec GBE, editors. Handbook of non-invasive methods and the skin. Boca Raton: CRC Press; 1995. p. 593–606.

Frimat P. Aspects médico-légaux de l'enquète en dermato-allergologie. In: Progrès en dermato-allergologie: 16e Cours d'actualisation en dermato-allergologie du GERDA, Arcachon. Paris: John Libbey Eurotext; 1995. p. 261–7.

Giordano-Labadie F, Rancé F, Pellegrin F, Bazex J, Dutau G, Schwarze HP. Frequency of contact allergy in children with atopic dermatitis: results of a prospective study of 137 cases. Contact Dermatitis. 1999;40:192–5.

Grace Y, Basketter DA, Smith Pease CK, Wilson K, et al. Further evaluation of quantitative structure-activity relationship models for the prediction of the skin sensitization potency of selected fragrances allergens. Contact Dermatitis. 2004;50:91–7.

Inerot A, Möller H. Symptoms and signs reported during patch testing. Am J Contact Dermatitis. 2000;11 (1):49–52.

Isolauri E, Turjanmaa K. Combined skin prick and patch testing enhances identification of food allergy in infants with atopic dermatitis. J Allergy Clin Immunol. 1996;97:9–15.

Kamphof WG, Kunkeler L, Bikkers SCE, Bezemer PD, Bruynzeel DP. Patch-test-induced subjective complaints. Dermatology (Basel). 2003;207(1):28–32.

Kligman AM, Basketter DA. A critical commentary and updating of the guinea pig maximization test. Contact Dermatitis. 1995;32:129–34.

Lachapelle JM. L'histoire contemporaine des batteries standard: une batterie standard 2: un réservoir utile? In: Progrès en dermato-allergologie: 16e Cours d'actualisation en dermato-allergologie du GERDA, Arcachon. Paris: John Libbey Eurotext; 1995. p. 217–27.

Lachapelle JM. Giant steps in Patch testing: an historical memoir. SmartPractice; 2010.

Lachapelle JM, Maibach H. Patch testing and prick testing. A practical guide. Official publication of the ICDRG. 3rd ed. London/New York: Heidelberg Dordrecht; 2012.

Lachapelle JM, Tennstedt D. Les tests epicutanés dans les toxidermies médicamenteuses. In: Progrès en dermato-allergologie: 19ème cours d'actualisation en dermatoallergologie du GERDA, Nancy. Paris: John Libbey Eurotext; 1998. p. 57–66.

Lachapelle JM, Frimat P, Tennstedt D, Ducombs G. Dermatologie professionnelle et de l'environnement. Paris: Masson; 1992.

Lauriere M, Pecquet C, Bouchez-Mahiuot I, Snegaroff J, Bayrou O, Raison-Peyron N, Vigan N. Hydrolyzed wheat proteins present in cosmetics can induce immediate hypersensitivities. Contact Dermatitis. 2006;54:284–9.

Mantoux C. Intradermo réaction de la tuberculine. Comptes rendus de l'académie des sciences. Paris. 1908;147:355–7.

Menardo JL, Bousquet J, Michel FB. Comparison of three prick test methods with the intradermal test and with the rats in the diagnosis of mite allergy. Ann Allergy. 1982;48:235–9.

Pepys J. Skin testing. Br J Hosp Med. 1975;14:412.

Pons-Guiraud A. Contre-indications des tests épicutanés. In: Progrès en dermato- allergologie: 16ème Cours d'actualisation en dermato-allergologie du GERDA, Arcachon. Paris: John Libbey Eurotext; 1995. p. 229–32.

Raison PN. Faut-il faire systématiquement des ajouts à la batterie standard d'épidermotests? Revue Française d'Allergologie. 2012;52(3):164–7.

Rancé F, Dutau G. Labial food challenge in children with food allergy. Ped Allergy lmmunol. 1997;8:41–4.

Salverda JG, Bragt PJC, de Wit-Bos L, Rustemeyer T, Coenraads PJ, Tupker RA, Kunkeler LC, et al. Results of a cosmetovigilance survey in The Netherlands. Contact Dermatitis. 2013;68:139–48.

Svedman C, Isaksson M, Björk J, Mowitz M, Bruze M. Calibration of our patch reading technique is necessary. Contact Dermatitis. 2012;66:180–7.

Van Ketel WG. Patch tests: methodology, standardization and significance of positive results. Arch Belg Dermatol. 1973;28:73–82.

Vigan M. Critères de lecture des tests epicutanés. In: Progrès en dermato-allergologie: 16e Cours d'actualisation en dermato- allergologie du GERDA, Arcachon. Paris: John Libbey Eurotext; 1995. p. 245–5.

Vigan M. La lecture tardive des patch- tests. In: Progrès en dermato-allergologie: 17e Cours d'actualisation en dermato-allergologie du GERDA, Bâle. Paris: John Libbey Eurotext; 1996. p. 109–17.

Vigan M, Brechat N, Girardin P, Vuitton DA, Laurent R. An alternative to animal testing active cosmetovigilance. In: Jadassohn Centenary Congress of the European Society of Contact dermatitis and the American contact dermatitis Society, London, 9–12 Oct 1996 (Abstract 166).

Vigan M, Girardin P, Adessi B, Laurent R. Late reading of patch tests. Eur J Dermatol. 1997;7:574–6.

Thermal Exchanges in Man

119

Jacques Bittel and Victor Candas

Contents

Keywords

Skin thermal exchange • Heat transfer • Heat balance equation • Cold environment • Hot environment

Man regulates his internal body temperature within a normal range, with limits around 37 °C. This endothermia relates only to the internal part of the body (core), as the peripheral part, represented by the skin, can vary greatly (from a few degrees up to 44 °C).

Regulation of the body temperature at a constant level is under the control of the thermoregulatory system located within the hypothalamus. The hypothalamic centers, which are also sensitive to the circulating blood temperature, are constantly informed of the thermal state of the various parts of the body. For that purpose there are peripheral (cutaneous) thermoreceptors, which respond specifically to warm or cold stimulation. Some of these sensors operate in static mode (temperature level), while others operate in dynamic mode (rate of temperature change) or both. The various thermal information is integrated inside the thermoregulatory center, which is, according to the thermostat principle (with a set point at 37 °C), sensitive to any perceived deviation compared to the set point (error signal) and triggers the thermoregulatory reactions involved in the adaptation to increased cold or heat.

The thermoregulatory adjustments required for the maintenance of endothermia aim toward

This chapter was originally published under the ISBN 978-3-540-01771-4 with the following book title Measuring the Skin. The content has not been changed.

J. Bittel (✉)
Cepa, CNRS, Strasbourg Cedex, France

V. Candas (✉)
Ex Research Director at CNRS, Strasbourg Cedex 2, France
e-mail: v.candas@orange.fr

P. Humbert et al. (eds.), *Agache's Measuring the Skin*,
DOI 10.1007/978-3-319-32383-1_69

equilibrating the heat gains and heat losses of the human body, and obtaining a heat balance of zero (thermal equilibrium). This balance (B) corresponds to the sum of the internal heat production (M, metabolic) and various heat fluxes (occurring at the skin surface at a pulmonary level): convective (C), conductive (K), radiative (R), and evaporative (E)

$$B = M \pm R \pm C \pm K - E$$

The metabolic heat production (M) associated with cellular activity in a resting condition is minimal (50 $W.m^{-2}$), but can be greatly increased (500 $W.m^{-2}$) during intense physical exercise. Heat, which is almost exclusively produced at the core level, is then carried away towards the skin, the site of thermal exchanges with the environment. This transportation is carried out by either tissue conduction or blood convection:

– *Tissue conduction* ($H_{k,t}$), is the transfer of heat by contact between different tissues, but this is of little importance as this process accounts for only 10–15 % and is reliant upon the formula:

$$H_{k,t} = h_{k,t}\left(T_{co} - \overline{T}_{sk}\right) \cdot A_k \text{ in W}$$

where $H_{k,t}$ represents the coefficient of the tissue conductance, T_{co} the core temperature, $\overline{T}_{sk}$ the mean skin temperature, and A_k the tissue area where heat exchange occurs by conduction.

– *Blood convection* represents the most important means of the core–skin heat transfer, and is reliant upon the following equation:

$$H_c = F_{sk} \cdot c_b \cdot \varrho \cdot (T_{ar} - T_v) \text{ in W}$$

where F_{sk} represents the global skin blood flow, c_b the specific heat of the blood, ϱ the blood density, and $(T_{ar} - T_v)$ the temperature difference between arterial blood and venous blood. Therefore the arterial-venous network is a true heat conducting system, removing heat from the muscles and active organs toward the other parts of the body, although it is mainly at the skin level that heat can be lost.

1 Heat Transfer between the Skin and the Environment

Heat transfer between the skin and the environment occurs by conduction (K), convection (C), radiation (R), and evaporation (E).

– *Heat exchanges by conduction* (K) occur by direct contact between the skin and the environment and are reliant upon the formula:

$$K = h_k\left(T_s - T_{sk}\right) \cdot A_k \text{ in W}$$

where h_k represents the thermal conductivity of body parts in contact with each other, T_s the temperature of those parts, T_{sk} the skin temperature in contact, and A_k the contact area.

– *Heat exchanges by convection* (C), used for instance when warming the air of a room (by an electric resistance heater), are reliant upon the formula:

$$C = h_c\left(T_{db} - \overline{T}_{sk}\right) \cdot A_c \text{ in W}$$

where h_c represents the heat exchange coefficient by convection, T_{db} the dry bulb (air) temperature, $\overline{T}_{sk}$ the mean skin temperature, and A_c the area where the exchange takes place. The air velocity increases these convective heat exchanges significantly by modifying h_c according to the formula:

$$h_c = K_c \cdot V_a^{0,6}$$

where K_c depends upon the shape of the body and V_a is the air velocity. In the absence of wind, convection is said to be natural convection; in the presence of wind it is said to be forced convection. Note that the reading of the dry bulb

thermometer gives us the exact value of the air temperature.

– *Heat exchanges by radiation* (R) are a little more complex to understand. Any body, living or inert, emits a radiation called radiance (R), which relies upon the formula: $R_t = \varepsilon\sigma T^4$, where R_t is the body emissivity, a is the Stefan-Boltzmann constant (5.67×10^{-8} $W.m^{-2} \cdot K^4$), and T the absolute body temperature in Kelvin (K).

Any body surface which faces any other surface exchanges heat by radiation. Knowing that for infrared heat exchange the skin has an emissivity of almost 1 (0.97), the intensity of the heat exchange between the skin and the environment can be rewritten as follows:

$$R = h_r\left(\overline{T}_r - \overline{T}_{sk}\right) \cdot A_r \text{ in } W$$

where h_r is the linearized heat exchange by radiation, $\overline{T}_r$ the mean radiant temperature of the environment, $\overline{T}_{sk}$ the mean skin temperature, and A_r the exchange surface.

As we generally do not know the value of A_r exactly, we express it as:

$$A_r = \frac{A_r}{A_d} \cdot A_d$$

where A_d is the DuBois area (total skin surface area) given by the formula:

$$A_d = 0,2025 \ M^{0,425} \cdot T^{0,725}$$

where M(kg) = body mass = weight/9.81 $m.s^{-2}$, and T(m) = height; $\frac{A_r}{A_d}$ corresponds to the percentage of the skin area which exchanges heat with the environment, generally 70 % (the remaining 30 % corresponds to the human body parts which exchange between themselves: the inside of the legs, the inside of the arms, between the chin and torso, etc.).

– *Heat exchanges by evaporation* (E) occur when sweat evaporates from the skin surface: for every gram of sweat that evaporates 2.42 kJ are eliminated. This is reliant upon:

$$E = h_c(P_a - P_{sk})A_e \text{ in } W$$

where h_e is the heat exchange coefficient by convective evaporation, which is linearly linked to the heat transfer coefficient, A_e is the evaporating surface, and ($P_a - P_{sk}$) is the difference between the ambient water vapor pressure and the saturated water vapor pressure at skin temperature. P_a generally being unknown, one can write

$$Ac = A_d \cdot \frac{A_e}{A_d}$$

where A_d is the DuBois area (total skin surface area; see above for calculation) and $\frac{A_e}{A_d}$ is the skin wettedness expressed as a percentage. The concept of skin wettedness is interesting because it describes fairly well the severity of the heat strain. A 30 % skin wettedness is associated with discomfort; at 50 % skin wettedness sweat starts to drip from the body; at levels higher than 85 % skin wettedness corresponds to very severe exposure. For any given situation (he, A_e fixed), the heat exchange by evaporation will be proportional to the water vapor pressure difference ($P_a - P_{sk}$). As a consequence, the closer P_a is to P_{sk} (5.8–6.6 kP_a), the less evaporation takes place and the more sweat drips from the body without any efficient thermolytic effect.

In summary, the heat exchanges by K, C, and *R* are called dry heat exchanges, because they are essentially proportional to the difference between the skin temperature and that of the environment (T_{sk}, T_{dh}, and T_r). Heat exchange by evaporation, also called latent heat exchange, is essentially proportional to the water vapor pressure difference between air and skin. These exchanges are linked to the skin temperature and therefore under the control of the thermoregulatory system. They can be assessed for the overall body (because thermal equilibrium is required for maintenance of endothermia) but they can also be assessed

locally (because they are at the origin of the thermal sensation and this may cause discomfort).

1.1 Additional Heat Exchanges Originating at the Level of the Respiratory System

Inspired air enters the respiratory tract at the dry bulb temperature, but leaves at approximately 35 °C, thus some heat exchange occurs by respiratory convection (C_{resp}). In the same way, inspired air enters the lungs at a humidity corresponding to the humidity level of ambient air. It leaves completely saturated at 35 °C; thus, some heat exchange also occurs by respiratory evaporation (E_{resp}). These heat exchanges ($C_{resp} + E_{resp}$) are not regulated because they are not under thermoregulatory control. Their intensity depends totally upon the ambient conditions and the respiratory ventilation rate. They are often negligible, except during intense physical exercise in dry environments.

2 Heat Balance Equation

The heat balance equation $B = M + K + C + R + E$ is defined as the sum of different components, which, by definition, will be allocated a positive (+) value if they correspond to a heat gain, and a negative (−) value in the case of heat loss. Given this, the equation is written:

$$B = M \pm K \pm C \pm R - E \quad \text{in } W.m^{-2}$$

So:

- M is always positive, as it is an internal heat production
- E is always negative, as it always heat loss (except in special cases where condensation could occur on the skin)
- K, R, and C can either be positive or negative depending upon the temperature difference between the skin and the environment.

Therefore, B can either be zero (thermoequilibrium), positive or negative.

In summary, when the heat balance equation is zero ($B = 0$), heat gains and heat losses are balanced and endothermia is maintained.

When heat gains and losses are unbalanced ($B \neq 0$), heat storage (S) can occur: this frequently happens during heat exposure and/or during physical exercise. On the other hand, heat debt (D) will take place especially during exposure to cold. In these two cases endothermia is at risk from the dangers of hyperthermia (heat) or hypothermia (cold).

2.1 Heat Balance in Cold Environments

The zero thermal balance in a cold environment dictates that $M = -R - C - K - E$, which means that the metabolic heat production Mmust offset all the heat losses (R, C, K, and E) to maintain endothermia. Therefore, two thermoregulatory reactions can be triggered against the cold:

- A reduction of heat losses by increasing the cutaneous insulation: peripheral vasoconstriction (diverting blood from the skin) leads to a decrease in the mean skin temperature, therefore reducing the temperature difference.
- An increase in internal heat production by either shivering, which corresponds specifically to muscular activity in the fight against the cold, and can reach between 200 and 250 $W.m^{-2}$, or by voluntary physical activity (up to 500 $W.m^{-2}$). Nevertheless, neither shivering nor physical activity can be maintained for long periods of time, rendering man particularly susceptible to the cold.
- Other heat sources may exist, notably the specific dynamic action of food intake, which has negligible importance. Regarding the non-shivering thermogenesis, well known in rodents, it is unlikely to occur and if so only in the case of developing adaptive mechanisms.

In summary, without the help of clothes or heated areas, in humans the cold climate often results in an unbalanced heat equation leading to a heat debt (hypothermia), the importance of which depends upon the intensity of the cold stress, its duration, and the type of environment the body is exposed to (water > air). The skin, thanks to the thermal insulation induced by peripheral vasoconstriction, plays a major role in the reduction of heat loss. It is the excessive physiological insulation that plays a part in the appearance of frostbite. Some adaptive mechanisms appear to reduce the intensity of the skin heat losses; for example, increased subcutaneous fat thickness which reduces peripheral thermal conductivity.

2.2 Heat Balance in Hot Environments

The balanced thermal equation in the heat is written $E = M \pm R \pm C \pm K$, which means that evaporation of sweat is the only means of heat loss compensating for the internal (M) and external ($R \pm C \pm K$) heat gains. Thus endothermia is maintained if $E = M \pm R \pm C \pm K$, and E represents the required evaporation (E_{req}) necessary to achieve zero thermal balance. The ambient evaporative capacity restricts the evaporation of sweat to an E_{max} value, which mainly depends upon the temperature and the humidity of the ambient air. Thus, when $E_{max} > E_{req}$ endothermia can be guaranteed, but when $E_{max} < E_{req}$, heat storage (S) will occur, leading to hyperthermia, the importance of which depends upon the severity of the climatic conditions, the activity level of the person, and the duration of heat exposure. Hyperthermia in the form of heat stroke is a serious condition which often results in death. A limitation of the thermolytic capacity depends upon the maximum sweating capacity of the subject. This can reach between 2 to 3 litres of sweat per hour, but this sweating rate can only be maintained for short periods of time. On the other hand, sweat losses, if not correctly counterbalanced by fluid intake, can lead to dehydration associated with hypothermia, tachycardia, and osmotic imbalance.

3 Conclusion

The skin is the site of heat exchanges between man and his environment. Its capacity to modify the intensity of these exchanges via vasomotor control means that it plays an essential role in the fight against environmental thermal stress. The development of millions of sweat glands allowing secretion and excretion of sweat makes it a unique location for heat loss in warm conditions.

References

General information on body temperature regulation will be found in the following books

Chapter 110 and 111: Cooper KE Basic thermo-regulation – Body temperature control and its disorders. In: Greger R, Windhorst U, editors. Comprehensive human physiology: from cellular mechanisms to integration, vol 2. Berlin/Heidelberg/New York: Springer; 1996. p. 2199–218.

Thermophysiological Parameters in Man

120

Victor Candas

Contents

This chapter was originally published under the ISBN 978-3-540-01771-4 with the following book title Measuring the Skin. The content has not been changed.

V. Candas (✉)
Ex Research Director at CNRS, Strasbourg Cedex 2, France
e-mail: v.candas@orange.fr

P. Humbert et al. (eds.), *Agache's Measuring the Skin*,
DOI 10.1007/978-3-319-32383-1_70

Keywords
Digestive tract temperature • Esophageal temperature • Hyperthermia • Mean skin temperature • Rectal temperature • Skin blood flow • Sublingual temperature • Sweat rate measurement • Thermal shivering • Tympanic temperature • Vaginal temperature

It is worth noting that an international standard (ISO 9886) provides guidelines for measurement and interpretation.

1 Thermal Shivering

1.1 Qualitative Aspect

Shivering corresponds to the isometric contraction of certain muscles, all the energy of which is converted into heat. It can easily be detected from the electromyographic activity of the muscles that are commonly involved. The detecting electrodes are generally located above the masseter muscles or on the scapular area. Shivering is at first localized and then tends to spread to meet the required heat. Electromyography permits accurate detection of the onset of shivering: this is interesting, for instance, when studying the cold adaptation process, although it does not allow quantitative analysis.

1.2 Quantitative Aspect

As muscular activity requires energy (see ▶ Chap. 121, "Functional Assessment of Thermoregulation in man"), shivering results in an increase in oxygen consumption. In normal conditions, when the respiratory quotient is normal (=0.8) (from combined oxidation of fats, carbohydrates, and proteins), each liter of oxygen consumed per hour in addition to the resting metabolism generates 5.6 W. Shivering assessment under hypothermic conditions is therefore carried out by measurement of the oxygen uptake and carbon dioxide elimination (knowledge of the respiratory quotient MCO_2/MO_2 gives a better estimation of the O_2 energy equivalent). For instance, a mild hypothermia which would require a heat production of 100 W corresponds to an additional oxygen consumption of 300 ml/min, which imposes an approximately twofold increase in the oxygen consumption observed at rest to maintain a stable core temperature.

2 Rectal Temperature

The thermosensor (with a disposable probe, or a probe which can be sterilized and used again with the same subject) is introduced into the rectum approximately 10–12 cm beyond the anal sphincter. Although inert, it is influenced by its location inside the rectum, i.e., whether it is in direct contact with the rectal wall, by the temperature of the venous blood returning from the inferior limbs. To avoid a possible injury it is essential to ensure that there are no hemorrhoids.

3 Esophageal Temperature

The thermosensor is introduced via the nose into the esophagus, aided by swallowing at the opportune moment small amounts of water stored in the mouth. Generally, a distance of about 40 cm between the probe and the nasal passage is necessary to give an accurate measurement. When located in the esophagus the sensor gives an accurate reading of the arterial blood temperature (due to the proximity of the heart and the aorta (Brengelmann et al. 1979)). This measure can be affected by a high respiratory rate (during effort) and is of course directly influenced by the temperature of ingested fluids and the resulting local evaporation.

4 Tympanic Temperature

In the case of a contact measurement (Brinnel and Cabanac 1989), the probe is usually at the tip of a very soft spring. Nevertheless the contact of the probe with the membrane is painful and is associated with the perception of a loud noise. The ear canal must be very clean (no wax) and well protected against external influences (e.g., ear

plugs and monaural headphones filled with isolating material) to avoid mistakes linked with the environmental temperature. Indirect measurement using an infrared thermometer seems easier because it is less invasive. However, it implies a rectilinear auditory canal, no obstruction, and expertise of the operator. Often an incorrect measure of the tympanic temperature is in fact a correct measure of the auditory canal temperature.

5 Sublingual Temperature

Sensors (with a disposable probe) are introduced underneath the tongue as deeply as possible. The subject must be asked to breath only through the nose to ensure a correct measure (Mairiaux et al. 1983). Any breathing through the mouth will lead to an underestimation of the temperature due to saliva evaporation. Measuring the oral temperature under physical activity is difficult; consequently it can be done during a short resting period between two phases of activity.

6 Digestive Tract Temperature

The sensor (consisting of a radiobattery) is ingested by the subject and moves along the digestive tract, allowing a radiologic tracing to be made. The sensor transmits variations in core temperature and is subject to fluctuations related to its location (contact/no contact with the feces or the intestinal walls).

7 Vaginal Temperature

This non-invasive measurement gives a correct value of the core temperature.

8 Mean Skin Temperature (Agache 2004)

Measurement of the local skin temperatures can be extrapolated to the total skin area, which is termed mean skin temperature. Local measurements are carried out by either contact or infrared thermometry. If the measurement is made by contact, the point of contact should not be under any pressure nor covered with anything that would insulate the sensor or restrict any evaporation that may occur locally. Calculation of the mean skin temperature is then carried out by averaging the local measures, each of them proportionally weighted to the percentage of the body surface it represents. Increase in the local skin temperature is usually lower than its decrease under cold stress. It does not depend upon internal heat production except in the case of intense physical exercise (see ▶ Chap. 121, "Functional Assessment of Thermoregulation in man"). Nevertheless, it is not totally independent of the adjustment of the hypothalamic thermostat, as demonstrated by the cutaneous hypothermia under fever conditions.

9 Heart Rate Measurement

Counting the QRS complexes on the electrocardiogram gives a measurement of the heart rate. This has become easy since personal, portable cardiofrequency meters (e.g., the Sport-tester model) became available. Ignoring the extracardiac activity associated with emotional influences, one can state that the heart rate is the sum of three components, each of which is subject dependent:

- A basal component, which can be assessed at rest under thermal neutrality
- An activity component linearly related to the intensity of the physical effort involved in carrying out a standard task
- A thermal component directly proportional to the heat storage, which originates from both environmental conditions and metabolic heat production

Indirect assessment of the thermal strain through heart rate measurement therefore requires previous knowledge of the subject's physical and thermal reactivity (Vogt et al. 1973).

10 Sweat Rate Measurement (Agache and Candas 2004a, b)

Assessments of the total sweat lost over a time interval can be achieved either by weighing the subject before and after, and eventually adding the quantity of sweat lost in the clothing, or by monitoring the subject's weight. The body mass variation is a reflection of the water losses due to sweating, after taking into account the body mass losses due to respiratory gas exchange and respiratory evaporation. Sweating can sometimes be divided into two parts; first the evaporative rate and second the dripping rate (the latter without cooling efficiency). To do this it is necessary to use two scales, one to measure the total body mass over time, the other to weight the dripped sweat (usually using an oil-containing tub located underneath the subject (Candas et al. 1980)). The evaporation rate is obtained by subtracting the dripping rate from the total sweat rate.

The measurement can be made at one body site only, either by collecting the sweat dripped from a determined surface area in a plastic pouch container (Risson et al. 1991), or by assessing the change in water content of a gas before and after it passes over the skin in a chamber (Graichen et al. 1982). However, extrapolating the results of such methods to the whole body area will usually give an overestimated figure. In the first method monitoring of the sweat rate is not possible, and the method is mostly used to estimate the electrolyte content of the collected sweat (detection of cystic fibrosis) (Boisvert et al. 1997). Furthermore, the obtained data are overestimated because the absence of evaporation increases the local skin temperature, which in turn stimulates the secretory process. But they could also be underestimated, because local excessive skin moisture can trigger a negative feedback of the sudomotor capacity (this phenomena is described as hidromeiosis) (Candas et al. 1979). In the second method the difference in water content of the gas entering and leaving the chamber is determined by a hygrometric technique. The method enables monitoring of the sweat rate. Such a technique is difficult to set up as it is not mobile and requires expensive devices (measurement of ventilation rate, of air temperature, and of its humidity content). However, the obtained results certainly represent the most accurate sweating intensity figure.

11 Skin Blood Flow (see ▶ Chaps. 48, "Skin Blood Flow: Histophysiology," ▶ 53, "Skin Capillaroscopy," ▶ 56, "Epicutaneous 133-Xenon Clearance," ▶ 58, "Transcutaneous Oxygen Pressure," ▶ 50, "Skin Microcirculation: Choosing the Appropriate Method," ▶ 49, "Photoplethysmography in the Evaluation of Skin Conditions," ▶ 52, "Assessment of Cutaneous Microvascular Function Using Laser Doppler Flowmetry and Acetylcholine Iontophoresis," Agache 2004a, b)

The individual capacity to withstand the heat is reliant upon vasomotor reactions. Indeed, exposure to heat, physical activity or both implies vasodilation in order to remove the internal heat towards the periphery, where it will be lost. Cutaneous blood flow (or more accurately, its variation) can be assessed either by plethysmography on a limb (for example a strain gauge placed around the arm) or on small skin areas by thermal clearance, or through the Doppler effect (laser-Doppler), which monitors local skin blood flow changes in arbitrary units.

12 Selecting a Method for Assessing Resistance to Hyperthermia

Selection of the appropriate thermal stimulus and physical parameters depends on what you are looking for and on financial constraints. To achieve hyperthermia in the absence of a climatic chamber, a heated room or a sauna can be used. It is simpler and more controllable to put the subject into

a hot bath. Ergometric bicycles, rowing machines, and treadmills are also able to induce thermoregulatory responses. The wearing of clothes, especially those that are impermeable, accelerates the process, leading to heat storage. Nevertheless, it is worth knowing that regardless of the mode of stimulation, at least 40 min are necessary in order to establish steady body temperature and associated thermophysical reactions. Finally, local sweat collection will take an additional 15–20 min for correct measurement of the sweat flow.

Therefore, the functional investigation of the thermoregulatory system requires a one-hour test for its complete implementation, except if the constraint is such that the heat storage is intense and continuous, in which case accidents may occur rapidly. During this time, all of the above-mentioned variables can be recorded. Whichever method is used, the internal temperature must not exceed 39 °C (102.2 °F) and the heart rate must permanently stay under the figure (190 minus age) for safety reasons. In such a case after 1 h, the total body water loss should not exceed 700–800 g. The local flow from the stimulated area is equal to or slightly lower than 1 $mg.min^{-1}.cm^{-2}$ at rest, and can reach 2–3 $mg.min^{-1}.cm^{-2}$ during intense exercise.

References

Agache P. Thermometry and remote thermography. In: Handbook of Measuring the skin. 1st edn. Berlin: Springer; 2004a. p. 354–62.

Agache P. Epicutaneous thermal clearance. In: Handbook of Measuring the skin. 1st edn. Berlin: Springer; 2004b. p. 352–53.

Agache P, Candas V. Eccrine sweat glands. In: Handbook of Measuring the skin. 1st edn. Berlin: Springer; 2004a. p. 302–9.

Agache P, Candas V. Sweat gland metrology. In: Handbook of Measuring the skin. 1st edn. Berlin: Springer; 2004b. p. 311–28.

Boisvert P, Desruelle A-V, Candas V. Comparison of sweat rate measured by a pouch collector and a hygrometric technique during exercise. Can J Appl Physiol. 1997;22 (2):161–70.

Brengelmann GL, Johnson JM, Hong PA. Electrocardiographic verification of esophageal temperature probe position. J Appl Physiol. 1979;147:638–42.

Brinnel H, Cabanac M. Tympanic temperature is a core temperature in humans. J Therm Biol. 1989;14:47–53.

Candas V, Libert JP, Vogt JJ. Influence of air velocity and heat acclimation on human skin wettedness and sweating efficiency. J Appl Physiol Respir Environ Exerc Physiol. 1979;47(6):1194–200.

Candas V, Libert JP, Vogt JJ. Effect of hidromeiosis on sweat drippage during acclimation to humid heat. Eur J Appl Physiol. 1980;44:123–33.

Graichen H, Rascati R, Gonzalez R. Automatic dew-point temperature sensor. J Appl Physiol Respir Environ Exerc Physiol. 1982;52(6):1658–60.

Mairiaux P, Sagot JC, Candas V. Oral temperature as an index of core temperature during heat transients. Eur J Appl Physiol. 1983;50:331–41.

Risson GR, Boisvert P, Peronnet P, Perrault H, Boisvert D, Lafond JS. A simple and disposable sweat collector. Eur J Appl Physiol. 1991;63:269–72.

Vogt JJ, Meyer-Schwertz MT, Foehr R, Metz B. Motor, thermal and sensory factors of heart rate variations: a methodology for indirect estimation of intermittent work and environmental heat loads. Ergonomics. 1973;356:131–42.

General Information on Body Temperature Regulation will be Found in the Following Book

Cooper KE. Chapters 110 &111: Comprehensive human physiology. From cellular mechanisms to integration. In: Greger R, Windhorst U, editors. Basic thermoregulation – body temperature control and its disorders, vol. 2. Berlin: Springer; 1996. p. 2199–218.

Functional Assessment of Thermoregulation in Man

121

Victor Candas and Jacques Bittel

Contents

Keywords

Resistance to heat • Sweat capacity • Heat tolerance • Cumulative Heat Stress Index (CHSI) • Heat storage • Hyperthermia • Hypothermia • Climatic chamber • Exogenous thermal strain • Endogenous thermal strain • Cold resistance • Combined heat strain

1 Resistance to Heat

With the exception of local sweating stimulation to determine the sweating capacity or the electrolyte content of the sweat, there is no simple test allowing assessment of the individual capacity to face thermal stress. All techniques require either the use of a climatic chamber or physical exercise of a certain duration so as to provoke an increase in core temperature, which elicits thermoregulatory processes.

It is obvious that it is the combination of both work and heat that triggers the most important responses. The exposure will be yet more severe if the ambient humidity level is higher, as the possible evaporation will be reduced.

This chapter was originally published under the ISBN 978-3-540-01771-4 with the following book title Measuring the Skin. The content has not been changed.

V. Candas (✉)
Ex Research Director at CNRS, Strasbourg Cedex 2, France
e-mail: v.candas@orange.fr

J. Bittel
Cepa, CNRS, Strasbourg Cedex, France

P. Humbert et al. (eds.), *Agache's Measuring the Skin*,
DOI 10.1007/978-3-319-32383-1_71

1.1 Parameters Involved in Assessing Heat Tolerance

Although the most interesting variable for the physician or the physiologist is the core temperature (because it is a regulated quantity and a survival factor), the skin temperature is also a major one. In fact, for a man at rest who has an internal metabolic production of around 100 W, internal heat transfer towards the periphery is possible only because there is a difference of a few degrees (3 or 4) between the core and skin temperatures. Any exposure to heat reduces the difference between the temperature of the core and that of the skin. This thermal difference is an index of heat tolerance (Pandolf and Goldman 1978). If the skin temperature became equal to or higher than the core temperature, the body would become unable to eliminate its own internal heat. Nevertheless, the thermal difference between the core and the skin can be as low as some tenths of a degree (2 or 3 tenths). In the more tolerant subjects, a more rapid sweating onset, a higher sweating rate, and a better vasomotor response allow this difference to remain around 1 °C. Passing from a non-adapted state (e.g., 0.2 °C difference between core and skin) to a more tolerant one (e.g., 0.6 °C) would reduce the cardiovascular cost by 300 %. The total metabolic heat must be transported by the blood from the active cells towards the periphery. The additional cardiac cost is a function of the core-skin thermal gradient amplitude because the heart rate has to compensate for the reduction in internal heat transfer due to a reduced thermal gradient. Therefore the heat rate is a good index for thermal stress assessment (Vogt et al. 1973) as far as the metabolic strain can be disregarded. Recently, Israeli colleagues have proposed an assessment of heat tolerance called cumulative heat stress index (CHSI), which integrates the heart rate variations and those of the core temperature (Frank et al. 1996).

The sweating rate is, of course, a good reflection of the thermoregulatory capacities. The higher the sweating rate, the greater is the evaporative capacity, capable of preventing excessive heat accumulation. An adequate distribution of sweat production is more beneficial than local oversweating because it is only the evaporated sweat that cools the body down. The evaporation is more effective if it takes place all over the body. It is because the sweat evaporation is faster and greater that the skin temperature increases less in a tolerant subject. And it is because the subject becomes more tolerant that the skin temperature increases less, therefore reducing the core temperature increase. All these thermophysiological parameters are interdependent, and this is the reason why one cannot favor the measurement of one or another.

The simplest parameter to measure is the heart rate. In a tolerant subject it increases on average by 30–35 beats per minute for each degree increase of the core temperature. In less-tolerant individuals, the increase in heart rate can be much higher. Next is the core temperature (rectal, esophageal, tympanic, vaginal, sublingual, auditory canal): it reflects the internal heat storage. Then comes the assessment of the sweating rate, which can easily be done by weighing the subject before and after heat exposure. Precise measurement of local sweating requires special laboratory equipment (Agache and Candas 2004a). Determination of the mean skin temperature is somewhat complex because it requires the use of several sensors (a minimum of four, an optimum of ten) to take into account the non-uniformity of the cutaneous thermal state. However, the core-skin temperature gradient may not be not a good predictor of the risk of hyperthermia in cool or cold conditions. While the core temperature may increase drastically due to high internal heat production, the skin temperature, which mainly depends on the thermal environment, may not change in such cases, and the core-skin thermal gradient can be high without avoiding the risk of hyperthermia. It is worth noting that certain hormones, notably those which regulate the body water content (ADH, renin-angiotensin, natriuretic factor), are also secreted in cases of severe heat exposure. Cortisol has been shown to be a good index of thermal stress in man exposed to heat (Follenius et al. 1982) but hormonal assessments are invasive and do not allow rapid diagnosis.

Finally, heat exposure often involves a large vasodilation; the non-resistant subject rapidly

reddens facially, does not exhibit complete wettedness (only some sweat droplets are visible instead of generalized sweating), and checking the pulse indicates an obvious tachycardia. Such simple observations make it possible to conclude that the subject exhibits poor heat tolerance. Conversely, the quantitative determination of heat tolerance requires more sophisticated methods.

1.2 Inducing Hyperthermia

Three types of thermal stress can be used and combined to induce heat storage:

- External strain: heat exposure
- Internal strain: performing physical exercise (both of these have a direct effect since they trigger an accumulation of heat either received or produced)
- Indirect external strain, which by reducing the likely evaporation will reduce the capacity to remove heat either received or produced.

1.2.1 Use of a Climatic Chamber (Exogenous Thermal Strain)

It is obvious that to increase the core temperature, exposure to heat is required. Climatic chambers are specially designed for this. If the experimenter (or the practitioner) wishes to control the hyperthermia, he or she must first control the experimental equipment. Existing climatic chambers are regulated by a collection of sensors that make the provided environment stable.

Air temperature is the most important factor to control. As for a heat source, any heat generator may be used. But to maintain a constant air temperature, air renewal is required. This can be achieved by injecting new air, at a rate that depends on air velocity (and vice versa). Determination of the air velocity is therefore important to ensure the correct renewal rate, but also because the air velocity modifies the convective and evaporative heat exchanges (see ► Chap. 119, "Thermal Exchanges in Man").

As explained in Agache (2004) heat exchange between man and his environment is also dependent upon the temperature of the surrounding surfaces. It is difficult to effectively control all of the wall surfaces of the climatic chamber. The simplest way is to use as a chamber a small enclosure such as a box or a tunnel constructed of two walls, between which water can be circulated. Control of the water temperature is easy provided the enclosure has suitable external thermal insulation. In the case of a larger room (similar to a normal-sized living room), an easy and cheap way of rapidly obtaining controlled wall temperatures is to force them to have the same temperature as the air. To do this, the walls are doubled inside the room by a polyurethane film which is stretched tight against all surfaces (except for the floor), the internal side of this film (the one facing the wall) being aluminized, thus reflecting the radiant heat, and then to actively circulate the room ambient air between this film and the walls.

The most difficult parameter to control is the air humidity level, corresponding to the ambient water vapor partial pressure. This parameter is very important for the evaporative rate (Agache and Candas 2004b). To humidify the air, it is necessary to vaporize water or to inject the vapor: this can be done by pouring water onto hot solids (as in a sauna), or by blowing overheated and water-saturated air onto temperature controlled surfaces (like the air escaping out of a pressure cooker valve). Nevertheless, maintenance of a constant level in the water vapor partial pressure is difficult and its regulation requires measuring tools, humidifiers and/or absorbers, which are expensive. Only specialized laboratories have them.

1.2.2 Thermal Strain Due to Effort (Endogenous Thermal Strain)

In the case of muscular exercise, heat is produced directly within the muscle and distributed inside the body. To be strictly endogenous, the strain should be imposed on a naked individual exposed to a thermal environment of 33 °C. In fact, in such a case the dry heat exchanges (convective and radioactive) are equal to zero. Since the difference between ambient and skin temperatures is zero, all the heat produced is of metabolic origin and must be eliminated by evaporation of sweat.

To carry out this physical and thermal strain, the tools generally used are:

- The ergometric bicycle
- The treadmill
- The rowing machine
- A staircase or a "step test"

The very low mechanical output of the human body at work (from a few to 22 %) implies that the majority of the effort results in heat production. The main physiological difference between the external heat load and the strictly internal heat load lies in the recruitment of the cardiovascular system. For the same resulting sweating intensity due to either of these two methods, the heart rate always increases more under effort because the redistribution needs of the blood supply are obviously more important when exercising.

1.2.3 Combined Heat Strain

The possibilities of combined heat stresses are numerous and result from the addition of heat exposure and effort. In everyday life conditions, the heat exposure is more radiative (the most frequent example in our climates is the presence of intense solar radiation), or sometimes more convective (in cases of warm air), but it is always combined.

1.2.4 Indirect Thermal Strain

The human body fights against hyperthermia by producing sweat and then evaporating it at the surface of the skin. Any increase in the ambient humidity level, or any hindrance of the evaporative capacity (for instance, by insulating some or all of the skin with non-permeable garments) will result in a more or less important reduction in the possible evaporation and therefore in some heat accumulation. The same is true in the case of exposure in warm water since no evaporation can occur in water.

1.3 Modifying Factors to Heat Tolerance

The acclimatization or acclimation (Acclimatization is increased tolerance to heat induced by a prolonged stay in hot climates. Acclimation is the same phenomenon artificially produced, for example by repeated exposures in a heat-controlled room) phenomenon (that is: heat adaptation) increases the capacity to fight against the thermal environment, as a result of:

- The time reduction of sweat onset (the subject sweats sooner)
- The increase in the sweating sensitivity (central and local effects allow the subject to sweat more)

The increased thermolytic capacity notably increases the difference in temperature between the core and the periphery, therefore reducing the cardiac cost linked to the internal heat transfer.

The electrolyte concentration of the excreted sweat decreases with heat acclimation but the total electrolyte losses are nevertheless increased due to a larger sweat loss. This higher water loss increases the risk of dehydration and is associated with detrimental consequences (tachycardia, hypovolemia, osmoconcentration, hyperthermia, and heat stroke).

2 Resistance to Cold

Man is relatively well equipped to fight against the heat, but his resistance to cold is weaker. In fact, without any technological help (houses, shelter, clothing) he would never be able to leave tropical or subtropical areas. Human resistance to cold (Bittel and Savourey 1995) is assessed using two criteria: pain and heat debt (hypothermia).

2.1 Cold Resistance and Pain

This resistance, or more precisely cold tolerance, is directly dependent upon the mean skin temperature level (T_{sk}). In fact, if T_{sk} is around 33 °C (i.e., within the thermal comfort range), any cold exposure induces a drop in the mean skin temperature by the direct cold effect and by peripheral vasoconstriction associated with cold exposure.

The intensity of this drop is a function of both the cold stress intensity and its duration. Thus a T_{sk} of 31 °C is felt as a cold sensation, a T_{sk} of 30 °C as an uncomfortable cold stress associated with shivering, and a T_{sk} of 28 °C as extremely cold. A T_{sk} of 25 °C represents a threshold limit of tolerance with intolerable pain and numbness.

Fortunately, some skin areas (notably those at the extremities; hands and feet) exhibit much lower thresholds. For instance, at the hand level, a 20 °C T_{sk} is felt as uncomfortably cold, 15 °C as extremely cold and 5 °C represents the threshold tolerance with an unsupportable pain. This 5 °C threshold is commonly used to determine the cold sensitivity of the extremities and to quantify the beneficial effect of the cold adaptation.

The skin temperature of the extremities may also reach negative values, leading to frostbite characterized by frozen tissues. This frostbite is enhanced by increased peripheral vasoconstriction limiting the heat losses.

2.2 Cold Tolerance and Heat Debt: Hypothermia

Hypothermia is an undesired decrease in the core temperature, below 35 °C and is generally measured in the rectum (T_{re}). It is a consequence of the heat imbalance, the heat production being lower than the heat losses (see ▶ Chap. 119, "Thermal Exchanges in Man") Again, the intensity of the hypothermia is a function of both the intensity of the cold stress and its duration. The cold tolerance, and as a consequence the survival prediction, is dependent upon the depth of the hypothermia. Hypothermia is said to be 'light' for a core temperature between 34 °C and 35 °C: the subject is conscious and shivering, the skin is pale and cold with gooseflesh, and the survival forecast is good. Hypothermia is 'moderate' for a T_{re} ranging between 32 °C and 34 °C and 'severe' or 'deep' for a T_{re} between 25 °C and 32 °C. Of course, the number of observed symptoms and their seriousness increase with the intensity of the hypothermia. Nevertheless, in each case the skin is cold and dry, sometimes thick with a waxy appearance, and the extremities are cyanotic.

Some obvious signs allow assessment of the intensity of hypothermia: shivering disappears below 32 °C and is replaced by muscular rigidity. At 30 °C the subject is unconscious and the stretch reflexes have disappeared. Between 28 °C and 30 °C ventricular fibrillation generally appears, which signals the beginning of death. Below 25 °C, the muscular rigidity disappears and the subject becomes limp. The assessment of the degree of hypothermia defined by the rectal temperature remains a subject of debate, as this temperature is only one of the local core temperatures. In fact, the temperatures of the vital organs (e.g., heart, brain) may not always be at this same level. Nevertheless, the rectal temperature remains the classic criterion to determine the degree of hypothermia.

2.3 Factors Affecting Cold Tolerance

Physical exercise, through metabolic heat production, is a beneficial factor favoring cold resistance (Bittel et al. 1988). In the same way, the calorie intake should be increased in relation to the intensity of the cold stress. On the other hand, contrary to popular belief and habits, alcohol intake under cold stress is contraindicated for preventative or therapeutic reasons. In fact, alcohol has an anesthetic effect on the thermoregulatory centers and is detrimental to the thermal balance. In addition, pain, which is an important alarm signal, is reduced or may even vanish under alcohol intoxication.

Finally, clothing insulation remains the main way for the human body to resist the cold. The insulation must be adapted to the intensity of the cold and to the physical activity of the subject. Some other physiological factors may favor resistance to cold: subcutaneous fat thickness (fat is three times more insulating than the skin) provides a real 'physiological garment', and the level of maximum oxygen uptake capacity (VO_2 max) corresponds to a heat quantity capacity related to the level of fitness.

2.4 General Cold Resistance Tests

The overall cold tolerance is measured during a whole-body cold exposure, which triggers the thermoregulatory responses. The peripheral vasoconstriction is sudden, thereby decreasing the skin temperatures and thus reducing the heat losses. Several minutes later, metabolic heat production is increased as a result of shivering (the time to onset of shivering $= d$). This time, and the intensity of shivering are both related to the intensity of cold stress and its duration. Nevertheless, the shivering heat production cannot exceed a maximum value corresponding to approximately five times the resting heat production, which means $5 \times 50 = 250$ W.m^{-2}. When the cold stress is relatively important the heat debt appears, revealing hypothermia. Cold tolerance tests can be carried out either in air or in water.

2.4.1 Cold Tests in Air

Cold tests in air are usually performed in laboratories capable of calculating the heat balance equation. A climatic chamber is used in which the ambient parameters are controlled and reproducible. There is no real standard cold test that has been widely adopted; however, the most widely used in France is that of the Centre de Recherches du Service de Santé des Armées (Army Health Research Center) thermophysiology department. It consists of exposing a naked subject, at rest in a supine position, for 2 h to a 1 °C ambient temperature, 30 % relative humidity and 0.8 m.s^{-1} air velocity, an environment leading to maximum shivering intensity.

During this overall exposure to cold, all the ambient parameters are measured (air temperature, air humidity, wall temperatures, air velocity) as well as the physiological variables required to calculate the heat balance (the methods for these assessments have been described in ▶ Chap. 120, "Thermophysiological Parameters in Man").

The core temperature usually considered is either the rectal or the esophageal temperature. It must be noted that the tympanic temperature and, even worse, the oral temperature are not reliable in the case of cold exposure. The local skin temperatures are measured at ten sites so as to calculate a mean skin temperature. Assessment of the muscular activity (shivering) against the cold is obtained by three cutaneous electrodes placed on the anterior aspect of the thigh (quadriceps) and at the thoracic level (pectoral muscles). Metabolic heat production produced by shivering is measured by respiratory techniques: ventilation rate measurement (Fleisch flow meter or ultrasound) and the CO_2 and O_2 concentration in expired air. It is then possible to calculate the oxygen uptake and the metabolic heat production once the oxygen energy equivalent is known from the respiratory quotient (CO_2/O_2). Finally, the electrocardiogram is continuously recorded to ensure the safety of the investigation. The cold test performed in air, in a thoroughly controlled environment, makes it possible to calculate an accurate heat balance equation and to precisely determine the heat debt (in kJ). The latter can be expressed in terms of a core temperature decrease on the following basis: 3.48 kJ.kg^{-1} correspond to a 1 °C drop in mean body temperature (i.e., a 244 kJ heat debt for a 70 kg man). On the other hand, this test never leads to a core temperature decrease below 35.5 °C, except in exceptional cases.

2.4.2 Cold Tests in Water

The resting naked subject is completely (except for the head) immersed in water, the temperature of which varies between 15 °C and 18 °C. This corresponds to a severe cold stress because water has a heat conductance 25 times that of the air. In these conditions, the heat debt occurs rapidly, and the threshold of 35.5 °C core temperature, signaling the suspension of immersion, is reached within a relatively brief time (between 15 and 45 min depending upon the subject's cold tolerance). The cold tolerance is then expressed as a duration corresponding to the time necessary to reach the 35.5 °C level. Repeated cold immersions are used to develop the overall cold adaptation phenomenon.

2.5 Local Tests for Cold Exposure

These tests are used to quantify the local tolerance of the extremities (mainly the hands). The most common one consists of hand exposure in stirred

water at 5 °C (Savourey et al. 1992). In this situation, taking certain technical precautions, it is possible to measure the local skin temperature (sites in hands and fingers) and also the local cutaneous and subcutaneous skin blood flow (laser Doppler technique).

As soon as the hand is immersed, its temperature drops rapidly, to stabilize within a few minutes around the level of the water temperature (5 °C). At this level, for subjects who are not locally adapted the pain is intense and becomes unsupportable after 5 min of immersion.

If immersion is sustained, paradoxical vasodilation, called cold-induced vasodilation (CIVD), occurs at the level of the immersed extremities (Lewis phenomenon, "hunting reaction"). This CIVD provokes an increase in the local skin temperature by a few degrees, leading to reduced pain intensity. CIVD lasts for a few minutes and is repeated at regular intervals more or less frequently depending upon the level of cold adaptation. Repeated immersions (once or twice a day) over a period of several weeks (1 month) leads to an efficient local adaptation and therefore a marked increase in cold tolerance. In this case, CIVD occurs sooner and is reproduced more frequently and more intensively. Therefore, local cold tolerance of the extremities can be characterized by a tolerance time (onset of unsupportable pain), and adaptation will be characterized by a longer time (1 h or more) associated with an increased local skin temperature (Savourey et al. 1996).

Thus, where the whole-body or local cold tolerance is concerned, skin behavior plays a major role in its level, not only through its insulation associated with vasoconstriction, but also through the pain generated under periods of intense cold.

References

Agache P. Thermometry and remote thermography. In: Handbook of Measuring the skin. 1st edn. Berlin: Springer; 2004. p. 354–62.

Agache P, Candas V. Sweat gland metrology. In: Handbook of Measuring the skin. 1st edn. Berlin: Springer; 2004a. p. 311–28.

Agache P, Candas V. Eccrine sweat glands. In: Handbook of Measuring the skin. 1st edn. Berlin: Springer; 2004b. p. 302–9.

Bittel J, Savourey G. L'Homme et le froid. Pour la Science. 1995;207:32–40.

Bittel J, Nonotte-Varly C, Livecchi-Gonnot G, Savourey G, Hanniquet AM. Physical fitness and thermoregulatory reactions in a cold air environment in men. J Appl Physiol. 1988;65(5):1984–98.

Follenius M, Brandenberger G, Oyono S, Candas V. Cortisol as a sensitive index of heat-in-tolerance. Physiol Behav. 1982;29:509–13.

Frank A, Morand EY, Belokopytov M, Shapiro Y. The estimation of heat tolerance by a new cumulative heat strain index. In: Shapiro Y, Moran DS, Epstein Y, editors. Environmental ergonomics: recent progress and new frontiers. Tel Aviv: Freund; 1996. p. 194–201.

Pandolf KB, Goldman RF. Convergence of skin and rectal temperatures as a criterion for heat tolerance. Aviat Space Environ Med. 1978;49:1095–101.

Savourey G, Vallerand AL, Bittel J. General and local cold adaptation after a ski journey in severe arctic environment. Eur J Appl Physiol. 1992;64:99–105.

Savourey G, Sendowski I, Bittel J. Biometrical characteristics and physiological responses to a local cold exposure of the extremities. Eur J Appl Physiol. 1996;74:85–90.

Vogt JJ, Meyer-Schwertz MT, Foehr R, Metz B. Motor, thermal and sensory factors of heart rate variations: a methodology for indirect estimation of intermittent work and environmental heat loads. Ergonomics. 1973;35:131–42.

General information on body temperature regulation will be found in the following book

Chapters 110 and 111: Cooper KE basic thermo-regulation – Body temperature control and its disorders. In: Greger R, Windhorst U, editors. Comprehensive human physiology: from cellular mechanisms to integration, vol 2. Berlin/Heidelberg/New York: Springer; 1996. p. 2199–218.

Distribution of Skin Thermal Sensitivity

122

Nicola Gerrett, Yacine Ouzzahra, and George Havenith

Contents

Keywords

Thermal sensitivity • Heat and cold • Body mapping • Gender • Exercise • Ethnicity • Regional thermal sensitivity

Abbreviations

ΔT_{sk}	Change in skin temperature (°C)
(EIA)	Exercise-induced analgesia
RH	Relative humidity (%)
s	Seconds
TRPV	Transient receptor potential vanilloid
TS	Transient response
T_{sk}	Skin temperature (°C)
VAS	Visual analogue scales
VO_{2max}	Maximal aerobic capacity ($ml \cdot kg^{-1} \cdot min^{-1}$)

1 Introduction

As an interface between the environment and the body core, the skin plays a vital role in protecting the body and maintaining a thermal equilibrium around 37 °C. Autonomic responses serve to maintain thermal balance by initiating several physiological responses. However behavioral thermoregulation reduces the need for autonomic thermoregulation as humans make a conscious decision to protect their thermal status. This is often based on emotional feelings associated

N. Gerrett (✉)
Institute of Sport and Exercise Science, University of Worcester, Worcester, UK
e-mail: n.gerrett@worc.ac.uk

Y. Ouzzahra
Institute for Health and Behaviour, University of Luxembourg, Walferdange, Luxembourg
e-mail: Yacine.Ouzzahra@uni.lu

G. Havenith
Environmental Ergonomic Research Centre, Loughborough Design School, Loughborough University, Loughborough, UK
e-mail: G.Havenith@lboro.ac.uk

P. Humbert et al. (eds.), *Agache's Measuring the Skin*,
DOI 10.1007/978-3-319-32383-1_72

with their thermal state and comfort/discomfort (Li 2001). It usually involves taking off or putting on clothing, moving into shaded areas, or adjusting indoor temperatures. This suggests that our sensation of temperature change is directly linked to our primary behavioral response.

The mechanisms associated with behavioral thermoregulation involve the thermoreceptors, which upon stimulation relay information to the brain about the surrounding environment. They are distributed around the periphery (skin) and central locations, including major organs and along the spinal cord (Bullock et al. 2001). The location, density, and distribution of thermoreceptors in the skin play an important role in our perception of temperature. These receptors transiently increase or decrease their firing rates depending upon the direction and magnitude of the change in skin temperature, and this ultimately influences the thermal sensation experienced (Bullock et al. 2001). Differences in perceptions of heat and cold are related to several factors including the reported larger numbers of cold-activated sensors than warm-activated sensors and a faster firing rate of the receptors upon cold stimulation compared to warm stimulation (Hensel 1981). The variation of thermoreceptors distribution across the body surface and the unequal number of warm and cold receptors helps explain why regional differences in thermal sensation exist.

2 Methodological Considerations

Different methodologies have been employed to investigate regional thermal sensitivity, and this can produce confounding results if the techniques used are not fully understood. The two main methods to assess thermal sensitivity are measurements of (1) thermal thresholds, which are the upper and lower limits for detection of cold or warm thermal sensations, and (2) thermal intensity rating (magnitude estimation) which is the estimation of the level of cold or warmth in response to a given stimulus. These methods produce different findings as one location may be sensitive enough to detect small temperature changes, but the degree of sensation it experiences for a given stimulus temperature may be lower than other locations. Both techniques can determine the sensitivity across regions, but the type of sensitivity is different and it is therefore important for researchers to define and differentiate between the methods used.

2.1 Thermal Thresholds

Three different types of thermal thresholds exist, namely, the absolute threshold, difference threshold, and terminal threshold.

Measuring the absolute threshold, also referred to as threshold detection, involves applying a stimulus, and participants respond to the stimulus once they sense a temperature change. It is the highest stimulus temperature capable of producing a cool sensation (cool threshold) or the lowest stimulus temperature capable of producing a warm sensation (warm threshold). Absolute thermal thresholds are measured with the method of limits, which consists of exposing a participant to a stimulus of changing intensity, starting from a neutral temperature. It is crucial that the stimulus temperature changes with a *low* and *constant* rate of change, as the measurement would be otherwise inaccurate due to the important influence of rate of change in temperature on thermoreceptors' activity. The participant is asked to indicate the first onset of a cool or warm sensation.

Difference threshold is the extent of change in a stimulus necessary to produce a noticeable difference. It is measured in the same way as the absolute threshold described above, but is presented as a change in temperature from neutrality needed to provoke a cool or warm thermal sensation (Lee et al. 2010).

Terminal threshold is the magnitude of a stimulus above which there is no further increase in the perceived intensity of the appropriate nature of that stimulus. For example, if thermal sensation values increase with an increasing stimulator temperature up to 40 °C, but do not increase any further with a further rise in temperature, then the terminal threshold is 40 °C. Above the terminal thermal threshold level, pain usually occurs.

In all thresholds discussed above, skin thermal sensitivity is related to a specific temperature; the lower the temperature for warmth and the higher the temperature threshold for cold, the more sensitive the area is. The values reported can be compared between body sites to a given temperature or one specific body site compared to a variety of different temperatures. One limitation of the method of limits is that a reaction time artifact exists, which can increase the value of the absolute threshold considerably (Yarnitsky and Ochoa 1990). The reaction time artifact is larger for warming than cooling, since the primary afferents are slower conducting, and is most extreme for more distal body sites. It can however be diminished by using a slow rate of temperature change (Yarnitsky and Ochoa 1990). Furthermore, another disadvantage of this method is that the subject may become accustomed to reporting that they perceive a stimulus and may continue reporting the same way even beyond the threshold (error of habituation). Conversely, the subject may also anticipate that the stimulus is about to become detectable or undetectable and may make a premature judgment (error of expectation) (Meilgaard et al. 2007). Hence the order of presenting stimuli should avoid any anticipatory knowledge.

2.2 Intensity Rating

The degree of the sensation experienced in response to a fixed stimulus is known as magnitude estimation or intensity rating. An area of the skin is stimulated with a thermal stimulus at a fixed temperature, and participants rate the degree of sensation experienced on a predetermined perceptual scale (see below for more information). The intensity rating is driven by the difference between skin temperature and stimulus temperature. As the skin temperature will change upon contact with the stimulator, the temperature difference between skin and stimulus will reduce over time. Apart from a strong response at the start of any stimulus (Hensel 1981), this initially stronger stimulus leads to a stronger "transient response" at the start and then a more stable "steady-state" response (typically after 10–20 s; Ouzzahra et al. 2012).

Transient responses must take into account initial skin temperature and the initial sensations reported expressed relative to that value. As skin temperature naturally varies across the body, one option to accommodate for this is to adjust the stimulus in order to create the same stimulus magnitude relative to the local skin temperature before the stimulus. This is done by measuring the local skin temperature before application of the stimulus and then setting the stimulus to a fixed temperature change in relation to the actual local skin temperature. Alternatively, a transient response (TS) could be divided by the difference between pre-stimulus skin temperature (T_{sk}) and stimulus temperature, often expressed as $TS/\Delta T_{sk}$. Both approaches will allow for comparison across multiple sites where T_{sk} is known to vary across the body in a variety of conditions (Choi et al. 1997; Fournet et al. 2013). When the stimulus is held for long enough to cause skin temperature to approach or reach stimulus temperature, this is referred to as a steady-state response (Ouzzahra et al. 2012). As a result this removes the effect of the initial T_{sk} and absolute values in thermal sensation should be reported and compared across regions. The choice for any of these approaches should be guided by the application of the research. This may be related to a fixed stimulus value (e.g., effects of a *constant* room or water temperature) or relative (e.g., effects of a *changing* room or water temperature). Finally, T_{sk} in some locations may not reach the stimulus temperature, depending on the interplay of insulative fat layers and local blood flow. For example, Nakamura et al. (2008) found that applying the same cold stimulus at different areas of the skin resulted in different levels of ΔT_{sk} and suggested that these regional differences in heat loss are likely caused by differences in skin blood flow due to vasomotor status and tissue vascularity. In that case, if one wants to calculate sensitivity in terms of $TS/\Delta T_{sk}$, one needs to track T_{sk} during the stimulus. This can be done using a very thin thermocouple which will determine "contact temperature" (Jay and Havenith 2003, 2004, 2006) or by measuring local T_{sk} immediately before and

after application of the stimulus (e.g., by an infrared thermometer; Ouzzahra et al. 2012; Gerrett et al. 2014).

In both cases, on a scale ranging from 0 to 10 or neutral to extremely hot/cold, a more intense absolute or relative local thermal sensation represents a more sensitive body site, and values can be compared between sites for intensity scores or individual sites compared to a variety of different temperature.

2.3 Perceptual Scales

The scales used in the literature vary but most often are unipolar or bipolar Likert scales ranging from 0 or "neutral" to extreme cases such as "extremely hot" or "extremely cold." The most frequently reported are modified versions of the ASHRAE thermal sensation scale (ASHRAE 1997). The original scale ranged from 1 (cold) to 7 (hot) with 4 designated as "comfortable." It has been modified by numerous researchers and typically ranges from −10 (extremely cold) to +10 (extremely hot) with a "neutral" zero (Gerrett 2012). The purpose of this was to allow assessment in extreme environments, and it can also be argued that this prevents a "ceiling effect" when rating thermal sensations. Scales have also been altered slightly and numbers have been inserted between each category vote to increase the sensitivity of the scale. More recently, visual analogue scales (VAS) are being used which involves presenting the participant a straight line (no numbers) with labels at either end. Participants are asked to rate a construct (sensation, comfort, regional sensations, etc.) by marking a point along the line which reflects their current status (Leon et al. 2008). They are reported to have a greater accuracy for detecting humans' perceptions as the participant is not forced to make ratings according to numbers or restricted to verbal categories which may not reflect their true current status (Leon et al. 2008). Davey et al. (2007) compared VAS with ASHRAE Likert scale in stable and dynamic thermal environments, and their evidence supports the notion that VAS has greater reproducibility and reflects body temperature more so than Likert scales. Research has also combined elements of a Likert scale with a VAS (see Fig. 2) to assess thermal sensations in response to a thermal stimulus (Ouzzahra et al. 2012; Gerrett et al. 2014).

2.4 Stimulation

Specific details about the stimulus used are extremely important and can influence reported thermal sensitivity. Of primary importance is the temperature of the stimulus as both direction and magnitude will influence thermal sensitivity when using intensity rating/magnitude estimation. A greater gap between the stimulus temperature and that of the stimulated skin will result in more intense thermal sensations. When deciding upon the stimulus temperature, consideration needs to be given to the range of temperatures stimulated by different thermoreceptors. Recent knowledge suggests that the principal temperature sensors in the nerve endings belong to the transient receptor potential (TRP) family which are activated by distinct temperatures (Schepers and Ringkamp 2008; Ständer and Luger 2009). Table 1 highlights the TRP family, the temperature range of stimulation, and the sensation they evoke once stimulated.

When using threshold detection techniques, the rate of change in stimulus temperature will have a strong influence upon thermal sensitivity. A fast temperature change causes the firing rate of the receptors to overshoot, sending strong signals to the brain. This has been shown to cause strong thermal sensations in comparison to slow continual changes in temperature (Hensel 1981). In addition, when the skin is exposed to changing temperatures, the thermal threshold is influenced by the initial temperature and the rate of change of temperature (Hensel 1950). The surface area exposed to the thermal stimulus will also impact thermal sensitivity. For example, when submerging a whole hand into a flask of warm water and a fingertip in another (of the same temperature), the water would feel warmer when it surrounds the

Table 1 Description of the transient receptor potential (TRP) family, the temperature range of stimulation, and the sensation they evoke once stimulated (Ständer and Luger 2009)[a] indicates myelinated fiber

Receptor	Stimulated by...	Sensation evoked
TRPV1	Noxious heat (>42 °C), protons, capsaicin, anandamide,	Cold, heat, burning pain
TRPV2	Noxious heat (>52 °C)	Pain induced by heat
TRPV3	Warmth (>33 °C)	Warmth
TRPV4	Warmth (~25 °C)	Warmth
TRMP8 (on Aδ fiber)[a];	Cold (8–28 °C and menthol)	Cold
TRPA1	Noxious cold (<17 °C), wasabi, horseradish	Pain induced by cold burning

whole hand in comparison to the fingertip (Ross and Murray 1996). Stevens et al. (1974) found the larger the area for a given stimulation, the greater the magnitude estimation. This condition refers to the spatial summation, in that the sensation is relative to the surface area stimulated and therefore to the number of thermoreceptors activated.

In the literature the thermal stimulus has been applied using contact or non-contact methods, such as thermal radiant lamps (Nadel et al. 1973), water-perfused suits (Cotter and Taylor 2005), thermal probes (Gerrett et al. 2014; Ouzzahra et al. 2012), or specialized clothing garments where the microclimate temperature is changed (Zhang et al. 2004). Non-contact methods are more difficult to implement, especially in regional sensitivity studies due to the difficultly in isolating specific areas on the body. However, they do ensure that only the thermoreceptors are stimulated. Contact methods such as thermal probe application or water-perfused suits are more common and easily implemented. However, the possibility of a "dual" neural stimulus between mechanoreceptors and thermoreceptors of any region cannot be excluded, particularly in areas sensitive to touch.

2.5 An Example Method

Regional differences in thermal sensitivity should provide specific instructions about assessing the exact locations for both dependent and independent samples. Recent research by Gerrett et al. (2014) measured 31 locations across the body and Fig. 1 provides an overview of potential measurement areas. Washable pen markings may be used on the body to indicate each measurement site for the application of the thermal probe. The testing sequence of the segments should be randomized or in small groups balanced using a Latin square type approach, to prevent any order effects.

Participants should be allowed to rest in the testing area to allow skin temperature and physiological responses to stabilize. During the rest period, participants should be familiarized with the sensation scales and allowed to practice rating their sensations to a range of stimuli strengths across different regions on the body to reduce response variability. After the rest period, the thermal sensitivity of each area to the desired stimulus should be determined. Each test area should be subjected to the following: the measurement of T_{sk} using an infrared thermometers or skin thermistors followed by probe application for the desired duration. The probe should be applied to the skin by the same investigator to ensure consistent pressure applied to each location and individual. Alternatively, a pressure gauge may be applied to the probe to ensure equal pressure during testing (see Filingeri et al. 2014). Participants should rate their thermal sensation on a predetermined perception scale (see Fig. 2 as an example) at designated times.

A thermal stimulator typically consists of a temperature controller and temperature stimulator. Some researchers have used patches of water-perfused tubes as stimulus (Nakamura et al. 2008) or water-perfused suits with local control (Ouzzahra 2012). Most recent studies have used an electrical stimulator (Fig. 2) (Fowler et al. 1987: Gerrett et al. 2014; Ouzzahra et al. 2012). The stimulator has a Peltier element which cools down or warms up the stimulator,

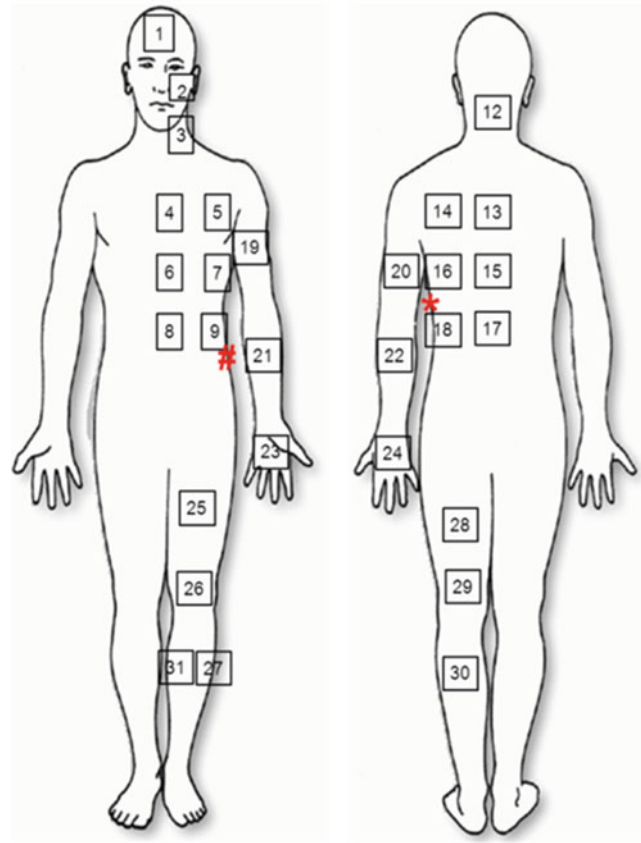

Fig. 1 Distribution of sample locations across the body in Gerrett et al. (2014) and Ouzzahra (2012)

depending on the direction of the current. The stimulator shown in Fig. 3, also referred to as thermal probe, is a metal block that comes in various sizes which can be set at temperatures ranging from 5 to 50 °C. Its cooling or warming depends upon the applied current direction, which can be changed by the controls situated on the temperature controller. The probe also encloses a temperature sensor for close control of the stimulus temperature, which is directly connected to the digital readout of the temperature controller.

To avoid an effect of surprise on transient responses, a verbal warning of the location of each out-of-sight body area prior to stimulation (e.g., "lateral lower back") should be given. Distractions should be minimized throughout any thermal sensitivity test. Any sweat produced during testing should be wiped away before the probe application to avoid the skin surface conductivity being affected.

3 Results: Body Mapping

Regional sensitivity data has been reported in tables or graphs (Cotter 1997; Nakamura et al. 2008), but this can be quite cumbersome to interpret, especially with a large number of regional comparisons. Gerrett et al. (2014) and Ouzzahra et al. (2012) generated body maps (similar to the body mapping of sweating by Smith & Havenith 2012) to display regional differences in thermal sensitivity to warmth (40 °C) and cold (20 °C). In order to generate the body maps, Ouzzahra et al. (2012) and Gerrett et al. (2014) used similar procedures detailed below.

After measuring skin temperature using infrared thermometer, a fixed temperature probe (Fig. 3) was placed directly onto the skin and participants were instructed to rate thermal sensation immediately after contact (*transient thermal sensation*), and/or 10 s after contact (*steady-state*

thermal sensation). The thermal sensation scale for innocuous cold or warmth stimuli shown in Fig. 2 was used. This procedure was repeated for numerous locations across the body at rest and during an exercise bout consisting of cycling at 30 % $\dot{V}$-$O_{2\ max}$. Results are presented as body maps assuming symmetry (e.g., Claus et al. 1987; Meh and Denišlič 1994) and are presented utilizing color codes to highlight the differences in thermal sensitivity (see Figs. 4, 5, 6, 7, and 8). A greater number has a darker color and represents a skin region which is more sensitive to warmth in terms of response magnitude.

	Thermal sensation
>10	Painfully hot/cold
10	Extremely hot/cold sensation
9	
8	
7	
6	
5	
4	
3	
2	
1	
0	No cold/heat sensation

Fig. 2 Example of a thermal sensation scale

3.1 Gender

Gender differences in thermal sensitivity to cold (20 °C) and warmth (40 °C) exist, not only in terms of the overall sensitivity but also in terms of its regional distribution. Females had significantly stronger thermal sensations (i.e., more sensitive) than males to both a warm (40 °C) and cold stimulus (20 °C) at all locations. This finding adds to the current body of literature surrounding the general concept of perception to a variety of stimuli between genders. Previous research has found females to be significantly more sensitive than males to cold and warmth using the method of limits (Golja et al. 2003; Lautenbacher and Strian

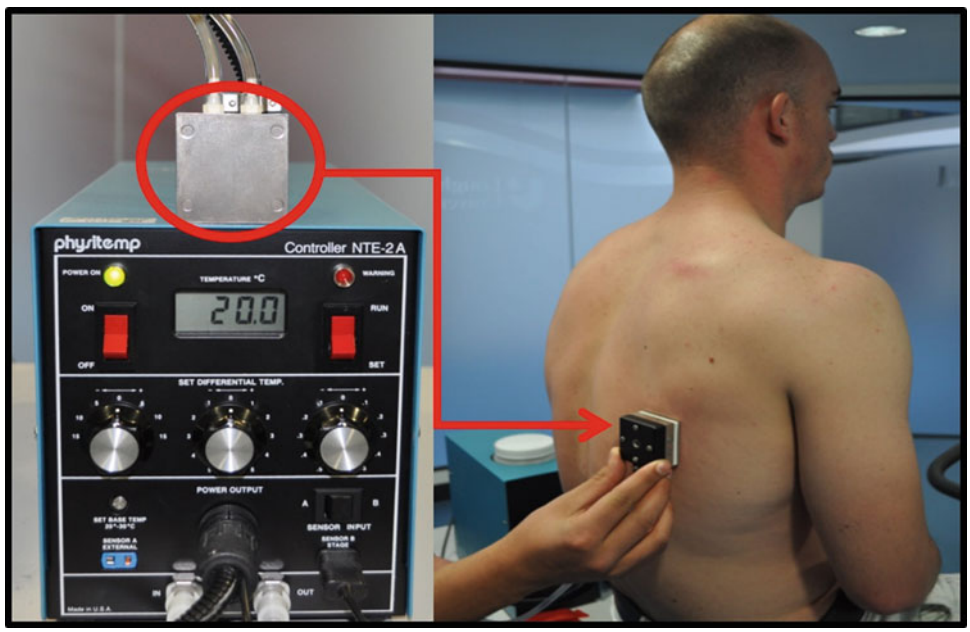

Fig. 3 Thermal sensitivity tester (*left*) and its application onto the skin (*right*)

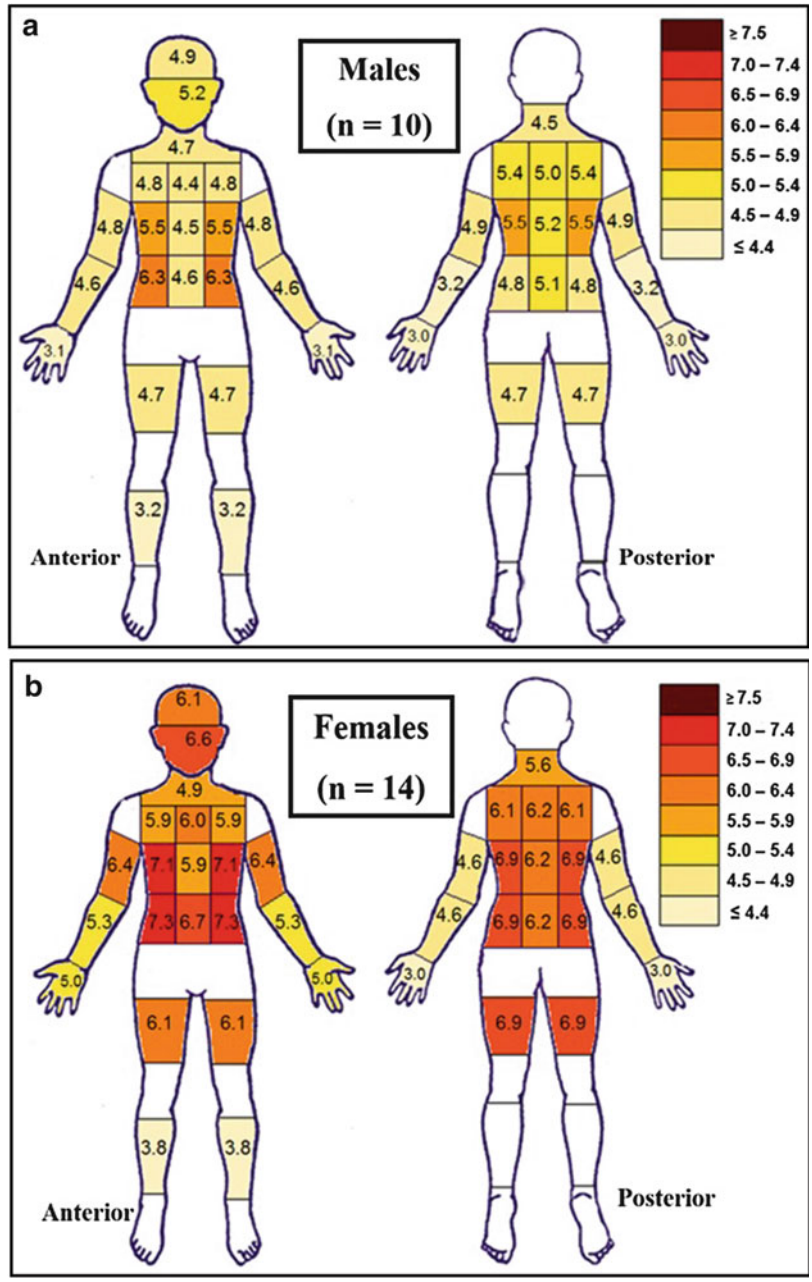

Fig. 4 Regional steady-state thermal sensations in response to a cold stimulus (20 °C) in males (**a**) and females (**b**) at rest (Ouzzahra et al. 2012)

1991; Kenshalo 1986), and this study confirms such gender differences using an intensity rating method. The greater thermal sensitivity to cold and warmth found in females may be attributed to several physiological and morphological differences between genders. Differences in the density of thermoreceptors are likely to play a major role in thermal sensitivity differences between genders. Using 3 mm punch biopsies, Gøransson et al. (2004) found that the density of epidermal nerve fibers at the leg is significantly greater in women compared with men. It is widely accepted that thermoreceptors distribution varies across the body (e.g., Strughold and Porz 1931), and it is possible that this regional distribution varies between genders, although no study has

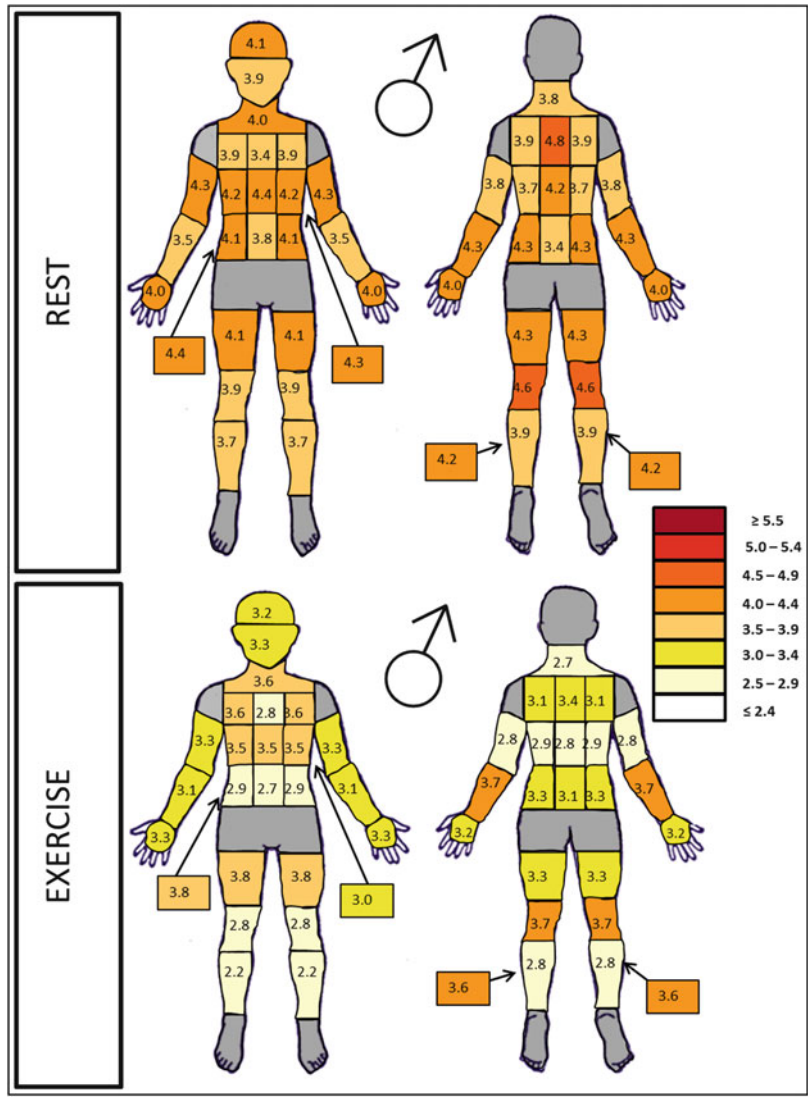

Fig. 5 Male regional steady-state thermal response to a warm stimulus (40 °C) during rest and exercise. All areas were significantly lower than females ($p < 0.05$). Areas shaded in black were not investigated

systematically investigated thermoreceptors distribution across the body in males and females.

Morphological factors such as hair density may also explain some of the differences found. Ouzzahra et al. (2012) showed some of the largest differences at the abdomen, posterior lower arm, and anterior thigh between males and females to a cold stimulus. Although females were not analyzed for hair density, these sites coincide with body areas which are naturally more hairy in men than women. Men's hair may have therefore acted as an insulator for the skin, introducing thermal resistance between the stimulus (thermal probe) and the skin. This would not be the case in the female participants who do not tend to have abdominal hair and usually shave their legs. Hair distribution and shaving have been previously mentioned as potential factors playing a role in the gender differences in thermal and pain sensitivity (Caissie et al. 2007). Moreover, skin thickness may also be a factor involved in the greater sensitivity in the female group (Golja et al. 2003). Indeed, it has been shown that females' skin is thinner than that of males (Sandby-Moller et al. 2003), and it is therefore possible that males' thicker skin act as a barrier between the

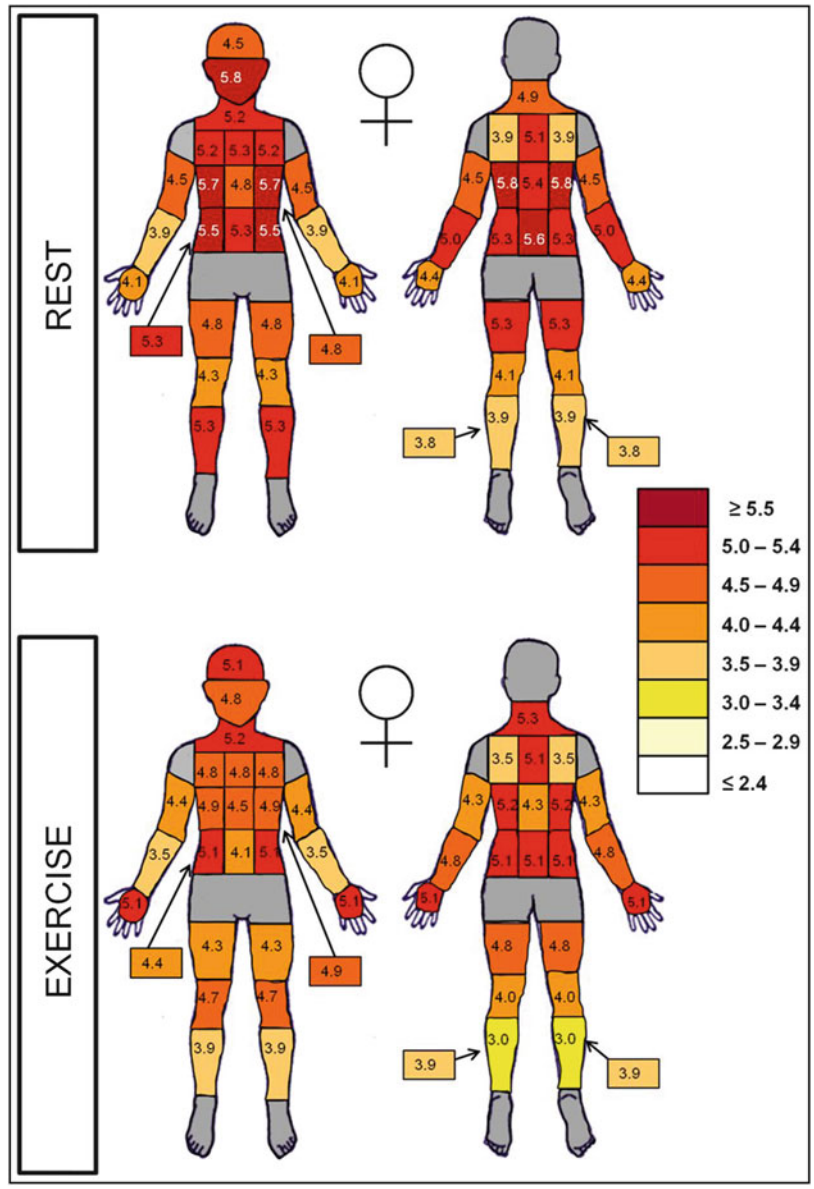

Fig. 6 Female regional steady-state thermal response to a warm stimulus (40 °C) during rest and exercise. All areas were significantly higher than males ($p < 0.05$). Areas shaded in black were not investigated

thermal stimulus and the thermoreceptors, thereby reducing the intensity with which these are effectively stimulated. Finally, the differences in thermal sensitivity to cold and warmth between males and females could perhaps be explained on the basis of previous observations in another cutaneous sensory system such as pain. In addition it has been suggested that the menstrual phase may have unique interacting effects on pain thresholds (Giamberardino et al. 1997). All things considered, it is likely that the complex interaction of these factors resulted in the differences between males and female across the body found in the present and previous studies.

3.2 Regional Distribution

The results from both Ouzzahra et al. (2012) and Gerrett et al. (2014) showed that regional

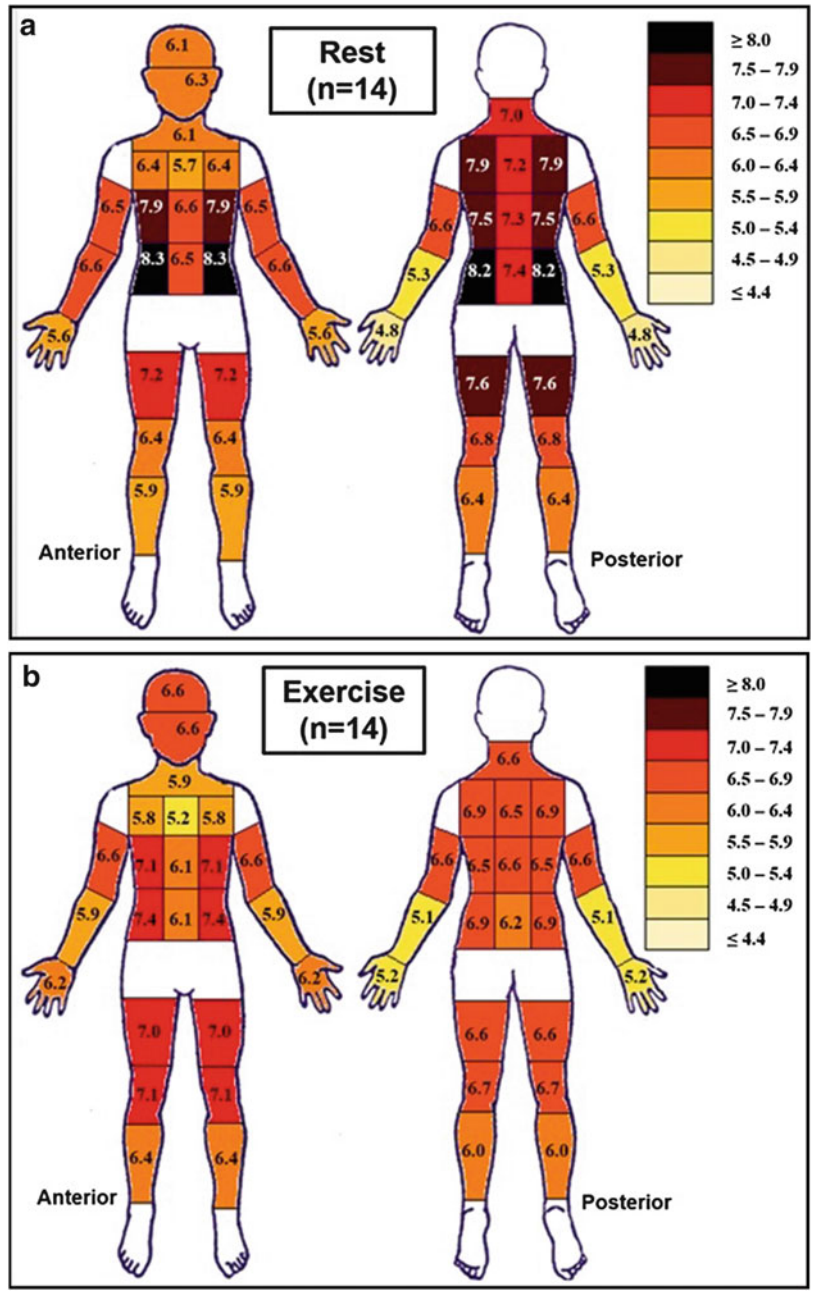

Fig. 7 Regional steady-state thermal sensations in response to a cold stimulus (15 °C) during rest (**a**) and exercise (**b**) in male participants (Ouzzahra et al. 2011)

variations in thermal sensation exist for both genders, but are more prominent for females. In agreement with the literature, the pattern over the body indicated a higher sensitivity at the head and the torso and the lowest at the extremities. This regional variation in thermal sensation may be due to several physiological variables. The two most commonly reported parameters are the uneven distribution of cutaneous thermoreceptors and the existence of a weighing of thermoafferent information by the integration center in the central nervous system (Burke and Mekjavić 1991). The rate of change in skin temperature (ΔT_{sk} rate) may also explain

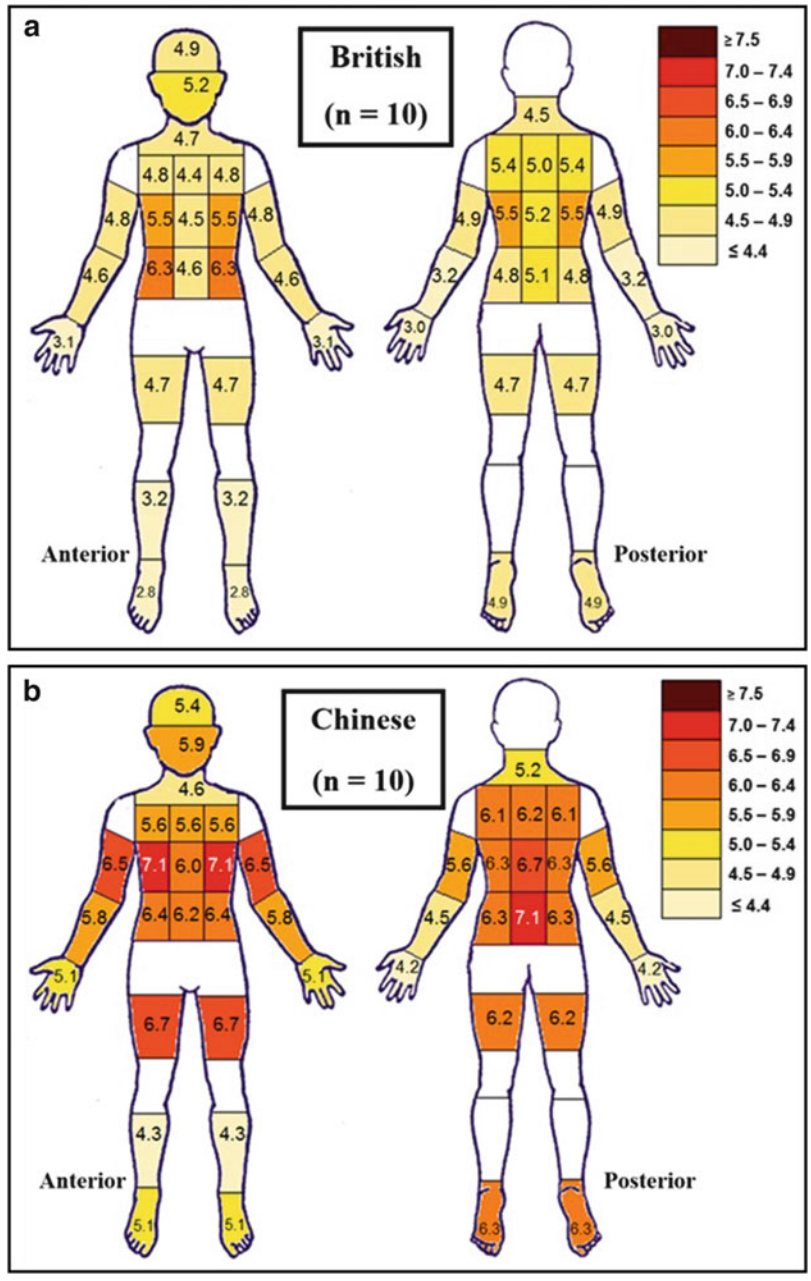

Fig. 8 (continued)

the differences in thermal sensitivity between body sites. Indeed, it is well established that different areas of the body lose their heat content more readily than others due to regional differences in skin blood flow (Nakamura et al. 2008).

Another similarity in these studies was that the lateral areas of the torso were more sensitive than the medial areas. As stated earlier, the thermal probe makes contact with the skin, and in doing so, it stimulates both thermoreceptors and mechanoreceptors simultaneously. The possibility of a

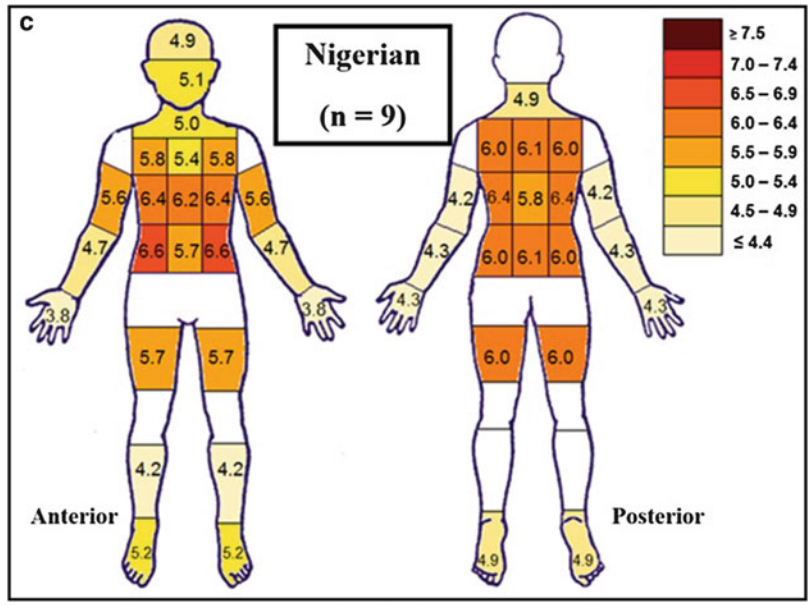

Fig. 8 Regional steady-state thermal sensations in response to a cold stimulus (20 °C) in males from three different ethnic groups: (**a**) British, (**b**) Chinese, (**c**) Nigerian (Ouzzahra et al. 2012)

"dual" neural stimulus between mechanoreceptors and thermoreceptors of any region cannot be excluded, particularly in areas such as the lateral torso which may be more sensitive to touch.

3.3 Rest and Exercise

In another study, Ouzzahra et al. (2011) investigated the effects of exercise on thermal sensitivity to cold (15 °C) on 28 sites across the upper and lower body (see Fig. 7). Participants were more sensitive to cold stimuli at rest than during exercise, and this was significant in 11 of the skin sites tested. One logical explanation for this is the increase in T_{sk} with exercise, resulting in thermoreceptors being stimulated with a greater ΔT_{sk}, which will increase the impulse frequency and in turn influence thermal sensation. The present data confirmed that T_{sk} may in part explain the decrease in sensitivity to cold, as suggested by a significant increase in mean T_{sk}. Similarly, Gerrett et al. (2014) found that exercise caused a reduction in thermal warmth sensation to a hot thermal stimulus in males but only at select locations for females (Figs. 5 and 6). Interestingly, the distribution of sensitivity to cold was more homogenous during exercise, but this was not observed in response to a warm stimulus.

Exercise itself has been reported to cause a reduction in perception to a variety of stimuli, particularly tactile and pain sensitivity due to exercise-induced analgesia (EIAs) (Guieu et al. 1992; Kemppainen et al. 1985, 1986; Pertovaara et al. 1984; Paalasmaa et al. 1991). EIA is thought to be due to a reduction in the transmission of sensory information to the thalamus and somatosensory cortex associated with one of the following: movement, increased activity in proprioceptive and muscles afferents, increase in arousal, and reduction in attention (Koltyn 2000). As the thermal state of the body did not change from rest to exercise in the presented study of Gerrett et al. (2014), changes in thermal sensitivity may be a result of EIA.

3.4 Ethnicity

Lastly, Ouzzahra (2012) also investigated differences in thermal sensitivity to cold between groups of individuals from different ethnic

backgrounds. A total of 29 participants all living in the UK were recruited: 10 Caucasians from Great Britain, 10 Asians from China, and 9 Africans from Nigeria. Thermal sensitivity to cold was tested at 27 body sites with a 20 °C thermal probe, and participants reported their local transient and steady-state cold sensations. Photos of the participants' front torso, arms, back, and legs were then taken, and local hairiness density was rated at nine sites using a five-point scale (Garn 1951). Body maps of cold sensations were created and are presented in Fig. 8 (steady state).

Results revealed that areas of high thermal sensitivity to cold included the lateral abdomen in all groups, the medial lower back in the Chinese group, and the medial upper abdomen in the Nigerian group. A total of 13 significant differences and trends ($0.05 \leq p \leq 0.1$) were found between ethnicities before Bonferroni corrections for the steady-state thermal sensations (see Ouzzahra (2012) for specific details). Most of these were between the British and the Chinese groups, with a greater (colder) thermal sensation found in the Chinese group. The Nigerian group was also more sensitive to cold than the British group at the central upper abdomen ($p = 0.052$) and the dorsal foot ($p = 0.017$).

The idea that thermal sensitivity may vary between humans of different geographical origins has been suggested before. For example, the extinct Fueguian tribes of South America were known to tolerate freezing conditions with minimal thermal protection. It is widely believed that selective forces within these populations favored extraordinary cold tolerance (Hernandez et al. 1997). Another example is the prehistoric Polynesians who, similarly to the Fueguians, lived in a cool and wet marine environment. Visser and Dias (1999) examined skulls of two prehistoric Polynesian groups from New Zealand, the Moriori and Maori, and of one contemporary Indian group. They analyzed the sensory nerve dimensions, based on the area of cranial nerve foramina. These features are of interest, because the cross-sectional area of a nerve is directly proportional to the number of axons and hence the number sensory receptors represented. Comparisons showed significantly lower cranial cutaneous sensory nerve foramina size in the prehistoric Polynesian groups, compared with the contemporary Indian group. This was interpreted as a lower facial cutaneous sensory nerve supply in the Polynesians. The authors proposed that reduced skin sensory nerve supply may have been selected as an adaptation to a cool and wet environment.

Besides these potential neurological differences, research has also explored several physiological characteristics which differ between ethnic groups and may result from environmental factors. These include adaptations in body mass, body shape and surface area, cranial morphology, skin color, body composition, metabolic rate, and peripheral vasoconstriction (see Lambert et al. 2008 for a complete review). One factor which may explain the thermal sensation differences found between ethnicities in the present study is the density of body hair. Despite the small sample used, the present results confirm the widespread notion that European individuals have a greater body hair density than their Asian and African counterparts. More importantly, the significantly higher body hair density found in the British group corresponds well with their lower thermal sensitivity, compared to the Chinese group. In humans, hair mainly has an insulation role and therefore serves to protect from the cold (Johnson et al. 1993). It seems reasonable to suggest that, in the present experiment, hair may have acted as an insulator for the skin, introducing thermal resistance between the stimulus (thermal probe) and the skin. This was in agreement with the significant correlation found in the cold sensation versus body hair density analysis, indicating that body regions with lower levels of local hairiness were associated with greater (colder) local thermal sensations. According to Hooton (1946), the loss of body hair in man must have taken place in a tropical climate, since such an adaptation is unlikely to take place in a cold environment. Other theories suggest that the loss of hairy covering in man is associated with an increase in subcutaneous fat layers. According to Keith (1912), humanization, which resulted in a richer variety and a more ample command of food all year round,

may be one of the reasons for the loss in human body hair. Indeed, such an improvement in pre- and postnatal nutrition may have brought about the increase in fat deposition, which in turn may have rendered body hair less needed, since a subcutaneous fat layer similarly preserves the warmth of the body (Hooton 1946). Prior to modernization, individuals indigenous to cold climates were typically relatively muscular, and the regional distribution of muscle and fat characteristics of these people is thought to maximize insulation (Beall and Steegmann 2000). As pointed out by Hooton (1946), it is also perfectly possible that some human groups may have retained, or even redeveloped, body hair at a late period of human evolution.

4 Conclusion

In order to test regional thermal sensitivity, the first step is to define sensitivity and determine whether a magnitude estimation or thermal threshold approach is most appropriate, and in the first case, whether to work with a fixed stimulus temperature or with a stimulus temperature relative to local skin temperature. Following this the desired temperature to stimulate designated TRP receptors must be determined. The duration of stimulation and the surface area will influence thermal sensitivity, but these should be standardized across regions. Transient responses can be expressed relative to the change in skin temperature. Steady-state responses should not be taken before skin temperature stabilizes and/or the response is stable. The correct timing for this should be determined during pilot studies. Strict care should be taken over assessing regional differences and ensuring precision over testing the same location within and between individuals. When presenting the data from multiple locations, body maps prove to portray this information most clearly.

References

ASHRAE. Thermal comfort. ASHRAE handbook of fundamentals. Atlanta: ASHRAE; 1997.

Beall CM, Steegmann AT. Human adaptation to climate: temperature, ultraviolet, radiation and altitude. In: Stinson S, Bogin B, O'Rourke D, editors. Human biology: an evolutionary and biocultural perspective. New York: Wiley; 2000. p. 163–224.

Bullock J, Boyle J, Wang MB. Physiology. 4th ed. Philadelphia: Lippincott Williams & Wilkins; 2001.

Burke WE, Mekjavić IB. Estimation of regional cutaneous cold sensitivity by analysis of the gasping response. J App Physiol. 1991;71:1933–40.

Caissie R, Landry PÉ, Paquin R, Champigny MF, Berthod F. Quantitative method to evaluate the functionality of the trigeminal nerve. J Oral Maxillofac Surg. 2007;65:2254–9.

Choi J, Miki K, Sagawa S, Shiraki K. Evaluation of mean skin temperature formulas by infrared thermography. Int J Biometeorol. 1997;41:68–75.

Claus D, Hilz MJ, Hummer L, Neundörfer B. Methods of measurement of thermal thresholds. Acta Neurol Scand. 1987;76:288–96.

Cotter JD, Taylor NA. The distribution of cutaneous sudomotor and alliesthesial thermosensitivity in mildly heat-stressed humans: an open-loop approach. J Physiol. 2005;565:335–45.

Cotter JD. The role of regional skin temperatures in thermoregulatory control during heat stress [PhD thesis]. University of Wollongong; 1997.

Davey S, Reily T, Newton M, Tipton M. The reproducibility and validity of visual analogue scales (VAS) that assess thermal perceptions in stable and dynamic, asymmetric environments. In: Mekjavic IB, Kounalakis SN, Taylor NSA, editors. Environmental ergonomics XII 2007: proceedings of the 12th International Conference on Environmental Ergonomics. Piran: Biomed D.O.O; 2007. p. 114–6. 2007 Aug 19–24.

Filingeri D, Redortier B, Hodder S, Havenith G. Thermal and tactile interactions in the perception of local skin wetness at rest and during exercise in thermo-neutral and warm environments. Neuroscience. 2014; 258:121–30.

Fournet D, Ross L, Voelcker T, Redortier B, Havenith G. Body mapping of thermoregulatory and perceptual responses of males and females running in the cold. J Therm Biol. 2013;38:339–44.

Fowler CJ, Carroll M, Burns D, Howe N, Robinson K. A portable system for measuring cutaneous thresholds for warming and cooling. J Neurol Neurosurg Psychiatry. 1987;50:1211–5.

Garn SM. Types and distribution of the hair in man. Ann N Y Acad Sci. 1951;53:498–507.

Gerrett N. Body mapping of perceptual responses to sweat and warm stimuli and their relation to physiological parameters [PhD thesis]. Loughborough University; 2012.

Gerrett N, Ouzzahra Y, Coleby S, Hobbs S, Redortier B, Voelcker T, Havenith G. Thermal sensitivity to warmth during rest and exercise. A sex comparison. Eur J Appl Physiol. 2014;114:1451–62.

Giamberardino MA, Affaitati G, Valente R, Iezzi S, Vecchiet L. Changes in visceral pain reactivity as a function of estrous cycle in female rats with artificial ureteral calculosis. Brain Res. 1997;774:234–8.

Golja P, Tipton MJ, Mekjavic IB. Cutaneous thermal thresholds – the reproducibility of their measurements and the effect of gender. J Therm Biol. 2003;28:341–6.

Gøransson L, Mellgren S, Lindal S, Omdal R. The effect of age and gender on epidermal nerve fiber density. Neurology. 2004;62:774–7.

Guieu R, Blin O, Pouget J, Serratrice G. Nociceptive threshold and physical activity. Can J Neurol Sci. 1992;19:69–71.

Hensel H. Temperaturempfindung und intracutane Wärmbewagung. Pflugers Arch. 1950;252:165–215.

Hensel H. Thermoreception and temperature regulation. Monogr Physiol Soc. 1981;38:1–321.

Hernandez M, Fox CL, Garcia-Moro C. Fueguian cranial morphology: the adaptation to a cold, harsh environment. Am J Phys Anthropol. 1997;103:103–17.

Hooton EA. Up from the ape. New York: The Macmillan Company; 1946.

Jay O, Havenith G. Skin cooling on contact with cold materials: a comparison between male and female responses during short-term exposures. Eur J Appl Physiol. 2003;93:1–8.

Jay O, Havenith G. Finger skin cooling on contact with cold materials: a comparison between male and female responses during short-term exposures. Eur J Appl Physiol. 2004;91(4):373–81.

Jay O, Havenith G. Differences in finger skin contact cooling response between an arterial occlusion and a vasodilated condition. J App Physiol. 2006; 100:1596–601.

Johnson EF, McClure J, Herron P, Baskerville KA. Anatomical variation, human diversity, and environmental adaptation. J Natl Med Assoc. 1993; 85:337–8.

Keith A. Man, a history of the human body. New York: Holt and company; 1912.

Kemppainen P, Pertovaara A, Huopaniemi T, Johansson G, Karonen SL. Modification of dental pain and cutaneous thermal sensitivity by physical exercise in man. Brain Res. 1985;360:33–40.

Kemppainen P, Pertovaara A, Huopaniemi T, Johansson G. Elevation of dental pain threshold induced in man by physical exercise is not reversed by cyproheptadine-mediated suppression of growth hormone release. Neurosci Lett. 1986;70:388–92.

Kenshalo Sr DR. Somesthetic sensitivity in young and elderly humans. J Gerontol. 1986;41:732–42.

Koltyn KF. Analgesia following exercise: a review. Sports Med. 2000;29:85–98.

Lambert M, Mann T, Dugas J. Ethnicity and temperature regulation. Med Sport Sci. 2008;53:104–20.

Lautenbacher S, Strian F. Sex differences in pain and thermal sensitivity: the role of body size. Atten Percept Psychophys. 1991;50:179–83.

Lee JY, Saat M, Chou C, Hashiguchi N, Wijayanto T, Wakabayashi H, et al. Cutaneous warm and cool sensation thresholds and the inter-threshold zone in Malaysian and Japanese males. J Therm Biol. 2010;35:70–6.

Leon GR, Koscheyev VS, Stone EA. Visual analog scales for assessment of thermal perception in different environments. Aviat Space Environ Med. 2008;79:784–6.

Li Y. The science of clothing comfort: a critical appreciation of recent developments. Oxford: The Textile Institute; 2001.

Meh D, Denišlič M. Quantitative assessment of thermal and pain sensitivity. J Neurol Sci. 1994; 127:164–9.

Meilgaard M, Civille GV, Carr BT. Sensory evaluation techniques. 4th ed. Boca Raton: CRC Press; 2007.

Nadel ER, Mitchell JW, Stolwijk JAJ. Differential thermal sensitivity in the human skin. Pflugers Arch Eur J Phys. 1973;340:71–6.

Nakamura M, Yoda T, Crawshaw LI, Yasuhara S, Saito Y, Kasuga M, Nagashima K, Kanosue K. Regional differences in temperature sensation and thermal comfort in humans. J App Physiol. 2008;105:1897–906.

Ouzzahra Y. Regional thermal sensitivity to cold at rest and during exercise [PhD thesis]. Loughborough University; 2012.

Ouzzahra Y, Redortier B, Voelcker T, Havenith G. Upper and lower body sensitivity to cold at rest and during exercise. In: Yokoyama S, editor. ICHES 2011: the Fourth International Conference on Human-Environment System; 2011 Nov 3–6; Sapporo, Japan. Japan: ICHES; 2011. p. 169–73.

Ouzzahra Y, Havenith G, Redortier B. Regional distribution of thermal sensitivity to cold at rest and during mild exercise in males. J Therm Biol. 2012;37:517–23.

Paalasmaa P, Kemppainen P, Pertovaara A. Modulation of skin sensitivity by dynamic and isometric exercise in man. Eur J Appl Physiol Occup. 1991;62:279–85.

Pertovaara A, Huopaniemi T, Virtanen A, Johansson G. The influence of exercise on dental pain thresholds and the release of stress hormones. Physiol Behav. 1984;33:923–6.

Ross HE, Murray DJ. E.H. Weber on the tactile senses. 2nd ed. Hove: Erlbaum, Taylor & Francis; 1996.

Sandby-Møller J, Poulsen T, Wulf H. Epidermal thickness at different body sites: relationship to age, gender, pigmentation, blood content, skin type and smoking habits. Acta Derma-Venereol. 2003;83(6):410–3.

Schepers RJ, Ringkamp M. Thermoreceptors and thermosensitive afferents. Neurosci Biobehav Rev. 2008;33:205–12.

Smith CJ, Havenith G. Body Mapping of Sweating Patterns in Athletes: A Sex Comparison. Med Sci Sports Exerc. 2012; 44:2350–2361.

Ständer S, Luger TA. Neuroreceptors & mediators. In: Granstein RD, Luger T, editors. Neuroimmunology of the skin. Berlin: Springer; 2009. p. 13–23.

Stevens JC, Marks LE, Simonson DC. Regional sensitivity and spatial summation in the warmth sense. Physiol Behav. 1974;13:825–36.

Strughold H, Porz R. Dia dichte der kaltpunkte auf der haut des men schlichen. Zeitschrift Biologie. 1931;91:563–571. Country. Optional translation of article title (MEDLINE/PubMed practice): the density of the cold spots on the skin of human. Z Biol. 1931;91:563–571.

Visser EP, Dias GJ. A case for reduced skin sensation in high latitude prehistoric polynesians. Ann Hum Biol. 1999;26:131–40.

Yarnitsky D, Ochoa JL. Studies of heat pain sensation in man: perception thresholds, rate of stimulus rise and reaction time. Pain. 1990;40:85–91.

Zhang H, Huizenga C, Arens E, Wang D. Thermal sensation and comfort in transient non-uniform thermal environments. Eur J Appl Physiol. 2004;92:728–33.

Skin Thermal Imaging

123

Francis J. Ring

Contents

Keywords
Skin temperature • Thermal imaging • Raynaud's phenomenon • Fever detection

1 Principle

The human body is endothermic. Human skin functions as an interface between the body core stable temperature (around 37 °C) and the variable environment temperature. Except in extreme cases such as strong sun-heat exposure, the skin surface is cooler than the blood. Therefore it should be possible to measure the variation of the skin blood perfusion by those of the skin surface temperature.

In normal conditions the latter depends on the outside temperature, the heat coming from the blood (variable with its location in the skin and transfer ability), and the heat generated by the skin (mostly the epidermis and appendages) metabolic activity. When inflammation or a high metabolic rate tumor develops within the skin or close deeper tissue, a heat conductive transfer is added. Practically the production of metabolic heat by healthy skin (0.16 cal min^{-1} cm^{-2}) (Houdas and Ring 1982) or even psoriatic skin (0.27 cal min^{-1} cm^{-2}) is too low to interfere.

F.J. Ring (✉)
Medical Imaging Research Unit, University of South Wales, Pontypridd, UK
e-mail: efring@glam.ac.uk

P. Humbert et al. (eds.), *Agache's Measuring the Skin*,
DOI 10.1007/978-3-319-32383-1_73

1.1 Contact Measurements: Thermometry

When a thermometer is applied on the skin, its temperature and the skin temperature are both modified at the point of contact (Stüttgen et al. 1989; Ring 1995). For the temperature at equilibrium to be very near the initial skin temperature, it is essential to comply with the following items: small contact area, low thermal sensor inertia, and moderate initial difference between temperatures. Furthermore, the skin heat being in continuous production induces its accumulation as soon as there is an occlusion of the skin surface. Contact skin temperature measurements must therefore be brief as possible.

1.2 Point Measurement

Thermometers use a variety of physical principles: thermocouples, electric resistance, thermistors, and semiconductors.

Thermocouples are an application of the thermal-electric effect. In a circuit made of two different metals (e.g., copper-constantan), a voltage is produced if the junctions are at different temperatures. This type of thermometer consists in a small applicator located at one of the junctions, the other being maintained at a stable temperature (reference temperature). A galvanometer records the generated voltage. The result is immediately displayed.

Metal resistance thermometers have an electric circuit consisting of a generator and a resistance (in nickel or platinum) which varies with temperature. The resistance is in the applicator which consequently has a large application area. However it is possible to find Pt sensors with a small contact area (less than 1 mm^2). The results are also displayed instantaneously.

Thermistors are also resistance thermometers, but provided with complex linearization electronics. Unfortunately they do not age well and it is necessary to recalibrate them regularly. Disposable probes are now available thus eliminating the need of cleansing and disinfection.

Semiconductors are based on a similar principle: the resistivity of the sensor varies with temperature. They are more durable and stable than thermistors and do not require frequent recalibration.

During application of contact thermometers, pressure must be avoided: this alters the blood flow, and the recorded temperature can be more like the interior of the skin, while the purpose of the measurement is to record the skin surface temperature.

For a point measurement, application should be made for 1 or 2 s only to prevent a disturbance of the temperature from occlusion or pressure. Metallic resistance and thermistor thermometers can have a preheated sensor, which may slightly modify the skin temperature. As a consequence they are preferably used for temperature monitoring over time, such as in intensive care.

The skin temperature in resting and neutral thermal conditions (i.e., the subject is naked, in resting position; in a room where the air and the walls are at the same temperature, close to 30 °C, the relative humidity is below 50 %, and the movement of the air is low (0.1 m to 0.2 m/s)) varies with body sites (Table 1), because each of them has its own vasculature pattern due to its anatomy and reactivity and has a specific thermal environment. Such diversity explains why the assessment of mean or average skin temperature requires measurements in numerous places. Modern infrared cameras can now image a whole body anterior and posterior from which total body mean temperatures can be readily calculated. Table 1 shows firstly the forehead as a relatively stable temperature and the large variability of the temperature in the extremities and then the homogenization of the temperatures in hot conditions and, in the opposite situation, great topographical diversity in cold conditions.

Skin temperature has a considerable inertia when compared to the variations in the arterial supply it depends on. For example, for a blood flow increase over 4 min followed by a plateau, the skin temperature rise may be seen only 6 min later and may plateau in 7 min.

Table 1 Current temperature on various body sites in an adult subject naked and lying supine in various environmental temperatures (Houdas and Ring 1982)

Body site	Cool (20 °C)	Thermal neutrality	Warm (40 °C)
Forehead	32.0	34.8	36.1
Palm	24.0	32.9	36.6
Volar forearm	27.7	33.6	36.7
Arm, anterior aspect	28.0	33.4	37.3
Chest, anterior	31.9	34.5	36.8
Close to umbilicus	31.3	34.4	36.2
Iliac fossa	30.7	34.7	36.1
Thigh anterior aspect	27.9	33.4	36.3
Leg, anterior aspect	25.8	32.7	36.4
Dorsum foot	20.0	31.1	37.0

1.3 Bidimensional Measurements (Mapping)

1.3.1 Noncontact Measurement: Thermography

Any warm surface emits an electromagnetic radiation whose energy is a function of the fourth power of its absolute temperature, according to the equation $E = \sigma\varepsilon T^4$ where σ is the Stefan-Boltzmann radiation constant and ε the surface emissivity. Between 32 °C and 36 °C (305–309 K), the skin surface emission is mainly at 10.5 μm, in the infrared (IR). It is therefore possible to measure, at a distance, the skin surface temperature by its IR radiation. Since water absorbs IR, the detected radiation is emitted by the stratum corneum, not by the underlying living tissues which are in a water environment. Like contact thermometry, thermography measures the skin superficial temperature. It provides the absolute temperature, but is mainly used to reveal topographical differences and follow variations on a quantitative image. Mapping of temperature distribution, absence of contact, and possibility of sustained observation provide many advantages over the contact methods. In recent years there has been a dramatic rise in the use of tympanic membrane radiometry, which has in many hospitals and clinics become more commonly used than contact thermometers for routine temperature assessment.

1.3.2 Thermal Imaging Cameras

IR cameras are of different types, depending on the IR detector, the image capture mode, and its processing (Ring et al. 2009). Cameras with cooled indium antimonide (AGA system) mainly detect 2–5.5 μm IR, which are wavelengths outside the absorbing zones of water. Mercury cadmium telluride IR cameras mainly detect 7–12.5 μm IR.

There are now a number of infrared cameras that use a focal plane array detector that can operate over a broader spectral band. Most of these do not need the cooling required for earlier detectors. There are continuous improvements and increasing numbers of detector elements. As a result modern systems are much easier to use in medicine. Excellent images can be obtained from 640 × 480 focal plane arrays. Compared to the earlier single-element scanners, they provide high resolution at high speed (real time). These improvements, together with a range of IR-transmitting lenses, also result in smaller compact cameras. In most cases now, a digital output signal can be directly fed to a small computer (earlier systems required the signal to pass through an analogue to digital converter, which increased the risk of calibration drift). With decreasing costs and improved reliability, thermal imaging is more available to clinicians who wish to use the technique. It is still recommended that the user purchases a blackbody temperature

reference source, which is needed to make regular checks on calibration of temperature, especially with the uncooled cameras. The thermographic signal is normally examined by computer image analysis.

1.3.3 Thermographic Image

The ranges of grays or colors indicate the difference of temperature (maximal thermal resolution 0.2 °C) in relation to a reference temperature selected by the operator. The larger the thermal resolution, the smaller the displayed temperature range. To obtain a good topographic discrimination, it is therefore necessary to choose the appropriate range, based on a reference temperature close to the average temperature of the zone investigated.

Finding both the temperature difference among body sites and especially hot or cold areas is easier in cool environmental conditions (Table 1), hence the choice of 22–23 °C as a usual examination room temperature.

For a selected ambient temperature, the skin temperature distribution is remarkably constant in the same individual. The fingertips are normally colder than the dorsal hands except in reactive hyperemia (Fig. 1a), but if the difference is over 2 °C, it indicates a vascular disease of the extremities (Fig. 1b). The warmest area is the head and the coldest the toes, and the difference is 4 °C in neutral thermal conditions, exceeding 10 °C in cold environmental conditions.

Reactive hyperemia, systemic or local cold test, heat test, and various pharmacological tests can be followed by thermography in real time with image registration at regular intervals or at some important times. For example, to measure the degree of a Raynaud syndrome and follow up the treatment, the generally used procedure is (Ring 1995):

- The patient remains seated in the examination room for 15 min, in neutral thermal conditions (in a room where the air and the walls are at the same temperature, close to 30 °C, the relative humidity is below 50 %, and the movement of the air is low (0.1 m to 0.2 m/s); in practice, the subject is neither cold nor too hot and does not feel any hot or cold air flow) with his forearms undressed.
- Thermogram of the dorsal side of both hands.
- The hands, in thin and transparent plastic gloves, are immersed up to the wrists in a 20 °C water bath for 1 min.
- Thermogram 10 min after removing the hands from the bath.

1.3.4 Interpretation

The thermograph image indicates an excessive or deficient heat supply to the skin surface. It may be due to a variation (increase or decrease) of the skin perfusion by the warm blood coming from the deeper parts or of a thermal transmission from underlying tissues.

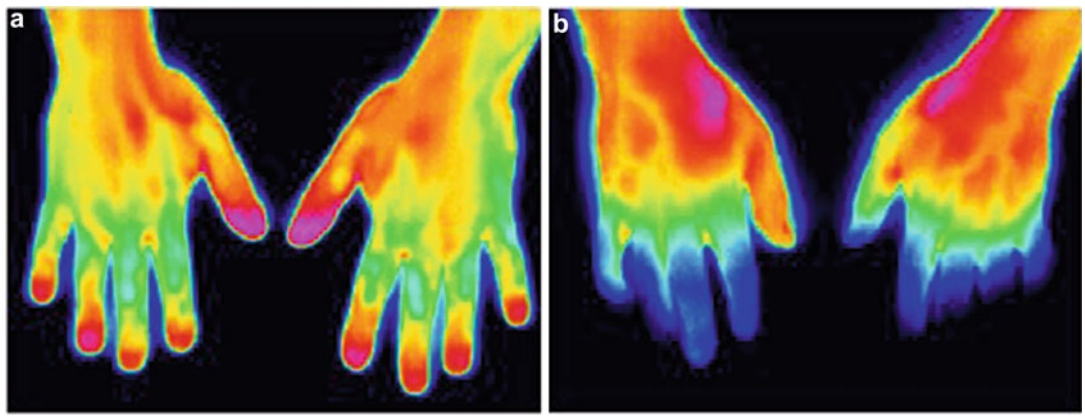

Fig. 1 (**a**) Reactive hyperemia in normal hands post-cooling by 1 min 20 °C water (hand protected by thin plastic gloves). (**b**) Thermogram of hands of a Raynaud's phenomenon patient after same water immersion as above

The first case applies to active (i.e., arteriolar) vasodilatation: opening of the "skin radiator" valve. A passive vasodilatation, for example, by increase of the venous pressure only (standing up from lying), remains invisible. The "skin radiator" is the subepidermal vascular plexus; therefore, any active erythema has a thermographic version. But the skin can be normally perfused and warm without erythema, and thermography can then show the topography of this invisible active vasodilatation. In inflammation, thermography is a means of assessing the extent of the process and its intensity (by the degree of thermal increase).

In the second case, a deeper source of heat, without involvement of the subepidermal plexus, is shown by thermography. The skin is warmer along the subcutaneous normal veins and varicose veins. The warm thermographic image of actively growing tumors depends on their intense angiogenesis, which usually connected with their proliferating activity.

Thermography detects the transmission to the skin surface of heat produced in deeper tissues. Any disruption in this transfer, such as edema or thickened tissues, impairs the image. A typical example is the papular urticaria. Accordingly a hyperthermia in an edematous zone would be most likely related to active vasodilatation of the subepidermal plexus.

These principles have resulted in some of the most interesting uses of thermography:

- Detection and delineation of invisible cutaneous, subcutaneous, or deeper tissue inflammation, since without erythema: for example, the persistent peri-lesion vasodilatation after healing in psoriasis, the lymph or blood drainage path of a tumor, and the degree of inflammation of a joint.
- Invisible vasoconstriction detection (Stüttgen and Flesch 1985) (e.g., in healed psoriasis lesions) or analysis (the blanched area induced by topical corticosteroids spreads beyond the area of hypothermia, which would indicate a preferential effect of the drug on capillaries rather than arterioles).
- Investigation of angiodysplasias in order to discern hyperperfused (warm), stagnant (cold), and normally perfused zones and to follow them up during treatment.
- Assessment of malignant tumor growth (generally associated with hyperthermia).
- The dermatological use of thermography is well developed and illustrated in the work of Stüttgen and Flesch (1985).

2 Good Practice

2.1 Examination Room

- An air lock is an ideal way to reduce temperature changes and drafts occurring on entrance or exit. This air lock may also be used as a cubicle for the patient to undress (Ammer and Ring 2013).
- The volume of the room must include air conditioning. Surface: 8–12 m^2. Maximal height 2.5 m in order to reduce temperature differences between the floor and the ceiling, which are reproduced between the patient's feet and head in standing position.
- Thermal insulation of the walls of the room can improve thermal stability.
- Air conditioning is essential, preferably set at 22–23 °C, so that the skin temperature differences are clearly revealed but allowing the undressed patient to feel comfortable. It is most efficient if left to operate day and night continuously. The relative humidity must not exceed 50 % since the stratum corneum hydration alters its emissivity.
- To reduce thermal currents to the minimum, it is recommended to block up the windows because they let the cold and the sun in.
- Avoid reflecting materials (aluminum, steel) or paint any reflecting surfaces. Walls should also be covered in nonreflecting paint.
- Room lighting should be operated by cold light or fluorescent tubes providing indirect lighting.

The central heating radiators should be placed as far as possible from the examination table, in any case not less than 2 m.

2.2 Method

- The subject should stay at least 15 min at room temperature before the examination takes place.
- Clothes strongly modify the thermal environment of the skin. The subject must therefore be undressed 15 min before the test.
- Alcohol or spicy food must be avoided 2 h prior to the examination to avoid the risk of facial, thorax, or extremity flush, in spite of the absence of erythema.
- The skin must be dry as humidity absorbs IR. Wet skin looks cold. A wound can appear to be 2 °C below its actual temperature.
- The subject must be placed at least 15 cm from the nearest wall, to avoid heat reflection, and 2 m from any source of heat.
- There should be no entrance or exit from the room during the examination.

2.3 Commercial Equipment

Most modern infrared cameras today are better equipped with faster detectors than the earlier systems of more than 30 years ago. Focal plane arrays are fast and efficient, providing images at real-time video speeds. There is now a wider range of cameras that operate successfully for medical applications without the need for detector cooling (Ring et al. 2009). However, it is always recommended that such systems should be used with an external blackbody reference temperature source. Time to reach stability can vary, and it is necessary to take a series of images for measurement from a known stable temperature reference source to verify when an individual camera is ready for image capture and temperature measurement. Modern systems also generate a digital thermal image, so that connection to a computer can be by fire wire or by wireless transmission. In many cases, a storage provision within the camera itself can be used, allowing the operator to download to the computer at a later time for detailed image analysis. In recent years the image and temperature resolution has increased. Currently many systems provide thermal images at 320 × 240 pixels, with 640 × 480 and upward becoming readily available at higher cost. Manufacturers and agencies exist now in many countries around the world. A large company that has integrated several well-known manufacturers is based in Sweden and the USA with a wide range of systems for many different applications in medicine science and industry. Whatever the choice of camera system selected for medical studies, it is important that regular maintenance by the company be undertaken. A thermal camera may perform to the manufacturer's specification for a period of time from leaving the factory, but is subject to offset drift, and multielement detectors can be affected by individual pixel and detector loss, which the manufacturer needs to deal with on a regular basis.

Reproducible results with thermal imaging depend on rigorous technique by the operator. Standardized procedures are now commonly adopted and can be found in the literature.

3 Clinical Applications

A number of modern reviews indicate that some applications have become more widely accepted in clinical medicine than others (Ring and Ammer 2012; Lahiri et al. 2012). Inflammatory lesions such as those found in the arthritides, rheumatoid arthritis, osteoarthritis, gout, psoriatic arthropathies, scleroderma, etc. can be effectively monitored by thermal imaging. The effect of anti-inflammatory treatments can be objectively monitored and has been documented in controlled clinical trials. Topical agents applied to the skin may be observed as a dynamic process (Fig. 2). In peripheral vascular diseases, skin temperature monitored by thermal imaging can be efficiently studied, particularly where a thermal or pharmacological challenge has been applied. Raynaud's phenomenon and vibration injury (hand-arm vibration syndrome) and complex regional pain syndrome are examples.

Due to the international concerns of pandemic influenza and the massive increase in air travel, attention has been focused on the use of thermal imaging in fever screening. The International

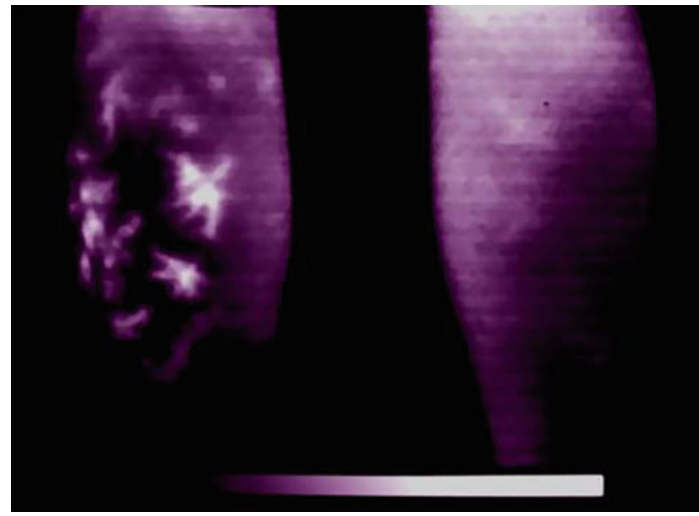

Fig. 2 Response to nicotinic acid spray to the calf

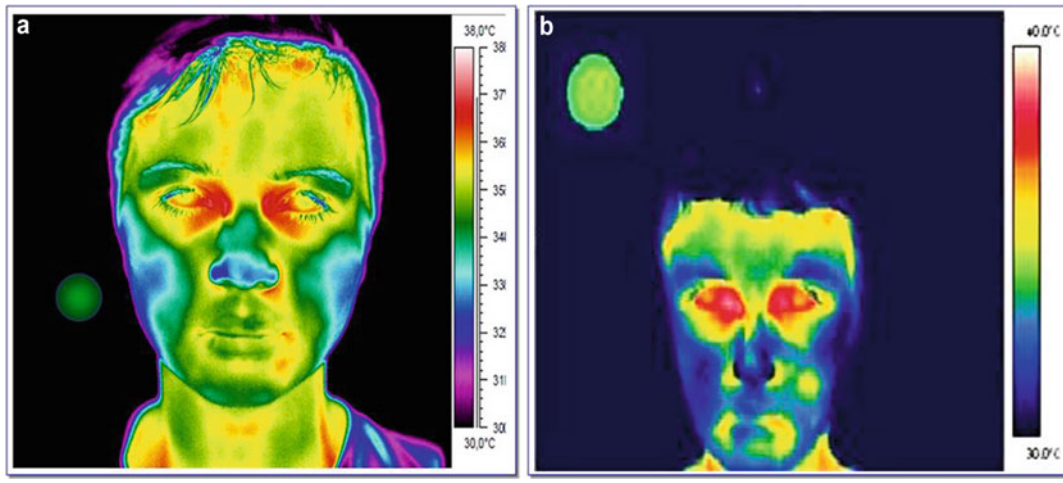

Fig. 3 (**a**) Thermogram of the face of a young male without fever. The checks and nose are the coolest areas. (**b**) Thermogram of the face of a young male with fever. The forehead checks and nose are cooler due to sweating. There is increased heat at the inner canthi of the eyes

Standards Organization has published two documents that specify the minimum technical requirements for this and also the required procedure to capture meaningful information from a close-up thermal image of the face. It is now shown that from such a close-up image, the temperature measured at the inner canthus of the eye can provide discriminatory evidence of systemic fever in children and adults compared to nonfebrile subjects (Fig. 3a, b) (Ring et al. 2013).

4 Conclusion

The technical performance of thermal imaging cameras, together with the power of computing and image processing, has transformed this technique in recent years. As a result the physiological knowledge of skin temperature in health and disease has also improved. From noninvasive monitoring of treatments to studies

in high-performance sport science, infrared thermal imaging has matured and when correctly performed can be a valuable and reliable objective imaging procedure in certain aspects of clinical medicine. The very high costs of the past have fallen, and performance has risen, making this technique more accessible than in the former years of its development.

References

Ammer K, Ring EFJ. Chapter 32.1–14, Standard procedures for infrared imaging in medicine. In: Diakides M, Bronzino JD, Petersen DR, editors. Medical infrared imaging principles and practices. Boca Raton/London/New York: CRC Press; 2013.

Houdas Y, Ring EFJ. Human body temperature, its measurement and regulation. New York: Plenum; 1982.

Lahiri BB, Bagasvathiappan S, Jayakumar T, Philip J. Medical applications of infrared thermography: a review. Infrared Phys Technol. 2012;55:221–35.

Ring EFJ. Thermal imaging of skin temperature. In: Serup J, Jemec GBE, editors. Handbook of non-invasive methods and the skin. Boca Raton: CRC Press; 1995. p. 457–71.

Ring EFJ, Ammer K. Infrared thermal imaging in medicine. Physiol Meas. 2012;33:R33–46.

Ring EFJ, Thomas RA, Howell KJ. Chapter 9, Sensors for medical thermography and infrared radiation measurements. In: Jones D, editor. Biomedical sensors. New York: Momentum Press; 2009.

Ring EFJ, Jung A, Kalicki B, Zuber J, Rusteka A, Vardasca R. New standards for fever screening with thermal imaging. J Mech Med Biol. 2013:1350045 (12 pp). doi:10.1142/S0219519413500450. World Scientific Publishing.

Stüttgen G, Flesch U, editors. Dermatological thermography. Weinheim: Verlag Chemie (VCH); 1985.

Stüttgen G, Ott A, Flesch U. Measurement of skin temperature. In: Leveque JL, editor. Cutaneous investigation in health and disease. New York: Marcel Dekker; 1989. p. 275–322.

Validity, Reliability, and Reproducibility of Skin Temperature in Healthy Subjects Using Infrared Thermography

124

Ismael Fernández-Cuevas, Joao Carlos Marins, Javier Arnáiz Lastras, Pedro Gómez Carmona, and Manuel Sillero Quintana

Contents

Keywords

Reliability • Reproducibility • Validity • Skin temperature • Infrared thermography • Humans • Healthy • Overweight • Patients • Software

By measuring the skin temperature (Tsk), there are a lot of factors, which could influence the results (Fernández-Cuevas et al. 2015). Among them, validity and reliability are two of the most important ones to take into account in order to obtain the more accurate and consistent results. Those adjectives – accurate and consistent – seem to be similar but they are not. On the one hand, accuracy is directly related to validity, and **validity** refers to whether a measurement is well founded and corresponds accurately to the real world. One the other hand, **reliability** is related to consistency because it refers to the degree to which the measurement gives the same result in repeated measurements.

Infrared thermography (IRT) is a rapid and noninvasive technology widely used to assess Tsk. In this case, the validity refers to how well IRT measures Tsk and, consequently, permits appropriate interpretation of Tsk scores. However, the reliability of IRT shows if this technology gives the same results in different situations (with different observers or software). Besides, Tsk reproducibility is related to the concept of reliability, and it is used here to describe the consistency of the temperature of the skin itself along the time.

In this chapter, a review of results about validity and reliability of IRT and reproducibility of Tsk will be shown, as well as a discussion about

I. Fernández-Cuevas (✉) • J. Arnáiz Lastras • P. Gómez Carmona • M. Sillero Quintana
Faculty of Sciences for Physical Activity and Sport (INEF), Universidad Politécnica de Madrid, Madrid, Spain
e-mail: ismael.fernandez@upm.es

J.C. Marins
Human Performance Laboratory – LAPEH, Universidade Federal de Viçosa (Brazil), Minas Gerais Código, Viçosa, Brazil

P. Humbert et al. (eds.), *Agache's Measuring the Skin*,
DOI 10.1007/978-3-319-32383-1_74

the convenience of using manual methods or software to analyze IRT images.

1 Infrared Thermography

Infrared thermography (IRT) is a safe, noninvasive, and low-cost technique that allows the rapid and noncontact recording of the irradiated energy released from the body (Akimov and Son'kin 2011; Merla et al. 2005; Ng 2009; Costello et al. 2012; Hildebrandt et al. 2012). IRT measures skin temperature (Tsk), and since it started to be used with human beings (the early 1960s), the development of this technique focused on discovering the validity of IRT to diagnose pathologies (Liu and Xu 2000). Due to conflicting results and a lack of methodological standards and quality assurance (Head and Elliott 2002), the IRT was replaced by emerging and more accurate technologies such as X-rays, ultrasound devices, or magnetic resonance: from initial enthusiastic interest to almost complete obscurity.

However, the technological improvements of IRT in the last years have made possible a resurgence of this technique (Jiang et al. 2005; Vainer 2005; Cheng et al. 2009; Spalding et al. 2008; Skala et al. 2011), paving the way to new applications of IRT for humans not only focused on the diagnosis (Marins et al. 2015). Even if IRT has been widely used in pathological conditions, there are much less data available from healthy subjects (Zaproudina et al. 2008). Moreover, the increase of interest on the application of IRT, not only in the medical sector but also in other fields as the physical activity with healthy subjects, makes it more necessary to increase the knowledge concerning the factors affecting the application of IRT on humans (Costello et al. 2012; Zaproudina et al. 2008; Ring and Ammer 2012), as well as the reproducibility of IRT measurements in different potential groups of application as children, elderly, overweight, disabled, or physically active subjects.

Ring recently defended and described the new features of IRT technology and the improvement on standardization protocols (Ring and Ammer 2012). Nevertheless, most research groups keep on analyzing IRT images using the software packages provided by the camera manufacturers, which are mainly created for industrial or architectural purposes, rarely adapted to human analysis (Murawski et al. 2003). Specific IRT software for humans is rare, but its reliability results are excellent by comparing with manual techniques. Therefore, there is a remarkable necessity of a larger supply on software to analyze IRT images of human beings.

2 Validity

As it was mentioned, validity refers to whether a measurement is well founded and corresponds accurately to the real world. In the case of IRT, validity would be the ability to estimate temperatures of an object's surface from its infrared radiation as recorded using a thermal camera. Burnham et al. (2006) demonstrated a good validity of a skin infrared thermometer ($r = 0.92$), but only Sherman et al. (1996) published a study of the validation of "video thermography."

Among the several technical improvements that have been made in IRT in the previous decades, certain aspects, such as the number of frames per seconds, the resolution, and the weight of the equipment, have notably improved.

Accuracy is directly related to the validity of IRT given that it refers to how close the thermal readings of an IRT camera are to the true temperature. Even if the accuracy has improved, IRT-based measurements are more than 1 °C (or 1 %) different from the actual temperature (in the best cameras). This is not a large error in the evaluation of a building or in an industrial setting. However, considering how important precision is in measuring human temperatures (more than 0.25 °C of side-to-side asymmetry is considered to be abnormal), poor accuracy could represent one of the weakest points of IRT. Nevertheless, since we work by comparing Tsk from bilateral ROIs on the same image, the potential error will be the same, and therefore it will not affect the final results in terms of asymmetry.

The validity of IRT as a diagnostic tool has been conclusively demonstrated in the context of several pathologies and injuries, including reflex

sympathetic dystrophy (Bruehl et al. 1996), stress fractures (Goodman et al. 1985), pneumothorax (Rich et al. 2004), dermatological pathologies (George et al. 2008), and diabetes (Sivanandam et al. 2012). However, studies of its validity have been performed only for specific applications (Owens et al. 2004; Roy et al. 2006).

Burnham et al. (2006) demonstrated a good validity of a skin infrared thermometer (ICC = 0.92) (see Table 1), but only Sherman et al. (1996) published a study of the validation of "video thermography," that is to say IRT.

To avoid the potential errors in IRT camera measurement accuracy (±2 % or ±1 % in the best cases), certain authors place a constant and known temperature source into the thermogram to calibrate the measurement of the thermal imager. Ring and Ammer (2000) assert that, despite the

Table 1 Reliability results (ICC) of several published articles about IRT validity

Year	Author	N	Sample	Pathology	Technique	ROI	ICC
1991	Plaugher	19	Healthy		IRT	Paraspinal	0.5–0.8
1999	Oerlemans	13	Patients	Reflex sympathetic dystrophy (RSD)	IRT thermometer	Hands	0.94
2003	Ammer	1	Healthy		IRT	Arm	0.48–0.87
2004	Owens	30	Healthy		IRT scanner	Paraspinal	0.92–0.97
2004	Varju	91	Patients	Hand osteoarthritis	IRT	Hands	0.899
2006	Burnham	17	Healthy		IRT thermometer	Different ROIs	0.97
2006	Selfe	9	Patients	Anterior knee pain	IRT	Knee	0.82–0.97
2007	Hart	30	Healthy		IRT scanner	Spine	>0.75
2008	Spalding	5	Patients	Wrist arthritis	IRT	Wrist	0.99
2008	Zaproudina	16	Healthy		IRT	Different ROIs	0.47
2009	Gold	45	Patients and healthy	Upper extremity musculoskeletal disorder (UEMSD)	IRT	Hands	0.46–0.85
2009a	Hildebrandt	15	Patients and healthy	Knee injuries	IRT	Knee	0.75–0.85
2010	Denoble	30	Patients and healthy	Knee osteoarthritis	IRT	Knee	0.5–0.72
2011	McCoy	100	Healthy		IRT scanner	Spine	0.95–0.97
2011	Pauling	15	Healthy		IRT	Hands	0.83–0.96
2012	Fernández-Cuevas	22	Healthy overweight		IRT	Different ROIs	0.989
2013	Costa	62	Patients and healthy	Temporomandibular disorder (TMD)	IRT	Face and neck	0.85–0.99
2012	Christensen	62	Healthy		IRT	Face	?
2012	Fernández-Cuevas	32	Healthy		IRT	Different ROIs	0.68–0.99
2013	Choi	28	Patients	Complex regional pain syndrome (CRPS)	IRT	Limbs	0.865
2013	Rodrigues-Bigaton	30	Patients and healthy	Temporomandibular disorder (TMD)	IRT	Face	0.84–0.87
2014	Rossignoli	24	Patients	Wheelchair users (WCUs)	IRT	Different ROIs	0.39–0.79
2015	Dibai-Filho	24	Healthy		IRT	Trapezius	0.62–0.92

internal reference temperature of many current thermal systems, using a reference source for calibration is highly recommended to improve the IRT results (Simpson et al. 2008). We therefore suggest the use of a calibration source for using IRT on humans until camera providers improve the imager's accuracy within the 20–50 °C range.

3 Reliability

Reliability refers to the degree to which the measurement gives the same result in repeated measurements. Likewise, repeatability and reproducibility are sub-terms of reliability, all of them related to consistency. In quantitative research, reliability studies aim to prove the consistency of analysis methods or instruments, as for example, if a manual analysis methodology gives the same results independently of the observer who takes the IRT image. Reproducibility is more related to the consistency of results along the time, which means, to investigate if Tsk is consistent now, in 5 s, 24 h, or 2 months (see Fig. 1). Repeatability is related to the consistency of findings obtained after the same procedure was repeated (Bartlett and Frost 2008).

However, both concepts are often mixed in the literature, and reliability is with no doubt the most used to describe the consistency of Tsk. According to statistics, there are different ways to investigate the reliability and reproducibility. Intra-class correlation coefficient (ICC) is the most common coefficient to describe the consistency (intra- and inter-examiner). In addition to this two-way mixed model, coefficient of variation (CV) represents another useful coefficient to show the dispersion of data, but less current in the literature. Lastly, Bland-Altman plots are an illustrative way to visualize the dispersion of data with agreement limits (see Fig. 2).

Although Tsk should be constant over time (Frim et al. 1990) and symmetric on both sides of the body (Uematsu et al. 1988; Niu et al. 2001), the list of the factors that affect the skin temperature is tremendously large (Ring and Ammer 2000) that the infeasibility of controlling for all of these factors could be considered one of the weakest points of IRT.

Therefore, to improve the applicability of IRT, better cameras with more advanced features should be developed, and the behavior of skin temperature due to the influence of different extrinsic and intrinsic factors should be studied.

3.1 IRT Software Reliability

Traditionally, human IRT images have been processed manually using IRT applications that were designed for other purposes or sectors (i.e., industry, construction, etc.). In this sense, certain authors reported inter-examiner variations (Plaugher et al. 1991; Zaproudina et al. 2008;

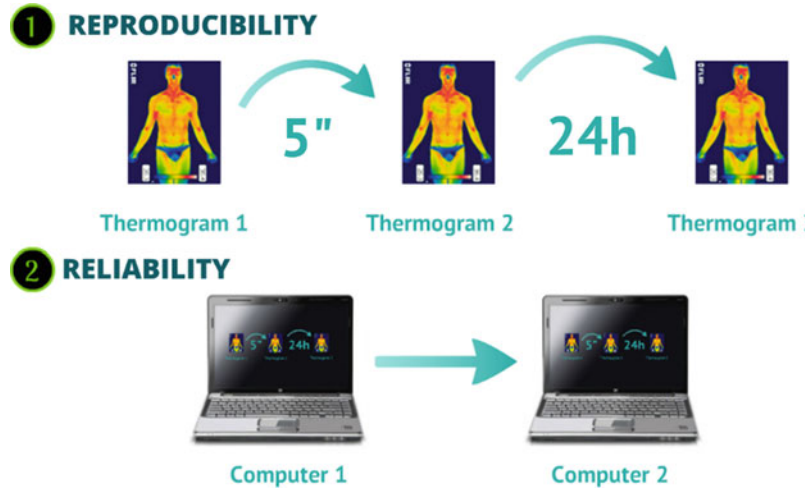

Fig. 1 Representation of the difference between reliability and reproducibility study design

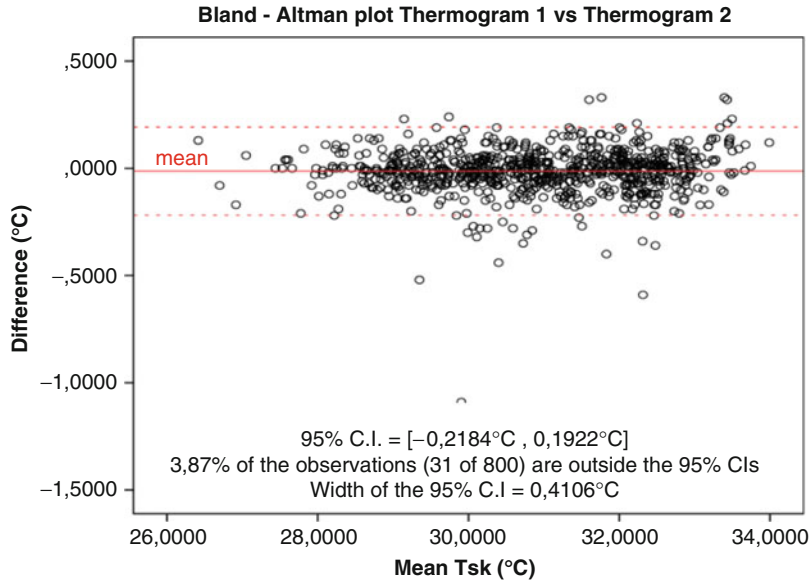

Fig. 2 Example of Bland-Altman plots for intra-examiner agreement between the same observer in two thermograms (separated by 5 s) showing dispersion of data (Fernández-Cuevas 2012)

Costa et al. 2013) due to the difficulty of manually selecting the region of interest (ROI) from the human IRT images (Ammer 2003).

Therefore, in addition to the efforts that have been made to create standardized protocols and guidelines (Ring and Ammer 2000; Schwartz 2006; Ammer 2008), there is a remarkable necessity of specific software program to make this difficult task more simple, efficient, and reliable. Nowadays, the supply of specific software is poor. On the one hand, there are some laborious solutions created by some research groups to analyze IRT images automatically (Murawski et al. 2003; Vardasca 2008; Fournet et al. 2013). On the other hand, a few specific software to investigate and analyze IRT images of humans are developed and sold by private companies, as TotalVision™ (infrared screening), Meditherm IRIS™ (breast cancer company), and Termotracker® and its new version ThermoHuman® (ThermoHuman, from sports sector).

From all of them, Termotracker® is the only one to have published reliable results (Fernández-Cuevas et al. 2012). This software uses a computer vision algorithm, which automatically identifies the body shape and ROIs from the IRT images, generating a database with the primary data of the considered ROI. The reliability results of Termotracker® are almost perfect (Fernández-Cuevas et al. 2012), and the new version ThermoHuman® will improve those results. By comparing the results with those that were obtained by manual methods (Zaproudina et al. 2008), the higher reliability, even with respect to the ICCs for the intra-examiner data, may be due to the automatic ROI identification process, a task that was performed by an observer in similar studies (Selfe et al. 2006; Hildebrandt et al. 2009b; Denoble et al. 2010).

In general terms, some studies that have examined inter- and intra-examiner reliability of IRT cameras reported good results (Selfe et al. 2006; Littlejohn 2008; Spalding et al. 2008; Zaproudina et al. 2008; Hildebrandt et al. 2009b; Denoble et al. 2010; Pauling et al. 2011), but none achieved such excellent ICCs as the results that are reported in Fernández-Cuevas (2012), and the reason lies surely in the fact of applying a computer vision. The automation on the process of determining the ROIs improves the IRT reliability and allows for a more rapid and more efficient IRT analysis of the thermograms from humans. Although the results reached by Termotracker® are not perfect (ICC = 0.999), there is no doubt that software solutions are faster and more accurate to analyze IRT images than manual methods, and therefore, there is a clear necessity of further investigation and supply of new specific software.

3.2 Reproducibility of IRT Values

IRT reliability has been examined in several works, both with patients (Selfe et al. 2006; Spalding et al. 2008; Hildebrandt et al. 2009b; Denoble et al. 2010; Costa et al. 2013; Choi et al. 2013) and healthy subjects (Zaproudina et al. 2008; Littlejohn 2008; Pauling et al. 2011). The majority of these studies achieved ICCs that ranged between 0.4 and 0.9 (see Table 1). However, certain of these studies reported the influence of factors, such as technical errors, the physiological variability from 1 day to another (Zaproudina et al. 2008), or the existence of previous injuries (Hildebrandt et al. 2009b). Recently, a study was performed (Fernández-Cuevas 2012) with only one examiner, following an adaptation of the guidelines from the European Association of Thermology (EAT) (Ammer 2008). Three consecutive thermograms from healthy subjects were taken, separating the first two thermograms by only 5 s and waiting 24 h to record the third thermogram under similar conditions as the two first assessments. With this study design, the aim was to identify the influence of time on Tsk variability and to avoid the potential influence of the factors that are mentioned in previous research.

According to the Littlejohn (2008) classification of ICC values (poor: 0–0.39, Fair: 0.40–0.59, Good: 0.60–0.79 and Excellent: 0.80–1.0), the results of this study (Fernández-Cuevas 2012) revealed excellent ICC values between the two first thermograms (5 s between readings), both in terms of the Tsk values (mean ICC = 0.991) and the side-to-side differences (ΔT) (mean ICC = 0.953); these results are nearly perfect. They suggest that the slight variation between the first two readings may be due not to the variability of Tsk but to small variations in the infrared camera; therefore, a calibration system with a black body was used (Plassmann et al. 2006). Moreover, when comparing the results of Tsk from thermograms 1 and 3 (separated by 24 h), which were conducted in similar conditions as other authors have used (Zaproudina et al. 2008; Hildebrandt et al. 2009b), the ICC outcomes differed depending on the ROI. With respect to Tsk values, the better ICCs were those from the muscle and central ROIs (i.e., abdominal, back, thigh, lumbar, dorsal), and the worst ICCs were for the joint ROIs (i.e., knee, ankle, elbow). These results are similar with those of Zaproudina et al. (2008), who demonstrated lower ICC values for the distal and joint ROI, such as the knee.

Moreover, there is a growing use of thermal asymmetries in the application of IRT on humans (Feldman and Nickoloff 1984; Uematsu et al. 1988; Niu et al. 2001; Vardasca 2008) to calculate the side-to-side differences (ΔT) in selected bilateral ROIs. A recent study (Fernández-Cuevas 2012) indicated that, when tracking a single ROI over time (e.g., monitoring an injury), muscular and central ROIs measurements are more reproducible. However, when examining asymmetries or bilateral values (ΔT), which are actually very useful tools with which to detect pathologies (Niu et al. 2001) or injury risks (Gómez Carmona 2012), the most reliable ΔT values are for the joints and the central ROI (i.e., the pectoral and shoulder ROIs).

4 Conclusions

The validity of IRT to assess Tsk has been proven, but it could improve if infrared cameras would be conceived to human applications. Although there are differences in the methodology among studies, most of them show good reproducibility results. However, it has been also demonstrated that the reproducibility of the Tsk measurements slightly decreased with some factors as the regions of interest (ROI) analyzed and the time between measurements. Regarding reliability results, specific software solutions seem to be the best option to analyze IRT images, but the supply of them is still poor.

References

Akimov E, Son'kin V. Skin temperature and lactate threshold during muscle work in athletes. Hum Physiol. 2011;37(5):621–8.

Ammer K. Need for standardisation of measurements in thermal imaging. In: Wiecek B, editor. Thermography and lasers in medicine. Lodz: Akademickie Centrum Graficzno-Marketigowe Lodar S.A; 2003. p. 13–7.

Ammer K. The glamorgan protocol for recording and evaluation of thermal images of the human body. Thermol Int. 2008;18(4):125–9.

Bartlett JW, Frost C. Reliability, repeatability and reproducibility: analysis of measurement errors in continuous variables. Ultrasound Obstet Gynecol: Off J Int Soc Ultrasound Obstet Gynecol. 2008; 31(4):466–75.

Bruehl S, Lubenow TR, Nath H, Ivankovich O. Validation of thermography in the diagnosis of reflex sympathetic dystrophy. Clin J Pain. 1996;12(4):316–25.

Burnham RS, McKinley RS, Vincent DD. Three types of skin-surface thermometers: a comparison of reliability, validity, and responsiveness. American journal of physical medicine & rehabilitation / Association of Academic Physiatrists. 2006;85(7):553–8.

Cheng VS, Bai J, Chen Y. A high-resolution three-dimensional far-infrared thermal and true-color imaging system for medical applications. Med Eng Phys. 2009; 31(9):1173–81.

Choi E, Lee P-B, Nahm FS. Interexaminer reliability of infrared thermography for the diagnosis of complex regional pain syndrome. Skin Research and Technology. 2013;19(2):189–93.

Christensen J, Vaeth M, Wenzel A. Thermographic imaging of facial skin – gender differences and temperature changes over time in healthy subjects. Dentomaxillofac Radiol. 2012;41(8):662–7.

Costa ACS, Dibai Filho AV, Packer AC, Rodrigues-Bigaton D. Intra and inter-rater reliability of infrared image analysis of masticatory and upper trapezius muscles in women with and without temporomandibular disorder. Braz J Phys Ther. 2013;17(1): 24–31.

Costello JT, McInerney CD, Bleakley CM, Selfe J, Donnelly AE. The use of thermal imaging in assessing skin temperature following cryotherapy: a review. J Therm Biol. 2012;37(2):245–74.

Denoble AE, Hall N, Pieper CF, Kraus VB. Patellar skin surface temperature by thermography reflects knee osteoarthritis severity. Clin Med Insights Arthritis Musculoskelet Disord. 2010;3:69–75.

Dibai-Filho AV, Guirro EC, Ferreira VT, Brandino HE, Vaz MM, Guirro RR. Reliability of different methodologies of infrared image analysis of myofascial trigger points in the upper trapezius muscle. Braz J Phys Ther. 2015;19(2):122–8.

Feldman F, Nickoloff EL. Normal thermographic standards for the cervical spine and upper extremities. Skeletal Radiol. 1984;12(4):235–49.

Fernández-Cuevas I. Effect of endurance, speed and strength training on skin temperature measured by infrared thermography. Madrid: Universidad Politécnica de Madrid; 2012.

Fernández-Cuevas I, Marins JC, Gómez Carmona PM, García-Concepción MÁ, Arnáiz Lastras J, Sillero Quintana M. Reliability and reproducibility of skin temperature of overweight subjects by an infrared thermography software designed for human beings. Thermol Int. 2012;22:130. Apendix 1 to number 3.

Fernández-Cuevas I, Bouzas Marins JC, Arnáiz Lastras J, Gómez Carmona PM, Piñonosa Cano S, García-Concepción MÁ, et al. Classification of factors influencing the use of infrared thermography in humans: a review. Infrared Phys Technol. 2015;71:28–55.

Fournet D, Ross L, Voelcker T, Redortier B, Havenith G. Body mapping of thermoregulatory and perceptual responses of males and females running in the cold. J Therm Biol. 2013;38(6):339–44.

Frim J, Livingstone SD, Reed LD, Nolan RW, Limmer RE. Body composition and skin temperature variation. J Appl Physiol. 1990;68(2):540–3.

George J, Bensafi A, Schmitt AM, Black D, Dahan S, Loche F, et al. Validation of a non-contact technique for local skin temperature measurements. Skin Res Technol. 2008;14(4):381–4.

Gold JE, Cherniack M, Hanlon A, Dennerlein JT,Dropkin J. Skin temperature in the dorsal hand of office workers and severity of upper extremity musculoskeletal disorders. Int Arch Occup Environ Health. 2009;82(10): 1281–92.

Gómez Carmona PM. Influencia de la información termográfica infrarroja en el protocolo de prevención de lesiones de un equipo de fútbol profesional español. Madrid: Universidad Politécnica de Madrid; 2012.

Goodman PH, Heaslet MW, Pagliano JW, Rubin BD. Stress fracture diagnosis by computer assited thermography. Physician Sportsmed. 1985;13(4):114

Hart J, Omolo B, Boone WR, Brown C, Ashton A. Reliability of three methods of computer-aided thermal pattern analysis. J Can Chiropr Assoc. 2007;51(3): 175–85.

Head JF, Elliott RL. Infrared imaging: making progress in fulfilling its medical promise. Eng Med Biol Mag IEEE. 2002;21(6):80–5.

Hildebrandt C, Raschner C. An intra-examiner reliability study of knee temperature patterns with medical infrared thermal imaging. Thermol Int. 2009a;19(3):73–6.

Hildebrandt C. Medical infrared thermography as a screening tool for knee injuries in professional junior alpine-ski-racers in Austria – Findings of a pilot study. In: Sciences EECoS, editor. 14th annual ECSS Congress; Oslo, Norway: ECSS European College on Sport Sciences; 2009b.

Hildebrandt C, Raschner C, Ammer K. An overview of recent application of medical infrared thermography in sports medicine in Austria. Sensors. 2010;10(5): 4700–15.

Hildebrandt C, Zeilberger K, Ring EFJ, Raschner C. The application of medical infrared thermography in sports medicine. In: Zaslav KR, editor. An international perspective on topics in sports medicine and sports injury. InTech; 2012. p. 534.

Jiang LJ, Ng EY, Yeo AC, Wu S, Pan F, Yau WY, et al. A perspective on medical infrared imaging. J Med Eng Technol. 2005;29(6):257–67.

Littlejohn RAN. Thermographic assessment of the forearm during data entry tasks: a reliability study. Virginia Tech.; Blacksburg, Virginia, USA 2008.

Liu J, Xu LX. Boundary information based diagnostics on the thermal states of biological bodies. Int J Heat Mass Transfer. 2000;43(16):2827–39.

Marins J.C.B, Fernández-Cuevas I, Arnaiz-Lastras J, Fernandes A.A. y Sillero-Quintana M. Aplicaciones de la termografía infrarroja en el deporte. Una revisión / Applications of Infrared Thermography in Sports. A Review. Revista Internacional de Medicina y Ciencias de la Actividad Física y el Deporte. 2015;60: 805–824. http://cdeporte.rediris.es/revista/revista60/artaplicaciones594.htm.

McCoy M, Campbell I, Stone P, Fedorchuk C, Wijayawardana S, Easley K. Intra-examiner and inter-examiner reproducibility of paraspinal thermography. PLoS One. 2011;6(2):e16535.

Merla A, Iodice P, Tangherlini A, De Michele G, Di Romualdo S, Saggini R, et al. Monitoring skin temperature in trained and untrained subjects throughout thermal video. Conf Proc IEEE Eng Med Biol Soc. 2005; 2(1):1684–6.

Murawski P, Jung A, Ring FEJ, Zuber J, Plassmann P, Kalicki B. "Image ThermaBase" – a software programme to capture and analyse thermographic images. Thermol Int. 2003;13(1):5–9.

Ng EYK. A review of thermography as promising non-invasive detection modality for breast tumor. Int J Therm Sci. 2009;48(5):849–59.

Niu HH, Lui PW, Hu JS, Ting CK, Yin YC, Lo YL, et al. Thermal symmetry of skin temperature: normative data of normal subjects in Taiwan. Zhonghua Yi Xue Za Zhi (Taipei). 2001;64(8):459–68.

Oerlemans HM, Perez RS, Oostendorp RA, Goris RJ. Objective and subjective assessments of temperature differences between the hands in reflex sympathetic dystrophy. Clin Rehabil. 1999;13(5):430–8.

Owens Jr EF, Hart JF, Donofrio JJ, Haralambous J, Mierzejewski E. Paraspinal skin temperature patterns: an interexaminer and intraexaminer reliability study. J Manipulative Physiol Ther. 2004;27(3):155–9.

Pauling JD, Shipley JA, Raper S, Watson ML, Ward SG, Harris ND, et al. Comparison of infrared thermography and laser speckle contrast imaging for the dynamic assessment of digital microvascular function. Microvascular Research. 2011;83(2):162–7.

Plassmann P, Ring EF, Jones CD. Quality assurance of thermal imaging systems in medicine. Thermol Int. 2006;16(1):10–5.

Plaugher G, Lopes MA, Melch PE, Cremata EE. The inter- and intraexaminer reliability of a paraspinal skin temperature differential instrument. J Manipulative Physiol Ther. 1991;14(6):361–7.

Rich PB, Dulabon GR, Douillet CD, Listwa TM, Robinson WP, Zarzaur BL, et al. Infrared thermography: a rapid, portable, and accurate technique to detect experimental pneumothorax. J Surg Res. 2004;120(2):163–70.

Ring E, Ammer K. The technique of infra red imaging in medicine. Thermol Int. 2000;10(1):7–14.

Ring EF, Ammer K. Infrared thermal imaging in medicine. Physiol Meas. 2012;33(3):R33–46.

Rodrigues-Bigaton D, Dibai Filho AV, Costa ACS, Packer AC, de Castro EM. Accuracy and reliability of infrared thermography in the diagnosis of arthralgia in women with temporomandibular disorder. J Manipulative Physiol Ther. 2013;36(4):253–8.

Roy R, Boucher JP, Comtois AS. Validity of infrared thermal measurements of segmental paraspinal skin surface temperature. J Manipulative Physiol Ther. 2006;29(2):150–5.

Schwartz RG. Guidelines for neuromusculoskeletal thermography. Thermol Int. 2006;16(1):5–9.

Selfe J, Hardaker N, Thewlis D, Karki A. An accurate and reliable method of thermal data analysis in thermal imaging of the anterior knee for use in cryotherapy research. Arch Phys Med Rehabil. 2006;87(12): 1630–5.

Sherman RA, Woerman AL, Karstetter KW. Comparative effectiveness of videothermography, contact thermography, and infrared beam thermography for scanning relative skin temperature. J Rehabil Res Dev. 1996; 33(4):377–86.

Simpson R, McEvoy H, Machin G, Howell K, Naeem M, Plassmann P, et al. In-field-of-view thermal image calibration system for medical thermography applications. Int J Thermophys. 2008;29(3):1123–30.

Sivanandam S, Anburajan M, Venkatraman B, Menaka M, Sharath D. Medical thermography: a diagnostic approach for type 2 diabetes based on non-contact infrared thermal imaging. Endocrine. 2012;42(2): 343–51.

Skala K, Lipic T, Sovic I, Gjenero L, Grubisic I. 4D thermal imaging system for medical applications. Period Biol. 2011;113(4):407–16.

Spalding SJ, Kwoh CK, Boudreau R, Enama J, Lunich J, Huber D, et al. Three-dimensional and thermal surface imaging produces reliable measures of joint shape and temperature: a potential tool for quantifying arthritis. Arthritis Res Ther. 2008;10(1):R10.

Uematsu S, Edwin DH, Jankel WR, Kozikowski J, Trattner M. Quantification of thermal asymmetry. Part 1: normal values and reproducibility. J Neurosurg. 1988;69(4): 552–5.

Vainer BG. FPA-based infrared thermography as applied to the study of cutaneous perspiration and stimulated vascular response in humans. Phys Med Biol. 2005; 50(23):R63.

Vardasca R, editor. Template based alignment and interpolation methods comparison of region of interest in thermal images. 3rd research student workshop. Glamorgan: The Research Office, University of Glamorgan; 2008.

Varju G, Pieper CF, Renner JB, Kraus VB. Assessment of hand osteoarthritis: correlation between thermographic and radiographic methods. Rheumatology (Oxford). 2004;43(7):915–9.

Zaproudina N, Varmavuo V, Airaksinen O, Narhi M. Reproducibility of infrared thermography measurements in healthy individuals. Physiol Meas. 2008; 29(4):515–24.

Potential Errors in Mean Skin Temperature Calculation Due to Thermistor Placement as Determined by Infrared Thermography

125

David D. Pascoe

Contents

Keywords
Mean skin temperature • Thermistor probes • Thermography • Infrared imaging • Temperature • Isotherms

1 Introduction

The skin is the largest organ of our body covering approximately 6 m^2 and providing us with a waterproof protective barrier between our body structures and the environment. However, as a thermal interface, the skin is remarkably adept at managing heat transfers between the metabolic core and the environmental conditions. In cold environments, vasoconstriction of the blood flow within the skin layers functions as an outer body insulator, protecting the core organs from hypothermia. In hot environments, blood flow can be dramatically increased to the skin to transform the tissue into a surface radiator that encourages heat transfers into the environment. The ratio of radiant heat emitted is 0.98 as compared to a black body perfect emitter of 1.0 (Flesch 1985), with no wavelength differences observed between skin colors as detected by infrared imaging (Jones and Plassmann 2008). Thus, the skin can be

D.D. Pascoe (✉)
School of Kinesiology, Auburn University, Aubur, Al, USA
e-mail: Pascodd@auburn.edu

P. Humbert et al. (eds.), *Agache's Measuring the Skin*,
DOI 10.1007/978-3-319-32383-1_75

thought of as a thermal chameleon, which alters its function in response to the core-environment heat transfers to provide precise core temperature regulation maintained within a small critical survival zone.

2 Neural Control of the Skin Surface

Neural vasomotor control of the vascular topography within the cutaneous skin layers regulates the appropriate core to skin to environment heat transfers for thermoregulation. The reflex neural regulation modulates the blood flow by way of sympathetic vasoconstriction or vasodilation of the arterial branches that feed the transverse (perforator) vessels which culminate in numerous cutaneous circulatory plexus. Further blood flow regulation occurs in the acral tissue regions (finger/toe digits, ears, nose, cheeks, lips, palmer surfaces of the hand and feet) that are structurally supplied with arteriovenous anastomoses (AVAs). The AVAs are thick-walled, low-resistance vessels that have a direct vascular pathway between the arterioles and venules that regulates plexus blood flow by sympathetic adrenergic vasoconstrictor activity. In the nonacral tissue regions (legs, arms, and chest), blood flow is under the dual control of adrenergic (vasoconstriction) and noradrenergic (vasodilation). For a more in-depth review of the regional sympathetic reflex regulation and skin blood flow, the reader is directed to Johnson and Proppe (1996), Charkoudian (2003), and Pascoe et al. (2006). It is important to recognize these differences in regional blood flow regulation when investigating, measuring, or interpreting the skin temperature surfaces across the various regions of the body.

3 Mean Skin Temperature Calculations

An understanding of the dynamic responses of the skin to internal and external thermal environments and measurements of a mean skin temperature has been a challenge due to the skin's contoured surface area and the constraints of the equipment used to measure the skin surface. The earliest published skin temperature measures were made by Davy in 1814 by holding a thermometer against the skin surface (Burton 1934). The advent of the skin thermocouple at the turn of the century provided greater measurement accuracy, improved testing procedures, and has been the dominant measurement device over the past century.

A "precise" mean skin temperature would require an accurate measurement device and would be derived from an infinite number of body temperature points. All mean skin temperature formulas rely on the assumption that a finite number of skin temperature measures can provide a correct and reliable estimate of mean skin temperature (Teichner 1958). Thermistor measures also assume that areas within the body regions are homogeneous in temperature and representative of the mean skin temperature for that surface area. Intuitively, the more sites a researcher measures, the more representative and reliable the measure of mean skin temperature will be for either regional or whole-body measures. To address this issue, Winslow et al. (1936) produced pivotal research that examined the convective and radiant exchanges of humans under varying environmental conditions. From this research, it has been advocated that 15 recommended sites could provide a "reasonable" maximum for conducting investigations related to the thermal exchanges from the skin surface area. The 15 recommended sites are located in seven regional areas defined as (Fig. 1):

$$\begin{aligned}\text{Mean Ts} = \;& \text{Ts Head}(A + B + L)/3 \\ & + \text{Ts Arms}(D + F)/2 + \text{Ts Hands}(G) \\ & + \text{Ts Trunk}\ (C + E + M + N)/4 \\ & + \text{Ts Thighs}\ (H\ + P0/2 + \text{Ts Legs}(J\ +\ Q)/2 + \text{Ts Feet}\ (K)\end{aligned}$$

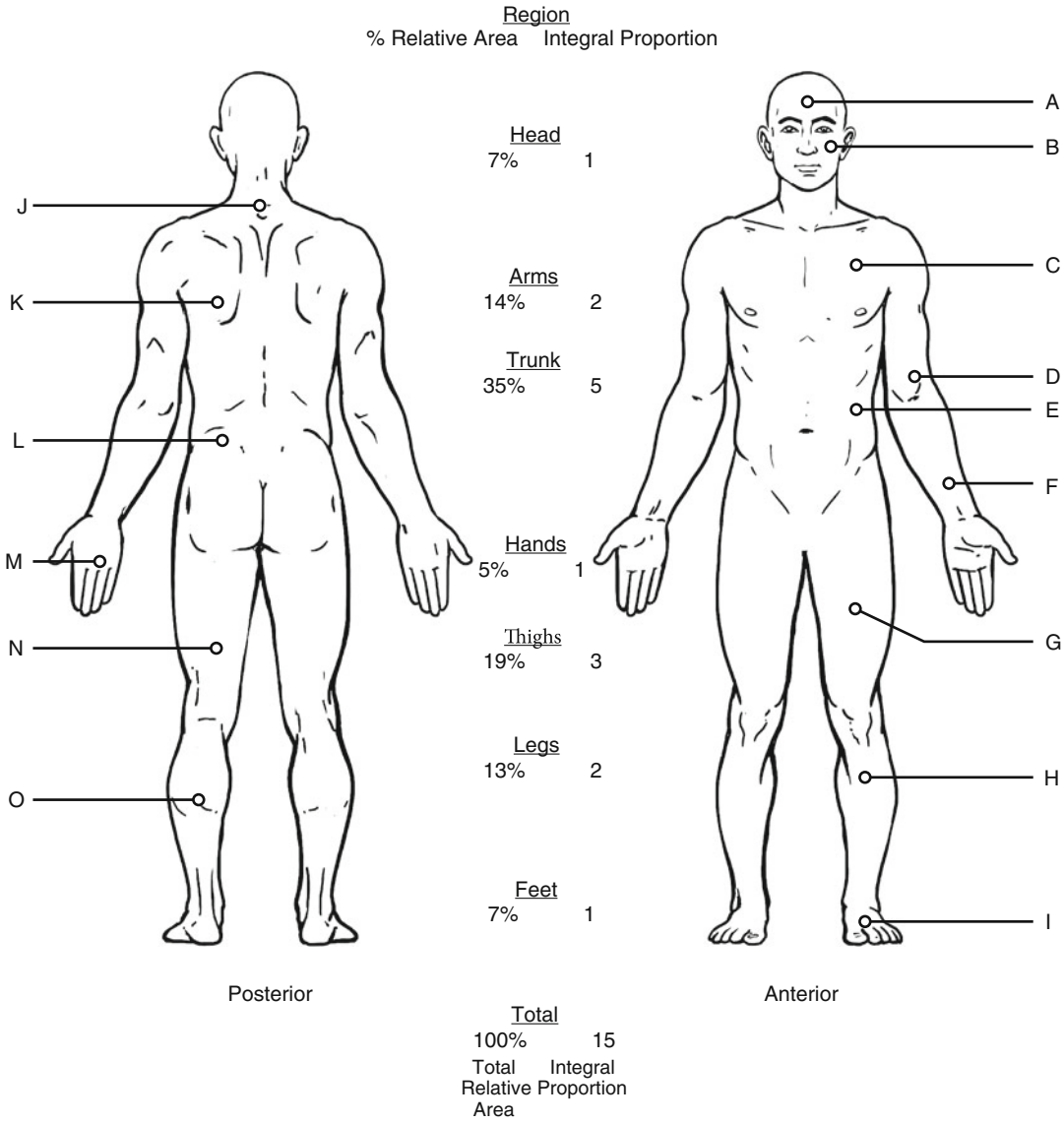

Fig. 1 Site locations, percent of relative area, and approximate integral proportions. Illustration of the 15 "optimal" measurement sites (Image drawn by Jason Adams, Auburn University)

This has been identified as the "optimal method" to determine whole-body mean skin temperature and the standard method used to compare the "accuracy" of other proposed formulas. The "accuracy" of the estimated mean skin temperature formula is determined by the agreement frequency percentage, which calculates the number of values that are within $\pm$ 0.2 °C when compared to standard measure, where the 0.2 °C allows for the error of the thermocouple device measurement. Using the same 15 sites, Winslow et al. (1936) proposed that the seven DuBois regions could be reduced to four by combining the arms and hands into the upper extremity and combining the thighs, legs, and feet into the lower extremity.

The research literature has focused on four basic formula approaches: (1) unweighted

average of the sites recorded; (2) weighted formulas based on regional surface averages as defined within population norms; (3) variable weighting based on individually determined surface areas, often determined by the DuBois linear formula; and (4) weighted formulas that incorporate factors that describe both the surface area and the thermoregulatory response to thermal stimuli (Nadel et al. 1973; Crawshaw et al. 1975). This fourth approach recognized that while the surface areas of the various regions help to explain the exposed surface available for heat exchange (conduction, convection, and radiation), differences in regional blood flow, temperature, and sweat gland distribution that contribute to measurable differences in the regional area's ability to dissipate heat through evaporation may not be adequately expressed. Comparative evaluations for various formulas used for mean skin temperature calculations can be found in the following research articles: Mitchell and Wyndham (1969), Lund and Gisolfi (1974), Olsen (1984), and Choi et al. (1997).

Due to the complexity of using 15 site measures, researchers have investigated the validity of monitoring fewer sites from which numerous mean skin temperature formulas have emerged. Mean skin temperature formulas have been devised using 3–15 measurement sites. Under resting conditions, the core environment is often considered homeothermic where the regional peripheral blood flow and temperatures are variable (poikilothermic) and more dependent upon environmental conditions. In colder external environmental conditions, regional skin temperatures are more heterogeneous, and variances across the region can be substantial. In warmer conditions, the skin temperature is more homogeneous and fairly consistent across the surface area. According to prevailing environmental conditions, some researchers have altered the number of measurement sites for the sake of convenience and reduced data handling to avoid measurement situations that would interfere with the research variables. Olsen (1984) used stepwise regression analysis of more than 800 tests from which he concluded that in warm environments 2–4 sites may be adequate, neutral conditions would require 4–8 sites, and cold environments would require between 8 and 12 sites to demonstrate a high degree of accuracy. Other researchers (Teichner et al. 1958; Veghte 1965; Jirak et al. 1975; Olsen 1984) have analyzed multiple data sources and have stated that at least six to seven sites need to be measured to assure accuracy of the estimated mean skin temperature. Some of the increased variance in regional skin temperatures in the cold can be attributed to the distribution of subcutaneous fat often associated with lower temperatures in areas of greater fat disposition (Livingston et al. 1987). Furthermore, the external environment, exercise metabolism, and clothing create an insulation effect (clo) that strongly influences thermal comfort and creates a microenvironment and thermal barrier that can alter or inhibit the skin surface thermoregulatory responses (Mairiaux et al. 1987; Mehnert et al. 2000). It is also important to recognize that these factors strongly influence the "accuracy" of mean skin temperature measures as determined by the agreement frequency percentage calculation such that a formula could be expected to perform differently under varying conditions, especially environmental temperature.

Potential errors in probe measurement can be attributed to poorly defined probe locations, regional point-to-point variations in temperature, different assigned numerical factoring values that try to account for regional contributions to the thermal status of the individual, and discrepancies created when comparing weighted calculations to the proportional unweighted measures of mean skin temperature. The regional point-to-point variation will be greatly influenced by the environment, where the magnitude of temperature variations has been reported from 7.2 °C to 3.6 °C (Jirak et al. 1975; Firm et al. 1990; Hunold et al. 1992) and deviations of microcirculation in the skin of 300 % within a few centimeters (Hunold et al. 1992). The accuracy of the probe, probe shape, mounting pressure, and adjoining wiring and the microenvironment created by skin surface attachment have provided methodological challenges. However, the thermocouple probe is still the favorite device for skin temperature measures under clothing.

4 Thermographic Measurements of the Skin Surface

In the 1960s, the development of infrared thermographic devices provided researchers with a method of obtaining a noncontact "thermal map" or thermal pictures of the skin surface area. In principle, this device detects the heat that is emitted (reminder: skin emissivity is 0.98) from the skin surface which greatly increases the number of measurement sites from a few probes to more than 10,000 digital pixel temperature-imaging points. The noncontact image removes researchers' concern over the influence of probe attachment to skin temperature measures while providing a very sensitive increment of measure (0.05 °C). From these images, thermography imaging programs can quickly provide the mean, high, low, and standard deviation of the selected skin surface region. While this imaging may appear to provide all thermal points of interest, there may be a 10 % loss of image accuracy around the border of the body image (projection angle more than 45°) and another 10 % that may be influenced by a thick hair cover (Choi et al. 1977). Additionally, the detection of heat emitted from the skin using infrared thermography is altered by clothing, more specifically the ability of heat transfers to pass through the clothing fabric.

The measured skin surface temperature is a combination of radiant heat from the core and environment and the influence of convective air movements, evaporative cooling during sweating, and conductive heat transfers when the skin is in contact with other surfaces. The radiant source of heat coming from the core is delivered to the skin via peripheral blood flow into the skin vascular plexus. Infrared imaging does not measure blood flow, but the skin temperature measures are strongly correlated to the anatomical distribution and blood flow to the surface area (Fig. 2).

These thermatomes, skin surface temperature patterns, allow the researchers to identify and understand the temperature distribution across the skin surface area, which negates the problem of probe placement. Within regional skin surface areas, the thermal image will have distinct areas with the same temperature (isotherms). These isotherms represent the blood flow distribution to the skin vascular plexus and the conduction of heat to the adjacent skin tissue layers. Within thermocouple research literature, researchers have observed regional skin surface areas that have a homogeneous temperature distribution that may practically be used to estimate the mean skin temperature of a region. This depends upon the proportional size of the isotherm in the region and the potentially sizeable variances in tissue temperatures across the skin surface that may shift the mean away from the isotherm mean temperature. These isotherms can change in accordance to exposures to varying environmental temperatures (see Fig. 3; Livingstone et al. 1988; Hunold et al. 1992), with greater heterogeneity in the surface temperatures observed when the skin is exposed to colder environments. As such, a same site probe location can provide discrepant measures due to the varying distribution of skin temperatures and fluctuating isothermal patterns.

Thermography is more adept than thermocouples when observing and measuring differences in local skin temperature as a result of radiant heat transfers due to posture and adjoining body parts (arms and torso) and the impact of convective air flow created by movement (mostly arms and legs). Additionally, the importance of the acral regions in heat transfers that modulate thermoregulation cannot be overlooked. As an example, if you feel hot while in bed at night, the simple act of sticking a foot outside of the bed covers changes your thermal status. A single thermal probe is unlikely to adequately describe the thermal response of acral regions (e.g., hands, feet), whereas thermography views the entire skin surface thermal response.

To understand the variances in skin temperature, Pascoe et al. (2012) investigated the mean skin temperatures within body regions in men and women while exposed to three environmental conditions (20, 30, 40 °C; all trials at 40 % relative humidity). Participants equilibrated on separate days within an environmental chamber for 20 min prior to thermographic measurements. The regional skin temperatures were determined from the mean temperature calculated (thermal image program)

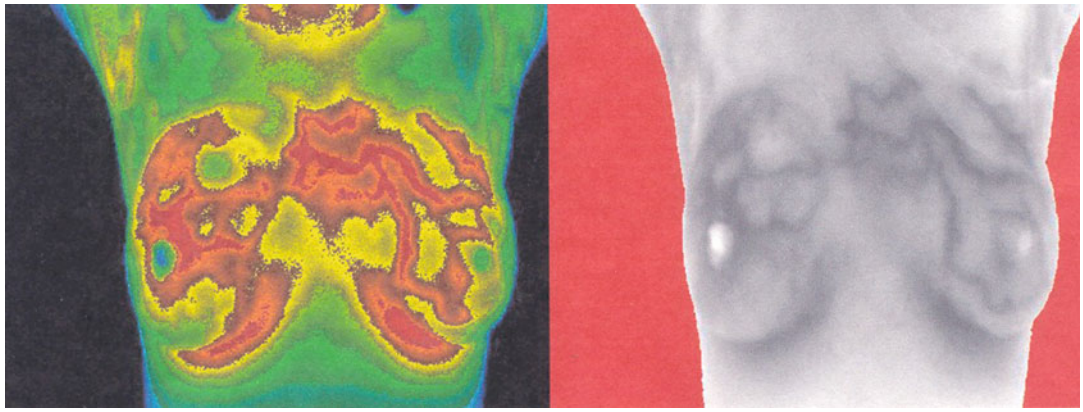

Fig. 2 Vascular image and thermal image. Images depicting the close correlation between the skin vascularity and skin temperature (Image provided by Dr. Robert Ensley)

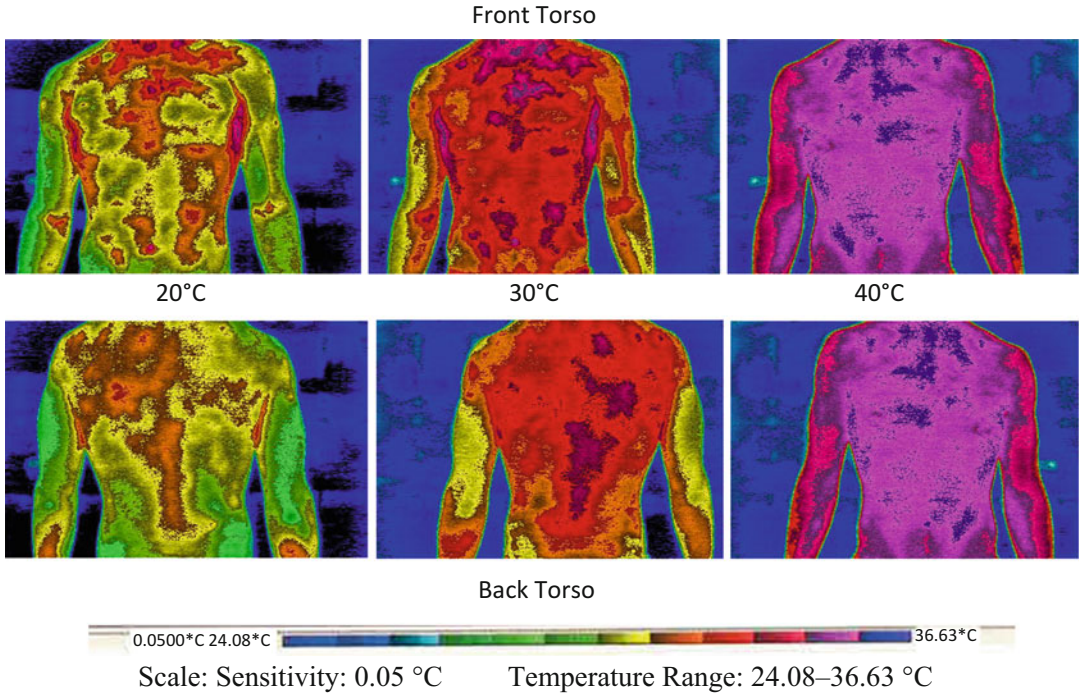

Fig. 3 Isotherm images. Images taken at 20, 30, and 40 °C to illustrate the different patterns in the thermal isotherms (Image taken by Khalil Lee, Vincent Santucci, and David Pascoe)

from the combined pixels within each regional surface area. No significant differences were found between men and women, so their data were combined. The regional skin temperatures in Figs. 4 and 5 demonstrate several key points:

1. The distribution and differences in regional thermal skin temperatures are linked to the environmental conditions.
2. The torso regional temperatures show a more homogeneous distribution when compared to

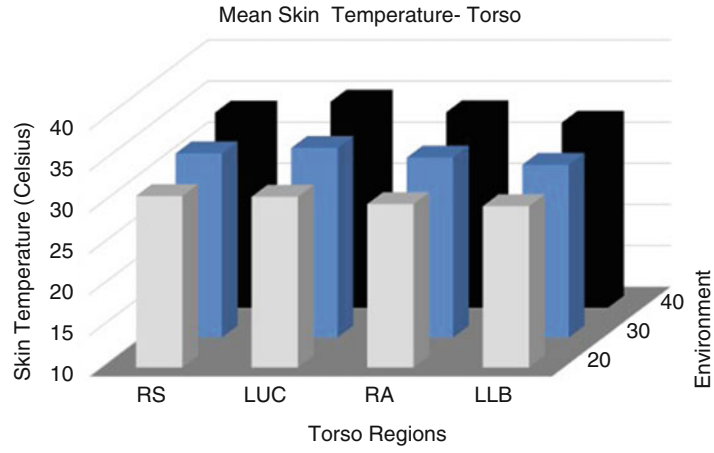

Fig. 4 Mean skin temperatures of torso across environmental conditions. Mean skin temperature of torso regions at 20, 30, and 40 °C as determined from thermographic images. *RS* right scapula, *LUC* left upper chest, *RA* right arm, *LLB* left lower back

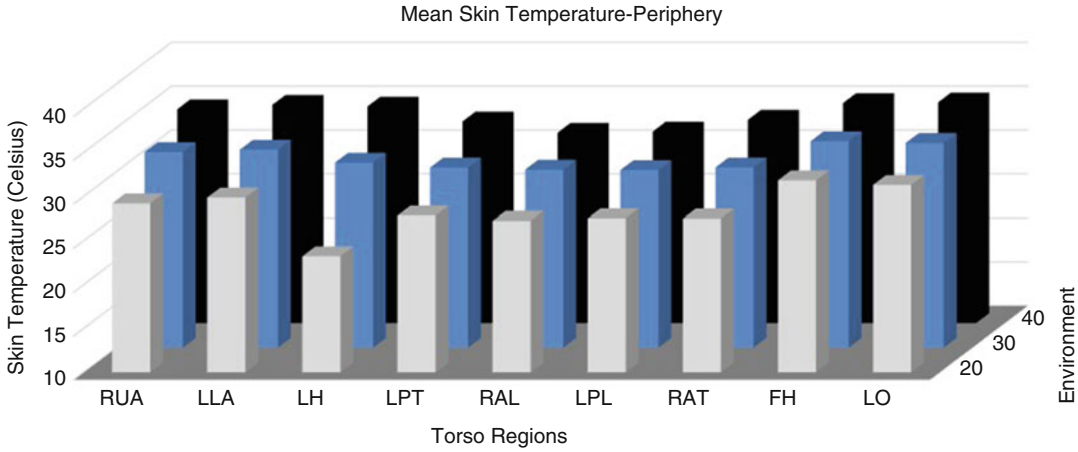

Fig. 5 Mean skin temperature of periphery across environmental conditions. Mean skin temperature of periphery regions at 20, 30, and 40 °C as determined from thermographic images. *RUA* right upper arm, *LLA* left lower arm, *LH* left hand (posterior view), *LPT* left posterior thigh, *RAL* right anterior leg, *LPL* left posterior leg, *RAT* right anterior thigh, *FH* forehead, *LO* lower occipital

heterogeneous thermal responses of the peripheral regions.

3. The greater variance of temperatures within the extremities can be attributed to the heat transfer properties of the acral regions (mostly hands and feet), which explains why the skin in the proximal portions of the limbs responds differently to the same environmental stressor (Clark). This observation illustrates the importance of the arteriovenous anastomoses within the acral regions for heat exchange and thermoregulation.
4. The variance in the temperature measures within and between regions suggests the potential for research error that can be observed when using formulas that vary in measurement site location, exposures to different environmental conditions, and the number of sites.

This potential error may be compounded by adding a "weighting" factor whose estimate of the mean skin temperature accuracy, as determined by the agreement frequency, varies according to environmental conditions and whether the individual is nude or clothed (Teichner 1958; Choi et al. 1977; Livingstone 1987).

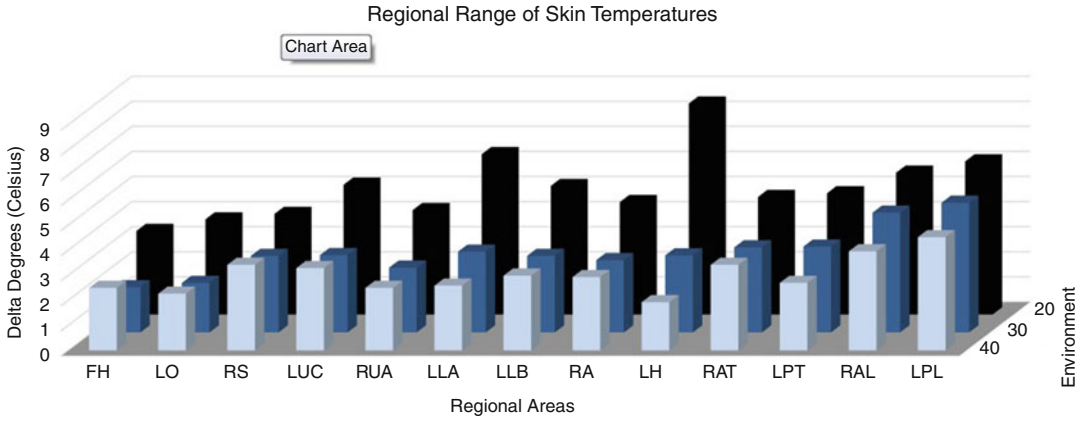

Fig. 6 Range of regional temperatures across environmental conditions. Variance of skin temperatures for optimal regions at 20, 30, and 40 °C as determined from thermographic images. *RUA* right upper arm, *LLA* left lower arm, *LH* left hand (posterior view), *LPT* left posterior thigh, *RAL* right anterior leg, *LPL* left posterior leg, *RAT* right anterior thigh, *FH* forehead, *LO* lower occipital, *RS* right scapula, *LUC* left upper chest, *RA* right arm, *LLB* left lower back

In Fig. 6, the range of temperatures within a region (high minus low measurement) demonstrates the variance in temperatures within and between regional skin temperatures surfaces. The figure clearly depicts the greater variance in regional areas during the colder exposure. This is consistent with the research literature and supports the need for using more thermistor probes when investigating mean skin temperature in colder environments (Olsen 1984). Unlike thermistors where a site may or may not represent the regional mean, thermographic skin temperature measures are able to capture all pixel sites from which a mean temperature is determined.

It is important to remember that the skin serves as an interface between the core thermal environment and the external environmental conditions. A majority of the research studies investigating mean skin temperature have been performed in the nude during resting conditions. Clothing can interfere with the normal regulatory processes, often creating a microenvironment that increases both temperature and humidity. The increased humidity reduces the skin to air vapor pressure which interferes with evaporative cooling. The wearing of loose clothing may reduce some of the thermal stress through clothing movement (pumping action) that increases the convective air movements. The insulation effect of clothing, clothing layers, and location of clothing all affect the distribution of skin temperatures (Nielsen and Nielsen 1984). In the clothed individual, the ability to access the skin surface area for infrared imaging may dictate whether the researcher uses thermistors or thermography. During work/exercise, the increase in the metabolic heat production must be regulated by skin heat transfers. Using thermography, Clark et al. (1977) observed an initial drop in skin temperatures with the initiation of exercise with a subsequent increase in skin temperatures over active muscle areas. They concluded the change in distribution patterns from the resting state were due to the direct heat transfer from the muscle tissue to the skin surface. While sweating would be expected to provide evaporative cooling, the wiping of sweat from the skin did change the thermal pattern. This demonstrated that the wetness of the skin does not significantly influence the skin surface emissivity.

5 Summary

When reviewing and interpreting the literature on mean skin temperature, the reader must be cognizant of the experimental influence of the following factors:

1. Measuring device and measuring accuracy: thermistor probes, attachment, infrared thermography-defined surface area, and sensitivity;
2. Environmental conditions: temperature, humidity, wind, and direct/indirect radiant heat sources [sunlight, incandescent lights, and heaters];
3. Activity level of the participants: passive or exercising [intensity, duration, mode of exercise, exercise or body movements that increase the convective air flow across the skin surface];
4. Layers of clothing, clothing fit, and heat transfer and moisture transport properties of fabric; and
5. Choice of mean skin temperature formulas: number of sites being evaluated, weight or unweighted.

All of these conditional factors explain the differences observed in the measures of mean skin temperature and research citations, but these factors also complicate our understanding of the thermoregulatory responses observed through the modulation of perfusion to our interactive skin tissue.

References

Burton AC. A new technic for the measurement of average skin temperature over surfaces of the body and the changes of skin temperature during exercise. J Nutr. 1934;7(5):481–91.

Charkoudian N. Skin blood flow in adult thermoregulation: how it works, when it does not, and why. Mayo Clin Proc. 2003;78:603–12.

Choi JK, Miki K, Sagawa S, Shiraki K. Evaluation of mean skin temperature formulas by infrared thermography. Inter J Biometeorol. 1977;4(2):68–75.

Clark RP, Mullian BJ, Pugh LGCE. Skin temperature during running – a study using infra-red colour thermography. J Physiol. 1977;267:53–62.

Crawshaw LI, Nadel ER, Stolwijk JAJ, Samford BA. Effect of local cooling on sweat rate and cold sensation. Pflugers Arch. 1975;354:19–27.

Flesch U. Physics of skin-surface temperature. In: Engel JM, Flesh U. Stüttgen G, editors Thermology methods (trans: Bierderman-Thorson MA). Federal Republic of Germany Weinheim; 1985. p 21–37.

Frim J, Livingstone S, Reed L, Nolan R, Limmer R. Body composition and skin temperature variation. J Appl Physiol. 1990;68:540–3.

Hunold S, Mietzsch E, Werner J. Thermographic studies on patterns of skin temperature after exercise. Eur J Appl Physiol. 1992;65:550–4.

Jirak Z, Jokl M, Stveràk, Pechlàt R, Coufalovà. Correction factors in skin temperature measurement. J Appl Physiol. 1975;38(4):752–6.

Johnson JM, Proppe DW. Cardiovascular adjustments to heat stress. In: Fregley MJ, Blattis CM, editors. Handbook of physiology. Oxford: Oxford University Press/ American Physiological Society; 1996. p. 215–43.

Jones BF, Plassmann P. Digital infrared imaging of human skin. IEEE Eng Med Biol. 2008;21:41–8.

Livingston SD, Nolan RW, Frim J, Reed DL, Limmer RE. A thermographic study of the effect of body composition and ambient temperature on the accuracy of mean skin temperature calculations. Eur J Appl Physiol. 1987;56:120–5.

Livingstone SD, Reed LD, Nolan RW, Cattroll SE. Measurement of torso skin temperature under clothing. Eur J Appl Physiol. 1988;57:225–9.

Lund DD, Gisolfi CV. Estimation of mean skin temperature during exercise. J Appl Physiol. 1974;36:625–8.

Mairiaux P, Malchaire J, Candas V. Prediction of mean skin temperature in warm environments. Eur J Physiol. 1987;56:686–92.

Mehnert P, Malchaire J, Kampmann B, Piette A, Griefahn B, Gebhardt H. Prediction of the average skin temperature in warm hot environments. Eur J Appl Physiol. 2000;82:52–60.

Mitchell D, Wyndham H. Comparison of weighing formulas for calculating mean skin temperature. J Appl Physiol. 1969;26:616622.

Nadel ER, Mitchell JW, Stowwijk JAJ. Differential thermal sensitivity in the human skin. Pflugers Arch. 1973;340:71–6.

Nielsen N, Nielsen B. Measurement of mean skin temperature of clothed persons in cool environments. Eur J Appl Physiol. 1984;53:231–6.

Olsen BW. How many sites are necessary to estimate a mean skin temperature? In: Hales JRS, editor. Thermal physiology. N.Y.: Raven Press; 1984. p. 33–8.

Pascoe DD, Mercer JB, DeWeerd L. Physiology of thermal signals. In: Bronzino J, editors The biomedical engineering handbook, 3rd ed. Taylor and Francis CRC Press; 2006 p 21.1–20.

Pascoe DD, Barberio MD, Elmer EJ, Laird RH. Potential errors in mean skin temperature calculation due to thermistor placement as determined by infrared thermography. European Association of Thermography Meeting Proceedings, Sept 2012.

Teichner WH. Assessment of mean body surface temperature. J Appl Physiol. 1958;12(2):169–76.

Veghte JH. Infrared thermography of subjects in diverse environments. Rept AAL-TR-65-18 AriticAeromeidcal Laboratory, Fort Wainwright; 1965.

Winslow CEA, Harrington LP, Gagge A. The determination of radiation and convection exchanges by partitional calorimetry. Am J Physiol. 1936;116: 669–84.

Skin Sensory Structural Component and Function

126

Laurent Misery

Contents

Keywords

Autonomic nervous system fibers • Cell innervation • Cutaneous innervation • Merkel cells • Neurotransmitters • Sensitive axons • Sensory epidermal formations

Sensory epidermal formations are mainly nerve fibers and Merkel cells. Skin innervation is highly dense, but with density and morphology variable with body site. Merkel cells (less than 1 % of epidermal cells) are neuroendocrine cells. Their distribution is also variable.

1 Cutaneous Innervation (Reznik 1996; Misery 2000; Saxod 1996)

In the skin, only axons are found, and especially nerve endings, whereas nerve cells which contain nuclei are localized in spinal nerve ganglions. These nerve fibers are immunoreactive for PGP9.5, neurofilaments, and some neurotransmitters. They are associated to Schwann cells, which express S100 protein and produce myelin. Skin nerve supply is double: from the sensitive or somatic nervous system and from the autonomic or vegetative nervous system.

1.1 Autonomic Nervous System Fibers

Autonomic nervous system fibers usually come from the sympathetic chains and are not myelinated.

This chapter was originally published under the ISBN 978-3-540-01771-4 with the following book title Measuring the Skin. The content has not been changed.

L. Misery (✉)
Department of Dermatology, University Hospital of Brest, Brest, France
e-mail: laurent.misery@chu-brest.fr

P. Humbert et al. (eds.), *Agache's Measuring the Skin*, DOI 10.1007/978-3-319-32383-1_76

They innervate vascular network, hair muscles, and sweat glands. They express tyrosine hydroxylase and contain many neurotransmitters (catecholamines, neuropeptides). Acetylcholine is only expressed by parasympathetic fibers and sympathetic fibers of sweat glands (the only case in the sympathetic system). The nervous network is superimposed on the vascular network. Sweat glands are surrounded by numerous nerve fibers, mainly around secretory coils but also along excretory ducts. Sebaceous glands are not innervated, and they are not neuropeptide- but hormone-dependent (Lever and Schaumburg-Lever 1983).

1.2 Sensitive Axons

Sensitive axons come from sensitive ganglions and define skin territories, which are named dermatomes (Figs. 1 and 2). They are myelinated in the dermis and not in the epidermis. From a plexus in the deep dermis, nerve fibers ascend toward the surface and form a second plexus at the junction between reticular and superficial dermis (Fig. 2a. Nerve endings can be free, dilated or corpuscular.

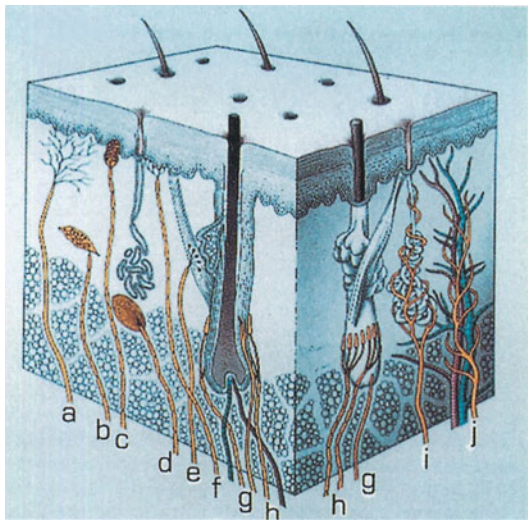

Fig. 1 Schematic view of the sensory corpuscles location within the skin. *a* Free nerve endings; *b* Ruffini corpuscle; *c* Meissner corpuscle; *d* Pacini corpuscle (above which a sweat gland is shown); *e* nerve of the piloarrector muscle; *f* nerve of a Merkel complex; *g* free nerve endings around a hair follicle; *h* perifollicular lanceolated corpuscle (above which piloarrector muscle and sebaceous gland are shown); *i* nerves to sweat glands; *j* perivascular sympathetic plexus (Courtesy of Professor Michel Reznik, University of Liège, Belgium)

In both dermis and epidermis, free nerve endings are very numerous (Figs. 1 and 2a, d, e). Their diameters vary from 1–2 μm (C fibers) to 2–5 μm (Aδ fibers). They express neuropeptides, such as substance P or calcitonin gene-related peptide (CGRP). Hairs are surrounded with a dense network of nerve fibers, which is modulated by hair cycle (Fig. 2c). Free nerve endings are found at the opening of sebaceous glands.

Dilated endings are lanceolated endings and Merkel-Ranvier disks. Lanceolated endings have a lance-shaped ending and are localized around the hair close to the outer root sheath. Merkel-Ranvier disks are in contact with Merkel cells but are localized at the dermal side of the dermo-epidermal junction (Fig. 2a, f).

Corpuscular endings are not numerous. They are mainly localized on the face, hands, feet, and genitalia. Several types are described. Ruffini endings are ovoid and 0.2–1 mm in length (Fig. 2a, b); they predominate around hair follicles and blood vessels. Wegner-Meissner corpuscles are bulboid endings (30 × 150 μm) in the dermal papillae (Fig. 2a). Vater-Pacini corpuscles are onion-like and reach 1–2 mm in length (see ▶ Chap. 118, "Cutaneous Testing: Detection and Assessment of Allergy"). They are located between the deep dermis and the hypodermis. Muco-cutaneous corpuscles, 50 μm in diameter, do not possess a well-defined capsule. They are found on the lips, anus, and genitalia. Golgi-Mazzoni corpuscles are bulboid; they are more frequent in the mucosae than in the skin.

2 Merkel Cells (Saxod 1996; Gaudillère and Misery 1994; Tachibana 1995) (Fig. 3)

Merkel cells are hybrid cells. They are neuroendocrine cells because they produce neurotransmitters and hormones, secreted in neurosecretory granules then excreted. They express neuroendocrine markers, such as neuronal specific enolase

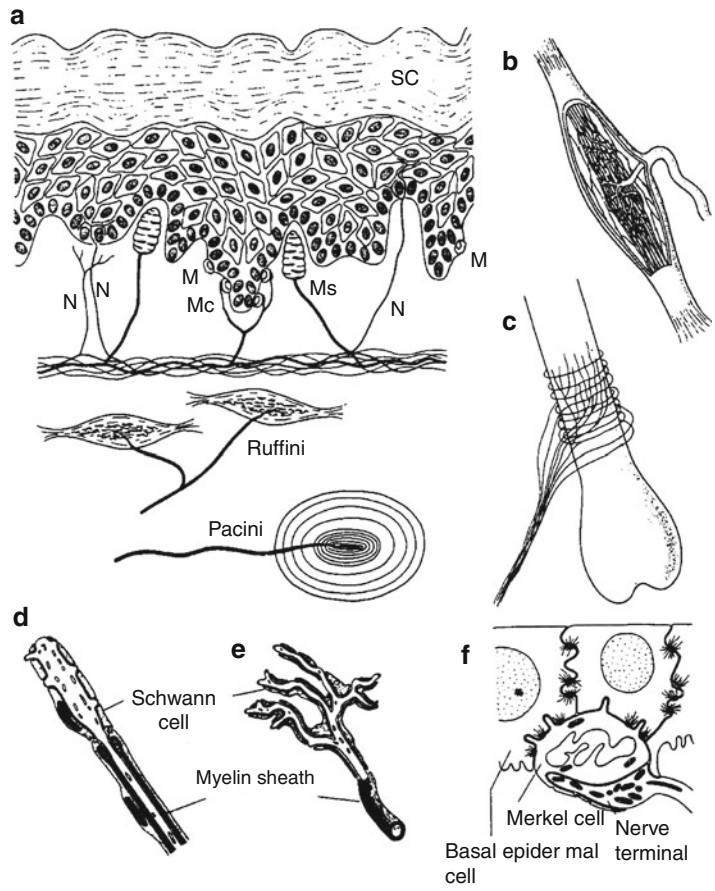

Fig. 2 (**a**–**f**) Cutaneous nerve endings: *A* in hairless skin. *M* Merkel cell, *Mc* Merkel corpuscle, *Ms* Meissner corpuscle, *P* upper dermis neural plexus, *SC* stratum corneum. Ruffini corpuscles (close to blood vessels). Pacini corpuscles are located in the subcutis. *B* Ruffini corpuscle (detail). *C* Hair follicle receptor. *D, E* Free nerve terminals. *F* Merkel corpuscle: note the Merkel cell convoluted nucleus and desmosomes (After (Brodal 1981), modified, with permission)

(NSE), S100 protein, PGP9.5, chromogranin A or synaptophysin. But they are also epithelial cells because they express cytokeratins 8, 18, 19, and 20 or epithelial membrane antigen (EMA). They probably originate from the same stem cells as do keratinocytes.

They are found in larger number on lips, palms, and finger extremities. Localized in the basal layer of the epidermis (Fig. 2a, f) and the epidermal appendages, they possess dendrites and neurosecretory granules (Fig. 3). They are usually single but can be arranged into Merkel corpuscles or complexes (Fig. 3a). During embryonic life, nerve fibers develop towards these cells to constitute Merkel-Ranvier disks (Fig. 2f). Merkel cells are usually associated with a nerve terminal (Fig. 3). The function of the association between the Merkel cell and the nerve ending remains unclear but seems to be sensory.

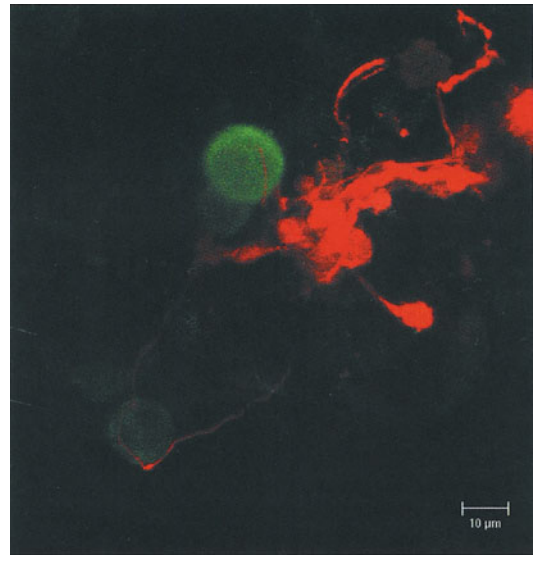

Fig. 3 Merkel cells (*green*) associated with nerve endings (*red*)

3 Cell Innervation (Chédotal and Hamel 1993; Misery 1997)

Nerve fibers are known to be in contact with cutaneous cells. These data are commonly accepted for skin vascular cells, sweat gland cells, and hair follicle cells. These contacts do not appear to be synapses. Neurotransmitter secretion is paracrine. True synapses are only observed with hair arrector muscles.

Synapse-like connections between an axon and a cutaneous or an immune cell have been described recently. Hence, close contacts between the membranes of nerve endings and non-neural cells are probably the sites where exchanges take place. Such connections have been observed with cells of the skin immune system: mast cells, dermal dendrocytes, and Langerhans cells. In the epidermis, most Langerhans cells, many melanocytes, and some keratinocytes have synapse-like connections with nerve terminals.

Skin is the organ of the fifth sense, rich in neurosensory formations. Hence, it is an important source of information for the nervous system. But the reverse also holds true.

References

Brodal A, editor. Neurological anatomy in relation to clinical medicine. 3rd ed. New York: Oxford University Press; 1981.

Chédotal A, Hamel E. L'innervation cholinergique de la paroi vasculaire. Méd/Sci. 1993;9:1035–42.

Gaudillère A, Misery L. La cellule de Merkel. Ann Dermatol Venereol. 1994;121:909–17.

Lever WF, Schaumburg-Lever G, editors. Histopathology of the skin. 6th ed. Philadelphia: Lippincott; 1983.

Misery L. Skin, immunity and the nervous system. Br J Dermatol. 1997;137:843–50.

Misery L. Vascularisation et innervation cutanées. Encycl Méd Chir. Elsevier, Paris (Cosmétologie et Dermatologie Esthétique, 50-020-E-10); 2000, 4 pp.

Reznik M. Structure et fonctions du système nerveux cutané. Path Biol. 1996;44:831–7.

Saxod R. Ontogeny of the cutaneous sensory organs. Micro Res Technique. 1996;34:313–33.

Tachibana T. The Merkel cell: recent findings and unresolved problems. Arch Histol Cytol. 1995;58:379–96.

Skin Sensorial Receptors

127

Loïc Rambaud and Laurence Kocher

Contents

Keywords

Autonomic nervous system • Cold/heat sensitivity • Dynamic sensitivity • Fast adaptating fibers • Low threshold mechanoreceptors • Mechanonociceptors • Nociceptors • Polymodal nociceptors • Slow adaptating fibers • Static sensitivity • Thermoreceptors

The functional characteristics of the various types of skin receptors are better known thanks to electrophysiological studies in animals and microneurographic studies in humans which allow to record the unitary fibers response to an electrical or sensitive stimulation.

Three types of receptors are distinguished: the low threshold mechanoreceptors, the thermoreceptors and the nociceptors. The functional characteristics of the skin autonomic nervous system will be briefly treated at the end of this chapter.

1 Low Threshold Mechanoreceptors

They are now well individualised (Iggo and Andres 1982) and their structural characteristics are described in ▶ Chap. 128, "Sensory Function of the Skin." Their distribution varies according to the type of skin, either hairless or hairy, and this is associated with their function. Microneurographic recordings and the study of the receptive fields have allowed to distinguish four types of primary

This chapter was originally published under the ISBN 978-3-540-01771-4 with the following book title Measuring the Skin. The content has not been changed.

L. Rambaud (✉)
French Institute for Public Health Surveillance, Saint Maurice, France
e-mail: l.rambaud@invs.sante.fr; l-rambaud@wanadoo.fr

L. Kocher
Service d'Explorations Fonctionnelles Neurologiques, Centre Hospitalier Lyon Sud, Hospices Civils de Lyon, Pierre-Bénite, France
e-mail: laurence.kocher@chu-lyon.fr

P. Humbert et al. (eds.), *Agache's Measuring the Skin*, DOI 10.1007/978-3-319-32383-1_77

afferent fibers (PAF) distributed in two units (Johansson and Vallbo 1983).

1.1 Type I Units

Type I units have small and distinct receptive fields. They have several high sensitivity zones because each PAF is connected to several mechanoreceptors in different places. Type I units comprise:

1. Fast adaptating fibers I (FA I): the discharge occurs only during stimulus initialization or interruption. Their response is therefore phasic and they code for low frequency sinusoidal stimuli perceived as a localized shiver. They are connected to the Meissner corpuscles
2. Slow adaptating fibers (SA I) which are active over the whole duration of the stimulus (tonic activity). They also respond on a phasic mode, with a lower and more constant threshold than the FA I. They are connected to the Merkel complexes.

1.2 Type II Units

On the opposite, type II units have wide receptive fields with imprecise limits and overlapping areas. The following fibers types are found:

– Fast adaptating fibers (FA II) which are activated by high frequency sinusoidal stimuli (100 Hz) and perceived as vibrations of the sub-cutaneous tissues. They are connected to the Pacini corpuscles;
– Slow adaptating fibers (SA II) which respond to sustained or phasic depressions of the skin surface. They are connected to the Ruffini corpuscles.

1.3 Distribution and Function

These physiological data must be correlated to the distribution of the different under-types of mechanoreceptors in order to understand their specific functions.

Type I units are more numerous on the palm with maximum density on the fingertips (FA I, 140/cm^2; SA I, 70/cm^2). On the opposite the type II units distribution is more uniform with a lower density (Knibestöl and Vallbo 1980).

FA I and SA I mechanoreceptors are particularly involved in tactile discrimination. In 1835, Weber showed that humans could perceive two distinct stimuli at a distance of 1–2 mm on the fingertips. Since then different experimental paradigms have shown that this distance could be reduced to 0.84 mm, even 0.17 mm (Johnson and Pkillips 1981; Loomis 1979). SA I are also plainly involved in the perception of shapes, roughness and surface sampling (Johnson and Hsiao 1992). Inversely, even when the FA I are activated by a moving stimulus, the perception of movement on the skin surface requires a sub-cortical and cortical somesthesic coding.

Finally types SA I and SA II units have a dynamic sensitivity (phasic activity proportional to the movement rapidity) and a static sensitivity (tonic activity which in case of a sustained joint position, for example, is proportional to the flexion angle) which can be compared to that of the neuromuscular units. They may therefore be able to inform the nervous system about the joints position and movement.

2 Thermoreceptors

The morphological aspect of the thermoreceptors does not allow to differentiate them from other neuron free endings. They can only be differentiated by their functional characteristics (Spray 1986). They have a low basal tonic activity associated with the skin temperature. However they do not respond to mechanical stimuli. Their response mode is of a phasic type with a low activation threshold, contrary to the nociceptors.

2.1 Sensitivity to Heat

The neuron free endings involved in heat sensitivity are mainly of type C. They are less numerous than those which code for cold. Their

receptive fields diameter is 1 mm. They are activated for temperature variations between 30 °C and 45 °C with a maximal sensitivity between 41 °C and 45 °C. Above 45 °C the thermal nociceptors are also activated while the thermoreceptors discharge frequency decreases.

2.2 Sensitivity to Cold

It corresponds to thermoreceptors activation (fibers Aδ and C). Their receptive fields are small, with a diameter of about 100 μm. They code for thermal variations within the range of 0.5–20 °C from the basal skin temperature. In this range they are activated by a sharp drop in temperature and inhibited when the temperature variation returns to basal state. There is therefore an overlapping zone between both types of thermal sensitivity (30–40 °C). In this range corresponding to the skin physiological temperature, both fibers types are active.

In some particular conditions receptors to cold can be activated by a warm stimulus. When a temperature of 45 °C is applied on a small area of the skin, the receptors to cold are activated with a perception of "paradoxical cold" (Vallbo et al. 1979).

3 Nociceptors

They are mainly constituted by slightly or not myelinated free ends. Contrary to mechanoreceptors, their activation threshold is high and their response increases parallel to the stimulus intensity. Two types of nociceptors are distinguished and their function is now better known (Chaouch and Besson 1986).

3.1 Mechanonociceptors

They are traditionally associated with the slightly myelinated Aδ fibers. Their receptive fields are large (1–2 cm) and separated by zones where stimulation is inefficient. They give a quick and well located stinging, pinching or cutting sensation. Their response is proportional to the stimulus intensity but reduced by its repetition (inactivation phenomenon).

3.2 Polymodal Nociceptors

Their primary afferent fibers are mainly of type C and not myelinated, but a smaller number of Aδ fibers has been described in monkeys and humans (Adriaensen et al. 1983, 1984; Torebjörk and Hallin 1974). Their receptive fields area varies from 1 mm^2 to 1 cm^2 and has either a homogenous sensitivity zone or maximal sensitivity zones. They respond to sharp and strong mechanical stimulations with functional characteristics identical to those of the mechanonociceptors. Then can also code temperature rises above 43 °C as painful. In this case the subject may feel a sharp sudden heat followed by a longer delayed heat sensation. This type of perception corresponds to the initial activation of fast conduction Aδ fibers (5–52 m/s) then slower C fibers (0.5–1.4 m/s). Finally they respond to chemical stimuli, especially to pain-generating substances which are found in inflammation (bradykinine, histamine) and to irritants.

As in the case of Aδ fibers, a repeated stimulus can cause an inactivation phenomenon, and especially sensitization. In this situation for a stimulus of a given intensity the response threshold decreases and the polymodal nociceptors discharge frequency increases.

Furthermore recent works have shown the presence of C fibers, called silent, in the skin, viscera and joints which are inactive in physiological conditions (Michaellis et al. 1996). Their activation may be induced by the inflammation neuromediators. Could they be a "new" type of nociceptors with a very high activation threshold? Or are they part of a peripheral physiological stage in the sensitization process of the central nervous system responsible for secondary hyperalgesia? Both hypotheses are still debated.

4 Role of the Autonomic Nervous System

As mentioned in ▶ Chap. 128, "Sensory Function of the Skin," the skin autonomic innervation belongs to the sympathetic nervous system (Reznik 1996; Vallbo et al. 1979). It regulates sweating, skin and muscular blood flow as well

as piloerection during sudden changes in our outer or inner environment ("fight and flight"). Finally, there is probably a physiological connection between the polymodal nociceptors and the autonomic nervous system, especially in the phenomenon of neurogenic inflammation.

References

Adriaensen H, Gybels J, Handwerker HO, Van Hees J. Response properties of thin myelinated (Aδ) fibers in human skin nerves. J Neurophysiol. 1983;49:111–22.

Adriaensen H, Gybels J, Handwerker HO, Van Hees J. Suppression of C fibre discharges upon repeated heat stimulation may explain characteristics of concomitant pain sensations. Brain Res. 1984;302:203–11.

Chaouch A, Besson JM. Mécanismes périphériques et médullaires de la nociception. Rev Neurol. 1986;142:173–200.

Iggo A, Andres HK. Morphology of cutaneous receptors. Annu Rev Neurosci. 1982;5:1–31.

Johansson RS, Vallbo AB. Tactile sensory coding in the glabrous skinof the human hand. Trends Neurosci. 1983;6:27–32.

Johnson KO, Hsiao SS. Neural mechanisms of tactual form and texture perception. Annu Rev Neurosci. 1992;15:227–50.

Johnson KO, Pkillips JR. Tactile spatial resolution. I. Two-point dicrimination, gap detection, grating resolution, and letter recognition. J Neurophysiol. 1981;46:1177–91.

Knibestöl M, Vallbo AB. Intensity of sensation related activityof slowly adapting mechanoreceptive units in the human hand. J Physiol. 1980;300:251–67.

Loomis JM. An investigation of tactile hyperacuity. Sens Processes. 1979;3:289–302.

Michaellis M, Häbler HJ, Jänig W. Silent afferents: a separate class of primary afferents? Clin Exp Pharmacol Physiol. 1996;23:99–105.

Reznik. Structure et fonctions du système nerveux cutané. Pathol Biol. 1996;44:831–7.

Spray DC. Cutaneous temperature receptors. Annu Rev Physiol. 1986;48:625–38.

Torebjörk HE, Hallin RG. Identification of afferent C units in intact human skin nerves. Brain Res. 1974;67:387–403.

Vallbo AB, Hagbarth KE, Torebjörk HE, Wallin BG. Somatosensory, proprioceptive, and sympathetic activity in human peripheral nerves. Physiol Rev. 1979; 59:919–57.

Sensory Function of the Skin

128

Laurent Misery

Contents

Keywords

Aδ fibers • Mechanoreceptors • Nociceptors • Pruriceptors • Silent C fibers • Skin sensory function • Anatomical classifications • Emotional experience • Gate control • Itch • Merkel cells • Nociceptors • Pain • Pruriceptors • Rapid accommodation • Thermoreceptors

Sensory function (touch) is one of the most important functions of the skin-nervous system but is not the only one (Misery 1997). Autonomic nervous system controls vasodilatation (and thus thermoregulation), pilo-arrection, sebaceous excretion, and sweat secretion and excretion. Sensory nerve fibers are also able to strongly modulate skin immunity, skin trophicity, hair growth, cutaneous effects of ultraviolet light (photoprotection and immunosuppression), keratinocyte differentiation or proliferation, and all other functions of the skin, thanks to an antidromic secretion of neuropeptides and neural growth factors. Hence, they also modulate wound healing and inflammation and exert effects on the time course of skin diseases.

1 The Cutaneous Sensitivity

Following an external stimulus, the signal generated in the skin is conveyed by activated C and Aδ fibers of the neurosensory system to the neuron cell (Reznik 1996; Boulais and Misery 2007). At this level the information is received through a

L. Misery (✉)
Department of Dermatology, University Hospital of Brest, Brest, France
e-mail: laurent.misery@chu-brest.fr

P. Humbert et al. (eds.), *Agache's Measuring the Skin*,
DOI 10.1007/978-3-319-32383-1_78

receptor, and then the electric potential of the cell membrane is altered and neurotransmitters are produced. The nervous impulse is conveyed to sensitive ganglions then to the spinal cord. A second neuron, via the spinothalamic funiculus, transmits the information to the thalamus, at the brain basis. A third neuron conducts the impulse to the temporal cortex. At all levels, the "gate control," exerted by intermediary neurons, regulates the system.

In the epidermis, Merkel cells (Boulais and Misery 2007) have a specific sensory function, especially in mechanoreception, in a close interaction with Aβ fibers. Other epidermal cells (mainly keratinocytes) could also have sensory functions because they express sensor proteins (Boulais and Misery 2008), and the epidermis can be considered as the forefront of the sensory system (Denda et al. 2007).

Anatomical and functional classifications of cutaneous neuroreceptors are not superimposable. Indeed, a same anatomical type of nerve endings is able to receive and transmit different types of information. Four functional types of receptors are defined: mechanoreceptors, thermoreceptors, nociceptors, and pruriceptors (Table 1).

1.1 Mechanoreceptors

There could have a slow accommodation (response over the whole duration of stimulus) or a rapid accommodation (response at the beginning and the end of the stimulus).

In non-hairy skin, type I receptors (Merkel cells and Meissner corpuscles) have small and well-limited receptive fields and the conduction velocity is 55–60 m/s. Type II receptors (Ruffini and Pacini corpuscles) have broader and less limited receptive fields and the conduction velocity is 45–50 m/s. In hairy skin, mechanoreceptors are perifollicular free nerve endings, Merkel complexes, lanceolated endings, and Ruffini corpuscles.

1.2 Thermoreceptors

They are mainly C fibers and have a very slow conduction velocity (0.5 m/s). The impulse frequency is proportional to the stimulus intensity and frequency. Two different receptors have been isolated: cold receptors (<30 °C) and heat receptors (32–48 °C). There is an overlap area around 30–40 °C, where variations of temperature are more important than temperature for activation of these receptors, which explains the possibility of paradoxical cold. Temperatures lower than 20 °C or higher than 45 °C are discerned as painful.

1.3 Nociceptors

They are unmyelinated free nerve endings (Cesaro 1994). Three types are described:

- Aδ fibers, sensitive to strong mechanical stimulations (bite, pinching, cut)
- Common C fibers, sensitive to mechanical, thermal, and chemical stimuli and to numerous mediators (neurotransmitters, cytokines, eicosanoids, etc.)
- "Silent" C fibers, activated only after a chemical or biochemical sensitization, especially by mediators of inflammation

Table 1 Sensory receptors in the skin

Type	Subtype	Stimuli	Type of nerve ending
Mechanoreceptor	Type I	Quivering, touch	Meissner, Aβ, C
	Type II	Vibration, pressure	Pacini, Ruffini, Aβ
Thermoreceptor	Cold	<30 °C	C, Aδ
	Heat	32–48 °C	C
Nociceptor	Mechano-	Excessive mechanostimulation	Aβ, Aδ
	Polymodal	Inflammatory mediators	C
Pruriceptor	See Table 2		

1.4 Pruriceptors

These receptors have been recently isolated (Schmelz et al. 1997) and are specific of pruritus or rather selective for pruritus. Itch is specific of the skin and some close mucosa and seems to originate in epidermal and maybe subepidermal nerve fibers, Aδ fibers, and mainly C fibers.

It has been initially shown that there were mechano-insensitive and heat-insensitive C fibers that discharged upon histamine iontophoresis and whose firing frequency paralleled the itch magnitude rating on a visual analog scale (Schmelz et al. 1997). Then histamine-sensitive mechano-insensitive spinal neurons with very low conduction velocity and conveying impulses to a distinct part of the hypothalamus were discovered in the cat (Andrew and Craig 2001). These data point to "a specific population of chemo-nociceptors responsible for itch forming a labeled line for itch processing" (Schmelz 2002).

Since these discoveries, many others have been performed and the following classification of pruriceptors can be proposed, dividing them in two types (Misery and Ständer 2010) (Table 2):

- Histamine-dependent pruriceptors
- Histamine independent that are mainly activated by cysteine or serine proteases like mucunain or tryptase, through PAR-2 receptors.

Table 2 Pruriceptors

Fibers C	Histamine (H1R)	Cowhage (PAR-2)
Mécano-insensibles (TRPV1−)	+	−
Mécano-sensibles (TRPV1+)	+	+

2 Pain

The international definition of pain is "a sensory and emotional experience, which is disagreeable and linked to a potential or existing tissular lesion, or described as such a lesion" (Cesaro 1994). It corresponds to an excess of nociception, and accordingly, pain appears beyond a threshold. Cutaneous pain is mainly acute, and generated by physical, chemical, or thermal traumas, but can be chronic. Pain is not so frequent in the course of skin diseases (mainly in leg ulcers or in de-epidermization processes like in Lyell's syndrome) but it can be present in the course of neurological or neuro-dermatological diseases. The central integration of pain plays an important part, through its psychological repercussions.

From nociceptive receptors, painful information is conveyed by the usual ways (see above). Intimate mechanisms of pain remain far from elucidated. External painful stimuli as well as numerous chemical substances, such as bradykinin, histamine, serotonin, prostaglandins, interleukin-1, etc., are able to modify or induce nociceptor activation. Substance P is the most well known and the most important mediator of pain, but others have been more recently described (CGRP, somatostatin, glutamate, etc.).

At all levels (the skin, spinal cord, brain), a "gate control" is permanently in operation. Serotonin and norepinephrine but particularly endorphins and enkephalins have endogenous analgesic effects. Pain is usually due to an excessive stimulus but can be also related to a lack of normal sensation gate control.

3 Itch

Pruritus or itch is an unpleasant sensation that causes a need to scratch (Misery and Ständer 2010; Bernhard 1994). Pruritus does not appear as a minimal pain, as it is often thought, because they are two different sensations. It occurs on the skin and external mucous membranes (genitalia, lips) rather than internal ones; it induces scratching, is exacerbated by heat or morphine-related drugs and soothed by cold, and can be triggered by very low stimuli. Pain is not specifically cutaneous, induces withdrawal, is exacerbated by cold and soothed by heat and morphine-related drugs, and is experienced beyond a relatively high threshold.

Pruritus can be acute or chronic. It occurs in a variety of circumstances: inflammatory skin

diseases, accumulation of toxins (related to liver or kidney diseases), and systemic diseases (mainly blood and endocrine diseases). Exogenous agents (chemical products, drugs) can induce itch. But it can be only neurogenic or psychogenic.

Central integration of pruritus is very important, but there is no one itch center because itch is related to interactions between sensory, motor, and affective areas in the brain. Gate control probably exists at different levels. Senile pruritus and maybe diabetic pruritus or certain neurological pruritus seem to be due to desafferentation.

Histamine is the most well-known mediator of itch, but it plays no role in most cases. That explains why antihistamines are usually ineffective. Substance P, serotonin, and prostaglandins are probably more important factors. Endogenous or exogenous morphine-related compounds can also induce pruritus, as well as cytokines such as interleukin-2 or interferon-α, some proteases (trypsin, papain), or kinins (kallikrein, bradykinin), and can be soothed by substances such as ciclosporin.

References

Andrew D, Craig AD. Spinothalamic lamina 1 neurons selectively sensitive to histamine: a central neural pathway for itch. Nat Neurosci. 2001;4:72–7.

Bernhard JD. Itch. Mechanisms and management of pruritus. New York: Mac Graw-Hill; 1994. 454 p.

Boulais N, Misery L. Merkel cells. J Am Acad Dermatol. 2007;57:147–65.

Boulais N, Misery L. The epidermis: a sensory tissue. Eur J Dermatol. 2008;18:119–27.

Cesaro P. La douleur. La Revue du Praticien. N° Spécial. 1994;44:1863–938.

Denda M, Nakatani M, Ikeyama K, Tsutsumi M, Denda S. Epidermal keratinocytes as the forefront of the sensory system. Exp Dermatol. 2007;16:157–61.

Misery L. Skin, immunity and the nervous system. Br J Dermatol. 1997;137:843–50.

Misery L, Ständer S. Pruritus. London: Springer; 2010. 348 p.

Reznik M. Structure et fonctions du système nerveux cutané. Path Biol. 1996;44:831–7.

Schmelz M. Itch: mediators and mechanisms. J Dermatol Sci. 2002;28:91–6.

Schmelz M, Schmidt R, Bickel A, Handwerker HO, Torebjork HE. Specific C-receptors for itch in human skin. J Neurosci. 1997;17(20):8003–8.

Quantitative Neurosensory Exploration of the Skin

129

Loïc Rambaud

Contents

Keywords

Boundaries method • Forced selection method • Laser stimulators • Levels method • Peltier's effect • Stairs method • Tactile sense • Thermal sensory analyser (TSA) • Threshold value

The clinical investigation of the skin sensory function is well codified. For long, a cotton pad, a needle, a diapason (100 or 128 Hz), hot or cold water have been the main tools used by clinicians. Pieces of different fabrics or other various objects in metal, wood, or plastic which can be calibrated can also be used. It is then possible to investigate the perception of shapes, weights and textures. However these tools are not standardised and their main drawback is their selection by the investigator. Quantitative exploration, more adapted to clinical research and psychophysiology, requires several standardised and reproducible techniques which necessitate a more costly and complicated equipment.

1 Tactile Sense

Blix and Von Frey were the first to develop a standardised method. They used human or horses hairs which are better because of their stiffness and changeable diameter and length. The pressure exerted by a hair on the skin, measured in g/m^2, allowed to test the skin low threshold receptors. Von-Frey (1897) developed a standardised system

This chapter was originally published under the ISBN 978-3-540-01771-4 with the following book title Measuring the Skin. The content has not been changed.

L. Rambaud (✉)
French Institute for Public Health Surveillance, Saint Maurice, France
e-mail: l.rambaud@invs.sante.fr; l-rambaud@wanadoo.fr

P. Humbert et al. (eds.), *Agache's Measuring the Skin*,
DOI 10.1007/978-3-319-32383-1_79

involving one hair placed in a graduated beaker. The pressure could be adjusted by the investigator. Depending on its intensity, a touch sensation, then a pressure sensation could be induced. Beyond a certain threshold and(or) according to the tested site (mucous membrane, cornea), it was possible to obtain a painful sensation. The interest of this method was to provide reliable and reproducible results. This technique is still valid, although its implementation is often time-consuming.

Since then, laboratories have developed more sophisticated stimulators using computer technology and robotics (Dotson 1997). These systems have been set up to meet the specific requirements of some groups working on peripheral neuropathies (reviewed in Dick et al. (1993)). The patient is placed in comfortable conditions in a quiet room and the stimulator is placed on different sites selected by the investigator (hand, foot, face, etc.). In these conditions :

1. The stimulus is measured by the device. Its physical characteristics are therefore constant from one experiment to the other;
2. The device proposes varied and reproducible experimental paradigms. They permit obtaining normative values established in each laboratory on healthy subjects. They are used as references to assess the sensitive thresholds in patients. These paradigms, independent from the stimuli physical characteristics, are described in the following chapter;
3. It is possible to select the type of stimulus (pressure, vibration, differentiation, shifting. . .) and its intensity, and therefore to study with accuracy the different types of receptors or fibers affected by a disease.

Sensitivity to skin mechanical distension has been measured using a suction device (Cutometer SEM 474, C + K Electronik, Köln, Germany) (Martalo et al. 2001). Two parameters were selected : the pull sensation threshold during a progressing suction force (25 mbar/s), and the pull sensation threshold following sudden suctions at increasing force. The latter was found significantly lower. The authors speculate that a progressive suction might stimulate slow adaptating nerve endings whereas sudden suction would involve fast adaptating nerve endings. Accordingly the method could permit measuring separately these two types of mechanoreceptors.

2 Temperature Perception and Pain

The most accessible method is the one using a Peltier's effect based thermode. Many authors use the Thermal Sensory Analyzer (TSA-2001®) developed by the MEDOC company. This stimulator, attached to the skin, consists of a contact plaque (30 × 30 mm), three thermistances and a water circuit. In the Peltier's effect, an electric current runs through a semiconductor and produces a temperature gradient in the contact plaque. The gradient direction depends on the current direction. The water circuit permits to cool down or heat up the surface opposite the contact plaque. The stimulator mechanism allows temperature changing rates of 0.3 °C/s up to a maximum of 2–4 °C depending on the type of stimulation, cold or heat respectively. The thermistances allow to continuously monitor the contact plaque and the hydraulic circuit temperatures, the latter acting as a safety device. The patient has at his disposal a response box with two buttons: one is for affirmative answers, the other for negative answers. The whole TSA-2001 system is connected to a computer which selects and rules the different stimulation methods

2.1 The Boundaries Method

The temperature applied on the skin rises gradually at a constant rate starting from a neutral temperature (no thermal sensation). When the patient feels the selected sensation (heat, cold, pain) he presses the YES key, thus establishing a threshold value. This test is repeated and the final threshold value is defined as the mean of all test. The thresholds obtained with this method are often over-evaluated.

2.2 The Levels Method

In this technique, prior to the test, the investigator chooses the temperature step which will be added to the adaptation temperature during the first stimulation. This step must be sufficiently high. If the subject answers YES, this step is divided by two and again added to the adaptation temperature. If the answer is NO, the temperature is increased by the full step. This operation is repeated in order to refine the threshold value which is defined as the mean of the last positive value and the last negative value.

The stairs method is a variant in which the investigator chooses three stimulation steps (large, intermediate and fine) to refine the threshold search.

2.3 Forced Selection Method

Its principle is to propose two stimulations to the subject, at random (one is significant, the other neutral) to which he must answer by yes or no. The efficient stimulation is generally selected among three pre-defined steps. The threshold admittedly corresponds to the intensity which generates 50 % of positive responses. This method takes longer than the previous ones, but is the most rigorous (Arendt-Nielsen 1990) because it reduces the bias obviously associated with both the subject and investigator.

The TSA 2001 device is therefore perfectly adapted to the study of threshold to heat and cold (whether painful or not). The radiant stimulator (Socrel Model DS 20® Ugo Basile, Varese, Italy) is used in some studies, however less frequently since it provides one type of stimulus only (heat).

Since its development by Mor et al. (1975), the laser (type CO_2 or Argon) has been of increasing interest in the investigation of nociception. Investigators have at their disposal a stimulation unit which controls the laser CO_2 activation intensity and frequency. However the constraints of this technique must be considered :

1. Stimulation of various sites is possible only if the device is equipped with an articulated arm comprising sophisticated mirror sets. This accessory is mandatory in skin exploration;
2. High intensity or high frequency stimulations generate an erythema, and sometimes a blister. The damage will appear even more easily if the stimulation is delivered to aged or fair skinned subjects.
3. Both the investigator and the control subject or the patient must wear protecting glasses. They prevent cornea lesions caused by the CO_2 laser if the beam accidentally veers off course. This type of laser cannot be responsible for retinal lesions because it is absorbed in the cornea.
4. Only the investigator and the patient should be allowed in the room.

The laser CO_2 generates a very steep rise in temperature (600 °C/s) in the most superficial layers of the epidermis thus activating in a synchronous manner the polymodal receptors to heat, either Aδ or C fibers. The skin basal temperature is reached again in 200 ms. The sensation perceived by the patient is either heat attributed to C fibers, or a more or less burning sting attributed to Aδ fibers. Above a certain intensity which varies according to individuals, the patient perceives two sensations, first a burning sting (Aδ fibers) followed by delayed heat involving the concomitant activation of the slow C fibers. A work by Bromm and Treede (1984) using microneurography showed that the Aα and Aβ fibers do not respond to this type of stimulus. Taking into account the distribution of the polymodal receptors, it is therefore possible to stimulate preferentially Aδ or C receptors according to the stimulus diameter (Bragard et al. 1996). The latter can be adjusted through lenses integrated in the stimulator.

Laser stimulators, still at a development stage, are mainly used to study the cortical projections of the spinothalamic paths in humans (Bromm et al. 1991; Valeriani et al. 1996). It is then possible: (1) to record evoked responses on the scalp using surface electrodes; (2) to observe metabolism modifications in functional imaging; (3) to test the efficiency of analgesics or topical preparations such as

EMLA ointment or capsaicin (Beydoun et al. 1996).

It is also possible to activate the mechanonociceptors with a stimulator which delivers a force expressed in g onto the skin surface (Basile algometer®; Ugo Basile, Varese, Italy).

3 Sympathetic Nerve Functioning

A direct correlation was found between firing rate and amplitude of the sympathetic nerves and the sweat response on palms and soles (Macefield and Wallin 1996), measured in terms of the number and amplitude of spontaneous skin conductance waves. This was used to investigate the development of the sympathetic nervous system associated with arousal in the first year of life. The mean skin conductance level at 88 Hz, the number of waves per second, and the amplitude of the waves were measured during spontaneous skin conductance changes, and after auditory stimulation (Hernes et al. 2002).

4 Conclusion

The various techniques to study the skin neurosensorial functions are more adapted to clinical research than current practice. Their implementation is heavy and requires important and costly logistics (computer scientists, technicians, engineers. . .). It often implies work in collaboration with people in the industry. Their interest is growing however, especially as they open the way to more accurate studies on the skin neurosensorial functions.

References

Arendt-Nielsen L. First pain event related potentials to argon laser stimuli: recording and quantification. J Neurol Neurosurg Psychiatry. 1990;53:398–404.

Beydoun A, Dyke DBS, Morrow TJ, Casey KL. Topical capsaicin selectively attenuates heat pain and A delta fiber-mediated laser-evoked potentials. Pain. 1996;65:189–96.

Bragard D, Chen ACN, Plaghki L. Direct isolation of ultralate (C fibre) eevoked brain potentials by CO_2 laser stimulation of tiny cutaneous surface areas in man. Neurosci Lett. 1996;209:81–4.

Bromm B, Treede RD. Nerve fibre discharges, cerebral potentials and sensations induced by CO_2 laser stimulation. Hum Neurobiol. 1984;3:33–40.

Bromm B, Treede RD. Laser-evoked cerebral potentials in the assessment of cutaneous pain sensitivity in normal subjects and patients. Rev Neurol. 1991;147:625–43.

Dick PJ, Karnes J, O'Brien PC. Zimmerman IR. Detection thresholds of cutaneous sensation in humans. In: Dick PJ, Thomas PK, editors. Peripheral neuropathy, WB Saunders, Philadelphia, 1993. pp 706–28.

Dotson RM. Clinical neurophysiology laboratory tests to assess the nociceptive system in humans. J Clin Neurophysiol. 1997;14:32–45.

Hernes KG, Moerkrid L, Fremming A, Oedegarden S, Martinsen OG, Storm H. Skin conductance changes during the first year of life in full-term infants. Pediatr Res. 2002;52:837–843.

Macefield VG, Wallin BG. The discharge behaviour of single sympathetic neurones supplying human sweat glands. J Auton Nerv Syst. 1996;14:277–286.

Martalo O, Henry F, Piérard GE. Seuil liminaire de perception d'un étirement cutané. Ann Dermatol Venereol. 2001;128:119–22.

Mor J, Carmon A. Laser emitted radiant heat for pain research. Pain. 1975;1:233–7.

Valeriani M, Rambaud L, Mauguière F. Scalp topography and dipolar source modelling of potentials evoked by CO2 laser stimulation of the hand. Electroencephalogr Clin Neurophysiol. 1996;100:343–53.

Von-Frey M. Untersuchungen über die Sinnesfunktion der menschlichen Haut. Erste Abhandlung : Druckenpfindung und Schmerz. Abh Mathem Phys Clas Kgl Sächs Ges Wiss. 1897:208–17:239–53: 261–66.

Thermal Sensory Analyzer and Skin 130

Iqbaljit Singh and Howard I. Maibach

Contents

I. Singh (✉)
Department of Dermatology, UCSF, Fremont, CA, USA
e-mail: gill1606@gmail.com

H.I. Maibach
Department of Dermatology, School of Medicine, University of California, San Francisco, CA, USA
e-mail: maibachh@derm.ucsf.edu

P. Humbert et al. (eds.), *Agache's Measuring the Skin*,
DOI 10.1007/978-3-319-32383-1_80

Keywords
Quantitative thermal testing • Thermal sensory analyzer • Warm sensation • Cold sensation • Cold pain • Warm pain • Itch magnitude • Itch duration • Thermoreceptors • Nocireceptors • Mechanoreceptors • Polymodal nociceptors • Diabetic neuropathy

1 The TSA-ii Model, and How It Works?

TSA-ii unit is connected to a laptop or computer for user interface and control of functions of the unit through the unit's software that can be loaded onto the CPU. A thermode that delivers temperature/pain sensations to the subject is also attached to the TSA-ii unit and is controlled by the software on a computer. Also attached to the TSA unit is a handheld control that can terminate the temperature signal coming in from the unit through the thermode if the subject feels pain in pain threshold testing as well as communicate sensation perception (hot/cold) to the machine once a sensation is appreciated, simply by pressing a button on the handheld control. The software records this threshold and also automatically compares the subject's threshold perception of sensation to his/her age-specific normal values.

The machine uses a Peltier's effect-based thermode and is, in effect, a thermal stimulator. This thermode is attached to the skin and has a contact plaque (or contact surface) of 30 × 30 mm, three thermistors (that measure the local skin surface temperature), and a water circuit. An electric current runs through a semiconductor and produces a temperature change in the contact surface of the thermode. The water circuit allows for cooling and heating of a surface opposite to the contact surface. Temperature can be changed at a rate of 0.3 °C, up to a maximum of 2–4 °C. The thermistors continuously check the temperatures of the contact surface and the hydraulic circuit temperatures (which act as a safety device). As described above, the patient has a control box with two buttons: one for affirmative responses and the other for negative responses. Finally, the whole TSA is also connected to a computer, which provides the interface to select and control different stimulation methods.

2 Receptors Involved in Thermal Sensation Induced by TSA Machine

Thermoreceptors: Contrary to nociceptors, thermoreceptors have a low activation threshold. The neuron-free endings that are sensitive to heat are comprised of type C fibers and are less numerous than those sensing for cold. Their diameters are 1 mm and activated for temperature variations between 30 °C and 45 °C with max sensitivity between 41 °C and 45 °C. Above 45 °C, nociceptor nerve endings are activated and the thermoreceptor decreases its firing.

Cold sensitivity is conveyed through the thermoreceptor nerve ending activation carried by fibers A-Delta and C. The receptive field is small as the free nerve ending has a diameter of 100 μm. They fire sensory signals when the temperature range is 0.5–20 °C; in this range they are activated especially if there is a sharp drop in temperature. They stop firing once the temperature range is back to the body's basal level. In the temperature range of 30–40 °C, both cold and warm fiber types can be active.

Nociceptor: These receptors are innervated by slightly or nonmyelinated nerve endings. These fiber types have a **high** threshold of activation, and their response increases in parallel to the intensity of the stimulus. Two types of nociceptors exist: mechanonociceptors and polymodal nociceptors.

Mechanonociceptors: These are slightly myelinated A-Delta fibers. Receptive fields are large (1–2 cm) and these are involved in quick and well-located stinging, pinching, and cutting sensations. Response is proportional to intensity but decreases on repetitive stimuli (inactivation phenomenon).

Polymodal Nociceptors: Primary afferent fibers are Type C and not myelinated; there are a

smaller number of A-Delta fibers as well. Receptive field is 1 mm^2 to 1 cm^2. These receptors respond to sharp and strong mechanical stimulations; they also code for temperature rising above 43 °C as painful. In this case, the subject feels a sharp, sudden heat followed by a longer delayed heat sensation. This is an example of initial fast conducting A-Delta activation and then activation of slower C fibers. C fibers respond to chemical stimuli such as bradykinin, histamine, and other irritants as well (Fig. 1 and 2).

3 Clinical Applications

Different medical conditions that utilize the TSA's abilities and testing are fibromyalgia, painful neuropathies, lumbar radiculopathies, small fiber allodynia in Complex Regional Pain Syndrome (CRPS), underlying central nervous system impairment in difficult-to-diagnose patients, **early detection of diabetic neuropathy of small caliber fibers**, entrapment and toxic neuropathies, testing to detect malingerers, and nerve root compression/inflammation.

4 Clinical Experiments Utilizing the TSA

4.1 Antipruritic and Thermal Sensation Effects of Hydrocortisone Creams in Human Skin

This experiment measured the effects of topical corticosteroids on thermal sensation and itch induced by histamine injections that were intradermal (Zhai et al.).

Itch was measured via (i) itch magnitude and (ii) duration; and thermal sensation was measured using the TSA unit, with categories of warm sensation (WS), cold sensation (CS), cold pain (CP), and warm pain (WP). Itch magnitude was measured each minute for 10 min using a Visual Analogue Scale (VSA). Histamine was injected in four separate areas spanning both forearms, and these four areas were each applied with (i) hydrocortisone 1 %, hydrocortisone 2.5 %, placebo, and histamine ONLY, which may have served as control. This was a double-blind, random, comparative, controlled, single-dose, and single-center study involving 18 subjects; 2.5 % hydrocortisone considerably reduced **itch duration** from 12.6 + or – 11.0 min (mean + or – SD) to 8.6 + or – 8.2 min (reducing rate being 32 %) as well as **itch magnitude** at minutes 3, 6, 7, and overall ($p = 0.03$). Placebo, 1 % and 2.5 % hydrocortisone significantly altered **cold sensation** threshold ($p < 0.05$).

The data suggest that topical application of 2.5 % hydrocortisone may be significantly beneficial for histamine-induced itch.

4.2 Quantitative Sensory Testing: Effect of Site and Skin Temperature on Thermal Thresholds

Objective was to determine the effect of different sites and local skin temperature on thermal thresholds. Cool and warm detection (coolDT, warmDT) and cold and heat pain thresholds (coldPT and heatPT) were compared in 46 normal volunteers at the (i) thenar eminence (TE), (ii) dorsum of hand (DH), (iii) volar surface of the wrist (VW), and (iv) dorsum of foot (DF) (Hagander et al.).

The hand was more sensitive to warm and cool sensation than the foot. In regards to the upper limb, TE was more sensitive for warm than DH and VW, although this difference is clinically negligible. DH and VW were equally sensitive to warm, and TE, DH, and VW are equally sensitive to cool sensation. Interindividual variance is least at TE. Warm and cool thresholds are independent of local skin temperature (range 27–37 °C). TE is less sensitive for cold *pain*, but otherwise the hand and foot are equally sensitive to thermal pain.

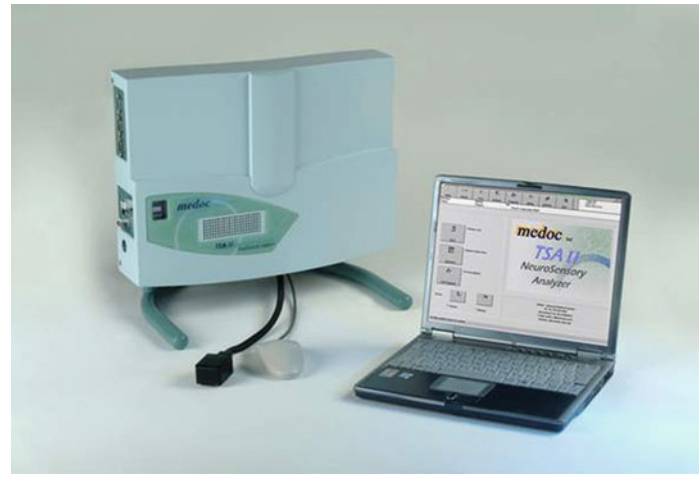

Fig. 1 TSA-iiNeuroSensory Analyzer System, with a laptop showing the loaded software interface (From: http://www.medoc-web.com/products/tsa-ii)

Fig. 2 (**a**) 30 × 30 mm thermode. (**b**) 16 × 16 mm thermode. (**c**) 5 × 5mm thermode (From: http://www.medoc-web.com/products/tsa-ii/tsa-ii-accessories)

TE is preferred for thermal sensation thresholds as it has least interindividual variability. TE is also preferred in evaluating hyperalgesia to cold due to the higher threshold to cold pain.

By determining the effect of different anatomical locations, as well as local skin temperature, on thermal thresholds, the goal is therefore to essentially compare and contrast the thermal thresholds at different sites of the human body: hand, wrist, and foot areas in general; and if there are any differences of thermal threshold sensation/pain at these sites, a preferred site of testing for a particular sensory threshold can be identified. Thus, four thermal modalities as mentioned above were tested (coolDT, warm DT, coldPT, and heatPT), and the effect of local skin temperature on cool and warm thresholds at the hand and the need to warm or cool the skin prior to testing was also tested.

4.3 Effect of Venlafaxine on Ongoing and Experimentally Induced Pain in Neuropathic Pain Patients: A Double-Blind, Placebo-Controlled Study

A randomized double-blind placebo controlled study investigated the effectiveness and safety of Venlafaxine XR (SNRI reuptake inhibitor) 75 and 150 mg, on ongoing pain and quantitative sensory testing in 60 patients with neuropathic pain for 8 weeks (Yucel et al. 2005).

Allodynia and pin-prick pain showed a significant decrease in venlafaxine groups compared to placebo. Pain threshold and summation threshold for electrical stimuli, as well as summation threshold for heat stimuli, showed that these thresholds increased significantly following treatment with venlafaxine, that is, more stimulus is required to produce the sensation.

Moreover, the degree of summation of electrical and heat stimuli decreased in the venlafaxine groups compared to placebo.

Therefore, Venlafaxine has significant effect on pain as well as electrical and thermal temporal summations.

4.4 Concentration-Effect Relationships for Intravenous Alfentanil and Ketamine Infusions in Human Volunteers: Effects on Acute Thresholds and Capsaicin-Evoked Hyperpathia

Ketamine and Alfentanil both decreased capsaicin-induced pain and increased the threshold of von Frey hair induced pain. Alfentanil also increased the thresholds for cool and warm sensation detection (Wallace et al. 2002).

Furthermore, the authors state that these studies provide a usefulness in human pain models for phase 1 clinical trials, as these experiments can help define efficacy of analgesics.

4.5 Oral Opioid Administration and Hyperalgesia in Patients with Cancer or Chronic Nonmalignant Pain

This study challenged the finding of previous research that after parenteral administration of opioids, animals had an increased latency for paw withdrawal to heat and mechanical stimuli, that is, after the opioid, they would more quickly withdraw their paws on painful stimulation and that, likewise, there is an increased pain sensitivity in humans after postoperative infusions of short-acting opioids, or in drug addicts (Reznikov et al. 2005).

This study explored any possibility of difference between opioid and nonopioid analgesic treatment in cancer-related or chronic nonmalignant pain subjects.

The results showed no differences were found for gender, age, duration of pain, or duration of treatment. No differences were found in punctuate, pressure, and heat pain thresholds or suprathreshold heat pain intensity.

Therefore, like nonopioid analgesics, common doses of opioid analgesics do not result in abnormal sensitivity to pain as purposed by previous research.

4.6 fMRI Measurement of CNS Responses to Naloxone Infusion and Subsequent Mild Noxious Thermal Stimuli in Healthy Volunteers

Using the fMRI machine (functional magnetic resonance imaging) and thermal stimuli via TSA, a study was done to understand the effects of naloxone on opioid systems and the drug's effect on the CNS response to mild noxious heat. Out of the two groups, normal saline and naloxone, naloxone group shows more cortical and subcortical activation. With a 46 °C stimulus, there was activation in insula, orbitofrontal cortex, thalamus, and hippocampus, in contrast to the normal saline group.

These results show that naloxone has effects in brain regions (cortical & subcortical) when given alone, that is, without psychophysical (heat) stimulation, and with heat stimulation has effects in different regions of the brain producing activation in regions with high levels of mu-opioid receptors that maybe involved in endogenous analgesia. Furthermore, the authors add that this study shows that fMRI can detect subtle changes in brain activation due to pharmacological agents without cognitive effects.

4.7 Dexmedetomidine Pharmacodynamics: Part II: Crossover Comparison of the Analgesic Effect of Dexmedetomidine and Remifentanil in Healthy Volunteers

Sigmoid curves shift to the right for both remifentanil and dexmedetomidine; however, the curve is less steep for dexmedetomidine (Cortinez et al. 2004).

In conclusion, dexmedetomidine is not as effective an analgesic as remifentanil, and the difference may be attributed to different mechanisms of actions of each drug. Dexmedetomidine does have a sedative effect, although authors conclude remifentanil is superior as an analgesic.

4.8 Effect of Remifentanil on the Heat Pain Threshold in Volunteers

This study investigated analgesic properties of remifentanil using heat pain threshold delivered via TSA, and it showed that there were dose-dependent increases in heat pain threshold with the drug. Analgesic effect was opioid mediated, and 0.05 μg Kg(−1) min(−1) was found to be an effective and safe increment in healthy volunteers. Remifentanil led to an increase in heat pain threshold differing significantly from placebo (Gustorff et al. 2001).

4.9 Placebo-Controlled Comparison of a Morphine/Dextromethorphan Combination with Morphine on Experimental Pain and Hyperalgesia in Healthy Volunteers

Both morphine alone and in combination with dextromethorphan decreased painful or noxious thermal stimuli delivered via TSA and had somewhat of an effect on secondary hyperalgesia delivered by brush and von Frey hair stimulation when compared with placebo. However, in clinical trials with humans, morphine/dextromethorphan combo did not provide superior analgesic effect, although this finding is opposite to the preclinical animal trials with the same drugs where there was a potentiation of analgesic effect with the combo.

Thus, adding 1:1 dextromethorphan and morphine combo does not improve analgesia over morphine alone in regards to noxious thermal stimuli and cutaneous sensitization.

This study allows for a possibility of determining optimal dosing or dose ratios in opioid analgesic combination studies.

4.10 Age Differences in Orofacial Sensory Thresholds

This study divides its subjects into two bimodal groups those <45 years of age and those >65 years of age and undertakes testing that aims to determine threshold differences between the two groups, involving thermal (executed by TSA) as well as pain and others. Therefore, thresholds for warm, cool, pain, touch, two-point discrimination, and taste were done (Heft and Robinson 2010).

All thresholds were elevated in the older individuals, and males were less sensitive to females to cool at the chin, touch, and sour taste. The study concludes that there are elevations in sense thresholds for multimodal somatosensory and gustatory senses.

4.11 Disturbances of C-Fiber-Mediated Sensibility in Lumbosacral Disk Disease

This study takes nine patients with lumbosacral disease and compares them with nineteen healthy individuals. Comparison is made between the sensory function of dermatomes in the feet ipsilateral to and contralateral to the leg with lumbosacral disk disease. These results were compared with 19 healthy individuals (Lautenbacher 1994).

Warmth threshold was increased ipsilateral to the lesion, but heat pain threshold is decreased contralateral to the lesion while normal ipsilateral to the lesion. Warmth threshold is normal in the contralateral dermatome. Hence, there is speculation that lumbosacral disk disease may increase sensitivity to pain due to nerve root compression.

4.12 Comparative Study of the Cutaneous Sensation of Leprosy-Suspected Lesions Using Semmes-Weinstein Monofilaments and Quantitative Thermal Testing

This study compared warm perception thresholds (WPT), cold perception thresholds (CPT), and warm and cold perception intervals (WCPI) with touch-pressure thresholds measured via Semmes-Weinstein monofilament (SWM), and hence, these thresholds are described using SWM. These tests were done on leprosy-suspected skin lesions (patch); 108 were total participants, 82 of which were diagnosed with leprosy. Further, the touch-pressure thresholds were measured at via SWN at 0.05 g, 0.2 g, 2 g, 4 g, 10 g, and 300 g (Villarroel et al. 2007).

The results showed a sensitivity of 81.7 % and specificity of 96.1 %, while warm perception threshold (WPT) was 90.2 % and cold perception 92.2 %, with combined 100 % specificity. In those diagnosed with leprosy, lesions that had SWN 0.05 g showed significantly different WPT, CPT, and WCPI values when compared to skin lesions of different etiologies.

In leprosy subjects, as the touch-pressure thresholds (SWN) rise, so do the WPT, CPT, and WCPI. Some exceptions with SWN of 0.05 and 0.2 g did not have increased WPT or CPT. However, all patients with SWN 2.0 g or above did have altered WPT and CPT. In regards to the WCPI, subjects with 0.05 g pressure thresholds had altered WCPI in the skin lesions.

In conclusion, although thermal testing is more sensitive, pressure thresholds also act as valid screening methods to detect cutaneous forms of leprosy, and these results can help extrapolate the thermal thresholds based on the results above.

4.13 A Comparison of Quantitative Sensory Testing with Skin Biopsy in Small Fiber Neuropathy

This study correlated QST testing and skin biopsies in small nerve fiber neuropathy. It determined that assuming skin biopsies are the gold standard for detecting small fiber neuropathy, the sensitivity of QST for detecting similar neuropathies is high provided that both warm and cold sense thresholds are tested, but the specificity is low at 46 % (Scott et al. 2003).

4.14 Clinical Applications of Quantitative Sensory Testing (QST)

4.14.1 Diabetes Mellitus

QST was used for evaluating and staging diabetic polyneuropathy (PNP). It was set of criteria for assessing severity of diabetic neuropathy based on warm and cold threshold abnormality that was suggested. A significant correlation was found between thermal abnormalities and clinical examination of small fiber function and suggested that these criteria can be used for long-term management of patients (Zaslansky and Yarnitsky).

Combining thermal and vibratory tests gave a joint sensitivity of 92–95 %, with specificity of 77–86 %.

A "warmth sensitivity index," the range between warmth sensory threshold and heat pain threshold, was suggested as a sensitive tool for detection of neuropathy in diabetics with no clinical evidence of neuropathy.

Natural history of diabetic neuropathy by QST parameters: 201 **well-established** NIDDM patients were followed for 2 years. The increase for vibratory and thermal thresholds during this period was significant between baseline and first year, and between first and second years; for example, warm sensory thresholds increased from 2.6 °C (median value) at baseline to 3 °C

after 1 year, and 3.4 °C after 2 years. Similarly, cold thresholds were 1.9 °C, 2.3 °C, and 2.7 °C, respectively, for baseline, first year, and second year. In contrast, 71 newly diagnosed NIDDM patients had only slight deterioration in VT at the feet over 5 years.

Polyneuropathy was assessed by a pain score, sensory clinical exam, NCS, autonomic function, and *thermal* and vibratory thresholds of the foot. The only parameters to change were a significant reduction in thermal scores that paralleled a decrease in pain scores, which confirms the importance of thermal sensation quantification in patients with diabetic neuropathy.

4.14.2 Alcoholic Polyneuropathy (PNP)

Fifty chronic alcoholics were examined for PNP. All had history of alcohol abuse for more than 7 years, daily alcohol consumption more than 100 g and a positive Munich Alcoholism Test. Six thermal sensation parameters were tested behind the internal malleolus, using the method of limits (Zaslansky and Yarnitsky).

Thresholds for cold sensation were raised in 62 % of patients, warmth sensation in 24 %, and heat pain in 22 %.

4.14.3 Vincristine and Cisplatin Neurotoxicity

Vincristine was seen to have vibratory and thermal sensation alterations, while cisplatin only had vibratory changes (Zaslansky and Yarnitsky).

4.14.4 Acute Inflammatory Demyelinating Polyradiculoneuropathy (Guillain-Barre Syndrome (GBS))

Twenty-two patients with GBS were tested with the TSA; average was 49 (range 17–49), being tested at outset of disease, at peak disease, and at resolution. At initial sensory testing, 68 % patients had at least one thermal threshold abnormality; at peak of disease, cold sensation at ankle and wrist was abnormal in 73 %, and heat thresholds at ankle and wrist were abnormal in 55 % and 50 % of patients (Zaslansky and Yarnitsky).

4.14.5 Myotonic Dystrophy

Myotonic dystrophy is a pure motor/muscular disorder without any sensory components, but thermal testing revealed otherwise. Twenty-four patients with 0.2–22 years duration of clinical symptoms were tested, and thermal thresholds

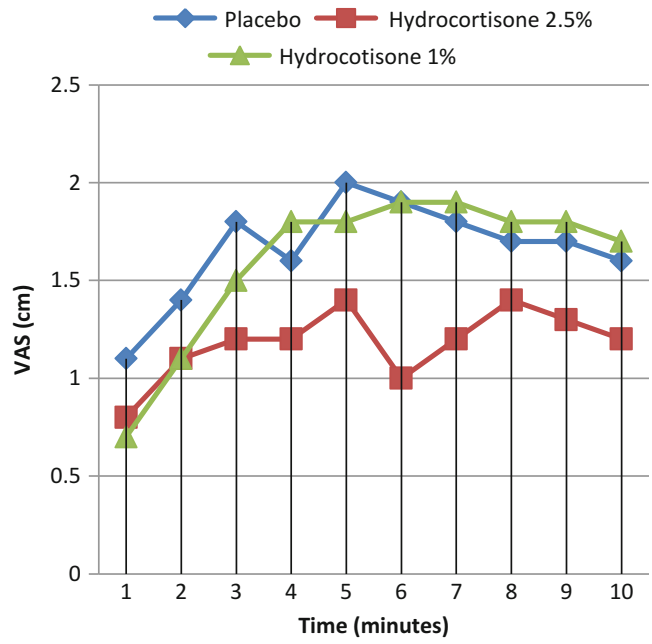

Fig. 3 This graph measures the effect on histamine-induced itch magnitude after application of placebo, 1 % hydrocortisone, and 2.5 % hydrocortisone. VAS measures itch magnitude (Modified from Zhai et al.)

were abnormal in 83 %, more at ankle (79 %) than wrist (50 %). Heat sensation was more frequently abnormal than cold sensation. Vibratory sensation at the foot was also deranged in 21 % of patients. Therefore, researchers conclude that Myotonic dystrophy is not a pure motor disease.

The TSA machine is of great use in understanding the thermal thresholds of subjects and more importantly these thresholds in patients with peripheral nerve disease. Not only thermal thresholds can be assessed, but nociceptive nerve function as well, by inducing heat and cold pain through the TSA machine: nerve endings can code for pain stimuli if the temperature rises above a certain threshold as described above through the different experiments.

This allows researchers and clinicians to assess a person's sensory function by comparing the person's threshold results to normative data, which is available in the software of the TSA machine. As a result, diabetic patients, others with peripheral neuropathies, and their physicians can have a better understanding of how a particular disease process is affecting the patient by picking up any deviations from normative thermal thresholds delineated by the TSA machine. This

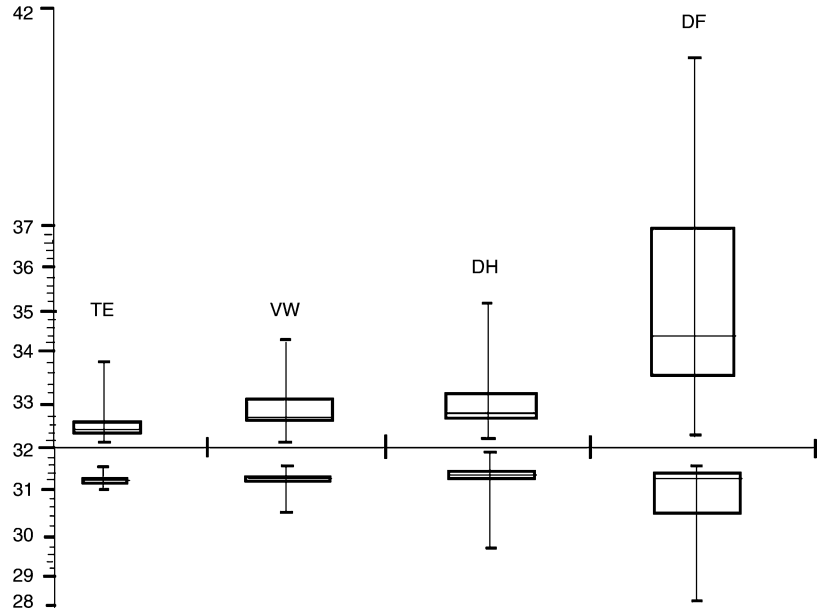

Fig. 4 Cool and warm detection thresholds for different anatomic sites. Rectangles measuring the median, 75th, 25th percentiles. Bars measuring 95th and 5th percentiles (Modified from Hagander et al.)

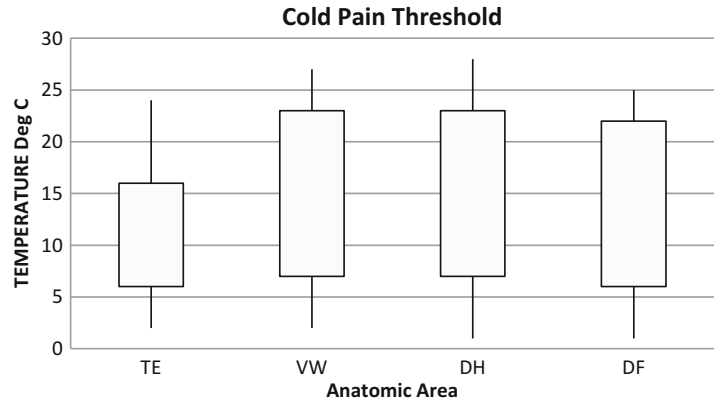

Fig. 5 Error bars measure 95th and 5th percentiles; rectangle measures 75th and 25th (Modified from Hagander et al.)

can be valuable for doctors and patients in diagnosing, managing, as well as prognosing the disease involving the peripheral sensory nerves. Hence, the TSA is an indispensable machine in medicine, and there is no doubt about its precision and accuracy as it inputs data based on the direct responses of the subject, by clicking of the controller, and therefore, the TSA provides an intimate measurement of thermal perception (Figs. 3, 4, and 5).

References

"Measuring the skin," Pierre Agache. Pages 660, 661, 667.

Borras C, Becerra L, Ploghaus A, Gostic JM, Da Silva A, Gonzalez RG, Borsook D. FMRI measurement of CNS responses to naloxone infusion and subsequent mild noxious thermal stimuli in healthy volunteers. J Neurophysiol. 2004;91:2723–33.

Cortinez LI, Hsu YW, Sum-Ping ST, Young C, Keifer JC, MacLeod D, Robertson KM, Wright DR, Moretti EW, Somma J. Dexmedetomidine pharmacodynamics: part II – crossover comparison of the analgesic effect of dexmedetomidine and remifentanil in healthy volunteers. Anesthesiology. 2004;101:1077–83.

Frymoyer AR, Rowbotham MC, Petersen KL. Placebo-controlled comparison of a morphine/dextromethorphan combination with morphine on experimental pain and hyperalgesia in healthy volunteers. J Pain. 2007;8(1):19–25.

Gustorff B, Felleiter P, Nahlik G, Brannath W, Hoerauf KH, Spacek A, Kress HG. The effect of remifentanil on the heat pain threshold in volunteers. Anesth Analg. 2001;92:369–74.

Hagander LG, Midani HA, Kuskowski MA, Parry GJG. Quantitative sensory testing: effect of site and skin temperature on thermal thresholds. Skin Pharmacol Appl Skin Physiol. 2000;13(6):352–7.

Heft MW, Robinson ME. Age differences in orofacial sensory thresholds. J Dent Res. 2010;89(10): 1102–5. doi:10.1177/0022034510375287. PMCID: PMC3318051.

Lautenbacher S. Disturbances of C-fiber-mediated sensibility in lumbosacral disc disease. J Neurol Neurosurg Psychiatry.1222–3. 1994. (Letter).

Reznikov I, Pud D, Eisenberg E. Oral opioid administration and hyperalgesia in patients with cancer or chronic nonmalignant pain. Br J Clin Pharmacol. 2005; 60(3):311–8.

Rodrigues Júnior IA, Silva IC, Gresta LT, Lyon S, Villarroel Mde F, Arantes RM, Editors. Degree of skin denervation and its correlation to objective thermal sensory test in leprosy patients. PLoS Negl Trop Dis. 2012;6(12): e1975. Published online 13 Dec 2012. doi: 10.1371/journal.pntd.0001975. PMCID: PMC3521713.

Scott K, Simmons Z, Kothari MJ. A comparison of quantitative sensory testing with skin biopsy in small fiber neuropathy. J Clin Neuromuscul Dis. 2003;4(3): 129–32.

Villarroel MF, Orsini MB, Lima RC, Antunes CM. Comparative study of the cutaneous sensation of leprosy-suspected lesions using Semmes-Weinstein monofilaments and quantitative thermal testing. Lepr Rev. 2007;78(2):102–9.

Wallace MS, Ridgeway III B, Leung A, Schulteis G, Yaksh TL. Concentration-effect relationships for intravenous alfentanil and ketamine infusions in human volunteers: effects on acute thresholds and capsaicin-evoked hyperpathia. J Clin Pharmacol. 2002; 42:70–80.

Yucel A, Ozyalcin S, Koknel Talu G, Kiziltan E, Yucel B, Andersen OK, Arendt-Nielsen L, Disci R. The effect of venlafaxine on ongoing and experimentally induced pain in neuropathic pain patients: a double blind, placebo controlled study. Eur J Pain. 2005; 9:407–16.

Zaslansky R, Yarnitsky D. Clinical applications of quantitative sensory testing (QST). J Neurol Sci. 1998; 153(2):215–38.

Zhai H, Frisch S, Pelosi A, Neibart S, Maibach HI. Antipruritic and thermal sensation effects of hydrocortisone creams in human skin. Skin Pharmacol Appl Skin Physiol. 2000;13(6):352–7.

Itch Metrology

131

Emilie Brenaut and Laurent Misery

Contents

Keywords

Electroencephalogram • Itch metrology • Definition • Experimental induction • Graphic rating scales • History specifies • Intensity measurement • Numerical rating scales • Perspectives • Qualitative aspects • Ratio estimation scales • Scratching intensity, measurement • Numerical rating scale (NRS) • Visual analogue scale (VAS)

Itch or pruritus is defined as "disagreeable cutaneous sensation inducing the need to scratch." These two words are nowadays used as synonyms, "pruritus" being more a medical word than "itch" (Bernhard 1994; Misery and Ständer 2010).

Pathophysiology remains partially unknown but huge breakthroughs have been recently performed (see chapter . . .). Therapeutic possibilities are relatively limited, except etiological treatments. Itch metrology is difficult. However, it is indispensable to evaluate itch in clinical and therapeutic studies. Itch is usually evaluated through human or animal in vivo models. The main instruments of measure are itch experience and scratching.

E. Brenaut • L. Misery (✉)
Department of Dermatology, University Hospital of Brest, Brest, France
e-mail: laurent.misery@chu-brest.fr

P. Humbert et al. (eds.), *Agache's Measuring the Skin*,
DOI 10.1007/978-3-319-32383-1_81

1 Experimental Induction of Pruritus

Itch can be induced by intradermal injection of histamine, serotonin, substance P, 48/80 compound, codeine, kallikrein, bradykinin, papain, or trypsin or by intravenous injection of morphinics or interleukin-2 (Wallengren 1993; Theunis et al. 2008). In practice, experimental induction of pruritus is usually obtained by intradermal or subcutaneous injection of 48/80 compound (3–100 μg), substance P (10–300 μg), or histamine (3–300 μg) or codeine (Theunis et al. 2008). There is a dose effect but too high doses lead to pain rather than pruritus. The induction of pruritus by cowhage (*Mucuna pruriens*) (Papoiu et al. 2011), which activates PAR-2+ pruriceptors, is a new used technique but a limitation is that the release of proteases is not controlled.

Pruritus can also be provoked by low electric currents. This technique is still discussed because electric currents should induce paresthesia (or pain) rather itch. They are also able to inhibit itch by stimulation of afferent nerve fibers (Ekbom 1995). However, electrical stimulation with stimulus durations $>$ or $=$ 2 ms and frequencies $>$ or $=$ 50 Hz seems to evoke a pure itch (Ikoma et al. 2005).

The mechanical induction of itch by esthesiometer (WEST-itch ™, Connecticut Bioinstruments Inc.) has been proposed. This device is formed by nylon fibers with different diameters (Weinstein et al. 1995). Five bundles of nylon fibers allow different levels of stimulation. This equipment is simple but somewhat expensive.

2 Qualitative Aspects of Pruritus

The evaluation of qualitative aspects of pruritus is based on clinical examination and anamnesis (Misery and Ständer 2010; Misery 2012). Clinical examination is focused on scratching lesions (quantity, deepness, localization, disposition), prurigo lesions, dermographism, and lichenification. Cutaneous or systemic symptoms can be associated and they can orientate etiological diagnosis. A glazed aspect of nails is in favor of intense and old itch. History specifies itch features:

- Date and mode of beginning (sudden or progressive)
- Course (acute, paroxystic, or chronic)
- Chronology (moment of the day, period of the year)
- Intensity (discomfort in working, everyday life, affective life, or sleep)
- Topography
- Aggravating factors (sweating, sport, bath, shower, meal) or soothing factors (cold, relaxation)
- Associated context (diseases, drugs, chemical products)
- Collective pruritus or not
- Effects of treatments

It is necessary to discriminate what is really pruritus and what is paresthesia, dysesthesia, or pain (that could be associated with itch, especially in neuropathic pruritus). It may be difficult in certain languages, especially in Africa or in Middle East, because there is no traditional word to differentiate these sensations.

There is no universally accepted questionnaire on pruritus (Weisshaar et al. 2012), whereas there is some on pain. In order to study qualitative aspects of itch, the Eppendorf itch questionnaire (Darsow et al. 1997) or the Brest questionnaire (Brenaut et al. 2013) could be used.

3 Intensity Measurement of Pruritus

The intensity of pruritus can be correctly evaluated only by the transcription of its experience by a human being. The appreciation by an observer is a bad method. Measurement of scratching intensity is possible with animals or humans but is only an indirect reflection of pruritus (see below). The measurement of itch intensity is difficult because it is subjective and dependent of experimental

conditions (e.g., deepness of injection of an itch inducer). Nonetheless, several methods have been proposed for the evaluation of itch intensity. They are inspired by pain evaluation scales.

Measurement scales are available. Some types are possible: nominal, ordinal, interval, or ratio scales. Nominal scales are the most simple (e.g., pruritus or not). Ordinal scales are semiquantitative (no pruritus, weak pruritus, moderate pruritus, severe pruritus). Interval scales are more accurate (from 1 to 8, from 1 to 10, from 0 to 11 for the Esthesiometer®). Ratio scale is more efficient because a true zero is defined and 2 means the double of 1. In therapeutic scales, the three first scales are the most often used. Statistical analysis of these scales is parametric (interval, ratio) or not (ordinal, nominal).

Ratio estimation scales allow comparisons of intensity of pruritus between themselves. The subject estimates intensities of itching induced by electric current of different intensities, saying, for example, "30 % more" or "30 % less." This method is criticized and is not used on itching induced by diseases.

With magnitude estimation scales, the subjects can choose a number without any limitation. This type of scale is relatively reliable and has been used in the measurement of various human sensations.

Graphic rating scales are simple, convenient, well validated, and the most commonly used. We personally prefer them. The subject indicates by a mark on a vertical or horizontal line the intensity of pruritus. Each extreme of the line represents "no itch" or "maximal itch." Most often a 10-cm scale is used, with or without cutoff points. The investigator converts the marking to a score by measuring the distance between the zero end (no itch) and the perpendicular mark on the line with a grid. The advantages of such scales are simplicity, sensitivity, and reproducibility. Nonetheless, some subjects may cluster their rating marks at the midpoint and the extremes of the scale. Others may have a decreased ability to think abstractly. Results are comparable in a same subject but not between several subjects.

Numerical rating scales are sometimes used for therapeutic studies. There is a need to propose a limited but discriminating quantity of numbers, as 3, 5, or 10 numbers. The validity of these scales has been shown for ratings of pain, but it is not yet the case for itch because numerical rating scales have been rarely evaluated for itch research.

Itch can be recorded by some proceedings. Itching is induced and then the subject indicates what he experiences with a pen or a plotter related to a potentiometer (Ekblom et al. 1984). The time interval between itch provocation and start/stop of itch is recorded as well as the perceived itch intensity. This allows the calculation of several itch variables: latency before itch, duration of itch, peak value of itch, and a total itch index (= area under the curve). This index reflects both the intensity of itch and its duration. A computerized system (PainTrack™ or SymTrack™, Styrex AB, Uppsala, Sweden) allows the continuous recording of itch sensation, as for arterial pressure. This proceeding could be the best to evaluate itching and to estimate efficacy of a treatment but it is little used.

The International Forum for the Study of Itch gives some recommendations (Ständer et al. 2013) to clarify the measurement of the intensity of itch:

- Visual analogue scale (VAS) is not an optimal instrument, but currently it cannot be dispensed with.
- Alternatively, numerical rating scale (NRS) can be used.
- VAS or NRS should be used in combination with verbal rating scale.
- Explanation and test run are recommended.

4 Measurement of Scratching Intensity

The appreciation of pruritus through scratching in humans or in animals is often used but its interest is limited. A weak pruritus does not induce scratching. Paresthesia, dysesthesia, or pain can induce scratching. The presence of probes on the

skin surface can induce pruritus or be embarrassment for movements. Nonetheless, some techniques are available to measure scratching (Savin 1995).

The intensity of scratching can be estimated by quantity and size of excoriations, prurigo lesions, or dermographism lesions. A video record can be useful to observe scratching.

The recording of scratching is not easy because scratching is not a regular activity. Duration, frequency, intensity, direction, amplitude, and localization of scratching actions are highly variable. It is difficult to separate one movement of scratching from the next. Several methods have been invented in order to measure one or several parameters of scratching.

The amplitude of movements can be registered, thanks to special wristwatches measuring the duration of scratching through movements in space by detectors of electromagnetic movements (Summerfiled and Welch 1980). This method is particularly interesting for studying pruritus during sleeping time.

Beds with detectors of vibrations can be used to detect movements of scratching. These movements are different from other movements by their irregular and repetitive characteristics (Felix and Shuste 1975).

Electrodes posed on forearms can measure muscular movements (Savin et al. 1973). This technique is convenient and reproducible. Beginning and end of the movements as their amplitude and their number can be assessed. This exam can be associated with registration of sleep to detect variations according to different phases of sleep.

Electroencephalogram can be coupled with measurements of pressure induced by scratching, thanks to probes on hands or nails (Brown and Kalucy 1975). More accurate measures are allowed by a proceeding inspired by this one and associating a computer and vibration transductors (using piezoelectric current) (Bergasa and Jones 1991).

Another proceeding has been recently proposed (Endo et al. 1997). Scratch-Monitor® is a little box with button which detects variations of pressure and a recording module attached to one hand. Number of movements is counted. Sensitivity is moderate.

5 Conclusions and Perspectives

Quantitative measurement of pruritus is difficult. Clinical examination and anamnesis allow an individual but inaccurate evaluation. For scientific working, especially therapeutic assays, there is a need to use simple techniques of measurement of pruritus or scratching. Scales of pruritus will probably remain the main methods to assess itch.

In our opinion, the methods revolutioning studies on pruritus in the future could be:

- In vitro studies, on a reconstructed skin associated with nerve fibers or on cocultures of nerve fibers and epidermal cells (Pereira et al. 2010)
- Studies on the cerebral integration of itch, by using positron emission tomography (PET) or functional resonance magnetic imagery (fRMI) (Bergeret et al. 2011)

References

Bergasa NV, Jones EA. Management of the pruritus of cholestasis: potential role of opiate antagonists. Am J Gastroenterol. 1991;86:1404–12.

Bergeret L, Black D, Theunis J, Misery L, Chauveau N, Aubry F, Gros H, Viallard G, Celsis P. Validation of a model of itch induction for brain positron emission tomography studies using histamine iontophoresis. Acta Derm Venereol. 2011;91:504–10.

Bernhard JD. Itch. Mechanisms and management of pruritus. New York: McGraw-Hill; 1994. 454 p.

Brenaut E, Garlantezec R, Talour K, Misery L. Itch characteristics in five dermatoses: non-atopic eczema, atopic dermatitis, urticaria, psoriasis and scabies. Acta Derm Venereol. 2013;93:573–4.

Brown RD, Kalucy RS. Correlation of neurophysiological and personality data in sleep scratching. Proc R Soc Med. 1975;68:528–32.

Darsow U, Mautner VF, Bromm B, Scharein E, Ring J. The Eppendorf itch questionnaire. Hautarzt. 1997;48:730–3.

Ekblom A, Fjellner B, Hansson P. The influence of mechanical vibratory stimulation and transcutaneous

electrical nerve stimulation on experimental pruritus induced by histamine. Acta Physiol Scand. 1984;122:361–7.

Ekbom A. Some neurophysiological aspects of itch. Sem Dermatol. 1995;14:262–70.

Endo K, Sumitsuji H, Fukuzumi T, Adachi J, Aoki T. Evaluation of scratch movements by a new scratch-monitor to analyze nocturnal itching in atopic dermatitis. Acta Dermatol Venereol. 1997; 77:432–5.

Felix R, Shuste S. A new method for the measurement of itch and the response to treatment. Br J Dermatol. 1975;93:303–12.

Ikoma A, Handwerker H, Miyachi Y, Schmelz M. Electrically evoked itch in humans. Pain. 2005;113:148–54.

Misery L. Prurit. Encycl Méd Chir. Paris: Editions Elsevier; 2012, Dermatologie, 98-140-A-10, 6p.

Misery L, Ständer S. Pruritus. London: Springer; 2010. 348p.

Papoiu AD, Tey HL, Coghill RC, Wang H, Yosipovitch G. Cowhage-induced itch as an experimental model for pruritus. A comparative study with histamine-induced itch. PLoS ONE. 2011;14:e17786.

Pereira U, Boulais N, Lebonvallet N, Pennec JP, Dorange G, Misery L. Mechanisms of the sensory effects of tacrolimus on the skin. Br J Dermatol. 2010;163:70–7.

Savin J. The measurement of scratching. Sem Dermatol. 1995;14:285–9.

Savin JA, Paterson WD, Oswald I. Scratching during sleep. Lancet. 1973;2:296–7.

Ständer S, Augustin M, Reich A, Blome C, Ebata T, Phan NQ, Szepietowski JC. Pruritus assessment in clinical trials: consensus recommendations from the International Forum for the Study of Itch (IFSI) special interest group scoring itch in clinical trials. Acta Derm Venereol. 2013;93:509–14.

Summerfiled JA, Welch ME. The measurement of itch with sensitive limb movement meters. Br J Dermatol. 1980;102:275–81.

Theunis J, Black D, Degouy A, Schmitt AM, Misery L. Comparison of perceived itch induced by skin prick-tests with histamine and codeine. Acta Derm Venereol. 2008;88:455–7.

Wallengren J. The pathophysiology of itch. Eur J Dermatol. 1993;3:643–7.

Weinstein CD, Drozdenko R, Weinstein S, Spivak H. A new noninvasive method to evaluate the antipruritic efficacy of over-the-counter skin care products. J Soc Cosmet Chem. 1995;46:53–65.

Weisshaar E, Gieler U, Kuepfer J, Furue M, Saeki H, Yosipovitch G, the International Forum for the Study of Itch. Questionnaires to assess chronic itch: a consensus paper of the international forum for the study of itch. Acta Derm Venereol. 2012;92:493–6.

Morphometry in Clinical Dermatology . . . or Measuring Without a Device

132

Pierre Agache

Contents

Keywords

Acetate sheets • Morphometry • Lesion surface • Point counting • Videocapillaroscopy

Morphometry embraces a number of methods aimed at measuring images or objects of irregular contour or shape as well as image density within a frame, using simple means associated with counting. As skin diseases mostly develop in the plane of the body surface, two-dimensional morphometry can be a valuable tool for the dermatologist who requires rapid and inexpensive measurement. However, the method is poorly known in dermatology because it was principally developed for research in tissue microscopy and ultrastructure.

1 Lesion Area

Point counting is the accurate method (Bahmer 1997). The rationale is that in a large area divided into equal squares, the center of each square can represent its area. Thus, when a squared grid with lines *d* cm apart is superimposed on a skin lesion, counting how many squares lie inside the lesion can be replaced by counting how many centers lie inside the lesion. As the square centers themselves can be replaced by the grid crossing points, the

Novices are advised to read Bahmer and Smolle (1992) and Loud and Anversa (1984) first.

This chapter was originally published under the ISBN 978-3-540-01771-4 with the following book title Measuring the Skin. The content has not been changed.

Pierre Agache: deceased.

P. Agache (✉)
Department of Dermatology, University Hospital of Besançon, Besançon, France
e-mail: aude.agache@free.fr; ferial.fanian@chu-besancon.fr; ferial.fanian@cert-besancon.com

P. Humbert et al. (eds.), *Agache's Measuring the Skin*, DOI 10.1007/978-3-319-32383-1_82

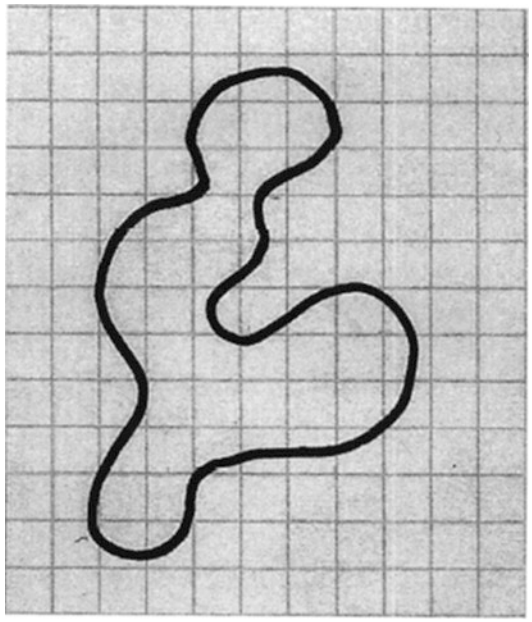

Fig. 1 Fictitious contour of a leg ulcer as seen through a 0.5-cm-spaced grid. As 31 crossing points lie inside the ulcer and 3 lie exactly on the border ($n = 34$), the ulcer area is 34×0.5^2 8.5 cm^2. As the grid crosses the outline 24 times vertically and 25 times horizontally, $n = 49$ and $P = 0.5 \times 49\pi/4 = 19.2$ cm. $RF = 64 \times 34/\pi 49^2 = 0.29\ cm^{-1}$

lesion area (A) is the count of crossing points (n) multiplied by the unit square area (d^2). The formula is straightforward:

$$A = n\ d^2$$

(points falling just on the outline should be taken).

Example To find the area of a leg ulcer, a transparent sheet on which a grid with lines 1 cm apart has been printed is applied on the lesion. If 26 crossing points have been counted inside the lesion or on its border, the ulcer area is 26 cm^2. See also Fig. 1.

Caution To avoid uncertainties with thick lines, a crossing point is defined as the precise outline of the upper right angle of the cross, and not its center, as shown below:

Accuracy The method is valid only if either the lesion has a random outline or the grid has been randomly superimposed on the lesion. The method is only an estimate, but surprisingly adequate. For a given object, the smaller the grid interval, and the higher the number of counted points, the more accurate the assessment is. Using a grid with lines 0.5 cm apart: for a circle 1.6 cm in diameter: $\pi^2 = 2.01\ cm^2$, $A = 0.25 \times 9 = 2.25\ cm^2$ (+12 %); for a circle 2.6 cm in diameter: $\pi r^2 = 5.31\ cm^2$, $A = 0.25 \times 21 = 5.25\ cm^2$ (−0.9 %). In the same way, using grids with small intervals favors more reliable measurement. The most appropriate grid spacing can be deducted from Weibel's nomogram (Weibel 1979). The theoretical efficiency of point counting has been studied by Gundersen (Gundersen et al. 1981; Gundersen and Jensen 1987).

2 Lesion (Line) Contour (Length)

A squared grid (interval width = d) is randomly applied on the lesion or the linear feature to be measured (Bahmer and Smolle 1992). Counting the number (N) of intersections of the grid's both horizontal and vertical lines with outline gives the perimeter (P) or the feature length, using the formula:

$$P = N\pi d/4$$

Examples Examples include measuring the perimeter of a leg ulcer (Fig. 1) or the length of telangiectasias (Fig. 2).

Accuracy Using a 0.5-cm interval grid, accuracy is as follows:

- For a circle 1.6 cm in diameter: $2\pi r = 5$ cm, $P = 0.5 \times 12\pi/4 = 4.7$ cm (−6 %)
- For a circle 2.6 cm in diameter: $2\pi r = 8.2$ cm, $P = 0.5 \times 20\pi/4 = 7.9$ cm (−3.7 %)

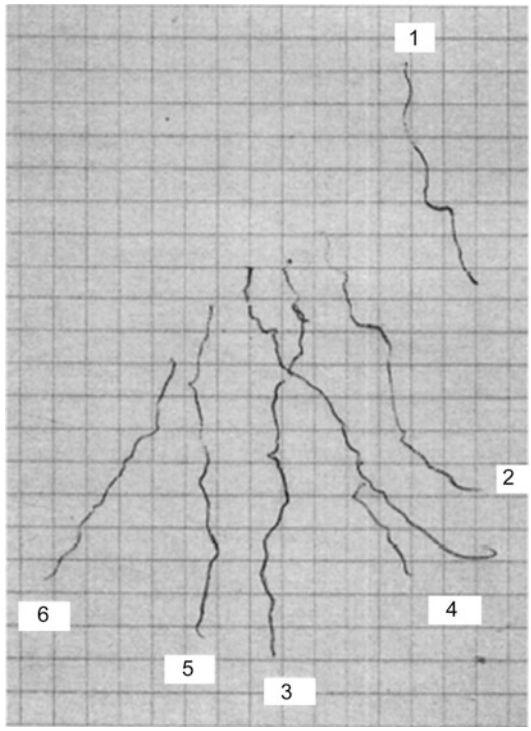

Fig. 2 Tracing of several telangiectasias in the medial aspect of the thigh as seen through a 0.5-cm-spaced grid. The lengths are: 1 4.3 cm, 2 5.5 cm, 3 6.3 cm, 4(ramified) 10.2 cm, 5 4.7 cm, 6 4.3 cm

3 Shape Regularity

A shape regularity factor RF (Bahmer and Smolle 1992) can be computed using the above-mentioned n and N parameters of the lesion irrespective of the grid interval, with the formula:

$$RF = 64n/\pi\ N^2$$

The RF lies between 0 (extremely irregular) and 1 (circle).

Example See Fig. 1.

Accuracy Using a 0.5-cm interval grid: for a circle 1.6 cm in diameter: $RF = 64 \times 9/12^2\pi = 1.27$; for a circle 2.6 cm in diameter: $RF = 64 \times 21/20\pi = 1.06$.

4 Area Fraction and Distribution

In disseminated lesions, counting their number and mean area is a way to assess the extent of the disease. A reference area, within which lesions will be counted, is determined on the grid. It may be the area of the printed sheet (e.g., 210 × 297 mm or a 7.25 × 10.5″ sheet) or any other whose number of crossing points is known or easy to compute. To prevent errors it has been stated that the boundaries of the reference area must be divided into two parts: upper and left sides (marked by thin lines in Fig. 3), and lower and right sides (marked by thick lines in Fig. 3). The latter should be extended beyond the boundaries in order to solve the problem of corner points (Weibel 1979; Bahmer and Smolle 1992).

The grid is put on the skin and all lesions located within the reference area, or crossing or touching its boundaries, except those touching the thick line (also called the forbidden lines (Gundersen et al. 1981)) even beyond the reference area, are counted. The ratio of this number to the number of crossing points in the reference area gives the lesion average area as a fraction of the reference area. As the latter is known, the lesion's absolute average area is obtained. If needed, the distribution of lesions according to area can be found by counting separately the lesions including one point (area = d^2), two points (area = 2 d^2), etc.

An imperative rule for counting is that only the lesions or features that do not touch or are not crossed by the limits of the reference area can be counted: accordingly, the latter should be clearly delineated on the grid.

Taking into account the biological variation and the frequent fuzziness of boundaries, counting approximately 100 points provides a satisfactory precision (Gundersen et al. 1981). The most appropriate grid spacing can be deducted from Weibel's nomogram (Weibel 1979). The theoretical efficiency of point counting has been studied by Gundersen (Gundersen et al. 1981; Gundersen and Jensen 1987).

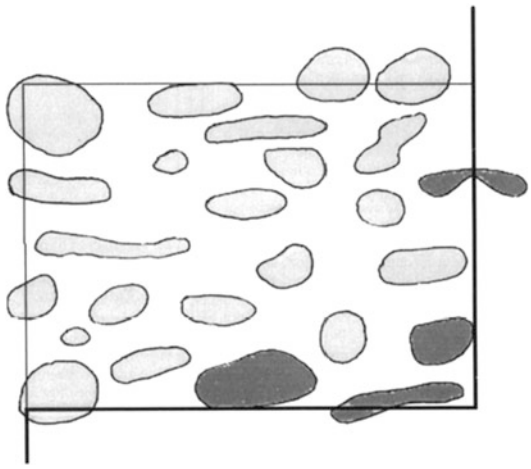

Fig. 3 Fictitious skin lesions. Assessment of area fraction and distribution. This figure is aimed at showing (1) the layout of the so-called forbidden lines (*thick lines*) and (2) the objects (lesions) that should be taken for counting crossing points, and those which should not be taken (*in gray*) because they touch the forbidden lines. The grid is omitted purposely to simplify the image

5 Field of Application

Disposable plastic or acetate sheets can easily be printed with a grid with adequate spacing using current squared paper (usually 5 mm spacing) or home-drawn (e.g., 2 mm spacing for small lesions, 10 mm and 20 mm spacing for larger ones).

Leg ulcer shape assessment takes only a few minutes, the main difficulty being determining the outline of the lesion. Such rapidity makes it possible to follow the progress of lesions over time in current practice as well as in drug trials. Changes in nail fungus involvement area with time is another possible application.

In psoriasis, showing a small number of lesions, following up plaque areas over time is easy and fast. The method has also been proposed to improve PASI rating (Bahmer 1989).

Atopic dermatitis extent can be assessed the same way, although lesion delineation is more difficult. Obviating the problem and in addition rating disease severity has been proposed by Bahmer et al. (1991) (see ▶ Chap. 136, "Clinical Scoring of Atopic Dermatitis").

Area is a parameter of positive prick or patch tests. Its quantification is quickly done using a 2-mm interval grid. The latter may easily be made on paper by the clinician and then photographed at the desired reduction on a transparent sheet.

Superimposing a grid on the computer screen displaying a videocapillaroscopy image can calculate the vessel diameters and lengths and the fraction of dermis occupied by blood vasculature.

Morphometry can also be performed on photographs, preferentially enlarged so that more points can be counted, or on slides projected on a grid printed screen. This is an easy task for clinicians. For example, following the number and size distribution of pigmented nevi during adolescence, quantifying the size and distribution of skin lesions in leprosy, following the number and size distribution of bullae in bullous diseases during treatment, quantifying vitiligo, etc., make this technique very useful in current dermatological practice.

In assessment of sweat or sebum excretion by mapping the gland output, the global area, average area, and size distribution of spots can be easily obtained using the area fraction and distribution method on an enlarged photograph or image. In the same way, microscopic dimensions, such as cell sizes, the size and shape of nuclei in malignant/benign tumors, etc. can be assessed rapidly. Indeed for decades, biological research was the only field of application for morphometry.

6 Other Morphometry Parameters

Point counting is especially useful for assessing morphological parameters of two-dimensional shapes or features, as is the case of most skin lesions. Morphometry can also be used to assess the three-dimensional morphology of microscopic objects; when focusing at various depths, each

plane can be considered as a slice and assessed separately. It is a fast and easy task (Loud and Anversa 1984).

Videocapillaroscopy images obtained at different depths in the skin can be processed in this way using point counting in a 3D setting; as the vessel diameters and lengths are known, the overall volume and size of the skin vasculature can be obtained. The same holds true for cutaneous innervation in health and sensory neuropathies. For histological preparations, special tools (dissector, fractionator, nucleator) have been designed (Gundersen et al. 1988a, b; Elias and Hyde 1983; Aherne and Dunhill 1982; Russ 1986).

References

Aherne WA, Dunhill MS, editors. Morphometry. London: Edward Arnold; 1982.

Bahmer FA. The size of lesions, or point counting as a step toward the solution of the PASI problem. Arch Dermatol. 1989;125:1282–3.

Bahmer FA. Morphometry in clinical dermatology. In: Wilhelm KP, Elsner P, Berardesca E, Maibach HI, editors. Bioengineering of the skin: skin surface imaging and analysis. Boca Raton: CRC Press; 1997. p. 229–40.

Bahmer FA, Smolle J. Morphometry in clinical dermatology. Acta Derm Venereol. 1992;72:52–7.

Bahmer FA, Schaefer HJ, Schubert HJ. Quantification of the extent and the severity of atopic dermatitis: the ADASI score. Arch Dermatol. 1991;127:1239–40.

Elias H, Hyde DM, editors. A guide to practical stereology. Basel: Karger; 1983.

Gundersen HJG, Jensen EB. The efficiency of systematic sampling in stereology and its prediction. J Microsc. 1987;147:229–63.

Gundersen HJG, et al. Comparison of semi-automatic digitizer tablet and simple point counting performance in morphometry. Virchows Arch B. 1981;37:317.

Gundersen HJG, Bentsen TF, Korbo L, et al. Some new, simple and effective stereological methods and their use in pathological research and diagnosis. APMIS. 1988a;96:379–94.

Gundersen HJG, Bagger P, Bentsen TF, et al. The new stereological tools: disector [sic], fractionator, nucleator and point sample intercepts and their use in pathological research and diagnosis. APMIS. 1988b;96:857–81.

Loud AV, Anversa P. Biology of disease: morphometric analysis of biological processes. Lab Invest. 1984;50:250–61.

Russ JC, editor. Practical stereology. New York: Plenum Press; 1986.

Weibel ER, editor. Stereological methods. Practical methods for biological morphometry, vol. 1. London: Academic; 1979.

Assessment of Erythema and Pallor 133

Pierre Agache

Contents

This chapter was originally published under the ISBN 978-3-540-01771-4 with the following book title Measuring the Skin. The content has not been changed.

Pierre Agache: deceased.

P. Agache (✉)
Department of Dermatology, University Hospital of Besançon, Besançon, France
e-mail: aude.agache@free.fr; ferial.fanian@chu-besancon.fr; ferial.fanian@cert-besancon.com

P. Humbert et al. (eds.), *Agache's Measuring the Skin*,
DOI 10.1007/978-3-319-32383-1_89

Keywords
Colorimetry • Erythema • Gray levels color chart • Hyperemia test • Minimal erythema dose (MED) • Pallor • Red color chart • Vasoconstriction

Healthy skin has a red component which comes from the subepidermal vascular plexus visible through the stratum corneum. The deeper vessels are invisible or look bluish if they are voluminous. The purpura is visible only if it is located in the superficial dermis. It is brighter in color because the red blood cells are extravascular. The red component of the skin depends on the subepidermal plexus volume, the vasodilatation level, and the overlying epidermal thickness and translucency. A thin epidermis above a rich plexus gives the skin color a homogeneous pink component, as in the case of newborn babies.

Erythema is defined by the accentuation of the skin's red component. Whether macular like in morbilliform or roseoliform rashes, or diffuse like in erythematous patches or scarlatiniform erythemas, the excessive coloring is induced by the vasodilatation of the subepidermal plexus, with or without deeper vasodilatation. As far as measurement is concerned, two main types of erythemas are distinguishable: those generated by the isolated vasodilatation of the subepidermal and perifollicular plexuses, and those which concern all of the skin's vascular networks, including the subcutaneous plexus.

- In the first category, only the skin color measurements are helpful, the assessment of the absorption wavelengths of hemoglobin, and capillaroscopy.
- In the second category (assessment of superficial and deep vasodilatation), it is possible to use photoplethysmography, laser Doppler, thermal clearance, epicutaneous xenon clearance, and skin thermometry (see the dedicated chapters).

Only valid methods for measuring isolated superficial vasodilatation are described below. Consequently, these are only the ones that can measure the erythematous component of global vasodilatation. Quantitative capillaroscopy, a most promising one, is detailed in ▶ Chap. 60, "Evaluation of Port-Wine Stains and Its Treatment."

1 Psychosensorial Techniques

It is common to assess erythema on a five point scale: 0, (+), +, ++, +++. Only four of them quantify the erythema, and the zero value describes the adjacent healthy skin. Some authors use a seven point scale (Westerhof et al. 1986) or a ten point scale (Kollias et al. 1997). The aim of the assessment is to work out two parameters: whether an erythema exists, and its intensity.

- To determine the *erythema threshold*, it is important, especially in photobiology, to find the minimal erythema dose (MED). In an investigation in 21 subjects and 42 photo tests, Lock-Andersen and Wulf (1996) studied the variability of two groups of four observers, well-trained people in one group and less trained people in the second one, working double blind with a five point scale. To detect the onset of a poorly delineated erythema, the variation coefficient was 4.6 % for the untrained group and 7.3 % for the other one, with 11.9 % and 23.2 % detected respectively for the MED (threshold dose for a well-defined erythema, as used in photobiology). These data tend to show that the poorly delineated erythema threshold is better detected with the naked eye than a well-defined erythema threshold and that training has no influence at this level. The intraindividual agreement in two double blind measurements of the same erythema threshold was 90.5 % in the untrained group and 92.9 % in the other.
- The measurement of the *erythema intensity*, following stepwise actinic exposures increasing by 25 % each time, was studied in the course of the same experiment. The agreement between observers decreased with the erythema intensity, reaching 54.8 % only in

the untrained group and 52.0 % in the other one, for class 5 (+++) erythemas; the agreement between two measurements by the same observer was 64.3 % and 71.4 %, respectively. These figures show the large variability of visual measurements, even done by specialists.

Erythema is the more difficult to detect and assess when the skin is pigmented. It is, therefore, essential to be aware of seasonal variations of pigmentation, even moderate, when comparisons are to be made. In black people, the measurement is only slightly reliable, especially since the basic color is often variable and nonhomogeneous.

In every psychosensorial assessment, the lower and upper limits of the measurement scale should be specified. For the measurement of the red component in healthy skin, zero is bloodless skin (pressure with a glass plate, proximal occlusion). To measure a localized redness (erythema), zero is the adjacent healthy skin. At the other end, what is a *very severe* erythema? It may be useful to set up reproducible conditions, but which ones?

The human eye is therefore not able to assess an erythema properly, but only to estimate its intensity. However, it is very sensitive in the detection of redness, but as visual memory is short and unreliable, to detect and grade small differences the areas need to be studied simultaneously and side by side.

2 Visual Assessment Using a Color Chart

2.1 Red Color Chart

A range (ten grades, increasing in 10 % increments) of saturated red Kodak gelatin films (CCR series) placed between two Plexiglas sheets was used as an erythema assessment scale in pig and mouse (Argenbright and Forbes 1982). The films were placed one after the other on the skin, beginning by the lowest grade (lightest color), and the first grade making the erythema limits invisible was considered the appropriate measure. The advantages and drawbacks of these color charts are described in ▶ Chap. 6, "The Measurement of Skin Color."

2.2 Gray Levels Color Chart

If the skin is examined through green glasses (which convert red into black) the erythema looks gray. When observed simultaneously, it can then be compared to the gray levels of a chart whose luminance (% of clearness) is known. Erythema is then quantified by its degree of luminance. The adaptation of a green filter on a pair of glasses does not present technical difficulty. The gray levels can be easily computer generated and calibrated with a colorimeter.

The advantages of this technique are the absence of contact with the skin, the possibility of eliminating the specular reflection by selecting the angle of vision, and the reference to international physical units which permits comparisons. However, the sensitivity of this method is poor because luminance is weakly influenced by erythema.

3 Photography

Color photography does not provide a reliable quantification of erythema (see ▶ Chap. 6, "The Measurement of Skin Color."). Monochromatic photography uses the same principle as the color chart with gray levels. The skin is photographed (annular flash) with white light through a green filter (540 nm) in the center of a circular chart of 21 levels of gray each varying by 2 % luminance (Breit et al. 1982). The filter and the color chart are attached to the camera so that the incidence angle of the light remains constant. The measurement consists of finding the level of gray matching the erythematous area on the photograph. The device can be achieved with any good camera. The chart has to be made and then calibrated by the user, as explained in the previous chapter. Unfortunately, this simple and cheap method does not measure the chromatic component of the erythema (red), which is its main element, but only the decrease in lightness of this chromatic component.

4 Colorimetry

The red component of healthy skin is measured by colorimeters from the reflectance of three wavelengths, located in the red, green, and blue, and then expressed by parameters L* and a* of the Commission Internationale de l'Eclairage (see ▶ Chap. 6, "The Measurement of Skin Color"). This absolute classification system determines the position in a 3D virtual space for any color. The vertical dimension L* defines its lightness (or value, or luminance) from zero (black) to 100 (maximal lightness). In each horizontal plane its hue (or chromaticity, or chroma) is defined along two perpendicular axes, one in abscissa (from -a* = green to + a* = red), and the other in ordinate (from −b* = blue to + b* = yellow). In the final plane, the distance to the origin characterizes its purity, or saturation, or brightness. An erythema increases the parameters a* which is a measure of the intensity of red, and reduces the parameter L* which expresses the skin lightness. However, L* is less correlated than a* to erythema. Measuring the parameter a* is equivalent to measuring the quantity of hemoglobin (HbO_2) in the superficial dermis. The erythematous component of 23 body areas studied in winter on ten subjects with the Minolta CR200 chromameter, using the parameters a* and L*, were measured by Serup's group (Takiwaki et al. 1994).

It is possible to study the red component of the skin by considering L* and a* simultaneously in a vertical plane formed by axes L* and a*. In this plane, all the red components of the normal skin of the back in Caucasians (established with the Minolta CR200 chromameter) were found located within a curvilinear area centered on a* = 12; its extreme coordinates were 53 and 75 % for L* and +2 to +17 for a* (Fig. 1) (Lock-Andersen et al. 1998). The more a subject's skin was pigmented, the darker the red component, and therefore located in the lower part of the area. Mediterranean type and black subjects show L* values less than 50 %. As each skin color is defined by its coordinates L*, a*, and b*, erythema and healthy skin can be distinguished by their coordinate differences (ΔL*, Δa* and Δb*). The difference in hue is $(\Delta a^{*2} + \Delta b^{*2})^{0.5}$ and the difference in lightness and redness is $(\Delta L^{*2} + \Delta a^{*2})^{0.5}$, formulas which are deduced easily from the orthogonal tridimensional structure of the colors' virtual space.

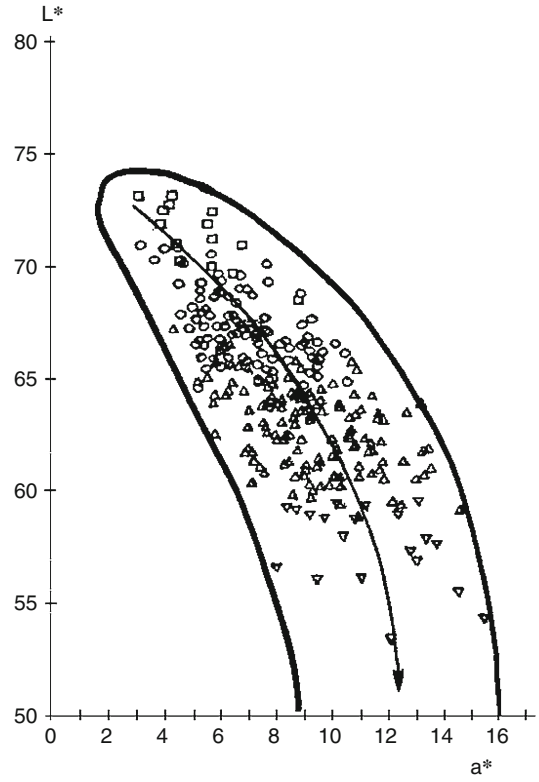

Fig. 1 Envelope in the L*a* plane of the skin's red component in Caucasians (dorsum foot). ◇ very light, ○ light, Δ intermediary, ▽ pigmented. *Arrow* pointing downward indicates the skin color shift when skin pigmentation increases (From Chardon et al. (1991), with permission)

5 Reflectometry (Takiwaki and Serup 1995)

Erythema is related to the dilatation of the subepidermal vessels, therefore to the increased amount of hemoglobin (HbO_2 and/or Hb) in the superficial dermis. As the pigment concentration varies like the inverse of the reflectance (IR), reflectometry is a way to assess this quantity. The technique uses the logarithm of IR (LIR). However, these

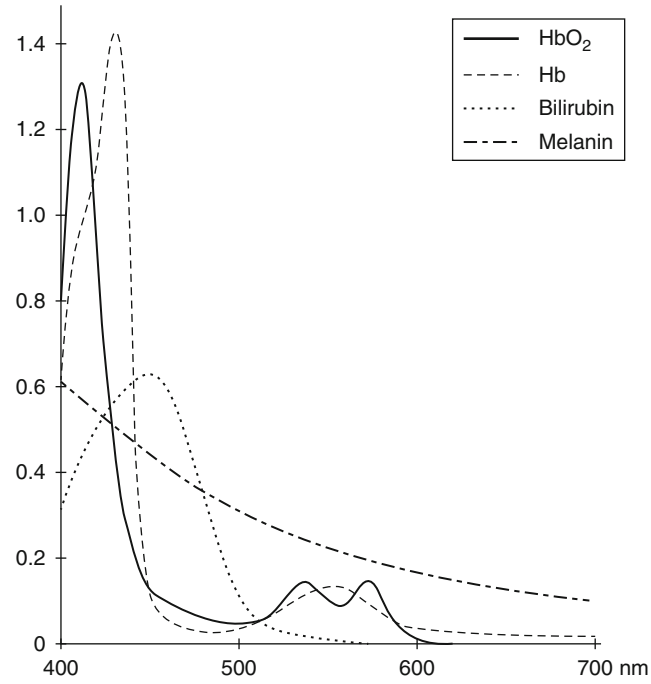

Fig. 2 Hemoglobins, bilirubin, and melanin absorption spectrums (Modified after Rox Anderson and Parrish (1981))

wavelengths are also absorbed by melanin. The amount of the latter is determined at wavelengths not absorbed by HbO_2, then subtracted from the LIR.

Reflectometers use green light (from 546 to 568 nm, depending on device), to measure LIR at 543 and 576 nm (HbO_2 absorption peaks), 554 nm (Hb absorption peak), and above 620 nm (red, melanin absorption) where absorption by HbO_2 is negligible but that of Hb, although low, is not (Fig. 2). These devices are small and portable and provide HbO_2 and melanin indices immediately. The Erythema Meter (Dia-Stron, Andover, UK) uses a white light (accordingly it is barely influenced by the ambient light) and measures the reflectance at 546 nm (green) and 672 nm (red). The Derma-Spectrometer (Cortex Technology ApS, Hadsund, Denmark) uses electroluminescent diodes emitting at 568 nm (green) and 655 nm (red). It adjusts the possible contamination by ambient light and allows the measurement at different temperatures. The Mexameter Mx 16 (Courage + Khazaka Electronic, Cologne, Germany) uses electroluminescent diodes emitting at 568 nm (green), 660 and 880 nm (red and infrared). The constant application pressure is ensured by a spring. A beep warns of any excessive penetration of exterior light into the probe. UV-Optimise (PBI Medical, Denmark) uses 555 and 660 nm wavelengths; it does not provide indices, but quantifies the pigmentation and the red component of the skin independently, each on a scale between 0 % and 100 %, with the zero corresponding to bloodless skin and 100 % a very dark facial nevus flammeus (purple).

The distribution of the erythema index on 23 body sites in ten subjects showed a remarkable correlation with the value of the parameter a* in the same location (Takiwaki et al. 1994; Takiwaki and Serup 1995).

6 Spectrophotometers and Spectrocolorimeters

These devices are based on the same principle as the reflectometers, but are more accurate and effective because they can use all the spectrum

wavelengths. According to Clarke et al. (1981), to assess the skin's red component (HbO_2 + Hb), the interval 415–425 nm (Soret's band) is the most reliable. They have thus evaluated the differences in complexion of 34 pairs of twins.

Andersen and Bjerring (1990) calculated the melanin index by using the interval 360–390 nm (near UVA). To distinguish HbO_2 from Hb he analyzed the reflectance at 543 and 576 nm (HbO_2 absorption peaks) and at 554 nm (Hb absorption peak) taking into account the melanin index. The skin received the polychromatic light of a xenon arc (Osram XBO 150), carried by an optic fiber (Hirschmann, Germany). The retrodiffused light was collected by an integration sphere and conducted by optic fiber to a monochromator (Jobin and Yvon H 20, France) which takes a measurement at every 5 nm between 355 and 700 nm. Each reflectance is detected by a photomultiplicator (Hamamatsu, Japan), digitalized, then computer analyzed.

Kollias calculated the melanin index from the 620 and 720 nm wavelengths (both in red) (Kollias and Baqer 1986), and the blood pigments apparent concentrations were measured at 560, 577 and 630 nm after correction for melanin. The light source of a spectrophotometer (HP 8452A DAS) was replaced by a tungsten halogen lamp, and the light conducted to the skin by optical fiber. The retrodiffused light collection was also carried out by a beam of quartz optical fibers. The device scanned the spectrum every 2 nm between 400 and 820 nm.

7 Green Light Laser Doppler

This device (Periflux 4001 Master; Perimed, Stockholm, Sweden) lights the skin with a 543 nm (green) monochromatic light and measures the wavelength shifted retrodiffused light due to contact with moving red blood cells (Doppler effect). The absorption of green by hemoglobin considerably reduces the signal and limits the investigation to the subepidermal plexus. An index of the subepidermal blood flow is provided through multiplication of the retrodiffused light amount (the moving blood cells' concentration) by the average wavelength shift (the cells average speed). This is the main interesting feature of this device, as no other equivalent equipment is available.

8 Conditions for a Reliable Measurement

- These devices are designed to be used on flat surfaces, which is not the case for skin. Relief may let ambient light penetrate the retrodiffused light collecting chamber. It is necessary to shave the hairy areas and place the subject in a position which reduces any risk of deep creases of the surface.
  - For the same reason, measurement in excessive light (direct sunlight, etc.) should be avoided.
  - Wet skin or skin with ointment may facilitate specular reflection and artificially alter the data provided by colorimeters and reflectometers. Between 5 % and 7 % of the incident light is diffused by the skin microrelief. The application of a topical that fills the furrows increases light penetration.
  - Hydration increases the stratum corneum translucency and can increase the erythema index as well as the parameters L*a*b*. This is more obvious for substances with a refraction index close to that of the stratum corneum (stratum corneum 1.54; air 1.00). As glycerol and acetic acid refraction indices are close to 1.54, these compounds are still more efficient than water (Solan and Laden 1977).
- The device needs to be recalibrated prior to each use with the standards provided:
  - It should be held perpendicular to the skin
  - Excessive pressure which could alter the erythema should be avoided
  - A control measurement on the adjacent nonerythematous skin is mandatory
  - As the skin color is often nonhomogeneous (lentigo, achromias, etc.), only average indices from three iterative measurements should be used

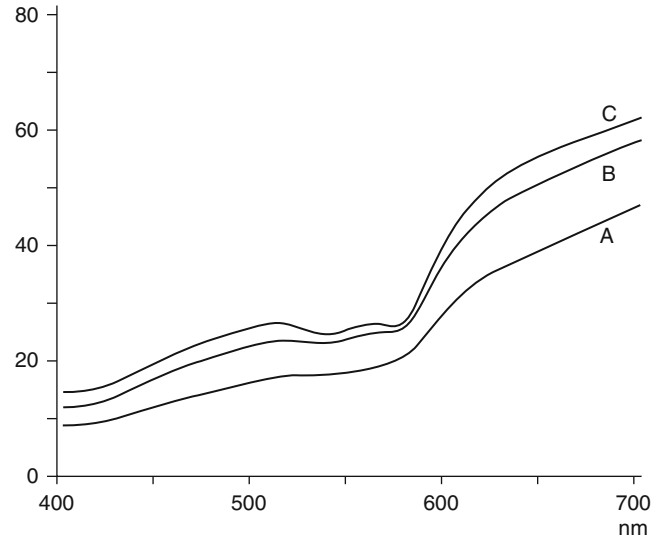

Fig. 3 Skin reflectance spectrum of black (*A*), Asian (*B*) and Caucasian (*C*) subjects (Koran et al. 1991), modified). *Ordinate:* % retro-diffused light. *Abscissa:* wavelength

- Erythema assessment using a reflectometer is valid only on barely pigmented skin, because the subtracted melanin index, which is measured in red light, is supposed to be identical in green light. However, this is not true, particularly with darker pigmentation, because the melanin spectrum linearly decreases from green to red, with a slope all the steeper because pigmentation is intense (Fig. 3). Consequently, it is not possible to compare the erythema indices of body sites with different melanin indices.
- As pigmentation reduces light retrodiffusion considerably, erythema measurements on dark skin are unsound.
- When interpreting the results, it is essential to consider the relative proportion of HbO_2 and Hb, their color being that of arterial and venous blood, respectively. In the absence of venous backflow or hindrance to normal venous flow, the skin blood is of arterial type. This is also the case in erythemas of active vasodilatation such as in inflammation or from a reactive hyperemia. The measurement of $(\Delta L^{*2} + \Delta a^{*2})^{0.5}$ or HbO_2 is then appropriate. Inversely, in case of blood stasis or venous backflow, the vasodilatation is passive and the reduced Hb fraction may be important, and induce some change of the color of erythema. Such is the case in dependent limbs or when the skin has been compressed over a long period of time by the body weight. The measurement of HbO_2 may then be insufficient. It is also important to remember that reduced Hb may augment the melanin index, while skin pigmentation stays unchanged (Agner 1992; Takiwaki and Serup 1994). Consequently, to detect the shift in skin hue due to higher Hb levels colorimetric measurement of $(\Delta a^{*2} + \Delta b^{*2})^{0.5}$ must supplement that of $(\Delta L^{*2} + \Delta a^{*2})^{0.5}$.

9 Choosing the Appropriate Method

The suitable method to assess a red component or an erythema will depend on its origin and the physical characteristics of the method.

9.1 Selection According to the Characteristics of the Device

- Colorimeters reconstitute the color of the erythema from reflectance and provide its L*a*b* components. Their capacity to characterize any color, thus erythemas of various hues, is their

main advantage. However, these parameters are indirectly associated with the chromophore skin content (Kollias et al. 1995) and are obtained from three wavelengths only.

- Inversely, the erythema indices given by reflectometers are directly associated with the amount of chromophore, both HbO_2 and Hb since their absorption peaks are very close. They should therefore theoretically be more specific. Comparative studies have shown their results strongly correlated with parameter a* (Takiwaki et al. 1994; Barel et al. 1998), but with a variation coefficient lower than that of a*.
- Spectrophotometers provide more accurate measurements than the above mentioned devices because many more wavelengths are used. They allow the measurement of Hb and HbO_2 separately.
- The green laser Doppler signal is associated with the amount of chromophores and the speed of the blood cells in the subepidermal vascular plexus (Ubbink et al. 1996a; Jünger et al. 1996).
- Instrumental techniques which measure the global skin blood flow rely more heavily on deep circulation whose volume and flow rate are much more important. Therefore, their results sometimes seem in conflict with those of reflectance based methods. The difference is obvious with the measurement of the skin temperature which is very sensitive to global active (arteriolar) vasodilatation, but seems to ignore the superficial blood flow when it is increased separately (Lock-Andersen et al. 1998).
- Since the laser Doppler only deals with circulating red blood cells, it may indicate an increased flow during skin blanching by vasoconstriction, a surprising result probably due to blood flow acceleration. When a limb is lifted higher than heart level its signal increases while the erythema index decreases, and inversely when the limb is lowered (Chardon et al. 1991). Laser Doppler is, therefore, not sensitive to blood stasis, even in deeper dermis or subcutis.
- Clearance methods (thermal clearance, epicutaneous xenon clearance) also based on the skin blood flow rate, ignore erythemas by passive vasodilatation.
- Conversely, photoplethysmography is an excellent method to measure global variations of the blood volume, associated with active or passive vasodilatation. However, this technique, which uses red or near infrared light, ignores superficial circulation.

9.2 Selection According to the Erythema

- All important active erythemas have a deep component, and therefore are measurable by all the skin blood flow measurement techniques. The relationship between the stimulus intensity and the ensuing signal is linear until clinical assessment grade (++). Beyond this, the signal is saturated, probably because vasodilatation is near its maximum.
- Actinic erythema implies superficial and deep vasodilatation, seemingly from the beginning. It can therefore be measured by all techniques. However, slight erythemas (below MED) seem more reliably measured by reflectance than by imaging laser Doppler (Lock-Andersen et al. 1998).
- Allergic erythemas also seem global and likely to be measured by all techniques. For example, thermography shows that skin temperature rises over allergic patch tests, but not always over irritation patch tests (Baillie et al. 1990).
- Irritative erythemas over a small area seem to mainly involve superficial microvasculature. In such cases, colorimetry (Gawkrodger et al. 1991), reflectometry, and spectrocolorimetry are preferable. For example, irritation induced by 1 % sodium lauryl sulfate under occlusion for 2 days increased the erythema index much more than the LDF signal, and the erythema index at D2 and D4 was more important than in allergic erythema (Gawkrodger et al. 1991). Moderate and intense irritations are associated with both superficial and deep vasodilatation. The green laser Doppler seems a promising

tool, but has not been used yet for this indication.
- To ascertain if an erythema has a deep component, thermography is a more appropriate technique because it seems insensitive to vasodilatation limited to the superficial dermis, and in particular to the red component changes (Lock-Andersen et al. 1998).
- To detect an infraclinical erythema, that is a vasodilatation of the subepidermal vessels without visible erythema, colorimetry, reflectometry, spectrophotometry and green laser Doppler are the favored methods. During irritation induced by 1 % sodium lauryl sulfate under occlusion for 2 days, the erythema index increased before the appearance of the clinical erythema [19]. The same was obtained after application of antipyrine 5 % in water under occlusion for 24 h (Nangia et al. 1996). However, remember that the increased signal may be also related to the sole increased permeability of the stratum corneum to light (especially when it is hydrated, as after occlusion), or to the sole reduction of regular reflectance from an attenuated skin microrelief, and/or from the furrows being filled with a substance whose refraction index is close to that of the stratum corneum (e.g., glycerol (Solan and Laden 1977)).
- Quantitative capillaroscopy (now useable on any body site, see ▶ Chap. 118, "Cutaneous Testing: Detection and Assessment of Allergy") together with green laser Doppler may become the reference method to assess superficial vasodilatation, especially at the preclinical stage. Capillaroscopy is sensitive to both active and passive vasodilatations (venular backflow) whereas green laser Doppler is sensitive only to active ones (Ubbink et al. 1996b). To our knowledge the use of these techniques to assess erythemas has not yet been published.
- Laser Doppler might be able to detect deep vasodilatations, such as in actinic or allergic erythema (Wahlberg 1989) and in some irritative erythemas, during their infraclinical stage (Wahlberg and Wahlberg 1984, 1985).
- Irritative erythemas (sodium lauryl sulfate (Kollias et al. 1995), retinoic acid (Kollias et al. 1997), trauma (e.g., after a slap) (Feather et al. 1988) are associated with the isolated increase of HbO_2. The actinic erythema is associated with the joint increase of HbO_2 and Hb (Andersen and Bjerring 1990). Stasis erythema, especially by increase of the hydrostatic pressure, is associated with the isolated increase of Hb (Kollias and Baqer 1986; Feather et al. 1988).

10 Pallor

Vasoconstriction is an important physiological phenomenon which is worth measuring in some diseases, such as excessive sensitivity to cold or arterial hypertension. It has also been used to assess the activity of topical corticosteroids or their cutaneous absorption in relation to the formulation (Poelman et al. 1984). All the methods used to measure vasodilatation are not valid to assess vasoconstriction. Laser Doppler particularly, which is only sensitive to moving blood cells, may not give out any signal although the clinical blanching is obvious (Noon et al. 1996). Furthermore, a pseudo skin blood flow increase has been shown by imaging laser Doppler (red light) during blanching induced by topical corticosteroids (Sommer et al. 1998), probably caused by blood cells acceleration under vascular narrowing.

10.1 Direct Measurement of Vasoconstriction

Assessment of blanching is reliable using reflectometry by the simple difference of the erythema indices (Noon et al. 1996; Feather et al. 1982; Lévêque et al. 1985). However, because of the time required before the appearance of vasoconstriction (several hours), time during which the blood flow may be altered, replacing the erythema index of the treated zone by the difference between this index and that of an adjacent untreated zone is recommended (Sommer et al. 1998).

Using a spectrophotometric (therefore more accurate) measurement of reflectance, Andersen et al. (Andersen et al. 1993) have shown that the blanching induced by corticosteroids of small and moderate strength came from a decrease of reduced Hb (venuloconstriction) and that the HbO_2 content (arteriolar constriction) was reduced only by the most powerful corticosteroids. The measurement must also consider the kinetics of the phenomenon, which is biphasic, following the application of betamethazone valerate. Venoconstriction begins about 3 h after cream removal, and peaks at about the 12th hour. By the 24th hour, the condition has gone back to normal. However, by the 32nd hour, a vasodilatation appears although the corticosteroids blood concentration is at its highest level, and peaks by the 72nd hour while the corticosteroids plasmatic concentration is still elevated (Andersen 1997; Andersen and Maibach 1995).

Colorimetry also detects blanching and provides a classification of corticosteroids similar to visual classification, but it seems less accurate (Queille-Roussel et al. 1991; Broby-Johansen et al. 1990).

Green laser Doppler seems a promising technique to measure blanching, but it has been used until now only to show superficial vasoconstriction to cold (Czastrau et al. 1996; Jepsen et al. 1996).

10.2 Reactive Hyperemia Test with Vasoconstrictor

Reactive hyperemia is easily measured by laser Doppler. Its reduction following topical corticosteroids can be measured by the same method (Bisgaard et al. 1986). Techniques based on reflectance measurement can also be used. However, the latter method is indirect, which introduces an additional risk of variability.

In conclusion, the whitening induced by topical corticosteroids is a venular vasoconstriction of the subepidermal plexus easily detectable with the naked eye and possibly accompanied by the acceleration of the skin blood flow. Reflectometry and spectrophotometry presently appear to constitute the most reliable measurement methods. Methods present too many hazards and should therefore be replaced, whenever possible, by instrumental techniques. To assess blanching in relation to deep vasoconstriction, such as the one induced by cold, all methods of skin blood flow measurement are usable because the phenomenon is global and concerns all types of vessels.

References

Agner T. Noninvasive measuring methods for the investigation of irritant patch test reactions. A study of patients with hand eczema, atopic dermatitis and controls. Acta Derm Venereol. 1992;173(Suppl):1–26.

Andersen P. Reflectance spectroscopic analysis of selected experimental dermatological models with emphasis on cutaneous vascular reactions. Skin Res Technol. 1997; 3[Suppl 1]:3–58.

Andersen PH, Bjerring P. Noninvasive computerized analysis of skin chromophores in vivo by reflectance spectroscopy. Photodermatol Photoimmunol Photomed. 1990;7:249–57.

Andersen PH, Maibach HI. Skin irritation in man: a comparative bioengineering study using improved reflectance spectroscopy. Contact Dermatitis. 1995;33:315–22.

Andersen P, Millioni K, Maibach H. The cutaneous corticosteroid vasoconstriction assay: a reflectance spectroscopic and laser-Doppler flowmetric study. Br J Dermatol. 1993;128:660–5.

Argenbright LW, Forbes PD. Erythema and skin blood content. Br J Dermatol. 1982;106:569–74.

Baillie AJ, Biagioni PA, Forsyth A, Garioch JJ, McPherson D. Thermographic assessment of patch-test responses. Br J Dermatol. 1990;122:351–60.

Barel AO, Clarys P, Lambrecht R, Manou I, Vanbeneden I. Skin surface color measurements: a comparison between the Chromameter CR 200 and the Mexameter MX16. In: Poster abstract, 12th International Symposium on Bioengineering and the Skin; 1998 June 25–27; Boston; 1998.

Bisgaard H, Kristensen JK, Sondergaard J. A new technique for ranking vascular corticosteroid effects in humans using laser-Doppler velocimetry. J Invest Dermatol. 1986;86:275–8.

Breit R, Kleber H, Will W. Measurement of erythemal response to ultraviolet radiation by "monochromatic" photography. Arch Dermatol Res. 1982;272:93–6.

Broby-Johansen U, Karlsmark T, Petersen LJ, Serup J. Ranking of the antipsoriatic effect of various topical corticosteroids applied under a hydrocolloid dressing: skin-thickness, blood-flow and colour measurements compared to clinical assessments. Clin Exp Dermatol. 1990;15:343–8.

Chardon A, Crétois I, Hourseau C. Skin color typology and suntanning pathways. Int J Cosmet Sci. 1991;13:191–208.

Clark SAE, Walsh RS, Jardine R, Martin NS. A twin study of skin reflectance. Ann Hum Biol. 1981;8:529–41.

Czastrau C, Klyscz T, Blazek V, Jünger M, Hahn M. Local cold exposure test with a new arterial photoplethysmographic sensor. Comparison with green and red laser-Doppler flux and capillary red blood cell velocity. In: Poster N°89, World Microcirculation Congress; 1996 Sept; Munich; 1996.

Feather JW, Ryatt KS, Dawson JB, Cotterill JA, Barker DJ, Ellis DJ. Reflectance spectrophotometric quantification of skin colour changes induced by topical corticosteroid preparations. Br J Dermatol. 1982;106:437–44.

Feather JW, Ellis DJ, Leslie G. A portable reflectometer for the rapid quantification of cutaneous haemoglobin and melanin. Phys Med Biol. 1988;33:711–22.

Gawkrodger DJ, McDonagh AJG, Wright AL. Quantification of allergic and irritant patch test reactions using laser-Doppler flowmetry and erythema index. Contact Dermatitis. 1991;24:172–7.

Jepsen H, Pries AR, Gaehtgens P, Schulte KL, Baumann G. Blood flow measurement in the skin: green and red laser-Doppler fluxmetry with improver video-microscopy. In: Poster N°316, World Microcirculation Congress; 1996 Sept; Munich; 1996.

Jünger M, Hahn M, Hauser J, Klyscz T. Green laser reflects dynamic changes of nutritive skin blood flow in men. In: Poster N°52, World Microcirculation Congress; 1996 Sept; Munich; 1996.

Kollias N, Baqer A. The assessment of melanin in human skin in vivo. Photochem Photobiol. 1986;43:49–54.

Kollias N, Gillies R, Muccini JA, Uyeyama RK, Phillips SB, Drake LA. A single parameter, oxygenated hemoglobin, can be used to quantify experimental irritant-induced inflammation. J Invest Dermatol. 1995;104:421–4.

Kollias N, Gillies R, Muccini JA, Phillips SB, Drake LA. Oxyhemoglobin is a quantifiable measure of experimentally induced chronic tretinoin in inflammation and accommodation in photo-damaged skin. Skin Pharmacol. 1997;10:97–104.

Koran A, Powers JM, Raptis CN, Yu R. Reflection spectrophotometry of facial skin. J Dent Res. 1991;60:979–82.

Lévêque JL, Poelman MC, Legall F, de Rigal J. New experimental approach to measure the skin-reflected light. Application to cutaneous erythema and blanching. Dermatologica. 1985;170:12–6.

Lock-Andersen J, Wulf HC. Threshold level for measurement of UV sensitivity: reproducibility of phototest. Photodermatol Photoimmunol Photomed. 1996;12:154–61.

Lock-Andersen J, Gniadecka M, de Fine OF, Dahlstroem K, Wulf HC. Skin temperature of UV-induced erythema correlated to laser Doppler flowmetry and skin reflectance measured redness. Skin Res Technol. 1998;4:41–8.

Nangia A, Andersen PH, Berner B, Maibach HI. High dissociation constants (pKa) of basic permeants are associated with in vivo skin irritation in man. Contact Dermatitis. 1996;34:237–42.

Noon JP, Evans CE, Haynes WG, Webb DJ, Walker BR. A comparison of techniques to assess skin blanching following the topical application of glucocorticoids. Br J Dermatol. 1996;134:837–42.

Poelman MC, Lévêque JL, Legall F. Objective determination of the bioavailability of dermocorticoids: influence of the formulation. Br J Dermatol. 1984;111 Suppl 27:158–62.

Queille-Roussel C, Poncet M, Schaefer H. Quantification of skin-colour changes induced by topical corticosteroid preparations using Minolta Chroma Meter. Br J Dermatol. 1991;124:264–70.

Rox Anderson R, Parrish JA. The optics of human skin. J Invest Dermatol. 1981;77:13–9.

Solan JL, Laden K. Factors affecting the penetration of light through the stratum corneum. J Soc Cosmet Chem. 1977;28:125–37.

Sommer A, Veraart J, Neumann M, Kessels A. Evaluation of the vasoconstrictive effects of topical steroids by laser-Doppler-perfusion-imaging. Acta Derm Venereol. 1998;78:15–8.

Takiwaki H, Serup J. Variation in color and blood flow of the forearm skin during orthostatic maneuver. Skin Pharmacol. 1994;7:226–30.

Takiwaki H, Serup J. Measurement of erythema and melanin indices. In: Serup J, Jemec GBE, editors. Handbook of non-invasive methods and the skin. Boca Raton: CRC Press; 1995. p. 377–84.

Takiwaki H, Overgaard L, Serup J. Comparison of narrow-band reflectance spectrophotometric and tristimulus colorimetric measurements of skin color. Skin Pharmacol. 1994;7:217–25.

Ubbink DT, Tulevski II, Jacobs JHM. Evaluation of red and green laser-Doppler perfusion measurements in leg ischemia. In: Poster N°380, World Microcirculation Congress; 1996 Sept; Munich; 1996.

Ubbink DT, Tulevski II, Jacobs JHM. Red and green laser-Dopler perfusion measurements compared with capillary microscopy in healthy subjects. In: Poster N°54, World Microcirculation Congress; 1996 Sept; Munich; 1996.

Wahlberg JE. Assessment of erythema: a comparison between the naked eye and Laser Doppler flowmetry. In: Frosch PJ, Dooms-Goossens A, Lachapelle JM, Rycroft RJG, Scheper RJ, editors. Current topics in contact dermatitis. Berlin/Heidelberg/New York: Springer; 1989.

Wahlberg JE, Wahlberg E. Skin irritancy from nickel sulfate and test patches. Contact Dermatitis. 1985;13:224–5.

Wahlberg JE, Wahlberg E. Patch test irritancy quantified by laser Doppler flowmetry. Contact Dermatitis. 1984;11:257–8.

Westerhof W, van Hasselt BAAM, Kammeyer A. Quantification of UV-induced erythema with a portable computer controlled chromameter. Photodermatology. 1986;3:310–4.

Cosmetic Facial Skin Type

134

Sang Woong Youn

Contents

Keywords

Cosmetic skin type • Sebum • Acne vulgaris • Bioengineering devices

Cosmetic facial skin type or cosmetic skin type is not a term that has been defined either scientifically or medically (Youn et al. 2002). Nevertheless, most people commonly use this term to explain their usual sebum-associated facial skin condition and to efficiently select facial cosmetics so as to prevent problems caused by skincare products that are not appropriate for their facial skin condition (Choi et al. 2013; Youn et al. 2013). This terminology was in the territory of myth, consisting of subjective feelings about the skin expressed by people with problematic skin and even by people with normal skin. Thus, the subjectivity inherent in the concept of cosmetic skin type always represented a hurdle for dermatologists. With recent improvements in bioengineering techniques for the skin, cosmetic skin type is now objectively measurable and classifiable (Youn et al. 2002; Youn 2010).

1 Definition of Cosmetic Facial Skin Type

In general, cosmetic facial skin is classified into three major types: oily, normal, and dry (Youn et al. 2005a). The oily and dry types are at the extremes of a subjective feeling of oiliness or dryness. The normal type is intermediate between the

S.W. Youn (✉)
Department of Dermatology, Seoul National University Bundang Hospital, Seongnam, Gyeonggi-do, South Korea
e-mail: swyoun@snu.ac.kr

P. Humbert et al. (eds.), *Agache's Measuring the Skin*,
DOI 10.1007/978-3-319-32383-1_90

Table 1 Skin type-related symptoms for the classification of cosmetic facial skin types

1. Dryness
2. Tightness
3. Coarseness
4. Washout of makeup
5. Quick production of sebum
6. Feeling differences in oiliness
7. Frequencies of acne lesions
8. Oiliness

oily and dry types. Cosmetic skin type is a term that was spontaneously developed by laypersons, as mentioned earlier. Consequently, clear-cut criteria for classification that exclusively fit each skin type did not exist. In the past, questionnaires describing skin type-related symptoms (STRS) (Choi et al. 2013) were used to differentiate cosmetic facial skin types (Table 1). Classification by these STRS questionnaires inevitably results in an overlap of skin types. The combination type is the fourth cosmetic skin type and is the most frequently encountered type (Youn et al. 2005a). Combination skin type indicates regional differences in sebum-associated skin type on an individual's face.

Following the development of sebum measuring devices, there have been some efforts to incorporate the concept of cosmetic skin type into the scientific field (Youn et al. 2002, 2005a; Choi et al. 2013; Youn 2010). The Sebumeter® is the most commonly used bioengineering device for sebum measurement. The SM 815 is the most recent model and can measure surface sebum secretion amounts in the range 0–350 μg/cm^2. To define a cosmetic skin type with the Sebumeter® or another sebum measuring device, one should keep in mind that regional sebum secretion amounts vary from one facial site to another. Thus, sebum measurement should be controlled and remeasured from time to time. Youn et al. suggested that sebum should be measured at five sites on the face, and the forehead (mid-glabella), nose (tip of the nose), both cheeks (the most protruding areas of the zygoma), and chin (mental prominence) are the controlled measurement points (Youn et al. 2002). Among these five sites, the forehead, nose, and chin constitute the high sebum-secreting zone (the so-called T zone), while the cheeks constitute the low sebum-secreting zone (the so-called U zone). By integrating these five points into a whole, we can simply calculate the sebum amounts at these five sites. This calculation is termed the mean facial sebum excretion (MFSE) (Youn et al. 2002). It can be easily memorized and calculated, but this arithmetic mean cannot reflect the exact areas of high sebum secretion or low sebum secretion contributing to whole face sebum secretion. Area weighting is needed to correct this inequality in sebum secretion. The new area-weighted formula for the evaluation of facial sebum secretion is as follows (Youn et al. 2013):

$$\text{AW whole face sebum excretion} = \frac{6 \times \text{forehead sebum} + 1 \times \text{nose sebum} + 2 \times \text{chin sebum} + 5 \times \text{right cheek sebum} + 5 \times \text{left chin sebum}}{19}$$

This equation was previously suggested for the calculation of mean facial pH (Youn et al. 2013) and was derived from the rule of fours (Yoon et al. 2008) for the estimation of regional facial areas. The rule of fours calculation introduced the area-weighted concept by considering the proportional area of the facial region and could also be applied to the mean of the facial sebum. However, the arithmetic mean has been used in most research dealing with sebum secretion.

In fact, when attempting to classify cosmetic facial skin types, the mean sebum secretion of the whole face is not meaningful. It is necessary to divide the face into a high sebum-secreting T zone and a low sebum-secreting U zone and calculate the mean of each zone (Youn et al. 2005a). The T zone and U zone have fundamentally different basal sebum secretion amounts, and the same standard values cannot be applied to each area. Choi et al. suggested a 95 % confidence interval of the casual sebum secretion amount in each area for the four cosmetic facial skin types (Table 2) (Choi et al. 2013). The definition of the combination

Table 2 The casual sebum level of four cosmetic skin types according to the facial zone (Adapted from the study by Choi et al.)

	Dry	Normal	Combination	Oily
T zone	120.8–174.9	139.8–206.7	190.4–223.6	204.6–235.4
U zone	55.4–113.6	78.8–150.8	109.8–145.5	120.6–153.7
Whole face	97.3–147.6	118.7–180.9	159.8–190.6	172.5–201.1

The unit of sebum amount is μg/cm^2 as measured by the Sebumeter®

type is different from those of the other three types (Youn et al. 2005a). The combination type should show a mismatch of sebum secretion amounts between the T zone and the U zone. Examples of combination skin types are an oily T zone with a normal U zone, a normal T zone with a dry U zone, and an oily T zone with a dry U zone. In general, the MFSE of combination skin types is in-between those of the oily skin type and the normal skin type (Youn et al. 2005a).

2 Factors Affecting Cosmetic Skin Type

Cosmetic skin type is always affected by the amount and change of facial sebum secretion and partly by the facial hydration status. In fact, the degree of hydration changes according to the environmental humidity and can also be changed by the application of moisturizers. Thus, facial sebum secretion, which can be affected by external factors to a relatively lesser degree than hydration status, is the main determining factor of cosmetic skin type.

Cosmetic facial skin type is not fixed throughout a person's lifetime because the sebum secretion amount is not steady. This variation in the sebum secretion amount is affected by either internal or external factors. The sebum secretion amount shows diurnal variations, and therefore set measurement conditions are needed to achieve precise sebum measurements in standard conditions for the purpose of comparing intra- or interpersonal changes. The major external factor that substantially impacts sebum secretion is seasonal change. Sebum secretion is highest in the summer, and summer sebum secretion values are statistically different from those of the other three seasons. This means that there is a certain possibility for facial skin type change, especially for a change into a more oily skin type in the summer season (Youn et al. 2005a; Sakuma and Maibach 2012). Interestingly, cosmetic skin type as measured by sebum amount does not show any change toward a more dry skin type in the winter season (Youn et al. 2005a).

Aging is a major internal factor that affects sebum secretion amount. Sebum secretion amounts in males remain stable with increasing age, whereas sebum secretion amounts in females progressively decrease (Luebberding et al. 2013; Choi et al. 2011). This means that aging women could show a change of cosmetic skin type from an oilier type to a drier type over their lifetimes.

3 Measurement by Bioengineering Devices

As mentioned earlier, the Sebumeter® is the most commonly used scientific device for measuring sebum amounts. The main strength of the Sebumeter® for cosmetic skin type classification is that it is a simple, fast, and easily quantifiable device. Other sebum measuring devices or tools like the Sebufix® (Dobrev 2007) or Sebutape® (Clarys and Barel 1995) cannot measure sebum numerically in a convenient way. The Sebumeter® is also valuable for cosmetic skin type determination because many reports exist on its use in the assessment of sebum-related normal skin physiology. Practically, this is a relatively expensive device for the routine assessment of cosmetic facial skin type. Cheaper informal devices are used in cosmetics shops for cosmetic facial skin type determination.

There are some imaging devices with CCD cameras and UV illumination that could be used to

determine cosmetic facial skin type (Kim et al. 2013) by analyzing sebum amounts from UV photographs using computer software. Most of these types of devices are not fully validated by clinical studies with large numbers of normal subjects.

4 Association with Acne Vulgaris

Two main interests triggered by the concept of cosmetic facial skin type are the selection of skin type appropriate cosmetics and the association of skin type with the development of facial skin lesions such as acne vulgaris (Youn 2010; Youn et al. 2005b; Kim et al. 2006).

Increased sebum secretion is one of the main pathogenetic mechanisms of acne, and it is usually observed that acne patients subjectively regard their facial skin type as oily without any objective evidences. In a study (Choi et al. 2013) of 709 acne patients, subjectively determined skin type results as assessed by STRS indicated 302 oily type patients, 303 combination type patients, 40 normal type patients, and 64 dry type patients. Most acne patients feel that they have oily or combination skin types. The study also objectively reevaluated the acne patients' cosmetic skin types with Sebumeter® measurements. This revealed a skin type distribution of 126 oily type patients, 379 combination type patients, 143 normal type patients, and 61 dry type patients. Interestingly, the number of objectively determined oily skin type patients was lower than the number of subjectively determined oily type patients. Combination type is the most common skin type in acne patients. This finding may be attributed to ordinary people's prejudice that acne patients have oilier skin compared with people with normal skin. Most combination types show an oily type T zone and a normal type U zone. This suggests that the increased sebum secretion caused by androgen activity is mainly located in the T zone area. Alternately, we can postulate that the sebaceous glands located in the T zone start functioning earlier than the sebaceous glands in the U zone. Regarding this assumption, it is worth noting that early-onset, adolescent type acne is mainly distributed in the T zone (Choi et al. 2011). By contrast, late-onset, postadolescent acne generally presents with more acne lesions in the U zone as compared with adolescent acne.

Additional very useful information provided by the former study (Choi et al. 2013) is that subjective skin type as determined by the subjective assumptions of general people is relatively well correlated with objective determinations made by bioengineering measurements. Therefore, even when expensive measuring devices are not available, we can simply determine subjects' cosmetic skin types by using reliable STRS questionnaires. To increase the validity of the questionnaire, clearer differentiation between the oily type and combination type is needed. Many people with combination type skin mischaracterize their skin as the oily type because they focus on the oilier T zone when evaluating their cosmetic skin type (Youn 2010).

5 New Cosmetic Skin Area: O Zone

When we attempt to measure facial sebum secretion in all regions of the face, it is obvious that there are regional differences in the amounts of sebum secretion. The concept of a high sebum-secreting T zone and a low sebum-secreting U zone existed even before facial sebum could be measured quantitatively. Differences in sebum secretion between these two zones are so obvious that laypersons may discriminate between them without measurement. However, in the current bioengineering era, we were able to identify a third, different zone that shows distinctive characteristics as compared with the other areas. The perioral area, which was formerly a part of the T zone, has intermediate sebum-secreting characteristics that fall between those of the T zone and the U zone. A study that described the perioral area as a new cosmetic zone named it the "O" zone (Youn et al. 2014). The mean sebum secretion amount of the T zone excluding the perioral area was

218.04 ± 126.28 μg/cm^2 and the U zone sebum secretion amount was 122.63 ± 110.99 μg/cm^2. The mean sebum secretion amount was 193.26 ± 125.84 μg/cm^2 for the O zone, and while this value was closer to the sebum secretion amount of the T zone than the U zone, it showed a statistical difference from the T zone amount. Therefore, the O zone is a moderate to high sebum-secreting zone that differs from the other areas, especially from the former T zone.

The difference of sebum secretion capability in the O zone would be somewhat affected by the age-related lesion distribution pattern in acne patients. Additionally, perioral dermatitis also implies that the O zone area possesses certain physiological and pathological differences. This regional difference of the O zone area should be elucidated in more detailed topographic studies.

6 Future of Cosmetic Skin Type Determination

Converting the general public's common sense beliefs into those based on academic science is always difficult. While cosmetic skin type is a measurable element that has been studied by many researchers, it remains in the layperson's domain. This is because subjective skin type assessment is very cheap and more easily accessible than objective assessment and because most people do not require further scientific evaluation for the selection of facial cosmetics. Thus, researchers who try to develop an easy way of measuring skin type should incorporate objectivity into subjective skin type determinations. Another important aspect of cosmetic skin type determination is simultaneous wide multifocal measurement. Current sebum measurements have been limited to the anatomical focus of the small application area of the Sebumeter® cassette. Direct contact quantitative measurement of all areas of interest is ideal for approaching the real sebum secretion amount. Innovative technological improvements will ultimately achieve this goal.

References

Choi CW, Lee DH, Kim HS, Kim BY, Park KC, Youn SW. The clinical features of late onset acne compared with early onset acne in women. J Eur Acad Dermatol Venereol: JEADV. 2011;25(4):454–61.

Choi CW, Choi JW, Youn SW. Subjective facial skin type, based on the sebum related symptoms, can reflect the objective casual sebum level in acne patients. Skin Res Technol. 2013;19(2):176–82.

Clarys P, Barel B. Quantitative evaluation of skin surface lipids. Clin Dermatol. 1995;13:307–21.

Dobrev D. Clinical and instrumental study of the efficacy of a new sebum control cream. J Cosmet Dermatol. 2007;6(2):113–8.

Kim MK, Choi SY, Byun HJ, Huh CH, Park KC, Patel RA, et al. Comparison of sebum secretion, skin type, pH in humans with and without acne. Arch Dermatol Res. 2006;298(3):113.

Kim BY, Choi JW, Park KC, Youn SW. Sebum, acne, skin elasticity, and gender difference – which is the major influencing factor for facial pores? Skin Res Technol. 2013;19(1):e45–53.

Luebberding S, Krueger N, Kerscher M. Skin physiology in men and women: in vivo evaluation of 300 people including TEWL, SC hydration, sebum content and skin surface pH. Int J Cosmet Sci. 2013;35(5):477–83.

Sakuma TH, Maibach HI. Oily skin: an overview. Skin Pharmacol Physiol. 2012;25(5):227–35.

Yoon HS, Choi JW, Youn JI. Method of assessing involved facial areas: rule of fours. Br J Dermatol. 2008; 158(5):1022–8.

Youn SW. The role of facial sebum secretion in acne pathogenesis: facts and controversies. Clin Dermatol. 2010;28(1):8–11.

Youn SW, Kim SJ, Hwang IA, Park KC. Evaluation of facial skin type by sebum secretion: discrepancies between subjective descriptions and sebum secretion. Skin Res Technol. 2002;8(2):168–72.

Youn SW, Na JI, Choi SW, Huh CH, Park KC. Regional and seasonal variations in facial sebum secretions: a proposal for the definition of combination skin type. Skin Res Technol. 2005a;11(2):189–95.

Youn SW, Park ES, Lee DH, Huh CH, Park KC. Does facial sebum excretion really affect the development of acne? Br J Dermatol. 2005b;153(5):919–24.

Youn SH, Choi CW, Choi JW, Youn SW. The skin surface pH and its different influence on the development of acne lesion according to gender and age. Skin Res Technol. 2013;19(2):131–6.

Youn SH, Choi CW, Choi JW, Kim BR, Byun SY, Youn SW. Novel facial cosmetic area 'O zone' shows unique characteristics in sebum excretion and acne lesion distribution. Skin Res Technol. 2014;20(2): 164–9.

Cellulite: Classification and Scoring 135

Doris Hexsel, Camile L. Hexsel, and
Fernanda Naspolini Bastos

Contents

Keywords

Cellulite • Classification • Depression-Flaccidity • Laxity • Measuring • Photonumeric • Scale • Scoring • Skin surface alteration • Validated • Validation

1 Introduction and Definition

Cellulite is a very common clinical condition in which there is modification of skin topography evident by skin dimpling and nodularity, giving an orange peel, cottage cheese, or mattress aspect to the skin (Segers et al. 1984; Scherwitz and Braun-Falco 1978; Hexsel et al. 2009a; Khan et al. 2010), more commonly presenting on the buttocks, lower limbs, and abdomen. It is a localized metabolic and a complex architectural multifactorial disorder of the subcutaneous tissue (Hexsel et al. 2009a; Khan et al. 2010). This condition can be found in different age groups and in both sexes, but the prevalence is higher in females after puberty and in obese patients, being reported as a normal manifestation of obesity (Hexsel and Mazzuco 2000). On the other hand, cellulite is also present in nonobese individuals (Hexsel et al. 2009a; Khan et al. 2010).

The pathophysiology of cellulite is complex, and there are many theories to elucidate it. The majority of the theories involve alterations to the adipose tissue and microcirculation causing fibrosclerosis of the connective tissue. It is considered a noninflammatory, degenerative

D. Hexsel (✉)
Brazilian Center for Studies in Dermatology, Department of Dermatology, Pontificia Universidade Catolica do Rio Grande do Sul (PUC-RS), Porto Alegre, RS, Brazil
e-mail: doris@hexsel.com.br

C.L. Hexsel
Brazilian Center for Studies in Dermatology, Porto Alegre, Brazil

F.N. Bastos
Universidade Luterana do Brasil, Canoas, Brazil

P. Humbert et al. (eds.), *Agache's Measuring the Skin*,
DOI 10.1007/978-3-319-32383-1_93

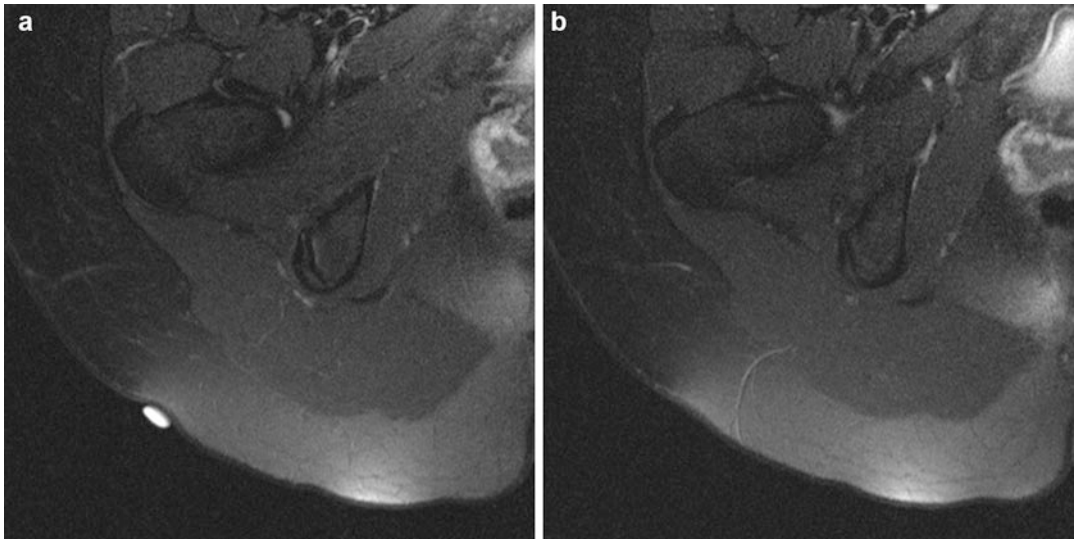

Fig. 1 Sequence of magnetic resonance imaging of a patient in an area with a cellulite depression. The first slice (**a**) shows a skin marker identifying the cellulite depression. The second slice (**b**) shows typical, thicker, ramified, and perpendicular fibrous septum

condition, producing alterations to the hypodermis producing irregular undulations on the skin overlying the affected areas (Hexsel et al. 2010).

Differences in subcutaneous tissue architecture between men and women may explain the female sex predominance of this condition (Nürnberger and Müller 1978). In women, bands of connective tissue are oriented radially or perpendicular to the skin surface (Nürnberger and Müller 1978; De la Casa et al. 2012). As the fat layer expands, herniation of subcutaneous fat within fibrous connective tissue occurs, leading to a puckered appearance of the skin (Querleux et al. 2002; Piérard et al. 2000). In men, these septa adopt an oblique zigzag pattern, which holds the fat layer and prevents the projection of the adipose tissue on the skin surface (De la Casa et al. 2012; Querleux et al. 2002; Piérard et al. 2000) (Fig. 1).

The skin surface alterations are comprised of depressed and raised areas, compared to normal adjacent skin. Depressed lesions occur due to the presence of fibrous septa that pull the skin surface down, and raised areas are the projection of underlying fat to the skin surface (Hexsel et al. 2009a). Recent studies have shown the anatomic structures involved in cellulite. One of those studies utilizing MRI analysis concludes that cellulite depressions on the buttocks are associated with the presence of underlying fibrous septa, (Hexsel et al. 2009b) which pulls the skin surface down, projecting the underlying fat to the skin surface and resulting in the raised areas (Hexsel 2001). It was found that all fibrous septa in the examined areas were perpendicular to the skin surface and most of them were ramified (Hexsel et al. 2009a).

Despite the morphological basis which explains the clinical presentation of cellulite, the pathophysiology of cellulite is still not fully elucidated. It seems to be a physiological phenomenon or at least that it has a physiological origin (De la Casa et al. 2012). It is a multi-causal disorder, with the coexistence of a number of factors that trigger, perpetuate, or exacerbate it (De la Casa et al. 2012). Flaccidity, laxity, or sagging of the skin further aggravates morphological alterations in the majority of patients (Hexsel et al. 2009a). Minor factors, such as weight gain or loss, localized tissue vascularity and postinflammatory changes, hormonal and genetic influences, and lifestyle, may also have an important role in cellulite's pathogenesis (Khan et al. 2010).

With the purpose of measuring cellulite severity and the effects of treatment modalities, a

comprehensive objective method of measuring cellulite was developed and is presented in this chapter, the new *Cellulite Severity Scale* (CSS) (Hexsel et al. 2009a). It considers important clinical and morphological aspects involved in the cellulite for its classification.

2 Classification and Scoring

Cellulite classification and scoring is of great relevance to accurately follow up treatment outcomes. This is also important to determine the more appropriate treatment for each patient. The evaluation of a patient with cellulite is mostly performed with clinical examination, and two classifications have already been developed aiming to determine different degrees of this condition. Cellulite must be evaluated with patients in standing position with relaxed muscles, so as to correctly identify the depressed and raised lesions of cellulite that are clearly apparent, regardless of pinch test or muscular contraction (Hexsel and Mazzuco 2000).

Nürnberger and Müller (1978) have described the most widely used classification until the last few years. They classified cellulite in degrees 0 to III, which varied from the complete absence of cellulite to its occurrence in a more severe degree (Table 1). A pinch test can be done to make the lesions more evident or to differentiate grades 0 from I.

Although largely used and practical, the abovementioned classification does not comprise all important additional morphologic aspects of cellulite and, thus, is not comprehensive enough to identify individual needs for treatment and to evaluate different treatment responses. Aiming to fulfill this gap, Hexsel, Dal'Forno, and Hexsel published the *Cellulite Severity Scale* (Hexsel et al. 2009a) (Table 2), which is based on five important clinical and morphological aspects of cellulite providing a more detailed classification for cellulite: (A) number of evident depressed lesions, (B) depth of depressions, (C) morphologic appearance of skin surface alterations, (D) grade of flaccidity or sagging skin, and (E) grade of cellulite. Each of these items is graded from zero to three. The total sum of the scores of each item indicates the cellulite grading as mild, moderate, or severe, as shown in Table 3.

The *Cellulite Severity Scale* (Hexsel et al. 2009a) is an alpha-photonumeric scale. Its main advantage is that it can indicate which morphological aspect is the most significant component of cellulite for each patient, allowing the physician to determine the most suitable treatment for the patient. For example, a patient with important laxity (e.g., grade 3 of letter D) and mild depressed lesions (e.g., grade 1 of letter B) should be treated for laxity to have an important improvement in cellulite grading rather than undergoing a Subcision®, which aims the treatment of depressed lesions.

De La Casa Almeida and cols (2013) assessed the intra- and interobserver reliability of the application of the CSS to a Spanish female population. They observed excellent reliability and internal consistency when used to evaluate cellulite on the buttocks and back of the thighs considered together. However, they considered that the dimension grade of laxity, flaccidity, or sagging skin does not contribute positively to the final consistency of the scale and suggested further analysis in greater depth in future studies.

The CSS has been used in some studies for the assessment of cellulite improvement after

Table 1 Classification of cellulite based on clinical criteria (Piérard et al. 2000)

Grade or stage	Clinical characteristics
0 (zero)	Skin surface is smooth
I	The skin surface is smooth while the subject is standing or lying, but the alterations to the skin surface can be seen by pinching the skin or with muscle contraction
II	The orange skin or mattress appearance is evident when standing, without the use of any manipulation (skin pinching or muscle contraction)
III	The alterations described in grade or stage II are present together with raised areas and nodules

Table 2 Hexsel, Dal'Forno, and Hexsel e Cellulite Severity Scale (CSS) (Hexsel et al. 2010)

(A) Number of evident depressions
This item refers to the total number of evident depressions by visual inspection in the area to be examined. The scores are expressed as follows:
ZERO = None/no depressions
1. A small amount: 1–4 depressions are visible
2. A moderate amount: 5–9 depressions are visible
3. A large amount: 10 or more depressions are visible
(B) Depth of depressions
This item evaluates the depth of depressions by visual inspection of the affected areas; comparison to the pictures of CSS is recommended
ZERO = No depressions
1. Superficial depressions
2. Medium depth depressions
3. Deep depressions
(C) Morphological appearance of skin surface alterations
Item C assesses the different morphological patterns of skin surface alterations; comparison with the pictures of CSS is recommended
ZERO = No raised areas
1. "Orange peel" appearance
2. "Cottage cheese" appearance
3. "Mattress" appearance
(D) Grade of laxity, flaccidity, or sagging skin
Laxity, flaccidity, or sagging skin confers the affected skin a draped appearance. This effect aggravates the appearance of cellulite. Item D assesses the grade of flaccidity, and comparison to the pictures of CSS is recommended
ZERO = Absence of laxity, flaccidity, or sagging skin
1. Slight draped appearance
2. Moderate draped appearance
3. Severe draped appearance
(E) Classification scale by Nürnberger and Müller
This item is based on the current classification of cellulite shown in Table 1. Patients should be evaluated in the standing position with relaxed gluteus muscles. However, if the patient has no evident depressions, they should be asked to contract their gluteus muscles or the *pinch test* should be applied (by pinching the skin between the thumb and index finger) in order to differentiate between scores 0 and 1 (see Fig. 1, item E – contracted)
ZERO = Zero grade
1. First grade
2. Second grade
3. Third grade

Table 3 New classification of cellulite based on the results of scores of Cellulite Severity Scale

Points	New classification of cellulite
1–5	Mild
6–10	Moderate
11–15	Severe

different treatments, being an objective and reliable tool to evaluate clinical trial outcomes (Hexsel et al. 2011, 2013; Knobloch et al. 2010).

Alexíades-Armenakas (Alexiades-Armenakas et al. 2008) and cols used a quantitative four-point grading scale to assess cellulite in a clinical trial that studied the use of unipolar radiofrequency treatment to improve the appearance of cellulite. However, there is no reference of validation of this scale (Table 4).

Table 4 Comprehensive cellulite grading scale

Grade	Contour	Dimple density	Dimple distribution	Dimple depth	Diameter % change
0	Smooth	0	0	0	100 × {[pre-post]/pre}
1	1 indentation	1–2/site	1 site	Shallow (1–2 mm)	
2	2 indentations	3–5/site	2 sites	Moderate (3–4 mm)	
3	3 indentations	6–8/site	3 sites	Advanced (5–6 mm)	
4	>3 indentations	>9/site	4≥ sites	Deep (>7 mm)	

Sites (graded individually): buttock, anterior thigh upper, anterior thigh lower, posterior thigh upper, posterior thigh lower; upper refers to upper one-half and lower to lower one-half of thigh length
Diameter: mean difference in diameter (mm) on photographic superimposition

References

Alexiades-Armenakas M, Dover JS, Arndt KA. Unipolar radiofrequency treatment to improve the appearance of cellulite. J Cosmet Laser Ther. 2008;10(3):148–53.

De la Casa Almeida M, Suarez Serrano C, Rebollo Roldán J, Jiménez Rejano JJ. Cellulite's aetiology: a review. J Eur Acad Dermatol Venereol. 2012;27:273–8.

De La Casa Almeida M, Suarez Serrano C, Jiménez Rejano JJ, Chillón Martínez R, et al. Intra- and inter-observer reliability of the application of the cellulite severity scale to a Spanish female population. J Eur Acad Dermatol Venereol. 2013;27(6):694–8.

Hexsel DM. Body repair. In: Parish LC, Brenner S, Ramos-e-Silva M, editors. Women's dermatology – from infancy to maturity. New York: Parthenon Publishing; 2001. p. 586–95.

Hexsel DM, Mazzuco R. Subcision: a treatment for cellulite. Int J Dermatol. 2000;39:539–44.

Hexsel DM, Dal'Forno T, Hexsel CL. A validated photonumeric cellulite severity scale. J Eur Acad Dermatol Venereol. 2009a;23(5):523–8.

Hexsel DM, Abreu M, Rodrigues TC, et al. Side-by-side comparison of areas with and without cellulite depressions using magnetic resonance imaging. Dermatol Surg. 2009b;35(10):1471–7.

Hexsel DM, Dal'Forno T, Mazzuco R. Definition, clinical aspects, classifications, and diagnostic techniques. In: Goldman MP, Hexel DM, editors. Cellulite pathophysiology and treatment. New York: Taylor & Francis; 2010. p. 14–21.

Hexsel DM, Siega C, Schilling-Souza J, Porto MD, et al. A bipolar radiofrequency, infrared, vacuum and mechanical massage device for treatment of cellulite: a pilot study. J Cosmet Laser Ther. 2011;13(6):297–302.

Hexsel D, Siega C, Schilling-Souza J, Oliveira DH. Noninvasive treatment of cellulite utilizing an expedited treatment protocol with a dual wavelength laser-suction and massage device. J Cosmet Laser Ther. 2013;15(2):65–9.

Khan MH, Victor F, Rao B, et al. Treatment of cellulite Part I. Pathophysiology. J Am Acad Dermatol. 2010;62(3):361–70.

Knobloch K, Joest B, Vogt PM. Cellulite and extracorporeal shockwave therapy (CelluShock-2009) – a randomized trial. BMC Womens Health. 2010;10:29.

Nürnberger F, Müller G. So-called cellulite: an invented disease. J Dermatol Surg Oncol. 1978;4(3):221–9.

Piérard GE, Nizet JL, Piérard-Franchimont C. Cellulite: from standing fat herniation to hypodermal stretch marks. Am J Dermatopathol. 2000;22:34–47.

Querleux B, Cornillon C, Jolivet O, et al. Anatomy and physiology subcutaneous adipose tissue by in vivo magnetic resonance imaging and spectroscopy: relationships with sex and presence of cellulite. Skin Res Technol. 2002;8:118–24.

Scherwitz C, Braun-Falco O. So-called cellulite. J Dermatol Surg Oncol. 1978;4(3):230–4.

Segers AM, Abulafia J, Kriner J, et al. Celulitis. Estudo histopatológico e histoquímico de 100 casos. Med Cut ILA. 1984;12:167–72.

Clinical Scoring of Atopic Dermatitis 136

Golara Honari

Contents

Keywords

Atopic dermatitis • Eczema outcome • Eczema area and severity index • Severity scoring of atopic dermatitis

1 Introduction

Atopic dermatitis (AD) is a common inflammatory skin disease, affecting approximately 10–30 % of children and 2–3 % of adults (Bieber and Bussmann 2012; Eichenfield et al. 2014; Williams et al. 1999). Atopic dermatitis is characterized by eczematous skin eruptions, often accompanied by other atopic disorders such as asthma and allergic rhinoconjunctivitis. Pathogenesis of AD involves genetic, immunologic, and environmental factors causing skin barrier dysfunction as well as immune dysregulation leading to the constellation of clinical findings. Pruritus, dry skin, erythema, edema, erosions and excoriations, oozing and crusting, and lichenification are key clinical manifestations of AD. AD, also known as atopic eczema, is a chronically relapsing course. Providing better care for affected individuals highlights the need for comprehensive evaluation of disease activity and measurements of disease severity. This chapter reviews validated scoring methods

G. Honari (✉)
Department of Dermatology, Stanford School of Medicine, Redwood City, USA
e-mail: Honari@stanford.edu

P. Humbert et al. (eds.), *Agache's Measuring the Skin*,
DOI 10.1007/978-3-319-32383-1_94

developed for comprehensive evaluation of disease severity in atopic dermatitis.

2 Diagnosis

AD is diagnosed clinically based on history, morphology, distribution, and other clinical signs. Hanifin and Rajka developed the first formal diagnostic criteria in 1980 (Hanifin and Rajka 1980). Several groups have proposed other diagnostic criteria, but the most widely accepted set of criteria is developed by the United Kingdom (UK) Working Party (Williams et al. 1994, 1999; Haileamlak et al. 2005; Gu et al. 2001). Both the Hanifin and Rajka and UK Working Party diagnostic principles have been validated and tested in different populations and are presented in Table 1 (De et al. 2006; Mevorah et al. 1988; Loden et al. 1998; Samochocki et al. 2000).

3 Clinical Scoring

Measurement of disease activity is key in clinical management and monitoring of individual patients. Standardization of measurement tools and harmonizing outcome measures is critical, in evidence-based practice. Considering high disease burden of AD, multiple scoring methods have been developed over the past decades (Table 2), but a few are considered reliable and validated.

Disease severity in atopic dermatitis can be measured based on subjective assessment of symptoms, objective measurements of clinical features, and tools to assess quality of life. Additional data may be obtained from epigenetic testing, bioengineering methods, and some inflammatory markers; however, these methods are not validated for measurements of disease activity (Gutgesell et al. 2002; Rodriguez et al. 2014).

The need for standard, reliable, and clinically meaningful outcome measures prompted foundation of the Harmonising Outcome Measures for Eczema (HOME) initiative in 2008, with the goal to facilitate evidence-based multidisciplinary consensus on core outcome sets (COS). Two levels of COS include outcome domains and outcome measures (The HOME (Harmonising Outcome Measures for Eczema) 2014). In general, outcome domains relate to the concept that needs to be measured (e.g., clinical signs of atopic eczema), and outcome measures relate to the methods that are used to measure them (e.g., the Eczema Area and Severity Index (EASI) to measure signs) (Fig. 1; The HOME (Harmonising Outcome Measures for Eczema) 2014; Schmitt et al. 2007, 2013, 2014; Sidbury et al. 2014).

In a recent systematic review on properties of outcome measures for clinical signs of AD, two scoring methods, namely, Eczema Area and Severity Index (EASI) (Tofte et al. 1998) and Severity Scoring of Atopic Dermatitis (SCORAD) index (*Severity scoring of atopic dermatitis: The SCORAD index. consensus report of the european task force on atopic dermatitis* 1993), were found to have the best measurement properties. The Six Area, Six Sign Atopic Dermatitis (SASSAD) (Berth-Jones 1996) severity score and Three-Item Severity (TIS) (Wolkerstorfer et al. 1999) score fulfill some quality criteria, but unclear about all required measures. Patient-Oriented Eczema Measure (POEM) (Charman et al. 2004) was found reliable and responsive but had inadequate content validity for assessing clinical signs of AD. This chapter focuses on these scoring methods.

4 Severity Scoring of Atopic Dermatitis (SCORAD) Index

Severity Scoring of Atopic Dermatitis is a composite scoring index based on objective data (extent and intensity of involvement) and subjective symptoms (itching and sleep loss) (Severity Scoring of Atopic Dermatitis 1993). SCORAD was developed in the early 1990s by the European Task Force on Atopic Dermatitis and remains a major scoring method. The score is calculated based on the following measures (Fig. 2):

Table 1 Diagnostic features of atopic dermatitis (Hanifin and Rajka 1980; Williams et al. 1994; Williams 2005)

Hanifin and Rajka criteria	UK Working Party's diagnostic criteria for AD[a]
Major features (3 out of 4 present)	Must have
Pruritus	An itchy skin condition (or parental report of scratching or rubbing in a child)
Typical morphology and distribution of skin lesions	
Chronic or chronically relapsing dermatitis	
Personal or family history of atopy	
Minor features (3 out of 23 present)	Three or more of the following
Xerosis	History of involvement of the skin creases such as folds of elbows, behind the knees, fronts of ankles, the neck, and around the eyes[b]
Ichthyosis/palmar hyperlinearity/keratosis pilaris	A personal history of asthma or hay fever (or history of atopic disease in a first-degree relative in children under 4 years of age)
Immediate (type I) skin test reactivity	A history of generally dry skin in the last year
Elevated serum IgE	Visible flexural eczema (or eczema involving the cheeks/forehead and extensor limbs in children under 4 years of age)
Early age of onset	Onset under 2 years of age (not used if child is under 4 years of age)
Tendency toward cutaneous infections/ impaired cell-mediated immunity	
Tendency toward nonspecific hand or foot dermatitis	
Nipple eczema	
Cheilitis	
Recurrent conjunctivitis	
Dennie–Morgan infraorbital fold	
Keratoconus	
Anterior subcapsular cataract	
Orbital darkening	
Facial pallor/erythema	
Pityriasis alba	
Anterior neck folds	
Pruritus when sweating	
Intolerance to wool and lipid solvents	
Perifollicular accentuation	
Food intolerance	
Course influenced by environmental/ emotional factors	
White dermographism/delayed blanch	

[a]Modified in 2005
[b]Original 1994 guidelines also included the cheeks in young children

(A) Extent of involvement; rule of 9 is applied in adults and modified in children (see Fig. 2). Score for each area is added up, and the total area is referred to as "A" (maximum score is 100 referring to100 % body surface area).
(B) Intensity of the signs in the representative area of eczema is scored as none (0), mild (1), moderate (2), or severe (3). The assessed signs are:
- Erythema
- Edema/papulation
- Oozing/crusting
- Excoriations
- Lichenification

Table 2 Named eczema outcome measures

ADAM (Charman et al. 1999b)	Atopic Dermatitis Assessment Measure
ADASI (Bahmer et al. 1991; Bahmer 1992)	Atopic Dermatitis Area and Severity Index
ADAS (Baek et al. 2015)	Atopic Dermatitis Antecubital Severity
ADSI (Van Leent et al. 1998)	Atopic Dermatitis Severity Index
BCSS (Verwimp et al. 1995)	Basic Clinical Scoring System
EASI (Tofte et al. 1998)	Eczema Area and Severity Index
FSSS (Mastrandrea et al. 2005)	Four-Step Severity Score
IGADA (Schachner et al. 2005)	Investigator's Global Atopic Dermatitis Assessment
Leicester (Berth-Jones and Graham-Brown 1993)	Leicester Index
NESS (Emerson et al. 2000)	Nottingham Eczema Severity Score
OSAAD (Sugarman et al. 2003)	Objective Severity Assessment of Atopic Dermatitis
POEM (Charman et al. 2004)	Patient-Oriented Eczema Measure
PO-SCORAD (Stalder et al. 2011)	Patient-Oriented Scoring of Atopic Dermatitis
RL Score (Rajka and Langeland 1989)	Rajka and Langeland Score
SA-EASI (Housman et al. 2002)	Self-Administered Eczema Area and Severity Index
SASSAD (Berth-Jones 1996)	Six Area, Six Sign Atopic Dermatitis severity score
SCORAD (*Severity scoring of atopic dermatitis: The SCORAD index. consensus report of the european task force on atopic dermatitis* 1993)	Severity Scoring of Atopic Dermatitis index
SIS (Kagi et al. 1992)	Skin Intensity Score
SSS (Costa et al. 1989)	Simple Scoring System
TBSA (vanJoost et al. 1994)	Six-Area Total Body Severity Assessment
TISS (Wolkerstorfer et al. 1999)	Three-Item Severity Score
WAZ-S (Silny et al. 2005)	(Polish acronym for atopic dermatitis severity score)

- Dryness (this is assessed in an area where there is no inflammation)

The intensity scores are added together to make "B" (maximum score is 18).

(C) Subjective symptoms for the last 3 days or nights include:
- Pruritus (visual analog scale 0–10)
- Sleep loss (visual analog scale 0–10)

These scores are added to give "C" (maximum score 20).

The SCORAD for each individual is calculated based on this formula $A/5 + 7B/2 + C$.

5 Eczema Area and Severity Index (EASI)

EASI is an objective scoring method that measures both extent and severity of involvement in four anatomical areas (Tofte et al. 1998). The intensity of clinical signs of inflammation including erythema, induration/papulation, excoriation, and lichenification is assessed as defined below. Symptoms like pruritus, as well as secondary signs like xerosis, and scaling are excluded from assessments. Anatomic regions include the head and neck, upper extremities, trunk, and lower

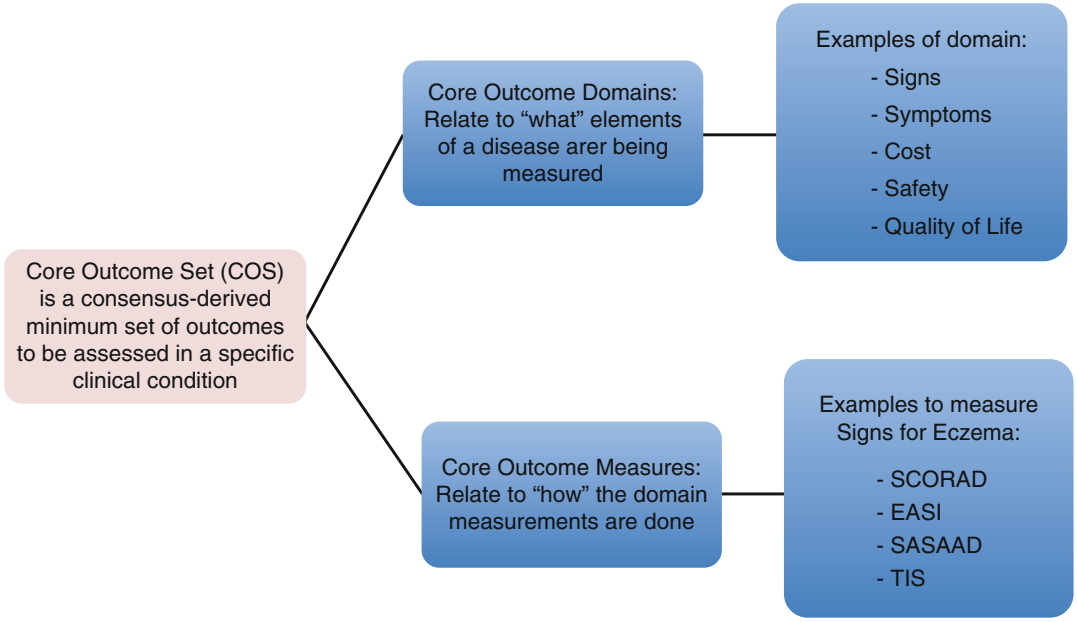

Fig. 1 Core outcome domains and core outcome measures (The HOME (Harmonising Outcome Measures for Eczema) 2014; Schmitt et al. 2015)

extremities. The percentage of areas involved in each of the four body regions is assigned a proportional score from 0 to 6 during the analysis: none (0), 1–9 % (1), 10–29 % (2), 30–49 % (3), 50–69 % (4), 70–89 % (5), and 90–100 % (6). The intensity of erythema, induration/papulation/edema, excoriation, and lichenification of the eczema is assessed as none (0), mild (1), moderate (2), and severe (3).

Calculation methods are summarized in Fig. 3, and case scenario is presented to better clarify these calculations:

> A 6 year old girl presents with a flare of atopic eczema. She has involvement of neck with mild erythema and scant excoriations (about 20 % of head and neck involved), bilateral antecubitals and forearms are involved with moderate erythema, several excoriations and moderate lichenification (about 15 % of upper limbs involved), on flexor knees she has deep dark erythematous plaques with moderate edema, several excoriations and moderate lichenification (9 % of lower limbs are involved). On trunk she has mild xerosis otherwise clear. The four intensity scores are added up for each body regions as follows:
>
> - Head and neck (mild erythema and scant excoriations) × (area of involvement 20% of head and neck) × (0.2 for age<7) = (1 + 0 +1+0) × 2 × 0.2 = 1.2
> - Upper Limbs (moderate erythema, several excoriations and moderate lichenification) × (15 % of upper limbs) × 0.2 = (2+0+2+2) × 2 × 0.2 = 2.4
> - Trunk (xerosis) = 0
> - Lower limbs with deep dark erythema, moderate edema, several excoriations and moderate lichenification) × (9% of lower limbs) × 0.3 = (3+2+2+2) × 1 × 0.3 = 2.7
>
> EASI = 1.2 + 2.4 + 2.7 = 6.3

The EASI is a valid and internally consistent scoring method with adequate intraobserver reliability, intermediate interobserver reliability, and adequate responsiveness (Schmitt et al. 2013). The use of (at least) EASI in future atopic eczema trials is recommended for improved evidence-based communications (Schmitt et al. 2015).

5.1 Three-Item Severity (TIS) Score

Three-Item Severity (TIS) score is a simple objective scoring method based on only three intensity

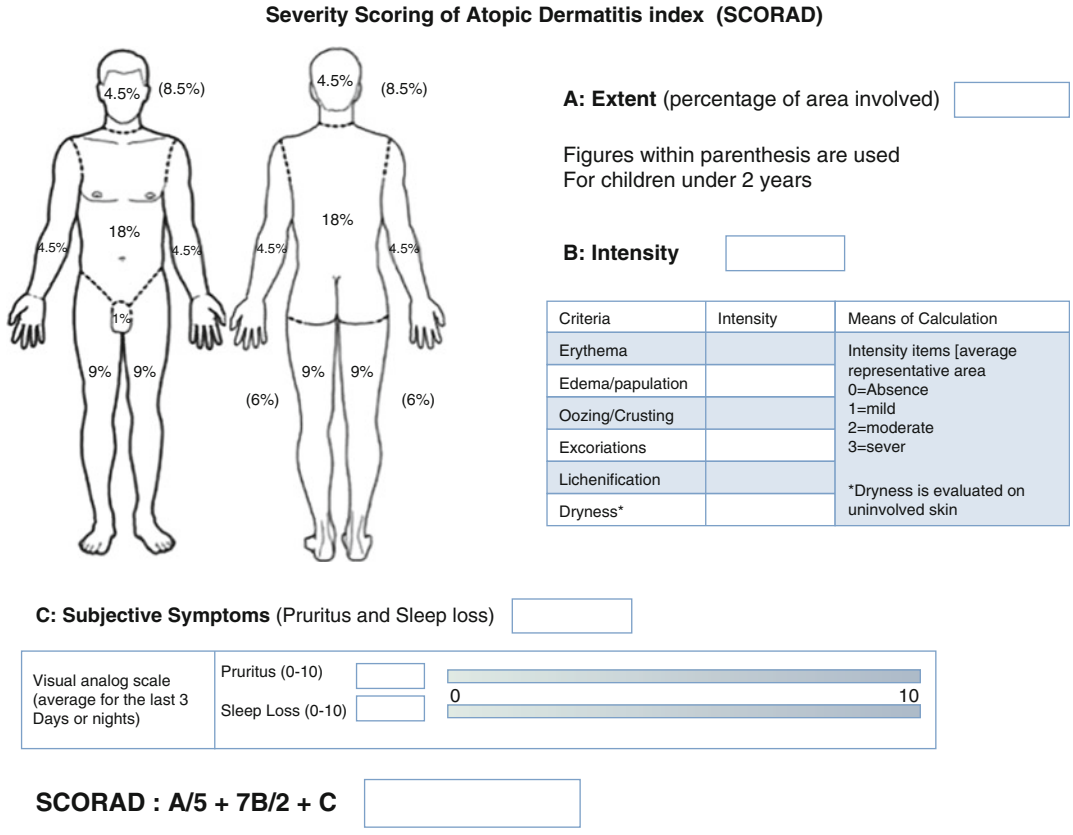

Fig. 2 Severity Scoring of Atopic Dermatitis (SCORAD) index (*Severity scoring of atopic dermatitis: the SCORAD index. consensus report of the european task force on atopic dermatitis* 1993)

items (erythema, edema/papulation, and excoriations) (Wolkerstorfer et al. 1999). Similar to SCORAD, each item is scored based on the most representative lesion, meaning that different items may be scored on different sites. Intensity of the signs in the representative area of eczema is scored as none (0), mild (1), moderate (2), or severe (3). The assessed signs are:

- Erythema
- Edema/papulation
- Excoriations

The range of TIS score lies between 0 and 9. TIS score is a reliable and simple scoring system with good content validity. It is applicable in routine clinical practice and for screening purposes in clinical trials (Wolkerstorfer et al. 1999).

6 Six Area, Six Sign Atopic Dermatitis (SASSAD) Severity Score

In this method, disease activity is assessed by grading six signs (erythema, exudation, excoriation, dryness, cracking, and lichenification), each on a scale of 0 (absent), 1 (mild), 2 (moderate), or 3 (severe), at each of six sites: arms, hands, legs, feet, head and neck, and trunk (Berth-Jones 1996). The maximum score is 108. This method eliminates risk of unreliable body surface area measurements by inexperienced observer (Berth-Jones 1996; Charman et al. 1999a). As an outcome measure, SASSAD meets some quality items and has the potential to be recommended in clinical trials, depending on further validation studies.

Eczema Area and Severity Index (EASI)

- **Body regions**
  - Head/neck
  - Upper limbs
  - Trunk
  - Lower limbs
- **Scoring of areas of Involvement in each anatomical region (Area)**

0	1	2	3	4	5	6
No eruption	<10%	10%-29%	30-49%	50-69%	70-89%	90-100%

- **Calculation of Intensity**

Criteria	0	1	2	3
Erythema (E)	None	Faintly detectable erythema, very light pink	Dull red, clearly distinguishable	Deep, dark red
Infiltration/Papulation (I)	None	Barely perceptible elevation	Clearly perceptible elevation	Extensive elevation
Excoriation (Ex)	None	Scant evidence of excoriation No erosion or crust	Several linear mark, some erosion or crust	Many erosive and/or crusty lesions
Lichenification (L)	None	Light thickening of skin discernable only by touch	Definite thickening of skin with exaggerated markings and markings and visible criss-cross pattern	Thickened Indurated skin and visible exaggerated criss-cross pattern

- **Calculations**

Head/Neck	(E+ I + Ex + L) x Area x 0.1 (In children 0-7 years (E+ I + Ex + L) x Area x 0.2)	
Upper limbs	(E+ I + Ex + L) x Area x 0.2	
Trunk	(E+ I + Ex + L) x Area x 0.3	
Lower limbs	(E+ I + Ex + L) x Area x 0.4 (In children 0-7 years (E+ 1 + Ex + L) x Area x 0.3)	
EASI	Sum of the above four body areas	Total score =

Fig. 3 Eczema Area and Severity Index (EASI) (Tofte et al. 1998)

7 Patient-Oriented Eczema Measure (POEM)

This is a subjective scoring system based on a questionnaire focusing on seven symptoms, using a simple 5-point scale of frequency of occurrence during the previous week (Charman et al. 2004). The maximum total score is 28. Patients are asked to circle one response for each question. Questions are as follows:

1. Over the last week, on how many days has your/your child's skin been **itchy** because of the eczema?				
No days	1–2 days	3–4 days	5–6 days	Every day
2. Over the last week, on how many nights has your/your child's **sleep been disturbed** because of the eczema?				
No days	1–2 days	3–4 days	5–6 days	Every day

(*continued*)

3. Over the last week, on how many days has your/your child's skin been **bleeding** because of the eczema?				
No days	1–2 days	3–4 days	5–6 days	Every day
4. Over the last week, on how many days has your/your child's skin been **weeping or oozing clear fluid** because of the eczema?				
No days	1–2 days	3–4 days	5–6 days	Every day
5. Over the last week, on how many days has your/your child's skin been **cracked** because of the eczema?				
No days	1–2 days	3–4 days	5–6 days	Every day
6. Over the last week, on how many days has your/your child's skin been **flaking off** because of the eczema?				
No days	1–2 days	3–4 days	5–6 days	Every day
7. Over the last week, on how many days has your/your child's skin been **felt dry or rough** because of the eczema?				
No days	1–2 days	3–4 days	5–6 days	Every day

POEM is a useful tool in clinical monitoring of patients with atopic eczema, but it is not recommended as a sole outcome measure in clinical trials.

8 Conclusion

The need to establish core outcome sets for atopic dermatitis is a priority for advancing evidence-based treatments. Harmonising Outcome Measures for Eczema (HOME) initiative has defined clinical signs, symptoms, quality of life, and long-term control of atopic dermatitis flares as core outcome domains for atopic dermatitis trials (Schmitt et al. 2015). In systematic review of measurement instruments for assessment of clinical signs of atopic dermatitis, EASI and SCORAD have been identified as extensively validated (Schmitt et al. 2015). However, the objective of SCORAD, despite providing adequate validity, responsiveness, and interobserver reliability, lacks clear intraobserver reliability. In a recent international consensus study, EASI was identified as the preferred measurement instrument to be used in future atopic eczema trial (Schmitt et al. 2015). Additional information and recourses are available and highly recommended through http://homeforeczema.org.

References

Baek JH, Park CW, Choi KM, Yang YS, Lee SY, Koh JS, Chung BY, Kim HO, Park GH, et al. The atopic dermatitis antecubital severity score: validity, reliability, and sensitivity to change in patients with atopic dermatitis. Int J Dermatol. 2015;54(12):1382–9. doi: 10.1111/ijd.12711.

Bahmer FA. ADASI score: atopic dermatitis area and severity index. Acta Derm Venereol Suppl (Stockh). 1992;176:32–3.

Bahmer FA, Schafer J, Schubert HJ. Quantification of the extent and the severity of atopic dermatitis: the ADASI score. Arch Dermatol. 1991;127(8):1239–40.

Berth-Jones J. Six area, six sign atopic dermatitis (SASSAD) severity score: a simple system for monitoring disease activity in atopic dermatitis. Br J Dermatol. 1996;135 Suppl 48:25–30.

Berth-Jones J, Graham-Brown RA. Placebo-controlled trial of essential fatty acid supplementation in atopic dermatitis. Lancet. 1993;341(8860):1557–60.

Bieber T, Bussmann C. Atopic dermatitis. In: Bolognia JL, Jorizzo JL, Schaffer JV, editors. Dermatology. 3rd ed. China: Elsevier; 2012. p. 203–17.

Charman CR, Venn AJ, Williams HC. Measurement of body surface area involvement in atopic eczema: an impossible task? Br J Dermatol. 1999a;140(1):109–11.

Charman D, Varigos G, Horne DJ, Oberklaid F. The development of a practical and reliable assessment measure for atopic dermatitis (ADAM). J Outcome Meas. 1999b;3(1):21–34.

Charman CR, Venn AJ, Williams HC. The patient-oriented eczema measure: development and initial validation of a new tool for measuring atopic eczema severity from the patients' perspective. Arch Dermatol. 2004;140(12):1513–9.

Costa C, Rilliet A, Nicolet M, Saurat JH. Scoring atopic dermatitis: the simpler the better? Acta DermVenereol. 1989;69(1):41–5.

De D, Kanwar AJ, Handa S. Comparative efficacy of hanifin and rajka's criteria and the UK working party's diagnostic criteria in diagnosis of atopic dermatitis in a hospital setting in north india. J Eur Acad Dermatol Venereol. 2006;20(7):853–9.

Eichenfield LF, Tom WL, Chamlin SL, et al. Guidelines of care for the management of atopic dermatitis: section 1. Diagnosis and assessment of atopic dermatitis. J Am Acad Dermatol. 2014;70(2):338–51.

Emerson RM, Charman CR, Williams HC. The Nottingham eczema severity score: preliminary refinement of the rajka and langeland grading. Br J Dermatol. 2000;142(2):288–97.

Gu H, Chen XS, Chen K, et al. Evaluation of diagnostic criteria for atopic dermatitis: validity of the criteria of Williams et al. in a hospital-based setting. Br J Dermatol. 2001;145(3):428–33.

Gutgesell C, Heise S, Seubert A, Stichtenoth DO, Frolich JC, Neumann C. Comparison of different activity parameters in atopic dermatitis: correlation with clinical scores. Br J Dermatol. 2002;147(5):914–9.

Haileamlak A, Lewis SA, Britton J, et al. Validation of the international study of asthma and allergies in children (ISAAC) and U.K. criteria for atopic eczema in ethiopian children. Br J Dermatol. 2005;152(4):735–41.

Hanifin JM, Rajka G. Diagnostic features of atopic eczema. Acta Derm Venereol Suppl (Stockh). 1980;92:44–7.

Housman TS, Patel MJ, Camacho F, Feldman SR, Fleischer Jr AB, Balkrishnan R. Use of the self-administered eczema area and severity index by parent caregivers: results of a validation study. Br J Dermatol. 2002;147(6):1192–8.

Kagi MK, Joller-Jemelka H, Wuthrich B. Correlation of eosinophils, eosinophil cationic protein and soluble interleukin-2 receptor with the clinical activity of atopic dermatitis. Dermatology. 1992;185(2):88–92.

Loden M, Andersson AC, Lindberg M. The number of diagnostic features in patients with atopic dermatitis correlates with dryness severity. Acta Derm Venereol. 1998;78(5):387–8.

Mastrandrea F, Pecora S, Scatena C, Cadario G. Methodology and potential pitfalls in allergic diseases study designs: measurements for the assessment of the overall severity of atopic dermatitis – the four step severity score (FSSS), SCORAD-related, electronic system, for the simple and rapid evaluation of the skin and mucosal allergic inflammation. Eur Ann Allergy Clin Immunol. 2005;37(9):357–61.

Mevorah B, Frenk E, Wietlisbach V, Carrel CF. Minor clinical features of atopic dermatitis. Evaluation of their diagnostic significance. Dermatologica. 1988;177(6):360–4.

Rajka G, Langeland T. Grading of the severity of atopic dermatitis. Acta Derm Venereol Suppl (Stockh). 1989;144:13–4.

Rodriguez E, Baurecht H, Wahn AF, et al. An integrated epigenetic and transcriptomic analysis reveals distinct tissue-specific patterns of DNA methylation associated with atopic dermatitis. J Invest Dermatol. 2014; 134(7):1873–83.

Samochocki Z, Paulochowska E, Zabielski S. Prognostic value of hanifin and rajka's feature sets in adult atopic dermatitis patients. J Med. 2000;31(3–4):177–82.

Schachner LA, Lamerson C, Sheehan MP, et al. Tacrolimus ointment 0.03% is safe and effective for the treatment of mild to moderate atopic dermatitis in pediatric patients: results from a randomized, double-blind, vehicle-controlled study. Pediatrics. 2005;116(3):e334–42.

Schmitt J, Langan S, Williams HC. European Dermato-Epidemiology Network. What are the best outcome measurements for atopic eczema? A systematic review. J Allergy Clin Immunol. 2007;120(6):1389–98.

Schmitt J, Langan S, Deckert S, et al. Assessment of clinical signs of atopic dermatitis: a systematic review and recommendation. J Allergy Clin Immunol. 2013;132(6):1337–47.

Schmitt J, Apfelbacher C, Spuls PI, Thomas KS, Simpson EL, Furue M, Chalmers J, Williams HC et al. The harmonizing outcome measures for eczema (HOME) roadmap: a methodological framework to develop core sets of outcome measurements in dermatology. J Invest Dermatol. 2015;135(1):24–30. doi: 10.1038/jid.2014.320.

Severity scoring of atopic dermatitis: the SCORAD index. consensus report of the european task force on atopic dermatitis. Dermatology. 1993;186(1):23–31.

Sidbury R, Davis DM, Cohen DE, et al. Guidelines of care for the management of atopic dermatitis: section 3. Management and treatment with phototherapy and systemic agents. J Am Acad Dermatol. 2014;71 (2):327–49.

Silny W, Czarnecka-Operacz M, Silny P. The new scoring system for evaluation of skin inflammation extent and severity in patients with atopic dermatitis. Acta Dermatovenerol Croat. 2005;13(4):219–24.

Stalder JF, Barbarot S, Wollenberg A, et al. Patient-oriented SCORAD (PO-SCORAD): a new self-assessment scale in atopic dermatitis validated in Europe. Allergy. 2011;66(8):1114–21.

Sugarman JL, Fluhr JW, Fowler AJ, Bruckner T, Diepgen TL, Williams ML. The objective severity assessment of atopic dermatitis score: an objective measure using permeability barrier function and stratum corneum hydration with computer-assisted estimates for extent of disease. Arch Dermatol. 2003;139(11):1417–22.

The HOME (Harmonising Outcome Measures for Eczema). http://www.homeforeczema.org. Accessed 05 Sept 2014.

Tofte SJ, Graeber M, Cherill R, Omoto M, Thurston M, Hanifin JM. Eczema area and severity index (EASI): a new tool to evaluate atopic dermatitis. J Eur Acad Dermatol Venereol. 1998;11 suppl 2:S197.

Van Leent EJ, Graber M, Thurston M, Wagenaar A, Spuls PI, Bos JD. Effectiveness of the ascomycin macrolactam SDZ ASM 981 in the topical treatment of atopic dermatitis. Arch Dermatol. 1998;134(7): 805–9.

vanJoost T, Heule F, Korstanje M, van den Broek MJ, Stenveld HJ, van Vloten WA. Cyclosporin in atopic dermatitis: a multicentre placebo-controlled study. Br J Dermatol. 1994;130(5):634–40.

Verwimp JJ, Bindels JG, Barents M, Heymans HS. Symptomatology and growth in infants with cow's milk protein intolerance using two different whey-protein hydrolysate based formulas in a primary health care setting. Eur J Clin Nutr. 1995;49 Suppl 1: S39–48.

Williams HC. Clinical practice. Atopic dermatitis. N Engl J Med. 2005;352(22):2314–24.

Williams HC, Burney PG, Hay RJ, et al. The U.K. working party's diagnostic criteria for atopic dermatitis. I. Derivation of a minimum set of discriminators for atopic dermatitis. Br J Dermatol. 1994; 131(3):383–96.

Williams H, Robertson C, Stewart A, et al. Worldwide variations in the prevalence of symptoms of atopic eczema in the international study of asthma and allergies in childhood. J Allergy Clin Immunol. 1999; 103(1 Pt 1):125–38.

Wolkerstorfer A, de Waard van der Spek FB, Glazenburg EJ, Mulder PG, Oranje AP. Scoring the severity of atopic dermatitis: three item severity score as a rough system for daily practice and as a pre-screening tool for studies. Acta DermVenereol. 1999;79(5):356–9.

Psoriasis Scoring

137

Yasser Afifi and Philippe Humbert

Contents

Keywords

Body surface area (BSA) • Dermatology Index of Disease Severity (DIDS) • Evaluation for Prognosis with Average PASI (E-PAP) • Lattice System Global Psoriasis Score (LS-GPS) • Psoriasis area and severity index (PASI) • Salford Psoriasis Index (SPI) • Self-administered psoriasis area and severity index (SAPASI)

1 The Body Surface Area

The main methods for assessing the severity of psoriasis incorporate an estimation of involved surface area (Ashcroft et al. 1999). One side of a flat closed hand is thought to represent an area of 1 % of the total body surface area. Nevertheless, planimetric investigations give another estimation of the hand surface, which in fact represents 0.70–0.76 % of the body surface area (BSA) (Long et al. 1992).

The rule of nines method assumes that the total BSA comprises the head (9 %), anterior trunk (upper, 9 %; lower, 9 %), posterior trunk (upper, 9 %; lower, 9 %), each leg (anterior, 9 %; posterior 9 %), each arm (9 %), and genitalia (1 %).

This chapter was originally published under the ISBN 978-3-540-01771-4 with the following book title Measuring the Skin. The content has not been changed.

Y. Afifi
Private Clinic, Rabat, Morocco
e-mail: yaafifi@yahoo.fr

P. Humbert (✉)
Department of Dermatology, University Hospital of Besançon, Besançon, France
e-mail: philippe.humbert@univ-fcomte.fr

P. Humbert et al. (eds.), *Agache's Measuring the Skin*,
DOI 10.1007/978-3-319-32383-1_95

2 The Psoriasis Area and Severity Index

Four main body areas are assessed by the Psoriasis Area and Severity Index (PASI) (Fredriksson and Pettersson 1978): head (h), trunk (t), upper extremities (u), and lower extremities (1), assumed to weigh 10 %, 20 %, 30 %, and 40 % of the total body area, respectively.

The extent of psoriatic involvement of these four main areas (A_h, A_t, A_u, and A_t) is given a numerical value: 0 = no involvement; 1 = <10 %; 2= >10 %, but <30 %; 3 = >30 %, but <50 %; 4= >50 %, but <70 %; 5= > 70 %, but <90 %, and 6 = 90–100 %.

In order to evaluate three clinical signs, erythema (E), infiltration (I), and desquamation (D) are assessed using a 0–4 scale, where 0 = no; 1 = slight; 2 = moderate; 3 = severe; 4 = very severe.

The PASI is the sum of each area score. The formula is as follows:

$$\begin{aligned}\text{PASI} = {} & 0,1A_h\ (E_h + I_h + D_h) \\ & + 0,3\ A_t(E_t + I_t + D_t) \\ & + 0,2\ A_u(E_u + I_u + D_u) \\ & + 0,4\ A_1(E_1 + I_1 + D_1)\text{Maximum} \\ = {} & (0,1 \times 6 \times 12) + (0,3 \times 6 \times 12) \\ & + (0,2 \times 6 \times 12) + (0,4 \times 6 \times 12) \\ = {} & 72\end{aligned}$$

Example:

1. Involvement × weight of area

Head	5 (75 % involved) × 0.1 = 0.5
Upper limbs	3 (1/3 area involved) × 0.3 = 0.9
Trunk	1 (less 10 % involved) × 0.2 = 0.2
Lower limbs	0 × 0.4 = 0

2. Clinical signs (maximum possible for each area: 4 × 3 = 12)

Head	Erythema (E): 2
Infiltration (I)	1
Desquamation (D)	2
Total	5
Upper limbs	Erythema (E): 2
Infiltration (I)	3
Desquamation (D)	4
Total	9
Trunk	Erythema (E): 2
Infiltration (I)	2
Desquamation (D)	2
Total	6
Lower limbs	0
Total for head	0.5 × 5 = 2.5
Total for upper limbs	0.9 × 9 = 8.1
Total for trunk	0.2 × 6 = 1.2
Total for lower limbs	0
Total PASI score	11.8

3 The Self-Administered Psoriasis Area and Severity Index

The Self-Administered Psoriasis Area and Severity Index (SAPASI) (Fleischer et al. 1994; Feldman et al. 1996) is a structured instrument for measuring the severity of psoriasis. It allows patients to assess the severity of psoriasis accurately.

Patients rate the color, induration, and scaliness of an average psoriatic lesion using three modified visual analog scales.

As in the original PASI score, the SAPASI weights the involvement of the head, upper extremities, trunk, and legs as 10 %, 20 %, 30 %, and 40 % of the total body area, respectively.

$$\begin{aligned}\text{SAPASI} = {} & (0,1 \times A_H) + (0,2 \times A_U) \\ & + (0,3 \times A_T) + (0,4 \times A_L)\ 4 \\ & \times (\text{VAS}_E + \text{VAS}_I + \text{VAS}_S)/\text{VAS len}\end{aligned}$$

where:

A_H: Head score
A_U: Upper extremity score
A_T: Trunk score
A_L: Lower extremity score
VAS: Visual analog scale
VAS_E: VAS erythema score (mm)
VAS_I: VAS induration score (mm)
VAS_S: VAS scale score (mm)

4 The Lattice System Global Psoriasis Score

The Lattice System Global Psoriasis Score (LS-GPS) (Ellis and Langley 2002) is a method for rating psoriasis. It correlates well with the PGA ($r > 0.8$). However, the LS-GPS is better defined and appears to be more reproducible.

The LS-GPS is proprietary, and there may be fees for its use.

5 The Evaluation for Prognosis with Average PASI

Evaluation for Prognosis with Average PASI (E-PAP). (Sugai et al. 1998) is derived from PASI. The authors modified PASI for evaluating clinical symptoms throughout the observation period by adding a time parameter (the number of days) to PASI.

The E-PAP value is calculated as follows. First the mean value of PASI for two consecutive observation days is calculated. The accumulated PASI for a short term (Apn) is determined by multiplying the mean PASI by the number of days in this short term. Then, all individually calculated Apn values during the entire observation period are summed. The accumulated Apn value is divided by the total number of observation days. The final value is the E-PAP value.

6 The Salford Psoriasis Index

The Salford Psoriasis Index (SPI) (Kirby et al. 2000) is derived from combining a score of current severity of psoriasis based on the PASI, a score indicating psychosocial disability, and a score based on historical information (Ellis and Langley 2002). The resultant three-figure SPI (signs, psychosocial disability, interventions) is a paradigm similar to the TNM classification for cancer staging.

The first figure of the SPI transforms the PASI into a number from 0 to 10, with each number corresponding to a band of PASI values.

PASI	Extent Score
0	0
0.1–3	1
3.1–5	2
5.1–8	3
8.1–11	4
11.1–14	5
14.1–18	6
18.1–23	7
23.1–29	8
29.1–36	9
>36	10

The second figure indicates the psychosocial impact of psoriasis on each patient using a 0–10 visual analog scale (VAS). Patients are asked to mark on the scale (10 = completely affected, and 0 = not at all affected) the extent to which they perceive that their psoriasis is affecting their day-to-day life at the time of assessment.

The third figure reflects historical disease severity as judged by the need for systemic treatment or admission to hospital and by the number of episodes of erythroderma.

Calculation of historical disease severity scores for the Salford Psoriasis Index

1 point for each individual systemic treatment including PUVA
1 extra point for each treatment received for >1 year
1 extra point if patient has received >200 treatments or >1000 J/cm^2 of PUVA
1 point for every five hospital admissions for the treatment of psoriasis
1 point for every episode of erythroderma

7 The Dermatology Index of Disease Severity

The Dermatology Index of Disease Severity (DIDS) (Faust et al. 1997) focuses on two factors: the percentage of involved BSA and functional limitation, in forming a five-stage scale ranging from stage 0 to stage IV.

0	No evidence of clinical disease
I	Limited disease
II	Mild disease
III	Moderate disease
IV	Severe disease

References

Ashcroft DM, Li Wan Po A, Williams HC, Griffiths CEM. Clinical measures of disease severity and outcome in psoriasis: a critical appraisal of their quality. Br J Dermatol. 1999;141:185–91.

Ellis CN, Langley RGB. A randomized comparative study of variability of Psoriasis Area and Severity Index., Psoriasis Global Assessment, and Lattice System Global Psoriasis Score in subjects with psoriasis. Br J Dermatol. 2002;147:1058.

Faust H, Gonin R, Chuang T, Lewis CW, Melfi CA, Farmer ER. Reliability testing of the Dermatology Index of Disease Severity (DIDS). Arch Dermatol. 1997;133:1443–8.

Feldman SR, Fleischer AB, Reboussin DM, Rapp SR, Lyn Exum M, Clark AR, Nurre L. The self-administered psoriasis area and severity index is valid and reliable. J Invest Dermatol. 1996;106:183–6.

Fleischer Jr AB, Rapp SR, Reboussin DM, Vanarthos JC, Feldman SR. Patient measurement of psoriasis disease severity with a structured instrument. J Invest Dermatol. 1994;102:967–9.

Fredriksson T, Pettersson U. Severe psoriasis-oral therapy with a new retinoid. Dermatologica. 1978;157:238–44.

Kirby B, Fortune DG, Bhushan M, Chalmers RJG, Griffiths CEM. The Salford Psoriasis Index: an holistic measure of psoriasis severity. Br J Dermatol. 2000;142:728–32.

Long CC, Finlay AY, Averill RW. The rule of hand: 4 hand areas = 2 FTU = 1 g. Arch Dermatol. 1992;128:1129–30.

Sugai J, Ozawa A, Kawakubo Y, Iizuka M, Miyahara M, Ohkido M. New method for determining prognosis of patients with psoriasis (E-PAP). J Dermatol Sci. 1998;16:165–9.

Acne Vulgaris Scoring

138

Devinder Mohan Thappa and M. Malathi

Contents

D.M. Thappa (✉)
Department of Dermatology and STD, The Jawaharlal Institute of Postgraduate Medical Education and Research, Pondicherry, Puducherry, India
e-mail: dmthappa@gmail.com

M. Malathi
Department of Dermatology, Jawaharlal Institute of Post Graduate Medical Education and Research, Gorimedu, Puducherry, India
e-mail: mmalathi.dr@live.com

P. Humbert et al. (eds.), *Agache's Measuring the Skin*,
DOI 10.1007/978-3-319-32383-1_96

Keywords
Acne vulgaris • Acne scars • Score • Grading system • Lesion counting • Photographic scales • Ideal scoring system • Quality of life scales

1 Introduction

Research on acne vulgaris, a common dermatosis encountered by dermatologists worldwide with significant individual and societal impact, is hindered owing to the absence of a universal, consistently applied standard for acne severity. Optimal patient care in the field of dermatology which predominantly relies on the clinical evaluation of patient necessitates a validated outcome measure which objectively monitors the disease severity over time without much inter- or intraobserver variability. As far as assessing the severity of acne vulgaris is concerned, more than 25 different grading systems exist in literature till date, indicating the lack of consensus on this issue resulting in the absence of a global standard grading system (Tan et al. 2013; Ramli et al. 2012). The difficulty in assessing acne severity and the presence of multiple assessment systems could be attributed to the polymorphic nature of acne vulgaris, its varied extent of involvement, and variations occurring during the natural course of the disease (Adityan et al. 2009). This limitation is likely to have an impact on patient care by hindering the translation of results from interventional studies

and epidemiologic research to clinical practice (Tan et al. 2013).

Cutaneous diseases have a significant impact on the quality of life (QOL) which can be as complex as those from more debilitating and life-threatening diseases, and acne vulgaris has been described to cause more psychic trauma and suffering that does other cutaneous diseases. Hence QOL measures which are not reflected in measures of skin disease severity, like psychologic stress, embarrassment, stigma, physical discomfort, etc., need to be assessed while assessing disease severity (Anderson and Rajagopalan 1997; Koo 1995). In addition, both active disease and damage from burnt out disease can cause significant patient morbidity. Hence scoring systems are essential for both acne vulgaris and its sequelae – post-acne scarring.

2 Classification of Scoring Systems in Acne

The scoring systems in acne can be classified into the following six types (Ramli et al. 2012; Faure et al. 2009; Barratt et al. 2009; Witkowski and Parish 2004):

- Qualitative scales – degrees of severity: minimal, moderate, and severe
- Semiquantitative scales – numerical score: ranging from 0 to 10
- Quantitative scales – based on lesion counting
- Photographic scales
- Acne-specific quality of life scales
- Post-acne scarring scoring system

Carmen Thomas of Philadelphia was the first person who used a scoring system for acne vulgaris by using lesion counting in the 1930s (Witkowski and Parish 1999). The various scoring systems for acne vulgaris published in literature are summarized in Tables 1, 2, and 3, and the scoring systems for acne scars are summarized in Table 4. The various quality of life (QOL) scales specific for acne vulgaris which can be used to monitor change during therapy include the following (Barnes et al. 2012):

- Acne Disability Index (ADI)
- The Cardiff Acne Disability Index (CADI)
- The APSEA (Assessment of the Psychological and Social Effects of Acne) from Leeds
- The acne QOL

3 Advantages and Disadvantages of Various Acne Scoring Systems

3.1 Grading System

Grading is based on observing the dominant lesions, evaluating the presence or absence of inflammation, and estimating the extent of involvement. It is simple, reproducible, and quick to use during serial clinic visits. It estimates the full extent of involvement and also allows the clinician to observe the dominant lesions and to evaluate the presence/absence of inflammation. It has also been suggested that an overall grading system can replace spot counting but it may not be so in the setting of therapeutic trials where lesion counting, a more sensitive method, would be preferred. The subjective nature and presence of multiple variables may result in interobserver variability with the grading system. In addition, grade assessment is complicated by the presence of erythema and scaling which might be attributed to the side effects of topical treatments rather than the worsening of acne per se. Some grading techniques use photographic standards as reference scales which have their own drawbacks which will be discussed later (Adityan et al. 2009; Barratt et al. 2009; Burke and Cunliffe 1984).

3.2 Lesion Counting

Lesion counting being an objective measure and a more sensitive technique by distinguishing small effects in therapeutic response far better than an

Table 1 Grading systems based on the description of lesions

S. no	Authors	Grading				
1.	Pillsbury et al. (1956) (Ramli et al. 2012)	Grade	Description			
		1	Comedones and occasional small cysts confined to the face			
		2	Comedones with occasional pustules and small cysts confined to the face			
		3	Many comedones and small and large inflammatory papules and pustules, more extensive but confined to the face			
		4	Many comedones and deep lesions tending to coalesce and canalize and involving the face and the upper aspects of the trunk			
2.	James and Tisserand (1958) (Ramli et al. 2012; Witkowski and Parish 2004)	Grade	Description			
		1	Simple noninflammatory acne comedones and a few papules			
		2	Comedones, pustules, and a few pustules			
		3	Larger inflammatory papules, pustules, and a few cysts; a more severe form involving the face, neck, and upper portions of the trunk			
		4	More severe, with cysts becoming confluent			
3.	Pochi et al. (1991) – Report of the Consensus Conference on Acne Classification	Grade	Papules/pustules (papules – inflammatory lesions <5 mm in diameter; pustules – visible central core of purulent material)	Nodules (inflammatory lesions ≥5 mm in diameter)		
		Mild	Few to several	None		
		Moderate	Several to many	Few to several		
		Severe	Numerous and/or extensive	Many		
4.	Doshi et al. (1997) – Global acne grading system (GAGS)	The face, chest, and back divided into six areas and assigned a factor based on size				
		Each type of lesion is given a value depending on severity				
		The score for each area is the product of the most severe lesion, multiplied by the area factor				
		Total score = sum of individual scores				
		Location	Factor	Severity	Local score	Acne severity
		Forehead	2	0 Nil	Factor X Severity	Mild 1–18
		Right cheek	2	1 Comedone		Moderate 19–30
		Left cheek	2	2 Papule		Severe 31–38
		Nose	1	3 Pustule		Very severe >39
		Chin	1	4 Nodule		
		Chest and upper back	3			

(*continued*)

Table 1 (continued)

S. no	Authors	Grading	
5.	Gollnick et al. (2003)	Grade	Description
		1	Mild comedonal
		2	Mild papulopustular, moderate papulopustular
		3	Moderate nodular
		4	Severe nodular/conglobate
6.	Leyden (2003)	Grade	Description
		Mild	Comedones
		Mild to moderate	Mild to moderate papular/pustular
		Moderate to severe	Severe nodulocystic
7.	US FDA-proposed investigator global assessment (IGA) (2005)	Static quantitative evaluation of overall acne severity	
		Grade	Description
		0	Clear skin with no inflammatory or noninflammatory lesions
		1	Almost clear; rare noninflammatory lesions with no more than one small inflammatory lesion
		2	Mild severity; greater than Grade 1; some noninflammatory lesions with no more than a few inflammatory lesions (papules/pustules only, no nodular lesions)
		3	Moderate severity; greater than Grade 2; up to many noninflammatory lesions and may have some inflammatory lesions but no more than one small nodular lesion
		4	Severe; greater than Grade 3; up to many noninflammatory and inflammatory lesions but no more than a few nodular lesions
8.	Thiboutot et al. (2009)	Grade	Description
		Mild	Comedonal; mixed and papular/pustular
		Moderate	Mixed and papular/pustular; nodular (<0.5 cm)
		Severe	Nodular/conglobate
9.	Layton (2010)	Grade	Description
		Mild	Mild to moderate papulopustular acne
		Moderate	Severe papulopustular acne, moderate nodular acne
		Severe	Severe nodular acne, conglobate acne
10.	European Guidelines group (2011) (European Dermatology Forum 2013)	Grade	Description
		1	Comedonal acne
		2	Mild – moderate papulopustular acne
		3	Severe papulopustular acne, moderate nodular acne
		4	Severe nodular acne, conglobate acne

overall grade would be a preferred technique in therapeutic trials. Lesion counting quantifies the types of lesion present and gives some insight into the morphogenesis and evolution of acne lesions before and during treatment. The major limitation is that it is time-consuming and requires practice, hence may not be practical to use in routine clinical evaluation. It is also dependent on external

Table 2 Scoring systems based on lesion counting

S. no	Authors	Scoring		
1.	Witkowski and Simons (1966) (Ramli et al. 2012; Witkowski and Parish 2004)	Number of closed comedones, open comedones, papules, pustules, and nodules counted on one side of face as time-saving measure		
		Number of lesions on the left side assumed to be nearly equal to those on the right side		
		Papules and pustules divided into small and large lesions.		
		Nodules or cysts termed as abscesses		
		This concept extended with the acne flow form (accurate method of entering and retrieving information and evaluating progress) and the acne questionnaire (to determine the reasons for acne flares or failures in response)		
		This method is more accepted by patients and improves the efficiency of the result		
2.	Frank (1971) (Ramli et al. 2012; Witkowski and Parish 2004) – numerical grading system	Numerical grading of 0–4 of each type of lesion on the face, chest, and back based on severity		
		The number of lesions based on types of lesion counted		
		James and Tisserand's method of grading used to provide grading		
3.	Plewig and Kligman (1975) (Ramli et al. 2012; Witkowski and Parish 2004)	Comedonal and inflammatory acne graded separately based on the number of lesions and type		
		Right side of the face, excluding the other side, chest, and back		
		Grade	Comedonal	Papulopustular
		1	<10 comedones	<10 inflammatory lesions
		2	10–25 comedones	10–20 inflammatory lesions
		3	25–50 comedones	20–30 inflammatory lesions
		4	>50 comedones	>30 inflammatory lesions
4.	Michaelson et al. (1977)	Number of lesions on the face, chest, and back counted		
		Score given to each lesion type		
		Severity index: comedones, 0.5; papules, 1; pustules, 2; infiltrates, 3; cysts, 4		
		Total score of acne severity = sum of product of number of each type of lesion by its severity index		
		Drawback scores ascribed to lesions are nonparametric, whereas absolute counts are parametric data, and hence these two types of data cannot be mixed		
5.	Christiansen et al. (1977) (Ramli et al. 2012; Witkowski and Parish 2004)	Lesion counting done in a test area and graded with a six-point scale 4 to −1		
		The area containing the most lesions used as the test area		
		Cardboard ring having an inner diameter of 5 cm used for counting		
		Scale	Percentage of reduction	Level
		4	100 % reduction	Excellent
		3	75–99 % reduction	Good
		2	50–74 % reduction	Moderate
		1	1–49 % reduction	Insufficient
		0	–	Unchanged
		−1	–	Worse

(*continued*)

Table 2 (continued)

S. no	Authors	Scoring		
6.	Burke and Cunliffe (1984) – leeds technique	Lesions divided into inflamed and noninflamed are as follows		
		Noninflamed lesions – blackheads and whiteheads (intermediate lesions counted according to their major component)		
		Inflamed lesions – superficial (papules and pustules) or deep (nodules, cysts, and deep pustules)		
		(i) *Superficial papules and pustules* – 0.1 cm (with minimal erythema) to 0.5 cm (with a marked macular flare). Smaller less inflammatory lesions were classified as "less active papules or pustules," the larger erythematous lesions as "active papules or pustules." The lesions were assigned according to its major component		
		(ii) *Deep inflamed lesions* – predominantly nodules 0.5 cm or larger		
		(iii) *Macules* – resolving phase of either superficial or deep lesions and were either large or small		
		Used for detailed work in therapeutic trials to distinguish between active and less active acne lesions		
7.	Lucky et al. (1996)	Counted each type of acne lesions, and then recorded on a special facial template that was divided into five segments, which are the right and the left forehead, the right and left cheek, and the chin		
		Hairline- and jawline-defined perimeters of the face and the nose area were excluded		
		Grade	Description	
		Very mild	Just a few comedones	
		Mild	More comedones and few papules and pustules	
		Moderate	Many papules and pustules	
		Severe	Many papules and pustules with a few nodules	
		Very severe	Several comedones, papules, pustules, and nodules	
8.	Dreno et al. (1999) Echelle de Cotation des Lésions d'Acné (ECLA) or ""Acne Lesion Score Scale""	Semiquantitative method		
		Three factors of severity considered based on the extent of involvement and scarring		
		Involvement of the face – based on the count of comedones (scored 0–5), papulopustules (scored 0–5), and inflamed nodules/cysts (counted not scored)		
		Involvement of other areas (the neck, chest, upper and lower back, and arms) – based on acne grading (comedones and papules/pustules all taken together) as 0, none; 1, mild; 2, moderate; 3, severe and counting inflamed nodules/cysts		
		The presence or absence of scarring is noted on the entire acne area		
		Advantages: entire acne-prone area covered, good intra- and interinvestigator's reliability, less time taken, can be used in clinics		
		Limitations: prior training mandatory		
9.	Lehmann et al. (2002)	Grade	Description	
		Mild	<20 comedones, <15 inflammatory lesions, or total lesion count<30	
		Moderate	20–100 comedones, 15–50 inflammatory lesions, or total lesion count 30–125	
		Severe	>5 cysts, total comedo count>100, total inflammatory count >50, or total lesion count>125	
10.	Tan et al. (2007) Comprehensive Acne Severity Scale (CASS)	Grade		Description
		Clear	0	No lesions to barely noticeable ones. Very few scattered comedones and papules
		Almost clear	1	Hardly visible from 2.5 m away. A few scattered comedones, few small papules, and very few pustules

(*continued*)

Table 2 (continued)

S. no	Authors	Scoring		
		Mild	2	Easily recognizable; less than half of the affected area is involved. Many comedones, papules, and pustules (0–5 papules-pustules)
		Moderate	3	More than half of the affected area is involved
				Numerous comedones, papules, and pustules (6–20 papules-pustules)
		Severe	4	The entire area is involved. Covered with comedones, numerous pustules, and papules, a few nodules and cyst (21–50 papules-pustules)
		Very severe	5	Highly inflammatory acne covering the affected area, with nodules and cyst present (>50 inflammatory lesions)

variables such as assessor's visual acuity and office lighting (Adityan et al. 2009; Barratt et al. 2009; Burke and Cunliffe 1984).

3.3 Photography

The major advantages of photography include a permanent record of acne severity and reliable recording of changes with time. Fluorescence and polarized light photography have some advantages over normal color photography in estimating the number of comedones and emphasizing erythema, but their major drawback is excessive time involvement and the need for more complicated and expensive equipment. Photography is associated with technical problems requiring constant lighting, constant distance between the patient and camera, and constant developing procedures which are difficult to standardize and maintain accurately. Moreover, photographs can never detect the small inflammatory lesions and comedones adequately and may not reflect disease activity. Residual erythema, pigmentary changes, tanning, and redness from natural or artificial light exposure and excoriations are minimized especially when the patient has additional pigment. Finally, photography being two dimensional can never replace palpation, resulting in errors in distinguishing deep lesions from active superficial lesions or macules (Adityan et al. 2009; Barratt et al. 2009; Burke and Cunliffe 1984).

3.4 Quality of Life Scales

Quality of life is considered an important outcome measure of treatment which guides treatment selection by both patients and physicians. With acne being a disorder associated with significant psychosocial issues, the improvement in quality of life should be considered a major outcome measure as they assess what the patient experiences (Anderson and Rajagopalan 1997; Koo 1995). But studies (Kokandi 2010; Dreno et al. 2007b; Ilgen and Derya 2005; Aktan et al. 2000) have shown that acne severity scores failed to correlate with the QOL scales, indicating that clinical severity alone does not affect quality of life and many other factors might play a role. Hence, each patient should be treated individually, taking into consideration that mild disease does not mean little effect on the quality of life, and scoring systems should include QOL measures also to assess response to treatment. In order for quality of life measures to be used more frequently in the routine clinical work, they need to be easy to use, meaningful, and readily accessible (European Dermatology Forum 2013).

4 Precautions to Be Followed

Whatever is the method used, certain precautions need to be followed while scoring the severity of acne in a patient. These include (Burke and Cunliffe 1984):

Table 3 Scoring systems based on photographic references and newer imaging modalities

S. no	Authors	Grading	
1.	Cook et al. (1979)	Grade	
		0	Up to small scattered comedones and/or small papules are allowed
		2	Very few pustules or three dozen papules and/or comedones; lesion are hardly visible from 2.5 m away
		4	There are red lesions and inflammation to a significant degree; worth treating
		6	Loaded with comedones, numerous pustules; lesions are easily recognized at 2.5 m
		8	Conglobata-, sinus-,or cystic-type acne; covering most of the face
		Both sides of a patient's face photographed on a single exposure using a front-surface mirror	
		Five reference photographs used	
		Proposed for use in larger clinical trials	
2.	Wilson (1980)	Elaborated on the scoring system devised by Blaney and Cookin 1976 and perfected at the 1978 American Academy of Dermatology meeting by inviting about 800 dermatologists to try his method for office application	
3.	Allen and Smith (1982)	A photonumeric method – both grading using lesion counting and photographic standards	
		Grade	Description
		0	The facial skin need not be perfectly clear. A few scattered comedones or papules may be present but should be visible only on close examination
		2	One fourth of the facial area involved, with small papules (about 6–12) and comedones (a few pustules or large prominent papules may be present)
		4	Half of the facial area involved, with small papules and large or small comedones. A few pustules or large prominent papules are usually present. (If lesions are generally large, then "grade 4" severity, even if less than half of facial area involved.)
		6	Three fourths of the facial area involved, with papules and/or large open comedones. (Lesser facial area of involvement is permissible if inflammatory lesions are large.) Numerous pustules are usually present, some of which may be large
		8	Whole facial area involved, with lesions. Large prominent pustules are usually visible. Lesions are usually highly inflammatory. Other types of acne (such as conglobata, including sinus and cystic types) may be present
		Grading scale for comedones	
		Grade	Description
		0	No comedones
		2	Mild comedonal acne
		4	Obvious comedonal acne
		6	Severe comedonal acne
		8	Extremely severe comedonal acne

(*continued*)

Table 3 (continued)

S. no	Authors	Grading	
4.	Gibson et al. (1982) (Gibson et al. 1984)	1. A 0–10 visual-tactile grading system – quick but thoughtful clinical assessment, overall impression of the clinical picture, both the types of lesions present, area of the skin involved are taken into account and given a score	
		2. Lesion counting – a careful count of less active and active papules, less active and active pustules, deep pustules, nodulo-cysts, and macules	
		3. Patient self-assessment – worse, no change, fair, good, excellent	
		4. Photographs (black and white and colour slides)	
		(1) Severity of acne according to a 0–4 scale with half point ratings	
		Grade	Description
		0	No acne
		1	Minimal acne
		2	Mild acne
		3	Moderate acne
		4	Severe acne
		(2) Change in acne severity using scoring system	
		Grade	Description
		−2	Much worse
		−1	Worse
		0	No change
		1	Minimal improvement
		2	Fair improvement
		3	Good improvement
		4	Excellent improvement
		Observed good correlation between lesion counts and the severity of acne as judged by both photographic methods and clinical grading	
		Lack of correlation between the photographic assessments and clinical grading with regard to the change in acne severity	
		Concluded that well-thought-out clinical grading system is the best overall method as it provides a meaningful assessment with speed and reasonable accuracy	
5.	Burke and Cunliffe (1984) – leeds technique	Graded acne lesions on a scale of 0 (no acne whatsoever) –10 (the most severe acne) and compared the results with reference photographs	
		Subdivided 0–2 into 7 subgroups – 0.25, 0.50, 0.75, 1, 1.25, 1.5, 1.75	
		Physiological acne or "acne minor" – 0.25–1	
		Clinical acne or "acne major" – ≥1.5 (1.5–10 subdivided into 0.50 subdivisions)	
		Three sites graded – the face including the chin and neck anterior to the stern mastoid muscles; the chest in men from the waist upward, but in women only the skin between the breasts and above the bra; back in both sexes from the waist upwards. Shoulders were included for both the back and chest assessment, but the arms were excluded	
		Accurate, reproducible, rapid, and suitable for use in the routine clinic	

(*continued*)

Table 3 (continued)

S. no	Authors	Grading			
6.	Samuelson (1985)	Graded based on a set of nine reference photographs			
		Both the patient and physician assessed the severity based on the reference on a nine-grade scale			
		The face, chest, and back are included			
		Degree of change	Description		
		Excellent	There was a decrease of three or more grade numbers with reduced redness and tenderness		
		Good	There was a decrease of two grades with reduced redness and tenderness		
		Moderate	There was a decrease of one grade with reduced redness and tenderness		
		None	There was no change		
		Worse	There was an increase of one grade or more or an increase in redness or tenderness with the same grade		
7.	Lucchina et al. (1996)	Fluorescence photography – Two filters were used for fluorescence photography for UVA transmittance and elimination of infrared light			
		Severity of comedonal acne assessed based on a four-point scale			
		Excluded the chest and back			
		Grade	Scale		
		0	None		
		1	Mild		
		2	Moderate		
		3	Extensive		
8.	Phillips et al. (1997)	Polarized light photography – the polarizing filter on the camera was oriented at a right angle with respect to the linear polarizer on the ring flash			
		Counts of comedones and inflammatory acne assessed			
		Enhanced visualization of the skin features, color, and lighting and framing made comedo counts easier			
9.	O'Brien et al. (1998) – The Leeds Revised Acne Grading System	Provides a photographic standard for acne grading of the face, back, and chest – representations selected over 1,000 photographs by an expert panel of three dermatologists and four acne assessors			
		12 grades for the face and 8 grades for the upper chest and back			
		Body part	Mild	Moderate	Severe
		Face	Grade 1–grade 4	Grade 5–grade 8	Grade 9–grade 12
		Upper chest and back	Grade 1–grade 3	Grade 4–grade 5	Grade 6–grade 8
10.	Rizova and Kligman (2001)	Parallel-polarized and cross-polarized photography with video microscopy and sebum production measurement			
		Since multiple modalities are used, it cannot be used for real-time analysis			
11.	Hayashi et al. (2008)	Standard photographs and lesion counting			
		First, acne classified based on the number of inflammatory eruption of half the face			
		Second, the lesions were counted and divided into four groups			
		The judgments on severity grades were then compared with those of an expert panel of three dermatologists, who evaluated half-face photographs of the same patients			
		Total number of lesions	Group		
		6–20	Moderate		
		21–50	Severe		
		>50	Very severe		

(*continued*)

Table 3 (continued)

S. no	Authors	Grading		
12.	Do et al. (2008)	Computer-assisted alignment and tracking of acne		
		Combined digital photography with photoediting software with alignment capabilities		
		Region of interest (ROI) with the most clinically major acne lesions selected – up to seven ROIs		
		The lesions were counted in each ROI and classified either as open or as closed comedones, papules, pustules, and nodules		
		From the first appearance, numbers were assigned to each new lesion after tracking inflammatory lesions		
		Lesion growth monitored every 2 weeks for 12 weeks		
		This technique eliminated photographic inconsistencies		
		such as variability of camera angle and framing		
13.	Fuji et al. (2008)	Multispectral imaging (MSI) – 16-band multispectral camera		
		The spectral information for various types of acne skin lesions, acquired from the MSI of the lesion used		
		Combination of several linear discriminant functions (LDFs) used for acne lesion classification		
		Three Fisher LDFs and three threshold values used to consider three classes to classify acne types		
		The Fisher LDFs were calculated from both reddish papule and pustule, both pustule and scar, and both reddish papule and scar, respectively		
		The threshold values for these LDFs were determined experimentally. MSI and the LDF classifier were able to differentiate several skin lesions such as comedo, reddish papule, pustule, and scar based on color image		
14.	Bae et al. (2008)	Multimodal facial color imaging modality for objective analysis of skin lesion		
		Used a conventional color image, parallel and cross-polarization color images, and a fluorescent color image		
		Proposed fluorescent image analysis methods for the quantitative evaluation of sebum-related parameters such as pattern, area and density, average size and diameter of spots		
15.	Dreno et al. (2011) Global Evaluation Acne (GEA) scale for France and Europe	Photographic and clinical assessment		
		Grade		Description
		0	Clear. No lesions	Residual pigmentation and erythema may be seen
		1	Almost clear. Almost no lesions	A few scattered open or closed comedones and very few papules
		2	Mild	Easily recognizable. Less than half of the face is involved. A few open or closed comedones and a few papules and pustules
		3	Moderate	More than half of the face is involved. Many papules and pustules; many open or closed comedones. One nodule may be present
		4	Severe	The entire face is involved, covered with many papules and pustules, open or closed comedones, and rare nodules
		5	Very severe	Highly inflammatory acne covering the face with the presence of nodules

(*continued*)

Table 3 (continued)

S. no	Authors	Grading
		Simple and practical tool designed for everyday use in routine clinical practice as well as in clinical trials Good inter- and intraobserver reliability
		Limitation validated for a homogeneous population of polymorphous juvenile acne of the face
16.	Choi et al. (2012)	3D image analysis system
		Skin surface roughness and volume of acnes protruding on the skin surface analyzed quantitatively
		Volume of acne lesions may provide more reliable criteria for the topographic classification of acne lesions because acne lesions usually have irregular shapes, and hence their diameter in any specific direction may not represent their size correctly
		3D image analysis system may supplement the counting or grading system of acne lesions
		Provides novel opportunities to address topographical changes of the skin from the cosmetic point of view
		Clinically less relevant than acne scoring based on pathological severity – could underestimate severe nodular and cystic acne if they show minimal protrusion above the level of the surrounding skin
		Requires additional methods including visual assessment, spectrophotometric determination and pathological examination

- The patient should be seated comfortably so that the observer can move around him easily to count each area.
- In addition to good background fluorescent lighting, Brighton l001 fluorescent lamp, which can be easily moved to illuminate both sides of the patient during the examination, is recommended.
- In the entire acne-prone area including the face, chest, back and in each site, the total area needs to be examined. When counting, the face should be divided into the right and left sides, and both sides need to be counted. In some patients, the lesions are clustered around the midline, making a right-left division difficult; in such cases, the forehead, the cheeks, and the chin should be counted separately and finally combined.
- Cosmetics should be removed at least 30 min prior to assessment as erythema due to washing needs to settle.
- Palpation (without stretching the skin) is mandatory in counting methods to enable detection of all comedones and nodules. Though stretching of the skin and use of magnifying lens would increase the number of visible whiteheads and blackheads, they are not permitted as the degree of stretching might vary.
- If a lesion is impalpable and not obvious with good lighting, then such a vague lesion should be best ignored.
- In clinical trials, baseline scoring is essential which should be after at least 3 months of washout period of the previous treatment.
- Trials should not be conducted in summer to avoid the anti-inflammatory effect of sun rays as ultraviolet radiation will camouflage the noninflamed lesions and make the inflamed lesions look less inflamed.
- All scales require a minimum observer training especially for counting methods as the secret of lesion counting is practice.
- Prior to clinical trials, the assessor's reliability needs to be checked – the novice assessor should select 30 patients and in groups of 10 should count the lesions (under standard conditions) on 1 day and then 24 h later. The more spot counting performed, the more spots will be seen until a plateau is reached. When this plateau is achieved, then comparison of

data collected on two consecutive days should give a correlation with a minimum value of 0.80. Only at this stage the physician will be considered ready to count spots in a clinical trial.
- Acne scores or grades are distributed on ordinal scale, and absolute counts are distributed on an interval scale, and these interval scales would be better for statistical analysis.

5 Problems Encountered

- Prominent follicles are likely to be confused with noninflamed lesions especially around the nose and on the chin, especially in mid-teenagers. Hence, in therapeutic trials, it is recommended that noninflamed lesions are not counted either on the nose or around the edge of the nose.
- Sandpaper acne covering the forehead (usually $\geq$100) are very superficial lesions, which are impossible to be classified correctly, and such patients should be excluded from clinical trials.
- Long, uncut hair may mask noninflamed lesions, and hence counting around the hairline should be avoided. However, there is usually no difficulty in recognizing inflamed lesions in this area.
- Growing mustache or beard during the trial would complicate the results, and these patients may develop low-grade folliculitis on the chin and neck as a result of shaving trauma. However, the papules and pustules associated with a folliculitis are much less easily felt than acne lesions. Patients should shave daily, preferably at a constant time, as stubble can affect the interpretation of all lesions.
- Other dermatoses like sycosis barbae which may occur in association with acne and low-grade seborrhoeic eczema may simulate a primary irritant dermatitis which can be seen commonly with treatments with benzoyl peroxide (Burke and Cunliffe 1984).

6 Ideal Scoring System

The essential components and features for ideal acne global grading scale (AGGS) have been currently established by consensus from clinical and investigative experts in acne by an online Delphi process (Tan et al. 2013, 2012). These include four clinical components and four features as follows:

6.1 Clinical Components

- Primary lesions (no inflammatory and inflammatory, evaluated separately)
- Quantity of lesions (evaluated through counting and numerical range)
- Extrafacial sites of involvement (specifically the chest, back, neck, and shoulders)
- Extent of involvement (evaluated using proportion descriptors such as one third or less)

6.2 Features

- Clinimetric properties (validity, reproducibility, discriminatory capacity, and responsivity)
- Efficiency (easy for clinicians, researchers, and nursing staff to use and easy to teach)
- Acceptability (by researchers, clinicians, and regulators)
- Categorization of severity (through descriptive text and/or photographic examples)

7 Future Prospects

Novel emerging techniques like computerized morphometric analysis of acne lesions and spectrophotometric dermoscopy to determine disruption of the dermal-epidermal junction and assess quantities of melanin, collagen, and blood within specific layers of skin to assess acne lesions may also help in assessing acne severity (Barratt et al. 2009).

Table 4 Scoring system for acne scars

S. no	Authors	Grading			
1.	Friedman et al. (2002)	Optical three-dimensional in vivo skin measurement device – grading device that focus on 3-dimensional grid-based mapping of lesions and molded skin replicas for comparison examination			
		Demonstrated a substantial correlation between subjective clinical assessment and objective 3D in vivo imaging			
		Not applicable in practical, daily use by the average physician			
2.	Dreno et al. (2006) (Dreno et al. 2007a) – ECCA grading scale (échelled'évaluation clinique des cicatrices d'acné)	Built on the model of the ECLA grading scale for acne. It is composed of six types of scar described and associated with a quantitative score (ranging from 0 to 4) and a weighting factor (ranging from 15 to 50)			
		This weighting factor is based on clinical approach and is based on the severity, the evolution, and the morphological aspect of the scars and hence is directly correlated with the clinical severity			
		Number of scars – semiquantitative estimation by a 4-point scale:			
		0 = no scar, 1 = a few scars (<5), 2 = limited number of scars (between 5 and 20), 3 = many scars (>20)			
		Grading of the different kinds of scars = product of the semiquantitative score and the weighting factor			
		V-shaped atrophic scars (weighting factor 15): diameter of <2 mm and punctiform;			
		U-shaped atrophic scars (weighting factor 20): diameter of 2–4 mm with sheer edges;			
		M-shaped atrophic scars (weighting factor 25): diameter of>4 mm, superficial and with irregular surface;			
		Superficial elastolysis (weighting factor 30);			
		Hypertrophic inflammatory scars (weighting factor 40): <2 years of age;			
		Keloid scars (weighting factor 50): hypertrophic scars,>2 years of age			
		Subgrading 1 – grading of the first 4 items			
		Subgrading 2 – grading of the last 2 items			
		Global score = subgradings 1 + 2 – varies between 0 and 540			
		Good interinvestigator reliability			
3.	Goodman and Baron (2006a, b)	Quantitative grading system: based on counting of scar type and severity (Goodman and Baron 2006a)			
		Reasonably accurate and reproducible with good interinvestigator reliability			
		(Grade) type	Number of lesions:	Number of lesions:	Number of lesions:
			1 (1–10)	2 (11–20)	3 (>20)
		Milder scarring (1 point each)	1 point	2 points	3 points
		Macular erythematous or pigmented			
		Mildly atrophic dish-like			
		Moderate scarring (2 points each)	2 points	4 points	6 points
		Moderately atrophic dish-like			

(*continued*)

Table 4 (continued)

S. no	Authors	Grading			
		Punched out with shallow bases small scars (<5 mm)			
		Shallow but broad atrophic areas			
		Severe scarring (3 points each)	3 points	6 points	9 points
		Punched out with deep but normal bases, small scars (<5 mm)			
		Punched out with deep abnormal bases, small scars (<5 mm)			
		Linear or troughed dermal scarring			
		Deep, broad atrophic areas			
		Hyperplastic papular scars	2 points	4 points	6 points
		Hyperplastic	Area <5 cm^2 6 points	Area 5–20 cm^2 12 points	Area >20 cm^2 18 points
		Qualitative grading system – simpler for quick, daily use (Goodman and Baron 2006b)			
		Grade	Level of disease	Characteristics	Examples of scars
		1	Macular	Erythematous, hyper- or hypopigmented flat marks visible to patient or observer irrespective of distance	Erythematous, hyper- or hypopigmented flat marks
		2	Mild	Mild atrophy or hypertrophy that may not be obvious at distances of ≥50 cm and may be covered adequately by makeup or the normal shadow of shaved beard hair in males or normal body hair if extra facial	Mild rolling, small soft papular

(*continued*)

Table 4 (continued)

S. no	Authors	Grading				
3.	Goodman and Baron (2006a, b)	3	Moderate	Moderate atrophic or hypertrophic scarring that is obvious at ≥50 cm and is not covered easily by makeup or the normal shadow of shaved beard hair in males or body hair if extra facial, but is still able to be flattened by manual stretching of the skin	More significant rolling, shallow "boxcar," mild to moderate hypertrophic or papular scars	
		4	Severe	Severe atrophic or hypertrophic scarring that is obvious at ≥50 cm and is not covered easily by makeup or the normal shadow of shaved beard hair in males or body hair (if extrafacial) and is not able to be flattened by manual stretching of the skin	Punched out atrophic (deep "boxcar"), "ice pick," bridges and tunnels, gross atrophy, dystrophic scars significant hypertrophy or keloid	
		Global acne scarring classification by area of involvement and major scar type (Goodman and Baron 2006b)				
		Grade	Description	Subgroup	A, focal, 1 cosmetic unit	B, discrete, 2–3 cosmetic units
		1	Macular	Erythematous	1A	1B
				Hyperpigmented		
				Hypopigmented		
		2	Mild	Atrophic	2A	2B
				Hypertrophic		
		3	Moderate	Atrophic	3A	3B
				Hypertrophic		
		4	Severe	Atrophic	4A	4B
				Hypertrophic		
4.	Chapas et al. (2008)	3D optical profilometry				
		Valid and reliable method for assessing improvement in acne scarring				
		Highly operator-dependent and may produce a variety of artifacts				
5.	Tan et al. (2010)-SCAR-S (2010)	Six-category global severity scale				
		For assessment of acne scarring at each of the face, chest, and back				
		Practical, validated, global system for acne scar evaluation				
		Clinically relevant in overall severity grading of acne				

Similarly, various methods and techniques developed for skin analysis can also be used as potential computational methods for acne grade assessment quantitatively. These include the following (Ramli et al. 2012):

- Xu et al. (1999) – automatic method for the segmentation of images of skin lesions
- Schmid-Saugeon et al. (2003) – computer-aided diagnosis system for skin lesion boundary detection and quantification of diagnostic features, the classification into different types of lesions, the visualization, etc.
- Masood et al. (2008) – unsupervised color segmentation procedure for skin lesion classification

Skin detection refers to a common preprocessing step for analyzing images or videos of humans aiming to track the human body for further recognition which includes face detection and recognition, image content classification, etc., and these include the following (Ramli et al. 2012):

- Skin color thresholding
- Neural network classifier
- Maximum entropy classifier
- Bayes classifier

The descriptions of these techniques are beyond the scope of this chapter. Readers may assess those papers to find the details.

8 Conclusion

A validated standard acne scoring system is essential to maintain objectivity in observations while evaluating the severity of acne, to monitor the response to therapy, and to evaluate the efficacy of new drugs. No universal standard exists for grading acne severity till date. In the absence of such a score, new therapies cannot be systematically assessed, and clinical trials conducted without such standardized outcome measures produce less reliable results. Essential clinical components and features for an ideal scale have been identified, and the current acne global scales can serve as foundations upon which an ideal standard can be developed.

References

Adityan B, Kumari R, Thappa DM. Scoring systems in acne vulgaris. Indian J Dermatol Venereol Leprol. 2009;75(3):323–6.

Aktan S, Ozmen E, Sanli B. Anxiety, depression, and nature of acne vulgaris in adolescents. Int J Dermatol. 2000;39(5):354–7.

Allen BS, Smith Jr JG. Various parameters for grading acne vulgaris. Arch Dermatol. 1982;118(1):23–5.

Anderson RT, Rajagopalan R. Development and validation of a quality of life instrument for cutaneous diseases. J Am Acad Dermatol. 1997;37(1):41–50.

Bae Y, Nelson JS, Jung B. Multimodal facial color imaging modality for objective analysis of skin lesions. J Biomed Opt. 2008;13(6):064007.

Barnes LE, Levender MM, Fleischer Jr AB, Feldman SR. Quality of life measures for acne patients. Dermatol Clin. 2012;30(2):293–300.

Barratt H, Hamilton F, Car J, Lyons C, Layton A, Majeed A. Outcome measures in acne vulgaris: systematic review. Br J Dermatol. 2009;160(1):132–6.

Burke BM, Cunliffe WJ. The assessment of acne vulgaris – the Leeds technique. Br J Dermatol. 1984;111(1):83–92.

Chapas AM, Brightman L, Sukal S, Hale E, Daniel D, Bernstein LJ, et al. Successful treatment of acneiform scarring with CO2 ablative fractional resurfacing. Lasers Surg Med. 2008;40(6):381–6.

Choi KM, Kim SJ, Baek JH, Kang SJ, Boo YC, Koh JS. Cosmetic efficacy evaluation of an anti-acne cream using the 3D image analysis system. Skin Res Technol. 2012;18(2):192–8.

Cook CH, Centner RL, Michaels SE. An acne grading method using photographic standards. Arch Dermatol. 1979;115(5):571–5.

Do TT, Zarkhin S, Orringer JS, Nemeth S, Hamilton T, Sachs D, et al. Computer-assisted alignment and tracking of acne lesions indicate that most inflammatory lesions arise from comedones and de novo. J Am Acad Dermatol. 2008;58(4):603–8.

Doshi A, Zaheer A, Stiller MJ. A comparison of current acne grading systems and proposal of a novel system. Int J Dermatol. 1997;36:416–8.

Dreno B, Bodokh I, Chivot M, Daniel F, Humbert P, Poli F, et al. ECLA grading: a system of acne classification for

every day dermatological practice. Ann Dermatol Venereol. 1999;126(2):136–41.
Dreno B, Khammari A, Orain N, Noray C, Mérial-Kieny C, Méry S, et al. ECCA grading scale: an original validated acne scar grading scale for clinical practice in dermatology. Dermatology. 2007a;214(1):46–51.
Dreno B, Alirezai M, Auffret N, Beylot C, Chivot M, Daniel F, et al. Clinical and psychological correlation in acne: use of the ECLA and CADI scales. Ann Dermatol Venereol. 2007b;134(5 Pt 1):451–5.
Dréno B, Poli F, Pawin H, Beylot C, Faure M, Chivot M, et al. Development and evaluation of a Global Acne Severity Scale (GEA Scale) suitable for France and Europe. J Eur Acad Dermatol Venereol. 2011;25(1):43–8.
European Dermatology Forum. Guideline on the Treatment of Acne. Available from http://www.isplad.org/data/efeaba2c91d7a63c211a093f3012a888.pdf. Last accessed on 30 Oct 2013.
Faure M, Pawin H, Poli F, Revuz J, Beylot C, Chivot M, et al. Factors influencing the clinical evaluation of facial acne. Acta Derm Venereol. 2009;89(4):369–71.
Friedman PM, Skover GR, Payonk G, Geronemus RG. Quantitative evaluation of nonablative laser technology. Semin Cutan Med Surg. 2002;21(4):266–73.
Fujii H, Yanagisawa T, Mitsui M, Murakami Y, Yamaguchi M, Ohyama N, et al. Extraction of acne lesion in acne patients from multispectral images. Conf Proc IEEE Eng Med Biol Soc. 2008;2008:4078–81.
Gibson JR, Harvey SG, Barth J, Darley CR, Reshad H, Burke CA. Assessing inflammatory acne vulgaris-correlation between clinical and photographic methods. Br J Dermatol. 1984;111 Suppl 27:168–70.
Gollnick H, Cunliffe W, Berson D, Dreno B, Finlay A, Leyden JJ, et al. Management of acne: a report from a Global Alliance to Improve Outcomes in Acne. J Am Acad Dermatol. 2003;49 Suppl 1:S1–37.
Goodman GJ, Baron JA. Postacne scarring-a quantitative global scarring grading system. J Cosmet Dermatol. 2006a;5(1):48–52.
Goodman GJ, Baron JA. Postacne scarring: a qualitative global scarring grading system. Dermatol Surg. 2006b;32(12):1458–66.
Hayashi N, Akamatsu H, Kawashima M. Establishment of grading criteria for acne severity. J Dermatol. 2008;35(5):255–60.
Ilgen E, Derya A. There is no correlation between acne severity and AQOLS/DLQI scores. J Dermatol. 2005;32(9):705–10.
Kokandi A. Evaluation of acne quality of life and clinical severity in acne female adults. Dermatol Res Pract. 2010;2010:1–3.
Koo J. The psychosocial impact of acne: patients' perceptions. J Am Acad Dermatol. 1995;32(5 Pt 3):S26–30.
Layton AM. Disorders of the sebaceous glands. In: Burns T, Breathnach S, Cosx N, Griffiths C, editors. Rook's textbook of dermatology. 8th ed. Oxford: Wiley-Blackwell; 2010. p. 42.1–88.
Lehmann HP, Robinson KA, Andrews JS, Holloway V, Goodman SN. Acne therapy: a methodologic review. J Am Acad Dermatol. 2002;47(2):231–40.
Leyden JJ. A review of the use of combination therapies for the treatment of acne vulgaris. J Am Acad Dermatol. 2003;49 Suppl 3:S200–10.
Lucchina LC, Kollias N, Gillies R, Phillips SB, Muccini JA, Stiller MJ, et al. Fluorescence photography in the evaluation of acne. J Am Acad Dermatol. 1996;35(1):58–63.
Lucky AW, Barber BL, Girman CJ, Williams J, Ratterman J, Waldstreicher J. A multirater validation study to assess the reliability of acne lesion counting. J Am Acad Dermatol. 1996;35(4):559–65.
Masood NA, Mashali HM, Mohamed AS. Color segmentation for skin lesions classification. Cairo International Biomedical Engineering Conference, Cairo, Egypt, 2008:1–4.
Michaelson G, Juhlin L, Vahlquist A. Oral zinc sulphate therapy for acne vulgaris. Acta Derm Venereol. 1977;57(4):372.
O'brien SC, Lewis JB, Cunliffe WJ. The Leeds revised acne grading system. J Dermatol Treat. 1998;9(4):215–20.
Phillips SB, Kollias N, Gillies R, Muccini JA, Drake LA. Polarized light photography enhances visualization of inflammatory lesions of acne vulgaris. J Am Acad Dermatol. 1997;37(6):948–52.
Pochi PE, Shalita AR, Strauss JS, Webster SB, Cunliffe WJ, Katz HI, et al. Report of the consensus conference on acne classification. Washington, D.C., March 24 and 25, 1990. J Am Acad Dermatol. 1991;24(3):495–500.
Ramli R, Malik AS, Hani AF, Jamil A. Acne analysis, grading and computational assessment methods: an overview. Skin Res Technol. 2012;18(1):1–14.
Rizova E, Kligman A. New photographic techniques for clinical evaluation of acne. J Eur Acad Dermatol Venereol. 2001;15 Suppl 3:13–8.
Samuelson JS. An accurate photographic method for grading acne: initial use in a double-blind clinical comparison of minocycline and tetracycline. J Am Acad Dermatol. 1985;12:461–7.
Schmid-Saugeon P, Guillod J, Thiran JP. Towards a computer-aided diagnosis system for pigmented skin lesions. Comput Med Imaging Graph 2003;27:65–78.
Tan JK, Tang J, Fung K, Gupta AK, Thomas DR, Sapra S, et al. Development and validation of a comprehensive acne severity scale. J Cutan Med Surg. 2007;11(6):211–6.
Tan JK, Tang J, Fung K, Gupta AK, Richard Thomas D, Sapra S, et al. Development and validation of a Scale for Acne Scar Severity (SCAR-S) of the face and trunk. J Cutan Med Surg. 2010;14(4):156–60.
Tan J, Wolfe B, Weiss J, Stein-Gold L, Bikowski J, Del Rosso J, et al. Acne severity grading: determining essential clinical components and features using a

Delphi consensus. J Am Acad Dermatol. 2012;67(2): 187–93.

Tan JK, Jones E, Allen E, Pripotnev S, Raza A, Wolfe B. Evaluation of essential clinical components and features of current acne global grading scales. J Am Acad Dermatol. 2013;69(5):754–61.

Thiboutot D, Gollnick H, Bettoli V, Dréno B, Kang S, Leyden JJ, et al. New insights into the management of acne: an update from the Global Alliance to Improve Outcomes in Acne group. J Am Acad Dermatol. 2009;60 Suppl 5:S1–50.

U.S.Department of Health and Human Services Food and Drug Administration Center for Drug Evaluation and Research (CDER). Guidance for Industry. Acne vulgaris: developing drugs for treatment (2005). Available from http://www.fda.gov/downloads/Drugs/GuidanceComplianceRegulatoryInformation/Guidances/UCM071292.pdf.Last. Accessed on 30 Oct 2013.

Wilson RG. Office application of a new acne grading system. Cutis. 1980;25(1):62–4.

Witkowski JA, Parish LC. From other ghosts of the past: acne lesion counting. J Am Acad Dermatol. 1999;40(1):131.

Witkowski JA, Parish LC. The assessment of acne: an evaluation of grading and lesion counting in the measurement of acne. Clin Dermatol. 2004;22(5):394–7.

Xu L, Jackowski M, Goshtasby A, Roseman D, Bines S, Yu C, Dhawan A, Huntley A. Segmentation of skin cancer images. Image Vis Comput 1999;17:65–74.

Photography in Acne: Skin Metrics

139

Audris Chiang, Farhaan Hafeez, and Howard I. Maibach

Contents

Keywords
Skin • Photo • Acne • Severity • Grading • Standards

1 Introduction

Optimal treatment of acne vulgaris depends on the accurate severity assessment (Rizova and Kligman 2001). Due to the polymorphic nature and varied involvement of acne, a simple evaluation is not easy (Adityan et al. 2009). Assessment has relied on text descriptions, lesion counting, and photographic methods. Clinical trials require valid and consistent measures, but with no universal method, trials rely on subjective assessments that complicate intertrial comparison (Barratt et al. 2009). An ideal grading system would be accurate and reproducible. Ease of use as well as time and monetary cost should also be considered. Photography approaches such a system and has a place in the measurement of acne severity (Tables 1 and 2).

2 Results

2.1 Photographic Standards

Photography has various uses in evaluating acne, from having a photographic standard for categorizing acne severity to using a patient's photographs to visualize their acne condition.

A. Chiang (✉)
UC Irvine School of Medicine, Berkeley, CA, USA

Department of Dermatology, University of California, San Francisco, CA, USA
e-mail: audrisc@uci.edu

F. Hafeez
Department of Dermatology, University of California, San Francisco, San Francisco, CA, USA
e-mail: farhaanhafeez@gmail.com; farhaan.hafeez@yale.edu

H.I. Maibach
Department of Dermatology, School of Medicine, University of California, San Francisco, CA, USA
e-mail: maibachh@derm.ucsf.edu

P. Humbert et al. (eds.), *Agache's Measuring the Skin*,
DOI 10.1007/978-3-319-32383-1_98

Cook et al. (1979) proposed an innovative and useful acne grading method: the first photographic standard. Lesion counting is not as simple a method as it sounds since size and redness of lesions are not considered and variance can be great. Even if lesion types are individually counted, classification still requires subjective judgment. To develop a user-friendly, precise, intergrader consistent grading system capable of documentation for retrospective verification, Cook proposed an overall acne severity scale of 0–8 with reference photos and text descriptions illustrating grades 0, 2, 4, 6, and 8. Both sides of the face were photographed on a single exposure by positioning the face parallel to a front-surface mirror. A 35-mm single-lens reflex camera fitted with lens of 85–105-mm focal length is placed 45° from the mirror. A strobe flashlight source above the camera provided sufficient depth of field to bring into focus both real and reflected images. A set of five reference photos that elicited the most consistent 2-4-6 response was selected from numerous patient photographs by trained graders and panelists.

This grading scheme was used by two judges in a trial involving treatment groups, each composed of 20 subjects: (1) placebo capsules and topical placebo, (2) oral tetracycline and topical placebo, and (3) topical tetracycline and placebo capsules. The greatest correlation between the judges was for overall severity grades for 1 week prior to treatment and after 8 weeks of treatment with coefficients 0.785 and 0.891, respectively. A similar earlier trial (Blaney and Cook 1976) was conducted with 75 subjects divided into groups: (1) topical active mixture and oral lactose capsules, (2) topical placebo and oral lactose capsules, and (3) topical placebo and oral tetracycline hydrochloride capsules. Three sets of five reference photos each were used to grade subjects. In addition, both sides of the face were photographed at each visit with the camera mirror setup described above. Other trials confirmed that grading overall severity provided a measurement of efficacy consistent between graders and more sensitive to differences between treatments than lesion counts. However, for studies on experimental drugs, affected lesions types should be defined and counted for precise results. For example, tetracycline has a greater effect on inflammatory lesions than comedonal acne. After initial efficacy trials, overall severity grading may be used for large-scale trials to save time. Cook concluded that photographic standards were useful and reliable, aiding consistency between sessions and graders. In addition, photographic documentation creates a regradable record for verification. Results showed that a 1.5 grade change constituted a clinically important difference. Since images are less powerful than on-site impressions, 1 grade change for photos was determined to be an important difference.

Through the years, Cook's photographic standard has been utilized and expanded on.

In 1980, Wilson (1980) commented on Cook's method revised at the 1978 American Academy of Dermatology meeting with a new set of chosen reference. Recording objective descriptions for later evaluation is often difficult, especially for acne with various lesion types. Patients improve more rapidly in certain areas than others, and if not observed for weeks, opinions on improvement may differ between physician and patient. Wilson found that while applying the system in clinic, grading agreed closely with the patient's opinion. In conclusion, Wilson praised Cook's method as a quick and accurate acne grading system in practice.

In 1985, Samuelson (1985) elaborated on Cook with a 9-grade scale of nine reference photos and descriptions. This scale was used to evaluate 62 patients in a 12-week study with half receiving minocycline and the other half tetracycline. Every 2 weeks, both the patient and on-site investigator evaluated patient condition, and patient photos were taken. Two reviewers retrospectively graded the photos twice: group 1 slides were completely randomized and group 2 slides were randomized for each patient. At baseline, the investigator and patients assigned comparable grades, but reviewers assigned grades averaging 1–2 units lower. By week 12, all grades agreed

Table 1 Photographic standards for grading acne severity

Author Reference	Method	Comment	References for trials testing methods
Cook et al. (1979)	Plain concave mirror (both sides of patient's face photographed on a single exposure)	Provided strong objective data, placebo versus active, permanent and regradable record, and documentation for verification	(Blaney and Cook 1976; Wilson 1980; Allen and Smith 1982; Leyden et al. 2005)
	Photonumeric 0–8 grading scale, standards given for grades 0, 2, 4, 6, 8	Standards aid consistency from session to session and from grader to grader	
		Allowed detection of 1-unit grade change	
		Cook's scale and lesion counting are at least equally reproducible grading methods	
Samuelson (1985)	Facial acne 1–9 grading scale with nine photographs and descriptions	Reasonable agreement within one grade unit between investigator, patients, and two independent retrospective reviewers	
	Color transparency of three-quarters left profile against surface mirror obtained	Disagreement seen for lower ratings by retrospective reviewers in early stages of study and agreement was best after 12 weeks of therapy	
	Strobe light adjusted to permit equal lighting of the reflected and opposite sides of the patient's face		
Burke and Cunliffe (1984)	Leeds technique: overall assessment of acne severity in area grade 0–10 scale. Graded sites include the face, back, and chest	Useful for routine clinical assessment	(Gibson et al. 1984; Bergman et al. 2009)
	Example black and white photographs of one side of face given for facial grades 0.5, 0.75, 1.0, 1.5, 2.0, 3.0, 5.0, and 8.0	Intradoctor correlation was good, especially for the face and back	
		Interdoctor correlation was numerically lower but still good, indicating importance of having the same rater evaluate a patient throughout a study or treatment	
		Meaningful assessment with speed and accuracy	
O'Brien et al. (1998)	Leeds revised: color photographs include a wide range of acne severity	Pictures easily demonstrate impact of inflamed lesions	(Tan et al. 2012a)
	Reference photographs for each grade in facial grades severity 1–12, back grades 1–8, and chest grades 1–8. Note for facial photographs that only right side is shown, and chest photographs are only of male subjects	Scale not suited to score noninflamed lesions, although photographs for a grading system 1–3 for noninflamed acne is introduced	
	Lighting necessary when assessing acne, especially with noninflamed lesions	Grading system is not all encompassing, for example for patients with disproportionately localized acne and sporadic and asymmetrical large nodular lesions	

(*continued*)

Table 1 (continued)

Author Reference	Method	Comment	References for trials testing methods
		Photographic grading cannot compensate for palpation to assess depth, but this pictorial assessment is still useful for standardization	
		Photographs inadequately represent milder acne grades; still a need for images that correspond to a categorical acne scale for the face, back, and chest	
Hayashi et al. (2008a)	Four rankings: mild, moderate, severe, and very severe. Photographs for half of the face taken at 70° angle from front	Standard photographs make adjustments for difference of judgments between estimators, increasing inter-rater conformity and precision	(Hayashi et al. 2008b)
	Nomination of standard photographs selected matched the counting-based classifications		
	Divisions of number inflammatory eruptions included in classifications for counting conversion to global estimation		

closely. Due to the difference in baseline grades, improvement was greater according to the investigator and patients. Investigator and reviewer grades were substantially different between groups 1 and 2, possibly since reviewers could not retain visual impressions. However, according to Samuelson, complete randomization for group 1 was an unreasonable test anyway. Samuelson concluded that the scale is a useful research tool, and disagreement between reviewers and investigator was caused by investigators having a 3D view, whereas reviewers had a flat perspective.

In 1984, Burke and Cunliffe (1984) presented the Leeds technique that included a clinical scale of 0–10 for the overall assessment of acne severity in particular areas: face, back, and chest. Grading between 0 and 2 was divided into 0.25 increments. Reference black and white facial photos were given for grades 0.5, 0.75, 1.0, 1.5, 2.0, 3.0, 5.0, and 8.0. However, the authors noted that black and white photos do not accurately reflect clinical assessment. Intra- and interdoctor comparisons were made for two physicians assessing patients with Pearson's coefficient correlation. Intradoctor was good with r-values for each of the doctors: face 0.92 and 0.94, back 0.89 and 0.89, and chest 0.81 and 0.94. Correlations between doctors were lower but still good with r-values: face 0.89, back 0.87, and chest 0.80. Three drawbacks of photography were mentioned: First, difficulty in maintaining constant lighting, distance to camera, and developing procedures; second, difficulty in detecting small noninflamed lesions; and third, because photos are 2D, difficulty in distinguishing deep lesions from active superficial lesions or macules. Grading is also complicated by erythema and scaling. The authors suggest that although Leeds is quick, reproducible, and suitable for clinical use, an overall grading system still cannot replace the counting technique that better distinguishes small differences, especially for trials. When patients have noninflamed and few inflamed lesions, inter- and intradoctor correlation is poor, and counting is a better assessment choice. However, Leeds is useful in clinic as it requires less practice, and if individual grading is consistent, interdoctor differences are of little concern.

In 1998, Cunliffe et al. (O'Brien et al. 1998) Leeds revised to include reference photos for each grade of facial 1–12, back 1–8, and chest 1–8. Standards were selected from 1,000 photographs

Table 2 Advanced methods for acne assessment

Author	Method	Comment	References
Lucchina et al.	Fluorescence photography	Fluorescence corresponds to protoporphyrin IX production by Propionibacterium acnes in open comedones, follicles, and inflammatory lesions	(Lucchina et al. 1996; Pagnoni et al. 1999)
Pagnoni et al.		Not sensitive enough to detect modest changes but is reliable when variation is clinically relevant	
		Culture still necessary when modest changes in P. acnes cannot be detected with fluorescence	
		Reliable, quick, and easy way to estimate suppressive effects of antibacterial agents on P. acnes	
Phillips et al.	Perpendicular (cross)-polarized and parallel-polarized light photography	Perpendicular-polarized photography enhances subsurface features to better visualize subtle features of acne that are often missed with clinical evaluation alone, such as small comedones, hyperpigmentation, and erythema, which is important for distinguishing inflammatory from noninflammatory lesions	(Rizova and Kligman 2001; Phillips et al. 1997)
Rizova and Kligman		Parallel-polarized photography enhances visualization of surface features such as greasiness, scaling, and degree of lesion elevation	
		Mean Leeds score from perpendicular photographs higher than scores from clinical assessments and flash photographs, indicating increased sensitivity for more accurate severity assessment	
Do et al.	Picture Window Pro 4.0 program	Used to align and track lesions, monitoring development of open/closed comedones, erythematous macules, papules, pustules, and nodules over time	(Do et al. 2008)
		The technology tracks effects of acne medication on lifespan of lesions and characterize natural history of acne	
Choi et al.	PRIMOS Compact	Skin surface measurements before and after treatment gave quantitative analysis of skin roughness and lesion volume	(Choi et al. 2012)
	3D image analysis system		
		While acne is usually classified by diameter, authors argue that lesions are often irregularly shaped. Thus, volume provides more reliable criteria for classification	
		Disadvantage: severity can be underestimated if lesions only have minimal protrusion	
Fuji et al.	Extraction method for lesion classification	Since inferior color reproduction provided by RGB cameras causes visual differentiation of lesion types to be difficult, in this computer-aided diagnosis system, detailed spectral features are acquired by multispectral images (MSIs) and lesion types such as papule, pustule, and scar are classified by applying a combination of linear discriminant functions (LDFs)	(Fuji et al. 2008)
Bae et al.	Multimodal imaging modality and objective image analysis methods	Independent modalities standard, parallel- and cross-polarized, and fluorescent photographs integrated into one modality to maximize clinical utility	(Bae et al. 2008)

(*continued*)

Table 2 (continued)

Author	Method	Comment	References
		Each image emphasizes different morphological and functional skin information, to more reliably evaluate severity	
		Polarized images used to analyze skin texture and compute erythema index and melanin index to evaluate vascular and pigmented lesions, respectively	
		Fluorescent images used to quantitatively evaluate sebum characteristics such as pattern, area and density, and average size and diameter of spots	

by the three authors and four assessors. Severity grading was based on inflammation, size of lesions, and erythema. Although the system is not for scoring noninflamed lesions, a 1–3 photographic scale for noninflamed acne was introduced. Other conditions such as irritant dermatitis or retinoid-induced dermatitis may complicate grading. Lighting is also important so as to not undergrade, especially noninflamed lesions. Photographic grading more easily demonstrates the impact of inflamed lesions but cannot easily assess lesion depth. However, the authors believe that the system's attempt at quantitative assessment of acne is useful in clinic and recommend that it complement counting.

In 2008, Hayashi et al. (2008a) established a photographic standard that matched lesion counts and text descriptions with the following categories: mild, moderate, severe, and very severe. Three dermatologists graded 390 half-face photographs. Complete accordance amongst grades was observed for 176 faces (45.1 %). Two hundred sixty-eight faces (68.7 %) had identical classifications by at least two dermatologists. One thousand one hundred seventy photographic evaluations were also compared: 770 decisions (65.8 %) showed conformity, and 1,165 decisions (99.6 %) were within one grade difference. After the comparison of counting lesion types and classification, counting was limited to inflammatory eruptions, papules, and pustules. Distribution of counts was analyzed and divisions were decided: 0–5 mild, 6–20 moderate, 21–50 severe, and 50 plus for very severe on half of the face. Standard photos that satisfied lesion counting-based classifications were selected and were believed to make classification more precise and adjust for differences between graders. Hayashi et al. (2008b) evaluated the validity of this method by calculating conformity for before and after grades. Eighty-seven members at the 104th meeting of the Japanese Dermatological Association and 82 members at the 11th Hunchun Symposium in Seoul were asked to participate, first grading six patient photos. After presenting the severity classification and reference photographs, the same six photos were presented in different orders for grading. The conformity rate rose from 67.0 % to 88.9 % in Japan and 68.0–79.8 % in Korea. A reference was made to Leeds revised (O'Brien et al. 1998) having an approximate conformity rate of 50 %. However, it was noted that Leeds grades into 16 groups rather than 4, so comparison cannot be easily done. The authors conclude that conformity data shows adequacy of their system and believe it is a candidate for acne severity classification at least for Asian patients.

2.2 Photographic Uses and Improvements

There have been many extensions of Cook's method using retrospective assessment of photos

and choosing parameters for grading and ways to increase accuracy of photographic methods.

In 1982, Allen and Smith (1982) used Cook's method in two acne treatment studies. One hundred ninety male college students participated in a first 12-week study, and 141 male college students enrolled in a second 10-week study. Three judges evaluated participants every 2 weeks, grading overall severity by Cook's method, papule count, pustule count, and comedo grade. Photos were taken every 4 weeks for documentation. Pearson's correlation coefficient was used to evaluate correlation of inter-judge evaluations and between the different grading methods. For the first study, severity grade versus papule count had high mean correlation coefficient of 0.84. Severity grade versus pustule count and severity grade versus comedo grade had correlation coefficients of 0.64 and 0.54, respectively. High mean correlation coefficients between graders were obtained for severity grade with 0.82 and papule count with 0.77. For the second study, severity grade versus papule count had high mean correlation coefficient of 0.89. Severity grade versus pustule count and severity grade versus comedo count had correlation coefficients of 0.59 and 0.67, respectively. High mean correlation coefficients between graders were obtained for severity grade with 0.82 and papule count with 0.86. The authors conclude that Cook's scale and counting are at least equally reproducible grading methods. Experience gained from study 1 improved correlation between judges for study 2. The authors believe that overall grading scales, with its ease of use and high reproducibility, are superior to laborious lesion counts for clinical evaluation of acne severity.

In 1984, Gibson et al. (1984) assessed correlation between clinical and photographic methods for assessing facial acne. Forty-five patients were evaluated clinically with Leeds (Burke and Cunliffe 1984) and lesion counting and retrospectively with photos from each visit. Retrospective assessment was conducted on a 0–4 scale with 0.5 increments and change in severity on a scale of −2 to 4. Correlation for clinical grading versus counts, correlation between the three judges grading photos, correlation for severity judged by photos versus clinical grading, and correlation for severity judged by photos versus counts were all significant ($p = 0.01$). Lesion counting appears objective but is tedious, whereas clinical grading can reflect disease severity more meaningfully but can lack objectivity. Photographic methods allow for a permanent record but lack palpation during retrospective assessment. The authors conclude that Leeds provides meaningful assessment with speed and accuracy.

In 2005, Leyden et al. (2005) presented findings from a retrospective photographic assessment study of topical retinoids for acne. Photos of 577 patients were collected from multiple trials comparing topical retinoids: tazarotene 0.1 % gel, adapalene 0.1 % gel, tretinoin 0.1 % microsponge, tretinoin 0.025 % gel, and tazarotene 0.1 % cream. Complete sets of right, front, and left view of patient photos before (week 0) and after treatment (week 12 or 15) were evaluated by five investigators. Overall severity was assessed with a 7-point modified version of Cook's method. 1 grade change indicated clinically meaningful, and grade change 2 or more indicated clearly clinically significant. This study showed intrainvestigator consistency with no significant differences. Interinvestigator consistency was also shown with correlation coefficients between investigators ranging from 0.648 to 0.836. The authors note that irritation in early phase of studies could not be observed since photos were only taken at the beginning and end of trials, implying that if photos were taken more frequently, a more complete record of results could be obtained.

In 2009, Bergman et al. (2009) conducted a study where 300 digital images from 20 patients were evaluated by two dermatology residents using total inflammatory lesion count (TILC) and Leeds (Burke and Cunliffe 1984). A set of front, right, and left views were taken by either subjects themselves or staff and reviewed for adherence to standardization. To test reliability, Pearson's coefficient correlation was calculated for TILC and κ-score for Leeds. Intra-rater reliability was excellent for TILC with $r = 0.989$ and 0.908, and Leeds $\kappa = 1.0$ and 0.879 for raters

A and B, respectively. Inter-rater reliability was high for TILC $r = 0.871$ but low for Leeds $\kappa = 0.381$. However, when agreement within 0.25 unit was considered for Leeds rather than absolute agreement, $\kappa = 0.74$. Although TILC was indicated as the best measure, since TILC reliability decreased with greater number of lesions and the patients studied had mild to moderate acne, a study evaluating a broader range of severity might indicate a better performance for Leeds. Inter-rater reliability was also less than intra-rater for all methods, reflecting the importance of having the same rater evaluate a patient throughout a study or course of treatment. The authors conclude that digital images can reliably be evaluated for diagnostic purposes and remotely monitor patient progress.

In 2012, Tan et al. (2012a) believed that text descriptions and photographs combined could accurately describe severity categories and would be more practical and time efficient than lesion counting in practice. The scales presented by Cook et al. (1979) and Hayashi et al. (2008a) included photos and text descriptions but are limited to facial acne. Therefore, the authors matched two acne scales that incorporated evaluation of the chest and back in addition to the face, assigning images from Leeds revised (O'Brien et al. 1998) to text description grades from the six-category comprehensive acne severity scale (CASS). Twenty-three dermatologists graded 56 photos of the face, chest, and back using CASS. Photographs included 25 patient photos and the set of 31 photographs from Leeds revised. Rater consensus was achieved for Leeds facial inflammatory 2 with CASS 3, 4 with CASS 4, 6 with CASS 4, and 9–12 all with CASS 5. Consensus was also obtained for Leeds facial comedonal A with CASS 2, Leeds chest 7 and 8 both with CASS 5, and Leeds back 7 and 8 both with CASS 5. The authors found that photos in Leeds revised inadequately represented milder CASS grades 1 and 2 for facial acne and all CASS grades of the chest and back except 5 for very severe. Thus, there is still a need for images that correspond to a categorical acne scale for the chest, back, and face.

2.2.1 Fluorescence and Polarized Photography Have Increased Accuracy of Acne Evaluation

In 1996, Lucchina et al. (1996) studied fluorescence photography for evaluating acne, as fluorescence corresponds to protoporphyrin IX production by P. acnes in open comedones, follicles, and inflammatory lesions. Thirty-two patients completed a 12-week study in which subjects applied either clindamycin 1 % topical or vehicle twice daily. Clinical evaluation with counting and Leeds (Burke and Cunliffe 1984) and evaluations of flash and fluorescence photographs were obtained at baseline and weeks 4, 8, and 12. Flash photographs were assigned a Leeds score at baseline and week 12. Fluorescence photographs were evaluated at baseline and week 12 for facial areas: overall, the nose only and face excluding nose. Each area was assigned a fluorescence score within 0–3 and an improvement score within −1 to 4. The treatment group had less fluorescence compared to baseline and statistically significant larger decreases in evaluations than the vehicle group. Fluorescence photography can evaluate acne therapy efficacy by charting the course of acne treatment.

In 1999, Pagnoni et al. (1999) also studied fluorescence photography as a quick and simple method to demonstrate P. acne population. Fourteen subjects, of which five were controls, participated in a study where 10 % benzoyl peroxide was applied twice daily for 7 days to measure efficacy. Fluorescence photos of the cheek and nose and cheek scrub culture samples were taken at baseline, day 3, day 7, and day 16. The area of fluorescence in the nose and cheek regions was calculated by Optimas 6.2 software. A decrease in fluorescence paralleled a decrease in cultured P. acnes with treatment. The recolonization of P. acnes after stopping treatment matched the reappearance of porphyrins. Correlation in the treatment group, mean = 0.80, between P. acnes and fluorescence was good, whereas correlation for control was poor. Fluorescence photography is not sensitive enough to detect modest changes but is reliable when variation is clinically relevant, at least one order magnitude. Thus, culture may still be necessary when modest changes in P. acnes

cannot be detected with fluorescence. The authors conclude that fluorescence photography is a reliable, quick, and easy way to estimate suppressive effects of antibacterial agents on P. acnes.

In 1997, Phillips et al. (1997) introduced the use of perpendicular polarized light photography (originally a method for enhancing subsurface features in photoaged skin) as a method to enhance visualization of acne. With standard photos, small comedones may be missed, and macular and elevated lesions cannot be differentiated. Features may also only change slightly during a 12-week trial. Polarized photography enhances visualization of features such as erythema, important for distinguishing inflammatory from noninflammatory lesions. Thirty-two subjects were treated with clindamycin 1 %, and clinical assessment using Leeds (Burke and Cunliffe 1984) was performed at baseline and after 12 weeks. Standard and perpendicular polarized photographs were also taken and retrospectively graded using Leeds. Because reproducible photographs were required for reliable retrospective evaluation, the authors concentrated on keeping consistent color, lighting, and framing with anatomic landmarks. Advantages of perpendicular polarized photos include enhancing visualization of subsurface erythema and hemoglobin-related structures and better identifying inflammatory lesions and open comedones by removing glare and surface topography. The mean Leeds score from perpendicular photos was higher than scores from clinical assessments and flash photos, indicating increased sensitivity. The difference in mean Leeds scores after 12 weeks for polarized photos was similar to clinical assessments but significantly higher than flash ($p = 0.03$). The authors conclude that clinical evaluations match retrospective grading with perpendicular more than with flash photos.

In 2001, Rizova and Kligman (2001) used polarized light photography as a noninvasive and reliable method to assess acne and track lesion development. Visual assessment is compromised by viewer subjectivity and is dependent on consistent standards. Although standard photography with consistent technique can be used for more objective assessment, visualization of small comedones and subtle cutaneous characteristics is inconsistent, and inflammatory lesions are difficult to differentiate from hyperpigmented macules. Polarized light photography can increase accuracy of acne evaluation. Five volunteers enrolled in a 16-week study with the folllowing phases: 4-week pretreatment phase to track the natural progression of lesions, 8-week treatment with adapalene gel 0.1 %, and 4-week follow-up after ending treatment to evaluate lesion evolution. Parallel- and cross (or perpendicular)-polarized photographs were taken at each visit to record lesion evolution. Parallel-polarized photography enhances visualization of surface features such as greasiness, scaling, and degree of lesion elevation, while cross-polarized photography improves visibility of subsurface erythema, hyperpigmentation, small lesions, and inflammation. The authors believe that serial photographs using polarized techniques to track lesions can provide more data for treatment efficacy and the changing landscape characteristic of acne.

2.2.2 Computational Methods Have Also Been Used to Improve Acne Evaluation

In 2008, Do et al. (2008) studied the program Picture Window Pro 4.0 used to align and track images of the night sky. Even with standardization, position inconsistencies are possible between photos. By manually selecting alignment points for anatomic landmarks such as the nose tip, successive photos could be superimposed to decrease angle and framing inconsistencies. Observations such as inflammatory lesions rising from comedones with a time course of 2–12 plus weeks were determined by monitoring development of lesion types open/closed comedones, erythematous macules, papules, pustules, and nodules. The authors conclude that such technology can track effects of acne medication on the lifespan of lesions and characterize the natural history of acne.

In 2012, Choi et al. (2012) used a 3D image analysis system (PRIMOS Compact) to evaluate skin texture and acne lesions objectively. From the successful use of 3D analysis to monitor wrinkles, the authors applied the method to quantify skin

surface roughness and acne volumes before and after 4 weeks of anti-acne cream (acure clarifying marks eraser®). Skin surface measurements before and after treatment using the 3D image system gave quantitative analysis of roughness and volume of lesions. Roughness was assessed by parameters: Ra average of values, Rmax maximum peak-to-valley value, Rz average of peak-to-valley values, and Rp maximum peak. Lesions were analyzed by total number and average volume. Results indicated that skin texture significantly improved after treatment with Ra, Rmax, Rz, and Rp, decreasing by 6.25 %, 7.50 %, 7.00 %, and 7.70 %, respectively. Volume of lesions decreased by 19.54 % after treatment, although lesion count was unchanged. While acne is usually classified by diameter, the authors indicate that volume provides more reliable criteria for the classification of lesions with irregular shapes. 3D analysis can supplement counting and grading systems. However, image analysis is less clinically relevant than grading based on severity since severity can be underestimated with minimal protrusion. Image-based analysis provides opportunities to address topographical changes in the skin and should be used with additional visual assessment methods to grade severity.

In 2008, Fuji et al. (2008) proposed an extraction method to classify lesion types such as comedo, reddish papule, pustule, and scar. Acne should be classified and counted for accurate grading, but this takes time. Inferior color reproduction of cameras causes visually detecting and differentiating lesion types to be difficult. Instead, accurate color reproduction of multispectral images (MSIs) is better. In the computer-aided diagnosis system, detailed spectral features are acquired by MSI, and lesions can be classified by applying linear discriminant functions (LDFs). Three LDFs were calculated from papule and pustule, pustule and scar, and papule and scar. Results of MSI and LDF classifier on clinical images showed viability of this method.

In 2008, Bae et al. (2008) introduced a multimodal imaging modality and objective image analysis methods. Independent modalities standard, parallel- and cross-polarized, and fluorescent images were integrated into one modality to maximize clinical utility. Each image emphasizes different morphological and functional skin information, and the images can be utilized to more reliably and efficiently evaluate severity. Polarized images are useful for analyzing skin texture, pigmentation, and vascularity and computing erythema index and melanin index to evaluate vascular and pigmented lesions, respectively. Fluorescent images are useful for quantitatively evaluating sebum characteristics such as pattern, area and density, and average size and diameter of spots.

There are also existing skin analysis methods that can be applied to quantitatively assess acne severity. In 1999, Xu et al. (1999) presented a segmentation method for images of skin cancer and pigmented lesions. Lesions are detected in an image to compute qualities such as diameter, color variation, etc. In 2003, Schmid-Saugeon et al. (2003) presented a computer-aided diagnosis system to assist physicians in analyzing pigmented skin lesions, such as lesion boundary detection, visualization, quantification of texture, shape, and color, and classification as benign or malignant. In 2008, Masood et al. (2008) introduced a segmentation procedure for lesions in atopic dermatitis. Improving accuracy of lesion boundary detection is important for obtaining objective evaluation of lesions through quantitative attributes and monitoring lesion evolution. Computerized analysis of position, size, shape, color, and other features can categorize lesions.

3 Conclusion

The photographic standard introduced by Cook et al. (1979) is precise, is easy to use, and has inter-grader consistency. Cook's method has been expanded in various ways, from including the back and chest evaluation to matching lesion counts with severity grades. Photography also documents progress for retrospective verification.

With lesion tracking, the natural history of lesion development can be determined. In addition, photographic methods have expanded from flash to fluorescence and polarized, to improve visualization and increase accuracy of assessing acne severity.

However, drawbacks of photography include not allowing palpation to determine depth and minimization of small lesions, comedones, and erythema. Photographs of patients with pigment are also difficult to evaluate (Witkowski and Parish 2004). Maintaining consistent settings such as lighting, distance to camera, framing, and angles can also be problematic (Burke and Cunliffe 1984). Although many agree that Cook's photonumeric method has good inter- and intra-rater reliability, some criticize that the method is inaccurate because photographic evaluation is inherently more subjective than lesion counting (Doshi et al. 1997). Pigmentation changes from healing lesions or tanning can affect grading. Dark skin tones also complicate the visualization and assessment of lesions (Witkowski et al. 1980). Some praise lesion counting as more objective and accurate, despite being tedious and time consuming.

Even so, there has been much support for a photographic standard, with trials showing reliability of such assessment and applicability to clinical practice. In addition, patient photos can be transferred to other physicians for a second opinion to ensure accurate assessment. As supported by Samuelson (1981), who concurrently used two methods of evaluation, there is a close correlation between lesion counting and overall assessment of photographs. While lesion count evaluations differed by as much as 20 %, the photographic method only had a 5 % difference, showing that the photographic method provides a more accurate evaluation of change. In addition, change in counts is meaningless if overall severity remains the same. With counting, a quantitative measure, statistical evaluation, must be handled carefully as a count of 10 reducing to 5 does not necessarily indicate 50 % severity reduction. Discrepancy between raters also increases as count rises (Bergman et al. 2009), indicating reliability issues as severity worsens. As evaluated in a survey conducted by Tan et al. (2012b), severity was selected as the most important clinical feature. In clinical practice, acne severity assessment must be time efficient, and although lesion counting is important, it is largely impractical in practice. Thus, severity is often measured by qualitative methods. Numerical range of lesions for severity categories with descriptive text and photographic standards are more appropriate for clinic use.

Methods such as fluorescence and polarized photography also offer more information about dermatological conditions than noticeable by clinical observation alone. Computer alignment, imaging modality, segmentation, quantitative analysis, and 3D analysis methods expand the use of images to track lesions and measure objective characteristics such as the extent of erythema and lesion attributes. Computational methods also address issues of inter- and intra-rater reliability, which can lead to effective acne treatment and contribute to existing grading systems (Ramli et al. 2012).

Since the introduction of Cook's standard, other photographic extensions and analysis techniques have helped improve accuracy of diagnosis. Photography is (1) an objective and usable technique for measuring acne and (2) a valuable technique for training and qualifying graders. Because of its reproducibility, the method can also help decrease subject sample size in research. Taken together, the combined experience summarized here strongly promotes the use of the photographic method – at least as an auxiliary method in phase 1 and 2 clinical trials. The small definitive intra-subject documentation achieved by Cook represents a major savings in resources.

References

Adityan B, Kumari R, Thappa DM. Scoring systems in acne vulgaris. Indian J Dermatol Venereol Leprol. 2009;75(3):323–6.

Allen BS, Smith JG. Various parameters for grading acne vulgaris. Arch Dermatol. 1982;118(1):23–5.

Bae Y, Nelson JS, Jung B. Multimodal facial color imaging modality for objective analysis of skin lesions. J Biomed Opt. 2008;13(6):064007.

Barratt H, Hamilton F, Car J, Lyons C, Layton A, Majeed A. Outcome measures in acne vulgaris: systematic review. Br J Dermatol. 2009;160(1):132–6.

Bergman H, Tsai KY, Seo SJ, Kvedar JC, Watson AJ. Remote assessment of acne: the use of acne grading tools to evaluate digital skin images. Telemed J E Health. 2009;15(5):426–30.

Blaney DJ, Cook CH. Topical use of tetracycline in the treatment of acne: a double-blind study comparing topical and oral tetracycline therapy and placebo. Arch Dermatol. 1976;112(7):971–3.

Burke BM, Cunliffe WJ. The assessment of acne vulgaris – the Leeds technique. Br J Dermatol. 1984;111(1):83–92.

Choi KM, Kim SJ, Baek JH, Kang SJ, Boo YC, Koh JS. Cosmetic efficacy evaluation of an anti-acne cream using the 3D image analysis system. Skin Res Technol. 2012;18(2):192–8.

Cook CH, Centner RL, Michaels SE. An acne grading method using photographic standards. Arch Dermatol. 1979;115(5):571–5.

Do TT, Zarkhin S, Orringer JS, et al. Computer-assisted alignment and tracking of acne lesions indicate that most inflammatory lesions arise from comedones and de novo. J Am Acad Dermatol. 2008;58(4):603–8.

Doshi A, Zaheer A, Stiller MJ. A comparison of current acne grading systems and proposal of a novel system. Int J Dermatol. 1997;36(6):416–8.

Fuji H, Yanagisawa T, Mitsui M, et al. Extraction of acne lesion in acne patients from Multispectral Images. 30th Annual IEEE EMBS Conference, Vancouver; 2008. p. 4078–81.

Gibson JR, Harvey SG, Barth J, Darley CR, Reshad H, Burke CA. Assessing inflammatory acne vulgaris – correlation between clinical and photographic methods. Br J Dermatol. 1984;111 suppl 27:168–70.

Hayashi N, Akamatsu H, Kawashima M. Establishment of grading criteria for acne severity. J Dermatol. 2008a; 35(5):255–60.

Hayashi N, Suh DH, Akamatsu H, Kawashima M, Acne Study Group. Evaluation of the newly established acne severity classification among Japanese and Korean dermatologists. J Dermatol. 2008b;35(5):261–3.

Leyden JJ, Shalita A, Thiboutot D, Washenik K, Webster G. Topical retinoids in inflammatory acne: a retrospective, investigator-blinded, vehicle-controlled, photographic assessment. Clin Ther. 2005;27(2):216–24.

Lucchina LC, Kollias N, Gillies R, Phillips SB, Muccini JA, Stiller MJ, Trancik RJ, Drake LA. Fluorescence photography in the evaluation of acne. J Am Acad Dermatol. 1996;35(1):58–63.

Masood NA, Mashali HM, Mohamed AS. Color segmentation for skin lesions classification. Cairo International Biomedical Engineering Conference, Cairo; 2008. p. 1–4.

O'Brien SC, Lewis JB, Cunliffe WJ. The Leeds revised acne grading system. J Dermatolog Treat. 1998;9(4): 215–20.

Pagnoni A, Kligman AM, Kollias N, Goldberg S, Stoudemayer T. Digital fluorescence photography can assess the suppressive effect of benzoyl peroxide on Propionibacterium acnes. J Am Acad Dermatol. 1999;41(5):710–6.

Phillips SB, Kollias N, Gillies R, Muccini JA, Drake LA. Polarized light photography enhances visualization of inflammatory lesions of acne vulgaris. J Am Acad Dermatol. 1997;37(6):948–52.

Ramli R, Malik AS, Hani AF, Jamil A. Acne analysis, grading and computational assessment methods: an overview. Skin Res Technol. 2012;18(1):1–14.

Rizova E, Kligman A. New photographic techniques for clinical evaluation of acne. J Eur Acad Dermatol Venereol. 2001;15 suppl 3:13–8.

Samuelson JS. Acne grading methods. Arch Dermatol. 1981;117(5):252.

Samuelson JS. An accurate photographic method for grading acne: initial use in a double-blind clinical comparison of minocycline and tetracycline. J Am Acad Dermatol. 1985;12(3):461–7.

Schmid-Saugeon P, Guillod J, Thiran JP. Towards a computer-aided diagnosis system for pigmented skin lesions. Comput Med Imaging Graph. 2003;27(1): 65–78.

Tan JK, Zhang X, Jones E, Bulger L. Correlation of photographic images from the Leeds revised acne grading system with a six-category global acne severity scale [published online ahead of print 28 Aug 2012. J Eur Acad Dermatol Venereol. 2012. http://onlinelibrary.wiley.com/doi/10.1111/j.1468-3083.2012.04692.x/abstract. Accessed Sept 2012.

Tan J, Wolfe B, Weiss J, et al. Acne severity grading: determining essential clinical components and features using a Delphi consensus. J Am Acad Dermatol. 2012b;67(2):187–93.

Wilson RG. Office application of a new acne grading system. Cutis. 1980;25(1):62–4.

Witkowski JA, Parish LC. The assessment of acne: an evaluation of grading and lesion counting in the measurement of acne. Clin Dermatol. 2004;22(5):394–7.

Witkowski JA, Parish LC, Guin JD. Acne grading methods. Arch Dermatol. 1980;116(5):517–8.

Xu L, Jackowski M, Goshtasby A, et al. Segmentation of skin cancer images. Image Vis Comput. 1999;17(1): 65–74.

Classification and Scoring of Androgenetic Alopecia (Male and Female Pattern)

140

Alireza Firooz, Ali Rajabi-Estarabadi, Hamed Zartab, Hournaz Hassanzadeh, and Yahya Dowlati

Contents

Keywords
Androgenetic alopecia • Male • Female • Classification • Hair loss scoring

Hair is a major visual demonstration of the human body, especially in social and sexual communications. Androgenetic alopecia (AGA) is the most common form of alopecia, affecting up to 80 % of men and 50 % of women in the course of their life (Piraccini and Alessandrini 2014; Shapiro et al. 2000; Blume-Peytavi et al. 2008). Today, hair loss is a common complaint in clinical dermatology. Hair growth assessment is based on the clinical experience and trichological knowledge of the assessor. Careful clinical examination is required in order to establish the differential diagnoses, which will then inform the choice of assessment technology made (Shapiro et al. 2000; Blume-Peytavi et al. 2008). The use of specific and reproducible scoring systems for scalp hair by the physician is best approached, as it facilitates the diagnosis and differential diagnosis with other diseases, allows staging of severity, and monitors the progress of the disease in time and response to treatment (Piraccini and Alessandrini 2014).

1 AGA Classification

The most well-known grading systems are those described by Hamilton-Norwood (for male) and Ludwig (for female) (Messenger

A. Firooz (✉) • A. Rajabi-Estarabadi • H. Hassanzadeh • Y. Dowlati
Center for Research and Training in Skin Diseases and Leprosy, Tehran University of Medical Sciences, Tehran, Iran
e-mail: firozali@sina.tums.ac.ir; dralirajabi@yahoo.com; hasanzadeh.hoornaz92@gmail.com; dowlatiy@yahoo.com

H. Zartab
Center for Research and Training in Skin Diseases and Leprosy, Tehran University of Medical Sciences, Tehran, Iran

Tissue Engineering and Wound Healing Lab, Department of Surgery, Division of Plastic Surgery, Brigham and Women's Hospital – Harvard Medical School, Boston, USA
e-mail: hzartabmd@yahoo.com; hzartab@partners.org; hzartabmd@gmail.com

P. Humbert et al. (eds.), *Agache's Measuring the Skin*,
DOI 10.1007/978-3-319-32383-1_101

Table 1 Different scalp hair assessment scores in androgenetic alopecia

Author	Year	Classification
Beek	1950	This study was done on 1,000 Caucasian with two aspect (frontal and front vertical baldness (Beek 1950)
Hamilton	1951	A classification based on the report of eight aspects and three subgroups for male pattern hair loss and further comparison of the incidence of baldness for Caucasians and Chinese (Hamilton 1951)
Ogata	1953	Fifteen types of baldness were distinguished from 20 different aspects and classified them to six groups (Ogata 1953)
Feit	1969	A more detailed classification than Hamilton version. He characterized 12 different varieties of 16 categorizes aspects (Feit 1969)
Setty	1970	A simplified three-group version of Hamilton's version: (1). Totopilosis (relates to Hamilton type I). (2). Indentato-pilosis (Hamilton type II–V). (3). Indentatocirculo-pilosis (more or less Hamilton VI–VII; confluent/nonconfluent) (Setty 1970)
Ebling and Rook	1972	Classification which differentiates alopecia into 5°: for grades I–III medical treatment is appropriate; for grade IV, surgical therapy; for grade V, no solution is available (Ebling and Rook 1972)
Rook and Dawber	1975	A classification of five evolving stages (Rook and Dawber 1982)
Norwood	1975	Norwood modified Hamilton classification, added more details for male pattern baldness, and described as Hamilton-Norwood classification (Fig. 1) (Norwood 1975)
Bouhanna and Nataf	1976	A simplified classification in three stages of evolution with or without vertex balding (Bouhanna and Nataf 1976)
Ludwig	1977	Ludwig classification (Fig. 3) (Ludwig 1977)
Blanchard and Blanchard	1984	Classification distributed into five stages of evolution by measuring the distance of fixed landmarks with the borders of alopecia (Blanchard and Blanchard 1984)
Camacho	1988	A classification of AGA which involves the hair loss pattern. Male AGA (MAGA.I–V) and male pattern female AGA (FAGA.M.I–V) are judged with the Ebling classification. Female AGA (FAGA.I–III) and female pattern male AGA (MAGA.F.I–III) are rated with the Ludwig classification (Camacho 1988)
Savin	1992	The Savin scale is a photographic depiction of gradations of scalp hair loss in women as determined by parting width. The patient's hair is compared with eight computer-generated pictorial representations of the central scalp hair parted in the middle (Savin 1992)
Bouhanna	2000	A presurgical method to determine the extent of bald and hairy areas, measured by five distances on the scalp: median sagittal distance, left and right paramedian distances, transverse supra-auricular distance, temporal anterior spacing distance (Bouhanna 2000; Camacho 1988).
Koo et al	2000	Classified the type of male pattern baldness into six types according to the English alphabetical letter shape of the bald area (Lee et al. 2007; Koo et al. 2000)
Sinclair	2004	Described more grade than the Ludwig scale (Fig. 4) (Messenger 2008; Sinclair et al. 2004; Gan and Sinclair 2005)
Olsen et al.	2004	The scalp is divided in four regions: frontal (F), bitemporal (T), midscalp (M), and vertex (V). These regions are each assigned a 7-point density scale of 0–6, with 0 being no loss and 6 being total or near-total terminal hair loss (Fig. 1) (Olsen et al. 2004)
Lee et al.	2007	Basic and specific (BASP) classification. There are four basic types (L, M, C, and U) and two specific types (F and V). The final type is decided by the combination of the assigned basic and specific types (Fig. 2) (Lee et al. 2007)

2008). However, various classifications for assessing hair loss score have been proposed for AGA (Table 1) (Blume-Peytavi et al. 2008; Lee et al. 2007; Olsen 2003; Thaysen-Petersen et al. 2015).

1.1 AGA in Men

In the majority of men, AGA involves the fronto-temporal and the vertex areas, and hair loss progresses to end-stage blading in 50–60 % of men

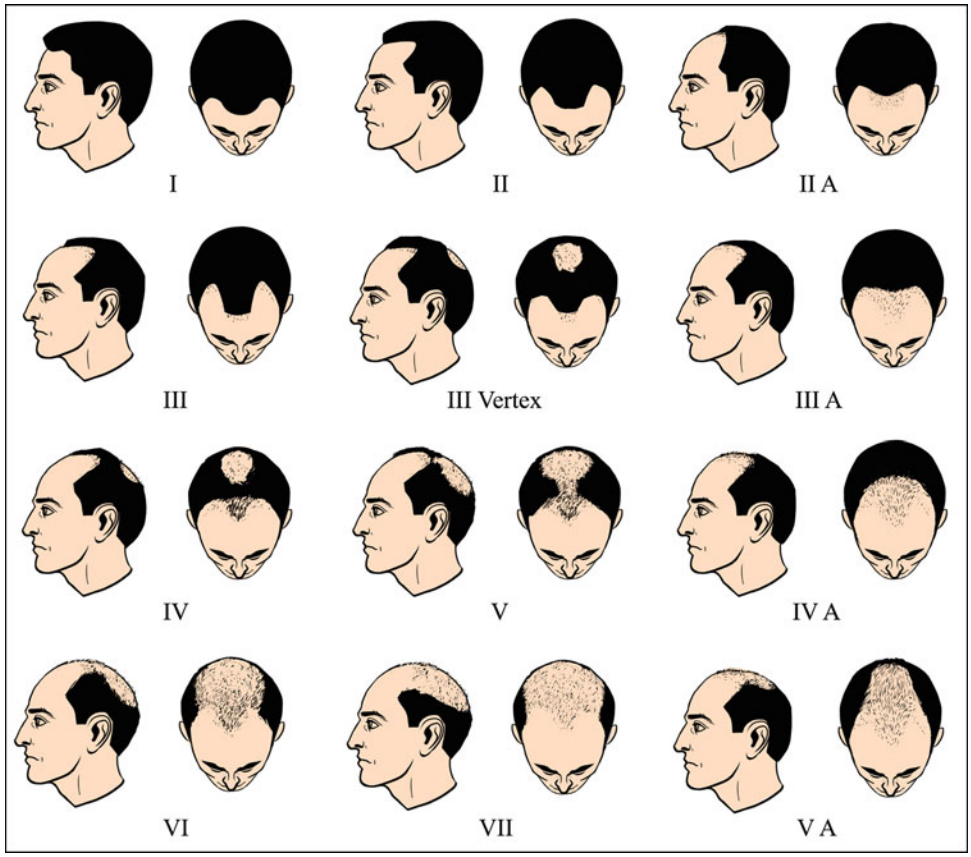

Fig. 1 Hamilton-Norwood classification of male balding (Drawing by Ali Rajabi Estarabadi based on Male pattern baldness classification published by Norwood) (Norwood 1975; Blume-Peytavi et al. 2011)

by age of 70 years (Fig. 1) (Hamilton 1951; Norwood 1975). This process may start at any time following puberty or sooner. The most widespread use classification method for male AGA is the one that described by Norwood in 1975, with refining Hamilton's classification (Blume-Peytavi et al. 2008; Lee et al. 2007; Norwood 1975). In some instances, however, men develop diffuse thinning of the crown with retention of the frontal hairline with a pattern that resembles the Ludwig type observed in women (Blume-Peytavi et al. 2011).

The basic and specific (BASP) classification is a new scoring method of hair loss which was introduced by Lee et al. in 2007. BASP was designed based on the pattern of hair loss, including four basic types (the shape of the anterior hairline) and two specific types (the density of hair on the frontal and vertex areas). The final type is decided by the combination of the basic and specific types (Fig. 2) (Lee et al. 2007).

1.2 AGA in Women

Female pattern hair loss (FPHL) is the most common hair loss disorder in women and has a complex mode of inheritance. The etiopathogenesis of FPHL is largely unknown; however, it is hypothesized that FPHL and male pattern baldness share common genetic susceptibility alleles (Nuwaihyd et al. 2014). It results from a progressive reduction in the ratio of terminal hairs to shorter, thinner vellus hairs, which is known as follicular miniaturization (Bouhanna and Nataf 1976; Blume-Peytavi et al. 2011). This miniaturization follows usually a pattern distribution. In women, FPHL typically presents as a diffuse reduction in hair density over the

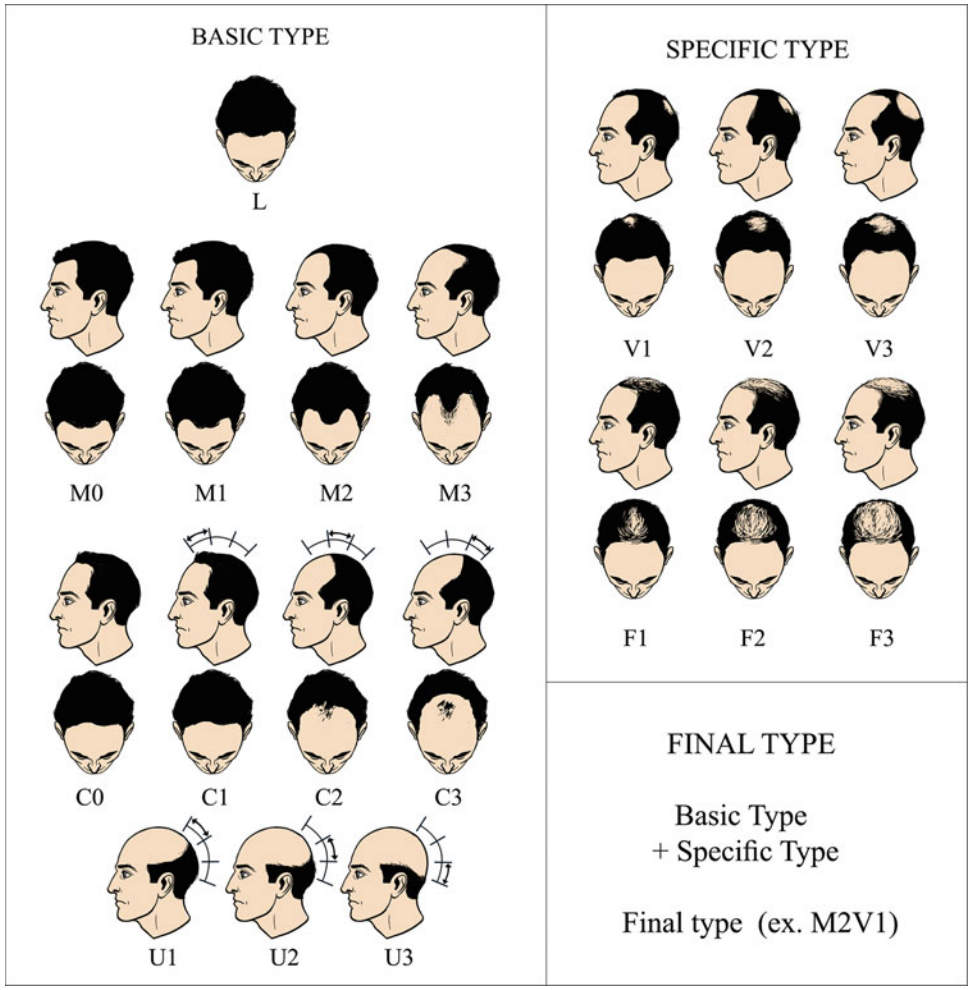

Fig. 2 The basic and specific (*BASP*) classification system. Four basic types (L, M, C, and U) and two specific types (V and F) are used in the BASP classification. The final type is defined by a combination of the basic and specific type (Drawing by Ali Rajabi Estarabadi based on BASP classification published by Lee and et al.) (Lee et al. 2007)

frontal and vertex areas, but parietal and occipital regions may be involved (Bouhanna and Nataf 1976; Blume-Peytavi et al. 2011). So FPHL may have three different patterns which is a term for decreasing in different regions of scalp hair density (Blume-Peytavi et al. 2008; Pragst and Balikova 2006):

1. Diffuse thinning of the crown region with preservation of the frontal hairline. There are two scales that describe this pattern: the commonly used 3-point Ludwig scale and the 5-point Sinclair scale (Blume-Peytavi et al. 2011).

The Ludwig classification uses three stages to describe female pattern genetic hair loss: type I (mild), type II (moderate), and type III (extensive). In all three Ludwig stages, there is hair loss on the front and top of the scalp with relative preservation of the frontal hairline. The back and sides may or may not be involved (Fig. 3) (Ludwig 1977; Olsen 2001, 2008).

2. Thinning and widening of the central part of the scalp with breach of frontal hairline described by Olsen scale: Christmas tree pattern (Fig. 5) (Olsen 2003, 2008). Olsen

Fig. 3 Ludwig pattern of hair loss-3-point (Drawing by Ali Rajabi Estarabadi based on Classification of alopecia in female published by Ludwig) (Ludwig 1977; Blume-Peytavi et al. 2011)

Fig. 4 Sinclair scale (5-point) for grading of female pattern hair loss (Drawing by Ali Rajabi Estarabadi based on the Sinclair scale) (Sinclair et al. 2004; Gan and Sinclair 2005)

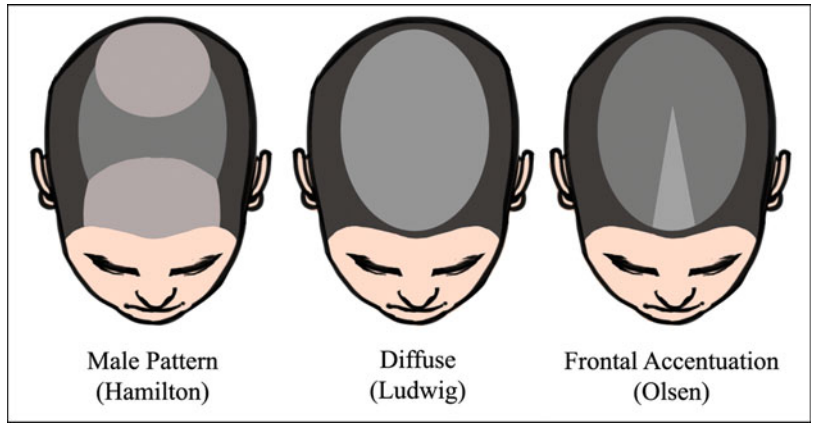

Fig. 5 Olsen scale: Christmas tree pattern in female pattern hair loss (Drawing by Ali Rajabi Estarabadi based on Female pattern hair loss published by Olsen) (Olsen 2008; Blume-Peytavi et al. 2011)

proposed that frontal accentuation (or the "Christmas tree" pattern) be considered another pattern of hair loss in women, which helps to distinguish hair loss from other potential hair loss mimicries in women (Lee et al. 2007; Olsen 2003; Vujovic and Del Marmol 2014).

3. Thinning associated with bitemporal recession the same as male hair loss pattern (Hamilton-Norwood type, Fig. 1) (Olsen 2003; Hamilton 1951; Norwood 1975).

Norwood-Hamilton's classification for male pattern of hair loss and Ludwig's classification

for female pattern of hair loss are the most commonly used classification methods for assessing AGA worldwide (Blume-Peytavi et al. 2008, 2011; Gan and Sinclair 2005).

References

Beek CH. A study on extension and distribution of the human body-hair. Dermatologica. 1950;101(6):317–31.

Blanchard G, Blanchard B. Proposition d'uneapprochetopographique de la transplantation capillaireet de reduction tonsurale. Ann Chir Plast Esthet. 1984;29:152–61.

Blume-Peytavi U, Hillmann K, Guarrera M. Hair growth assessment technique. In: Blume-Peytavi U, Tosti A, Whiting DA, Trüeb RM, editors. Hair growth and disorders. Berlin/Heidelberg: Springer; 2008. p. 125–57.

Blume-Peytavi U, Blumeyer A, Tosti A, Finner A, Marmol V, Trakatelli M, et al. S1 guideline for diagnostic evaluation in androgenetic alopecia in men, women and adolescents. Br J Dermatol. 2011;164(1):5–15.

Bouhanna P. Multifactorial classification of male and female androgenetic alopecia. Dermatol Surg. 2000;26(6):555–61.

Bouhanna P, Nataf J. A propos des transplantations des cuirchevelu: critiques et propositions. Rev Chir Esthet. 1976;7:17–23.

Camacho F. Clínica de lasalopecias. Clasificación general. Monogr Dermatol. 1988;1:33–72.

Ebling FJG, Rook A. Hair. In: Rook AJ, Wilkinson DS, Ebling FJ, editors. Textbook of dermatology. 2nd ed. Oxford: Blackwell Scientific; 1972. p. 1588.

Feit LJ. Pathogenic classification of male pattern baldness. New innovations in surgical techniques. Int Surg. 1969;51(1):58–67.

Gan DCC, Sinclair RD. Prevalence of male and female pattern hair loss in Maryborough. J Investig Dermatol Symp Proc. 2005;10:184–9.

Hamilton JB. Patterned loss of hair in man; types and incidence. Ann N Y Acad Sci. 1951;53(3):708–28.

Koo S-H, Chung H-S, Yoon E-S, Park S-H. A new classification of male pattern baldness and a clinical study of the anterior hairline. Aesthet Plast Surg. 2000;24:46–51.

Lee WS, Ro BI, Hong SP, Bak H, Sim WY, do Kim W, et al. A new classification of pattern hair loss that is universal for men and women: basic and specific (BASP) classification. J Am Acad Dermatol. 2007;57(1):37–46.

Ludwig E. Classification of the types of androgenetic alopecia (common baldness) occurring in the female sex. Br J Dermatol. 1977;97(3):247–54.

Messenger A. Male androgenetic alopecia. In: Blume-Peytavi U, Tosti A, Whiting DA, Trüeb RM, editors. Hair growth and disorders. Berlin/Heidelberg: Springer; 2008. p. 159–70.

Norwood OT. Male pattern baldness: classification and incidence. South Med J. 1975;68:1359–65.

Nuwaihyd R, Redler S, Heilmann S, Drichel D, Wolf S, Birch P, et al. Investigation of four novel male androgenetic alopecia susceptibility loci: no association with female pattern hair loss. Arch Dermatol Res. 2014;306(4):413–8.

Ogata T. Development of patterned alopecia. Sogo Rinsho. 1953;2:101–6.

Olsen EA. Female pattern hair loss. J Am Acad Dermatol. 2001;45:70–80.

Olsen EA. Current and novel methods for assessing efficacy of hair growth promoters in pattern hair loss. J Am Acad Dermatol. 2003;48(2):253–62.

Olsen EA. Female pattern hair loss. In: Blume-Peytavi U, Tosti A, Whiting DA, Trüeb RM, editors. Hair growth and disorders. Berlin/Heidelberg: Springer; 2008. p. 171–86.

Olsen EA, Hordinsky MK, Price VH, Roberts JL, Shapiro J, Canfield D, et al. Alopecia areata investigational assessment guidelines – part II. National Alopecia Areata Foundation. J Am Acad Dermatol. 2004;51(3):440–7.

Piraccini BM, Alessandrini A. Androgenetic alopecia. G Ital Dermatol Venereol. 2014;149(1):15–24.

Pragst F, Balikova MA. State of the art in hair analysis for detection of drug and alcohol abuse. Clin Chim Acta. 2006;370(1–2):17–49.

Rook A, Dawber R. Hair follicle structure, keratinization and the physical properties of hair. In: Rook A, Dawber R, editors. Disease of the hair and scalp. Oxford: Blackwell Scientific; 1982. p. 18–48.

Savin RC. A method for visually describing and quantitating hair loss in male pattern baldness. J Invest Dermatol. 1992;98:604 [abstract].

Setty LR. Hair patterns of scalp of white and Negro males. Am J Phys Anthropol. 1970;33(1):49–55.

Shapiro J, Wiseman M, Lui H. Practical management of hair loss. Can Fam Phys. 2000;46:1469–77.

Sinclair R, Jolley D, Mallari R, Magee J. The reliability of horizontally sectioned scalp biopsies in the diagnosis of chronic diffuse telogen hair loss in women. J Am Acad Dermatol. 2004;51:189–99.

Thaysen-Petersen D, Barbet-Pfeilsticker M, Beerwerth F, Nash JF, Philipsen PA, Staubach P, et al. Quantitative assessment of growing hair counts, thickness and colour during and after treatments with a low-fluence, home-device laser: a randomized controlled trial. Br J Dermatol. 2015;172:151–159.

Vujovic A, Del Marmol V. The female pattern hair loss: review of etiopathogenesis and diagnosis. Biomed Res Int. 2014;2014:767628.

Hirsutism

141

Ferial Fanian

Contents

Keywords

Hirsutism scoring system-Ferriman • Gallwey scale

1 Introduction

Hirsutism is a condition where a female develops a male pattern growth of thick, pigmented androgen-dependent terminal hair. This is to be differentiated from overgrowth of nonsexual (vellus) hair, which is the fine, lightly pigmented hair covering most areas of the body during the prepubertal years and is known as hypertrichosis. Although hirsutism is generally thought to affect 5–10 % of women of reproductive age, it is important to bear in mind that the incidence is highly affected by location and ethnicity being higher in those of African or Mediterranean descent (Metwally 2012).

The first semiquantitative assessment method was developed for the of body hair growth by *D. Ferriman* and *J.D Gallwey*, published in 1961 by D. Ferriman and J.D. Gallwey in the *Journal of Clinical Endocrinology*. Five gradings based on densities and areas involved (0–4) were determined for each of 11 sites: upper lip, chin, chest, upper back, lower back, upper abdomen, lower abdomen, upper arms, forearms, thighs, and legs

F. Fanian (✉)
Center for Study and Research on the Integuments, Department of Dermatology, University Hospital of Besançon, Besançon, France
e-mail: ferial.fanian@chu-besancon.fr; ferial.fanian@cert-besancon.com; fanian@gmail.com

P. Humbert et al. (eds.), *Agache's Measuring the Skin*,
DOI 10.1007/978-3-319-32383-1_111

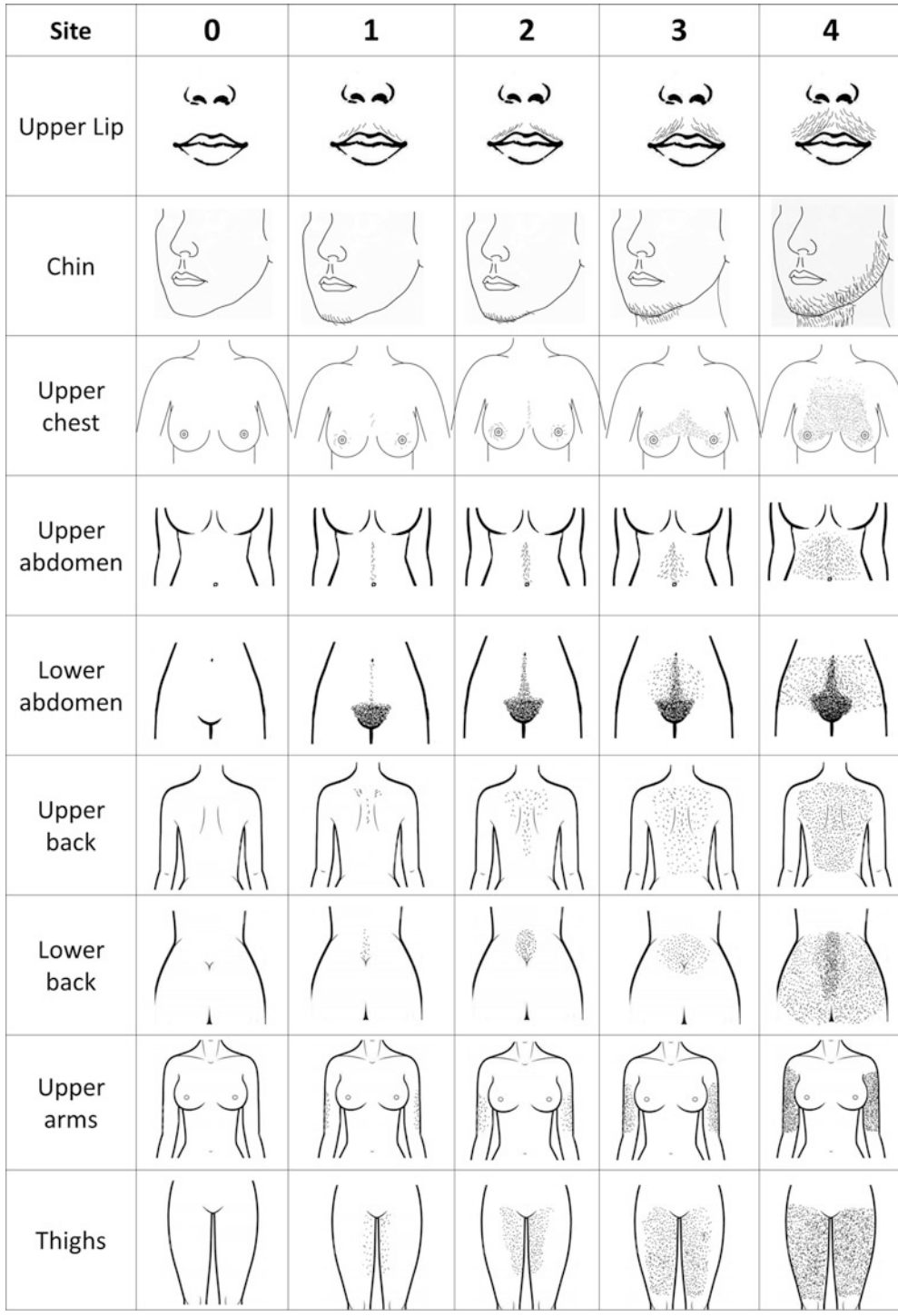

Fig. 1 The modified Ferriman-Gallwey scoring model for quantifying the extent and severity of hair growth in women. Hair growth is graded using a scale from 0 (no terminal hair) to 4 (maximal growth) in nine different areas. The maximum score is 36. A score more than 8 could be considered as hirsutism and indicated the hyperandrogenic state (Reproduced from Hatch R, Rosenfield RS, Kim MH, Tredway D. Hirsutism: implications, etiology and management. Am J Obstet Gynecol 1981; 140: 815. Copyright ©1981 Elsevier)

Table 1 Suggested cutoffs for the mFG hirsutism score according to the 95 percentile in different unselected populations of premenopausal women (Escobar-Morreale HF et al. Hum Reprod Update. 2012) (Escobar-Morreale et al. 2012)

Author, year	Year	Country	Race	Ethnicity	Sample size	Suggested mFG cutoff[a]
Tellez and Frenkel (1995)	1995	Chile	White	Hispanic	236	≥6
Asuncion et al. (2000)	2000	Spain	White	Mediterranean	154	≥8
Sagsoz et al. (2004)	2004	Turkey	White	Middle Eastern	204	≥9
Cheewadhanaraks et al. (2004)	2004	Thailand	Asian	Thai and Chinese	531	≥3
DeUgarte et al. (2006)	2006	USA	White	Caucasian and Hispanic	283	≥8
			Black	African-American	350	≥8
Zhao et al. (2007)	2007	China	Asian	Chinese Han	623	≥2
Api et al. (2009)	2009	Turkey	White	Middle Eastern	121	≥11
Moran et al. (2010)	2010	Mexico	White	Hispanic	150	≥10
Noorbala and Kefaie (2010)	2010	Iran	White	Middle Eastern	900	≥10
Kim et al. (2011)	2011	Korea	Asian	Chinese	1010	≥6
Gambineri (2011, personal communication)	2011	Italy	White	Mediterranean	200	≥9
Escobar-Morreale (2011, personal communication)	2011	Spain	White	Mediterranean	291	≥10

[a]As defined by the 95th percentile of an unselected population of premenopausal women (Escobar-Morreale et al. 2012)

(Ferriman and Gallwey 1961). In 1981, Hatch et al. provided the modified FG scoring model with nine zones by eliminating forearms and thighs and legs (Hatch et al. 1981) (Fig. 1).

2 Cutoff Score for Defining Hirsutism

According to the different studies, the women with the score of more than 8 are considered to be hirsute (Hertweck et al. 2012; Hassa et al. 2005; Rosenfield 2005); however, the Rong Li et al. considered 4 as the cutoff score for nonhirsute/hirsute women (Li et al. 2012). *Escobar-Morreale* et al. suggested a table of cutoffs for the modified FG hirsutism score according to the 95 percentile in different unselected populations of premenopausal women based on their systematic review published on 2012 (Table 1) (Escobar-Morreale et al. 2012).

3 How Modified Ferriman-Gallwey Scale is Applicable?

Although the Ferriman-Gallwey scale is a useful clinical scoring system, there are a number of potential limitations, one of which is the fact that the existing scoring system does not take into account the fact that abnormal amounts of hair growth may be confined to only a few areas without exceeding the cutoff value in total hirsutism score. Also it does not include areas such as the neck, sideburns, and buttocks/perineum where increased hair growth may be a concern in some women. Moreover, it is also less prominent in adolescents and older women and regresses as women age (Azziz 2004). *Hassa* et al. in 2005 showed that the areas not considered in FG scale like buttocks/preneum, sideburn, and neck have a high score in accordance with the hyperandrogenic state (Hassa et al. 2005). They

also revealed that the upper arm, upper back, and upper abdomen have a low impact on the total hirsutism score. Although the study population was too small, the author believes the existing scoring is open to intra- and interobserver variations and he proposed to include these three zones in the visual scoring of hirsutism (Hassa et al. 2005).

4 Is It Any Concordance Between Clinicians' and Patients' Self Scoring?

According to the study of *Espinos J* et al. in 2010 (Espinós et al. 2010), patients' self-scoring of hirsutism using the mFG system showed a mean (SEM) score of 15.1, compared with 12.0 for clinicians' scoring ($P = .01$). For the most androgen-sensitive areas, patients' scores were also significantly higher than clinicians' scores (9.4 vs. 8.1; $P = .04$). A relationship between patients' scores and clinicians' scores was observed ($r = 0.502$, $P < .007$), with a stronger relationship occurring when only the most androgen-sensitive areas were considered ($r = 0.599$, $P < .001$). In the logistic regression analysis, clinicians' scores of clinical hirsutism were significantly associated with BMI and TFI. In contrast, patients' self-scorings of hirsutism were not associated with any of the analyzed parameters. In the multivariable analysis, clinicians' scoring of hirsutism was the only independent variable significantly associated with increased total plasma T levels, with an area under the ROC curve of 0.939 (95 % confidence interval, 0.851–1.028) and a sensitivity of 100 % and specificity of 82.6 % for a mFG score >13 (Espinós et al. 2010).

References

Api M, Badoglu B, Akca A, Api O, Gorgen H, Cetin A. Interobserver variability of modified Ferriman-Gallwey hirsutism score in a Turkish population. Arch Gynecol Obstet. 2009;279:473–9.

Asuncion M, Calvo RM, San Millan JL, Sancho J, Avila S, Escobar-Morreale HF. A prospective study of the prevalence of the polycystic ovary syndrome in unselected Caucasian women from Spain. J Clin Endocrinol Metab. 2000;85:2434–8.

Azziz R. PCOS: a diagnostic challenge. Reprod Biomed Online. 2004;8(6):644–8.

Cheewadhanaraks S, Peeyananjarassri K, Choksuchat C. Clinical diagnosis of hirsutism in Thai women. J Med Assoc Thai. 2004;87:459–63.

DeUgarte CM, Woods KS, Bartolucci AA, Azziz R. Degree of facial and body terminal hair growth in unselected black and white women: toward a populational definition of hirsutism. J Clin Endocrinol Metab. 2006;91:1345–50.

Escobar-Morreale HF, Carmina E, Dewailly D, Gambineri A, Kelestimur F, Moghetti P, et al. Epidemiology, diagnosis and management of hirsutism: a consensus statement by the Androgen Excess and Polycystic Ovary Syndrome Society. Hum Reprod Update. 2012;18(2):146–70.

Espinós JJ, Calaf J, Estadella J, Checa MA. Hirsutism scoring in polycystic ovary syndrome: concordance between clinicians' and patients' self-scoring. Fertil Steril. 2010;94(7):2815–6.

Ferriman D, Gallwey JD. Clinical assessment of body hair growth in women. J Clin Endocrinol Metab. 1961;21:1440–7.

Hassa H, Tanir HM, Yildirim A, Senses T, Eskalen M, Mutlu FS. The hirsutism scoring system should be population specific. Fertil Steril. 2005;84(3):778–80.

Hatch R, Rosenfield RL, Kim MH, Tredway D. Hirsutism: implications, etiology, and management. Am J Obstet Gynecol. 1981;140(7):815–30.

Hertweck SP, Yoost JL, McClure ME, Siow Y, Brock GN, Wintergerst KA, et al. Ferriman-Gallwey scores, serum androgen and mullerian inhibiting substance levels in hirstute adolescent girls. J Pediatr Adolesc Gynecol. 2012;25(5):300–4.

Kim JJ, Chae SJ, Choi YM, Hwang SS, Hwang KR, Kim SM, Yoon SH, Moon SY. Assessment of hirsutism among Korean women: results of a randomly selected sample of women seeking pre-employment physical check-up. Hum Reprod. 2011;26:214–20.

Li R, Qiao J, Yang D, Li S, Lu S, Wu X, et al. Epidemiology of hirsutism among women of reproductive age in the community: a simplified scoring system. Eur J Obstet Gynecol Reprod Biol. 2012;163(2):165–9.

Metwally M. Hirsutism. Obstet Gynaecol Reprod Med. août 2012;22(8):211–4.

Moran C, Tena G, Moran S, Ruiz P, Reyna R, Duque X. Prevalence of polycystic ovary syndrome and related

disorders in Mexican women. Gynecol Obstet Invest. 2010;69:274–80.
Noorbala MT, Kefaie P. The prevalence of hirsutism in adolescent girls in Yazd, Central Iran. Iran Red Crescent Med J. 2010;12:111–7.
Rosenfield RL. Clinical practice. Hirsutism. N Engl J Med. 2005;353(24):2578–88.
Sagsoz N, Kamaci M, Orbak Z. Body hair scores and total hair diameters in healthy women in the Kirikkale Region of Turkey. Yonsei Med J. 2004;45:483–91.
Tellez R, Frenkel J. [Clinical evaluation of body hair in healthy women]. Rev Med Chil 1995;123:1349–1354.
Zhao JL, Chen ZJ, Shi YH, Geng L, Ma ZX, Li Y, Tang R. [Investigation of body hair assessment of Chinese women in Shandong region and its preliminary application in polycystic ovary syndrome patients]. Zhonghua Fu Chan Ke Za Zhi. 2007;42:590–4.

Skin Scoring for Mycosis Fungoides and Sézary Syndrome

142

Julia J. Scarisbrick

Contents

J.J. Scarisbrick (✉)
Department of Dermatology, Queen Elizabeth Medical Centre, University Hospitals Birmingham NHS Foundation Trust, Queen Elizabeth Hospital, Birmingham, UK
e-mail: juliascarisbrick@doctors.net.uk

P. Humbert et al. (eds.), *Agache's Measuring the Skin*,
DOI 10.1007/978-3-319-32383-1_112

Keywords
Skin scoring • Modified skin-weighted severity score • mSWAT • Cutaneous T-cell lymphoma • CTCL • Mycosis fungoides • Sézary syndrome

1 Part I: Primary Cutaneous T-Cell Lymphoma

Primary cutaneous T-cell lymphoma (CTCL) is typically an indolent lymphoma. Mycosis fungoides is the most common form of CTCL and 70 % of patients present with patches and plaques limited to the skin (stage I). Within 10 years from diagnosis, approximately 40 % of patients will progress to more advanced stages (stage II–IV) with development of skin tumors, erythroderma, or lymphadenopathy (Whittaker et al. 2003). Thirty percent present with advanced disease and have a poor prognosis with a median survival of 1-5 years. Sézary syndrome is a leukemic form of CTCL which presents with a triad of erythroderma, lymphadenopathy, and circulating atypical lymphocytes (Sézary cells).

In mycosis fungoides and Sézary syndrome, the skin is staged T1-T4 where T1 is defined by patches or plaques covering less than 10 % of the body surface area (BSA), T2 as patches and/or plaques covering greater than 10 % of BSA), T3 as presence of skin tumors, and T4 denotes erythroderma where greater than 80 % of BSA is involved. This staging system is used with staging

Table 1 Bunn and Lamberg staging system (Bunn and Lamberg 1979)

Stage	Tumor (T)	Lymph node (N)	Metastasis (M)
IA	T1: patches/plaques over <10 % of body surface	N0: no palpable nodes or histological evidence of MF	M0: no visceral involvement
IB	T2: patches/plaques over >10 % of body surface	N0	M0
IIA	T1 or T2	N1: palpable node; no histological evidence of MF	M0
IIB	T3: tumors	N0 or N1	M0
III	T4: erythroderma	N0 or N1	M0
IVA	T1–T4	N2, no palpable nodes but histological evidence of MF, or N3, palpable nodes and histological evidence of MF	M0
IVB	T1–T4	N0–N3	M1: histological visceral involvement

of lymph nodes (N0-3), and the presence or absence of metastasis (M0–1) to produce a TNM stage which is used to calculate a Bunn and Lamberg stage I-IVB (Table 1) (Bunn and Lamberg 1979). This staging system has been shown to have prognostic significance (Table 2) (Scarisbrick et al. 2014). The TNM staging has recently been revised by EORTC to include a blood stage (B0-B2) as well as to differentiate patches and plaques (T1a/b and T2a/b where "a" denotes patches and "b" plaques) and to record T-cell receptor clonality in blood and lymph node (where "a" denotes polyclonality and "b" monoclonality) (Table 3) (Olsen et al. 2007a). When more than one T rating might be applied, the highest is used for staging purposes, but in situations where both tumors and erythroderma exist simultaneously, both T ratings should be recorded (e.g., T4(3)). This provides a means of tracking patients with erythroderma plus tumors that may impact a poorer prognosis.

To skin score in MF/SS, the lesion type must be clearly defined prior to calculating BSA involved with each lesion type.

2 Part II: Defining Patch, Plaque, and Tumor Disease in MF

2.1 Patch

A patch disease is defined as flat erythema. A patch may be any size lesion without induration or significant elevation above the surrounding uninvolved skin. A patch must be flat and barely palpable but there may be light scaling (Figs. 1 and 2). The presence/absence of scale, crusting, poikiloderma (Fig. 3), and/or of hypo- or hyperpigmentation (Fig. 4) should be noted.

2.2 Plaque

Plaque disease is defined as any size lesion which is indurated, scaly, and possibly excoriated and includes keratoderma which is raised above the surface of the skin. It should be palpable with induration but without vertical growth or deep infiltration. Plaques are typically pink or red and maybe scaly (Fig. 5). Presence or absence of scale, crusting, ulceration, and/or poikiloderma should be noted. Histological features such as folliculotropism or large-cell transformation (25 % large cells defined as >4× diameter of normal lymphocytes), CD30+ or CD30−, and clinical features such as ulceration are also important to document.

2.3 Tumors

Tumors are any solid or nodular lesion greater than 1 cm in diameter with evidence of deep infiltration in the skin and/or vertical growth. Ulceration may occur with significant loss of superficial skin, including the entire epidermis and some portion of the upper dermis. Tumor

Table 2 Prognosis in mycosis fungoides and Sézary syndrome (Scarisbrick et al. 2014)

Stage	IA	IB	IIA	IIB	III	IVA	IVB
OS at 5 years	91–100 %	72–86 %	49–73 %	40–65 %	40–57 %	15–40 %	0–15 %
OS at 10 years	80–100 %	58–75 %	45–49 %	20–39 %	20–40 %	5–20 %	0–5 %
DSS at 5 years	96–100 %	96 % (81 %[a])	68 %	52–80 %	52 %	25–40 %	0 %
DSS at 10 years	92–98 %	83 % (36 %[a])	68 %	39–42 %	39 %	13–20 %	0 %
Median survival	35.5 years	12.1–26 years	10–15.8 years	2.9–4.7 years	3.6–4.7 years	13–25 months	13 months
Disease progression at 5 years	4 %	21 %	65 %	32 %		70 %	100 %
Disease progression at 10 years	10 %	39 %	65 %	60 %		70 %	100 %
Overall disease progression	9 %	20 %	34 %				
FFR at 5 years	50 %	36 %	9 %				
FFR at 10 years		31 %	3 %				

OS overall survival, *DSS* disease-specific survival, *FFR* freedom from relapse, *y* years, *mo* months
IB[a] Indicates DSS at 5 years and 10 years for stage IB patients with folliculotropic MF

Table 3 Revised TNMB staging for mycosis fungoides and Sézary syndrome (Olsen et al. 2007a)

Stage	Tumor (T)	Lymph node (N)	Blood (B)	Metastasis (M)
IA	T1: patches/plaques over <10 % of body surface	N0: no palpable nodes or histological evidence of MF	B0: <5 % peripheral blood lymphocytes atypical	M0: no visceral involvement
	T1a patches only	N0a clone negative	B0a clone negative	
	T1b plaques only	N0b clone positive	B0b clone positive	
			B1: >5 % of peripheral blood lymphocytes are atypical but <1,000/μl	
			B1a clone negative	
			B1b clone positive	
IB	T2: patches/plaques over >10 % of body surface	N0	B0–1	M0
	T2a patches only			
	T2b plaques only			
IIA	T1 or T2	N1: no histological evidence of MF (dermatopathic)	B0–1	M0
		N1a clone negative		
		N1b clone positive		
		N2: early involvement with MF, aggregates of atypical cells with preservation of nodal architecture		
		N2a clone negative		
		N2b clone positive		
IIB	T3: tumors, lesions >1 cm diameter with deep infiltration	N0–2	B0–1	M0
IIIA	T4: erythroderma >80 % BSA involved	N0–2	B0	M0
IIIB	T4: erythroderma	N0–2	B1	M0
IVA1	T1–T4	N0–2	B2: >1,000/μl circulating atypical lymphocytes (Sézary cells)	M0
IVA2		N3: lymph nodes involved with effacement of normal architecture	B0–2	M0
IVB	T1–T4	N0–N3	B0–2	M1: histological visceral involvement

lesions are often dome-shaped. There may be loss of epidermotropism and no scale (Fig. 6).

The total number of lesions, total BSA of lesions to include the largest size lesion, and region of body involved may be noted, but the significance of this finding is not known. Histological evidence of large-cell transformation and CD30 positivity is encouraged.

The distinction between patch and thin plaque lesions and between thick plaques and tumors is subjective (Olsen et al. 2007a; Oliver et al. 1978; Lamberg et al. 1984). Whether there should be a

Fig. 1 Patch of mycosis fungoides

Fig. 2 Patches of mycosis fungoides over the buttocks

minimum histological depth of infiltrate to distinguish plaque from tumor in order to corroborate this important assignment of T stage based on a single lesion has not been yet been determined.

2.4 Erythroderma

The ISCL criteria of erythroderma (T4 skin classification) is at least 80 % BSA involvement with

Fig. 3 Poikilodermatous MF – patch stage showing dyspigmentation, telangiectasia, and atrophy

patch/plaque disease (Fig. 7). In erythroderma the extent of skin tumor burden may be assessed with macular erythema equivalent to patch stage MF, erythema with induration/edema equivalent to plaque, and the presence of tumors noted.

3 Part III: Assessment of BSA Involvement in Dermatological Disease

Estimating BSA has been used in the assessment of burns for more than 60 years. Burn surface area determines fluid resuscitation volumes and allows triage of patients to specialist burn units. Accurate measurement of burn BSA is therefore critical for burn assessment.

There are various methods of calculating BSA which act as guides to assess the percentage of the

total body surface area affected. The three commonly used methods of estimating BSA are (1) palmar surface (Kirby and Blackburn 1981), (2) Wallace's "rule of nines" (Wallace 1951), and (3) the Lund and Browder chart (Lund and Browder 1944).

Fig. 4 Patches of hypopigmented MF over legs

3.1 Palmar Surface

Palmar surface assessment uses the palmar surface area of the patient's hand as an estimation guide (Kirby and Blackburn 1981). The surface area of the patient's palm including the fingers is assumed to be 1.0 % of the total body surface area. This method is useful to estimate relatively small affected BSA (less than 15 % of the total surface area) or larger areas (greater than 85 % when normal skin is counted), but in the middle ranges, this method is less accurate, because if the hand alone is used to assess the BSA affected, this may be overestimated as actual palmar surface is typically less than 1 % (Lee et al. 2007). This method is liable to further inaccuracies as textbook teaching of the definition of the palm or palmar surface varies (palm +/− fingers +/− thumb) and is assigned between 0.5 % and 1.5 % of the total body surface area.

This technique may be used to calculate affected skin or in a subtraction method by calculating the unaffected skin.

3.2 Wallace's "Rule of Nines" (Wallace 1951)

The "rule of nines" initially defined by Pulaski and Tennison in 1947 and published by Wallace in 1951 divides BSA into regions of 9 % or multiples of 9 %, leaving 1 % for the genitalia/perineum. The

Fig. 5 Plaque of mycosis fungoides

Fig. 6 Tumors of mycosis fungoides

Fig. 7 Erythroderma defined as skin involvement greater than 80 % BSA

percentage of involved skin for each body part is recorded, and the sum of affected areas is calculated. This tool is convenient when estimating BSA involvement in an adult, but is less applicable in young children because of proportion differences.

3.3 The Lund and Browder Chart (Lund and Browder 1944)

The Lund and Browder chart consists of two body diagrams, one of the anterior and one of the posterior body, to allow mapping of the affected skin. The percentage SA of body parts are shown on a table that varies according to age to reflect body parts affected by growth. This chart provides comprehensible and accurate estimation for both children and adults (Hettiaratchy and Papini 2004).

Measuring BSA is subjective and vulnerable to errors due to inaccurate percentages assigned to body parts or errors in calculation of body surface area affected. The latter has been shown to be particularly vulnerable due to inconsistencies in published methods of measuring BSA. The palmar method of calculating BSA has proven preferable in many studies because of the relative speed of calculations. However, review of the literature shows discrepancies exist over the percentage BSA of the hand/palm. The original Lund and Browder publication designated each surface of hand as 1.5 %; this was later reduced in the modified Lund and Browder detailing each surface of hand as 1.25 %. The palmar method defines the surface of the hand to equal 1 %.

While UK teaching has been that the patient's palm represents 1 % of BSA, definition of the palm is lacking (Jose et al. 2004). The Advanced Trauma Life Support (ATLS) guidelines define the palm to exclude fingers and equal to 1 % (American College of Surgeons 1993) which

contradicts UK teaching where the distal wrist creases to top of the finger tips (palm plus digits is equal to 1 %) (Kirby and Blackburn 1981).

Planimetry involves using an instrument to measure the area of a plane figure. Planimetry may be used to measure hand/palmar surface area. A review of the literature (Scarisbrick and Morris 2013) identified several planimetry studies investigating palm surface area and found the palm alone to be consistently 0.5 % men, although may be affected by stature and is relatively smaller in women (0.4 %) and larger in children (~0.6 %), and there is also variation with race and BMI. The palmar surface plus fingers is approximately 0.8 %, while palm alone is 0.5 %. Using the palm and fingers to equate to 1 %, BSA will result in overscoring and inaccurate calculation of BSA which will be accentuated by a weighted scoring system as used in CTCL.

Even with a constant BSA assessment method, there is significant inter-user variability in scoring. Constant scoring methods are required for future studies. Where possible the same scorer should score any individual.

4 Part IV: Skin Scoring in Dermatology

Measuring BSA affected by skin diseases has allowed various methods of skin scoring to be developed in dermatological diseases. These skin scoring methods have been developed to aid assessment of disease severity and for use in clinical trials to measure disease response. Scoring systems for inflammatory diseases such as psoriasis and atopic eczema have been developed. The PASI (Psoriasis Area Severity Index) was first published in 1978 for quantifying skin disease in psoriasis (Fredriksson and Pettersson 1978). The body is divided into four sections (head, trunk, arms, and legs). The percentage involvement of each of these areas is scored by itself, and then the four scores are combined into the final PASI. The Atopic Dermatitis Severity Index (ADSI) (Bahmer et al. 1991) involves mapping disease onto body diagrams and evaluating using grid-point counting (this involves mapping areas of affected skin onto diagrams and is time-consuming). SCORAD (SCORing Atopic Dermatitis) is a clinical tool used to assess the extent and severity of eczema (Scorad Index 1993). The sites affected by eczema are shaded on a drawing of a body and the rule of nines is used to calculate the affected area.

4.1 Skin Scoring in MF/SS

Distinction between stage T1 and T2 disease is dependent on the involvement of more than 10 % of BSA, while T4 is defined as greater than 80 % involvement. In T3 there is no minimum BSA involvement and the presence of one tumor >1 cm diameter defines disease. Skin scoring provides adjuvant information to staging in mycosis fungoides and Sézary syndrome by determining BSA involved with patch, plaques, and tumor. Skin scoring utilizes the measurement of affected BSA and type of skin lesion (patch, plaque, or tumor) and is used to allow quantification of skin tumor burden. Stevens et al. (2002) published a severity-weighted assessment tool (SWAT) which has been modified to produce the mSWAT which is now the preferred method of skin scoring in mycosis fungoides and Sézary syndrome. The mSWAT calculates BSA involved with patch, plaque, and tumor separately and then weights patch $\times 1$, plaque $\times 2$, and tumor $\times 4$ to produce a numerical value out of 400.

The overall mSWAT may not correlate with survival as a patient with widespread patches may have a high-percentage body surface area involved but a normal life expectancy, whereas tumors may be small 1-2 cm and cover a much smaller surface area but portray a poor prognosis and median survival of 3-5 years. However, the mSWAT score does allow responses to treatments to be quantified which is essential in clinical trials.

4.2 Lesion Weighting

For mSWAT calculations, the BSA of patch lesions are weighted $\times 1$, while BSA of plaque

lesions are weighted ×2 to reflect the heavier dermal infiltrate in plaques and higher skin tumor burden. Tumor BSA is multiplied by ×4. However, the thickness of the dermal infiltrate of tumors is far greater than four times that of patches (Rieger et al. 1989). However, multiplication ×4 was agreed because of the variability of investigators in assigning a lesion to plaque versus tumor (Olsen et al. 2011). Thus, any change in tumor BSA may be underscored in the total mSWAT compared to changes in patch and plaques. A skin scoring for erythroderma may also be calculated using the mSWAT with summation of BSA involvement with macular erythema ×1, equivalent to patch, plus erythema with induration/edema ×2, equivalent to plaque, and the BSA of tumors ×4. In this way the mSWAT may quantify extent of tumor burden in erythroderma while maintaining the ability to simultaneously track any tumors that may be present but does not track fissures or scale/exfoliation separately (Olsen et al. 2011).

4.3 SWAT

The original paper by Steven et al. in 2002 mapped clinical disease onto body diagrams distinguishing patch, plaque, and tumor. A 1 cm grid was randomly placed on the drawing, and the number of grid intersections overlying each lesion was counted to produce the percentage total BSA for each type of lesion (a method known as grid-point counting). Multiplication of patch ×1, plaque ×2, and tumor ×3 produced a numerical value or SWAT out of 300. This method was verified in a study of 1,194 records from 323 (Stevens et al. 2002).

4.4 mSWAT

This SWAT has been modified (modified SWAT or mSWAT) in a number of studies using assessment of BSA by rule of nines or Lund and Browder charts as opposed to grid mapping, and multiplication of tumors has been used as ×4 in some papers (Olsen et al. 2001, 2007b). This higher value for tumors is suggested as the infiltrative depth of a tumor is relatively greater than ratios 1:3 patch or 2:3 plaque, but higher than ×4 may further increase any discrepancies in BSA calculation. This modified SWAT is recommended as the skin scoring tool of choice to provide a global skin assessment of BSA weighted to skin lesion type and suggests the palmar method as the preferred method of calculating BSA. However, the total BSA of the hand in the modified Lund and Browder charts used is 5 %. If the palmar surface is taken as 1 % to represent palm plus fingers minus thumb, then each thumb would account for 0.5 % which is disproportional and may make this calculation invalid. Ensuring an accurate and robust measure of BSA is essential particularly as this scoring system is weighted and will multiply inconsistencies.

The mSWAT may be calculated using a chart (Fig. 8) showing the % BSA for the body regions. The BSA for patch, plaque, and tumor is calculated separately and then multiplied by the weighting factor.

It is recommended that in clinical trials mSWAT calculations should be performed by the same investigator at all time points to eliminate interobserver variability for a given patient (Olsen et al. 2011). If the same investigator cannot perform all the assessments, then all personnel grading the same patient must have completed prior training, ideally before study initiation. Standardized photographs of the skin are recommended to document the appearance of skin lesions at baseline and times of response/progression.

The recent international consensus paper from the EORTC (European Organisation for Research and Treatment of Cancer Cutaneous Lymphoma Task Force) and International Society for Cutaneous Lymphoma (ISCL) provides end points and response criteria for CTCL and recommends the mSWAT as the preferred method for determining skin tumor burden for both mycosis fungoides and Sézary syndrome (Olsen et al. 2011).

An iPhone application (CL-App) has been developed with Guy's and St Thomas' NHS Trust (2012) to aid skin scoring in CTCL by providing interactive body diagrams to score BSA involved as opposed to standard charts.

Body region (%BSA)	Patch*	Plaque*	Tumor*
Head (7 %)			
Neck (2%)			
Anterior trunk (13%)			
Arms (8%)			
Forearms (6%)			
Hands (5%)			
Posterior trunk (13%)			
Buttocks (5%)			
Thighs (19%)			
Legs (14%)			
Feet (7%)			
Groin (1%)			
Subtotal of lesion BSA			
Weighting factor	x1	x2	x4
Subtotal lesion BSA x weighting factor			
mSWAT score = summation of each column line above =			

Fig. 8 The body surface area of different body parts for calculating modified SWAT

This has the advantage over charts as mSWAT calculations are made electronically and this is likely to reduce user error. This application allows more rapid scoring of mSWAT within the clinical setting. The application also provides information on how to perform scoring. However, the availability requires access to an iPhone/iPad.

4.5 Discussion

In mycosis fungoides and Sézary syndrome, the mSWAT is the preferred method of skin scoring. The palmar surface of 0.5 % should be used as the measurement tool to skin score as this is relatively constant with age, stature, and different races (Scarisbrick and Morris 2013). A constant training method should be used to teach mSWAT calculations as there is significant inter-user variability. Where possible the same scorer should score any individual. Clinical photography is a useful adjuvant to represent skin involvement but skin scoring from photos is difficult.

The mSWAT should be used for skin scoring in mycosis fungoides and Sézary syndrome and may allow more accurate comparisons between centers which is essential for future clinical trials.

References

American College of Surgeons. Committee on trauma advanced. Trauma life support manual for physicians. Chicago: American College of Surgeons; 1993.

Bahmer FA, Schafer J, Schubert HJ. Quantification of the extent and the severity of atopic dermatitis: the ADASI score [letter]. Arch Dermatol. 1991;127:1239–40.

Bunn PA, Lamberg SI. Report of the committee on staging and classification of cutaneous T-cell lymphomas. Cancer Treat Rep. 1979;63:725–8.

Consensus Report of the European Task Force on Atopic Dermatitis. Severity scoring of atopic dermatitis: the SCORAD index. Dermatology. 1993;186:23–31.

Fredriksson T, Pettersson U. Severe psoriasis – oral therapy with a new retinoid. Dermatologica. 1978;157(4): 238–44.

Hettiaratchy S, Papini R. ABC of burns: initial management of a major burn: II – assessment and resuscitation. Br Med J. 2004;329:101–3.

Jose RM, Roy DK, Vidyadharan R, Erdmann M. Burns area estimation-an error perpetuated. Burns. 2004; 30(5):481–2.

Kirby NG, Blackburn G. Field surgery pocket book. London: HMSO; 1981. p. 85.

Lamberg SI, Green SB, Byar DP, et al. Clinical staging for cutaneous T-cell lymphoma. Ann Intern Med. 1984;100:187–92.

Lee JY, Choi JW, Kim H. Determination of body surface area and formulas to estimate body surface area using the alginate method. J Physiol Anthropol. 2007;26 (4):475–83.

Lund C, Browder N. The estimation of areas of burns. Surg Gynecol Obstet. 1944;79:352–8.

Oliver HB, Carr DT, Rubin P, et al. American Joint Committee on Cancer: AJCC cancer staging manual. 1st ed. Chicago: Whiting Press; 1978.

Olsen E, Duvic M, Frankel A, et al. Pivotal phase III trial of two dose levels of denileukin diftitox for the treatment of cutaneous T-cell lymphoma. J Clin Oncol. 2001;19:376–88.

Olsen E, Vonderheid E, Pimpinelli N, et al. Revisions to the staging and classification of mycosis fungoides and Sézary syndrome: a proposal of the International Society for Cutaneous Lymphomas (ISCL) and the cutaneous lymphoma task force of the European Organization of Research and Treatment of Cancer (EORTC). Blood. 2007a;110:1713–22.

Olsen EA, Kim YH, Kuzel TM, et al. Phase IIb multicenter trial of vorinostat in patients with persistent, progressive, or treatment refractory cutaneous T-cell lymphoma. J Clin Oncol. 2007b;25:3109–15.

Olsen EA, Whittaker S, Kim YH, et al. Clinical end points and response criteria in mycosis fungoides and sézary syndrome: a consensus statement of the international society for cutaneous lymphomas, the united states cutaneous lymphoma consortium, and the cutaneous lymphoma task force of the european organisation for research and treatment of cancer. Clin Oncol. 2011; 29(18):2598–607.

Rieger E, Smolle J, Hoedl S, et al. Morphometrical analysis of mycosis fungoides on paraffin-embedded sections. J Cutan Pathol. 1989;16:7–13.

Scarisbrick J, Morris SJ. How big is your hand & should you use it to skin score. Br J Dermatol. 2013;169(2): 260–5.

Scarisbrick JJ, Kim YH, Whittaker SJ, Wood GS, Vermeer MH, Prince HM, Quaglino P. Prognostic factors, prognostic indices and staging in mycosis fungoides and sézary syndrome: where are we now? Br J Dermatol. 2014;170(6):1226–36.

Stevens SR, Ke MS, Parry EJ, et al. Quantifying skin disease burden in mycosis fungoides-type cutaneous T-cell lymphomas: the severity-weighted assessment tool (SWAT). Arch Dermatol. 2002;138(1):42–8.

Wallace AB. The exposure treatment of burns. Lancet. 1951;257:501–4.

Whittaker SJ, Marsden JR, Spittle M, Russell Jones RJ. Joint British Association of Dermatologists and U.K. Cutaneous Lymphoma Group guidelines for the management of primary cutaneous T-cell lymphomas. Br J Dermatol. 2003;149:1095–107.

Impact of Excess Body Weight on Skin Hydration and Biomechanics

143

Liliana Tavares, Lídia Palma, Osvaldo Santos, MªAngélica Roberto, Mª Julia Bujan, and Luís Monteiro Rodrigues

Contents

L. Tavares • L. Palma
CBIOS – Research Center for Health Science and Technologies, Universidade Lusófona, Lisbon, Portugal

O. Santos
Faculty of Medicine, Public Health Preventive Medicine Institute and Environmental Health Institute, Universidade de Lisboa, Lisbon, Portugal

M. Roberto
Plastic Surgery Service, Rua José António Serrano, Lisboa, Lisbon, Portugal

M.J. Bujan
Faculty of Medicine and Health Science, Universidad de Alcalá de Henares, Campus Universitario, Ctra. Barcelona, Madrid, Spain

L.M. Rodrigues (✉)
CBIOS – Research Center for Health Science and Technologies, Universidade Lusófona, Lisbon, Portugal

Department of Pharmacological Sciences, Universidade de Lisboa – School of Pharmacy, Lisbon, Portugal
e-mail: monteiro.rodrigues@ulusofona.pt; monteirorodrigues@sapo.pt

P. Humbert et al. (eds.), *Agache's Measuring the Skin*, DOI 10.1007/978-3-319-32383-1_113

Keywords
Overweight • BMI • Skin physiology • Epidermal water • Skin biomechanics

1 Introduction

The term "obesity" suggests several images that illustrate different personal, social, and/or professional impacts, explaining the diversity of definitions found for this disease (Longo et al. 2012). Obesity can be defined as a condition involving an excess of fatty tissue, which increases the risk of premature illness and mortality (Villareal et al. 2005). This definition requires the quantification of adipose tissue by the Quetelet index (weight/height^2) kg/m^2 (Garrow and Welster 1985), commonly known as the body mass index (BMI) (Weigley and Adolphe 1976).

The available data on the prevalence of obesity is substantially affected by its definition, and the data is not always representative, often hindering comparison between different studies and groups (Wang et al. 2007). The most recent studies on the prevalence of obesity in the United States show that more than one third of adults and almost 17 % of children and adolescents were obese in 2009–2010 (Ogden et al. 2007, 2012). It is also suggested that differences in prevalence between men and women decreased between 1999–2000 and 2009–2010, with prevalence of male obesity reaching the same level of the female (Ogden et al. 2012). Regarding age, the prevalence of

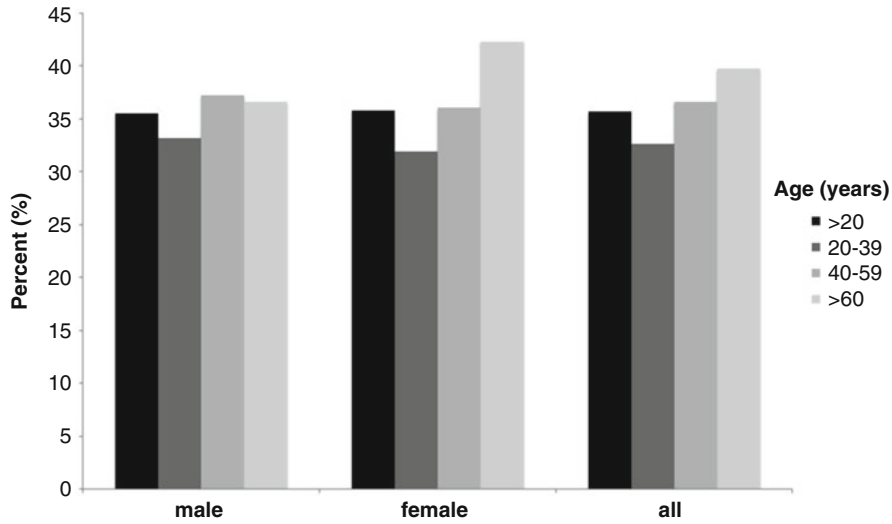

Fig. 1 Prevalence of obesity in adults over age 20 in the United States (2009–2010), stratified by age and gender (Adapted from Ogden et al. 2007)

obesity was higher among older women compared with younger. These age differences were not detected in males. In children and adolescents, the prevalence of obesity was higher among adolescents than preschool children. According to this same study, no change in the prevalence of obesity was noted in recent years or even in the last decade for male (children and adults), but the same is not true for females (Ogden et al. 2012) (Fig. 1).

According to the WHO, in Europe in 2008, over 50 % of men and women were overweight, and about 23 % of women and 20 % of men were obese (WHO Europe 2012). Based on the latest European Union previews, up to 70 % of adults may be considered overweight, while obesity can reach 30 % in adults (WHO Europe 2012). The WHO estimates that the number of overweight children in Europe has increased steadily between 1990 and 2008, and over 60 % of children who are overweight before puberty will be overweight in early adult age (WHO Europe 2012).

Morbidity is well known and documented (Bray et al. 2009; Shipman and Millington 2011; Guida et al. 2010), and in most cases, obesity amplifies the effects of other pathologies such as skin diseases (e.g., ulcers and healing, or infections). Specifically, beyond stretch marks, lymphedema, cellulitis, intertrigo, and lower limb stasis pigmentation, it has also been related to scleroderma, gangrene, and acanthosis nigricans (Shipman and Millington 2011). Nevertheless, it is not clear whether obesity per se is a cause of skin disease, although biomechanical and barrier modifications maybe present.

In general, the epidermal barrier is designed to prevent the loss of water and other components through the skin (Darlenski and Fluhr 2012; Venus et al. 2010). It is an essential property, especially dependent on the outermost layer, the stratum corneum (SC). Due to its constitution, the stratum corneum is also responsible for the mechanical strength of the skin. Thus, this barrier function seems to be closely related to the "envelope" function, and it has been demonstrated that when the skin barrier function is compromised, the biomechanical properties of the skin are also altered (Pederson et al. 2006) (Table 1). From the structural point of view, this biomechanical behavior allows the definition of the body contour even during dramatic shape variations such as in pregnancy, or when a marked increase or loss of weight occurs (Darlenski and Fluhr 2012). These properties illustrate a complex anisotropic

Table 1 Relationship between variables representing the "envelope" and the epidermal "barrier" functions

	Barrier function	Envelope function
TEWL	– – –	* * *
Epidermal hydration	+++	* * *
Biomechanical properties	* * *	+++

TEWL transepidermal water loss, +++ positive influence, – – – negative influence, *the published data determine a connection – see text

viscoelastic behavior that determines a nonlinear response when submitted to a force (physiological or not, such as the application of suction) (Darlenski and Fluhr 2012; Wu et al. 2006).

These properties change with age or gender, and also with many different pathological conditions. However, regarding obesity, modifications of skin physiology are still poorly described. TEWL changes have been related to the BMI in obese patients (Darlenski and Fluhr 2012; Guida et al. 2010; Löffler et al. 2002). A relationship between obesity and skin hydration (xerosis), increased TEWL, and sweat activity has been reported (Wu et al. 2006). However, most of these studies still provide insufficient information, and the information is difficult to compare when applying different methodologies and individuals. Therefore, in the present study, the focus is centered in comparing skin behavior of normal and overweight individuals in regard to these two basic properties of in vivo skin – barrier function and biomechanical behavior.

2 Material and Methods

2.1 Subjects

A convenience sample of 30 healthy female volunteers aged between 29 and 46 (36 ± 4) years old, was selected after informed consent, in accordance with previously established inclusion criteria. The applied protocols were in full compliance with all ethical standards set by the Declaration of Helsinki and its amendments (World Medical Association declaration of Helsinky 2004).

In order to minimize individual variability and to make the sample as homogeneous as possible, noninclusion criteria regarded pregnancy or lactation, cutaneous signs, pigmentation or scarring in the experimental area, history of allergy, any skin treatments and regular practice of sport.

Restrictions were also imposed to reduce external interference:

- Application of cosmetics on the skin areas involved
- Washing the study areas with soap or shower gel on the day of laboratory measurements
- The use of tight underwear or any cause of friction in the area under study
- Oral and/or topical medication potentially interfering with measurements (mandatory to inform the investigator about any dermatological and/or ongoing pharmacological treatments)
- Sporadic utilization of antihistamines or vitamins (vitamin A) preceding the study and during its course
- Vaccination in the 3 weeks prior to the study
- Exposure to water via sauna/Turkish bath or immersion in an ocean/pool in the 2 days before the study
- Intense sun exposure in the 2 weeks before the study
- Consumption of coffee and/or tea in the 48 h prior to the study

2.2 Instrumentation

Taking into account the announced objectives, the "barrier" function was characterized by the TEWL, obtained with the Tewameter TM300 (CK electronics, FRG), expressed in $g/m^2/h$, and by the epidermal hydration, measured by the Moisture Meter SC (Delphin Technology D) system, which is based on the measurement of the "capacitance" and expressed in AU (arbitrary units). The "envelope" function was measured by the Cutometer CM575 systems (in mm) (Rodrigues and EEMCO 2001; Seidenari et al. 2006; Darlenski et al. 2009) from CK Technologies, FRG by several utility

descriptors. The chosen descriptors were the full recovery of the deformation at the end of the stress period (Ua), total elasticity of the skin (Ua/Uf, including pulse stretching and recovery), total elasticity or elastic function (Ur/Ue), and the viscoelastic ratio (Uv/Ue, e.g., the relationship between the elastic and the viscoelastic extension).

2.3 Experimental Design

This study was conducted at the Research Centre in Biosciences and Health Technologies (CBIOS from Universidade Lusófona) and the Plastic Surgery Department of the Hospital S. José, in collaboration with the service of General Surgery from the same hospital.

The sample was divided into three groups – Group I with BMI between 19.9 and 24.9 kg/m^2, Group II with BMI between 25 and 29.9 kg/m^2, and Group III with BMI between 30 and 39.9 kg/m^2.

After confirming all inclusion and noninclusion criteria, volunteers were submitted to the evaluations required for the quantitative description of the respective "barrier" and "envelope" function characterizations. Volunteers were allowed to acclimatize for a period of about 20 min to ensure full adaptation of their skin functions to ambient conditions. All evaluations were conducted in the laboratory under controlled temperature and humidity (21 ± 1 °C, 45 ± 5 %), in the absence of heat sources and forced convection, according to methodology and previously published recommendations (Rogiers and EEMCO Group 2001; Piérard 1999).

2.4 Statistics

Statistical analysis (descriptive and comparative) was performed using the SPSS (v 20.0) software by univariate analysis with calculation of measures of central tendency and dispersion. Pearson and Spearman tests were also applied, according to the (normal or non-normal, respectively) distribution of variables, confirmed via the t-student and Mann-Whitney tests, and a 95 % confidence level was adopted. An adjustment for age was also applied.

3 Results and Discussion

3.1 TEWL and Epidermal Hydration

Some studies indicate that TEWL increases with BMI, while others suggest that TEWL decreases in obese individuals, although not stratified by classes (obese and overweight individuals including class I and II, and morbidly obese individuals) (Guida et al. 2010; Löffler et al. 2002; Nino et al. 2012; Sotoodian and Maibach 2012). In our experimental conditions, overweight and obese individuals have shown lower TEWL values than individuals with a normal body mass (Table 2). Until now, the lack of studies with sample stratification by BMI class has not allowed comparisons, but our results seem to favor related previously published data in this direction (Guida et al. 2010; Nino et al. 2012; Yosipovich et al. 2007; Millington 2012; Hidalgo 2002; Brown et al. 2004; Boza et al. 2012). These individuals (overweight and obese) also show higher epidermal hydration values than individuals with lower (normal) BMIs.

Dry skin is a well-known common problem in obese patients, necessarily related to a poor epidermal hydration (Nino et al. 2012; Yosipovich et al. 2007). However, our results have consistently shown that individuals with a BMI between 25 and 39.9 kg/m^2 had higher values of epidermal hydration. It appears that increased TEWL values always correspond to lower values of surface hydration. Since higher TEWL values correspond to greater water loss through the skin, this seems also to reflect lower water retention capacity and thus lower epidermal surface hydration.

Potentially related, a recent study demonstrated for the first time a clear influence of dietary habits, in particular the consumption of water, on skin hydration and elasticity (Palma et al. 2012a, b).

Table 2 Descriptive statistics regarding evaluated variables related with the barrier function (TEWL and epidermal hydration) in different anatomical areas (see text)

		N	Mean	Std. deviation	Std. error	95 % confidence		Minimum	Maximum
						Lower bound	Upper bound		
TEWL zygomatic	Normal	10	11.5	4.3	1.4	8.4	14.5	6.6	19.0
	Excess weight	10	7.8	3.3	1.0	5.4	10.1	5.4	16.7
	Obese	10	8.4	2.6	0.8	6.5	10.2	5.6	11.8
TEWL forehead	Normal	10	10.1	4.1	1.3	7.2	13.0	4.5	17.9
	Excess weight	10	8.0	2.9	0.9	6.0	10.1	1.5	12.4
	Obese	10	8.5	2.4	0.7	6.8	10.2	6.0	14.1
TEWL breast	Normal	10	13.6	20.8	6.6	−1.3	28.4	2.3	72.4
	Excess weight	10	7.5	5.8	1.8	3.4	11.7	2.8	20.1
	Obese	10	9.8	5.4	1.7	5.9	13.6	4.1	18.7
TEWL abdomen	Normal	10	7.1	2.7	0.9	5.1	9.0	3.4	11.4
	Excess weight	10	3.5	1.4	0.4	2.6	4.5	1.9	5.9
	Obese	10	4.7	2.9	0.9	2.6	6.8	2.1	12.1
Epidermal hydration zygomatic	Normal	10	58.6	16.0	5.0	47.2	70.0	30.0	80.0
	Excess weight	10	59.2	22.7	7.2	43.0	75.4	22.0	91.0
	Obese	10	67.9	11.9	3.8	59.4	76.4	47.0	86.0
Epidermal hydration forehead	Normal	10	57.8	19.8	6.3	43.6	72.0	16.0	86.0
	Excess weight	10	61.7	19.4	6.1	47.8	75.6	18.0	80.0
	Obese	10	67.4	17.5	5.5	54.9	79.9	35.0	92.0
Epidermal hydration breast	Normal	10	53.3	24.3	7.7	35.9	70.7	14.0	83.0
	Excess weight	10	66.5	15.0	4.8	55.7	77.3	43.0	89.0
	Obese	10	75.5	20.8	6.6	60.6	90.4	48.0	105.0
Epidermal hydration abdomen	Normal	10	51.8	23.8	7.5	34.8	68.8	18.0	91.0
	Excess weight	10	47.9	10.4	3.3	40.5	55.3	33.0	68.0
	Obese	10	40.7	15.6	4.9	29.5	51.9	15.0	61.0

3.2 Biomechanics

Previous studies allowed us to consider variables Ua and the ratios Ua/Uf, Uv/Ue, and Ur/Ue, as well as the most relevant descriptors of the skin biomechanical condition. Some of these studies correlate these descriptors with weight variation and with subcutaneous adipose tissue. These seem to be better fitted to approach the ability of the skin to distend and retract in an immediate or delayed form, allowing an overview of its mechanical condition and also a quantitative description of its plastic, elastic, and viscoelastic characteristics (Krueger et al. 2011; Ryu et al. 2008; Verhaegen et al. 2010; Xin et al. 2010; Paye et al. 2007; Ezure and Amano 2010).

Table 3 shows the results for the registered biomechanical descriptors. Ua corresponds to the maximum contractile recovery of the skin

Table 3 Descriptive statistics regarding evaluated variables related with the envelope function (biomechanical descriptors indentified in the text) in different anatomical areas

		N	Mean	Std. deviation	Std. error	95 % confidence		Minimum	Maximum
						Lower bound	Upper bound		
Ua/Uf zygomatic	Normal	10	0.430	0.299	0.095	0.216	0.644	0.132	0.774
	Excess weight	10	0.130	0.036	0.011	0.105	0.156	0.063	0.187
	Obese	10	0.119	0.042	0.013	0.089	0.150	0.072	0.219
Ua/Uf forehead	Normal	10	0.801	0.100	0.032	0.729	0.873	0.689	1.000
	Excess weight	10	0.083	0.068	0.021	0.035	0.132	0.048	0.273
	Obese	10	0.063	0.020	0.006	0.049	0.077	0.041	0.098
Ua/Uf breast	Normal	10	0.884	0.094	0.030	0.817	0.951	0.705	0.980
	Excess weight	10	0.120	0.041	0.013	0.091	0.150	0.076	0.217
	Obese	10	0.138	0.049	0.015	0.103	0.173	0.058	0.242
Ua/Uf abdomen	Normal	10	0.794	0.229	0.072	0.631	0.958	0.233	0.959
	Excess weight	10	0.164	0.046	0.015	0.131	0.197	0.116	0.250
	Obese	10	0.149	0.024	0.008	0.132	0.166	0.109	0.187
Ur/Ue zygomatic	Normal	10	0.436	0.369	0.117	0.171	0.700	0.084	1.005
	Excess weight	10	0.080	0.021	0.007	0.065	0.095	0.043	0.115
	Obese	10	0.076	0.024	0.008	0.058	0.093	0.047	0.133
Ur/Ue forehead	Normal	10	1.032	0.444	0.140	0.715	1.350	0.661	2.043
	Excess weight	10	0.062	0.064	0.020	0.017	0.108	0.034	0.243
	Obese	10	0.041	0.011	0.003	0.033	0.049	0.026	0.062
Ur/Ue breast	Normal	10	1.199	0.378	0.119	0.929	1.469	0.705	1.809
	Excess weight	10	0.086	0.040	0.013	0.058	0.115	0.047	0.187
	Obese	10	0.094	0.037	0.012	0.067	0.120	0.037	0.165
Ur/Ue abdomen	Normal	10	0.980	0.396	0.125	0.696	1.263	0.185	1.480
	Excess weight	10	0.119	0.040	0.013	0.090	0.148	0.071	0.195
	Obese	10	0.102	0.028	0.009	0.082	0.122	0.064	0.146
Uv/Ue zygomatic	Normal	10	0.352	0.334	0.106	0.113	0.592	0.076	1.070
	Excess weight	10	0.073	0.015	0.005	0.063	0.083	0.037	0.085
	Obese	10	0.068	0.013	0.004	0.059	0.077	0.043	0.087
Uv/Ue forehead	Normal	10	0.970	0.614	0.194	0.531	1.409	0.338	2.277
	Excess weight	10	0.072	0.116	0.037	−0.011	0.155	0.028	0.402
	Obese	10	0.038	0.011	0.004	0.030	0.046	0.020	0.057
Uv/Ue breast	Normal	10	0.867	0.315	0.100	0.641	1.093	0.449	1.487
	Excess weight	10	0.070	0.026	0.008	0.052	0.089	0.037	0.117
	Obese	10	0.077	0.033	0.010	0.054	0.101	0.036	0.134

(*continued*)

Table 3 (continued)

		N	Mean	Std. deviation	Std. error	95 % confidence		Minimum	Maximum
						Lower bound	Upper bound		
Uv/Ue abdomen	Normal	10	0.614	0.296	0.094	0.403	0.826	0.102	1.128
	Excess weight	10	0.086	0.030	0.009	0.065	0.108	0.043	0.133
	Obese	10	0.056	0.014	0.005	0.046	0.066	0.035	0.072
Ua zygomatic	Normal	10	0.361	0.119	0.038	0.276	0.446	0.198	0.583
	Excess weight	10	0.307	0.097	0.031	0.237	0.377	0.124	0.467
	Obese	10	0.276	0.128	0.040	0.184	0.367	0.144	0.565
Ua forehead	Normal	10	0.353	0.245	0.077	0.177	0.528	0.126	0.840
	Excess weight	10	0.173	0.156	0.049	0.061	0.284	0.098	0.609
	Obese	10	0.136	0.048	0.015	0.101	0.171	0.077	0.223
Ua breast	Normal	10	0.517	0.215	0.068	0.363	0.670	0.259	0.980
	Excess weight	10	0.255	0.102	0.032	0.182	0.328	0.148	0.488
	Obese	10	0.307	0.141	0.044	0.207	0.408	0.111	0.613
Ua abdomen	Normal	10	0.738	0.245	0.077	0.563	0.913	0.419	1.070
	Excess weight	10	0.372	0.140	0.044	0.272	0.472	0.226	0.650
	Obese	10	0.296	0.054	0.017	0.258	0.335	0.208	0.371

(in mm), showing higher values for the normal weight individuals. Skin adapts to a new body contour following weight increase, apparently denoting greater distensibility. Therefore, we would expect that this recovery could be also higher in groups corresponding to a higher BMI. However, in our sample, values obtained in higher BMIs are lower than those from the normal weight group. This might imply some loss of resilience, given that the strain skin has been subjected for so long. In any case, our results agree with a previously published study (although performed in mice), suggesting a negative correlation of Ua with weight (Ezure and Amano 2009).

Concerning the ratios Ua/Uf, corresponding to biological elasticity (given by the correlation between the recovery and the maximum extensibility of the skin), and Ur/Ue, corresponding to the elastic function variables (the ratio between the immediate recovery Ur and immediate distension of the skin Ue), we normally consider for both ratios. The higher the ratio, the better its biomechanical behavior. Our results have shown higher values for the normal weight group for both ratios.

An inverse correlation between the Ua/Uf ratio and sagging has been described in obesity (Krueger et al. 2011; Ryu et al. 2008; Verhaegen et al. 2010; Xin et al. 2010; Paye et al. 2007; Ezure and Amano 2009, 2010; Barbenel 2006; Blaak et al. 2011). According to these authors, the larger the value, the lower the sagging and hence higher firmness and better biomechanical behavior of the skin.

Another study identified a decrease of Ur/Ue in obese mice previously subjected to a high-fat diet, and this parameter correlated well with the degradation of the biomechanical behavior (Xin et al. 2010).

With weight gain, a better biomechanical behavior of the skin is expected, in view of the adaptability to new body contour. Here there is a negative change in biomechanical behavior with increasing weight.

Regarding the viscoelasticity, e.g., the ratio between the immediate and the delayed distension Uv/Ue, the higher its value, the better the ability of the skin to react after stretching, and therefore, the better its viscoelastic behavior. It would be expected that the skin's ability to react after stretching, i.e., its viscoelastic behavior, might improve with the weight gain as a consequence of the skin's progressive adaptation, to a new body contour. However, our results have shown that the viscoelastic behavior decreases with the weight gain.

Previous studies identified statistically significant differences among different age groups and as well as different anatomical areas (Krueger et al. 2011; Ezure and Amano 2010; Wa and Maibach 2010). The age adjustment performed helps to avoid the influence of this factor. Furthermore, our results are consistent with those studies referring significant differences among anatomical sites. Nevertheless, our results do not identify any significant statistical difference between the BMI groups for most of the anatomical areas. This is likely due to sample size limitations.

4 Conclusions

Our study clearly demonstrates that excess body weight alters the in vivo epidermal barrier function, superficial hydration, and biomechanical behavior of the skin, depending on the considered anatomical area. The magnitude of excess body weight seems to determine different changes – more pronounced deterioration of the skin biomechanical condition is registered with higher BMI, which also corresponds to higher TEWL. This might be related with the variety of dermatoses and other related skin problems observed in obese individuals when compared to normal weight individuals. Further studies involving wider populations, with all classes of BMI, are needed to better understand the pathophysiological impact of this condition on the skin's normal physiology.

References

Barbenel JC. Identification of Langer's lines. In: Serup J, Jemec G, Grove G, editors. Handbook non-invasive methods and the skin. 2nd ed. Texas: C.H.I.P.S; 2006. p. 565–9.

Blaak J, Lüttje D, John SM, Schürer NY. Irritability of the skin barrier: a comparison of chronologically aged and photo-aged skin in elderly and young adults. Eur Geriatr Med. 2011. doi:10.1016/j.eurger.2011.05.011.

Boza JC, Trindade EN, Peruzzo J, Sachett L, Rech L, Cestari TF. Skin manifestations of obesity: a comparative study. JEADV. 2012;26:1220–3.

Bray G, Clearfield M, Fintel D, Nelinson D. Overweight and obesity: the pathogenesis of cardiometabolic risk. Clin Cornerstone. 2009;9(4):30–42.

Brown J, et al. Skin problems in people with obesity. Nurs Stand. 2004;18(35):38–42.

Darlenski R, Fluhr J. Influence of skin type, race, sex, and anatomic location on epidermal barrier function. Clin Dermatol. 2012;30:269–73.

Darlenski R, Sassning S, Tsankov N, Fluhr JW. Non-invasive in vivo methods for investigation of the skin barrier physical properties. Eur J Pharm Biopharm. 2009;72:295–303.

Ezure T, Amano S. Increased subcutaneous adipose tissue impairs dermal function in diet-induced obese mice. Exp Dermatol. 2009;19:878–82.

Ezure T, Amano S. Influence of subcutaneous adipose tissue mass on dermal elasticity and sagging severity in lower cheek. Skin Res Technol. 2010;16:332–8.

Garrow JS, Welster J. Quetelet's index (W/H2) as a measure of fatness. Int J Obes. 1985;9:147–53.

Guida B, Nino M, Perrino NR, Laccetti R, Trio R, Labella S, Balato N. The impact of obesity on skin disease and epidermal permeability barrier status. J Eur Acad Dermatol Venereol. 2010;24(2):191–5.

Hidalgo L. Dermatological complications of obesity. Am J Clin Dermatol. 2002;3(7):497–506.

Krueger N, Luebberding S, Oltmer M, Streker M, Kerscher M. Age-related changes in skin mechanical properties: a quantitative evaluation of 120 females subjects. Skin Res Technol. 2011;17:141–8.

Löffler H, Aramaki J, Effendy I. The influence of body mass index on skin susceptibility to sodium lauryl sulfate. Skin Res Technol. 2002;8:19–22.

Longo DL, Fauci AS, Kasper DL, Hauser SL, Jameson JL, Loscalzo J. Harrison's principles of internal medicine. 18th ed. New York: McGraw-Hill; 2012.

Millington G. Obesity, genetics and the skin. Clin Exp Dermatol. 2012;38:50–6.

Nino M, Franzese A, Ruggiero Perrino N, Balato N. The effect of obesity on skin disease and epidermal permeability barrier status in children. Pediatr Dermatol. 2012;29(5):567–570.

Ogden C, Yanovski S, Carroll M, Flegal K. The epidemiology of obesity. Gastroenterology. 2007;132:2087–102.

Ogden CL, Carroll MD, Kit BK, Flegal KM. Prevalence of obesity in the United States, 2009–2010, NCHS data brief, vol. 82. Hyattsville: National Center for Health Statistics; 2012.

Palma ML, Monteiro C, Tavares L, Bujan MJ, Rodrigues LM. Relationship between the dietary intake of water and skin hydration. Biomed Biopharm Res. 2012a; 2(9):173–81.

Palma L, Tavares L, Monteiro C, Bujan MJ, Rodrigues LM. Diet water seems to influence skin hydration and biomechanics. World Congress of the International Society for Biophysics and Imaging of the Skin (ISBS), Copenhagen, 28–30 Nov 2012.

Paye M, Mac-Mary S, Elkhyat A, Tarrit C, Mermet P, Humbert PH. Use of the Reviscometer for measuring cosmetics-induced skin surface effects. Skin Res Technol. 2007;13:343–9.

Pederson L, Jemec GB. Mechanical properties and barrier function of healthy human skin. Acta Derm Venereol.2006;86:308–311. In: Menon GKK, editor. Barrier functions of human skin: a holistic view. Skin Pharmacol Physiol. 2009;22:178–89.

Piérard GE. EEMCO guidance to the in vivo assessment of tensile functional properties of the skin. Part 1: relevance to the structures and ageing of the skin and subcutaneous tissues. Skin Pharmacol Appl Skin Physiol. 1999;12(6):352–62.

Rodrigues L, EEMCO. EEMCO guidance to the in vivo assessment of tensile functional properties of the skin. Part 2: instrumentation and test modes. Skin Pharmacol Appl Skin Physiol. 2001;14(1):52–67.

Rogiers V, EEMCO Group. EEMCO guidance for the assessment of transepidermal water loss in cosmetic sciences. Skin Pharmacol Appl Skin Physiol. 2001; 14(2):117–28.

Ryu HS, Joo YH, Kim SO, Park KC, Youn SW. Influence of age and regional differences on skin elasticity as measured by the Cutometer. Skin Res Technol. 2008;14:354–8.

Seidenari S, Giusti F, Pellacani G. Non-invasive methods and assessment of skin diseases. In: Serup J, Jemec G, Grove G, editors. Handbook non-invasive methods and the skin. 2nd ed. Texas: C.H.I.P.S; 2006. p. 37–46.

Shipman AR, Millington GWM. Obesity and the skin. Br J Dermatol. 2011;165:743–50.

Sotoodian B, Maibach H. Noninvasive test methods for epidermal barrier function. Clin Dermatol. 2012;30:301–10.

Venus M, Waterman J, McNab I. Basic physiology of the skin. Surgery. 2010;28(10):469–72.

Verhaegen PDHM, Res EM, Engelen AV, Middelkoop E, Zuijlen PPMV. A reliable, non-invasive measurement tool for anisotropy in normal skin and scar tissue. Skin Res Technol. 2010;16:325–31.

Villareal DT, Apovian CM, Kushner RF, Klein S. Obesity in older adults: technical review and position statement of the American Society for Nutrition and NAASO, the Obesity Society. Am J Clin Nut. 2005;82:923–4, citado por Kuczmarski R. In: Kumanyika S, Brownson R, Hanbook of obesity prevention – a resource for health professionals, Springer science + Business Media, LLC., 2007, 2:25–44.

Wa C, Maibach H. Mapping the human face: biophysical properties. Skin Res Technol. 2010;16:38–54.

Wang Y, Kumanyika S. Descriptive epidemiology of obesity in the United States. In: Hanbook of obesity prevention – a resource for health professionals. Springer science + Business Media, LLC, USA, 2007;3:45–71.

Weigley ES, Adolphe Quetelet (1976–1874): pioneer anthropometrist. Nutr. Today. 1989;24:12–16, citado por Kuczmarski R. in Kumanyika S, Brownson R. Hanbook of obesity prevention – a resource for health professionals. Springer science + Business Media, LLC, USA, 2007, 2:25–44.

WHO Europe: facts and figures. In http://www.euro.who.int, 30 de Junho de 2012.

World Medical Association declaration of Helsinky. Ethical Principles for Medical Research Involving Human subjects, amended until 2004.

Wu K, Osdol W, Dauskardt R. Mechanical properties of human stratum corneum: effects of temperature, hydration, and chemical treatment. Biomaterials. 2006;27:785–95.

Xin S, Man W, Fluhr J, Song S, Elias PM, Man MQ. Cutaneous resonance running time varies with age, body site and gender in a normal Chinese population. Skin Res Technol. 2010;16:413–21.

Yosipovich G, De Vore A, Dawn A. Obesity and skin: skin physiology and skin manifestations of obesity. J Am Acad Dermatol. 2007;6:901–16.

Development and Diagnostic Accuracy and Reliability of a Teledermatology Tool for Occupational Skin Surveillance

144

Markus F. C. Steiner

Contents

Keywords

Occupational contact dermatitis • Occupational health surveillance • Teledermatology • Reliability • Diagnostic accuracy • HECSI • HEROS • Hand eczema • Hand dermatitis

Abbreviations

HE	Hand eczema
HECSI	Hand eczema severity index
HEROS	Hand eczema score for occupational screenings
HSE	Health and Safety Executive
ITU	Intensive care unit
OCD	Occupational contact dermatitis
OHSI	Osnabruck hand eczema severity index
S&F	Store-and-forward technology
UK	United Kingdom
VC	Videoconferencing link

1 Introduction

1.1 Occupational Skin Health Surveillance

Occupational skin diseases are very common and some occupations have a far higher risk than others. Occupational contact dermatitis (OCD) of the hands is the most common form and

M.F.C. Steiner (✉)
GO Health Services, NHS Grampian, Aberdeen, UK
e-mail: m.steiner@abdn.ac.uk; m.steiner@nhs.net

P. Humbert et al. (eds.), *Agache's Measuring the Skin*,
DOI 10.1007/978-3-319-32383-1_117

accounts for about 80 % of all cases (Andersen 2003). The economic consequences due to days lost at work from absenteeism and related costs for industries are significant. Brown summarized the strategies for prevention of OCD in the workplace following the hierarchy of control to minimize or eliminate exposure hazards: elimination, substitution, engineering controls, administrative controls, and personal protective equipment (Brown 2004). Despite the lack of supporting evidence, health and safety legislation requires that employers offer regular skin surveillance for their staff where the hazard cannot be eliminated or adequately controlled (HSE 2011). This includes workers exposed to chemicals (e.g., solvents), wet work, biological agents, and physical agents such as low humidity, cold, or heat. The current UK recommendation is to screen the workforce at risk on a regular basis (annual or more frequent depending on the likelihood of adverse health outcomes) using regular questionnaire surveys or visual inspection by a responsible person such as a supervisor or line manager (HSE 2008).

Both approaches have their limitations:

- Despite the widespread use of questionnaires asking about both skin symptoms in the past and current symptoms, these have not been validated against clinical assessment. Both recall bias and the individual's perception of their health status and what is normal skin make these instruments open to misclassification and under- or overreporting. In some industries, workers see changes in their skin as "something that comes with the job" and consider these changes as normal, and so they are not reported.
- On the other hand, there is also no validation of screening the workforce by a responsible person. Ideally, this would be done by an occupational health professional with the appropriate resources, but in most cases this is done by someone with no health background. We don't know how valid such screening programs are, and whether underreporting to protect colleagues from unwanted job changes or loss of job occurs.

1.2 Teledermatology

Telehealth (long-distance professional health education, public health, and health administration) and telemedicine (long-distance clinical health care for diagnosis and treatment) (Gershon-Cohen and Cooley 1950; Strehle and Shabde 2006; WHO Group Consultation on Health Telematics 1998) have evolved and gained widespread use since their origins around 1910 (Romero et al. 2008; Senel 2010; Preston et al. 1992). Nowadays, the change from analogue to digital technologies allows fast transmission and storage of clinical data around the world. Teledermatology has been shown to give accurate results with concordant results of between 80 % and 90 % when compared to face-to-face consultation (High et al. 2000) but do not always reduce costs compared with traditional face-to-face consultations with dermatologists, when using expensive videoconferencing systems (Loane et al. 2001; Hailey et al. 2002).

Teledermatology implements three different approaches of telemedicine:

- Store-and-forward technology (S&F) where digital photographs are taken and sent (with clinical information) to a specialist for assessment at a convenient time. This method only requires a digital camera (or even mobile phone with camera) and an internet connection to transfer the images.
- The second approach uses a real-time videoconferencing link (VC) between patient or local health professional and a dermatologist. This method is far more resource intensive in terms of the equipment needed; however, recent technical developments have reduced equipment costs considerably. This method would now be feasible in any practice with a PC and internet connection. However, this method requires that both patient and/or local health professional and the specialist are available at the time of consultation with the requirement of scheduled appointments. On the positive side, the direct interaction between patient and specialist makes it possible to obtain clinically useful information for diagnosis and management (Loane et al. 2000).

- The third approach applies both approaches, S&F and VC, where photographic images are transferred before or during a VC consultation so combining the advantages of both systems.

In recent years studies looking into the feasibility, acceptance by patients and specialists, cost-effectiveness, and reliability of teledermatologic assessments and treatment outcomes have been published. These studies were in settings providing support to rural areas where direct consultation is time consuming and expensive (Loane et al. 2001; Baba et al. 2005; Bergmo 2000; Burgiss et al. 1997; Finch et al. 2007; Finch 2008; Du Moulin et al. 2003; Eminovic et al. 2010; Chambers et al. 2012). However, they have had their emphasis on specific skin condition like psoriasis, melanoma, or other skin tumors (Kroemer et al. 2011; Singh et al. 2011; Warshaw et al. 2009a, b, 2010), or looking into the treatment success in other specific conditions (e.g. treatment of leg ulcers) (Binder et al. 2007). Other studies were conducted in settings where a multitude of different skin conditions were seen.

Recent studies in these areas suggest a good agreement between clinical face-to-face examination and S&F teledermatology, reporting a kappa – the chance-corrected agreement between two modalities – of 0.71 and 0.86 for S&F teledermatology (Edison et al. 2008; Rubegni et al. 2011). Parsi et al. reported cost reductions in teledermatologic care of psoriasis patients of 1.7 times less compared to face-to-face consultations (Parsi et al. 2012), and Moreno-Ramirez et al. reported a similar cost reduction of 1.6 times for skin cancer patients (Moreno-Ramirez et al. 2009).

All these conditions were looking into clinically ill patients for various dermatological conditions, examining the reliability to make the correct diagnosis and/or to monitor treatment progress and outcomes. Only one study was identified looking into the diagnostic accuracy of teledermatologic assessment of dermatitis and skin rashes, a condition probably closest to what one would expect to see in an occupational health clinic. Heffner et al. reported the diagnostic concordance in 137 pediatric patients with skin rashes between direct visual assessment and teledermatologic assessment with history and digital images alone by a board-certified dermatologist. The intra-rater concordance by the primary dermatologist was 82 % with a kappa of 0.8 (95 %-CI, 0.73–0.88); the inter-rater concordance between two dermatologists was reported for photographs only and photograph versus inpatient assessment with 73 % respective 69 % and a kappa of 0.69 (95 %-CI, 0.61–0.77) respective 0.65 (95 %-CI, 0.58–0.73). Clinically relevant disagreement occurred in 12–16 % of cases depending on modality. However, this study included many different diseases and aimed to make a correct differential diagnosis for these conditions.

2 Results

In occupational medicine and specifically in occupational health surveillance for skin diseases, the signs for skin lesions are often minor, but their recognition is important to avoid progression to more severe or chronic disease. The early detection of workers with damaged skin can also support the health and safety processes in a company to identify areas and work tasks with an increased risk and implement preventive measures according to the hierarchy of risk control. Apart from many examples of telemedical applications in an occupational context, especially in the maritime environment (Schlaich et al. 2009), teledermatologic applications are almost nonexistent.

However, two recent studies have been identified using a teledermatologic approach to occupational health surveillance (Steiner 2011; Baumeister et al. 2009). Both studies were looking into the early detection of occupational hand dermatitis.

Baumeister et al. reported teledermatological skin examinations using digital images in 100 metal workers. All workers were assessed for hand dermatitis in their workplace by a physician including completing an initial interview-based questionnaire related to working conditions, the use of protective equipment, and

medical history. The skin was then examined and classified into four categories no, discrete, moderate, or severe skin change. Subsequently the skin was assessed using a quantitative scoring system developed by the authors (Weistenhofer et al. 2011) where 54 areas of the hands were scored for several primary (erythema, vesicles, papules) and secondary skin changes (scaling, erosions, fissures, lichenification) and the corresponding severity between 0 (absent) and 3 (severe). The hand eczema score for occupational screenings (HEROS) has been validated in a separate study for its intra-observer and inter-observer validity and shown to have a comparable reliability to three other scoring systems for distinct hand eczema, namely, the hand eczema severity index (HECSI) (Held et al. 2005), the Osnabrueck hand eczema severity index (OHSI) (Skudlik et al. 2006), and Manuscore (John 2001). After the examination digital photographs using an Olympus SP-350 camera mounted on a tripod against a green background were taken of the dorsal and palmar aspect of both hands. After several weeks, the digital images were analyzed by two physicians using the same scoring system. The results in their study showed that the mean scores were significantly higher in the teledermatological examination (16.3) compared to the face-to-face examination (13.1) with a predominance of higher scores for secondary skin lesions. No difference was found for the primary lesions. Mean scores for the four subjective categories of skin damage were reported as 5.6 in the face-to-face examination respective 6 in the teledermatologic assessment for no skin changes, 14.6 respective 16.7 for discrete changes, and 33.8 respective 9 (only one case) for moderate skin damage. No assessment of concordance and reliability for the agreement in the subjective categories "no skin change," "discrete," "moderate," and "severe" between the two modalities of face-to-face examination and teledermatologic assessment, but a calculation from the numbers provided in the paper the kappa (quadratic weighted kappa) was 0.1 (95 %-CI, -0.09–0.23) providing only a poor intra-agreement between both modalities.

The second study in the field of teledermatologic assessment of occupational skin diseases has been conducted by this author and was looking into the development of a toolkit taking standardized photographs regardless of environmental influences and its assessment for diagnostic accuracy and reliability using calibrated equipment (Steiner 2011). Despite proven reliability and technical advances, the reasons teledermatology is not widely practiced are (Armstrong et al. 2010, 2011):

- Lack of appropriate training in taking photographs to high standards
- Costly and inefficient software platforms
- Need for better integration in existing practice systems
- Lack of reimbursement for telemedical services but also cost-attractive implementation models

This study aimed to address the first two points with the development of a cost-effective photographic tool for taking standardized photographs without the need for specialist training.

Elimination for the need of user interaction controlling camera settings and taking reproducible photographs independent of time, location, and operator in workplaces where no control over lighting conditions was guaranteed led to the development of a toolkit under the following premise:

- Easy to transport, robust, and set up as the toolkit was for use in different workplaces
- Use of standard components to keep the costs low
- A compact digital camera which could be remotely controlled by a laptop or PC (tethered shooting)
- Give reproducible lighting condition and reduce environmental influences from other light sources
- Assessment of the digital images using a standardized setup with color-calibrated equipment avoiding differences in classification of skin damage and scoring results due to technical issues

Standardized lightning conditions were achieved by a setup blocking out environmental light sources and using a reproducible light output of defined light quality (camera flash). The camera was controlled via tethered shooting in the following aspects: (a) live preview of the picture on the PC, (b) zoom control, (c) autofocus, (d) flash output control, and (e) full control over the exposure settings (ISO, shutter speed, aperture, and white balance). Figure 1 shows the final toolbox in its dismantled and fully setup stage.

For the second objective to assess the diagnostic validity and reliability between face-to-face and teledermatologic assessment in occupational skin health surveillance, a web platform was developed presenting the photographs on color-calibrated monitors. Four occupations at increased risk of hand dermatitis (Forrester and Roth 1998; Meyer et al. 2000) were selected: health-care workers in an intensive care unit (ITU), engineering workers from engineering workshops in the Aberdeen area, hairdresser apprentices from several colleges in North East Scotland, and due to anecdotal evidence of increased hand dermatitis, nursery nurses from several children's nurseries in the region were included.

Next to a qualitative assessment into "normal skin," "dry skin," or "dermatitis," the quantitative hand eczema severity index (HECSI) (Held et al. 2005) was used.

The participants were examined during their working hours so the time for the face-to-face assessment had to be kept short, and the quantitative HECSI and qualitative assessment was blinded to additional information. Arrangements were made to examine the participants on a monthly basis over a 7-month period if available.

Three pictures of the hands were taken at each time point from every participant: (1) dorsal aspect of the hand, (2) palmar aspect of the hand with fingers stretched out, and (3) fingers lifted to see the fingertips. Toward the end of the study, a fourth picture (4) was added displaying the inner lateral aspect of the fingers. Figure 2 gives an overview over the four positions of the hands which took only about 1–2 min including checking and entering the participant identifier. A standard reference color card (Gretag Macbeth Color Checker Mini-Chart, X-Rite Inc.) was used

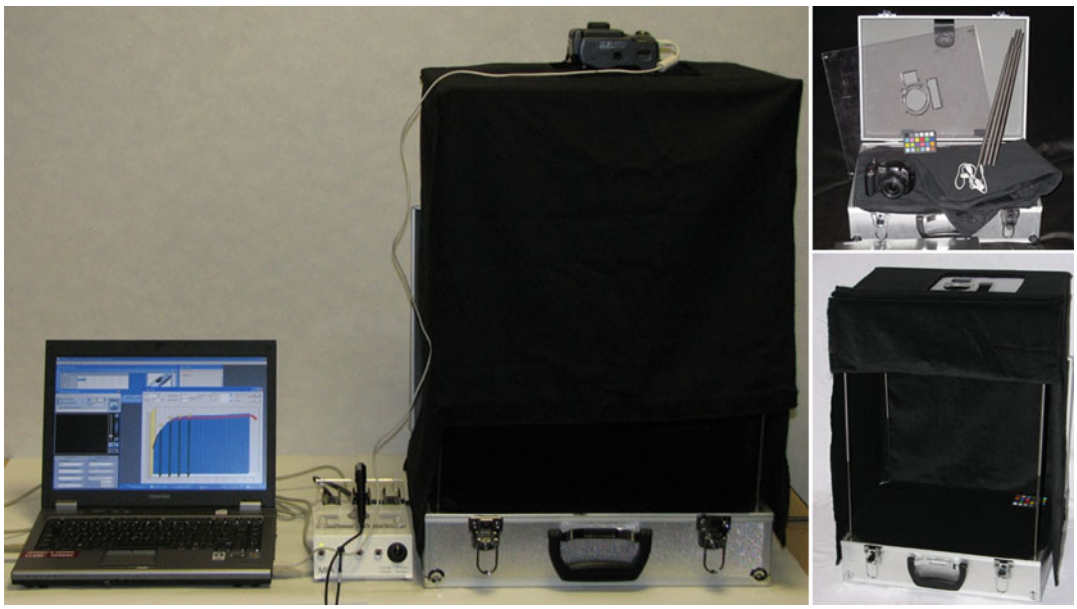

Fig. 1 Photographic toolbox used for taking standardized photographs in the workplace

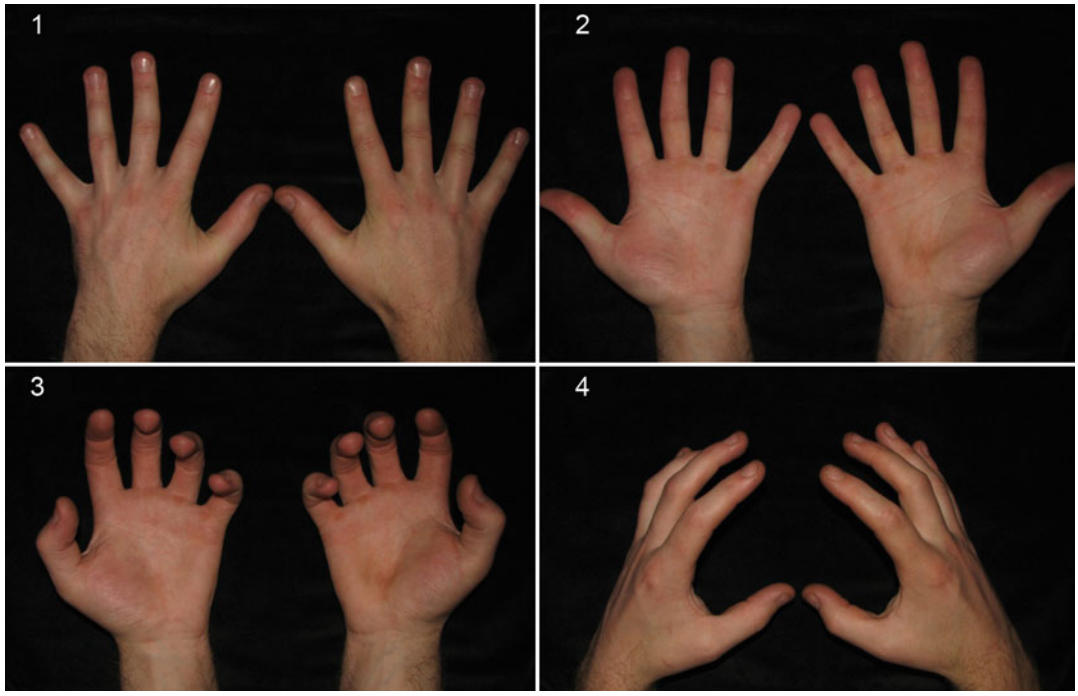

Fig. 2 Example of photographs taken from each participant at each session

regularly to permit checking of the photographs for correct exposure settings (with regard to color casts).

Overall 1,217 face-to-face assessment in 332 participants were available for analysis of intra- and inter-observer agreement. The teledermatologic assessment was based solely on the visual appearance of the hands in the photographs without additional supporting information. Analysis for agreement between face-to-face inspection and teledermatologic assessment for the subjective categories "normal skin," "dry skin/minor dermatitis," and "dermatitis" using unweighted kappa gives intra-rater agreement of 87.8 % with a kappa of 0.79 (95 %-CI, 0.76–0.82) and an inter-rate agreement between the physician and the dermatologist of 57.2 % with a corresponding kappa of 0.16 (95 %-CI, 0.12–0.21). Using quadratic weighted kappa, the intra-rater agreement increases to 95.1 % with a weighted kappa of 0.82 (95 %-CI, 0.78–0.85) and respective 80.1 % with a weighted kappa of 0.27 (95 %-CI, 0.20–0.33). HECSI scores were only complete for the intra-rater assessment and showed a spearman correlation of coefficient of 0.76 HECSI discriminated well between the three categories of skin health independent from factors like occupation, age, or sex. Overall this study has shown a very good intra-rater agreement between face-to-face and teledermatologic assessments in occupational skin surveillance for hand dermatitis but presented a poor inter-rater agreement.

3 Discussion

Teledermatology has been established and widely used in clinical settings supporting the general practitioner in rural areas with dermatology input, reducing costs and times for patients and specialists specifically when using S&F technology. Teledermatology has also shown a good diagnostic agreement between face-to-face consultation and teledermatologic assessment for several skin conditions, mainly skin tumors, melanomas, or psoriasis, and to monitor treatment success in specific disease conditions (Pak et al. 2007). Baumeister et al. presented a case

study where teledermatology was successfully used supporting an occupational physician to make a diagnosis and identify the probable source for an inflammatory condition in six railroad workers (Baumeister et al. 2007) and later tested the performance and correlation of two hand eczema scoring systems for early hand eczema in teledermatological settings (Baumeister et al. 2010). Only two studies to date have used teledermatology in the setting of occupational health surveillance despite its potential attractiveness to offer a method which is quick and wouldn't disturb the work process. The results from both studies are inconclusive as one showed a poor intra-rater reliability (Baumeister et al. 2009), the other promising results in terms of intra-rater agreement, but a poor inter-rater reliability (Steiner 2011). What are the potential reasons for these results and how can they be addressed? Diagnostic concordance in other studies between dermatologists in face-to-face consultations is about 78 % (Ribas et al. 2010), and one would expect that teledermatology would offer a similar reliability.

The first study doesn't report if the settings for taking photographs have been standardized and if precautions had been taken to avoid misclassification due to technical issues. This can be a major issue in failing an accurate assessment in a teledermatological setting. Figure 3 shows an example of the same photograph presented on the same monitor when viewed at different angles and illustrates the importance to standardize every step in the pathway using teledermatology for occupational screening for skin conditions.

The second study addressed all possible issues around the standardization taking hand photographs and the assessment, and similar suggestions can now be found in the practice guidelines for teledermatology published by the American Telemedicine Association (Krupinski et al. 2008). The study was able to show a very good agreement between face-to-face and teledermatologic assessment but showed only a poor to moderate inter-rater agreement between clinical RF and the dermatology consultant. Both trained the scoring for hand dermatitis in a clinical outpatient setting on patients with distinct hand dermatitis. The presentation of the photographs was randomized and blinded, and bias was reduced to a possible minimum. Two probable reasons for the disagreement between both assessors are likely (a) the dermatologist scored only participants when subjectively identified with hand dermatitis and therefore relied on the first overview of the hands not looking closer for specific signs and (b) different threshold when assessing patients with minor skin changes or skin damage between specialties. The dermatologist consultant only sees patients in the clinic with moderate to severe hand dermatitis, and rarely patients present with minor skin changes on the hands which would require clinical treatment. In contrast the clinical RF and occupational physician is confronted with workers where the hands show only minor skin changes, which need to be addressed to avoid their deterioration with possible time off work or job loss and to suggest preventive measures for the workforce. This makes it likely that both assessors had a different view

Fig. 3 Appearance of the same photograph under minimal changes of the viewing angle on a calibrated laptop screen

according to the settings in which they normally work. Another drawback in the performance of the teledermatologic method is the fact that some skin lesions might be too subtle to be easily recognized in photographs. This is true to some extent for minor scaling as presented, for example, in occupations exposed to wet work. Such skin changes are only recognized by experienced assessors and can easily be missed. The provision of additional occupational and clinical data is likely to increase the accuracy in the assessment of such minor changes.

Both studies showed that skin conditions are scored worse in the teledermatological setting compared to the face-to-face inspection. A likely reason for this might be the ability to zoom into the picture into greater detail than possible by visual inspection, and minor changes are studied in more detail with more time in the digital images. This does lead to higher scores in using established scoring tools but didn't have an effect on the subjective assessment for dermatitis in the second study.

Based on the very good intra-rater agreement using standardized equipment, teledermatology offers an attractive method for occupational skin surveillance for signs of hand dermatitis, with the advantage that it wouldn't take much of a workers time (minutes only) or disrupt working processes and that it can be done at convenient times for the worker and employer. It also offers the advantage that the assessment can be done at convenient times by a health professional without blocking valuable clinical times and that the progress of preventive measures or treatments can be monitored over time and documented using a reproducible method. The easy standardized setup allows to produce photographs which are repeatable and which can be integrated in the documentation process of occupational skin surveillance but also allows frequent follow-up in the clinical setting or clinical studies in the treatment of hand dermatitis.

For the assessment of hand dermatitis, several scoring systems are available and validated, and despite some of these were developed to monitor clinical treatment progress of distinct HE (HECSI, Manuscore), the studies have shown that they are able to distinguish also for minor skin changes like their alternatives (HEROS, OHSI). The methods for taking photographs and for the remote assessment however have to be standardized all the way through to allow for reproducible results. Further studies into the inter-rater reliability of teledermatologic occupational skin surveillance should be initiated to identify further shortcomings or prove the validity of this concept.

Important factors for a toolkit to be used for occupational skin surveillance are:

- A setup that does not need user interaction controlling camera settings and lighting conditions for reproducible photographs
- An assessment environment using standardized workstation settings and calibrated equipment
- Assessors which are sufficiently trained in recognizing minor skin damage; later might be best achieved in assessment centers with trained staff, regular training, and cross-validation of random samples between assessors

Future developments of such toolkits might include:

(a) A setup where staff cards can be used to start up the system for the specific staff member without further user input and real-time user instructions as to how to position their hands for a set of four photographs
(b) The use of polarized light sources to allow a more detailed inspection of either surface structures (e.g. for scaling using parallel-polarized photographs)

Due to the fact that all camera manufacturers discontinued compact camera models which allow tethered shooting, new alternatives are necessary: either one could make use of more expensive digital SLR cameras which would increase the costs for the teledermatologic tool or the development of a solution using a credit card-sized computer (Raspberry Pi) with a camera module or a mobile phone app making the use of

a dedicated laptop for controlling the camera and storing the photographs obsolete.

References

Andersen KE. Occupational issues of allergic contact dermatitis. Int Arch Occup Environ Health. 2003;76(5):347–50.

Armstrong AW, Sanders C, Farbstein AD, Wu GZ, Lin SW, Liu FT, et al. Evaluation and comparison of store-and-forward teledermatology applications. Telemed J E Health. 2010;16(4):424–38.

Armstrong AW, Kwong MW, Ledo L, Nesbitt TS, Shewry SL. Practice Models and Challenges in Teledermatology: A Study of Collective Experiences from Teledermatologists. PLoS ONE. 2011;6(12):e28687. doi:10.1371/journal.pone.0028687.

Baba M, Seckin D, Kapdagli S. A comparison of teledermatology using store-and-forward methodology alone, and in combination with Web camera videoconferencing. J Telemed Telecare. 2005;11(7):354–60.

Baumeister T, Drexler H, Kutting B. Teledermatology – a hitherto underestimated tool in occupational medicine – indications and limitations. J Occup Health. 2007;49(6):504–8.

Baumeister T, Weistenhofer W, Drexler H, Kutting B. Prevention of work-related skin diseases: teledermatology as an alternative approach in occupational screenings. Contact Dermatitis. 2009;61(4):224–30.

Baumeister T, Weistenhofer W, Drexler H, Kutting B. Spoilt for choice – evaluation of two different scoring systems for early hand eczema in teledermatological examinations. Contact Dermatitis. 2010;62(4):241–7.

Bergmo TS. A cost-minimization analysis of a realtime teledermatology service in northern Norway. J Telemed Telecare. 2000;6(5):273–7.

Binder B, Hofmann-Wellenhof R, Salmhofer W, Okcu A, Kerl H, Soyer HP. Teledermatological monitoring of leg ulcers in cooperation with home care nurses. Arch Dermatol. 2007;143(12):1511–4.

Brown T. Strategies for prevention: occupational contact dermatitis. Occup Med (Lond). 2004;54(7):450–7.

Burgiss SG, Julius CE, Watson HW, Haynes BK, Buonocore E, Smith GT. Telemedicine for dermatology care in rural patients. Telemed J. 1997;3(3):227–33.

Chambers CJ, Parsi KK, Schupp C, Armstrong AW. Patient-centered online management of psoriasis: a randomized controlled equivalency trial. J Am Acad Dermatol. 2012;66(6):948–53.

Du Moulin MF, Bullens-Goessens YI, Henquet CJ, Brunenberg DE, de Bruyn-Geraerds DP, Winkens RA, et al. The reliability of diagnosis using store-and-forward teledermatology. J Telemed Telecare. 2003;9(5):249–52.

Edison KE, Ward DS, Dyer JA, Lane W, Chance L, Hicks LL. Diagnosis, diagnostic confidence, and management concordance in live-interactive and store-and-forward teledermatology compared to in-person examination. Telemed J E Health. 2008;14(9):889–95.

Eminovic N, Dijkgraaf MG, Berghout RM, Prins AH, Bindels PJ, de Keizer NF. A cost minimisation analysis in teledermatology: model-based approach. BMC Health Serv Res. 2010;10:251.

Finch T. Teledermatology for chronic disease management: coherence and normalization. Chron Illn. 2008;4(2):127–34.

Finch TL, Mair FS, May CR. Teledermatology in the UK: lessons in service innovation. Br J Dermatol. 2007;156(3):521–7.

Forrester BG, Roth VS. Hand dermatitis in intensive care units. J Occup Environ Med. 1998;40(10):881–5.

Gershon-Cohen J, Cooley AG. Telognosis. Radiology. 1950;55(4):582–7.

Hailey D, Roine R, Ohinmaa A. Systematic review of evidence for the benefits of telemedicine. J Telemed Telecare. 2002;8 Suppl 1:1–30.

Held E, Skoet R, Johansen JD, Agner T. The hand eczema severity index (HECSI): a scoring system for clinical assessment of hand eczema. A study of inter- and intraobserver reliability. Br J Dermatol. 2005;152(2):302–7.

High WA, Houston MS, Calobrisi SD, Drage LA, McEvoy MT. Assessment of the accuracy of low-cost store-and-forward teledermatology consultation. J Am Acad Dermatol. 2000;42(5 Pt 1):776–83.

HSE. Skin at work: work-related skin disease – legal requirements. Available at: http://www.hse.gov.uk/skin/professional/legal.htm. Accessed 10 Dec 2011.

HSE. Topic inspection pack – work related contact dermatitis (Disease Reduction Programme (DRP) Skin Disease Programme). 2008 Version 4, March 2008:1–35.

John SM. Diagnostics in the investigation of occupational skin diseases – I:operationalisation of the clinical findings (Manuscore). In: John SM, editor. Clinical and experimental studies of the diagnostics in occupational dermatology. Osnabrueck: Universitaetsverlag Rasch; 2001. p. 133–41.

Kroemer S, Frühauf J, Campbell TM, Massone C, Schwantzer G, Soyer HP, et al. Mobile teledermatology for skin tumour screening: diagnostic accuracy of clinical and dermoscopic image tele-evaluation using cellular phones. Br J Dermatol. 2011;164(5):973–9.

Krupinski E, Burdick A, Pak H, Bocachica J, Earles L, Edison K, et al. American Telemedicine Association's Practice Guidelines for Teledermatology. Telemed J E Health. 2008;14(3):289–302.

Loane MA, Bloomer SE, Corbett R, Eedy DJ, Hicks N, Lotery HE, et al. A comparison of real-time and store-and-forward teledermatology: a cost-benefit study. Br J Dermatol. 2000;143(6):1241–7.

Loane MA, Bloomer SE, Corbett R, Eedy DJ, Evans C, Hicks N, et al. A randomized controlled trial assessing the health economics of realtime teledermatology

compared with conventional care: an urban versus rural perspective. J Telemed Telecare. 2001;7(2):108–18.

Meyer JD, Chen Y, Holt DL, Beck MH, Cherry NM. Occupational contact dermatitis in the UK: a surveillance report from EPIDERM and OPRA. Occup Med (Lond). 2000;50(4):265–73.

Moreno-Ramirez D, Ferrandiz L, Ruiz-de-Casas A, Nieto-Garcia A, Moreno-Alvarez P, Galdeano R, et al. Economic evaluation of a store-and-forward teledermatology system for skin cancer patients. J Telemed Telecare. 2009;15(1):40–5.

Pak H, Triplett CA, Lindquist JH, Grambow SC, Whited JD. Store-and-forward teledermatology results in similar clinical outcomes to conventional clinic-based care. J Telemed Telecare. 2007;13(1):26–30.

Parsi K, Chambers CJ, Armstrong AW. Cost-effectiveness analysis of a patient-centered care model for management of psoriasis. J Am Acad Dermatol. 2012;66(4): 563–70.

Preston J, Brown FW, Hartley B. Using telemedicine to improve health care in distant areas. Hosp Community Psychiatry. 1992;43(1):25–32.

Ribas J, Cunha Mda G, Schettini AP, Ribas CB. Agreement between dermatological diagnoses made by live examination compared to analysis of digital images. An Bras Dermatol. 2010;85(4):441–7.

Romero G, Garrido JA, Garcia-Arpa M. Telemedicine and teledermatology (I): concepts and applications. Actas Dermosifiliogr. 2008;99(7):506–22.

Rubegni P, Nami N, Cevenini G, Poggiali S, Hofmann-Wellenhof R, Massone C, Bilenchi R, Bartalini M, Cappelli R, and Fimiani M. Geriatric teledermatology: store-and-forward vs. face-to-face examination. Journal of the European Academy of Dermatology Venereology, 2011;25:1334–1339.

Schlaich C, Reinke A, Savenich C, Reimer T, Oldenburg M, Baur X, et al. Guidance to the International Medical Guide for Ships 3(rd) edition: interim advice regarding the best use of the medical chest for ocean-going merchant vessels without a doctor onboard: joint statement of WHO Collaborating Centres for the health of seafarers and the International Maritime Health Association – 2009 version. Int Marit Health. 2009;60(1–2):51–66.

Senel E. History of teledermatology: a technique of the future in dermatology. Skinmed. 2010;8(3):167–70.

Singh P, Soyer HP, Wu J, Salmhofer W, Gilmore S. Tele-assessment of Psoriasis Area and Severity Index: a study of the accuracy of digital image capture. Australas J Dermatol. 2011;52(4):259–63.

Skudlik C, Dulon M, Pohrt U, Appl KC, John SM, Nienhaus A. Osnabrueck hand eczema severity index – a study of the interobserver reliability of a scoring system assessing skin diseases of the hands. Contact Dermatitis. 2006;55(1):42–7.

Steiner MFC. Workplace health surveillance for occupational skin diseases: diagnostic accuracy and reliability of a teledermatology tool. PHD thesis. University of Aberdeen; 2011.

Strehle EM, Shabde N. One hundred years of telemedicine: does this new technology have a place in paediatrics? Arch Dis Child. 2006;91(12):956–9.

Warshaw EM, Lederle FA, Grill JP, Gravely AA, Bangerter AK, Fortier LA, et al. Accuracy of teledermatology for nonpigmented neoplasms. J Am Acad Dermatol. 2009a;60(4):579–88.

Warshaw EM, Lederle FA, Grill JP, Gravely AA, Bangerter AK, Fortier LA, et al. Accuracy of teledermatology for pigmented neoplasms. J Am Acad Dermatol. 2009b;61 (5):753–65.

Warshaw EM, Gravely AA, Bohjanen KA, Chen K, Lee PK, Rabinovitz HS, et al. Interobserver accuracy of store and forward teledermatology for skin neoplasms. J Am Acad Dermatol. 2010;62(3):513–6.

Weistenhofer W, Baumeister T, Drexler H, Kutting B. How to quantify skin impairment in primary and secondary prevention? – HEROS – a proposal of a hand eczema score for occupational screenings. Br J Dermatol. 2011;164(4):807–13.

WHO Group Consultation on Health Telematics A health telematics policy in support of WHO's health-for-All strategy for global health development: report of the WHO group consultation on health telematics. Geneva: World Health Organization; 1998. p. 1–39.

Sodium Lauryl Sulfate-Induced Irritation in the Human Face: Regional and Age-Related Differences

145

Slaheddine Marrakchi and Howard I. Maibach

Contents

Keywords
Irritation • Face • Sodium lauryl sulfate • TEWL • Age • Regional variation • Capacitance

1 Introduction

Although extensively studied (Agner 1992), sodium lauryl sulfate (SLS) has been rarely used on the face to investigate mechanisms of irritation (Cua et al. 1990).

Because of the particular skin sensitivity of the face and the neck and because of the regional and age-related variabilities detected in these areas to compounds inducing contact urticaria (Shriner and Maibach 1996; Marrakchi and Maibach 2006), we conducted this study with SLS 2 % under occlusion for 1 h.

Because baseline TEWL has been speculated as a predictive parameter to skin susceptibility to SLS (Tupker et al. 1989) and changes in hydration of superficial epidermis suspected to be responsible for the seasonal variability of skin irritation induced by SLS (Agner and Serup 1989), we measured the baseline TEWL and capacitance before SLS application and studied their correlation with changes in TEWL (∂TEWL), 1 h and 23 h after patch removal (Agner 1992).

S. Marrakchi (✉)
Department of Dermatology, Hedi CHAKER Hospital, Sfax, Tunisia
e-mail: slaheddine.marrakchi@tunet.tn

H.I. Maibach
Department of Dermatology, School of Medicine, University of California, San Francisco, CA, USA
e-mail: maibachh@derm.ucsf.edu

P. Humbert et al. (eds.), *Agache's Measuring the Skin*,
DOI 10.1007/978-3-319-32383-1_144

2 Material and Methods

2.1 Subjects

Two age groups were examined: ten young subjects, aged 25.2 ± 4.7 years ranging from 19 to 30, and ten older subjects, aged 73.7 ± 3.9 years ranging from 70 to 81.

2.2 Methods

Eight areas of the skin (forehead, nose, cheek, nasolabial and perioral areas, chin, neck, and volar forearm) were studied.

After 15 min of rest, necessary to suppress excess water evaporation, baseline TEWL was measured using an evaporimeter, Tewameter TM 210* (Courage + Khazaka, Cologne, Germany), and baseline capacitance was measured with a Corneometer CM 820 PC (Courage + Khazaka, Cologne, Germany).

Sodium lauryl sulfate (Sigma, St Louis, MO) 2 % (w/v) in water was then applied to each of the eight areas for 1 h under occlusion using a saturated absorbent filter paper disk (0,8 cm diameter) in Finn Chamber aluminum disks (Epitest Ltd Oy, Finland). On the contralateral side, water was applied in the same conditions as control.

To assess skin irritation, TEWL was measured 1 h and 23 h after patch removal.

Transepidermal water loss values of the areas tested were corrected according to the changes in the control areas:

$$\text{TEWL} = \text{TEWL measured} - \partial\text{TEWL } H_2O$$

where TEWL measured is the measured TEWL in the tested area at 1 h or 23 hand ∂TEWL H_2O = TEWL control − baseline TEWL H_2O where TEWL control is the measured TEWL value in the control area at 1 h or 23 h.

The skin reactivity to SLS was assessed by the changes in TEWL (∂TEWL = TEWL – baseline TEWL)

2.3 Statistical Analysis

To compare the skin reactivity (∂TEWL) of the regions within each group, the two-tailed Student *t* test for paired data was used. The two-tailed Student *t* test for unpaired data was used to compare the two age groups.

Simple linear regression and correlation analysis between basal TEWL and skin irritation (∂TEWL) and between baseline capacitance and ∂TEWL for each skin location combining the data of the two age groups was used. ∂TEWL was considered as the dependent variable.

3 Results

3.1 Skin Reactivity

Sodium lauryl sulfate 2 % under occlusion for 1 h induced in most of the cases a subclinical irritation and sometimes minimal erythema.

The absolute TEWL values taken after 1 h and 23 h did not show significant differences. Since the 23 h measurements demonstrated lower standard deviation values, only the irritation assessed at 23 h will be considered.

3.1.1 Comparison Between the Regions

In the young group, all the areas reacted to SLS except the forearm. Skin irritation induced by SLS and assessed by ∂TEWL was greater in the cheek and chin when compared to the neck and forearm ($p < 0.05$).

The highest ∂TEWL mean values were found in the cheek and chin (Table 1), but no statistically significant differences with the remaining regions of the face were detected.

All the other regions except the forehead showed a significantly higher irritation than the forearm.

In the old group, all regions reacted to SLS except the nose, perioral area, and forearm. The cheek and chin showed the highest ∂TEWL mean values (Table 1). Significantly ($p < 0.05$) higher

reactivity of these two areas was found when compared to the forearm and when the chin is compared to the forehead.

3.1.2 Comparison Between the Two Age Groups

The mean ∂TEWL values were higher in all the areas studied in the young than in the older group (Table 1). Only in the chin ($p = 0.035$) and nasolabial area ($p = 0.005$) were the differences significant.

4 Correlation Study

4.1 Correlation Between Baseline TEWL and ∂TEWL

Table 2 summarizes the correlations in each area between baseline TEWL and ∂TEWL 23 h after patch removal.

The forehead and the neck showed the strongest correlations ($r = 0.6474$, $p = 0.002$ in the forehead; $r = 0.6273$, $p = 0.003$ in the neck).

Table 1 Reactivity of regions in the young and old group

Area	∂TEWL (Mean ± SD) g/m^2 h		p value
	Young group	Old group	
Cheek	15.1 ± 12.8	6.8 ± 7.3	0.093
Chin*	13.5 ± 9.9	6.0 ± 3.3	0.035
Forearm	1.9 ± 2.1	1.1 ± 1.5	0.354
Forehead	10.4 ± 13.9	2.3 ± 2.3	0.086
Neck	6.8 ± 6.0	3.6 ± 3.7	0.165
Nasolabial area*	12.4 ± 6.3	4.4 ± 4.8	0.005
Nose	8.6 ± 7.6	5.0 ± 6.0	0.251
Perioral area	10.7 ± 10.0	4.2 ± 4.1	0.074

∂TEWL = TEWL 23 h after patch test removal corrected to the control – baseline TEWL
*Difference between the young and old group statistically significant ($p < 0.05$)

Table 2 Correlations in each area between baseline TEWL (BTEWL) and reactivity of the skin to SLS, 23 h after patch removal (∂TEWL)

	BTEWL (Mean ± SD)	TEWL 23H (Mean ± SD)	∂TEWL (Mean ± SD)	r	p
Cheek*	15.63 ± 6.70	26.63 ± 15.30	10.96 ± 11.01	0.4616	0.040
Chin*	20.87 ± 6.37	30.47 ± 12.08	9.77 ± 8.13	0.3535	0.126
Forearm	8.64 ± 3.97	9.70 ± 4.92	1.51 ± 1.83	–	–
Forehead*	14.10 ± 5.71	20.40 ± 14.96	6.39 ± 10.53	0.6474	0.002
Neck*	11.55 ± 4.35	16.63 ± 8.54	5.18 ± 5.12	0.6273	0.003
Nasolabial*	28.74 ± 8.56	36.93 ± 13.44	8.40 ± 6.78	0.4831	0.031
Nose*	19.04 ± 6.03	25.27 ± 11.15	6.77 ± 6.92	0.3218	0.166
Perioral	24.25 ± 8.93	29.98 ± 14.6	7.47 ± 8.17	0.4547	0.044

Areas which reacted to SLS: statistically significant ($p < 0.05$) difference baseline TEWL and TEWL 23 h after patch removal
r coefficient of correlation
p significance (significant correlation when $p < 0.05$)

The nose and chin did not demonstrate a significant correlation between basal TEWL and TEWL changes induced by SLS. The forearm was not studied since this area did not react to the surfactant.

4.2 Correlation Between Baseline Capacitance and ∂TEWL

The baseline capacitance was not correlated to the skin irritation induced by SLS in any area studied.

5 Discussion

Sodium lauryl sulfate, an anionic surfactant, is widely used to study the sensitivity of the skin to irritants. Little information on the susceptibility of the face to SLS is available (Cua et al. 1990).

It has also been demonstrated that SLS could greatly increase the capacity of rigid nanoparticles to serve as transdermal drug carriers (Lopez et al. 2011).

In this study, we investigated the influence of age and regional variability on SLS irritation with a focus on the skin of the face.

We considered only TEWL 23 h after patch removal because of the lower SD when compared to the 1 h values. This difference in SD might be explained by the "transient damage to the water barrier of the skin" described by Agner and Serup (1993) and induced by exposure to water. This transient increase of TEWL not related to SLS nor to the evaporation of additional water lasts between 1 and 3 h after patch removal.

Considering the increase of TEWL after SLS exposure (∂TEWL), the young group had a higher irritant response than the old group in the chin and nasolabial area. In the remaining regions including the neck, ∂TEWL mean values were higher in the young group although the differences were not significant. This lack of significant differences might be explained by the high SD values (Table 1) in these regions. Previous studies (Cua et al. 1990; Elsner et al. 1990) investigated the influence of age on the susceptibility to SLS and reported a decrease of the sensitivity in the elderly which is in concordance with our results.

Various protocols (concentrations, application time) use SLS in water solution to induce skin irritation (Wilhelm et al. 1989; Van Neste and De Brouwer 1992). In our study, since the face was suspected to be more sensitive than the remaining regions of the body, and for a practical purpose, SLS 2 % was applied only for 1 h under occlusion. This protocol was sufficient to induce subclinical irritation in most of the areas of the face but not in the forearm confirming that the face is more sensitive than the forearm.

Although the cheek and chin showed the highest ∂TEWL mean values, no regional variations were detected between the various regions of the face in both age groups, but the cheek and chin were more sensitive than the neck in the young group. This lack of significant differences between regions might be explained by the high SD observed in ∂TEWL values.

To see whether significant differences in skin irritation induced by surfactant exist between the regions of the face, higher SLS concentrations should be tested as well as repeated open applications which may better reflect the common use of potential irritants on the face.

The correlation study showed a significant correlation between basal TEWL and ∂TEWL in five of the seven areas which have reacted to SLS (Table 2).

The correlations between baseline TEWL and TEWL 23 h after patch removal were more obvious. All the areas which reacted to SLS (all the areas studied except the forearm) showed a strong correlation coefficient varying between 0.76 and 0.88 with a highly significant p value < 0.001.

However, we think that the correlation between basal TEWL and the absolute TEWL value after irritation does not imply that higher basal TEWL values predispose to higher skin sensitivity, but only the correlation between baseline TEWL and the changes in

TEWL after irritation (∂TEWL) may have this significance. Even if for different basal TEWL values, the changes in TEWL are the same, a positive correlation could be found because

TEWL is considered as a stable parameter (Oestmann et al. 1993).

The tendency that reactivity of the human face to SLS decreases with age is sustained by findings in the literature that TEWL measured in the face of a large group of Asian volunteers decreases with age (Tagami 2008).

Not only the face but also volar forearm, a seemingly homogeneous skin area, demonstrated regional variability to react to SLS (Bock et al. 2007).

Further studies are needed to detect the participation, with baseline TEWL of biophysical, biochemical, or anatomical parameters in the susceptibility of the face to irritants.

References

Agner T. Noninvasive measuring methods for the investigation of irritant patch test reactions: a study of patients with hand eczema, atopic dermatitis and controls. Acta Derm Venereol (Stockh). 1992;173(Suppl):1–26.

Agner T, Serup J. Seasonal variation of skin resistance to irritants. Br J Dermatol. 1989;121:323–8.

Agner T, Serup J. Time course of occlusive effects on skin evaluated by measurement of transepidermal water loss (TEWL): including patch tests with sodium lauryl sulphate and water. Contact Dermatitis. 1993;28:6–9.

Bock M, Wulfhorst B, John SM. Site variations in susceptibility to SLS. Contact Dermatitis. 2007;57:94–6.

Cua AB, Wilhelm KP, Maibach HI. Cutaneous sodium lauryl sulphate irritation potential: age and regional variability. Br J Dermatol. 1990;123:607–13.

Elsner P, Wilhelm D, Maibach HI. Irritant effect of a model surfactant on the human vulva and forearm. J Reprod Med. 1990;35:1035–9.

Lopez RF, Seto JE, Blankschtein D, Langer R. Enhancing the transdermal delivery of rigid nanoparticles using the simultaneous application of ultrasound and sodium lauryl sulphate. Biomaterials. 2011; 32:933–41.

Marrakchi S, Maibach HI. Functional map and age related differences in the human face: nonimmunologic contact urticaria induced by hexyl nicotinate. Contact Dermatitis. 2006;55:15–9.

Oestmann E, Lavrijsen AP, Hermans J, Ponec M. Skin barrier function as assessed by transepidermal water loss and vascular response to hexyl nicotinate: intra- and inter-individual variability. Br J Dermatol. 1993;128:130–6.

Shriner DL, Maibach HI. Regional variation of nonimmunologic contact urticaria: functional map of the human face. Skin Pharmacol. 1996;9:312–21.

Tagami H. Location-related differences in structure and function of the stratum corneum with special emphasis on those of the facial skin. Int J Cosmet Sci. 2008;30:413–34.

Tupker RA, Coenraads P-R, Pinnagoda J, Nater JP. Baseline transepidermal water loss (TEWL) as a prediction of susceptibility to sodium lauryl sulfate. Contact Dermatitis. 1989;20:265–9.

Van Neste D, De Brouwer B. Monitoring of skin response to sodium lauryl sulphate: clinical scores versus bioengineering methods. Contact Dermatitis. 1992;27:151–6.

Wilhelm KP, Surber C, Maibach HI. Quantification of sodium lauryl sulfate irritant dermatitis in man: comparison of four techniques: skin color reflectance, transepidermal water loss, laser Doppler flow measurement and visual scores. Arch Dermatol Res. 1989;281:293–5.

Friction Foot Blisters: The Effect of Hydration on the Risk of Blister Creation

146

Farina Hashmi

Contents

Keywords

Foot • Skin • Blister • Hydration • Tissue mechanics • Friction • Compression • Textiles

1 The Risk Factors Associated with Foot Blister Creation

Foot blisters can form in people of all ages and activity levels, but those at increased risk are athletes (Institute for Preventative Foot Health [Internet]. National Foot Health Assessment; [cited 2014]; Brennan 2002), hikers (Kogut and Rodewald 1994), those wearing incorrect footwear and hosiery (Dai et al. 2006) and military staff (Akers and Sulzberger 1972; Mailler-Savage and Adams 2006; Sian-Wei Tan et al. 2008). Moreover, the formation of blisters during endurance training can be the cause of further injury (Van Tiggelen et al. 2009; Bush et al. 2000). The primary risks associated with foot blisters are local sepsis and consequent cellulitis (Hoeffler 1975; Knapik et al. 1995).

There are a range of suspected (but not fully verified) factors that place foot skin at increased risk of blister. Some of these factors can be manipulated in order to reduce the risk; others are intrinsic to the nature of the skin (Table 1). Proactive measures to reduce the risk of blistering can be successful to a degree, the primary target being that of moisture reduction within the shoe and

F. Hashmi (✉)
School of Health Sciences Research, University of Salford, Manchester, UK
e-mail: F.Hashmi@salford.ac.uk

P. Humbert et al. (eds.), *Agache's Measuring the Skin*,
DOI 10.1007/978-3-319-32383-1_145

Table 1 Risk factors associated with blister creation

Differences in structure and function of skin	References	Susceptibility to high pressure points during walking	References	Inshoe microclimate	References
Sex: females are more likely to blister compared to males	Patterson et al. (1994)	Structural or bony foot deformity: flat feet (pes planus)	Knapik et al. (1998)	Inshoe humidity: increased during exercise	Hennig et al. (2005)
	(Van Tiggelen et al. 2009)				
Race: increased risk in Caucasian skin type	Reynolds et al. (2000)	Altered biomechanics of the foot during walking: forefoot varus alignment	Reynolds et al. (2000)	Sock fiber: fibers that allow for wicking of moisture way from the skin reduces risk	Herring and Richie (1993)
	Patterson et al. (1994)				Knapik et al. (1996)
					(Dai et al. 2006)
					Bogerd et al. (2011, 2012)
Inherent differences in moisture, i.e., hyperhidrosis	Reynolds et al. (1995)	Footwear fit: too tight or too loose	Manna et al. (2001)		
			Bush et al. (2000)		

sock and consequently the surface of the skin. A number of other risk factors have been referred to in the literature but have not yet been tested in the context of foot skin blister, such as skin elasticity and thickness.

The majority of foot blister research studies have focused largely on prevalence and severity of blisters in response to specific activities as the sole outcome measure. Such studies have not been conducted in controlled conditions, but "in the field," for example, obtaining blister counts from groups of people after military training exercises or at the end of hiking sessions. Due to the practical nature of these studies, and the consequent methodological limitations, the physiological events (and the causes) that take place prior to the visible appearance of the blisters are overlooked. As a result, advances in the development of effective, preventative interventions are stunted. There are some seminal pieces of work in the field of tribology that have contributed to a greater understanding of how foot skin might respond to specific external forces. The next section describes the early works that formed the foundations of knowledge in this area.

2 Early Work on the Measurement of Skin Trauma Due to External Forces

It was the detrimental impact of foot blisters on military staff that motivated the research conducted by Naylor and Sulzberger in the 1950s and 1960s (Naylor 1955; Sulzberger et al. 1966). Naylor reported an inverse relationship between the number of 'rubs' required to form a blister and the frictional force applied (Naylor 1955). Sulzberger and associates generated a large body of evidence that corroborated and added to Naylor's findings (Akers 1977). Both authors conducted laboratory-based research on anterior shin, forearm, and palmar skin sites (in vivo), by systematically rubbing the skin to the point of pain, blister, and/or abrasion. Akers and Sulzberger (1972) further explored the effects of temperature and moisture on blister formation on these skin sites using strain gauge technology to allow for the precise quantification of forces applied to the skin. The apparatus used a system of weights and pulleys to apply a loading probe that could be moved

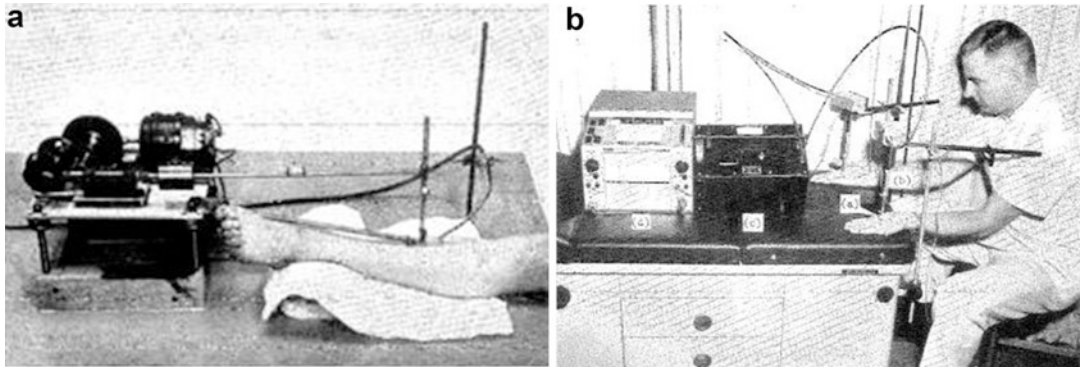

Fig. 1 The friction measurement devices designed by (**a**) Naylor (1952) and (**b**) Sulzberger et al. (1966)

manually in a linear direction across the surface of the skin allowing for the simultaneous measurement of friction loads at the interface of the probe and the skin (Fig. 1). The elegance of this work involved altering the frictional loads while maintaining constant normal (or perpendicular) loads. This was achieved by systematically applying substances to the skin that would alter the coefficient of friction (CoF), for example, oil or talcum powder. Their results showed that a greater number of load cycles were required to cause tissue trauma, using these substances, compared to skin without any substance being applied. Conversely, Naylor found that increased skin surface moisture caused an increase in CoF (Naylor 1955), and El Shimi (1977) later found that dry skin has a relatively low friction response (Shimi 1977). On closer inspection of Naylor's data, it is plausible to suggest that a reduction in CoF of approximately 30 % could increase the number of load cycles required to cause skin trauma by threefold. He therefore demonstrated that by keeping the compressive forces constant and manipulating only the friction loads, skin damage could still occur.

This early work paved the way for the science of tribology, where a range of motorized, laboratory-based devices were developed that primarily involved the application of a controlled normal load to a skin site on the body and the detection of the resistance of the skin to the movement of that applied load. The direction of the load movement of these devices tended to be either linear (Comaish and Bottoms 1971; Koudine et al. 2000; Asserin et al. 2000; Sivamani et al. 2003a, b) or rotational (Shimi 1977; Highley et al. 1977; Prall 1973; Cua et al. 1990; Elsner et al. 1990). During this time the focus of research shifted from testing skin on the lower limb to sites elsewhere on the body, mainly skin on the forearm. In fact, published work of this nature on foot skin is rare, and many blister prevention interventions are informed by the work conducted on skin other than on the foot.

3 The Application of Knowledge in Tribology and Tissue Mechanics to Foot Skin Function and Blistering

In the 1970s, the basic principles of friction in relation to skin were beginning to be challenged. According to Amonton's law, the dynamic friction coefficient, generated when two relatively stiff materials (with smooth surfaces) pass across one another, remains constant despite changes in normal load and velocity of the relative movement. However, in the case of a stiff material in contact with viscoelastic skin, at the contact phase between the two materials, there is a nonlinear deformation of the skin with increasing load transfer to the deeper tissues. This load is referred to as shear load (Fig. 2). Several investigators have tested this behavior of the skin and have concluded that it does not follow Amonton's law

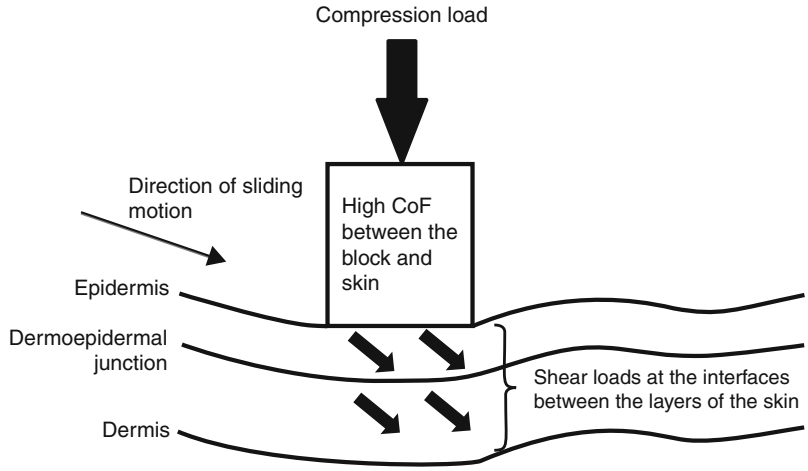

Fig. 2 Diagram illustrating the generation of shear loads in response to compression and friction forces

(Shimi 1977; Comaish and Bottoms 1971; Koudine et al. 2000). This scenario of increased shear forces within the skin places the dermoepidermal junction vulnerable to physical rupture. It follows that increased friction can lead to increased shear forces in the deeper tissues. This is even more relevant in the case of foot skin where the friction and shear components of contact loading are influenced by the repetitive forces generated not only between the shoe and foot skin during walking but also between the contoured bony prominence (of the heel or metatarsal head) and the adjacent subcutaneous tissue. It is these additional factors that influence friction and shear forces to reach a critical level causing abrasion, blistering, or ulceration of foot skin.

During walking, each area of the skin on the foot (in particular plantar and posterior heel skin) is subjected to a combination of perpendicular and parallel loads. The generation and decline of these loads relate to the changes in the gait cycle as well as the nature of the soft tissues that respond to these loads. These loads vary greatly from site to site on the foot and between different stages of the gait cycle. The peak compression and shear loads do not necessarily take place at the same time. The majority of the research focusing on the reduction of skin trauma from repetitive loading has concentrated on peak compression levels only. However, it is clear that the true nature of repetitive loading involves a friction and shear element, for example, low, repetitive peak loads are damaging when a significant component of the load is parallel to the surface of the skin. An example of this is chaffing of the skin. When this shear component is large, damage to the skin can take place relatively early (i.e., after a few load cycles). Conversely, when the friction component is small, it takes more load repetitions to cause skin damage. The level of friction loads is governed by the CoF and the direct contact pressure. To add to this complex picture, there is considerable variability in CoF measures within the general population, i.e., the skin of one person may respond to loads differently to that of another.

With these factors in mind, Hashmi et al. (2013) designed a series of experiments on posterior heel skin (in vivo), where the incidence of foot blisters is most common, and the architecture of the underlying bone is likely to influence tissue damage (Hashmi et al. 2013). The authors generated 30 heel blisters from a population of healthy adults, using a device that applied a standard, intermittent load/unload pattern on the skin that mimicked the contact between the posterior heel skin and the counter of the shoe during walking (Fig. 3). The degree of tissue trauma during load application was monitored and quantified using medical thermography (Fig. 4). This acted as a surrogate measure for trauma due to friction and shear loads. The experimental design was similar to those of other devices used in tribological studies but with a focus on effectively applying load to the contoured, bony surface of the

posterior aspect of the heel while being able to visually inspect and measure the degree of inflammation in response to tissue trauma. The results showed that the initiation of friction heel blisters took place at a temperature of approximately 5 °C above the normal skin temperature of the foot.

Fig. 3 Load application mechanism for applying intermittent normal and friction loads to the posterior aspect of the heel (Hashmi et al. 2013)

Although understanding the architecture of the foot and its relationship to the biomechanical properties of soft tissues is vital, the common factor that increases the susceptibility of skin to blistering on any site on the body is that of increased moisture. Therefore, in the context of foot blistering, the interaction between the skin and footwear materials and the accumulation of moisture within the shoe is an important consideration when implementing clinical solutions.

4 The Effect of Hydration on Foot Skin Friction and Shear Forces

Water on the surface of skin has the effect of making the skin more pliable when in contact with the loading surface. This in turn allows for closer contact between the skin and the material

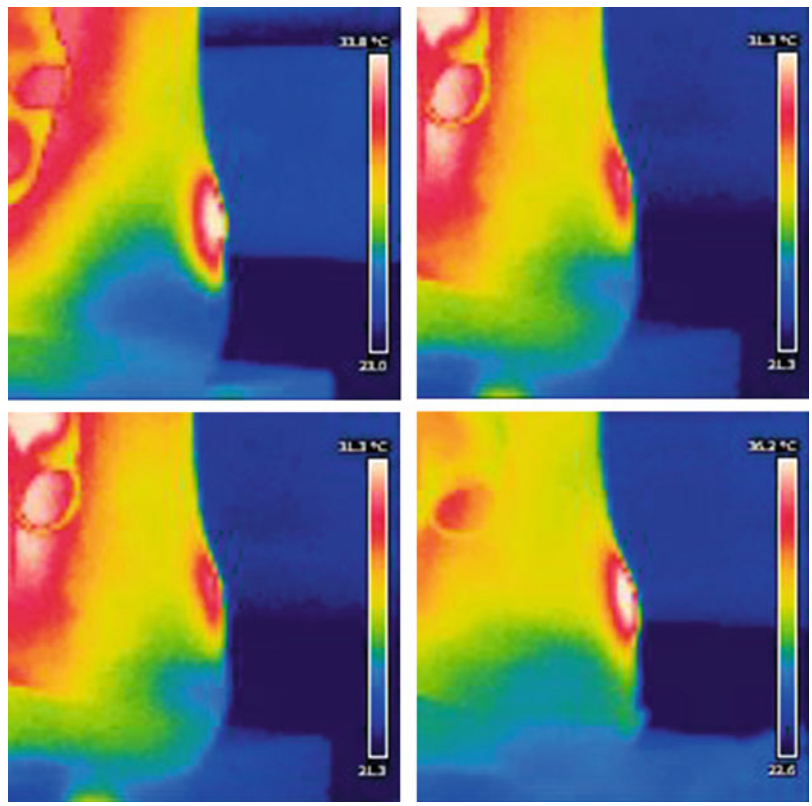

Fig. 4 Thermal images of four different heels at the point of blister creation. Each image depicts a 'hot spot' (*in red*) representing the area where the blister has formed

and therefore increases the CoF. The converse is the case with dry skin in that the loading surface does not achieve as much contact with the skin and slides more easily over the surface. This has been tested in skin dried using isopropyl alcohol (Sivamani et al. 2003a) and in patients with clinically dry skin (Lodén et al. 1992). However, the maintenance of constant moisture on the skin surface under experimental conditions is difficult to achieve, therefore producing varied CoF results (Shimi 1977; Sivamani et al. 2003a; Highley et al. 1977; Nacht et al. 1981).

A similar observation was made by Kirkham et al. (2014), who hydrated foot skin using a water foot bath and subjected the skin to the same compression and friction loads, as reported by Hashmi et al. (2013). These data were compared to the skin on contralateral feet that were not hydrated and showed that the time taken to achieve skin trauma (akin to a preblistered state) was significantly less in the hydrated foot skin compared to the relatively dry skin. Contrary to the data generated from other skin sites, Kirkham et al. found no significant, positive correlation between heel skin hydration and elasticity (Kirkham et al. 2014). This is not surprising as the measurement of elasticity was conducted using suction pressure; therefore, the inclusion of the dermis in the measure could not be avoided, whereas the hydration readings were that of the superficial skin layers. Also, it may be reasonable to assume that the evaporation of the water from the surface of the skin may occur relatively quickly compared to the time taken to conduct the experiment, as well as water being absorbed into the deeper layers of the skin. The changes in hydration of foot skin during exercise have not been reported; therefore, the work by Kirkham cannot be put into the context of the behavior of skin within the shoe.

In addition, a clearer understanding of how the friction, compression, and shear forces act collectively on the skin around bony prominences of the foot is necessary. Researchers in the field of prosthetics and orthotics have tried to address this question in the context of pressures applied at the interface between a limb stump and a prosthetic. The most notable research in this area is that conducted by Sanders and colleagues (1992, 1993, 1997, 1998, 2004; Sanders and Daly 1993), who designed shear load sensors that quantified shear/friction forces at various prosthetic socket wall locations. This technology has allowed peak friction loads on "at-risk" locations to be varied by making known changes in the interface CoF at those locations using a variety of common cushioning materials with known CoF (Sanders et al. 1998, 2004). From their data, a number of material combinations could be selected, representing a significant range of CoF values. It would be helpful to apply these methods to exploring the interaction between the foot and shoe in order to understand and interpret foot skin mechanics during walking. It is only when translation of this knowledge is achieved that the development (based on scientific evidence) of efficacious prevention treatments for blisters, calluses, and ulcers can truly be successful.

5 Hydration and the Inshoe Environment

Skin trauma as a result of changes in the microclimate within the skin – clothing system and the transfer of heat and moisture within it – has been extensively reviewed (Zhong et al. 2006); however, minimal work has been generated with regard to the inshoe microclimate and foot skin irritation. The degree of foot skin hydration is largely influenced by two factors: inherent susceptibility to the production of sweat and the accumulation of moisture within the shoe. Therefore, the appropriate choice of footwear, socks, and topical preventative therapies is imperative for those who are prone to hyperhidrosis and blistering. The few papers published in this area have concentrated on measuring the prevalence and size of blisters in response to different types of sock materials. For example, the outcomes of a double-blind study by Herring and Richie showed that acrylic fiber socks reduced the prevalence and size of foot blisters after long-distance running (Herring and Richie 1993). Knapik et al. (1996) conducted a similar study on military trainees and found that the denser sock materials increased the prevalence and size of foot blisters (Knapik et al. 1996), the implication being that the denser the material, the greater the

potential for accumulating moisture within it. Others have attempted to test the effects of antiperspirants on the incidence and severity of friction foot blisters (Reynolds et al. 1995; Knapik et al. 1998). These works showed no positive effects of preventing blisters after hiking activities. In fact, an increased rate of irritant dermatitis was reported. Despite these works, the prevalence and severity of blisters in response to activities and preventative treatments are poorly understood. This will remain the case until a more detailed identification of the specific changes in the functional behavior of foot skin in different microclimates is made. In short, more sensitive measures of change in skin are required to counteract the variations seen between people.

There are several approaches that can be implemented to combat the challenges of predicting inshoe responses of foot skin to changes in microclimate and force generation during walking. In the absence of designing controlled laboratory studies and the presence of multiple variables, finite element modeling (FEM) may be the future direction for research in this field. An example of one such work is that conducted by Dai and colleagues, who used FEM to understand the effects of specific sock materials on friction forces at the skin to sock and sock to shoe interfaces (Dai et al. 2006). These researchers found that wearing a sock with low friction against foot skin was more effective in reducing plantar shear force than on the skin than with a sock with low friction against the insole of the shoe. This is valuable knowledge when considering the motion of the foot within the shoe. As the philosophy behind the design of blister prevention treatments focuses on the reduction of moisture at the skin material interface, it would be valuable to develop models to test this and further apply the results to predicting the efficacy of blister prevention treatments.

6 Conclusions and Future Directions

The importance of hydration as a risk factor for friction blisters is evident. What is agreed among all researchers in this field is the multifarious etiology of foot blisters and the limitations that these place on study designs. It must be acknowledged that the work conducted to date, by researchers in all scientific disciplines, has endorsed the impact of hydration on foot blister risk. However, it is evident that the data generated from these studies may now have reached a saturation point, and in order to be able to translate these data to have meaningful clinical impact, the use of modeling technology may be the logical progression. Incorporation of existing clinical study data into specific foot skin models may bring us closer to predicting the efficacy of interventions. Advances in this direction may also prove fruitful avenues for investigating the role of friction and the potential value of friction management in reducing foot ulceration and excessive callus formation.

References

Akers WA. Sulzberger on friction blistering. Int J Dermatol. 1977;16(5):369–72.

Akers WA, Sulzberger MB. The friction blister. Mil Med. 1972;137(1):1–7.

Asserin J, Zahouani H, Humbert PH, Couturaud V, Mougin D. Measurement of the friction coefficient of the human skin in vivo: quantification of the cutaneous smoothness. Colloids Surf B Biointerfaces. 2000;19(1):1–12.

Bogerd CP, Rechsteiner I, Wüst B, Rossi RM, Brühwiler PA. The effect of two sock fabrics on physiological parameters associated with blister incidence: a laboratory study. Ann Occup Hyg. 2011;55(5):510–8.

Bogerd CP, Niedermann R, Brühwiler PA, Rossi RM. The effect of two sock fabrics on perception and physiological parameters associated with blister incidence: a field study. Ann Occup Hyg. 2012;56(4):481–8.

Brennan Jr FH. Managing blisters in competitive athletes. Curr Sports Med Rep. 2002;1(6):319–22.

Bush RA, Brodine SK, Shaffer RA. The association of blisters with musculoskeletal injuries in male and marine recruits. JAMA. 2000;90(4):194–8.

Comaish S, Bottoms E. The skin and friction: deviations from Amonton's laws, and the effects of hydration and lubrication. Br J Dermatol. 1971;84(1):37–43.

Cua AB, Wilhelm KP, Maibach HI. Frictional properties of human skin: relation to age, sex and anatomical region, stratum corneum hydration and transepidermal water loss. Br J Dermatol. 1990;123(4):473–9.

Dai XQ, Li Y, Zhang M, Cheung JT. Effect of sock on biomechanical responses of foot during walking. Clin Biomech (Bristol, Avon). 2006;21(3):314–21.

Elsner P, Wilhelm D, Maibach HI. Frictional properties of human forearm and vulvar skin: influence of age and

correlation with transepidermal water loss and capacitance. Dermatologica. 1990;181(2):88–91.
Hashmi F, Richards BS, Forghany S, Hatton AL, Nester CJ. The formation of friction blisters on the foot: the development of a laboratory-based blister creation model. Skin Res Technol. 2013;19(1):e479–89.
Hennig E, et al. The influence of sock construction on foot climate in running shoes. Cleveland: Footwear Biomechanics Symposium, Footwear Biomechanics Group (International Society of Biomechanics); 2005.
Herring KM, Richie Jr DH. Comparison of cotton and acrylic socks using a generic cushion sole design for runners. J Am Podiatr Med Assoc. 1993;83(9):515–22. Erratum in: J Am Podiatr Med Assoc 1993 Nov;83(11):624.
Highley KR, Coomey M, DenBeste M, Wolfram LJ. Frictional properties of skin. J Invest Dermatol. 1977;69(3):303–5.
Hoeffler DF. Friction blisters and cellulitis in a navy recruit population. Mil Med. 1975;140(5):333–7.
Institute for Preventative Foot Health [Internet]. National foot health assessment; [cited 2014 May 9]. Available from http://www.ipfh.org/images/research_materials/2012_National_Foot_Health_Assessment_June_2012.pdf
Kirkham S, Lam S, Nester CJ, Hashmi F. The effect of hydration on the risk of friction blister formation on the heel of the foot. Skin Res Technol. 2014;20(2):246–53.
Knapik JJ, Reynolds KL, Duplantis KL, Jones BH. Friction blisters: pathophysiology, prevention and treatment. Sports Med. 1995;20(3):136–47.
Knapik JJ, Hamlet MP, Thompson KJ, Jones BH. Influence of boot-sock systems on frequency and severity of foot blisters. Mil Med. 1996;161(10):594–8.
Knapik JJ, Reynolds K, Barson J. Influence of an antiperspirant on foot blister incidence during cross-country hiking. J Am Acad Dermatol. 1998;39(2):202–6.
Kogut KT, Rodewald LE. A field survey of the emergency preparedness of wilderness hikers. J Wilderness Med. 1994;5(2):171–8.
Koudine AA, Barquins M, Anthoine PH, Aubert L, Lévêque JL. Frictional properties of skin: proposal of a new approach. Int J Cosmet Sci. 2000;22(1):11–20.
Lodén M, Olsson H, Axéll T, Linde YW. Friction, capacitance and transepidermal water loss (TEWL) in dry atopic and normal skin. Br J Dermatol. 1992;126(2):137–41.
Mailler-Savage EA, Adams BB. Skin manifestations of running. J Am Acad Dermatol. 2006;55(2):290–301.
Manna I, Pradhan D, Ghosh S, Kar SK, Dhara P. A comparative study of foot dimension between adult male and female and evaluation of foot hazards due to using of footwear. J Physiol Anthropol Appl Human Sci. 2001;20(4):241–6.
Nacht S, Close J, Yeung D, Gans EH. Skin friction coefficient: changes induced by skin hydration and emollient application and correlation with perceived skin feel. J Soc Cosmet Chem. 1981;32:55–65.
Naylor P. The measurement of epidermal strength. Trans St John Hosp Dermatol Soc. 1952;31:29–33.
Naylor PFD. Experimental friction blisters. Br J Dermatol. 1955;67(10):327–42.
Patterson HS, Woolley TW, Lednar WM. Foot blister risk factors in an ROTC summer camp population. Mil Med. 1994;159(2):130–5.
Prall JK. Instrumental evaluation of the effects of cosmetic products on skin surfaces with particular reference to smoothness. J Soc Cosmet Chem. 1973;24:693–707.
Reynolds K, Darrigrand A, Roberts D, Knapik J, Pollard J, Duplantis K, Jones B. Effects of an antiperspirant with emollients on foot-sweat accumulation and blister formation while walking in the heat. J Am Acad Dermatol. 1995;33(4):626–30.
Reynolds K, Williams J, Miller C, Mathis A, Dettori J. Injuries and risk factors in an 18-day Marine winter mountain training exercise. Mil Med. 2000;165(12):905–10.
Sanders JE, Daly CH. Normal and shear stresses on a residual limb in a prosthetic socket during ambulation. J Rehabil Res Dev. 1993;30:191–204.
Sanders JE, Daly CH, Burgess EM. Interface shear stresses during ambulation with a below-knee prosthetic limb. J Rehabil Res Dev. 1992;29(4):1–8.
Sanders JE, Daly CH, Burgess EM. Clinical measurement of normal and shear stresses on a trans-tibial stump: characteristics of waveform shapes during walking. Prosthet Orthot Int. 1993;17:38–48.
Sanders JE, Lam D, Dralle A, Okumura R. Interface pressures and shear stresses at 13 socket sites on two persons with transtibial amputation. J Rehabil Res Dev. 1997;34:19–43.
Sanders JE, Greve JM, Mitchell SB, Zachariah SG. Material properties of commonly-used interface materials and their static coefficients of friction with skin and socks. J Rehabil Res Dev. 1998;35(2):161–76.
Sanders JE, Nicholson BS, Zachariah SG, et al. Testing of elastomeric liners used in limb prosthetics: classification of 15 products by mechanical performance. J Rehabil Res Dev. 2004;41(2):175–86.
Shimi AF E –. In vivo skin friction measurements. J Soc Cosmet. 1977;28:37–51.
Sian-Wei Tan S, Kok SK, Lim JK. Efficacy of a new blister prevention plaster under tropical conditions. Wilderness Environ Med. 2008;19(2):77–81.
Sivamani RK, Goodman J, Gitis NV, Maibach HI. Friction coefficient of skin in real-time. Skin Res Technol. 2003a;9(3):235–9.
Sivamani RK, Wu GC, Gitis NV, Maibach HI. Tribological testing of skin products: gender, age, and ethnicity on the volar forearm. Skin Res Technol. 2003b;9(4):299–305.
Sulzberger MB, Cortese TA, Fishman L, Wiley HS. Studies on blisters produced by friction. I. Results of linear rubbing and twisting techniques. J Invest Dermatol. 1966;47(5):456–65.
Van Tiggelen D, Wickes S, Coorevits P, Dumalin M, Witvrouv E. Sock systems to prevent foot blisters and the impact on overuse injuries of the knee joint. Mil Med. 2009;174(2):183–9.
Zhong W, Xing MM, Pan N, Maibach HI. Textiles and human skin, microclimate, cutaneous reactions: an overview. Cutan Ocul Toxicol. 2006;25(1):23–39.

Use of "Connectivity Map" (Cmap) to Identify Novel, Safe, Effective Antiaging Ingredients for Topical Use

147

Johanna M. Gillbro, Eve Merinville, Mia Nilsson, Eva Hagforsen, Garrett Moran, Tamara Al-Bader, and Alain Mavon

Contents

J.M. Gillbro (✉) • E. Merinville • M. Nilsson • E. Hagforsen • G. Moran • T. Al-Bader • A. Mavon
Oriflame Skin Research Institute, Stockholm, Sweden

Oriflame R&D Ltd, Bray, Co Wicklow, Ireland

Department of Medical Sciences, Dermatology and Venereology, Uppsala University, Uppsala, Sweden
e-mail: johanna.gillbro@oriflame.com

P. Humbert et al. (eds.), *Agache's Measuring the Skin*,
DOI 10.1007/978-3-319-32383-1_146

Keywords
Retinoids • Connectivity map • Organoculture • Skin • Gene array

Abbreviations

A-A-A	Acetyl aspartic acid
Cmap	Connectivity map
COLIV	Collagen IV
CYPs	Cytochrome P450-dependent enzymes
DEJ	Epidermal–dermal junction
ECM	Extracellular matrix
HRIPT	Human repeat insult patch
MMPs	Matrix metalloproteinases
RA	All-trans retinoic acid/ tretinoin
RALDH	Retinol dehydrogenases (RDH) and retinal dehydrogenases
RAR	Retinoic acid receptors
RHE's-SkinEthic model	Human reconstructed epidermis
ROI	Region of interest
RXRs	9-*cis*-retinoic acid receptors

1 The Use of the Connectivity Map in Drug Development

In 2006, an innovative method, named the "connectivity map" (Cmap), was reported by Lamb et al. (2006). The investigators created a large public database containing hundreds of gene expression profiles, called "reference gene signatures," of cultured human cells treated with >1,000 bioactive small molecules, attached to a pattern-matching tool.

The most recent version contains 7,056 gene expression profiles from 1,309 bioactive compounds, representing 6,100 individual treatments in five different human cell lines.

Researchers can access that database via the Internet and can compare gene signatures of interest with the Cmap database. The pattern-matching software scores and ranks similarities between the researcher's and the reference signatures and can lead to unexpected connections between the researcher's gene profiling data and small molecules and therefore lead to new treatment strategies in a number of diseases.

2 Applications of Cmap in Drug Discovery

In this section, we discuss some of the applications of Cmap in the context of therapeutic research. With the use of this method, novel agents have been identified mainly for use in the treatment of cancer (Sirota et al. 2011; Chen et al. 2011; Yang and Agarwal 2011; Siu et al. 2008; Claerhout et al. 2011; Hassane et al. 2008; Wang et al. 2011; Reka et al. 2011). Recently agents have also been identified for drug development within Gaucher disease (Chen et al. 2011), pain management (Chang et al. 2010), muscle atrophy (Kunkel et al. 2011), inflammatory bowel disease (Dudley et al. 2011), smoking cessation (Boyle et al. 2010), and Alzheimer's disease (Chen et al. 2013) (as outlined in Table 1). Within the dermatology field, however, there is only one study published so far on the use of connectivity mapping. The Shiseido research group has identified a potential repurposing opportunity for the promiscuous antipsychotic drug, fluphenazine, to be used as a novel hair-growth inducer candidate by means of Cmap analysis (Ishimatsu-Tsuji et al. 2010).

3 The Use of Retinoids as an Antiaging Strategy

One of the most studied classes of skin-targeted compounds is all-trans retinoic acid (RA) also referred to as tretinoin. RA and its synthetic or natural derivatives (retinoids) affect epidermal

Table 1 Drugs identified and key findings through gene arrays with corresponding connectivity mapping and the disease that these drugs could be used as a treatment

Disease	Drug identified	Key finding	Validation	Reference
Muscle atrophy	Ursolic acid	Identified opportunity to repurpose ursolic acid to, for example, muscle atrophy	In vitro and in vivo (rodent)	(Kunkel et al. 2011)
Lung cancer	Cimetidine (an antiulcer drug)	Predicted new indications for the 164 drugs in the Cmap and validated cimetidine as a candidate therapeutic for lung adenocarcinoma	In vitro and in vivo (rodent)	(Sirota et al. 2011)
Hepatocellular carcinoma (HCC)	Chlorpromazine and trifluoperazine	Identified therapeutic candidates for HCC, with in vitro anti-tumor activities validated for 28 drugs and in vivo for 2 drugs (Chlorpromazine and trifluoperazine)	In vitro and in vivo (rodent)	(Chen et al. 2011)
Hair growth	Fluphenazine (an antipsychotic drug)	Identified a list of candidate agents with mimic patterns to the hair growth inducer cyclosporine and validated fluphenazine in vivo	In vivo (rodent)	(Ishimatsu-Tsuji et al. 2010)
Osteoarthritic pain	Phenoxybenzamine (an antihypertensive drug)	Predicted analgesic activity for phenoxybenzamine	In vivo (rodent)	(Chang et al. 2010)
Inflammatory bowel disease	Topiramate (an anticonvulsant drug)	Predicted new use option for topiramate as a drug to treat IBD	In vivo (rodent)	(Dudley et al. 2011)
Lung cancer	Polyphyllin D (a potent cytotoxic saponin)	Predicted polyphyllin D as a potential endoplasmic reticulum stress inducer to be used for anticancer treatment	In vitro	(Yang and Agarwal 2011)
Breast cancer (tamoxifen resistant)	Phenothiazines (antipsychotic and antihistaminic drugs)	Identified and validated three compounds from phenothiazine family as potential therapeutics for drug-resistant breast cancers	In vitro	(Siu et al. 2008)
Gastric cancer	Vorinostat (for cutaneous T-cell lymphoma)	Identified vorinostat as a candidate drug for gastric cancer	In vitro	(Claerhout et al. 2011)
CNS injury	Piperazine (antipsychotic drug)	Identified piperazine as promoters of CNS neurite growth	In vitro	(Johnstone et al. 2012)
Acute myelogenous leukemia (AML)	Celastrol and 4-hydroxy-2-nonenal	Predicted and discovered new agents that can effectively improve AML	In vitro	(Hassane et al. 2008)
Smoking cessation	Geldanamycin (HSP90 inhibitor)	Predicted that geldanamycin may suppress smoking-induced transcriptome changes as an antiemetic of tobacco	In vitro	(Boyle et al. 2010)
Cancer	Terpineol (a bioactive component from essential oil extract)	Elucidated cytotoxicity and potential antitumor utility and mechanism of NF-kappaB inhibition for terpineol	In vivo	(Hassan et al. 2010)

(*continued*)

Table 1 (continued)

Disease	Drug identified	Key finding	Validation	Reference
Lung cancer	HDAC inhibitors, HSP90 inhibitors, PI3K inhibitors, and others	Predicted HDAC inhibitors such as 17-AAG among several other compounds as potential candidates for treating lung cancer	In vitro	(Wang et al. 2011)
Cancer metastasis	LY294002, 17-AAG, rapamycin	Identified potential epithelial–mesenchymal transformation inhibitors of rapamycin, 17-AAG, LY294002 that may be used in preventing metastasis	In vitro	(Reka et al. 2011)
Gaucher disease	Comparison of signature from microarray profiling of spleen and liver cells obtained from GD1 and wild-type mice	Use of Cmap to query signature to yield a hierarchical list of novel compounds that share common mechanisms with GBA1	In vivo rodents	(Zhao et al. 2012)
Colon cancer	Mebendazole (anthelmintic drug)	Repositioning of the anthelmintic drug mebendazole for the treatment for colon cancer	In vitro	(Nygren et al. 2013)
Alzheimer's disease	Comparison of different brain regions in AD and the corresponding gene signatures	Identified small molecules, such as histone deacetylase (HDAC) inhibitor, may be candidate drugs in the treatment of AD	In vivo rodents	(Chen et al. 2013)

growth and differentiation (Eckert and Rorke 1989). Synthetic retinoids are today used widely in the treatment of psoriasis and other disorders of keratinization (Saurat 1999; Pavez Loriè et al. 2009a). Acne has been widely treated with various forms of natural and synthetic retinoids for more than 40 years (Kligman et al. 1986; Titus and Hodge 2012). Retinoids have also been used in the treatment of hyperpigmentation disorders such as post-inflammatory hyperpigmentation and melasma (Griffiths et al. 1993). Separate from the effect of retinoids in skin disease, Kligman and Willis were the first to introduce retinoids for use as anti-photoaging agents (Kligman and Willis 1975). After its application, the authors noticed improvement of skin depigmentation and rejuvenation (Kligman et al. 1984, 1986). Today, retinoids are extensively used for this indication (Babamiri and Nassab 2010; Bellemère et al. 2009).

Further studies have shown that RA's clinical effects include improvement of wrinkles, surface roughness, mottled pigmentation, and skin appearance as a whole when used on photodamaged skin (Kang et al. 1997; Liu et al. 2009). At a cellular level, retinoids are known to modulate the proliferation and differentiation of epidermal keratinocytes (Fuchs 2007; Fuchs and Green 1981; Asselineau et al. 1989) by binding to nuclear retinoic acid receptors (RAR) and 9-*cis*-retinoic acid receptors (RXRs) which results in upregulation or downregulation of the transcription of target genes (Ghyselinck et al. 2002).

RA is the biologically active form of vitamin A (retinol). Endogenous production of RA by epidermal keratinocytes involves the uptake of preformed vitamin A from the surroundings followed by a series of metabolic activation steps involving retinol dehydrogenases (RDH1, RDH4, RDH10, and DHRS9) and retinal dehydrogenases (RALDH1, RALDH2, and RALDH3) (Kurlandsky et al. 1996; Vahlquist 1999; Napoli 2012).

While endogenously produced or exogenously applied, RA is transported through the cytoplasm by specific intracellular retinoic-binding proteins (CRABP2) (Bellemère et al. 2009).

Once synthesized, the cellular levels of RA are controlled by several cytochrome P450-dependent enzymes (CYPs), CYP26A1, B1, and C1, which

metabolize RA into 4-hydroxy-RA, 4-oxo-RA, and 18-OH-RA (White et al. 1997; Taimi et al. 2004). CYP26B1 is known to be expressed higher than both CYP26A1 and CYP26C1 in human keratinocytes (Pavez Loriè et al. 2009b).

Over the last quarter century, 532 genes have been validated to be regulated by RA (Balmer 2002). In some cases this control is direct, driven by a liganded RAR:RXR heterodimer bound to a DNA response element; in others, it is indirect, reflecting the actions of intermediate transcription factors, nonclassical associations of receptors with other proteins, or even more distant mechanisms.

Cell cultures have been studied extensively to characterize and prophesy the effect of retinoids on epidermal differentiation and growth (Fuchs and Green 1981; Asselineau et al. 1989; Eckert and Green 1984; Gilfix and Eckert 1985; Varani et al. 1989; Asselineau and Darmon 1995).

In addition, a selection of genes using RT–PCR has been studied in full-thickness skin treated with retinoids.

Today, recent gene array techniques allow the characterization of the mRNA expression status of a large number of genes in cells or tissues after retinoid treatments with more than 170 studies conducted.

Some studies using gene arrays to evaluate the effect of RA have also been carried out on reconstructed epidermis and human epidermis in vivo (Bernard et al. 2002). In 2013, the first gene arrays were conducted investigating the effect of RA in organocultures of human skin (Gillbro et al. 2014).

4 Retinoic Acid as a Lead Compound to Find New Active Antiaging Ingredients

Due to the well-known and studied activity of RA, this has been used as a lead compound to identify new active ingredients for antiaging purposes (Gillbro et al. 2014).

To investigate the effect of RA on 30,000 genes with corresponding Cmap analysis, an organoculture of human skin was firstly conducted (Fig. 1). Briefly, the skin from surgical waste material from breast reductions was

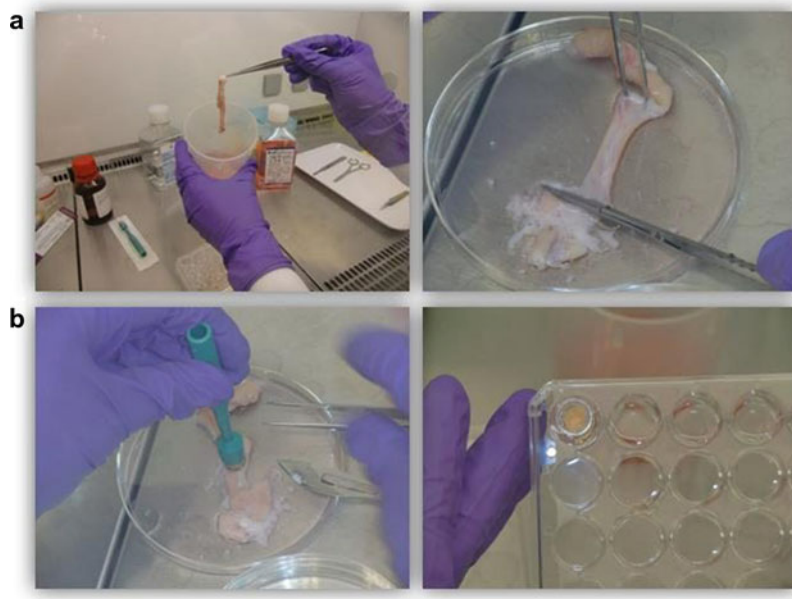

Fig. 1 Establishment of a skin organoculture. Briefly, the skin from surgical waste material from breast reductions was collected directly after surgery and immediately put in DMEM (**a**). All subcutaneous fat was removed with a scalpel to ensure full diffusion nitrification of the tissue. Eight millimeter punch biopsies were taken from the skin and referred to as full-thickness skin explants. Thereafter, the explants were put on Millipore Millicell culture plate inserts (12 mm Ø) (**b**)

collected and immediately put in DMEM at 8 °C (Gillbro et al. 2014). All subcutaneous fat was removed with a scalpel to ensure full diffusion nitrification of the tissue. Eight millimeter punch biopsies were taken from the skin and referred to as full-thickness skin explants. Thereafter, the explants were put on Millipore Millicell culture plate inserts (12 mm Ø) (Millipore Corporation, Stockholm, Sweden). Inserts containing skin explants were put in six-well plates (one insert/well) and supplemented with keratinocyte medium (M154) (Life Technologies, Stockholm, Sweden) to allow survival of the explants. Cream containing RA (tretinoin) (0,05 %) (Aberela®, Janssen-Cilag) at a concentration of 5 mg/cm^2 was applied topically on each explant, using positive displacement pipettes. Five milligram per square centimeter is a typical finite dose applied on skin penetration tests and considered as a nonocclusive dose (*OECD guidance notes on dermal absorption* 2010; Scientific committee on consumer safety SCCS Basic criteria for the in vitro assessment of dermal absorption of cosmetic ingredients 2010). The study was vehicle controlled with a cream containing all ingredients except for RA, referred to as placebo.

The explants were incubated with the RA cream for 24 h at 37 °C in 5 % CO_2 humidified air. At the end of the incubation period, two Ø 3 mm biopsies were taken from each explants for RNA extraction. Total RNAs were extracted from skin samples using QIAzol Lysis Reagent (Qiagen) according to the manufacturer's protocol. Two-hundred fifty nanograms of total RNA from each sample was used to prepare biotinylated fragmented cRNA according to the GeneChip® 3′ IVT Express Kit Manual (Affymetrix Inc., Santa Clara, CA). Affymetrix GeneChip® expression arrays (Human Genome U133 Plus 2.0) were hybridized for 16 h in a 45 °C incubator, rotated at 60 rpm. The arrays were washed and stained using the Fluidics Station 450 and finally scanned using the GeneChip® Scanner 3000 7G (Affymetrix).

Subsequent analysis of the gene expression data was carried out in the freely available statistical computing language R (http://www.r-project.org) using packages available from the Bioconductor project (www.bioconductor.org). The raw data was normalized using the robust multi-array average (RMA) method (Irizarry et al. 2003; Li and Wong 2001). In order to search for the differentially expressed genes between the **X** sample and the **Y** sample groups, an empirical Bayes moderated *t*-test was then applied using the "limma" package (Smyth 2004). To address the problem with multiple testing, the p-values were adjusted using the method of Benjamini and Hochberg (Benjamini et al. 2001). The enrichment analysis was performed to determine the probability that gene ontology groups are specifically overexpressed in RA-treated skin as compared to vehicle-treated skin. For this analysis investigators are often using DAVID bioinformatics database (http://david.abcc.ncifcrf.gov/). The enrichment score of each gene is determined by calculating the relative expression in the RA-treated skin compared to placebo-treated skin (Gillbro et al. 2014).

To do subsequent enrichment analysis, researchers normally compare gene expression between control and experimental cells with fold changes $2\geq$ and p-values ≤ 0.05) for selection (Huang et al. 2009).

5 The Identification of Genes and Biological Groups Affected by RA in an Organoculture of Human Skin

Microarrays simultaneously measure the levels of 22,000 mRNAs. We showed that 93 genes were significantly regulated by RA. Out of these 93 genes, 60 genes were upregulated and 33 downregulated (Gillbro et al. 2014). The clusters with the smallest p-value ($p < 0.05$) which were retrieved after 24 h stimulation with RA are presented in Fig. 2 and Table 2.

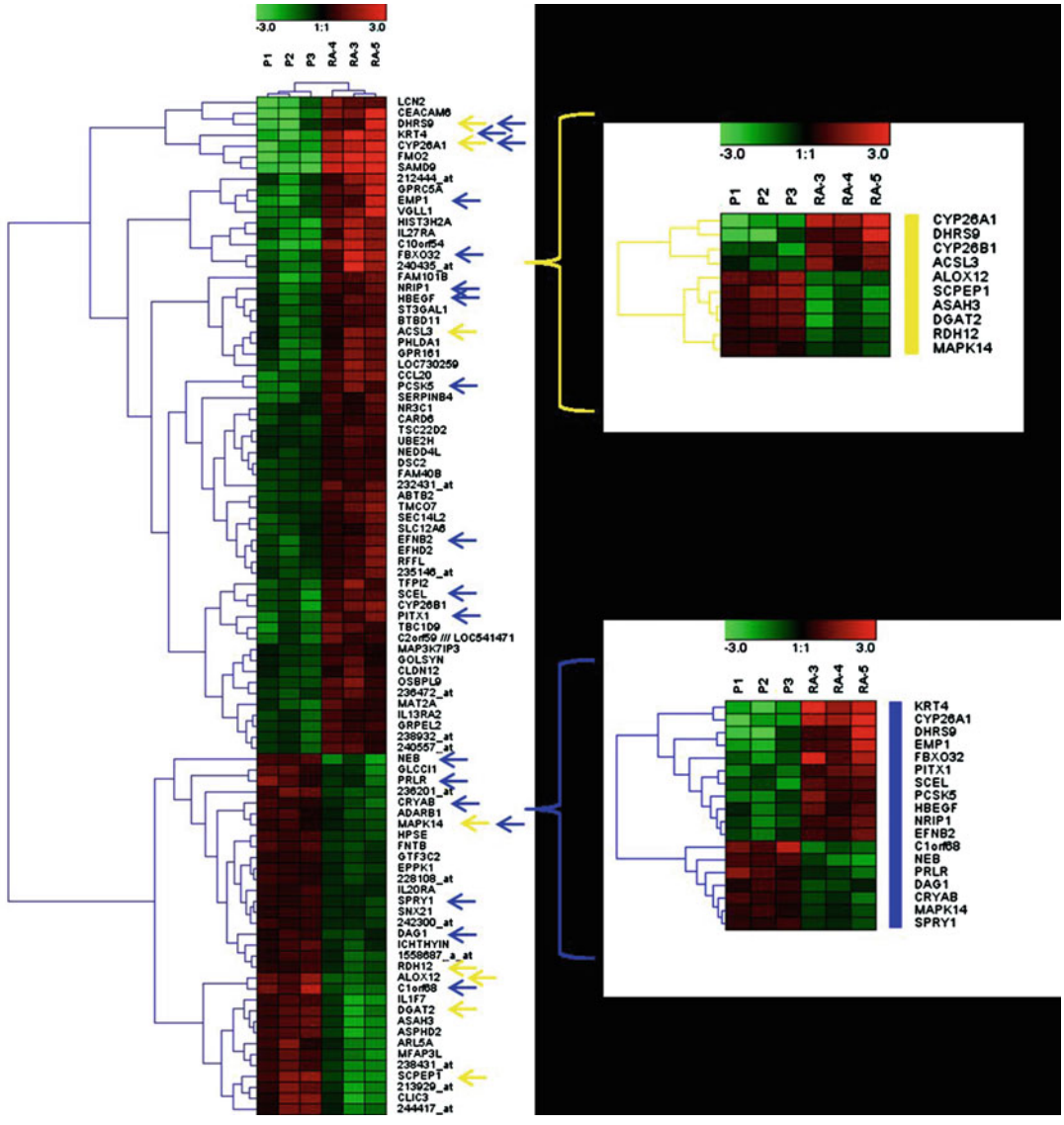

Fig. 2 Heat map of hierarchical clustering of 93 genes in RA-treated explants compared to placebo. Hierarchical clustering was performed using the Genesis software, with default settings (e.g., Euclidean distance, average linkage) of genes differentially expressed more than twofold, i.e., 93 genes. *Green* indicates reduced expression, *black* indicates the unaltered expression, and *red* indicates increased expression in RA-treated as compared to placebo-treated explants ($n = 3$). The *color scale bar* is shown at the top of each figure

When summarized, the functional categories of the genes upregulated by RA were found to be more than 30 % within one of the following ontological categories: clusters (lipid, hormone, and retinoid metabolism) and in development (organ, tissue, and epithelial development) (Gillbro et al. 2014).

Table 2 The corresponding genes to the clusters shown in Fig. 2, with gene name, gene symbol, gene ID, and fold change compared to placebo

Gene name	Gene symbol	Gene ID	Fold change
Cluster 1a, metabolism			
Cytochrome P450, family 26, subfamily A, polypeptide 1	CYP26A1	206424_at	22,61
Dehydrogenase/reductase (SDR family) member 9	DHRS9	224009_×_at	11,96
Cytochrome P450, family 26, subfamily B, polypeptide 1	CYP26B1	219825_at	5,26
Acyl-CoA synthetase long-chain family member 3	ACSL3	201662_s_at	3,66
Proprotein convertase subtilisin/kexin type 5	PCSK5	213652_at	2,69
Nuclear receptor subfamily 3, group C, member 1	NR3C1	201866_s_at	2,36
Mitogen-activated protein kinase 14	MAPK14	211561_×_at	−2,13
Retinol dehydrogenase 12 (all-trans/9-cis/11-cis)	RDH12	242998_at	−2,42
Diacylglycerol O-acyltransferase homolog 2 (mouse)	DGAT2	226064_s_at	−4,58
Arachidonate 12-lipoxygenase	ALOX12	207206_s_at	−4,73
Serine carboxypeptidase 1	SCPEP1	218217_at	−6,41
Cluster 1b, retinoic acid metabolism			
Cytochrome P450, family 26, subfamily A, polypeptide 1	CYP26A1	206424_at	22,61
Dehydrogenase/reductase (SDR family) member 9	DHRS9	224009_×_at	11,96
Cytochrome P450, family 26, subfamily B, polypeptide 1	CYP26B1	219825_at	5,26
Retinol dehydrogenase 12 (all-trans/9-cis/11-cis)	RDH12	24998_at	−2,42
Serine carboxypeptidase 1	SCPEP1	218217_at	−6,41
Cluster 2, development			
Keratin 4	KRT4	213240_s_at	26,97
Cytochrome P450, family 26, subfamily A, polypeptide 1	CYP 26A1	206424_at	22,61
Dehydrogenase/reductase (SDR family) member 9	DHRS9	224009_×_at	11,96
Epithelial membrane protein 1	EMP 1	213895_at	7,31
F-box protein 32	FBXO32	241762_at	6,39
Paired-like homeodomain 1	PITX1	209587_at	4,54
Sciellin	SCEL	1554921_a_at	4,06
Nuclear receptor-interacting protein 1	NRIP1	202600_s_at	3,70
Heparin-binding EGF-like growth factor	HBEGF	38037_at	10,8
Ephrin-B2	EFNB2	202669_s_at	3,18
Proprotein convertase subtilisin/kexin type 5	PCSK5	213652_at	2,69
Nuclear receptor subfamily 3, group C, member 1	NR3C1	201865_×_at	2,11
Sprout homolog 1, antagonist of FGF signaling (*Drosophila*)	SPRY1	212558_at	−2,12
Mitogen-activated protein kinase 14	MAPK14	211561_×_at	−2,13
Dystroglycan 1 (dystrophin-associated glycoprotein 1)	DAG1	205417_s_at	−2,28
Crystalline, alpha B	CRYAB	209283_at	−2,66
Prolactin receptor	PRLR	227629_at	−3,28
Nebulin	NEB	205054_at	−4,53
Chromosome 1 open reading frame 68	C1orf68	217087_at	−5,92

6 The Identification of New Novel Cmap Compounds Mimicking the Gene Profile of RA Treatment in an Organoculture

As for the identification of new compounds stimulating hair growth using cyclosporine as lead compounds (Ishimatsu-Tsuji et al. 2010), the gene signatures of the RA-treated skin were queried in the Cmap database to identify novel antiaging actives. Agents that were highly ranked in Cmap were identified as potential antiaging ingredients. Solely compounds of natural origin were selected for further analysis. One example of an identified agent through this approach was quercetin (unpublished

data). The use of quercetin as an antiaging compound has also been noted previously, but RA mimicking action has not been investigated (Chondrogianni et al. 2010; Casagrande et al. 2006).

7 Identification of New Novel Cmap Compounds Mimicking the Gene Profile of Topical RA Treatment in a Clinical Study on Nine Female Subjects

In addition, the gene profile of RA treatment was investigated in an in vivo study conducted on nine healthy Caucasian female volunteers aged 56.78 ± 6.87 (Mean ± SEM) exhibiting moderate to severe photodamage on their lower outer forearms. Tretinoin (Retin-A®, 0.025 %) and placebo were applied once daily on randomly assigned left or right forearm test sites for 7 days (Gillbro et al. 2015a).

Topical stimulation of nine females for 7 days with RA resulted in less significant gene alteration compared to the explant study on three subjects.

Eighteen genes were upregulated and one downregulated according the selection criteria. As for the study on topical application of RA in an organoculture (Gillbro et al. 2014), the in vivo study showed genes overrepresented in development process (Fig. 3 and Table 3).

Within the cluster of development process, KRT4 was highly upregulated.

Interestingly, genes involved in retinoid metabolism such as CYP26 were not induced in the clinical study as for the study in organocultures (Gillbro et al. 2015a). This could be due to greater variance between the subjects in the clinical in vivo study compared to the study in organocultures. Another explanation could be that mRNA levels of CYP26 are induced after acute short-term treatment and not after long-term treatment.

The gene signature of this in vivo study was then queried in the Cmap database.

8 Cmap Analysis Connects the Gene Signature of RA-Treated Skin to Acetyl Aspartic Acid (A-A-A)

The genes that were significantly upregulated (18 genes) or downregulated (1 gene) more than twofold were entered into the Cmap. Forty-eight compounds (data not shown) were highly ranked as comparable to the RA gene signature. Importantly, tretinoin (RA) was ranked highest (1) in the Cmap list with highest specificity (p-value 0,00002) which was an important proof that the gene expression profile for RA in the tested cell lines was similar for RA-treated skin in this study. Interestingly, also compounds with antibiotic character were listed among the identified compounds. This is in line with recent discoveries on inhibition of retinoid catabolism/metabolism by antibiotic drugs (Regen et al. 2015).

In total, six natural compounds were identified out of in total 48 RA mimicking agents.

Once we had identified the RA gene signature in photodamaged human skin, we conducted corresponding Cmap analysis which revealed six natural compounds showing similar activity on the gene level compared to the applied RA. These were tomatidine, cyanocobalamin (vitamin B12), docosahexaenoic acid ethyl ester, riboflavin (vitamin B2), *N*-acetylmuramic acid (peptidoglycan), and *N*-acetyl-L-aspartic acid (A-A-A).

Further restrictions on low molecular weight (<500 g/mol), chemical properties, and potential sourcing resulted in selection of *N*-acetyl aspartic acid (A-A-A) with the enrichment score 0,673 (p-value 0,02) (Table 4).

A-A-A is a derivative of aspartic acid. The actual chemical name is (2S)-2-acetamidobutanedioic acid; cas number is "997-55-7," with a formula of C6H9NO5 and a molecular weight of 175 g/mol, and a log P of −1.1. In the Cmap, the dose which other scientists worldwide have used to get the expression profile was also revealed (i.e., 23 μM). Therefore we continued using a range of 2,3–230 uM for further activity testing in vitro.

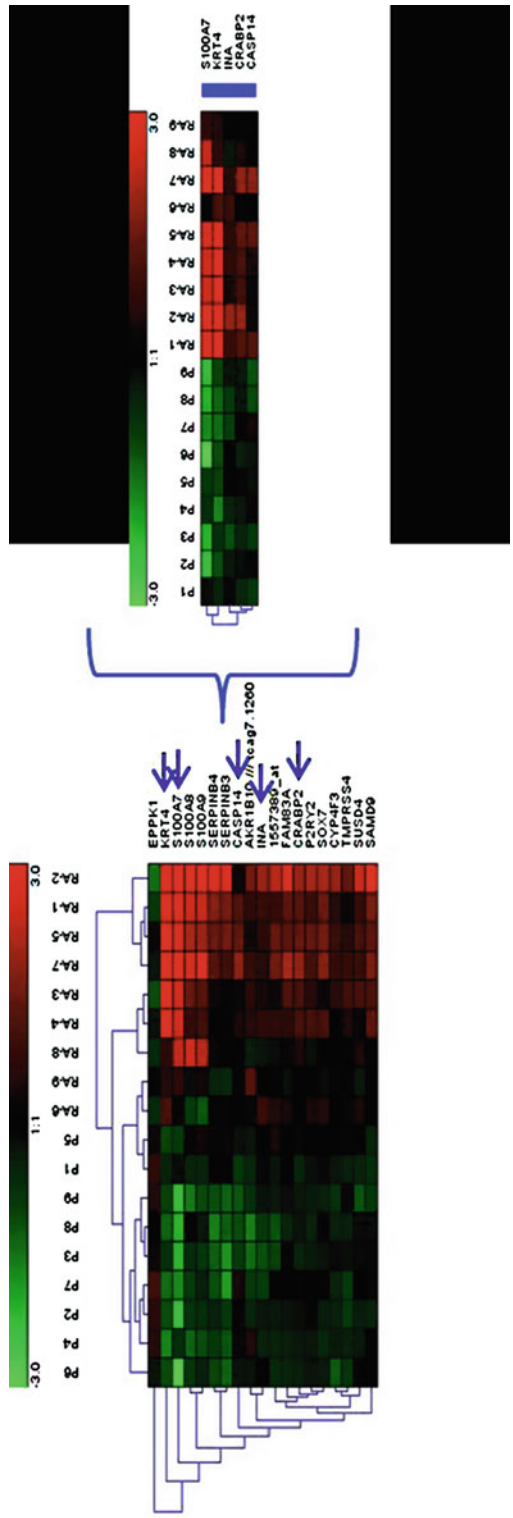

Fig. 3 Heat map of hierarchical clustering of 19 genes in nine RA-treated volunteers compared to placebo. Cluster analyses of genes encoding genes involved in development genes (*blue arrows*). These subsets of genes were clustered hierarchically on the basis of the similarity of their expression profiles (cluster 1: enrichment score 2.0). *P* placebo, *R4* retinoic acid treatment. Table 2 shows the corresponding genes to the clusters shown in Fig. 3

Table 3 The corresponding genes to the clusters shown in Fig. 3, with gene name, gene symbol, gene ID, and fold change compared to placebo

Development			
Gene name	Gene symbol	Gene ID	Fold change
Keratin 4	KRT4	213240_s_at	4,72
S100 calcium-binding protein A7	S100A7	205916_at	4,04
Cellular retinoic acid-binding protein 2	CRABP 2	202575_at	1,33
Caspase 14, apoptosis-related cysteine peptidase	CASP14	231722_at	1,14
Internexin neuronal intermediate filament protein, alpha	INA	204465_s_at	1,12

Table 4 The connectivity scores for RA and A-A-A identified through Cmap, through the transcriptional activity to RA in a clinical study of nine healthy Caucasian female volunteers

Cmap name	Connectivity score (enrichment)	*P*-value
Tretinoin (RA)	0,512	0.00002
A-A-A	0,673	0.02

The next step was to investigate whether A-A-A could be used as a cosmetic ingredient. In vitro studies showed relief of the fibroblast stiffness marker (F-actin) together with increased keratinocyte regeneration and inhibition of matrix metalloproteinases (MMPs) (Gillbro et al. 2015b).

Safety studies were conducted (see section below on "Safety Testing of A-A-A") as well as testing the skincare benefits in terms of skin firmness. Skin firmness was used as a testing parameter since RA is known to increase skin firmness (Ho et al. 2012), and RA was used as the lead compound in the Cmap studies described herein.

9 Safety Testing of A-A-A

The first stage in the safety assessment of A-A-A was a complete literature review of its toxicological profile. There was sufficient data in the literature to give a complete picture of its hazard potential with the exception of skin irritation and skin sensitization.

An in vitro skin irritation study on human reconstructed epidermis (RHE's-SkinEthic model) according to OECD Guideline 439 was therefore conducted in the first instance. After application of the test substance (pure) on RHE's for 42 min and a 42 h posttreatment incubation, cellular viability was measured by the transformation of MTT into blue formazan crystal. Under the conditions of the assay, the test substance tested pure was classified as nonirritant.

The lack of sensitization potential of A-A-A was confirmed in a Human Repeat Insult Patch (HRIPT) study after review of structurally similar materials. The study was a single-center, evaluator-blinded, within-subject randomized patch application study. The objective was to confirm, in a panel of healthy adult subjects, that the application of A-A-A tested neat, under maximizing conditions of exposure, did not induce delayed contact sensitization (Daly and Moran 2015).

Healthy men or nonpregnant women ages 18–68 of Caucasian origin with skin phototypes I–III were screened to enroll a sufficient number to achieve a minimum completion rate of 100, a sample size standard for these studies (Jordan and King 1977).

The methodology used was an adaptation of that described by Marzulli and Maibach (1976). The volunteers were treated with neat A-A-A under occlusive patch nine times to the same site (induction site) over a period of 3 consecutive weeks followed by a challenge phase after a minimal 2-week rest period, under patch, to the induction site and to a virgin site for 48 h.

In conclusion, under the experimental conditions adopted, the repeated application of A-A-A, tested neat, under occlusive patch on a panel of 107 test subjects with all types of skin on the body, induced no allergic reaction. The studies were conducted in accordance with the Declaration of

Helsinki and good clinical practice (GCP) guidelines.

10 Clinical Testing of the Antiaging Effect of A-A-A

As a first effort to investigate the antiaging effect of A-A-A, a clinical study on 16 Caucasian healthy female volunteers age range 55–75 years (mean age 64) with visible signs of moderate photodamage on the skin of the lateral forearms was conducted (Gillbro et al. 2015c).

The study was designed as a placebo-controlled, assessor-blinded, within-subject comparison of 12-day treatment phase of three test sites under occlusion (Finn Chambers 12 mm in diameter). One site was a blank chamber that was used as negative control.

Two extracellular matrix (ECM) proteins, collagen IV (COLIV) and fibrillin-1 were investigated using histological analysis of the 3 mm Ø punch biopsies taken from the sites. One of the ECM proteins, COLIV, expressed in the epidermal–dermal junction (DEJ) is important for dermal support to protect against wrinkle formation (Uitto 1986; Mays et al. 1995; Boisnic et al. 1999). Fibrillin-1 is a glycoprotein and shown to be important for the formation of elastic fibers (Sakai et al. 1986).

After 12-day topical application with A-A-A, both ECM proteins, COLIV and fibrillin-1, were statistically significantly increased compared to placebo and untreated skin, visualized by immunohistochemical stainings using diaminobenzidine (DAB) in brown (Fig. 4a). A-A-A treatment increased COLIV protein expression with 13,2 % versus placebo and 17,6 % versus untreated skin. Fibrillin expression increased with 6,4 % compared to placebo-treated skin (Fig. 4b).

COLIV was primarily expressed in the DEJ which separates the epidermis from dermis. Fibrillin-1 showed strong staining in DEJ as well as throughout the dermis. The DEJ was defined as region of interest (ROI) in the analysis of COLIV, and for fibrillin-1, DEJ plus 200 μm in dermis was defined as ROI.

Since the lead compound RA is known to improve skin firmness (Ho et al. 2012; Tucker-Samaras et al. 2009), we investigated the effect of the identified Cmap compound, A-A-A, on skin firmness using a Cutometer MPA580 (Courage + Khazaka Electronic GmbH, Cologne, Germany) on the inner forearm of 12 healthy female volunteers aged 50–65 years. In this double-blind vehicle-controlled study, three products were tested. All products were based on the same simple formulation only further characterized by the addition of A-A-A (1 %) in Product A and of retinol (0.1 %) in Product B. Product C was the vehicle (no active compound). Retinol was chosen as the cosmetically used precursor of RA, i.e., retinol (Tucker-Samaras et al. 2009).

In preparation of the study, volunteers followed a strict washout phase for 7 days during which no topical products could be used on the forearms. That restriction was observed for the whole length of the study.

On the first day of the study, four standard sites were identified and marked on the forearms of each volunteer (two on each forearm), leaving one site as untreated control. The assignment of each test products to a particular test site was randomized via a standard procedure prior to the start of the study. A baseline measurement of skin firmness was performed on all sites after a 30 min acclimatization in controlled conditions (T°: 21 ± 1 °C; RH 50 ± 5 %). Subsequently to the baseline, measurement products were applied at an approximate dose of 2 mg/cm^2, twice daily for 28 days. Final Cutometer measurements were performed on all test sites at the end of the study.

The Cutometer enables the investigation of the viscoelastic properties of the skin via the principle of repeated cycles of suction and release of the skin through the aperture of the probe (2 mm). It is an established standard technique for the measurement of skin firmness and elasticity (Barel and Courage 1995). The F4 area parameter represents skin firmness, i.e., the resistance of the skin to suction over the set of repeated cycles (20 in total). A decrease in F4 corresponds to an increase in skin firmness.

Changes in F4 after 28 days of product application in the treated areas were compared to the changes in the untreated control (shown in Fig. 5).

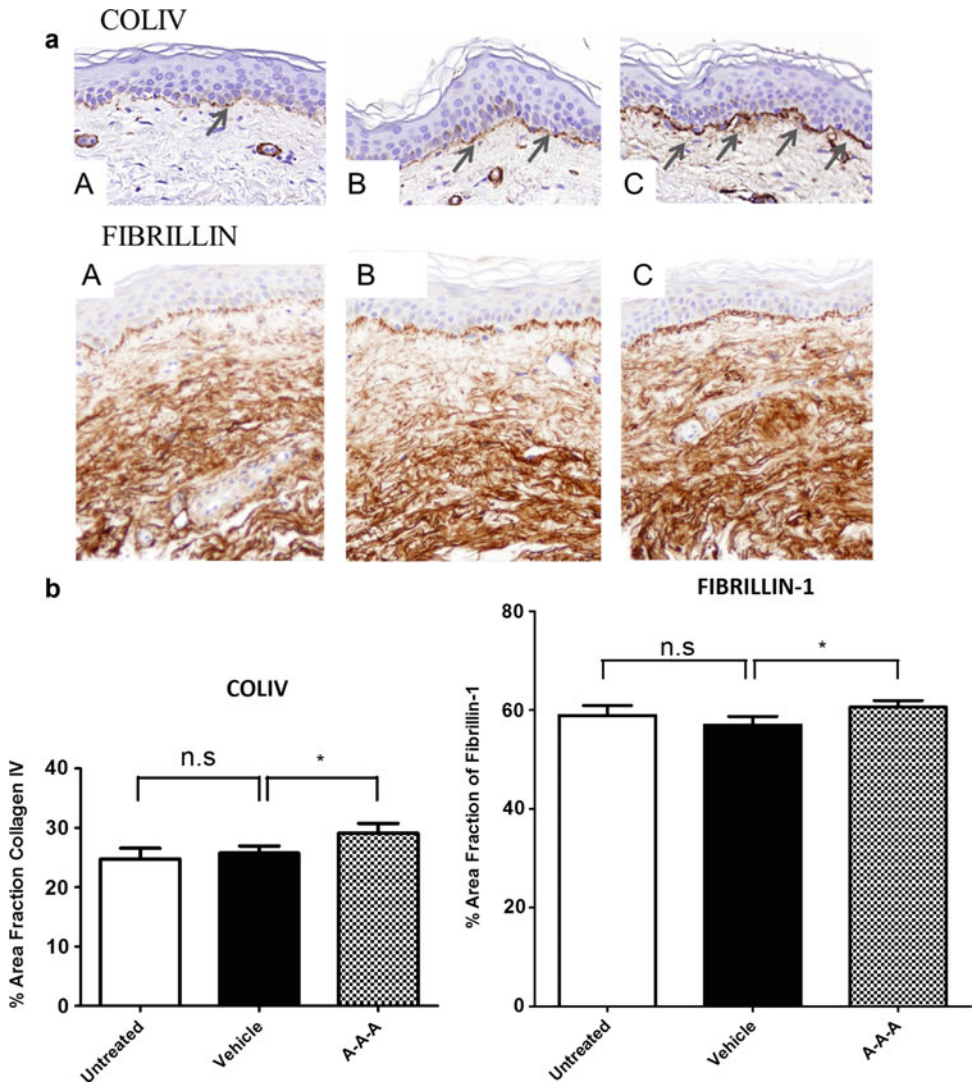

Fig. 4 **a** Application of A-A-A resulted in increased expression of COLIV, the basement membrane of the dermo-epidermal junction of photoaged skin (**c**) compared to vehicle (**b**) and untreated skin (**a**). *Arrows* indicate the location of the presence of this staining. Fibrillin-1 expression was also increased after 12-day treatment with A-A-A (**c**) compared to vehicle (**b**) and untreated skin (**a**). (**b**) Quantification of immunostaining in (**a**) represented in graph. A-A-A treatment increased COLIV protein expression by 13.2 % vs vehicle and 17.6 % vs untreated skin. Fibrillin-1 expression increased by 6.4 % compared to vehicle-treated skin. Statistical analysis using paired *t*-test; $*p = 0.02$, $**p = 0.004$, mean ± SEM

Both retinol- and A-A-A-containing products were found to enhance significantly skin firmness after 28 days of treatment, whereas the vehicle did not. Further comparison of the active products with the vehicle showed that A-A-A significantly increased skin firmness compared to placebo after 28 days of treatment. This effect was comparable to retinol (Gillbro et al. 2015c).

11 General Conclusion

The studies presented in this chapter show the Cmap approach is highly functional to identify novel antiaging ingredients. This chapter described studies using Cmap to identify new compounds of medical and cosmetic interest. To our knowledge,

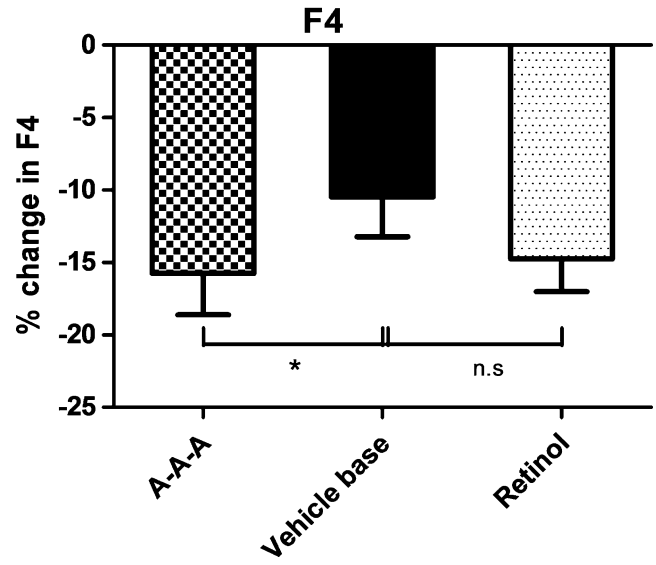

Fig. 5 Increase of skin firmness (associated with a decrease of F4) corrected to baseline after the use of the test products. Statistical analysis using paired *t*-test, $***p < 0.0001$; $*p = 0.0104$. Mean ± SEM

Oriflame Cosmetics is the first company using the Cmap approach to identify new ingredients for antiaging purpose. Organocultures of human skin and a preclinical clinical study on photoaged skin of human forearm were used to identify new compounds with antiaging benefits. A-A-A was identified and based on our criteria continued in in vitro screening where it was shown to have activity on both keratinocytes and fibroblasts. In vitro irritation study confirmed A-A-A to be nonirritant and HRIPT testing confirmed lack of sensitization potential. Furthermore, A-A-A was clinically tested in a vehicle-controlled study and shown to significantly increase protein expression of two ECM proteins, COLIV and fibrillin-1, which was translated in improved skin firmness in a similar manner to retinol using Cutometer assessment on human forearm.

In conclusion, Affymetrix® gene arrays with corresponding connectivity mapping have been proven to be a useful method to identify new lead compounds with antiaging activities.

References

Asselineau D, Darmon M. Retinoic acid provokes metaplasia of epithelium formed in vitro by adult human epidermal keratinocytes. Differ Res Biol Divers. 1995;58:297–306.

Asselineau D, Bernard BA, Bailly C, Darmon M. Retinoic acid improves epidermal morphogenesis. Dev Biol. 1989;133:322–35.

Babamiri K, Nassab R. Cosmeceuticals: the evidence behind the retinoids. Aesthet Surg J Am Soc Aesthet Plast Surg. 2010;30:74–7.

Balmer JE. Gene expression regulation by retinoic acid. J Lipid Res. 2002;43:1773–808. doi:10.1194/jlr.R100015-JLR200.

Barel AO, Courage WCP. Suction method for measurement of skin mechanical properties: the Cutometer®. In: Jemec SJ, editor. Handb. non-invasive methods Ski. Boca Raton: CRC Press; 1995. p. 335–40.

Bellemère G, Stamatas GN, Bruère V, et al. Antiaging action of retinol: from molecular to clinical. Skin Pharmacol Physiol. 2009;22:200–9.

Benjamini Y, Drai D, Elmer G, et al. Controlling the false discovery rate in behavior genetics research. Behav Brain Res. 2001;125:279–84. doi:10.1016/S0166-4328(01)00297-2.

Bernard F-X, Pedretti N, Rosdy M, Deguercy A. Comparison of gene expression profiles in human keratinocyte mono-layer cultures, reconstituted epidermis and normal human skin; transcriptional effects of retinoid treatments in reconstituted human epidermis. Exp Dermatol. 2002;11:59–74.

Boisnic S, Branchet-Gumila MC, Le Charpentier Y, Segard C. Repair of UVA-induced elastic fiber and collagen damage by 0.05% retinaldehyde cream in an ex vivo human skin model. Dermatology. 1999;199:43–8.

Boyle JO, Gümüs ZH, Kacker A, et al. Effects of cigarette smoke on the human oral mucosal transcriptome. Cancer Prev Res Phila Pa. 2010;3:266–78.

Casagrande R, Georgetti SR, Verri WA, et al. Protective effect of topical formulations containing quercetin against UVB-induced oxidative stress in hairless

mice. J Photochem Photobiol B. 2006;84:21–7. doi:10.1016/j.jphotobiol.2006.01.006.

Chang M, Smith S, Thorpe A, et al. Evaluation of phenoxybenzamine in the CFA model of pain following gene expression studies and connectivity mapping. Mol Pain. 2010;6:56. doi:10.1186/1744-8069-6-56.

Chen M-H, Yang W-LR, Lin K-T, et al. Gene expression-based chemical genomics identifies potential therapeutic drugs in hepatocellular carcinoma. PLoS One. 2011;6:e27186. doi:10.1371/journal.pone.0027186.

Chen F, Guan Q, Nie Z-Y, Jin L-J. Gene expression profile and functional analysis of Alzheimer's disease. Am J Alzheimers Dis Other Dement. 2013. doi:10.1177/1533317513500838.

Chondrogianni N, Kapeta S, Chinou I, et al. Anti-ageing and rejuvenating effects of quercetin. Exp Gerontol. 2010;45:763–71. doi:10.1016/j.exger.2010.07.001.

Claerhout S, Lim JY, Choi W, et al. Gene expression signature analysis identifies vorinostat as a candidate therapy for gastric cancer. PLoS One. 2011;6:e24662. doi:10.1371/journal.pone.0024662.

Daly P, Moran G. Safety assessment of a novel active ingredient, acetyl aspartic acid, according to the EU Cosmetics Regulation and the Scientific Committee on Consumer Safety guidelines. Int J Cosmet Sci Suppl. 2015;1:21–7.

Dudley JT, Sirota M, Shenoy M, et al. Computational repositioning of the anticonvulsant topiramate for inflammatory bowel disease. Sci Transl Med. 2011;3:96ra76.

Eckert RL, Green H. Cloning of cDNAs specifying vitamin A-responsive human keratins. Proc Natl Acad Sci U S A. 1984;81:4321–5.

Eckert RL, Rorke EA. Molecular biology of keratinocyte differentiation. Environ Health Perspect. 1989;80:109–16.

Fuchs E. Scratching the surface of skin development. Nature. 2007;445:834–42.

Fuchs E, Green H. Regulation of terminal differentiation of cultured human keratinocytes by vitamin A. Cell. 1981;25:617–25.

Ghyselinck NB, Chapellier B, Calléja C, et al. Genetic dissection of retinoic acid function in epidermis physiology. Ann Dermatol Venereol. 2002;129:793–9.

Gilfix BM, Eckert RL. Coordinate control by vitamin A of keratin gene expression in human keratinocytes. J Biol Chem. 1985;260:14026–9.

Gillbro JM, Al-Bader T, Westman M, et al. Transcriptional changes in organoculture of full thickness human skin following topical application of all-trans retinoic acid. Int J Cosmet Sci. 2014;36:1–9. doi:10.1111/ics.12121.

Gillbro JM, Merinville E, Olsson M, et al. The use of gene arrays and corresponding connectivity mapping (Cmap) to identify novel anti-aging ingredients. Int J Cosmet Sci. 2015a;37:9–14.

Gillbro JM, Lundahl M, Westman M, et al. Structural activity relationship analysis (SAR) and in vitro testing reveal the anti-aging potential activity of acetyl aspartic acid. Int J Cosmet Sci. 2015b;37:15–20.

Gillbro J, Merinville E, Cattley K, et al. In vivo topical application of acetyl aspartic acid increases fibrillin-1 and collagen IV deposition leading to a significant improvement of skin firmness. Int J Cosmet Sci. 2015c;37 Suppl 1:41–6.

Griffiths CE, Finkel LJ, Ditre CM, et al. Topical tretinoin (retinoic acid) improves melasma. A vehicle-controlled, clinical trial. Br J Dermatol. 1993;129:415–21.

Hassan SB, Gali-Muhtasib H, Göransson H, Larsson R. Alpha terpineol: a potential anticancer agent which acts through suppressing NF-kappaB signalling. Anticancer Res. 2010;30:1911–9.

Hassane DC, Guzman ML, Corbett C, et al. Discovery of agents that eradicate leukemia stem cells using an in silico screen of public gene expression data. Blood. 2008;111:5654–62. doi:10.1182/blood-2007-11-126003.

Ho ET, Trookman NS, Sperber BR, Rizer RL, Spindler R, Sonti S, Gotz VMR. A randomized, double-blind, controlled comparative trial of the anti-aging properties of non-prescription tri-retinol 1.1% vs. prescription tretinoin 0.025%. J Drugs Dermatol. 2012;11:64–9.

Huang DW, Sherman BT, Lempicki RA. Systematic and integrative analysis of large gene lists using DAVID bioinformatics resources. Nat Protoc. 2009;4:44–57. doi:10.1038/nprot.2008.211.

Irizarry RA, Hobbs B, Collin F, et al. Exploration, normalization, and summaries of high density oligonucleotide array probe level data. Biostatistics. 2003;4:249–64. doi:10.1093/biostatistics/4.2.249.

Ishimatsu-Tsuji Y, Soma T, Kishimoto J. Identification of novel hair-growth inducers by means of connectivity mapping. FASEB J Off Publ Fed Am Soc Exp Biol. 2010;24:1489–96.

Johnstone AL, Reierson GW, Smith RP, et al. A chemical genetic approach identifies piperazine antipsychotics as promoters of CNS neurite growth on inhibitory substrates. Mol Cell Neurosci. 2012;50:125–35. doi:10.1016/j.mcn.2012.04.008.

Jordan WP, King SE. Delayed hypersensitivity in females. The development of allergic contact dermatitis in females during the comparison of two predictive patch tests. Contact Dermatitis. 1977;3:19–26.

Kang S, Fisher GJ, Voorhees JJ. Photoaging and topical tretinoin: therapy, pathogenesis, and prevention. Arch Dermatol. 1997;133:1280–4.

Kligman AM, Willis I. A new formula for depigmenting human skin. Arch Dermatol. 1975;111:40–8.

Kligman LH, Duo CH, Kligman AM. Topical retinoic acid enhances the repair of ultraviolet damaged dermal connective tissue. Connect Tissue Res. 1984;12:139–50.

Kligman AM, Grove GL, Hirose R, Leyden JJ. Topical tretinoin for photoaged skin. J Am Acad Dermatol. 1986;15:3271–4.

Kunkel SD, Suneja M, Ebert SM, et al. mRNA expression signatures of human skeletal muscle atrophy identify a

natural compound that increases muscle mass. Cell Metab. 2011;13:627–38.
Kurlandsky SB, Duell EA, Kang S, et al. Auto-regulation of retinoic acid biosynthesis through regulation of retinol esterification in human keratinocytes. J Biol Chem. 1996;271:15346–52.
Lamb J, Crawford ED, Peck D, et al. The connectivity map: using. Science. 2006;313:1929–35. doi:10.1126/science.1132939. 80-.
Li C, Wong W. Model-based analysis of oligonucleotide arrays: model validation, design issues and standard error . . .. Genome Biol. 2001.
Liu P, Tan S, Wang Q, Wang Y. Effects of all-trans retinoic acid and tazarotene on MMP-1 and TIMP-1 expression in cultured human fibroblasts after heat shock. Nan fang yi ke da xue xue bao. J South Med Univ. 2009;29:217–9.
Marzulli FN, Maibach HI. Contact allergy: predictive testing in man. Contact Dermatitis. 1976;2:1–17.
Mays PK, McAnulty RJ, Campa JS, Laurent GJ. Age-related alterations in collagen and total protein metabolism determined in cultured rat dermal fibroblasts: age-related trends parallel those observed in rat skin in vivo. Int J Biochem Cell Biol. 1995;27:937–45. doi:10.1016/1357-2725(95)00056-U.
Napoli JL. Physiological insights into all-trans-retinoic acid biosynthesis. Biochim Biophys Acta. 2012;1821:152–67. doi:10.1016/j.bbalip.2011.05.004.
Nygren P, Fryknäs M, Agerup BLR. Repositioning of the anthelmintic drug mebendazole for the treatment for colon cancer. J Cancer Res Clin Oncol. 2013;139:2133–40.
OECD guidance notes on dermal absorption 10-22-2010. 2010.
Pavez Loriè E, Gånemo A, Borgers M, et al. Expression of retinoid-regulated genes in lamellar ichthyosis vs. healthy control epidermis: changes after oral treatment with liarozole. Acta Dermatovenereologica. 2009a;89:12–20.
Pavez Loriè E, Li H, Vahlquist A, Törmä H. The involvement of cytochrome p450 (CYP) 26 in the retinoic acid metabolism of human epidermal keratinocytes. Biochim Biophys Acta. 2009b;1791:220–8.
Regen F, Hildebrand M, Le Bret N, et al. Inhibition of retinoic acid catabolism by minocycline: evidence for a novel mode of action? Exp Dermatol. 2015;24:473–6.
Reka AK, Kuick R, Kurapati H, et al. Identifying inhibitors of epithelial-mesenchymal transition by connectivity map-based systems approach. J Thorac Oncol. 2011;6:1784–92. doi:10.1097/JTO.0b013e31822adfb0.
Sakai LY, Keene DR, Engvall E. Fibrillin, a new 350-kD glycoprotein, is a component of extracellular microfibrils. J Cell Biol. 1986;103:2499–509. doi:10.1083/jcb.103.6.2499.
Saurat JH. Retinoids and psoriasis: novel issues in retinoid pharmacology and implications for psoriasis treatment. J Am Acad Dermatol. 1999;41:S2–6.
Scientific committee on consumer safety SCCS. Basic criteria for the in vitro assessment of dermal absorption of cosmetic ingredients 6-22-2010.
Sirota M, Dudley JT, Kim J, et al. Discovery and preclinical validation of drug indications using compendia of public gene expression data. Sci Transl Med. 2011;3:96ra77–7. doi:10.1126/scitranslmed.3001318.
Siu F-M, Ma D-L, Cheung Y-W, et al. Proteomic and transcriptomic study on the action of a cytotoxic saponin (Polyphyllin D): induction of endoplasmic reticulum stress and mitochondria-mediated apoptotic pathways. Proteomics. 2008;8:3105–17.
Smyth G. Linear models and empirical Bayes methods for assessing differential expression in microarray {. . .}. Stat Appl Genet Mol Biol. 2004;3
Taimi M, Helvig C, Wisniewski J, et al. A novel human cytochrome P450, CYP26C1, involved in metabolism of 9-cis and all-trans isomers of retinoic acid. J Biol Chem. 2004;279:77–85.
Titus S, Hodge J. Diagnosis and treatment of acne. Am Fam Physician. 2012;86:734–40.
Tucker-Samaras S, Zedayko T, Cole C, et al. A stabilized 0.1% retinol facial moisturizer improves the appearance of photodamaged skin in an eight-week, double-blind, vehicle-controlled study. J Drugs Dermatol. 2009;8:932–6.
Uitto J. Connective tissue biochemistry of the aging dermis. Age-related alterations in collagen and elastin. Dermatol Clin. 1986;4:433–46.
Vahlquist A. What are natural retinoids? Dermatol Basel Switz. 1999;199(Suppl):3–11.
Varani J, Nickoloff BJ, Dixit VM, et al. All-trans retinoic acid stimulates growth of adult human keratinocytes cultured in growth factor-deficient medium, inhibits production of thrombospondin and fibronectin, and reduces adhesion. J Invest Dermatol. 1989;93:449–54.
Wang G, Ye Y, Yang X, et al. Expression-based in silico screening of candidate therapeutic compounds for lung adenocarcinoma. PLoS One. 2011;6:7. doi:10.1371/journal.pone.0014573.
White JA, Beckett-Jones B, Guo YD, et al. cDNA cloning of human retinoic acid-metabolizing enzyme (hP450RAI) identifies a novel family of cytochromes P450. J Biol Chem. 1997;272:18538–41.
Yang L, Agarwal P. Systematic drug repositioning based on clinical side-effects. PLoS One. 2011;6:e28025. doi:10.1371/journal.pone.0028025.
Zhao H, Zhu L-L, Zaidi M, et al. Disease-drug pairs revealed by computational genomic connectivity mapping on GBA1 deficient, Gaucher disease mice. Biochem Biophys Res Commun. 2012;422:573–7. doi:10.1016/j.bbrc.2012.05.027.

Measuring Skin Cell Stiffness

148

Christian Schulze and Soeren Jaspers

Contents

Keywords

Elasticity • Stiffness • Optical stretcher • Cell mechanics

Abbreviations

ECM Extracellular matrix

SFM Scanning-force microscopy

1 Introduction

Active and passive cellular biomechanics based on the stability provided by the cytoskeleton impact many essential cellular functions such as motility, division, and mechanosensitivity (Bereiter-Hahn et al. 1994; Fletcher and Mullins 2010). Previous studies have shown that biomechanical properties are connected to cell functions that are regulated by mechanical forces (Ingber 1997; Janmey and Weitz 2004). Individual cells are able to sense mechanical signals and transduce them into a biochemical response. There is a link between the fibroblasts' collagen production and mechanical forces acting on the cells when comparing the cells' synthesis activity in stressed versus relaxed collagen gels (Kessler et al. 2001; Fluck et al. 2003). Moreover, it has been shown that a functionally intact cytoskeleton is crucial to build up contraction forces in a three-dimensional collagen lattice (Kolodney and Wysolmerski 1992; Brown et al. 1996). All these cell functions are essentially needed for the homeostasis of the skin.

C. Schulze (✉) • S. Jaspers
Research and Development, Beiersdorf AG, Hamburg, Germany
e-mail: Christian.Schulze@beiersdorf.com; Soeren.Jaspers@beiersdorf.com

P. Humbert et al. (eds.), *Agache's Measuring the Skin*,
DOI 10.1007/978-3-319-32383-1_147

Considering the importance of cellular biomechanics for correct physiologic functioning, the mechanical behavior of isolated skin cells is accessible by new sophisticated biotechnological tools.

2 Biomechanical Characterization of Cells

Different types of measurement techniques have been developed to quantify the mechanical properties of biological cells and to investigate the relation between structural response and cytoskeletal composition. The majority of these studies imply a correlation of cellular stiffness to cell status.

In general, a defined force or stress is applied to the cells and the resulting deformation is analyzed. Most techniques deform local regions of the cell, while only a few methods are capable of assessing the cells' whole structural response (global deformation techniques). One of the most common methods is the micropipette aspiration (Hochmuth 2000) that works by applying locally a negative pressure to adherent cells while measuring the linear extension into the pipette. Using this method, it was shown that malignantly transformed fibroblasts are significantly softer than their normal counterparts (Ward et al. 1991). In addition micropipette aspiration was used to determine the elastic properties of polymer gels (Boudou et al. 2009) and cell adhesion forces (Sung et al. 1996). A more recently developed technique is scanning-force microscopy (SFM) that allows the measurement of biomechanical properties of cells, tissues, and even molecules (Rotsch and Radmacher 2000). Besides imaging biological samples at nanometer resolution, an SFM is capable of probing cellular elasticity by using a hard indentor to measure the relation between applied force and local deformation of adherent cells. Thereby, defined forces are exerted to the cell membrane by a fine tip that is attached to a flexible cantilever. When in contact with the sample, the cantilever deflection is detected by a laser beam reflected from the back of the cantilever to a photodiode detector (Fig. 1a). Figure 1b shows a typical force-distance curve measured by a SFM. The cantilever tip is pushed into the cell (approach) and then retracted again, while recording the height and deflection. Based on a theoretical model developed by Heinrich Hertz, which analytically describes the elastic deformation of two homogeneous spheres pressed against each other (Hertz 1881), the cell's local Young's modulus can be calculated if the force constant of the cantilever is known. The SFM technique has been improved by attaching micron-sized beads to the cantilever tip that prevent penetration of the plasma membrane and

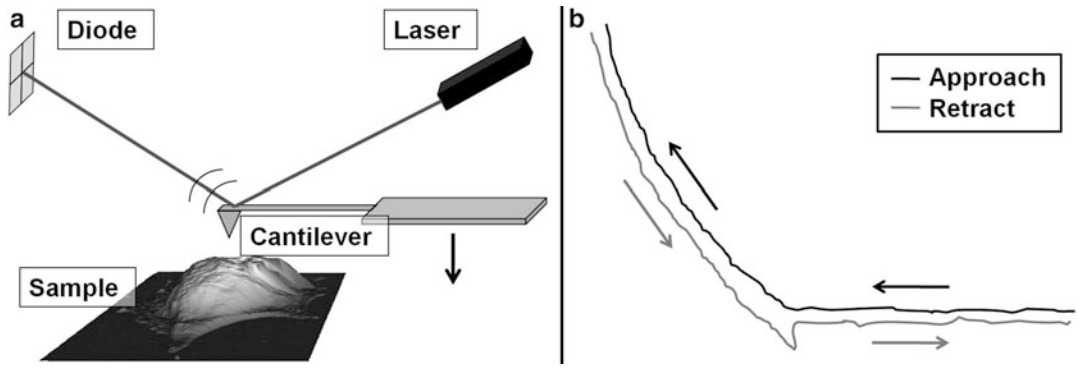

Fig. 1 Elasticity measurement by scanning-force microscopy. (**a**) The SFM basically consists of a flexible cantilever that is deflected by the sample. The reflected IR laser beam changes its position, which is detected by the photodiode. (**b**) The force exerted by the cantilever can be calculated from the deflection signal. Fitting the measured data of applied force and sample indentation with an appropriate analytical model allows for extracting cell elasticity

assures a well-defined geometrical shape (Mahaffy et al. 2000). Since the Hertz model assumes linear elastic materials and does not consider the cells' cytoplasmic viscosity, it was extended by Mahaffy et al. to obtain information about the frequency-dependent viscoelastic response.

Using the so-called force mapping mode, the SFM can provide two-dimensional elasticity maps of a sample by scanning the cantilever over the cell and measuring a force-distance curve for each point of the map. A disadvantage of this method is the high measurement duration.

In case of magnetic bead microrheology, the viscoelastic properties of adherent cells are measured by exerting forces via micron-sized magnetic beads that are coated and bound specifically to integrin receptors at the cell membrane (Fabry et al. 2001). The microbeads are twisted by an external homogeneous magnetic field that is varying sinusoidally in time. Analysis of the bead displacement allows to calculate viscoelastic material properties. Optical tweezers can also be used for cell deformation experiments when beads with appropriate optical properties are bound to the membrane and serve as handles for the force application (Sleep et al. 1999). Besides an active deformation of the sample, there are also passive methods where the cytoskeleton is interspersed by fluorescent beads. Here, the Brownian motion, which is influenced by the mechanical properties of the polymer network, is measured. A disadvantage that all bead experiments have in common is the fact that it cannot be known if and how the beads are attached to the sample. In case of active deformation techniques, differences in contact area would cause a varying mechanical stress. In addition, coating of the beads with antibodies makes these methods tedious and cost intensive. Another critical point, which also applies for the micropipette aspiration technique, is that the displacement of microspheres can provide inaccurate measurement data if the plasma membrane detaches from the cytoskeleton during deformation.

While the already mentioned methods probe cell elasticity predominantly over a relative small area of the surface (local deformation), the mechanical response of whole cells can be assessed by microplate manipulation, where the rheological properties of cell monolayers are measured by shear experiments (Fernandez et al. 2007). Nevertheless, these measurements can only provide an average value rather than the true single cell behavior and suffer from artifacts due to the influence of cell-cell and cell-substrate adhesion.

The optical stretcher is a recently developed technique that permits measuring large numbers of individual cells without any mechanical contact (noninvasively). Deformation experiments by direct contact can cause problems due to an unsymmetric stress distribution or not predictable active cell reactions. The microfluidic optical stretcher is an optical trap that allows trapping and controlled deformation of single suspended cells by using two counter-propagating laser beams (Guck et al. 2000). Cellular extension is caused by a momentum transfer acting on the cell surface. The applied global stress permits the measurement of whole cell elasticity that characterizes the integral effects of molecular changes on the cytoskeleton. A disadvantage of this technique is that probing rheological properties of cells in suspension may be considered as unphysiological, because of the lack of cellular contact to the extracellular matrix. Nevertheless, the symmetric shell-like structural design, the broad and continuous distribution of stress over the cell surface, and the avoidance of artifacts due to mechanical contact are the reasons for the low variability within the measured properties of the cell populations and the reproducibility of this method. The use of optical deformability as a sensitive cell marker has already been demonstrated for the characterization of individual dermal fibroblasts at different donor ages (Schulze et al. 2010).

3 Optical Cell Stretcher

Optical traps have been used to exert forces and manipulate dielectric particles for quite a long time (Ashkin 1970). Soon, the great potential to use optical techniques like optical tweezers to

noninvasively analyze biological samples was realized (Ashkin et al. 1987). The forces that can be exerted on biological matter by light are in the range between pico- and nanonewtons, which might appear small compared to other micromanipulation tools like SFM. However, these forces are perfectly suited to noninvasively hold and manipulate individual biological cells without causing damage and contamination. The optical stretcher is a recently developed two-laser beam trap that uses two counter-propagating divergent beams integrated into a microfluidic system to probe the viscoelastic behavior of suspended cells. Since the laser beams are not focused, there is no problem with radiation damage, which minimizes the light flux through the cells in comparison to other optical traps.

In this paragraph, first the basic working principle of stretching dielectric particles with light is introduced, followed by the experimental setup of the optical stretcher and a description of data analysis.

3.1 Basic Principle

When light hits the surface of an object with higher optical density, forces are generated that act normal to the surface and point away from the optical denser medium. This physical effect can be used to exert forces on single biological cells in suspension to analyze their deformation behavior. The optical stretcher basically consists of two laser beams with Gaussian intensity distribution that form a symmetric trap geometry. The cells are typically deformed by a constant stress profile causing a characteristic, passive, viscoelastic response. The surface forces can be attributed to a transfer of momentum at the interface between the cell (high refractive index) and surrounding medium (low refractive index) according to Newton's second law. The theoretical description of the interaction between laser radiation and small dielectric particles strongly depends on the ratio of particle size and the used wavelength λ. In case of optical traps, the wavelength is usually in the range of 600–1200 nm, whereas the cell diameter d is an order of magnitude larger d >20 μm. For that reason the surface forces can be quantitatively explained using the Mie regime, which is also called ray-optics regime. The approach in this regime is to decompose the laser beam into individual rays that propagate in a straight line and are described by geometric optics. The theoretical explanation in case of $d \approx \lambda$ is highly nontrivial and requires the exact solution of the Maxwell equations, whereas problems in the limit $d << \lambda$ are specified by the Rayleigh regime.

At first, one might expect that a soft dielectric particle hit by two counter-propagating laser beams is rather compressed than stretched. In the Mie regime, the ability of light to exert forces on dielectric samples can be explained by simple momentum transfer. To illustrate the basic principle of cell stretching, the following section outlines changes of momentum when a light ray passes at normal incidence through an optically denser object. For each ray or photon with the energy $E = h \cdot \nu$ the relativistic energy-momentum relation predicts the momentum p as (Ashkin and Dziedzic 1973)

$$p = n \cdot \frac{E}{c_0} \tag{1}$$

where n is the refractive index of the medium, c_0 is the speed of light in vacuum, h is the Planck constant, and ν is the frequency. Since the momentum is directly proportional to the refractive index, the light gains momentum as it enters the object. According to the law of conservation of momentum, the same amount of momentum change is transferred to the surface in the opposite direction. As the light exits the optical denser medium, it loses momentum which causes a transfer of momentum to the surface at the back in the direction of light propagation. Further, at both interfaces, a fraction of light is reflected, which leads to additional transfer of momenta in the direction of light propagation. In case of biological cells interacting with an infrared laser, the fraction of reflected light is less than 0.5 %. Therefore, the contribution of reflected light to the surface forces is considerably smaller. The resulting forces acting on the front and back

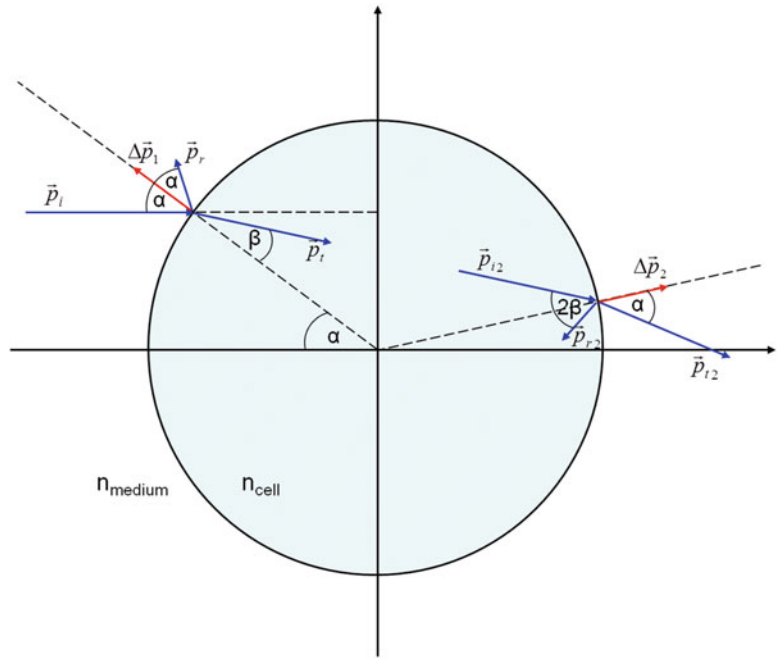

Fig. 2 Schematic of a light ray incident on a spherical object with refractive index n_{cell}, which is refracted and reflected at the intersurfaces according to Snell's law

surface are directed in opposite directions and will cause a stretching of soft objects.

In this example the asymmetry between both surface forces would cause a net force acting on the center of mass and pushing the cell away from the laser source (so-called scattering force). A second light ray passing through the object from the opposite site would compensate this net force, so that only surface forces are left, which are additive.

If a light ray with momentum $p_i = n_{\text{medium}} \cdot E/c_0$ hits the surface of a spherical object like a cell under arbitrary angle of incidence, it has to be considered that not only the absolute value of momentum but also its direction changes (Fig. 2). This is described by Snell's law:

$$n_{\text{medium}} \cdot \sin\alpha = n_{\text{cell}} \cdot \sin\beta \tag{2}$$

where n_{medium} and n_{cell} are the refractive indices and α and β the angles of incidence and refraction. The angle of reflection is identical to the angle of incidence.

The momenta of the reflected light ray p_r and the refracted (transmitted) light ray p_t are given by

$$p_r = \frac{n_{\text{medium}} \cdot E}{c} \cdot R(\alpha) \tag{3}$$

$$p_t = \frac{n_{\text{cell}} \cdot E}{c} \cdot (1 - R(\alpha)) \tag{4}$$

where $R(\alpha)$ is the reflection coefficient, which represents the ratio of reflected and incident intensity and can be calculated by Fresnel's equations.

The magnitudes of momentum at the backside of the cell are accordingly given by

$$p_{i2} = p_t \tag{5}$$

$$p_{t2} = p_t \cdot (1 - R(\beta)) \tag{6}$$

$$p_{r2} = p_t \cdot R(\beta) \tag{7}$$

Taking the vector nature of momentum into account, the resulting momenta transferred to the surfaces calculate as

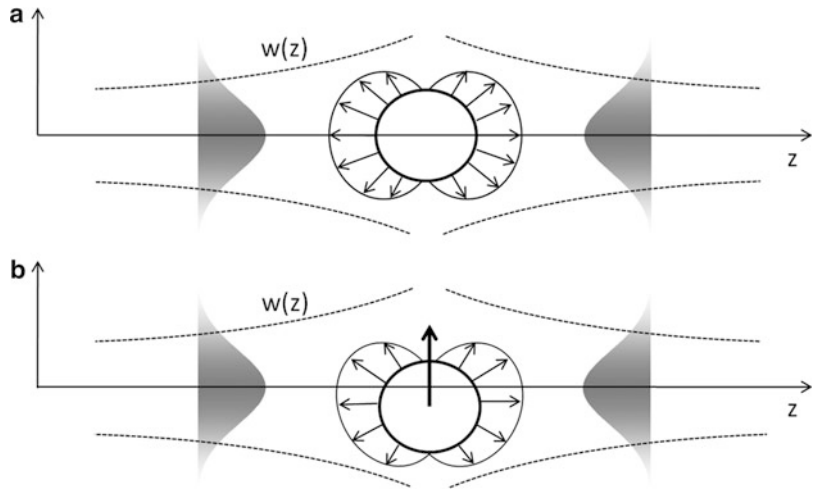

Fig. 3 (**a**) Rotational symmetric stress profile acting on a cell trapped in a two -laser beam geometry with Gaussian intensity distributions. (**b**) When the cell is out of the center of the trap, restoring gradient and scattering forces will move it back

$$\Delta\vec{p_1} = \vec{p_i} - \vec{p_r} - \vec{p_t} \tag{8}$$

$$\Delta\vec{p_2} = \vec{p_{i2}} - \vec{p_{r2}} - \vec{p_{t2}} \tag{9}$$

A dual beam laser trap, such as the optical stretcher, consists of two counter-propagating, divergent Gaussian laser beams that function as stable optical trap where cells can be held between the two beams and stretched along the laser beam axis at increasing power. Based on this simple ray-optics model, the total stress profile σ(α) acting on the surface of the object can be calculated by considering the total transferred momentum of the incident beam (Guck et al. 2000) (Fig. 3):

$$\sigma(\alpha) = \frac{F(\alpha)}{A} = \frac{\Delta p(\alpha)}{\Delta t \cdot A} = \frac{\Delta p(\alpha)}{E}\frac{E}{\Delta t \cdot A} = \frac{\Delta p(\alpha)}{E} \cdot I(z, r, \alpha) \tag{10}$$

where $\Delta p(\alpha)$ is the total momentum transferred on a single surface element, $I(z, r, \alpha)$ is the local light intensity that can be calculated at distance z from the source fiber as follows, and r is the radius of the particle:

$$I(z, r, \alpha) = \frac{2P}{\pi\omega(z)^2}\exp\left(-\frac{2(r\sin\alpha)^2}{\omega(z)^2}\right). \tag{11}$$

Here, P is the total power of the laser beam and $\omega(z)$ is the beam width. The latter describes the circumstance that the beam diverges as it exits the optical fiber with increasing distance and can be calculated by

$$w(z) = w_0\sqrt{1 + \left(\frac{\lambda z}{n_{\text{medium}}\pi w_0^2}\right)^2} \tag{12}$$

with the beam waist at the exit of the optical fiber ω_0. The peak stress σ_0 acting along the laser beam axis can be calculated by insertion of $\alpha = 0$:

$$\sigma_0 = \frac{n_{\text{medium}} I}{c}\left(R^2 - R - 2\right)\left(\frac{n_{\text{cell}}}{n_{\text{medium}}} - 1\right) \tag{13}$$

The shape of the stress profile and the magnitude of peak stress depend on the ratio between beam width ω and sphere radius r, as well as the ratio of refractive indices $n_{\text{cell}}/n_{\text{medium}}$. Figure 3 shows the total stress profiles for a cell that is stable trapped between the two divergent beams and a cell that is displaced from the beam axis. All forces act normal to the surface. In the first case, the profile has rotational symmetry with respect to the beam axis and the total force on the center of mass is zero. When the cell gets displaced, the symmetry is broken and it experiences a restoring net force perpendicular to the axis (so-called gradient

force). The gradient force pulls the cell in direction of the highest light intensity at the center of the beam.

3.2 Experimental Setup and Data Analysis

In typical optical stretcher experiments, suspended cells are trapped by the opposing laser beams at low power (i.e., 0.1 W per fiber) and stretched by increasing the laser power to 1.0–1.4 W per fiber. The setup basically consists of the fiber laser, a microfluidic delivery system, an inverted microscope, and a charge-coupled device (CCD) camera to monitor the deformation over time. As infrared laser light source, an ytterbium-doped single-mode fiber laser can be used emitting at a wavelength of $\lambda = 1064$ nm. At this wavelength, light is barely absorbed by proteins. The two fibers of the laser are integrated into a microfluidic system that guides the cells serially into the trap through a microfluidic flow channel (Fig. 4). The microfluidic chamber is positioned on the stage of a phase contrast microscope where a digital CCD camera is connected via C-mount adapter recording the stretching experiments.

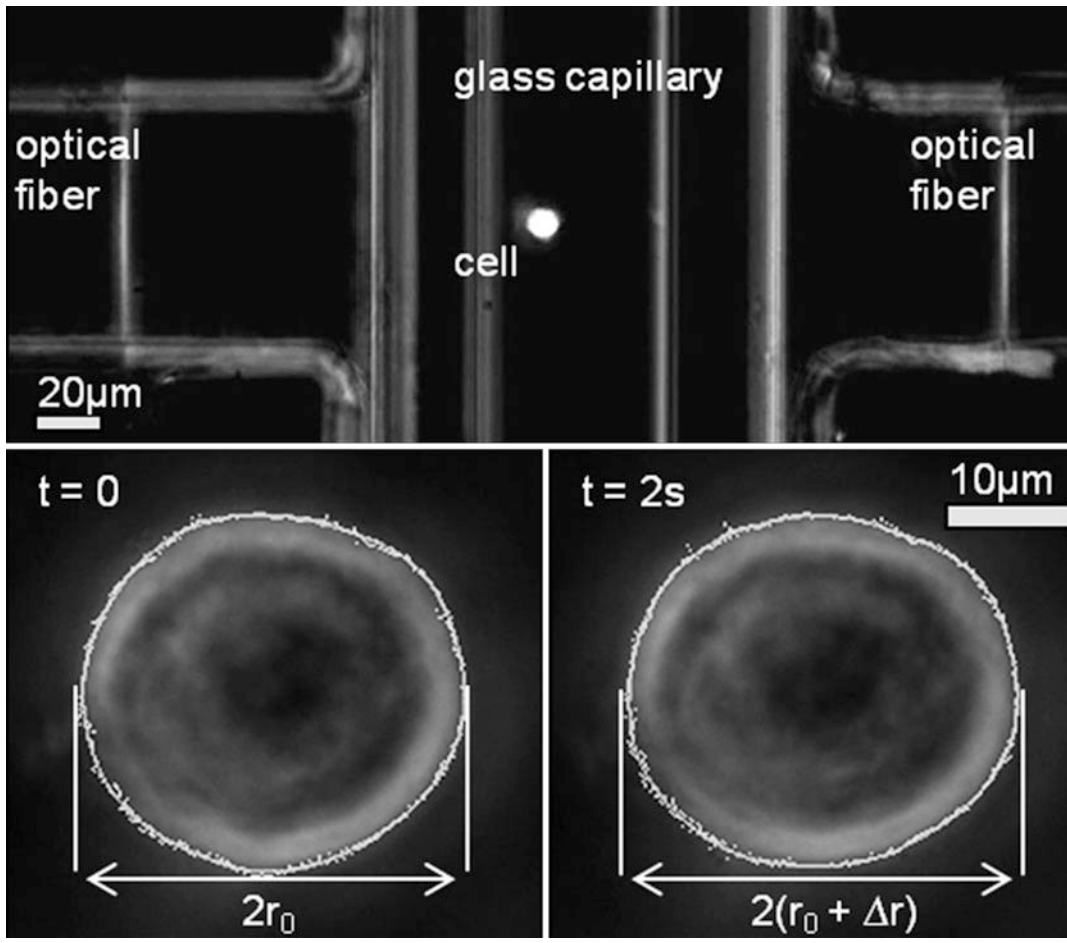

Fig. 4 Microfluidic chamber. Using photo-lithographic structures (SU-8), the optical fibers are aligned perpendicular to a glass capillary that has an inner diameter of 80 µm. Suspended cells are trapped at low laser power and can be deformed along the laser beam axis by increasing the power

The setup can be automated using a computer-controlled microfluidic pump and image-processing software that allows for live detection of cells in the trapping region of the flow chamber. Automated optical stretcher setups enable trapping and stretching of about 150–300 cells per hour.

In order to quantify cellular deformation, it is necessary to detect the cell boundaries by image processing. When the time development of the cell boundaries is given in an analytical form, the relative deformation along the laser beam axis $\Delta x/x$ can be derived (Fig. 5). During a "step stress" experiment, the cell is stretched for 2 s at constant laser power, followed by a relaxation phase, when the laser is switched back to trapping power. The temporal development of strain can be further analyzed to extract physical material properties. The mechanical behavior of biological cells under stress can be quantified using a simple model that illustrates the viscoelastic response of the cell to external forces, as they arise in the optical stretcher. The stress-strain behavior can be explained by a mechanical analogon that combines elastic and viscous components and describes the deformation of the cell under stress to a sufficient approximation (Wottawah et al. 2005a, b). This model implies that the deformation and relaxation is passive and due to a transiently cross-linked isotropic actin cortex, which is only given for a relative small strain (linear viscoelastic regime) and short times of applied stress. Any active cell behavior like actomyosin interactions as well as the glassy material properties and metastability of

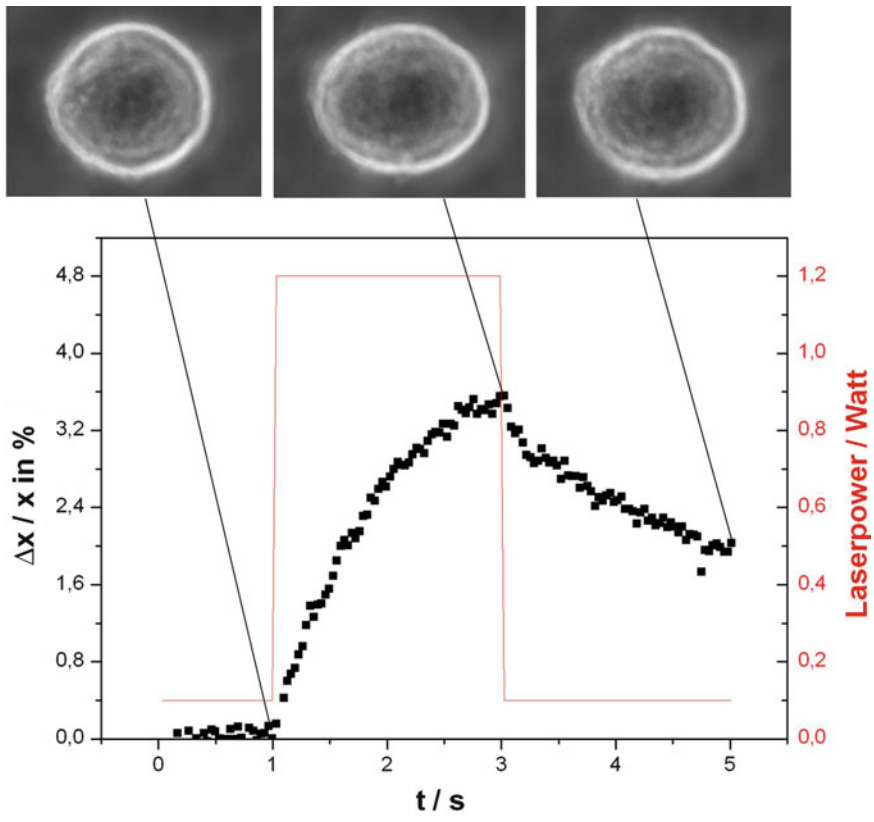

Fig. 5 Viscoelastic deformation of a fibroblast (*black*). The cell is trapped at a laser power (*red*) of 0.1 W per fiber and then stretched for 2 s at 1.2 W per fiber. When the laser is switched back to trapping power, the cell's relaxation behavior can be observed

the polymer network (Kollmannsberger and Fabry 2009; Semmrich et al. 2007) is not considered in this simple model. Based on the three-element model described by Wottawah et al., the relation between applied stress and resulting strain can be described by the constitutive equation:

$$\sigma + \frac{\eta_0 + \eta_1}{E_0}\dot{\sigma} = \eta_1\dot{\gamma} + \frac{\eta_0\eta_1}{E_0}\ddot{\gamma} \qquad (14)$$

where η_0, η_1 and E_0 are the viscosities and Young's modulus of the mechanical elements (Fig. 6a). Solving this differential equation for a constant stress σ between $t_0 = 1$s and $t_1 = 3$s gives the temporal development of extension and relaxation:

$$\gamma(t) = \frac{\sigma}{E_0}\left(1 - e^{-\frac{E_0}{\eta_0}(t-t_0)}\right) + \frac{\sigma}{\eta_1}(t - t_0) \quad \text{for } 1 \leq t \leq 3 \qquad (15)$$

$$\gamma(t) = \frac{\sigma}{E_0}\left(1 - e^{-\frac{E_0}{\eta_0}(t_1-t_0)}\right)e^{-\frac{E_0}{\eta_0}(t-t_1)} + \frac{\sigma}{\eta_1}(t_1 - t_0) \quad \text{for } 3 \leq t \qquad (16)$$

Fitting these equations to the strain data (Fig. 6b) allows for the calculation of several physically relevant values. When the analytical expression of the compliance $D(t) = \gamma(t)/\sigma$ is known, the time-dependent Young's modulus $E(t)$ can be derived (Wotottawah et al. 2005b) using the substitutions:

$$b_1 = \frac{(\eta_0 + \eta_1)}{E_0},\ a_1 = \eta_1,\ \textit{and}\ a_2 = \frac{\eta_0 \cdot \eta_1}{E_0}. \qquad (17)$$

Young's modulus can be calculated by

$$E(t) = \frac{a_1 b_1 - a_2}{b_1^2}e^{-\frac{t}{b_1}} + \frac{a_2}{b_1}\delta(t). \qquad (18)$$

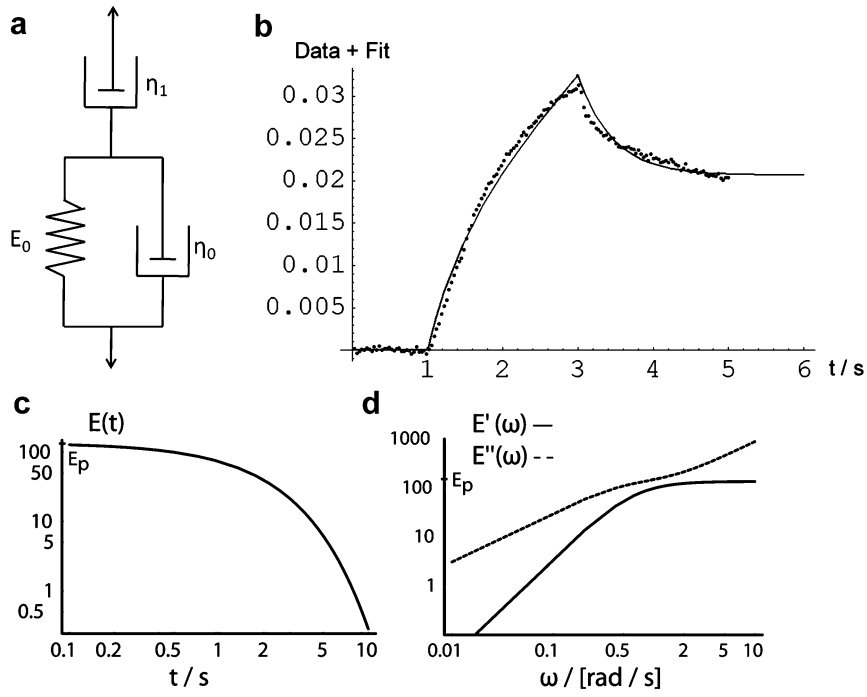

Fig. 6 (**a**) Scheme of the three-element model used to fit optical stretcher data. (**b**) Fitting of the strain function to the measured cell extension. The parameters can be used to calculate the cells' viscoelastic properties such as the time-dependent relaxation modulus E(t) (**c**) and the frequency-dependent Young's modulus $E^*(\omega) = E'(\omega) + i\,E''(\omega)$ (**d**)

Fourier integration gives the frequency-dependent complex Young's modulus describing the behavior in case of an oscillatory deformation:

$$E^*(\omega) = E'(\omega) + iE''(\omega) \quad \text{with} \tag{19}$$

$$E'(\omega) = \omega \int_0^\infty E(t)\,\sin(\omega t)dt = \frac{\omega^2(a_1 b_1 - a_2)}{1+\omega^2 b_1^2} \quad \text{and} \tag{20}$$

$$E''(\omega) = \omega \int_0^\infty E(t)\,\cos(\omega t)dt = \frac{\omega a_1 + \omega^3 a_2 b_1}{1+\omega^2 b_1^2} \tag{21}$$

E', which is also called storage modulus, is a measure for the part of energy stored during a periodic strain and corresponds to the elastic part of the stress response. E'' describes the part associated with the viscous dissipation of energy and is called loss modulus. Typical results obtained for the dynamic material properties are shown in Fig. 6c, 6d. Equations 19 and 20 allow for the calculation of characteristic rheological parameters like the plateau Young's modulus at high frequencies:

$$E_p = \lim_{\omega\to\infty} E'(\omega) = \frac{a_1 b_1 - a_2}{b_1^2} \tag{22}$$

and the steady-state viscosity:

$$E_{sts} = \lim_{\omega\to 0} \frac{E''(\omega)}{\omega} = a_1 \tag{23}$$

References

Ashkin A. Acceleration and trapping of particles by radiation pressure. Phys Rev Lett. 1970;24(4):156–9.

Ashkin A, Dziedzic JM. Radiation pressure on a free liquid surface. Phys Rev Lett. 1973;30(4):139–42.

Ashkin A, Dziedzic JM, Yamane T. Optical trapping and manipulation of single cells using infrared laser beams. Nature. 1987;330(6150):769–71.

Bereiter-Hahn J, Lüers H. In: Akkas N, editor. Biomechanics of active movement and division of cells. Berlin: Springer; 1994. p. 181–230.

Boudou T, Ohayon J, Picart C, Pettigrew RI, Tracqui P. Nonlinear elastic properties of polyacrylamide gels: implications for quantification of cellular forces. Biorheology. 2009;46(3):191–205.

Brown RA, Talas G, Porter RA, McGrouther DA, Eastwood M. Balanced mechanical forces and microtubule contribution to fibroblast contraction. J Cell Physiol. 1996;169(3):439–47.

Fabry B, et al. Scaling the microrheology of living cells. Phys Rev Lett. 2001;87(14):148102.

Fernandez P, Heymann L, Ott A, Aksel N, Pullarkat PA. Shear rheology of a cell monolayer. New J Phys. 2007;9:419.

Fletcher DA, Mullins RD. Cell mechanics and the cytoskeleton. Nature. 2010;463(7280):485–92.

Fluck M, Giraud M-N, Tunc V, Chiquet M. Tensile stress-dependent collagen XII and fibronectin production by fibroblasts requires separate pathways. Biochim Biophys Acta. 2003;1593:239–48.

Guck J, Ananthakrishnan R, Moon TJ, Cunningham CC, Käs J. Optical deformability of soft biological dielectrics. Phys Rev Lett. 2000;84(23):5451–4.

Hertz H. Über die Berührung fester elastischer Körper. J Reine Angew Math. 1881;92:156–71.

Hochmuth RM. Micropipette aspiration of living cells. J Biomech. 2000;33:15–22.

Ingber DE. Tensegrity: the architectural basis of cellular mechanotransduction. Annu Rev Physol. 1997;59:575–99.

Janmey PA, Weitz DA. Dealing with mechanics: mechanisms of force transduction in cells. Trends Biochem Sci. 2004;29(7):364–70.

Kessler D, Dethlefsen S, Haase I, Plomann M, Hirche F, Krieg T, Eckes B. Fibroblasts in mechanically stressed collagen lattices assume a "synthetic" phenotype. J Biol Chem. 2001;237:159–72.

Kollmannsberger P, Fabry B. Active soft glassy rheology of adherent cells. Soft Matter. 2009;5:1771–4.

Kolodney MS, Wysolmerski RB. Isometric contraction by fibroblasts and endothelial cells in tissue culture: a quantitative study. J Cell Biol. 1992;117:73–82.

Mahaffy RE, Shih CK, MacKintosh FC, Käs J. Scanning probe-based frequency-dependent microrheology of polymer gels and biological cells. Phys Rev Lett. 2000;85(4):880–3.

Rotsch C, Radmacher M. Drug-induced changes of cytoskeletal structure and mechanics in fibroblasts: an atomic force microscopy study. Biophys J. 2000;78(1):520–35.

Schulze C, Wetzel F, Kueper T, Malsen A, Muhr G, Jaspers S, Blatt T, Wittern KP, Wenck H, Käs JA. Stiffening of human skin fibroblasts with age. Biophys J. 2010;99(8):2434–42.

Semmrich C, Storz T, Glaser J, Merkel R, Bausch AR, Kroy K. Glass transition and rheological redundancy in F-actin solutions. Proc Natl Acad Sci U S A. 2007;104(51):20199–203.

Sleep J, Wilson D, Simmons R, Gratzer W. Elasticity of the red cell membrane and its relation to hemolytic disorders: an optical tweezers study. Biophys J. 1999;77:3085–95.

Sung KL, Yang L, Whittemore DE, Shi Y, Jin G, Hsieh AH, Akeson WH, Sung LA. The differential adhesion forces of anterior cruciate and medial collateral ligament fibroblasts: effects of tropomodulin, talin, vinculin, and alpha-actinin. Proc Natl Acad Sci U S A. 1996;93(17):9182–7.

Ward KA, Li WI, Zimmer S, Davis T. Viscoelastic properties of transformed cells: role in tumor cell progression and metastasis formation. Biorheology. 1991;28:301–13.

Wottawah F, Schinkinger S, Lincoln B, Ananthakrishnan R, Romeyke M, Guck J, Käs J. Optical rheology of biological cells. Phys Rev Lett. 2005a;94(9):098103.

Wottawah F, Schinkinger S, Lincoln B, Ebert S, Müller K, Sauer F, Travis K, Guck J. Characterizing single suspended cells by optorheology. Acta Biomater. 2005b;1(1):263–27.

Electron Paramagnetic Resonance Spectroscopy to Evaluate the Radical Scavenging Activity of the Skin

149

Martina C. Meinke, Anna-Christina Lauer, Annette Friedrich, Sophia Arndt, Stefan F. Haag, and Jürgen Lademann

Contents

Keywords
TEMPO • PCA • Antioxidant status • Hyperforin • Chokeberry • Aronia • Curly kale

1 Introduction

Our skin is surrounded by reactive oxygen species (ROS) and other free radicals. This is due to environmental hazards such as UV irradiation (Thiele et al. 2001), ozone gas, air pollutants, xenobiotics, or microorganisms (Sander et al. 2004; Vermeij et al. 2011) but also endogenous radical formation, e.g., by the mitochondrial respiratory chain (Berger 2005), antimicrobial mechanisms of leucocytes, and inflammatory responses (Sander et al. 2004; Berger 2005). Reactive oxygen species occur during important physiological processes, e.g., immune defense and cell signalling (Vermeij et al. 2011; Vermeij and Backendorf 2010). If an unbalance of oxidants and antioxidants appears in the skin, oxidative stress is the consequence, and the excess production of ROS can cause severe cell damage associated with skin carcinogenesis and accelerated skin aging (Sander et al. 2004; Richelle et al. 2006; Packer and Valacchi 2002). Therefore, antioxidants are of high importance for the maintenance of skin health. The skin provides a variety of enzymatic and nonenzymatic antioxidants (Thiele et al. 2001; Richelle et al. 2006).

M.C. Meinke (✉) • A.-C. Lauer • A. Friedrich • S. Arndt • S.F. Haag • J. Lademann
Department of Dermatology, Venereology and Allergology, Center of Experimental and Applied Cutaneous Physiology, Charité - Universitätsmedizin Berlin, Berlin, Germany
e-mail: martina.meinke@charite.de; juergen.lademann@charite.de

P. Humbert et al. (eds.), *Agache's Measuring the Skin*,
DOI 10.1007/978-3-319-32383-1_148

Superoxide dismutase, catalase, and glutathione peroxidase are examples for enzymatic antioxidants. Important nonenzymatic antioxidants in the human body and the skin are carotenoids (beta-carotene, lycopene, lutein); coenzyme Q10; glutathione; and the vitamins A, C, E, and D (Thiele et al. 2001; Shindo et al. 1994). These antioxidants form protective chains, i.e., they protect each other against the destructive effects of free radicals (Valko et al. 2007; Wrona et al. 2003). Most of these antioxidants cannot be produced in the human body but have to be taken in with food, especially with a diet rich in fruit and vegetables.

Darvin et al. showed that women of comparable age (around 50 years) with a high concentration of lycopene in the skin have less wrinkles and furrows compared to women with low values (Darvin et al. 2008). For the prevention of skin aging and cancer development, a diet rich in antioxidants is important. So far the antioxidant status can be measured in blood samples (Tong et al. 2013). These invasive investigations only give information about the short-term antioxidant status, because blood clearance is fast for most antioxidants. In the skin, antioxidants such as carotenoids can be stored over a longer time period (Meinke et al. 2010). For routine investigations, noninvasive methods that measure the antioxidant status of the skin are more suitable. One noninvasive method is resonance Raman spectroscopy, which measures cutaneous carotenoids. Carotenoids can be used as a marker substance of the exogenous skin antioxidants (Haag et al. 2011), if the nutrition is well-balanced and no acute changes in nutrition or life style (e.g., sudden stress) appeared. Should the endogenous antioxidants be of interest, electron paramagnetic resonance (EPR) spectroscopy can be applied to measure the antioxidant status of the skin, effects of nutrition, or topically applied antioxidants and the effect of stress can also be studied.

The EPR spectroscopy is a method, which can detect paramagnetic species such as free radicals in the skin. Therefore, it can be used to investigate the radical scavenging activity of the skin. This can be performed in two ways:

1. Direct reaction of antioxidants with a topically applied test radical
2. Radical formation induced by irradiation or other forms of stress

In the first method, a test radical is applied, whereby the cutaneous antioxidants react with the test radical and the EPR signal decreases over time. Regarding the second method, another test radical, which does not react directly with the cutaneous antioxidants, is applied and a stress is induced to form short-lived radicals. These short-lived radicals cannot be measured directly. They react with the applied test radical and decrease its initial signal. Existing cutaneous antioxidants can also neutralize induced short-lived radicals and act as a competitive mechanism.

The two methods can provide information about:

- Antioxidant potential of the skin
- Sun protection properties
- Lifestyle (nutrition, sleeplessness, smoking, etc.)
- Topically applied antioxidants

These properties can be measured in vivo without an intervention but also to determine the effect of supplements, creams, or possible stress effects such as irradiation in the UV, visible, or near-infrared spectral range.

In this chapter, the application of EPR spectroscopy will be shown to investigate the effect of supplements containing a fruit and vegetable extract. Moreover, topically applied antioxidants are evaluated with regard to their protection properties against stress such as sunlight.

2 Materials and Methods

2.1 Electron Paramagnetic Resonance (EPR) Spectroscopy

EPR spectroscopy is based on the resonant absorption of microwave radiation by paramagnetic species exposed to a magnetic field.

Microwave absorption occurs when the applied radiation matches the energy difference of the spin state, so that characteristic absorption spectra are obtained from specific substances (Haag et al. 2011).

The measurements were performed with the L-Band EPR spectrometer LBM MT 03 (Magnettech, Berlin, Germany) using the following EPR parameters: microwave frequency (1.3 GHz), central magnetic field (46 mT), sweep width (8 mT), sweep time (10 s), and modulation amplitude (0.15 mT).

2.1.1 Direct Reaction of Antioxidants with a Topically Applied Test Radical

In vivo EPR investigations of the direct radical scavenging activity was performed using the spin probe TEMPO (2,2,6,6-tetramethyl-1-piperidinyloxy; Sigma-Aldrich, Steinheim, Germany). Using a 30 mM TEMPO solution, the spectral shape is optimal for intensity evaluation by measuring the height of the central line, as previously described by Haag et al. (Haag et al. 2011). A typical spectrum of the nitroxide in the skin is shown in Fig. 1.

Measuring spots were chosen from the middle third of the inner forearm. All measurements from one volunteer were performed on the same arm. The measurement area was prepared by carefully clipping off all terminal hairs and cleaning the skin with an ethanol-soaked cotton pad. TEMPO solution (50 μL) was applied onto a filter paper (diameter 11 mm; Epitest Ltd Oy, Tuusula, Finland) and occluded with a Finn Chamber (Epitest Ltd Oy, Tuusula, Finland) for 10 min. The Finn Chamber and filter paper were then removed, and the skin was wiped with a paper towel. The arm was placed on a splint in the EPR and lifted up to the surface coil with soft pressure. A thin cover glass (Menzel-Gläser, Braunschweig, Germany) separated the skin from the surface coil. To increase the signal-to-noise ratio, four scans per minute were recorded for a total of 20 min and the mean spectrum of eight scans covering 2 min of reaction time was evaluated. The intensities of the central lines were plotted over time as exemplified in Fig. 2 and fitted by the equation $I = I_0 \exp -kt$, whereas k represents the rate constant of the function, which characterizes the individual radical scavenging properties of the skin. The exponential decay was normalized to the baseline EPR signal height (Fig. 2). On each visit, measurements were performed in duplicate.

2.1.2 Radical Formation Induced by Irradiation

For the determination of radical formation, the nitroxide 3-carboxy-2,2,5,5-tetramethyl-1-pyrrolidinyloxy (PCA; Sigma-Aldrich) was

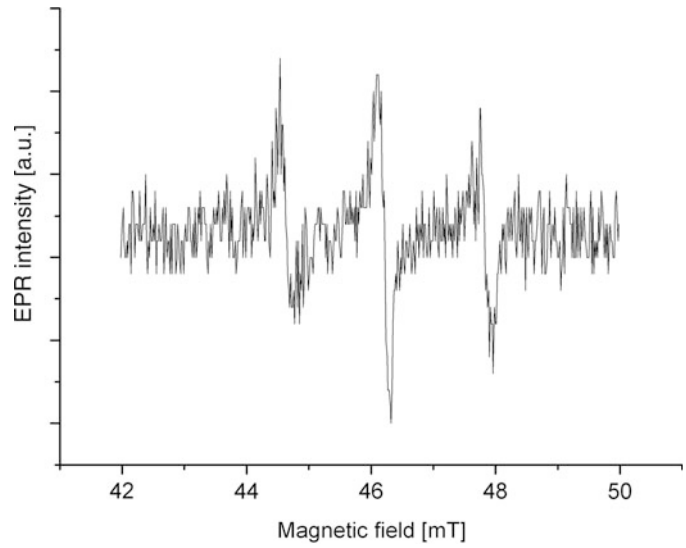

Fig. 1 Typical EPR spectrum of the nitroxide TEMPO after penetration into the skin

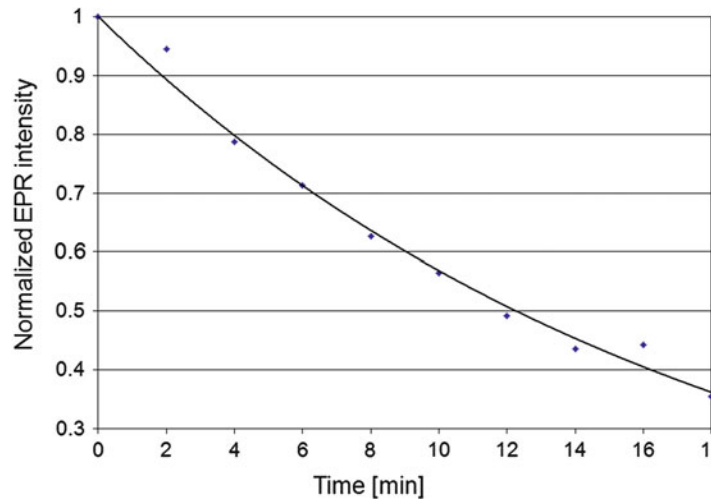

Fig. 2 Peak-to-peak intensity decay of TEMPO in the skin over time following a first order exponential decay

used. Compared to TEMPO, PCA hardly reacts with the skin's antioxidant system at the concentration used (Haag et al. 2010). However, PCA reacts well with short-lived free radicals, e.g., irradiation induced radicals, which transform the EPR marker to EPR-silent. This reduction in EPR signal intensity can be correlated with free radical formation (Darvin et al. 2010; Herrling et al. 2003). Preparation of measurement areas on the right inner forearm was performed as described above, for the section regarding the determination of radical scavenging capacity. PCA solution (100 µL) (43 mM, water:ethanol, 1:1, v:v) was applied to the skin on two paper filter disks (Epitest Ltd Oy), occluded with a Finn chamber (Epitest Ltd Oy) and allowed to penetrate the skin for 40 min. Subsequently, the arm was placed in the EPR spectrometer and measurements were started without irradiation for 10 min. Since the reduction of PCA was below 5 % without irradiation, the same measurement spot was used for the irradiation experiment. A solar simulator (Low Cost Solar Simulator, LS0104, LOT-Oriel Group, Darmstadt, Germany, wavelength: 420–2000 nm; output: 120 mW/cm^2) was used for in situ irradiation of the skin. Measurements were continued during irradiation for a further 10 min. To increase the signal-to-noise ratio, four scans per minute were recorded and the mean spectrum of eight scans covering 2 min of reaction time was evaluated. PCA intensity was derived from the central line of the spectrum. Measurements were performed in duplicate on each volunteer.

Measurements After Topical Application

In Vivo

The volunteers applied the verum and placebo cream to either one of the inner forearms twice daily for a period of 4 weeks. One-third of the placebo cream-treated forearm remained untreated. The last application of the test creams was, on average, 8.5 h (range 5–12 h) prior to the measurements, in order to avoid optical influences of the creams due to occlusive layer development or different penetration behavior of placebo and verum cream.

The measurements were performed as described above.

Ex Vivo

Comparable to the in vivo measurements, the following samples were prepared from each pig ear: two samples each without any cream applied, treated with placebo cream or with verum cream. The pig ears were first washed, shaved, and cleaned with ethanol.

Afterwards, the skin samples (d = 19 mm), fixed onto glass slides, were treated as in vivo

with slight modifications (50 μL PCA solution, 20-min penetration time, no glass slide) in order to achieve similar EPR intensities as in vivo. Thereafter, the cream, if any, was applied (2 mg/cm^2 according to the Colipa standard) and measurements started one hour after penetration.

Measurements without irradiation were performed for 20 min and subsequently for 20 min under NIR/VIS irradiation. All measurements were performed in duplicate.

3 Results and Discussion

3.1 Cutaneous Antioxidant Status Before and After Supplementation

3.1.1 Supplementation of Water Soluble Antioxidants

In this study, vitamin C (calcium ascorbate) or chokeberry extract (Aronia energy, Privatinstitut Galenus, Berlin, Germany) was taken by 33 healthy volunteers. Aronia energy is a powder, which consists of dextrose, Aronia berry peel extract, Topinambur extract, and calcium ascorbate (<3 %). The major antioxidant part is the chokeberry peel extract (>70 %). For the vitamin C sample, calcium ascorbate was prepared in dextrose, and as placebo, pure dextrose was taken. All samples were randomly numbered.

The placebo controlled double blind study consisted of three groups with 11 volunteers in each group of placebo, vitamin C (Vit C), and Aronia (Meinke et al. 2012a).

The antioxidant activity of the samples of the vitamin C and the Aronia group was adjusted to the same radical protection factor (RPF, 3600×10^{14} radicals/mg) (Herrling et al. 1998). This resulted in approximately 100 mg vitamin C per day.

All volunteers were measured before (visit 1) and after 28 days with supplementation (visit 2). The volunteers were measured by EPR spectroscopy on the inner forearm.

Each volunteer was instructed to take the study powder by dissolving one spoonful of the powder in water twice daily, in the morning and in the evening. After 14 days, nine volunteers of the vitamin C group were investigated in addition to the visits 1 and 2. The nine volunteers had been selected by the study coordinator, whereby the investigator was not informed as to which group the volunteers had been allocated, in order to ensure double blindness.

The radical scavenging of the skin was enhanced after supplementation, the decrease in TEMPO is faster and the rate constant increases. Although the individual values of rate constant differ strongly in all groups, with the exception of placebo, significant differences after the intake of the antioxidants were obtained. Significant differences could be found between the differences in rate constants before and after the intake of both verum groups compared to placebo (Fig. 3)

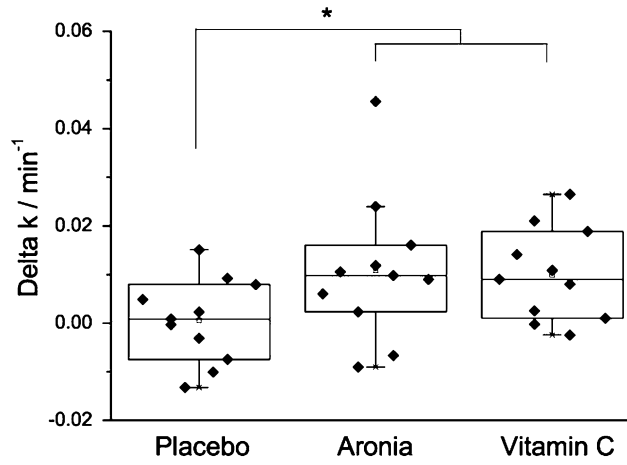

Fig. 3 Rate constants after a 4-week intake of the different products related to the initial values before intake; taken from (Meinke et al. 2012a)

No significant differences could be found between Aronia and Vit C. The relative increase is 23 % for Aronia and 20 % for Vit C.

Additionally, cutaneous carotenoids were measured but no significant change could be observed. Nine volunteers from the Vit C group were measured after 14 and 28 days with supplementation. The rate constants increased significantly after 14 days, whereas no further significant increase appeared after 28 days.

This indicates that both vitamin C and chokeberry extract increase the antioxidant status of the skin. The appearance in the skin is within 14 days, perhaps even faster and did not increase with further intake.

The intestinal absorption capacity for ascorbate is limited by the amount of transporters present. In healthy adults almost maximal absorption is achieved by a single 200 mg dose (Levine et al. 1996); vitamin C bioavailability decreases after further increasing oral doses. The amount of 125 mg per day vitamin C in two portions can be considered to be a moderate dose. This amount is already sufficient to considerably enhance the radical scavenging capacity in the skin.

Furthermore, the natural extract, with the same RPF consisting of different polyphenolic compounds also increases the antioxidant capacity to the same amount, although the absorption of dietary polyphenols is, in general, very low (plasma concentrations of total metabolites are in the nM to low μM range) and the time to reach maximum concentration ranges between 30 min and several hours, depending on the site of absorption (Manach et al. 2003). However, EPR spectroscopy does not provide the identity of the antioxidants, which are responsible for the increased radical scavenging activity. It could be demonstrated that polyphenols from chokeberry contribute to the radical scavenging effect in the skin.

3.1.2 Supplementation of Lipohilic Antioxidants

In the following study, the effect of a curly kale extract was investigated (Meinke et al. 2013a). The supplements were provided for a time period of 8 weeks. The verum capsules LutexskinTM (BioActive Food GmbH, Bad Segeberg, Germany) consist of a curly kale extract (*Brassica oleracea* convar. *acephala* var. *sabellica* L.), sea buckthorn oil (*Hippophae rhamnoides* L.), and olive oil, containing a high amount of carotenoids. The dosage for 1 day provided the following moderate amounts of carotenoids: 2200 μg lutein, 1000 μg beta carotin, 50 μg alpha carotin, 400 μg lycopin, 700 μg zeaxanthin, and 100 μg cryptoxanthin. As a control, a placebo capsule containing olive oil with almost no antioxidants was given.

Twenty-four healthy volunteers were recruited. The study included four visits and lasted 20 weeks. As starting time, autumn was chosen in order to reduce a possible influence of the sun. The volunteers took the supplements for a time period of 8 weeks. On visit 1 the volunteers were randomly assigned to either the verum group or to the placebo group. Supplementation started in the evening of visit 1. The second visit took place after 4 weeks, the third visit 8 weeks after administration of the supplements. After a further 12 weeks without supplementation, the fourth and final visit took place.

The following measurements were performed at each visit: (1) Resonance Raman spectroscopy was conducted to determine cutaneous carotenoids. (2) By means of EPR spectroscopy the radical scavenging capacity of the skin was determined. (3) Determination of radical formation in the VIS/NIR spectral range in order to acquire information about the photoprotection of the skin against oxidative stress.

At visits 1 and 4, the volunteers completed a questionnaire in order to ensure that neither their life style nor their eating habits had changed.

Radical Scavenging Activity

In order to determine the radical scavenging activity of the supplement itself, the RPF value was determined using the highly reactive test radical 2,2-diphenyl-1-picrylhydrazyl (DPPH), which resulted in 180×10^{14} radicals/mg. However, the supplement did not react with the test radical TEMPO that is used for the determination of the skin radical scavenging capacity in a time frame of 6 h.

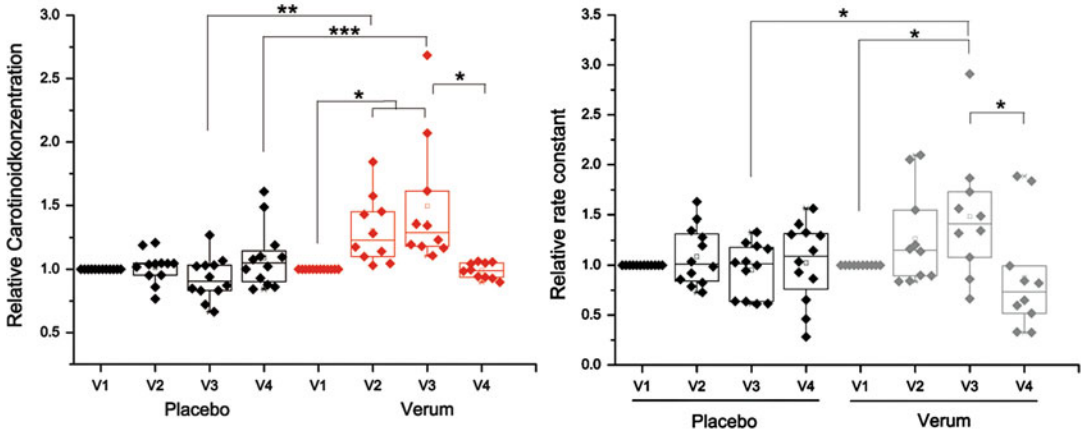

Fig. 4 *Left*: Cutaneous carotenoid concentration relative to initial value, *right*: rate constant relative to initial value, V1 – before intake, V2 – after a 4-week intake, V3 – after an 8-week intake, V4 – 12 weeks after stop of intake; taken from (Meinke et al. 2013a)

Nevertheless, the radical scavenging capacity of the skin changed after the supplementation with the curly kale extract. A stronger decrease of the test radical TEMPO in the verum group was observed at V3 with an increase in rate constant (Fig. 4, right).

The bioavailability of the curly kale extract in the skin was measured using resonance Raman spectroscopy. Regarding the rate constants, as a measure of the antioxidant capacity determined by EPR spectroscopy, the data obtained show a similar behavior as the increase of the additionally measured cutaneous carotenoids; however, the differences were less pronounced. The increase in the rate constant of the verum group is 27 % after 4 weeks and significantly 48 % after 8 weeks; furthermore, the difference between the rate constants of verum and placebo groups at V3 is significant. After the end of supplementation, the k-values decreased significantly from V3 to V4 to their initial values at V1 within the verum group. Moreover, no differences between verum and placebo at V4 could be observed.

Prevention of Radical Formation

Radical formation after VIS/NIR irradiation can be reduced by topically applied antioxidants. The question was whether orally applied antioxidants, such as the administered curly kale extract, can reduce the radical formation during a 10-min VIS/NIR irradiation.

Prevention of radical formation induced by VIS/NIR irradiation was observed after 8 weeks of supplementation at V3. After 10 min of VIS/NIR irradiation, the radical formation in the verum group was significantly reduced by 34 %. At other time points no significant differences between both groups were observed.

The estimation of the daily total carotenoid intake of all volunteers resulted in 2.13 mg ± 1.97 mg (range: 0.25–6.39 mg).

The RPF value of 180×10^{14} radicals/mg is rather low compared to other values of antioxidants. This is due to the low reaction efficacy of carotenoids with the used test radical DPPH (Herrling et al. 1998). Carotenoids also do not react with the cutaneously used test radical TEMPO within 6 h. Nevertheless, the investigations could show that the topically applied TEMPO was reduced much faster in the verum group after supplementation with carotenoids for 8 weeks. Significance could also be achieved within the verum group between the k-values before the beginning and after the end of supplementation. This indicates that the radical scavenging activity of the skin is enhanced on the whole, implying that antioxidants interact with each other and that carotenoids in a natural matrix affect other antioxidants in such a way

that they increase the antioxidant properties of the skin.

The reduction in radical formation after irradiation in the VIS/NIR range is in agreement with the increase in the antioxidant capacity of the skin. Studies which applied the antioxidants topically have shown that radical formation was reduced after irradiation in the VIS/IR range (Meinke et al. 2011) Furthermore, this result corresponds to results from UV irradiation with reduced erythema or photodamage in cells after consumption of carotenoids or other antioxidants (Meinke et al. 2012b; Heinrich et al. 2003; Bayer et al. 2011) In this context, synergistic effect should be mentioned (Wölfle et al. 2013).

3.2 Antioxidant Status After Topical Application of Antioxidants

3.2.1 In vivo

The aim of these in vivo measurements was to evaluate a method that measures radical protection by a cream, containing the *Hypericum perforatum* extract (1.5 %), which is rich in hyperforin and known to reduce radical formation in the skin ex vivo after IR irradiation. The radical protection factor (RPF) of the verum cream was 425 [10^{14} radicals/mg] and the verum cream without HP extract was 39 [10^{14} radicals/mg]. The investigated creams were applied in vivo several times by the volunteers, in order to detect the long-term effect of the application. EPR measurements were performed during irradiation and the changes in radical formation of the in vivo investigations after 4 weeks of cream application are shown in Fig. 5 left (Arndt et al. 2013).

The increase in radical production decreases along with time. During the first 2 min, the radical production is maximal (Haag et al. 2013). A longer irradiation time than 10 min of the untreated skin did not increase the radical formation significantly (data not shown). Untreated skin shows the highest radical production followed by a significant decrease to 55.7 ± 8.7 % after a 12-min irradiation of placebo-pretreated skin and a further significant reduction to 24.9 ± 8.7 % when verum was applied.

The analysis of the questionnaires did not show any significant differences in stress, smoking, and intake of fruit and vegetables.

The topical application increases the neutralization of ROS in a more pronounced manner than the so far investigated oral application. A possible reason is that for topical applications the concentration could be much higher than the recommended physiological concentration for supplementation. So far no side effects of topically applied antioxidants have been reported (Darvin et al. 2006).

3.2.2 Ex vivo

Ex vivo, the measurements were performed 1 h after one single application of the creams.

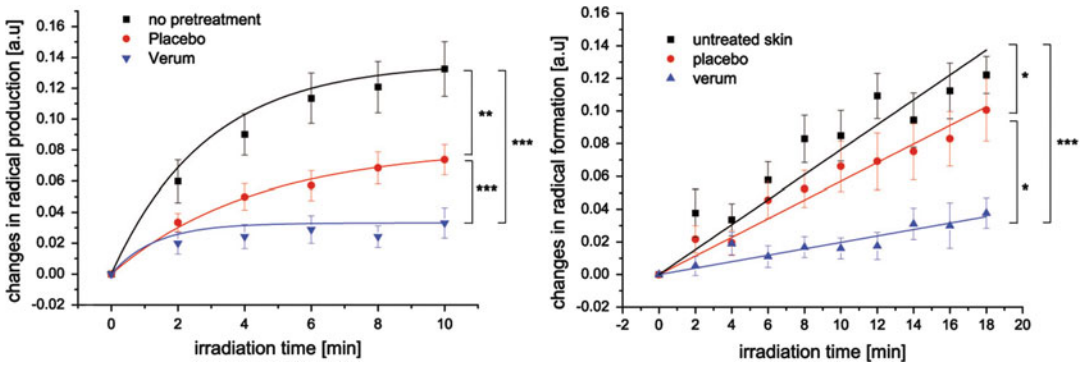

Fig. 5 Changes in radical formation during VIS/NIR irradiation (120 mW/cm^2), on untreated, placebo, and verum-treated skin; *left*: in vivo on a volunteer's forearm, and *right* ex vivo on porcine ear skin; taken from (Arndt et al. 2013)

Untreated skin was used as control. In contrast to in vivo measurements, the measurement time can be extended to longer irradiation times. The ex vivo results on porcine ear skin are presented in Fig. 5, right. The radical production did not decrease within the performed time frame. The change in radical production could be fitted by a linear equation. This means that the production of radicals has a constant value over the irradiation time, however, this value differs, depending on pretreatment.

As with in vivo, the untreated skin produced the highest number of radicals. Taking the fitted values, placebo and verum reduced the radical production to $75 \pm 20\%$ and 26.3 ± 8.5 %, respectively.

A direct comparison of results after a 10-min irradiation of excised porcine ear skin and the forearm of the volunteers in vivo showed that the radical production, due to irradiation in the VIS/NIR range, is more pronounced in vivo. For the same irradiation time of 10 min in vivo, the radical production is 1.9 times higher compared to ex vivo. This difference can be reduced by a longer irradiation time ex vivo.

The results have shown that both verum and placebo cream applied in vivo or ex vivo protect the skin from VIS/NIR induced radicals. The effect of placebo could be due to the optical properties of the cream. Besides antioxidants, high scattering properties of the creams can reduce radical formation in the infrared region as shown for sunscreens applied ex vivo (Meinke et al. 2013b). This method is also applicable to the investigations of sunscreens from the UV to the NIR spectral range.

The fact that in human skin in vivo more radicals are produced in the first minutes compared to ex vivo in porcine ear skin can be explained by the oxygen supply in living tissue. Nevertheless, this should be investigated in more detail using excised human skin as comparison. The decrease in radical formation in vivo with time could be explained by an up regulation of the endogenous antioxidant network, which neutralizes induced free radicals (Thiele et al. 2001). This defense mechanism cannot be studied ex vivo.

4 Conclusion

The different investigations have shown that EPR spectroscopy is well suited to investigate the antioxidant status and stress of the skin. The investigation can be performed ex vivo as well as in vivo. The results have shown that during in vivo and ex vivo investigations the radical formation due to irradiation is different.

The uptake of hydrophilic and lipophilic supplements could be followed, with the result that both products increase the radical scavenging activity in the skin. This even occurs when the investigated product does not react directly with the test radical TEMPO, indicating that the cutaneous antioxidants interact and protect each other. It could be shown that compounds which increase the rate constant also provide protection against stress induced radicals as formed during VIS/NIR irradiation.

The effects of water soluble antioxidants were observed faster in the skin (a saturation is visible within 2 weeks) compared to carotenoids (saturation not visible after 2 months) which is plausible due to different transport mechanisms of water and lipid soluble vitamins.

In comparison to orally applied antioxidants in physiological concentrations, topical application of antioxidants in a cream provided higher protection against stress induced radicals as formed during VIS/NIR irradiation.

This leads to the conclusion that a moderate protection distributed over the whole body could be achieved by oral application of antioxidants, and for high protection on sun-exposed areas, an additional topical application of antioxidants can be recommended.

Acknowledgments This work was supported by the Federal Land of Berlin within the Program to Promote Research, Innovation and Technologies (ProFIT, grant n# 10142343 and 10149524) for granting subsidies from the innovation promotion fund, with cofinancing by the European Fund for Regional Development (ERDF). We would also like to thank the companies Privatinstitut Galenus, Bioactive Food, and Klosterfrau Healthcare Group for providing the investigated products containing the different antioxidants.

References

Arndt S, Haag SF, Kleemann A, Lademann J, Meinke MC. Radical protection in the visible and infrared by a hyperforin-rich cream – in vivo versus ex vivo methods. Exp Dermatol. 2013;22:354–7.

Bayer M, Proksch P, Felsner I, Brenden H, Kohne Z, Walli R, Duong TN, Gotz C, Krutmann J, Grether-Beck S. Photoprotection against uvar: effective triterpenoids require a lipid raft stabilizing chemical structure. Exp Dermatol. 2011;20:955–8.

Berger MM. Can oxidative damage be treated nutritionally? Clin Nutr. 2005;24:172–83.

Darvin M, Zastrow L, Sterry W, Lademann J. Effect of supplemented and topically applied antioxidant substances on human tissue. Skin Pharmacol Physiol. 2006;19:238–47.

Darvin M, Patzelt A, Gehse S, Schanzer S, Benderoth C, Sterry W, Lademann J. Cutaneous concentration of lycopene correlates significantly with the roughness of the skin. Eur J Pharm Biopharm. 2008;69:943–7.

Darvin ME, Haag SF, Lademann J, Zastrow L, Sterry W, Meinke MC. Formation of free radicals in human skin during irradiation with infrared light. J Invest Dermatol. 2010;130:629–31.

Haag SF, Bechtel A, Darvin ME, Klein F, Groth N, Schafer-Korting M, Bittl R, Lademann J, Sterry W, Meinke MC. Comparative study of carotenoids, catalase and radical formation in human and animal skin. Skin Pharmacol Physiol. 2010;23:306–12.

Haag SF, Taskoparan B, Darvin ME, Groth N, Lademann J, Sterry W, Meinke MC. Determination of the antioxidative capacity of the skin in vivo using resonance raman and electron paramagnetic resonance spectroscopy. Exp Dermatol. 2011;20:483–7.

Haag SF, Tscherch K, Arndt S, Kleemann A, Gersonde I, Lademann J, Rohn S, Meinke MC. Enhancement of skin radical scavenging activity and stratum corneum lipids after the application of a hyperforin-rich cream. Eur J Pharm Biopharm. 2013;86:227–33.

Heinrich U, Gartner C, Wiebusch M, Eichler O, Sies H, Tronnier H, Stahl W. Supplementation with beta-carotene or a similar amount of mixed carotenoids protects humans from uv-induced erythema. J Nutr. 2003;133:98–101.

Herrling T, Zastrow L, Groth N. Classification of cosmetic products – the radical protection factor (RPF). SÖFW-Journal. 1998;5:282–4.

Herrling T, Fuchs J, Rehberg J, Groth N. Uv-induced free radicals in the skin detected by esr spectroscopy and imaging using nitroxides. Free Radic Biol Med. 2003;35:59–67.

Levine M, Conry-Cantilena C, Wang Y, Welch RW, Washko PW, Dhariwal KR, Park JB, Lazarev A, Graumlich JF, King J, Cantilena LR. Vitamin c pharmacokinetics in healthy volunteers: evidence for a recommended dietary allowance. Proc Natl Acad Sci U S A. 1996;93:3704–9.

Manach C, Morand C, Gil-Izquierdo A, Bouteloup-Demange C, Remesy C. Bioavailability in humans of the flavanones hesperidin and narirutin after the ingestion of two doses of orange juice. Eur J Clin Nutr. 2003;57:235–42.

Meinke MC, Darvin ME, Vollert H, Lademann J. Bioavailability of natural carotenoids in human skin compared to blood. Eur J Pharm Biopharm. 2010;76:269–74.

Meinke MC, Haag SF, Schanzer S, Groth N, Gersonde I, Lademann J. Radical protection by sunscreens in the infrared spectral range. Photochem Photobiol. 2011;87:452–6.

Meinke MC, Lauer A, Haag SF, Darvin ME, Groth N, Lademann L. Cutaneous radical scavenging effects of orally administered antioxidants measured by electron paramagnetic resonance spectroscopy. e-SPEN Journal. 2012a;7:e160–6.

Meinke MC, Schanzer S, Haag SF, Casetti F, Müller ML, Wölfle U, Kleemann A, Lademann J, Schempp CM. In vivo photoprotective and anti-inflammatory effect of hyperforin is associated with high antioxidant activity in vitro and ex vivo. Eur J Pharm Biopharm. 2012b;81:346–50.

Meinke MC, Friedrich A, Tscherch K, Haag SF, Darvin ME, Vollert H, Groth N, Lademann J, Rohn S. Influence of dietary carotenoids on radical scavenging capacity of the skin and skin lipids. Eur J Pharm Biopharma. 2013a;84:365–373.

Meinke MC, Syring F, Schanzer S, Haag SF, Graf R, Loch M, Gersonde I, Groth N, Pflücker F, Lademann J. Radical protection by differently composed creams in the uv/vis and ir spectral ranges. Photochem Photobiol. 2013b;89:1079–84.

Packer L, Valacchi G. Antioxidants and the response of skin to oxidative stress: Vitamin e as a key indicator. Skin Pharmacol Appl Skin Physiol. 2002;15:282–90.

Richelle M, Sabatier M, Steiling H, Williamson G. Skin bioavailability of dietary vitamin e, carotenoids, polyphenols, vitamin c, zinc and selenium. Br J Nutr. 2006;96:227–38.

Sander CS, Chang H, Hamm F, Elsner P, Thiele JJ. Role of oxidative stress and the antioxidant network in cutaneous carcinogenesis. Int J Dermatol. 2004;43:326–35.

Shindo Y, Witt E, Han D, Epstein W, Packer L. Enzymic and non-enzymic antioxidants in epidermis and dermis of human skin. J Invest Dermatol. 1994;102:122–4.

Thiele JJ, Schroeter C, Hsieh SN, Podda M, Packer L. The antioxidant network of the stratum corneum. Curr Probl Dermatol. 2001;29:26–42.

Tong TK, Kong Z, Lin H, Lippi G, Zhang H, Nie J. Serum oxidant and antioxidant status following an all-out

21-km run in adolescent runners undergoing professional training – a one-year prospective trial. Int J Mol Sci. 2013;14:15167–78.

Valko M, Leibfritz D, Moncol J, Cronin MT, Mazur M, Telser J. Free radicals and antioxidants in normal physiological functions and human disease. Int J Biochem Cell Biol. 2007;39:44–84.

Vermeij WP, Backendorf C. Skin cornification proteins provide global link between ros detoxification and cell migration during wound healing. PLoS One. 2010;5:1–7.

Vermeij WP, Alia A, Backendorf C. ROS quenching potential of the epidermal cornified cell envelope. J Invest Dermatol. 2011;131:1435–41.

Wölfle U, Haarhaus B, Schempp CM. The photoprotective and antioxidative properties of luteolin are synergistically augmented by tocopherol and ubiquinone. Planta Med. 2013;79:963–5.

Wrona M, Korytowski W, Rozanowska M, Sarna T, Truscott TG. Cooperation of antioxidants in protection against photosensitized oxidation. Free Radic Biol Med. 2003;35:1319–29.

Mechanical Properties of Three Different Types of Skin Graft

150

J. Pauchot, Alexandre Guichard, Thomas Lihoreau, Ahmed Elkhyat, Sophie Mac-Mary, and Philippe Humbert

Contents

J. Pauchot (✉)
Orthopedic Surgery, Traumatology, Plastic Aesthetic, Reconstructive Surgery, and Hand Surgery Department, EA 4268, IFR 133 INSERM I4S, Besançon University Hospital, Besançon, France
e-mail: julien.pauchot@gmail.com

A. Guichard • T. Lihoreau
Center for Research and Studies on the Integument (CERT), Department of Dermatology, Clinical Investigation Center (CIC INSERM 1431), Besançon University Hospital; INSERM UMR1098, FED4234 IBCT, University of Franche-Comté, Besançon, France
e-mail: guichard.alexandre@gmail.com; tlihoreau@chu-besancon.fr

A. Elkhyat
Center for Research and Studies on the Integument (CERT), Department of Dermatology, Clinical Investigation Center (CIC BT506), Besançon University Hospital, INSERM UMR1098, FED4234 IBCT, University of Franche-Comté, Besançon, France
e-mail: aelkhyat@chu-besancon.fr

S. Mac-Mary
Skinexigence SAS, Bioparc, Besançon, France
e-mail: asmac@skinexigence.com

P. Humbert
Department of Dermatology, University Hospital of Besançon, Besançon, France
e-mail: philippe.humbert@univ-fcomte.fr

P. Humbert et al. (eds.), *Agache's Measuring the Skin*, DOI 10.1007/978-3-319-32383-1_149

Keywords
Artificial dermis • Skin substitute • Defects • Cancer • Negative-pressure therapy

1 Introduction

Artificial dermis is widely used in the treatment of excessive burn injuries and is also more and more used in reconstructive surgery. It is an excellent option for reconstructing defects created by tumor excision. After an overall description of the properties of DE, their relevance in the treatment of oncologic surgical defects is assessed through a review of the literature and our own experience.

2 Artificial Dermis

2.1 Presentation

Since the 1970s, various types of dermal skin substitutes have been developed and used as models in in vitro studies and for therapeutic use. Thanks to the development of techniques of cell culture, the reconstruction of the epidermis (Rheinwald and Green 1975) and the reconstruction of dermal equivalents (DEs) are now possible. DE can be cellularized, like the model by Bell et al. (1981) consisting of a matrix of collagen contracted by the fibroblasts it contains (Apligraf®), or constituted by a synthesized matrix and integrated by the fibroblasts themselves (TransCyte®). Other types of DE are in acellular form, such as the model developed by Yannas and Burke (1980; Yannas et al. 1980). The latter (Integra® (Integra LifeSciences®)) is made of collagen supplemented with chondroitin-6-sulfate and is available in single layer or double layer types, covered by a silicone film. Integra® was the first dermal substitute on the market and remained the only product available for 10 years. Since 2007, new acellular dermal equivalents have been available in France: Matriderm® (Medical Z®) is made of a collagen and elastin matrix; Renoskin® (Perouse Plastie®) consists of a collagen matrix covered with a silicone film; Hyalomatrix® (Addmedica®) is composed of esterified hyaluronic acid covered with a flexible elastomer film.

Whereas the implantation of the first products was performed in a two-stage procedure, substitutes allowing to perform the skin graft and the implantation of the dermal equivalent simultaneously have been developed (Integra® single layer, Matriderm® 1 mm). In research, models are continuously becoming more complex: either endothelialized reconstructed dermis, or immunocompetent substitute, or reconstructed skin including the hypodermis (Auxenfans et al. 2009). In this article, only acellular DE will be reviewed.

2.2 Mode of Action of Acellular Dermal Equivalents

The DE is implanted on a site where it is susceptible to be colonized by fibroblasts and the process of vascularization is possible. As a simplified model of the extracellular matrix of the dermis, it is integrated in the healing process in order to recreate the mechanical and nutritional support of the epidermis. Histological studies have showed four stages in the process (Moiemen et al. 2006):

- A phase of inhibition
- A phase of migration of the fibroblasts
- A phase of revascularization lasting 4 weeks (without associated negative pressure therapy)
- A phase of remodeling and maturation

The 3-D structure of the acellular DE acts like a frame in the process of connective healing with the de novo synthesis of a tissue similar to mature human dermis within a few weeks, without proliferation of the anarchic granulation tissue (Lakhel-Le Coadou et al. 2000). The colonized DE behaves like neodermis, not like scar tissue, thus accounting for aesthetic and functional results which are similar to the normal cutaneous layer and superior to those of an isolated split skin

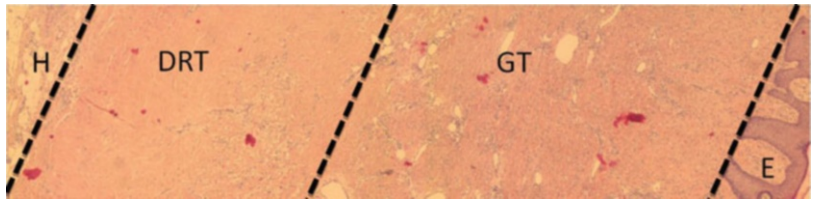

Fig. 1 Histological section 1 year after application of dermis equivalent followed by a granulation phase and then a split-thickness skin graft (patient 2 of the series). *H* hypodermis, *DRT* dermal regeneration template, *GT* granulation tissue, *E* epidermis. Note the rich vascularization and the cell infiltrate within the granulation tissue in contrast to the organization of the collagen fibers of the corresponding area on application of the dermal equivalent. Standard HES stain, objective X 2.5

graft (Dantzer and Braye 2001). From a histological point of view, the recolonized dermal skin substitute is distinct from the original dermis by the absence of pilosebaceous annexes, the absence of elastin fibers (absent in Integra®, but present in Matriderm®), the absence of nerve ending, and a straight dermis-epidermis junction without the papilla (Fig. 1) (Moiemen et al. 2006). This accounts for the sensation of dryness sometimes reported by patients and the absence of superficial sensitivity. In histology it is however impossible to differentiate new collagen from collagen of the local dermis. Regarding the two most frequently used DE types in France, no evidence has been found of a difference between Integra® and Matriderm® in animals in terms of revascularization or integration of the substitute (Schneider et al. 2009).

When the implantation of a dermal equivalent is to be followed by a skin graft in a two-stage procedure, it is temporarily covered with a silicon film. This film limits liquid leaks by allowing gas exchanges and is also a barrier to bacteria. Dermal substitutes implanted together with a skin graft in a one-stage procedure are thinner (1 mm) to accelerate nutrition of the epidermis from the capillaries before the death of the keratinocytes.

2.3 Legislation

Dermal skin substitutes are medical devices (MD). In the French *Code de la Santé Publique* (Public Health Regulations) (Art L5221-1 and R5211-1), MD are defined as "any instrument, device, piece of equipment, matter, product, [. . .] designed by the manufacturer to be used in humans for medical purposes and whose main intended action is obtained through neither pharmacological, nor immunological means, nor metabolism. . ." (Article L5211). Contrary to medicine, their commercialization does not need the authorities' approval (*Autorisation de Misesur le Marché* – AMM), but requires CE marking which guarantees its conformity to essential exigencies in conception, manufacturing, performances, and safety. The main drawback of CE marking is the quasi absence of exigency in terms of efficacy demonstrated by clinical evaluation. CE marks are delivered by a certified organization or by the manufacturer's self-certification for class I MD.

There are four classes of MD (I, IIa, IIb, III) corresponding to increasing levels of risks (Table 1). This classification is based on the product's length of use (from temporary to implantable), its invasive or noninvasive characteristics, its surgical or nonsurgical features, its active or non-active characteristics, and the part of the body in contact with the MD. Dermal equivalents are class III medical devices (very serious potential risk). In addition, since dermal equivalents are considered implantable MD, they are submitted to compulsory sanitary traceability according to the procedures of the *Code de la Santé Publique* (Article R5212-36 to 5212-42). The aim is the rapid identification of patients exposed to risks from a specific batch or series and the identification of batches of MD used by a patient.

Table 1 Classification of medical devices and risks

Class	Type of device	Examples	Risk
Class I	Noninvasive device	Medical beds, wheelchairs	Low risk ↓ High risk
	Invasive device – continuous use for less than 1 h		
Class IIa	Invasive device – continuous use between 1 h and 30 days	Urinary catheter	
		Tracheal tube	
Class IIb	Invasive device – long-term use (>30 days)	Articular prosthesis, bone cements, non-resorbable sutures	
Class III	Invasive device – long-term use (implantable device) designed to be in direct contact with the heart, the central circulatory system, or the central nervous system, to have a biological effect, containing medicine or manufactured from tissue of animal origin	Vascular stents, bone cements with antibiotics, mammary prosthesis, etc.	

2.4 Technical Applications of Artificial Dermis

2.4.1 Dermal Equivalents and Burns

Integra®, the first dermal substitute on the market, was initially developed to improve the management of acute burns (Burke et al. 1981). Its monopolist position and free availability in the management of burn injuries in many countries account for the vast amount of literature on this particular MD, even though recent articles also show the efficacy of other DE in the same indications, such as Matriderm® (Haslik et al. 2007; Ryssel et al. 2008; Kolokythas et al. 2008) and Hyalomatrix (Gravante et al. 2007).

In the management of severe burns, the free-of-charge availability of Integra® has been justified by its specific qualities (Heimbach et al. 1988, 2003):

- Reduced duration of hospitalization (Ryan et al. 2002)
- Advantageous replacement of allograft of the skin bank
- Association with split skin grafts allowing quicker healing of donor sites
- Better quality of skin grafts (texture, suppleness, glide space)
- Reduction of hypertrophic scars (Dantzer and Braye 2001; Branski et al. 2007; Clayman et al. 2006)

In the treatment of burn sequelae, the use of Integra® also allows the diminution of contractures and bridges (Chou et al. 2001; Groos et al. 2005; Unglaub et al. 2005; Stiefel et al. 2009); however, usual prevention means by immobilization and pressure therapy are still necessary (Hunt et al. 2000; Haertsch 2002). In some cases, the use of DE avoids implanting skin flaps after exposure of structures without spontaneous healing potential (Boyce et al. 2009).

Patients with burns have reported the following problems:

- Sensitivity to infection with two peaks of frequency, on D3 (by accumulation of fluid and hematoma) and on D14 (Molnar et al. 2004). The rate of infection in burned patients varies between 16.3 % (Heimbach et al. 2003) and 40 % (Branski et al. 2007; Muangman et al. 2006). Infection is mainly due to one germ (83 %) with predominance of Gram-negative bacillus.
- The rate of Integra® integration is lower than with skin grafts (Molnar et al. 2004) and evaluated at 76.2 % in the largest series (Heimbach et al. 2003).
- The cost, which is approximately 5 €/cm^2 in France for Integra®, and the absence of free-of-charge availability and valorization in some countries like France.

The infection risk must however be put in perspective. The bacterial ecosystem and the immunity of burned patients managed in specialist care centers are specific, and grafted surfaces are often large (Bargues et al. 2009).

However, it justifies the use of dressings with antiseptic properties in very rigorous asepsis conditions. The risk of complications can be reduced by two treatments which can be associated:

- Negative-pressure therapy (NPT)
- Skin grafting and DE implantation performed in a one-stage procedure

The possibility to implant the thin skin graft together with the DE in a one-stage procedure (DE (Matriderm® 1 mm, Integra® single layer) also has several advantages (Ryssel et al. 2008):

- Single surgical operation
- Reduced risk of bacterial contamination
- Reduced healing time

However, as in full-thickness skin grafts, the presence of dermis delays the nutrition of the epidermis from the capillaries and can be at the origin of a delay in the successful take of the skin graft. We were able to show this phenomenon in our investigations with perfusion laser Doppler imaging and capillaroscopy (Fig. 2).

2.4.2 The Use of Dermal Equivalents in Cases Other than Burns

The use of DE for loss of substance in plastic surgery in cases other than the treatment of burns is more recent. In France it is used in this indication only occasionally because of a problem of cost, since no study has shown the economic benefits of the products. The properties put forward to justify their prescription in plastic surgery are:

- Improvement of the quality of split skin grafts
- Possibility of glide plane in the mobile areas or in contact with tendons (Haslik et al. 2008; Aquilina et al. 2009; Yurugi et al. 2002; Wang and To 2000)
- Possibility of integration of DE implanted on tissue without granulation power such as bone without periosteum (bridge phenomenon)

The latter property makes DE a possible alternative to skin flaps, as a structure independent from the vascular network, and a good option in this indication. For some authors, DEs are already an alternative to skin flaps in civilian (Molnar et al. 2004; Pu 2008) and military (Helgeson et al. 2007) practice. Clinical cases have shown successful implants of artificial dermis to cover loss of substance in cases of skull exposure (Simon et al. 2008), after purpura fulminans (Besner and Klamar 1998; Pollard et al. 2008), on myelomeningocele (Nakazawa et al. 2005), on tendons (Wetzig et al. 2009), and after breast reconstruction (Namnoum 2009).

3 Artificial Dermis in Skin Cancer

3.1 Overview

DE can be used in skin cancer:

- To help understand cancer in research with in vitro models (Meier et al. 2000; Satyamoorthy et al. 1999; Berking and Herlyn 2001)
- To treat sequelae on donor sites of skin flaps used in cancer treatment, especially radial forearm free flap (Wax et al. 2002) and forehead skin flap (Wang and To 2000)
- To perform primary cover for loss of substance after excision of cancer lesions

In the latter case, DEs are used:

- To improve the quality of the skin graft
- As an alternative to a skin flap

Aside from any aesthetic consideration, cancer-related losses of substance have specific features:

- Elderly patients in most cases
- Multi-operated sites
- Lower risk of infection (compared to patients with burns)
- Absence of compromise with the excision margins that are sometimes important and necessity of total independence from reconstruction (except on the face in some cases)

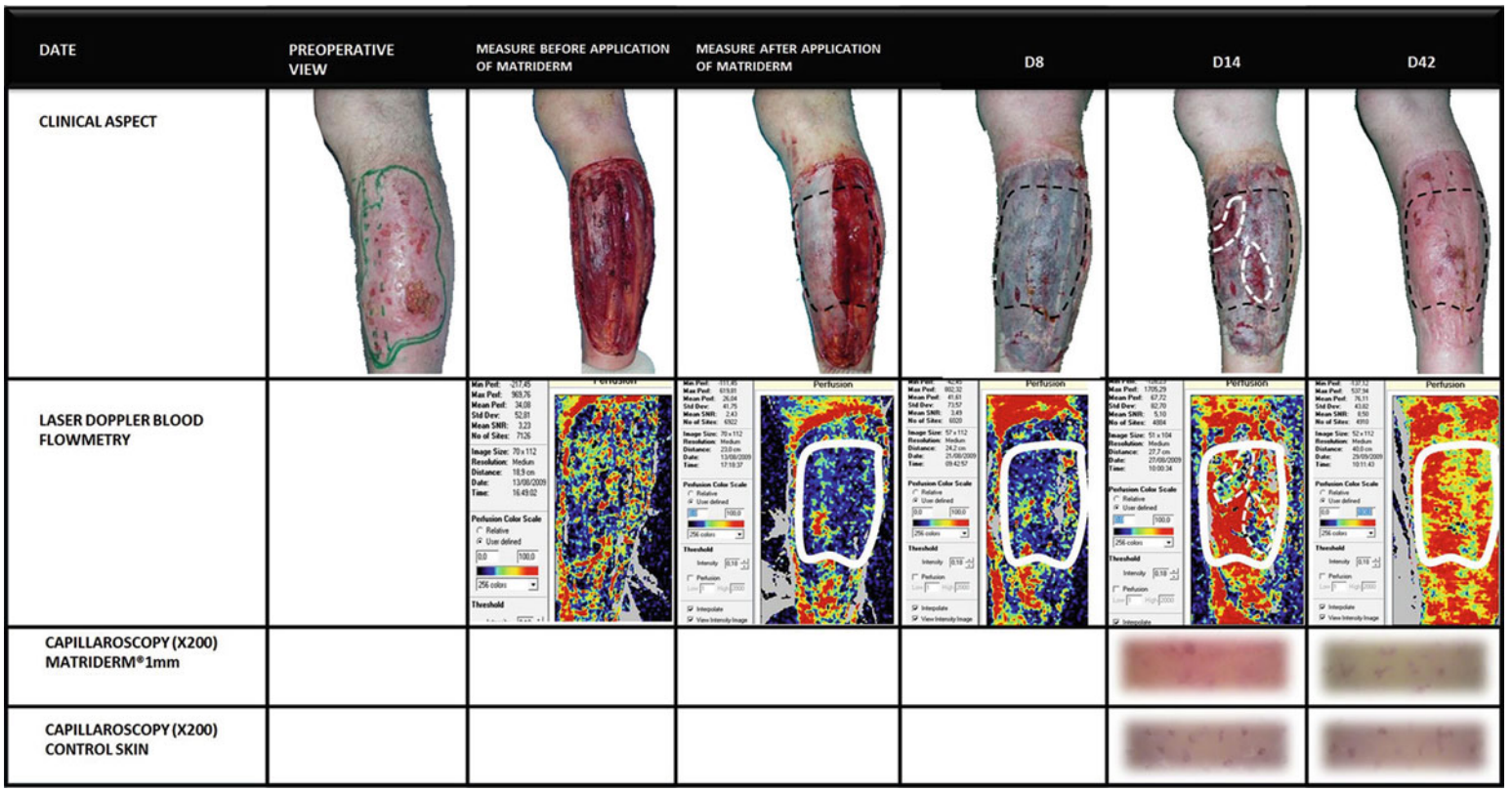

Fig. 2 Patient 4 of the series: demonstration of distress of a split-thickness skin graft applied at the same time as a dermal substitute related to the inevitable delay in revascularization inherent to the presence of the DE (*dotted white lines* on D14). Patient with a squamous cell carcinoma with fungoid mycosis of the left leg. Skin excision including muscular aponeurosis. Application of a layer of Matriderm® 1 mm partially covering the loss of substance (*dotted black line*) and application at the same time of a 2/10th millimeter split-thickness skin graft. The use of negative pressure therapy from D0 to D14 with a change of dressing on D8. As the laser Doppler perfusion imager (laser Doppler PeriScan PIM 3 imager, Perimed) visualizes the vascular flow at a depth of about 1 mm, it objectivates the delay in perfusion within the dermal substitute on D8 with a predominance of blue, the image being comparable to the appearance on D0. From D14, there is no obvious difference in vascularization between the dermal substitute and the skin graft applied directly to the muscle, with a comparable red color in both cases. Conversely, the delay in revascularization of the skin graft because of the presence of the DE explains the epidermolysis of part of the skin graft (*dotted white lines*). At the same time, capillaroscopy within the dermal substitute shows an increase in the number of capillaries within the substitute between D14 and week 6 (W6), so that it is comparable in terms of density to that of healthy skin

- Possibility of adjuvant or neoadjuvant radiotherapy, chemotherapy, and adjuvant immunotherapy requiring fast healing process so as not to delay treatment
- Possibility to have to differ covering of the loss of substance while waiting for results from anatomo-pathological analyses of edges and deep plane
- Non-recommendation of prolonged NPT (Labler et al. 2009; Jacobs et al. 2008)
- Possibility of local recurrence and relevance of early detection
- Significant psychological impact

The covering of loss of substance, depending on its extent, is performed by procedures that can be simple when it is possible or more complex when it is necessary: direct suture, skin graft, and local, regional, or free flaps. In all types of skin tumor, the skin graft, when it is necessary and possible, is an option as a cover and has many advantages:

- Low morbidity, especially in full-thickness skin graft procedure.
- Its thinness makes local follow-up easy.
- It can be removed and repeated if surgical revision is required for pathological excision margins.
- It does not induce an additional scar to the tumor site.

However:

- The bed that receives it must be able to revascularize it.
- Its thinness makes it sensitive to mechanical constraints, to adjuvant radiotherapy.
- It can be unaesthetic because of dyschromia or depression, depending on the location.

When full-thickness skin grafting is not possible, a skin flap is the obvious option, but its implantation can be difficult because of the patient's age and susceptibility, the presence of scars from previous surgery, or a history of previous radiotherapy. Furthermore, when it is local or regional, it results in scars near the tumor site that can alter lymphatic drainage pathways. Finally it causes additional morbidity associated with the donor site morbidity that can justify the recourse to other covering procedures.

3.2 Review of Literature

Dermal substitutes can present the advantages of both skin graft and skin flap with the possibility to be revascularized in bridges in case of partial implantation on a poorly vascularized bed. In Tufaro's series (Tufaro et al. 2007), Integra® double layer was used without NPT for cancer-related losses of substance with skin grafts performed on D21. The mean age of the 17 patients was 54 years old and the defect surface was 172 $cm^2 \pm 260$ (20–1,080). In six cases, Integra® was placed on the bone and in seven cases on the periosteum, and in three cases the patients received neoadjuvant radiotherapy. The author does not report any complication except premature loosening of less than 10 % of the silicone film from the surface in two patients and the successful take of the skin graft superior to 97 % in all cases. Three patients out of five who underwent radiotherapy presented with phlyctenules (ophtalmic terme) for blistering and ulcerations of favorable evolution in controlled healing.

The Corradino's series (Corradino et al. 2009) refers to the cases of eight elderly patients (mean age 81.5) presenting with scalp tumors. A two-stage procedure of excision and skin grafting was performed under local anesthesia (average loss of substance = 143 cm^2). The success of the graft was very satisfactory in all patients without using NPT. Two local recurrences were found at an early stage because of the fineness of the layer and were treated successfully using the same procedure. In this series, no removal of the outer table of the skull was performed contrary to other authors' recommendations (Komorowska-Timek et al. 2005; Koenen et al. 2008).

Giant congenital nevi are particular cases. They are not actually malignant cutaneous tumors, but

the risk of degenerescence, recently reevaluated at 0.7 % (Krengel et al. 2006), requires excision and poses the same problems of reconstruction in a younger population (Abai et al. 2004). Schiestl reports the cases of 12 children (mean age 3.8 years, extremes 7 months and 11 years) with giant congenital nevi representing 1–12 % of body surface treated with Integra® double layer (Schiestl et al. 2009). NPT was used in the last treated patients and biological glue was used in all cases. In two-third of children, the two-stage procedure was a success. In a third of the patients, implantation of Integra® was not successful, among them one patient with complete failure in a gluteal and perianal location treated without NPT. The benefits of NPT, colic preparation, and parenteral nutrition are herein reminded for gluteal and perianal sites.

In the literature the use of DE after excision of facial skin carcinoma in patients with xeroderma pigmentosum (Herlin et al. 2009) is also reported.

3.3 Preliminary Experience in Our Department

In our department, five patients could benefit from the use of dermal equivalents after excision of malignant or degenerative skin lesions: two melanoma, one Darier-Ferrand dermatofibrosarcoma, one spinocellular carcinoma, and one giant congenital nevus (Table 2) (Figs. 3, 4, 5, 6, 7, 8, 9, and 10). In four patients the lesions were located on the lower limbs and in one patient on the supraclavicular region. DE was selected as the appropriate option for the following reasons:

- To avoid the use of a skin flap because of bone or tendon exposure after excision (patients 1, 2, and 3)
- To improve the quality of the skin graft by the addition of dermis (patients 4 and 5)

The mean surface of losses of substance was 216 cm^2 (extremes 20 and 330 cm^2). The patients are listed in Table 1 in chronological order of treatment in the department. This was our first experience of the use of DE in the department. The first three patients received Integra® double layer without NPT and the last two Matriderm® 1 mm with split skin graft associated with NPT in a one-stage procedure. After implantation of DE, the patients without NPT were followed in an outpatient setting for the renewal of dressings three times a week. Patients with NPT were hospitalized for the whole duration of the treatment (15 days) because of circumstances impeding their follow-up at home. Although implantation of DE was not complete in two patients for both types of dermal substitutes, final healing was always obtained by controlled wound healing.

3.4 Discussion

Our preliminary series reveals the following issues:

- The management of DE in hospitals in France
- The complications of our series and the learning curve inherent in the acquisition of a new technique
- The relevance of the association with NPT

3.4.1 Dermal Substitutes in Hospital Practice

Hospital funding in France is based on T2A (*Tarification A l'Activité*: fees in connection with activity) defining GHS (*Groupe Homogène de Séjour*: homogeneous group of hospitalization) representing fees for all the costs associated with the patients' hospitalization defined by the GHM (*Groupe Homogène de Maladies*: homogeneous group of diseases). These fees include the costs of dermal equivalents except those described in the "list of implantable medical devices funded in addition to GHS fees."

The decision to cover these costs in addition to GHS fees and the funding of a medical device belongs to the Ministry of Health, based on:

- The medical and technical recommendations of the National Committee for the evaluation of medical devices and health technology (*Commission nationale d'évaluation des dispositifs médicaux et des technologies de santé* (CNEDiMTS)) (e.g., *Commission*

Table 2 Patients having received artificial skin for the cover of loss of substance after excision of skin tumors or giant congenital nevus

Patient	Age	Pathology	Comments	Exposure bone or tendon	Localization	Surface	Dermal substitute	Dressing	Integration of de	Integration of skin graft	Complications
Patient 1	48	Melanoma	Breslow 1,36 mm	Achilles tendon	Posterior aspect Lower third of leg	20 cm^2	Integra ® double layer	UrgoTulSAg®	100 %	100 %	NO
Patient 2	35	Achromic melanoma	Breslow 23 mm	Bone and tendon	Volar aspect lower third of leg	180 cm^2	Integra® double layer	UrgoTulSAg®	100 %	100 %	Infection and removal of silicone film on D17
Patient 3	32	Darier-Ferrand dermatofibrosarcoma	Excision margin 3 cm (Mohs)	Bone	Supraclavicular	300 cm^2	Integra® double layer	UrgoTulSAg®	90 %	95 %	Infection on D10, premature removal of silicone film, controlled wound healing
Patient 4	70	Spinocellular carcinoma on mycosis fungoides		No	Leg	250 cm^2	Matriderm® single layer	TPN 15 days	100 %	85 %	Controlled healing
Patient 5	15	Giant congenital nevus	Expansion and dermal substitute	No	Buttock	330 cm^2	Matriderm® single layer	TPN 15 days	75 %	75 %	Controlled healing

Fig. 3 Patient 2 of the series. Excision of an achromic melanoma (Clark level V, Breslow index 23 mm). Sentinel node procedure with metastatic lymph node (T4b N2c M0). Loss of substance exposing the inner aspect of the tibia and the tendons of the anterior tibial muscle, long extensor muscle of the great toe, and long extensor muscle of the toes after excision with 3 cm safety margins. Coverage with Integra® DL

Fig. 4 Patient 2 of the series. Premature application of the silicone film on D17 because of *Staphylococcus aureus* superinfection, but revascularization of the whole DE. Split-thickness skin graft applied 20 days after application of the silicone film

d'Evaluation des Produits et Prestations (CEPP) *de la Haute Autorité de Santé* (HAS))
- The medical and economic recommendations of the Economic Committee for Health Products (*Comité Economique des Produits de Santé* (CEPS))

It is then listed in the List of Refundable Products and Services (*Liste des Produitset Prestations Remboursables* (LPPR)). The CNEDiMTS gives scientific and independent recommendations on the expected service determined from the severity of the pathology, the disability and the quality of life, the ratio efficacy/risk, the place in the therapeutic strategy, and the interest for public health and on the improvement of the expected service. Among the skin substitutes currently marketed in France (Integra®, Matriderm®, Renoskin®, Hyalomatrix®), none is on the LPPR list. Only Integra® has had, since May 27, 2008, a positive recommendation by the CNEDiMTS with an expected service estimated to be sufficient and a moderate improvement of the expected service (ASA III) in severe burns when a classic skin graft (autograft or allograft) is not available, technically possible or presents important risks of failure and an absence of improvement of the expected service (ASA V) in the losses of total cutaneous substance (Haute Autorité de Santé 2008). In conclusion, to this day, the cost of all the dermal substitutes is included in the GHS.

In 2008, national funding was provided through the National Program in Favor of Innovating and Expensive Techniques (*Programme National de Soutien aux Techniques Innovantes et Coûteuses* (STIC)) for the medical and economic evaluation of Integra® in the cover of trauma-induced losses of skin substance of the lower limbs. At the University Hospital of Besancon, the funding of Integra® has been guaranteed since June 2009 by this STIC in the evaluation of treatments in post-trauma losses of

Fig. 5 Patient 2 of the series. Outcome at 12 months and locoregional recurrence with multiple cutaneous and subcutaneous lesions. Note the extension by contiguity of the melanoma within the DE and the quality of the skin graft

Fig. 6 Patient 3 of the series with neglected dermatofibrosarcoma protuberans of the supraclavicular region. Outline of the excision limits with 3 cm margins and exhaustive analysis of the edges using modified Mohs technique

cutaneous substances of the lower third of the leg and foot in comparison with the skin flap technique and by the GHS for the other indications. Funding of DE has also been obtained from the Department of Clinical Research and Innovation (*Département de la Recherche Clinique et de l'Innovation* (DRCI)) of the hospital in the treatment of cancer-related losses of substances allowing the treatment of eight to ten patients each year in the department.

With regard to other countries, Integra® is funded in the United States of America, Greece, and Hungary for the treatment of burns. In Hungary, the government also provides funding for Integra® used in reconstructive surgery.

3.4.2 Our Series

Our experience of the use of dermal substitutes related in this article corresponds to our first patients treated with DE in our department. In all our patients, the objectives at the basis of DE indication have been filled, i.e., to avoid the use of skin flaps and to improve skin graft quality. However, the learning curve which is inherent to the acquisition of any new technique probably explains the high infection rate (2/5) found in the first treated cases and the use of controlled wound healing in some cases. Infection has however not been detrimental to the success of the implantation of DE when it occurred after revascularization (patient n°2). This differs from the results obtained by some authors who may already be experienced in the use of the product (Tufaro et al. 2007; Corradino et al. 2009). These infections are probably prompted by the absence of NPT in our first cases, with changes of dressings three times a week in an outpatient setting, and by the absence of knowledge of clinical follow-up for the detection and early treatment of infections and effusion. If a patient shows

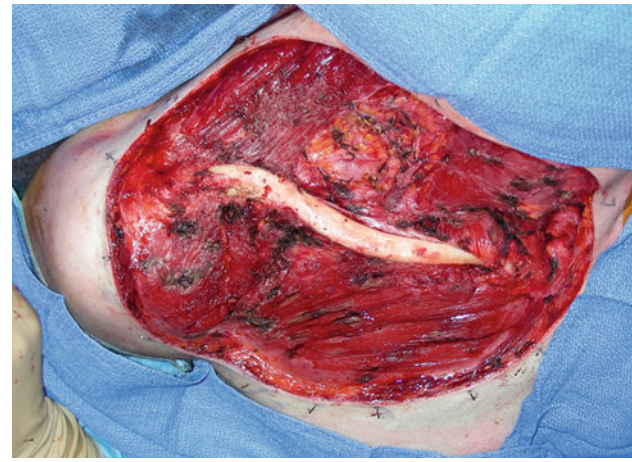

Fig. 7 Patient 3 of the series. Loss of substance with exposure of the periosteum clavicle

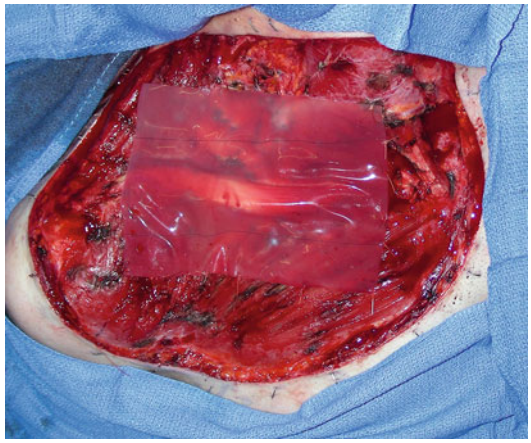

Fig. 8 Patient 3 of the series. Application of an Integra® DL film to cover the exposed bone

Fig. 9 Patient 3 of the series. Premature application of silicone film on D15 for infection (*Pseudomonas aeruginosa*)

signs of local infection, the centers specialized in the treatment of severely burned patients recommend local care with dressings humidified with alcohol chlorhexidine (Bargues et al. 2009), local antibiotics such as neomycin and polymyxin B (Muangman et al. 2006), and irrigations of mafenide solution every 8 h (Bargues et al. 2009).

3.4.3 Interest of Negative Pressure Therapy

The combination of dermal substitute and NPT was suggested in 2004 (McEwan et al. 2004) and has several advantages (Sinna et al. 2009):

- Reduction of exogene bacterial contamination due to the reduced number of dressing changes (changed every 4 (Molnar et al. 2004) or even 7 days (Schiestl et al. 2009)) and the adhesive film which isolates the wound from the exterior environment
- Acceleration of revascularization inside the dermal substitute with split skin grafts possible between D4 and D11 for Integra® double layer (Molnar et al. 2004), whereas the manufacturer recommends grafting around the 21st day without NPT (Burke et al. 1981; Heimbach et al. 1988; Clayton and Bishop 1998; Sheridan et al. 2001)

Fig. 10 Patient 3 of the series. Outcome at 2 years

- Application of homogeneous "pressure" on the DE by depression on the whole surface of the DE with diminution of the risk of collection (recommended depression – 125 mmHg (Molnar et al. 2004))
- Possibility to organize NPT at home, hence shortened hospitalization

Some authors use biological glue, either isolated or combined with NPT (Tufaro et al. 2007; Schiestl et al. 2009; Greenhalgh et al. 1999; Currie et al. 2001; Jeschke et al. 2004).

The last two patients in our series received the association of DE and skin graft at the same time and NPT with excellent results and moderate results for gluteal and perianal locations; the problems related to these locations have already been mentioned (Schiestl et al. 2009).

4 Conclusion

DE is beneficial in skin cancer therapy and is well adapted to this type of pathology. It should not be substituted to full-thickness skin graft when it is possible but it can be an alternative to skin flaps. As is the case in the acquisition of knowledge of any new technique, it implies a learning curve. The simultaneous association DE, skin graft, and NPT seems to be the ideal solution, but the combination of the three techniques increases the cost whose total amount is included in the GHS, thus limiting its indications.

Acknowledgments The author thanks the companies Skinexigence and Perimed, as well as the laboratory of anatomo-pathology, in particular Professor Kantelip and Dr Algros for their contribution to this article.
There is no conflict of interest.

References

Abai B, Thayer D, Glat PM. The use of a dermal regeneration template (Integra) for acute resurfacing and reconstruction of defects created by excision of giant hairy nevi. Plast Reconstr Surg. 2004;114(1):162–8.

Aquilina D, Darmanin FX, Briffa J, Gatt D. Chest wall reconstruction using an omental flap and Integra. J Plast Reconstr Aesthet Surg. 2009;62(7):e200–2.

Article L5211-1 du Code de la Santé Publique. In. https://www.legifrance.gouv.fr/affichCodeArticle.do?cidTexte=LEGITEXT000006072665&idArticle=LEGIARTI000006690281

Auxenfans C, Fradette J, Lequeux C, Germain L, Kinikoglu B, Bechetoille N, et al. Evolution of three dimensional skin equivalent models reconstructed in vitro by tissue engineering. Eur J Dermatol. 2009;19(2):107–13.

Bargues L, Boyer S, Leclerc T, Duhamel P, Bey E. Incidence and microbiology of infectious complications with the use of artificial skin Integra in burns. Ann Chir Plast Esthet. 2009 Dec;54(6):533–9. doi:10.1016/j.anplas.2008.10.013. Epub 2009 Feb 14.

Bell E, Ehrlich HP, Sher S, Merrill C, Sarber R, Hull B, et al. Development and use of a living skin equivalent. Plast Reconstr Surg. 1981;67(3):386–92.

Berking C, Herlyn M. Human skin reconstruct models: a new application for studies of melanocyte and melanoma biology. Histol Histopathol. 2001;16(2):669–74.

Besner GE, Klamar JE. Integra Artificial Skin as a useful adjunct in the treatment of purpura fulminans. J Burn Care Rehabil. 1998;19(4):324–9.

Boyce A, Atherton DD, Tang R, Jawad M. The use of Matriderm((R)) in the management of an exposed Achilles tendon secondary to a burns injury. J Plast Reconstr Aesthet Surg. 2009.

Branski LK, Herndon DN, Pereira C, Mlcak RP, Celis MM, Lee JO, et al. Longitudinal assessment of Integra in primary burn management: a randomized pediatric clinical trial. Crit Care Med. 2007;35(11):2615–23.

Burke JF, Yannas IV, Quinby Jr WC, Bondoc CC, Jung WK. Successful use of a physiologically acceptable artificial skin in the treatment of extensive burn injury. Ann Surg. 1981;194(4):413–28.

Chou TD, Chen SL, Lee TW, Chen SG, Cheng TY, Lee CH, et al. Reconstruction of burn scar of the upper extremities with artificial skin. Plast Reconstr Surg. 2001;108(2):378–84. discussion 385.

Clayman MA, Clayman SM, Mozingo DW. The use of collagen-glycosaminoglycan copolymer (Integra) for the repair of hypertrophic scars and keloids. J Burn Care Res. 2006;27(3):404–9.

Clayton MC, Bishop JF. Perioperative and postoperative dressing techniques for Integra Artificial Skin: views from two medical centers. J Burn Care Rehabil. 1998;19(4):358–63.

Corradino B, Lorenzo SD, Leto Barone AA, Maresi E, Moschella F. Reconstruction of full thickness scalp defects after tumour excision in elderly patients: our experience with Integra((R)) dermal regeneration template. J Plast Reconstr Aesthet Surg. 2009.

Currie LJ, Sharpe JR, Martin R. The use of fibrin glue in skin grafts and tissue-engineered skin replacements: a review. Plast Reconstr Surg. 2001;108(6):1713–26.

Dantzer E, Braye FM. Reconstructive surgery using an artificial dermis (Integra): results with 39 grafts. Br J Plast Surg. 2001;54(8):659–64.

Gravante G, Delogu D, Giordan N, Morano G, Montone A, Esposito G. The use of Hyalomatrix PA in the treatment of deep partial-thickness burns. J Burn Care Res. 2007;28(2):269–74.

Greenhalgh DG, Gamelli RL, Lee M, Delavari M, Lynch JB, Hansbrough JF, et al. Multicenter trial to evaluate the safety and potential efficacy of pooled human fibrin sealant for the treatment of burn wounds. J Trauma. 1999;46(3):433–40.

Groos N, Guillot M, Zilliox R, Braye FM. Use of an artificial dermis (Integra) for the reconstruction of extensive burn scars in children. About 22 grafts. Eur J Pediatr Surg. 2005;15(3):187–92.

Haertsch P. Reconstructive surgery using an artificial dermis (Integra). Br J Plast Surg. 2002;55(4):362–3.

Haslik W, Kamolz LP, Nathschlager G, Andel H, Meissl G, Frey M. First experiences with the collagen-elastin matrix Matriderm as a dermal substitute in severe burn injuries of the hand. Burns. 2007;33(3):364–8.

Haslik W, Kamolz LP, Manna F, Hladik M, Rath T, Frey M. Management of full-thickness skin defects in the hand and wrist region: first long-term experiences with the dermal matrix Matriderm((R)). J Plast Reconstr Aesthet Surg. 2008.

Haute Autorité de Santé. Avis de la Commission des Produits et Prestations, 27 mai 2008. Consulté le 01/09/2009 sur http://www.has-sante.fr/portail/upload/docs/application/pdf/2008-06/cepp-1753integra.pdf

Heimbach D, Luterman A, Burke J, Cram A, Herndon D, Hunt J, et al. Artificial dermis for major burns. A multicenter randomized clinical trial. Ann Surg. 1988;208(3):313–20.

Heimbach DM, Warden GD, Luterman A, Jordan MH, Ozobia N, Ryan CM, et al. Multicenter postapproval clinical trial of Integra dermal regeneration template for burn treatment. J Burn Care Rehabil. 2003;24(1):42–8.

Helgeson MD, Potter BK, Evans KN, Shawen SB. Bioartificial dermal substitute: a preliminary report on its use for the management of complex combat-related soft tissue wounds. J Orthop Trauma. 2007;21(6):394–9.

Herlin C, Sauniere D, Huertas D. Xeroderma pigmentosum: radical therapeutic procedure on the face using artificial dermal. Ann Chir Plast Esthet. 2009.

Hunt JA, Moisidis E, Haertsch P. Initial experience of Integra in the treatment of post-burn anterior cervical neck contracture. Br J Plast Surg. 2000;53(8):652–8.

Jacobs S, Simhaee DA, Marsano A, Fomovsky GM, Niedt G, Wu JK. Efficacy and mechanisms of vacuum-assisted closure (VAC) therapy in promoting wound healing: a rodent model. J Plast Reconstr Aesthet Surg. 2008.

Jeschke MG, Rose C, Angele P, Fuchtmeier B, Nerlich MN, Bolder U. Development of new reconstructive techniques: use of Integra in combination with fibrin glue and negative-pressure therapy for reconstruction of acute and chronic wounds. Plast Reconstr Surg. 2004;113(2):525–30.

Koenen W, Goerdt S, Faulhaber J. Removal of the outer table of the skull for reconstruction of full-thickness scalp defects with a dermal regeneration template. Dermatol Surg. 2008;34(3):357–63.

Kolokythas P, Aust MC, Vogt PM, Paulsen F. Dermal substitute with the collagen-elastin matrix Matriderm in burn injuries: a comprehensive review. Handchir Mikrochir Plast Chir. 2008;40(6):367–71.

Komorowska-Timek E, Gabriel A, Bennett DC, Miles D, Garberoglio C, Cheng C, et al. Artificial dermis as an alternative for coverage of complex scalp defects following excision of malignant tumors. Plast Reconstr Surg. 2005;115(4):1010–7.

Krengel S, Hauschild A, Schafer T. Melanoma risk in congenital melanocytic naevi: a systematic review. Br J Dermatol. 2006;155(1):1–8.

Labler L, Rancan M, Mica L, Harter L, Mihic-Probst D, Keel M. Vacuum-assisted closure therapy increases local interleukin-8 and vascular endothelial growth factor levels in traumatic wounds. J Trauma. 2009;66(3):749–57.

Lakhel-Le Coadou A, Cantaloube D, Carsin H. Indications des substituts cutanés chez le brûlé. In: Encyclopédie Médico Chirurgicale. Paris: Elsevier; 2000.

McEwan W, Brown TL, Mills SM, Muller MJ. Suction dressings to secure a dermal substitute. Burns. 2004;30(3):259–61.

Meier F, Nesbit M, Hsu MY, Martin B, Van Belle P, Elder DE, et al. Human melanoma progression in skin reconstructs: biological significance of bFGF. Am J Pathol. 2000;156(1):193–200.

Moiemen NS, Vlachou E, Staiano JJ, Thawy Y, Frame JD. Reconstructive surgery with Integra dermal regeneration template: histologic study, clinical evaluation, and current practice. Plast Reconstr Surg. 2006;117(7 Suppl):160S–74.

Molnar JA, DeFranzo AJ, Hadaegh A, Morykwas MJ, Shen P, Argenta LC. Acceleration of Integra incorporation in complex tissue defects with

subatmospheric pressure. Plast Reconstr Surg. 2004;113(5):1339–46.
Muangman P, Deubner H, Honari S, Heimbach DM, Engrav LH, Klein MB, et al. Correlation of clinical outcome of integra application with microbiologic and pathological biopsies. J Trauma. 2006;61(5):1212–7.
Nakazawa H, Kikuchi Y, Honda T, Isago T, Nozaki M. Successful management of a small infant born with a large meningomyelocele using a temporary artificial dermis. Scand J Plast Reconstr Surg Hand Surg. 2005;39(1):53–6.
Namnoum JD. Expander/implant reconstruction with AlloDerm: recent experience. Plast Reconstr Surg. 2009;124(2):387–94.
Pollard RL, Kennedy PJ, Maitz PK. The use of artificial dermis (Integra) and topical negative pressure to achieve limb salvage following soft-tissue loss caused by meningococcal septicaemia. J Plast Reconstr Aesthet Surg. 2008;61(3):319–22.
Pu LL. An alternative approach for soft-tissue coverage of a complex wound in the foot and ankle with vacuum-assisted closure over artificial dermis and subsequent skin graft. J Plast Reconstr Aesthet Surg. 2008.
Rheinwald JG, Green H. Serial cultivation of strains of human epidermal keratinocytes: the formation of keratinizing colonies from single cells. Cell. 1975;6(3):331–43.
Ryan CM, Schoenfeld DA, Malloy M, Schulz 3rd JT, Sheridan RL, Tompkins RG. Use of Integra artificial skin is associated with decreased length of stay for severely injured adult burn survivors. J Burn Care Rehabil. 2002;23(5):311–7.
Ryssel H, Gazyakan E, Germann G, Ohlbauer M. The use of MatriDerm in early excision and simultaneous autologous skin grafting in burns – a pilot study. Burns. 2008;34(1):93–7.
Satyamoorthy K, Meier F, Hsu MY, Berking C, Herlyn M. Human xenografts, human skin and skin reconstructs for studies in melanoma development and progression. Cancer Metastasis Rev. 1999;18(3):401–5.
Schiestl C, Stiefel D, Meuli M. Giant naevus, giant excision, eleg(i)ant closure? Reconstructive surgery with Integra Artificial Skin((R)) to treat giant congenital melanocytic naevi in children. J Plast Reconstr Aesthet Surg. 2009.
Schneider J, Biedermann T, Widmer D, Montano I, Meuli M, Reichmann E, et al. Matriderm versus integra: a comparative experimental study. Burns. 2009;35(1):51–7.
Sheridan RL, Morgan JR, Cusick JL, Petras LM, Lydon MM, Tompkins RG. Initial experience with a composite autologous skin substitute. Burns. 2001;27(5):421–4.
Simon E, Sellal S, Chassagne J, Stricker M, Duroure F. Total, nonreplantable scalp avulsion: utility of artificial dermis. Eur J Plast Surg. 2008;30:233–7.
Sinna R, Qassemyar Q, Boloorchi A, Benhaim T, Carton S, Perignon D, et al. Role of the association artificial dermis and negative pressure therapy: about two cases. Ann Chir Plast Esthet. 2009.
Stiefel D, Schiestl C, Meuli M. Integra Artificial Skin((R)) for burn scar revision in adolescents and children. Burns. 2009.
Tufaro AP, Buck 2nd DW, Fischer AC. The use of artificial dermis in the reconstruction of oncologic surgical defects. Plast Reconstr Surg. 2007;120(3):638–46.
Unglaub F, Ulrich D, Pallua N. Reconstructive surgery using an artificial dermis (Integra): results with 19 grafts. Zentralbl Chir. 2005;130(2):157–61.
Wang JC, To EW. Application of dermal substitute (Integra) to donor site defect of forehead flap. Br J Plast Surg. 2000;53(1):70–2.
Wax MK, Winslow CP, Andersen PE. Use of allogenic dermis for radial forearm free flap donor site coverage. J Otolaryngol. 2002;31(6):341–5.
Wetzig T, Gebhardt C, Simon JC. New indications for artificial collagen-elastin matrices? Covering exposed tendons. Dermatology. 2009.
Yannas IV, Burke JF. Design of an artificial skin. I. Basic design principles. J Biomed Mater Res. 1980;14(1):65–81.
Yannas IV, Burke JF, Gordon PL, Huang C, Rubenstein RH. Design of an artificial skin. II. Control of chemical composition. J Biomed Mater Res. 1980;14(2):107–32.
Yurugi S, Hatoko M, Kuwahara M, Tanaka A, Iioka H, Niitsuma K. Usefulness and limitations of artificial dermis implantation for posttraumatic deformity. Aesthet Plast Surg. 2002;26(5):360–4.

Dynamic Infrared Thermography of Infantile Hemangiomas

151

Marty O. Visscher, Denise M. Adams, and Shona A. Burkes

Contents

M.O. Visscher (✉)
Skin Sciences Program, Division of Plastic Surgery, Cincinnati Children's Hospital Medical Center, Cincinnati, OH, USA

Department of Surgery, College of Medicine, University of Cincinnati, Cincinnati, OH, USA
e-mail: marty.visscher@gmail.com

D.M. Adams
Hemangioma and Vascular Malformation Center, Cincinnati Children's Hospital Medical Center, Cincinnati, OH, USA

Department of Pediatrics, College of Medicine, Cincinnati Children's Hospital Medical Center, Cincinnati, OH, USA

S.A. Burkes
Skin Sciences Program, Division of Plastic Surgery, Department of Surgery, Cincinnati Children's Hospital Medical Center, College of Medicine, University of Cincinnati, Cincinnati, OH, USA

James L. Winkle, College of Pharmacy, University of Cincinnati, Cincinnati, OH, USA

P. Humbert et al. (eds.), *Agache's Measuring the Skin*,
DOI 10.1007/978-3-319-32383-1_150

Keywords
Infantile hemangiomas (IHs) • Control skin • Dynamic response • Rapid IH growth • Region of involvement (ROI) • Infrared (IR) thermography • Dynamic IR • Static IR • Matlab®

1 Introduction

1.1 Infrared Thermography

The skin emits infrared radiation as a result of physiological processes. Temperature distribution depends upon blood perfusion, metabolism, thermal conductivity, drug effects, sympathetic nervous system activity, and environmental conditions (Wu et al. 2007; Jones 1998; Fujimasa et al. 2000). Cellular metabolic activity is distributed at the skin surface as heat and may change as a result of physiological abnormality (Wu et al. 2007). In addition, heat exchange occurs between circulating blood and tissue. External factors, e.g., thermal energy, also impact skin surface temperature (Thomas et al. 2000). Skin lesions result from abnormal processes including increased cell proliferation, excess metabolism, and disordered structure and respond differently from normal, healthy tissue (Wu et al. 2007). Infrared thermography has been used to ascertain the physiology for tumors, lesions, vascular function, and vascular disease (Fujimasa et al. 2000; Garcia-Romero et al. 2014; Janicek et al. 2003; Saxena and Willital 2008). Surface temperature is influenced by tumor size, i.e., higher with increasing size, and depth, i.e., inversely with distance of the vasculature from the skin surface (Wu et al. 2007; Draper and Boag 1971; Deng and Liu 2004).

Infrared (IR) thermography records 7.5–13-μm emitted radiation and provides an intensity map of thermal energy at the skin surface (Jones 1998). Static IR captures steady-state conditions at a point in time. Dynamic IR applies a stress (e.g., cooling, heating, pressure) to the skin and alters the subsurface structures (vasculature). They respond and restore equilibrium. The patterns, such as time to prestress temperature, provide functional tissue information (Pirtini Çetingül and Herman 2011; Di Carlo 1995; Santa Cruz et al. 2009). As a result, dynamic IR provides information about metabolism, depth, structure, and circulatory effects, more information than can be obtained from static IR (Renkielska et al. 2006). The time course to return to initial conditions following a specific stress, reveals physiological abnormalities (Cetingul and Herman 2010; Jiang et al. 2005). The use of IR thermography in the dynamic mode eliminates environmental effects on the physiological response (Fujimasa et al. 2000).

Measurement of skin temperature over time in the dynamic IR mode has been used to quantify vascular and neurological conditions such as diabetic neuropathy (Jiang et al. 2005; Bagavathiappan et al. 2010; Lahiri et al. 2012). IR thermal imaging differentiated superficial from deep areas in pediatric burns and was used to estimate graft sizes needed for treatment (Medina-Preciado et al. 2013). Dynamic IR methods have been used effectively to determine burn depth and to predict which burns will heal within 3 weeks. The quantitative results were more accurate than clinical assessment of burn depth (Renkielska et al. 2014). Thermal imaging over time following skin prick testing has been evaluated for quantifying and understanding the mechanisms involved with allergic cutaneous responses (Rokita et al. 2011). Melanoma lesions exhibited higher temperatures during recovery from cold stress compared to benign lesions and healthy skin using dynamic IR (Pirtini Çetingül and Herman 2011; Ruminski et al. 2007; O'Reilly and Taylor 1992). Skin erythema resulting from boron neutron capture therapy for melanoma was detected as a more rapid

rewarming response to cold stress compared to normal tissue (Santa Cruz et al. 2009).

1.2 Infantile Hemangiomas

Infantile hemangiomas (IHs) are benign rapidly proliferating vascular neoplasms occurring in up to 12 % of births (Mueller and Mulliken 1999). They exhibit increased angiogenesis, disorganized structure, increased perfusion, and resultant higher temperatures than uninvolved tissue. They are most commonly located on the head and neck (60 %) (Adams and Lucky 2006). They appear shortly after birth and undergo rapid growth via endothelial cell proliferation for 8–18 months, followed by stabilization (plateau), then slowly involute with diminishing cellular activity, reduced blood flow, and fat deposition for 7–10 years (Marler and Mulliken 2005; Mulliken and Glowacki 1982). About 50 % have involuted by 5 years. Up to 24 % develop life- or function-threatening complications including ulcerations, infection, heart failure, vision impairment, airway obstruction, and disfigurement (Haggstrom et al. 2006; Holland and Drolet 2010). They are classified as superficial, deep, or mixed based on dermal involvement and exhibit wide heterogeneity. Superficial IHs are bright red, slightly elevated, and noncompressible reaching maximal size by 6–8 months. Deep IHs are soft, warm, and slightly bluish and may proliferate for up to 2 years (Drolet et al. 1999). Most IHs are both superficial and deep. They are diagnosed by history and examination of size, color, depth, tactile characteristics, and morphologic subtype (Beck and Gosain 2009; Chang et al. 2008).

In the clinic, IHs are examined visually and palpated for temperature and deformation. Color photographs may be used to judge color and size and treatment response. These are indirect measures of IH status as the extent of proliferation or involution must be inferred. Size, vasculature, and direction of blood flow can be measured with gray-scale and color Doppler ultrasound (Verity et al. 2006), but experienced operators are required (Spierer et al. 2012). Magnetic resonance imaging and computed topography are rarely used due to risks of sedation and radiation exposure (Spierer et al. 2012; Dubois and Garel 1999; Baker et al. 1993; Burrows et al. 1998; Argenta et al. 2006). Conventional histology is impractical for most cases.

2 IR Thermography Methods

Subjects equilibrated to room conditions for at least 15 min prior to measurements. To quantify the characteristics of hemangiomas, or other cutaneous conditions of interest, IR images of the region of interest (ROI), including adjacent regions and uninvolved contralateral control sites, were taken at 60 cm and perpendicular to the site with an emissivity of 0.98 (Jones 1998). A FLIR T400 (FLIR Systems Inc., Wilsonville, OR, USA) was used for this work. The infrared range was 7.5–13 μm, and the camera used an uncooled microbolometer focal plan array detector, 320 × 240 pixel resolution, sensitivity of $< 0.05\ ^{\circ}C$ at 30 °C, and accuracy of $\pm 2\ ^{\circ}C$ (<2 %) in either the static or dynamic mode. To relate the thermal information to the IH as visualized clinically, a static IR image was co-registered with a high-resolution color image. Color images were taken 30 cm perpendicular to the site with a digital camera (Nikon D90, Micro Nikkor 60-mm lens, Nikon R1 Wireless Close-Up flash (Nikon Inc., Nikon Corporation, Tokyo, Japan)), standardized lighting, and color correction (Canning et al. 2009).

2.1 Static IR

The region of involvement (ROI) was extracted from the IR image with an algorithm to segment

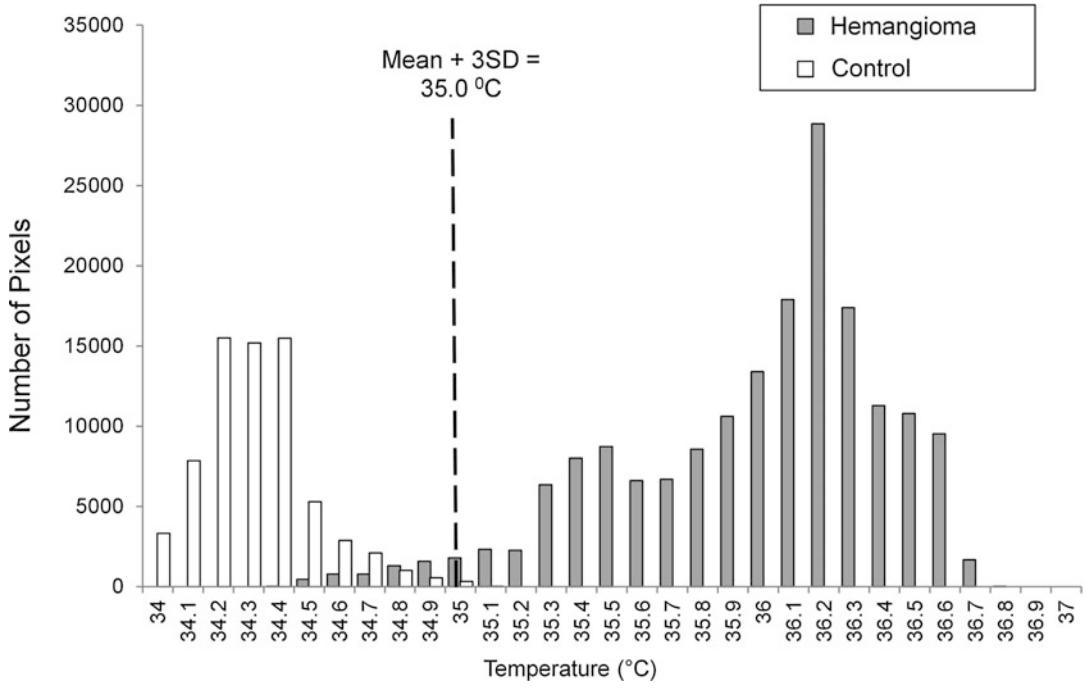

Fig. 1 Static IR threshold determination. Histograms for a typical hemangioma and contralateral uninvolved control site are shown. A threshold of three standard deviations above the control mean temperature was selected to isolate the thermal activity attributable to the IH

the region of higher temperature from uninvolved control skin (ExaminIR software). A threshold of three standard deviations above the control IR image mean temperature was used to isolate the IH features (Fig. 1) following an evaluation of multiple IHs and control sites.

2.2 Dynamic IR

In the dynamic IR mode, a cold stress was applied at 18 ± 0.2 °C for 30 s (Jack Frost™ insulated cold pack, Cardinal Health, McGaw Park, IL). The consistency and reproducibility of cooling were determined (subject coefficient of variation (%CV) of 0.49–1.27 % and cool pack %CV of 2.59 %). The cold stress was removed and rewarming temperature video recorded (7 frames/s) for 30 s. The behavior of the uninvolved contralateral site and that of an area adjacent to the IH (within the cooled region) were similar ($n = 24$, cooled 32.5° ± 1.4 °C; contralateral 32.7° ± 1.2 °C; $p = 0.36$). Therefore, adjacent sites served as the control to minimize the number of cooling procedures (Pirtini Çetingül and Herman 2011; Hassan et al. 2004).

For extraction of quantitative outcomes, the ROI was the IH thermal area above the temperature of uninvolved tissue at the end of rewarming (30 s). This ROI was used for the analysis of all other time points during rewarming (ExaminIR software, FLIR). Distributions of thermal intensity and area were determined using Matlab® (R2012a, MathWorks, Natick, MA, USA). A threshold of the highest 10 % of thermal pixels immediately after cooling was selected (Janicek et al. 2003; Symonds et al. 2012; Wojciech et al. 2010). This procedure isolates the highest thermal activity

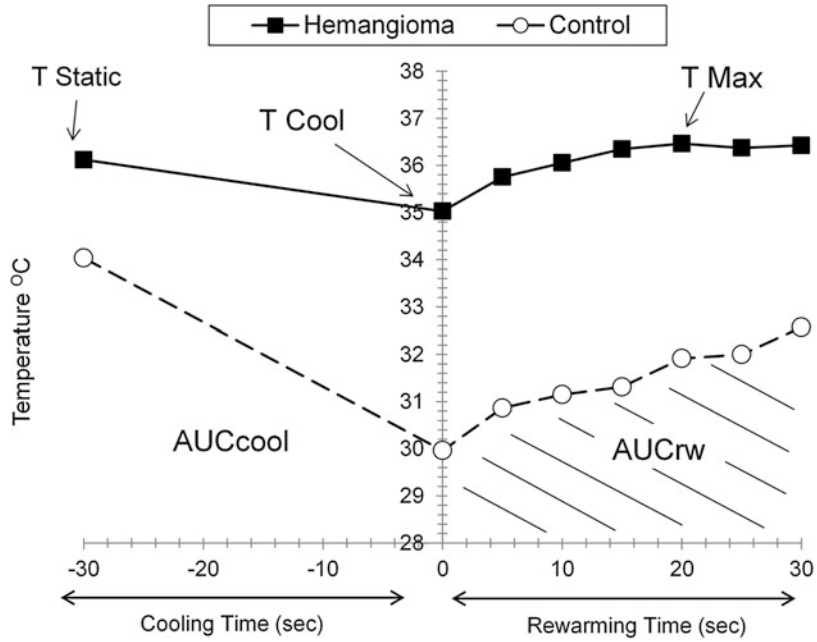

Fig. 2 Dynamic IR imaging outcomes. The dynamic IR imaging outcome measures are shown. In this example, the IH temperature prior to cooling for 30 s is higher than the control site (T static), indicating greater thermal activity. The temperature decrease with cooling (T cool – T static) is greater for the control than the IH, resulting in a lower area under the curve (AUCcool). The area under the curve during rewarming (AUCrw) is greater for the IH, and T max is reached about 20 s after the cool stress is removed

within the IH, segments it from surrounding uninvolved skin, and provides a better signal to noise ratio versus thresholds based on the control value. Video frames at baseline (cooling removed) and 5-s intervals for 30 s were used to generate rewarming curves (Meyer et al. 2013).

Quantitative outcomes were distribution maps of thermal area and intensity, temperature change with cooling (after cooling – static), area under the curve during cooling (AUCcool), area under the curve during rewarming (AUCrw), time to maximum temperature (Tmax) during rewarming, and difference in cooling and rewarming (AUCcool-AUCrw) (Fig. 2). In this example, the IH temperature prior to cooling for 30 s was higher than the control site (T static), indicating greater thermal activity. The temperature decrease with cooling (T cool – T static) was greater for the control than the IH, resulting in a lower AUCcool. The AUCrw is greater for the IH, and T max is reached about 20 s after the cool stress is removed.

3 IR Thermography of Infantile Hemangiomas

Static and dynamic IR thermography coupled with color imaging was used to evaluate the features of IHs over time in a group of patients with superficial or mixed IHs.

3.1 Subjects

Twenty-five subjects were recruited from the patient population of the Hemangioma and Vascular Malformation Center of Cincinnati Children's Hospital Medical Center. This multidisciplinary clinic was composed of specialists from hematology/oncology, surgery, dermatology, pathology, cardiology, orthopedics, and radiology and is a national referral center. The Institutional Review Board approved the study, and parents/guardians provided written

informed consent. Clinic physicians determined the appropriate treatment as propranolol, topical timolol, or observation (untreated). The 25 subjects with 26 IHs were assessed at each clinic visit over 17 months The mean age at enrollment was 7.4 ± 8.4 months (range 1.3–38.3) with six males and 19 females, reflecting the expected gender distribution. There were 59 evaluation sessions (mean 3.8 per subject, range 2–9). Rapid IH growth occurs from 6 to 9 weeks (Tollefson and Frieden 2012), early proliferation before 3 months, most growth before 5 months, and on the plateau for ~7 months and involution takes place after 10–12 months (Chang et al. 2008). Therefore, the data were stratified by age at evaluation into four groups: 1–2 months, 3–5 months, 6–9 months, and 10–18 months.

3.2 Region of Involvement

An example of IR (A) and color images (B) of an IH is shown in Fig. 3a–e. Both images are from

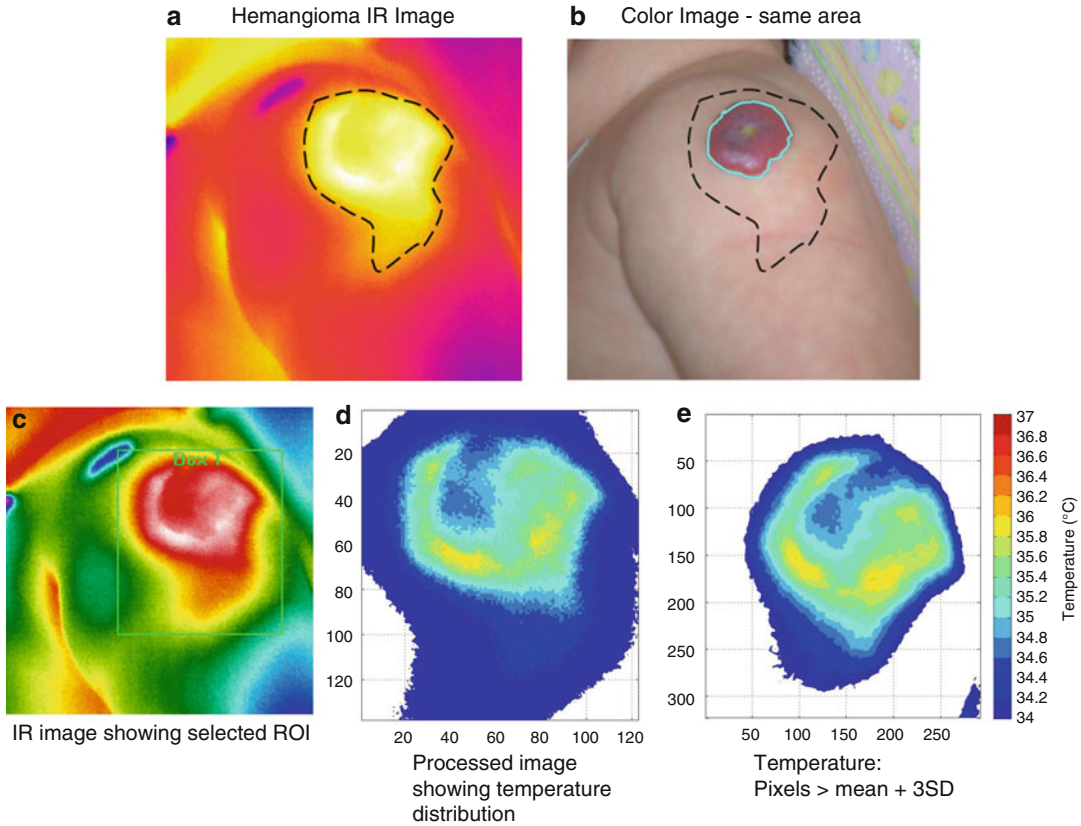

Fig. 3 IR and color images of the same region. An example of IR (**a**) and color images (**b**) of an IH is shown here. Both images are from the same area on the patient. Areas of highest temperature are *white*, followed by *yellow*, *orange*, and *red* in the IR image. The color image shows the visible area of the lesion. The IR area of involvement extends beyond the visible borders in the color image. The IR image has a larger area of elevated temperature as outlined by the *black dashed line*. The area visible upon inspection is outlined in *blue*. The thermal area of involvement selected with the IR software is shown in (**c**). Image processing creates a temperature distribution map (**d**). The map in (**e**) is for thermal pixels greater than the control mean plus 3SD threshold

the same area on the patient. Areas of highest temperature are white, followed by yellow, orange, and red in the IR image. The color image shows the visible area of the lesion. The IR area of involvement extends beyond the visible borders in the color image. The IR image has a larger area of elevated temperature as outlined by the black dashed line. The area visible upon inspection is outlined in blue (Fig. 3b). Figure 3c shows the thermal area of involvement selected with the IR software. Image processing creates a temperature distribution map (D). Figure 3e is the map for thermal pixels greater than the control mean plus three standard deviation (SD) threshold. The color area/IR area ratio for the 59 evaluations averaged 36 % ± 19 %, suggesting that the relevant information about the IH is not readily visible, i.e., upon clinical examination.

3.3 IH and Control Skin

For the study population, the IHs differed from uninvolved (control) skin for all of the dynamic IR outcomes ($p < 0.05$, data not shown). The behavior of the IH and control sites during cooling and rewarming (Fig. 2) is representative of the overall results for the 59 evaluations.

3.4 Dynamic IR Responses

An example of the dynamic response to a cold stress is shown in Fig. 4 for a mixed IH in a 6-month subject. The color and thermal images were co-registered (Fig. 4a). The IR temperature distribution maps are shown for the static image (before cooling) above threshold of mean + 3SD with an area of 353 pixels (Fig. 4b) and for the highest 10 % of thermal pixels (Fig. 4c). Figures 4d, e, f and g show maps at 30 s, immediately after removal of the cold pack (area 325 pixels), 33 s (area 496), 36 s (area 932), and 39 s (area 1190), respectively. The area of thermal activity increases from 325 pixels after cooling to 1190 pixels 9 s later. Note that the highest temperature was at the top of the IH prior to cooling (Fig. 4c) but that the portion at the bottom responded more quickly (Figs. 4d, e, f, g). Specifically, the highest thermal activity is at the bottom, as indicated by the red color. The lowest temperature is in the center and regions of remaining thermal activity are toward the outside of the hemangioma.

The IH was then surgically excised. Histological evaluation showed involvement throughout the dermis but not into the subcutaneous tissue and closely packed capillary blood vessels lined with flattened or hobnailed endothelial cells (Fig. 5a) with pericytes in some regions. Medium-sized feeding vessels were noted in lower regions. There was nonuniform proliferation, some capillary vessel dilatation and slightly increased paucicellular fibrous stroma, both suggesting early involution. The response to the cold stress is shown in Fig. 5b and consistent with rapid rewarming, presumably due to capillary blood flow.

3.5 Dynamic Response – IH Changes Over Time

The mean strata ages were 2.2, 4.5, 8.0, and 12.8 months. The AUCrw decreased over time ($p < 0.05$) indicating a slower response to cooling (Fig. 6). AUC was higher for subjects aged 1–2 months than all older groups and higher for infants of 3–5 months (mean 4.5) than 10–18 months.

The dynamic response over time (two visits) is shown for two subjects. Figure 7 shows an untreated mixed IH at 5.1 (Fig. 7a) and 22 months (Fig. 7f). There was a visibly detectable change. IH height from three-dimensional scans (data not shown) and decreased from 5.1 mm to 3.4 mm. At 5.1 months, the area increased from 359 pixels immediately after cooling (Fig. 7b) to 1100 pixels within 7 s (Fig. 7c). There were pixels at higher temperatures, i.e., ≥ 36.5 °C, 14 s (area 1365, Fig. 7d) and 27 s (area 1482,

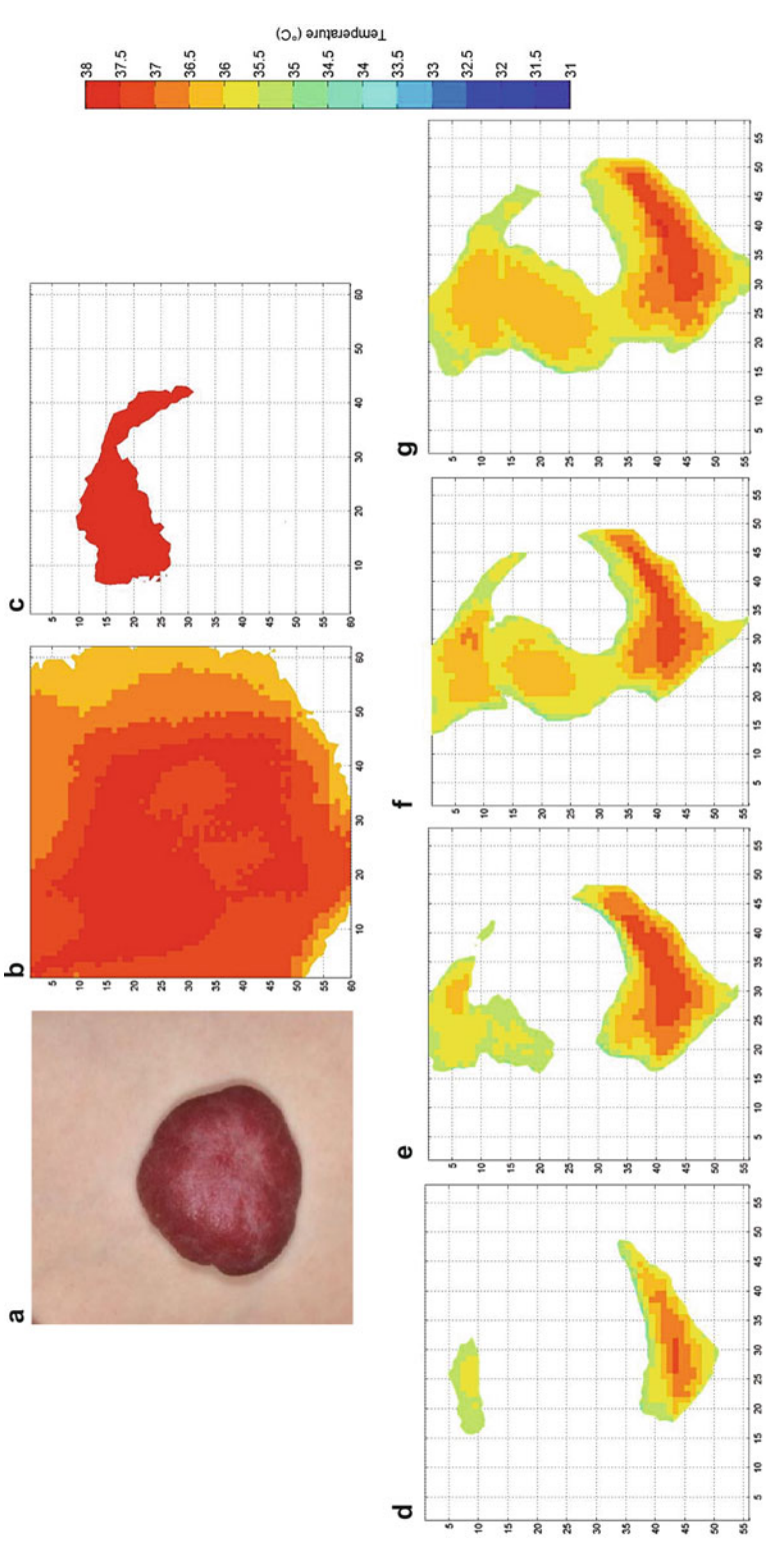

Fig. 4 IH dynamic response to cold stress. An example of the dynamic response to a cold stress is shown for a mixed IH in a 6-month-old subject. The color and thermal images were co-registered **(a)** The static IR temperature distribution maps are prior to cooling and show values above the mean + 3SD **(b)** and the highest 10 % of thermal pixels (area 353) **(c)**. The maps in **(d), (e), (f), and (g)** are at 30 s, immediately after removal of the cold pack (area 325), 33 s (area 496), 36 s (area 932), and 39 s (area 1190). The area of thermal activity increases from 325 pixels after cooling to 1190 pixels 9 s later. Note that the highest temperature was at the *top* of the IH prior to cooling but that the region at the *bottom* responded more quickly. Specifically, the region of highest thermal activity is at the *bottom*, as indicated by the *red* color. The lowest temperature is in the *center* and regions of remaining thermal activity to be toward the outside

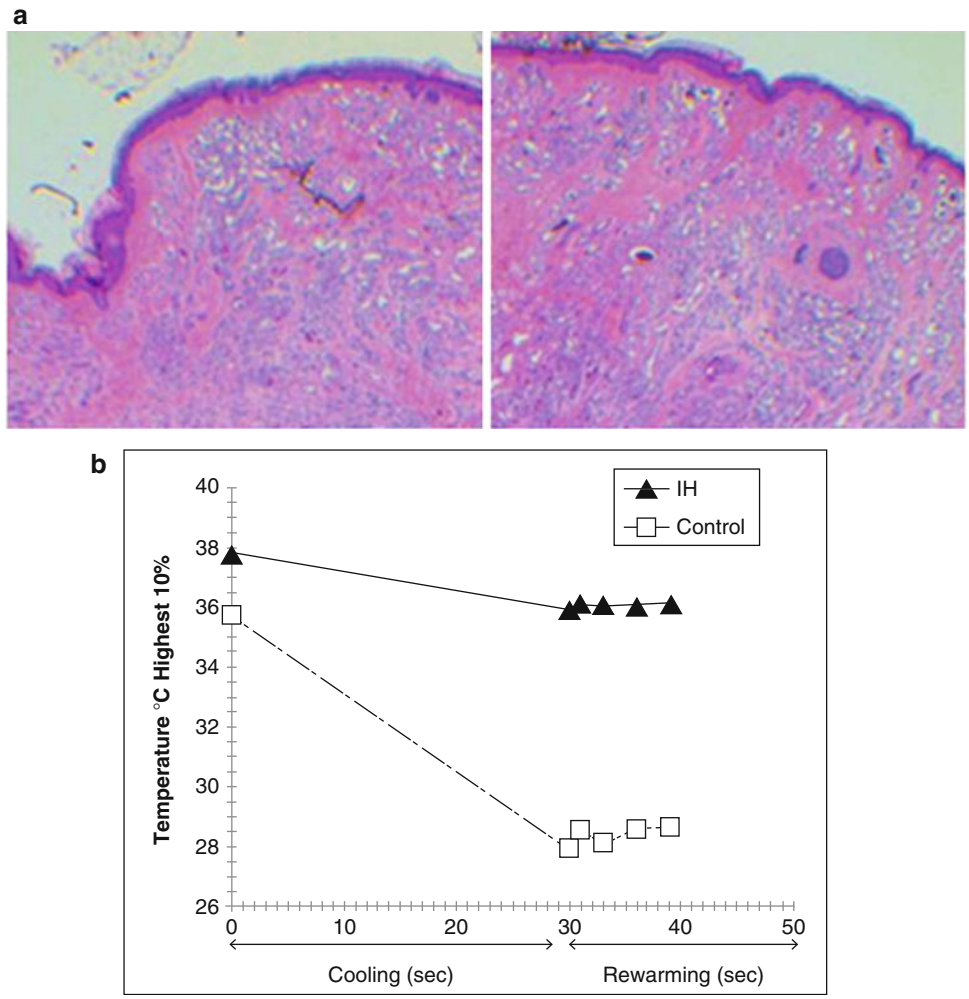

Fig. 5 Histology and dynamic IR outcomes. **(a)** Histological evaluation of the IH in Fig. 4 showed involvement throughout the dermis but not into the subcutaneous tissue. The IH had closely packed capillary blood vessels lined with flattened or hobnailed endothelial cells with pericytes in some regions. Medium-sized feeding vessels were noted in lower regions. There was nonuniform proliferation, some capillary vessel dilatation and slightly increased paucicellular fibrous stroma, both suggesting early involution. The response to the cold stress (**b**) is consistent with rapid rewarming, presumably due to capillary blood flow

Fig. 7e) after cooling. The highest temperatures are generally outside the superficial portion (color image, Fig. 7a), suggesting they are from deeper components. At 22 months (Fig. 7f), the central areas were slowest to rewarm (Figs. 7g, h, i, j). The areas were 418 immediately after cooling (Fig. 7g), 868 at 5 s (Fig. 7h), 1169 at 11 s (Fig. 7i) and 1579 at 24 sec (Fig. 7j). While the areas were similar, the temperatures were lower, i.e., indicated by yellow (35.5-36.5 °C) and green (34-35.5 °C) regions in Figs. 7g, h, i and j.

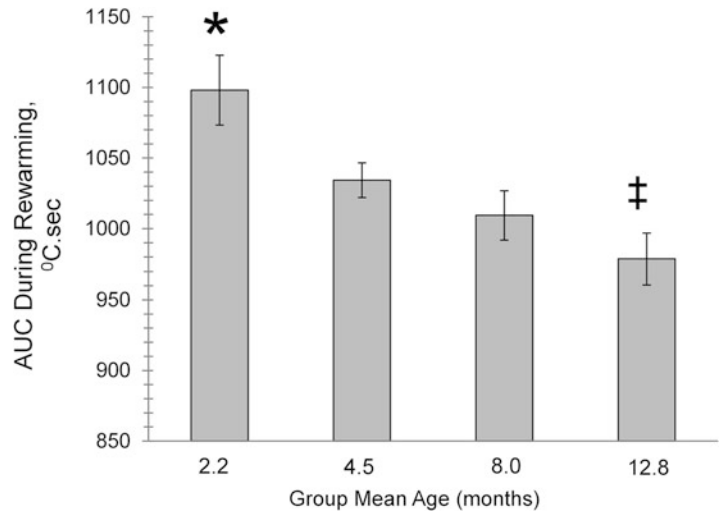

Fig. 6 Dynamic IR response over time. The AUCrw decreased over time indicating a slower response to cooling. AUCrw was higher for subjects aged 1–2 months than all older groups and higher for infants of 3–5 months (mean 4.5) than 10–18 months. * indicates different versus all other groups ($p < 0.05$). ‡ indicates different from mean age of 4.5 months ($p < 0.05$)

Figure 8 shows a mixed IH treated with propranolol. From 11.7 to 15.7 months, the height decreased from 10.3 to 6.5 mm and lightness increased (Figs. 8a, f). The thermal area increased from 769 immediately after cooling to 2047 at 2 sec (Fig. 8c), 4207 at 9 s (Fig. 8d) and 6358 pixels at 25 s (Fig. 8e), with the highest temperature in the lower portion (Fig. 8e). Four months later, the areas were much lower, i.e., 190 pixels immediately post cooling (Fig. 8g), 456 at 4 s (Fig. 8h), 728 at 11 s (Fig. 8i) and 1131 at 27 s (Fig. 8j). The highest activity was toward the center.

4 Summary

Dynamic IR thermography was used to investigate the physiological response to stress, namely, cooling, among subjects with IHs at varying ages. The slower recovery from this stress over time is taken to be due to a reduction in perfusion, blood supply, and/or metabolic activity as proliferation decreases and involution occurs. A relatively small decrease in temperature and area after cooling suggests that sources of thermal activity are robust. IR thermography does not quantify blood flow as volume per time but may be correlated with it (Pascoe et al. 2007). The method provides physiological information about IH status that is not visible upon clinical inspection or with standard color imaging. Therefore, it shows promise as a viable tool for the quantitative evaluation of infantile hemangiomas and has potential application for other cutaneous conditions.

Acknowledgments This research was funded by the Society of Pediatric Dermatology, American Foundation of Pharmaceutical Education Pre-Doctoral Fellowship, Center for Clinical and Translational Science and Training, and Imaging Research Center. It was supported by the National Center for Research Resources and the National Center for Advancing Translational Sciences, National Institutes of Health, through Grant 8 UL1 TR000077-05. The content is solely the responsibility of the authors and does not necessarily represent the official views of the NIH.

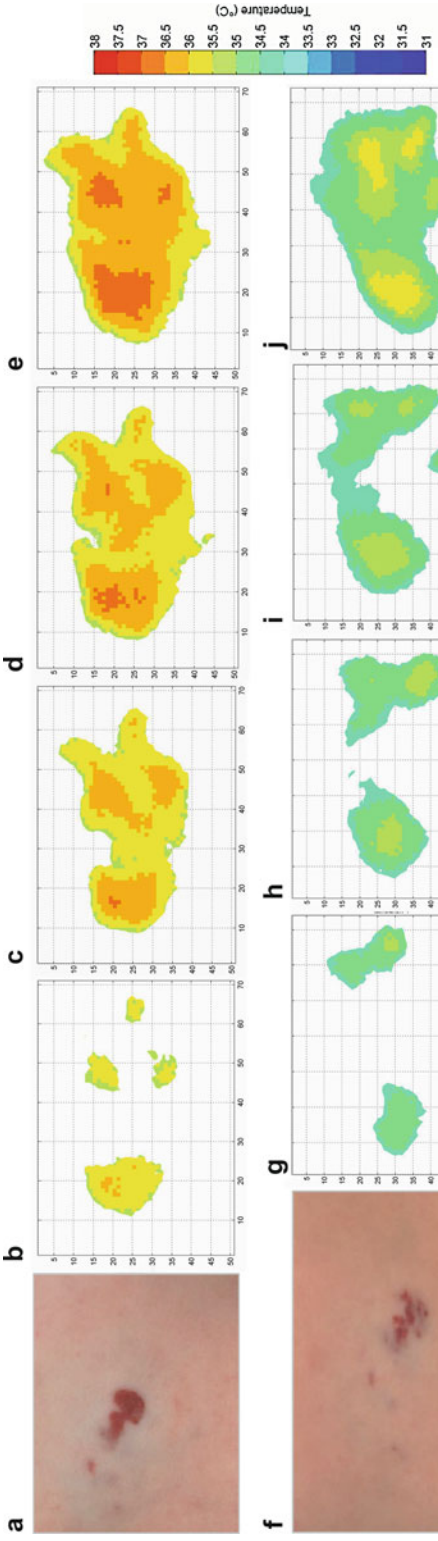

Fig. 7 Example of IR response – untreated mixed IH over time (Fig. 7a). At 5.1 months, the area increased from was 359 pixels immediately after cooling to 1100 within 7 s (Fig. 7c). Areas were 1365 1169 at 14 s (Fig. 7d) and 1482 at 27 sec (Fig. 7e). The highest temperatures were generally outside the superficial portion (Fig. 7f), At 22 months, the central area was the slowest to rewarm. The areas were 418 immediately after cooling (Fig. 7g), 868 at 5 s (Fig. 7h), 1169 at 11 s (Fig. 7i) and 1579 at 24 sec (Fig. 7j). While the areas were similar, the temperatures were lower, i.e., indicated by yellow (35.5-36.5 °C) and green (34-35.5 °C) regions in Figs. 7g, h, i and j

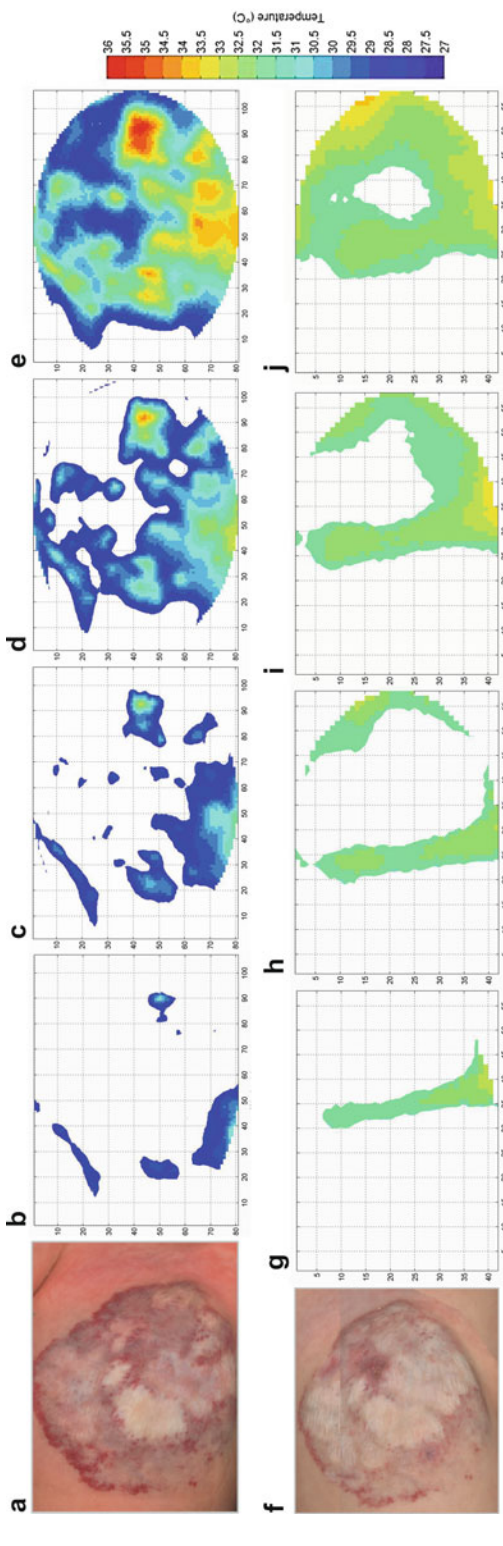

Fig. 8 Example of IR response – propranolol treated mixed IH over time. The lightness decreased (Fig. 8a, f) as did height. The 769 pixels area increased after cooling (Fig. 8b) to 2047 at 2 sec (Fig. 8c), 4207 at 9 s (Fig. 8d) and 6358 pixels at 25 s (Fig. 8e), with the highest temperature in the lower portion (Fig. 8e). Four months later, the areas were much lower, i.e., 190 pixels immediately post cooling (Fig. 8g), 456 at 4 s (Fig. 8h), 728 at 11 s (Fig. 8i) and 1131 at 27 s (Fig. 8j)

References

Adams DM, Lucky AW. Cervicofacial vascular anomalies. I. Hemangiomas and other benign vascular tumors. Semin Pediatr Surg. 2006;15(2):124–32.

Argenta LC, David LR, Sanger C, Park C. Advances in hemangioma evaluation and treatment. J Craniofac Surg. 2006;17(4):748–55.

Bagavathiappan S, Philip J, Jayakumar T, Raj B, Rao PN, Varalakshmi M, et al. Correlation between plantar foot temperature and diabetic neuropathy: a case study by using an infrared thermal imaging technique. J Diabetes Sci Technol. 2010;4(6):1386–92.

Baker LL, Dillon WP, Hieshima GB, Dowd CF, Frieden IJ. Hemangiomas and vascular malformations of the head and neck: MR characterization. AJNR Am J Neuroradiol. 1993;14(2):307–14.

Beck DO, Gosain AK. The presentation and management of hemangiomas. Plast Reconstr Surg. 2009;123(6): 181e–91.

Burrows PE, Laor T, Paltiel H, Robertson RL. Diagnostic imaging in the evaluation of vascular birthmarks. Dermatol Clin. 1998;16(3):455–88.

Canning J, Barford B, Sullivan D, Wickett R, Visscher M. Use of digital photography and image analysis techniques to quantify erythema in health care workers. Skin Res Technol. 2009;15(1):24–34.

Cetingul MP, Herman C. A heat transfer model of skin tissue for the detection of lesions: sensitivity analysis. Phys Med Biol. 2010;55(19):5933–51.

Chang LC, Haggstrom AN, Drolet BA, Baselga E, Chamlin SL, Garzon MC, et al. Growth characteristics of infantile hemangiomas: implications for management. Pediatrics. 2008;122(2):360–7.

Deng ZS, Liu J. Mathematical modeling of temperature mapping over skin surface and its implementation in thermal disease diagnostics. Comput Biol Med. 2004;34(6):495–521.

Di Carlo A. Thermography and the possibilities for its applications in clinical and experimental dermatology. Clin Dermatol. 1995;13(4):329–36.

Draper JW, Boag JW. Skin temperature distributions over veins and tumours. Phys Med Biol. 1971;16(4):645–54.

Drolet BA, Esterly NB, Frieden IJ. Hemangiomas in children. N Engl J Med. 1999;341(3):173–81.

Dubois J, Garel L. Imaging and therapeutic approach of hemangiomas and vascular malformations in the pediatric age group. Pediatr Radiol. 1999;29(12): 879–93.

Fujimasa I, Chinzei T, Saito I. Converting far infrared image information to other physiological data. IEEE Eng Med Biol Mag. 2000;19(3):71–6.

Garcia-Romero MT, Chakkittakandiyil A, Pope E. The role of infrared thermography in evaluation of proliferative infantile hemangiomas. Results of a pilot study. Int J Dermatol. 2014;53(3):e216–7.

Haggstrom AN, Drolet BA, Baselga E, Chamlin SL, Garzon MC, Horii KA, et al. Prospective study of infantile hemangiomas: clinical characteristics predicting complications and treatment. Pediatrics. 2006;118(3):882–7.

Hassan M, Little RF, Vogel A, Aleman K, Wyvill K, Yarchoan R, et al. Quantitative assessment of tumor vasculature and response to therapy in kaposi's sarcoma using functional noninvasive imaging. Technol Cancer Res Treat. 2004;3(5):451–7.

Holland KE, Drolet BA. Infantile Hemangioma. Pediatr Clin North Am. 2010;57(5):1069–83.

Janicek MJ, Demetri G, Janicek MR, Shaffer K, Fauci MA. Dynamic infrared imaging of newly diagnosed malignant lymphoma compared with Gallium-67 and Fluorine-18 fluorodeoxyglucose (FDG) positron emission tomography. Technol Cancer Res Treat. 2003; 2(6):571–8.

Jiang LJ, Ng EY, Yeo AC, Wu S, Pan F, Yau WY, et al. A perspective on medical infrared imaging. J Med Eng Technol. 2005;29(6):257–67.

Jones BF. A reappraisal of the use of infrared thermal image analysis in medicine. IEEE Trans Med Imaging. 1998;17(6):1019–27.

Lahiri B, Bagavathiappan S, Jayakumar T, Philip J. Medical applications of infrared thermography: a review. Infrared Phys Technol. 2012;55:221–35.

Marler JJ, Mulliken JB. Current management of hemangiomas and vascular malformations. Clin Plast Surg. 2005;32(1):99–116. ix.

Medina-Preciado JD, Kolosovas-Machuca ES, Velez-Gomez E, Miranda-Altamirano A, Gonzalez FJ. Noninvasive determination of burn depth in children by digital infrared thermal imaging. J Biomed Opt. 2013;18(6):061204.

Meyer J, Gorbach AM, Liu WM, Medic N, Young M, Nelson C, et al. Mast cell dependent vascular changes associated with an acute response to cold immersion in primary contact urticaria. PLoS One. 2013;8(2), e56773.

Mueller BU, Mulliken JB. The infant with a vascular tumor. Semin Perinatol. 1999;23(4):332–40.

Mulliken JB, Glowacki J. Hemangiomas and vascular malformations in infants and children: a classification based on endothelial characteristics. Plast Reconstr Surg. 1982;69(3):412–22.

O'Reilly D, Taylor L, el-Hadidy K, Jayson MI. Measurement of cold challenge responses in primary Raynaud's phenomenon and Raynaud's phenomenon associated with systemic sclerosis. Ann Rheum Dis. 1992;51(11):1193–6.

Pascoe DD, Mercer JB, de Weerd L. Physiology of thermal signals. In: Diakides NA, Bronzino JD, editors. Medical infrared imaging. Boca Raton: CRC Press; 2007. p. 6.1–20.

Pirtini Çetingül M, Herman C. The assessment of melanoma risk using the dynamic infrared imaging technique. J Therm Sci Eng Appl. 2011;3(3):031006.

Renkielska A, Nowakowski A, Kaczmarek M, Ruminski J. Burn depths evaluation based on active dynamic IR thermal imaging–a preliminary study. Burns. 2006; 32(7):867–75.

Renkielska A, Kaczmarek M, Nowakowski A, Grudzinski J, Czapiewski P, Krajewski A, et al. Active dynamic infrared thermal imaging in burn depth evaluation. J Burn Care Res. 2014;35(5):e294–303.

Rokita E, Rok T, Taton G. Application of thermography for the assessment of allergen-induced skin reactions. Med Phys. 2011;38(2):765–72.

Ruminski J, Kaczmarek M, Renkielska A, Nowakowski A. Thermal parametric imaging in the evaluation of skin burn depth. IEEE Trans Biomed Eng. 2007; 54(2):303–12.

Santa Cruz GA, Bertotti J, Marin J, Gonzalez SJ, Gossio S, Alvarez D, et al. Dynamic infrared imaging of cutaneous melanoma and normal skin in patients treated with BNCT. Appl Radiat Isot. 2009;67(Suppl 7-8):S54–8.

Saxena AK, Willital GH. Infrared thermography: experience from a decade of pediatric imaging. Eur J Pediatr. 2008;167(7):757–64.

Spierer O, Neudorfer M, Leibovitch I, Stolovitch C, Kessler A. Colour Doppler ultrasound imaging findings in paediatric periocular and orbital haemangiomas. Acta Ophthalmol. 2012;90(8):727–32.

Symonds ME, Henderson K, Elvidge L, Bosman C, Sharkey D, Perkins AC, et al. Thermal imaging to assess age-related changes of skin temperature within the supraclavicular region co-locating with brown adipose tissue in healthy children. J Pediatr. 2012;161(5):892–8.

Thomas RA, Donne K, Clement M, Kernan M. Thermography in dermatology. InfraMation Conference, Orlando, Fla, Sept 24-27, 2000.

Tollefson MM, Frieden IJ. Early growth of infantile hemangiomas: what parents' photographs tell us. Pediatrics. 2012;130(2):e314–20.

Verity DH, Restori M, Rose GE. Natural history of periocular capillary haemangiomas: changes in internal blood velocity and lesion volume. Eye (Lond). 2006; 20(10):1228–37.

Wojciech T, Gerald S, Tomoharu N, Lukasz M. Applications of fuzzy rule-based systems in medical image understanding. Rough fuzzy image analysis. Boca Raton: CRC Press; 2010. p. 6-1–31.

Wu Z, Liu HH, Lebanowski L, Liu Z, Hor PH. A basic step toward understanding skin surface temperature distributions caused by internal heat sources. Phys Med Biol. 2007;52(17):5379–92.

Body Surface Area

152

Pierre Agache and Ferial Fanian

Keywords

Body surface area (BSA) • Body height • Body weight • Dubois formula • Sendroy and Collision Chart

There are many equations available in order to calculate the body surface area (BSA) based on the height and weight (Sendroy and Collison 1966). Some of them are as follow:

$$\mathrm{BSA}\ (\mathrm{m}^2) = \frac{\sqrt{\text{height (cm)} \times \text{weight(kg)}}}{3600}$$

Dubois formula:

$$\mathrm{BSA}\ (\mathrm{m}^2) = 0.007184\ \times \mathrm{Weignt}^{0.425} \times \mathrm{Height}^{0.725}$$

$$\mathrm{BSA}\ (\mathrm{m}^2) = \frac{\sqrt{\text{Height (in.)} \times \text{weight (lb)}}}{3131}$$

In 1960, J Sendroy et al. constructed a chart for calculating the BSA based on the weight and height. This chart has been adapted for children shorter than 95 cm (Fig. 1) and the subjects as tall as 85–200 cm (Fig. 2) (Sendroy and Collison 1966).

This chapter was originally published under the ISBN 978-3-540-01771-4 with the following book title Measuring the Skin. The content has not been changed.

Pierre Agache: deceased.

P. Agache
Department of Dermatology, University Hospital of Besançon, Besançon, France
e-mail: aude.agache@free.fr; ferial.fanian@chu-besancon.fr; ferial.fanian@cert-besancon.com

F. Fanian (✉)
Center for Study and Research on the Integuments, Department of Dermatology, University Hospital of Besançon, Besançon, France
e-mail: ferial.fanian@chu-besancon.fr; ferial.fanian@cert-besancon.com; fanian@gmail.com

P. Humbert et al. (eds.), *Agache's Measuring the Skin*,
DOI 10.1007/978-3-319-32383-1_151

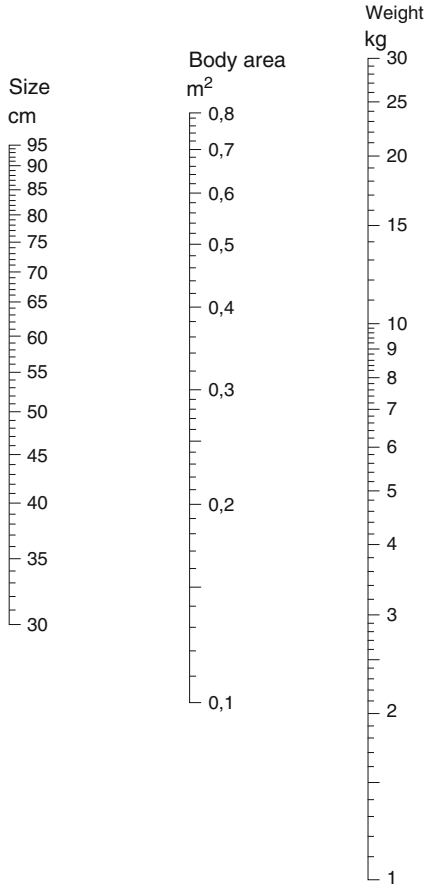

Fig. 1 Total body area in small children

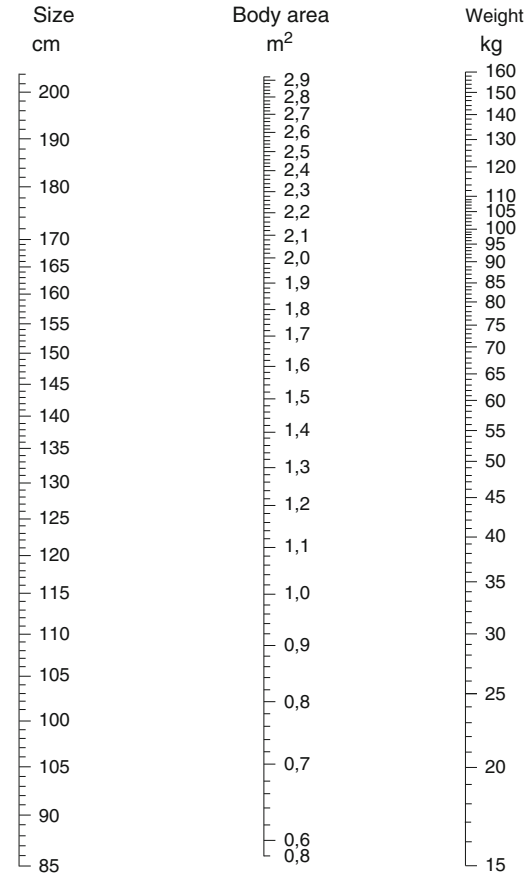

Fig. 2 Total body area in children and adolescents

References

Sendroy Jr J, Collison HA. Determination of human body volume from height and weight. J Appl Physiol. 1966;21(1):167–72.

Blaschko Lines

153

Pierre Agache

Keywords
Blaschko's lines • Skin mosaicism

This chapter was originally published under the ISBN 978-3-540-01771-4 with the following book title Measuring the Skin. The content has not been changed.

Pierre Agache: deceased.

P. Agache (✉)
Department of Dermatology, University Hospital of Besançon, Besançon, France
e-mail: aude.agache@free.fr; ferial.fanian@chu-besancon.fr; ferial.fanian@cert-besancon.com

P. Humbert et al. (eds.), *Agache's Measuring the Skin*,
DOI 10.1007/978-3-319-32383-1_152

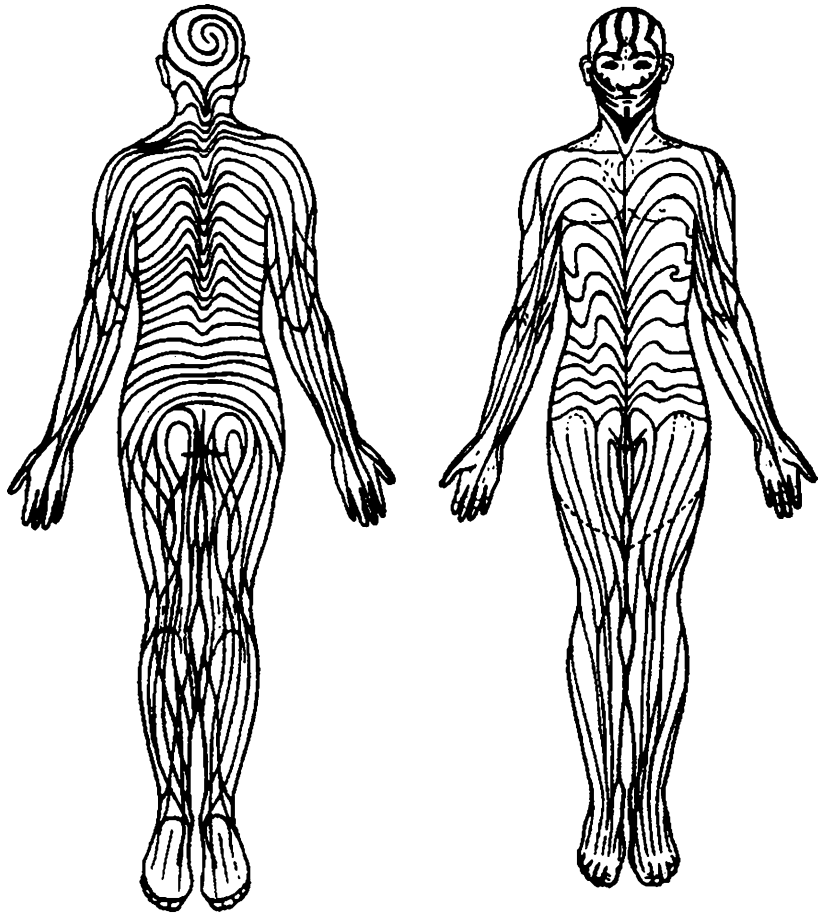

Fig. 1 Original Blaschko's drawing (Blaschko 1901), completed on the scalp by Happle data (Happle et al. 1984) (From Happle (1993), with permission)

Fig. 2 Blaschko's lines of the face, as modified by Bolognia et al. (1994) and Restano et al. (1998) (Modified from Restano et al. (1998), with permission)

References

Blaschko A. Die Nervenverteilung in der Haut In ihrer Beziehung zu den Erkrankungen der Haut. In: Beilage zu den Verhandlungen der Deutschen Dermatologischen Gesellschaft, VII Kongress zu Breslau, Mai 1901. Vienna: Braunmüller; 1990.

Bolognia JL, Orlow SJ, Glick SA. Lines of Blaschko. J Am Acad Dermatol. 1994;31:157–90.

Happle R. Mosaicism in human skin. Arch Dermatol. 1993;129:1460–70.

Happle R, Fuhrmann-Rieger A, Fuhrmann W. Wie verlaufen die Blaschko-Linien am behaarten Kopf? Hautarzt. 1984;35:366–9.

Restano L, Cambiaghi S, Tadini G, Cerri A, Caputo R. Blaschko lines of the face: a step closer to completing the map. J Am Acad Dermatol. 1998;39:1028–30.

Dermatomes

154

Pierre Agache

Keywords

Human Dermatome map • Spinal cord segmentation • Segmental sensory innervation

This chapter was originally published under the ISBN 978-3-540-01771-4 with the following book title Measuring the Skin. The content has not been changed.

Pierre Agache: deceased.

P. Agache (✉)
Department of Dermatology, University Hospital of Besançon, Besançon, France
e-mail: aude.agache@free.fr;
ferial.fanian@chu-besancon.fr;
ferial.fanian@cert-besancon.com

P. Humbert et al. (eds.), *Agache's Measuring the Skin*,
DOI 10.1007/978-3-319-32383-1_153

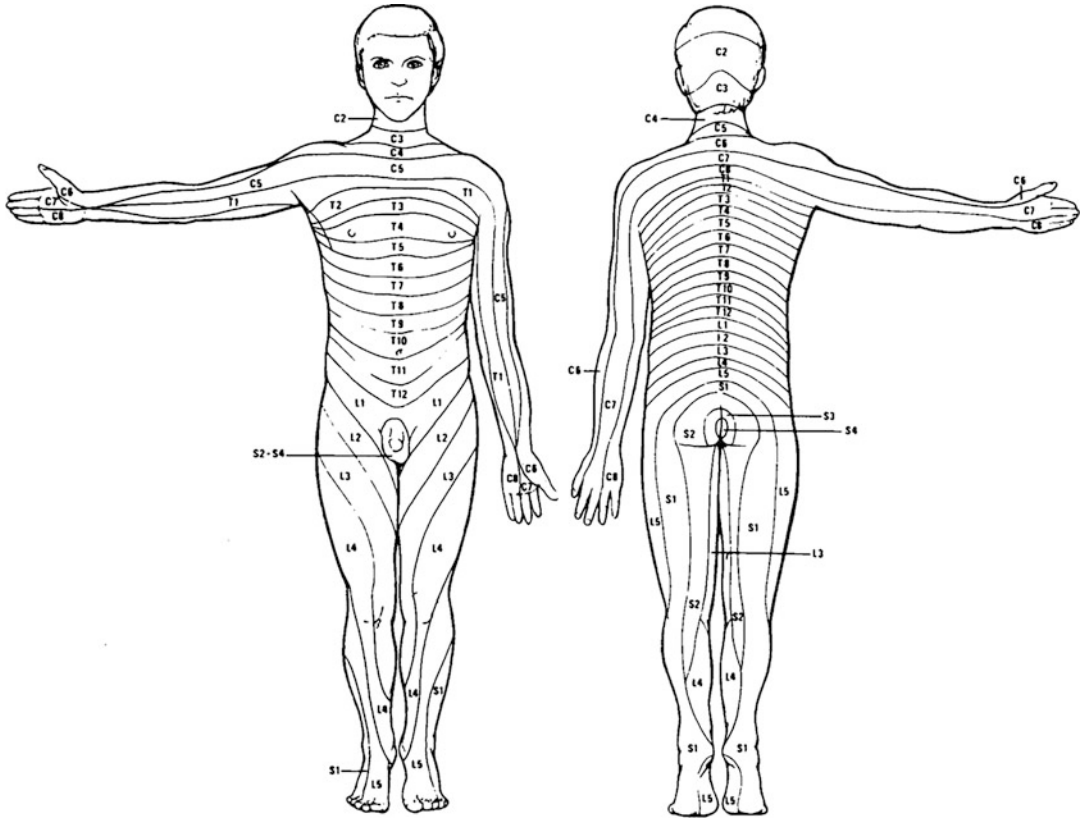

Fig. 1 Dermatomes of the human body surface and their relation to spinal cord segments: *C* cervical, *D* thoracic, *L* lumbar, *S* sacral (From Martin and Jessell (1991), with permission)

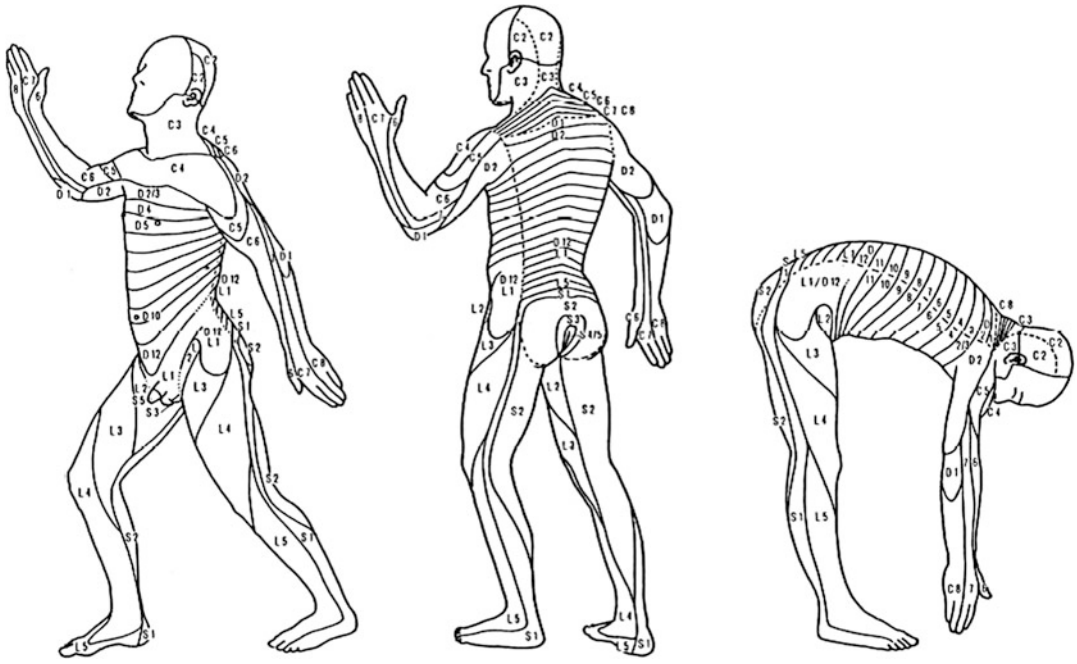

Fig. 2 Dermatomes of the human body surface and their relation to spinal cord segments: *C* cervical, *D* thoracic, *L* lumbar, *S* sacral (From Windhorst (1996), with permission)

References

Foerster O. The dermatomes in man. Brain. 1933. 56:353–523.

Martin JH, Jessell TM. Anatomy of the somatic sensory system. In: Kandel ER, Schwartz JH, Jessell TM, editors. Principles of neuronal science. London: Prentice-Hall; 1991. p. 353–66.

Keegan JJ, Garrett FD. The segmental distribution of the cutaneous nerves in the limbs of man. Anat Rec. 1948. 102(4):409–37.

Lee MW, McPhee RW, Stringer MD. An evidence-based approach to human dermatomes. Clin Anat, 2008. 21(5):363–73.

Standing S, Gray H. Grey's Anatomy of the Human Body. 39th ed. Philadelphia, Pa: Lea & Febiger; 2005. p. 435–7.

Windhorst U. Central projections of cutaneous and enteroceptive senses. In: Greger R, Windhorst U, editors. Comprehensive human physiology, From cellular mechanisms to integration, vol. 1. Berlin/Heidelberg/New York: Springer; 1996. p. 623–46 (Fig. 78.2 from p 636).

Langer's Lines

155

Pierre Agache

Keywords

Cleavage lines • Dermis collagen orientation • Langer's lines • Topological skin lines

This chapter was originally published under the ISBN 978-3-540-01771-4 with the following book title Measuring the Skin. The content has not been changed.

Pierre Agache: deceased.

P. Agache (✉)
Department of Dermatology, University Hospital of Besançon, Besançon, France
e-mail: aude.agache@free.fr;
ferial.fanian@chu-besancon.fr;
ferial.fanian@cert-besancon.com

P. Humbert et al. (eds.), *Agache's Measuring the Skin*,
DOI 10.1007/978-3-319-32383-1_154

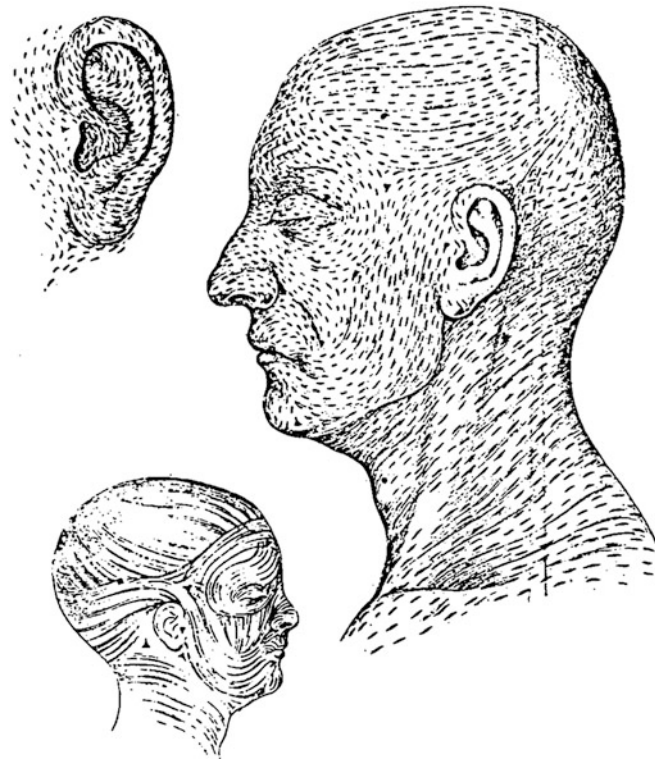

Fig. 1 Face profile and ear (From Langer (1861))

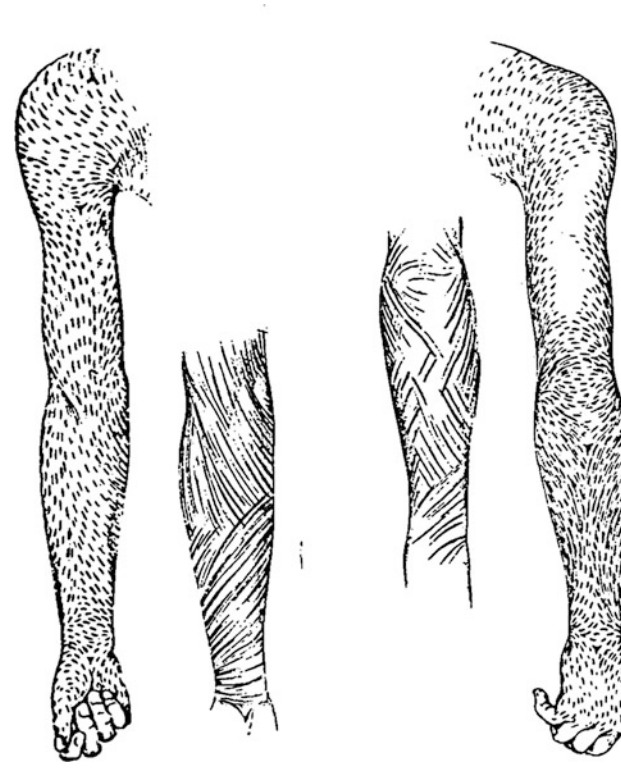

Fig. 2 Arm and forearm (From Langer (1861))

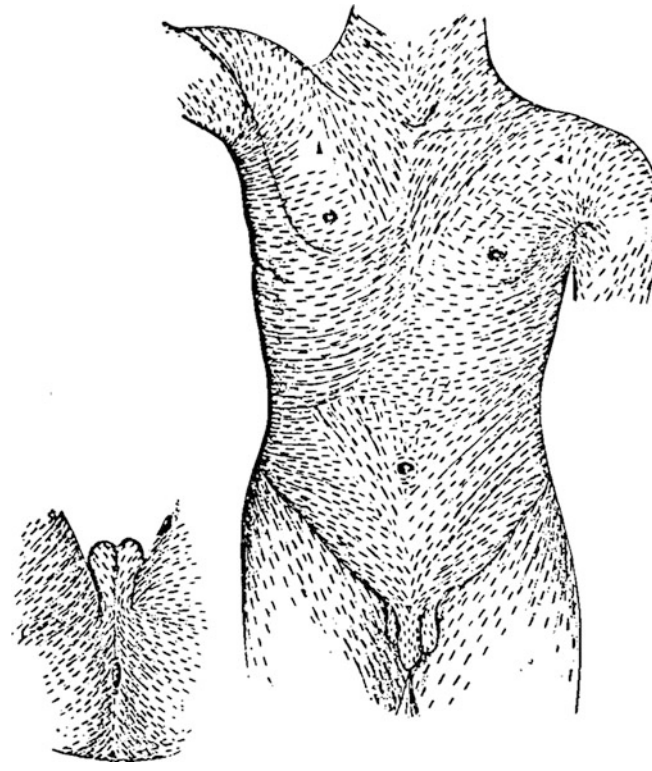

Fig. 3 Anterior trunk and perineum (From Langer (1861))

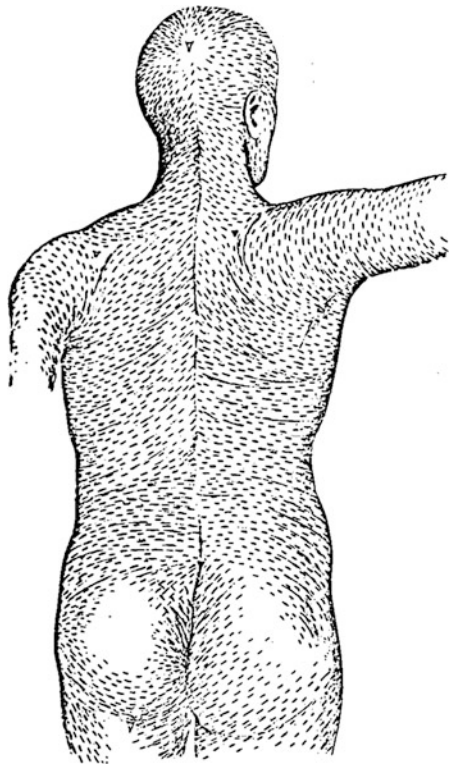

Fig. 4 Posterior trunk and scalp (From Langer (1861))

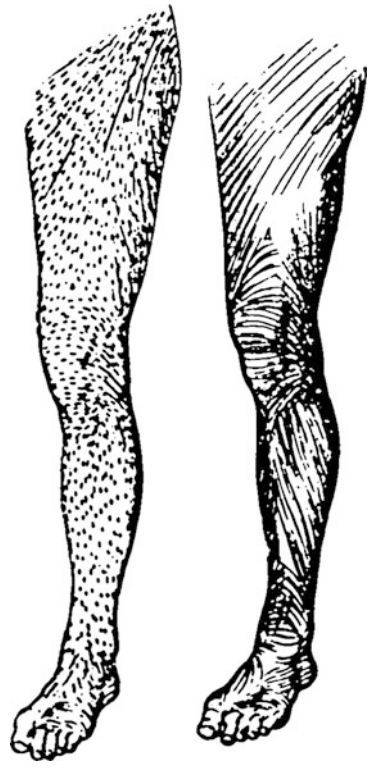

Fig. 5 Anterior leg (From Langer (1861))

Fig. 6 Leg, medial aspect (From Langer (1861))

Fig. 7 Hand and foot (From Langer (1861))

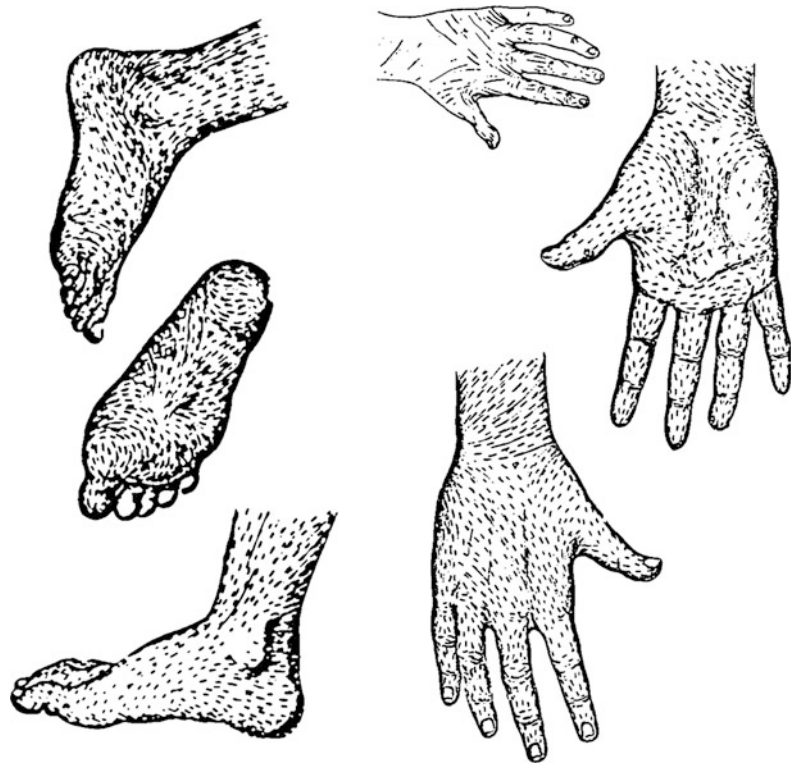

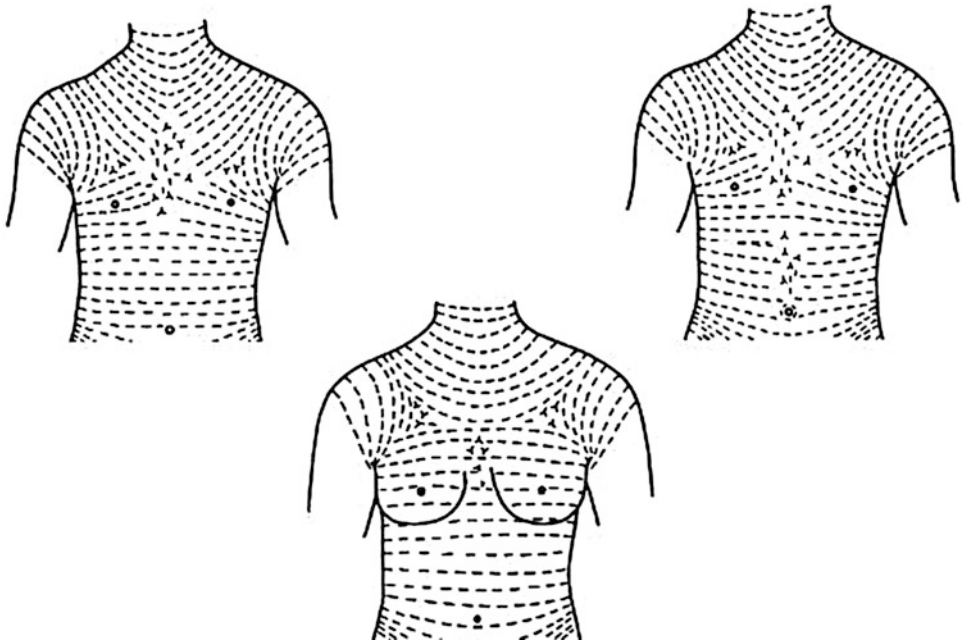

Fig. 8 Anterior chest (From Namikawa et al. (1986))

References

Langer K. Zur Anatomie und Physiologie der Haut. 1. Über der Spaltbarkeit der Cutis [On the skin splitting capacity]. Sitzungsberichte der kaiserlichen Akademie der Wissenschaften/Mathematisch-Naturwissenschaftlichen Classe; 1861 Apr 25. Vienna: K.K. Hof- und Staatsdruckerei; 1862, 44: 19–45.

Langer, K. On the anatomy and physiology of the skin. Brit J Plast Surg. 1978;31(1):3–8.

Namikawa A, Sakai H, Motegi K, Oka T. Cleavage lines of skin. In: Bibliotheca Anatomica, vol. 27. Basel: Karger; 1986. p. 1–60.

Wilhelmi BJ, Blackwell SJ, Phillips LG. Langer's lines: to use or not to use. Plast Reconstr Surg. 1999;104 (1):208–14.

Main Skin Biological Constants

156

Pierre Agache

Contents

This chapter was originally published under the ISBN 978-3-540-01771-4 with the following book title Measuring the Skin. The content has not been changed.

Pierre Agache: deceased.

P. Agache (✉)
Department of Dermatology, University Hospital of Besançon, Besançon, France
e-mail: aude.agache@free.fr; ferial.fanian@chu-besancon.fr; ferial.fanian@cert-besancon.com

P. Humbert et al. (eds.), *Agache's Measuring the Skin*,
DOI 10.1007/978-3-319-32383-1_156

Keywords

Anatomical constants (averages) • Body surface area • Circadian rhythms (solar time) • Dermis thickness • Dermis composition • Eccrine sweat glands number • Hair composition • Hair follicle proliferation index • Lymphatic capillaries diameter • Minimal erythema dose (MED) for Caucasians • Nail composition • Nail growth rate • Nails thickness • Neonates skin thickness • Pilo-sebaceous follicles • Sebum composition • Skin capillaries diameter • Skin collagen content • Skin blood flow volume • Skin Functional constants • Skin lymphatics • Skin metabolism • Skin microbial density • Skin relief • Skin thickness • Skin volume in vivo • Skin weight in vivo • Stratum corneum thickness • Stratum corneum composition • Stratum corneum renewal rate • Stratum malpighi renewal rate • Subcutaneous fat thickness • Sweat chemical composition • Tissue retraction • Viable epidermis thickness (stratum Malpighi)

1 Anatomical Constants (Averages)

1.1 Tissue Retraction Following Processing for Histology (Jouanny et al. 1993)

Young people	38–58 %
Aged people	12 %

1.2 Body Surface Area

- Standard figure in adults ≈ 1.8 m^2
- Du Bois and du Bois' formula $A = 71.84 \approx Weight^{0.425} \approx Height^{0.725}$ (Du Bois and du Bois 1916) (weight in kg, height in cm, and area in cm^2) Example: for 63 kg and 1.61 m the skin area is 1.66 m^2

When the body surface area is less than 0.6 m^2, Boyde's formula would be more accurate (Pittet et al. 1979):

- Boyde's formula $A = 3.207 \times 10^{-4} \times Weight^{(0.7285 - 0.0188 \log weight)} \times Height^{0.3}$ (Pittet et al. 1979)

  (weight in g, height in cm, and area in cm^2)
- Wallace's fractional distribution (Wallace 1951):

  Head and neck 9 %, each upper limb 9 %, each lower limb 18 %, anterior trunk 18 %, posterior trunk 18 %, genitalia 1 %
- Lund and Browder's fractional distribution (% of total body surface area) (Lund and Browder 1944):

Age (years)	Head	Trunk, neck, genitalia	Upper limbs	Lower limbs
0	19	34	19	28
1	17	34	19	30
5	13	34	19	34
10	11	34	19	36
15	9	34	19	38
Adult	7	34	19	40

At all ages palm area ≈ 1 % of body area

Berkow's fractional distribution (Berkow 1931):

Body anterior aspect (total = 51%)	
Face	3 %
Anterior trunk (total = 20%)	
Neck + upper third	7 %
Middle third	6 %
Lower third + genitalia	7 %

(*continued*)

Upper limbs anterior aspect (total = 9%)	
Arms	3.5 %
Forearms	3.25 %
Hands	2.25 %
Lower limbs anterior aspect (total = 19%)	
Thighs	9.5 %
Legs	6.5 %
Feet	3 %
Body posterior aspect (total = 49 %)	
Head	3 %
Posterior trunk (total = 18 %)	
Neck + upper half	9 %
Lower half	9 %
Upper limbs posterior aspect (total = 9 %)	
Arms	3.5 %
Forearms	3.25 %
Hands	2.25 %
Lower limbs posterior aspect (total = 19 %)	
Thighs	9.5 %
Legs	6.5 %
Feet	3 %
Children (see also maps, ▶ Chap. 152, "Body Surface Area")	
Trunk	40 %
Head	6 % + (12 minus age) %
Lower limbs	38 % + (12 minus age) %

1.3 Special Areas

Scalp area, 400–500 cm^2

Palm area (Mahler et al. 1983):

	Male (n = 22)	Female (n = 18)
Area (cm^2)	146 ± 14	118 ± 10
% Body area	0.76 ± 0.10	0.70 ± 0.07

Forefinger last phalange (ventral aspect) length (Long and Finlay 1991):

Male	2.6 ± 0.15 cm (n = 16)
Female	2.4 ± 0.10 cm (n = 14)

1.4 Skin Volume In Vivo (Calculated for 18,000 cm^2 Body Area)

Male	3.8 dm^3	for 1.3 mm (mean skin thickness)
Female	3.2 dm^3	for 1.1 mm (mean skin thickness)

1.5 Skin Weight in Vivo (Calculated for 18,000 cm^2 Body Area)

Skin weight in vivo = [in vitro skin density (d = 1.18) × volume] + blood density (d = 1.06) × 500 ml

Male	5.0 kg	(of which 0.5 kg blood)
Female	4.3 kg	(of which 0.5 kg blood)

1.6 Skin Thickness

1.6.1 Ultrasound (20 MHz) Measurement (mm) (Black 1969)

Site	Male	Female
Forehead	2.19	1.79
Cheek	1.83	1.49
Neck	1.61	1.34
Nape	2.09	1.92
Site	Male	Female
Anterior chest	1.92	1.77
Abdomen	1.88	1.62
Back	2.62	2.33
Loins	2.21	2.09
Arm, anterior aspect	1.53	1.45
Arm, posterior aspect	1.21	1.05
Forearm, anterior aspect	1.31	1.12
Forearm, posterior aspect	1.42	1.36
Dorsum hand	1.50	1.26
Palm	1.48	1.50
Thigh, anterior aspect	1.59	1.42
Thigh, posterior aspect	1.51	1.46
Leg, anterior aspect	1.42	1.34
Leg, posterior aspect,	1.34	1.30
Ankle	2.01	2.08
Dorsum foot	1.74	1.49
Sole	1.60	1.53

	Males, 28.3 ± 6.2 years (n = 30)	Females (Spalteholz 1927), 27.8 ± 8.0 years (n = 30)
Forehead	1.78 ± 0.14 (±SD)	1.55 ± 0.20
Volar forearm	0.92 ± 0.09 (±SD)	0.90 ± 0.11

1.6.2 Xeroradiography (Black 1969) (mm)

Volar forearm

Male	1.3 mm
Female	1.1 m

1.6.3 Magnetic Resonance Imaging (Querleux et al. 2002)

Upper dorsal thigh	
Male	1.71 ± 0.24 ($n = 23$)
Female without cellulite	1.58 ± 0.21 ($n = 20$)
Female with cellulite	1.87 ± 0.39 ($n = 21$)

1.6.4 Neonates Skin Thickness (A-mode Echography) ($n = 48$) (Petersen et al. 1995)

Weight (g)	Abdomen (±SD)	Back (±SD)
1095	0.47 ± 0.05	0.52 ± 0.06
1810	0.55 ± 0.05	0.71 ± 0.04
1940	0.61 ± 0.09	0.65 ± 0.06
2900	0.65 ± 0.09	0.76 ± 0.05
3390	0.67 ± 0.08	0.78 ± 0.06
3890	0.67 ± 0.08	0.76 ± 0.09
4750	0.80 ± 0.08	0.85 ± 0.06

1.7 Skin Relief

First order furrows	70–200 μm
Second order furrows	20–70 μm
Small wrinkles	0.2–1 mm
Common wrinkles	>1 mm

1.8 Stratum Corneum

Thickness	8–20 μm	(Holbrook et al. 1974)
Volar forearm	16.8 ± 1.1 μm	(Corcuff et al. 1993)
Hip	11.8 ± 1.4 μm (SE) (Anderson and Cassidy 1973)	
Palms and soles	0.5–1 mm	

(*continued*)

Number of cell layers	19 ± 1.2 (SE)	(Anderson and Cassidy 1973)
Face	9 ± 2 (84) (Japanese) (M ± SD, *n*)	Holbrook et al. (1974)
Eyelid	9 ± 1 (8)	
Cheek	10 ± 3 (43)	
Nose	10 ± (2)	
Nasolabial fold	7 ± (2)	
Lip	10 ± (2)	
Ear	7 ± 2 (8)	
Periauricular	10 ± 3 (3)	
Scalp	12 ± 2 (12)	
Neck	10 ± 2 (5)	
Shoulder	13 ± 2 (3)	
Chest	13 ± 4 (9)	
Back	13 ± 3 (18)	
Abdomen	14 ± 4 (44)	
Buttock	12 ± 4 (20)	
Genitalia	6 ± 2 (9)	
Arm, outer	13 ± 4 (13)	
Arm, inner	14 ± (2)	
Forearm volar	16 ± 4 (4)	
Thigh	16 ± 4 (31)	
Leg posterior	18 ± 5 (5)	
Hand dorsum	25 ± 11 (10)	
Palm	50 ± 10 (8)	
Foot dorsum	30 ± 6 (7)	
Sole	55 ± 14 (12)	
Heel	86 ± 36 (5)	
Corneocytes number	0.7×10^6 to	(Hunter et al. 1956)
(volar forearm)	$1.5 \times 10^6/cm^2$	
Corneocytes thickness	0.3 μm	(Holbrook et al. 1974) (Plewig et al. 1983) (Ya-Zian et al. 1999)
Corneocyte diameter	26–45 μm	(Bartolone et al. 1991)
Corneocyte area	1000 μm^2	(Plewig et al. 1983)
Corneocyte thickness of keratin filaments	10–15 nm	
Intercellular spaces width	25 nm	(Lundström et al. 1994)
	0.1 μm	(Ya-Zian et al. 1999)
Corneodesmosomes		
Length	290 nm	(Lundström et al. 1994)
Thickness	25 nm	(Lundström et al. 1994)
Corneodesmosomes	Involved fraction of cell membranes, 6.8 %	(Lundström et al. 1994)

1.9 Viable Epidermis (Stratum Malpighi)

Thickness	30–80 μm	
Volar forearm	36 ± 4 μm	(Corcuff et al. 1993)
Volar forearm (23–34 years)	64.2 ± 4.9 (n = 7) (histology)	(Timar et al. 2000)
Volar forearm (44–54 years)	72.2 ± 14.1(n = 7) (histology)	(Timar et al. 2000)
Buttocks	69.6 ± 10.2 (n = 67) (histology)	(Therkildsen et al. 1998)
Number of cell layers	5–10	
Volar forearm (23–34 years)	4.4 ± 0.5 (n = 7) (histology)	(Timar et al. 2000)
Volar forearm (44–54 years)	4.6 ± 0.4 (n = 7) (histology)	(Timar et al. 2000)
Epidermal cells number/ mm^2	73,952 ± 19,426 (from 24 biopsies)	(Bauer et al. 2001)
Keratinocytes number/ mm^2		(Corcuff et al. 1993)
Stratum basale	7000	
Stratum spinosum	4000	
Stratum granulosum	1500	
Langerhans cells density	2–4 % of cells	(Banchereau et al. 1998)
	1/53 other epidermal cells (1.86 %)	(Bauer et al. 2001)
Langerhans cells number/ mm^2	460–1000	(Oxholm et al. 1987)
	1394 ± 321 (breast, from 24 biopsies)	(Bauer et al. 2001)
Melanocytes	0.3–2.4 % of epidermal volume	(Zelickson and Mottaz 1968)
Cell diameter	30–40 μm	
Melanosome dimensions	~1 × 0.4 × 0.4 μm	
Intercellular spaces	1.5–1.9 % of epidermal volume	(Zelickson and Mottaz 1968)
Histologic section:	1.1–1.2	(Frost and van Scott 1966)
dermo-epidermal junction:		
length versus a straight line		
Histologic section:	44 10^{-4} μm^2	(Frost and van Scott 1966)
epidermis area along 1 cm		
Histologic section:	9 × 10^{-4} μm^2	(Frost and van Scott 1966)
dermal papillae area along 1 cm		
Keratinocyte nucleus average diameter	4.60 μm	(Barton 1988)

(*continued*)

Keratinocyte nucleolus average diameter	1.22 µm	(Barton 1988)
Desmosomes length		(Lundström et al. 1994)
Basal layer	0.13 µm	
Spinous and granular layers	0.26 µm	
Hemi-desmosomes	0.19 µm	
Desmosomes: involved fraction of cell membranes		(Lundström et al. 1994)
Basal layer	4 %	
Spinous and granular layers	11 %	
Dermo-epidermal junction length over a straight line (interdigitation index) (histology)		(Timar et al. 2000)
Volar forearm (23–34 years)	1.333 ± 0.153 ($n = 7$)	
Volar forearm (44–54 years)	1.106 ± 0.090 ($n = 7$)	

1.10 Dermis

Subpapillary dermis thickness	50–100 µm	
Peri-adnexial dermis thickness	20–70 µm	
Reticular dermis thickness	0.8–1.2 mm	
% Area of elastic fibers (by histology)		(Timar et al. 2000)
23–34 years ($n = 7$)	4.9 ± 1.9	
44–54 years ($n = 7$)	11.6 ± 1.6	
% Area of intercellular GAGs (by histology)	23–34 years ($n = 7$)	(Timar et al. 2000)
44–54 years ($n = 7$)	10.7 ± 2.2	
Collagen fibers thickness	2–20 µm	
Collagen fibrils wavelength	3 µm	
Collagen fibrils thickness	50–70 nm	
Reticular dermis		
24 weeks fetus	≅50 nm	(Quaglino et al. 1996)
At birth	≅100 nm	
Adults	110–115 nm	
Beyond 60 years	≅100 nm	
Elastic fibers thickness	0.1–0.4 µm	(Pope 1998)
Oxytalan fibers	13–14 nm	(Pope 1998)
Fibrillin fibrils	1.0–1.3 nm	(Pope 1998)
Basement membrane thickness	50–100 nm	(Timpl and Brown 1996)
Dendritic cells	2–3 % of dermal cells	(Banchereau et al. 1998)

Table 1 Subcutaneous fat thickness, mm mean +/−2 SE, skin fold (Carpentier and Maricq 1990)

Age group	Males Upper arm	Hip	n	Females Upper arm	Hip	n
5–9	5.4 ± 0.7	14.8 ± 1.8	17	6.7 ± 0.8	18.4 ± 2.2	9
10–14	5.5 ± 0.6	16.3 ± 1.9	24	8.3 ± 1.0	26.4 ± 3.2	17
15–19	5.8 ± 0.6	10.0 ± 1.2	22	10.9 ± 1.2	30.5 ± 3.8	25
20–29	6.3 ± 0.7	9.7 ± 1.1	42	10.9 ± 1.3	31.3 ± 3.5	53
30–39	6.2 ± 0.7	8.6 ± 1.0	22	10.4 ± 1.2	31.5 ± 3.9	21
40–49	6.3 ± 0.7	9.1 ± 1.1	27	10.6 ± 1.2	31.6 ± 4.0	20
50–69	6.4 ± 0.9	9.4 ± 1.0	13	11.1 ± 1.4	29.1 ± 4.1	14
70–91	5.8 ± 0.8	8.3 ± 1.0	13	9.1 ± 1.1	13.3 ± 1.8	22

1.11 Subcutis

Subcutaneous fat thickness, mm mean ± 2 SE, skin fold (Lever et al. 1983) (Table 1):

Subcutaneous fat thickness at upper dorsal thigh (magnetic resonance imaging) (Uitto et al. 1989):

Males	6.64 ± 3.16 (SE)
Females without cellulite	8.34 ± 2.44 (SE)
Females with cellulite	34.02 ± 5.42 (SE)

Neonate subcutis thickness (mm) ultrasound A mode (n = 7) (Petersen et al. 1995):

Body weight (g)	Abdomen	Back
1095	0.65 ± 0.07	0.77 ± 0.10
1810	0.78 ± 0.13	0.95 ± 0.13
1940	1.52 ± 0.20	1.53 ± 0.16
2900	1.67 ± 0.17	1.87 ± 0.19
3390	1.80 ± 0.16	1.74 ± 0.23
3890	1.95 ± 0 − 31	1.84 ± 0.27
4750	2.90 ± 0.22	2.45 ± 0.24

Dermis-subcutaneous tissue irregularity index (Querleux et al. 2002):

Males	1.91 ± 0.24	(n = 20)
Females without cellulite	2.08 ± 0.12	(n = 17)
Females with cellulite	2.29 ± 0.32	(n = 16)

1.12 Blood Capillaries

Nail-fold		
Papillary loops number/mm	8.4 ± 1 (n = 118)	(Jouanny et al. 1993)
	7.2 ± 1.5 (n = 20)	(Gasser and Buhler 1992)

(*continued*)

Ascending loop internal diameter (i.e. of RBC column)	10.8 ± 30 μm (n = 396)	(Mahler et al. 1983)
Descending loop internal diameter (i.e. of RBC column)	12.0 ± 2.7 μm (n = 396)	(Mahler et al. 1983)
Ascending loop internal diameter (plasma, FITC-alb)	15.0 ± 2.5 μm (n = 396)	(Mahler et al. 1983)
Descending loop internal diameter (plasma, FITC-alb)	16.7 ± 3.0 μm (n = 396)	(Mahler et al. 1983)
Papillary loop		
Length	0.3–0.4 mm	(Spalteholz 1927)
Papillary loop width	62.6 μm	(Spalteholz 1927)
Papillary loop involved skin area	0.027–0.040 mm^2	(Spalteholz 1927)
Volar forearm capillaries number/mm^2		(Prasad et al. 1995)
Using capillaroscopy	31.2 ± 7.0 (n = 10)	
Using plasma, FITC-alb	28.9 ± 5.4 (n = 10)	
Subepidermal plexus vessels external diameter		(Braverman and Keh-Yen 1977)
Horizontal capillaries	10–15 μm	
Ascending arteriole	17–26 μm	
Post-capillary venule	18–35 μm	
Deeper vessels (transfer vessels) external diameter		
Arterioles	30–150 μm	
Venules	50–300 μm	

1.13 Lymphatic Capillaries (Limbs)

Mean diameter	91 ± 22 μm	(Bollinger et al. 1981)

1.14 Pilo-Sebaceous Follicles

Total number		(Ebling et al. 1979)
Whole body	5×10^6	
Head and face	1×10^6	
Scalp	1×10^5	
Number/cm^2	(mean ± SEM)	(Cunliffe et al. 1976)
Forehead	330 ± 20	
Chest (medial)	59 ± 10	
Upper back (medial)	72 ± 2	
Upper back (lateral)	84 ± 4	
Hair density (per cm^2)		
Scalp		
Terminal hair	200–300	(Ebling et al. 1979)

(*continued*)

Vellus hair	5–15 %	(Guarrera et al. 1997) (Hayashi et al. 1991)
Forehead	439 ± 24 (±SEM)	(Blume et al. 1998)
Cheek (female)	416 ± 37 (±SEM)	(Blume et al. 1998)
Shoulder (male)	68 ± 5 (±SEM)	(Blume et al. 1998)
Chest	57 ± 3 (±SEM)	(Blume et al. 1998)
Back	85 ± 4 (±SEM)	(Blume et al. 1998)
Scalp terminal hair thickness		
Caucasians	50–90 μm (oval in section)	
Mongoloids	120 μm (round)	
Scalp vellus hair thickness	<30 μm	
Scalp hairs oval in section diameters' ratio	0.63–0.91	(Van Neste et al. 1985)
Scalp hair bulb volume		
Papilla	338×10^3 μm^3	(Van Scott et al. 1958)
Matrix	3370×10^3 μm^3	
Scalp hair daily growth	>0.2 mm/day	
Keratin production	0.2–0.3 g/day	

Body hairs

Mean length (Dawber et al. 1998):

	Males (mm)	Females (mm)
Thigh	17.0	5.5
Arm (outer)	9.0	6.0

Maximum length (Blume et al. 1998):

	15–20 years (mm) (±SEM)	25–30 years (mm) (±SEM)
Forehead	2.0 ± 0.3	1.6 ± 0.5
Cheek (female)	4.1 ± 0.5	3.4 ± 0.4
Shoulder (male)	6.0 ± 0.4	4.3 ± 0.4
Chest	4.6 ± 0.2	3.9 ± 0.4
Back	6.2 ± 0.4	5.0 ± 0.4

Pilo-sebaceous duct exit size (mm^2) (mean ± SEM), (Cunliffe et al. 1976):

Forehead	2.0 ± 0.1
Chest (medial)	4.3 ± 0.3
Upper back (medial)	3.0 ± 0.2
Upper back (lateral)	3.9 ± 0.2

Hair cells dimensions:

Cuticle	0.5–1 μm × 45 μm
Cortex	2–5 μm80 × 115 μm

Hair cortex internal components, (Atkins et al. 1974):

×Helix	1 nm
Protofibril	3–5 nm
Microfibril	8–15 nm
Macrofibril	200–500 nm

1.15 Nails

Total thickness at distal margin:

Fingers	0.3 mm (d5), 0.5 mm (thumb)
Toes	0.5 mm (d5), 0.8 mm (dl)

Nail thickness contributions (Achten and Parent 1983):

Upper dorsal nail	33 % of total nail thickness
Lower dorsal nail	66 % of total nail thickness

Big toe-nail (measurements on eight normal avulsed nails) (Johnson and Shuster 1993):

	Proximal end	End of lunula	Onychodermal band
% of total length	0	34.8	100
% of maximal thickness	27	19	100

Nail thickness contributions:

Nail bed	22 %
Matrix	78 %

Big toe-nail (measurements on 54 normal avulsed nails) (Johnson and Shuster 1994):

– Mean thickness:

Male	1.65 ± 0.43
Female	1.38 ± 0.20

	Proximal end	End of lunula	Onychodermal band
Thickness mean (mm)	0.37 ± 0.0004	1.08 ± 0.0008	1.38 ± 0.01
Thickness range	0.26–0.55	0.85–1.31	0.85–1.76

Onychocytes diameter, (Achten and Parent 1983):

Upper dorsal nail	2.2 µm
Lower dorsal nail	5.5 µm

1.16 Eccrine Sweat Glands

Total number: 3–4 × 10^6

Regional counts (Szabo 1962):

Soles	620 ± 120
Forehead	360 ± 50
Cheeks	320 ± 60
Dorsum foot	250 ± 5
Forearm	225 ± 25
Abdomen and groin	190 ± 5
Chest	175 ± 35
Back and buttocks	160 ± 30
Calf	150 ± 15
Arm	150 ± 20
Thigh	120 ± 10

Eccrine tube:

Length	5 mm
Diameter	0.02–0.05 mm

2 Chemical Composition

2.1 Whole Skin (% Abdomen Skin Dry Weight) (Weinstein and Boucek 1960)

Collagen (both sexes)	76.8 ± 9.1 (n = 83)	
Elastin		
Males:	4.45 ± 1.4 (n = 17)	
Females:	3.95 ± 0.9 (n = 10)	
Reticulin:	0.4 % skin dry weight	(Lundström et al. 1994)
Collagen content (g/cm^2 skin)	234 ± 72 (SE)	(Shuster et al. 1969)

2.2 Sebum: Standard Composition (in Weight) (▶ Chap. 47, "Skin Wound Healing Assessment", Ref. 9)

Squalene	12.0 %
Wax esters	26.0 %
Glycerides and free fatty acids	57.5 %
Sterols (free and esters)	4.5 %

2.3 Skin Surface Lipids of Epidermal Origin (in Weight) (▶ Chap. 47, "Skin Wound Healing Assessment", Ref. 9)

Glycerides and free fatty acids:	65 %
Cholesterol esters:	15 %
Cholesterol:	20 %

2.4 Stratum Corneum

Proteins (corneocytes)	2.92 ± 0.89 μg cm^{-2} (n = 6)	(Elias 1983)
Cystine	2.9 %	Fraser, in (Leveque 1994)
Other amino acids		see Fraser, in (Leveque 1994)
Lipids	10 %	(Leveque 1994)
Lipid fractions (of weight)		(De Rigal et al. 1992)
Cholesterol esters	15 %	
Cholesterol	32 %	
Saturated fatty acids	16 %	
Ceramides	37 %	
Water (for 20–60 % atmospheric relative humidity)		
35 % of volume		(Blank et al. 1984)
0.05–0.15 g cm^{-3}		(Blank 1952)
0.12 ± 0.01 g cm^{-3} ($n = 6$)		(Tagami et al. 1994)

2.5 Dermis

Reticular dermis (Quaglino et al. 1996) (all figures represent percentages) (Table 2):

2.6 Subcutis

Composition: upper dorsal thigh, (magnetic resonance spectroscopy) ($n = 67$) (Querleux et al. 2002):

Water	4.7 ± 5.6 %
Unsaturated lipids	3.7 ± 2.3 %
Saturated lipids	85.3 ± 5.9 %

Table 2 Reticular dermis (Quaglino et al. 1996)

	24 weeks fetus	At birth	Adults	Beyond 60 years
Collagen/tissue ratio	24	≅60	≅70	≅40
Elastic fibers/ tissue	Absent	3–4	3–4	7–8
Mesenchymal cells	20	4	1.5	1.5
Type I collagen	80 % of total collagen			(Uitto et al. 1989)
Type III collagen	15 % of total collagen			(Uitto et al. 1989)
Collagen type I/type III	5:1 to 6:1			(Uitto et al. 1989)
Mature elastic fiber		(Braverman and Fonferko 1982)		
90 % elastin				
10 % microfibrils				
Interstitial fluid	2 % proteins			
Suction blister fluid				
4.2 % proteins	55 % albumin, 45 % globulins	(Stüttgen 1965)		
3.9 ± 0.4 g/dl ($n = 6$)	=54 % of concentration in plasma (Braun-Falco and Rupec 1964)			

Fatty acid ratio within lipids (gas liquid chromatography) ($n = 22$ obese women) (Timpl and Brown 1996):

	Arm	Thigh	Abdominal wall
Saturated fatty acids	39.4 ± 5.1 %	33.9 ± 4.3 %	35.9 ± 4.8 %
Unsaturated fatty acids	60.6 ± 4.7 %	66.0 ± 4.1 %	67.1 ± 4.6 %

Major fatty acids: % within lipids (gas liquid chromatography) ($n = 22$ obese women) (Timpl and Brown 1996):

	Arm	Thigh	Abdominal wall
12:0	6.7 ± 2.9	6.4 ± 2.9	8.4 ± 3.4
14:0	50.1 ± 10.6	44.7 ± 11.7	50.9 ± 9.6
15:0	5.1 ± 1.4	5.0 ± 1.4	4.9 ± 1.4
16:0	278.0 ± 40.0	245.5 ± 29.3	273.2 ± 32.4
16: I	80.3 ± 17.7	107.8 ± 21.9	82.3 ± 23.9
17:0	3.5 ± 1.1	3.0 ± 1.5	3.5 ± 1.1
17:1	4.3 ± 0.9	5.1 ± 1.3	4.6 ± 1.6
18:0	50.7 ± 12.2	34.1 ± 18.1	48.3 ± 16.6
18:1	464.8 ± 9.7	485.6 ± 31.7	465.5 ± 20.2
18:2	48.0 ± 30.9	51.9 ± 27.5	48.9 ± 25.5
20:1	8.4 ± 2.4	9.4 ± 3.6	9.4 ± 4.3

2.7 Hair

Standard composition (in weight)

Keratins	85–90 %	
Water	10–13 %	
Lipids	2 %	(Leveque 1994)
Trichochromes		
Cystine	7.6 %	Fraser, in (Leveque 1994)
Other amino acids		see Fraser, in (Leveque 1994)

2.8 Nails: Mean Composition

Cystine	7.4 %	Fraser, in (Leveque 1994)
Other amino acids		see Fraser, in (Leveque 1994)
Water	9–10 % of weight (in vitro big toe-nail, $n = 8$)	(Johnson and Shuster 1993)

Nota bene: Dehydration does not change nail thickness.

Relative humidity (%)	Water content (% of weight)	(Finlay et al. 1980)
15–20	5–6	
35–45	8–10	
60	13	
80	16	
90	17–21	
100	29	

Lipid (% of dry weight) (Helmdach et al. 2000):

	Male ($n = 31$)	Female ($n = 40$)
Cholesterol sulphate	1.45 ± 0.50	1.98 ± 0.72**
4–6 ceramides	6.12 ± 0.08	9.94 ± 1.96**
1–3 ceramides[a, b]	26.92 ± 5.78	25.60 ± 4.14
Cholesterol	8.93 ± 2.95	13.16 ± 2.83**
Free fatty acids[a]	30.83 ± 9.65	24.20 ± 6.53*
Triglycerides	7.34 ± 2.20	5.79 ± 1.53**
Sterol and wax esters	7.47 ± 1.08	8.44 ± 0.34**
Squalene	2.71 ± 0.48	1.50 ± 1.28**
Unidentified	7.56 ± 2.38	8.11 ± 3.08

Difference between males and females significant at 0.01 (*) and 0.001 (**) levels
[a]Infants excluded (two males and four females)
[b]Infants: 1–3 ceramides: mean = 4.59 %; free fatty acids: mean = 12.07 %

2.9 Sweat (▶ Chap. 76, "Scalp Sebaceous Function Assessment", Ref. 7)

Na^+ (mM)	<40
K^+ (mM)	4–20
Cl^- (mM)	<20
$CO3H^-$ (mM)	15–20
Ammonia (mM)	0.5–8
Lactates (mM)	10–15
Urea (mg/ml)	0.15–0.25
Glucose (:g/ml)	2–5
Proteins (mg/ml)	0.15–0.25

3 Functional Constants

3.1 Current Minimal Erythema Dose (MED) for Caucasians

UVB	30 mJ cm^{-2}
UVA	30 J cm^{-2}

3.2 Stratum Corneum Renewal

Daily production	1.15 ± 0.09 new layer	(Johannesson et al. 1978)
Desquamation		
Forearm	1309 ± 328 cells cm^{-2} h^{-1}	(Edwards et al. 1995)
Forehead	2083 ± 481 cells cm^{-2} h^{-1}	(Christensen et al. 1978)
Other body sites		See ▶ Chap. 25, "Stratum Corneum Desquamation", Sec ▶ 4
Daily protein loss forehead	12.1 ± 4.7 μg cm^{-2}	(Christensen et al. 1978)
Renewal time		
Overall	15 days	
Forearm	18.5 ± 4.6 days	(Roberts et al. 1980)
Forehead	6.3 ± 1.4 days	(Baker et al. 1967)
Abdomen	25.9 ± 5.4 days	(Roberts et al. 1980)
Other body sites		(Jansen et al. 1974)

3.3 Stratum Malpighi Renewal

Renewal time	15 days	
Basal cells distribution		(Mommers et al. 2000)
G0 phase	30 %	
Cycling	10 %	

(*continued*)

Number of mitoses in basal layer		
7.7 per cm length		(Frost and van Scott 1966)
1 out of 600 cells		(Fischer and Maibach 1971)
Mitotic index	1.59	(Fischer and Maibach 1971)
Proliferation index (thymidine or BrdU)	▶ Chap. 36, "Epidermal Physiology", Ref. 22	
Basal layer only	5–6 % of cells in S-phase	
Basal + 3 suprabasal layers	46 % of cells in S-phase	
Proliferation index (thymidine)		(Marks et al. 1987)
Sun unexposed sites	4.7 ± 2.2 (n = 19)	
Sun exposed sites	8.6 ± 2.1 (n = 19)	
Cell cycle duration		
G1 phase	7.6 h	(Mommers et al. 2000)
S phase	5.3–10.3 h	(Galand et al. 1989)
G2 + M phases	11 h	(Knaggs et al. 1994)
M phase	1.5 h	(Knaggs et al. 1994)
Whole cycle	50–282 h	(Knaggs et al. 1994)
28 h		(Mommers et al. 2000)
Transit time from basal layer to stratum corneum	6–27 days	(Knaggs et al. 1994)

3.4 Hair Follicle

Proliferation index, 11 % (Knaggs et al. 1994)

Scalp hair common stage formula: Anagen 80–90 %, telogen 10–20 %, catagen <1 %

Scalp hair stages:

	Male	Female	
Anagen with sheath	>55 %	>65 %	
Anagen without sheath	>20	>20	
Dystrophic anagen	<1,5	<1	
Catagen	<1	1 %	
Telogen	<25	<15	
% anagen hairs	Male (±SEM)	Female (±SEM)	
Body site (▶ Chap. 44, "In Vivo Magnetic Resonance Imaging of the Skin", Ref. 10)			
Forehead	49.5 ± 4.8	48.5 ± 4.5	
Cheek		46.4 ± 4.8	
Chest	34.7 ± 2.9	42.2 ± 2.4	
Shoulder	32.8 ± 2.2		

(*continued*)

	Male	Female	
Back	32.0 ± 2.0	30.9 2.5	
	Anagen	Telogen	
Stage duration			(Saitoh et al. 1970)
Scalp, terminal hair	3–7 years	3 months	
Scalp, vellus hair	4–26 weeks		(Ebling et al. 1979)
Arm	9 weeks	15 weeks	
Leg	16 weeks	22 weeks	
Dorsum finger	8 weeks	10 weeks	
Thigh(male)	8 weeks		(Saitoh et al. 1970)
Thigh (female)	3 weeks		(Saitoh et al. 1970)
Forehead	60.8 ± 4.9 days (±SEM)		(Blume et al. 1998)
Cheek (female)	78.6 ± 14.6 days (±SEM)		(Blume et al. 1998)
Shoulder (male)	51.2 ± 4.6 days (±SEM)		(Blume et al. 1998)
Back (female)	41.8 ± 1.8 days (±SEM)		(Blume et al. 1998)
Back (male)	49.4 ± 2.9 days (±SEM)		(Blume et al. 1998)
Chest	45.6 ± 1.9 days (±SEM)		(Blume et al. 1998)

Anagen duration (days) (▶ Chap. 44, "In Vivo Magnetic Resonance Imaging of the Skin", Ref. 12):

	Males	Females
Thigh	54	22
Arm (outer)	28	22

Daily growth (mm)

Scalp	0.3–0.5 mm	(Saitoh et al. 1970)
Thigh (male)	0.38 mm	
Thigh (female)	0.21 mm	
Chest	0.44 mm	
Beard	0.27 mm	
Back	0.134 ± 0.010 (SEM)	(Blume et al. 1998)
Forehead (male)	0.037 ± 0.005 (SEM)	
Forehead (female)	0.037 ± 0.005 (SEM)	
Cheek (female)	0.060 ± 0.007 (SEM)	
Shoulder (male)	0.119 ± 0.011 (SEM)	

Scalp: daily hair length production, 30–50 m (i.e., 0.3 –0.5 g)

Scalp: current (normal) daily hair loss, <70 (Kligman 1961)

Resistance to plucking (g):

Scalp hair	48 ± 18 (n = 10)	(Cunliffe et al. 1976)
Chest hair	71 ± 10 (n = 110)	(Chapman 1992)

3.5 Sebum

Casual level (forehead)	100–200 μg cm^{-2}	
Other body sites		see ▶ Chap. 13, "Sebaceous Physiology"
Casual level recover time	3–4 h; 50 % within 33 min	(Downing et al. 1981)
Infundibulum reservoir content	80 % of casual level	
Skin surface sebum spreading coefficient	1–10 mJ m^{-2}	
Maximal *spontaneous* sebum creep up the hair shaft	2 cm	
Sebaceous gland: cell transit time from basal layer to excretory canal	3 sem	
Sebaceous gland secretion rate	6–25 mg cm^{-2} h^{-1}	(Jani 1992) (Downing et al. 1981)

3.6 Nails

Daily linear growth:

Standard figures		
Hands	0.1 m	
Feet	0.05 mm	
Maximal rate (25 years)		(Orentreich et al. 1979)
Male	0.9 mm/week	
Female	0.7 mm/week	
Rate over life	0.5 % decrease per year, to 50 % reduction by 60 years of age, then stable	(Orentreich et al. 1979)
Temperature dependence	0.08 mm/week at 16 °C 2.0 mm/week at 32 °C	(Orentreich et al. 1979)
Circadian rhythm	5 μm h^{-1} by midday 1 μm h^{-1} by midnight	(Orentreich et al. 1979)

Thickness increase rate, (Johnson and Shuster 1993):

Lunula	0.13 mm/1.41 % length increment
Bed	0.02 mm/0.22 % length increment

3.7 Eccrine Sweat Glands

Fraction of active glands	50 %	(Knip 1969)
Sweat excretion frequency	0.3–12 min^{-1}	
Excretion rate per gland	4–28 nl min^{-1}	
Global sweating rate	1–3 mg min^{-1} cm^{-2}	(Cotter et al. 1995)
Heat loss per gland working as a heat pipe	9.68 × 10^{-6} W	
Sweating threshold	Max. by 18 h	(Crockford et al. 1970)

3.8 Skin Metabolism

Metabolic oxygen consumption at 37 °C	2.6×10^{-3} ml g^{-1} min^{-1}	(Severinghaus et al. 1978)
Metabolic oxygen consumption at 45 °C (as in $tcPO_2$ measurement)		
Normal skin	3.7×10^{-3} ml g^{-1} min^{-1}	(Severinghaus et al. 1978)
Psoriasis (diseased skin)	5.4×10^{-3} ml g^{-1} min^{-1}	(Ott et al. 1984)
Metabolic heat produced by epidermis		
Normal skin	0.16 cal $min^{-}1$ cm^{-2}	▶ Chap. 58, "Transcutaneous Oxygen Pressure"
	(4 % increase per °C)	
Psoriasis (diseased skin)	0.27 cal min^{-1} cm^{-2}	(Ott et al. 1984)
Total heat loss[a] at rest and in thermal neutrality	30 g h^{-1} m^{-2}	

[a]From skin and lung

Skin temperature (naked subject) (▶ Chap. 123, "Skin Thermal Imaging"):

	At 20 °C	At thermal neutrality
Forehead	32.0 °C	34.8 °C
Forearm	27.7 °C	33.6 °C
Dorsum foot	20.0 °C	31.1 °C
Other body sites, see ▶ Sect. 2.1		

3.9 Skin Microbiology (▶ Chap. 4, "The Skin Surface Ecosystem: A Presentation")

Microbial density at the skin surface (for details, see ▶ Chap. 4, "The Skin Surface Ecosystem: A Presentation", Tables 3 and ▶ 4):

Scalp	$1.0 \times 10^6/cm^2$ to $1.2\times$ $106/cm^2$
Forehead	$4.4 \times 10^6/cm^2$
Upper limbs (extremity)	$1.7 \times 10^3/cm^2$
Lower limb (extremity)	$4.4 \times 10^3/cm^2$
Axilla	$4.8 \times 10^3/cm^2$
Perineum	$4.3 \times 10^7/cm^2$
Toe webs	$1.4 \times 10^7/cm^2$
Staphylococcus aureus carriage,	$>10^6/cm^2$

3.10 Skin Blood Flow

Skin blood volume		(Martineaud et al. 1977)
At rest	9 % of total blood volume	
Vasodilated skin	12 % of total blood volume	
Global skin blood flow		(Martineaud et al. 1977)
At rest	0.5 l min^{-1}	
Moderate exercise	0.9 l min^{-1}	
Intense exercise + high outside temperature	7 l min^{-1}	
Subpapillary dermisa skin blood flow (volar forearm)	30–45 ml min^{-1} per 100 g tissue	
Resting skin blood flow (xenon clearance)		
Forearm	5.1 ± 1.7 ml min^{-1} per 100 g tissue	(Sejrsen 1969)
Lateral Malleola	6.2 ± 1.1 ml min^{-1} per 100 g tissue[b]	(Cardot et al. 1977)
Cheek with beard	15.2 ± 3.0 ml min^{-1} per 100 g tissue	(Sejrsen 1969)
Capillary perfusion pressure (nail-fold capillaries)		
Ascending limb	35.3 ± 6.5 torr	(Stüttgen et al. 1989)
Descending limb <?1>	20.8 ± 5.6 torr	(Stüttgen et al. 1989)
	16–21 torr	(Hahn et al. 1998)
Capillary pulse amplitude	2–5 torr	(Hahn et al. 1998)

[a]100 g subpapillary dermis – 5000 cm^2 skin area (Coleman et al. 1986)
[b]100 g skin tissue – 850 cm^2 skin area

Capillary perfusion pressure (forehead capillaries), (Agache et al. 1993) (Table 3):

3.11 Skin Lymphatics

Lymphatic flow rate (dorsum foot)	10.3 ± 4.1 μm s^{-1}	(Franzeck et al. 1996)
Intralymphatic pressure (dorsum foot)		(Spiegel et al. 1992)
Subject lying	3.9 ± 4.2 torr	
Subject sitting	9.3 ± 3.0 torr	

3.12 Circadian Rhythms (Solar Time)

See Table 4.

Table 3 Capillary perfusion pressure (Tur et al. 1983)

	Children	Young adults	Elderly
Capillary systolic pressure (csp)	25 ± 4 torr	65 ± 8 torr	150 ± 10 torr
Ratio csp/arterial pressure (arm)	42 %	42 %	54 %
Diastolic pressure	15 torr	18 torr	16 torr
Arterioles compliance index (▶ Sect. 2)	6.0	3.5	1.8
Skin blanching pressure	30 torr		(Agache et al. 1993)
Red blood cells velocity (nail-fold capillaries)	0.7–1.1 mm/s		(Hahn et al. 1998)
At 23 °C	0.65 ± 0.27 ($n = 20$)		(Gasser and Buhler 1992)
After warming	0.87 ± 0.30 ($n = 20$)		(Gasser and Buhler 1992)
After cooling	0.21 ± 0.08 ($n = 20$)		(Gasser and Buhler 1992)
Vasomotion frequency	6–10 min^{-1} (∀ waves); 1–2 min^{-1} (∀ waves)		(Kastrup et al. 1989)
Cutaneous intravascular partial			(Hansen et al. 1980)
pressure (forearm, 44 °C)			
O_2	64.3 ± 18.4 torr (n = 10)		
CO_2	46.8 ± 3.6 torr (n = 10)		
Transcutaneous oxygen partial			▶ Chaps. 57, "Carbon Dioxide Transcutaneous Pressure" and ▶ 58, "Transcutaneous Oxygen Pressure"
pressure ($tcPO_2$) at 44 °C			
Chest	80 torr		
Dorsum foot	72 torr		
Forearm	70 torr		
Other body sites, variation with sex and age			▶ Sect. 2.2
Transcutanous oxygen index			(Versmold et al. 1979)
(TCI) = $tcPO_2/PaO_2$			
Premature	−1		
Child	−0.9		
Adult	−0.8		
Mouth-skin (forearm) transit time			(Hansen et al. 1980)
O_2	51 s		
CO_2	61 s		
N2	94 s		
He	52 s		
$tcPO_2$ decreasing rate under			
arterial occlusion (forearm)			
At 44 °C	130 torr min^{-1}		
At 37 °C	90 torr min^{-1}		(Severinghaus et al. 1978)
Cutaneous veins filling time (plethysmography)	35 ± 12 s		

Table 4 Circadian rhythms (solar time) of the skin biometrologic parameters

Event	Max. by	Min. by	Site	Reference
Stratum corneum renewal time	17 h	09 h	Forearm	(Takahashi et al. 1987)
Sweating threshold	18 h			(Crockford et al. 1970)
Growth of nails	12 h			(Orentreich et al. 1979)
TEWL	24 h	12 h	Forehead	(Clarys et al. 1997)
TEWL	18 h	06 h	Forearm	(Clarys et al. 1997)
TEWL (95 % c.i.)	6.00 ± 4.30 h		Forearm	(Le Fur et al. 2001)
TEWL (95 % c.i.)	11.38 ± 2.30 h		Face	(Le Fur et al. 2001)
Skin temperature	23 h	10 h	Forehead	(Le Fur et al. 2001)
Skin temperature (95 % c.i.)		0.48 ± 3.50 h	Forearm	(Le Fur et al. 2001)
Skin temperature	24 h	14 h	Forearm	(Le Fur et al. 2001)
Skin temperature	02 h	12 h	Shin	(Le Fur et al. 2001)
pH	14 h	02 h	Forearm	(Le Fur et al. 2001)
pH	11 h	24 h	Shin	(Le Fur et al. 2001)
pH	Morning	Afternoon	Axilla	(Burry et al. 2001)
Sebum casual level (95 % c.i.)	13.18 ± 3.30 h		Forehead	(Le Fur et al. 2001)
Sebum casual level	13.30–15.30 h	05.30 h	Forehead	(Downing et al. 1981)

References

This list includes those publications not cited in preceding chapters. There are cross-references in this chapter to references cited elsewhere.

Achten G, Parent D. The normal and pathologic nail. Int J Dermatol. 1983;22:556–65.

Agache P, De Rigal J and Leveque JL. Influence of an external pressure on skin microcirculation. In: Boccalon H, editor. Vascular medicine. Amsterdam: Excerpta Medica; 1993. p. 527–33.

Anderson RL, Cassidy JM. Variations in physical dimensions and chemical composition of human stratum corneum. J Invest Dermatol. 1973;61:30–2.

Atkins EDT, Keller A. Structure of fibrous biopolymers. London: Butterworths; 1974.

Baker H, Kligman AM. Technique for estimating turnover time of human stratum corneum. Arch Dermatol 1967; 95:408–411.

Banchereau J, Steinman RM. Dendritic cells and the control of immunity. Nature 1998;392:245–252.

Bartolone J, Doughty D, Egelrud T. A non-invasive approach for assessing comeocyte cohesion: immunochemical detection of desmoglein 1. J Invest Dermatol. 1991;96:596.

Barton SP, Polack DR. Surface contour: variability, significance and measurement. In: Marks R, Barton SP, Edwards C, editors. The physical nature of the skin. Lancaster: MTP Press; 1988. p. 23–30.

Bauer J, Bahmer FA, Wörl J, Neuhuber W, Schuler G, Fartasch M. A strikingly constant ratio exists between Langerhans cells and other epidermal cells in human skin. A stereologic study using the optical dissector method and the confocal laser scanning microscope. J Invest Dermatol. 2001;116:313–8.

Berkow SG. Values of surface area proportions in the prognosis of cutaneous burns and scalds. Am J Surg. 1931;11:315.

Black MM. A modified radiographic method for measuring skin thickness. Br J Dermatol. 1969;81:661–6.

Blank I.H. : *Factors which influence the water content of the S.C;* J. Invest. Dermatol., 1952, 18, 433–440

Blank IH, Moloney J, Emslie AG, Simon I, Apt C. The diffusion of water across the stratum corneum as a function of its water content. J Invest Dermatol, 1984, 82:188–194.

Blume U, Ferracin J, Verschoore M, Czernielewski JM, Schaefer H. Physiology of the vellus hair follicle: hair growth and sebum excretion. Br J Dermatol 1998;124:21–28.

Bollinger A, Jäger K, Sgier F, Seglias J. Fluorescence microlymphography. Circulation. 1981; 64(6): 1195–2000.

Braun-Falco O, Rupec M. Some observations on dermal collagen fibrils in ultra-thin sections. J Invest Dermatol. 1964;42:15–9.

Braverman IM, Fonferko E. Studies in cutaneous aging: I. The elastic fiber network. J Invest Dermatol. 1982;78:434–43.

Braverman IM, Keh-Yen A. Ultrastructure of the human dermal microcirculation II. The capillary loops of the dermal papillae. J Invest Dermatol. 1977;68:44–52.

Burry J, Coulson HF, Roberts G. Circadian rhythms in axillary skin surface pH. Int J Cosmet Sci. 2001;23:207–10.

Cardot JC, Bazin R, Baud M, Agache P, Bidet R. Etude de la microcirculation cutanée par diffusion épicutanée du xénon 133. C.R. Soc Biol. 1977;171:340–4.

Carpentier PH, Maricq HR. Microvasculature in systemic sclerosis. Rheum Dis Clin N Am. 1990;16:75–91.

Chapman D. The anchoring strengths of various chest hair root types. Clin Exp Dermatol. 1992;17:421–23.

Christensen MS, Nacht S, Kantor SL, Gans EH. A Method for measuring desquamation and its use for assessing the effects of some common exfoliants. J Invest Dermatol 1978;71:289–294.

Clarys P, Manou I, Barel A. Relationship between anatomical site and response to halcinonide and methyl nicotinate studied by bioengineering techniques. Skin Res Technol. 1997;3:161–8.

Coleman LS, Dowd GSE, Bentley G. Reproducibility of tcPO2 measurements in normal volunteers. Clin Phys Physiol Meas. 1986;7:259–63.

Corcuff P, Bertrand C, Lévêque JL: Morphometry of human epidermis in vivo by real-time confocal microscopy. Arch Dermatol Res 1993; 285:475–481

Cotter JD, Patterson MI, Taylor NAS. The topography of eccrine sweating in humans during exercice. Eur J Appl Physiol. 1995;71:549–54.

Crockford GW, Davies CTM, Wiener LS. Circadian changes in sweat threshold. J Physiol. 1970;207:26–7.

Cunliffe WJ, Perera WHD, Thackray P, Williams M, Forster RA, Williams SM. Pilo-sebaceous duct physiology: observations on the number and size of pilosebaceous ducts in acne vulgaris. Br J Dermatol. 1976;95:153–6.

Dawber RPR, de Berker D, Wojnarowska F. Disorders of hair. In Champion RH et al. (eds) Rook, Wilkinson, Ebling Textbook of Dermatology, 6th edition, 1998, pp 2869–2974

Denda M, Sato J, Tsuchiya T, Elias PM, Feingold KR. Low humidity stimulates epidermal DNA synthesis and amplifies the hyperproliferative response to barrier disruption: implication for seasonal exacerbations of inflammatory dermatoses. J Invest Dermatol. 1998;111:873–8.

de Rigal J, Losch MJ, Bazin R, Camus C, Sturelle C, Descamps V, Lévêque JL. Near infra-red spectroscopy: A new approach to the characterization of dry skin. In: IFSCC. Yokohama : IFSCC, 1992;3:1131–1146.

Downing DT, Stewart ME, Strauss JS. Estimation of sebum production rates in man by measurement of the squalene content of skin biopsies. J Invest Dermatol. 1981;77:358–60.

Du Bois D, du Bois EF. A formula to estimate the approximate surface area if the weight and height be known. Arch Intern Med. 1916;17:863–71.

Ebling FJ, Rook A. Hair. Cyclic activity of the follicle. In: Rook A, Wilkinson DS, Ebling FJG, editors. Textbook of dermatology. 3rd ed. Oxford: Blackwell; 1979. p. 1743–46.

Ebling FJ, Rook A. Hair. Development and distribution of hair follicles. In: Rook A, Wilkinson DS, Ebling FJG, editors. Textbook of dermatology. 3rd ed. Oxford: Blackwell; 1979. p. 1733–35.

Edwards C, Marks R : Methods to determine the desquamation rate. In Serup J & Jemec GBE (eds) Handbook of non-invasive methods and the skin. CRC Press, Boca Raton, 1995, pp 143–148.

Elias PM : Epidermal lipids, barrier function, and desquamation. J Invest Dermatol 1983 80: 44s–49s

Finlay AY, Frost P, Keith AD et al. An assessment of factors influencing flexibility of human fingernails. Br J Dermatol. 1980;103:357–365.

Fischer LB, Maibach HI. The effect of corticosteroids on human epidermal mitotic activity. Arch Dermatol. 1971;103:39–44.

Franzeck UK, Fisher M, Costanzo U, Herrig I, Bollinger A. Effect of postural changes on human lymphatic capillary pressure of the skin. J Physiol. 1996;494:595–600.

Frost P, van Scott EJ. Ichthyosiform dermatoses. Classification based on anatomic and biometric observations. Arch Dermatol. 1966;94:113–26.

Galand P and Degraef C. Cyclin/PCNA immunostaining as an alternative to tritiated thymidine pulse labeling for marking S phase cells in paraffin sections from animal and human tissues. Cell. Tissue. Kinet, 1989, 22, 383–392.

Gasser P, Buhler FR. Nailfold microcirculation in normotensive and essential hypertensive subjects, as assessed by video-microscopy. J Hypertens. 1992;10:83–6.

Guarrera M, Semino MT, Rebora A. Quantitating hair loss in women: a critical approach Dermatology 1997;194: 12–16.

Hahn M, Heubach T, Steins A, Jünger M. Hemodynamics in nailfold capillaries of patients with systemic scleroderma: synchronous measurements of capillary blood pressure and red blood cell velocity. J Invest Dermatol. 1998;110:982–5.

Hansen TN, Sonoda Y, McIlroy MB. Transfer of oxygen, nitrogen, and carbon dioxide through normal adult human skin. J Appl Physiol. 1980;49:438–43.

Hayashi S, Miyamoto I, Takeda K. Measurement of human hair growth by optical microscopy and image analysis. Br J Dermatol 1991;125:123–129.

Helmdach M, Thielitz A, Roepke KE, Gollnick H. Age and sex variation in lipid composition of human fingernail plates. Skin Pharmacol Appl Skin Physiol. 2000;13: 111–9.

Holbrook KA, and Odland GF. Regional differences in the thickness (cell layers) of the human Stratum corneum: an ultrastructural analysis. J Invest Dermatol 62: 415–422. 1974.

Hunter R, Pinkus H, Steele CH. Examination of the epidermis by the strip method. III The number of Buatin cells in the human epidermis. J Invest Dermatol. 1956;27:31–4.

Jani M. Le mécanisme de l'excrétion sébacée chez l'homme (The mechanism of sebum secretion in man). Thesis of "Life Sciences and Healthcare", Besançon, 1992, N°92014.

Jansen IH, Hojyo-Tomoko MT, Kligman AM. Improved fluorescence staining technique for estimating turnover of the human stratum corneum. Br J Dermatol. 1974;90:9–12.

Johnson M, Shuster S. Continuous formation of nail along the bed. Br J Dermatol. 1993;128:277–80.

Johnson M, Shuster S. Determinants of nail thickness and length. Br J Dermatol. 1994;130:195–8.

Johannesson A, Hammar H. Measurement of the horny layer turnover after staining with dansyl chloride: Acta Derm. Venereol 1978;58:76–9

Jouanny P, Schmidt C, Feldmann L, Schmitt J. Capillaroscopie périunguéale: Intérêt dans le diagnostic des maladies systémiques. Presse Med. 1993;22:1256–60.

Kastrup J, Bulow J, Lassen NA. Vasomotion in human skin before and after local heating recorded with laser Doppler flowmetry. Int J Microcirc Clin Exp. 1989;8:205–15.

Kligman AM. Pathologic dynamics of human hair loss. Arch Dermatol. 1961;83:175–8.

Knaggs HE, Holland DB, Morris C, Wood EJ, Cunliffe WJ. Quantification of cellular proliferation in acne using the monoclonal antibody Ki67. J Invest Dermatol. 1994;102:89–92.

Knip A S. Measurement and regional distribution of functioning eccrine sweat glands in male and female caucasians. Hum Biol. 1969;41:380.

Le Fur I, Reinberg A, Lopez S, Morizot F, Mechkouri M, Tschachler E. Analysis of circadian and ultradian rhythms of skin surface properties of face and forearm of healthy women. J Invest Dermatol. 2001;117:718–24.

Lever WF, Schaumburg-Lever G (eds) Histopathology of the skin. 6th ed. Lippincott, Philadelphia, 1983, p 655.

Leveque JL. Water–keratin interactions. In: Elsner P, Berardesca E, Maibach HI, editors. Bioengineering of the skin: water and the stratum corneum. Boca Raton: CRC Press; 1994. p. 13–22.

Long CC, Finlay AY. The finger-tip unit: a new practical measure. Clin Exp Dermatol. 1991;16:444–7.

Lund CC, Browder NC. The estimation of the area of burns. Surg Gynecol Obstet. 1944;79:352–8.

Lundström A, Serre G, Haftek M, Egelrud T. Evidence for a role of corneodesmosin, a protein which may serve to modify desmosomes during cornification, in stratum corneum cell cohesion and desquamation. Arch Dermatol Res 1994;286:369–375.

Mahler F, Nagel G, Saner H, Kneubühl F. In vivo comparison of the nailfold capillary diameter as determined by using the erythrocyte column and FITC-labelled albumin. Int J Microcirc Clin Exp. 1983;2:147–55.

Marks R, Berth-Jones J, Black DR, Gaskell SA. The effects of photoaging and intrinsic aging on epidermal structure and function. G Ital Chir Dermatol Oncol. 1987;2 (3/4):252–63.

Martineaud JJ, Seroussi 5. Physiologie de la circulation cutantée. Paris: Masson; 1977.

Mavon A. Energie libre de surface de la peau humaine in vivo: une nouvelle approche dela séborrhée. Besançon: Thèse Sciences de la Vie et de la Santé; 1997. p. N°259706.

Mommers JM, Goossen JW, van De Kerkhof PC and van Erp. Novel functional multiparameter flow cytometric assay to characterize proliferation in skin. Cytometry, 2000, 42, 43–49.

Orentreich N, Markowsky J, Vogelman JH. The effect of aging on the rate of linear nail growth. J Invest Dermatol. 1979;73:126–30.

Ott A, Stüttgen G. Microcirculation in psoriasis. Acta Derm-Venereol. 1984;1135:90–102.

Oxholm A, Oxholm P, Staberg B. Reduced density of T6-positive epidermal Langerhans cells in uninvolved skin of patients with psoriasis. Acta Derm Venereol. 1987;67:8–11.

Petersen JS, Petersen S, Serup J. High-frequency ultrasound measurement of dermis and subcutaneous fat in the newborn infant. Skin Res Technol. 1995;1:86–9.

Pittet PG, Halliday D, Bateman PE. Site differences in the fatty acid composition of subcutaneous adipose tissue of obese women. Br J Nutr. 1979;42:57–61.

Plewig G, Scheuber E, Reuter B, Waidelich W: Thickness of comeocytes. In Marks R & Plewig G (eds) Stratum Corneurn. Springer-Verlag, Berlin Heidelberg, 1983, pp 171–174.

Pope FM. Dermis. In Champion RH, Burton JL, Burns DA, Breathnagh SM (eds) Textbook of Dermatology: Blackwell 6th ed. 1998, pp 59–92

Prasad A, Dunnill GS, Mortimer PS, MacGregor GA. Capillary rarefaction in the forearm skin in essential hypertension. J Hypertens. 1995;13:265–8.

Quaglino D, Bergamini G, Boraldi F, Pasquali Ronchetti I. Ultrastructural and morphometrical evaluations on normal human dermal connective tissue – the influence of age, sex and body region. Br J Dermatol. 1996;134:1013–22.

Querleux B, Cornillon C, Jolivet O, Bittoun J. Anatomy and physiology of subcutaneous adipose tissue by in vivo magnetic resonance imaging and spectroscopy: relationships with sex and presence of cellulite. Skin Res Technol. 2002;8:118–24.

Roberts D, Marks R. The determination of regional and age variations in the rate of desquamation: a comparison of four techniques. J Invest Dermatol 1980;74:13–16.

Saitoh M, Uzuka M, Sakamoto M. Human hair cycle. J Invest Dermatol. 1970;54:65–81.

Sejrsen, P. Blood flow in cutaneous tissue in man studied by washout ofxenon-133. Circ Res. 1969;25: 215–29.

Severinghaus JW, Stafford M, Thunstrom AM. Estimation of skin metabolism and blood flow with tcpO2 and tcpCO2 electrodes by cuff occlusion. Acta Anaesth Scand. 1978;68(Suppl):9–15.

Shuster S, Raffle EJ, Bottoms E. Quantitative changes in skin collagen in morphoea. Br J Dermatol. 1969;82:456–9.

Spalteholz W. Blutgefäss in der Haut. In: Jadassohn J, editor. Handbuch der Haut- und Geschlechtskrankheiten. Berlin: Springer; 1927. p. 379–433.

Spiegel M, Vesti B, Shore A, Franzeck UK, Becker F, Bollinger A. Pressure of lymphatic capillaries in human skin. Am J Physiol. 1992;262:H1208–10.

Stüttgen G, editor. Die normale und pathologische Physiologie der Haut. Stuttgart: Fischer; 1965. p. 259.

Stüttgen G, Ott A, Flesch U. Measurement of skin microcirculation. In: Lévèque LJ, editor. Cutaneous investigation in health and disease. New York: Marcel Dekker; 1989. p. 359–84.

Szabo G. The number of eccrine sweat glands in human skin. In: Montagna W, Ellis RA, Silver AF, editors. Advances in biology of the skin. Eccrine sweat glands and eccrine sweating, vol 3. Oxford: Pergamon Press; 1962. p. 1–5.

Tagami H. Quantitative measurements of water concentration of the stratum corneum in vivo by high-frequency current. Acta Derm Venereol. 1994;185(Suppl):29–33.

Takahashi M, Black D, Hughes B, Marks R. Exploration of a quantitative dansyl chloride technique for measurement of the rate of desquamation. Clin Exp Dermatol. 1987;12:246–49.

Therkildsen P, Haedersdal M, Lock-Andersen J, de Fine OF, Poulsen T, Wulf HC. Epidermal thickness measured by light microscopy: a methodological study. Skin Res Technol. 1998;4:174–9.

Timar JF, Soos G, Szende B, Horvath A. Interdigitation index: a parameter for differentiating between young and older skin specimens. Skin Res Technol. 2000;6:17–20.

Timpl R, Brown JC. Supramolecular assembly of basement membranes. Bioessays. 1996;18:123–32.

Tur E, Tur M, Maibach HI, Guy RH. Basal perfusion of the cutaneous microcirculation: measurements as a function of anatomic position. J Invest Dermatol. 1983; 81:442–6.

Uitto J, Olsen DR, Fazio MJ. Extracellular matrix of the skin: 50 years of progress. J Invest Dermatol. 1989;92 suppl 41:61–77.

Van Neste D. Une technique simple pour l'étude de la cuticule de la tige pilaire en microscopie optique. Ann. Dermatol. Venereol. 1985;112:231–233.

Van Scott EJ, Ekel TM. Geometric relationships between the matrix of the hair bulb and its dermal papilla. J Invest Dermatol 1958;31:281–285.

Versmold HT, Tooley WH, Severinghaus JW. Increase of skin O2 diffusion resistance with birthweight. Birth Defects: Original Article Series, Vol XV N° 4, The National Foundation 1979, pp 271–272.

Wallace AB. Exposure treatment of burns. Lancet. 1951;1:501–4.

Weinstein GD, Boucek RJ. Collagen and elastin of human dermis. J Invest Dermatol. 1960;35:227–9.

Ya-Xian Z, Suetake T, Tagami H : Number of cell layers of the stratum corneum in normal skin – relationship to the anatomical location on the body, age, sex and physical parameters. Arch Dermatol Res 1999; 291:555–559.

Zelickson AS, Mottaz JH. Epidermal dendritic cells: a quantitative study. Arch Dermatol. 1968;98:652–9.

Main Skin Physical Constants

157

Pierre Agache

Contents

This chapter was originally published under the ISBN 978-3-540-01771-4 with the following book title Measuring the Skin. The content has not been changed.

Pierre Agache: deceased.

P. Agache (✉)
Department of Dermatology, University Hospital of Besançon, Besançon, France
e-mail: aude.agache@free.fr; ferial.fanian@chu-besancon.fr; ferial.fanian@cert-besancon.com

P. Humbert et al. (eds.), *Agache's Measuring the Skin*,
DOI 10.1007/978-3-319-32383-1_157

Keywords

Chemicophysical constants • Connective tissue fibers in vitro • Corneocyte • Corneodesmosome • Dermis and subcutis • Elastic phase • Electrical constants • Hair • Mass density in vitro • Nails • Optical constants • Sebum • Skin • Stratum corneum • Sweat • Thermal constants • Ultrasound (25 MHz) attenuation • Ultrasound (25 MHz) impedance • Ultrasound (25 MHz) velocity • Viable epidermis • Whole skin in vitro • Whole skin in vivo • Skin acoustic constants • Skin Mecahnical constants • Skin optical constants • Skin thermal constants • Skin electrical constants • Skin chemicophysical constants

1 Mass Density In Vitro (kg/dm^3)

Whole skin	1.176	Edwards (1988)
Epidermis	1.106	Edwards (1988)
Dermis	1.274	Edwards (1988)
Stratum corneum	1.30 and	Weigand et al. (1974)
	1.20 ± 0.57 (±SEM)	Anderson and Cassidy (1973)
Hair shaft	2.32 (60 % relative humidity)	
Nail	1.115	Orentreich et al. (1979)
	1.33	Finlay et al. (1980)
Sebum	0.910 ± 0.048	Butcher et al. (1949)
Subcutaneous fat	0.9007 at 37 °C	▶ Chap. 67, "Subcutis Metrology"
Sweat	<1,006	

2 Acoustic Constants

2.1 Ultrasound (25 MHz) Velocity

Epidermis + dermis	−1600 m s^{-1}	Edwards (1988), Escoffier et al. (1986)
Epidermis	1500 m s^{-1}	Edwards (1988)
Dermis	1660 m s^{-1}	Edwards (1988)
Adipose tissue	1450 m s^{-1}	
Stratum corneum	−2600 m s^{-1}	Agache and Humbert (2004)
Whole skin		
Forearm	1566 ± 26 m s^{-1}	Guittet (1997)
Face	1598 ± 19 m s^{-1}	Escoffier et al. (1986)
Breast	1640 ± 16 m s^{-1}	Escoffier et al. (1986)
Whole nail	2459 m s^{-1}	Jemec and Serup (1988)
Nail dorsal	3103 m s^{-1}	Jemec and Serup (1988)
Nail ventral	2125 m s^{-1}	Jemec and Serup (1988)

2.2 Ultrasound (25 MHz) Impedance

1 Rayleigh $= 10^6$ kg m^{-2} s^{-1}		
Whole skin	1.863 Rayleigh	Edwards (1988)
(With respect to hydration)	Rayleigh 1.5–1.9	
Epidermis	1.659 Rayleigh	Edwards (1988)
Dermis	2.115 Rayleigh	Edwards (1988)
Stratum corneum	1.534 Rayleigh	Edwards (1984)

2.3 Ultrasound (25 MHz) Attenuation

Whole skin	2.95 ± 0.46 dB cm^{-1} MHz^{-1}	Guittet (1997)
Dermis	4 ± 1 dB cm^{-1} MHz^{-1}	Querleux (1994)

3 Mechanical Constants

3.1 Whole Skin In Vivo (Elastic Phase)

Elastic strain limit	25 %	
Volar forearm	10 %//and 27 % ζ Langer's lines	Ehring (1960)
Quasi-static Young's modulus in vivo (extension, calf)		
//to Langer's lines	1–4 MPa	Wijn et al. (1981)
ζ Langer's lines	0.06–0.25 MPa	Wijn et al. (1981)
Mechanical anisotropy coefficient (A) 16.0		Wijn et al. (1981)
Young's modulus at elastic limit (posterior calf)		
//to Langer's lines	0.22 MPa	Manschot et al. (1986)
ζ Langer's lines	0.6 MPa	Manschot et al. (1986)
Tangent modulus	3.0 MPa	Vasselet et al. (1987)
(extension 1 %/s, forearm)		
Tangent modulus (suction)	0.8 MPa	Panisset et al. (1993,1994)

	Male	Female	
Volar forearm	0.11 MPa	0.12 MPa	Barel et al. (1998)
Forehead	0.21 MPa	0.25 MPa	
Volar forearm	0.14 MPa	0.16 MPa	Tokumura et al. (1999)
Forehead	0.23 MPa	0.27 MPa	

Tangent modulus (torsion)	1.1 MPa	Escoffier et al. (1989)
Dynamic modulus	600 MPa	Takahashi et al. (1981)
Shear wave (5600 Hz) propagation velocity		Bader et al. (1983)
Volar forearm ($n = 34$)		
//arm axis	50 ms^{-1}	
ζ arm axis	40–50 ms^{-1}	
Breast ($n = 20$)		
//breast contour	62.0 ± 2.2 ms^{-1}	
ζ breast contour	36.6 ± 1.4 ms^{-1}	
Shear modulus (volar forearm)	1–2 kPa	Bader et al. (1983)
Stiffness coefficient (E/σ) (calf)	0.244	Wijn et al. (1981)
Poisson's coefficient	0.3–0.4	see ▶ Chap. 95, "Skin Mechanical Function" sect. 2.4
Ballistometry		
Restitution coefficient		Tosti et al. (1977)
Forehead	0.5	
Dorsum of hand	0.6	
Thigh	0.7	
Absorption coefficient	0.4–1.1 with respect to age	Tosti et al. (1977)

3.2 Whole Skin In Vitro

In saline (▶ Chap. 95, "Skin Mechanical Function", Ref. 30)	
Elongation <40 % (elastic phase) Young's modulus	<7 kPa
Elongation 40 %–70 % yield phase modulus	510 kPa
Rupture: elongation 90 %	
In air (▶ Chap. 95, "Skin Mechanical Function", Refs. 32 and 33)	
Young's modulus:	7–50 MPa

3.3 Connective Tissue Fibers In Vitro

Young's modulus		
Elastic fibers	−0.3 MPa	Burton et al. (1968) Caro et al. (1978)
Collagen fibers	−100 MPa	Caro et al. (1978)
	−1000 MPa	Lapière et al. (1988), Burton (1968)

3.4 Stratum Corneum

3.4.1 Stratum Corneum

In vivo dynamic (sonic) Young's modulus	12.4–13.4 MPa	Weigand et al. (1974)
In vitro strain tangent modulus (volar forearm)	50–210 MPa	Koutroupi et al. (1990), Ferguson et al. (1980), Vasselet (1989)
In vitro strain elastic limit (volar forearm)	10 %	Agache and Humbert (2004)
Resistance to stripping (kPa)		Marks et al. (1972)

1. Surface layer

	Male	Female
Forearm	20.07 ± 3.20	17.15 ± 3.49
Wrist	22.23 ± 4.41	20.21 ± 3.94
Back	15.30 ± 2.18	15.30 ± 2.18

2. ≥18th strip: cohesion twice as strong

		Marks (1986)
Resistance to vertical peeling (1 m min^{-1}) (Leveque 1994):		
	Force (N)	Pressure (kPa) as calculated for a 15 × 70 mm area
February	2.69 ± 0.15	2.56 ± 0.14
August	1.65 ± 0.16	1.57 ± 0.15

3.4.2 Corneocyte

In vitro (in water) elastic modulus (volar forearm)	450 MPa	Lévêque et al. (1988)

3.4.3 Corneodesmosome

Stress at rupture (in water) (volar forearm)	26 GPa	Lévêque et al. (1988)

3.5 Hair

Hair shaft mechanical parameters when elongated at a constant rate (25 %/min) at 20 °C (Pierard et al. (1993)) (Table 1):

Table 1 Hair shaft mechanical parameters when elongated at a constant rate (25 %/min) at 20 C (Piérard et al. 1993)

Relative humidity	Young's modulus (kPa)	σ at elastic limit (kPa)	ε at elastic limit (%)	σ at yield limit (kPa)	Post-yield modulus (kPa)	σ at rupture (kPa)	ε at rupture (%)
30 %	5100	51	1.02	110	416	196	40
60 %	4500	45	1	91	425	190	43
85 %	3300	30	0.93	65	442	186	48

σ, stress; ε, strain

3.6 Nails

Young's modulus (GPa)	Deflection method	Sound velocity method	Finlay et al. (1980)
//keratin fibers (i.e., ⊥ finger axis)	4.3 ± 0.6 ($n = 7$)	4.3 ± 0.4 ($n = ?$)	
ζ keratin fibers (i.e., //finger axis)	4.0 ± 0.7 ($n = 2$)	2.1 ± 0.3 ($n = ?$)	

4 Optical Constants

Non-specular reflection at the skin surface	<8 %	Anderson et al. (1981)
Skin reflectance (for a perpendicular beam of any wavelength)	4 %–7 %	Anderson and Parrish (1981)
Wavelength emitted by the skin at 32–36 °C	$\lambda \cong 10.5$ μm (i.e., IR ray)	
Skin emittance (in IR)		
	$\varepsilon = 0.97$ for $7 < \lambda < 12.5$ μm	
	$\varepsilon = 0.7$ for $2 < \lambda < 5.5$ μm	
Refractive index		
Stratum corneum	1.52–1.54	Greger (1996), See ▶ Chap. 158, "Physical, Biological and General Constants of the Skin"
When strongly hydrated	1.33	Agache and Humbert (2004)
	Between 1.36 and 1.50 from Optical Coherence Tomography	Knüttel et al. (2000)
Viable epidermis	1.39	Hulsbergen et al. (1977)
Scattering coefficient		Knüttel et al. (2000)
Stratum corneum	1–1.5	
Epidermis volar forearm	1.5–2	
Palm		
Basal layer	4–5	

(*continued*)

Granular layer	6–7	
Upper dermis	8–10	
Transmittance beyond dermis	$1300 > \lambda > 600$ nm, and <1 % of received light	Anderson and Parrish (1981)

5 Thermal Constants

Current skin temperature (Other body sites, (Agache 2004a))	32 °C (extremities) to 36 °C (forehead) see ▶ Chap. 123, "Skin Thermal Imaging" sect. 1.2, ▶ table 1	Houdas et al. (1977)
		Houdas et al. (1977)
Radiant fraction of the skin surface area (relative to body surface area)		▶ Chap. 119, "Thermal Exchanges in Man"
Sitting or squatting	0.7	
Standing	0.8	
Saturating watervapor pressure at skin temperatures	5.8–6.6 kPa	Houdas et al. (1977)
Energy produced by evaporation of 1 g sweat	2.42 kJ	
Thermal conductivity (K)		see ▶ Chap. 158, "Physical, Biological and General Constants of the Skin"
Of skin in vivo (volar forearm)	0.2–0.6 W m^{-1} °C^{-1}	Dittmar et al. (1991)
	0.2 W m^{-1} °C^{-1} (ischemia by tourniquet)	Dittmar et al. (1991)
	0.9 W m^{-1} °C^{-1} (intense vasodilation)	Dittmar et al. (1991)
Of stratum corneum free water	0.6 W m^{-1} °C^{-1}	see ▶ Chaps. 29, "Physical Methods to Measure Stratum Corneum Water Content In Vivo" and ▶ 30, "Stratum Corneum Dynamic Hydration Test"
Of stratum corneum bound water	0.18 W m^{-1} °C^{-1}	see ▶ Chaps. 29, "Physical Methods to Measure Stratum Corneum Water Content In Vivo" and ▶ 30, "Stratum Corneum Dynamic Hydration Test"
Of adipose tissue	0.0278 W m^{-1} °C^{-1}	
Thermal inertia (KDC)	cal^2 cm^{-4} °C^{-2} s^{-1}	Houdas et al. (1977)
Skin	90×10^{-5}–400×10^{-5} with respect to the degree of vasodilation	
Skin (ischemia)	90×10^{-5}	see ▶ Chap. 158, "Physical, Biological and General Constants of the Skin"

(*continued*)

Skin in vitro (see Annex 5)	55×10^{-5} (dry skin) to 75×10^{-5} (wet skin)	
Adipose tissue	22×10^{-5}–32×10^{-5} (with respect to temperature)	
Thermal skin–atmosphere		Houdas and Guieu (1977)
convection coefficient		
No wind	3.7–6.0 W m^{-2} °C^{-1}	
Wind	8.3 U0.5 W m^{-2} °C^{-1} (U is the wind speed)	
Thermal core–skin convection coefficient		Houdas and Guieu (1977)
By thermal neutrality	12 W m^{-2} °C^{-1}	
In the cold state	6.5 W m^{-2} °C^{-1}	
In the warm state	80–150 W m^{-2} °C^{-1}	

6 Chemicophysical Constants

6.1 Skin Surface

6.1.1 pH

Adults overall, 4.2–6.1 (▶ Chap. 4, "The Skin Surface Ecosystem: A Presentation" sect. 3.1)

Forehead	*n*	Median	5th–95th percentiles	Zlotogorski (1987)
Males	282	4.6	4.0–5.5	
Females	292	4.6	4.0–5.6	
Cheek				
Males	282	5.1	4.2–5.8	
Females	292	5.2	4.2–6.1	

Forearm (volar)	5.4–5.9		Braun-Falco et al. (1986)
	4.5 ± 0.2	$n = 7$	Öhman et al. (1998)
	4.87–5.44	$n = 16$	Yosipovitch et al. (1998)
Forehead	4.93–5.29	$n = 16$	Yosipovitch et al. (1998)
Back (upper)	5.14–5.50	$n = 16$	Yosipovitch et al. (1998)
Shin	4.8–5.5	$n = 16$	Yosipovitch et al. (1998)
Axilla		$n = 20$	Krönauer et al. (2001)
Morning	5.87 ± 0.23		
Evening	5.49 ± 0.23		
Tongue	6.65 ± 0.61	$n = 32$	Yosipovitch et al. (2001)
Bucca	6.68 ± 0.65	$n = 32$	Yosipovitch et al. (2001)
Palate	7.23 ± 0.88	$n = 32$	Yosipovitch et al. (2001)
Lip	6.61 ± 0.60	$n = 32$	Yosipovitch et al. (2001)
Neonates (first day)	7.08 ± 1.70	$n = 44$ (no difference between sites)	Yosipovitch et al. (2000)
Infants	6.6 ± 0.25	$n = 40$	Gfatter et al. (1997)

6.1.2 Surface Energy Parameters

Critical surface wetting tension

Volar forearm	27.5 ± 2.4 dyn/cm	see ▶ Chap. 4, "The Skin Surface Ecosystem: A Presentation" sect. 3.2
Forehead	>50 dyn/cm	see ▶ Chap. 4, "The Skin Surface Ecosystem: A Presentation" sect. 3.2
Free energy		
Volar forearm	38.7 ± 6.4 mJ/m^2	see ▶ Chap. 4, "The Skin Surface Ecosystem: A Presentation" sect. 3.2
Forehead	42.5 ± 3.9 mJ/m^2	see ▶ Chap. 4, "The Skin Surface Ecosystem: A Presentation" sect. 3.2

6.2 Viable Epidermis

Water content	88–99 %	Blank et al. (1984)
	86.4 % (48 mol)	Wilson et al. (1989)
	83 % (0.83 g ml^{-1})	Diridollou et al. (2000)
Resistance to transepidermal O_2 diffusion		Versmold et al. (1979)
Term infants	1.59 ± 0.32 103 atm ml^{-1} min cm^2 ($n = 7$)	
Premature	0.58 ± 0.27 103 atm ml^{-1} min cm^2 ($n = 7$)	
Adults	1.67 ± 0.66 103 atm ml^{-1} min cm^2 ($n = 10$)	
O_2 solubility "in skin" (assumed to equal that of water)		Severinghaus et al. (1978)
At 45 °C	0.0219 ml g^{-1} atm^{-1}	
At 37 °C	0.0238 ml g^{-1} atm^{-1}	
CO_2 solubility "in skin" at 45 °C and 40 Torr:		Severinghaus et al. (1978)
1.48 ml g^{-1} atm^{-1} (estimated) (0.47 the value in blood, 3 times the value in water)		

6.3 Dermis and Subcutis

Mean water concentration	88 %	Blank et al. (1984)
Interstitial pressure (limbs)	0.18–0.27 Torr	McMaster (1946)
	1.10–1.67 Torr after	
	>15 min venous occlusion	
Suction blister oncotic pressure	4.70–6.84 Torr	Schwindt et al. (1998)

(*continued*)

Interstitium/blood partition coefficient (skin is likened to water)		Severinghaus et al. (1978)
O_2	8 = 0.90	
CO_2	8 = 0.47	
Xenon	8 = 0.7 (adipose tissue 8 = 10)	Sejrsen (1969)
O_2 and CO_2 solubility "in skin"		See sect. 6.2

6.4 Stratum Corneum

6.4.1 Water Content

In vitro, dry stratum corneum: strongly bound water		
5 % of dry stratum corneum		Gournay et al. (1995), Gilard et al. (1998)
7 % of dry stratum corneum		Hansen and Yellin (1972), Leveque et al. (1987)
In vitro, saturated stratum corneum		
Total water	30–50 % of saturated stratum corneum	Warner and Lilly (1994)
Bound water	25–40 % of saturated stratum corneum	Warner and Lilly (1994)
	20–30 % of saturated stratum corneum	Walkley (1972), Inoue et al. (1986)
Increase in volume when in water:	>100 % (hair shaft: <5 %)	Fluhr et al. (2000)
stratum corneum		
In vivo		
Water content in uppermost stratum corneum	5.2 % (ambient air at 22 °C and 31 % RH)	Diridollou et al. (2000)
	22 % (ambient air at 31 °C and 40 % RH)	Wilson and Maibach (1989)
	10–30 % in the 1/3 upper layers (4–20 % in case of "dry skin")	Hensen et al. (1980)
Water content in the 2/3	30–35 % (20–35 % in case of "dry skin")	Hensen et al. (1980)
deeper layers		
Mean water content during bathing	23.7 %	Pirot (1996)

6.4.2 Diffusion Parameters

Water partition coefficient at the skin surface		
Stratum corneum/air	0.413 (if 93 % relative humidity)	Blank et al. (1984)
Stratum corneum/water	0.9	Scheuplein (1980)

(*continued*)

Water partition coefficient at stratum corneum/viable tissue interface		
Stratum corneum/viable tissue	0.162 (if 60 % relative humidity)	Blank et al. (1984)
Stratum corneum intercellular lipid/viable tissue	0.06	Potts and Francoeur (1991)
Water diffusion coefficient	2.15 (0.2–7.7) × 10–9 $cm^2\ s^{-1}$	Schwindt et al. (1998)
	3 × 10–10 $cm^2\ s^{-1}$	Liron et al. (1994)
Forearm	6 × 10–10 $cm^2\ s^{-1}$	Scheuplein (1983)
Forearm	2.54 ± 1.2 × 10^{-9} $cm^2\ s^{-1}$ ($n = 5$)	Burry et al. (2001)
Back	2.34 ± 0.82 × 10^{-9} $cm^2\ s^{-1}$ ($n = 5$)	Burry et al. (2001)
Abdomen	1.38 ± 0.42 × 10^{-9} $cm^2\ s^{-1}$ ($n = 5$)	Burry et al. (2001)
Thigh (Other body sites, see ▶ Chap. 101, "Skin Photoprotection Function", Table 1)	2.37 ± 1.6 × 10^{-9} $cm^2\ s^{-1}$ ($n = 5$)	Burry et al. (2001)
Water permeability coefficient (If 60 % HR)	500 × 10^{-6} cm h^{-1}	Scheuplein (1980)
	21.0 × 10^{-8} cm s^{-1}, or 756 × 10^{-6} cm h^{-1}	Horii et al. (1989)
Permeability coefficients for various products: see ▶ Chap. 106, "In vivo Skin Absorption and Skin", Table 2		
Ethanol in water permeability coefficient (Other permeability coefficients: see ▶ Chap. 106, "In vivo Skin Absorption and Skin", Table 1)	500 × 10^{-6} cm h^{-1}	Scheuplein (1980)
Resistance to transepidermal diffusion (i.e., 1/permeability coefficient) (forearm)		Wu et al. (1983)
O_2	1.79 ± 0.92 atm cm^2 $min{:}1^{-1}$	
CO_2	62.8 ± 28.7 atm cm^2 min ml^{-1}	
N_2	8.49 ± 1.81 atm cm^2 $min{:}1^{-1}$	
Resistance to O_2 transepidermal diffusion at 44 °C (as in $tcPO_2$ measurement)		Versmold et al. (1979)
Premature	0.58 ± 0.27 atm cm^2 min μl^{-1} ($n = 7$)	
Term infants	1.59 ± 0.32 atm cm^2 min μl^{-1} ($n = 7$)	
Adults	1.67 ± 0.66 atm cm^2 min μl^{-1} ($n = 10$)	

6.4.3 Transepidermal Water Loss

Adults			
Forehead	20.1 ± 4.8 g m^{-2} h^{-1}	($n = 16$)	see ▶ Chap. 108, "Transepidermal Water Loss"
	10.34 ± 0.70	($n = 7$ males 20–30 years)	Torp et al. (1975)
	9.39 ± 0.73	($n = 8$ females 20–30 years)	Torp et al. (1975)
Post-auricular	8.35 ± 0.41	($n = 8$) (males 20–30 years)	Torp et al. (1975)
Chest	10.7 ± 1.3	($n = 16$)	see ▶ Chap. 108, "Transepidermal Water Loss"
	4.73 ± 0.26	($n = 8$) (males 20–30 years)	Torp et al. (1975)
Abdomen	9.9 ± 1.8	($n = 16$)	see ▶ Chap. 108, "Transepidermal Water Loss"
	4.40 ± 0.51	($n = 7$) (males 20–30 years)	Torp et al. (1975)

(*continued*)

Adults			
Arm (upper outer)	4.24 ± 0.35	(n = 8 males 20–30 years)	Torp et al. (1975)
	5.07 ± 0.23	(n = 8 males 45–55 years)	Torp et al. (1975)
	4.73 ± 0.45	(n = 7 males 65–80 years)	Torp et al. (1975)
	5.12 ± 0.35	(n = 7 females 20–30 years)	Torp et al. (1975)
Volar forearm	10.4 ± 3.1	(n = 16)	see ▶ Chap. 108, "Transepidermal Water Loss"
Elbow	2.50 ± 0.30	(n = 7) (males 20–30 years)	Torp et al. (1975)
Mid	4.00 ± 0.32	(n = 8) (males 20–30 years)	Torp et al. (1975)
Wrist	7.19 ± 0.39	(n = 7) (males 20–30 years)	Torp et al. (1975)
Back	4.51 ± 0.57	(n = 8) (males 20–30 years)	Torp et al. (1975)
Thigh	4.39 ± 0.32	(n = 7) (males 20–30 years)	Torp et al. (1975)
Calf	9.6 ± 1.8	(n = 16)	see ▶ Chap. 108, "Transepidermal Water Loss"
First day of life			Bork (1977)
Palms	31.3 ± 8.5		
Soles	16.8 ± 4.7		
Back	11.0 ± 2.9		
Abdomen	11.0 ± 3.4		
Forearm	27.5 ± 14.8	(n = 44)	
Children 1–6 years			Yosipovitch et al. (2000)
Volar forearm	6.2 ± 3.5 g m^{-2} h^{-1}	(n = 44) (not different from their parents)	

6.5 Sebum

Surface tension	24.16 ± 1.29 dyn cm^{-1}	Mathot et al. (1976)
Surface free energy	−34 N m^{-2}	Mavon (1997)
Freezing point	15–17 °C	Burton (1970)
Melting point of free fatty acids and triglycerides	20–30 °C	Dünner et al. (1946)
Viscosity at 32 °C	0.855 P	Butcher et al. (1949)
Between 38 °C and 31 °C	η = 4.969–0.047 °C (for details, See chapter 26 sect. 1.2 (Agache 2004b)	

6.6 Sweat

pH	5.0 (moderate sweating) to 7.0 (profuse sweating)	Sato et al. (1991)
	6.55 ± 0.32 (SE)	Shelley et al.(1953)
Osmolality (mOsmol/1)	154 ± 40	Dahlgren and Elsnau (1984)
Cryoscopic delta (°C)	−0.32	
Surface tension	32.2 ± 2.5 mN/m^{-1} (n = 6)	Mavon (1997)
Interface tension sebum-sweat	−1.5 mN/m^{-1}	Mavon (1997)

6.7 Nails

Transonychial water loss			
Median	Range	*n*	
12.4 g m^{-2} h^{-1}	7.9–18.7	10	Jemec et al. (1989)
75 %–25 % percentile interval	10.1–14.7	10	Jemec et al. (1989)
19.4 g m^{-2} h^{-1}	11.7–33.5	21	Rougier et al. (2002)

7 Electrical Constants

7.1 Skin

DC resistance of stratum lucidum/corneum interface, 8700 ± 3500 Ω (n = 50), Zesch et al. (1972)

Current frequency (Hz)	10^2	10^4	10^6	
Dielectric constant				Yamamoto and Yamamoto (1976)
Stratum corneum	31	15.5	6.8	
Viable epidermis	7700	930	80	
Resistivity ρ (Ωm)				Yamamoto and Yamamoto (1976)
Stratum corneum	50 × 10^6	84 × 10^5	79 × 10^3	
Viable epidermis	680	680	170	
Stratum corneum dielectric constant at 10^3 Hz				see ▶ Chaps. 29, "Physical Methods to Measure Stratum Corneum Water Content In Vivo"
Dry	−8			
Very hydrated	−80			

7.2 Hair

Resistivity	10^{12} Ωm	Zviak et al. (1988)

References

Agache P (2004a) Thermometry and remote thermography. In: Handbook of Measuring the skin, 1st edn. Springer, Berlin p. 354–62.

Agache P (2004b) Sebaceous physiology. In: Agache P, Humbert P (eds) Measuring the skin, 1st edn. Springer, Berlin.

Agache P, Humbert P (eds) (2004) Measuring the skin, 1st edn. Springer, Berlin.

Anderson RL, Cassidy JM. Variations in physical dimensions and chemical composition of human stratum corneum. J Invest Dermatol. 1973;61:30–2.

Anderson RR, Parrish JA. The optics of human skin. J Invest Dermatol. 1981;77:13–19.

Bader DL, Bowker P. Mechanical characteristics of skin and underlying tissue in vivo. Biomaterials. 1983;4:305–308.

Barel AO, Lambrecht R, Clarys P. Mechanical function of the skin: state of the art. In: Elsner P, Barel AO, Berardesca E, Gabard B, Serup J, editors. Current problems in dermatology, Skin bioengineering techniques and applications in dermatology and cosmetology, vol. 26. Basel: Karger; 1998. p. 69–83.

Blank IH, Moloney IJ, Emslie AG, Simon I, Apt C. The diffusion of water across the stratum corneum as a function of its water content. J Invest Dermatol. 1984;82:188–94.

Bork K. Physikalische Grundlagen der Blasenbildung. Arch Dermatol Res. 1977;260:217–26.

Braun-Falco O, Korting HC. Der normale pH-Wert der menschlichen Haut. Hautarzt. 1986;7:126–29.

Burry J, Coulson HF, Roberts G. Circadian rhythms in axillary skin surface pH. Int J Cosmet Sci. 2001;23:207–10.
Burton AC. Les parois des vaiseaux sanguins et leurs fonctions. In: Burton AC, editor. Physiologie et Biophysique de la circulation. Paris: Masson; 1968. pp. 63–75.
Burton JL. The physical properties of sebum in Acne vulgaris. Clin Sci. 1970;39:757–67.
Burton A, editor. Physiology and biophysics of the circulation. Chicago: Year Book Medical; 1968.
Butcher EO, Coonin A. The physical properties of human sebum. J Invest Dermatol. 1949;12:249–54.
Caro C, Pedley T, Schroter R, Seed W, editors. The mechanics of the circulation. Oxford: Oxford University Press; 1978.
Dahlgren RM, Elsnau WH. Measurement of skin condition by sonic velocity. J Soc Cosmet Chem. 1984;35:1–19.
Diridollou S, Berson M, Vaillant L, Vabre V, Black D, Lagarde JM, Gall Y, Patat F. Sex- and site-dependent variations in the thickness and mechanical properties of human skin in vivo. Int J Cosmet Sci. 2000;22:421–35.
Dittmar A, Delhomme G, Vernet-Maury E, Pauchard T. Estimation of skin blood flow from the measurement of thermal conductivity. Innov Tech Biol Med. 1991; 12(N°spécial 1):121–37.
Dünner M. Der Einfluss physikalischer Faktoren (Druck, Temperatur) auf die Talgabsonderung des Menschen. Dermatologica. 1946;93:249–71.
Edwards C. The acoustic properties of the epidermis and stratum corneum. In: Marks RM, Barton SP, Edwards C, editors. The physical nature of the skin. Lancaster: MTP Press; 1988. p. 201–7.
Edwards C. The use of high frequency ultrasound to study dimensions and properties of skin. PhD thesis, University of Manchester, Faculty of Technology; 1984.
Ehring F. Die Technik der Vitalmikroskopie an der Haut. Bibl Anat. 1960;1:222–8.
Escoffier C, Querleux B, De Rigal J, Lévêque JL. In vitro study of the velocity of ultrasound in the skin. Bioeng Skin. 1986;2:87–94.
Escoffier C, De Rigal J, Rochefort A, Vasselet R, Lévêque J-L, Agache P. Age-related mechanical properties of human skin: an in vivo study. J Invest Dermatol. 1989;93:353–357.
Ferguson J, Barbenel JC. Skin surface patterns and the directional mechanical properties of the dermis. In: Payne P, Marks R, editors. Bioengineering and the skin. Lancaster: MTP Press; 1981. p. 83–92.
Ferguson J. The structural and mechanical properties of human stratum corneum. Thesis University of Strathclyde, Glasgow; 1980.
Finlay AY, Frost P, Keith AD, et al. An assessment of factors influencing flexibility of human fingernails. Br J Dermatol. 1980;103:357–65.
Fluhr JW, Pfisterer S, Gloor M. Direct comparison of skin physiology in children and adults with bioengineering methods. Pediatr Dermatol. 2000;17:436–9.
Gfatter R, Hackl P, Braun F. Effects of soap and detergents on skin surface pH, stratum corneum hydration and fat content in infants. Dermatology. 1997;195:258–62.
Gilard V, Martino R, Malet-Martino M, Rivière M, Gournay A, Navarro R. Measurement of total water and bound water contents in human stratum corneum by in vitro proton nuclear magnetic resonance spectroscopy. Int J Cosmet Sci. 1998;20:117–25.
Gournay A, Navarro R, Mathieu J, Rivière M. Water retention of treated stratum corneum measured by a coupling method: thermal desorption-mass spectrometry. Int J Cosmet Sci. 1995;17:165–72.
Greger R. The formation of sweat. In: Greger R, Windhorst U, editors. Comprehensive human physiology, vol. 2. Berlin/Heidelberg/New York: Springer; 1996. Chap. 112.
Guittet C. Echographie haute-résolution et estimation du paramètre d'atténuation ultrasonore dans les tissus humains: application à la peau. Thèse en Sciences de la Vie et de la Santé, Université de Tours; 1997.
Hansen JR,Yellin W. NMR and Infra-red spectroscopic studies of Stratum Corneum hydration. In: Jellinek E, editor. Water structure and the water polymer interface. New York: Plenum; 1972.
Hensen TN, Sonoda Y, McIlroy MB. Transfer of oxygen, nitrogen, and carbon dioxide through normal adult human skin. J Appl Physiol. 1980;49:438–43.
Horii I, Nakayama Y, Obota M, Tagami H. Stratum corneum hydration and aminoa acid content in xerotic skin. Br J Dermatol. 1989;121:587–92.
Houdas Y, Guieu JD. La fonction thermique. Villeurbanne: Simep-Editions; 1977.
Hulsbergen Henning JP, Beerens EGJ, Van der Leun JC. A non-invasive microscopic method for measuring epidermal thickness in vivo. Arch Derm Res. 1977;258:25–32.
Inoue T, Tsujii K, Okamoto K, Toda K. Differential scanning calorimetric studies on the melting behaviour of water in Stratum Corneum. J Invest Dermatol. 1986; 86(6):689–93.
Jemec GBE, Serup J. Ultrasound structure of the human nail plate. Arch Dermatol. 1988;125:643–6.
Jemec GBE, Agner T, Serup J. Transonychial water loss: relation to sex, age and nail-plate thickness. Br J Dermatol. 1989;121:443–6.
Knüttel A, Boehlau-Godau M. Spatially confined and temporally resolved refractive index and scattering evaluation in human skin performed with optical coherence tomography. J Biomed Opt. 2000;5:83–92.
Koutroupi KS, Barbenel JC. Mechanical and failure behaviour of the stratum corneum. J Biomech. 1990;23: 281–87.
Krönauer C, Gfesser M, Ring J, Abeck D. Transonychial water loss in healthy and diseased nails. Acta Derm Venereol. 2001;81:175–7.
Lapière ChM, Nusgens BV, Pierard GE. The architectural organization and function of the macromolecules in the dermis. In: Marks RM, Barton SP, Edwards C, editors. The physical nature of the skin. Lancaster: MTP Press; 1988. p. 163–76.
Leveque JL. Water-keratin interactions. In: Elsner P, Berardesca E, Maibach HI, editors. Bioengineering

and the skin: water and the stratum corneum. Boca Raton: CRC Press; 1994. p. 13–22.
Leveque JL, Escoubez M, Rasseneur l. Water-keratin interaction in human Stratum Corneum. Bioeng Ski. 1987;3:227–42.
Lévêque JL, Poelman MC, de Rigal J, Kligman AM. Are corneocytes elastic? Dermatologica. 1988;76:65–9.
Liron Z, Wright RL, McDougal JN. Water diffusivity in porcine stratum corneum measured by a thermal gravimetric analysis technique. J Pharm Sci. 1994;83:457–62.
Manschot JFM, Brakkee AJM. The measurement and modelling of the mechanical properties of human skin in vivo: the model. J Biomechanics. 1986;19:517–21.
Marks R, Nicholls S, Fitzgeorge D. Measurement of intracorneal cohesion in man using in vivo techniques. J Invest Dermatol. 1972;69:299–302.
Marks R. The epidermal engine. A commentary on epidermopoiesis, desquamation and their interrelationships. Int J Cosmet Sci. 1986;8:134–44.
Mathot MA. La tension superficielle du sébum. Thèse Med Besançon, n°7669; 1976.
Mavon A. Energie libre de surface de la peau humaine, in vivo: une nouvelle approche de la séborrhée. Thèse Sciences de la Vie et de la Santé, Besançon, N°259706; 1997.
McMaster PD. The effects of venous obstruction upon interstitial pressure in animal and human skin. J Exp Med. 1946;84:495–509.
Öhman H, Vahlquist A. The pH gradient over the stratum corneum differs in X-linked recessive and autosomal dominant ichthyosis: a clue to the molecular origin of the "Acid Skin Mantle"? J Invest Dermatol. 1998;111:674–77.
Orentreich N, Markofsky J, Vogelman JH. The effect of aging on the rate of linear nail growth. J Invest Dermatol. 1979;73:120–30.
Panisset F, Varchon D, Agache P. Non invasive assessment of stratum corneum Young's modulus in vivo. In: XIVth International Congress on Biomechanics. Paris, 4–8 July, 1993., Congrès Annuel de Recherche Dermatologique, Nimes, 14–16 octohre 1993, et 10th International Symposium of Bioengineering and the Skin, Cincinnati, Ohio, June 13–15, 1994.
Piérard GE, Piérard-Franchimont C. Topical anti-acne drugs. Evaluation of sebum delivery by a combined photometric-multistep samplings with Sebutape. Clin Exp Dermatol. 1993;18:410–13.
Pirot F. Analyse, mesure et prédiction de la diffusion dans le stratum corneum humain. Thèse Sciences de la Vie et de la Santé, Besançon, 1996.
Potts RO, Francoeur ML. The influence of stratum corneum morphology on water permeability. J Invest Dermatol. 1991;96:495–9.
Querleux B. Imagerie et caractérisation de la peau in-vivo par échographie ultrasonore à haute résolution spatiale. In: Journées d'études "Interaction entre les ultrasons et les milieux biologiques," Université de Valenciennes; 1994 avril 6–8; 1994.
Rougier A, Lotte C, Maibach HI. In vivo relationship between percutaneous absorption and transepidermal water loss. In: Bronaugh RL, Maibach HI, editors. Topical absorption of dermatological products. New York: Marcel Dekker; 2002. p. 115–28.
Sato K, Kang WH, Sato F. Eccrine Sweat Glands. In: Goldsmith LA, editor. Physiology, biochemistry and molecular biology of the skin. 2nd ed. Oxford: Oxford University Press; 1991. p. 741–62.
Scheuplein RJ. Percutaneous absorption: theoretical aspects. In: Mauvais-Jarvis P, Vickers CF, Wepierre J, editors. Percutaneous absorption of steroids. London: Academic; 1980. p. 1–17.
Scheuplein RJ, Bronaugh RJ. Percutaneous absorption. In: Goldsmith LA, editor. Biochemistry and biology of the skin. Oxford: Oxford University Press; 1983. p. 1255–95.
Schwindt DA, Wilhelm KK, Maibach HI. Water diffusion characteristics of human stratum corneum at different anatomical sites in vivo. J Invest Dermatol. 1998;111:385–89.
Sejrsen P. Blood flow in cutaneous tissue in man studied by washout of xenon-133. Circ Res. 1969;25:215–29.
Severinghaus JW, Stafford M, Thunstrom AM. Estimation of skin metabolism and blood flow with tcpO2 and tcpCO2 electrodes by cuff occlusion. Acta Anaesth Scand. 1978;Suppl. 68;9–15.
Shelley WB, Hurley HJ, Jr. The physiology of the human axillary apocrine sweat gland. J Invest Dermatol. 1953:20; 285.
Takahashi M, Kawasaki K, Tanaka M, Ohta S, Tsuda Y. The mechanism of stratum corneum plasticization with water. In: Marks R, Payne PA, editors. Bioengineering and the skin. Lancaster: MTM Press; 1981. p. 67–76.
Takenouchi M, Suzuki H, Tagami H. Hydration characteristics of pathologic stratum corneum. Evaluation of bound water. J Invest Dermatol. 1986;87:574–6.
Tokumura F, Ohyama K, Fujisawa H, Nukatsuka H. Seasonal variation in adhesive tape stripping of the skin. Skin Res Technol. 1999;5:208–12.
Torp S, Arridge R, Armenades C, Bare E. Structure properties relationships in tendon as a function of age. In: Atkins E, Keller A, editors. Structure of fibrous polymers. London: Butterworth; 1975.
Tosti A, Compagno G, Fazzini ML, Villardita S. A ballistometer for the study of the plastoelastic properties of skin. J Invest Dermatol. 1977;69:315–17.
Vasselet R, Agache P. Perspectives de modélisation des propriétés mécaniques de la peau humaine in vivo. In: Vasselet R, editor. Étude in vitro des propriétés mécaniques du stratum corneum humain à partir des essais de traction-relaxation et fluage: identification de son comportement viscoélastique à un modèle rhéologique non linéaire avec écrouissage. Besançon: Thèse Sciences pour l'Ingénieur; 1987. p. 213–33.
Vasselet R. Etude mécanique du stratum corneum humain in vitro [thesis]. France: University of Besançon; 1989.

Versmold HT, Tooley WH, Severinghaus JW. Increase of skin O2 diffusion resistance with birthweight. Birth Defects Orig Artic Ser. 1979;XV(4):271–72. The National Foundation.

Walkley K. Bound water in Stratum Corneum measured by differential scanning calorimetry. J Invest Dermatol. 1972:59;225–27.

Warner RR, Lilly NA. Correlation of water content with ultrastructure in the stratum corneum. In: Elsner P, Berardesca E, Maibach HI, editors. Bioengineering of the skin: water and the stratum corneum. Boca Raton: CRC Press; 1994. p. 3–12.

Weigand DA, Haygood C, Gaylor JR. Cell layers and density of Negro and Caucasian stratum corneum. J Invest Dermatol. 1974;62:563–86.

Wijn PFF, Brakkee AJM, Kuiper JP, Vendrik AJH. The alinear viscoelastic properties of human skin in vivo related to sex and age. In: Marks R, Payne PA, editors. Bioengineering and the skin. Lancaster: MTP Press; 1981. pp. 135–46.

Wilson DR, Maibach, HI. Transepidermal water loss: A review. In: Cutaneous investigation in health and disease: Noninvasive methods and instrumentation, Chapter 6. In: Lévêque JL, editor. New York: Marcel Dekker; 1989. p. 113–33.

Wu MS, Yee DJ, Sullivan ME. Effect of a skin moisturizer on the water distribution in human stratum corneum. J Invest Dermatol. 1983;81:446–8.

Yamamoto T, Yamamoto Y. Electrical properties of the epidermal stratum corneum. Med Biol Eng. 1976;14:151–8 (fig 8).

Yosipovitch G, Xiong GL, Haus E, Sackett-Lundeen L, Ashkenazi I, Maibach HI. Time-dependent variations of the skin barrier function in humans: transepidermal water loss, stratum corneum hydration, skin surface pH, and skin temperature. J Invest Dermatol. 1998; 110:20–3.

Yosipovitch G, Maayan-Metzger A, Merlob P, Sirota L. Skin barrier properties in different body areas in neonates. Pediatrics. 2000;106:105–8.

Yosipovitch G, Kaplan I, Calderon S, David M, Chan YH, Weiinberger A. Distribution of mucosal pH on the bucca, tongue, lips and palate: a study in healthy volunteers and patients with lichen planus, Behcet's disease and Burning Mouth syndrome. Acta Derm Venereol. 2001;81:178–80.

Zesch A, Nordhaus R, Schaefer H. Zur Kontrolle des Hornschichtabrisses durch Widerstandsmessungen. Arch Dermatol Forsch. 1972;242:398–402.

Zlotogorski A. Distribution of skin surface pH on the forehead and cheek of adults. Arch Dermatol Res. 1987;279:398–401.

Zviak C, Dawber RPR. Structure, fonctions et propriétés physico-chimiques du cheveu. In: Zviak C, editor. Science des traitements capillaires. Paris: Masson; 1988. p. 1–47.

Physical, Biological and General Constants of the Skin

158

Pierre Agache

Contents

Keywords

Acoustic constants • Biological constants • Blood density • Plasma density • Energy • Optic constants • Thermal constants • Thermal neutrality

Avogadro number	6.06×10^{23}	
Absolute temperature (K)	°C + 273	
Gravitational constant	$g = 9.806\ m\ s^{-2}$ at altitude zero and latitude 45°	
(Usual figure	$g = 9.81\ m\ s^{-2}$)	
Water surface tension	72.8 dyn/cm	
Water dielectric constant	≈80	
Water diffusion coefficient		
Water into itself	$3 \times 10^{-5}\ cm^2\ s^{-1}$	▶ Chap. 105, "Skin Barrier Function," Rutter et al. (1979)
Water vapor into air	$670\ g\ m^{-1}\ h^{-1}\ Pa^{-1}$	▶ Chap. 105, "Skin Barrier Function," Schwindt et al. (1998)
Oxygen solubility in water		▶ Chap. 58, "Transcutaneous Oxygen Pressure," Severinghaus et al. (1978)

(*continued*)

This chapter was originally published under the ISBN 978-3-540-01771-4 with the following book title Measuring the Skin. The content has not been changed.

Pierre Agache: deceased.

P. Agache (✉)
Department of Dermatology, University Hospital of Besançon, Besançon, France
e-mail: aude.agache@free.fr; ferial.fanian@chu-besancon.fr; ferial.fanian@cert-besancon.com

P. Humbert et al. (eds.), *Agache's Measuring the Skin*, DOI 10.1007/978-3-319-32383-1_158

At 37 °C	31.3 10^{-6} ml g^{-1} $Torr^{-1}$	
At 44 °C	28.8 10^{-6} ml g^{-1} $Torr^{-1}$	

1 Energy

Metabolic rate (basal) (= minimal energy production)	~50 Wm^{-2} ▶ Chap. 119, "Thermal Exchanges in Man"
Metabolic rate (resting)	59 Wm^{-2}
Oxygen originated energy (for a respiratory quotient 0.84)	5.6 Wl^{-1}
Oxygen thermal coefficient (for a respiratory quotient 0.84)	20.27 kJl^{-1} ▶ Chap. 58, "Transcutaneous Oxygen Pressure," Houdasy et al. (1977)

2 Thermal Constants

Thermal conductivity	Wm^{-1} °C^{-1}
Air	25 × 10^{-3}
Free water	624 × 10^{-3} at 37 °C[a]
Protein-bound water	180 × 10^{-3}
Thermal inertia (KDC)	cal^2 cm^{-4} °C^{-2} s^{-1}
Human tissues (with respect to temperature)	
Muscle	56 × 10^{-5} to 113 × 10^{-5}
Bone	44 × 10^{-5} to 68 × 10^{-5}
Materials	
Concrete	170 × 10^{-5}
Oak	13 × 10^{-5}
Steel	9 × 10^{-1}
Blood specific heat capacity	3.64 J °$C^{-1}g^{-1}$

[a] ▶ Chap. 2, "Measurements of the Human Skin: Why and How?," Sect. 2.3

Thermal neutrality: subject naked in a room in which air and walls have the same temperature, close to 30 °C, relative humidity is below 50 %, and where air is barely in motion (0.1–0.2 m/s)

Saturating water pressure with respect to temperature (under 760 Torr atmospheric pressure) (Houdas and Guieu 1977): for given outside relative humidity (RH_{ext}), outside temperature (T_{ext}) and room temperature (T_{int}), the room relative humidity (RH_{int}) is calculated as follows: $RH_{int} = RH_{ext} \times Psat_{ext}/Psat_{int}$, where $Psat_{ext}$ is the outside saturating water pressure, and $Psat_{int}$ is the room saturating water pressure.

Example: If RH_{ext} = 30 %, Text = 9 °C, and T_{int} = 21 °C, then $HR_{int} = 30 \times 8.65/18.71 = 13.9$

Temperature (°C)	Saturating pressure (torr)	Temperature (°C)	Saturating pressure (torr)
−10	2.16	31	33.76
−9	2.34	32	35.72
−8	2.52	33	37.79
−7	2.73	34	39.95
−6	2.94	35	42.23
−5	3.17	36	44.61
−4	3.42	37	47.12
−3	3.68	38	49.75
−2	3.96	39	52.50
−1	4.26	40	55.38
0	4.58	41	58.40
1	4.96	42	61.55
2	5.33	43	64.86
3	5.72	44	68.31
4	6.14	45	71.92
5	6.58	46	75.69
6	7.05	47	79.64
7	7.55	48	83.76
8	8.09	49	88.06
9	8.65	50	92.55
10	9.25	51	97.23
11	9.89	52	102.12
12	10.56	53	107.22
13	11.28	54	112.53
14	12.03	55	118.07
15	12.84	56	123.84
16	13.68	57	129.85
17	14.58	58	136.11
18	15.53	59	142.62
19	16.53		
20	17.59		
21	18.71		
22	19.88		
23	21.13		
24	22.43		
25	23.81		
26	25.27		
27	26.80		
28	28.42		

(*continued*)

Temperature (°C)	Saturating pressure (torr)	Temperature (°C)	Saturating pressure (torr)
29	30.12		
30	31.89		

3 Acoustic Constants

Ultrasound (25 MHz) velocity in water	1480 m s^{-1}
Ultrasound (25 MHz) acoustic impedance in water	1.48 Rayleigh ▶ Chap. 157, "Main Skin Physical Constants," Edwards et al. (1984)

4 Optic Constants

Stefan Bolzmann universal radiation constant	$\Phi = 5.6710^{-8}$ $Wm^{-2}K^{4}$
Refraction indexes	
Air	1.00
Glycerol	1.54
Acetic acid	1.54
Water	1.33
Irradiance: midday mean solar UV-A in summer (mediterranean countries)	3.5 mW cm^{-2}

Solar energy reaching the ground (normalized to equator):

Town	21 June	Equinox	21 December
Besançon	91.5	68.0	33.5
Nice	93.9	72.6	39.6
Casablanca	98.4	83.5	55.0

Solar energy reaching the ground (normalized to a blue sky):

	Blue "milky" sky	Cirrhus	Stratus	Stratocumulus
UVB	100	100	80	40
UVA	100	100	80	40
visible	100	95	80	30
IR	95	80	60	10

(*continued*)

Light reflection	
Snow	85 %
Sand and light colored soil or walls	17 %
Water	5 %
Grass	3 %
Absorption peaks	
Hb	415, 553 nm
HbO_2	415, 543 and 577 nm
Light wavelengths seen by the human eye	560, 530, 420 nm (orange, green, blue, respectively)

Infrared main absorption bands

Wavelength		Stretched bonds	Measured substance	Reference
μm	cm^{-1}			
9.65	1036	OH	Water	
8.94	1118		Protein	
6.47	1545 (amide II)	C-N	Protein	
6.10	1640	OH	Water	
6.08	1645 (amide I)	C═O	Protein	
5.85	1710	C═O	Free fatty acids	Brancaleon et al. (2001)
5.75	1740	C═O	Fatty acids esters	Brancaleon et al. (2001)
4.76	2101	OH	Water	
4.3	2326	CO_2	Carbon dioxide	Thiele and Van Kempen (1972)
3.42	2920	CH_2 asymmetrical	Lipids	Brancaleon et al. (2001)
3.51	2850	CH_2 symmetrical	Lipids	Brancaleon et al. (2001)
3.03	3300	OH	Water	Brancaleon et al. (2001)
1.95	5128	OH	Water	

5 Biological Constants

Blood density	1.058–1.062
Plasma density	1.025–1.027
Plasma osmolality	302–308 mOsm l^{-1}
Plasma cryoscopic delta	−0.56 to −0.57 °C
Blood pH	7.38
Plasma composition	
Na + (mM)	140
K+ (mM)	4–5
Cl − (mM)	103
CO_3H- (mM)	20–25
Ammonia (mM)	0.025–0.16
Lactates (mM)	<2
Urea (mg ml^{-1})	0.15–0.25
Glucose (:g ml^{-1})	700–1000
Proteins (mg ml^{-1})	70–80
Triglycerides density	0.92

References

Brancaleon L, Bamberg MP, Sakamaki T, Kollias N. Attenuated total reflection-Fourier transform infrared spectroscopy as a possible method to investigate biophysical parameters of stratum corneum in vivo. J Invest Dermatol. 2001;116:380–6.

Houdas Y, Guieu JD. La fonction thermique. Villeurbanne: Simep Editions; 1977.

Thiele FAJ, Van Kempen LHJ. A micro method for measuring the carbon dioxide release by small skin areas. Br J Dermatol. 1972;86:463–71.

Pressure Units of the Skin

159

Pierre Agache

Keywords

Pressure units • Bar • torr • MSW (metres sea water) • Atmosphere • Pascal

Presently or formerly popular pressure units include the following:

- Atmosphere (atm)
- Manometric units:
  - Centimeter, inch, millimeter (Torr) and micrometer (mTorr, micron) of mercury
  - Height of equivalent column of water, including millimetre (mm H2O), centimetre (cm H2O), metre, inch, and foot of water
- Imperial and customary units:
  - Kip, short ton-force, long ton-force, pound-force, ounce-force, and poundal per square inch
  - Short ton-force and long ton-force per square inch
  - FSW (feet sea water) used in underwater diving, particularly in connection with diving pressure exposure and decompression
- Non-SI metric units:
  - Bar, decibar, millibar
- MSW (meters sea water), used in underwater diving, particularly in connection with diving pressure exposure and decompression
  - Kilogram-force, or kilopond, per square centimeter (technical atmosphere)
  - Gram-force and tonne-force (metric ton-force) per square centimeter
  - Barye (dyne per square centimetre)
  - Kilogram-force and tonne-force per square meter
  - Sthene per square metre (pieze)

This chapter provides the correspondence between different standard pressure units.

The table should be read from left to right (Table 1). Example: 1 cm H_2o is equal to 0.7356 torr and equal to 10^{-3} kg-force cm^{-2}

This chapter was originally published under the ISBN 978-3-540-01771-4 with the following book title Measuring the Skin. The content has not been changed.

Pierre Agache: deceased.

P. Agache (✉)
Department of Dermatology, University Hospital of Besançon, Besançon, France
e-mail: aude.agache@free.fr; ferial.fanian@chu-besancon.fr; ferial.fanian@cert-besancon.com

P. Humbert et al. (eds.), *Agache's Measuring the Skin*,
DOI 10.1007/978-3-319-32383-1_159

Table 1 Correspondance between different pressure units

	Pascal (MKSA)	Bar (CGS) = 10^6 barye	torr (mm Hg)	cm H_2O	kg-force/cm^2	Atmosphere
1 Pascal=	1	10^{-5}	7.498×10^{-3}	10.19×10^{-3}	1.020×10^{-5}	9.865×10^{-6}
1 bar=	10^5	1	749.8	1.019×103	1.020	0.9865
1 torr=	133.4	1.334×10^{-3}	1	1.359	1.358×10^{-3}	1.316×10^{-3}
1 cm H_2O=	98.11	98.11×10^{-5}	0.7356	1	10^{-3}	9.679×10^{-4}
1 kg-force cm^{-2}=	9.807×10^4	0.9807	736.4	10^3	1	9.686
1 atm=	10.13×10^4	1.013	760	1.033×10^3	1.032	1

Correspondence Between International System Units (MKSA) and CGS Units

160

Pierre Agache

Keywords
International System of Units- MKS system • CGS system

This chapter was originally published under the ISBN 978-3-540-01771-4 with the following book title Measuring the Skin. The content has not been changed.

Pierre Agache: deceased.

P. Agache (✉)
Department of Dermatology, University Hospital of Besançon, Besançon, France
e-mail: aude.agache@free.fr;
ferial.fanian@chu-besancon.fr;
ferial.fanian@cert-besancon.com

P. Humbert et al. (eds.), *Agache's Measuring the Skin*,
DOI 10.1007/978-3-319-32383-1_160

Correspondence between international system units (MKSA) and CGS units

Physical quantity	MKSA system	Ratio MKSA/CGS	CGS system
Length	Meter (m)	$=10^2$	Centimeter (cm)
Mass	Kilogram (kg)	$=10^3$	Gram (g)
Time	Second (s)	$=1$	Second (s)
Electric current	Ampere (A)	$=1$	Ampere (A)
Surface	m^2	$=10^4$	cm^2
Volume	m^3	$=10^6$	cm^3
Mass density	kg m^{-3}	$=10^{-3}$	g cm^{-3}
Speed	m s^{-1}	$=10^2$	cm s^{-1}
Acceleration	m s^{-2}	$= 10^2$	cm s^{-2}
Force	Newton (N) = kg m s^{-2}	$=10^5$	dyne = g cm s^{-2}
Work	Joule (J) = N m	$=10^7$	erg = dyne cm
Power	Watt (W) = J s^{-1}	$=10^7$	erg s^{-1}
Pressure	Pascal (Pa) = N m^{-2}	$=10$	Barye = dyne cm^{-2}
Surface tension	N m^{-1}	$=10^3$	dyne cm^{-1}
Torque moment	N m	$=10^7$	dyne cm
Viscosity	Poiseuille = kg m^{-1} s^{-1}	$=10$	Poise = g cm^{-1} s^{-1}

1 kg force (=1 kg weight) = 10^3 g force = 9,81 N. It is the *force* exerted by gravity (9,81 m s^{-2}) on a 1 kg mass

Index

P. Humbert et al. (eds.), *Agache's Measuring the Skin*,
DOI 10.1007/978-3-319-32383-1